The interaction of Bromophenol Blue with proteins in acidic solution

Yong-ju Wei, Ke-an Li *, Shen-yang Tong

Department of Chemistry, Peking University, Beijing 100871, China

Received 31 March 1995; revised 23 June 1995; accepted 6 July 1995

Abstract

The interactions of Bromophenol Blue (BPB) with bovine serum albumin and γ-globulin in acidic solutions were investigated by a spectrophotometric method. It was considered that the electrostatic force is the main binding force, and that the color change during the combination is due to the transformation of dye species of free acidic form into bound basic form as well as to the bathochromic and hyperchromic effects of conjugation. The formation of an isosbestic point in the absorption spectra was explained based on a new consideration about the solution equilibria. Two conditional constants, apparent binding constant and maximum binding number, were defined to express the binding ability of a dye to a certain protein under a given set of conditions, and two linear regression equations were derived to determine these two parameters and the molar absorptivity of bound dye. The Scatchard model is not appropriate in the treatment of data obtained here. The factors which influence the sensitivity of a dye binding protein assay were discussed, and the Sandell index was used to express the sensitivity of protein detection. It was found that sodium chloride concentration and acidity of the solutions have significant effect on the sensitivity of BPB protein assay.

Keywords: Bromophenol Blue; Bovine serum albumin; γ-Globulin; Acidic solutions

1. Introduction

Dye binding protein assays are commonly used in biochemical and clinical laboratories, but they are not well understood at the molecular level. A further theoretical study on this kind of reaction should be benficial not only with regard to the

quantitation of proteins but also to a deep understanding of the interaction between proteins and small ions or molecules.

Scatchard et al. [1] treated the reaction of small ions with albumin as a true combination of the ligand with specific sites on the macromolecule. Since then, this model has been widely used to describe this kind of reaction. However, Pesavento and Profumo [2] reported that the Scatchard model was not appropriate for the

* Corresponding author.

treatment of data obtained in the study of the combination of T-azo-R with bovine serum albumin (BSA) in acidic solutions. They considered that there were no evident specific combination sites on the BSA molecule, and proposed a two-phase distribution model to interpret their experimental findings. Congdon et al. [3] recently employed a modified Scathard equation and Hill equation to study the high-affinity dye binding sites of the interaction between Coomassie Brilliant Blue and proteins at high protein/dye concentration ratios, but they failed in their attempt to use these equations to estimate the total number of dye binding sites under normal conditions. Therefore, the question of whether the Scatchard model is suitable for the description of dye binding reactions still remains unanswered.

In this paper, a new attempt is made to interpret the interaction of Bromophenol Blue (BPB) with proteins [4,5]. BPB has been used as a staining reagent in the determination of urinary proteins [6,7], yet no theoretical study on its staining reaction has been found in the literature. It will be shown that the BPB–protein binding reaction can be successfully treated by using a new method proposed in this paper, and that the Scatchard plot obtained here is completely different from that expected.

2 Experimental

2.1. Reagents

BSA 99%, was obtained from Sigma and used without further purification. All calculations reported by BSA are in terms of a molecular weight of 65 000. The aqueous BSA solution $(2.0 \times 10^{-5} \, \text{mol} \, l^{-1})$ was prepared by dissolving 0.262 g BSA reagent in 200 ml deionized water. γ-Globulin Human (γ-G) was obtained from Serva (Germany). Calculations reported for γ-G are in terms of a molecular weight of 160 000. The aqueous γ-G solution $(6.25 \times 10^{-6} \, \text{mol} \, l^{-1})$ was prepared by solving 0.100 g γ-G reagent in 100 ml deionized water. BPB was purchased from BDH and purified by recrystallization from boiling glacial acetic acid [8]. The BPB stock solution

$(1.5 \times 10^{-3} \, \text{mol} \, l^{-1})$ was prepared by dissolving 0.100 g purified dye in 20 ml 95% ethanol, and then diluting it to 100 ml with water. The operating solution of BPB was prepared by diluting the stock solution with water. Britton–Robinson buffer was prepared by adding a given amount of $0.2 \, \text{mol} \, l^{-1}$ NaOH to 100 ml of mixed-acid solution containing phosphoric acid, acetic acid, and boric acid each with a concentration of $0.04 \, \text{mol} \, l^{-1}$. All other reagents were of analytical or guaranteed reagent grade.

2.2. Apparatus

A Shimadzu Model UV-265 double-beam spectrophotometer was used for recording absorption spectra, and a Shimadzu UV-120-02 spectrophotometer for the measurement of absorbance at a given wavelength. A Model 821 pH/mV meter (Zhongshan University, China) was used for the pH measurements.

2.3. Method

Aliquots of 5% NaCl solution, pH buffer or HCl solution, and BPB operating solution were transferred into a series of 25 ml volumetric flasks, and then protein solution was added to each flask in different amounts. The mixtures were diluted to the mark with water and mixed thoroughly. After 20 min [4–7], spectra or absorbances of these solutions were measured with reference to water.

3. Results and discussion

3.1. Absorption spectra and binding mechanism

Fig. 1 shows the absorption spectrum of BPB. It was obtained by keeping the BPB concentration constant and changing the pH of the solutions. In Fig. 1, two absorption peaks appear at 435 nm and 591 nm. A well-defined isosbestic point is observed at 494 nm. This spectral feature corresponds to the proton dissociation of BPB:
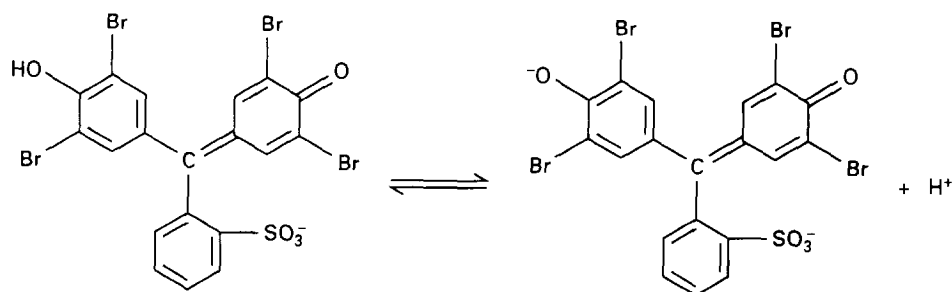
and its dissociation constant is $pK_a = 3.85$.

For simplicity, the above equation can be written as

$$HL^- \rightleftharpoons L^{2-} + H^+ \qquad (1)$$

Fig. 2 shows the absorption spectra of BPB–BSA mixtures. They were obtained by keeping the BPB concentration and pH constant and increasing the BSA concentration. With the increase in BSA concentration, the absorption peak at 591 nm increases strikingly and shifts to 604 nm, while the absorption peak at 435 nm decreases and shifts to 440 nm. An isosbestic point is formed at 502 nm. Fig. 2 indicates that there are interactions between BPB and BSA.

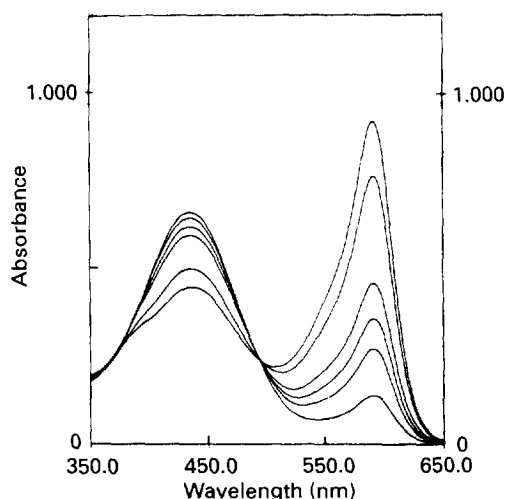In view of the molecular structure of BPB and BSA, it is not possible to reach a conclusion that

BPB combines preferentially with a particular group on BSA to form a complex. Compton and Jones [9] suggested that the binding of Coomassie Brilliant Blue G-250 on protein is a result of Van der Waals forces and hydrophobic interactions. This mechanism is not convincing in this study, because the hydrophobic groups on the BPB molecule were not predominant compared with the hydrophilic groups, although the Van der
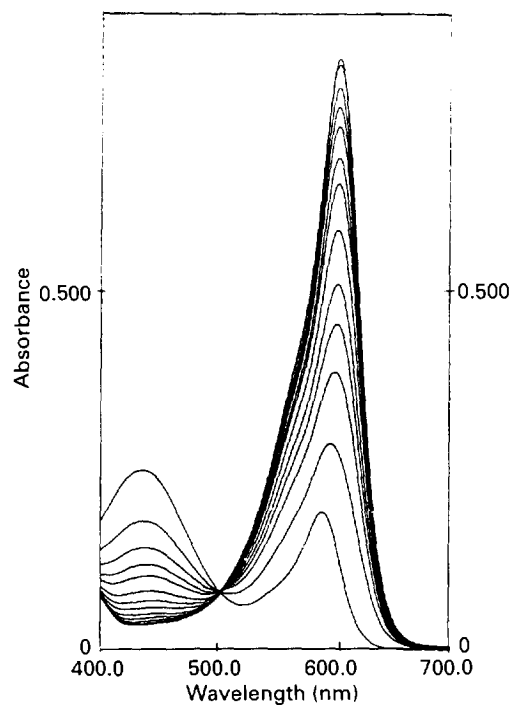

Fig. 1. BPB absorption spectra at various pH values. BPB concentration constant at 3.01×10^{-5} mol l^{-1}. In order of increasing peak absorbances at 591 nm. pH values are 2.67, 2.98, 3.12, 3.28, 3.56 and 3.72.

Fig. 2. Absorption spectra of BPB–BSA mixtures. BPB concentration constant at 1.2×10^{-5} mol l^{-1}, pH 3.28, 0.5% NaCl. In order of increasing peak absorbances at 600 nm, BSA concentrations are 0.0, 4.0×10^{-7}, 8.0×10^{-7}, 1.2×10^{-6}, 1.6×10^{-6}, 2.4×10^{-6}, 3.2×10^{-6}, 4.0×10^{-6}, 5.2×10^{-6}, 6.4×10^{-6}, 8.0×10^{-6}, 1.2×10^{-5} and 1.36×10^{-5} mol l^{-1}.

Waals forces and hydrophobic interactions may play a part in the binding process. A reasonable explanation of these molecular events is that BPB interacts with BSA by non-specific, electrostatic forces [2,4,5,10]. Under the conditions of Fig. 2, the pH (3.28) is lower than the isoelectric point of BSA ($pI = 4.8$). Lysine, arginine and other amino acid residues on the BSA molecular chain are in the protonated form and therefore the whole BSA molecules are positively charged. However, the BPB species, HL^- and L^{2-}, have negative charge. Therefore, BSA and BPB species should be bound together by electrostatic forces:

$$L^{2-} + P^+ \rightleftharpoons L' \qquad (2)$$

$$HL^- + P^+ \rightleftharpoons HL' \qquad (3)$$

where P^+ represents the non-specific binding sites on protein, and the primed symbols, L' and HL', refer to bound L^{2-} and HL^- respectively. Since L^{2-} has more negative charges than HL^-, it takes priority in binding to protein. As the free L^{2-} species is used up in the binding process, equilibrium (1) shifts to the right to restore the concentration of L^{2-}, thereby resulting in an increase of absorbance in the vicinity of 600 nm. However, as BSA is in the positively charged state, the bound HL^- should more easily lose H^+ than free HL^-:

$$HL' \rightleftharpoons L' + H^+ \qquad (4)$$

This reaction also results in an increase of absorbance in the vicinity of 600 nm.

Considering all the four possible reactions in the binding process, the overall solution equilibria may be expressed as

$$HL^- \rightleftharpoons L^{2-} + H^+$$
$$P^+ \,\big\updownarrow \quad P^+ \,\big\updownarrow \qquad\qquad (5)$$
$$HL' \rightleftharpoons L' + H^+$$
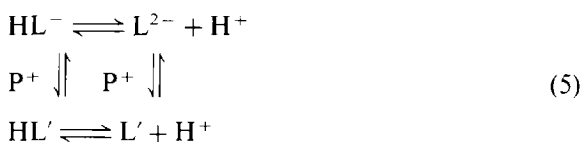
There are two paths to carry the binding process through according to this equilibria model: either the free HL^- first dissociates its H^+ and then binds to BSA; or else it first binds to BSA and then dissociates H^+. Both paths have the same final state and therefore the same free energy change, so both paths have no difference in terms

of thermodynamics. Adding Eq. (1) to Eq. (2) or adding Eq. (3) to Eq. (4) gives the same total reaction equation

$$HL^- + P^+ \rightleftharpoons L' + H^+ \qquad (6)$$
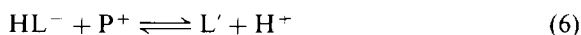
An increase in BSA concentration will shift equilibrium (6) from the left to the right, causing spectral changes as can be seen in Fig. 2.

The red shift and hyperchromic effect observed in Fig. 2 can be explained by the conjugation theory [3]. Binding of dye to lysine and arginine side-chains may allow donation of electrons by an auxochromic amino or guanidino group to the π electron system, thereby increasing the degree of conjugation and lowering the energy of a π^* state of the dye. Such electron donation provides an explanation for the hyperchromicity, while the lower-energy excited state explains the bathochromicity.

3.2. Explanation of the formation of the isosbestic point

The formation of an isosbestic point in Fig. 1 is due to the transformation of two BPB color species from one into another [11]. In the conditions of Fig. 2, however, there are four color species in solution according to the equilibrium model (5). The existing theory [11] cannot give an explanation in this case. In the following discussion, an attempt will be made to give an interpretation for the formation of the isosbestic point in Fig. 2. This discussion will also lead to a new method for the treatment of dye binding reactions.

Define $\{L\}$ as the total concentration of free BPB, $\{L'\}$ as the total concentration of bound BPB, and c_L as the analytical concentration of BPB, that is (omitting electrical charges):

$$\{L\} = [HL] + [L] \qquad (7)$$

$$\{L'\} = [HL'] + [L'] \qquad (8)$$

$$c_L = \{L\} + \{L'\} \qquad (9)$$

The absorbance of the dye–protein mixtures is (with a 1 cm cell)

$$A = \varepsilon_{HL}[HL] + \varepsilon_L[L] + \varepsilon_{HL'}[HL'] + \varepsilon_{L'}[L'] \qquad (10)$$

where ε_{HL}, ε_L, $\varepsilon_{HL'}$ and $\varepsilon_{L'}$ are molar absorptivities of HL, L, HL', and L' respectively. Define distribution coefficients as

$$\delta_{HL} = [HL]/\{L\} \tag{11}$$

$$\delta_L = [L]/\{L\} \tag{12}$$

$$\delta_{HL'} = [HL']/\{L'\} \tag{13}$$

$$\delta_{L'} = [L']/\{L'\} \tag{14}$$

Substitution of Eq. (7) into Eq. (11) gives:

$$\delta_{HL} = [HL]/([HL] + [L])$$
$$= [HL]/([HL] + k_a[HL]/[H]) = [H]/([H] + k_a) \tag{15}$$

Similar substitution leads to

$$\delta_L = k_a/([H] + k_a) \tag{16}$$

$$\delta_{HL'} = [H]/([H] + k_a') \tag{17}$$

$$\delta_{L'} = k_a'/([H] + k_a') \tag{18}$$

where k_a and k_a' are the dissocation constants of HL and HL':

$$k_a = [H][L]/[HL] \tag{19}$$

$$k_a' = [H][L']/[HL'] \tag{20}$$

k_a' is an unknown constant. Note that distribution coefficients are merely the functions of pH and are independent of BSA concentration.

Substituting Eqs. (11–14) into Eq. (10) yields

$$A = (\varepsilon_{HL}\delta_{HL} + \varepsilon_L\delta_L)\{L\} + (\varepsilon_{HL'}\delta_{HL'} + \varepsilon_{L'}\delta_{L'})\{L'\} \tag{21}$$

Let

$$\varepsilon = \varepsilon_{HL}\delta_{HL} + \varepsilon_L\delta_L \tag{22}$$

$$\varepsilon' = \varepsilon_{HL'}\delta_{HL'} + \varepsilon_{L'}\delta_{L'} \tag{23}$$

where ε and ε' are the mean molar absorptivities of free and bound dye $(mol^{-1} l\,cm^{-1})$ respectively. They are constants when pH and measuring wavelength are given. So Eq. (21) may be simplified as

$$A = \varepsilon\{L\} + \varepsilon'\{L'\} = \varepsilon c_L + (\varepsilon' - \varepsilon)\{L'\} \tag{24}$$

If $\varepsilon' = \varepsilon$ at a certain wavelength (502 nm in Fig. 2), Eq. (24) becomes $A = \varepsilon c_L$, which is a constant,

unchanging with increase of BSA concentration, and so the isosbestic point appears.

3.3. A new method for the treatment of the dye binding reaction

Apparent binding constant

According to Eq. (6), the equilibrium constant of the total binding reaction should be

$$K = [L'][H]/[HL][P] \tag{25}$$

where [P] represents the concentration of unoccupied binding sites on protein

$$[P] = Nc_P - \{L'\} = (N - \bar{n})c_P \tag{26}$$

where c_P is the anlaytical concentration of protein, N the total number of binding sites per protein molecule (it is an unknown constant, since there are 60 lysines, 26 arginines, and other aromatic amino acids on BSA molecule, the total number of binding sites on BSA should be more than 86) [12], $\bar{n}$ the average binding number of die molecules per protein molecule (see Eq. (36)). If $\bar{n}$ can be omitted when compared with N (see Table 1), then Eq. (26) may be written approximately as

$$[P] = Nc_P \tag{27}$$

This approximation leads to an easy mathematical treatment, and it holds under normal conditions.

From Eqs. (11–14), we have $[HL] = \delta_{HL}\{L\}$, and $[L'] = \delta_{L'}\{L'\}$. Substituting these two equations and Eq. (27) into Eq. (25) gives

$$K = \delta_{L'}\{L'\}[H]/\delta_{HL}\{L\}Nc_P \tag{28}$$

If [H] (or pH) has been given (as in Fig. 2), then $\delta_{L'}$, δ_{HL}, and N have fixed values. Thus, we can define a new constant:

$$K_c = NK\delta_{HL}/\delta_{L'}[H] = \{L'\}/\{L\}c_P \tag{29}$$

K_c is a conditional constant. It is a measure of the dye binding ability of a protein under certain conditions. Similar to the apparent stability constant used in the treatment of complexation equilibria, we call K_c the apparent binding constant.

Theoretically, K_c is a constant when experimental conditions are given; it has been proved by experiment that K_c is indeed a constant under certain conditions (see Table 1).

Table 1
Data used for linear regressions. $c_P \sim \Delta A$ data were obtained from Fig. 2. $c_L = 1.2 \times 10^{-5}\,\text{mol}\,l^{-1}$, pH = 3.28, 0.5% NaCl, $\Delta A_{max} = 0.804$ at 605 nm

c_P (mol l^{-1})	ΔA	$\Delta A/c_P$	$\bar{n}$	$\bar{n}c_P$	$\bar{n}/\{L\}$	$\log K_c$
0.4×10^{-6}	0.144	3.60×10^5	5.38	2.15×10^{-6}	5.46×10^5	5.737
0.8×10^{-6}	0.254	3.18×10^5	4.75	3.80×10^{-6}	5.79×10^5	5.763
1.2×10^{-6}	0.322	2.68×10^5	4.01	4.81×10^{-6}	5.58×10^5	5.747
1.6×10^{-6}	0.378	2.36×10^5	3.53	5.65×10^{-6}	5.56×10^5	5.745
2.4×10^{-6}	0.456	1.90×10^5	2.84	6.82×10^{-6}	5.48×10^5	5.739
3.2×10^{-6}	0.520	1.63×10^5	2.43	7.77×10^{-6}	5.74×10^5	5.759
4.0×10^{-6}	0.556	1.39×10^5	2.08	8.31×10^{-6}	5.64×10^5	5.751
5.2×10^{-6}	0.598	1.15×10^5	1.72	8.94×10^{-6}	5.62×10^5	5.750
6.4×10^{-6}	0.628	9.81×10^4	1.47	9.39×10^{-6}	5.63×10^5	5.751
8.0×10^{-6}	0.654	8.18×10^4	1.22	9.78×10^{-6}	5.50×10^5	5.740

Determination of apparent binding constant

A method for the determination of the apparent binding constant K_c may be developed from Eq. (24). Rearranging Eq. (24) yields

$$\{L'\} = (A - \varepsilon c_L)/(\varepsilon' - \varepsilon) \qquad (30)$$

where A is the absorbance of dye–protein mixtures, and εc_L the absorbance of a zero-protein solution. Both A and εc_L can be measured. Let

$$\Delta A = A - \varepsilon c_L \qquad (31)$$

$$\Delta \varepsilon = \varepsilon' - \varepsilon \qquad (32)$$

then Eq. (30) may be simplified as

$$\{L'\} = \Delta A/\Delta \varepsilon \qquad (33)$$

If ε' and ε are determined previously from the absorbance of solutions with an excess of BSA and without BSA, then $\Delta \varepsilon$ is a known quantity. Therefore $\{L'\}$ can be calculated according to Eq. (33). Furthermore, since $\{L\} = c_L - \{L'\}$, K_c may be calculated directly by using Eq. (29).

The above method for the determination of K_c is simple in principle but inconvenient in use, because the values of ε' and ε have to be determined in advance. For this reason the following linear regression method was developed.

Substituting Eq. (33) and Eq. (9) into Eq. (29) gives

$$K_c = (\Delta A/\Delta \varepsilon)/[(c_L - \Delta A/\Delta \varepsilon)c_P]$$

Rearranging this equation yields

$$\Delta A = \Delta \varepsilon c_L - Kc^{-1}\Delta A/c_P \qquad (34)$$

where K_c is a constant, and $\Delta \varepsilon c_L$ has a fixed value. In fact, $\Delta \varepsilon c_L$ is the maximum value of ΔA, which can be measured directly at high protein/dye concentration ratios. Therefore, we write

$$\Delta A_{max} = \Delta \varepsilon c_L \qquad (35)$$

There is a linear relationship between ΔA and $\Delta A/c_P$ according to Eq. (34). From the slope $(-Kc^{-1})$ and intercept $(\Delta \varepsilon c_L)$ of the regression line, Kc and $\Delta \varepsilon$ (and then ε') can be calculated.

Binding number and maximum binding number

Define the (average) binding number of dye molecules per protein molecule as

$$\bar{n} = \{L'\}/c_P \qquad (36)$$

Substituting Eq. (33) into Eq. (36) yields

$$\bar{n} = \Delta A/\Delta \varepsilon c_P \qquad (37)$$

Since $\Delta \varepsilon$ has been determined, $\bar{n}$ can be calculated by using Eq. (37).

Multiplying Eq. (34) by $K_c/\Delta \varepsilon$, we get

$$K_c\Delta A/\Delta \varepsilon = K_c c_L - \Delta A/\Delta \varepsilon c_P$$

Substituting Eq. (37) into this equation and rearranging gives

$$\bar{n} = K_c c_L - K_c \bar{n}c_P \qquad (38)$$

Since K_c is a constant and c_L is a fixed value, a plot of $\bar{n}$ vs. $\bar{n}c_P$ should give a straight line with slope $-K_c$ and intercept $K_c c_L$.

Table 2
Effect of NaCl concentration on binding of BPB on BSA. pH = 3.1, $c_L = 1.2 \times 10^{-5}$ mol l^{-1}, at 605 nm

NaCl (%)	log K_c	n	ε ($\times 10^3$)	ε' ($\times 10^4$)	S	R
0	6.18	18.0	4.45	7.01	0.054	−0.997
0.04	6.10	14.8	5.13	6.90	0.069	−0.997
0.10	6.01	12.1	5.63	6.69	0.088	−0.996
0.20	5.94	10.3	6.13	6.45	0.11	−0.997
0.50	5.80	7.5	7.22	6.44	0.15	−0.993
1.00	5.67	5.5	7.82	6.33	0.21	−0.996
2.00	5.49	3.7	8.74	6.57	0.31	−0.996

Note that the physical meaning of the intercept $K_c c_L$ on the $\bar{n}$ axis is the maximum value of $\bar{n}$ under the experimental conditions. Therefore we call this extrapolated value the maximum binding number n:

$$n = K_c c_L \qquad (39)$$

The maximum binding number n is also a conditional constant. As will be seen later on, it is a useful parameter for expressing the dye binding ability of a protein under certain conditions.

Table 1 gives a group of data taken from Fig. 2. Using these data, a $\Delta A \sim \Delta A / c_p$ regression equation and a $\bar{n} \sim \bar{n} c_P$ regression equation were obtained:

$$\Delta A = 0.804 - 1.79 \times 10^{-6} \Delta A / c_P \quad R = -0.998$$

$$n = 6.63 - 5.57 \times 10^5 \bar{n} c_P \qquad R = -0.998$$

From the slopes and intercepts of these two equations, $\log K_c = 5.75$, $\Delta A_{max} = 0.804$, and $n = 6.63$ are obtained.

It is shown in this example that the theory discussed above is coincident with the experimental findings.

A question which must be asked is that with more than 86 binding sites on the BSA molecule, why do so few of these sites bind to dye? This question may be addressed from the position that the dye binding is indeed a process of competition between the dye species and anions for the same binding sites on protein [1]. For controlling the acidity and the ion strength, buffer and salt must be added to the solution. The concentrations of the anions are usually 1000 ~ 10 000-fold higher than that of the dye species, so the binding sites

are actually surrounded by anions which prevent the die species from binding to protein. The higher the concentration of the anions, the fewer the binding numbers (see Table 2).

3.4. Test of Scatchard model

In the Scathard model, the binding equation is given by [3]

$$\bar{n} / \{L\} = kN - k\bar{n} \qquad (40)$$

where k is the intrinsic binding constant.

Using the data listed in Table 1, a plot of $\bar{n} / \{L\}$ vs. $\bar{n}$ was drawn, and it was found that the plot does not conform to Eq. (40), because the $\bar{n} / \{L\}$ values are essentially constant. Actually, the term $\bar{n} / \{L\}$ in Eq. (40) is just the apparent binding constant K_c defined in this paper. Therefore the Scatchard model is unsuitable for this study.

3.5. Sensitivity of a dye binding protein assay

Define the molar absorptivity of a dye–protein complex as

$$\varepsilon_p = n\varepsilon' \qquad (41)$$

According to Beer's law, the absorbance of a solution of dye–protein complex may be expressed as (with a 1 cm cell)

$$A = \varepsilon_p c_p \qquad (42)$$

The absorbance of a solution containing protein and an excess of dye is

$$A = \varepsilon_p c_p + \varepsilon(c_L - n c_p) \qquad (43)$$

In the practice of a proetin assay, the absorbance of a dye–protein mixture is measured against the blank solution of dye, so the net absorbance is

$$\Delta A = [\varepsilon_P c_P + \varepsilon(c_L - nc_P)] - \varepsilon c_L \tag{44}$$

Using Eq. (41), this equation may be simplified as

$$\Delta A = n(\varepsilon' - \varepsilon)c_P \tag{45}$$

Eq. (45) indicates the factors which influence the sensitivity of a dye binding protein assay. For a given amount of protein, the net absorbance depends on three factors: the maximum binding number n; the mean molar absorptivity of bound die ε'; and the mean molar absorptivity of free dye ε.

It should be noted that Eq. (45) has been obtained before [12] from a simpler consideration not involving the binding of protonated forms of the dye to protein. It is interesting that essentially the same result is found by this more complex treatment.

The Sandell index (S, $\mu g\, cm^{-2}$) [13], which represents the number of micrograms of the determinand per millilitre of a solution having an absorbance of 0.001 for the path length 1 cm, is a suitable parameter for expressing the sensitivities of a protein assay under different conditions and for comparing the variability of color development among proteins with different molecular weights. The relationship between the Sandell index and the above three parameters is

$$S = F/n(\varepsilon' - \varepsilon) \tag{46}$$

where F is the molecular weight of the protein assayed.

3.6. Influence of experimental conditions on dye binding reaction

It is shown in Table 2 that an increase in salt concentration causes a significant decrease in $\log K_c$ and n values, thus decreasing the sensitivity of the BPB protein assay. This effect may be explained as a competition between anions and dye species for the same binding sites on BSA [1]. Even when no salt was added to the solutions, the concentrations of anions coming from the addi-

Table 3
Effect of pH on binding of BPB on BSA. $c_L = 1.2 \times 10^{-5}\, mol\, l^{-1}$, 0.5% NaCl, at 605 nm

pH	$\log K_c$	n	$\varepsilon\,(\times 10^3)$	$\varepsilon'(\times 10^4)$	S	R
2.12	5.74	6.5	0.76	1.99	0.52	−0.995
2.49	5.79	7.3	2.02	3.60	0.26	−0.999
2.80	5.83	8.0	4.20	4.88	0.18	−0.995
3.10	5.80	7.5	7.23	6.44	0.15	−0.993
3.28	5.75	6.7	10.6	7.75	0.15	−0.997
3.42	5.72	6.2	14.9	8.20	0.16	−0.998

tion of buffer are still much higher than that of the dye species. This is probably the reason why the maximum binding numbers determined in this paper are no more than 18.

The influence of acidity on BPB binding reaction is shown in Table 3. From Table 3 we know that in the tested pH range the change of pH has no great influence on $\log K_c$ and n values, but has significant influence on ε and ε' values. The Sandell index S has the best value at pH 3.2.

The influence of BPB concentration on the binding reaction is shown in Table 4. From this test we know that an increase in BPB concentration causes a decrease in $\log K_c$ but an increase in n values, while ε and ε' remain practically constant. However, the dye concentration cannot be too high because of the restriction of spectral measurement.

3.7. Combination between BPB and γ-G

The combination of BPB with γ-G was investigated by using the above method. Fig. 3 shows the absorption spectra of BPB–γ-G mixtures. Using the spectral data measured at 610 nm, a

Table 4
Effect of BPB concentration on binding of BPB on BSA. 0.5% NaCl, pH = 3.1 at 605 nm

$c_L\,(mol\, l^{-1})$	$\log K_c$	n	$\varepsilon\,(\times 10^3)$	$\varepsilon'(\times 10^4)$	S	R
0.6×10^{-5}	6.01	6.1	7.39	6.45	0.19	−0.997
0.9×10^{-5}	5.90	7.1	7.40	6.38	0.16	−0.991
1.2×10^{-5}	5.80	7.5	7.23	6.44	0.15	−0.993
1.5×10^{-5}	5.76	8.4	7.16	6.24	0.14	−0.994
1.8×10^{-5}	5.68	8.6	7.08	6.26	0.14	−0.995

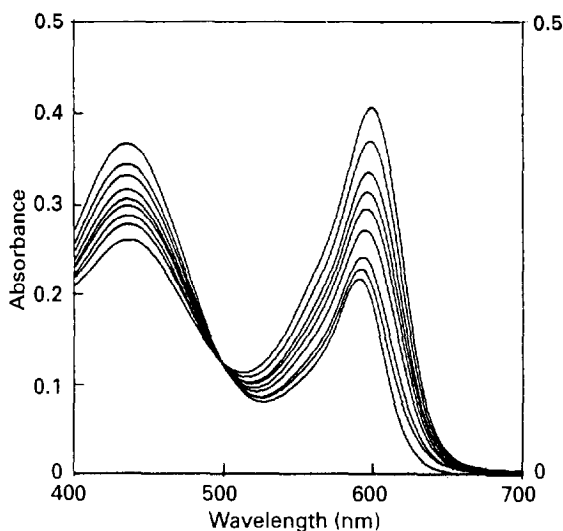Fig. 3. Absorption spectra of BPB–BSA mixtures. BPB concentration constant at 1.2×10^{-5} mol l^{-1}, pH 3.28, 0.5% NaCl. In order of increasing peak absorbances at 600 nm, BSA concentrations are 0.0, 4.0×10^{-7}, 8.0×10^{-7}, 1.2×10^{-6}, 1.6×10^{-6}, 2.4×10^{-6}, 3.2×10^{-6}, 4.0×10^{-6}, 5.2×10^{-6}, 6.4×10^{-6}, 8.0×10^{-6}, 1.2×10^{-5} and 1.36×10^{-5} mol l^{-1}.

$\Delta A \sim \Delta A / c_P$ linear regression equation was obtained:

$$\Delta A = 0.384 - 1.50 \times 10^{-6} \Delta A / c_P \qquad R = -0.993$$

From the slope and intercept of this equation, $\log K_c = 5.83$, $\Delta A_{max} = 0.384$, and $n = K_c c_L = 11.8$ were obtained.

4. Conclusions

The combination of BPB species with proteins in acidic solutions is due mainly to the non-specific electrostatic forces. This kind of combination allows a transformation of BPB species from free acidic form into bound basic form and allows a donation of electrons by the protein to the π electron system of BPB, thereby causing bathochromicity and hyperchromicity. These spectral effects establish the foundation of the BPB protein assay.

The Scatchard model is not appropriate for this study. Instead a new linear regression method based on a new consideration about the solution equilibria is able to give a reasonable description

of the dye–protein combination under different conditions. Both the apparent binding constant and the maximum binding number proposed in this paper depend on experimental conditions. Therefore they are different from the Scatchard intrinsic binding constant and the number of binding sites.

It seems that this method is useful and convenient for the investigation of dye-binding protein assays, because the parameters defined in this paper describe the conditions of the dye–protein binding reaction, and these parameters can be determined easily.

To use the method, the experiment should be carried out under proper conditions. That is to say, the dye/protein concentration ratios should not be too high or too low so that the free dye species and the unoccupied protein binding sites are substantially coexistent under experimental conditions.

The intercept ($\Delta \varepsilon c_L$) of the $\Delta A \sim \Delta A / c_P$ regression equation and the intercept ($K_c c_L$) of the $\bar{n} \sim \bar{n} c_P$ regression equation have definite physical meaning—$\Delta \varepsilon c_L$ is the maximum net absorbance ΔA_{max} and $K_c c_L$ is the maximum binding number n. These two parameters had to be determined under extreme dye/protein concentration ratios (with an excess of protein or an excess of dye) using the previous method. Now, they can be determined by using the linear regression (extrapolation) method under proper concentration ratios.

Experimental conditions such as acidity, ion strength, and concentration of dye have different effects on the maximum binding number and the molar absorptivities of free and bound dye, thereby influencing the sensitivity of a protein assay.

Acknowledgement

References

[1] G. Scatchard, I.H. Scheinberg and S.H. Armstrong, J. Am. Chem. Soc., 72 (1950) 535.

[2] M. Pesavento and A. Profumo, Talanta, 38 (1991) 1099.

[3] R.W. Congdon, G.W. Muth and A.G. Splittgerber, Anal. Biochem., 213 (1993) 407.

[4] K.E. Lind, U. Kragh-Hansen and J.V. Moller, Biochim. Biophys. Acta, 871 (1974) 451.

[5] R. Flores, Anal. Biochem., 88 (1978) 605.

[6] K.H. Schosinsky, M. Vargas, A.L. Esquivel and M.A. Chavarria, Clin. Chem., 33 (1987) 223.

[7] K. Jung, E. Nikel and M. Pergande, Clin. Chim. Acta, 1987 (1990) 163.

[8] E.C. White and S.F. Acree, J. Am. Chem. Soc., 41 (1919) 1205.

[9] S.J. Compton and C.J. Jones, Anal. Biochem., 151 (1985) 369.

[10] G.V. Kaler and V.B. Gavrilov, Mol. Biol. 28 (No. 1, Part 2) 140.

[11] W.A.E. McBryde, Talanta, 21 (1974) 982.

[12] H.J. Chial and A.G. Splittgerber, Anal. Biochem., 213 (1993) 362.

[13] B.E. Sandell, Colorimetric Determination of Traces of Metals, 3rd edn., Interscience, New York, 1959, p. 83.

Potentiometric study of the protonation and distribution equilibria of 2-chlorophenol in NaCl medium at 25°C. Construction of a thermodynamic model

Ainoa Rios, Gorka Arana*, Nestor Etxebarria, Luis A. Fernández

Kimika Analitikoaren Saila, Euskal Herriko Unibertsitatea (UPV/EHU), P.K. 644, E-48080 Bilbao, Basque Country, Spain

Abstract

The potentiometric determination of the protonation constant of 2-chlorophenol in NaCl media at different ionic strengths and its distribution coefficient between these media and two organic solvents at 25°C are presented. An automated potentiometric system was used, and the determination of the constants was carried out using both graphical and numerical methods. A thermodynamic model using the modified Bromley methodology has been constructed for the prediction of protonation constants and distribution coefficients in NaCl media. The relevance of this study to the development of supported liquid membrane recovery systems is discussed.

Keywords: Protonation equilibria; Distribution equilibria; Potentiometry; Thermodynamic model; 2-Chlorophenol

1. Introduction

2-Chlorophenol is a priority pollutant phenol and, like many other phenols, may be found in the wastewaters of some manufacturing industries, such as coke production, paper and pulp processing, oil refining, coal gas liquefaction, etc. Some of the consequences of the uncontrolled disposal of this kind of compound are toxicity to water-life, increase in chemical and biological oxygen demand, and bad taste and smell in water [1–4].

As the toxicity of chlorophenols is high they are used as disinfectants; however, some of them are suspected of being carcinogenic, and a concentration of phenols of higher than $2\,mg\,dm^{-3}$ is dangerous to water-life. For the reasons, chlorophenols containing wastewaters have to be controlled [4]. By improving analytical methods, these pollutants have been detected and reported in industrial and city wastes.

There are several methods for treating phenolic wastes and their choice depends on the concentration levels of the phenols. For high concentrations, recovery and reuse or disposal by incineration is possible. Intermediate concentrations can be treated biologically or by adsorption onto active surfaces. In more diluted wastes chemical oxidation can be used. Apart from these methods,

---

* Corresponding author.

recovery using membrane processes is possible [5]. One of these membrane processes, the use of supported liquid membranes, has proved to be a valid option [6]. Such processes require knowledge of the chemical model, and some thermodynamic studies have been carried out in order to simulate and model the separation and recovery of these compounds [7].

Since membrane processes are based on the extraction of chlorophenol into an organic phase and the driving force of the transport is the concentration gradient, it is necessary to know the acid–base and distribution equilibria of the species involved in order to design selective liquid membrane separation processes and to interpret the permeation results obtained. One of the main requirements for an organic solvent to be part of a liquid membrane is that it is immiscible with water. It also needs to have a high boiling point in order to avoid evaporation of the membrane. Kerosene or aliphatic solvents are normally used for these purposes. However, it might also be interesting to try aromatic solvents in order to enhance the separation, since the solutes are aromatic in nature and thus should have higher distribution coefficients. As well as the liquid membrane itself, the influence of the aqueous media in the permeation process should be taken into account. In a previous work [8], the distribution coefficients of several phenols between 1.0 mol dm^{-3} NaCl and different organic solvents were determined. NaCl has been reported as a common medium in the wastewater of epoxy resin manufacturing; therefore, in this work the acid–base and distribution equilibria were determined in this medium at different ionic strengths (0.5, 2.0 and 3.0 mol dm^{-3}) in order to build a thermodynamic model, taking 2-chlorophenol as an example to demonstrate the usefulness of the methodology used. One-phase potentiometric titrations were used for the determination of the acid–base equilibria. This is one of the commonest techniques, together with spectrophotometry, although some other methods, such as liquid chromatography, are used for the study of the acid–base equilibria of chlorophenols [9]. Two-phase potentiometric titrations were used for the distribution equilibria, as described in Refs. [10]–[12].

2. Experimental

2.1. Chemicals and solutions

2-Chlorophenol (Aldrich, >99%), sodium chloride (Merck, p.a.), sodium hydroxide (Merck p.a.) and hydrochloric acid (Fluka, p.a.) were used without further purification.

The organic solvents n-decane (Fluka, 98%) and 95 A 16/18 — an industrial aromatic mixture manufactured and kindly supplied by CEPSA, in Bilbao, Spain — were washed several times with 0.1 mol dm^{-3} NaOH and 0.1 mol dm^{-3} HCl in order to eliminate the acid and basic impurities, and were finally saturated in the corresponding ionic medium.

All solutions were prepared using MilliQ water. The NaOH solutions were prepared in N_2 atmosphere and standardized against potassium phthalate with phenolphthalein as indicator. These solutions were used as titrants. The HCl solutions were standardized against Tris(hydroxymethyl)-aminomethane with bromocresol green as indicator. Different solutions of the phenols were prepared with the following general composition:

$$B \text{ mol dm}^{-3} \text{ 2-chlorophenol} + 0.01 \text{ mol dm}^{-3}$$

$$\text{HCl} + (I - 0.01 - B) \text{ mol dm}^{-3} \text{ NaCl}$$
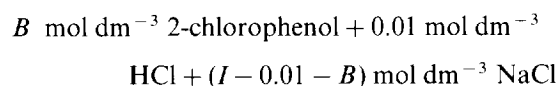
where B is 0.01 or 0.03 and I is the concentration of the ionic medium. I was checked by weighing the solid residue after evaporation of a known volume of the solution.

2.2. Procedure

Potentiometric one-phase or two-phase titrations of 2-chlorophenol were carried out using an automated system developed in this laboratory [13] and a thermostatic bath at $25.0 \pm 0.1°C$ by measuring the emf of the cell:
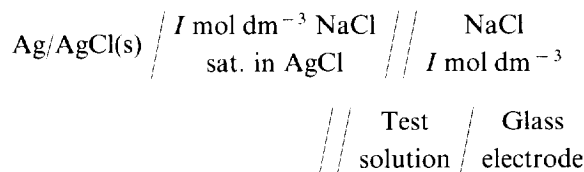
$$\text{Ag/AgCl(s)} \left| \begin{array}{c} I \text{ mol dm}^{-3} \text{ NaCl} \\ \text{sat. in AgCl} \end{array} \right| \left| \begin{array}{c} \text{NaCl} \\ I \text{ mol dm}^{-3} \end{array} \right|$$

$$\left| \begin{array}{c} \text{Test} \\ \text{solution} \end{array} \right| \begin{array}{c} \text{Glass} \\ \text{electrode} \end{array}$$

Table 1
Values of j_{ac}, j_{bas} and K_w for the different ionic strengths and electrode systems used in this work

I/NaCl (mol dm^{-3})	j_{ac} (mV mol^{-1} dm^3)	j_{bas} (mV mol^{-1} dm^3)	log K_w
0.5	-90 ± 1	250 ± 4	-13.69 ± 0.01
2	-28.5 ± 0.3	110 ± 2	-13.72 ± 0.01
3	0	42 ± 1	-13.93 ± 0.02

where I is the concentration of the ionic medium (0.5, 2.0 and 3.0 mol dm^{-3}) and the test solutions were

B mol dm^{-3} 2-chlorophenol/h mol dm^{-3} H$^+$/

$(I - h - B)$ mol dm^{-3} Na$^+$/$(I - B)$ mol dm^{-3} Cl$^-$

where B is 0.01 or 0.03.

For the two-phase titrations, 0.070 dm^3 of the test solution was equilibrated with 0.025 dm^3 of one of the organic solvents, which was in contact with the aqueous phase. However, there was no contact with the electrodes in order to obtain more stable readings of emf from the electrodes.

The values of h were varied by stepwise addition of the titrant using a Metrohm 665 automatic burette connected to the computer via a RS-232C interface. The emf of the cell was measured using a glass electrode (Metrohm 6.0101.100) and an Ag/AgCl (s) double junction reference electrode (Metrohm 6.0726.100). The signals from the electrodes, preamplified by an operational amplifier in order to adequate the electric signal, were measured by a Hewlett-Packard HP-E1326B voltmeter incorporated into the VXI data acquisition system connected to the computer. When the standard deviation of the emf over a preset period of time (about 3 min) was less than 0.04 mV, or a certain number of measurements were taken (more than 20), an instruction for new addition was given by the computer to the burette. Each titration took between 12 and 72 h to be completed, depending on the number of chemical phases and the solvent used, and all of them were repeated at least three times.

Throughout the titrations N$_2$, presaturated in the corresponding ionic medium, was bubbled through the solution in order to avoid the pres-

ence of CO$_2$. The solution was continuously stirred making use of a magnetic stirrer immersed in an oil bath at a constant temperature of 25°C.

2.3. Determination of h

The free hydrogen ion concentration (h) was determined by measuring the emf of the cell, which at 25°C can be expressed as follows:

$$E(\text{mV}) = E° + 59.16 \log h + E_j(h) \tag{1}$$

where $E_j(h)$, the liquid junction potential, can be expressed as

$$E_j(h) = j_{ac} h + j_{bas} K_w \cdot h^{-1} \tag{2}$$

Therefore, in order to be able to determine the value of h in the phenolic solutions, the values of the acid liquid junction potential coefficient (j_{ac}), the basic liquid junction potential coefficient (j_{bas}) and the autoprotolysis constant of water in this medium (K_w) must be previously known, whereas the standard potential of the glass electrode, $E°$, is determined for each titration since it may vary from day to day [14].

The values of j_{bas}, j_{ac} and K_w can be considered constant, since the ionic strengths of the solutions were kept constant throughout the titrations and were determined by means of $E°$ titrations as explained elsewhere [15]. The values of these constants for the different ionic strengths are shown in Table 1.

Once the values of these constants are known and $E°$ is calculated for each titration using Gran's method [16], h can be calculated for each experimental point. Since the equation to calculate the value of h cannot be analytically solved, an iterative procedure such as the Newton–Raphson method is used.

3. Results and discussion

3.1. Acid–base equilibria

The chemical systems studied in the one-phase titrations can be described by the following equilibrium:

$$H^+ + B^- \rightleftharpoons HB \tag{3}$$

where HB is 2-chlorophenol with the stochiometric constant

$$\beta = \frac{[HB]}{[H^+][B^-]} \tag{4}$$

For each titration, the total concentrations of 2-chlorophenol (B_{tot}) and hydrogen ions (H_{tot}) were known, and the free hydrogen ion concentration can be calculated from Eq. (1). H_{tot} is calculated using the following expression:

$$H_{tot} = \frac{C_0 \cdot V_0 + C_a \cdot V_0 - C_b \cdot V}{V_0 + V} \tag{5}$$

where C_0 is the initial HCl concentration, C_a is the initial 2-chlorophenol concentration and C_b is the titrant concentration. V_0 is the initial volume and V is the titrant volume.

The average number of protons bound to the phenol is evaluated as follows:

$$Z = \frac{[HB]}{B_{tot}} = \frac{H_{tot} - h + K_w \cdot h^{-1}}{B_{tot}} = \frac{h\beta}{1 + h\beta} \tag{6}$$

The results obtained were treated both graphically and numerically. A normalized variable method was used to carry out the graphical treatment. The following normalized variable is defined:

$$u = h\beta \tag{7}$$

Therefore, Eq. (6) can be transformed into

$$Z = \frac{h\beta}{1 + h\beta} = \frac{u}{1 + u} \tag{8}$$

Comparing the experimental formation curves Z vs. $-\log h$ (Fig. 1) with the theoretical curves Z vs. $-\log u$, the value of $\log \beta$ can be calculated from the point along the pH-axis at which both curves overlap. This method allows estimation of the errors in the fit by shifting the theoretical

curve to the left and to the right while the curves still overlap, as well as the systematic errors that may arise. Moreover, it was proved that there is no aggregation of 2-chlorophenol since the Z curves corresponding to the two different concentrations of phenol overlap.

Numerical treatment, in order to refine the results from the graphical method, was carried out using the NYTIT version of the LETAGROP program [17] and the BSTAC program [18]. For all N_p experimental points the sum of square errors U, defined as

$$U = \sum_{N_p} (X_{calc} - X_{exp})^2 \tag{9}$$

was minimized, where $X = H_{tot}$ in NYTIT and $X = E$ in BSTAC. Using NYTIT, H_{exp} and H_{calc} are the experimental and calculated total concentrations of protons for each experimental point based on a set of formation constants and E°, j_{ac}, j_{bas} and K_w values. This program allows the detection and correction of any possible systematic error arising in the titrations, such as the concentration of 2-chlorophenol, H_{tot}, etc. Using BSTAC, E_{calc} and E_{exp} are calculated and experimental potentials of the cell. Systematic errors can be detected and corrected using this program, but the basic liquid junction potential cannot be considered. It is also possible to treat all the titrations corresponding to the same ionic strength together. The results of the graphical and numerical calculations are the same, and the values of the formation constants for the different ionic strengths with the statistical parameters given by NYTIT are
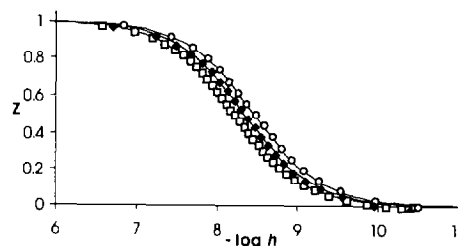

Fig. 1. Graphical representations of Z vs. $-\log h$ of 2-chlorophenol with the theoretical curves Z vs. $-\log u$ in the position showing the best fit in the one-phase titrations at different ionic strengths: □, 0.5 mol dm^{-3}; ◆, 2.0 mol dm^{-3}; ○, 3.0 mol dm^{-3}.

Table 2
Values of formation constants of 2-chlorophenol in different ionic media

	I/NaCl(mol dm^{-3})			I/(mol dm^{-3})			
	0.5	2.0	3.0	1.0 [15]	$\rightarrow$0 [19]	0.1 NaClO$_4$ [20]	0.1 NaClO$_4$ [21]
log β	8.23 ± 0.01	8.36 ± 0.01	8.46 ± 0.01	8.22 ± 0.01	8.53	8.25	8.33
σ^a	0.025	0.088	0.031				
R^b	5.94×10^{-3}	1.21×10^{-2}	3.10×10^{-3}				

^{a} $\sigma = [U_H/(N_p - N_k)]^{1/2}$; $N_p =$ number of experimental points; $N_k =$ number of parameters.
^{b} R (Hamilton's factor) $= (U/\Sigma H_{tot}^2)^{1/2}$.

summarized in Table 2 together with the data found in the literature.

There is not much possibility of comparing the results obtained in this work with bibliographic data, since the values found in the literature are determined in different ionic media.

3.2. Distribution equilibria

In the case, together with the acid–base equilibria showed in Eq. (3), it is necessary to consider the distribution equilibria, which can be described as follows:

$$HB \rightleftharpoons \overline{HB} \tag{10}$$

where HB is the 2-chlorophenol and $\overline{HB}$ is the phenol in the organic phase. This equilibrium has the corresponding equilibrium constant:

$$K_d = \frac{[\overline{HB}]}{[HB]} \tag{11}$$

The distribution of the phenol into the organic phase affects the acid–base equilibrium as a side-reaction.

As in the one-phase titration, for each titration point B_{tot}, H_{tot} and h can be calculated.

The average number of protons bound to the phenol, taking into account the distribution equilibrium, is evaluated as follows:

$$Z = \frac{[HB] + [\overline{HB}]V_r}{B_{tot}} = \frac{H_{tot} - h + K_w h^{-1}}{B_{tot}}$$

$$= \frac{h\beta(1 + K_d \cdot V_r)}{1 + h\beta(1 + K_d \cdot V_r)} \tag{12}$$

where V_r is the organic phase to aqueous phase volume ratio (V_{org}/V_{aq}). The results obtained were treated both graphically and numerically. A normalized variable method with one parameter was used to carry out the graphical treatment. As well as the normalized u variable defined in Eq. (7), the following parameter is expressed:

$$p = K_d \tag{13}$$

Therefore, Eq. (12) can be transformed into

$$Z = \frac{u(1 + pV_r)}{1 + u(1 + pV_r)} \tag{14}$$

Comparing the experimental formation curves Z vs. $-\log h$ with the theortical curves Z vs. $-\log u$, since β is already known, an approximate value of K_d can be calculated as that which makes both curves overlap (Figs. 2 and 3). Again, it was proved that, in the range of concentrations studied, there is no aggregation equilibrium in the organic phase, since the Z curves corresponding to the two different concentrations of phenol
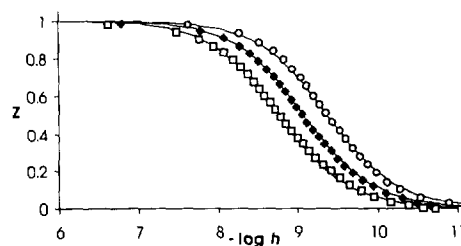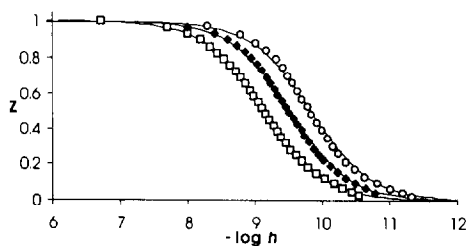
Fig. 2. Graphical representations of Z vs. $-\log h$ of 2-chlorophenol with the theoretical curves Z vs. $-\log u$ in the position showing the best fit in the two-phase titrations containing n-decane at different ionic strength: $\square$, 0.5 mol dm^{-3}; $\blacklozenge$, 2.0 mol dm^{-3}; $\bigcirc$, 3.0 mol dm^{-3}.

Fig. 3. Graphical representations of Z vs. $-\log h$ of 2-chlorophenol with the theoretical curves Z vs. $-\log u$ in the position showing the best fit in the two-phase titrations containing 95 A 16/18 at different ionic strength: $\square$, 0.5 mol dm^{-3}; $\blacklozenge$, 2.0 mol dm^{-3}; $\bigcirc$, 3.0 mol dm^{-3}.

overlap. Once these values were obtained they were refined using numerical methods.

The numerical calculations were carried out using the MODEL FUNCTION version of the LETAGROP program [22]. This program allows all the titrations corresponding to the same solvent to be treated together. The calculations were carried out minimizing the sum of square errors:

$$U_Z = \sum_i (Z_{i,\text{calc}} - Z_{i,\text{exp}})^2 \tag{15}$$

were Z_{calc} is defined as follows:

$$Z_{\text{calc}} = \frac{h\beta(1 + K_d \cdot V_r)}{1 + h\beta(1 + K_d \cdot V_r)} \tag{16}$$

and $Z_{i,\text{exp}}$ is calculated as in Eq. (12). The final values of the distribution coefficients corresponding to both solvents and the different ionic strengths are compiled in Table 3.

No data have been found in the literature of the distribution equilibria for the solvents used and 2-chlorophenol. It is noteworthy that many of the distribution data are determined in batch experiments on measuring the concentration of the distributed substances in both phases after equilibrium has been reached. However, there are other methods in the literature such as the technique of countercurrent distribution [23] or gas chromatography [24], mainly chromatographic methods based on the relation of the chromatographic capacity factor and the distribution coefficient [25], with the advantage that a very small amount of the substance is needed. The two-phase titration technique is not new, but is not very

common either; it allows the detection and correction of systematic errors both in the graphical and numerical treatment of the data. This is possible because the distribution coefficient is determined from a fairly large number of measurements (i.e. emf readings) transformed into the Z function, rather than from a single measurement of concentration, in which a minor error can give rise to large errors in the distribution coefficients.

3.3. Thermodynamic model

The behaviour of the chemical system studied, the acid-base and distribution equilibria of 2-chlorophenol in NaCl media at different ionic strengths, can be explained by a thermodynamic model. In order to construct this model, when the stoichiometric formation constants and distribution coefficients at different ionic strengths are known and making use of a model of the calculation of the activity coefficients, the thermodynamic constant of the system at infinite dilution can be calculated. The calculation is not direct, and numerical methods must be used. Unknown parameters, which depend on the model, are calculated in order to adjust the experimental values to the theoretical function.

A modification of Bromley's methodology [26] for the calculation of activity coefficients, which can be applied to molar as well as to molal concentrations, has been successfully used with both inorganic and organic solutes in aqueous systems [27–30] for the calculation of thermodynamic formation constants at infinite dilution $(°\beta)$ and of the interaction parameters between the species taking part in the equilibria and the ions of the ionic media.

Considering the activities, Eq. (4) can be rewritten as

$$°\beta = \frac{\{HB\}}{\{B^-\}\{H^+\}} = \beta \frac{\gamma_{HB}}{\gamma_{B^-}\gamma_{H^+}} \tag{17}$$

and taking logarithms

$$\log \beta = \log °\beta - \log \gamma_{HB} + \log \gamma_{B^-} + \log \gamma_{H^+} \tag{18}$$

According to the modified Bromley methodology, the individual activity coefficient of a charged species can be expressed as

Table 3
Values of the distribution coefficients corresponding to both organic solvents at different ionic strengths

Solvent		I/NaCl(mol dm^{-3})			
		0.5	2.0	3.0	1.0 [8]
n-Decane	K_d	7.5 ± 0.01	12.29 ± 0.01	19.4 ± 0.3	8.97 ± 0.08
	σ [a]	0.0008	0.01	0.016	
	R [b]	1.18×10^{-2}	1.61×10^{-2}	1.66×10^{-2}	
95 A 16/18	K_d	21.6 ± 0.1	39.6 ± 0.2	70 ± 1	19.6 ± 0.2
	σ [a]	0.01	0.01	0.02	
	R [b]	1.57×10^{-2}	1.44×10^{-2}	3.07×10^{-2}	

[a] $\sigma = (U_z/(N_p - N_k))^{1/2}$; N_p = number of experimental; N_k = number of parameters.
[b] R (Hamilton's factor) = $(U/\Sigma Z^2_{exp})^{1/2}$.

$$\log \gamma_M = -\frac{A Z^2_M \sqrt{I}}{1 + \sqrt{I}} + \sum_X \dot{B}_{M.X}(|Z_M| + |Z_X|)^2 \frac{c_X}{4}$$

$$(19)$$

where $A = 0.5109 \text{ dm}^{2/3} \text{ mol}^{-1/2}$, I is the ionic strength on the molar scale, Z_M is the ionic charge of M, Z_X is the charge of the ionic species with opposite sign to M, and c_X is its molar concentration. The parameter $\dot{B}_{M.X}$ can be expressed as

$$\dot{B}_{M.X} = \frac{(0.06 + 0.6_{M.X})|Z_M Z_X|}{\left(1 + \frac{1.5}{|Z_M Z_X|} I\right)^2} + B_{M.X}$$

$$(20)$$

where $B_{M.X}$ is the interaction parameter of the ion pair M and X on the molar scale. In this case, using Eqs. (19) and (20), the activity coefficient of B^-(γ_{B-}) is a function of the concentration of Na$^+$ in the ionic media, and the contribution of H$^+$ can be neglected as its concentration is much lower. The ionic medium, NaCl, is a 1:1 salt; thus, the concentration of Na$^+$ is the same as the ionic strength, and γ_{B-} can be expressed as a function of I and the interaction parameter B_{B^-,Na^+}. Similarly, the activity coefficient of H$^+$ is a function of the ionic strength and the interaction parameter B_{H^+,Cl^-}, which has been previously determined using values from the literature of activity coefficients of solutions containing hydrochloric acid, its value being 0.1648 [31]. The activity coefficient of the neutral species HB in the ionic medium NaCl is expressed by means of the salt coefficient proposed by Long and McDevit [32] where, in this case, C_{NaCl} equals the ionic strength:

$$\log \gamma_{HB} = S_{HB.NaCl} C_{NaCl}$$

$$(21)$$

Considering activities, Eq. (11) can be rewritten as

$$°K_d = \frac{\{\overline{HB}\}}{\{HB\}} = K_d \frac{1}{\gamma_{HB}}$$

$$(22)$$

where the activity coefficient of the neutral species in the organic phase is considered constant since only the ionic strength in the aqueous solution changes and therefore it is taken as part of the stoichiometric distribution coefficient. Taking logarithms gives

$$\log K_d = \log °K_d + \log \gamma_{HB}$$

$$(23)$$

where there are no interaction parameters the salt coefficient $s_{HB.NaCl}$ being the only parameter.

In order to relate the distribution to the acid–base data we can consider the acid–base and distribution equilibrium together, obtaining the following equilibrium:

$$H^+ + B^- \rightleftharpoons \overline{HB}$$

$$(24)$$

with the corresponding formation constant

$$°K = °\beta °K_d = \frac{\{\overline{HB}\}}{\{B^-\}\{H^+\}} = \frac{K}{\gamma_{B-} \gamma_{H+}}$$

$$= \frac{\beta K_d}{\gamma_{B-} \gamma_{H+}}$$

$$(25)$$

Taking logarithms in Eq. (25) gives

$$\log K_d = \log °K_d + \log °\beta - \log \beta + \log \gamma_{B-}$$
$$+ \log \gamma_{H+}$$

$$(26)$$

Substituting Eqs. (19), (20) and (21) into Eqs. (18) and (26) leads to

$$\log \beta = \log {}^{\circ}\beta - S_{\mathrm{HB,NaCl}}I - 2\frac{0.5109\sqrt{I}}{1+\sqrt{I}}$$

$$+ \left[\frac{(0.06 + 0.6B_{\mathrm{B^-,Na^+}})}{(1+1.5I)^2} + B_{\mathrm{B^-,Na^+}}\right]I$$

$$+ \left[\frac{(0.06 + 0.6B_{\mathrm{H^+,Cl^-}})}{(1+1.5I)^2} + B_{\mathrm{H^+,Cl^-}}\right]I \quad (27)$$

$$\log K_{\mathrm{d}} = \log {}^{\circ}K_{\mathrm{d}} + \log {}^{\circ}\beta - \log \beta - 2\frac{0.5109\sqrt{I}}{1+\sqrt{I}}$$

$$+ \left[\frac{(0.06 + 0.6B_{\mathrm{B^-,Na^+}})}{(1+1.5I)^2} + B_{\mathrm{B^-,Na^+}}\right]I$$

$$+ \left[\frac{(0.06 + 0.6B_{\mathrm{H^+,Cl^-}})}{(1+1.5I)^2} + B_{\mathrm{H^+,Cl^-}}\right]I \quad (28)$$

The correlation of the experimental β and K_{d} values with ionic strength was made with both Eqs. (27) and (28), making use of the MODEL FUNCTION version of the LETAGROP program. The results of the formation and distribution thermodynamic constants at infinite dilution and the interaction parameters obtained are collected in Table 4. Figs. 4 and 5 show the fit between the experimental data and the theoretical curves (Eqs. 27 and 28) of the acid–base equilibria and distribution equilibria, respectively. The slope of the plots in Fig. 5 is the salt coefficient of 2-chlorophenol. The fact that the representation of $\log K_{\mathrm{d}}$ vs. ionic strength follows a linear trend with the same slope for both organic solvents as predicted in Eq. (23) confirms the previously made assumption that the activity coefficients of the neutral species in the organic phase are constant. Therefore, making use of the salt co-
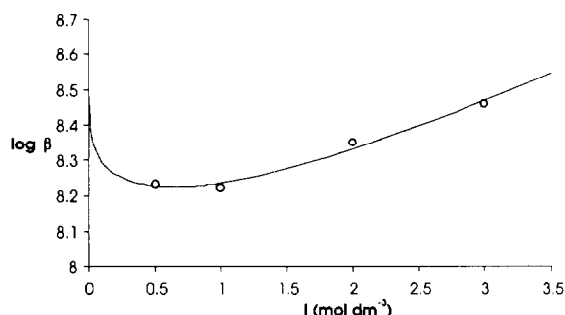

Fig. 4. Variation of $\log \beta$ with ionic strength together with the theoretical function (Eq. 27).

efficients found in the literature [32], values of K_{d} at a given ionic strength can be predicted once the value of K_{d} is known at another ionic strength of the same salt for any organic solvent. The salt coefficients can be determined either by determining distribution coefficients using any of the techniques available at different ionic strengths of the corresponding ionic medium or by measuring activity coefficients of the substance under study as a function of ionic strength in the corresponding ionic media, making use of Eq. (21). It should be taken into account that these salt coefficients depend on the ionic medium to be used, i.e. the salt coefficient is different for KCl and NaCl media, but is independent of the organic solvent, as long as the activity coefficient of the substance in the organic phase is kept constant, which is feasible for low concentrations.

In order to be able to predict the stoichiometric formation constants of 2-chlorophenol or any other substance it is necessary to know the values
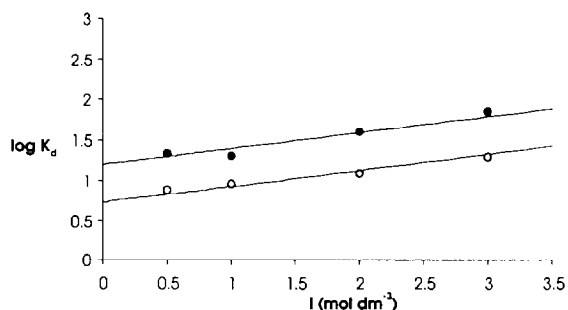
Table 4
Thermodynamic constants in infinite dilution and parameters calculated in the construction of the thermodynamic model

$\log {}^{\circ}\beta$	8.49 ± 0.05
${}^{\circ}K_{\mathrm{d}}$ (n-decane)	5.5 ± 0.1
${}^{\circ}K_{\mathrm{d}}(95\ \mathrm{A}\ 16/18)$	15.7 ± 0.5
S_{HB}	0.196 ± 0.004
$B_{\mathrm{B^-,Na^+}}$	0.228 ± 0.02
σ	0.056
R	8.04×10^{-3}

Fig. 5. Variation of $\log K_{\mathrm{d}}$ for both organic solvents with ionic strength together with the corresponding theoretical functions (Eq. 28): ●, 95A 16/18, ○, n-decane.
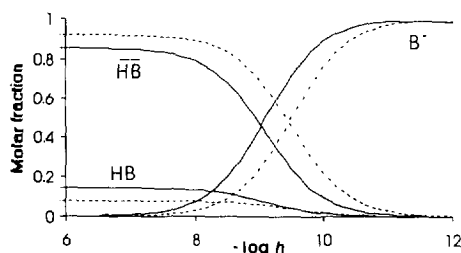
Fig. 6. Distribution diagram of the system 2-chlorophenol/ H_2O/n-decane for two different ionic strengths in NaCl: solid line, 0.2 mol dm^{-3}; broken line, 2.5 mol dm^{-3}.

of the corresponding B parameters, which depend on the ionic medium and the substance itself. A further discussion on the values of calculated B parameters for many ion pairs is under preparation in a different work. Thus, it is possible to predict the values of the stochiometric formation constants of many chemical equilibria for any ionic strength within an appropriate range (it should be an interpolation and not an extrapolation) in many ionic media, once the corresponding thermodynamic formation constant at infinite dilution is known.

The value of the thermodynamic formation constant of 2-chlorophenol obtained is similar to that found in the literature, although it is not very clear how this was determined. The value obtained for the salt coefficient of 2-chlorophenol is close to that given by Long and McDevit [32] for phenol in the same ionic medium.

Using the values collected in Table 4 and the value of B_{H^+,Cl^-} it is possible to calculate the stoichiometric formation constants and distribution coefficients for any value of ionic strength of NaCl in the range 0–3 mol dm^{-3}. Fig. 6, the distribution diagram of the system 2-chlorophenol/H_2O/n-decane for two different ionic strengths, shows the different behaviour of the system as a function of ionic strength.

As was pointed out above, the aim of this work is the construction of a thermodynamic model for application to a supported liquid membrane system for the separation of phenols as well as seeking practical aspects of the membrane technique, we are interested in its basic chemistry. The correct interpretation of the permeation results

requires a good knowledge of the chemical system, i.e. acid–base equilibria and distribution equilibria, in such a way that it is possible to predict the optimum experimental conditions, pH, organic solvent to be used or ionic strength, for the best separation of the corresponding phenols. It is also possible to use the model in the interpretation or prediction of the permeation results obtained with wastewaters of varying concentration of NaCl, since a significant proportion of the parameters needed are from the model. However, apart from the interest in the elimination or separation of the priority pollutant 2-chlorophenol, the model constructed shows the usefulness of the procedure employed and can be applied to any other chemical system with different applications, e.g. sample preparation using solvent extraction, etc.

Acknowledgements

References

[1] J.M. Carron and B.K. Afghan, in B.K. Afghan and A.S.Y. Chau (Eds.), Analysis of Trace Organics in the Aquatic Environment, CRC Press, Boca Raton, FL, 1989, p. 119.

[2] A.I. Hafez, G.I. El Diwani and S. Hawash, Afinidad, 44 (1987) 471.

[3] R.E. Pauls, M.E. Bambacht, C. Bradley, S.E. Schepple and D.C. Cronauer, Energ. Fuels, 4 (1990) 236.

[4] K.H. Lanouette, Chem. Eng., Oct. 17 (1977) 99.

[5] J.A. Garcia-Portilla, F.V. Díez and J. Coca, Ing. Quím., 21 (1989) 151.

[6] A.M. Urtiaga, M.I. Ortiz and A. Irabien, Environ. Sci. Res., 42 (1991) 647.

[7] J.R. Campbell and R.G. Luthy, in Report DOE/FFC/ 10157-1600, Order no. DE84016077, 1984.

[8] G. Arana, N. Etxebarria and L.A. Fernández, Mikrochim. Acta, 117 (1994) 31.

[9] P. Chaminade, A. Billet, D. Ferrier, B. Bourgvignon and D.L. Massart, Anal. Chim. Acta, 280 (1993) 93.

[10] E. Högfeldt and F. Fredlund, Trans. R. Inst. Technol., (1964) 226.

[11] F.F. Cantwell and D.J. Pietrzyk, Anal. Chem., 46 (1974) 344.

[12] P.A. Johansson and S. Thelander, Anal. Chim. Acta, 192 (1987) 17.

[13] R. Cazallas, L.A. Fernández, N. Etxebarria and J.M. Madariaga, Lab. Robotic Autom., 5 (1993) 161.

[14] H.S. Rossotti, in The Study of Ionic Equilibria. An Introduction, Longman, London, 1978.

[15] G. Arana, N. Etxebarria and L.A. Fernández, Fresenius' J. Anal. Chem., 349 (1994) 703.

[16] G. Gran, Analyst, 77 (1952) 661.

[17] N. Ingri and L.G. Sillén, Acta Chem. Scand., 16 (1962) 173.

[18] C. De Stefano, P. Mineo, C. Rigano and S. Sammartano, Annal. Chim., 83 (1993) 243.

[19] Z.L. Ernst and F.G. Herring, Trans. Faraday Soc., 61 (1965) 454.

[20] A.G. Desai and R.M. Milburn, J. Am. Chem. Soc., 91 (1969) 1958.

[21] K.E. Jabalpurwala and R.M. Milburn, J. Am. Chem. Soc., 88 (1966) 3224.

[22] J.L. Fonseca, B. Sc. Thesis, UPV-EHU, Bilbao, 1989.

[23] N.C. Saha, A. Bhattacharjee, N.G. Basak and A. Lahiri, J. Chem. Eng. Data, 8 (1963) 405.

[24] T.M. Xie and D. Dyrssen, Anal. Chim. Acta, 160 (1984) 21.

[25] A.D. Kossoy, D.S. Risley, R.M. Kleyle and D. Nurok, Anal. Chem., 64 (1992) 1345.

[26] L.A. Bromley, AIChE J., 19 (1973) 313.

[27] N. Etxebarria, M.J. Zapatero, J.M. Castresana, M.A. Olazabal, L.A. Fernández and J.M. Madariaga, J. Sol. Chem., 20 (1991) 1213.

[28] R. Castaño, N. Etxebarria and J.M. Madariaga, J. Chem. Soc., Dalton Trans., (1994) 2729.

[29] N. Etxebarria, L.A. Fernandez and J.M. Madariaga, J. Chem. Soc., Dalton Trans. (1994) 3055.

[30] R. Cazallas, M.J. Citores, N. Etxebarria, LA. Fernández and J.M. Madariaga, Talanta, 41 (1994) 1637.

[31] J.M. Madariaga, Unpublished results, 1995.

[32] F.A. Long and W.F. McDevit, Chem. Rev., 51 (1952) 119.

PA·FPNS: its synthesis and use in spectrophotometric determination of magnesium

Hui-Min Ma *, Yue-Xian Huang, Shu-Chuan Liang

Institute of Chemistry, Chinese Academy of Sciences, Beijing 100080, China

Received 19 April 1995; revised 19 July 1995; accepted 21 July 1995

Abstract

A new polymeric chromogenic reagent PA·FPNS has been synthesized by condensing polyallylamine (PA) with 3-(4-formylphenylazo)-4,5-dihydroxynaphthalene-2,7-disulfonic acid (FPNS) and its properties studied. In alkaline media, PA·FPNS reacts with magnesium to form a water-soluble blue complex, whose absorption maximum is at 604 nm. The molar absorptivity (ε) of the complex is $5.2 \times 10^4 \, l \, mol^{-1} \, cm^{-1}$, which is four times that of the FPNS–Mg complex, and Beer's law is obeyed over the range $0–0.35 \, \mu g \, ml^{-1}$ magnesium. Compared to the corresponding low-molecular-weight FPNS and other chromogenic reagents, PA·FPNS offers considerably improved sensitivity and selectivity for magnesium, which may be attributed to incorporating FPNS into a water-soluble polymer and the effect of the polymeric chain on the reaction microenvironment. Also, a simple and sensitive spectrophotometric method for the determination of magnesium has been developed and applied to water and human fluid samples with satisfactory results.

Keywords: PA·FPNS; Magnesium; Spectrophotometry

1. Introduction

Water-soluble polymers such as poly(vinyl alcohol) have been widely used in photometric analysis to improve the sensitivity, stability and solubility of reaction systems, which may be described as enhancing effects. It is interesting to see whether by incorporating a chromogenic group into a water-soluble polymer, the resulting polymeric reagents will have simultaneously chromogenic and enhancing functions. Such an idea

has been realized for the first time in our laboratory. For example, we had synthesized two polymeric chromogenic reagents, PV·FPNS and PV·FPAQ, by condensing poly(vinyl alcohol) (PV) with 3-(4-formylphenylazo)-4,5-dihydroxynaphthalene-2,7-disulfonic acid (FPNS) and 7-(4-formylphenylazo)-8-quinolinol (FPAQ) respectively. The two reagents did have the predicted desirable properties such as greatly improved sensitivities and stabilities of color reactions with some metal ions [1,2]. However, they are somewhat unselective. According to the rule of soft and hard acids and bases, the condensation prod-

* Corresponding author.

ucts contain a large number of hard base ligands such as hydroxy, and hence their reactivities are strengthened for other hard acid metal ions.

Obviously, in order to improve the reagent selectivities it is necessary to link the low-molecular-weight reagents to some other water-soluble polymers. Although there are a lot of photometric reagents for magnesium, few of them are superior to chromotrope 2R in terms of both sensitivity and selectivity [3–7]. Therefore, in this paper FPNS with an active formyl group and the structure feature of chromotrope 2R is chosen as a constituent to be incorporated. The water-soluble polymer employed is polyallylamine rather than poly (vinyl alcohol), because the former has active amino groups which condense easily with aldehydes, and the nitrogen donors intrinsically show more preference than oxygen for Mg^{2+} over Ca^{2+} [8]. This is conducive to improvements in reagent selectivity. Thus in this work the new polymeric chromogenic reagent PA·FPNS has been synthesized by incorporating FPNS into polyallylamine with different weight ratios of the two reactants. Furthermore, its analytical properties and applictions have been studied. The results show that PA·FPNS has a large advantage over PV·FPNS and other chromogenic reagents for magnesium determination, indicating that incorporation of the chromogenic part into water-soluble polymers can be used as an important measure for improving analytical functions of photometric reagents.

2. Experimental

2.1. Apparatus and reagents

Spectral and absorbance measurements were made with a Hitachi-340 ultraviolet–visible spectrophotometer and a Model 721 spectrophotometer (Shanghai, China). The pH values were obtained with a Model 25 pH meter (Shanghai, China). Infrared spectra were taken with a Perkin-Elmer 683 spectrometer. Microanalysis was performed on a Carlo Erba 1102 elemental analyzer.

Poly(allylamine hydrochloride) with average M_n 8500–11 000 was purchased from Aldrich,

and chromotropic acid(disodium salt) and p-aminobenzaldehyde were obtained from Beijing Chemical Factory, China. Magnesium stock solution (1.0 mg ml^{-1}), 0.1% (w/v) of FPNS and PA·FPNS (9.8% amino groups substituted) solutions, and 0.1 mol l^{-1} of Na_2HPO_4–NaOH buffer solution (pH 11.50) were used. Deionized-distilled water was employed throughout. All other chemicals used were of analytical grade.

2.2. Synthesis of PA·FPNS

Poly(allylamine hydrochloride) (2.0 g) was dissolved in 100 ml of pH 11 aqueous buffer (Na_2CO_3–$NaHCO_3$). To this was slowly added a solution of 2 g FPNS (prepared following our previous method [1c]) in 100 ml of water with stirring at room temperature. After 1 h the reaction solution was neutralized to pH 8–9 with dilute HCl. The resulting precipitate was filtered off, washed thoroughly with water, and dried in vacuo. The crude product was purified by dissolving in aqueous NaOH and reprecipitating with dilute HCl to give 2.0 g of PA·FPNS as a dark red solid. The product is soluble in alkaline solution (purplish red color) and slightly in water, but not in ethanol, acetone or dioxane. The alkaline solution of PA·FPNS is stable for 20 days at room temperature. After that its concentration decreases slowly. IR (KBr pellets): 3600–3300 cm^{-1} (brs, OH, NH); 1640 cm^{-1} (C=N); 1600, 1570, 1495 cm^{-1} (C=C, N=N); 1240–1150 cm^{-1} (brs, C–O, S=O); 1040 cm^{-1} (S=O). A 6.32% sulfur content was determined by barium salt titration. Absorption spectra of PA·FPNS were recorded against the corresponding reagent blank.

2.3. Procedure for magnesium determination

2.5 ml of pH 11.50 aqueous buffer (Na_2HPO_4–NaOH) and 2.0 ml of 0.1% PA·FPNS were added to a sample solution containing not more than 3.5 μg of magnesium and the final volume adjusted to 10 ml with water. The absorbances were measured at 604 nm in 1 cm cells against the reagent blank.

3. Results and discussion

3.1. Synthesis of PA·FPNS and its infrared and UV–visible spectra

A 1% solution of poly(allylamine hydrochloride) has a pH of 4 and an isoelectric point at ≈pH 9, at which polyallylamine has low solubility and precipitates easily. Accordingly, the condensation products of polyallylamine with aldehydes are conveniently purified by reprecipitation. Moreover, in alkaline media aromatic aldehydes react readily with aliphatic amines to give Schiff's bases [9]. Thus, neither the preparation nor the purification of PA·FPNS are difficult. In addition, by using different weight ratios of the two reactants, PA·FPNS with different degrees of substitution of amino groups could be prepared. For example, by using the three different weight ratios (2, 1 and 0.5) of PA to FPNS, PA·FPNS with three different sulfur contents (4.93%, 6.32% and 8.39%) could be obtained, and their degrees of substitution by amino groups were 6.6%, 9.8% and 17.3% respectively.

IR spectral analysis showed that, after reacting with PA, the carbonyl absorption peak (1685 cm^{-1}) of FPNS disappeared and a new one for the C=N double bond was observed at 1640 cm^{-1}, indicating that the condensation reaction between FPNS and PA did take place.

UV–visible spectra of PA·FPNS and its magnesium complex are shown in Fig. 1. Compared with FPNS [2c], PA·FPNS has a similar absorption spectrum except for the absorption maximum at 530 nm with a 5 nm red shift, which may be attributed to the increased conjugation of the whole molecule in the presence of a C=N double bond. The magnesium complex absorbs maximally at 604 nm.

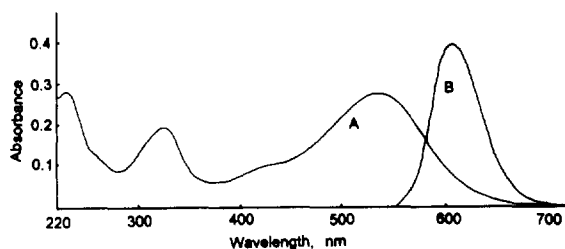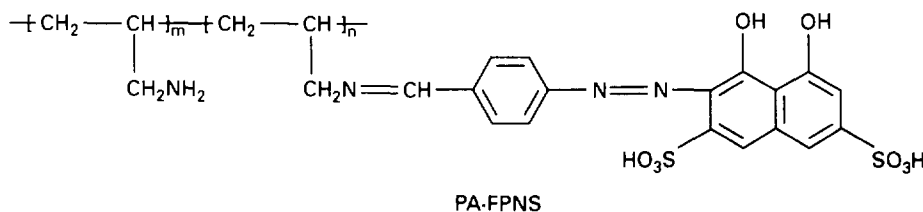The PA·FPNS structure is proposed as follows:

Fig. 1. Absorption spectra of PA·FPNS and its magnesium complex at pH 11.5. Experimental conditions: (A) 0.0015% of PA·FPNS solution against water blank; (B) the solution containing 0.15 μg ml^{-1} of Mg^{2+} and 0.02% of PA·FPNS against the corresponding reagent blank.

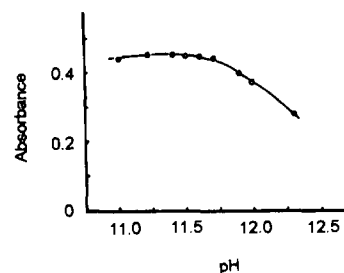Fig. 2. Effect of pH on the determination of magnesium (0.2 μh ml^{-1}).

It should be pointed out that the distribution of the chromogenic group in the polymer is uncertain.

3.2. Effect of amino group substitution

PA·FPNS with the three different degrees of substitution prepared above has little effect on the sensitivity of determining magnesium. Higher substitutions do not enhance the sensitivity except by giving stronger background absorbance. In this work, PA·FPNS with a moderate substitution (9.8%) was chosen to study the spectrophotometric determination of magnesium.

PA·FPNS

3.3. Conditions for spectrophotometric determination

Effects of pH and buffer systems

PA·FPNS is apt to precipitate in media with $7 < pH < 11.0$ and hardly reacts with magnesium at $pH < 7$. However, at higher pH ($\geqslant 11.0$) it gives a very sensitive color reaction with magnesium. The optimum pH range for the color reaction is 11.0–11.7, and at pH values higher than 11.7 the absorbance of the complex decreases (Fig. 2). Therefore, a pH of 11.5 ± 0.2 was used and maintained with aqueous Na_2HPO_4–NaOH buffer in this study, the optimum amount of which was 2.5 ml. No difference was observed with other buffers such as $Na_2B_4O_7$–NaOH.

Effect of PA·FPNS concentration

For the determination of 0.2 µg ml^{-1} Mg^{2+}, the absorbance reached a maximum value in the volume range 1.5–2.5 ml of 0.1% PA·FPNS solution, and 2.0 ml of PA·FPNS was used.

Characteristics of the color reaction

The blue PA·FPNS–Mg complex is immediately formed and the absorbance remains constant for at least 12 h. Variation of the temperature within the range 15–35°C does not affect the absorbance of the complex. Beer's law is obeyed over the range 0–0.35 µg ml^{-1} of magnesium and the linear regression equation is $A_{(absorbance)} = 2.122 \cdot C$ (µg Mg^{2+} ml^{-1}) $- 0.007$, $n = 6$, $r = 0.9960$. The molar absorptivity (ε) of the complex has been found to be 5.2×10^4 l mol^{-1} cm^{-1}, and according to IUPAC's recommendation [10] the detection limit is 14 ng ml^{-1}, based on 15 blank measurements ($k = 3$).

Effects of ethanol and surfactants

Ethanol and nonionic surfactants such as Triton X-100 and poly(vinyl alcohol)-1750 do not interfere with the determination of magnesium. Anionic surfactant (sodium dodecyl sulfate) leads to a negative error (-13%), whereas cationic surfactants, such as cetyltrimethylammonium bromide, associate with the reagent anion to form a precipitate and thus influence magnesium determination.

Effects of foreign ions

The potential interferences of more than 30 ions were examined for the determination of 2 µg of magnesium in the presence of each foreign ion. The tolerable amount was that of a species which gives a relative error of less than $\pm 5\%$ in the analytical signal(absorbance) of magnesium, i.e. for 2 µg of magnesium in 10 ml of solution, the tolerable amounts of the foreign ions are: at least 50 µg of A(III) and La(III); 5 µg of Ag(I), Au(III), Cr(VI)*, Ga(III), Mo(VI), Sc(III), Sn(IV), Sr(II) and Ti(IV); 2.5 µg of As(V); 10 µg of Ba(II)*, Cd(II), Co(II), Cu(II), Ge(IV), Hg(II), In(III), Pb(II), W(VI) and Zn(II); 0.5 µg of Be(II)*; 20 µg of Ca(II)*, Mn(II) and V(V); 30 µg of Fe(III); 400 µg of K(I); 2 µg of Ni(II)*, Pd(II) and Pt(IV); 1 µg of Rh(III); 500 µg of Cl$^-$, NO$_3^-$ and SiO$_3^{2-}$; 200 µg of SO$_4^{2-}$ (where an asterisk indicates that an ion with the given amount causes a maximum error of $\pm 5\%$). The tolerable amounts of Be(II) and Ni(II) are small, but concentrations of these two ions are naturally much lower than that of magnesium.

3.4. Comparison with FPNS

Under its optimum condition (pH 11.0), FPNS reacts with magnesium to form a complex with a maximum absorption at 600 nm and a molar absorptivity of 1.3×10^4 l mol^{-1} cm^{-1}, whereas the molar absorptivity of PA·FPNS–Mg complex is 5.2×10^4 l mol^{-1} cm^{-1}, which is four times that of the FPNS–Mg complex.

3.5. Comparison with other methods

There are few spectrophotometric methods for determining magnesium which possess simultaneously high sensitivity and selectivity. The methods with good selectivity are usually less sensitive [11,12]. Although increased sensitivities are achieved by using extraction or the formation of a multicomponent complex, the procedures become tedious and some suffer from nonselectivity [13,14]. Fortunately, the new polymeric reagent PA·FPNS could be directly used to determine magnesium in many samples without separation and masking treatment.

Table 1
Analytical results of magnesium in samples and recovery tests

Sample [a]		Volume used (µl)	Mg added (µg)	Mg found [b] (µg)	Mg concn. in sample (µg ml^{-1})	Recovery (%)	Mg concn. in sample detd. by AAS (µg ml^{-1})
Serum	1	120	0	3.02 ± 0.23(5)	25.2 ± 1.9	–	24.3
		60	1.0	2.55 ± 0.23(3)	–	104	
	2	150	0	3.15 ± 0.24(5)	21.0 ± 1.6	–	20.8 (certified value)
Urine	1	40	0	3.37 ± 0.28(3)	84.3 ± 7.0	–	90.0
		20	1.5	3.08 ± 0.26(3)	–	93	
	2	30	0	1.90 ± 0.21(3)	63.3 ± 7.0	–	60.3
	3	20	0	2.68 ± 0.23(3)	134.0 ± 11.5	–	132.5
Tap water	1	60	0	2.16 ± 0.18(5)	36.0 ± 3.0	–	35.0
		30	1.0	2.03 ± 0.21(3)	–	95	–
	2	60	0	2.25 ± 0.22(3)	37.5 ± 3.7	–	37.3
	3	60	0	1.00 ± 0.23(3)	16.7 ± 3.8	–	15.0

[a] Serum 1: serum mixtures of normal humans were provided by Zhongguancun Hospital, Beijing; serum 2: a human serum reference material (GBW 09135) was obtained from the National Research Center for Certified Reference Materials (Beijing, China). Fresh urine and tap water were acidified with a few drops of dilute HCl. Appropriate volumes of these samples were taken and analyses were then conducted following the procedure given in the text.
[b] Mean $\pm t S_{y_0}(m)$ [21] at the 95% confidence level, $S_{y_0} = S_{y \cdot x} \cdot 1/b \cdot \{1/m + 1/n + 1/b^2 \cdot (y_0 - \bar{y})^2/\Sigma(x_i - \bar{x})^2\}^{1/2}$, m = the number of determinations.

3.6. Analytical applications

Atomic absorption spectrometry is considered to be the best method for the assay of magnesium in water and human fluids such as serum and urine, but spectrophotometric methods are more often used because of their simplicity and low cost [15–18]. Different chromogenic reagents such as Methylthymol Blue, formazan dye, magon and especially Calmagite have been proposed for determining Mg^{2+} in biological fluids [16,19]. In practical applications, Calmagite needs a nonionic surfactant and masking agents (e.g. NaCN and EGTA) to improve its selectivity for Mg^{2+}. Most sensitive spectrophotometric methods for determining Mg^{2+} in water also require previous treatments such as separation or masking [15,18,20]. Compared with those methods described above, however, the present proposed method is simple, needs no masking and can be satisfactorily applied to the direct determination of magnesium in water and human fluids (Table 1). The results, given in Table 1, were evaluated by the paired t-test [21] and showed that there was no significant difference between the proposed method and AAS at the 95% confidence level.

4. Conclusions

The present results further demonstrate that incorporation of a chromogenic group into water-soluble polymers can be used as an effective way for improving the analytical properties of photometric reagents. By replacing the hydroxy group in the polymer used with an amino group, the resulting condensed product PA·FPNS provides better analytical properties than PV·FPNS in terms of both sensitivity and selectivity. PA·FPNS is one of the best chromogenic reagents for determining magnesium. When applied to the analysis of human fluids, it requires only small sample volumes and needs no previous treatment. Of course, the presented method may also be adapted for improvements in other analytical reagents such as fluorimetric reagents. We are currently focusing on such an attempt.

Acknowledgment

References

[1] S.-C. Liang and E. Zang, Fresenius' Z. Anal. Chem., 334 (1989): (a) 511; (b) 636. (c) Huaxue Shiji, 13 (1991) 323.

[2] E. Zang and S.-C. Liang, Trace Analysis (in Chinese): (a) 5 (1989) 7; (b) 6 (1990) 67. (c) Huaxue Shiji, 14 (1992) 129.

[3] K. Ueno, T. Imamura and K.L. Cheng, Handbook of Organic Analytical Reagents, 2nd edn., CRC Press, Boca Raton, FL, 1992, p. 192.

[4] A. Young, T.R. Sweet and B.B. Baker, Anal. Chem., 27 (1955) 356.

[5] Z. Ji, J. Huang and Z. Mao, Yejin Fenxi, 13 (1993) 50.

[6] S. Shibata, A. Uchiumi, S. Sasaki and K. Goto, Anal. Chim. Acta, 44 (1969) 345.

[7] J. Marcos, A. Rios and M. Valcarcel, Analyst, 117 (1992) 1629.

[8] R.J.P. Williams, Q. Rev. Chem. Soc., 24 (1970) 331.

[9] M.M. Sprung, Chem. Rev., 26 (1940) 308.

[10] G.L. Long and J.D. Winefordner, Anal. Chem., 55 (1983) 712A.

[11] T. Pal, N.R. Jana and P.K. Das, Analyst: (a) 117 (1992) 791; (b) 118 (1993) 1337.

[12] N. Peerzada and E. Kozllik, Anal. Lett., 23 (1990) 1087.

[13] J. Zhuang, Z. Su, J. Li and Q. Pan, Fenxi Huaxue, 17 (1989) 731, 766.

[14] K. Fukamachi, H. Kohara and N. Ishibashi, Bunseki Kagaku, 19 (1970) 1529.

[15] H. Wada, G. Nakagawa and K. Ohshita, Anal. Chim. Acta, 159 (1984) 289.

[16] R.J. Elin, Magnesium Trace Elem., 10 (1991/1992) 60.

[17] G.V. Iyenger, Elemental Analysis of Biological Systems, Vol. 1, CRC Press Inc., Boca Raton, FL, 1989, p. 96.

[18] D.T.E. Hunt and A.L. Wilson, The Chemical Analysis of Water, General Principles and Techniques, 2nd edn., Royal Society of Chemistry, London, 1986, p. 367.

[19] J. Savory, K.S. Margrey, Jr., J.R. Shipe, M.G. Savory, M.H. Margrey, T.E. Miffin, M.R. Wills and J.C. Boyd, Clin. Chem., 31 (1985) 487.

[20] X. Qiu and Y. Zhu, Mikrochim. Acta, Part III (1983) 1.

[21] J.C. Miller and J.N. Miller, Statistics for Analytical Chemistry, 2nd edn., Ellis Horwood, Chichester, 1988, pp. 58, 101–115.

Determination of glycerol in alcoholic beverages using packed bed reactors with immobilized glycerol dehydrogenase and an amperometric FIA system

M.I. Prodromidis, C.D. Stalikas, S.M. Tzouwara-Karayanni, M.I. Karayannis*

University of Ioannina, Laboratory of Analytical Chemistry, Ioannina, Greece

Abstract

A flow injection analysis system incorporating amperometric detection and enzyme reactor for glycerol determination in alcoholic beverages is described. The reactor is based on the glycerol dehydrogenase system, and the enzyme was immobilized through chemical modification on several supporting materials such as aminopropyl and isothiocyanate controlled pore glass, aminopolystyrene resin and m-aminobenzyloxymethyl cellulose. NADH, the product of the enzymatic reaction, was monitored amperometrically with a three-electrode wall-jet type flow through cell, at $+0.5$ V vs. Ag/AgCl. The method was evaluated in the presence or absence of potassium and the following linear dynamic ranges were found: $2 \times 10^{-5} - 2 \times 10^{-4}$ mol l^{-1} and $4 \times 10^{-5} - 4 \times 10^{-4}$ mol l^{-1}, respectively. The interference effects of various compounds were also studied. The relative standard deviation was found to be better than 1.0% ($n = 6$). The reactors are stable for over a period of 3 months and after about 2500 injections. Under optimum working conditions the sampling frequency was 30 samples h^{-1}. The successive application of the method was confirmed by comparison with a reference method. The mean relative error is 2.2% and the recovery 95–102%.

Keywords: Amperometric FIA; Glycerol determination; Isothiocyanate CPG; Immobilized enzyme

1. Introduction

Glycerol in grape juice has been shown to be an indicator of defects in harvested grapes [1]. It is also a secondary fermentation product in wine contributing to the sensory properties, while it is added to the beer and other alcoholic beverages in order to improve their taste. Therefore, a rapid, sensitive, reliable and at the same time economical

*Corresponding author.

method is desired for the determination of this analyte. The official methods for determining glycerol are that recommended by the AOAC and also liquid chromatography [2,3]. Both methods are either very time-consuming and tedious or expensive and not suited to routine analysis. However, several enzymatic methods have been developed for the analysis of glycerol, combining the selectivity of the enzymes involved with different detection systems [4–11]. In these cases the shortcomings of the methods arise from the use of

more than one enzymatic pathway, the tedious pretreatment of the sample, the need for preparation of many reagents and the use of complicated instrumentation. Here we present a simple, precise and reproducible procedure which links a reactor bearing immobilized glycerol dehydrogenase (GDH) and the amperometric detection of the produced NADH, using a graphite electrode mounted on a wall-jet type flow through cell. A fully automated flow injection analysis (FIA) manifold is used for performing the determinations. The GDH is immobilized on several inorganic and organic polymeric supporting materials for the construction of packed bed reactors (PBRs). The resulting enzymatic reactors are evaluated and the superior one is used for the determination of glycerol. Moreover, the proposed method does not use additional reagents, such as mediators or other co-immobilized enzymes, except the NAD^+ required for the operation of the immobilized enzyme. Many attempts have led in the past to similar enzymatic schemes, but to our opinion without the analytical advantages of the present work [4,9].

The glycerol concentration is proportional to the yield of NADH, the product of the enzymatic reaction:

$$Glycerol + NAD^+ \xrightarrow{GDH} dihydroxyacetone$$

$$+ NADH + H^+ \qquad (1)$$
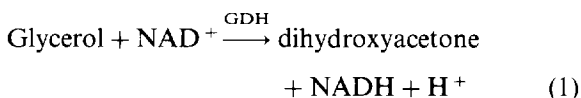
2. Experimental

2.1. Apparatus

An automated dual-channel, in-house built FIA manifold was used for the determinations. The FIA system consists of a four-way pneumatically actuated injection valve (Rheodyne, Type 50 Teflon, Cotati, CA, USA) and an in-house electronic actuator, assembled from a transformer (DC, 5–12 V, 2 A, 5 W) and a 12 V coil. The coil is actuated by resident software developed in our laboratory which controls the passage of compressed air through the valve as well as a four-channel peristaltic pump (Gilson Minipuls 3, Villiers-le-Bel, France). The three-electrode elec-

trochemical detector, model 656 (Metrohm, Herisau, Switzerland) comprises a wall-jet type thermostatted cell (volume < 1 μl), a graphite working electrode (RW001, 3.0 mm i.d., Ringsdorff-Werke GmbH), a built-in gold auxiliary electrode and a Ag/AgCl reference electrode. The potentiostat is the Autolab Electrochemical Analyser (Eco Chemie, Utrecht, The Netherlands).

2.2. Reagents

A glycerol dehydrogenase, (glycerol:NAD^+ 2-oxidoreductase; EC 1.1.1.6, cellulomonas species, 49 U mg^{-1} solid) was purchased from Sigma, Cat. No. G-3512 (St. Louis, MO, USA). The aminopropyl and isothiocyanate controlled pore glass (CPG, 500 A, 200–400 mesh) as well as the aminopolystyrene resin (APSR) and m-aminobenzyloxymethyl cellulose (m-ABMC) were also purchased from Sigma. Boehringer (Mannheim, Germany) was the supplier of the enzymatic Test Kit which was used as a reference method. All the other chemicals were of analytical-reagent grade and were obtained from Sigma. Tris–HCl buffer 0.05 mol l^{-1}, pH 9.0 was prepared by dissolving 0.76 g Tris–HCl and 5.47 g Trizma base in 1 l distilled water.

2.3. Preparation of the immobilized enzyme reactors

Before immobilizing the enzyme, the supporting materials are chemically modified. The isothiocyanate CPG was purchased preactivated with thiophosgene [12]. The PBRs were prepared by packing the derivatives (80 mg) in glass tubes (2 mm i.d × 30 mm length). A 0.05 mol l^{-1} solution based on a phosphate buffering system of suitable pH (Table 1), containing 2.5% v/v glutaraldehyde, was pumped through the columns of aminopropyl-CPG and APSR at a flow rate 0.2 ml min^{-1} for 2 h at room temperature in order to preactivate the support, followed by washing of the columns with doubly-distilled water for 2 h. The m-ABMC was activated by diazotation with $NaNO_2$ as described elsewhere [13]. GDH (343 U) was loaded onto the supporting materials by cir-

culating the enzyme in phosphate buffer solution of appropriate pH for 36 h at a flow rate of 0.2 ml min^{-1}, and 4°C. The solution with the enzyme was directed along the reactor by reversing the flow for time intervals (15 min) specified by means of a computer program, in order to achieve better efficiency of immobilization. The support was then washed with water (5 min), NaCl 0.5 mol l^{-1} (60 min), water (60 min) and finally with the phosphate buffer solution 0.05 mol l^{-1} (30 min). An increase in circulation time up to 48 h did not significantly improve the efficiency of immobilization. The reactors were stored at 4°C filled with the buffer of immobilization. In all cases the concentration of the enzyme solution was 7 mg GDH/3.5 ml of 0.05 mol l^{-1} phosphate. The immobilization on APSR and m-ABMC was carried out at pH 7.0 and 7.8, respectively [14,15]. Higher concentrations of GDH did not improve the response.

2.4. Procedure

The flow diagram of the FIA system is shown in Fig. 1. The streams of the carrier (Tris–HCl 0.05 mol l^{-1} pH 9.0, containing 1.45×10^{-2} mol l^{-1} K^+) and the NAD^+ solution (1×10^{-2} mol l^{-1}) in the working buffer solution were continu-
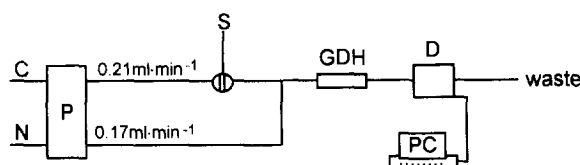

Fig. 1. Schematic representation of the FIA manifold for glycerol determination. GDH, glycerol dehydrogenase; C, carrier; N, NAD^+; P, pump; S, sample; D, detector; and PC, personal computer.

ously pumped at flow rates of 0.21 ml min^{-1} and 0.17 ml min^{-1}, respectively. Standards or real samples were introduced automatically as shots of 170 μl via the loop injection valve. The peak height of the current response was taken as a measure of the glycerol concentration.

According to previous investigations, the graphite electrodes proved to be very efficient with respect to stability, reproducibility and sensitivity for the determination of NADH [16]. They were maintained and regenerated as follows: graphite rods were first polished using wet emery paper (Nr.240), washed thoroughly with deionized water and finally dried at 60°C for 30 min prior to heating in a muffle furnace at 700°C for 90 s, in order to remove tiny particles from their surface [17]. After cleaning, the electordes were pretreated by cycling between + 1.0 and − 1.0 V at a scan rate of 100 mV s^{-1} for about 20–30 scans in 10% H_2SO_4.

Table 1
Efficiencies of GDH immobilization on different supports for different pH values

Support	pH	Immobilization yield (%)	Relative activity (%) [a]
CPG/Glu [b]	7.0	74	91
CPG/Glu [b]	8.0	67	86
CPG/ThC [c]	7.0	81	95
CPG/ThC [c]	8.0	84	100
APSR [d]	7.0	22	9
m-ABMC [e]	7.8	28	16

[a]Measurements under standard conditions related to the most active preparation.
[b]CPG activated with 2.5% glutaraldehyde in phosphate.
[c]Isothiocyanate-CPG (preactivated with 10% thiophosgene in chloroform).
[d]Aminopolystyrene resin.
[e]m-Aminobenzyloxymethyl cellulose.

3. Results and discussion

The amount of immobilized enzyme was determined as proteinic molecules by measuring the absorbance of the GDH solutions at 280 nm before and after the immobilisation [18]. The use of APSR and m-ABMC did not give considerable yields of immobilization. The immobilization of GDH on CPG was performed with efficiencies between 67 and 85% (Table 1). The results prove that these materials are very good functionalized supports for the immobilization of GDH, and, to the best of our knowledge, this is the first time they have been used as such. The response of the system was high enough to avoid the use of

diaphorase which has been previously used as a link in reaction schemes given by Eq. (1) [4].

Parameters such as immobilization and working pH, concentrations of NAD^+ and flow rates of the reagents were optimized. The different parameter variations were implemented with a glycerol standard solution of 1×10^{-4} mol 1^{-1}.

The optimum pH for the activation of GDH has been previously reported to be 9.0 and 8–10 [19,20], while pH 11 leads to inactivation of the enzyme. The effect of pH on the system was also investigated. Several buffering systems of different concentration and pH were used. Fig. 2 illustrates that Tris–HCl buffer 0.05 mol 1^{-1}, pH 9.0, is the most suitable for the operation of the system. The buffer based on the glycine system yielded slightly higher responses but in a narrower range of pH, which restricted the operational conditions of the system.

Several flow rates in the range 0.10–0.60 ml min^{-1} were used in the experiments. An overall flow rate of 0.38 ml min^{-1} gave fairly high peak intensities and satisfactory sampling throughput (30 samples h^{-1}). A 9:7 flow ratio (buffer carrier to NAD^+ solution) offered low dilution of the sample and therefore satisfactory peak current. A sample volume of 170 μl was selected for performing the experiments which compensates for
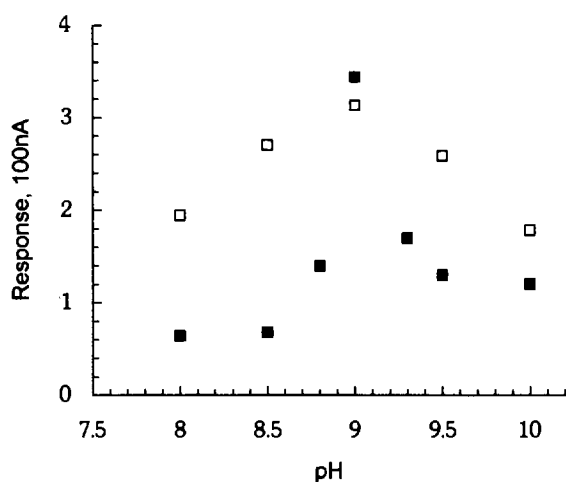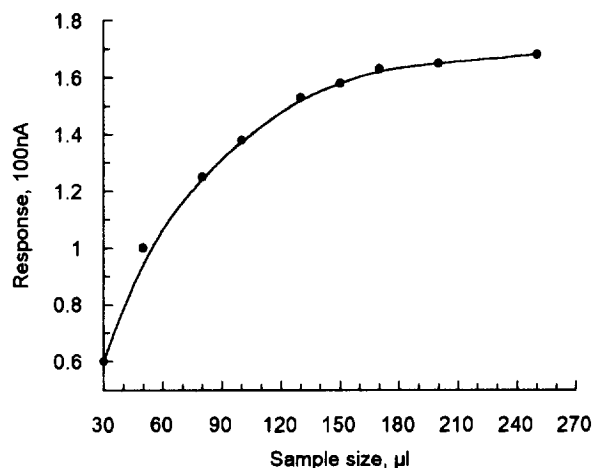
Fig. 3. Effect of sample size on the response of the system. Buffer concentration 0.05 mol ml^{-1}; glycerol concentration 1×10^{-4} mol 1^{-1}.

no peak broadening and fairly high sensitivity (Fig. 3). No influence on the system was observed by positioning a plain reactor beyond the meeting point of the sample with NAD^+ for better mixing.

Since the equilibrium of the employed reaction favours glycerol breakdown only in the case of NAD^+ being in large excess [21], a final concentration of 4.5×10^{-3} mol 1^{-1} was chosen for the experiments, providing high sensitivity.

Systems using the electrochemical oxidation of NADH at electrode surfaces need special emphasis on the use of mediators, which allow operation at lower potentials. The system described here is without mediators since no interference of ascorbic acid or other electrochemically active compounds is encountered in the tested real samples. In addition, most of the mediators are strongly pH dependent [16]. The majority of commonly used mediators such as Meldola Blue, Nile Blue, p-benzoquinone, ferrocenes and Methylene Blue are inactive in alkaline media (> 8) [22]. Ferricyanide and DCIP tested at pH 9.0 showed good electrochemical behaviour, but their analytical performance was limited in the absence of the enzyme diaphorase.

According to the literature [23], it is possible to regenerate NAD^+ from NADH at naked electrodes under ideal conditions (0.1 M NADH, pH

Fig. 2. Effect of pH on the response of the system. □, Tris–HCl; ■, glycine. Buffer concentration 0.05 mol 1^{-1}; glycerol concentration 1×10^{-4} mol 1^{-1}.

7) although a large overvoltage is needed, i.e. + 1.1 V vs. SCE, and prolonged usage results in fouling of the electrode surface. However, the direct anodic oxidation of NADH has been reported by Laval et al. using a Blaedel and Wang type pretreatment of the electrode [24], by Eggers et al. using diluted NADH [25], and by Blaedel and Engstrom at + 0.875 V vs. SCE using an NAD$^+$ concentration of 1–5 mM [26]. As noticed, the NAD$^+$ was shown not to cause fouling of the electrode [26]. In the present work, a lower potential of + 0.5 V vs. Ag/AgCl was applied in order to improve the stability of the baseline while minimizing the graphite surface fouling. Replicate measurements of a glycerol standard solution during our experiments showed no fouling effect at the electrode surface.

The behaviour of commonly considered interferents, normally present in real samples, was also investigated. All the tested compounds (metals, amino acids and organic acids) were present at concentrations of 1×10^{-3} mol l^{-1} in mixtures containing 1×10^{-4} mol l^{-1} of glycerol. As expected, the results displayed in Table 2 show that only potassium and ascorbic acid give positive interferences. In this case, potassium functions as an activator of the enzyme [19] leading to an increase in the system sensitivity. For routine experiments, the potassium is led to the FIA

Table 2
Interference effect of various compounds on the assay of glycerol in a standard solution of 1×10^{-4} mol l^{-1}. The concentration of interfering compound in all cases was 1×10^{-3} mol l^{-1}

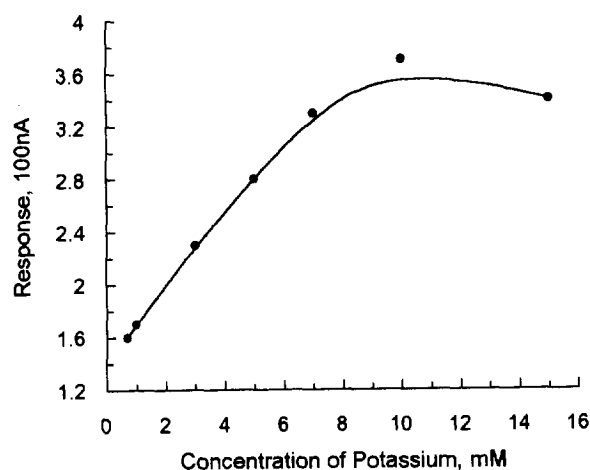| Interfering compound	Relative activity (%)
None	100
KCl	270
NaCl	101
CaCl$_2$	100
Leucine	102
Alanine	102
Tartaric acid	100
Citric acid	104
Malic acid	103
Ethylene glycol	112
Ascorbic acid	440

Fig. 4. Effect of potassium on the response. Tris–HCl 0.05 mol l^{-1}, pH 9.0; glycerol concentration 1×10^{-4} mol l^{-1}.

system along with the carrier at a concentration of 8×10^{-3} mol l^{-1} as indicated in Fig. 4. Owing to the high concentrations of glycerol in real samples large dilutions were performed, thus minimizing the interferences present.

Under the optimum working conditions, good linearity was achieved in the follow concentration ranges of glycerol: 4×10^{-5}–4×10^{-4} mol l^{-1} without potassium and 2×10^{-5}–2×10^{-4} mol l^{-1} in the presence of potassium. The correlation coefficients were 0.997 and 0.998, respectively. The relative standard deviation for both reactors was 0.8% for a 1×10^{-4} mol l^{-1} standard glycerol solution (six replicate measurements). The detection limit (for signal-to-noise ratio = 3) in the presence of potassium was 5×10^{-6} mol l^{-1}.

The reactors displayed very good operational and storage stability if kept in the buffer of immobilization at 4°C when not in use. Under the conditions described above, after more than 2500 injections over a period of 3 months, the reactor retained 85% of its initial activity.

Although several methods have been suggested for the determination of glycerol in food samples, the proposed method surpasses those previously given in the literature in terms of simplicity and low cost.

The method was applied to the determination of glycerol in several types of wines, beers and champagne. Dilutions of 1:100 to 1:500 are neces-

Table 3
Determination of glycerol in several alcoholic beverages. The standard deviation of the means ranges from 0.03 to 0.06

Sample	Reference method [a] (g l^{-1})	With K$^+$ [b] (g l^{-1})	Relative error (%)	Without K$^+$ [b] (g l^{-1})	Relative error (%)
Red wine (Boutari)	7.55	7.45	1.3	7.32	3.0
White wine (Tsantali)	6.78	6.88	1.5	6.69	1.3
White wine (Zitsa)	5.19	5.11	1.5	5.35	3.1
Red wine (local)	6.38	6.28	1.6	6.10	4.4
Retsina	6.31	6.46	2.4	6.25	1.0
Champagne	7.89	7.76	1.6	7.65	3.0
Beer (Heineken)	1.24	1.25	0.8	1.21	2.4
Beer (Henninger)	1.39	1.37	1.4	1.32	5.3
Beer (Amstel)	1.28	1.31	2.3	1.30	1.6

[a]Boehringer–Mannheim Test Kit.
[b]Average of five runs.

Table 4
Recovery of glycerol surplus added to some of the real samples given in Table 3

Sample	Glycerol added (g l^{-1})	Glycerol found (g l^{-1})	Recovery (%)
Red wine (Boutari)	0.46	0.45	98
Retsina	0.46	0.45	98
Champagne	0.40	0.38	95
Beer (Amstel)	0.40	0.41	102

sary, depending on the glycerol concentration of the sample. The accuracy of the FIA method was evaluated by comparing it to the enzymatic standard method using the Boehringer Test Kit. The results as well as the relative errors are presented in Table 3, and are in good agreement with those obtained by the reference method. The original samples normally contained high concentrations of potassium, but the performed dilutions kept its content to a minimum. The matrix effect was studied for different samples by recovery experiments. The recoveries attained were in the range 95–102% as shown in Table 4.

References

[1] A.S. Kupina, Am. J. Enol. Vitic., 35 (1984) 59.
[2] Official Methods of Analysis, 12th edn., AOAC, Arlington, VA, 1975, Sect. 11.010–11011.
[3] A. Caputi, E. Christensen, N. Biedenweg and S. Miller, J. Assoc. Off. Anal. Chem., 75 (1988) 379.
[4] A.S. Attiyat and G.D. Christian, Anal. Chim. Acta, 106 (1979) 225.
[5] M. Masoom and P.J. Worsfold, Anal. Chim. Acta, 188 (1986) 281.
[6] T.A. Kelly and G.D. Christian, Analyst, 109 (1984) 453.
[7] N. Kiba, H. Maruyama and M. Furusawa, J. Chromatogr., 456 (1988) 398.
[8] B. Merchie, A. Girard, B. Maisterrena, P. Michalon and R. Couturier, Anal. Chim. Acta, 263 (1992) 85.
[9] M. Kiyoshi, M. Hiroaki, H. Masashi, D. Toyohiko and O. Yutaka, Agric. Biol. Chem., 55 (1991) 1055.
[10] I.L. Mattos, J.M.F. Romero, M.D.L de Castro and M. Valcarcel, Analyst, 120 (1995) 179.
[11] L.J. Murphy and P.T. Galley, Anal. Chem., 66 (1994) 4345.
[12] H.H. Weetall, Biochim. Biophys. Acta, 212 (1970) 1.
[13] H.H. Weetall, in K. Mosbach (Ed.), Methods in Enzymology, Vol. XLIV, Academic Press, New York, 1976, p. 134.
[14] I. Karube, K. Hara, I. Satoh and S. Suzuki, Anal. Chim. Acta, 106 (1979) 243.
[15] B.P. Surinov and S.E. Manoilov, Biochemistry (USSR), 31 (1966) 337.
[16] G. Palleschi, H.S. Rathore and M. Mascini, Anal. Chim. Acta, 209 (1988) 223.

[17] G. Jonsson and L. Gorton, Anal. Lett., 20 (1987) 839.

[18] W.J. Waddell, J. Lab. Clin.Med., 48 (1956) 311.

[19] L.A. Decker (Ed.), Worthington Enzyme Manual, Freehold, NJ, 1977.

[20] J.E. Strickland and D.N. Millen, Biochim. Biophys. Acta, 159 (1968) 221.

[21] M. Burton, in S.P. Colowick and N.O. Kaplan (Eds.), Methods in Enzymology, Vol. 1, Academic Press, New York, 1955, p. 397.

[22] S.A. Wring and J.P. Hart, Analyst, 117 (1992) 1215.

[23] A.P.F. Turner, I. Karubeand and G.S. Wilson (Eds.), Biosensors. Fundamentals and Applications, Oxford Science Publications, Oxford, 1987, pp. 265, 325.

[24] J.M. Laval, C. Bourdillon and J. Moiroux, J. Am. Chem. Soc., 106 (1984) 4701.

[25] H.M. Eggers, H.B. Halsall and W.R. Heineman, Clin. Chem., 28 (1982) 1848.

[26] W.J. Blaedel and R.C. Engstrom, Anal. Chem., 52 (1980) 1691.

Study of chemical modifiers for direct determination of silver in sea water by ETA-AAS with deuterium background correction

P. Bermejo-Barrera*, J. Moreda-Piñeiro, A. Moreda-Piñeiro, A. Bermejo-Barrera

Department of Analytical Chemistry, Nutrition and Bromatology, Faculty of Chemistry, University of Santiago de Compostela 15706, Santiago de Compostela, Spain

Abstract

Methods for the direct determination of silver in sea water samples by ETA-AAS using different chemical modifiers were studied. The effect of salinity was studied using synthetic sea water of high (72.8‰) and low (34.2‰) salinity, and the results were compared with aqueous standard solutions. The charring temperatures achieved were 800 and 900°C for magnesium nitrate and ammonium dihydrogen phosphate respectively, being 1100 °C for palladium nitrate and their mixtures. The best sensitivity obtained in the peak-height measurement mode was achieved by using reduced palladium (limit of detection (LOD) between 0.5 and 1.1 μg l^{-1} for an injection volume of 20 μl) with analytical recoveries close to 100% for synthetic and real sea water samples. The use of ammonium dihydrogen phosphate (LOD of 1.3 μg l^{-1} for an injection volume of 20 μl) produced good recoveries for low salinity; at high salinity an increase of around 25% was obtained, the method being unsuitable for sea water analysis. Finally, an interference study of the major components of sea water was carried out and applied to the analysis of surface sea water from the Galicia coast.

Keywords: ETA-AAS; Silver determination; Sea water; Chemical modifiers

1. Introduction

Silver has been recognized as a toxic element owing mainly to its abundance in marine environments [1]. Therefore, it is necessary to know the concentrations of silver in sea water. Despite the fact that silver determination is one of the most sensitive determinations by ETA-AAS, there are only a few reports on its implementation in sea water using a graphite furnace [2-6]. A reason for this could be the strong interference of chloride [7] and the high silver volatility. In fact, losses of silver were reported [8] at temperatures higher than 400°C, and also incomplete volatilization of the inorganic matrix of the sea water samples at these relatively low charring temperatures.

The above problems could be reduced considerably with the use of chemical modifiers, ensuring silver stabilization at higher charring temperatures, and hence allowing better elimination of the sea water matrix resulting in a decrease in the

---

* Corresponding author.

Table 1
Different procedures for silver separation from sea water

Preconcentration method	LOD	Ref.
Complexation with dithizone and extraction of the complex formed in IBMK	–	[3]
Complexation with dithizone and extraction of the complex formed in bencene	–	[4]
Complexation with ammonium pyrrolidine-1-yl dithioformate and diethylcarbamic acid, extraction with IBMK and re-extraction with nitric acid	$0.02 \, \mu g \, l^{-1}$	[9]
Coprecipitation of silver with mercury(II) sulfate	0.5 pg	[5]
Coprecipitation using cobalt pyrrolidine dithiocarbamate	$0.1 \, ng \, l^{-1}$	[6]
Coprecipitation with sodium tetrahydroborate	$0.7 \, ng \, l^{-1}$	[10]
Complexation with dithizone and sorption of the complex on activated carbon; elution with nitric acid	$1.6 \, \mu g \, l^{-1}$	[11]
Complexation with ammonium dithiophosphoric acid O,O-diethyl ester and sorption on carbon; elution with nitric acid	$1.0 \, ng \, l^{-1}$	[12]

matrix interference effects. For this reason, Rettberg and Holcombe [2] used tantalum as a second atomization surface. To avoid the matrix effect, the separation of silver from sea water using extractive procedures or by coprecipitation methods was also carried out; these procedures are summarized in Table 1. However, the use of analyte separation methods presents some disadvantages because of the laborious procedures required, and the possible loss of analyte and sample contamination during these procedures. Thus, a direct method with chemical modifiers appears more suitable.

Among the different chemical modifiers previously proposed for silver determination, ammonium dihydrogen phosphate [6], ascorbic acid [13,14], nitric acid [15] and EDTA, alone or combined with ammonium dihydrogen phosphate [16], were used for silver determination in oyster, sea water, mineral water and geological samples. Recently, Bhattacharyya [17] studied the effect of platinum, iridium, palladium, cadmium, magnesium, vanadium and titanium modifiers, and proposed the use of palladium acetate as a chemical modifier for silver determination in coal fly ash.

Some authors have successfully used palladium reduced by different reducing agents such as ascorbic acid and hydroxylamine hydrochloride, with 5% hydrogen as purge gas [18]. The addition of a reducing agent ensures that palladium is reduced to the metal early in the temperature program, improving the sensitivity for metals such

thallium and lead [18], and mercury [19] in sea water samples.

Thus, in the present work, a comparative study of palladium nitrate, alone or combined with magnesium nitrate and reducing reagents, and ammonium dihydrogen phosphate will be carried out for the direct determination of silver in real and synthetic sea water samples of low and high salinity, using a deuterium background correction system.

2. Experimental

2.1. Apparatus

Silver absorbance was measured with a Perkin-Elmer 1100 B atomic absorption spectrotometer equipped with a deuterium lamp for background correction, a HGA-700 graphite furnace atomizer and an AS-70 autosampler. The operating conditions are shown in Table 2.

2.2. Reagents

All solutions were prepared from analytical-reagent grade chemicals using ultrapure water, resistivity 18 MΩ cm^{-1}, which was obtained from a Milli-Q water purification system (Millipore).

The solutions used were: silver nitrate stock standard solution, 1.000 g l^{-1} (BDH chemicals, Poole, UK); palladium stock standard solution,

3.000 g l⁻¹ (99.999%, Aldrich, Milwaukee, WI, USA), prepared according to Welz et al. [20]; magnesium nitrate stock standard solution, 2.000 g l⁻¹, prepared from magnesium nitrate (Merck, Darmstadt, Germany); ammonium dihydrogen phosphate, 2.000 g l⁻¹, prepared from ammonium dihydrogen phosphate (BDH Chemical Ltd.); hydroxylamine hydrochloride (HONH₃Cl), 1.000 g l⁻¹, prepared from hydroxylamine hydrochloride (Merck); L(+)-ascorbic acid, 1.000 g l⁻¹, prepared from L(+)-ascorbic acid (Merck); citric acid, 1.000 g l⁻¹, prepared from citric acid (Merck).

Two synthetic sea water (SSW) samples [21] were prepared from the following components. SSWI: 30 g l⁻¹ of sodium chloride (Merck), and 10 g l⁻¹ each of magnesium chloride, potassium chloride, calcium chloride and strontium chloride (Merck), giving a salinity of 72.8 ‰. SSWII: 32 g l⁻¹ of sodium chloride, 14 g l⁻¹ of magnesium sulfate heptahydrate (Merck) and 0.15 g l⁻¹ of sodium hydrogencarbonate (Merck), giving a salinity of 34.2‰.

Ammonium nitrate, 1.000 g l⁻¹, was prepared from ammonium nitrate (Merck), and argon N-50 purity (99.999%) was obtained from SEO, Madrid, Spain.

2.3. Procedure for sample collection

Sea water samples, with a salinity between 28 and 30‰, were collected from coastal surface water of Galicia (north–west, Spain) in 100 ml glass bottles and immediately acidified with 200 μl of concentrated nitric acid [22]; this gave pH < 1.6, avoiding silver adsorption onto the glass bottle walls.

2.4. Procedure for measurements

Each real or synthetic sea water sample (200 μl), along with the appropriate volumes of the different chemical modifiers to obtain a concentration that will be referred to in the next section, was transferred into the autosampler cup. The volume was then made up to 1 ml and the solution stirred before measurements. Volumes of 20 μl were injected into the atomizer. A sequential dry–ash–atomize–clean electrothermal program (Table 2) was run and the integrated absorbances recorded.

3. Results and discussion

3.1. Charring and atomization temperatures

A study on silver stabilization in sea water samples, i.e. synthetic sea water spiked with 10 μg l⁻¹ of Ag⁺ and an aqueous standard solution of 10 μg l⁻¹ of Ag⁺ using (a) nitric acid (3.5%, v/v), (b) palladium nitrate (20 μg l⁻¹), (c) magnesium nitrate (20 μg l⁻¹), (d) palladium (20 μg l⁻¹)–magnesium nitrate (20 μg l⁻¹), (e) palladium (20 μg l⁻¹)–ascorbic acid (200 μg l⁻¹), (f) palladium (20 μ l⁻¹)–hydroxylamine hydrochloride (200 μg l⁻¹), (g) palladium (20 μ l⁻¹)–citric acid (200 μg l⁻¹) and (h) ammonium dihydrogen phosphate (20 μg l⁻¹), was performed. The optimum charring temperatures obtained are shown in Table 3. As can be observed, when aqueous standard solutions were used, optimum charring temperatures of 1000 and 1100°C were reached when using palladium nitrate, palladium–magnesium nitrate and reduced palladium; in contrast, for nitric acid, magnesium nitrate and ammonium dihydrogen phosphate, loss of silver was observed at charring temperatures of 600, 800 and 900°C respectively.

Table 2
Graphite furnace temperature program and spectrometer operating conditions [a]

Step	Temperature	Ramp	Hold	Argon flow
Drying	150	15	20	300
Charring	700–1500	15	30	300
Atomization	1800–2500	0	3	0 (read)
Cleaning	2500	1	3	300

[a] Ag hollow cathode lamp; wavelength = 328.1 nm; lamp current = 4 mA; spectral bandwidth = 0.7 nm; integration time = 3 s; peak-area and peak-height measurements; pyrolytically coated graphite tubes and pyrolytic platform; deuterium background correction; injection volume = 20 μl.

Table 3
Optium charring and atomization temperatures (°C) corresponding to each chemical modifier, obtained for aqueous standard, synthetic and real sea water samples spiked with Ag^+ $(10 \mu g l^{-1})$

Chemical modifier	Aqueous standard		Sea water		SSWII (34.2‰)		SSWI (72.8‰)	
	Char. temp.	Atom. temp.	Char. temp.	Atom. temp.	Char. temp.	Atom. temp.	Char. temp.	Atom. temp.
Pd (20 mg l^{-1})	1100	2200	1100	2200	1200	2200	1100	2000
Pd (20 mg l^{-1})–Mg(NO$_3$)$_2$ (20 mg l^{-1})	1000	2100	1100	2100	1100	2100	1100	2100
Pd (20 mg l^{-1})-L(+)-ascorbic acid (200 mg l^{-1})	1100	2100	1100	2100	1100	2200	1100	2000
Pd (20 mg l^{-1})–HONH$_3$Cl (200 mg l^{-1})	1100	2000	1100	2100	1100	2100	1000	2000
Pd (20 mg l^{-1})–citric acid (200 mg l^{-1})	1000	2200	1100	2100	1000	2200	1000	2000
Mg(NO$_3$)$_2$ (20 mg l^{-1})	800	2200	800	2200	800	2300	900	2100
(NH$_4$)H$_2$PO$_4$ (20 mg l^{-1})	900	2200	900	2200	900	2200	1000	1900
HNO$_3$ (3.5%, v/v)	600	2100	–	–	–	–	–	–

When real and synthetic sea water samples of low salinity (SSWII) were used, similar results to those found when using aqueous standard solutions were obtained for all the chemical modifiers tested (except when nitric acid was used). For synthetic sea water samples of high salinity (SSWI), an increase in charring temperature of about 100°C was observered when palladium nitrate, magnesium nitrate and ammonium dihydrogen phosphate were used as chemical modifiers. This could be due to some beneficial effect of the high content of sodium chloride matrix on silver stabilization.

For all the chemical modifiers tested, real and synthetic sea water samples gave a scatter of silver absorbance signals for charring temperatures lower than 700°C; this is due to the incomplete salt volatilization at these temperatures. The use of HNO$_3$ as a chemical modifier is thus inadequate, owing to the low charring temperatures obtained.

The atomization temperature was also studied for these chemical modifiers, using the corresponding optimum charring temperatures obtained previously. The atomization temperature was varied between 1800 and 2500°C. Similar optimum atomization temperatures, around 2200°C, were achieved (Table 3) for all chemical modifiers and samples. However, the peak profile related to the use of palladium reduced by ascorbic acid was better (higher peak height) when the atomization temperature was increased to over 2200°C. For palladium alone or combined with magnesium nitrate, hydroxylamine hydrochloride and citric acid, the improvement to the peak profile was small. For ammonium dihydrogen phosphate and magnesium nitrate, the increase in atomization temperature did not modify the peak profiles. This can be also seen in Fig. 1, for different silver absorbance–time profiles obtained using palladium nitrate, palladium–magnesium nitrate, palladium reduced by ascorbic acid, magnesium nitrate and ammonium dihydrogen phosphate. In addition, early appearance times were obtained when atomization temperatures were increased for all the chemical modifiers tested. For lower atomization temperatures, the peaks present tailed off, owing to poorer precision in the measurements, and the peak heights were correspondingly lower.

It may be concluded that the use of nitric acid as a chemical modifier does not allow the direct determination of silver in sea water samples, and that magnesium nitrate and ammonium dihydrogen phosphate produce poorer silver stabilization compared with palladium nitrate and their mixtures.

3.2. Background signal

The background signal values obtained previously for the optimum charring temperatures and

for each chemical modifier, when a real sea water sample was used, were low (around 0.010 absorbance units (a.u.)), except in the cases of magnesium nitrate and ammonium dihydrogen phosphate. For these chemical modifiers, the
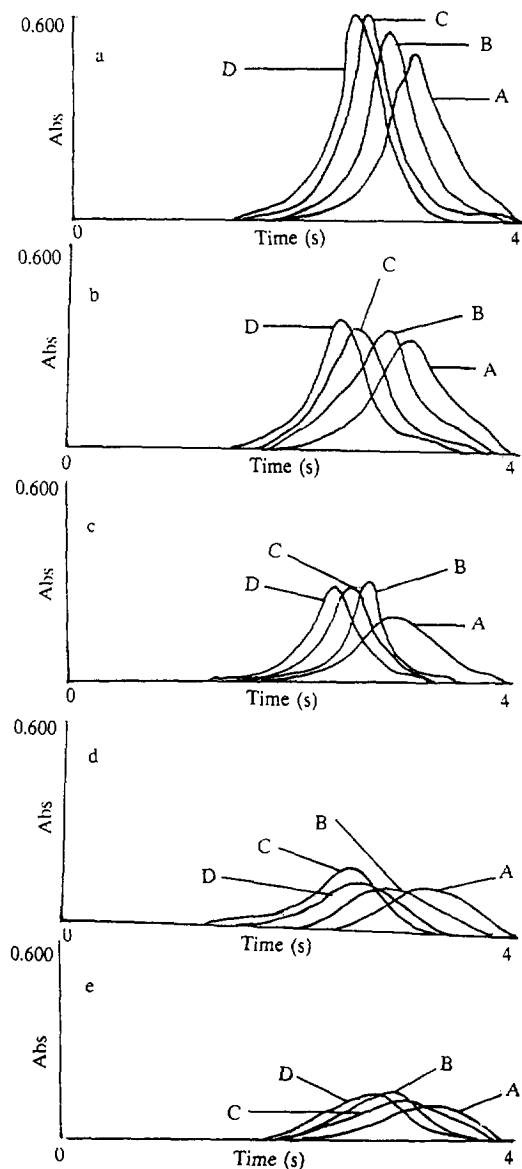

Fig. 1. Peak profiles obtained for a real sea water sample when (a) palladium–ascorbic acid, (b) palladium nitrate, (c) palladium–magnesium nitrate, (d) magnesium nitrate, and (e) ammonium dihydrogen phosphate were used as chemical modifier for different atomization temperatures: (A) 2100°C, (B) 2200°C, (C)2300 °C and (D) 2400°C.
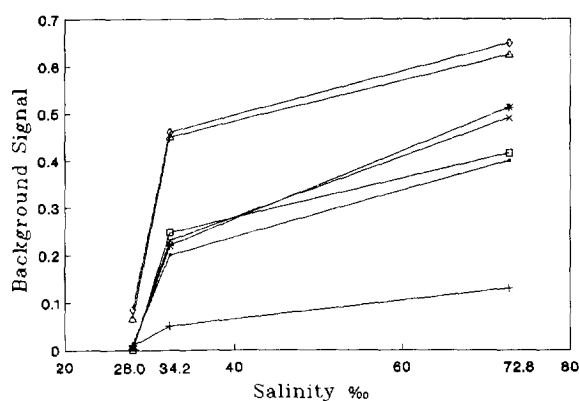
Fig. 2. Background values related to different salinities for several chemical modifiers: palladium nitrate (■), palladium–magnesium nitrate (|), palladium–ascorbic acid (□), palladium–hydroxylamine (*), palladium–citric acid (×), magnesium nitrate (△) and ammonium dihydrogen phosphate (◇).

background signal values were 0.090 and 0.070 a.u. respectively, due to the lower admissible charring temperatures (800 and 900°C), which do not allow efficient removal of the sea water matrix.

When synthethic sea water of low and high salinity was used, the background signal values increased strongly (Fig. 2) for all chemical modifiers, except the mixture palladium–magnesium nitrate. The use of palladium nitrate and reduced palladium offered background signal values of around 0.200 and 0.400 a.u. for low and high salinities respectively, while the highest background signal values obtained were for ammonium dihydrogen phosphate, i.e. 0.450 and 0.600 a.u. for low and high salinities respectively.

The addition of ammonium nitrate to real and synthetic sea water samples was carried out to increase the removal of sodium chloride from samples when magnesium nitrate and ammonium dihydrogen phosphate were used. From the results obtained, it can be said that the addition of ammonium nitrate does not offer sufficient volatilization of sodium chloride, which necessitates a charring temperature higher than 900°C [23].

Finally, when palladium nitrate plus magnesium nitrate was used the background signal values obtained were considerablely low, around 0.050 and 0.130 a.u. for low and high salinity
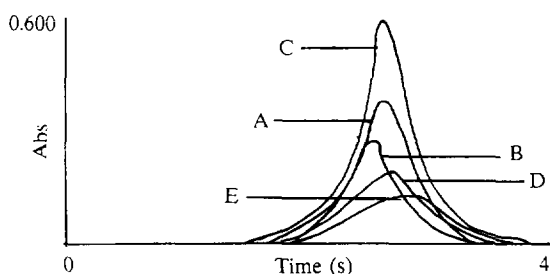
Fig. 3. Peak profiles obtained for a sea water sample spiked with Ag^+ (10 μg l^{-1}) corresponding to the use of (A) palladium nitrate (20 mg l^{-1}), (B) palladium (20 mg l^{-1})-magnesium nitrate (20 mg l^{-1}), (C) palladium (20 mg l^{-1})-ascorbic acid (200 mg l^{-1}), (D) magnesium nitrate (20 mg l^{-1}) and (E) ammonium dihydrogen phosphate (20 mg l^{-1}).

respectively. Thus, the addition of $Mg(NO_3)_2$ has some beneficial effects, problably due to matrix oxidation, which increase the advantages of the use of palladium [24].

3.3. Peak profiles

The peak profiles obtained for a sea water sample spiked with 10 μg l^{-1} of Ag^+ and for each chemical modifier, at a concentration referred to previously, are shown in Fig. 3. As can be seen, the best peak profile (highest peak height and smallest tails) corresponds to the use of palladium reduced by ascorbic acid. The other reducing reagents (hydroxylamine hydrochloride and citric acid) did not improve the peak profile when added to palladium nitrate. Finally, the worst

peak profiles correspond to the use of magnesium nitrate and ammonium dihydrogen phosphate.

3.4. Calibration and standard addition graphs

A study of the calibration and addition graphs with the chemical modifiers tested for silver determination was performed. The charring temperature was an optimum one related to a real sea water sample and the atomization temperature employed was 2300 °C, as the best peak profiles were obtained for some of the chemical modifiers at this atomization temperature. The calibration and addition slopes obtained using peak-area and peak-height measurements are shown in Table 4. As can be seen, these slopes, related to all kinds of samples for each chemical modifier (except when ammonium dihydrogen phosphate was used), are very similar, no statistical differences being found when the F-test [25] was applied for a confidence level of 99.5%. Thus, it can be assumed that the matrix effect for high salinity is small. Consequently, the calibration method using aqueous standard solution may be used independently of the salinity of the sea water sample. When $(NH_4)H_2PO_4$ was used, an increase of about 100% in the slope value was obtained for synthetic sea water of high salinity (SSWI), the calibration method employing aqueous standard solutions being unsuitable in this case. For this situation a standard addition method will be carried out.

The increase in the slope values obtained when peak-height measurements were used (Table 4)

Table 4
Slopes expressed as a.u./μg of $Ag\,l^{-1}$ of calibration and addition graphs for different chemical modifiers

Chemical modifier	Aqueous standard		Sea water		SSWII 34.2‰		SSWI 72.8‰	
	Area mode	Height mode	Area mode	Height mode	Area mode	Height mode	Area mode	Height mode
Pd (20 mg l^{-1})	0.021	0.023	0.020	0.022	0.018	0.020	0.022	0.025
Pd (20 mg l^{-1})-$Mg(NO_3)_2$ (20 mg l^{-1})	0.022	0.020	0.020	0.020	0.019	0.021	0.021	0.022
Pd (20 mg l^{-1})-L(+)-ascorbic acid (200 mg l^{-1})	0.036	0.041	0.035	0.044	0.030	0.044	0.035	0.040
Pd (20 mg l^{-1})-$HONH_3Cl$ (200 mg l^{-1})	0.020	0.021	0.022	0.023	0.015	0.019	0.021	0.020
Pd (20 mg l^{-1})-citric acid (200 mg l^{-1})	0.022	0.028	0.020	0.027	0.016	0.025	0.021	0.021
$Mg(NO_3)_2$ (20 mg l^{-1})	0.019	0.021	0.020	0.018	0.018	0.022	0.020	0.026
$(NH_4)H_2PO_4$ (20 mg l^{-1})	0.011	0.013	0.013	0.011	0.011	0.017	0.021	0.019

Table 5
Characteristic mass (m_0), detection limit (LOD), quantification limit (LOQ) and mean RSD (%) corresponding to each chemical modifier

Chemical modifier	m_0 (pg)		LOD (µg l^{-1})		LOQ (µg l^{-1})		Mean RSD (%)	
	Area mode	Height mode	Area mode	Height mode	Area mode	Height mode	Area mode	Height mode
Pd (20 mg l^{-1})	4.6	4.3	1.2/0.4[a]	1.0/0.3[a]	4.0	3.3	1.4	0.6
Pd (20 mg l^{-1})–Mg(NO$_3$)$_2$ (20 mg l^{-1})	4.4	4.5	1.5/0.5[a]	1.6/0.5[a]	5.0	5.3	1.9	1.6
Pd (20 mg l^{-1})-L(+)-ascorbic acid (200 mg l^{-1})	2.5	1.8	0.7/0.2[a]	0.5/0.1[a]	2.3	1.7	1.3	0.4
Pd (20 mg l^{-1})–HONH$_3$Cl (200 mg l^{-1})	4.3	4.3	1.3/0.4[a]	1.1/0.3[a]	4.3	3.7	1.3	1.4
Pd (20 mg l^{-1})–citric acid (200 mg l^{-1})	4.5	3.6	1.4/0.4[a]	1.0/0.3[a]	4.7	3.3	1.5	0.5
Mg(NO$_3$)$_2$ (20 mg l^{-1})	4.4	5.0	1.2	1.0	4.0	3.3	1.9	1.1
(NH$_4$)H$_2$PO$_4$ (20 mg l^{-1})	8.8	7.3	2.3	2.1	7.7	7.0	2.7	3.2

[a] These detection limits were obtained using 400 µl of sea water sample (filled to 1 ml) and by hot injection of 40 µl aliquot into the atomizer.

was strong when palladium reduced by ascorbic acid and citric acid was utilized. This is due to the good peak profile (high peak height) of the silver signal for these chemical modifiers. When palladium nitrate was used alone, a smooth increase in the slope values was obtained using the peak-height measurement mode, while for palladium–magnesium nitrate, magnesium nitrate, palladium–hydroxylamine hydrochloride and ammonium dihydrogen phosphate some improvement of the slope values was achieved.

3.5. Precision

The within-batch precision of the methods, obtained for 11 replicates of a sea water sample solution spiked with 0, 5 and 10 µg l^{-1} of Ag$^+$, was studied for all the chemical modifiers tested. The mean RSD (%) values are shown in Table 5. The precision obtained using peak-area and peak-height measurement modes is acceptable, RSD < 3.2%, corresponding to the best within-batch precision when the peak-height mode was used.

3.6. Sensitivity

A study of the sensitivity achieved for each chemical modifier was performed. The sensitivity was examined using the following parameters: limit of detection (LOD), limit of quantification (LOQ) and characteristic mass (m_0) [26]. Table 5

shows the values of these parameters obtained with each chemical modifier, and related to the use of both measurement modes (peak height and peak area). The slopes in each case were the calibration graphs using SSWII, and the standard deviation (SD) was related to 11 replicates of the blank of the calibration using SSWII.

As can be seen (Table 5), the use of the peak-height measurement mode for palladium nitrate, palladium–ascorbic acid and palladium–citric acid offers better LODs than the use of the peak-area measurement mode. When the other chemical modifiers were used, similar LODs were obtained in both measurement modes. In addition, for both measurement modes, the use of palladium reduced by ascorbic acid offers the best sensitivity, giving LODs of 0.7 and 0.5 µg l^{-1} for the peak-area and peak-height modes respectively.

These detection limits can be improved by introducing a large volume of sea water into the autosampler cup and by increasing the volume introduced into the graphite tube. Thus, when 400 µl of sea water sample was used to prepare the final solution and 40 µl aliquot was introduced into the atomizer by the hot injection technique (at 120°C), the detection limits could be reduced as shown in Table 5. Thus, when palladium–ascorbic acid was used the LOD obtained was reduced to 0.2–0.1 µg l^{-1} for each measurement mode. When magnesium nitrate and ammonium dihydrogen phosphate were used, the increase in

Table 6
Analytical recovery corresponding to each chemical modifier

Chemical modifier	Sea water		SSWII (34.2‰)		SSWI (72.8‰)	
	Area	Peak	Area	Peak	Area	Peak
Pd (20 mg l^{-1})	91.3	96.7	93.0	109.0	103.7	98.6
Pd (20 mg l^{-1})–Mg(NO$_3$)$_2$ (20 mg l^{-1})	93.3	103.0	97.8	102.0	104.2	107.4
Pd (20 mg l^{-1})-L(+)-ascorbic acid (200 mg l^{-1})	96.0	98.6	97.0	101.3	95.8	105.6
Pd (20 mg l^{-1})–HONH$_3$Cl (200 mg l^{-1})	105.7	97.5	102.1	102.5	105.3	103.3
Pd (20 mg l^{-1})–citric acid (200 mg l^{-1})	102.7	102.5	94.8	104.7	102.3	98.7
Mg(NO$_3$)$_2$ (20 mg l^{-1})	104.5	104.0	103.0	97.4	102.1	100.7
(NH$_4$)H$_2$PO$_4$ (20 mg l^{-1})	105.0	97.6	103.5	105.8	157.5	130.7

salt content obtained for a large injection volume produced a scatter in the silver absorbance signal due to inefficient volatilization of the sea water matrix and more pronounced matrix effects.

3.7. Accuracy

Owing to the fact that a reference material of sea water with certified silver concentration is not available, the accuracy was studied by analysis of a reference material (plant materials of aquatic origin) BCR-61, with an indicative silver concentration of 2.0 mg kg^{-1}. The results expressed for a confidence level of 95% as mean $\pm$ confidence limit were 2.5 $\pm$ 0.4, 2.3 $\pm$ 0.4, 2.6 $\pm$ 0.3, 2.4 $\pm$ 0.3, 2.4 $\pm$ 0.4, 2.5 $\pm$ 0.4 and 2.6 $\pm$ 0.4 mg kg^{-1} for palladium, palladium–magnesium nitrate, palladium–ascorbic acid, palladium–hydroxylamine hydrochloride, palladium–citric acid, magnesium nitrate and ammonium dihydrogen phosphate, respectively. In addition, the accuracy was studied

through the analytical recovery. As can be seen (Table 6), the use of palladium nitrate, magnesium nitrate, palladium–magnesium nitrate and reduced palladium ensures excellent recoveries, close to 100% for all silver concentrations and all salinities when both measurement modes were used. However, when ammonium dihydrogen phosphate was employed, only acceptable recoveries were obtained for low salinity; at high salinity (with respect to Milli-Q water), the analytical recovery increased to 150%, owing to the significant interference of salts from the sea water which will be discussed in the next section.

3.8. Interference study of the major components of sea water

The influence of the increasing concentration of sodium chloride and potassium sulfate (the major components of sea water) on the integrated absorbance signal of a sea water sample spiked

Table 7
Percentage of silver absorbance variation produced with the addition of NaCl and K$_2$SO$_4$ on a sea water sample spiked with Ag$^+$ (10 µg l^{-1})

Interferent	Conc. added (g l^{-1})	Pd	Mg(NO$_3$)$_2$	Pd–Mg(NO$_3$)$_2$	Pd–ascorbic acid	Pd–HONH$_3$Cl	Pd–critic acid	(NH$_4$)H$_2$PO$_4$
NaCl	5	−7.1	−10.3	+5.5	−4.6	−10.8	−8.2	−11.3
	10	−16.7	−25.3	+11.7	−9.6	−20.0	−22.1	−25.1
	15	−35.1	−51.6	+22.3	−23.7	−36.7	−33.5	−56.7
K$_2$SO$_4$	0.5	−7.2	−10.6	−10.8	−7.7	−10.6	−9.7	−13.2
	1	−10.7	−41.9	−55.3	−16.2	−30.6	−31.6	−35.4
	2	−20.6	−55.5	−68.5	−23.6	−48.1	−53.0	−55.9

with Ag^+ (10 μg l^{-1}) for each chemical modifier tested is shown in Table 7. We assume that these species begin to interfere at a concentration corresponding to a 10% increase or decrease in the signal in their absence.
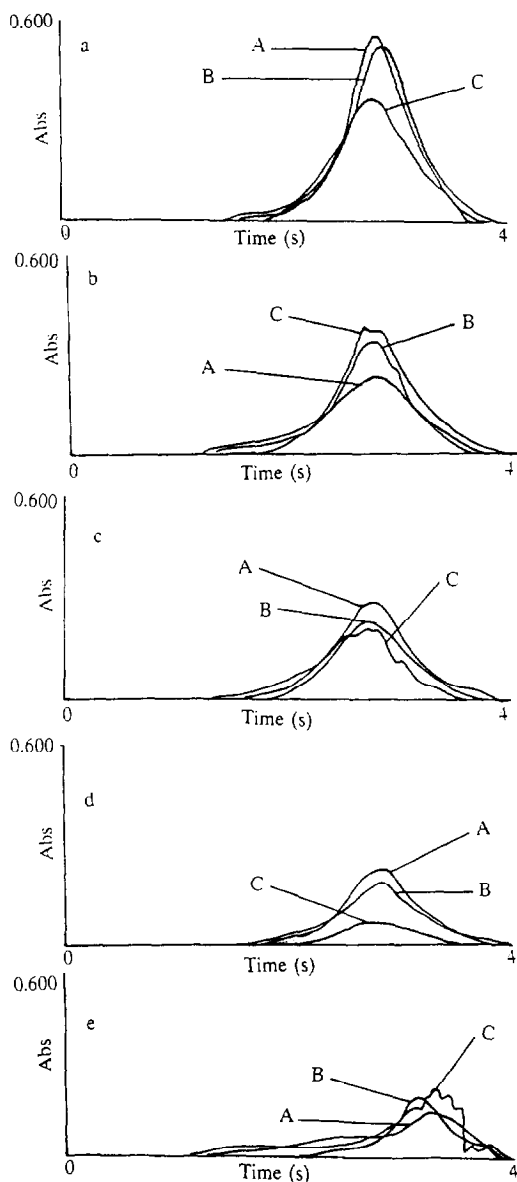

Fig. 4. Effect of increasing concentration of NaCl, (A) 0 g l^{-1}, (B) 5 g l^{-1} and (C) 10 g l^{-1}, on the peak profile of a real sea water sample spiked with 10 μg l^{-1} of silver when (a) palladium–ascorbic acid, (b) palladium–magnesium nitrate, (c) palladium nitrate, (d) magnesium nitrate and (e) ammonium dihydrogen phosphate were used as chemical modifiers.

At concentrations of sodium chloride of up to 5 g l^{-1} there was no effect on the silver signal for the different chemical modifiers used, except in the case of palladium reduced by ascorbic acid for which a sodium chloride concentration of 10 g l^{-1} did not exhibit significant interference.

The increase in sodium chloride concentration (Fig. 4) produces the worst peak profile (small peak height) for all the chemical modifiers, except for the mixture palladium–magnesium nitrate for which an increase in the peak height was obtained. Finally, as can be seen in Fig. 4, a scatter of the silver peak was obtained for high sodium chloride concentration when ammonium dihydrogen phosphate was used as chemical modifier.

The addition of potassium sulfate did not produce any interference at concentrations higher than 0.5 g l^{-1} for all the chemical modifiers tested. However, the addition of this species produced a distorted peak profile, as was also observed on addition of sodium chloride.

4. Application

The method using the mixture palladium–ascorbic acid as chemical modifier was applied to the determination of silver in sea water samples from the Galicia coast (north–west Spain) using the peak-height mode and a calibration method with standard aqueous solution. Two sub-samples for each sea water sample were then analyzed. A volume of sea water of 200 μl was transferred into the autosampler cup with the appropiate volume of palladium and ascorbic acid to obtain the concentration referred to previously; it was then diluted to 1 ml. A 20 μl aliquot was injected into the atomizer. Owing to the low silver concentration of the sample 6, a 40 μl aliquot was introduced into the atomizer by hot injection at 120°C. The silver concentrations obtained are given in Table 8, together with the RSDs, and are seen to vary between 0.4 and 11.7 μg l^{-1}.

5. Conclusions

Palladium reduced by ascorbic acid was found to be the most adequate chemical modifier, with

Table 8
Silver levels in sea water samples [a]

Sample	Silver concentration ($\mu g\, l^{-1}$)	RSD (%)
1	7.8	2.1
2	2.9	2.5
3	5.3	1.8
4	11.7	3.4
5	5.9	1.4
6	0.4	3.1
7	3.3	2.6

[a] $n = 4$.

the lowest LOD (0.5 μg l^{-1}) obtained using the peak-height mode, for the direct determination of silver in sea water samples of low and high salinity. The other reducing reagents did not provide a more consistent performance. Thus, the behavior of the palladium modifier depends on the reduction method used. The analytical recoveries were close to 100% for all salinities and chemical modifiers, except for $(NH_4)H_2PO_4$ at high salinity. Thus, a single calibration curve using aqueous standard solution may be used for the analysis of sea water samples. When $(NH_4)H_2PO_4$ is employed for sea water of high salinity, the standard addition method must be used, owing to the matrix effect observed with this chemical modifier. Finally, the peak-height measurement mode was found to be more adequate when palladium, both alone and combined with reducing agents, was used, because better detection limits and within-batch precision are observed.

References

[1] E. Merian (Ed.), Metals and their Compounds in the Environmemt, VCH, New York, 1991, p. 1195.

[2] T.M. Rettberg and J.A. Holcombe, Spectrochim. Acta, Part B, 39 (1984) 249.

[3] F.H. Chermann, M.J. Spencer, W.B. Lyons and P.A. Mayewski, Chem. Geol., 53 (1985) 25.

[4] Y. Shijo, T. Shimizu and T. Tsunoda, Anal. Sci., 5 (1989) 65.

[5] M.N. Quigley and F. Vernon, Anal. Proc., 29 (1992) 1.

[6] N.S. Bloom and E.A. Crecelius, Anal Chim. Acta, 156 (1984) 139.

[7] W. Frech, E. Lundgerg and A. Cedergrem, Progr. Anal. Atom. Spectrosc., 8 (1985) 257.

[8] J.B. McHugh, At. Spectrosc., 5 (1984) 123.

[9] T.K. Jan and D.R. Young, Anal. Chim. Acta, 50 (1978) 1250.

[10] S. Nakashima, R.E. Sturgeon, S.N. Willie and S.S. Berman, Anal. Chim. Acta, 207 (1988) 291.

[11] E. Beinrohr. J. Rojcek and J. Garaj, Analyst, 113 (1988) 1831.

[12] A.K. Avila and A.J. Curtius, J. Anal. At. Spectrom., 9 (1994) 543.

[13] S.A. Sheuchuk, A.S. Alemasova and E. Trejos-Espinosa, Zavod Lab., 52 (1986) 1.

[14] N.E. Karmanova, Zh. Prikl. Spektrosk., 40 (1985) 904.

[15] B. Welz, Atomic Absorption Spectrometry, Verlag Chemie, Weinheim, 1985.

[16] Y.S. Zheng and X.G. Su, Can. J. Appl. Spectrosc., 38 (1993) 109.

[17] S.S. Bhattacharyya, At. Spectrosc., 15 (1994) 242.

[18] L. Voth-Beach and D. Shrader, J. Anal. At. Spectrom., 2 (1987) 45.

[19] P. Bermejo-Barrera, J. Moreda-Piñeiro, A. Moreda-Piñeiro and A. Bermejo-Barrera, Mikrochim. Acta, in press.

[20] B. Welz, G. Schlemmer and J.R. Mudakavi, J. Anal. At. Spectrom., 3 (1988) 695.

[21] D.C. Baxter and W. Frenh, Anal. Chim. Acta, 225 (1989) 175.

[22] K.C. Jones, P.J. Peterson and B.E. Davis, Int. J. Environ. Anal. Chem., 20 (1985) 247.

[23] G. Schlemmer and B. Welz, Spectrochim. Acta, Part B, 41 (1986) 1157.

[24] P. Bermejo-Barrera, J. Moreda-Piñeiro, A. Moreda-Piñeiro and A. Bermejo-Barrera, Anal. Chim. Acta, 296 (1994) 181.

[25] J.C. Miller and J.N. Miller, Statistics for Analytical Chemistry, Wiley, New York, 1984.

[26] L.H. Keith, W. Crummett, J. Deegan, R.A. Libby, J.K. Taylor and G. Wenther, Anal. Chem., 55 (1983) 2210.

Trace level voltammetric determination of manganese, iron and chromium in real samples in the presence of each other

Clinio Locatelli

Department of Chemistry "G. Ciamician", University of Bologna, Via F. Selmi 2, I-40126 Bologna, Italy

Abstract

The determination of manganese in the presence of iron and chromium by differential pulse voltammetry and fundamental harmonic alternating current voltammetry was compared, including the case of very high element concentration ratios. The voltammetric measurements were carried out using a stationary mercury electrode in ammonia–ammonium chloride buffer (pH 9.6). The analytical procedure was verified by the analysis of the standard reference materials Portland Cement BCS 372, Spectrographic Zinc Spelter NBS-SRM 631, Stainless Steel (AISI 321) NBS-SRM 121d and Highly Alloyed Steel Eurostandard 281-1. Precision and accuracy, expressed as relative standard deviation and relative error respectively, were of the order of 3–5%, while the detection limit for each element was around 1×10^{-9} M. The standard addition technique improved the resolution of the voltammetric methods, within a maximum experimental error of 5%, even in the case of very high concentration ratios, that is outside the non-interference concentration ratios $69:1 > c_{Fe}:c_{Mn} > 1:74$; $35:1 > c_{Fe}:c_{Cr} > 1:30$ and $63:1 > c_{Fe}:c_{Mn} > 1:65$; $32:1 > c_{Fe}:c_{Cr} > 1:31$ for the differential pulse and alternating current techniques respectively, extrapolating the linear section of the i_p vs. concentration analytical calibration function for the element present at the lowest concentration. In contrast, the element with the greatest concentration was determined by the relevant calibration curve.

Keywords: Voltammetry; Manganese; Iron; Chromium; Reference materials

1. Introduction

The simultaneous determination of several elements at trace and ultratrace level concentrations in real matrices is one of the main aims of an analytical procedure, which however must always have both good selectivity and very high sensitivity. In the metal determination, several techniques are employed such as neutron activation analysis, atomic absorption spectrometry, atomic emission spectrometry with inductively-coupled plasma excitation and X-ray fluorescence. Usually such techniques need enrichment steps and, furthermore, as regards selectivity and sensitivity, often favour only one of these two aspects. For the above reasons, the voltammetric techniques appear to be very suitable, versatile and rapid for multicomponent determinations, having good selectivity and sensitivity without requiring metal enrichments before the analytical measurements

[1,2]. In previous works [3,4] sensitive and selective voltammetric methods were employed for the simultaneous determination of various elements in real matrices. The present work, regarding the determination of manganese in the presence of chromium and iron—these three elements are often present together in various real matrices—is the continuation of that endeavour.

Manganese is an essential micronutrient: in fact it is very important in various biochemical cycles regarding man, animals and plants. In addition, it is present in a great deal of inorganic matrices, in which chromium and iron are also almost always present. Adsorptive stripping voltammetry was proposed for the determination of manganese in the presence of several interferents [5] and in real samples [6]. Also, differential pulse anodic stripping voltammetry was employed successfully for determining manganese in natural water [7-9] and in sea water [10,11]. Finally, manganese was also determined in real matrices by a potentiometric stripping technique [12], taking into account either interference problems [13] or batch and flow procedures [14-16].

In the literature a lot of papers, using PIPES together with a chelating agent as supporting electrolyte, appeared to determine the various metal species by adsorptive voltammetry. Often such a technique suffers the effects of interferent ions, either as peak overlaps or as voltammetric signal depression, with consequent sensitivity reduction of the analytical method. In the specific case of manganese, employing PIPES and Eriochrome Black T as chelating agent, the presence of iron, chromium, nickel, copper, titanium, etc. produces considerable signal depression up to 35%, depending on their concentration. With regard to this, the results obtained by Wang and Mahmoud [5] have also been generally confirmed in our laboratory. For this reason a new selective and sensitive method has been set up to determine manganese, iron and chromium in real samples in the presence of each other, employing differential pulse voltammetry (DPV) and fundamental harmonic alternating current voltammetry (ACV); such analytical procedures require ammonia–ammonium chloride buffer (pH 9.6) as supporting electrolyte.

2. Experimental

2.1. Apparatus

Voltammetric measurements were carried out with an AMEL Mod. 433 instrument employing, as working electrode, a hanging mercury drop electrode (HMDE) consisting of a glass capillary having an internal diameter of 0.1 mm and a cone-shaped tip. An Ag/AgCl, KCl sat. electrode and a platinum wire were used as the reference and auxiliary electrodes respectively. The voltammetric cell was thermostatted at $25.0 \pm 5°C$. The solution was deaerated with pure nitrogen for 15 min prior to measurements, while a nitrogen blanket was maintained above the solution during the analysis. Standard additions were made with Gilson micropipettes with diposable plastic tips. The solutions were deaerated for 2 min after each standard addition.

2.2. Reagents and reference solutions

All solutions were prepared with deionized water (Millipore, Milli-Q). Suprapure grade acids, ammonia and sodium hydroxide were used. Ammonia–ammonium chloride buffer solution (pH 9.6) was prepared by mixing an appropriate amount of hydrochloric acid and ammonia solutions. Aqueous stock solutions of manganese, iron and chromium were prepared by dilution of the respective standard 1000 mg l^{-1} BDH solutions. The Teflon voltammetric cell was rinsed every day with suprapure concentrated nitric acid in order to prevent any contamination.

The following standard reference materials were chosen for the analyses: Portland Cement BCS 372, Spectrographic Zinc Spelter NBS-SRM 631, Stainless Steel (AISI 321) NBS-SRM 121d and Highly Alloyed Steel Eurostandard 281-1.

3. Results and discussion

3.1. Aqueous reference solutions

Prior to the analysis of standard reference materials, a preliminary study was carried out

employing aqueous reference solutions. The experimental conditions are reported in Table 1. The solution pH affects the peak height of each element; the pH vs. i_p behaviours of Mn, Cr and Fe (Fig. 1), employing the differential pulse technique, show that the best pH value compromise for all three elements is 9.6. When considering ACV the best analysis pH is also 9.6 (the pH vs. i_p behaviour is practically the same). The standard addition method was used for the measurements of the analytical calibration functions for both DPV and ACV (Tables 2 and 3). The correlation coefficient was found to be satisfactory in all cases, while the precision of the techniques, expressed in terms of the residual standard deviation, was excellent ($s_r < 5\%$). Tables 2 and 3 also report the detection limits for each element.

The simultaneous determination of manganese, iron and chromium was studied in a large range of concentration ratios of the components. More precisely, employing the experimental conditions of Table 1, the element concentration ratios, within which each single element could be determined without mutual interference, were investigated. To a fixed, but very small, concentration of
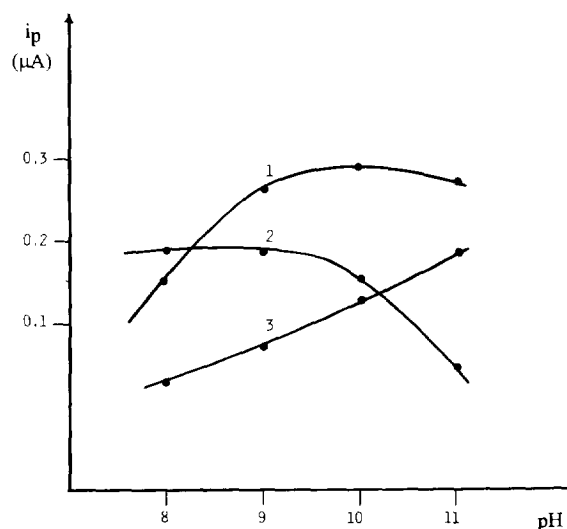
Fig. 1. Behaviours (i_p vs. pH) of Mn (curve 1), Fe (curve 2) and Cr (curve 3) with ammonia–ammonium chloride buffer (pH 9.6) as supporting electrolyte; $c = 2.5 \times 10^{-7}$ M for all the elements. Voltammetric technique: DPV. Experimental conditions: see Table 1.

Table 1
Experimental conditions for the determination of Mn, Fe and Cr by DPV and ACV. Supporting electrolyte: 1.0 M ammonia–ammonium chloride buffer (pH 9.6)

Experimental condition [a]	Method	Mn, Fe, Cr
E_i	–	−1.300
ΔE	ACV	10
	DPV	50
ϕ	ACV	270 + 88 (Mn)
		270 + 83 (Fe)
		270 + 84 (Cr)
f	ACV	100
dE/dt	–	10
τ	DPV	0.065
v	DPV	0.250

[a] E_i = initial potential (V/SCE); ΔE = amplitude of alternating current voltage (ACV) and pulse (DPV) superposed (mV); ϕ = demodulation phase angle (degrees); f = frequency (Hz); dE/dt = potential scan rate (mV s^{-1}); τ = pulse duration (s); v = pulse repetition (s).
Experimental peak potentials E_p (V/SCE): −1.665 ± 0.005 (Mn); −1.495 ± 0.005 (Fe); −1.420 ± 0.005 (Cr).

the element of interest, standard additions of the interfering element were added in such a way as to change their concentration ratios. Then the peak current values of the former element were compared to those determined by using the analytical calibration function of the individual element (cf. Tables 2 and 3) and the relative errors were calculated. Such errors are plotted in Figs. 2 and 3. It is apparent that the determination of the metals is possible, within a maximum error of 5%, in the concentration ranges $69:1 > c_{Fe}:c_{Mn} > 1:74$, $35:1 > c_{Fe}:c_{Cr} > 1:30$ and $63:1 > c_{Fe}:c_{Mn} > 1:65$, $32:1 > c_{Fe}:c_{Cr} > 1:31$ employing DPV and ACV techniques respectively. Such concentration ratios have also been confirmed by mono- and bivariate [3,4,17,19–21] analyses. In all cases, within the considered concentration ratios interval, the slopes of the statistical functions were practically equal to the analytical calibration function of the single element, and, moreover, the slope of the interfering element (bivariate analysis) was negligible, thus indicating non-interference between neighbouring species (Tables 2 and 3). The same Tables 2 and 3 also emphasize that there were no significant differences in the employment of the

Table 2
Analytical calibration functions[a] and relative mono and bivariate analyses (DPV)

	Mn	Fe	Cr
Calibration functions of each single element	$i_p = (0.02 \pm 0.03) + (1.18 \pm 0.05) \times 10^6 c$ $r = 0.9993^b$ $s_r = 2.8\%^c$ D.L. $= 8.47 \times 10^{-9}$ M^d	$i_p = (0.01 \pm 0.01) + (4.57 \pm 0.06) \times 10^5 c$ $r = 0.9996$ $s_r = 1.9\%$ D.L. $= 2.19 \times 10^{-8}$ M	$i_p = (0.02 \pm 0.02) + (7.41 \pm 0.05) \times 10^5 c$ $r = 0.9992$ $s_r = 3.6\%$ D.L. $= 1.35 \times 10^{-8}$ M
Monovariate analysis[e]	$i_p = (0.01 \pm 0.01) + (1.15 \pm 0.04) \times 10^6 c$ $r = 0.9995$ $s_r = 4.1\%$ D.L. $= 8.70 \times 10^{-9}$ M	$i_p = (0.02 \pm 0.02) + (4.68 \pm 0.09) \times 10^5 c$ $r = 0.9996$ $s_r = 3.8\%$ D.L. $= 2.14 \times 10^{-8}$ M	$i_p = (0.02 \pm 0.03) + (7.20 \pm 0.07) \times 10^5 c$ $r = 0.9989$ $s_r = 4.7\%$ D.L. $= 1.39 \times 10^{-8}$ M
Bivariate analysis[e]	$i_p = (0.01 \pm 0.02) + (1.14 \pm 0.03) \times 10^6 c_{Mn} + (2.0 \pm 0.2) \times 10 c_{Fe}$ $r = 0.9993$ $s_r = 3.1\%$ $e = -3.4\%$ D.L. $= 8.77 \times 10^{-9}$ M	$i_p = (0.01 \pm 0.01) + (4.79 \pm 0.12) \times 10^5 c_{Fe} + (8.3 \pm 0.2) c_{Mn}$ $r = 0.9993$ $s_r = 2.8\%$ $e = +4.8\%$ D.L. $= 2.09 \times 10^{-8}$ M $i_p = (0.01 \pm 0.02) + (4.67 \pm 0.11) \times 10^5 c_{Fe} + (6.2 \pm 0.4) \times 10 c_{Cr}$ $r = 0.9992$ $s_r = 4.0\%$ $e = +2.2\%$ D.L. $= 2.14 \times 10^{-8}$ M	$i_p = (0.01 \pm 0.02) + (7.56 \pm 0.11) \times 10^5 c_{Cr} + (8.6 \pm 0.7) \times 10 c_{Fe}$ $r = 0.9990$ $s_r = 3.9\%$ $e = +2.0\%$ D.L. $= 1.32 \times 10^{-8}$ M

[a] The errors correspond to a probability of 95%; i_p = peak current (μA); c = concentration of the electroactive species (M).
[b] r = correlation coefficient.
[c] s_r = mean standard residual deviation.
[d] Limit of detection (D.L.) is expressed according to IUPAC [18] and corresponds to a probability of 99%.
[e] In monovariate analysis, interferences from neighbouring elements are neglected; they are considered, however, in bivariate analysis [19–21].

Table 3
Analytical calibration functions[a] and relative mono and bivariate analyses (ACV)

	Mn	Fe	Cr
Calibration functions of each single element	$i_p = (0.01 \pm 0.01) + (0.88 \pm 0.07) \times 10^6 c$ $r = 0.9994^{b}$ $s_r = 3.0\%^{c}$ D.L. $= 1.14 \times 10^{-8}$ M^{d}	$i_p = (0.01 \pm 0.02) + (3.95 \pm 0.06) \times 10^5 c$ $r = 0.9990$ $s_r = 3.7\%$ D.L. $= 2.53 \times 10^{-8}$ M	$i_p = (0.02 \pm 0.02) + (5.71 \pm 0.08) \times 10^5 c$ $r = 0.9995$ $s_r = 3.1\%$ D.L. $= 1.75 \times 10^{-8}$ M
Monovariate analysis[e]	$i_p = (0.02 \pm 0.03) + (0.84 \pm 0.06) \times 10^6 c$ $r = 0.9988$ $s_r = 4.6\%$ D.L. $= 1.19 \times 10^{-9}$ M	$i_p = (0.01 \pm 0.02) + (4.12 \pm 0.08) \times 10^5 c$ $r = 0.9990$ $s_r = 3.8\%$ D.L. $= 2.43 \times 10^{-8}$ M	$i_p = (0.01 \pm 0.02) + (5.86 \pm 0.11) \times 10^5 c$ $r = 0.9988$ $s_r = 5.2\%$ D.L. $= 1.71 \times 10^{-8}$ M
Bivariate analysis[e]	$i_p = (0.01 \pm 0.01) + (0.82 \pm 0.03) \times 10^6 c_{Mn} + (4.9 \pm 0.5) \times 10 c_{Fe}$ $r = 0.9991$ $s_r = 4.0\%$ $e = -6.8\%$ D.L. $= 1.22 \times 10^{-8}$ M	$i_p = (0.02 \pm 0.02) + (3.73 \pm 0.11) \times 10^5 c_{Fe} + (9.8 \pm 0.3) c_{Mn}$ $r = 0.9996$ $s_r = 1.8\%$ $e = -5.6\%$ D.L. $= 2.68 \times 10^{-8}$ M $i_p = (0.01 \pm 0.01) + (4.09 \pm 0.05) \times 10^5 c_{Fe} + (8.1 \pm 0.7) \times 10 c_{Cr}$ $r = 0.9989$ $s_r = 4.2\%$ $e = +3.5\%$ D.L. $= 2.44 \times 10^{-8}$ M	$i_p = (0.02 \pm 0.02) + (5.99 \pm 0.14) \times 10^5 c_{Cr} + (9.2 \pm 0.8) \times 10 c_{Fe}$ $r = 0.9993$ $s_r = 2.8\%$ $e = +4.9\%$ D.L. $= 1.67 \times 10^{-8}$ M

[a] The errors correspond to a probability of 95%; i_p = peak current (μA); c = concentration of the electroactive species (M).
[b] r = correlation coefficient.
[c] s_r = mean standard residual deviation.
[d] Limit of detection (D.L.) is expressed according to IUPAC [18] and corresponds to a probability of 99%.
[e] See Table 2.

ELECTROLYTE: 1.0 M AMMONIA-AMMONIUM CHLORIDE BUFFER
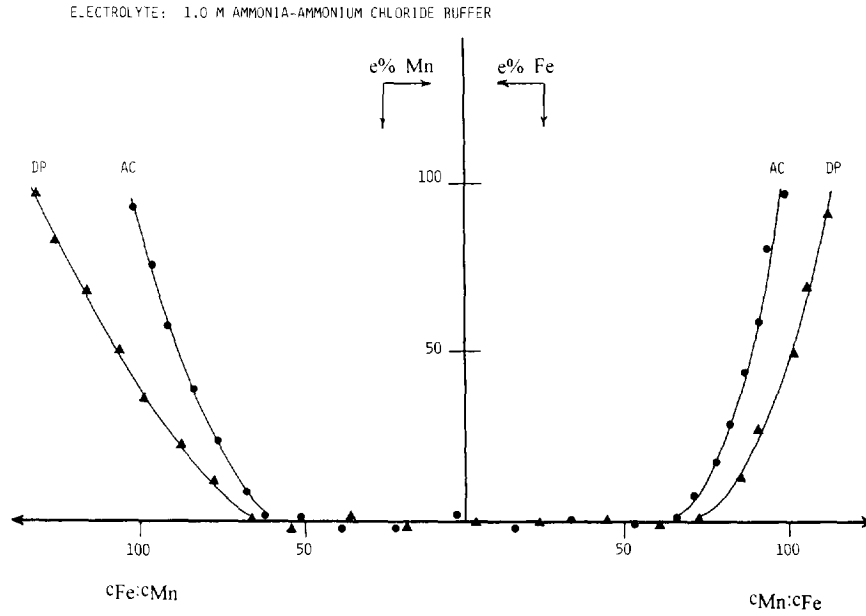
Fig. 2. Relationship between the metal concentration ratios (Mn/Fe) and the relative errors in the determination of the element present at the lowest concentration. Supporting electrolyte: 1.0 M ammonia–ammonium chloride buffer (pH 9.6). AC: alternating current voltammetric technique; DP: differential pulse voltammetric technique.

ELECTROLYTE: 1.0 M AMMONIA-AMMONIUM CHLORIDE BUFFER
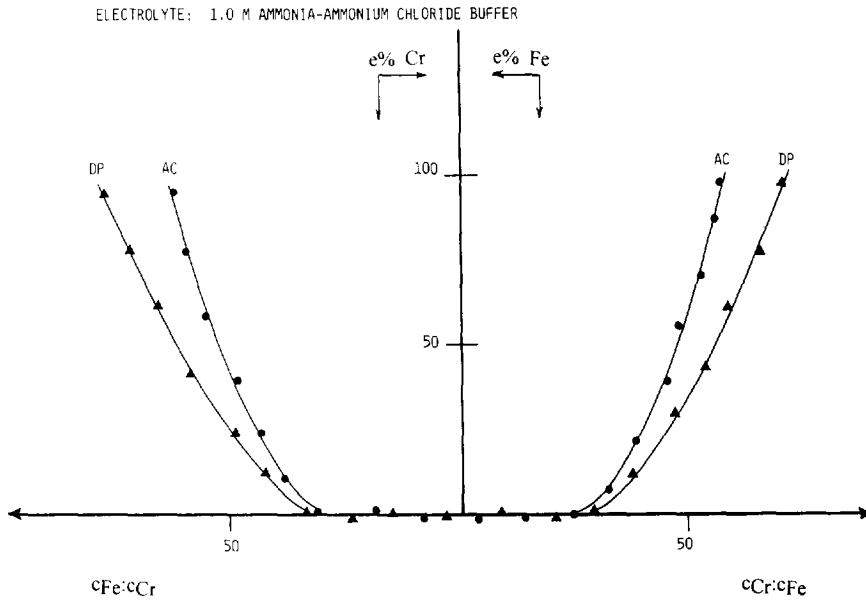
Fig. 3. Relationship between the metal concentration ratios (Cr/Fe) and the relative errors in the determination of the element present at the lowest concentration. Supporting electrolyte: 1.0 M ammonia–ammonium chloride buffer (pH 9.6). AC: alternating current voltammetric technique; DP: differential pulse voltammetric technique.

Table 4
Slopes (μA M^{-1}) of the analytical calibration functions in the real samples

Element	Method	Portland cement BCS 372	Spectrographic Zinc Spelter NBS-SRM 631	Stainless Steel (AISI 321) NBS-SRM 121d	Highly Alloyed Steel Eurostandard 281-1	Analytical calibration functions[a]
Mn	DPV	$(1.23 \pm 0.06) \times 10^6$	$(1.20 \pm 0.5) \times 10^6$	$(1.24 \pm 0.08) \times 10^6$	$(1.12 \pm 0.08) \times 10^6$	$(1.18 \pm 0.05) \times 10^6$
	ACV	$(0.84 \pm 0.06) \times 10^6$	$(0.93 \pm 0.07) \times 10^6$	$(0.89 \pm 0.05) \times 10^6$	$(0.91 \pm 0.09) \times 10^6$	$(0.88 \pm 0.07) \times 10^6$
Fe	DPV	$(4.69 \pm 0.11) \times 10^5$	$(4.72 \pm 0.14) \times 10^5$	$(4.66 \pm 0.15) \times 10^5$	$(4.31 \pm 0.08) \times 10^5$	$(4.57 \pm 0.06) \times 10^5$
	ACV	$(4.15 \pm 0.12) \times 10^5$	$(4.01 \pm 0.06) \times 10^5$	$(3.79 \pm 0.11) \times 10^5$	$(3.98 \pm 0.09) \times 10^5$	$(3.95 \pm 0.09) \times 10^5$
Cr	DPV		$(7.16 \pm 0.19) \times 10^5$	$(7.43 \pm 0.08) \times 10^5$	$(7.06 \pm 0.28) \times 10^5$	$(7.41 \pm 0.05) \times 10^5$
	ACV		$(5.69 \pm 0.23) \times 10^5$	$(6.00 \pm 0.35) \times 10^5$	$(5.47 \pm 0.21) \times 10^5$	$(5.71 \pm 0.08) \times 10^5$

[a]See Tables 2 and 3.

two voltammetric techniques: DPV is slightly more sensitive than ACV.

The most interesting aspect of the work concerns the determination of the metal with the lowest concentration and an unfavourable concentration ratio as to the interferent species, that is, outside the concentration ratios interval where the regression function obtained from bivariate analysis of the data was valid. In this situation, bringing the concentration ratio within the interval valid for bivariate analysis by appropriately adding the standard solution of the metal with the lowest concentration was enough to determine the metal itself. In fact, the i_p vs. concentration plots showed non-linear behaviour. A linear section was obtained when the concentration ratios attained values within the validity of the bivariate analysis. An extrapolation of this linear section permitted the evaluation of the metal content in the mixture with acceptable accuracy (behaviour as in Fig. 5 in the following section). The limit within which linearity prevails was statistically evaluated according to the method of Liteanu et al. [22] using the t-test criteria.

3.2. Practical application

Once established for aqueous reference solutions, the method was transferred to real matrices in order to confirm the applicability of the analytical procedure.

Sample preparation and analytical results

Portland Cement BCS 372 was prepared according to Riley [23]. Approximately 0.1 g cement, weighed accurately in a platinum crucible, was dissolved in 1 ml of 60% (m/m) perchloric acid, 3 ml of 40% (m/m) hydrofluoric acid was added, and the mixture was evaporated almost to dryness. After cooling, the soluble salts were dissolved in 250 ml of 1.0 M ammonia–ammonium chloride buffer solution (pH 9.6).

Spectrographic Zinc Spelter NBS-SRM 631, Stainless Steel (AISI 321) NBS-SRM 121d and Highly Alloyed Steel Eurostandard 281-1 were prepared as described by Thomerson and Price [24]. According to the metal content of the standard reference material employed, approximately

Table 5
Analytical results[a]

Element	Value	Method	Portland cement BCS 372	Spectrographic Zinc Spelter NBS-SRM 631	Stainless Steel (AISI 321) NBS-SRM 121d	Highly Alloyed Steel Eurostandard 281-1
Mn	Certified (%)		0.6×10^{-1}	1.5×10^{-3}	1.80	0.786
	Determined (%)	DPV	$(0.58 \pm 0.03) \times 10^{-1}$	$(1.54 \pm 0.55) \times 10^{-3}$	1.74 ± 0.07	0.818 ± 0.035
		ACV	$(0.56 \pm 0.04) \times 10^{-1}$	$(1.44 \pm 0.82) \times 10^{-3}$	1.69 ± 0.15	0.766 ± 0.029
	e (%)[b]	DPV	-3.3	$+2.7$	-3.3	$+4.1$
		ACV	-6.7	-4.0	-6.1	-2.5
	RSD (%)[b]	DPV	3.5	3.8	2.8	3.6
		ACV	3.2	4.3	4.5	4.2
Fe	Certified (%)		2.49	0.5×10^{-2}	68.263	70.307
	Determined (%)	DPV	2.58 ± 0.13	$(0.52 \pm 0.02) \times 10^{-2}$	66.318 ± 2.094	66.598 ± 4.049
		ACV	2.60 ± 0.14	$(0.48 \pm 0.03) \times 10^{-2}$	66.039 ± 2.792	73.439 ± 3.211
	e (%)[b]	DPV	$+3.6$	$+4.0$	-2.8	-5.3
		ACV	$+4.4$	-4.0	-3.2	$+4.5$
	RSD (%)[b]	DPV	2.8	4.3	5.1	3.2
		ACV	2.8	3.4	2.1	3.7
Cr	Certified (%)			1.0×10^{-4}	17.40	18.17
	Determined (%)	DPV		$(0.97 \pm 0.04) \times 10^{-4}$	18.32 ± 1.17	18.98 ± 1.04
		ACV		$(0.97 \pm 0.02) \times 10^{-4}$	18.09 ± 1.12	17.55 ± 0.91
	e (%)[b]	DPV		-3.0	$+5.3$	$+4.5$
		ACV		-3.0	$+4.0$	-3.4
	RSD (%)[b]	DPV		4.2	3.9	4.7
		ACV		4.9	2.9	2.6

[a] Number of samples: 5.
[b] e: relative error; RSD: relative standard deviation.

0.1–0.3 g, weighed accurately in a platinum crucible, was dissolved in 1 ml of 37% (m/m) hydrochloric acid, and 1 ml of 69% (m/m) nitric acid was added. After the initial reaction had subsided, 2 ml of 60% (m/m) perchloric acid was added and the solution evaporated until the sample was fully oxidized and fumes of perchloric acid appeared. After cooling, the soluble salts were dissolved in 250 ml of 1.0 M ammonia–ammonium chloride buffer solution (pH 9.6). The solutions were analyzed under experimental conditions listed in Table 1.

Table 4 shows the slopes of the analytical calibration functions calculated in the real samples for each element, together with those determined in the aqueous reference solutions (cf. Tables 2 and 3). Their comparison emphasizes that, in all cases, no matrix interferences were present, there being no significant differences at 5% error level.

The simultaneous determination of Fe, Mn and Cr was not difficult in the cases of the Portland Cement BCS 372—in such a matrix Cr is not present—and the Stainless Steel (AISI 321) NBS-SRM 121d, since the concentration ratios in the sample solution did not exceed the values of reciprocal interference at the 5% error level reported above. Then, each element was determined by the respective calibration curves (cf. Tables 2 and 3). The analytical results are listed in Table 5.

Spectrographic Zinc Spelter NBS-SRM 631, however, contains an excess of Fe, which interferes with the chromium peak ($c_{Fe}:c_{Cr} = 46.6$). The subsequent chromium standard additions enabled the analytical calibration function to show linear behaviour as soon as the concentration ratio $c_{Fe}:c_{Cr}$ equal to 35 and 32 for DPV and ACV respectively was attained. An extrapolation of this linear portion allowed the determination of
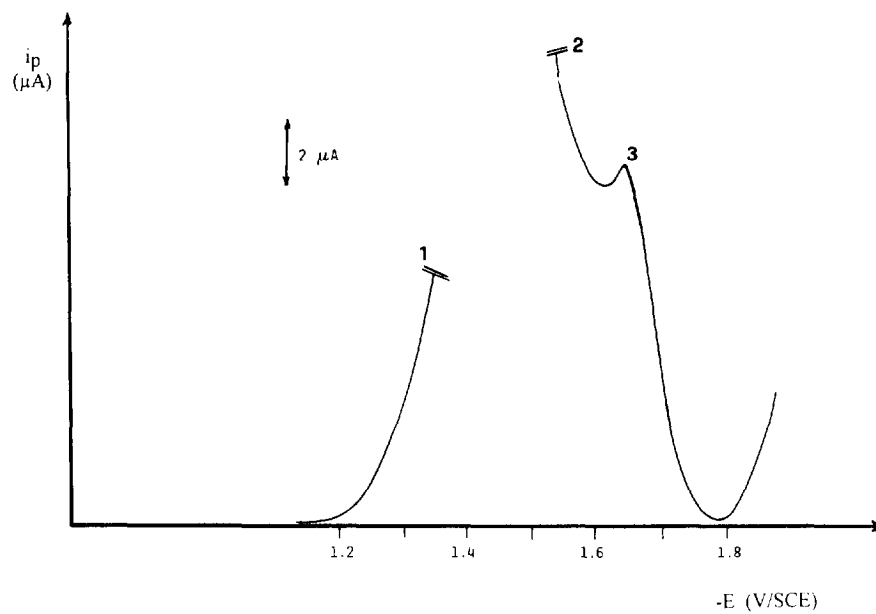
Fig. 4. Differential pulse voltammogram of the sample of Highly Alloyed Steel Eurostandard 281-1. 1: Cr (peak anodic side); 2: Fe (peak catohodic side); 3: peak of Mn. Experimental conditions: see Table 1.
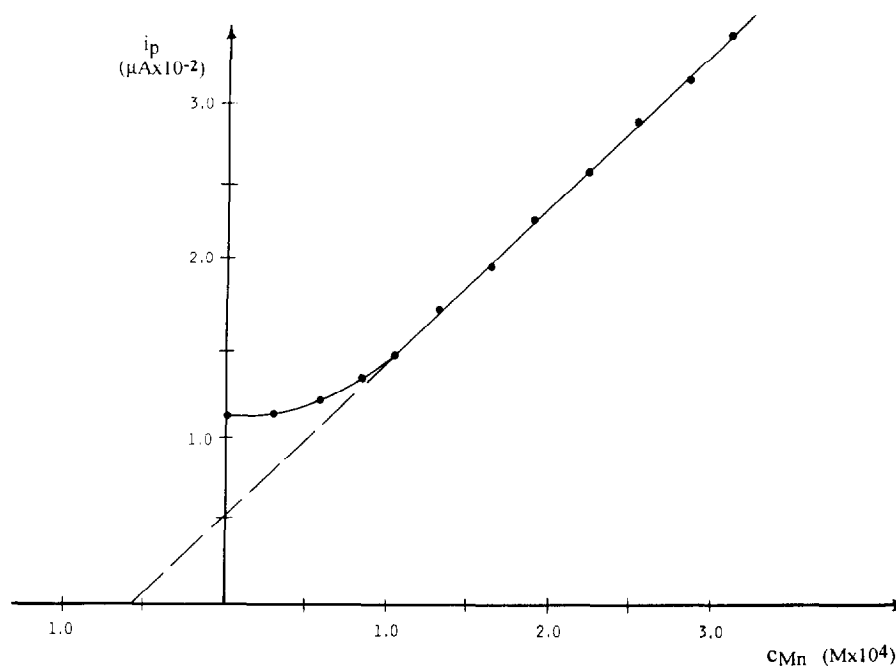

Fig. 5. Analytical calibration function of Mn in Highly Alloyed Steel Eurostandard 281-1. Voltammetric technique: differential pulse voltammetry. Experimental conditions: see Table 1.

chromium, while iron and manganese were determined using the respective analytical calibration functions (Tables 2 and 3).

The manganese determination was also difficult for the Highly Alloyed Steel Eurostandard 281-1 ($c_{Fe}:c_{Mn} = 88.1$ vs. a maximum concentration ratio equal to 69), but, employing the same method described above, it is possible to evaluate the metal content and Figs. 4 and 5 show, as examples, the relevant differential pulse voltammogram and the manganese analytical calibration function. In this case, manganese (Fig. 4, peak 3), being outside the non-interference concentration ratio interval, has been determined by extrapolating the linear section of the i_p vs. concentration fitting (Fig. 5). Chromium and iron (Fig. 4, peaks 1 and 2), however, were determined by the respective analytical calibration curves (cf. Tables 2 and 3), since the concentration ratio is inside the non-interference interval ($c_{Fe}:c_{Cr} = 3.9$). The experimental data fall in the confidence interval of the certified values for each element of the standard reference materials (cf. Table 5). The precision of the analyses, expressed as relative standard deviation, and accuracy, expressed as relative error, were less than 5% in all cases, confirming the validity of the proposed method.

It can be concluded that an appropriate employment of voltammetric techniques, supporting electrolytes and the standard addition method can be a selective and sensitive procedure, suitable for a multicomponent determination in real samples.

Acknowledgement

References

[1] A.M. Bond, Modern Polarographic Methods in Analytical Chemistry, M. Dekker, New York, 1980.

[2] J. Wang, Stripping Analysis—Principles, Instrumentation and Applications, VCH, Deerfield Beach, FL, 1985.

[3] F. Fagioli, C. Locatelli, S. Landi and R. Vecchietti, Electroanalysis, 1 (1989) 449.

[4] C. Locatelli, F. Fagioli and T. Garai, Anal. Chem., 63 (1991) 1409.

[5] J. Wang and J.S. Mahmoud, Anal. Chim. Acta, 182 (1986) 147.

[6] L. Wang, C. Ma, X. Zhang and J. Wang, Anal. Lett., 26 (1993) 1711.

[7] M.P. Colombini and R. Fuoco, Talanta, 30 (1983) 901.

[8] D. Kalavská, Int. J. Environ. Anal. Chem., 45 (1991) 159.

[9] V. Stara and M. Kopanica, Electroanalysis, 5 (1993) 595.

[10] R.J. O'Halloran and H.J. Blutstein, J. Electroanal. Chem., 125 (1981) 261.

[11] R.J. O'Halloran, Anal. Chim. Acta, 140 (1982) 51.

[12] J.K. Christensen and L. Kryger, Anal. Chim. Acta, 118 (1980) 53.

[13] Y. Zhang, K. Jiao, C. Liu and X. Liu, Anal. Chim. Acta, 282 (1993) 125.

[14] H. Eskilsson and D.R. Turner, Anal. Chim. Acta, 161 (1984) 293.

[15] M. Betti, L. Almestrand, D. Jagner and L. Renman, Ann. Chim. (Rome), 82 (1992) 339.

[16] E. Beinrohr, P. Csemi, F.J. Rojas and H. Hofbauerova, Analyst, 119 (1994) 1355.

[17] C. Locatelli, F. Fagioli, T. Garai, C. Bighi and R. Vecchietti, Anal. Chim. Acta, 204 (1988) 189.

[18] IUPAC, Analytical Chemistry Division, Spectrochim. Acta, Part B, 33 (1978) 219.

[19] A. Hald, Statistical Theory with Engineering Applications, Wiley, London, 1952.

[20] H.L. Youmans, Statistics for Chemistry, Charles E. Merrill, Columbus, OH, 1973.

[21] F. Fagioli, T. Garai and J. Devay, Ann. Chim. (Rome), 64 (1974) 633.

[22] C. Liteanu, I.C. Popescu and E. Hopirtean, Anal. Chem., 48 (1976) 2010.

[23] J.P. Riley, Anal. Chim. Acta, 19 (1958) 413.

[24] D.R. Thomerson and W.J. Price, Analyst, 96 (1971) 825.

Sodium di-*n*-propyldithiophosphinate and activated carbon used for the concentrating of bismuth and its determination by atomic emission spectroscopy with inductively-coupled plasma

Hr.G. Malakova *, Z.M. Mateva

Centre of Analytical Chemistry, University of Plovdiv, 24, Tsar Assen Street, 4000 Plovdiv, Bulgaria

Abstract

Sodium di-*n*-propyldithiophosphinate has been proposed as a reagent to improve the sorption properties of activated carbon. The conditions for sorption concentration and separation of bismuth from aqueous solutions were studied. Possibilities for desorption and subsequent determination of bismuth by atomic emission spectroscopy with inductively-coupled plasma were shown.

1. Introduction

Activated carbon is widely used as a sorbent for concentrating micro-impurities. Its sorbtion properties can be improved by adding complexing compounds. Very few complexing agents to be used together with activated carbon are given in the literature. The reagents proposed are dithizone and sodium diethyldithiocarbamate but they have some disadvantages such as low stability of the reagent solutions and the fact that they reduce the degree of extraction of some elements [1]. Pre-concentration of bismuth, lead and cadmium for their determination in sea water was carried out by sorption of the respective diethyl- and

di-*n*-propyldithiophosphate complexes [2,3] on activated carbon. Ammonium diethyldithiophosphate and activated carbon were used in the analysis of pure aluminium and gallium [4]. Dithiophosphinic acids are compounds having the same functional group as dithiophosphoric acids and form complexes with a great number of elements (at various pHs and under different conditions) [5]. The alkali salts of dithiophosphinic acid are stable in acid medium and in storage. In the literature the most frequently proposed methods for determination of elements after being concentrated are atomic absorption spectroscopy and spectrophotometry.

In order to expand the range of organic compounds suitable for sorption concentrating, the conditions and possibilities of sorption concen-

---

* Corresponding author.

trating and separating of small amounts of bismuth from solutions by means of sodium di-*n*-propyldithiophosphinate and activated carbon and its subsequent atomic emission spectroscopy—inductively-coupled plasma (AES–ICP) determination were studied.

2. Experimental

A solution of 5×10^{-2} M Bi was prepared by dissolving $Bi(NO_3)^{3\cdot}5 H_2O$ (Fluka) in 1 M HNO_3. The exact concentration was determined by complexometry using EDTA [6]. Sodium di-*n*-propyldithiophosphinate was synthesized by a known procedure [7], and the purity was controlled by thin layer chromatography [8]. Aqueous solutions with a concentration of 5×10^{-2} M were used The activated charcoal, pure granular form (Riedel-de-Haenag, Seelze Hannover) was treated before use as follows: activated charcoal granules were ground to powder in a china mortar, treated with HCl (1:1), filtered through a fritted glass filter and rinsed with doubly-distilled water until the pH was 7. It was dried in a drying furnace at 60°C [2].

The required pH of the solution was achieved using the following buffer systems [9]: universal buffer mixture (0.04 M solutions of acetic, boric and phosphoric acids, and a 0.04 M solution of sodium hydroxide); the system of aminoacetic acid–0.1 M HCl; acetate buffer; borate buffer. All the reagents used were of analytical grade.

Spectral grade dichlorethane (Merck) was used for extraction.

The abosrption of the extracts was read on a Specord UV VIS (K. Zeiss) spectrophotometer; pH of the solutions was measured with a pH meter (Radelkis 208).

The analysis of the solution obtained after the respective treatment of the activated carbon was done on a AES-ICP instrument (Spectro flame, Spectro Analytical Instruments), with quartz plasma-torch and a Cross-Flow pulverizer. Air light optics and a monochromatic system were used. The bismuth analytical signal was measured at $\lambda = 223.049$ nm. The optimal instrumental parameters were $E = 1$ kW; Neb = 2.4 bars;

Aux = 0.8 1 min^{-1}; Cool = 17 1 min^{-1}; peristaltic pump with a sample consumption of 1 ml min^{-1}.

The content of bismuth in the aqueous phase was determined by EAAS with Zeeman correction, with a Perkin-Elmer 5100-Zeeman spectrophotometer with AS-40. The determination was carried out directly: 20 ml of the solution was dosed with AS-40 in a graphite furnace equipped with a pyrolith platform of Lvov. Parameters of the analysis: a nullode Bi = 8 mA; wavelength = 223.0 nm; slit = 0.2; integration time = 3 s; non-selective absorption corrector = Zeeman.

The procedure for adsorption concentration of bismuth on activated carbon with the aid of sodium di-*n*-propyldithiophosphinate was as follows. A portion of the standard solution of bismuth (20–150 µg) was placed in a beaker of 300 ml. It was diluted up to 100 ml with buffer solution or water (pH 1–7). A reagent solution in a quantity relevant to the proportion Bi:L = 1:10 and 0.05g of activated carbon were consecutively added. The mixture was left to stand for 30 min, being stirred at regular intervals, and then filtered. The desorption of bismuth di-*n*-propyldithiophosphinate was carried out by treating the activated carbon with nitric acid (1:3) [2] and the analysis of the solution was done on a AES–ICP instrument. The content of bismuth in the filtrate was determined by EAAS or by extraction with 10 ml dichloroethane.

3. Results and discussion

As pointed out in the literature, the most appropriate element in studying adsorptioin processes is the one that shows amphoteric properties [10]. A selection of elements with these properties, allowing one to study the adsorption over a wide range of acidity led us to the study of bismuth. When a solution of bismuth and an aqueous solution of di-*n*-propyldithiophosphinate are mixed, a yellow precipitate soluble in organic solvents is obtained. In the electronic spectrum of a dichloroethane solution of the complex there are two clearly pronounced maxima, at 340 and 420 nm (Fig. 1). Kabanova et al. [11] studied the interaction between bismuth and sodium di-
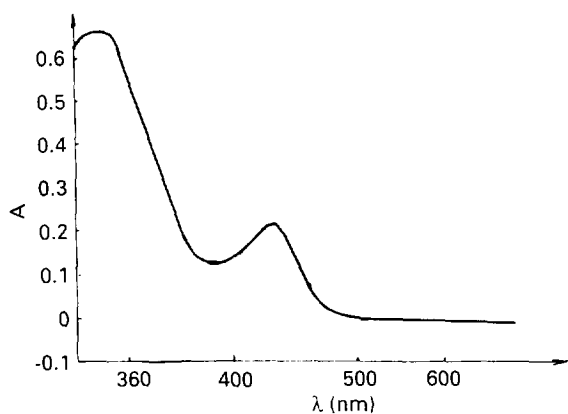
Fig. 1. Absorbance spectrum of bismuth di-n-propyldithiophosphinate in dichloroethane.

ethyldithiophosphinate and found the conditions for extraction-spectrophotometric determination of this element. Sodium di-n-propyldithiophosphinate can be expected to have similar behaviour, because the length of its alkyl radical carbon chain is not much different from that of diethyldithiophosphinate. The optimal acidity for complexation to take place was experimentally determined to be pH 1–6. The buffer composition exerts a certain effect. The universal buffer was found to be appropriate. A ten-fold excess of reagent and 1 min extraction at a ratio of water phase to organic phase of 1:10 and 1:20 are needed. The bismuth determination limit established in this way was 1–20 μg ml^{-1}. The study of the possibility of extracting bismuth with sodium di-n-propyldithiophosphinate allows the control of its content in the aqueous phase after the adsorption. The distribution coefficient and extraction degree in

dichloroethane have been calculated (log $D = 2.3$; $R = 99.50$).

Depending on the acidity of the medium the ions of the elements were adsorbed on activated carbon to a different degree. In strongly acid medium the adsorption was negligible. For this reason, the adsorption of the element without addition of the reagent was studied before the adsorption of the complex of bismuth with sodium di-n-propyldithiophosphinate on activated carbon. The results showed that the process is strongly dependent on the composition of the aqueous phase. In the pH range 1–9, achieved with the buffers mentioned above, the degree of adsorption did not exceed 75%. When the acidity of the medium was adjusted with solutions of hydrochloric acid and ammonium hydroxide, the degree of adsorption was 80–90%. Besides the acidity of the medium the effect of the amount of bismuth and sodium di-n-propyldithiophosphinate as complexing agent were also studied (Table 1). The results obtained agree with those in the literature for Cu, Fe and Ni [12]. For quantitative evaluation of adsorption we have determined q [2] by the formula:

$$q = \frac{(C_0 - C_p) \cdot V}{m}$$

where C_0 is the total concentration of Bi in the water phase, C_p is the equilibrium concentration of Bi in the water phase after adsorption, V is the volume of the water phase and m is the mass of the activated carbon.

The above-mentioned procedure was also used in the study of the adsorption of bismuth on

Table 1
Adsorption of bismuth on activated carbon (pH = 1; $V = 300$ ml; $m = 0.05$ g, complexing agent = sodium di-n-propyldithiophosphinate)

Bi content in the solution analyzed (μg)	Content on activated carbon without complexing agent		Content on the activated carbon with complexing agent	
	Bi (μg)	$10^3 q$ (mmol g^{-1})	Bi (μg)	$10^3 q$ (mmol g^{-1})
100	80	7.8	100	9.6
200	120	11.4	200	19.2
300	134	12.6	300	28.8
400	150	14.4	400	38.4

activated carbon in the presence of the proposed organic reagent. In the literature there are two methods proposed. One of them requires the complex compound to be prepared first and then adsorbed on activated carbon. In the second, the activated carbon is modified with a complexing reagent before contact with the ions of the metal. We used the former method which ensures a greater excess of the reagent and a quantitative completion of the complexation process.

The adsorption of bismuth on activated carbon in the presence of sodium di-n-propyldithiophosphinate was studied at pH 1–9. Though the complexation with alkali dithiophosphinate takes place at pHs up to 7, the adsorption process was studied in the alkali region in order to find whether adsorption of bismuth hydroxide was possible. The results suggest that the quantitative extraction is achieved at a pH of the aqueous phase up to 7, accompanied by a significant effect of the buffer composition. Preference should be given to buffer systems free from organic compounds. The quantitative extraction of bismuth ions from the aqueous phase is possible at the milligram level too. An amount of 0.05 g of activated carbon was found to be sufficient for extraction of microgram levels of bismuth from an aqueous phase of up to 500 ml under the above-mentioned experimental conditions. The adsorption time, with occasional stirring, was 15–30 min. The ionic strength of the aqueous phase had an effect on the degree of extraction of the bismuth complex. The increase in the ionic strength leads to a decrease in the degree of extraction regardless

chloride, ammonium chloride, sodium sulphate and sodium nitrate.

Various methods for metal chelate desorption from activated carbon have been pointed out in the literature. Some of them do not involve destruction of the comlex adsorbed. Attempts to extract bismuth di-n-propyldithiophosphinate by treating activated carbon with an organic solvent which dissolves the complex well, such as CCl_4, $C_2H_4Cl_2$, and $CHCl_3$, did not give a good result. This shows that bismuth dithiophosphinate is adsorbed and not mechanically held on the activated carbon. Another method for metal chelate desorp-

Table 2
Desorption of $[(n-C_3H_7)_2PSS]_3Bi$ with EDTA

Bi (µg)		$R(\%)$
Taken	Found	
50.0	34.7	69.5
100.0	57.1	57.1
150.0	77.4	51.6

tion from activated carbon involves a competitive complexation by adding a reagent to the activated carbon collector which forms more stable complexes than the respective chelates. The new complexes obtained are not adsorbed on activated carbon [13]. Such reagents are the metal complexonates with EDTA and DTPA. Usng a procedure proposed by the authors, the possibility of desorption of bismuth di-n-propyldithiophosphinate with a solution of EDTA was studied. The amount of bismuth after the desorption was determined by AES-ICP (Table 2). An appropriate method for desorption by treating the activated carbon with nitric acid was proposed [2,14–16]. Experiments for desorption of bismuth dithiophosphinate were carried out by this procedure (Table 3) [1]. The most appropriate reagent for this purpose was nitric acid at a concentration of 1:3.

The concentration of bismuth ions by the procedure proposed is also possible with an aqueous phase volume of 500ml.

The alkaline and alkali earth elements as well as the aluminium, zinc and tin compounds do not have an interfering effect. Cu, Ag and Hg do have an inter-

Table 3
Desorption of $[(n-C_3H_7)_2PSS]_3Bi$ with nitric acid

Bi (µg)	$R(\%)$		
	1.390 HNO_3	1:3 HNO_3	1:1 HNO_3
20.0	94.0	99.8	81.2
40.0	88.0	98.9	83.1
100.0	89.5	96.7	85.4
150.0	84.0	97.9	81.4

fering effect because they form the most stable complexes with the complexing agent. The effect of other coexisting metal ions has not been studied in detail but a possibile interfering action can be avoided by selecting an appropriate acidity of complexation.

References

[1] E. Heuss and K. Lieser, J. Radioanal. Chem., 50 (1979) 289.

[2] T.V. Rodionova, V.M. Ivanov, M.S. Sheih and G.V. Kosireva, Vestm. MGU, Khim., 26 (1985) 398.

[3] T.V. Rodionova and V.M. Ivanov, Zh. Anal. Khim., 41 (1986) 2181.

[4] H. Berndth and I. Messerschmidt, Fresenius' Z. Anal. Chem. B, 308 (1981) 104.

[5] W. Kuchen and H. Hertel, Angew. Chem., 81 (1969) 127.

[6] R. Christova, St. Alexandrov, D. Zalev, B. Zheljzkova and Michailova, Handbook of Quantitative Analysis, Nauka i izkustvo, Sofia, Bulgaria, 1986.

[7] W. Kuchen, K. Strolenberg and J. Metten, Chem. Ber., 96 (1963) 1733.

[8] A.N. Shishkov and Hr.G. Malakova, Universite de Plovdiv, Travaux Scientifiques, Chimie, 17 (1979) 55.

[9] U.U. Lurie, Reference Book of Analytical Chemistry, Khimiya, Moscow, 1979, p. 231.

[10] P.I. Artuhin, D.V. Andreev and B.M. Shavinski, Izv. SO. Akad. Nauk, SSSR, Ser. Khim., 1 (1990) 16.

[11] L.K. Kabanova, S.V. Usova and P.M. Solojenkin, Izv. Akad. Tadz. SSR 1 (1971) 39.

[12] N.A. Fitkova, Zh. Anal. Chim., 32 (1977) 1776.

[13] N. Vracheva, Dissertation, Institute of Non-ferrous Metallurgy, Plovdiv, Bulgaria, 1989.

[14] H. Berndth, U.H. Arms and M. Sonneborn, Fresenius' Z. Anal. Chem., 3 (1985) 322.

[15] M. Kumura and K. Kawanami, Talanta, 26 (1979) 401.

[16] D.Y. Howeel and B.R. Dohnt, Talanta, 29 (1982) 391.

Liquid–liquid distribution of ion associates of hexachloroplatinate(IV) with quaternary ammonium counter ions

Koichi Yamamoto *, Shinichi Katoh

Department of Materials Science, Yonago National College of Technology 4448, Hikona-cho, Yonago-shi, Tottori 683, Japan

Abstract

The distribution behavior of ion associates of $PtCl_6^{2-}$ with quaternary ammonium cations (Q^+) between aqueous phase and two organic phases (chloroform and carbon tetrachloride) was examined, and the extraction constants ($\log K_{ex}$) were determined. A linear relationship was found between $\log K_{ex}$ and the total number of carbon atoms in Q^+; from the slope of the line, the contribution of a methylene group to $\log K_{ex}$ was calculated to be 0.6. The extractability with alkyltrimethylammonium cations was larger than that with symmetrical tetraalkylammonium cations. From the extraction constants obtained, an extraction method based on the ion association of $PtCl_6^{2-}$ with Q^+ can be used for the separation and determination of platinum at the 10^{-6} M level.

Keywords: Liquid–liquid distribution; Hexachloroplatinate(IV); Quaternary ammonium ion

1. Introduction

An extraction of platinum from an aqueous halide medium into an organic solvent has been frequently used for both the separation and spectrophotometric determination of platinum. Spectrophotometric methods for the determination of platinum by an extraction into nitrobenzene as an ion associate formed between a 1,10-phenanthroline–iron(II) chelate cation and a hexachloroplatinate(IV) anion [1], and by a dissolution of an ion associate of a platinum(IV)–chloro complex with

* Corresponding author.

Crystal Violet precipitated by flotation with benzene in ethanol [2] have been reported. Mirza [3] studied an extraction of platinum metals with tri-iso-octylamine from hydrochloric and hydrobromic acids, and methods were devised for a separation of gold from platinum and its determination and also for the simultaneous determination of palladium and platinum. Hara et al. [4] investigated a solvent extraction of gold and platinum by zephiramine (tetradecyldimethylbenzylammonium)–iodoaurate(III) or iodoplatinate(IV)–chloroform systems, which were used for a pretreatment in the simultaneous atomic absorption spectrometric determination of gold and plat-

Table 1
Salts of quaternary ammonium cations examined

Salt (abbreviation)	Formula	Supplier [a]	Purity (%)
Tetraalkylammonium salts			
Tetrabutylammonium chloride (TBA)	$(C_4H_9)_4NCl$	A	>98
Tetraamylammonium chloride (TAA)	$(C_5H_{11})_4NCl$	B	>95
Alkyltrimethylammonium salts			
Octyltrimethylammonium chloride (OTMA)	$C_8H_{17}N(CH_3)_3Cl$	A	>98
Decyltrimethylammonium chloride (DTMA)	$C_{10}H_{21}N(CH_3)_3Cl$	A	>95
Dodecyltrimethylammonium chloride (DDTMA)	$C_{12}H_{25}N(CH_3)_3Cl$	A	
Tetradecyltrimethylammonium chloride (TDTMA)	$C_{14}H_{29}N(CH_3)_3Cl$	A	>98
Cetyltrimethylammonium chloride (CTMA)	$C_{16}H_{33}N(CH_3)_3Cl$	A	>95
Stearyltrimethylamonium chloride (STMA)	$C_{18}H_{37}N(CH_3)_3Cl$	A	>97
Alkyldimethylbenzylammonium salts			
Tetradecyldimethylbenzyl-ammonium chloride (Zeph)	$C_{14}H_{29}N(CH_3)_2(CH_2C_6H_5)Cl$	C	>98

[a] A, Tokyo Kasei Co., Ltd.; B, Wako Pure Chem. Ind.; C, Dojindo Laboratories.

inum. Several aspects of the extraction of a platinum(IV)-chloro complex by salts of trioctylamine and organic acids [5], alcohols [6] and tributylphosphate [7] from hydrochloric-sulphuric acid solutions, NTAB-182 from hydrochloric acid solution [8], a mixture of amines and organophosphoric acids [9], and high molecular weight amines [10] have also been reported.

In the present work, the authors studied the extraction of ion associates of hexachloroplatinate(IV) anion with various quaternary ammonium cations (Q^+) and proposed an extraction method for the separation and determination of platinum by using Q^+ as counter ions of hexachloroplatinate(IV).

2. Experimental

2.1. Apparatus

A Japan Spectroscopic (Uvidec-430) spectrophotometer was used for recording spectra and absorbance measurements in quartz cells of 10 mm light pathlength. An Iwaki (Model V-SX type KM) shaker was used for horizontal shaking of the 25 ml stoppered test-tubes for extraction. An Iwaki (Model V-DN type KM) shaker was used for vertical shaking of the 50 ml separatory funnel for extraction.

2.2. Reagents

A standard platinum(IV) solution (1.03×10^{-4} M) was prepared by diluting 4 ml of a 1000 ppm standard platinum(IV) solution (5.13×10^{-3} M hydrogen hexachloroplatinate(IV) in 1 N hydrochloric acid solution, Wako Pure Chem.) to 200 ml with 1 N hydrochloric acid solution.

Quaternary ammonium ion (Q^+) solutions were prepared from the salts listed in Table 1, which were dried under reduced pressure. Accurately weighed amounts of the dried salts were dissolved in distilled water to give stock standard solutions, which were diluted before use.

Commercially available chloroform was used without further purification, and was saturated with distilled water before use.

All of the reagents were of analytical-reagent grade and were used without further purification.

2.3. Standard procedure for stoichiometry measurement

Two milliliters of a 1.03×10^{-4} M platinum (IV) solution were transferred to a 25 ml stoppered test-tube; then 1 ml of a 3 N hydrochloric acid solution and an appropriate amount of aqueous quaternary ammonium salt solution were added. The solution was diluted to 5 ml with distilled water. This brought the ionic strength to 1.0. The aqueous solution was mechanically shaken with 5 ml of an extracting solvent for 40 min at 25°C. After phase separation, the absorbance of the aqueous phase was measured at 262 nm against distilled water as a reference; the concentration of platinum in the aqueous phase was then calculated from the molar absorptivity of the hexachloroplatinate(IV).

2.4. Recommended procedure for spectrophotometric determination of platinum

A 44 ml portion of a sample solution containing platinum up to 4.66×10^{-6} M and 1 N hydrochloric acid was transferred to a separating funnel (about 65 ml). To this 4 ml of a 1.5 N hydrochloric acid solution and 2 ml of 6×10^{-3} M tetraamylammonium chloride (TAA) solution were added. To this mixture, 5 ml of chloroform was added; the funnel was then shaken for 40 min. After phase separation, the absorbance of the organic phase was measured at 269 nm against chloroform.

3. Results and discussion

3.1. Absorption spectra

The absorption spectra of the hexachloroplatinate(IV) ion in aqueous solution are shown in Fig. 1. The maximum absorbance of the hexa-

chloroplatinate(IV) ion was at 262 nm, where the absorbance of the reagent blank was negligibly small. A calibration graph obtained for platinum was linear over the $0-4.1 \times 10^{-5}$ M range. The molar absorptivity for platinum was about 2.4×10^4 l mol^{-1} cm^{-1} at 262 nm.

3.2. Effect of conditions

5.13×10^{-3} M hydrogen hexachloroplatinate-(IV) stock solution (in 1 N hydrochloric acid solution) was diluted 50 times with distilled water, 0.5 M sulphuric acid and 1 N hydrochloric acid to prepare a 1.03×10^{-4} M standard platinum(IV) solution. In both distilled water and 0.5 M sulphuric acid, the absorbance at 262 nm in the aqueous solution gradually decreased as the time after preparation passed. In 1 N hydrochloric acid, the absorbance remaind constant. Therefore, 1 M chloride was used for the formation of the hexachloroplatinate(IV) ion.

3.3. Determination of extraction constants and some considerations of extractability of ion associates

In the aqueous phase, platinum(IV) reacts with chloride to form $PtCl_6^{2-}$. This complex anion distributes between the aqueous and organic phases:

$$PtCl_6^{2-} + 2Q^+ \rightleftharpoons ((Q^+)_2 \cdot PtCl_6^{2-})_{org} \qquad (1)$$
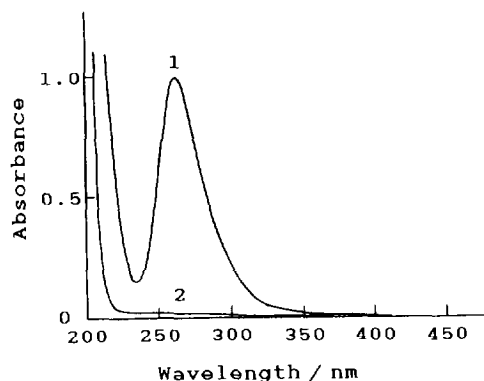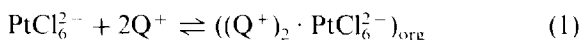
Fig. 1. Absorption spectra of the platinum(IV) chloro complex in water. Platinum(IV): (1) 4.1×10^{-5} M, (2) 0 M; chloride ion, 1 M; reference, distilled water.

and

$$K_{ex} = [(Q^+)_2 \cdot PtCl_6^{2-}]_{org}/[Q^+]^2[PtCl_6^{2-}] \qquad (2)$$

where K_{ex} is the extraction constant; the subscript "org" refers to the organic phase and the absence of a subscript indicates the aqueous phase. The distribution ratio of platinum between the aqueous and organic phases (D_{Pt}) is given by

$$D_{Pt} = \frac{[(Q^+)_2 \cdot PtCl_6^{2-}]_{org}}{[PtCl_6^{2-}]} \qquad (3)$$

Hence, the following equation can be derived from Eqs. (2) and (3):

$$D_{Pt} = K_{ex} \cdot [Q^+]^2 \qquad (4)$$

where

$$\log D_{Pt} = \log K_{ex} + 2 \log[Q^+] \qquad (5)$$

The side-reaction coefficient for the quaternary ammonium ion ($\alpha(Q^+(Cl^-))$) is given by

$$\alpha(Q^+(Cl^-)) = \frac{[Q^+]'}{[Q^+]} = \frac{[Q^+] + [Q^+ \cdot Cl^-]_{org}}{Q^+]}$$

$$= 1 + K_{ex}(Q^+ \cdot Cl^-) \cdot [Cl^-] \qquad (6)$$

where $[Q^+]'$ is the total concentration of the quaternary ammonium ion that is not bound in ion associates with hexachloroplatinate(IV), and $K_{ex}(Q^+ \cdot Cl^-)$ is the extraction constant of a quaternary ammonium ion with a chloride ion. $[Q^+]$ can be calculated by

$$[Q^+] = [Q^+]'/\alpha(Q^+(Cl^-)) \qquad (7)$$

In the extraction for hexachloroplatinate(IV), the distribution ratios of platinum at different concentrations of the quaternary ammonium ions were determined. The values of $\log D_{Pt}$ were plotted against $\log[Q^+]$. The results obtained for chloroform and carbon tetrachloride are shown in Figs. 2 and 3 respectively. The plots for all quaternary ammonium cations were linear with slopes equal to two, calculated by the least-squares method. This means that the extraction equilibrium shown in Eq. (1) holds and that the extracted species was $(Q^+)_2 \cdot PtCl_6^{2-}$. The extraction constants calculated from Eq. (5) are summarized in Table 2; the standard deviation is very small.
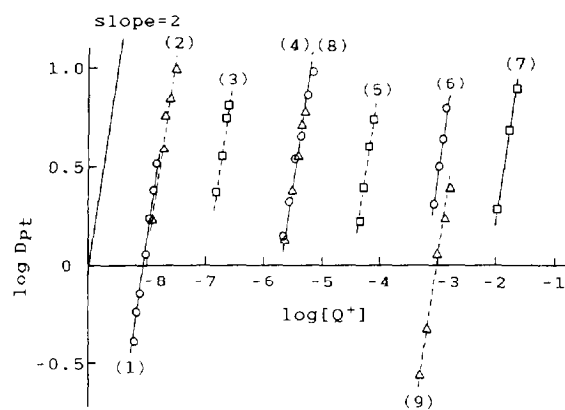
Fig. 2. Plots of $\log D_{Pt}$ vs. $\log[Q^+]$. Q^+: 1 (○) Zeph, 2 (△) STMA, 3 (□) CTMA, 4 (△) TDTMA, 5 (□) DDTMA, 6 (○) DTMA, 7 (□) OTMA, 8 (○) TAA, 9 (△) TBA; extracting solvent: chloroform.

3.4. Relationship between the extraction constants and the number of carbon atoms in the quaternary ammonium ion

The values of the extraction constants ($\log K_{ex}$) were plotted against the number of carbon atoms in the quaternary ammonium ion (N_c). The results obtained for chloroform and carbon tetrachloride extraction systems are shown in Figs. 4 and 5 respectively. For the same carbon number, the extractability ($\log K_{ex}$) with long-
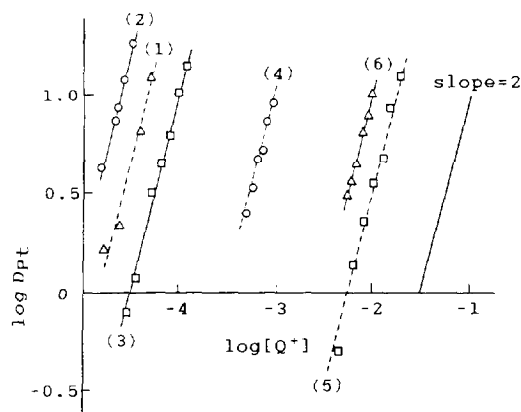
Fig. 3. Plots of $\log D_{Pt}$ vs. $\log[Q^+]$. Q^+: 1 (△) STMA, 2 (○) CTMA, 3 (□) TDTMA, 4 (○) DDTMA, 5 (□) DTMA, 6 (△) TAA; extracting solvent: carbon tetrachloride.

Table 2

Extraction constants (log K_{ex}) obtained between aqueous and organic phases

Q^+ cation	Extracting solvent [a]	log K_{ex}	
		PtCl$_6^{2-}$ [b]	Cl$^-$ [c]
TAA	CTC	5.01 ± 0.01(6)	−5.18
DTMA	CTC	4.49 ± 0.06(7)	−8.11
DDTMA	CTC	7.04 ± 0.02(6)	−6.93
TDTMA	CTC	9.02 ± 0.04(7)	−5.75
CTMA	CTC	10.24 ± 0.01(5)	−4.57
STMA	CTC	9.68 ± 0.08(4)	−3.60
TBA	CF	6.04 ± 0.03(5)	0.16
TAA	CF	11.36 ± 0.06(6)	2.52
OTMA	CF	4.22 ± 0.02(3)	−1.59
DTMA	CF	6.49 ± 0.02(4)	−0.41
DDTMA	CF	8.97 ± 0.03(4)	0.77
TDTMA	CF	11.39 ± 0.03(5)	1.95
CTMA	CF	13.97 ± 0.01(4)	3.13
STMA	CF	15.95 ± 0.09(5)	4.10
Zeph	CF	16.11 ± 0.02(7)	4.68

[a] Solvent: CTC, carbon tetrachloride; CF, chloroform.
[b] Mean value ± standard deviation. The figures in parentheses are the numbers of measurements.
[c] Ref. [11].

Fig. 5. Relation between log K_{ex} and number of carbon atoms in quaternary ammonium ion. Alkyltrimethylammonium cations: (a) STMA, (b) CTMA, (c) TDTMA, (d) DDTMA, (e) DTMA; extracting solvent: carbon tetrachloride.

Fig. 4. Relation between log K_{ex} and number of carbon atoms in the quaternary ammonium ion. Alkyltrimethylammonium cations (●): (a) STMA, (b) CTMA, (c) TDTMA, (d) DDTMA, (e) DTMA, (f) OTMA; tetraalkylammonium cations (○): (g) TAA, (h) TBA; extracting solvent: chloroform.

chain alkyltrimethylammonium cations (group I) is larger than that with symmetrical tetraalkylammonium cations (group II) for the chloroform extraction system, and the difference in log K_{ex} values between these groups is about 3.9 for an identical carbon number. This indicates that the electrostatic attraction of the cations in group I for the anionic complex is larger than that of the cations in group II. In the log K_{ex}-N_c plot for the carbon tetrachloride extraction system, the points for the quaternary ammonium ions having more than 17 carbon atoms (group I-II) deviate from the straight line for those up to 17 (group I-I), which may be because the increment in spread of the hydrophobic alkyl chain of the cations in group I-II is smaller than that of the cations in group I-I. The slopes of all the lines in Figs. 4 and 5 were identical, and by dividing the slope by two, the contribution of a methylene group to the extraction constants (log K_{ex}) was found to be about 0.6 on average, in good agreement with the value previously reported [12-16].
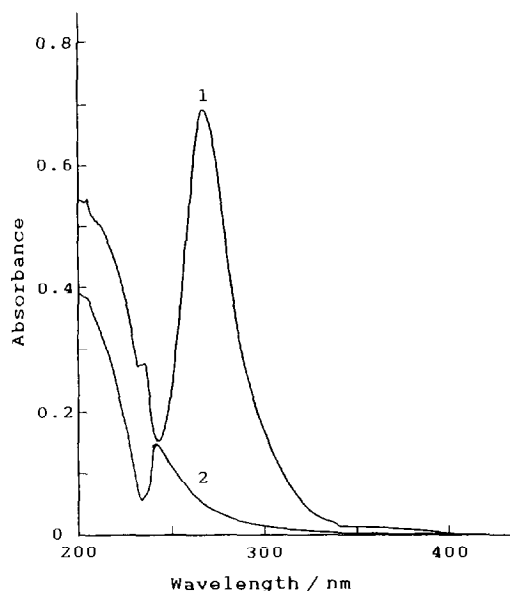
Fig. 6. Absorption spectra of the ion associate of hexachloro-platinate(IV) with TAA in chloroform. Volumes of the aqueous and organic phases were 50 ml and 5 ml respectively; initial concentrations in aqueous phase of platinum(IV): (1) 4.1×10^{-6} M, (2) 0 M, TAA 2.4×10^{-4} M, chloride ion 1 M; reference. chloroform.

3.5. Separation and determination of platinum based on the formation of an ion associate of hexachloroplatinate(IV) with quaternary ammonium cations

For example, we consider the chloroform extraction of the ion associate of $PtCl_6^{2-}$ with TAA, in which the initial concentrations of platinum, TAA and chloride ion are 4.1×10^{-5} M, 2.4×10^{-3} M and 1 M respectively, and the volumes of the aqueous and organic phases are equal. For more than 90% of the platinum to be extracted into the organic phase, the logarithm of the extraction constant must be greater than 11.3, which can be calculated by using Eqs. (2), (6) and

(7). This extraction constant agrees closely with that given in Table 2. Experimentally platinum could be extracted almost quantitatively into chloroform under the experimental conditions described above. Fig. 6 shows the absorption spectra of the ion associate $[(TAA^+)_2 \cdot PtCl_6^{2-}]$ and of the reagent blank in chloroform obtained by the recommended procedure. This proposed method can be applied to the determination of trace amounts of platinum up to 4.1×10^{-6} M by measuring the absorbance at 269 nm. This extraction procedure can be used for the separation and determination of platinum.

References

[1] Y. Yamamoto, M. Tsubouchi, I. Okimura and T. Takaki, Nippon Kagaku Zasshi, 88 (1967) 745.
[2] Z. Marczenko and J. Maruszak, Chem. Anal. (Warsaw), 24 (1979) 341.
[3] M.Y. Mirza, Talanta, 27 (1980) 101.
[4] S. Hara, H. Matsuo and T. Kumamaru, Bunseki Kagaku, 35 (1986) 503.
[5] V.V. Belova, A.I. Khol'kim, P. Muehl, K. Gloe and V.N. Khol'kina, Zh. Neorg. Khim., 36 (1991) 141.
[6] L.N. Moskvin, G.L. Grigor'ev and V.M. Krasnoperov, Zh. Prikl. Khim. (Leningrad), 56 (1983) 1153.
[7] L.N. Moskvin, G.L. Grigor'ev, V.M. Krasnoperov and S.A. Simanova, Zh. Prikl. Khim. (Leningrad), 53 (1980) 1938.
[8] X. Dai and Y. Song, Guijinshu, 13 (1992) 1.
[9] Deptula and J. Czeslaw, Inorg. Nucl. Chem., 29 (1967) 1097.
[10] Khattak, M. Akram and R.J. Magee, Recl. Trav. Chim. Pays-Bas, 88 (1969) 584.
[11] S. Motomizu, Dojin News, 38 (1987) 3.
[12] S. Motomizu, S. Hamada and K. Tôei, Bunseki Kagaku, 32 (1983) 648.
[13] K. Yamamoto, T. Fujibayashi and S. Motomizu, Solvent Extr. Ion Exch., 10 (1992) 459.
[14] K. Yamamoto and M. Endo, Anal. Sci., 10 (1994) 755.
[15] I. Kasahara, Y. Ohgaki, K. Matsui, K. Kano, S. Taguchi and K. Goto, Nippon Kagaku Kaishi, (1986) 894.
[16] H. Matsunaga and T. Yotsuyanagi, Nippon Kagaku Kaishi, (1982) 785.

Study of complex formation in the manganese(II)/azide system

Horacio Dorigan Moya [a], Eduardo Almeida Neves [b,*], Maria Encarnación Vázquez
Suárez-Iha [a], Nina Coichev [a]

[a] *Institute de Química, Universidade de São Paulo, Caixa Postal 26077, CEP 05599-970, São Paulo, Brazil*
[b] *Departamento de Química, Universidade Federal de São Carlos, Caixa Postal 676, Cep 13.565-905, São Carlos, Brazil*

Abstract

The complex formation between Mn(II) cations and N_3^- anions was studied in aqueous medium at 25°C and ionic strength 2.0 M ($NaClO_4$). Data of average ligand number, $\bar{n}$ (Bjerrum's function), were obtained from pH measurements on the $Mn(II)/N_3^-/HN_3$ system followed by integration to obtain Leden's function, $F_0(L)$. Graphical treatment of data and a matrix solution of simultaneous equations have given the following overall formation constants of mononuclear stepwise complexes: $\beta_1 = 4.15 \pm 0.02\ M^{-1}$, $\beta_2 = 6.61 \pm 0.04\ M^{-2}$, $\beta_3 = 3.33 \pm 0.02\ M^{-3}$, $\beta_4 = 0.63 \pm 0.01\ M^{-4}$. A linear plot of $\log K_n$ vs. $(n-1)$ shows no change in the configuration during complex formation. Slow spontaneous oxidation of solutions to Mn(III) occurs when the N_3^- concentration is greater than 1.0 M.

Keywords: Complex formation; Manganese; Azide

1. Introduction

Studies of azide complex formation with several metal ions, such as Co(II) [1], Co(III) [2], Cu(II) [3], Ni(II) [4], Fe(III) [5] and U(VI) [6], have been done by our research group in recent years, with special interest in determining the stability constants and analytical applications.

Some of our studies were concentrated on the autoxidation of Co(II) azide complexes induced by S(IV) in order to develop one alternative method for analytical determination of S(IV) of

environmental interest [7–13].

The complexes of Co(II) formed in aqueous solutions of N_3^-/HN_3 buffer were slowly oxidized to a mixture of complexes of Co(III) by dissolved oxygen, with a marked colour change from blue to brown–yellowish. It has been found by Senise [13] that S(IV), as SO_2, HSO_3^- or SO_3^{2-}, accelerates these oxidation processes significantly instead of hindering them, leading to a spot-test.

The synergistic effect of Mn(II) on sulfite autoxidation of metal ions was investigated for the $Co(II)/N_3^-$ and aquated Fe(II) systems [2]. The results indicate that Mn(II) has a significant catalytic effect, but that the synergistic effect actually

---

* Corresponding author. Fax: (55) 011-815-5579.

occurs in the presence of Co(III) and Fe(III) respectively. These metal ions, in the oxidation state (III), can rapidly oxidize sulfite to $SO_3^{\bullet-}$ radical, which in turn initiates a series of free radical propagation reactions in which sulfite is oxidized by the dissolved oxygen to mainly sulfate.

A thorough study of the mechanism of the autoxidation of Mn(II) and Co(II) azide complexes and Fe(II) in aqueous solutions was done by some of the authors [9–12].

The determination of the stability constants of Mn(II)/N_3^- complexes brings additional information about the distribution complex species, according to the azide concentration, and more contributions to the elucidation of the above synergistic effect of Mn(II).

2. Experimental

2.1. Reagents and standard solutions

All reagents were of AR or CP specification (Merck or Fluka Chemie A.G.).

Sodium azide solution was prepared directly from the salt. Standardization was carried out by adding a known volume of standard sulfuric acid, boiling to remove volatile hydrazoic acid (HN_3) and then back titrating with standard sodium hydroxide solution.

Sodium perchlorate solution, used for making up the ionic strength of working solutions, was standardized by taking a small volume of solution and then drying in an oven at 120 °C until constant weight.

Standard perchloric acid solution was used in the working solutions to displace HN_3 from the azide ions.

Manganese(II) perchlorate solution was prepared from the direct reaction of excess carbonate with 6 M perchloric acid for 2 days, with stirring at room temperature. After filtering, free perchloric acid was used to adjust the pH to 5.5, in order to avoid hydrolysis. Standardization was carried out by complexometric titration with EDTA [14].

2.2. Working solutions

Several series of working solutions were prepared by adding different volumes of 1.002 M $Mn(ClO_4)_2$ solution to 10.06 cm³ of several N_3^-/ HN_3 buffer solutions with $NaClO_4$ (ionic strength, I, 2.0 M). Five additions of Mn(II) solution changed its concentration in the final solution from 0.02 M to 0.1 M. The azide concentration in the working solution was in the range 0.025–1.8 M.

In order to keep such working solutions free from oxygen, with no volatile hydrazoic acid being lost, all standard solutions were previously bubbled with purified nitrogen before mixing.

2.3. Potentiometric measurements and data treatment

A Metrohm 654 pHMeter adapted to a glass electrode (Metrohm AG Herisau) combined with an Ag/AgCl reference electrode filled with 3 M NaCl was used in the pH measurements at $(25.0 \pm 0.1)°C$. To standardize the glass electrode, a 0.05 M potassium phthalate buffer solution (conditional pH = 3.795) was used, at the same ionic strength of the working solution (2.00 M $NaClO_4$), in order to measure hydrogen ion concentration instead of activity. This buffer had previously been calibrated from free strong acid (0.01 M) at the same ionic strength (held at 2.0 M with $NaClO_4$).

The change of pH measured from initial pH_1 to final pH_2 by adding manganese(II) to N_3^-/HN_3 buffer was followed potentiometrically with the calibrated glass electrode (see experimental data in Table 1).

QUICK BASIC programs were used to make the calculations on an IBM PC-AT desk computer.

3. Results and discussion

The Henderson–Hasselbalch equation for buffer systems and mass balances was applied to the present system, where N_3^- acts as both ligand for the metal cation and as a component of the buffer solution [15].

Table 1
Calculated values of Leden's function, $F_0(L)$, from the integration of selected $\bar{n}$ vs. $\log[N_3^-]$ data for the manganese(II)/azide system. ($I = 2.0$ M $NaClO_4$ and $T = 25.0°C$.)

pH_1	$[N_3^-]_1 (\times 10^{-2})$ (M)	$[Mn(II)](\times 10^{-2})$ (M)	pH_2	$[N_3^-]_2 (\times 10^{-2})$ (M)	$\bar{n}$	$F_0(L)$
4.507	2.503	10.00	4.536	1.609	0.06394	1.068
4.507	2.503	7.997	4.388	1.766	0.06644	1.075
4.507	2.503	5.999	4.414	1.912	0.07309	1.081
4.507	2.503	3.976	4.446	2.097	0.07564	1.088
4.549	5.003	10.00	4.395	3.190	0.1309	1.137
4.549	5.003	7.997	4.422	3.463	0.1416	1.149
4.549	5.003	5.999	4.453	3.793	0.1513	1.165
4.549	5.003	3.976	4.483	4.142	0.1639	1.181
4.549	5.003	2.000	4.515	4.543	0.1793	1.200
4.863	10.00	10.00	4.715	6.465	0.2534	1.295
4.863	10.00	7.997	4.747	7.097	0.2618	1.326
4.863	10.00	5.999	4.770	7.635	0.2944	1.354
4.863	10.00	3.976	4.799	8.319	0.3187	1.390
4.863	10.00	2.000	4.829	9.082	0.3587	1.432
5.230	20.00	10.00	5.090	13.16	0.4838	1.674
5.230	20.00	7.997	5.115	14.23	0.5202	1.741
5.230	20.00	5.999	5.142	15.44	0.5604	1.819
5.230	20.00	3.976	5.171	16.82	0.5910	1.911
5.230	20.00	2.000	5.200	18.33	0.6358	2.015
5.534	40.00	10.00	5.414	27.54	0.8470	2.730
5.534	40.00	7.997	5.438	29.69	0.8861	2.914
5.534	40.00	5.999	5.462	32.02	0.9326	3.121
5.534	40.00	3.976	5.485	34.41	0.9920	3.345
5.534	40.00	2.000	5.509	37.07	1.065	3.612
5.654	60.00	10.00	5.543	42.15	1.186	4.173
5.654	60.00	7.997	5.565	45.25	1.241	4.549
5.654	60.00	5.999	5.587	48.57	1.309	4.978
5.654	60.00	3.976	5.610	55.20	1.343	5.899
5.654	60.00	2.000	5.632	55.98	1.410	6.014
5.785	80.00	7.997	5.705	61.56	1.502	6.906
5.785	80.00	5.999	5.725	65.78	1.574	7.648
5.785	80.00	3.976	5.746	70.34	1.595	8.505
5.899	100.0	3.976	5.864	88.78	1.796	12.63
6.038	140.0	3.976	6.009	126.0	1.094	28.04
6.167	180.0	10.00	6.102	140.2	2.181	31.47
6.167	180.0	7.997	6.116	147.8	2.215	35.34
6.167	180.0	5.999	6.129	155.5	2.289	39.62
6.167	180.0	2.000	6.155	171.8	2.321	49.88

An initial conditional equilibrium was reached. for which measurement of PH_1 provided the equilibrium concentrations of $[N_3^-]_1$ and its acid $[HN_3]_1$. Subsequent addition of a volume of a metal cation solution resulted in a new conditional equilibrium for pH_2 and $[N_3^-]_2$ and $[HN_3]_2$ [1]. A conditional pK value of the N_3^-/HN_3 system, at ionic strength 2.00 M ($NaClO_4$) and

$25.0 \pm 0.1°C$, was determined for each pH experiment. The use of the pK value from each experiment proved to be a reliable procedure because it corrects any drift in junction potentials, small losses of volatile hydrazoic acid and eventual slope deviation of the glass electrode. The average pK of the hydrazoic acid at this strength was 4.530.

The average number of ligands, $\bar{n}$ (Bjerrun's function) [15], was obtained as described elsewhere [1,15].

Since the same curve of $\bar{n}$ vs. $[N_3^-]_2$ (Fig. 1) was obtained for four different manganese(II) concentrations, no significant polynuclear complexation was evident in the metal cation concentration range employed.

Table 1 shows the experimental data of pH and the calculated values of $\bar{n}$, free ligand concentrations and metal ion analytical concentration for each equilibrium condition. An appropriate computer program was used to obtain data of the Leden function, $F_0(L)$ [15], by integration of the curve of $\bar{n}$ vs. log $[N_3^-]_2$ from several consecutive small increments of ligand concentration [1].

The treatment of $F_0(L)$ data, to find the stability constants, was done by two different methods. The first was the familiar graphical procedure, extrapolating the subsidiary $F_n(L)$ function to zero ligand concentration [1,15]. The graphical treatment has clearly shown the existence of four stepwise complexes. Computer methods of calculation, based on properly weighted simultaneous equations, were also used for the final results [16].

Both solutions gave very similar values. However, the best set of constants came from matrix calculations [16], by solving the following system of weighted simultaneous equations:
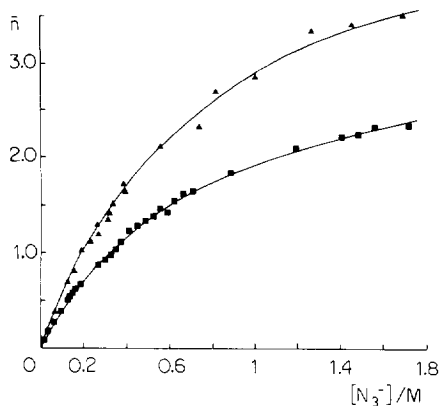
Fig. 1. Formation curves for (■) the Mn(II)/N_3^- system at several metal concentrations (see Table 1) and (▲) the Co(II)/N_3^- [1] system.
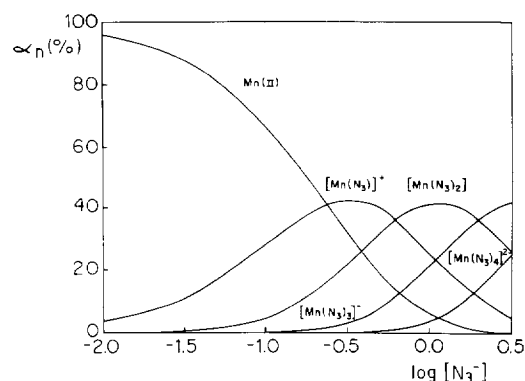
Fig. 2. Distribution diagram of the species in the Mn(II)/N_3^- system calculated from the equilibrium constants.

$$6.838 \times 10^3 = (8.078 \times 10^2 \times \beta_1) + (3.667$$
$$\times 10^2 \times \beta_2) + (2.681 \times 10^2$$
$$\times \beta_3) + (2.707 \times 10^2 \times \beta_4)$$
$$4.404 \times 10^3 = (3.667 \times 10^2 \times \beta_1) + (2.681$$
$$\times 10^2 \times \beta_2) + (2.707 \times 10^2$$
$$\times \beta_3) + (3.348 \times 10^2 \times \beta_4)$$
$$4.307 \times 10^3 = (2.681 \times 10^2 \times \beta_1) + (2.707$$
$$\times \beta_2) + (3.348 \times 10^2 \times \beta_3)$$
$$+ (4.58 \times 10^2 \times \beta_4)$$
$$5.320 \times 10^3 = (2.707 \times 10^2 \times \beta_1) + (3.348$$
$$\times 10^2 \times \beta_2) + (4.658 \times 10^2$$
$$\times \beta_3) + (6.942 \times 10^2 \times \beta_4)$$

The solution for a 95% confidence level in the values is $\beta_1 = 4.15 \pm 0.02$ M^{-1}, $\beta_2 = 6.61 \pm 0.04$ M^{-2}, $\beta_3 = 3.33 \pm 0.02$ M^{-3}, $\beta_4 = 0.63 \pm 0.01$ M^{-4}. The distribution diagram is represented in Fig. 2.

The β_1 value is in good agreement with the literature data (Table 2). The complexes are weak and follow the Irving–Williams rule:

$$Mn^{2+} < Fe^{2+} < Co^{2+} < Ni^{2+} < Cu^{2+} > Zn^{2+}$$
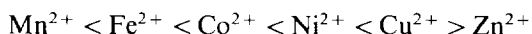
The coordination of one or two ligands is quite easy as can be inferred from the values of the constants. This behaviour suggests that a larger entropic factor favours the initial steps. In fact the formation of the less hydrated neutral species from highly hydrated ions does affect the reaction. On this basis, the formation of the third species

Table 2
Some literature data for the stability constants for mononuclear complexes of several metal ions with azide complexes

Metal ion	Method	I (M)	T (°C)	β_1 (M^{-1})	β_2 (M^{-2})	β_3 (M^{-3})	β_4 (M^{-4})	β_5 (M^{-5})	Ref.
Mn^{2+}	Spectr.	1.0	25.0	4.2	–	–	–	–	[18]
	Spectr.	1.0	25.0	4.6	–	–	–	–	[18]
	Potent.	1.0	25.0	4.4	1.5	–	–	–	[19]
	Potent.	1.0	25.0	3.8	4	–	–	–	[20]
	Potent.	2.0	25.0	4.2	6.6	3.3	0.63	–	a
Fe^{2+}	–	–	–	4.9	–	–	–	–	[19]
Co^{2+}	Potent.	2.0	25.0	5.7	19	7.0	16	4.4	[1]
	Spectr.	1.0	25.0	5.3	–	–	–	–	[21]
Ni^{2+}	Spectr.	1.0	25.0	6.9	–	–	–	–	[21]
	Potent.	1.0	25.0	7.4	18	20	–	–	[22]
	Potent.	2.0	25.0	5.8	9.7	7.5	5.3×10^2	–	[4]b
Cu^{2+}	Spectr.	0.2	20.0	230	–	–	–	–	[23]
	Spectr.	4.0	25.0	–	2.90×10^4	3.02×10^6	–	–	[3]
	Potent.	1.0	25.0	244	1.20×10^4	1.45×10^5	3.18×10^7	–	[24]
Zn^{2+}	Potent.	1.0	25.0	5.7	21	145	280	–	[25]

a Present work.

b Results are also given for the polynuclear complexes.

should be unfavoured, consistent with the low β_3 value.

The linear relationship of $\log K_n$ vs. $(n - 1)$, Fig. 3, means that the magnitude of the free energy involved in complex formation linearly decreases for each ligand introduced. On this basis, no configuration change has been found to occur, as could happen with other systems
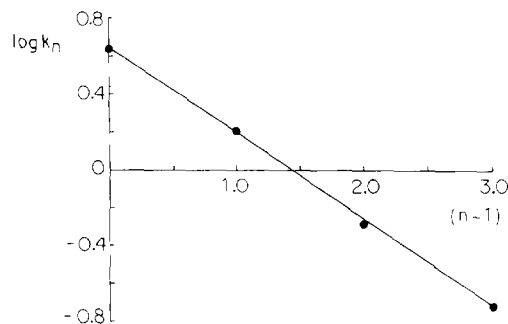
Fig. 3. Log K_n as a function of $(n - 1)$ for $Mn(II)/N_3^-$ complexes: $K_1 = 4.2$ M^{-1}; $K_2 = 1.6$ M^{-1}; $K_3 = 0.5$ M^{-1}; $K_4 = 0.18$ M^{-1}.

such as $Co(II)/SCN^-$, where a change from octahedral to tetrahedral geometry is observed [17].

All the experiments were carried out in the absence of oxygen. At ligand concentrations higher than 1.0 M conditions exist for a slow spontaneous autoxidation of manganese(II) to manganese(III) complexes, with remarkable spectral changes. The manganese(III) complexes have a maximum absorbance peak at 428 nm [9,10].

As was pointed out previously a synergistic effect of the manganese ions [7,8,12] on the induced autoxidation of metal ions by S(IV) occurrs and, it is important to compare the formation curves of complexes of Co(II) [1] and Mn(II) azide complexes. It was found that the 0.5 M azide concentration is the best experimental condition for analytical purposes for determination of S(IV), based on the cobalt(II)-induced autoxidation. At this azide concentration the average number of ligands is 2 and 1.3 for Co(II) and Mn(II) complexes respectively (Fig. 1).

References

[1] E.A. Neves, R. Tokoro and M.E.V. Suárez, J. Chem. Res. (S), (1979) 376; J. Chem. Res. (M), (1979) 4401.

[2] N. Coichev and E.A. Neves, Polyhedron, 8 (1989) 641.

[3] E.A. Neves, E. de Oliveira and Z.L. Santos, Talanta, 27 (1980) 609.

[4] M.E.V. Suárez and E.F.A. Neves, Polyhedron, 11 (1992) 759.

[5] E.A. Neves and J.F. Andrade, Polyhedron, 5 (1986) 717.

[6] G.O. Chierice and E.A. Neves, Polyhedron, 2 (1983) 31.

[7] J. Gebert, E.A. Neves and D. Klockow, Fresenius' Z. Anal. Chem., 331 (1988) 260.

[8] E.A. Neves, N. Coichev, J. Gebert and D. Klockow, Fresenius' Z. Anal. Chem., 335 (1989) 386.

[9] N. Coichev and R. Van Eldik, Inorg. Chim. Acta, 185 (1991) 69.

[10] N. Coichev, E.A. Neves and R. Van Eldik, Inorg. Chim. Acta, 179 (1991) 133.

[11] N. Coichev and R. Van Eldik, Inorg. Chem., 30 (1991) 2375.

[12] N. Coichev, K. Bal Reddy and R. Van Eldik, Atmos. Environ., Part A, 26 (1992) 2295.

[13] P. Senise, Mikrochim. Acta, 5 (1957) 640.

[14] H.A. Flaschka, EDTA Titrations, Pergamon Press, London, 1989, p. 77.

[15] M.T. Beck, Chemistry of Complex Equilibria, Van Nostrand, London, 1970, pp. 32–81.

[16] E.F.A. Neves, I.G.R. Gutz and R.G. Tavares, J. Electroanal. Chem., 179 (1984) 91.

[17] E.F.A. Neves, N.C.F. Velloso and I.G.R. Gutz, Polyhedron, 4 (1985) 2043.

[18] O.E.S. Godinho and L.M. Aleixo, J. Coord. Chem., 6 (1977) 245.

[19] O.E.S. Godinho and L.M. Aleixo, J. Coord. Chem., 10 (1980) 207.

[20] E. Avsar, J. Inorg. Nucl. Chem., 42 (1980) 881.

[21] P. Senise and O.E.S. Godinho, J. Inorg. Nucl. Chem., 32 (1970) 3641.

[22] S. Ahrland and E. Avsar, Acta. Chem. Scand., Ser. A, 29 (1975) 881.

[23] G. Saini and G. Ostacoli, J. Inorg. Nucl. Chem., 8 (1957) 346.

[24] J.F. De Andrade and O.M. Guimarães, Anal. Chim. Acta, 271 (1993) 149.

[25] S. Ahrland and E. Avsar, Acta. Chem. Scand., Ser. A, 29 (1975) 890.

Differential pulse anodic stripping voltammetric determination of ziram (a dithiocarbamate fungicide)

L. Mathew, M.L.P. Reddy, T.P. Rao *, C.S.P. Iyer, A.D. Damodaran

Regional Research Laboratory (CSIR), Trivandrum 695 019, India

Received 30 May 1995; revised 20 July 1995; accepted 7 August 1995

Abstract

A d.c. polarographic technique has been used previously for the determination of the pesticide, ziram, in aqueous samples. this paper reports differential pulse anodic stripping voltammetric determination of ziram zinc in rice samples using a static mercury drop electrode. The procedure developed distinguishes inorganic zinc and ziram zinc in sodium acetate–sodium chloride media. The procedure developed is suitable for the determination of concentrations as low as 10 ppb of ziram with a precision of 2.1% for five successive determinations of 150 ppb of ziram.

Keywords: Ziram; Zinc: Anodic stripping voltammetry

1. Introduction

Ziram, or cuman L, is the common name for zinc dimethyl-dithiocarbamate and is used as an agricultural fungicide because of its low phytotoxicity, and as a vulcanization accelerator and antioxidant in the rubber industry. Ziram is relatively non-toxic to plants and is particularly useful in controlling diseases of vegetable crops such as anthracnose of tomatoes and cucurbits and early blight of tomatoes and potatoes. Ziram causes irritation to the mucous membrane in the dust or powder form [1].

Common methods of determination of ziram are spectrophotometry [2–7], head space CG [8]

and HPLC [9]. Electrochemical techniques have not been widely used. One method [10] reported for zineb (a related dithiocarbamate fungicide) is based on the d.c. polarographic studies at −0.18 V vs. SCE. Our studies on differential pulse anodic stripping voltammetry (DPASV) determination of ziram revealed that inorganic zinc and ziram zinc could be differentiated as they give well-resolved peaks at −1.18 and −1.08 V vs. the Ag/AgCl electrode in sodium acetate–NaCl media. Based on this, a simple and sensitive DPASV procedure is described for the determination of ziram. The method is free from interference due to other dithiocarbamate pesticides and can be used for the determination of concentrations as low as 10 ppb of ziram in rice samples.

---

* Corresponding author. Fax: (91)471-490186.

2. Experimental

2.1. Apparatus

Stripping voltammograms were recorded with a Princeton Applied Research Model 174 with Model 303 static mercury drop electrode (SMDE). Deaeration was done with purified nitrogen. The reference electrode was Ag/AgCl with an auxillary Pt electrode. The recordings were made on an Omniscribe XY/T recorder.

2.2. Reagents

Ziram stock solution (Hindustan Ciba-Geigy Ltd.; 10^{-3} M) was prepared by dissolving 0.0762 g ziram in hot 0.01 N HCl and making up with water to 250 ml. Sodium acetate (1.0 M) and sodium chloride (1.0 M) were prepared in distilled water.

2.3. Procedure

Transfer a suitable aliquot of sample solution containing 0.1–6 µg ziram (up to 8 ml) into a 10 ml calibrated flask. Add 1 ml of sodium acetate and 1 ml of sodium chloride, dilute to volume with water, transfer the solution into the electrochemical cell and place the SMDE in it. After deaeration, deposit for 4 min at −1.4 V vs. Ag/AgCl with stirring, switch off the stirrer, allow 30 s for the turbulence to cease and anodically scan the potential from −1.4 to −0.8 V with a scan rate of 2 mV s^{-1} and a pulse amplitude of 25 mV. Construct a calibration graph for various concentrations of ziram by plotting peak current vs. concentration of ziram.

2.4. Analysis of rice samples

Rice samples (100 g) were sprayed with known amounts of zinc and ziram and left for 2–4 h. The extracts were prepared by extraction of a crushed sample with 100 ml of acetone. The extract was evaporated to dryness. The residue was dissolved in 5 ml of 0.01 M HCl and transferred to a 50 ml volumetric flask.

3. Results and discussion

Preliminary studies were carried out to determine ziram by following the DPASV stripping peak of zinc. These studies revealed that ziram zinc gives a stripping peak at −1.08 V after deposition at −1.4 V for 4 min (curve B, Fig. 1). In contrast, for inorganic zinc the stripping peak occurs at −1.18 V under identical conditions (curve A, Fig. 1). This indicates that DPASV studies can distinguish ziram zinc and inorganic zinc in sodium acetate–NaCl medium. This shift in the E_p value of zinc in ziram is possibly due to the formation of a complex. Detailed optimization studies for the determination of ziram were conducted and the results obtained are described below.

3.1. Effect of supporting electrolyte

The determination of 5×10^{-7} M ziram using the SMDe with deposition for 4 min at −1.4 V was studied in different supporting electrolytes. The results are shown in Table 1, from which it is clear that the acetate–chloride medium gives the maximum stripping current signal compared to acetate or chloroacetate or NaCl. Furthermore, the stripping peaks of ziram zinc and inorganic zinc are resolved in NaCl or acetate–chloride but
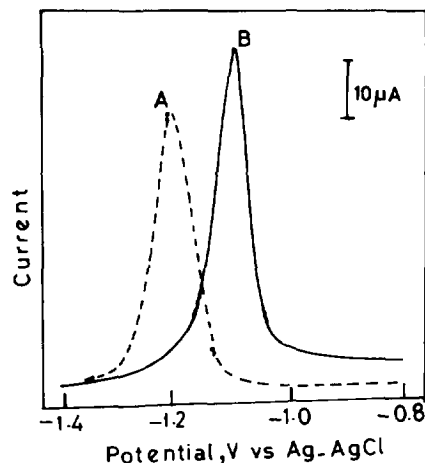
Fig. 1. Differential pulse anodic stripping voltammograms recorded for 5×10^{-7} M inorganic zinc (curve A) and ziram zinc (curve B) after deposition at −1.4 V vs. Ag/AgCl for 4 min (0.1 M sodium acetate + 0.1 M sodium chloride, scan rate 2 mV s^{-1}).

Table 1
Stripping current obtained for ziram in various supporting electrolytes

(Ziram concn. = 5 × 10^{-7} M, t_d = 4 min, E_d = −1.4 V vs. Ag/AgCl, scan rate = 2 mV s^{-1}, pulse amplitude = 25 mV)

Supporting electrolyte	I_p (μA)
HCl (0.1 M)	4.2
Chloracetic acid (0.1 M)	34.0
Ammonium acetate (0.1 M)	37.8
Sodium chloride (0.1 M)	39.6
Sodium acetate (0.1 M)	41.6
Sodium acetate (0.1 M) + NaCl (0.1 M)	55.0

not in acetate solutions. An acetate–sodium chloride medium (pH 5) was chosen for further studies.

3.2. Variation of deposition potential

In order to ascertain the optimum deposition potential (E_d) the cathodic limit of the deposition potential was varied in the range −1.0 to −1.5 V vs. Ag/AgCl in steps of 0.1 V with deposition for 4 min at each deposition potential, followed by a DPASV scan rate of 2 mV s^{-1} and a modulation amplitude of 24 mV. The magnitude of the stripping signal attains a maximum at a deposition potential of −1.3 V vs. Ag/AgCl and remains unaltered on further increase. −1.4 V was chosen as the deposition potential in subsequent studies.

3.3. Variation of deposition time

The effect of deposition time (30–480 s) on the magnitude of the stripping signal was studied. The stripping signal varied linearly with the deposition time and a deposition time of 240 s was chosen to offer reasonable sensitivity and a reasonable number of samples that can be determined in a given time.

3.4. Variation of scan rate

The effect of scan rate in the range 0.1–100 mV s^{-1} was studied during DPASV determination of ziram. At 2 mV s^{-1} the sensitivity and resolution of the ziram zinc and inorganic zinc were found to be optimum. The stripping signal

was found to be the same for successive determinations.

3.5. Variation of modulation amplitude

The modulation amplitude was varied from 5 to 50 mV during DPASV determination of ziram. At 25 mV the resolution of ziram zinc and inorganic zinc was optimum and reasonably sensitive.

3.6. Effect of other interferents

The influence of other coexisting interferents on DPASV determination of ziram was investigated. Ten-fold amounts of Thiram, Mn^{2+}, Fe^{3+}, Pb^{2+}, Cd^{2+}, Ni^{2+} and sodium diethyldithiocarbamate did not interfere in the DPASV determination of ziram.

3.7. Sensitivity and precision

The DPASV signal was found to be linear in the range 10–600 ppb of ziram at a deposition potential of −1.4 V vs. Ag/AgCl for 4 min with a scan rate of 2 mV s^{-1}. The coefficient of variation of 150 ppb of ziram was 2.1% for five successive determinations.

3.8. Application of the method to rice samples

Suitable aliquots were analysed according to the procedure described in the Experimental. The results obtained are shown in Table 2. The recoveries on addition of known amounts of ziram and inorganic zinc to the rice samples are also given in Table 2. Rice samples were spiked with known amounts of ziram and inorganic zinc prior to

Table 2
Analysis of rice samples (100 g)

Amount of ziram added (ng)	Amount of zinc added (ng)	Amount of ziram found (ng)	Amount of zinc found (ng)
100	50	98.0	49.5
200	20	199.0	19.5
400	40	395.0	38.0

extraction with acetone. A blank was also run to check whether there were any interferences present at the same current signal. The recoveries were found to be in the range 95–99%. From these results, it is evident that the developed DPASV procedure can be reliably used for the determination of zinc in rice samples.

4. Conclusion

In general, the analysis of ziram by spectrophotometry is based on the determination of zinc. These methods therefore cannot distinguish from the zinc naturally present in rice or soil samples. Conventional spectrophotometric methods are not adequately sensitive. Head space GC and HPLC methods are used only for the determination of ziram. In contrast, by using the present method, it is possible to determine inorganic and ziram zinc simultaneously in rice samples. The present procedure is free from the interference of other dithiocarbamate fungicides.

References

[1] E.H.F. Donald (Ed.), Chemistry of the Pesticides, 3rd edn., Van Nostrand, New York, 1955, p. 294.
[2] D.K. Clark, H. Baum, E.L. Stanley and W.F. Hesta, Anal. Chem., 23 (1951) 1842.
[3] B.C. Verma, R.V. Sood and M.S. Sindu, Talanta, 30 (1983) 784.
[4] A.K. Malik and A.L.J. Rao, Talanta, 37 (1990) 1205.
[5] A.L.J. Rao and N. Verma, Talanta, 36 (1989) 1041.
[6] A.K. Malik and A.L.J. Rao, Talanta, 38 (1991) 941.
[7] L. Mathew, T.P. Rao, C.S.P. Iyer and A.D. Damodaran, Talanta, 42 (1995) 41.
[8] Reports by the Panel on Determination of Dithiocarbamate Residues, Analyst, 106 (1981) 782.
[9] K.H. Gustafsson and R.A. Thompson, J. Agric. Food Chem., 29 (1981) 729.
[10] A.L.J. Rao and N. Verma, Bull. Electrochem., 6 (1990) 435.

Determination of traces of chromium in cocaine and heroin by flameless atomic absorption spectrometry

Pilar Bermejo-Barrera*, Antonio Moreda-Piñeiro, Jorge Moreda-Piñeiro, Adela Bermejo-Barrera

Department of Analytical Chemistry, Nutrition and Bromatology, Faculty of Chemistry, University of Santiago de Compostela, 15706-Santiago de Compostela (A Coruña), Spain

Abstract

A method for the determination of total chromium in cocaine and heroin by flameless atomic absorption spectrometry is presented. Cocaine samples were dissolved in 2 ml of HNO_3 35.0% (v/v) and diluted to 10 ml with ultrapure water; heroin samples were dissolved in ultrapure water, adding 0.4 ml of HNO_3 35.0% (v/v) to dissolve inert species, and also diluted to 10 ml. $Mg(NO_3)_2$ and HNO_3, as chemical modifiers, were compared in terms of sensitivity, precision and accuracy, a lower detection limit being obtained for the use of $Mg(NO_3)_2$, 5.77 μg kg^{-1} (7.23 μg kg^{-1} for HNO_3). Within-batch precision was found to be 6.19% and 1.48% for drug solution spiked with 0 and 10 μg l^{-1} of Cr^{3+}, respectively, when using $Mg(NO_3)_2$, and 7.45 and 1.19% for the same respective concentration levels when using HNO_3. Similar results on analytical recovery were obtained for both $Mg(NO_3)_2$ and HNO_3. $Mg(NO_3)_2$ was selected as the more adequate of the two chemical modifiers. A study of the introduction of a cooling-down step of 50°C was carried out and compared in terms of sensitivity to the programme without a cooling-down step, but no advantage was observed. Studies on the variation in precision and analytical recovery with the amount of sample, and interferent effects of different species on chromium determination were developed. Finally, chromium concentrations obtained in cocaine samples varied between 0.02 and 0.14 mg kg^{-1}, the levels in the heroin samples being in the 0.05-0.59 mg kg^{-1} range.

Keywords: Chromium; Cocaine; Heroin; Chemical modifiers; Magnesium nitrate modifier; Flameless absorption spectrometry

1. Introduction

The remarkable increase in the improper use of cocaine and heroin, two of the more dangerous

narcotics, has led to the imposition by the International Community of a control on the trade and utilization of these drugs. Therefore, it is very important to determine whether a confiscated drug comes from a certain geographical area. In this way, it is possible to discover its trading routes. Such studies are usually based on organic

---

*Corresponding author.

compounds present in drugs, and thus extensive information is available on the organic constituents in cocaine and heroin. However, knowledge about the inorganic constituents of these substances is very poor. In this sense, only few data have been found in the literature on metallic species [1], chromium being one of the metals whose presence has been reported. According to the chromium concentration found [1], it can be concluded that it is a trace constituent in cocaine, being present in levels between 0.2 and 1.6 mg kg^{-1}. The concentration interval reported for heroin [1] is 0.2–140 mg kg^{-1}. The chromium concentration in a great number of samples cannot be determined easily by inductively coupled plasma-atomic emission spectrometry, which is the technique employed by Violante et al. [1] in their studies, because it is lower than the detection limit of the technique.

Flameless atomic absorption spectrometry (FAAS) has been recognized as one of the best techniques for determining metal content, chromium being one of the metallic species requiring very sensitive detection [2].

As there is no literature on the determination of chromium in samples such as cocaine and heroin, in order to select the most adequate chemical modifier, a bibliographic search was carried out on the determination of chromium in biological and environmental materials and waters [3–28]. It should be mentioned that as a consequence of the refractory behaviour of chromium [2,29], it has been proposed not to add a chemical modifier [3–5]. However, it is evident that the low charring temperatures obtained in the absence of a matrix modifier do not offer satisfactory matrix volatilization when the samples contain complex matrices; thus, the addition of a chemical modifier appears to be necessary. The use of nitric acid [6–8] as a chemical modifier was therefore proposed, charring occurring at 1300°C. The addition of Na$_2$WO$_4$, in solution [7–9] or the use of W-coated graphite tubes [10,11], has also been reported; the former was of more advantage, owing to the large difference in charring temperatures reported, i.e. 1600°C for addition in solution and 900°C for the use of coated graphite tubes. The use of graphite tubes coated with Zr [9], Ta

[11,12] and La [13,14] has also been reported. Vanadium and molybdenum [15] have been proposed for chromium determination, achieving a charring temperature of 1400°C. Finally, NH$_3$ [16] and ascorbic acid [17] have also been used as chemical modifiers for chromium.

Magnesium nitrate alone [7,9,18–24], or in conjuction with palladium [25] or calcium [26,27], appears to be the most adequate chemical modifier for chromium, owing to the higher charring temperatures reported. In this sense, palladium has also been proposed as an adequate chemical modifier [14,28]. In addition, these species present the advantage, in comparison with the other chemical modifiers cited, that their content is not frequently determined by FAAS; hence, their use in large amounts, mg l^{-1}, as chemical modifiers does not lead to contamination of the graphite furnace.

In this paper, the use of nitric acid and magnesium nitrate as chemical modifiers for chromium determination is compared, investigating also palladium and the mixture palladium–magnesium nitrate proposed by Welz et al. [30]. Finally, a method for chromium determination in cocaine and heroin was developed and applied to different samples.

2. Experimental

2.1. Apparatus

AAS measurements were performed with a Perkin-Elmer model 1100B atomic absorption spectrometer equipped with an HGA 700 graphite furnace, an AS-70 autosampler and a deuterium arc background corrector. A Cr hollow cathode lamp (Perkin-Elmer) operated at 25 mA, which provided a 357.9 nm resonance line, was used. The spectral bandwidth was 0.7 nm. Pyrolytically graphite-coated graphite tubes and L'vov graphite platforms were used throughout.

2.2. Reagents

All the solutions were prepared from analytical-reagent grade chemicals using ultrapure water,

resistivity 18 MΩ cm^{-1}, which was obtained by means of a Milli-Q (Millipore, USA) water purification system.

Nitric acid stock standard solution, 35.0% (v/v), was prepared from nitric acid Aristar, 69.0–70.5% (v/v) (BDH Chemicals, Poole, UK) with a maximum chromium content of 0.05 mg l^{-1}.

Chromium nitrate stock standard solution, 1.000 g l^{-1}, was obtained from Merck (Darmstadt, Germany).

Magnesium nitrate stock standard solution, 2.000 g l^{-1}, was prepared by dissolving 2 g of magnesium nitrate (Analar, BDH Chemicals) in 1 l of ultrapure water.

Palladium stock standard solution, 3.000 g l^{-1}, was prepared according to Welz et al. [31] by dissolving 300 mg of palladium (99.999%, Aldrich, Milwaukee, WI, USA) in 1 ml of concentrated nitric acid and diluting to 100 ml with ultrapure water. If the dissolution was incomplete, 10 μl of hydrochloric acid (Aristar, 35.0% (v/v), BDH Chemicals, with a maximum chromium content of 0.005 mg l^{-1}) was added to the cold nitric acid and heated to gentle boiling in order to volatilize the excess chloride.

2.3. Procedure

Cocaine samples, 0.5 g, were dissolved in 2 ml of nitric acid 35.0% (v/v), diluting to 10 ml with ultrapure water. For heroin samples, 0.25 g of sample was dissolved in ultrapure water, and 0.4 ml of nitric acid 35.0% (v/v) was added to dissolve any remaining undissolved inert substances. The solutions were then diluted to 10 ml with ultrapure water. All samples were kept in polyethylene vials at 4°C.

0.5 or 0.25 ml of cocaine and heroin solution, respectively, was transferred to an autosampler cup, adding an adequate volume of magnesium nitrate to obtain a concentration of 15 mg l^{-1} after dilution to 1 ml. Calibration was performed over the 0–10 μg l^{-1} range, injecting 20 μl into the atomizer, and running the sequential dry–charring–atomization–cleaning programme of the graphite furnace shown in Table 1.

3. Results and discussion

3.1. Comparative study of palladium, magnesium nitrate, palladium–magnesium nitrate and nitric acid as chemical modifiers

A comparative study on the use of palladium, magnesium nitrate, palladium–magnesium nitrate and nitric acid as chemical modifiers for the determination of chromium in cocaine and heroin was developed. Charring curves corresponding to each chemical modifier were obtained for a cocaine sample solution spiked with 10 μg l^{-1} of Cr^{3+}, for a heroin sample solution and for an aqueous standard solution of 15 μg l^{-1} of Cr^{3+}, Figs. 1(a), 1(b) and 1(c), respectively. The atomization temperature used was 2500 °C (Table 1) and the concentration of the chemical modifier in these experiments was 10 mg l^{-1} of palladium and magnesium nitrate, and 3.5% (v/v) of nitric acid, i.e. the concentration of nitric acid obtained after dissolution and dilution of the cocaine in the autosampler cups, according to Section 2.3. As can be seen in Figs. 1(a)–1(c), the optimum charring temperatures ranged between 1500 and 1700°C for the different chemical modifiers and solutions. A lower charring temperature, 1500°C, was found for heroin solutions than for cocaine and aqueous standard solutions, 1600 °C, when using palladium–magnesium nitrate. Therefore,

Table 1
Graphite furnace temperature programmes and spectrometer operating conditions[a]. Values in brackets correspond to the use of nitric acid as a chemical modifier

Stage	Temperature (°C)	Ramp (s)	Hold (s)	Ar flow (ml min^{-1})
Drying	150	15	15	300
Charring	1600	10	15 (20)	300
Atomization	2500	0	4	0 read
Cleaning	2600	2	3	300

[a]Cr hollow cathode lamp operating at 25 mA; wavelength 357.9 nm; spectral bandwidth 0.7 nm; integration time 4s; peak-area measurements; injection volume 20 μl; pyrolytic graphite tubes and L'vov platforms.
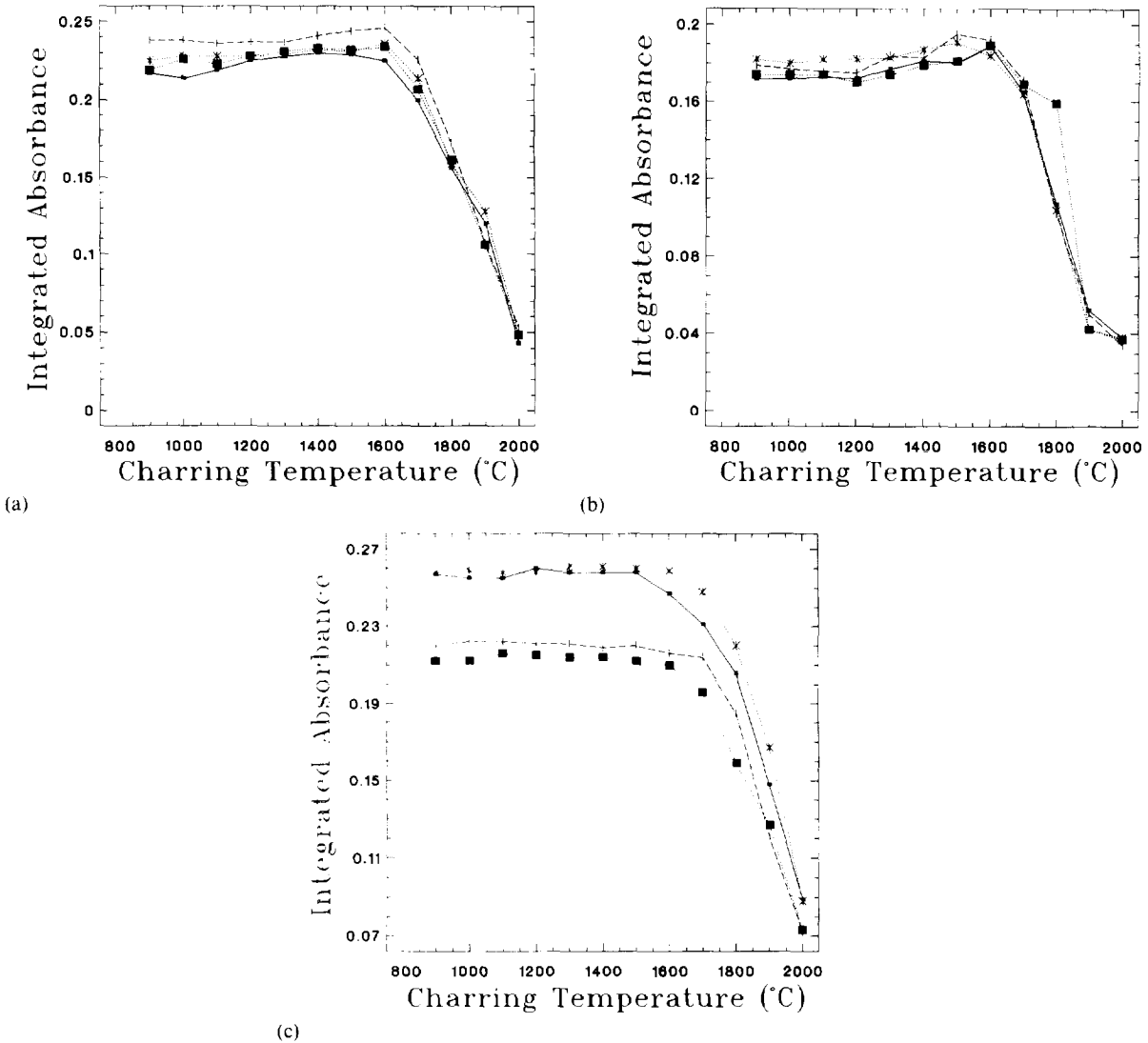
Fig. 1. Charring curves corresponding to (a) cocaine sample solution spiked with 10 μg l^{-1} of Cr^{3+}, (b) heroin sample solution and (c) aqueous standard solution of 15 μg l^{-1} of Cr^{3+}, obtained for 10 mg l^{-1} of palladium (■), 10 mg l^{-1} of palladium and magnesium nitrate (*), 10 mg l^{-1} of magnesium nitrate (|) and 3.5% (v/v) of nitric acid (■).

for the use of this chemical modifier, an optimum charring temperature of 1500°C was selected. Similarly, the charring temperature observed for the aqueous standard of Cr^{3+}, 1500 °C, was selected as optimum for palladium. Finally, an optimum charring temperature of 1600°C was chosen when using magnesium nitrate and nitric acid.

Because chromium levels are lower for cocaine than for heroin samples, and hence a greater amount of cocaine is required to prepare the solutions, the following studies were performed on cocaine solutions, considering the results obtained for cocaine solutions are applicable to heroin sample solutions owing to their greater dilution.

(a)   (b)
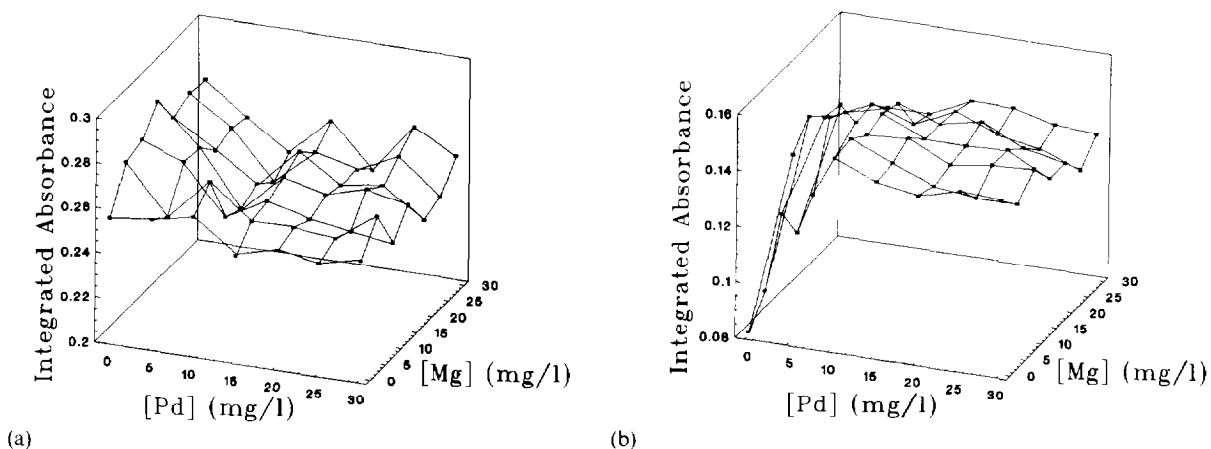
Fig. 2. Dependence of the chromium absorbance signal on the combined effects of various amounts of palladium and magnesium nitrate added to (a) cocaine sample solution spiked with 10 $\mu g\ l^{-1}$ of Cr^{3+} and (b) aqueous standard solution of 15 $\mu g\ l^{-1}$ of Cr^{3+}.

3.2. Optimization of the amount of chemical modifier

In order to investigate the use of magnesium nitrate, palladium–magnesium nitrate and palladium as chemical modifiers, and to determine their optimum amounts, a study involving different combinations of palladium and magnesium was performed. The charring temperature used was the optimum found for palladium–magnesium nitrate, 1500 °C, and the atomization temperature was 2500 °C. These experiments were carried out on cocaine sample solutions spiked with 10 $\mu g\ l^{-1}$ of Cr^{3+}, Fig. 2(a), and Cr^{3+} aqueous standard solutions of 15 $\mu g\ l^{-1}$, Fig. 2(b). The addition of palladium does not have any influence, as shown in Fig. 2(a). However, chromium absorbance values increase slightly, in the absence of palladium, until a concentration of 15 mg l^{-1} of magnesium nitrate is reached. These facts can also be observed in Figs. 3 and 4, where different peak schemes, corresponding to 0 mg l^{-1} of palladium and various amounts of magnesium, and 15 mg l^{-1} of magnesium and different amounts of palladium, respectively, are represented. In Fig. 2(b), which shows the results obtained for aqueous standards of Cr^{3+}, it can be seen that the addition of palladium increases the chromium absorbance signal. However, it should

be mentioned that the higher chromium absorbance signals correspond to combinations between $Mg(NO_3)_2$ and Pd, where the amount of magnesium nitrate is greater than that of Pd. Therefore, the highest chromium absorbance is obtained for concentrations of 10 and 15 mg l^{-1} for palladium and magnesium nitrate, respectively. Because the addition of palladium to cocaine sample solutions does not offer a significant increase in chromium absorbance, we select magnesium alone, at a concentration of 15 mg l^{-1}, as adequate for stabilizing chromium.

The amount of nitric acid was optimized in the same way, increasing the concentration up to 10% (v/v) for aqueous standard solutions of 15 $\mu g\ l^{-1}$
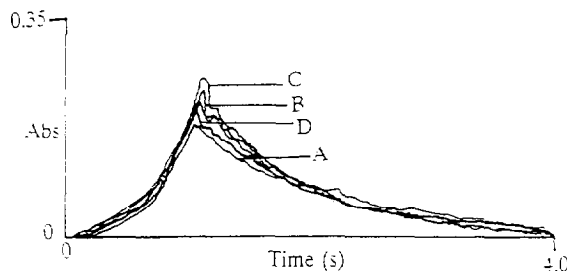
Fig. 3. Effect of 0 mg l^{-1} of palladium and different amounts of magnesium nitrate on the peak scheme corresponding to a cocaine sample solution spiked with 10 $\mu g\ l^{-1}$ of Cr^{3+}: (A) 0 mg l^{-1} (0.254 A.s.); (B) 5 mg l^{-1} (0.272 A.s.); (C) 15 mg l^{-1} (0.285 A.s.); (D) 25 mg l^{-1} (0.272 A.s.).
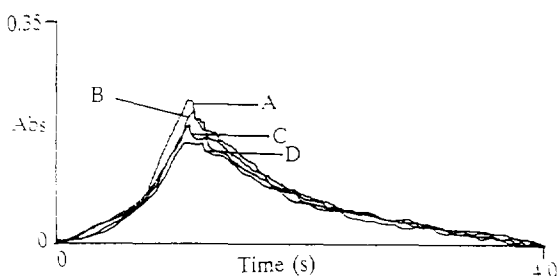
Fig. 4. Effect of 15 mg l^{-1} of magnesium nitrate and different amounts of palladium on the peak scheme corresponding to a cocaine sample solution spiked with 10 μg l^{-1} of Cr^{3+}: (A) 0 mg l^{-1} (0.285 A.s.); (B) 5 mg l^{-1} (0.267 A.s.); (C) 10 mg l^{-1} (0.243 A.s.); (D) 20 mg l^{-1} (0.246 A.s.).

of Cr^{3+} and a cocaine sample solution spiked with 10 μg l^{-1} of Cr^{3+}. Chromium absorbance was not statistically varied in the range studied and no variation in the peak scheme was found with larger amounts of nitric acid for both cocaine and aqueous solutions. Therefore, because an increase in the concentration of nitric acid results in faster damage of graphite tubes, we selected an optimum concentration of nitric acid of 3.5% (v/v), i.e. the concentration obtained after dissolution and dilution of cocaine samples in the autosampler cups (Section 2.3).

3.3. Optimization of the graphite furnace temperature programmes

Although chromium absorbance is stronger when magnesium nitrate is used instead of nitric acid, a temperature programme for nitric acid has also been developed and compared in terms of sensitivity, precision and accuracy to that for magnesium nitrate. The use of nitric acid as a chemical modifier is simpler than the use of magnesium nitrate because the optimum concentration of nitric acid, 3.5% (v/v), is that obtained after dissolution and dilution of cocaine in the autosampler cups; thus, it is only necessary to dilute the cocaine samples, without the addition of other species.

As mentioned previously, in the cases of nitric acid and magnesium nitrate a charring temperature of 1600°C was found to be optimal. Optimum values of the ramp and hold times for the charring step, corresponding to the use of magnesium nitrate and nitric acid, are shown in Table 1.

In order optimize the atomization temperatures for each chemical modifier, a range of temperatures between 1800 and 2600°C was studied for a cocaine sample solution spiked with 10 μg l^{-1} of Cr^{3+} and an aqueous solution of 15 μg l^{-1} of Cr^{3+}; these were the optimum temperatures for each chemical modifier and solution shown in Table 2.

Optimum drying conditions, temperatures and times, for each chemical modifier, were determinated by observing the sample in the graphite tube. In order to provide smooth evaporation of the solvent with no sputtering of the sample, an optimum temperature of 150°C with ramp and hold times of 15 s was achieved for both chemical modifiers.

3.4. Linear range, and calibration and standard addition graphs

The linear range was established for the use of magnesium nitrate and nitric acid, being 0.15-15 and 0.18-15 μg l^{-1} of Cr^{3+}, respectively. In order to determine the matrix effects for both methods, the standard addition method was applied over the same range of concentrations. The equations obtained for the use of magnesium nitrate were

calibration graph:

$$Q_A = 0.008 + 0.017[Cr^{3+}] \quad r = 0.999$$

standard addition graph:

$$Q_A = 0.049 + 0.020[Cr^{3+}] \quad r = 0.999$$

Table 2
Optimum atomization temperatures corresponding to different chemical modifiers

Chemical modifier	Atomization temperature (°C)	
	Cocaine sample solution	Aqueous Cr standard
Palladium	2600	2600
Palladium-magnesium nitrate	2600	2600
Magnesium nitrate	2500	2600
Nitric acid	2500	2600

Table 3
Analytical recovery ($n = 11$) corresponding to the use of magnesium nitrate and nitric acid as chemical modifiers

Cr^{3+} concentration added (μg l^{-1})	$Mg(NO_3)_2$			HNO_3		
	Cr^{3+} concentration found (μg l^{-1})	Analytical recovery (%)	RSD (%)	Cr^{3+} concentration found (μg l^{-1})	Analytical recovery (%)	RSD (%)
5.0	4.87 ± 0.07	96.4 ± 1.4	2.3	5.23 ± 0.09	104.5 ± 2.0	2.8
7.5	7.32 ± 0.09	97.6 ± 1.2	1.8	7.53 ± 0.05	100.4 ± 0.7	1.0
10.0	10.3 ± 1.2	103.5 ± 1.2	1.7	9.88 ± 0.09	98.8 ± 0.9	1.4

and for the use of nitric acid were

calibration graph:

$$Q_A = 0.011 + 0.017[Cr^{3+}] \quad r = 0.997$$

standard addition graph:

$$Q_A = 0.041 + 0.014[Cr^{3+}] \quad r = 0.999$$

where Q_A is the integrated absorbance and $[Cr^{3+}]$ is in units of μg l^{-1}.

The F-test [32] was applied to comparison of the slopes in each graph and for each chemical modifier; in both cases, the slopes of the calibration and standard addition graphs were statistically the same, and thus there are no matrix effects in the determination of chromium when using magnesium nitrate or nitric acid. Aqueous calibration was found to be a real possibility for developing the analysis for the use of both chemical modifiers.

3.5. Sensitivity

The sensitivity of magnesium nitrate and nitric acid as chemical modifiers was studied for the two programmes (Table 1). The limit of detection (LOD), limit of quantification (LOQ) and characteristic mass (m_0) [33] were the parameters used in the study.

The blanks were solutions of 3.5% (v/v) nitric acid when using nitric acid as a chemical modifier, and 3.5% (v/v) of nitric acid and 15 mg l^{-1} of magnesium nitrate when using magnesium nitrate as a modifier. The values obtained, for 11 replicate injections, were 0.008 ± 0.001 and 0.006 ± 0.001 A.s. for magnesium nitrate and nitric acid, respectively.

The LODs, corresponding to 0.5 g of drug sample, were 5.77 and 7.23 μg^{-1} for the use of magnesium nitrate and nitric acid, respectively, the LOQs being 19.24 μg kg^{-1} for magnesium nitrate and 24.20 μg kg^{-1} for nitric acid. The values of m_0 obtained were 5.2 ± 0.34 and 4.6 ± 0.67 pg for magnesium nitrate and nitric acid, respectively. As can be seen, the sensitivity is better for magnesium nitrate as a chemical modifier.

3.6. Precision and accuracy

Precision was studied for the use of both chemical modifiers, magnesium nitrate and nitric acid. The within-batch precisions obtained for 11 replicate injections of cocaine sample solutions spiked with 0, 5, 7.5 and 10 μg l^{-1} of Cr^{3+}, expressed as RSDs, were 7.45, 2.21 0.86 and 1.19%, respectively, for nitric acid, and 6.19, 1.78, 1.52 and 1.48%, respectively, for magnesium nitrate. As can be seen, similar precision is achieved by both chemical modifiers.

The accuracy of the methods was studied by analytical recovery. This parameter was obtained for cocaine solutions spiked with 5, 7.5 and 10 μg l^{-1} of Cr^{3+}, which were injected into the atomizer 11 times. The results are shown in Table 3. As can be seen, analytical recoveries close to 100% were achieved for all concentration levels for both chemical modifiers.

Good precision and analytical recovery were discovered for both the chemical modifiers investigated, and a similar linear range was achieved. Therefore, owing to the lower LOD obtained with the use of magnesium nitrate, we consider magnesium nitrate to be a more suitable chemical

modifier than nitric acid. In the following studies, magnesium nitrate, at the optimum concentration of 15 mg l^{-1}, will be used.

3.7. Study of the introduction of a cooling-down step

The introduction of a cooling-down step, which has been reported for the determination of lead and aluminiun [34], has also been implemented in the determination of chromium in foodstuffs [24]. Therefore, in this section a graphite furnace temperature programme incorporating a cooling-down step, just before atomization, with ramp and hold times of 10 s for each and cooling temperatures between 50 and 350°C, was studied. The within-run precision, for seven replicate injections of a cocaine sample solution spiked with 10 μg l^{-1} of Cr^{3+}, was studied for each cooling temperature, obtaining good precision (< 10%) for measurements in the peak-area and peak-height modes. However, the RSD (%) values for higher cooling temperatures were larger than those for lower cooling temperatures and those similar to the values obtained without the introduction of a cooling-down step (Table 1). An increase in chromium absorbance, measured in the peak-area mode, compared to that obtained using the former programme, was obtained for all cooling temperatures.

A cooling temperature of 50°C was selected as the most adequate cooling temperature owing to good within-run precision and the peak scheme attained. However, the sensitivity achieved was poorer than that obtained using the former programme (Table 1), the LOD being three times higher (19.24 μg kg^{-1}) than the standard programme (5.77 μg kg^{-1}).

3.8. Interferences

A study on the effects of species that could interfere with the chromium absorbance signal was carried out. We assume a species to be an interferent when, at a specified concentration, it produces a variation in the chromium absorbance signal of ± 10% of the signal measured in the absence of the species. Therefore, several different

cations, Al^{3+}, Ba^{2+}, Ca^{2+}, Cd^{2+}, Co^{2+}, Cu^{2+}, Fe^{3+}, K^+, Li^+, Mn^{2+}, Na^+, NH_4^+, Ni^{2+}, Pb^{2+} and Zn^{2+}, and anions, Cl^-, PO_4^{3-}, SO_4^{2-}, SiO_3^{2-} and citrate, were studied. Different amounts of each species were added to a cocaine sample solution spiked with 10 μg l^{-1} of Cr^{3+}; the results obtained are shown in Table 4, which gives the lowest concentration corresponding to 0.5 g of the drug sample, the percentage chromium absorbance variation and the levels for some species reported in the literature [1]. As can be seen, species that can be considered as major constituents, such as Ca^{2+}, Mg^{2+} and Zn^{2+}, do not exhibit interfering behaviour. Similarly, for anions such as Cl^-, PO_4^{3-} and SO_4^{2-}, that could also be considered as major constituents, the addition of 100 mg l^{-1} (4000 mg kg^{-1} corresponding to sample) does not statistically vary the ab-

Table 4
Effects of different elements on the chromium absorbance signal of a cocaine sample solution spiced with 10 μg l^{-1} of Cr^{3+}

Interferent	Lowest concentration with respect to sample (mg kg^{-1})	Concentration interval (mg kg^{-1})	% Chromium absorbance variation
Al^{3+}	2000	0.5-2700	+ 10.2
Ba^{2+}	120	0.1-26	- 3.6
Ca^{2+}	4000	$-^a$	+ 5.1
Cd^{2+}	120	0.1-2.1	- 1.6
Co^{2+}	120	$-^a$	- 1.1
Cu^{2+}	400	0.7-270	- 6.4
Fe^{3+}	4000	2.7-2200	+ 14.7
K^+	4000	$-^a$	+ 3.0
Li^+	1200	$-^a$	+ 7.5
Mg^{2+}	4000	$-^a$	+ 3.4
Mn^{2+}	1200	0.5-220	- 0.5
Na^+	4000	$-^a$	- 7.5
NH_4^+	1200	$-^a$	- 0.5
Ni^{2+}	80	0.0-77	- 4.8
Pb^{2+}	80	0.3-2.1	- 0.5
Zn^{2+}	4000	0.1-2600	- 0.4
Citrate	4000	$-^a$	- 1.1
Cl^-	4000	$-^a$	- 2.2
PO_4^{3-}	4000	$-^a$	- 0.5
SiO_3^{2-}	1200	$-^a$	+ 4.3
SO_4^{2-}	4000	$-^a$	- 6.6

^{a} Data not available.

sorbance signal. Interfering behaviour is only obtained at concentrations of Fe^{3+} and Al^{3+} greater than 2000 mg kg^{-1}. Although this fact has been observed by several authors [7,8,35,36], no explanation has been reported. Finally, for the other species whose concentration levels are available, there are no observed interfering effects at the highest concentration tested, which is greater than that reported in these kinds of samples.

3.9. Study of precision and analytical recovery with the amount of sample

A study on the precision and analytical recovery for different amounts of drug samples was developed in order to reduce the LOD and LOQ, and to verify if the amount of drug sample chosen, 0.5 g, is a representative mass to carry out the analysis. Therefore, 0.25, 0.5, 1.0 and 2.0 g cocaine samples were prepared as indicated in Section 2.3, obtaining sample concentrations of 2.5, 5.0, 10.0 and 20.0% (m/v), respectively, after dilution to 10 ml. The volume of nitric acid used to dissolve the samples was 2 ml (Section 2.3); however, for an amount of sample of 2 g, it was necessary to increase the volume of nitric acid to 2.5 ml to totally dissolve the sample.

The effect of the different sample concentration precisions was studied through the within-run precision, for 11 replicate injections of the solutions prepared from each amount of sample. To obtain similar chromium absorbance values, different volumes of an aqueous standard solution of Cr^{3+} were added to the solutions of lower sample concentrations. The RSD values obtained were 2.03, 0.72, 1.38 and 1.36% for 2.5, 5.0, 10.0 and 20.0% (m/v), respectively. As can be seen, the increase in the amount of sample does not impair the precision.

To study the effect of the amount of sample on the analytical recovery, each cocaine sample solution, corresponding to each amount of sample, spiked with 5 and 10 μg l^{-1} of Cr^{3+}, was injected 11 times into the graphite furnace, and the analytical recoveries were determined. The results are shown in Table 5, where it can be seen that for all sample concentrations and for the two concentra-

Table 5
Analytical recovery ($n = 11$) corresponding to different sample concentrations

Sample concentration (% (w/v))	Analytical recovery (%)	
	$+5\ \mu g\ l^{-1}\ Cr^{3+}$	$+10\ \mu g\ l^{-1}\ Cr^{3+}$
2.5	102.4 ± 1.0	99.6 ± 0.9
5.0	97.4 ± 1.4	103.5 ± 1.2
10.0	96.6 ± 2.6	101.6 ± 1.6
20.0	92.8 ± 3.6	102.0 ± 1.9

tion levels tested, analytical recoveries closed to 100% were achieved.

Therefore, the amount of sample can be increased to 2 g of drug sample without a loss of analytical performance, attaining a LOD of 1.44 μg kg^{-1}.

However, 0.5 g of drug sample can be considered as an adequate and representative mass for developing the analysis due to precision, and analytical recovery is not statistically varied in the 0.25–2.00 g range, obtaining an adequate LOD for the determination of chromium in a great number of samples.

3.10. Application

The method, using magnesium nitrate as a chemical modifier, was applied to the determination of chromium content in cocaine and heroin samples from various geographical areas. One subsample was taken from each sample and prepared as in Section 2.3, and two subsamples from each were subjected to FAAS twice. The results obtained are shown in Table 6, together with the SDs for four analyses of each drug sample. The obtained concentrations of chromium are low, those in heroin (0.05–0.59 mg kg^{-1}) being slightly bigger than those in cocaine (0.02–0.14 mg kg^{-1}). This can be attributed to the lower purity of the heroin samples compared to the cocaine samples. It can be said that the chromium levels found for cocaine and for some heroin samples are lower than 0.2 mg kg^{-1}, which is the lowest concentration of chromium reported by Violante et al. [1].

Table 6
Chromium levels found in several heroin and cocaine samples

Sample		Chromium level (mg kg^{-1})	SD^a (mg kg^{-1})
Heroin	1	0.33	0.05
	2	0.15	0.10
	3	0.05	0.04
	4	0.32	0.12
	5	0.59	0.08
Cocaine	1	0.14	0.05
	2	0.07	0.03
	3	0.09	0.06
	4	0.06	0.04
	5	0.07	0.04
	6	0.08	0.04
	7	0.06	0.04
	8	0.13	0.06
	9	0.06	0.05
	10	0.06	0.05
	11	0.06	0.03
	12	0.02	0.03

$^a n = 4$.

4. Conclusions

The results of this work confirm the advantageous application of magnesium nitrate as a chemical modifier for the determination of chromium. With the use of this chemical modifier, matrix effects are satisfactorily removed and aqueous calibration is a real possibility. In addition, magnesium nitrate offers the lowest LOD and LOQ, thus giving acceptable precision and accuracy. Finally, it should be mentioned that the introduction of a cooling-down step before atomization, recommended by several authors for chromium determination [24], does not offer any advantage in terms of sensitivity.

References

[1] N. Violante, M.G. Quaglia, A. Lopez and S. Caroli, Microchem. J., 45 (1992) 79.

[2] B. Welz, Atomic Absorption Spectrometry, 2nd edn., VCH, Weinheim, 1985, p. 279.

[3] Y.Q. Zhang, D.J. Wang, J.C. Cui, L.M. Zhang, Y.L. Ren and Y.S. Zheng, Guangpuxue Yu Guangpu Fenxi, 12 (1992) 71.

[4] H. Minami, Q. Zhang, H. Itoh and I. Atsuya, Microchem. J., 49 (1994) 126.

[5] V.A. Granadillo, L. Parra de Machado and R.A. Romero, Anal. Chem., 66 (1994) 3624.

[6] D.C. Paschal and G.G. Bailey, At. Spectrosc., 12 (1991) 151.

[7] E. Beceiro-González, J. Barciela-García, P. Bermejo-Barrera and A. Bermejo-Barrera, Fresenius' J. Anal. Chem., 344 (1992) 301.

[8] E. Beceiro-González, P. Bermejo-Barrera, A. Bermejo-Barrera, J. Barciela-García and C. Barciela-Alonso, J. Anal. At. Spectrom., 8 (1993) 649.

[9] S.C. Apte, S.D.W. Comber, M.J. Gardner and A.M. Gunn, J. Anal. At. Spectrom., 6 (1991) 169.

[10] K. Pyrzynska, Anal. Lett., 22 (1989) 2847.

[11] S. Chen, S. Lin, G. Zhou, W. Qi and Y. Qian, Fenxi Huaxue, 18 (1990) 645.

[12] S. Xiao-Quan, Z. Yan and N. Zhe-Ming, At. Spectrosc., 11 (1990) 116.

[13] G. Tan, M. Liu and Lihua Jianyan, Huaxue Fence, 27 (1991) 7.

[14] R. Liu, D. Yan and Z. Zheng, Fenxi Shiyanshi, 11 (1992) 43.

[15] J.L. Manzoori and A. Saleemi, J. Anal. At. Spectrom., 9 (1994) 337.

[16] Y.Z. Ma, B.W. Li, Z.K. Li, J.Z. Wang and Y.Q. Li, Fenxi Huaxue, 21 (1993) 745.

[17] R.F.J. Stobbaerts and H.A. Deelstra, Bull. Soc. Chim. Belg., 98 (1989) 513.

[18] U. Völlkopf, Z. Grobenski and B. Welz, At. Spectrosc., 4 (1983) 165.

[19] Z. Grobenski, R. Lehmann, B. Radziuk and U. Völlkopf, At. Spectrosc., 5 (1984) 87.

[20] W. Slavin and G.R. Carnrick, At. Spectrosc., 6 (1985) 157.

[21] K.S. Subramanian, Prog. Anal. Spectrosc., 9 (1986) 237.

[22] F. Betts and A. Yau, Anal. Chem., 61 (1989) 1235.

[23] D. Wagley, G. Schmiedel, E. Mainka and H.J. Ache, At. Spectrosc., 10 (1989) 106.

[24] N.J. Miller-Ihli and F.E. Greene, J. Assoc. Off. Anal. Chem., 75 (1992) 354.

[25] S. Cuo, C. Wang and G. Sheng, Fenxi Huaxue, 17 (1989) 937.

[26] G. Benling and L. Yongming, At. Spectrosc., 11 (1990) 229.

[27] E. Álvarez-Cabal Cimadevilla, K. Wróbel, J.M. Marchante-Gayón and A. Sanz-Medel, J. Anal. At. Spectrom., 9 (1994) 117.

[28] M. Hoeing, P. Regnier and R. Wollast, At. Spectrosc., 5 (1984) 87.

[29] R.C. Weast, CRC Handbook of Chemistry and Physics, 65th edn., CRC Press, Boca Raton, FL, 1984, p. B-88.

[30] G. Schlemmer and B. Welz, Spectrochim. Acta, Part B, 41 (1986) 1157.

[31] B. Welz, G. Schlemmer and R.G. Mudakavi, J. Anal. At. Spectrom., 3 (1988) 695.

[32] J.C. Miller and J.N. Miller, Statistics for Analytical Chemistry, 2nd edn., Wiley, New York, 1986, p. 57.

[33] L.H. Keith, W. Crummett, J. Deegan, R.A. Libby, J.K. Taylor and G. Wenther, Anal. Chem., 55 (1983) 2210.

[34] M.W. Hinds, M. Katyal and K.W. Jackson, J. Anal. At. Spectrom., 3 (1988) 83.

[35] K. Matsusaki, T. Yoshino and Y. Yamamoto, Anal. Chim. Acta, 124 (1981) 163.

[36] D.C. Manning, W. Slavin and G.R. Carnrick, Spectrochim. Acta, Part B, 37 (1982) 331.

Stabilisation of tetravalent cerium in perchloric acid medium and measurement of the stability constants of its fluoride complexes using ion selective potentiometry

R.M. Sawant, R.K. Rastogi, M.A. Mahajan, N.K. Chaudhuri *

Fuel Chemistry Division, Bhabha Atomic Research Centre, Trombay, Bombay 400 085, India

Received 1 March 1995; revised 14 August 1995; accepted 17 August 1995

Abstract

The stability constants of the fluoride complexes of cerium(IV) in 1 M $(HClO_4, NaClO_4)$ medium have been measured potentiometrically using a fluoride ion-selective electrode. Quantitative oxidation of cerium to its tetravalent state and its stabilisation in the perchlorate medium were accomplished by oxidation with AgO followed by quick addition of a known amount of fluoride ion. This procedure ensures stability of the oxidation state and prevents hydrolysis and polymerisation of Ce(IV). Logarithms of the average values of β_1, β_2, β_3 and β_4 were estimated to be 7.57 ± 0.04, 14.50 ± 0.03, 20.13 ± 0.37 and 24.14 ± 0.10 respectively.

Keywords: Cerium(IV); Stability constants; Fluoride complexes; Ion selective potentiometry

1. Introduction

The oxidation state of cerium(IV) is not stable in aqueous perchloric acid medium (standard electrode potential of the Ce(IV)/Ce(III) couple is 1.61 V). Ce(IV) is slowly reduced to Ce(III) as water is decomposed to liberate oxygen. In addition, Ce(IV) is very susceptible to hydrolysis and polymerisation like other tetravalent cations and a high acidity must be maintained in the medium. Stability constant data for Ce(IV) complexes are

* Corresponding author. Fax: 91-22-5560750; E-mail: fuelchem@magnum.barct1.emet.in.

very scarce mainly due to these difficulties. We are interested in the stability constant values of Ce(IV) fluoride complexes in perchlorate medium, which have not been reported in the literature so far, for correlating the stability constants of the tetravalent actinides [1] with the values of other cations in general [2] and tetravalent cations in particular.

In a preliminary study we established that AgO (standard electrode potential of the Ag(II)/Ag(I) couple is 1.98 V) could be used for quantitative oxidation of Ce(III) to Ce(IV) in 3–4 M perchloric acid medium and that the reduction of Ce(IV) could be arrested by immediate addition of some

known quantity of fluoride ion. The addition of fluoride before dilution prevented the hydrolysis and polymerisation of Ce(IV). Ion selective potentiometry using a lanthanum fluoride membrane electrode has been recommended as the best method for the study of fluoride complexes [3]. In the presence of cations forming strong complexes with fluoride, the lanthum fluoride electrode responds to free fluoride ion concentration three decades below 10^{-6} M, the accepted detection limit in non-complexing solutions. This has been validated experimentally and theoretically by several workers [4,5]. Various difficulties associated with the study of fluoride complexing in a highly acidic medium and the procedure developed by us to overcome these difficulties have been discussed in our earlier papers on the fluoride complexes of actinides [1,6]. In the present work the same experimental procedure has been followed while ensuring the stabilisation of the tetravalent state in the perchloric acid medium.

2. Experimental

2.1. Reagents

Cerium perchlorate stock solution

G.R. grade ammonium cerric nitrate, $(NH_4)_2$-$Ce(NO_3)_6$, from LOBA Chemie was dissolved in 1:1 $HClO_4$, evaporated to near dryness and fumed repeatedly with $HClO_4$. Finally a stock solution was made in 4 M $HClO_4$. During this process some of the Ce(IV) was reduced to Ce(III). Ce(IV) was determined by potentiometry after adding an excess of ferrous sulphate and then back titrating excess ferrous ions with standard potassium dichromate solution. Total Ce was determined by potentiometry after oxidation of Ce(III) to Ce(IV) with AgO in sulphuric acid medium. An aliquot of the stock solution containing 3-4 mg of Ce was taken in dilute sulphuric acid medium. Excess silver(II) oxide powder (about double the amount theoretically required) was added with constant stirring. After about 3 min, when the redox potential reached a stable maximum the excess AgO was destroyed with sluphamic acid. Ferrous sulphate solution was

then added and excess ferrous ions were back titrated with standard dichromate solution. It was observed that about 50% of the cerium in the stock solution was in the trivalent state. An aliquot of the stock solution was analysed for nitrogen at the trace level and showed complete absence of nitrogen. The hydrogen ion concentration of the stock solution was determined by titration with standard NaOH in a citrate medium using a glass pH electrode for end-point detection.

AgO

Silver(II) oxide was prepared in our laboratory following the procedure of Milner et al. [7]. The dry silver oxide powder was analysed for Ag(II) content by adding a known weight of the powder in standard ferrous sulphate solution and back titrating excess ferrous ions potentiometrically with standard potassium dichromate solution. 57% of silver was found to be in the bivalent state.

Standard $NaClO_4$ and NaF solutions were prepared as given in our earlier communication [1].

2.2. Apparatus and equipment

A combination fluoride electrode from Orion Research Inc. (Model-9609) coupled to a digital ion analyser (EA 940) was used for the determination of equilibrium free fluoride concentration. A polyethylene weight burette was used for precise addition of the titrant by weight which was converted to volume using the density of the solution. The temperature of the titration vessel was maintained at $23 \pm 1°C$ using a thermostat. A Teflon-coated bar magnet was used for stirring. A digital potentiometer with a freshly cleaned platinum electrode and a saturated calomel electrode was used for measurement of the redox potential in redox titrations. All labware used was made of polypropylene. Water used was double quartz distilled.

2.3. Procedure

Before each experiment for the determination of the stability constant, the fluoride electrode was freshly calibrated using standard fluoride solution

to obtain the standard electrode potential (E_F^0) and the electrode slope (S). The relation between $[H^+]$ and liquid junction potential (E_j) was evaluated using the procedure described in our earlier work [1,6]. For the determination of the stability constant an aliquot of cerium stock solution containing about 10 mg Ce was taken in a thermostated polypropylene beaker. About 30–40 mg AgO powder (at least twice the amount theoretically needed for complete oxidation) was added and immediately a known weight of NaF solution was added with constant stirring. Dilute perchloric acid solution was then added to the solution to bring the acidity below 1 M while maintaining the ionic strength at 1 M. Small increments of fluoride solution were added and the potentials (stable to within ± 0.2 mV) were noted. About 35–40 readings were taken in each experiment. The experiment was repeated with different quantities of total cerium. The electrode was washed thoroughly immediately after each experiment and kept in a very dilute fluoride solution for conditioning.

3. Results and discussion

3.1. total conversion to Ce(IV) and its stabilisation

At the outset it was necessary to ascertain that Ce(III) was completely oxidised to Ce(IV) by AgO. It was observed that in perchloric acid medium Ag(II) decomposed rapidly and almost completely within 10 min. Ce(IV), obtained by the oxidation of Ce(III) by AgO in perchloric acid medium, also underwent reduction to Ce(III) slowly. The recovery of Ce(IV) on potentiometric analysis decreased with waiting time. However, when an amount of fluoride was added immediately after addition of AgO, the oxidation state of Ce(IV) remained stable. Fluoride prevented the reduction as it brought down the reduction potential by preferably complexing with Ce(IV). This was confirmed by analysis of Ce(IV) in the presence of small amounts of fluoride (with varying waiting time) which showed 100% recovery. The amount of fluoride

thus added initially was taken into account of the total fluoride added during titration. Ag^+ introduced in the solution and the H^+ consumed by the oxide were taken into account in adjusting the total ionic strength of the medium of 1 M. Total H^+ concentration of the medium, H_T, was corrected for the H^+ consumed by the dissolution of the silver oxide.

3.2. Prevention of hydrolysis and polymerisation of Ce(IV)

As Ce(IV) is extremely susceptible to hydrolysis and polymerisation the stock solution had to be made in very highly acidic medium and used within a few days. It must not be stored for a long time. Even in 4 M $HClO_4$ medium problems were encountered when the solution was aged for a few weeks. It was very important to treat the aliquot of metal ion stock solution in 4 M $HClO_4$ medium with AgO and NaF solutions before diluting to below 1 M with respect to $HClO_4$. The role of F^- in preventing hydrolysis and polymerisation is well known [8]. In an experiment the redox potential of the Ce(IV)/Ce(III) couple in the presence of fluoride (the same amount as added initially before dilution in our titration) was noted while adding micro drops of NaOH solution with vigorous stirring. As Ce(IV) is more susceptible to hydrolysis a drop in potential is expected when hydrolysis begins. The potential remained constant (at 1.265 V vs. standard calomel electrode) up to the addition of a certain amount of NaOH. The addition was stopped at the point where the potential started falling (1.254 V) with the appearance of a faint turbidity in the medium. The H^+ concentration of the medium determined at this point by titration with standard NaOH in citrate buffer was 0.6 M. The initial acidity of the medium in our experiments was maintained higher than 0.7 M with respect to $HClO_4$. In the absence of fluoride a much higher acidity (much exceeding the desired ionic strength of the medium) might be required, which was found to be detrimental to the life and performance of the fluoride-sensing electrode.

Table 1
Equilibrium data for cerium(IV) fluoride system ($I = 1.0$ M) (standard potential = -247.85 mV, slope = 58.32 mV)

E_F (mV)	M_T (mM)	H_T (mM)	F_T (mM)	E_j (mV)	H^+ (mM)	F^- (mM)	$\bar{n}$
246.0	7.075	856.127	0.697	−27.9	856.124	0.113246×10^{-5}	0.0985
182.0	6.920	837.435	2.862	−27.4	837.424	0.143946×10^{-4}	0.4120
167.0	6.826	825.981	4.188	−27.1	825.962	0.257230×10^{-4}	0.6108
155.4	6.725	813.818	5.597	−26.8	813.786	0.423409×10^{-4}	0.8276
139.9	6.583	796.596	7.591	−26.3	796.540	0.795009×10^{-4}	1.1445
133.4	6.523	789.343	8.430	−26.1	789.270	0.103545×10^{-3}	1.2813
123.9	6.434	778.579	9.677	−25.8	778.470	0.152381×10^{-3}	1.4876
114.9	6.356	769.029	10.783	−25.6	768.879	0.219588×10^{-3}	1.6730
103.8	6.268	758.433	12.084	−25.3	758.251	0.344166×10^{-3}	1.8780
92.3	6.186	748.543	13.155	−25.0	748.178	0.547687×10^{-3}	2.0676
84.4	6.132	742.056	13.906	−24.8	741.559	0.753356×10^{-3}	2.1866
76.2	6.076	735.294	14.689	−24.7	734.698	0.104897×10^{-2}	2.3045
67.9	6.017	723.156	15.515	−24.5	727.206	0.146705×10^{-2}	2.4206
61.1	5.966	721.990	16.229	−24.3	720.749	0.193186×10^{-2}	2.5124
54.2	5.910	715.126	17.024	−24.1	713.529	0.255613×10^{-2}	2.6059
48.1	5.856	708.638	17.775	−23.9	706.589	0.327583×10^{-2}	2.6835
42.9	5.806	702.633	18.471	−23.8	700.112	0.404971×10^{-2}	2.7463
37.0	5.743	695.018	19.352	−23.6	691.849	0.515258×10^{-2}	2.8168
30.6	5.667	685.743	20.426	−23.3	681.678	0.670723×10^{-2}	2.8861
21.2	5.531	669.341	22.325	−22.8	663.493	0.991440×10^{-2}	2.9771
15.5	5.430	657.111	23.742	−22.4	649.829	0.126016×10^{-1}	3.0290
10.9	5.337	645.817	25.049	−22.1	637.137	0.153201×10^{-1}	3.0646
5.4	5.214	630.979	26.767	−21.6	620.286	0.193858×10^{-1}	3.0792
1.0	5.104	617.590	28.318	−21.2	604.974	0.234491×10^{-1}	3.0723

3.3. Calculation of concentration stability constants

The measured fluoride electrode potential, E_F (corresponding to each addition of fluoride to the metal ion solution), was used for the determination firstly of approximate and then of more corrected values of free fluoride ion, free hydrogen ion and the liquid junction potential using the iterative procedure described in the earlier work [1]. The total hydrogen ion concentration, H_T, and the free fluoride ion concentration, $[F^-]$, at each point were used for the evaluation of the fluoride attached to H^+ as HF and HF_2^- using their stability constant values [1]. The average number of F^- ions attached to the metal ion ($\bar{n}$) was then calculated. Stability constants were obtained by non-linear least-squares fitting to Bjerrum's equation for mononuclear complexes (program BETA). The MINIQUAD program [9] using least-squares fitting to mass balance equations was also used to obtain another set of results on the same experiments. A typical set (set I) of

primary and processed data is presented in Table 1. The concentrations of HF and free F^- in the equilibrium mixture increased with the increasing amount of added fluoride leading to a progressive decrease in the tendency of Ce(IV) to undergo hydrolysis and polymerisation. As evident from Table 1, towards the end of the titration the free H^+ ion concentration dropped appreciably. However, by then, large concentrations of HF and free F^- had accumulated, the value of $\bar{n}$ was above two and almost all the Ce(IV) ions were attached to one or more fluoride ions. These factors combined to prevent hydrolysis at the lower acidity encountered towards the end of titration. Average log values of the overall stability constants obtained for the three sets by the two methods of calculation are presented in Table 2. A speciation plot is shown in Fig. 1. The best fit was obtained when four constants (β_1–β_4) were included. Inclusion of higher constants decreased the goodness of fit and increased the standard deviation. The possibility of some fluoride ion being attached to silver ion and its effect on the final results were

Table 2
Stability constants of the fluoride complexes of Ce(IV) in perchloric acid mediuim ($I = 1$ M, Temp. $= 23 \pm 1°C$)

Set No.	$\log \beta_1$	$\log \beta_2$	$\log \beta_3$	$\log \beta_4$
I[a]	7.561 ± 0.025	14.427 ± 0.021	20.249 ± 0.028	24.229 ± 0.075
I[b]	7.558 ± 0.040	14.417 ± 0.034	20.230 ± 0.055	24.243 ± 0.176
II[a]	7.572 ± 0.136	14.508 ± 0.091	20.083 ± 0.136	24.170 ± 0.240
II[b]	7.580 ± 0.096	14.504 ± 0.046	20.098 ± 0.118	24.159 ± 0.255
III[a]	7.588 ± 0.123	14.554 ± 0.061	20.015 ± 0.128	24.309 ± 0.154
III[b]	7.581 ± 0.158	14.556 ± 0.074	20.025 ± 0.164	25.138 ± 0.117
Mean	7.573 ± 0.045(6)	14.498 ± 0.026(6)	20.126 ± 0.037	24.141 ± 0.099(5)

[a] By program BETA.
[b] By program MINIQUAD (R factors: Set I, 0.000102; Set II, 0.000148; Set III, 0.000799).

examined by including silver fluoride complex in fluoride mass balance equation in the MINIQUAD program. Though the concentration of Ag^+ was high the amount of fluoride attached to it was very negligible. The value of $\log \beta_1$ for AgF is
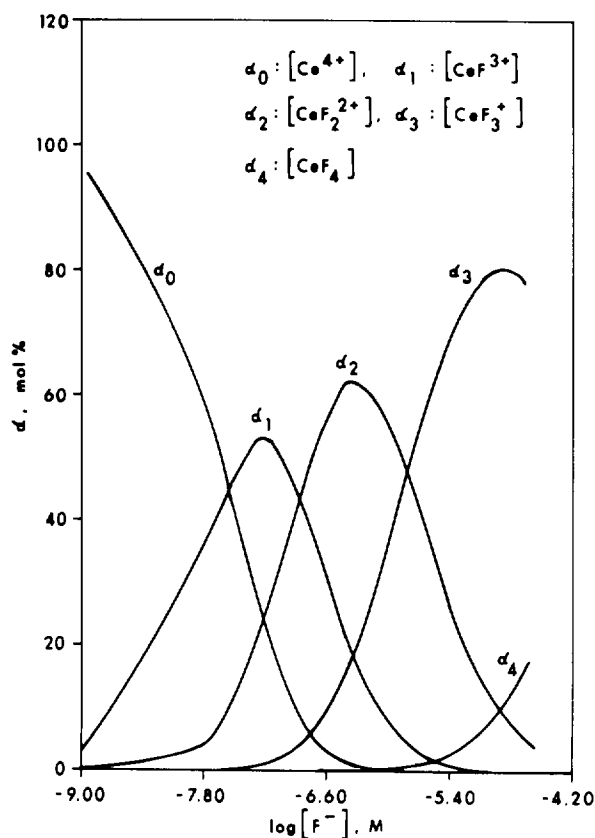
Fig. 1. Speciation plot of cerium(IV)–fluoride system.

reported [3] to be -0.32. The values for Ce(IV)–fluoride complexes remained unchanged after the correction. Only one work [10] in 3.8 M ionic strength medium containing 3 M H_2SO_4, in which Ce(IV) is stable, is reported in the literature. However, sulphate also forms a strong complex with Ce(IV). No measurement in the perchloric acid medium was reported in the literature, mainly because of the instability of the oxidation state. This has been taken care of by the particular procedure followed in the present work. Close agreement of the β values in different sets of experiments with varying metal ion concentration indicated that only mononuclear complexes were formed in this experimental condition.

An attempt was made to examine whether this value of the stability constant of the Ce(IV)–F complex agrees with the general trend of the fluoride complexes of other cations as correlated with their fundamental properties such as charge and radius [11] and, in a more generalised way, their electronic structure as well (Brown–Sylva–Ellis or BSE equation) [12]. Values of stability constants [3] of monofluoro mononuclear complexes of various metal ions were collected. Generally values obtained in perchlorate medium of 1 M and, in a few cases, 0.5 M ionic strength and at temperature $298 \pm 5°C$ were taken and converted to so-called thermodynamic values at zero ionic strength using the Debye–Hückel equation modified by Davies [13] as given below:

$$\log \beta_1^\circ = \log \beta_1 - A\,\Delta Z_i^2 [\mu^{1/2}/(1 + \mu^{1/2}) - 0.3\mu]$$

where
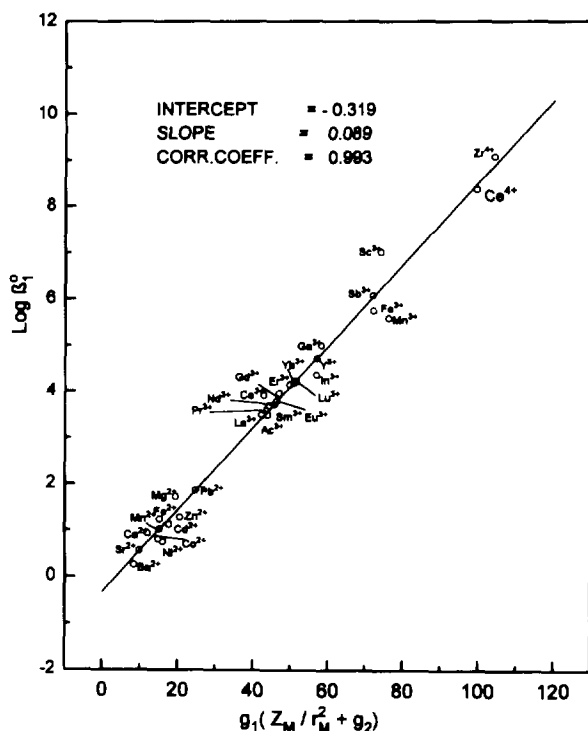
Fig. 2. Position of Ce(IV) in the linear correlation of thermodynamic stability constants of the monofluoro complexes of metal ions with the BSE parameter [12] involving charge, radius and electronic structure.

$$\Delta Z_i^2 = \sum Z_{i\,(\text{products})}^2 - \sum Z_{i\,(\text{reactants})}^2$$

The value of "A" was taken as 0.5115. The values of ionic radii were obtained from the compilation of Shannon [14]. Among the various relations, the columbic attraction parameter, $[Z_M \cdot Z_L/(r_M + r_L)]$, and the BSE parameter, $g_1(Z_M/r_M^2 + g_2)$, gave good linear relations with β_1° (regression coefficients 0.9686 and 0.9928 respectively). The slope and intercept of the former were 7.965 and −6.11 respectively. A plot of the latter is presented in Fig. 2. The measured value of Ce(IV)

fits in very well in both the plots. However, unlike Zr^{4+}, the values of Hf^{4+} could not be compared as the values reported in the literature are obtained only in very high acidity and ionic strength media.

Acknowledgments

References

[1] R.M. Sawant, N.K. Chaudhuri and S.K. Patil, J. Radioanal. Nucl. Chem. Articles, 143 (1990) 295.

[2] P.L. Brown, Talanta, 36 (1989) 351.

[3] A.M. Bond and G.T. Hefter, Critical Survey of the Stability Constants and Related Thermodynamic Data of Fluoride Complexes in Aqueous Solution, Pergamon Press, Oxford, 1980.

[4] E.W. Bauman, Anal. Chim. Acta, 54 (1971) 189.

[5] D. Midgley, Analyst, 104 (1979) 248.

[6] R.M. Sawant, G.H. Rizvi, N.K. Chaudhuri and S.K. Patil, J. Radioanal. Nucl. Chem., 96 (1985) 41.

[7] G.W.C. Milner, A.J. Wood and G.E. Cassie, A.E.R.E.-R4975, Atomic Energy Research Establishment, Harwell, UK, 1965.

[8] N.E. Ivory and D.R. Williams, Polyhedron, 4 (1985) 1883.

[9] A. Sabatini, A. Vacca and P. Gans, in D.J. Leggett (Ed.), Computational Methods for the Determination of Formation Constants, Plenum Press, New York, 1985, p. 99.

[10] V.I. Bogovina, Yu. I. Usatenko and V.E. Maltsev, Zh. Anal. Khim., 23 (1968) 115.

[11] G. Hefter, Coord. Chem. Rev., 12 (1974) 221.

[12] P.L. Brown and R.N. Sylva, J. Chem. Res. (s), 4 (1987) 110.

[13] C.W. Davies, Ion Association, Butterworths, London, 1992.

[14] R.D. Shannon, Acta. Crystallogr., 32 (1976) 751.

Studies on the formation of Cu(II) and Ni(II) complexes of 1,2-dihydroxy-9,10-anthraquinone and lack of stimulated superoxide formation by the complexes

Saurabh Das, A. Saha, P.C. Mandal *

Nuclear Chemistry Division, Saha Institute of Nuclear Physics, 1/AF, Bidhannagar, Calcutta-700 064, India

Abstract

Formation of Cu(II) and Ni(II) complexes of 1,2,-dihydroxy-9,10-anthraquinone (DHA) has been studied by the spectrophotometric method. Both the metals form stable complexes of the type $[M(LH)_3]^-$ where LHH_1 represents DHA. The effective stability constant of the Cu(II) complex is 5.135×10^{29} while that of the Ni(II) complex is 3.446×10^{25}. These complexes, unlike free DHA, do not catalyze the flow of electrons from NADH to molecular O_2 through NADH dehydrogenase.

Keywords: 1,2-Dihydroxy-9,10-anthraquinone(DHA); Cu(II)–DHA; Ni(II)–DHA; Stability constant; Cardiotoxicity

1. Introduction

Anthracyclines constitute an important class of chemical compounds. The presence of a quinone chromophore which acts as a mediator in electron transport processes in many living systems has prompted an extensive study of these compounds. Techniques such as spectrophotometry, fluorescence studies and circular dichroism have been applied as probes [1–5] to understand the nature and chemical characteristics of such molecules. These compounds gained more importance with the discovery that they could be used as drugs in the treatment of cancer. Among the chemotherapeutic drugs in use today, quinone anti-tumor agents such as daunorubicin and adriamycin are important [6–13]. However, the principal drawback from which these drugs suffer is that they are cardiotoxic [14–19] and should not be applied to patients for a prolonged period of time. These compounds are reduced to semiquinone [20–23] by enzymatic systems and then reoxidised by molecular oxygen to give superoxide radicals and other reactive oxygen species [24–26]. In fact these radicals are responsible for the anti-tumor activity and cytotoxic properties of these compounds. Earlier studies [27,28] have shown that formation of metal complexes with these drugs greatly influences the toxicity imparted by them. In fact, complexation of adriamycin and carminomycin by Fe(III) gives complexes which are less

---

* Corresponding author. Fax: (91)033-374-637.

cardiotoxic [29–31] than the parent drug but quite
effective as an anti-tumor agent against P 388
leukemia.

A number of metal complexes [27,32–34] of the
anthracyclines have been tried for the treatment
of cancer and their use has aroused growing inter-
est in the study of the role of metal ions in these
compounds. It is now well established from vari-
ous studies conducted on model nucleic acid bases
[35–39] and hypoxic tumor cells [40,41] that tran-
sition metal ions are quite effective as radiosensi-
tizers. These metal ions are also good binding
agents for cellular target DNA [42–44]. Hence
complexation of these drug molecules with suit-
able transition metals [45,46] to give a soluble
complex would result in a compound which
would be less cardiotoxic [27,28] but could be
better targetted to cellular DNA. However, there
is also a possibility that due to complexation with
metal ions the drugs may lose a certain amount of
their chemotherapeutic significance.

Previous studies have shown that metal ions
such as Fe^{3+} form complexes with quinizarin
derivatives [47,48] while the formation of long-
chain polymers was observed for Cu^{2+} and vari-
ous dihydroxyquinoid ligands [49] in the solid
state. A very recent study [2] has indicated that
Al^{3+} ions show a profound tendency to bind
molecules such as quinizarin and quinizarin-2-sul-
phonic acid which are essentially the core
molecules of the anthracycline antibiotics. The
stability of these compounds has been reported to
be comparable to those of the Al^{3+}-adriamycin
complexes. Studies on the complexation of 1,2-di-
hydroxy-9,10-anthraquinone with metal ions have
not been reported. In this investigation we have
studied the complexation of this molecule with the
transition metal ions Cu(II) and Ni(II) and have
determined their stability constants.

Furthermore, we have prepared the Cu(II)
and Ni(II) complexes of 1,2-dihydroxy-9,10-an-
thraquinone (DHA) and characterized them by
spectroscopic techniques. Also, their ability to be
reduced by enzymatic processes was assessed by
following their catalytic role in the flow of elec-
trons from nicotinamide adenine dinucleotide
(NADH) to molecular oxygen, forming superox-
ide radical through the enzyme NADH dehydro-
genase [29].

2. Materials and methods

2.1. Materials

DHA (BDH) was purified by recrystallization
from pure ethanol and was used in the present
investigation. Concentrations of solutions used
were of the order of 10^{-5} M. Substances contain-
ing the quinone moiety being sensitive to light, all
solutions used were prepared just before the ex-
periments or if required were stored in a dark
place. Standard Cu(II) and Ni(II) solutions were
prepared using analytical reagent grade $CuSO_4 \cdot
5H_2O$ and $NiSO_4 \cdot 7H_2O$ respectively. Sodium ni-
trate of analytical grade was used to maintain the
proper ionic strengths in the medium. Cy-
tochrome c (extrapure) was purchased from the
Sisco Research Laboratories, India. β-Nicotin-
amide adenine dinucleotide, reduced form (β-
NADH), and NADH dehydrogenase were pur-
chased from Sigma. The enzyme activity was
assayed [50] by following the increase in ab-
sorbance at 550 nm of cytochrome c in the pres-
ence of NADH dehydrogenase at pH 7.4.
Superoxide dismutase (SOD) was obtained as a
gift from the Department of Biochemistry, Uni-
versity of Calcutta. The specific activity of the
enzyme was 6500 units mg^{-1} of protein. Hepes
buffer [51] (4-(-hydroxyethyl)-1-piperizine ethane-
sulphonic acid; 0.05 M) was used for maintaining
the pH of the solutions. All solutions were pre-
pared in triply-distilled water.

Absorption spectra were taken on a UV-2101
Shimadzu spectrophotometer.

3. Elemental analysis of the complexes

Analyses of carbon and hydrogen were carried
out at the Central Drug Research Institute, Luc-
know, India. Estimations of copper and nickel in
the DHA complexes were carried out by the
methods described in the literature [52].

3.1. NADH dehydrogenase assay

The enzymatic assay was done at 25°C by a
method described earlier [50] where cytochrome c

was used as the electron acceptor. DHA and complexes of DHA with Cu(II) and Ni(II) were assayed for their NADH–cytochrome c reductase activity by following the reduction of cytochrome c at 550 nm. The reaction mixture contained 0.05 M Hepes buffer (pH 7.4), 80.5 μM cytochrome c, 157.5 μM NADH, 3 U l^{-1} NADH dehydrogenase and the substance of interest. The concentrations of the compounds which included DHA, Cu(II)–DHA and Ni(II)–DHA were varied from 0 to 15.75 μM. The activity of the enzyme NADH dehydrogenase is expressed in units where one unit of activity reduces 1.0 μ mole of oxidized cytochrome c per minute at pH 7.4 at 25°C. The formation of superoxide radical anion catalyzed by the DHA and its complexes was measured from the cytochrome c reduction [29,53,54] inhibited by SOD in the presence of NADH and NADH dehydrogenase. The enzymatic assay was carried out using kinetics software (Shimadzu Corporation).

4. Results and discussion

4.1. Acid dissociation of DHA

DHA can exist in three distinctly different forms depending on the pH of the solution. These forms can be represented as LHH_1, LH_1^- and L^{2-}. In LHH_1, H corresponds to the hydrogen present on the $-OH$ group at the C_2 carbon atom while H_1 represents the hydrogen on the $-OH$ group at the C_1 atom of the carbon of DHA.

$$LHH_1 \rightleftharpoons H^+ + LH_1^- \qquad K_1 = \frac{[H^+][H_1L^-]}{[H_1HL]} \qquad (1)$$

$$LH_1^- \rightleftharpoons H_1^+ + L^{2-} \qquad K_2 = \frac{[H_1^+][L^{2-}]}{[H_1L^-]} \qquad (2)$$
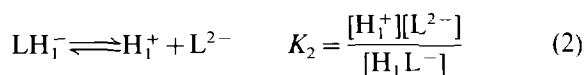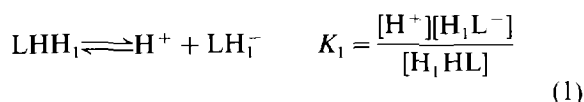
Fig. 1 shows the absorption spectra of an aqueous solution of DHA at different pH values. At pH 5.1, the absorption spectrum shows two peaks at 307 nm and 433 nm respectively (Fig. 1). On further decreasing the pH by 2.0 to 3.1 there was no significant change in the absorption spectrum indicating that the protonation of DHA to the form
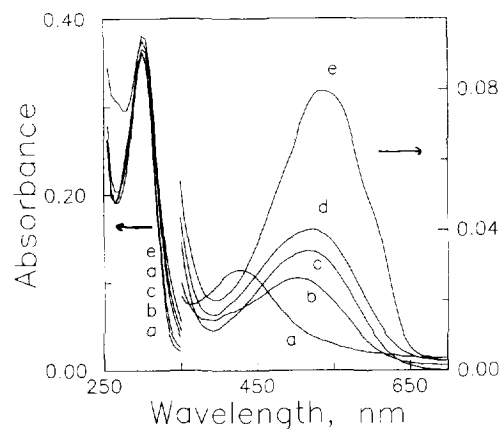
Fig. 1. Absorption spectra of DHA in aqueous solution at different pH values: (a) 5.16; (b) 6.35; (c) 7.10; (d) 9.0; (e) 11.07. [DHA] = 12 μM, [NaNO$_3$] = 0.04 M, T = 25°C.

LH_3^+ [55] takes place at much higher acid concentration. When the pH of the solution is increased beyond 5.1, there is a little increase in the absorbance of the UV peak at 307 nm, but the absorbance of the 433 nm peak decreased. However, with further increase of pH to 6.4, the peak at 433 nm disappeared and a new peak at ≈ 500 nm appeared. With further increase in pH the peak is further red-shifted to 520 nm with gradual increase in the absorbance at this wavelength. This red shift of the peak and gradual increase of the absorbance, therefore, indicate that the ligand DHA has undergone some prominent changes in its structure. The changes can be attributed to the dissociation of a proton from a phenolic-OH group on the ligand. With further increase of the pH beyond 11.07, it was observed that the peak is shifted further to 550 nm. This shift with wavelength is due to the dissociation of a second phenolic-OH proton from a ligand. The dissociation of the first proton from a phenolic-OH group present on the ligand corresponds to the phenolic-OH at the C_2 position. The second dissociation then corresponds to the proton on the phenolic-OH at C_1. To determine the proton dissociation constants, the absorbance of the compound at 520 nm was followed in the pH range 4–12. The observed absorbance, A_{obs}, at 520 nm would be given by

$$A_{obs} = A_1/(1 + 10^{pH - pK_1} + 10^{pH - pK_2})$$

$$+ A_2/(1 + 10^{pK_1 - pH} + 10^{pH - pK_2})$$

$$+ A_3/(1 + 10^{pK_1 - pH} + 10^{pK_2 - pH}) \qquad (3)$$

where A_1, A_2, and A_3 refer to the absorbances attributed to the forms LHH_1, LH_1^- and L^{2-} respectively and pK_1, pK_2 are the pK values corresponding to dissociation of LHH_1 given by relations (1) and (2) respectively. By fitting the experimental data according to Eq. (3), as shown in Fig. 2, we obtained the pK_1 and pK_2 values at 5.98 ± 0.05 and 9.88 ± 0.05 respectively.

The dissociations of the two protons from DHA can be explained if one carefully examines the structure of the molecule. DHA exists in two canonical forms I and II [56]:
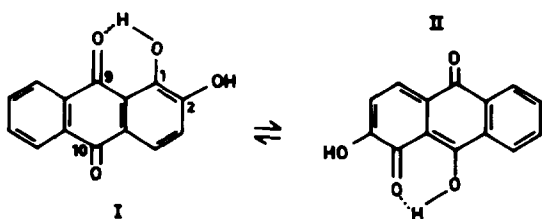
The phenolic-OH at C_1 in structure I is associated by strong hydrogen bonding with the neighboring carbonyl at C_9. In the other canonical form II the hydrogen bonding exists but in this structure the
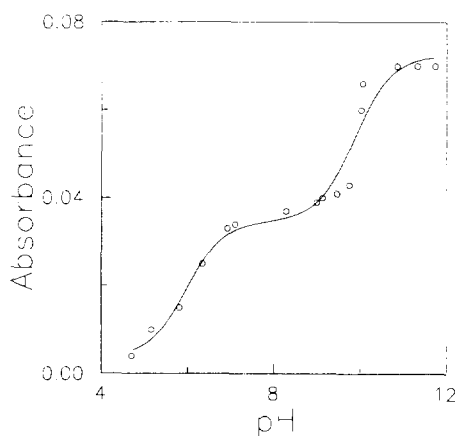
Fig. 2. Spectrophotometric titration of DHA, shown by the variation of absorbance at 520 nm; [DHA] = 12 μM, [NaNO₃] = 0.04 M, $T = 25$ °C. The solid line represents the fitted data according to Eq. (3).

carbonyl is in C_1, thus rendering an electron withdrawing effect on the phenolic-OH at C_2. As a consequence of this the phenolic-OH at C_2 becomes more acidic than one would normally expect ($pK = 5.98$) and dissociates first. Owing to the presence of the intramolecular hydrogen bonding, the phenolic-OH at C_1 dissociates later and this therefore corresponds to the pK of 9.88. Similar values for the pK (10.0) of phenolic-OH at C_{11} of the anthraquinone moiety have been reported for such molecules as doxorubicin and daunorubicin [33].

It was further seen that upon complexation of the ligand with metal ions through the carbonyl group at C_9 and the phenolate anion at C_1 the I structure for the ligand molecule predominates. As a result it was found as expected that in the complexed state the dissociation of the phenolic-OH at C_2 is decreased and it now has a $pK \approx 8.2$ (discussed later). The dissociation of the ligand in the presence of metal ions therefore occurs as shown by the following equation:

$$LHH_1 = H_I^+ + LH^- \qquad (4)$$

where H_I^+ corresponds to the dissociation of a proton from $-OH$ at C_1. This deprotonation step of $-OH$ at C_1 has been characterized by pK_2 for the free ligand.

4.2. Formation of the Cu(II) and Ni(II) complexes of DHA

When $CuSO_4$ was added to a solution of DHA at neutral pH an absorbance peak at 520 nm was observed. In order to determine the stoichiometry of the complex formed between DHA and Cu^{2+} a fixed concentration of the metal ion was taken and the concentration of the ligand (DHA) in solution was varied. The pH was maintained at 7.0 using Hepes buffer. It was found that with a gradual increase in the concentration of the ligand (DHA) with respect to a fixed concentration of the metal ion absorbance of the solution measured at 520 nm gradually increased. When the molar concentration ratio of the metal ion to ligand reached 1:3, the absorbance at this wavelength reached a maximum value and it remained unchanged even after subsequent increase in the
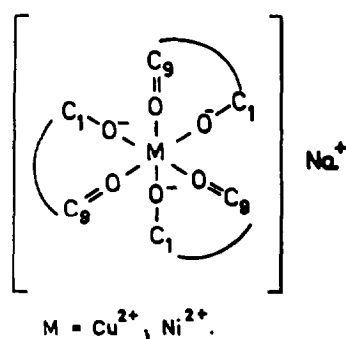
Fig. 3. Schematic diagram of the Na [M(DHA)₃] complex.

ligand (DHA) concentration for a fixed concentration of the metal ion. Thus one can suggest that Cu^{2+} forms a 1:3 complex with DHA in solution which may be represented by the schematic diagram (Fig. 3). However, it was also seen that when the concentration of Cu^{2+} in solution was increased with respect to DHA a purple to violet coloured polymeric insoluble substance resulted. The polymeric material precipitated out of the solution as soon as it was formed.

For accurate characterization of the complex, spectrophotometric titration of the Cu(II)–DHA system at 1:3 molar ratio was performed at an ionic strength of 0.05 M. The pH of the DHA solution was first lowered to 2.9 and Cu(II) solution was added to it. Then the solution was slowly titrated with 0.1 M NaOH solution. Fig. 4 shows the absorption spectra at various pH values. At
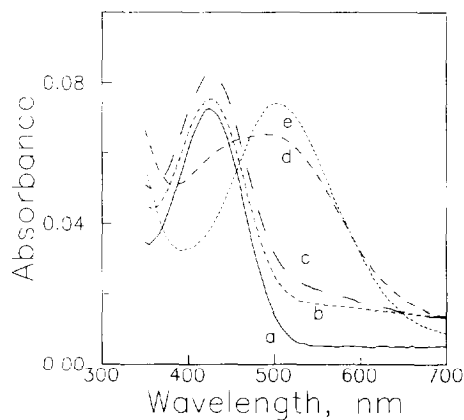
Fig. 4. Absorption spectra of DHA in the presence of Cu^{2+} at different pH values: (a) 2.90; (b) 4.16; (c) 4.70; (d) 5.50; (e) 7.20. [DHA] = 19.84 μM, [CuSO₄] = 6.613 μM, T = 25°C.
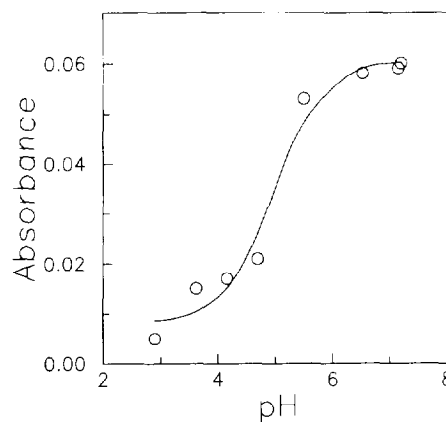
Fig. 5. Spectrometric titration of DHA in the presence of Cu^{2+} as shown by the variation of absorbance, at 520 nm; [DHA] = 19.84 μM, [CuSO₄] = 6.613 μM, [NaNO₃] = 0.04 M, T = 25°C. The solid line represents the fitted data according to Eq. (10).

pH 2.9, the solution shows an absorption peak at 423 nm which, however, increases in intensity with increasing pH until it reaches a pH ≈ 5.50. At this pH, the intensity of this peak decreased with the formation of a new absorption peak at 520 nm. This change in peak indicates deprotonation of one of the OH groups of the DHA molecule. For a further increase in pH, the intensity at 520 nm increases. The change in absorbance at 520 nm with an increase in pH was followed as shown in Fig. 5. It was observed that in the pH range 5–6 one of the protons from the OH groups has been released. The formation constants for the complex, β^* and β, can be described as follows:

$$Cu^{2+} + 3HH_1L \rightleftharpoons \{Cu(LH)_3\}^- + 3H_1^+ \qquad (5)$$

$$\beta^* = \frac{[\{Cu(LH)_3\}^-][H_1^+]^3}{[Cu^{2+}][HH_1L]^3} \qquad (6)$$

$$Cu^{2+} + 3LH^- \rightleftharpoons \{Cu(LH)_3\}^- \qquad (7)$$
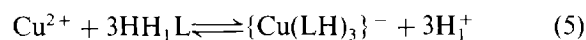
$$\beta = \frac{[\{Cu(LH)_3\}^-]}{[Cu^{2+}][LH^-]^3} \qquad (8)$$

From Eqs. (4) and (8) one gets

$$\beta = \frac{\beta^*}{K_2^3} \qquad (9)$$

where K_2 is the equilibrium constant for the dissociation of the proton of DHA as shown in Eq. (4).

The release of the proton from the phenolic-OH at C_2 corresponding to K_1 occurs later during the course of complexation. The formation constant β^* of the Cu(II) complex was determined from the above spectrophotometric titration. The absorbance A_{obs} at 520 nm could then be described as

$$A_{obs} = A_1/(1 + 10^{pH - pK}) + A_2/(1 + 10^{pK - pH}) \quad (10)$$

where A_1 and A_2 are the absorbances corresponding to the forms LHH_1 and LH^- respectively. Fitting the experimental data as shown in Fig. 5, one gets a pK value of 4.98 ± 0.05. The value of the formation constant β for $[Cu(II)(LH)_3]^-$ can then be determined from relation (9) and was found to be 5.135×10^{29}. This stability constant value obtained by us is almost the same $(10^{31}-10^{34})$ as that for the Fe(III) [27,29,32] complexes of anthracyclines having identical stoichiometry. However, the reported stability constant value of the 1:2 Cu(II)–doxorubicin [45,46] complex is 2×10^{17}. Pd(II) [34] ions also bind to anthracyclines with stability constants of the order of 10^{22}.

When formation of the Ni(II) complex with DHA was followed, it was observed that, similar to the behavior of the Cu(II) species, Ni(II) also forms a 1:3 complex of DHA represented by $[Ni(II)(LH)_3]^-$ (Fig. 3). The value of pK for the Ni(II) complex of DHA was obtained as 6.47 ± 0.05. the formation constant of this complex was then evaluated and found to be 3.446×10^{25}.

4.3. Preparation of the Cu(II) and Ni(II) complexes with DHA

The Cu(II) complex of DHA was prepared by mixing $CuSO_4$ and DHA in the molar ratio 1:3 in an aqueous medium at $\approx 30°C$ at neutral pH. The solution was then heated to about 60°C with constant stirring and allowed to react. It was then reduced to a smaller volume and allowed to stand for some time until a purple-coloured solid gradually separated out. The solid complex thus obtained was then filtered and recrystallized from an ethanol–water mixture.

Formation of the complex was ascertained by studying its UV absorption and IR spectra. The IR spectrum of pure DHA indicates a band at $3350\ cm^{-1}$ which is usually attributed to the presence of a strong intramolecular hydrogen bonding that occurs between a carbonyl group and an –OH group [57]. There are also sharp bands at $1190\ cm^{-1}$ and $1280\ cm^{-1}$ which are attributed to the O–H deformation and C–O stretching combinations due to the presence of the phenolic-OH functional group. The bands obtained at $1450\ cm^{-1}$ and $1580\ cm^{-1}$ may be assigned to the interactions of the keto group with the neighbouring –OH on the C_1 atom. The peak at $1665\ cm^{-1}$ is characteristic of the carbonyl group (C=O) stretching in quinones (with both carbonyl groups in the same ring) [57]. In the Cu(II)–DHA complex the band in the $3350\ cm^{-1}$ region flattened due to the absence of interaction of the phenolic –OH at C_1 with the carbonyl group, indicating the introduction of the metal ion. At the same time the appearance of a peak at about $1530\ cm^{-1}$ indicates the formation of a metal chelate with participation of one of the carbonyl groups. Thus the IR spectrum of the complex indicates that metal–DHA complex is formed with the Cu^{2+} coordinated by the carbonyl group and the phenolate anion at the C_1 carbon atom. The appearance of a new band at $830\ cm^{-1}$ in the IR spectrum of the complex which was not present in the IR spectrum of DHA suggests the formation of an octahedral Cu(II)–DHA complex.

The Ni(II)–DHA complex was also prepared by a very similar method as has been described for Cu(II). The solid was isolated from an aqueous solution and recrystallized from ethanol–water mixtures. In a similar solution the formation of a Ni(II)–DHA complex was ascertained by comparing its IR spectrum with that of the free ligand.

The molecular formulae of the complexes prepared were determined from their elemental analyses and it was found that both Cu(II) and Ni(II) formed complexes which can be represented as $[Cu(LH)_3]^-$ and $[Ni(LH)_3]^-$ respectively.

4.4. Effect of the compounds on the superoxide formation by NADH dehydrogenase

It has been pointed out that the cardiotoxicity [14–19] induced by the anthraquinone anticancer drugs is related to the formation of reduced oxygen radicals such as superoxide radical anion [20–24] and other oxygen radical species by enzymatic reduction processes. We have tested the ability of these complexes to be reduced by NADH through NADH dehydrogenase. For this purpose the formation of superoxide anion radical in the presence of the compounds was followed by measuring the cytochrome c reduction inhibited by SOD. The results are shown in Fig. 6. It is evident from this figure that with an increase in the concentration of DHA, the yield of O_2^- increased, indicating that DHA catalyzes the flow of electrons from NADH to molecular oxygen through NADH dehydrogenase. However, when the ligand is complexed with Cu(II) and with Ni(II), the formation of O_2^- is greatly reduced. In fact the Cu(II) complex is more effective in comparison to the Ni(II) complex in reducing the formation of O_2^-. Thus the reduction in car-
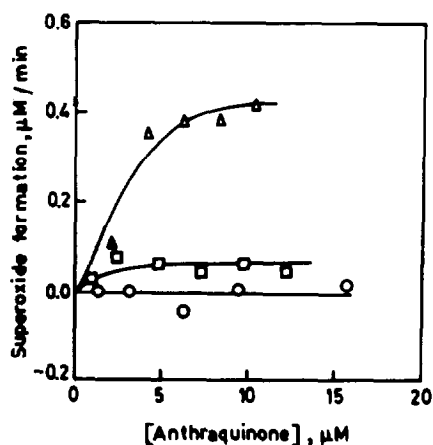
Fig. 6. Effect of DHA and complexes of DHA on superoxide formation by NADH dehydrogenase. Superoxide formation was determined spectrophotometrically by the rate of superoxide dismutase–inhibitable cytochrome c reduction. Reaction mixture composition was 0.05 M Hepes buffer (pH 7.4), 80.5 µM cytochrome c, 157.5 µM NADH, 3 U l^{-1} NADH dehydrogenase, 0 or 39.2 µg ml^{-1} SOD and the indicated amount of compound. ($\triangle$, DHA; $\square$, Ni(II)–DHA; $\bigcirc$, Cu(II)–DHA.)

diotoxicity would be greater with the Cu(II) complex than with the Ni(II) complex.

As already mentioned the formation of superoxide (O_2^-) in such enzymatic reactions occurs when the semiquinones are oxidized by molecular oxygen (O_2). As a result of complexation the carbonyl at C_9 of DHA is engaged in coordinating the metal ions Cu(II) and Ni(II) in their respective complexes. Consequently one of the quinone carbonyls in DHA is unable to form semiquinone any more. This therefore decreases the chances of formation of superoxide (O_2^-) to a considerable extent in the case of the complexes. However, semiquinones may form through the reduction of C_{10} carbonyl. Due to the presence of a metal ion in the complex an electron will be transferred from the semiquinone centre to the metal ion in the complex which will therefore decrease the ability of the semiquinone to interact with molecular oxygen (O_2). Thus there is observed an overall decrease in the superoxide (O_2^-) formation in the case of the complexes in comparison to free DHA. That the Cu(II) complex is more effective in reducing the formation of O_2^- over the Ni(II) complex can be attributed to the higher redox potential of Cu(II) over that of Ni(II). It can be concluded from the above observations that the complexes would be less cardiotoxic than the parent drug and could be safely used for cancer therapy.

Acknowledgments

References

[1] E. Fantine and A. Garnier-Suillerot, Biochem. Biophys. Acta, 856 (1986) 130.

[2] E. Pereira, M.M.L. Fiallo, A. Garnier-Suillerot, T. Kiss and H. Kozlowski, J. Chem. Soc., Dalton Trans., (1993) 455.

[3] P.K. Dutt and J.A. Hutt, Biochemistry, 25 (1986) 691.

[4] A. Moustatih and A. Garnier-Suillerot, Inorg. Chim. Acta, 135 (1987) L17.

[5] M. Manfait, A.J.P. Alix, P. Jeanneson, J.C. Jardiller and T. Theophanides, Nucleic Acids Res., 10 (1982) 3803.

[6] R.H. Blum and S.K. Carter, Ann. Int. Med., 80 (1974) 249.

[7] S.K. Carter, J. Natl. Cancer Inst., 55, (1975) 1265.

[8] R.A. Beckman, P.J. McFall, B.I. Sikic and S.D. Smith, J. Natl. Cancer Inst., 80 (1988) 361.

[9] M.J. Ehrke and E. Mihich, in M.S. Mitchell and J.L. Fahey (Eds.), Clinics in Immunology and Allergy, Vol. 4, No. 2, W.B. Saunders, London, 1984, p. 259.

[10] J.J. Wang, E. Cortes, L.F. Sinks, T.F. Holland et al., Cancer, 28 (1971) 837.

[11] A.M. Casazza, in F.M. Muggia, C.W. Young and S.K. Carter (Eds.), Anthracycline Antibiotics in Cancer Therapy, Martinus Nijhoff Publishers, The Hague, 1982, p. 13.

[12] M.G. Brazhnikova, V.B. Zbarsky, M.K. Kudinova, L.I. Muravieva, V.I. Ponomarenko and V.P. Potapova, Antibiotik, 18 (1973) 678.

[13] R.L. Commis, B.F. Issel, K. Pittman, S.J. Ginsberg, A. Rudolf, J.C. Aust, S.M. Difino, R.W. Tinsley, B.J. Poiesz and S.T. Crooke, Cancer Res., 42 (1982) 2944.

[14] R.A. Minow, R.S. Benjamin and J.A. Gottlieb, Cancer Chem. Rep., 6 (1975) 195.

[15] J.F. Van Vleet, V.J. Ferrans and W.E. Weirich, Am. J. Pathol., 99 (1980) 13.

[16] R. Bossa, I. Galatulas and E. Mantovani, Neoplasma, 24 (1977) 405.

[17] E.A. Lefrak, J. Pitha, S. Rosenheim and J.A. Gottlieb, Cancer 32 (1973) 302.

[18] F.P. Mettler, D.M. Young and J.N. Ward, Cancer Res., 37 (1977) 2705.

[19] J.W. Lown, H.H. Chen, J.A. Plambeck and E.M. Acton, Biochem. Pharmacol., 28 (1979) 2563.

[20] J. Butler, B.M. Hoey and A.J. Swallow, FEBS Lett., 182 (1985) 95.

[21] E.J. Land, T. Mukherjee, A.J. Swallow and J.M. Bruce, Br. J. Cancer, 51 (1985) 515.

[22] J.W. Lown, H.H. Chen, J.A. Plambeck and E.M. Acton, Biochem. Pharmacol., 31 (1982) 575.

[23] V. Berlin and W.A. Haseltine, J. Biol. Chem., 256 (1981) 4747.

[24] H.A.O. Hill, in R.J.P. Williams and J.R.R.F. Da Silva (Eds.), New Trends in Bio-Inorganic Chemistry, Academic Press, London, 1978, Chapter 6, p. 173.

[25] J.H. Doroschow, Cancer Res., 43 (1983) 460.

[26] E.J. Land, T. Mukherjee and A.J. Swallow, J. Chem. Soc., Faraday Trans. 1, 79 (1983) 391.

[27] H. Beraldo, A. Garnier-Suillerot, L. Tosi and F. Lavelle, Biochemistry, 24 (1985) 284.

[28] M. Gosalvez, M.F. Blanco, G. Vivero and F. Valles, Eur. J. Cancer, 14 (1978) 1185.

[29] M.M.L. Fallio and A. Garnier-Suillerot, Biochem. Biophys. Acta, 840 (1985) 91.

[30] M. Inaba, H. Kobayashi, Y. Sakurai and R.K. Johnson, Cancer Res., 39 (1979) 2200.

[31] A. Ramu, T.C. Shan and D. Glaubiger, Cancer Treat Rep., 67 (1983) 895.

[32] P.M. May, G.K. Williams and D.R. Williams, Inorg. Chim. Acta., 46 (1980) 221.

[33] R. Kiraly and R.B. Martin, Inorg. Chim. Acta., 67 (1982) 13.

[34] M.M.L. Fiallo and A. Garnier-Suillerot, Biochemistry, 25 (1986) 924.

[35] S.N. Bhattacharyya, P.C. Mandal and S. Chakrabarti, Radiat. Phys. Chem., 37 (1991) 347.

[36] S. Chakrabarti, P.C. Mandal and S.N. Bhattacharyya, Can. J. Chem., 71 (1993) 307.

[37] S.N. Bhattacharyya and P.C. Mendal, J. Chem. Soc., Faraday trans. 1, 79 (1983) 2613.

[38] S.N. Bhattacharyya, P.C. Mandal and S. Chakraborty, Anticancer Res., 9 (1989) 1181.

[39] S. Chakrabarti, P.C. Mandal and S.N. Bhattacharyya, Talanta, 42 (1995) 55.

[40] E.B. Douple, C.J. Gren and M.G. Simic, Int. J. Radiat. Oncol. Biol. Phys., 6 (1980) 1545.

[41] K.A. Skov, H. Adomat and N.P. Farrell, in M. Nicolini (Ed.), Platinum Co-ordination Compounds in Cancer Chemotherapy, Martinus-Nijhoff, The Hague, 1987, p. 733.

[42] G.L. Eichhorn, J.J. Butzow, P. Clark, H.P. Von Hahn, G. Rao, J.M. Heim, E. Tarien, D.R. Craper and S.J. Karlik, in A.E. Martell (Ed.), Inorganic Chemistry in Biology and Medicine, ACA Symp. Ser. 140, American Chemical Society, Washington, DC, 1980, p. 75.

[43] A. Monneron and Y. Moule, Exp. Cell Res., 51 (1968) 531.

[44] J. Hurwitz, L. Yarbrough and S. Wickner, Biochem. Biophys. Res. Commun., 48 (1972) 628.

[45] F.T. Greenaway and J.C. Dabrowiak, J. Inorg. Biochem., 16 (1982) 91.

[46] H. Beraldo, A. Garnier-Suillerot and L. Tosi, Inorg. Chem., 22 (1983) 4117.

[47] M.J. Maroney, R.O. Day, T. Psyris, L.M. Fleury and J. Whitehead, Inorg. Chem., 28 (1989) 173.

[48] S.S. Massoud and R.B. Jordan, Inorg. Chem., 30 (1991) 4851.

[49] H.D. Coble and H.F. Holtzclaw, J. Inorg. Nucl. Chem., 36 (1974) 1049.

[50] H.R. Mahler, in S.P. Colowick and N.O. Kaplan (Eds.), Methods in Enzymology II, Academic Press, New York, 1955, p. 668.

[51] R.H. Steele, J. Sabik, R.R. Benerito and S.W. O'Dea, Arch. Biochem. Biophys., 267 (1988) 125.

[52] Solvent Extraction, in Vogel's Textbook of Quantitative Chemical Analysis, Revised by G.H. Jeffery, J. Bassett, J. Mendham and R.C. Denney, 5th edn., ELBS/Longman, Great Britain, 1989, pp. 178–182.

[53] J. Butler, G.G. Jayson and A.J. Swallow, Biochim. Biophys. Acta, 508 (1975) 215.

[54] W.W. Koppenol, K.J.H. van Buuren, J. Butler and R. Braams, Biochim. Biophys. Acta, 449 (1976) 157.

[55] F.G. Bordwell, Organic Chemistry, The Macmillan Company, New York, 1963, p. 867.

[56] J. Schmidt, in N. Campbell (Ed.), Organic Chemistry, 7th edn., Oliver and Boyd, London, 1955, p. 598.

[57] I.L. Finar, Organic Chemistry, Vol. 1: The Fundamental Principles, 6th edn., ELBS/Longman, Singapore, 1990, p. 698.

The use of chlorophenol red for the selective determination of chlorine dioxide in drinking water

Deborah L. Sweetin, Elizabeth Sullivan, Gilbert Gordon*

Hughes Laboratories, Miami University, Oxford, OH 45056, USA

Abstract

In recent years, the use of chlorine dioxide as an alternative disinfectant for drinking water has become increasingly attractive. As a result, an accurate method for the determination of mg l^{-1} concentrations of chlorine dioxide is needed. Improvements to chlorophenol red (CPR) spectrophotometry result in a selective method for ClO_2 with few interferences. CPR selectively reacts with $0.1–1.9$ mg l^{-1} ClO_2 at pH 7, yielding a linear response (0.9994) with a limit of detection of 0.12 mg l^{-1} ClO_2. Several species, ClO_2^-, ClO_3^-, NH_2Cl, and free available chlorine (FAC), were studied as potential interferents using this method. There was found to be less than 2% interference due to 1.38 mg l^{-1} ClO_2^-, 9.87 mg l^{-1} ClO_3^-, and 5.31 mg l^{-1} NH_2Cl. The interference from up to 1.19 mg l^{-1} FAC was $\leqslant 3.7\%$ and could be further reduced by the addition of oxalic acid, sodium cyclamate or thioacetamide.

*Keywords:*Chlorine dioxide; Chlorophenol red; Drinking water

1. Introduction

The primary goal of water disinfection is to remove or inactivate pathogens that exist in our water supply. At present, chlorine is the most widely used chemical for disinfection of water and wastewater in the United States. However, it was reported in 1974 that chlorination of drinking water [1] often results in the formation of trihalomethanes (THMs). THMs [2] are known carcinogens, and in order to comply with the maximum contaminant level for total THM content, many water utilities are switching to alternative oxidants [3] for water disinfection.

In recent years, the use of chlorine dioxide as an alternative disinfectant for drinking water has become increasingly attractive. In addition to removing some of the THM precursors [4,5] from drinking water, the use of chlorine dioxide does not result in the formation of THMs. Because there are some health effects [6] associated with chlorine dioxide and its inorganic byproducts, chlorite and chlorate ions, accurate methods for the determination of these species are required.

There are very few specific and accurate colorimetric methods [7] available for the determination of chlorine dioxide. In 1978, Wheeler et al. [8] developed titrimetric and spectrophotometric procedures for the determination of chlorine dioxide, based on the oxidation of chlorophenol red (CPR). Both procedures were carried out at pH 7.0, and the titrimetric procedure required a com-

*Corresponding author. Fax: (513) 529-5715.

plex standardization procedure for CPR. The authors reported no interferences due to OCl^-, ClO_2^-, ClO_3^-, Fe^{3+}, MnO_4^- or CrO_4^{2-} in the ClO_2 determination. This method is suggested for a 0.05–2.5 mg l^{-1} ClO_2 concentration range.

Harp et al. [9] developed improvements to the CPR spectrophotometric method. A pH 5.2 citrate buffer and a pH 10 2-amino-2-methyl-1-propanol buffer were used in this procedure, which was developed for three concentration ranges of chlorine dioxide: 0–1.0 mg l^{-1}, 0–0.2 mg l^{-1}, and 0–0.1 mg l^{-1}.

In 1985, Fletcher and Hemmings [10] reported additional improvements to the CPR spectrophotometric method, carried out using a pH 7.0 phosphate buffer. The authors reported no interferences from ClO_2^-, ClO_3^-, NH_2Cl, $NHCl_2$ or NO_2^-. However, FAC was found to react with CPR at FAC concentrations as low as 0.5 mg l^{-1}. The FAC interference was removed by the addition of sodium cyclamate and thioacetamide to the sample. This method is recommended by the authors for ClO_2 concentrations of up to 0.4 mg l^{-1}.

As a follow up to the previously reported results, we carried out preliminary experiments in order to improve the CPR method. Initially, the standardization procedure for the CPR titrimetric method was studied, requiring acidification of CPR with concentrated sulfuric acid prior to titration of the solution with 0.01 N potassium dichromate. Because this reaction is slow [8], the titration was carried out at 100°C. The stoichiometry of the $K_2Cr_2O_7$–CPR reaction was found to be 2:1. Because the standardization procedure is complex, the spectrophotometric method was studied. The molar absorptivity of CPR is 1.51×10^4 M^{-1} cm^{-1} at 574 nm. In this work, experiments were carried out in order to improve the analytical characteristics of the CPR spectrophotometric method and to determine the extent of interferences from selected species.

2. Experimental

All of the solutions were prepared using deionized triply-distilled water. Three different CPR

reagents were studied: MC/B indicator grade (3.40×10^{-4} M), Aldrich indicator grade (3.54×10^{-4} M), and Aldrich water soluble, 70% dye content (2.51×10^{-4} M–2.67×10^{-4} M). Sodium chlorite from Eastman Kodak was triply recrystallized [11,12] and the purity was greater than 99%. FAC (35.78 mg l^{-1} Cl_2) and NH_2Cl (48.02 mg l^{-1} Cl_2) were prepared [8] and delivered directly into the sample cell via 50.00 ml burets. The N,N-diethyl-p-phenylenediamine (DPD) titrimetric method [13] was used in order to determine the concentrations of the FAC and NH_2Cl solutions.

Chlorine dioxide was prepared [14] with a laboratory scale generator. Owing to its volatility, chlorine dioxide was added directly to the pH 7.3 buffer in the sample cell using a Metrohm Herisau E535 Autoburet and placing the tip of the titrator below the surface of the solution in the cell. The resulting stock solution was kept in a brown bottle in ice in order to minimize any loss of chlorine dioxide over time. Its concentration was calculated from its absorbance using a molar absorptivity [15] of 1250 M^{-1} cm^{-1} at 360 nm.

The CPR species at different pH values are shown in Fig. 1. Because the spectrophotometric method is based on the absorbance of the red species at 574 nm, it was necessary to keep the reaction conditions at pH 7 or higher to ensure the presence of only one CPR species in the solution. Therefore, in this work a 1 M, pH 7.3 phosphate buffer was used in order to maintain a stable pH between 7.0 and 7.5. The buffer concentration at the time of the CPR–ClO_2 reaction was 0.06–0.22 M. This was shown to be high enough to minimize any effects of variations due to water hardness and the like.
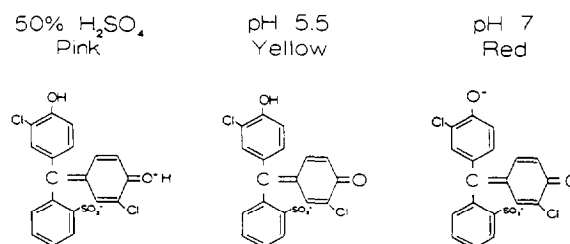
Fig. 1. CPR species [8] at different pH values.

Table 1
Comparison of absorbance values at pH 7.3–7.5 for different CPR reagents without chlorine dioxide in solution

CPR reagent	CPR concentration (M)	Absorbance ($\lambda = 574$ nm)
Indicator, MC/B	1.26×10^{-5}	0.0509
Indicator, Aldrich	1.31×10^{-5}	0.2370
Water Soluble, Aldrich	9.30×10^{-6}	1.557

An HP8450A UV/visible spectrophotometer was used to measure the absorbances of the solutions. A 3.00 cm fused-silica cell of 9.048 ± 0.007 ml volume was used. All solutions were delivered directly into the sample cell. The absorbances for the solutions in the CPR method were measured at the maximum wavelength of 574 nm.

3. Results and discussion

3.1. CPR reagent quality

In order to determine if the quality and/or source of the CPR reagent are factors in this method, the absorbances of the diluted CPR solutions (pH 7.3–7.5) were measured; the results are shown in Table 1. Although the concentration of the water soluble reagent solution was less than those of the indicator grade reagent solutions, the former has a higher absorbance value.

The higher absorbance value for the water soluble reagent solution may be attributed to the greater solubility of CPR in the solution or to a higher purity of CPR in the reagent. Since the water soluble CPR reagent has the highest absorbance value without chlorine dioxide in the solution and the CPR method is based on the decrease in absorbance of the CPR indicator solution when CPR reacts with chlorine dioxide, the water soluble CPR reagent was used in the optimization and interference studies of the CPR method.

3.2. Optimized CPR method

1 mol of CPR reacted with 2 mol of ClO_2 in basic solution to form a colorless product. In the absence

of sufficient CPR, the absorbance of the CPR–ClO_2 solution increased over time. In other words, less of an overall absorbance change occurred than expected from competitive side-reactions. Therefore, the concentration of CPR must be kept in excess. This effect is reflected in the %SD column of the results shown in Table 2.

When the concentration of CPR was greater than that of chlorine dioxide (0.23 mg l^{-1}), the absorbance change over time was only 0.4%. However, when the ClO_2 concentration (0.92 mg l^{-1}) was greater than that of CPR, the absorbance change was 12.1%. Therefore, it is necessary to have an excess of CPR in solution in order to minimize the errors associated with the determination of the ClO_2 residual by this method.

For the determination of ClO_2, a CPR concentration of 1.18×10^{-5} M was used. The pH 7.3 buffer concentration was 0.22 M in order to maintain a constant pH for all of the solutions studied, and the CPR absorbances were measured.

Typical absorbance values for the CPR–chlorine dioxide reaction with a 0.13–1.94 mg l^{-1} ClO_2 concentration range are depicted in Fig. 2. A plot of absorbance change versus chlorine dioxide concentration (mg l^{-1}) yields a linear response ($R = 0.9994$) with a slope of 0.7899 and a y-intercept of -3.119×10^{-2}. This results in an LOD [13] of 0.12 mg l^{-1} ClO_2.

Interferences

Experiments were carried out in order to determine if chlorite ions, chlorate ions, monochloramine, and FAC react directly with CPR, and if these species interfere with the determination of the chlorine dioxide concentration.

Table 2
Comparison of absorbance changes over 11 min for 11 samples with decreasing concentration ratios of CPR to ClO_2 at pH 7.3–7.5

ClO_2 (M)	CPR (M)	Average absorbance	%SD[a]
3.425×10^{-6}	4.15×10^{-6}	1.940 ± 0.008	0.4
1.023×10^{-5}	4.15×10^{-6}	0.635 ± 0.017	2.7
1.368×10^{-5}	4.15×10^{-6}	0.354 ± 0.043	12.1

[a]Standard deviation.
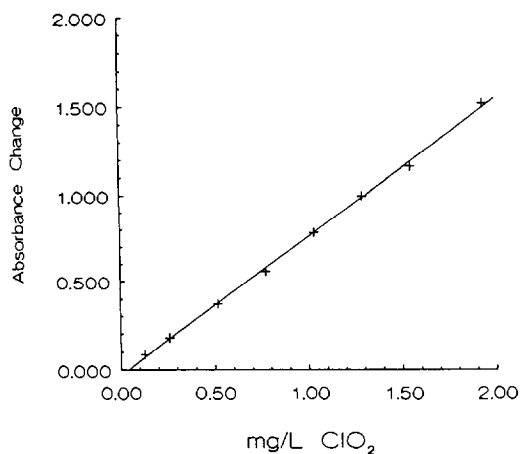
Fig. 2. Plot of CPR–ClO_2 absorbance data.

Fig. 3. Absorbance spectra of ClO_2, ClO_2^-, and ClO_2–ClO_2^- solutions without CPR.

Because the chlorite ion is a byproduct of ClO_2 decomposition, it will almost certainly be present in ClO_2 samples. The direct reaction of chlorite ions with CPR was studied by mixing a 41.4 mg l^{-1} chlorite ion solution with CPR. The absorbance change was 0.011, which is only a 0.5% difference from the blank absorbance value (CPR only).

The interference of chlorite ions in a solution of ClO_2 was also studied. Table 3 shows the results obtained for various concentrations of chlorite ions with 1.03 mg l^{-1} chlorine dioxide in solution. When the chlorite ion concentration is equivalent to or less than the chlorine dioxide concentration, the percentage difference is $\leqslant 2.0\%$ which is an acceptable level of error. However, as the chlorite ion concentration is increased, the percentage difference also increases.

Because the absorbance increases with increasing chlorite ion concentration and, as a result, the

change in absorbance is negative, it appears that the concentration of chlorine dioxide is less than that originally added to the CPR solution. However, when both chlorite ions (41.44 mg l^{-1}) and chlorine dioxide (1.03 mg l^{-1}) are present in solution without CPR, there is no decrease in the ClO_2 absorbance at 360 nm. This is shown in the absorbance spectra in Fig. 3. Therefore, the ClO_2 concentration in the CPR solution is unchanged.

The results obtained in Table 3 and shown in Fig. 3 can be attributed to the formation [16] of a $ClO_2 \cdot ClO_2^-$ complex. When the chlorite ion concentration is greater than that of ClO_2, a significant amount of $ClO_2 \cdot ClO_2^-$ complex is formed. The formation of this stable complex under pH 7 conditions was observed by Gordon and Emmenegger in 1966 [16], and is reported in considerably more detail by Crawford [17]. When the $ClO_2 \cdot ClO_2^-$ complex is in solution, the stoichiometry of the ClO_2–CPR reaction appears to change.

Based on the results obtained in this work, it can be concluded that chlorite ions do not interfere in the CPR method as long as the chlorite ion concentration is equivalent to or less than the chlorine dioxide concentration. However, at high concentrations, chlorite ions are potential interferents.

The direct reaction of chlorate ions with CPR was studied by mixing a 9.87 mg l^{-1} chlorate ion

Table 3
Chlorite ion interference in the CPR method

ClO_2 (mg l^{-1})	ClO_2^- (mg l^{-1})	Average absorbance	Change in absorbance	% difference
1.03	—	1.290 ± 0.012	—	—
1.03	0.55	1.285 ± 0.006	0.005	0.4
1.03	1.38	1.316 ± 0.025	−0.026	2.0
1.03	5.53	1.333 ± 0.012	−0.043	3.3
1.03	8.28	1.361 ± 0.011	−0.071	5.5
1.03	13.81	1.424 ± 0.015	−0.134	10.4
1.03	41.44	1.497 ± 0.008	−0.207	16.0

Table 4
FAC interference in the CPR method

ClO_2 (mg l^{-1})	FAC (mg l^{-1} Cl$_2$)	Average absorbance	Change in absorbance	% difference
—	—	2.403	—	—
—	0.40	2.392 ± 0.012	0.011	0.5
—	1.19	2.345 ± 0.022	0.058	2.4
—	4.74	2.219 ± 0.069	0.184	7.7
—	9.89	2.144 ± 0.050	0.259	10.8
—	19.77	2.072 ± 0.062	0.331	13.8
0.99	—	1.714 ± 0.018	—	—
0.99	0.40	1.658 ± 0.007	0.056	3.3
0.99	1.19	1.650 ± 0.030	0.064	3.7
0.99	4.75	1.578 ± 0.063	0.136	7.9
0.99	9.89	1.561 ± 0.052	0.153	8.9

solution with CPR. The absorbance change was −0.014 which is only a 0.7% difference from the blank absorbance value (CPR only). At chlorate ion concentrations of up to 49.33 mg l^{-1} with 1.03 mg l^{-1} ClO_2, the percentage difference is 1.4–2.4%. Therefore, it can be concluded that chlorate ions do not significantly interfere in the CPR method.

Monochloramine was also studied as a potential interferent in the CPR method. A 5.31 mg l^{-1} Cl$_2$ solution of monochloramine was mixed with CPR in order to study the direct reaction of NH_2Cl with CPR. The absorbance change was −0.005 which is only a 0.2% difference from the blank absorbance value (CPR only).

The interference of monochloramine in a solution of chlorine dioxide was studied for monochloramine solutions of 5.31 mg l^{-1} Cl$_2$ and 10.61 mg l^{-1} Cl$_2$ concentrations with 0.99 mg l^{-1} ClO_2 in solution. At monochloramine concentrations of up to 10.61 mg l^{-1} Cl$_2$, the percentage difference is 0.3–0.5%. Therefore, it can be concluded that monochloramine does not interfere in the determination of chlorine dioxide by the CPR method.

Fletcher and Hemmings [10] reported that FAC was an interferent in the CPR method. As a result, experiments were carried out in order to determine the extent of FAC interference. The direct reaction of FAC with CPR was investigated for concentrations of FAC ranging from 0.40 to 19.77 mg l^{-1} Cl$_2$, and the results are shown in Table 4.

As the concentration of FAC is increased the change in absorbance also increases, reflecting the direct reaction of FAC with CPR. At low FAC concentrations (0.40–1.19 mg l^{-1} Cl$_2$), the percentage difference is 0.5–2.4%, there being a minimal degree of reaction between FAC and CPR. However, as the FAC concentration is increased, the reaction between FAC and CPR becomes significant.

The interference of FAC in a solution of chlorine dioxide was also studied. Table 4 shows the results obtained for various concentrations of FAC with 0.99 mg l^{-1} ClO_2 in solution, all of which exhibit interference in chlorine dioxide determination. The extent of this interference increases with increasing FAC concentration. However, at FAC concentrations of 0.40 mg l^{-1} Cl$_2$ and 1.19 mg l^{-1} Cl$_2$, the percentage differences are only 3.3% and 3.7%, respectively. These errors may be acceptable in situations in which only an estimation of the chlorine dioxide residual concentration is needed, rather than an exact determination.

In order to eliminate FAC interference in this method, oxalic acid was studied as a masking agent for FAC. The concentration of oxalic acid was 3.5×10^{-3} M in the sample, and it was allowed to react with the FAC–ClO_2 solution for 10 min prior to the addition of the pH 7 buffer and CPR reagent. When 1.19 mg l^{-1} Cl$_2$ and 4.75 mg l^{-1} Cl$_2$ from the FAC solution was added to a 0.99 mg l^{-1} ClO_2 solution along with oxalic acid,

the error in the CPR method was less than 1.3–1.5%.

4. Conclusions

Improvements to the CPR method for the accurate and specific determination of chlorine dioxide are presented. The use of water soluble CPR indicator solution with a stock concentration of 2.1×10^{-4} M is recommended. In addition, the pH of the reaction should be maintained between 7.0 and 7.5 using a high-capacity buffer.

All reagents should be added directly to a 3.00 cm cell and a blank absorbance of a diluted, buffered CPR solution measured. The procedure developed for this method is as follows:

(1) add 1.0 ml of a pH 7.3 buffer (1 M) to a 3.00 cm cell;

(2) add sample or water;

(3) add 0.5 ml of a 2.1×10^{-4} M CPR solution;

(4) dilute to the cell volume and measure the absorbance at 574 nm.

The CPR method for the selective and accurate determination of chlorine dioxide is linear in the 0.13–1.94 mg 1^{-1} ClO_2 concentration range with an LOD of 0.12 mg 1^{-1}. The interferences from $\leqslant 10$ mg 1^{-1} chlorate ions and $\leqslant 5$ mg 1^{-1} monochloramine are minimal. In addition, when the concentration of chlorite ions is less than or equivalent to that of chlorine dioxide, the interference is less than 2.0%. When the FAC concentration is $\leqslant 1.2$ mg 1^{-1} Cl_2, the interference is only 3.7%. In order to further reduce the FAC interference, oxalic acid, sodium cyclamate or thioacetamide can be used as an effective chemical mask. The CPR method for the determination of chlorine dioxide warrants further study, and automation of this method is recommended.

References

[1] T.A. Bellar, J.J. Lichtenberg and R.C. Kroner, The occurrence of organohalides in chlorinated drinking waters, J. Am. Water Works Assoc., 66 (1974) 703–706.

[2] National Cancer Institute, Report on the Carcinogenesis Bioassay of Chloroform, NTIS No. PB264018/AS, National Cancer Institute, Washington, DC, 1976.

[3] P.C. Singer, Alternative Oxidant and Disinfectant Treatment Strategies for Controlling Trihalomethane Formation, EPA Project Report, EPA-600/S2-88/044, US Environmental Protection Agency, Cincinnati, OH, October 1988, 5 pp.

[4] R.J. Miltner, The Effect of Chlorine Dioxide in Drinking Water, M.S. Thesis, University of Cincinnati, Cincinnati, OH, 1976.

[5] J.M. Symons, J.K. Carswell, R.M. Clark, P. Dorsey, E.E. Geldreich, N.P. Hefferman, J.C. Hoff, U.T. Luve, Jr., L.J. McCabe and A.A. Stevens, Ozone, Chlorine Dioxide and Chloramines as Alternatives to Chlorine for Disinfection of Drinking Water, in R.L. Jolley, H. Gorchev, D.H. Hamilton, Jr., (Eds.), Water Chlorination: Environmental Impact and Health Effects, Vol. 2, Ann Arbor Science, Ann Arbor, MI, 1979, pp. 555–560; Complete Report entitled "State of the Art...", US EPA, Cincinnati, OH, November 1977, 84 pp.

[6] Drinking Water and Health: Disinfectants and Disinfectant By-Products, Vol. 7, National Academy Press, Washington, DC, 1987, 207 pp.

[7] G. Gordon, W.J. Cooper, R.G. Rice and G.E. Pacey, Disinfectant Residual Measurement Methods, American Water Works Association Research Foundation, AWWARF ISBN 0-89867-408-5, Denver, CO, 1987, 815 pp.

[8] G.L Wheeler, P.F. Lott and F.W. Yau, A rapid microdetermination of chlorine dioxide in the presence of active chlorine compounds, Microchem. J., 23 (1978) 160–164.

[9] D.L. Harp, R.L. Klein, Jr., and D.J. Schoonover, Spectrophotometric determination of chlorine dioxide, J. Am. Water Works Assoc., 73 (1981) 387–388.

[10] I.J. Fletcher and P. Hemmings, Determination of chlorine dioxide in potable waters using chlorophenol red, Analyst, 110 (1985) 695–699.

[11] G. Peintler, I. Nagypál and I.R. Epstein, Kinetics and mechanism of the reaction between chlorite ion and hypochlorous acid, J. Phys. Chem., 94 (1990) 2954–2958.

[12] I. Fábián and G. Gordon, Complex formation reactions of the chlorite ion, Inorg. Chem., 30 (1991) 3785–3787.

[13] A.E. Greenberg, L.S. Clesceri and A.D. Eaton (Eds.), Standard Methods for the Examination of Water and Wastewater, 18th edn., American Public Health Association, Washington, DC, 1992, pp. 10–137.

[14] M.L. Granstrom and G.F. Lee, Generation and use of chlorine dioxide in water treatment, J. Am. Water Works Assoc., 50 (1958) 1453–1466.

[15] R.G. Kieffer and G. Gordon, Disproportionation of chlorous acid. Part I. Stoichiometry, Inorg. Chem., 7 (1968) 235–239.

[16] G. Gordon and F. Emmeneger, Complex ion formation between ClO_2 and ClO_2^-, Inorg. Nucl. Chem. Lett., 2 (1966) 395–398.

[17] L.F. Crawford, Novel Methods of Generation of Chlorine Dioxide. Ph.D. Thesis, Miami University, Oxford, OH, 1995.

Fabrication and features of a Methylene Green-mediating sensor for hydrogen peroxide based on regenerated silk fibroin as immobilization matrix for peroxidase

Haiying Liu [a], Yongcheng Liu [b], Jianghong Qian [a], Tongyin Yu [b], Jiaqi Deng [a],*

[a] Department of Chemistry, Fudan University, Shanghai 200433, People's Republic of China
[b] Department of Macromolecular Science, Fudan University, Shanghai 200433, People's Republic of China

Abstract

Regenerated silk fibroin prepared from waste silk was employed as immobilization matrix for peroxidase and the structures of the blend membranes of regenerated silk fibroin and peroxidase were first investigated with IR and scanning electron microscopy. There was intermolecular interaction between peroxidase and regenerated silk fibroin in the immiscible state. Cyclic voltammetry and constant applied potential measurement showed that Methylene Green efficiently mediated electron transfer from oxidized horseradish peroxidase in regenerated silk fibroin membrane to a glassy carbon electrode. A sensor coupling immobilized peroxidase with Methylene Green responded rapidly to low H_2O_2 concentration and achieved 95% of the steady-state current in less than 25 s with a detection limit of 1.0×10^{-7} M H_2O_2. The sensor was stable in continuous operation, indicating that peroxidase was entrapped in regenerated silk fibroin membrane and did not freely diffuse away from the sensor surface into solutions.

1. Introduction

Horseradish peroxidase (HRP) can catalyze four kinds of reactions: peroxidation, oxidation, dismutation and hydroxylation [1]. Peroxidation is the predominant reaction in the presence of a hydrogen donor such as phenols, aromatic amines and certain other heterocyclic compounds. The enzymatic reaction of horseradish peroxidase involves compound I (HRP-I) containing Fe(IV) and a porphyrin-radical cation, and compound II (HRP-II) with one Fe(IV) in the following sequential reaction [2–6].

$$HRP + H_2O_2 \longrightarrow HRP\text{-}I + H_2O \qquad (1)$$

$$HRP\text{-}I + AH \longrightarrow HRP\text{-}II + A \qquad (2)$$

$$HRP\text{-}II + AH \longrightarrow HRP + A^{\bullet} \qquad (3)$$
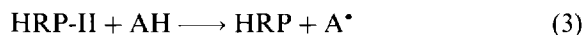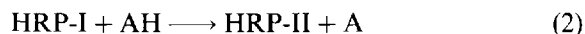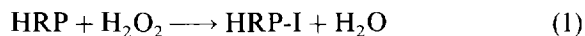
where AH represents the hydrogen donor and $A^{\bullet}$ the free radical formed during the reaction. The radicals are bound to the enzyme throughout the enzymatic process and dimerize before they are

* Corresponding author.

reduced at a certain potential. The mediatorless activation of electroreduction of H_2O_2 in the presence of horseradish peroxidase at carbon black [6], spectrographic graphite [7], non-platinized activated carbon electrodes [8] and pyrolytic graphite [9] has been reported. Entrapment of horseradish peroxidase in carbon paste [10] or in polypyrrole [9] has been investigated. However, they are insensitive to submicromolar H_2O_2. Amperometric coupling of peroxidase with mediators is a highly sensitive detection method for H_2O_2, in which peroxidases provide electrochemical H_2O_2 sensors with a detection limit as low as 10^{-8}–10^{-7} M by employing a dissolved electron mediator [11] such as (2-aminoethyl)ferrocene [12], $[Ru(NH_3)_5py]^{2+}$ [12], o-phenylenediamine [13], ferrocene [14], or tetrathiafulvalene [15].

Although silk fibroin obtained directly from silk larvae has been applied to immobilization of peroxidase [16], it is only available several times a year. In this paper, we employed regenerated silk fibroin prepared from waste silk to entrap peroxidase and first investigated the structures of the blend membrane of regenerated silk fibroin and peroxidase. We have shown for the first time the feasibility of Methylene Green mediating electron transfer between horseradish peroxidase in regenerated silk fibroin membrane and a glassy carbon electrode. Sensor stability and the dependence of the steady-state current on pH, temperature of the supporting electrolyte and applied potential were investigated.

2. Experimental

2.1. Materials

Peroxidase from horseradish (POD) (EC 1.11.1.7, type VI) was obtained from Sigma and Methylene Green (MG) was purchased from Aldrich. Hydrogen peroxide (30% w/v solution) was purchased from Shanghai Chemical Reagent Company. The concentration of more dilute peroxide solutions prepared from this material was determined by titration with cerium(IV) to a ferroin endpoint [17]. All other chemicals were analytical grade. All the solutions were prepared with doubly distilled water.

Silk fibroin solution

The waste silk of a silk mill was degummed with 0.5% $NaHCO_3$ solution at 100°C for 30 min and then washed with distilled water. The degummed silk was dissolved in 9.3 M LiBr aqueous solution. After dialysis against distilled water for 3 days, the solution was purified by filtering and the regenerated silk fibroin solution was collected.

Membranes were cast by using the regenerated silk fibroin solution or the mixture solution of the given weight of the silk fibroin and horseradish peroxidase on glass plates at room temperature in air.

2.2. Apparatus

Cyclic voltammetry and amperometric measurements were carried out with FDH 3204 and FDH 3206 cyclic voltammetry apparatus (Scientific Equipment Company of Fudan University, China) in line with a type 3086 x–y recorder (Tokyo, Japan). All experiments were carried out in a thermostatted, stirred electrochemical 5 ml cell at $20.0 \pm 0.5°C$, which is equipped with a H_2O_2 sensor as working electrode, a saturated calomel reference electrode and a platinum wire auxiliary electrode. All experimental solutions were thoroughly deoxygenated by bubbling nitrogen through the solution for at least 10 min. In the constant potential experiments, successive additions of stock H_2O_2 solution in the buffer were made and the current–time data were recorded after a constant residual current had been established. Changes in the measured reduction current were recorded as a function of time, following the addition of H_2O_2. The sensor response was measured as the differences between total and residual current.

IR spectra were recorded using an FT-IR 5DX spectrometer (Nicolet) at room temperature. The spectra of the membranes in the dry state were obtained by the reflection method and those of the peroxidase KBr disc were run by the transmission method.

Scanning electron micrographs were recorded on a Hitachi S-520 instrument operating at 20.0 kV.

2.3. Construction of H_2O_2 sensor

Glassy carbon electrodes (4 mm in diameter) were polished to a mirror-like finish with 0.3, 0.1 and 0.05 μm Al_2O_3 paste, rinsed thoroughly in deionized water between each polishing step sonicated in 1:1 nitric acid, acetone and doubly distilled water successively and dried in air before use. 20 mg peroxidase in 0.25 ml regenerated silk fibroin was completely mixed. Aliquots (8 μl) of the mixture were deposited on a glassy carbon electrode and allowed to dry in ambient conditions for 20 h. A 5 μl aliquot of 75% ethanol was syringed onto the sensor and allowed to dry in air for about 5 min. The sensor was kept in air at 4°C in a refrigerator between the measurements.

2.4. Calculation of Michaelis–Menten constant

The apparent Michaelis–Menten constant K_M^{app} can be obtained from the electrochemical Eadie–Hofstee form of the Michaelis–Menten equation [18]

$$j_{ss} = j_{max} - K_M^{app}(j_{ss}/C)$$

where j_{ss} is the steady-state catalytic current, j_{max} refers to the maximum current measured under saturating substrate conditions, C is the H_2O_2 concentration and K_M^{app} represents the apparent Michaelis–Menten constant of the system as a whole, not that of peroxidase itself, and provides a measure of the H_2O_2 concentration range over which the response of the sensor is approximately linear.

3. Results and discussion

3.1. IR spectra of membranes

Without ethanol treatment, the regenerated silk fibroin in the membrane exists in silk structure 1, because its absorption bands are $1706\ cm^{-1}$ (amide I), $1571\ cm^{-1}$ (amide II) and $1293\ cm^{-1}$ (amide III). With ethanol treatment, the regenerated silk fibroin in the membrane ex-

ists in a mixed structure of silk I and silk II because the absorption bands are split into two groups. One is the same as that characteristic of silk structure 1 and the other is $1687\ cm^{-1}$ (amide I), $1559\ cm^{-1}$ (amide II), $1275\ cm^{-1}$ (amide III), characteristic of silk structure II. This indicates that part of silk structure I is transferred into silk structure II after ethanol treatment. Before ethanol treatment the regenerated silk fibroin in the blend membrane containing peroxidase shows a red shift of absorption bands to 1660^{-1} (amide I), $1537\ cm^{-1}$ (amide II), $1240\ cm^{-1}$ (amide III), attributable to a characteristic of silk structure 1. After ethanol treatment, the regenerated silk fibroin in the blend membrane containing peroxidase also possesses two kinds of structure: silk structure 1, as it has absorption bands at $1668\ cm^{-1}$ (amide I), $1550\ cm^{-1}$ (amide II) and $1240\ cm^{-1}$ (amide III) and silk structure II as it has absorption bands at $1625\ cm^{-1}$ (amide I), $1531\ cm^{-1}$ (amide II) and $1265\ cm^{-1}$ (amide III). In both cases of the blend membrane, the corresponding absorption bands of regenerated silk fibroin are of smaller wavenumbers than those in pure regenerated silk fibroin membrane. This is attributed to intermolecular interaction between peroxidase and regenerated silk fibroin. Immobilization of peroxidase in regenerated silk fibroin is based on its conformation transformation from silk structure I to silk structure II resulting from ethanol treatment.

3.2. SEM of the blend membrane

SEM (Fig. 1) indicates that the blend membrane containing 10% peroxidase has a sea island-like structure which is attributed to the microphase segregation between both macromolecules in the blend membrane. The bright islands are peroxidase domains distributed randomly (Fig. 1(a)). Fig. 1(b) shows that the enzyme in the blend membrane has relatively free microenvironments because there are many empty spaces in the enzyme domains and that the enzyme can change its conformation to the favourable state in which its activity is maintained.

3.3. Cyclic voltammetry

Fig. 2 depicts typical cyclic voltammograms of Methylene Green in 0.1 M phosphate buffer (pH 7.0) containing 0.25 mM Methylene Green. In the absence of H_2O_2, the enzyme contributes no response and only Methylene Green generated voltammograms complying with a reversible electron redox agent because a linear plot of peak current vs. square root of scan rate $(i_p/V^{1/2})$ at constant concentration of Methylene Green was observed for the oxidation and reduction of Methylene Green in aqueous solution under diffusion control.

(a)
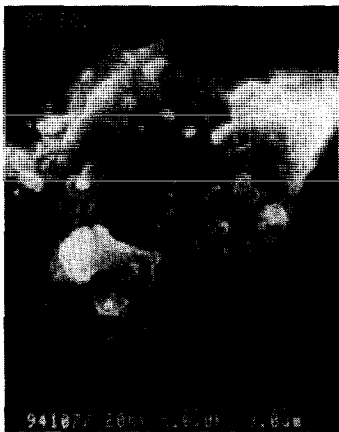
(b)

Fig. 1. Scanning electron micrograph of the regenerated silk fibroin membrane surface containing 10% peroxidase.
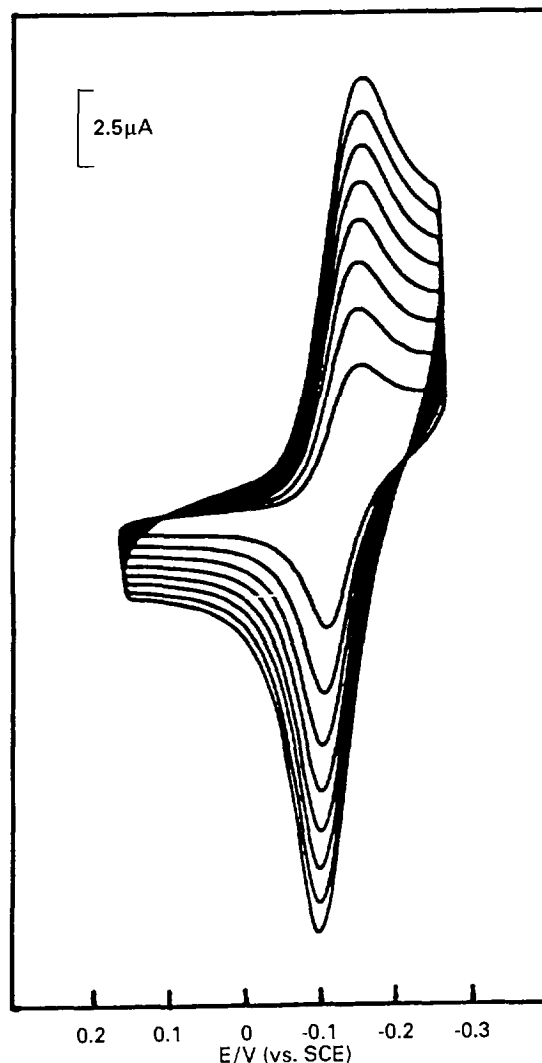
Fig. 2. Cyclic voltammograms of the H_2O_2 sensor at various scan rates (from inner curve to outer one): 15, 25, 45, 65, 85, 105, 125, 145, 165 mV s^{-1} in 0.1 M phosphate buffer containing 0.3 mM Methylene Green.

3.4. Electrocatalytic reduction of H_2O_2 at the sensor

No electrocatalytic reduction current is found at a glassy carbon electrode when H_2O_2 is added to the phosphate buffer containing 0.25 mM Methylene Green. Fig. 3 shows characteristic cyclic voltammetric results for the H_2O_2 sensor. In the absence of H_2O_2, the peroxidase yields no response and only typical oxidation and reduction peaks for Methylene Green in solution are ob-

served in Fig. 3 (curve a). Adding H_2O_2 to the cell produces a dramatic change in the cyclic voltammogram with an increase in cathodic current and a concomitant decrease in anodic current (Fig. 3 (curve b)). At slow scan speeds (<1 mV^{-1}) the anodic peak disappears completely and the cathodic peak appears as a plateau. Comparison of the voltammograms with and without H_2O_2 demonstrates that Methylene Green can effectively shuttle electrons between peroxidase in regenerated silk fibroin membrane and a glassy carbon electrode. The peroxidase (POD) reduces hydrogen peroxide to water:

$$H_2O_2 + POD(red) \longrightarrow H_2O + POD(ox)$$
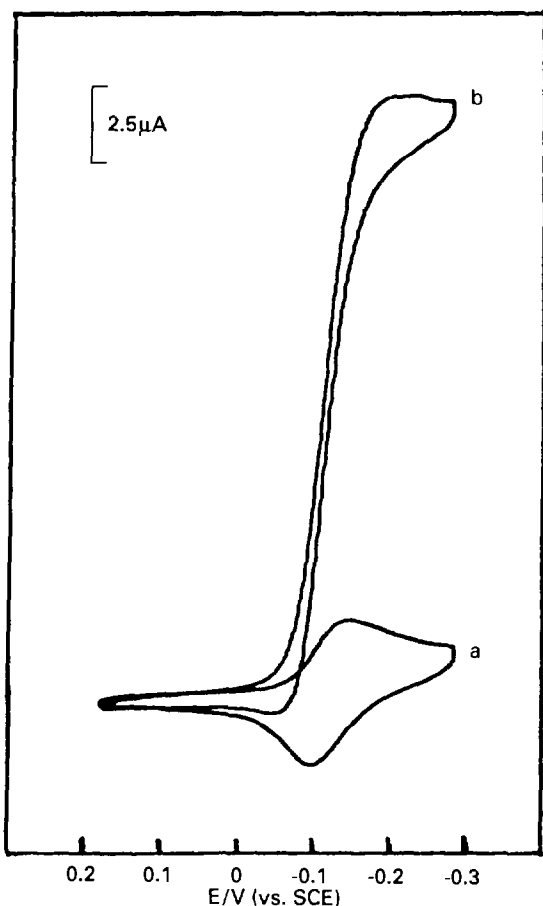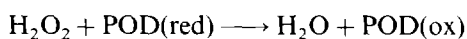
Fig. 3. Cyclic voltammograms of the H_2O_2 sensor at a scan rate of 15 mV s^{-1} in 0.1 M phosphate buffer (pH 7.0) containing 0.3 mM Methylene Green in absence of H_2O_2 (curve a) and presence of 0.5 mM H_2O_2 (curve b).
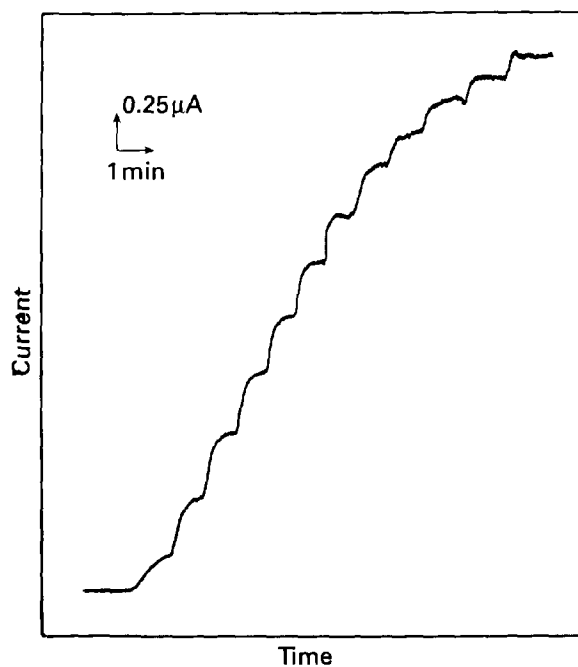
Fig. 4. Amperometric response of the H_2O_2 sensor to successive increase of H_2O_2 of 80 μM in solution containing 0.3 mM Methylene Green at an applied potential of -0.20 V.

and then oxidized peroxidase converts the Methylene Green (MGH) to MG$^+$:

$$POD(ox) + MGH \longrightarrow POD(red) + MG^+ + H^+$$
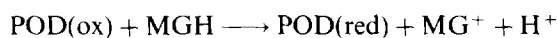
Finally MG$^+$ is reduced at the sensor, resulting in cathodic current:

$$MG^+ + H^+ + 2e \longrightarrow MGH$$
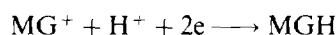
3.5. Steady-state amperometric response of the sensor to H_2O_2

Fig. 4 displays calibration data for H_2O_2 at the sensor. A well-defined and fast amperometric response is observed at -0.20 V with successive injections of H_2O_2 and the time required to reach 95% of maximum response is less than 25 s. Fig. 5 shows the calibration plot of the sensor response. The linear response is observed up to 4.0 mM. An extremely low detection limit of 1.0×10^{-7} M H_2O_2, at a signal-to-noise ratio of 3, can be estimated.
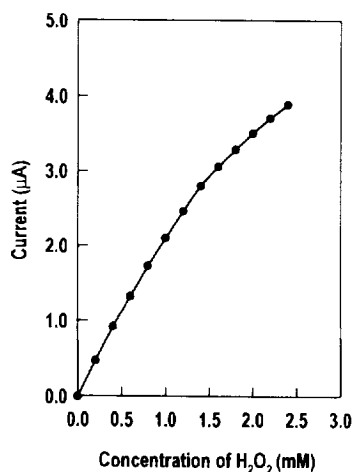
Fig. 5. Calibration plot for the H_2O_2 sensor. Steady-state current was measured in 0.1 M phosphate buffer (pH 7.0) containing 0.3 mM Methylene Green at 20°C.
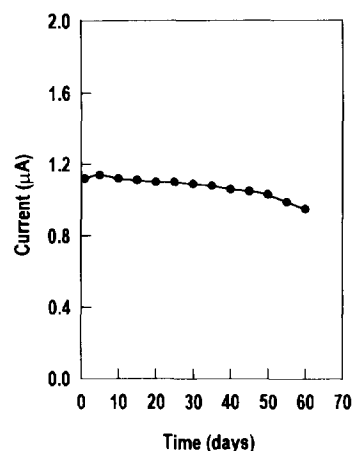
3.6. Effect of applied potential on sensitivity of the sensor

The steady-state response to 0.5 mM H_2O_2 was measured at several applied potential values in the buffer containing 0.25 mM MG (Fig. 6). The cathodic current increased with decreasing positive applied potential and reached limiting values at approximately -0.35 V vs. SCE, which indicates that the sensitivity and Michaelis–Mentens con-
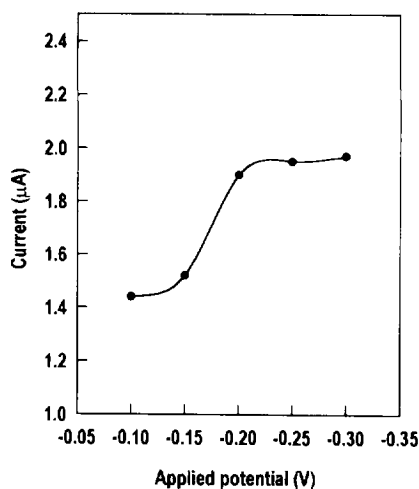
Fig. 6. Effect of applied potential on the response of sensor to H_2O_2.
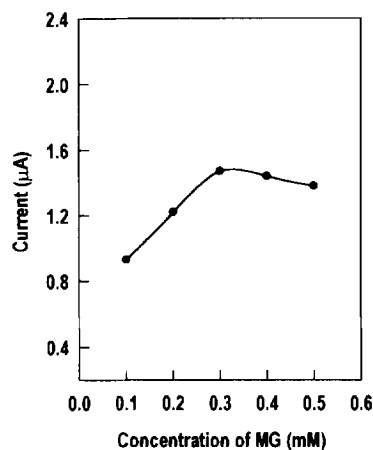
Fig. 7. The influence of the amount of Methylene Green on sensitivity of the sensor in the presence of 0.5 mM H_2O_2.

stant are dependent on the working potential. Michaelis–Mentens constants at -0.15, -0.20, -0.25 and -0.30 V are 4.6, 6.1, 7.2 and 8.4 mM H_2O_2 respectively. The increased sensitivity with applied potential can be assigned to an increased driving force for the fast reduction of POD (ox).

3.7. Influence of concentration of Methylene Green on sensitivity of the sensor

The effect of amount of mediator on the response of the sensor to H_2O_2 is shown in Fig. 7.

The reduction current increases substantially with increased amount of Methylene Green in solution from 0.1 to 0.3 mM. Further increasing the mediator concentration results in a decrease in the sensor response. Moreover, the higher concentration of Methylene Green causes an increase in background current.

3.8. Effect of pH and temperature on the H_2O_2 sensor

The pH dependence of the sensor was as shown in Fig. 8, exhibiting an optimum between pH 6.0 and 6.5, which indicates that the pH profile is controlled by the enzymatic activity.

The effect of temperature on the sensor has been examined between 15 and 60°C. The immobilized enzyme loses about 50% of its activity at

50°C after 3 h operation. The experiment shows that the current response increases with increasing temperature between 15 and 55°C, and that further increase in temperature gives rise to a decrease of the response current because of the partial denaturation of the enzyme.

3.9. Studies of interference

Several substances have been examined as possible interferents for the hydrogen peroxide sensor. Analyses of phosphate buffers containing 0.5 mM H_2O_2, to which the possible interferents are added, were executed. L-Tyrosine (0.2 mM), L-lactate (0.5 mM), glucose (5.0 mM), uric acid (0.2 mM), galactose (5.0 mM), L-leucine (0.2 mM), L-cysine (0.2 mM), L-tryptophan (0.2 mM), L-cysteine (0.2 mM), L-aspartic acid (0.2 mM), L-histidine (0.2 mM), and L-glutamic acid (0.2 mM) do not cause any observable interference to the determination of H_2O_2. However, L-proline (0.5 mM) and ascorbic acid (0.5 mM) decrease response currents by 0.8% and 27.5% of the initial values respectively. The decrease in response current results from consumption of H_2O_2 involved in oxidation of ascorbic acid because the sensor displays no response to adding ascorbic acid (5 mM) to phosphate buffer without H_2O_2.

Fig. 9. Stability of the H_2O_2 sensor under dry storage at 4°C.

3.10. Stability of the sensor

The reproducibility of the current response of the sensor is tested at an H_2O_2 concentration of 0.5 mM and the relative deviation is 1.5% ($n = 9$). The sensor possesses good storage characteristics. The H_2O_2 sensor was stored in air at 4°C when not in use. The response of the sensor decreased about 13% after storing for 2 months (Fig. 9).

4. Conclusion

Entrapment of peroxidase in regenerated silk fibroin offers a useful retention of enzyme and there is intermolecular interaction between regenerated silk fibroin and peroxidase. The enzyme in the membrane surface maintains a relatively free microenvironment. The advantages of the H_2O_2 sensor employing Methylene Green as electron transfer mediator between peroxidase in regenerated silk fibroin membrane and a glassy carbon electrode include high stability and sensitivity of the electrochemical signal. The simple method of sensor construction should be applicable to other enzyme–substrate systems for a variety of practical situations. In addition, we have found that organic mediators such as Meldola Blue, phenazine methosulphate, cresyl fast biolet, Catechol Violet, Methylene Violet, Brilliant Cresyl Blue, Toluidine Blue and Methylene Blue effectively mediate electron transfer between peroxidase and

Fig. 8. Effect of pH on H_2O_2 sensor. Steady-state current measured in the presence of 0.5 mM H_2O_2 in phosphate buffer (pH 7.0) containing 0.3 mM Methylene Green at 20°C.

a glassy carbon electrode. These results will be reported in the future.

Acknowledgments

This work is supported by the National Science Foundation of China and the Electroanalytical Chemistry Open Laboratory of Changchun Institution of Applied Chemistry, Chinese Academy of Sciences.

References

[1] J. Wang and M.S. Lin, Electroanalysis, 1 (1989) 43.

[2] H. Durliat, A. Courteix and M. Comptat, Bioelectrochem. Bioenerg., 22 (1989) 197.

[3] H.B. Dunford and J.S. Stillman, Coord. Chem. Rev., 19 (1976) 187.

[4] A.C. Maehly, Methods Enzymol., 2 (1955) 801.

[5] D.J. Danner, P.J. Brignac, Jr., D. Arceneaux and V. Patel, Arch. Biochem. Biophys. 156 (1973) 759.

[6] A.L. Yaropolov, V. Malovik, S.D. Varfolomeev and I.V. Berrzin, Dokl. Akad. Nauk SSSR, 249 (1979).

[7] G. Jonsson and L. Gorton, Electroanalysis, 1 (1989) 465.

[8] W.O. Ho, D. Athey, C.J. Mcneil, H.J. Hager, G.P. Evans and W.H. Mullen, J. Electroanal. Chem., 351 (1993) 185.

[9] U. Wollenberger, V. Bogdanovskaya, S. Bobrin, F. Scheller and M. Tarasevich, Anal. Lett., 23 (1990) 1795.

[10] U. Wollerberger, J. Wang, M. Ozsoz, E.G. Romero and F. Scheller, Bioelectrochem. Bioenerg. 36 (1991) 287.

[11] T. Tatsuma and T. Watanabe, Anal. Chem., 63 (1991) 1580.

[12] J.E. Frew, M.A. Harmer, H.A.O. Hill and S.I. Libor, J. Electroanal. Chem., 201 (1986) 1.

[13] N. Oyyama, T. Ohsaka and T. Shimizu, Anal. Chem., 57 (1985) 1526.

[14] L. Chen, M. Lin, M. Hara and G.A. Rechnitz, Anal. Lett., 24 (1991) 1.

[15] L. Bifulco, C. Cammaroto, J.D. Newman and A.P.F. Turner, Anal. Lett., 27 (1994) 1443.

[16] M. Demura, T. Asakura, E. Nakamura and H. Tamura, J. Biotechnol., 10 (1989) 113.

[17] E.C. Hurdis and H. Romeyn, Jr., Anal. Chem., 26 (954) 320.

[18] R.A. Kamin and G.S. Wilson, Anal. Chem., 52 (1980) 1198.

Chemiluminescence flow sensor for the determination of ascorbic acid with immobilized reagents

Zhujun Zhang *, Wei Qin

Department of Chemistry, Shaanxi Normal University, Xian 710062, China

Received 26 May 1995; accepted 4 August 1995

Abstract

A novel flow sensor based on chemiluminescence (CL) for the determination of ascorbic acid has been proposed. The analytical reagents, luminol and ferricyanide, were both immobilized on an anion-exchange resin column. The CL signal produced by the reaction between luminol and ferricyanide, which were eluted from the column through sodium phosphate injection, was decreased in the presence of ascorbic acid. The CL emission intensity was linear with ascorbic acid concentration in the range $0.01-0.8$ $\mu g\ ml^{-1}$; the detection limit was 5.5×10^{-3} $\mu g\ ml^{-1}$. The whole process, including sampling and washing, could be completed in 1 min with a relative standard deviation of less than 5%. The sensor could be reused more than 100 times and has been applied successfully to the analysis of ascorbic acid in pills and vegetables.

Keywords: Chemiluminescence; Flow sensor; Ascorbic acid; Immobilized reagents

1. Introduction

Ascorbic acid (vitamin C), found in citrus fruits and vegetable products, is mainly a cure for scurvy, drug poisoning, liver disease, allergic reaction and atherosclerosis. In addition, it is helpful for building up one's resistance to disease. Various methods have been proposed for determination of ascorbic acid, such as titrimetry [1], spectrophotometry [2,3], fluorimetry [4], chromatography [5] and electrochemical detection [6,7] by a manual technique or by flow injection analysis. Each has its advantages and disadvantages [8].

In recent years, biosensors with high selectivity based on an electrode coated with ascorbate oxidase or plant tissue for ascorbic acid determination have appeared especially attractive [9–12]. In these sensors, the consumption of dissolved oxygen takes place in an enzymatic reaction and is detected by an oxygen electrode. However, these sensors still suffer from stability problems.

Chemiluminescence (CL) has been successfully applied to deterine ascorbic acid with excellent sensitivity over a wide linear dynamic range and with the use of simple instrumentation [13–15]. Recently, various CL biosensors have been investigated [16–19]. Most of them are based on immobilized enzymes with dissolved CL reagents

---

* Corresponding author.

which react with hydrogen peroxide released from the enzymatic reactions to produce a CL light signal. In this paper, a novel CL flow biosensor for ascorbic acid determination is presented. It is based on the inhibition of vitamin C in the CL reaction between luminol and ferricyanide and the CL light decrement is related to the amount of ascorbic acid. The two CL reagents, luminol and ferricyanide, used in this sensor, are both immobilized on Amberlyst A-27 anion-exchange resin. Through injection of a volume of sodium phosphate, the reagents on the anion-exchange resin column are eluted from the resins and in the presence of ascorbic acid the CL reaction is inhibited, by which ascorbic acid can be sensed. Compared with electrodes and other methods, the sensor offers potential advantages of simplicity, rapidity and high sensitivity for ascorbic acid determination.

2. Experimental

2.1. Reagents and ion-exchange resin

All the reagents were of analytical grade; doubly-distilled water was used for the preparation of solutions of all dilutions. A stock solution of ascorbic acid $(1 \times 10^{-2} \text{ g ml}^{-1}$ in water) was stored in the refrigerator. Working standards were prepared daily from the stock solution by appropriate dilution. A 0.25 M luminol solution was prepared by dissolving 44.3 g of luminol in 1 l of 0.5 M NaOH solution. Other solutions were $\text{Na}_3\text{PO}_4 (2 \times 10^{-4}$ M), $\text{K}_3\text{Fe(CN)}_6 (0.2$ g ml^{-1}) and NaOH (0.6 M). Amberlyst A-27 anion-exchange resin (20 + to 50 − mesh) purchased from Rohm and Haas Co. was used for reagent immobilization.

2.2. Preparation of immobilized reagents

Amberlyst A-27 (0.5 g) was stirred with 25 ml of 0.25 M luminol or 0.2 g ml^{-1} potassium ferricyanide for 12 h, then the resin was filtered, washed with doubly-distilled water and dry-stored. The most convenient method to determine the amounts of luminol and ferricyanide immobi-

lized is to measure the losses of these reagents from the immobilization solutions. This was done by UV–Vis absorbance. The concentration was monitored at 360 nm for luminol and at 420 nm for ferricyanide. The amounts of luminol and ferricyanide immobilized were 1.64 mmol g^{-1} and 1.18 mmol g^{-1} resin respectively.

2.3. Apparatus

The flow injection system used in this work is shown in Fig. 1. A peristaltic pump was used to deiver all flow streams at a flow rate of 2 ml min^{-1} on each flow line. PTFE tubing (0.8 mm i.d.) was used between all components in the flow system. The anion-exchange resins containing immobilized luminol (0.06 g) and ferricyanide (0.12 g) were mixed together and packed into a glass column with an internal diameter of 4 mm and total volume of about 0.6 ml, and plugged with glass wool at both ends to prevent the resins from leaking. Sodium phosphate solution (200 µl) was injected by an injection valve. Before reaching a flow cell (200 µl), the streams of luminol, ferricyanide, sodium hydroxide and analyte were combined in mixing tubing (80 mm in length). The light signal produced in the flow cell was detected with an R456 photomultiplier tube (PMT) and recorded with an XWT-204 recorder (Shanghai Dahua Instrument and Meter Plant).

Absorbance monitoring was done using a UV-spectrophotometer Model-752 (Shanghai Third Analytical Instrument Plant).
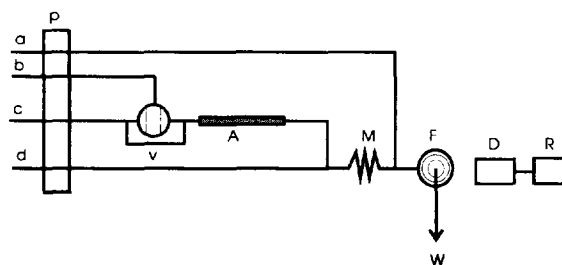
Fig. 1. Schematic diagram of the flow system for ascorbic acid determination: (a) NaOH; (b) Na$_3$PO$_4$; (c) H$_2$O; (d) sample; (A) anion exchange column; (p) pump; (v) valve; (M) mixing tubing; (F) flow cell; (W) waste; (D) detector; (R) recorder.

Table 1
Character of eluants for ascorbic acid determination [a]

Type of CL intensity	Relative CL intensity						
	NaCl	NaAc	NaOH	$NaNO_3$	Na_2SO_4	Na_2CO_3	Na_3PO_4
I	23	16	14	37	55	49	100
II	11	10	10	14	20	18	24
III	12	6	4	23	35	31	76

[a] The concentration of each eluant was 2×10^{-4} M. The relative CL intensity corresponds to the normalized maximum light intensity. (I): CL intensity in the absence of ascoribc acid; (II): CL intensity in the presence of 0.1 μg ml^{-1} ascorbic acid; (III): decreased CL intensity.

2.4. Procedures

Flow lines (a), (b), (c) and (d) were inserted into NaOH solution, eluant solution of sodium phosphate, water carrier and sample solution respectively. The pump was started to wash the whole flow system until a stable baseline was recorded. Then 200 μl of eluant containing 2×10^{-4} M or 8×10^{-4} M sodium phosphate was injected into the carrier stream and luminol and ferricyanide were released quantitatively. The concentration of ascorbic acid was quantified by the CL intensity.

3. Results and discussion

3.1. Influence of eluant

Different amounts of luminol and ferricyanide could be released by anions with different eluting abilities being injected through the resin columns, which had an effect on the CL intensity. The results are shown in Table 1. The eluant sodium phosphate with the highest relative CL intensity (type II) and decreased CL intensity (type III) was chosen for subsequent work.

3.2. Effect of ratio between resins with immobilized luminol and ferricyanide

To examine the influence of the mixing ratio, resins (0.18 g) with different mixing ratios were packed into the glass column. By injection of sodium phosphate at a fixed concentration of 2×10^{-4} M, different amounts of luminol and

ferricyanide were eluted from the resins and caused a CL intensity, which is shown in Table 2. The mixing ratio 1:2 between the amount of luminol resin and that of ferricyanide resin was selected in the present work not only for the relatively high CL intensity but also for the most effective inhibiting effect of ascorbic acid.

3.3. Effect of eluant concentration

The release of luminol and ferricyanide was determined by the concentration of sodium phosphate. Various concentrations of sodium phosphate were injected through the anion-exchange resin column. The immobilized luminol and ferricyanide released were measured by UV–Vis absorbance and by the CL reaction with 2.5×10^{-4}

Table 2
Effect of mixing mass ratio between resins with immobilized luminol and ferricyanide [a]

Mass ratio (luminol:ferricyanide)	Relative CL intensities		Decreased CL intensity
	Blank [b]	Signal [c]	
1:4	84	40	44
1:2	100	24	74
1:1	60	20	40
2:1	18	6	12
4:1	9	3	6

[a] The concentration of each eluant was 2×10^{-4} M. The relative CL intensity corresponds to the normalized maximum light intensity.
[b] CL intensity in the absence of ascorbic acid.
[c] CL intensity in the presence of 0.1 μg ml^{-1} ascorbic acid.
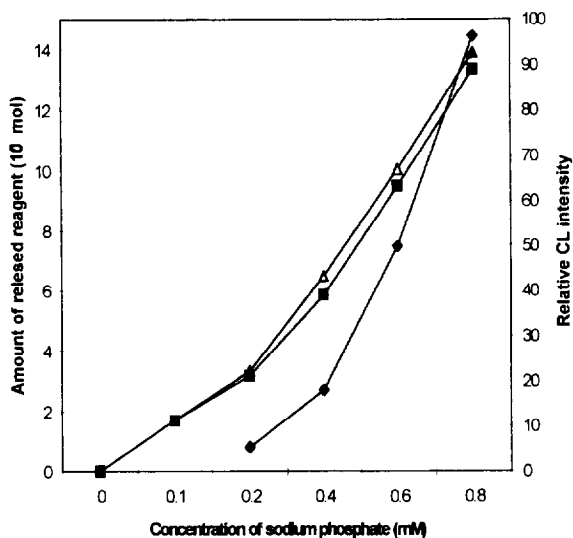
Fig. 2. Effects of eluant concentration on (▲) amount of luminol released ($n = -8$) amount of ferricyanide released ($n = -10$) and (♦) CL intensity in the presence of 0.1 μg ml^{-1} ascorbic acid.

M luminol (pH 12) respectively. The results are shown in Fig. 2. It can be seen that the amounts of luminol and ferricyanide released both increased linearly with the concentration of sodium phasphate injected. Naturally, it can be predicted that increasing the eluant concentration gives an increased CL intensity. This situation is also illustrated in Fig. 2. Considering lifetime and linear range of the sensor (discussed in detail below), 2×10^{-4} M or 8×10^{-4} M sodium phosphate was used for the linear range 0.01–0.1 μg ml^{-1} ascorbic acid respectively.

3.4. Effect of sodium hydroxide concentration

Luminol reacts with ferricyanide to produce CL light in basic solution. Therefore, sodium hydroxide was added in flow line (a) to improve the sensitivity of the sensor. Since the sodium hydroxide concentration versus CL intensity plot shows a maximum for sodium hydroxide levels around 0.6 M, this concentration was used in subsequent experiments (Fig. 3).

3.5. Performance of the sensor for ascorbic acid measurements

Since ascorbic acid is detected as an inhibitor, it is obvious that small amounts of ascorbic acid can be sensed linearly by the CL reaction with small amounts of luminol and ferricyanide, and vice versa. Therefore, the linear range of the sensor is determined by the amounts of luminol and ferricyanide released, and is in turn determined by the eluant concentration. To gain a relatively long lifetime of over 100 times, 2×10^{-4} and 8×10^{-4} M sodium phosphate was chosen for ascorbic acid determination over the range 0.01–0.1 μg ml^{-1} with a correlation coefficient of 0.9991 and over the range 0.1–0.8 μg ml^{-1} with a correlation coefficient of 0.9986 respectively (Fig. 4). At a concentration of >0.8 μg ml^{-1}, the linearity disappears because of smaller amounts of luminol and ferricyanide being released as a result of the eluant concentration used. Increasing the sodium phosphate concentration can widen the linear range of the sensor, but unfortunately may shorten the sensor's lifetime. At a flow rate of 2.0 ml min^{-1}, the determination of ascorbic acid could be performed in 1 min including sampling and washing, giving a throughput of about 60
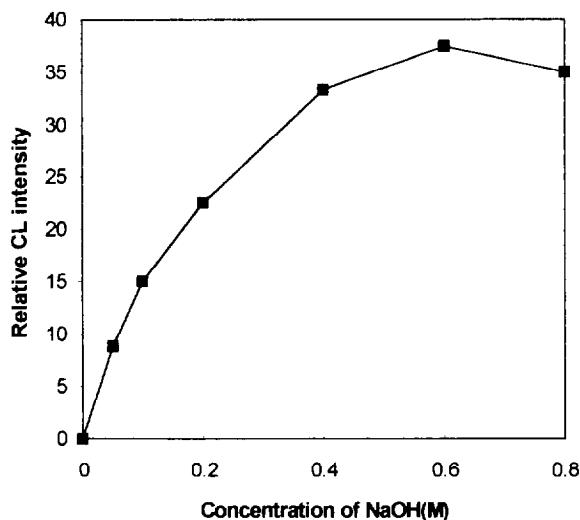
Fig. 3. Effect of NaOH concentration on CL intensity in the presence of 0.1 μg ml^{-1} ascorbic acid with 2×10^{-4} M Na$_3$PO$_4$ as eluant.
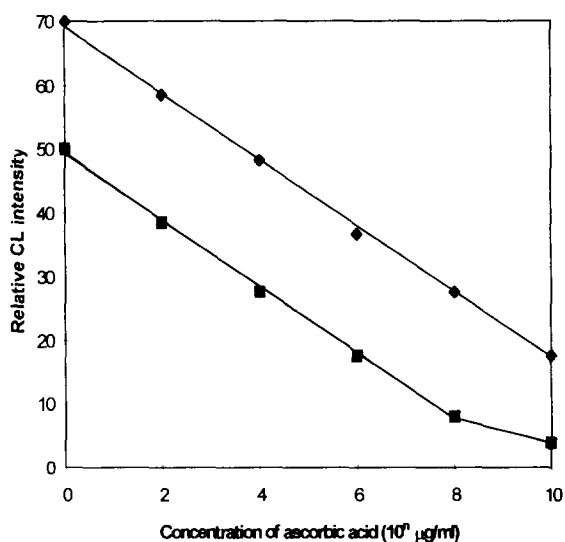
Fig. 4. Relative CL intensity vs. ascorbic acid concentration (type II): ($\blacklozenge$) $n = -2$, ($\blacksquare$) $n = -1$.

times h. The detection limit of the sensor was $5.5 \times 10^{-3}\ \mu g\ ml^{-1}$ (3σ), and the relative standard deviation was less than 5% for $5 \times 10^{-2}\ \mu g\ ml$ ($n = 7$).

3.6. Interferences

Interferences of foreign substances were tested by analysing a standard solution of ascorbic acid ($0.3\ \mu g\ ml^{-1}$). The tolerable concentrations of some interfering inorganic ions and organic compounds are listed in Table 3.

Table 3
Tolerable concentration ratios with respect to ascorbic acid for some interfering species ($< 5\%$ error)

Substance	Tolerable concentration ratio
K^+, Na^+, Cl^-, Br^-, F^-, SO_4^{2-}, HCO_3^-, HPO_4^{2-}, NO_3^-, amylum, acetic acid, tartaric acid, citric acid	> 1000
I^-, sucrose	500
Zn^{2+}, Sn^{2+}, Al^{3+}, Pb^{2+}, Ca^{2+}, Mg^{2+}, Ni^{2+}, S^{2-}, NO_2	100
Glucose, maltose, oxalic acid, dehydroascorbic acid	100
SO_3^{2-}	50
Vitamin B_2	20
Mn^{2+}, cholesterol	10
Cu^{2+}, thiourea, uric acid, Vitamin B_1	1
Fe^{3+}, Fe^{2+}	0.1

4. Application

4.1. Analysis of vitamin C in pills

Several commercial vitamin C tablets or capsule multivitamins were ground to powder and a portion of the powder was weighted and dissolved in 100 ml doubly-distilled water. After filtering, aliquots of the solution were diluted by a factor of 10 000 for the analysis. The results are given in Table 4. It is shown that the results obtained by

Table 4
Results of vitamin C in pills and vegetables

Sample[a]	Results by proposed method[a]		Recovery results			Result by iodimetry[a] (mg g^{-1})
	In diluted sample solution (10^{-5} mg ml^{-1})	In real sample (mg g^{-1})	Added (10^{-5} mg ml^{-1})	Found[a] (10^{-5} mg ml^{-1})	Recovery (%)	
Vitamin C tablet	10.1	505	10.0	19.9	98	512
Multi vitamin capsule	6.8	136	5.0	12.0	104	140
Tomato	4.0	0.500	2.0	5.8	90	0.506
White gourd	1.9	0.253	2.0	4.0	95	0.246
Mung bean sprouts	5.7	0.019	2.0	7.9	110	0.022

[a] Average of four measures.

the sensor agreed well with those obtained by iodimetric analysis [1].

4.2. Analysis of vitamin C in vegetables

Tomato (20 g), mung bean sprouts (30 g) and white gourd (15 g) were cut into small pieces and homogenised with 100 ml acetic acid buffer solution (pH 4.0), then filtered and diluted with doubly-distilled water by factors of 2500, 100 and 2000 respectively for the determination. The results are given in Table 4. Again, the values obtained by the present sensor agreed well with those obtained by iodimetric analysis.

Acknowledgement

References

[1] M.Z. Barakat, S.K. Shehab, N. Darnish and A. El-Zoheivy, Anal. Biochem., 53 (1973) 245.

[2] O.W. Lau, S.F. Luk and K.S. Wang, Analyst, 112 (1987) 1023.

[3] M.I. Karayannis and D.I. Farasoglou, Analyst, 112 (1987) 767.

[4] H. Huang, R. Cai, Y. Du and Y. Zeng, Anal. Chim. Acta, 309 (1995) 271.

[5] N. Moll and J.P. Joly, J. Chromatogr., 405 (1987) 347.

[6] S. Uchiyama, Talanta 39 (1992) 1289.

[7] K. Matsumoto, J.J. Baeza and H.A. Mottola, Anal. Chem., 65 (1993) 1658.

[8] P.W. Washko, R.W. Welch and K.R. Dhariwal, Anal. Biochem., 204 (1992) 1.

[9] K. Matsumoto, K. Yamada and Y. Osajima, Anal. Chem., 53 (1981) 1974.

[10] S. Uchiyama, Y. Hasebe and S. Suzuki, Electroanalysis, 5 (1993) 653.

[11] S. Uchiyama and Y. Umetsu, Anal. Chim. Acta, 255 (1991) 53.

[12] Q. Wang and J.Q. Deng, Fenxi Huaxue, 21 (1993) 1018.

[13] T. Pere-Ruiz, C. Martinez-Lozaro and A. Sanz, Anal. Chim. Acta, 308 (1995) 299.

[14] K. Sato, Y. Chiba and S. Tanaka, Anal. Chim. Acta, 277 (1993) 61.

[15] A.A. Alwarthan, Analyst, 118 (1993) 639.

[16] M.S. Abde-Latif and G.G. Guilbault, Anal. Chem., 60 (1988) 2671.

[17] M.V. Cattaneo, K.B. Male and J.H.T. Luong, Biosens. Bioelectron., 7 (1992) 569.

[18] X.F. Xie, A.A. Ahmad, G.G. Guilbault, Z.M. Yang and Z.A. Sun, Anal. Chim. Acta, 266 (1992) 325.

[19] L.J. Blum, Enzyme Microb. Technol., 15 (1993) 407.

A polypyrrole-based amperometric ammonia sensor

Ilkka Lähdesmäki, Andrzej Lewenstam, Ari Ivaska*

Laboratory of Analytical Chemistry, Åbo Akademi University, FIN-20500 Turku-Åbo, Finland

Abstract

An ammonia sensor is described in this work. The sensing membrane is a thin layer of oxidized polypyrrole (PPy) on a platinum substrate. This sensor is used as the working electrode in a conventional three-electrode system for amperometric measurement of ammonia in aqueous solutions in the potential range of $+0.2$ to $+0.4$ V (vs. Ag/AgCl). Contact with ammonia causes a current to flow through the electrode. This current is proportional to the concentration of free ammonia in the solution and ammonium ions do not contribute to the measured signal. The signal is due to reduction of PPy by ammonia with subsequent oxidation of PPy by the external voltage source. The sensor is able to detect ammonia reproducibly at the μM level. The main interference is the doping effect of small anions such as Cl^- and NO_3^-, also giving a response on PPy at the mM level. This anionic response can, to a certain degree, be reduced by covering the polymer surface with dodecyl sulfate. The sensor gradually loses its activity when exposed to ammonia concentrations greater than 1 mM. The sensor has been tested by the flow injection analysis technique.

Keywords: Ammonia sensor; Polypyrrole; Conductive polymer; Amperometry; Flow injection analysis

1. Introduction

Gaseous ammonia is known to reduce the oxidized form of the conducting polymer polypyrrole (PPy) [1]. Josowicz and Janata [2] utilized this property to prepare a sensor for gaseous ammonia where oxidized PPy formed the active membrane. They used the conductivity of PPy as a measure of the concentration of ammonia in gaseous samples.

Trojanowicz et al. [3] described an amperomet-

ric ammonia sensor for the determination of dissolved ammonia in aqueous samples, where PPy deposited on platinum is the working electrode in a three-electrode system. They also presented the optimized conditions for preparation of the sensor and for measurement of ammonia. The influence of some common interfering species in clinical samples on the response of the sensor was also studied. The sensor was found to be deactivated in the process of detecting ammonia. In this work, we have further studied and tried to eliminate the interfering effect of common inorganic anions and cations. Sensor preparation and ammonia measurements were carried out under optimized conditions, as given in Ref. [3].

---

2. Experimental

2.1. Chemicals

Pyrrole (Aldrich, 99%) was purified by distillation and stored in a refrigerator under a N_2 or Ar atmosphere. Sodium dodecyl sulfate (NaDS) (Fluka, p.a.), 25% aqueous ammonia solution (Riedel-de Haën, p.a.), and NaCl, NaOH, sodium borate ($Na_2B_4O_7 \cdot 10H_2O$) and NH_4Cl (Merck, p.a.) were all used as received. Distilled deionized water was used to prepare the solutions.

2.2. Instrumentation

Electrochemical polymerization of pyrrole was carried out using a PAR model 273 potentiostat–galvanostat in a single compartment three-electrode electrochemical cell. The working electrode was a Pt electrode (area 0.16 mm^2) and the reference electrode was a Ag/AgCl/3 M KCl electrode. The counter electrode was a graphite electrode.

Amperometric measurements were performed using a BAS model CV-37 potentiostat connected to a three-electrode cell, where both the reference and the counter electrodes were the same as above, but the working electrode was a Pt electrode modified by a PPy film on top of it. The three-electrode cell was used as a detector in a Tecator FIAstar 5010 flow injection analyzer. An ABB Goerz model SE 120 strip chart recorder was used to record the signal given by the detector. Cyclic voltammetric measurements were carried out with either of the potentiostats using a scan rate of 20 mV s^{-1}. Energy dispersive analysis of X-rays (EDAX) was performed with a Leica Cambridge S 360 scanning electron microscope.

2.3. Sensor preparation

Before polymerization of the PPy layer, the Pt electrode was polished with 0.3 μm alumina and rinsed with water and methanol. Polymerization was carried out in a stagnant aqueous solution containing 0.1 M NaCl and 0.1 M pyrrole monomer. The polymerization was performed at a constant potential of +0.80 V for 3 min. The electrolyte solution was deareated by purging with

N_2 for 15 min prior to addition of the monomer, and an inert environment was maintained in the cell during the polymerization by a N_2 atmosphere.

2.4. Amperometric measurements in the flow injection analysis (FIA) system

The PPy ammonia sensor was used as an amperometric detector in an electrochemical wall-jet cell in the flow injection analysis (FIA) system shown in Fig. 1. A sample volume of 100 μl was injected into a water carrier stream, which was then mixed with a stream of borate buffer (pH 9.2) to convert a substantial amount of NH_4^+ in the sample into NH_3 and to keep the $[NH_3]/[NH_4^+]$ ratio constant. The flow rates of the carrier and the buffer were both 1.15 ml min^{-1}. The current was normally measured at +0.30 V, but +0.35 V was also used in some experiments.

2.5. EDAX measurements

PPy samples for EDAX measurements were prepared by polymerizing pyrrole for 10 min on indium–tin oxide (ITO) glass. The procedure of polymerization was as described above. The ITO glass pieces had been cleaned with ethanol and water prior to use. After preparation, the PPy samples were treated as shown in Table 1. The supporting electrolyte in all experiments where the PPy sensor was used at +0.3 V in a NH_3 solution was 0.05 M Na_2SO_4 (i.e. treatment of samples #2 and #4). Likewise, in all these experiments, 5 M H_2SO_4 was used to acidify the solution before switching off the potential in order to avoid reduction of PPy by NH_3 during removal of the electrode from the cell. All samples were then rinsed with water and dried in a flow of N_2 before the EDAX measurements.

2.6. IR measurements

PPy samples for IR measurements were prepared on pieces of ITO glass in the same way as described above for the EDAX measurements. A total of three samples were prepared: one of them was treated by applying +0.30 V to the PPy–
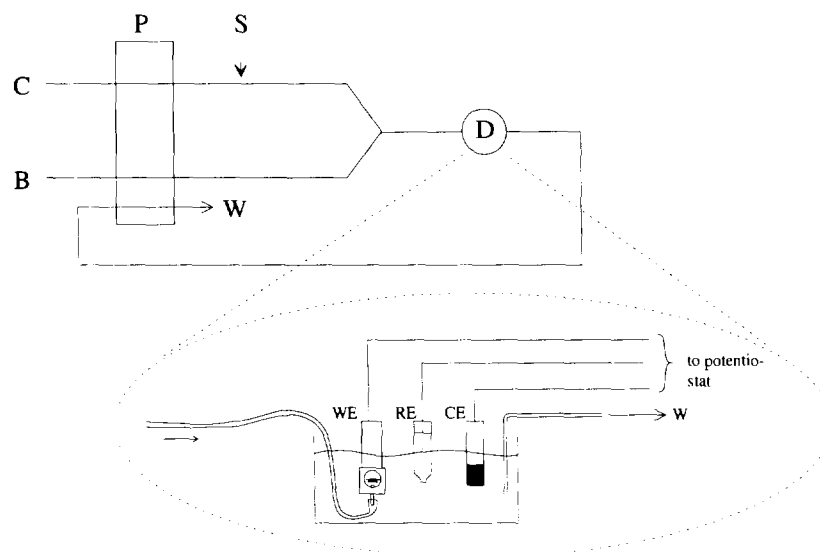
Fig. 1. The FIA system used in the ammonia measurements. C, carrier (deionized water); B, buffer (0.05 M borate, pH 9.2); S, sample injection point; D, wall-jet amperometric detector; P, pump; W, waste. The flow rates of the carrier and the buffer stream were both 1.15 ml min^{-1}. The volume of the injected sample was 100 μl.

ITO electrode in an aqueous 0.15 M solution of NH$_3$ for 15 min, another was soaked in the same solution of NH$_3$ for the same time but at open circuit potential and the third sample was left untreated. A cyclic voltammetric measurement in 0.1 M NaCl was performed to confirm that the first sample, i.e. that treated in ammonia at + 0.30 V, was completely deactivated. After rinsing the samples with water and drying them in N$_2$, the PPy films were peeled off the ITO glass and their transmission spectra were taken using a Bruker IFS66 FT-IR spectrometer.

Table 1
Treatment of PPy by ammonia in different solutions. The EDAX spectra are shown in Fig. 6. The background electrolyte used in experiments #2–4 was 0.05 M Na$_2$SO$_4$

Sample #	Treatment
1	Soaked in water for 15 min
2	Kept at +0.3 V in 0.15 M NH$_3$ for 10 min
3	Soaked in 0.15 M NH$_3$ for 15 min (at open circuit potential)
4	Kept at +0.3 V in 0.003 M NH$_3$ for 1 min
5	Kept at +0.3 V in 0.15 M H$_2$SO$_4$ for 0.5 min

3. Results and discussion

3.1. Sensor operation

The response of the Pt/PPy sensor to ammonia in aqueous solutions was tested by injecting 100 μl of different concentrations of NH$_4$Cl into the FIA system. The recorder trace is shown in Fig. 2. The calibration line within the studied concentration range 10–120 μM was linear with $r = 0.995$, and RSD = 2.2% and 1.1% at the lower and upper limit, respectively. These RSD values were determined by ten injections of the 10 μM and 120 μM NH$_4$Cl solutions. As can be seen in Fig. 2, the limit of detection is well below 5 μM NH$_3$ ($\approx$ 10 μM NH$_4$Cl at pH 9.2). The short-time stability of the sensor was tested by injecting 60 times 100 μl of 100 μM NH$_4$Cl. The signal was found to be stable with RSD = 0.7%.

In order to study the intefering effect due to small ions on the ammonia response at the PPy electrode, NaCl was selected as the model compound. Since NaCl levels in clinical samples normally fall within 0.08–0.18 M, concentrations of 0.05 M and 0.2 M were chosen in the interference studies. The current responses of injections of 100 μl of the solutions are shown in Fig. 3A. As can
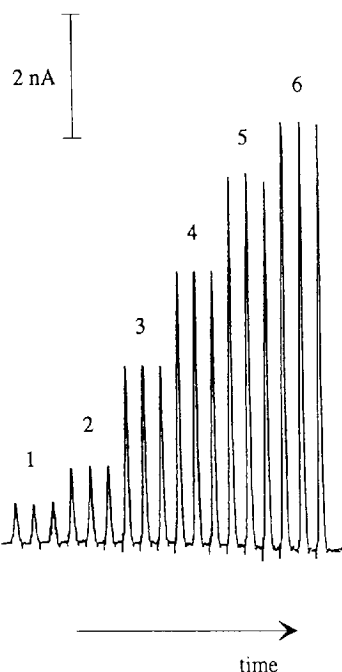
Fig. 2. Injections of ammonia at different concentrations: (1) 10 μM, (2) 20 μM, (3) 50 μM, (4) 70 μM, (5) 100 μM and (6) 120 μM NH$_4$Cl.

be seen, NaCl at these concentrations really does interfere since, for example, 0.05 M NaCl gives an approximately equally strong response as 50 μM NH$_4$Cl. The interfering signal is due to the involvement of small anions such as chloride in the doping process of PPy:

$$PPy^0 + Cl^- \rightleftharpoons PPy^+Cl^- + e^-$$
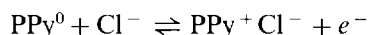
The participation of small anions in the doping process has been used to construct conducting polymer-based amperometric anion sensors [4-7].

In order to diminish the effect of chloride ions on the signal at the PPy electrode, the concentration of NaCl in the buffer stream was set at 0.4 M. This procedure did not give any great improvement to the interfering effect of chloride. The buffer stream was then adjusted to 60 μM with respect to the anionic surfactant sodium dodecyl sulfate, NaDS. This compound is adsorbed at the electrode and forms an anionic layer on the surface. A similar experiment to that shown in Fig. 3A was performed but, as explained above, now with DS$^-$ in the buffer stream. The

results are shown in Fig. 3B and, as can be seen, the interference from Cl$^-$ is considerably decreased. The ratio of signals (120 μM NH$_4$Cl):(0.2 M NaCl) is 1:2.2 before and 1:0.56 after the addition of 60 μM NaDS. The decreased interference of Cl$^-$ is probably due to the fact that the DS$^-$ surfactant anions form a negatively charged layer on the *surface* of the PPy film. Owing to their bulky size, the DS$^-$ ions are not capable of penetrating the polymer film and doping it [8]. The DS$^-$ layer repels anions and thus creates a strong diffusional barrier to the flux of Cl$^-$ to the PPy film. This hypothesis is confirmed by the cyclic voltammograms shown in Fig. 4. The cyclic voltammogram of PPy in 0.2 M NaCl + 0.05 M borax (pH 9.2) shows that there are two different redox processes taking place in the PPy film: one at -0.05 V and another at -0.4 V. Li and Qian [9] observed similar behavior in PPy(NO$_3^-$) and attributed the two processes to anion and cation insertion. More specifically, the more anodic process corresponds to anion insertion and the more cathodic process to cation insertion. After addition of 0.05 M NaDS to the electrolyte solution, the redox peak pair at -0.05 V disappeared, which means that anion insertion was no longer taking place. The cation insertion, in contrast, could still be observed. This confirms our assumption that DS$^-$ forms a permselective layer on the electrode that prevents Cl$^-$ entering the PPy film by charge exclusion.

As can be seen in Figs. 3A and 3B, there are negative peaks (those pointing downwards) preceding the Cl$^-$ signal. These may originate from small changes in the potential of the working electrode that are not immediately compensated by the potentiostat. The current observed obviously has contributions both from Faradaic and charging currents.

The interfering signal from injections of NaCl could further be diminished by increasing the concentrations of NaDS and NaCl in the borax buffer stream to 0.05 M and 0.4 M, respectively (see Fig. 3C). The negative peaks, however, are an interfering phenomenon in the determination of ammonia, and although addition of NaDS and NaCl to the buffer stream clearly reduced these peaks, NaCl levels of 0.1-0.2 M still interfered to
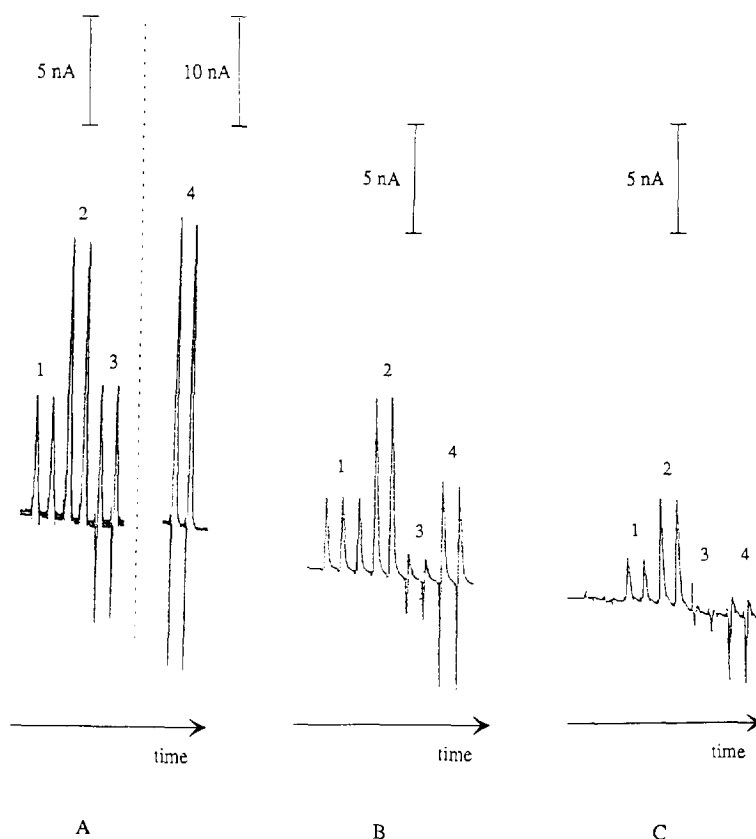
Fig. 3. Interference caused by NaCl: (A) under normal measuring conditions; (B) after the concentration of NaDS in the buffer stream had been set at 60 μM; (C) after the buffer stream had been adjusted to 0.05 M with respect to NaDS and 0.4 M with respect to NaCl. The injected solutions were: (1) 50 μM NH$_4$Cl, (2) 120 μM NH$_4$Cl, (3) 0.05 M NaCl, (4) 0.2 M NaCl.

some extent in the determination of ammonia at low, i.e. μM, ammonia concentrations.

3.2. Response mechanism

The exact mechanism behind the ability of a PPy electrode to detect ammonia is not clear. The response is obviously based on the capability of ammonia to reduce PPy. Gustafsson et al. [10] reported that when PPy was exposed to gaseous ammonia at low concentrations and for short times, the conductivity of the PPy film was decreased but was reversibly recovered after flushing with Ar. However, when the PPy film was exposed to 1 atm gaseous ammonia for a long period (14 days) an irreversible increase in the resistivity of the polymer film was observed. Gustafsson et al. also explained that the reversible

change in conductivity is due to a compensation effect where ammonia acts as an electron donating species. In addition, the authors discuss the possibility of proton transfer between the polymer and ammonia as the compensation reaction. The irreversible change of conductivity was explained as a nucleophilic attack by ammonia or hydroxide on the polymer, which leads to loss of conjugation in the polymer structure and thus to increased resistivity.

Trojanowicz et al. observed a continuous decrease in the amperometric response of PPy for repetitive injections of ammonia. The rate of the signal decrease was found to be proportional to both the potential of the measurement and the concentration of ammonia in the solution. This was confirmed by our experiments in which repeated injection of a solution where [NH$_3$] > 1
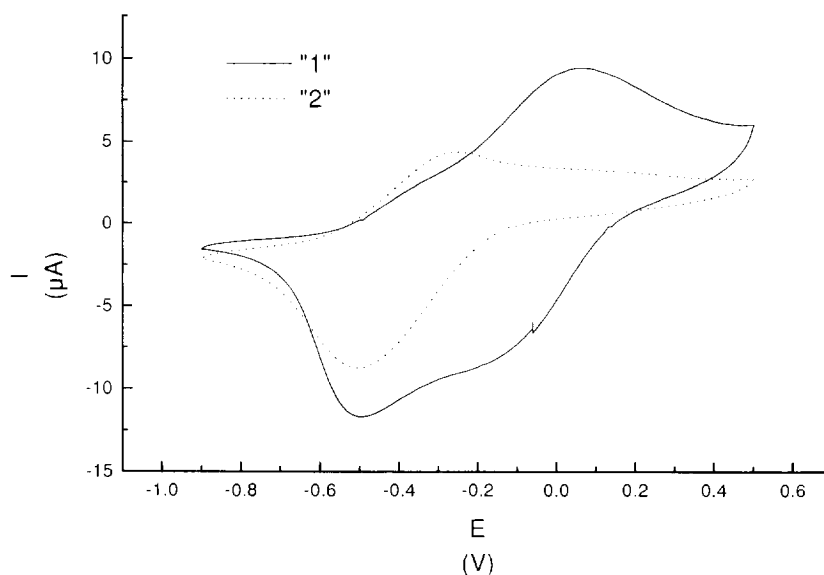
Fig. 4. Cyclic voltammograms at a Pt–PPy electrode (area 0.16 mm²) in two different media. Medium "1" is 0.05 M borax + 0.2 M NaCl (pH 9.2). Medium "2" is 0.05 M borax + 0.2 M NaCl + 0.05 M NaDS (pH 9.2). The sweep rate is 50 mV s⁻¹.

mM resulted in sensor deactivation as shown in Fig. 5. The signal was partly restored when only the carrier solution was pumped past the electrode for 10 min. This is also demonstrated in Fig. 5. These results suggest that sensor deactivation is not an entirely irreversible process.

The IR spectra of three identically prepared but differently treated PPy samples were measured. One of the PPy samples was not treated with ammonia, one was treated for 15 min at open circuit potential and the other for 15 min at +0.3 V. No big differences could be found between the spectra. The only variation was a shift in the baseline, such that the untreated sample showed the lowest transmission and that treated in 0.15 M NH₃ at +0.30 V showed the highest transmission. Gustafsson et al., on the contrary, found big changes in the IR spectrum of their PPy samples when treated with gaseous ammonia. These changes were explained by chemical variations in the structure of PPy. The most important result in our measurements is that the chemical structure of PPy remained virtually the same after exposure to ammonia in aqueous solution. Deactivation of the sensor was therefore to be the result of another type of attack by ammonia on PPy. Since the degree of IR transmission of a conducting

polymer decreases with its conductivity, the observed shift in baseline reflects the change in the degree of doping. The untreated sample had the lowest transmission and therefore the highest degree of doping. The sample treated with ammonia at +0.3 V was most reduced. Our IR measurements indicate that ammonia is capable of reducing doped PPy.

The EDAX measurements were used to study the content of counterions in PPy after different kinds of treatment with ammonia. The procedures are shown in Table 1 and the results in Fig. 6. These results can be interpreted by looking at the peaks for Cl and S. It can clearly be seen that the content of Cl⁻ in the PPy film was unaffected when the film was not treated with ammonia (samples # 1 and # 5). It should be pointed out that a quantitative analysis of the curves in Fig. 6 is not possible owing to the fact that, although all they were prepared in exactly the same way, there are always some morphological differences between the individual films. Therefore, the doping and undoping processes of the different films are not exactly comparable. Some clear trends, however, can be observed. Sample # 2 was treated with 0.15 M ammonia for 10 min at +0.3 V in 0.05 M Na₂SO₄ supporting electrolyte. As can be

seen in Fig. 6, the Cl peak decreased and a clear
S peak appeared, indicating a decrease in Cl
content and increase in S content in the PPy film.
The film doped with Cl^- was reduced when ex-
posed to ammonia, i.e. undoped, and Cl^- ions
were expelled from the film. Because the film was
continuously held at $+0.3$ V it would have been
reoxidized immediately, i.e. doped with anions of
the electrolyte, SO_4^{2-}. Therefore, the peak for S
appears in the EDAX spectrum of sample #2.

In experiment #3, the PPy film doped with
Cl^- ions was soaked in 0.15 M ammonia with
0.05 M Na_2SO_4 at open circuit potential. The film
was reduced by ammonia but was not reoxidized.
Therefore, the Cl peak decreasesd but no S peak
could observed. In experiment #4, the film was
soaked in a solution of 0.003 M ammonia and 0.05
M Na_2SO_4 for 1 min, and a potential of $+0.3$ V
was applied. The Cl peak decreased and a clear
peak for S appeared, indicating undoping of Cl^-
and redoping with SO_4^{2-}. Experiment #4 was
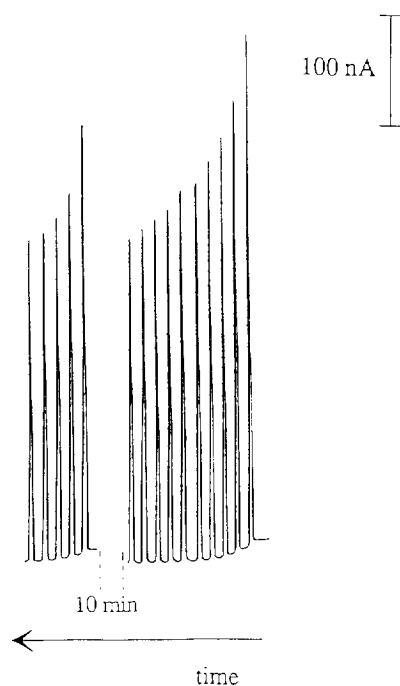
Fig. 5. Signal degradation caused by measuring relatively high
ammonia concentrations. A standard solution of 0.01 M
NH_4Cl was injected into the FI analyzer as follows: ten
injections, 10 min break, five injections. The volume of the
injected sample was 100 μl.

similar to #2, but the ammonia concentration
was lower and the soaking time shorter. By study-
ing the curve for #4, it can be seen that the Cl
peak decreased to the same level as in experiment
#2, but the S peak did not increase as much as in
#2. This is obviously due to the physical differ-
ences between films #2 and #4. In experiment
#5, the PPy film was soaked in 0.15 M H_2SO_4 for
30 s. No change compared to curve #1 can be
observed. This indicates that the PPy film doped
with Cl^- remained doped at this potential and
that Cl^- could not be exchanged for SO_4^{2-} with-
out first undoping the PPy film. The results in Fig.
6 indicate that the reaction behind the amperomet-
ric PPy-based ammonia sensor is — at least for
the most part — the ordinary, reversible redox
reaction of PPy rather than an irreversible reaction
between ammonia and PPy.

The redox characteristics of ammonia were ex-
amined further by cyclic voltammetry at a bare Pt
electrode. Fig. 7 shows the cyclic voltammogram
of a solution of 0.15 M NH_3 in 0.2 M NaCl at pH
11.2. There is also a reference voltammogram
taken in a solution whose ionic strength and pH
were identical to the ammonia solution, but that
did not contain any ammonia. It can be seen that
an increase in oxidation current is observed in the
ammonia solution even at the bare electrode.
Since Pt is a chemically inert material, there is no
possibility of an oxidation reaction between am-
monia and the electrode material, and the current
has to originate from an oxidation process of
ammonia alone. This experiment clearly proves
that an irreversible reaction between PPy and
ammonia is not necessarily needed for oxidation
of ammonia and reduction of PPy. Of course, it
does not prove that such an irreversible reaction
does *not* take place, but it makes reversible un-
doping–doping more plausible as the reaction for
the signal observed with the PPy electrode.

When the PPy electrode comes into contact
with an aqueous solution of ammonia, the ammo-
nia — according to the undoping–doping model
— reduces PPy. If a potentiostat is used to keep
the potential of the PPy electrode at a constant
positive potential, the PPy film is immediately
reoxidized, doped, to its original redox state. In
experiments #2 and #4, it can be seen that Cl^-
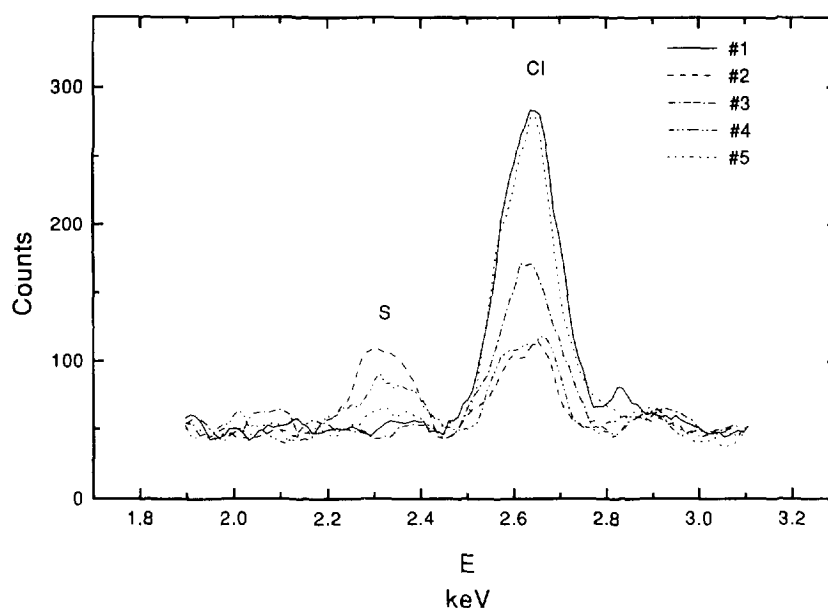
Fig. 6. EDAX spectra of PPy samples treated in different ways. The treatment procedures are given in Table 1.
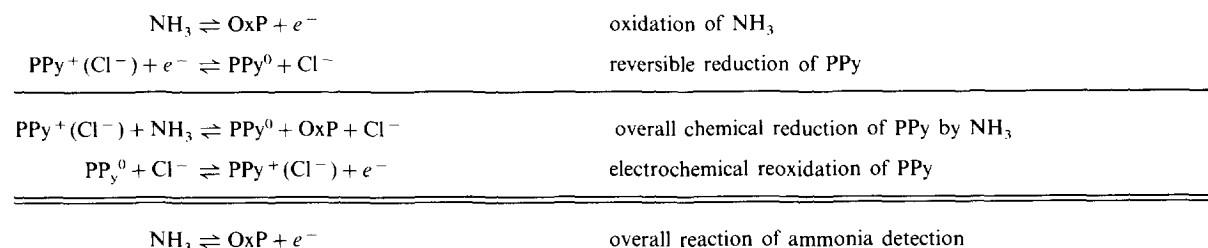
was exchanged with SO_4^{2-}. The electrochemical reoxidation step produced an oxidation current that was the signal of the sensor. A representation of the model for the results in Figs. 2–4 is given in Scheme 1.

The oxidation product of ammonia is denoted by OxP. Fig. 8 shows a cyclic voltammogram where the catalytic oxidation of ammonia at a PPy electrode is clearly seen: the presence of only 5 mM ammonia resulted in an increase of 3.2 μA mm^{-2} in the oxidation current on the PPy-coated electrode. The same concentration of ammonia, however, increased the oxidation current by only 0.071 μA mm^{-2} when measured at a bare Pt electrode. We have not been able to identify the oxidation product. It may also be somehow at-

tached to the polymer as described by Gustafsson et al. in their mechanisms. It should be pointed out that the reaction mechanism as presented above refers to the reversible reduction of PPy describing the response of the sensor at the μM concentration level. The mechanism for the irreversible reduction, however, is not yet clear and is therefore not discussed further in this paper. A proposal for the irreversible reaction mechanism is presented elsewhere [11].

4. Conclusions

The PPy-based ammonia sensor is shown to work satisfactorily. However, it has two major

$$NH_3 \rightleftharpoons OxP + e^-$$	oxidation of NH_3

$$PPy^+(Cl^-) + e^- \rightleftharpoons PPy^0 + Cl^-$$	reversible reduction of PPy

$$PPy^+(Cl^-) + NH_3 \rightleftharpoons PPy^0 + OxP + Cl^-$$	overall chemical reduction of PPy by NH_3

$$PP_y^0 + Cl^- \rightleftharpoons PPy^+(Cl^-) + e^-$$	electrochemical reoxidation of PPy

$$NH_3 \rightleftharpoons OxP + e^-$$	overall reaction of ammonia detection

Scheme 1.
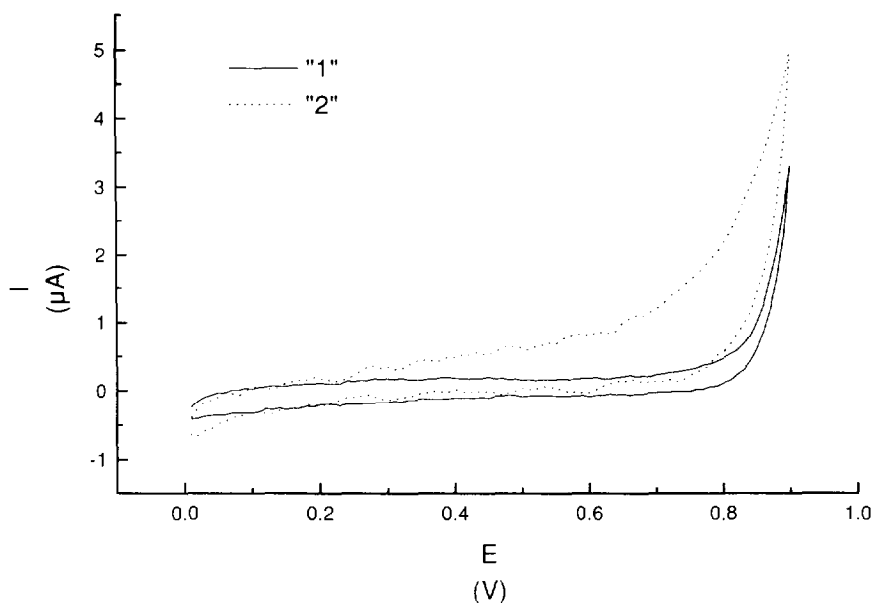
Fig. 7. Cyclic voltammograms at a bare Pt electrode (area 2.4 mm^2) in two different media. Medium "1" is 0.2 M NaCl (pH adjusted to 11.2 with NaOH). Medium "2" is 0.2 M NaCl + 0.15 M NH$_3$ (pH 11.2). The sweep rate is 50 mV s^{-1}.

problems. Firstly, high concentrations of small inorganic anions such as Cl$^-$ cause considerable interference by giving rise to false signals. Secondly, the sensor is deactivated when measure-

ments at high ammonia concentrations are performed. The first problem can be diminished to a certain extent by adding the anionic surfactant dodecyl sulfate to the buffer stream. This
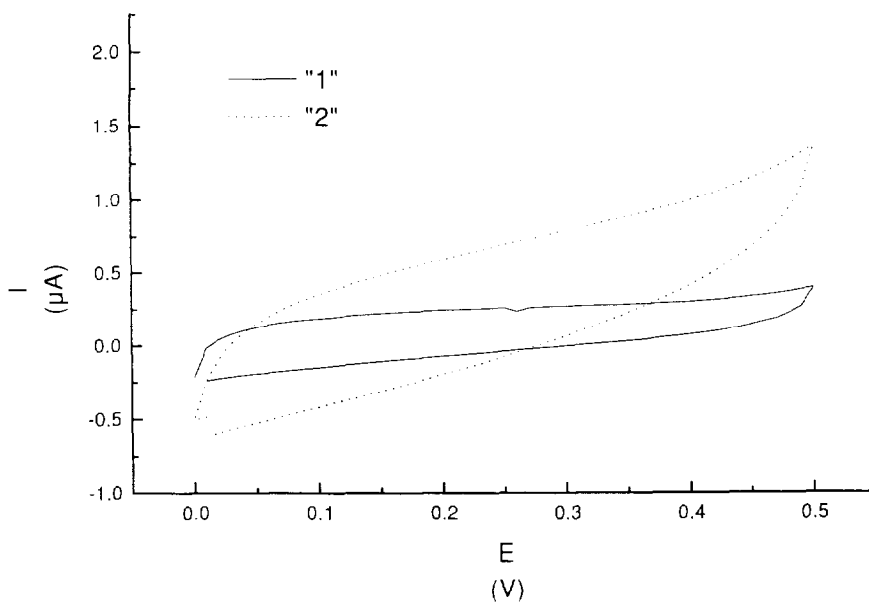
Fig. 8. Cyclic voltammograms at a Pt–PPy electrode (area 0.16 mm^2) in two different media. Medium "1" is 0.05 M borax (pH 9.2). Medium "2" is 0.05 M borax + 5 mM NH$_3$. The sweep rate is 50 mV s^{-1}.

procedure, however, results in a new interference caused by cations, which can be reduced to a certain extent by addition of sodium chloride to the buffer stream. These measures do not remove the problem completely, but they do make it much less severe.

The second problem is the deactivation of the sensor, when measuring relatively high concentrations of ammonia. EDAX and IR studies of ammonia-deactivated PPy samples supported the theory that PPy remains virtually chemically intact in the ammonia measurements. Exposing the sensor to ammonia concentrations greater than 1 mM resulted in a decrease of the sensor signal that was partly reversible and partly permanent. The deactivation may thus be thought of as being due partly to the oxidation product(s) of ammonia sticking to the electrode surface, and partly to irreversible electrochemical degradation of PPy.

Acknowledgment

References

[1] K.K. Kanazawa, A.F. Diaz, R.H. Geiss, W.D. Gill, J.F. Kwak, J.A. Logan, J.F. Rabolt and G.B. Street, J. Chem. Soc., Chem. Commun., (1979) 854.
[2] M. Josowicz and J. Janata, Anal. Chem., 58 (1986) 514.
[3] M. Trojanowicz, W. Matuszewski, B. Szczepanczyk and A. Lewenstam, in G.G. Guibault and M. Mascini (Eds.), Uses of Immobilized Biological Compounds, Kluwer Academic, Dordrecht, 1993, p. 141.
[4] Y. Ikariyama and W.R. Heineman, Anal. Chem., 58 (1986) 1803.
[5] Y. Ikariyama, C. Galiatsatos, W.R. Heineman and S. Yamauchi, Sensors and Actuators, 12 (1987) 455.
[6] J. Ye and R.P. Baldwin, Anal. Chem., 60 (1988) 1979.
[7] P. Ward and M.R. Smyth, Talanta, 40 (1993) 1131.
[8] R.C.D. Peres, M.A. De Paoli and R.M. Torresi, Synth. Met., 48 (1992) 259.
[9] Y. Li and R. Qian, J. Electroanal. Chem., 362 (1993) 267.
[10] G. Gustafsson, I. Lundström, B. Liedberg, C.R. Wu, O. Inganäs and O.Wennerström, Synth. Met., 31 (1989) 163.
[11] M. Trojanowicz, A. Lewenstam, T. Krawczynski vel Krawczyk, I. Lähdesmäki and W. Szczepek, Electroanalysis, in press.

Development of long-term stable reference electrode with fluoric resin liquid junction

Satoshi Ito [a,b,*], Fumie Kobayashi [a], Keiko Baba [a], Yasukazu Asano [a], Hiroko Wada [b]

[a] Research Center, DKK Corp., 4-13-14, Kichijoji Kitamachi, Musashino, Tokyo 180, Japan
[b] Department of Applied Chemistry, Nagoya Institute of Technology, Gokiso, Showa, Nagoya 466, Japan

Abstract

A porous polytetrafluoroethylene (PTFE) junction reference electrode with an air-tight inner solution chamber containing saturated potassium chloride (KCl) was developed for flow analysis. This reference electrode is not influenced by a change in the sample pressure, and is not necessary to supply the KCl inner solution. The pore size of the porous PTFE junction is about 150 μm, although the conventional porous ceramic junction is 0.1 ~ 0.3 μm. The large pore size of the porous PTFE junction promotes the continuous exudation of KCl from the liquid junction and the higher surface tension of PTFE is effective to prevent the overflow of KCl. The porous PTFE was made by putting 74% of PTFE powder and 26% of KCl powder in a mold, pressing with a pressure of 200 kgf cm^{-2}, and sintering at 365°C. The quantity of KCl exuded from the disposable reference electrode is closely related to the life of the electrode. The relationship between the diffusion rate of the PTFE reference electrode and its characteristics was investigated. The quantity of KCl exuded from this reference electrode was initially of the order of 10^{-5} mol h^{-1} and decreased to the order of 10^{-6} mol h^{-1} after a year. This is approximately one-tenth of that exuded in a conventional reference electrode with a ceramic junction. The junction potential of the developed reference electrode was stable in the pH range 2 ~ 12 with a total ionic strength of more than 10^{-3} mol l^{-1}. This reference electrode containing 8 ml of the KCl inner solution was able to be used continuously for one or two years.

Keywords: Stable reference electrode; PTFE; Liquid junction

1. Introduction

One of the most important performances in the use of the reference electrode is continuous outflow of the potassium chloride (KCl) inner

* Corresponding author. Fax: (81)422-52-2042.

solution from the liquid junction [1]. In the conventional reference electrode, 0.1 ~ several ml day^{-1} of the KCl internal solution exudes constantly through the liquid junction of the reference electrode. If the outflow of the KCl internal solution from the inside of the reference electrode to the outside (into the sample solution) was stopped, the KCl concentration at the surface of

S. Ito et al./Talanta 43 (1996) 135–142

the liquid junction would become low, the reference electrode would lose its normal function and liquid junction potential errors would occur. As a result, the liquid junction potential would become unstable or fluctuating. Generally, to get a stable junction potential, a technique of pressing the KCl inner solution against the sample pressure has been used when the sample has some pressure or else the KCl inner solution for KCl consumption has been supplied using a head tank of the KCl solution. This is a very annoying matter in the treatment of the reference electrode. It is an obstacle to the miniaturization of a reference electrode in the case of flow analysis in which the sample pressure is particularly changeable. If we simply make a smaller-sized electrode by making the KCl chamber airtight, the continuous outflow of the KCl solution from the liquid junction become impossible and its performance is lost.

Up to now, many attempts to improve the reference electrode have been done for flow analysis. As an example, a solid-state reference electrode of the coated-wire type based on the silver/silver chloride (Ag/AgCl) electrode was reported. It is easy to miniaturize and is not influenced by the sample pressure, furthermore it is free from the direction in case of installation [2–6]. An example of an ion-selective field effect transistor with a inert polymer membrane has also been reported [7]. However, in our experiences, the solid-state reference electrodes do not give satisfactory stability and reproducibility of the reference electrode potential. As a reference which belongs between the conventional reference electrode and the solid-state reference electrode, we have developed an air-tight structured reference electrode with a KCl inner solution. As mentioned above, in an air-tight structured reference electrode with a ceramic junction, continuous outflow of the KCl inner solution could not be expected. At first, we tried to use a ceramic junction (5 mm in diameter and 5 mm in length) with an air-tight structure. However, the outflow of the KCl inner solution from the reference electrode was too high. We decided that a plastic with higher surface tension than an alumina or a silica ceramic was a good material to use. We adopted polytetrafluoroethylene (PTFE) because of the

easy plastic molding operation and its anti-corrosion ability in the various sample solutions. To make small holes to exude the KCl inner solution through PTFE, a mixture of PTFE powder and KCl powder was molded, and when it was washed by water after a cutting process, it became porous PTFE. The KCl powder was selected to give porosity to the PTFE junction because it was easy to arrange the uniformed particles, stable above 365°C and soluble in water. This reference electrode with the porous PTFE junction has an air-tight KCl inner solution chamber, and the KCl inner solution should be packed so as not to allow any air in this chamber. In this reference electrode, there is not outflow of the KCl inner solution but diffusion of K^+ and Cl^- ions from the reference electrode to the sample solution. By the diffusion of K^+ and Cl^- ions, the liquid junction potential is kept stable. We studied the processes for producing the porous PTFE liquid junction and its performances. A long-term stable and maintenance-free reference electrode with porous PTFE liquid junction was developed and applied to flow analysis with the ion electrode.

2. Experimental

2.1. Apparatus and reagents

A DKK Model IOL-50 ion-meter, a DKK Model EL7020 chloride ion electrode, and a DKK Model EL4083 reference electrode were used for outflow or diffusion rate measurements of Cl^- ion from the reference electrode.

PTFE powder for molding Model M12 (grain size = 20 μm) and Model M33 (grain size = 750 μm) were purchased from Daikin Industries (Osaka, Japan). All chemicals used were of analytical reagent grade. Potassium chloride, hydrochloric acid, acetic acid, trimethanolamine and sodium hydroxide were obtained from Wako Chemicals (Osaka, Japan). The KCl was sieved using a sieve of 40 ~ 80 mesh to get uniform particles. Pure water obtained by a MILLI-Q SP Reagent Water System was used in this work. A model F11 porous ceramic was purchased from Kyocera (Kyoto, Japan), and was used as the

ceramic junction by molding and cutting to 2 mm in diameter and 10 mm in length. The material, mean porosity and pore rate of this ceramic junction are 99.9% of alumina (Al_2O_3), 0.3 mm and 47% respectively, according to the maker.

2.2. Manufacture of porous PTFE junction

The KCl powder of uniform size was obtained as follows. The KCl was dried for about 1 h in an oven at 120°C, ground to find powder by a mortar, and was sieved in two ranks: 100 ~ 60 mesh (147 ~ 246 μm grain size); and 80 ~ 48 mesh (175 ~ 295 μm grain size). If the grain size is less than 147 μm, the outflow of KCl solution through the PTFE junction was not observed. Furthermore, if it is more than 295 μm, the outflow of KCl solution is too much to use at the liquid junction. The standard deviation of the outflow rate of this PTFE junction for the grain size or the content of KCl is not small, i.e. about 30%. The KCl grain size of 147 ~ 246 μm with smaller standard deviation was adopted practically.

As the grain size of PTFE powder did not influence the outflow rate of this PTFE junction, PTFE of finer size was used for Model M12.

The developed reference electrode consisted of the PTFE body and the PTFE junction which were pressed and sintered together. PTFE powder only was used in the part of the body, the mixture of PTFE powder and KCl powder was used in the part of the junction. The PTFE–KCl mixture was made, that is, the PTFE powder was mixed with KCl powder for 10 min at 1520 rev min^{-1}. Firstly, 80 g of the PTFE–KCl mixture was stuffed in the bottom part of the stainless-steel cylinder mold (25 mm in diameter and 250 mm in length). Next, 200 g of the PTFE powder was stuffed in the upper part of it. The PTFE powder and mixture were pressed for 5 min at 200 kgf cm^{-2}. In this way a stick 25 mm in diameter and 70 mm in length was obtained. One part of this stick consists of the PTFE, another part consists of the mixture. This stick was sintered for 2.5 h at 365°C, and was cut by a lathe in the shape of the reference electrode body. The part of the liquid junction (porous PTFE) consists of the sides of 12 mm diameter and 10 mm in length, and the

bottom. Its surface area is about 5 cm^2. The relationship between the wall thickness and the outflow of KCl through the PTFE junction was observed to be inversely proportional. When the wall thickness was less than 1.5 mm, the outflow of KCl was too much to use for a long period. When it was more than 2.5 mm, the outflow of KCl was too low for the junction potential to become unstable. The wall thickness of the sides and the bottom was made to be 2 mm. At the end of the process, the reference electrode body was left in water overnight at room temperature for making porous PTFE by solving and removing the KCl powder.

2.3. Structure of reference electrode

The structure of the reference electrode is shown in Fig. 1. The reference electrode and the liquid junction are in a body, and there is a screw for installation of a flow cell. The inner electrode used is the silver/silver chloride electrode. As an inner solution, the saturated KCl solution and the KCl sludge are enclosed in it. The super-saturated KCl enclosed in the electrode body would decrease by diffusion to the sample solution in practical use as the source of KCl.

2.4. Measurement of diffusion rate of KCl

The diffusion rate of KCl in the PTFE reference electrode to the sample solution was measured as follows. A junction part of each reference electrode was soaked in 40 ml of water at room temperature. After 24 h exactly, the 40 ml of water-diffused KCl was made up to 50 ml exactly, and the molar concentration of Cl^- ion was measured by a chloride ion electrode. The diffusion rate was calculated as the number of moles of KCl diffused in a unit time (1 h). This measurement was made using ten developed reference electrodes and the percent standard deviation was calculated. It was measured once a month, and was continued for 12 months. The first measurement was made a week after manufacture. During the test terms, the junction part of the reference electrode was soaked in water, which was renewed once a week to keep its electrtonic conductivity low.
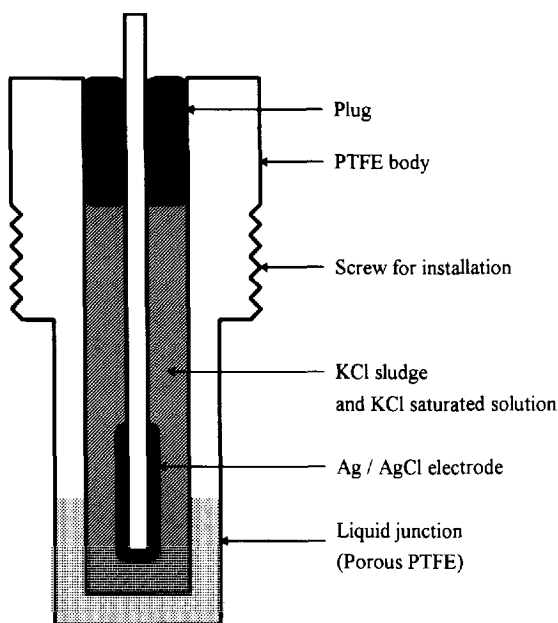
Fig. 1. The structure of the PTFE reference electrode.

Fig. 3. The ionic strength effect of the PTFE reference electrode.

The change in the KCl diffusion rate is shown in Fig. 2. The open circles show the KCl diffusion rate of the PTFE junction. The filled circles show the KCl diffusion rate of the ceramic junction. The reference electrode with ceramic junction prepared for the test was manufactured by holding the porous ceramic (2 mm in diameter and 10 mm
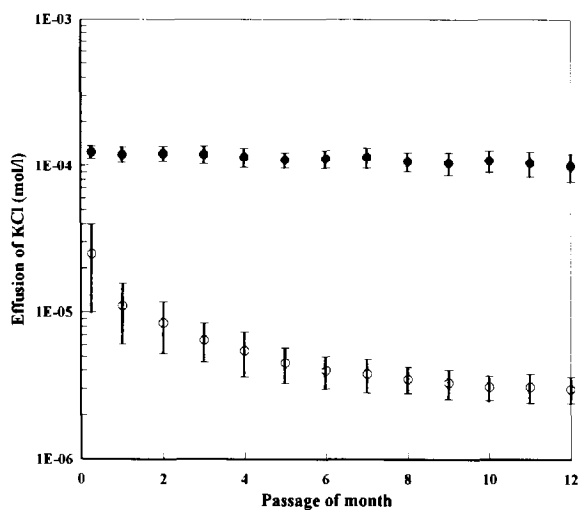

Fig. 2. The change in the KCl diffusion rate of the PTFE reference electrode.

in length) with rubber packing at one end of the glass tube (12 mm in diameter). The head pressure of the KCl inner solution was kept at 0.1 kgf cm^{-2} (about 1 m in a column of water) by supplying another KCl inner solution occasionally. In the case of the PTFE junction, the KCl diffusion rate was 2.5×10^{-5} mol h^{-1} initially and it became 3.0×10^{-6} mol h^{-1} after a year. However, in the case of the ceramic junction, it was 1.25×10^{-4} mol h^{-1} throughout the year. The relative standard deviation of the KCl diffusion rate was $\pm 60\%$ after a week, $\pm 45\%$ after a month, and $\pm 20\%$ after a year in the PTFE junction. It was $\pm 10\%$ after a week, $\pm 20\%$ after a month and $\pm 20\%$ after a year in the ceramic junction.

2.5. Measurement of ionic strength effect

Generally in the reference electrode, the liquid junction potential is growing when the outflow of the diffusion of KCl is scant, because it is being blocked by particles of dirt or soil in the sample solution [8]. The PTFE liquid junction is influenced by the ionic strength of the sample solution when the diffusion of KCl is in short supply too.

Fig. 3 shows the ionic strength effect of this PTFE reference electrode. The ionic strength was adjusted by KCl. The liquid junction potential was measured against the standard Model 4083 reference electrode with a glass sleeve junction. The measurement was performed on each of ten pieces a month, six months and a year after manufacture. There was a slight tendency for the junction potential to become large with the lapse of time after manufacture. The magnitude of the junction potentials mostly corresponded to a little diffusion of KCl. It was 3.3 ± 2 mV at 10^{-4} mol l^{-1} and 1.1 ± 0.5 mV at 10^{-3} mol l^{-1} of the ionic strength. When the ionic strength was above 10^{-2} mol l^{-1}, the junction potential was nearly zero.

2.6. Measurement of pH effect

The PTFE liquid junction is also influenced by the hydrogen ion activity (H$^+$ or pH). In Fig. 4, pH 0–3 was adjusted by addition of hydrochloric acid, pH 4–7 with acetic acid and sodium hydroxide, pH 8–12 with triethanolamine and hydrochloric acid, and pH 13–14 with sodium hydroxide, using a pH meter. The ionic strength of each solution was adjusted in 0.01 mol l^{-1} steps by KCl. The liquid junction potential was measured against the standard Model 4083 reference electrode with a glass sleeve junction. The measurement was performed on ten pieces a month, six months and a year after manufacture. The magnitudes of the junction potentials correspond to the diffusion of KCl mostly. They were 10.5 ± 4.9 mV, 4.2 ± 1.8 mV, 1.1 ± 0.4 mV, -0.5 ± 0.2 mV, -1.4 ± 0.4 mV and -4.1 ± 1.4 mV at pH 0, 2, 12, 13, and 14 respectively. In the pH range 3–11, they were almost zero.

2.7. Relationship between KCl diffusion rate and temperature

The diffusion rate of KCl seems to increase with a rise in temperature. Fig. 5 shows the relationship between the diffusion rate and the temperature. The measurements were made at 5, 10, 20, 30, 40 and 50°C with the same reference electrode after six months. A junction part of each

reference electrode was soaked in 40 ml of water at each temperature. After 24 h exactly, the sample of 40 ml including diffused KCl was made up to 50 ml exactly, and Cl$^-$ ion molar concentration was measured by the chloride ion electrode. The diffusion rate was calculated as the number of moles of KCl diffused in a unit time (1 h). Although it was 4×10^{-6} mol h^{-1} at 5 or 10 °C, it increased to 8×10^{-6} mol h^{-1} at 40°C. When the temperature exceeds 40°C, the diffusion rate increased to 1.5×10^{-5} mol h^{-1} at 50°C.

2.8. Aplication to flow analysis

In order to apply this PTFE reference electrode to flow analysis with the ion electrode, the flow cell and the system were devised. Fig. 6 shows a flow cell and a flow system. The flow cell was made from a transparent polyacrylate resin. The ion electrode and the reference electrode were mounted on the cell by a screw, and were shielded by a rubber O-ring. A fluoride ion electrode was used, and a fluoride ion electrode membrane (lanthanum fluoride, LaF$_3$, single crystal) which is not as easily influenced by the sample pressure change as a solid state membrane, and has very good characteristics among many sorts of ion electrode membrane such as stability, high sensitivity, good reproducibility and response. The fluoride ion electrode was manufactured by pasting an epoxy resin tube with a LaF$_3$ single crystal membrane (8 mm in diameter and 2 mm in length), by putting 1 mol l^{-1} sodium chloride and 0.01 mol l^{-1} sodium fluoride as an inner solution in it, and by leading out the silver/silver chloride inner electrode. The sample was admitted to the cell with the peristaltic pump or could be sucked in by the peristaltic pump behind the flow cell. Inner diameters of the sampling tube and the passage in the flow cell are 1 mm. The sample flows through a very small region of the ion electrode membrane. The size of this region is 5 mm in diameter and 0.2 mm in depth, i.e. the volume is about 0.04 ml, and the cross-section of the sample passage in the neighborhood of the ion electrode membrane is about 0.01 cm^2. When the sample flow rate is 5 ml min^{-1}, the line flow rate of the ion electrode membrane surface becomes
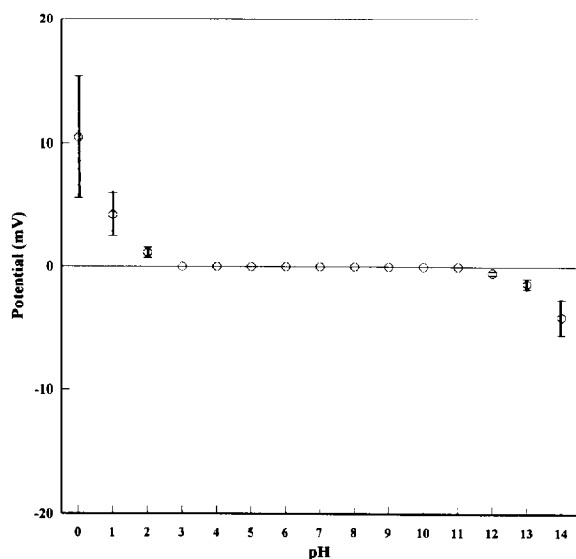
Fig. 4. The pH effect of the PTFE reference electrode.

8.3 cm s^{-1}. However, in the neighborhood of the liquid junction of the reference electrode, the passage diameter is 14 mm as against the liquid junction diameter of 12 mm. The line flow rate of the liquid junction surface becomes about 0.05 cm s^{-1}. It is about two orders of magnitude smaller than that of the ion electrode.

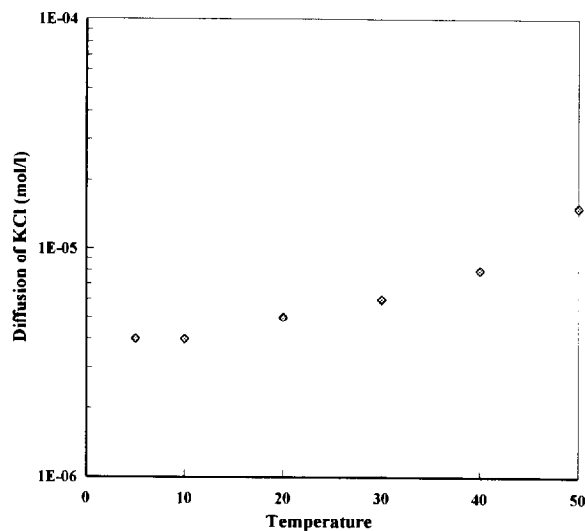To study the performance of the flow system

Fig. 5. The relationship between the diffusion rate and the temperature.

with the PTFE reference electrode in Fig. 6, the batch cell measurement was used as a reference standard method. The fluoride ion electrode and the Model 4083 (with glass sleeve junction) reference electrode are placed in a 200 ml beaker. The sample of 100 ml in a beaker was stirred by a 30 mm length of magnet on a magnetic stirrer at 400 rev min^{-1}. The line flow rate of the fluoride ion membrane surface becomes about 63 cm s^{-1} if its membrane is located very close to the magnet edges and the viscosity of a sample is neglected. As the sample solution, F$^-$ standard solution— NaF of 10^{-2}, 10^{-3}, 10^{-4}, 10^{-5} and 10^{-6} mol l^{-1}—were prepared based on KCl solutions of 10^{-2}, 10^{-3} and 10^{-4} mol l^{-1}, respectively. However in the batch cell, F$^-$ standard solutions only based on 10^{-2} mol l^{-1} KCl were used as the concentration of the sample solution increases owing to exudation of KCl from the liquid junction. Table 1 shows the reproducibility of this reference electrode in the F$^-$ measurement of different concentrations. The measurement was performed as follows. Before use, electrodes and cell were sufficiently conditioned with the blank solution (based on the same concentrated KCl solution with each standard solution, did not contain the F$^-$ ion). With four kinds of F$^-$ standard solution and the blank solution, measurements were repeated several times, from 10^{-6} mol l^{-1} F$^-$ solution to 10^{-5} mol l^{-1} F$^-$ solution, from 10^{-5} to 10^{-4} mol l^{-1}, from 10^{-4} to 10^{-3} mol l^{-3} to 10^{-2} mol l^{-1}, from 10^{-2} to 10^{-3} mol l^{-1}, from 10^{-3} to 10^{-4} mol l^{-1}, from 10^{-4} to 10^{-5} mol l^{-1}, from 10^{-5} to 10^{-6} mol l^{-1}, from blank solution to 10^{-6} mol l^{-1}, from blank solution to 10^{-3} mol l^{-1} and from blank solution to 10^{-2} mol l^{-1}. All data were obtained when the measuring value was constant within 0.1 mV for 30 s as a final value. Reproducibility shows double the standard deviation of the final values. It is important that the sample solution is stirred powerfully in the low level measurement by the fluoride ion electrode. In Table 1, the reproducibility of the 10^{-6} mol l^{-1} F$^-$ standard solution may be caused not by the reference electrode but by the F$^-$ ion electrode. However, it can be said that a flow cell measurement with the PTFE reference electrode is equal to a batch measure-
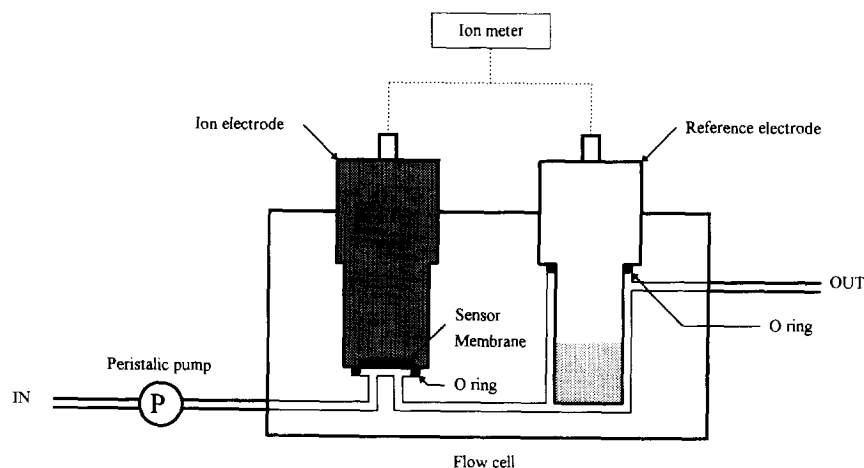
Fig. 6. The structure of the flow cell system for ion analysis.

ment when the ionic strength of the sample solution is over 10^{-3} mol 1^{-1}.

3. Results and discussion

3.1. Performance of PTFE reference electrode

The results of the fluoride ion measurement are shown in Table 1. In the case of measurements with the conventional reference electrode (with glass sleeve junction), the reproducibility of the potential could be said to be within ±1 mV. A potential error of 1 mV causes ≈4% concentration error in fluoride ion (mono-ion) measurements, and a ≈8% concentration error in divalent-ion measurements. These are regarded as adequate for the ion electrode measurements. In the measurements with the PTFE reference electrode, when the total ionic strength of the sample solution is more than 10^{-3} mol 1^{-1}, the performance can be said to be nearly equal to that with the conventional reference electrode.

3.2. Restriction of application and errors

In the practical use of the solid-state reference electrode or the disposable reference electrode, occurrence of the unnecessary liquid junction potential should be paid attention to when considering the pH or the total ionic strength of the

sample solution. In the case of using this PTFE reference electrode in pH measurement with a glass pH electrode, errors of about +0.1 pH in the sample with liquid resistance of about 20 mS m^{-1}, +0.3 pH in the sample of 0 pH, +0.1 pH with 1 pH and −0.1 pH with 14 pH had to be expected respectively, at 25°C, as shown in Figs. 3 and 4.

3.3. Amount of inner KCl in reference electrode and electrode life

The content of the inner solution in a manufactured reference electrode such as that shown in Fig. 1 is about 10 ml. Though the amount of KCl contained in a saturated KCl solution is 3.1 g, 10 g of KCl can be contained in it when KCl sludge is considered. This amount of KCl (10 g) is equivalent to 0.134 moles. If the average diffusion rate from the PTFE junction is 5×10^{-6} mol h^{-1}, the electrode could be durable for 3.1 years of use with 10 g KCl. If it is 10^{-5} mol h^{-1}, its life could be about 1.5 years under continuous measurement conditions.

3.4. Mechanism of porous PTFE liquid junction

In the reference electrode, errors in the liquid junction potential seem to occur by decrease in KCl concentration on the liquid junction surface [9]. Essentially, the surface of the liquid junction

Table 1
Reproducibility of fluoride ion measurement

Concentration of standard solution	Batch cell measurement (with Model 4083) 10^{-2} mol l⁻¹ of KCl		Flow cell measurement (with PTFE reference electrode)					
			10^{-4} mol l⁻¹ of KCl		10^{-3} mol l⁻¹ of KCl		10^{-2} mol l⁻¹ of KCl	
	Potential (mV)	Reproducibility (mV)	Potential (mV)	Reproducibility (mV)	Potential (mV)	Reproducibility (mV)	Potential (mV)	Reproducibility (mV)
10^{-2} mol l⁻¹ of F⁻	−20.3	±0.3	−20.1	±1.3	−20.5	±0.5	−21.7	±0.3
10^{-3} mol l⁻¹ of F⁻	38.8	±0.3	38.0	±1.7	38.6	±0.6	37.4	±0.3
10^{-4} mol l⁻¹ of F⁻	97.6	±0.5	95.5	±1.6	97.3	±0.8	96.2	±0.4
10^{-5} mol l⁻¹ of F⁻	156.1	±0.7	152.5	±2.7	155.9	±1.1	154.8	±0.6
10^{-6} mol l⁻¹ of F⁻	212.2	±2.1	208.3	±4.2	213.6	±2.1	212.3	±1.1

should be filled with concentrated KCl. The conventional type of reference electrode has a KCl supply system (head tank or compressed air); the fresh KCl inner solution exuded through the liquid junction keeps the concentration of KCl high on the liquid junction surface. However, in the solid-state type of reference electrode or the reference electrode with an air-tight structured inner solution chamber, such as this PTFE reference electrode, decrease of KCl concentration on the liquid junction surface cannot be prevented. As this decrease of KCl concentration is caused by the dilution of the inner solution (concentrated KCl) with the sample solution, ease of replacement or supply of KCL becomes important in the junction material and the inner solution. An aqueous inner solution is easily replaceable compared with the solid-state electrolyte, the gel or high viscosity solution. Furthermore, as the porous PTFE junction has a larger pore size compared to the porous ceramic junction, quicker replacement or supply of KCl can be expected.

We noticed that a stable liquid junction potential of this reference electrode with the PTFE junction does not lead to outflow of KCl solution but to diffuse K⁺ and Cl⁻ ions. Though the porous PTFE junction has larger pore size and wider junction surface than the ceramic junction, diffusion of K⁺ ion and Cl⁻ ion from the inside to the outside of the reference electrode is much less than for a ceramic junction. In addition, as it has higher surface tension then ceramics, miscibility between the inner solution and the sample solution became smaller. As a result, it can be said that this PTFE reference electrode is compact, disposable, long-lived, and has good performance compared to the conventional reference electrode.

References

[1] A.K. Covington and P.D. Whalley, Anal. Chim. Acta, 169 (1985) 221.

[2] I. Cukrowski and A.L. Dawidowics, Chem. Anal., 37 (1992) 87.

[3] M. Omine and S. Katsube, Institute of Electronics, Information and Communication Engineers Technical Report on Organic Material Electronics, 91 (29) (1991) 1.

[4] A. Bettelheim, R. Harth and D. Ozer, J. Electrochem. Soc., 135 (1988) 1041.

[5] S. Hettiarachchi and D.D. Macdonald, J. Electrochem. Soc., 134 (1987) 1307.

[6] K. Suzuki, H. Ishiwada, K. Saito and T. Shirai, Bunseki Kagaku, 30 (1981) 722.

[7] S. Tahara, M. Yoshii and S. Oka, Chem. Lett., 3 (1982) 307.

[8] Y. Asano, S. Ito and F. Kobayashi, Nippon Kagaku Kaishi, 10 (1980) 1516.

[9] R.G. Bates, Determination of pH: Calculation of the Liquid-junction Potential, John Wiley & Sons, New York, 1964, pp. 39–47.

Talanta

Aliphatic polyurethane as a matrix for pH sensors: effects of native sites and added proton carrier on electrical and potentiometric properties

Vasile V. Cosofret [a], Miklos Erdosy [a], James S. Raleigh [a], Timothy A. Johnson [a], Michael R. Neuman [b], Richard P. Buck[a],*

[a] Departments of Chemistry and Medicine, University of North Carolina, Chapel Hill, NC 27599, USA
[b] MetroHealth Medical Center, Case Western Reserve University, Cleveland, OH 44109, USA

Abstract

The potentiometric and impedance characteristics of polymeric membranes, based on aliphatic polyurethane (Tecoflex) as a matrix, are described and interpreted by theory and experiments for H^+ and alkali metal ion-sensitive sensors. Both dummy plasticized membranes and proton carrier-loaded membranes can show pH response. The pH response of dummy membranes is due to protonated natural negative sites in the polyurethane matrix. The electrodes with added proton carrier show improved rejection of Li^+, Na^+, and K^+ responses and give useful analytical responses. Optimal performance requires control of negative site concentration by addition of lipophilic salt (e.g. tetraphenylborate derivatives). Impedance analyses show surface-rate semicircles and, depending on the bathing electrolyte solution, appearance of a diffusional Warburg impedance. In addition to these time-dependence surface region effects, changes in the bulk membrane resistance with soaking time can be well correlated with equilibrium water content of plasticized membranes.

1. Introduction

In recent years, there has been an increasing interest in the design and fabrication by solid-state technology of electrochemical sensors that respond to blood gases and ions as well as various organic substrates such as lactate and glucose in blood [1-7]. In these sensors, the poly-meric membranes are cast on solid surfaces with no internal electrolyte solution [8] or with very small volumes of isotonic buffer solution [1,2,9] incorporated into a thin hydrogel layer. The substrate (platform) of these devices is either silicon, alumina or polyimide (Kapton), which often includes integrated electronics. The hydrogel layer (e.g. poly (2-hydroxyethyl methacrylate); poly-HEMA) is loaded with a buffered aqueous solution containing a required

*Corresponding author.

salt that ensures a thermodynamically defined interface.

While several polymeric matrices have been used in macro ion-selective electrodes (conventional type with a large volume of inner solution), poly (vinyl chloride) (PVC) remains one of the best membrane matrices. A few other materials, such as silicone rubber [10], ethylene vinyl acetate [11], and polyimide [12], were proposed as membrane matrices in polymeric ion-selective electrodes. However, reduction of macro- to micro-electrodes has uncovered new problems with these materials. One of the main causes of failure in the miniature probes has been the poor adhesion of these membranes to the substrate surface, leading to electrolyte shunts around the membrane making the sensor inoperative. The lifetime of the sensor can be enhanced significantly with improved membrane adhesion. Thus, the problem of adhesion of different polymeric ion-selective membranes to the substrates (platforms) determines which of many suggested materials is optimal.

Additional polymer materials have been suggested by Meyerhoff and his co-workers [13–16] and by others [17–20]. Some of these materials have improved adhesion to various substrates but may show inferior electrochemical performances when compared to PVC. Carboxylated PVC (PVC-COOH) and aminated PVC (PVC-NH$_2$) have found many applications in biosensor fabrication and in planar ion-selective sensors produced by microelectronic technologies [1–3,7,20,21,23]. In two recent papers Meyerhoff and co-workers [15,16] showed that both biocompatibility and adhesion may be improved by using a mixture of polyurethane (PU) and hydroxylated PVC (PVC-OH) or PU-terpoly(vinyl chloride/vinyl acetate/vinyl alcohol). However, they showed that the response slope and selectivity of potassium selective membranes prepared with pure polyurethane matrix were inferior to those of the standard PVC matrix membranes [15]. In contrast to this observation, we found that aliphatic polyurethane (Tecoflex) have very good analytical performances in Ca^{2+} and K$^+$ selective sensors with normal and reduced amounts of plasticizer [24,25]. Additionally, the membranes with reduced plasticizer content had better adhe-

sive properties, less anion interference, extended lifetime and better biocompatibility [24].

Recently, our work has focused on using unmodified aliphatic PU as a polymeric matrix for pH sensors with possible biomedical applications. We were surprised to find that dummy membranes (matrix + plasticizer) showed pH responses as PVC-COOH or PVC-NH$_2$ do. In this paper, we demonstrate the ion-exchange properties of PU membranes and interpret the ion exchange for H$^+$- and M$^+$-sensitive membrane sensors theoretically and experimentally. The nature of anionic sites in the plasticized PU membranes remains unknown, but they are believed to be residual ionic components from the manufacturing process. Additionally, PU may be protonated by acidic electrolytes, and this phenomenon is responsible for leveling the pH response and introducing anion responses of these plasticized membranes. By incorporating a proton carrier in the PU plasticized membrane, the pH response range is significantly improved. Addition of both controlled sites (tetraphenylborate) and proton carriers produces a superior pH sensor. Impedance analysis was used to understand the behavior of the membranes in various bathing electrolyte solutions, over 2 days of electrolyte contact.

2. Experimental

2.1. Reagents and solutions

For all experiments, deionized water (Barnstead NAN-O-Pure II) and chemicals of p.a. grade were used. Most of the products were supplied by Fluka (Ronkonkoma, NY): H$^+$ carrier ETH 5294 (Chromoionophore I, Ch1, #27086); 2-nitrophenyl octyl ether (o-NPOE, #27086); bis (2-ethyl-hexyl) sebacate (DOS, #84818); potassium tetrakis (4-chlorophenyl) borate (KTpClPB), #60591). The material used for the membrane matrix was aliphatic polyurethane (Tecoflex 85A) supplied by Thermedics Inc. (Woburn, MA). During this work, the following buffer solutions were used for the determination of pH sensitivity and potentiometric selectivities of the electrodes based on PU matrix: (1) citrate–borate buffer with

60 mM Li⁺ ion background; (2) a Tris buffer with 140 mM Na⁺ ion background; and (3) a Tris buffer with 200 mM K⁺ ion background [18]. The pH values of the solutions were adjusted using a hydrogen-selective glass electrode (Orion, Model 91-57). Solutions of alkali metal chlorides (10^{-1}–10^{-5} M) were prepared by serial dilutions from the respective 10^{-1} M stock solution and were used for both potentiometric calibrations and selectivity coefficient determinations.

2.2. Membrane and electrodes

The solvent polymeric membranes were cast as described elsewhere [26] Dummy membranes contained only aliphatic PU, and the plasticizer in a weight ratio of 1:2. Additionally, membranes containing about 3% proton carrier (ETH 5294), and 2% proton carrier plus 1% potassium tetrakis p-chlorophenyl borate respectively, were prepared and investigated. All studied membranes were incorporated into Phillips IS-560 liquid membrane electrode bodies (Moller- Glassblaserei, Zürich, Switzerland) and evaluated for their electroanalytical properties. The inner filling solution varied, depending on the performed experiment. For pH sensors, containing 'normal' membranes (e.g. carrier and added sites), a Tris buffer of pH 7.0 was used throughout.

2.3. EMF measurements

Measurements of emf were performed at room temperature in an air-conditioned laboratory at $25.0 \pm 0.5°C$ with an Orion pH/mV meter (Model 701A) connected to an Orion Model 605 electrode switch box. As a reference electrode, an Orion Model 90-02 Ag/AgCl double junction was used throughout (1.0 M lithium acetate solution in the outer compartment). The measured emf values were corrected for changes in the liquid junction potential according to the Henderson equation [27].

2.4. Selectivity coefficients

The selectivity coefficients, $K_{H,M}$, for dummy membranes were determined by the separate so-

lution method at the 10^{-3} M concentration level [28]. The mean activity coefficients were calculated with the extended Debye-Huckel equation [27] and the measured emf values were corrected for changes in the liquid junction potential according to the Henderson equation [27]. The selectivity coefficients, $K_{H,M}$, for "normal" membranes containing proton carrier and TPB⁻ derivative were evaluated by using the calibration curves obtained with the three buffer solutions listed above.

2.5. Impedance spectra of dummy and "normal" membranes

The bulk and surface resistances (R_{bulk} and R_{surf} respectively) were determined from the impedance plots for each membrane using a Solartron 1250 frequency response analyzer (FRA), a Solartron 1186 electrochemical interface, and a Hewlett-Packard 85B computer. The amplitude of the applied sinusoidal voltage was in all cases 0.25 V. Membranes with 0.5 cm² active surface areas were tested in Philips electrode bodies with an Ag/AgCl double junction reference electrode as an external reference element.

2.6. Equilibrium water content

The equilibrium water content (EWC) of aliphatic PU membranes based on both o-NPOE and DOS as plasticizers was evaluated using the gravimetric method. Dry membranes weighing about 125 mg (w_1) were immersed in the appropriate soaking medium for 5 days, and the swollen membranes were blot-dried with a paper towel and immediately weighed (w_2). Then, the swollen membranes were dried at room temperature to a constant weight (w_3). The EWC values were calculated using the following equation:

$$EWC(\%) = [(w_2 - w_3)/w_2] \times 100$$

The loss of plasticizer from the membrane into the water phase was evaluated from the difference between w_1 and w_3.

3. Results and Discussion

3.1. Properties of PVC Membranes for comparison with PU membranes

Poly (vinyl chloride) (HMW-PVC) has been considered as an inert matrix for the plasticizer to yield a structureless organic membrane that dissolves the neutral carrier [29]. Later, this matrix was found to possess a more heterogeneous structure [30] and to contain various anionic sites. The exact nature and origin of anionic sites in PVC has not been well established in spite of the interesting study and postulates of van den Berg et al. [31]. In order to identify the ionic components in PVC polymer, these authors used impedance measurements, X-ray fluorescence, secondary ion mass spectrometry and X-ray photoelectron spectroscopy. They postulate that sulfate or sulfonate groups act as the anionic sites. Frequency response analysis measurements indicated that these sites may be present in the form of emulsifier residues and are not bound to the polymer matrix [31]. From conductivity measurements [30,31] it was shown that ionic sites gradually leach out from the plasticized membrane. This finding does not prevent carboxylate from remaining immobilized in the membrane, covalently attached to the PVC backbone structure. These anionic sites create permselectivity for cations in ionophore-free membranes and are crucial for the performance of ion sensors [32,33]. Neutral carrier-based ion sensors can be optimized by the addition of lipophilic salt additives such as tetraphenylborate- and tetraalkylammonium derivatives for cation- and anion-selective sensors respectively.

3.2. Dummy PU-based membranes: potentiometric cationic response due to residual sites

Aliphatic PU used in our studies is a commercial product manufactured by Thermedics Inc. (type 80A). It is specially formulated for medical applications and it is synthesised from methylene bis (cyclohexyl) diisocyanate (HMDI), poly (tetramethylene ether glycol) (PTMEG), and 1,4-bu-

tane diol chain extender [34]. Generally, from the manufacturing process of polyurethanes, it is possible to have in the finished product traces of isocyanates, metalloorganic compounds used as catalysts, as well as various surfactants [35].

Dummy membranes (aliphatic PU and plasticizer only; weight ratio of 1:2) show cationic potentiometric responses when placed in solutions of different alkaline or alkaline-earth salts of varying activities. This response is also observed with non-modified PVC [36]. In the case of modified PVC (aminated or carboxylated) the potentiometric response to H^+ and to H^+ or M^+ respectively, is clearly understandable and it was theoretically and experimentally described [13,22,37].

Surprisingly, PU shows a much better selectivity than PVC-COOH for H^+ over Na^+, K^+, Li^+, NH_4^+ and Ca^{2+} [22]. For an electrode containing a dummy membrane of PU-NPOE, the following selectivity coefficients ($-\log K_{H,M}$) were calculated: 2.08, 1.95, 2.19, 2.04 and 2.47 respectively. This much better potentiometric response to protons (pH linear range between 3 and 5; slope of 43.3 mV pH^{-1}) is probably due to the presence of natural protonated sites in PU. The process of protonation by solvent acid to form a conjugated acid of urethane is a predominant factor in the dissociation [38]. Under extreme conditions (concentrated acid, high temperature and pressure), the dissociation proceeds by eliminating isocyanate from the positively charged conjugated acid of urethane, which donates a proton to the solvent molecule (a termolecular mechanism):

(I)

$$\rightleftharpoons S^+H_2 + R_1\text{-}N\text{=}C\text{=}O + R_2\text{-}OH + S^-$$
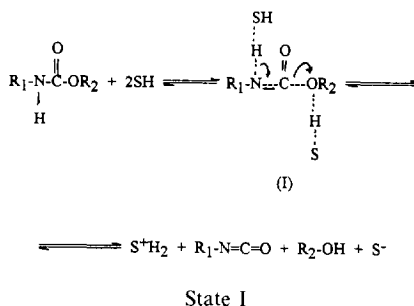
State I

In state I, simultaneously, one solvent S acts as a base to accept a proton and the other acts as an acid to donate a proton. By the shift of an

electron pair, state **I** may dissociate to a very
small extent, but enough to create negative sites
for protonation by ion exchange in the system.
The latter could be responsible for H^+ potentio-
metric response. At pH < 3 the anion effect inter-
ference (Donnan failure) was observed as the case
of aminated PVC or proton carrier-based mem-
branes [37]. This process is protonation of nitro-
gen or oxygen atoms to create NH^+X^- from the
extracted HX.

3.3. Water uptake by dummy aliphatic PU membranes

We found that the aliphatic PU takes up water
as other polymers do [21,39–43]. The water up-
take depends on the polarity of the plasticized
membrane as well as on the aqueous solvent
(solution) used to hydrate the membrane. Higher
EWC values were observed in pure water, when a
polar solvent, such as o-NPOE, was used as the
solvent plasticizer ($\varepsilon\varepsilon_0 = 23.9$). With DOS
($\varepsilon\varepsilon_0 = 3.9$) the water uptake was less from pure
water than from 10^{-3} M NaCl solution (Table 1).
Interesting is the fact that a non-polar solvent
such as DOS showed poor "compatibility" with
the aliphatic PU. Freshly prepared membranes
were "oily" and this plasticizer was exuded when
the membrane was placed in contact with aqueous
solutions. The exuded plasticizer surface layer was
greater for DOS than for o-NPOE plasticizer
(Table 1). Confirmation came from dummy mem-
branes with DOS that showed a very high surface
layer resistance as evaluated by impedance analy-
sis (see below). These membranes also showed
unstable potentiometric readings. This effect was
also found in membranes containing a proton
carrier, namely the phenoxazine derivative ETH
5294. The high surface membrane resistance
could be and was, reduced significantly by
adding the lipophilic salt additive potassium te-
trakis (4-chlorophenyl) borate in our optimal
compositions.

3.4. Impedance analysis of PU dummy membranes

Impedance analysis with dummy membranes

showed that o-NPOE-based membranes revealed
a second, so-called "kinetic", semicircle at
medium frequencies lying between the geometric
bulk semicircle at highest frequencies and the
Warburg impedance at lowest frequencies. As was
shown by Buck [44], the second semicircle occurs
for two well-known reasons: (i) slow, potential-
dependent transfer rates for ions that cross the
interface; and (ii) slow, potential-dependent trans-
fer of ions through a high-resistance (relative to
bulk) surface film. Both processes cause a second
semicircle that disappears when surface rates be-
come fast compared to bulk bathing electrolyte
transport rates. Both processes are equivalent to a
surface resistance (R_{surf}) in parallel with a low-fre-
quency capacitance, approximating the double-
layer value at each membrane/electrolyte interface
[32].

Because of the very high surface resistance of
PU-DOS membranes, reflected in the unstable
potential measurements as well, we investigated
only the polar membranes with o-NPOE as plas-
ticizer (polymer:plasticizer ratio of 1:2 by
weight). Interesting is the fact that in many situ-
ations (different symmetric concentrations of
bathing electrolyte) the second semicircle dimin-
ished or disappeared, but in all cases the 45°
line, indicating a Warburg impedance (current is
controlled by diffusion of the counterions from
bathing electrolyte), was observed (see Fig. 1
(a–c)). Because counterions must be combined
with sites, this feature indicates that mobile sites
are present in dummy membranes, possibly from
intrinsic charged impurities, and that concen-
tration changes of sites, and corresponding
diffusion, may occur. Alternative explanations
seem less likely: (1) a porous surface layer
through which solution species diffusion occurs;
(2) an organic layer or site-free layer extracts
whole salts that then diffuse to the bulk mem-
brane.

The size of the bulk resistance depends on the
concentration of the bathing electrolyte. During
48 h soaking (symmetric electrolyte concentration,
i.e. 0.1 M or 0.01 M NaCl) the bulk resistance
decreased gradually with elapsed time, as shown
in Fig. 2. In an acidic medium (0.1 M NaCl of
pH 2.0), the bulk resistance of the dummy mem-

brane was about 25% less than in the neutral pH range. This may be explained by HX extraction and by protonation of the PU in the membrane, creation of positive sites and anions X^- that lower the membrane resistance.

In an asymmetric bathing solution (internal, 10^{-3} M; external, H_2O), the impedance plane plots consistently showed two semicircles (bulk and surface resistances) with the first one approximately constant (3.2 MΩ) and the second (surface resistance) progressively increasing up to 25 MΩ during a 48 h soaking period (Fig. 3). This can be explained by the leaching of sites from the surface region.

3.5. Membranes containing a proton carrier

Addition of ETH5294 chromoionophore I (a proton carrier) to fresh, unsoaked membranes, decreased initial bulk resistance to about a half, and this value remained approximately constant during the 48 h soaking period. The second semicircle showed a high resistance for the first 3 h and then it decreased dramatically. After 24 h of membrane soaking the surface resistance disappeared and was replaced with a Warburg impedance (Fig. 4). We can surmise that the presence of ionophore and counterions (bound together as $ChlH^+$) retains the original mobile sites. The ionophore–counterion sites are much more hydrophobic species and so are favored in the membrane. Extraction of sites into bathing

Table 1
Equilibrium water content (EWC%) and loss of plasticizer (LP%) from dummy PU-based membranes [a]

	PU/o-NPOE membrane	PU/DOS membrane
EWC (%)		
in H_2O	2.0	0.4
in 10^{-3} M NaCl	0.9	2.2
in 10^{-1} M NaCl	0.3	–
LP (%)		
in H_2O	0.06	5.1
in 10^{-3} M NaCl	0.18	1.3
in 10^{-1} M NaCl	0.22	–

[a] All values are the averages of two measurements.
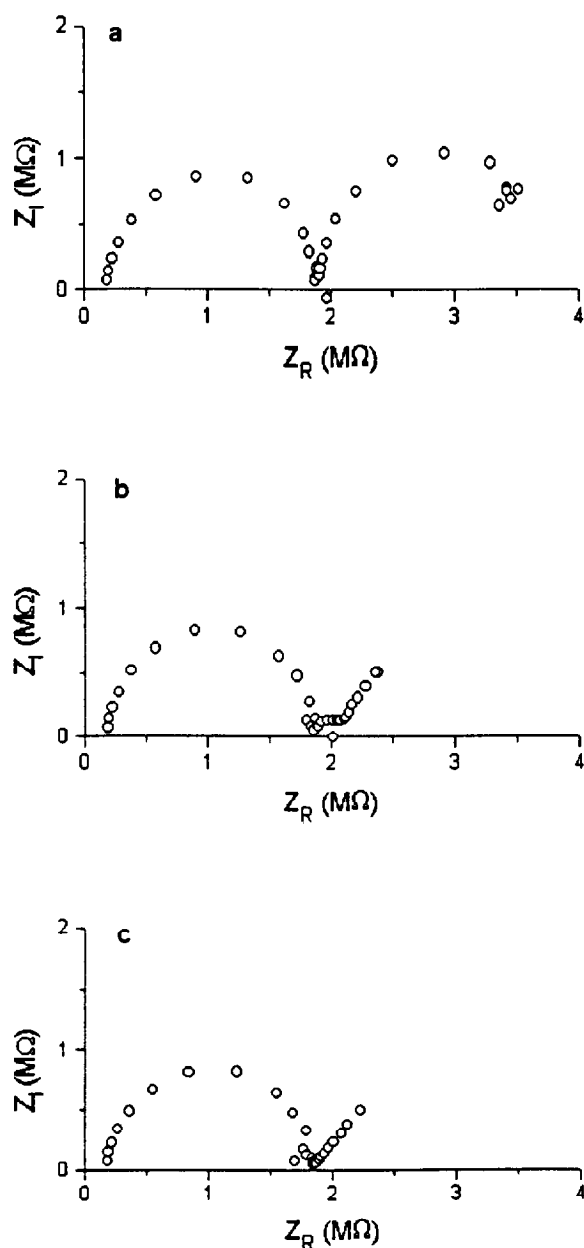
Fig. 1. Impedance plane plots of a dummy membrane made with aliphatic PU and o-NPOE as plasticizer (wt. ratio, 1:2); frequency range from 65 000 Hz to 0.1 Hz; symmetric bathing solution of 0.1 M NaCl. (a) after 2 h soaking; (b) after 3 h soaking; (c) after 4 h soaking.

solutions as H^+Site^- occurs from dummy membranes because partitioning into membranes is not highly favored. Thus, our hypothesis that
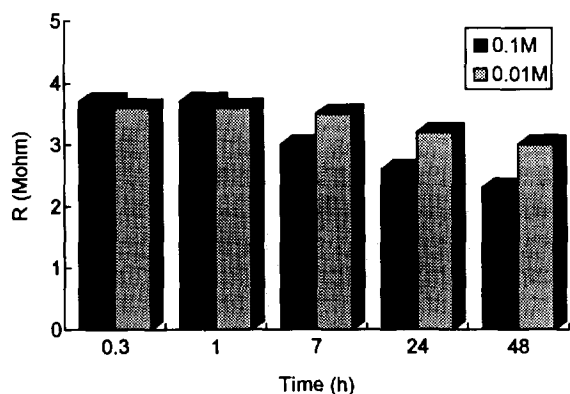
Fig. 2. Variation of the bulk resistances of dummy membranes (PU-NPOE) during a 48 h soaking period in symmetric electrolyte solutions.

H^+ Site$^-$ does extract from dummy membranes is realistic.

The electrode containing the proton carrier ETH5294 (Ch1) in its PU-based membrane showed a linear pH response in the range 4–10, but the emf readings were not stable enough for practical use, and the electrode drifted badly in the alkaline pH region. Subsequent addition of potassium tetrakis (*p*-chlorophenyl) borate had three important advantages, namely, increasing the stability of potential measurements, reducing the membrane resistance and reducing the anion interference effect. As shown in Fig. 5, the electrode with "normal" membrane composition, i.e. polymer–plasticizer–ion carrier–lipophilic salt,
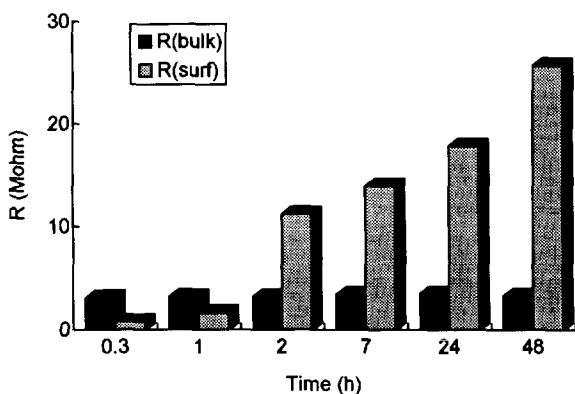
Fig. 3. Variation of the bulk resistance and surface resistance of a PU-NPOE membrane with soaking time; asymmetric bathing solutions (internal, 10^{-3} M NaCl; external, H_2O).
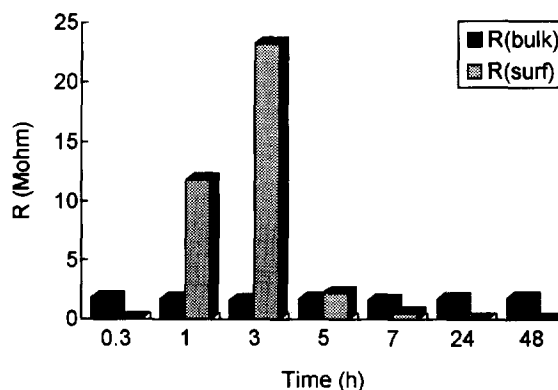
Fig. 4. Variation of the bulk resistance and surface resistance of a PU-NPOE-Ch1 membrane with soaking time; symmetric bathing solutions of 0.1 M NaCl.

displayed a linear pH response in the range pH 4–11, with near-Nernstian sensitivity. The impedance plots of "normal" membranes with *o*-NPOE as a plasticizer showed one very small semicircle (bulk resistance of about 140 kΩ) and relative large surface resistance (about 5 MΩ) after 2–3 h of soaking in symmetric bathing electrolyte (0.1 M NaCl). Leaching of the plasticizer from the membrane surface region again produced site-free surface resistive films which have, as a consequence, the appearance of the second "kinetic" semicircle. As in the case of dummy PU membranes, the size of the second, surface-rate
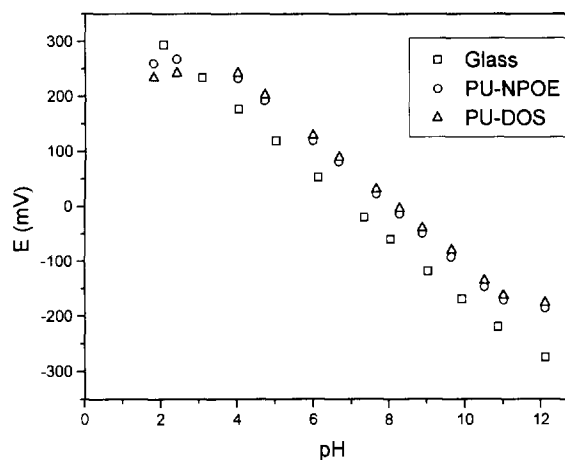
Fig. 5. pH potentiometric response of PU-based membranes containing chromoionophore I (Ch1) as a proton carrier and lipophilic salt additive (KTpClPB).

Table 2
Analytical performance of pH sensors based on aliphatic PU
as matrix and two different plasticizers (H⁺ carrier: ETH5294
phenoxazine derivative; salt additive: KTpClPB)[a]

Parameter	Electrode 1 (o-NPOE)	Electrode 2 (DOS)
pH range	4-11	4-11
Intercept (mV)	464.7 ± 9.8	475.5 ± 10.2
Slope (mV pH⁻¹)	58.1	57.8
Bulk membrane resistance (MΩ) (after 24 h soaking in pH 7, Tris)	0.125	13.1
Selectivity coefficients ($-\log K_{H,M}$)		
Li⁺	10.7	10.2
Na⁺	10.6	10.4
K⁺	10.6	10.4
Potential reproducibility (mV)	0.3	1.2
Drive (mV h⁻¹)	0.05	0.12

[a] Data based on four electrodes of each type.

semicircle depends on the polarity of the plasticizer as well as on the concentration of the bathing electrolyte. The same behavior was observed with "normal" DOS-based membranes. In this later case, the bulk resistance was much higher (about 7 MΩ); the surface resistance varied continuously and reached a value of 12.9 MΩ after 24 h soaking time.

Table 2 lists additional data showing the good analytical performance of pH sensors based on aliphatic PU as a polymeric matrix. Both potential reproducibility and drift were smaller for o-NPOE-based relative to DOS-based membrane electrodes. These membranes will be investigated in planar microsensors for biomedical applications and the results reported later.

4. Conclusions

This work shows that aliphatic PU contains mobile and fixed residual sites which are responsible for the H⁺ and M⁺ potentiometric response of plasticized membranes in the solvent polymeric membrane type of sensor. The dummy membranes (PU-plasticizer) show much better responses to H⁺ than towards alkali and alkaline-earth cations. The relatively wide range, but sub-Nernstian, pH response of dummy mem-

branes is attributed to the ion exchange of protons into the PU. In the acidic medium, however, acid extraction (with anions) produces sub-Nernstian responses as predicted by theory. The electrodes with proton carrier-containing membranes and added mobile sites show good pH response, potential reproducibility and small potential drift. Both dummy membranes and "normal" membranes (containing proton carrier and added sites) show, by low frequency impedance measurements, surface-rate (so called "kinetic") semicircles and can also show a Warburg impedance which occurs when the current is controlled by diffusion of different ionic species into the membrane phase. Detailed interpretation postulates different extents of mobile site extraction depending on the hydrophobicity of the counterion-carrier complex compared to uncomplexed counterions, as well as differing dielectric constants of plasticizers.

References

[1] V.V. Cosofret, M. Erdosy, T.A. Johnson, R.P. Buck, R.B. Ash and M.R. Neuman, Anal. Chem., 67 (1995) 1647.
[2] E. Lindner, V.V. Cosofret, S. Ufer, R.P. Buck, R.P. Kusy, R.B. Ash and H.T. Nagle, J. Chem. Soc., Faraday Trans., 89 (1993) 361.
[3] H.S. Yim, C.E. Kibbey, S.C. Ma, D.M. Kliza, D. Liu, S.B. Park, C.E. Torre and M.E. Meyerhoff, Biosens. Bioelectron., 8 (1993) 1.
[4] J. Janata, Principles of Chemical Sensors, Plenum Press, New York, 1989.
[5] C.C. Liu and Z.R. Zhang, Selective Electrode Rev., 14 (1992) 147.
[6] Q. Wu, K.M. Lee and C.C. Liu, Sens. Actuat. B, 13-14 (1993) 16.
[7] M.R. Neuman, R.P. Buck, V.V. Cosofret, E. Lindner and C.C. Liu, IEEE-EMBS, 13 (1994), 409.
[8] P. Bergveld and A. Sibbald, Analytical and biomedical applications of ion-sensitive field effect transistors, in G. Svehla (Ed.), Wilson and Wilson's Comprehensive Analytical Chemistry, Vol. 23, Elsevier, Amsterdam, 1988.

[9] V.V. Cosofret, E. Lindner, T.A. Johnson and M.R. Neuman, Talanta, 41 (1994) 931.

[10] D.N. Reinhoudt and P.D. van der Wal, Proc. ACS Div. Polym. Sci., Vol. 64, Spring Meeting, Atlanta, GA, 1991, p. 296.

[11] A. El-Jammal, A.A. Bouklouze, G.J. Patriarche and G.D. Christian, Talanta, 38 (1991) 929.

[12] G.S. Cha and R.B. Brown, Sens. Actuat., B1 (1990) 281.

[13] S.C. Ma, N.A. Chaniotakis and M.E. Meyerhoff, Anal. Chem., 60 (1988) 2293.

[14] G.S. Cha and M.E. Meyerhoff, Talanta, 36 (1989) 271.

[15] G.S. Cha, D. Liu, M.E. Meyerhoff, H.C. Cantor, A.R. Midgley, H.D. Goldberg and R.B. Brown, Anal. Chem., 63 (1991) 1666.

[16] D. Liu, M.E. Meyerhoff, H.D. Goldberg and R.B. Brown, Anal. Chim. Acta, 274 (1993) 37.

[17] T. Satchwill and D.J. Harrison, J. Electroanal. Chem., 202 (1986) 75.

[18] V.V. Cosofret, E. Lindner, R.P. Buck, R.P. Kusy and J.Q. Whitley, J. Electroanal. Chem., 345 (1993) 169.

[19] E. Lindner, V.V. Cosofret, R.P. Kusy, R.P. Buck, T. Rosatzin, U. Schaller, W. Simon, J. Jeney, K. Toth and E. Pungor, Talanta, 40 (1993) 957.

[20] V.V. Cosofret, E. Lindner, R.P. Buck, R.P. Kusy and J.Q. Whitley, Electroanalysis, 5 (1993) 725.

[21] V.V. Cosofret, M. Erdosy, R.P. Buck, W.J. Kao, J.M. Anderson, E. Lindner and M.R. Neuman, Analyst, 119 (1994) 2283.

[22] V.V. Cosofret, R.P. Buck and M. Erdosy, Anal. Chem., 66 (1994) 3592.

[23] V.V. Cosofret, M. Erdosy, T.A. Johnson, D.A. Bellinger, R.P. Buck, R.B. Ash and M.R. Neuman, Anal. Chim. Acta, 314 (1995) 1.

[24] E. Lindner, V.V. Cosofret, S. Ufer, R.P. Buck, W.J. Kao, M.R. Neuman and J.M. Anderson, J. Biomed. Mater. Res., 28 (1994) 591.

[25] P. D'Orazio, I. Laios and G.N. Bowers, Jr., Development of a reference method for serum ionized calcium: understanding the requirements of the measurement system, in Electrolytes, Blood Gases, and Other Critical Analytes: the Patient, the Measurement and the Government, Vol. 14, Proc. Int. Symp., Chatham, MA, May 17–20, 1992, pp. 21–34.

[26] G.J. Moody, R.B. Oke and J.D.R. Thomas, Analyst, 95 (1970) 910.

[27] P.C. Meier, D. Ammann, W.E. Morf and W. Simon, in J. Koryta (Ed.), Medical and Biological Applications of Electrochemical Devices, Wiley, Chichester, 1980, pp. 13–91.

[28] E. Pungor, K. Toth and A. Hrabeczy-Pall, Pure Appl. Chem., 51 (1979) 1913.

[29] W.E. Morf, in Studies in Analytical Chemistry, Vol. 2, Elsevier, Amsterdam, 1981.

[30] G. Horvai, E. Graf, K. Toth, E. Pungor and R.P. Buck, Anal. Chem., 58 (1986) 2735.

[31] A. van den Berg, P.D. Van den Wal, M.S. Ptasinska, E.J.R. Sudholter, D.N. Reinhoudt and P. Bergveld, Anal. Chem., 59 (1987) 2827.

[32] K. Toth, E. Graf, G. Horvai, E. Pungor and R.P. Buck, Anal. Chem., 58 (1986) 2741.

[33] E. Lindner, E. Graf, Z. Niegreisz, K. Toth, E. Pungor and R.P. Buck, Anal. Chem., 60 (1988) 295.

[34] Thermedics, Inc., Tecoflex Resin: Material Description and Specification, Woburn, MA, 1992.

[35] D.J. David and H.B. Staley, Analytical Chemistry of Polyurethanes, Wiley-Interscience, New York, 1969.

[36] S. Bouen, J. Dale and W. Lund, Anal. Chim. Acta, 185 (1986) 347.

[37] R.P. Buck, V.V. Cosofret and E. Lindner, Anal. Chim. Acta, 282 (1993) 273.

[38] T. Mukaiyama and Y. Hoshino, J. Am. Chem. Soc., 78 (1956) 1946.

[39] A.D.C. Chan, X. Li and D.J. Harrison, Anal. Chem., 64 (1992) 2512.

[40] Z. Li, X. Li, S. Petrovich and D.J. Harrison, Anal. Methods Instrum., 1 (1993) 30.

[41] D.J. Harrison, X. Li and S. Petrovich, Water and ion-selective electrode membrane, in P.G. Edelmen and J. Wang (Eds.), Biosensors and Chemical Sensors–Optimizing Performance Through Polymeric Materials, American Chemical Society, Washington, DC, 1992.

[42] W.T.K. Stevenson and M.V. Seften, J. Appl. Polym. Sci., 36 (1988) 1541.

[43] J. Anzai and C.C. Liu, Polym. Commun., 31 (1990) 375.

[44] R.P. Buck, Ion-Selective Electrode Rev., 4 (1982) 3.

Accumulation and voltammetric determination of complexed metal ions at zeolite-modified sensor electrodes

Chen Bing, Lars Kryger*

School of Science, National Institute of Education, Nanyang Technological University, 469 Bukit Timah Road, Singapore 1025, Singapore

Abstract

Chemically modified electrodes based on zeolite-containing graphite pastes were constructed and evaluated as sensor electrodes for the voltammetric determination of traces of metallic species in solution. Zeolite molecular sieves with pore sizes of 3, 4, 5, and 10 Å were all suitable for chemical deposition and subsequent voltammetric quantitation of traces of Cu(II), Cd(II), and Zn(II). The highest sensitivity was obtained using the zeolite with the 10 Å pore size. The detection limit obtained for Cu(II) was 0.3 μM following a 2 min chemical deposition. The detection limits for Cd(II) and Zn(II) following a 4 min chemical deposition were 87 nM and 145 nM, respectively. The effects on the zinc signal of coexisting metallic species in the ammonia deposition medium were studied. While the addition of Hg(II) gave rise to increasing zinc signals, the addition of Ag(I), Cu(II), Cd(II), Ni(II), and Co(II) resulted in decreasing zinc signal amplitudes. Most notably, the magnitude of the interference from these latter metal ions correlated well with the coordination numbers of their ammonia complexes. Thus the electrode acted as a device which was sensitive to the size and shape of the interfering metal complex.

Keywords: Chemically modified electrodes; Voltammetric determination; Zeolite

1. Introduction

Chemically modified electrodes (CMEs) [1] with chemically selective groups attached to their surfaces are potentially useful as sensor electrodes in electroanalysis, in particular in conjunction with electrochemical stripping procedures where they offer the possibility for introducing an additional dimension of selectivity in the preconcentration

---

* Corresponding author. Present address: Department of Chemistry, Århus University, Langelandsgade 140, DK-8000 Århus C, Denmark.

step [2–11]. In such procedures, the analyte is first accumulated on the electrode via a non-electrochemical interaction with the modifier, e.g. a covalent linkage [2], complexation [3–7], or ion exchange [8–11], and is subsequently quantitated by a voltammetric approach. Cage structures, such as zeolites, which may act as ion exhangers, and which may exhibit selectivity according to molecular size and shape, offer interesting possibilities as electrode modifiers [12,13]. However, while several reports on mechanistic studies of zeolite-modified electrodes have been published [14–18], only a few workers have investigated the

analytical possibilities of such electrodes. Hernandez et al. [10] have constructed an Hg(II)-sensitive electrode based on a natural zeolite obtained from volcanic rock. Furthermore, Wang and Martinez [11] have described the accumulation and voltammetric determination of Ag(I) at a carbon-paste electrode modified with the zeolite Linde 4A, with an effective pore diameter of 4 Å. In the present investigation, the possibilities afforded by zeolite CMEs with smaller and larger pore diameters were studied. The electrodes were constructed using graphite paste modified with four different zeolites having pore diameters of 3, 4, 5, and 10 Å. Cu(II), Cd(II), and Zn(II) were chosen as target analytes. The study included a series of experiments in which suitable experimental conditions for the determination of the metal ions were established, including the composition of the electrode matrix, and of the solutions for chemical deposition, voltage scanning and regeneration of the electrode surface. Furthermore, the sensitivity and detection limits for the target analytes were evaluated. Finally, since the accumulation of metallic species in the zeolite cage structure might potentially reflect the size and shape of these species, experiments were carried out to study whether such effects could be observed.

2. Experimental

2.1. Apparatus

Voltammetric measurements were carried out using a computerized potentiostat/galvanostat (model 273A, EG&G, Princeton Applied Research with model 270/250 Research Electrochemistry software 4.0). The three-electrode assembly included a 50 ml glass cell, a saturated calomel electrode, a platinum wire counter electrode, and a rotating disk electrode assembly (model 616, EG&G, Princeton Applied Research).

2.2. Equipment, chemicals, and reagents

Ultrafiltered deionized water (model D 4755, Barnstead, USA) was used for all solutions of complexing agents and electrolytes. Dilute solutions (100 mg l^{-1} or lower) of metal ions were prepared daily by dilution from 1000 mg l^{-1} stock solutions. Before use, flasks and containers were soaked in 6 M HNO_3 for at least 24 h, then rinsed with deionized water. Molecular sieves, types 3A, 4A, 5A, and 13X (Union Carbide, BDH) were used as received. Extra-pure graphite fine powder (Merck), silicone oil DC 350 (Merck), DC 710 (Fluka) and nujol oil (Specac, UK) were used as bonding agents for the graphite pastes.

2.3. Preparation of electrodes

Mixtures (1:1 and 1:2 (w/w)) of the zeolite modifier and graphite were prepared in a mortar by grinding and mixing 2.5 g portions of zeolite molecular sieve pellets with 2.5 g and 5 g of graphite powder, respectively. Graphite pastes, 1:1 and 1:2, were prepared from these powders by further mixing with silicone or nujol oils; 3 ml and 4 ml of the oil were added to the 1:1 and 1:2 mixtures, respectively. Plain (unmodified) carbon paste was prepared in the same fashion from 5 g of plain graphite powder and 3 ml of silicone oil. Electrode bodies were made by removing the tips from disposable 1 ml polyethylene syringes using a razor blade, thus producing tubes (0.5 cm i.d.). The CMEs were prepared by filling the tubes with modified or plain graphite paste and polishing the surfaces on paper until a shiny surface appeared. The CMEs were attached to the disk arbor via rubber tubing filled with graphite paste using a copper wire inserted in both pastes to establish electrical contact between the CME and the rotating electrode assembly.

2.4. Analytical procedure

The analytical procedure included chemical deposition of the analyte in question (by exposure of the electrode surface to a solution of the analyte), transfer of the electrode to the electrochemical cell, and voltammetric quantitation of the deposit. Furthermore, in order to regenerate the electrode surface, the CME was finally exposed to a purging solution under open-loop conditions. Prior to the voltammetric measurements, the electrolytic medium was deaerated for at least 5 min using

nitrogen gas which had first been passed through a vanadous chloride scrubber solution then through 50 ml of the electrolyte solution. During the voltammetric measurements, a flow of nitrogen was passed over the electrolytic medium. Several variations of this procedure were evaluated, using different materials and media for the above-mentioned steps. These included the construction of CMEs using representative combinations of graphite powder, and the different zeolite molecular sieves and bonding agents. Furthermore, the effects on sensitivity of a CME conditioning programme were studied. This programme included a 30 s exposure of the CME to 0.1 M HNO_3 under convective conditions then exposure to blank ammonia medium (pH 9) followed by a CME polarization programme which included at least five cyclic scans of the CME potential beginning and ending at $+0.6$ V and shifting at a vertex potential of -1.2 V.

The experimental conditions for chemical deposition and voltammetric quantitation were optimized for Cu(II), Cd(II), and Zn(II) separately using chemical deposition from and square wave voltammetric scanning in several combinations of media. Voltammetric scanning was carried out first in 0.1 M HNO_3 mixed with increasing amounts of concentrated ammonium hydroxide then in Na_2HPO_4–NaH_2PO_4 buffers. Chemical depositions were carried out from dilute solutions of the three metal ions in the above-mentioned media. Regeneration of the CME after chemical deposition and voltage scanning was also attempted by exposing the CME surface to different media including H_2O, 0.05 M Na_2CO_3, HOAc–NaOAc (pH 4.2), and 0.1 M HNO_3.

In addition, the effects of variations in the square-wave voltage excitation frequency, and hence the scan rate, were studied, using constant values for the scan increment (2 mV) and for the amplitude of the superimposed square wave (50 mV). Moreover, the suitability of procedures which included a constant potential reduction step, carried out in unspiked electrolytic medium, between the chemical deposition and the voltage scanning quantitation was investigated.

Finally, the effects of Ag(I), Cu(II), Cd(II), Hg(II), Ni(II), and Co(II), on the CME accumula-

tion of Zn(II) from ammonia medium were studied.

3. Results and discussion

3.1. Sensitivity to Cu(II)

The experiments showed that all types of CME could be used for the chemical accumulation and voltammetric quantitation of Cu(II). However, since the highest sensitivity was obtained using silicone oil DC710 and the 1:1 mixture of graphite powder and zeolite 13X, this type of CME was chosen for the remaining part of the study. Experiments also revealed that the highest sensitivity was obtained if the CME was conditioned using the above-mentioned acid/ammonia/polarization programme. Thus the exchange of H^+ ions (in ZO^-H^+) or NH_4^+ ions (in $ZO^-NH_4^+$) with Cu^{2+} ions was more efficient than the exchange of Na^+ ions (in ZO^-Na^+) with Cu^{2+} ions. Fig. 1 shows the cyclic square-wave voltammogram obtained using the conditioned CME following exposure to ammonia buffer spiked with Cu^{2+}. Analogous experiments with unmodified electrodes and with unspiked media resulted in featureless voltammograms. The most efficient accumulation of Cu^{2+} (judged by the magnitudes of the currents resulting from both the reduction and oxidation of the copper deposit) was achieved for $4 < pH < 8$ with a maximum at pH 6. As a consequence of these observations, the remaining part of the study was carried out with chemical deposition from Na_2HPO_4–NaH_2PO_4 buffer (pH 6). While the reduction of the copper deposit invariably gave rise to single peaks, the oxidations were typically more complex, with double peaks, presumably because of stepwise oxidation (oxidation states 1 and 2) of the metallic copper generated by the reduction. Consequently, the reduction signal was chosen for quantitation. Since the maximum reduction current was obtained when ammonia buffer (pH 9) was used as a medium for voltage scanning, this medium was chosen for the remaining part of the study. The experiments also revealed that the analyte deposit formed by chemical deposition could be partially
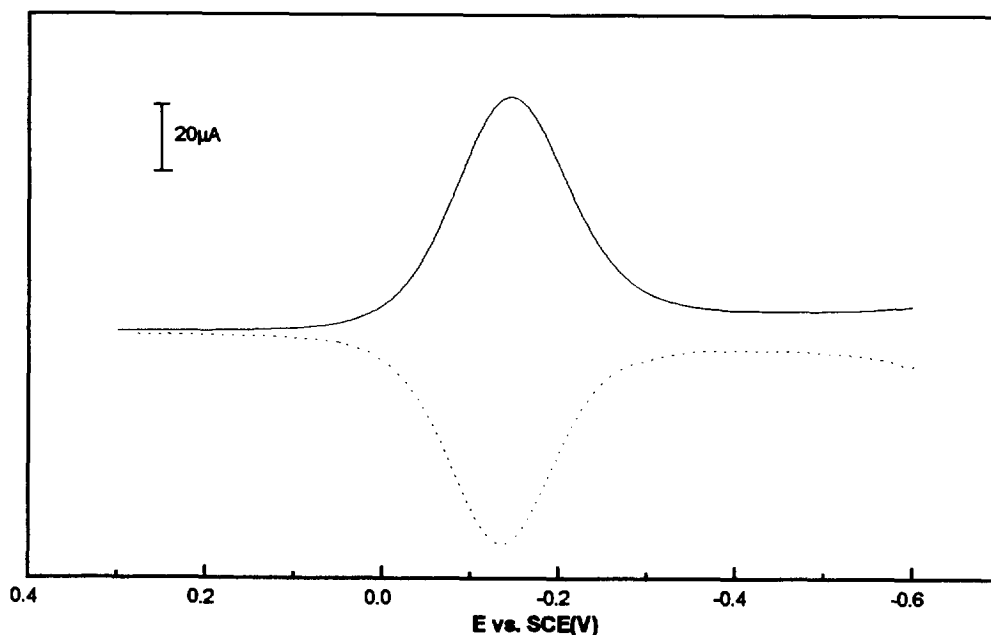
Fig. 1. Cyclic square-wave voltammogram obtained after 1 min open-loop exposure of the CME to ammonia buffer (pH 9) spiked with 0.002 M Cu(II), (solid curve, cathodic scan; broken curve, anodic scan). (Medium for voltammetry, ammonia buffer (pH 9); square-wave frequency, 60 Hz; pulse amplitude, 50 mV; scan increment, 2 mV.)

dissolved by long-term exposure of the CME to H_2O, to 0.05 M Na_2CO_3, or to HOAc–NaOAc (pH 4.2). However, since a 40 s exposure to 0.1 M HNO_3 removed all evidence of previous chemical deposition/voltage scanning cycles, this purging solution was used for further experiments, such that a single CME surface could be used for several deposition/scanning cycles. Experiments in which the square-wave frequency was gradually increased (10, 20, 30, 60, and 100 Hz) showed that the width of the reduction signal increased with frequency, leading to poorer resolution. The reduction peak current, on the other hand, initially increased and reached a maximum at 30 Hz. Going to higher frequencies, and hence to higher scan rates, resulted in a gradual decrease of the current, presumably due to non-exhaustive reduction of the deposit. In view of these observations, a frequency of 30 Hz was chosen for the remaining part of the study. Table 1 summarizes the experimental conditions for the determination of Cu(II) thus established. Using these conditions, the copper reduction peak current increased with deposition time and, as shown in Fig. 2, with

concentration of Cu(II). Moreover, when the voltammogram obtained after CME regeneration (broken curve in Fig. 2) was used as a reference baseline, the baseline-corrected signal amplitudes obtained in the standard addition experiment correlated well with the added concentrations of Cu(II) (correlation coefficient, 0.9992). The limit of detection for a 2 min chemical deposition was estimated from eight consecutive analyses of a solution which contained 30 μM Cu(II). The mean value and 95% confidence limits for the analytical signal obtained under these conditions were 28.05 μA $\pm$ 0.30 μA; thus the detection limit was estimated as $30 \times 0.30/28.05$ μM, which equals 0.3 μM.

3.2. Sensitivity to Cd(II)

Table 1 gives the experimental conditions for the determination of Cd(II), as established by optimizing the cadmium signal by variations of the media used for chemical deposition and voltage scanning. In contrast to the observations for Cu(II), no well-developed reduction peak for

Table 1
Experimental conditions for the determination of Cu(II), Cd(II), and Zn(II) using the modified electrode[a]

Experimental conditions	Cu^{2+}	Cd^{2+}	Zn^{2+}
Deposition medium	Phosphate buffer, pH 6	Ammonia buffer, pH 9	Ammonia buffer, pH 9
Voltage scanning medium	Ammonia buffer, pH 9	Phosphate buffer, pH 6	Phosphate buffer, pH 6
CME regeneration medium, time	0.1 M HNO_3, 40 s	0.1 M HNO_3, 40 s	0.1 M HNO_3, 40 s
Analytical electrode process	Reduction	Oxidation[b]	Oxidation[c]
Square-wave frequency (Hz)	30	60	60

[a] Graphite paste composition: 2.5 g graphite powder, 2.5 g zeolite 13X, 3 ml silicone oil DC 710.
[b] After reduction of the deposit for 120 s at -1200 mV.
[c] After reduction of the deposit for 150 s at -1300 mV.

the cadmium deposit was observed, regardless of the combination of media chosen. Consequently, the procedure for Cd(II) was modified to include an additional step in which the cadmium deposit was reduced to oxidation state 0 immediately after transfer of the CME from the cadmium-containing sample to a fresh solution of electrolyte. Quantitation of the analyte was subsequently carried out by oxidation of the deposit. Using these conditions, the cadmium oxidation peak current increased with deposition time, and, as shown in Fig. 3, with concentration of

Cd(II). Moreover, the signal amplitudes obtained in the standard addition experiment correlated well with the added concentrations of Cd(II) (correlation coefficient, 0.9998). The limit of detection for a 4 min chemical deposition was estimated from 10 consecutive analyses of a solution which contained 600 μg 1^{-1} Cd(II). The mean value and 95% confidence limits for the analytical signal obtained under these conditions were 1.84 μA $\pm$ 0.03 μA; thus the detection limit was estimated as 600 × 0.03/1.84 μg 1^{-1}, equal to 87 nM.
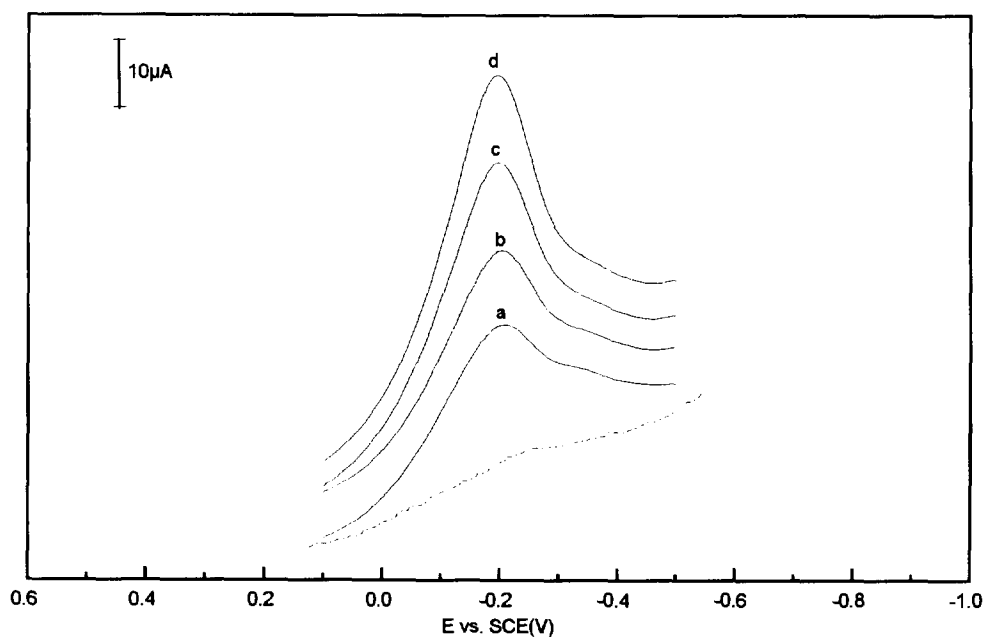
Fig. 2. Standard addition experiment for Cu(II). (Chemical deposition time, 5 min.) Curve a, 0.30 mg 1^{-1} Cu(II); curve b, 0.50 mg 1^{-1} Cu(II); curve c, 0.70 mg 1^{-1}; curve d, 1.00 mg 1^{-1} Cu(II). Broken curve, baseline.
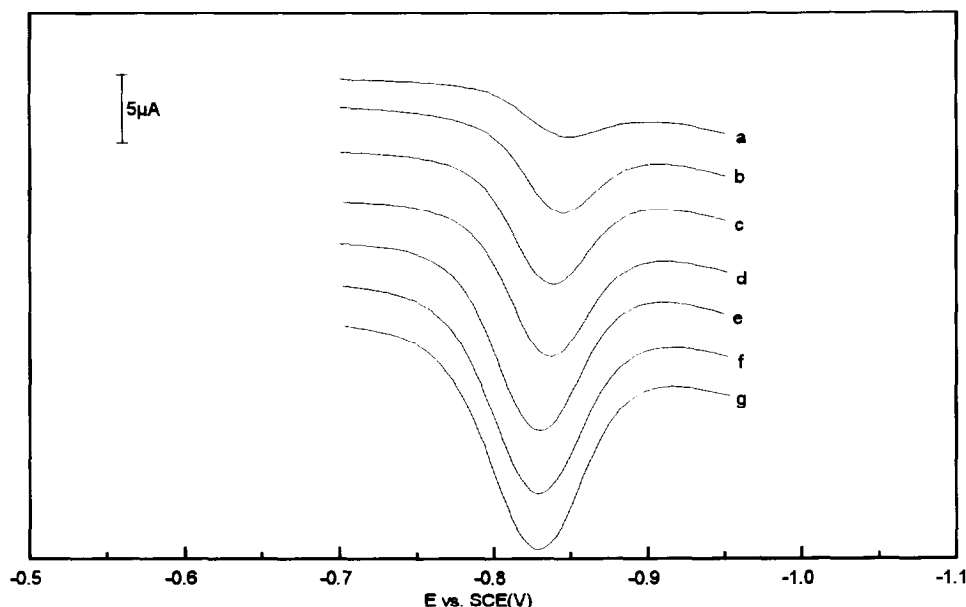
Fig. 3. Standard addition experiment for Cd(II). Concentrations: curve a, 0.2 mg l^{-1}; curve b, 0.4 mg l^{-1}; curve c, 0.6 mg l^{-1}; curve d, 0.8 mg l^{-1}; curve e, 1.2 mg l^{-1}; curve f, 1.6 mg l^{-1}; curve g, 2.0 mg l^{-1}. (Chemical deposition time, 5 min; electrolytic reduction, 150 s.)

3.3. Sensitivity to Zn(II)

Suitable experimental conditions for the determination of Zn(II) are given in Table 1. As for Cd(II), regardless of the combination of media, no well-developed reduction signal was observed for the zinc deposit. Therefore the voltammetric quantitation of Zn(II) was preceded by a reduction step, and the oxidation signal was used as the analytical response. Using these conditions, the zinc oxidation peak current increased with deposition time and with concentration of Zn(II). Furthermore, the signal amplitudes obtained in a standard addition experiment (0.00, 0.20, 0.50, 0.80, and 1.20 mg l^{-1} Zn(II), chemical deposition for 5 min, electrolytic reduction for 5 min) correlated well with the added concentrations of Zn(II) (correlation coefficient, 0.9997). The limit of detection for a 4 min chemical deposition was estimated from 10 consecutive analyses of a solution which contained 200 μg l^{-1} Zn(II). The mean value and 95% confidence limits for the analytical signal obtained under these conditions were 2.10 μA $\pm$ 0.10 μA; thus the detection limit was estimated as 200 × 0.10/2.10 μg l^{-1}, equal to 145 nM.

3.4. Competing species in the zeolite accumulation of Zn(II)

The zinc signal obtained following a 4 min chemical deposition from 1 mg l^{-1} Zn(II) in ammonia medium was significantly affected by additions of milligram per litre concentrations of Ag(I), Cu(II), Cd(II), Hg(II), Ni(II), and Co(II) to the deposition solution. The additions of Hg(II) gave rise to steadily increasing zinc signal amplitudes, an effect which could be attributed to the reduction of Hg(II) and hence the formation of metallic mercury, such that the zinc oxidation took place by the oxidation of zinc amalgam. On additions of Ag(I), Cu(II), and Cd(II), the zinc signal initially increased (compare Fig. 4 for Ag(I)). This observation was explained by the possibility of the linear Ag(NH$_3$)$_2^+$, planar Cu(NH$_3$)$_4^{2+}$, and tetrahedral Cd(NH$_3$)$_4^{2+}$ ions entering the 10 Å zeolite pores simultaneously with the tetrahedrally coordinated Zn(NH$_3$)$_4^{2+}$ ion such that elemental silver, copper, and cadmium, formed during the reduction step, exerted a catalytic effect on the reduction of the zinc complex. However, the overall trend was a decrease in the
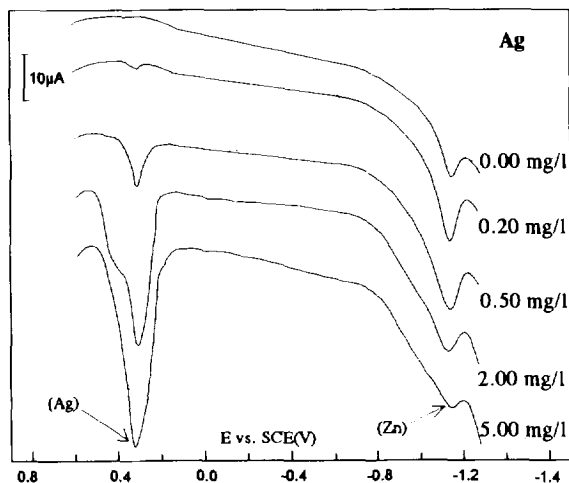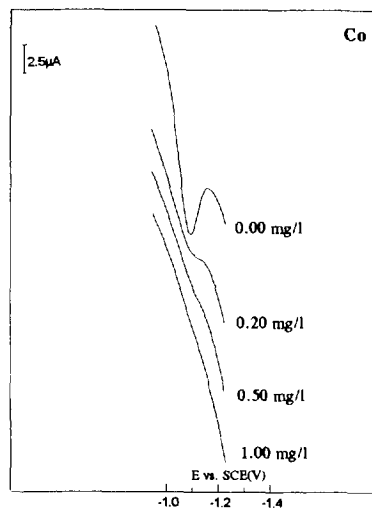
Fig. 4. Effects of Ag(l) additions on the zinc signal obtained following a 4 min chemical deposition from 1 mg l^{-1} Zn(II).

zinc signal. Since the concentrations in the deposition medium of the analyte Zn(II) and the interfering species Ag(I), Cu(II), and Cd(II) were all of the same order of magnitude, and, since the electrode was transferred to a clean electrolyte medium and reduction of the deposits was carried out before voltammetric quantitation, Zn(II) as well as the interfering species (e.g. Cd(II)) existed in oxidation state 0, before the anodic potential scan was started. Consequently, the decreasing zinc signals could not be explained by a simple

redox exchange (e.g. between Cd(II) and Zn(0)), which would be possible only if voltage scanning was carried out in the the bulk of the deposition medium. The decrease in the zinc signal and the increasing silver signal observed upon the addition of Ag(I) were therefore attributed to an increasing competition from $Ag(NH_3)_2^+$ ions for available sites in the zeolite. Qualitatively, the effects on the zinc signal of the addition of Cu(II) and Cd(II) were analogous to those observed for Ag(I). However, quantitatively, the decreases were more pronounced. This latter observation could be explained by the increased size of the competing ions $Cu(NH_3)_4^{2+}$ (planar coordination), and $Cd(NH_3)_4^{2+}$ (tetrahedral coordination). The $Ni(NH_3)_6^{2+}$ and the $Co(NH_3)_6^{2+}$ complexes were not reducible at the potentials covered in this experiment; thus no oxidation signals for nickel and cobalt were observed. However, the effects of both Ni(II) and Co(II) were significant. Most notably, as shown in Fig. 5, the addition of 1 mg l^{-1} Co(II) completely eliminated the zinc signal. This dramatic effect was attributed to the ability of the octahedrally coordinated ions to enter the zeolite pores and thereby, because of their size, efficiently prevent simultaneous accumulation of $Zn(NH_3)_4^{2+}$. Figs. 6 and 7 shows the changes in

Fig. 5. Effects of Co(II) additions on the zinc signal obtained following a 4 min chemical deposition from 1 mg l^{-1} Zn(II).
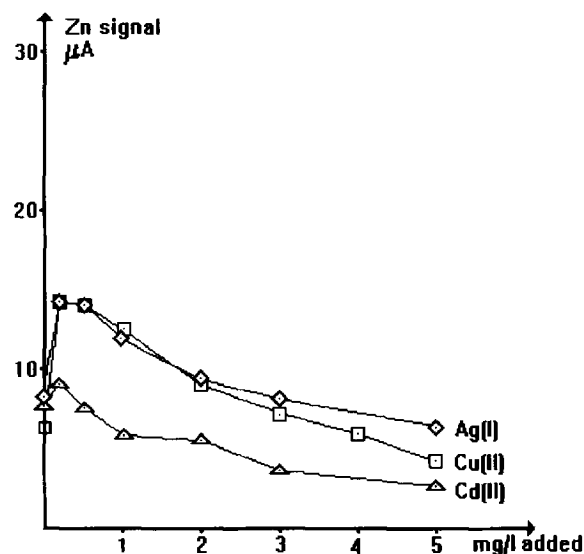
Fig. 6. Effects on the zinc signal (following a 4 min chemical deposition from 1 mg l^{-1} Zn(II)) of additions of Ag(I), Cu(II) and Cd(II).
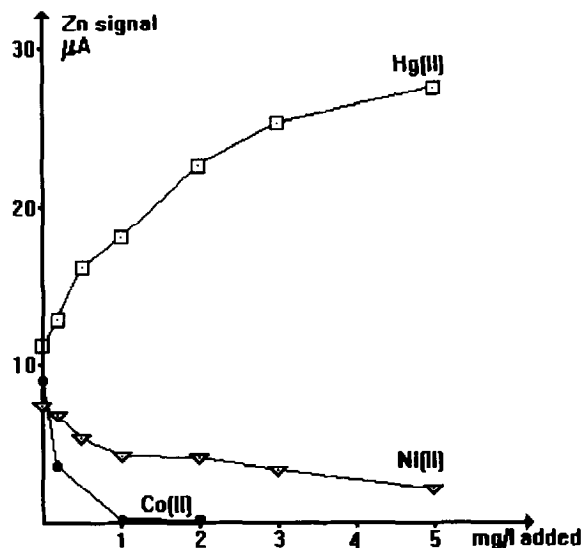
Fig. 7. Effects on the zinc signal (following a 4 min chemical deposition from 1 mg l^{-1} Zn(II)) of additions of Hg(II), Ni(II) and Co(II).

the zinc signal amplitude (obtained following a 4 min chemical deposition from 1 mg l^{-1} Zn(II)) as a result of the addition of the above-mentioned species. If expressed as the average percentage decrease of the zinc reduction current per μM added of the interfering species, the effects of the interferences were as follows: Ag(I), 0.65; Cu(II), 0.93; Cd(II), 2.35; Ni(II), 2.39; Co(II), 3.20.

Thus, if the metallic species were placed in order according to their suppression of the zinc signal, the following order was obtained: Co > Ni > Cd > Cu > Ag.

This order was identical to the trend of the metal ions when listed according to decreasing coordination number with ammonia. Thus the results underline the ability of the zeolite modifier to discriminate according to size. Conversely, if the zinc concentration in the ammonia medium and the deposition time were kept constant, and if the attenuation of the zinc response was taken as the analytical signal, the CME acted as a device

which was sensitive to the size and geometry of the interfering species.

References

[1] R.W. Murray, in A.J. Bard (Ed.), Electroanalytical Chemistry, Vol. 13, Marcel Dekker, New York, 1984, pp. 191–368.
[2] J.F. Price and R.P. Baldwin, Anal. Chem., 52 (1980) 1940.
[3] G.T. Cheek and R.F. Nelson, Anal. Lett., 11 (1978) 393.
[4] J.A. Cox and M. Majda, Anal. Chem., 52 (1980) 861.
[5] R.P. Baldwin, J.K. Christensen and L.Kryger, Anal. Chem., 58 (1986) 1790.
[6] S.V. Prabhu, R.P. Baldwin and L.Kryger, Electroanalysis, 1 (1989) 13.
[7] L.D. Kong, L.Kryger, J.K. Christensen and K.N. Thomsen, Talanta, 38 (1991) 101.
[8] J.A. Cox and P.J. Kulesza, Anal. Chim. Acta, 154 (1983) 71.
[9] J. Wang, B. Greene and C. Morgan, Anal. Chim. Acta, 158 (1984) 15.
[10] P. Hernández, E. Alda and L Hernández, Fresenius' Z. Anal. Chem., 327 (1987) 676.
[11] J. Wang and T. Martinez, Anal. Chim. Acta, 207 (1988) 95.
[12] C.G. Murray, R.J. Nowak and D.R. Rolison, J. Electroanal. Chem., 164 (1984) 205.
[13] D.R. Rolison, R.J. Nowak, T.A. Welsh and C.G. Murray, Talanta, 38 (1991) 27.
[14] M.V. Susic, Electrochim. Acta, 24 (1979) 535.
[15] N. El Murr, M. Kerkeni, A. Sellami and Y. Ben Taarit, J. Electroanal. Chem., 246 (1988) 461.
[16] O. Enea, Electrochim. Acta, 34 (1989) 1647.
[17] A. Walcarius, L. Lamberts and E.G. Derouane, Electrochim. Acta, 38 (1993) 2267.
[18] Jian-Wei Li and G. Calzaferri, J. Electroanal. Chem., 377 (1994) 163.

Determination of trace nitrite ion in water by spectrophotometric method after preconcentration on an organic solvent–soluble membrane filter

Xuexin Gu [a], Tianze Zhou [a,*], Dayong Qi [b]

[a] *Capital Normal University, Beijing 100037, China*
[b] *Research Centre of Eco-environment, Academia Sinica, Beijing 100085, China*

Abstract

A simple and rapid preconcentration technique, based on collecting trace nitrite on a membrane filter and dissolving the membrane filter in an organic solvent, has been applied to its spectrophotometric determination in water. At pH 2.0, nitrous acid diazotizes with p-aminoacetophenone, which is then coupled with N-(1-naphthyl)-ethylenediamine, at the same pH. The azo dye formed is collected on a 0.45 μm nitrocellulose filter at pH 4.7 as its ion associate with dodecyl sulfate. The ion associate and filter are dissolved in a small volume of 2-methoxyethanol (methylcellosolve), and acidized with 0.05 ml of 2 M hydrochloric acid and the absorbance of the resulting solution is measured at 555 nm against a reagent blank. Detection limits better than 0.1 μg/dm^{-3} as NO_2^- can be achieved. The ions normally present in water do not interfere when sodium metaphosphate is added as a masking agent. The proposed method has been applied to the analysis of water samples from several sources, the recoveries of the nitrite added to the samples are quantitative, and results found are satisfactory.

Keywords: Nitrite; Photometric determination; Preconcentration; Soluble filter

1. Introduction

It has become very important to determine trace amounts of nitrite in environmental protection, some chemical processes, the food industry and hygiene applications. Many reagents for the spectrophotometric determination of nitrite at very low concentrations have been reviewed and

_____
* Corresponding author. Fax: (86)10-841-6837.

usually employed with one of the modifications of the Griess–Ilosvay reactions [1]. The procedure using the Griess–Ilosvay reaction seems to be a satisfactory one, but in order to enhance sensitivity extraction has been proposed. It was reported [2] that nitrous acid diazotizes p-aminoaceto-phenone, which is then coupled with m-phenyl-enediamine; the 2,4-diamino-4'-acetyl-azobenzene formed is extracted into toulene at pH 9, and the absorbance measured at 450 nm. The molar absorptivity is about 2.3×10^4 l mol^{-1}. An improve-

ment to this extraction system was later suggested by Zhou and Xie [3]. It was reported that nitrite diazotizes with p-aminoacetophenone at pH 2.0, and is then coupled with N-(1-naphthyl)-ethyldiamine; the azo dye formed is further associated with β-naphthyl sulfonic acid in acid medium and extracted into n-butanol in the presence of aluminium nitrate and salted-out at the same pH; the absorbance of the extract is measured at 555 nm and the molar absorptivity is about 4.8×10^4 l mol^{-1} cm^{-1}.

Though solvent extraction of the nitrite has achieved considerable success in increasing the sensitivity and improving the detection limit to better than 10 μg dm^{-3}, the enrichment factor is usually limited by the mutual solubility of organic solvent and water. It is also especially tedious to twice introduce pollution of the solvent.

Recently, solvent-soluble membrane filters (MFs) have been reported for the rapid and simple preconcentration of trace components in water [4–6]. This new pre-concentration technique, which is based on collecting the analyte on a membrane filter and dissolving the membrane in an organic solvent, resembles solvent extraction but has many advantages over solvent extraction. Maximum possible concentration factors are not limited by the mutual solubility of water and organic solvent. Concentration factors greater than 100 can easiy be obtained.

In previous studies, this preconcentration technique has been used by one of the authors in place of solvent extraction for the determination of nitrite in water [7]. A ten-fold preconcentration (with 50 ml sample volume) can be done in a short time (with high sample throughout >50 ml min^{-1}) with a detection limit of 0.5 μg dm^{-3} as NO$_2^-$. Nitrite ion is converted to 4-sulfobenzenediazonium ion and then coupled with 1-aminonaphthalene to form an azo dye, which is collected on a nitrocellulose membrane filter as its ion-associate with benzyldimethyltetradecylammonium ion at about pH 4.7. The resulting compound is dissolved in methyl-cellosolve.

In the present investigation, the authors developed a more sensitive and selective preconcentration-spectrophotometric method for trace nitrite

ion in water samples by applying the principle mentioned above. The main improvements on this method have been suggested.

The conditions for the formation of a coloured ion associate are similar to those reported in earlier work on extraction of nitrite [3]. The volumes of reagent added are varied in proportion to the sample volume. The most attractive features of the new pre-concentrated methods are diazotizing with p-aminoacetophenone which has a hydrophobic substitutive group, associating with an anion surfactant having a long-chain alkyl such as sodium dodecyl sulfate and collecting the ion associate in a acid medium. Therefore the sensitivity and selectivity of the present method are enhanced. The detection limit is 0.1 μg dm^{-3}NO$_2^-$ on a 3σ basis under 100-fold preconcentration (with 500 ml sample volume), and Beer's law is obeyed in the range 0.1–1.0 μg NO$_2^-$ in 5 ml of solvent with excellent reproducibility. In this paper optimum conditions of the experiment and analytical results are reported.

2. Experimental

2.1. Reagents

Standard nitrite solution

Dissolve 0.492 g anhydrous sodium nitrite (dried in desiccator for 4 h) in 100 ml water (1.00 mg nitrogen or 3.28 mg nitrite per ml). Prepare a working solution by suitable dilution and store in a brown bottle in a refrigerator. Standardize iodometrically before using.

p-Aminoacetophenone hydrochloride solution

Prepare a 0.5% (w/v) solution in 1 + 9 hydrochloric acid, and store in a brown bottle: N-(1-naphthyl)-ethylenediamine dihydrochloride solution.

Dissolve 0.5 g N-(1-naphthyl)-ethylenediamine dihydrochloride in 100 ml of 1 + 99 hydrochloric acid.

Sodium dodecyl sulfate solution

Prepare a 1.00×10^{-3} M aqueous solution. Dissolve 0.288 g sodium dodecyl sulfate in 1 l water.
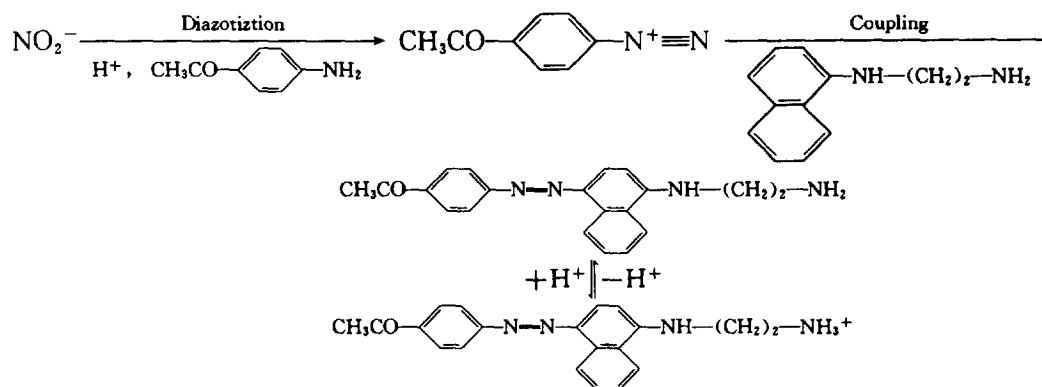
Fig. 1. Azo dye formation from nitrite, *p*-amino acetophenone and *N*-(1-naphthyl)-ethylenediamine.

β-Naphthyl sulfonic acid 0.5% (w/v)

Dissolve 0.5 g *β*-naphthyl sulfonic acid in 100 ml water. Adjust to pH 6.0 with sodium hydroxide solution.

Sodium metaphosphate solution: 5.0% (w/v).

Unless stated otherwise, all reagents used are of analytical pure grade, and all solutions are diluted with nitrite-free water, which is obtained by distilling alkaline permanganate–distilled water using an all-glass distillation apparatus.

2.2. Apparatus

A UV–visible spectrophotometer UV-265 Model (Shimadzu, Japan), visible spectrophotometer 723 Model (Shanghai Third Analytical Instruments Factory, China), a pH Meter pHs-2 Model (Shanghai Second Analytical Instruments Factory, China) were used.

Membrane filters and holder: Most of the data presented in this paper were obtained with a nitrocellulose membrane (25 mm in diameter, 0.45 μm pore size, Adjective Factory of Chemical Engineering College of Beijing, Beijing 100029). A Toyo KG-25 filter holder (effective filtration area 1.3 cm²) was used.

2.3. Procedure

Add about 50 ml of sample solution containing 0.1–1.0 μg nitrite-N to a 150 ml beaker. Add 1.0 ml of *p*-aminoacetophenone hydrochloride

solution and adjust to pH 2.0 with either sodium acetate solution or hydrochloric acid. After 15 min standing at room temperature, add 1.0 ml of *N*-(1-naphthyl)-ethylenediamine dihydrochloride solution and swirl. Add 2.0 ml of sodium dodecyl sulfate solution and mix thoroughly again. Filter off the ion associate on the membrane filter, and wash the membrane with about 10 ml of water. Dissolve the filter in 5 ml of 2-methoxyethanol and acidize with 0.05 ml 2 M hydrochloric acid. Absorbance due to the associate in the solvent is measured in a 10 mm cell at 555 nm against a reagent blank.

3. Results and discussion

3.1. Reactions for colour development

In an acidic solution, nitrite reacts with a primary aromatic amine to produce diazonium salt, which in turn couples with an aromatic amine or phenol to form a coloured azo dye. In the orignal Griess reaction, sulfanilic acid was used and diazotized, but the azo compound formed cannot be collected quantitatively by the membrane filter becauase of the hydrophilic nature of the sulfonic group. By using *p*-aminoacetophenone in place of sulfanilic acid [2], the hydrophobic ability of the azo compund is enhanced, favouring collection on a membrane filter. The reactions for colour development are as shown in Fig. 1.

3.2. Absorption spectra

Absorption maximum of the azo compound formed by diazotization of nitrous acid with p-aminoacetophenone and its coupling with N-(1-naphthyl)-ethylenediamine in aqueous solution is 543 nm; that of the ion associate in organic solvent is at 480 nm and that of the species in organic solvent after acidation is at 555 nm. All absorbance measurements of the extract are made at the latter wavelength. Absorption spectra are shown in Fig. 2.

3.3. Selection of counter ion

In previous work [7] nitrite is converted to 4-sulfobenzendiazonium ion, which is then coupled with 1-aminonaphthalene to form an azo dye as in the conventional method, and the azo dye formed is collected on a nitrocellulose filter as its ion associate with a larger cation, benzyl-dimethyltetradecyl ammonum ion, at about pH 4.7 (acetate buffer). Collection is poor at pH lower than 4, where most of the azo dye is in the pink, zwitterionic form and the selectivity of the reaction is not good. In the present investigation the azo dye obtained by diazo coupling with p-aminoacetophenone and N-(1-naphthyl)-ethylenediamine is protonated in the acidic media as the
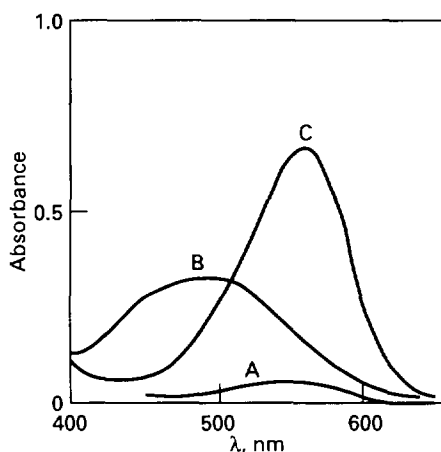

Fig. 2. Absorption spectra of the azo dye. Nitrite in aqueous solution: 1.0 μg per 50 ml. (A) No concentration, pH 2.0. (B) Membrane concentration, not acidified. (C) Membrane concentration, acidified.

cation form. By using a large anion, the dye cation can be collected on the membrane filter as an ion association complex. Hexoic acid, benzene sulfonic acid, naphthyl sulfonic acid and sodium dodecyl sulfate were investigated as sources of large anions. It was found experimentally that sodium dodecyl sulfate is preferable for obtaining efficient collection.

3.4. Effect of pH

A study of the effect of pH on the relevant diazo coupling reaction and collecting on the membrane filter disclosed that diazotization of p-aminoacetophenone should be carried out in acidic solution and a constant and maximum absorbance is obtained at pH 0–3; in the coupling of the diazonium cation with N-(1-naphthyl)-ethylenediamine, the coloured compound has a constant absorbance in the pH range 1.0–3.0; the ion associate of azo dye with dodecyl sulfate can be collected on the membrane filter at a pH between 1.0 an 5.0 without adjusting that of the solution. In practice, when 1.0 ml of p-aminoacetophenone hydrochloride solution is added to a sample, the pH becomes about 2.0, it remains almost the same even when N-(1-naphthyl)-ethylenediamine is added and after adding sodium dodecyl sulfate the pH of the aqueous solution is about 4–5 (4.7 in practice). In order to minimize the effect of foreign ions in diazo coupling a pH of 2.0 is preferred.

3.5. Effect of temperature

Diazotization and coupling are usually carried out at 0–5°C. However, reactions in this case proceed quantitatively at 10–30°C. Therefore the reactions may be carried out at room temperature.

3.6. Effect of standing time

A complete diazotization requires at least 5 min, and the coupling reaction requires 15 min or more. The azo compound formed in the aqueous phase is stable for at least 2 h, and in the organic phase for 24 h.

Table 1
Effect of other factors on formation and collection of azo dye (for 50 ml water sample)

Variable	Tested	Optimum	Preferred
Amount of p-aminoacetophenone (ml)	0.1–2.0	0.8–2.0	1.0
Amount of N-(1-naphthyl)-ethylenediamine (ml)	0.1–2.0	0.2–2.0	1.0
Amount of sodium dodecyl sulfate (ml)	0.5–3.0	1.5–2.5	2.0
Amount of solvent (ml)	5	5	5
Volume of washing water (ml)	10 × (1–5)	10 × (1–3)	10 × 3
Standing time after diazo coupling (min)	5	10–30	15
Stirring time after addition of surfactant (min)	1.0–4.0	2.0–4.0	3.0

3.7. Membrane filter for collection

Several filters of different types and with different pore sizes were examined for their usefulness for collecting the azo ion associate with nitrite. Nitrocellulose membrane filters are suitable because they readily dissolve in 2-methoxyethanol. Although any nitrocellulose membrane filter with pore sizes between 0.2 and 0.6 μm can be used, 0.45 μm filters are recommended because of their more stable absorbance of colour compound and acceptable filtration rate of about 50 ml min^{-1}.

The analyte on a membrane filter should be washed three times with water to decrease the reagent blank.

3.8. Solvent

Water-miscible organic solvents were tested as solvents for the wet membranes. Dimethyl sulfoxide (DMSO), N-N-dimethylformamide (DMF), acetone and 2-methoxyethanol readily dissolve the nitrocellulose and acetylcellulose membranes, but acetone is not recommended because of its high volatility. The colour intensity weakens obviously and decreases rapidly with time in DMSO and DMF. Absorbance of the colour compound is almost constant in 2-methoxyethanol for 24 h and is recommended as a proper solvent in the determination of nitrite. Other water-miscible solvents, such as ethanol, methanol and acetonitrile, will not dissolve the membrane under normal conditions.

3.9. Effects of other factors

Other factors, such as the amounts of reagents, time etc., recommended for the formation of azo dye and its collection on a membrane filter are shown in Table 1.

The volume of aqueous phase can be increased to 1000 ml and good concentration is still obtained on condition that the amount of reagents should be increased in proportion to the 50 ml water sample. For example, for treating a 250 ml sample of water the amount of reagents should be increased five fold. For convenience 500 ml sample of water is often used.

3.10. Sensitivity, precision and linear relation

Table 2 shows that microgram quantities of nitrite-nitrogen in 50 ml of sample can be determined with satisfactory precision. The lower limit of determination (taken as three times the standard deviation of the blank) is about 0.002 μg of nitrite-nitrogen per 100 ml of sample

3.11. Precision

Absorbances of 11 runs for 0.6 μg NO$_2^-$-N(50 ml) are 0.423, 0.424, 0.403, 0.417, 0.416, 0.406, 0.416, 0.406, 0.417. $X = 0.415$; $S = 9.0 \times 10^{-3}$; C.V. = 2.17%.

3.12. Linear relation

The regression equation in the range 0.1–1.0 μg NO$_2^-$-N is $y = -0.023 + 0.76X$ with a relative coefficient of 0.9997.

Table 2
Reproducibility at different nitrite levels[a]

Nitrite taken (µg) NO$_2^-$-N	Concn. of nitrite (µg dm^{-3})		Absorbance at 555nm		
	as N	as NO$_2^-$	$\bar{X}$	s	RSD (%)
0.2	4.0	13.1	0.121	0.005	3.8
0.4	8.0	26.3	0.254	0.006	2.4
0.6	12	39.4	0.403	0.007	1.7
0.8	16	52.6	0.542	0.010	1.9
1.0	20	65.7	0.636	0.011	1.7

[a] Volume of sample: 50 cm^3; concentration factor: 10; No. of runs: 5.

Table 3
Analyses of water samples and recovery of nitrite added to water sample

Sample	Nitrite added (µg dm^{-3} as nitrite)	Absorbance at 555 nm	Nitrite found (µg dm^{-3}, as nitrite)	Recovery of nitrite (µg dm^{-3} as nitrite)	%
Ground water	0	0.270	25.2	–	–
	13.1	0.419	38.2	13.0	99
	26.3	0.554	49.9	23.6	94
River water	0	0.210	20.1	–	–
	13.1	0.348	32.1	12.0	92
Tapwater	0	0.090	9.7	–	–
Wellwater	0	0.434	39.5	–	–

3.13. Effect of diverse components

The effect of diverse components on the formation of azo dye and collecting of the ion associate by membrane filter was examined. In this study, the tolerance limit was set as the amount which caused an error of ±5% in the recovery of 1 µg of nitrite in a 50 ml sample. At the nitrite level no interference was found with the following ions (where present the amount in milligrams and the form in which they were added are given in parantheses): Na$^+$ (200, NaCl); K$^+$ (200, KCl); NH$_4^-$ (200, NH$_4^+$Cl); Ca^{2+} (5, CaCl$_2$); Mg^{2+} (5, MgCl$_2$); Sr^{2+} (2, SrCl$_2$); Mn^{2+} (2, MnSO$_4$); Cd^{2+} (2, CdCl$_2$); Cu^{2+} (1, CuSO$_4$); Pb^{2+} (1, Pb(NO$_3$)$_2$); Zn^{2+} (1, ZnSO$_4$); Hg^{2+} (0.5 Hg (NO$_3$)$_2$); Co^{2+} (0.1 CoCl$_2$); Mo(VI) (0.1, Na$_2$MoO$_4$); Al^{3+} (2000, Al(NO$_3$)$_3$); Ga^{3+} (1, Ga(NO$_3$)); Cr^{3+} (1, CrCl$_3$); As(III) (0.1, Na$_3$AsO$_3$); Sb(V) (1, Sb(NO$_3$)$_5$); Cl$^-$ (500, HCl); F$^-$ (40, NaF); CH$_3$COO$^-$ (30, CH$_3$COONa); BO$_2^-$ (14, Na$_2$B$_4$O$_7$); Br$^-$ (8, NaBr); I$^-$ (1, KI); PO$_4^{3-}$ (200, (NaPO$_3$)$_6$); citrate (30, citric acid); tartrate (30, tartric acid). Interference by large amounts of 5 mg or more of Fe^{3+} can be masked by addition of sodium metaphosphate.

3.14. Application of natural water samples

The proposed method was applied for the analysis of river water and groundwater samples filtered through a 0.45 µm membrane filter. Table 3 shows the analytical results of original samples and samples to which known quantities of nitrite has been added. Recovery of the added nitrite was nearly quantitative as shown in this Table.

Acknowledgement

References

[1] D.F. Boltz and J.A. Hoell, Colorimetric Determination of Nonmetals, Interscience, New York, 1978, p. 232.

[2] K. Toei and K. Kiyose, Anal. Chim. Acta, 88 (1977) 125.

[3] Tianze Zhou and Yongming Xie, Int. J. Environ. Anal. Chem., 15 (1983) 213.

[4] S. Taguchi, E. Ito-oka, K. Masuyama, I. Kasahara and K. Goto, Talanta, 32 (1985) 391.

[5] C. Matsubara, Y. Yamamoto and K. Takamura, Analyst, 112 (1987) 1256.

[6] K. Goto and S. Taguchi, Anal. Sci., 9 (1993) 1.

[7] N. Hata, Q.Y. Lu, X.X. Gu, I. Kasahara, S. Taguchi and K. Goto, Bunseki Kagaku, 43 (1994) 461.

[8] APHA, AWWA and WPCF, Standard Methods for the Examination of Water and Wastewater, 14th edn., Washington, DC. 1976, p. 434.

Equilibrium studies of the diorganotin(IV) complexes with some amino acids and related compounds

Mohamed M. Shoukry

Department of Chemistry, Faculty of Science, University of Cairo, Giza, Egypt

Abstract

The interaction of dimethyltin(IV) and diethyltin(IV) cations with water and some amino acids and related compounds was investigated at 25°C and ionic strength 0.1 M $NaNO_3$ using a potentiometric technique. The results showed the formation of 1:1 and 1:2 (organotin:ligand) complexes and the corresponding stability constants were determined. The participation of different ligand functional groups in binding to organotin is discussed. The effect of the pK_a value of the respective ligand on the stability constant of its complex species was elucidated. The concentration distribution of the complexes in solution was evaluated.

Keywords: Diorganotin(iv); Complexes; Amino acids

1. Introduction

A variety of organotin complexes structurally related to *cis*-platin and its derivatives [1,2] have been investigated for antitumour properties [3-6]. Recent studies [7-9] of compounds of the type $R_2SnX_2 \cdot L$, where L is generally a bidentate ligand, have suggested a relationship between their antitumour activity and stability. In the case of nitrogen-bearing ligands [10], incresing stability is thought to reduce activity by hindering the dissociation of the ligand that is necessary for binding between tin and DNA. In view of this, encouraging results on the antitumour activity of diorganotin(IV) complexes with bipyridyl [7] and 2,2′-bi-imidazole [11] have led us to investigate the solution equilibria of organotin complexes. As part of our project dealing with the study of metal complexes of expected antitumour activity [12-14] and as a continuation of our previous studies on triorganotin(IV) complexes [15-17], the present investigation aims to characterize the complex formation equilibria of diorganotin(IV) with amino acids and related compounds.

2. Experimental

2.1. Materials and reagents

Dimethyltin(IV) and diethyltin(IV) chlorides were received from Alfa Inorganics Chem. Co.

The ligands used were glycine, alanine, phenylalanine, valine, leucine, serine, proline, hydroxyproline, methionine, histidine·HCl, histamine·2HCl, ornithine·HCl, lysine·HCl, bipyridyl and phenanthroline·HCl. These materials were supplied by Fluka Chem. Co. Carbonate-free sodium hydroxide stock solutions were prepared by diluting the contents of BDH concentrated volumetric solution vials. These solutions were systematically checked by titration against potassium hydrogen phthalate. All solutions were prepared in deionized water.

2.2. Procedure and measuring techniques

Potentiometric titrations were carried out using a Metrohm 686 titroprocessor equipped with a 665 Dosimat (Switzerland). The buffer solutions (pH 6.86 and 4.01) based on the NBS scale [18], now U.S. National Institute of Standards and technology (NIST), were used for calibration. The following mixtures (A)–(C) were prepared and titrated potentiometrically with sandardized NaOH solution:

(A) 0.02 mol dm^{-3} ligand (10 cm^3) + 0.13 mol dm^{-3} NaNO$_3$ (30 cm^3).

(B) 0.02 mol dm^{-3} organotin(IV) (10 cm^3) + 0.13 mol dm^{-3} NaNO$_3$ (30 cm^3).

(C) 0.02 mol dm^{-3} organotin(IV) (10 cm^3) + 0.02 mol dm^{-3} ligand (20 cm^3) + 0.40 mol dm^{-3} NaNO$_3$ (10 cm^3).

The titrations were performed in a special vessel described previously [19] at 25°C in a purified N$_2$ atmosphere. The ionic strength remained almost constant during titration, $\mu = 0.1$ M. The acid dissocation constants of the ligands were determined by titrating mixture (A), where the ligand is in the protonated form. The stability constants of the hydroxo complexes [R$_2$Sn(OH)$_n$] were determined by titrating mixture (B). The stability constants of the organotin(IV) complexes were determined by titrating mixture (C).

The species formed in the systems studied were characterized by the general equilibrium process (1), while the formation constants for these generalized species are given by Eq. (2):

$$p(M) + q(L) + r(H) \rightleftharpoons (M)_p(L)_q(H)_r \qquad (1)$$
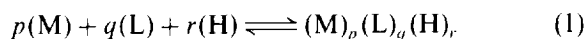
$$\beta_{pqr} = \frac{[(M)_p(L)_q(H)_r]}{[M]^p[L]^q[H]^r} \qquad (2)$$

where M, L and H stand for organotin(IV), ligand and proton respectively. The calculations were performed using the computer program MINIQUAD-75 [20] loaded on an IBM-4336 computer. The stoichiometries and stability constants

Table 1
Formation constants and the maximum proportions of dimethyltin(IV) (DMT) complexes

System	p	q	r^a	log β^b	n^c	S^d	% proportion of species	pH
DMT–OH	1	0	−1	−3.15(0.01)	66	1.0×10^{-8}	86	4.3
	1	0	−2	−8.44(0.01)			81	6.1
Glycine	0	1	1	9.61				
	0	1	2	11.92				
	1	1	0	8.76(0.01)	68	2.7×10^{-7}	74	4.2
	1	2	0	15.92(0.02)			76	6.3
Proline	0	1	1	10.52				
	0	1	2	12.03				
	1	1	0	9.63(0.01)	68	3.1×10^{-7}	73	4.3
	1	2	0	17.77(0.02)			77	6.3
Alanine	0	1	0	9.69				
	0	1	2	11.89				
	1	1	0	8.83(0.01)	68	3.1×10^{-7}	74	4.2
	1	2	0	16.21(0.02)			75	6.2
Valine	0	1	1	9.57				
	0	1	2	11.71				
	1	1	0	8.74(0.01)	68	2.8×10^{-7}	72	4.1
	1	2	0	15.99(0.02)			75	6.2

(continued opposite.)

Table 1 (continued)

System	p	q	r_a	$\log \beta^b$	n^c	S^d	% proportion of species	pH
Leucine	0	1	1	9.76				
	0	1	2	10.22				
	1	1	0	9.04(0.01)	68	2.8×10^{-7}	76	4.2
	1	2	0	16.44(0.02)			74	6.2
Serine	0	1	1	9.14				
	0	1	2	11.40				
	1	1	0	8.37(0.01)	68	2.6×10^{-7}	76	4.2
	1	2	0	15.11(0.02)			77	6.2
Hydroxyproline	0	1	1	8.97(0.02)				
	0	1	2	11.18(0.03)				
	1	1	0	8.28(0.01)	68	2.9×10^{-7}	77	4.1
	1	2	0	14.84(0.02)			73	6.3
Phenalalanine	0	1	1	9.12				
	0	1	2	11.12				
	1	1	0	8.25(0.01)	68	3.0×10^{-7}	72	4.2
	1	2	0	15.01(0.02)			75	6.2
Methionine	0	1	1	9.10				
	0	1	2	11.09				
	1	1	0	8.22(0.01)	68	3.0×10^{-7}	71	4.3
	1	2	0	14.96(0.02)			76	6.2
Histidine	0	1	1	9.53				
	0	1	2	15.81				
	0	1	3	17.81				
	1	1	0	10.38(0.02)	68	5.0×10^{-8}	74	5.6
	1	1	1	15.33(0.01)			82	4.1
	1	2	0	16.83(0.02)			75	7.0
Histamine	0	1	1	9.86				
	0	1	2	15.93				
	1	1	0	10.21(0.01)	66	2.7×10^{-8}	72	5.8
	1	1	1	15.32(0.01)			82	4.1
	1	2	0	16.67(0.01)			61	6.9
Lysine	0	1	1	10.73				
	0	1	2	20.00				
	0	1	3	22.14				
	1	1	0	14.04(0.03)	68	1.3×10^{-7}	99	7.3
	1	1	1	19.35(0.02)			84	4.2
	1	2	0	18.52(0.03)			62	9.8
Ornithine	0	1	1	10.58				
	0	1	2	19.44				
	0	1	3	21.39				
	1	1	0	13.50(0.03)	68	1.2×10^{-7}	99	7.4
	1	1	1	18.78(0.03)			84	4.2
	1	2	0	18.19(0.02)			67	9.5
Bipyridyl	0	1	1	4.42				
	1	1	0	4.18(0.03)	68	7.4×10^{-7}	50	3.1
	1	2	0	7.68(0.03)			51	4.1
Phenanthroline	0	1	1	4.96				
	1	1	0	4.39(0.02)	68	3.6×10^{-7}	55	3.6
	1	2	0	7.94(0.02)			51	4.1

[a] The symbols p, q and r are the stochiometric coefficients corresponding to organotin(IV), ligand and H^+ respectively.
[b] Standard deviations are given in parentheses.
[c] Number of data points.
[d] Sum of square of residuals.

Table 2
Formation constants and the maximum proportions of dimethyltin(IV) (DMT) complexes

System	p	q	r	$\log \beta$	n	S	% proportion of species	pH
DMT–OH	1	0	−1	−3.23(0.01)	66	3.7×10^{-7}	89	4.4
	1	0	−2	−8.90(0.01)			86	6.6
Glycine	1	1	0	8.76(0.02)	66	1.2×10^{-7}	80	4.3
	1	2	0	15.61(0.03)			73	6.5
Proline	1	1	0	9.50(0.01)	68	2.5×10^{-7}	79	4.5
	1	2	0	17.18(0.02)			83	7.0
Alanine	1	1	0	8.78(0.01)	68	2.3×10^{-7}	79	4.3
	1	2	0	15.75(0.02)			79	6.8
Valine	1	1	0	8.70(0.02)	68	9.9×10^{-8}	80	4.4
	1	2	0	15.57(0.03)			73	6.4
Leucine	1	1	0	9.01(0.01)	68	2.4×10^{-8}	81	4.3
	1	2	0	16.04(0.02)			79	6.8
Serine	1	1	0	8.30(0.01)	68	2.4×10^{-7}	80	4.4
	1	2	0	14.71(0.02)			77	6.7
Hydroproline	1	1	0	8.23(0.01)	68	2.7×10^{-7}	83	4.4
	1	2	0	14.43(0.02)			79	6.8
Phenylalanine	1	1	0	8.18(0.01)	68	2.4×10^{-7}	80	4.5
	1	2	0	14.57(0.02)			79	6.8
Methionine	1	1	0	8.20(0.01)	68	1.9×10^{-7}	80	4.4
	1	2	0	14.53(0.02)			79	6.8
Histidine	1	1	0	10.03(0.02)	68	4.6×10^{-8}	67	5.8
	1	1	1	15.23(0.01)			84	4.1
	1	2	0	16.37(0.02)			72	7.0
Histamine	1	1	0	9.77(0.01)	66	2.6×10^{-8}	65	5.9
	1	1	1	16.07(0.01)			84	4.3
	1	2	0	15.17(0.01)			61	7.0
Lysine	1	1	0	13.56(0.03)	68	1.3×10^{-7}	99	8.2
	1	1	1	19.22(0.02)			87	4.5
	1	2	0	18.00(0.03)			61	9.9
Ornithine	1	1	0	13.05(0.03)	68	9.5×10^{-8}	99	7.8
	1	1	1	18.68(0.02)			87	4.4
	1	2	0	17.66(0.03)			65	9.6
Bipyridyl	1	1	0	3.97(0.02)	68	3.4×10^{-7}	44	3.2
	1	2	0	7.51(0.02)			51	4.2
Phenanthroline	1	1	0	4.56(0.02)	68	8.1×10^{-7}	68	3.7
	1	2	0	7.83(0.05)			43	4.8

of the complexes formed were determined by trying various composition models for the system studied. The model selected was that which gave the best statistical fit and which was chemically consistent with the titration data without giving any systematic drifts in the magnitudes of various residuals, as described elsewhere [20]. The fitted model was tested by comparing the experimental titration data points and the theoretical curve calculated from the values of acid dissociation constants of the ligand and formation constants

of the corresponding complexes. Tables 1 and 2 list the stability constants together with their standard deviations and the sum of the square of residuals as output by the program MINIQUAD-75.

3. Results and discussion

The acid dissociation constants of the ligands were determined under the same experimental conditions of ionic strength and temperature
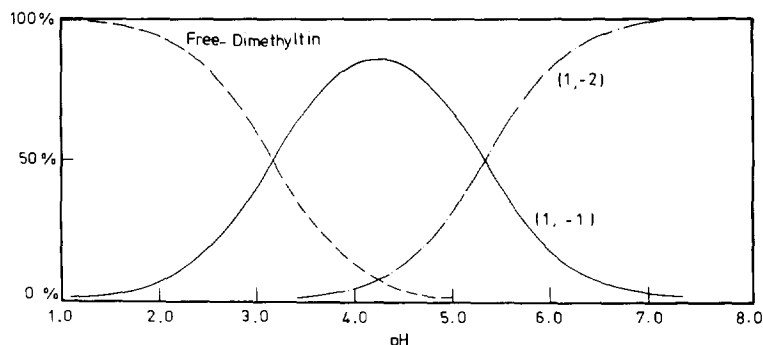
Fig. 1. Concentration distribution diagram for the dimethyltin(IV)–OH system.

which are used for the study of organotin(IV) complex equilibria. The results obtained are in good agreement with literature values [21].

The acid–base chemistry of diorganotin(IV) has been characterized by fitting the potentiometric data (mixture B) to various acid–base models.
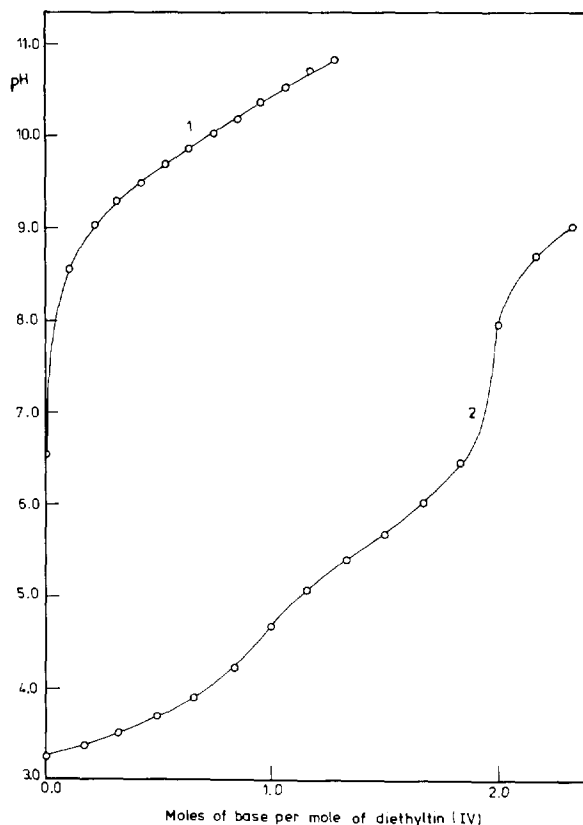
Fig. 2. Potentiometric titration curves in diethyltin(IV)–glycine system: (1) Glycine; (2) 1:2 DET–glycine.

The fitted model, according to the aforementioned method of calculation, was found to be consistent with the mono- and dihydroxo-organotin(IV) $[R_2Sn(OH)_n$, where $n = 1$ and 2]. The concentration distribution of the hydroxy-species is shown in Fig. 1.

The potentiometric titration curve of a solution mixture of dimethyltin(IV) and glycine (mixture C), taken as a representative, is given in Fig. 2. The curve starts at pH 3.2 and passes two inflections at $a = 1$ and $a = 2$ (a is the number of moles of base added per mole of organotin(IV)), corresponding to the formation 1:1 and 1:2 complex species respectively.

Diorganotin(IV) compounds form complexes with various structural geometries. It was concluded that the trigonal bipyramidal tin environment [22] characterizes the diaorganotin(IV)–mercaptocarboxylato complexes. It was demonstrated that 2-(arylazo)pyridine [23] and β-diketones [24] form octahedral complexes with diorganotin(IV). Seven-coordinate pentagonal bipyramidal tin stereochemistry [25] was observed in the 1:1 adduct of diphenyltin(IV) with triphenylphosphine. Accordingly, it is assumed that tin has an octahedral configuration with an equatorial alkyl group. The amino acid coordinates via the amino nitrogen and carboxylate oxygen atoms in the axial position. It should be mentioned that the carboxylate group may bind as bidentate [22,26]. However, if the amino acid interacts with diorganotin(IV) by the two carboxylic oxygen atoms, leaving the amino group non-coordinating, the amino group will be protonated. However, the fitted model, in this investi-
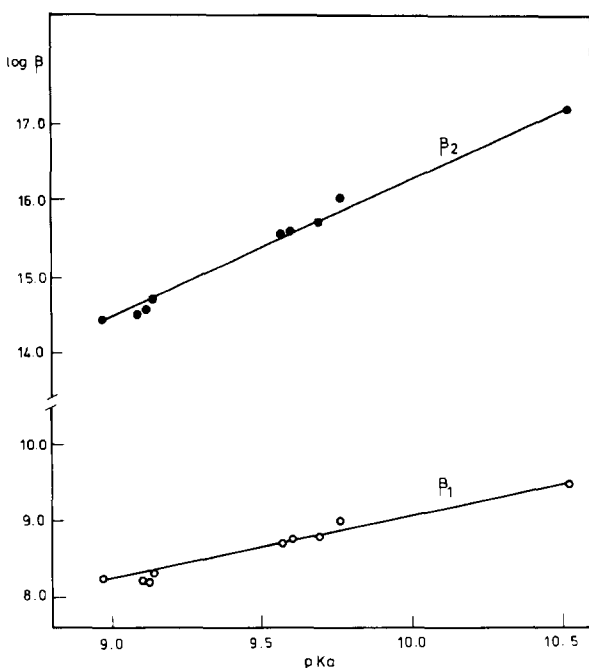
Fig. 3. Relation between pK_a value of the ligand and $\log \beta$ value of the complex.

gation, is found to consist of the deprotonated complex only. This reveals that the amino group is not free and is involved in the complex formation with $R_2Sn(IV)$.

Further studies are needed to support the structural elucidation of the coordination geometry of the organotin(IV) complexes, e.g. the crystal structure of the solid complexes. However, such studies are not yet available and will be considered in the future.

The amino acids methionine and serine have extra binding centres on the thioether and β-alcoholato groups. The thioether group in methionine [27] and β-alcoholato group in serine [28] were reported to participate in transition metal ion complex formation. The stability constants of organotin(IV) complexes of serine and methionine are in fair agreement with those of other amino acids studied, if the difference in the acid dissociation constants of the amino acids is considered. This indicates that serine and methionine chelate diorganotin(IV) as substituted glycinates.

Histidine is a tridentate ligand that has amino, imidazole and carboxylate groups as metal ion

binding sites. With metal ions having a square-planar coordination sphere, for steric reasons, only two of the three binding sites [29,30] i.e. either histamine-like or glycine-like complexes have to be formed. With regard to the protonated complex of histidine the question arises as to where the proton is located? This problem has been discussed by considering the acid dissociation constant of this species, given by Eq. (3) [15]:

$$pK^H = \log K^M_{MLH} - \log K^M_{ML} \qquad (3)$$

The values of pK^H are 4.95 and 5.20 for dimethyl- and diethyltin(IV) complexes respectively. These values compare favourably with the acid dissociation constants of the imidazole residue of histidine ($pK^H = 6.28$) if the increase in its acidity as a result of organotin(IV) complex formation is considered. Furthermore, it should be recognized that the stability constants of the deprotonated complexes of histidine are in fair agreement with the stability constants obtained for the other amino acid complexes. This provides further support for the view that histidine coordinates to organotin(IV) in an amino acid-like form. Lysine and ornithine may coordinate as bidentate ligands either by (N, N) or (N, O) donor sets. The stability constants of their complexes are higher than those of α-amino acids by about four logarithmic units. This may indicate that lysine and ornithine chelate by the (N, N) donor set.

It is reported that for metal complexes with a series of structurally-related ligands, a linear relationship holds between the stability constant of the complex and the acid dissociation constant of the ligand [31]. The importance of these plots is that they afford a means of estimating the stabilities of complexes that have not yet been studied. Fig. 3 demonstrates a relationship between $\log \beta_1$ and $\log \beta_2$ for the diethyltin(IV) complexes of α-amino acids. Lysine and ornithine complexes do not fall on these straight lines, providing further evidence for their different mode of coordination.

It is found (Tables 1 and 2) that the dimethyltin(IV) complexes are more stable than the corresponding diethyltin(IV) complexes. This is explained in terms of steric crowding between the ethyl group and the incoming ligand.

The concentration distribution diagrams in terms of formation precentage as a function of pH were obtained for complexes formed in solutions, using the program SPECIES [32]. The maximum percentages of formation of the various complexes given in Tables 1 and 2 are obtained under the prevailing experimental conditions. In all the species distributions the concentration of the complexes increases with increasing pH, thus making $R_2Sn(IV)$ biologically available in the physiological pH range.

Acknowledgments

References

[1] B. Rosenber, L. van Camp and T. Kringas, Nature, 205 (1965) 698.

[2] J.L. van der Weel and J. Reedijk, Chem. Ber., 20 (1988) 775.

[3] M. Gielen, P. Lelieveld, D. de Vos and R. Willem, In vitro antitumour activity of organotin compounds, in M. Gielen (Ed.), Metal-Based Antitumour Drugs, Vol. 2, Freund Publishing House, Tel Aviv, 1992, p. 29.

[4] M. Gielen, P. Lelieveld, D. de Vos and R. Willem, In vitro antitumour activity of organotin(IV) derivatives of salicylic acid and related compounds, in B.K. Keppler (Ed.), Metal Complexes in Cancer Chemotherapy, VCH, Weinheim, 1993, p. 383.

[5] M. Gielen, Tin-Based Antitumour Drugs, NATO ASI Series H: Cell Biology, Vol. 37, Springer-Verlag, Berlin, 1990.

[6] R. Barbieri, Inorg. Chim. Acta, 191 (1992) 253.

[7] A.J. Crowe, P.J. Smith and G. Atassi, Inorg Chim. Acta, 93 (1984) 171.

[8] A.J. Crowe, P.J. Smith and G. Atassi, Chem. Biol. Interact., 32 (1980) 171.

[9] M. Gielen, C. Vanbellinghen, J. Gelan and R. Willem, Bull. Soc. Chim. Belg., 97 (1988) 873.

[10] A.J. Crowe, P.J. Smith, C.J. Cordin, H.E. Parge and F.E. Smith, Canc. Lett., 24 (1984) 45.

[11] A.S. Gonzalez, J.S. Casas, J. Sordo, U. Russo, M.I. Lareo and B.J. Regueiro, J. Inorg. Biochem., 39 (1990) 227.

[12] M.M. Shoukry, H. Hohmann and R. van Eldik, Inorg. Chem. Acta, 198–200 (1992) 187.

[13] M.M. Shoukry, I.M. Kenawy and I.H. El-Haj, Transition Met. Chem., 16 (1991) 637.

[14] M.M. Shoukry, E.M. Khairy and A. Saeed, J. Coord. Chem., 17 (1988) 305.

[15] M.M. Shoukry, Bull. Soc. Chim. Fr., 130 (1993) 117.

[16] M.M. Shoukry, J. Inorg. Biochem., 48 (1992) 484.

[17] M.M. Shoukry, J. Coord. Chem., 25 (1992) 111.

[18] R.G. Bates, Determination of pH—Theory and Practice, 2nd edn., Wiley-Interscience, New York, 1973, p. 73.

[19] M.M. Shoukry, M.M. Khater and E.M. Shoukry, Indian J. Chem., 25A (1986) 488.

[20] P. Gans, A. Sabatini and A. Vacca, Inorg. Chim. Acta, 18 (1976) 237.

[21] D.D. Perrin, Stability Constants of Metal–Ion Complexes: Part B, Organic Ligands, Pergamon Press, Oxford, 1979.

[22] C.D. Hager, F. Huber, A. Silvestri, A. Barbieri and A. Barbieri, Gazz. Chim. Ital., 123 (1993) 583.

[23] D. Dey, T.S. Basu Baul and E. Rivarola, Bull Chem. Soc. Jpn., 66 (1993) 1556.

[24] D.F.S. Natusch and L.J. Porter, J. Chem. Soc. A, (1971) 2527; Chem. Commun., (1970) 596.

[25] M. Nordelli, C. Pelizzi and G. Pelizzi, J. Chem. Soc., Dalton trans., (1978) 131.

[26] M. Gielen, A. El-Khloufi, M. Biesemans, R. Willem and J. Meunier-Piret, Polyhedron, 11 (1992) 1861.

[27] H. Kozlowski, B.R. Decock, J.L. Delarulle, C. Loucheux and B. Ancian, Inorg. Chim. Acta, 78 (1983) 31.

[28] L.D. Pettit and J.L.M. Swash, J. Chem. Soc., Dalton Trans., (1976) 2416.

[29] D.D. Perrin, I.G. Sayce and V.S. Sharma, J. Chem. Soc. A, (1967) 1755.

[30] J.L. Meyer and J.E. Bauyman, Jr., J. Am. Chem. Soc., 92 (1970) 4210.

[31] H. Siegel, J. Inorg. Nucl. Chem., 37 (1975) 507.

[32] L. Pettit, University of Leeds, personal communication.

First-derivative solid-phase spectrophotometric determination of molybdenum at the ng ml^{-1} level

A. Molína-Diaz[a,*], M.I. Pascual-Reguera[a], E. Liñán-Veganzones[a], M.L. Fernández de Córdova[a], L.F. Capitán-Vallvey[b]

[a]*Department of Analytical Chemistry, Faculty of Experimental Sciences, University of Jaén, E-23071 Jaén, Spain*
[b]*Department of Analytical Chemistry, Faculty of Sciences, University of Granada, E-18071 Granada, Spain*

Abstract

Derivative spectrophotometry was applied to solid-phase spectrophotometry in order to enhance its sensitivity and remove the large background noise caused by the absorption of the resin layer itself, and avoid the necessity of preparing a blank. The determination of micro-amounts of molybdenum (at the ng ml^{-1} level) with pyrocatechol violet to form a 1:1 blue complex in acid medium, which is fixed on a dextran-type anion-exchange resin (Sephadex QAE-A-25), is described as an example of the application of this technique. The absorbance of the resin, packed in a 1 mm spectrophotometric cell, was measured directly. The characteristic peak amplitude of the signal at 716 nm in the first-derivative spectra is useful for quantitative determination of molybdenum (2–8 ng ml^{-1}; RSD = 4, 30%) in natural and industrial water samples, plant tissues and soil extracts.

Keywords: Solid-phase spectrophotometry; Derivative spectrophotometry; Pyrocatechol violet; Molybdenum determination; Natural water; Industrial water; Plant tissues; Soil extracts

1. Introduction

Molybdenum is an essential element in plants, having important biochemical functions in nitrate reduction, biosynthesis of nucleic acids and biochemical processes related to the fixation of molecular nitrogen by micro-organisms and bacteria. As either a deficiency or an excess of molybdenum can cause damage to plants, its routine control is highly recommended for healthy plant growth.

Molybdenum is also present in soils and waters [1,2], but generally at lower levels than in plants. Therefore, very sensitive and accurate methods for its determination are required, which are crucial to the understanding of the status and fate of Mo in the environment, and for the detection of

* *Corresponding author.

Mo pollution in order to take timely control measures.

The spectrophotometric methods most commonly used for the determination of Mo require a previous step of pre-concentration. Generally, ion exchangers and other solid supports are used for pre-concentration, but the analyte has to be eluted if a spectrophotometric method is going to be employed and consequently an undesirable dilution is carried out. When spectrophotometry is used in combination with a solid phase, the analytical signal being provided by direct measurements of the absorbance of the species of interest sorbed on the solid support (solid-phase spectrophotometry, SPS), a large increase in sensitivity is achieved [3-8]. This operating technique proposed by Yoshimura et al. [9] was later applied using spectrofluorimetry [10-13]. The large background produced because of strong absorption of the solid phase could be avoided by using derivative solid-phase spectrophotometry (DSPS). This technique has been applied to the determination of both inorganic and organic compounds, but there are only a few cases cited in the literature [14-17].

In this paper, we propose a method for the determination of Mo at trace level by DSPS using pyrocatechol violet (PV) as a chromogenic reagent. The derivative signal of the blank is zero at the measurement wavelength; hence, the necessity of preparing a blank is avoided, reducing both the amount of work and the time required for carrying out the analysis.

2. Experimental

2.1. Reagents

All chemicals used were of analytical grade and the water was doubly distilled.

Molybdenum(VI) standard solution 1.000 ± 0.002 g l^{-1} was prepared from a Titrisol Merck solution of $(NH_4)_6Mo_7O_{24} \cdot 6H_2O$ in 0.7% aqueous NH_3. Solutions of lower concentration were prepared by dilution with doubly distilled water.

The ion exchanger was a Sephadex QAE A-25 (Aldrich). Anion-exchange resin was used in the chloride form and without pre-treatment.

Buffer solutions of pH 2.9 were prepared by dissolving 20.0190 g of KHphthalate in 1000 ml of doubly distilled water containing 257 ml of 0.2 M HCl solution.

PV solutions of various concentrations were prepared by dissolving analytical grade PV (Aldrich) in water.

2.2. Apparatus

A single beam GBC 911 microcomputer-controlled UV/vis spectrophotometer, from GBC Scientific Equipment Ply Ltd. which can store as many as 32 spectral scans and 15 operating programs, with 1 mm glass cells was employed for all spectral measurements. The GBC 911A UV/vis spectrophotometer was connected to a BRAVO AST/30 286 microcomputer by means of a serial port. The GBC SCAN MASTER V 1.62 and Data Leader Software (Beckman) were used for data acquisition and treatment. The spectra were recorded at a scan rate of 250 nm min^{-1}. A COMX PL80 plotter was used for graphical representations. The pH measurements were made using a Crison Model 2002 pH-meter fitted with a glass-saturated calomel electrode assembly and a temperature probe. An Agitaser 2000 rotating bottle agitator was also used.

2.3. Absorbance and first-derivative signal measurements

The absorbance (really attenuation) of the complex species sorbed on the resin (when the normal zero-order absorption spectra of the complex were used) was measured in a 1 mm cell at 663 nm (corresponding to the absorption maximum of the coloured species) and 800 nm (the wavelength at which the sample species no longer absorbs). The net absorbance for the complex was calculated as in a previous report [3].

The first-derivative spectra were recorded; in this case only a single wavelength was required for carrying out the measurements. The negative peak height at 716 nm is related to the concentration of Mo(VI).

2.4. Procedures

(I) A 100 ml water sample containing between 10 and 80 ng ml^{-1} of Mo(VI) was transferred into a 1 l polyethylene bottle, and 5 ml of 7.76×10^{-5} M PV, 15 ml of pH 2.9 KHphthalate/HCl buffer solution ($C_T = 0.2$ M) and 30 mg of Sephadex QAE A-25 resin were added. The mixture was stirred for 30 min, the resin beads collected by filtration and the resin slurry transferred to the spectrophotometric cell with the aid of a pipette. For absorbance measurements, a blank was required and values were obtained as indicated above. The signals of the first derivative were measured as described above.

The calibration graph was constructed in the same way using molybdenum solutions of known concentration.

(II) A 500 ml sample solution containing 5–18 ng ml^{-1} of Mo(VI) was transferred into a 1 l polyethylene bottle, and 5 ml of 2.06×10^{-4} M PV solution, 75 ml of pH 2.9 KHphthalate/HCl buffer solution and 30 mg of Sephadex QAE A-25 resin were added. The agitation time was 1 h, operating as indicated in the above procedure.

(III) To a 1000 ml sample solution containing 2–8 ng ml^{-1} of Mo(VI) (placed in a 2 l polyethylene bottle) was added 10 ml of 1.29×10^{-4} M PV solution, 150 ml of pH 2.9 KHphthalate/HCl buffer solution and 30 mg of ion exchanger. The mixture was agitated for 2 h, in the same way as in the above procedures.

2.5. Treatment of samples

Waters

Natural and industrial waters were filtered through a filter with a pore size of 0.45 μm (Millipore), and the analyses were performed immediately. The usual general precautions were taken to avoid contamination.

Vegetal tissue

Potato leaves were picked during the flowering period. The sample comprised the third or fourth leaves from the apex [18]. It was immediately dried in a forced draft oven for 24 h at 65°C to prevent decomposition or weight loss. After the

sample had been divided into pieces and ground with a small mill, a suitable portion was weighed (9 g dry material) into a quartz crucible; mineralization was carried out by heating slowly to 450°C over 2 h and holding at this temperature for other 2 h. The ashes were wetted down carefully with a fine stream of doubly distilled water, followed by the addition of 1 ml of concentrated HCl and heating until the first vapours were formed. The solution was filtered through Whatman no. 42 paper over a 25 ml standard flask. The filter paper was stored in a quartz crucible and heated in a furnace for 30 min at 550°C. The ashes were then treated with 5 ml of HF in a teflon crucible, taken to dryness, and finally 1 ml of concentrated HCl and warm water were added. The solution was filtered through Albet no. 242 paper in the same 25 ml standard flask and made up to volume with distilled water.

Soil extracts

A sample of soil was taken from 0–20 cm depth in the University Campus of Jaén. 50 g of sieved and air-dried material were weighed and placed in a 200 ml polyethylene bottle, adding 100 ml of water. After 12 h agitation, the solution was filtered through Albet no. 242 paper.

3. Results and discussion

3.1. Spectral characteristics

(a) Zero-order spectra

PV reacts with Mo(VI) in solution to give a chelate that is fixed on Sephadex anion-exchange resin, showing an absorption maximum at 663 nm and a green or blue colour (depending on the amount of reagent sorbed on the resin). PV is also fixed on Sephadex QAE A-25, showing a sharp absorption peak (basic medium) at about 630 nm (540 nm in solution); this peak disappears when the pH decreases to about 3. The spectra of the complex in solution and the solid phase are shown in Fig. 1. A strong increase in sensitivity in the solid phase compared to in solution can be seen.

(b) Derivative spectra

Derivative spectra of different orders were obtained from stored zero-order spectra using numerical differentiation with the program GBC SCAN MASTER V 1.62, being selected as more appropriate for the determination of first-order spectra. A scan speed of 250 nm min^{-1} was selected after verifying that this parameter did not influence the intensity or shape of the derivative spectra. A smoothing function was used in order to reduce the noise levels in the derivative spectra. This function was based on the Savitzky–Golay method [19]. The first-derivative spectra were smoothed using 25 experimental points.

The influence of the $\Delta\lambda$ value on the derivative spectra was tested between 0.5 and 11.5 nm. 5.7 nm was considered as suitable for the first-derivative spectrum.

Using the zero-crossing technique, we can avoid the necessity of preparing a blank by measuring the signal at $^1D_{716.0}$ ($^1D_{716.0} = 0$ for blank).
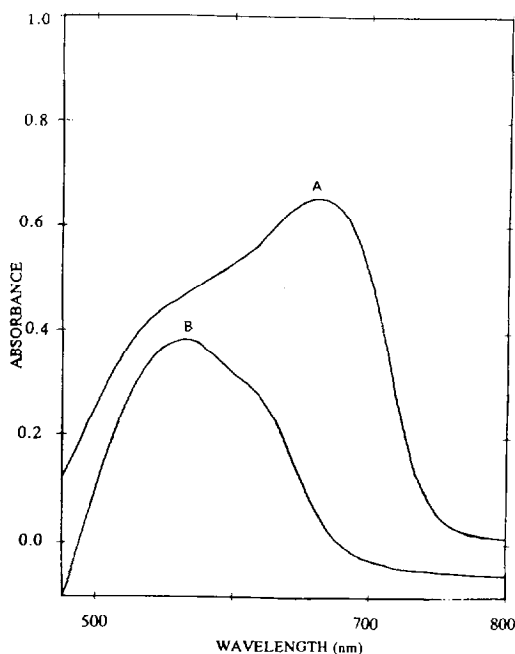
Fig. 1. Net absorption spectra of the Mo(VI)–PV complex: (A) on the resin (resin as reference), [Mo(VI)] = 1.04 × 10^{-6} M, [PV] = 6.47 × 10^{-6} M, pH 2.9, 100 ml sample, 30 mg resin, 1 mm glass cell; (B) in aqueous solution, [Mo(VI)] = 6.25 × 10^{-5} M, [PV] = 6.00 × 10^{-4} M, pH 2.9, 10 mm glass cell.

3.2. Optimization of variables

The optimum pH for the formation and fixation of the species was found within the range 2.5–3.0. The values of the first-derivative signal of the blank can be considered as zero at pH 3; at pH values above 3.0 this signal increases significantly. A 0.03 M concentration of pH 2.9 KHphthalate/HCl buffer was selected to obtain an adequate buffering capacity. The working wavelength selected was 716 nm corresponding to a maximum value of the first-derivative signal.

The effect of PV concentration was studied for 100 ml, 500 ml and 1000 ml samples, and the optimal values found were 3.88 × 10^{-6} M, 2.06 × 10^{-6} M and 1.29 × 10^{-6} M for a PV to molybdenum ratio of about 12, 16 and 16 respectively.

The optimum stirring times were 30, 60 and 120 min for 100, 500 and 1000 ml respectively. 30 mg of resin, the amount required to fill the cell and ease handling, was used in all measurements. The fixed complex was stable for at least 16 h after equilibration.

3.3. Nature and distribution of the fixed complex

The stoichiometry of the complex formed and sorbed on the resin at pH 2.9 was studied by the methods of Asmus and Job. In both instances, the ligand to metal ratio found was 1:1. This result agrees with that found in the literature [20].

The global complexation–fixation process can be represented by the following scheme:

$$MoO_2^{2+} + H_3L^- \rightleftharpoons MoO_2HL^- + 2H^+$$

(complexation process)

$$MoO_2HL^- + Cl_m^m \cdot R^{m+} \rightleftharpoons$$

$$MoO_2HL^- Cl_{m-1}^{(m-1)} \cdot R^{m+} + Cl^-$$

(fixation process)

$$MoO_2^{2+} + H_3L^- + Cl_m^m \cdot R^{m+} \rightleftharpoons$$

$$MoO_2HL^- Cl_{m-1}^{1)} \cdot R^{m+} + Cl^- + 2H^+$$

(global process)
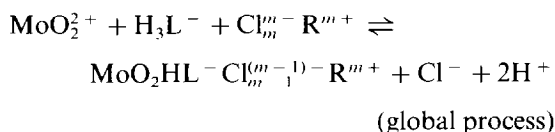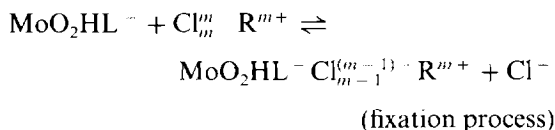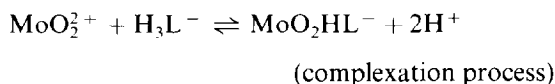
Table 1
Analytical parameters

Parameter	Volume of sample system		
	100 ml	500 ml	1000 ml
Intercept	-2.11×10^{-3}	-4.986×10^{-3}	-5.031×10^{-3}
Slope	3.064×10^{-4}	1.602×10^{-3}	2.605×10^{-3}
Linear dynamic range (ng ml^{-1})	10–80	5–18	2–8
Correlation coefficient	0.9999	0.9971	0.9979
Detection limit (ng ml^{-1}) [26]	0.114	0.032	0.024
Quantification limit (ng ml^{-1}) [27]	0.377	0.107	0.080
RSD (%)	3.52	3.14	4.30

The distribution ratio of the complex was determined and an average value of $D = (4.9 \pm 0.2) \times 10^5$ ml g^{-1} was obtained from four replicate experiments.

4. Analytical parameters

The linear dynamic ranges of the calibration graphs of the first-derivative signal and the reproducibility (RSD%), for each proposed method, are shown in Table 1. It is noticeable that the system does not rigorously follow Beer's law, as a threshold concentration seems to exist below which there is no signal. We can verify that this also happens in the solution method. Other analytical parameters are shown in Table 1. It can be observed that the values of the limit of detection (LOD) and limit of quantification (LOQ) are lower than those reported by Vilchez et al. [13] for the determination of Mo by solid-phase spectrofluorimetry, and similar to those found by us for other elements by SPS [3,6,7]. Nevertheless, the LOD and LOQ values shown in this table are really apparent due to the mentioned threshold concentration. Consequently, in practice, these values should be increased in the corresponding threshold concentration, i.e. 6.89, 3.11 and 1.93 ng ml^{-1} for 100, 500 and 1000 ml respectively.

The sensitivity, expressed as apparent molar absorptivity, of the proposed methods was compared with that of spectrophotometric procedures (including extractive procedures and formation of ternary complexes with surfactants) described in the literature [21–24]. Whereas the sensitivity of

these methods is between 1.60×10^4 and 1.3×10^5 l mol^{-1} cm^{-1}, the procedures proposed in this paper offer a sensitivity 10^3–10^4 higher than these and also higher than another method of determination of Mo by SPS [25].

This effect is expected to be more intense when the distribution ratio has a high value. In our case, D is especially high (4.89×10^5 ml g^{-1}). Hence, the increase in sample volume will produce an increase in sensitivity if the amount of resin stays constant. Thus, one of the main advantages of SPS methods is the potential increase in sensitivity with an increase in the sample volume taken for analysis. This effect can be calculated by measuring the first-derivative signal of resin equilibrated with different volumes of solutions containing the same concentration of Mo(VI) and proportional amounts of the other reagents. Fig. 2 shows that the signal increases with sample volume up to a value of 1500 ml and becomes
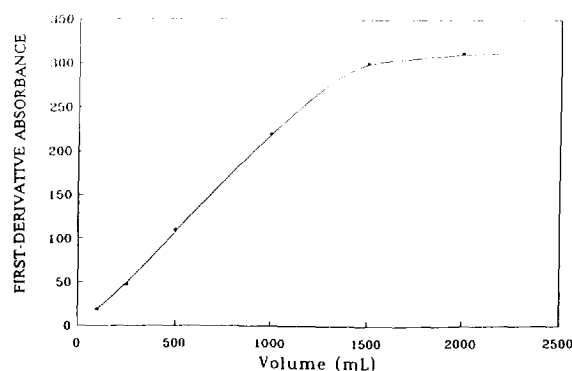
Fig. 2. Influence of the sample volume on colour development. [Mo(VI)] = 1.04×10^{-7} M, [PV] = 3.88×10^{-6} M, pH 3, 30 mg resin.

Table 2
Effect of foreign ions on the determination of 50 ng ml^{-1} of molybdenum

Foreign ion	Tolerance level (ng ml^{-1})
SO_4^{2-}	2000
NO_3^-	1500
Ca^{2+}, PO_4^{3-}	1000
F^-	900
Al^{3+}, EDTA, Zn^{2+}, Mn^{2+}	500
Cu^{2+}	300
Mg^{2+}	250
Cl^-	100
W^{6+}	25
Fe^{3+}	5

independent of the volume at higher values, as usually found in SPS.

The increase in sensitivity with increase in volume of the sample can be calculated from the slope of the calibration graphs. The calculated values of the sensitivity ratio (S) for the samples analysed in this paper are $S_{1000-100} = 8.5$, $S_{1000-500} = 1.62$ and $S_{500-100} = 5.23$, where the subscripts represent the sample volume (ml).

4.1. Effect of foreign ions

A detailed study of interference effects on the determination of molybdenum at the 50 ng ml^{-1} level was carried out following the general procedure for a 100 ml sample system. A maximum level of potentially interfering ions of 2000 ng ml^{-1} was tested. Ions were considered as non-interfering when they produced an error of less than 5% in the determination of analyte. The tolerance limits for the ions studied are summarized in Table 2. The most severe interference was caused by iron and tungsten. The latter causes a positive error because tungsten forms a complex with PV that absorbs at the wavelength used in the procedures. With respect to Fe(III), the interference could be suppressed by using 1,10-phenanthroline after reduction to Fe(II) with hydrogen in acidic medium. The cationic complex Fe(II)–phenanthroline re-

mained in solution and was not absorbed onto the anionic resin.

4.2 Analytical applications

The proposed method was applied to the determination of molybdenum in natural and industrial waters, vegetal tissues and a soil extract.

As representative samples of natural waters, we selected tap water from the Jaén city supply (higher ionic content) and natural water from Ortigosa del Monte (Segovia) (lower ionic content). The molybdenum content in all waters was lower than the detection limit of the most sensitive proposed method in this paper (1000 ml).

A recovery study was therefore carried out. The mean percentage recovery obtained for Ortigosa del Monte water was 97.8 for a 500 ml sample volume, and for tap water was 98.3, 98.3 and 97.1 for 100, 500 and 1000 ml sample volumes respectively.

The results obtained for an industrial water from a manufacturer of steel (Insisur S.A.), potato leaves and soil extracts are summarized in Table 3. A matrix effect was found in Insisur S.A. water and soil extracts which was evaluated by the ratio of slopes between the standard and standard-addition calibration graphs, found to be 0.91 and 0.69 respectively.

The average value of the molybdenum content in potato leaves and soil extracts referred to the original sample was 0.47 mg kg^{-1} (0.51 mg kg^{-1} by EAAS) and 235 μg kg^{-1} (230 μg kg^{-1} by EAAS).

The average value of the molybdenum content in industrial water (Insisur S.A.) agrees with that found by EAAS (31 ng ml^{-1}).

Acknowledgements

Table 3
Determination of Mo in real samples (100 ml sample procedure)

Sample	Molybdenum content added (ng ml^{-1})	Molybdenum content found[a] (ng ml^{-1})	Mean recovery (%)
Industrial water	--	29.06	—
(Insisur S.A.)[c]	10	40.20	111.4
	20	48.30	96.2
Potato leaves[b]	--	22.47	—
	10	32.46	99.9
	20	43.42	104.8
	30	52.85	101.3
Soil extract[c]	—	23.53	—
	10	33.2	96.7
	20	42.9	96.8

[a] Average values of three determinations.
[b] Standard calibration graph method. Analysis carried out on an aliquot of 20 ml of mineralized sample.
[c] Standard addition calibration graph method. Analysis carried out on an aliquot of 20 ml of mineralized sample.

References

[1] A. Kabata-Pendias and H. Pendias, Trace Elements in Soils and Plants, CRC Press. Boca Raton, FL, 1985, p. 203.

[2] J. Rodier, Análisis de las aguas, Omega, Barcelona, 1978, p. 838.

[3] A. Molina-Diaz, J.M. Herrador-Mariscal, M.I. Pascual-Reguera and L.F. Capitán-Vallvey, Talanta, 40 (1993) 1059.

[4] A. Molina-Diaz, J.J. Vida-Sagrista, M.I. Pascual-Reguera and L.F. Capitán-Vallvey, Int. J. Environ. Anal. Chem., 45 (1991) 219.

[5] M.I. Pascual-Reguera, A. Molina-Diaz, N. Ramos-Martos and L.F. Capitán-Vallvey, Anal. Lett., 24 (1991) 2245.

[6] M.L. Fernández de Córdova, A. Molina-Diaz, M.I. Pascual-Reguera and L.F. Capitán-Vallvey, Anal. Lett., 25 (1992) 1961.

[7] M.L. Fernández de Córdova, A. Molina-Diaz, M.I. Pascual-Reguera and L.F. Capitán-Vallvey, Fresenius' J. Anal. Chem., 349 (1994) 722.

[8] M.L. Fernández de Córdova, A. Molina-Diaz, M.I. Pascual-Reguera and L.F. Capitán-Vallvey, Talanta, 42 (1995), 1057.

[9] K. Yoshimura, H. Waki and S. Ohashi, Talanta, 23 (1976) 449.

[10] F. Capitán, E. Manzano, J.L. Vilchez and L.F. Capitán-Vallvey, Anal. Sci., 5 (1989) 549.

[11] F. Capitán, E. Manzano, A. Navalón, J.L. Vilchez and L.F. Capitán-Vallvey, Talanta, 39 (1992) 21.

[12] F. Capitán, G. Sánchez-Palencia, A. Navalón, L.F. Capitán-Vallvey and J.L. Vilchez, Anal. Chim. Acta, 259 (1992) 345.

[13] J.L. Vilchez, G. Sánchez-Palencia, R. Blanc, R. Avidad and A. Navalón, Anal. Lett., 27 (1994) 2355.

[14] H. Ishiih, Fresenius' Z. Anal.Chem., 319 (1984) 23.

[15] L.F. Capitán-Vallvey, I. de Orbe, M. Valencia and J.J. Berzas-Nevado, Anal. Chim. Acta, 282 (1993) 75.

[16] L.F. Capitán-Vallvey, I. de Orbe, J.J. Berzas-Nevado and F. Salinas, Quim. Anal., 13 (1994) 126.

[17] M.I. Pascual-Reguera, A. Molina-Diaz, M.C. Pacheco-Castillo, M.C. Anguita-Fernández, M.L. Fernández de Córdova and L.F. Capitán-Vallvey, Mikrochim. Acta, 112 (1994) 225.

[18] E. Esteban-Velasco and A. Aguilar, Proc. 4e Coll. Int. sur le Contrôle de l'Alimentation des Plantes Cultivées. Gent, Vol., 1976, p. 219.

[19] A. Savitzky and M.J.E. Golay, Anal. Chem., 36 (1964) 1627.

[20] A.K. Majumdar and C.P. Savariar, Naturwissenschaften, 45 (1958) 84.

[21] Z. Marczenko, Separation and Spectrophotometric Determination of Elements, Ellis Horwood, Chichester, 1986, pp. 383-384.

[22] B.W. Bailey, J.E. Chester, R.M. Dagnall and T.S. West, Talanta, 15 (1968) 1395.

[23] M.B. Shustova and V.K. Nazarenko, Zh. Anal. Khim., 18 (1963) 964.

[24] L.I. Ganago and I.F. Ivanova, Zh. Anal. Khim., 35 (1980) 1138.

[25] F. Capitán, L.F. Capitán-Vallvey and M.C. Gómez, Quim. Anal., 6 (1987) 343.

[26] IUPAC, Nomenclature, symbols, units and their usage in spectro-chemical analysis. Pure Appl. Chem., 45 (1976) 105.

[27] Guidelines for data acquisition and data quality evaluation in environmental chemistry, Anal. Chem., 52 (1980) 2242.

ELSEVIER

Talanta

Flow-injection fluorimetric determination of nabam and metham

Tomás Pérez-Ruiz*, Carmen Martínez-Lozano, Virginia Tomás, Rocio Casajús

Department of Analytical Chemistry, Faculty of Chemistry, University of Murcia, 30071 Murcia, Spain

Abstract

A simple and sensitive flow-injection fluorimetric method was developed to determine nabam or metham in water and cereal samples. The procedure is based on the oxidation of these pesticides by thallium(III) with the concomitant formation of fluorescent thallium(I). Lineal calibration graphs were obtained between 0.25 and 2.56 μml^{-1} for nabam, and between 0.26 and 2.65 μg ml^{-1} for metham. The sampling rate was 80 samples h^{-1}. The method was satisfactorily applied to the direct analysis of water, wheat, barley and oat samples spiked with nabam or metham.

Keywords: Nabam; Metham; Flow injection; Fluorimetry

1. Introduction

Metham (sodium N-methyldithiocarbamate) and nabam (disodium ethylenebis[dithiocarbamate]) are two well-known dithiocarbamate fungicides widely used against a variety of plant pathogenic fungi. They are highly mobile in soil and can leach into groundwater. Although dithiocarbamate pesticides are used primarily on field crops and cereals, appreciable amounts of lettuce and other vegetables and fruits are also treated. The maximum residue limits for dithiocarbamates (expressed as carbon disulphide) which are being considered by the European Union are 2–7 mg kg^{-1}.

Dithiocarbamates are generally determined on the basis of their decomposition by hot mineral acid to amines and carbon disulphide. This is then absorbed in methanolic potassium hydroxide solution and the potassium methyl xantate thus formed is titrated iodometrically [1]. Alternatively, carbon disulphide is absorbed in an ethanol solution containing copper(II) and an alkylamine to form copper dialkyldithiocarbamate chelates, which can be determined photometrically [2,3]. Gas chromatography, including head-space analysis [4,5] and liquid chromatographic methods [6,7], has also been used to determine dithiocarbamate residues.

Analytical methods which use processes other than acid decomposition include iodometry in anhydrous solvents [8,9], indirect titration with EDTA [9,10], polarography [11] and determination of the metallic component of herbicides using different approaches [12,13].

Flow-injection analysis has proved to be a very useful and versatile automated technique for the determination of a large number of inorganic and

---

*Corresponding author.

organic analytes [14,15]. However, no flow-injection method has been found to deal with the determination of the dithiocarbamates.

In this paper the development of a fluorimetric flow-injection method for the determination of metham and nabam is described. The determination is based on the oxidation of these pesticides by thallium(III) and the parameter measured is the fluorescence of thallium(I) formed during the reaction. This violet fluorescence has been attributed to the existence of the anionic $TlCl_4^{3-}$ complex [16,17] and hence the reaction is carried out in the presence of hydrochloric acid.

The proposed method is simple and sensitive, and enables these two pesticides to be determined in waters and cereals.

2. Experimental

2.1. Apparatus

A SLM-Aminco (Urbane, Illinois, USA) Series 2 spectrofluorimeter was used for recording spectra; excitation and emission spectra were corrected. A Perkin-Elmer (Norwalk, CA, USA) Model 3000 spectrofluorimeter equipped with a Hellma (Müllheim, Baden, Germany) 176.052 QS flow cell (inner volume 25 μl) and connected to a Linseis (Selb, Germany) 6512 recorder was used as the detector in the flow-injection system.

A Gilson (Villiers Le Bell, France) Minipuls HP4 peristaltic pump and an Omnifit (Cambridge, UK) injection valve were also used.

2.2. Reagents

All chemicals used were of analytical-reagent grade; doubly distilled water was used for the preparation of solutions and all dilutions.

Metham and nabam were obtained from Riedel-de Haën (Seelze, Germany) and used as received. Stock solutions (200 mg 1^{-1}) of these pesticides were prepared by dissolving 20.0 mg of each compound in doubly distilled water and diluting to 100 ml in a calibrated flask. Working solutions of lower concentration were freshly prepared by appropriate dilution with water.

Thallium(III) stock solution $(1.0 \times 10^{-3}$ M) was prepared by dissolving the required amount of $TlCl_3$ (Fluka, Buchs, Switzerland) in 0.5 M hydrochloric acid. Solutions of lower concentration were prepared from the stock solution by appropriate dilution with 0.5 M hydrochloric acid.

2.3. Manifold design

The configuration of the flow-injection (FI) manifold used is shown in Fig. 1 with the optimum conditions as stated. With the exception of the pump tubing (Tygon), PTFE tubing (0.5 mm i.d.) was used throughout the manifold. The fluorescence intensity of thallium(I) formed in the reaction between thallium(III) and the pesticides was measured at 419 nm with excitation at 227 nm. The spectrofluorimeter was set with 10 nm excitation and emission slits.

2.4. Basic procedure

The samples containing between 0.25 and 2.56 μg ml^{-1} of nabam or between 0.26 and 2.65 of metham were aspirated into the sample loop (200 μl) of the injection valve by means of the peristaltic pump, and injected into the pre-mixed hydrochloric acid and the thallium streams of the FI manifold (see Fig. 1). The concentration of these pesticides was evaluated from the peak height with a calibration graph prepared using freshly prepared nabam or metham standard solutions.
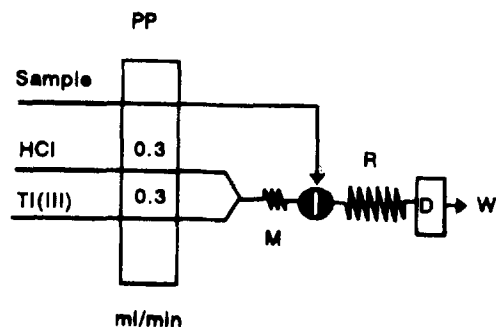
Fig. 1. Manifold for the determination of nabam and metham: PP, peristaltic pump (with flow rates given in ml min^{-1}); M, mixing coil (20 cm); R, reaction coil (100 cm for nabam and 150 cm for metham); D, detector; W, waste.
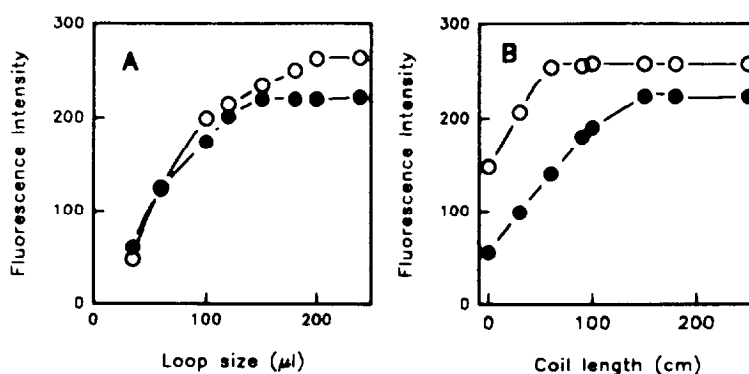
Fig. 2. Effect of the loop size (A) and the reaction coil (B) on peak height for nabam ( ) and metham (●).

2.5. Determination of nabam or metham in water

The samples were diluted as appropriate with doubly distilled water and analysed following the basic procedure.

2.6. Determination of nabam or metham in grains

About 10 g of accurately weighed wheat, barley or oat was sprayed with 5 ml of an aqueous solution containing between 5 and 100 μg ml^{-1} of nabam or metham. The samples were then allowed to dry in the sun for 1 h and thereafter in the shade for 24 h to remove extraneous moisture. For each determination a blank assay was carried out by spraying the same amount of grain with 5 ml of water. The samples were weighed again in order to determine the amount of pesticide retained. The previously ground samples were treated with 50 ml of 0.1 M sodium hydroxide, sonified for 10 min and centrifugated at 2000 rpm for 5 min. Aliquots of the resulting solutions were filtered and processed following the basic procedure.

3. Results and discussion

We have found that nabam and metham are oxidized by thallium(III) to form fluorescent thallium(I). These reactions seemed more quantitative when performed in acid media. The nature of the acid proved important because the fluorescence intensity of thallium(I) increases with increasing

chloride and ion hydrogen concentrations [16–19]. A maximum, stable fluorescence intensity was obtained when the concentration of hydrochloric acid was 0.6 M for nabam and 0.3 M for metham.

Alternatively, both nabam and metham can be oxidized in a flow system by injection into a thallium(III) solution flowing on-line. A two-line FI manifold with fluorimetric detection is suitable for the determination of both pesticides. The manifold represented in Fig. 1 was used to investigate the effect of chemical and FI variables on the peak height.

3.1. Optimization of manifold parameters

The variables studied were volumed of injected sample, flow rate and length of the reaction coil. The reagent concentrations used in the experiments were as follows: thallium(III) line, 2.0 × 10^{-4} M; hydrochloric acid line, 0.3 M. The mixing ratio between both streams was always 1:1.

The sample volume was varied between 35 and 240 μl (Fig. 2A). A sample volume of 200 μl was pre-selected for both pesticides in order to obtain maximum peak heights.

The peak height obviously depends on the residence time of the sample zone in the system, i.e. on the total flow rate and the tube length. The effect of the flow rate was checked over the range 0.4–2.4 ml min^{-1}. The lower flow rates gave higher fluorescence intensities although, up to 0.5 ml min^{-1}, the peak-height reproducibility was poor and the peaks were so broad that the sample
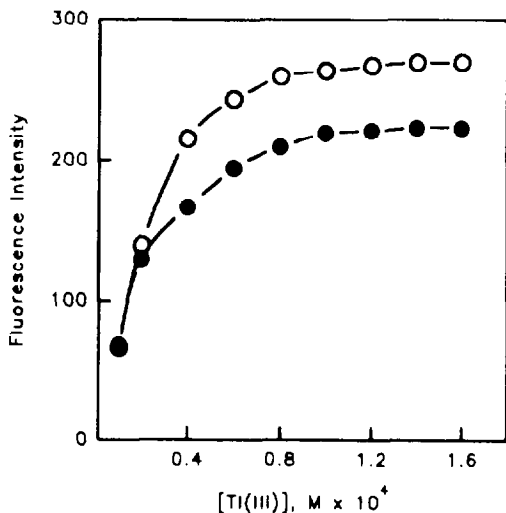
Fig. 3. Influence of Tl(III) on peak height for nabam (○) and metham (●).

3.2. Optimization of reagent concentration

The effect of varying the concentrations of thallium(III) and hydrochloric acid was tested in the optimized flow system.

The peak heights for both pesticides increased with increasing thallium(III) concentration up to 9.0×10^{-5} M, above which they remained virtually constant (Fig. 3). The concentration selected was 1.0×10^{-4} M.

The concentration of hydrochloric acid used as a carrier was selected to obtain the required optimum level when the sample zone merged with the thallium(III) stream, which was 0.5 M in HCl. The carrier selected for nabam and metham was 0.7 and 0.1 M hydrochloric acid, respectively.

3.3. Calibration graph

A series of standard solutions of nabam and metham were injected into the manifold under the optimized conditions to test the linearity of the calibration graphs. The figures of merit corresponding at these two analytes are summarized in Table 1, from which the excellent sensitivity of the proposed method is evident. The sample throughput was about 80 samples h^{-1}.

3.4. Interferences

An interference study to determine nabam or metham in real samples was performed. Samples containing a fixed concentration of each pesticide and various concentrations of foreign substances were injected into the FI system. Tolerance was defined as the amount of foreign substance induc-

throughput was very low. A flow rate of 0.6 ml min^{-1} was pre-selected as a compromise between reproducibility, sensitivity and sample throughput.

The length of the reaction coil was examined over the range 0–240 cm. Fig. 2B shows that a coil of 100 cm for nabam and of 150 cm for metham permitted the maximum peak height to be obtained.

An iterative procedure was followed, in that after the first round of experiments the best conditions were taken as the starting point for a further optimization cycle. This resulted in only a very small improvement; thus, the new values can be considered as very close to the optimum: sample volume injected, 220 μl; flow rate, 0.6 ml min^{-1}; coil length, 110 cm for nabam and 170 cm for metham.

Table 1
Features of the calibration graphs for the determination of nabam and metham

	Nabam	Metham
Determination range	1.0×10^{-6}–1.0×10^{-5} M	1.0×10^{-6}–1.0×10^{-5} M
Slope (L_F M^{-1})	37.8×10^6	18.5×10^6
Intercept (L_F)	6.7	3.4
Correlation coefficient[a]	0.999	0.998
RSD (%)[b]	1.4; 0.8	1.2; 0.5

[a]The correlation coefficient was calculated using 11 different concentrations of each analyte.
[b]Relative standard deviation (n = 10). Concentration levels: 3×10^{-6} M; 7×10^{-6} M.

Table 2
Tolerance to different substances in the determination of nabam and metham

Substance added	Tolerance molar ratio Interferent: pesticide	
	Nabam	Metham
Urea. sulphate. chloride, acetate, perchlorate, sodium(I), potassium (I). ammonium	1000	1000
Phosphate, tartrate	1000	800
Calcium(II), magnesium(II), zinc(II)	800	500
Citric acid, glucose, alanine	800	100
Glycine, aluminium(III), cadmium(II), manganese(II)	50	20
Oxalate, nitrate	10	10
Thiamine, cysteine, ascorbic acid, uric acid	5	1
Lead(II), iron(III)	1	0.5
Copper(II), bismuth(III), mercury(II)	0.1	0.1

Pesticide concentration: 2.5×10^{-6} M.

ing errors lower than 3% in the determination of the analyte. Table 2 shows the results obtained.

The interference of metallic ions can be eliminated by passing the solution through strongly a acidic cation-exchange (sodium form) column. The interference of ascorbic acid can be minimized by heating the solution to 60°C in the presence of 0.1 M sodium hydroxide.

Nabam or metham, if present in other common dithiocarbamate pesticides such as thiram, disulphuram, zineb, maneb and ziram, can easily be separated by extraction with chloroform: nabam or metham will remain in the aqueous phase which can then be analysed following the basic procedure.

3.5. Analysis of real samples

To investigate the applicability of the proposed FI method to real samples, nabam and metham were determined in water and cereal grain. The results in Tables 3 and 4 show that the method is applicable to water and grains sprayed with solutions of these pesticides. Taking into account that the recoveries obtained are close to 100%, it may be assumed that no interfering substances were encountered.

The determination of residues of nabam in wheat grains under field conditions is summarized in Table 5. The results show that nabam residues as measured by the proposed FI procedure were in excellent agreement with those obtained by the manual carbon disulphide spectrophotometric method.

Table 3
Recovery of nabam from treated water and grain samples

Sample	Added	Found[a]	Recovery (%)
Water ($\mu g \ ml^{-1}$)			
Tap water	0.30	0.29 ± 0.02	96.6
	0.40	0.39 ± 0.01	97.5
Irrigation water	0.40	0.41 ± 0.01	102.5
	0.50	0.52 ± 0.01	104.0
Grain ($\mu g \ g^{-1}$)			
Wheat	2.5	2.6 ± 0.2	104.0
	10.0	9.9 ± 0.2	99.0
Barley	4.0	4.1 ± 0.1	102.5
	8.0	7.93 ± 0.06	99.1
Oat	4.0	3.83 ± 0.06	95.75
	10.0	9.9 ± 0.2	99.0

[a]Average $\pm$ SD of three analyses.

Table 4
Recovery of metham from treated water and grain samples

Sample	Added	Found[a]	Recovery (%)
Water ($\mu g \ ml^{-1}$)			
Tap water	0.30	0.29 ± 0.02	96.6
	0.50	0.51 ± 0.02	102.0
Irrigation water	0.40	0.42 ± 0.01	105.0
	0.50	0.52 ± 0.01	104.0
Grain ($\mu g \ g^{-1}$)			
Wheat	4.0	3.8 ± 0.1	95.0
	8.0	7.86 ± 0.06	98.2
Barley	2.5	2.43 ± 0.06	97.2
	5.0	4.8 ± 0.1	96.0
Oat	4.0	3.83 ± 0.05	101.5
	6.0	6.1 ± 0.1	101.6

[a]Average $\pm$ SD of three analyses.

Table 5
Determination of nabam residues from wheat

	Fl method[a] (mg kg^{-1})	Reference method[a] (mg kg^{-1})
Sample 1[b]	2.2 ± 0.2	2.1 ± 0.1
Sample 2[b]	2.4 ± 0.1	2.2 ± 0.1
Sample 3[c]	4.3 ± 0.2	4.1 ± 0.2
Sample 4[c]	4.1 ± 0.1	4.2 ± 0.2

[a]Average ± SD of five analyses.
[b]Samples 1 and 2 from an experimental greenhouse treated with 20 l of 2 g l^{-1} nabam solution. Harvested 20 days after nabam application.
[c]As for footnote b but treated with 20 l of 4 g l^{-1} nabam solution.

Acknowledgements

References

[1] Official Methods of Analysis, in W. Horwith (Ed.), AOAC, 30th edn., Arlington, VA, 1980, p. 110.
[2] D.G. Clarke, H. Baum, E.L. Stanley and W.F. Hester, Anal. Chem., 23 (1951) 1842.
[3] W.K. Lowen, Anal. Chem., 23 (1951) 1846.
[4] H.A. McLeod and K.A. McCully, J. Assoc. Off. Anal. Chem., 52 (1969) 1226.
[5] Panel on Determination of Dithiocarbamates Residues of the Committee for Analytical Methods for Residues of Pesticides and Veterinary Products in Foodstuffs of the Ministry of Agriculture, Fisheries and Foods, Analyst, 106 (1981) 782.
[6] F.J. Lawrence, F. Iverson, H.B. Hanekamp, P. Bos and R.W. Frei, J. Chromatogr., 212 (1981) 245.
[7] H. Irth, G.J. de Jong, R.W. Frei and U.A. Th. Brinkman, Int. J. Environ. Anal. Chem., 39 (1990) 129.
[8] A.F. Grand and M. Tamres, Anal. Chem., 40 (1968) 1904.
[9] D.D. Clyde, J. Assoc. Off. Anal. Chem., 66 (1983) 646.
[10] A.S. Hyman, Analyst, 94 (1969) 152.
[11] D.J. Halls, A. Townshend and P. Zuman, Analyst, 93 (1968) 219.
[12] M.C. Quintero, M. Silva and D. Pérez-Bendito, Anal. Chim. Acta, 222 (1989) 269.
[13] M.C. Quintero, M. Silva and D. Pérez-Bendito, Talanta, 38 (1991) 359.
[14] J. Ruzicka and E.H. Hansen, Flow Injection Analysis, Wiley, New York, 1988.
[15] M. Valcarcel and M.D. Luque de Castro, Flow Injection Analysis: Principles and Applications, Ellis Horwood, Chichester, 1987.
[16] G.F. Kirkbright, T.S. West and C. Woodwards, Talanta, 12 (1965) 517.
[17] G.H. Schenk, Absorption of Light and Ultraviolet Radiation: Fluorescence and Phosphorescence Emission, Allyn and Bacon, Inc., Boston, MA, 1973, p. 221.
[18] R.E. Curtice and A.B. Scott, Inorg. Chem., 3 (1964) 1383.
[19] P.J. Mayne and G.F. Kirkbright, J. Inorg. Nucl. Chem., 137 (1975) 1527.

Quantitation of the global secondary structure of globular proteins by FTIR spectroscopy: comparison with X-ray crystallographic structure[1]

Thomas F. Kumosinski*, Joseph J. Unruh

U.S. Department of Agriculture, ARS, Eastern Region Research Center, 600 East Mermaid Lane, Philadelphia, PA 19118, USA

Abstract

Fourier transform infrared spectroscopy (FTIR) is potentially a powerful tool for determining the global secondary structure of proteins in solution, providing the spectra are analyzed using a statistically and theoretically justified methodology. We have performed FTIR experiments on 14 globular proteins and two synthetic polypeptides whose X-ray crystal structures are known to exhibit varying types and amounts of secondary structures. Calculation of the component structural elements of the vibrational bands was accomplished using nonlinear regression analysis, by fitting both the amide I and amide II bands of the Fourier self-deconvoluted spectra, the second-derivative spectra, and the original spectra.

The methodology was theoretically justified by comparing (via nonlinear regression analysis) the global secondary structure determined after deconvolving into component bands the vibrational amide I envelopes with the calculated structure determined by first principles from Ramachandran analysis of the X-ray crystallographic structure of 14 proteins from the Brookhaven protein data bank. Justification of the nonlinear regression analysis model with respect to experimental and instrumental considerations was achieved by the decomposition of all the bands of benzene and an aqueous solution of ammonium acetate into component bands while floating the Gaussian/Lorentzian character of the line shapes. The results for benzene yield all pure Lorentzian line shapes with no Gaussian character while the ammonium acetate spectra yielded all Gaussian line shapes with no Lorentzian character. In addition, all-protein spectra yielded pure Gaussian line shapes with no Lorentzian character. Finally, the model was statistically justified by recognizing random deviation patterns in the regression analysis from all fits and by the extra sum of squares F-test which uses the degrees of freedom and the root mean square values as a tool to determine the optimum number of component bands required for the nonlinear regression analysis.

Results from this study demonstrate that the globular secondary structure calculated from the amide I envelope for these 14 proteins from FTIR is in excellent agreement with the values calculated from the X-ray crystallographic data using three-dimensional Ramachandran analysis, providing that the proper contribution from GLN and ASN side chains to the 1667 and 1650 cm^{-1} component bands has been taken into account. The standard deviation of the

---

regression analysis for the per cent helix, extended, turn and irregular conformations was found to be 3.49%, 2.07%, 3.59% and 3.20%, respectively.

1. Introduction

Previous studies comparing the global secondary (2°) structure of globular proteins calculated from their X-ray crystal structure with those determined from Fourier self-deconvolution (FSD) FTIR spectroscopy were performed in D_2O. However, D_2O may cause increased hydrophobic interactions which could lead to spurious 2° structural changes in some proteins [1]. Using D_2O also results in the elimination of the amide II peptide band, which may be helpful for validation of the amide I assignments. With the use of an extremely short path length (6–12 μm) and accurate water vapor subtraction [2], the determination of protein secondary structure in H_2O, using both the amide I and amide II regions, is now possible. However, controversy exists among researchers concerning the deconvolution of the FTIR amide I and II envelopes into their component bands. Not only the number of bands, but also the character of the bands (whether they are of pure Gaussian, pure Lorentzian, or a combination of Gaussian and Lorentzian character) is suspect. In addition, when using FSD to ascertain the number of bands, the magnitude of the half-width at half-height of the band and the value of the resolution enhancement factor (REF) are also open to discussion. Additionally, when experiments are performed in H_2O, the amide II band, while present, is not always deconvolved. Analysts also routinely apply conservatively low values for the REF with large half-width at half-height values of 13–18 cm^{-1}, in order to not overdeconvolute the spectrum, and in the next step (nonlinear regression analysis), only the smallest number of component bands are used for the nonlinear regression analysis.

The rational for these procedures is to avoid the possibility of distorting the experimental spectrum. However, no studies analyzing the same spectrum using nonlinear regression analysis with varying FSD parameters have as yet been performed; thus the optimum parameter limits to use without causing distortion are unknown. Using higher REFs and narrower half-widths during FSD increase the number of component bands. We will attempt to show that properly choosing to use this increased number of bands (with equal half-widths at half-height) in the nonlinear regression fit of the experimental spectrum results in much lower root mean square (RMS) values (i.e. the square root of the average of the squares of the differences between the experimental spectra and the nonlinear regression fitted spectra).

While nonlinear regression analysis using an increased number of component bands is more difficult and more time consuming (and cannot be easily performed on older microcomputers), the correct number of peaks must be obtained to insure the correct band assignments to the secondary structure of the protein. If one band is used when two are predicted from theory, then a larger amount of disordered, helical or extended structure could be calculated because of incorrect assignments. With the methodology employed herein, the researcher can use the maximum number of component bands to fit the theoretical curve to the experimental data. This in fact yields the lowest RMS value, and the amide II envelope is fit simultaneously with the amide I envelope. It is critical to allow a zero slope baseline to vary to a calculated value. It is noted that during the calculations, the use of too many bands may result in the heights of the excess bands approaching a zero or negative value. The number of bands were controlled by use of the F-test as well as the agreement of calculated frequencies with previously reported experimental and theoretical assignments. Thus, the statement that excessive numbers of bands always yield better fits to the data is not valid. This statement only applies to the use of polynomial curve fitting algorithms and not to nonlinear regression analyses.

In this work we measure FTIR spectra in H_2O of 14 globular proteins and two polypeptides — with varying types and amounts of 2° structures — whose X-ray crystal structures are known. A more complete theoretically, experimentally, and statistically based analysis of the spectral data in H_2O using FSD, second-derivative spectra, and band curve-fitting techniques is presented. The analysis allows the individual 2° structural components to be distinguished and then compared with results in D_2O [3,4] and with the global 2° structural parameters calculated from the protein X-ray crystallographic data. Previous frequency assignments of structural components are also assessed and contrasted with the new information in H_2O.

2. Methods

2.1. Infrared measurement

The individual proteins were prepared as 4 solutions (by weight) in a 20 mM imidazole buffer, pH 6.7. All protein solutions and buffers were filtered using a HVIP 0.45 μm Millipore low-protein retention filter prior to the FTIR experiments. The protein concentrations after filtration were calculated from their respective absorptivities at 280 nm. All samples were introduced into a demountable cell with CaF_2 windows and a 12 μm Teflon spacer. Spectra were obtained using a Nicolet 740 FTIR spectrometer equipped with the Nicolet 660 data system. Data collection was carried out following a 30 min nitrogen purge of the sample chamber. Eight data sets of 512 drift and intensity correlated interferograms were collected, coadded (net for each spectrum was 4096 double-sided interferograms with 16 384 data points), phase-corrected, apodized (Happ-Genzel function), and fast-Fourier transformed. The eight data sets were routinely checked for drift using calculated second derivatives before summing. Nominal instrument resolution was 2 cm^{-1} with one data point every 1 cm^{-1}. Water vapor absorption was routinely subtracted from all spectra using the second-derivative method [2].

To reduce the water vapor in the sample chamber, the FTIR spectrometer is purged with nitro-

gen which has been passed through a Balston model 75-52 FTIR purge gas generator, drying the nitrogen to a dew point of $-100°F$. In addition, three additional nitrogen purging lines were added to the sample compartment of the FTIR spectrometer, the net effect being a purge rate of 60 l min^{-1}. The total amount of water vapor observed by the IR detector in the course of a typical protein solution scan is illustrated in Fig. 1A, where the water vapor spectrum is represented by crosses. For comparison purposes, the FTIR amide I and II envelopes of the FSD spectra of trypsin, the component bands obtained from the nonlinear regression fit of the amide I and II envelopes, and the resulting sum of the component bands are also illustrated (as single lines). (The use of nonlinear regression analysis for decomposition of the amide I and II envelopes into component bands will be discussed in another section of this manuscript.) As can be seen in Fig. 1A, the water vapor spectrum is significantly smaller than the actual protein amide I and II envelopes as well as the component bands derived from nonlinear regression analysis. The heights are 50–100 times smaller and the half-widths at half-height are also significantly smaller in magnitude. Thus, even if no vapor subtraction is performed on the protein FTIR spectrum, the water vapor spectrum cannot be a source of the component bands attributed to the protein. Hence, the proposition that the component bands derived from nonlinear regression analysis are useful in defining unique populations of protein vibrating molecular groups is valid.

It is important to emphasize that to obtain acceptable FTIR spectra of proteins in water, a good signal-to-noise ratio (SN) is mandatory. SN is dictated by the sensitivity, resolution and stability of the FTIR spectrometer and its computer. For our system, only a resolution of 2 cm^{-1} is possible due to the long scanning times required for a 1 cm^{-1} resolution spectrum, i.e. four times as long or approximately a 2 h scan. However for researchers having a quicker, more sensitive and stable instrument (such as a Nicolet 800 series spectrophotometer), a resolution of 1 cm^{-1} should be possible to attain, although for comparison purposes, an FTIR spectrum of one protein (with corresponding buffer, background and vapor spec-

(A)   WAVENUMBER, cm⁻¹

(B)   WAVENUMBER, cm⁻¹

(C)   WAVENUMBER, cm⁻¹
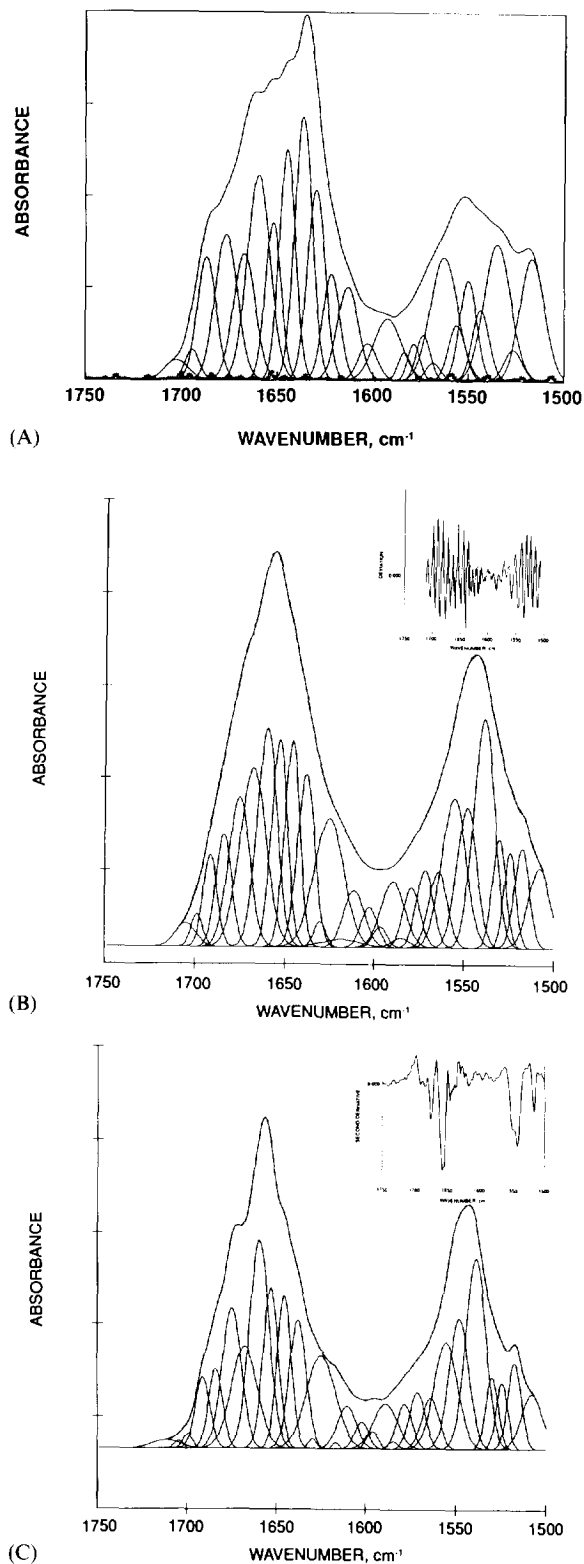
tra) was accumulated at a resolution of 1 cm^{-1}. Decomposition of this spectrum into component bands by nonlinear regression analyses yielded fractional areas for both the amide I and II envelopes in agreement to within 1% with fractional areas from the spectrum of the same protein solution collected at a resolution of 2 cm^{-1}. Also, using the 2 cm^{-1} resolution parameters, a protein solution was diluted to a concentration of 3% with buffer, and its FTIR spectrum was accumulated. Comparison of the areas of the component bands from nonlinear regression analysis agreed to within 1% with those determined using a 4% solution. These two tests add confidence to the methodology used in this study.

To ascertain whether the FTIR instrumental parameters yield line shapes that are Lorentzian, Gaussian or composites of both line shapes, FTIR spectra were obtained for benzene using KBr windows and an aqueous solution of ammoniuim acetate using CaF_2 windows. Our regression analysis program contains line shape parameters for the amount of Gaussian character (i.e. pure Gaussian, 1; pure Lorentzian, 0), the line shape is varied along with the frequency position, height, and half-width at half-height variables. The results conclusively show that all component bands

Fig. 1. (A) FSD FTIR spectra of the amide I and II envelopes of trypsin in H_2O, represented by the solid line; component bands from nonlinear regression analysis, and the composite sum of the bands are also represented as solid lines (note: the composite sum and the FSD overlap). The crosses denote the atmospheric water vapor FTIR spectrum experienced during a typical protein accumulation if no second-derivative water vapor subtraction is performed. The crosses also represent all instrumental and phase errors (see Section 2 of text). (B) FTIR spectrum showing the amide I and amide II envelopes of lysozyme in aqueous solution. The outer envelope double line represents the original spectrum. The single line on the outer envelope and the individual component bands underneath are the results of nonlinear regression analysis, as described in the text. The inset shows a plot of connected residuals or deviations between calculated and experimental absorbances vs. frequency. (C) Fourier self-deconvolution of the FTIR spectrum of lysozyme in Fig. 1. The single line on the outer envelope and the individual component bands underneath were found by nonlinear regression analysis as described in the text. The double line represents connected experimental data. The inset shows the unsmoothed second derivative of the original spectrum.

of benzene have pure Lorentzian line shapes —
the theoretical line shape for most pure condensed
phase samples and gases [5]. While the aqueous
ammonium acetate solution spectra yield pure
Gaussian line shapes — theoretically predicted by
Beer's law for the absorbance of a solid dissolved
in a liquid [5]. In addition, all residual plots had a
pseudorandom character, with a magnitude equiv-
alent to an instrument residual plot.

2.2. Data analysis

Protein spectra (amide I and II regions) were
obtained by subtracting the buffer spectra from
the respective protein solution spectra in the
$2000-1350$ cm^{-1} region. Subtractions were per-
formed interactively using the subtraction func-
tion in the Sx software of the Nicolet 660 data
system. The scaling factor (FCR) was individual-
ized during each subtraction by adjusting the
FCR parameter value until the region from 2000
to 1800 cm^{-1} was as flat as possible. The sub-
tracted region from 1800 to 1350 cm^{-1} was then
saved as the protein spectrum. This method for
subtraction does not take into account the spec-
tral modifications due to water–protein interac-
tions. Previous NMR studies by Kakalis and
Kumosinski [6] have shown that the water–
protein interaction is small on a molar basis (wa-
ter to protein), and therefore should not interfere
with this type of subtraction. The protein spectra
thus obtained were then used to calculate the
second-derivative spectra by a simple analytical
procedure that employs every data point [3]. Sec-
ond-derivative spectra served as sensitive indica-
tors for the identification of individual peak
positions, and the initial number of bands to be
used in subsequent nonlinear regression analysis.
The unresolved spectra were subjected to FSD
using an algorithm developed from that described
by Kauppinen et al. [7].

FSD was undertaken with a number of resolu-
tion enhancement factors. Qualitatively, under-
FSD was judged by the absence of peak positions
indicated in the spectra and over-FSD by the
appearance of side lobes in the flat portions of the
spectra [4]. Over-FSD also resulted in excessively
low baselines computed by the regression routine.

The methodology used will be illustrated for
lysozyme.

All spectra were deconvolved (decomposed into
their component structural elements) using a
Gauss–Newton nonlinear iterative curve-fitting
program ABACUS developed at this laboratory [8],
which can assume Gaussian, Lorentzian shapes or
a combination of both for the band envelope
shape of the resolved component bands. The de-
convolving curve-fitting program was applied only
to the amide I and II envelopes, which consisted
of at least 200 experimental points. In practice,
the four parameters of each component band
(Lorentzian character, height, peak frequency,
and half-width at half-height) were allowed to
float during the iterations, as was the baseline.
Integrated areas were calculated for those peaks
that correspond to conformational elements, e.g.
helices, sheets, turns, and loops [9]. This proce-
dure yielded the relative areas of the component
bands, which serve to estimate the fraction of the
various 2° structural elements in the protein
molecule.

3. Results

3.1. Sample calculation: analysis of lysozyme

A typical FTIR spectrum of hen's egg white
lysozyme showing the amide I and amide II re-
gions is shown as the outer envelope in Fig. 1B.
This spectrum can be considered to be the sum of
a variety of individual bands arising from the
specific structural components of the protein, such
as α-helix, β-sheets and turns. Identification of all
the components of the spectrum by fitting it di-
rectly with an undefined number of peaks by
nonlinear regression would be a daunting task. To
alleviate this dilemma, we first examine the second
derivative of the spectrum (inset, Fig. 1C) to find
the number of component bands and the approxi-
mate positions of those bands, and to compare
these assignments with those of Byler and Susi [3].

The next step in the analysis is to enhance the
resolution of the original spectrum via an FSD
algorithm. Care must be taken to choose the
proper half-width and REF values used in the

algorithm so that the FTIR spectrum is not over or under FSD.

Initially, all amide I component band assignments of Byler and Susi [3] are used to fit the FSD spectra, along with comparable theoretical amide II bands and side-chain assignments from Krimm and Bandekar [10]. Initial half-width at half-height values are assigned as 2 or 2.5 cm^{-1}, while the initial heights are assigned values higher than the FSD experimental data. The number of bands fit to the amide I and amide II envelopes is also controlled via the statistical F-test, which will be discussed later.

For faster convergence of the nonlinear regression analysis, the investigator may initially float only the heights, the half-widths at half-height, or the peak positions and the Gaussian/Lorentzian parameter in an alternating fashion during the process of the fitting program. Later, three of the parameters can be floated in an alternating fashion. And finally, all four parameters are floated simultaneously until the nonlinear regression analysis converges. The criteria for progress in the nonlinear regression analysis is a continually decreasing RMS value. If divergence takes place, the iteration factor that determines the step increase in the parameter values for the next iteration should be lowered. It is mandatory that the baseline value be allowed to vary during all of the above iterations. The imposition of a fixed baseline value adds error to the results, slows the convergence process, and in some cases causes calculations which ultimately diverge.

In addition, to alleviate the local minima problem, the whole process should be repeated starting with heights of the components that are lower in value than the FSD experimental data. The results of these two calculatons should be in agreement. Failure of these two calculations from different starting points to agree for all component bands indicates local minima resulting from use of a lower number of component bands. It is noted that all calculations using nonlinear regression analysis should be performed in this manner.

Fig. 1C shows the fit of 29 component Gaussian bands for the Fourier self-deconvoluted amide I and II FTIR envelope of lysozyme using deconvolution values of 13 cm^{-1} and 2 REF. The

RMS value for this fit is 0.000125 which is well within the criteria for acceptability as stated above. This lack of Lorentzian character is in agreement with the conclusions of Byler and Susi [3] that only Gaussian component band shapes occur in FSD spectra.

The use of a high REF value results in over-FSD of the FTIR spectra, usually an unacceptable RMS value, and a baseline value far below that expected from the experimental data. Repeating the above nonlinear regression process at a variety of FSD parameters for all the proteins in our database yielded the optimum FSD parameter values of 2.3 for the REF and 9 cm^{-1} for the half-width at half-height (see Fig. 4A).

After fitting the FSD spectrum of lysozyme, the next step was to use these results to fit the original spectrum shown in Fig. 1B. Here, the frequency positions from the FSD FTIR envelope of Fig. 1C were initially not allowed to iterate. Only the heights, half-widths at half-height, and the fraction of Lorentzian/Gaussian character of the band shape were allowed to alternately vary. For lysozyme as for all proteins in our database, the fraction of Lorentzian character vanished. Even when the peak positions were allowed to vary, only Gaussian band shapes were found to be present. A final convergent deconvolved original spectrum of lysozyme is presented in Fig. 1B. A plot of the difference between the experimental and the fit absorbences vs. frequency is presented in the inset of Fig. 1B. This deviation plot is seen to be pseudorandom in shape, which further adds validity to the analysis. Furthermore, the fractional areas of the component bands of the amide I envelope in Fig. 1B were in excellent agreement with those determined from the FSD spectra in Fig. 1C. These findings (random deviation plot and agreement of the original and FSD FTIR spectral fits) for lysozyme were used as criteria of acceptability for all the proteins analyzed in the presented database.

Since the lack of Lorentzian character in the original FTIR spectrum has not been reported, we initiated further studies on other systems to aid in the validation of this conclusion. Recently, we inherited the previously reported [3] FTIR spectra of proteins in D$_2$O. Fig. 2A shows the FSD

(A)   (B)
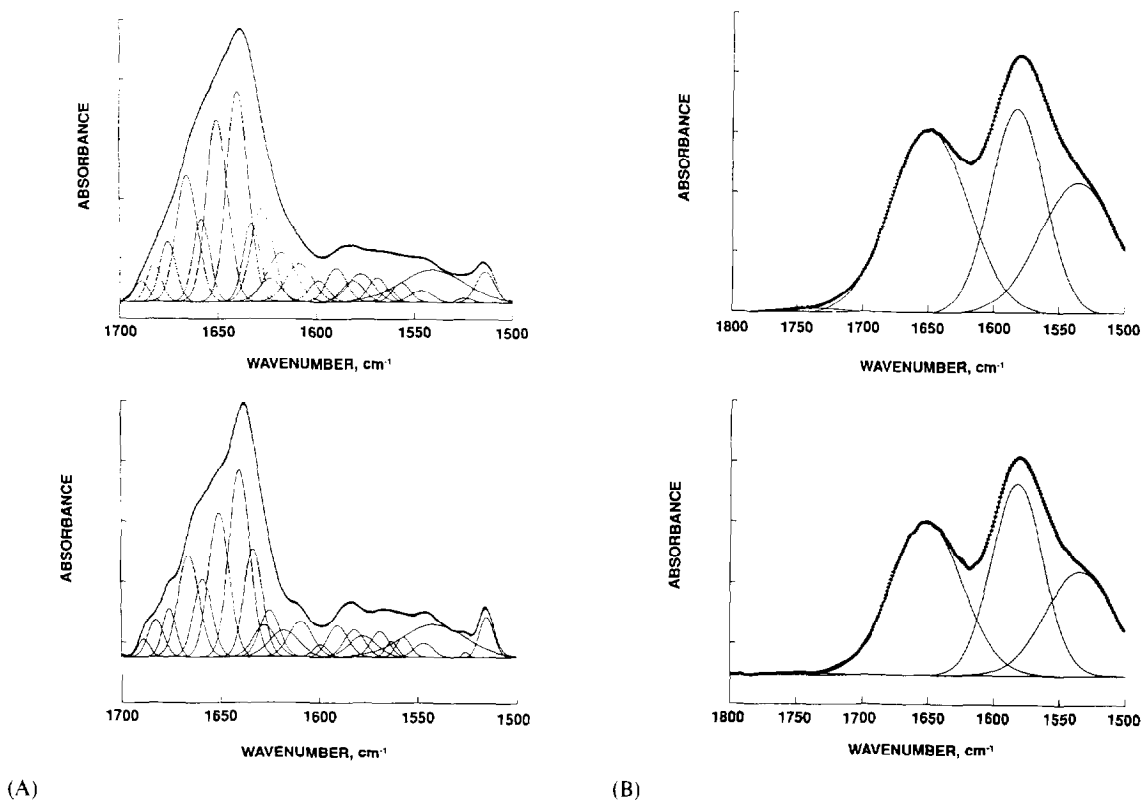
Fig. 2. (A) FTIR spectrum showing the amide I and II envelopes of ribonuclease in D_2O from the previously published work of Byler and Susi [3]. The outer envelope double line represents connected experimental data. The solid line on the outer envelope is the sum of component bands (solid line) calculated from nonlinear regression described in the text. The upper spectrum is the original FTIR spectrum; the lower spectrum is the Fourier self-deconvoluted spectrum. (B) FTIR spectra showing the amide I and II envelopes of polyaspartic acid under environmental conditions where the polymer adopts a disordered conformation. Same representation as in (A). The upper spectrum is the original FTIR spectrum; the lower spectrum is the Fourier self-deconvoluted spectrum.

(lower) and original (upper) FTIR spectra of ribonuclease A in D_2O [3]. In both cases a small amide II envelope due to incomplete exchange of the D_2O still exists. Using the above methodology for fitting both the amide I and II envelopes for both the FSD and the original spectra using Gaussian component bands was extremely successful, as seen in Fig. 2A. Ten amide I component bands for the FSD and original spectra with both fractional areas yielding equivalent global secondary structure result. No Lorentzian character bands were found by the nonlinear regression fitting analysis of either the FSD or the original spectra. Other FTIR spectra in D_2O, i.e. lysozyme, cytochrome C, conconavalin A, etc., yielded the same results.

Finally, FTIR studies of polyaspartic acid and polylysine at pH 7 in 0.08 M KCl and H_2O were initiated to further test the above results. At pH 7 in 0.08 M KCl, both polymers exist in a nonperiodic or random conformation. The above methodology presented for lysozyme was carried out on each of the spectra for each of the two polymers. For the FSD spectra, a half-width at half-height of 9 cm^{-1} and an REF of 2.3 was used. The nonlinear regression analysis was started with 29 component bands, and the Lorentzian/Gaussian character of the bands was permitted to vary. For polyaspartic acid, only three major bands at 1648 cm^{-1}, 1581 cm^{-1} and 1534 cm^{-1} with fractional area of 40%, 32% and 28%, respectively, were present. The nonlinear

regression program caused the excess bands to converge to the lower boundary of zero for the height, then these bands were removed from the calculation. The program's result also had all the bands with pure Gaussian character. The results of these calculations for the FSD and original FTIR spectra of polyaspartic acid are presented in Fig. 2B (lower spectra are FSD; the upper are original). Excellent fits for both spectra can be observed, and the fractional areas are equivalent for both spectra. Results for polylysine yielded only two major bands at 1646 cm^{-1} and 1536 cm^{-1} with fractional areas of 70% and 30%, respectively. A small band at 1745 cm^{-1} with a less than 0.4% fraction of the total area was also present for both of these polypeptide samples. The total study was also repeated at a lower salt concentration, which yielded the same results. It is apparent from these studies that the amide I assignment of 1646–1648 cm^{-1} for a random coil or irregular conformation is appropriate [3]. Also, the 1581 cm^{-1} band is most likely due to unprotonated side chain carboxyl groups.

Thus, the validity of the methodology for deconvolving FTIR spectra into component bands using nonlinear regression analysis is consistent for proteins in H_2O, proteins in D_2O, and polypeptides in H_2O. Even the number of component bands decreased markedly from 29 bands observed for lysozyme to 2 or 3 for the two polypeptides in irregular conformations. Also, no Lorentzian character is observable in any of the FTIR spectra.

Further validation of the calculated components of the amide I and II bands can be obtained by mathematical comparison of the second-derivative FTIR spectrum obtained from the original spectrum with the calculated second derivative obtained from the model fit. The result of such a fit to a second-derivative spectrum of lysozyme is shown in Fig. 3, where the irregular line represents the second-derivative spectrum of the fitted model and the smooth line that of the experimental data. The inset of this figure shows a pseudorandom plot of the connected residuals which further establishes the reliability of this methodology for quantitatively resolving FTIR spectra of proteins into component bands.

3.2. Number of parameters for the nonlinear regression analysis

To evaluate the effects of fitting a protein with too few component bands, let us examine the spectrum of lysozyme. Fig. 4A shows the fit of the Fourier self-deconvoluted amide I and II envelopes of lysozyme with 28 component Gaussian bands. The fit is excellent with no discernible difference between the resulting theoretical and experimental curves. However, when the band at 1659 cm^{-1} is removed and only 27 peaks ($N-1$) are utilized, nonlinear regression analysis yields a poor fit, with some component bands becoming much broader than others (see Fig. 4B). Also, it can be seen that the fit in the amide II envelope is affected even though no band was removed from that range of frequencies. In addition, as seen in Table 1, the RMS for 27 peaks is six times larger than for 28 peaks, i.e. 0.00157 versus 0.000251, respectively. If additional bands are removed
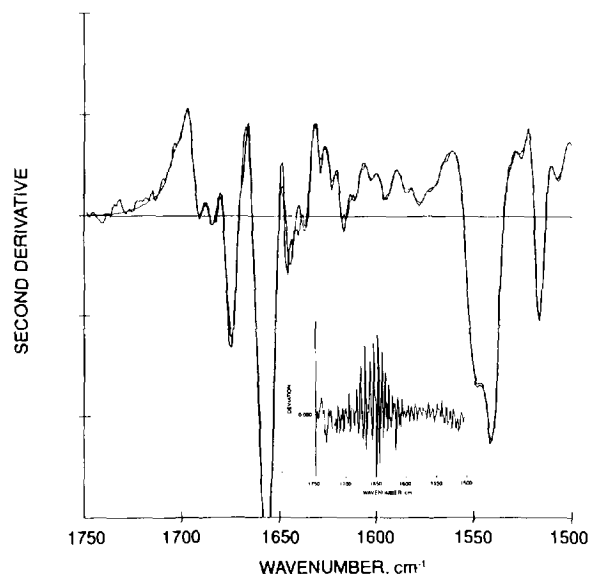
Fig. 3. Second-derivative FTIR spectrum of the amide I and II bands of lysozyme in aqueous solution. The single smooth line represents connected experimental data. The irregular line is the second derivative of the composite sum of the individual component bands from the nonlinear regression analysis as described in the text. The inset shows a plot of connected second-derivative residuals between calculated (composite sum of nonlinear regression analysis) and experimental second derivatives vs. frequency.

(A)   (B)
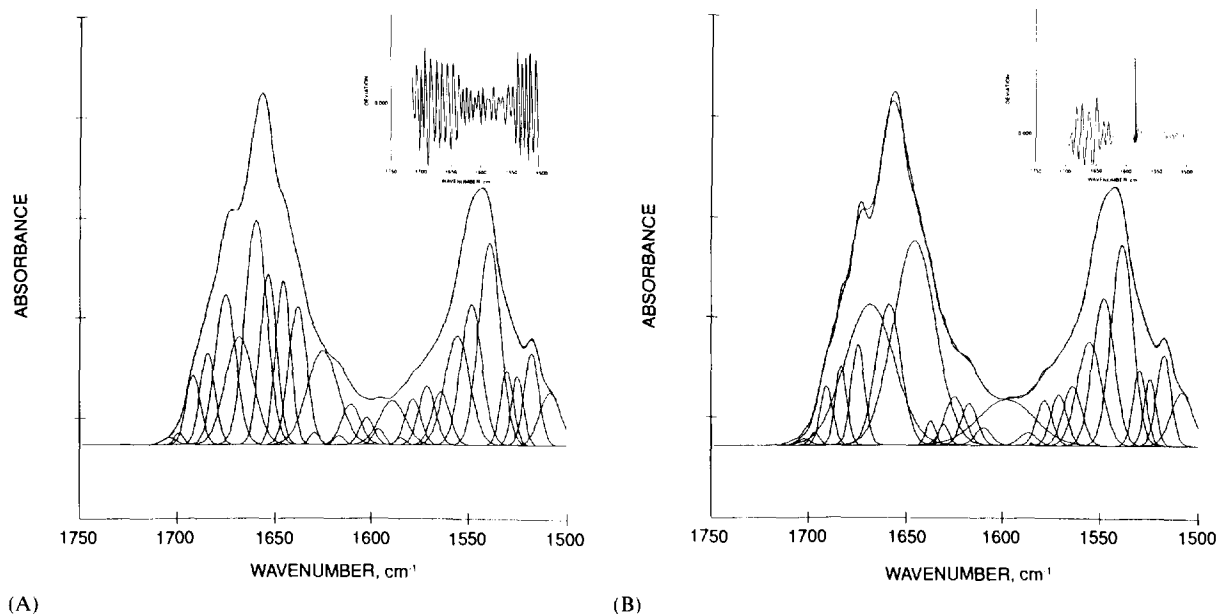
Fig. 4. Best fit for Fourier self-deconvoluted lysozyme FTIR spectrum using nonlinear regression analysis, a half-width at half-height (W) of $9\,cm^{-1}$, and a resolution enhancement factor, (REF) of 2.5. The light line represents connected experimental points; the dark line represents the theoretical sum of component bands shown by the light lines. (A) For 28 peaks; (B) for 27 peaks. Inserts in each show plots of connected residuals between spectra and composite nonlinear fit.

($N-2$ and $N-3$), the RMS continues to increase but at a smaller rate (see Table 1).

The above comparison is also observed for all the proteins reported here but is only illustrated in Table 1 for the fits of trypsin, elastase, and myoglobin. In all cases the fits after removing peaks ($N-1$, $N-2$, $N-3$) in the area of $1659\,cm^{-1}$ are extremely poor. Removing the peaks results in some extremely broad peaks in the amide I region, which in turn influences the fit of the amide II region. It should be noted that FSD causes the component bands to have almost equal half-widths at half-heights, and in the work of Byler and Susi [3], the appearance of overly broad component bands in the nonlinear regression analysis results were considered unacceptable. The RMS values of the unacceptably poor fits are on the order of three to six times higher than the best fits (see Table 1). Despite the improved fits (better RMS values), the number of peaks which exist under the amide I or II envelope should be based upon more theoretically and statistically sound concepts to prove the above hypothesis.

Rusling et al. [11] have successfully used the sum of squares principle and the extra sum of squares F-test to determine the confidence level of whether an electrochemically active compound binds to a detergent micelle according to a monophasic or biphasic mechanism. In our study, Eq. (1) (Eq. (14) of Rusling et al. (11)) relates the RMS and the degrees of freedom (which is defined as the number of data points (n) minus

$$F_{(p_2-p_1,n-p_2)} = \frac{(S_1-S_2)/(p_2-p_1)}{S_2/(n-p_2)} \tag{1}$$

the number of parameters (bands, p) in the nonlinear regression analysis) to an F-ratio, which in turn can be used in conjunction with standard F-test tables to obtain the confidence level with which the model with the smaller number of degrees of freedom fits the data better.

In the third column of Table 1, the probabilities (p) are calculated for N number of bands from the RMS values in the N and $N-1$ columns. In all cases, it is noted that the probability of N bands yields a confidence level of over 99%. Therefore using N bands is well-determined on a

Table 1
Influence of number of Gaussian peaks on RMS values

Protein	N	RMS_N p [a] (%)	RMS_{N-1}	RMS_{N-2}	RMS_{N-3}
Lysozyme	28	0.000251, >99	0.00157	0.00176	0.00187
Trypsin	25	0.000362, >99	0.00140	0.00222	0.00281
Elastase	24	0.000624, >99	0.00174	0.00191	0.00197
Myoglobin	17	0.000306, >99	0.00154	0.00161	0.00166
Papain	26	0.000759, >99	0.00201	0.00213	0.00236

[a] Probability confidence level with which RMS_N can be considered significantly smaller than RMS_{N-1} after correction for degrees of freedom in each nonlinear regression fit analysis.

statistical basis. This calculation has been used for the remaining proteins in our database (see Table 2 for the list of proteins) which gives a statistical confidence for the number of component bands found for each protein. Such statistical tests should be utilized by all investigators when performing nonlinear regression analysis. The use of this statistical method clearly adds confidence to the choice in the number of component bands.

The above discussion deals with the error in choosing too few bands in the nonlinear regression analysis to fit the amide I and II envelopes. The opposite consideration would be choosing too many bands. One could argue that choosing an infinite number of infinitely narrow bands would lead to an exact fit. For an integral in calculus, this would be true, but in FTIR there are certain theoretical and realistic constraints available which control the maximum number of bands chosen. Theoretically, the number and position of bands should correlate with the calculated theoretical values of Krimm and Bandekar [10]. Realistically, the number of bands and their positions should approximate the number of bands observed in the second-derivative and FSD spectra. The approximate number of bands indicated by the second-derivative and FSD spectra will vary with the parameters chosen to carry out those analyses (e.g. the degree of smoothing chosen for the second-derivative spectra, or the REF and half-width at half-height chosen for the FSD spectra), so these values should not limit the number of bands in the nonlinear regression analysis, but should represent a good number to begin the regression analysis. The above theoretical and

realistic constraints should be considered when adding bands to the regression analysis.

An additional theoretical and realistic concern is that there can be no negative bands in fits for vibrational spectra. A feature of the ABACUS software we use for our nonlinear regression analysis is our ability to set a lower boundary for the heights of the bands at zero. So when we add too many bands, we have found the unnecessary bands $(N+1, N+2, \ldots)$ approach zero height. When this occurs, they are removed from the analysis and no additional bands are added.

3.3. Secondary structure assignment and theoretical justification

Controversy also exists in the literature concerning the assignment of the frequency of peaks to unique protein secondary structure. Studies attempting to resolve this issue have ranged from the theoretical to the experimental, as well as combinations of both.

Because of discrepancies with peak assignments, we have tentatively assigned our secondary structural elements to agree with the assignments of the following investigators: Byler and Farrell [4], Dong et al. [2], Dousseau et al. [12], Dousseau and Pezolet [9], Krimm and Bandekar [10], Kumosinski and Farrell [13], noting of course, that these assignments can change in the future. We shall assign the α-helix structure to 1650–1660 cm⁻¹, the irregular or disordered structure to 1642–1648 cm⁻¹, the strand or extended structure to 1624–1638 cm⁻¹, and the turn conformations to all frequencies above 1670 cm⁻¹ up to 1695 cm⁻¹. No attempt will be made to distinguish the

Table 2
Percent influence of side chain - glutamine and asparagine

Protein	1651 cm^{-1} (C–N)	1667 cm^{-1} (C–O)	% Glutamine and asparagine
Hemoglobin	19.8 ± 0.7	7.2 ± 0.3	5.4
Myoglobin	31.2 ± 0.6	5.5 ± 0.4	3.4
Cytochrome C	18.3 ± 2.2	6.1 ± 0.4	3.6
Lysozyme	11.4 ± 0.3	14.6 ± 0.4	8.6
Ribonuclease	6.4 ± 0.5	13.6 ± 1.3	8.9
Papain	12.3 ± 1.2	22.8 ± 0.8	8.3
Pancreatic trypsin inhibitor	4.0 ± 0.4	5.1 ± 1.3	5.4
α-Chymotrypsin	11.6 ± 1.2	11.5 ± 0.3	7.0
Trypsin	8.4 ± 0.5	9.3 ± 1.1	7.9
Elastase	8.0 ± 0.5	10.0 ± 0.3	8.7
Carbonic anhydrase	11.3 ± 0.6	8.6 ± 0.5	6.1
β-Lactoglobulin	9.7 ± 0.3	10.0 ± 0.4	6.3
Concanavalin A	11.0 ± 0.9	8.3 ± 0.6	5.5

type of turns assigned to frequency ranges in this study.

To add a theoretical basis for the nonlinear regression model and the tentative frequency assignments that were chosen, we turn our attention to the theoretical work of Torii and Tasumi [14–16]. In a series of papers they have developed a model for the calculation of amide 1 envelopes from the X-ray crystallographic data of proteins. Their model consists of assigning one oscillator with a transition dipole to each peptide group. Coupling between these oscillators is then introduced through a transition dipole coupling mechanism. While this method allows for faster computational times, contributions from disulfide bonds and side chain–side chain and side chain–backbone are nonexistent. In one paper by Torii and Tasumi [14], the theoretical FTIR amide I spectrum of lysozyme was calculated using the X-ray crystallographic data. In their calculation, they utilized a Gaussian envelope with a half-width at helf-height of 3.0 cm^{-1} for each peptide oscillator. Their calculations were used to qualitatively compare theoretical spectra of several proteins with their experimental counterparts in D$_2$O, so the force constants used were optimized to agree with D$_2$O and not H$_2$O results. For all the above reasons we cannot exactly compare our experimental results for lysozyme with their theoretical spectrum. We can, however, deconvolve their spectrum for lysozyme into the component

Gaussian peaks using nonlinear regression analysis and compare the number of peaks and fractional areas with our experimental FTIR spectrum. Here, it must be stressed that the theoretical spectrum must contain at least but not less than the same number of bands in our experimentally analyzed spectrum.

Fig. 5 shows the deconvolved theoretical FTIR spectra from Torii and Tasumi [14] with the best fit of the sum of 14 Gaussian bands for the amide I region. Attempts to use less than 14 bands resulted in poor fits, while the addition of more
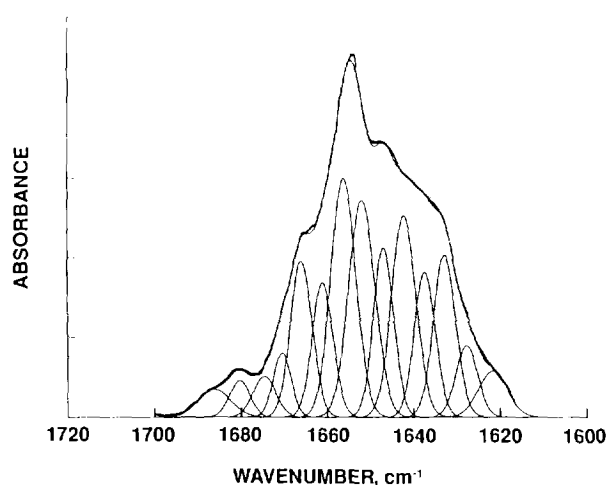
Fig. 5. Best fits by nonlinear regression analysis using the amide 1 band of lysozyme. (From theoretical calculations of Torii and Tasumi [14].)

peaks caused the height of the extra bands to approach a zero or negative value. Calculation of the percentage of extended, helix, turn and irregular structure from the fractional areas of Fig. 5, and using the above assignments, yields values of 25.2%, 26.0%, 36.3% and 12.5%, respectively. Inspection of Tables 3, 4 and 5 yields experimental values of 28.9%, 23.4%, 32.6% and 15.3% for the percentage of extended, helix, turn and irregular conformation of lysozyme, respectively. The agreement between the theoretical calculations and the experimental data is acceptable because of the assumptions in the calculation of Torii and Tasumi [14]. Other proteins which were common to both studies (myoglobin, concanavalin A, trypsin, and ribonuclease) also yielded comparable results well within a 5% deviation. It also should be noted that the model of Torii and Tasumi [14–16] does not take into account any water interactions or internal dynamic motion of the structure which would occur for a protein in solution.

4. Discussion

4.1. Contribution of asparagine (ASN) and glutamine (GLN) side chains

Recently, Venyaminov et al. [19] performed FTIR experiments on amino acids in water and deconvolved the spectra into component bands to ascertain the influence of side chains on the overall amide I envelope. They found that large bands due to the side chains of arginine (ARG), ASN and GLN exist within the amide I envelope. In subsequent articles [17,18], they attempted to eliminate side-chain contributions to the amide I and II envelopes by subtracting, on a molar basis, the amino acid side-chain absorptions from the amide I and II regions of the protein absorptions. They assumed that the absorptivity of the side chains of free amino acids and those in proteins were equivalent. This assumption may not be valid, when the dipolar coupling and energy changes are considered for the side chain which now is part of a compact globular protein structure. Finally, the DuPont curve analyzer used in

Table 3
Percent extended structure

Protein	FTIR [a] result	R [b] result
Hemoglobin	7.7	8.2
Myoglobin	10.4	5.9
Cytochrome C	10.5	11.6
Lysozyme	29.6	30.5
Ribonuclease	41.3	37.5
Papain	22.2	19.8
Pancreatic trypsin inhibitor	31.8	29.5
α-Chymotrypsin	38.8	37.9
Trypsin	40.6	39.6
Elastase	36.6	33.6
Carbonic anhydrase	41.7	36.0
β-Lactoglobulin	44.5	44.2
Concanavalin A	44.2	44.5
Oxytocin	0	0
Polylysine	0	0
Polyaspartic	0	0

[a] Average error, ± 1.6 cm^{-1}.
[b] Ramachandran.

the latter study has a limited range of applicability to FTIR experimental data.

Basing our starting point on their results, we obtained spectra of ARG, polyARG, ASN, polyASN, GLN, and polyGLN in order to analyze the results for side-chain contributions. We fit the spectra using our nonlinear regression methodology. For the free amino acids we found some differences in the frequencies for the proposed contributions. These differences are probably due to the fact that Venyaminov et al. [19] subtracted the spectrum of alanine to arrive at the possible side-chain contributions of the amino acids. The frequency and the ratio of height to half-width at half-height need to be the same for spectral subtractions to be valid; this is not the case when subtracting alanine from ARG, ASN, or GLN spectra. Our methodology permits the identification of the side-chain contributions without the subtraction of the aniline spectrum. We found that the possible contribution for ASN and GLN is the same at 1668 cm^{-1} with a small band at 1650 cm^{-1}, while the possible contribution for ARG is at 1679 cm^{-1}. Further differences are noted for the polyamino acids. Here the influence of dipolar coupling is observed for the side-chain

Table 4
Percent helix structure

Protein	x		3 10, Bent strand	
	FTIR [a] result	R [b] result	FTIR [a] result	R [b] result
Hemoglobin	76.7	81.6	1.2	.
Myoglobin	76.4	78.1	1.9	–
Cytochrome C	46.2	44.6	2.2	4.0
Lysozyme	25.6	27.1	4.2	5.5
Ribonuclease	10.0	18.0	10.3	8.8
Papain	15.2	18.8	17.4	15.6
Pancreatic trypsin inhibitor	4.2	12.0	0	6.9 BE [c]
x-Chymotrypsin	11.9	12.4	3.5	6.8
Trypsin	17.4	10.4	0	8.3
Elastase	14.1	9.7	0	8.2
Carbonic anhydrase	14.2	14.2	1.7	7.1 BE [c]
β-Lactoglobulin	15.8	5.0	3.1	9.2 BE [c]
Concanavalin A	13.6	1.7	2.2	8.8 BE [c]
Oxytocin	0	0	0	0
Polylysine	0	0	0	0
Polyaspartic	0	0	0	0

[a] Average error x-helix, ± 0.8 cm^{-1}.
[b] Ramachandran.
[c] BE, bend strand.

contributions of ASN and GLN but not for ARG. The contributions of ASN and GLN side chains relative to the amide I carbonyl band remains relatively the same while the ARG side-chain contribution relative to the amide I carbonyl decreases dramatically. Despite these differences we attempted to correlate the appropriate side-chain contribution to band area with their percent content in the proteins in our data base. We only found significant contribution and correlation for ASN and GLN combined. While the contribution of ARG appears to be negligible, it should not be discounted until further analysis is carried out on other proteins which have a higher ARG content than our proteins; in the latter case the results might correlate well.

Table 2 lists the area percent for the 1651 cm^{-1} and 1667 cm^{-1} bands in the first and second columns, respectively, for the indicated proteins in our database. Column 3 lists the combined percentage content of GLN and ASN residues present in the respective proteins. As can be seen, even though the global secondary structures of these proteins change with increasing row num-

bers (i.e. ranging from almost pure helix to turn, and then to strand structures), the percentage areas of the 1651 and 1667 cm^{-1} bands are relatively invariant, with the exception of myoglobin, hemoglobin and cytochrome C. Higher percent values of the 1651 cm^{-1} band for these first three helical proteins occurs as a result of the overlap of the E band of the x-helix structure. If the 1651 cm^{-1} bands of the three helical proteins are not considered, then a reasonable correlation exists between the experimental bands and the percentage of ASN and GLN residues. The results of the linear regression analysis of the area percent of the 1651 and 1667 cm^{-1} bands versus the percent GLN and ASN, where the percent areas of the 1651 cm^{-1} for the first three predominately helical proteins (hemoglobin, myoglobin and cytochrome C) are eliminated from this analysis, yielded an intercept value of 2.83 (standard error, 2.06; $\sigma = 0.184$) and a slope of 0.948 (standard error 0.292; $\sigma = 0.00388$). Thus, it appears that the intercept value could statistically have a zero value, with the slope having a value near unity. While the analysis suggests a correlation, it should

Table 5
Percent non-periodic structure

Protein	Turn or twisted strand		Irregular	
	FTIR [a] result	R [b] result	FTIR [a] result	R [b] result
Hemoglobin	4.3	7.5	10.1	10.8
Myoglobin	2.3	2.1	8.8	14.6
Cytochrome C	37.9	35.8	3.1	3.1
Lysozyme	28.1	26.6	12.5	9.6
Ribonuclease	24.2	26.0	14.2	9.7
Papain	43.3	39.6	15.7	6.2
Pancreatic trypsin inhibitor	60.5	49.6	3.5	8.9
x-Chymotrypsin	25.2	22.8	20.6	20.1
Trypsin	26.3	28.8	15.7	16.7
Elastase	31.8	33.6	17.4	16.0
Carbonic anhydrase	22.3	26.0	20.1	16.3
β-Lactoglobulin	17.3	21.2	19.3	20.4
Concanavalin A	22.2	22.7	17.7	22.3
Oxytocin	100.0	100.0	0	0
Polylysine	0	0	100.0	100.0
Polyaspartic	0	0	100.0	100.0

[a] Average error: turn or twisted strand, ± 1.4 cm^{-1}; loop ± 0.8 cm^{-1}.
[b] R, Ramachandran.

be viewed as an assumption. Only when the analysis of at least 50 proteins yields similar results would this assumption be considered proven. In addition, new studies of deaminated proteins in H_2O could help resolve this issue.

For this report, we will assign these bands to GLN and ASN side-chain modes. Most likely the 1651 cm^{-1} band is assigned to a C–N deformation and the 1667 cm^{-1} band is assigned to C=O stretch. The true fraction of GLN and ASN should be subtracted from the fractional areas of these bands and any excess area arising should be assigned to the appropriate global secondary structure. If the percentage of area is less than the percentage of GLN and ASN residues present, then the experimental areas should be subtracted from the amide I envelope and all the remaining bands should be normalized.

4.2. Ramachandran analysis

Of paramount importance to predicting the global secondary structure of proteins (by correctly interpreting the assignments of the FTIR amide I bands) is the correct calculation of the

secondary structure from the results of X-ray crystallography. Not only is the amount of α-helix, turn and extended conformation important, but the length of the helix and extended conformation is important as well. In addition, whether or not internal backbone hydrogen bonding exists may also be relevant descriptors for correlation with the percent areas of the component bands of the amide I region. Until recently, researchers in this field used the values provided in the Brookhaven Protein Data Bank. However, no quantitative algorithm has been used for subdividing the periodic structure. The values depend on the definitions of conformation adopted by each crystallographer. The definitions can, also, change over a period of time. What is needed, is an algorithm consistent with FTIR results to be used on all X-ray crystallographic structures. To date, no consensus in the scientific community for the appropriate algorithm has been found.

Kalnin et al. [18] have recently subdivided both the helices and sheets into hydrogen-bonded and non-hydrogen-bonded conformations, which along with the turn and all other conformations form a basis of six instead of four conformations.
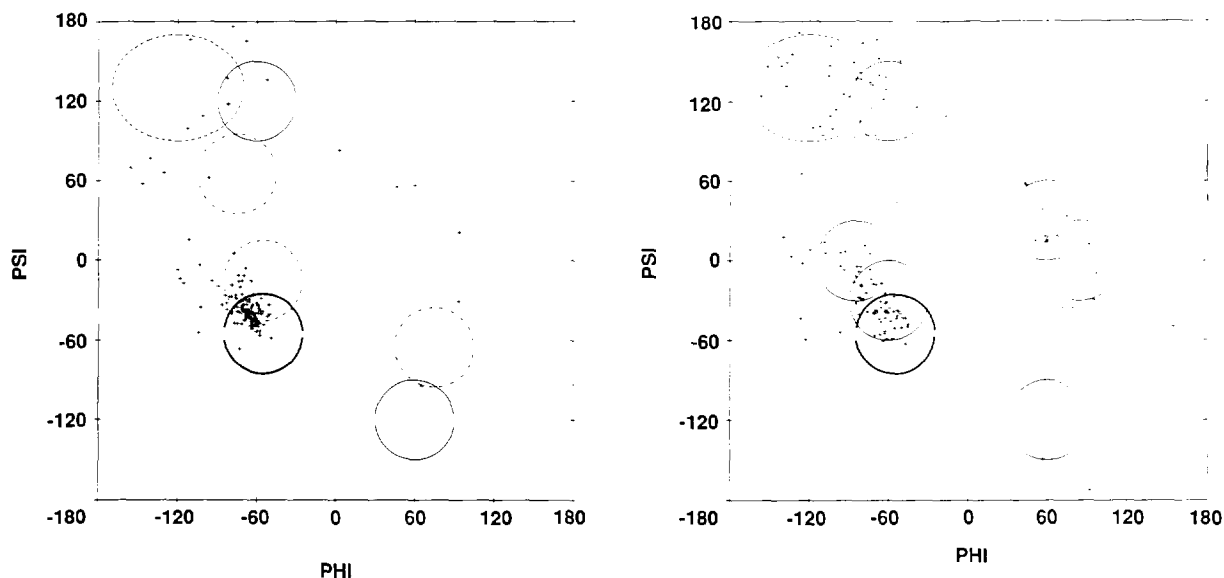
Fig. 6. Ramachandran plot from X-ray crystallographic structure of (A) myoglobin, and (B) lysozyme.

Their calculations, however, are correlated with FTIR results using factor analysis instead of non-linear regression analysis. They normalize the structures in their analyses (i.e. the total conformation of an individual protein adds up to 100%) and show reasonable correlation with FTIR results. Other researchers using factor analysis (e.g. Pancoska et al. [20,21], Pancoska and Keiderling [22]) do not achieve the same good correlations — they use only four conformations and do not normalize structures to 100%.

An algorithm developed recently in Liebman's laboratory [23,24] shows good agreement with FTIR results when deconvolving the amide I into component bands. However, these experiments were performed only for serine proteases in D_2O and were correlated with helix and extended structures. While this method appears to be promising, it is still in its infancy and more correlations between experimental results and calculated fractions of conformations must be reported, and may ultimately be correlated with the Gaussian components described above. In this study, we use the traditional Ramachandran plot calculated from the X-ray crystallographic structure of proteins in conjunction with the secondary conformations reported in the protein data banks. We strongly stress at this time that the adoption of Ramachan-

dran analysis does not in any way imply that the transitional dipolar coupling mechanisms of Krimm and Bandekar [10] or Torii and Tasumi [14–16] do not apply here to the vibrational spectroscopy of proteins. We believe their mechanisms are valid.

Here, we use the Ramachandran plot as a method for corroborating the reported fractional values. If discrepancies exist, we use other molecular modeling techniques available in the Sybyl Molecular Modeling software (such as inspection by ribbon) in conjunction with the Ramachandran analysis. The latter analysis, of course, does not take into account the required minimum number of sequential residues to sustain a periodic conformation. In Figs. 6A and 6B the Ramachandran plots are given for myoglobin and lysozyme, respectively. Fig. 6A shows a template Ramachandran with theoretical curves for predominately helical proteins. The broken lines in the upper left are for a β sheet structure. The solid circle next to it is defined as the second position for a β turn type II. Directly under this circle is the theoretical envelope for a one-residue inverse "a" (γ) turn. Directly under the inverse "a" turn is the area which defines the 3/10 helix; the double line area represents the α-helix region. At the lower right hand region is an area representative

of a type II β turn, and above it is the area common for an "a" (γ) turn.

Fig. 6B uses a template plot which is more consistent with proteins containing a large amount of turn conformation. Here the broken lines and double lines represent the sheet and α-helix regions, respectively, as in Fig. 6A. Adjacent to the sheet region is the second position for the type II β turn and directly under that region is the envelope for the one-center inverse "a" turn. The third position for a type I and II β turn region is below the inverse "a" turn. Directly above the double-line acceptable region for an α-helix is the envelope for the second position of the type III β turn. In the lower right hand quadrant and proceeding upward are the acceptable regions for the conformations of the second position of a type II β turn, an "a" turn, the third position of type I and II β turn, and the second position of type III β turn, respectively. Also shown in Fig. 6B (as + symbols) are the calculated dihedral angles ϕ and ψ, from the Sybyl modeling program analysis of the X-ray crystallographic structure of lysozyme (6LYZ).

A three-dimensional Ramachandran plot, where the residue number is plotted on the third axis, can also be calculated using the Sybyl molecular modeling software. With this plot, adjacent residues within a periodic structure as well as those residues which are part of a turn conformation can easily be determined. With all the above analyses, the global secondary structure calculated from the crystallographic data for each of the proteins studied in the FTIR was calculated. The results along with the corresponding experimental values are presented in Tables 3, 4 and 5 for strand, helix, and turn with irregular, respectively. The results for each conformation will be discussed in the following sections of this report.

4.3. Extend (strand) content

Table 3 shows a comparison between the experimentally determined global 2° structure of the extended conformation (column 2, headed FTIR) along with values calculated by the composite Ramachandran analysis (column 3, headed R). The amount of extended conformation was deter-

mined from FTIR amide I results by summing the component bands from 1638 to 1623 cm^{-1}. Bands at frequencies lower than 1623 cm^{-1} and closer to 1615 cm^{-1} are presumed to be caused by unprotected side-chain carboxyl groups [10]. Note that we assumed the bands (1638–1623 cm^{-1}) quantitate not only the amount of sheet conformation but also extended or strand non-hydrogen-bonded structures, as did Prestrelski et al. [23–24]. For a proper comparison, we sum all the points in the upper left hand quadrant of the Ramachandran plot for ϕ values above 130°, as well as those within the sheet region. Connectivity for any extended structure was determined using a three-dimensional Ramachandran plot (not shown).

As shown in Table 3, comparison between the experimental (FTIR) and calculated (R) extended conformation is excellent. Only in carbonic anhydrase, a high helical protein, is the deviation greater than 4%. Quantitative correlation of the amount of extended structure determined via FTIR and Ramachandran analyses of the X-ray crystal structure for the 16 proteins in this database was accomplished using linear regression analysis and polynomial curve fitting analysis. Using the F-test, it was found for the helix, turn and irregular structure as well as the extended structure that linear regression analysis was the most statistically significant methodology. For the extended structure, linear regression analysis yielded an intercept of 0.65 ± 0.95 ($\sigma = 0.49$) and a slope of 1.03 ± 0.03 ($\sigma = 0.0001$). The standard deviation for the regression analysis was 2.07%. In addition, this good correlation for the extended structures is supported by the fact that all proteins except for carbonic anhydrase lie within the 0.95 confidence level in the linear regression analysis. For carbonic anhydrase, if the excess amount of bent extended structure (calculated from Ramachandran analysis in Table 4, last two columns) minus the amount from FTIR at 1667–1669 cm^{-1} (i.e. $7.1 - 1.7 = 5.4$) is added to the amount of extended structure from Ramachandran analysis in the last column of Table 3 (i.e. $36.0 + 5.4 = 41.4$), then good agreement is obtained with the experimental amount of extended structure via FTIR, 41.7. Thus, the need for better mathematical algorithms for the calculation of

global secondary substructure from the X-ray crystal structure is imperative for correlating with FTIR global secondary structure.

We compared our results for trypsin, α-chymotrypsin and elastase with those reported by Liebman's group — calculated and experimentally determined values in D_2O [23,24]. Values calculated using the Liebman algorithms were 42, 42 and 37. Their experimental results were 39, 45, and 46, while our experimental values were 41, 39 and 37, (all values respective to trypsin, α-chymotrypsin, and elastase). While both our experimental values for trypsin and α-chymotrypsin agree equally with the calculated values, our elastase value of 37 is more in agreement with the calculated value of 37 than the experimental value of 46% in D_2O [23,24]. This adds further support for our methodology and the supposition that the amount of GLN and ASN side-chain residues must be subtracted from the 1667 and 1651 cm^{-1} component amide I bands.

4.4. Helix content

Table 4 lists the calculated and experimental results for the α-helix (columns 1–3), 3/10 helix (columns 5, 6). Linear regression analysis of the amount of helical structure determined via FTIR versus the amount calculated from three-dimensional Ramachandran analysis of the X-ray structure for these 16 proteins yielded an intercept of 2.13 ± 1.81 ($\sigma = 0.26$) and a slope of 0.92 ± 0.06 ($\sigma = 0.0001$). The standard deviation of the regression analysis was 5.6%, which is significantly larger than the error calculated for the amount of extended structure, especially for the low content helical proteins. In fact, five proteins did not fall within the 95% confidence region. Close inspection of these differences may provide a rationale for the change. Not counting the high helical proteins (hemoglobin and myoglobin) we observe that the largest differences occur for ribonuclease, the serine protease system (i.e. pancreatic trypsin inhibitor (PTI), and trypsin), concanavalin A (CON A) and β-lactoglobulin. The last two proteins in this series contain significant amounts of β-barrel structures. Such structures appear as antiparallel β-sheets which are highly bent. The

Ramachandran plots of these proteins also yield points in the lower left quadrant which is normally considered a forbidden region. The Ramachandran plots for the serine proteases also contain some ϕ, ψ angles in this region. Hence, the discrepancy in the experimental and calculated helical content for concanavalin A, β-lactoglobulin and perhaps the serine proteases may be caused by β-barrels which could have bands at 1658 ± 2 cm^{-1}. More experimental and theoretical studies must be performed before this hypothesis can be concluded. But since ribonuclease contains no β-barrel, inspection of the work of Kalnin et al. [18] may provide an answer to the discrepancy. In their study, the α-helix was subdivided into an ordered and unordered class as was the sheet structure. They calculated values of 13% and 10% for their ordered and unordered α-helix and found experimental values of 11% and 8%, respectively. Upon inspection of the ribbon structure, a major distortion of the helical region of ribonuclease is found. In addition, a value of 10.3% has been obtained from the excess area of the 1667 cm^{-1} band which we have assigned as a 3/10 helix, in accordance with the results of Krimm and Bandekar [10]. If the α-helix and 3/10 helix values are summed they add up to more acceptable values. However, the Ramachandran plot for ribonuclease shows 11 residues within the type III or 3/10 helix region which calculates to a theoretical value of 8.8% for these possible conformations. It should also be stressed that Kalnin et al. [18] calculates an ordered α-helix conformation of 27% for lysozyme which agrees well with our experimental and theoretical values of 25.6% and 27.1%. Therefore, we believe that the discrepancy for the ribonuclease helical structure is the result of its structure, which our Ramachandran analysis could not adequately calculate.

The discrepancy between the amount of helix determined from Ramachandran analysis and FTIR experiments for trypsin can be easily explained by closer inspection of Table 4. Ramachandran analysis of trypsin yields 10.4% α-helix, and 8.3% 3/10 helix content where the experimentally determined values from FTIR are 17.4% and 0%, respectively. As can be seen in the Ramachandran plot for myoglobin (Fig. 6A),

there is a large overlap between the acceptable regions for the α and 3/10 helixes. This is due to the small differences between their respective ϕ and ψ values. For this reason it is not possible by this method to precisely determine the differences between these two structures. Moreover, a protein in solution does not adopt a static structure but an average dynamic structure. The dynamic structure, due to thermal fluctuations, causes internal motions within the solvated protein configuration. Under these circumstances, the ϕ, ψ angles for a 3/10 helix may easily change to those for an α-helix. Only intense molecular dynamics calculations of a protein in water can attempt to approximate the dynamic motions of a protein. However, for this study it will be assumed that the 3/10 helix calculated via Ramachandran analysis closely approximates an α-helix. Therefore, we now change the value of the α-helix calculated from Ramachandran analysis to 18.7% ($= 10.4\% + 8.3\%$) which more closely agrees with the experimental value of 17.4%.

It should be stated that the 1676 cm^{-1} band was also summed along with the excess area for the 1651 cm^{-1} band, and the 1658 cm^{-1} band for obtaining the total α-helix content of hemoglobin and myoglobin. The 1676 cm^{-1} band represented approximately 17% of the total helical structure. The areas of the 1658 cm^{-1} and 1651 cm^{-1} bands summed to 63%, and a value of 63% was also calculated as the amount of unordered helix content in myoglobin by Kalnin et al. [18]. Moreover, close inspection of the ribboned structures of hemoglobin and myoglobin reveal highly distorted helical segments which could not be observed using Ramachandran analysis. The 1676 cm^{-1} band, assigned by Krimm and Bandekar [10] as a turn may be reflective of a type III β-turn. Such a turn would have ϕ, φ values seriously overlapping the α-helical region of a Ramachandran plot (see Fig. 6B). Nevertheless, for high helical proteins (i.e. above 55%) it may be more prudent for investigators to utilize UV circular dichroism analysis, because as Torii and Tasumi [14–16] have recently reported, a serious overlap of E and A bands for α-helices with varying lengths occurs, thus resulting in theoretical amide I envelopes which contain bands well

below the 1650 cm^{-1} region. With lower helical proteins, FTIR correlates much better than circular dichroism since the turn conformation can be more easily determined.

Finally, the excess areas in the 1667 cm^{-1} band above the GLN and ASN side-chain contribution is shown in Table 4 as a 3/10 helix or bent strand, i.e. a possible "a" turn. These small values cannot be easily correlated with Ramachandran analysis and no firm assignments are made. Excellent correlation between three-dimensional Ramachandran analysis and FTIR determination of the α-helix at 1659 cm^{-1} and the 3/10 helix at 1667 cm^{-1} is obtained for papain (see Table 4). However, we do not observe any large amounts of 3/10 helix in lysozyme, especially in the 1638 cm^{-1} region where Prestrelski et al. [23,24] have concluded that such 3/10 helical bands exist. While we have not performed any experiments on α-lactalbumin, we still concur with the assignment of Krimm and Bandekar [10] that the 3/10 helix is in the range of 1665 cm^{-1} rather than in the low range of 1638–1640 cm^{-1} as reported by Prestrelski et al. [23,24]. Perhaps this discrepancy may be explained by the fact that their experiments were performed in D_2O rather than in H_2O.

With the above changes in the α-helix percentages, we can now recalculate the correlation (via linear regression analysis) between the experimentally determined FTIR values and the Ramachandran calculated amount of α-helix.

4.5. Turn and irregular content

Table 5 shows the turn and irregular content determined experimentally from analysis of the FTIR amide I band and calculated from the three-dimensional Ramachandran analysis of X-ray crystallographic structures of the 16 listed proteins. The turn content was determined from the sum of all amide I bands from 1670 to 1694 cm^{-1}. The irregular content was calculated from the normalized area of the 1646 $\pm$ 2 cm^{-1} band. The irregular theoretical structure was calculated as all other structure not defined by this analysis. Good agreement between the experimental and theoretical values is observed with the standard deviations from the regression analysis of 3.6%

and 3.2% calculated for the turn and irregular content, respectively. Linear regression analysis of the FTIR values vs. the Ramachandran values yielded an intercept of 0.97 ± 1.39 ($\sigma = 0.49$) and a slope of 1.00 ± 0.04 ($\sigma = 0.0001$) calculated for the turn conformation, and an intercept of -0.75 ± 1.02 ($\sigma = 0.98$) and a slope of 1.01 ± 0.03 ($\sigma = 0.0001$) calculated for the irregular or "all other" conformation. These values for the turn and irregular conformations are well within the standard deviations observed in the strand and α-helix content, i.e. 2.1% and 5.5%. However, it should be noted that in the case of cytochrome C and β-lactoglobulin, ϕ and ψ values exist in the upper right hand region of the Ramachandran plot. Although this region has been considered forbidden, closer inspection shows that these ϕ and ψ values are a result of twisted sheets. Hence, since no other proteins in this database exhibited ϕ and ψ values in this region, we have concluded that the 1676 cm^{-1} band may also be assigned to a twisted strand. However, more studies must be performed before a definite assignment can be made.

5. Conclusions

Calculation of the component 2° structural elements of the vibrational bands, i.e. approximately 25 Gaussian bands, was accomplished by fitting both the amide I and II bands using nonlinear regression analysis of the Fourier self-deconvoluted spectrum, the second-derivative spectrum, and the original spectrum. Fixed frequencies initially used in the original spectral analysis were obtained from both the FSD spectrum and the second-derivative analyses. The criterion for the acceptance of any analysis was that the fractional areas calculated from all three methods were in agreement (within experimental error calculated from the nonlinear regression analysis). Results clearly show that 2° structural conformations determined in water were in better agreement with global 2° structural analysis of X-ray structures than the previously reported values determined in D_2O. Also, with H_2O, the 2° structural elements can be calculated from the amide II envelope to

be used for validation of amide I assignments. In addition, the resolution of amide I spectra in water is greater than that in D_2O as observed in comparable second-derivative spectra and lower half-width values of 9 instead of 13–18 cm^{-1} for the H_2O and D_2O spectra, respectively. The deterioration of resolution of FTIR spectra in D_2O may result primarily from the incomplete exchange of protein protons to deuterons. These results lay the foundation for the study of conformational changes in proteins induced by ligands, consolutes or perhaps structural changes from site-directed mutagenesis [7], and in other system applications where for example D_2O may obscure water–protein interactions.

In this study, we have presented a method for analyzing the FTIR of proteins in water and determining their global secondary structure. Analysis of 16 proteins whose X-ray crystallographic structures are known showed agreement of secondary structure content to within 2–6% between the experimental FTIR and the X-ray coordinate calculations. The bands which are assigned to these structures are shown in Table 6 along with their tentative structural assignments. These assignments differ from previous assignments for only the GLN and ASN side-chain contributions and the 1675 cm^{-1} band which is now assigned to a turn rather than to an extended conformation. The high frequency β structure band at 1675 cm^{-1} reported by Byler and Susi [3] was not observed in this study. In our data base we have tentatively assigned this frequency as a turn conformation. This discrepancy may have arisen from the fact that Byler and Susi [3] did not consider turn conformations in their study, nor did they account for GLN or ASP side-chain contributions. In this study we tentatively assign the 1676 cm^{-1} band to the "a" turn conformation. While these results are quite promising, it must be stressed that only after a database of at least 50 proteins is obtained can any definite conclusions be reached. It is hoped that this study will inspire other investigators to adopt this methodology and add more information to increase this database above 16 proteins.

There are recent reports in the literature on the potential of FTIR to evaluate the global 2° struc-

ture of proteins which discuss the limitations of "band-narrowing" methodologies used to analyze FTIR spectra of proteins [25,26]. Our methodology addresses some of these limitations.

(1) We have eliminated atmospheric water completely with a thorough dry nitrogen purge and an accurate vapor spectra subtraction.

(2) We have considered the influence of side-chain absorptions, and recommend compensating for ASN and GLN side-chain absorptions as described above.

(3) We obtain a large number of interferograms to insure a high signal-to-noise ratio (S/N). A high S/N is necessary to ensure accurate vapor and buffer subtractions. A high S/N also reduces the influence of the instrumental noise.

(4) The ABACUS nonlinear regression program eliminates the operator influence on band shape — the relative Gaussian/Lorentzian contribution is determined by the fit.

(5) We statistically choose the number of bands used to fit the spectral data with the use of the extra-sum-of-squares F-test and the ABACUS program's ability to lower-bound all bands at zero height.

(6) Although we only use the amide I results for assignments, we fit both the amide I and II envelopes simultaneously. This improves the amide I fit compared to fitting the arbitrarily terminated amide I envelope alone.

(7) We use and analyze the original, the FSD, and the second-derivative spectra, accepting results only when all three regression fits statistically agree. This addresses the question of unique fits.

(8) We fit the spectra from two different starting values — small heights and large heights — requiring both analyses to come to the same answer. This eliminates the possibility of local minima being reached and ensures a unique fit.

(9) In general our methodology eliminates as much operator influence on the nonlinear regression fitting process as possible.

(10) Spectra are obtained in H_2O. This is the natural environment of proteins and the environment in which most X-ray crystal structures are analyzed. This eliminates any possible conformational distortions which may occur with the use of D_2O.

(11) We reanalyze each protein's X-ray crystal structure data using three-dimensional Ramachandran analysis. This ensures a consistent 2° structural X-ray analysis procedure from which to compare the protein structures obtained by FTIR.

(12) Finally, we recommend the use of amino acid secondary-sequenced-based prediction algorithms in conjunction with FTIR to analyze proteins with unknown structure.

References

[1] S.N. Timasheff, in H. Peeters (Ed.), Protides of the Biological Fluids, 20th Colloquium, 1973, pp. 511–519.

[2] A. Dong, P. Huang and W.S. Caughey, Biochemistry, 29 (1990) 3303.

[3] D.M. Byler and H. Susi, Biopolymers, 25 (1986) 469.

[4] D.M. Byler and H.M. Farrell, Jr., J. Dairy Sci., 72 (1989) 1719.

[5] P.R. Griffiths and J.A. de Haseth, Fourier Transform Infrared Spectrometry, Wiley, New York, 1986, pp. 102–103.

[6] L.T. Kakalis and T.F. Kumosinski, Biophys. Chem., 43 (1992) 39.

[7] J.K. Kauppinen, D.J. Moffatt, H.H. Mantasch and D.G. Careron, Appl. Spectros., 35 (1981) 271.

[8] W. Damert, Quantum Chem. Program Exchange Bull., 14(4) (1994) 61. (Note: Version F.1 is available on the Internet from QCPE (their program number 652) or directly from ERRC. Persons desiring the program may use FTP, connect to "ishtar.arserrc.gov", and use the account "anonymous" which requires no password. They would then select directory "abacusf" and download all files. Installation instructions and user documentation are also provided.)

[9] R. Dousseau and M. Pezolet, Biochemistry, 29 (1990) 8771.

[10] S. Krimm and J. Bandekar, Adv. Protein Chem., 38 (1986) 181.

[11] J.F. Rusling, C.-N. Shi and T.F. Kumosinski, Anal. Chem., 60 (1988) 1260.

[12] F. Dousseau, M. Therrien and M. Pezplet, Appl. Spectrosc., 43 (1989) 538.

[13] T.F. Kumosinski, H.M. Farrell, Jr., J. Protein Chem., 10 (1991) 3.

[14] H. Torii and M. Tasumi, J. Chem. Phys., 96 (1992) 3379.

[15] H. Torii and M. Tasumi, J. Chem. Phys., 97 (1992) 86.

[16] H. Torii and M. Tasumi, J. Chem. Phys., 97 (1992) 92.

[17] S.Yu. Venyaminov and N.N. Kalnin, Biopolymers, 30 (1990) 1259.

[18] N.N. Kalnin, I.A. Baikalov and S.Yu. Venyaminov, Biopolymers, 30 (1990) 1273.

[19] S. Yu. Venyaminov and N.N. Kalnin, Biopolymers, 30 (1990) 1243.

[20] P. Pancoska, S.C. Yasui and T.A. Keiderling, Biochemistry, 30 (1991) 5089.

[21] P. Pancoska, L. Wang and T.A. Keiderling, Protein Sci., 2 (1993) 411.

[22] P. Pancoska and T.A. Keiderling, Biochemistry, 30 (1991) 6885.

[23] S.J. Prestrelski, A.L. Williams and M.N. Liebman, Proteins, Structure, Function and Genetics, 14 (1992) 430.

[24] S.J. Prestrelski, A.L. Williams and M.N. Liebman, Proteins, Structure, Function and Genetics, 14 (1992) 440.

[25] W.K. Surewicz, H.H. Mantsch and D. Chapman, Biochemistry, 32 (1993) 389.

[26] E. Goormaghtigh, V. Cabiaux and J.M. Ruysschaert, in H.J. Hilderson and G.B. Ralston (Eds), Subcellular Biochemistry, Vol. 23, Physicohemical Methods in the Study of Biomembranes, 1994, p. 405–450.

Quantitative determination of silicon in silica dust by FT-Raman spectroscopy

D.N. Phillips*, T.M. Suckling, W. van Bronswijk

School of Applied Chemistry, Curtin University of Technology, P.O. Box U1987, Perth, W.A. 6001, Australia

Received 20 June 1995; revised 21 August 1995; accepted 25 August 1995

Abstract

Silicon was quantitatively determined in respirable silica dusts and silica fume by FT-Raman spectroscopy using barium sulfate as an internal standard. Barium sulfate was selected as the standard as its Raman spectrum does not overlap with that of silicon and its scattering cross-section is significantly lower. This allowed silicon admixed with barium sulfate in ratios as low as 0.00003 to be detected. The laser beam was defocussed to cover the sample area. 128 scans at 4 cm^{-1} resolution with 600 mW of power at the sample achieved a detection limit of 0.1 μg of silicon in a 5 mg sample. Silicon to $BaSO_4$ ratios in the range 0.00003–0.06 showed a near linear response with any decade change being linear. The RSD for this analytical method was $\pm 2\%$. Silica fume and respirable silica dust showed silicon concentrations to be in the range 2.6–51.5 ppm and 0.05–0.7 mg m^{-3} respectively.

Keywords: Silicon; Silica dust; FT-Raman spectroscopy

1. Introduction

Silicon is manufactured by the reduction of high grade quartzite with charcoal and coal at temperatures of up to 1780°C using graphite electrodes in a submerged electric arc furnace. While there are a few less important reactions, the following represents the main reaction sequence [1]:

$$SiO_2(l) + C(s) \rightarrow SiO(g) + CO(g)$$

$$SiO(g) + 2C(s) \rightarrow SiC(s) + CO(g)$$

$$SiC(s) + SiO_2(l) \rightarrow Si(l) + SiO(g) + CO(g)$$
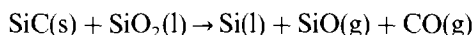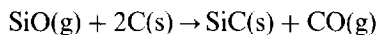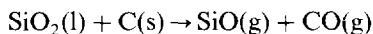
A by-product of the process is silica fume which is formed when unreacted silicon monoxide is oxidised in the upper reaches of the furnace:

$$2SiO(g) + O_2(g) \rightarrow 2SiO_2(s)$$
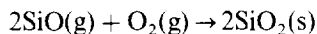
The silica fume is mainly comprised of amorphous silica but also contains approximately 4% free carbon, 2% silicon carbide, 4% crystalline silica and very low levels of silicon [2,3]. A knowledge of the silicon content of silica fume and respirable silica dusts is important for two reasons. There have been three reports of explosions when the levels of silicon in silica fume have exceeded 1%. The presence of silicon in silica fume leads to the formation of hydrogen gas

---

* Corresponding author. Fax: (61) 9-351-2300.

Table 1
Pressed powder standards

Standard	Wt. Si (mg)	Wt. $BaSO_4$ (mg)	Mass ratio Si:$BaSO_4$	Intensity ratio Si:$BaSO_4$
1	13.25000	231.66000	0.0571960	46.0629
2	4.0400	397.0400	0.0101753	10.0241
3	2.16731	297.98269	0.0072733	7.2341
4	0.16384	228.23616	0.0007179	0.9153
5	0.16980	338.19020	0.0005022	0.5549
6	0.00998	341.95002	0.0000292	0.0616
7	0.00051	275.92949	0.0000018	0.0279

when the metal comes in contact with the alkaline environment. To prevent such occurrences, the maximum permissible quantity of silicon in silica fume has been set at 0.2% [4]. Occupational Health and Safety requirements demand that the air quality at the plant is regularly sampled near the tapping floor. While crystalline silica has a greater potential for causing silicosis [5–7], it has been shown that crystalline silicon can also induce silicosis [8]. The current exposure limit set for silicon in respirable silica dusts in Western Australia is 5 mg m^{-3} [9].

Current methods for determining low concentrations of silicon are complex and time-consuming [10,11]. Crystalline silicon has a tetrahedral diamond-like structure and its Raman-active symmetrical stretch occurs at 519 cm^{-1}. In the present paper the viability of this stretch was evaluated for quantitative solid state analysis. The major problems addressed, as with any solid state Raman method, were the selection of a suitable standard, homogeneous sample dispersion and full Raman illumination of the entire sample.

2. Experimental

2.1. Samples

The silica fume and respirable silica dust samples were provided by Simcoa Operations, Kemerton, W.A. The eight silica fume samples were taken at irregular intervals from the fume discharge line to the baghouse and the five respirable silica dust samples were collected at irregular in-

tervals by filtering 0.8 m^3 of air at the tapping floor.

2.2. Reagents

Barium sulfate, AR Grade, BDH, dried at 90°C for 24 h. Hydrofluoric acid, 48%, AR Grade, Merck. Silicon, 99.8%, Simcoa Operations, ground to <100 μm.

2.3. Internal standard

Barium sulfate was chosen as the internal standard as it possesses an intense sharp Raman peak at 986 cm^{-1}, sufficiently removed from the silicon peak at 519 cm^{-1}. The pressed powder standards were prepared by homogenising various ratios of the silicon and barium sulfate as shown in Table 1.

2.4. Preparation of samples for Raman analysis

The respirable silica dust and silica fume samples were analysed as pressed powders. The respirable silica dust samples were prepared by intimately hand-mixing, in an agate mortar and pestle, the required amount of barium sulfate to make the total weight of sample 30 mg. 5 mg of sample was then compressed, by hand, into a stainless-steel sample holder with a 1.7 mm diameter, 0.5 mm deep, conical sample cavity.

The silica fume samples were treated with hydrofluoric acid prior to Raman analysis to remove amorphous and crystalline silica. They were also heated to remove all the free carbon. Approxi-
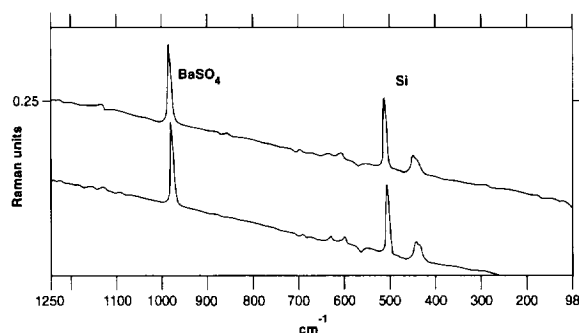
Fig. 1. Duplicate Raman spectra of typical pressed powder standard.

mately 10 g of silica fume, in duplicate, was accurately weighed in a 500 ml Teflon beaker and treated with 40 ml of hydrofluoric acid. The solution was diluted to 400 ml and filtered through a Whatman 541 filter paper, dried at 110°C and weighed. The residue was then ashed in a porcelain crucible at 550°C for 2 h and reweighed when cool. The samples were determined in the same manner as the respirable samples.

2.5. Instruments

All spectra were obtained with a Bruker RFS100 FT-Raman Spectrometer using a 1064 nm excitation laser in the 180° back-scatter mode. 128 scans were taken at 4 cm^{-1} resolution using 600 mW of laser power at the sample. The software package was OPUS Version 1.5c Beta, enabling peak heights and areas to be determined with high accuracy. Standards were weighed using a Sartorius R200D semi-micro balance accurate to five decimal places.

3. Results and discussion

The Raman spectrum of pressed powder standard 4, in duplicate, is shown in Fig. 1. The sharp peaks of barium sulfate and silicon are seen at 986 cm^{-1} and 519 cm^{-1} respectively. The figure shows the high degree of precision that can be obtained by this method.

The calibration plot for the whole range of the intensity ratio versus the concentration ratio showed curvature, and thus calibration plots were established for low (0.0001–0.0008), middle (0.002–0.012) and high (0.01–0.06) range standards. The calibration plots for the low, middle and high standards all showed excellent linearity with correlation coefficients of 0.9987, 0.9999 and 0.9989 respectively. The equations for each line are:

$$I = 1.4542 + 806.875C \quad \text{(high)}$$

$$I = 0.1191 + 970.365C \quad \text{(middle)}$$

$$I = 0.01996 + 1137.550C \quad \text{(low)}$$

where I is the intensity of silicon(519 cm^{-1})/intensity of barium sulfate(986 cm^{-1}) and C is the weight of silicon/weight of barium sulfate. Acquiring 256 scans at 4 cm^{-1} resolution with 600 mW of defocussed laser power and a 5 mg sample mixed with 10 mg of barium sulfate gave a detection limit ratio of Si/BaSO$_4$ = 0.00002, which corresponds to 0.1 μg of silicon in the sample (i.e. 20 ppm). A greater number of scans could be used to improve this detection limit if required. A reduction of resolution to 8 cm^{-1} may then be useful to reduce acquisition times.

The results for the silicon content of the respirable dust samples are shown in Table 2. The

Table 2
Silicon content of respirable dusts

Sample	Intensity ratio Si/BaSo$_4$	Conc. ratio Si/BaSO$_4$	Wt. Si (mg)	Si in dust (%)	Si in air (mg m^{-3})
1	0.0154	0.1140	0.0037	0.15	0.19
2	0.0249	0.1707	0.0072	0.55	0.69
3	0.0135	0.0951	0.0026	0.04	0.05
4	0.0072	0.2692	0.0043	0.14	0.17
5	0.0133	0.0823	0.0026	0.13	0.16

Table 3.
Silicon content of silica fume

Sample	Intensity ratio Si/BaSO$_4$	Conc. ratio Si/BaSO$_4$	Wt. Si (mg)	Si in dust (ppm)
1	0.7509	0.00071	0.05	2.6
2	1.9243	0.00191	0.21	5.3
3	4.5988	0.00465	0.49	4.0
4	9.8677	0.01003	1.06	51.5
5	2.4029	0.00234	0.33	5.9
6	2.3069	0.00230	0.54	21.7
7	0.8924	0.00086	0.13	5.5
8	3.4886	0.00351	0.30	4.5

silicon content of the respirable dusts was found to range from 0.04 to 0.55%, corrresponding to a silicon content in air of 0.05–0.7 mg m^{-3} respectively. A typical respirable dust weight of 10.6 mg gave a Si/BaSO$_4$ ratio of 0.000083 from a Raman intensity ratio of 0.114. The data obtained for the respirable dusts were well within the Occupational Health and Safety requirement of 5 mg m^{-3} [9].

The results for the silicon content of the silica fume samples are shown in Table 3. The silicon content was found to range from 2.6 to 51.5 ppm. A typical fume sample of about 100 mg gave a Si/BaSO$_4$ ratio of 0.0024 from a Raman intensity ratio of 2.403. The data for the fume samples indicated only trace levels of silicon in the fume and no cause for concern in relation to explosions in alkaline cement environments [4].

4. Conclusions

A quantitative method for the determination of low levels of silicon in respirable silica dust and silica fume has been developed. The method has good sensitivity, a good dynamic range and very good reproducibility. Concentrations of silicon in the respirable dusts and silica fume were found to range from 0.05–0.7 mg m^{-3} and 2.6–51.5 ppm

respectively. The detection limit for the analytical method was 0.1 μg of silicon in a 5 mg sample. The RSD for the analytical method was $\pm 2\%$. The values obtained for the respirable dusts were well within the Western Australian Occupational Health and Safety Standard for exposure to such dusts of 5 mg m^{-3}, while the values obtained for silica fume were also within the prescribed limit.

References

[1] D.M. Spratt, R.A. Leupen and P.A. Bibby, Conf. Australian Inst. Mining Metall., Perth, Australia, 1989, p. 123.

[2] I.S. Barrow, S.T. Dye, D.N. Phillips and D.E. Woodford, Talanta, 40 (1993) 909.

[3] I.S. Barrow, A.C. Fletcher and D.N. Phillips, Talanta, 41 (1994) 1663.

[4] Safety Bulletin No.6, Formation of Hydrogen Gas from Silicon Metal, Department of Minerals and Energy, Perth, Australia, 1994.

[5] Encyclopaedia of Occupational Health and Safety, 3rd edn, International Labor Office, Geneva, 1983, p. 2037.

[6] E. Raask and C.J. Schilling, Ann. Occ. Hygiene, 23 (1980) 147.

[7] R.S. Bottrill, Silica Fume Analysis—A Preliminary Report, Tasmania Department of Resources and Energy, Tasmania, Australia, 1991.

[8] Y.N. Golodnikov, Gigiena Truda I Professional'nye Zabolevaniya, 78 (1978) 31.

[9] Maunsell and Partners Pty. Ltd., Western Australian Silicon Trust for the Western Australian Silicon Project: Environmental Review and Management Program, Environmental Protection Authority, Perth, Australia, 1986.

[10] C.R. Ivanova, S.P. Bratinova and S.A. Popova, Dok. Bolgarskoi Akad. Nauk, 45 (1992) 61.

[11] M. Ordogh, G. Miskovits, J. Appel and E. Szabo, Int. J. Appl. Rad. Isotopes, 25 (1973) 61.

Determination of ATP using chelation-enhanced fluorescence

Gregory P. Foy, G.E. Pacey*

Department of Chemistry, Miami University, Oxford, OH 45056,USA

Received 23 June 1995; revised 1 September 1995; accepted 1 September 1995

Abstract

A method for the direct determination of ATP that exhibits reasonable sensitivity, and responds to very few interferants, has been developed. The chelation-enhanced fluorescence between N-(anthracen-9'-yl methyl)tris(3-aminopropyl)amine and adenosine 5'-triphosphate is utilized in this determination. The method was tested in batch and flow-injection analysis (FIA) modes. The typical detection limit for FIA determination of ATP is 1 μM, with a linear range of 0.5-100 ppm. A typical relative standard deviation at 20 ppm is 2.3%.

Keywords: ATP; Chelation-enhanced fluorescence; Flow-injection analysis

1. Introduction

Determination of the adenosine phosphate compounds (ATP, ADP, AMP) is performed in many biological systems. The current methods for this determination are the widely used firefly luciferase [1-6] chemiluminescent method and the spectrophotometric monitoring of the enzymatic conversion of ATP to ADP [1,7,8]. In general these methods suffer from numerous interferants as well as limited linear range. Typically, the detection limits are in the 10 μM region for the spectrophotometric methods [1], and at the 10^{-10} M level for direct detection with luciferase in a flow-injection system [3], with a level of 10^{-14} M having been reported [4]. These levels of detection are only achieved after separation from similar

compounds, or minimization of other interferants.

The ideal method for ATP determination would not destroy the ATP in the sample, providing the possibility of further analysis, and would provide a large range for determination as well as a low level of detection without stringent requirements for pH and temperature. The method would also be selective for ATP without prior separation. One approach would be to use an anthrylmethylpolyamine, N-(anthracen-9'-yl methyl)tris(3-aminopropyl)amine, and the chelation-enhanced fluorescence effect (CHEF) reported by Czarnik [9]. The CHEF effect measures the increase in fluorescence due to the formation of a chelate between the amine and the anion of interest. The magnitude of the formation constant for the chelation of the anion is proportional to the observed enhancement. This paper describes the investigation of the anthrylmethylpolyamine, N-(an-

* Corresponding author. Fax: (513) 529-7284.

thracen-9′-yl methyl)tris(3-aminopropyl) amine as an analytical reagent for ATP determinations.

2. Experimental

All starting materials were purchased from Aldrich. The amine, *N*-(anthracen-9′-yl methyl)tris(3-aminopropyl)amine was prepared by using tris(cyanoethyl)amine in the procedure of Van Winkle et al. [11]. The next step is hydrogenation over Raney Nickel following the procedure of Chin et al. [12]. In the synthesis of *N*-(anthracen-9′-yl methyl)tris(3-aminopropyl)amine the procedure of Hutson [10] was used, but with the following modifications. After the reaction was complete, the washing steps were performed, and the organic layer was dried over sodium carbonate. This was followed by solvent removal and drying on a rotovap. The elution through and alumina plug was not performed, because increased purity did not result from this step. The key to purity was the drying of the HCl salt under vacuum. The salt was dried in a drying pistol which was loaded with drying agent and held under vacuum for 24 h. If the sample was not completely dried, crystals would not form. Verification of the product was accomplished using 200 MHz NMR data which were compared to the reported proton and ^{13}C data of Czarnik [9]. The melting point of the crystals also matched Czarnik's reported data.

The general procedure for preparation of the amine for analysis was as follows. *N*-(anthracen-9′-yl methyl)tris(3-aminopropyl)amine (2.79 mg) was dissolved in 1 l of triply-distilled water to make 5 μM amine. 4-Morpholineethane-sulfonic acid (MES) (10.66 g) was dissolved in 1 l triply-distilled water to make 0.05 M buffer which was adjusted to pH 6.0 by addition of 50% NaOH. Standard concentrations of ATP were prepared by dissolving an appropriate amount of adenosine 5′-triphosphate, disodium salt hydrate, in triply-distilled water followed by appropriate dilution. The batch measurements were made by mixing 3 ml of amine, 5 ml of MES, and 4 ml of ATP. The relative fluorescence intensity (excitation 335 ± 3 nm, emission 417 ± 3 nm) was recorded. All batch

fluorescence measurements were performed on a LS-50 Perkin-Elmer luminescence spectrometer.

pH studies were performed using the above standard procedures, and by varying the pH of the MES buffer through addition of concentrated hydrochloric acid, or 50% NaOH. pH measurements were performed on a Fisher Scientific Accumet pH meter. A blank fluorescence measurement was performed for each pH by addition of 3 ml amine, 5 ml MES, and 3 ml of triply-distilled water.

The study of interferents was performed in several different ways. The initial screening of anions was done with many of the common anions at various concentrations to determine which compounds exhibited CHEF. The anions showing the largest enhancement (ADP and phosphate) were studied further by adding different concentrations of the possible interferant to a standard sample containing 10 ppm ATP, and recording the relative intensity of the signal.

Flow-injection analysis (FIA) was used to automate the determination of ATP using the manifold shown in Fig. 1. All FIA experiments were performed using a Tecator 5020 FIA analyzer with a Waters 470 flowthrough fluorescence detector with excitation at 335 ± 3 nm and emission at 417 ± 3 nm. The system is held at a constant pH by pumping a 0.5 M MES buffer (1.2 ml min^{-1}) which is mixed into a carrier stream of triply–distilled water (1.2 ml min^{-1}). The two streams are then mixed in a 60 cm × 0.5 mm i.d. mixing coil, and merged into a stream of 5 μM amine (1.2 ml min^{-1}). The final mixing is done in a 30 cm × 0.5 mm i.d. mixing coil. A 200 μL sample loop containing ATP is directly injected

Reagent 1 = Amine
Reagent 2 = MES Buffer
Carrier 1 = Triply distilled water
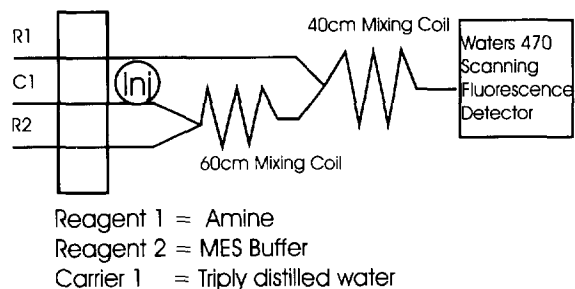
Fig. 1. Flow-injection manifold design.

Table 1

Responses of different anions relative to ATP. The relative responses have been normalizd to the response of a 10 ppm ATP sample

Anion	Relative response
ATP	17000
ADP	4035
Phosphate	12
Citrate	8
Potassium hydrogen phthalate	4
Morpholine ethane sulfonic acid	2
Sulfate	1.9
Chloride	0.3
Nitrate	< 0.1
Bromate	< 0.01

into the carrier stream. Interferant studies in the FIA system were performed by adding the possible interferant in varying concentrations directly to the ATP standard. Output from the fluorescence detector was recorded on a Linear® strip chart recorder. All reported data are based on peak height.

The pK_a values of the anthrylmethylpolyamine were determined by titrating a sample of the amine adjusted to pH 2.2 with standardized 0.005 M NaOH. Titrations were performed on a Radiometer Titrilab automated titrator.

3. Results and discussion

The work began with the characterization of N-(anthracen-9'-yl methyl)tris(3-aminopropyl)amine as an anion reagent. Initial studies based on the work described by Czarnik [9] suggested that phosphate ion produced the most intense response with the reagent. In Czarnik's work, no analytical data were presented; therefore, the capability of the reagent with phosphate was investigated. After optimization a linear range from 10–100 ppm was observed with a detection limit around 10 ppm. Given this level of detection it was clear that the compound was not particularly applicable to phosphate ion determinations. In fact given the overall response of the reagent to anions (Table 1) it was clear that the common anions did not produce significant CHEF. However, the data for

ATP and ADP show that the CHEF was significant and that a thorough investigation of the potential for ATP determination should be performed.

Current methods for ATP determination involve the use of firefly luciferase which is a very expensive reagent. In addition, the luciferase method suffers from a number of interferents. The method measures the amount of $MgATP^{2-}$, but responds to free ATP as a competitive inhibitor at 50% of the $MgATP^{2-}$ complex [8]. There is also an inhibitory effect of salts ($NaCl$, KCL, NH_4Cl, $LiCl$, $NaBr$, $MgCl_2$, and $NaHCO_3$) [13], which follows the Hofmeister series. The method also shows some inhibition by ADP which has been described in this manner: "... AMP and $MgATP^{2-}$ are bound 40 times more strongly than adenosine and MgADP is only fourfold as strongly bound as adenosine." [1]. The most logical interpretation of this statement is that adenosine does not respond to firefly luciferase, and ADP responds at a level which is approximately a 10% intereference in ATP determination at similar concentrations.

The initial CHEF studies with phosphate ion resulted in a determination of a set of optimized conditions. It was found that these conditions were also optimal for the investigation of CHEF with ATP. Amine concentrations at micromolar levels produced the lowest background fluorescence with the greatest possible enhancement. The background fluorescence signal was affected by pH (Fig. 2). The background signal is large at lower pHs, presumably due to the protonation of the amine. This point is critical because the most likely mechanism for CHEF is an electrostatic interaction between the protonated amine sites and the negative sites of the anion. Therefore, a compromise between a pH to ensure proper protonation of the amine and a pH to ensure deprotonation of the anion is necessary. The measured pK_a values of the amine are 5.95 (two terminal amines) and 9.4 (benzyl amine) with the terminal amines at the lower pK_a value. The initial studies with phosphate resulted in the optimum enhancement of the fluorescence at a pH of 6.05. The ATP study was therefore begun in the batch mode, holding the pH at 6.05 with MES as the

Fluorescence Response of Amine vs pH
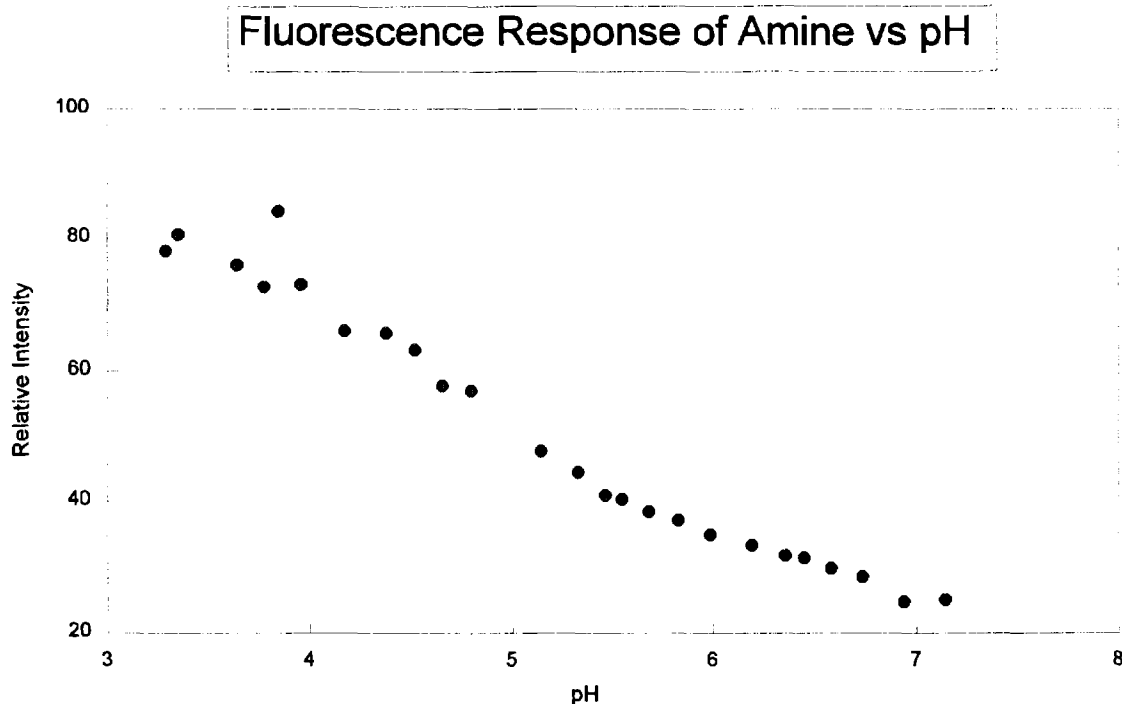
Fig. 2. Change in relative intensity of fluorescence of the regeant amine with change in pH.

buffer and a 10 μM amine concentration. ATP was easily decected down to a 10 ppm level which was adequate for any interference or pH studies which were needed in the batch mode.

The method was converted for use in FIA. The adaptation to the flow-injection system was relatively straightforward. All flow streams were pumped at the same rate, with triply-distilled water as the carrier, MES buffer as reagent 1, and the amine as reagent 2 (see Fig. 1 for manifold details). The optimum conditions were the same as the batch method except for the amine concentration which was lowered to 5 μM in order to decrease the background signal of the amine. The decrease in background signal of the amine was necessary because of the increased sensitivity of the flowthrough detector. An enhancement in the signal was seen, thus allowing a lower level of detection. A typical calibration plot in the flow-injection system for ATP was $y = 0.8106(x)$ $(\pm 0.10) + 0.214$ (± 0.235) with a r^2 value of 0.9997. The calculated detection limit of 1 μM with a linear range of 0.5–100 ppm was observed.

At 10 μM, the percent recovery was 96.8%. A typical calibration curve is shown in Fig. 3.

The interferences in this method are minimal. The biggest possible interferents with this system can be identified from the enhancements seen in Table 1. The addition of phosphate to the 50 ppm ATP–amine system did not interfere until a concentration of 1000 ppm phosphate was added. At equivalent 50 ppm concentrations of ATP and ADP a 14% increase in the signal is observed.

The enhancement in the signal varied tremendously with a change in the pH, which should have an impact on the complexing properties of the host amine. Czarnik's [9] explanation of the CHEF effect describes an electrostatic interaction between the host amine and the anion which participates in the chelating. This interaction then results in an increase in the rigidity of the pendant arm of the amine which subsequently favors the fluorescence process. The enhancement of the signal is directly related to the concentration of the anion in solution. The signal should increase when the amine–anion interaction is favorable,

Low Level Det of ATP

R Squared=0.0999603

Lowest ppm Range

R Squared=0.998171
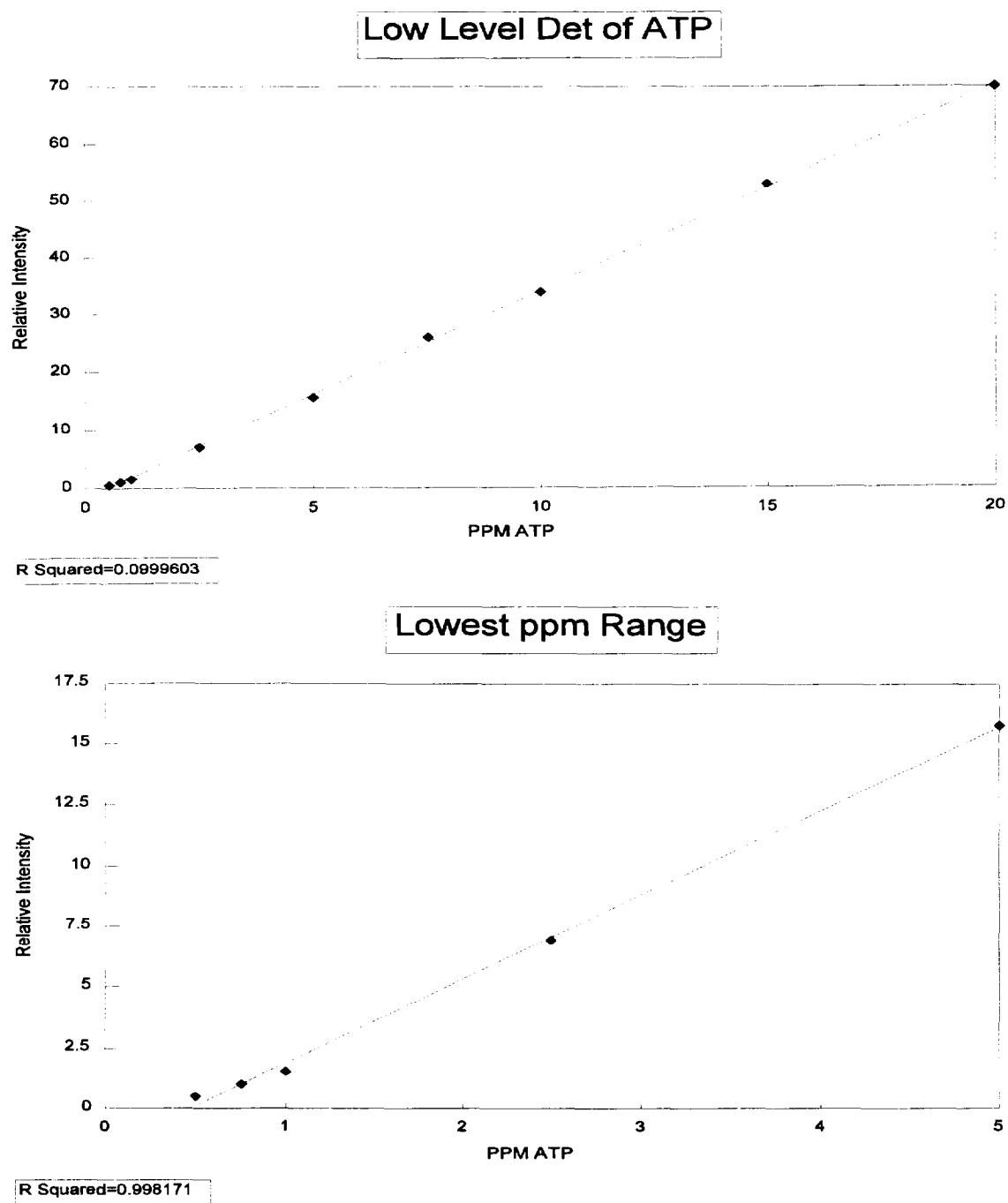
Fig. 3. Typical calibration curves for ATP CHEF.

but the anion should have no effect on the signal when it no longer possesses a negative charge, as is the case at low pH. This is not the observed trend at lower pH as can be seen from Fig. 4. ATP actually reproducibly quenches the signal at lower pH. Fig. 4 also indicates that ADP has

ATP and ADP Enhancements with Changing pH

with and without Buffer
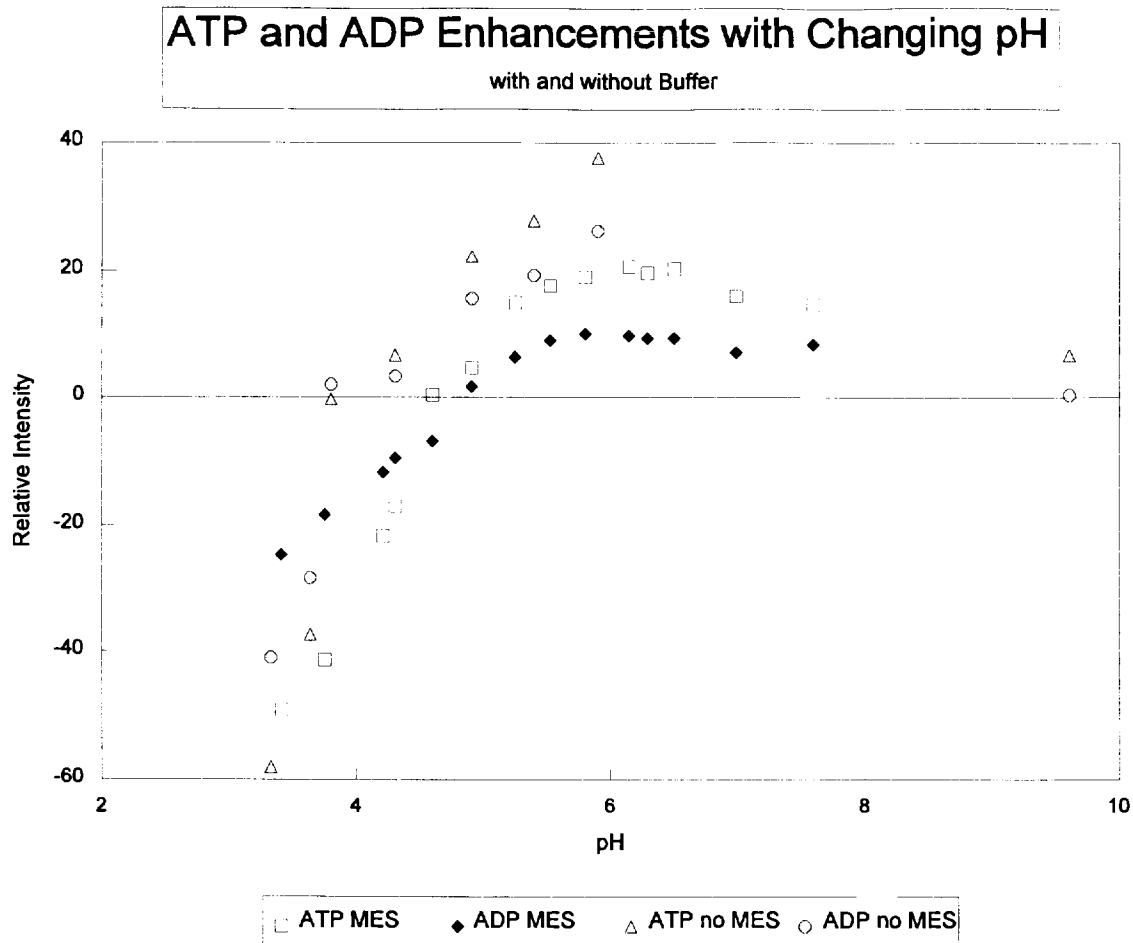
Fig. 4. Change in CHEF of ATP and ADP with and without MES buffer with change in pH.
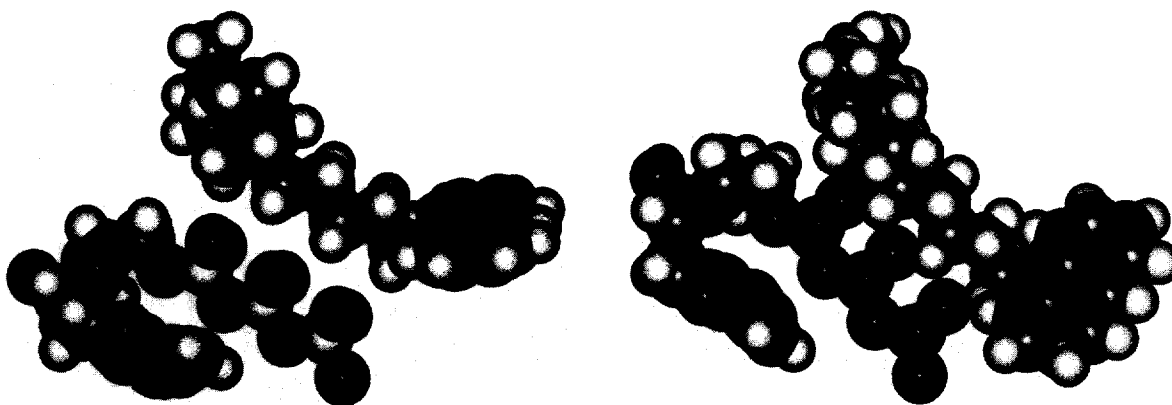
Fig. 5. Possible amine-ATP electrostatic interaction. These orientations result from the use of molecular mechanics simulation. The phosphate chain of ATP (below) aligns with the amine "arm" of the anthrylmethylpolyamine (above).
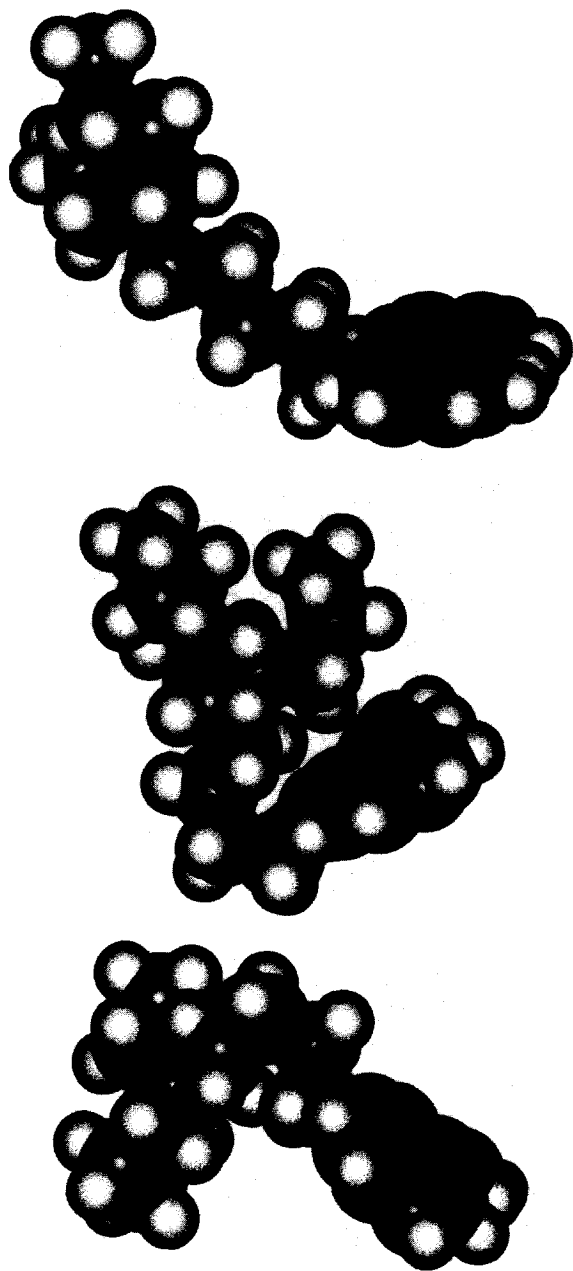
Fig. 6. The N-(anthracen-9'-yl methyl)tris(3-amino-propyl)amine molecule with movement of the pendant arm relative to anthracene over a 10 ps time scale. The movements are the result of a molecular mechanics simulation.

The explanation which Czarnik [9] has given in his description of CHEF is very straightforward, and it is the best description of the amine-anion interaction available. In order to strengthen this position, some molecular mechanics calculations (Hyperchem Version 3.0) were performed. Fig. 5 shows the results of the interaction between the host amine and ATP. The phosphate groups align themselves in the amine pocket for the best possible interaction between the protonated amines and the negative charges of the unprotonated phosphate groups. The longer chain of the ATP triphosphate group is able to interact more fully with the amine than the diphosphate group of ADP, and this reasoning rules out any interaction with AMP. There is the possibility of an increase in the electrostatic attraction as well as a decrease in the steric interaction of the bulky adenosine portion of the molecule. The initial calculations used when the host amine is allowed to move freely in space (Fig. 6) show that the amine arm of anthracene rotates from a position away from the pi face of anthracene to one close to the pi face in a matter of picoseconds. This free rotation of the arm promotes dissipation of energy which quenches the native fluorescence of the molecule. When ATP is chelated by the host amine, the free rotation of the arm is impeded by the steric bulk of ATP, and the fluorescence of the system is enhanced.

4. Conclusions

Determination of ATP at biological pH levels is a critical issue. The method described in this work is a simple, automated method for the detection of ATP with very little interference. The study of the CHEF effect with changing pH reveals a possible way to lower the small interference of ADP while improving the sensitivity. The detection limit of 1 μM and the linear range of an order of magnitude both compare favorably with current methods of ATP determination. The use of CHEF for ATP determination does not rely on enzymatic reactions, and can be used over a large range of pH including the biological pH region. All of the common interferants which

similar quenching properties at a much lower level. We have not been able to adequately explain this phenomenon, but can only present these data and assure their reproducibility.

have been tested show minimal interference. The method allows determination over a wide concentration range coupled with a low level of detection. Materials needed for synthesis of the anthrylmethylpolyamine are inexpensive, and synthesis of this compound is straightforward. The anthrylmethylpolyamine is readily soluble in water and stable for more than a week when stored below 5°C.

References

[1] F.R. Leach, J. Appl. Biochem., 3 (1981) 473.

[2] R.T. Lee, J.L. Denburg and W.D. McElroy, Arch. Biochem. Biophys., 141 (1970) 38.

[3] G. Gamborg and E.H. Hansen, Anal. Chim. Acta, 285 (1994) 321.

[4] J.N. Miller, M.B. Nawawi and C. Burgess, Anal. Chim. Acta, 266 (1992) 339.

[5] K.-D. Gunderman and F. McCapra, Chemiluminescence in Organic Chemistry, Springer-Verlag, New York, 1987, p. 151.

[6] R.E. Hodson, O. Holm-Hansen and F. Azam, Mar. Biol., 34 (1976) 143.

[7] M.R.L. Stratford and M.F. Dennis, J. Chromatogr. B., 662 (1994) 15.

[8] R.M. Bock, N. Ling, S.A. Morell and S.H. Lipton, Arch. Biochem. Biophys., 62 (1956) 253.

[9] A.W. Czarnik, in H. Schneider and H. Duerr (Eds.), Frontiers in Supramolecular Organic Chemistry and Photochemistry VCH, Weinheim, 1991, p. 109.

[10] M.E. Huston, Synthesis and Study of Anthrylmethyl-polyamine Conjugate Fluorescence Probes for Metal and Non-metal Ion Detection in Aqueous Solutions, PhD. Thesis, Ohio State University, 1990.

[11] J.L. Van Winkle, J.D. McClure and P.H. Williams, J. Org. Chem., 31 (1966) 3300.

[12] J. Chin, M. Banaszczyk, V. Jubian and X. Zou, J. Am. Chem. Soc., 111 (1989) 186.

[13] H. Holmsen, I. Holmsen and A. Bernhardsen, Anal. Biochem., 17 (1966) 456.

Homogeneous liquid–liquid extraction method for spectrofluorimetric determination of chlorophyll a

Takahito Sudo, Shukuro Igarashi*

Department of Materials Science, Faculty of Engineering, Ibaraki University, Nakanarusawa 4-12-1, Hitachi, Ibaraki 316, Japan

Abstract

A new homogeneous liquid–liquid extraction using a fluorocarbon ionic surfactant, Zonyl FSA (FSA), having a diethylthioether group as a spacer between the perfluoroalkyl group and carboxyl group has been developed. In this FSA method, the phase separation phenomena were observed at mild pH (below pH 6). Moreover, by using this extraction method as a preconcentration, a highly sensitive spectrofluorometric determination of chlorophyll a was established. The results for the standard chlorophyll a were as follows. The concentration factor (V_w/V_o) was 200 (water phase, V_w, 20 cm^3, water-immiscible phase, V_o, 100 μl), the distribution ratio, $\log D$, was 4.85, the extraction percentage, E, was 99.7%, and the procedure time was ≈ 30 min. The calibration curve was linear in the concentration range 2×10^{-11}–3×10^{-7} mol dm^{-3} and the detection limit $(S/N = 3)$ was 1×10^{-11} mol dm^{-3}. The relative standard deviation was 0.72% for 10^{-8} mol dm^{-3} (five determinations).

1. Introduction

Recently, we have found that the neutralization of perfluorooctanate ion (PFOA$^-$) in an aqueous water-miscible organic solvent solution induces a new type of phase separation which provides a small volume of an oily, transparent, water-immiscible liquid phase from a large volume of aqueous solution. By using this phenomenon, a new homogeneous liquid–liquid extraction based on pH-dependent phase separation was reported [1]. As a result, porphyrin chelates were rapidly

extracted into the water-immiscible precipitated phase, and were then easily concentrated by a factor of about 10^4. However, a strongly acidic condition (below pH 0.6) was necessary for this method, because the acid dissociation constant of the carboxyl group in PFOA$^-$ was low (i.e. the pK_a value of PFOA was 1.01 at 20°C and the ionic strength, $I = 0.1$) due to the electron withdrawing force of fluorine atoms in the perfluoroalkyl chain, which was a serious problem in the previous method. Therefore, we postulated the use of Zonyl FSA (FSA), which introduced a methylene chain (e.g. diethylthioether group) as a spacer between the perfluoroalkyl group and car-

* Corresponding author.

boxyl group in order to negate the effect of fluorine. As a result, phase separation at mild pH is possible. Compared with the PFOA method, important information from this FSA method is possibly applicable to homogeneous liquid–liquid extraction for many environmental samples or vital samples concerning denaturation under strongly acidic conditions. Details of homogeneous liquid–liquid extraction method based on the pH-dependent phase separation with FSA and the spectrofluorimetric determination for chlorophyll a (chl.a) in pond water will be discussed in this paper.

2. Experimental

2.1. Apparatus

The fluorescence measurement was made with a Hitachi Model F-4500 fluorescence spectrophotometer. The fluorescence spectrometer was equipped with a 150 W xenon lamp source. A Hitachi model 200-10 double beam spectrophotometer was used for the measurement of absorption spectra. A Toa HM-18B pH meter was used for the measurement of pH. A Karl–Fisher titrator (Mitsubishi Kasei Co., Type CA-06, Version 3.0) was used for the water content measurement in the precipitated phase. A Tomy LC-100 centrifugal machine was used for the phase separation. A Sibata CS-20 supersonic washer was used for the destruction of the phytoplankton cell.

2.2. Reagents

FSA was used as received from Du Pont and was a mixture that contained components with carbon numbers in the alkyl group from 6–10 (Fig. 1). In this study, FSA diluted to 25 wt.%

FSA

$$CF_3\text{-}(CF_2)_n\text{-}CH_2\text{-}CH_2\text{-}S\text{-}CH_2\text{-}CH_2\text{-}COOH \qquad n = 6 \sim 8$$
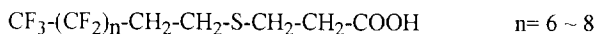
Fig. 1. Structure of FSA.

with water was used. Chl.a as a standard sample was then used as a biochemical reagent from spirulina which was obtained from Wako Pure Chemical Industry. The pH buffer aqueous solution was prepared at pH 4 by mixing 4 mol dm^{-3} acetic acid solution and 4 mol dm^{-3} sodium acetate solution. THF was obtained from the Kanto Chemicals Corporation. All other chemicals used were of analytical reagent grade.

2.3. Procedure

2.3.1. Homogeneous liquid–liquid extraction

A 12 cm^3 sample solution containing each type of solute, 6 cm^3 of water-miscible organic solvent such as THF or acetone, and 1 cm^3 of 25 wt.% FSA aqueous solution, was placed in a 50 cm^3 cylindrical glass vial fitted with a plastic cap. Acetic acid–sodium acetate mixture buffer solution (1 cm^3) was then added in order to adjust the pH value of the mixture to below pH 5. After centrifuging at 2500 rev min^{-1} for 15 min, the volume of the precipitated phase was determined using a 0.1 cm^3 micro-syringe. The concentrations of solutes in the precipitated phase were then determined spectrophotometrically or spectrofluorimetrically after dilution using 0.5 cm^3 of THF.

2.3.2. Determination of chlorophyll a

This procedure was similar to the previous procedure. Namely, 12 cm^3 of sample solution (e.g. pond water) containing chl.a, 6 cm^3 of THF and 1 cm^3 of 25 wt.% FSA aqueous solution was placed in a 50 cm^3 cylindrical glass vial fitted with a plastic cap. Next, the mixture was exposed to a 46 kHz supersonic vibration for 10 min using the supersonic washer. The phytoplankton cell was then destroyed, and chl.a was solubilized. Then, 1 cm^3 of pH buffer solution at pH < 5 was added. After centrifuging at 2500 rev min^{-1} for 15 min, the concentration of the extracted chl.a in the precipitated phase was spectrofluorimetrically determined by measuring the fluorescence intensity at λ(em) = 666 nm (λ(ex) = 430 mm) after dilution using 0.5 cm^3 of THF.
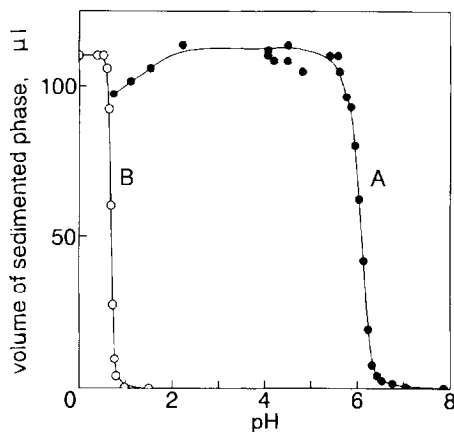
Fig. 2. Relationship between pH and the volume of sedimented phase: (curve A) FSA method; (curve B) PFOA method. $[FSA]_T = 1.25$ wt.%, $[THF]_T = 30$ vol.%, temperature = 20°C.

Fig. 3. Ternary phase diagram for water/THF/FSA solution. Point A: experimental condition. $[FSA]_T = 1.25$ wt.%, temperature = 20°C.

3. Results and discussion

3.1. Mechanism of pH-dependent phase separation

A fluorosurfactant such as PFOA or FSA dissolves in water at a higher pH value than its acid dissociation constant of the carboxylic acid group. If the pH of this aqueous solution is lower than its acid dissociation constant, the fluorosurfactant is precipitated as a needle-like crystalline solid due to the charge neutralization of the carboxyl ion. However, if small amounts of a water-miscible organic solvent such as THF or acetone coexisted in this system, the fluorosurfactant precipitated in the water-immiscible liquid phase. The solute was then extracted into the precipitated phase. The reaction formula in this phase separation phenomenon and the acid dissociation constant (K_a) are expressed as follows:

$$R_f-COO^- + H^+ \rightleftharpoons R_f-COOH \tag{1}$$

$$K_a = \frac{[R_f-COO^-][H^+]}{[R_f-COOH]} \tag{2}$$

where R_f in PFOA is C_7F_{15}. The R_f group in FSA is shown in Fig. 1.

The effect of pH during the phase separation is shown in Fig. 2. The acid dissociation constant (pK_a) of FSA was 6.5 in the 50 vol.% THF

solution. The precipitated phase was produced at below pH 6. Also, this phase separation phenomenon was reversible depending upon pH.

3.2. Effect of FSA concentration

A ternary diagram is shown in Fig. 3. It expresses the relationship between the volume content of the water/THF/FSA ternary component solution and the state of the phase separation. In this Figure, point A is the proposed experimental condition. The relationship between the concentration of FSA and the precipitated phase volume
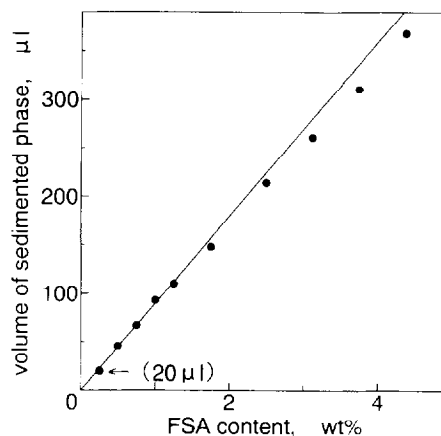
Fig. 4. Relationship between the FSA content and the volume of sedimented phase. $[THF]_T = 30$ vol.%, temperature = 20°C.

is shown in Fig. 4. The volume of the precipitated phase increased in proportion with the amount of added FSA. However, if the concentration of FSA exceeded 2.5 wt.%, the experimental point deviated from a straight line that passes through the origin. In order to have a quantitative phase separation the amount of added FSA must be below 2.5 wt.%. The maximum concentration factor (the volume ratio between the water phase and the precipitated phase after the phase separation) was 1000. In practice, it was possible to concentrate the solute from 20 cm³ of aqueous solution to 20 μl of the water-immiscible liquid phase.

3.3. Effect of water-miscible organic solvent

The properties of the water-miscible organic solvent significantly influenced the phase separation behaviour. As previously mentioned, this phase separation occurred due to the existence of the fluorosurfactant and some types of water-miscible organic solvent. Water-miscible organic solvents such as THF, acetone, N,N-dimethylformamide, acetonitrile, 1,4-dioxane, dimethylsulfoxide and ethanol were then examined. Amongst these solvents, THF and acetone were best suited for this extraction method. In the case of acetone, however, the volume and viscosity of the precipitated phase were both greater than when using THF. Based on these findings, THF was selected for this extraction method. The effect of THF concentration on the phase separation is shown in Fig. 5 (curve A). When THF was added over the volume range 10–50 vol.%, the precipitated phase became oily and transparent. Also, when THF was added below 10 vol.%, FSA precipitated as a solid. Furthermore, when THF was added above 50 vol.%, the precipitated phase was not produced.

3.4. Composition ratio in the water-immiscible precipitated phase

The change in composition of the precipitated phase was examined using the following method. The water content was measured by coulometric titration with Karl-Fisher reagent. The FSA content was measured by weighing after the evapora-
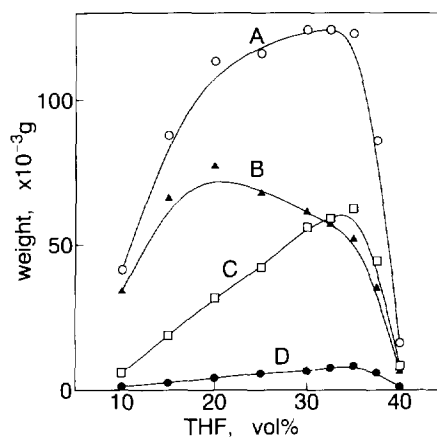
Fig. 5. Relationship between the volume of THF added and the weight of components in the sedimented phase: (A) total weight; (B) FSA; (C) THF; (D) water. $[FSA]_T = 1.25$ wt.%, temperature $= 20°C$.

tion of water and THF using a vacuum dryer. Also, the content of THF was obtained by calculating the difference from the total weight. The results are shown in Fig. 5. The content of THF in the precipitated phase increased with increasing THF concentration. The water content of the precipitated phase in the FSA system was 5%, and this value was lower than that of the PFOA method (e.g. 23% when using acetone) [1]. As a result, the most suitable hydrophobic solute for the proposed method was postulated.

3.5. Extraction of some kinds of solute

The extraction of various porphyrin compounds was examined. The distribution ratio (D) and the volume ratio are given by

$$D = C_o/C_W, \qquad V = V_W/V_o \qquad (3)$$

where C_o and C_W are the concentrations of the precipitated phase and the water phase respectively and V_W and V_o are the volumes of the water phase and the precipitated phase respectively. The extraction percentage is given by Eqs. (3) and (4).

$$E = 100D/(D + V) \quad (\%) \qquad (4)$$

The extraction result is shown in Table 1. The extraction percentage of the hydrophilic compounds having a carboxyl or phenol group was

Table 1

The distribution ratio and extraction percentage for various solutes ([FSA]$_T$ = 1.25 wt.%, pH = 4.8, $V = V_W/V_o$ = 100 ~ 200)

Sample	Water-miscible Organic solvent	log D	E (%)
Copro III	THF	1.99	49.9
TCPP[a]	THF	2.06	54.1
TCPP[a]	Acetone	2.21	45.1
THPP[b]	THF	1.82	33.8
THPP[b]	Acetone	2.88	81.3
TPP[c]	THF	3.77	98.8
TPP[c]	Acetone	3.14	91.9
Cu–chlorophyllin	Acetone	2.41	59.7
Chl.a	THF	4.85	99.7

[a] 5,10,15,20-Tetrakis(4-carboxylphenyl)porphine.
[b] 5,10,15,20-Tetrakis(4-hydroxylphenyl)porphine.
[c] 5,10,15,20-Tetraphenylporphine.

low. However, the extraction of chl.a (i.e. log D = 4.85, E = 99.7) was much better than for the other solutes.

3.6. Determination of chlorophyll a

The spectrofluorimetric determination of standard chl.a was then developed by combination with this extraction method. As a result, the calibration curve was linear in the concentration range 2×10^{-11}–3×10^{-7} mol dm^3, the detection limit (S/N = 3) was 1×10^{-11} mol dm^{-3}, and the coefficient of correlation for the calibration curve was 0.998. The relative standard deviation was 0.72% for 10^{-8} mol dm^{-3} (five determinations). For the determination of chl.a in an environmental water sample at concentrations of 10^{-11} mol dm^{-3}–10^{-8} mol dm^{-3}, the supersonic washer was used in order to disrupt the phytoplankton cell. As a result of the examination to determine the exposure time, 5 min was found to be insufficient. Also, the transformation of the cell occurred after 20 min. Hence, the exposure time was chosen to be 10 min in this study. The results, which were determined using this proposed method, correlated very well with those using a conventional extraction method [2,3] (Table 2). In the results, the RSD (4.99%) of the practical sample is much larger than that (0.72%) of the standard chl.a, because the

Table 2

Comparison with conventional method for pond water from Ibaraki University

Method	Chl.a (mol dm^{-3})	Relative standard deviation [a] (%)
This method	1.72×10^{-8}	4.99
Acetone extraction method	1.81×10^{-8}	4.87

[a] Five determinations.

former contains the determination procedure for destroying the cells, etc. This method remarkably reduced the processing time (i.e. the previous standard extraction method with acetone [2,3] was approximately 200 min, while that with the FSA method was approximately 30 min) because it did not require a filtration procedure. Therefore, this method is superior to the conventional method with respect to the treatment of many samples.

4. Conclusions

It is well known that chl.a is an important indicator for environmental evaluations. Chl.a is the magnesium complex of porphyrin, and the pheophitin is produced from chl.a by dissociating magnesium ion at approximately pH 3. Also, the phytole group is hydrolyzed under more acidic conditions (i.e. below pH 3). However, the FSA method was able to operate at near neutral pH suited for the extraction of chl.a. In addition, complicated procedures such as filtration or crushing were not needed in the proposed method. In conclusion, it is expected that this method will be extensively applied to various environmental waters in rivers, lakes, seas, etc. as a rapid, simple and highly sensitive determination of chl.a.

References

[1] S. Igarashi and T. Yotsuyanagi, Mikrochim. Acta, 106 (1992) 37.
[2] J.D.H. Strickland and T.R. Parsons, Fish. Res. Board Can. Bull., 167 (1968) 185.
[3] The SCOR/UNESCO Working Group on Photosynthetic Pigments, Monogr. Oceanogr. Methodol., 1 (1966) 69.

Flow-injection analysis–spectrophotometric determination of nitrite and nitrate in water samples by reaction with proflavin

R. Segarra Guerrero[a], C. Gomez Benito[a], J. Martínez Calatayud[b],*

[a]Departamento de Química Analítica, Universitat de València, València, Spain
[b]Departamento de Química, Colegio Universitario CEU, Moncada, València, Spain

Abstract

A flow-injection manifold is proposed for determination of nitrite based on the reaction with 3,6-diamino acridine (proflavin sulfate) in hydrochloride acid medium. The assembly is adapted for nitrate determination by including a reductive column filled with copperized cadmium. The influence of foreign substances is also studied. The method gives a linear calibration graph over the range $0.06-4 \text{ mg l}^{-1}$ nitrite, with an RSD $<0.5\%$. The method was applied to nitrite and nitrate determinations in either waste water or coastal marine water samples.

1. Introduction

Nitrite and nitrate concentrations are routine parameters to be determined in different types of sample water (waste, underground, marine, etc.). Flow-injection analysis is a suitable methodology when a great number of samples are to be considered. A number of analytical papers have been published dealing with nitrite determination by a flow-injection assembly, mainly with the aid of spectrophotometric [1, 2] detection; electrochemical [3], fluorimetric [4] and chemiluminiscence [5] detectors have also been proposed.

Nitrate determinations have been based on direct spectrophotometric methods or on measurement after derivatization, usually as reduction to nitrite; these methods utilize a homogeneous reduction process or a heterogeneous reduction with amalgamated zinc [6], zinc [7], amalgamated cadmium [9], copperized cadmium [10] or copperized cadmium silver [11]. UV irradiation in a homogeneous system has also been proposed [12].

This paper deals with a simple flow-injection analysis (FIA) assembly for the spectrophotometric determination of nitrites and nitrates by reaction with a non-cancerous reagent, which is easily water-soluble, resulting in solutions which are stable for a long time; the reagent is the sulfate of

* Corresponding author.

3,4-diamino acridine (or proflavin sulfate). The acridine is a linear dibenzopyridine, with a molecular structure similar to anthracene and with pharmaceutical applications as a topical antiseptic. A relevant feature of this family of compounds is the chemical stability; they can be boiled without decomposition and no reaction occurs with NaOH fusion; they can be partially converted into the acridinic acid by permanganate. The proflavin is a white, hygroscopic compound, soluble in water (300 parts in cold water), slightly soluble in alcohol and insoluble in chloroform and ether [13]. In a previous paper we reported the reaction of nitrite with proflavin and some related compounds [14]. In the present paper we study the analytical characteristics of the reaction to be applied to nitrate and nitrite determination in a FIA assembly.

2. Experimental

2.1. Reagents and apparatus

Aqueous solutions of 3,6-diamino acridine sulfate (Sigma), sodium nitrite (Panreac), sodium nitrate (Panreac), metallic cadmium (Merck) and copper sulfate (Panreac) were used. All reagents used were of analytical-reagent grade unless stated otherwise. The buffer solution for the conversion of nitrates into nitrites was prepared by dissolving 13 g of NH_4Cl (Panreac) and 1.7 g of Na_2EDTA (Panreac) in pure distilled water, then the pH was adjusted to 8.5 by adding NH_3 solution dropwise, and finally the resulting mixture was diluted to 1 l with distilled water.

2.2. FIA manifold

Fig. 1 shows the continuous-flow manifold used. The sample injector was from Rheodyne, model 5041 and a Gilson Minipuls 2 pump was used. The determination of nitrite was carried out by means of a Lambda 3B spectrophotometer from Perkin-Elmer at 328 nm; the cell was provided with a quartz flow-cell of 18 μl and 1 cm pathlength (from Hellma). The PTFE tubing was of 0.5 mm i.d. A copperized-cadmium column

was used for the "in-situ" reduction of nitrates to nitrides to provide the determination of nitrates in water samples; the column (10 cm length and 0.5 cm i.d.) was filled with particles with a mean size of 4 mm.

3. Analytical characteristics of the system 3,6-diamino acridine–nitrite

The aqueous solutions of proflavin at pH 1 gave absorption spectra with maximum absorbances at wavelengths 236, 282, 362 and 452 nm; changes in absorption spectra were observed when the pH was increased, two absorption bands appearing in the regions 260–265 and 400–450. The acidic proflavin solutions remained stable against time or temperature changes (they were mostly protected from daylight).

A violet colour was developed by mixing solutions of nitrite and 3,6-diamino acridine in acidic media, mainly at pH < 3. The formed compound (stoichiometry 1:1) remains unchanged for more than 2 h at temperatures <40°C. Fig. 2 depicts the corresponding absorption spectra of the reagent in hydrochloride acid medium and the nitrite–proflavin compound in the same medium. The highest absorbances were observed in strong acid media. The absorption spectra of this compound (kinetic stability) remained unchanged for long periods of time.

Different configurations of the FIA assembly were tested to select the most suitable. The selected manifold is depicted in Fig. 1. The selection procedure was carried out by performing series of experiments in which the reaction was studied under different chemical (pH) and manifold conditions. Different mixing chamber configurations were tested, the one giving the higher sample throughput (Fig. 1) was selected. The selected manifold allows a mixture of the nitrite (in pure distilled water) and the hydrochloride solution of proflavin to be formed by means of a mixing chamber. The resulting mixture is injected into a carrier stream of pure distilled water. The influence of the ratio flowrate of nitrite solution/ flowrate of the proflavin was studied and the
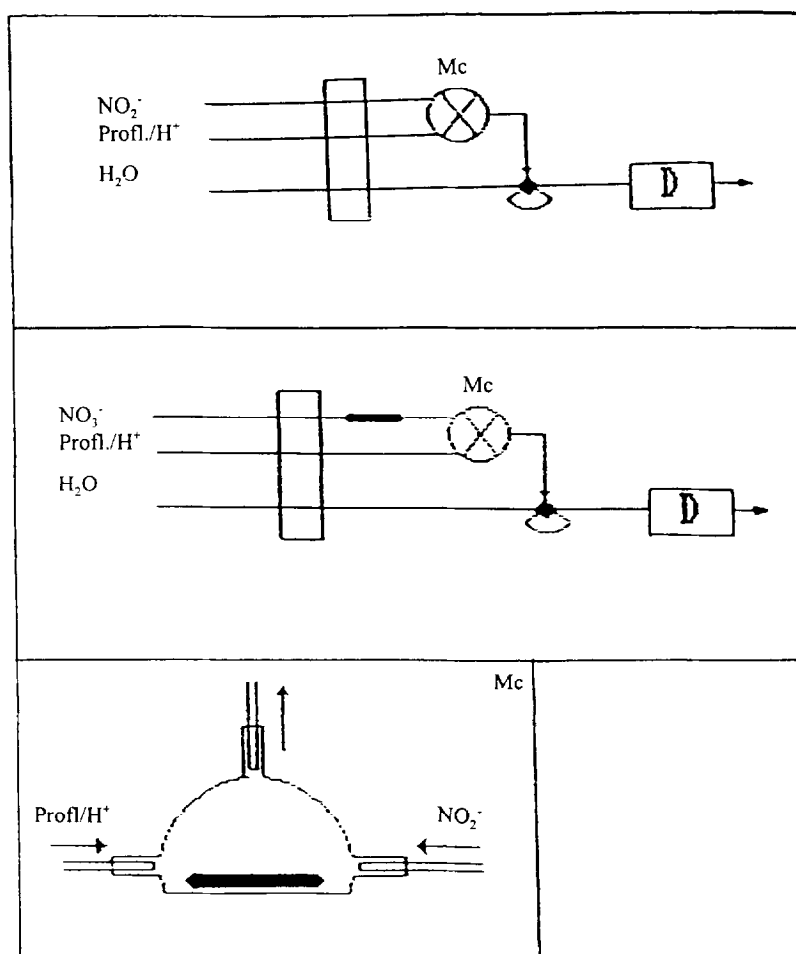
Fig. 1. Flow manifolds for determination of nitrite (upper panel) and nitrate (middle panel). The selected mixing chamber is also depicted (lower panel): height, 1 cm; diameter, 1.5 cm.

results are shown in Fig. 3; the ratio 1.45 was selected as the optimum that could be obtained.

Once the FIA assembly was selected, the chemical and FIA parameters influencing the degree of reaction and the sample dispersion were studied. The influence of acidity was important, according to the preliminary batch experiments where hydrochloric acid seemed to be the most suitable. Different concentrations of this acid were studied (2×10^{-4} mol 1^{-1} acridine, 2.0 mg 1^{-1} nitrite and distilled water as carrier) over the range 0.05–2.0 mol 1^{-1}. Best results (by considering both peak height and width of peak base) were observed with the solution containing 1 mol 1^{-1} HCl. The influence of other acids (acetic, perchloric and

phosphoric, all at 1 mol 1^{-1}) was also tested by means of the selected FIA manifold; the obtained transient signals, in absorbance units, were as follows: HCl, 0.502; $HClO_4$, 0.405; HAc, 0.018; H_3PO_4, 0.229. 1.0 mol 1^{-1} HCl was the medium selected for further work.

The influence of the proflavin content on the transient outputs was studied and the results are depicted in Fig. 4. The concentration 2×10^{-4} mol 1^{-1} (in 1 mol 1^{-1} hydrochloric acid) was selected for further work. A suitable carrier solution was selected from experiments with the following series: (a) 1 mol 1^{-1} HCl; (b) 2×10^{-4} mol 1^{-1} proflavin in 1.0 mol 1^{-1} HCl; (c) distilled water. Best outputs were observed with distilled water.
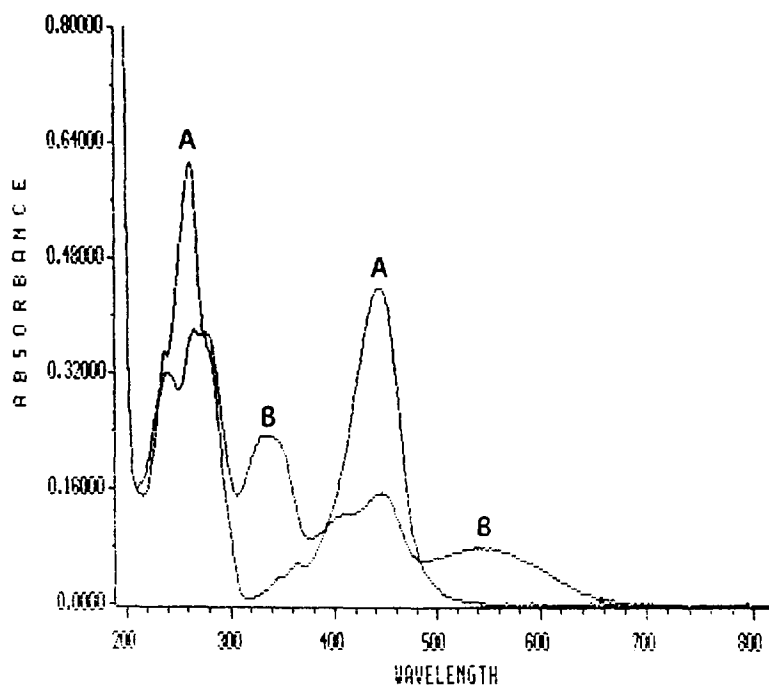
Fig. 2. Absorption spectra of the system nitrite–proflavin. (A) Reagent spectrum: 10^{-4} mol 1^{-1} proflavin solution in 0.1 mol 1^{-1} HCl. (B) Spectrum of the system nitrite–proflavin: nitrite (2.8 μg ml^{-1}) and proflavin (10^{-1} mol 1^{-1}) in 0.1 mol 1^{-1} HCl.

The influence of the temperature was tested up to 80°C, by introducing the sample loop into a water bath. The influence of temperature was

Fig. 3. Influence on the FIA output of the flow rate ratio nitrite solution/reagent stream.

shown to be irrelevant; peak height increased less than 2% (at 80°C) vs. the FIA peaks at room temperature. The formation of bubbles and lower reproducibility (as RSD, %) of the transient outputs lead us to select room temperature for further work.

The kinetic behavior of the system was studied by varing the contact time of the sample reagent in a stopped-flow mode and by changing the carrier flow rate and the distance from the injection valve to the flow cell. The reaction proved to be very quick (it was completed in the mixing chamber) and the carrier flow rate and the length of the injection valve flow cell only influenced the dispersion of the derivatized sample (increasing the base peak width), which lead us to select an injector to detector length as short as possible.

The influence of the sample volume was shown to be a relevant parameter. The increase of this parameter up to 457 μl resulted in increased peak heights; higher volumes resulted in higher absorbances (output height) with wider peak base (see Fig. 5). The set of influences studied, the
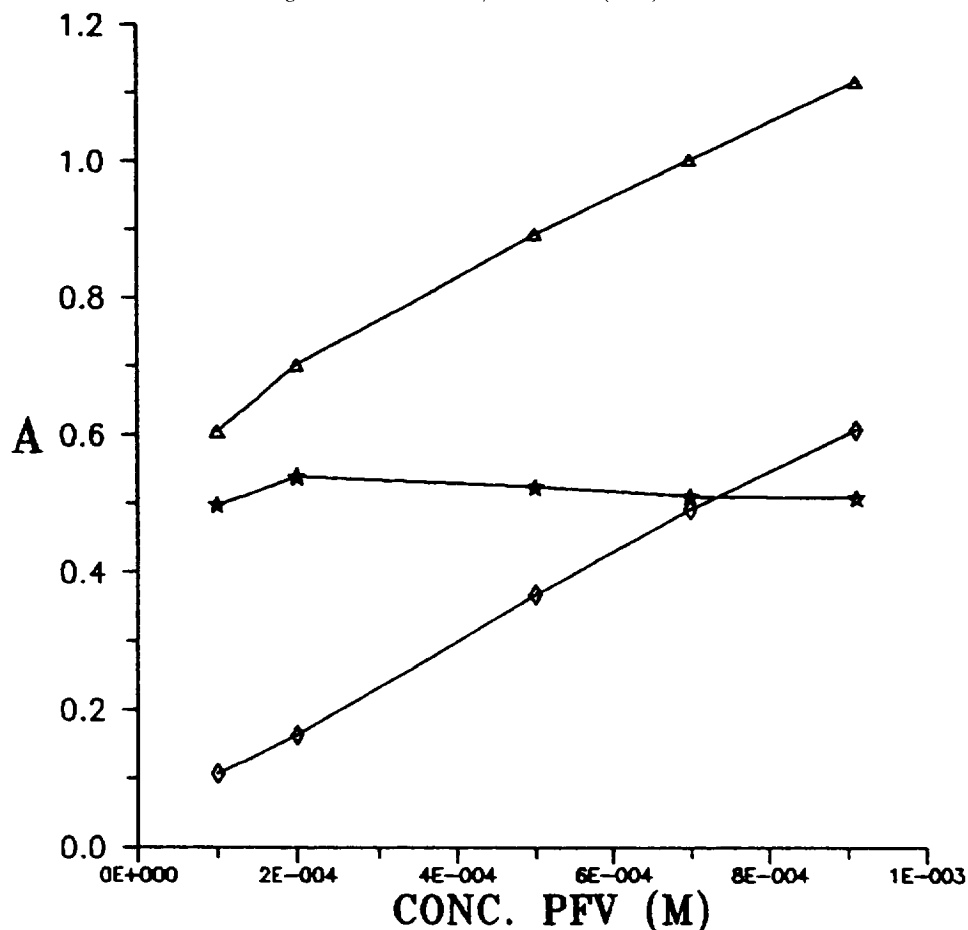
Fig. 4. Influence on the FIA output of the proflavin concentration: ($\triangle$) nitrite; ($\diamondsuit$) blank (H_2O); ($\star$) difference between nitrite and water outputs. 1 M HCl medium; carrier, water; carrier flow rate 1.79 ml min^{-1}; concentration of proflavin, 2×10^{-4} M.

tested range for each parameter and the values selected as the optimum that could be obtained are summarized in Table 1.

3.1. Application to the determination of nitrates

The proposed FIA manifold can be applied to determination of nitrate contents by adding a reductive column packed with cadmium-copperized particles and placed prior to the mixing chamber (Fig. 1). The chemical and FIA parameters influencing the conversion into nitrite (medium, flow rate, length and internal diameter of the column) were studied.

The conversion into nitrite was carried out in ammonia–ammonia chloride–Na_2EDTA medium

(pH 8.5) and different concentrations of the buffer were studied. The tested range was (millilitres of buffer solution/millilitres final volume) from 1/20 to 1/2. The influence of this parameter was shown to be irrelevant and the selected concentration was 1/4. The influence of the HCl content in the reagent solution was also tested over the range 0.1–2.0 mol l^{-1}, 1.0 being the most suitable.

The influence of the FIA parameters affecting the nitrate reduction (flow rate and reactor length) was studied by varying the reactor length (from 5 to 15 cm) at different flow rates (from stopped flow to 2.89 ml min^{-1}). The size (4 mm) of the solid particles packed into the reactor tubing was selected according to preliminary experiments. The obtained results showed a relevant
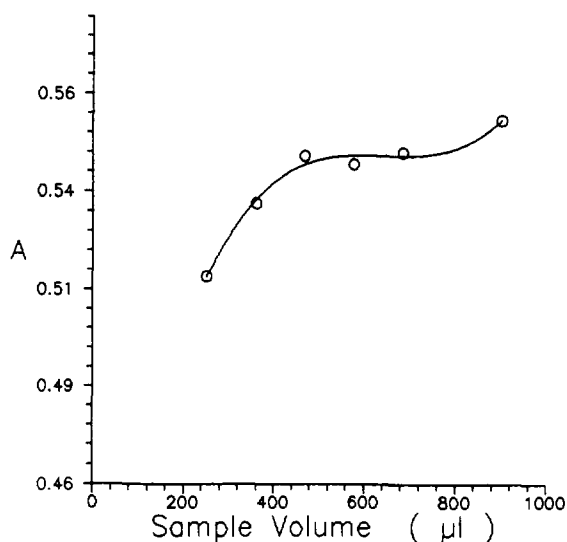
Fig. 5. Influence of the sample volume on the transient output. Conditions as in Fig. 4.

influence of the contact time between the sample and solid-phase reductor on the conversion degree and offered the possibility of working with different sensitivities (different linear calibration graphs and detection limits). The plot of absorbance vs. flow rate (in ml min^{-1}, 2 μg ml^{-1} nitrite) for a column 10 cm long, was as follows: 0.284, 2.89; 0.320, 2.16; 0.388, 1.43; 0.498, 0.70; 0.560, 0.21.

4. Analytical figures of merit

4.1. Determination of nitrites

The calibration graph was linear over the range 0.06–4 mg l^{-1} of nitrite with the equation $A = 0.277 + 0.184c$, with a correlation coefficient of 0.9995. The reproducibility and sample throughput were tested by injecting solutions containing

Table 1

Optimization of experimental parameters influencing the nitrite–proflavin FIA–spectrophotometric system

Parameter	Studied range	Selected value
Flow rate (nitrite–proflavin) ratio	0.379–1.872	1.450
Wavelength (nm)	324–332	328
HCl concentration (M)	0.05–2.0	1.0
Proflavin concentration (M)	1×10^{-4}–9.2×10^{-4}	2×10^{-4}
Carrier flow rate (ml min^{-1})	0.63–2.66	1.79
Stopped flow time (min)	0–5	0
Sample volume (μl)	246–881	457
Reaction coil length (cm)	25–175	25

Table 2

Influence of foreign compounds on the determination of nitrites. Concentration of sodium nitrite = 2.0 μg ml^{-1}

Compound[a]	Conc. (ppm)	Error (%)	Compound[b]	Conc. (ppm)	Error (%)
Br$^-$	1010	0.37	Na$^+$	1201	0.86
SO$_4^-$	1001	0.41	K$^+$	1308	0.37
PO$_4^-$	990	0.92	Cd^{2+}	1016	0.88
Cl$^-$	1053	2.70	Zn^{2+}	1001	2.60
HCO$_3^-$	940	0.63	NH^{4+}	975	2.50
CO$_3^{2-}$	992	1.70	Ca^{2+}	1008	2.30
NO$_3^-$	987	2.66	Cu^{2+}	500	3.60
SiO$_2$	909	1.10	Al^{3+}	800	2.50
			Mg^{2+}	260	2.60
			Fe^{3+}	1	0.80

[a] From sodium or potasium salts.
[b] From chloride or nitrate salts.

Table 3
Analytical figures of merit from the determination of nitrate for two different sets of sample flow rates through the solid-phase reductive reactor

Flow rate 1.79 ml min^{-1}	Flow rate 0.19 ml min^{-1}
Equation ($r = 0.9995$)	Equation ($r = 0.9999$)
Abs. $= 0.003757$ (μg l^{-1}) $+ 0.1506$	Abs. $= 0.1165$ (μg l^{-1}) $+ 0.1481$
Range $0.1-25$ μg l^{-1}	Range $0.075-10$ μg l^{-1}
Detection limit 0.1 μg l^{-1}	Detection limit 0.075 μg l^{-1}
Sample throughput (h^{-1}) 68 (5 μg l^{-1})	Sample throughput (h^{-1}) 24 (5 μg l^{-1})
Reproducibility (RSD) 0.68	Reproducibility (RSD) 0.763

0.60 or 2.0 mg l^{-1} of nitrite and the calculated results were 0.5%–37 h^{-1} and 0.1%–26 h^{-1} respectively.

The influence of foreign compounds (inorganic ions) that are commonly found in water samples containing nitrites was investigated. To solutions containing 2.0 μg ml^{-1} of nitrite were added various concentrations of the possible interfering substances up to 1000 μg ml^{-1} or when the relative error (by comparison with pure nitrite solution, 2 μg ml^{-1}) was about 3%. The results in terms of concentration (μg l^{-1}) and relative error (5) are depicted in Table 2. Fe(III) was the most serious interferent; however, it is not interfering at concentrations lower than 1 mg l^{-1} which means that it is not an interferent for drinking water samples (Spanish legal regulations allow no more than 0.05 ppm of iron in tap water).

4.2. Determination of nitrates

Table 3 depicts the analytical figures of merit obtained with the two different flow rates through the column (column length, 10 cm; carrier flow rate, 1.79 ml min^{-1}), 2.89 and 0.21 ml min^{-1}, in order to test the analytical applications with high sample throughput and high sensitivity respectively.

The method was applied to the determination of nitrate or nitrite contents in water samples (industrial waste water and coastal marine samples) and the results compared with: (a) the standard colorimetric procedure of Griess (for the nitrite content); (b) the direct spectrophotometric procedure (for the nitrate content). Nitrite contents in a waste water sample: proposed FIA

method, 1.47 (sample 1) and 2.26 μg l^{-1} (sample 2); Griess, 1.50 and 2.30 μg l^{-1}; relative error, 2.0 and 1.7% respectively. Nitrate contents in a coastal water sample: proposed FIA method, 1.73 μg l^{-1}; UV measurement, 1.75 μg l^{-1}; relative error, 1.1%.

5. Conclusions

A simple and quick FIA spectrophotometric procedure is proposed for nitrite determination. The method is based on the reaction of nitrite ion with the non-cancerous reagent, 3,6-diamino acridine. The acridine aqueous solutions are stable for long time periods. The method shows competitive precision and selectivity and a wider linear range than many other FIA procedures. The method can also be applied to determination of the nitrate by adding a suitable reductive copperized-cadmium column to the proposed FIA manifold.

References

[1] A.C. Ariza, P. Linares, M.D. Luque de Castro and M. Valcarcel, J. Autom. Chem., 14 (1992) 181.
[2] M. Yaqoob, M.A. Siddiqui and M. Massoom, J. Chem. Soc. Pak., 13 (1991) 248.
[3] M. Trojanowicz and W. Matuszewski, Anal. Chim. Acta, 261 (1992) 391.
[4] T. Perez-Ruiz, C. Martínez-Lozano and V. Tomas, Anal. Chim. Acta, 265 (1992) 103.
[5] A.T. Pilipenko and O.V. Zui, J. Water Chem. Technol, 13 (1991) 52.
[6] S.J. Bajic and B. Jaselskis, Talanta, 32 (1985) 115.

[7] M.A. Koupparis, K.M. Walczak and H.V. Malmstad, Anal. Chim. Acta, 142 (1982) 119.

[8] J.H. Margeson, J.C. Suggs and M.R. Midgett, Anal. Chem., 52 (1980) 1955.

[9] Z. Marczenko, Spectrophotometric determination of Elements, Ellis-Horwood, Chichester, 1976, pp. 397–399.

[10] J.F. Van Staden, Anal. Chim. Acta, 138 (1982) 403.

[11] R.B. Willis, Anal. Chem., 52 (1980) 1376.

[12] K. Takeda and K. Fujiwara, Anal. Chim. Acta, 276 (1993) 25.

[13] M. Windholz (Ed.), The Merck Index. An Encyclopedia of Chemicals, Drugs and Biologicals, 10th edn., Merck and Co, Inc., Rahway, NJ, 1983.

[14] F. Bosch Reig, J. Martinez Calatayud and J.R. Picó Puchades, Quím. Anal., 31 (1977) 347.

Ammonium tetraphenylborate–naphthalene adsorbent for the preconcentration and trace determination of iron in alloys and biological samples using 2-(5-bromo-2-pyridylazo)-5-diethylaminophenol by third derivative spectrophotometry

Mohammad Ali Taher, Bal Krishan Puri*

Department of Chemistry, Indian Institute of Technology, Hauz Khas, New Delhi 110 016, India

Abstract

A solid ion-pair material produced from ammonium tetraphenylborate on naphthalene (ATPB–naphthalene) provides a simple, rapid, economical and selective technique for preconcentrating iron from ≈ 500 ml of aqueous solution of standard alloys and biological samples. Iron reacts with 2-(5-bromo-2-pryidlazo)-5-diethylaminophenol (5-Br-PADAP) to form a water-soluble cationic complex. When the aqueous solution of this cationic species in the pH range 3.2–8.5 is passed over the adsorbent ATPB–naphthalene at a flow rate of 1 ml min^{-1}, it is quantitatively retained on naphthalene as an uncharged ion-associated complex. The solid mass from the column was dissolved out with 5 ml of dimethylformamide (DMF) and iron is determined by third derivative spectrophotometry by measuring the signal $d^3A/d\lambda^3$ between λ_2(773 nm) and λ_3(737 nm). The calibration curve is linear over the concentration range 0.10–25.0 μg of iron in 5 ml of DMF solution. Eight replicate determinations of 5 μg of iron gave a mean intensity (peak-to-peak signal between λ_2 and λ_3) of 1.534 with a relative standard deviation of 0.90%. The sensitivity of the method is 0.307 (d^3A/dnm^3)/μg found from the slope of the calibration curve. The interference of a large number of anions and cations has been studied and the optimized conditions developed were utilized for the trace determination of iron in various standard alloys and biological samples.

1. Introduction

Sodium tetraphenylborate (TPB) and its derivatives have been used in the estimation of alkali

*Corresponding author. Fax: (91)11-686-2037.

and univalent metal ions [1–3]. It has also been used as a counter-ion in the extraction and adsorption of some metal complexes into molten naphthalene [4–6] and microcrystalline naphthalene respectively [7–9]. A survey of the literature reveals that metal ions may be preconcentrated on various adsorbents such as thiol cotton [10], silanized glass beads [11], silica gel [12], Amberlite XAD-4 resin [13], cellulose [14], green tea leaves [15] and polythioether foams [16]. Some of these adsorbents may be fairly effective for preconcentration of metal ions, but their methods of preparation are lengthy and involve rigid control of conditions. The desorption of the metal is carried out by the slow process of elution (the metal complex is probably held by the interior surfaces of the adsorbent and thus the absorbed complex is not eluted easily), hence the procedure is time-consuming.

The reagent 2-(5-bromo-2-pyridylazo)-5-diethylaminophenol(5-Br-PADAP) has been tried for the estimation of some metal ions by zero order spectrophotometry [17–20]. In the present work it has been tried for the trace determination of iron in various standard alloys and biological samples using third derivative spectrophotometry after preconcentration of the cationic complex on ammonium tetraphenylborate–naphthalene adsorbent from a large volume of the aqueous solution (≈ 500 ml preconcentration factor 100). The proposed reagent is fairly sensitive and more selective than most of the recently reported reagents in the literature for the estimation of iron [21–24]. The use of the preconcentration technique and third derivative spectrophotometry further enhance the sensitivity and selectivity of the method [25]. The interference of a number of metal ions and anions on the estimation of iron has been studied in detail and the developed method is found to be highly sensitive and selective and has been employed for the estimation of iron in complex materials. Iron may also be estimated by directly aspirating the DMF solution of the metal complex into the flame of the atomic absorption spectrometer after the preconcentration step, but the instrument is relatively expensive, day-to-day maintenance is high and it is not free from the matrix effect.

2. Experimental

2.1. Apparatus and reagents

A Shimadzu UV 160 spectrophotometer and Hitachi UV–vis model 330 spectrophotometer with 1.0 cm quartz cell were used. An Elico pH meter was employed for pH measurements. A funnel-tipped glass tube (60 mm × 6 mm) was used as a column for preconcentration. It was plugged with polypropylene fibres and then filled with the adsorbent to a height of 1.0–1.2 cm after pressing lightly with a flat glass rod. All glassware and the column were washed with a mixture of concentrated sulphuric and nitric acids (1 + 1) before use. All chemicals used were of analythical reagent grade. A 0.01% solution of 5-Br-PADAP was prepared in ethanol. Iron(III) chloride solution was prepared in distilled water in the presence of a few millilitres of hydrochloric acid and standardized by known methods. A more dilute solution of iron (5 ppm) can be prepared by diluting the standard solution. A buffer solution of pH ≈ 5 was prepared by mixing 50 ml of 0.5 M acetic acid and 100 ml of 0.5 M sodium acetate solutions.

2.2. Preparation of naphthalene–NH_4–TPB absorbent

A solution of naphthalene was prepared by dissolving 20 g of naphthalene in 40 ml of acetone on a hot-plate stirrer at 30–35°C. This solution was transferred into 1500 ml of distilled water containing 25 ml of 1 mol 1^{-1} ammonium acetate and 75 ml of 1 mol 1^{-1} ammonia solution (pH 9.5), in a fast stream continuous flow with continuous stirring at room temperature. Then, to this solution, 500 ml of an aqueous solution containing 1.7 g of TPB was added. The naphthalene coprecipitated with NH_4^+ and TBP^- was stirred for about 2 h and then allowed to stand for 2 h. The supernatant solution was decanted off and the remaining solid mass was washed twice with distilled water. The adsorbent in the form of a slurry was stored in a bottle for subsequent use.

2.3. General procedure

An aliquot of the solution containing 0.1–25 μg of iron was taken in a 25 ml beaker and 2.0 ml of 0.01% alcoholic solution of 5-Br-PADAP and 1.0 ml of acetate buffer of pH $\approx$ 5 were added to it and the final volume in the beaker was made up to approximately 15 ml with water if required. The column loaded with the adsorbent NH$_4$-TPB–naphthalene was conditioned to pH $\approx$ 5 by passing 2–5 ml of the acetate buffer solution at a flow rate of 1 ml min^{-1}. The iron sample solution prepared above was then passed at a flow rate of 1 ml min^{-1}. The packing in the column was washed with a few millilitres of distilled water and then aspirated strongly for 2–3 min, pushing down the solid mass in the column with a glass rod in order to eliminate the excess water attached to the adsorbent. The metal complex was dissolved out of the column along with napthalene with 5 ml of DMF. The third derivative absorption spectra in the range 650–850 mm were recorded against a blank solution prepared in the same way. The signal was measured between $\lambda_2 = 773$ nm and $\lambda_3 = 737$ nm. A calibration curve was prepared by taking various known amounts of iron under the conditions given above.

3. Results and discussion

3.1. Spectrophotometric measurements

The zero order and first, second and third order derivative spectra of the complex are shown in Figs. 1 and 2 respectively. As can be seen, the higher wavelength peaks of the third derivative spectra are more significant. The sensitivity of the third order derivative is much higher than for zero, first and second orders (zero order = A/μg = 0.10, first order = $(dA/dnm)/\mu$g = 0.08, second order = $(d^2A/dnm^2)/\mu$g = 0.19, and third order = $(d^3A/dnm^3)/\mu$g = 0.31). Third derivatization leads to sharper zero order bands and gives higher signals on the resulting spectra. The characteristics of derivative spectra, such as peak height and noise level, depend on the choice of parameters such as order of derivative, scan speed
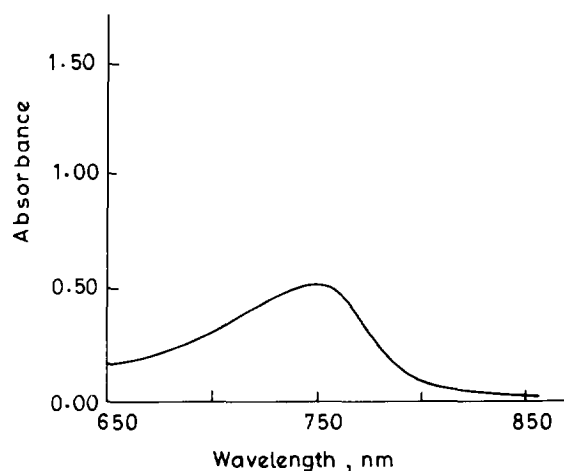
Fig. 1. Zero order spectrum of the naphthalene–Fe(III)–(5-Br-PADAP)–TPB complex. Fe(III): 5 μg; buffer: 1.0 ml; pH: 5.0; 5-Br-PADAP: 2.0 ml(0.01%); flow rate: 1 ml min^{-1}; solvent: 5 ml DMF; reference: reagent blank.

and integration time during recording of the spectra. The optimum parameters were chosen from preliminary experiments. The best results were obtained from third derivative spectra due to high
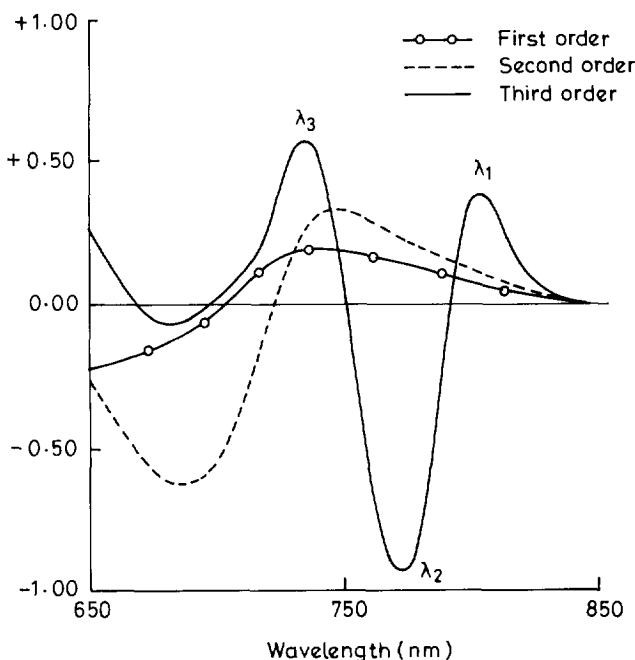
Fig. 2. First, second and third derivative spectra of the naphthalene–Fe(III)–(5-Br-PADAP)–TPB complex. For conditions, see Fig. 1.

signals at $\lambda_1 = 806$ nm, $\lambda_2 = 773$ nm, $\lambda_3 = 737$ nm, with a length interval of 9 nm. Iron could be determined by measuring the signal between the baseline and the corresponding peaks. It could also be determined from the signal between λ_1 and λ_2 or λ_3 and λ_2. In the present work a peak-to-peak method between λ_3 and λ_2 was applied.

3.2. Retention characteristics of NH_4-TPB

The TPB^- forms a weakly bonded ion-pair with NH_4^+ in aqueous solution and coprecipitates with microcrystalline naphthalene as follows:
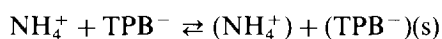
$$NH_4^+ + TPB^- \rightleftarrows (NH_4^+) + (TPB^-)(s)$$

From the experimental observation, the NH_4-TPB ion-pair produced from TPB^- and ammonium acetate in aqueous solution when supported on naphthalene was unstable and partly desorbed from the surface of the naphthalane in the column on passage of the buffer of pH 5. However, the NH_4-TPB ion-pair prepared in acetate buffer of pH 9.5 is highly stable and TPB^- is not desorbed even on washing with water or the buffer of pH ≈ 5. The adsorbent shows excellent absorption characteristics for various cationic metal complexes such as $Fe(1,1\text{-phen})_3^{2+}$. In this work, TPB^- has been selected as the counter-ion because of its purity and moderate price.

3.3. Reaction conditions

These were established with the use of 5 μg iron. The adsorption of iron on this adsorbent was found to be a maximum in the pH range 3.2–8.5 (Fig. 3). In subsequent studies, the pH was maintained at approximately 5.0. Addition of 0.5–15 ml of the buffer did not aflect the retention of iron and the use of 1.0 ml is recommended. Various amounts of 0.01% alcoholic solution of 5-Br-PADAP were tried. Iron was quantitatively absorbed on the absorbent over the range 1.0–4.0 ml of the reagent. Therefore, 2.0 ml of the reagent is recommended in the present study. The flow rate was varied from 0.5 to 8 ml min^{-1}. It was found that the flow rate did not affect adsorption within this range. A flow rate of 1 ml min^{-1} was recommended for all experiments. In the case of a
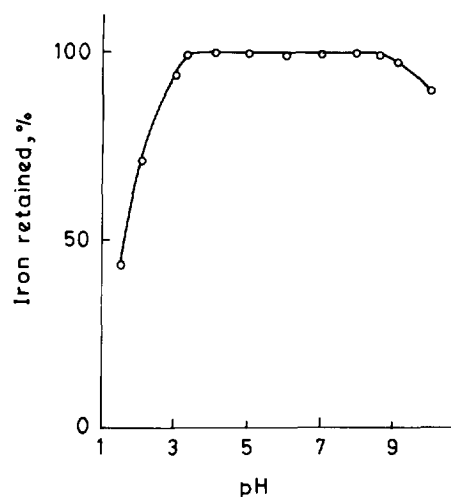
Fig. 3. Effect of pH. For conditions, see Fig. 2.

large volume of the aqueous phase, a flow rate of 5–8 ml min^{-1} may be used. The adsorption was constant and maximal when the volume of the aqueous phase did not exceed 500 ml, resulting in a preconcentration factor of ≈ 100. The retention started to decrease slowly as the volume of the aqueous phase was increased beyond 500 ml. The solid mass can be completely dissolved out of the column with less than 3 ml of the solvent (DMF); thus a preconcentration factor of ≈ 170 may be achieved. In subsequent study, 20 ml of the aqueous phase was used for convenience.

3.4. Choice of solvent

A number of solvents were tried to dissolve the metal complex along with naphthalene from the column. Since the solid mass is dissolved in a small volume (3–5 ml) of solvent from the column, it is essential to select a solvent in which the chelate is highly soluble and also sensitive for UV–vis spectrophotometric measurements. The solid material is insoluble in ordinary organic solvents such as toluene, 1,2-dichloroetane, n-hexane, nitrobenzene, isoamyl alcohol, n-amyl alcohol, ethyl acetate, methyl isobutyl ketone, chloroform and dioxane, but soluble in dimethyl sulfoxide, DMF, and propylene carbonate. DMF

was preferred because of its high solubility and stability. It was found that 2–3 ml of this solvent was sufficient to dissolve the entire mixture, thus further enhancing the sensitivity of the method. Since only a small volume (3–5 ml) of the solvent is required to dissolve the solid mass from the column, it was essential to study the effect of the surplus water attached to the absorbent. It was found that the surplus water caused the absorbance to decrease by 10–12% and led to an error in the determination. Thus it was necessary to eliminate the water attached to naphthalene in the column completely by aspirating it for 2–3 min.

3.5. Calibration, sensitivity, precision, stability and column capacity

On the basis of the optimum conditions developed above a calibration graph was constructed according to the standard procedure. It was linear over the concentration range 0.1–25 μg of iron in 5 ml of DMF solution (Fig. 4). Eight replicate determinations of 5.0 μg of iron gave a mean intensity in the third derivative spectrum, measured from the peak-to-peak signal between λ_2 and λ_3, of 1.534 with a relative standard deviation of 0.9%. The sensitivity was 0.307 $(d^3A/dnm^3)\mu$g from the slope of the calibration curve, the detection limit was 0.01 μg ml^{-1} (signal-to-noise ra-
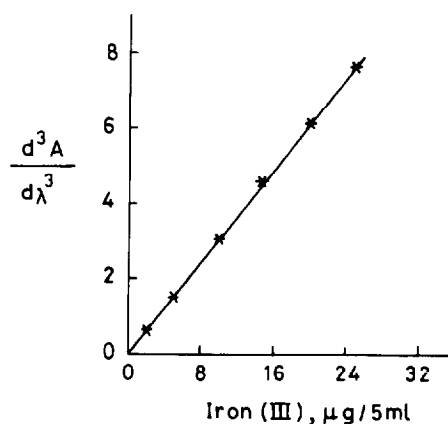
Fig. 4. Calibration curve for Fe(III) by third derivative spectrophotometry from signal peak-to-peak measurements between λ_2 and λ_3. For conditions, see Fig. 2.

Table 1
Effect of foreign salts and metal ions

Salt or ion	Tolerance limit
$CH_3COONa \cdot 3H_2$, NaCl, KNO_3	1 g
NH_4Cl, $(NH_4)_2 SO_4$, NH_4Br	500 mg
Thiourea	600 mg
KI	400 mg
K_2CO_3	100 mg
Potassium sodium tartrate	50 mg
KSCN	10 mg
Na_2 EDTA	5 μg
Al(III)	20 mg
Mg(II), Ca(II)	5 mg
Ti(IV)	1 mg
Pb(II)	1.5 mg
Cr(III)	600 μg
Cd(II), Cu(II), Mn(II), Zn(II)	250 μg
Ni(II)	400 μg
Zr(IV)	300 μg
Bi(III), Pd(II), W(VI), Ru(III)	200 μg
Mo(VI)	150 μg
Co(II)	100 μg

tio $= 2$), the solution was stable for over 6 days and the capacity of the column was 1.1 mg Fe g^{-1} of adsorbent.

3.6. Interference of foreign ions

Various salts and metals ions were added individually to a solution containing 5 μg of iron and the general procedure was applied. The tolerance limit (error < 3%) is given in Table 1. Among the salts examined, most did not interfere at the gram per milligram level with the exception of EDTA. Among the metal ions studied, many did not interfere even at the milligram level. Thus the method is highly selective without the use of masking agents. The proposed procedure has therefore been applied to the determination of iron in alloys and biological samples without any prior separations.

3.7. Determination of iron in standard aluminium and zinc alloys

The proposed method has been applied to determination of iron in Nippon Keikinzoku Kogyo (NKK) CRM 916 NKK 3A30 aluminium alloys,

Table 2
Analysis of samples for iron

Sample	Composition(%)	Concentration of iron (%)	
		Certified value	Found[a]
NKK 916 Aluminium Alloy	Si,0.41;Cu,0.27;Mn,0.11; Mg,0.10;Cr,0.05;Ni,0.06; Zn,0.30;Ti,0.10;Sn,0.05; Pb,0.04;V,0.02;Zr,0.05; Bi,0.03;Co,0.03;Sb,0.01; B,0.0006	0.54	0.53 ± 0.03
NKK 3A30 Aluminium Alloy	Si,9.96;Cu,0.059;Mn,0.042; Mg,0.01;Zn,0.43;Ni,0.042; Ti,0.038;Sn,0.038	0.633	0.630 ± 0.015
NIST SRM 629 Zinc Alloy	Cu,1.50;Al,5.15;Mg,0.094; Pb,0.0135;Cd,0.0155; Sn,0.012;Cr,0.0008; Mn,0.0017;Ni,0.0075; Si,0.078	0.017	0.017 ± 0.003
NIES No. 3 Cholorella	K,1.24 ± 0.06;Ca,0.49 ± 0.03 Mg,0.33 ± 0.02;P,(1.7)%; Mn,69 ± 5;Zn,20.5 ± 1.0; Sr,40 ± 3;Co,0.87 ± 0.05; Cu,3.5 ± 0.3;Cd,(0.026); Pb,(0.60);Sc,(0.013)μg g^{-1}	0.185 ± 0.010	0.182 ± 0.012
NIES No. 6 Mussels	Na,1.00 ± 0.03;K,0.54 ± 0.02; Ca,0.13 ± 0.01;Mg,0.21 ± 0.01; P,(0.77)%;Zn,106 ± 6;Mn,16.3 ± 1.2; As,9.2 ± 0.5;Cu,4.9 ± 0.3; Ni,0.93 ± 0.06;Pb,0.91 ± 0.04; Cd,0.82 ± 0.03;Cr,0.63 ± 0.07; Ag,0.027 ± 0.003;Al,(220); Sr(17),Se,(1.5);Co,(0.37); Hg(0.05)μg g^{-1}	158 ± 8[b]	155 ± 9[b]
NIES No. 2 Pond Sediment	Al,10.6 ± 0.5;Ca,0.81; K,0.68;Na,0.57%; Zn,343;Cu,210;Pb,105; Cr,75;Ni,40;Co,27; As,12;Cd,0.82μg g^{-1}	6.53 ± 0.35	6.47 ± 0.39

[a] Mean of four determinations.
[b] μg g^{-1}, ± SD.
The composition values in parentheses are uncertified values.

and National Institute of Standards Technology Standard Reference Materials NIST, SRM 929 Zinc Alloy. A 0.1 g sample of the standard alloy was completely dissolved in 4–5 ml of hydrochloric acid (1 + 1) by heating on a waterbath and then 1 ml of 30% hydrogen peroxide was added to the solution. The excess of peroxide was decomposed by heating the solution on a waterbath. The solution was cooled and filtered if needed and the filtrate was diluted to 100 ml with doubly-distilled water in a calibrated flask. An aliquot (1–2 ml) of this solution was taken and iron was determined by the general procedure (Table 2).

3.8. Determination of iron in chlorella, mussel and pond sediment

The proposed method has been applied to the determination of iron in National Institute for Environmental Studies (NIES) No. 3 Chlorella, NIES No. 6 Mussels and NIES No. 2 Pond Sediment. Chlorella or pond sediment (0.1 g) or mussel (0.5 g) were taken individually in a beaker and dissolved in concentrated nitric acid (≈ 5 ml) with heating. The solution was cooled, diluted and filtered. The filtrate was made up to 100 ml with water in a calibrated flask. An aliquot (1–2 ml) of the sample solution was taken individually and iron was determined by the general procedure. The results are given in Table 2 and are in good agreement with the certified values.

4. Conclusion

A solid ion-pair compound produced from NH_4^+ and TPB^- on naphthalene provides a simple and economical method for the preconcentration of iron from large volumes of alloys and biological samples using 5-Br-PADAP as the complexing agent. This reagent is fairly sensitive and selective for iron but with the preconcentration step and the use of derivative spectrophotometry its sensitivity and selectivity have been further improved and thus the developed method can be used safely for the estimation of iron in a number of complex materials such as environmental samples. Since the adsorbent provides TPB^- as the counter anion, the absorbent may therefore be used for the preconcentration of various types of cationic metal complexes. Although the metal may be estimated by AAS after the preconcentration step, AAS is however a relatively expensive instrument and day-to-day expenses and maintenance are high. Another, cheaper, technique is differential pulse polarography which could be tried for the estimation of iron after the precon-

centration step. As a whole the proposed method is highly sensitive, selective, simple and highly economical (it requires simple glassware, and a small volume of the organic solvent to dissolve the solid mass from the column) for the estimation of iron.

References

[1] A.J. Barnard, Jr., Chemist-Analyst, 44 (1955) 104.
[2] A.J. Bernard, Jr., Chemist-Analyst, 47 (1958) 46.
[3] C.N. Reilly, Advances in Analytical Chemistry, Vol. 1, Interscience, New York, 1960.
[4] M. Satake, T. Nagahiro and B.K. Puri, Analyst, 109 (1984) 31.
[5] T. Nagahiro, K. Uesugi, M. Satake and B.K. Puri, Bull. Chem. Soc. Jpn., 85 (1985) 1115.
[6] L.F. Chang, M. Satake, T. Kuwamoto and B.K. Puri, Microchem. J., 33 (1986) 46.
[7] T. Nagahiro, M. Satake, J.L. Lin and B.K. Puri, Analyst, 109 (1984) 163.
[8] J.L. Lin, M. Satake and B.K. Puri, Analyst, 110 (1985) 1351.
[9] M.C. Mehra, T. Nagahiro and M. Satake, Microchem. J., 33 (1986) 198.
[10] Y.M. Quig and L.G. Quin, Talanta, 30 (1983) 265.
[11] S. Taguchi, T. Yal, Y. Shimada and K. Goto, Talanta, 30 (1983) 169.
[12] M. Kubota, K. Matseemoto and K. Terada, Anal. Sci., 3 (1987) 45.
[13] Y. Sakai and N. Mori, Talanta, 33 (1986) 161.
[14] P. Burba and P.G. Willmer, Talanta, 30 (1983) 381.
[15] M. Kimura, H. Yamashita and J. Komada, Bunseki Kagaku, 35 (1986) 400.
[16] A.S. Khan and A. Chow, Talanta, 33 (1986) 182,
[17] G.V. Rathala and M.C. Eshwar, Analyst, 111 (1986) 61.
[18] L.D. Martinez, E. Perino, E.J. Marchensky and R.A. Olsina, Talanta, 40 (1993) 385.
[19] M. Jarosz, S. Oszwaldowski and Z. Marczenko, Chem. Anal. (Warsaw), 37 (1992) 335.
[20] S.D. Hartenstein, Anal. Chim. Acta, 228 (1990) 279.
[21] T. Nagahiro, K. Uesugi and M. Satake, Analyst, 111 (1986) 1389.
[22] H. Ishii and K. Kohata, Analyst, 112 (1987) 1121.
[23] L. Vladescu and R.L. Gurguta, Talanta, 40 (1993) 1127.
[24] I. Mori, M. Toyoda, Y. Fujita, T. Matsuo and K. Taguchi, Talanta, 41 (1994) 251.
[25] J.A. Murillo and J.M. Lemus, Analyst, 113 (1988) 1479.

Catalytic-adsorptive stripping voltammetry of cobalt in the presence of 2,2'-bipyridine and nitrite

Zhiqiang Gao*, Kok Siong Siow

Department of Chemistry, National University of Singapore, Kent Ridge, Singapore 0511, Singapore

Received 7 June 1995; revised 20 September 1995; accepted 25 September 1995

Abstract

A highly sensitive and selective procedure is presented for the voltammetric determination of cobalt. The procedure involves an adsorptive accumulation of cobalt-2,2'-bipyridine complex on a hanging mercury drop electrode, followed by a stripping voltammetric measurement of the catalytic reduction current of nitrite at -1.25 V (vs. Ag/AgCl). The optimum conditions for the analysis of cobalt include 0.1 M ammonium buffer (pH 8.55–9.25), 2.0–5.0 μM 2,2'-bipyridine, 0.20 M sodium nitrite and an accumulation potential between -0.75 and -0.90 V (vs. Ag/AgCl). An accumulation time of 30 s results in a very low detection limit of 9.5 pM (0.56 p.p.t.) and a linear current–concentration relationship up to 2.0 nM. The relative standard deviation at 0.10 nM is 4.9%. Possible interferences from co-existing ions are also investigated.

Keywords: Cobalt; 2,2'-Bipyridine; Adsorptive voltammetry; Nitrite

1. Introduction

Interest in cobalt found in biological systems is due to the importance of this metal as an essential trace element; it is a component of vitamin B_{12} and participates in a number of enzymatic reactions [1–3]. Since the concentration of cobalt is extremely low in various natural samples (usually at sub-p.p.b. levels), a sufficiently sensitive and selective analytical procedure for the reliable de-

termination of cobalt in natural samples would be of great interest. Consequently, a large number of papers have been published on the determination of cobalt. The most commonly used methods for the determination of cobalt include spectrophotometry [4], atomic absorption spectrometry (AAS) [5], high performance liquid chromatography [6], neutron activation analysis [7], mass spectrometry [8] and fluorescence spectrometry [9]. Among these methods, only the highly costly neutron activation analysis and mass spectrometry have sufficient sensitivty for direct measurements of trace amounts of cobalt. AAS,

* Corresponding author. Fax: (65) 779-1691;
e-mail: CHMGAOZ@leonis.nus.sg.

which is frequently used for the determination of trace amounts of metals, is not highly reliable for analyzing cobalt at sub-p.p.b. levels, because such levels are comparable to the detection limit of the technique.

Electroanalytical methods for the determination of traces of cobalt, mainly involving the formation and adsorptive collection of cobalt complexes with various dioximes, such as dimethylglyoxime [10,11], nioxime [12,13], α-benzil dioxime [14], and α-furil dioxime [10], on a hanging mercury drop electrode (HMDE), have also been proposed. Further improvement in sensitivity has been reported by the application of the catalytic effect of cobalt–dioximes complexes on the reduction of nitrite [10–12,14]. Among those procedures, the most sensitive one for the determination of cobalt is based on the formation of cobalt-α-benzil dioxime complex coupling with the catalytic reduction of nitrite in ammonium medium. The detection limit of 41 pM was obtained following a short accumulation period (30 s). Furthermore the cobalt-α-benzil dioxime approach has been used to determine cobalt in zinc plant electrolyte [15] and in metallic zinc [16]. Some other complexing agents, including 1,10,-phenanthroline [17], 1-nitroso-1-naphthol [18], 4-[2-(5-bromopyridyl)azo]-1,3-dihydroxynaphthalene [19] and 2-quinolinethiol [20] have also been studied in attempts to develop highly sensitive methods for cobalt analysis. However, all those procedures are not so sensitive as the cobalt-α-benzil dioxime system.

The polarographic behaviour of cobalt-2,2'-bipyridine (Co(II)–BPY) complexes has previously been reported by Fungaro and Tokoro [21]. In acidified aqueous medium, the reduction product of Co(II)–BPY, Co(I)–BPY, catalyzes the reduction of hydrogen ions. Preliminary studies in our laboratory have shown that no obvious catalytic effect on the reduction of hydrogen ions is observed in alkaline solutions. Instead, remarkable improvement in sensitivity is observed using the catalytic effect of the Co(II)–BPY complex by adding sodium nitrite to the solution. In this paper the catalytic-adsorptive stripping voltammetry of the Co(II)–BPY complex at the HMDE was investigated. Compared to the adsorptive

stripping procedure, this method provides much better sensitivity and selectivity.

2. Experimental

2.1. Apparatus and reagents

A PAR Model 174A polarographic analyzer was employed in connection with a Model 303 SMDE (EG&G, PAR, USA) and a Graphtec X–Y recorder. A medium-sized HMDE electrode, with a surface area of 1.8 mm^2 was used. An Ag/AgCl (in saturated KCl) reference electrode was used in all experiments. All potentials reported in this paper are referred to the Ag/AgCl electrode. Solutions were deoxygenated with high-purity nitrogen for 4 min prior to each experiment and all experiments were performed under nitrogen atmosphere.

Water purified in a Milli-Q water purification system (Millipore) was used for all solutions and sample preparations. All chemicals were of certified analytical grade and above. Working solutions of cobalt (Co(II)) were prepared from a 1000 p.p.m. stock solution of Co(II) (atomic absorption standard, Aldrich). Stock solutions of 0.010 M BPY and 1.0 M nitrite were prepared by directly dissolving required amounts of BPY and sodium nitrite in water, respectively. Traces of cobalt in blank electrolyte were removed using Chelex-100 resin. Cobalt found in the purified electrolyte is generally less than 0.030 nM. Reagent containers and sample bottles were cleaned by soaking in 1:1 nitric acid for a few days. Then they were thoroughly rinsed with water and stored in 0.01 M nitric acid.

2.2. Procedure

The supporting electrolyte solution (10 ml 0.1 M ammonium buffer pH 9.2) containing 5.0 μM BPY and 0.20 M sodium nitrite was pipetted into the cell and purged with nitrogen for 4 min. The accumulation potential (-0.80 V) was applied to a fresh mercury drop while the solution was stirred (400 rev min^{-1}). Following the accumulation, a linear scan voltammogram was recorded

from -0.80 to -1.5 V, with a scan rate of 100 mV s^{-1}. After obtaining the background voltammogram, aliquots of the cobalt standard solutions were introduced into the cell while maintaining a nitrogen atmosphere over the solution. All data were obtained at room temperature in a clean environment.

3. Results and discussion

3.1. Voltammetric properties of Co(II)–BPY in nitrite medium

Fig. 1 shows cyclic voltammograms for BPY, NO_2^-, BPY–NO_2^-, and BPY–NO_2^-–Co(II) in 0.1 M pH 9.2 ammonium buffer solution. As can be seen in Fig. 1A, for the solution containing BPY alone, a couple of waves were observed at -1.4 V, which is due to the redox reaction of BPY at the HMDE. As shown in Fig. 1B, in the ammonium buffer containing nitrite alone, no obvious current peaks were observable between -0.50 and -1.5 V. Beyond -1.5 V a sharp increase in reduction current was observed, which is attributed to the reduction of nitrite. For the solution containing nitrite and BPY, two small cathodic peaks were observed (Fig. 1C). The one at less negative potential is due exclusively to

Fig. 1. Cyclic voltammograms for (A) 5.0 μM BPY, (B) 0.20 M nitrite, (C) A + B and (D) C + 2.0 nM cobalt in 0.1 M pH 9.2 ammonium buffer. Accumulation potential, -0.50 V, accumulation time, 0 s (dotted line) and 30 s (solid lines); potential scan rate, 100 mV s^{-1}.

traces of cobalt in the purified electrolyte. Voltammetric properties of Co(II)–BPY complex in slightly alkaline medium were investigated by several groups [22–24]. The Co(II)–BPY complex shows strongly adsorptive character at the mercury electrode. The reduction of the adsorbed Co(II)–BPY complex takes place around -1.53 V (vs. SCE) and the stripping peak current was used to determine trace amounts of cobalt with a detection limit of 5 nM after a few minutes of adsorptive accumulation [22,23]. On the other hand, as indicated in Fig. 1D, with the addition of a small amount of Co(II), a new cathodic peak located at -1.25 V was obtained when scanning the electrode potential in the negative direction, and the reverse scan gave another cathodic peak at -1.1 V, suggesting a catalytic process. In the absence of nitrite, no catalytic current was observed for the electrode process. As we know, nitrite may disproportionate to nitrate and nitrogen monoxide in aqueous medium [25]. When nitrate was substituted for nitrite, no obvious current peaks were observable between -0.50 and -1.5 V except the redox responses of BPY, indicating that nitrate is not involved in the catalytic reaction. The fact that a well-defined and intensive signal was obtained in cyclic voltammetry for 2.0 nM cobalt indicates the remarkable sensitivity associated with the catalytic process. The short accumulation period (stirred) resulted in a significant enhancement of the sensitivity, as compared with that of the non-accumulated response (broken line in Fig. 1D). The peak current decreased rapidly upon repetitive potential cycling and after a few cycles the peak currents approached that of the non-accumulated response, suggesting desorption of the complex from the HMDE surface.

The strongly adsorptive character of the Co(II)–BPY complex can thus be used as an effective means of an analyte accumulation step, prior to voltammetric measurement, making possible a highly sensitive voltammetric procedure for cobalt analysis. Fig. 2A displays linear scan voltammograms for 0.30 nM cobalt after different accumulation periods, ranging from 5 to 40 s. The longer the accumulation time, the more the Co(II)–BPY complex was accumulated and the
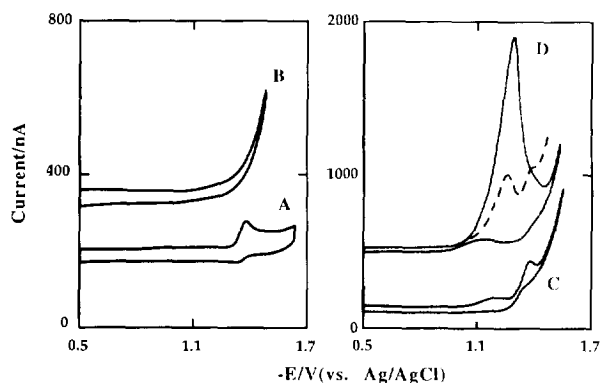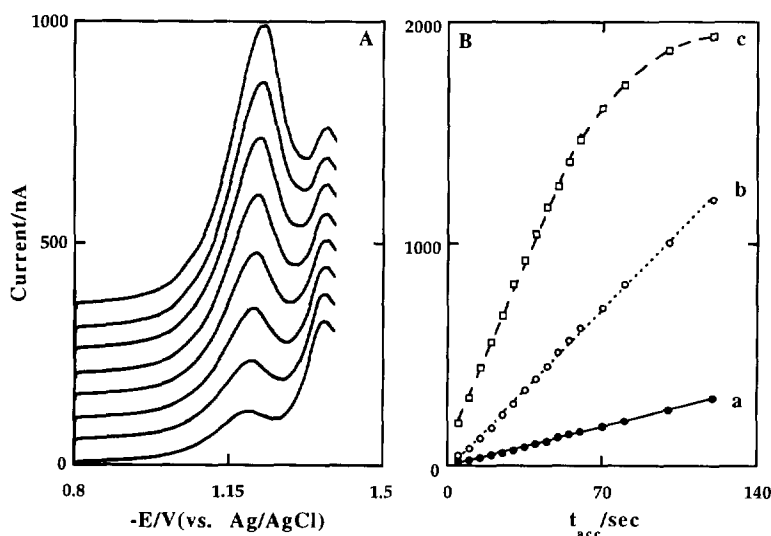
Fig. 2. (A) Catalytic-adsorptive stripping voltammograms for 0.30 nM cobalt following different accumulation periods: from bottom to top, 5–40 s in 5 s steps. (B) Stripping peak current versus accumulation time plots for (a) 0.050 nM, (b) 0.30 nM and (c) 1.0 nM cobalt. Accumulation at − 0.80 V; other conditions as in Fig. 1D.

higher was the current sensitivity, which again suggests the involvement of adsorption in the electrode process. As a consequence, the voltammetric measurement of cobalt at sub-nanomolar levels is feasible after a very short accumulation period. Fig. 2B shows plots of the stripping peak current against the accumulation time at different cobalt concentrations, namely, 0.050, 0.30 and 1.0 nM. In all cases, the stripping peak current increased linearly with increasing accumulation time from 0 to 60 s. For an accumulation time between 80 and 120 s, further gain in sensitivity is very small at 1.0 nM. In addition, non-linear behavior between the concentration and the stripping peak current was also observed after prolonged accumulation, which reflects the adsorption equilibrium at different concentrations.

3.2. Effects of various experimental parameters

Various experimental parameters affecting the stripping peak current of the Co(II)–BPY complex in linear scan voltammetry were explored and the results are presented in Fig. 3. Variation of pH produced a maximum in the stripping peak

current between 8.55 and 9.25. Substantial decreases in the stripping peak current were observed at both lower and higher pH values (Fig. 3A). Since BPY is an essential component for the formation of the adsorptive complex, it is expected that the stripping peak current is strongly dependent upon the BPY concentration. As shown in Fig. 3B, the stripping peak current increased sharply upon increasing the BPY concentration from 0.0 to 1.5 μM and then started to level off between 2.0 and 6.0 μM. Slight decrease in the stripping peak current was obtained for higher BPY concentrations, presumably due to the competitive adsorption of BPY. The nitrite concentration also had a strong effect on the stripping peak current. For example, the response for 1.0 nM cobalt increased linearly with increasing nitrite concentration (Fig. 3C). Due to the reduction of nitrite at potentials more negative than − 1.5 V, a rather broad reduction peak was observable at much higher nitrite concentration which was found to interfere with the determination of cobalt at low concentration levels. In addition, due to the cobalt impurity in purified electrolyte, especially in nitrite, increasing the ni-
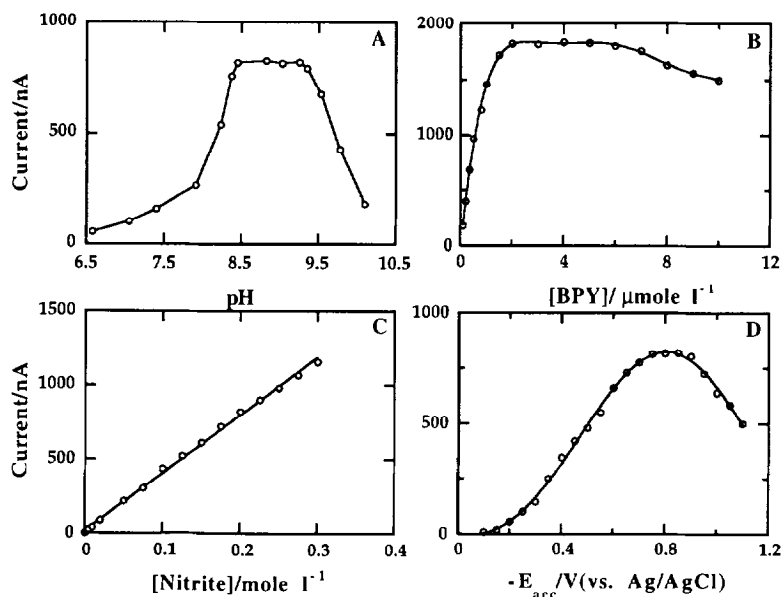
Fig. 3. Dependence of the catalytic-adsorptive stripping current on (A) pH, (B) BPY concentration, (C) nitrite concentration and (D) accumulation potential. Accumulation time, 30 s; other conditions, as in Fig. 2B(b).

trite concentration resulted in a larger background current. Therefore 0.20 M nitrite was selected as the optimal concentration for a fairly good sensitivity.

The influence of adsorption potential on the stripping peak current was examined over the range -0.1 V to -1.1 V. As illustrated in Fig. 3D, the stripping peak current increased gradually when the adsorption potential became increasingly negative. The highest stripping peak current was attained at -0.75 V and remained practically unchanged for accumulation potentials between -0.75 and -0.90 V. This pattern somehow reflects the charging state of the electrical double at the electrode–solution interface. For mercury electrodes, the potential of zero charge (PZC) is roughly around -0.4 V. On the positive side of the PZC, the electrode is positively charged. As we know, the Co(II)–BPY complex is cationic $(CO(BPY)_3^{2+})$; therefore the repulsive interaction between the Co(II)–BPY complex and the electrode surface prevents the Co(II)–BPY complex from accumulating onto the electrode surface at less negative accumulation potentials. As the accumulation potential becomes more negative, less net possitive charges are found at the electrode

surface and eventually the electrode is negatively charged once the accumulation potential is on the negative side of the PZC. Consequently, dramatic increase in the stripping peak current is observed. Due to the partial reduction of the accumulated complex, substantial decrease in the stripping peak current is expected when accumulation potentials are more negative than -1.0 V, indicating that only the Co(II)–BPY complex is accumulated at the HMDE surface, whereas the reduction product has no catalytic-adsorptive property.

Subsequent experiments were, therefore, performed using 0.1 M pH 9.2 ammonium buffer containing 5.0 μM BPY and 0.20 M sodium nitrite, and the accumulation time of 30 s at -0.80 V, taking into account the speed of the measurement and the performance.

3.3. Linearity, detection limit and reproducibility

Under these conditions, by taking advantage of the catalytic-adsorptive nature of the system, the sensitivity of the linear scan voltammetric method was improved significantly. The stripping peak current of the Co(II)–BPY complex was found to

be proportional directly to the cobalt concentration in the range of 0.050 to 2.0 nM (correlation coefficient 0.998) with a current sensitivity of 0.81 μA nM^{-1}, which is over ten thousand times higher than that of the simple diffusion-controlled current of cobalt ions. The detection limit, estimated from three times the standard deviation of repetitive measurements of 0.050 nM cobalt under optimal conditions, was found to be 9.5 pM (0.56 p.p.t.) using the adsorption time of 30 s, which is comparable with or better than various Co(II)–dioxime systems [10–14]. Further lowering of the detection limit through extending the accumulation time was limited by the cobalt impurity ($\leqslant 0.030$ nM) in the purified electrolyte. The reproducibility of the procedure was established by a prolonged series of 25 repetitive determinations of 0.10 nM cobalt with the 30 s accumulation period. Parts of these determinations are shown in Fig. 4. The mean stripping peak current was 107 nA, with a variation range from 102 to 114 nA and a relative standard deviation of 4.9%.

3.4. Interferences

In the voltammetric determination of cobalt in the catalytic-adsorptive systems, other trace ele-
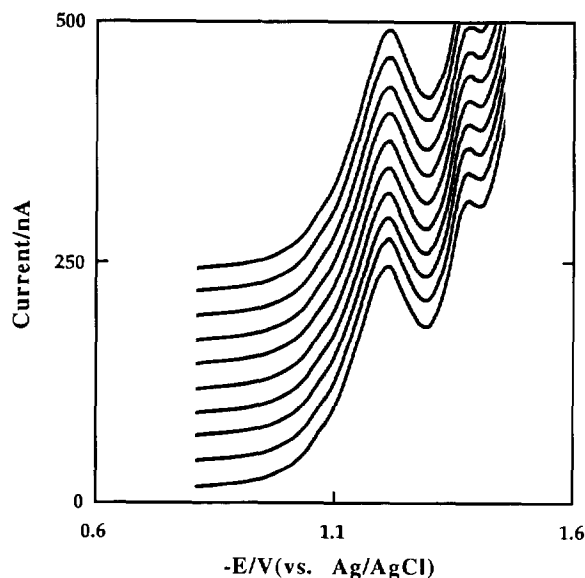
Fig. 4. Catalytic-adsorptive stripping voltammograms for 0.10 nM cobalt. Conditions as in Fig. 3.

ments can interfere if they from a complex with BPY, adsorb on the HMDE, or produce a reduction current at potentials near that of the Co(II)–BPY complex. Because of the extremely high current sensitivity, it is expected that the influence of a large excess of another reducible species on the determination of cobalt with be minute, even with a similar peak potential to that of the Co(II)–BPY complex. The effect of co-existing ionic species and surface-active substances on the determination of cobalt was investigated. More than fifty ions were examined for their possible interferences in the determination of 1.0 nM cobalt. It was found that large amounts of alkali, alkaline earth metal and common anions have no effect on the determination of cobalt. Amounts of less than 5000-fold Al^{3+}, Sn^{2+}, Mn^{2+}, SbO^+, Ce^{3+}, Pb^{2+}, ZrO^{2+}, MoO_4^{2-}, VO^{2+}, WO_4^{2-}, Cd^{2-} and Hg^{2+}; 2000-fold In^{3+}, Bi^{3+}, Tl^+, Ti^{3+}, Ga^{3+}, Pd^{2+}, Cu^{2+} and Ag^+; and 1000-fold Fe^{2+} and Fe^{3+} had little effect on the determination of cobalt. Moreover, excellent selectivity was observed against zinc. It was found that the determination of cobalt is free from the interference of zinc up to 50 μM. The fact that zinc was not interfering is of particular significance considering its major interference in most of the Co(II)–dimethylglyoxime systems [26–32]. But it is inferior to the Co(II)–α-benzil dioxime procedure in terms of selectivity against zinc [14].

In ammonium buffer solution containing BPY and nitrite, however, nickel and chromium each produced a catalytic-adsorptive stripping current peak at -1.13 and -1.40 V, respectively. They were found to interfere with the measurement of cobalt at concentrations higher than 100 nM and 60 nM of nickel and chromium, respectively. Furthermore, owing to the adsorptive properties of the Co(II)–BPY complex, surface-active substances, such as natural organic surfactants, Triton X-100, sodium dodecyl sulfate and cetyl trimethyl ammonium bromide may interfere as a result of competitive adsorption at the electrode surface. For example, additions of 5.0 p.p.m. cetyl trimethyl ammonium bromide, Triton X-100 and sodium dodectyl sulfate resulted in 11–18% depressions of the stripping peak current. High concentration of complexing agents, such as EDTA

was also found to suppress the response. For example, only slight suppression (< 5%) was observed in the presence of 0.50 μM EDTA. However the signal was almost completely eliminated by the addition of 0.10 mM EDTA. Depending on the complexity of the sample, for direct determinations of cobalt, complexing agents and natural surface-active substances must be removed before the determination. Therefore necessary sample pretreatments, such as wet digestion and UV-irradiation, are strongly recommended.

4. Conclusions

In summary, the results obtained indicate that the procedure developed here offers a simple, fast, selective and sensitive method for the determination of trace amounts of cobalt by means of the coupling of catalytic and adsorptive effects in the system Co(II)–BPY–nitrite. Catalytic-adsorptive voltammetry of the Co(II)–BPY complex may serve as an inexpensive and convenient alternative for highly costly mass spectrometry and neutron activation analysis. The proposed method gives extreme sensitivity and a much lower detection limit compared to AAS. Good selectivity against nickel and zinc adds to the versatility of the procedure.

References

[1] I.T.T. Davis, The Clinical Significance of the Essential Biological Metals, Thomas, Springfield, IL, 1972.

[2] M.J. Kendrick, M.T. May, M.J. Plishka, K.D. Robinson, Metals in Biological Systems, Ellis Horwood, London, 1992.

[3] A. Kabata-Pendias and H. Pendias, Trace Elements in Soils and Plants, CRC Press, Boca Raton, FL, 1985.

[4] J. Zbiral and L. Sommer, Fresenius J. Anal. Chem., 306 (1981) 129.

[5] B.J. Sampson, J. Anal. At. Spectrom., 3 (1988) 456

[6] N. Uehara, A. Katamine and Y. Shijo, Analyst, 119 (1994) 1333.

[7] G. Nicolaou, R. Pietra, E. Sabbioni and R.M. Parr, Sci. Total Environ., 80 (1989) 167.

[8] C. Haraldsson, B. Lyvén, M. Pollak and A. Skoog, Anal. Chim. Acta, 284 (1993) 327.

[9] B. Armitage and H. Zeitlin, Anal. Chim. Acta, 53 (1971) 47.

[10] A. Bobrowski, Anal. Chem., 61 (1989) 2178.

[11] R. Heinrich and J. Angerer, Int. J. Environ. Anal. Chem., 16 (1984) 305.

[12] A. Bobrowski, Anal. Lett., 23 (1990) 1487.

[13] J.R. Donat and K.W. Bruland, Anal. Chem., 60 (1988) 240.

[14] A. Bobrowski and A.M. Bond, Electroanalysis, 3 (1991) 157.

[15] R.I. Mrzljak, A.M. Bond, T.J. Cardwell, R.W. Cattral, R.W. Knight, O.M.G. Newman, B.R. Champion, J. Hey and A. Bobrowski, Anal. Chim. Acta, 281 (1993) 281.

[16] A. Bobrowski, Talanta, 41 (1994) 725.

[17] V.J. Bebeki and A.N. Voulgaropoulos, Fresenius J. Anal. Chem., 342 (1992) 352.

[18] V. Genmer-Colos, G. Scollary and R. Neeb, Fresenius J. Anal. Chem., 313 (1982) 412.

[19] Z.Q. Zeng, Mikrochim, Acta, 1 (1991) 89.

[20] M. Paneli and A. Voulgaropoulos, Fresenius J. Anal. Chem., 341 (1991) 716.

[21] D.A. Fungaro and R. Tokoro, Anal. Lett., 28 (1995) 493.

[22] H. Kavel and F. Umland, Fresenius J. Anal. Chem., 325 (1986) 191.

[23] H. Suwamoto, Daigaku Kyoikygakubo Kenkyn Hokoku, 33 (1981) 9.

[24] L. Pospisil and J. Kuta, J. Electroanal. Chem., 101 (1979) 391.

[25] D.T. Chow and R.J. Robinson, Anal. Chem., 25 (1953) 1493.

[26] J. Golimowski and M. Cendrowska, Chem. Anal., 30 (1985) 777.

[27] S.B. Adeloju, A.M. Bond and M.H. Briggs, Anal. Chim. Acta, 164 (1984) 181.

[28] H. Chen and R. Neeb, Fresenius J. Anal. Chem., 314 (1983) 657.

[29] A. Meyer and R. Neeb, Fresenius J. Anal. Chem., 315 (1983) 118.

[30] K. Torrance and C. Gatford, Talanta, 32 (1985) 273.

[31] M.J.M. Gilbert, H.K.I. Powell and J.J. Farry, Anal. Chim. Acta, 207 (1988) 181.

[32] A. Romanus, H. Müller and D. Kirsch, Fresenius J. Anal. Chem., 340 (1991) 363.

ELSEVIER

Talanta

Extraction of azo dyes by polyurethane foam

R. Werbowesky, A. Chow*

Department of Chemistry, University of Manitoba, Winnipeg, Manitoba, R3T 2N3, Canada

Abstract

The extraction of 12 closely related mono-azo dyes by polyester- and polyether-type polyurethane foams was studied to gain more information regarding the mechanism of the extraction of organic compounds. The effects on extraction of solution pH, dye concentration and salt concentration were investigated. It was found that the extraction of the dyes involved a neutral zwitterionic species and is highly dependent on the parameters studied. The dependency of the extraction on these parameters can be explained in a manner consistent with solvent extraction; however, the dual-mode sorption mechanism seems a more likely model. This mechanism involves both absorption related to solvent extraction, and an added component for surface adsorption. While the dual-mode sorption model explains the observed extraction behaviour, the data suggest that surface adsorption plays a much larger role than previously considered.

Keywords: Azo dyes; Polyurethane foam; Extraction

1. Introduction

With a heightened sense of environmental responsibility comes a need for more economical methods of testing for, and removal of, organic pollutants. It is this area which has been a focus of research in organic applications of polyurethane foams. Because of its desirable characteristics, polyurethane foam has been evaluated for its use to remove preconcentrate, and separate a variety of organic substances including phenols [1,2], phthalates [3], PCBs [4], carboxylic acids [5], and insecticides [2,6–12]. The quasi-spherical and open cell structures offer much higher flow rates

___
* Corresponding author. Fax: (204) 275 0905.

and higher concentrating ability compared to other solid sorbents [1].

Polyurethane foams have been used for more than 20 years to extract and separate both organic and inorganic substances from liquid and gaseous media. The development of this field, since its beginning with Bowen's paper [13] in 1970, has been very well summarized by a number of reviewers [14–20]. However, aside from the work with insecticides, there has not been widespread acceptance and use of polyurethane foams for the extraction of organics from aqueous solutions, despite the number of advances made and the number of years for which this technology has been known. It is thought that the slow development of the area is at least partially due to the

lack of understanding regarding the mechanism of extraction.

Over the years a number of possible mechanisms have been proposed, namely surface adsorption, solvent extraction, ligand exchange, anion exchange and cation chelation. The cation chelation mechanism was first proposed by Hamon et al. [21] in 1981, for the extraction of metal ions. In this mechanism, cations are effectively solvated by the oxygen atoms of the poly(ethylene oxide) portion of the foam. These sections of polymer adopt a helical structure with inwardly-directed oxygen atoms and appear to have a cation selectivity similar to the crown ether, 18-crown-6. The polymer in polyester foam does not easily assume a helical structure which is thought to explain the lower observed extractions. For the extraction of organics, solvent extraction, also referred to as phase distribution, is the most commonly proposed mechanism. In this mechanism the foam acts simply as a solid phase organic layer, into which the analyte is diffused.

Much of the work done on the mechanism of extraction with organics has come in just a few papers. Schumack and Chow [22] were among the first to investigate this area. In their study they investigated the extraction of a variety of aromatic organic compounds and how the extractions were affected by extraction time, salt addition, solution pH, ethanol concentration and solution temperature. They concluded that the extraction of organic compounds occurs by an ether-like solvent extraction mechanism, and there was no evidence of a mechanism requiring an ionic species, as would be the case for ion exchange or cation chelation. In addition they found that hydrogen bonding was a significant factor in the extractions, and that compounds containing phenolic or carboxylic groups were better extracted with polyether-type polyurethane. The preference for polyether-type foam was attributed to its ability to form stronger hydrogen bonds than those formed with polyester-type foam.

Chow et al. [23] looked at the extraction of 59 organic dyes into polyurethane foams. Using a smaller subset of those dyes, they looked at the effects of salt addition, extraction from 50% methanol solutions, extractions using diethyl ether

and ethyl acetate, and ordered the dyes in terms of polarity using thin layer chromatography. While broad in scope, this study was fairly inconclusive and reported that the extraction of the organic dyes tested showed support for both solvent extraction and cation chelation mechanisms. It is currently thought that much of the confusion with their results is related to the researchers' use of the distribution ratio, D, for comparisons among the dyes. Such comparisons are only valid if the distribution ratio is a good approximation of the distribution coefficient, K_d. For organic acids and bases, this only occurs when the predominant species is in the neutral form [24,25]. Because the researchers did not optimize the extractions with regard to solution pH, the distribution ratio did not approximate the distribution coefficient. Results from the current study suggest that even when the predominant species is in its neutral form, additional factors must be considered before the distribution ratio is suitable for making direct comparisons.

Fong and Chow [26-28] published three papers studying the extraction of organic compounds into polyurethane foams. They first looked at the extraction of salicylic acid, 8-hydroxyquinoline, 1-amino-2-naphthol-4-sulphonic acid, and cinnamic acid. Based on salting-out effects and pH studies they concluded that the compounds were extracted as neutral molecules via a solvent extraction mechanism. Their work also confirmed the importance of hydrogen bonding as reported previously [22]. The second paper involved the extraction of alkali metal tetraphenylborates. Based on the extraction sequence of the alkali metals, they concluded that these extractions could be explained using the cation chelation mechanism. However in their following paper [28], which looked at the extraction of alkylammonium tetraphenylborates and dipicrylaminates, they could find no conclusive evidence to support the cation chelation mechanism. They concluded that the selectivity for the alkylammonium ions is affected by a combination of effects which are steric, inductive, and hydrophobic in nature.

While there seems to be a general consensus that the mechanism of extraction is a solvent extraction of a neutral species, cation chelation

remains a possibility. There are still many unanswered questions, especially regarding the role of functional groups attached to the analyte. Despite the shortcomings of the earlier dye study [23] it is thought that the wide variety of organic dyes available could be valuable probes into the sorption mechanism of organic species.

2. Experimental

2.1. Apparatus

Spectra and absorbance readings were taken using a Hewlett-Packard Model 8452A diode-array spectrophotometer. Solution pH was measured with an Orion Expandable Ion Analyser EA 940. A Burrell Wrist-Action shaker was used for sample agitation.

2.2. Reagents

All chemicals used were of reagent grade and water was obtained from a Barnsted Nanopure II™ purifiction sustem fed with water purified by reverse osmosis. The majority of the dyes used were obtained from the companies Sigma and Aldrich and were used without further purification. Polyether foam used was obtained by Union Carbide Corporation and the polyester foam was purchased as diSPo™ plugs from Baxter, Canlab, Canada.

2.3. Procedure

Both types of foam were cleaned before use. In order to remove inorganic contaminants, the foam was soaked and periodically squeezed in a 1 M hydrochloric acid bath for 6 h. The foam was then repeatedly soaked, squeezed and rinsed in water until the pH of the rinse water was unchanged after an hour of soaking. After removal of excess water, the foam was Soxhlet-extracted with acetone for 6 h to remove any soluble organic contaminants. The majority of the acetone was then squeezed out of the foam, which was then dried in a vacuum desiccator overnight. Finally the foam was ground into a coarse powder

by freezing the foam pieces in liquid nitrogen and grinding them in a metal container with a Waring blender. The ground foam was then stored in brown glass jars.

Stock dye solutions were prepared on the day of an experiment by accurately weighing a chosen amount of dye, dissolving it in water and quantitatively transferring it with water to a 500 mL or 1 L volumetric flask which was then filled to volume. Sample dye solutions of approximately 10^{-5} M were prepared by transferring a 60 mL aliquot of dye stock solution to a 100 mL volumetric flask. Parameters such as pH and salt concentration were then adjusted before dilution to volume.

Each extraction was performed using approximately 0.1 g of foam accurately weighed into a 20 mL sample vial. A 15 mL aliquot of 10^{-5} M dye solution was added to the vial which was then sealed with plastic wrap and a screw cap. A comparison standard was prepared following the same method but omitting the foam. The vials were shaken for 24 h using an automatic shaker. After filtration through a #4 Whatman filter the pH and UV–visible spectrum (190–820 nm) of the aqueous layer were taken.

The degree of dye soprtion was reported as the distribution ratio, D:

$$D = (VE)/W(100 - E) \tag{1}$$

$$E = 100(C_0 - C_{eq})/C_0 \tag{2}$$

where E is the percentage extraction, C_0 is the initial molar concentration of solution (M), C_{eq} is the concentration of solution after sorption (M), V is the volume of solution (L) and W is the mass of foam (kg).
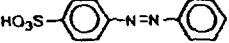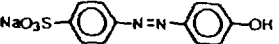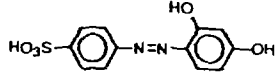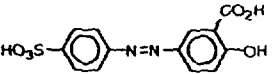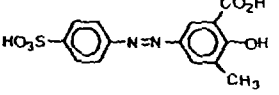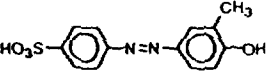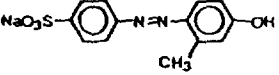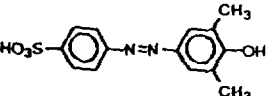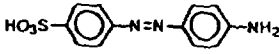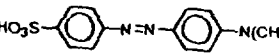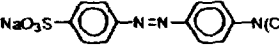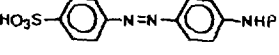
3. Results and discussion

3.1. Neutral species extraction

The effect of solution pH on extraction was studied in order to confirm that neutral species extraction was occurring. The results were analysed by plotting the distribution ratio of the extraction against the equilibrium pH of the solu-

Table 1

Summary of the sorption results of the 12 dyes. (Conditions: $\approx 10^{-5}$ M dye solutions, 0.1 g foam, 15 mL solution, 24 h extraction time)

Dye[a]	Maximum distribution ratio[b] ($L\ kg^{-1}$)		pH at maximum extraction	
	Polyester	Polyether	Polyester	Polyether
4-Phenylazobenzenesulfonic acid	1100	1000	1.5	2.5
4'-(4-hydroxyphenylazo)benzenesulfonic acid *	2100	5000	2.0	3.0
Tropaeolin O	4500	9500	2.5	4.5
Mordant Yellow 10	7500	9500	2.0	2.5
Mordant Yellow 7	9500	12000	2.5	3.5
4'-(4-hydroxy-3-methylphenylazo)benzenesulfonic acid	4500	7000	2.0	3.5
4'-(4-hydroxy-2-methylphenylazo)benzenesulfonic acid *	5500	11500	2.0	2.5
4'-(2,6-dimethyl-4-hydroxyphenylazo)benzenesulfonic acid	5000	8500	1.5	3.5
4'-(4-aminophenylazo)benzenesulfonic acid	400	3000	3.0	4.5
Methyl orange	500	–	3.0	5.5
Ethyl Orange *	4500	∞	3.5	4.5
Orange IV	∞	∞	3.5	5.5

[a]The dyes that have been assigned an asterisk, *, were used as sodium salt.
[b]Values above 12 000 L kg^{-1} are listed as ∞.

tion, producing what will be called an *extraction profile*. Fig. 1 shows the extraction profile of 4-phenylazobenzenesulfonic acid (4-PABSA). An obvious trend can be seen in this and the profiles of the other 11 dyes, all of which are summarized in Table 1. The results of the extractions for all 12 dyes seem to follow a pK_a-type curve. There was little or no extraction from solutions more basic than pH 6. As the solutions became more acidic there was an increase in extraction, which was always followed by a decrease in extraction as the solutions became increasingly more acidic. This decrease in extraction generally begins to occur with solutions at about a pH of 2. Notable exceptions were those dyes containing an amino group, where the decrease in extraction occurred in solutions with a pH of 4 or less.

The results of this pH survey can be easily interpreted as showing only neutral species extraction. To aid in this interpretation, two of the dyes were chosen for further examination. Although the following arguments hold true for all of the dyes investigated, only these more extensively studied dyes will be discussed. For basic solutions of 4-PABSA, a large percentage of the species would be expected to be negatively charged be-
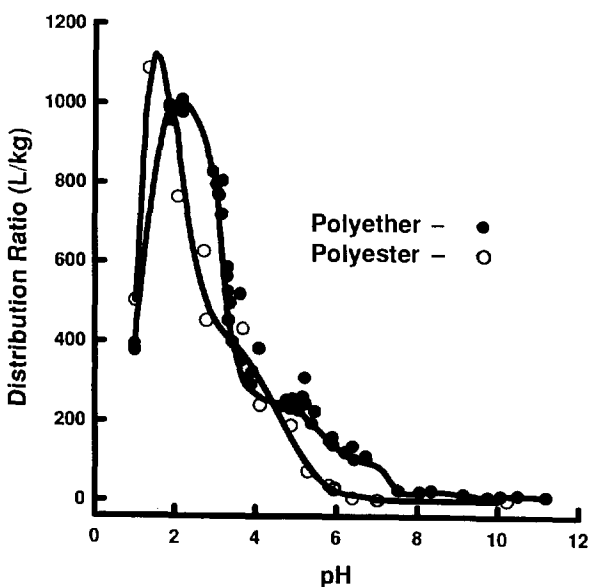
Fig. 1. Extraction profile of 4-PABSA. Conditions: $\approx 10^{-5}$ M dye solutions, 0.1 g foam, 15 mL solution, 24 h extraction time.

cause of the unprotonated sulfo groups (Fig. 2a). As the solutions become more acidic, the azo groups are expected to become protonated, and the molecules become zwitterions with an overall neutral charge (Fig. 2b). Such species therefore become extractable, as was observed. As solutions become very acidic (pH < 2) some of the sulfo groups also become protonated (Fig. 2c) producing an unextractable species (because of its overall positive charge); therefore a decrease in extraction is expected.

In order to further test the idea of neutral species extraction, the first pK_a value of 4-PABSA, that of the azo group, was experimentally determined and estimated to be 2.55. Using this pK_a value the percentage of monoprotonated species was plotted vs. the corresponding pH to produce the protonation profile shown in Fig. 3. When the sulfo group is unprotonated, upon protonation of the azo group the molecule becomes a neutral zwitterion. Because above a pH of 1 the vast majority of the sulfo groups are in an unprotonated state, a plot of the percentage of protonated azo groups is therefore also a plot of the neutral species available.

The relationship between the protonation profile and the extraction profile of 4-PABSA is emphasised by overlaying Figs. 1 and 3 as shown in Fig. 4. Although the extraction proceeds to some extent in solutions where there should only be a small percentage of neutral species, the sharp rise in extraction and the extraction maxima seem to correspond with the amount of neutral species available. These results suggest that the extraction mechanism can also explain the sharp decrease in the extraction in acidic solutions. This decrease is thought to occur because as the sulfo group becomes protonated, it gives an overall positive charge to the molecule. Unfortunately, because of the acidity of the solution and therefore the instrumental error associated with measuring such low values of pH, attempts to experimentally determine the pK_a value of the sulfo group were unsuccessful. Literature values for the acid constant in aqueous solutions of this or any similar dye were also unavailable.

The reliance of the mechanism on the presence of a neutral species can be more clearly illustrated

(a)

(b)

(c)
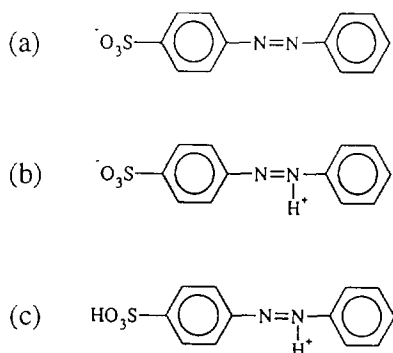
Fig. 2. Charge states of 4-PABSA.

by analysing the results of the extraction of Ethyl Orange. The first pK_a value of Ethyl Orange is for the amino group and as with 4-PABSA, the monoprotonation of the dye yields an overall neutral, extractable, zwitterion (Fig. 5b). As with 4-PABSA, upon being doubly protonated, this time with the protonation of the azo group, the molecule becomes positively charged (Fig. 5c) and unextractable. In this case the neutral species involves a protonated amino group and an unprotonated azo group. Therefore to graphically represent the percentage of neutral species
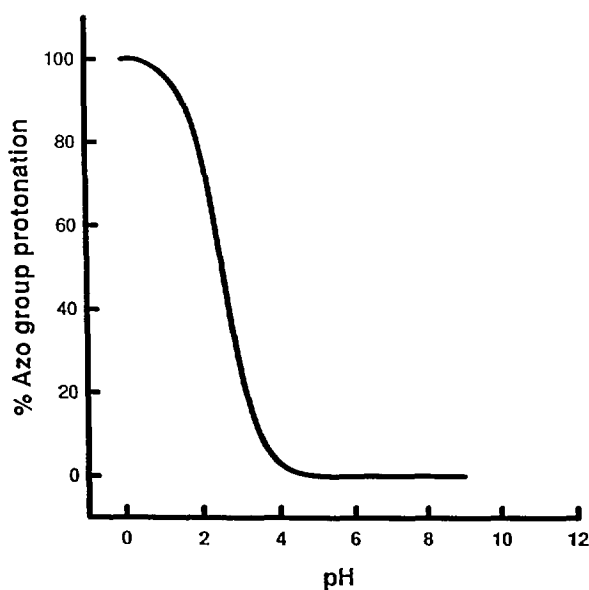
Fig. 3. Protonation profile of 4-PABSA showing the percentage of dye species with a protonated azo group.
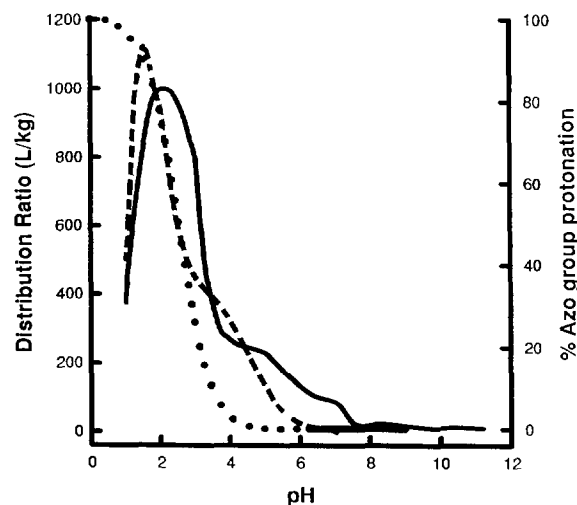
Fig. 4. Overlay of Figs. 1 and 3 emphasizing the correlation between extraction of 4-PABSA and the percentage of neutral species available. Note: data points have been removed for clarity.

present, the percentages of both protonated amino groups and protonated azo groups need to be plotted. In Fig. 6 the two percentage curves are shown; the neutral species is represented by the protonated azo group curve on the acidic side of their intersection (pH < 4), and the protonated amino group curve on the basic side of their intersection (pH > 4)

The overlay of the extraction profile of Ethyl Orange and the protonation profile is shown in Fig. 7. Although the curves are shifted by 0.5 pH, the extraction using polyether-type polyurethane closely follows the percentage of Ethyl Orange that is predicted to be present as a neutral species.

(a)

(b)

(c)
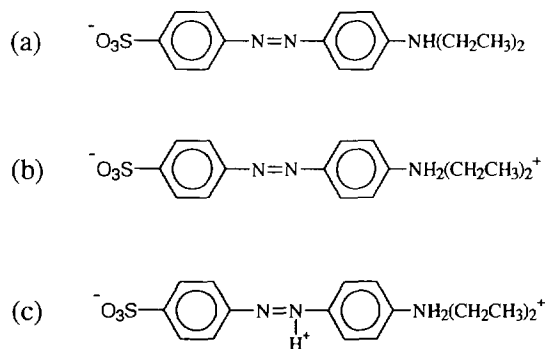
Fig. 5. Charge states of Ethyl Orange.
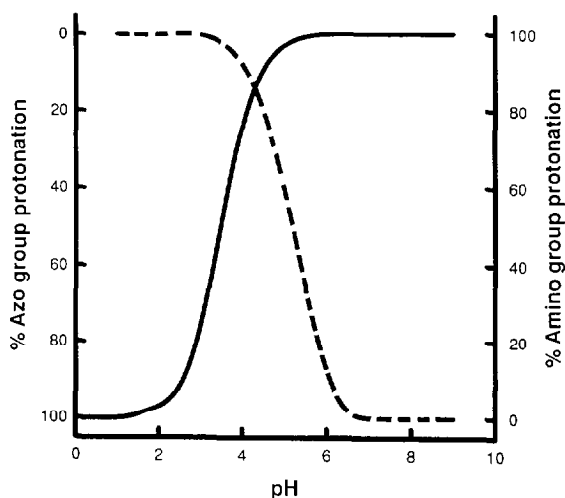
Fig. 6. Protonation profile of Ethyl Orange. The percentage of neutral species is represented by the solid line, the percentage of protonated azo groups to the left of the intersection, and the broken line shows the percentage of protonated amino groups to the right of the intersection.

The increase and decrease of the Ethyl Orange extraction mimic those percentages, which leaves little doubt that the extraction is of a neutral species.

There is additional evidence that the majority
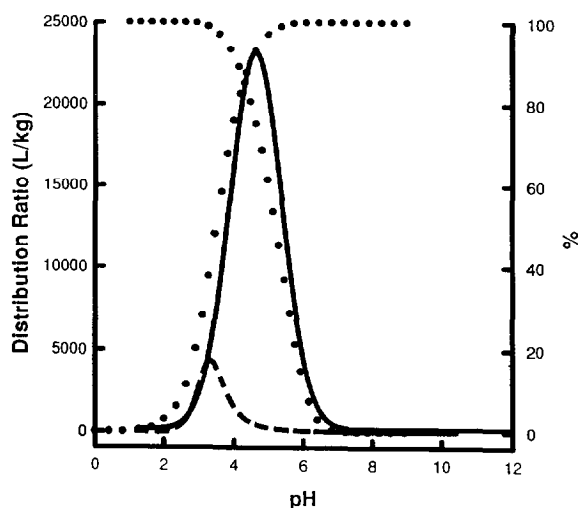
Fig. 7. Overlay of the extraction profiles of Ethyl Orange, polyester (broken line), and polyether (solid line) with Fig. 6 (dotted line). This emphasizes the correlation between the extraction of Ethyl Orange and the amount of neutral species present. Note: data points have been removed for clarity.

of the extraction is dependent on the charge of the dye species, and not on a foam-related phenomenon. This comes from the fact that the increase in extraction, from basic to acidic solutions, follows the pK_a curve of the dye being extracted. Specifically, this can be seen by comparing the extraction profiles of 4-PABSA and Ethyl Orange. If this were a foam-related phenomenon, the extraction increase would be expected to occur in solutions with similar pH regardless of the dye being extracted. Instead, the extraction appears to follow the pK_a curve of the dye being extracted.

It seems clear that the overriding mechanism involves the sorption of an overall neutral species. There is however some evidence of an additional extraction mechanism which has a less significant effect on the extraction. In Fig. 1, the slow increase in extraction of 4-PABSA as the solution is changed from pH 5 to 8, could be interpreted as showing two minor increases in extraction, between pH 7 and 8, and between pH 5 and 6. These small increases in extraction are not easily explained using a neutral species extraction. One possible explanation for this behaviour lies in the protonation of nitrogen- and oxygen-containing groups of the foam; as the foam group becomes protonated it might act as a ion exchange site. However, given the small amount of extraction attributable to this mechanism when compared to neutral species extraction, this hypothesis was not further explored.

3.2. Polyester vs. polyether

The composition and structure of a polyester-type polyurethane are quite different from those of the polyether-type, so it is not surprising that they have different extraction characteristics. Although the extraction profiles have the same general shape, extractions with polyester foam are usually different from those using polyether. The two main differences are in the maximum amount of dye extracted and the solution conditions necessary for extraction to occur.

The extraction profiles show that the increase in extraction from basic to acidic solutions, and the maximum extraction, occur in more acidic solutions with polyester than with polyether foam.

There seems to be a consistent need for solutions to be generally 1–3 pH units more acidic for a comparable extraction into polyester compared to polyether foam (see Table 1). This suggests that the above effect is not a dye-related phenomenon, but rather is probably due to the differences in the dielectric constants of the two foams [29]. This shift of two pH units does not apply for the decrease in extraction, which occurs in the same pH range for the two foams. Since the extraction with both foams decreases as the percentage of neutral species declines, this can be interpreted as further proof of a neutral species extraction by both types of foam.

Another difference, seen throughout the results, is that the extractions with polyether foam often have a higher maximum distribution ratio than with polyester. The extractions showing this behaviour involve dyes with either a hydroxyl or amino functional group. Trends similar to this have been reported by previous researchers [22,26]. Schumack and Chow [23] found that compounds containing phenolic or carboxylic groups were extracted more efficiently by polyether than polyester foam. Through a comparison of ortho-, meta- and para-nitrophenols they determined that the difference in extraction can be attributed to the presence of hydrogen bonding. Hydrogen bonds are likely to be much stronger with a polyether than with a polyester foam [30] and therefore compounds containing hydrogen bonding functional groups are likely to be better extracted by a polyether than a polyester foam.

From Table 1 it can be seen that differences between polyether and polyester extractions are greater with those dyes containing an amino group than with hydroxyl-containing dyes. Fong and Chow [26] reported similar results using 1-amino-2-naphthol-4-sulfonic acid. In their extraction, it is likely that the amino group was protonated; they suggested that an additional ion–dipole interaction might explain the greater differences in their distribution ratios. This interaction could also explain the extraction behaviour of the amino-containing dyes found in this study.

3.3. Comparison of maximum extractions

One of the aims of this study was to gain some insight into the role that functional groups play in the extraction process. This was to be done by comparing the maximum distribution ratios, D_{max}, of the similar dyes. It was thought that these comparisons would be valid since the maximum distribution ratio should be a good approximation of the distribution coefficient [24,25]. However, the strength of such comparisons is weakened, perhaps even invalidated, by the discovery of the dependence of the extraction on the equilibrium dye concentration, described next.

3.4. Equilibrium dye concentration

The discovery of an interesting trend was made while constructing the extraction profiles using data from several separate experiments. It appeared that the amount of extraction was somehow linked to the concentration of dye present during an extraction. In order to study this effect, an experiment was designed which varied the initial dye concentration from 5 mg L^{-1} to 500 mg L^{-1}.

The results of this experiment showed that the distribution ratio is very dependent on the equilibrium dye concentration. Fig. 8 shows the results using polyether foam; the results for the polyester-type (not shown) were similar. Initially, it was thought that this behaviour might be an indication that the foam was reaching capacity, i.e. it was becoming saturated with dye. To examine this, data were used to plot the actual amount of dye being sorbed per gram of foam. Fig. 9 shows that the polyether foam appears to approach its capacity, estimated to be approximately 12 mg of 4-PABSA per gram of foam. However, the experiments showing the greatest dependence on dye concentration occur under conditions well below this saturation level. In addition the polyester-type foam did not appear to become saturated. It was therefore concluded that the dependency of the sorption on equilibrium dye concentration was not related to the capacity of the foam.
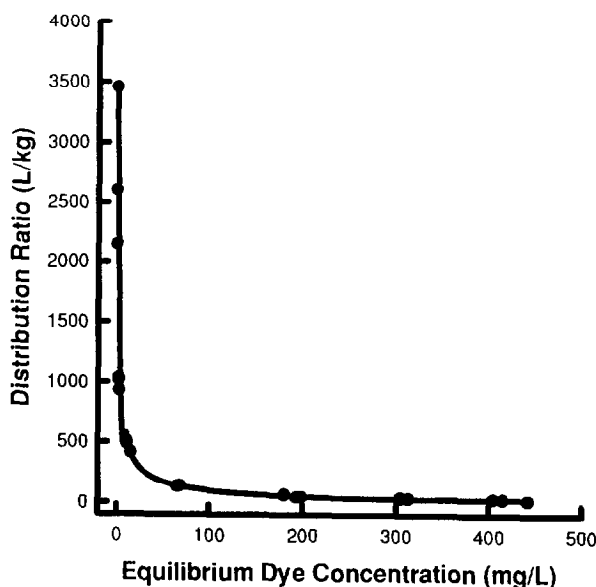
Fig. 8. The effect of dye concentration on the extraction of 4-PABSA. Conditions: 0.1 g foam, 15 mL dye solution ($\approx 10^{-5}$ M, pH ≈ 2.5), 24 h extraction time.

To explain these results two models were evaluated; one involves the solvent extraction mechanism and how it is affected by the ionic strength of the solution, the other, called the dual-mode
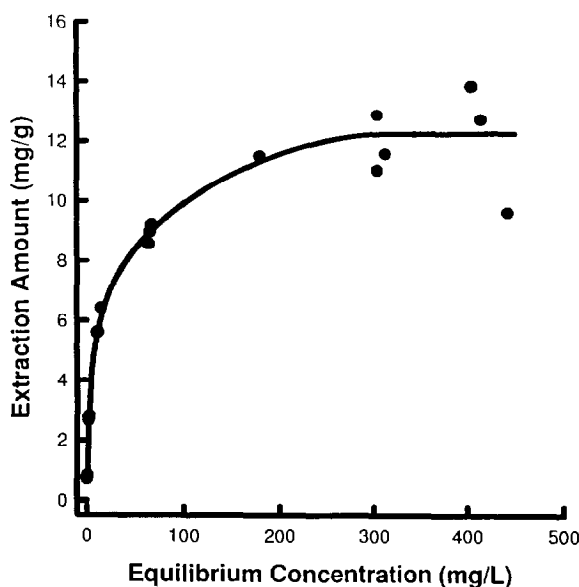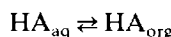

Fig. 9. Amount of 4-PABSA extracted per gram of foam. Conditions: 0.1 g foam, 15 mL solution, 24 h extraction time.

sorption model [31], involves the solvent extraction mechanism and the adsorption mechanism.

3.4.1. Ionic strength

Examining the solvent extraction model shown below, we can better understand what might be occurring.

$$HA_{aq} \rightleftharpoons HA_{org}$$

$$K_d = \frac{a_{HA \cdot org}}{a_{HA \cdot aq}} = \frac{[HA_{org}]f_{HA \cdot org}}{[HA_{aq}]f_{HA \cdot aq}} = D\frac{f_{HA \cdot org}}{f_{HA \cdot aq}} \qquad (3)$$

where HA is a neutral dye species, K_d is the distribution coefficient, a_{HA} is the activity of the dye in the corresponding phase, and f_{HA} is the activity coefficient of the dye in the corresponding phase.

In this model there is an equilibrium between the neutral species in the aqueous phase and the neutral species in the organic phase, in this case the foam. This equilibrium can be expressed as a ratio of the activities of the dye in each phase, which in turn can be expressed as the distribution ratio multiplied by the ratio of the activity coefficients of the dyes in each phase. It is usual to assume for dilute solutions that the activity coefficients are both near unity and constant [32]. Therefore the distribution coefficient K_d is approximately equal to the distribution ratio and it is generally assumed that solvent extraction is concentration independent.

The problem then is to explain the extraction results using this solvent extraction model. One plausible explanation involves the assumption made regarding the activity coefficients. From Eq. (3) it can be seen that if either of the activity coefficients were not constant, the distribution ratio, D, would have to change since K_d, the distribution coefficient, is a thermodynamic constant. One thing that would change the aqueous activity coefficient of the dye is the ionic strength of the solution.

Although it has been shown that the extraction is largely of neutral species, the species involved are actually zwitterions. Therefore it might be possible that changing the concentration of the dye would also change the ionic strength of the solution, although no information regarding such
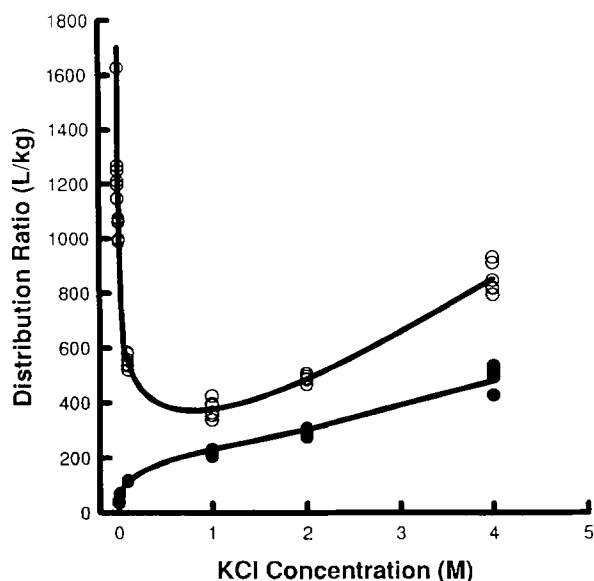
Fig. 10. Effect of potassium chloride concentration on the extraction of 4-PABSA with polyether foam. Conditions: 15 ml dye solution ($\approx 10^{-5}$ M, 0.001-4 M KCl), 0.1 g foam, 15 mL solution, 24 h extraction time. $\bigcirc$, Acidic conditions; $\bullet$ basic conditions.

effects was found in the literature. As the ionic strength of the solution increases, the activity coefficient of the dye in solution would decrease [32]. Again, looking at Eq. (3), it can be seen that this would cause the ratio of the activity coefficients to increase. Since K_d is a thermodynamic constant, the distribution ratio would have to decrease as the aqueous activity coefficient decreased. This is the exact behaviour observed in these experiments. While there is some doubt as to whether such small increases in dye concentration could affect its activity coefficient, additional strength is added to this argument by the salt concentration results shown in Fig. 10. This Figure shows that under acidic conditions, very small salt concentrations have a large effect on the extraction efficiency. The behaviour observed is similar to that with increasing dye concentration, and can be explained in the same way. As the salt concentration increases, the ionic strength of the solution will increase.

The behaviour observed in basic solutions is quite different from that found with acidic solutions. In this pH range there is originally no

extraction without salt present; upon the addition of salt there is an increase in extraction. These results are similar to the salting-out effect, where upon addition of a salt the extraction of a non-ionic solute increases. However, at the basic pH of the experiment, only charged species should exist. In this case it is possible that the potassium ion could associate with either the negatively charged sulfo group or with the pair of electrons on one or both of the nitrogens of the azo group. These possible associations would yield neutral species which could be extractable, as was observed.

Based on this model, as a solution approaches infinitely dilute conditions, the distibution ratio should become a closer approximation of the distribution coefficient and the maximum distribution ratio for an extraction should become more constant. However, even when the equilibrium dye concentration approaches the limits of detection, the distribution ratio showed no signs of levelling off, therefore no estimation of K_d can be made.

3.4.2. Dual-mode sorption

Dual-mode sorption is the second model used to try and explain the dependence of the extraction on the equilibrium dye concentration. In this model, the sorbed dye is classified into two groups: the absorbed dye (solvent extraction mechanism), and the adsorbed dye (surface adsorption described by the Langmuir equation). This model is mathematically represented as

$$C_{org} = C_{ab} + C_{ad} = K_d C_{aq} + \frac{SK_L C_{aq}}{1 + K_L C_{aq}} \qquad (4)$$

where C_{org} and C_{aq} are the equilibrium dye concentrations on the polyurethane foam and in solution, C_{ab} and C_{ad} are the equilibrium dye concentrations on the foam as an absorbed species and as an adsorbed species, S is the saturation value for the Langmuir adsorption, K_d is the distribution coefficient, and K_L is the Langmuir constant.

Eq. (4) can be solved for the distribution ratio, D as

$$D = K_d + \frac{SK_L}{1 + K_L C_{aq}} \qquad (5)$$

From Eq. (5) it is now obvious that the distribution ratio is not independent of the dye concentration. The equation can be fitted to the extraction data, shown in Fig. 11, giving the values $K_d = 30$ L kg^{-1}, $S = 0.012$ mol kg^{-1}, and $K_L = 300\,000$ L mol^{-1}. From Eq. (5) it can be seen that as the concentration of the dye increases, the contribution to D approaches the value of K_d. As the concentration approaches zero, D should approximate $K_d + SK_L$. No levelling off of D was observed as C_{aq} approached zero; however, as C_{aq} increased, a levelling off of D was observed. Therefore according to this model, the data obtained suggest that the absorption coefficient, K_d, is much smaller than previously thought.

Future studies will need to focus on soluble non-ionic dyes or other organic compounds to test these findings. This approach should eliminate any effect on the ionic strength of the solution but should not affect the amount of adsorption occurring.

4. Conclusions

The study of the extraction of 12 closely related mono-azo dyes shows that these compounds are extracted as neutral zwitterions and that their
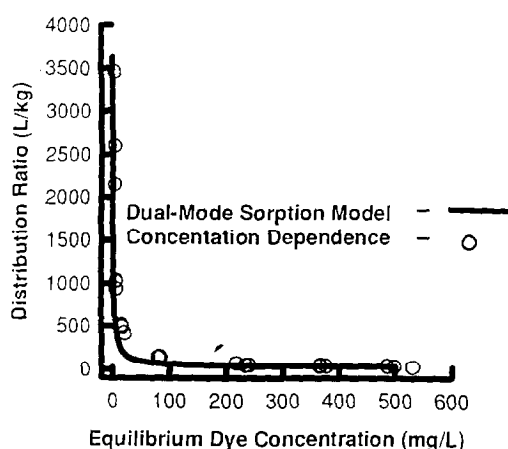
Fig. 11. Graphical representation of the dependence of the distribution ratio on equilibrium dye concentration according to the dual-mode sorption model. Eq. (5) fitted to data from Fig. 8.

extraction may involve a number of mechanisms. When anionic species are present below a pH of 8, there is some evidence to support some form of ion-exchange mechanism. However, even when this mechanism is thought to be operating, its contribution to the overall extraction seems to be small. The extreme sensitivity of the extraction to dye concentrations which was found can be explained using either a solvent extraction model or a dual-mode sorption model.

The solvent extraction model requires that very small increases in the dye concentration will have large effects on the ionic strength of the solution. While doubtful, this idea is supported by the salt concentration experiments done under acidic conditions. However, the salt concentration results may also be explained by the cation being chelated or ion paired with the dye producing an unextractable dye species, mechanisms unrelated to ionic strength.

The dual-mode sorption model offers an excellent description of the observed behaviour and of the two models presented seems the most plausible. According to this model when analyte concentrations are low adsorption is responsible for the majority of the sorption, but when analyte concentrations are higher, absorption becomes the dominant mechanism because of its higher capacity. Although the model implies a much greater role of adsorption than previously considered, this seems logical given the large surface area of a foamed polymer.

The inability to confidently obtain the distribution coefficient for the extractions of the dyes has reduced our ability to make the comparisons between dyes that are necessary to study the effect of various functional groups. Despite this limitation the results show that there can be large differences in the extractions due to the presence and position of functional groups on the ring structure of the dyes. The cause of these differences and other extraction behaviour are not fully understood and need further study.

Previous researchers have relied heavily on the solvent extraction model to explain the extraction of organic compounds using polyurethane foam. The distribution ratio, while useful for describing the results of liquid–liquid extractions, has been

shown not to be adequate for comparisons between extractions using polyurethane foam, especially when dealing with low analyte concentrations. Once the dual-mode sorption mechanism is confirmed in future experiments, further studies will be able to easily estimate the extraction constants of both absorption and adsorption. Using those values researchers can then begin to make the proper comparisons necessary to study the mechanisms of extraction and the roles of the functional groups of the analytes.

Acknowledgements

References

[1] M.S. El-Shahawi, A.B. Farag and M.R. Mostafa, Sep. Sci. Technol., 29 (1984) 289.
[2] M.S. El-Shahawi, Chromatographia, 36 (1993) 318.
[3] K.M. Gough and H.D. Gesser, J. Chromatogr., 115 (1975) 383.
[4] H.D. Gesser, A. Chow and F.C. Davis, Anal. Lett., 4 (1971) 883.
[5] S.R. Ahmad, H.S. Rathore, I. Ali and S.K. Sharma, J. Indian Chem. Soc., 62 (1985) 786.
[6] A.B. Farag, A.M. El-Wakil, M.S. El-Shahawi and M. Mashaly, Anal. Sci., 4 (1989) 415.
[7] A.B. Farag, A.M. El-Wakil and M.S. El-Shahawi, Fresenius' Z. Anal. Chem., 324 (1986) 59.
[8] A.B. Farag, A.H. Al-Kubaisi, A.M. El-Wakil and W.M. Abo-El-Maaty, Int. J. Chem., 3 (1992) 135.
[9] A.B. Farag and M.S. El-Shahawi, J. Chromatogr., 552 (1991) 371.
[10] A.B. Farag, M.S. El-Shahawi, A.M.A. Helmy and S. Farag, Bull. Soc. Chim. Fr., 92 (1991) 641.
[11] J.F. Uthe, J. Reinke and H. Gesser, Environ. Lett., 3 (1972) 117.
[12] P.R. Musty and G. Nickless, J. Chromatogr., 100 (1974) 83.
[13] H.J.M. Bowen, J. Chem. Soc. A, (1970) 1082.
[14] T. Braun and A.B. Farag, Anal. Chim. Acta, 99 (1978) 1.
[15] G.J. Moody and J.D.R. Thomas, Analyst, 104 (1979) 1.
[16] T. Braun, Fresenius' Z. Anal. Chem., 314 (1983) 652.
[17] T. Braun, Cell. Polym., 3 (1984) 81.
[18] T. Braun, Fresenius' Z. Anal. Chem., 333 (1989) 785.
[19] G.J. Moody and J.D.R. Thomas, Chromatographic Separation and Extraction with Foamed Plastics and Rubbers, M. Dekker, New York, 1982.
[20] T. Braun, J.D. Navratil and A.B. Farag, Polyurethane foam Sorbents in Separation Science, CRC Press, Boca Raton, FL, 1985.
[21] R.F. Hamon, A.S. Khan and A. Chow, Talanta, 29 (1982) 313.
[22] L. Schumack and A. Chow, Talanta, 34 (1987) 957.
[23] A. Chow, W. Branagh and J. Chance, Talanta, 37 (1990) 407.
[24] B.L. Karger, L.R. Snyder and C. Horvath, An Introduction To Separation Science, John Wiley, New York, 1973.
[25] J.A. Dean, Chemical Separation Methods, Van Nostrand, New York, 1969.
[26] P. Fong and A. Chow, Talanta, 39 (1992) 497.
[27] P. Fong and A. Chow, Sep. Sci. Technol., 27 (1992) 1291.
[28] P. Fong and A. Chow, Anal. Chim. Acta, 260 (1992) 123.
[29] R.F. Hamon, Ph. D. Thesis, University of Manitoba, 1981.
[30] J. March, Advanced Organic Chemistry, 3rd edn., John Wiley, New York, 1985.
[31] T. Shibusawa and Y. Chigira, J. Polym. Sci., Part B, 30 (1992) 563.
[32] D.A. Skoog, D.M. West and F.J. Holler, Analytical Chemistry: An Introduction, 5th edn., Saunders College Publishing, Philadelphia, PA, 1990.

Application of the first derivative spectra method for investigation of the complexation of some aza-15-crown-5-containing chromoionophores with Sr^{2+}

N. Mateeva[a], L. Antonov[b], M. Mitewa[a,*], S. Miteva[a]

[a]University of Sofia, Department of Chemistry, Sofia 1126, Bulgaria
[b]Higher Forestry Institute, Division of Chemistry & Biochemistry, Sofia 1756, Bulgaria

Abstract

An approach for quantitative spectrophotometric analysis of binary mixtures based on first derivative spectra is developed. The proposed method is used for investigation of the complex formation of some aza-15-crown-5-containing ligands with Sr^{2+}, where the stability constant is low and the absorption spectrum of the complex cannot be obtained directly. The described general approach can be applied for quantitative analysis of any other two-component mixture where the absorption spectra of the components cannot be obtained experimentally.

Keywords: UV–Vis spectroscopy; Derivative spectroscopy; Complex formation; Aza-15-crown-5

1. Introduction

It is well known that the quantitative spectrophotometric analysis of complex mixtures where the spectra of the individual components is unknown is generally an impossible task [1], except in cases where some additional information allows the creation of a non-linear optimization model. Recently, some methods for analysis of binary systems based on such non-linear regression models [2], analysis of overlapped absorption bands [3,4] or by finding the individual absorption ranges of the components [5,6] have been developed, but it should be noted that these methods employ complicated mathematical algorithms and sometimes require massive computations.

* Corresponding author.

The application of these methods for investigation of complexation processes of the type

$$n\mathrm{L} + q\mathrm{M} = \mathrm{M}q\mathrm{L}n \equiv \mathrm{C}$$
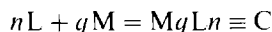
is possible, but a simpler mathematical procedure could be used because in these cases the ligand (L) spectrum is known. At the same time the complexation process is very often characterized by a low stability constant, i.e. the equilibrium is not shifted totally to the complex (C) and so its spectrum cannot be obtained experimentally. Thus quantitative analysis is impossible, especially if the structure of the complex formed is unknown (i.e. n and q are unknown).

In order to overcome such problems the aim of this study is to modify the first derivative spectra method [7] and to use it for quantitative analysis of binary mixtures composed of individual pure

components with unknown spectra, and then to apply it to spectrophotometric investigation of complexation of aza-15-crown-5-containing chromoionophores with Sr^{2+}. During the last few years we have designed a series of such chromoionophores and studied their complexation with alkali and alkaline-earth ions [4,5,8–10].

2. Experimental

2.1. Synthetic procedure

The chromoionophores I–V (Scheme 1) are synthesized as previously described [8].
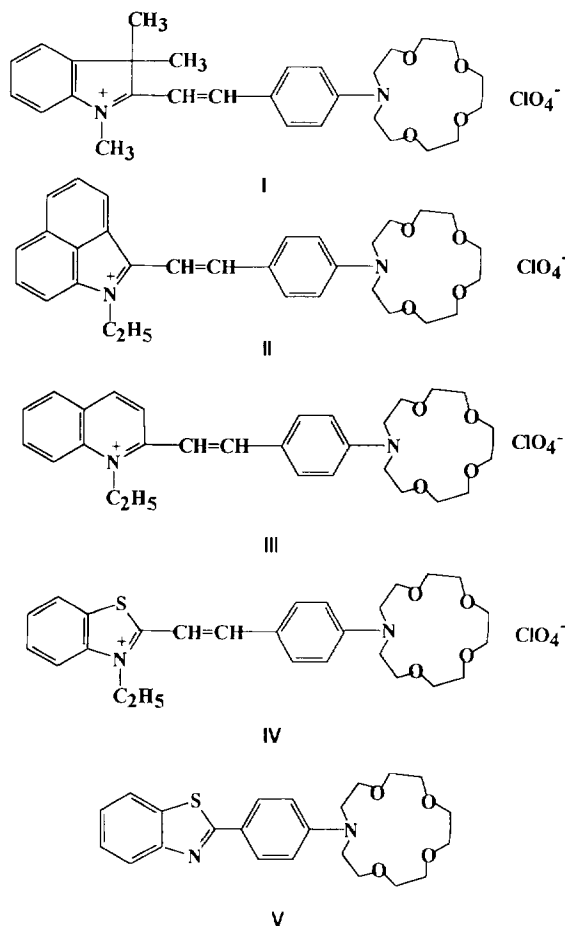
Scheme 1.

2.2. Analytical procedure

Absorption spectra were recorded on a Perkin-Elmer Lambda 17 UV–Vis spectrophotometer in dry acetonitrile (Uvasol). Acetonitrile used was dried as follows: after 4 h boiling over CaH_2 it was distilled and stored over a molecular sieve. $Sr(ClO_4)_2$ was obtained by treating SrO with concentrated $HClO_4$ (Merck).

The experimental spectra obtained were processed using a special program DERGSK for MATHCAD 3.0 (Windows version), based on the algorithm described above.

3. Theory

The quantitative analysis of a binary isomolar system is based on the additivity principle:

$$A(\lambda) = x_1 \cdot A_1(\lambda) + x_2 \cdot A_2(\lambda) \qquad (1)$$

where $A(\lambda)$ is the absorbance measured at the wavelength λ, x_1 and x_2 are the molar fractions of the components and $A_1(\lambda)$ and $A_2(\lambda)$ are the individual absorbances of the components at the wavelength λ. By differentiation Eq. (1) is transformed as follows:

$$\frac{dA(\lambda)}{d\lambda} = x_1 \cdot \frac{dA_1(\lambda)}{d\lambda} + x_2 \cdot \frac{dA_2(\lambda)}{d\lambda} \qquad (2)$$

Evidently when $A_1(\lambda)$ $(dA_1(\lambda)/d\lambda$ respectively) or $A_2(\lambda)$ $(dA_2(\lambda)/d\lambda$ respectively) are unknown the analysis of the system is generally impossible. However, if the absorption maxima λ_1 and λ_2 in both spectra are known then Eq. (2) is transformed into

$$\text{at } \lambda = \lambda_1 \Rightarrow \frac{dA_1(\lambda_1)}{d\lambda} = 0$$

$$\frac{dA(\lambda_1)}{d\lambda} = x_2 \cdot \frac{dA_2(\lambda_1)}{d\lambda}$$

$$\text{at } \lambda = \lambda_2 \Rightarrow \frac{dA_2(\lambda_2)}{d\lambda} = 0$$

$$\frac{dA(\lambda_2)}{d\lambda} = x_1 \cdot \frac{dA_1(\lambda_2)}{d\lambda} \tag{4}$$

Using the mass balance $(x_1 + x_2 = 1)$ and substituting for relations (3) and (4) in Eq. (2), a linear relationship for the first derivatives of a series of isomolar solutions at λ_1 and λ_2 is obtained:

$$\frac{dA'(\lambda_2)}{d\lambda} = \frac{dA_1(\lambda_2)}{d\lambda} - \frac{dA'(\lambda_1)}{d\lambda} \cdot \frac{(dA_1(\lambda_2)/d\lambda)}{(dA_2(\lambda_1)/d\lambda)} \tag{5}$$

From the intercept and slope of Eq. (5) the $dA_1(\lambda_2)/d\lambda$ and $dA_2(\lambda_1)/d\lambda$ values are estimated and using Eqs. (3) and (4) the molar fractions of both components can be calculated.

It is evident that the main problem for the successful application of this approach is the determination of λ_1 and λ_2, which could be made using:

— visual evaluation of the absorption spectra of the isomolar solution. This method, however, is very uncertain, especially in cases of strong overlapping of the bands of the individual components and when weak spectral changes are observed.

— estimation using the second derivative spectra. This estimation could be incorrect if the electronic bands have a vibrational structure [11,12].

4. Results and discussion

The complex formation between alkali and alkaline-earth metal ions and aza-15-crown-5-containing dyes can be described with the relation [13,14]:

$$L + M \rightleftharpoons C$$

If the ligand concentration is constant (i.e. the system is isomolar for the ligand) and the metal salt concentration (C_M^i) is different in each solution the following relations are valid:

Mass balance:

$$x_L^i + x_C^i = 1 \tag{6}$$

Stability constant:

$$\beta = \frac{x_C^i}{x_L^i \cdot C_M^i} \tag{7}$$

Additivity of the first derivatives:

$$\frac{dA'(\lambda_C)}{d\lambda} = \frac{dA_L(\lambda_C)}{d\lambda} - \frac{dA'(\lambda_L)}{d\lambda} \cdot \frac{dA_L(\lambda_C)/d\lambda}{dA_C(\lambda_L)/d\lambda} \tag{8}$$

where $i = 1-p$, p is the number of isomolar solutions, λ_L and λ_C are the absorption maxima of the ligand and the complex respectively, x_L and x_C are the molar fractions of the ligand and the complex respectively, and C_M is the concentration of the metal salt.

The experimental spectra obtained by adding different amounts of $Sr(ClO_4)_2$ to the solution of **I** are shown in Fig. 1a. It is evident that the complexation results in decrease of the ligand band intensity at approximately 540 nm and the appearance of a new band at approximately 450 nm due to the complex formed. On the whole, however, the spectral changes are rather weak. As long as the ligand spectrum is known the absorption maximum can be easily estimated (i.e. $\lambda_L = 537$ nm) and by means of the Golay–Savitzky method [15] the $dA_L(\lambda)/d\lambda$ value can be calculated. The value of λ_C cannot be determined
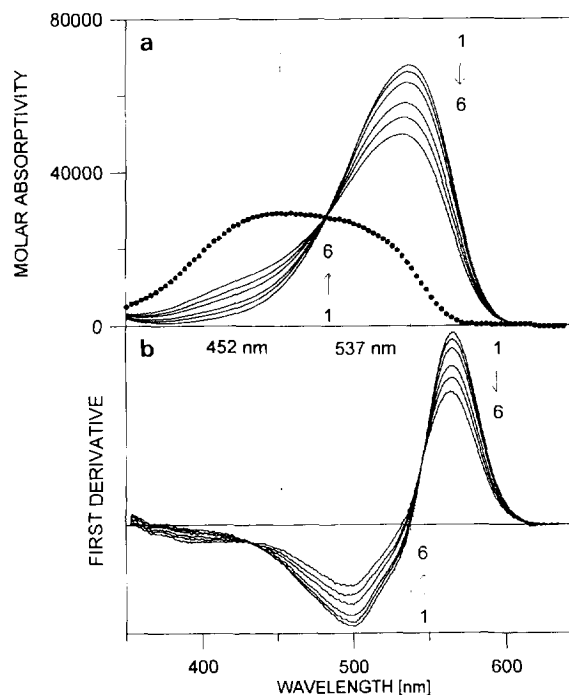
Fig. 1. Absorption spectra of **I** in dry acetonitrile in the presence of different amounts of $Sr(ClO_4)_2$. $C_{Sr(ClO_4)_2}$ ($\times 10^2$ mol l^{-1}): 1, 0; 2, 1.04; 3, 1.39; 4, 2.20; 5, 2.78; 6, 3.47. Calculated spectrum of the complex ($\cdots$). (b) The first derivative spectra of the solutions shown in Fig. 1(a).

Table 1
The stability constants of the Sr^{2+} complexes and the spectral characteristics of the corresponding ligands and complexes

Compound	lgβ	Ligand		Complex	
		λ_{max}	ϵ_{max}	λ_{max}	ϵ_{max}
I	1.32 ± 0.17	537	68160	452	29160
	1.33 ± 0.10[a]				
II	1.08 ± 0.29	650	69460	536	40950
	1.06 ± 0.21[a]				
III	2.07 ± 0.12	517	56480	404	32570
	2.05 ± 0.08[a]				
IV	1.67 ± 0.14	518	57010	417	26840
	1.67 ± 0.10[a]				
V	3.26 ± 0.08	358	42990	321	26420
	3.25 ± 0.04[b]				

[a] Using the method described in Ref. [5].
[b] Using classical multicomponent analysis, because the spectrum of the complex can be obtained experimentally.

from the spectra shown in Fig. 1a because the spectral changes in the range 400–500 nm are rather weak.

In Fig. 1b the first derivatives of the absorption spectra of Fig. 1a are shown. As is seen the spectral changes are rather weak. The situation for the second derivatives is the same and at about 450 nm no definite maximum characteristic for λ_C is observed. For this reason the following procedure was used to determine λ_C:

(1) The change in λ in the spectral range 400–500 nm with a small step, i.e. $\lambda^j = 400 + j \cdot \Delta\lambda$ ($\Delta\lambda = 1$ nm), was determined.

(2) For every j value the dependence $dA'(\lambda^j)/d\lambda = f[dA'(\lambda_L)/d\lambda]$ was obtained and the corresponding intercept (IY^j) was calculated according to Eq. (8).

(3) Calculation of the square (S) of the difference between the estimated IY^j value and the value calculated from the ligand spectrum $dA_L(\lambda^j)/d\lambda$:

$$S_j = \left(\frac{dA_L(\lambda^j)}{d\lambda} - IY^j\right)^2 \tag{9}$$

Evidently when $\lambda^j = \lambda_C$ then $IY^j = dA_L(\lambda^j)/d\lambda$ according to Eq. (8) and S_j tends to 0, i.e. $\lambda^j = \lambda_C$ S_j has a minimal value.

Using this procedure it was estimated that $\lambda_C = 452 \pm 1$ nm and in accordance with relations (8), (3) and (4) the molar fractions of the ligand in every solution were determined.

Using the dependence

$$\lg\frac{x_L^i}{1 - x_L^i} = \lg\beta + \lg C_M^i \tag{10}$$

which follows from Eqs. (6) and (7) the value of $\lg\beta = 1.32 \pm 0.17$ was obtained with a good regression coefficient (0.998). The same value was obtained by treatment of the spectral curves (Fig. 1a) with another approach as described in Ref. [5], thus confirming the reliability of the procedure described above (Table 1).

Using the data obtained for x_L in accordance with Eq. (1) the spectrum of the complex was calculated and is shown in Fig. 1a.

Similarly, using the same procedure, the stability constants for the Sr^{2+} complexes with the other ligands were estimated and the data obtained together with the spectral characteristics of the corresponding ligands and complexes are collected in Table 1. As seen in Table 1 standard deviations of $\lg\beta$ determined according to the present approach are bigger than those estimated according to Ref. [5] and this fact could be explained by the increase in the signal/noise ratio in the first derivative spectra. In spite of the relatively low accuracy of the present approach its application might be useful in cases where the classical spectrophotometric analysis could not be used.

5. Conclusion

An approach for quantitative spectrophotometric analysis of binary mixtures based on first derivative spectra has been developed. The proposed method is used for investigation of the complex formation of some aza-15-crown-5-containing ligands with Sr^{2+} where the stability constant is low and the absorption spectrum of the complex cannot be obtained directly. The results obtained are in good agreement with those obtained for complexation of these ligands with Ca^{2+} and Ba^{2+} described previously [9,10].

Acknowledgements

References

[1] H.-H. Perkampus, UV–VIS Spectroscopy and Its Applications, Springer-Verlag, Berlin, 1992, Chapter 4.2.
[2] P. Gans, Data Fitting in the Chemical Sciences by the Method of Least Squares, Wiley, Chichester, 1992. F. Peral, J. Mol. Struct., 266 (1992) 373.
[3] L. Antonov and St. Stoyanov, Anal. Chim. Acta, 314 (1995) 225.
[4] L. Antonov and N. Mateeva, Talanta, 41 (1994) 1489.
[5] M. Mitewa, N. Mateeva, L. Antonov and T. Deligeorgiev, Dyes and Pigments, 27 (1995) 219.
[6] I.Ya. Berstein and Yu.L. Kaminskii, Opt. Spektrosk, 15 (1963) 705.
[7] J.J.B. Nevado, C.C. Cabanillas and A.M.C. Salcedo, Analusis, 22 (1994) 5.
[8] N. Mateeva, T. Deligeorgiev, M. Mitewa and S. Simova, Dyes and Pigments, 20 (1992) 271.
[9] N. Mateeva, T. Deligeorgiev, M. Mitewa and S. Simova, J. Inclus. Phenom., 17 (1994) 81.
[10] N. Mateeva, V. Enchev, L. Antonov, T. Deligeorgiev and M. Mitewa, J. Inclus. Phenom., 20 (1995) 323.
[11] L. Antonov and St. Stoyanov, Appl. Spectrosc., 47 (1993) 1030.
[12] L. Antonov and St. Stoyanov, Appl. Spectrosc., 47 (1993) 1712.
[13] S.A. Jonker, F. Ariese and J.W. Verhoeven, Recl. Trav. Chim. Pays-Bas, 108 (1989) 109.
[14] S.A. Jonker, J.W. Verhoeven, C.A. Reiss, K. Goubitz and D. Heijdenrijk, Recl. Trav. Chim. Pays-Bas, 109 (1990) 154.
[15] A. Savitzky and M.J.E. Golay, Anal. Chem., 36 (1964) 1627.

Enzyme sensors for determination of fish freshness

G. Volpe, M. Mascini

Dipartimento di Sanità Pubblica, Epidemiologia e Chimica Analitica Ambientale, Sezione di Chimica Analitica, Via G. Capponi 9, 50121 Firenze, Italy

Abstract

A simple and rapid procedure for the determination of fish freshness was developed and applied to the determination of the K_1 parameter (freshness indicator): $K_1 = ([HXR] + [HX])/([IMP] + [HXR] + [HX]) \times 100$, where [IMP], [HXR] and [HX] are inosine monophosphate, inosine and hypoxanthine concentrations, respectively. A platinum electrode is used to detect hydrogen peroxide produced by the enzymatic reaction catalysed by xanthine oxidase immobilised on the electrode surface. The determination of inosine and inosine monophosphate was performed by the addition of nucleoside phosphorylase, 5'-nucleotidase or alkaline phosphatase to the buffer solution. Parameters such as type of buffer, amount of enzymes and sample treatment were optimised. With this procedure a linear response was obtained in the concentration range $1 \times 10^{-6} - 2 \times 10^{-5} \, \text{mol} \, 1^{-1}$ for hypoxanthine, inosine and inosine monophosphate. The detection limit was $5 \times 10^{-7} \, \text{mol} \, 1^{-1}$.

1. Introduction

The establishment of a simple, rapid and accurate method for the determination of fish freshness is required in the food industry. Various indicators of spoilage such as volatile basic nitrogen [1], ammonia [2], amines [3], volatile acids [4], and pH [5] have been reported. However, fish freshness is difficult to measure satisfactorily from these indicators and, further, they require pretreatment and complicated procedures. In recent years, considerable attention has been focused on nucleotide degradation in fish muscle as a reliable indicator of the freshness of raw fish [6, 7]. Imme-

diately after the death of fish, ATP in fish muscles starts to degrade to uric acid through the following autolytic pathway:

$$ATP \rightarrow ADP \rightarrow AMP \rightarrow IMP$$
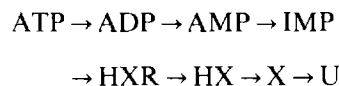
$$\rightarrow HXR \rightarrow HX \rightarrow X \rightarrow U$$

where ATP, ADP, AMP, IMP, HXR, HX, X and U represent adenosine triphosphate, adenosine diphosphate, adenosine monophosphate, inosine monophosphate, inosine, hypoxanthine, xanthine and uric acid respectively. To indicate fish freshness a K value, based on the degradation of these compounds in fish meat, is defined [8]:

$$K =$$

$$\frac{[HXR] + [HX]}{[ATP] + [ADP] + [AMP] + [IMP] + [HXR] \, [HX]}$$

$$\times \, 100$$

It has been shown that fishes with $K < 20$ are very fresh, fishes with $20 < K < 40$ must be cooked and those with $K > 40$ are not suitable for human consumption [9]. Since ATP, ADP and AMP disappear around 24 h after the death of the fish, the K value is defined as [10]

$$K_1 = \frac{[HXR] + [HX]}{[IMP] + [HXR] + [HX]} \times 100$$

It is then possible to estimate the fish freshness by measuring only three of the six parameters.

2. Proposed method for determination of fish freshness

The biochemical pathways of IMP degradation are:

$$IMP \overset{NT}{\to} HXR + P_i$$

$$HXR + P_i \overset{Np}{\to} HX + \text{ribose-1-phosphate}$$

$$HX + 2O_2 \overset{XO}{\to} UA + 2H_2O_2$$
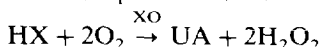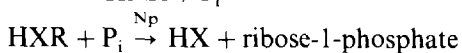
where NT, NP, XO and P_i are 5′-nucleotidase, nucleoside phosphorylase, xanthine oxidase and phosphate respectively. IMP, HXR and HX can be determined by using oxygen or hydrogen peroxide electrodes coupled to the enzymes mentioned above.

The oxygen consumed or hydrogen peroxide formed on the electrode surface produce a current variation which is correlated to the concentration of these metabolites in solution. The determination of the K_1 value by oxygen-based probes has been reported in the literature. Analysis was carried out by immobilisation of the enzymes onto the electrode surfaces which were inserted in a flow cell [10], or by enzyme linkage on chitosan porous bead reactors [11]. The first method requires a software-controlled instrumentation, while the second is based on two reactors and two oxygen electrodes in a flow injection system. Moreover, for both the devices a calibration curve

for each metabolite is necessary.

In this study a fast and simple procedure based on a hydrogen peroxide probe was developed. Hypoxanthine was determined by immobilisation of xanthine oxidase on the electrode surface. Inosine monophosphate and inosine were measured by adding, in solution, 5′-nucleotidase and nucleoside phosphorylase using an end-point procedure. The method of determination is shown in Fig. 1: the first current variation upon the addition of fish extract was related to hypoxanthine, then nucleoside phosphorylase and 5′-nucleotidase were added and the relative current variations due to HXR and IMP were recorded. With this procedure the K_1 value can be measured as follows:

$$K_1 = \frac{\Delta_1 + \Delta_2}{\Delta_1 + \Delta_2 + \Delta_3}$$

Therefore, in principle, no calibration curve is required. Alternatively, the determination of IMP has also been performed by replacing 5′-nucleotidase (which is quite expensive) with much cheaper alkaline phosphatase (AP). Results are compared.

3. Experimental

3.1. Materials

5′-Nucleotidase (EC 3.1.3.5) from Crotalus
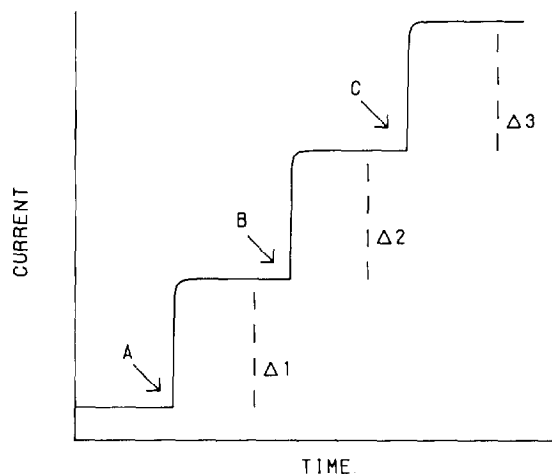
Fig. 1. Determination of the K_1 value using XO, NP and NT. A = sample addition, B = NP addition, C = NT addition; $\Delta_1, \Delta_2, \Delta_3$ = current variations due to HX, HXR and IMP respectively.

Adamanteus, alkaline phosphatase (EC 3.1.3.1) from bovine intestinal mucosa, nucleoside phosphorylase (EC 2.4.2.1) bacterial, xanthine oxidase (EC 1.1.3.22) from buttermilk, hypoxanthine, inosine, and inosine monophosphate were purchases from Sigma Chemical Co. (St. Louis, MO). The "Immunodyne Immunoaffinity" membrane (0.45 μm pore) was from Pall Biosupport Division (Glen Clove, NY). Cellulose acetate membrane (approximate molecular weight cut-off 100) was prepared in the authors, laboratory; the procedure is reported in the literature [12].

Polycarbonate membrane (0.03 μm pore size, 6 μm thick) was from Nucleopore Plesanton, CA).

3.2. Apparatus

The hydrogen peroxide-based platinum electrode (0.3 mm^2 nominal surface area) and the amperometric biosensor detector (ABD) were from Universal Sensors Inc., (Metairie, LA). The current output was recorded with an Amel model 868 recorder (Milan).

3.3. Electrode assembly

The biosensor probe consists of a platinum electrode polarised at +650 mV vs. a built-in silver/silver chloride reference electrode. This probe was assembled by placing the following membranes on an inverted electrode jacket in the given order: cellulose acetate (which protects the platinum electrode from electrochemical interferences), the enzyme membrane, and a polycarbonate membrane (which protects the enzyme from proteins or bacterial attack). The cellulose acetate membrane gives the advantage of selective measurement of H_2O_2. A solution of uric acid gives a current variation of only 3.5% of the current variation obtained by the same concentration of hydrogen peroxide. Xanthine oxidase produces from hypoxanthine two moles of hydrogen peroxide and one of uric acid. Therefore, with this membrane in place, we measure only hydrogen peroxide formation. The membranes were then secured with an O-ring. The electrode jacket was filled with a solution of 0.1 M potassium chloride,

the electrode was then inserted into the jacket and screwed down until the tip of the platinum was firmly in contact with the membranes.

3.4. Enzyme immobilisation

Xanthine oxidase was immobilized on the "Immunodyne Immunoaffinity" membrane. This membrane is intrinsically hydrophilic and contains functional groups which form covalent linkages with a variety of nucleophilic groups of enzymes/proteins. For a single membrane of 1 cm diameter, 0.1 U of dry enzyme was placed on the membrane, 10 μl of 0.05 M phosphate buffer pH 7.8 was added and the resulting mixture was homogeneously spread over the membrane with a glass stick. The membrane was air-dried for about 2 h, then washed in the same buffer and finally washed in the same buffer +KCl 1 M to remove the unbound enzyme. The enzymatic membrane was stored at 4°C in 0.05 M phosphate buffer pH 7.8 until used.

3.5. Preparation of fish extract

Two groups of authors [13, 14] proposed a treatment of fish sample according to the method of Ehira and co-workers [15, 16]: (1) deproteinization of fish fillet by precipitation with trichloroacetic acid; (2) centrifugation; (3) neutralization of supernatant with sodium hydroxide. A simpler method [17] was based on the homogenization of 5 g of fish meat with 15 ml of distilled water. The homogenate was then filtered through a membrane filter (0.2 μm pore size). The filtrate was made up to 20 ml with distilled water and used immediately as the sample.

After the preliminary experiments it was realised that the tedious procedure of deproteinization was not necessary for the measurement of current variation due to hypoxanthine. Therefore a simpler procedure was adopted for the rest of the work: a few microliters of liquid obtained by squeezing fish fillet was used directly. A small piece of fish fillet was packed into a hydrophobic nylon-net membrane and squeezed, preferably with a meat squeezer. No effort by the operator is required, even when the fish samples are fresh and high retention of water in tissues occurs.
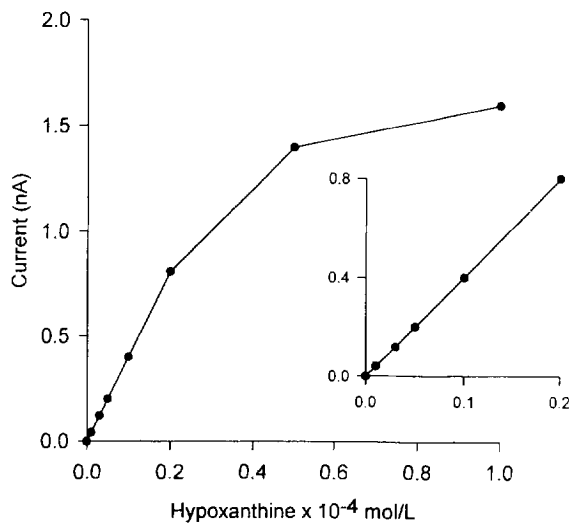
Fig. 2. Calibration curve of hypoxanthine.

4. Results and discussion

4.1. Parameter optimisation

Different buffers were tested at room temperature, fixing the pH at 7.8, which represent a compromise for the three enzymes [17]. The buffers were Hepes, Mops, Tris and Imidazol. The latter gave a low and reproducible background current, and was therefore selected to calibrate the probe using standard solutions of hypoxanthine. As shown in Fig. 2 the linear range was from 1×10^{-6} to $2 \times 10^{-5} \, \text{mol} \, l^{-1}$ with a detection limit of $5 \times 10^{-7} \, \text{mol} \, l^{-1}$ of hypoxanthine. For the detection of inosine monophosphate and inosine it was necessary to optimize the amount of phosphate in the buffer; phosphate is a substrate of nucleoside phosphorylase and a product of 5'-nucleotidase. As is shown in Fig 3., for all three enzymes we obtained a response of 100% using a phosphate concentration of $20 \, \text{mmol} \, l^{-1}$. Total volume, buffer concentration and enzyme units of NT and NP added were optimized. When the volume of the buffer was decreased, keeping constant the enzyme amounts, the response time decreased. Using 0.4 U of NP and a concentration of $\text{HXR} = 2 \times 10^{-5} \, \text{mol} \, l^{-1}$ we obtained the following response times with different volumes of buffer: 20 ml, 10 min; 10 ml, 5 min; 3 ml, 3 min.

Keeping a constant volume of 3 ml and 0.4 units of NP the amount of NT was varied. At a concentration of $2 \times 10^{-5} \, \text{mol} \, l^{-1}$ IMP we obtained the following response times with different amounts of NT: 0.56 U, 6 min, 1.0 U, 4 min. One unit of NT gave an acceptable response time.

When 5'-nucleotidase was replaced with alkaline phosphatase we observed that the reaction time was too slow with a concentration of $20 \, \text{mmol} \, l^{-1}$ of phosphate, so we decided to eliminate phosphate during the reaction of alkaline phosphatase. Phosphate and then NP were added at the end of this reaction. It was observed that using standard solutions of IMP, 4 U of AP in 3 ml buffer converted $2 \times 10^{-5} \, \text{mol} \, l^{-1}$ of IMP to HXR completely in 1 min. With this procedure the determination of the K_1 value is obtained by analysing the fish sample twice (Fig. 4). The first measurement was performed in imidazol buffer $+20 \, \text{mmol} \, l^{-1}$ of phosphate with addition of a few microliters of fish extract and then NP (Fig. 4a). The current signals of HX and HXR are measured in this step. In the second measurement after addition of fish extract to the imidazol buffer, AP was added and after 1 min $\text{NP} + 20 \, \text{mmol} \, l^{-1}$ of phosphate were injected. In this step the current signals of HX and HXR + IMP were obtained (Fig. 4b). With this procedure the K_1 value can be defined as follows:

$$K_1 = \frac{\Delta_1 + \Delta_2}{\Delta_1 + \Delta_2 + \Delta_3}$$
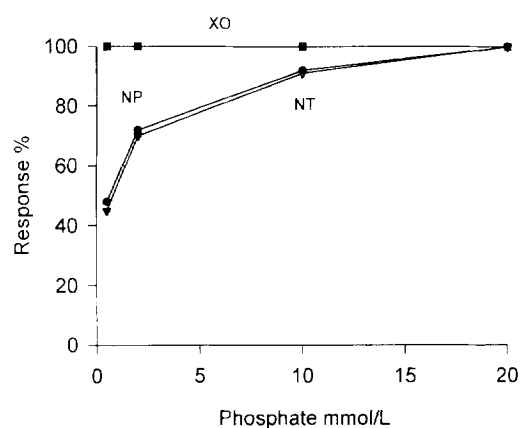
Fig. 3. Optimization of phosphate concentration. [HX] = [HXR] = [IMP] = $2 \times 10^{-5} \, \text{mol} \, l^{-1}$.
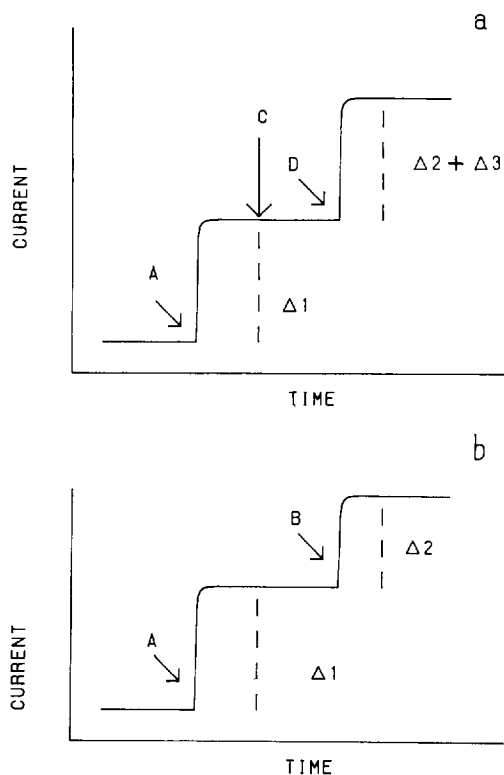
Fig. 4. Determination of the K_1 value using XO, NP, AP. A = sample addition, B = NP addition, C = AP addition, D = NP and phosphate addition; $\Delta_1, \Delta_2, \Delta_3$ = current variations due to HX, HXR and HXR + IMP respectively.

4.2. Response of the biosensors to HX, HXR, IMP

In Fig. 5 three calibration curves are reported, with all parameters optimized, in the range $1 \times 10^{-6} - 2 \times 10^{-5}$ mol l^{-1}. As shown, these calibration curves established by using three different metabolites resulted in only one line, an indication of total conversion of inosine monophosphate and inosine to hypoxanthine.

5. Analysis of fish samples

For most measurements the procedure for determination of K_1 was realised with NT enzyme, which is more rapid. To 3 ml of imidazol buffer (0.05 M, pH 7.8) with phosphate (20 mM) 5 μl of fish extract was added and according to Fig. 1 a
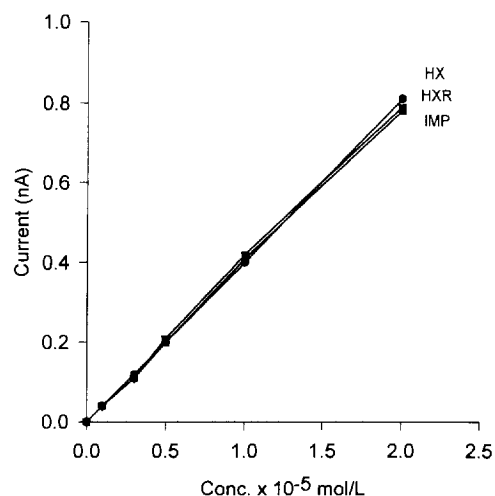
Fig. 5. Calibration curves of HX, HXR and IMP with all parameters optimized.

current variation due to HX was recorded. Then NP (0.4 U) and finally NT (1 U) were added and the relative current variations due to HXR and IMP were recorded. The total analysis time is less than 10 min which is acceptable. Recovery studies were carried out by adding HX, HXR and IMP to the buffer after the fish extract addition. The results, reported in Table 1, show good recoveries of between 98% and 106%.

The determination of K_1 values in 12 fish samples is reported in Table 2. Two different species

Table 1
Recovery studies of HX, HXR and IMP added to three fish extracts

Sample	Added (10^{-6} mol l^{-1})	Expected (10^{-6} mol l^{-1})	Found (10^{-6} mol l^{-1})	Recovery
1	HX 5.0	6.8	7.2	106
	HXR 5.0	8.2	8.4	102
	IMP 5.0	19.4	19.4	100
2	HX 5.0	6.6	6.8	103
	HXR 5.0	8.5	8.3	98
	IMP 5.0	17.0	17.0	100
3	HX 3.2	5.4	5.6	104
	HXR 3.2	10.3	10.8	105
	IMP 3.2	10.7	11.0	103

Table 2
Results obtained with real samples stored under different conditions

Sample	Storage method	time from death	Enzymes: XO, NP, NT HX Current (nA)	HX Conc. $mmol\,l^{-1}$	HXR Current (nA)	HXR Conc. $mmol\,l^{-1}$	IMP Current (nA)	IMP Conc. $mmol\,l^{-1}$	Enzymes: XO, NP, AP HX Current (nA)	HX Conc. $mmol\,l^{-1}$	HXR+IMP Current (nA)	HXR+IMP Conc. $mmol\,l^{-1}$	K_i (%) (XO, NP, NT)	k_i (%) (XO, NP, AP)
Common carp	3°C with ice	0	0.05 ±0.01	0.29 ±0.06	0.24 ±0.02	1.4 ±0.1	0.84 ±0.03	4.9 ±0.2	0.04 ±0.01	0.23 ±0.06	1.07 ±0.04	6.23 ±0.20	26 ±3	25 ±4
Mirror carp	3°C with ice	0	0.09 ±0.01	0.52 ±0.06	0.30 ±0.02	1.75 ±0.1	1.01 ±0.04	5.9 ±0.2	0.09 ±0.01	0.52 ±0.06	1.04 ±0.04	6.05 ±0.20	28 ±3	34 ±4
Common carp	3°C with ice	24	0.14 ±0.01	0.82 ±0.06	0.56 ±0.03	3.26 ±0.20	0.59 ±0.03	3.44 ±0.20	0.12 ±0.01	0.70 ±0.06	1.07 ±0.04	6.23 ±0.20	54 ±4	57 ±5
Mirror carp	3°C with ice	24	0.09 ±0.01	0.52 ±0.06	0.27 ±0.02	1.57 ±0.10	0.89 ±0.03	5.18 ±0.20	0.09 ±0.01	0.52 ±0.06	1.09 ±0.04	6.35 ±0.20	29 ±3	30 ±4
Mirror carp	3°C with ice	48	0.13 ±0.01	0.76 ±0.06	0.25 ±0.02	1.46 ±0.10	1.21 ±0.04	7.05 ±0.20	0.11 ±0.01	0.64 ±0.02	1.25 ±0.04	7.28 ±0.20	24 ±3	26 ±3
Mirror carp	3°C with ice	66	0.10 ±0.01	0.58 ±0.06	0.20 ±0.02	1.16 ±0.10	0.95 ±0.03	5.53 ±0.20	—	—	—	—	24 ±3	—
Common carp	3°C with ice	234	0.16 ±0.01	1.05 ±0.07	0.76 ±0.03	5.02 ±0.20	0.03 ±0.01	0.20 ±0.07	—	—	—	—	97 ±5	—
Common carp	−80°C	352	0.02 ±0.01	0.13 ±0.07	0.18 ±0.01	1.19 ±0.10	0.90 ±0.03	5.94 ±0.20	—	—	—	—	18 ±2	—
Common carp	−30°C	352	0.14 ±0.01	0.92 ±0.07	0.33 ±0.01	2.18 ±0.07	0.53 ±0.03	3.5	—	—	—	—	47 ±4	—
Common carp	+3°C for 112 hours then at −80°C	352	0.25 ±0.01	1.65 ±0.07	0.67 ±0.01	4.42 ±0.07	0.04 ±0.01	0.26	—	—	—	—	96 ±6	—
Common carp	−80°C	352	0.05 ±0.01	0.33 ±0.07	0.16 ±0.01	1.06 ±0.07	0.73 ±0.03	4.82 ±0.20	—	—	—	—	22 ±3	—

of carp (common carp and mirror carp) were stored under different conditions and analysed. Five samples were analysed with both procedures using NT and AP. Both species showed an initial K_1 value of about 25–26%. During storage at 3°C the K_1 value increased to about 57% for common carp after 24 h, while it remained constant for mirror carp until 66 h. After 352 h of storage, if the fish fillet of common carp was kept at $-30°C$ the K_1 value reached 47%, while it is was stored at $-80°C$ the K_1 value remained constant.

6. Conclusions

A method for the determination of fish freshness was developed by measuring the K_1 parameter with a xanthine oxidase probe based on a hydrogen peroxide electrode. Measurement of HXR and IMP concentrations were carried out by NP, NT or AP addition in solution. The resultant procedure was fast and simple and moreover the biosensor technology allows the miniaturisation of the system for a field instrument.

References

[1] T. Kawabata and H. Terui, Bull. Jpn. Soc. Sci. Fish, 19 (1953) 741.

[2] F. Ota and T. Nakamura, Bull. Jpn. Soc. Sci. Fish, 18 (1952) 15.

[3] K. Yamada, Bull. Jpn. Soc. Sci. Fish, 34 (1968) 541.

[4] T. Suzuki, Bull. Jpn. Soc. Sci. Fish, 19 (1953) 102.

[5] M. Yamanoto and M. Sonehara, Bull. Jpn. Soc. Sci. Fish, 19 (1953) 761.

[6] D.I. Fraser, D. Pitts and W. J. Dyer, Fisheries Research Board of Canada, 25 (1963) 239.

[7] R. Hughes and N.R. Jones, J. Sci. Food Agric., 17 (1966) 434.

[8] E. Gruger, J. Agric. Food Chem., 20 (1972) 781.

[9] Instruction Manual of the Freshness Meter KV-101, Oriental Electric Co. Ltd., Niiza, Saitama 352, Japan.

[10] E. Watanabe and M. Tanaka, in D.L. Wise (Ed.), Bioinstrumentation and Biosensors, 1991, pp. 39–73.

[11] H. Okuma, H. Takahashi, S. Yazawa, S. Sekimukai and E. Watanabe, Anal. Chim. Acta, 260 (1992) 93.

[12] M. Mascini, F. Mazzei, D. Moscone, G. Calabrese and M. Massi Benedetti, Clin. Chem., 33 (1987) 591.

[13] E. Watanabe, K. Ando, I. Karube, H. Matsuoka and S. Suzuki, J. Food Sci., 48 (1983) 496.

[14] J.H.T. Luong, K.B. Male and A.L. Nguyen, Enzym. Microb. Technol., 11 (1989) 277.

[15] S. Ehira and H. Uchiyama, Bull. Jpn. Soc. Sci. Fish, 35 (1969) 1080.

[16] S. Ehira, H. Uchiyama, F. Ulda and H. Matsumija, Bull. Jpn. Soc. Sci. Fish, 36 (1970) 491.

[17] E. Watanabe, A. Nagumo, M. Hoshi, S. Conagaya and M. Tanaka, J. Food Sci., 52 (1987) 592.

Book reviews

The Directory of Controlled Release Technologies: Products and Organizations, by David Williams, Elsevier, Oxford, 1995, Diskette, £190. ISBN 1-85617-239-2.

This new diskette from Elsevier contains details of the major manufacturers, researchers and their products in the controlled release field across the world, in an easily accessible, flexible directory format. The diskette provides an overview of the technology, materials and future developments of controlled release products, as well as an alphabetical list of companies and products.

The overview technology section deals with the concepts, terminology and regulatory matters used in controlled release technologies together with diagrams and schemes to illustrate the types of mechanisms involved. The three main methods of containment are discussed, namely reservoir, matrix (oral and subdermal) and carrier. These mechanisms are well illustrated. As controlled release technology involves a combination of a drug with a type of device, the legal and regulatory position is also discussed. The text also elaborates on the methods of environmentally mediated release, such as osmotic pressure, vapour pressure, hydrodynamic pressure, pH activation and physically activated systems, namely infusion pumps, magnetic control and iontophoresis. Details are also provided of microcapsule, nanosphere and liposome technology. The section of the overview dealing with materials discusses polymers under the headings of types, biocompatability, biodegradation and permeability. The structures of both biodegradable and non-biodegradable polymers are illustrated. The overview section concludes with a discussion of future developments, and a list of references for further reading.

An A–Z list of companies comprises a further section, as well as being listed by geographical location and by application area. Selection of a letter will give companies beginning with that letter. Further selection of a particular company will provide various business details such as address, telephone and fax numbers, parent company and application areas. Personnel details and products are also provided.

The products section is also listed A–Z. This comprises a selected list of products manufactured by the companies. The uses, description and company are provided. The products are also listed according to application area, namely whether agricultural, cosmetic, household, pharmaceutical or veterinary.

There is also a search facility whereby a word or topic can be traced in the list of products and companies. This new diskette is certainly a useful means of gaining access to details of products and companies specialising in controlled release technology.

D.L. Munday

Chemometrics: Experimental Design, by E. Morgan, Wiley, Chichester, 1991, (paperback 1995), xviii + 275 pp., £19.50. ISBN 0-471-95832-8.

I reviewed the hardback version of this book 4 years ago (Talanta, 38 (1991) 1204–1205), and recommended it as a clear introduction to chemometrics, as well as being a very good self-teach manual for which it had the market largely to itself. The book has obviously stood the test of time well, since it now appears in paperback unchanged from the hardback version except that it is about £5.00 cheaper (which is not really a great price reduction).

Book reviews

The Directory of Controlled Release Technologies: Products and Organizations, by David Williams, Elsevier, Oxford, 1995, Diskette, £190. ISBN 1-85617-239-2.

This new diskette from Elsevier contains details of the major manufacturers, researchers and their products in the controlled release field across the world, in an easily accessible, flexible directory format. The diskette provides an overview of the technology, materials and future developments of controlled release products, as well as an alphabetical list of companies and products.

The overview technology section deals with the concepts, terminology and regulatory matters used in controlled release technologies together with diagrams and schemes to illustrate the types of mechanisms involved. The three main methods of containment are discussed, namely reservoir, matrix (oral and subdermal) and carrier. These mechanisms are well illustrated. As controlled release technology involves a combination of a drug with a type of device, the legal and regulatory position is also discussed. The text also elaborates on the methods of environmentally mediated release, such as osmotic pressure, vapour pressure, hydrodynamic pressure, pH activation and physically activated systems, namely infusion pumps, magnetic control and iontophoresis. Details are also provided of microcapsule, nanosphere and liposome technology. The section of the overview dealing with materials discusses polymers under the headings of types, biocompatability, biodegradation and permeability. The structures of both biodegradable and non-biodegradable polymers are illustrated. The overview section concludes with a discussion of future developments, and a list of references for further reading.

An A–Z list of companies comprises a further section, as well as being listed by geographical location and by application area. Selection of a letter will give companies beginning with that letter. Further selection of a particular company will provide various business details such as address, telephone and fax numbers, parent company and application areas. Personnel details and products are also provided.

The products section is also listed A–Z. This comprises a selected list of products manufactured by the companies. The uses, description and company are provided. The products are also listed according to application area, namely whether agricultural, cosmetic, household, pharmaceutical or veterinary.

There is also a search facility whereby a word or topic can be traced in the list of products and companies. This new diskette is certainly a useful means of gaining access to details of products and companies specialising in controlled release technology.

D.L. Munday

Chemometrics: Experimental Design, by E. Morgan, Wiley, Chichester, 1991, (paperback 1995), xviii + 275 pp., £19.50. ISBN 0-471-95832-8.

I reviewed the hardback version of this book 4 years ago (Talanta, 38 (1991) 1204–1205), and recommended it as a clear introduction to chemometrics, as well as being a very good self-teach manual for which it had the market largely to itself. The book has obviously stood the test of time well, since it now appears in paperback unchanged from the hardback version except that it is about £5.00 cheaper (which is not really a great price reduction).

It is a book concerned with experimental design moving at a leisurely pace, suitable for self-teaching, through a review of the necessary basic statistics, full factorial designs, fractional factorials, and response surfaces. Throughout there are summaries, aims and objectives clearly stated, all coupled with numerous self-assessment questions. Often large spaces (up to one page) are left blank for the students to write in their answers, but this is not always the case, and this is somewhat inconsistently used. However, it is an excellent book for the self-teaching environment, but would also provide a useful text to accompany a first course in experimental design. It is a pity that not more students learn about such design methods either as undergraduates or as postgraduates.

C.J. Gilmore

TrAC — Trends in Analytical Chemistry, Reference Edition, Vol. 13, edited by Y. Gohshi, J.F.K. Huber and A. Townshend, Elsevier, Amsterdam, 1994, 478 pp. +171 pp. (Supplement), US$400.00. ISBN 0-444-82110-4.

I have always had the sneaking suspicion that publishers never take any notice of my book reviews. Two years ago (Talanta, 41 (1994) 166) I wrote a review of the 1992 edition of TrAC in which my only concern was the steep price hike (14%) on the previous year. Imagine my surprise when this edition arrived on my desk costing $400 (a rise of only 3% over two years) and containing an extra 76 pages. So thanks are due to Elsevier. If this situation remained the norm I would not be faced with the miserable task of identifying titles we can no longer afford with our inflation linked budgets. Other publishers please note!

Most readers will not be aware of the philosophy behing the *Trends in* series. TrAC is a compilation of the archival material reprinted from the 10 issues of the journal published in 1994. Every year that I get the happy task of reviewing TrAC I point out that for little extra cost you can subscribe to the journal and obtain the reference edition *gratis*. This year's edition contains the usual mixutre of readable reviews of recent devel-

opments in instrumentation by established researchers (between 6 and 10 per issue). These include multidimensional GC, multidimensional protein NMR spectroscopy, atmospheric pressure ionisation mass spectrometry, Shpol'skii spectroscopy, scanning tunnelling microscopy, and capillary electrophoresis. There are a number of excellent articles specifically targeted at the analysis of environmental samples: pollution and pesticide analysis; stripping electroanalytical techniques; supercritical fluid extraction and enzyme immunoassay of soil pesticides; multivariate sensor arrays and analysis of complex environmental data using chemometric methods. Of general interest to analytical chemists are articles on Internet resources and quality assurance. Most issues contain a random mixture of the above, but in keeping with previous years, two issues are devoted to specific areas (June/July concentrating on Fourier transform mass spectrometry and October on water analysis).

The quality of TrAC is consistently high and is a superb resource for all teachers of University level analytical chemistry. The emphasis is always on relevance and accessibility. For the research worker, TrAC is a useful way of staying in touch with modern developments in areas outside one's own speciality. The only annoying feature of this edition is the supplement (171 pages) that contains the *'Directory of Hyphenated Techniques'*. I have reviewed this separately for Talanta and am still of the opinion that it serves no useful purpose.

B.A. McGaw

Quantitative X-ray Spectrometry, Second Edition, edited by R. Jenkins, R.W. Gould and D. Gedcke, Dekker, New York, 1995, xi + 484 pp., US$150.00. ISBN 0-8247-9554-7.

The appearance of the second edition of Quantitative X-ray Spectrometry, as Volume 20 in the Practical Spectroscopy Series, is both timely and welcome. Timely, in that it is complementary to Volume 14 ("Handbook of X-ray Spectrometry"), and welcome because it is some 15 years since the

It is a book concerned with experimental design moving at a leisurely pace, suitable for self-teaching, through a review of the necessary basic statistics, full factorial designs, fractional factorials, and response surfaces. Throughout there are summaries, aims and objectives clearly stated, all coupled with numerous self-assessment questions. Often large spaces (up to one page) are left blank for the students to write in their answers, but this is not always the case, and this is somewhat inconsistently used. However, it is an excellent book for the self-teaching environment, but would also provide a useful text to accompany a first course in experimental design. It is a pity that not more students learn about such design methods either as undergraduates or as postgraduates.

C.J. Gilmore

TrAC — Trends in Analytical Chemistry, Reference Edition, Vol. 13, edited by Y. Gohshi, J.F.K. Huber and A. Townshend, Elsevier, Amsterdam, 1994, 478 pp. +171 pp. (Supplement), US$400.00. ISBN 0-444-82110-4.

I have always had the sneaking suspicion that publishers never take any notice of my book reviews. Two years ago (Talanta, 41 (1994) 166) I wrote a review of the 1992 edition of TrAC in which my only concern was the steep price hike (14%) on the previous year. Imagine my surprise when this edition arrived on my desk costing $400 (a rise of only 3% over two years) and containing an extra 76 pages. So thanks are due to Elsevier. If this situation remained the norm I would not be faced with the miserable task of identifying titles we can no longer afford with our inflation linked budgets. Other publishers please note!

Most readers will not be aware of the philosophy behing the *Trends in* series. TrAC is a compilation of the archival material reprinted from the 10 issues of the journal published in 1994. Every year that I get the happy task of reviewing TrAC I point out that for little extra cost you can subscribe to the journal and obtain the reference edition *gratis*. This year's edition contains the usual mixutre of readable reviews of recent devel-

opments in instrumentation by established researchers (between 6 and 10 per issue). These include multidimensional GC, multidimensional protein NMR spectroscopy, atmospheric pressure ionisation mass spectrometry, Shpol'skii spectroscopy, scanning tunnelling microscopy, and capillary electrophoresis. There are a number of excellent articles specifically targeted at the analysis of environmental samples: pollution and pesticide analysis; stripping electroanalytical techniques; supercritical fluid extraction and enzyme immunoassay of soil pesticides; multivariate sensor arrays and analysis of complex environmental data using chemometric methods. Of general interest to analytical chemists are articles on Internet resources and quality assurance. Most issues contain a random mixture of the above, but in keeping with previous years, two issues are devoted to specific areas (June/July concentrating on Fourier transform mass spectrometry and October on water analysis).

The quality of TrAC is consistently high and is a superb resource for all teachers of University level analytical chemistry. The emphasis is always on relevance and accessibility. For the research worker, TrAC is a useful way of staying in touch with modern developments in areas outside one's own speciality. The only annoying feature of this edition is the supplement (171 pages) that contains the '*Directory of Hyphenated Techniques*'. I have reviewed this separately for Talanta and am still of the opinion that it serves no useful purpose.

B.A. McGaw

Quantitative X-ray Spectrometry, Second Edition, edited by R. Jenkins, R.W. Gould and D. Gedcke, Dekker, New York, 1995, xi + 484 pp., US$150.00. ISBN 0-8247-9554-7.

The appearance of the second edition of Quantitative X-ray Spectrometry, as Volume 20 in the Practical Spectroscopy Series, is both timely and welcome. Timely, in that it is complementary to Volume 14 ("Handbook of X-ray Spectrometry"), and welcome because it is some 15 years since the

It is a book concerned with experimental design moving at a leisurely pace, suitable for self-teaching, through a review of the necessary basic statistics, full factorial designs, fractional factorials, and response surfaces. Throughout there are summaries, aims and objectives clearly stated, all coupled with numerous self-assessment questions. Often large spaces (up to one page) are left blank for the students to write in their answers, but this is not always the case, and this is somewhat inconsistently used. However, it is an excellent book for the self-teaching environment, but would also provide a useful text to accompany a first course in experimental design. It is a pity that not more students learn about such design methods either as undergraduates or as postgraduates.

C.J. Gilmore

TrAC — Trends in Analytical Chemistry, Reference Edition, Vol. 13, edited by Y. Gohshi, J.F.K. Huber and A. Townshend, Elsevier, Amsterdam, 1994, 478 pp. + 171 pp. (Supplement), US$400.00. ISBN 0-444-82110-4.

I have always had the sneaking suspicion that publishers never take any notice of my book reviews. Two years ago (Talanta, 41 (1994) 166) I wrote a review of the 1992 edition of TrAC in which my only concern was the steep price hike (14%) on the previous year. Imagine my surprise when this edition arrived on my desk costing $400 (a rise of only 3% over two years) and containing an extra 76 pages. So thanks are due to Elsevier. If this situation remained the norm I would not be faced with the miserable task of identifying titles we can no longer afford with our inflation linked budgets. Other publishers please note!

Most readers will not be aware of the philosophy behing the *Trends in* series. TrAC is a compilation of the archival material reprinted from the 10 issues of the journal published in 1994. Every year that I get the happy task of reviewing TrAC I point out that for little extra cost you can subscribe to the journal and obtain the reference edition *gratis*. This year's edition contains the usual mixutre of readable reviews of recent devel-

opments in instrumentation by established researchers (between 6 and 10 per issue). These include multidimensional GC, multidimensional protein NMR spectroscopy, atmospheric pressure ionisation mass spectrometry, Shpol'skii spectroscopy, scanning tunnelling microscopy, and capillary electrophoresis. There are a number of excellent articles specifically targeted at the analysis of environmental samples: pollution and pesticide analysis; stripping electroanalytical techniques; supercritical fluid extraction and enzyme immunoassay of soil pesticides; multivariate sensor arrays and analysis of complex environmental data using chemometric methods. Of general interest to analytical chemists are articles on Internet resources and quality assurance. Most issues contain a random mixture of the above, but in keeping with previous years, two issues are devoted to specific areas (June/July concentrating on Fourier transform mass spectrometry and October on water analysis).

The quality of TrAC is consistently high and is a superb resource for all teachers of University level analytical chemistry. The emphasis is always on relevance and accessibility. For the research worker, TrAC is a useful way of staying in touch with modern developments in areas outside one's own speciality. The only annoying feature of this edition is the supplement (171 pages) that contains the '*Directory of Hyphenated Techniques*'. I have reviewed this separately for Talanta and am still of the opinion that it serves no useful purpose.

B.A. McGaw

Quantitative X-ray Spectrometry, Second Edition, edited by R. Jenkins, R.W. Gould and D. Gedcke, Dekker, New York, 1995, xi + 484 pp., US$150.00. ISBN 0-8247-9554-7.

The appearance of the second edition of Quantitative X-ray Spectrometry, as Volume 20 in the Practical Spectroscopy Series, is both timely and welcome. Timely, in that it is complementary to Volume 14 ("Handbook of X-ray Spectrometry"), and welcome because it is some 15 years since the

first edition was published. There are thirteen chapters, six appendices and an index, the main addition to the first edition being a chapter on special applications of the XRF method.

The scope of the book is quite considerable, ranging from description of the interaction of X-rays with matter, excitation sources, instrumentation, statistics, general computer applications, specimen preparation, and trace analysis to discussion of the main subject material — problems in quantitative analysis and methods and models for quantitative analysis. The authors quite rightly go into considerable detail in the latter two topics and here, as in all other chapters, very sensibly divide discussion between wavelength dispersive and energy dispersive methods. The book is very readable and interesting because every theoretical aspect is backed up with experimental results, usually displayed in graphical or tabular form. Another appealing aspect about the book is that it is written from a practical, no-nonsense standpoint, and contains a wealth of *practical* advice. For example, under Specimen Preparation the reader is not only provided with specific methods of specimen preparation, but is urged to use a common sense approach before even laying hands on a specimen (e.g. "...have analytical goals clearly in mind — precision, accuracy, concentration range, cost, speed...").

There are a few typographical errors, fortunately most are obvious, and one diagram is labelled incorrectly. A surprising feature in the chapter on radiation hazards in spectrometry is the authors' use of outdated terminology when referring to units of measurement for ionizing radiation, e.g. the *rad* and the *rem* as opposed to the ICRU- and ICRP-approved units, the *gray* and the *sievert*. Notwithstanding these remarks, Jenkins et al. have produced a work of considerable value to all current practitioners of XRF. In the preface to this edition, they state that they hope that it will enjoy the same success as the first, and take its place in the literature on X-ray materials analysis. I have no doubt that this will be the case.

D.F. Rendle

Photochemical-fluorimetric method for the determination of total chlorophenoxyacid herbicides[1]

Sergei A. Eremin[2], Belkacem Laassis, Jean-Jacques Aaron*

*Institut de Topologie et de Dynamique des Systèmes de l'Université Paris, 7 Denis-Diderot, Associé au CNRS, URA 34
1, Rue Guy de la Brosse, 75005 Paris, France*

Abstract

A room temperature photochemically-induced fluorescence (RTPF) method is proposed for the quantitative analysis of seven widely-used chlorophenoxyacid herbicides. The influence of organic solvent, pH (in aqueous solutions), methanol percentage, and UV irradiation time on the excitation and emission wavelengths and fluorescence intensity was investigated. It was found that the largest fluorescence signals were obtained in a mixture of methanol and pH 5 buffer (50/50, v/v), while organic solvents and water produced generally lower signals. The tri- and bichlorinated phenoxyacid herbicides were photolysed significantly more slowly than the monochlorinated derivatives, and the derivatives of 2-propionic acid were photodegraded more quickly than the corresponding derivatives of acetic and butyric acid. Selected UV irradiation times were found to be 15 min for all herbicides under study. Linear calibration graphs were established over about one to two orders of magnitude in the interval 0.1–10 μg ml^{-1}. The RTPF limits of detection were between 36 ng ml^{-1} and 179 ng ml^{-1}, according to the compound. Analytical application of RTPF to river water samples containing chlorophenoxyacid herbicides is discussed.

Keywords: Photochemically-induced fluorescence; Chlorophenoxyacid herbicides

1. Introduction

Monitoring of environmental samples for pesticide residues has become very important. The detection of their presence in surface water is a convenient indicator of contamination. Chlorophenoxyacid herbicides are of particular concern because of their potential toxicity towards animals and humans [1]. Some of them, such as 2,4-dichlorophenoxyacetic acid (2,4-D) and 2-(2-methyl-4-chlorophenoxy) propionic acid (MCPP or mecoprop), are still widely-used herbicides for broadleaf weed conrol, while another, 2,4,5-trichlorophenoxyacetic acid (2,4,5-T), has been restricted since 1969.

---

* Corresponding author.

[1] Presented at the Symposium on Analytical Sciences, held in Paris, France, March 1995.

[2] On leave from: Division of Chemical Enzymology, Department of Chemistry, M.V. Lomonosov Moscow State University, Moscow 000958, Russian Federation.

Established screening procedures for detection of these herbicides include gas chromatography [2], used after extraction of samples, or liquid chromatography with on-line selective preconcentration [3]. However, immunoassay methods provide simpler, cheaper, and more robust methods for the direct analysis of a large number of samples. Several radioimmunoassays [4,5] and enzyme-linked immunosorbent assays (ELISA) for specific determination of 2,4-D [6] and most phenoxyacid herbicides have been described [7,8]. Recently, more rapid, but less sensitive, polarization fluoroimmunoassays have been proposed for specific measurement of 2,4-D and 2,4,5-T [9].

The continued application of herbicides and growing concern about the potential contamination of ground water require regulations, such as the European Community drinking water ordinance, which set a very low upper limit for pesticide concentrations of 0.1 ng ml^{-1} for a single substance, and 0.5 ng ml^{-1} for total pesticides [10]. The higher, and more reasonable, detection limits in drinking water proposed as health advisory levels for individual pesticides have been established by the Office of Water of the US Environmental Protection Agency. For example, for 2,4-D, this limit is 70 ng ml^{-1}. However, real water samples can occasionally contain up to a hundred times higher concentrations. Moreover, high 2,4-D concentrations of about 2.5 μg ml^{-1} could be measured in the urine of workers involved in spraying this herbicide, 3 days after exposure [11].

Many pesticides are persistent and should be continuously monitored. Traditional analytical methods used in pesticide analysis are expensive because they require costly laboratory equipment, and they are generally time-consuming. The initial screening of pesticides should be technically simple, inexpensive, and useful for routine analysis of a large number of samples. Recently, we developed a simple method of detection of some aromatic pesticides based on a photodegradation reaction, which may be applicable to the very simple and quick preliminary monitoring of water samples [12]. The main advantages of the method, named room temperature photochemically-induced fluorescence (RTPF), are its simplicity, ra-

pidity, and the low cost of the required equipment [13].

The aim of this paper was to investigate the photochemically-induced fluorescence properties of a series of chlorophenoxyacid herbicides (Fig. 1) in different solvents, and to develop a rapid RTPF screening method for the determination of the chlorophenoxyacid herbicide total concentration in a bulk solution.

2. Experimental

2.1. Reagents

Chlorophenoxyacid herbicides were obtained from Sigma or Merck (analytical grade). The solvents (spectroscopic grade) were purchased from Merck. The buffer solutions were obtained from Janssen Chimica. Deionized water was utilized for preparing binary mixtures.

2.2. Apparatus

Fluorescence measurements were performed on a Kontron SFM-25 spectrofluorimeter, using a Kontron SFM-25 data control and acquisition program. The high voltage level on the instrument lamp was 600 V, and the gain factor varied from 1 to 10. A 200 W HBO Osram high-pressure mercury lamp with an Oriel model 8500 power supply was utilized for the photodegradation reaction. The photochemical set-up included a light box, consisting of a fan, a mercury lamp and a convenient quartz lens. A standard Hellma 1 cm^2 quartz reaction cuvette (sample cell) was placed on an optical bench at 45 cm from the mercury lamp [13].

2.3. Procedure

Standard stock solutions of chlorophenoxyacid herbicides (0.1–0.5 mg ml^{-1}) were prepared from the corresponding compounds by dissolving them in ethanol, and were stored at room temperature. Serial dilutions were freshly done for the working solutions. The photolysis reaction was performed by irradiating with UV light a 3 ml volume of
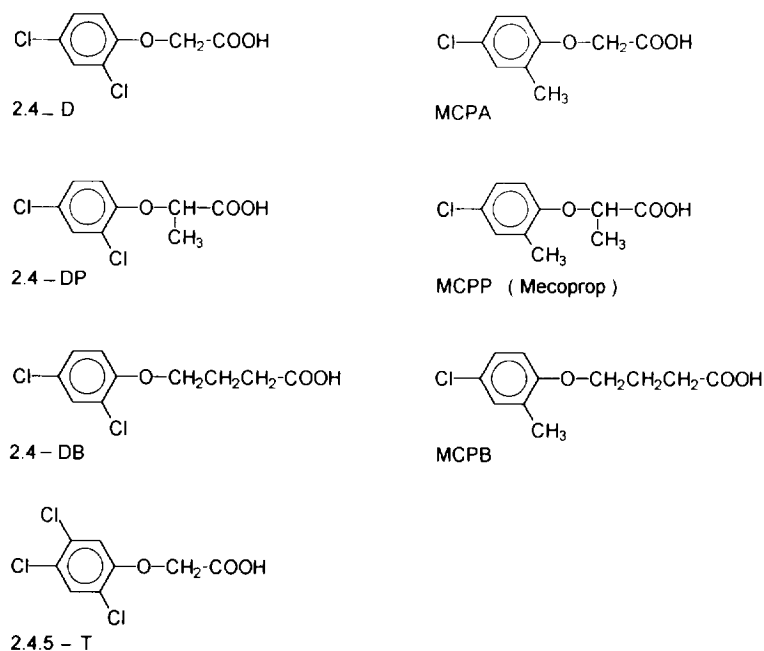
Fig. 1. Names and chemical structures of the chlorophenoxyacid herbicides under study.

dilute herbicide solution which was magnetically stirred at room temperature. For the analytical applications, a 50/50 v/v mixture of methanol and a pH 5 buffer and a 15 min irradiation time were chosen. The curves of the fluorescence intensity (I_F) vs. the various parameters (time, methanol percentage, pH) were plotted at constant excitation (276 nm) and emission (292 nm) wavelengths of the pesticide photoproducts.

3. Results and discussion

3.1. Photochemically-induced fluorescence properties

The chlorophenoxyacid herbicides have no native fluorescence, but they can be photolysed into strongly fluorescent photoproducts. The fluorescence intensity of photodegraded herbicide increased with negligible change in the shape of the emission spectra during UV irradiation (Fig. 2). For all chlorophenoxyacid herbicides, the excitation spectra of photoproducts presented a broad maximum centered near 276 nm. The latter value

was selected as the analytical excitation wavelength. The emission spectra varied slightly with the compound, its concentration, and the type of solvent (Table 1). To develop a screening method, we chose an emission wavelength of 292 nm for all chlorophenoxyacid herbicides under study. The photoproducts have an unknown structure, but they probably consist of a mixture of photodegradation products, including derivatives produced by hydrolysis, dechlorination and polymerization reactions. As is well known, the chlorinated phenols are very quickly (20-160 s) photodegraded [14]. The main identified products are lower chlorinated phenols, polymeric and dihydroxylated products, and phenol, which present excitation and emission wavelengths at 270 and 290-300 nm respectively [14].

3.2. Effect of solvent

The effect of several solvents on the photochemically-induced fluorescence properties of 2, 4-D was investigated. As can be seen in Table 1, no significant shift of the emission wavelengths occurred upon changing solvent but the fluorescence
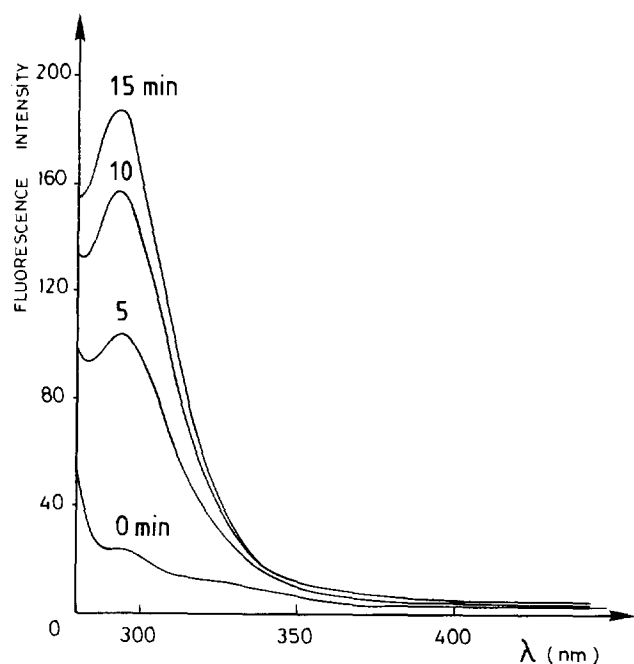
Fig. 2. Effect of the ultraviolet irradiation on the fluorescence emission spectra of 5.0 μg ml^{-1} 2,4-D in 2-propanol, at room temperature. Irradiation times were 0, 5, 10, and 15 min.

Fig. 3. Effect of the percentage of methanol on the fluorescence intensity of 2,4-D (5 μg ml^{-1}) in a methanol/water mixture after 15 min irradiation.

signal was increased considerably in alcohols compared to water. Similarly, a strong influence of solvents on the fluorescence intensity of photoproducts was found in the case of other pesticides [12,15]. For analytical purposes, methanol was

Table 1
Photochemically-induced fluorescence properties of 2,4-D (5 μg ml^{-1}) in various solvents

Solvent	λ_{em} (nm)[a]	I_F^{b}
Water	296	1.0
Methanol	290	3.9
2-Propanol	293	4.3
Ethanol	292	3.8
Dimethylsulfoxide	295	0.8
Dimethylformamide	291	1.4
Acetonitrile	297	0.8
Buffer (pH 4)	296	0.7
Buffer (pH 10)	294	0.5

[a] λ_{em} = maximum emission wavelength.
[b] I_F = relative fluorescence intensity, normalized relative to the fluorescence intensity in water. A 15 min irradiation time was used for all solvents.

selected as the solvent giving the largest fluorescence signal, and for economic reasons.

3.3. Effect of the percentage of methanol

In order to evaluate the influence of water in binary mixtures on the fluorescence intensity of the photoreaction, we tested the effect of the percentage of methanol on the photochemically-induced fluorescence intensity of 2,4-D. As can be observed in Fig. 3, the photochemically-induced fluorescence signal in a 50/50 v/v methanol–water mixture is higher than in pure methanol or water.

3.4. Effect of pH

The influence of pH on the photochemical reaction of 2,4-D was investigated. The fluorescence intensity of the photoproducts changed considerably with the pH of the reaction medium (Fig. 4). A pH value of 5, corresponding to the maximum photochemically-induced fluorescence signal, was considered as optimum for analytical applications. The unbuffered water samples present pH values varying between 4 and 7. For all further analytical experiments we chose a methanol/pH 5 buffer mixture (50/50 v/v) as the ideal solvent for photodegradation of chlorophenoxyacid herbicides.
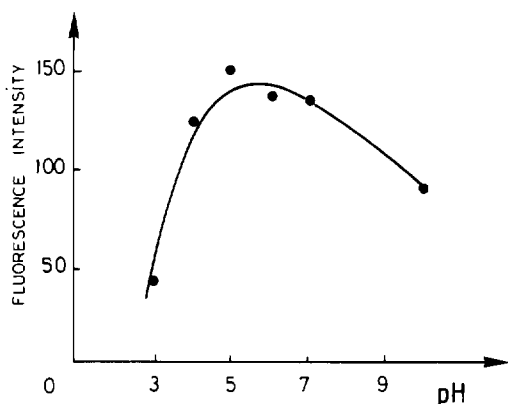
Fig. 4. Effect of the buffer pH on the fluorescence intensity of 2,4-D (5 μg ml⁻¹) in a 50/50 v/v methanol/pH 5 buffer mixture after 15 min irradiation.

3.5. Effect of irradiation time

The I_F vs. irradiation time curves exhibited two types of shape. For 2,4-D and 2,4,5-T the curves were characterized by a continuous increase of the fluorescence signal, no well-defined maximum value being reached up to a 30 min irradiation time (Fig. 5). However, in the case of MCPP and MCPA, the fluorescence intensity increased, reached a maximum value, and then a small decrease in intensity occurred (Fig. 5). For all compounds studied, the kinetics of photodegradation are rather slow. A very small influence of the herbicide initial concentration on the kinetics of photodegradation was observed. Generally, for
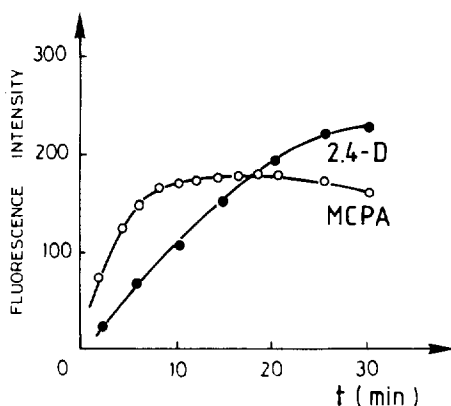
Fig. 5. Effect of the ultraviolet irradiation time on the fluorescence intensity of 5 μg ml⁻¹ 2,4-D (●) and 3 μg ml⁻¹ MCPA (○) in a 50/50 v/v methanol/pH 5 buffer mixture.

low herbicide concentrations the fluorescence intensity maximum was reached more quickly. For this reason, we chose an optimal irradiation time of 15 min for the RTPF detection of all chlorophenoxyacid herbicides, in order to achieve shorter analysis times with a minimum decrease in sensitivity. The tri- and bichlorinated phenoxyacid herbicides (2,4,5-T and 2,4-D) were photodegraded significantly more slowly than the monochlorinated derivatives (MCPP and MCPA), a behaviour which was also found for chlorophenols [14]. The derivatives of 2-propionic acid (MCPP and 2,4-DP) were more quickly photodegraded than the corresponding derivatives of acetic acid (MCPA and 2,4-D) and butyric acid (MCPB and 2,4-DB).

3.6. Analytical figures of merit

Linear log–log plots of the photochemically-induced fluorescence intensity of chlorophenoxyacid herbicides vs. initial concentration were established in the range 0.1–10 μg ml⁻¹ with good correlation coefficients (Table 2). As indicated by the slope values of the calibration plots, the sensitivity of the method was higher for the monochlorinated acetic acid derivatives than for the di- and trichlorinated derivatives.

The limits of detection (LODs) varied between 36 and 179 ng ml⁻¹, according to the compound. The lowest LOD value (36 ng ml⁻¹) was obtained for mecoprop. These RTPF LOD values were close to those determined by the polarization fluoroimmunoassay method [9], for which a specific reagent is needed.

The precision of RTPF measurements was satisfactory. For example, the relative standard deviation (RSD) found for a 2,4-D concentration of 1 μg ml⁻¹ was 1.3% (n = 5).

3.7. Application to river water

Water samples were collected from the Marne river, near Paris, at 1 month intervals, and were filtered through a Whatman filter paper. A pH value of 7.8 was measured for these samples. 5 ml portions of filtered river water samples were spiked with 0, 30, 60, 90, 120, and 150 μl meco-

Table 2
Analytical figures of merit for the RTPF determination of chlorophenoxyacid herbicides[a]

Herbicide	Concentration range (μg ml^{-1})	Regression equation[b]		r[c]	LOD[d] (ng ml^{-1})
		A	B		
2,4-D	0.2–2.5	1.56	0.74	0.997	103
2,4-DP	0.1–5.0	1.83	0.74	0.991	55
2,4-DB	0.3–10.0	1.50	0.80	0.992	179
2,4,5-T	0.3–10.0	1.50	0.65	0.992	119
MCPA	0.3–5.0	1.85	0.84	0.998	74
MCPP	0.1–5.0	2.13	0.85	0.999	36
MCPB	0.1–5.0	1.87	0.79	0.996	59

[a] In a 50/50 v/v MeOH/pH 5 buffer mixture
[b] $\log I_f = A + B \log C$; I_f = relative fluorescence intensity; C = analyte concentration (μg ml^{-1})
[c] r = correlation coefficient.
[d] LOD = limit of detection, defined as the concentration of analyte giving a signal-to-noise ratio of 3.

prop stock solution (166 μg ml^{-1} in ethanol), and a 5 ml methanol volume was added to each spiked solution. The final mecoprop concentrations were 0, 0.5, 1.0, 1.5, 2.0, and 2.5 μg ml^{-1} respectively. These samples were treated ultrasonically to remove dissolved air, and their fluorescence signal was measured after a 5 min irradiation time.

In order to evaluate the analytical usefulness of the RTPF method, recovery experiments of mecoprop were performed on the spiked Marne river samples, using the direct measurement procedure. Analytical results are shown in Table 3. It can be seen that satisfactory recoveries of mecoprop were obtained, with values ranging from 92 to 116%. In most cases, no interference was found in real samples, although one of the Marne river water samples showed the presence of residual mecoprop, or some other interfering compound, at the 100 ng ml^{-1} level. Therefore, our results demonstrate that RTPF does not suffer significantly from interferences due to the river matrix used.

In some "real" cases, the presence of other pesticides or different types of organic matter in the samples may interfere in the RTPF determination of chlorophenoxyacid herbicides. However, we feel that it is possible to improve considerably the selectivity of our method by selecting different UV irradiation times for other pesticides, or by applying to RTPF specific techniques such as

derivative spectra or partial least-squares (PLS) multivariate calibration [16,17]. Also, on-line liquid chromatography is adaptable to RTPF detection [13], and can be used for separation of the various chlorophenoxyacid herbicides, if more selectivity is required.

Table 3
Recovery of mecoprop in spiked Marne river samples by RTPF[a]

Sample[b]	Mecoprop (μg ml^{-1})		Recovery (%)
	Added	Found	
1	–	0.00	–
	0.50	0.47	94
	1.00	1.03	103
	1.50	1.56	104
	2.00	1.94	97
	2.50	2.56	102
2	–	0.00	–
	0.50	0.58	116
	1.00	0.92	92
	1.50	1.42	95
	2.00	2.06	103
	2.50	2.51	101

[a] The direct measurement procedure was used.
[b] The Marne river samples were collected at 1 month intervals. See text for details of the treatment of samples.

4. Conclusion

We can conclude that RTPF is a simple, precise, and rather sensitive method for the determination of the chlorophenoxyacid herbicide total content of samples. Therefore, RTPF may be used for preliminary, rapid screening of waste water or environmental samples and for pesticide control.

Acknowledgements

References

[1] S.A. Hoar, A. Blair, F.F. Holmes, C.D. Boysen, R.J. Robel, R. Hoover and J.F. Fraumeni, Jr., J. Am. Med. Assoc., 256 (1986) 1141.

[2] J. Hodgeson, J. Collins and W. Bashe, J. Chromatogr., 659 (1994) 395.

[3] V. Coquart and M.-C. Hennion, Sci. Total Environ., 132 (1993) 349.

[4] D.F. Rinder and J.R. Fleeker, Bull. Environ. Contam. Toxicol., 26 (1981) 375.

[5] D. Knopp, P. Nuhn and H.-J. Dobberkau, Arch. Toxicol., 58 (1985) 27.

[6] M. Franek, V. Kolar, M. Granatova and Z. Nevorankova, J. Agric. Food Chem., 42 (1994) 1369.

[7] J. Fleeker, J. Assoc. Off. Anal. Chem., 70 (1987) 874.

[8] J.C. Hall, R.J.A. Deschamps and K.K. Krieg, J. Agric. Food Chem., 37 (1989) 981.

[9] S.A. Eremin, in J.O. Nelson, A.E. Karu and R.B. Wong (Eds.), Emerging Technologies in Immunoanalysis of Agrochemicals, ACS Symposium Series 586, American Chemical Society, Washington, DC, 1995, Chapter 16, p. 223.

[10] D. Barcelo, J. Chromatogr., 643 (1993) 117.

[11] D. Knopp and S. Glass, Int. Arch. Occup. Environ. Health, 63 (1991) 329.

[12] A. Coly and J.-J. Aaron, Analyst, 119 (1994) 1205.

[13] J.-J. Aaron, in S.G. Schulman (Ed.), Molecular Luminescence Spectroscopy: Methods and Application, Vol. 3, Wiley, New York, 1993, p. 85.

[14] C.E. Werkhoven-Goewie, W.M. Boon, A.J.J. Pratt, R.W. Frei, U.A.Th. Brinkman and C.J. Little, Chromatographia, 16 (1982) 53.

[15] A. Coly and J.-J. Aaron, Talanta, 41 (1994) 1475.

[16] M.C. Mahedero, F. Salinas, M. Jimenez-Arrabal and J.-J. Aaron, Anal. Lett., 27 (1994) 1543.

[17] M. Sanchez-Peña, A. Muñoz de la Peña, F. Salinas, M.C. Mahedero and J.-J. Aaron, Analyst, 119 (1994) 1177.

Synthesis and analytical properties of a chelating resin functionalised with bis-(*N*,*N'*-salicylidene)1,3-propanediamine ligands

Kapil Dev, G.N. Rao*

Department of Chemistry, Indian Institute of Technology, Delhi, Hauz Khas, New Delhi-110 016, India

Abstract

A polystyrenedivinylbenzene-based macroreticular resin was functionalised with bis-(*N*,*N'*-salicylidene)1,3-propane-diamine ligands and its analytical properties have been investigated. The pH dependence of metal resin chelation has been determined for Cu(II), Ni(II), Co(II), Zn(II), Fe(II), Mn(II), Pb(II), Cd(II) and Cr(III). Trace amounts of these metal ions were quantitatively retained on the resin at neutral pH and easily recovered by elution with 1 N hydrochloric acid. The resin exhibits good chemical stability and fast equilibration with the metal ion making it useful for rapid concentration of trace amounts of metal ions on the resin columns.

Keywords: Chelating resin; Bis-(*N*,*N'*-salicylidene)1,3-propanediamine

1. Introduction

Chelating resins have found widespread applications in the enrichment of metals from a variety of matrices. A large number of chelating resins incorporating a variety of ligands (e.g. ethylenediamine tetraacetic acid [1,2], iminodiacetic acid [3,4]) have been prepared and their analytical properties investigated. Fritz and co-workers synthesised and applied resins containing sulphonic acid, amide and hexylthioglycolate groups [5–7]. Sughi et al. reported polystyrene resin containing phenylalanine groups [8]. In our earlier communi-

cations we have reported resins containing *N*,*N*-bis(2-hydroxyethyl)glycine and *N*-hydroxyethylethylene-diamine groups [9,10].

Polymeric Schiff's bases constitute an important class of chelating resins. A number of such resins have been propared and studied for their ion-selective properties. Bayer [11,12] was first to introduce such polymeric ligands and reported relative stabilities of complexes formed with different metal ions. Bottino et al. [13] reported preferential complexation of nickel(II) over other metal ions with a polymeric Schiff's base chelating resin. A renewed interest developed for such chelating polymers with N,O-donor atoms, as they have been found to possess very good selectivity for

* Corresponding author. Fax: (91) 11-686-2037.

transition metals and show negligible affinity for alkali and alkaline earth metals. Most of these chelating resins have been prepared by polycondensation reactions. Though they possess high selectivity and capacity, their mechanical and chemical stability is not good [14].

In the present investigation we have prepared a Schiff's base of salicylaldehyde and 1,3-propanediamine (Bis-(N,N'-salicylidene)1,3-propanediamine) and incorporated it on a macroreticular polystyrene divinyl benzene-based resin (XAD-4). Polystyrene divinyl benzene support is expected to give additional stability while retaining the analytical properties of the Schiff's base ligand. The resin has been characterised, and the sorption behaviour of different metal ions on the resin has been studied.

2. Experimental

2.1. Instrumentation

An ECIL India 4139 flame atomic absorption spectrometer was used for monitoring the concentration of the metals. An Elico (India) digital pH meter LI-120 was used for pH measurements. Infrared spectra were recorded on a Nicolet DX FTIR spectrophotometer with KBr pellets. A Perkin 240C elemental analyser was used for elemental analysis. A mechanical shaker (Scientific Instruments, India) with an incubator, which had a speed of 200 strokes min^{-1}, was used for batch equilibration.

2.2. Reagents

The stock metal ion solutions were prepared by dissolving the reagent grade nitrate and chloride salts of the metal in water or the matrix acid and they were standardised by appropriate methods. XAD-4 was obtained from Fluka. Salicylaldehyde and 1,3-propanediamine were obtained from E. Merck and were used after distillation. The following buffer solutions were used to control the pH of the metal ion solution: hydrochloric acid–glycine (pH 1–3); acetic acid–sodium acetate (pH 3–5); disodium hydrogen phosphate–potassium

dihydrogen phosphate (pH 5–8); and sodium borate–hydrechloric acid (pH 8–9).

2.3. Preparation of bis-(N,N'-salicylidene)1,3-propanediamine (Salpen) [15]

1,3-Propanediamine (1.7 ml) in 50 ml of freshly distilled ethanol was taken in a round-bottomed flask and salicylaldehyde (3.81 ml) in 30 ml of freshly distilled ethanol was added dropwise with vigorous stirring. The mixture was cooled in an ice bath and the product was filtered and recrystallised from chloroform. On analysis of Salpen, the following elemental compositions (%) were found: C, 72.22; H, 6.24; N, 9.79. The calculated values are C, 72.34; H, 6.38; N, 9.92.

2.4. Preparation of XAD₄–Salpen resin

XAD-4 was functionalised via esterification. XAD-4 beads (10g) were refluxed with acetic anhydride (20 ml) and anhydrous aluminium trichloride (1 g) in petroleum ether (60–80°C) at 70°C for 30 h. The product was filtered off and washed with 50 ml hexane. The intermediate product (II, Scheme 1) was then stirred in 500 ml water containing 8.5 g potassium permanganate and 10 g sodium hydroxide at 40°C for 1 h. The product was filtered off, washed with water and then treated with hydrochloric acid (1:1). It was then refluxed with 50 ml thionyl chloride at 60°C for 30 min. The intermediate resin(IV) was refluxed with Salpen (2.5 g) and sodium ethoxide (11.3 mM) in DMF at 90°C for 8 h. A light yellow resin
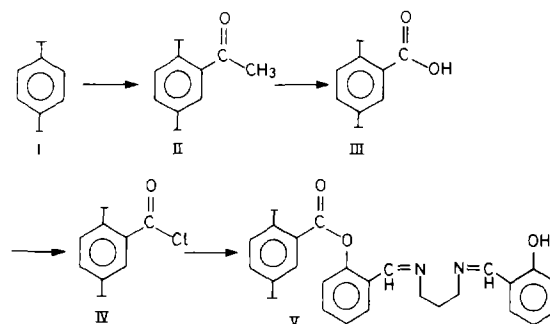
Scheme 1. Synthesis of the resin.

was obtained. A total of 20 g resin was perpared and 200–250 mesh fraction of the resin was used for metal sorption studies.

2.5. pH dependence of metal ion uptake

The optimum pH of metal ion uptake was determined by batch equilibration technique. Excess metal ion (50 ml, 50 μg ml^{-1}) was shaken with 100 mg of resin for two hours. The pH of the metal ion solution was adjusted prior to equilibration over a pH range of 2–9 with buffer solutions. For determining the effect of pH on the trace metal ion uptake, a buffered solution (50 ml) containing 5μg ml^{-1} of metal ion was equilibrated with 100 mg of resin. The concentration of the adsorbed metal ion was determined after eluting with 1 N hydrochloric acid by atomic absorption spectrometry (AAS). Sorption experiments were carried out in duplicate each time.

2.6. Resin capacity

The capacity of the resin was determined by shaking the excess metal ion (50 ml, 100 μg ml^{-1}) with 100 mg resin (50 mg for cadmium and lead) for 6 h at the optimum adsorption pH. The resin was filtered off, and the concentration of the remaining metal ion in the solution was determined by AAS. The capacity was also checked after soaking the resin in 1 N HCl/1 N alkali for one day.

2.7. Equilibration time

To determine the time of equilibrium for the metal under investigation, the metal ion solution (50 ml, 10 μg ml^{-1}), at a constant pH, was sampled in six bottles. The first bottle was removed from the shaker after 5 min and the remaining bottles at intervals of 15 min. The last bottle was removed after 2 h. The concentration of the metal ion was determined by AAS. The time of equilibration for all the metal ions was determined in a similar manner. The duplicate values agreed with a precision of ± 2%.

2.8. Effect of diverse ions

Standard solutions of 50 ml of Cu, Ni, Co, Zn and Pb (1–5 μg ml^{-1} each) containing sodium chloride, Mg and Ca ions as interferents were analysed.

2.9. Enrichment of metal ions

Both batch as well as column methods were used to concentrate the trace metal ions. For batch equilibration, the sample solution (250–500 ml) containing (0.1 μg ml^{-1}) metal ion was adjusted at optimum pH of adsorption with buffer solution and then shaken with 100 mg of resin for about 15 min. Sorbed metal ions were eluted with 1 N hydrochloric acid (10 ml) and the concentration of the metal ion in the eluent was determined with AAS.

For the column method, the dry resin (0.5 g) was packed into a glass column (0.5 × 6 cm) and conditioned with the buffer solution. The metal ion solution (0.05 to 0.1 μg ml^{-1}) was passed through the column at a flow rate of 2.0 ml min^{-1}. The adsorbed metal ion was desorbed from the resin with 1 N hydrochloric acid (5 ml).

3. Results and discussion

The resin was synthesised according to Scheme 1. Spherical macroreticular styrenedivinyl benzene beads were used as starting material.

The coordination of the Salpen ligand to the polymer by the displacement of the –Cl is indicated by the absence of the ν_{C-Cl} band at 670 cm^{-1} in the spectrum of the final resin V (Scheme 1, Fig. 1). Another feature in the spectrum of resin IV is the absorption band at 1740–1765 cm^{-1}, probably resulting from Fermi resonance between the carbonyl band and the overtone of a longer wavelength band near 875 cm^{-1} [16]. This band appears in the spectrum of intermediate resin IV and disappears in final resin V. The presence of the all major absorption bands corresponding to the Salpen ligand in the final resin V with reduced intensities, confirms the incorporation of the ligand.
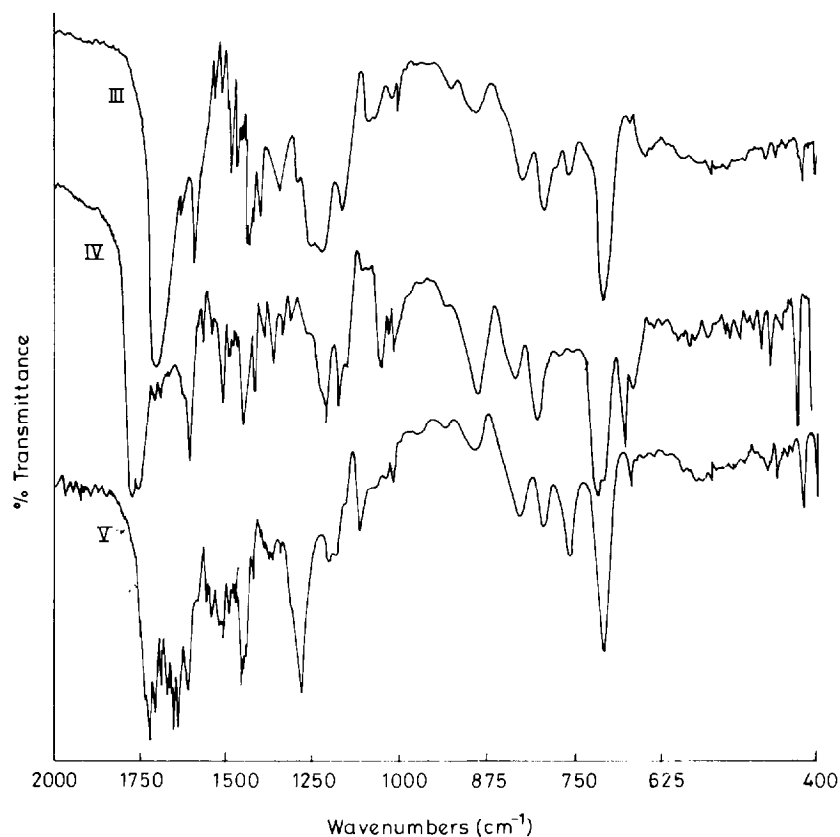
Fig. 1. Infrared spectra of resins (KBr disks): (III) carboxylated resin; (IV) acid chloride resin; (V) Salpen resin.

Salpen acts as a tetradentate ligand, coordinating with the metal ion through hydroxyl group oxygens and tertiary nitrogens [17]. However in polymer-bound Salpen, one of the hydroxyl group oxygens is used for binding to the polymer, leaving one free hydroxyl group and two tertiary nitrogens as binding sites for the metal ions.

Nitrogen analysis of the resin gave 1.72% nitrogen. Assuming that all the nitrogen is part of the intact Salpen groups, the capacity for the metal ion should be 0.61 mmol g^{-1} of resin. The values actually obtained are reported in Table 1. The lower values could be due to the rigidity of the polymeric matrix and the inability of all the Salpen groups to participate in chelation, due to steric restriction.

The resin was found to be fairly stable on successive treatment with dilute acid and alkaline solutions. The stability was checked by the change

of the hydrogen metal exchange capacity and the nitrogen content.

In a preliminary experiment, the sorption behaviour of some metal ions on XAD$_4$–Salpen resin at different pH values has been examined by

Table 1
Metal uptake capacities

Metal	Optimum pH	Capacity (± SD) (mmol g^{-1} resin)
Cu(II)	8.52	0.46(0.01)
Ni(II)	8.10	0.42(0.01)
Co(II)	8.03	0.43(0.01)
Zn(II)	8.05	0.38(0.02)
Cd(II)	6.59	0.40(0.02)
Pb(II)	6.04	0.39(0.01)
Fe(II)	5.05	0.24(0.02)
Mn(II)	8.01	0.36(0.02)

SD, Standard deviation
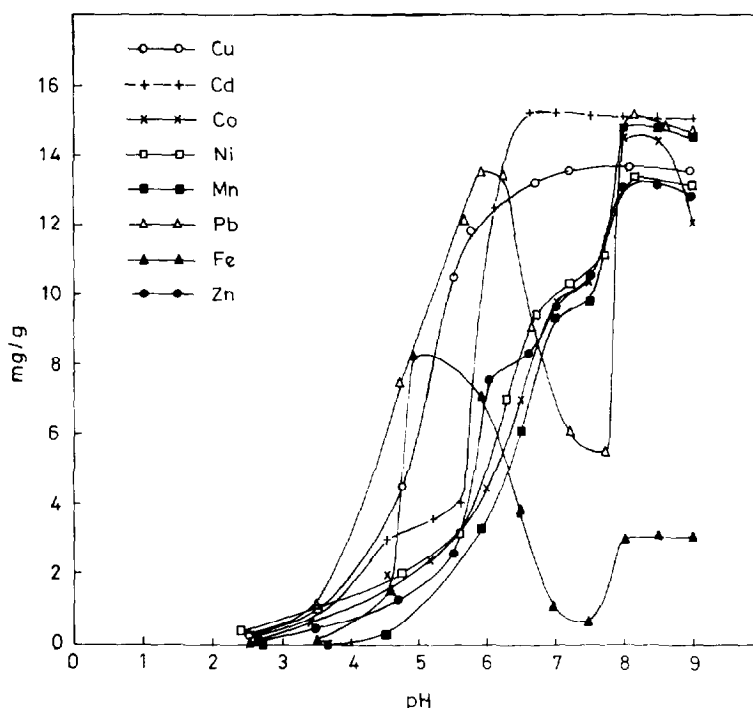
Fig. 2. Effect of pH on metal sorption with Salpen resin.

the batch method and the results are shown in Fig. 2. In most of the cases the sorption increases with increasing pH, reaching a limiting value in each instance, followed by a decrease in sorption, beyond the limiting value. Sorption of copper and cadmium reaches the limiting value at around neutral pH while for manganese, zinc, cobalt and nickel the maximum sorption is beyond pH 7.5. The XAD_4–Salpen resin shows relatively low affinity towards iron(II) and it does not interact with Cr(III) at any pH.

The capacity of the resin is an important factor to determine and is the quantity of resin required to remove quantitatively a specific metal ion from the solution. The capacity of each metal ion is reported in Table 1.

The sorption behaviour of the trace amount of metal ion on the resin is shown in Fig. 3. The sorption is quantitative for the trace metal ions in the region of pH 6.5–9 for Cu(II); 7.5–9 for Ni(II); 7–8.5 for Co(II); 7–9 for Zn; 7–9 for Mn(II); 5.5–6.5 and 8–9 for Pb(II); and 6–9 for Cd(II). Sorption of Fe(II) is 92% in the pH range

5–6. The time of equilibration was determined for all the metal ions at the optimum pH of sorption and the results are plotted in Fig. 4.

The kinetics of the resin–metal interaction is sufficiently rapid for most of the metal ions. Sorption reaches a 80–90% extraction level within 5–7 min of the interaction of the metal ions with the resin. This allows the resin to be used in a packed column as it requires fast equilibration because of the short contact time between the resin and the solution.

Manifold amounts of NaCl, Ca and Mg do not effect the recovery of the metal ions from the solution. The results in Table 2 show the recovery rates in the presence of excess of these foreign ions. This makes the resin useful for trace concentration of metal ions from natural samples which contain large concentrations of alkali and alkaline earth metals

The resin shows good stability towards dilute acids and bases and its metal uptake capacity was not affected after regenerating it several times.
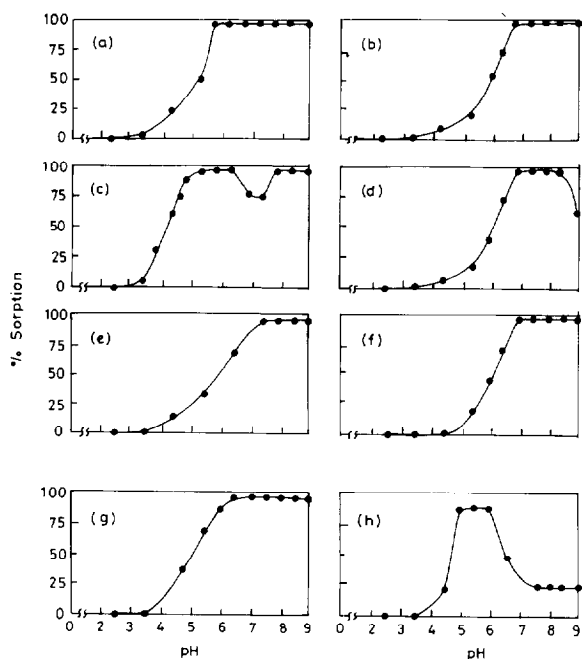
Fig. 3. pH dependence of the uptake of trace metals: (a) Cd(II); (b) Zn(II); (c) Pb(II); (d) Co(II); (e) Ni(II); (f) Mn(II); (g) Cu(II); (h) Fe(II).

Preconcentration of all metal ions on the resin-was carried out by batch and column methods, and the results are shown in Tables 3 and 4. Metal ions could be enriched up to 40–50 times with XAD_4-Salpen resin. The column method was
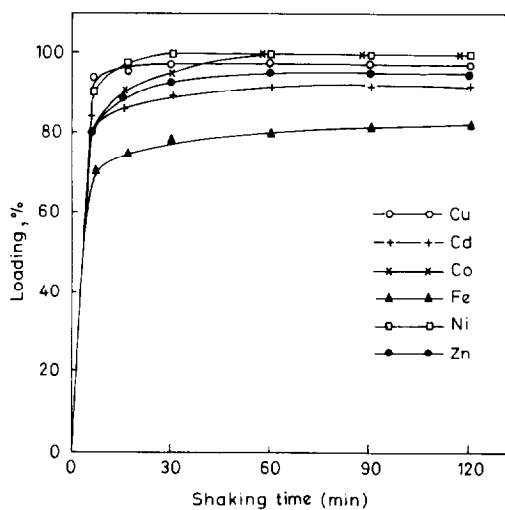
Fig. 4. Rate of uptake of metal ions.

found to be better for enrichment of the metal ions as the sorption is more complete and subsequent elution is easier. But the column method is more time consuming than the batch method for XAD_4-Salpen resin.

Table 2
Effect of diverse ions

Interfering ions[a]	Recovery (%)				
	Cu(II)	Ni(II)	Co(II)	Zn(II)	Pb(II)
Ca	99.3	99.4	100.2	98.9	100.9
Mg	99.7	99.2	99.8	98.7	99.1

[a] Concentration $= 50~\mu g~ml^{-1}$.

Table 3
Preconcentration of metal ions (amount of metal ion taken, $0.1~\mu m~ml^{-1}$) by the batch method

Metal ion	Sample volume (ml)	Metal found[a] ($\mu g~ml^{-1}$)
Cu(II)	250	2.43
Cu(II)	500	4.88
Ni(II)	250	2.47
Ni(II)	500	4.99
Co(II)	250	2.44
Co(II)	500	5.02
Zn(II)	250	2.52
Zn(II)	500	5.01
Pb(II)	250	2.49
Pb(II)	500	4.92

[a] Values agree with a precision of $\pm 1\%$.

Table 4
Preconcentration of metal ions by the column method

Metal ion	Amount of metal ion ($\mu g~ml^{-1}$)	Sample volume (ml)	Metal found[a] ($\mu g~ml^{-1}$)
Cu(II)	0.05	250	2.45
Cu(II)	0.10	250	4.98
Ni(II)	0.05	250	2.48
Co(II)	0.05	250	2.42
Zn(II)	0.05	250	2.41
Pb(II)	0.05	250	2.51

[a] Values agree with a precision of $\pm 1\%$.

4. Conclusions

XAD$_4$-Salpen resin has been found useful for the concentration of trace metals from aqueous solutions. Fast equilibration of the metal on the resin makes it applicable for the conventional column method also. The capacity of the resin is also high enough for use in the simultaneous concentration and determination of several metals. Low affinity of the resin towards alkali and alkaline earth metals indicates its use for natural samples.

Acknowledgement

References

[1] E.M. Moyers and J.S. Fritz, Anal. Chem., 49 (1977) 418.

[2] M. Marhol and K.L. Cheng, Talanta, 21 (1974) 751.

[3] S. Tomoshige, M. Hirai and H. Ueshima, Anal. Chim. Acta, 115 (1980) 285.

[4] P. Figura and B. McDuffie, Anal. Chem., 49 (1977) 1950.

[5] M.D. Arguello and J.S. Fritz, Anal. Chem., 49 (1977) 1595.

[6] G.M. Orf and J.S. Fritz, Anal. Chem., 50 (1978) 1328.

[7] E.M. Moyers and J.S. Fritz, Anal. Chem., 48 (1976) 1117.

[8] A. Sughi, N. Ogawa, I. Katayama and T. Hida, Talanta, 29 (1982) 263.

[9] Kapil Dev and G.N. Rao, Talanta, 42 (1995) 591.

[10] Kapil Dev and G.N. Rao, Analyst, 120 (1995) 2509.

[11] E. Bayer, Angew. Chem., 69 (1957) 107.

[12] E. Bayer, Chem. Ber., 90 (1957) 2325.

[13] F.A. Bottino, P. Finocchiaro, E. Lebertini, A. Mamo and A. Recca, Polym. Commun., 24 (1983) 63.

[14] D. Wochrie, Adv. Polym. Sci., 50 (1983) 45.

[15] J.R. Dilworth, C.A. McAuliffe and B.J. Sayle, J. Chem. Soc., Dalton Trans., (1977) 849.

[16] R.M. Silverstein, G.C. Bassler and T.C. Morrill, Spectrometric Identification of Organic Compounds, 5th ed., John Wiley, New York, 1991, p. 120.

[17] W. Sawondy, M. Riederer and E. Urban, Inorg, Chim. Acta, 29 (1978) 63.

Development of a monitoring system for vinyl chloride gas in air by using an HCl monitoring tape and pyrolyzer

Nobuo Nakano[a],*, Akihiro Yamamoto[a], Kuino Nagashima[b]

[a]*Riken Keiki Co., Ltd., 2-7-6, Azusawa, Itabashi-ku, Tokyo 174, Japan*
[b]*Faculty of Engineering, Kogakuin University, 1-24-2, Nishishinjuku, Shinjuku-ku, Tokyo 160, Japan*

Abstract

A continuous monitoring system for vinyl chloride gas in air has been developed using an HCl monitoring tape and pyrolyzer consisting of a heater around a quartz tube. It is based on the color change of the tape by reaction with HCl gas produced by decomposition of vinyl chloride gas in the heated quartz tube. The conversion efficiency of vinyl chloride into HCl depends on the temperature of the pyrolyzer. The tape impregnated with a coloring solution that includes Metanil Yellow (pH indicator; pH 1.2–2.3, red–yellow), glycerin and methanol is a highly sensitive means of detecting HCl gas. When vinyl chloride gas was passed through the heated quartz tube (910°C) and the HCl gas produced was passed through the tape, the color of the tape changed from yellow to red. The degree of color change was proportional to the concentration of vinyl chloride gas with a constant sampling time and flow rate. The degree of color change could be recorded by measuring the intensity of reflecting light (555 nm). This method is scarcely affected by other gases with the exception of chlorinated hydrocarbons such as trichloroethylene and chloroform or strong acids such as HCl gas. Reproducibility tests showed that the relative standard deviation of the relative intensity ($n = 10$) was 4.5 for 5 ppm vinyl chloride. The detection limit was 0.4 ppm for vinyl chloride with a sampling time of 40 s and a flow rate of 300 ml min^{-1}.

Keywords: Vinyl chloride; HCl monitoring tape; Pyrolyzer

1. Introduction

Exposure to vinyl chloride gas in the workplace often occurs because of leakage or discharge during its storage, transportation or production. Vinyl Chloride (1000 ppm) is a colorless gas, with a distinctive chloroform-like smell and causes narcotic symptoms. Its threshold limit value (TLV) has been defined as 5 ppm by the American Conference of Governmental Industrial Hygienists [1].

The monitoring of vinyl chloride gas efficiently and reliably at levels below 5 ppm is needed. To achieve widespread routine use, the method

---
* Corresponding author.

should be simple, capable of unattended operation and inexpensive. However, while various methods have been developed [2–4] for the determination of vinyl chloride gas in air, few, if any, exhibit all these desirable characteristics. Although several methods have been used for the detection of vinyl chloride gas, including gas chromatography, absorptiometry and use of a gas detection tube, they are batchwise procedures and unsuitable for a continuous method. The chlorinated hydrocarbon can be determined by measuring HCl gas produced by its decomposition through a pyrolyzer [5,6]. We have already developed a continuous monitoring system for 1,1-dichloro-2,2,2-trifluoroethane in air by using a pyrolyzer consisting of a heater around a quartz tube and an electrochemical HCl sensor [7]. At first, we investigated this system for vinyl chloride gas, but it could not detect low concentrations (5 ppm). Furthermore, the lifetime of the electrochemical HCl sensor is short owing to the degradation of the catalyst and contamination of the electrolyte solution.

In this experiment, we tried to produce a new monitoring system using a pyrolyzer and the sensitive tape for HCl gas that had already been developed, instead of an electrochemical HCl gas sensor. Because the tape monitor [8–10] is highly sensitive and selective, easy to maintain and of low running cost it was thought to be suitable for our purpose. The sampling spot of the tape is renewed for every measurement. Thus the base level and sensitivity are constant for all measurements.

As no suitable reagents react with vinyl chloride gas to produce a color stain, we have developed a continuous monitoring system for vinyl chloride gas in air using a pyrolyzer consisting of a heater wound around a quartz tube and an HCl monitoring tape [9]. It is based on the color change of the tape by reaction with HCl gas produced by decomposition of vinyl chloride gas in passing through the heated quartz tube. We had investigated the tape using pH indicator (Metanil Yellow), with a color change from yellow to red for HCl, because of the high response. This method has the desirable attributes of high sensitivity, wide range of concentration, simplicity, portabil-

ity, and ease of adaptation to automatic, unattended operation. In this paper, we describe a study of the development of a continuous monitoring system for vinyl chloride gas in the range 0.4–10 ppm. The conversion efficiency of vinyl chloride gas to HCl gas at various heater temperatures, gas flow rates and sampling times and the reproducibility of response were investigated to evaluate the characteristics of the system for the determination of vinyl chloride gas.

2. Experimental

2.1. Gas samples

The standard vinyl chloride gas mixtures were prepared by controlling the flow rates of streams of primary standard 21 ppm vinyl chloride (N_2 balance; Nippon Sanso) and air from a cylinder (99.9%; Taiyo Sanso). Various standard chlorinated hydrocarbon gas mixtures were generated continuously by purging the diffusion tube containing various chlorinated hydocarbons (analytical reagent grade; Tokyo Kasei Kogyo) with a constant flow of purified air. The gas concentration was calculated from the flow rate and the mass loss of the chlorinated hydocarbons. The diffusion tube in a gas generating system (PD-1B; Gastec) was kept at $30 \pm 0.1°C$ in a thermostatically controlled water bath.

2.2. Pyrolyzer

The pyrolyzer consists of a quartz tube (4 mm i.d, 6 mm o.d. and 180 mm length), in which a cylindrical mass (4 mm diameter and 5 mm length) of gold wire (50 μm diameter and 10 m length) is packed at the center. Heater wire of 900 mm length ($\approx 13\Omega$) is wound around the quartz tube of 34 mm length. The distance between the windings is 0.5 mm.

When the applied voltage is 13.0 V the temperature in the quartz tube, which is measured by a Pt–Rh thermometer, is 910°C. The construction of the pyrolyzer is shown in Fig. 1.
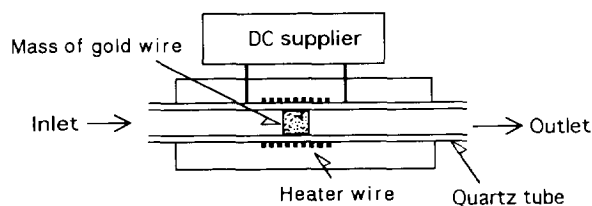
Fig. 1. Cross-section of pyrolyzer.

2.3. Monitoring tape

The processing solution used had the same composition as that used previously [9]. The monitoring tape for HCl gas was prepared as follows: the porous cellulose tape (Whatman 1Chr papers, 20 mm wide, 0.18 mm thick, 25 m long) was immersed in the processing solution for 1 min, oven-dried at 40°C and stored in a desiccator.

2.4. Apparatus

Samples were introduced to the pyrolyzer and then to the monitoring tape for HCl gas with an air-pump as shown in Fig. 2. The tape monitor was connected to the pyrolyzer with Teflon tubing (4 mm i.d and 6 mm o.d.).

The end (approximately 2 cm in diameter) of the tube from the pump was attached tightly to the tape. The sample gas was sucked at a constant flow rate (300 ml min^{-1}) for a constant sampling time (40 s). The Metanil Yellow on the tape reacted with HCl produced by decomposition of vinyl chloride gas passing through the pyrolyzer to give a change in its homogeneous color. The
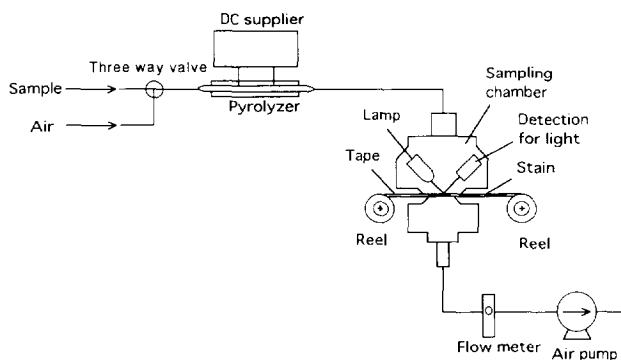
Fig. 2. Schematic diagram of monitoring system.

Table 1
Effect of weight of Au wire on response (Concentration of vinyl chloride. 5 ppm; sampling time, 40 s)

Weight (g)	Response
0.2	0.011
0.3	0.076
0.4	0.108
0.5	0.105

degree of color change was recorded by measuring the relative reflectance at 555 nm. The tape exposed was renewed by moving it 10 mm every 40 s. The response is defined by $A = -\log V_1/V_0$, where V_0 and V_1 are the outputs of a blank (atmospheric air) and the sample respectively. A period of 30 min was required to measure the responses after the tape was set in the apparatus. All measurements were carried out at 25 ± 2°C.

3. Results and discussion

3.1. Effect of mass of gold wire

To imporve the sensitivity for vinyl chloride gas, the effect of a cylindrical mass of gold wire packed at the center of the quartz tube was examined (Table 1). The response increased with increase in weight of the cylindrical mass ($\approx$ 4 mm diameter and 5 mm length) of gold wire and became nearly constant in the region 0.4–0.5 g. The optimum weight of the mass was found to be 0.4 g.

3.2. Effect of temperature of pyrolyzer on response

It was found that the system responded to vinyl chloride gas when the temperature of the pyrolyzer was greater than 600°C. Table 2 shows the effect of the temperature of the pyrolyzer on the response and conversion efficiency of vinyl chloride gas to HCl gas. The conversion efficiency is defined by (response of 5 ppm of vinyl chloride)/(response of 5 ppm HCl) × 100. As the temperature of the pyrolyzer increased, the concentration

Table 2
Effect of temperature of pyrolyzer on response and conversion efficiency (Concentration of vinyl chloride, 5 ppm; sampling time, 40 s)

Temperature (°C)	Response	Conversion efficiency (%)
670	0.051	3.7
720	0.073	5.2
770	0.086	6.1
820	0.099	6.8
870	0.106	7.2
910	0.113	7.7
970	0.116	7.9

of HCl (the detectable product) increased, but the response for vinyl chloride gas increased and became nearly constant above 910°C. Thus 910°C was chosen as the optimum temperature of the pyrolyzer.

3.3. Gas flow rate

Table 3 shows the effect of sample gas flow rate on the response. The response did not change very much in the region 200–400 ml min⁻¹. Thus 300 ml min⁻¹ was chosen as the optimum sample gas flow rate.

3.4. Calibration graph

Typical calibration graphs for vinyl chloride gas using the optimum experimental conditions are shown in Fig. 3. The detection limit (signal-to-noise ratio = 3) was 0.4 ppm for vinyl chloride gas with a sampling time of 40 s. Reproducibility tests ($n = 10$) showed that the relative standard deviation was 4.5% for 5 ppm vinyl chloride.

Table 3
Effect of sample gas flow rate on response (Concentration of vinyl chloride, 5 ppm; sampling time, 40 s)

Gas flow rate (ml min⁻¹)	Response
100	0.057
200	0.106
300	0.113
350	0.106
400	0.088
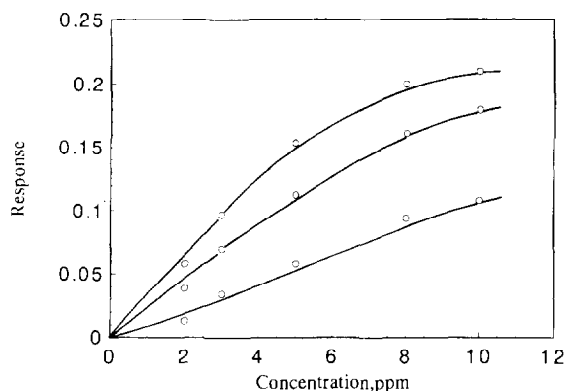
Fig. 3. Calibration graphs for vinyl chloride gas. Sampling time: (a) 60 s; (b) 40 s; (c) 20 s.

3.5. Selectivity

The responses of the monitoring system to various gases are given in Table 4. The responses for acetone, toluene, nitrogen dioxide, sulfur dioxide, carbon dioxide, hydrogen, acetic acid, hydrogen sulfide and hydrogen fluoride were less than 0.005. Hydrogen chloride and chlorinated hydrocarbons such as trichloroethylene and chloroform gave a high response. Consequently, this monitoring system for vinyl chloride gas in air is applicable to the working air in the manufacture of vinyl chloride polymer.

Table 4
Response for various gases

Gas examined	Concentration of gas (v/v)	Response
Acetone	5%	<0.005
Toluene	1%	<0.005
Nitrogen dioxide	105 ppm	<0.005
Sulfur dioxide	15.2	<0.005
Carbon dioxide	4.9%	<0.005
Hydrogen	5%	<0.005
Acetic acid	24 ppm	<0.005
Hydrogen sulfide	32 ppm	<0.005
Hydrogen fluoride	6.0 ppm	<0.005
Hydrogen chloride	1 ppm	0.081
Trichloroethylene	3 ppm	0.092
Chloroform	1 ppm	0.080
Vinyl chloride	5 ppm	0.113

Table 5
Long-term stability of the tape and pyrolyzer (Concentration of vinyl chloride, 5 ppm; sampling time, 40 s)

Day	Response
0	0.113
5	0.108
10	0.102
15	0.097

3.6. Long-term stability

The stability for long-term operation is a very important characteristic for monitoring systems. The responses for 5 ppm vinyl chloride were recorded every few days (Table 5). The result demonstrates that this monitoring system gives a reliable quantitative response to vinyl chloride even after two weeks under normal conditions. It is considered that the response factor decrease depends on the deterioration of the pH indicator and/or the change in concentration of reagents on the tape.

In conclusion, the continuous monitoring system using an HCl monitoring tape and a pyrolyzer consisting of a heater around a quartz tube is very suitable for the determination of vinyl chloride gas concentrations in the range 0.1–15 ppm. The method is simple, specific, capable of unattended operation and recommended for both laboratory and field operation.

References

[1] ACGIH, Threshold Limit Values for Chemical Substances and Biological Exposure Indices for 1993–94, American Conference of Governmental Industrial Hygienists, Cincinnati, OH, 1993.

[2] L.A. Gonzalez and M.V. Sefton, Am. Ind. Hyg. Assoc. J., 46 (1995) 591.

[3] F. Poy, L. Cobelli, S. Banfi and F. Fossati, J. Chromatogr., 395 (1987) 281.

[4] J. Wittsiepe, F. Selenka and E. Jackwerth, Fresenius' J. Anal. Chem., 336 (1990) 322.

[5] J. Unwin and P.T. Walsh, Sens. Actuat., 17 (1989) 45.

[6] J. Unwin and P.T. Walsh, Sens. Actuat., 18 (1989) 575.

[7] H. Matsuda, N. Nakano and K. Nagashima, Bunseki Kagaku, 43 (1994) 545.

[8] N. Nakano, A. Yamamoto, Y. Kobayashi and K. Nagashima, Bunseki Kagaku, 42 (1993) 537.

[9] N. Nakano, A. Yamamoto, Y. Kobayashi and K. Nagashima, Analyst, 118 (1993) 1539.

[10] N. Nakano, A. Yamamoto, Y. Kobayashi and K. Nagashima, Analyst, 119 (1994) 2009.

Determination of ruthenium and osmium in each other's presence in chloride solutions by direct and third-order derivative spectrophotometry

Maria Balcerzak*, Elżbieta Święcicka

Department of Analytical Chemistry, Warsaw University of Technology, ul. Noakowskiego 3, 00-664 Warsaw, Poland

Abstract

Ruthenium and osmium (up to 20 μg Ru(Os) ml^{-1}) can be determined in chloride solutions directly after absorption of RuO_4 and OsO_4 in hydrochloric acid. In 9 M HCl, RuO_4 and OsO_4 are quantitatively converted into $RuCl_6^{2-}$ ($\lambda_{max} = 480.0$ nm, $\epsilon = 4.8 \times 10^3$ l mol^{-1} cm^{-1}) and $OsCl_6^{2-}$ ($\lambda_{max} = 334.8$ nm, $\epsilon = 8.4 \times 10^3$ l mol^{-1} cm^{-1}) respectively. Osmium does not interfere with the determination of ruthenium in the form of the $RuCl_6^{2-}$ complex by direct spectrophotometry. The absorbance of the obtained solution at $\lambda_{max} = 480.0$ nm corresponds only to the concentration of ruthenium. A derivative spectrophotometric method using numerical calculation of absorption spectra of the $RuCl_6^{2-}$ and $OsCl_6^{2-}$ complexes has been developed for the determination of osmium in a mixture with ruthenium. The interfering effect of ruthenium on the determination of osmium can be eliminated by measuring the value of a third-order derivative spectrum of the $OsCl_6^{2-}$ complex at 350.0 nm ("zero-crossing point" of ruthenium). Simple and rapid determination of ruthenium and osmium in a calibration standard solution of the noble metals (Ru, Rh, Pd, Os, Ir, Pt and Au) for plasma spectroscopy using the proposed methods has been achieved.

Keywords: Noble metal analysis; Ruthenium; Osmium; Derivative spectrophotometry

1. Introduction

Interest in the development of analytical techniques for determination of the noble metals is still growing as a result of rapid growth of their applications, e.g. in chemical engineering, microelectronics and medicine. Because of the great chemical similarity of the noble metals, small concentrations of the metals which are encountered in many types of samples and heterogeneity of the examined materials, chemical pretreatment of the samples and separation of the metals prior to their determination is necessary.

Selective isolation of ruthenium and osmium by distillation in the form of volatile RuO_4 and OsO_4

* Corresponding author.

is generally a preliminary step for analysis of multicomponent samples of the noble metals [1,2]. Ruthenium and osmium are converted into Ru(VIII) and Os(VIII) respectively in the presence of strong oxidizing agents (e.g. $HClO_4 + H_2SO_4$, $KMnO_4$) and escape from the samples as RuO_4 and OsO_4. Simultaneous determination of ruthenium and osmium directly in solutions obtained after absorption of both the tetroxides is still a challenge for analytical chemists. The very close chemical similarity of the complexes formed by ruthenium and osmium in various media [3,4] mostly necessitates separation of the elements from each other prior to their determination. Osmium can be selectively oxidized to OsO_4 and quantitatively separated from ruthenium in the presence of weak oxidation agents, e.g. dilute HNO_3 or H_2O_2 [1,2,4].

Simultaneous determination of ruthenium and osmium in chloride solutions obtained by absorption of RuO_4 and OsO_4 in hydrochloric acid is the aim of this work. Hydrochloric acid is the most frequently used absorption medium for volatile RuO_4 because the latter is easily reduced to lower oxidation states in this medium [4,5]. The $RuCl_6^{2-}$ complex ($\lambda_{max} = 485$ nm, $\epsilon = 4.8 \times 10^3$ l mol^{-1} cm^{-1}), the most stable reduction product of RuO_4 in 6–10 M HCl at room temperature, was obtained earlier [5]. Reduction of OsO_4 in hydrochloric acid requires more drastic conditions. For quantitative conversion of OsO_4 into the stable $OsCl_6^{2-}$ complex it was necessary to use 8–10 M HCl and 20 min heating at 100°C [6].

In this work detailed studies on simultaneous reduction of Ru(VIII) and Os(VIII) to Ru(IV) and Os(IV) in hydrochloric acid and their quantitative conversion into the $RuCl_6^{2-}$ and $OsCl_6^{2-}$ complexes have been carried out. The experiments have shown that osmium does not interfere with the determination of ruthenium in solutions obtained by absorption of RuO_4 and OsO_4 in hydrochloric acid using direct spectrophotometry, while ruthenium seriously interferes with the determination of osmium.

Attempts to eliminate the band-overlap interference of ruthenium on the determination of osmium using derivative spectrophotometry are described in the paper. Derivative spectrophoto-

metry [7–12] makes it possible to resolve the absorption band of a particular compound by analogue differentiation and mathematical processing of overlapping UV and visible absorption spectra. Very closely positioned absorption maxima that cannot be separated by conventional spectrophotometry appear as separated bands in the derivative spectra. These spectra can be recorded with the aid of new generation commercial spectrophotometers capable of operating in the derivative mode or by numerical calculation of zero-order absorption spectra. The absorbance value, the shape of the zero-order spectrum and the method of computing affect the quality of the obtained signals. Suitable selection of the wavelength range and the derivative order allow one to eliminate interfering signals. Second-order derivative spectrophotometry was used earlier [13] for determination of ruthenium (in the presence of osmium) and osmium (in the presence of ruthenium) after conversion of their chloride complexes into complexes with tin(II) chloride.

In this work rapid methods of simultaneous determination of ruthenium and osmium in chloride solutions, based on direct and third-order derivative spectrophotometry using numerical calculation of spectra of the $RuCl_6^{2-}$ and $OsCl_6^{2-}$ complexes, have been developed.

2. Experimental

2.1. Apparatus and reagents

The absorption spectra were recorded with a Hitachi U-3300 spectrophotometer (Japan) with 1 cm cells. Derivative spectra were obtained by numerical calculation with the aid of the GRAMS/386 program of Galactic Industries Corporation using the Savitzky–Golay algorithm.

Ruthenium standard solution (1 mg Ru ml^{-1}) was prepared according to an earlier procedure [5].

Osmium standard solution (1 mg Os ml^{-1}) was prepared by dissolving 0.2529 g of potassium hexachloroosmate (IV) (K_2OsCl_6) in 100 ml of 4 M HCl.

2.2. Procedures

2.2.1. Distillation of ruthenium and osmium

Place the test solution containing ruthenium and osmium in a distillation flask. Add 2 ml of concentrated $HClO_4$ and 6 ml of concentrated H_2SO_4. Attach the flask to a distillation apparatus equipped with two receivers in series. Place 10 ml and 5 ml of 9 M HCl in the first and second receivers respectively. Pass nitrogen continuously (2–3 bubbles per second) through the distillation apparatus and heat the solution in the flask until intense fumes of perchloric acid appear. Stop heating the solution and continue to pass nitrogen until the distillation apparatus has cooled to room temperature. Transfer the contents of the receivers into a 25 ml volumetric flask and dilute to the mark with 9 M HCl.

2.2.2. Determination of ruthenium

Measure the absorbance of the solution obtained at $\lambda_{max} = 480.0$ nm against the blank. Calculate the concentration of ruthenium using the appropriate regression equation.

2.2.3. Determination of osmium

Heat the obtained solution for 30 min at 90°C. Allow it to cool to room temperature. Record the absorption spectrum of the solution against the blank with the following instrumental parameters: wavelength 300–650 nm; slit 1 nm; scan speed 120

Fig. 2. Spectra of the $RuCl_6^{2-}$ complex (16 μg Ru ml^{-1}) in (a) 6 M HCl, (b) 8 M HCl, (c) 9 M HCl and (d) 10 M HCl (directly after absorption of RuO_4, curve 1; after 30 and 60 min, curves 2 and 3 respectively; after 24 h curve 4).

nm min^{-1}; sampling interval (interpoint distance) 0.2 nm. Calculate (with 55 points and 2nd degree polynomial) the third-derivative absorption spectrum of the solution. Measure the value of the third derivative of osmium at 350.0 nm. Calculate the osmium concentration using the appropriate regression equation.

Fig. 1. Spectra of $RuCl_6^{2-}$ complex (16 μg Ru ml^{-1}) in 6 M, 8 M, 9 M and 10 M HCl (curves 1–4 respectively) and OsO_4 (16 μg Os ml^{-1}) in 6 M, 8 M, 9 M and 10 M HCl (curves 5–8 respectively) at room temperature.
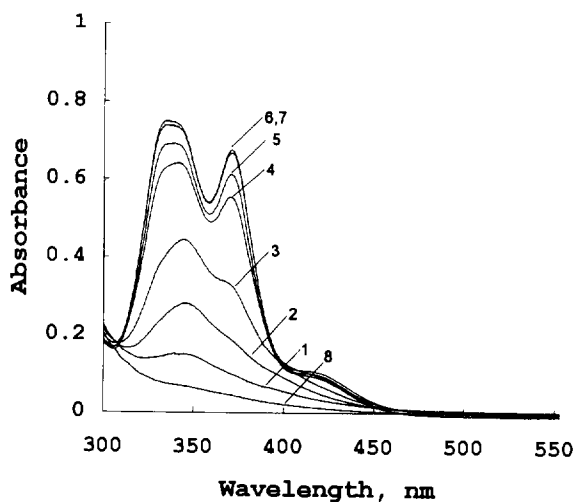
Fig. 3. Effect of temperature on the reduction of OsO_4 (16 μg Os ml^{-1}) in 9 M HCl. Curves 1–8 correspond respectively to the temperatures 50, 60, 70, 80, 85, 90, 95°C and room temperature. Heating time (constant), 20 min.

3. Results and discussion

3.1. Studies on the reduction of RuO_4 and OsO_4 in hydrochloric acid.

Ruthenium and osmium are quantitatively oxidized to Ru(VIII) and Os(VIII) in a medium of
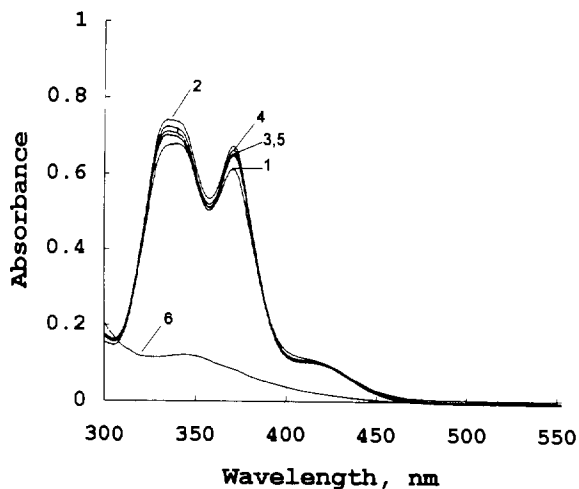
Fig. 4. Effect of the heating time on the reduction of OsO_4 (16 μg Os ml^{-1}) in 10 M HCl (5, 10, 15, 20 and 25 min at 90°C, curves 1–5 respectively; spectrum of OsO_4 solution in 10 M HCl at room temperature, curve 6).
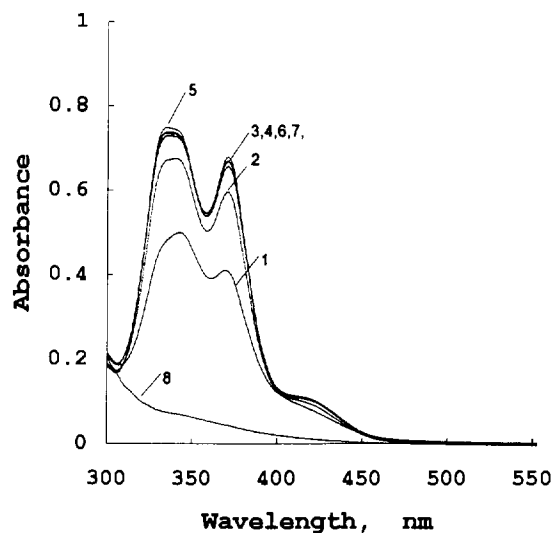
Fig. 5. Effect of the heating time on the reduction of OsO_4 (16 μg Os ml^{-1}) in 9 M HCl (5, 10, 15, 20, 30, 45 and 60 min at 90°C, curves 1–7 respectively; spectrum of OsO_4 solution in 9 M HCl at room temperature, curve 8).

hot concentrated $HClO_4 + H_2SO_4$ (1 + 3) and selectively volatilized as RuO_4 and OsO_4 from the examined samples. The experiments carried out in this work have shown that both the tetroxides are quantitatively absorbed in hydrochloric acid medium with the formation of chloride complexes of the elements in lower oxidation states. The reduction rates of RuO_4 and OsO_4 and the type of complexes formed depend on the HCl concentration, temperature and reaction time.

It has been found that in 6–10 M HCl RuO_4 is easily reduced to Ru(IV) and the complex $RuCl_6^{2-}$ with λ_{max} at 480.0 nm is formed (Fig. 1; curves 1–4). Quantitative conversion of Ru(VIII) into this complex takes place at room temperature. Large amounts of decomposition products of $HClO_4$ and H_2SO_4 acids that pass during distillation into the absorbing solution may cause slight differences in the maximum absorbance of the solution obtained by distillation of ruthenium from a dilute $KMnO_4$ solution ($\lambda_{max} = 485.0$ nm) [5]. The maximum stability of the $RuCl_6^{2-}$ complex is observed in 8 M hydrochloric acid (Fig. 2b). The absorbance of the obtained complex at $\lambda_{max} = 480.0$ nm does not change significantly over a period of 24 h. Slow partial reduction of
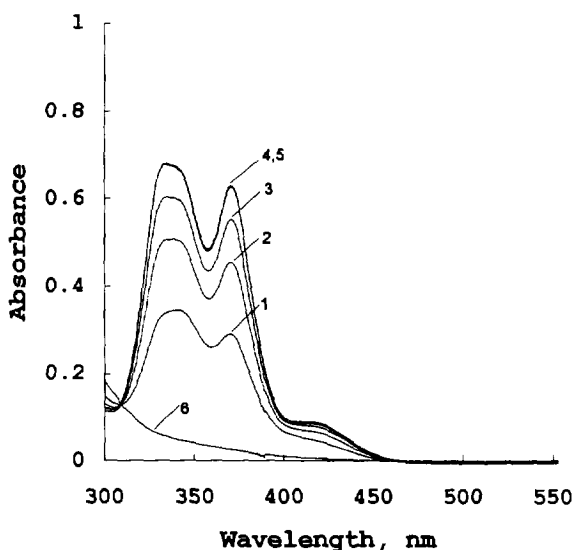
Fig. 6. Effect of the heating time on the reduction of OsO_4 (16 μg Os ml^{-1}) in 8 M HCl (10, 20, 30, 60 and 120 min at 90°C, curve 1–5 respectively; spectrum of OsO_4 solution in 8 M HCl at room temperature, curve 6).

Ru(IV) to Ru(III) and the formation of the $RuCl_6^{3-}$ complex with maximum absorbance at 350 nm may take place with increasing HCl concentration. The maximum absorbance of the $RuCl_6^{2-}$ complex at 480 nm in 9 M and 10 M HCl decreases by about 9% and 11% respectively, within 24 h (Fig. 2c,d). The absorbance of the complex is practically constant 60 min after absorption of RuO_4 in both the examined media.

The experiments have shown that OsO_4 is very slowly reduced in hydrochloric acid medium at

room temperature. No chloride complexes containing osmium in lower oxidation states are formed directly after absorption of OsO_4 in 6–10 M hydrochloric acid (Fig. 1; curves 5–8). In 6 M and 8 M HCl solutions no reduction of OsO_4 was observed after 24 h at room temperature. Slow reduction of Os(VIII) to Os(VI) and the formation of the $OsO_2Cl_4^{2-}$ complex [4] with λ_{max} at 346.8 nm take place in 9 and 10 M HCl.

It has been found that the reduction of osmium(VIII) can be considerably accelerated by heating OsO_4 solutions in hydrochloric acid (Fig. 3). On heating OsO_4 solutions in 8–10 M hydrochloric acid Os(VIII) is rapidly reduced to Os(IV) and the stable $OsCl_6^{2-}$ complex ($\lambda_{max} = 334.8$ nm, $\epsilon = 8.4 \times 10^3$ l mol^{-1} cm^{-1}) is formed. Quantitative conversion of osmium into the $OsCl_6^{2-}$ complex takes place after 10 min, 15 min and 1 h heating of OsO_4 solutions in 10 M HCl (Fig. 4), 9 M HCl (Fig. 5) and 8 M HCl (Fig. 6) at 90°C respectively. In this work reduction of Os(VIII) to Os(IV) was carried out in 9 M hydrochloric acid upon heating for 30 min at (90 ± 1)°C.

3.2. Determination of ruthenium

Osmium does not interfere with direct spectrophotometric determination of ruthenium in all the examined media (Fig. 1; curves 5–8). OsO_4 in hydrochloric acid and the $OsCl_6^{2-}$ complex obtained after the reduction of Os(VIII) to Os(IV) have no effect on the absorbance of ruthenium at

Table 1
Statistical evaluation of the results of the determination of ruthenium by direct spectrophotometry

Ruthenium added (μg)	Ruthenium found[a] (μg)	Standard deviation (s) (μg)	Relative standard deviation (RSD) (%)	Confidence limits ($\alpha = 0.05$)
100.0	102.1	6.17	6.0	102.1 ± 6.6
	(96.7)[b]	(6.25)	(6.4)	(96.7 ± 6.4)
200.0	196.8	6.43	3.3	196.8 ± 6.8
	(197.8)	(5.90)	(3.0)	(197.8 ± 6.2)
400.0	399.5	6.52	1.6	399.5 ± 6.9
	(396.9)	(7.99)	(2.0)	(396.9 ± 8.3)

[a] $n = 6$.
[b] Data obtained in the presence of 200 μg of Os in examined solution.

Wavelength, nm
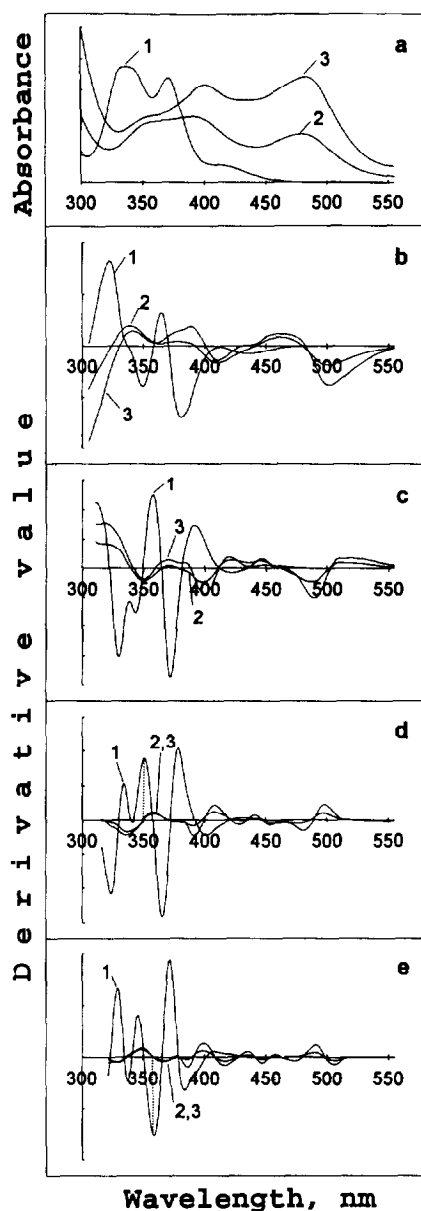
Fig. 7. Direct (a) and derivative (first-, second-, third- and fourth-order, b–e respectively) spectra of the $OsCl_6^{2-}$ (16 μg Os ml^{-1}, curve 1) and $RuCl_6^{2-}$ complexes (8 and 16 μg Ru ml^{-1}, curves 2 and 3 respectively) in 9 M HCl after heating for 30 min at $(90 \pm 1)°C$.

480.0 nm. It has been found that osmium in concentrations of up to 100 μg ml^{-1} does not interfere with the determination of ruthenium. The maximum absorbance of the solution at 480.0 nm corresponds only to the concentration of

ruthenium. The molar absorptivity of the $RuCl_6^{2-}$ complex in 9 M HCl medium amounts to 4.8 1 mol^{-1} cm^{-1}. The linear concentration range for ruthenium determination with the examined conditions amounts to 0.07–20 μg Ru ml^{-1}. The regression equation is $y = 0.0472c - 0.0144$ where y is the absorbance measured and c is the concentration of ruthenium (μg ml^{-1}); correlation coefficient $R^2 = 0.9999$. Sensitivity of the method ($u = s_{y/x}/m$; where $s_{y/x}$ and m are the average deviation from the regression line and the slope of the calibration curve respectively) amounts to 0.073 μg Ru ml^{-1}. The precision and accuracy of the results of the determination of ruthenium in the absence of osmium in the examined solutions and in mixtures with osmium are shown in Table

Wavelength, nm
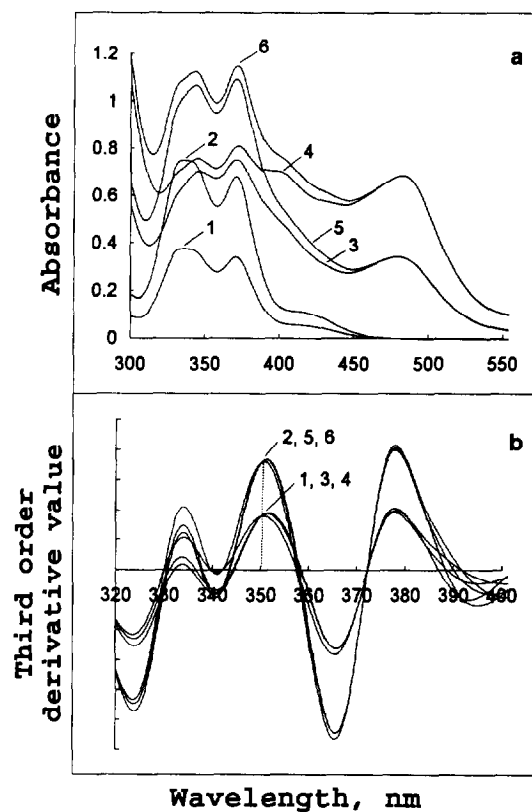
Fig. 8. Direct (a) and third-order derivative (b) spectra of $OsCl_6^{2-}$ complex (8 μg Os ml^{-1}, curve 1; 16 μg Os ml^{-1}, curve 2) and mixtures of $OsCl_6^{2-}$ and $RuCl_6^{2-}$ complexes (8 μg Os ml^{-1} + 8 μg Ru ml^{-1}, curve 3; 8 μg Os ml^{-1} + 16 μg Ru ml^{-1}, curve 4; 16 μg Os ml^{-1} + 8 μg Ru ml^{-1}, curve 5; 16 μg Os ml^{-1} + 16 μg Ru ml^{-1}, curve 6).

Table 2
Statistical data on the results of the determination of osmium by third-order derivative spectrophotometry

Osmium added (μg)	Osmium found[a] (μg)	Standard deviation (s) (μg)	Relative standard deviation (RSD) (%)	Confidence limits (x = 0.05)
100.0	101.5 (97.5)[b]	2.08 (4.98)	2.1 (5.1)	101.5 ± 2.19 (97.5 ± 5.2)
200.0	204.3 (201.3)	4.47 (4.09)	2.2 (2.0)	204.3 ± 4.67 (201.3 ± 4.3)
400.0	398.9 (402.5)	4.01 (2.94)	1.0 (0.7)	398.9 ± 4.21 (402.5 ± 3.1)

[a] $n = 6$.

[b] Data obtained in the presence of 200 μg of Ru in examined solution.

Table 3
Results of the determination of ruthenium and osmium in standard plasma solution of the noble metals (100 μg Ru ml^{-1}, 100 μg Rh ml^{-1}, 100 μg Pd ml^{-1}, 100 μg Os ml^{-1}, 100 mg Ir ml^{-1}, 100 μg Pt ml^{-1} and 100 μg Au ml^{-1} in 20 % HCl)

Sample examined (ml)	Element determined[a] (μg ml^{-1})	Standard deviation (s) (μg ml^{-1})	Relative standard deviation (RSD) (%)	Condidence limits (x = 0.05)
Ruthenium				
1	99.4	3.83	3.8	99.4 ± 4.0
2	99.8	1.83	1.8	99.8 ± 1.9
3	99.6	2.51	2.5	99.6 ± 2.6
Mean (μg ml^{-1})	99.6			
Osmium				
1	100.4	3.25	3.2	100.4 ± 3.4
2	100.3	4.36	4.3	100.3 ± 4.5
3	98.5	2.23	2.2	98.5 ± 2.3
Mean μg ml^{-1}	99.7			

[a] $n = 6$.

1. The relative standard deviation (RSD) does not exceed 6.0% and 6.4% respectively.

3.3. Determination of osmium

Ruthenium interferes with the spectrophotometric determination of osmium in hydrochloric acid media (Fig. 7a). The results of the determination of osmium are higher by about 50% when the concentrations of ruthenium and osmium in examined solutions are equal. It has been found that the interferences of ruthenium (up to 100 μg Ru ml^{-1} examined) can be completely eliminated when numerical calculation of absorption spectra

of the OsCl$_6^{2-}$ and RuCl$_6^{2-}$ complexes is carried out and derivative spectra are recorded. The derivative absorption band of ruthenium is partially reduced when considering the first-, second-, third- and fourth-order (Fig. 7b–e respectively) derivative spectra. The third- and fourth-order derivative spectra of ruthenium cross the zero line at 350.0 nm and 359.0 nm respectively (Fig. 7d,e) independently of the ruthenium concentration. The value of the corresponding derivative spectrum of osmium at these wavelengths depends only on the osmium concentration in the examined solution (Fig. 8b). The calibration curve for osmium determination by the third-order deriva-

tive values at 350.0 nm ("zero-crossing point" of ruthenium) is linear in the 0.02–20 μg Os ml^{-1} concentration range. The regression equation is $y = 2.22 \times 10^{-5}c - 1.6 \times 10^{-6}$ where y is the measured derivative value and c is the concentration of osmium (μg ml^{-1}); correlation coefficient $R^2 = 0.9992$. Sensitivity of the method ($u = s_{y/x}/m$) amounts to 0.015 μg Os ml^{-1}. The RSD does not exceed 2.2% in the absence of ruthenium in the final solution and 5.1% for a mixture of $OsCl_6^{2-}$ and $RuCl_6^{2-}$ complexes (Table 2).

4. Analytical application

The developed methods were applied to the determination of ruthenium and osmium in a calibration standard solution for plasma (ICP and MIP) spectroscopy (MBH Analytical LTD product), containing 100 μg ml^{-1} each of the noble metals Ru, Rh, Pd, Os, Ir, Pt and Au in 20% HCl. Ruthenium and osmium were selectively separated from the solution by distillation of RuO_4 and OsO_4 from $HClO_4 + H_2SO_4$ (1 + 3) medium. Both the tetroxides were absorbed in 9 M HCl and the ruthenium and osmium contents were determined according to the above procedure. The results are presented in Table 3. The RSDs for ruthenium and osmium were 1.8–3.8% and 2.2–4.3% respectively.

References

[1] F.E. Beamish and J.C. Van Loon, Recent Advances in the Analytical Chemistry of the Nobel Metals, Pergamon Press, Oxford, 1972.

[2] J.C. Van Loon and R.R. Barefoot, Determination of the Precious Metals, Selected Instrumental Methods, Wiley, Chichester, 1991.

[3] S.E. Livingstone, The Chemistry of Ruthenium, Rhodium, Palladium, Osmium, Iridium and Platinum, Pergamon Press, Oxford, 1973.

[4] S.I. Ginsburg, N.A. Ezerskaya, I.V. Prokof'eva, N.F. Fedorenko, V.I. Shlenskaya and N.K. Belskii, Analytical Chemistry of Platinum Metals, Izd. Nauka, Moscow, 1972.

[5] M. Balcerzak, Mikrochim. Acta Part II, (1985) 389.

[6] Z. Marczenko, M. Balcerzak and H. Pasek, Mikrochim. Acta, Part II, (1982) 371.

[7] A. Savitzky and M.J.E. Golay, Anal. Chem., 36 (1964) 1627.

[8] T.C. O'Haver and G.L. Green. Anal. Chem., 48 (1976) 312.

[9] H. Ishii and K. Satoh, Fresenius' Z. Anal. Chem., 312 (1982) 114.

[10] G. Heidecke, J. Kropf and G. Stork, Fresenius' Z. Anal. Chem., 316 (1983) 405.

[11] R. Łobiński and Z. Marczenko, Crit. Rev. Anal. Chem., 23 (1992) 55.

[12] G. Talsky, Derivative Spectrophotometry, VCH, Weinheim, 1994.

[13] M. Balcerzak and S. Kuś, Anal. Sci. (Japan), 10 (1994) 65.

Behaviour of the dithiocarbamate complexes of arsenic, antimony, bismuth, mercury, lead, tin and selenium in methanol with a hydride generator

L. Vuchkova, S. Arpadjan*

Faculty of Chemistry, University of Sofia, 1126 Sofia, Bulgaria

Abstract

A study was carried out with a continuous hydride generator coupled to an atomic emission spectrometer with inductively-coupled plasma to determine whether hydrides of As, Bi, Pb, Sb, Sn and Se and mercury vapor could be generated in methanol solutions of their dithiocarbamate complexes. It was found that (with the exception of Pb) hydride generation with sufficient efficiency for simultaneous multi-element determination is achieved using 0.25% $NaBH_4$–0.6 mol l^{-1} HCl as reaction medium. The detection limit was found to be 0.2 ng ml^{-1} for As, 30 ng ml^{-1} for Bi, 0.03 ng ml^{-1} for Se, Sb and Sn.

Keywords: Inductively-coupled plasma atomic emission spectrometry; Continuous hydride generator; Dithiocarbamate complexes in methanol; Solid phase extraction

1. Introduction

The generation of volatile covalent hydrides and mercury vapor has become a widely-used technique in atomic spectrometry for analysis of As, Sb, Se, Sn, Ge, Te, Bi, Hg and Pb in various matrices. For the determination of extremely low element concentrations and for the elimination of matrix interferences a preliminary preconcentration is necessary. Liquid–liquid extraction preconcentration methods have been described in combination with subsequent hydride generation

(HG) directly in non-aqueous media without any mineralisation or re-extracting procedures [1–11]. However, the solvent extraction method offers limited enrichment factors and is unsuitable for automation of the analysis and for preservation and transportation of pretreated samples. This is the reason for the recent enhanced interest in preconcentration methods using column solid phase extraction. An effective preconcentration technique allowing higher concentration factors than with liquid extraction was developed using a water-insoluble ligand, such as ammonium hexahydroazepine-1-dithiocarboxylate (ammonium hexamethylenedithiocarbamate) (HMDC), physically immobilized on polyurethane foam, and dis-

---

* Corresponding author.

posable syringes as microcolumns [12]. In a pre-liminary study optimum conditions were estab-lished for quantitative solid phase extraction of As, Bi, Hg, Sb, Se, Sn and Pb. A complete elution was achieved by total dissolution of the sorbed analyte dithiocarbamate complexes in organic sol-vents [12,13]. The application of a water-miscible solvent such as methanol simplifies the analytical procedure due to the possibility of using the con-ventional hydride generator for aqueous solutions without any changes. However, no data are avail-able on whether elemental hydrides and mercury vapor could be generated from methanol solu-tions of chelate complexes of the analytes and then followed by inductively-coupled plasma atomic emission spectrometry (ICP-AES) mea-surements.

The aims of the present work are: (i) to investi-gate the hydride generation of As, Sb, Sn, Se, Bi and Pb when present as dithiocarbamate com-plexes in methanol solutions; (ii) to investigate the behaviour of Hg under the same conditions; and (iii) to optimize the working conditions for combi-nation of the HG in methanol solutions of the analyte dithiocarbamate complexes with an induc-tively-coupled plasma optimized for simultaneous determination of the above elements by atomic emission spectrometry.

2. Experimental

2.1. Reagents and apparatus

All reagents used were of analytical-reagent grade. Redistilled water was used throughout. Stock solutions of 0.25% and 0.5% $NaBH_4$ (Merck) in 0.4% NaOH were prepared daily and stored in a polyethylene bottle before use. The multielement standard solutions for all the studied elements were prepared from Titrisol (Merck, Germany). HMDC (Merck) was used as received. The solvent methanol (Merck) was additionally purified by distillation.

The ICP-AES measurements were performed with a simultaneous ICP spectrometer Spec-troflame combined with a continuous hydride generator 341-ARL. The ICP and HG operating conditions are given in Table 1.

The HMDC-immobilized polyurethane foam and the sorbent columns for solid phase extrac-tion were prepared as described earlier [12].

2.2. Preparation of test solutions

To 20.00 ml of a standard solution containing 50 ng ml^{-1} As(III), Sb(III), Bi(III), Se(IV); 60 ng ml^{-1} Sn(IV); 20 ng ml^{-1} Hg(II) and 100 ng ml^{-1} Pb 5 ml acetic buffer at pH 4.66 was added. This solution was pumped through a sorbent column filled with HMDC-immobilized polyurethane foam using the conditions reported previously [12]. Then the organic chelating ligand, HMDC, together with the analyte–dithiocarbamate com-plexes formed were completely dissolved in 9.0 ml methanol or in 9.0 ml aqueous methanol solution with 66% methanol (6.0 ml $CH_3OH + 3.0$ ml H_2O).

2.3. Recommended procedure

In 150 ml of a water sample 3 g KI is dissolved and heated gently at 60°C for 1 h to ensure that the analytes are present in their lower oxidation states. The pH is adjusted to 4.5 ± 0.5 with ac-

Table 1
ICP operating parameters and HG conditions

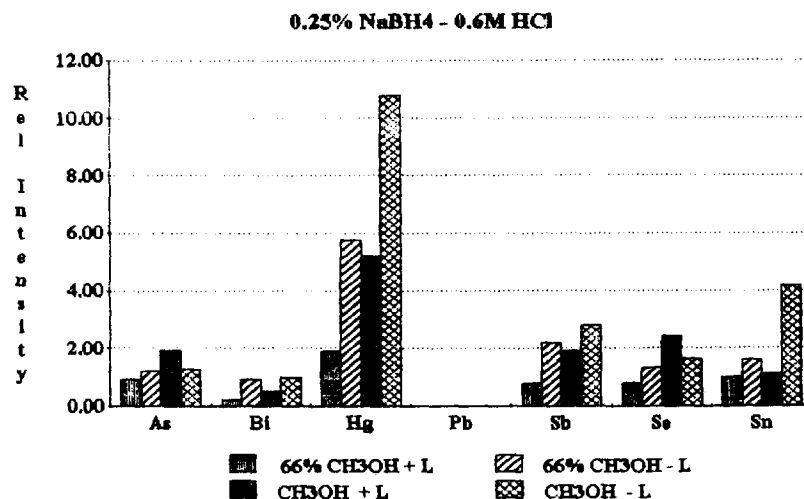|	
Incident power (kW)	1.25
Argon flow rates (l min^{-1}):	
coolant	17
carrier	0.9
sheath	0.85
Observation height (mm)	15
Pre-integration time (s)	30
Integration time (s)	5
Wavelengths (nm):	
As I	189.04
Bi I	230.0
Hg I	184.95
Pb II	220.35
Sb I	206.8
Se I	196.09
Sn II	189.98
Reductant	$NaBH_4$ solution in 0.4% NaOH
Reductant flow rate (ml min^{-1})	2.4
Acid flow rate (ml min^{-1})	1.2
Sample flow rate (ml min^{-1})	6.0

0.25% NaBH4 - 0.6M HCl

Fig. 1. Analyte line intensity relative to aqueous reference solutions using 0.25% NaBH₄–0.6 M HCl as reaction medium for hydride generation: + L in presence of HMDC; − L in absence of HMDC.
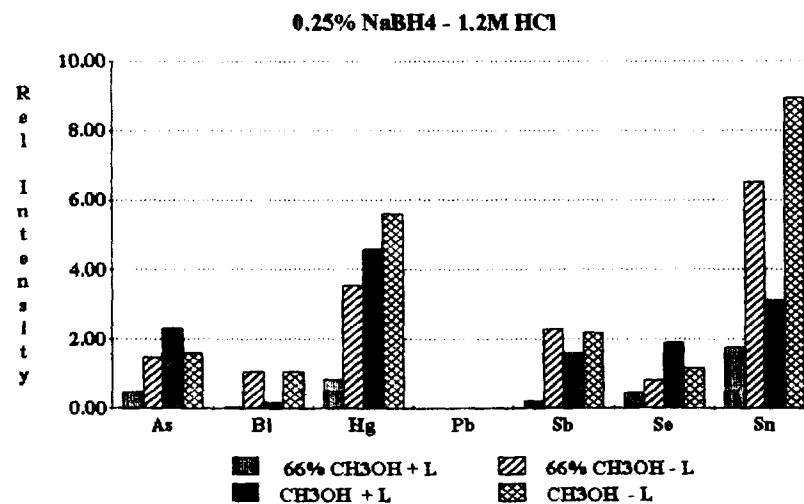
0.25% NaBH4 - 1.2M HCl

Fig. 2. As Fig. 1 but with 0.25% NaBH₄–1.2 M HCl as reaction medium.

etate buffer or if necessary with some drops of dilute ammonia or HCl. The sample is pumped through the sorbent column at a flow rate of 2 ml min⁻¹. Then 5.0 ml CH₃OH is placed in a dry quartz beaker and passed six times through the sorbent with the aid of the syringe plunger. This methanol solution of the analyte–dithiocarbamate complexes is connected to the sample channel of the hydride generator. The calibration solutions were prepared from aqueous multielement standard solutions by appropriate dilution with a methanol solution of HMDC (10 g l⁻¹).

3. Results and discussion

The influence of methanol and of the chelate-forming ligand HMDC on the yield of hydride was investigated for the following reaction systems: A, 0.25% NaBH₄–0.6 M HCl; B, 0.25% NaBH₄–1.2 M HCl; C, 0.25% NaBH₄–0.6 M HNO₃; D, 0.25% NaBH₄–1.2 MHNO₃; E, 0.25% NaBH₄–2 M HNO₃; F, 0.5% NaBH₄–2 M HNO₃.

The intensity of the emission signal of the analytes when present as dithiocarbamate complexes
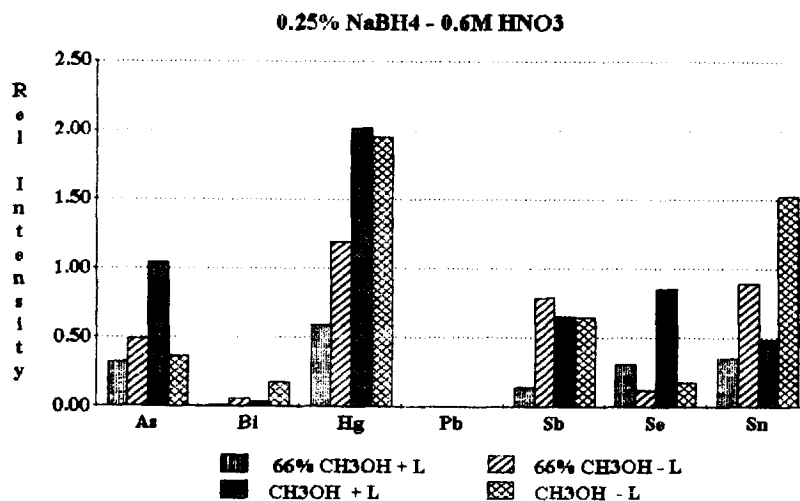
0.25% NaBH4 - 0.6M HNO3

Fig. 3. As Fig. 1 but with 0.25% $NaBH_4$–0.6 M HNO_3 as reaction medium.
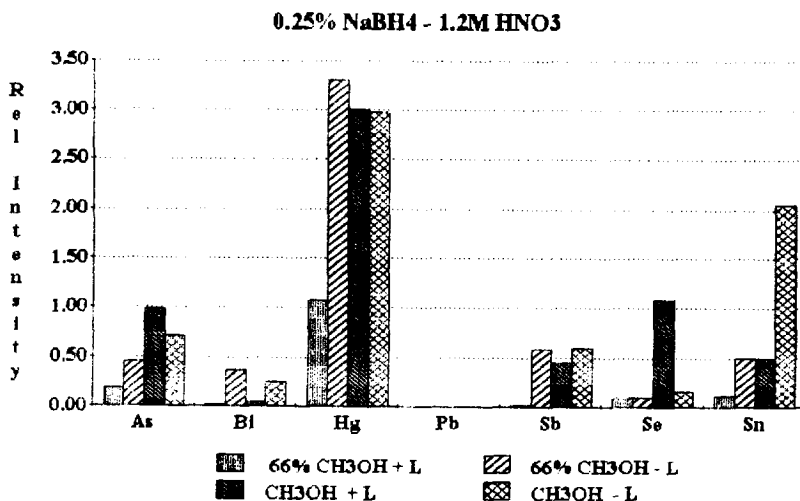
0.25% NaBH4 - 1.2M HNO3

Fig. 4. As Fig. 1 but with 0.25% $NaBH_4$–1.2 M HNO_3 as reaction medium.

in methanol (I_o) was compared with that obtained for aqueous solutions (I_w) at the same experimental conditions. The results obtained for the relative intensity, I_r ($= I_o/I_w$), are shown in Figs. 1–6. The chelate-forming ligand HMDC affects the process of hydride generation. The HG reaction was realised with higher efficiency in methanol solutions without ligand than in those with ligand. The influence of HMDC depends on the stability of the dithiocarbamate complexes of the analytes in methanol and on the rate of hydride formation or reduction to the elemental state (Hg). In the

presence of methanol and HMDC Pb cannot form a volatile covalent hydride at all. The ligand HMDC strongly suppresses the formation of bismuthine in all the investigated reaction systems (Figs. 1–6) due to the high stability of the Bi–dithiocarbamate complex and the relatively slow rate of bismuthine formation. The determination of Bi in the presence of HMDC is possible only in 0.25% $NaBH_4$–0.6 M HCl with twice as poor sensitivity ($I_r = 0.5$).

Arsenic forms a volatile hydride independent of the presence of ligand and in the applied reaction
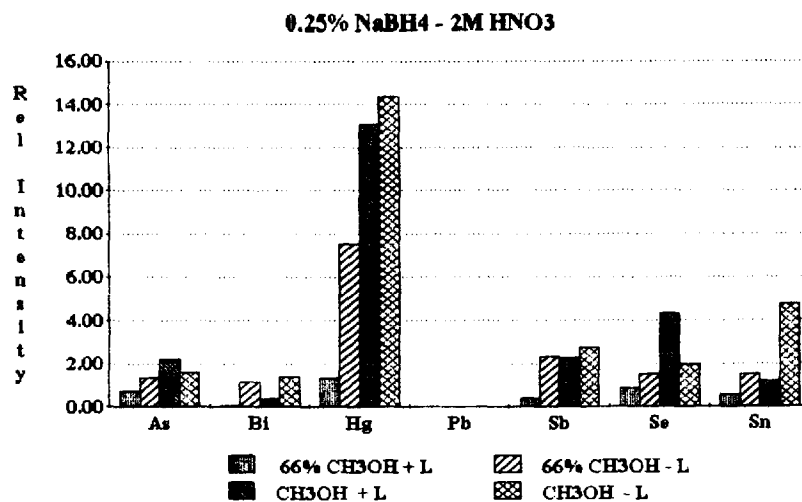
0.25% NaBH4 - 2M HNO3

Fig. 5. As Fig. 1 but with 0.25% $NaBH_4$–2 M HNO_3 as reaction medium.
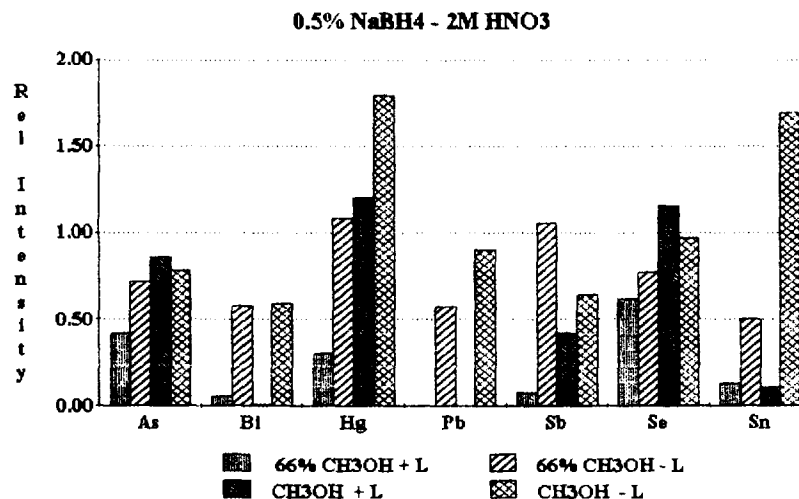
0.5% NaBH4 - 2M HNO3

Fig. 6. As Fig. 1 but with 0.5% $NaBH_4$–2 M HNO_3 as reaction medium.

system in pure CH_3OH as well as in 66% CH_3OH (Fig. 1).

Selenium forms a volatile hydride in methanol solutions of HMDC with all the studied reduction systems. The efficiency of H_2Se formation is higher in HCl medium ($I_r \approx 1.9$–2.4, Figs. 1 and 2) than in HNO_3 medium ($I_r \approx 0.85$–1.15, Figs. 3, 4 and 6), except for the system 0.25% $NaBH_4$–2 M HNO_3 where $I_r = 4.3$ (Fig. 5).

In the case of antimony the efficiency of stibine formation is higher ($I_r \approx 2$) in hydrochloric acid-containing reaction systems (Figs. 1, 2) than in nitric acid medium ($I_r < 1$, Figs. 3, 4 and 6).

A strong depression of SnH_4 formation was observed in the presence of HMDC in the methanol solution for all reaction systems with HNO_3.

Mercury forms stable dithiocarbamate complexes. Nevertheless, the efficiency of mercury vapor formation is high in the reaction systems containing HCl ($I_r \approx 4.5$) and HNO_3 ($I_r \approx 1.13$). This is probably due to the high reduction rate of mercury to the elemental state.

The higher intensity signals for As, Hg, Sb, Se and Sn in methanol in the absence of the chelate-

Table 2
Detection limits (3 σ) for HG with ICP-AES for methanol solutions of dithiocarbamate complexes of the analytes

Reaction medium	Detection limit (ng ml^{-1})					
	As	Bi	Hg	Sb	Se	Sn
0.25% NaBH$_4$-0.6 M HCl	0.2	30	0.03	3	3.3	2.7
0.25% NaBH$_4$-1.2 M HCl	0.5	–	0.1	–	–	–
0.25% NaBH$_4$-0.6 M HNO$_3$	0.8	–	0.2	1.8	9	4
0.25% NaBH$_4$-1.2 M HNO$_3$	0.7	–	0.1	–	7	–
0.25% NaBH$_4$-2 M HNO$_3$	–	–	0.2	–	9	–
0.5% NaBH$_4$-2 M HNO$_3$	0.4	–	0.2	3	8.5	–

forming ligand HMDC (Figs. 1 and 2) than for their aqueous reference solutions could be explained by a lowering of the surface tension, promoting a higher rate of hydride or cold vapor liberation from the liquid phase. This is presumably the explanation for the higher efficiency in pure methanol than in 66% methanol. An exception is observed for bismuth and lead. The generation of bismuthine in HCl medium does not depend ($I_r \approx 1$) on the replacement of water by CH$_3$OH.

3.1. Choice of working conditions

A higher sensitivity and a more stable plasma were obtained for methanol solutions of HMDC in comparison to aqueous methanol solutions (66% CH$_3$OH).

Table 3
Comparison of the detection limits (3 σ) of HG–ICP in aqueous solutions and in methanol solutions of the analyte dithiocarbamate complexes after preconcentration by column solid phase extraction (recommended procedure)

Element	HG-ICP in aqueous solutions (ng ml^{-1})	Recommended procedure (ng ml^{-1})
As	0.2	0.008
Bi	0.35	1
Hg	0.02	0.001
Sb	0.5	0.1
Se	0.6	0.1
Sn	0.3	0.1

The optimum conditions for single element determination can be seen from the calculated limits of detection presented in Table 2. For simultaneous multi-element analysis, elution by total dissolution of the analyte–dithiocarbamate complexes in pure methanol and HG using the reaction system 0.25% NaBH$_4$-0.6 M HCl is recommended as the optimal compromise decision. In comparison with work with aqueous solutions under these experimental conditions the background signal for Bi does not change, but for As, Se, Sb and Sn it is enhanced 1.5-fold and for Hg it is enhanced 2.3-fold. The relative standard deviations of the measurements in methanol and aqueous media do not differ significantly, varying between 1 and 4%.

Table 3 presents the achievable best sensitivity for HG–ICP determination of the investigated elements in aqueous solutions using the optimal experimental conditions for aqueous media (0.5% NaBH$_4$-0.3 M HCl). It can be seen that whereas for As and Hg no substantial change in the sensitivity of their determinations was observed, for selenium the sensitivity in methanol solution of its dithiocarbamate complex is approximately five times worse than by HG from aqueous Se(IV) solutions. This lowering in sensitivity is about a factor of nine for Sn and almost two orders of magnitude for Bi. However, the combination of HG with preliminary 30 fold preconcentration of the traces by column solid phase extraction, as described in the recommended procedure, permits the determination of extremely low analyte concentrations with the exception of Bi (Table 3).

Table 4
Recovery (%) from spiked water samples (n-number of samples)

Sample	Recovery (%)					
	As	Bi	Hg	Se	Sb	Sn
Tap water (n = 4)	97 ± 5	95 ± 5	99 ± 2	97 ± 3	95 ± 4	96 ± 5
Mineral water (n = 3)	97 ± 3	96 ± 6	97 ± 3	96 ± 3	97 ± 3	97 ± 4
Ground water (n = 3)	96 ± 6	97 ± 5	98 ± 4	95 ± 4	96 ± 5	98 ± 2
Waste water (n = 4)	95 ± 4	95 ± 7	96 ± 5	93 ± 5	97 ± 4	95 ± 4
Sea water (n = 7)	96 ± 6	96 ± 6	97 ± 5	92 ± 6	94 ± 4	93 ± 5

3.2. Application of the method

The recommended procedure was applied to a number of water samples: sea water, waste water, tap water, mineral water and ground water. The recovery studies were performed by adding known amounts of the analytes to the samples prior to adjustment of the pH value to 4.5 ± 0.5. The results are shown in Table 4. The high recoveries obtained indicate that the foreign ions present in the samples do not interfere to any significant extent with the determination of As, Bi, Sb, Se and Sn after HG in methanol solutions of the analyte dithiocarbamate complexes. The highest concentrations of coexisting ions in the water samples analysed were 0.4 μg l^{-1} Cd, 2 μg l^{-1} Cr, 100 μg l^{-1} Cu, 300 μg l^{-1} Fe, 200 μg l^{-1} Mn, 1.2 μg l^{-1} Ni, 5 μg l^{-1} Pb and 150 μg l^{-1} Zn. The alkali and alkaline earth elements, aluminium and the anions are not sorbed and hence could not be present in the methanol solution.

The results for water samples with higher analyte content were compared with those of HG in aqueous solutions as shown for two cases in Table 5. The agreement is good and the difference between the standard deviations of both methods is not statistically significant. HG-ICP in aqueous solutions is undoubtedly a faster and simpler technique, but the proposed column solid phase extraction preconcentration in combination with subsequent HG in methanol solutions for simultaneous determination by ICP-AES allows higher sensitivity for As, Hg, Sb, Se and Sn, and permits better possibilities for the preservation and transportation of the water samples.

4. Conclusion

The conversion of the analytes from their dithiocarbamate complexes in methanol to covalent hydrides or cold vapor (Hg) through direct

Table 5
Results (μg l^{-1}) of the analysis of waste-water and sea-water samples (n = number of parallel determinations)

| Element	Waste water (n = 4)		Sea water (n = 5)	
	Recommended procedure	HG-ICP in aqueous solutions	Recommended procedure	HG-ICP in aqueous solutions
As	2.8 ± 0.3	2.8 ± 0.2	1.27 ± 0.08	1.32 ± 0.07
Bi	9.7 ± 0.8	9.3 ± 0.7	<1	<0.35
Hg	<0.001	<0.02	2.5 ± 0.3	2.3 ± 0.2
Se	6.4 ± 0.5	6.2 ± 0.3	<0.1	<0.6
Sb	17.2 ± 1.2	16.6 ± 0.8	0.37 ± 0.05	<0.5
Sn	46 ± 3	47.2 ± 2.4	<0.1	<0.3

reduction in the organic solvent permits the development of an effective solid phase extraction preconcentration procedure prior to HG for simultaneous determination of As, Bi, Sb, Se and Sn.

Acknowledgement

References

[1] J. Aznarez, F. Palacios, M.S. Ortega and J.C. Vidal, Analyst, 109 (1984) 123.

[2] J. Aznarez, F. Palacios, J.C. Vidal and J. Galvan, Analyst, 109 (1984) 713.

[3] J. Aznarez, J.M. Rabadan, A. Ferrer and P. Cipres, Talanta, 33 (1985) 458.

[4] J. Aznarez, J.C. Vidal and J.M. Gascon, At. Spectrosc., 7 (1986) 59.

[5] J. Aznarez, J.C. Vidal and R. Carnicer, J. Anal. At. Spectrom., 2 (1987) 55.

[6] J.R. Castillo, J.M. Mir, J. Val, M.P. Colon and C. Martinez, Analyst, 110 (1985) 1219.

[7] M. Chikuna and N. Aoki, J. Anal. At. Spectrom., 8 (1993) 415.

[8] S. Zhang, H. Han and G. Ni, Anal. Chim. Acta, 221 (1989) 85.

[9] M.R. Rezende, R.C. Campos and A.J. Curtius, J. Anal. At. Spectrom., 8 (1993) 247.

[10] B. Huang, X. Zeng, Z. Zhang and J. Liu, Spectrochim. Acta, Part B, 43 (1988) 381.

[11] A.G. Menendez, J.E.S. Uria and A. Sanz-Medel, J. Anal. At. Spectrom., 4 (1989) 581.

[12] A. Alexandrova and S. Arpadjan, Analyst, 118 (1993) 1309.

[13] L. Vuchkova and S. Arpadjan, Analyst, (1996) submitted.
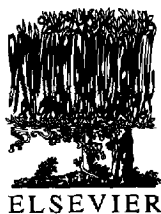
Comparison of two extraction methods for determination of PCBs and PCTs in mussels from Galicia

Mª Elena Alvarez Piñeiro[a], Jesús Simal Lozano[b], Mª Asunción Lage Yusty[a,b,*], Susana T. Carril González-Barros[b]

[a]Instito de Investigacion y Análisis Alimentarios, Laboratorio de Bromatologia, Facultad de Farmacia, Campus s/n 15706, Santiago, Spain

[b]Departamento de Química Analítica, Nutrición y Bromatología, Area de Nutrición y Bromatología, Facultad de Farmacia, Universidad de Santiago de Compostela, 15706 Santiago de Compostela, Spain

Abstract

We compared two extraction methods for use in GC-ECD determination of polychlorinated bi- and terphenyl contaminants (PCBs and PCTs respectively) in mussels (*Mytilus galloprovincialis*). Mussels spiked with standard PCB and PCT mixtures Aroclor 1260 and Aroclor 5460 were extracted with cold acetonitrile, or with 1:1 n-hexane/ dichloromethane in a Soxhlet extractor, which gave the better mean recoveries of $99.0 \pm 2.5\%$ and $59.5 \pm 8.3\%$ for PCBs and PCTs respectively.

Keywords: PCBs; PCTs; GC/ECD; Mussels

1. Introduction

Polychlorinated bi- and terphenyls (PCBs and PCTs respectively) constitute a family of environmentally persistent, synthetic chlorinated hydrocarbons which are highly lipophilic and are consequently water-insoluble [1] and tend to bioaccumulate in fatty tissues [2].

Both PCBs and PCTs have been used as insulating materials in electrical capacitors and transformers, and as components in hydraulic and lubricating fluids, plasticizers, paints adhesives and waxes. Use of both types of compound is now restricted [3]. However, although PCBs and particularly PCTs are subject to bio- and photodegradation [4], these compounds are highly stable in the environment and are now so widely distributed that detectable levels of PCBs [5–13] and PCTs [14–19] (although few studies are available) have been found in types of sample ranging from molluscs to mothers' milk.

Determination of PCBs and PCTs in environmental samples generally uses gas chromatography with electron-capture detection (GC-ECD), analysing organic solvent extracts of samples fol-

---

* Corresponding author.

lowing pre-analysis clean-up on any one of a variety of solid phases [5–19]. In this work we compared two different extraction methods for determination of PCB and PCT mixtures (Aroclor 1260 and Aroclor 5460 respectively) in mussels (*Mytilus galloprovincialis*) from Galicia, N.W. Spain.

2. Experimental

2.1. Reagents

Pesticide-residue-analysis grade acetonitrile was purchased from Carlo Erba, pesticide-residue-analysis grade n-hexane and analysis-grade diethyl ether from Scharlau, pesticide-residue-analysis grade dichloromethane and residue-analysis grade anhydrous sodium sulphate from Merck and washed sea-sand from Panreac. Minicolumns (Sep-Pak® Florisil) were from Waters. Aroclor 1260 was from Monsanto Ibérica, S.A. and Aroclor 5460 from Chem Service; stock solutions containing 10 μg ml^{-1} and 7 μg ml^{-1} respectively were prepared in n-hexane. A working solution of 20 g l^{-1} sodium chloride was prepared with distilled water previously extracted with n-hexane.

2.2. Apparatus

Samples were homogenized with an Omni-mixer homogenizer 17106 and partially dried in a Heraeus T-340 laboratory oven. We used a Perkin-Elmer 8500 gas chromatograph, equipped with a 63 Ni ECD connected to a capillary column (Alltech RSL-200 0.25 mm × 25 mm; film thickness 0.2 μm) and samples were injected automatically (Perkin-Elmer AS-8300 autosampler).

2.3. Samples

Mussels were removed from their shells and homogenized. Aliquots (25 g) of mussel homogenate were then spiked with Aroclor 1260 (5–160 μg kg^{-1}) and 5460 (26–280 μg kg^{-1}) so as to roughly double the levels found in unspiked samples.

2.4. Extraction procedures

2.4.1. Extraction with acetonitrile [20]

Each spiked aliquot of mussel homogenate was extracted by stirring it for 30 min with 2 × 25 ml portions of acetonitrile. The liquid extracts were isolated by vacuum filtration through a Buchner funnel (AFORA Fef. 884/73, 20–40 μm), combined into a single sample and mixed with 150 ml of the NaCl solution. This mixture was sequentially extracted with 2 × 25 ml portions of n-hexane, and the combined hexane-soluble extracts were washed with 15 ml and 10 ml portions of distilled water (previously extracted with n-hexane) before drying them over anhydrous Na$_2$SO$_4$. Finally, the hexane solution was concentrated to 1 ml in a Kuderna–Danish type evaporator.

2.4.2. Soxhlet extraction [21]

Each spiked aliquot of mussel homogenate was mixed with 25 g of washed sea-sand and left at 40°C in a laboratory oven for 24 h. Next, the mixture was placed in a Soxhlet extractor and extracted with 200 ml of 1:1 n-hexane/ dichloromethane. After 6 h, the extractant was cooled, dried over anhydrous Na$_2$SO$_4$ and concentrated to 1 ml in a Kuderna–Danish type evaporator.

2.5. Clean-up

Suitable samples for GC-ECD analysis were obtained by passing the concentrate from each extraction method through Sep-Pak® Florisil minicolumns, eluting in each case with 5 ml of n-hexane, and then concentrating the eluates to 1 ml in a Kuderna–Danish type evaporator.

2.6. Gas chromatography

Gas chromatography was performed in the split/splitless injection mode (vent flow, 20 ml min^{-1}; splitless period, 1 min) on the apparatus described above. The injector and detector temperatures were 300°C. The oven temperature followed the following temperature programme: 1 min at 50°C, increasing at 20°C min^{-1} to 175°C, then at 3°C min^{-1} to 320°C. The carrier gas was
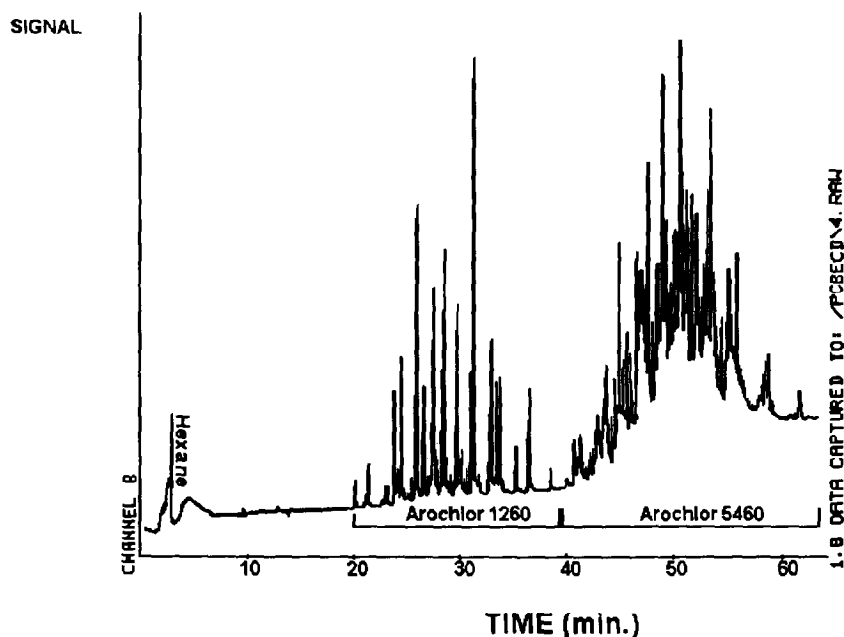
Fig. 1. Gas chromatogram showing optimal separation of standard mixtures of polychlorinated bi- and terphenyls (Aroclor 1260 and 5460 respectively).

nitrogen (N-50 grade) and the flow rate was 0.5 ml min^{-1}. Make-up gas was also nitrogen with a flow rate of 200 kPa.

2.7. Quantification

Quantification of the PCBs and PCTs was by the external standard method, using the following equation

$$C_m = \frac{C_s \times A_m}{A_s} \times 40$$

where C_m is the concentration (μg kg^{-1}) of the analyte (PCB or PCT) in the mussel sample; C_s is the concentration (μg ml^{-1}) of the Aroclor 1260 or Aroclor 5460 external standard, A_m is the total area of the peaks due to PCBs or PCTs in the sample, and A_s is the total area of the peaks due to the Aroclor 1260 or Aroclor 5460 external standard.

3. Results and discussion

Separation of the peaks due to the Aroclor

1260 and the Aroclor 5460 standards was optimized in a series of experiments in which mixtures of these standards were injected and the temperature programme was systematically varied. Fig. 1 shows the chromatogram obtained using the selected temperature programme.

Calibration curves were constructed by regressing the detector response at standard concentration for six mussel samples spiked with between 5 and 160 μg kg^{-1} of Aroclor 1260 (PCBs) or between 26 and 280 μg kg^{-1} of Aroclor 5460 (Table 1). Correlation coefficients (0.999$_8$ for PCBs, and 0.996 for PCTs) were high in both cases.

3.1. Efficiency of the extraction method

Twenty aliquots of homogenized mussel tissue were spiked with 160 μg kg^{-1} of Aroclor 1260 and 280 μg kg^{-1} of Aroclor 5460. Ten of these samples were then extracted using the acetonitrile method, and ten with 1:1 n-hexane/dichloromethane in a Soxhlet extractor; sample clean-up and GC-ECD analysis were the same for each series of samples. The realative efficiencies of the

Table 1
Correlation coefficient (r) and regression parameters for the calibration curves $y = bx + a$

Standard	Concentration range (μg kg^{-1}) in the six spiked samples	r	b	a
Aroclor 1260	5–160	0.999$_8$	5.29×10^5	1.65×10^4
Aroclor 5460	26–280	0.996	6.39×10^5	1.60×10^5

Table 2
PCB and PCT contents of mussels from the four major Galician estuarine bays (μg kg^{-1})

Source of mussels	No. of samples	Arithmetic PCB mean		Arithmetic PCT mean	
		Soxhlet	Acetonitrile	Soxhlet	Acetonitrile
Muros-Noya	11	183	165	0.60	nd[a]
Arosa	52	98	47	9.02	nd
Pontevedra	18	80	43	4.83	nd
Vigo	26	138	69	7.36	nd

[a] nd = not detected.

two extration methods were assessed by comparison of recoveries. The Soxhlet extraction method was the superior method, with recoveries of $99.0 \pm 2.5\%$ in the case of Aroclor 1260 (PCBs), and $59.5 \pm 28.3\%$ in the case of Aroclor 5460 (PCTs).

3.2. PCB and PCT content of Galician mussels

The results for the samples by estuarine bays are listed in Table 2. Using Soxhlet extraction high levels of PCBs are found, being, approximately, half those in the same samples extracted with acetonitrile (except in mussels from Muros-Noya). PCTs were not detected in samples extracted with acetonitrile and were detected in all the samples analyzed with hexane: dichloromethane although mean levels were low.

4. Conclusions

On the basis of these results, we suggest that levels of PCB and PCT contaminants in mussels should be determined using extraction with 1:1

n-hexane/dichloromethane in Soxhlet appartus, followed by sample clean-up on Sep-Pak Florisil minicolumns and GC-ECD using the external standard method.

Since recoveries were low for PCTs (59.5%) more extraction time may be required.

References

[1] J.F. Brown Jr. and R.E. Wagner, Environ. Toxicol. Chem., 6 (1987) 579.
[2] A. Södergren, P. Larsson, J. Knulst and C. Bergquist, Mar. Pollut. Bull., 21 (1990) 18.
[3] Council of European Communities.
[4] J.F. Fawell and S. Hunt, Water and Wastewater Technology, Ellis Horwood, England, 1988.
[5] C.L. Stratton and J.B. Sosebee Jr., Environ. Sci. Technol., 10 (1976) 1229.
[6] R. Kruse and K.E. Krüger, Arch. Lebensmitte lhyg., 140 (1989) 99.
[7] O. Osibanjo and O. Bamgbose, Mar. Pollut. Bull., 21 (1990) 581.
[8] B. Krauthacker, Bull. Environ. Contam. Toxicol., 46 (1991) 797.
[9] B. Crathone, M. Fielding, C.P. Steel and C.D. Watts, Environ. Sci. Technol., 18 (1984) 797.

[10] J. Volgelgesang, Fresenius' J. Anal. Chem., 34 (1991) 384.

[11] S.A. Wise, B.A. Benner Jr., R.J. Christensen, B.J. Koster, J. Kurtz, M.M. Schantz and R. Zeisler, Environ. Sci. Technol., 25 (1991) 1695.

[12] M.X. Petreas, T. Wiesmueller, F.H. Palmer, J.J. Winkler and R.D. Stephens, Chemosphere, 25 (1992) 621.

[13] M.T. Galceran, F.J. Santos, J. Caixach and J. Rivera, Chemosphere, 27 (1993) 1183.

[14] M.M. Schantz, R.M. Parris, J.K. Kurtz, K. Ballschmitter and S.A. Wise, Fresenius' J. Anal. Chem., 346 (1993) 766.

[15] S. Freudenthal and P.H. Greve, Bull. Environ. Contam. Toxicol., 10 (1973) 108.

[16] G.F. Fries and G.S. Marrow, J. Assoc. Off. Anal. Chem., 56 (1973) 1002.

[17] J.C. Sosa-Lucero and F.A. de la Iglesia, Bull. Environ. Contam. Toxicol., 10 (1973) 248.

[18] D.C. Villeneuve, L.H. Reynolds, G.H. Thomas and W.E. Philips, J. Assoc. Off. Anal. Chem., 56 (1973) 999.

[19] M.T. Galceran, F.J. Santos, J. Caixach, F. Ventura and J. Rivera, J. Chromatogr., 43 (1993) 399.

[20] M. Fernàndez Muiño, J. de la Montaña Miguelez and J. Simal Lozano, Chromatographia, 31 (1991) 453.

[21] M.E. Alvarez Piñeiro, J. Simal Lozano and M.A. Lage Yusty, J. Assoc. Off. Anal. Chem. Int., 77 (1994) 985.

Determination of trace heavy metals in biological samples by inductively-coupled plasma atomic emission spectrometry after extraction with 1,5-bis-(di-2-pyridylmethylene)thiocarbonohydrazide

E. Vereda Alonso*, A. Garcia de Torres, J.M. Cano Pavon

Department of Analytical Chemistry, Faculty of Sciences, University of Málaga, 29071 Málaga, Spain

Abstract

A sensitive inductively-coupled plasma atomic emission spectrometric sequential method for the determination of trace heavy metals (cadmium, cobalt, copper and nickel) in biological samples after extraction of the metals into isobutyl methyl ketone (IBMK) containing 1,5-bis-(di-2-pyridylmethylene)thiocarbonohydrazide (DPTH) is described. A systematic study was made to determine the optimum conditions for extraction of the metals into IBMK. The complexes formed are quite soluble in IBMK, so much so that this allows the use of aqueous-to-organic phase volume ratios of up to 40 and hence the determination of concentrations down to 40 times lower than those afforded by the direct non-extractive method. The method has been used for the determination of these elements in various biological materials with good results.

Keywords: Biological samples; Extraction; Inductively-coupled plasma spectrometry; 1,5-bis-(di-2-pyridyl-methylene)thiocarbonohydrazide

1. Introduction

Analysis of metals in biological samples is of appreciable interest due to the toxicity of some elements. Although various analytical techniques are available, electrothermal atomic absorption spectrometry (ETA-AAS) is adopted by most

trace metal analysts because of its speed, minimal sample preparation, automation possibilities and sensitivity for most of the commonly determined metals. However, there are several disadvantages associated with the use of AAS as the detection method. These result from the limited linear calibration range, the large matrix interferences, the very small amounts of sample that can be introduced into the graphite tube and the fact that it is a single-element technique.

---

* Corresponding author.

Inductively-coupled plasma atomic emission spectrometry (ICP-AES) has been widely recognized [1] as a suitable technique for the determination of trace elements, its particular advantages being multi-element capability, large dynamic range and effective background correction. However, several problems have been indicated by researchers, e.g. spectral interferences owing to matrix components, nebulizer blockage owing to the high solids content of the solution, and analyte emission enhancement. In addition, ICP-AES has a significant drawback because the detection limit is sometimes inadequate to comply with requirements for the determination of trace elements in biological samples.

Adequate detection power can be achieved using electrothermal vaporisation for sample introduction [2,3], but a number of interferences arise from the vaporisation and transport of the analyte to the plasma which have yet to be elucidated fully. The alternative to increasing the detection limit of the ICP-AES system is to pre-concentrate the elements of interest prior to their determination. Liquid–liquid extraction is one of the most frequently used sample pre-treatment techniques for the determination of trace metals by ICP-AES [4–9]. The extraction serves the dual purposes of concentrating the metals of interest and separating them from an interfering matrix. The extent of the concentration achieved depends on the ratio of the aqueous to organic phase volumes. However, isolation from the matrix significantly decreases the solids content of the solution, thus avoiding the nebulizer blockage.

Although there have been relatively few literature reports of solvent extraction combined with ICP spectrometry, solvent extraction procedures initially developed for atomic absorption spectrometry (AAS) can often be used in ICP-AES. The theoretical principles underlining these methods and compilations of numerous illustrative applications can be found [10–12]. In general, ammonium pyrrolidine-1-carbodithioates [13–17] and sodium diethyldithiocarbamate [18–22] are the most frequently used reagents, although other reagents such as 1-(2-pyridylazo)-2-naphthol (PAN) [23], dithizone [24] and 8-hydroxyquinoline [25], have been proposed. Normally, prior extrac-

tion increases the selectivity of the determination, but an adequate increase in sensitivity may not be obtained. In addition, only a few studies are available dealing with the suitability for preconcentration of digests of biological materials obtained with specific sample digestion procedures. However, since the major metallic elements that constitute the matrix of both animal material and seawater are of the same nature, procedures that are suitable for trace element preconcentration and matrix separation of seawater may also be applicable to solutions of mineralized biological fluids and tissues.

Watanabe et al. [26] described a preconcentration method for Cd, Cu, Fe, Mn, Ni, Pb and Zn from seawater prior to determination by ICP-AES. The method involved complexation of the metal ions with 8-hydroxyquinoline followed by (column) absorption of C_{18}-bonded silica gel. The authors reported excellent rejection of Cu, Fe, Mn and Ni, but, owing to high blanks, Cd, Pb and Zn could not be determined.

A method based on dithiocarbamate preconcentration for the simultaneous determination of Cd, Cu, Fe, Mo, Ni, V and Zn in seawater by ICP-AES was described by McLeod et al. [27]. The trace metals were extracted from the sample with a mixture of ammonium tetramethylene dithiocarbamate and diethylammonium diethyldithiocarbamate in chloroform and back-extracted into nitric acid. The concentrations of Cd, Cu, Ni and Zn, found at the ng ml^{-1} level, were consistent with the results of independent AAS analysis.

1,5-bis-(di-2-pyridylmethylene)thiocarbonohydrazide (DPTH) is a suitable complexing reagent for a number of metal ions. Most of the complexes it forms are coloured and can be extracted into a variety of organic solvents. Its synthesis and properties have been described in detail [28], as well as its use in the determination of nickel [29] and mercury [30]. In this work an ICP-AES method is described for the determination of trace amounts of three essential trace elements (Co, Cu, Ni) and one toxic heavy metal (Cd) in biological materials after extraction of these metals into isobutyl methyl ketone (IBMK) containing DPTH. The complexes formed are quite soluble

in IBMK, so much so that it allows the use of aqueous-to-organic phase ratios up to 40 and hence the determination of concentrations down to 40 times lower than afforded by the direct non-extractive method is possible. In addition, the extraction step enhances the selectivity. The method thus developed was applied to the determination of Cd, Co, Cu and Ni in various biological materials.

2. Experimental

2.1. Apparatus

The ICP-AES measurements were made on a Perkin-Elmer 40 sequential emission spectrometer controlled by an IBM XT-286 computer which was used to develop the method and for acquiring and storing the data. A standard torch and Meinhard concentric glass nebulizer (controlled by a peristaltic pump fitted with silicone pump tubes working at a flow rate of 1 ml min^{-1}) were used during the experiments. The r.f. generator of the nebulizer is internally mounted as a "free-running" oscillator-type with a nominal central frequency of 40 MHz and a nominal operating power level of 900 W. The measurements were made with the aid of a Crison Digit-501 pH meter furnished with a combined glass-calomel electrode. Separating funnels were shaken on a Gallenkamp flask agitator with variable rate and programmable time.

All glassware used was soaked in 10% nitric acid for 1 day and rinsed with water just before use.

2.2. Reagents

All chemicals were of at least analytical-reagent grade, and doubly-distilled deionised water was used throughout.

The ligand for the DPTH solution was synthesized as described elsewhere [29]. A stock solution in IBMK was prepared by dissolving 0.1 g of DPTH in 9 ml of N,N-dimethylformamide and diluting to 100 ml with IBMK. The solution was found to remain stable for at least 1 week in a refrigerator.

Stock solutions of cadmium (II), cobalt (II), copper (II) and nickel (II) were prepared from their commercial salts (nitrate or sulphate) and standardized titrimetrically or gravimetrically. Standards of working strength were made by appropriate dilution daily as required.

A glycine–HCl buffer of pH 3.6 was prepared by mixing 25 ml of 0.2 mol l^{-1} glycine and 2.5 ml of 0.2 mol l^{-1} HCl in a 100 ml volumetric flask and diluting to the mark with distilled water. A 1 mol l^{-1} solution of NaClO$_4$ was also used.

2.3. Procedures

2.3.1. Choice of optimum extraction conditions

The metal ions were extracted as follows: in 250 ml separatory funnels were placed 10 μg of each metal ion and variable volumes of HCl, NaOH and NaClO$_4$ solutions and the mixture was diluted to variable volumes of aqueous phase. Then 10 ml of DPTH solution in IBMK at different concentrations was added and the mixture was shaken vigorously on the mechanical agitator for different periods of time. Once both phases had been separated, the aqueous phase was collected and the equilibrium pH measured. The organic phase was introduced into the plasma by means of a peristaltic pump, the content of metals was determined using appropriate calibration graphs (the standards were prepared in water-saturated IBMK). Appropriate blanks were prepared and were run in the same manner.

2.3.2. Recommended procedure

Aliquots of samples or standard solutions containing the metal ions at pH 3.6 were placed in 250 ml separating funnels. Then, 10 ml of 0.1% DPTH in IBMK was added (the maximum volume ratio of the aqueous to organic phases was 20:1 for a single-stage extraction of 99–100%). The mixture was shaken vigorously on the mechanical agitator at 3000 rev min^{-1} for 5 min. The phases were allowed to separate, and the organic solvent layer (approximately 5 ml, when the volume ratio of the aqueous to organic phases was 20:1) was transferred into a polypropylene centrifuge tube (some samples needed centrifugation for up to 5–10 min to improve separation

between the layers). The organic phase was inserted into the plasma by means of a peristaltic pump and the metals were determined according to the instrumental conditions given in Table 1.

Two replicate measurements of the three individual sample preparations of the reference material were made and the metals were determined from the calibration graph, constructed with standard solutions treated in the same way, and for each sample examined the value of the blank was subtracted (blanks were always run in the same way); alternatively the standard addition method was also satisfactorily applied.

2.3.3. Sample preparation

The certified reference materials (CRMs) analysed were: Community Bureau of Reference (BCR), CRM 061 Platihypnidium Ripariodides (Aquatic Moss), 176 City Waste Incineration Ash, 186 Pig Kidney; National Research Council Canada (NRCC), CRMs TORT-1 Lobster Hepatopancreas, DOLT-1 Dogfish Liver; and National Institure of Standards and Technology (NIST), Standard Reference Material (SRMs) 2670 Human Urine Elevated Level. These samples were first dried in accordance with the norms of the respective analysis certificates. Three replicates of each dried sample were prepared according to the following procedure. In a reaction flask were placed 0.500 g of weighed sample and 10 ml of concentrated nitric acid, and the mixture was heated under reflux until the disappearance of nitrous fumes. Then, 2 ml of hydrogen peroxide was added and the mixture was evaporated to a small volume by heating on a hot plate to remove

Table 1
Operating conditions for ICP

R.f. generator frequency	40 MHz, incident power 1.1 kW
Photomultiplier voltage	600 V
Plasma gas flow rate	12 l min^{-1}
Auxiliary gas flow rate	0.5 l min^{-1}
Nebulizer gas flow rate	0.35 l min^{-1}
Plasma viewing height	15 mm above induction coil
Integration time	100 ms
Read delay	20 s
Peristaltic pump flow rate	1 ml min^{-1}

the nitric acid. Next, the mixture was neutralized with NaOH solution, and was transferred to a 500 ml standard flask. The pH was adjusted by means of glycine–HCl buffer solution (pH 3.6) and 12.5 ml of 1 mol ml^{-1} NaClO$_4$ solution was added; finally the contents were diluted with distilled water to the mark. The analysis of each sample was completed as described under "recommended procedure".

The SRM 2670 did not require mineralization and the sample was prepared from concentrates according to the directions supplied.

3. Results and discussion

3.1. Optimization of extraction conditions

Extraction of metal ions by an organic reagent is known to be dependent on several factors, such as type and amount of reagent, organic solvent, pH of solution, shaking time, etc. We have investigated the extraction process in order to obtain optimum conditions. IBMK has a significant solubility in water but was chosen as the organic solvent because of its high extraction efficiency for Cd(II), Co(II), Cu(II) and Ni(II)–DPTH complexes.

In a general previous study [31], the influence of the pH on the extraction of Cd(II), Cu(II), Co(II) and Ni(II) into IBMK containing DPTH was investigated. The results obtained showed that the optimum pH range for the quantitative extraction is different for each ion: Cadmium, 3.3–11.4; cobalt, 1.5–8.0; copper, 2.8–9.8 and nickel, 2.0–5.0. Therefore, pH 3.6, provided with glycine–HCl buffer, is adopted in all subsequent experiments. The volume of this buffer added had no effect.

The influence of the NaClO$_4$ concentration in the aqueous phase was examined. No appreciable variation in the percentage of extraction was observed, except for the Cu–DPTH complex; in this case and increase in the extraction was observed when the sodium perchlorate concentration was increased up to 0.025 M (Fig. 1). The optimal concentration of the anion was found to be 0.025 mol l^{-1} which was obtained by adding 5 ml of 1 mol l^{-1} NaClO$_4$ to 200 ml of aqueous phase.
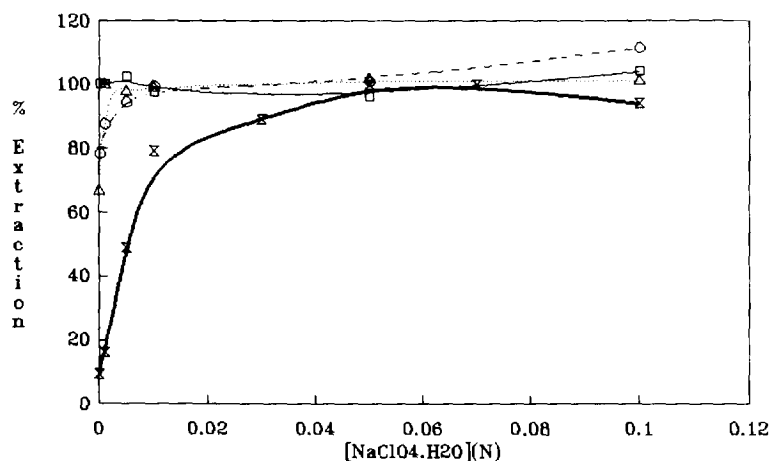
Fig. 1. Influence of perchlorate concentration on the extraction. Concentration of each ion in the aqueous phase: 50 ng ml^{-1}. Concentration of DPTH in the organic phase: 2.3×10^{-3} M. Shaking time: 10 min. Aqueous to organic phase volume ratio: 20. □, Cd; △, Co; ⨉, Cu; ○, Ni.

The minimum shaking time was determined by varying the shaking time from 0 to 10 min (Fig. 2); 3 min was found to be sufficient, however, prolonged shaking had no adverse effect on the extraction of metal ions and 5 min was selected for subsequent experiments.

The reagent concentration in the organic phase was varied while keeping its final volume at 10 ml. The results obtained (Fig. 3) showed that the extracted fraction remains constant for DPTH concentrations equal to or greater than 1.37×10^{-3} mol l^{-1} (0.06%). A concentration of 2.3×10^{-3} mol l^{-1} (0.1%) was used in practice in order to prevent depletion by other extractable ions potentially occurring in the aqueous medium.

The extraction of metal ions was found to be quantitative up to an aqueous-to-organic phase volume ratio of 20, above which the organic phase volume was insufficient for the sequential determination of the four metal ions, because when the volume of the aqueous phase was increased, the volume of the organic phase after extraction decreased, for the reason that IBMK is not totally immiscible with water; however, the quantitative extraction of the metal ions could be verified from the analysis of the aqueous phase. When a phase ratio of 20 was used (200 ml of aqueous phase and 10 ml of organic phase), only approximately 5 ml of organic phase was ob-

tained after extraction hence the phase ratio is actually 40. This phase ratio allows the sensitivity of the direct non-extractive method to be increased by a factor of approximately 40.

3.2. Selection of measurement conditions

Several wavelengths were investigated for each metal. The following ICP lines were selected: 228.802 nm for cadmium, 237.862 nm for cobalt, 324.754 nm for copper and 352.454 nm for nickel. These wavelengths were selected using the minimum background equivalent concentration (BEC) as the optimization criterion. Other operating variables such as type of nebulizer, nebulizer flow rate, photomultiplier voltage and plasma observation height were established to achieve the best signal-to-noise (S/N) ratios. The operating conditions for the spectrometer are recorded in Table 1.

3.3. Calibration graph: precision and detection limit

The relationship between each metal concentration and emission intensity was studied in the range 0–1000 ng ml^{-1} of metal ion in the aqueous phase. A linear calibration graph was obtained for every metal ion in this range when an aqueous-to-organic phase volume ratio of 20
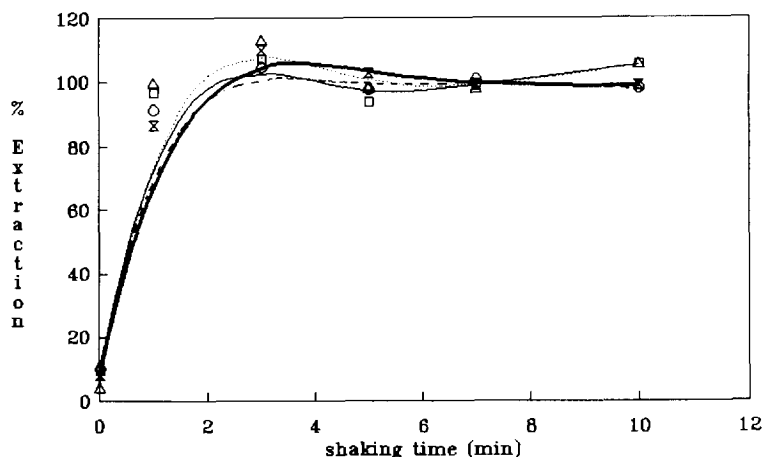
Fig. 2. Influence of shaking time on the extraction of 50 ng ml^{-1} of Cd, Co, Cu, and Ni in the presence of perchlorate (0.025 M). Concentration of DPTH: 2.3×10^{-3} M. Aqueous to organic phase volume ratio: 20. Symbols as in Fig. 1.

was used with a slope of 86.6 for Cd, 36.3 for Ni, 44.8 for Co and 418.9 for Cu. The blank levels for the analytes were: 1.9 ± 0.2 ng ml^{-1} for Cd, 10 ± 1.0 ng ml^{-1} for Ni (the presence of IBMK in the extractant produced a considerable background at the Ni lines), 1.7 ± 0.9 ng ml^{-1} for Co and 0.3 ± 0.1 ng ml^{-1} for Cu.

The limits of detection and determination of the method were established according to American Chemical Society Committee of Environmental Improvement definitions [32]. The values found for each metal when an aqueous-ot-organic phase volume ratio of 20 was used are listed in Table 2.

Under the optimum conditions, ten determinations of standard solutions containing 10 ng ml^{-1} of each metal ion in the aqueous phase gave a relative standard deviation of 3.6% for Cd, 4.0% for Co, 3.0% for Cu and 4.4% for Ni; and for 100 ng ml^{-1} (aqueous phase) gave 1.9%, 1.8%, 2.1% and 0.8% respectively.

3.4. Effect of foreign ions

The effect of various ions on the sequential determination of cadmium, cobalt, copper and nickel by the proposed method was examined under the optimum working conditions. For this study, different amounts of the ionic species tested were added to 25 ng ml^{-1} solutions of Cd, Co, Cu and Ni in the aqueous phase, the volume of

which was 200 ml, whereas the organic phase was 10 ml. The starting point was an interferent-to-metal ion ratio of 4000 m/m; if any interference occurred, the ratio was gradually lowered until the interference disappeared. The tolerance limits found (Table 3) show that these ions can be sequentially determined in the presence of a variety of foreign ions including most of those which commonly occur with them in natural and synthetic samples. The tolerance level for some metal ions can be increased by addition of a masking agent (see Table 3). However, some interferences were minimized by the addition of glycine as a masking agent. For this reason the glycine–HCl buffer was chosen for the determination of these metal ions.

3.5. Sample analysis

In order to test the accuracy and applicability of the proposed method to the analysis of real samples, six biological reference materials mineralized as described under "Sample preparation" were analysed. The standard additions method was used and the results were obtained by extrapolation (similar results were obtained from the calibration graphs). These results, as the average of three separate determinations, are shown in Table 4. As can be seen, the metal concentrations determined by the proposed method are in close agreement with the certified values.
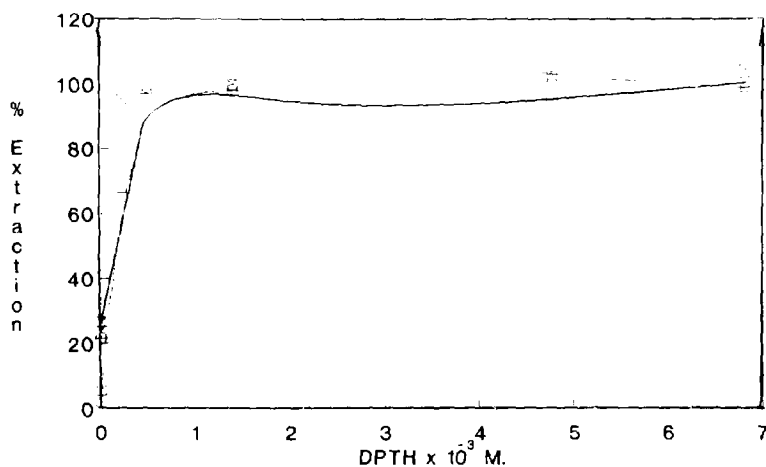
Fig. 3. Effect of reagent concentration (organic phase) on the extraction of 10 μg of Cd, Co, Cu and Ni. Aqueous to organic phase volume ratio: 20. Shaking time: 5 min. Symbols as in Fig. 1.

4. Conclusions

Two of the most frequently stated advantages of ICP as a source for emission spectrometry are its multi-element capability and low detection limits. However, in certain instances, detection limits possible with the ICP are still inadequate, especially when the sample has a complex matrix. There are also many sample matrices that present difficulties in their own right. Problems may arise due to the high dissolved solid content of the sample solution, which can cause erratic nebulization and salt build-up on the torch aerosol injector tip. In these circumstances, solvent extraction can provide valuable analyte separation from an interfering matrix. This study has shown that the

ICP method described enables the determination of Co, Cd, Cu and Ni in biological materials. Detection limits for Cu, Cd, Co and Ni ranged from 0.25 to 3.7 ng ml^{-1}, which compares favourably with other ICP-AAS methods [33].

Table 2
Limits of detection and determination

Element	Limit of detection (ng ml^{-1}; aqueous phase)	Limit of determination (ng ml^{-1}; aqueous phase)
Cadmium	0.7	2.2
Cobalt	3.0	10.5
Copper	0.25	0.8
Nickel	3.7	10.8

Table 3
Tolerated levels of foreign species

Species	Tolerated ratio (m/m)
Alkali metal ions, alkaline earth metal ions except Sr(II), sulfate, nitrate, iodide, bromide, fluoride, ascorbic acid	>4000
Sr(II)	2500
Cr(III), Mo(VI), oxalate, phosphate, thiosulphate	2000
Mn(II), As(III), As(V), thiourea	1500
Pb(II)	1000
Zn(II), Hg(I), Fe(III)[a], Fe(II)[b]	500
Al(III)	400
Hg(II)	250
Sb(III), Ag(I)	200
Bi(III)	150

[a] Using NaF at a concentration 3000 times higher than that of Cd, Co, Cu, Ni.
[b] As for [a] plus 1 drop of H_2O_2.

Table 4
Determination of metal ions in biological samples

Sample	Metal	Certified (μg g^{-1})	Found (μg g^{-1})[a]
BCR CRMs 061	Cd	1.07 ± 0.08	0.96 ± 0.52
Platihypnidium	Co	(43)	43 ± 2
ripariodides (aquatic moss)	Cu	720 ± 31	717 ± 34
	Ni	(420)	412 ± 31
BCR CRMs 176	Cd	470 ± 9	495 ± 1
City wast incineration ash	Co	30.9 ± 1.3	25.1 ± 2.2
	Cu	1302 ± 26	1288 ± 80
	Ni	123.5 ± 4.2	87.8 ± 4.2
NRCC CRMs TORT-1	Cd	26.3 ± 2.1	22.6 ± 0.1
Lobster hepatopancreas	Co	0.42 ± 0.05 + 50 added	51.73 ± 2.41
	Cu	439 ± 22	471 ± 7
	Ni	2.3 ± 0.3 + 50 added	59.3 ± 2.2
BCR CRMs 186	Cd	2.71 ± 0.15	3.12 ± 1.36
Pig kidney	Co	49.3 added	46.6 ± 1.3
	Cu	31.9 ± 0.4	29.8 ± 5.8
	Ni	(0.42) + 48.13 added	50.65 ± 5.88
NRCC CRMs DOLT-1	Cd	4.18 ± 0.28	4.53 ± 1.50
Dogfish liver	Co	0.157 ± 0.037 + 49.348 added	43.425 ± 1.430
	Cu	20.8 ± 1.2	22.8 ± 8.3
	Ni	0.26 ± 0.06 + 50.22 added	50.51 ± 3.24
NIST SRM 2670	Cd	0.088 ± 0.003	0.077 ± 0.013
Human urine elevated level	Co	0.26 added	0.33 ± 0.03
(μg ml^{-1})	Cu	0.37 ± 0.03	0.37 ± 0.01
	Ni	(0.30)	0.31 ± 0.15

[a] Mean ± standard deviation for two replicate measurements of three individual sample preparations.

Acknowledgements

References

[1] A.A. Brown, S.J. Halls and A. Taylor, J. Anal. At. Spectrom., 3 (1988) 45.

[2] A. Aziz, J.A.C. Broekaert and F. Leis, Spectrochim. Acta, Part B, 37 (1982) 369.

[3] V. Karanassios, J.M. Ren and E.D. Salin, J. Anal. At. Spectrom., 6 (1991) 527.

[4] R.V. Whiteley and R.M. Merril, Fresenius'Z Anal. Chem., 311 (1982) 7.

[5] A. Miyazaki, A. Kimura, K. Banzho and Y. Umezaki, Anal. Chim. Acta, 114 (1982) 214.

[6] J.S. Jones, D.E. Harrington, B.A. Leone and W.R. Bramstedt, At. Spectros., 4 (1983) 49.

[7] M. Roura, G. Rouret, F.R. Inern and P. Sánchez, Quim. Anal., 3 (1984) 229.

[8] V.Z. Krasil'shchik, E.I. Voropaev, G.A. Voronina, G.G. Butrimenko and M.S. Chupakhin, Zh. Anal. Khim., 43 (1988) 1170.

[9] K. Yamagaki, T. Takahashi, K. Yamada, M. Yoshii and T. Suzuki, Bunseki Kagaku, 37 (1988) T181.

[10] K. Bachmann, Crit. Rev. Anal. Chem., 12 (1981) 1.

[11] J. Minczewski, J. Chwastowska and R. Dybczynski, Separation and Preconcentration Methods in Inorganic Trace Analysis, Wiley, New York, 1982.

[12] M.S. Cresser, Solvent Extraction in Flame Spectroscopic Analysis, Butterworths, London, 1978.

[13] D. Tsalev and I. Petrov, Anal. Chim. Acta, 111 (1979) 1555.

[14] K.M. Bone and W.D. Hibbert, Anal. Chim. Acta, 107 (1979) 219.

[15] R. Rubio, J. Huguet and G. Rauret, Water Res., 18 (1984) 243.

[16] R.P. Sharma, J.M. Mckenzie and T. Kjellstrom, J. Anal. Toxicol., 6 (1982) 135.

[17] R.T. Tulley and H.P. Lehmann, Clin. Chim. Acta, 122 (1982) 189.

[18] M. Tominge and Y. Umezaki, Bunseki Kagaku, 28 (1979) 2495.

[19] E.E. Kaminiski, Anal. Chem., 46 (1974) 1304.

[20] D. Chakraborti, F. Adams, W. Van Mol and K.J. Irgolic, Anal. Chim. Acta, 196 (1987) 23.

[21] P.W. Bearpre, W.W. Holland and D.J. Mckenney, Mikrochim. Acta, Part II, (1983) 415.

[22] M. Stoeppler and K. Brandt, Fresenius'Z. Anal. Chem., 300 (1980) 372.

[23] Z. Zhov, Gaodeng Xuexiao Huaxue Xuebao, 4 (1983) 179.

[24] G. Severin, E. Schumacher and F. Umland, Fresenius'Z. Anal. Chem., 311 (1982) 205.

[25] R.E. Sturgeon, S.S. Berman and S.N. Willie, Talanta, 29 (1982) 167.

[26] H. Watanabe, K. Goto, S. Taguchi, J.W. McLaren, S.S. Berman and D.S. Russell, Anal. Chem., 53 (1981) 738.

[27] C.M. McLeod, A. Otsuki, K. Okamoto, H. Haraguchi and K. Fuwa, Analyst, 106 (1981) 419.

[28] J.R. Bonilla Abascal, A. García de Torres and J.M. Cano Pavón, Microchem J., 26 (1981) 55.

[29] E. Vereda Alonso, A. García de Torres and J.M. Cano Pavón, Analyst, 117 (1992) 1157.

[30] P. Cañada Rudner, A. García de Torres and J.M. Cano Pavón, J. Anal. At. Spectrom., 8 (1993) 705.

[31] J.M. Cano Pavón, E. Vereda Alonso, C. Bosch Ojeda and A. García de Torres, Anal. Lett., 24 (1991) 153.

[32] ACS Committee on Environmental Improvement, Anal. Chem., 52 (1980) 2242.

[33] V. Porta, C. Sarzanini, O. Abollino, E. Mentasti and E. Carlini, J. Anal. At. Spectrom., 7 (1992) 21.

Review

Electrochemical analysis of surfactants: An overview

M. Gerlache[a], J.M. Kauffmann[a,*], G. Quarin[a], J.C. Vire[a], G.A. Bryant[b], J.M. Talbot[b]

[a]Institut de Pharmacie, Université Libre de Bruxelles, Campus Plaine 205/6, Bvd du Triomphe, 1050 Bruxelles, Belgium
[b]Colgate–Palmolive, Research & Development Inc., Avenue du Parc Industriel, 4041 Herstal, Belgium

Abstract

This work presents an overview of electrochemical techniques, namely potentiometry, amperometry, tensammetry, electrocapillary measurements and biosensors, recently applied for the determination of surfactants.

Keywords: Surfactant; Electrochemistry; Analysis

1. Introduction

Surface-active agents (surfactants) are produced worldwide in large amounts. The total world consumption was 4 500 000 tonnes in 1993 [1]. A surfactant is an amphiphilic molecule which contains in its structure a hydrophobic non-polar part and a polar part whose structures may differ according to the nature of the tensio-active molecule. Table 1 shows the global repartition between the four groups of surfactant [2].

Surfactants are widely used in household or industrial cleaners, cosmetics, research laboratories, etc. Even though at the present time most tensio-active products used are biodegradable, their accumulation, or the accumulation of their

biodegradation products in natural waters, induces water pollution which can, in extreme conditions, lead to the destruction of the surface water fauna and flora [3–8]. The literature devoted to the determination of surfactants is greatly expanding and a number of applications are oriented towards the analysis of environmental samples [9–11] and in the quality control of manufactured products [9,11].

The most widely used technique in surfactant analysis is the so-called two-phase titration. In this method, the surfactant is extracted in an organic hydrophobic solvent ($CHCl_3$) as a lipophilic ion-pair formed with the titrant. The latter is generally a surfactant of opposite charge. The titration is carried out in the presence of an ionic dye (or a mixture of ionic dyes) which colours the organic layer differently in the presence of an excess of anionic or cationic surfactants [9,12–16]. This procedure is currently used

---

as a standard method; however, it suffers from several drawbacks (Table 2).

Alternative analytical methods have been developed such as spectrophotometry [17-20], ion pairing [21] and thin-layer chromatography [22,23], gas chromatography after derivatisation or thermal decomposition [24,25], HPLC coupled with conductimetric detection or post-column extraction and UV detection [11,26-32] capillary electrophoresis with UV detection and electrochemistry [11,33]. This review is intended to provide an overview of recent electroanalytical methods devoted to surfactant analysis.

2. Potentiometry

Volumetric titration of a surfactant can be carried out in the presence of an ion-selective electrode (ISE) with potentiometric end-point detection. During the assay, the titrant and the surfactant to be analyzed form an ion-pair insoluble in water. Before the equivalent point, the analyte is in excess and, afterwards, the titrant is in excess. The electrode may be sensitive to the analyte or to the titrant. Basically, the electroactive part of an ISE membrane consists of an association of an ion-pair (C^+A^-): where A^- is an anionic surfactant (AS) and C^+ is a positively charged counter ion, e.g. a cationic surfactant (CS). This kind of ISE is suitable for the detection of A^- and C^+.

Three different types of ISEs have been developed: liquid impregnated inert membrane ISEs, conventional polymeric membrane ISEs (comprising an internal reference cell), and polymeric-coated wire ISEs.

2.1. Liquid impregnated membrane electrodes

The shape of this kind of electrode is approximately the same for all ISEs (Fig. 1a). A glass tube is stoppered at one end with a Teflon membrane or a hydrophobic glass frit impregnated by the sensing solution [9]. This solution is an ion-pair, e.g. hexadecyltrimethyl ammonium-dodecylsulphate [9], dissolved in a hydrophobic organic solvent often belonging to the nitroaromatic derivatives. The inner body of the electrode is filled with a

Table 1
World surfactant consumption by surfactant type [2]

Surfactant type	Consumption (%)
Anionic surfactant (AS)	59
Non-ionic surfactant (NS)	33
Cationic surfactant (CS)	7
Amphoteric surfactant (ZS)	1

Table 2
Drawbacks of the two-phase titration technique used in surfactant analysis.

Formation of an emulsion during titration (the interface between the two phases is not well defined)
Turbidity of the solution when analyzing a complex sample
Interferences by many other components (ClO_4^- , SCN^-, NO_3^- , . . .)
Toxicity of the chlorinated organic solvent ($CHCl_3$)
Time-consuming
The ion-pair must be lipophilic, i.e. the procedure is not applicable to NS or ZS titration
Automation is difficult

chloride solution of a diluted anionic surfactant and a Ag/AgCl reference electrode is dipped into this internal solution. The measurements are realized versus a second reference electrode (Ag/AgCl or SCE). Other liquid-membrane-based ISEs have been developed [9,34-37]. Ishibashi et al. [34] used a Crystal Violet salt (Fig.
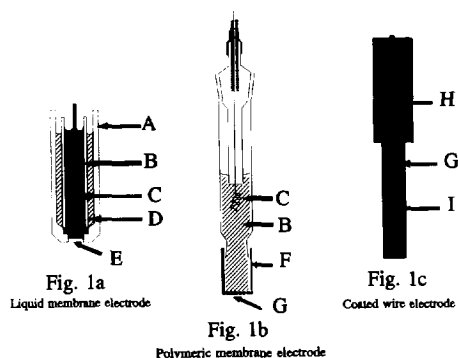

Fig. 1. Potentiometric electrodes. A: electrode body; B: inner solution; C: internal reference electrode; D: inner body; E: glass frit; F: PVC tube; G: polymeric membrane; H: electric insulating body; I: metallic or graphite wire.

Fig. 1a
Liquid membrane electrode

Fig. 1b
Polymeric membrane electrode

Fig. 1c
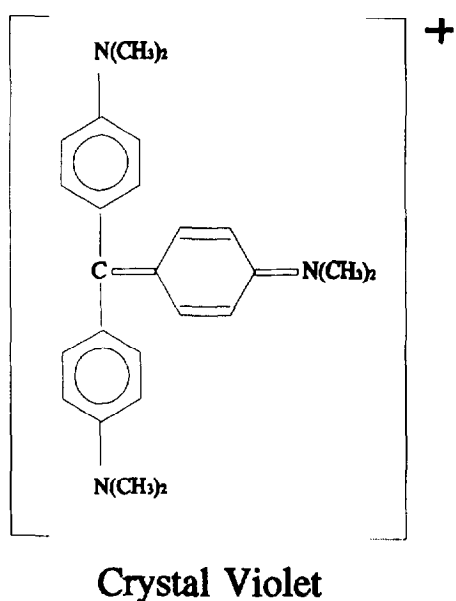Coated wire electrode

Crystal Violet

Fig. 2. Structure of the Crystal Violet ion.

2) in a nitrobenzene or 1,2-dichloromethane matrix as the active sensing part. This electrode is sensitive to aromatic sulfonates. The advantage of this membrane is the presence of hydrophobic groups in the Crystal Violet molecule which limit the dissolution of the sensing solution in aqueous samples. Sap et al. [37] used an Fe(II) bis [2,4,6-tri(2-pyridyl)]-1,3,5-triazine complex embedded in the sensor for the analysis of ASs such as dodecyl sulphate (DS^-). The authors reported a linear response range between 7×10^{-6} and 1.5×10^{-3} mol l^{-1} without any interference from inorganic salts. This ISE, however, is also sensitive to other organic ions. In such titrations, the end point is detected by a potential jump whose magnitude increases with the alkyl chain length of the surfactant (formation of a more hydrophobic ion-pair). A successful ISE for the titration of CS with sodium tetraphenylborate has also been developed [9]. The reaction mechanism will be discussed below.

Two major problems encountered with all liquid membrane electrodes are the drift of the potentiometric signal with time and a risk of membrane dissolution in the aqueous phase when the concentration of the surfactant approaches the critical micelle concentration (CMC). Actu-

ally, it is practically impossible to use liquid membranes in direct potentiometric measurements of surfactants. The electrodes are generally applied for end-point detection in volumetric titrations. A comparison of the results obtained with the electrode of Anghel et al. [35] and the two-phase titration procedure reveals great accuracy for both techniques. However, the analysis of commercial cosmetic products and washing powders gives better results with the potentiometric titration method [35].

2.2. Conventional polymeric membrane ISEs

Liquid membranes have been replaced by plasticised polymeric membranes. These electrodes are more robust and less sensitive to solubilization in aqueous media. The success of this kind of electrode is related to its simple membrane design (Fig. 1b) [38]. The first step of the fabrication consists of dissolving a polymer (generally PVC), a large amount of plasticiser, and the sensing component in an organic solvent (e.g. THF or cyclohexanone). The latter is allowed to evaporate, leaving a dry membrane. Then, the membrane is adjusted onto the body of the electrode. Using a plasticiser:PVC ratio of 70:30, this type of membrane can be regarded as a single phase homogeneous mixture [12]. The choice of the plasticiser is of considerable importance. The nature of this compound will influence the slope and the linear range of the ISE response. The amount of plasticiser determines the stability and the longevity of the electrode. Ortho-nitrophenyl octyl ether (NPOE) [2,12,36,39–53] and nitrophenyl phenyl ether (NPPC) [12,39,46,54–56] are currently the most commonly-used plasticisers. The polymeric substance must be insoluble in water and chemically compatible with the plasticiser and the sensing material. Moreover, the glassy transition temperature (T_g) of the membrane mixture must be below the working temperature. Note that the T_g of PVC is $+81°C$, but it falls to $-65°C$ when mixed with 70% of NPOE. However, due to the deleterious effect of the surfactants, direct measurements using polymeric membrane ISEs still suffer from instability of the electrode potential [9].

The first PVC-based ISEs used in surfactant titrations were nitrate and calcium ISEs, sensitive to AS and AS or CS respectively. However, it can be understood that these electrodes suffer from many interferences such as bivalent cations (Mg^{2+}, Sr^{2+}, ⋯) for the calcium ISE and anions (Cl^- or SCN^-) for the nitrate ISE. As explained above, the electrodes are sensitive to the variation of either the analyte or the titrant concentration. This explains why the nature of the titrant used can greatly influence the evolution of the titration. The titrant is usually sodium dodecylsulfate or tetraphenylborate for the determination of ASs. It is N-benzyl-N,N-dimethyl-N-[4-1,1,3,3-tetramethyl-butyl) - phenoxyethoxyethyl] - ammonium chloride (commercial name: Hyamine 1622), cetylpyridinium chloride or 1,3-dodecyl-2-methyl imidazolium [2,51,57] (commercial name: TEGOtrant A100; Metrohm) for the determination of CSs. The molecule of TEGOtrant A100 is more hydrophobic than Hyamine 1622 (Fig. 3) and its use gives higher potential jumps than with Hyamine. Moreover, the TEGOtrant permits the detection of alkyl sulphates with shorter chain lengths and less lipophilic molecules [57].

Today, it is possible to find some commercial ISEs specifically constructed for surfactant analysis, e.g. Orion model 93-42 [49,53], ASTEC model TSE 01/91 [48,51] and, more recently, the Metrohm "High Sense Tenside" ISE [2,41,42,51] whose sensing part is based on PVC + NPOE + an appropriate ionophore. The latter electrode is

Hyamine 1622
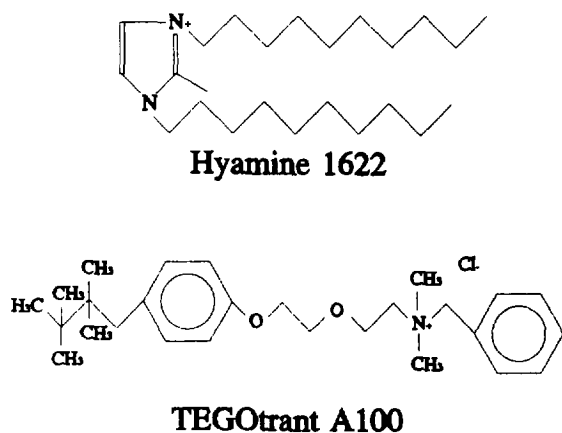
TEGOtrant A100

Fig. 3. Structure of Hyamine 1622 and TEGOtrant A100.

able to work for more than 7 months with a relative standard deviation (RSD) of between 0.2 and 1.3% for ASs [51]. The High Sense Electrode is stable over a wide pH range [1–12] and its use permits differentiation between some detergents in mixtures simply by changing the pH of the analyzed sample [57]. The successful analysis of a soap/alkyl sulfonate or amine/quaternary ammonium mixture has been reported [57]. Another important advantage of this electrode is its linear response over a large range of surfactant concentration. Recently, Szczepaniak and co-worker [48,50] proposed a mercurated organometallic polystyrene (R–Hg–Acetate) as the active sensing part in a PVC-ISE for AS determination. The plasticiser is a 1:1 mixture of NPOE and dodecyl phthalate. This electrode shows a Nernstian response (59 mV per decade of surfactant concentration) for many surfactants with response times of 10 s and 1 min for 1×10^{-3} and 1×10^{-6} mol l^{-1} of SDS respectively.

Buschmann and co-workers [2,41] have demonstrated that a PVC–NPOE–ionophore ISE is suitable for the determination of amphoteric (ZS) and cationic (CS) surfactants. Amphoteric surfactants are composed of a hydrophobic chain ending in two different polar groups, e.g. an amido or ammonium group at one site and a carboxylate or sulfonate group at the other. At pH < 1.5, the ZS reacts as a CS and can be titrated by a bulky counter ion such as tetraphenyl borate. Here, the ionophore is a TPB$^-$ – TPP$^+$ (tetraphenyl phosphate) or a TPB$^-$ –CP$^+$ (cetylpyridinium) ion-pair [41]. Using this procedure it is possible to detect a ZS in the presence of a CS by volumetric titration because the potential jumps are significantly distinct, the RSDs being 2 and 7.5% respectively.

Non-ionic surfactants (NS) have also been analyzed by potentiometric titration. Moody and co-workers [54,55] and Buschmann and co-workers [41,51] take advantage of the fact that the ethoxylated part of NSs can be complexed with a bivalent cation such as Ba^{2+}. The positive complex is titrated with TPB$^-$. Jones et al. [54] report a detection limit of 1×10^{-7} mol l^{-1} for Antarox 880. However, the analysis takes more than 1 h. Modified PVC electrodes with functional end

groups have also been tested [58,59] but, up to now, these probes do not seem to be as effective as the others.

All the described PVC membranes are homogeneous. The sensing material, e.g. an organic anion in the case of an electrode sensitive to CSs, is dissolved in this membrane. However, homogeneity is not an absolute criterion and an electrode sensitive to CSs can be constructed with a carrier insoluble in the membrane matrix. A synthetic clay, laponite, has been recently used as active material for such a membrane. The results obtained with this configuration are similar to those obtained with a "classical" membrane, e.g. a linear response of the potential is observed between 5×10^{-7} mol 1^{-1} and the CMC for dodecyltrimethylammonium with a response time of 1 s. An extended electrode life time of more than 1 month is reported [60].

2.3. Polymeric-coated wire electrodes

The titration of surfactants with an ISE having no inner solution (Fig. 1c), the so-called coated wire electrode (CWE), has been performed. In a CWE, a metallic or a carbon wire is coated with a plasticized polymer/ionophore solution. The electrode is ready after solvent evaporation. The nature of the metallic wire may interfere with the electrode response if the coating is non-uniform [61], and it also has to be chemically inert towards the membrane components [45]. Aluminium [12,43–45,47,56], graphite [62–64] and platinum [9] are commonly used as substrates. CWEs exhibit interesting properties, they can be machined in any shape, and they are characterized by a fast response time due to the reduced thickness of the membrane layer. They do exhibit, however, a shorter life time and a higher potential drift. For this reason, CWEs are better applied under hydrodynamic conditions, e.g. in flow-injection analysis, where the contact of the sample plug with the electrode surface is brief.

An interesting membrane has been constructed by Dowle and co-workers [63–65]. It is prepared by coating a graphite rod with a PVC solution containing tritonyl phosphate (TTP) plus an appropriate ionophore (0.1%). The latter is tetrade-

Table 3
Characteristics of the electrode of Dowle et al. [63] in a potentiometric titration

Linear range (SDS)	1×10^{-2}–1×10^{-6} mol 1^{-1}
Reproducibility:RSD	2% for 1×10^{-4} mol 1^{-1} SDS
Potential jump	80–250 mV
Response time	30 s
Insensitive to inorganic salts	
Not influenced by the presence of ethanol	(max. 20%)

cylammonium dodecyl sulphate which is sensitive to ASs. The characteristics of this electrode are summarised in Table 3. This electrode operated well in ethanolic solutions (20% v/v) and can be used under flow conditions such as in HPLC. Later, this CWE was redesigned and integrated into a flow-through system [64]. The inner side of a graphite tube was coated with the active membrane. The disadvantages are a relatively poor life time and the need to calibrate the electrode several times per day.

The group of Vytras [43,44] has elaborated a CWE able to follow titration of CSs and ZSs by TPB$^-$. The addition of Ba^{2+} in the membrane permitted titration of NS. Results reported for the determination of the mean oxyethylene unit numbers per one TPB$^-$ ion are in the same range as those obtained by Gallegos [49] using an Orion electrode. The electrode appears to be stable for more than 7 months of intensive use [44].

A recent communication of Lowy et al. [62] shows the utilization of heteropolyanions (HPAs) for quaternary ammonium titrations. HPAs (α-P$_2$CoMoW$_{16}$O$_{61}$(H$_2$O)$^{8-}$) exhibit a high symmetry, high stability and are not influenced by the presence of inorganic salts, neutral and anionic organic molecules (alcohol, acrylonitrile, propanenitrile). The characteristics of HPAs in surfactant titration are reported in Table 4.

All of the above-mentioned electrodes are based on polymer membranes that dissolve when used in organic solvents. Actually, solid state and conventional polymeric electrodes which do not dissolve in mixed aqueous–organic titration systems are still needed.

3. Amperometry

The general measuring principle in amperometric analysis of surfactants is based on the monitoring of a faradaic current at an electrode, for a selected potential, due to the electrolysis of an electroactive species. Usually, the surfactant is not electroactive and it is necessary to use an indirect amperometric technique. In this case, the solution contains a certain amount of an electroactive species (a marker) which is oxidized or reduced amperometrically at the working electrode. The current due to the marker decreases in the presence of surfactant, which inhibits the electronic transfer at the electrode surface, and the concentration of surfactant can be related to the magnitude of the current decrease.

3.1. Indirect amperometric techniques

Polarographic maximum suppression by a surface-active substance can be used to determine, at a mercury electrode, the concentration of surfactants in solution. In polarographic measurements, faradaic current begins to flow as the electrode approaches the reduction or oxidation potential of the electroactive species involved. A classical polarogram has a sigmoidal shape and the electrochemical process is, at the wave plateau, usually controlled by adsorption, diffusion or kinetic parameters [66]. However, often, a greater current than the limiting current may appear; this is called a polarographic maximum. The amplitude of the maximum is affected by the presence of surfactants and it is possible to correlate the amount of a surfactant to the decrease of the maximum current, i.e. maxima of Hg(II) or oxygen [67–69]. The technique of polarographic maxima suppres-

Table 4
HPA as CS titrant [62]

Slope	55–58 mV per decade
Linear range (CS)	2×10^{-5}–1×10^{-2} mol l^{-1}
Limits of detection of the order of	1×10^{-6} mol l^{-1}
RSD lower for HPA than for SDS or TPB⁻	

sion (TPMS) shows, however, limited selectivity. Actually, all impurities which are able to be adsorbed at a given potential on the electrode, such as those present in distilled water, in reagent-grade chemicals, in mercury, in containers, can be a source of interferences [66]. For this reason, the analysis of surfactants by the TPMS requires preferably one or more separation steps. Moreover, the experimentation is not always easy to perform. If the concentration of the surfactant is too high, the polarographic maximum is totally suppressed but the polarographic wave may be affected as well [66,70]. In fact, the total maximum suppression corresponds to a coverage of the electrode surface by 1/20 or 1/100 of the amount able to modify the faradaic process. This corresponds to 0.1% coverage of the surface [71]. The theory of TPMS can be found in the books by Bard [66] or Heyrovsky and Kuta [70]. The restricted useful concentration domain plus the lack of specificity are the main disadvantages of the TPMS and probably explain the limited interest devoted to this technique. However, the inhibition of a faradaic process can be advantageously exploited by other techniques.

The adsorption of a surfactant on the electrode surface can be monitored by its influence on the voltammetric response of an electroactive species at this electrode. For instance, the study of the reduction of a metal ion at a hanging mercury drop electrode (HMDE) through the adsorbed layer can lead to information on the surfactant concentration in solution [72]. In a similar approach, using a modified graphite working electrode, Skoog et al. [73] studied ASs, CSs and NSs by their influence on the amperometric and cyclic voltammetric responses of hexacyanoferrate. In a flow system, they noted that the presence of NSs has an irreversible blocking effect on the electrode response which required tedious surface reconditioning before further analysis.

The suppression by a surfactant of the adsorptive voltammetric response of the nickel–dimethylglyoxime complex at an HMDE, a glassy carbon mercury-film-coated electrode or a dropping mercury electrode was also reported [74,75]. Here, in contrast to the theory, the current decrease is approximately proportional to the sur-

factant concentration. However, the response is linear only within a narrow range of surfactant concentration: 0.5–3 mg l^{-1}, 0–65 mg l^{-1}, 0–300 μg l^{-1} for linear alkylbenzene sulfonate [74], hexadecyltrimethylammonium bromide [75] and cetyl pyridinium chloride [75] respectively. With the same method, it is possible to analyze both types of ionic surfactants. The reported limit of detection is 100 ppb for alkybenzene sulfonates. Tested in environmental and industrial conditions, this technique has the drawback of being influenced by some interfering materials which are also able to be adsorbed [74,75]. The study of the inhibition of *para*hydroquinone oxidation at a graphite electrode in the presence of a surfactant (phospholipid) was recently reported [76]. A decrease of the oxidation peak is observed by raising the surfactant concentration. Phospholipids in amniotic fluids were also determined by their inhibition of the oxygen reduction at the DME [77].

3.2. Modified gold electrode

In commercial formulations, surfactants are mixed in matrices which are becoming more and more complex. A first separation step is often required to eliminate interfering species (e.g. chromatography, BiAS precipitation, etc). For routine analysis, however, it is of interest to develop techniques which are able to work directly in such complex media. A self-assembled monolayer (SAM) modified gold electrode may be used for this purpose. Recently, Kawaguchi et al. [78] took advantage of the perturbation of a lipidic membrane structure fixed at a gold electrode to elaborate a new electrochemical assay for surfactants. The authors modified the surface of a clean gold electrode by chemisorbing a monolayer of alkane thiol [78]. The pretreatment of the surface is essential as it will define the characteristics of the SAM electrode [79–82]. The cleaning consists of polishing the gold surface with alumina or diamond paste and rinsing with a solvent (water, chloroform, ethanol, etc.) [77,79–83]. The structure of the alkane thiol SAM is quasi-crystalline [80,82], the alkyl chains are oriented primarily in an all-trans configuration and are nearly close packed (a $\sqrt{3}$x$\sqrt{3}$ $R30°$ adlattice forms on

Au) [79,84]. This monolayer represents a physical barrier between the electrode surface and an electroactive marker in solution (e.g. hexacyanoferrate) (Fig. 4a). The sensitivity of the SAM–Au electrode to the redox behaviour of Fe^{3+} [77], $Fe(CN)_6^{3-}$ [77,78,85], ferrocene dimethanol [85] and $Ru(NH_3)_6^{3+}$ [85] marker ions is very poor. However, the presence of a surfactant in solution will change the organisation of the SAM allowing one to observe the electroactivity of the marker (Fig. 4b). For instance, no reduction current of $Fe(CN)_6^{3-}$ ions is detected by cyclic voltammetry at an alkylthiol-modified SAM gold electrode (Fig. 5a, b) [86]. The introduction of a CS into the solution gives an increase of the reduction current (Fig. 5c). This current increase is related to the CS concentration and can be exploited by amperometry in flow-injection analysis (FIA) (Fig. 6) [86]. A linear response is obtained for cetyltrimethylammonium chloride solution (CS) between 5×10^{-6} and 1×10^{-3} mol l^{-1} with a response time of less than 2 s. The precise reaction mechanism of the observed phenomenon is not yet explained. It might be related to the formation of an ion-pair between the CS and the redox tracer which could diffuse through the monolayer and could be reduced at the gold electrode surface [77]. The electrode response is quite selective, i.e. by replacing CS by AS or NS only a weak baseline current decrease is observed. This can be the result of a steric effect and/or electrostatic repulsion [77].

The advantage of using a gold electrode modified with alkane thiol is related to the strong covalent bond between gold and the modifier sulphur head [87]. Methanol can be present in the solution since its presence is not affecting the SAM layer and it is possible to perform flow-injection or HPLC analysis [79]. The SAM electrode may be functionalized by judicious selection of the thioalkyl modifier allowing improved selectivity [85,88–90].

3.3. Carbon paste electrode

Recently, other sensor matrices have been investigated. Carbon paste electrodes (CPEs) have been considered since they are readily modified
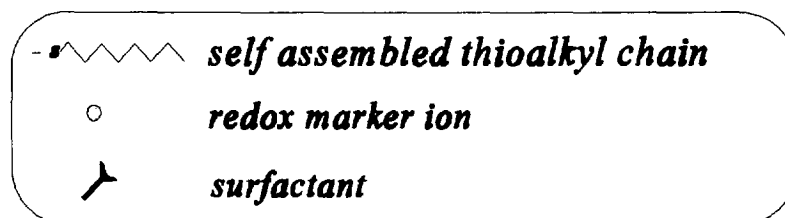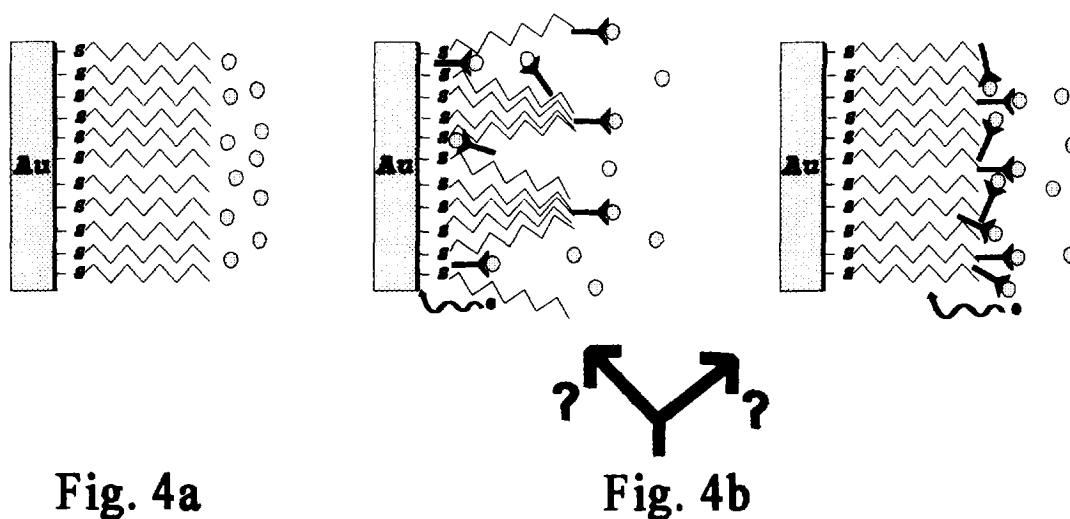
Fig. 4. Schematic of the alkane thiol SAM gold electrode: (a) in the absence of surfactant; (b) in the presence of surfactant.

and display a very low residual current in a large potential range. Kim et al. [91] use ferrocene in the CPE as a redox tracer. They report a modification of the redox behaviour in the presence of different surfactants. In the presence of sodium dodecylsulphate, the oxidation peak current of ferrocene is enhanced by a factor of 3.5 [91]. A limitation of the technique is its duration since the electrode–solution contact time is 1 h. Change in the CPE surface area (erosion) is likely to occur in the process but clear explanation of the observed behaviour is not reported.

4. Tensammetry

The determination of electroinactive molecules which are surface active can be performed by another indirect technique, tensammetry. Tensammetry is the study of the differential capacity–potential curves and of parameters which are able to modify the double layer capacity, such as:

nature and concentration of an adsorbed species (here surfactant);

applied electrode potential (corresponding or not to the potential of maximum adsorption);

kinetic parameters (mass transport, adsorption rate, stirring, frequency of the superimposed alternative potential, ···).

The capacitative curves measured under conditions of adsorptive equilibrium present, in the ideal case, five different potential domains [92]. There is one central domain where the capacity passes through a minimum value which diminishes when the concentration of surfactant increases (domain III in Fig. 7). This corresponds to the maximum of adsorption for one concentration. There are two domains (I and IV) at extreme potentials where no more adsorption takes place. And, between these minimum and maximum potentials of adsorption, there are two domains (II and IV) which are characterized by an increase of the capacity with the increase of the surfactant

concentration. Cases II, III and IV are of analytical interest and the relation between the capacitative values and the surfactant concentration depends on the type of adsorption isotherm (Henry, Langmuir, ...) [92]. It follows that the relation between C_d and C is complex and depends on the frequency of the alternating current used.

In the ideal case [92] of a HMDE, i.e. where the adsorptive parameters (concentration C, charge q, interfacial tension γ and relative superficial excess Γ) can be determined with good accuracy, the differential capacity (C_d) can be expressed, at the state of adsorption equilibrium, as

$$C_d = \frac{dq}{dE} = \left(\frac{\partial q}{\partial E}\right)_\Gamma + \left(\frac{\partial q}{\partial \Gamma}\right)_E \frac{d\Gamma}{dE} \qquad (1)$$

and, in the case of the Henry isotherm, the relative superficial excess is proportional to the concentration

$$R \cdot T \cdot \Gamma = B(E) \cdot C \qquad (2)$$

where B is a function of the applied potential and C is the concentration of the surfactant [92,93]. By combining Eqs. (1) and (2), it appears that the differential capacity is thus related to the concentration of surfactant by a complex relation
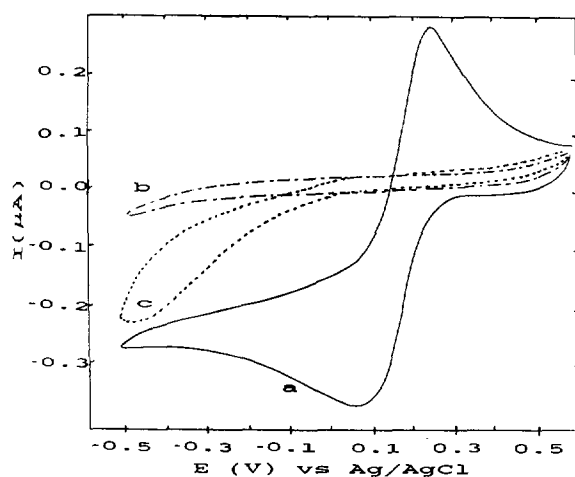
Fig. 5. Cyclic voltammograms of 1×10^{-4} mol l^{-1} Fe(CN)$_6^{3-}$ in 0.1 mol l^{-1} KCl. 0.025 mol l^{-1} acetate buffer pH 4.74 and 20% acetone at a bare gold electrode (a), at the SAM-modified gold electrode (b) and at the SAM-modified gold electrode in the presence of a CS (c). Scan rate 100 mV s^{-1}.
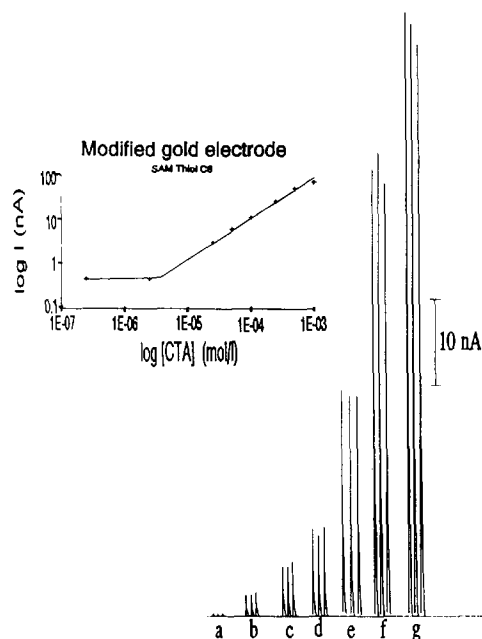
Fig. 6. FIA of cetyltrimethylammonium chloride (CTA). Amperometric reduction at a SAM-modified gold electrode (at 0.0 V vs. Ag/AgCl reference electrode). 20 μl injection of CTA at concentrations of (a) 2.5×10^{-6}; (b) 2.5×10^{-5}; (c) 5×10^{-5}; (d) 1×10^{-4}; (e) 2.5×10^{-4}; (f) 5×10^{-4}; (g) 1×10^{-3} mol l^{-1}. Carrier as in Fig. 5 plus 1×10^{-5} mol l^{-1} hexacyanoferrate.

$$C_d = \text{cte} + \left(\frac{\partial q}{\partial \Gamma}\right)_E \cdot \frac{C}{R \cdot T} \cdot \left(\frac{dB(E)}{dE}\right)_\Gamma \qquad (3)$$

where cte is equal to $(\partial q/\partial E)_\Gamma$ and corresponds to the value of the capacity for a given coverage. As it appears in Eq. (3), C_d is directly proportional to the surfactant concentration C provided that
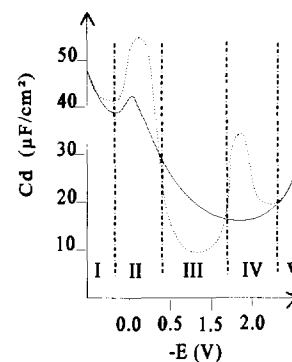
Fig. 7. Typical capacitance–potential curve for an aqueous solution of an analyte (——) and for an analyte in the presence of a surface-active substance (⋯).

the adsorption phenomenon follows the Henry isotherm. In other isotherms, e.g. Langmuir, Frumkin, ... the relationship is much more complex with no direct relation between C_d and C.

The presence of other compounds which are able to be adsorbed on the electrode surface reduces the selectivity and thus the applicability of tensammetry. Actually, one or more separation steps are necessary in complex sample analysis.

Bos et al. [94] used a gold electrode covered by a mercury film in a flow-injection system to analyze ionic and non-ionic surfactant solutions in the range 1×10^{-5}–1×10^{-4} mol l^{-1}. Generally, they applied a potential of -0.85 V (vs. Ag/AgCl) which corresponds to the analytically interesting domain.

One interesting application is the analysis of phospholipids [76] at the HMDE in acetonitrile–water–methanol media in the presence of LiClO$_4$ as support electrolyte. The C_d–E curves present a maximum at -1.65 V. This corresponds to the adsorption of the solvent at the HMDE. The diminution of the maximum of capacity at this potential with the increase of the concentration of phospholipids is the analytical information used to determine the quantity of phospholipids in solution. The variation of C_d with the concentration follows a sigmoidal curve. In FIA, a tensammetric peak is obtained which is the result of a "temporary" substitution of the solvent molecules by the phospholipids. The reported detection limit is 150–400 ng per 20 μl injection of phospholipid [76]. In their work, Schmidt and Emons [76] distinguish another domain of potential which can be used (corresponding to the central domain discussed before), but the range of concentration is less extended because of the formation of a limited superficial excess.

Szymanski and co-workers [95–99] have developed an indirect tensammetry method (ITM). Here, the analytical signal is the depreciation of the ethyl acetate peak current (at -1310 mV) by a competitive adsorption of NS at an HMDE. In this case, other molecules, i.e. AS, can be adsorbed but the authors took advantage of the fact that AS cannot be adsorbed at the HMDE if the potential is more negative than -1300 mV. They realised their tensammetric measurements from a starting

potential of -1400 mV and then scanned anodically [95]. A general discussion of mixed adsorption problems can be found in the paper by Jehring [93]. A single calibration curve, established with Triton X-100, can be used for the determination of many NSs [95,96]. The response of different NSs are roughly additive [100]. However, if the NS has less than five oxyethylene units, the method cannot be employed. Moreover, the response is highly affected by matrix effects. In a different strategy, Szymanski and co-workers [99,100] developed adsorptive stripping tensammetry (AST). They realised a preconcentration of the surfactant, at a required potential, before recording the tensammetric curves. In this technique, the observed tensammetric peak is a desorption peak. The results obtained are similar to those obtained using the standard bismuth-active substance (BiAS) method [101,102]. In a recent paper, Wyrwas et al. [98] combined the BiAS–ITM techniques for the selective determination of NSs having 3–30 oxyethylene subunits. An application of the ITM for the determination of NSs in surface water is given by the authors [103]. The latter also improved the BiAs precipitation and washing steps allowing better sensitivity (2–1000 μg of NS in the sample) and recovery [104].

Many other examples of tensammetric (and polarographic) analysis of surfactants have been described; a good review has been given by Bersier and Bersier in 1988 [105].

We may also point out that double-layer capacitance measurements have been realised using a SAM gold electrode [106,107]. Here the surfactant effect is due to a change of the magnitude of the electrode inlayer capacity.

5. Biosensor

During the last few years, many biosensors have been developed for monitoring the fluctuation of environmental parameters [10]. In this way, a novel bioreactor-type electrochemical sensor for the determination of linear alkylbenzene sulfonates (LASs) has been described [10]. The principle of this biosensor is based on the fact that, when the LASs are biodegraded by LAS degrad-

ing bacteria, their respiratory activity in solution increases with concomitant decrease in dissolved oxygen. The latter can be followed by an oxygen electrode positioned on-line in an appropriate flow set-up. Using this novel microbial sensor, a linear response up to 6 mg l^{-1} of LAS can be achieved in less than 15 min. Applications to surfactant analysis in river pollution are foreseen.

6. Electrocapillary measurements

The quantification of a surfactant can be realized by electrocapillary measurements [108]. In the presence of a surfactant, the interfacial tension (γ) of a mercury drop electrode changes and can be estimated by measuring the mercury drop time. Thus, the change of the drop time will give, at a potential corresponding to the maximum of adsorption, information about the amount of surfactant present in solution [108,109]. This kind of measurement is difficult to perform because many parameters have to be controlled, such as the state of the electrode capillary and the adsorption equilibrium. The latter can be achieved by convective adsorption accumulation. In the ideal case the equation relating γ to the drop time (t) can be expressed by the equation [109]

$$\gamma_{E,C} = K \cdot t \qquad (4)$$

Under standard conditions of capillary internal diameter, if the length of the capillary is lower than 100 cm, K is also a function of γ. The superficial excesses (Γ), which are representative of the quantity adsorbed, are functions of the concentration and applied potential, and are related to the interfacial tension by the equation

$$-\frac{1}{R \cdot T} \cdot \left(\frac{\partial(\Delta\gamma)}{\partial(\ln C)} \right)_E = \Gamma_{E,C} \qquad (5)$$

In this relation, concentration is equivalent to the activity. Electrocapillary mesurements, like all adsorptive techniques, are subject to interferences by other species able to be adsorbed on the mercury electrode. Due to these limitations and a tedious analysis time, the electrocapillary technique is applicable only with difficulty in routine analysis of surfactants. However, it is an interesting tool for fundamental studies.

References

[1] B. Fabry and D. Nickel, J. Com. Esp. Deterg., 25 (1994) 65.
[2] N. Buschmann, personal communication, 1994.
[3] R.S. Boethling, Water Res., 18 (1984) 1061.
[4] A. Grammo, R. Ekelund, K. Magnusson and M. Berggren, Environ. Pollut., 59 (1989) 115.
[5] M.A. Lewis, Water Res., 25 (1991) 101.
[6] M. Ahel, J. McEvoy and W. Giger, Environ. Pollut., 79 (1993) 243.
[7] M. Ahel, W. Giger and M. Koch, Water. Res., 28 (1994) 1131.
[8] J.A. Field, T.M. Field, T. Poiger, H. Siegrist and W. Giger, Water Res., 29 (1994) 1301.
[9] T.M. Schmitt, Analysis of Surfactants, M. Dekker, New York, 1992.
[10] Y. Nomura, K. Ikebukuro, K. Yokoyama, T. Takeuchi, Y. Arikawa, S. Ohno and I. Karube, Anal. Lett., 27 (1994) 3095.
[11] J. Cross and E.J. Singer, Cationic Surfactants, Analytical and Biological Evaluation, M. Dekker, New York, 1994.
[12] J.D.R. Thomas, Anal. Chim. Acta, 180 (1986) 289.
[13] Z.P. Li and M.J. Rosen, Anal. Chem., 53 (1981) 1516.
[14] P.A. Johansson, U. Stefansson and G. Hoffmann, Anal. Chim. Acta, 151 (1983) 49.
[15] V.W. Reid, G.F. Longman and E. Heineth, Tenside, 4 (1967) 292.
[16] H. Koenig and E. Walldorf, Fresenius' Z. Anal. Chem., 189 (1978) 177.
[17] S. Motomizu, M. Oshima and T. Kuroda, Analyst, 113 (1988) 747.
[18] S. Motomizu and M. Kobayashi, Anal. Chim. Acta, 261 (1992) 471.
[19] H. Liu and P.K. Dasgupta, Anal. Chim. Acta, 288 (1994) 237.
[20] S. Motomizu, Y.H. Gao, K. Uemura and S. Ishibara, Analyst, 119 (1994) 473.
[21] M.Y. Ye, R.G. Walkup and K.D. Hill, J. Liq. Chromatogr., 17 (1994) 4087.
[22] E.R. Michelsen, Tenside Deterg. 15 (1978) 169.
[23] A. Kruse, N. Buschmann and K. Cammann, J. Planar Chromatogr., 7 (1994) 22.
[24] H. König and W. Stroebel, Fresenius' Z. Anal. Chem., 314 (1983) 143.
[25] K. Linhart and K. Wrabertz, Tenside Deterg., 15 (1978) 19.

[26] V.T. Wee, Water Res., 18 (1984) 223.

[27] J. Kawase, Y. Takao and K. Tsuji, J. Chromatogr., 262 (1983) 293.

[28] K. Levsen, M. Emmrich and S. Behnert, Fresenius' Z. Anal. Chem., 346 (1993) 732.

[29] J. Kawase, Y. Takao and K. Tsuji, J. Chromatogr., 262 (1983) 408.

[30] J. Kawase, H. Veno and K. Tsuji, J. Chromatogr., 264 (1983) 415.

[31] J. Kawase, H. Veno and K. Tsuji, J. Chromatogr., 267 (1984) 133.

[32] J. Kawase, H. Veno and K. Tsuji, J. Chromatogr., 267 (1984) 149.

[33] S. Chen and D.J. Pietrzyk, Anal. Chem., 65 (1993) 2770.

[34] N. Ishibashi, H. Kohara and K. Horinouchi, Talanta, 20 (1973) 867.

[35] D.F. Anghel, G. Popescu and F. Niculescu, Tenside Deterg. 17 (1980) 171.

[36] T.K. Christopopoulos, E.P. Diamandis and T.P. Hudjii Oannou, Anal. Chim. Acta, 143 (1982) 143.

[37] P. Sap, D.F. Anghel and C. Luca, Rev. Roum. Chim., 28 (1983) 883.

[38] A. Craggs, G.J. Moody and J.D.R. Thomas, J. Chem. Educ., 51 (1974) 541.

[39] A.S. Attiyat, G.D. Christian, J.L. Hallman and R.A. Bartsch, Talanta, 35 (1988) 789.

[40] H.H.Y. Oei, I. Mai and D.C. Toro, J. Soc. Cosmet. Chem., 42 (1991) 309.

[41] N. Buschmann and R. Schulz, Tenside Surf. Deterg., 29 (1992) 128.

[42] N. Buschmann and R. Schulz, Tenside Surf. Deterg., 30 (1993) 18.

[43] K. Vytras, J. Kalous and J. Symersky, Anal. Chim. Acta, 177 (1989) 219.

[44] K. Vytras, V. Dvorakova and I. Zeman, Analyst, 114 (1989) 1435.

[45] K. Vytras, Electroanalysis, 3 (1991) 343.

[46] G.J. Moody, B.B. Saad and J.D.R. Thomas, Sel. Electr. Rev., 10 (1988) 71.

[47] E. Halamek, T. Capoun and J. Soucek, Collect. Czech. Chem. Commun., 53 (1988) 912.

[48] W. Szczepaniak, Analyst, 115 (1990) 1451.

[49] R.D. Gallegos, Analyst, 118 (1993) 1137.

[50] W. Szczepaniak and M. Ren, Electroanalysis, 6 (1994) 341.

[51] N. Buschmann, U. Görs and R. Schulz, J. Com. Esp. Deterg., 24 (1993) 469.

[52] R.A. Lienado, Anal. Chem., 47 (1975) 2243.

[53] J. Baro-Roma, J. Sanchez, M. del Valle, J. Alonso and J. Bartroli, Sens. Actuat. B, 15–16 (1993) 179.

[54] D.L. Jones, G.J. Moody, J.D.R. Thomas and B.J. Birch, Analyst, 106 (1981) 974.

[55] P.H.V. Alexander, G.J. Moody and J.D.R. Thomas, Analyst, 112 (1987) 113.

[56] S.S.M. Hassan and I.H.A. Badr, Talanta, 41 (1994) 523.

[57] R. Schulz and R. Gerhards, Int. Lab., 10 (1994) 10.

[58] C.J. Davidson, P. Meares and D.G. Hall, J. Membr. Sci., 36 (1988) 511.

[59] S.G. Cutler, P. Meares and D.G. Hall, J. Chem. Soc., Faraday Trans. 1, 74 (1978) 1758.

[60] C. Baillarger, A. Mayaffre, M. Turmine, P. Letellier and H. Suquet, Electrochim. Acta, 39 (1994) 813.

[61] A. Bouklouze, A.El Jammal, J.C. Viré and G.J. Partiarche, Anal. Chim. Acta, 257 (1992) 41.

[62] D.A. Lowy, A. Patrut and M.E. Walter, Process Control and Quality, 4 (1993) 125.

[63] C.J. Dowle, B.G. Cooksey, J.M. Ottaway and W.C. Campbell, Analyst, 112 (1987) 1299.

[64] C.J. Dowle, B.G. Cooksey and W.C. Campbell, Anal. Proc., 25 (1988) 78.

[65] C.J. Dowle, B.G. Cooksey, J.M. Ottaway and W.C. Campbell, Analyst, 113 (1988) 117.

[66] H.H. Bauer, in A.J. Bard (Ed.), Electroanalytical Chemistry, Vol. 8, M. Dekker, New York, 1975.

[67] V. Zutic, B. Cosovic and Z. Kozarac, J. Electroanal. Chem., 78 (1977) 113.

[68] Z. Kozarac, V. Zutic and B. Cosovic, Tenside Deterg., 13 (1976) 260.

[69] T. Zvonaric, V. Zutic and M. Branica, Thalassia Jugosl., 9 (1973) 65.

[70] J. Heyrovsky and J. Kuta, Principles of Polarography, Academic Press, New York, 1966.

[71] E. Blomgran and J.M. Backris, J. Phys. Chem., 63 (1959) 1475.

[72] N. Batina, B. Cosovic and N. Filipovic, J. Colloid Interface Sci., 25 (1988) 69.

[73] M. Skoog, K. Kronkvist and G. Johansson, Anal. Chim. Acta, 269 (1992) 59.

[74] S.B. Adeloju and S.J. Shaw, Electroanalysis, 6 (1994) 639.

[75] S.B. Adeloju and S.J. Shaw, Electroanalysis, 6 (1994) 645.

[76] T. Schmidt and H. Emons, Electroanalysis, 3 (1994) 543.

[77] A. Sanchez Perez, J. Armesto Gomez and J. Hernandez Mendez, Anal. Lett., 23 (1990) 1291.

[78] T. Kawaguchi, Y. Yamauchi, H. Maeda and H. Ohmori, Chem. Pharm. Bull., 41 (1993) 1601.

[79] L.H. Dubois and R.G. Nuzzo, Ann. Rev. Phys. Chem., 43 (1992) 437.

[80] H. Ron and I. Rubinstein, Langmuir, 10 (1994) 4566.

[81] L.H. Guo, J.S. Facci, G. McLendon and R. Mosher, Langmuir, 10 (1994) 4588.

[82] Z. Yang, A. Gonzalez-Cortès, G. Jourquin, J.C. Viré, J.M. Kauffmann and J.L. Delplancke, Biosens. Bioelectr., 10 (1995) 789.

[83] C. Schonenberger, J.A.D. Sondag-Huethorst and J. Joristma, Langmuir, 10 (1994) 611.

[84] S.E. Creager, L.A. Hockett and G.K. Rowe, Langmuir, 8 (1992) 854.

[85] K. Takehara, H. Takemure and Y. Ide, Electrochim. Acta, 39 (1994) 817.

[86] M. Gerlache, unpublished work.

[87] C.A. Widrig, C. Chung and M.D. Porter, J. Electroanal. Chem., 310 (1991) 335.

[88] S.E. Creager and G.K. Rowe, J. Electroanal. Chem., 370 (1994) 203.

[89] L. Sun, B. Johnson, T. Wade and R.M. Crooks, J. Phys. Chem., 94 (1990) 8869.

[90] F. Malem and D. Mandler, Anal. Chem., 65 (1993) 3741.

[91] O.S. Kim, S. Shiragami and K. Kusuda, J. Electroanal. Chem., 367 (1994) 271.

[92] A.J. Bard and L.R. Faulkner, Electrochemical Methods. Fundamentals and Applications, John Wiley, New York, 1980.

[93] H. Jehring, J. Electroanal. Chem., 21 (1969) 77.

[94] M. Bos, J.H.H.G. Van Willigen and W.E. van der Linden, Anal. Chim. Acta, 156 (1984) 71.

[95] A. Szymanski and Z. Lukaszewski, Anal. Chim. Acta, 260 (1992) 25.

[96] A. Szymanski and Z. Lukaszewski, Anal. Chim. Acta, 273 (1993) 313.

[97] A. Szymanski and Z. Lukaszewski, Anal. Chim. Acta, 293 (1994) 77.

[98] B. Wyrwas, A. Szymanski and Z. Lukaszewski, Anal. Chim. Acta, 278 (1993) 197.

[99] A. Szymanski and Z. Lukaszewski, Anal. Chim. Acta, 281 (1993) 443.

[100] R. Wyrwas, A. Szymanski and Z. Lukaszewski, Talanta, 42 (1995) 1251.

[101] R. Wickbold, Tenside Deterg., 17 (1972) 173.

[102] J. Waters, J.T. Garriyan and A.M. Paulsin, Water Res., 20 (1986) 247.

[103] A. Szymanski, B. Wyrwas and Z. Lukaszewski, Anal. Chim. Acta, (1995) in press.

[104] B. Wyrwas, A. Szymanski and Z. Lukaszewski, Talanta, 41 (1994) 1529.

[105] P.M. Bersier and J. Bersier, Analyst, 113 (1988) 3.

[106] J.A.M. Sondag-Huethorst and L.G.J. Fokkink, J. Electroanal. Chem., 367 (1994) 49.

[107] A. Swietlow, M. Skoog and G. Johansson, Electroanalysis, 4 (1992) 921.

[108] L. Novotny and R. Kalvoda, Collect. Czech. Chem. Commun., 51 (1986) 1595.

[109] B.B. Damaskin, O.A. Petrii and V.V. Batrakov, Adsorption of Organic Compounds on Electrodes, Plenum Press, New York, 1971.

Review

Combination of classical dry ashing with stripping voltammetry in trace element analysis of biological materials: review of literature published after 1978

Pavel Mader*, Jiřina Száková, Eva Čurdová[1]

Faculty of Agronomy, Czech University of Agriculture, 165 21 Prague 6-Suchdol, Czech Republic

Abstract

Critical statements have appeared recently in the literature concerning the need for classical dry ashing in trace element analysis of biological materials. In contrast, respected institutions (AOAC, Nordic Committee on Food Analysis, etc.) as well as numerous other laboratories have developed, verified, and/or successfully used classical dry ashing in practical analyses of a number of materials of biological origin. Hence, it is desirable to find out under which conditions the latter decomposition technique yields good and accurate results. Since electroanalytical techniques are among the most demanding with regard to the completeness of the biological matrix removal, we decided to critically review the literature published after 1978 in which classical dry ashing is combined with some version of electroanalytical measurement. It emerged from this review that in particular the charring step requires careful performing. When performed well, classical dry ashing leads to complete removal of the organic matrix and to accurate analytical results for a number of determined elements.

Keywords: Classical dry ashing; Stripping voltammetry; Trace element analysis; Biological materials; Literature review

"A number of sample preparation procedures used today have been in use for more than 100 years. For example, heating samples in open beakers over flames or burners, a technique that doubtless predates the era of the alchemists, is still widely used today, especially when the modern hot plate is added to the list of applicable heating sources. However, the experimental conditions that prevail in open-beaker digestions are, at best, empirical." [1].

"Decomposition of organic matter by dry ashing is often chosen for its seeming simplicity, especially by less experienced working places. From the general point of view, the dry ashing decomposition is very problematic especially in determinations of trace contents of heavy metals. ...Decomposition of organic matter by dry ashing

* Corresponding author. Tel: + 42-2-338-2747 or 338-2716; Fax: + 42-2-344-418; e-mail: MADER@agro.VSZ.CZ
[1]Present address: Institute of Chemical Technology, 166 28 Prague, Czech Republic.

is in no case suitable for determination of mercury, selenium, arsenic, lead, cadmium, and zinc." [2].

"For the oxidation of organic materials with air or pure oxygen a variety of techniques has been established which produce very good results. Dry ashing however, though widely used in the past and still in use to a certain extent, should be completely abandoned from the protocols of trace analysis. The experimental parameters are poorly reproducible and make dry ashing very error prone." [3].

The essentiality of a number of trace elements for animal and/or plant organisms has been recognized long ago. Other (supposedly non-essential) trace elements such as Cd, Pb, or Hg, are also closely monitored in various environmental compartments including plants and animals in connection with growing awareness of their harmful effects as a consequence of environmental pollution. A number of sensitive analytical techniques has been developed and there exists powerful instrumentation capable of detecting trace or ultratrace amounts of these elements. The majority of these analytical methods belong to the group of so-called destructive methods, i.e. they require biological samples to be solubilized and at the same time mineralized as far as possible prior to the measuring step. There are at least three good reasons for solubilization and mineralization of biological tissues:

(1) In biological tissues, determined trace elements are present in several chemical forms; some of them do not give any signal during measurement, others give signals of different intensities. Mineralization transforms the analyte into a single chemical form with uniform response.

(2) Organic components of biological materials greatly interfere during measurement in many measuring techniques.

(3) Heterogeneity is a typical property of many biological materials. The possibility of using a larger amount of analyzed sample which, upon mineralization, turns into an homogeneous digest, helps to overcome this complicating factor.

In parallel with a great number of measuring techniques, there also exists a broad spectrum of decomposition methods in trace element analysis of biological materials. General evaluation of these methods as such is not possible. Other factors, namely the analyte(s), the matrix, and the technique

to be used for measurement must also be taken into consideration in such an evaluation. Thus for example, pressurized wet digestion with nitric acid at temperatures lower than 200°C in a number of instances was shown to be an inappropriate preparation step for anodic stripping voltammetry since it frequently leaves an interfering residue of incompletely degraded organic matrix in (and sometimes introduces very resistant nitro forms into) the digests [4–8], while for ICP-AES this is a very convenient method because chemical interferences practically do not exist here due to the very high temperature of the inductively-coupled plasma which removes all organics present in the digests very efficiently.

Classical dry ashing (i.e., dry ashing performed in air, in open vessels, and at atmospheric pressure) was, and to a lesser extent still is, one of the extensively used and popular means of organic matrix destruction in trace element analysis of biological materials. Recent criticism, however (see the opening quotes of this paper), pointed out several fundamental drawbacks of classical dry ashing and in a few instances it even requested the complete abandonment of this method of sample preparation [3]. However, a great number of authors have successfully used this method and repeatedly furnished accurate results, as demonstrated for example in interlaboratory testing of candidate certified reference materials. Hence, we decided to go through the literature and see in detail how successful laboratories proceed when applying classical dry ashing as their sample preparation step. In this literature survey, we have used the following two restrictions.

(1) In 1979, an excellent monograph by Bock [9] was published in which dry ashing, as well as a number of other decomposition techniques, was thoroughly and critically evaluated and discussed. Two years later, an important update review paper was published by Sansoni and Panday [10]. Hence, we restricted our literature survey only to papers published in 1979 and thereafter.

(2) From measuring techniques, we have selected electroanalytical methods. All versions of the technique require that the analyzed sample is solubilized prior to the measurement. As concerns the requirement for complete removal of the

organic matrix of biological samples (mineralization), individual versions differ to a large degree. In the case of liquid samples such as body liquids, just dilution of the sample and addition of suitable detergent without any mineralization is often sufficient. The best known example of such a procedure is stripping voltammetric determination of lead in whole blood according to Morell and Girvidhar [11]. The commercially available ASV instrument (Model 3010B by Environmental Science Associates, [12]) requires that the blood sample be diluted by a factor of 30 into an acidified medium containing Ca^{2+} and Cr^{3+} among other ingredients (Hg^{2+}, Bi^{3+}, EDTA, Triton X-100, cf. e.g. Refs. [13, 14]). According to Feldman et al. [15], this large dilution factor reduces accuracy and precision. Morell and Girvidhar [11] used only heparinized blood samples which were sonicated for 15 s and 100 μL was then transferred to 2.9 ml of the Metexchange reagent in a cell. Portable stripping analyzers are currently being developed in Wang's laboratory for clinical screening of blood lead levels in children; the procedure again uses simple sample pre-treatment without complete digestion [16]. According to Ostapczuk [17], for determination of lead and cadmium in blood by potentiometric stripping analysis it is even sufficient to dilute the blood sample with an appropriate supporting electrolyte (0.5 mol L^{-1} HCl), avoiding the use of any complexing agent, detergent, or other ingredients. Thus, this version of the electroanalytical measuring technique seems to be the least sensitive to the presence of small amounts or organic constituents during the steps of lead plating and dissolution.

For solid biological samples, digestion of the sample is very often necessary prior to electroanalytical determination [18]. However, here also in several instances mere solubilization of solid tissue with suitable detergent was demonstrated to be sufficient. An alcoholic solution of tetramethylammonium hydroxide is the detergent of choice for solubilization of solid animal and human tissues in atomic absorption and emission spectrometry (e.g. Refs. [19, 20]). In stripping voltammetry, a broader spectrum of detergents has been applied. Thus, benzyltrimethylammonium methoxide was used for Zn determination in SRMs bovine liver

and oyster tissue [21], and 2,5-dimercapto-1,3,4-thiadiazole was used as a ligand in adsorptive stripping voltammetry for Cd, Zn, Ni, As, Al and Se determination in SRMs oyster tissue and spinach [22, 23]. Wahdat et al. [24] used sodium dodecyl sulphate for Cd, Pb and Cu determination in muscle, fish and blood. In this case, prior to stripping the original sample solution was replaced by another electrolyte (diluted HCl). Without medium exchange, the voltammograms exhibited undesirable adsorption peaks caused by organic compounds present in the solution.

Various sample treatments and stripping modes for the determination of trace elements in blood, urine and solid biological samples have been summarized and discussed by Wang [25].

It can be concluded from the voluminous literature that, *in instances when the biological material is mineralized*, the remnants of the organic matrix and its degradation products *must be completely removed* from the digest prior to anodic stripping measurements. Hence, for the estimation of the mineralization efficiency of various *decomposition* techniques, anodic stripping voltammetry is very suitable.

Of the total of 35 papers which we found in the above survey, 20 ([26–45]) more or less differed from each other. Of the remaining 15 papers ([46–60]), one of the procedures published in the former group of papers was repeated. Ten parameters have been selected which give detailed insight into the proper procedure: M, analyzed material; A, sample weight; B, ashing aid (if applied before charring); C, temperature + time regime of charring; D, temperature + time regime of ashing; E, ashing aid (if applied after ashing); F, repeated ashing with ashing aid (if the latter was added after ashing); G, ash leaching; H, elements determined electrochemically; QA/QC, quality assurance/quality control system.

Table 1 gives details of classical dry ashing decomposition which were used in the more or less independent procedures published in Refs. [26–45]. In Table 2 frequencies and values of the chosen parameters from all 35 reviewed papers (i.e. from Refs. [26–45] given in Table 1 as well as from Refs. [46–60] in which some of the previous procedures were repeated) are summarized. The

Table 1
Details of classical dry ashing procedure used before determination of given elements in biological materials by electrochemical method. (Key: M, material; A, weight of sample; B, ashing aid before charring; C, temperature program of charring; D, final temperature + time of ashing; E, ashing aid after ashing; F, additional ashing; G, ash leaching; H, elements determined by electrochemical method; QA/QC, quality assurance/quality control system applied; ? not mentioned; – not used)

Ref.	Country	Code	Procedure
26	USA	M	sludge, plant, animal
		A,B,C	?
		C	475°C
		D-G	?
		H	Cd, Cu, Pb, Zn
		QA/QC	no
27	USA	M	animal, plant, food
Method AOAC,		A	5–10 g
1982		B	5 ml K_2SO_4, evap. in the oven (120°C)
		C	cold furnace, set 500–550°C, avoid excessive overshooting of temperature
		D	500–550°C, >4 h (may be ashed overnight)
		E	2 ml HNO_3 (if ash contains carbon)
		F	500°C, 30 min. (repeat E,F until white ash)
		G	1 ml HNO_3, 10 ml H_2O, hotplate (if necessary) H_2O to 50 ml, do not filter
		H	Cd, Pb
		QA/QC	yes
28	USA	M	food (canned)
		A	5–10 g
		B	–
		C	furnace, 200°C, slowly increase up to 500°C
		D	500°C, overnight
		E	1 ml H_2O
		F	furnace 200°C, gently up to 500°C, then overnight
		G	1 ml H_2O, 2 ml HCl (1 + 1), filtration, H_2O, 25 ml
		H	Pb
		QA/QC	yes
29	USA	M	plant, food
		A	1–3 g
		B	3–4 ml 40% H_2SO_4 + 3–4 ml H_2O, furnace 115°C, 3 h
		C	furnace, 1h up to 275°C, then 3 h; 2 h up to 500°C
		D	500°C for 8–20 h (depending on sample type)
		E	1 ml HNO_3 + 0.5 ml H_2O, hotplate, evap. to dryness
		F	furnace 200°C, then 450°C for 30 min. (repeat, if necessary)
		G	dissolve in 1 ml HNO_3 + 5 ml H_2O, H_2O to 25 ml
		H	Cd, Pb
		QA/QC	yes
30	USA	M	food
		A	5–10 g
		B	5 ml 10% K_2SO_4 or 20% $MgSO_4$
		C	cold furnace, slowly bring temp. up to 500–550°C
		D	500–550°C, overnight

Table 1 (continued)

Ref.	Country	Code	Procedure
		E	5 ml H_2O + 2 ml HNO_3 conc. (if a carbon residue remains)
		F	re-ash for 30 min. at 300°C
		G	HNO_3 + H_2O (25 ml)
		H	Pb
		QA/QC	no
31	Australia	M	animal
Method of		A	0.5 g
Adeloju		B_1	–
et al., 1984		B_2	5 ml 20% H_2SO_4
		B_3	5 ml 5% HNO_3
		C_1	–
		$C_{2,3}$	water bath for 3 h, then hotplate, heat until white fumes created (or dryness)
		D_1	450 or 500°C, overnight
		D_2	500°C, overnight
		D_3	450°C, overnight
		E, F	–
		G	5 ml 5% HNO_3 or 5 ml 2.5% HCl, H_2O to 10 ml
		H	Cd, Pb
		QA/QC	yes
32	Australia	M	animal, plant
		A	0.5 g, silica dish
		B	–
		C	hotplate, gently 30–60 min, then furnace, 450°C
		D	450°C, 8 h or overnight
		E, F	
		G	3 ml of 6 M HCl, hotplate, H_2O to 10 ml
		H	Co, Ni
		QA/QC	yes
33	Italy	M	plant
Method of		A	0.5 g, Pt crucible
Locatelli,		B, C	–
1984		D	500°C, 2 h
		E	10 drops of H_2O + 3 ml HNO_3 (1:1) hotplate, evap. at 120°C
		F	500°C, 1 h
		G	2 ml 1 M $HClO_4$, to 50 ml
		H	Cd, Cu, Fe, Mn, Pb, Zn
		QA/QC	yes
34	Germany	M	animal, plant, food
		A	1–10 g
		B, C	–
		D	furnace, 580–780°C, 12–16 h
		E, F	–
		G	0.2–0.5 ml conc. HCl, H_2O to 10–20 ml
		H	Co, Ni
		QA/QC	yes

Table 1 (continued)

Ref.	Country	Code	Procedure
35	Czech Republic	M	animal
		A	1–2 g
		B	–
		C	furnace, 1 h 200°C, 1 h 300°C, 1 h 400°C
		D	500°C, overnight (16 h)
		E	1 ml conc. HNO_3
		F	500°C, 1 h
		G	7 ml 1% HNO_3
		H	Cd, Pb
		QA/QC	yes
36	Netherlands	M_1	feed
		M_2	food, animal
		A	feed 5g, milk 25 g f.w., blood + tissues 1 g d.m.
		B	–
		C	furnace, 50°C per 1 h
		D	450°C, 16 h
		E	$HNO_3 + H_2O$ (1:1) or 0.1 mol. 1^{-1} $Mg(NO_3)_2$
		F	450°C until white ash was obtained
		G	M_1:15 ml 3 M HCl, then to 100 ml flask, add 20 ml citrate buffer (pH 8.5) and 10 ml sat. NaCl
			M_2:0.5 ml HCl (12 M) + 5 ml H_2O + 5 ml acetate buffer (pH 3.5)
		H	Cd, Pb
		QA/QC	no
37	Netherlands	M	animal, feed
Method of		A	1 g
RIKILT, 1986		B	2.5 ml 65% HNO_3 + 2.5 ml 10% $Mg(NO_3)_2$ furnace, 50°C h^{-1}, up to 450°C
		D	450°C, 8–9 h
		E	1 ml 65% HNO_3
		F	450°C, 30 min, repeat E,F until white ash
		G	0.5 ml 30% HCl + 4.5 ml H_2O, stirring
		H	Cd, Pb
		QA/QC	no
38	Netherlands	M	animal
		A	5 g f.w.
		B	1 ml 70% HNO_3 + 1 ml 25% $Mg(NO_3)_2$
		C	furnace, slowly from 150 up to 450°C
		D	450°C, overnight
		E	1 ml 70% HNO_3
		F	450°C, 1h
		G	0.5 ml 37% HCl, then 5 ml H_2O, gently heat on the hotplate
		H	Cd, Pb
		QA/QC	no
39	Netherlands	M	plant, soil
		A,B	?
		C	quartz, stepwise up to 450°C
		D	450°C
		E	HNO_3
		F	until white ash
		G	3 M HCl
		H	Cd, Pb
		QA/QC	yes

Table 1 (continued)

Ref.	Country	Code	Procedure
40	Czech Republic	M	animal
		A	1 g
		B	–
		C	220°C 1 h, 280°C 1 h, 340°C 1 h, 390°C 1 h (hotplate); 350°C 30 min, 400°C 30 min, (muffle furnace)
		D	500°C 16 h (muffle furnace)
		E	1 ml conc. HNO_3
		F	1 h 500°C
		G	10 ml 1.5% HNO_3
		H	Cd, Pb
		QA/QC	yes
41	Czech Republic	M	food
		A	?
		B	$Mg(NO_3)_2$
		C	furnace, max. 480°C
		D-F	?
		G	dil. HNO_3
		H	Cd, Pb
		QA/QC	no
42 Standard CSFR Procedure ČSN 56 0065 effective from 1987	Czech Republic	M	food
		A	5–20 g f.w.
		B	2 ml 5% $Mg(NO_3)_2$, evaporate to dryness
		C	burner, IR lamp, or electrical heater
		D	cold furnace, grandually up to 450°C, until white ash
		E	1 ml HNO_3
		F	cold furnace, gradually up to 450°C, then 30 min
		G	0.1 M HCl
		H	Cd, Pb
		QA/QC	no
43	Poland	M	plant, food
		A	0.3 g, quartz crucible
		B, C	–
		D	muffle furnace, 550°C, 2–3 h
		E	0.1–0.2 ml H_2O_2
		F	550°C, 2–3 h
		G	0.5 ml 0.4 M HNO_3, water to 10 ml
		H	Cd, Cu, Pb, Zn
		QA/QC	yes
44	USA	M	ash, ash–soil mixture, plant, animal
		A	5–10 g
		B	5 ml 10% K_2SO_4
		C	cold furnace, set temp. at 450°C
		D	450°C, overnight
		E, F	–
		G	HNO_3
		H	Cd
		QA/QC	no
45	Netherlands	M	food
		A	1 g, quartz crucible

P. Mader et al. / Talanta 43 (1996) 521–534

Table 1 (continued)

Ref.	Country	Code	Procedure
		B	2–3 ml H_2O, 2 ml H_2SO_4 (20%)
		C	hotplate, evap. SO_3, then muffle furnace (increase of temp. 50°C h⁻¹), at 300°C prolongation for 2 h, then 50°C h⁻¹ up to 500°C
		D	500°C, 6 h
		E	1 ml H_2O, 1 ml conc. HNO_3 (if ash contains carbon)
		F	hotplate, muffle furnaces 350°C, increase of temp. 50°C h⁻¹ up to 500°C, then 30 min
		G	0.5 ml conc. HCl + 1 ml H_2O, water to 10 ml
		H	Cd, Pb
		QA/QC	yes

following conclusions can be drawn as to how classical dry ashing should be performed in order to yield good results.

(A) With one exception, the dry weight of the sample did not fall below 0.5 g, it mostly being between 1 and 5 g. The possibility to utilize relatively large amounts of biological material in classical dry ashing helps to overcome the heterogeneity of the analyzed material, and also results in increased concentrations of the analytes in the digest.

(B) An ashing aid was applied before charring in ≈50% of cases. When applied at this stage, it was almost exclusively in the form of a salt. H_2SO_4 used in five cases served not to increase the oxidation power but to bind analytes (especially Pb) into the less volatile chemical form. Magnesium nitrate, sometimes combined with nitric acid, was the reagent of choice.

(C) Charring is the most critical step of classical dry ashing. Slow continual or stepwise increase of temperature during charring is considered to be very important.

(D) Nobody ashes above 550°C, and even 550°C is something of an exception. The most frequently used ashing temperature is 450°C or 500°C. (In Ref. [34], where 580°C to 780°C ashing temperatures were used, only Co and Ni have been determined and the risk of losses due to volatilization at higher temperatures is not questioned.) Ashing time is rarely shorter than 8 h, the majority of laboratories ash overnight (16 h).

(E) In instances when an ashing aid was applied only after ashing, it was almost exclusively nitric acid. Since the ash of most biological materials contains several units to several tens of percent carbonates, nitrates are formed in situ after adding nitric acid to the ash. Additional ashing is then in fact melting with nitrates and should help to remove the most resistant degradation products of the organic matrix of biological samples.

(F) The temperature of additional ashing is again most often 450°C or 500°C, and the time of additional ashing is 30 min to 1 h.

(G) In about half of the cases, diluted hydrochloric acid and in the other half, diluted nitric acid are the favorite leaching media. Anodic stripping voltammetry (ASV) works well with both acids, HCl solutions yielding somewhat higher differential pulse (DP) peaks and higher reproducibility [31].

(H) The spectrum of determined elements reflects those elements which are more or less easily determined by electroanalytical techniques. Lead and cadmium by far exceed all the rest.

(QA/QC) Two-thirds of the reviewed papers [26–60] applied some form of quality assurance/quality control (reference material, round-robin test, recovery test, independent method). Seven of them (Refs. [40,50,51,53,54,58,59]) used two such forms simultaneously, while 12 papers (Refs. [26,30,36–39,41,42,44,48,57,60]) do not mention any such support of their analytical data.

Table 2
Summary of the dry ashing methods reported in Refs. [26–60] (f.w. = fresh weight)

M (material)
animal = 15 ×
plant = 13 ×
food = 16 ×
feed = 3 ×
sludge = 1 ×
soil = 2 ×

A (sample weight)
not mentioned = 4 ×
0.3 g = 4 ×
0.5 g = 1 ×
1.0 g = 9 ×
1–2 g = 1 ×
1–3 g = 1 ×
5.0 g = 2 ×
1–10 g = 1 ×
10.0 g = 3 ×
5–10 g = 4 ×
5–20 g f.w. = 1 ×
5 g f.w. = 3 ×
25 g f.w. = 2 ×

B (ashing aid before charring)
not mentioned = 3 ×
not used = 11 ×
HNO_3 only = 1 ×
H_2SO_4 only = 3 ×
$H_2O + H_2SO_4$ = 2 ×
$HNO_3 + Mg(NO_3)_2$ = 7 ×
$Mg(NO_3)_2$ = 4 ×
sulphate (K, Mg) = 6 ×

F (additional ashing)
not used = 5 ×

Temperature:
not mentioned = 6 ×
300°C = 1 ×
450°C = 11 ×
500°C = 11 ×
550°C = 1 ×

Time:
not mentioned = 5 ×
30 min = 15 ×
1 h = 6 ×
2–3 h = 1 ×
overnight = 1 ×
until white ash = 2 ×

QA/QC
not mentioned = 12 ×
RM = 17 ×
Round robin test = 3 ×
Recovery test = 9 ×
Independent method = 1 ×

C (temperature program of charring)
not mentioned = 1 ×
not used = 9 ×
one or more prolongations = 5 ×
slow continuous increase = 20 ×
fast increase = 1 ×

D (final temperature + time of ashing)
Temperature:
450°C = 15 ×
475°C = 1 ×
480°C = 1 ×
450–500°C = 1 ×
500°C = 12 ×
500–550°C = 5 ×
550°C = 1 ×
580–780°C = 1 ×

Time:
not mentioned = 6 ×
2 h = 2 ×

2–3 h = 1 ×
6 h = 1 ×
8–9 h = 6 ×
16 h = 14 ×
12–16 h = 1 ×
8–20 h = 1 ×
until white ash = 3 ×

E (ashing aid after ashing)
not mentioned = 4 ×
not used = 5 ×
H_2O = 1 ×
HNO_3 = 24 ×
H_2O_2 = 1 ×
$Mg(NO_3)_2$ = 1 ×

G (ash leaching)
not mentioned = 2 ×
HCl = 17 ×
HNO_3 = 15 ×
$HClO_4$ = 2 ×
HCl buffer = 2 ×

H (elements determined)
Pb = 30 ×
Cd = 28 ×
Cu = 5 ×
Zn = 5 ×
Ni = 3 ×
Co = 3 ×
Fe = 2 ×
Mn = 2 ×
Se = 1 ×

Below, we discuss in more detail several publications in which various modifications of classical dry ashing were methodologically tested, while the electroanalytical technique was selected to be a measuring step.

At the 95th Annual Meeting of the AOAC (October 19–22, 1981), a special symposium was held on "Analytical Methodology for Lead in Foods". Results of this symposium were presented in J. Assoc. Off. Anal. Chem., 65(4) (1982). Here, the results of a collaboration study of classical dry ashing and differential pulse anodic stripping voltammetry for lead and cadmium determination in foods were also presented by Capar et al. [27]. The procedure described schematically in Table 1 of Ref. [27] forms the basis of the AOAC method of classical dry ashing combined with voltammetry, which was published in 1984 in the 14th edition of *Official Methods of Analysis* [61] and reprinted virtually without change in 1990 and 1995 in the 15th and 16th editions [62]. It has been routinely used during the period (e.g. in Refs. [46,48,52,55,58]). In the AOAC procedure a controllable hotplate is used, but only for drying the samples after adding concentrated HNO_3 as an ashing aid. It was also found useful to carry out the ash leaching step (with diluted HNO_3) on the hotplate. The charring step is performed entirely in the muffle furnace. The procedure has been verified [27] for green beans, beef, fish, dried milk, apple juice, and cereals.

In 1984, Adeloju et al. [31] used very resistant liver tissue (Bovine Liver NBS 1577) and compared direct dry ashing without any ashing aid with two versions in which either nitric or sulfuric acid were used as an ashing aid; in both cases, they were applied before the charring step. (Magnesium nitrate was not tested "because purification of this reagent is often necessary for accurate determination of trace elements" [31].) Details of decomposition procedures are given in Table 1 of Ref. [31]. A controllable hotplate has been used for drying samples. Charring (or at least a substantial part of it, see below) and ashing were performed in a muffle furnace, and the ashing temperature was either 450°C or 500°C. Ashing was done overnight. As an ash leaching reagent either dilute nitric or dilute hydrochloric acid was used. Ash leaching was supported by heating on a water

bath. Reproducibility of the three dry ashing methods considered was excellent. Comparison with the certified values for Cd and Pb suggests that the method with sulfuric acid as ashing aid is superior. For ash leaching, the authors prefer dilute HCl over dilute nitric acid since it gives more reproducible results, and also somewhat higher sensitivity.

In 1989, Adeloju [63] considerably extended a previous investigation [31] from 1984 by also including magnesium nitrate as an ashing aid, and comparing all four procedures above with three versions of wet digestion. The spectrum of voltammetrically determined elements was considerably extended as well (besides Cd and Pb also As, Bi, Co, Cu, Ni, Se, V, and Zn). One plant and three animal standard reference materials from IAEA and NBS were used in this study. All four modifications of classical dry ashing were found to be suitable the only problem being an increased blank level when an ashing aid was applied. As a consequence, direct dry ashing without an ashing aid is preferred except for As and Se determination; here, $Mg(NO_3)_2$ as an ashing aid is necessary.

In 1987, Stryjewska et al. [64] published a statistical estimation of the influence of mineralization methods including classical dry ashing (0.5 g sample, 450°C for 2 h, H_2O_2 as ashing aid, additional ashing at 450°C for 1 h, HNO_3 for ash leaching), wet digestion, and pressurized wet digestion, on the results of heavy metals determination in cereals by the DPASV method. Dry ashing gave satisfactory results.

Since atomic absorption spectrometry (AAS) and inductively-coupled plasma atomic emission spectrometry (ICP-AES) are today by far the most frequently used measuring techniques in trace element analysis of biological materials, we also include brief discussion of several papers in which classical dry ashing in combination with AAS or ICP was used.

In 1984, Muys [65] described a procedure in which 1–5 g of sample was weighed into a quartz dish and 5 ml of magnesium nitrate solution added. After drying on a hotplate by gently raising the temperature, the samples were placed in the muffle furnace where stepwise charring was performed (2 h at 150°C, 2 h at 250°C, 3 h at

350°C). Ashing took place for 6 h at 450°C. If necessary, 1 ml of 65% nitric acid was then applied as another ashing aid, dried on a hotplate and reashed for 30 min at 350°C. For ash leaching, 1 ml of water and 5 ml of 65% nitric acid were added and the mixture was heated for a few minutes on a hotplate, and then rinsed with 25 ml of demineralized water into a 50 ml polyethylene bottle. Cd and Pb were then determined by ETA-AAS. The method was found to give accurate results for chicken meat, eggs, milk powder, fish products, bread, vegetables, and animal feedstuffs.

In 1986, Friel and Nguyen [66] described classical dry ashing of hair which gave good results for Cu, Mn, and Zn when flame (Cu,Zn) or flameless (Mn) AAS was used. Hair samples were ashed in a muffle furnace for 12 h at 450°C, after oven-drying at 250°C for 2 h. After they had cooled for 1 h, five drops of concentrated nitric acid were added and samples were returned to the muffle furnace, where they were heated at 250°C for an additional 8 h. Dilute HNO_3 was used for ash leaching.

In 1988, Miller-Ihli [67] compared four methods (wet ashing, dry ashing, microwave dissolution, direct solid analysis), all with the NBS SRM 1577 Bovine Liver. She used magnesium nitrate as an ashing aid in dry ashing and applied it before charring. The latter was performed in a muffle furnace under the following regime: 100°C, 1 h; 150°C, 1 h; 200°C, 1 h; 250°C, 1 h. Ashing temperature and time were 450°C and overnight respectively. For ash leaching, 5% HNO_3 was used. All sample preparation methods provided accurate analytical data for the four elements (Cu, Fe, Mn, Zn) determined.

For ICP-AES we will mention one paper which is according to our opinion of fundamental importance (considerable parts of it were reprinted in van Loon's monograph [68]). In 1983, de Boer and Maessen [69] compared classical dry ashing of the NBS SRM 1577 Bovine Liver (1 g sample in quartz beaker, cold muffle furnace, temperature increase 50°C h^{-1} until 520°C, then ashing for 14 h, ash dissolved in 30% HCl, dilution and filtration) with six other procedures: low temperature ashing in oxygen plasma; two direct approaches (extraction with dilute HNO_3; solubilization with tetramethylammonium hydrox-

ide); and three acid digestions (HNO_3 + $HClO_4$ in microwave oven; H_2O_2 + H_2SO_4; HNO_3 in Teflon-lined steel bomb). According to these authors, "muffle furnace ashing yielded accurate and precise results for Mn, Zn, Cd, and Pb. The principle source of error associated with this procedure is the loss of analytes by evaporation or by retention. Systematic error can be avoided or reduced by application of an experimentally well established temperature–time regime and by careful selection of the crucible material. The use of sulfuric acid for avoiding losses of the volatile elements Cd and Pb appeared to be superfluous. Small retention losses were observed for Cu and Fe.".

As follows from the above, the majority of laboratories which use classical dry ashing have applied an ashing aid (either before charing, or after ashing), and many of them also felt that the charring step should be performed with special care. The ashing aid serves more purposes than just to increase the oxidizing power which facilitates decomposition. It can transform the analyte into the less volatile form (e.g. Pb and sulfuric acid or sulfate), suppress the interaction between the analyte and reaction vessel walls (salts which form voluminous ash), or can also act mechanically (water drops which help to destroy the crust on the top of the ashed sample which hinders the approach of oxygen to the lower layers). Moderation of charring is realized by slow continuous or stepwise increase of temperature in the muffle furnace with extended prolongations at individual temperatures. All four above-quoted AAS papers [65–67,69] used only HNO_3 (mostly dilute) for ash leaching, obviously to avoid the well-known interferences by halides during the AAS measurement. In contrast, the ICP work [69] used HCl as an ash leaching medium (the chemical interferences practically do not exist during the ICP-AES measurement).

Our own practical experience with classical dry ashing began in 1983 with platinum dishes as reaction vessels, a sand bath for drying, and a muffle furnace for both charring and ashing. Since at that time we had at our disposal only electroanalytical instrumentation for measurement, we often ran into the problem of severe interferences

caused by the incompletely destroyed organic matrix of biological samples [70,71]. Replacement of Pt dishes with borosilicate glass Simax beakers and introduction of a stepwise increase of temperature in the muffle furnace during charring plus HNO_3 as an ashing aid (applied after ashing) in 1984 lead to considerable improvement in efficacy of decomposition in many cases (e.g. muscle and kidney [35]) but definitive solution of all the problems came only in 1985 when we decided to totally remove the charring step from the muffle furnace and transfer it instead to a hotplate located in a fume hood. A specially designed hotplate has been prepared and tested (for photographic documentation see Ref. [72]) and a standard operation procedure SOP-1 (cf. e.g. Ref. [73]) developed for soft animal tissues. The latter procedure was later gradually slightly modified in various steps to be optimized for decomposition of a number of other materials of biological origin (higher plants, yeast, green and blue–green algae, gelatine, meat-bone meals, various body liquids, sugar and sugar-containing foods, egg white and egg yolk, sewage sludge, etc.). The procedure has been tested by a number of quality control protocols. The facts that (i) all our laboratory means submitted so far in interlaboratory trials have been accepted [74]; (ii) analyses of many foreign (NBS/NIST, IAEA, BCR, etc.) biological RMs which were performed as a part of the quality assurance/quality control system of our Trace Element Laboratory repeatedly yielded results which agreed well with certified or recommended values for which the determined elements; as well as (iii) our continually good performance in external quality controls of our laboratory lead us to the conclusion that the introduction of the hotplate into the classical dry ashing procedure and adaptation of the details of the time–temperature program of charring to individual types of decomposed biological materials is a fundamental contribution which brings about dramatic improvement in its whole performance. In this connection it was of our great interest to learn at the end of 1992 about the standard operation procedure developed recently by the Nordic Committee for Food Analysis for determination of metals in foodstuffs by AAS [75]. Classical dry ashing is the only recommended procedure

for sample decomposition here, and it has two versions, depending on the availability of a programmable muffle furnace in the user's laboratory. If only an ordinary muffle furnace is available (which is still often the case), charring is performed on a hotplate, using a regime which is almost identical to that which we arrived at a few years earlier. With a programmable muffle furnace, both charring and ashing are done in the furnace, using a carefully selected time–temperature program. There are, however, cases when even laboratories which possess a programmable muffle furnace are strongly advised to pre-ash samples on a hotplate. Two mineral acids are used in the procedure: 6 mol l^{-1} hydrochloric acid as an ashing aid applied after ashing, and 0.1 mol l^{-1} nitric acid for leaching. The reliability of the method has been tested by collaborative study with 16 participating laboratories. It has been verified for the elements Cd, Cr, Cu, Fe, Ni, Pb, and Zn and recommended for their determination in all kinds of food products by AAS; it has also been used for the determination of Ca, Co, K, Mg, Mn, and Na.

All the above facts lead to the conclusion that classical dry ashing can perform well, if it is done well. Well-performed classical dry ashing requires in particular careful and moderate performance of the charring step. The words of deBoer and Maessen [69] deserve repetition at this time: "Systematic error [of classical dry ashing] can be avoided or reduced by application of an experimentally well established temperature–time regime...".

Pikhart [2] unfortunately disqualified himself from obtaining good results even before he begun his investigation. His extraordinarily high selected ashing temperature of 800°C and complete neglect of the need to moderate the charring step prevented him from being successful.

Even the experimentally well-established procedures of classical dry ashing largely lack an exact and objective interpretation in physico-chemical terms. Hence, Boardman [1] is right when he calls for greater elucidation of so far mostly empirically established procedures of classical dry ashing. We fully agree with this need and have performed a separate study [72] in which we studied how classical dry ashing actually proceeds in terms of dynam-

ics and chemistry of organic matrix degradation. Results revealed the strong exothermic character of decomposition during charring and great variability depending on the individual type of biological material. The former finding calls for sufficient moderation of the charring step in order to prevent local overheating of the sample and subsequent risk of loss of part of the analyte due to its mechanical removal from the sample in the form of solid particles of smoke. The latter finding explains why the time–temperature program for charring must be optimized for each type of biological material which is to be decomposed by dry ashing. Under the *controlled* conditions, classical dry ashing has the potential to yield accurate results.

As with every method, classical dry ashing, besides its advantages, also has limitations which have to be respected. Comparison of various decomposition techniques including classical dry ashing has been done many times (see e.g. Refs. [9,10,72,76–85]) and it is not the purpose of this paper to repeat what has been already said. What we cannot accept, however, is the attempt to create suspicion that classical dry ashing cannot give good analytical results under *any* circumstances. It is obvious from the above text that the statement [3] that classical dry ashing should be completely abandoned from the protocols of trace analysis is more of a wish than an actual need and it may well be that such statements should be removed from the scientific literature.

References

[1] S. A. Boardman, in H.M. Kingston and L.B. Jassie (Eds.), Introduction to Microwave Sample Preparation, ACS Professional Reference Books, Washington, DC, 1988, p. XVII.

[2] J. Pikhart, Chem. Listy, 82 (1988) 881.

[3] P.B. Stockwell and G. Knapp, Int. Labmate, 14 (1989) 47.

[4] J. Hertz and R. Pani, Fresenius' Z. Anal. Chem., 328 (1987) 487.

[5] P. Schramel, S. Hasse and G. Knapp, Fresenius' Z. Anal. Chem., 326 (1987) 142.

[6] M. Wuerfels, E. Jackwerth and M. Stoeppler, Fresenius' Z. Anal. Chem., 329 (1987) 461.

[7] G. Knapp, Mikrochim. Acta, Part II, (1991) 445.

[8] E. Šucman, M. Šucmanová, O. Čelechovská and S. Zima, in B. Welz (Ed.), 6. Colloquium atomspektrometrische Spurenanalytik, Ueberlingen, 1991, p. 617.

[9] R. Bock, A Handbook of Decomposition Methods in Analytical Chemistry, International Textbook Co., London, 1979.

[10] B. Sansoni and V.K. Panday, in S. Facchetti (Ed.), Analytical Techniques for Heavy Metals in Biological Fluids, Elsevier, Amsterdam, 1981, p. 91.

[11] G. Morell and G. Girvidhar, Clin. Chem., 22 (1976) 221.

[12] Model 3010A Trace Metal Analyzer Instruction Manual, Environmental Science Associates, Bedford, Ma, 1986.

[13] M. Oehme and W. Lund, Fresenius' Z. Anal. Chem., 298 (1979) 260.

[14] D. Jagner, L. Renman and Y. Wang, lecture delivered at the 4th European Conference on Electroanalysis, Noordwijkerhout, The Netherlands, May 31–June 3, 1992. No abstract had been submitted by these authors.

[15] B.J. Feldman, J.D. Osterloh, B.H. Hata and A. D'Alessandro, Anal. Chem., 66 (1994) 1983.

[16] J. Wang, Analyst, 119 (1994) 763.

[17] P. Ostapczuk, Clin. Chem., 38 (1992) 1995.

[18] P. Ostapczuk, Anal. Chim. Acta, 273 (1993) 35.

[19] J.L.M. De Boer and F.J.M.J. Maessen, Spectrochim. Acta, Part B, 38 (1983) 739.

[20] J.V. Van Loon, Selected Methods of Trace Metal Analysis. Biological and Environmental Samples, J. Wiley, New York, 1985, p. 98.

[21] N. Peerzada, Mikrochim. Acta Part III, (1986) 43.

[22] C. Li, B.D. James, J. Rumble and R.J. Magee, Microchim. Acta, Part III, (1988) 175.

[23] C. Li, B.D. James and R.J. Magee, Microchim. Acta, Part II, (1989) 149.

[24] F. Wahdat, Z. Lukaszewski and R. Neeb, Fresenius' J. Anal. Chem., 338 (1990) 163.

[25] J. Wang, Electroanalytical Techniques in Clinical Chemistry and Laboratory Medicine, VCH, New York, 1988, p. 31.

[26] A.K. Furr, T.F. Parkinson, J. Ryther and C.A. Bache, Bull. Environ. Contam. Toxicol., 26 (1981) 54.

[27] S.G. Capar, R.J. Gajan, E. Madzsar, R.H. Albert, M. Sanders and J. Zyren, J. Assoc. Off. Anal. Chem., 65 (1982) 978.

[28] E.R. Elkins, J. Assoc. Off. Anal. Chem., 65 (1982) 965.

[29] R.D. Satzger, CH.S. Clow, E. Bonnin, and F.L. Fricke, J. Assoc. Off. Anal. Chem., 65 (1982) 987.

[30] W. Thornburg, J. Assoc. Off. Anal. Chem., 65 (1982) 992.

[31] S.B. Adeloju, A.M. Bond and M.L. Noble, Anal. Chim. Acta, 161 (1984) 303.

[32] S.B. Adelju, A.M. Bond and M.H. Briggs, Anal. Chim. Acta, 164 (1984) 181.

[33] C. Locatelli, F. Fagioli, C. Bighi and L. Scanavini, in P. Braetter and P. Schramel (Eds.), Trace Elem.—Anal. Chem. Med. Biol., Vol. 3, W. de Gruyter, Berlin, 1984, p. 529.

[34] A. Mayer and R. Neeb, Fresenius' Z. Anal. Chem., 321 (1985) 235.

[35] P. Mader, J. Musil, J. Cibulka, J. Korečková and E. Čurdová, in Mikroelementy '85, Proc. 19th Seminar on

Microelements, Brno, 7 May, 1985, pp. 18–26,
P. Mader, J. Musil, E. Čurdová, J. Korečková and J. Cibulka, Chem. Listy, 81 (1987) 1190.

[36] K. Vreman, N.G. Veen, E.J. Molen and W.G. Ruig, Nethl. J. Agric. Sci., 34 (1986) 129.

[37] N.G. Veen and K. Vreman, Nethl. J. Agric. Sci., 34 (1986) 145.

[38] J.B. Luten, W. Bouquet, M.M. Burgraaff and A.B. Rauchbaar, Bull. Environ. Contam. Toxicol., 36 (1986) 770.

[39] D. Wiersma, B. Van Goor and N.G. Van Der Veen, J. Agric. Food Chem., 34 (1986) 1067.

[40] P. Mader, in Mikroelementy '87, Proc. 21th Seminar on Microelements, Prague, 6 May, 1987.
P. Mader, J. Kučera, J. Cilbulka and D. Miholová, Chem. Listy, 83 (1989) 765.

[41] J. Lukačka, Hydina, 1 (1987) 3.

[42] A. Prugarová and M. Kováč, Nahrung, 31 (1987) 635.

[43] E. Stryjewska, J. Staniszewska and S. Rubel, in 6th Int. Trace Element Symp., Leipzig, Germany, 1989, p. 490.

[44] G. Stoewsand, L.J. Anderson, A.C. Bache and D.J. List, Sci. Total Environ., 94 (1990) 253.

[45] G. Ellen and J.W. Wanloon, Food Addit. Contam., 7 (1990) 265.

[46] S.G. Capar and C.A. Subjoc, J. Assoc. Off. Anal. Chem., 65 (1982) 1025.

[47] C. Locatelli, F. Fagioli, C. Bighi, S. Landi and T. Garai, Ann. Chim. (Rome), 74 (1984) 521.

[48] K.A. Wolnik, F.L. Fricke, S.G. Capar, M.W. Meyer and E.B. Satzger, J. Agric. Food Chem., 33 (1985) 807.

[49] S.B. Adeloju and A.M. Bond, Anal. Chem., 57 (1985) 1728.

[50] G. Vos, J.J.M.H. Teeuwen and W. Van Delft, Z. Lebensm.—Unters. Forsch., 183 (1986) 397.

[51] G. Vos, J.J.M.H. Teeuwen and K. Vreman, J. Agric. Sci., 34 (1986) 437.

[52] S.G. Capar and M. Loges, J. Food Saf., 8 (1987) 187.

[53] G. Vos, J.P.C. Hovens and W. Van Delft, Food Addit. Contam., 4 (1987) 73.

[54] G. Vos, J.J.M.H. Teeuwen, O.C. Knottnerus and B.L. Wijers, Nethl. J. Agric. Sci., 36 (1988) 167.

[55] S.G. Capar and E.J. Rigsby, J. Assoc. Off. Anal. Chem., 72 (1989) 416.

[56] J. Cibulka, D. Miholová, J. Píša, Z. Sova, P. Mader, S. Jandurová, J. Száková and J. Pytloun, in 7th Int. Conf. Heavy Metals in the Environment, Geneva, Switzerland, 1989, p. 145.

[57] A. Prugarová, M. Kováč and P. Karol, Rostl. Vyroba, 35 (1989) 719.

[58] S.G. Capar, J. Assoc. Off. Anal. Chem., 73 (1990) 357.

[59] G. Vos, H. Lammers and C.A. Kan, Food Addit. Contam., 7 (1990) 83.

[60] I. Poláček, V. Greco, S. Králová, J. Biskupičová, A Lalcíková and E. Korčeková, krmivarstvi Sluzby, 26 (1990) 203.

[61] Official Methods of Analysis, 14th edn., AOAC, Arlington, VA, 1984, Sections 25.008–25.015.

[62] Official Methods of Analysis, 15th edn., AOAC, Arlington, VA, 1990, Section 982.23; 16th edn., 1995, Section 9.1.02.

[63] S.B. Adeloju, Analyst, 114 (1989) 455.

[64] E. Stryjewska, S. Rubel, A. Henrion and G. Henrion, Fresenius' Z. Anal. Chem., 327 (1987) 679.

[65] T. Muys, Analyst, 109 (1984) 119.

[66] J.K. Friel and C.D. Nguyen, Clin, Chem., 32 (1986) 739.

[67] N.J. Miller-Ihli, J. Res. Natl. Bur. Stand. (U.S.), 93 (1988) 350.

[68] J.C. Van Loon, Selected Methods of Trace Metal Analysis: Biological and Environmental Samples, J. Wiley, New York, 1985.

[69] J.L.M. de Boer and F.J.M.J. Maessen, Spectrochim. Acta., Part B, 38 (1983) 739.

[70] P. Mader, J. Cibulka, M. Prousková, Z. Sova and M. Hájková, in Mikroelementy '83, Proc. 17th Seminar on Microelements, Rožnov pod Radhoštěm, 26–28 April, 1983, pp. 51–56.

[71] P. Mader, J. Cibulka, M. Prousková and M. Dostálová, in Mikroelementy '84, Proc. 18th Seminar on Microelements, Prague, 3 May, 1984, pp. 24–30.

[72] P. Mader, in J. Cibulka (Ed.), Pohyb olova, kadmia a rtuti v zemědělské výrobě a biosféře (Movement of Lead, Cadmium and Mercury in Agricultural Production and in the Biosphere), State Agricultural Publishing House SZN, Prague, 1986, pp. 117–156.

[73] P. Mader, V. Haber and J. Zelinka, Fresenius J. Anal. Chem., submitted.

[74] D. Miholová, P. Mader, J. Száková, A. Slámová and Z. Svatoš, Fresenius' J. Anal. Chem., 345 (1993) 256.

[75] Nordic Committee on Food Analysis, Metals. Determination by Atomic Absorption Spectrophotometry in Foodstuffs, No. 139, 1991.
L. Jorhem, J. Assoc. Off. Anal. Chem. Int., 76 (1993) 798.

[76] T.T. Gorsuch, The Destruction of Organic Matter, Pergamon Press, Oxford, 1970.

[77] J.G. van Raaphorst, A.W. van Weers and H.M. Haremaker, Analyst, 99 (1974) 523.

[78] M. Blanuša and D. Breški, Talanta, 28 (1981) 681.

[79] J.K. Friel and C.D. Nguyen, Clin. Chem., 32 (1986) 739.

[80] P. Schramel, S. Hasse and G. Knapp, Fresenius' Z. Anal. Chem., 326 (1987) 142.

[81] M. Stoeppler, in G.F. Nordberg and P.R. Sager (Eds), Biological Monitoring of Toxic Metals, Plenum New York, 1988, pp. 481–497.

[82] J. Angerer, M. Fleischer, G. Machata, W. Pilz, M. Stoeppler and H. Zorn, in J. Angerer and K.H. Schaller (Eds.), Analyses of Hazardous Substances in Biological Materials. Methods for Biological Monitoring, Vol. 2, Verlag Chemie, Wechheim, 1988, pp. 1–30.

[83] J.E. Rechcigl and G.G. Payne, Commun. Soil. Sci. Plant Anal., 21 (1990) 2209.

[84] N. Ybáñez, M.L. Cervera and R. Montoro, J. Anal. At. Spectrom., 6 (1991) 379.

[85] H.-M. Kuss, Fresenius' J. Anal. Chem., 343 (1992) 788.

Flow-injection on-line column preconcentration for low powered microwave plasma torch atomic emission spectrometry

Dongmei Ye, Hanqi Zhang, Qinhan Jin*

Department of Chemistry, Jilin University, Changchun 130023, China

Abstract

This paper describes an improvement in detection capability of microwave plasma torch atomic emission spectrometry by using a flow-injection on-line column preconcentration system. The analytical performances of Cd, Cu, Mn and Zn were studied. The analytes were preconcentrated with a thiol resin. The preconcentration period, the pH of the sample solution and the HCl concentration in the eluant were examined in detail. Operating conditions were optimized as follows: sample uptake, 1.2 ml min^{-1}; preconcentration period, 1 min; pH of sample solution, 9; HCl concentration in the eluant, 1 mol l^{-1}. The experimental results show that flow-injection on-line column preconcentration can not only eliminate the effect of some concomitant elements, such as Li, Na and K, on the determination of analyte, but also enhance the sensitivity.

Keywords: Flow-injection; Preconcentration; Microwave plasma torch AES

1. Introduction

Microwave induced plasma (MIP) has been of interest as an excitation source for atomic emission spectrometry (AES) because it is a powerful emission source for a wide range of elements, and inexpensive and easy to operate. One of the major limitations of MIP for AES is its low tolerance to the introduction of aqueous sample. To perform aqueous sample analysis, the amount of water vapor entering the MIP must be restricted

through desolvation, or the power applied to the discharge must be increased. A low power applied to the microwave discharge does not provide sufficient energy to desolvate, atomize and excite the analyte for a large aqueous loading. However, a higher applied power can result in plasma device heating and microwave leakage. Therefore a water-cooled plasma device must be used [1]. Another approach to solving this problem is to improve the plasma device. Okamoto and co-workers [2,3] reported a circularly polarized wave mode cavity that facilitates the production of a high power (> 1 kW) annular atmospheric pressure plasma. The microwave plasma

* Corresponding author

torch (MPT) developed by Jin et al. [4] showed great promise for direct solution analysis. Since the plasma obtained with the MPT has a central channel and the analyte is forced to pass through the central channel, the analyte is efficiently vaporized, atomized, excited and ionized and causes minimal perturbation to the plasma. Matusiewicz [5] reported a new microwave cavity assembly: an integrated microwave plasma cavity/magnetron combination (MPCM). The introduction of wet aerosols can be accomplished by using direct nebulization with no desolvation system. Ng and Chen [6] used a dual, low-powered (<200 W total power) MIP system for direct liquid aerosol introduction. The MIPs are sustained in two Beenakker cavities arranged in tandem. The first plasma performs the major task of desolvation, volatilization, and atomization; the second plasma performs the major task of excitation.

Compared with an inductively-coupled plasma (ICP) source the MIP seems to be prone to interelement effects, especially when an easily ionized element (EIE) is also introduced. This is another major disadvantage of the MIP (the so-called matrix effect). The reason for the existence of the matrix effect is that the gas temperature of the MIP is lower than that for the ICP. There are two ways to overcome the matrix effect. One is to increase the microwave forward power. The other is to separate the matrix from the analyte prior to its introduction into the MPT.

It has long been recognized that off-line preconcentration and separation of trace constituents by using ion-exchange, adsorption or solvent extraction batch procedures are effective in improving the sensitivity and selectivity of atomic spectrometric methods [7]. Principal drawbacks of off-line separation procedures are that they are often time-consuming, frequently require a large sample volume, the sample may be contaminated, and the sample throughput is very low. With the implementation of on-line flow-injection techniques for separation and preconcentration, such drawbacks no longer exist, while the beneficial effects are further enhanced: sampling frequency can be increased by one or two orders of magnitude and consumption of sample and

reagent can be decreased by one or two orders of magnitude. On-line flow-injection techniques also have better precision and are easy to operate automatically [8].

The objectives for on-line pretreatment may be either to remove the interfering matrix or to enhance the sensitivity, or both. Of the different approaches, separations and preconcentrations based on column techniques seem to have undergone the most rapid development, probably owing to the simplicity of operation and the existence of a wealth of knowledge on related batch procedures. When a sample is introduced into an on-line column, the interest of the operator is focused on the complete collection of the analyte, while releasing the matrix to waste, and later on, the complete release of the analyte from the column into the detector. Although flow-injection (FI) on-line column preconcentration has been extensively applied to atomic spectrometry, such as atomic absorption spectrometry (AAS) and inductively-coupled plasma atomic emission spectrometry (ICP-AES)[9], very little has been done so far on coupling it with MIP systems[10]. Madrid et al. [10] determined Cu by applying FI on-line column preconcentration to MPT-AES with an ultrasonic nebulization system.

In this paper, the elements determined are preconcentrated using a thiol resin and introduced into the MPT with an FI-pneumatic nebulization system and the solvent is removed by a desolvation system. The results indicated that FI on-line column preconcentration can eliminate the EIE effects without causing losses in sensitivity or precision.

2. Experimental

2.1. Apparatus

The FI-MPT-AES system was built in this laboratory. The block diagram of the system is shown in Fig. 1. The components of the system are listed in Table 1 and are described below in some detail. The operating conditions are listed in Table 2 unless otherwise stated.
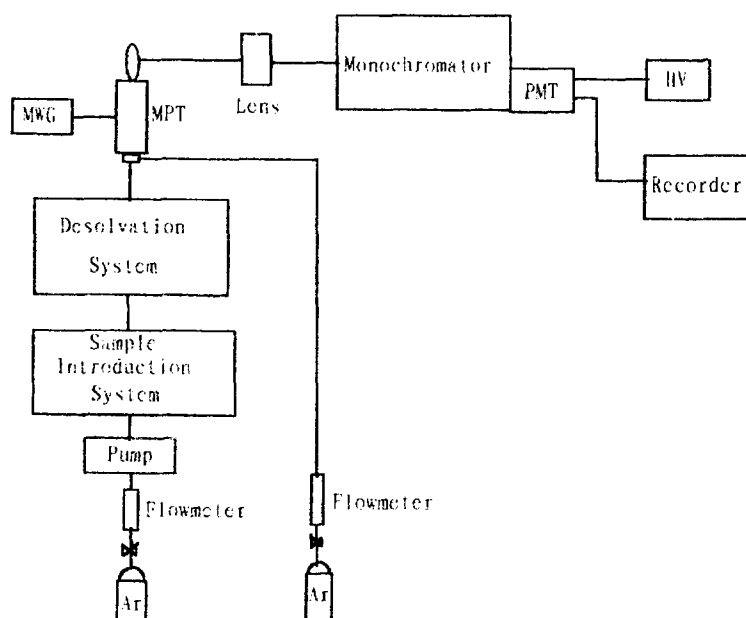
Fig. 1. Block diagram of instrumentation: MWG, microwave generator; MPT, microwave plasma torch; PMT, photomultiplier tube; HV, high voltage.

2.1.1. FI on-line column preconcentration system.

The block diagram of the sample introduction system is shown in Fig. 2. The sorbent extraction

Table 1
Experimental instrumentation

Component	Model	Manufacturer
Torch	MPT	Laboratory built
Nebulizer	Concentric nebulizer	Laboratory built
Spray chamber	Diameter 25 mm, length 200 mm	Laboratory built
Microwave generator	DW-1, 0–100 W	Beijing Geological Instrument Factory
Monochromator	WDG30 $F = 30$ cm, grating 1200 grooves mm^{-1}	Beijing Optical Instrument Factory
Strip-chart recorder	XWT-164	Shanghai Dahua Instruments
Flow injection analyzer	LZ-1010	Shenyang Zhaofa Institute of Automatic Analysis
Lens	Diameter 30 mm, focal length 70 mm, quartz	Beijing Optical Instrument Factory

column (3 mm i.d., 3.5 cm long) was made in this laboratory. The packing filled two-thirds of the volume of the column and was held in place by two small plugs of plastic foam at either end.

Aqueous sample solutions were introduced into the plasma with a pneumatic concentric nebulizer with a desolvation system. In the load position of the actuated injection value, the carrier liquid (distilled water) flows from a peristaltic pump

Table 2
Operating conditions

Parameter	Value
Microwave frequency	2450 MHz
Forward power	60 W
Reflected power	2 W
Plasma viewing mode	Side-on
Plasma viewing position	0–15 mm above top of torch
Carrier gas flow rate	700 ml min^{-1}
Support gas flow rate	400 ml min^{-1}
Sample introduction rate	1.3 ml min^{-1}
Entrance slit height	2 mm
Entrance slit width	20 μm
Exit slit height	1 cm
Exit slit width	20 μm
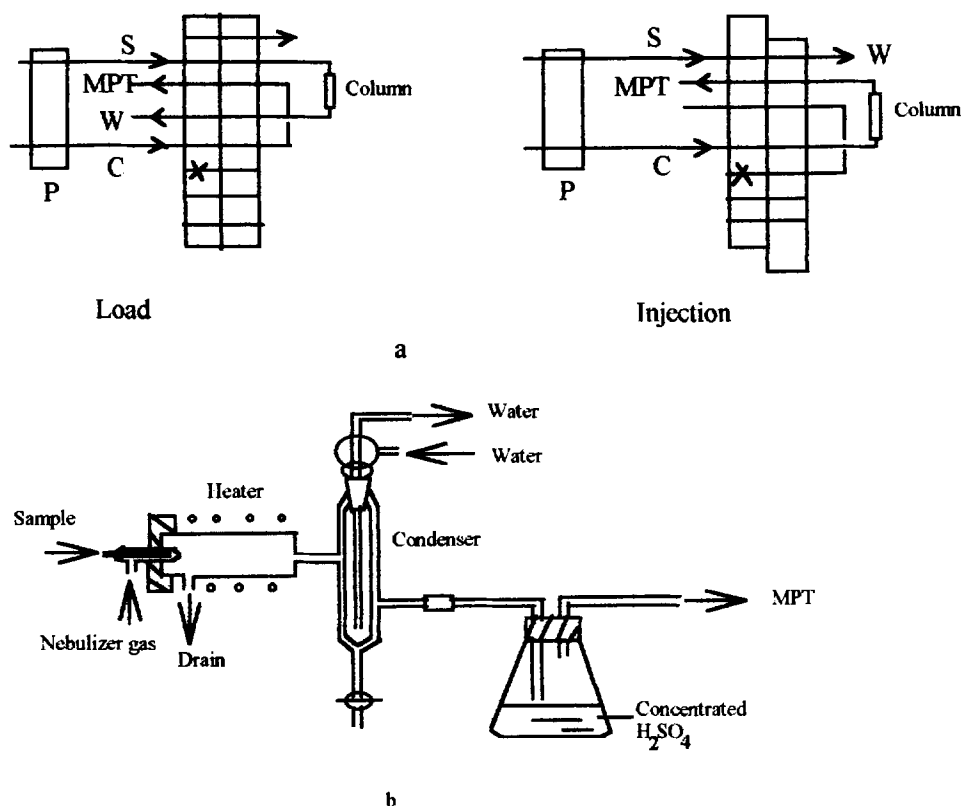
Fig. 2. Schematic diagram of sample introduction system. (a) Flow injection system: S, sample; C, carrier; W, waste; P, pump; X, block line. (b) Nebulization and desolvation system.

directly through the pneumatic nebulizer into the plasma while the sample is simultaneously drawn into the sorbent extraction column. When the valve is rotated, the path of the carrier liquid is redirected to flow through the sorbent extraction column thereby carrying the sample plug into the MPT. The loading solution flow rate is 1.7 ml min^{-1} and the eluant flow rate is 1.3 ml min^{-1}.

2.1.2. Desolvation system

Although the MPT discharge will operate stably with a wet aerosol, a simple desolvation system consisting of a heated glass tube, a water-cooling condenser and a concentrated sulfuric acid desiccator is used. It was shown that the system effectively removed the water from the sample solution. Only 0.3% of water entered into the plasma [11].

2.1.3. Torch

The torch used in this study is similar to an ICP torch, consisting of three concentric metal tubes [4]. The plasma support gas is introduced through the intermediate tube and sample aerosol is introduced through the central tube by a carrier gas. The plasma forms between the intermediate tube and central tube near the top of the torch and extends into the surrounding air to form a flame-like discharge with a central channel. The microwave energy is coupled into the plasma via a 6 mm i.d. cylindrical antenna which surrounds the intermediate tube. The plasma can be ignited easily with a short burst from a Tesla coil or by a touch of a screwdriver on the top of the central tube.

2.2. Gas and reagents

Argon (99.99%) was used as carrier gas and support gas. All reagents used were of suprapure

grade or analytical grade. The stock solutions (1 mg ml^{-1}) of all elements were prepared according to standard procedures. To obtain desired concentration of different working solutions, volumetric dilutions of the stock solutions were made. Double-distilled water was used throughout the experiments. The resin used is a thiol resin (Type 190, produced by Nankai University, China) whose active group is -SH. It is similar to Duolite ES-465.

2.3. Intensity measurement

In this study, transient emission signal (peak-shaped plots of intensity vs. time) were recorded with a strip-chart recorder. The peak heights of the signals recorded were measured and taken as the relative intensities. Peak height was used to measure emission intensities and three replicate measurements (RSDs < 3%) were made each time unless otherwise stated. In Figs. 3-7, the intensity is plotted relative to the first signal and in Fig. 8 the intensity is plotted relative to that without an EIE at respective power levels.
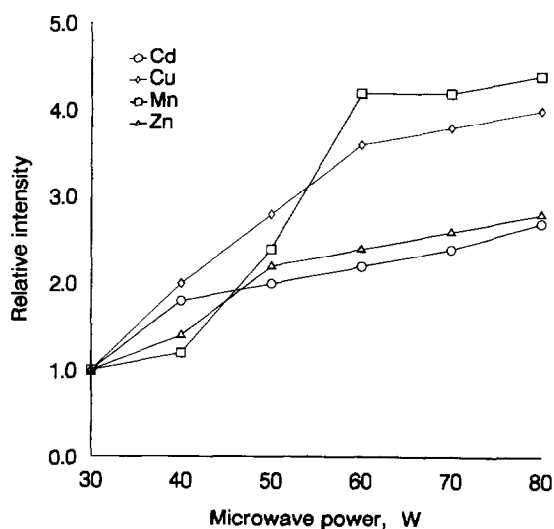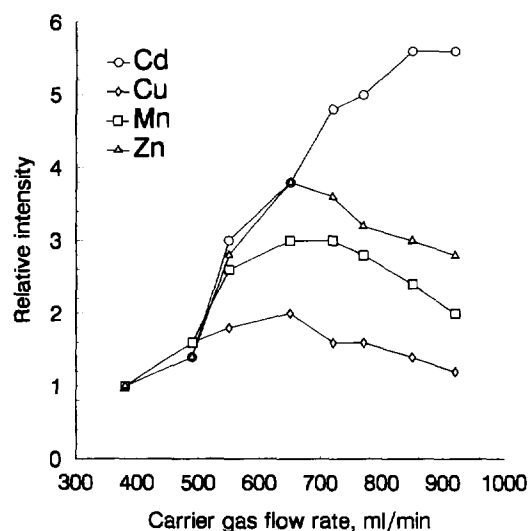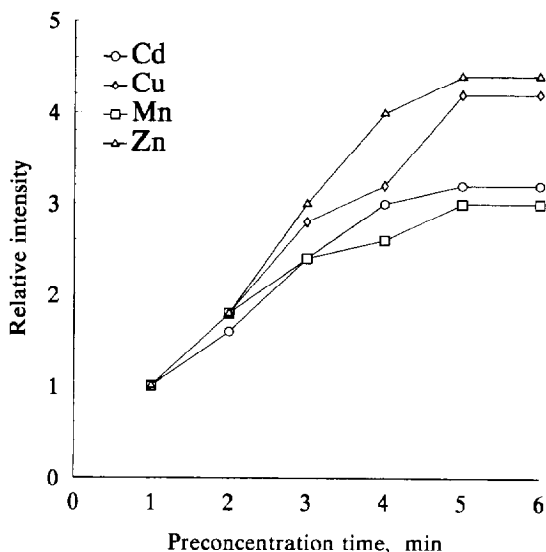

Fig. 3. The effect of microwave forward power on emission intensity. Analytical line and analyte concentration in loaded sample: Cd 228.8 nm, 0.3 μg ml^{-1}; Cu, 324.7 nm, 0.3 μg ml^{-1}; Mn 257.6 nm 1.0 μg ml^{-1}; Zn, 213.9 nm, 0.3 μg ml^{-1}; HCl concentration of the eluent, 1 mol l^{-1}.

3. Results and discussion

3.1. Optimization of experimental parameters

To achieve the best analytical performance, the experimental parameters, such as microwave forward power, support and carrier gas flow rates, preconcentration time, preconcentration conditions, and HCl concentration in the eluant, were optimized by using a univariate optimization procedure for simplicity. Because the experimental parameters are known to be inter-dependent, the procedure may not yield the most optimal conditions.

3.1.1. Forward power

As shown in Fig. 3, at lower microwave power (< 60 W), the emission intensities of analytical lines increase as the microwave power increases, and at higher power (> 60 W) an increase in the applied power causes only a slight change in the emission intensities. It is also evident from Fig. 3 that the effects of microwave power on intensities of the ionic lines and atomic lines are very similar. These results are very similar to those obtained with an ultrasonic nebulizer [11] and very different from those obtained with a surfatron (a microwave device) under similar experimental conditions. When a surfatron is used and the experimental conditions are as follows: inner diameter of discharge tube 2-5 mm; carrier gas flow rate 200-800 ml min^{-1}; microwave power, 30-80 W; the emission intensity always increases with the microwave power and at higher power levels (> 60 W) the emission intensities of the "hard lines" (ionic lines and atomic lines with excitation potentials greater than 5 eV) increase more significantly than at lower power levels (< 60 W) [4]. The reason for this phenomenon is probably because for surfatron the plasma is sustained in a discharge tube, so that when the power increases the plasma becomes longer and the power density does not increase significantly. However, the plasma viewing mode is end-on, so the residence time of analytes in the plasma will by prolonged and the emission intensities of the analytical lines will increase. However, for the MPT the plasma is formed between the intermediate and central tubes near the top of
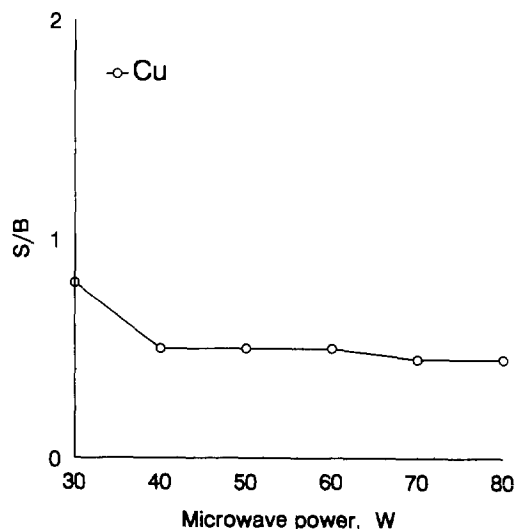
Fig. 4. The effect of microwave forward power on S/B. Analytical line and analyte concentration in the sample solution: Cu, 324.7 nm, 0.3 μg ml^{-1}; HCl concentration of the eluent, 1 mol l^{-1}.

the torch and extends into the surrounding air, so that the plasma expands with the applied power and the power density does not increase sharply.

The effect of microwave forward power on signal-to-background ratio (S/B) has also been studied. Since it was shown that the blank signal was identified with the background signal in this case, the blank signal was measured as background as described in the literature [12]. To measure the blank signal, the recorder is first adjusted to the zero position by blocking all radiation from entering the monochromator at the analytical wavelength. The blank signal is then measured by replacing the analytical sample with a blank that is identical to the analytical sample except that there is no analyte being studied at the same wavelength. The results are shown in Fig. 4. It is evident from Fig. 4 that the effect of microwave forward power on S/B is not significant. The reason is evident. As the power increases, the emission intensities of analytical lines and background emission increase simultaneously, so that S/B does not change with power. Because the concentration of the analyte is very low (0.3 μg ml^{-1}), the analyte signal is always smaller than that of the background.

3.1.2. Gas flow rate

Either carrier gas (central) or support gas (outer) has influence on the stability of the plasma and emission intensity of analytical lines. It is evident that the carrier gas flow rate has more significant influence on the analytical signals than the support gas flow rate [11]. As shown in Fig. 5, for the elements examined an increase in carrier gas flow rate initially causes significant increase in the emission intensities of analytical lines, and then levels off or decreases slightly. The results can be explained in the light of the effect of carrier gas flow rate on the nebulization efficiency, the temperature of the plasma and the residence time of the analyte in the MPT. The nebulization efficiency increases as the carrier gas flow rate increases, but the temperature of the plasma and the residence time of the analyte in the MPT decrease.

3.1.3. Preconcentration time

The effects of preconcentration time on emission signals are shown in Fig. 6. It is evident that an increase in preconcentration time causes an increase in the signal, but when the preconcentration time is greater than 5 min, the signal in-

Fig. 5. The effect of carrier gas flow rate on emission intensity. Analytical lline and analyte concentration in loaded sample: Cd, 228.8 nm, 0.3 μg ml^{-1}; Cu, 324.7 nm, 0.3 μg ml^{-1}; Mn, 257.6 nm, 1.0 μg ml^{-1}; Zn, 213.9 nm, 0.3 μg ml^{-1}; HCl concentration of the eluent, 1 mol l^{-1}.

Fig. 6. The effect of preconcentration time on emission intensity. Analytical line and analyte concentration in loaded sample: Cd, 228.8 nm, 0.3 μg ml^{-1}; Cu, 324.7 nm, 0.3 μg ml^{-1}; Mn, 257.6 nm, 1.0 μg ml^{-1}; Zn, 213.9 nm, 0.3 μg ml^{-1}; HCl concentration of the eluent, 1 mol l^{-1}.

creases slightly or does not increase at all. It is shown that under such circumstances the thiol resin is saturated and with the increase in preconcentration time the competition between analyte ion and other ions becomes more significant. In order to speed up the sample throughput, the preconcentration time used in this study is 1 min.

3.1.4. Preconcentation conditions

In order to preconcentrate the analyte completely, the effect of pH (1–14) of sample solution on preconcentration was studied. The results show that when the pH is about 9, the analyte is preconcentrated completely. The pH of the sample solution is, therefore, adjusted to about 9 with a buffer solution of NH_3–NH_4Cl. However, the concentration of NH_3–NH_4Cl was shown to have no significant effect on emission intensity. In this study the NH_3–NH_4Cl concentration used is 0.05 mol l^{-1}.

3.1.5. HCl concentration in eluant

The effect of the HCl concentration in the eluant (0–2 mol l^{-1}) was also studied. The results show that the effect of HCl concentration in

eluant on peak height is not significant. The only effect is on eluating time. The lower the HCl concentration, the longer the eluating time. In order to reduce the eluating time, an HCl concentration in eluant of 1 mol l^{-1} was selected in this work.

3.2. Detection limits and linear dynamic ranges

The detection limits (3σ) for selected elements obtained by this method under optimized conditions are listed in Table 3. The preconcentration time used here is also 1 min. For comparison, the results obtained by FI-MPT-AES without preconcentration are also included. It is clear from Table 3 that the detection limits obtained by this method are lower than those obtained by FI-MPT-AES under similar experimental conditions. The method appears particularly attractive in view of the enrichment factor and its simplicity of operation.

Enrichment factor (EF) is the criterion used most frequently for the evaluating preconcentration systems. However, the precise meaning of the term is often not defined. There are three different ways in the literature of defining EF. Some workers deduce enrichment factors by comparing the peak height before and after preconcentration [13,14], others do so by finding from a calibration graph of the unprocessed standard solution the concentration which gives the same peak height as the processed sample [15]. Yet another approach is to do the evaluation by comparing slopes of the linear portion of the calibration curves before and after the preconcentration [16]. The first approach is very straightforward, so we used it in this study. In order to obtain the peak height before preconcentration, a regular FI set-up was used, the volume of the sample loop being 150 μl. The EFs obtained are listed in Table 3.

For all elements studied, the linear dynamic ranges determined experimentally are over three orders of magnitude (see Table 3).

It is evident that the detection limits, linear dynamic ranges and EFs are relevant to the experimental conditions, especially the preconcentration time. The sample throughout is 20 per hour.

Table 3
The detection limits, dynamic linear ranges and enrichment factors

Element	line (nm)	Detection limit (ng ml^{-1})		Dynamic linear range (μg ml^{-1})	EF
		This method	FI-MPT-AES		
Cd	I 228.3	3.6	10	0.01–20	4.9
Cu	I 324.7	2.2	9.3	0.01–20	4.4
Mn	II 257.6	3.1	9.1	0.05–20	4.2
Zn	I 213.9	1.8	7.8	0.01–20	4.3

3.3. Precision

The RSDs for determination of selected elements are shown in Table 4. It is clear that the RSDs for selected elements are acceptable.

3.4. Effect of easily ionized elements (EIEs)

There are a large amount of EIEs, especially K and Na, in many natural samples. Study of the effect of EIEs on microwave plasma emission is of significance for developing MWP-AES and improving its application to real sample analysis. The effect of EIEs on emission intensities in MWP-AES has been studied by using TM_{010} (a specific operating mode of a microwave resonant cavity) [1,17–21], surfatron [22] plasma sustained devices and with various sample introduction systems, such as electrothermal vaporization [23–26], pneumatic nebulizer [27,28] and ultrasonic nebulizer [29,30]. The results indicated that the effect of EIEs is very closely related to the discharge system and sample introduction system. When

TM_{010} or surfatron is used, the plasma is sustained in a discharge tube, but for MPT the plasma is formed between the intermediate and central tubes near the top of the torch and extends into the surrounding air and hence the EIE effect may have different behavior. Madrid et al. [10] studied the effect of K and Na on emission of Cu, and a reduction in the K and Na effect by the use of the FI system was observed. In this study a similar reduction of the effect of EIEs on signals of Cu by using the FI pneumatic nebulization sample introduction system was also observed (Fig. 7). It should be noted that the on-line preconcentration is not applied in the EIE effect study. For the EIE effect study, the "column" in Fig. 2 was replaced by a 150 μl sample loop and the sample solution containing analyte and EIEs are introduced into the MPT by using the FI sample introduction system. It was observed that the existence of a large quantity of EIE caused a depression in analyte emission (EIE effect). However, this EIE effect can be reduced simply by an increase in the applied microwave power (Fig. 8).

Table 4
The RSDs for some elements

Element	Line (nm)	Added (μg ml^{-1})	Found (μg ml^{-1})	RSD (%)
Cd	I 228.8	0.30	0.29, 0.30, 0.29, 0.31, 0.30, 0,30, 0.30	0.69
Cu	I 324.7	0.30	0.29, 0.29, 0.30, 0.32, 0.30, 0.31, 0.30	1.1
Mn	II 257.6	1.00	1.0, 1.0, 1.0, 1.0, 0.98, 1.0, 1.0	0.76
Zn	I 213.9	0.30	0.30, 0.32, 0.30, 0.30, 0.30, 0.28, 0.30	1.2
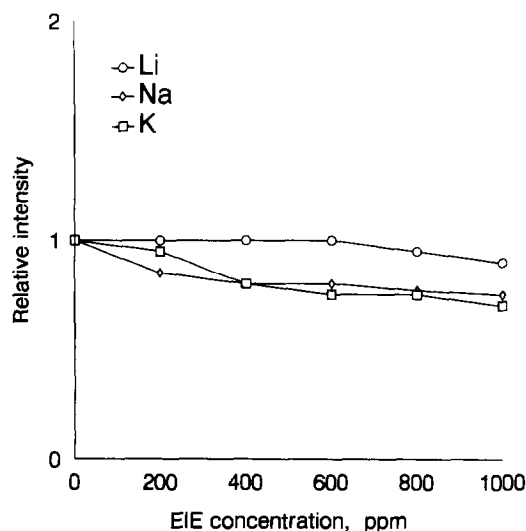
Fig. 7. The effect of EIE using the FI sample introduction system. Analytical line and analyte concentration in the sample solution: Cu, 324.7 nm, 1 μg ml^{-1}; HCl concentration in the sample solution: 1 mol l^{-1}.
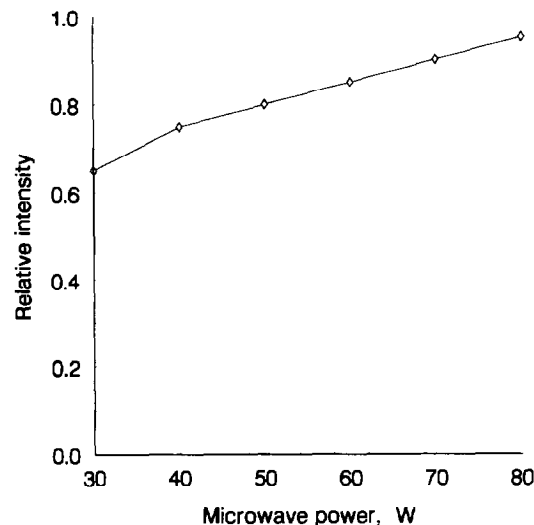
Fig. 8. The effect of microwave forward power on EIE interference. Analytical line and analyte concentration in the sample solution: Cu, 324.7 nm, 1 μg ml^{-1}; EIE concentration in the sample solution: Li, 1000 μg ml^{-1}; HCl concentration in the sample solution: 1 mol l^{-1}.

Table 5
The effects of EIE on relative emission intensities

EIE (μg ml^{-1})	Cd		Cu		Mn		Zn	
	a	b	a	b	a	b	a	b
Li (1000)	1.0	0.98	1.0	1.0	1.0	0.99	1.0	1.0
Na (1000)	1.0	0.98	1.0	1.0	1.0	0.99	1.0	1.0
K (1000)	1.0	0.99	1.0	1.0	1.0	0.99	1.0	1.0

[a] Without EIE.
[b] With EIE.

It is clear from Fig. 8 that as the power increases the effect of Li (1000 μg ml^{-1}) on Cu emission decreases. This is because the higher the applied power (energy), the more efficient the volatilization and atomization of the analytes and therefore the EIE effect is decreased. To eliminate the effect of EIE, an on-line column preconcentration technique as described above was adopted and it was shown (Table 5) that when the concomitant EIE concentration reaches 1000 μg ml^{-1}, the EIE still has no significant effect on the analyte emission intensity. The reason for this phenomenon is probably that the thiol resin preconcentrates the

analyte selectively. When a sample solution containing EIEs is pumped through the thiol resin, only the analyte can be preconcentrated and EIEs go to waste, not being introduced into the plasma, so there is no effect of EIEs on the emission intensity of the analyte.

4. Conclusion

The FI on-line column preconcentration technique has provided a first close connection between chemical modification of the sample and the final physical process of MPT-AES detection. It eliminates the matrix interference efficiently and enhances the sensitivity of MPT-AES for elements studied significantly. The FI on-line column preconcentration MPT-AES instrument is simple and fast in operation, and the running cost is low.

Acknowledgement

References

[1] G.L. Long and L.D. Perkins, Appl. Spectrosc., 41 (1987) 980.

[2] Y. Okamoto, M. Yasuda and S. Murayama, Jpn. J. Appl. Phys., 29 (1990) 2670.

[3] Y. Okamoto, Anal. Sci., 7 (1991) 283.

[4] Q. Jin, C. Zhu, M.W. Borer and G.M. Hieftje, Spectrochim. Acta, Part B, 46 (1991) 417.

[5] H. Matusiewicz, Spectrochim. Acta, Part B, 47 (1992) 1221.

[6] K.C. Ng and S. Chen, Microchem. J., 48 (1993) 383.

[7] Yu.A. Zolotov and N.M. Kuzmin, in G. Svehle (Ed.), Preconcentration of Trace Elements, Vol. XXV of Wilson and Wilson's Comprehensive Analytical Chemistry, Elsevier, Amsterdam, 1990.

[8] Z. Fang, Spectrochim. Acta Rev., 14 (1991) 235.

[9] Z. Fang, Flow Injection Separation and Preconcentration, VCH, Weinheim, 1993.

[10] Y. Madrid, M. Wu, Q. Jin and G.M. Hieftje, Anal. Chem. Acta, 227 (1993) 1.

[11] Q. Jin, H. Zhang, Y. Wang, X. Yuan and W. Yang, J. Anal,. At. Spectrom., 9 (1994) 851.

[12] P.W.J.M. Boumans, F.J. De Boer, F.J. Dahmen, H. Hoelzel and A. Meier, Spectrochim. Acta, Part B, 30 (1975) 449.

[13] Z. Fang and B. Welz, J. Anal. At. Spectrom., 4 (1989) 543.

[14] Y. Liu and J.D. Ingle, Jr., Anal. Chem., 61 (1989) 520.

[15] F. Malamas, M. Bengtsson and G. Johansson, Anal. Chim. Acta, 160 (1984) 1.

[16] J. Ruzicka and G.D. Christian, Analyst, 115 (1990) 475.

[17] K.G. Michlewicz and J.W. Carnahan, Anal. Chem., 58 (1986) 3122.

[18] K.G. Michlewicz and J.W. Carnahan, Anal. Chem., 57 (1985) 1092.

[19] C.I.M. Beenakker, B. Bosman and P.W.J.M. Boumans, Spectrochim. Acta, Part B, 33 (1978) 373.

[20] L.D. Perkins and G.L. Long, Appl. Spectrosc., 43 (1989) 499.

[21] D. Kollotzeu, P. Tschopel and G. Tolg, Spectrochim. Acta, Part B, 39 (1984) 625.

[22] L.J. Galante, M. Selby and G.M. Hieftje, Appl. Spectrosc., 42 (1988) 559.

[23] J.P. Matousek, B.J. Orr and M. Selby, Spectrochim. Acta, Part B, 41 (1986) 415.

[24] H. Kawaguchi and B.L. Valke, Anal. Chem., 47 (1975) 1029.

[25] H. Kawaguchi, I. Astmya and B.L. Vallee, Anal. Chem., 49 (1977) 226.

[26] M. Selby, R. Rezaniyaan and G.M. Hieftje, Appl. Spectrosc., 41 (1987) 761.

[27] C.I.M. Beenakka, B. Bosman and P.W.I.M. Bouman, Spectrochim. Acta, Part B, 37 (1978) 373.

[28] R.K. Skogerboe and G.N. Coleman, Appl. Spectrosc., 130 (1976) 504.

[29] M.H. Abdallah, S. Coulombe and J.M. Mermet, Spectrochim. Acta, Part B, 37 (1990) 873.

[30] Q. Jin, H. Zhang, Y. Duan, A. Yu, Y. Ren, X. Zhang, H. Lu and S. Yu, Microchem. J., 44 (1991) 153.

Studies on the extraction of Copper(II) with 4-alkyldithiocarboxylate derivatives of 1-phenyl-3,5-dioxopyrazolidine

Aurora Molinari, Raúl Ariz, Alfonso Oliva**

Institute of Chemistry, Catholic University of Valparaiso, Casilla 4059, Valparaiso, Chile

Received 5 May 1995; revised 15 September 1995; accepted 21 September 1995

Abstract

The extraction behaviour of copper(II) from acid solutions (pH 0–6) was studied with the new reagent 4-alkyldithiocarboxylate-3,5-dihydroxy-1-phenylpyrazol (HL; alkyl = n-butyl, n-dodecyl). The species extracted was found to be ML_2. The reagent was used to separate copper(II) from iron(III) in an acidic lixiviation solution of a mineral sample composed of enarguite (Cu_3AsS_4) and pyrite (FeS_2). Additionally, the extraction efficiency of this new reagent was compared with the commercially available LIX 984 N extractant of copper (II).

Keywords: Copper(II); Minerals; 1-Phenyl-3,5-dioxopyrazolidine

1. Introduction

It is known that 4-acyl-5-pyrazolones are good extractants for a wide variety of transition metals, actinides, lanthanides and other ions [1–5]. A few years ago we initiated a program concerning the synthesis and extractive properties of related compounds, where the acyl group is replaced by the alkyldithiocarboxylate. We have described the Cu(II) and Ni(II) complexes of 4-alkyldithiocarboxylate-5-pyrazolones [6] and shown that these ligands are good extractants for Cu(II) at pH 4–6 [7].

Looking for new extractants which can be efficiently used under more drastic acidic conditions with Cu(II), we have turned our attention to alkyldithiocarboxylate derivatives of five-membered heterocyclic diones. In this paper, we report the results of the extraction of Cu(II) in the presence of Fe(III) with ligands derived from 1-phenyl-3,5-dioxopyrazolidine which is also named 1-phenyl-3-hydroxy-5-pyrazolone in the literature [8,9]).

2. Experimental

2.1. Reagents

The ligands 4-butyldithiocarboxylate-3,5-dihy-

---

* Corresponding author. Fax: (56) 32-212 746.

droxy-1-phenylpyrazol (HBDTP) and 4-dode-cyldithiocarboxylate-3,5-dihydroxy-1-phenylpyra-zol (HDDTP) were synthesized by the reaction of 1-phenyl-3,5-dioxopyrazolidine with sodium acetate, carbon disulfide and butyl or dodecyl bromide in dimethylformamide (DMF) as the solvent. Stock solutions containing 0.01 M copper (II) acetate and 0.1 M potassium nitrate at fixed pH 0–6 or 0.01 m iron(III) chloride and 0.1 M potassium nitrate at pH 0–2 were used in the extraction studies. Stock solutions of 0.01 M copper(II) acetate, 0.01 M iron(III) chloride and 0.1 M potassium nitrate at pH 0–2 were used for extractive separation studies at pH 0.

The initial metal content of the stock solutions was determined by complexometric titration with EDTA [10]. All the extraction experiments were performed by the batch method with a variable-speed vortex mixer (Orbital Shaker). A mineral mixture of enarguite (Cu_3AsS_4) and pyrite (CuS_2) containing 16.5% Cu and 23.7% Fe, analyzed according to standard ASTM methods and lixiviated with bromine electrogenerated in situ [11], was supplied by El Indio Mining Company (La Serena, Chile) to study the separation of Cu(II) in real mineral samples.

2.2. Extraction and analytical procedure

2.2.1. Extraction of Cu(II) from a 0.01 M copper(II) acetate solution as a function of pH

A portion of the stock solution 10.0 ml was acidified with HCl to a fixed pH and shaken for 10 min in a separatory funnel with an equal volume of a 0.02 m chloroform solution of the ligand. After the extraction, the pH of the aqueous phase was measured with a pH meter and its Cu(II) content was evaluated with 0.1 M EDTA and murexide as indicator. The amount of Cu(II) extracted into the organic phase was calculated from the difference between the metal concentration in the aqueous phase before and after extraction. The same procedure was used in the extraction studies of Fe(III) but with the use of 5-sulfosalicylic acid as indicator in the titration step.

2.2.2. Separation of Cu(II) from an aqueous solution 0.01 M in Cu(II) and Fe(III) at pH0

A portion of stock solution (10.0 ml) was acidified to pH 0 with HCl and shaken for 10 min with an equal volume of 0.03 M chloroform solution of HDDTP. The Fe(III) was precipitated from the aqueous phase with concentrated NH_3 and after filtration the Cu(II) content was evaluated as before.

2.2.3. Separation of Cu(II) from a lixiviation solution of enarguite and pyrite

A portion of the lixiviation solution (2.0 ml) was neutralized to pH 0 with concentrated NH_3 and extracted for 10 min with 3.0 ml of a 0.067M chloroform solution of HDDTP. After the separation of the organic phase, the extraction was repeated five more times, after which all the Cu(II) was transferred, free of Fe(III), to an organic phase. The Cu(II) content after each extraction was determined as follows: 1 ml of the aqueous phase was diluted to 100.0 ml and 10.0 ml of this solution was titrated with EDTA as before.

3. Results and discussion

According to the spectroscopic and analytical data, previously reported IR studies of tautomerism of five-membered heterocyclic ketones [12,13], and the reported ^1H or ^{13}C chemical shifts in related structures [14–17], the production of the reaction between 1-phenyl-3,5-diox-opyrazolidine, carbon disulfide and alkyl bromides is present in polar solvents as a dienolic form (Fig. 1). Chelation of copper(II) must occur through the thiono sulfur atom and 3-hydroxy or 5-hydroxy group.

The extraction of aqueous copper(II) solutions with chloroform solutions of both ligands was studied as a function of pH and the results are shown in Fig. 2. The following features of this study are of interest.

(1) A nearly constant 88–94% yield of extraction is observed in the pH range 0–6 and the best results are observed at pH 0 or 1. This can be seen as an important advantage, considering the strong acidity of the lixiviation solution from copper minerals.
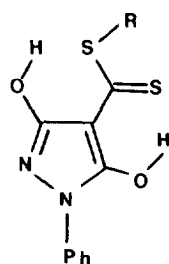
Fig. 1. Dienolic form of 4-alkyldithiocarboxylate-1-phenyl
3,5-dioxopyrazolidine.

Compound	R
HBDTP	n-C$_4$H$_9$
HDDTP	n-C$_{12}$H$_{25}$

(2) There is not significant difference in the extractive properties of HBDTP and HDDTP in 0.02 M chloroform solutions. However, the better solubility of HDDTP in this solvent allows study of the extraction with a 0.067 M solution.

(3) In general, these ligands are better extractants than alkyldithiocarboxylate derivatives of 3-methyl-5-pyrazolones also studied in our laboratory. For example, 1-dodecyl-4-dodecyldithiocarboxylate-5-hydroxy-3-methylpyrazol extracts only 26% of copper(II) at pH 0 [7].

(4) The nature of the extracted species was

established by plotting log of distribution ratio (K_d) vs. log of ligand concentration at fixed pH (Fig. 3). This gave slopes close to two and similar values were observed for plots of log K_d vs. pH at constant ligand concentration. From these results it can be inferred that the main equilibrium in the extraction process is

$$Cu^{2+} + 2HL \rightarrow CuL_2 + 2H^+$$
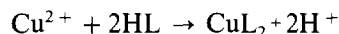
The deduced stoichimoetry is in agreement with the elemental analyses of both copper(II) complexes.

In order to explore the use of HDDTP in the extraction of copper from minerals with a high content of iron in a strong acidic medium, the extraction of Fe(III) at pH 0 and 1 was also studied. Under these conditions Fe(III) is only 8–12% extracted and Cu(II) is 95% selectively extracted with a 0.03 M HDDTP chloroform solution from an aqueous 0.01 M solution of Cu(II) and Fe(III)

Using a lixiviation solution from a mineral mixture of enarguite and pyrite with 16.5% Cu and 23.7% Fe, Cu(II) was completely separated from Fe(III) at pH 0 with a chloroform solution of HDDTP. The results and conditions employed are summarized in Table 1.

If the extraction of the lixiviation solution is performed under the same conditions but replacing the chloroform solution of HDDTP by a 15% kerosene solution of LIX 984N, the amount of
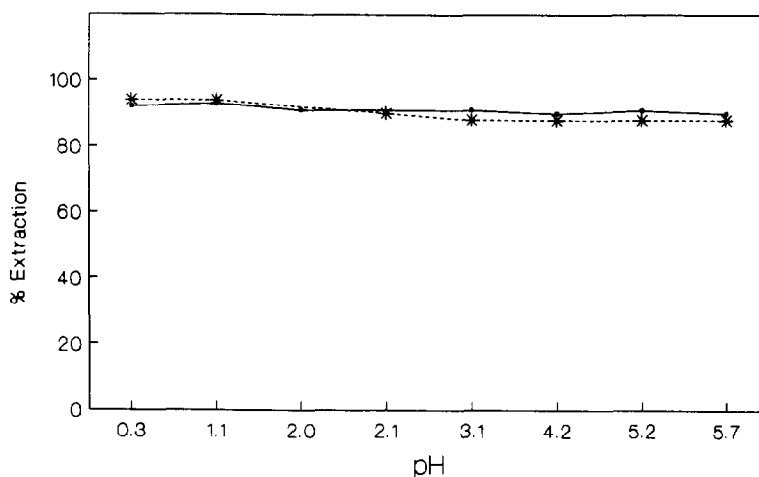
Fig. 2. Plot of % extraction vs. pH. —■—, HBDTP, --*--, HDDTP.
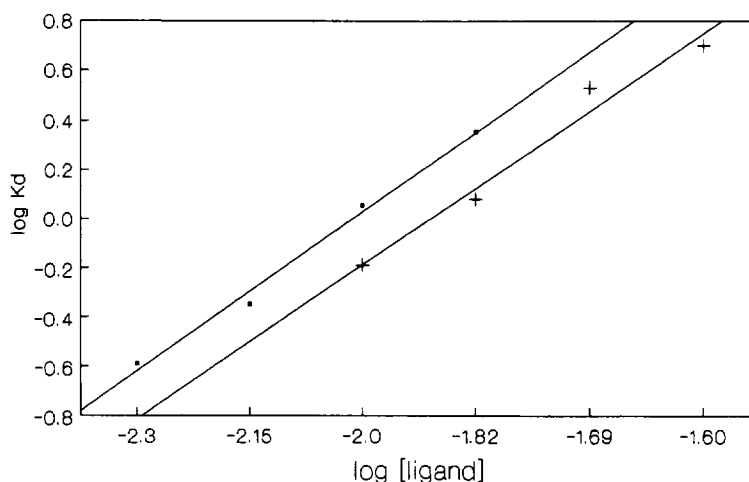
Fig. 3. Plot of log K_d vs. log [ligand] (■, HBDTP: pH = 4.78; m = 2.04; +, HDDTP: pH = 4.32; m = 2.38).

Cu(II) extracted in each step is 8.0 mg and the process requires five steps.

Finally, and according to the results with analyzed mineral samples, this procedure can be succesfully applied to sulfide-type minerals with similar composition (bornite, cubanite, chalcopyrite, chalcosite and others) as well as to oxidized copper minerals (chrysocolla, brochantite, malachite and others).

In conclusion, under the experimental conditions of this study, these new compounds show extractive and selective properties closely related to industrial LIX resins which are used in solvent extractions of copper from lixiviated solutions with a high iron content. Ligands with this kind of β-hydroxydithioester structure could become an alternative to the β-hydroxyoxime arrangement of the commercial extractants mentioned. Studies on this matter are in progress.

Acknowledgements

Table 1
Extraction of Cu (II) from a lixiviation solution of enarguite and pyrite

Volume of the aqueous lixiviation solution of mineral	2.0 ml
Concentration of Cu(II) in the lixiviation solution	16.5 mg ml^{-1}
Concentration of Fe(III) in the lixiviation solution	23.7 mg ml^{-1}
Volume of the chloroform ligand solution	3.0 ml
Concentration of the ligand in the organic solution	28.0 mg ml^{-1}
Number of steps for quantitative extraction of Cu(II)	6
Amount of Cu(II) extracted in each step	6.0 mg
Yield of the extraction in each step	95%
Concentration of Fe(III) in the remaining aqueous solution	23.6 mg ml^{-1}

References

[1] M. Mirza, Talanta, 25 (1978) 685.
[2] A. Roy and K. Nag, J. Inorg. Nucl. Chem., 40 (1978) 331.
[3] H.C. Arora and G.N. Rao, Indian J. Chem., 21A (1982) 335.
[4] F.T. Coronel, St. Marera and N. Yordanov, Talanta, 29 (1982) 119.
[5] Y. Akama, K. Sato, M. Ukaji, T. Kawata and M. Kajitami, Polyhedron, 4, (1985) 59.
[6] R. Maurelia, G. León and A. Oliva, Polyhedron, 8 (1989) 2723.
[7] R. Maurelia, P, Villalobos, C. Bahamondes, D. Carrillo, G. León and A. Oliva, Bol. Soc. Chil. Quim, 37 (1992) 175.

[8] J. Büchi, J. Amman, E. Lieberherr and E. Eichenberger, Helv. Chim. Acta, 36 (1953) 75.

[9] A. Weissberger and H.D. Porter, J. Am. Chem. Soc., 65 (1943) 52.

[10] R. Belcher, D. Gibbons and T.S. West, Anal. Chim. Acta, 13 (1955) 226.

[11] H. Lizama, R. Schrebler, G. Cote, D. Bauer and R. Córdova, Analusis, 23 (1995) 68.

[12] A.J. Boulton, A.R. Katritzky, A. Majid-Hamid and S. Oksne, Tetrahedron, 20 (1964) 2835.

[13] P.E. Gagnon, J.L. Boivin, R. MacDonald and L. Yaffe, Can. J. Chem., 32 (1954) 823.

[14] R. Maurelia, G. León and A. Oliva, Synth. Commun., 20 (1990) 477.

[15] A. Oliva, G. León and R. Maurelia, Org. Prep. Proced. Int., 22 (1990) 511.

[16] J. Bartulin, J. Belmar and G. León, Bol. Soc. Chil. Quim., 37 (1992) 13.

[17] A. Oliva, I. Castro, C. Castillo and G. León, Synthesis, (1991) 481.

Rapid, selective, direct and derivative spectrophotometric determination of titanium with 2,4-dihydroxybenzaldehyde isonicotinoyl hydrazone

O. Babaiah, C. Kesava Rao, T. Sreenivasulu Reddy*, V. Krishna Reddy

Department of Chemistry, Sri Krishnadevaraya University, Anantapur-515 003, A.P., India

Received 17 May 1995; revised 20 September 1995; accepted 25 September 1995

Abstract

A simple and sensitive spectrophotometric method is developed for the determination of titanium in aqueous medium. The metal ion forms a reddish brown coloured complex with 2,4-dihydroxybenzaldehyde isonicotinoyl hydrazone (2,4-DHBINH) in the pH range 1–7. The complex shows two absorption maxima, one at 430 nm and the other at 500 nm. The reagent shows appreciable absorbance of 430 nm and negligible absorbance at 500 nm at pH 1.5. Beer's law is obeyed in the range 0.09 to 2.15 μg ml^{-1} of titanium(IV). The molar absorptivity and the Sandell's sensitivity of the method are 1.35×10^4 l mol^{-1} cm^{-1} and 0.0049 μg cm^{-2}, respectively. A method for the determination of titanium by first-order derivative spectrophotometry is also proposed. The methods have been employed successfully for the determination of titanium in several alloy and steel samples.

Keywords: Spectrophotometry; Titanium; 2,4-Dihydroxybenzaldehyde isonicotinoyl hydrazone

1. Introduction

The potential of the analytical application of hydrazone derivatives for the spectrophotometric determination of metal ions has been reviewed by R.B. Singh et al. [1]. Very few hydrazones are reported for the spectrophotometric determination of titanium [2–5]. Among the sensitive methods reported, most of them involve extraction processes [6–12] and suffer from lack of selectivity. Classical methods using hydrogen peroxide [13] and chromotropic acid [14] suffer from the

disadvantages of interference and critical pH maintenance, respectively.

In the present paper a simple, rapid, selective, sensitive and direct spectrophotometric method is reported for the determination of micro amounts of titanium in aqueous medium by complexing with 2,4 dihydroxybenzaldehyde isonicotinoyl hydrazone (2,4-DHBINH).

Derivative spectrophotometry is a very useful approach for determining the concentration of single components in mixtures with overlapping spectra as it eliminates much of the interference. It has recently been used to eliminate interference during spectrophotometric analysis [15–25]. It has

---

* Corresponding author. Fax: (91) 08554-22150.

been widely used in pharmaceutical analysis, amino acid and protein analysis, clinical chemistry, environmental analysis etc., [26] but less often in inorganic analysis [27,28].

In this paper a first-order derivative spectrophotometric method is described for the determination of titanium(IV) in which the interference seen with the zero-order method is eliminated.

2. Experimental

A Shimadzu UV–visible spectrophotometer model UV-160A equipped with 1 cm quartz cells and a Phillips Digital pH meter model PP 9046 were used for absorbance and pH measurements, respectively. Suitable settings for first-order derivative are as follows: spectral band width 2 nm; wavelength readability, 0.1 nm increment; scan speed, fast (nearly 2400 nm min^{-1}); wavelength accuracy, ± 0.5 nm with automatic wavelength correction; recorder, computer controlled thermal graphic printer with cathode ray tube, and with nine degrees of freedom in the wavelength range 800–400 nm.

3. Reagents

3.1. 2,4-Dihydroxybenzaldehyde isonicotinoyl hydrazone

The reagent was prepared by condensing 2,4-dihydroxybenzaldehyde and isonicotinic acid hydrazide in methanol using a general procedure [29] (m.p. 290°C). The structure of the reagent is as follows:
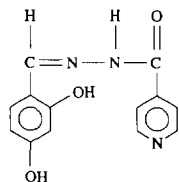
A 0.01 M solution in dimethyl formamide is used in the studies.

3.2. Stock solution of Ti(IV)

This was prepared by dissolving the requisite quantity of $K_2TiO(C_2O_4)_2\cdot 2H_2O$ (AR, BDH) in doubly distilled water and made up to the mark in a 100 ml volumetric flask to give a 0.01 M solution. The resulting titanium solution was standardized gravimetrically [30]. Working solutions were prepared daily by diluting the stock solution to an appropriate volume. All other chemicals used were of analytical reagent grade.

3.3. Buffer solutions

For the preparation of buffer solutions, 1 M HCl and 1 M sodium acetate (pH 1 to 3), and 0.2 M acetic acid and 0.2 M sodium acetate (pH 3.2 to 7.0) were used.

4. Procedures

4.1. Direct spectrophotometry

In each of a set of different 10 ml standard flasks, 5 ml of buffer solution (pH 1.5) various volumes of 5×10^{-4} M titanium(IV) solution, 1 ml of n-butanol, 1 ml of dimethylformamide (DMF) and 1 ml of 2,4-DHBINH (1×10^{-2} M) in DMF were added and made up to the mark with distilled water. The absorbance was measured at 500 nm against the reagent blank. The calibration curve was prepared by plotting the absorbance against the amount of titanium.

4.2. First derivative spectrophotometry

For the above solutions, first-order derivative spectra were recorded with a scan speed of fast (nearly 2400 nm min^{-1}), slit width of 1 nm, with degrees of freedom 9, in the wavelength range from 800 to 400 nm. The derivative peak height was measured by peak-zero method at 580 nm. The peak height was plotted against the amount of titanium to obtain the calibration curve.

The calibration graphs follow the straight line equation $y = mx + b$ where x is the concentration of the solution, y is the measured absorbance or
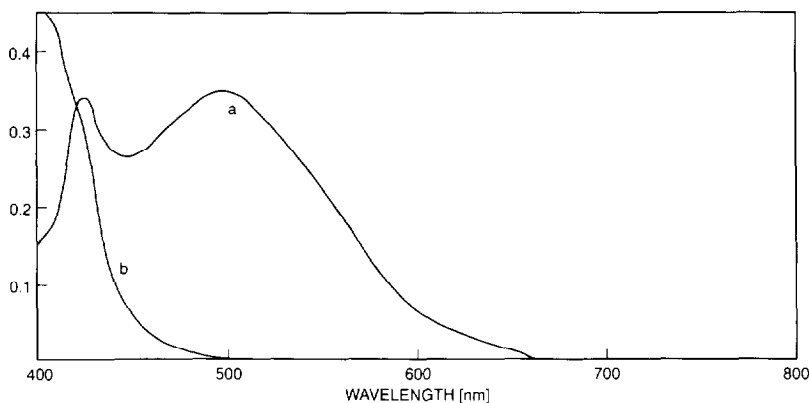
Fig. 1. Absorption spectra of (a) Ti(IV)-2,4-DHBINH complex (2.5 × 10⁻⁵ M); (b) 2,4-DHBINH (1 × 10⁻³ M).

peak height, and m and b are constants. By substituting the corresponding experimental data into the above equation, calibration equations were calculated as $y = 0.292x + 0$ for the zero order data and $y = 0.076x + 0.001$ for the derivative data.

5. Results and discussion

5.1. Absorption spectra

The absorption spectra of the reagent and the complex were recorded in the wavelnegth range 400–800 nm at pH 1.5 against the buffer solution and reagent blank, respectively (Fig. 1). The complex shows two absorption maxima, one at 430 nm and the other at 500 nm. The reagent has appreciable absorbance at 430 nm and negligible absorbance at 500 nm. Hence analytical studies were made at 500 nm.

5.2. pH effect

It is observed that the reddish brown precipitate is instantaneously formed between Ti(IV) and 2,4-DHBINH in the pH range 1–7. The study of the effect of pH on the colour intensity of the reaction mixture showed that maximum colour is obtained in the pH range 1.2–3.5. The analytical studies were carried out at pH 1.5, as the interference due to foreign ions is at a minimum at this pH.

5.3. Effect of 2,4-DHBINH concentration

The studies revealed that a 30-fold molar excess of 2,4-DHBINH is essential for complete and constant colour development. Excess of the reagent has no effect on the absorbance of the complex.

5.4. Effect of solvent

It is observed that the reddish brown precipitate of Ti(IV)–2,4-DHBINH complex dissolves in 20% aqueous DMF. But there is a decrease in the colour intensity of the complex. The intensity of the colour is stabilized by adding 1 ml of n-butanol to the reaction mixture. Hence further studies are carried out in a 20% + 10% DMF–n-butanol mixture.

5.5. Colour and stability of the complex

The colour reaction between Ti(IV) and 2,4-DHBINH was instantaneous at room temperature. The absorbance of the complex was found to be constant for more than 24 h.

5.6. Order of addition of reactants

It is observed that the intensity of the coloured solution is independent of the order of addition of the reactants. However the reagent was added after the addition of n-butanol and DMF to avoid the precipitate formation.

5.7. Applicability of Beer's law

From the calibration plot, it is observed that in the present method Beer's law is obeyed in the concentration range 0.09–2.15 μg ml^{-1} of Ti(IV). The molar absorptivity of the complex at 500 nm and at pH 1.5 is calculated as $(1.35 \pm 0.05) \times 10^4$ l mol^{-1} cm^{-1}. The Sandell's sensitivity of the method in the determination of 1.2 μg of Ti(IV) is found to be 0.0049 μg cm^{-2}.

Other statistical data derived for the present method are as follows. The standard deviation of the method for ten determinations of 1.2 μg of Ti(IV) is 0.005. The zero-order calibration plot passes through the origin. The correlation coefficient (γ) of the calibration equation of the experimental data is 0.990.

5.8. Composition and stability of the complex

The composition of the complex was determined by the Job and mole ratio methods and found to be 1:2 (Ti(IV):2,4-DHBINH). The stability constant of the complex was determined by Job's method as 8.04×10^8.

5.9. Effect of foreign ions

The effect of various diverse ions on the determination of Ti(IV) was studied to find out the tolerance levels of these diverse ions in the present method. The tolerance limit of a foreign ion was taken as the amount that caused an error in the absorbance value by $\pm 2\%$. The data are presented in Table 1. Large numbers of commonly associated cations and anions do not interfere in the determination of titanium.

In the presence of ascorbic acid (6000 μg), Fe(III) (1764 μg), Cu(II) (30 μg) and V(V) (25 μg) are tolerable. Mo(VI) can be masked up to 10 μg by adding 440 μg of tartrate.

5.10. Determination of titanium(IV) by first derivative spectrophotometry

In the zero-order spectrophotometric determination of titanium with 2,4-DHBINH, the commonly associated metals interfere and have to be masked with masking agents. To avoid the use of masking agents, we have applied the first derivative technique. The technique enhances the detectability of minor spectral features as weak shoulders.

The first-order derivative spectrum of the Ti(IV)–2,4-DHBINH complex was recorded for the solutions of zero order as described before and is presented in Fig. 2. The peak-zero (h) method is followed for the preparation of the analytical calibration plot. The maximum peak is at 560 nm. However, it was observed that at 580 nm, many of the interfering ions do not interfere. The peak height at 580 nm is also proportional to the concentration of Ti(IV). Therefore 580 nm is chosen for analytical studies. Beer's law is obeyed between 0.048 and 2.39 μg ml^{-1} of titanium(IV).

Table 1
Tolerance limit of diverse ions in the determination (1.2 μg ml^{-1}) of titanium(IV)

Diverse ion	Tolerance limit (μg ml^{-1})	Diverse ion	Tolerance limit (μg ml^{-1})
Ascorbic acid	17600	Ba(II)	4110
Iodate	5730	Zn(II)	1950
Bromate	4317	Fe(III)	1764[a]
Thiourea	2283	Co(II)	1740
Nitrate	1860	Mn(II)	1650
Thiocyanide	1770	Ni(II)	1160
Iodide	1170	Mg(II)	720
Chloride	1065	Hg(II)	600
Citrate	472	Pb(II)	104
Tartrate	444	Pb(II)	414[b]
Oxalate	132	Cd(II)	336
Phosphate	48	Ce(IV)	210
Fluoride	10	Cr(III)	208
		Tc(IV)	127
		Cu(II)	95[b]
		Cu(II)	32[a]
		Al(III)	25
		Cu(II)	5[c]
		V(V)	25[a]
		V(V)	5[c]
		Zr(IV)	27[c]
		Mo(VI)	10[cd]

[a] Masked by 6000 μg ml^{-1} ascorbic acid.
[b] Masked by 2283 μg ml^{-1} thiourea.
[c] Masked by 132 μg ml^{-1} oxalate.
[d] Masked by 444 μg ml^{-1} tartrate.
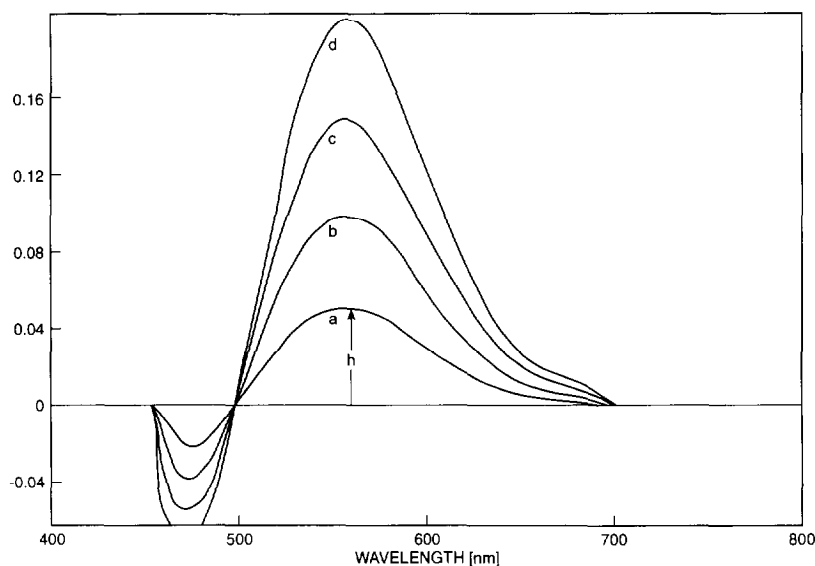
Fig. 2. First-derivative spectra of Ti(IV): (a) Ti(IV) 0.48 μg ml^{-1}; (b) Ti(IV) 0.96 μg ml^{-1}; (c) Ti(IV) 1.44 μg ml^{-1}; (d) Ti(IV) 1.92 μg ml^{-1}.

Other statistical data derived for the present method are as follows. The standard deviation of the method for ten determination of 1.2 μg of titanium(IV) is 0.004. The intercept and the correlation coefficient (γ) of the calibration equation for the experimental data are +0.001 and 0.996, respectively.

5.10. Interference due to foreign ions

The interference of a 100-fold excess of Al(III) and a 20-fold excess of Cu(II), Mo(VI), Th(IV), V(V), U(VI) and Zr(IV) can be avoided by carrying out the determination of 1.2 μg Ti(IV) in the derivative mode.

6. Applications

6.1. Analysis of alloys and steel samples

Titanium present in various alloy and steel samples was determined by the zero-order and first-order derivative methods.

6.2. Preparation of sample solutions

Solutions of the nickel-based high temperature alloys, titanium alloy and low alloy steel were prepared by following the precedure reported by Busev et al. [31]. A weight of 0.1–0.5 g of sample was dissolved in 2 ml HCl + 10 ml HNO$_3$. The resulting solution was evaporated to a small volume. To this, 5 ml of 1:1 H$_2$O:H$_2$SO$_4$ mixture was added and evaporated to dryness. The residue was dissolved in 15 ml of distilled water and filtered through Whatman filter paper No. 41. The filtrate was collected in a 100 ml volumetric flask and made up to the mark with distilled water. The sample solutions were appropriately diluted to obta-in the titanium concentration in the required range.

The amount of titanium present in the sample solutions was calculated from the predetermined calibration plots. In zero order spectrophotometry, 1 ml of 1 M ascorbic acid was added to mask iron(III) and copper(II) and 0.5 ml of 0.03 M oxalate to mask molybdenum(VI). In the derivative technique, 1 ml of 1 M ascorbic acid was added to mask iron(III). The results obtained in these studies are presented in Table 2.

Table 2
Determination of titanium in alloy and steel samples

Sample	Taken (μg ml^{-1})	Found (μg ml^{-1})					
		Direct method*	Error (%)	RSD (%)	First derivative method*	Error (%)	RSD (%)
Nickel-base high temperature alloy[a]							
(i) Udimet — 500	0.51	0.50	− 1.96	0.020	0.50	− 1.96	0.020
	1.02	1.04	+ 1.96	0.020	1.03	+ 0.98	0.019
	1.53	1.54	+ 0.65	0.026	1.55	+ 1.30	0.020
(ii) Udimet — 700	1.00	1.01	+ 1.00	0.018	1.00	–	0.019
	1.50	1.48	− 1.33	0.017	1.49	− 0.67	0.017
	2.00	2.04	+ 2.00	0.021	2.02	+ 1.00	0.021
Titanium-based alloy[b]	0.62	0.63	+ 1.61	0.025	0.64	+ 3.22	0.026
	1.20	1.26	+ 1.61	0.026	1.25	+ 0.81	0.018
	1.86	1.88	+ 1.07	0.015	1.87	+ 0.54	0.010
BAS No. 387[c]	0.50	0.51	+ 2.00	0.022	0.51	+ 2.00	0.021
	1.00	1.02	+ 2.00	0.024	1.02	+ 2.00	0.025
	2.00	1.98	− 1.00	0.026	2.01	+ 0.50	0.022
Low alloy steel[d]	0.70	0.68	− 2.85	0.029	0.71	+ 1.42	0.019
	1.40	1.42	+ 1.43	0.021	1.39	+ 0.71	0.016
	2.10	2.12	+ 0.95	0.023	2.09	− 0.48	0.019

* Average of five determinations.

Composition of samples (%) is as follows:

[a] (i) Cr, 18; Co, 18.5; Al, 2.9; Mo, 4.8; C, 0.08; B, 0.006; Zr, 0.05; Ti, 2.9 (ii) Cr, 15; Co, 18; Al, 4.3; Mo, 5.21; C, 0.08; B, 0.003; Ti, 3.5;

[b] Ti, 70.14; Ni, 15.03; Cu, 14.83;

[c] Ni, 41.9; Fe, 36.0; Cr, 12.46; Mo, 5.83; Ti, 2.95; Si, 0.28; Al, 0.24; Co, 0.21; Mn, 0.08; Cu, 0.032; C, 0.03;

[d] C, 0.1; Cr, 0.1; Cu, 0.3; W, 0.1; Mo, 0.1; Ti, 0.1; Fe, 99.

7. Comparison with other methods

The present method is compared with the standard hydrogen peroxide method, chromotropic acid method and other hydrazone methods and the results are presented in Table 3.

The hydrogen peroxide method is less sensitive than the present method and suffers from the interference of many cations. Although the sensitivity of the chromotropic acid method is slightly higher than that of the present method, it suffers from the disadvantage of critical pH and the separation of large amounts of Fe(III). Furthermore most of the other sensitive methods involve extraction. The present method has the advantage of high selectivity in the presence of ascorbic acid and is more sensitive than the other hydrazone methods.

The first-order derivative spectrophotometric method eliminates the interference of V(V), Cu(II), Zr(IV), Mo(VI), U(VI) and Th(IV), which causes problems in the zero order method. The only interfering cation, Fe(III), is easily masked, up to 1000-fold, with ascorbic acid. Thus the first-order derivative method is selective for the determination of Ti(IV) in the presence of ascorbic acid.

Table 3
Comparison with other methods

Reagent	ε^a ($\times 10^4$ l mol^{-1} cm^{-1})	λ_{max} (nm)	pH of medium	M:L	Beer's law range (μg ml^{-1})	Interference/ remarks	Ref.
Hydrogen peroxide	0.07	–	Acid	–	–	V, Mo, U, Nb, Cr	[13]
Chromotropic acid	1.7	–	3.5	–	–	The pH is critical and large amounts of Fe(III) should be separated	[14]
Acyl hydrazones of aromatic carbonyl compounds	0.7–1.4	–	2.0–6.0	1:1	–	Extraction	[10]
2-Methyl isonicotinic salicylal hydrazone	–	425	1.0–2.5	1:2	–	Extraction V(V) U and Fe(III)	[5]
Hydrazo-'T'	–	525	1.5–2.5	–	0.1–20	Extraction	[8]
Diphenylglyoxal bis (2-hydroxy-benzoyl)-hydrazone	1.5	500	0.1N H$_2$SO$_4$	1:3	0.5–2.5	Medium is different	[4]
Pyridoxal salicylal hydrazone	0.39	450	0.9–2.5	1:1	1.0–10	–	[32]
Pyridoxal-3-hydroxy-2-naphthyl-hydrazone	–	430	2.7	–	0.5–7.0	–	[3]
Pyridoxal-nicotinoyl hydrazone	0.69	410	2.1–2.3	1:1	–	–	[34]
1,2-Cyclohexane dione bis(benzoyl)-hydrazone	1.0	477	1.75–3.0	1:2	–	–	[35]
Present method (2,4-DHBINH)	1.35	500	1.2–3.5	1:2	0.90–2.15	Selective in presence of ascorbic acid	Present method

^{a} ε, molar absorptivity.

References

[1] R.B. Singh, P. Jain and R.P. Singh, Talanta, 29 (1982) 77–84.

[2] N. Urmanov, R. Kh. Dzhiyanbaeva, L.V. Chaprasova, A. Inoyatov, L. Biktimirow and L. Tsoi, Nauch Trudy Taskhent Gos Univ., (1973) 34; Anal. Abstr., 28 (1975) 6, B 126.

[3] V.N. Podchainova and L.N. Dzyubo, Trudy Vses Nauchno Issled Inst. Standart Obraztsov Sppektr Etabonov 7 (1971) 44; Anal. Abstr; 24 (1973) 99.

[4] M. Silva and M. Valcarcel, Microchem. J., 25 (1980) 117.

[5] A.V. Dolgorev, Zh. Analit. Khim., 28 (1973) 1093.

[6] Sh. T. Talipov and K. G. Nigai, Zh. Anal. Khim., 18 (1963) 178–181.

[7] A.K. Sankar and D. Jyotirmoydas, Anal. Chem., 39 (1967) 1608–1612.

[8] A.V. Dolgarov, Zovod Lab., 39 (1973) 772–774.

[9] R. Moro Garcia, J.E. Sanchez Uria and S. Arribas, J. Imeno; Quin. Anal., 30 (1976) 385–388.

[10] L.N. Dzymbo, I.N. Matenkova and V.N. Pochainova, Zn. Anal. Khim., 27 (1972) 2386–2391.

[11] S. Tribalat and J.M. Caldero, Bull. Soc. Chim. France, (1964) 3187.

[12] M.M. Tananaiko and S.L. Nebylits Kaya, Zavodsk Lab., 28 (1962) 263.

[13] A.K. Babko and A.I. Volkova, Zh. Obshch. Khim., 21 (1951) 1949.

[14] W.W. Brandt and A.e. Preiser, Anal. Chem. 25 (1957) 567.

[15] S. Shibata, M. Furukawa and K. Goto, Anal. Chim. Acta, 65 (1973) 49.

[16] A.C. Davidson and H. Elsheikh, Analyst, 107 (1982) 879.

[17] A.M. Wahbi, H. Abdine and S.M. Blaih, J. Assoc. Off. Anal. Chem., 60 (1977) 1175.

[18] A.F. Fell, Proc. Anal. Div. Chem. Soc., 15 (1978) 260.

[19] A.F. Fell, UV, Spectrum, Group Bull., 8 (1980) 5.

[20] H.L. Purdue, A.E. McDowell, M.D. Fast and J.M. Milano, Clin., Chem., 21 (1975) 1192.

[21] J. Travest, V. Such, R. Gonzalo and E. Gelpi, J. Pharm. Sci., 69 (1980) 629.

[22] A.G. Davidson, J. Pharm. Pharamacol., 30 (1978) 410.

[23] S.M. Hassan and A.G. Davidson, J. Pharm. Pharmacol., 36 (1984) 7.

[24] K. Kitamura and R. Majima, Anal. Chem., 55 (1983) 54.

[25] V. Such, J. Travest, R. Gonzalv and E. Gelpi, Anal. Chem., 52 (1980) 412.

[26] F. Sanchez Rojas, C. Bosch-Ojeda and J.M. Cano Pavon, Talanta, 35 (1988) 753.

[27] A. Bermejo-Barrera, P. Bermajo-Barrera and F. Bermejo Martinez, Analyst, 110 (1985) 1313.

[28] R. Kuroda, M. Kurosaki and Hayashibe, Talanta, 77 (1990) 619.

[29] P.P.T. Sah and S.A. Peoples, J. Am. Pharm. Assoc. Sci. Edn., 43 (1954) 513.

[30] A.I. Vogel, A Text Book of Quantitative Inorganic Analysis, 4th edn., ELBS and Longman, 1978, p. 750.

[31] A.I. Busev and V.M. Ivanov, Zh. Analytica Khim., 18 (1963) 208.

[32] M. Gallego, M. Valcarcel and M. Vargas, Mikro Chim. Acta, 1 (1983) 289.

[33] M.C. Gutierrez, A. Genez-Hens and M. Valcarcel, Mikro Chim. Acta, 3 (1984) 17.

[34] M.A. Cejas, A. Gomez-Hens and M. Valcarcel, Quim. Anal., 3 (1984) 164.

[35] M. Garcia-Vargas, S. Frvilla and M. Milla, Talanta, 33 (1986) 209.

Sequential injection technique employed for stoichiometric studies, optimization and quantitative determination of some fluoroquinolone antibiotics complexed with iron(III) in sulfuric acid media

Fakhr Eldin O. Suliman, Salah M. Sultan*

Chemistry Department, King University of Petroleum and Minerals, KFUPM Box 2026, Dhahran 31261, Saudi Arabia

Abstract

A sequential injection spectrophotometric method for stoichiometric studies, optimization and quantitative determination of ciprofloxacin and norfloxacin was developed. The work is based on the complexation reaction of ciprofloxacin and norfloxacin with iron(III) in sulfuric acid media and a spectrophotometric measurement of absorbances of the corresponding complexes at 447 and 430 nm respectively. The stoichiometries and formation constants were determined. A 1:2 iron(III) to drug mole ratio was found to give the most predominant complexes for both drugs with 5.00×10^{-3} M H_2SO_4 and at 0.20 M ionic strength utilizing Job's method and the molar ratio method. A numerical method was utilized for the calculation of the formation constants, the logarithms of which were found to be 7.756 ± 0.121 and 7.839 ± 0.056, for ciprofloxacin and norfloxacin respectively. A factorial design together with the all-model-search method was utilized for the optimization of the concentration and aspiration volume of iron(III) as these were the variables which most affected peak absorbance. Working dynamic ranges of 50–500 ppm and 50–400 ppm were obtained for ciprofloxacin and norfloxacin respectively. The method was found to be suitable for the determination of these compounds in pharmaceutical preparations.

Keywords: Sequential injection spectrophotometry; Ciprofloxacin; Norfloxacin; Complexation

1. Introduction

Apart from the original papers describing the principles of sequential injection analysis (SIA) [1–5] few publications [6–11] have appeared in the literature so far. It is apparent that the SI technique is still in its infancy and that its full versatility and capacity have yet to be explored. The SI technique involves one pump, one valve, and a single channel, making it simpler than the conventional flow injection (FI) technique. Once constructed, the mechanical flow system of an SI

---

* Corresponding author. Fax: + 966 03-860-4277.

apparatus does not have to be reconfigured for different injection volumes, reaction times or mutual zone dispersion, because these parameters can be controlled directly by changing the volumes of flow reversals and the forward flow rate from the computer keyboard [12].

Cumbersome jobs which usually bother experimenters can be performed with some ease using SI. For instance, the determination of stoichiometries and formation constants of complexation reactions involves the preparation of a large series of solutions under carefully adjusted conditions and precise repetition of the procedure until acceptable results are obtained. When a valuable and expensive reagent is used, the above operations become difficult to repeat and usually the reporting of poor data is the ultimate result. Formation constants, or equilibrium constants for complexation reactions, are effective measures of the affinity of a ligand for a metal ion in solution and are used to provide valuable information essential to many other fields, e.g. medicine, electrochemistry, geochemistry, and pollution [13,14]. The advent of computers has enabled advanced mathematical treatment of huge equilibrium data to be carried out and has also encouraged amateurish chemists to determine the formation constants by making use of advanced computerized numerical methods rather than just studying the position of equilibria they encounter during the course of their investigation of a chemical reaction [13].

The aim of this paper is to demonstrate the versatility of the SI technique in conjunction with numerical methods for the determination of stoichiometries and stability constants for the complexation of two members of the flouroquinolone family of drugs, ciprofloxacin and norfloxacin. Two FI methods based on the complexation reaction of iron(III) with ciprofloxacin and norfloxacin have been reported by the present authors [15,16]. Therein, no detailed information was given on the stability and no stoichiometry studies were carried out on line by the FI micro-technique. The present work demonstrates the advantages of SI over FI, thus showing the inevitability of the utilization of SIA for such investigations. A method for the determination of ciprofloxacin and

norfloxacin, based on their complexation with iron(III) in sulfuric acid medium, is also proposed. A chemometric optimization approach is employed to select the best experimental conditions for the assay of these two drugs.

Fluoroquinolones, a group of synthetic antibacterial agents currently employed as broad spectrum antibiotics, are structurally related to nalidixic acid. It is believed that the mode of action of this family of drugs is through binding DNA-gyrase enzyme [17–19]. It is also reported that there is a direct correlation of fluoroquinolone bonding with inhibition of DNA-gyrase enzyme activity and induction of DNA breakage [19]. Because of this special mechanism of action, flouroquinolones are considered to be the most effective Gram-positive-Gram-negative pathogens to combat infections caused by microorganisms that are resistant to other microbials, such as tetracycline. Most of the methods available in the literature for the determination of ciprofloxacin and norfloxacin are suitable for the assay of these drugs in biological fluids [20–27]. It is interesting to note that no official methods have been reported so far by the British Pharmacopoeia (BP) or United States Pharmacopoeia (USP) for the assay of these two drugs in pharmaceutical products.

2. Experimental

2.1. Apparatus

The SI apparatus described recently [11] was used for SI measurements. The apparatus consists of a peristaltic pump (C4v, Alitea USA, Medina, WA), a Valco 10-port selector valve (Cheminert, Valco Instruments, Houston, TX), a holding coil, a reaction coil, and a Spectronic Mini-20 spectrophotometer (Milton Roy, Rochester, NY). All the tubing connecting the different units was made of Teflon (0.8 mm i.d.). The holding coil and the reaction coil were 1.5 m and 0.5 m long respectively. Pump tubings were Par-Med 1.02 mm i.d. (Upchurch) held on pump rollers by FI peristaltic pump tubing adapters (Upchurch). A personal computer (Austin Computer Systems, Austin,

TX) together with FIAlab software (Alitea USA, Medina, WA) was used to control the peristaltic pump, the valve and data acquisition. The communication between the computer and the other components of the apparatus was expanded by a general purpose I/O board (Model ADA-110, Real Time Devices (RTD), State College, PA).

A Perkin-Elmer lambda 5 UV–visible spectrophotometer equipped with 10.00 mm cells was used for preliminary investigations.

2.2. Reagents

2.2.1. Fluoroquinolones standard solutions

Stock standard solutions (2000 ppm) of the two fluoroquinolones were prepared by dissolving the appropriate amounts of the pure analytical reagent grade products in pure water for ciprofloxacin (supplied by Bayer representative, Batch No. (09867) for the east province of Saudi Arabia) and dilute sulfuric acid (5.0×10^{-3} M) for norfloxacin (Merck Sharp and Dohme, Haarlem, The Netherlands). Working solutions were prepared by appropriate dilutions.

2.2.2. Norfloxacin tablets

Five tablets of the proprietary drug Noroxin (Merck Sharp and Dohme, Haarlem, The Netherlands), claimed to contain 400 mg norfloxacin, were carefully weighed out. An amount of the powder equivalent to 400 mg was dissolved in about 300 ml dilute sulfuric acid (5.0×10^{-3} M) in a 500 ml volumetric flask. The mixture was warmed at 50°C in a water bath for 15 min, agitated by an electrical shaker for 15 min and filtered through an ordinary filter paper; it was then washed several times with warm dilute sulfuric acid and the filtrate plus the washings were made up to the mark with the dilute sulfuric acid solution after cooling to room temperature. Appropriate solutions were then obtained from this stock by dilution.

2.2.3. Ciprofloxacin tablets

Ten tablets of Ciprobay (Bayer), claimed to contain 250 mg ciprofloxacin, were weighed out and crushed. An exact amount of this powder equivalent to about 250 mg was dissolved in water

in a 250 ml volumetric flask. Working solutions were obtained by diluting appropriate portions of this stock.

2.2.4. Ciprofloxacin infusion

The solution of the proprietary drug Cibrobay (Bayer), claimed to contain 2000 ppm ciprofloxacin, was tested by appropriate dilution of the infusion in acidified water to make the required concentration of ciprofloxacin in a final solution of 5.00×10^{-3} M sulfuric acid and the ionic strenght was then adjusted to 0.20 M with ammonium sulfate solution.

2.2.5. Ammonium sulfate

A 0.20 M solution was prepared by dissolving about 13.4 g of AnalaR ammonium sulfate in water in a 500 ml flask.

2.2.6. Iron(III) solution

0.100 M iron(III) solution was prepared in 0.050 M sulfuric acid by dissolving exactly about 24.9 g of pre-dried ammonium ferric sulfate $NH_4Fe(SO_4)_2 \cdot 12H_2O$ in 0.050 M sulfuric acid in a 500 ml volumetric flask. This solution is only used after at least 24 h, to guarantee complete dissolution.

2.2.7. Sulfuric acid

1.0 M solution was prepared by diluting AnalaR concentrated acid.

2.3. Experimental design

The variables included in the optimization were aspiration volume and concentration of iron(III) which were found to greatly influence the peak absorbance. Preliminary investigations have revealed that other performance criteria, such as the precision, are of acceptable levels. Three levels of the aspiration volume were included, 29.5 μl, 88.5 μl and 147.5 μl, whereas five levels of iron (III) were selected in the range 2.0×10^{-3}–10.0×10^{-3} M. Iron(III) concentration was varied at each level of aspiration volume until no further improvement in the peak absorbance was observed, then five levels of iron(III) were selected to construct a factorial design. The factorial design

was then repeated by nesting the selected iron(III) solutions around the selector valve in a random manner in an attempt to minimize any possible bias. In all of these experiments 88 μl of 200 ppm solution of the appropriate drug was aspirated, and all experiments for each drug were run within 1 h.

2.4. Procedure

The SI manifold is shown in Fig. 1. The procedure starts by nesting the drug and iron(III) solutions around the selector valve. 80 μl of each solution was first aspirated into the lines from the ports by selecting one port at a time. The excess of the solutions introduced in the holding coil was then pumped through port 9 to waste. The steps of the procedure were then fed into the computer as follows. (1) The carrier solution (5.0×10^{-3} M sulfuric acid) is pumped through port 1, by setting
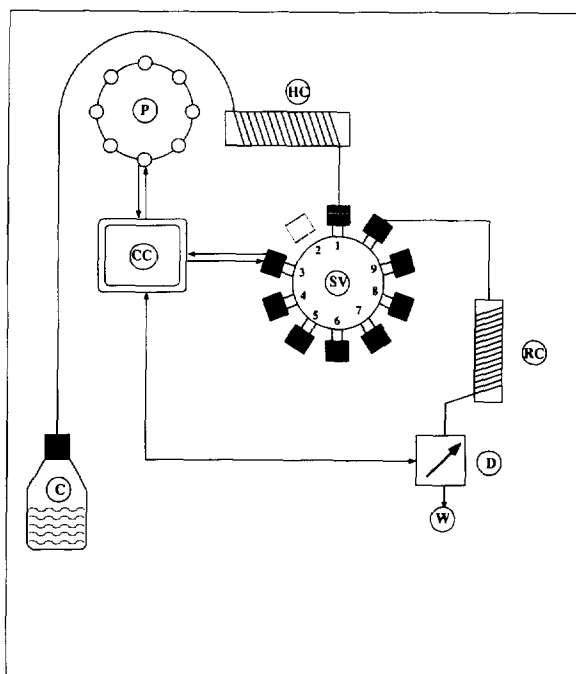
Fig. 1. Schematic diagram of the sequential analysis apparatus used: C, carrier solution; PP, peristaltic pump; HC, holding coil; SV, selector valve; 2, iron(III) solution; 3–8, drug solution; 9, auxiliary waste; RC, reaction coil; SP, spectrophotometer; W, waste; CM, computer.

the pump in the forward mode, for 25 s. (2) 147.5 μl of 1.0×10^{-3} M iron(III) solution is aspirated into the holding coil via port 2. (3) 88 μl of the appropriate drug solution is aspirated into the holding coil via ports 3–8. Both of the last two steps are achieved by setting the pump in the reverse mode. (4) Finally the carrier solution is propelled through port 1 to the reaction coil and then into the detector. The data were then acquired by the computer and transferred to a plotting software package for further manipulation. The volumes of the solutions were determined from the time of aspiration and the volumetric flow rate of the pump [11], which was 29.5 μl s^{-1} in this study.

Following Job's method of continuous variation, different aliquots of equimolar solutions of iron(III) and the drug were mixed to give solutions of identical total concentration (iron(III) + drug) but different mole fractions. Therefore, a total volume of aspiration of 162.0 μl was constantly maintained by adjusting the aspiration times. The volume of each reagent was varied between 14.8 μl (0.5 s) and 147.5 μl (5.5 s).

In the molar ratio method the total volume of the ligand was maintained constant by aspirating 147.5 μl into the holding coil by flow reversal, whereas the iron(III) solution was varied between 14.8 μl (0.5 s) and 192.0 μl (6.5 s). The ionic strength of all solutions was adjusted to 0.20 M with ammonium sulfate and the sulfuric acid concentration was 5.00×10^{-3} M.

3. Results and discussion

3.1. Determination of stoichiometry

In the sulfuric acid concentration range 5.0×10^{-3}–0.60 M, a deep yellow color is formed instantaneously when iron(III) solution is added to ciprofloxacin and norfloxacin solutions, indicative of complex formation. The spectra of the complex show absorption bands at 350 nm for ciprofloxacin and 370 nm for norfloxacin with shoulders extending into the visible region. The shoulder, which is responsible for the yellow color of the complex, shows a maximum absorbance at

447 nm for ciprofloxacin and 430 nm for norflox-acin. At these wavelengths the two drugs and iron(III) show negligible absorbance. It has also been observed that the intensity of the colored complex increases with a decrease in the concentration of sulfuric acid, which may be due to the dissociation of the complex at high acid concentration. The Job plot of continuous variation was used to determine the stoichiometry of the complexation of ciprofloxacin and norfloxacin with iron(III) in sulfuric acid media. Fig. 2(a) is a typical Job plot generated by using equimolar solutions of iron(III) and ciprofloxacin of 1.00×10^{-3} M, whereas Fig. 2(b) shows a Job plot for equimolar solutions of iron(III) and norfloxacin of 2.00×10^{-3} M. Both plots were produced using 5.00×10^{-3} M sulfuric acid and an ionic strength of 0.20 M. It is clear that the curves $A = f(X_{drug})$ exhibit a maximum for the mole fractions close to 0.66, indicating that the ratio of iron(III):drug in the complex is 1:2. Similar plots made at sulfuric acid concentrations greater than 0.025 M gave different results, and the 1:1 iron(III):fluoroquinolone complex was found to be the dominant species. These findings are in agreement with the results published by two independent groups, where a 1:1 complex was obtained by one group [15] when iron(III) was complexed with ciprofloxacin at acidities higher than 0.025 M, and a 1:2 complex was obtained for the complexation of norfloxacin by the other group [28] when 5.00×10^{-3} M sulfuric acid was used. It can also be observed that only 10 min at most is needed to generate the Job plot using SIA and less than 10 ml is enough to repeat the procedure as many times as necessary.

In the molar ratio method ideally two straight lines are obtained when the absorbance is plotted versus the iron(III) to drug ratio, and the point of intersection of these two lines corresponds to the stoichiometric ratio upon interpolation to the mole ratio axis. Fig. 3(a) shows a typical molar ratio plot for the complexation of iron(III) with ciprofloxacin, with peaks 1–11 being produced by varying the molar ratio of iron(III) to drug from 0.1 to 1.1 in steps of 0.1. In contrast Fig. 3(b) represents a molar ratio method for the complexation of norfloxacin with iron(III); here the molar

(a)

(b)
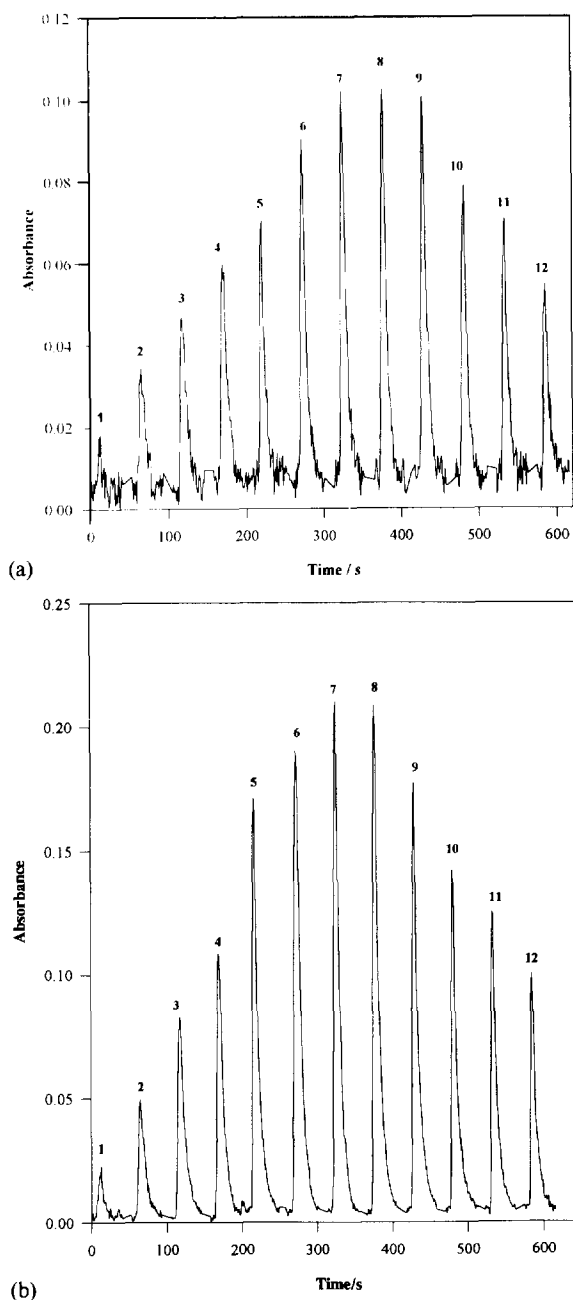
Fig. 2. SIAgram representing Job's plot: (a) [iron(III)] = [ciprofloxacin] = 1.00×10^{-3} M; (b) [iron(III)] = [norfloxacin] = 2.00×10^{-3} M; [H$_2$So$_4$] = 5.00×10^{-3} M; ionic strength = 0.20 M; total volume is equivalent to 162.0 μl and aspiration volumes were varied between 14.5 μl and 147.5 μl. Mole fractions of the drug were: (1) 0.0; (2) 0.10; (3) 0.20; (4) 0.3; (5) 0.40; (6) 0.50; (7) 0.60; (8) 0.70; (9) 0.80; (10) 0.90; (11) 0.95; (12) 0.97.

ratio of iron(III) to drug was varied from 0.1 (peak 1) to 1.3 (peak 13) in steps of 0.1. These plots were produced using equimolar solutions of iron(III) and the corresponding drug. The ionic strength was adjusted to 0.020 M and the sulfuric
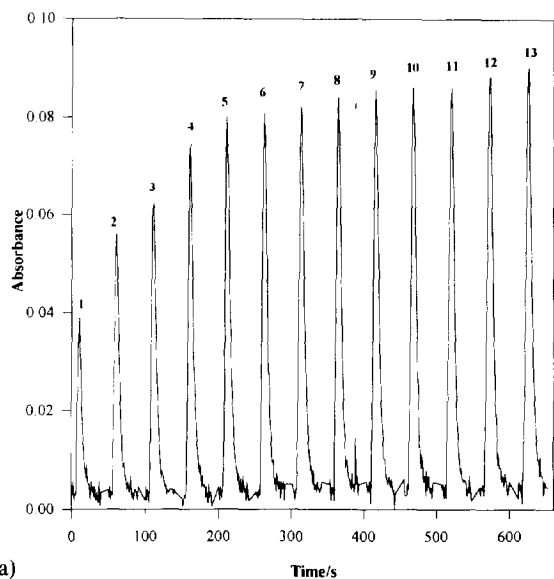
(a)
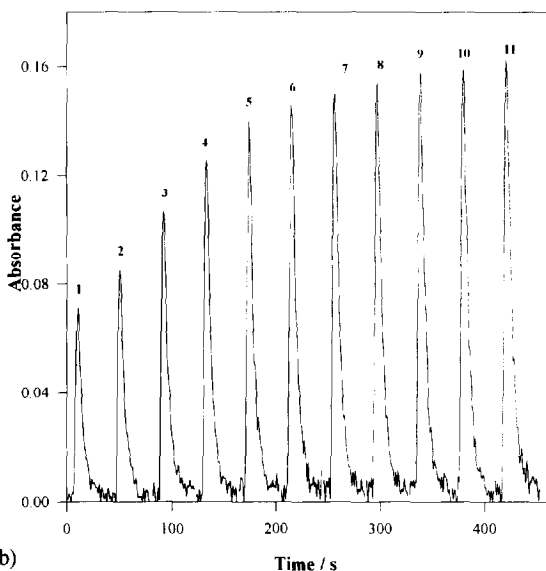
(b)

Fig. 3. SIAgram representing molar ratio plots: (a) [iron(III)] = [ciprofloxacin] = 1.00 × 10⁻³ M; (b) [iron(III)] = [norfloxacin] = 2.00 × 10⁻³ M; [H₂SO₄] = 5.00 × 10⁻³ M; ionic strength = 0.20 M; total volume of the drug was 147.5 µl; aspiration volumes of iron(III) solution were varied between 14.5 µl (peak 1) and 192 µl (peak 13).

acid concentration was 5.00×10^{-3} M. It is obvious from these plots that the point of intersection of the two lines is close to 0.5 when extrapolation is made to the molar ratio axis, indicating a 1:2 ratio for iron(III):drug.

It is likely that incomplete mixing of the reagents with the drug might take place due to dispersion and zone penetration; however, nesting the solutions around the valve, followed by getting rid of the excess, plus automated aspiration with exact computer control of timing would certainly minimize this problem. If mixing was still not complete it would lead to a constant error in both the drug and reagent concentrations that would pose no problem with the data obtained and in calculating the mole ratio. However, the correction factors which can be introduced from the zone penetration and dispersion were found to have a very minor effect on the data obtained.

It is well known that iron(III) has its greatest affinity for ligands that coordinate via oxygen [29]. It has also been reported [30,31] that fluoroquinolones are present in different forms in aqueous media, including neutral molecules and zwitterions, as well as monoprotonated and diprotonated species depending on the pH of the medium. For instance, at low acid concentrations the neutral species together with the monoprotonated species are the predominant forms, whereas at highly acidic concentrations the proportion of the diprotonated form increases greatly. Therefore it can be suggested that iron(III) complexes ciprofloxacin and norfloxacin by binding to the carboxylate group and to the adjacent keto group in the 3 and 4 positions respectively, thus forming a six-membered ring, as shown previously [12].

3.2. Formation constants

The formation constant and the composition of the complex of iron(III) with ciprofloxacin and norfloxacin were also investigated by numerical methods. The Jobcon program [32] was used to analyze the continuous variation data whereas the MRLET program was utilized to treat the molar ratio data [33]. Both programs were modified by the authors, were rewritten in C language and applied on a PC/AT computer. The calculations

are based on fitting a function $f(x, \beta)$ to a set of experimental data, using a least-squares method. Unknown parameters are estimated by minimizing U, the sum of squares of residuals defined by Eq. (1):

$$U = \sum_{i=1}^{n} (A_{\exp i} - A_{\text{calc} i})^2 \qquad (1)$$

where n represents the number of experimental points, $A_{\exp}$ the experimental absorbance, and $A_{\text{calc}} = f(x, \beta)$, the absorbance calculated by the program from the formation constants and stoichiometric ratios. Therefore, various equilibrium models could be fitted to the experimental data iteratively by varying the values of formation constants and the stoichiometric ratios.

In this study different total concentrations of iron(III) and drug were used to determine the equilibrium constants. The mean values of the logarithms of formation constants (log K_f) obtained for ciprofloxacin and norfloxacin in 5.00 × 10^{-3} M sulfuric acid and at 0.20 M ionic strength were 7.756 ± 0.121 and 7.839 ± 0.056 respectively. The value reported earlier for norfloxacin was 8.60 [28]. It is apparent from these results that the value of the formation constant for the 1:2 iron(III)–norfloxacin complex is close to the value reported earlier [28]. It was also observed that the stoichiometry and the value of the formation constant are independent of the total concentration of the metal ion and the ligand.

3.3. Optimization

The factorial design experimental data for ciprofloxacin and norfloxacin systems are given in Table 1. In order to determine the optimum experimental condition for the assay of these drugs, based on their complexation with iron(III) in sulfuric acid media, an ordinary least-squares method [33] was used together with an exhaustive search for the best regression model (all-model search) to find a model which correlates peak absorbance with the concentration and aspiration volume of iron(III). Before undertaking any statistical analysis the factors were scaled within the range ± 1 to simplify the interpretation of the regression coefficients when the relative impor-

Table 1
Factorial design for optimization of iron(III) concentration and aspiration volume

[Iron(III)][a]	Aspiration volume[a]	Peak height (mm)	
		Ceprofloxacin	Norfloxacin
−1.0	1	50	46
−0.5	1	58	58
0.0	1	62	68
0.5	1	65	73
1.0	1	64	76
−1.0	0	47	34
−0.5	0	57	50
0.0	0	62	61
0.5	0	65	68
1.0	0	65	72
−1.0	−1	36	17
−0.5	−1	48	32
0.0	−1	55	42
0.5	−1	59	51
1.0	−1	56	56

[a] Coded levels

tance of factors is compared.

The all-model search was utilized to investigate all possible models with 1,2,..., k parameters. Quadratic, cubic and two-factor interactions were included to obtain the best model. The test statistic used here is an F ratio of the form [34]

$$F = \frac{(\text{SSE}_R - \text{SSE}_C)/r}{\text{SSE}_C/(N - P)}$$

where SSE_R and SSE_C are the residual sum of squares associated with the reduced model and the complete model, i.e. models with $i - 1$ and i parameters, respectively, r is the difference in the number of parameters in the reduced and complete models, P is the number of parameters in the complete model and N is the number of experiments. The best models, ones that are significant to the F test at the 97.5% level and characterized by the highest coefficient of multiple regression R^2, were found to be five parameter models for both ciprofloxacin and norfloxacin systems and are given as follows:

$$\text{PH} = 62.63 + 8.67I + 4.40V - 6.86I^2$$

$$- 4.00V^2 \quad (R^2 = 0.973) \qquad (3)$$
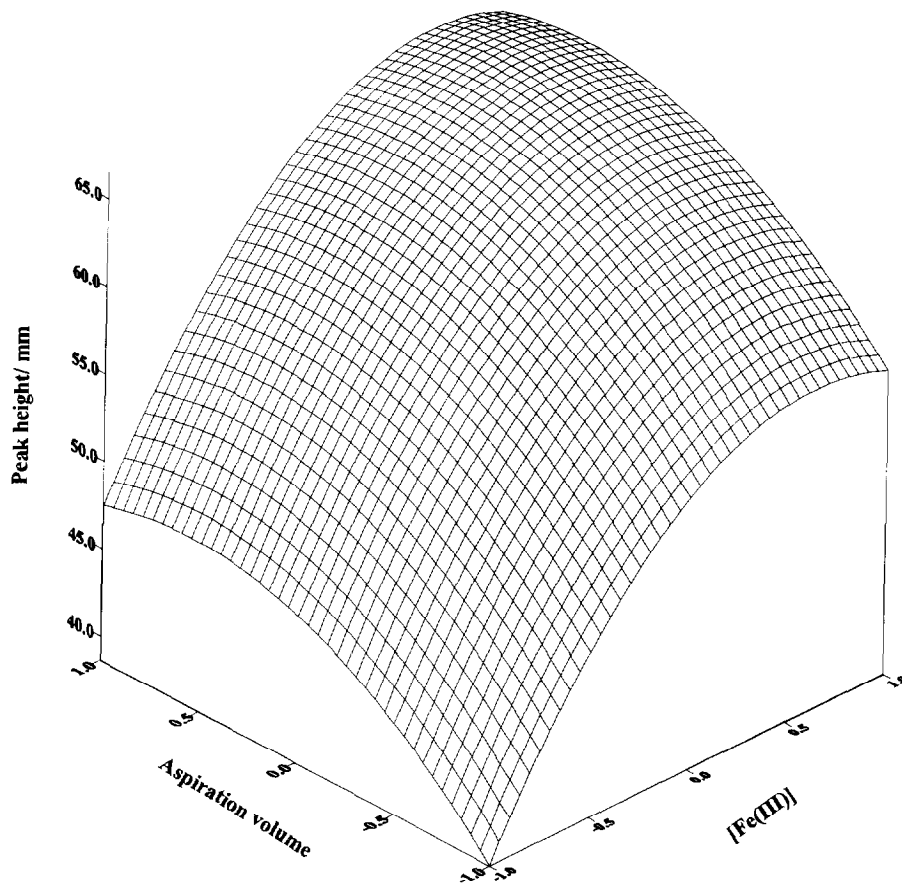
Fig. 4. Response surface plot as a function of iron(III) concentration and aspiration volume.

$$PH = 60.94 + 17.87I + 12.91V - 6.29I^2$$

$$- 5.30V^2 \quad (R^2 = 0.964) \tag{4}$$

for ciprofloxacin and norfloxacin systems respectively, where PH is the peak height (mm), I is the iron(III) concentration and V is the aspiration volume. When the five parameter (four independent variables and an intercept) model was compared with the four parameter model, using the F test described by Eq. (1), the F values obtained were 20.5 and 8.99, for ciprofloxacin and norfloxacin systems respectively, and were found to be highly significant at the 97.5% level ($F_{1,9} = 6.94$).

The predictive ability of the selected model was evaluated by the leave-one-out cross validation method [34]. The values obtained for the coefficient of multiple determination in prediction for ciprofloxacin and norfloxacin systems were

0.972 and 0.967 respectively suggesting that the models can be used for optimization purposes. Determination of the optimum experimental conditions for the assay of the two drugs was then executed using a modified simplex algorithm as a search method and the regression models obtained by this strategy were 147.5 μl for the aspiration volumes for both systems whereas 1.00×10^{-2} M and 8.0×10^{-3} M values were obtained for iron(III) concentrations for ciprofloxacin and norfloxacin systems respectively. Fig. 4 shows a surface plot as a function of iron(III) concentration and aspiration volume for the ciprofloxacin system. It is apparent from this figure that higher levels of both iron(III) concentration and aspiration volumes are favorable for the assay of this drug as the peak absorbance reaches a plateau region.
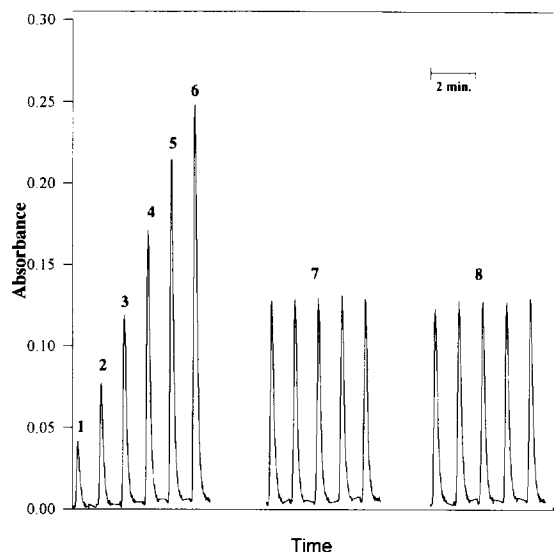
Fig. 5. Typical SI results of ciprofloxacin standard solutions of: (1) 50; (2) 100; (3) 200; (4) 300; (5) 400; (6) 500 ppm; (7) five runs of 215 ppm Ciprobay tablets; (8) 210 ppm Ciprobay infusion.

3.4. Analytical appraisal

Series of standard solutions were run for the two drugs as typically shown in Fig. 5 for ciprofloxacin. A weighted regression line [35] was plotted for absorbance vs. concentration by giving minimum weighting for the lower and upper concentrations and full weighting for the others. The linear range was found to be between 50 and 500 ppm for ciprofloxacin and between 50 and 400 ppm for norfloxacin with the following calibration equations:

$$A = 0.0280 + 4.592 \times 10^{-4}C \quad (R^2 = 0.995) \quad (5)$$

$$A = 0.0115 + 6.451 \times 10^{-4}C \quad (R^2 = 0.999) \quad (6)$$

where A is the peak absorbance and C is the concentration (ppm).

3.5. Application

The proposed method was applied to the assay of some proprietary drugs containing ciprofloxacin and norfloxacin and the results are shown in Table 2. Ciprobay tablets and ciprobay infusion (Bayer) with five runs are represented by the groups of peaks 7 and 8 respectively in Fig. 5. The method was statistically compared to the previous FIA methods [15,16] and the results obtained (Table 2) indicate that a similar degree of accuracy can be obtained with the SIA and FIA methods. In the FIA method both drugs were injected into a continuous stream of iron(III) solution to form a brown–red complex which is monitored at 447 nm and 430 nm for ciprofloxacin and norfloxacin respectively. It can also be suggested from these results that the proposed method is suitable for the determination of these two drugs in pharmaceutical products without any interferences from compounds usually added to such fomulations. The SIA method is superior to the FIA method with respect to considerably lower reagent consumption. Although FIA is characterized by a high sampling frequency SIA is easier to operate and optimize because only a single pump and a single valve are used. Also the ease of use of the automated SI system rendered the generation of plenty of data in a short period of time a simple task.

Table 2
Results obtained by the proposed SIA method an by FIA [15,16] for analysis of ciprofloxacin an norfloxacin in proprietary drugs.

Drug	Supplier	Active material	Mean recovery $\pm$ SD(%)[a]		t[b]
			SIA	FIA	
Ciprobay tablets	Bayer	Ciprofloxacin, 250 mg	100.8 ± 0.94	101.8 ± 0.96	2.38
Ciprobay infusion	Bayer	Ciprofloxacin, 2000 ppm	99.4 ± 1.00	100.3 ± 0.68	2.01
Noroxin tablets	Merck Sharp and Dohme	Norfloxacin, 400 mg	99.8 ± 0.67	100.7 ± 0.55	2.31

[a] $n = 5$.
[b] Calculated t test value [theoretical value = 2.78 ($p = 0.05$)].

Acknowledgements

References

[1] J. Ruzicka and G.D. Marshall, Anal. Chim. Acta, 237 (1990) 329.

[2] J. Ruzicka and T. Gubeli, Anal. Chem., 63 (1991) 1680.

[3] T. Gubeli, G.D. Christian and J. Ruzicka, Anal. Chem., 63 (1991) 2407.

[4] C.H. Pollema, J. Ruzicka, G.D. Christian and A. Lernmark, Anal. Chem., 64 (1992) 1356.

[5] A. Baron, M. Guzman, J. Ruzicka and G.D. Christian, Analyst, 117 (1992) 1839.

[6] M. Guzman, C. Pollema, J. Ruzicka and G.D. Christian, Talanta, 40 (1993) 81.

[7] M. Guzman, C. Pollema, J. Ruzicka and G.D. Ghristian, Fresenius' J. Anal. Chem., 346 (1993) 1813.

[8] M. Guzman and B.J. Compton, Talanta, 40 (1993) 1943.

[9] H.C. Shu, H. Hakanson and B. Mattiasson, Anal. Chim. Acta, 283 (1993) 727.

[10] P.J. Baxter, G.D. Christian and J. Ruzicka, Analyst, 119 (1994) 1807.

[11] S.M. Sultan, F.O. Suliman and B.S. Bahruddin, Analyst, 120 (1995) 561.

[12] G.D. Christian and J. Ruzicka, Anal. Chim. Acta, 261 (1992) 11.

[13] A.E. Martell and R.J. Motekaitis, Determination and Use of Stability Constants, 2nd edn., VCH, New York, 1992.

[14] F.R. Hartley, C. Burgess and R.M. Alcock, Solution Equilibria, Ellis Horwood, Chichester, 1980.

[15] S.M. Sultan and F.O. Suliman, Analyst, 117 (1992) 1523.

[16] S.M. Sultan and F.O. Suliman, Analyst, 118 (1993) 573.

[17] K. Grohe, Chem. Br., (1992) 34.

[18] H. Zeiler and K. Grohe, J. Clin. Microbiol., 3 (1984) 339.

[19] L.L. Shen, W.E. Kohlbrenner, I.D. Weig and J. Baranowski, J. Biol. Chem., 264 (1989) 1973.

[20] A. Lagana, M. Rotatori, R. Curini, G.D. Ascenzo and L. Miano, J. Pharm. Biomed. Anal., 6 (1988) 221.

[21] I. Nelson-Ehle, J. Chromatogr., 416 (1987) 207.

[22] A. Lagana, M. Rotatori, R. Curini, G.D. Ascenzo and L. Miano, J. Chromatogr., 417 (1987) 135.

[23] C.M. Myers and J.L. Blumer, J. Chromatogr., 422 (1987) 153.

[24] W.M. Awani, J. Clarkson and D.R.P. Guay, J. Chromatogr., 419 (1987) 414.

[25] C.E. Fasching and L.R. Peterson, J. Liq. Chromatogr., (1985) 555.

[26] K. Borner, H. Lode, G. Hoeffken, C. Prinzing, P. Glatzel and R. Wiley, J. Clin. Chem. Biochem., 24 (1986) 325.

[27] G.J. Krol A.J. Noe and D. Beerman, J. Liq. Chromatogr., 9 (1986) 2897.

[28] P.B. Issopoulos, Analyst, 114 (1989) 627.

[29] F.A. Cotton and G. Wilkinson, Advanced Inorganic Chemistry, 3rd edn., Wiley, New York, 1962.

[30] D.A. Buckingham, C.R. Clark and A. Nagia, Aust. J. Chem., 43 (1990) 301.

[31] A.M.Y. Jaber and A. Lounici, Anal. Chim. Acta, 291 (1994) 53.

[32] W. Likussar, Anal. Chem., 45 (1973) 1926.

[33] M. Meloun and J. Cermak, Talanta, 31 (1984) 947.

[34] J.A. Cornell, Experiments with Mixtures, Wiley, New York, 1981.

[35] D.C. Montogomery, Design and Analysis of Experiments, 2nd edn., Wiley, New York, 1994.

Talanta

High performance liquid chromatographic method for the separation and quantification of some psychotherapeutic benzodiazepines optimized by the modified simplex procedure

Salah M. Sultan*, Aarif H. El-Mubarak

The Chemistry Department, King Fahd University, KFUPM Box 2026, Dhahran 31261, Saudi Arabia

Abstract

An accurate high performance liquid chromatography method for the separation and quantification of a solution mixture of nitrazepam, diazepam and medazepam and medazepam was developed. The modified simplex program has been utilized for the optimization of the chemical and chromatographic parameters using the chromatographic response function as the quality criterion and a photodiode array as a detector. The separation was achieved in 2 min using a 20 cm long, 4.6 mm diameter Lichrosorb C18 reverse phase column. A 5 μl solution mixture containing 10 ppm of each drug was injected into a mobile phase containing 89:11 v/v acetonitrile: acetate buffer and a flow rate of 3.44 ml min^{-1} was found to be optimal. The method was found to be suitable for the determination of these compounds in proprietary drugs without suffering interferences.

Keywords: High performance liquid chromatography; Diode array detector; Modified simplex optimization; Benzodiazepines

1. Introduction

High performance liquid chromatography (HPLC) in combination with a diode array detector (DAD) is now considered the most powerful multicomponent mixture separation technique. This paper demonstrates the novelty of this technique for the separation and quantification of an important family of drugs, the benzodiazepines.

Benzodiazepines, mainly nitrazepam (NZP), diazepam (DZP) and medazepam (MZP), are psychotherapeutic agents. They have hypnotic, tranquilizing, anti-depressive, sedative and anticonvulsant properties. Benzodiazepines are chemically characterized by the presence of a phenyl ring fused to a saturated seven-membered ring with nitrogen at the 1 and 4 positions. They undergo extensive metabolism, therefore it is essential that the assay method be sensitive, specific and capable of separating and determining parent

* Corresponding author. Fax: (966) 03-860-4277.

drugs and major metabolites. However, various methods for the separation of the benzodiazepines have been reported in the literature [1–12], most of which are HPLC methods. Different mobile phase combinations such as methanol–water and acetonitrile–water with and without phosphate or acetate buffer were used. In some cases triethylamine was added to the mobile phase to act as a modifier [11]. However, many workers have not used state-of-the-art technology for efficient, reliable optimization but have mainly relied on conventional one-factor-at-a-time methods. This paper utilizes the modified simplex program for successful optimization of instrumental as well as system parameters such as acetonitrile/acetate buffer comination ratio, flow rate of elution and sample volume, thus affecting the quality of the separation and the quantification of these compounds. It is important to note here that simplex optimization was first introduced with HPLC separation in 1973 by Morgan and Deming [14,15] and is now considered mandatory by virtue of its availability, simplicity and rapidity in obtaining proper optimal conditions in a pre-selected time.

2. Experimental

2.1. Apparatus

A Water system equipped with a Waters Model 600E multi-solvent delivery system, a Waters 991 series photodiode array detector, a Waters Intelligent Sample Processor (WISP) model 712, and an NEC Powermate 2 Data Station, equipped with Waters 5200 printer plotter, were used.

2.2. Stationary phase

A Lichrosorb RP-18 (C18), 10 μ, 20 cm × 4.6 mm i.d. stainless-steel column from Hewlett-Packard was used.

2.3. Mobile phase

Acetonitrile (Burdick & Jackson, HPLC grade) filtered through a 0.22 mm GV Millipore filter was used together with 0.1 M ammonium acetate

buffer (pH 6.0, adjusted with acetic acid) prepared with triply-distilled, organic-free water from a Milli-Q system (Millipore) and filtered through a 0.45 mm Millipore filter. The mobile phase was sparged with He gas at a rate of 20 ml min^{-1} prior to, and throughout, the analysis.

2.4. Standard stock solutions and drug tablets

Analytical grade samples of the drugs NZP (1,3-dihydro-7-nitro-5-phenyl-2H-1,4-benzodiazepine-2-one), DZP (7-chloro-1,3-dihydro-1-methyl-5-phenyl-2H-1,4-benzodiazepine-2-one) and MZP (7-chloro-2,3-dihydro-1-methyl-5-phenyl-1H-1,4-benzodiazepine) were supplied by Roche Co. (Switzerland). Standard stock solutions of NZP, DZP and MZP were prepared by dissolving exactly about 0.1 g in CH_3CN and making the volume up to 100 ml. To give a concentration of 1 mg ml^{-1}, working standards were prepared by appropriate dilutions.

Drug tablets were prepared by crushing to powder five tablets after accurate weighing. A weighed portion of powder, equivalent to 5 mg nitrazepam and 10 mg diazepam, was carefully transferred to a beaker. Then about 40 ml of mobile phase of acetonitrile: acetate buffer, 89:11, was added, sonicated while heating for 30 min and filtered through a 0.45 mm filter (Millipore). The filtrate was washed several times with warm mobile phase, and the volume was made up to 100 ml with the mobile phase to give a concentration of 50 ppm nitrazepam and 100 ppm diazepam. Further dilutions were made to yield claimed concentrations of 5 and 10 ppm respectively. A mixture of 10 ppm of each was used throughout the analysis.

2.5. System conditioning

All lines were degassed, the column was conditioned by passing the mobile phase for 30 min, the on-column pressure limit was set to 0–6000 psi, and the DAD was warmed up for 10–15 min prior to analysis to condition the optics, flow cell and diode array. The sampling time was adjusted to 55–63 × 8 ms to give maximum sensitivity, the wavelength range was 230–282 nm with a resolu-

Table 1
Simplex optimization of HPLC variables for method development for the mixture of benzodiazepines (10 ppm each). Steps of 4, 4, 0.6 and 98 were taken for CH_3CN, buffer, flow rate and drug concentration respectively.

Expriment No.[a]	%CH_3CN	% Buffer	Flow rate (ml min^{-1})	Conc. (ng)	CRF
1	85.00	15.00	2.50	100	14.03
2	87.83	12.17	2.62	111	12.94
3	85.71	14.29	2.97	111	15.51
4	85.71	14.29	2.62	145	13.42
5 R	83.11	16.89	2.78	126	14.20
6 R	83.51	16.49	2.88	80	15.13
7 R	83.22	16.78	3.25	112	11.34
8 R	84.56	15.45	2.69	103	14.13
9 R	83.66	16.34	3.06	109	15.09
10 R	85.47	14.53	3.17	74	15.55
11 E	86.65	13.35	3.36	47	17.15
12 R	86.91	13.09	3.08	50	15.48
13 R	89.34	10.66	3.40	59	18.97
14 R	87.55	12.45	3.41	95	17.68
15 C	86.78	13.22	3.18	89	16.49
16 C	87.31	12.69	3.29	78	16.72
17 R	88.38	11.62	3.50	56	20.35
18 C	87.54	12.46	3.40	59	18.24
19 R	89.29	10.71	3.45	21	19.41
20 R	90.47	9.53	3.50	32	24.09
21 C	89.36	10.64	3.44	48	24.64
22 C	89.34	10.66	3.47	33	22.25
23 R	91.07	8.94	3.44	19	23.37
24 R	91.25	8.75	3.45	33	21.20
25 C	89.82	10.18	3.46	33	21.02

[a] R = reflection; C = contraction; E = expansion.

tion of 1.4 nm, the analysis time range was a minimum of 0–3.5 min, with an interval of 1.96 s, accumulation and smoothing was for seven points, drift was 0.002 AU min^{-1}, the baseline was corrected from 0.03–3.5 min, and the Y-scale was 0.185 AU FS and then adjusted automatically by the system. These conditions enable peak detection of a minimum height of 1×10^{-4} AU and a minimum area of 1×10^{-5} AU min^{-1}.

2.6. Procedure

The mobile phase of acetonitrile: acetate buffer (89:11 v/v) was allowed to flow at a rate of 3.44 ml min^{-1} at room temperature for about 30 min to condition the column and the detector cell. A 5 μl solution mixture was injected into the column. The separated compounds were allowed

to pass the DAD through a 1 cm flow cell for a fixed time of 3 min. The absorbance was monitored in the range 230–282 nm but requested only at 254 nm on the screen, and finally recorded on the flow chart printer.

3. Results and discussion

3.1. Optimization

The modified simplex method [16–20] of the COPS (Chemometrical Optimization by Simplex) program (Elsevier, Amsterdam, was used for the optimization of the variables considered to be most affecting the separation of the mixture components. These are: the percentage of acetonitrile and the percentage of the acetate buffer combined
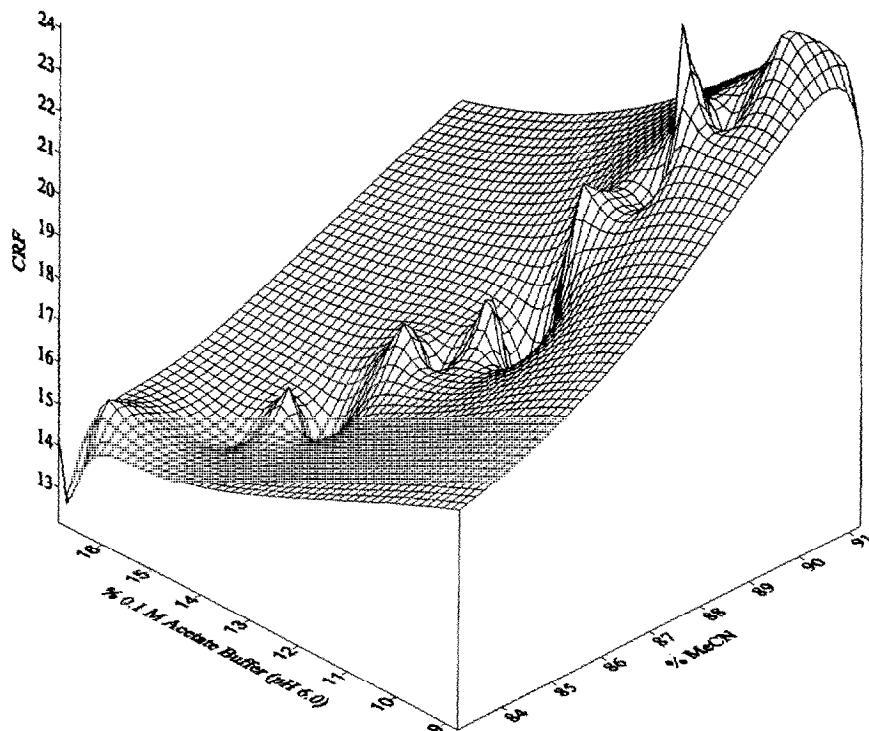
Fig. 1. Three-dimensional surface diagram showing the effect of the binary mobile phase (acetonitrile: acetate buffer) on the CRF.

and depending on each other, thus constituting a binary mobile phase as one variable. The other two variables are the flow rate of elution and the sample volume injected for a specific known concentration. The optimization procedure was carried out for a wide range (5–50 ppm) of concentration of each drug in the mixture and run at room temperature using a Lichrosorb C18 column of 4.6 mm diameter and 20 cm length, with absorption measured at 254 nm using the DAD.

The modified simplex program was started by introducing upper and lower boundary conditions for the above three factors, determined by conducting preliminary experiments as follows: 100–80% for CH_3CN; 0–20% for the buffer; 4.0–1.0 ml min^{-1} for the flow rate and 1–50 μl sample volumes of 10 ppm each results in 10–500 ng for the drug concentration. Experiments 1–4 in Table 1 show the values of the three parameters designated as the initial simplex conditions.

The chromatographic response function (CRF) earlier adopted by Wright et al. [21] of the follow-

ing form was chosen as the quality criterion:

$$CRF = \sum_{i=1}^{n-1} R_i + n - |T_A - T_L| \qquad (1)$$

where R_i is the resolution between adjacent peak pairs, n is the number of peaks detected, T_A is the target retention time in seconds for the last peak, and T_L is the retention time for the last peak. However, a computer program has been written in BASIC for the calculation of the CRF. It includes all necessary equations. The program ensures that any retention time for the last peak, that occurs within ± 1 min of the target time, T_A, is equally acceptable, since the last term in the CRF is only included if it exceeds 1 min. The target retention time used in the present work is 2 min.

In the modified simplex program, the reduction step is simply one experiment and not $(n + 1)$, where n is the number of optimized parameters, as in the case of the normal simplex method. In the contraction step, the worst point is replaced by one in the middle of the worst and best points. In
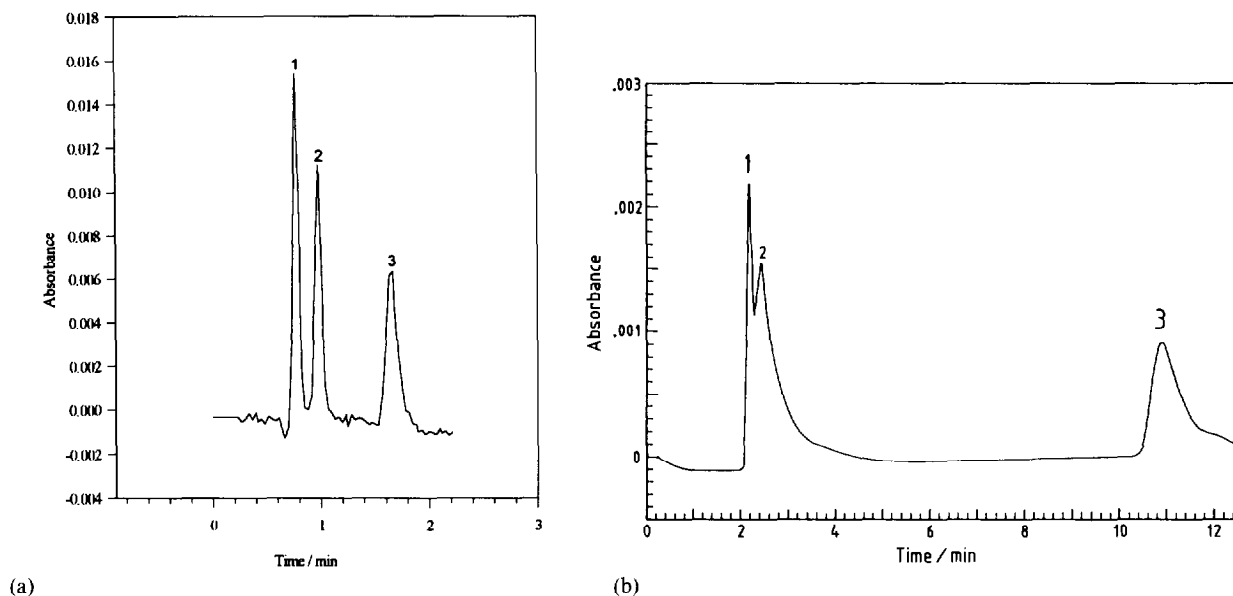
Fig. 2. (a) An optimized chromatogram for experiment No. 21 during the simplex search for method development. (1) nitrazepam; (2) diazepam; (3) medazepam; column, Lichrosorb C18; mobile phase, acetonitrile: acetate buffer, 89:11; flow rate, 3.44 ml min^{-1}; detection, DAD at 254 nm; concentration, 10 ppm each. (b) An un-optimized chromatogram in the early investigation for method development. (1) nitrazepam; (2) diazepam; (3) medazepam; column, Lichrosorb C18; mobile phase, acetonitrile:acetate buffer, 50:50; flow rate, 2.50 ml min^{-1}; detection, DAD at 254 nm; concentration, 10 ppm each.

reduction, contraction, reflection and expansion steps, the modified simplex program uses the differences in the responses at the vertices to estimate the vertex with a better response. When the vertex with the worst response is reflected through the centroid of the simplex, three vertices are located on a straight line. After contraction or expansion the new vertex will also be on the same line. Measuring the response in the centroid results in three responses. An estimation of the position of the next vertex on the line, which probably gives a better response, is formed by fitting a second order model or a Gaussian model through these three responses. The position of the maximum of the fitted function provides the location of the next vertex. The results of the modified simplex progress are introduced in Table 1 and experiment number 21 indicates optimum conditions with the highest CRF value. The simplex was halted at experiment 25 as there was no further significant improvement towards the maximization of the CRF value. The data obtained indicate that the effect of variation of acetoni-

trile–buffer concentration ratio is more significant on the CRF value than the other two parameters are. This could be attributed to the acetonitrile being a highly dipolar aprotic solvent with a small autoprotolysis constant ($pK_{HS} = 33.6$) and a relatively high dielectric constant of $\epsilon = 36.0$ [22]. Fig. 1 shows the interactive effect of this binary mobile phase on the CRF on a three-dimensional surface, thus visualizing the movement of the simplex towards the optima in a hill-climbing way as the mobile phase combination changes, i.e. the CRF increases as actonitrile increases and the acetate buffer decreases.

It is worth mentioning here that.the mechanism of the retention of benzodiazepines in the reverse bulky hydrocarbonaceous moiety of Lichrosorb C18 stationary phase is stronger (London forces) than in the mobile phase [23]. The reverse holds true when considering parameters reflecting the ability of the solute to take part in different, stronger types of bonding such as charge transfer, hydrogen bonding, etc. With all the above considerations together with the help of the modified

Table 2
Analytical appraisal for standard solutions of nitrazepam and diazepam using the external addition method.

Compound	Calibration equation[a]	r^{2b}	Concentration (ppm)
Nitrazepam	$A = 6.3557 \times 10^{-5} + 1.0656 \times 10^{-4} C$	0.9993	0.2–200
Diazepam	$A = 1.0082 \times 10^{-5} + 1.0238 \times 10^{-4} C$	0.9991	0.2–200

[a] A = absorbance; C = compound concentration (ppm). [b] Correlation coefficient.

simplex optimization, it was feasible to separate the three components in the mixture in less than the 2 min predetermined initially. Fig. 2(a) shows the optimized chromatograms obtained around the optimum conditions; in comparison Fig. 2(b) shows a chromatogram under other conditions (same as optimum except an acetonitrile: acetate buffer ratio of 50:50 and a flow rate of 2.5 ml min^{-1} were used). Note that the run was carried out in 12 min and the separation was poor.

The optimum conditions are as follows: acetonitrile: acetate buffer, 89:11; flow rate, 3.44 ml min^{-1}; injected volume of 5 μl of each 10 ppm mixture; ambient temperature; a Lichrosorb C18 column of 4.6 mm diameter and 20 cm length; and UV DAD monitored at 254 nm. These conditions were used in the analytical appraisal as well as the application. Peaks were identified by the method of iterative elution of the drugs at the same optimum conditions. The order of elution was found to be nitrazepam, diazepam and medazepam.

4. Analytical appraisals

The external addition method was used to judge the analytical appraisal by using different series of standard solutions of the drugs. The results obtained are to be found in Table 2, and indicate excellent linearity and reasonable dynamic range.

For application and determination of the drugs in proprietary forms either the above external method or the internal addition method could be used as long as any of these compounds could be used as an internal standard.

The benzodiazepine drugs are controlled and the only two made available for our investigation

was Mogadon (Roche) containing 5 mg nitrazepam and Valume (Roche) containing 10 mg diazepam. A solution mixture was prepared as in the method above and used under the optimized conditions. No interference peak from excipients present with the tablets could be detected indicating successful application of the method to the dosage forms. The results of analysis of these proprietary drugs (see Table 3) were statistically compared with those obtained using the standard official method [24,25]. The parameters and conditions of both methods are summarized in Table 4. The Student t-test values obtained indicated no significant difference in the mean recovery results for diazepam between the official and developed methods.

The results obtained showed that our present method is precise, accurate and suitable for the determination of these compounds in drug formulations. It is faster (analysis time is 2 min) and more specific than the other existing methods.

5. Conclusion

The modified simplex program and the sophistication of the DAD system resulted in successful chromatographic and chemical optimization conditions thus giving an excellent separation in a reasonable requested time. This makes the current method the fastest of those adopted for these compounds. The modified simplex program could be used for the optimization of similar chromatographic separations.

Table 3

Statistical analysis of the results obtained by the present method compared with those obtained by the official method for the analysis of nitrazepam and diazepam proprietary drugs

Drug	Active ingredient	Supplier	Mean recovery ± SD (%)[a]		t[b]
			Present	Official[c]	
Mogadon	Nitrazepam 5 mg	Roche, Switzerland	101.4 ± 1.4	–	–
Valume	Diazepam 10 mg	Roche, Switzerland	101.6 ± 1.6	100.2 ± 1.5	1.53

[a] $n = 5$.
[b] Theoretical value = 2.31; $n = 5$.
[c] Ref. [19].

the research institute for allowing him to use their facilities and to read for an M. Sc. degree in the chemistry department.

Table 4

Comparison of the developed HPLC method with the official adopted method [20] for the assay of diazepam in tablets.

Parameter	Official method	Developed method
HPLC system column	Tracor 950 solvent pump C18 Bondapack, 10μ, stainless-steel, 30 cm × 3.9 mm i.d. (Waters Associates, Inc.)	Waters 600E solvent pump C18 Lichrosorb, 10 μ, stainless-steel, 20 cm × 4.6 mm i.d. (Hewlett-Packard)
Mobile phase	MeOH: water, 65:35	MeCN:acetate buffer, 89:11
Flow rate	1.2 ml min⁻¹	3.44 ml min⁻¹
Temperature	Ambient	Ambient
Injection system, inj. vol.	Auto-manual, 10–20 μl	Autoinjection, 5 μl
Detector, wavelength	Tracor 970A UV, 254 nm	Photodiode array 991, 254 nm
Detector sensitivity	60–90% AUFS	80–90% AUFS
Diazepam standard, solvent	USP Ref. Std., MeOH	Roche Generic Std., MeCN
Diazepam tablets	Unknown	Valume, Roche, Switzerland
Calibration method	Internal Std., p-tolualdehyde	External Std.
Diazepam retention time	>8.0 min	<1.0 min
Detection limit	Unknown	200 ppb
Recovery	103.2%	101.6%
Accuracy	0.20 ppm	0.11 ppm

References

[1] J.K. Lawrence, A.K. Larsen and I.R. Tebbett, Anal. Chim. Acta., 288 (1994) 123.

[2] F.T. Noggle, C.R. Clark and J. De Ruiter, J. Liq. Chromatogr., 13 (1990) 4005.

[3] I.S. Lurie, D.A. Cooper and R.F.X. Klein, J. Chromatogr., 598 (1992) 59.

[4] P.C. Ho, E.J. Triggs, V. Heazlewood and D.W.A. Bourne, Ther. Drug Monit., 5 (1983) 303.

[5] B. Kinberger and P. Wahrgren, Anal. Lett., 15 (1982) 549.

[6] H.B. Greizerstein and C. Wojtowicz, Anal. Chem., 49 (1977) 2235.

[7] U.R. Tjaden, M.T.H.A. Meeles, C.P. Thys, and M. Van Der Kaay, J. Chromatogr., 181 (1980) 227.

[8] H.M. Stevens, J. Forensic Sci. Soc., 25 (1985) 67.

[9] F. Mubhoff and T. Daldrup, International Journal of Legal Medicine 105 (1992) 105.

[10] D. Carvalho and V.L. Lanchote, Ther. Drug Monit., 13 (1991) 55.

[11] A. Sioufi and J.P. Dubois, J. Chromatogr., 531 (1990) 459.

[12] M. Japp, K. Garthwaite, A.V. Geeson and M.D. Osselton, J. Chromatogr., 112 (1975) 267.

[13] W.D. Hopper, J.A. Roome, A.R. King, M.T. Smith, M.J. Eadie and R.G. Dickinson, Anal. Chim. Acta, 177 (1985) 267.

[14] S.L. Morgan and S.N. Deming, J. Chromatogr., 112 (1975) 267.

[15] S.N. Deming and S.L. Morgan, Anal. Chem., 45 (1973) 278A.

[16] J.C. Berridge, Analyst, 109 (1984) 291.

[17] S.M. Sultan, Analyst, 117 (1992) 773.

[18] S.M. Sultan, F.O. Suliman, S.O. Daffuaa and I.I. Abu-Abdoun, Analyst, 117 (1992) 1179.

[19] M.W. Routh, P.A. Swartz and M.B. Denton, Anal. Chem., 49 (1977) 1422.

[20] P.B. Ryan, R.L. Barr and H.D. Todd, Anal. Chem., 52 (1980) 1460.

[21] A.G. Wright, A.F. Fell and J.C. Berridge, Chromatographia, 24 (1987) 533.

[22] J. Barbosa and V. Sanz-Nebot, Talanta, 36 (1989) 837.
[23] R. Kaliszan, A. Kaliszan, T.A.G. Noctor, W.P. Purcell and I.W. Wainer, J. Chromatogr., 609 (1992) 69.

[24] K. Helrich, Official Method of Analysis, Vol. 1, 15th edn., Association of Official Analytical Chemists Inc., Arlington, Virginia, 1990.
[25] M. Tsougros, J. Assoc. Off. Anal. Chem., 68 (1985) 545.

Spectrophotometric determination of Isoproturon and Metoxuron using ethylacetoacetate and application to technical and formulation grade samples[1]

K. Ramakrishnam Raju, S.R.K.M. Akella, J.V.S. Murthy, U.T. Bhalerao*

Indian Institute of Chemical Technology, Hyderabad 500 007, India

Abstract

A simple and rapid spectrophotometric method for the determination of Isoproturon and Metoxuron is described based on alkaline hydrolysis of the compounds to their corresponding primary amines, followed by diazotization and coupling with ethylacetoacetate in alkaline medium. The chromogenic species obeys Beer's law up to 15 and 9 μg ml^{-1} for Isoproturon and Metoxuron respectively. The method is successfully applied for technical and formulation samples with RSD in the ranges 0.48–0.72, 0.86–1.32 and 0.66–0.74, 0.27–0.69 for technical and formulation grade samples of Isoproturon and Metoxuron respectively. The advantages over the earlier methods are discussed.

Keywords: Spectrophotometry; Isoproturon; Metoxuron

1. Introduction

Among the phenylurea herbicides, *N,N*-dimethyl-*N'*-[4-(1-methyl ethyl) phenyl] urea and *N'*-(3-chloro-4-methoxy phenyl)-*N,N*-dimethyl urea popularly known as Isoproturon (IPN) and Metoxuron (MTN) respectively, are widely used for the control of different weed species in cereals and carrots. The need for a simple method for their routine analysis and quality evaluation in technical and formulation grade samples is acknowledged. Titrimetric [1], GC [2] and UV spec-

trophotometric [3] methods are available for this purpose and are unsuitable for routine use for the reasons previously outlined [4,5]. The use of coupling reactions of diazo derivatives of primary amines with phenols, amines and carbanions is known for their analysis. Coupling reactions with carbanions have been by far the least explored, and in particular application to pesticides has not been reported. Ethylacetoacetate, with an active hydrogen atom, is a simple useful carbanion-yielding reagent that can be used for coupling with diazonium salts [6–8]. During further investigations on analytical methods, we developed yet another simple and rapid spectrophotometric method based on the coupling reaction of ethyl-

---

* Corresponding author.
[1] IICT Communication No. 3538.

acetoacetate, a common chemical, in strong alkali medium with the diazonium salt obtained after hydrolysis and subsequent diazotization and the results are presented here.

2. Experimental

2.1. Apparatus

A Parkin-Elmer Model Lambda-2 UV–Visible spectrophotometer with 1 cm matched quatrz cells was used.

2.2. Reagents and materials

All the chemicals used were of AnalaR grade. The following solutions were prepared: 0.5 N and 0.8 N sulfuric acid (Loba Chemicals, Bombay) in water; 1.0% w/v sodium nitrite (Qualigens, Bombay) in water; 5.0% sulfamic acid (Loba Chemicals, Bombay) in water; 0.5 and 5.0% v/v ethylacetoacetate (Reidel, Germany) in methanol; 50.0% w/v sodium hydroxide (Qualigens, Bombay) in water; 0.5 N sodium hydroxide in methanol.

Standard IPN was supplied by M/s Bharat Pulverising Mills, Bombay and used as received. MTN was supplied by the Pesticides Division, IICT, Hyderabad and was used after recrystallization in hot water.

2.3. Preparation of standard herbicide solutions

Standard herbicide solutions were prepared by dissolving 80 mg herbicide in methanol and diluting to 50 ml in a standard flask from which 3.0 ml was taken and diluted further to 50 ml with methanol and then used as working solutions.

2.4. General procedure

A 1.0 ml portion of working sample solution was transferred into a 10 ml standard flask to which 1.0 ml 0.5 N methanolic sodium hydroxide was added and allowed to stand for 5 min to ensure complete hydrolysis. After evaporating the solvent, 1.25 ml 0.8 N and 0.75 ml 0.5 N sulfuric

acid were added for IPN and MTN respectively and the flasks were heated in a water bath for about 30 min (IPN) and 5 min (MTN). The flasks were then removed from the water bath and cooled to room temperature after which 1.0 ml and 0.75 ml of 1.0% sodium nitrite solution were added for IPN and MTN respectively and the flasks allowed to stand for 5 min. Then 0.5 ml (IPN) and 0.25 ml (MTN) 5.0% sulfamic acid solution were added, the flasks were stood for 5 min, 1.0 ml 0.5% ethyl acetoacetate solution and 2.0 ml 50.0% sodium hydroxide solution were added to each flask and distilled water was added to 10 ml. The absorbances of the solutions were measured at 398 nm (IPN) and 400 nm (MTN) against distilled water blank.

2.5. Technical grade samples

About 80 mg of technical grade sample was weighted accurately and dissolved in 50 ml methylene chloride. The solution was treated with 1 N hydrochloric acid and the organic layer was evaporated. The residue was dissolved in methanol and diluted to 50 ml in a standard flask. A 3.0 ml portion of solution was further diluted to 50 ml with methanol and then 1.0 ml was extracted and subjected to analysis using the general procedure.

2.6. Formulation samples

About 160 mg and 110 mg of formulations of IPN and MTN respectively were weighed accurately, 50 ml of methylene chloride was added and the samples were centrifuged. The organic layer was evaporated after treatment with 1 N hydrochloric acid. The residue was dissolved in methanol, diluted to 50 ml, and 3.0 ml portions of the solutions were diluted to 50 ml with methanol and 1.0 ml was used for subsequent analysis using the general procedure.

Synthetic formulations (80%) as wettable powders for MTN were prepared [9] and analysed owing to the non-availability of commercial formulations.

3. Results and discussion

3.1. Optimisation of reaction variables

Typical absorption spectra of IPN and MTN are shown in Fig. 1. The reaction variables have been optimised to obtain maximum colour development by varying one variable at a time while keeping the others constant. The optimum concentrations of the various reagents for IPN and MTN respectively are found to be 1.0 ml 0.5 N methanolic sodium hydroxide, 1.25 ml 0.8 N and 0.75 ml 0.5 N sulfuric acid, 30 min and 5 min heating time, 1.0 ml and 0.75 ml 1% sodium nitrite, 0.5 ml and 0.25 ml 5% sulphamic acid and 1.0 ml 0.5% ethylacetoacetate followed by 2.0 ml 50% sodium hydroxide.

Although methanolic sodium hydroxide brings about rapid hydrolysis [10,11] of the present herbicides, methanol affects the colour development
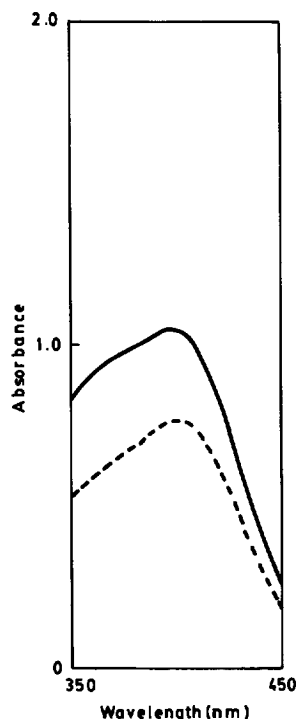
Fig. 1. Absorption spectra of IPN and MTN: (——) IPN; (-----) MTN. (1.0 ml 0.025% IPN/MTN + 1.0 ml 0.5 N methanolic NaOH + 1.0 ml 0.8 N H₂SO₄ + 1.0 ml 1.0% NaNO₂ + 0.5 ml 5.0% sulfamic acid + 1.0 ml 0.5% ethylacetoacetate + 2.0 ml 50% NaOH against distilled water blank.)

Table 1
Beer's law, precision and accuracy

Parameter	IPN	MTN
λ_{max} (nm)	398	400
Beer's law limit ($\mu g \ ml^{-1}$)	15	9
Molar absorptivity (E) (1 $mol^{-1} \ cm^{-1}$)	1.37×10^4	2.33×10^4
Slope	0.0608	0.0963
Intercept	0.0351	0.0192
Correlation coefficient	0.9995	0.9958
Regression equation	$y = 0.0608x + 0.0351$	$y = 0.0963x + 0.0192$

and therefore its evaporation is recommended for further procedure after hydrolysis.

Variations in absorption measurements are observed when made against reagent blank. Upon further investigation it is found that the reagent blank is not stable. It is found that the variation in the absorbance of the blank is due to insufficient quantity of sulfamic acid being used to destroy the excess nitrite [12]. However, with the use of further excess of sulfamic acid, although the blank absorption is found to be constant, the absorbance of the sample decreases (vide optimum conditions). However, the absorption measurements for samples are stable and reproducible when made against distilled water blank and hence the present work is carried out accordingly.

3.2. Beer's law, precision and accuracy

The absorption maxima (λ_{max}), the molar absorptivities, Beer's law limits and correlation coefficients are given in Table 1. Although the reaction is fast, 3 min standing time is necessary to obtain reproducible results and the colour is stable for 30 min in both cases.

3.3. Reaction mechanism

Compounds containing active methylene groups such as ethylacetoacetate can be used as reagents for the determination of primary amines as it is known that diazo derivatives undergo coupling reactions by means of electrophilic sub-

Scheme 1.
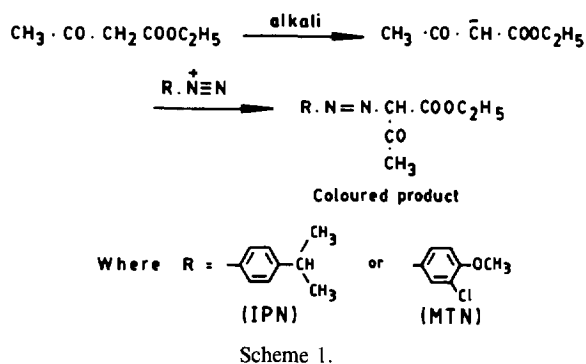
stitution with phenols, amines, and carbanions with active methylene groups [7]. Thus, the authors are also of the opinion that diazo derivatives of the amines formed after alkaline hydrolysis of IPN and MTN [10,11] are likely to couple with the carbanions of ethylacetoacetate, as reported earlier [8], yielding the yellow chromogenic species shown in Scheme 1.

3.4. Application

A series (7) of standard samples of IPN and MTN has been analysed and the average percent relative error is found to be 0.74 [1.04, 0.44] for IPN and 0.68 [0.99, 0.37] for MTN at the 95% confidence level. A number of technical and formulation grade samples of IPN and MTN are analysed using the present method and the data are shown in Table 2. The RSDs were in the ranges 0.48–0.72, 0.86–1.32 and 0.66–0.74, 0.27–0.69 for technical and formulation grade samples of IPN and MTN respectively. The recoveries with respect to a comparison method [1] are also given in Table 2 to indicate the applicability of the method.

3.5. Advantages

The present method does not involve time-consuming distillation, thermal and photo-decomposition as reported earlier [1–3]. Furthermore, the present method is superior to our earlier methods [4,5] in terms of the simplicity of the reagent and is much more sensitive than the latter method and comparable with the former. Therefore, the

present method is simple, sensitive, rapid and useful for routine analysis.

Acknowledgement

Table 2
Assay of IPN and MTN[a]

Sample	Comparison method (Ref. [1])	Present method	Recovery (%)	RSD (Present method)
IPN				
Technical grade	99.80	99.10	99.50	0.48
	98.40	98.90	100.50	0.58
	99.30	99.10	99.80	0.37
	98.70	98.30	99.60	0.72
Formulation	50.20	50.00	99.60	0.86
(labelled 50%)	49.40	49.60	100.80	1.03
	49.70	49.30	99.20	1.32
MTN				
Technical grade	93.30	93.18	99.83	0.66
	98.90	99.13	100.17	0.73
	99.72	99.37	99.67	0.74
Formulation	80.60	80.30	99.60	0.69
	79.40	79.60	100.20	0.27
	79.20	79.70	100.60	0.52

[a] Averages of seven determinations.

References

[1] Z. Günthar, Analytical Methods for Pesticides and Plant Growth Regulators, Vol. 8, Academic Press, New York, 1976, p. 417.
[2] H. Buser and K. Grolimund, J. Assoc. Off. Anal. Chem., 57 (1974) 1294.
[3] Indian Standards Institution, Delhi, IS No. 12004, 1987.
[4] K. Ramakrishnam Raju, T.N. Parthasarathy and S.R.K.M. Akella, Analyst, 115 (1990) 455.
[5] K. Ramakrishnam Raju, T.N. Parthasarathy, S.R.K.M. Akella and U.T. Bhalerao, Talanta, 39 (1992) 1387.
[6] S. Belal, E.A. El Neanaey and S. Soliman, Talanta, 25 (1978) 290.
[7] A.K. Connors, Reaction Mechanisms in Organic Chemistry, Wiley Interscience, New York, 1973, p. 244.

[8] S.M. Hassan, F. Belal, M. Sharaf El-Din and M. Sultan, Analyst, 113 (1988) 1087.

[9] W.V. Valkenburg, Pesticide Formulations, Marcel Dekker, New York, 1973, p. 178.

[10] D. Hartley and H. Kidd, The Agrochemicals Handbook, 2nd edn., Royal Society of Chemistry, London, 1987.

[11] C.S.P. Sastry, D. Vijaya and K. Ekambareswara Rao, Food Chem., 20 (1986) 157.

[12] M.I. Walash, M. Rizk and A. El-Brashy, Talanta, 35 (1988) 895.

Simultaneous first-derivative spectrophotometric determination of iron(III) and molybdenum(VI) in cobalt–chromium and nickel–chromium alloys

A. Youssef El-Sayed[a]*, M.M.H. Khalil[b]

[a]Department of Chemistry, Faculty of Science, Al-Azhar University, Assiut, Egypt
[b]Department of Chemistry, Faculty of Science, Ain Shams University, Cairo, Egypt

Abstract

A method is proposed for the simultaneous determination of iron(III) and molybdenum(VI) by first-derivative spectrophotometry based on the absorption spectra of their complexes with morin in the presence of a cationic surfactant. The zero-crossing measurement technique is found sutiable for the direct measurement of the first-derivative value at the specified wavelengths. Iron(III) $(0.9–1.5\ \mu g\ ml^{-1})$ and molybdenum(VI) $(0.3–4.2\ \mu g\ ml^{-1})$ in different ratios have been determined simultaneously. A critical evaluation of the proposed method is performed by statistical analysis of the experimental data. The method was applied to determine iron and molybdenum in different alloys.

Keywords: Iron; Molybdenum; Alloys; First-derivative spectrophotometry

1. Introduction

The development of spectrometric methods has allowed the resolution of the complex spectra of multicomponent mixtures [1–3]. The resolution of binary mixtures of compounds with overlapped spectra by derivative spectrophotometry is greatly simplified and their reliability is increased by the determination of the individual components without the need for chemical separation. Derivative

spectrophotometric procedures have been applied for simultaneous determination of aluminum and iron with 8-hydroxyqunioline [4], molybdenum and titanium with hydrogen peroxide [5], aluminum and beryllium with 5,8-dihydroxy-1,4-napthaquinone [6], iron and bismuth with EDTA [7], palladium and platinum with dithizone [8], palladium and ruthenium with 2-thiobarbituric acid [9], beryllium and magnesium with 1-hydroxy-2-carboxyanthraquinone [10], copper and magnesium with emodin [11], copper and iron with cyanide [12], nickel and manganese with 2-(2-

---

* Corresponding author.

pyridylmethyleneamino)phenol [13], and gold and silver as rhodanine derivatives [14]. In contrast, morin has been used as a sensitive reagent for determination of iron [15,16] and molybdenum [17] in micellar media. It had been reported that molybdenum(VI) interferes strongly in the determination of iron(III), where their morin complexes show very close overlapping bands. The low seletivity of these methods makes them unsuitable for direct application without masking or a preliminary separation.

This paper reports a rapid and simple derivative spectrophotometric method for simultaneous determination of iron(III) and molybdenum(VI) in their mixtures. The method is based on the formation of colored complexes with morin in the presence of cetylpyridinum bromide. The first-derivative spectrum $(d_1A/d\lambda)$ is determined using the zero-crossing technique. The reported method was successfully applied to determine iron and molybdenum simultaneously in a range of diverse alloys.

2. Experimental

2.1. Apparatus

A Perkin-Elmer Lambda 3B spectrophotometer fitted with Perkin-Elmer Pecss software (controlled by a Mitsuba 368/33DX computer in conjunction with an HP Laser Jet 4L printer) and equipped with a 1 cm quartz cell was used for all measurements. The software was used to obtain the first-derivative spectra and to select the differential wavelength $(\Delta\lambda)$. The auto-option uses a width of $\Delta\lambda$ calculated by the method of Savitzky and Golay [18] at a scan speed of 120 nm min^{-1}. The pH measurements were made on an Orion Ionalyzer Model 920E fitted with a combined glass–calomel electrode.

2.2. Reagents

All materials used were of analytical grade and doubly-distilled water was used throughout. The certified cobalt/chromium, nickel/chromium, cobalt/chromium/nickel and ferromolybdenum al-
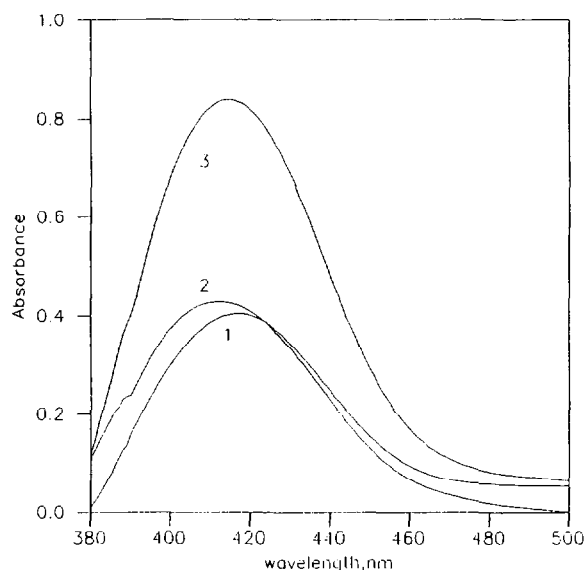
Fig. 1. Zero-order absorption spectra of (1) iron(III)–morin–CPB; (2) molybdenum(VI)–morin–CPB; (3) mixture of iron(III)– and molybdenum(VI)–morin–CPB complexes. [Iron(III)] = 0.46 μg ml^{-1}; [molybdenum(VI)] = 1.35 μg ml^{-1}; [morin] = 4 × 10^{-4} M; [CPB] = 2 × 10^{-3} M; reference reagent blank.
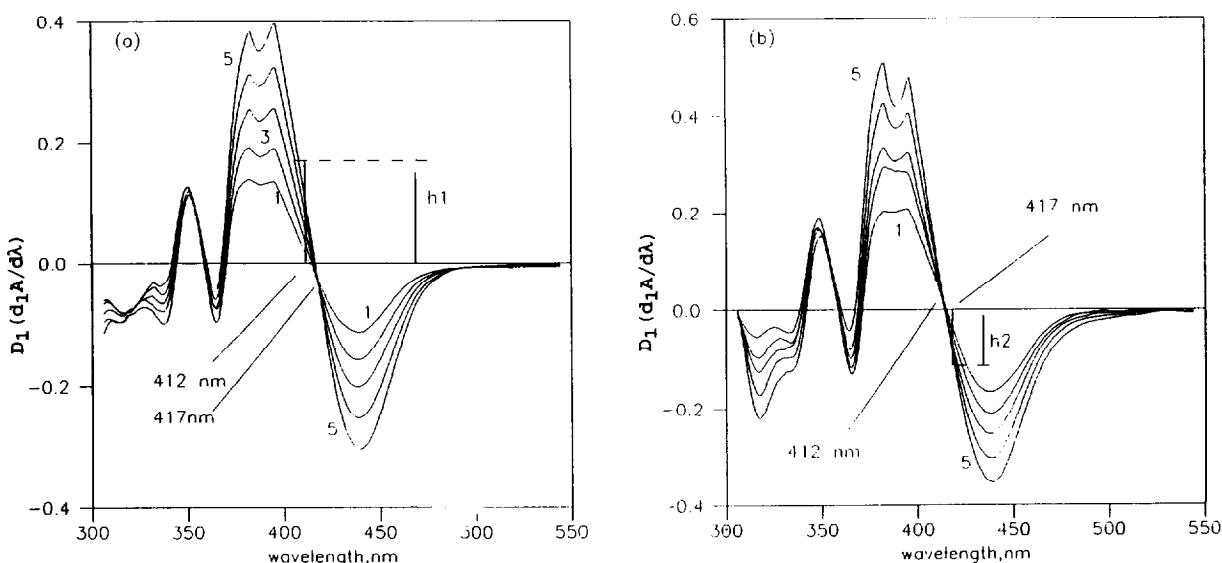
loys were provided by the General Metal Co. (Cairo) and Helwan Engineering Industries Co. (Cairo). The certified data were obtained by quantometer model 3400 (Applied Research Co.,

Fig. 2. First-order derivative spectra of (1) iron(III)–morin–CPB; (2) molybdenum(VI)–morin–CPB; (3) mixture of iron(III)– and molybdenum(VI)–morin–CPB complexes. [Iron(III)] = 0.46 μg ml^{-1}; [molybdenum] = 1.35 μg ml^{-1}; [morin] = 4 × 10^{-4}; [CPB] = 2 × 10^{-3} M; reference reagent blank.

Fig. 3. First-derivative spectra of a mixture of iron(III)– and molybdenum(VI)–morin–CPB complexes: (a) [molybdenum] = 1.35 μg ml^{-1}; [iron(III)] = 0.11, 0.34, 0.57, 0.8 and 1.03 μg ml^{-1} for curves (2)–(5) respectively; (b) [iron(III)] = 0.46 μg ml^{-1}; [molybdenum] = 0.63, 1.35, 2.69, and 3.36 μg ml^{-1} for curves (1)–(5) respectively.

Switzerland) and by a standard chemical method [19].

A stock solution of iron(III) (1 mg ml^{-1}) was prepared by dissolving 0.7234 g Fe$_2$(NO$_3$)$\cdot$H$_2$O (Aldrich) in 100 ml 0.1 N HNO$_3$. The solution was standardized by direct EDTA titration [20].

A stock solution of molybdenum(VI) (1 mg ml^{-1}) was made by dissolving 0.2522 g of Na$_2$MoO$_4\cdot$2H$_2$O (Aldrich) in 250 ml of water and standardized by titration with EDTA [20].

Morin (2′,3,4′,5,7-pentahydroxyflavone) solution (5 × 10^{-3} M) was prepared by dissolving 0.3778 g of the reagent (Merck) in 250 ml of absolute ethanol.

Cetylpyridinium bromide (CPB) aqueous solution (10^{-2} M) was prepared by dissolving 1.006 g of CPB (Fluka) in 250 ml of water.

Potassium chloride–hydrochloric acid buffer solution of pH 2.5 was prepared by adjusting the pH of 0.2 M KCl solution with 1 N HCl. Iron-free hydrochloric acid (1:1) was prepared according to the procedure of Jackson and Phillips [21].

Potassium fluoride solution (0.2 M) was prepared by dissolving 2.9 g of KF in 250 ml water.

2.3. Procedures

2.3.1. Simultaneous determination of iron(III) and molybdenum(VI) as morin–CPB complexes with first-derivative spectrophotometry

Transfer aliquots of iron(III) (2–26 μg) and molybdenum(VI) (5–100 μg) to separate 25 ml volumetric flasks. Add 1 ml of morin solution and 5 ml of CPB and dilute to the mark with acid buffer solution. Record the D_1 spectra of the mixture against a reagent blank after 10 min of mixing. Measure the absolute $D_1(d_1A/d\lambda)$ values at 412 and 417 nm for determination of iron and molybdenum respectively.

2.3.2. Simultaneous determination of iron and molybdenum in diverse alloys

Weigh 0.4 g of the alloy sample into a 150 ml beaker. Treat with 40 ml concentrated HCl (1:1) and 10 ml of concentrated HNO$_3$. Heat on a steam bath to near dryness and then cool to room temperature. Dissolve the residue in 50 ml HCl and boil the mixture to dissolve the salt, followed by dilution to 100 ml with water. Transfer a suitable aliquot of sample to a 25 ml volumetric flask and add 2 ml of 0.2 M KF. The iron and

Table 1

Statistical analysis of the simultaneous determination of iron and molybdenum in their mixtures with morin and CPB by first-derivative spectrophotometry[a]. Standard specimens; $n = 10$; first-derivative value D_1

Metal ion	λ (nm)	Regression equation	Linear range (μg ml^{-1})	r	$S_{y/x}$	S_b	S_x	Detection limits (μg ml^{-1})
Iron(III)	412	$D_1 = 8.64 \times 10^{-2}C - 6.28 \times 10^{-4}$	0.07–1.5	0.9997	9.72×10^{-4}	2.1×10^{-3}	1.18×10^{-3}	0.07
Molybdenum (VI)	417	$D_1 = 1.61 \times 10^{-2}C - 1.21 \times 10^{-2}$	0.2–4.2	0.9984	1.12×10^{-3}	1.05×10^{-2}	1.72×10^{-3}	0.2

[a] $C = \mu$g ml^{-1}, r = correlation coefficient, $S_{y/x}$ = standard deviation of residuals, S_b = standard deviation of slope of regression line, S_x = standard deviation of mixture containing 0.34 μg ml^{-1} iron(III) and 2 μg ml^{-1} molybdenum(VI).

molybdenum contents are simultaneously determined as before starting from "Record the D_1 spectra . . . . ." in the previous section.

3. Results and discussion

Morin forms colored complexes with iron and molybdenum in aqueous media. A hyperchromic effect is usually observed in the presence of surfactants [15–17].

Fig. 1 shows the zero-order absorption spectra of morin–CPB complexes of iron(III) (curve 1) with a maximum at ≈ 417 nm and molybdenum(VI) (curve 2) with a maximum at ≈ 412 nm.

Table 2

Interference levels of diverse ions in the simultaneous determination of iron and molybdenum. Concentration of iron(III) = 0.46 μg ml^{-1}; concentration of molybdenum(VI) = 1.35 μg ml^{-1}

Ion added	Tolerance limits [Ion]/[Iron]
Na$^+$, K$^+$, NH$_4^+$, NO$_3^-$, SO$_4^{2-}$, Cl$^-$, F$^-$, Br$^-$, I$^-$	2000
Ba^{2+}, Ca^2, Mg^{2+}	1000
Au^{3+}, Cd^{2+}, Hg^{2+}, Rh^{3+}, Ru^{3+}, Pd^{2+}, Cr^{3+}	100
Co^{2+a}, Gd^{3+}, La^{3+}, Mn^{2+a}, Ni^{2+a}, Pr^{3+}, Sn^{2+a}, Zn^{2+a}, Cu^{2+b}	80
Al^{3+a}, Be^{2+a}, Ta^{5+a}, Nb^{5+a}, Th^{4+a}, W^{5+a}, Zr^{4+a}	50
V^{5+}	3

[a] 2 ml of 0.2 M potassium fluoride.
[b] 1 ml of 0.5 M thiourea.

The total absorption spectrum of iron and molybdenum complexes is given in curve 3. However, the maximum absorption of morin reagent in acidic medium was 350 nm [15]. Consequently the absorption of iron(III) and molybdenum(VI) complexes and their mixture appeared as negative absorbance in the range 380–300 nm.

The complexation of iron and molybdenum with morin in the presence of CPB occurs over a wide pH range; the maximum absorption intensity is between 2 and 3 for iron and between 1.5 and 3 for the molybdenum complexes. The concentrations of morin (4×10^{-4} M) and CPB (2×10^{-3} M) in the final solution are selected to ensure that an excess of the reagent is present. Full color development is obtained 10 min after addition of acidic buffer to a mixture of iron(III)– and molybdenum(VI)–morin–CPB complexes. The absorbance remains constant for about 2 h.

Because of the large band overlap of the spectra of the two complexes, the determination of iron and molybdenum in their mixture by normal spectrophotometry is subject to considerable difficulties. For this reason, it was found to be more convenient and simple to resolve the problem of closely overlapped spectra by making use of the derivative spectra of the mixutre of both complexes.

A study of the first-, second-, third-, and fourth-derivative spectra of the mixture of iron and molybdenum complexes demonstrated that the first-derivative spectra gave results of highest accuracy and lowest detection limits. Fig. 2 shows the first-derivative spectra of the complexes shown

Table 3
Simultaneous determination of iron and molybdenum in diverse alloys using first-derivative spectrophotometry

Sample	Composition (%)	Certified (%)		Found[a] (%)		RSD (%)	
		Fe	Mo	Fe	Mo	Fe	Mo
Cobalt–chromium alloy	C: 0.9, Si: 0.37; Mn: 0.48; Ni: 4.16; Cr: 29.32; W: 4.16; Co: 59.52	2.77	0.42	2.76	0.43	0.92	1.05
Nickel–chromium alloy	C: 0.06; Si: 0.44; S: 0.03; Mn: 1.23; Cr: 22.08; Ni: 63.01	6.80	6.12	6.78	6.14	0.75	0.91
Cobalt–chromium–nickel alloy	C: 0.05; Si: 0.38; Ni: 14.9; Cr: 26.86; Mn: 0.06; Co: 50.63	1.52	5.39	1.51	5.41	1	0.86
Ferromolybdenum alloy	C: 2.1; S: 0.23; Si: 0.04; Cu: 0.09	27.02	72.2	27.03	72.91	0.53	0.48

[a] Average of five determinations.

in Fig. 1. It can be seen that the first-derivative spectra of the mixture of both complexes (Fig. 2, curve 2) are not sufficiently resolved to generate two distinct peaks. Therefore the zero-crossing measurement technique was utilized for resolving the mixture of the named complexes.

Fig. 3 (a)(b) shows series of first-derivative spectra of a mixture of iron(III)– and molybdenum(VI)–morin–CPB complexes. A series of first-derivative spectra of a mixture of 0.46 μg ml^{-1} iron(III) plus increasing amounts of molybdenum(VI) (0.63–3.36 μg ml^{-1}) are given in Fig. 3(a). Fig. 3(b) shows a series of first-derivative spectra of mixtures of 1.35 μg ml^{-1} molybdenum(VI) and increasing concentrations of iron(III) (0.1–1.0 μg ml^{-1}). The heights h_1 and h_2 in the first-derivative spectrum of the mixtures corresponding to values taken at wavelengths of 417 nm (zero-crossing wavelength of iron complex) and 412 nm (zero-crossing wavelength of molybdenum complex) are proportional to iron(III) and molybdenum(VI) concentrations respectively.

3.1. Calibration graphs and statistical treatment of results

The calibration graphs obtained by the recommended procedure are linear over the ranges 0.07–1.5 μg ml^{-1} of iron in the presence of 1.35 μg ml^{-1} molybdenum and 0.2–4.2 μg ml^{-1} of molybdenum in the presence of 0.46 μg ml^{-1} iron. The calibration graphs prepared by plotting the first-derivative values (h) vs. iron or molybdenum concentration all gave significant linearity with negligible intercepts, confirming the mutual independence of the derivative signals of the two complexes.

In Table 1 the statistical parameters for calibration graphs are given. The high values of correlation coefficients and intercepts on the y-axis (close to zero) indicate the good linearity of all calibration graphs and the conformity of Beer's law of first-derivative measurements. The precision of the method is determined for 10 samples, each containing 0.34 μg ml^{-1} iron(III) and 2 μg ml^{-1} molybdenum(VI). The values of $d_1\varepsilon$ for determi-

nation of iron and molybdenum at 412 and 417 nm are calculated from computing the corresponding values of d_1A and the results are given in Table 1. The $d_1\varepsilon$ value was equal to 8.64×10^{-2} and 1.61×10^{-2} μg ml^{-1} (the slopes of the regression lines in Table 1) for determination of iron and molybdenum respectively. The relative standard deviation is 1.5 and 1.7% for iron and molybdenum respectively. Moreover, the detection limits [22] are 0.04 and 0.2 μg ml^{-1} for iron and molybdenum respectively. The results in Fig. 3 and Table 2 suggest that a satisfactory resolution of two overlapping spectra is obtained by the first-derivative zero-crossing method.

3.2. Interference studies

The influence of the presence of diverse ions on the simultaneous determination of 0.46 μg ml^{-1} iron(III) and 1.35 μg ml^{-1} molybdenum(VI) was investigated by applying the recommended procedure to a solution containing a 2000-fold (mol/mol) ratio of interfering ion to iron; if interference occurred, this ratio was reduced until the interference ceased. Metal ions are added as the nitrate, chloride or sulfate, while the anions are added as ammonium, potassium or sodium salts. The criterion for interference was a deviation of more than ± 3% from the concentration of iron and molybdenum. The tolerance limits of some cations increased by addition of 2 ml of 0.2 M potassium fluoride. The results are given in Table 2.

The method has been applied to the simultaneous determination of iron and molybdenum in diverse alloys. The results obtained are presented in Table 3 and are in quite good agreement with those obtained by a standard chemical method [20] and by X-ray fluorescence.

References

[1] F. Salinas, J.J. Berzas Nevado and A. Espinosa Mansilla, Talanta, 37 (1990) 347.
[2] B. Morelli, Analyst, 113 (1988) 1077.
[3] H. Ishii and K. Satoh, Fresenius' Z. Anal. Chem., 312 (1982) 144.
[4] M. Blanco, J. Coello, F. Gonzalez, H. Iturriaga and S. Maspoch, Anal. Chim. Acta, 226 (1989) 271.
[5] N. Suzuki and R. Kuroda, Mikrochim. Acta, Part II, (1987) 47.
[6] N.K. Agnihotri, H.B. Singh, R.L. Sharma and V.K. Singh, Talanta, 40 (1993) 415.
[7] M. Adela Bermejo-Barrera, M. Pilar Bermejo-Barrera, M. Manuella Guisasola-Escudere and F. Bermejo-Martinez, Analyst, 112 (1987) 481.
[8] S. Kus and Z. Marczenko, Analyst, 112 (1987) 1503.
[9] B. Morelli, Analyst, 108 (1983) 1506.
[10] F. Salinas, A. Munoz da la Pana and J.A. Murillo, Analyst, 112 (1987) 1391.
[11] T. Pal and N.R. Jana, Talanta, 40 (1993) 1519.
[12] W. Naixing and L. Weian, Talanta, 40 (1993) 897.
[13] Z. Grabaric, Z. Lazarevic and N. Koprivanac, Anal. Lett., 26 (1993) 2455.
[14] A. Youssef El-Sayed, Bull. Chem. Soc. Jpn., 67 (1994) 3216.
[15] M.T.M. Zaki, A.M. El-Atrach, W.H. Mahmoud and A. Youssef El-Sayed, Analyst, 113 (1988) 937.
[16] F.H. Hernandez, J.M. Escriche, R.M. Saze and M.C.R. Barreda, Analyst, 111 (1986) 1045.
[17] M.T.M. Zaki, A.K. Abdel-Kader and M.M. Abdalla, Fresenius' J. Anal. Chem., 339 (1991) 197.
[18] A. Savitzky and M.J.E. Golay, Anal. Chem., 36 (1964) 1627.
[19] 1971 Annual Book of ASTM Standards, Part 32: Chemical Analysis of Metals; Sampling and Analysis of Metal-bearing Ores, American Society for Testing and Materials, Philadelphia, PA, 1971.
[20] T.S. West (Ed.), Complexometry with EDTA and Related Reagents, 3rd edn. Broglia Press, London, 1969.
[21] H. Jackson and D.S. Phillips, Analyst, 87 (1962) 712.
[22] J.C. Miller and J.N. Miller (Eds.), Statistics for Analytical Chemistry, 3rd edn. Ellis Horwood, Chichester, 1993.

Simultaneous determination of neodymium, erbium and holmium in rare earth mixtures with 2-phenyltrifluoroacetone and octylphenol poly(ethyleneglycol) ether by third-derivative spectrophotometry

Nai-Xing Wang*, Zhi-Kun Si, Jing-He Yang, Ai-Qin Du, Zhen-Dong Li

Department of Chemistry, Shandong University, 250100, Jinan, People's Republic of China

Received 13 April 1995; revised 5 October 1995; accepted 9 October 1995

Abstract

The complexes of the rare earth metals with 2-phenyltrifluoroacetone in the presence of TX-100 are reported. The characteristic absorbances of neodymium, holmium and erbium complexes can be increased by factors of 8.5, 31 and 15 respectively, compared to those of the cholrides. The third-derivative spectra have been used to eliminate the interference of cerium, and the sensitivities are increased again by factors of 7.4, 5.5 and 6.5. A method for the direct determination of neodymium, erbium and holmium in rare earth mixtures is proposed.

Keywords: Neodymium; Erbium; Holmium; Third-derivative spectrophotometry

1. Introduction

As colour-producing agents for the rare earth ions, there are a lot of highly sensitive reagents including arsenazo III [1] 1-(2-pyridylazo)-2-naphthol [2], chlorophosphonazo III [3] etc., but the determination of the individual rare earths in their mixture with these reagents is almost impossible because these reagents lack selectivity. There has

always been interest in the determination of individual rare earths, based on the absorption bands of their 4f electron transitions [4–12].

However, the determination of the rare earth elements with 2-phenyltrifluoroacetone has hardly been described. In this paper, we have discovered that 2-phenyltrifluoroacetone can form stable complexes with rare earth methal in the presence of TX-100. In the absorption spectra, the peaks of neodymium, holmium and erbium in the visible region are enhanced, the absorbances at λ_{max} being increased by factors of 8.5, 31 and 15 respec-

* Corresponding author.

tively, compared with those of the chlorides. However, direct determination by conventional spectrophotometry is still subject to interference from other rare earths. Accordingly, derivative spetra were studied, and the use of the third-derivative spectra was found to eliminate the interference and to enhance the sensitivity. On this basis, a method was developed for the determination of neodymium, erbium and holmium in rare earth mixtures. The analytical results obtained are quite satisfactory.

2. Experimental

2.1. Apparatus

A Shimadzu UV-3000 recording spectrophotometer with 4.0 cm cells was used.

2.2. Reagents

Standard solutions of rare earth metals were prepared from the pure oxides (Johnson Matthey) and mixed as required.

2-Phenyltrifluoroacetone (PTA) solution (0.05 M) was prepared by dissolving 1.080 g of PTA (Shanghai Chemical Reagent Plant) in ethanol and diluting to 100 ml with ethanol.

A solution of octylphenol poly(ethylengelycol) ether (TX-100; 2.0% v/v) was prepared by dissolving 5.00 ml of TX-100 (Rohm & Hass, Philadelphia, PA) in 250 ml of water.

Ammonium chloride solution (0.5 M) of pH 9.26 was used as a buffer.

All other reagents used were of analytical grade.

2.3. Procedure

Transfer a known volume of the lanthanide solution into a 10.0 ml volumetric flask, add 3.00 ml of PTA, 2.5 ml of TX-100 and 2.0 ml of buffer solution, dilute to volume with distilled water and mix. Record the absorption spectrum or its derivative spectrum against a reagent blank as reference.

3. Results and discussion

The absorption spectra of lanthanide ions and their complexes in the presence of TX-100 are shown in Fig. 1. It can be seen that curves 1 and 2 show some changes in the spectral features. The absorption band for the neodymium complex is shifted to longer wavelengths compared to the spectrum of the neodymium ion in the chloride, while those of erbium and holmium are shifted to shorter wavelengths. The sensitivity is enhanced considerably. A very sharp absorption band is found at 574 nm for neodymium, at 449 nm for holmium and at 521 nm for erbium, which allows their determination by means of their derivative spectra. Table 1 gives the spectral characteristics of the systems.

Fig. 2 shows that the normal spectrophotometric determination for neodymium, erbium and holmium is subject to interference by other rare earths. Cerium interferes to the greatest extent.
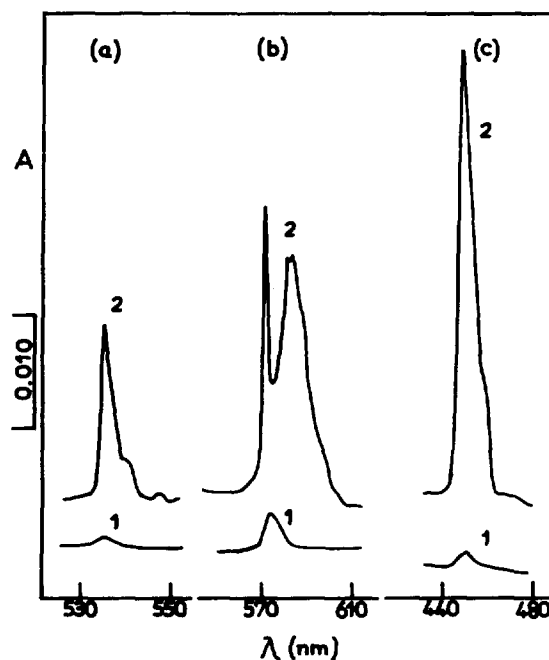
Fig. 1. Absorption spectra of ions and complexes. $[Nd] = 1.2 \times 10^{-4}$ M; $[Er] = [Ho] = 1.0 \times 10^4$ M; $[PTA] = 5.0 \times 10^{-3}$ M; $[TX-100] = 0.4\%$ v/v; pH 9.26; 4.0 cm cells. (1) Nd^{3+} (Er^{3+}, Ho^{3+}) ($LnCl_3$, pH 6.0) against water as a reference. (2) $Nd(Er, Ho)$–PTA–TX-100 against PTA–TX-100 as a reference.

Table 1
Spectral characteristics of Nd^{3+}, Ho^{3+} and Er^{3+} species in different systems

Characteristic	System						
	Nd^{3+}	Nd–PTA–TX-100		Ho^{3+}	Ho–PTA–TX-100	Er^{3+}	Er–PTA–TX-100
λ (nm)	575	572	584	450	449	523	521
ϵ (l mol^{-1} cm^{-1})	6.5	53	44.7	3.7	97	2.2	33
Spectral transition [2]	$^4I_{9/2} \rightarrow {}^2G_{7/2} + {}^4G_{5/2}$			$^5I_6 \rightarrow {}^5F_2 + {}^5F_1$		$^4I_{15/2} \rightarrow {}^2H_{11/2} + {}^4S_{3/2}$	

Therefore, in order to eliminate the interference and improve the sensitivity, the 1st–4th derivative spectra of the lanthanide complexes were investigated along with the variable measuring parameters of the instrument. It is found that the optimum instrumental conditions for neodymium, erbium and holmium proved to be the use of the third-derivative spectrum with $\Delta\lambda = 3.5$ nm, bandpass = 1.0 nm, scan rate = 50 nm min^{-1}.

Fig. 3 shows the third-derivative spectra of the representative lanthanide complexes, from which it is clear that the optimal analytical signals are at 572.2(+) and 569(−) nm for neodymium, at

513(+) and 516(−) nm for erbium and at 451.5(+) and 449(−) nm for holmium, where other lanthanides produce only constant absorption signals and cause no interference.

Fig. 4 shows the effect of pH on the absorption of the complexes. In the pH range 6.5–11.0, the highest absorption was obtained. Hence, a pH 9.26 buffer solution was chosen in subsequent experiments.

Fig. 5 shows the effect of the amount of reagent. In view of this, the amount of PTA used in the determinations was always at least 50 times that of the lanthanides present.
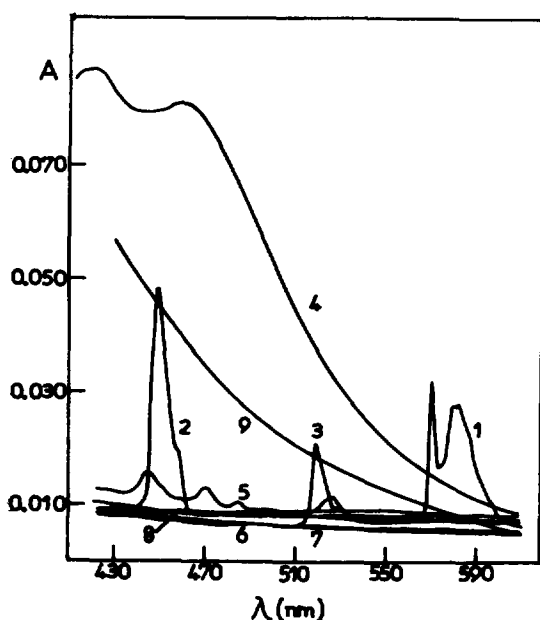
Fig. 2. Absorption spectra of complexes. $[Nd^{3+}] = 1.2 \times 10^{-4}$ M; $[Ln^{3+}] = 1.0 \times 10^{-4}$ M; other conditions as in Fig. 1, curve 2. (1) Nd; (2) Ho; (3) Er; (4) Ce(IV); (5) Pr; (6) Sm; (7) Y; (8) Eu; (9) PTA–TX-100 against water as a reference.
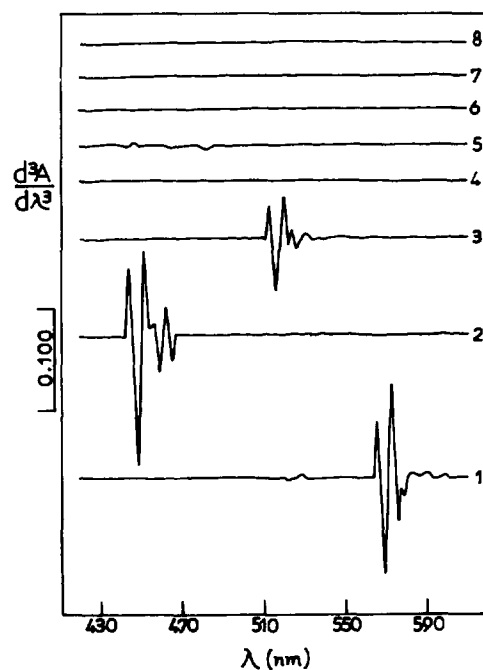
Fig. 3. Third derivative spectra of complexes. $\Delta\lambda = 3.5$ nm; bandpass = 1.0 nm; scan rate = 50 nm min^{-1}; other conditions as in Fig. 2, curves 1–8.
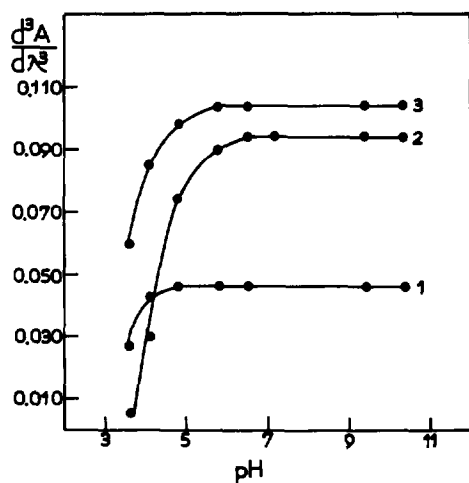
Fig. 4. Effect of pH on the third derivative absorption of the complexes. [Nd] = 6.1 × 10^{-5} M; [Er] = [Ho] = 5.0 × 10^{-5} M; instrumental parameters as in Fig. 3. Other conditions as in Fig. 1, curve 2. (1) Er peak-to-valley amplitude measurements are at 513(+) and 516(−) nm; (2) Nd peak-to valley amplitude measurements are at 572.2(+) and 569(−) nm; (3) Ho peak-to-valley amplitude measurements are at 451.5(+) and 449(−) nm.

As regards the effect of the amount of TX-100 on the absorption of the complexes, the experimental results showed that precipitation would occur at TX-100 < 0.1% v/v. Variation of the amount of TX-100 solution between 0.1 and 1.0%
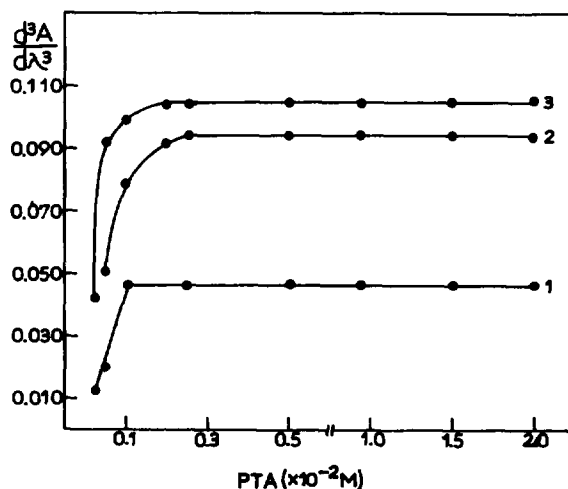
Fig. 5. Effect of PTA on the third derivative absorption of the complexes. pH = 9.26; other conditions as in Fig. 4, except for the change in the PTA concentration.

Table 2

Compositions of synthetic samples (oxides; % m/m) and analytical results

Prestent	Found[a]	RSD[b]
La 21/04, Ce(IV) 50.20, Pr 3.70, Nd 15.80, Sm 0.80,	15.40[c]	0.8[c]
Eu 0.73, Gd 1.21, Tb 0.20, Ho 1.42	3.12[d]	2.2[d]
Er 3.00, Y 2.10 Y 2.10	1.48[e]	3.0[e]
La 1.85, Ce(IV) 3.62, Pr 5.50, Nd 3.25, Sm 1.89,	3.40[c]	2.8[c]
Eu 1.13, Gd 10.27, Tb 5.78, Ho 4.22,	6.13[d]	2.4[d]
Er 6.00, Y 56.49	4.36[e]	2.8[e]

[a] Average of five determinations.
[b] $n = 5$.
[c] Result of neodymium.
[d] Result of erbium.
[e] Result of holmium.

v/v had no effect on the derivative absorption of the complexes.

The complexes formed quickly and were stable for more than 6 h.

The calibration graphs are linear up to ≈ 30 μg ml^{-1} for Nd$_2$O$_3$ and ≈ 35 μg ml^{-1} for Ho$_2$O$_3$ and Er$_2$O$_3$. The sensitivities for neodymium, holmium and erbium are 7.5, 5.5 and 6.5 times greater than those achieved with the ordinary method.

The precision of the studied methods was evaluated using ten samples, each containing 5.0 μg ml^{-1} of Nd, Er and Ho. The relative standard deviations are 1.2%, 1.6% and 1.9% for Nd, Er and Ho respectively. The detection limits (signal-to-noise ratio = 2) are 0.25 μg ml^{-1}, 0.70 μg ml^{-1} and 1.1 μg ml^{-1} for Nd, Ho and Er respectively.

In order to test the applicability of the method, two synthetic samples were prepared on the basis of the relative contents of rare earth oxides in Earth's crust [13]. The analytical results obtained are listed in Table 2.

Table 3
Analytical results of Nd, Ho and Er in the different samples (oxides; % m/m)

Present	Found[a]			
	This work	RSD[b]	XRF[c]	RSD[b]
1 La 27.11, Ce(IV) 49.21, Pr 5.18, Nd 16.75, Sm 1.29, Eu 0.23, Gd 0.40, Tb 0.03, Dy 0.09, Ho 0.023, Er 0.027, Y 0.27, Tm 0.0095, Yb 0.013, Lu 0.003	16.51[d]	1.2[d]	16.55[d]	1.4[d]
2 La 13.50, Ce(IV) 3.12, Pr 2.43, Nd 7.28,	7.19[d]	1.8[d]	7.20[d]	1.5[d]
Sm 2.31, Gd 3.44, Dy 6.10, Ho 1.63, Er 8.25, Yb 2.42, Lu 6.30, Y 20.30	8.38[e]	1.8[e]	8.22[e]	1.2[e]
	1.78[f]	2.7[f]	1.43[f]	2.1[f]

[a] Average of five determinations.
[b] $n = 5$
[c] XRF = X-ray fluorescence methods.
[d] Result of neodymium.
[e] Result of erbium.
[f] Result of holmium. 1, From Baotou Rare Earths Academy, People's Republic of China. 2, From Jiangxi Dingnan lanthanide base rock sample, People's Republic of China.

In addition, the reference material and lanthanide base samples were also analysed. The results are listed in Table 3. These show that the accuracy and precision of the method are reasonably satisfactory.

References

[1] I.G. Surin, P.K. Spitsyn and V.F. Barkovskij, Zh. Anal. Khim., 34 (1979) 1103.
[2] S. Shibata, Anal. Chim. Acta, 28 (1963) 388
[3] J. Zhao, Yejin Fenxi, 6 (1985) 54.
[4] Z.X. Yang, Fenxi Huaxue, 3 (1975) 133.
[5] I.R. Efimov and A.K. Nurtaeva, Zh. Anal. Khim., 32 (1977) 1735.
[6] J.W. Kang, R.Y. Chen and G.B. Bei, Acta. Chim. Sin., 42 (1984) 921.
[7] T. Taketatsu and C.V. Banks, Anal. Chem., 38 (1966) 1524.
[8] Y. Ren, Z.J. Lin and H.P. Zhou, Fenxi Huaxue, 13 (1985) 6.
[9] T. Taketatsu and N. Toriumi, Talanta, 17 (1970) 465.
[10] Y. Ren and P.X. Zhang, Acta. Chim. Sin., 44 (1986) 920.
[11] M.T.M. Zaki, A.F. Shouky and M.B. Hafez, Analyst, 108 (1983) 531.
[12] J.Z. Gao, J.W. Kang and G.B. Bei, Kexue Tongbao, 24 (1979) 1119.
[13] Y.E. Zeng, J.K. Cheng and Q.Y. Luo, Analytical Chemistry of Rare Earth Elements, Part I, Science Press, Beijing, 1981, p. 6.

Talanta

Determination of serum selenium by hydride generation flame atomic absorption spectrometry

Da-Qing Hao*, Guo-Hong Xie, Yi-Min Zhang, Guo-Jun Tian

Institute of Occupational Diseases, Xinxiang, Henan 453003, People's Republic of China

Abstract

Serum is rapidly digested with a mixture of nitric and perchloric acids at a temperature of $180 \pm 10°C$, and hydrochloric acid is used to reduce selenium(VI) to selenium(IV). Selenium is determined by hydride generation flame atomic absorption spectrometry. The results show that this method has the advantages of being sensitive, accurate, rapid and simple. After the serum is digested and diluted, 4.0 ml is taken for the determination. The characteristic concentration, detection limit, variation coefficient, recovery rate and linear range are 2.93 μg l^{-1}, 1.55 μg l^{-1}, 1.6–5.0%, 97.3–99.2% and 0.0–320.0 μg l^{-1} respectively. Serum at 4°C and in frozen state can be preserved for at least 7 and 14 days, respectively.

Keywords: Serum; Selenium; Hydride generation flame atomic absorption spectrometry

1. Introduction

Selenium is an essential trace element [1]. With the development of science and technology, the selenium content in serum has become an important monitoring index in clinical medicine. Selenium is not only a nutritional anticancer element [2] but also a strong antioxidant. It can suppress the effect of chemical cancerogenic substances. Selenium plays a part in the study of tumours, cancer, cardiology, liver diseases [3] and endemic diseases [4], and has received great attention in the medical field.

* Corresponding author.

Many investigators have reported the determination of serum selenium using fluorimetry, polarography [5,6], neutron activation, graphite furnace atomic absorption spectrometry [7] and hydride generation atomic absorption spectrometry. Fluorimetry is a classical method with high sensitivity, but the preprocessing of samples is prolix and laborious. Polarography is a handy method but suffers from poor reproducibility. Neutron activation and graphite furnace atomic absorption spectrometry are seldom used in the determination of serum selenium due to the volatilization loss of selenium in the measurement process. Hydride generation atomic absorption spectrometry is a sensitive and accurate method;

the detection limit of the method is in the range 1–5 ng ml^{-1}, and it is often used in the determination of selenium [8–12]. In this paper, we use a mixture of nitric and perchloric acids to digest the samples, and then use $NaBH_4$ to reduce the tetravalent selenium to H_2Se in the acidic medium. The generated H_2Se was transported into a heated quartz tube by carrier gas for atomization, and the determination of selenium was performed by using atomic absorption spectrometry at a wavelength of 196.0 nm. To prevent the loss of selenium, special attention should be paid to the conditions of digestion and reduction. We used this method to quantitatively determine the selenium content of serum. The samples were collected from various cancerous and non-cancerous patients. Some attractive results were found and are reported in this paper.

2. Experimental

2.1. Sampling, shipment and storage

Wash skin with 3% nitric acid and then 75% ethanol. Take 2 ml venous blood into a stoppered plastic tube. Store for 1 h and then centrifuge the sample at 2000 rev min^{-1} for 10 min. Remove all the serum slowly and place it in a stoppered plastic tube to be stored at a temperature of 4°C or frozen. The serum has to be mixed homogeneously before analysis.

2.2. Procedure

2.2.1. Blood blank sample
Take serum from a calf or several normal people, and mix the serum for use.

2.2.2. Sample preparation
Place 0.5 ml serum in a small weighing bottle, add 1.0 ml mixed acid, mix homogeneously and cover with a glass coverslip. Heat on an electric hot plate at 180 ± 10°C until the digested solution becomes colourless and transparent with white fumes given off; cool to room temperature. Carefully wash the coverslip into a weigh-

ing bottle with 1.0 ml of deionized water. Add 0.6 ml of concentrated hydrochloric acid, mix homogeneously and heat for 20 min without covering. Cool. Transfer the remaining solution and wash the weighing bottle several times with heated deionized water into a 10 ml test tube, dilute to volume and mix homogeneously for determination. At the same time run a reagent blank with 0.5 ml water instead of serum.

2.2.3. Calibration
Take six small weighing bottles and fill them with 0.5 ml of standard selenium solutions of different concentrations and 0.5 ml of serum blank sample. Mix homogeneously and process as for the sample.

2.2.4. Measurement
Under the working conditions of the apparatus, place 4.0 ml of solution into an atomization reaction bottle, and cover the bottle. Add a fixed amount (2.0 ml) of sodium borohydride $NaBH_4$ alkaline solution. Determine the selenium concentration of the sample by reference to the absorbance values obtained concurrently for the calibration solutions. The absorbance value of the sample is corrected by subtracting that obtained for the blank solution.

2.3. Apparatus

The following apparatus was used. A Shimadzu model AA-670 atomic absorption spectrometer, equipped with a single-slot 10 cm air–acetylene burner. A selenium hollow cathode lamp (Hebei, People's Republic of China). A model VA-90 hydride generation system with quartz tube atomizer (Tong-Ji Medical University, Wuhan, People's Republic of China). ϕ 25 × 40 mm hard glass weighing bottle. The following spectrometer conditions were used: wavelength, 196.0 nm; slit width, 0.3 nm; lamp current, 8 mA; flow rate of acetylene, 1.9 l min^{-1}; flow rate of air, 8.0 l min^{-1}; burner height, 18 mm; flow rate of argon, 0.8 l min^{-1}; measurement mode, peak height.

2.4. Reagents

All glassware and plasticware were soaked overnight in 30% (v/v) nitric acid, thoroughly rinsed with water and dried. Deionized water is used throughout. The following reagents were used: hydrochloric acid, high purity grade; nitric acid, high purity grade; perchloric acid, high purity grade; mixed acid, nitric acid and perchloric acid (1 + 1); hydrochloric acid solution, 6% (v/v); nitric acid solution, 3% (v/v); ethanol solution, 75% (v/v).

2.4.1. Sodium borohydride solution

Dissolve 0.6 g sodium borohydride (high purity grade) and 0.5 g sodium hydroxide (analytical reagent) in water and dilute to 100 ml.

2.4.2. Standard solutions

Standard solution of 100 mg 1^{-1}. Working solutions of 40.0, 80.0, 160.0, 240.0 and 320.0 μg 1^{-1} prepared by dilution of the stock solution with 6% hydrochloric acid solution before use.

3. Results

3.1. Choice of conditions for reducing selenium(VI) to selenium(IV)

While serum is being digested, quite a lot of the selenium exists in the form of selenium(VI) as a result of heating and the action of oxidizing acid. In the determination with hydride generation atomic absorption spectrometry, it is very hard to reduce selenium(VI) to hydrogen selenide by sodium borohydride. Therefore, it is necessary to reduce selenium(VI) to selenium(IV) in heated hydrochloric acid medium before hydrogenates are generated and then carry out the determination [13]. Otherwise, the determination accuracy of serum selenium will be directly affected. We added a certain amount of selenium to the samples. It was digested in the same way the samples are treated. When the samples became colourless and transparent they were taken away for cooling. 0.2, 0.3, 0.4, 0.5, 0.6. 0.7 and 0.8 ml of concentrated hydrochloric acid was added to the sam-

ples. After digesting and diluting, under the working conditions of the apparatus the absorbance values of each sample were determined repeatedly six times. When the addition of hydrochloric acid was increased from 0.2 ml to 0.4 ml, the absorbance value of the sample was obviously increased. The maximum absorbance value was reached when addition of hydrochloric acid was increased to 0.6 ml. After that the absorbance was stable with further addition of hydrochloric acid (as seen in Fig. 1). It was found that choosing the addition of hydrochloric acid as 0.6 ml did not only reduce selenium(VI) to selenium(IV), but also satisfied the acid conditions demanded in the determining process.

3.2. Choice of amount of sodium borohydride solution

Sodium borohydride reduces selenium(IV) to hydrogen selenide in acid medium. The amount of sodium borohydride will affect the sensitivity of determination directly. We prepared a mixed serum sample with a high selenium concentration. The samples were treated with the aforementioned sample preparation method and different volumes of 0.6% sodium borohydride solution were added. It was found that, after four determinations, the relevant absorbance value reached a maximum when the amount of sodium borohydride was increased to 2.0 ml. With further increase the absorbance value increased slightly (as Fig. 2 shows), but as there is a booming sound as
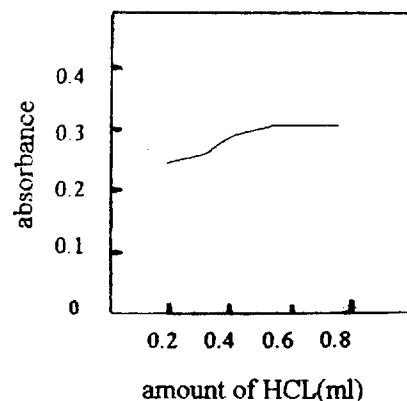
Fig. 1. Relationship between amount of hydrochloric acid and absorbance value.
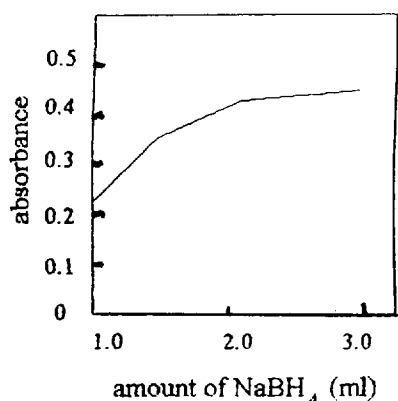
Fig. 2. Choice of amount of sodium borohydride.

a result of the high concentration of hydride in the reaction process, choosing 2.0 ml of sodium borohydride solution can satisfy the determination demand.

3.3. Choice of the flow of carrier gas

In this method, argon is used as the carrier gas to lead hydrogen selenide generated in the reaction bottle into the heated quartz tube atomizer. When the addition of hydrochloric acid is 0.6 ml, the samples are determined with the same concentration of selenium. The flow of argon was adjusted from 0.4 l min^{-1} to 1.2 l min^{-1}, when the flow rate of argon reached 0.8 l min^{-1}, the absorbance value reached a maximum. With four determinations, it was found that the result was stable and the RSD was 1.4%. Therefore, a flow of 0.8 l min^{-1} of argon was chosen.

3.4. Linear range, characteristic concentration and detection limit

Take standard selenium solutions of different concentration and 0.5 ml serum blank sample. Digest as for the samples and determine against a serum blank similarly prepared. Then carry out linear regression of the relevant concentration with the average absorbance value. When the determination range is 0.0-320.0 μg l^{-1}, the regression equation is $y = 0.0012x + 0.0056$, and the correlation coefficient is $r = 0.9994$. According to the requirement of atomic absorption spectrome-

Table 1
Precision of experiment ($n = 6$)

Addition of selenium into serum (μg l^{-1})	Absorbance value ($\bar{x} \pm s$)	RSD (%)
60.0	0.120 ± 0.006	5.0
100.0	0.170 ± 0.004	2.4
300.0	0.376 ± 0.006	1.6

try, it is found by experiment that this method's characteristic concentration is 2.93 μg l^{-1} and the detection limit is 1.55 μg l^{-1}.

3.5. Precision and method validation

3.5.1. Precision

Take serum of normal people, mix homogeneously and then into three groups. Add standard selenium solutions of different concentration; three samples with low, medium and high concentrations were prepared. Determine selenium six times. The results are shown in Table 1.

3.5.2. Method validation

Take serum of three different concentration—low, medium and high—and add different amounts of standard selenium solutions and then determine selenium six times. When the addition of selenium is 40.0-160.0 μg l^{-1}, the relevant recovery rates are 97.3-99.2%, as shown in Table 2.

3.5.3. Determination of standard matter

Cow serum standard matter (GBW 09131) from the Institute of Environmental Sanitation Moni-

Table 2
Method validation ($n = 6$)

Concentration of serum selenium (μg l^{-1})			Recovery rate (%)
Base value	Addition value	Determination value ($\bar{x} \pm s$)	
49.23	40.0	88.15 ± 2.01	97.3
81.15	80.0	160.5 ± 4.24	99.2
131.20	160.0	288.8 ± 6.66	98.5

Table 3
Preservation of samples ($n = 6$)

Preservation time (days)	4°C		Frozen	
	Determination value (μg l^{-1})	Recovery rate (%)	Determination value (μg l^{-1})	Recovery rate (%)
1	4.258	–	4.258	–
3	4.263	100.1	–	–
7	4.047	95.0	4.127	96.9
14	2.944	69.1	4.048	95.1

tor of Chinese Academy of Preventive Medicine was determined six times. The standard value was 38.9 ± 2.3 μg l^{-1}, the determination value was 37.57 ± 1.21 μg l^{-1}, and the relative deviation was -3.4%.

3.6. Interference experiment

In this method of determining serum selenium, only elements which are likely to form hydrogenates and some transition elements are likely to produce interference. In this experiment four metal ions of different concentrations are added to samples with a content of 113.2 μg l^{-1} selenium. Determinations show that 0.028 mg l^{-1} Ni^{2+}, 16.0 mg l^{-1} Fe^{3+}, 0.1 mg l^{-1} As^{3+} and 4.5 mg l^{-1} Cu^{2+} produce no interference.

3.7. Preservation of samples

Take serum from normal people and store it in two plastic bottles. Preserve at 4°C and in frozen state and determine selenium six times on the first day, the third day, the seventh day and the fourteenth day. The findings are shown in Table 3.

3.8. Applications

The method is used to determine serum selenium concentration in 101 normal people (age 19–63) and in 43 cancer patients of nine types, e.g. liver cancer, etc. The concentration of serum selenium in normal people is 81.6–140.4 μg l^{-1} (the average concentration is 97.4 μg l^{-1} and in

cancer patients it is 38.7–88.3 μg l^{-1}, average concentration (66.6 μg l^{-1}) which is remarkably lower than that of the normal people ($p < 0.001$). The serum selenium concentrations of both normal people and cancer patients correspond with those reported in the literature [14,15].

4. Discussion

A key problem in determining serum selenium is to control the digesting conditions of the samples to prevent selenium from being volatilized in the digesting process. We have compared several frequently used wet methods and decided to use the method of rapid digestion with nitric and perchloric acids. Attention should be paid to the digestion and in particular to the completion of the digestion of the samples. Preferably, digestion should be stopped when a white smoke separates from the transparent liquid. Never evaporate the samples to dryness.

As an acid medium for the sample solution, hydrochloric acid has characteristics of high sensitivity, a low blank value and good coincidence. The best hydrochloric acid concentration is decided according to the hydrogenate generation device used in the experiment.

According to the requirement of hydride generation atomic absorption spectrometry, the procedures of treating the samples and standards have to agree with each other so as to reduce errors.

After determining different types of serum samples, it is found that this method applies to sam-

ples whose basal body and selenium concentration vary greatly.

5. Conclusions

This paper has established a method for determining serum selenium by hydride generation flame atomic absorption spectrometry. When the concentration of selenium is in the range 60.0–300.0 μg l^{-1}, the RSDs are 1.6–5.0%, the recovery rates are 97.3–99.2%, the characteristic concentration is 2.93 μg l^{-1}, the detection limit is 1.55 μg l^{-1}, and the linear range of calibration is 0.0–320.0 μg l^{-1}. This method is sensitive, accurate, rapid and simple, and can satisfy the health monitoring requirements of normal persons and the clinical diagnosis of cancer patients.

References

[1] X.-R. Kong, Essential Trace Element, Science and Technology Press, Anhui, China, 1982, p. 296.
[2] G.N. Schrauzer, Foreign Med. Sci., 7 (1986) 103.
[3] Z. Wang, Stud. Trace Elem. Health, 11 (1994) 15.
[4] Z. Wang, Nutr. Rev., 38 (1980) 278.
[5] B.V. Trivedi and N.V. Thakkar, Talanta, 36 (1989) 786.
[6] T. Ferri, R. Morabito, B.M. Petronio and E. Pitti, Talanta, 36 (1989) 1259.
[7] P.-J. Li et al., Chin. J. Prev. Med., 27 (1993) 368.
[8] W. Lin et al., Phys. Testing Chem. Anal., 25 (1989) 33.
[9] Z.-X. Wang et al., Med. Anal., 5 (1985) 368.
[10] B. Welz and M. Melcher, Anal. Chem., 57 (1985) 427.
[11] J. Fairhurst et al., Anal. Chim. Acta, 197 (1987) 97.
[12] W.G. Brumbaugh and M. Walther, J. Assoc. Off. Anal. Chem., 72 (1989)484.
[13] R.-H. Mi. Spectrosc. Spectral. Anal., 13 (1993) 105.
[14] Trace Element Reference Values in Tissues from Inhabitants of the European Community, Joint Research Centre, Commission of European Communities, 1990.
[15] J. Ladon, Occupational Medicine, Appleton and Lange, Norwalk, CT/San Matec, CA, 1990, pp. 459–466.

ELSEVIER

Anion-exchange preparation of a ^{232}U radiotracer for α-particle liquid scintillation counting

Colin G. Ong*, James O. Leckie

Environmental Engineering and Science, Department of Civil Engineering, Stanford University, Stanford, CA 94305, USA

Received 7 August 1995; revised 19 September 1995; accepted 17 October 1995

Abstract

Daughter product ingrowths, which could act as analytical interferences, are removed from ^{232}U(VI) stock solutions prior to use as an α-particle emitting radiotracer in conjunction with detection by liquid scintillation counting. The preparative benchtop separation procedure employs elution with HCl through a BioRad AG1-X8 anion-exchange resin column, and fraction collection. The importance of the separation of the ^{232}U isotope from daughter products, characterized by high recovery, is illustrated by liquid scintillation energy spectra. Rapid ingrowth in the purified fraction also limits the period of time after purification in which the radiotracer is usable.

Keywords: Anion-exchange preparation; ^{232}U radiotracer; Liquid scintillation counting

1. Introduction

The environmental impact of uranyl ion UO_2^{2+}, one of several radionuclide species potentially released from a hypothetically breached radioactive waste repository [1], is being investigated with respect to ion sorption onto a variety of mineral surfaces representative of the surrounding geological material. Uranium radioisotopes in wastes likely to be stored in such a repository include ^{238}U and ^{234}U. An analytical methodology developed for experimental sorption studies involves the dosing of a mineral suspension with a radiolabelled uranyl solution principally comprising depleted naturally occurring uranium, and also containing a trace quantity of radioactive uranium which is detected with a liquid scintillation counter (LSC). ^{232}U, in the uranyl form, is employed as the radiotracer because it is artificial, and therefore absent from the depleted U solution. Daughter products in the ^{232}U stock standard solution which also emit α-particles (Fig. 1) typically have to be removed just prior to sorption experiments to eliminate interference with the ^{232}U α-particle scintillation energy spectrum during analytical detection.

* Corresponding author. Fax: 415 725 3162; e-mail: cgong@leland.stanford.edu

It has long been known that anion-exchange resins can be used with HCl eluent to effect U(VI) solution cleanup by initial selective retention followed by elution [2-4]. Empirical partition coefficients on anion-exchangers indicate that U(VI) is strongly sorbed in 9-12 M HCl, and poorly retained in 0.1 M HCl [5,6]. Cation-exchange methods [7-9] and the use of other eluents for U separation [10-12] have also been published. A recently developed anion-exchange resin, U/ TEVA (EiChrom, Darien, IL), has been applied to cleanup of U-containing solutions [13,14], but did not improve U/Th separation over prior anion-exchange resins [15].

A brief description is presented here as an update of the basic anion-exchange preparative procedure for isolating the ^{232}U isotope in aqueous HCl media, and this illustrates the successful separation with α-particle scintillation energy spectra of the eluted fractions. Previous works differ in the radioisotope (i.e. ^{238}U and ^{233}U), and analytical instrumentation (e.g. neutron activation analysis, Geiger-Muller radiometric counter, laser kinetic phosphorimetry, mass spectrometry) used.

2. Experimental

A preparative ion-exchange column was set up by packing a 0.7 cm i.d. × 10 cm length borosilicate chromatography column (Kontes, Vineland, NJ) with a slurry made up of 100 mg 100-200 mesh AG1-X8 chloride-form anion exchange resin (Bio-Rad, Richmond, CA) and MilliQ-grade distilled-deionized water. A stopcock was attached to the column outlet for flow control. The resin was conditioned for storage until use by passing through 15 ml of 0.1 N HCl in 2 ml aliquots.

$$^{232}_{92}U \xrightarrow[68.9\,y]{\alpha} {}^{228}_{90}Th \xrightarrow[1.912\,y]{\alpha} {}^{224}_{88}Ra$$

$$\alpha \downarrow 3.66\,d$$

$$^{212}_{82}Pb \xleftarrow[0.15\,s]{\alpha} {}^{216}_{84}Po \xleftarrow[55.6\,s]{\alpha} {}^{220}_{86}Rn$$
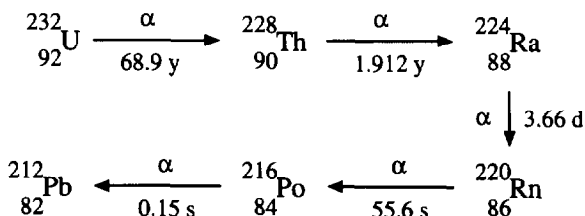
Fig. 1. The α-particle radioactive decay series of ^{232}U.

In preparation for the ion-exchange procedure, the resin was conditioned by passing through 2 ml of concentrated HCl. Unless otherwise noted, all eluents in this procedure were added in 0.5 ml aliquots to minimise upwards diffusion of solutes. 25 μl of a nominal 100 μCi ^{232}U stock solution not in equilibrium with daughters (Isotope Products Laboratories, Burbank, CA) in 0.28 ml 2 N HCl was diluted with 10 ml of 2 N HCl, to produce a lower radioactivity reagent solution for handling in regular use for the preparative ion-exchange step. 0.5 ml of the diluted ^{232}U stock (≈ 0.45 μCi) was combined with 2 ml of concentrated HCl, then passed through the resin. The outflow was collected as fraction I. The resin column was then flushed with an additional 2 ml of 0.1 N HCl. The outflow was collected as fraction II. The pH was then raised by passing through 2 ml of concentrated HCl. The outflow was collected as fraction III. The stopcock was closed. The first 0.5 ml aliquot of another 2 ml portion of 0.1 N HCl was added, and the column was allowed to stand for 15 min. The stopcock was then reopened, and the remaining 0.1 N HCl portion was passed through. Outflow was collected as fraction IV. The resin was then washed by adding 5 ml of 0.1 N HCl. Before the last 0.5 ml aliquot was added, the stopcock was closed and the cap twisted on to prevent the resin drying out.

To determine that the separation was performed satisfactorily, 50 μl of each fraction was combined with 15 ml of Ultima Gold XR scintillation cocktail (Packard Instrument Company, Meriden, CT), and analyzed on a Packard TR2500/AB Liquid Scintillation Analyzer set to CPM mode. All analyses were performed with a count time of 60 min.

3. Results and discussion

Scintillation spectra in the instrument's full scale detector range of 0-2000 keV of the collected fractions are shown in Fig. 2. It is important to note that experimentation with a variety of commercial cocktails showed that peak positions and height/width may differ. In practice, a more
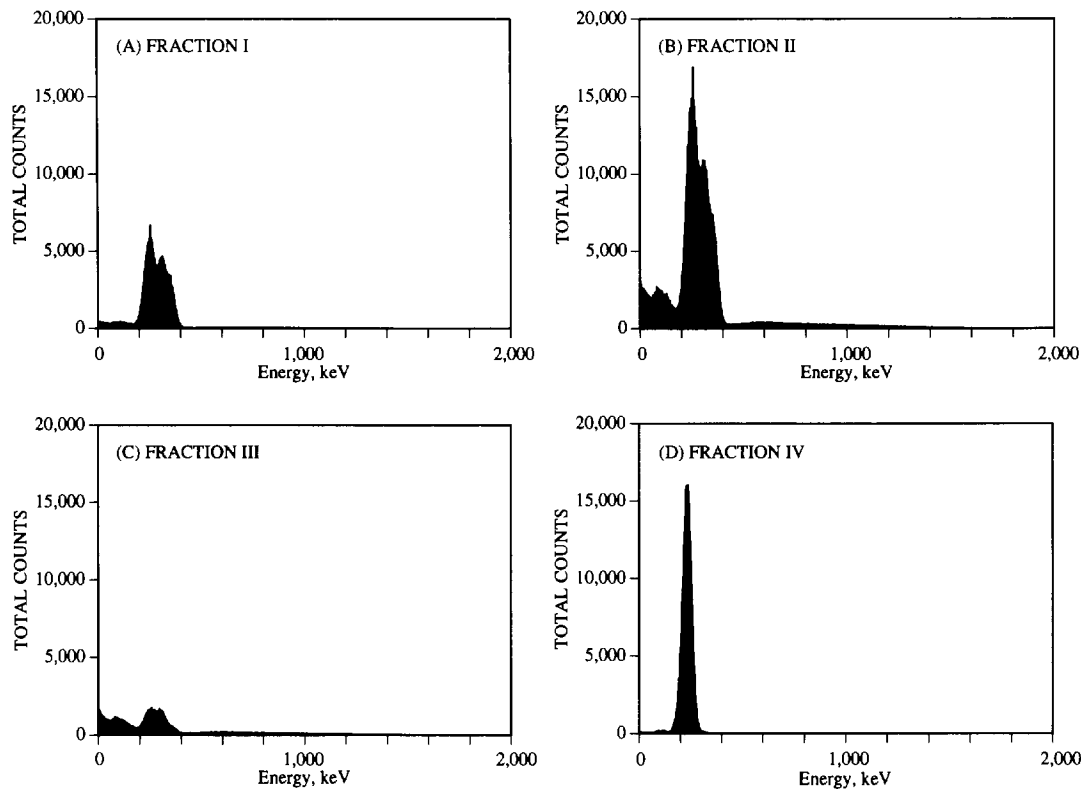
Fig. 2. Liquid scintillation counting energy spectra of fractions from ^{232}U ion-exchange separation. Total counting time = 60 min.

narrow energy window is used for counting after establishing peak variations under a range of applicable experimental conditions [16], in order to ignore remaining low energy interferences, and relatively higher energy ingrowths that may occur before actual use of the purified radiotracer.

Fraction IV, characterized by a single peak over a narrow energy range in the energy distribution spectrum, indicates the successful separation of U(VI) from daughter products. The daughter products are also shown to have been mostly eluted in fractions I and II. The relatively low profile in the fraction III spectrum indicates that little U(VI) is eluted with the first 2 ml pass of 0.1 N HCl. A trace of β activity is observed in fraction IV, but it is much less than that found in other fractions.

The activity of daughter products is comparatively significant to the ^{232}U parent activity. ^{232}U decay accounts for about 2% disintegration of the parent atoms, and the supplier reported a small

(< 1%) error in the nominal starting activity. The extent of ^{228}Th ingrowth can be estimated from the equation [17]:

$$A_{\text{Th-228}} = A_{\text{U-232(0)}}(1 - e^{-\lambda_{\text{Th-228}}t}) \tag{1}$$

where

$$\lambda = \frac{0.693}{t_{1/2}} \tag{2}$$

and λ, $t_{1/2}$, A and $A_{(0)}$ respectively represent the decay constant, half-life, activity at time t, and activity at time $t = 0$. The anion-exchange separation was performed at approximately $t = 2.1$ years, which with Eq. (1) yields a $A_{\text{Th-228}}/A_{\text{U-232(0)}}$ value of about 53%. Additionally, since the decay series comprises daughter products with decreasingly smaller half-lives, and daughter products have had adequate time to be established in detectable quantities, each ^{232}U decay is essentially manifested as five α-particle emissions. Therefore, total α-particle activity due to daughter products
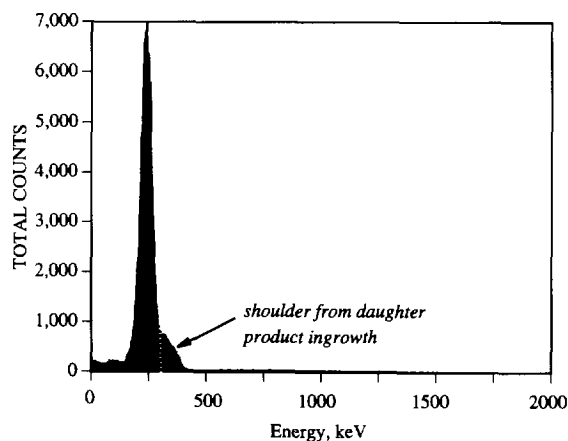
Fig. 3. Liquid scintillation counting energy spectra of ^{232}U radiotracer 2.1 months after purification.

is expected to be approximately 2.5 times greater than that of ^{232}U which is qualitatively illustrated by the data, and further iterates the importance of the preparative treatment.

To illustrate the significance of short-term ingrowth, 20 μl of fraction IV was analyzed about 2.1 months after purification. A shoulder to the ^{232}U peak is shown in Fig. 3. The ratio $A_{Th-228}/A_{U-232(0)}$ is calculated to be approximately 6%. In our isotope dilution procedure, we have typically discarded or repurified the radiotracer 1 month after purification when the calculated $A_{Th-228}/A_{U-232(0)}$ ratio is 3%.
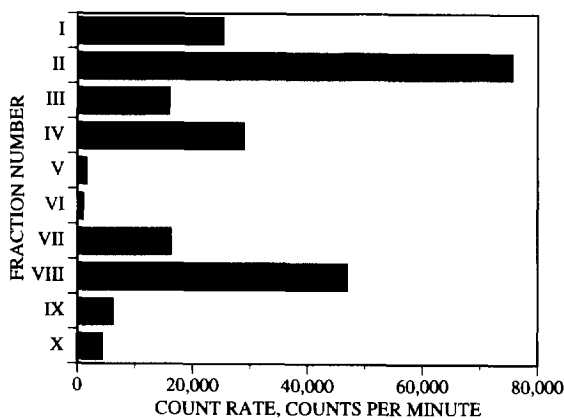
Fig. 4. Count rate data from liquid scintillation analysis of ^{232}U anion-exchange preparation fractions.

In Fig. 4, the count rates are compared for the sequence of elutions including the initial separation (fractions I–IV), a pair of 2 ml washes with 0.1 N HCl (fractions V and VI), and the separation of fraction II using the same anion-exchange procedure (fractions VII–X). From analyzing post-separation wash fractions, it was found that up to 5% may elute with each wash. The minor quantity of ^{232}U retained on the resin might be attributed to mobile phase–stationary phase partitioning. Furthermore, the repeat of the ion-exchange separation procedure with fraction II showed that up to 13% of total ^{232}U activity (or 3% of the total activity) was subject to pass-through. All of the activity of fraction II is balanced by the activities observed in fractions VII–X, illustrating recoverability of the radioactive components.

4. Conclusions

^{232}U(VI) is purified on Bio-Rad AG1-X8 anion exchange resin using HCl as the eluent. The necessity for the preparative procedure in the use of ^{232}U(VI) as a radiotracer is illustrated by liquid scintillation detection of the anlayte of interest and daughter product ingrowth interferences overlapping in the α-particle energy region. ^{232}U(VI) not recovered was either passed through the column in earlier elutions or retained by the resin due to mobile phase–stationary phase partitioning.

References

[1] K. Krauskopf, Radioactive Waste Disposal and Geology, Chapman and Hall, New York, 1988, Chapter 2.

[2] K.A. Kraus, G.E. Moore and F. Nelson, J. Am. Chem. Soc., 78 (1956) 2692.

[3] S.S. Berman, L.E. McKinney and M.E. Bednas, Talanta, 4 (1960) 153.

[4] E.S. Gladney, J.W. Owens and J.W. Starner, Anal. Chem., 48 (1976) 973.

[5] T.N. van der Walt, F.W.E. Strelow and R. Verheij, Solvent Extr. Ion Exch., 3 (1985) 723.

[6] H.A. Laitinen and W.E. Harris, Chemical Analysis, 2nd edn., McGraw-Hill, New York, 1975, Chapter 25.

[7] E.A.C. Crouch and G.B.J. Cook, Inorg. Nucl. Chem., 2 (1956) 223.

[8] F. Nelson and D.C. Michelson, J. Chromatogr., 25 (1966) 414.

[9] F. Nelson, T. Murase and K.A. Kraus, J. Chromatogr., 13 (1964) 503.

[10] Y. Sasaki, H. Takeishi, T. Adachi and K. Izawa, J. Radioanal. Nucl. Chem., 139 (1990) 143.

[11] S.J. Usuda, Radioanal. Nucl. Chem., 123 (1988) 619.

[12] F.W.E. Strelow, Talanta, 35 (1988) 385.

[13] E.P. Horwitz, M.L. Dietz, R. Chiarizia, H. Diamond, S.L. Maxwell III and M.R. Nelson, Anal. Chim. Acta, 310 (1995) 63.

[14] J.J. Hines, H. Diamond, J.E. Young, W. Mulac, R. Chiarizia and E.P. Horwitz, Sep. Sci. Technol., 30 (1995) 1373.

[15] A.G. Adriaens, J.D. Fassett, W.R. Kelly, D.S. Simons and F.C. Adams, Anal. Chem., 64 (1992) 2945.

[16] C.G. Ong, A. Prasad and J.O. Leckie, Anal. Chem., 67 (1995) 3893.

[17] W.D. Ehmann and D.E. Vance, Radiochemistry and Nuclear Methods of Analysis, Wiley-Interscience, New York, 1991, Chapter 5.

Estimation of the ionization pK_a of pharmaceutical substances using the computer program SPARC

S.H. Hilal[a], Y. El-Shabrawy[b], L.A. Carreira[c,*], S.W. Karickhoff[a],
S.S. Toubar[b], M. Rizk[b]

[a]*Environmental Research Laboratory, U.S. Environmental Protection Agency, Athens, GA 30605, USA*
[b]*Department of Analytical Chemistry, Faculty of Pharmacy, University of Mansoura, Mansoura 35516, Egypt*
[c]*Department of Chemistry, University of Georgia, Athens, GA 30602, USA*

Abstract

The computer program SPARC was used to calculate the pK_a values of some important pharmaceutical substances. The SPARC models proved to be suitable for estimating the pK_a values of beta-adrenergic blocking agents and benzodiazepine drugs. Ionization macroconstants, microconstants, zwitterionic equilibria, speciation curves as a function of the pH and the isoelectric points of a semi-essential amino acid, arginine, and an anti-inflammatory, niflumic acid, were calculated.

Keywords: SPARC computer program; pK_a; Pharmaceuticals

1. Introduction

Knowledge of the aqueous ionization of a substance is of great importance in drug design and environmental regulatory compliance in the pharmaceutical industry. For example, the pK_a value of a compound controls many aspects of drug metabolism, including the fate of the drug in the body and transport through membranes which are frequently permeable only to a particular species. In chemistry, pK_a values can be used to select conditions for synthesis by considering the effects of pH on reaction products and on the properties of postulated intermediates that may not be measurable. The pK_a values may also assist in the interpretation of pH titration curve measurements where multiple acidic and/or basic sites are present.

With sensitive electrodes, potentiometric measurements can be a rapid technique for the determination of pK_a, provided that the solubility of a substance is at least 10^{-5} M. If the substance is less soluble than this but possesses an analytically useful chromophore, then spectroscopic methods can be employed. When solubilities become extremely low, below 10^{-6}, experimental determination of many physical/chemical properties becomes difficult. In such cases, calculation

* Corresponding author. Fax: + 706-542-9454.

schemes may become the best alternative to characterize thermodynamic properties including ionization pK_a.

Recently, we have developed mathematical models for predicting chemical reactivity parameters and physical properties of a wide range of organic compounds using SPARC [1–5] (SPARC Performs Automated Reasoning in Chemistry). SPARC uses computational algorithms based on fundamental chemical structure theory to estimate ionization pK_a values of a wide range of molecules strictly from their molecular structure. SPARC predictive methods are based on a blending of the well-known, established methods of linear free energy reltionships [6] (LFER) and perturbed molecular orbital theory [7] (PMO). In general, SPARC utilizes LFER to compute thermodynamic or thermal properties and PMO theory to describe quantum effects such as delocalization energies or polarizabilities of π electrons. In reality, every chemical property involves both quantum and thermal contributions and necessarily requires the use of both of these methods for prediction.

2. Calculation of ionization pK_a

The details of the SPARC pK_a computational methods were presented in previous publications [1–5] and hence only a brief description will be given here. SPARC seeks to analyze chemical structure relative to a specific reactivity query in much the same manner as an expert chemist would. Molecular structures are factored into functional units called reaction center and perturber. The reaction center, C, is the smallest subunit that has the potential to ionize and lose a proton to the solvent. The perturber, P, is the molecular structure appended to the reaction center, C. The perturber structure is assumed to be unchanged in the reaction. The pK_a value of the reaction center is either known from direct measurement or is inferred indirectly from pK_a measurements. The pK_a of the reaction center is adjusted for the molecule in question using the mechanistic perturbation models described previ-

ous [1–4]. The pK_a value for a molecule of interest is expressed in terms of the contributions of both P and C.

$$pK_a = (pK_a)_C + \delta_P(pK_a)_C \qquad (1)$$

where $(pK_a)_C$ describes the ionization behaviour of the reaction center, and $\delta_P(pK_a)_C$ is the change in ionization behaviour brought about by the perturber structure. SPARC computes reactivity perturbations, $\delta_P(pK_a)_C$, which are then used to "correct" the ionization behaviour of the reaction center for the compound in question in terms of potential "mechanisms" for interaction of P and C as

$$\delta_P(pK_a)_C = \delta_{ele}(pK_a)_C + \delta_{res}(pK_a)_C + \delta_{solv}(pK_a)_C$$
$$+ \delta_{H-bond}(pK_a)_C \qquad (2)$$

where $\delta_{res}(pK_a)_C$, $\delta_{ele}(pK_a)_C$, $\delta_{sol}(pK_a)_C$ and $\delta_{H-bond}(pK_a)_C$ describe the differential resonance, electrostatic interaction, solvation and H-bonding of P with the protonated and unprotonated states of C respectively. Electrostatic interactions are derived from local dipoles or charges in P interacting with charges or dipoles in C. δ_{res} describes the change in the delocalization of π electrons of the two states due to P. H-bonding and solvation effects are derived from interactions of the structural elements of P that are contiguous to C with the two states through H-bonding or steric blockage of solvent access to C respectively.

Resonance effect models (including steric twisting and its impact on the π-resonance integrals) were developed and calibrated on light absorption spectra using PMO theory [4,7]. Electrostatic, solvation and H-bonding models were developed and calibrated using ionization pK_a values based on both LFER and PMO theory. These reactivity models have been used to estimate both ionization pK_a and electron affinity for a large number of molecular structures [2–5]. More recently, the SPARC pK_a calculator was rigorously tested on 4338 pK_a values for some 3685 compounds including multiple pK_a values up to the eight pK_a spanning a range of over 30 pK_a units [5]. The RMS deviation for this large set of values was found to be 0.37 pK_a units.

3. Results and discussion

Although β-adrenergic blockers were originally developed for the treatment of angina pectoris, they have numerous other clinical applications for the treatment of hypertension, arrhythmia, thyrotoxicosis, hypertrophic cardiomyopathy, migraine and glaucoma. According to Perrin et al. [8], beta-blockers are ionized and are not absorbed through the stomach. In the intestine, the pH is elevated and this will promote the absorption of these drugs. β-blockers are classified into two major groups according to their chemical structure: (i) amino alcohol derivatives such as amosulalol, bufuralolol, nifenalol and sotalol with the general structure

$$\underset{\substack{| \\ R_1CHCH_2NHCH}}{OH} \underset{\substack{\diagdown \\ R_3}}{\overset{\diagup R_2}{}}$$

I
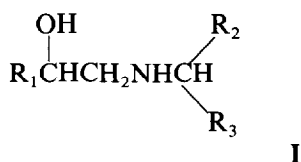
(ii) phenylethers with amino-2-propanol such as propranolol, pindolol and practolol, with the general structure:

$$\underset{\substack{| \\ R_2OCH_2CHCH_2NHCR_1}}{OH} \underset{\substack{\diagdown \\ CH_3}}{\overset{\diagup CH_3}{}}$$

II
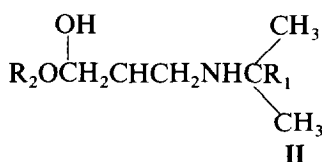
The pK_a value for the OH group in both structures is greater than 14 and is of less importance to this study. The acid–base characteristics of these chemical structures are mainly due to the ionization of the N atom in the N-terminal isopropyl group, which is necessary for the pharmacological action. The pK_a values for structures I and II (R = H) are 10.1 and 9.7 respectively. The $(pK_a)_C$ value of the N atom $(pK_a$ for ammonia including statistical correction of 0.6 (log 4) where there are four equivalent ionizable H sites and only one protonation site) is 9.2 and the perturbations in both structures are relatively small. Sigma induction from the two hydrophilic groups attached to the N atom tend to raise the pK_a while differential solvation effects tend to lower the pK_a. Direct electrostatic interaction of the dipole mo-

ment of the OH and ROR' groups will stabilize both the structures, making each one more acidic. For all the β-adrenergic blockers shown in Table 1 the pK_a values range from 8.9 to 10.1 depending on the strength of the dipole moment of the substituents in the structure R. The case for prizidilol is somewhat more complicated. There are five basic ionizable sites (three aliphatic N groups and two in-ring N groups) and one acidic–OH site. There are four major distinguishable microscopic species (concentration above 1%) between pH 2 and 12, as shown in Fig. 1. At pH values greater than 9.1 and less than 14 the prizidilol exists in solution as a neutral. At pH values below 9 the N atom begins to protonate. Below pH 4.6, both the in-ring N atoms start to convert from the basic to the acidic form.

The benzodiazepine drugs have hypnotic, tranquillizing, anticonvulsant and anxiolytic properties. The main chemical characteristic of bezodiazepines is the presence of a benzene ring fused with a seven-member ring with nitrogen atoms at the 1 and 4 positions. The acid–base properties of benzodiazepines are due to the nitrogen atom in position 4 (=N). The structural formula and calculated/observed pK_a values of some benzodiazepines are given in Table 2. These compounds have a low pK_a value and can be absorbed rapidly from the gastrointestinal tract to the blood where they become un-ionized. Such compounds are usually administered orally. However, if very rapid action is required they can be administered by intravenous injection.

4. Zwitterionic equilibria

There is not a huge body of literature on zwitterionic equilibria constants of drugs, although many molecules contain both acid and base functionality where both the base and the acid sites may be simultaneously ionized to form an internal salt. These substances are referred to as zwitterionic. At low and high pH, the cationic species and anionic species predominate respectively. The internal salt predominates as an intermediate over a wide range of pH. Actually, the zwitterion and the uncharged molecule are in equilibrium in
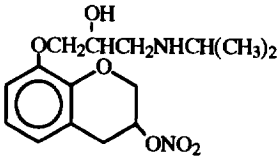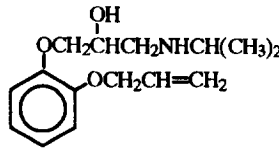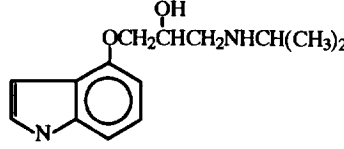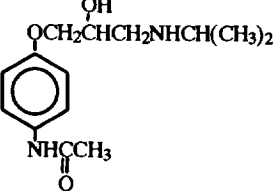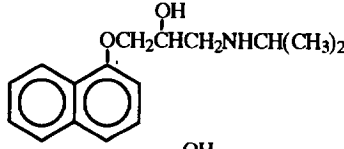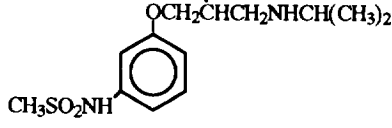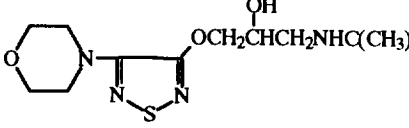
Table 1

Ionization pK_a values of the beta blockers in aqueous media

Structure	Name	Calc.	Obs.[a]
$CH_3CH_2CH_2CONH$—(ring, COCH$_3$)—$OCH_2CHCH_2NHCH(CH_3)_2$, OH	Acebutolol	9.2	9.4
(ring, CH$_2$CH=CH$_2$)—$OCH_2CHCH_2NHCH(CH_3)_2$, OH	Alprenolol	9.3	9.5
CH_3—(ring, SO$_2$NH$_2$)—$CHCH_2NHCH_2CH_2O$—(ring, OCH$_3$), OH	Amosulalol	10.1	10.2
NH_2COCH_2—(ring)—$OCH_2CHCH_2NHCH(CH_3)_2$, OH	Atenolol	9.4	9.6
CH_3—(ring)—$OCH_2CHNHCH_2CH_2$—(ring, OCH$_3$, OCH$_3$), OH	Bevantolol	8.9	·····
(indole ring, N, CH$_3$)—$OCH_2CHCH_2NHC(CH_3)_3$, OOCC$_6$H$_5$	Bopindolol	9.0	·······
(coumarin ring, CH$_3$)—$OCH_2CHCH_2NHC(CH_3)_3$	Bucumolol	9.1	·······
(benzofuran ring, CH$_2$CH$_3$)—$CHCH_2NHC(CH_3)_3$, OH	Bufuralol	9.2	·······
(tetrahydrofuran–CH$_2$O–ring)—$OCH_2CHCH_2NHC(CH_3)_3$, OH	Bufetolol	9.3	·······

Table 1 (contd.)

Structure	Name	Calc.	Obs.[a]
	Bupranolol	9.4	.....
	Butofilolol	9.2	....
	Carazolol	9.4	.....
	Carbuterol	9.1	......
	Esmolol	9.4	....
	Labetalol	9.0	....
	Mepindolol	9.3	....
	Nadolol	9.5	9.7
	Nifenalol	9.0	....

Table 1 (contd.)

Structure	Name	Calc.	Obs.[a]
OH OCH₂CHCH₂NHCH(CH₃)₂ ... ONO₂ structure	Nipradilol	9.2	....
OH OCH₂CHCH₂NHCH(CH₃)₂ ... OCH₂CH=CH₂ structure	Oxprenolol	9.4	9.5
OH OCH₂CHCH₂NHCH(CH₃)₂ ... indole structure	Pindolol	9.5	....
OH OCH₂CHCH₂NHCH(CH₃)₂ ... NHCCH₃ O structure	Practolol	9.4	....
OH OCH₂CHCH₂NHCH(CH₃)₂ ... naphthalene structure	Propranolol	9.4	9.5
OH OCH₂CHCH₂NHCH(CH₃)₂ ... CH₃SO₂NH structure	Sotalol	9.4	9.8
OH OCH₂CHCH₂NHC(CH₃)₃ ... morpholine/thiadiazole structure	Timolol	8.9	....

[a] Observed values are from Ref. [14,15].

aqueous solution. In such cases, the ionization macroconstants which describe the overall acidity or basicity of these molecules cannot be assigned to individual species or fully describe such an

equilibrium. However, the microscopic constants are the equilibrium constants for equilibria involving individual species in solution. When two or more such species exist in solution, the micro-
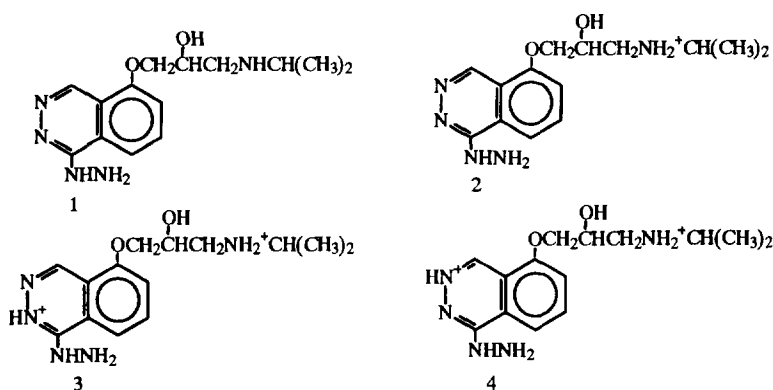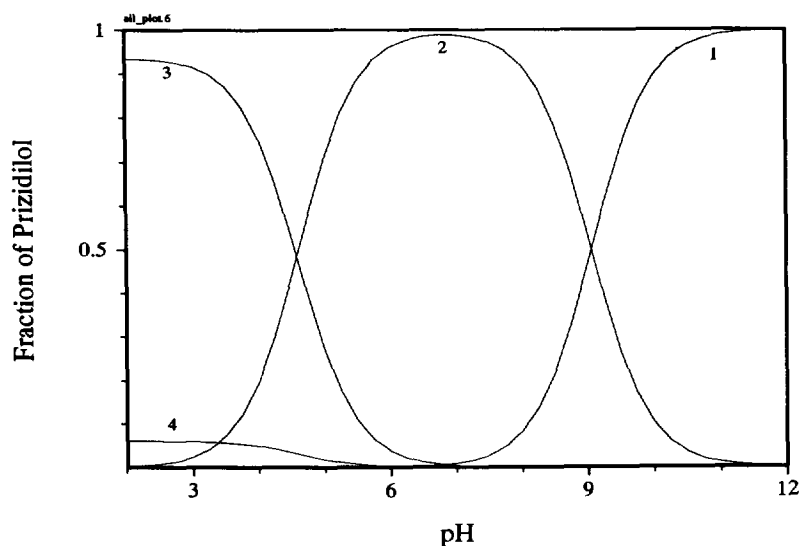
Fig. 1. The fraction of the four major microscopic species of prizidilol between pH 2 and 12. The ionization of the OH group and any pK_a values < 2 were neglected (see text).

scopic constants may not be able to be determined distinctly. These constants provide informtion on the individual proton-binding sites and their interactions with other sites in the molecule. Thus, microconstants are the proper terms for exact characterization of both the speciation and basicity/acidity of multiple acidic/basic ligands. Estimation of these microconstants is useful in calculating the pH-dependent concentrations of the different microspecies, and in the calculation of zwitterionic equilibria.

Niflumic acid is a potent drug used in the treatment of inflammatory and rheumatic disor-

ders. The molecule contains three possible ionizable sites: two basic sites (in-ring N, NH_2) and the acidic CO_2H site. There are 12 possible microscopic species or states. Table 3 shows the observed vs. SPARC calculated microscopic and macroscopic constants for niflumic acid. The notation for the microconstants follows the scheme first proposed by Hill [9] and is shown in Fig. 2. The ionizing group of interest is indicated in the microscopic pK by the last number in the subscript. Any numbers preceding this in the subscript denote other groups in the molecule which already exist in the basic form when the ionization

S.H. Hilal et al. / Talanta 43 (1996) 607–619

Table 2

Ionization pK_a values of benzodiazepines in aqueous media
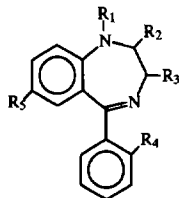
Molecule	R1	R2	R3	R4	R5	SPARC	Obs.[a]
Medazepam	Me	H	H	H	Cl	5.05	4.4–6.2[b]
Diazepam	Me	=O	H	H	Cl	3.02	3.4
Nitrazepam	H	=O	H	H	H	2.58	3.2
Flurazepam	$C_2H_4NEt_2$	=O	H	F	Cl	1.82	2.00
Flunitrazepam	Me	=O	H	F	NO_2	2.35	1.80
Clonazepam	H	=O	H	Cl	NO_2	2.30	1.57
Oxazepam	H	=O	OH	H	Cl	1.70	1.70
Lormetazepam	Me	=O	OH	Cl	Cl	0.92	1.30
Lorazepam	H	=O	OH	Cl	Cl	0.97	1.00
7-Aminonitrazepam	H	=O	H	H	NO_2	3.62	4.51
7-Acetamidonitrazepam	H	=O	H	H	$NHCOCH_3$	3.00	3.20
7-Aminoflunitrazepam	Me	=O	H	F	NO_2	3.44	3.55
N-1-Desalkylflurazepam	H	=O	H	F	Cl	2.79	2.57
Delorazepam	H	=O	H	Cl	Cl	2.70	2.17
Fludiazepam	Me	=O	H	F	Cl	2.58	2.22
Nimetazepam	Me	=O	H	H	NO_2	2.58	2.63
Nordazepam	H	=O	H	H	Cl	3.10	3.48

[a] Observed values are from Ref. [15–17]

[b] Protonation of NH_2 not =N

under consideration is taking place. Thus pK_{23} denotes the pK value for the ionization of the in-ring N group when the NH_3^+ group has already been converted to the conjugate base, NH_2. Since the number 1 does not appear in the subscript 23, its absence denotes that group 1, the carboxyl, is still in the un-ionized form for the reaction in question. Only four of the eight possible microscopic species (indicated by an asterisk in Fig. 2) have appreciable concentration in the pH range between 0–10 as shown in Fig. 3. Hence, only four microscopic constants are needed to describe the equilibria as was suggested by Takacs-Novak et al. [10]. The zwitterionic equilibrium constant, k_{zw}, may be determined using the left or right path of the cycle of the major species in Fig. 2. Since both thermodynamic paths give the same zwitterion product, k_{zw} may be expressed as a function of the microscopic con-

stants within any loop as

$$K_{zw} = \frac{K_{23}}{K_{21}} = \frac{K_{123}}{K_{231}} \tag{3}$$

The integrity of the SPARC pK_a calculator can be checked by calculating k_{zw} using the two different loops. For niflumic acid, pK_{zw} is found to be 1.3 and 1.4 for the first and second paths respectively. k_{zw} values calculated from different thermodynamic paths ($pK_{zw} = 1.36$).

The fraction of each of the microscopic species formed by a molecule of interest with multiple ionizable sites can be expressed as function of pH in terms of the microconstants. If we start from the neutral species (uncharged species) rather than from the positively charged species, the fraction of any microscopic species for a molecule having N ionizable sites can be expressed in general as $D_{ij\cdots k}/D$ where D can be expressed as
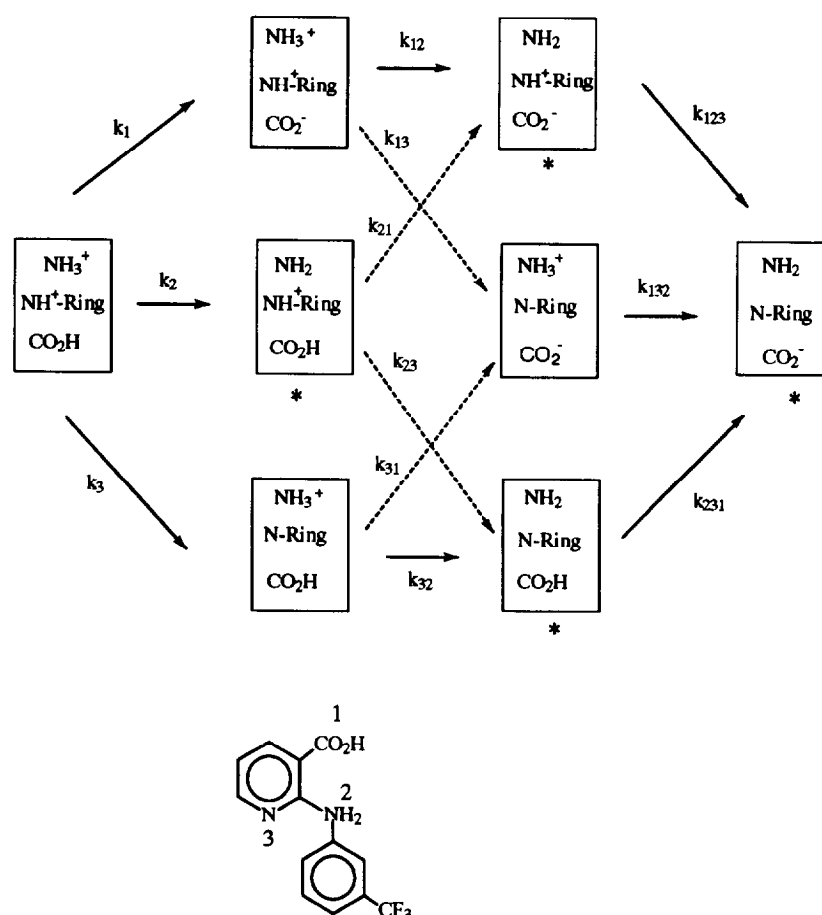
Fig. 2. The eight microscopic states of niflumic acid and the 12 ionization constants which interrelate them. Asterisks identify the four major microscopic species.

$$D = \frac{1}{0!} + \frac{\sum_i k_i[H]^{L_i}}{1!} + \frac{\sum_i \sum_{j \neq i} k_i k_{ij}[H]^{L_{ij}}}{2!} + \ldots + $$

$$\times \frac{\sum_i \sum_{j \neq i} \cdots \sum_{k \neq i,j} k_i k_{ij} \ldots k_{ij \cdots k}[H]^{L_{ij \cdots k}}}{N!} \qquad (4)$$

where $L_{ij \cdots k}$ is the charge of the final state ($ij \cdots k$ state). The factorial is the number of different thermodynamic paths that lead to the $ij \cdots k$ state and $D_{ij \cdots k}$ is one of the terms in the denominator. For example, the fraction of neutral species would be $1/D$ and the fraction of a singly ionized species would be $k_i[H]^{L_i}/D$.

In addition, the isoelectric point can be estimated by plotting the fraction of neutral or zwit-

terionic species versus pH. The pH at the middle of the zwitterionic (or any other species where the total net charge of the molecule is zero) range is the isoelectric point. At the isoelectric point more than 90% of the niflumic acid exists in solution as a zwitterion. Because of this niflumic acid can be absorbed rapidly and distributed well in the body.

Arginine is a semi-essential amino acid which plays an important role in the binding of proteins, and as a metal-complexing agent. Due to its biological significance, the acid–base properties of arginine have been studied in detail [11]. It has five different ionizable sites: an acidic CO_2H site, a basic =N site and three NR_2 groups acting as a base (NR_2 as an acid was not ionized). Since each of the five groups may exist in either the acidic or basic state, there are 32 possible microscopic spe-

Fig. 3. Fraction of the four major microscopic species of niflumic acid as a function of pH: (1) the neutral species; (2) negatively charged species; (3) zwitterionic species; (4) positively charged species.

cies or states. The most positive of these 32 states is the cation, with net charge $z = +3$; the most negative is the anionic species, with $z = -1$. Each of the ionizable groups in arginine is characterized by 16 microconstants, since the tendency of each group to accept or donate a proton depends on the ionization state of the other four groups. Hence, there are 80 microscopic ionization constants connecting the 32 possible microscopic species.

SPARC calculates the 80 microconstants required to describe the fraction (population) of the varius microscopic species. Only four of the 32 possible microscopic species are calculated to have appreciable concentration (above 1%) in the pH range 0–15. The fraction of each of these microscopic species as a function of pH is shown in Fig. 4. At pH > 15 all five sites are completely ionized and the arginine is negatively charged. At pHs between 15 and 8.5 arginine exists in solution as a zwitterionic species where both the =N and CO_2H groups are simultaneously charged positively and negatively respectively. In addition, the titration curve (charge curve) in Fig. 5 can be determined by multiplying the fraction-species curve by the charge on the species and summing over all species.

The observed vs. SPARC-calculated ionization macroconstants of arginine are shown in Table

3. The estimated ambiguity of the observed values according to Noszal and Kassai-Tanczos [11] is 0.02–0.06 log K units except for the pK_1 value of arginine which was estimated to be 15 at $I = 2.0$ M, where the measurement error is 0.1–0.2 pK units. Although the measurement error may be as small as 0.2 pK_a units we believe that the ionic strength perturbation may make the actual error much larger and that it can be as high as 1.1 pK_a units for pK_1. It is expected that pK_1 would be higher than the pK_a value for guanidine (13.6 [12,13]), H_2NC (=NH) NH_2, by only a few tenths of a pK_a unit. The dipole field effect of the NH_2 group in the structure $(CH_2)_3C(NH_2)CO_2^-$ should stabilize arginine and make it more acidic than guanidine while the CO_2-charge field effect will raise the pK_1 value. For example, compare the pK_a values at 25°C for 3-hydroxybenzoic acid (10.2) and 3-hydroxyaniline (9.8), where the OH group is the ionizable site, to that of phenol (10.0). At a distance of separation r between the guanidine group and the CO_{2-}/NH_2 groups in the arginine, the effect of CO_{2-} will definitely oercome the effect of NH_2 because charge field effects depend on $1/r$ while the dipole field effect is $1/r^2$ (see Refs. [3, 4]). Because r is so large both effects are small and pK_1 is more basic than the pK_a value for guanidine by only a few tenths. In addition, pK_C^G, where the arginine is in the neu-
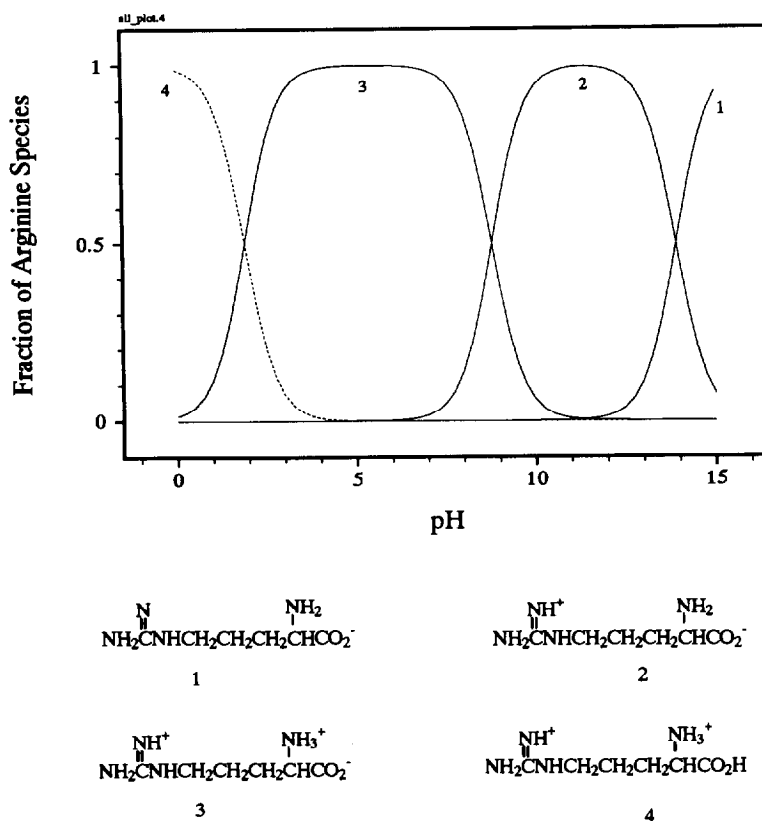
Fig. 4. Fractions of the four major microscopic species of arginine as a function of pH. The four major microscopic species are shown below the plots.

tral state (see Ref. [11]), is certainly expected to be lower than the pK_a value of guanidine because of the field effects of both dipole groups (CO_2H and NH_2) and not higher as reported by Noszal and Kassai-Tanczos [11]. Finally, the macroscopic pK_a ranges in all the other reported measurements [11], 11.5–12.6, 8.8–9.3 and 1.9–2.2 for pK_1, pK_2 and pK_3 respectively, are lower than their measured pK_a values. Even the upper limit of this range for pK_1 is still much lower than 15. Because of this, calculated values for pK^G_C, pK^G_{AC}, pK^G_A and pK^G of the =N group for the neutral, NH_3^+, NH_3^+/CO_2^- and CO_2^- species are expected to be higher than the actual values.

5. Summary

In this paper we applied the SPARC computational algorithms to estimate ionization pK_a values of several important pharmaceutical substances. The SPARC technique allows the calculation of all the microscopic ionization constants for complex molecules. The ability to calculate these microconstants allows this technique to calculate complex speciation as a function of pH. From this complex speciation several other important physical properties such as zwitterionic equilibrium constants and isoelectric points can be extracted.
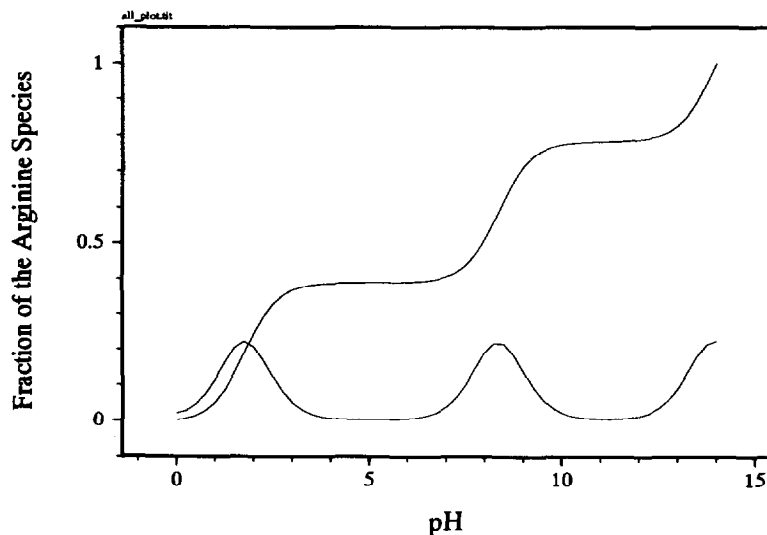
Fig. 5. Titration curve for arginine (top) and its derivative (bottom). The three macroscopic pK_a values are shown in the bottom curve.

Table 3
(a) Ionization of Microconstants of Niflumic Acid and Arginine

pK	Niflumic acid		pK	Arginine	
	SPARC[a]	Obs. [10][b]		SPARC	Obs. [11][b]
pK_1	0.4	–	pK^G	14.0	15.0
pK_{12}	<0	–	pK^A	9.23	9.51
pK_{123}	4.4	4.41	pK^C	3.95	4.48
pK_{231}	2.8	3.18	pK_A^G	13.2	14.8
pK_{13}	<0	–	pK_C^G	13.5	14.9
pK_{132}	<0	–	pK_G^A	8.32	9.30
pK_2	<0	–	pK_{GA}^C	1.73	2.14
pK_{21}	1.8	2.28	pK_C^A	8.00	7.33
pK_{23}	3.2	3.52	pK_G^C	3.70	4.35
pK_3	<0	–	pK_A^C	2.01	2.30
pK_{31}	1.4	–	pK_{AC}^G	12.7	14.7
pK_{32}	<0	–	pK_{GC}^A	7.02	7.12

[a] Ionization forms of the corresponding constants as shown in Fig. 2.
[b] Observed values of niflumic acid were determined by NMR, while the observed values for arginine were determined by potentiometric titration.

Table 3
(b) Ionization macroconstants, Isoelectric Points and Zwitterionic Constants of Arginine and Niflumic Acid at 25°C

pK	Niflumic acid		Arginine	
	SPARC	Obs. [10]	SPARC	Obs. [11]
pK_1	4.31	4.44	13.9	11.4–15
pK_2	1.80	2.26	8.80	8.8–9.4
pK_3	–	–	1.90	1.8–2.2
pK_{zw}	1.39	1.36	7.90	–
Isoelectric point	3.01	3.30	11.40	–

Acknowledgements

References

[1] S.W. Karickhoff, V.K. McDaniel, C.M. Melton, A.N. Vellino, D.E. Nute and L.A. Carreira, Environ. Toxicol. Chem., 10 (1991) 1405.

[2] S.H. Hilal, L.A. Carreira, C.M. Melton and S.W. Karickhoff, Quant. Struct. Act. Relat., 12 (1993) 389.

[3] S. Hilal, L.A. Carreira, C.M. Melton, G.L. Baughman and S.W. Karickhoff, Phys. Org. Chem., 7 (1994) 122.

[4] S.H. Hilal, L.A. Carreira and S.W. Karickhoff, in P. Polizer and J.S. Murray (Eds.), Quantitative Treatment of Solute/Solvent Interactions: Theoretical and Computational Chemistry, Vol. 1, Elsevier, Amsterdam, 1994, Chapter 9.

[5] S.H. Hilal, L.A. Carreira and S.W. Karickhoff, Quant. Struct. Act. Relat., 14 (1995) 348.

[6] L.P. Hammett, Physical Organic Chemistry, 2nd edn., McGraw-Hill, New York, 1970.

[7] M.J.S. Dewar, The Molecular Orbital Theory of Organic Chemistry, McGraw-Hill, New York, 1969.

[8] D.D. Perrin, B. Dempsey and E.P. Serjeant, pK_a Prediction for Organic Acids and Bases, Chapman and Hall, New York, 1981.

[9] T.L. Hill, J. Phys. Chem., 101 (1944) 48.

[10] K. Takacs-Novak, A. Avdeef, K.J. Box, B. Podanyi and G. Szasz, J. Pharm. Biomed. Anal., 12 (1994) 1369.

[11] B. Noszal and R. Kassai-Tanczos, Talanta, 38 (1991) 1439.

[12] A. Albert and E.P. Serjeant, The Determination of Ionization Constants, 3rd edn., Chapman and Hall, New York, 1984.

[13] D.D. Perrin, Dissociation Constants of Organic Bases in Aqueous Solution, Butterworths, London, 1965.

[14] W. Martindale, The Extra Pharmacopoeia, 29th edn., The Pharmaceutical Press, London, 1989.

[15] J. Barbosa, D. Barron and Ma. E. Torrero, Analusis, 19 (1991) 1.

[16] J. Barbosa and V. Sanz-Nebot, Talanta, 36 (1989) 837–842.

[17] L.A. Berrueta, B. Gallo and F. Vicente, J. Pharm. Biomed. Anal., 10 (1992) 109–136.

Talanta

Formation of dinuclear copper(II) complex with N,N,N',N'-tetrakis(2-pyridylmethyl)-1,2-ethanediamine in aqueous solution

Naoki Hirayama[a,*], Shinji Iimuro[a], Koji Kubono[b], Hisao Kokusen[c], Takaharu Honjo[a]

[a]Department of Chemistry, Faculty of Science, Kanazawa University, Kakuma-machi, Kanazawa 920-11, Japan
[b]Department of Living Science, Shohoku College, Nurumizu, Atsugi 243, Japan
[c]Department of Chemistry, Faculty of Education, Tokyo Gakugei University, Nukui-Kita-machi, Koganei 184, Japan

Abstract

The polynuclear complexation of divalent 3d transition metal cations with N,N,N',N'-tetrakis(2-pyridylmethyl)-1,2-ethanediamine (tpen) in aqueous solution was investigated. It was found that copper(II) forms a dinuclear complex with tpen in an aqueous solution containing chloride. The composition of the complex was determined as $Cu_2Cl_2(tpen)^{2+}$. Furthermore, the stability constant of the complex was determined and its structure was postulated to be $(\mu\text{-Cl})_2$.

Keywords: Polynuclear complexation; Transition metal cations; Copper(II); Tpen

1. Introduction

The formation of stable charged complexes of metal cations with multidentate ligands in aqueous solution is very effective as a pretreatment method for separation and determination of the cations by capillary electrophoresis [1–8] or ion-interaction chromatography [9–16]. However, it is well known in the field of inorganic chemistry that the cations and ligands often form polynuclear complexes. These complexes can be regarded

as by-products and interfere with the determination of the cations using the formation reaction of mononuclear complexes. Therefore, to be able to use these mononuclear complexation reactions analytically it is very important to obtain information concerning the polynuclear complexations, such as stability constants.

N,N,N',N' - Tetrakis(2 - pyridylmethyl) - 1,2 - ethanediamine (tpen) [17] is an uncharged sexadentate ligand. This ligand forms very stable charged complexes with many divalent transition metal cations in aqueous solution [18], but it sometimes acts as a pentadentate ligand [18]. Although the

* Corresponding author. Fax: (81) 762-64-5742.

only analytical use of tpen reported previously [19,20] was as a masking agent of heavy metal cations for the measurement of Ca^{2+} in a cell, it can be expected that tpen is a useful ligand in analytical chemistry.
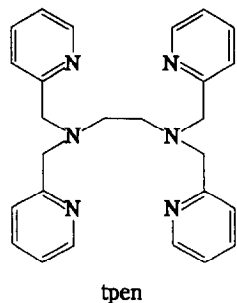
tpen

In this paper, the authors investigated the formation of polynuclear complexes of divalent 3d transition metal cations with tpen in aqueous solution. As a result, it was found that copper(II) forms a dinuclear complex with tpen, and the stability constant of the complex was determined.

2. Experimental

All reagents and solvents were of analytical-reagent grade and were used without further purification.

The synthesis of tpen was performed by modifying the method of Anderegg and Wenk [17] as follows. To a solution of 2-(chloromethyl)pyridine hydrochloride (3.3 g; 20 mmol) in water (8 cm³) previously neutralized with sodium hydroxide, 1,2-ethanediamine (0.34 cm³; 5 mmol) was added with stirring. The reaction mixture was heated (65°C) and more 4 M NaOH (5 cm³; 20 mmol) was added over a period of 1 h in small portions. The red solution was cooled and extracted with chloroform (5 × 10 cm³). The combined organic phases were dried over anhydrous sodium sulfate. After removal of the chloroform with a rotary evaporator, a red oily residue was obtained. By adding diethyl ether (10 cm³) to the residue, a brown precipitate was obtained. The precipitate was recrystallized twice from acetone (30 cm³).

Table 1
Several equilibrium constants relevant to tpen [18] (20°C, $I = 0.1$ (KNO₃))

Acid dissociation constants	
$H_4tpen^{4+} \rightleftharpoons H_3tpen^{3+} + H^+$	$pK_{a_3} = 2.95$
$H_3tpen^{3+} \rightleftharpoons H_2tpen^{2+} + H^+$	$pK_{a_4} = 3.35$
$H_2tpen^{2+} \rightleftharpoons Htpen^+ + H^+$	$pK_{a_5} = 4.86$
$Htpen^+ \rightleftharpoons tpen + H^+$	$pK_{a_6} = 7.19$

Stability constants of mononuclear complexes	
$tpen + Mn^{2+} \rightleftharpoons Mn(tpen)^{2+}$	$\log \beta_1 = 10.27$
$tpen + Fe^{2+} \rightleftharpoons Fe(tpen)^{2+}$	$\log \beta_1 = 14.61$
$tpen + Co^{2+} \rightleftharpoons Co(tpen)^{2+}$	$\log \beta_1 = 16.59$
$tpen + Ni^{2+} \rightleftharpoons Ni(tpen)^{2+}$	$\log \beta_1 = 21.55$
$tpen + Cu^{2+} \rightleftharpoons Cu(tpen)^{2+}$	$\log \beta_1 = 20.54$
$tpen + Zn^{2+} \rightleftharpoons Zn(tpen)^{2+}$	$\log \beta_1 = 15.58$

Finally, a white precipitate of the desired chelating agent (tpen) was formed, filtered off, washed with cold acetone and diethyl ether, and dried under vacuum. Yield: 50%. ¹H NMR (CDCl₃); δ 2,76 (s, 4H, en), 3.78 (s, 8H, N–CH₂–R), 7.11 (m, 4H, py), 7.45 (d, 4H, py), 7.57 (m, 4H, py), 8.48 (d, 4H, py). Anal: calc. for C₂₆H₂₈N₆: C, 73.56; H, 6.65; N, 19.79; found: C, 73.41; H, 6.75; N, 19.87.

The synthesis of N,N,N',N'-tetrakis(2-pyrazolylmethyl)-1,2-ethanediamine (tpzen) and N,N,-N',N'-tetrakis(3,5-dimethyl-1-pyrazolylmethyl)-1,2-ethanediamine (tdmpzen) was performed by using the method of Driessen [21].

The absorption spectra of solutions at 20°C were recorded on a JASCO U-best 30 UV-visible spectrophotometer in the range 200–900 nm using 1 cm matched quartz cells. pH values were obtained using a Horiba F-12 pH meter with a Horiba 6366-10D combined glass electrode.

3. Results and discussion

3.1. Composition and stability of Cu^{2+}–tpen dinuclear complex

Table 1 shows the acid dissociation constants of tpen, which is a hexa-acidic base, and the stability constants of mononuclear divalent 3d metal complexes with tpen [17]. From these constants, the influence of protonation of tpen on the following study is obviously negligible.

First, Job's continous variation method [22,23] was applied to confirm the compositions of M^{2+}-tpen complexes (M = Mn, Fe, Co, Ni, Cu, Zn) in aqueous solutions containing 0.1 M NaCl, $NaNO_3$ or $NaClO_4$ to adjust the ionic strength $I = 0.1$. With the exception of the Cu^{2+}-tpen complex in 0.1 M NaCl, all of these compositions were confirmed as 1:1. However, as shown in Fig. 1, it was not confirmed that Cu^{2+} and tpen form only $Cu(tpen)^{2+}$ in the aqueous solution containing Cl^-. This result suggests the formation of a relatively unstable polynuclear Cu^{2+}-tpen complex containing Cl^-.

To study the composition of the polynuclear complex, the continuous variation plot for Cu^{2+}-$Cu(tpen)^{2+}$ was performed. In this experiment, the formation of $Cu(tpen)^{2+}$ was regarded as being complete. From the result shown in Fig. 2, it was proved that the polynuclear complex species having a ratio of Cu^{2+}:$Cu(tpen)^{2+}$ of 1:1, i.e. Cu^{2+}:tpen = 2:1, is formed in aqueous solution containing Cl^-. In other words, the polynuclear species is shown as $Cu_2Cl_n(tpen)^{(4-n)+}$.

To determine n, the following experiment was performed. In considering the equilibrium

$$Cu^{2+} + Cu(tpen)^{2+}$$

$$+ nCl^- \overset{K_{di}}{\rightleftharpoons} Cu_2Cl_n(tpen)^{(4-n)+} \qquad (1)$$
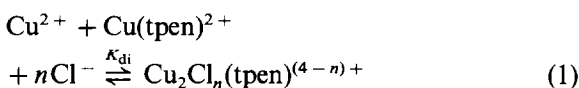
$$K_{di} = \frac{[Cu_2Cl_n(tpen)^{(4-n)+}]}{[Cu^{2+}][Cu(tpen)^{2+}][Cl^-]^n} \qquad (2)$$
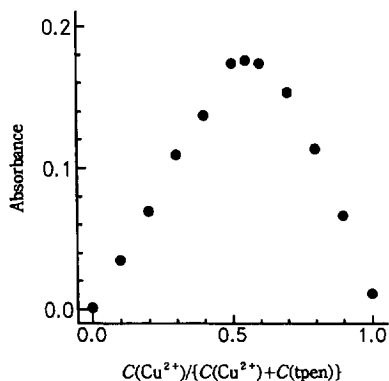
Fig. 1. Continous variation plots for Cu^{2+}-tpen complex in 0.1 M NaCl aqueous solution ($I = 0.1$). $C(Cu^{2+}) + C(tpen) = 2 \times 10^{-3}$ M; pH 4.5; $\lambda = 685$ nm.
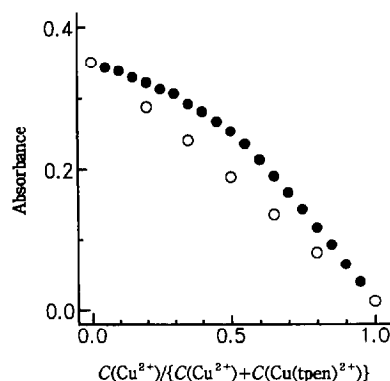
Fig. 2. Continous variation plots for Cu^{2+}-$Cu(tpen)^{2+}$ complex in aqueous solution ($I = 0.1$). $C(Cu^{2+}) + C(Cu(tpen)^{2+}) = 2 \times 10^{-3}$ M; pH 4.5; $\lambda = 685$ nm. (●) 0.1 M NaCl; (○) 0.1 M $NaNO_3$.

taking $C(Cu^{2+}) = C(Cu(tpen)^{2+}) = C_0$, there is the folllowing relationship concerning the concentration of each species in the equilibrium:

$$[Cu^{2+}] = [Cu(tpen)^{2+}]$$

$$= C_0 - [Cu_2Cl_n(tpen)^{(4-n)+}] \qquad (3)$$

Therefore the absorbance (A) of the solution is as follows:

$$A = \{\varepsilon_1[Cu_2Cl_n(tpen)^{(4-n)+}] + \varepsilon_2[Cu^{2+}]$$

$$+ \varepsilon_3[Cu(tpen)^{2+}]\}l$$

$$= \{(\varepsilon_2 + \varepsilon_3)C_0$$

$$+ (\varepsilon_1 - \varepsilon_2 - \varepsilon_3)[Cu_2Cl_n(tpen)^{(4-n)+}]\}l \qquad (4)$$

where l is the cell length and ε_1, ε_2 and ε_3 are molar decadic absorption coefficients for $Cu_2Cl_n(tpen)^{(4-n)+}$, Cu^{2+} and $Cu(tpen)^{2+}$ respectively. (The value of ε_1 can be obtained from Fig. 2.) By taking $A_1 = \varepsilon_1 C_0 l$ and $A_2 = (\varepsilon_2 + \varepsilon_3)C_0 l$

$$A_1 - A = (\varepsilon_1 - \varepsilon_2 - \varepsilon_3)\{C_0 - [Cu_2Cl_n(tpen)^{(4-n)+}]\}$$

$$\times l \qquad (5)$$

$$A - A_2 = (\varepsilon_1 - \varepsilon_2 - \varepsilon_3)[Cu_2Cl_n(tpen)^{(4-n)+}]l \qquad (6)$$

$$A_1 - A_2 = (\varepsilon_1 - \varepsilon_2 - \varepsilon_3)C_0 l \qquad (7)$$

$$K_{di} = \frac{(A - A_2)(A_1 - A_2)}{(A_1 - A)^2 C_0[Cl^-]^n} \qquad (8)$$

$$\log\left\{\frac{(A - A_2)(A_1 - A_2)}{(A_1 - A)^2}\right\}$$

$$= \log K_{di} + \log C_0 + n \, \log[Cl^-] \tag{9}$$

Therefore, by plotting $\log\{(A - A_2)(A_1 - A_2)/(A_1 - A)^2\}$ vs. $\log[Cl^-]$, the values of n and $\log K_{di}$ can be obtained.

Fig. 3 shows this plot for $C_0 = 1 \times 10^{-3}$ M, pH 4.5 and $I = 0.1$ (NaNO$_3$). From the slope of the line in the figure, n was determined as 2 and the dinuclear species was shown to be $Cu_2Cl_2(tpen)^{2+}$. Furthermore, the value of $\log K_{di}$ was determined to be 5.66 (20°C, $I = 0.1$) and the overall stability constant (β_{22}) for $Cu_2Cl_2(tpen)^{2+}$ was calculated as follows:

$$2Cu^{2+} + tpen + 2Cl^- \overset{\beta_{22}}{\rightleftharpoons} Cu_2Cl_2(tpen)^{2+} \tag{10}$$
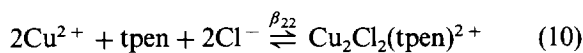
$$\beta_{22} = \frac{[Cu_2Cl_2(tpen)^{2+}]}{[Cu^{2+}]^2[tpen][Cl^-]^2} = \beta_1 K_{di} \tag{11}$$

$$\log \beta_{22} = \log \beta_1 + \log K_{di} = 20.54 + 5.66$$

$$= 26.20 \,(20°C, \, I = 0.1) \tag{12}$$

As mentioned above, this dinuclear complexation reaction proceeds only under the conditions of excess Cu^{2+} and a large excess of Cl^-. Therefore, the reaction can be avoided by paying attention to the experimental conditions.

Fig. 4. Reported coordination structure of Cu(tpen)$^{2+}$ (a) [18] and proposed structure of Cu$_2$Cl$_2$(tpen)$^{2+}$ (b).

3.2. Estimation of the structure of $Cu_2Cl_2(tpen)^{2+}$

It was reported previously [18] that the coordination number of copper in Cu(tpen)$^{2+}$ is five and that the mononuclear complex has a square pyramidal structure having one uncoordinating pyridine N atom, as shown in Fig. 4(a). Possibly, the structure causes the deviation of $\log \beta_1$ for M(tpen)$^{2+}$ (shown in Table 1) from the Irving–Williams stability series.

Fig. 5 shows the absorbance spectrum of $Cu_2Cl_2(tpen)^{2+}$ calculated from the spectrum un-

Fig. 3. Relationship between the absorbance of Cu(tpen)$^{2+}$ – Cu^{2+} solution and the concentration of Cl$^-$ ($I = 0.1$(NaNO$_3$)). C(Cu^{2+}) + C(Cu(tpen)$^{2+}$) = 1 × 10^{-3} M; pH 4.5; $\lambda = 685$ nm. See text for details.
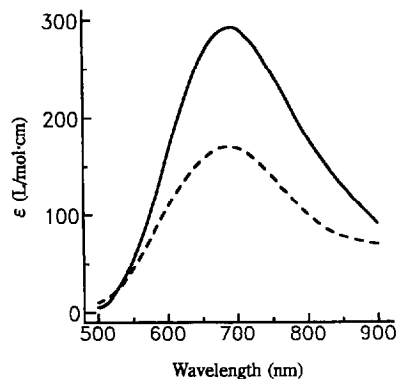
Fig. 5. Calculated absorbance spectrum of Cu$_2$Cl$_2$(tpen)$^{2+}$ (solid curve) and measured spectrum of Cu(tpen)$^{2+}$ (broken curve) in aqueous solution.

der several different conditions and the values of K_{di}. This spectrum is very similar to that of Cu(t-pen)$^{2+}$. From the result, it is considered that the coordination structures around the two Cu atoms are very similar to the structure in Cu(tpen)$^{2+}$, i.e. square pyramidal.

By regarding Cu$_2$Cl$_2$(tpen)$^{2+}$ as the (μ-Cl)$_2$ complex shown in Fig. 4(b), all of the above-mentioned criteria can be satisfied. In the proposed structure, it is considered that each Cu atom is surrounded by two pyridine N atoms, one amine N atom and two Cl atoms and these atoms adopt the square pyramidal structure.

Another supposed structure is that each Cu atom is surrounded in square planar fashion by two pyridine N atoms, one amine N atom and one Cl atom. However, the sturcture is obviously unsuitable from the viewpoint of the structural change around the Cu atom that occurs with the formation of the dinuclear complex.

tpzen

tdmpzen
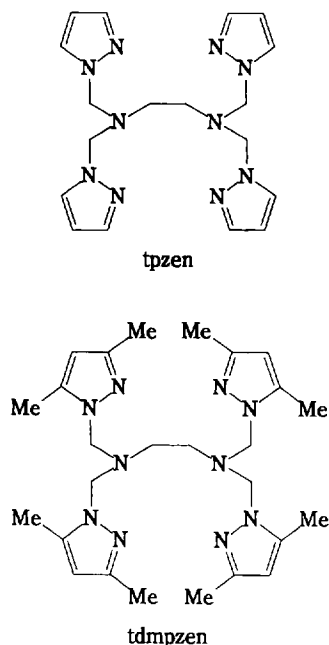
For the strict study of the coordination structure, crystallographic characterization of the dinuclear complex is very effective. However, the isolation of the complex has not yet been accomplished. Accordingly, to prove the appropriateness of the (μ-Cl)$_2$ structure, continuous variation
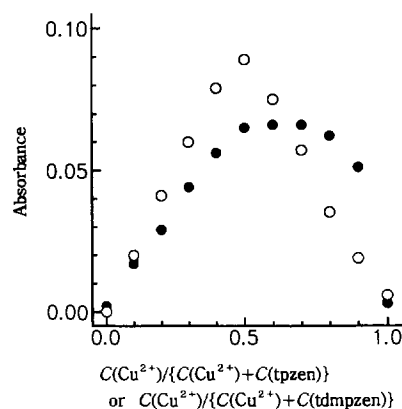
Fig. 6. Continous variation plots for Cu^{2+}–tpzen and Cu^{2+}–tdmpzen complexes in 0.1 M NaCl aqueous solution ($I = 0.1$). (●) C(Cu^{2+}) + C(tpzen) = 2 × 10^{-3} M; pH 6.0; $\lambda = 635$ nm; (○) C(Cu^{2+}) + C(tdmpzen) = 1 × 10^{-4} M; pH 6.0; $\lambda = 655$ nm.

plots for Cu^{2+}–tpzen and Cu^{2+}–tdmpzen complexes in aqueous solution containing Cl$^-$ were performed. Fig. 6 shows the result. The plot for Cu^{2+}–tpzen suggested the formation of Cu$_2$Cl$_2$(tpzen)$^{2+}$. In contrast, that for Cu^{2+}–tdmpzen suggested the absence of Cu$_2$Cl$_2$(tdmpzen)$^{2+}$. It is supposed that the 3-methyl groups on the pyrazole rings in tdmpzen disturb the formaton of the μ-Cl bridge by steric hinderance. These results support the formation of Cu$_2$Cl$_2$(tpen)$^{2+}$ and Cu$_2$Cl$_2$(tpzen)$^{2+}$ complexes having two μ-Cl bridges. The Cu^{2+}–tpzen and Cu^{2+}–tdmpzen complexes are less stable than the Cu^{2+}–tpen complex, and a structural study concerning these complexes will be described in a forthcoming paper.

Acknowledgment

References

[1] S. Motomizu, S. Nishimura, Y. Obata and H. Tanaka, Anal. Sci., 7 (suppl.) (1991) 253.

[2] S. Motomizu, M. Oshima, S. Matsuda, Y. Obata and H. Tanaka, Anal. Sci., 8 (1992) 619.

[3] A.R. Timerbaev, W. Buchberger, O.P. Semenova and G.K. Bonn, J. Chromatogr., 630 (1993) 379.

[4] M. Iki, H. Hoshino and T. Yotsuyanagi, Chem. Lett., (1993) 701.

[5] W. Buchberger, O.P. Semenova and A.R. Timerbaev, J. High Resolut. Chromatogr., 16 (1993) 153.

[6] M. Aguilar, A. Farran and M. Martinez, J. Chromatogr., 635 (1993) 127.

[7] A.R. Timerbaev, O.P. Semenova, P. Jandik and G.K. Bonn, J. Chromatogr., 671 (1994) 419.

[8] A.R. Timerbaev, O.P. Semenova, G.K. Bonn and J.S. Fritz, Anal. Chim. Acta, 296 (1994) 119

[9] J.W. O'Laughlin, Anal. Chem., 54 (1982) 178.

[10] I. Albiaty and J.S. Fritz, Anal. Chim. Acta, 146 (1983) 191.

[11] J.N. King and J.S. Fritz, Anal. Chem., 59 (1987) 703.

[12] J.N. King and J.S. Fritz, Anal. Chim. Acta, 207 (1988) 137.

[13] M.D. Palmieri and J.S. Fritz, Anal. Chem., 59 (1987) 2226.

[14] M.D. Palmieri and J.S. Fritz, Anal. Chem., 60 (1988) 2244.

[15] M.V. Main and J.S. Fritz, Anal. Chem., 61 (1989) 1272.

[16] M.V. Main and J.S. Fritz, Anal. Chim. Acta, 229 (1990) 101.

[17] G. Anderegg and F. Wenk, Helv. Chim. Acta, 50 (1967) 2330.

[18] G. Anderegg, E. Hubmann, N.G. Podder and F. Wenk, Helv. Chim. Acta, 60 (1977) 123.

[19] P. Arslan, F. Virgilio, M. Beltrame and R.Y. Tsien, J. Biol. Chem., 260 (1985) 2719.

[20] H. Komulainen and S.C. Bondy, Neurochem. Int., 10 (1987) 55.

[21] W.L. Driessen, Recl. Trav. Chim. Pays-Bas, 101 (1982) 441.

[22] P. Job, Ann. Chim., 8 (1928) 113.

[23] W.C. Vosburgh and G.R. Cooper, J. Am. Chem. Soc., 63 (1941) 437.

Pulsed photothermal phase-shift spectroscopy for weak absorption measurement

Bincheng Li[a,1], Yanzhuo Deng[b,*], Jieke Cheng

[a]*Department of Chemistry, Wuhan University, Wuhan 430072, Hubei, People's Republic of China*
[b]*Center of Analysis and Testing, Wuhan University, Wuhan 430072, Hubei, People's Republic of China*

Abstract

A novel photothermal phase-shift spectroscopy configuration based on the retro-reflected beam interference has been developed and its operational principle is described. The weak absorption measurement ability of this technique is experimentally proven with a water/ethanol solution of standard Pyronine G dye and the limit of detection is found to be 1.8×10^{-6} absorbance. Potential applications of the technique are discussed.

1. Introduction

Photothermal spectroscopy is a sensitive spectroscopic technique for weak absorption measurement. Unlike conventional beam-transmittance spectrophotometry, photothermal methods directly measure the absorbed radiation of an excitation beam by monitoring temperature fluctuations produced within the medium. Absorbances as low as 10^{-7} are determined by thermal lensing (TLS) [1], photothermal deflection (PTDS) [2], and photothermal phase-shift spectroscopy (PTPS) [3] techniques. Photothermal phase-shift spectroscopy measures the phase change caused by absorption of the excitation beam by placing the sample under investigation in one arm of an interferometer. This technique was discovered by Stone [4] and by Davis and Petuchowski [5], who refer to it as phase fluctuation optical heterodyne (PFLOH) spectroscopy. Subsequently, many theories and applications of this technique have been investigated [3,6,7].

In this paper, we describe a novel photothermal phase-shift spectroscopy technique—retro-reflected beam photothermal interference spectroscopy. Fig. 1 shows the proposed photothermal interference spectroscopy technique schematically. Our proposed configuration differs from all other existing photothermal phase-shift or interferometric spectroscopy techniques in that we utilize the light of a focused probe laser beam reflected from the

---

* Corresponding author.
[1] Present address: Laboratory of Photoacoustic Science, Institute of Acoustics, Nanjing University, Nanjing 210093, Jiangsu, People's Republic of China.

front surface of a sample (or a cell containing the sample) as the reference beam, while the light passing through the sample and reflected from the rear surface of the sample (or the cell) is used as the signal beam. Due to the divergence of the focused probe laser beam, both reflected beams overlap in the far field and, as both originate from the same wave, they interfere, leading to a regularly spaced interference fringe pattern. The change in refractive index (RI) of the sample, resulting in a temperature rise within the sample caused by absorption of the energy of the excitation beam, induces phase shifts in the signal beam which, in turn, translate into lateral shifts of the interference fringes. Because the fringes are approximately equally spaced, shifts are conveniently detected with a position-sensitive detector. Upon calibration, the absorbance of the sample can be determined from the photothermal signal.

2. Experimental

The experimental photothermal interference spectroscopy configuration is illustrated in Fig. 2. A Nd:YAG frequency-doubled pulsed laser (Quantel, France) operated at a wavelength of 532.1 nm is used as the excitation beam, illuminating the sample from the rear surface. The pulse duration is 8 ns and the repetition rate is 10 Hz.
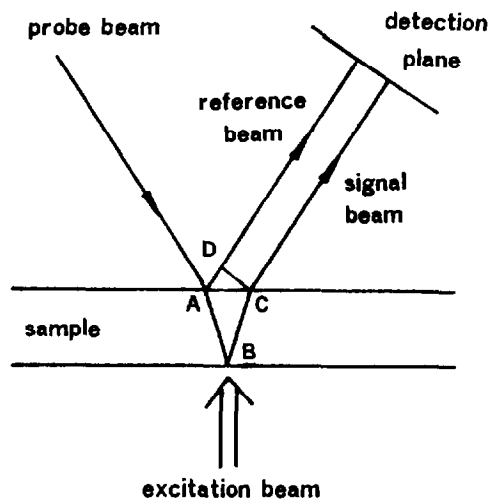
Fig. 1. Schematic diagram of the proposed retro-reflected beam photothermal interference configuration.
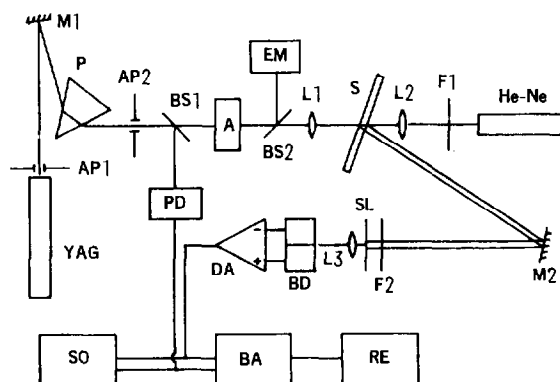
Fig. 2. Experimental arrangement of photothermal interference spectroscopy: YAG, Nd:YAG frequency-doubled pulsed laser; AP1, AP2, apertures; M1, M2, mirrors; P, prism; BS1, BS2, beamsplitters; PD, photodiode; A, attenuator; EM, energy meter; L1, L2, spherical lenses; S, sample; F1, F2, filters; He–Ne, He–Ne laser; SL, slit; L3, cylindrical lens; BD, bicell photodiode detector; DA, differentiating amplifier; SO, storage oscilloscope; BA, boxcar average; RE, recorder.

The output energy per pulse is adjustable from zero to a maximum of about 300 mJ. A 2 mW He–Ne laser operated at a wavelength of 632.8 nm is used as the probe beam. A bicell photodiode detector (Chongqing Institute of Photoelectronics, China) is used as a position-sensitive detector to measure the fringe shift in the interference field. The output of the detector is fed into the input end of a boxcar averager (EG&G Model 165/162, USA) after differentiation and amplification by a differential amplifier. The signal is monitored by a storage oscilloscope (Tektronix Model 446, USA) and the output of the boxcar averager is recorded by a recorder.

After propagating through an aperture of 5 mm diameter, a prism and another aperature of 6 mm diameter for improving beam quality and eliminating the light at a wavelength of 1.06 μm, and a variable attenuator for energy adjustment, the excitation beam is focused by a spherical lens (focal length 140 mm) onto the sample from the rear surface. A fraction of the laser energy is sampled by means of a beamsplitter and monitored by an energy meter. Another small part of the excitation beam is split and received by a photodiode to trigger the boxcar averager and the storage oscilloscope. Care is taken to adjust the energy of the excitation beam illuminating the

sample to prevent the occurrence of non-linear effects [2]. The probe beam is focused with a lens of 46 mm focal length onto the sample from the front surface. To maximize the interaction length of the excitation and probe beams and therefore the photothermal signal magnitude, the collinear photothermal configuration is used. The two beams are not paralled, but intersect with a small angle of about 4°; therefore the contribution of the cell wall absorption to the photothermal signal is eliminated. The relative position of the excitation and probe beams is adjusted by carefully moving the focusing lens L1 mounted on a micrometer-driven translation stage. The probe beam (and also the excitation beam) are incident on the sample surface with an incident angle of 15°; therefore the reflected probe beams do not pass through the focusing lens L2 again. A filter is used before the He–Ne laser to prevent the excitation beam from entering the resonator of the probe laser.

The reflected probe beams from the two surfaces of the sample interfere as they propagate away from the sample and an interference fringe pattern is formed at the far field. A slit with width approximately equal to the fringe spacing is used to select a suitable fringe for detection. The slit position is adjusted with a micrometer-driven translation stage to allow only one fringe to pass through the slit (in this case the two edges of the slit are located at the two minimum intensity points (destructive interference) of the selective fringe) and be detected by a bicell photodiode detector [8,9]. To gather more light at the detector, the fringe is compressed along the vertical direction by a cylindrical lens (focal length 40 mm). A 632.8 nm bandpass filter is placed at the front of the slit to eliminate the excitation laser light. The position-sensitive detector is mounted on a micrometer-driven two-dimensional translation stage for accurate alignment. The position of the bicell detector is adjusted vertically and laterally so that the center of gravity of the fringe is centered on the detector. A null complementary output current of the detector is produced, therefore the common-mode amplitude noise (such as intensity fluctuation of the probe beam) is eliminated and the measurement sensitivity is maxi-

mized. Because the present detection arrangement satisfies the optimum detection condition [8] (the detection point is located midway between constructive and destructive interference) the maximum linear measurement range is obtained.

The standard Pyronine G dye, purchased from Fluka (Buchs, Switzerland) is used in this experiment. Pyronine G dye is dissolved in 40/40 water/ethanol solution to required concentrations. The ethanol is added to enhance the photothermal signal [10]. Fig. 3 shows the absorbance spectrum of a 5.0×10^{-6} mol l^{-1} 40/60 water/ethanol solution of Pyronine G, measured with a UV–Vis spectrometer (Shimadzu UV-240, Japan). With a 10 mm pathlength cell, the absorbance of the Pyronine G solution at 532.1 nm is 0.132; therefore the molar absorbance of a 40/60 water/ethanol solution of Pyronine G is 2.64×10^4 cm^{-1} (mol $l^{-1})^{-1}$. The sample cell used in the experiment is a commercially available fused-silica tube (1.0 mm i.d., 1.7 mm o.d) used without additional optical processing for smoothing the tube walls (the surfaces). The sample is introduced into the tube by flowing with a constant-flow pump.

3. Results

Fig. 4 shows the interference fringe pattern of a 40/60 water/ethanol filled fused-silica tube, recorded using a photodiode and a pinhole of 0.2
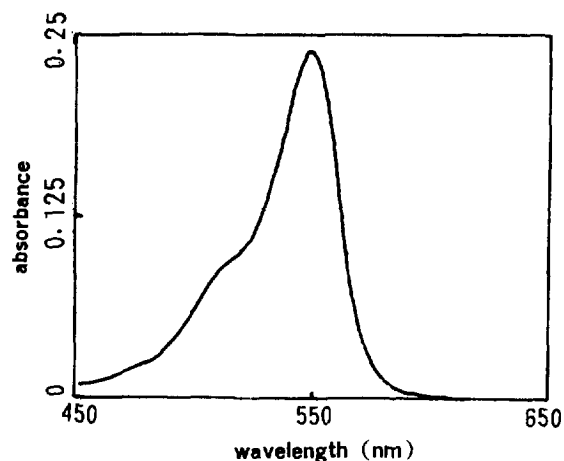

Fig. 3. Absorbance spectrum of 5.0×10^{-6} mol l^{-1} 40/60 water/ethanol solution of Pyronine G.
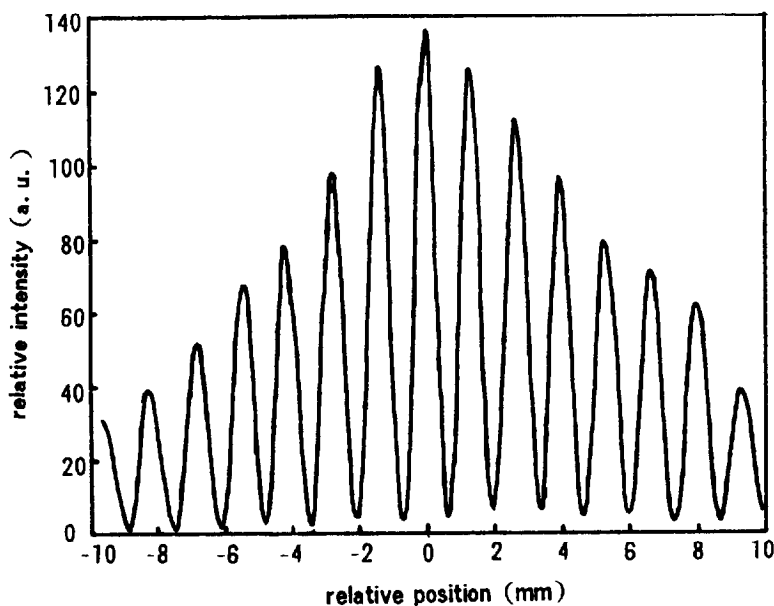
Fig. 4. Interference fringe pattern of fused-silica tube (1.0 mm i.d., 1.7 mm o.d.) recorded at a plane 143 cm away from the sample.

mm diameter placed in front of the detector, at a plane 143 cm away from the fused silica tube. The recorded fringe pattern is a typical high-contrast interference pattern produced by the interference of two Gaussian laser beams having approximately identical intensities. This simple, regularly-spaced, high-contrast interference fringe pattern is ideal for measuring the phase shift caused by the refraction index change of the measured sample [8]. In this experiment, the fringe located near the central area of the interference fringe pattern, which has the maximum intensity and measurement sensitivity, is chosen for detection.

Fig. 5 shows the photothermal phase-shift signal transients of 1.0×10^{-8} mol l^{-1} Pyronine G 40/60 water/ethanol solution, recorded with different signal processing time constants of the boxcar averager. Taking the optical pathlength of the sample into account, the absorbance of the sample solution at this concentration is 2.64×10^{-5}. The curve in Fig. 5 (top) represents the photothermal phase-shift signal transient recorded when the time constant is set to be 1 s. The noise level of the photothermal signal transient is relatively high. To reduce the noise level, a longer signal processing time constant is chosen when recording the signal transient. Lengthening the time con-

stant increases the measurement data points and the signal-to-noise ratio is therefore improved. Fig. 5 (bottom) is the result obtained with a 10 s
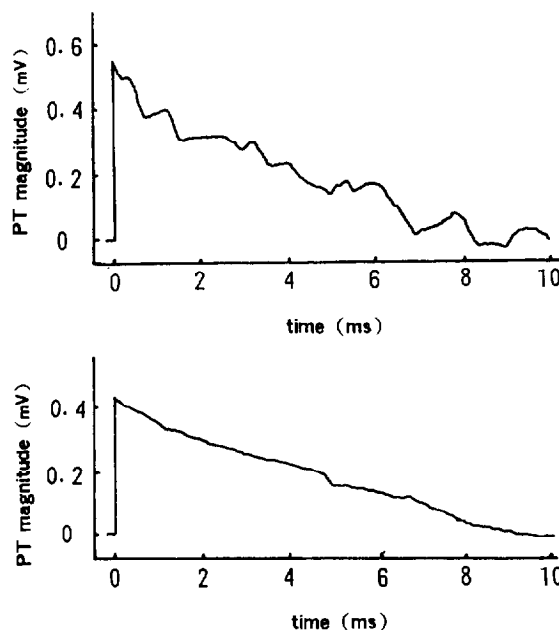
Fig. 5. Photothermal signal transients of 1.0×10^{-8} mol l^{-1} Pyronine G 40/60 water/ethanol solution. The energy of the laser pulse is about 0.1 mJ. The signal processing time constant of the boxcar averager is (top) 1 s, (bottom) 10 s.
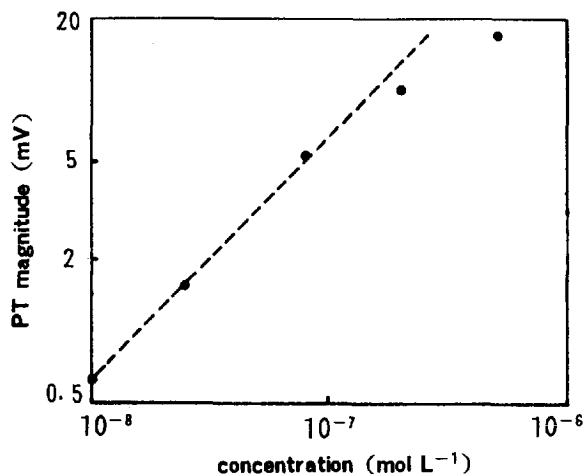
Fig. 6. Photothermal signal magnitude vs. concentration of Pyronine G solution. The energy of the laser pulse is about 0.1 mJ (●, experimental data).

time constant. Although the signal transient is distorted due to the long signal processing time constant, the noise level is considerably reduced and therefore the measurement sensitivity is improved. Increasing the signal processing time constant of the boxcar averager by a factor of N produces a factor of $\sqrt{N}$ improvement in the signal-to-noise ratio, resulting in a $\sqrt{N}$ improvement in measurement sensitivity. Because the blank absorbance caused by the water and ethanol is in the range $1 \times 10^{-7} - 1 \times 10^{-8}$ in this experiment [10], much lower than the absorbance detection limit determined by the photothermal signal measurement noise, the effect of the blank absorption is neglected when calculating the detection limit of absorbance. By using the IUPAC definition, the limit of detection (LOD) is determined to be 5.7×10^{-6} absorbance from Fig. 5 (top). With a factor of $\sqrt{10}$ improvement in Fig. 5 (bottom), the absorbance detection limit is 1.8×10^{-6}. A lower LOD can be obtained by setting a longer signal processing time constant of the boxcar averager, until the LOD determined by the blank absorbance is achieved.

Fig. 6 shows the photothermal signal magnitude as a function of sample concentration. For each measurement, the positions of the slit and bicell decector are carefully readjusted to maintain the optimum detection condition, so as to ensure identical detection response and sensitivity

at each measurement. At low sample concentration, the linear dependence of the phothermal signal on concentration is quite good. As the sample concentration increases, the phototermal results exhibit a marked non-linear response, which does not agree with the theoretical prediction of the conventional photothermal experiment. There are several reasons for the unexpected non-linear response. The most likely of these is the poor mechanical stability of the experimental system and environmental vibrations, which degenerate the performance of the photothermal system during the experimental procedure, especially when the measurements at different concentrations are made at widely separated times, resulting in a continuous decrease in the measurement sensitivity. Repeated experiments demonstrate the decline of the system performance with time. The photophysical and photochemical properties of the sample, such as photodecomposition, may be an important factor in the non-linearity. The photodecomposition phenomenon becomes very apparent when the sample concentration is increased to about 1.0×10^{-5} mol 1^{-1} and can be easily observed from the oscilloscope display by flowing the sample solution. The photothermal signal amplitude of the flowing sample is much higher than that of the static sample.

4. Discussion

Although the absorbance LOD obtained with the retro-reflected beam photothermal interference configuration is comparable with the values recently reported by Waldron and Dovichi [11] using the crossed-beam thermo-optical configuration and by Krattiger and co-workers [12,13] using a hologram-based thermo-optical configuration, accounting for the 1.0 mm i.d. of the fused-silica tube and the collinear photothermal configuration used in our experiment, the resulting probing volume is much larger than that using 50 μm and 20 μm i.d. capillaries and a crossed-beam configuration. It seems that our results are only moderately successful. However it should be pointed out that the experimental ap-

paratus reported on here is far from optimal. As the interference technique is extremely sensitive to environmental vibrations, the poor mechanical stability and poor vibration-isolation ability of the experimental system are the main factors limiting the measurement sensitivity in our experiment. The use of a short-duration pulse laser (the pulse duration is 8 ns in our experiment) as the excitation beam also severely limits further improvement in sensitivity of the photothermal measurement. Due to the high power of the pulse laser, the maximum pulse energy used in the experiment is relatively low ($\leqslant 0.1$ mJ), to avoid damage of the sample cell wall and occurrence of non-linear effects, and the waist radius of the excitation beam used is much larger than that used in photothermal experiments employing the continuous wave excitation laser. As the photothermal signal magnitude increases linearly with excitation beam energy or power, and decreases rapidly with the increase of the excitation beam radius, increasing the excitation beam energy or power and decreasing the excitation beam radius will effectively improve the sensitivity of the photothermal measurement. In this respect, use of a continuous wave laser of moderate power as the excitation beam in a photothermal experiment is more profitable in improving the measurement sensitivity and reducing the probing volume than the use of a pulse laser. Another source of noise which limits the sensitivity improvement is the electromagnetic radiation interference in the detector electronics, caused by the discharge of the pump lamp of the pulsed Nd:YAG laser. It is reasonable to believe that the sensitivity of the photothermal measurement reported here would be very much improved if all the limitation factors were eliminated and the experimental system optimized.

The most promising application of the proposed retro-reflected beam interference configuration should be as a universal RI decector in HPLC and capillary electrophoresis (CE) separation. This RI detector could also be readily used to perform sensitive absorption detection using a photothermal method with CE detection. Compared to the RI detection method based on transmitted beam interference developed by Bornhop and Dovichi [14], the retro-reflected beam inter-

ference method has the advantages that the interference fringe pattern is simple, well-spaced an of high contrast, while the optical arrangement is relatively simple. This high-contrast fringe pattern allowed us to conveniently select the fringe having the optium sensitivity for detection. Krattiger co-workers introduced the use of an index-matching fluid (RIMF) [8,15] and a holographic optical element (HOE) [16] to simplify the fringe pattern in order to improve the detection and improve the measurment sensitivity. In so doing the detection system was complicated. In the retro-reflected beam configuration, the sampling arm of the probe beam crosses the capillary through its center where the optical path is longer than that in the transmitted beam configuration, and if the probe beam is perpendicularly incident on the capillary wall (in this case a well-spaced, high-contrast circular fringe pattern is formed at the far field), the retro-reflected probe beam from the rear surface crosses the capillary twice in the same path, the optical path is doubled, and therefore the measurement sensitivity is further improved. The retro-reflected beam interference configuration has been successfully used as the on-column detector for CE separation of amino acids [17] with a 50 μm i.d. fused-silica capillary. The results are very encouraging. Employing both the transmitted and retro-reflected beam configurations in photothermal experiments, as the optical path in the retro-reflected beam configuration is longer than that in the transmitted beam configuration, we can safely predict that if all other experimental conditions are identical in the two photothermal experiments, the retro-reflected beam photothermal interference configuration has potentially higher measurement sensitivity than the transmitted beam photothermal interference configuration. As the capillaries usually employed in CE separations have enough good surfaces to form high-quality interference fringe patterns after the protective polymide coatings of the capillaries are removed, this retro-reflected beam interference method and its photothermal configurations are likely to find wide applications in CE detection. Further investigation on the performance optimization of the retro-reflected beam interference experimental system to improve the measurement

sensitivity and applications to CE detection are being undertaken in our laboratory.

5. Conclusions

We have demonstrated that a novel photothermal phase-shift spectroscopy configuration should be a sensitive detection technique for extremely weak absorption measurement. In common with other photothermal techniques, this photothermal technique based on retro-reflected beam interference is also useful for determination of optical and thermal properties of transparent materials. This sensitive detection technique is especially suitable for measurement on small volume samples. It may find extensive applications in trace analyses and HPLC and CE detections and thermo-optical characterization of optical materials. This configuration can be used for samples or sample cells having two approximately parallel, smooth surfaces of appropriate thickness, or a capillary with appropriate diameter.

Acknowledgement

References

[1] C.D. Tran, in D. Bicanic (Ed.), Photoacoustic and photothermal Phenomena III, Springer-Verlag, Berlin, 1992, p. 463.

[2] S.E. Bialkowski, X. Gu, P.E. Poston and L.S. Powers, Appl. Spectrosc., 46 (1992) 1335.

[3] D.L. Mazzoni and C.C. Davis, Appl. Opt., 30 (1991) 756.

[4] J. Stone, Appl. Opt., 12 (1973) 1828.

[5] C.C. Davis and S.J. Petuchowski, Appl. Opt., 20 (1981) 2539.

[6] W.K. Lee, A. Gungor, P-T. Ho and C.C. Davis, Appl. Phys. Lett., 47 (1985) 916.

[7] B. Monson, R. Vyas and R. Gupta, Appl. Opt., 28 (1989) 2554.

[8] A.E. Bruno, B. Krattiger, M. Maystre and H.M. Widmer, Anal. Chem., 63 (1991) 2689.

[9] J. Vattulainen and R. Hernberg. Rev. Sci. Instrum., 64 (1993) 1451.

[10] N.J. Dovichi, CRC Rev. Anal. Chem., 17 (1987) 357.

[11] K.C. Waldron and N.J. Dovichi, Anal. Chem., 64 (1992) 1396.

[12] B. Krattiger, A.E. Bruno, H.M. Widmer and R. Dändliker, Anal. Chem., 67 (1995) 124.

[13] J.M. Saz, B. Krattiger, A.E. Bruno, J.C. Diez-Masa and H.M. Widmer, J. Chromatogr. A, 699 (1995) 315.

[14] D.J. Bornhop and N.J. Dovichi, Anal. Chem., 58 (1986) 504.

[15] B. Krattiger, A.E. Bruno, H.M. Widmer, M. Geiser and R. Dändliker, Appl. Opt., 32 (1993) 956.

[16] B. Krattiger, G.J.M. Bruin and A.E. Bruno, Anal, Chem., 66 (1994) 1.

[17] Y. Deng and J. He, Gaodeng Xuexiao Hauxue Xuebao (Chem. J. Chin. Univ.), 15 (1994) 667 (in Chinese).

Electroanalytical characteristics of enoxacin and their analytical application

Zheng-Qi Zhang*, Yan-Fei Li, Xiao-Mei He, Hong Zhang

Department of Chemistry and Chemical Engineering, Hunan University, Changsha, People's Republic of China

Abstract

In a 0.050 M HCl solution containing 0.12 M KCl, enoxacin yields a sensitive polarographic wave at -1.05 V, which can be used to determine trace amounts of the drug, the linear range being from 1.6×10^{-8} to 1.6×10^{-5} M with a detection limit of 6.25×10^{-9} M. The electrochemical characteristics of the drug were studied by normal polarography, cyclic voltammetry and potentiostatic coulometry. A single-sweep polarographic procedure for the determination of enoxacin has been worked out and applied to urine and serum samples.

1. Introduction

Polarography and voltammetry are widely applied to the determination of drugs. Several reviews have appeared covering the voltammetric determination of drugs [1–4]. In the first polarographic study of quinolone derivatives, the reduction and polarographic behaviour of nalidixic acid was investigated by d.c. polarography [5]. Van Oort et al. [6] used differential pulse polarography to determine nalidixic acid. Hoffman and Dybowski [7] reported a d.c. polarographic assay of pipemidic acid. Stripping voltammetric procedures were recommended for determination of ciprofloxacin [8], rufloxacin [9], ofloxacin [10,11] and norfloxacin

[12] drugs in tablets, urine and serum samples. Recently, we used a surfactant as a sensitizer to achieve higher sensitivity and better selectivity in a polarographic assay of ofloxacin [13].

Enoxacin (1-ethyl-6-fluoro-1,4-dihydro-4-oxo-7-(1-piperazinyl)-1,8-naphthyridine-3-carboxylic acid) is a new quinolone carboxylic acid derivative which shows a broad antimicrobial spectrum. Its primary effect is the inhibition of bacterial DNA-gyrase (topoisomerase II). After oral administration, the drug is rapidly absorbed and widely distributed to the body tissues and fluids. Various techniques, including HPLC, reversed-phase HPLC, ion chromatography, spectrophotometry and spectrofluorimetry, have been proposed for the determination of enoxacin. Squella et al. [14] used differential pulse polarography for the determination of enoxacin in tablet samples. However, other

* Corresponding author.

electroanalytical techniques for the determination of enoxacin have not been reported yet. The aim of this work was to develop a method for the determination of enoxacin by single-sweep oscillopolarography. The proposed method has been used for the determination of trace amounts of enoxacin in urine samples, no sample pretreatment being necessary. The detection limit is 6.25×10^{-9} M.

enoxacin
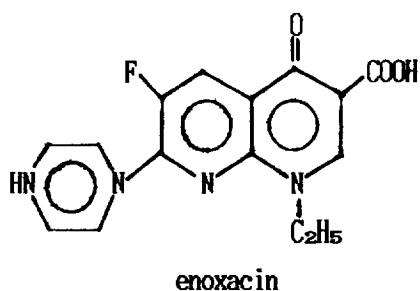
2. Experimental

2.1. Apparatus

The single-sweep polarograms were recorded on a JP-1A oscillopolarograph (Chengdu Instrumental Factory). The polarographic cell has the three-electrode system: a dropping mercury electrode (DME) as working electrode, a saturated calomel electrode (SCE) reference electrode and a platinum wire auxiliary electrode. A drop time of 7 s was selected using a knocker, with a rest time of 5 s and a scan time of 2 s, the scan rate being 250 mV s^{-1}. An XJP-821 neopolarograph (Jiangsu Electroanalytical Instrumental Factory) in connection with an LZ3-100 X-Y recorder (Dahua Instrumental Factory) and a JM-01 (manual micrometric screw delivery) hanging mercury drop electrode (HMDE) were used for cyclic voltammetry measurements. A static mercury drop electrode (SMDE), J-shaped capillary, was used for medium-exchange measurements. A PAR Model 273 potentiostat/galvanostat with a PAR Model 303 SMDE, controlled by PAR Model 270 software, was used for normal pulse polarography and other electrochemical measurements. For pulse polarography the instrumental parameters were as follows: accumulation time, 120 s; accumulation potential, -0.70 V; drop size, medium; pulse amplitude, 50 mV; pulse period, 2

s; equilibrium time, 15 s. Potentiostatic coulometry was carried out on an apparatus consisting of an M179 coulometer, an M273 potentiostat and an electrolytic cell with a mercury pool as cathode, a platinum electrode anode and an SCE reference electrode.

2.2. Reagents

2.2.1. Standard enoxacin solution

A stock solution (1.0×10^{-3} M) of enoxacin was prepared by dissolving 0.080 g of enoxacin (99.8%, from Hunan Institute for the Control of Pharmaceutical Products) in 25 ml of 0.10 M HCl solution, followed by dilution to 250 ml.

2.2.2. HCL solution, 0.50 M

42 ml of concentrated HCL was dissolved in 1000 ml of water, and titrated with Na$_2$CO$_3$ to prepare the standard solution.

2.2.3. Buffer solution

The test solutions under study were buffered using universal buffer for the pH range 2-11, containing 0.1 M citric acid, 0.1 M sodium phosphate and 0.1 M boric acid. The pH was adjusted with NaOH or HCl.

Other reagents were of suprapure or analytical-reagent grade. Water, redistilled in a fused-silica apparatus, was used throughout.

2.3. Procedures

2.3.1. Polarography of pure enoxacin solution

1.0 ml of 0.50 M HCl solution was mixed with 1.20 ml of 1.0 M KCl solution and various amounts of standard enoxacin solution. The mixture was diluted to 10 ml with water. The solution was transferred to the polarographic cell, and purged with oxygen-free nitrogen for 10 min. A flow of nitrogen was maintained over the cell throughout the analysis to prevent interference from oxygen. The derivative polarograms were recorded, starting the potential scan at -0.70 V. The peak potential is -1.05 V.

2.3.2. Serum and urine sampling

After 12 h of overnight fasting, rabbits received an oral dose of enoxacin (8.0 mg Kg^{-1}). After 2 h

the rabbits were killed and blood samples were taken. The samples were then centrifuged three times, and the blood serum was collected and kept at −10°C.

After the rabbits received the dose as described above, spontaneously voided urine was collected for 24 h. All samples were kept frozen at −10°C.

2.3.3. Analysis of urine samples

Urine was diluted 10 times with water. 0.50 ml of the solution was transferred to a 10 ml standard flask, and the procedure continued as described in the section on polarography of pure enoxacin solution above.

2.3.4. Analysis of serum samples

The enoxacin in serum samples was extracted by chloroform [15]. To 1.0 ml of serum were added 9.0 ml of chloroform and 2.0 ml of pH 7.50 phosphate buffer solution, and the solution was mixed thoroughly on a vortex mixer. The mixture was allowed to stand for 15 min and centrifuged at 4000g for 10 min. The aqueous phase was removed and the chloroform phase was filtered. The filtrate was evaporated to dryness at 50°C. The residue was dissolved with 1.00 ml of 0.50 M HCl solution. 1.20 ml of 1.00 M KCl solution was added to the solution and the procedure was continued as described in the section on polarography of pure enoxacin solution.

2.3.5. Recovery experiment

The amounts of enoxacin shown in Table 2 were added to a 50 ml beaker containing the No. 4 serum sample or the No. 4 urine sample and they were then treated as described above.

3. Results and discussion

3.1. Single-sweep polarography

In a pH 2–11 buffer solution, enoxacin yields a sensitive oscillopolarographic wave, the peak potential shifting in the negative direction with increasing pH value of the test solution. In a 0.050 M HCl solution containing 0.12 M KCl the peak potential of the drug is −1.05 V (Fig. 1(b)). In the

range 1.60×10^{-8}–1.60×10^{-5} M, the peak currents are linearly proportional to the concentration of the drug. The detection limit is 6.25×10^{-9} M, which was taken as the concentration that gave a signal equal to three times the standard deviation of the blank signal, calculated from the calibration slope. The reproducibility was evaluated by 15 repetitive experiments on a 5.0×10^{-7} M enoxacin solution. The relative standard deviation was 1.1%.

3.2. Effect of HCl concentraion

In a pH 2–11 buffer solution, the peak current of enoxacin increases with decreasing pH value of the test solutions. In a dilute acidic solution such as H_2SO_4, H_3PO_4, HNO_3 or HCl, enoxacin gives a good polarographic wave, and the best results were obtained in a HCl solution, so we used it as a background solution. The effect of HCl concentration on the peak current is shown in Fig. 2a. The optimal HCl concentration was from 0.040 to 0.060 M. Accordingly, a HCl concentration of 0.050 M was used throughout for maximum sensitivity.

3.3. Effect of KCl concentration

Support electroytes such as KCl, NaCl, KNO_3 and $NaNO_3$ were examined in 5.0×10^{-7} M

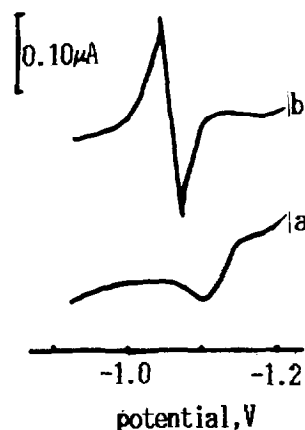

Fig. 1. Derivative single-sweep polarograms of enoxacin: (a) 0.050 M HCl, 0.12 M KCl; (b) 0.050 M HCl, 0.12 M KCl, 1.60×10^{-6} M enoxacin.
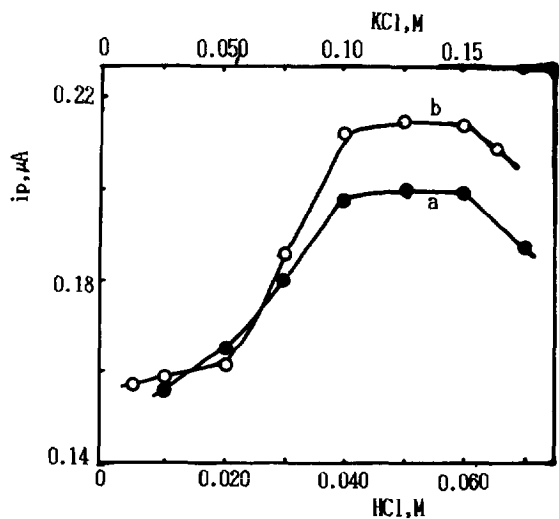
Z.-Q. Zhang et al. / Talanta 43 (1996) 635–641

Fig. 2. Effects on solutions of 1.0×10^{-6} M enoxacin: (a) effect of HCl concentration: 0.030 M KCl; (b) effect of KCl concentration: 0.050 M HCl.

enoxacin solution. The best results were obtained with KCl support electrolyte. The effect of its concentration on the peak current is shown in Fig. 2b. The peak current increases rapidly with increasing KCl concentration from 0.050 to 0.10 M and decreases greatly when the concentration of KCl exceeds 0.15 M. A concentration of 0.12 M for KCl was chosen for subsequent studies.

3.4. Adsorptive characteristic of enoxacin

The adsorption of enoxacin at the DME was demonstrated by constructing electrocapillary curves and by carring out medium-exchange experiments.

The electrocapillary curve of a solution containing enoxacin (Fig. 3(b,c) is lower than that of the background (Fig. 3(a)), indicating that enoxacin is adsorbed at the DME.

For medium-exchange studies, the SMDE with J-shaped capillary, used as a working electrode, was kept in contact with a solution containing enoxacin for 180 s with stirring. Following this, the electrode was cleaned in water for 15 s while stirring and transferred to another cell containing the background solution only. In the voltammogram obtained with the new cell there is a voltammetric peak at -1.05 V, and the peak

current is close to that obtained with the original cell.

The normal pulse polarogram of enoxacin $(3.0 \times 10^{-6}$ M) has a maximum, indicating that the adsorption process of enoxacin on the mercury electrode is reactant adsorption [16].

3.5. Dependence of peak current (i_p) on the potential scan rate (v)

Assume that $i_p = Av^x$; when the electrode process is diffusion-controlled, x should take a value of 0.5 [17], and for an adsorption-controlled process it should take a value of 1.0 [18]. As diffusing and adsorbed species were reduced simultaneously, the peak current had contributions from both diffusion and adsorption currents [19], so the value of x varied between 0.5 and 1.0. The dependence of peak current of enoxacin on the potential scan rate is affected by the concentration of the drug. The cycle voltammograms were recorded at constant rest times before the appearance of the peak and with different scan rates to estimate the value of x in the enoxacin concentration range from $1.0 \times 10^{-10}–1.0 \times 10^{-5}$ M. The peak cur-
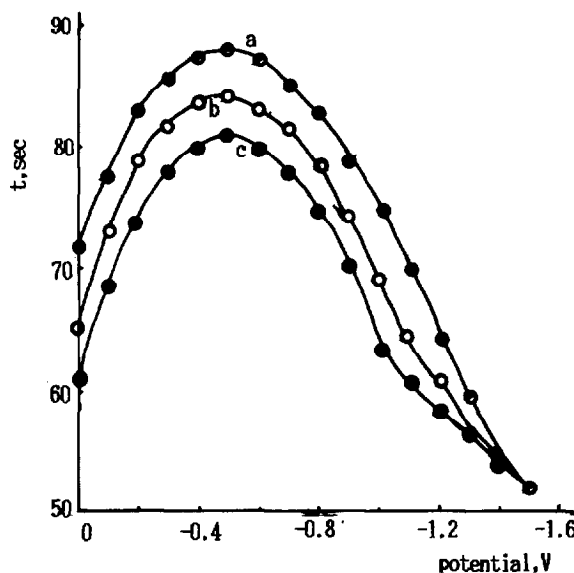

Fig. 3. Electrocapillary curves of enoxacin: (a) 0.050 M HCl, 0.12 M KCl; (b) 0.050 M HCl, 0.12 M KCl, 5.0×10^{-7} M enoxacin; (c) 0.050 M HCl, 0.12 M KCl, 1.0×10^{-7} M enoxacin.

Table 1

Relationship between the value of x and the concentration of enoxacin[a]

Concentration of enoxacin ($\times 10^7$ M)	x
0.0010	0.97
0.0080	0.92
0.010	0.83
0.050	0.72
0.10	0.60
0.50	0.58
1.0	0.55
5.0	0.54
10.0	0.54
50.0	0.50
100	0.48

[a] 0.050 M HCl; mercury drop area of 0.0117 cm^2; rest time of 180 s; potential scan rate from 20 to 800 mV s^{-1}.

rent was measured and the regression of $\log i_p$ vs. $\log v$ gave the value of x listed in Table 1. Table 1 shows that the electrode process of enoxacin was essentially diffusion-controlled at a concentration of enoxacin greater than 5.0×10^{-6} M (diffusion region), whereas at the enoxacin concentrations below 8.0×10^{-10} M the electrode reaction was essentially adsorption-controlled (adsorption region) [20]. In the intermediate concentration range 1.0×10^{-9}–1.0×10^{-6} M the peak current includes both diffusion and adsorption components. These results were also supported by the a.c. impedance spectra of corresponding solutions.

3.6. Cyclic voltammetry

Fig. 4 shows the cyclic voltammograms for the enoxacin–KCl system. The drug gives a cathodic peak at about −1.05 V due to its reduction, and no peak was observed on the anodic branch, indicating the the reduction of enoxacin is irreversible. The width at the mid-peak of the drug was determined (curve a) and found to be 35 mV. The αn_α value was calculated and found to be 1.78 [21]. In Fig. 4 subsequent repetitive scans yielded significantly smaller (but stable) cathodic peaks corresponding to the reduction of dissolved species. This behaviour indicates that the adsorption of the drug on the mercury electrode is reactant adsorption [22], which agrees with normal pulse polarographic data.

3.7. Potentiostatic coulometry

Under optimum conditions the solution containing enoxacin was electrolyzed at −1.15 V until the electrolytic current was close to zero, and the expended charge Q_1 was measured. Similarly, the background solution was electrolyzed under the same conditions and charge Q_2 was obtained. The charge difference ΔQ ($Q_1 - Q_2$) is the charge expended by enoxacin:

$$\Delta Q = nFCV \qquad (1)$$

where C and V are the concentration and volume of the enoxacin solution respectively, and n and F have their usual meanings. From Eq. (1) the electron number of the electrochemical reaction can be found. For enoxacin $n = 1.96 \pm 0.05$.

The pH value strongly affects the position of the potential peak of the drug. The obtained dependence of E_p on the pH values of the test solution is the same as that described in the literature [14]. Over the HCl concentration range 0.50 to 0.010 M (pH 0.3–2.0), the coefficient of the regression equation of peak potential E_p vs. pH was 0.059, indicating that the molecules of the drug combined with one H^+ as soon as the drug obtained one electron. In acidic solution the drug is protonated. The possible electrode process could be assumed to be as follows:
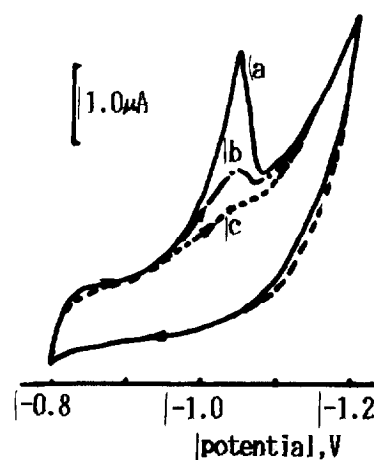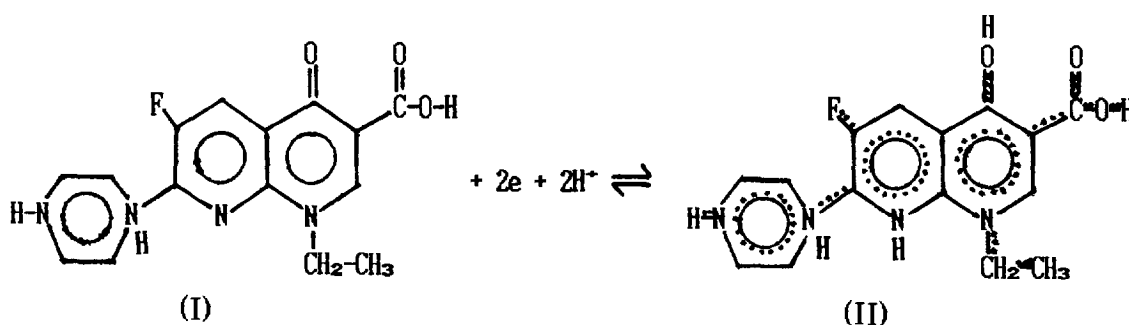

Fig. 4. Cyclic voltammograms of enoxacin. 0.050 M HCl, 0.12 M KCl, 1.6×10^{-6} M enoxacin, scan rate 200 mV s^{-1}, accumulation time 120 s. (a) First scan; (b) second scan; (c) background solution.

(I)   + 2e + 2H⁺ ⇌   (II)

From the quantum-chemical point of view, the enoxacin was reduced, and the two electrons captured from the electrode belonged to the whole of the conjugated system and could move freely along the conjugated system [23] to form product (II).

3.8. Application

The main metabolite of the drug is 4-oxo enoxacin [24]. Its content in plasma is less than

Table 2
Determination of enoxacin in urine and serum samples

Sample	Enoxacin added (μg ml^{-1})	Enoxacin found[a] (μg ml^{-1})	Recovery (%)	Content[b] (μg ml^{-1})
Urine				
No. 1	0	129.2	–	130.0
No. 2	0	101.4	–	100.1
No. 3	0	162.4	–	159.5
No. 4	0	148.0	–	155.6
No. 4	60.0	211.0	105	–
No. 4	120.0	263.0	95.8	–
No. 4	180.0	322.3	96.8	–
No. 4	240.0	391.2	101	–
Serum				
No. 1	0	1.57	–	1.63
No. 2	0	2.58	–	2.55
No. 3	0	4.26	–	4.31
No. 4	0	2.53	–	2.45
No. 4	1.50	4.06	102	–
No. 4	3.00	5.42	96.4	–
No. 4	4.50	7.23	104	–
No. 4	5.50	7.92	97.9	–

[a] Mean of three parallel determinations.
[b] Determination by HPLC.

15% of that of enoxacin so its interference was ignored.

We examined the interference of vitamins such as vitamin C, vitamin B_2 and vitamin B_{12}, which did not affect the determination of the drug.

3.8.1. Analysis of urine samples

Using the single-sweep polarographic procedure proposed in this paper to determine enoxacin in urine samples, no sample pretreatment was required, other than a dilution with the supporting electrolyte.

The standard enoxacin solutions used for the preparation of the calibration line were treated as described in the section on polarography of pure enoxacin. The regression equation of the calibration line has the form:

$$Y = 0.263X + 0.036 \qquad (2)$$

where Y is the peak current in μA and X is the enoxacin concentration in μg ml^{-1}. The correlation coefficient was 0.998. The results of the determination of enoxacin in the urine samples are summarized in Table 2.

3.8.2. Analysis of serum samples

The enoxacin in serum samples was extracted by chloroform because the proteins interfere in the determination of the drug in serum. The standard enoxacin solutions used for the preparation of the calibration line was treated as described in the section on analysis of serum samples. The slope of the calibration line is 0.110 μA ml μg^{-1}, and the intercept is 0.007 μA.

The results of the determination of enoxacin in serum samples are also summarized in Table 2.

References

[1] A.J. Bard, Electroanalytical Chemistry, Vol. 11, Marcel Dekker, New York, 1979, pp. 141–343.

[2] P.T. Kissinger and W.R. Heineman, Laboratory Techniques in Electroanalytical Chemistry, Marcel Dekker, New York, 1983, pp. 569–609.

[3] G.J. Patriarche and J.C. Vire, Anal. Chim. Acta, 196 (1987) 193.

[4] X.K. Kong and J.H. Pang, Yaoxue Xuebao, 26 (1991) 627; Chem. Abstr., 116 (1991) 28247y.

[5] R. Starosak, I. Prachowska and J. Sulkowska, Pharmazie, 29 (1974) 387.

[6] W.J. Van Oort, R.H.A. Sorel, D. Brussee, S.G. Schulman, P. Zuman and J. Den Harugh, Anal. Chim. Acta, 149 (1983) 175.

[7] H. Hoffman and M. Dybowski, Fresenius' Z. Anal. Chem., 313 (1982) 625.

[8] P. O'Dea, A. Costa Garcia, A.J. Miranda Ordiers, P. Tunon Blanco and M.R. Smyth, Electroanalysis 3 (1991) 337.

[9] S. Furlanetto, P. Gratteri, S. Pinzauti, R. Leardi, E. Dreassi and Santoni, J. Pharm. Biomed. Anal., 13 (1995) 431.

[10] A. Tamer, Anal. Chim. Acta, 231 (1990) 129.

[11] G. Zhou and J. Pan, Anal. Chim. Acta, 307 (1995) 49.

[12] X. Liu, G. Chen, D. Xie, S. Wang, J. Zhang, R. Jiang, L. Ding and L. Ming, Yaowu Fenxi Zazhi, 15 (1995) 30.

[13] Y.F. Li, Electroanalytical Characteristics of Quinolone Drugs, Thesis, Hunan University, 1995.

[14] J.A. Squella, A. Alvarez-Lucjc, J.C. Sturm and L.J. Nunez-Vergara, Anal. Lett., 26 (1993) 1943.

[15] L.J. Notarinni and R.W. Jones, J. Chromatogr., 431 (1988) 461.

[16] M. Lovric, J. Electroanal. Chem., 170 (1984) 143.

[17] R.S. Nicholson and I. Shain, Anal. Chem., 36 (1964) 709.

[18] A.J. Band and L.R. Faulkner, Electrochemical Methods, John Wiley, New York, 1980, p. 522.

[19] X.X. Gao and Z.D. Wang, Zhongguo Kexue, Series B, (6) (1987) 582.

[20] R.H. Wopschall and I. Shain, Anal. Chem., 39 (1967) 1514.

[21] E. Laviron, J. Electroanal. Chem., 52 (1974) 355.

[22] S. Dong, Fenxi Yiqi, 1 (1984) 1.

[23] M. Zong, Hückel Molecular Orbital Theory and its Application, Vol. 1, Science Press, Beijing, 1982, pp. 437–449.

[24] T.B. Vree and A.M. Baars, J. Chromatogr., 343 (1985) 449.

ELSEVIER

Acid–base equilibria in γ-butyrolactone studied by use of pH-ISFETs

Kosuke Izutsu*, Masayuki Ohmaki

Department of Chemistry, Faculty of Science, Shinshu University, Matsumoto 390, Japan

Abstract

pH-ISFETs were used in the study of acid–base equilibria in γ-butyrolactone (GBL). After the spectrophotometric determination of the pK_a value of 3,5-dichloropicric acid, the pK_a values and homo-conjugation constants of various acids (including the conjugate acids of bases) were determined potentiometrically using a Ta_2O_5-type pH-ISFET. The values of pK_a in GBL were in a linear relation with those in propylene carbonate (PC) and 1.0 units smaller on average. The difference in pK_a between GBL and PC was mainly attributable to the difference in proton solvation. The autoprotolysis constant of GBL, roughly estimated by a rapid titration with a Si_3N_4-ISFET, was about 30 on the pK_{SH} scale. A comparative study was made of the response speeds of the Ta_2O_5- and Si_3N_4-type pH-ISFETs and a conventional pH-glass electrode. The result was Si_3N_4-ISFET > Ta_2O_5-ISFET > glass electrode. Because GBL is not stable against acids and bases, the use of pH-ISFETs was much more convenient than the use of the conventional glass electrode.

1. Introduction

γ-Butyrolactone (GBL) is a dipolar aprotic solvent with a dielectric constant of 39, a donor number of 18 [1] and an acceptor number of 17.3 [2]. Because GBL is often used as a solvent for lithium batteries, aluminum electrolytic capacitors and electrical double-layer capacitors, the behavior of electrolyte solutions in GBL has been studied to a considerable extent [3]. Coetzee et al. [4] reported on the potentiometric characterization of

GBL using ion-selective electrodes. Though the acid–base behaviour in GBL is also important, detailed study of it does not seem to have appeared. In the present paper, we studied the acid–base equilibria in GBL. In the study, we used pH-ISFETs, which we recently found useful as pH-sensors in nonaqueous solutions [5]. The pH-ISFETs responded faster than a conventional glass electrode and their use in GBL was especially convenient because GBL tended to hydrolyze in the presence of acids and bases. The acid dissociation constants in GBL were compared with those in propylene carbonate (PC) [6,7].

---

* Corresponding author. Fax: + 81 263 35 1085.

Table 1
Spectrophotometric pK_a determination of $HPicCl_2$ in GBL

C_{HA} (mM)	Absorbance (430 nm)	$[PicCl_2^-]$ (mM)	$[HPicCl_2]$ (mM)	γ	pK_a
0.100	0.049	0.0114	0.0886	0.989	5.85
0.200	0.073	0.0169	0.183	0.986	5.82
0.400	0.101	0.0234	0.377	0.984	5.85
0.500	0.117	0.0271	0.473	0.983	5.82
1.00	0.153	0.0355	0.965	0.980	5.90
10.0	0.477	0.1107	9.89	0.966	5.94
				Average	5.86 ± 0.05

2. Experimental

2.1. Apparatus

Ta_2O_5- and Si_3N_4-type pH-ISFETs, both obtained from Shindengen Industry Co. Ltd., were used. Because the contact between the ISFET tip and the leadwire was often attacked by the solvent, that part was protected by fixing with polyethylene. The reference electrode was Ag|5 mM AgClO₄ + 5 mM Et₄NClO₄‖10 mM Et₄NClO₄‖ and the gate voltage was measured with Shindengen ISFET mV/pH meter to 0.1 mV. The response of the ISFETs in GBL was compared with that of a conventional glass electrode (Horiba 1826A-06T9). The potential of the glass electrode was measured with a conventional pH/mV meter. The potential–time relations and titration curves were recorded with a Yokogawa two-pen recorder LR4110-3711 and a Metrohm 665 Dosimat autoburet. The titration data could be stored in a memory card inserted in the slot of the recorder and could be processed with a personal computer. A Shimadzu UV–visible recording spectrophotometer UV-260 was used in spectrophotometric measurements. All measurements were made at 25 ± 1°C.

2.2. Reagents

γ-Butyrolactone was a pure product (F-GBL, water content < 50 ppm) and was a gift of Mitsubishi Petrochemical Co. Ltd. It was used after further purification by adding p-toluenesulfonic acid to neutralize trace basic impurities and distilling under reduced pressure. The solution ≈ 0.1 M Bu₄NOH in MeOH–toluene (1:10 v/v) was prepared by the method of Selig [8] and used for titrating acids. Trifluoromethanesulfonic acid used for titrating bases was the reagent-grade Wako product. 3,5-Dichloropicric acid ($HPicCl_2$) and its tetraethylammonium salt were prepared by the method of Ref. [7]. Other acids and bases and their salts were also obtained as described in Ref. [7].

3. Results and discussion

3.1. Spectrophotometric determination of the pK_a value of 3,5-Dichloropicric acid

The absorption spectra of $Et_4NPicCl_2$ and undissociated $HPicCl_2$ were recorded and the molar absorption coefficient of the $PicCl_2^-$ ion at 430 nm was determined to be 4.31×10^3. The undissociated $HPicCl_2$ was obtained by adding trifluoromethanesulfonic acid to the $HPicCl_2$ solution. Then, measuring the absorbance of $HPicCl_2$ solutions between 10^{-4} M and 10^{-2} M at 430 nm, the dissociation constant K_a of $HPicCl_2$ was determined by the relation $K_a = \gamma^2[H^+][PicCl_2^-]/[HPicCl_2]$, where $[H^+] = [PicCl_2^-]$, and the ionic activity coefficient γ was obtained from the Debye–Hückel equation. As shown in Table 1, the pK_a value of $HPicCl_2$ was 5.86 ± 0.05 and there was no indication of a homo-conjugation reaction.

3.2. Potentiometric determination of pK_a values and homo-conjugation constants

The Nernstian response $(59.2 \pm 1.0 \text{ mV } pa_H^{-1})$ of the Ta_2O_5-type pH-ISFET was confirmed by titrating 20 ml of 5 mM $HPicCl_2$ in GBL with 0.1 M Bu_4NOH solution in MeOH–toluene (1:10 v/v). The ISFET showed an equilibrium potential 1 min after each addition of titrant. The effect of the MeOH–toluene on the proton activity (a_H) was neglected and the pH of the solution during titration was obtained by

$$a_H^2\gamma^2 C_s - a_H\gamma K_a[(C_s + C_a) + K^f(HA_2^-)(C_s - C_a)^2]$$

$$+ K_a^2 C_a = 0 \qquad (1)$$

where C_a and C_s are the concentrations of the acid and its salt and, for $HPicCl_2$, the homo-conjugation constant $K^f(HA_2^-)$ was equal to zero.

Using the Ta_2O_5-type pH-ISFET calibrated in the solution 1:1 mixture of $HPicCl_2$ and $Et_4NPicCl_2$, the solution of 5 mM picric acid (HPic) in GBL was titrated with the Bu_4NOH solution. The pK_a value of HPic was determined from the half-neutralization potential to be 8.35. Then the experimental results for the relation between $(pH - pK_a - \log \gamma)$ and (% titrated) were plotted and compared with the theoretical curves of the same relation for various $K^f(HA_2^-)$ values. Personal computer software Katto-Pro from the Ever Green Co. Ltd., Japan, was used in the data processing. With HPic, the best fit was obtained when no homo-conjugation reaction was assumed.

For other acids of the HA-type, the relations of $(pH - pK_a - \log \gamma)$ vs. (% titrated) were obtained by titrating the acids with the Bu_4NOH solution. For the acids of BH^+-type, the bases B were titrated with the trifluoromethanesulfonic acid solution in GBL. The pH-ISFET was calibrated before and after each titration with a buffer solution of 3 mM HPic–3 mM Et_4NPic. The pK_a values of the acids were obtained from the half-neutralization potentials while the homo-conjugation constants were obtained by fitting the theoretical titration curves to the experimental results. Eq. (1) was used for obtaining theoretical
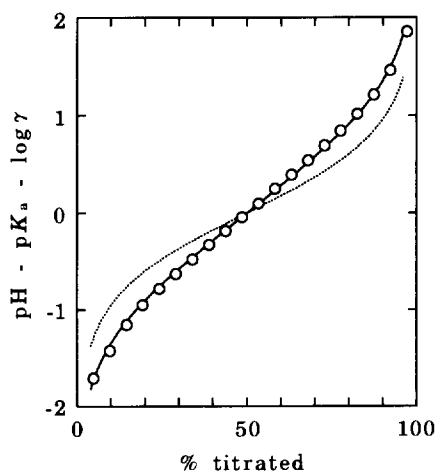
Fig. 1. Relations of $(pH - pK_a - \log \gamma)$ vs. (% titrated) for the titration of 20 ml of 5 mM oxalic acid in GBL with 0.1 M Bu_4NOH in MeOH–toluene. Circles are experimental results and solid and dotted lines are theoretical relations for $K^f(HA_2^-) = 400$ and 0 respectively.

pH values during titration.

Some of the theoretical and experimental titration curves are shown in Figs. 1 and 2. The values of pK_a and $K^f(HA_2^-)$ are summarized in Table 2. For BH^+-type acids no appreciable homo-conjugation reaction occurred.
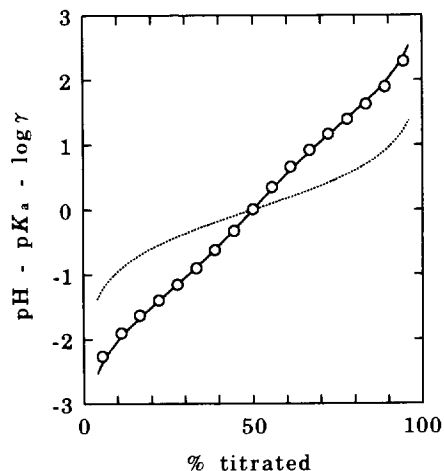

Fig. 2. Relations of $(pH - pK_a - \log \gamma)$ vs. (% titrated) for the titration of 20 ml of 5 mM 3,5-dinitrobenzoic acid in GBL with 0.1 M Bu_4NOH in MeOH–toluene. Circles are experimental results and solid and dotted lines are theoretical relations for $K^f(HA_2^-) = 3000$ and 0 respectively.

Table 2

pK_a values and homo-conjugation constants of acids and conjugate acids of bases in GBL

Acids[a]	pK_a^b	$K^f(HA_2^-)^{b,c}$
3,5-Dichloropicric acid (1)	5.8_6	≈ 0
Picric acid (3)	8.3_5	≈ 0
p-Toluenesulfonic acid	7.1_5	1.9×10^2
Salicylic acid (7)	14.5_4	5.7×10^2
Oxalic acid	12.4_4	4.7×10^2
Phthalic acid	12.4_0	≈ 0
Methanesulfonic acid (2)	8.05	1.7×10^3
Trifluoroacetic acid	10.8_0	5.0×10^3
3,5-Dinitrobenzoic acid	15.0_6	3.5×10^3
2,4-Dinitrophenol (6)	13.6_6	≈ 0
Anilinium (4)	9.1_3	≈ 0
1,3-Diphenylguanidinium (8)	15.5_0	≈ 0
Triethylammonium (10)	16.6_0	≈ 0
Tributylammonium (9)	16.5_7	≈ 0
Pyridinium (5)	10.7_6	≈ 0

[a] For the numbers in parentheses, see Fig. 3.

[b] Average of 2–5 measurements.

[c] ≈ 0 means $K^f(HA_2^-) < 50$. For conjugate acids of bases, $k^f(B_2H^+)$ values are shown.

3.3. Comparison of the pK_a values in GBL and PC

The relation between the pK_a values in GBL and PC [7] are plotted in Fig. 3. There is a linear relation with unit slope. The average difference between the pK_a values in the two solvents is 0.96.
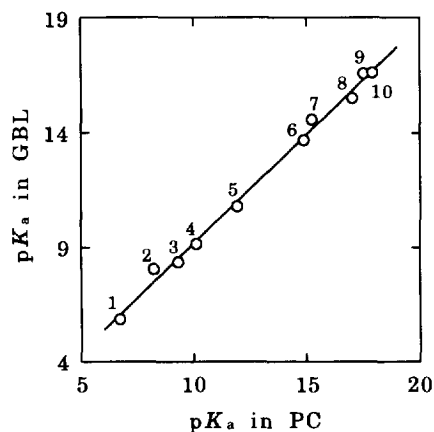
Fig. 3. Relation between pK_a values in GBL and those in PC. Numbered circles refer to the acids listed in Table 2.

The solvent effect on pK_a can be represented by

$$pK_a(HA,S) - pK_a(HA,R)$$

$$= \log \gamma_t(H^+,R \to S) + \log \gamma_t(A^-,R \to S)$$

$$- \log \gamma_t(HA,R \to S) \qquad (2)$$

$$pK_a(BH^+,S) - pK_a(BH^+,R)$$

$$= \log \gamma_t(H^+,R \to S) + \log \gamma_t(B,R \to S)$$

$$- \log \gamma_t(BH^+,R \to S) \qquad (2')$$

where γ_t shows the transfer activity coefficient from solvent R to S. If $\log \gamma_t(A^-,R \to S) \doteqdot \log \gamma_t(HA,R \to S)$ or $\log \gamma_t(B,R \to S) \doteqdot \log \gamma_t(BH^+, R \to S)$, we can expect $pK_a(HA,S) - pK_a(HA,R) \doteqdot \log \gamma_t(H^+,R \to S)$ or $pK_a(BH^+,S) - pK_a(BH^+, R) \doteqdot \log \gamma_t(H^+,R \to S)$. In the previous paper [5], we confirmed that both pH-ISFETs and the glass electrode responded in near-Nernstian ways to $\log \gamma_t(H^+,R \to S)$. We determined $\log \gamma_t(H^+,GBL \to PC)$ using the ISFETs and the glass electrode, under the extrathermodynamic assumption of negligible liquid junction potential [9] which was considered to be reliable enough from our detailed study [10] on the liquid junction potential between different solvents. The values of $\log \gamma_t(H^+,GBL \to PC)$ obtained were between 1.0 and 1.5 and fairly near to the difference between pK_a values in PC and GBL. Thus the difference between pK_a values in PC and GBL can mainly be attributed to the difference in proton solvation. The donor numbers of PC and GBL are 15.1 and 18 respectively, and GBL is somewhat more basic than PC. However, the structures and properties of PC and GBL are somewhat similar to each other. Therefore, it seems reasonable that the relations $pK_a(HA,PC) - pK_a(HA,GBL) \doteqdot \log \gamma_t(H^+,GBL \to PC)$ and $pK_a(BH^+,PC) - pK_a(BH^+,GBL) \doteqdot \log \gamma_t(H^+,GBL \to PC)$ were obtained.

3.4. Comparison of the response of the pH-ISFETs and the glass electrode in GBL and rough estimation of the autoprotolysis constant of GBL

In the determination of pK_a values and homo-conjugation constants above, the Ta_2O_5-type pH-ISFET was mainly used. When the glass electrode
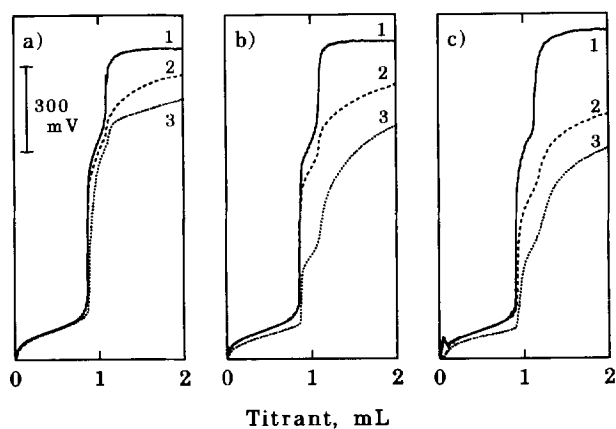
Fig. 4. Titration curves of 20 ml of 5 mM picric acid in GBL with 0.1 M Bu_4NOH in MeOH–toluene, obtained with three kinds of pH sensor and at three different speeds of titrant addition. Speed of titrant addition: (a) 0.075; (b) 0.5; and (c) 4.5 ml min^{-1}. pH sensor: (1) Si_3N_4-ISFET; (2) Ta_2O_5-ISFET; and (3) glass electrode.

was used, it took a few hours or more to get a whole titration curve and some distortion occurred in the curve mostly as the result of hydrolysis of GBL by acids and bases. Thus it was difficult to get reliable information with the glass electrode. The response of the Ta_2O_5-type ISFET was fast enough in so far as the titration curves were measured *manually*, waiting, after each addition of titrant, until the equilibrium potentials were reached.

In order to get titration curves more rapidly, the use of a pH sensor with higher response speed was essential. We ran a comparative study concerning the response speeds of the Si_3N_4- and Ta_2O_5-type pH-ISFETs and the glass electrode. Typical results are shown in Fig. 4. The titration curves of picric acid with Bu_4NOH were obtained at three different titration speeds using an autoburet. The recording of a titration curve took approximately 27 min for (a), 4 min for (b) and approximately 27 s for (c). It is apparent that the response speed is in the order Si_3N_4-ISFET > Ta_2O_5-ISFET > glass electrode. With the Si_3N_4-ISFET, the titration curve was almost satisfactory even in case (c) and the pH reached after the end point was the highest in this case. In cases (a) and

(b), the pH after the end point was lower than in case (c) because of the reaction of OH^- ions with GBL. In addition to the rapid response, the Si_3N_4-ISFET could respond in the Nernstian way to the pH in GBL.

The curve for the rapid titration of picric acid with Bu_4NOH obtained with Si_3N_4-ISFET (curve 1 of Fig. 4c) was used for the rough estimation of the autoprotolysis constant (K_{SH}) of GBL. It was between 29 and 30 on the pK_{SH} scale. The pK_{SH} of PC has been reported to be ≈ 29 [6,11]. This result also supports the fact that the acid–base property of GBL is close to that of PC.

4. Conclusions

In the present work, we used a Ta_2O_5-type pH-ISFET to determine the pK_a values and homo-conjugation constants of acids in GBL and a Si_3N_4-type pH-ISFET to estimate the pK_{SH} value of GBL. This seems to be the first use of pH-ISFETs for the practical study of acid–base equilibria in nonaqueous solvents. Due to their rapid response, the pH-ISFETs gave results which could not be obtained with a conventional glass electrode. pH-sensors with high response speeds are very important in nonaqueous solutions. They are applicable to unstable acid–base systems in nonaqueous solvents. They can also be used for pH measurements of flow systems as well as for high speed nonaqueous acid–base titrations. Systematic studies are now in progress in our laboratory to develop highly reliable pH-sensors for use in nonaqueous systems.

References

[1] Y. Marcus, Ion Solvation, Wiley, New York, 1985, p. 143.

[2] C. Reichardt, Solvents and Solvent Effects in Organic Chemistry, 2nd. edn., VCH, New York, 1988, p. 23.

[3] M. Ue, J. Electrochem. Soc., 141 (1994) 3336. M. Ue, K. Ida and S. Mori, J. Electrochem. Soc., 141 (1994) 2989 (and references cited therein).

[4] J.F. Coetzee, T.-H. Chang, B.K. Deshmukh and T. Fonong, Electroanalysis, 5 (1993) 765.

[5] K. Izutsu, T. Nakamura and S. Hiraoka, Chem. Lett., (1993) 1843. K. Izutsu, T. Nakamura, T. Arai and M. Ohmaki, Electroanalysis, 7 (1996) 884.

[6] K. Izutsu, Acid–Base Dissociation Constants in Dipolar Aprotic Solvents, IUPAC Chemical Data Series No. 35, Blackwells, Oxford, 1990.

[7] K. Izutsu, I.M. Kolthoff, T. Fujinaga, M. Hattori and M.K. Chantooni, Jr., Anal. Chem., 49 (1977) 503. K. Izutsu, T. Nakamura and I. Iijima, Bull. Chem. Soc. Jpn., 59 (1979) 2721.

[8] W. Selig, Microchem. J., 23 (1978) 466.

[9] R. Alexander, A.J. Parker, J.H. Sharp and W.E. Waghorne, J. Am. Chem. Soc., 94 (1972) 1148.

[10] K. Izutsu, Anal. Sci., 7 (1991) 1 (and references cited therein).

[11] N.A. Baranov, G.B. Manukhina and N.A. Vlasov, Zh. Fiz. Khim., 53 (1979) 2634; Russ. J. Phys. Chem., 53 (1979) 1503.

Dialkylphosphoric acids as carriers in separation of lanthanides and thorium on supported liquid membranes

A. Hrdlička*, I. Fialová, J. Doležalová

Department of Analytical Chemistry, Masaryk University, Kotlářská 2, 611 37 Brno, Czech Republic

Abstract

Permeation of seven lanthanides (Ln) and thorium through a supported liquid membrane containing di-(n-octyl)phosphoric (DOPA) or di-(n-pentyl)phosphoric (DPPA) acid as a carrier has been studied as a function of the chemical composition of the system. The results have been compared with a previous study in which di-(2-ethyl-hexyl)phosphoric acid was used.

Metal cations were transported from feed solutions of pH 1.1–4.8 (HNO_3) into strip solutions of 0.015–0.1 mol l^{-1} nitric acid. The ionic strength was kept constant at 0.1 mol l^{-1} (HNO_3, KNO_3). The initial lanthanide concentration and carrier concentration in the liquid membrane were varied from 0.5 to 500 μmol l^{-1} and from 0.01 to 0.5 mol l^{-1} respectively. To describe the mass transfer of metal cations, permeability coefficients have been determined by inductively-coupled plasma atomic emission spectroscopy or by on-line flow-injection analysis of metal concentrations in strip or feed solution.

Probably as the result of a higher solubility of the carrier in aqueous media, transport of Ln with DPPA was not observed. By using DOPA, La, Ce, Pr, and Nd permeated through the membrane while transport of heavier Ln was partly or totally suppressed. This enables these four Ln (separation factor $\alpha = 3.0$ for Nd and Sm) to be separated from the others. Furthermore, at a very low acidity gradient, only La (III) is transported over the membrane ($\alpha \geq 3.4$ for La, Ce and next Ln). The seven elements from La to Tb can be separated from Th(IV) because no evidence of its permeation through the membrane was found under the conditions of Ln transport. In contrast to previous studies on Ln transport with dialkylphosphoric acid carrier, the possibility of participation of species other than $Ln(AHA)_3$ in the transport has been discussed. The decrease of permeability observed at higher Ln concentrations and higher pH of the feed solution has been explained as the result of formation of species, e.g. polymeric ones, that are unable to permeate through the membrane.

Keywords: Lanthanides; Thorium; Membrane separation

* Corresponding author.

1. Introduction

The commercial-scale separation and refining of rare earth elements (REE) have been mainly carried out by solvent extraction with di-alkylphosphoric acids (DAPAs), particularly with di-(2-ethylhexyl)phosphoric acid (DEHPA) [1,2]. Recently, new DAPA extractants, such as di-(4-ethylcyclohexyl)phosphoric acid [3] and isopropyl-3-pentadecylphenylphosphoric acid [4], have been investigated with the aim of improving extraction efficiency. Generally, better extraction properties were found with DAPAs with long and straight alkyl chains than with those with short and branched chains [5]. The extraction separation of adjacent lanthanides (Ln) follows the trend n-octyl < 2-ethyl-hexyl < 3-octyl, i.e. in the order of increasing steric hindrance by the alkyl group [6]. Another feature of lanthanide extraction with organophosphoric acids is an increase of extraction efficiency with atomic number owing to lanthanide contraction [3,6,7].

Among DAPA extractants for Ln, di(n-pentyl)phosphoric (DPPA) and di(n-octyl)phosphoric acid (DOPA) have been employed. In agreement with the conclusions reported above, considerably higher values of extraction constants of Ln with DOPA were found than those with DEHPA and the values of separation factors for adjacent Ln were lower when DOPA was used [5].

A new approach for selective extraction and enrichment is the supported liquid membrane (SLM) technique that is employed in both chemical technology and analytical chemistry [8,9]. The analytical application of this technique consists of sample preparation before analysis and field sampling. The basic principle is a continuous extraction from an aqueous phase (feed solution) into a liquid membrane, followed by a continuous stripping to aqueous acceptor phase (strip solution) on the other side of the membrane. The membrane is formed by an organic solvent of low polarity, immobilised in a thin porous hydrophobic support.

Application of DEHPA in the transport of REE through SLMs is currently under study [10–13]. In previous work [14–16], transport of Ln has been investigated as a function of hydrody-namic conditions, feed solution acidity and carrier concentration.

Here we present the results of our detailed study on the transport of Ln through SLMs containing DPPA or DOPA as a function of the chemical composition of the system, aimed at comparison of these carriers with DEHPA and the explanation of transport processes of Ln with dialkylphosphoric acid carriers. Furthermore, the transport of Th(IV) that coexists with Ln, e.g. in monazite and thorite, has been investigated. Separation of Th from REE is important in analysis and production of these elements which may be of particular interest in the future regarding the possible use of thorium in nuclear power plants.

2. Experimental

2.1. Reagents and solutions

Nitrates of La (Merck, Germany), Ce (Carlo Erba, Italy), Nd, Eu and Tb_4O_7 (Fluka, Switzerland) of analytical-grade purity as well as pure nitrates of Pr and Sm (Fluka) were dissolved in nitric acid. Stock solutions of 2.5 mmol l^{-1} Ln or $Th(NO_3)_4$ (analytical grade; Lachema, Czech Republic) in 0.1 or 0.15 mol l^{-1} HNO_3 respectively, were standardised by chelatometric titration.

DPPA and DOPA were synthesized and purified in the Department of Inorganic Chemistry of the University. Their purity was verified by ^{1}H-NMR and ^{31}P-NMR spectroscopy. Stock solutions of the dialkylphosphoric acids were prepared in kerosene (Lachema) which was previously purified by extraction with 0.5 mol l^{-1} sodium hydroxide, water, and 0.5 mol l^{-1} hydrochloric acid.

Feed solutions of pH 1.1–4.8 (pH adjusted with dilute nitric acid or ammonia) contained lanthanide or thorium at an initial concentration of 4.2 μg ml^{-1} with the exception of the study of the effect of metal concentration where the concentration of La, Pr, or Eu was varied in the range 0.5–500 μmol l^{-1}, i.e. between 0.07 and 76 μg ml^{-1}. As a strip solution, 0.015–0.1 mol l^{-1} nitric acid was used. The ionic strength of the feed and strip solutions was kept constant at 0.1 mol l^{-1} (HNO_3, KNO_3).

The reagent solution used in the flow-injection analysis (FIA) determination of Ln [17,18] contained 0.06 mmol l^{-1} Xylenol Orange (Lachema), 0.6 mmol l^{-1} cetylpyridinium bromide monohydrate (pure; Aldrich, USA) and 4% v/v ethanol (distilled; Lachema) in 0.2 mol l^{-1} acetate buffer pH 4.5.

Isothermally-distilled ammonia was used. All other reagents were of analytical grade purity and were purchased from Lachema.

2.2. Procedure and apparatus

Durapore GVHP 04700 (Millipore, USA), a laminar microporous poly(vinylidenedifluoride) film of 125 μm thickness and with an effective pore diameter of 0.22 μm, was used as a solid support for liquid membranes. The effective area of the liquid membrane, i.e. the product of the nominal porosity coefficient of the support (0.75) and its cross-sectional area in contact with solutions, was 8.51 cm^2.

SLMs were prepared, treated and reimpregnated by the method described earlier [14]. One membrane was reused up to 50 times without the observation of any inconsistency in the results. When not in use the purified membrane was stored in kerosene.

Transport experiments were performed in a two-compartment cell described elsewhere [19], in which the flat sheet membrane separated the feed from the strip solution (200 ml of each). Both solutions were stirred at 1300 rev min^{-1} [14].

Lanthanide concentrations in feed and/or strip solution were on-line monitored using a FIA spectrophotometric method [17] based on the reaction of Ln with Xylenol Orange and cetylpyridinium bromide at pH 4.5 which was adjusted by acetate buffer. By injecting samples of acidic strip solution, a negative signal was obtained due to insufficient capacity of the acetate buffer. The determination of lanthanide in the strip solution was established as the linear decrease of the absolute value of this negative signal with increasing metal concentration. The data used to determine the permeability coefficient values were collected at 3 min intervals 3–30 min from the beginning of the transport experiment. Feed solution acidity was monitored during the run.

A Model PCR 01 four-path peristaltic pump equipped with Tygon tubing (Labeco, Slovak Republic) was used to maintain the flows of the FIA reagent, carrier, and sampled solution each at 0.8 ml min^{-1}. As the carrier solution, 0.2 mol l^{-1} acetate buffer pH 4.5 was employed. The FIA manifold consisted of a Model 5020, six-port injection valve (Rheodyne, USA) with a sample loop of 72 ml volume, a Model VD 104 on-capillary photometric detector (Labeco), and a TZ4620 recorder (Laboratory Instruments Prague, Czech Republic). Transport lines, a 0.5 m mixing coil and a 1 m reaction coil were made with 0.8 mm i.d. Teflon tubing. Lanthanide concentration was monitored at 610 nm with 40 nm bandwidth.

To follow the effect of metal concentration on membrane transport of Ln and to study the transport of Th(IV), 1 ml aliquots were taken from the feed and strip solution at 5 min intervals during a 30 min membrane experiment and diluted 1:1 with nitric acid solution. A Model PU 7000 inductively-coupled plasma sequential atomic emission spectrometer with grid nebulizer and plasma generator working at a power input of 0.9 kW (Philips-Unicam, UK) was employed to determine the metal concentration. The samples in 0.1 mol l^{-1} HNO_3 were introduced at a flow rate of 1 ml min^{-1} by means of a peristaltic pump. The measurement of Th, La, Pr, and Eu was performed at wavelengths of 283.730, 333.749, 390.844 and 381.967 nm respectively. Nitric acid, 0.1 mol l^{-1}, was used as a reference solution.

A Model OP-208 pH-meter equipped with an OP-0808-P glass–Ag/AgCl combined electrode and phthalate and phosphate standard buffers (all Radelkis, Hungary) was used for acidity measurements.

3. Results and discussion

Mass transport of metal cations has been expressed in terms of permeability coefficients, P (cm min^{-1}). Their values were determined from sets of primary data in the form of a metal concentration vs. time dependence by using the linear relationship introduced by Danesi [20]:

$$\ln \frac{c_{f,0}}{c_f} = \frac{Q}{V_f} \cdot P_f t \tag{1}$$

where Q is the membrane effective area, V_f is the volume of feed solution, and $c_{f,0}$ and c_f are time-dependent bulk concentrations of the metal species in the feed solution at time zero and time t respectively. P_f represents the value of the permeability coefficient determined from the measurement of c_f.

In previous studies [14–16] on the permeation of lanthanide cations through SLMs containing di-(2-ethylhexyl)phosphoric acid, a decrease in permeability at pH > 2.5–3 and/or at higher DEHPA concentrations was noted. The presence of a waxy-gelled, metal-containing substance in the feed solution and at the feed–membrane interface has been interpreted in terms of chemical speciation and blockage of the membrane surface. The presence of the gel-like substance in the feed solution has also been observed by other authors [21,22]. To avoid discrepancies arising from formation of this substance, variations of metal concentration in the feed solution have been monitored as the difference between the initial concentration of the metal, $c_{f,0}$, and its concentration in the strip solution at time t, c_s. Therefore, the values of permeability coefficients P_s have been estimated by using the linear Eq. (2) [15]:

$$\ln \frac{c_{f,0}}{c_{f,0} - c_s} = \frac{Q}{V_f} \cdot P_s t \tag{2}$$

Thus, for the determination of P_s values, the separation function of the membrane has been considered for the strip–membrane interface.

3.1. DPPA

The application of DPPA as a carrier has been investigated under the conditions that have been found favourable for the membrane transport of lanthanides with DEHPA [14–16]. The DPPA and initial Nd(III) concentrations were kept at 50 mmol l^{-1} and 4.2 μg ml^{-1} respectively. The strip solution consisted of 0.1 mol l^{-1} HNO$_3$ and the feed solution acidity was varied in the range pH 2.8–5.5. In successive experiments, the carrier concentration was increased up to 250 mmol l^{-1} and the acidity gradient over the membrane,

which is a driving force in membrane transport with acidic carriers, was enhanced by using 0.5 mol l^{-1} HNO$_3$ as a strip solution (ionic strength in solutions kept at 0.5 mol l^{-1} (HNO$_3$, KNO$_3$). However, no evidence for the transport of Nd(III) cations into and/or through the liquid membrane was found during the 95 min experiments, probably due to the solubility of DPPA in the aqueous phase. In a SLM, the volume of the liquid membrane is negligible in comparison to those of the feed and strip solutions and thus higher solubility of the carrier in aqueous media has a detrimental effect on the transport process. Subsequent application of DOPA as a carrier possessing longer alkyl chains and hence having lower solubility in water media, resulted in a noticeable transport of Ln through the SLM under the experimental conditions mentioned above.

3.2. DOPA

3.2.1. Effect of acidity

In previous studies on lanthanide permeation through SLMs with DEHPA [10–16], which mostly used a dialkylphosphoric acid carrier, the effect of the strip solution acidity on transport has been investigated rarely or not at all. In Fig. 1,
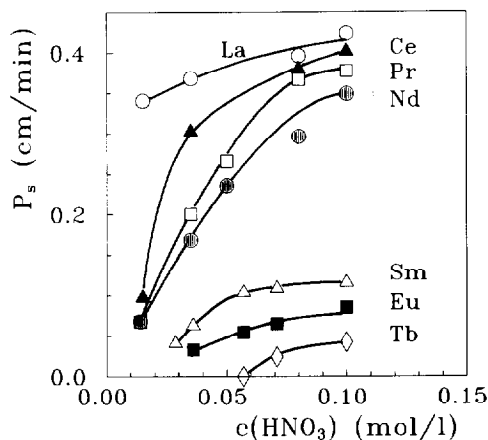

Fig. 1. Effect of strip solution acidity on permeability coefficients. Feed solution: initial lanthanide concentration 4.2 μg ml^{-1}; pH: La, 3.10 $\pm$ 0.01; Ce, 3.08 $\pm$ 0.02; Pr, 3.04 $\pm$ 0.02; Nd, 2.90 $\pm$ 0.04; Sm, 2.87 $\pm$ 0.05; Eu, 3.12 $\pm$ 0.02; Tb, 3.10 $\pm$ 0.05. Ionic strength in feed and strip solutions: 0.1 mol l^{-1} (HNO$_3$, KNO$_3$). SLM: 50 mmol l^{-1} DOPA in kerosene.
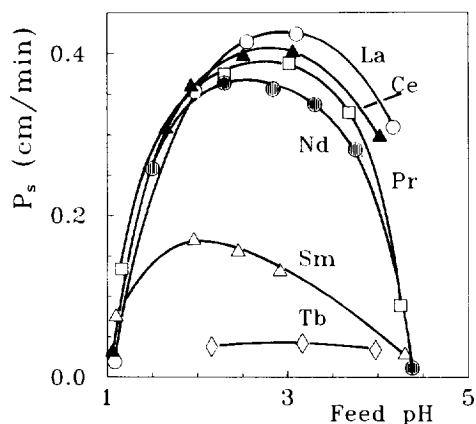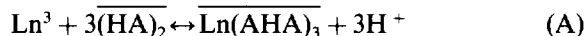
Fig. 2. Effect of feed solution pH at higher acidity gradient. Strip solution acidity given by 0.1 mol 1^{-1} HNO_3. Other conditions as in Fig. 1.

the behaviour of Ln in transport with DOPA carrier is shown in terms of dependence on nitric acid concentration in the strip solution. The permeability coefficients decrease with increasing atomic number and those of light Ln from La to Nd are considerably higher than the values found for Sm, Eu, and Tb. The difference increases with acidity of the strip solution and at 0.1 mol 1^{-1} HNO_3 the membrane separation factor of the couple Nd–Sm, $\alpha = P_{s,Nd}/P_{s,Sm}$, equals 3.0, which can be used in separation of the groups of Ln. In contrast, permeability coefficients rapidly decrease in the case of nitric acid concentrations lower than about 70 mmol 1^{-1} (Tb) or 40 mmol 1^{-1} (Ce). However, La(III) permeability remains high even at 15 mmol 1^{-1} HNO_3. Thus, La(III) can be separated from adjacent cerium ($\alpha = P_{s,La}/P_{s,Ce} = 3.4$) or from the other Ln at low acidity of the strip solution.

The P_s vs. feed solution pH curves of light Ln presented in Fig. 2 (0.1 mol 1^{-1} HNO_3 as strip solution) exhibit maxima. With increasing atomic number, the maxima are lower and their position changes from pH 3.2 for La to pH 2.1 for Sm. The transport of Tb, a representative of the heavy Ln, practically does not proceed and the curve of Tb is flat. If the acidity gradient is decreased by lowering the concentration of nitric acid in the strip solution to 35 mmol 1^{-1} (Fig. 3), i.e. at lower force driving the transport, a plateau and

maximum appear on the curves of La, Ce, and Pr (maxima: pH 3.1 for La, 3.0 for Ce, 1.9 for Pr; plateau: pH 1.9–2.5 for La and Ce, 2.5–3.0 for Pr). The curves of Nd and Sm show maxima at pH 1.9 and 2.1 respectively. Only a slight deformation can be found on the Nd curve at pH ≈ 2.8 where the plateau should appear by analogy with praseodymium. The permeability of the next lanthanide, Sm, is already low and Tb is not transported over the membrane due to the low acidity gradient. The position of the maxima on the curves of La, Ce, and Sm and that of the plateau or deformation on the curves of Pr or Nd corresponds approximately to the maxima found at higher acidity gradient in Fig. 2.

The appearance of the plateau and maxima on pH curves measured at lower acidity gradient could be explained by the transport of two species with different permeability which are formed due to dependence on feed solution pH. This, of course, means that the commonly suggested [5,21,22] extraction equilibrium (A)

$$Ln^3 + 3\overline{(HA)_2} \leftrightarrow \overline{Ln(AHA)_3} + 3H^+ \qquad (A)$$

where overbars denote the species present in the organic phase of low polarity and HA represents DAPA extractant, is not the only one which could take place in the membrane transport processes. It is well known that LnA_3 species are formed in the solvent extraction with deficient amount of
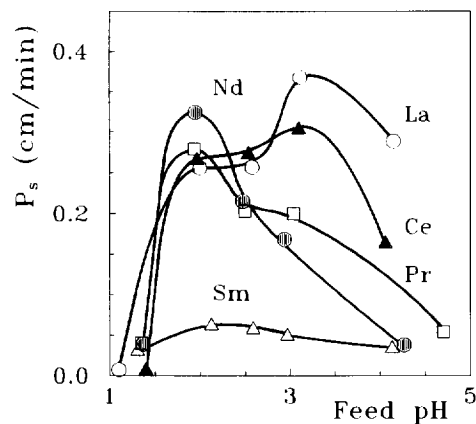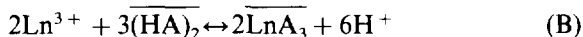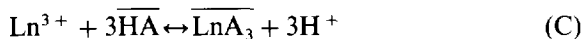

Fig. 3. Effect of feed solution pH at lower acidity gradient. Strip solution acidity given by 0.035 mol 1^{-1} HNO_3. Other conditions as in Fig. 1.

DAPA [5] where the extraction equilibria could follow scheme (B):

$$2Ln^{3+} + 3\overline{(HA)_2} \leftrightarrow 2\overline{LnA_3} + 6H^+ \quad (B)$$

or scheme (C):

$$Ln^{3+} + 3\overline{HA} \leftrightarrow \overline{LnA_3} + 3H^+ \quad (C)$$

if the dimerization of DAPA does not proceed. Explanation of membrane transport of Ln by equilibrium (C) has been suggested in the literature [11]. However, the DOPA concentration in the liquid membrane in our study was about three orders of magnitude higher than the initial Ln concentration in the feed solution and, thus, the conditions were more favourable for equilibrium (A).

In contrast, the equilibria producing mixed-ligand complexes $Ln(AHA)_x(NO_3)_y(HA)_z$, where $x + y = 3$, could also proceed for the extraction from nitrate solutions. Taking into account the coordination number (six) of Ln(III) cation and the presence of dimeric $(HA)_2$ and anionic $(AHA)^-$ species, the complexes, e.g. $Ln(AHA)_2$-$(NO_3)(HA)_2$, could be formed in the membrane separation process and the equilibrium (D) could proceed with dependence on pH:

$$\overline{Ln(AHA)_2(NO_3)(HA)_2} \leftrightarrow \overline{Ln(AHA)_3} + H^+ + NO_3^-$$

$$(D)$$
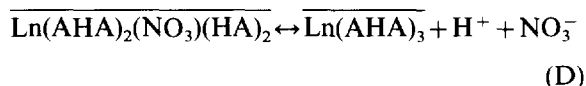
The formation of similar mixed-ligand complexes in acetone solutions, referred to as Eu-$A(NO_3HA)_2$, and their decomposition to EuA_3 polymeric species appearing as a solid phase after dilution with water, have been described elsewhere [23].

3.2.2. Effect of carrier concentration

The effect of DOPA concentration in the liquid membrane on the permeation of Ln into strip solutions of 100 mmol l^{-1} (Fig. 4) and 35 mmol l^{-1} nitric acid (Fig. 5) was studied at pH 3.0 $\pm$ 0.1 of the feed solution, i.e. near the maxima (or plateau) observed in the pH curves in Figs. 2 and 3. All the plots of P_s vs. DOPA concentration have maxima at 50 mmol l^{-1} DOPA. In Fig. 5, i.e. at lower acidity gradient, lower P_s values are attained and the decrease of La and Ce perme-
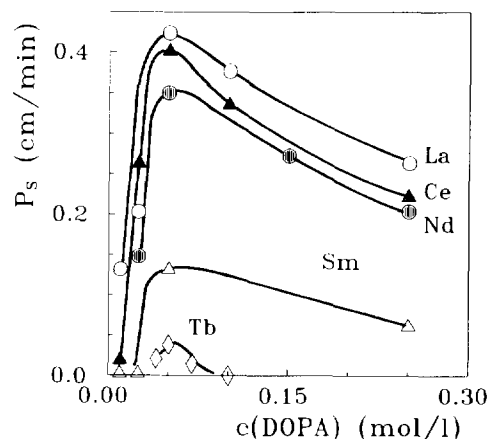

Fig. 4. Effect of carrier concentration at higher acidity gradient. Feed solution pH: La, 3.07 ± 0.03; Ce, 3.03 ± 0.03; Nd, 2.95 ± 0.05; Sm, 2.93 ± 0.02; Tb, 3.13 ± 0.03. Strip solution acidity given by 0.1 mol l^{-1} HNO$_3$. Other conditions as in Fig. 1.

ability coefficients at $c(DOPA) > 50$ mmol l^{-1} is sharper.

3.2.3. Effect of lanthanide concentration

Studies on membrane transport involving the effect of metal concentration are few [12,24,25] although this variable can play an important role as shown in Fig. 6. The permeability coefficients of La and Pr determined from Eqs. (1) and (2) are
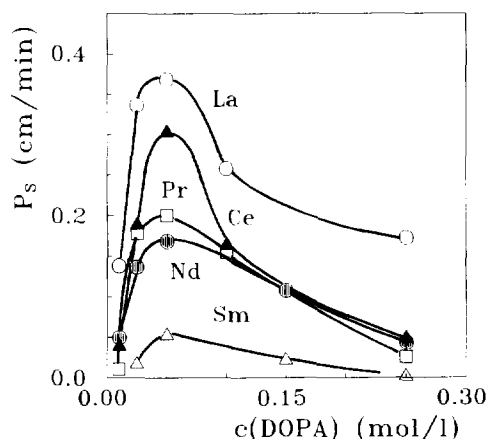

Fig. 5. Effect of carrier concentration at lower acidity gradient. Feed solution pH: La, 3.12 ± 0.01; Ce, 3.08 ± 0.01; Pr, 3.03 ± 0.03; Nd, 2.91 ± 0.03; Sm, 2.98 ± 0.03. Strip solution acidity given by 0.035 mol l^{-1} HNO$_3$. Other conditions as in Fig. 1.
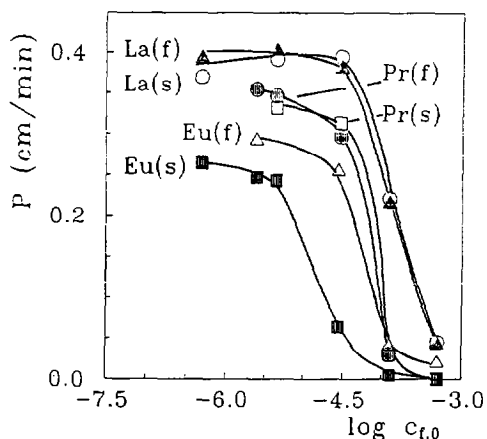
Fig. 6. Effect of initial lanthanide concentration (mol l^{-1}) on permeability coefficients measured in feed and strip solutions. Feed solution pH: La, 2.83 ± 0.05; Pr, 2.80 ± 0.06; Eu, 2.84 ± 0.06. Other conditions as in Fig. 1.

practically independent of initial concentrations $c_{f,0} < 30$ μmol l^{-1}. For Eu, representing the group of heavier Ln, this limit is valid only for P_f values while those of P_s decrease even at $c_{f,0} > 5$ μmol l^{-1}. Furthermore, P_s values are lower than P_f values over the whole concentration range studied.

At $c_{f,0} > 30$ μmol l^{-1}, the ratio of c(DOPA)/$c_{f,0}$ is still high, ranging between 1.6×10^3 and 1×10^2. Thus Eq. (1) should be valid and the initial membrane flux, J_0, should vary with $c_{f,0}$ in compliance with the relation $J_0 = P \cdot c_{f,0}$ [20,25], where the permeability coefficient P is a proportionality constant. The curves of log J_0 vs. log $c_{f,0}$ in Fig. 7 (J_0 calculated by using the relation introduced above) show that this is valid only at lower concentrations and that the decrease of permeability in Fig. 6 is greater than could be explained by saturated flux through the membrane.

The observed decrease of permeability at higher lanthanide concentrations can be explained due to formation of species that are unable to permeate through the membrane. The heavier lanthanide species remain partially in the membrane or block the feed–membrane interface. As a result, P_s values lower than P_f are obtained.

In previous work on membrane transport of Eu(III) with DEHPA [21], formation of polymeric Eu–DEHPA species was presumed as an explana-

tion for both the origin of the gel-like coating found on the membrane surface and the drop in transmembrane conductivity. However, in contrast to studies [14–16,21,22] on Ln transport with DEHPA as a carrier, the presence of any gel-like material was not observed using DOPA.

3.2.4. Transport of thorium(IV)

Thorium(IV) can be extracted from its nitrate solutions in the form of mixed ligand complexes with DEHPA [2]:

$$Th^{4+} + NO_3^- + 3\overline{(HA)_2} \leftrightarrow \overline{Th(NO_3)(AHA)_3} + 3H^+$$

(E)
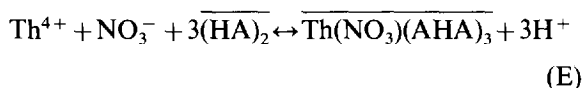
As assumed, Th(IV) extraction with DOPA would follow an identical scheme. The pH of feed solutions containing Th(IV) was varied between 1.1 and 3.0 to maintain sufficient acidity gradient over the membrane and to prevent Th(IV) hydrolysis [26,27], leading to the formation of Th(OH)$^{3+}$ and Th(OH)$_2^{2+}$ species at pH > about 3. The membrane containing 50 mmol l^{-1} DOPA and 0.1 mol l^{-1} nitric acid was used as a strip solution. The concentration of thorium in the feed solution remained at the initial level, $c_{f,0}$, and no evidence for transport of Th(IV) was found under conditions favourable for permeation of Ln. As a consequence, Th(IV) could be separated from the Ln studied under the given conditions.
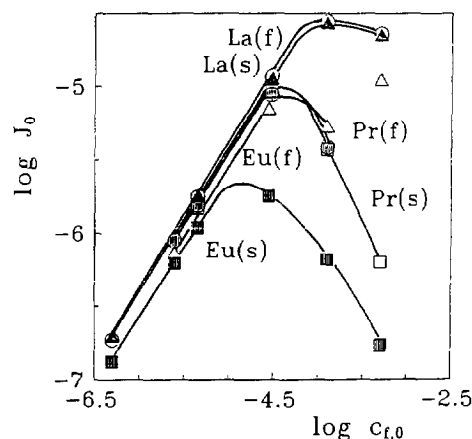

Fig. 7. Initial flux through the membrane as a function of initial lanthanide concentration (mol l^{-1}). Conditions given in Fig. 6.

4. Conclusions

The dependences of P_s on carrier concentration and P_s on pH of the feed solution, which have been measured under identical experimental conditions using DEHPA [15,16] as carrier, are very similar to those with DOPA and their maxima are situated at identical or comparable values of carrier concentration and pH respectively. In the case of membrane transport with DEHPA, Ln are divided into two groups: light (inclusive of Tb), and heavy lanthanides which differ significantly in their permeability as can be demonstrated by the value of the membrane separation factor $\alpha = P_{s,Tb}/P_{s,Ho} = 1.4$ [16].

With DOPA carrier, the values of permeability coefficients of the Ln from La to Nd are comparable to those obtained with DEHPA. However, the permeation of heavier Ln is suppressed and a separation factor of 3.0 is achieved for the Nd, Sm couple. In contrast to DEHPA, the formation of any gel-like substance in solutions or on membrane interfaces has not been observed using DOPA.

This work shows that the transport efficiency of Ln with dialkylphosphoric acid carrier is not only a strong function of feed pH and carrier concentration, as observed in previous studies with DEHPA but that the strip solution acidity and initial lanthanide concentrations also play an important role. Furthermore, it was shown that $Ln(AHA)_3$ are not the only species which can take part in Ln transport through the membrane. However, the decrease of permeability at higher lanthanide concentrations and higher pH of the feed solution can probably be explained by formation of species which are unable to permeate through the membrane. The decrease of permeability observed at higher carrier concentrations, i.e. in the range $0.05-0.25$ mol 1^{-1} DOPA, could only be partially explained by the decrease of diffusion coefficients with increasing viscosity of the liquid membrane.

Acknowledgements

References

[1] S. Motomizu and H. Freiser, Solvent Extr. Ion Exch., 3 (1985) 637.

[2] E.B. Sandell and H. Onishi, Photometric Determination of Traces of Metals, General Aspects, John Wiley, New York, 1978, p. 998.

[3] K. Yoshizuka, M. Koba and K. Inoue, in D.H. Logsdail and M.J. Slater (Eds.), Solvent Extraction 1993, Proc. Int. Solv. Extr. Conf., ISEC '93, Vol. 1, Elsevier Applied Science, London, 1993, p. 242.

[4] S. Sreelatha, T.P. Rao, C.S. Narayanan and A.D. Damodaran, Anal. Lett., 26 (1993) 573.

[5] J. Starý, Ekstrakciya Khelatov, Mir, Moscow, 1966, p. 259.

[6] J.S. Preston and A.C. Du Preez, in T. Sekine (Ed.), Solvent Extraction 1990, Proc. Int. Solv. Extr. Conf., ISEC '90, Part A, Elsevier, Amsterdam, 1992, p. 883.

[7] K. Akiba, K. Yamada and S. Nakamura, Nippon Kagaku Kaishi, 5 (1993) 555; Current Contents on Disketta with Abstracts, 25 (1993).

[8] T. Araki and H. Tsukube (Eds.), Liquid Membranes: Chemical Applications, CRC Press, Boca Raton, FL, 1990.

[9] J.A Jönsson and L. Mathiasson, Trends Anal. Chem., 11 (1992) 106.

[10] Y. Hirashima, S. Kohri and G. Adachi, in T. Sekine (Ed.), Solvent Extraction 1990, Proc. Int. Solv. Extr. Conf., ISEC '90, Part B, Elsevier, Amsterdam, 1992, p. 1499.

[11] K. Scott and A. Ibhadon, in D.H. Logsdail and M.J. Slater (Eds.), Solvent Extraction 1993, Proc. Int. Solv. Extr. Conf., ISEC '93, Vol. 2, Elsevier Applied Science, London, 1993, p. 856.

[12] R. Kopunec and T. Ngo Manh, J. Radioanal. Nucl. Chem., Articles, 170 (1993) 51.

[13] J.S. Gill, U.R. Marwah and B.M. Misra, Sep. Sci. Technol., 29 (1994) 193.

[14] C. Moreno, A. Hrdlička and M. Valiente, J. Membr. Sci., 81 (1993) 121.

[15] J. Doležal, C. Moreno, A. Hrdlička and M. Valiente, Fundamental study of solid supported liquid membranes containing di-(2-ethylhexyl)phosphoric acid (DEPHA) as a carrier for selective transport of lanthanides, Int. Solv. Ext. Conf., ISEC '93, York, UK, 9–15 September 1993.

[16] J. Doležal, C. Moreno, A. Hrdlička and M. Valiente, unpublished work.

[17] J. Havel, C. Moreno, A. Hrdlička and M. Valiente, Talanta, 41 (1994) 1251.

[18] A. Hrdlička, J. Havel, C. Moreno and M. Valiente, Anal. Sci., 7 (1991) 925.

[19] V. Salvadó, A. Masana, M. Hidalgo, M. Valiente and M. Muhammed, Anal. Lett., 22 (1989) 2613.

[20] P.R. Danesi, Sep. Sci. Technol., 19 (1984–1985) 857.

[21] T.-M. Hung and Ch.-J. Lee, in T. Sekine (Ed.), Solvent Extraction 1990, Proc. Int. Solv. Extr. Conf., ISEC '90, Part B, Elsevier, Amsterdam, 1992, p. 1469.

[22] Y. Hirashima, S. Kohri and G. Adachi, in T. Sekine (Ed.), Solvent Extraction 1990, Proc. Int. Solv. Extr. Conf., ISEC '90, Part B, Elsevier, Amsterdam, 1992, p. 1499.

[23] Yu.I. Trifonov, E.K. Legin and D.N. Suglobov, in T. Sekine (Ed.), Solvent Extraction 1990, Proc. Int. Solv. Extr. Conf., ISEC '90, Part A, Elsevier, Amsterdam, 1992, p. 279.

[24] R. Kopunec and T. Ngo Manh, J. Radioanal. Nucl. Chem., Articles, 163 (1992) 131.

[25] R. Chiarizia, A. Castagnola, P.R. Danesi and E.P. Horwitz, J. Membr. Sci., 14 (1983) 1.

[26] H.S. Du, D.J. Wood, S. Elshani and C.M. Wai, Talanta, 40 (1993) 173.

[27] J. Kragten, Atlas of Metal–Ligand Equilibria in Aqueous Solution, Ellis Horwood, Chichester, 1978, p. 648.

Determination of Benzo[a]pyrene in smoking-flavour agents (water-soluble liquid smoke) by second derivative constant-wavelength synchronous spectrofluorimetry

S. García Falcón*, S. González Amigo, M.A. Lage Yusty,
M.J. López de Alda Villaizán, J. Simal Lozano

*Department of Analytical Chemistry, Nutrition and Bromatology, Area of Nutrition and Bromatology, Faculty of Pharmacy,
University of Santiago de Compostela, E-15706 Santiago de Compostela, La Coruña, Spain*

Abstract

We have developed a simple, rapid, inexpensive method for the determination of benzo[a]pyrene (BP, a known carcinogen) in smoking-flavour agents (water-soluble liquid smoke; WSLS). After purification of the WSLS by a single passage through a Sep Pak C18 Plus cartridge, BP in the hexane eluate was determined by second derivative constant-wavelength synchronous spectrofluorimetry. Method precision (RSD < 6%) and recovery ($\approx$ 92%) were satisfactory, and the detection and quantification limits (1.05 and 2.28 μg kg^{-1} respectively) indicated that the current maximum permissible concentration of BP in smoke flavourings (10 μg kg^{-1}) can be monitored by this method.

1. Introduction

Polycyclic aromatic hydrocarbons (PAHs) are formed when organic matter undergoes incomplete pyrolysis and then condensation. In recent years, their toxicology and analysis have been of interest because of the carcinogenicity of many of them, and the general ubiquity of PAHs in the environment due to the following factors: (a) aerial transport of PAHs from combustion sources and their subsequent deposition in bodies of water and in soil and into plants, from which they propagate along the food chain; (b) pyrolysis of food components (mainly carbohydrates, lipids and proteins) during food preparation involving high temperatures (500-700°C); (c) food processing, when food comes into contact with hydrocarbon-based materials such as agricultural and industrial lubricants or food packaging; (d) during the smoking of foods by natural or artificial methods (water-soluble liquid smoke; WSLS) [1-3].

Benzo[a]pyrene (BP) in particular is frequently sought as an indicator of the presence of other

* Corresponding author.

PAHs in such diverse matrices as water [4] and foodstuffs [5]. Human exposure to BP and PAHs in general can occur through ingestion of food, contaminated air and water [4]. Thus several legal measures aimed at limiting the levels of BP in foodstuffs have been adopted. In Council Directive 88/388/EEC [5], the EC (now the EU) set the maximum permissible level of BP in foods, derived from smoke flavouring, at 0.03 μg kg^{-1}. However, no limits are currently stated for other foods, although the EU intends to set a maximum level of 1 μg kg^{-1}, as well as introducing restrictions on cooking foods on an open flame [3]. In contrast, the FAO/WHO Joint Committee on Food Additives [6] has provisionally authorized the use of smoke flavourings when deemed necessary—which are typically used at a dose of between 1 and 2 g kg^{-1} of foodstuff—to levels of BP no higher than 10 μg kg^{-1}.

The analyses of smokes absorbed in liquids for commercial handling involve various analytical methods (GC, HPLC, etc.) [7–12]. In this work we develop a simple, rapid, inexpensive method for the determination of BP from "water-soluble liquid smoke" (WSLS). The method precision and recovery are satisfactory, and the quantification limit is considerably lower than the 10 μg kg^{-1} minimum suggested by the FAO/WHO Joint Committee.

2. Experimental

2.1. Reagents

WSLS was supplied free of change by a manufacturer of smoke flavourings; BP standard was purchased from Aldrich, residue-analysis-grade n-hexane was from Merck, and routine-grade acetonitrile for HPLC was from Scharlau. Stock solutions containing 100 μg l^{-1} and 100 mg l^{-1} of BP were prepared in n-hexane and acetonitrile/water (1:2), and were stable under refrigeration at 4°C; BP standards (0.5, 1, 2, 4, 8 and 16 μg l^{-1}) were prepared by appropriate dilutions of these stock solutions with n-hexane and with acetonitrile/water.

Table 1
Optimization of the polarity of the initial eluent used in the purification step ($n = 6$)

Solvent ratio		% R
Acetonitrile	Water	
1	1.0	59.6
1	1.2	78.1
1	1.4	94.2
1	1.6	98.0
1	1.8	99.6
1	2.0	100

2.2. Apparatus

All spectrofluorimetric measurements were performed with a Perkin-Elmer LS-50 luminescence spectrometer equipped with a xenon discharge lamp, Monk–Gillieson monochromators and 1 cm quartz cuvettes, and provided with Fluorescence DM software for acquisition and processing of spectral data. Moreover, the LS-50 was serially interfaced (RS232C) to a Handok HNS-286 PC linked to an HP Laserjet IIP printer for hard copies.

2.3. Procedure

2.3.1. Purification

A sample of the WSLS (2 g) was spiked with 15 or 30 ng of benzo[a]pyrene, mixed into 15 ml of a 1:2 mixture of acetonitrile/water in a beaker, and passed through a Sep Pak C18 Plus cartridge that had previously been activated by passage of 5 ml of acetonitrile followed by 10 ml of distilled wa-

Table 2
Precisions (% RSD) and recoveries (%R) obtained when 5 ml of n-hexane was used to elute the BP sorbed onto a Sep Pak Plus Cartridge during passage of 15 ml of a 1, 4 or 8 μg l^{-1} solution of BP in 1:2 CH$_3$CN/H$_2$O ($n = 6$)

BP in 15 ml of standard (ng)	BP determined in eluent (ng)	% RSD	%R
5	5.30	2.6	106
20	20.8	1.8	104
40	36.9	0.6	92

ter. The sides of the beaker were washed with a further 15 ml of 1:2 acetonitrile/water, which was then passed through the cartridge to complete the purification process. The aqueous acetonitrile eluate was discarded, and the BP retained on the cartridge was eluted into a volumetric flask with *n*-hexane (final volume 5 ml). A sample was transferred to a quartz cuvette for subsequent spectrofluorimetric determination of BP.

2.3.2. Spectrofluorimetry

Synchronous fluorescence spectra of the hexane solution obtained above were recorded between 200 and 500 nm at a scan speed of 240 nm min^{-1} and with excitation and emission slit-widths both

set to 5 nm. The excitation–emission wavelength difference was either 20 or 110 nm (see Results and discussion). Second derivative spectra were then generated by the data handling system of the spectrofluorimeter.

3. Results and discussion

Constant-wavelength synchronous spectrofluorimetry is a selective and sensitive analytical technique that is both rapid and easy to apply. As such, it has been widely used for the determination of BP in a variety of matrices [13–16], usually after an extraction/purification step that
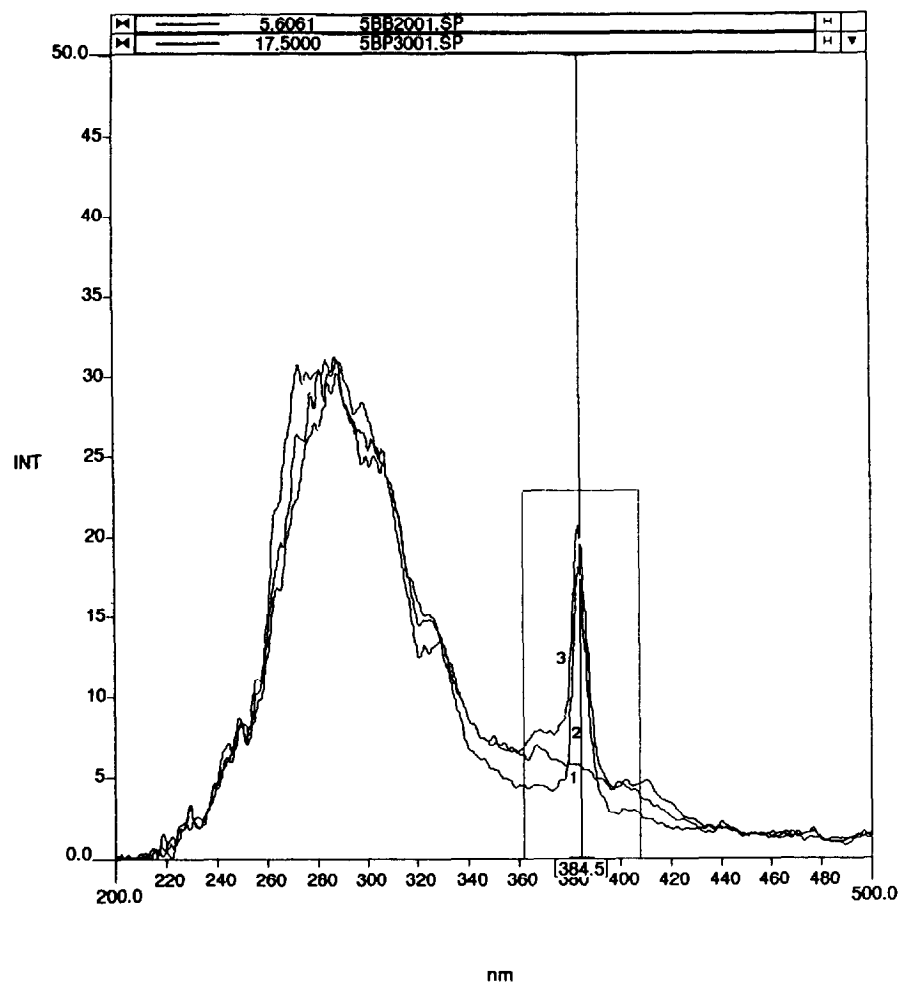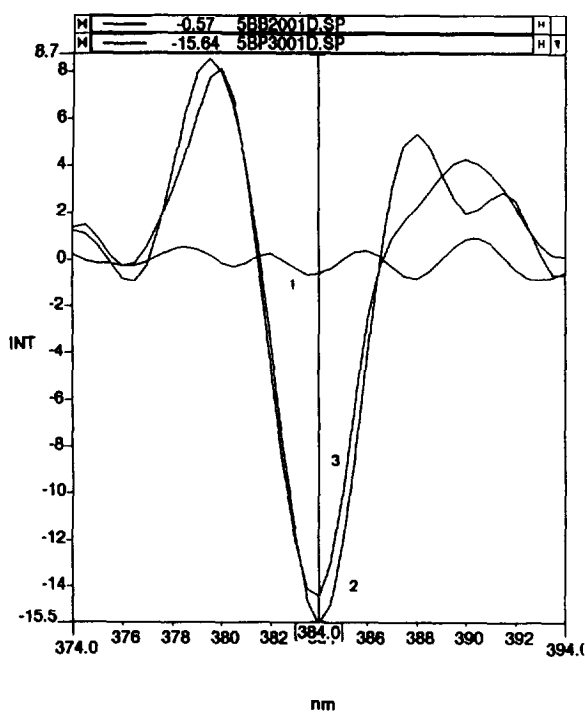

Fig. 1 (a).

Fig. 1(a) Synchronous fluorescence spectra with $\Delta\lambda = 20$ nm of hexane solutions of an unspiked sample of WSLS (1); 3 μg l^{-1} BP standard (2) and WSLS spiked with 15 ng of benzo[a]pyrene (3). (b) Zoom-like expansion of the second derivative of the marked region in (a).

removes interferents present in the matrix. Such a step is necessary in the case of WSLS: it cannot be analysed directly due its inherent opacity, while its solutions in water or polar organic solvents show single broad peaks that mask the signal due to BP.

In the purification step elaborated in this work, the BP in the WSLS was separated from hydrophilic components and most of the interfering fluorescent compounds except other PAHs (these, however, do not interfere in the subsequent spectrofluorimetric determination [17]) by a single passage through a Sep Pak C18 Plus cartridge. The key to this step was careful balancing of the polarity of the initial eluent so that all the BP in the liquid smoke was retained on the cartridge. The optimum result was achieved using the 1:2 acetonitrile/water mixture described (Table 1). Subsequently, hexane was chosen to elute the BP because it was sufficiently apolar to allow com-

plete elution; it afforded a solution that was transparent in the wavelength region in which BP fluoresced; and it is the recommended solvent for determination of BP and PAHs in general by spectrofluorimetry [18]. A recovery of approximately 100% was attained by eluting the BP in 5 ml of hexane (Table 2).

For the spectrofluorimetric determination of the BP, the spectrometer settings were adjusted so that, as far as possible, the instrumental sensitivity and resolution were optimized. The wavelength interval $(\Delta\lambda)$ between the emission and excitation monochromators that afforded the best signal (i.e. that maximized signal intensity while minimizing interference) was evaluated from the results of 50 assays in which $\Delta\lambda$ was varied, in 5 nm increments, between 10 and 255 nm. A 20 or 110 nm interval gave the best results: the maximum peak intensity was obtained with a 110 nm interval (see Fig. 2); however, interference was less evident in the peak obtained with a 20 nm interval (Fig. 1(a)), and so this peak was used for quantification. The small amount of residual interference due to background absorption was effectively eliminated by taking the second derivatives of these spectra.

Having established $\Delta\lambda$, several combinations of slit widths were examined: the greatest sensitivity was obtained with widths of 2.5 (excitation) and 20 nm (emission); however, a cleaner spectrum resulted when both slits were set at 5 nm. The selected scan speed of 240 nm allowed rapid spectral acquisition without excessive noise.

3.1. Quantification and linearity of the instrumental response

Quantification of the BP was by measurement of the peak-to-trough height of the signal corresponding to the second derivative between 379 and 384 nm (Fig. 1(b)) of the direct spectrum obtained with $\Delta\lambda = 20$ nm (Fig. 1(a)). The presence of a signal at 296 nm in the direct spectrum obtained with $\Delta\lambda = 110$ nm served to confirm that the analyte being determined was indeed BP (Fig. 2).

The calibration line, constructed by regressing peak-to-trough height (I) of the second derivative
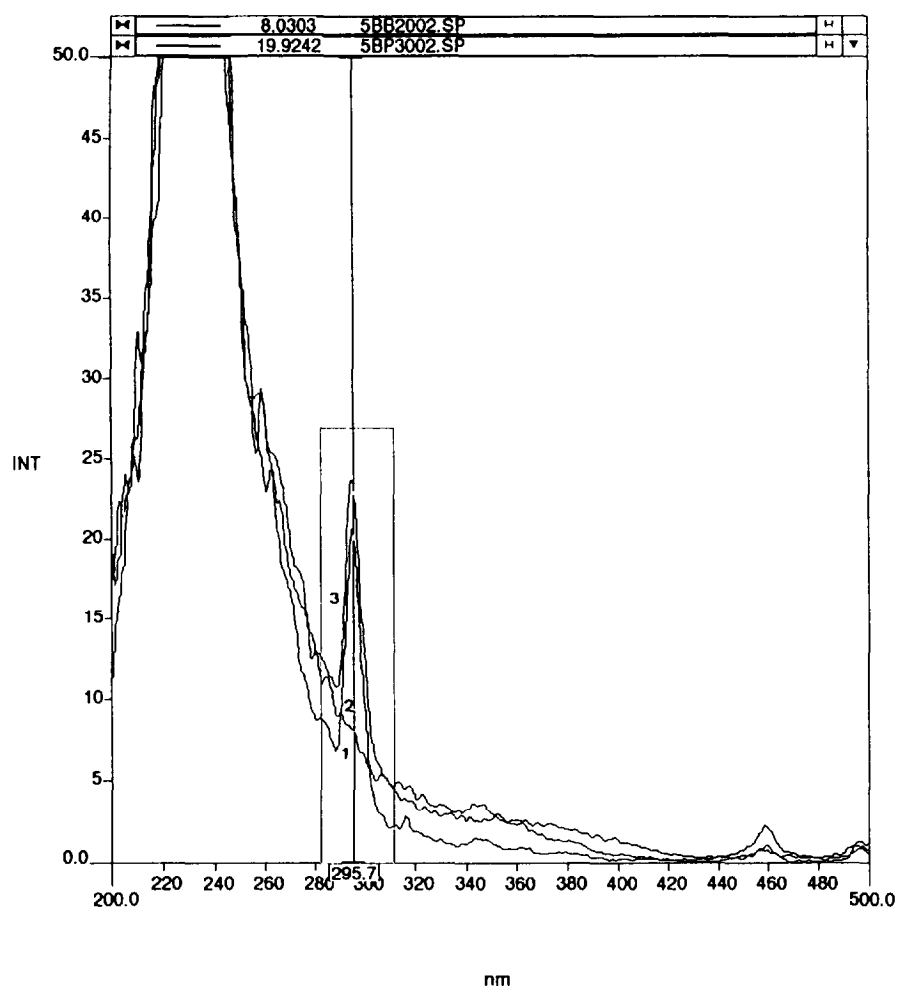
Fig. 2. Synchronous fluorescence spectra with $\Delta\lambda = 110$ nm of hexane solutions of an unspiked sample of WSLS (1); 3 μg l^{-1} BP standard (2) and WSLS spiked with 15 ng of benzo[a]pyrene (3).

signal due to BP on its concentration (c) for five of the standards (1–16 μg l^{-1}), gave the equation $c = 0.1146I + 0.0023$ with a correlation coefficient (r) of 0.9998.

The concentration (in μg kg^{-1}) of ben-

Table 3
Precisions (% RSD) and recoveries (%R) obtained for six replicate samples of WSLS spiked with 15 and 30 ng of BP

Amount added (ng)	Amount measured	% RSD	%R
15	13.7	5.2	91
30	28.0	5.9	93

zo[a]pyrene in the WSLS was obtained by multiplying its concentration (μg l^{-1}) in the hexane eluate by a factor of 2.5, which value was deduced from the purification process carried out [i.e. (15 ng/2 g)/(15 ng/5 ml)]. No BP was detected in unspiked WSLS (see Fig. 2).

3.2. Detection and quantification limits

Detection and quantification limits (calculated, following ACS guidelines [19], as the concentration corresponding to the signal (i.e. its peak-to-trough height) equal to the mean signal for 6

blanks plus respectively, three and ten standard deviations) were 0.42 and 0.91 μg l^{-1} respectively, for BP in the hexane eluate. These equate to a detection limit of 1.05 μg kg^{-1} and a quantitation limit of 2.28 μg kg^{-1} for BP in the WSLS. Clearly, the latter concentration limit is much lower than the 10 μg kg^{-1} maximum set by the FAO/WHO Joint Committee on Food Additives [6], which they considered to be the minimum concentration that could be quantified in smoke flavourings. In the light of these results, the maximum permissible concentration of BP in smoke flavourings should be reviewed, and accordingly reduced.

3.3. Precision and recovery

Method precision and recovery were determined by applying the full procedure to six replicate samples of WSLS (2 g) spiked with BP (15 or 30 ng). Table 3 lists the precisions (%RSD) and recoveries (%R) obtained.

4. Conclusions

The combination of a straightforward purification step and analysis by constant-wavelength synchronous spectrofluorimetry provides a simple, rapid, inexpensive method for the determination of benzo[a]pyrene in WSLS, a widely-used food additive. Method precision (%RSD < 6) and recovery ($\approx$ 92%) are satisfactory, and the quantitation limit (2.28 μg kg^{-1}) is considerably less than the maximum permissible concentration of BP in smoke flavourings (10 μg kg^{-1}), which, according to the FAO/WHO Joint Committee on Food Additives [6], corresponds to the minimum concentration of benzo[a]pyrene that can be quantified in such flavourings. In the light of these results, we recommend that the maximum permissible concentration of BP in smoke flavourings be reviewed, and accordingly reduced, in order to lessen human exposure to benzo[a]pyrene through ingestion of foodstuffs treated with smoke flavourings.

References

[1] J.W. Howard and T. Fazio, J. Assoc. Off. Anal. Chem., 63 (1980) 1077.
[2] J.M. Concon, Food Toxicology, Part A, M. Dekker, New York, 1988.
[3] R. Derache, Toxicología y seguridad de los alimentos, Ed. Omega, Barcelona, 1990, p. 295.
[4] World Health Organization, Guidelines for Drinking-water Quality, Vol. 2, World Health Organization, Geneva, 1984.
[5] Council of the European Communities, Directive 88/388/EEC, Off. J. Eur. Communities, L184 (1988) 61.
[6] 31st report of the FAO/WHO Joint Committee on Food Additives, World Health Organisation, Geneva, 1987.
[7] W. Lijinsky and P. Shubik, Toxicol. Appl. Pharmacol., 7 (1965) 337.
[8] V.M. Gorbatov, N.N. Krilova, V.P. Volovinskaya, Yu. N. Lyaskovskaya, K.I. Bazarova, R.I. Khalamova and G. Ya. Yakovleva, Food Technol., 25 (1971) 71.
[9] R.H. White and C.J. Barnes, Agric. Food Chem., 1 (1971) 143.
[10] E.A. Gomaa, J.I. Gray, S. Rabie, C. López-Bote and A.D. Booren, Food Addit. Contam., 10 (1993) 503.
[11] H. Yuco Yabicu, M. Satou Martins and M. Yamasaki Takahashi, Food Addit. Contam., 10 (1993) 399.
[12] M.D. Guillén, M.J. Manzanos and L. Zabala, J. Agric. Food Chem., 43 (1995) 463.
[13] R. Law and E. Andrulewicz, Mar. Pollut. Bull., 14 (1983) 289.
[14] K. Tanaka and M. Saito, Analyst, 113 (1988) 509.
[15] J.J. Santana Rodríguez, J. Hernández García, M.M. Bernal Suárez and A. Bermejo Martín-Lazaro, Analyst, 118 (1993) 917.
[16] M.J. López de Alda-Villaizán, S. García-Falcón, M.A. Lage-Yusty and J. Simal-Lozano, J. Assoc. Off. Anal. Chem., 78 (1995) 402.
[17] J. Simal Lozano, M.A. Lage Yusty, L. Vázquez Odériz and M.J. López de Alda-Villaizán, J. Fr. d'Hydrologie, 23 (1992) 37.
[18] M.J. López de Alda Villaizán, E. Álvarez Piñeiro, S. García Falcón, M.A. Lage Yusty and J. Simal Lozano, Analusis, 22 (1994) 495.
[19] American Chemical Society Subcommittee on Environmental Analitical Chemistry, Anal. Chem., 52 (1980) 2242.

Kinetic analysis of arginase–urease coupled reaction with a surface acoustic wave enzyme sensor system

Dezhong Liu, Lihua Nie, Shouzhuo Yao*

Department of Chemistry and Chemical Engineering, Hunan University, Changsha 410082, People's Republic of China

Abstract

An extended set of equations which describe coupled arginase–urease reactions is presented. The mathematical treatment leads to the development of new equations which relate the lag-time required for the concentration of urea to reach a defined fraction of its steady-state concentration to the kinetic parameters of the enzymes, when the steady-state concentration of urea is small compared to its Michaelis constant value. the coupled arginase–urease reaction was monitored with a surface acoustic wave (SAW) enzyme sensor system, to couple the biochemical selectivity of enzymes with the sensitivity of SAW sensors. The proposed theoretical expressions were verified experimentally. The kinetic parameters of urease and arginase (extracted directly from bovine liver) were examined under theoretical guidance. Dependence of the lag-time of the coupled enzyme reaction on the concentrations of urease and arginase is also described.

Keywords: Arginase–urease reactions; Kinetic analysis; Mathematical treatment; Surface acoustic wave enzyme sensor system

1. Introduction

As analytical reagents, enzymes offer the characteristic of high selectivity (and occasionally specificity). Enzymes have been widely used in analytical chemistry owing to their substrate specificity. Enzyme-based analytical procedures may be designed to determine the concentrations of substrates, coenzymes, activators and inhibitors.
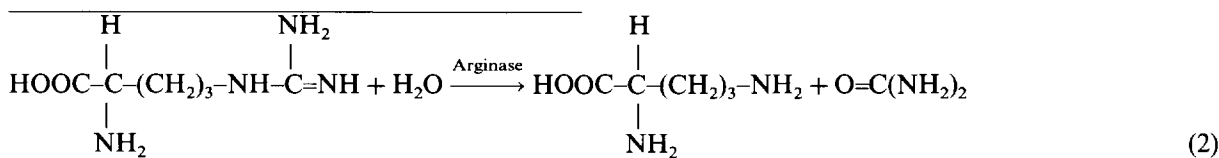
All of these possible applications, together with enzymatic kinetic assay, are included in the term enzymatic analyses.

The equations relating the rate of an enzyme to the rate of appearance of a detectable product resulting from subsequent (auxiliary) enzyme reactions were first developed by McClure [1] for systems involving two auxiliary enzymes. These were later extended by others to include multienzyme systems and methods to minimize the cost of a two auxiliary enzyme system [2–4] were developed. So far there is no report on the deriva-

* Corresponding author.

tion of kinetic equations for an arginase–urease coupled reation. Kinetic procedures for the estimation of arginine or the activity of arginase have only been reported [5–7].

The purpose of this paper is to provide a theoretical derivation of the kinetic equations for an arginase–urease coupled reaction and to make an experimental evaluation. The kinetic parameters

$$
\underset{\substack{|\\ NH_2}}{\overset{\substack{H \qquad\qquad NH_2\\ |\qquad\qquad\ |}}{HOOC-C-(CH_2)_3-NH-C=NH}} + H_2O \xrightarrow{\text{Arginase}} \underset{\substack{|\\ NH_2}}{\overset{\substack{H\\ |}}{HOOC-C-(CH_2)_3-NH_2}} + O=C(NH_2)_2
\tag{2}
$$

of the arginase for arginine as substrate are also determined based on the proposed kinetic theory.

2. Theory

The derivations rely on the fulfillment of the following three assumptions: (1) the enzyme reaction obeys Michaelis–Menten kinetics; (2) the steady-state concentration of the substrate (urea) produced from the hydrolysis of arginine by arginase is much less than the apparent Michaelis constant for the subsequent urease; and (3) only the initial rate conditions are considered (the reverse reactions are negligible). Whereas none of the above conditions are necessary for the development of the kinetic theory for the coupled enzyme reactions, the last two conditions are easily achieved by selecting appropriate substrate concentrations.

In a previous paper [8], the correlation between the frequency shift of the SAW (surface acoustic wave) sensor system and the conductivity of the test solution was derived by using circuit network theory, and was also verified experimentally. There is a relationship between the frequency-shift (ΔF) of the SAW enzyme sensor system and the conductivity change of the test solution ($\Delta\kappa$) durint the enzymatic reactions:

$$
\Delta F = a\Delta\kappa + b
\tag{1}
$$

where a and b are constants resulting from the SAW oscillator, the detection cell, the solution conductivity range and other experimental condi-

tions. The sensor possesses a sensitive response to the change of ion species in the test solution. In addition, interferences caused by mass, viscoelastic properties can be avoided. Only the alteration of conductivity in the test solution can produce a frequency shift in the sensor system.

The enzymatic catalytic reaction proceeds via arginase as shown below:

Conductivity is not affected by the reaction. However, the reaction may be monitored with the SAW enzyme sensor system if it is coupled to a second reaction, in which the urea formed in the first reaction acts as a substrate for urease to hydrolyze:

$$
O=C(NH_2)_2 + 3H_2O \xrightarrow{\text{Urease}} HCO_3^- + 2NH_4^+ + OH^-
\tag{3}
$$
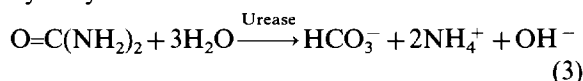
The second reaction involves the production of three kinds of charged species from a neutral compound (urea), resulting in an abrupt change in the concentration of ions, so the course of the reaction may be followed by measuring the frequency-shift response with time according to Eq. (1) by means of the SAW enzyme sensor system. The kinetic frequency-shift response of the SAW enzyme sensor system to the above coupled enzyme reaction was recorded and the reaction rate obtained. With careful selection of the reaction conditions, the rate of the second reaction will be an indicator of the rate of the first reaction.

The above-mentioned reactions can be considered as the general situation:

$$
A \xrightarrow[v_1]{E_1} B \xrightarrow[v_2]{E_2} C
\tag{4}
$$

The substrate A that has to be determined reacts under the catalysis of the enzyme E_1 to give B. The product is also hydrolyzed in the presence of enzyme E_2 and B can be easily detected. In the kinetic process of this system, the concentration of A is initially A_0, and drops to zero; the concentration of B is initially zero, rises until it achieves

a maximum and then drops to zero again. In the experiment, the response signal (frequency shift, ΔF), which is proportional to the concentration of B, is read at several intervals.

In general, the rate of [B] is given by

$$\frac{d[B]}{dt} = v_1 - v_2 \tag{5}$$

where v_1 is the rate of the first (primary) reaction and v_2 the rate of the second (indicator) reaction. As with the rate of any single-enzyme system, v_1 should reach a constant value almost instantaneously and remain at this value over the period of interest (the next few minutes). In contrast, v_2 will have an initial value of zero (since [B] is initially zero) and will rise as [B] rises, according to the Michaelis–Menten equation [9,10]:

$$v_2 = \frac{V_B[B]}{[B] + K_B} \tag{6}$$

where V_B is the maximum reaction rate for the enzyme E_2 and K_B is the Michaelis constant for the substrate B. Similarly, the following equation can also be obtained:

$$v_1 = \frac{V_A[A]}{[A] + K_A} \tag{7}$$

where V_A is the maximum reaction rate for the enzyme E_1 and K_A is the Michaelis constant for the substrate A.

The observed steady-state rate (v_{obs}) of the coupled enzyme reaction is simply the rate of enzyme E_2:

$$v_{obs} = V_B[B]_{ss}/(K_B + [B]_{ss}) \tag{8}$$

When the steady-state concentration $B([B]_{ss})$ is less than 0.01 K_B, Eq. (8) simplifies to the relationship:

$$v_{obs} = V_B[B]_{ss}/K_B \tag{9}$$

In order to calculate the elapsed time before the onset of the steady state, an expression for formation of B in terms of time (t) must be obtained. Combining Eqs. (5) and (6) gives the following expression:

$$\frac{d[B]}{dt} = v_1 - \frac{V_B[B]}{[B] + K_B} \tag{10}$$

The above equation is the difference between the rate of formation of $B(v_1)$ and the rate of its destruction. At steady state, when $d[B]/dt = 0$, Eqs. (10) and (8) predict:

$$v_1 = v_{obs} = d[C]/dt \tag{11}$$

Eq. (11) implies that, when the reaction reaches the steady state, the observed rate will be that of enzyme E_1. this is illustrated in Fig. 1. A plot of v_{obs} vs. v_1 gives a straight line with a slope of one until the rate of enzyme E_1 is equal to the rate of enzyme E_2; at this point and at all values of v_1 in excess of V_B, the observed rate equals V_B.

By assuming [B] = 0 at $t = 0$ and holding v_1 and V_B constant with respect to time, integration of Eq. (10) gives:

$$\int \frac{(K_B + [B])}{v_1 K_B + [B](v_1 - V_B)} d[B] = \int dt \tag{12}$$

From Eq. (12), the following equation for [B] at any time t is obtained:

$$(K_B v_1 - \phi[B]) \exp[\phi[B]/(K_B V_B)]$$
$$= K_B v_1 \exp[-t\phi^2/(K_B V_B)] \tag{13}$$

where $\phi = V_B - v_1$. When $v_1 \ll V_B$ and $[B] \ll K_B$, Eq. (13) gives:

$$[B] = K_B v_1/V_B(1 - \exp[-tV_B/K_B]) \tag{14}$$

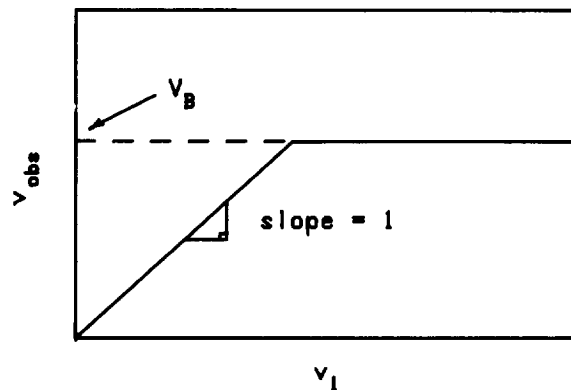By defining

$$\beta = [B]/[B]_{ss} \times 100\% \tag{15}$$

Fig. 1. Theoretical prediction from Eq. (11). Note that $v_1 = v_{obs}$ for all values of $v_1 < V_B$. The Figure presupposes measurements at infinite time.
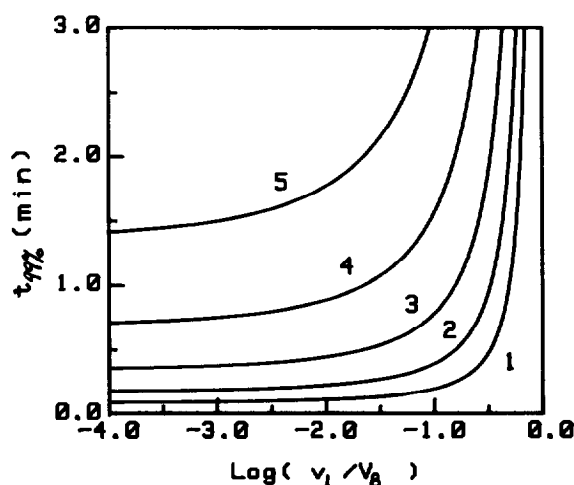
Fig. 2. Theoretical relationship between $\log(v_1/V_B)$ and the time required for B to reach 99% of its steady-state value calculated from Eq. (17). Each curve represents a different value of V_B: (1) 16.0; (2) 8.00; (3) 4.00; (4) 2.00; (5) 1.00 kHz min^{-1}. K_B value (Michaelis constant for urease) was experimentally estimated as 1.65 mM.

where [B] is the concentration of the substrate B at any time t and $[B]_{ss}$ is the concentration of B in the steady state given by

$$[B]_{ss} = \frac{v_1 K_B}{(V_B - v_1)} = \frac{v_1 K_B}{\phi} \qquad (16)$$

We can combine Eqs. (13), (15) and (16) to obtain:

$$t_\beta = \frac{-K_B}{\phi^2}[\beta v_1 + V_B \ln(1 - \beta)] \qquad (17)$$

where t_β is the lag-time before B reaches a defined fraction of its steady-state concentration as given by Eq. (15). Provided that $v_1 \ll V_B$, Eq. (17) can be simplified as

$$t_\beta = -\frac{K_B}{V_B}\ln(1 - \beta) \qquad (18)$$

Fig. 2 shows the relationship between the lag-time (t_β, with $\beta = 99\%$) calculated from Eq. (17) and the ratio (v_1/V_B). Note that, as the ratio v_1/V_B increases above 0.1, the time required for B to achieve 99% of its steady-state concentration increases dramatically. If β is selected as 95%, the actual lag-times are shorter, but follow the same trends as seen for $\beta = 99\%$. Thus v_1/V_B should be

less than 0.1 if the steady-state rate is to be reached under conditions where the steady-state assumptions are still valid. This is particularly important when kinetic data for enzyme E_1 are examined at concentrations of substrate which are less than the value of the Michaelis constant. In addition, the t_β value reflects the time required for the substrate (B) concentration to achieve a defined fraction (β) of its steady-state concentration ($[B]_{ss}$). In order to determine the kinetic parameters of E_1 accurately, the amount of enzyme E_2 must be in as great an excess as possible so that the observed rate is directly proportional to the amount of substrate A or enzyme E_1 added. Therefore, the kinetic parameters of enzyme E_1 can be estimated by using a Lineweaver–Burke plot [10] which was derived from Eq. (7):

$$\frac{1}{v_1} = \frac{1}{V_A} + \frac{K_A}{V_A[A]} \qquad (19)$$

3. Experimental

3.1. Apparatus

The apparatus used in this work was in principle identical to that described previously [11], where 10 ml detection cell was used. The whole experimental set-up is illustrated in Fig. 3. In order to maintain constant temperature, the whole assembly was thermostated in a double-lay-
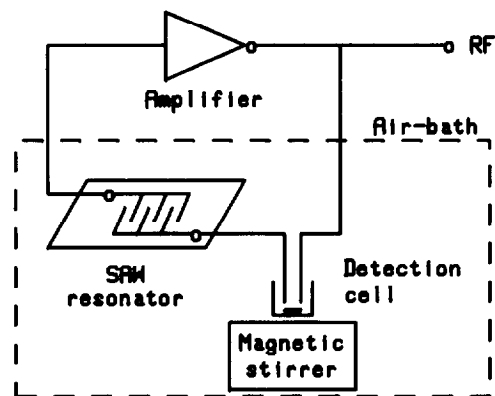

Fig. 3. Sketch of the whole experimental set-up.

ered air-bath thermostating equipment (laboratory made) which was monitored and controlled by a temperature controller (Modes WMZK-01, Shanghai Medical Instrument Corporation). This arrangement permitted the temperature of the system to be maintained within $\pm 0.2°C$.

3.2. Reagents

Urease (E.C. 3.5.1.5, from jack bean) was obtained from BDH Chemicals Ltd., Poole, UK. The enzyme activity, determined by the standard procedure [12], was found to be 1.7 E.U. mg^{-1}. Arginase (L-arginine urea hydrolase, E.C. 3.5.3.1, from bovine liver) was obtained from Shanghai Biochemical Institute of Chinese Scientific Academy. The enzyme activity, determined by the standard procedure [13], was found to be 25.0 E.U. mg^{-1}.

Arginase was also extracted from bovine livers (freshly obtained from a local slaughter house) using the following procedure. A fresh bovine liver (≈ 250 g) was sliced with a razor blade and kept frozen for several hours in a refrigerator. The frozen liver slices were disrupted carefully with a universal mincer. A portion (100 g) of the liver paste was mixed with 200 ml of 0.02% sodium azide–20% glycerol (all in w/v, pH was adjusted to 7.5 with a small volume of 0.1 M NaOH). The mixture was shaken on an oscillating machine for 30 min (275 times per minute) at room temperature and kept in a refrigerator for 6 hs. It was stirred periodically. Finally, the mixture was filtered with a vacuum pump and two phases were separated. The crude extract was directly used in the measurements below without further purification. The enzyme activity of arginase in the extract, estimated by the standard procedure [13], was found to be 3.0 E.U. ml^{-1}. When not in use, the arginase extract should be kept cold (4°C).

All other chemicals used were of analytical grade. Distilled–deionized water was used for preparing all solutions. 1.0 mM Tris-EDTA (pH 8.5) was used as working reagent. The stock arginine solution was 0.10 M in 1.0 mM Tris-EDTA working reagent. Urease was dissolved in 0.02% sodium azide–20% glycerol (pH 7.5) to yield a final concentration of 17 E.U. ml^{-1}.

3.3. Procedure

Working reagent, arginase solution and urease solution were prewarmed at 30°C just before use. In a typical experiment, 8.70 ml working reagent, 0.50 ml urease solution and 0.80 ml arginase extract were pipetted into the detection cell. The cell was placed in a thermostated air-bath chamber and incubated for 4 min. This allowed any side-reactions to reach completion since there is a small content of urea in the arginase extract. The platinum electrode was inserted into the cell. The reaction was started by the addition (with a microsyringe) of 50 μl of standard arginine solution into the cell (total volume of test solution was 10 ml). Frequency was recorded with time. The blank frequency-shift response was made in the same way but without adding arginine solution. The temperature of the test solution was kept at $30.0 \pm 0.2°C$ during measurements.

4. Results and discussion

4.1. Kinetic parameters of urease and arginase

To test the theoretical expressions proposed in the previous section, the coupled enzyme system involving both arginase and urease was examined. It is necessary to know the kinetic parameters of urease prior to the present study. Therefore, a kinetic assay was conducted to determine the value of K_B under the following conditions: 1.0 mM Tris-EDTA; pH 8.5; 30°C; 0.85 E.U. ml^{-1} urease; urea standards varying from 0.042 to 0.50 mM. The Lineweaver–Burke plot yields a K_m value for urease of 1.65 $mM(K_B)$, which is of the same order of magnitude as that reported for jack bean [14], and a corresponding maximum initial rate, V_B, of 6.25 kHz min^{-1}.

According to Eq. (17), a short lag-time is desirable when measuring the kinetic parameters of arginase. Hence an excess of urease was necessary in order to ensure prompt conversion of all the urea formed and that the observed rate is directly proportional to the concentration of arginine. Kinetic parameters of arginase were measured by using the SAW enzyme sensor system according

to Eq. (19). Under the selected conditions (1.0 mM Tris-EDTA; pH 8.5; 30°C; 0.24 E.U. ml⁻¹ arginase; 2.55 E.U. ml⁻¹ urease) arginine standards varied from 0.050 to 0.50 mM. Experimental results give $K_A = 12.0$ mM and $V_A = 4.78$ kHz min⁻¹. the K_m value of arginase is of the same order of magnitude as literature values of 10–20 mM (for rat liver arginase) [15,16].

4.2. Selection of reaction conditions

The reaction mixture must be buffered, and the buffer will contribute a background conductance. A low concentration of Tris-EDTA buffer (1.0 mM), with its low intrinsic conductivity, was selected as the reaction medium. One further factor which needs to be taken into account is the pH profiles of the various enzymes involved. Clearly, it is essential that all the component enzymes are active at the pH used for assay, and the narrow ranges of activity of some enzymes pose problems in this respect. However, in practice, arginase is active around pH 8–10 and urease around pH 7–8. Both enzymes are sufficiently active at about pH 8.5, but at no pH value are both enzymes active enough to be coupled together. Experimental results showed that the optimum pH was 8.5 and an especially sharp decrease of the reaction rate was observed above pH 9.0. Therefore, all supsequent investigations were performed at pH 8.5. The influence of temperature on the coupled reaction was similarly studied in the range 10–50°C. The reaction rate increases with increasing temperaure in the range 10–37°C, but decreases rapidly with increasing temperature above 40°C. 30°C was therefore selected for further experiments.

4.3. Response of the SAW enzyme sensor system

Typical responses of the SAW enzyme sensor system to different concentrations of arginine solution are depicted graphically in Fig. 4. It can be seen that frequency-shift response, or the reaction rate, increases with increase in arginine concentration. The slopes of the curves at any given time are related to the rates of the coupled enzyme reactions at that point in time. As described previously [11], there is a correlation between fre-
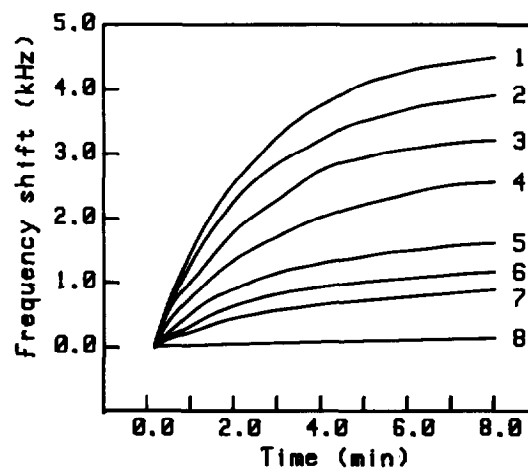

Fig. 4. Typical frequency-shift response curves for various concentrations of arginine: (1) 0.50; (2) 0.40; (3) 0.30; (4) 0.20; (5) 0.15; (6) 0.10; (7) 0.05; (8) 0.00 mM. The determination was carried out under the following conditions: 0.24 E.U. ml⁻¹ arginase extracted from bovine liver, 2.55 E.U. ml⁻¹ urease, 8.50 ml working reagent. Total volume of the detection solution was 10.0 ml and pH in the reaction medium was 8.5.

quency-shift (ΔF) and urea concentration ($\Delta F = 107.5$[Urea] + 3), or a relationship between the rate of urea hydrolysis (v_2) and urea concentration ($v_2 = 60.5$[Urea] + 13), where [Urea] is expressed in μg ml⁻¹, ΔF in Hz, and v_2 in Hz min⁻¹. The response curve of the SAW enzyme sensor system is analogous to that of a normal enzyme kinetic reaction [17]. Only about 10 s of lag-time was observed in this procedure since the concentration of urease was quite large (2.55 E.U. ml⁻¹ in 10 ml of test solution).

4.4. Dependence of lag-time of the coupled enzyme reaction on urease concentration

For the arginase–urease coupled reaction, the observed reaction rate changes over the time course of the experiment. The final steady-state rate is achieved after a definite lag-time. Hence it is important to calculate or measure the lag-time because the observed initial rate does not accurately reflect the rate of the arginase before a lag period has elapsed. Investigations show that the observed lag-time ($t_{99\%}$) depends on the kinetic constant of urease—maximum reaction rate of urease—which is directly proportional to its con-

centration. A short lag-time is desirable since the shorter the lag-time, the lower the steady-state concentration of urea in the coupled reaction and the less substrate is consumed before the steady state is observed. At the same time, it is worth noting that the shorter the lag-time, the more coupled enzyme is required (Table 1).

The arginase-urease coupled reaction has an appreciable lag-time (about 1 min) before the steady state is reached. The lag-time depends mainly on the concentration of urease. In addition, complete mixing of the sample and reagents cannot be achieved instantaneously and it may take seconds to reach the linear phase. Hence it should be possible to choose reaction conditions which ensure that the procedure gives a reasonable estimation of the initial rate.

Fig. 5 shows the frequency-shift response of the SAW enzyme sensor system to arginine with different concentrations of urease. It can be seen that the lag-time of the coupled enzyme reaction was reduced and the frequency-shift response increased with increasing urease concentration. The experimental and calculated results of lag-time are listed in Table 1. The values coincide with each other. As can be seen from Table 1, the lag-time
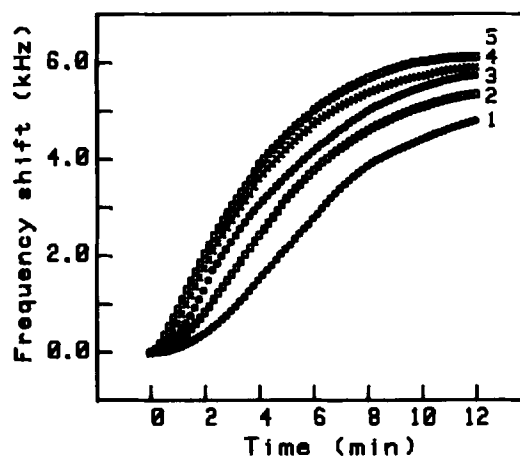

Fig. 5. Frequency-shift response of SAW enzyme sensor system for different amounts of urease: (1) 3.40; (2) 8.50; (3) 13.6; (4) 17.0; (5) 25.5 E.U. in 10 ml test solution. 0.15 E.U. ml^{-1} arginase and 0.50 mM arginine were selected in this procedure.

of the coupled enzyme reaction was reduced with increasing urease concentration. However, the reaction rate decreases when the concentration of urease added is greater the 1.70 E.U. ml^{-1}. This phenomenon shows that the excess urease has been added under these conditions.

4.5. Dependence of lag-time of the coupled enzyme reaction on arginase concentration

Fig. 6 shows the frequency-shift response of the SAW enzyme sensor system to arginine with arginase in different concentrations. It can be seen that the frequency-shift response, i.e. the reaction rate, increases with increase in arginase concentration. At the same time, the reaction rate is reduced provided that the concentration of arginase is greater than 0.24 E.U. ml^{-1}. This phenomenon shows that excess arginase has been added under these conditions. However, with the increase in arginase concentration, the lag-time of the coupled enzyme reaction changes only slightly as shown in Table 1. According to Eq. (18), the lag-time depends only on the values of K_B and V_B if $v_1 \ll V_B$. Hence the lag-time will not alter while the reaction conditions and the concentration of urease are kept constant. The experimental results are consistent with the theoretical prediction.

Table 1
Comparison between the experimental and theoretical lag-time results for the arginase-urease coupled reaction

Enzyme concentration (E.U. ml^{-1})		Lag-time, $t_{99\%}$ (s)	
Urease	Arginase	Experimental value[a]	Theoretical value[b]
0.34	0.15	105.2 ± 7.5	100.2
0.85	0.15	54.3 ± 5.0	58.5
1.36	0.15	42.9 ± 4.6	42.4
1.70	0.15	27.4 ± 2.9	30.0
2.55	0.15	11.5 ± 2.5	9.7
0.85	0.03	45.8 ± 4.5	43.4
0.85	0.09	47.4 ± 4.6	44.6
0.85	0.24	49.5 ± 4.4	47.1
0.85	0.30	40.5 ± 4.5	44.0

[a] The experimental results were obtained under the conditions: 1.0 mM Tris-EDTA; pH 8.5; 30°C; 0.50 mM arginine standard.
[b] Theoretical values were calculated according to Eq. (17) where $K_B = 1.65$ mM, $V_B = 6.25$ kHz min^{-1} and $\beta = 99\%$.
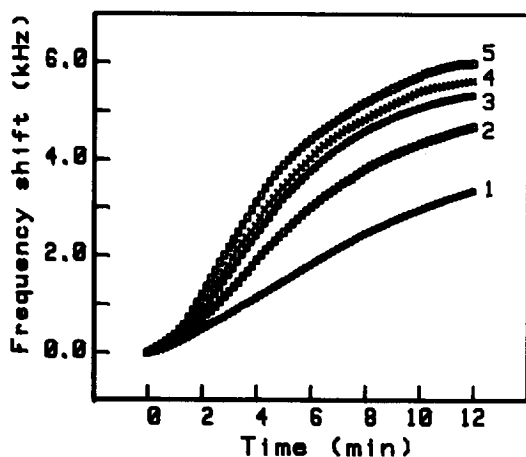
Fig. 6. Frequency-shift response of SAW enzyme sensor system for different amounts of arginase which was extracted from bovine liver: (1) 0.30; (2) 0.90; (3) 1.50; (4) 2.40 (5) 3.00 E.U in 10 ml test solution. 0.85 E.U. ml^{-1} and 0.50 mM arginine were selected in this procedure.

4.6. Reproducibility

The reproducibility of the lag-time was examined. For 0.85 E.U. ml^{-1} urease, 0.24 E.U. ml^{-1} arginase and 0.50 mM arginine, five measurements gave a relative standard deviation of 8.9%. As can be seen in Table 1, the absolute error of the lag-time becomes larger with the decrease of the lag-time (experimental values of lag-time given in this Table are obtained from three measurements).

In conclusion, the kinetic equations for the arginase–urease coupled reaction are derived. The theoretical results are verified experimentally. The kinetic parameters of the arginase (extracted directly form bovine liver) and the lag-time of the coupled enzyme reaction have been estimated satisfactorily under the theoretical guidelines.

References

[1] W.R. McClure, Biochemistry, 8 (1969) 2782.
[2] F. Garcia-Carmona, F. Garcia-Canovas and J.A. Lozano, Anal. Biochem., 113 (1981) 286.
[3] I. Takagahara, J. Yamauti, K. Fujii, J. Yamashita and T. Horio, J. Biochem. (Tokyo), 93 (1983) 1145.
[4] S.P.J. Brooks, T. Espinola and C.H. Suelter, Can. J. Biochem. Cell Biol., 62 (1984) 945.
[5] C.H. Konings, Clin. Chim. Acta, 176 (1988) 185.
[6] N.R. Larsen, E.H. Hansen and G.G. Guilbault, Anal. Chim. Acta, 79 (1975) 9.
[7] C.L. Garganta and J.S. Bond, Anal. Biochem., 154 (1986) 388.
[8] S. Yao, K. Chen, D. Liu and L. Nie, Anal. Chim. Acta, 294 (1994) 311.
[9] D.V. Roberts, Enzyme kinetics, Cambridge University Press, Cambridge, 1977, pp. 26–36.
[10] T. Palmer, Understanding Enzymes, Ellis Horwood, Chichester, 1981, pp. 326–334.
[11] D. Liu, K. Ge, K. Chen, L. Nie and S. Yao, Anal. Chim. Acta, 307 (1995) 61.
[12] G. Gorin, E. Fuchs, L.G. Butler, S.L. Chopra and R.T. Hersh, Biochemistry, 1 (1962) 911.
[13] Worthington Enzyme Manual, Worthington Biochemical Corp., NJ, 1972.
[14] P.C. Pandey and A.P. Mishra, Analyst, 113 (1988) 329.
[15] G.G. Guilbault, Handbook of Enzymatic Methods of Analysis, Science and Technology Press, Shanghai, 1983, pp. 63–65 (translated into Chinese by F. Miao and S. Cheng).
[16] G. Musznska and E. Ber, Int. J. Biochem., 9 (1979) 757.
[17] I. Tinoco, Jr., K. Sauer and J.C. Wang, Physical Chemistry, Principles and Applications in Biological Sciences, Prentice-Hall, Englewood Cliffs, NJ, 1985, p. 365.

Talanta

A thin liquid film thickness shear mode bulk acoustic wave sensor for determination of *Proteus mirabilis*

Lili Bao, Le Deng, Lihua Nie, Shouzhuo Yao, Wanzhi Wei*

Department of Chemistry and Chemical Engineering, Hunan University, Changsha 410082, People's Republic of China

Received 26 May 1995; accepted 2 October 1995

Abstract

A thickness shear mode bulk acoustic wave sensor coated with a thin liquid culture medium film was developed and applied to determine the concentration of *Proteus mirabilis* (*P. mirabilis*). Experiments demonstrated that there was a good linear relationship between the turning point time and the logarithm of the *P. mirabilis* concentration in the range 2.0×10^2–2.0×10^6 cells ml^{-1}. The detection was fast and accurate because of the sharp turning point of the response due to the thin culture film on the sensor surface. Other problems concerning the experiments are discussed in detail.

Keywords: Acoustic wave sensor; Thickness shear mode; Thin film; *Proteus mirabilis*

1. Introduction

The successful oscillation of the thickness shear mode (TSM) bulk acoustic wave sensor in the liquid phase in the 1980s initiated an entirely new field of research for the TSM sensor [1–3]. Since then, the TSM sensor, as a fast, convenient and sensitive analysis tool, has been used more extensively in various areas, e.g. for determining microcomponents in solution [4], for determining bio-macromolecules [5] and for monitoring blood clotting [6].

Recently, research concerning the use of the TSM sensor as a powerful tool for the determination of bacteria was reported [7,8]. These new methods, mainly based on mass or conductivity response, are faster and more sensitive compared with conventional methods such as the pour plate counts (PPC) technique, the most probable number technique, and the turbidity method, all of which are cumbersome and time-consuming. Therefore, these new methods are important in practice. However, when the techniques are used, the antibodies are usually difficult to acquire in the immune methods and in the conductivity response methods the accurate determination of frequency detection time (FDT) is not easy since the response curve change near the FDT is very slow,

* Corresponding author.

so the analysis precision strongly relies on the experience of the analysts. In addition, the amount of sample needed is considerable. Because of the above reasons, it is imperative to develop a better method.

P. mirabilis is Gram-negative, is a member of the genus *Proteus* within the family Enterobacteriaceae, occurs widely in humans, animals and in the environment, and can be readily recovered from sewage, soil, garden vegetables and many other materials. It is often found as a contaminant of shigellae, appears in the stools of patients recovering from bacillary dysentery, and occurs as a secondary invader in wounds and bedsores. Hence the determination of *P. mirabilis* is of practical importance in food hygiene, clinical medicine and environmental monitoring.

Usually, the TSM sensor, as a non-mass sensor, can response to viscosity and density changes of liquid. Kanzawa and Gordon's research [9] indicated that the following equation is effective under certain experimental conditions:

$$\Delta F = -F_s^{3/2}(\eta\rho_L/\pi\mu\rho_Q)^{1/2} \tag{1}$$

where ΔF is the resonant frequency change of the crystal, F_s is the resonant frequency, η is the viscosity of the liquid, ρ_L is the density of the liquid, μ is the shear modulus of quartz, and ρ_Q is the density of quartz. The detection of *P. mirabilis* with the TSM sensor presented in this paper was mainly based on the changes in viscosity and density. The response also included mass and surface stress effects. When the medium coagulated, the viscosity and density of the medium changed; meanwhile, complicated mass and surface stress changes took place. After some bacteria were added and grew in the liquid medium, the coagulation character of the medium was changed. The change was related to the initial bacteria concentration and so the gelation process was used to detect the bacteria concentration on the coagulation frequency curve, the time at which the frequency begins to increase was a sharp turning point. It was defined as turning point time (TT) and was found to be linearly related to the logarithm of the initial concentration of bacteria. The TT was very easy to determine because of the sharp turning point on the

response curve. Detection time and amount of sample needed were also reduced further. Only a micro-medium and less than 4 h detection time were needed.

2. Experimental

2.1. Stock medium

The composition of stock medium is as follows: beef extract, 1 g; yeast extract, 2 g; peptone, 5.0 g; NaCl, 5.0 g; doubly-distilled water, 1000 ml. The medium was dispensed into bottles and sterilized by autoclaving at 121°C for 15 min.

2.2. Stock culture

A 20 ml volume of medium was placed in a 50 ml sterilized conical vial and four loops of *P. mirabilis* on slant agar were inoculated with an inoculating loop. After incubation for 16 h at 37°C, the conical vial was removed from the incubator and stored in a refrigerator. The culture gave and approximate concentration of 3.1×10^7 cells ml^{-1}.

2.3. Coating solution of medium film

The composition of incubating medium is as follows: beef extract, 1.5 g; peptone, 2.5 g; gelatin, 0.4 g; doubly-distilled water, 1000 ml. The medium was sterilized before use. One aliquot of incubating medium and two aliquots of bacteria solution were mixed and, after incubation, the mixture was coated on the sensor surface and then the coagulation process was determined.

2.4. Incubation of P. mirabilis

The optimum temperature of a bacterium is approximately that of its natural habitat, i.e. about 37°C in the case of organisms that are parasitic in humans and warm-blooded animals [10], and the majority of commensal and pathogenic bacteria grow best in a neutral or very slightly alkaline reaction medium (pH 7.2–7.6) [10]. In order to ensure that the *P. mirabilis* grows

well and rapidly, and so as to obtain good reproducibility, the incubation was performed under the same conditions described in the literature [10].

2.5. Apparatus

The TSM sensor used was a 9 MHz AT-cut quartz crystal (diameter 12.5 mm) with silver electrodes (diameter 5.5 mm) on both sides. One side of the electrode was sealed and the other side was coated with liquid film. A thermostat was used to control the temperature at 37°C. A Model SC7200 Isutax universal frequency counter was employed to record frequency.

2.6. Frequency curve measurement

In a sterilized bottle, two aliquots of bacteria solution were added to one aliquot of medium and thoroughly mixed. Then, after incubation at 37°C for 4 h, the bottle was removed from the incubator and stored in a refrigerator. For the detection, 50 μl of mixture was coated on the sensor surface and the sensor was then placed in a thermostat and the frequency was recorded every 10 min or for a shorter time interval near the TT. At the end of the experiment it was observed that the film coagulated and a flat solid membrane formed.

2.7. Comparison of TT detection with standard PPC technique

P. mirabilis was inoculated in pure cultures of various concentrations and the TTs were determined with the TSM sensor. From Eq. (2), which will be discussed below, the numbers of cells were obtained. At the same time, the same amount of P. mirabilis was also measured by the standard PPC.

3. Results and discussion

3.1. Conditions of determination

The volume of coating solution was a key factor in the coating process of the film. Experimentally, 50 μl was suitable for practical deter-

minations. Firstly, 30–40 μl of solution was coated. It was found that the solution was not able to spread over the whole sensor surface. When 80 μl was coated, the solution was arched on the sensor surface (that is to say, the solution was able to spread over the sensor surface) and the film was apparently flat. Thus the reproducibility of the result was influenced in both cases. However, the use of 50 μl of solution made it easy for the solution to spread over the whole sensor surface and the film was not as arched. As a result, good reproducibility was obtained and a 50 μl volume was employed in the following experiments.

The composition of the medium film and the temperature and humidity of the coagulating process were related to the coagulation time.

When 50 μl of film, containing one aliquot of medium and three aliquots of water was coated on the sensor surface no obvious frequency change was observed after 6 h and it could be seen that the coated film did not coagulate. However, when a film with a mixture of one aliquot of medium and one aliquot of water was employed, although the coagulation time shortened, oscillation of the sensor was found to be difficult and so the TT could not be determined accurately. This was probably because the solid membrane formed at the end of the coagulation process was too thick. The film with the composition of one aliquot of medium and two aliquots of water provided quick coagulation and easy oscillation and was therefore used in the following experiments.

In order to study the effect of coagulating temperature, a mixture of one aliquot of medium and two aliquots of bacteria solution was coated on the sensor surface and the coagulation process was investigated at different temperatures. Results shown in Fig. 1 indicate that the increase in temperature reduces coagulation time. This may be because at higher temperature water in the medium is volatilized more rapidly. A coagulation temperature of 37°C was chosen because a higher temperature made the oscillation of the sensor unstable and at a lower temperature the coagulation time was too prolonged.

To test the effect of humidity on coagulation, a mixture of medium and water was used to observe
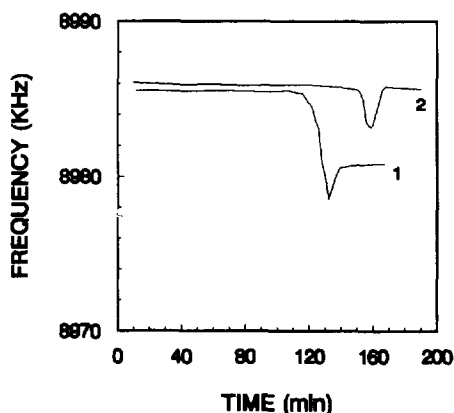
Fig. 1. Effect of coagulating temperature on detection. Coagulation of mixture of medium and water: (1) $T = 37°C$; (2) $T = 28°C$.

the coagulation process at different humidities. The TT was found to increase with the increase in humidity. The reason was that the decrease in humidity made the volatilization of water from the medium easier and more rapid. Thus the coagulation was performed at a relative humidity of about 50%.

3.2. Typical response curve

Typical response curves are shown in Fig. 2; it can be seen that the coagulation process of the medium was rather complicated. When no bacteria were added, the frequency decreased very slowly at first, then dropped quickly, and finally,
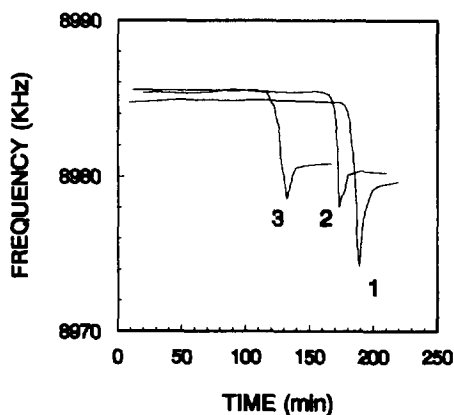

Fig. 2. Typical response curves. Initial concentration of P. mirabilis (cells ml^{-1}): (1) 2.0×10^6; (2) 2.0×10^4; (3) 0.
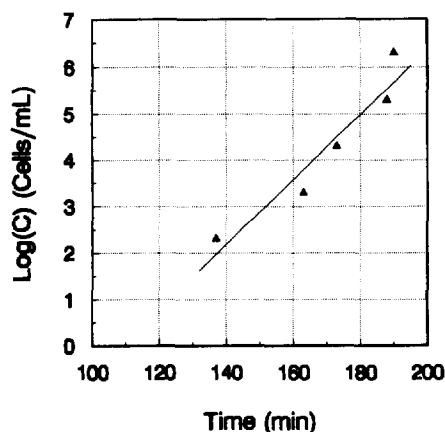

Fig. 3. TT calibration graph for the determination of P. mirabilis.

after an increase, reached a stable value. The time at which the frequency began to increase, i.e. the TT, was 132 min. After the growth of bacteria in the medium, the gelation curve shape was the same but the TT was delayed: the increase in the bacteria concentration results in an increase in the time delay. As the TT was sharp and the linear relationship between the TT and the logarithm of the bacteria concentration was good, the TT was employed in the practical determinations.

3.3. Determination of P. mirabilis

Various concentrations of P. mirabilis were inoculated in the medium and incubated at 37°C for 4 h, after which the mixture was stored in a refrigerator. When P. mirabilis was detected, it was coated on the TSM sensor and the frequency was recorded at different time intervals. Frequency curves were constructed and the TTs were measured, then a calibration graph of TT vs. logarithm of P. mirabilis concentration was constructed. The results (Fig. 3) showed that the TT was linearly related to the logarithm of the initial concentration (C) of the P. mirabilis, with C in the range of $2.0 \times 10^2 - 2.0 \times 10^6$ cells ml^{-1}. The regression equation is

$$\log C = 0.07 \,(\text{TT}) - 7.62 \qquad (2)$$

where C is the initial concentration of P. mirabilis in cell ml^{-1} and TT is the turning point time in

Table 1
Comparison of the bacteria concentration predicted by the TT tehcnique with that obtained from the PPC method

No.	Concentration predicted by TT method[a] (cells ml^{-1})	Logarithm of predicted value	Concentration obtained from PPC method (CFU[b] ml^{-1})	Logarithm of pour plate value
1	2.7×10^2	2.43	3.0×10^2	2.48
2	7.5×10^3	3.88	3.7×10^3	3.57
3	3.3×10^3	3.52	3.8×10^3	3.58
4	3.9×10^4	4.59	4.3×10^4	4.63
5	3.7×10^5	5.57	1.8×10^5	5.26
6	5.1×10^5	5.71	5.8×10^5	5.76
7	1.2×10^6	6.08	2.3×10^6	6.36

[a] Calculated by Eq. (2).
[b] CFU = colony forming units.

min; the correlation coefficient is 0.96 ($n = 5$). Hence, if the TT is determined the concentration of *P. mirabilis* can be calculated according to Eq. (2).

The standard error of the regressioin line is $S = 0.525$.

$$\log C = 0.07 \, (\text{TT}) - 6.57 \tag{3}$$

$$\log C = 0.07 \, (\text{TT}) - 8.67 \tag{4}$$

The area between the two lines plotted from Eqs. (3) and (4) is the 95% confidence range.

The concentration of the stock culture bacteria solution of *P. mirabilis* was obtained by the PPC technique. The solutions used in the determination were obtained by a series dilution of the stock culture solution. Therefore, the initial concentrations of the series bacteria solutions were calculated according to the dilution.

3.4. Comparison of the TT technique with the PPC method

The proposed method was compared with the conventional PPC method for determining *P. mirabilis*. The results are given in Table 1. It can be seen that all the PPC values fall inside the 95% confidence area of the TT predicted concentrations. Therefore it can be concluded that the TT method agrees well with the PPC technique.

3.5. Two further response parameters

After a thorough investigation of the response curve, two further response curve parameters were found to be related to the initial concentration of *P. mirabilis*. As shown in Fig. 2, after a horizontal portion of the curve, the frequency decreased very slowly at first, then dropped quickly, and finally, after an increase, reached a stable value. The time at which the frequency begins to decrease was defined as the decrease time (DT) and was found to be delayed when the concentration of *P. mirabilis* rose. There was a linear relationship between the DT and the logarithm of the *P. mirabilis* concentration (Fig. 4). The regression equation is as follows:
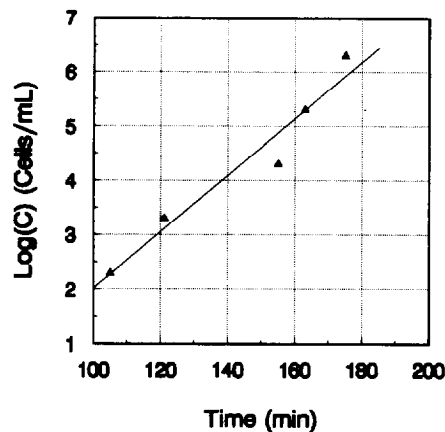

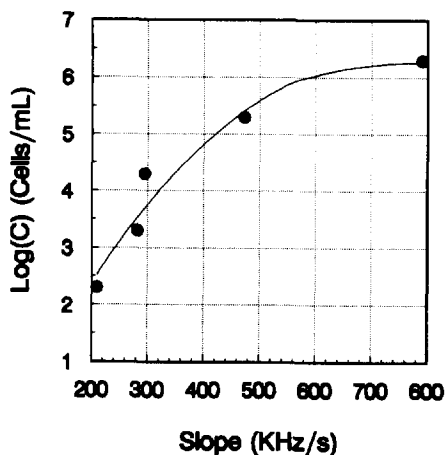Fig. 4. DT calibration graph for the determination of *P. mirabilis*.

Fig. 5. Relationship between the increase in the slope of frequency and the logarithm of the P. mirabilis concentration.

$$\log C = 0.05\,(DT) - 3.19 \tag{5}$$

where C is the same as in Eq. (2) and DT is the time at which the frequency begins to decrease (min). The correlation coefficient is 0.97 ($n = 5$).

The slope of the increase of the frequency after the TT of the curve was also related to the initial P. mirabilis concentration. With the increase in the P. mirabilis concentration, the slope of the frequency increase was found to become more steep (Fig. 5).

The precision of the DT and TT methods when determining P. mirabilis was approximately the same and so both methods could be used for the quantitative detection of P. mirabilis. However, the DT was not so obvious on the frequency curve compared with the TT and thus was not so easy to determine. As for the slope of the increase in the frequency after the TT on the curve, the relationship between the slope and the logarithm of the P. mirabilis concentration was complicated. Therefore, the TT was preferred for quantitative detection in these experiments when considering its ease of determination and the simplicity of its relationship with the logarithm of the P. mirabilis concentration.

In conclusion, this method employed the evident coagulation process of the medium to detect microorganisms indirectly. The TT used for quantitative determination was easy to determine because of the sharp turning point of the response curve and was in good linear relationship with the logarithm of the bacteria concentration. This method is rapid and simple with high sensitivity, and only a micro-sample is needed. It can be used to determine the concentration of bacteria, to study the coagulation process of biomolecules and the influence of microorganisms on biomolecules. It can also be used in bacteria growth monitoring.

Acknowledgements

References

[1] T. Nomura and A. Minemura, Nipon Kagaku Kaishi, 104 (1980) 1681.

[2] P.L. Konash and G.J. Bastiaans, Anal. Chem., 52 (1980) 1929.

[3] T. Nomura and M. Okahara, Anal. Chim. Acta, 142 (1982) 281.

[4] S.Z. Yao, S.L. Dan and L.H. Nie, Anal. Chim. Acta, 209 (1988) 213.

[5] H. Muramatsu, E. Tamiya and I. Karube, Anal. Chim. Acta, 215 (1988) 741.

[6] S.H. Si, T.A. Zhou, D.Z. Liu, L.H. Nie and S.Z. Yao, Anal. Lett., 11 (1994) 2027.

[7] H. Muramatsu, Y. Watanabe, M. Hikuma, T. Ataka, I. Kubo, E. Tamiya and I. Karube, Anal. Lett., 22 (1989) 2155.

[8] F.J. He, Q. Geng, W.H. Zhu, L.H. Nie, S.Z. Yao and C.M. Feng, Anal. Chim. Acta, 289 (1994) 313.

[9] K.K. Kanazawa and J.G. Gordon II, Anal. Chim. Acta, 175 (1985) 99.

[10] R. Cruickshank, J.P. Duguid, B.P. Marmion and R.H.A. Swain, Medical Microbiology, Vol. 1: Microbial Infections, Churchill Livingstone, Edinburgh, 1973.

Novel use of a fiber-optic-based on-line trichloroethylene sensor in a column retardation experiment

F. Hoffman[a,c,*], D. Ronen[c], H. Rosin[c], F. Milanovich[b]

[a]*Environmental Protection Department, Lawrence Livermore National Laboratory, Livermore, CA 94551, USA*
[b]*J. Division, Lawrence Livermore National Laboratory, Livermore, CA 94551, USA*
[c]*Department of Environmental Sciences and Energy Research, Weizmann Institute of Science, Rehovot 76100, Israel*

Abstract

A newly developed fiber-optic-based trichloroethylene (TCE) sensor previously described [F.P. Milanovich, S.B. Brown, B.W. Colston, Jr., P.F. Daley and K. Langry, Talanta, 41 (1994) 2189], was used to provide analyses of TCE in laboratory tests of retardation of TCE in ground water. The sensor enabled inexpensive real time analyses of TCE in retardation tests conducted in a sand-filled flow-through column. The simultaneous data analysis of TCE, ^{18}O and Cl^- breakthrough curves enabled the calculation of an estimated retardation coefficient which was found to be in good agreement with that predicted by the octanol/water partitioning K_d method. The fiber-optic sensor was demonstrated to be a fast and reliable method for conducting on-line laboratory analyses of TCE at the parts per billion level in a small volume of contaminated water, thus providing excellent temporal resolution of the data as well as minimizing volatile losses during sample collection and analysis.

1. Introduction

Throughout the world, major economic and public health decisions are being made in the investigation and attempted cleanup of aquifers contaminated by volatile organic compounds (VOCs), many of which are classified as probable human carcinogens, such as trichloroethylene (TCE).

In addition to the determination of the extent and degree of ground water contamination, the prediction of contaminant movement in aquifers is often required. The analysis of contaminant transport in ground water is very sensitive to the retardation factor, i.e. the relationship of the linear velocity of the ground water to the linear velocity of the contaminant. The retardation factor (R) for a ground water contaminant is calculated by [2]

$$R = V_w/V_c = 1 + (\rho_b/n)(K_d) \qquad (1)$$

where V_w is the velocity of the ground water, V_c is the velocity of the contaminant, ρ_b is the bulk density of the porous medium, n is the porosity of

*Corresponding author.

the porous medium, and K_d is the distribution coefficient.

Of the variables in Eq. (1) K_d is the most difficult to measure in permeable unconsolidated sediments. In addition, K_d is also sensitive to the amount of organic carbon present in the sediment. Schwarzenbach and Westall [3] have proposed 0.1% organic carbon as the lower limit for sorption of VOCs to be dominated by the organic carbon. Above this limit, a number of researchers have presented methods for estimating K_d values based upon the amount of organic carbon present in the sediments and the octanol/water partitioning coefficient of the VOC of concern. Several of these methods have been presented and compared by Domenico and Schwartz [4]. Using a series of laboratory batch K_d experiments, Piwoni and Banerjee [5] proposed a method for estimating K_d values of VOCs, in low organic carbon (< 0.1%) sediments, that they claim should be accurate within a factor of two or three:

$$\log K_d = 1.01 \log K_{ow} - 3.46 \qquad (2)$$

where K_{ow} is the octanol/water partition coefficient. Applying the values of K_{ow} for TCE taken from Schwarzenbach and Giger [6] to Eq. (2) provided an estimated K_d for TCE of 0.07 ml g^{-1}.

Laboratory batch K_d tests are commonly conducted by immersing a small amount of solid material in water containing the contaminant. The mixture is then agitated for a specified period of time, the solid removed, and the remaining water analyzed. The difference between the original concentration in the water and the concentration at the end of the test is assumed to be the amount retained by the solid. Because of the sample disturbance in the laboratory batch K_d experiments, the resulting K_d value does not account for the retardation mechanisms that are inherent in undisturbed sediments.

Among the mechanisms which contribute to apparent retardation are (not in order of priority): adsorption to the surfaces of inorganic materials; hydrodynamic dispersion; biotic and/or abiotic degradation; partitioning to organic carbon; diffusion into, and entrapment/retention in, constricted or dead-end pores; and diffusion into relatively immobile waters in lenses of finer-

grained materials. For some of these mechanisms we can assume instantaneous local equilibrium, some are destructive of the VOCs, and some are rate-limited. A retardation experiment using a column packed to approximate aquifer conditions can measure the sum of many of these retardation mechanisms, hereafter referred to as sorption. The experiments described here are the initial efforts in a longer term research project designed to evaluate the relative contributions of the various retardation mechanisms.

Fundamental to the investigation and remediation planning for VOCs is the ability to perform accurate and precise chemical analyses. To provide rapid and inexpensive TCE analyses a fiber-optic-based TCE sensor was designed and developed at Lawrence Livermore National Laboratory (LLNL) [1,7–9]. This paper reports on the laboratory utilization of this newly developed fiber-optic-based sensor to provide real time analyses of TCE in retardation tests conducted in a flow-through column. These column experiments were conducted at low flow rates designed to approximate ground water flow velocities. As a result, samples for TCE analysis had to be collected over a relatively long period of time, at atmospheric pressure, during which they were subject to volatile losses. The volatile losses could be minimized by the collection of the smallest possible sample over the shortest time period. In addition, greater temporal resolution of the data would be achieved by taking the smallest possible sample. The fiber-optic-based sensor allowed immediate analysis of a 7.5 ml sample with acceptable precision at concentration levels of 10 parts per billion or less.

2. Methods

2.1. Fiber-optic TCE analytical technique

The TCE analyses were conducted using a fiber-optic-based sensor where the concentration of TCE is determined by the rate of change of 560 nm light absorption, in basic pyridine reagent. This reagent develops a red color by reacting with TCE [1,7–9].

When the sensor is placed in a vapor stream containing the contaminant, or in the headspace of a water sample, as is the case in this experiment, the contaminant diffuses through a semipermeable membrane tubing, contacts the reagent, and produces the colored product. The onset of the color change is monitored remotely with optical fibers.

When the analysis begins, the computer attached to the control center of the system monitors the rate of change of light absorption, caused by the color production in the reagent. The rate of the color reaction is proportional to the concentration of the contaminant in the sample. The sensor itself is constructed from porous membrane tubing, which holds the reagent during the analysis [1]. The instrument is also equipped with syringe pumps for the reagent feed and reagent waste. When the analysis is complete, the computer controls the injection of new reagent into the sensor and the evacuation of the old, colored reagent. The sensor is then ready for the next analysis.

The daily calibration of the sensor, for this experiment, was accomplished by the analysis of standard solutions of TCE, prepared by dilution, at concentrations of 25 ppb, 100 ppb, 250 ppb, and 500 ppb. The light absorbance curves were plotted against the concentrations and the linear regression was calculated. The resulting linear relationships had correlation coefficients (r^2) that commonly varied between 0.97 and 0.99. All calibration and experimental analyses were conducted in vials containing 7.5 ml of sample with 7.5 ml of headspace. The estimated analytical error of this new methodology, in the 25–500 ppb range, is 10% [10]. Comparisons of TCE analytical results from a series of ground water samples using the fiber-optic-based sensor and purge and trap gas chromatography are included in Ref. [9].

2.2. The experimental column

A sand-filled column was designed to perform retardation tests on geological materials. Since the tests were to be evaluated based on the retardation of the contaminant through the column, the column was designed to approach complete and uniform contact of the contaminated water with the sediment and to minimize preferential flow through the sediments or along the boundaries of the column. In addition, the sediment was to be compacted to approximate field conditions. Another design constraint of the column was to minimize contaminant adsorption on the column construction materials.

To meet these design criteria, the column was constructed entirely of Teflon. The Teflon serves two important purposes: (1) many contaminants are minimally sorbed to Teflon [11]; and (2) under the compacting forces on the sediments, the sediment grains are forced into the softer Teflon, thereby minimizing the possibility of preferential flow along the walls of the column. The only exception to the Teflon materials is a 230 μm pore size nylon membrane placed at either end of the sediment ot help retain the sand (Fig. 1). A Teflon screen extends beyond the threads of the end-cap to allow the application of mechanical pressure to the sediments to assist in compaction. The nominal outside dimensions of the column are 6.75 cm in diameter and 15 cm in length and the nominal dimensions of the sediment chamber are 5 cm in diameter and 9.5 cm in length.

The distribution of the influent and effluent flows is through three ports equally spaced 120° apart at either end of the column (Fig. 1). Immediately inside the column is a void mixing space followed by a Teflon screen with 39 equally spaced 3 mm diameter holes.

The sediment used in the column was designed to approximate a low organic carbon (< 0.1%), fine-to medium-grained sand of known grain-size distribution. To achieve this, the sand was acid-washed and sieved into three fractions. The first fraction passed a 1000 μm sieve and was retained on a 500 μm sieve, the second was retained on a 250 μm sieve and the third on a 125μm sieve. The three fractions were then recombined in equal parts by weight and homogenized. The homogenization process consisted of combining the three fractions, splitting the result into another three fractions, and recombining. This process was repeated until there was no visible sorting of the different grain sizes.
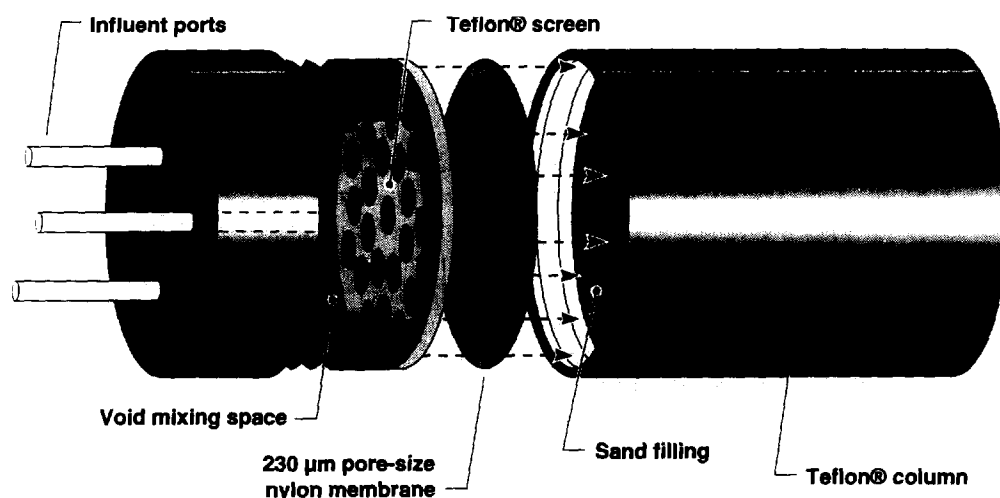
Fig. 1. Diagram of the construction features of the influent end of the sand-filled column. The effluent end of the column (not shown) is similar to the influent end without the threaded end-cap.

After the sand was poured and compacted, the column was saturated by slowly applying water from the bottom up. Water was then drawn through the column using a vacuum system which also helped to remove any entrained air bubbles. To ensure that the column met its design requirements, flow tests were evaluated using magnetic resonance imaging (MRI) [12].

The bulk density and porosity of the sand were determined gravimetrically and the hydraulic conductivity was measured with a constant head flow test. The bulk density of the column was found to be 1.84 g cm^{-3} and the porosity 0.27. The hydraulic conductivity was 2.1 × 10^{-2} cm s^{-1}.

2.3. Retardation test procedures

The contaminant used in the experiments was TCE dissolved in water. Conservative tracers (Cl– and ^{18}O-depleted water) were also added to the solution. The velocities of the advective fronts for the TCE and the tracer were calculated from the breakthrough curves and retardation and distribution coefficients were determined from Eq. (1).

The experimental set-up is illustrated in Fig. 2. The influent water was made up in a 500 ml glass volumetric flask and was drawn into the syringe pump through a Y valve through PVC tubing. The Y valve was then turned such that the syringe

pump would pump the water to the column at 30 ml h^{-1}. Ahead of the column was a glass tee with a valve which allowed the collection and release of any air bubbles prior to the flow entering the column. This device was utilized only during the initial filling of the distribution system, since the syringe pump produced no bubbles. The column was held in a vertical position and the TCE-bearing water was introduced from the bottom up to avoid any buoyancy-induced fingering of the contaminant. The effluent from the column was then directed by a Y valve to one of two sample collection cells. When the cell had received 7.5 ml of effluent (after 15 min of operation) the flow was switched to the second cell and the fiber-optic TCE sensor was inserted into the first cell. Following the analyses for TCE, the effluent was poured from the cell into a sample collection vial for analysis of the conservative tracer. The procedure was then repeated for the second cell.

2.3.1. Experiment 1

In the first experiment a solution of 136 ppm NaCl and 500 ppb TCE was delivered to the column, which was saturated with deionized water. Each sample was analyzed for TCE using the fiber-optic-based sensor, as soon as it was collected, and was then stored for later chloride analysis by high performance liquid chromatogra-
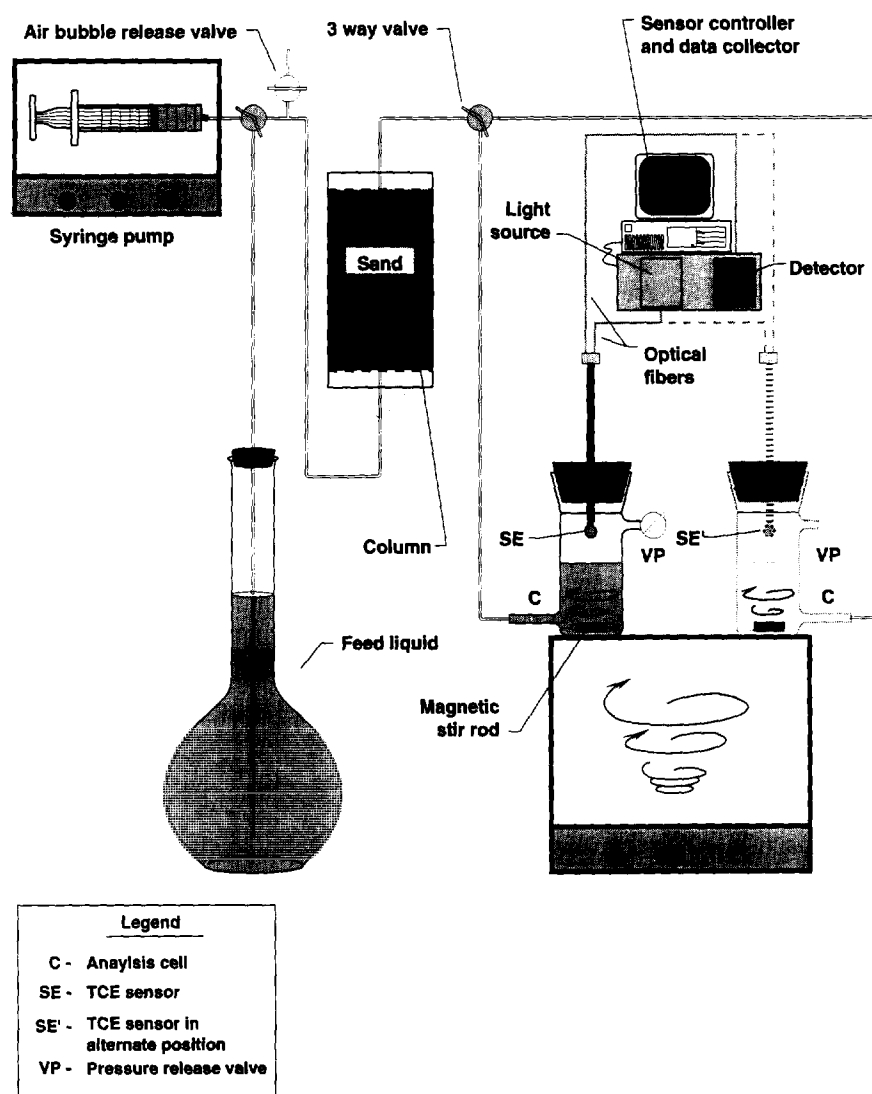
Fig. 2. Schematic diagram of the sand-filled column experiment apparatus used to measure retardation and to estimte the K_d value of TCE in an acid-washed sand.

phy (HPLC) with a precision of 4%. The experiment was terminated after 500 min.

2.3.2. Experiment 2

The procedures for the second experiment were essentially the same as the first with the following exceptions. The influent water contained 500 ppb TCE, 128.5 ppm chloride and was made up with ^{18}O-depleted water (δ = 60%). When the concentration of TCE appeared to begin to level off, the influent water was replaced with distilled water with no detectable TCE, a chloride concentration of less than 10 ppm, and a $\delta^{18}O$ content of – 4‰. At this point, the column was inverted such that the influent entered the column at the top and moved to the bottom, to minimize buoyancy-induced fingering. The collected samples were analyzed for TCE and for chloride, as in experiment 1, and for [18]O by mass spectrometry with a precision of 0.2‰.
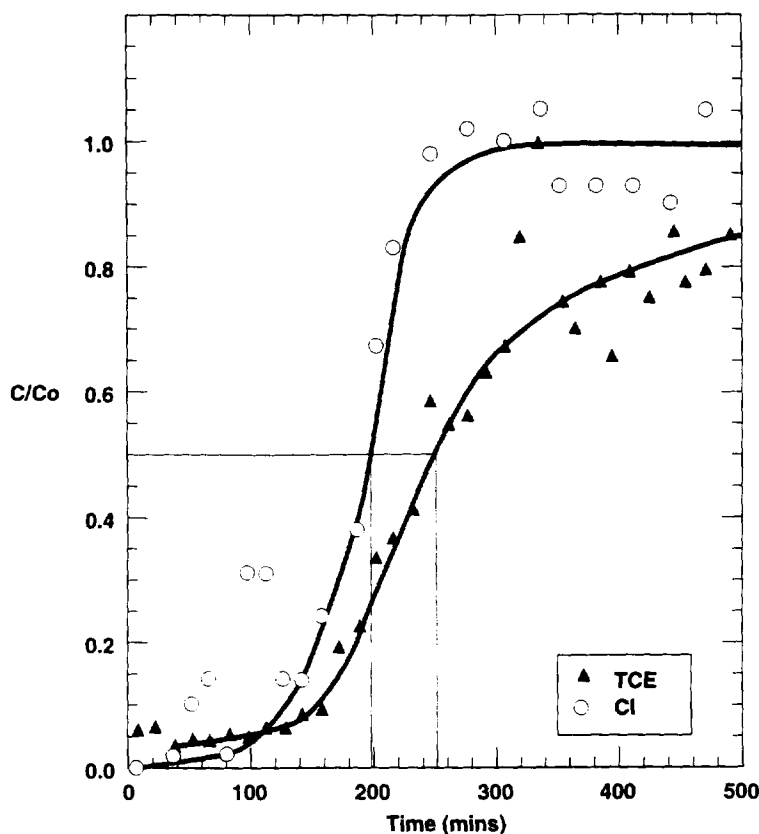
Fig. 3. TCE and chloride breakthrough curves from the first TCE sorption experiment. Application of Eq. (2) yields an R value of 1.34 and a K_d value of 0.05 ml g^{-1}.

During the course of this experiment the influent water was sampled and analyzed for TCE periodically. Some TCE was lost to volatilization during the experiment, and the value of the concentration of the influent was corrected accordingly.

3. Results and discussion

Most contaminant transport models assume that sorption is an equilibrium process. However, over the past decade, work on VOC plumes appears to indicate that sorption is a slow process, most notably in low organic carbon sediments, and that the kinetics and rates of VOC sorption/desorption remain poorly understood. At the Borden aquifer, monitoring of an injected VOC plume indicated that sorption was continuing to increase even 2 years after the experiment com-

menced [13]. In addition, in studies with field columns (columns pushed into sediment at the bottom of an augured hole and studied in place) at the same site, retardation coefficients varied inversely with the average pore water velocities indicating non-equilibrium transport conditions [14]. Knox et al. [15] discussed the differences in sorption rates between sediments which contain organic carbon (fast sorption) and those which do not (slow sorption). Since the sands in this column were acid-washed, resulting in low organic carbon content, we anticipated slow sorption.

In estimating the velocity differences of the water and of the contaminant, in this experiment we used the common convention [4] of selecting $C/C_0 = 0.5$ as the arrival of the advective front, where $C =$ the concentration of the solute at time t, and $C_0 =$ the concentration of the solute in the
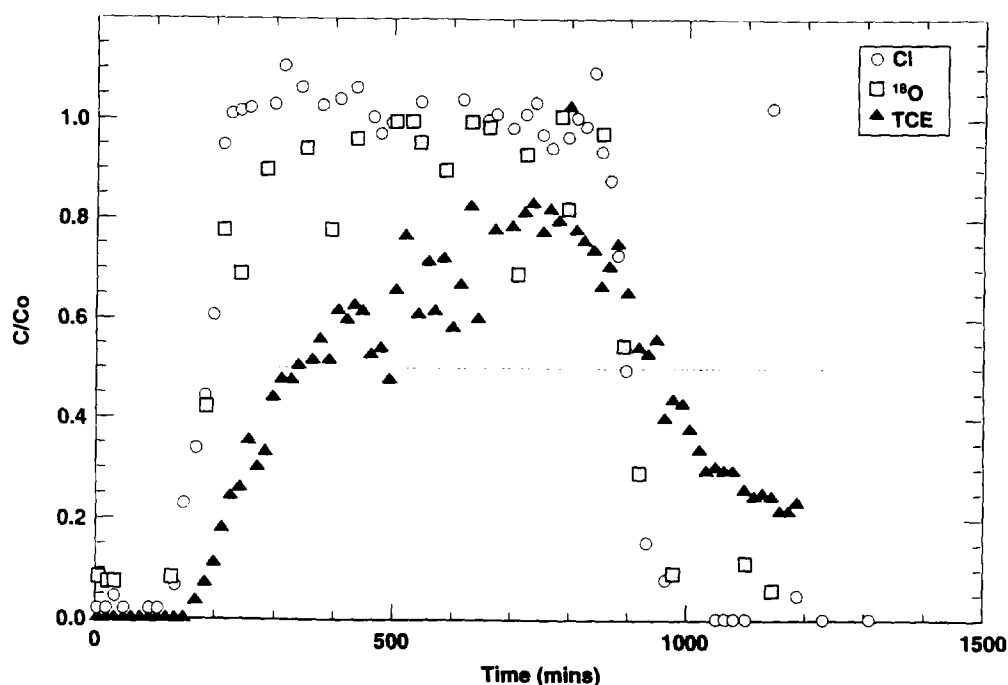
Fig. 4. TCE, chloride, and ^{18}O breakthrough curves from the second TCE sorption experiment. Application of Eq. (2) yields an R value of 1.72 and a K_d value of 0.11 ml g^{-1}. At approximately $t = 668$ min, the influent water was replaced with distilled water.

influent. In both experiments (Figs. 3 and 4), it is apparent that sorption was continuing to occur, although at a decreasing rate, at the time that we terminated the injection of the TCE-containing influent. Although sorption is continuing to take place, at a rapidly decreasing rate, behind the advective front, this sorption does not have a significant effect on the velocity of the leading edge of the plume.

3.1. Experiment 1

Prior to the experiment, several hundred pore volumes of deionized water were slowly pumped through the column in an effort to ensure that no TCE was present at the start of the test. The breakthrough curves for this experiment are shown in Fig. 3. The initial analyses for TCE indicated that there was a small amount of TCE, approximately 20 ppb, present in the column at the beginning of the experiment. This TCE may

be residual TCE sorbed to the sand in the column from preliminary tests. About 120 min into the experiment, the TCE analyses indicated the beginning of a steady rise in concentrations until approximately 350 min. At that time, the rate of increase of the TCE concentrations began to decrease.

The analyses for chloride in the early portion of the experiment were erratic, possibly the result of analytical error or inadequate flushing of the column prior to the experiment. However, these results were followed by a smooth steady increase in concentration until the analyses leveled off near the C/C_0 ratio of 1.0.

The retardation and K_d value for the TCE in this low organic carbon sand was calculated using Eq. (1). The resulting retardation was 1.34 and K_d was 0.05 ml g^{-1}. This K_d value agrees closely with the value of 0.07 ml g^{-1} determined by the Piwoni and Banerjee method [5] with a log K_{ow} value for TCE of 2.29 [6].

3.2. Experiment 2

Prior to conducting the second experiment, the column was rapidly flushed with several hundred pore volumes of hot tap water followed by several hundred pore volumes of deionized water to ensure the removal of the residual contaminants seen in experiment 1. Following the flushing, the initial TCE analyses indicated no TCE and the chloride analyses were low and steady, supporting the hypothesis that the variations seen in the early parts of the first experiment were the result of inadequate flushing prior to beginning the test. As in the first experiment, the breakthrough curves were smooth and steady for all three tracers, and as the concentrations for each constituent approached a C/C_0 ratio of 1.0, they became more variable (Fig. 4).

At times 428 min, 593 min, and 668 min the feed water was analyzed for TCE. The sample at 668 min was taken as the feed water was switched to deionized water. These analyses indicated a steady loss of TCE throughout the experiment. To prepare the plot for TCE shown in Fig. 4, the volatile loss was assumed to be linear between analyses and the C_0 value was corrected for each syringe filling, since the volatile loss must have taken place in the feed water flask, and no appreciable further volatilization would have occurred after the water was drawn into the syringe. It is worthwhile noting that the volatilization that occurred in the first 300 min is relatively minor, i.e. less than 10%, and is within the range of analytical error. In future experiments with influent-containing volatile compounds, a collapsible bag as an influent supply reservoir, such as that used by Szecsody and Bales [16], or simultaneous injection of water and the VOC as described by Priddle and Jackson [17] would be preferable, to help reduce volatile loss.

The retardation and K_d value were calculated as in the first experiment. In this case, the retardation was 1.72 and the K_d value was 0.11 ml g^{-1}. This value is also similar to the value of 0.07 ml g^{-1} given by the Piwoni and Banerjee method [5].

The increased variability in concentrations near the top of the breakthrough curves for each of the constituents in the two experiments may be the result of the small scale heterogeneities in the sand seen in the MRI experiments [12].

Although sorption was continuing to take place, the feed water was switched to deionized water at 668 min to accommodate the time constraints of the experiment. The chloride breakthrough curve for the deionized water is a mirror image of the steep chloride and ^{18}O breakthrough curves for the contaminated feed water, while the TCE curve starts off steep and then begins to level off at a C/C_0 ratio of 0.3.

4. Conclusion

The fiber-optic-based TCE sensor developed at LLNL shows promise as an inexpensive rapid method for conducting TCE analyses in the field as well as in the laboratory. In this experiment, it enabled real time accurate analysis of TCE in tests conducted in a sand-filled flow-through column and was sufficiently sensitive to detect residual parts per billion TCE contamination in the column at the beginning of experiment 1.

The sensor is capable of accurate analysis of samples as small as 7.5 ml, which increased the temporal resolution of the data and minimized volatile losses. In addition, the real time analyses provided the opportunity to make adjustments in the experiment once it was underway.

This study used the sensor to examine the retardation of the leading edge of a relatively low concentration TCE plume in a low organic carbon fine- to medium-grained sand. The experiment is part of a longer term research project designed to study the relative contributions of the various mechanisms that result in apparent retardation of VOCs in ground water. On-line laboratory studies of contaminant retardation may be of major importance in planning and predicting the restoration of contaminated ground water. The use of the sensor in further experiments of this type may help to advance our understanding of TCE behaviour in ground water, and to inspire new cleanup technologies.

Acknowledgements

References

[1] F.P. Milanovich, S.B. Brown, B.W. Colston, Jr., P.F. Daley and K. Langry, Talanta, 41 (1994) 2189–2194.

[2] R.A. Freeze and J.A. Cherry, Groundwater, Prentice-Hall, Inc., NJ, 1979.

[3] R.P. Schwarzenbach and J. Westall, Environ. Sci. Technol., 15 (1981) 1360–1367.

[4] P.A. Domenico and F.W. Schwartz, Physical and Chemical Hydrogeology, John Wiley, New York, 1990.

[5] M.D. Piwoni and P. Banerjee, J. Contam. Hydrol., 4 (1989) 162–179.

[6] R.P. Schwarzenbach and W. Giger, Behavior and fate of halogenated hydrocarbons in ground water, in C.H. Ward, W. Giger and P.L. McCarty (Eds.), Ground Water Quality, Wiley-Interscience, New York, 1985.

[7] F.P. Milanovich, D.G. Garvis and S.M. Angel, Anal. Instrum., 15 (1986) 137.

[8] S.M. Angel, M.N. Ridley, K. Langry, T.J. Kulp and M.L. Myrick, New developments and applications of fiber optic sensors, in R.W. Murray, R.E. Dessy, W.R. Heineman, J. Janata and W.R. Seitz (Eds.), American Chemical Society Symposium Series 403, Vol. 23, Washington, DC, American Chemical Society, 1989, p. 345.

[9] F.P. Milanovich, P.F. Daley, K. Langry, B.W. Colston, Jr., S.B. Brown and S.M. Angel, A fiber optic sensor for the continuous monitoring of chlorinated hydrocarbons, in Proc. 2nd Int. Conf. Field Screening Methods for Hazardous Wastes and Toxic Chemicals, 12–14 February, 1991, EPA, Las Vegas, NV, 1991, p. 43.

[10] B.W. Colston, Jr., Lawrence Livermore National Laboratory, Livermore, CA, personal communication, 1994.

[11] M.J. Barcelona, J.P. Gibb and R.A. Miller, A Guide to the Selection of Materials for Monitoring Well Construction and Groundwater Sampling, SWS Contract Report #327. Illinois Department of Energy and Natural Resources, Water Survey Division, Champagne, IL, 1983, p. 78.

[12] F. Hoffman, R. Ronen and Z. Pearl, J. Contam. Hydrol., (1996) in press.

[13] P.V. Roberts, M.N. Goltz and D.M. Mackay, Water Resour. Res., 22 (1986) 2047.

[14] C.J. Ptacek and R.W. Gillham, J. Contam. Hydrol., 10 (1992) 119.

[15] R.C. Knox, D.A. Sabatini and L.W. Canter, Subsurface Transport and Fate Processes, Lewis Publishers, Boca Raton, FL, 1993.

[16] J.E. Szecsody and R.C. Bales, J. Contam. Hydrol., 4 (1989) 181.

[17] M.W. Priddle and R.E. Jackson, Ground Water, 28 (1991) 260.

Short Communication

Investigation of the detection limit of a series piezoelectric sensor

Qi Kang[a], Zechang Liu[a], Jintian Hu[b], Dazhong Shen[b],*

[a]*Chemical Engineering Department, Jinan Branch of Shandong Institute of Mining and Technology, Jinan 250031, People's Republic of China*
[b]*Chemistry College, Shandong University, Jinan 250100, People's Republic of China*

1. Introduction

Recently, there has been increasing interest in the application of piezoelectric sensors in solution chemistry [1–3]. In most of the applications, a piezoelectric sensor is used as a microbalance due to its high sensitivity to the mass change on the surface of the quartz crystal [4]. Besides the mass effect, applications based on the response modes in viscosity [5,6], conductivity [7,8] and permittivity [9] were reported.

To improve the stability and selectivity of the frequency response of piezoelectric sensors in the liquid phase, a type of series piezoelectric quartz crystal (SPQC) was reported recently [10–12]. It was shown that the SPQC possesses a selective frequency response to permittivity and conductivity with excellent frequency stability [13,14]. In this paper, the detection limit of the SPQC to conductivity is reported.

---

* Corresponding author.

2. Experimental

2.1. Apparatus and reagents

The construction of the SPQC was described in detail previously [10,12]. The appartus used was the same as that in Ref. [10]. Analytical reagent grade chemicals and doubly-distilled water were used throughout.

2.2. Procedure for measurements

Before the experiment, 30 min was required to allow the oscillator to stabilize. Then a KCl solution of known conductivity was introduced into the detection cell. A stable oscillating frequency of the SPQC was recorded with a time window of 10 s. The average value of 30 oscillating frequencies in 5 min was recorded as the oscillating frequency; the standard deviation of the 30 oscillating frequencies was taken as the noise level.

3. Results and discussion

Generally, the detection ability of a chemical sensor is described by its detection limit, which is determined by the signal-to-noise ratio. For a change in conductivity $(\Delta\chi)$ due to the analyte concentration, the frequency shift signal in the SPQC, ΔF_{signal}, can be estimated as $\Delta F_{signal} = |S_\chi \cdot \Delta\chi|$, where S_χ is the sensitivity to conductivity (χ). By using the S_χ values measured experimentally, the ΔF_{signal} values with $\Delta\chi = 10^{-4}$ S m^{-1} are depicted in Fig. 1. It can be seen that the ΔF_{signal} values decrease with increasing cell constant and depend greatly on the background conductivity. In a solution of medium conductivity, there is a maximum of ΔF_{signal}.

If only ΔF_{signal} is considered, it seems that the detection ability of the SPQC can be improved by using a smaller cell constant. Detection ability in solutions of medium conductivity is better than that in low conductivity solutions. This statement is somewhat questionable, because the detection ability of a sensor depends not only on the signal but also on its noise level.

Fig. 2 shows the standard deviations of 30 oscillating frequencies recorded in KCl solutions, which are used as the noise level of the SPQC, ΔF_{noise}. Fig. 2 reveals that ΔF_{noise} is also related

Fig. 2. Dependence of ΔF_{noise} on background conductivity.

significantly to the background conductivity. In addition, ΔF_{noise} decreases with increasing cell constant. This result can be explained as follows.

In the SPQC, the noise level may be expressed as

$$\Delta F_{noise} = (\Delta F_{tem}^2 + \Delta F_{osc}^2 + \Delta F_{ins}^2)^{1/2}$$

where $\Delta F_{tem} = \partial F/\partial t \cdot \Delta t$ is the solution temperature noise, $\partial F/\partial t$ is the frequency–temperature coefficient of the SPQC [10], and Δt is the variation in solution temperature. $\Delta F_{osc} \approx 10^6 Q^{-2}$ is the noise level of the oscillator, where Q is the quality factor of the SPQC [14]. ΔF_{ins} is the noise level of the frequency counter, its typical value being less than 0.1 Hz.

Under general experimental conditions, the solution temperature can be controlled within $\pm 0.1°C$. According to the frequency–temperature coefficient of the SPQC discussed in detail previously [10], the ΔF_{noise} values arise mainly from ΔF_{tem}, except in the case of $\partial F/\partial t \approx 0$. Comparing the ΔF_{noise} value with the frequency–temperature coefficient, the variation in solution temperature is about $\pm 0.04°C$ during the measurement time under our experimental conditions.

In solutions of low conductivity, $\Delta F_{osc} \approx 0$, as the SPQC has a much greater Q value [14]. With increasing conductivity, the $\partial F/\partial t$ value decreases [10], and hence a decrease in ΔF_{noise} is obtained.
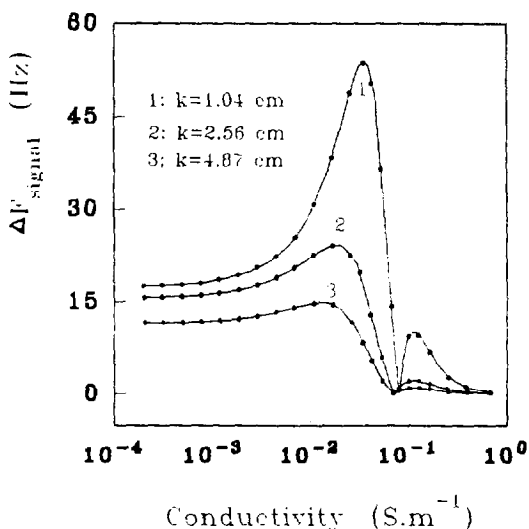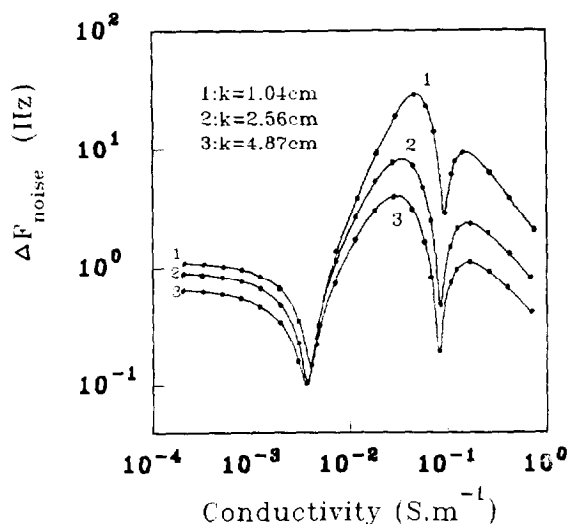

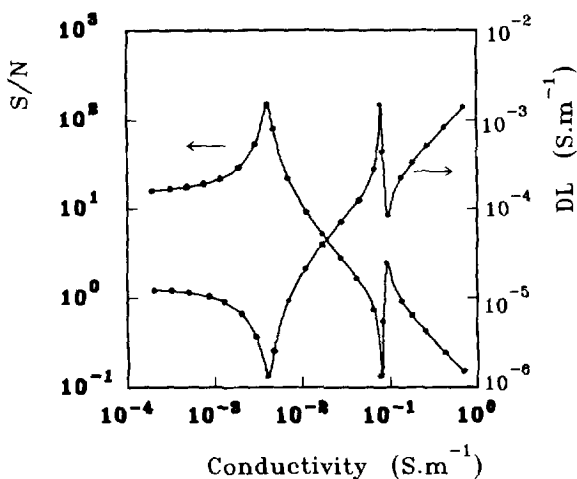Fig. 1. Theoretical dependence of ΔF_{signal} on background conductivity; $\Delta\chi = 10^{-4}$ S m^{-1}.

Fig. 3. Dependence of signal-to-noise ratio ($\Delta_\chi = 10^{-4}$ S m^{-1}) and detection limit to conductivity on background conductivity.

The ΔF_{noise} value reaches its minimum in solution with $\chi \approx 4 \times 10^{-3}$ S m^{-1}, where $\partial F/\partial t \approx 0$, and the value of ΔF_{noise} is close to ΔF_{ins}.

In a solution of medium conductivity, ΔF_{noise} has a maximum that corresponds to the maximum frequency–temperature coefficient. In the solution with $\chi \approx 8 \times 10^{-2}$ S m^{-1}, there is a second minimum for ΔF_{noise}, where $\partial F/\partial t \approx 0$ again. As discussed previously [14], the Q values of the SPQC decrease significantly in medium conductivity solutions, and so ΔF_{noise} is determined mainly by ΔF_{osc} here.

With increasing background conductivity in highly conductive solutions, the $\partial F/\partial t$ value decreases, and hence a decrease in ΔF_{noise} is observed again as $\Delta F_{osc} \approx 0$.

Using the values of ΔF_{signal} and ΔF_{noise}, the signal-to-noise ratio (S/N) of the SPQC is illustrated in Fig. 3. As the S/N values depend only slightly on the cell constant, for clarity only the results in the SPQC with a cell constant of 1.04 cm are shown. With S/N = 2, the detection limit (DL) to conductivity is also shown in Fig. 3. It can be seen that the S/N and DL values are significantly dependent on the background conductivity.

In low conductivity solutions, the ΔF_{signal} values are nearly constant, while the ΔF_{noise} values de-

crease with increasing background conductivity. As a result, S/N increases and DL decreases with increasing background conductivity. The lowest DL value can be obtained in the solution with $\Delta F_{tem} \approx 0$. As the background conductivity continues to grow, ΔF_{signal} and ΔF_{noise} increase. Because the increase in ΔF_{noise} is more rapid than that in ΔF_{signal}, S/N decreases and DL increases with increasing background conductivity in medium conductivity solutions. The minimum S/N value corresponds to the point where $S_\chi \approx 0$.

With increasing background conductivity in high conductivity solutions, ΔF_{noise} and ΔF_{signal} decrease. The decrease in ΔF_{signal} is more obvious than that in ΔF_{noise}. Consequently, S/N decreases and DL increases as background conductivity increases.

4. Conlcusions

The noise level of the SPQC in electrolyte solutions arises mainly from the variation in solution temperature. The detection limit to conductivity is not influenced by the cell constant, but it depends significantly on the background conductivity. The detection limit in solutions of low background conductivity is much lower than that in medium conductivity solution, despite a higher sensitivity in the latter.

References

[1] M. Thompson, A.L. Kipling, W.C. Duncan-Hewitt, L.V. Rajaković and B.A. Čavić-Vlasak, Analyst, 116 (1991) 881.

[2] D.A. Duttry, in A.J. Bard (Ed.), Electroanalytical Chemistry, Vol. 17, M. Dekker, New York, 1991, pp. 1–85.

[3] D.A. Buttry and M.D. Ward, Chem. Rev., 92 (1992) 1355.

[4] G. Sauerbrey, Z. Phys., 155 (1959) 206.

[5] H. Endo, K. Sode, I. Karube and H. Muramatus, Biotechnol. Bioeng., 36 (1990) 636.

[6] H. Muramatus, E. Tamiya, M. Suzuki and I. Karube, Anal. Chim. Acta, 215 (1988) 91.

[7] S.Z. Yao and Z.H. Mo, Anal. Chim. Acta, 193 (1987) 97.

[8] Z.H. Mo, L.H. Nie and S.Z. Yao, Sci. Chin. (Ser. B), 1 (1991) 1.

[9] W.H. Zhu, W.Z. Wei, Z.H. Mo, L.H. Nie and S.Z. Yao, Anal. Chem., 65 (1993) 2568.

[10] D.Z. Shen, W.H. Zhu, L.H. Nie and S.Z. Yao, Anal. Chim. Acta., 276 (1993) 87.

[11] T. Nomura, T. Yanagihara and T. Mitsui, Bunseki Kagaku, 41 (1992) 307.

[12] D.Z. Shen, Y.J. Xu, L.H. Nie and S.Z. Yao, Talanta, 41 (1994) 1993.

[13] D.Z. Shen, L.H. Nie and S.Z. Yao, J. Electroanal. Chem., 360 (1993) 71.

[14] D.Z. Shen, M.S. Huang, L.H. Nie and S.Z. Yao, J. Electroanal. Chem., 371 (1994) 117.

A nonlinear regression model applied to kinetic studies of ester hydrolysis with a surface acoustic wave sensor

Quingyun Cai, Ronhgui Wang, Liying Wu, Lihua Nie, Shouzhuo Yao*

Department of Chemistry and Chemical Engineering, Hunan University, Changsha 410082, , People's Republic of China

Abstract

A non-linear regression model was derived for the simultaneous determination of the rate constant in alkaline hydrolysis of esters and the initial concentration of esters based on the linear relationship between the frequency response of the surface acoustic wave sensor system and the conductivity of the solution. The model was tested theoretically and experimentally with the methyl-, ethyl-, and n-propyl-acetate systems. The corresponding rate constants estimated at 25°C are 0.147, 0.103 and 0.0671 respectively.

Keywords: Nonlinear regression model; Kinetic studies; Ester hydrolysis; Surface acoustic wave sensor

1. Introduction

Surface acoustic wave (SAW) devices are very sensitive chemical sensors and considerable attention has been devoted to them [1–4]. SAW devices are most frequently used for the determination of low concentrations of species in the gas phase [5,6]. Although the application of SAW devices to liquid systems is of interest, many problems exist owing to the large energy loss in the propagation of the Rayleigh wave [7] when the SAW sensors are immersed in liquid.

By combining conductive electrodes with a SAW device, a new SAW sensor system for liquids was proposed by Yao et al. [8]. This SAW sensor system is very sensitive to the physical properties of the solution that will cause variations in the loop parameters in the oscillation circuit, such as conductivity and permittivity. Under certain experimental conditions, there exists a linear relation between the frequency response of the SAW device and the conductivity of the solution studied [8]. Compared to the normal conductivity method, the sensitivity is improved by employing a SAW device and the polarization potential that seriously affects normal conductivity measurements in a high background conductance solution does not exist owing to the high oscillation frequency of the SAW devices. As the SAW device is not in contact with the solution, the frequency stability of the sensor system is

* Corresponding author.

much better than that of normal SAW sensors operated directly in the analyte vapor or gas, where a large amount of energy dissipates from the SAW surfaces to polymer coatings. Some applications of the modified SAW sensor system have been reported [9,10].

The study of reaction mechanisms is important and usually involves a kinetic investigation of the factors that influence the rate of reaction. Such investigations have often been undertaken using a linear method of data analysis (e.g. a pseudo-first-order approach). Since only a small amount of information from the response curves is used, the precision relies strongly on the experience of the analyst and the experimental conditions. In contrast, regression analysis makes full use of information from the entire response curve, so that more parameters can be determined simultaneously and the precision is higher than using linearisation. For nonlinear least-square problems, the Levenberg–Marquardt–Fletcher (LMF) algorithm [11], a modification of the Levenberg–Marquardt (LM) method [12], is believed to be one of the most powerful methods. Owing to a powerful combination of the Steepest Descent algorithm and the Newton–Gauss algorithm and adjustment of the Marquardt parameter based on the ratio of the practical decrease of the residual sum of the squares, QS, to its decrease expected when QS is assumed to be a quadratic function, the LMF algorithm can rapidly converge to the minimum without good initial estimates of the parameters. Several applications of the LM algorithm have been reported [13,14] and a few reports have been published on the application of the LMF algorithm in chemistry.

The purpose of this work was to derive a nonlinear regression model for the simultaneous determination of the hydrolysis rate constant of ester in basic solution and its initial concentration, based on the linear relationship between the frequency shifts of the SAW sensor and the conductivity of the solution to be studied. The systems methyl-, ethyl- and n-propyl-acetate were investigated with the model. The rate constants, concentrations, and system parameters have been determined simultaneously.

2. Theory

The alkaline hydrolysis of esters is a second-order reaction [15] expressed as Eq. (1) and the rate equation is expressed as

$$CH_3COOR + OH^- \rightleftharpoons CH_3COO^- + ROH \quad (1)$$
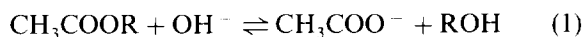
$$dC_t/dt = k(C_0 - C_t)(C_{OH^-}) \quad (2)$$

where C_0 denotes the initial concentration of ester, C_t is the concentration of hydrolyzed ester at time t and k is the rate constant.

In alkaline solution the dissociation of acetic acid is almost complete, the presence of HAc can be neglected (this assumption is reasonable for an acid whose dissociation constant is greater than 10^{-9}), and the concentration of H^+ is far less than that of OH^-. Then:

$$C_{OH^-} = C_B - C_t \quad (3)$$

$$C_{Ac^-} = C_t \quad (4)$$

where C_B denotes the concentration of base (KOH) added. The integral of Eq. (2) is expressed as below. When $C_0 \neq C_B$:

$$C_t = C_B \cdot C_0 \cdot \{\exp[kt(C_B - C_0)] - 1\}/$$
$$\{C_B \exp[kt(C_B - C_0)] - C_0\} \quad (5)$$

When $C_0 = C_B$:

$$C_t = ktC_0^2/(1 + ktC_0) \quad (6)$$

With a set of initial estimates of k and C_0, C_t can be calculated. The frequency shift Δf and the residual sum of squares sum QS can then be calculated from Eqs. (7) and (8):

$$f = S'(r_{OH^-}C_{OH^-} + r_{Ac^-}C_{Ac^-} + r_{K^+}C_B) + f^{0\prime}$$
$$= -S'(r_{OH^-} - r_{Ac^-})C_t + S'(r_{OH^-} + r_{K^+})C_B + f^{0\prime} \quad (7)$$

$$\Delta f = f^0 - f = SC_t$$

$$QS = \sum_{points} (\Delta f^{calc} - \Delta f^{exp})^2 \quad (8)$$

where f^0 is the initial frequency (kHz) where $t = 0$, S is the sensitivity of the sensor system (kHz mol^{-1}), r is the molar conductivity of ions, and C is the concentration of corresponding ions (mol l^{-1}).

This is a nonlinear regression model. To obtain the model parameters S, C_0 and k, the partial derivatives of the parameters must be calculated:

$$\partial \Delta f / \partial k = S \partial C_t / \partial k \qquad (9)$$

$$\partial \Delta f / \partial C_0 = S \partial C_t / \partial C_0 \qquad (10)$$

$$\partial \Delta f / \partial S = C_t \qquad (11)$$

Once the partial derivatives $\partial \Delta f / \partial S$, $\partial \Delta f / \partial k$ and $\partial \Delta f / \partial C_0$ have been calculated, the Hessian matrix is directly built up and the standard LMF algorithm [11] is used to compute the parameters.

3. Experimental

3.1. Apparatus and reagents

The 62 MHz one-port resonator was used in the study with a y,z-cut $LiNbO_3$ crystal. The detection cell and the complete assembly were described previously [8]. The detection cell was suspended in a brass thermostatic bath at constant temperature. The frequency was measured using a SC7201 Universal Counter at a resolution of 1 Hz and data were collected at more than 12 points min^{-1}.

All chemicals used were of analytical-reagent grade. The concentration of KOH was prepared at about 5 mmol l^{-1} and calibrated with guaranteed-reagent-grade potassium biphthalate. Doubly-distilled water was used throughout.

3.2. Procedure

Under the protection of N_2, 10 ml of 0.005 mol l^{-1} KOH solution was transferred to a detection cell and stirred with a magnetic stirrer at a constant speed. The baseline noise was determined by using frequency data collected for 5 min before the experiment. Several microliters of ester were injected into the solution with a micro-syringe and the frequency shift vs. time was recorded. All experiments were repeated at least three times and for each curve at least 100 points were acquired.

3.3. Computation and analysis of data

A program written in FORTRAN 77 was compiled and run on an IBM PC/386 computer. The data were input from a data file by the DOS pipe command. All computations were in double precision. The run time for a set of data was less than 1 min. The program is available from the authors.

4. Validation of the non-linear regression model

The simultaneous determination of the concentration C_0 and the rate constant k relies on them being linearly correlated. The parameters C_0 and k occur in the form $C_0 k$ in Eq. (2). To test their correlation, the response of frequency shift with time is given in Fig. 1 for different k values, keeping $C_0 k$ constant. We can see that the effects of k and C_0 on the response are different. Therefore the simultaneous determination of k and C_0 can be achieved with the model.

To test the ability of the algorithm estimating parameters, synthetic frequency response curves vs. time were computed according to Eq. (7) for given parameters, and a random noise of 1% of the maximum frequency shift was added to the theoretical data. The parameters were then computed with the theoretical data with added noise. The regression results are listed in Table 1. The residual given by the program showed that all the
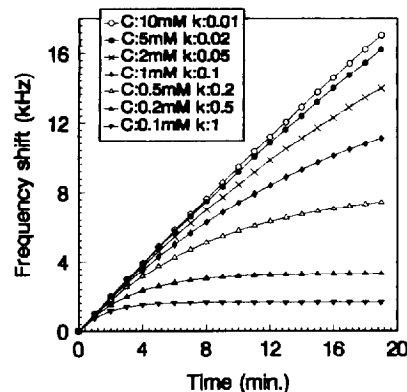

Fig. 1. Response curves of frequency shifts vs. time at different concentrations of ester, keeping kC_0 constant at 0.1; $C(KOH) = 10$ mmol l^{-1}.

Table 1
Regression analysis of synthetic data with random noise of 1% of the maximum frequency shift

k (1 mol^{-1} s^{-1})		C_0 (mmol 1^{-1})		S [(kHz $\pm$ Hz) 1 mol^{-1}]	
Actual	Estimated ($\pm$ SD)	Actual	Estimated ($\pm$ SD)	Actual	Estimated ($\pm$ SD)
8.75×10^{-3}	$(8.75 \pm 0.18) \times 10^{-3}$	1.00	1.005 ± 0.076	19250	19250 ± 19
2.77×10^{-2}	$(2.69 \pm 0.17) \times 10^{-2}$	1.00	1.03 ± 0.064	19250	19250 ± 23
8.75×10^{-2}	$(8.74 \pm 0.11) \times 10^{-2}$	1.00	1.01 ± 0.002	19250	19250 ± 18
2.77×10^{-1}	$(2.75 \pm 0.16) \times 10^{-1}$	1.00	1.004 ± 0.007	19250	19250 ± 14
8.75×10^{-2}	$(8.67 \pm 0.20) \times 10^{-2}$	0.50	0.497 ± 0.016	19250	19250 ± 17
8.75×10^{-2}	$(8.62 \pm 0.26) \times 10^{-2}$	0.10	0.101 ± 0.0061	19250	19250 ± 24

Table 2
Effect of the initial estimates on the results

Actual		Initial		Estimated	
k	C_0 (mmol 1^{-1})	k	C_0 (mmol 1^{-1})	k	C_0 (mmol 1^{-1})
0.0875	1.00	0.00875	5.00	0.08749	0.999
0.0875	1.00	0.0360	5.00	0.08751	0.999
0.0875	1.00	8.75	5.00	0.08751	0.999
0.0875	1.00	0.036	0.050	0.08751	0.999
0.0875	1.00	0.036	50.00	0.08751	0.999

deviations were of random distribution, indicating a good fit of the theoretical model to the data. In all cases, the S parameters calculated were close to the expected values with small deviations. For k and C_0, if they are not too small, the technique can give accurate estimations. When they are too small, the response of the sensor is too low and no accurate k and C_0 values can be determined.

For non-linear regression, a good initial estimate of the parameter is generally important. The effect of the initial estimates of k and C_0 on the regression has been tested with the synthetic frequency response curve. The results are listed in Table 2. Owing to the use of analytical derivatives together with the LMF algorithm, there are no strict demands on the initial estimates, and they may be varied in a range of 100–0.1 times the true values for k and 50–0.05 times for C_0. The initial estimate of S has no limitation since it is linear.

If the dissociation constant K_a of the acid produced by hydrolysis of esters is small (e.g. $K_a < 10^{-9}$), the hydrolysis of RCOO$^-$ should be taken into account. Fig. 2 gives the response curves of

frequency shifts vs. time with different dissociation constants K_a. It shows that when $K_a > 10^{-9}$, there is little influence of K_a on the response, when K_a is in the range 10^{-9}–10^{-15}, the influence of K_a on the response is large, and when $K_a < 10^{-15}$ little response can be observed even with large rate constants and high initial concentrations of base. Since the dissociation of the acid is so small, no notable change of the conductivity can be observed. Therefore when $K_a > 10^{-9}$ the presence of RCOOH can be neglected (set $C_t = [RCOO^-]$); when $K_a = 10^{-9}$–10^{-15} neglect of RCOOH can influence the results seriously, and when $K_a < 10^{-15}$ no accurate results can be given by methods based on conductivity response.

5. Results and discussion

5.1. Relationship between frequency shifts and conductivity

In order to investigate the relationship between

the frequency shifts and conductivity, the re-
sponse of the SAW sensor system to conductivity
has been determined by titrating water with 0.1
mol l^{-1} KOH solution at 25°C. The result shows
that a linear relationship exists in a certain con-
ductance region where the corresponding KOH
concentration is up to 20 mmol l^{-1}. The linear
region can be changed by adjusting the loop
parameter in the oscillation circuit [8]. In this
work, the linear region was adjusted to that where
the corresponding KOH concentration was 1–6
mmol l^{-1} ($S_{Y/X} = 78$ Hz, $R = 0.999$, $n = 7$).

Fig. 4. The variation of apparent reaction rate ($d\Delta f/ dt$) with
time calculated from the experimental data in Fig. 3.

5.2. Estimation of the initial concentration of esters and the rate constant

The hydrolysis of methyl-, ethyl- and n-propyl-
acetate was done at four different concentrations
(0.05, 0.10, 0.50 and 1.0 mmol l^{-1}) of the ester.
The concentration of potassium hydroxide was
kept constant at 5.00 mmol l^{-1}. During the reac-
tion the variation of the ionic strength is slight
and the molar conductivity and sensitivity S can
be assumed to be constant. The experimental
temperature was kept constant at 25°C and 40°C
respectively. A part of the calculated and experi-
mental response curves is given in Fig. 3. The
apparent rate ($d\Delta f/ dt$ in Hz s^{-1}) at time t calcu-
lated from the experimental response curves in
Fig. 3 is given in Fig. 4. The estimated results of
the ethyl-acetate system are shown in Table 3.
The rate constants determined for methyl-, ethyl-
and n-propyl-acetate, together with the literature
values, are given in Table 4. The residual distribu-
tion for ethyl-acetate is shown in Fig. 5, indicating
that the residual distribution was random. Table 3
shows that the estimated concentrations agree
well with the actual values. The lowest concentra-
tion that can be determined simultaneously with k
is about 1×10^{-5} mol l^{-1}. The lower limit de-
creases with the increase of the rate constant k.
From Table 4 we can see that the rate constant k
estimated is higher than that published in the
literature [15,16], which results from the different
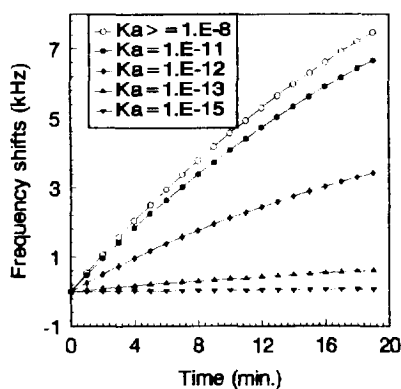experimental conditions and the different rate

Fig. 2. Response curves of frequency shifts vs. time with
different acid dissociation constants K_a; C(KOH) = 10 mmol
l^{-1}; $C_0 = 1.0$ mmol l^{-1}, $k = 0.11$.
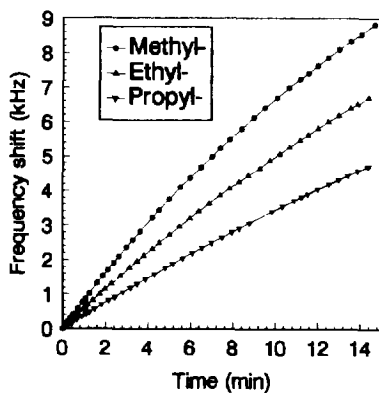

Fig. 3. Part of the calculated and experienced response curves
for the methyl-, ethyl- and n-propyl-acetate systems:
C(KOH) = 5 mmol l^{-1}; $C_0 = 1.0$ mmol l^{-1}, $T = 25$°C.

Table 3
Regression analysis of the response data for ethyl acetate; $C(KOH) = 0.005$ mol l^{-1}

No.	T (°C)	Actual	Estimated		
		C_0 (mmol l^{-1})	C_0 (mmol l^{-1})	k (l mol^{-1} s^{-1})	S (kHz l mol^{-1})
1	25.0	0.050	0.0487	0.112	18985
2	25.0	0.10	0.11	0.0998	18760
3	25.0	0.50	0.49	0.0892	18420
4	25.0	1.00	0.987	0.109	18394
5	40.0	0.05	0.0482	0.231	19635
6	40.0	0.10	0.109	0.234	19563
7	40.0	0.50	0.513	0.226	19434
8	40.0	1.00	1.07	0.213	19056

$k(25°C) = 0.103 \pm 0.010$; $k(40°C) = 0.224 \pm 0.01$; $E_a = 40.15$ kJ mol^{-1}

Table 4
The rate constants determined for methyl-, ehtyl- and n-propyl-acetate

Ester	$k(25°C)$ (this paper)	k	$T°C$	Rate equation	Medium
Methyl-acetate	0.147	0.066[a]	20	$k[e][H^+]$[c]	62% acetone 0.02 mol l^{-1} OH$^-$
Ethyl-acetate	0.103	0.0723[b]	19	$k[e][OH^-]$[c]	0.02 mol l^{-1} OH$^-$
n-Propyl-acetate	0.0671				

[a] Ref. [16].
[b] Ref. [15].
[c] e denotes the concentration of esters.

equation. From Fig. 4 we can clearly see that the reaction rate increases with the decrease in the number of $-CH_2-$ units.

5.3. A comparison of the SAW-sensing method with conductometry

The hydrolysis of ethyl-acetate was monitored with the SAW-sensing method and with conductometry for comparison. The response curves are given in Fig. 6. For the first 10 min the signal-to-noise ratio of the SAW-sensing method is 4000 with a noise level of 1 Hz and the signal-to-noise ratio of conductometry is 400 with a noise level of 0.1 μS cm^{-1} under our experimental conditions. The proposed method is more sensitive than conductometry. The lower limit of the concentration is 1×10^{-5} mol l^{-1} (SAW-sensing method). The similar form of the response curves demonstrates

the linear relationship between the frequency shift and the conductivity.

5.4. A comparison of the nonlinear regression analysis method with the normal linear method

With the proposed method, the concentration can be estimated with only one response curve. The concentration range that can be determined is only dependent on the linear region of frequency shifts vs. conductivity as well as the signal-to-noise ratio of the response curve. Owing to this the linear region can be changed by adjusting the loop parameters in the oscillation circuit; theoretically the concentration that can be determined has no limitation if the signal-to-noise ratio is large. For the normal linear method, however, a calibration curve of rate vs. concentration is usually needed so the concentration that can be deter-
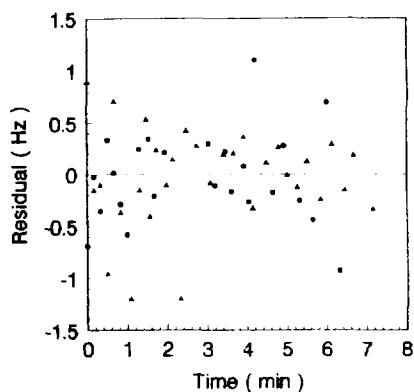
Fig. 5. Residual plot from regression analysis of the experimental data at 25°C (●) and 40°C (▲) for the ethyl-acetate system $C(KOH) = 5$ mmol l^{-1}, $C_0 = 1.0$ mmol l^{-1}.
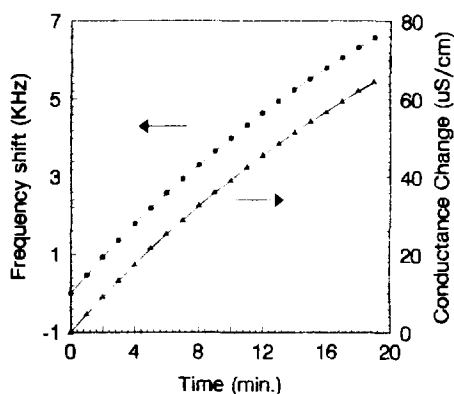

Fig. 6. Comparison of the SAW-sensing method with conductometry under the same experimental conditions for the ethyl-acetate system. $C(KOH) = 5$ mmol l^{-1}; $C_0 = 1.0$ mmol l^{-1}; $T = 25$°C.

mined is dependent on the linear region of the calibration curve. Therefore, a great deal of work needs to be done and the precision of the result strongly relies on the experience of the analyst.

5.5. Usefulness and applications

The technique introduced in this paper can be used as a simple and accurate method for determining hydrolysis rate constants of an ester and its initial concentration simultaneously. That the concentration and kinetic constant can be determined

simultaneously is a novel advantage, especially in biochemical systems where the accurate concentrations of reactants are usually unknown. With only a slight modification, the technique can be used to study the kinetic procedure in enzyme-catalysis reactions. Such works will be reported later.

Acknowledgements

References

[1] J.W. Grate, S.J. Martin and R.M. White, Anal. Chem., 65 (1993) 940A, 987A.

[2] L.J. Kepley, R.M. Crooks and A.J. Ricco, Anal. Chem., 64 (1992) 3191.

[3] D. Hauden, M. Hoummady, A. Choujaa and F. Bastien, Sens. Actuat. A, 33 (1992) 99.

[4] A.J. Ricco and S.J. Martine, Sens. Actuat. B, 10 (1993) 123.

[5] M.S. Nieuwenhuizen and A.J. Nederlof, Anal. Chem., 60 (1988) 230.

[6] D.S. Ballantine, S.L. Rose, J.W. Grate and H. Wohltjen, Anal. Chem., 58 (1986) 3058.

[7] G.S. Calabrese, H. Wohltjen and M.K. Roy, Anal. Chem., 59 (1987) 833.

[8] S.Z. Yao, K. Chen, F. Zhu, D.Z. Shen and L.H. Nie, Anal. Chim. Acta., 287 (1994) 65.

[9] S.Z. Yao, K. Chen and L.H. Nie, Anal. Chim. Acta., 289 (1994) 47.

[10] K. Chen, D.Z. Liu, L.H. Nie and S.Z. Yao, Talanta, 41 (1994) 2195.

[11] R. Fletcher, Report No. R6799, AERE, Harwell, UK, 1971.

[12] D.W. Marquardt, J. Soc. Ind. Appl. Math., 11 (1963) 431.

[13] A.D. Zuberbuhler and Th. A. Kaden, Talanta, 29 (1982) 201.

[14] R.M. Alcock, F.R. Hartley and D.E. Rogers, J. Chem. Soc. Dalton Trans., 123 (1978).

[15] J.E. Potts and E.S. Amis, J. Am. Chem. Soc., 71 (1949) 2112.

[16] J.E. Potts and E.S. Amis, J. Am. Chem. Soc., 72 (1950) 287.

ELSEVIER

Talanta

Formation and stability of pyrophosphate complexes with aliphatic amines in aqueous solution

Concetta De Stefano*, Claudia Foti, Ottavia Giuffrè, Silvio Sammartano

Dpt. Chimica Inorganica, Analitica e Struttura Molecolare dell'Università, Salita Sperone 31, I-98166, Villa S. Agata, Messina, Italy

Abstract

The complex formation between pyrophosphate ($P_2O_7^{4-}$) and protonated methylamine, ethylenediamine, diethylenetriamine, triethylenetetramine, tetraethylenepentamine and pentaethylenehexamine, has been studied potentiometrically, in aqueous solution, at 25°C. It was found that the species ALH_q (A = amine, $L = P_2O_7^{4-}$) are formed with $q = 1 \ldots n$ ($n = 3, 5, 6, 7, 7$ and 8 for the above amines respectively). Mono- and di-amines form species A_pLH_q too. The stability of these species is quite high [e.g. $H_4A^{4+} + HL^{3-} \rightleftarrows ALH_5^+$: $\log K = 8.1$ (A = pentaethylenehexamine)] and depends strictly on the charges involved in the formation reaction. Charges of reactants being equal, the stability trend is penten > tetren > trien > dien > en > meta and cationic mixed species are more stable than anionic ones. These results are discussed in relation to speciation problems in natural and biological fluids.

Keywords: Aliphatic amines; Pyrophosphate complexes; Formation constants; Potentiometry

1. Introduction

Pyrophospate (diphosphate, $P_2O_7^{4-}$) is involved in many natural reactions. Owing to its high charge, pyrophosphate is mainly present in biological and natural fluids as an ion pair or complex with different metal ions, which, in turn, may be of great importance in biochemical processes. As an example, the catalytic activity of PPase requires Mg^{2+} ions for the formation of the substrates $Mg(P_2O_7)^{2-}$ and $Mg_2(P_2O_7)^0$. Poly-

phosphates are also involved in eutrophization phenomena and it has been demonstrated that intracellular accumulation of phosphorus takes place in the form of polyphosphate granules, which have been recognised in algal cells. In all cases it is necessary to know as rigorously as possible the speciation of polyphosphates in order to study biochemical reaction mechanisms.

Metal pyrophosphate complexes have been studied extensively, in particular where alkali and alkaline earth cations are concerned. Recently it has been reported that pyrophosphate forms quite stable complexes with protonated polyamines [1],

---

* Corresponding author.

Table 1
Experimental details of potentiometric measurements $(T = 25°C)$[a]

A	C_A	$C_{P_2O_7}$	pH	I_{range}	No. titrations[b]	No. points
Meta	0.1–0.3	0.015–0.04	2.0–11.2	0.18–0.42	7	677
En	0.025–0.1	0.009–0.035	1.5–11.2	0.11–0.35	6	897
Dien	0.02–0.06	0.009–0.035	1.5–11.2	0.10–0.33	6	960
Trien	0.009–0.035	0.009–0.035	1.5–10.0	0.10–0.31	6	662
Tetren	0.006–0.025	0.009–0.035	2.5–11.0	0.09–0.28	6	509
Penten	0.05–0.016	0.009–0.035	2.5–11.1	0.08–0.27	6	702

[a] Concentrations (C) and ionic strength (I) in mol dm^{-3}; titrant solution: 1.119 mol dm^{-3} NaOH.
[b] Number of duplicate titrations.

and, in kinetic studies [2], it has been suggested that polyamines can substitute for Mg^{2+} as an activator in vitro. The complexation of $P_2O_7^{4-}$ with polyguanidine cations and some diamines has also been reported [3].

In order to make a contribution to work on the speciation of this ligand in natural and biological fluids, we thought it interesting to investigate its complexing ability towards polyamines. In this work we report a potentiometric study of the formation and stability of pyrophosphate complexes with methylamine (meta), ethylenediamine (en), diethylenetriamine (dien), triethylenetetramine (trien), tetraethylenepentamine (tetren) and pentaethylenehexamine (penten), in aqueous solution, at 25°C.

2. Experimental

2.1. Materials

Amines (methylamine, ethylenediamine, diethylenetriamine, triethylenetetramine, tetraethylenepentamine and pentaethylenehexamine, Fluka products) were purified by transformation into the corresponding hydrochlorides [4], and were used in this form. Tetrasodium diphosphate (Analar, BDH) was used without further purification. Solutions of NaOH and HCl were prepared by diluting concentrated Fluka ampoules and were standardised against potassium biphthalate and sodium carbonate respectively. Grade A glassware and doubly-distilled water were used for all solutions.

2.2. Appartus

Potentiometric measurements were carried out with two different sets of equipment: (a) an Amel 631 potentiometer coupled with Metrohm glass saturated calomel electrodes; the titrant was delivered by an Amel 231 dispenser; (b) an automatic system using a Metrohm E654 potentiometer coupled with a combination Ross-type electrode 8102 and connected to a Metrohm dosimat 665 dispenser; a computer program was used for the acquisition of the potentiometric data. The titration program for the equipment (b) allows the evaluation of equilibrium potential values and determines the amount of titrant based on the actual buffering properties of the titrated solution, so that there is a difference in pH values of 0.05–0.08 between two successive readings; the e.m.f. was considered to be stable when the variation was less than 0.1 mV within 5 min.

2.3. Procedure

25–50 ml of the solution containing $P_2O_7^{4-}$, HCl (in order to have the full protonated ligand) and the amine hydrochloride under study were titrated with standard NaOH up to 80–90% neutralisation. Other experimental details are reported in Table 1. Separate titrations of HCl at about the same ionic strength (adjusted with NaCl) as the sample under study were carried out for determining the standard electrode potential E^0. A stream of purified and presaturated N_2 was bubbled through all solutions in order to exclude the presence of CO_2 and O_2.

2.4. Calculations

The computer program ESAB2M [5] was used to calculate the purity of the reagents and to refine all the parameters related to the calibration of the electrode system. The computer programs BSTAC [6] and STACO [7] were used to calculate the formation constants from measurements carried out at variable ionic strengths. The ionic strength dependence of formation constants was taken into account by using the Debye–Hückel-type equation [6,8].

$$\log \beta = \log{}^T\!\beta - z^* \sqrt{I}/(2+3\sqrt{I}) + CI + DI^{3/2} \qquad (1)$$

$$C = c_0 p^* + c_1 z^*$$

$$D = d_1 z^*$$

$$p^* = \sum p_{\text{reactants}} - \sum p_{\text{products}};$$

$$z^* = \sum z^2_{\text{reactants}} - \sum z^2_{\text{products}}$$

where β = formation constants; ${}^T\!\beta$ = formation constant at zero ionic strength; p and z are the stoichiometric coefficients and the charges respectively. As previously reported [6,8], when weak interactions are taken into account [sodium complexes of $P_2O_7^{4-}$, anion (Cl^-) complexes of protonated amines, association of background salt], such as in this work, the empirical parameters of Eq. (1), i.e. values of C and D, can be considered independent of the type of reaction, and dependent on the charges only (for $I < 1$ mol dm^{-3}). For the calculations performed in this work we used the values $c_0 = 0.10$, $c_1 = 0.23$ and $d_1 = -0.1$ (these values are taken from Ref. [9], and are in good agreement with those reported in other works [6,8]). In some cases, when $I_{\text{max}} > 0.3$ mol dm^{-3}, the parameter C was refined together with the formation constants, and D was kept constant at $-0.1z^*$. The computer programs BSTAC and STACO can be used when dealing with measurements performed at variable ionic strength, by using Eq. (1) for the dependence of log β on I. Formation constants were expressed as follows (charges omitted):

$$\beta_{pq} = [ACl_p H_q]/([A][Cl]^p[H]^q) \qquad (2a)$$

$$\beta_{pq} = [Na_p LH_q]/([Na]^p[L][H]^q) \qquad (2b)$$

for the protonation constants and for the formation of amine–Cl^- or $P_2O_7^{4-}$–Na^+ complexes, and

$$\beta_{pq} = [A_p LH_q]/([A]^p[L][H]^q) \qquad (2c)$$

$$K_{[\text{reactants}]} = [\text{product}]/\Pi[\text{reactants}] \qquad (2d)$$

$$K_{ij} = [ALH_{i+j}]/([AH_i][LH_j]) \qquad (2e)$$

where A = amine and $L = P_2O_7^{4-}$. The overall formation constant β_{pq} is the constant obtained in the least-squares refinement, whilst $K_{[\text{reactants}]}$ are the equilibrium constants calculated according to the most probable formation reaction, in general $AH_i + LH_j \rightleftarrows ALH_{i+j}$ (K_{ij}). Concentrations and formation constants are given on the molar scale.

3. Results

3.1. Protonation constants of the ligands

Protonation of amines and pyrophosphate has already been studied, together with weak complexes with Cl^- and Na^+. Pyrophosphate forms [10], in addition to the five protonated species, weak complexes with Na^+ of the type $Na_p LH_q^{(p+q-4)}$ ($p, q = 1, 0$; 1, 1; 1, 2; 2, 0; 2, 1). Amines [1,11–14] form, in addition to the n protonated species (n = number of amino groups), weak complexes with Cl^- of the type $ACl_p H_q^{(q-p)}$ ($q = 1 \ldots n$, $1 \leqslant p \leqslant n - 2$). Protonation and weak complex formation constants are reported in Table 2. As can be seen, some formation constants of Na^+–$P_2O_7^{4-}$ and AH_i^+–Cl^- complexes are greater than one log unit and therefore NaCl interferences may mask other complex formation reactions, when $C_{\text{NaCl}} \gg C_{\text{reactants}}$.
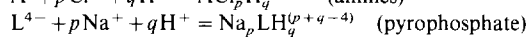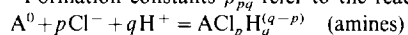
3.2. Proton mixed-ligand systems

Experimental data of mixed systems (potentiometric titrations) cannot be explained by considering the protonation constants of the two ligands only. Therefore, the formation of mixed proton amine–pyrophosphate complexes must be taken into account. Least-squares calculations were con-

Table 2
Protonation constants and Na^+ or Cl^- complex formation constants for the ligands considered in this work, at $I = 0$ mol dm^{-3} and $T = 25°C$

p	q	log β_{pq}[a]						
		$P_2O_7^{4-}$ [10][b]	Meta [1]	En [11]	Dien [12]	Trien [13]	Tetren [13]	Penten [14]
0	1	8.77	10.63	9.91	9.80	9.67	9.83	9.89
0	2	14.87		16.77	18.54	18.54	18.84	18.95
0	3	16.76			22.20	24.66	26.57	27.04
0	4	17.46				27.04	30.47	32.86
0	5						32.35	35.94
0	6							37.54
1	0	1.5						
1	1	9.8	10.40	9.80	9.70	9.36	9.31	10.01
1	2	15.3		17.43	19.33	19.32	19.36	19.79
1	3				23.73	26.08	27.73	28.77
1	4					28.78	32.15	35.00
1	5						34.53	38.26
1	6							40.10
2	0	2.6						
2	1	9.7						
2	3				24.05	26.43	27.99	
2	4					30.39	33.37	35.89
2	5						36.00	40.00
2	6							42.19
3	5						37.05	40.32
3	6							43.40
4	6							43.22

[a] Formation constants β_{pq} refer to the reactions [see Eqs. (2a), (2b)]:
$A^0 + pCl^- + qH^+ = ACl_pH_q^{(q-p)}$ (amines)
$L^{4-} + pNa^+ + qH^+ = Na_pLH_q^{(p+q-4)}$ (pyrophosphate)
[b] $I = 0.25$ mol dm^{-3}.

sistent with the formation of ALH_q species ($q = 1 \ldots n$; $n = 3, 5, 6, 7, 7$ and 8, for meta, en, dien, trien, tetren and penten respectively). In Table 3 we report the formation constants of mixed species as both overall and partial (according to the most probable formation reaction) constants. As one can see, the stability of these complexes is relevant and in some cases very high. Now, let us examine each system in detail.

3.2.1. $P_2O_7^{4-}$ –meta

In this system, six species are formed: ALH_q^{q-4} ($q = 1 \ldots 3$), $A_2LH_2^{2-}$, $A_2LH_3^-$ and $A_4LH_4^0$. Formation constants increase with increasing charge in both cation and anion. This rule is confirmed quantitatively for the formation of the species

ALH_2^{2-} and $A_2LH_2^{2-}$ (the same charges are involved in the formation reaction) for which very similar values of constants (log $K = 2.10$ and 2.06 respectively) are observed. In some cases, it is difficult to assign the correct partial formation reaction to each species. This is the case for the tetramine species $A_4LH_4^0$, for which only a semi-overall formation constant had been calculated. In Fig. 1a we report the distribution of the species vs. pH. At relatively high concentrations of reactants and with ratios $C_A/C_L \gg 1$ all the species are formed in significant amounts. If the above ratio is equal to one and with concentrations of the order of mmol dm^{-3}, only some species are significant [ALH_q ($q = 1, 2, 3$)] with formation percentages $< 15\%$. Therefore, at concentration levels

Table 3
Formation constants for the $P_2O_7^{4-}$ amine complexes at 25°C and $I = 0$ mol dm^{-3}

p	q	$\log \beta_{pq} \pm 3s$ [a]	Reaction	$\log K$ [b]
Meta				
1	1	13.65 ± 0.15	$HA^+ + L^{4-} \rightleftarrows ALH^{3-}$	3.0
1	2	22.26 ± 0.06	$HA^+ + HL^{3-} \rightleftarrows ALH_2^{2-}$	2.1
1	3	28.23 ± 0.05	$HA^+ + H_2L^{2-} \rightleftarrows ALH_3^-$	1.4
2	2	26.34 ± 0.03	$ALH^{3-} + HA^+ \rightleftarrows A_2LH_2^{2-}$	2.1
2	3	33.88 ± 0.13	$ALH_2^{2-} + HA^+ \rightleftarrows A_2LH_3^-$	1.0
4	4	48.97 ± 0.14	$4HA^+ + L^{4-} \rightleftarrows A_4LH_4^0$	6.4
Dien				
1	1	13.0 ± 0.3	$HA^+ + L^{4-} \rightleftarrows ALH^{3-}$	3.2
1	2	23.99 ± 0.02	$H_2A^{2+} + L^{4-} \rightleftarrows ALH_2^{2-}$	5.4
1	3	32.30 ± 0.03	$H_2A^{2+} + HL^{3-} \rightleftarrows ALH_3^-$	4.2
1	4	38.64 ± 0.04	$H_2A^{2+} + H_2L^{2-} \rightleftarrows ALH_4^0$	3.9
1	5	42.96 ± 0.05	$H_3A^{3+} + H_2L^{2-} \rightleftarrows ALH_5^+$	4.6
1	6	44.05 ± 0.08	$H_3A^{3+} + H_3L^- \rightleftarrows ALH_6^+$	3.4
Tetren				
1	1	12.5 ± 0.3	$HA^+ + L^{4-} \rightleftarrows ALH^{3-}$	2.7
1	2	23.50 ± 0.05	$H_2A^{2+} + L^{4-} \rightleftarrows ALH_2^{2-}$	4.7
1	3	33.54 ± 0.03	$H_2A^{2+} + HL^{3-} \rightleftarrows ALH_3^-$	5.2
1	4	41.61 ± 0.03	$H_3A^{3+} + HL^{3-} \rightleftarrows ALH_4^0$	5.5
1	5	47.98 ± 0.05	$H_3A^{3+} + H_2L^{2-} \rightleftarrows ALH_5^+$	5.2
1	6	52.35 ± 0.07	$H_4A^{4+} + H_2L^{2-} \rightleftarrows ALH_6^{2+}$	5.7
1	7	54.61 ± 0.10	$H_5A^{5+} + H_2L^{2-} \rightleftarrows ALH_7^{3+}$	6.1

p	q	$\log \beta_{pq} \pm 3s$ [a]	Reaction	$\log K$ [b]
En				
1	1	12.98 ± 0.11	$HA^+ + L^{4-} \rightleftarrows ALH^{3-}$	3.1
1	2	22.86 ± 0.02	$HA^+ + HL^{3-} \rightleftarrows ALH_2^{2-}$	3.4
1	3	30.32 ± 0.04	$H_2A^{2+} + HL^{3-} \rightleftarrows ALH_3$	4.0
1	4	35.52 ± 0.06	$H_2A^{2+} + H_2L^{2-} \rightleftarrows ALH_4^0$	2.6
1	5	36.6 ± 0.2	$H_2A^{2+} + H_3L \rightleftarrows ALH_5^+$	1.4
2	4	42.42 ± 0.03	$ALH_2^{2-} + H_2A^{2+} \rightleftarrows A_2LH_4^0$	2.8
2	5	48.52 ± 0.15	$A_2LH_3 + H_2A^{2+} \rightleftarrows A_2LH_5^+$	1.4
Trien				
1	1	12.5 ± 0.3	$HA^+ + L^{4-} \rightleftarrows ALH^{3-}$	2.8
1	2	24.07 ± 0.03	$H_2A^{2+} + L^{4-} \rightleftarrows ALH_2^{2-}$	5.5
1	3	33.38 ± 0.05	$H_2A^{2+} + HL^{3-} \rightleftarrows ALH_3^-$	5.3
1	4	40.80 ± 0.06	$H_3A^{3+} + HL^{3-} \rightleftarrows ALH_4^0$	6.6
1	5	46.33 ± 0.04	$H_3A^{3+} + H_2L^{2-} \rightleftarrows ALH_5^+$	5.6
1	6	49.61 ± 0.12	$H_4A^{4+} + H_2L^{2-} \rightleftarrows ALH_6^{2+}$	6.4
1	7	49.8 ± 0.2	$H_4A^{4+} + H_3L \rightleftarrows ALH_7^{3+}$	4.3
Penten				
1	1	13.52 ± 0.11	$HA^+ + L^{4-} \rightleftarrows ALH^{3-}$	3.6
1	2	23.95 ± 0.09	$H_2A^{2+} + L^{4-} \rightleftarrows ALH_2^{2-}$	5.0
1	3	33.87 ± 0.04	$H_2A^{2+} + HL^{3-} \rightleftarrows ALH_3$	5.4
1	4	43.02 ± 0.05	$H_3A^{3+} + HL^{3-} \rightleftarrows ALH_4^0$	6.4
1	5	50.50 ± 0.10	$H_4A^{4+} + HL^{3-} \rightleftarrows ALH_5^+$	8.1
1	6	56.25 ± 0.15	$H_4A^{4+} + H_2L^{2-} \rightleftarrows ALH_6^{2+}$	7.2
1	7	59.9 ± 0.2	$H_5A^{5+} + H_2L^{2-} \rightleftarrows ALH_7^{3+}$	7.8
1	8	61.6 ± 0.3	$H_6A^{6+} + H_2L^{2-} \rightleftarrows ALH_8^{4+}$	7.9

[a] Overall formation constants β_{pq} relate to the reaction [see Eq. (2c)]

$$pA + L + qH = A_pLH_q$$

[b] Partial formation constants [see Eqs. (2d), (2e)].

of natural and biological fluids these complexes are not very important.

3.2.2. $P_2O_7^{4-}$ -en

Seven species are formed in this system: ALH_q^{q-4} ($q = 1 \ldots 5$), $A_2LH_4^0$ and $A_2LH_5^+$. Also in this case one can observe a check (in the same system) for the strict dependence of the stability on the charges involved in the formation reaction. In fact the species ALH_4^0 and $A_2LH_4^0$ have partial formation constants which are quite close to each other. In Fig. 1b the distribution of the species vs. pH is reported. The speciation of this system, as a function of concentration and pH, is qualitatively very similar to that of meta. When the concentration of reactants is 1 mmol dm^{-3}, complex species A_pLH_q, with $q > 1$ disappear, but the formation percentages of the other species, in the range $2 \leqslant pH \leqslant 8$, are always > 35%. This means that this system can be consid-

ered fairly significant for natural and biological fluids.

3.2.3. $P_2O_7^{4-}$ -dien

Six species are formed in this system: ALH_q^{q-} $4(q = 1 \ldots 6)$. The ratio log K/z_t ($z_t = z_{cation} + |z_{anion}|$) is fairly constant ($0.9 \pm 0.2$), further confirming the strict dependence of formation constants on charges. However, the difference between positively and negatively charged species becomes relevant; in fact the formation constant for the species ALH_3^- is significantly lower than that of ALH_5^+ (even if charges involved in the reaction are the same absolute value). This indicates that the charge on the protonated amine is more important than the charge of the anion in determining the stability of mixed proton complexes. In Fig. 1c we report the distribution of the species vs. pH. Formation percentages are very high, and also, when the concentration of reactants is < 1 mmol dm^{-3}, significant presence of mixed complexes is observed.

3.2.4. $P_2O_7^{4-}$ -trien

Seven species are formed in this system: $ALH_q^{q-4}(q = 1 \ldots 7)$. Since all the species are formed in the range $3 \leqslant pH \leqslant 9$, in some cases it is difficult to detemine the correct formation reaction. For example, the formation of the species ALH_4^0 can be described by the reactions:

$H_3A^{3+} + HL^{3-} \rightleftarrows ALH_4^0$ (log $K = 6.6$)

$H_2A^{2+} + H_2L^{2-} \rightleftarrows ALH_4^0$ (log $K = 6.1$)
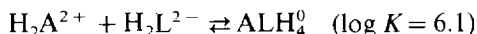
In Table 3 we report the formation constant relative to the first reaction since in the real conditions of our experiments the third protonation constant of trien is significantly higher than the second one of pyrophosphate. However, at $I = 0$ mol dm^{-3}, log K_3^H (trien) $\cong$ log $K_2^H(P_2O_7^{4-})$, and under these conditions it is right to write the second reaction too. In Fig. 1d we report the distribution of the species vs. pH. When $C_L = C_A = 10$ mmol dm^{-3}, mixed species are predominant; at pH < 9 the sum of the percentages of ALH_q complexes is always > 90%. For $C_L = C_A = 1$ mmol dm^{-3}, the sum of the percentages in the above range is not lowered too much.
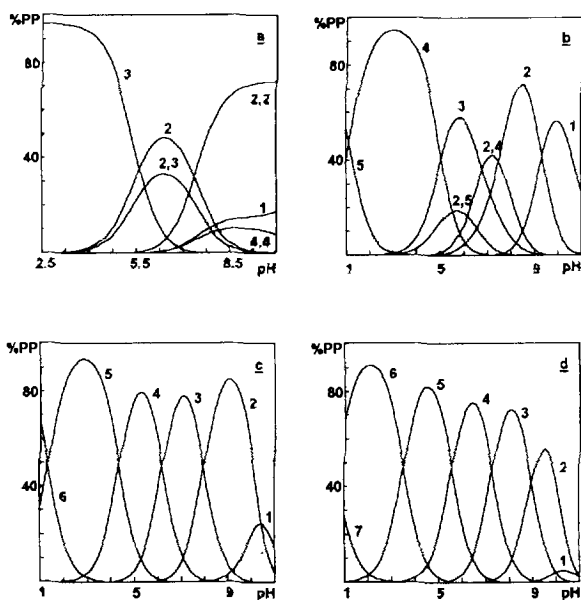
Fig. 1. Distribution of the species vs. pH in the systems H^+-$P_2O_7^{4-}$-meta (a), H^+-$P_2O_7^{4-}$-en (b), H^+-$P_2O_7^{4-}$-dien (c) and H^+-$P_2O_7^{4-}$-trien (d). Numbers which locate complexes (q) refer to the species ALH_q [or (pq) for A_pLH_q]. (a) $C_A = 0.25$, $C_L = 0.02$ mol dm^{-3}; (b) $C_A = 0.05$, $C_L = 0.01$ mol dm^{-3}; (c) $C_A = 0.025$, $C_L = 0.01$ mol dm^{-3}; (d) $C_A = 0.01$, $C_L = 0.01$ mol dm^{-3}; $T = 25°C$, $I = 0.15$ (NaCl) mol dm^{-3}.
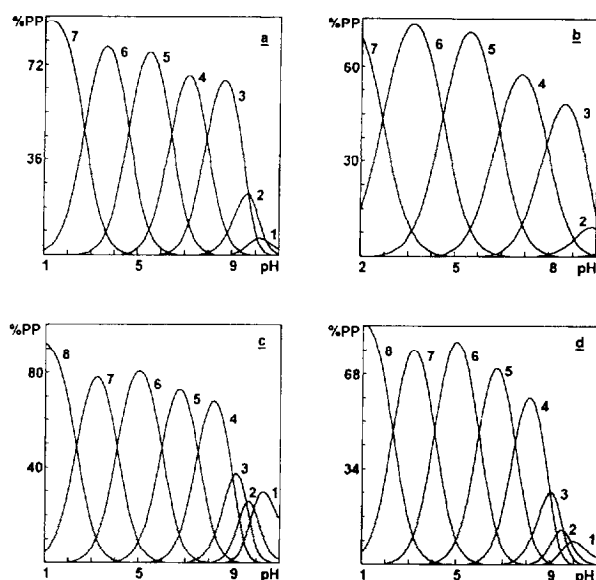
Fig. 2. Distribution of the species vs. pH in the systems $H^+-P_2O_7^{4-}$-tetren (a, b) and $H^+-P_2O_7^{4-}$-penten (c, d). Numbers which locate complexes (q) refer to the species ALH_q. (a, c) $C_L = C_A = 0.01$ mol dm^{-3}; (b, d) $C_L = C_A = 0.001$ mol dm^{-3}; $T = 25°C$, $I = 0.15$ (NaCl) mol dm^{-3}.

3.2.5. $P_2O_7^{4-}$ –tetren and penten

In these systems seven [ALH_q ($q = 1...7$)] and eight [$ALH_q(q = 1...8)$] species are formed respectively. Apart from the values of formation constants, the same considerations as for trien apply to these systems. In Fig. 2a–2c the distribution diagrams of the species vs. pH are shown. In these systems, the formation of mixed species is almost quantitative for $C_L = C_A > 1$ mmol dm^{-3}. For the system penten–$P_2O_4^{4-}$, when the concentration is 1 μmol dm^{-3}, 40–45% of ligands are still present as mixed complexes in the pH range 3–6, and 20% at pH 7.

4. Discussion

4.1. General stability trends

Taking the formation constants of the different systems together, some general trends can be evidenced.

(a) The charges of the reactants being equal, formation constants for the amine–$P_2O_7^{4-}$ com-
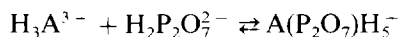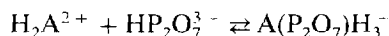
plexes follow the trend: meta < en < dien < tetren < penten.

(b) The stability is in general directly proportional to the charges involved in the formation reaction.

(c) The sum of charges in the protonated amine and in pyrophosphate being equal the stability of mixed proton complexes follows the trends:

(i) cationic species > anionic species;

(ii) the stability of complexes is higher when the differences between charges in the amine and in pyrophosphate are smaller, i.e. log $K(\Delta|z_1|) >$ log $K(\Delta|z_2|)$, when $\Delta|z_2| > \Delta|z_1|$.

In Fig. 3 we report log K vs. n (number of amino groups in the amine) for the reactions:

$$H_2A^{2+} + HP_2O_7^{3-} \rightleftarrows A(P_2O_7)H_3^-$$

$$H_3A^{3-} + H_2P_2O_7^{2-} \rightleftarrows A(P_2O_7)H_5^-$$

As can be seen, a significant linear trend is observed with positive slope [point (a)] for both types of complex, whilst the relative stability is in favour of cationic species [points (c), (i)].

Trends (a)–(c) can be expressed quantitatively by the simple relationship (all formation constants of different mixed systems are taken simultaneously into account):

$$\log K = 1.05z_{cation} + 0.67|z_{anion}| + 0.36n$$

$$- 0.28\Delta z - 0.90 \tag{3}$$

Where n = number of amino groups in the amine, with a mean deviation ε (log K) = 0.6.
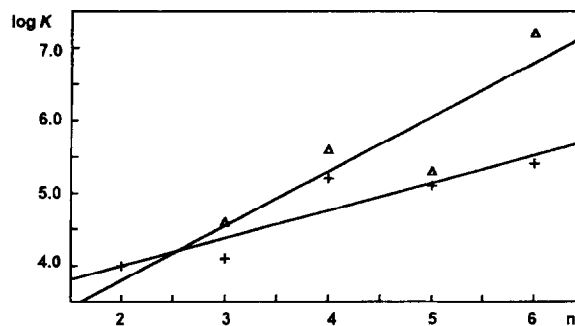

Fig. 3. Dependence of log K on n (number of amino groups): (Δ) $H_2A^{2+} + HL^{3-} \rightleftarrows ALH_3^-$; (+) $H_3A^{3+} + H_2L^{2-} \rightleftarrows ALH_5^-$.

Steric factors influence the stability of ligand–ligand complexes, as observed in other investigations [1], but the electrostatic factor, namely the charges involved in the complexation reaction, plays a much more important role.

4.2. Ionic strength and medium dependence of formation constants

Formation constants of mixed systems were calculated under the assumption that all significant interactions among all the components have been taken into account, i.e. "true" formation constants were obtained. In particular, we took into account the formation of $Na^+–P_2O_7^{4-}$ and Cl^-–amine complexes, as reported in Table 2. Different assumptions are generally made in the literature: (a) Na^+ and Cl^- complexes are neglected altogether; (b) only Na^+ complexes are taken into account (c) the formation of Na^+ complexes is avoided by using tetrealkylammonium cations for the background salt and/or for the titrant strong base. The formation of Cl^- complexes has been neglected in most cases. Different assumptions (i.e. different complexation models) give rise to very different values of formation constants, in particular with Na^+ and Cl^- complexes with $K > 10$ mol^{-1} dm^3, as for many systems studied here. In order to show the magnitude of differences in log K_{ij} for the formation of mixed proton complexes due to the choice of different assumptions, we calculated formation constants at three different ionic strengths ($I =$ 0.1, 0.25 and 0.5 mol dm^{-3}) by (i) considering both Na^+ and Cl^- complexes; (ii) taking into account only Na^+ complexes; (iii) neglecting both Na^+ and Cl^- interactions. As can be seen (Table 4), in some cases the differences are very significant; for example log K_{62} (penten–$P_2O_7^{4-}$) is lowered by more than four units on going from (i) to (iii).

Empirical parameters of Eq. (1) were checked randomly for their dependence on ionic strength for different systems and complexes studied here. In particular, the value of c_1 was calculated for all systems and the obtained mean value was $c_1 =$ 0.225 ± 0.021 [the error in log K_{ij} introduced into the calculations, due to the use of Eq. (1), is $z^* \times 0.021 \times I$, i.e. in most cases < 0.05].

4.3. Comparison with similar systems

Very few amine–anion complexes have been studied quantitatively. Most studies in this field relate to the complexation of polyanions by cyclic protonated amines [15–20]. In this laboratory, different amine–anion systems have been investigated [1,21–26], and in all cases, a strict dependence between stability and charges has been found. As an example, we may compare the stability of tetren–$P_2O_7^{4-}$ complexes with the analogous complexes tetren–$Fe(CN)_6^{4-}$ [24] and tetren–btC^{4-} [4–25] (btc = butanetetracarboxylate): for log K_{20} we have 4.4 and 4.0 respectively (4.7 for $P_2O_7^{4-}$). The system en–$P_2O_7^{4-}$ has been studied by Dietrich et al. [3] at $I = 0.1$ mol dm^{-3} in Me$_4$NCl; they found log $K_{10} = 1.5$, log $K_{11} =$ 2.5 and log $K_{21} = 2.6$. These values are intermediate between our values (b) and (c) reported in Table 4. This is consistent with some observations already made, according to which Cl^- forms complexes with protonated amines [11–14] and Me$_4$N$^+$ forms very weak complexes with unprotonated amines [11,12], whilst N^{a+} forms fairly strong complexes with $P_2O_7^{4-}$ [10].

4.4. Statistical analysis and errors

The speciation model for each system was obtained by using some simple rules, including the statistical ones. Briefly, the procedure for selecting the best model includes these main points: (a) check for the absence of systematic errors (all the experimental conditions were randomised); (b) choose a suitable weighing scheme;(c) use the F test for the selection of the most suitable speciation model; (d) check for the absence of systematic trends in the residuals in order to avoid bias in the selecion of species. Nevertheless, it is important to bear in mind that the speciation models, together with formation constants obtained for each system, are strictly valid only within experimental conditions; in fact, it is not possible to exclude the formation of other species when the concentrations of reactants is higher than that used in the present work. Moreover, it is possible that some quaternary species such as AL(Cl)H$_q$ or AL(Na)H$_q$ are formed at higher Na^+ and Cl^- concentrations.

Table 4
Dependence on ionic strength of formation constants in NaCl, under different assumptions about the formation of Na^+ and Cl^- complexes[a]

i	j	$I = 0$	$I = 0.1$			$I = 0.25$			$I = 0.5$		
			b	c	d	b	c	d	b	c	d
Metam											
1	0	2.9	2.2	2.2	1.5	2.1	2.1	1.1	2.2	2.1	0.8
1	1	2.1	1.6	1.6	0.7	1.5	1.5	0.2	1.6	1.5	e
1	2	1.4	1.1	1.1	0.1	1.0	1.0	c	1.1	1.0	e
En											
1	0	3.1	2.4	1.4	1.7	2.3	2.2	1.2	2.4	2.3	1.0
1	1	3.4	2.9	2.9	2.0	2.9	2.8	1.5	2.9	2.8	1.0
2	1	4.0	3.0	2.9	2.0	2.9	2.7	1.4	3.0	2.7	0.9
2	2	2.6	1.9	1.8	0.8	1.8	1.6	0.1	1.9	1.6	e
2	3	1.4	1.1	1.0	0.0	1.0	0.8	e	1.1	0.8	e
Dien											
1	0	3.2	2.5	2.5	1.8	2.4	2.3	1.3	2.5	2.4	1.1
2	0	5.5	4.1	4.0	3.3	3.9	3.7	2.3	4.0	3.6	2.3
2	1	4.1	3.1	3.0	2.1	3.0	2.8	1.5	3.1	2.7	0.9
2	2	3.9	3.2	3.1	2.1	3.2	3.0	1.5	3.2	2.8	0.6
3	2	4.6	3.5	3.2	2.2	3.4	2.6	1.1	3.5	2.5	0.3
3	3	3.4	2.9	2.6	1.6	2.8	2.0	0.5	2.9	1.9	e
Trien											
1	0	2.8	2.1	2.1	1.4	2.0	2.0	1.0	2.1	2.0	0.7
2	0	5.5	4.1	4.0	3.3	4.0	3.8	2.8	4.1	3.7	2.4
2	1	5.2	4.2	4.1	3.2	4.1	3.9	2.6	4.2	3.8	2.0
3	1	6.6	5.0	4.7	3.8	4.9	4.4	3.1	5.0	4.1	2.3
3	2	5.6	4.5	4.2	3.2	4.4	3.9	2.4	4.5	3.6	1.4
4	2	6.4	5.0	4.5	3.5	4.8	3.8	2.3	5.0	3.4	1.2
4	3	4.3	3.6	3.1	2.1	3.5	2.5	1.0	3.6	2.0	e
Tetren											
1	0	2.8	2.1	2.1	1.4	2.0	2.0	1.0	2.1	2.0	0.7
2	0	4.7	3.3	3.2	2.5	3.1	3.0	2.0	3.2	2.9	1.6
2	1	5.1	4.0	3.9	3.0	3.9	3.8	2.5	4.0	3.7	1.9
3	1	5.5	3.9	3.7	2.8	3.8	3.5	2.2	3.9	3.3	1.5
3	2	5.3	4.3	4.1	3.1	4.2	3.9	2.4	4.3	3.7	1.5
4	2	5.7	4.3	3.9	2.9	4.2	3.5	2.0	4.3	3.0	0.8
5	2	6.1	4.4	3.7	2.7	4.2	3.0	1.5	4.3	2.3	0.1
Penten											
1	0	3.6	2.9	2.9	2.2	2.8	2.7	1.7	2.9	2.7	1.4
2	0	5.0	3.6	3.5	2.8	3.5	3.3	2.3	3.6	3.2	1.9
2	1	5.4	4.4	4.3	3.4	4.2	4.0	2.7	4.3	3.9	1.1
3	1	6.5	4.9	4.5	3.6	4.7	4.0	2.7	4.8	3.8	1.0
4	1	8.1	6.0	5.4	4.5	5.8	4.8	3.5	5.9	4.4	2.6
3	2	7.2	6.1	5.7	4.7	6.0	5.3	3.8	6.1	5.1	2.9
4	2	7.2	5.8	5.2	4.2	5.7	4.7	3.2	5.8	4.3	2.1
5	2	7.8	6.1	5.2	4.2	5.9	4.6	3.1	6.0	3.9	1.7
6	2	7.9	5.8	4.7	3.7	5.6	4.0	2.5	5.7	3.1	0.9

[a] I in mol dm^{-3}; i and j refer to the formation constant K_{ij} [see Experimental section, Eq.(2e)].
[b] Formation constants calculated by considering the formation of both Na^+ and Cl^- complexes.
[c] Formation constants calculated by neglecting Cl^- complexes.
[d] Formation constants calculated by neglecting both Na^+ and Cl^- complexes.
[e] $\log K_{ij} < 0$.

Errors associated with overall formation constants β_{pq} are reported in Table 3 as three times the standard deviation. In general these uncertainties can be considered satisfactory, but we must consider that by including small systematic errors, formation constants may be affected by substantially higher uncertainties. Values of log K_{ij} are reported to only one decimal place since they are affected by an error $0.1 \leqslant 3s \leqslant 0.4$.

4.5. Concluding remarks

The most important finding of this work relates to the quite high strength of pyrophosphate–amine complexes, in particular for polyamines with more than two amino groups. In some cases the formation constants of mixed proton–$P_2O_7^{4-}$–amine species are comparable with those of $P_2O_7^{4-}$–alkaline earth metal complexes [27], and in the case of penten higher log K_{ij} values are also observed.

The second remark to be made concerns the dependence of the medium of formation constants of complexes studied here. In fact, as reported in the text and in Table 4, different ionic strengths and different background conditions may cause a substantial lowering of formation constants. This is due to the high charges of pyrophosphate and protonated polyamines and to the strong interferences of Na^+ and Cl^-. Therefore, care must be taken when using these formation data in the speciation of different biological and natural fluids.

Finally it must be stressed that, in the light of present results, interaction of $P_2O_7^{4-}$ with polyamines may play an important role in natural systems, since it occurs also at very low concentrations. Semi-quantitative information for the stability of other complexes with biologically important amines can be obtained using Eq. (3).

Acknowledgements

References

[1] P.G. Daniele, C. De Stefano, E. Prenesti and S. Sammartano, J. Solution Chem., 24 (1995) 325.

[2] R. Lahti, R. Hannukainen and H. Lönnberg, Biochem. J., 259 (1989) 55.

[3] B. Dietrich, D. Fyles, T.M. Fyles and J.M. Lehn, Helv. Chim. Acta, 62 (1979) 2763.

[4] D.D. Perrin, W.L.F. Armarego and D.R. Perrin, Purification of Laboratory Chemicals, Pergamon Press, Oxford, 1966.

[5] C. De Stefano, P. Princi, C. Rigano and S. Sammartano, Ann. Chim. (Rome), 77 (1987) 643.

[6] C. De Stefano, P. Mineo, C. Rigano and S. Sammartano, Ann. Chim. (Rome), 83 (1993) 243.

[7] C. De Stefano, C. Foti, O. Giuffrè, P. Mineo, C. Rigano and S. Sammartano, Ann. Chim. (Rome), submitted for publication.

[8] P.G. Daniele, A. De Robertis, C. De Stefano, S. Sammartano and C. Rigano, J. Chem. Soc., Dalton Trans., (1985) 2353.
P.G. Daniele, A. De Robertis, C. De Stefano and S. Sammartano, in S. Alegret, J.J. Arias, D. Bercelo', J. Casal and G. Rauret (Eds.), Miscellany of Scientific Papers Offered to Enric Casassas, Publicacions de la Universitat Autonoma de Barcelona, Bellaterra, Spain, 1991 (and references cited therein).

[9] A. Casale, P.G. Daniele, A. De Robertis and S. Sammartano, Ann. Chim. (Rome), 78 (1988) 249.

[10] C. De Stefano, C. Foti and A. Gianguzza, J. Chem. Res. (S), (1994) 464; J. Chem. Res. (M), (1994) 2639.

[11] A. Casale, A. De Robertis, F. Licastro and C. Rigano, J. Chem. Res. (S), (1990) 204; J. Chem. Res. (M), (1990) 1601.

[12] A. De Robertis, C. De Stefano and G. Patane', Thermochim. Acta, 209 (1992) 7.

[13] A. De Robertis, C. De Stefano, G. Patane' and S. Sammartano, J. Solution Chem., 22 (1993) 927.

[14] A. De Robertis and O. Giuffrè, unpublished results.

[15] E. Kimura, A. Sakonaka, T. Yatsunami and M. Kodama, J. Am. Chem. Soc., 103 (1981) 3041.

[16] M.W. Hosseini and J.M. Lenh, J. Am. Chem. Soc., 104 (1982) 3535.

[17] E. Kimura, M. Kodama and T. Yatsunami, J. Am. Chem. Soc., 104 (1982) 3182.

[18] B. Dietrich, J.M. Lehn, C. Pascard and E. Sonveaux, Helv. Chim. Acta, 67 (1984) 91.

[19] M.W. Hosseini and J.M. Lehn, Helv. Chim. Acta, 69 (1986) 587.

[20] M.W. Hosseini and J.M. Lehn, Helv. Chim. Acta, 70 (1987) 1312.

[21] P.G. Daniele, A. De Robertis, C. De Stefano, D. Gastaldi and S. Sammartano, Ann. Chim. (Rome), 83 (1993) 575.

[22] C. De Stefano, A. Gianguzza and S. Sammartano, Talanta, 40 (1993) 629.

[23] A. De Robertis, A. Gianguzza, G. Patane' and S. Sammartano, J. Chem. Res. (S), (1994) 182.

[24] C. De Stefano, C. Foti and O. Giuffrè, J. Solution Chem., in press.

[25] A. De Robertis, C. De Stefano, O. Giuffrè and S. Sammartano, unpublished work.

[26] A. De Robertis, C. De Stefano, C. Foti, A. Gianguzza and S. Sammartano, J. Chem. Soc., Faraday Trans., 91 (1995) 1619.

[27] E. Högfeldt, Stability Constants of Metal–Ion Complexes, Part A: Inorganic Ligands, Pergamon Press, Oxford, 1982.

Catalytic–adsorptive stripping voltammetric determination of molybdenum in plant foodstuffs

Zhiqiang Gao*, Kok Siong Siow

Department of Chemistry, National University of Singapore, Kent Ridge, Singapore 0511, Singapore

Abstract

In acetate buffer solution (pH 3.5) containing oxine and chlorate, ultratrace amounts of molybdenum can be determined after adsorptive accumulation of the Mo(VI)–oxine complex on a hanging mercury drop electrode, coupled with the catalytic effect on the reduction of chlorate. Under optimized conditions, the catalytic–adsorptive stripping voltammetric procedure gives excellent selectivity and an extremely low detection limit of 1.7 pM molybdenum (60 s accumulation). The stripping peak current increases linearly with molybdenum concentration between 10 pM and 5.0 nM. The procedure is applied to determine traces of molybdenum in plant foodstuffs.

Keywords: Adsorptive voltammetric determination; Molybdenum; Plant foodstuffs

1. Introduction

Molybdenum is a biologically essential trace element [1–3]. It always occurs in the hexavalent form (Mo(VI)) in aqueous solutions. Depending on the acidity of the solution, it may be cationic, anionic or polymeric [4]. Molybdenum plays an important role in a wide variety of plants and animals, particularly ruminants. Molybdenum deficiency eventually results in a diminished number of flowers on plants and severe interference in the development of pollen. In contrast a high concentration of molybdenum in soil causes abnormal growth of some plants [5,6]. Molybdenum also affects self-purification processes of natural

water. At about 5 ppm it inhibits biochemical self-purification processes. An even higher content of molybedenum in water prevents the growth of the appropriate microorganisms [7]. Since the concentrations of molybdenum in plants, water and soil are generally at parts per billion levels, sufficient sensitivity is therefore required for the determination of molybdenum.

Many electroanalytical procedures have been proposed for the determination of trace amounts of molybdenum [8–14]. On the basis of the adsorptive accumulation of a molybdenum complex, such as Mo(VI)–tropolone [8], Mo(VI)–oxine [9] or Mo(VI)–mandelic acid [10], on a hanging mercury drop electrode (HMDE), nanomolar amounts of molybdenum in various samples can be successfully determined. Further improvement in the sensitivity has been reported by the applica-

* Corresponding author. Fax: + 65 779 1691.

tion of catalytic effects of Mo(VI)–cupferron [11], Mo(VI)–mandelic acid [12] and Mo(VI)–3-methoxy-4-hydroxymandelic acid complexes [13] on the reduction of chlorate, and Mo(VI)–2-(2'-thiozolylazo)-p-cresol complex on the reduction of nitrate [14]. Picomolar detection limits have been achieved after a few minutes of adsorptive accumulation.

This paper describes an extremely sensitve and highly selective catalytic–adsorptive stripping voltammetric procedure for the determination of traces of molybdenum in plant foodstuffs. The procedure is based on the catalytic reduction of chlorate by the accumulated molybdenum complex with oxine. The voltammetric behavior of Mo(VI)–oxine complex in slightly acidic medium was first reported by van den Berg [9]. The reduction current of the adsorbed Mo(VI)–oxine complex was used for the direct determination of molybdenum in sea water with a detection limit of 0.10 nM (10 min accumulation). The catalytic–adsorptive procedure developed in this paper lowers the detectability further to the picomolar level with a relatively short adsorptive accumulation time.

2. Experimental

2.1. Apparatus and reagents

A PAR Model 174A polarographic analyzer equipped with a Model 303 static mercury drop electrode (EG&G, PAR, Princeton, NJ) and a Graphtec 2400 X–Y recorder were used for voltammetric study. A conventional three-electrode system, comprising an HMDE, a platinum wire counter electrode and an Ag/AgCl (in saturated KCl) reference electrode, was used in all experiments. All potentials reported in this paper were referred to the Ag/AgCl electrode. All experiments were performed under a nitrogen atmosphere in a clean environment.

Water purified in a Milli-Q water purification system (Millipore) was used for all solution and sample preparations. All chemicals were of certified analytical grade and above. A 1000 ppm stock Mo(VI) solution (atomic absorption stan-

dard, Aldrich) was diluted as required. Stock solutions of 1.0 mM oxine and 1.0 M chlorate were prepared by directly dissolving required amounts of oxine and sodium chlorate in water respectively.

2.2. Procedure

The supporting electrolyte solution (10 ml 0.050 M acetate buffer, pH 3.5), containing 0.20 M sodium chlorate and 50 μM oxine, was pipetted into a voltammetric cell and purged with nitrogen for at least 4 min. The accumulation potential was applied to a fresh mercury drop while the solution was stirred. After 60 s of accumulation, a period of quiescence of 10 s was allowed whereafter a linear scan voltammogram was recorded from -0.10 to -0.70 V, with a potential scan rate of 100 mV s^{-1}. After the background voltammogram had been obtained, aliquots of the Mo(VI) standard solution were introduced into the cell while maintaining a nitrogen atmosphere over the solution. All data were obtained at room temperature.

2.3. Reagent purification

All containers were thoroughly cleaned by soaking in 1:1 HNO$_3$ for several days. They were then rinsed and stored in 0.10 M HNO$_3$. All experiments were performed in a clean environment. Trace amounts of molybdenum in the electrolyte solution were removed by Chelex-100 ion-exchanger at pH 3.5. The ion-exchanger was purified according to the proposed procedure [10,12]. The contribution of molybdenum to the supporting electrolyte from the thus purified reagents was generally less than 5.0 pM.

2.4. Sample analysis

For the determination of molybdenum in plant foodstuffs, samples (0.50–1.0 g) were first ashed for 5–7 h at 500°C in a quartz crucible. After cooling, the ashes were carefully moistened with 2 ml of 1:1 nitric acid and the mixture was heated on a hotplate to near dryness. The residue was dissolved in 1.0 mM nitric acid. The solution was filtered and collected in a clean polyethylene bot-
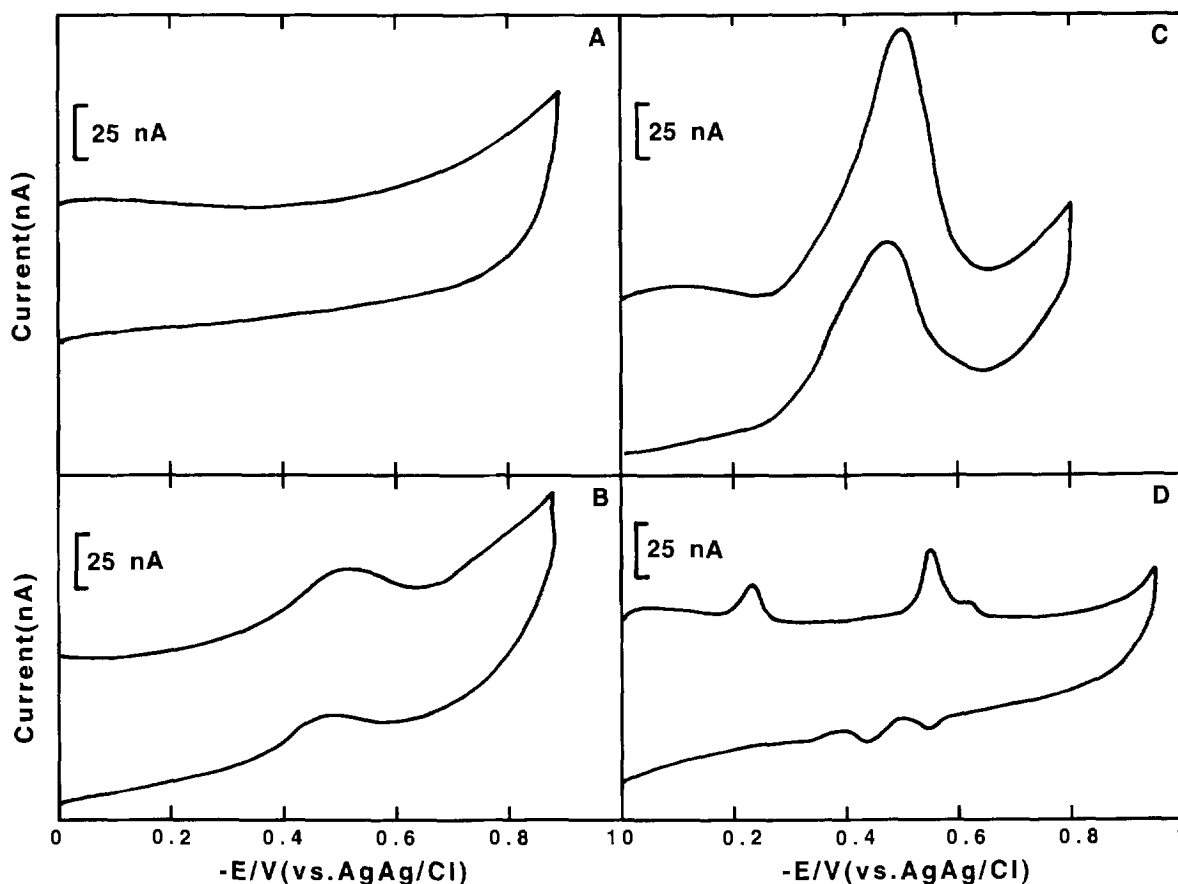
Fig. 1. Cyclic voltammograms of molybdenum in different solutions: (A) 0.20 M NaClO₃ + 0.050 M acetate buffer (pH 3.5); (B) same as (A) + 0.50 μM Mo(VI); (C) same as (A) + 0.20 nM Mo(VI) + 50 μM oxine; (D) 50 μM oxine + 0.10 μM Mo(VI) + 0.050 M acetate buffer (pH 3.5). Accumulation potential 0.0 V, accumulation time 60 s, scan rate 100 mV s⁻¹.

tle. Aliquots of the solution were pipetted into the voltammetric cell and the concentrations of molybdenum were determined using the standard additions method.

3. Results and discussion

Fig. 1 shows cyclic voltammograms for different combinations of Mo(VI), oxine and chlorate in 0.050 M acetate buffer solution (pH 3.5). As illustrated in Fig. 1A, for a solution containing chlorate alone, no obvious current peaks were observed between 0.0 and − 1.0 V. However, in an acidic medium contining Mo(VI), chlorate gave a catalytic current peak at approximately

− 0.5 V (Fig. 1B). This catalytic current increased linearly with increasing molybdenum concentration in the range 0.10–1.0 μM [15]. When mixing Mo(VI) with oxine in the buffer solution, three adsorptive stripping current peaks were obtained (Fig. 1D). The first stripping current peak at approximately − 0.2 V corresponds to the reduction of Mo(VI) in the complex to Mo(V). The second current peak at approximately − 0.5 V should be the reduction of Mo(V) to Mo(IV). The last one represents the reduction of Mo(IV) to Mo(III). The peak current increased with increasing accumulation time prior to the potential scan, indicating that the Mo(VI)–oxine complex is readily adsorbed onto the HMDE. The stripping peak current was directly proportional to the

concentration of molybdenum up to 0.30 μM, with a detection limit of 4.0 nM, following 1 min of accumulation [9]. As indicated in Fig. 1C, upon adding chlorate to the Mo(VI)–oxine complex solution, a dramatic increase in peak current was observed. Furthermore, the catalytic current did not commence until the potential became considerably more negative than that of the first current peak of the Mo(VI)–oxine complex, suggesting that both Mo(VI) and Mo(V) have no catalytic activity towards the reduction of chlorate. As the electrode potential approached the peak potential of the second current peak, more and more Mo(IV) ions were generated at the HMDE surface upon the reduction of Mo(V), which catalyzes the reduction of chlorate in the solution.
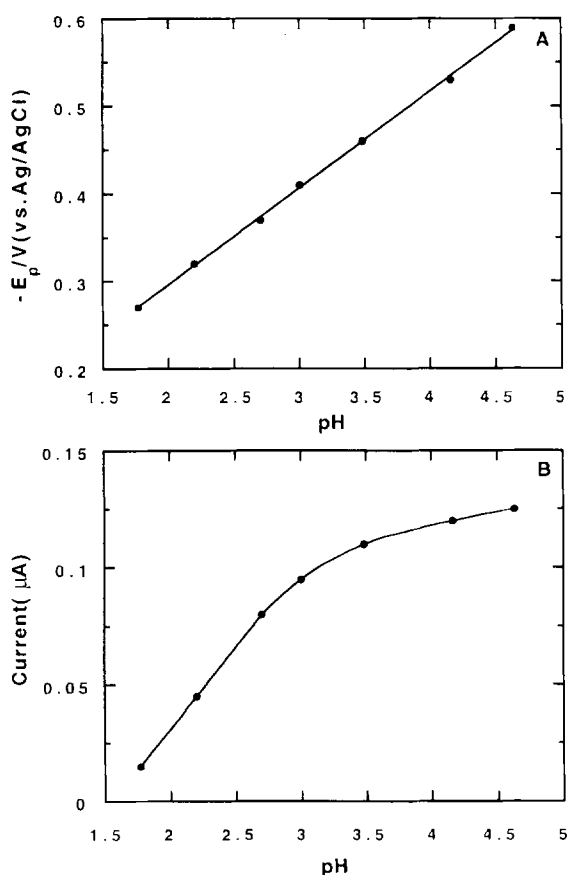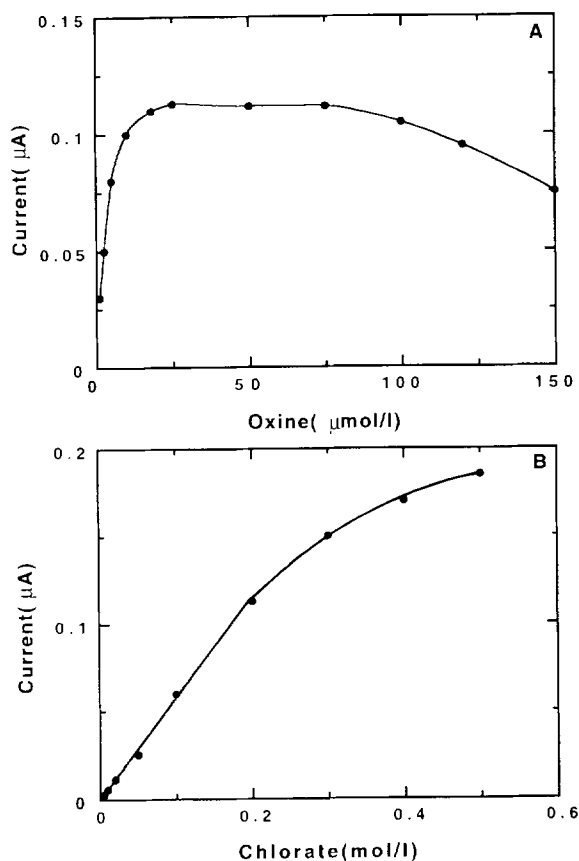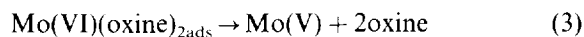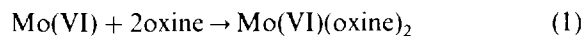

Fig. 3. Variations in the peak current for 0.20 nM Mo(VI) as functions of (A) oxine and (B) NaClO₃ concentration. Accumulation potential −0.10 V, other conditions as in Fig. 1C.

Fig. 2. Effect of pH on (A) peak potential and (B) peak current of Mo(VI)–oxine. Accumulation potential −0.10 V, other conditions as in Fig. 1C.

Referring to the well-known mechanism of the catalytic reduction of chlorate by molybdenum [15,16], a possible reaction mechanism is that uncomplexed Mo(IV), generated at the HMDE surface upon the reduction of the Mo(VI)–oxine complex, reduces chlorate, and in the mean time the regenerated Mo(V) is re-reduced at the electrode surface to Mo(IV), therefore contributing repeatedly to the reduction current. This is a typical EC process and the possible mechanism is as follows:

$$Mo(VI) + 2oxine \rightarrow Mo(VI)(oxine)_2 \qquad (1)$$

$$Mo(VI)(oxine)_2 \rightleftharpoons Mo(VI)(oxine)_{2ads} \qquad (2)$$

$$Mo(VI)(oxine)_{2ads} \rightarrow Mo(V) + 2oxine \qquad (3)$$

$$Mo(V) \rightarrow Mo(IV) \tag{4}$$

$$\boxed{6Mo(IV) + ClO_3^- + 6H_+}$$

$$\rightarrow 6Mo(V) + Cl^- + 3H_2O \tag{5}$$
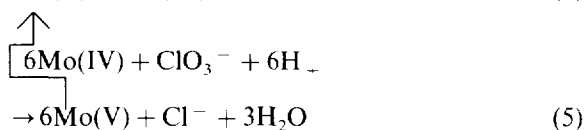
The pH dependences of the catalytic peak po tential and peak current are shown in Fig. 2. As illustrated in Fig. 2A, the peak potential varied with the pH and was shifted in the negative direction by 112 mV pH^{-1}. A larger peak current was observed at higher pH. Good sensitivity was attained in the pH range 3.5–4.0. A substantial decrease in peak current was observed when the pH was lower than 3.0. The largest current was obtained at a pH of about 4.6 (Fig. 2B). However, a dramatic increase in the peak width was also observed at pH 4.6, which may cause inaccuracy in current measurements, especially at very low

Fig. 5. Catalytic–adsorptive stripping voltammograms for solutions of increasing Mo(VI) concentration: (1) 0.020; (2) 0.050; (3) 0.10; (4) 0.20; (5) 0.50 nM. Conditions as in Fig. 3.

concentrations, since the broadening of the current peak overlaps the reduction currents of oxine and traces of oxygen.

Since oxine is an essential component for the formation of the adsorptive complex, the oxine concentration would be expected to strongly affect the peak current. The peak current increased sharply upon increasing the oxine concentration between 1.0 μM and 20 μM, and then leveled off between 20 μM and 75 μM. Only a slight decrease in the peak current was observed for higher oxine concentrations (Fig. 3A). Chlorate concentration also had a profound effect on the peak current (Fig. 3B). For example, the peak current for 0.20 nM molybdenum increased linearly with increasing chlorate concentration up to 0.20 M, and then more slowly. A chlorate concentration higher than 0.40 M resulted in a larger background current, presumably due to the reduction of chlorate.

The influence of the variation of the accumulation potential on the peak current, examined over the range 0.0 to −0.40 V, is shown in Fig. 4A. The largest peak current was obtained for accumulation potentials between −0.050 and −0.15 V. The peak current decreased when accumulation potentials were more negative than −0.15 V and diminished substantially if an accumulation

Fig. 4. Dependence of peak curent for Mo(VI)–oxine on (A) accumulation potential and (B) accumulation time. (A) 0.20 and (B) 2.0 nM Mo(VI), other conditions as in Fig. 3.

Fig. 6. Catalytic–adsorptive stripping voltammograms for 0.085 nM Mo(VI) (solid lines) and 0.085 nM Mo(VI) + 0.50 μM Cu^{2+} (broken lines) in the presence of (A) mandelic acid, (B) oxine and (C) cupferron. Accumulation time 60 s, other conditions as in Ref. [12], Fig. 3 and Ref. [11] respectively.
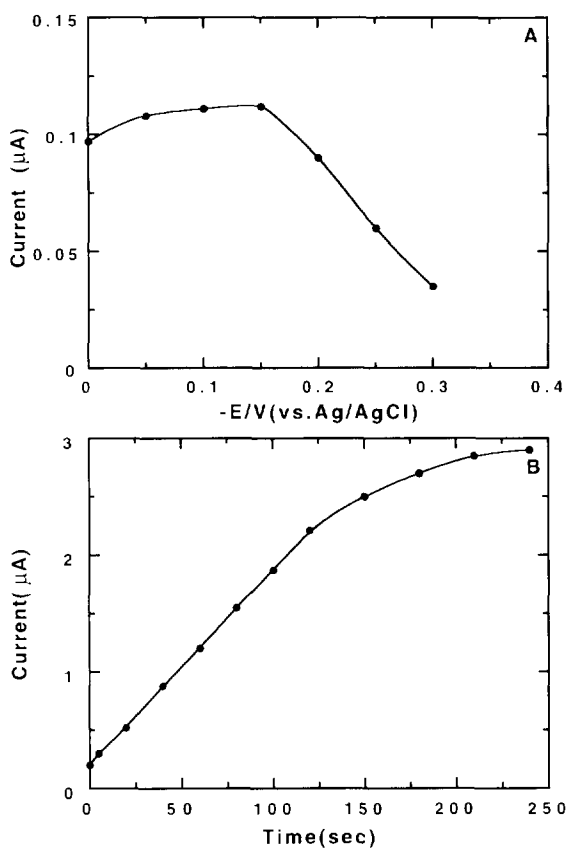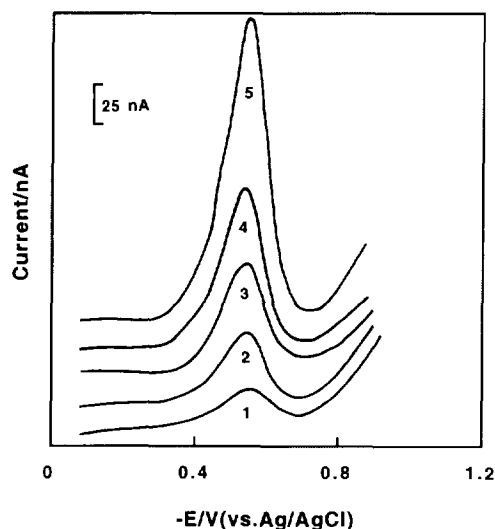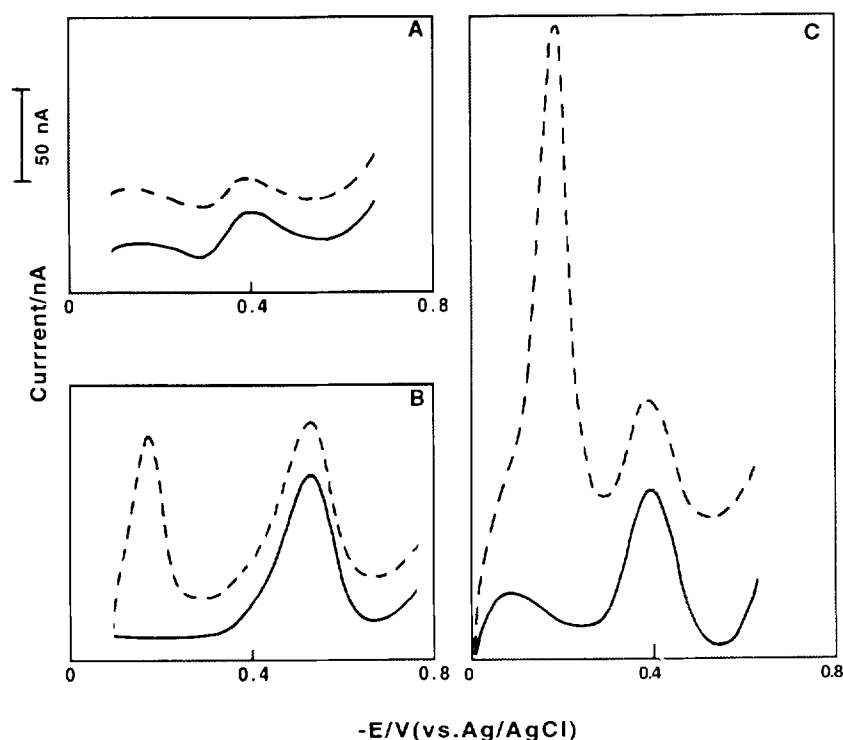
potential was selected on the negative side of the first current peak, indicating that only the Mo(VI)–oxine complex is accumulated at the electrode surface, whereas the reduction product has no adsorptive property. The strong adsorptive character of the Mo(VI)–oxine complex can be used as an effective collection step, prior to voltammetric measurement, and provides an extremely sensitive procedure for molybdenum analysis. As shown in Fig. 4B, the longer the accumulation time, the more the Mo(VI)–oxine complex was accumulated and the higher was the current sensitivity. The peak current increased linearly with increasing accumulation time from 0 to 120 s. For accumulation times above 150 s, the gain in sensitivity was very small. Subsequent experiments were, therefore, performed using 0.050 M acetate buffer solution (pH 3.5) containing 50 μM oxine and 0.20 M sodium chlorate, and an accumulation time of 60 s at − 0.10 V, taking into account the speed of the measurement

and the performance.

Under these conditions, by taking advantage of the adsorptive–catalytic nature of the Mo(VI)–oxine complex, the sensitivity of the linear scan voltammetric method is improved significantly. The dependence of the catalytic–adsorptive stripping peak current on the concentration of molybdenum is shown in Fig. 5, which displays parts of the catalytic–adsorptive stripping voltammograms in calibration experiments. Well-defined peaks were obtained despite the very low molybdenum concentrations (subnanomolar levels). The catlaytic–adsorptive stripping peak current of the Mo(VI)–oxine complex was found to be directly proportional to the Mo(VI) concentration in the range 10 pM–5.0 nM (correlation coefficient 0.998), with a sensitivity of 0.56 μA nM^{-1}, which is more than 10 000 times higher than that for a simple diffusion-controlled current of molybdenum ions in an acidic medium. As shown in Fig. 6 (solid lines), the sensitivity obtained in this work

Table 1
Determination of molybdenum in plant foodstuffs (average of six determinations)

Sample	Mo content (ppb)	Mo added (ppb)	Mo after addition (ppb)	Recovery (%)
Cucumber	52	50	100	96
Cabbage	74	50	126	104
Tea[a]	210	200	398	94
Tomato	38	50	87	98
Wheat[a]	510	500	985	95
Potato	31	50	79	96

[a] Air-dried sample.

was higher than the most sensitive catalytic–adsorptive procedure, the Mo(VI)–cupferron system [11], and much higher than those of other catalytic–adsorptive stripping voltammetric procedures [12–14]. The detection limit, estimated from three times the standard deviation of repetitive measurements of 10 pM molybdenum under optimal conditions, was found to be 1.7 pM, which is about three orders of magnitude lower than that of the corresponding adsorptive stripping procedure [9] and is comparable with that of the most sensitive catalytic–adsorptive stripping voltammetric procedures [11–14]. The reproducibility of the procedure was established by two sets of 20 repetitive determinations of 20 pM and 2.0 nM molybdenum. The mean peak currents were 11.8 nA and 1.12 μA with relative standard deviations of 5.1% and 1.9% respectively.

In the voltammetric determination of molybdenum in the catalytic–adsorptive systems, interferences may be caused by the competitive adsorption of ions and their complexes on the electrode surface and competitive participation in the catalytic reaction. They may also be the result of the appearance of reduction peaks next to the Mo(VI)–oxine complex current peak. Owing to the extremely high sensitivity of the catalytic–adsorptive stripping current, it is expected that the influence of a large excess of another reducible species on the determination of molybdenum will be minor, even with a similar peak potential to the catalytic current peak potential. The effect of co-existing ions was tested at a concentration of 1.0 nM molybdenum. It was found that up to 1.0 mM of SO_4^{2-}, NO_3, F, BO_3^{3-}, CO_3^{2-}, Cl, NH_4^+, K^+, Sr^{2-}, Li^+, Be^{2+}, Ba^{2+}, Ca^{2+} and

Mg^{2-}; 0.10 mM of BrO_3^-, NO_2, SCN^-, Al^{3-} and Ga^{3-}; 10 μM of Cd^{2-}, Co^{2-}, Fe^{2+}, Fe^{3+}, Cr^{3+}, CrO_4^{2-}, $AuCl_4^-$, Pb^{2+}, Ag^+, Hg^{2+}, Zn^{2+}, Ni^{2+}, Mn^{2+} and Ce^{4+}; 5.0 μM of Cu^{2-}, Bi^{3-} and In^{3+}; and 2.0 μM VO^{2+} have little effect on the determination of molybdenum. However, SbO^- has a reduction current peak in the region of the stripping peak of molybdenum which interferes at concentrations of 1.0 μM. Additions of 3.0 μM I^- and 0.20 μM WO_4^{2-} lower the Mo(VI)–oxine peak by 12% and 15% respectively. In addition, due to the adsorptive nature of the Mo(VI)–oxine complex, surface-active substances, such as natural organic sufactants, Triton X-100, Tween-80, sodium dodecylsulfate (SDS) and cetyltrimethylammonium bromide (CTAB), may interfere as a result of competitive adsorption at the electrode surface. For example, additions of 0.50 μM CTAB and SDS resulted in 12 and 15% depressions of the peak current respectively. Depending on the complexity of the sample, for direct determination of molybdenum, necessary sample pretreatments, such as UV irradiation, ashing, acid digestion and microwave digestion, are recommended. Compared to other catalytic-adsorptive stripping voltammetric procedures, for example Mo(VI)–cupferron [11] and Mo(VI)–mandelic acid [12], better selectivity against copper was observed (Fig. 6, broken lines). In addition, better selectivity against tungsten was also observed.

The proposed method was sucessfully applied to detemine molybdenum in a number of plant foodstuffs. In order to eliminate the matrix effect, molybdenumm contents were determined using the standard additions method. The results are

listed in Table 1. The recoveries obtained by this method were good enough for practical use.

In conclusion, linear scan voltammetry offers a simple, fast and convenient method for the determination of ultratrace amounts of molybdenum by means of the coupling of adsorptive and catalytic effects of the molybdenum–oxine complex on the reduction of chlorate. The extremely high sensitivity and good selectivity, which are comparable with the most sensitive procedures, adds to the versatility of the proposed method.

References

[1] E.J. Underwood, Trace Elements in Human and Animal Nutrition, Academic Press, New York, 1977.

[2] L.L Hopkins, Jr. and H.E. Mohr, in W. Mertz and W.E. Cornatzer (Eds.), New Trace Elements in Nutrition, M. Dekker, New York, 1971.

[3] I.T.T. Davis, The Clinical Significance of the Essential Biological Metals, Thomas, Springfield, IL, 1972.

[4] D.V. Ramano Rao, Anal. Chim. Acta, 12 (1955) 211.

[5] C.R. Millican, Proc. R. Soc. Victoria, 61 (1949) 25.

[6] A. Petrosek and E. Steven, Ind. Water Eng., 10 (1971) 26.

[7] T.A. Asmangulan, Gig. Sanit., 4 (1965) 6.

[8] S.H. Khan and C.M.G. van den Berg, Mar. Chem., 27 (1989) 31.

[9] C.M.G. van den Berg, Anal. Chem., 57 (1985) 1532.

[10] J. Pelzer, F. Scholz, G. Henrion and P. Heininger, Fresenius' Z. Anal. Chem., 334 (1989) 331.

[11] K. Jiao, W. Jin and H. Metzer, Anal. Chim. Acta, 260 (1992) 35.

[12] K. Yokoi and C.M.G. van den Berg, Anal. Chim. Acta, 257 (1992) 293.

[13] J. Wang, J. Lu and Z. Taha, Analyst, 117 (1992) 35.

[14] P.A.M. Farias, A.K. Ohara, A.W. Nobrega and J.S. Gold, Electroanalysis, 9 (1994) 333.

[15] G.P. Haight, J. Am. Chem. Soc., 76 (1954) 4718.

[16] I.M. Kolthoff and I. Hodara, J. Electroanal. Chem., 5 (1963) 2.

Determination of trace amounts of iron by catalytic–adsorptive stripping voltammetry

Zhiqiang Gao*, Kok Siong Siow

Department of Chemistry, National University of Singapore, Kent Ridge, Singapore 0511, Singapore

Received 19 May 1995; revised 1 November 1995; accepted 2 November 1995

Abstract

A highly sensitive and selective voltammetric procedure is described for the determination of trace amounts of iron. The procedure is based on the adsorptive collection of an iron–thiocyanate–nitric oxide complex on a hanging mercury drop electrode. The adsorbed complex catalyzes the reduction of nitrite in solution, which gives a detection limit of 40 ppt iron (30 s accumulation). The stripping current increases linearly with iron concentration up to 80 ppb. The relative standard deviations are 4.2% and 1.6% at 0.5 ppb and 40 ppb respectively. Most of the common ions, except cobalt, do not interfere with the determination of iron. The procedure is applied to determine iron in biological samples, natural waters and analytical-grade chemicals.

Keywords: Iron; Adsorptive stripping voltammetry; Iron–thiocyanate–nitric oxide complex

1. Introduction

In recent years, substantial efforts have been devoted to the development of catalytic–adsorptive voltammetric procedures, which are based on the adsorptive accumulation of metal complex on a hanging mercury drop electrode (HMDE) followed by a homogeneous catalytic reaction [1–12]. This interest is due to the excellent sensitivity, selectivity, accuracy, precision and the low cost of instrumentation. The detection limit of catalytic–adsorptive voltammetry is usually lower than 0.1 ppb, making it one of the most sensitive analytical methods for ultratrace analysis.

A number of metals, including cobalt [1,2], chromium [3,4], molybdenum [5–8], titanium [8], platinum [9], tungsten [10,11], and vanadium [12] have been successfully analyzed using catalytic–adsorptive voltammetric procedures. The electrochemical behavior of iron makes its polarographic determination very difficult. Therefore, for the analysis of trace amounts of iron, most of the reported electroanalytical procedures are based on adsorptive stripping voltammetry. For example, in the presence of catechol [13], 1-nitro-2-naphthol [14], solochrome violet RS [15] or 2-(5-bromo-2-pyridylazo)-5-diethylaminophenol [16], trace amounts of iron can be determined after adsorptive accumulation of the iron complexes with these ligands. Depending on the accumula-

* Corresponding author. Fax: + 65 779 1691.

tion time, iron at ppb levels in various samples has been determined following a few minutes of accumulation. However determination of iron by catalytic–adsorptive voltammetry has rarely been attempted. Golimowski [17] proposed a catalytic–adsorptive voltammetric procedure for measuring iron in the presence of triethanolamine and potassium bromate, but the detection limit (4 ppb) is relatively poor. A more sensitive catalytic–adsorptive voltammetric procedure was reported by Lu et al. [18]. A detection limit of 10 ppt was achieved after 10 min accumulation.

In this paper a novel method of catalytic–adsorptive stripping voltammetry of the iron–thiocyanate–nitric oxide complex at the HMDE is investigated and applied to the determination of trace amounts of iron in a number of samples. Compared to the adsorptive stripping voltammetric procedures, this method provides a very low detection limit (40 ppt) for a very short accumulation period and excellent selectivity against most co-existing ionic species.

2. Experimental

2.1. Apparatus and reagents

A PAR Model 174A polarographic analyzer was employed in connection with a Model 303 static mercury drop electrode (EG & G, PAR, Princeton, NJ) and a Graphtec X–Y recorder. A medium-sized HMDE electrode, with a surface area of 2.0 mm², was used. An Ag/AgCl (in saturated KCl) reference electrode was used in all experiments. All potentials reported in this paper are referred to the Ag/AgCl electrode. Solutions were deoxygenated with high purity nitrogen for 4 min prior to each experiment and all experiments were performed in a clean environment under a nitrogen atmosphere.

Water purified in a Milli-Q water purification system (Millipore) was used for all solutions and sample preparations. All chemicals were of certified analytical grade and above. A stock solution of 1000 ppm iron was prepared by directly dissolving the required amount of ammonium ferrous sulfate in acidified water. Traces of iron in

blank electrolyte were removed according to the procedure developed by Lazaro et al. [19]. Reagent containers and sample bottles were cleaned by soaking in 1:1 nitric acid for a few days. They were then thoroughly rinsed with water and stored in 0.01 M nitric acid.

2.2. Procedure

The supporting electrolyte solution (10 ml 0.1 M pH 4.0 acetate buffer), containing 0.1 M sodium nitrite and 0.05 M potassium thiocyanate, was transferred by pipette into a voltammetric cell and purged with nitrogen for 4 min. The adsorption potential (−0.15 V) was applied to a fresh mercury drop in quiescent solution. A linear scan voltammogram was recorded from −0.15 to −0.75 V following 30 s accumulation, with a potential scan rate of 100 mV s⁻¹. After the background voltammogram had been obtained, aliquots of the iron standard solution were introduced into the cell while maintaining a nitrogen atmosphere over the solution. All data were obtained at room temperature.

2.3. Sample analysis

Biological samples were first ashed for 5 h at 450°C in quartz crucibles. After cooling, the ashes were carefully moistened with 2 ml of 4.0 M ultrapure nitric acid and the mixtures were heated on a hotplate to near dryness. The residues were dissolved in purified acetate buffer. The resultant solutions were filtered and collected in clean polyethylene bottles. Water samples (15–25ml) were filtered through a 0.40 μm cellulose acetate membrane filter into a quartz crucible and the pH was adjusted to about 3.0 with acetate buffer. They were then UV-irradiated for 5–8 h. Analytical grade chemicals were directly dissolved in water and the pH of the sample solution was adjusted to 3.5–4.0 with acetate buffer solution. An aliquot of the sample solution was pipetted into the voltammetric cell and the concentration of iron was determined using the procedure described above.
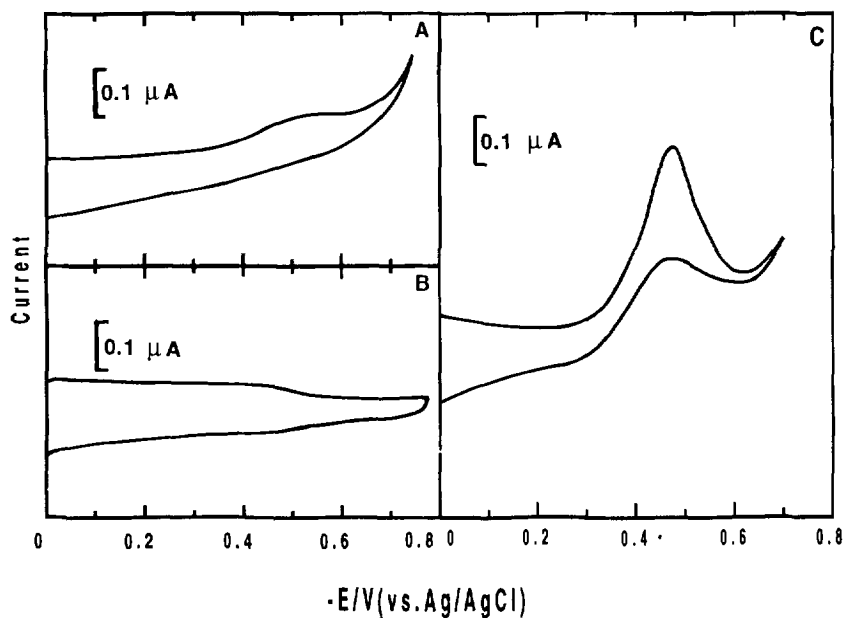
Fig. 1. Cyclic voltammograms of iron in different solutions: (A) 0.05 M KSCN + 0.1 M NaNO$_2$ + 0.1 M pH 4.0 acetate buffer; (B) 0.05 M KSCN + 1.0 ppm Fe^{2+} + 0.1 M pH 4.0 acetate buffer; (C) as for (A) with the addition of 5.0 ppb Fe^{2+}. Accumulation potential 0 V; accumulation time 30 s; potential scan rate 100 mV s^{-1}.

3. Results and discussion

Fig. 1 shows cyclic voltammograms for NO$_2^-$ – SCN$^-$, Fe^{2+}–SCN$^-$ and NO$_2^-$–SCN$^-$–Fe^{2+} in 0.1 M pH 4.0 acetate buffer solution. As can be seen in Fig. 1A, for solutions containing nitrite and thiocyanate, a small current peak is observed,
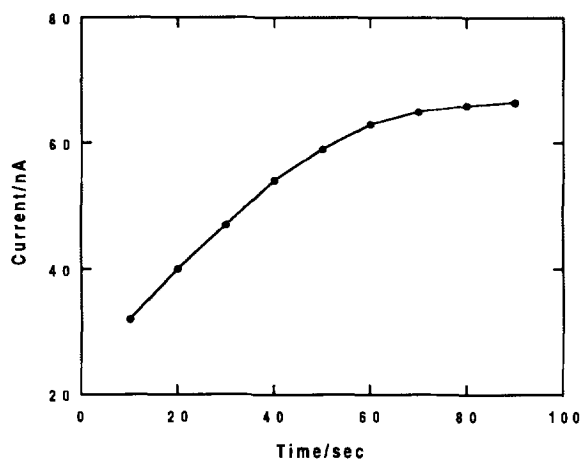

Fig. 2. Dependence of peak current for 0.5 ppb iron on the accumulation time at – 0.15 V. Other conditions as in Fig. 1C.

which is due exclusively to traces of iron in purified electrolyte (see also Fig. 6, broken line). In the acetate buffer containing iron and thiocyanate, no obvious current peaks are observable between 0.0 and – 0.7 V (Fig. 1B). As we know, thiocyanate can only cause an oxidation current by forming Hg(SCN)$_2$ at the mercury electrode surface, which is oxidized at positive potentials. Previous study has shown that in an acidic medium containing thiocyanate, nitrite gives a catalytic reduction wave with a peak potential of about – 0.35 V [20]. The cayalytic current increases linearly with increasing nitrite concentration in the range from parts per million to 0.1%. However, this catalytic current disappears almost completely when increasing the pH of thiocyanate solution to about 3.8. In thiocyanate medium, ferrous iron exists mainly as thiocyanate complexes, Fe(SCN)$_n^{2-n}$. Depending on the concentration of thiocyanate, they may be cationic (FeSCN$^+$), neutral (Fe(SCN)$_2$) or anionic (Fe(SCN))$_n^{2-n}$, $n \geq 3$). However, none of these complexes are reducible in the studied potential range. However, with the addition of a small amount of iron to the solution containing NO$_2^-$
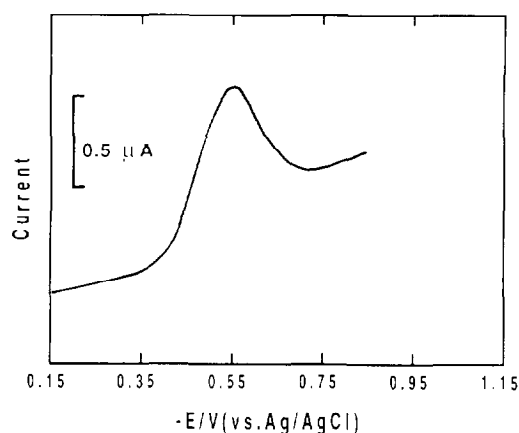
Fig. 3. Normal pulse polarogram for 30 ppb iron in 0.1 M pH 4.0 acetate buffer containing 0.05 M KSCN and 0.1 M NaNO₂. Potential scan rate 10 mV s⁻¹; drop time 1 s; pulse width 25 mV.

and SCN^-, one reduction peak appears at approximately -0.45 V during the negative-going scan. Scanning in the positive direction also produces a reduction peak, indicating a catalytic process. The fact that a well-defined and intense signal is obtained in cyclic voltammetry with iron concentration at ppb levels indicates the remarkable sensitivity associated with the catalytic process. Additional gains in sensitivity can be obtained with an adsorption period prior to the potential scan. As shown in Fig. 2, the peak current increases substantially when the accumulation period preceded the potential scan, suggesting the involvement of adsorption in the electrode process. Supportive evidence for the adsorptive character of the complex can also be found from normal pulse polarography (NPP). As demonstrated in Fig. 3, the appearance of the Barker–Bolzan peak in NPP indicates that the iron complex is strongly adsorbed on the mercury

electrode surface [21]. Furthermore, identical response was observed when adding Fe^{3+} to the solution instead of Fe^{2+}. Apparently, ferric iron in the iron–thiocyanate complex is reduced to ferrous iron at the initial potential, leading to the accumulation of the ferrous iron complex. Subsequent experiments were therefore conducted using ferrous iron solutions.

In addition, when nitrate was substituted for nitrite, no obvious current peaks were observable between 0.0 and -0.7 V, indicating that nitrate is not involved in the catalytic reaction. It is known that the reduction potential of nitrite is more negative than -1.0 V in acidic media. It is also known that in acidic media, nitrite disproportionates to nitrate and nitric oxide [22]. Nitrate cannot be reduced before the reduction of hydrogen ions. A plausible explanation for the reduction current is that nitric oxide is involved in the electrode process, most probably by forming a complex with $Fe(SCN)_n^{2-n}$, namely $[Fe(SCN)_nNO]^{2-n}$. It has been demonstrated that a ternary complex, $[FeSCNNO]^+$, is formed under the experimental conditions [23]. After potential-controlled electrolysis at -0.6 V, the resulting solution was tested qualitatively according to the proposed procedure [24]. A positive indication of the existence of hydroxyamine in the solution was observed.

On the basis of the above results and discussion, the catalytic reduction of nitrite in 0.1 M pH 4.0 acetate buffer solution containing iron and thiocyanate is typical electrochemical–chemical process and can be represented as follows:

$$Fe^{2+} + SCN^- + NO \rightarrow [FeSCNNO]^+_{ads} \qquad (1)$$

$$[FeSCNNO]^+_{ads} + e^- \rightarrow [FeSCNNO]_{ads} \qquad (2)$$

$$4[FeSCNNO]_{ads} + NO_2^- + 5H^+ \rightarrow 4[FeSCNNO]^-_{ads} + NH_2OH + H_2O \qquad (3)$$

Great sensitivity improvement is due to the co-existence of the adsorptive nature of the complex (Eq. (1)) and the electrochemical–chemical process of the catalytic reduction of nitrite (Eqs. (2) and (3)).
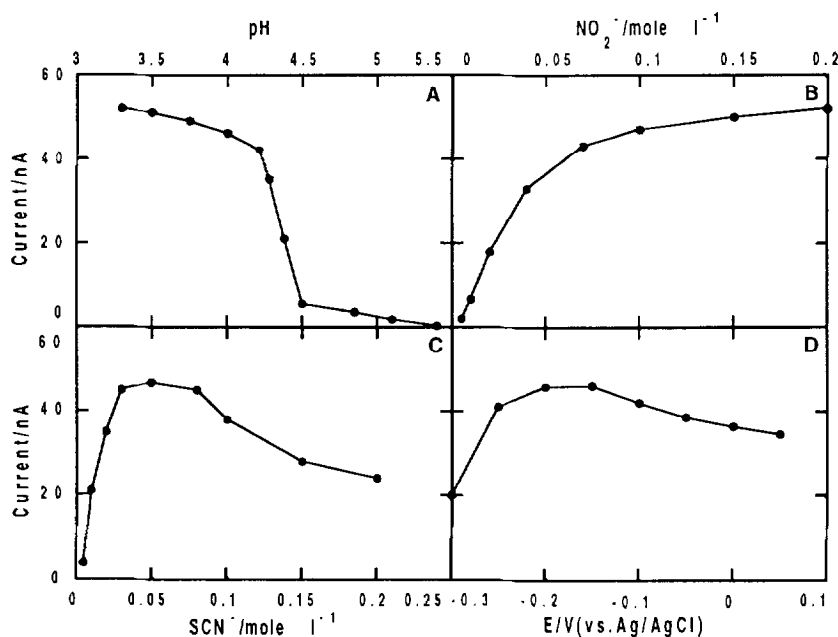
Fig. 4. Dependence of the peak current for 0.5 ppb iron on pH (A), $NaNO_2$ concentration (B), KSCN concentration (C) and accumulation potential (D). Conditions as in Fig. 2.

The dependence of the peak current on the pH of acetate buffer is shown in Fig. 4A: the stripping peak current is strongly dependent on the acidity of the solution. Decreasing the pH from 5.4 to 4.3 results in a sharp increase in peak current. Good sensitivity is attained in the pH range 4.0–4.3. Although the largest peak current is obtained at pH 3.5, this pH is not suitable for trace analysis of iron, due to interference from the co-existing catalytic reduction of nitrite by thiocyanate [20].

The concentration of nitrite has a profound effect on the catalytic–adsorptive stripping current. As can be seen in Fig. 4B, the stripping peak current for 0.5 ppb iron increases almost linearly with increasing nitrite concentration up to 0.05 M and then more slowly. Increases in response are obtained even at very low nitrite concentrations, namely less than 2.0 mM, but the optimal condition for good sensitivity was found to be in the range 0.1–0.2 M. Due to the reduction of nitrite at a potential of approximately −0.9 V [25], a broad reduction peak was observable at higher nitrite concentrations and was found to interfere with the determination of iron, especially at very low concentrations.

As expected, the stripping peak current exhibits a strong dependence on the concentration of thiocyanate (Fig. 4C). The peak current increases with increasing thiocyanate concentration up to 0.03 M and then starts to level off. In contrast, higher thiocyanate concentrations result in a considerable decrease in peak current, presumably because of competitive adsorption.

The dependence of the stripping peak current on the adsorption potential was examined over the range 0.05 to −0.3 V (Fig. 4D). The peak current increases as the adsorption potential becomes more negative up to −0.15 V, reaches a maximum between −0.15 and −0.2 V, and then decreases again until the potential of the onset of the reduction peak at −0.3 V is reached.

Optimal conditions for the determination of iron were therefore 0.1 M pH 4.0 acetate buffer as the supporting electrolyte, 0.1 M nitrite, 0.05 M thiocyanate and an accumulation period of 30 s at −0.15 V.

The dependence of the stripping peak current on the concentration of iron is shown in Fig. 5, which displays linear scan voltammograms for successive increases in the iron concentration in 1
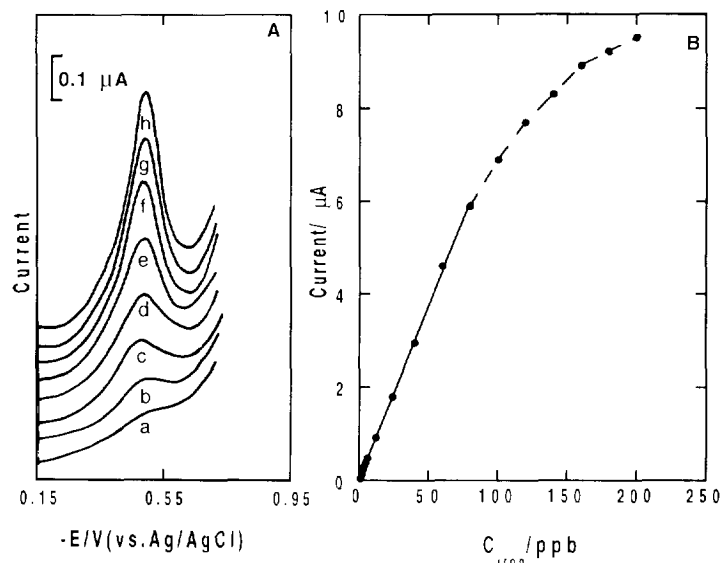
Fig. 5. Catalytic–adsorptive stripping voltammograms (A) for solutions of increasing iron concentration: (a) 0; (b) 1; (c) 2; (d) 3; (e) 4; (f) 5; (g) 6; (h) 7 ppb and (B) the resulting calibration plot in the range 0.0–200 ppb. Conditions as in Fig. 2.

ppb steps. Well-defined peaks are obtained despite the very short accumulation time (30 s). The peak current is directly proportional to the iron concentration up to 80 ppb. The resulting calibration plot is also shown in Fig. 5. The slope of the initial linear portion is 76 nA ppb^{-1}, with a correlation coefficient of 0.998. The precision was estimated from two series of 20 repetitive mea-

surements of 0.5 and 40 ppb iron solution with the 30 s accumulation period. The mean stripping peak currents were 46.8 nA and 2970 nA and relative standard deviations were 4.2% and 1.6% respectively. For the 30 s accumulation, the detection limit, estimated from three times the standard deviation of repetitive measurements of 0.25 ppb iron under optimal conditions (Fig. 6, solid line), was found to be 40 ppt, which is limited by iron impurities in the purified electrolyte solution (Fig. 6, broken line).

In the catalytic–adsorptive stripping voltam-metric measurement of iron, interferences may be
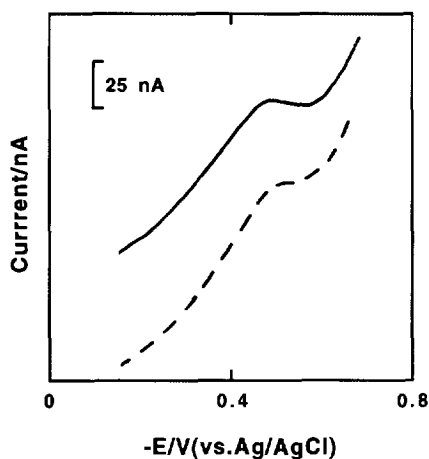
Fig. 6. Catalytic–adsorptive stripping voltammograms for 0 (broken line) and 0.25 ppb iron (solid line) in 0.1 M pH 4.0 acetate buffer containing 0.05 M KSCN and 0.1 M NaNO$_2$. Conditions as in Fig. 2.

Table 1
Results of sample analysis (average of six determinations)

Sample	Iron found (ppm)	Reference value (ppm)	Recovery (%) (+0.5 ppm)
Apple	0.772	0.781	95.3
Potato	3.25	3.35	98.2
Tap water	0.135	0.131	102
River water	0.173	0.167	97.5
KNO$_3$	0.852	≤1.00	99.1
NaOAc	4.82	≤5.00	103
Na$_2$SO$_4$	4.36	≤5.00	96.2

[a]Obtained by AAS analysis.

caused by the competitive adsorption of ions and their complexes on the electrode surface and competitive participation in the catalytic reaction. They may also be the result of the appearance of reduction peaks next to the stripping current peak. Due to the high sensitivity, it is expected that the influence of a large excess of another reducible species on the determination of iron will be minor, even with a similar peak potential to that of the stripping peak potential of iron. The effect of co-existing ionic species and surface-active substances on the determination of iron was investigated. More than 50 ions were examined for their possible interferences in the determination of 0.50 ppb iron. It was found that large amounts of alkali, alkaline earth metal, halide ions, NH_4^-, SiO_3^{2-}, $C_2O_4^{2-}$, BO_3^{3-}, SO_4^{2-}, ClO_3^-, NO_3^-, ClO_4^-, CO_3^{2-}, PO_4^{3-}, citrate and tartrate have no effect on the determination of iron. Amounts of less than 2000-fold (w/w) Al^{3+}, Sn^{2+}, Zn^{2+}, Mn^{2+}, Hg^{2+}, Ce^{3+} and WO_4^{2-}: 1000-fold Bi^{3-}, ZrO^{2+}, Tl^+, Ti^{3+}, VO^{2+}, MoO_4^{2-}, Ga^{3+}, Pd^{2-}, Cr^{3+}, CrO_4^{2-}, Ag^+ and Se^{4-}; and 200-fold Ni^{2+} have little effect on the determination of iron. However, Cd^{2-}, SbO^+, Cu^{2+}, In^{3+} and Pb^{2+} each have a reduction current peak in the vicinity of the stripping peak of iron which interfered at concentration of 0.50, 0.60, 0.13, 0.4 and 1.0 ppm of Cd^{2-}, SbO^- Cu^{2+}, In^{3+} and Pb^{2+} respectively. In thiocyanate medium containing nitrite, cobalt produces a catalytic–adsorptive current peak with a similar peak potential to that of iron [20], which severely interfered with the measurement of iron at concentrations higher than 5.0 ppb. Furthermore, owing to the adsorptive properties of the iron–thiocyanate–nitrite system, surface-active substances, such as natural organic surfactants, Triton X-100, Tween-80, sodium dodecylsulfate (SDS) and cetyltrimethylammonium bromide (CTAB) may interfere as a result of competitive adsorption at the electrode surface. For example, additions of 2.0 ppm CTAB, Triton X-100, Tween-80 and SDS resulted in 9, 13, 12 and 16% depressions of the stripping peak current respectively. Depending on the complexity of the sample, for direct determinations of iron, necessary sample pretreatments are strongly recommended.

The proposed method was successfully applied to determine iron in biological samples, natural waters and purified chemicals. The results are listed in Table 1. The results are in good agreement with the reference values for iron in the samples. The recoveries obtained by this method are also good enough for practical use.

In conclusion, the method developed in this paper provides a simple and fast procedure for the measurement of trace amounts of iron. The catalytic–adsorptive nature of the system results in a significant improvement in the detectability of iron, permitting convenient analysis of iron at sub-ppb levels. Good selectivity (which is better than that of adsorptive stripping voltammetric procedures) adds to the versatility of the proposed method.

References

[1] A. Bobrowski, Anal. Chem., 61 (1989) 2178.
[2] Z. Gao and K.S. Siow, Talanta, in press.
[3] J. Wang and J. Lu, Analyst, 117 (1992) 1913.
[4] Z. Gao and K.S. Siow, Electroanalysis, in press.
[5] J. Wang, J. Lu, and Z. Taha, Analyst, 117 (1992) 35.
[6] Z. Gao and K.S. Siow, Talanta, in press.
[7] K. Jiao, W. Jin and H. Metzner, Anal. Chim. Acta, 260 (1992) 35.
[8] K. Yokoi and C.M.G. van den Berg, Anal. Chim. Acta, 257 (1992) 293.
[9] C.M.G. van den Berg and G.S. Jacinto, Anal. Chim. Acta, 211 (1988) 129.
[10] B. Magyer, H.R. Elsener and S. Wunderli, Mikrochim. Acta, Part III, (1990) 179.
[11] J. Wang and J. Lu, Talanta, 39 (1992) 801.
[12] J. Wang, B. Tian and J. Lu, Talanta, 39 (1992) 1273.
[13] C.M.G. van den Berg and Z.Q. Huang, J. Electroanal. Chem., 177 (1984) 269.
[14] C.M.G. van den Berg, M. Nimmo, O. Abollino and E. Mentasti, Electroanalysis, 3 (1991) 477.
[15] J. Wang and S. Mannino, Analyst, 114 (1989) 643.
[16] Z. Zhao and W. Jin, J. Electroanal. Chem., 267 (1989) 271.
[17] J. Golimowski, Anal. Lett., 22 (1989) 481.
[18] J. Lu, J. Wang and C. Yarnitzhy, Electroanalysis, 7 (1995) 79.
[19] F. Lazaro, M.D. Luque De Castro and M. Valcarcel, Anal. Chim. Acta, 219 (1989) 231.
[20] Z. Gao and S.K. Siow, Anal Chim. Acta, in press.
[21] G.C. Barker and J.A. Bolzan, Fresenius' Z. Anal. Chem., 216 (1966) 215.
[22] D.T. Chow and R.J. Robinson, Anal. Chem., 25 (1953) 1493.
[23] Z. Zhao and X. Cai, J. Electroanal. Chem., 252 (1988) 361.
[24] F. Feigl and M. Steinhauser, Mikrochim. Acta, 35 (1950) 553.
[25] W.M. Graven, Anal. Chem., 31 (1959) 1197.

Simultaneous determination of lithium, sodium and potassium in blood serum by flame photometric flow-injection analysis

George Narh Doku, Victor P.Y. Gadzekpo*

Department of Chemistry, University of Cape Coast, Cape Coast, Ghana

Received 13 February 1995; revised 30 October 1995; accepted 30 October 1995

Abstract

A simultaneous flow-injection analysis (FIA) manifold that could analyse three ions from a single injection was designed, constructed, calibrated and used successfully to analyse Li^+, Na^+ and K^+. This FIA method was 10 times faster than the batch technique. The sample volume required was a fraction of about 1/110 to 1/75 that of the batch technique. The outputs were quite reproducible and calibration curves were linear. Results obtained for artificial sera compared favourably with the actual known concentrations of ions and results obtained in the analysis of eight natural human blood sera compared well with those obtained by the traditional batch technique.

Keywords: Flow-injection analysis; Blood serum; Lithium; Sodium; Potassium

1. Introduction

Blood electrolytes are cations and anions present in sera which perform various functions [1] for human health. Regular monitoring of these ions is important because deficiency or excess of these ions can cause serious health defects. The routine determination of these ions is by separate batch techniques [2–4] where fresh blood serum is taken to determine each ion, i.e. one sample for every ion analysis. This is time-consuming, wasteful in terms of blood serum and labour-intensive. In this paper, the description of the design, construction and use of a flow-injection analysis

(FIA) manifold [5–7], involving sample zone splitting [8,9], which could analyse three blood ions simultaneously from just one sample injection, is given. The process involves the splitting of the injected sample zone into three different coils of different coil lengths, the three sample portions reach the detector at different times and are used to determine the ions in turn by moving the filter on the detector from one ion to another.

2. Experimental

2.1. Apparatus and manifold construction

The manifold designed to serve the purpose of one sample–three ion analysis is shown in Fig. 1.

---

* Corresponding author.

An air compressor system was used to force distilled water (carrier stream) out of an enclosed container to flow through the tubings. The tubings were made of PVC and had an internal diameter (i.d.) of 1.0 mm. An injection valve, equipped with a simple syringe, was used to introduce the sample, reproducibly, into the carrier stream. A splitting system split the sample zone at point S into three separate coils C_1, C_2 and C_3. Due to the different coil lengths, the sample portions reach the detector at different times and are used to determine the different ions in turn.

The splitting system, constructed on a perspex plate, is shown in Fig. 2. S, E, 1, 2 and 3 are smooth holes of 0.25 cm depth and 2.00 mm i.d. drilled on a perspex plate of 0.5 cm thickness. These holes sit on smaller holes of 0.25 cm depth and 1.0 mm i.d on the underside of the plate. On the underside of the plate, S is connected to the adjacent holes 1, 2 and 3 by smooth route paths of 1.0 mm i.d. The underside of the plate is sealed completely with PVC tape without blocking the holes and route paths. PVC tubings of 0.7 cm length and 1.0 mm i.d. were fixed into the larger holes on the upperside of the plate with a glue prepared by dissolving perspex powder in a 50:50 mixture of $CHCl_3$ and THF. The holes 1, 2 and 3 on one side are connected to 1, 2 and 3 respectively on the other side by PVC tube coils C_1, C_2 and C_3 respectively. Point E is a point of confluence which all sample portions pass before reaching the detector. Thus it was possible to determine one ion from one sample portion and then to turn the filter to another ion to be determined from the next sample portion. The detector used was the single window PFP 7 flame photometer manufactured by Jenway Ltd., UK. The Endim 621-02 recorder, produced by the "Neptum" Schlothin Company in Germany, was used in conjunction with the detector.

2.2. Reagents

Li^+, Na^+, and K^+ standard stock solutions, used to prepare calibration curves, were provided by Jenway Ltd. The concentrations of the standard stock solutions used were Li^+, 1.0 mmol l^{-1}; Na^+, 140.0 mmol l^{-1}, and K^+, 5.00 mmol
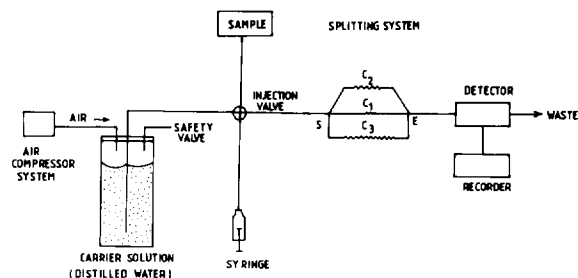

Fig. 1. Manifold design for one sample-three ion analysis.

l^{-1}. Doubly-distilled water was used as the blank/carrier solution. LiCl, NaCl, NaH_2PO_4, KCl and $MgSO_4 \cdot H_2O$ used for preparation of artificial blood sera were of reagent grade and were products of BDH (UK).

2.3. Calibration of analytical system (Optimum flow conditions)

The relative coil lengths C_1, C_2 and C_3 were optimised by successive injections of a 14.0 mmol l^{-1} Na^+ standard solution and adjustment of the lengths until the sample portions did not merge at the point of exit, E. The differences between the times when the sample portions reached the detector were sufficient to change the filter position from one ion to another and for a stable baseline to be obtained.

The respective dispersions D_1, D_2 and D_3 in the coils were determined by first aspirating directly a 14.0 mmol l^{-1} Na^+ standard solution and recording the detector output, then injecting this solution using doubly-distilled water as the carrier stream and recording the output from the coils,
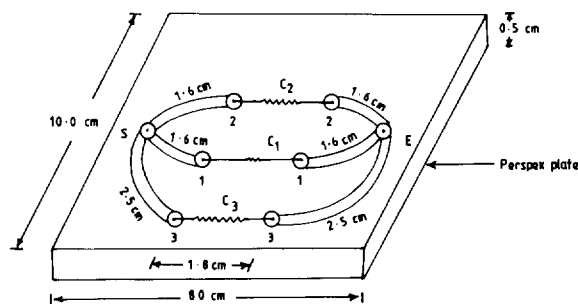

Fig. 2. Diagram showing construction of splitting system.

and then calculating the dispersion, D, from the formula

$$D = \frac{\text{output of direct pumping}}{\text{output of coil after injection}} \quad (1)$$

Each coil had its own residence time [7] which was measured with a stop-clock, as the time from injection to output maximum.

Optimum sample volume range was obtained by injecting various sample volumes of a 14.0 mmol l^{-1} Na^+ standard solution, recording the output, determining the corresponding dispersions in coils and the various differences between the times when the sample portions reached the detector, choosing the optimum sample volume range as that which gave good dispersions in coils for reliable output and optimum time separations for changing filter positions, zeroing the instrument, and having good resolution of peaks.

The optimum flow rate [7] was also determined after varying only the flow rate on subsequent injections of the 14.0 mmol l^{-1} Na^+ standard solution until a good output, time separations for changing filter positions, zeroing of the instrument and good resolution of peaks were obtained. To measure the sampling rate [7], the time from injection to detection of the third ion was noted and the sampling rate was calculated as the number of ions analysed per hour. Different concentration levels of the standard stock solution were then prepared and aspirated directly to obtain batch calibration plots [10,11] and these were then injected to obtain FIA calibrations plots for Li^+, Na^+ and K^+.

2.4. Preparation of standard solutions

The required volumes of the standard stock solution were taken and diluted to different levels to obtain concentration ranges of 0.01–1.0 mmol l^{-1} for Li^+; 14.0–140.0 mmol l^{-1} for Na^+; and 0.5–5.00 mmol l^{-1} for K^+ which were used for calibration curves for Li^+, Na^+ and K^+ respectively.

2.5. Pretreatment of natural blood serum samples

Eight blood serum samples were obtained from

the Cape Coast central hospital. The serum samples were diluted ten-fold by adding 1 ml of 1.0 mmol l^{-1} Li^+ and 8 ml of doubly-distilled water to 1 ml of blood serum sample. The lithium was added to enhance the sensitivity of the flame photometer for Li^+ since the concentration of lithium in natural blood serum is very low (0.001 mmol l^{-1}).

2.6. Preparation of artificial serum

An artificial blood serum was prepared by taking 4.24×10^{-2} g of LiCl, 8.0716 g of NaCl, 0.1304 g of NaH_2PO_4, 0.381 g of KCl, 0.2792 g of $CaCl_2$ and 0.1408 g of $MgSO_4 \cdot H_2O$, dissolving in doubly-distilled water and diluting the mixture to the 1 l mark [12]. This gave concentrations of Li^+, 1.000 mmol l^{-1}; K^+, 5.113 mmol l^{-1}; and Na^+, 146.3 mmol l^{-1}. Similar preparations of other solution mixtures was done to obtain four other solutions with concentrations as follows:

Li^+ (mM)	K^+ (mM)	Na^- (mM)
0.500	3.00	138.0
0.700	3.50	140.0
0.800	4.00	142.0
0.900	4.50	144.0

These five solutions were used for the analysis.

2.7. Analysis of blood serum samples

2.7.1. Batch process

The various standard solutions were first aspirated directly into the flame photometer and the results were used to obtain batch calibration plots for Li^+, K^+ and Na^-. The volume aspirated in each case was 3.0×10^3 μl, giving a total of 9.0×10^3 μl for the three ions. The eight different natural sera were aspirated directly and the concentrations of the ions were determined.

2.7.2. FIA process

100 μl portions of the standard solutions were injected into the carrier stream and the readings obtained were used to plot calibration curves for Li^+, K^- and Na^+. After sample injection, the sample splits into the coils C_1, C_2 and C_3. The

Table 1
Actual concentration of Li^+ vs. FIA results for artificial serum

Actual conc. (mmol l^{-1})	FIA conc. (mmol l^{-1})	% Deviation
0.500	0.503	0.60
0.700	0.701	0.14
0.800	0.795	0.63
0.900	0.902	0.22
1.000	1.005	0.50

Table 3
Actual concentration of K^+ vs. FIA results for artificial serum

Actual conc. (mmol l^{-1})	FIA conc. (mmol l^{-1})	% Deviation
3.000	3.02	0.67
3.500	3.50	0.11
4.000	4.00	0.03
4.500	4.49	0.22
5.113	5.25	2.7

output reading for Li^+ was taken from the sample portion in C_1. When all the sample in C_1 had passed through, the filter knob was turned from Li^+ to Na^+ within 10 s and the instrument zeroed again to obtain a stable baseline as the carrier stream passed. The sample portion in C_2 reached the detector 5 s later and a reading was taken for Na^+. When the sample in C_2 had passed through, the filter knob was turned from Na^+ to K^+ within 10 s and the instrument zeroed again. The sample portion in C_3 reached the detector 10 s later and a reading was taken for K^+.

The artificial sera [2] containing the different concentrations of Li^+, K^+ and Na^+ were injected, after ten-fold dilution, to determine the ions with the FIA system in order to compare the FIA results with the actual known concentrations in the artificial sera. Percentage deviation and correlation curves [12] were used to compare the two sets of values.

The eight different natural sera were then injected and the ions determined by the simultaneous FIA method.

Table 2
Actual concentration of Na^+ vs. FIA results for artificial serum

Actual conc. (mmol l^{-1})	FIA conc. (mmol l^{-1})	% Deviation
138.0	136	1.1
140.0	141	0.57
142.0	142	0.14
144.0	145	1.0
146.1	146	0.34

3. Results and discussion

The i.d. of the tubings used was 1.0 mm. Optimised coil lengths were found to be $C_1 = 6.0$ cm, $C_2 = 100$ cm, $C_3 = 210$ cm, and the differences between the times when sample portions reached the detector were C_1 to $C_2 = 15$ s and C_2 to $C_3 = 20$ s. The dispersions in the coils were $D_1 = 3.46$ (limited dispersion), $D_2 = 13.2$ (about medium dispersion) and $D_3 = 25.7$ (large dispersion). After considering the relative sensitivities of the flame photometer for the ions Li^+, Na^+ and K^-, the allocations of the coils to the ions were C_1 for Li^-, C_2 for Na^+ and C_3 for K^+ so as to enhance the sensitivity of the flame photometer for all three ions. The residence times (T) for coils C_1, C_2 and C_3 were $T_{C1} = 8.0$ s, $T_{C2} = 31$ s and $T_{C3} = 100$ s.

For FIA, the optimum sample volume range was 80.0–120 μl whilst the batch method required 9.0×10^3 μl (9.0 cm^3) for three ions. Thus, the FIA sample volume was about 1/110 to 1/75 times smaller than that required for the batch technique. The optimum flow rate obtained and used in the process was 5.0 ml min^{-1}. The FIA sampling rate was 108 samples per hour whilst that of the batch technique was 10.5 samples per hour. Thus, the FIA method was 10.3 times faster than the batch technique. Data obtained for each ion in various standard solutions were quite reproducible and calibration plots were considerably linear, showing that the FIA design was reliable. FIA results compared with actual known concentrations of ions in artificial blood sera are shown in Tables 1–3. The correlation plots of actual concentrations versus FIA concentrations were

Table 4
Batch and FIA results for natural sera

Blood serum	Li$^+$ conc. (mmol l^{-1})			K$^+$ conc. (mmol l^{-1})			Na$^+$ conc (mmol l^{-1})		
	Batch	FIA	% Deviation	Batch	FIA	% Deviation	Batch	FIA	% Deviation
1	0.001	0.0011	10	3.80	4.00	5.3	144	142	0.90
2	0.002	0.002	0.00	3.70	3.40	8.1	135	134	0.96
3	0.001	0.001	0.00	3.75	3.40	9.3	110	107	2.7
4	0.000	0.000	0.00	3.90	3.80	2.6	120	118	2.1
5	0.002	0.002	0.00	3.50	3.00	14.0	130	30	0.08
6	0.002	0.0019	5.0	3.30	3.00	9.1	121	20	0.91
7	0.003	0.0029	3.3	4.80	4.72	8.0	130	134	2.8
8	0.000	0.000	0.00	4.00	4.0	0.00	122	122	0.41

straight lines passing through the origin with slopes of 0.99, 1.40 and 0.98. These results show the reliability and acceptability of the simultaneous FIA design.

The batch and FIA results of eight natural sera and the percentage deviations are shown in Table 4. The Li$^+$ concentrations for the eight natural sera were obtained after the added lithium was subtracted from the total lithium concentration.

4. Conclusions

FIA results for the artificial blood sera were quite similar to the actual known concentrations of ions. Also, FIA results for the natural blood sera were quite similar to those obtained with the batch technique.

The FIA method was 10 times faster than the batch method and required a sample volume that was 1/110 to 1/75 times smaller that that for the batch technique. Hence the FIA method saved time and sample.

References

[1] M.B.V. Roberts, Biology, A Functional Approach, 2nd edn., English Language Books Society and Nelson, Kenya, 1976, p. 219.

[2] P.C. Hanser, S.S. Tan, J.J. Cardwell, R.W. Catrall and P.C. Hamilton, Analyst, 113 (1988) 1551.

[3] P.M. Hald, Sodium and potassium by flame photometry, in D. Seligson (Ed.), Standard Methods of Clincial Chemistry, Vol. 2, Academic Press, New York, 1958, pp. 165–185.

[4] H.H. Bauer, G.D. Christian and J.E. O'Rielly, Instrumental Analysis, Allyn and Bacon, Boston, MA, 1978.

[5] E.H. Hansen, J. Ruzicka and A.K. Ghose, Anal. Chim. Acta, 108 (1979) 241.

[6] J. Ruzicka, E.H. Hansen and E.A. Zagatto, Anal. Chim. Acta, 88 (1977) 1.

[7] J. Ruzicka and E.H. Hansen, Flow injection analysis, John Wiley, New York, 1981.

[8] M.K. Schwart, Anal. Chem., 45 (1973) 741A.

[9] J. Ruzicka, J.W.B. Stewart and E.A. Zagatto, Anal. Chim. Acta, 81 (1975) 389.

[10] H.H. Willard, L.L. Merrit and J.A. Dean, Instrumental Methods of Analysis, 5th edn., Van Nostrand, New York, 1974, p. 83.

[11] M.T. Kumah, Flame photometric determination of Na, K, and Ca in blood serum employing FIA, Undergraduate Project Report, University of Cape Coast, 1988, p. 8.

[12] G.D. Christian, Analytical Chemistry, 5th edn., John Wiley, New York, 1994.

Colour reaction of free chlorine with p-amino-N,N-diethylaniline in the presence of alcohol and its analytical application

Minghao Zhang[a],*, Quanru Zhang[a], Zheng Fang[b]

[a]Department of Chemical Engineering, Changsha Industrial College, Changsha 410012, People's Republic of China
[b]Department of Chemistry, Central South University of Technology, Changsha 410083, People's Republic of China

Abstract

A simple, precise, rapid-colour-forming and stable spectrometric method has been developed for determining free chlorine in water. p-Amino-N,N-diethylaniline reacts with free chlorine almost instantaneously in the presence of alcohol to form a red oxidized product with absorption maximum at 513 nm. Beer's law is obeyed in the free chlorine concentration range of 0–2 μg ml^{-1}. The molar absorptivity is 1.79×10^4 l mol^{-1} cm^{-1}, limit of detection 0.0036 μg ml^{-1}, relative standard deviation 1.51%, and amount of free chlorine 7 μg. The colour reaction rate and absorbance are independent of temperature in the range 3–45°C and the stable absorptivity lasts for at least 1 h. The method is satisfactory for the determination of free chlorine in aqueous solution.

Keywords: Chlorine determination; p-Amino-N,N-diethylaniline; Colour reaction

1. Introduction

The methods of determining free chlorine were critically reviewed by Nicolson [1] early in 1965. Although a lot of methods, such as ion-selective electrode [2], pneumatic current [3], chromatography [4] and some new amperometry [5–7] and spectrophotometry [8–13] methods have been established, the most frequently used method is still N,N'-diethyl-p-phenylenediamine (DPD) spectrophotometry [14]. However, this method re-

quires modification as the colour fades with time, the absorbance is affected by temperature and some oxidizing agents interfere greatly with measurement [1]. In the present paper, a new method is reported for determining free chlorine based on its colour reaction with p-amino-N,N-diethylaniline sulfate (TSS) [15] in the presence of ethyl alcohol. Its principal advantages are the rapid colouring at room temperature, stable absorbance, the non-temperature dependence of the reaction rate and absorbance, wide linear range, simple and convenient procedure, and relatively high sensitivity and reproducibility.

---

* Corresponding author. Fax: (86) 731-8882461.

2. Experimental

2.1. Apparatus

A spectrophotometer (Model 72G, Shanghai Analytical Instrument Factory) with a stoppered comparison cell of 1 cm optical path and a pH meter (Model 25, Shanghai Kanchuan Metals Factory) were used.

2.2. Reagents

The following reagents were used.
Alcohol (anhydrous).
EDTA solution (pH 4.5) 0.3 mol l^{-1}.

TSS alcohol solution. A mixture of 1.3 g TSS and 2.0 ml of 1:9 H_2SO_4 was dissolved in alcohol and diluted to 100 ml. The solution was stable for up to 9 months in a light-proof bottle in a refrigerator.

HAc-NaAc buffer solution of pH 4.7 (25°C). 20 g anhydrous sodium acetate was dissolved in a small amount of water, pH was adjusted to 4.7 with glacial acetic acid and the solution was diluted to 1000 ml with alcohol.

Chlorine solution. 8 g manganese dioxide and 8 g potassium permanganate were ground together in a mortar. 60 ml of 36% hydrochloric acid was slowly added to the mixture in a conical flask. The chlorine liberated was passed into 400 ml of 1 mol l^{-1} sodium hydroxide solution, whose pH had to be kept above 10 to prevent the formation of chlorate. The hypochlorite solution, whose concentration was determined by iodimetric titration to be in the range 0.19-0.25 mol l^{-1}, was placed in a light-proof bottle in a refrigerator. The stock standard solution should maintain its titre for 6 months in an amber-coloured polypropylene bottle. The 1.70 mg l^{-1} solution was obtained by subsequent dilution. Redistilled water was used. Other reagents were of analytical grade.

2.3. Procedure

Add 2.0 ml of the buffer solution, 1.0 ml of TSS solution and 3-4 drops (≈ 0.18 ml) of the EDTA solution to 12.5 ml comparison tubes. Shake the mixture, and then take a known volume of aqueous solution containing about 12 μg of free

chlorine in the tubes. After shaking the mixture, add 2.5 ml of the alcohol immediately and shake vigorously. Then dilute the solution to the mark with water and shake again. Measure the absorbance at 513 nm against the reagent blank prepared in the same manner.

3. Results and discussion

3.1. Absorption spectra

As shown in Fig. 1, under the experimental conditions the colour product exhibited maximum absorption at 513 nm. Pure TSS showed no peak in the wavelength range 400-600 nm.

3.1.1. Effect of acidity

The experimental results showed that pH 3.5-4.9 is suitable for colouring acidity (that is, the acidity having influence on the colour reaction) (see Fig. 2). As is well known, free chlorine in water exists primarily as Cl_2, HClO or ClO$^-$, depending on pH. Their distribution calculated
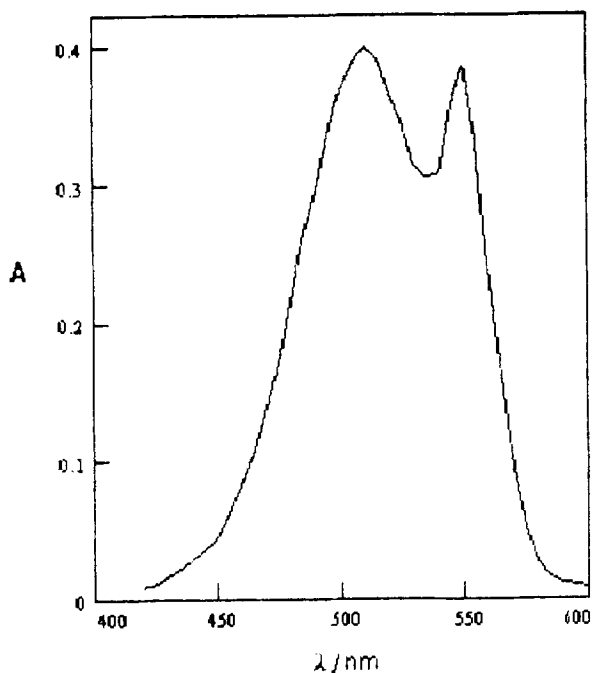

Fig. 1. Absorption spectrum of the colour reaction products (against reagent blank as reference).
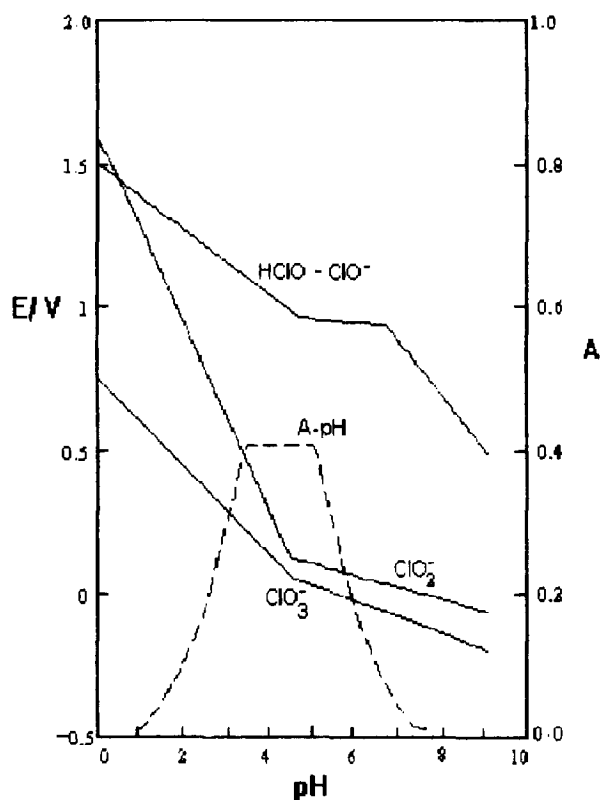
Fig. 2. The absorbance and redox potentials of chlorine species as functions of pH. The potentials (SHE) were obtained by cyclic voltammetry at a Pt electrode [11].

from equilibrium constants [16] as a function of pH illustrates that free chlorine exists primarily in the form of HClO in the pH range 3.5–4.9. From Fig. 2 it can be seen that pH should be controlled in the range 4.5–4.9 in order to maintain the relative high potential relating to HClO, which influences the colour sensitivity, and to prevent interference from such non-free chlorine species as ClO_2^- and ClO_3^-. Hence, pH 4.7 was selected in the experiment.

3.1.2. Effect of reagent amounts

3.1.2.1. TSS Solution. The maximum, stable absorbance was attained as 0.5–2.0 ml TSS solution was added under the selected conditions. Therefore, 1.0 ml was selected.

3.1.2.2. HAc–NaAc buffer solution. The experiment showed that 1.0–8.0 ml buffer solution was suitable and 2.0 ml was recommended.

3.1.2.3. Alcohol. The colouring rate in the non-alcohol medium was slightly slower than in the alcohol medium and the absorbance was not stable. The colour compound is the more stable, the greater the alcohol content. The absorbance was stable for at least 1 h and increased by 10% in a
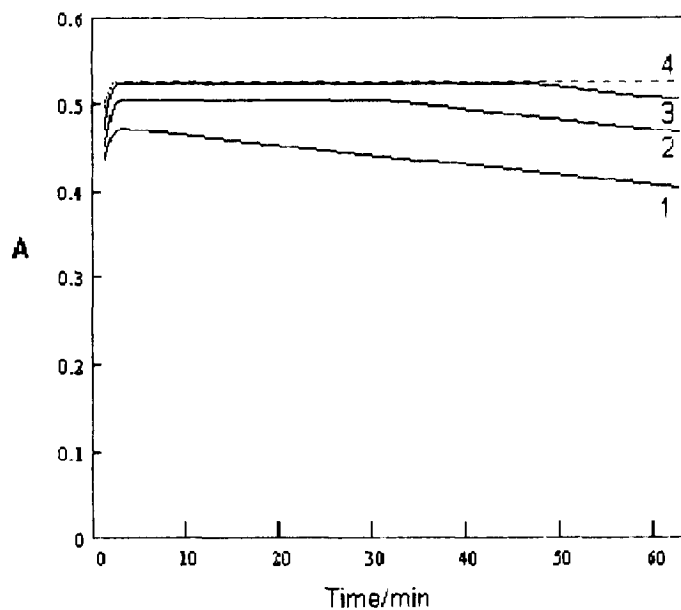

Fig. 3. Curves showing the dependence of the stability of the coloured product on alcohol content (volume ratio: (1) 0%; (2) 15%; (3) 30%; (4) ≥ 45%).

Table 1
The tolerance limits in the determination of 10 μg free chlorine with TSS in the presence of alcohol

Ion added	Amount tolerated (μg)
As(V), Pb(IV)	1600
Ni(II)	1200
Zn(II), Hg(II)	1000
Al(III), Mo(VI), W(VI)	800
Pb(II)	600
Fe(III), Cu(II), Sn(IV), Co(II)	400
ClO_3^-	75
NO_2^-	70
V(V)	40
ClO_2^-	38
Mn(VII)	2
Cr(VI)	0.4

solution of $\geq$ 45% alcohol (volume ratio). The results are shown in Fig. 3. Therefore a volume ratio of 45% was chosen.

3.1.2.4. EDTA. Some metal ions such as Fe^{3+} and Al^{3+}, which can oxidize TSS or produce hydroxide precipitation, will form complexes with EDTA. Maintaining 0.16% EDTA in the medium

was recommended. The absorbance will decrease as the concentration of EDTA increases.

3.2. Temperature

The experiment showed that the colouring rate and absorbance were virtually unaffected by temperature in the 3–45°C range.

3.3. Analytical characteristics

A calibration graph, shown in Fig. 4, was plotted. Beer's law is obeyed over the concentration range 0–2 μg free chlorine in 1 ml of the final solution. The molar absorptivity is 1.79×10^4 l mol^{-1} cm^{-1} and the limit of detection 0.0036 μg ml^{-1}.

3.4. Interferences

The influences of 39 diverse ions were examined. The ions were added individually to the tested solution. Ions such as Cl^-, Br^-, I^-, NO_3^-, SO_4^{2-}, Ac^-, $C_2O_4^{2-}$, HPO_4^{2-}, $H_2PO_4^-$, AsO_3^{3-}, H_2Y^{2-}, K^+, Na^+, NH_4^+, Ca^{2+}, Mg^{2+}, Ba^{2+},
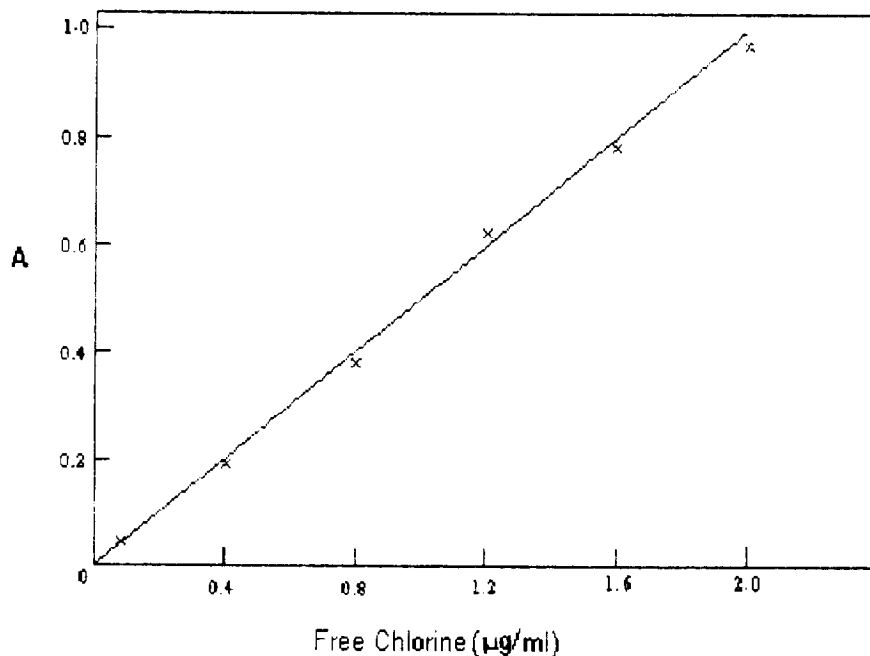

Fig. 4. Calibration graph.

Table 2
Free chlorine in tapwater (μg ml^{-1})

Sample	Parallel measurements with (A)						Av. of (A)	RSD (%)	Av. of (B)[a]
1	0.93	0.95	0.93	0.92	0.96	0.95	0.94	1.65	0.93
2	0.83	0.84	0.84	0.83	0.85	0.85	0.84	2.26	0.84
3	0.99	0.96	1.00	0.99	0.98	0.97	0.98	1.51	0.97

[a] A reference method: O - toluidine method [17].

Bi^{3+}, Mn^{2+} and Fe^{2+} did not influence the determination of free chlorine. The tolerance limits (error $\leqslant$ 5%) of other ions are listed in Table 1. The interference of Cr(VI) and Mn(VII) was serious. However, it might be eliminated by the use of a hydrophobic, gas-ventilating membrane such as a microporous poly(tetrafluoroethylene) separator through which the free chlorine can pass into the solution of TSS, which will, as a colour reagent, react with it after the tested solution is acidified with hydrochloric acid because the free chlorine exists as Cl_2 in the medium.

3.5. Applications

The method (A) has been applied to tapwater samples. The results are shown in Table 2.

4. Conclusion

The colour reaction of free chlorine with TSS in the presence of ethyl alcohol provides a simple and rapid spectrophotometric approach for determining free chlorine. The method has a wide linear range, good reproducibility and excellent colour stability. The molar absorptivity is 1.79×10^4 1 mol^{-1} cm^{-1}, limit of detection 0.0036 μg ml^{-1}, relative standard deviation 1.51%, and amount of free chlorine 7 μg. The colouring is almost instantaneous and both its rate and absorbance are independent of temperature in the range 3–45°C.

References

[1] N.J. Nicolson, Analyst, 90 (1965) 187.

[2] N.A. Dimmock and D. Midgley, Talanta, 29 (1982) 57.

[3] Du. Tongguang, Fenxi Huaxue, 16 (1988) 467.

[4] J.M. Cheplen, C. Banow and E.L. White, Anal. Chem., 56 (1983) 209.

[5] N.A. Dimmock and D. Midgeley, Water Res., 13 (1979) 1101.

[6] N.A. Dimmock and D. Midgeley, Water Res., 13 (1979) 1317.

[7] E.M. Aieta, P.V. Roberts and M. Hernandez, J. Am. Water Works Assoc., 76 (1984) 64.

[8] L. Balt, E.J. Stamhuls and G.E.H. Joosten, Anal. Chem., 53 (1981) 1799.

[9] J.C. Patton and S.R. Crouch, Anal. Chem., 49 (1977) 466.

[10] R. Bauer and C. Rupe, Anal. Chem., 43 (1971) 421.

[11] K.R. O'Halloran, Ph.D. Thesis, University of Queensland, 1990.

[12] B. Chiswell and K.R. O'Halloran, Analyst, 116 (1991) 657.

[13] B. Chiswell and K.R. O'Halloran Anal. Chim. Acta, 249 (1991) 519.

[14] C. Barry and K.L. Beatrice, Analyst, 118 (1993) 1457.

[15] Liang Shiyi and Chen Bencheng, Higher Organic Chemistry, Higher Education Press, Beijing, 1993, p. 233.

[16] G.R. Nelson, in R.L. Jolley (Ed.), Water Chlorination, Ann Arbor Science, Ann Arbor, MI, 1978, pp. 345–378.

[17] Institution of Water Engineers, Approved Methods for the Physical and Chemical Examination of Water, 3rd edn., The Institution of Water Engineers, London, 1960, p. 37.

Synthesis of 5-(5-nitro-2-pyridylazo)-2,4-diaminotoluene and its application to spectrophotometric determination of microamounts of palladium

Heqing Yang*, Guang Zhang, Linlin Zhang, Genqi Liu, Xinhuai Zhang

Experimental Centre, Shaanxi Normal University, Xi'an 710062, People's Republic of China

Abstract

A new pyridylazo reagent, 5-(5-nitro-2-pyridylazo)-2,4-diaminotoluene (5-NO_2-PADAT) has been synthesized, and found to be a good chromogenic reagent for palladium. In sulfuric acid, hydrochloric acid and perchloric acid palladium reacts with 5-NO_2-PADAT to form a 1:1 chelate, exhibiting an absorption maximum at 592 nm. The apparent molar absorptivity is 1.25×10^5 1^{-1} mol^{-1} cm^{-1}. Beer's law was obeyed in the range 0–0.9 μg ml^{-1} Pd. Relatively large amounts of co-existing elements, including all other noble metals, can be tolerated. The method is simple and rapid, with high sensitivity and good selectivity and was applied to the determination of palladium in some industrial samples with satisfactory results.

Keywords: 5-Nitro-PADAT; Palladium; Spectrophotometry

1. Introduction

A heterocyclic azo reagent is a good chromogenic reagent for spectrophotometric determination of palladium [1–6]. Its good selectivity is well known, but its sensitivity is not so good. Therefore, one would expect to obtain a new chromogenic reagent for palladium with high sensitivity and good selectivity by introduing a nitro group in the heterocyclic ring. In this paper, the preparation of 5-(5-nitro-2-pyridylazo)-2,4-di-aminotoluene (5-NO_2-PADAT), and the chromogenic reaction of this reagent with palladium in aqueous solution are reported. Its structure is
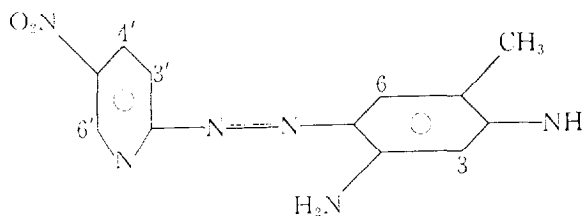
* Corresponding author.

Table 1
Sensitivities of some typical reagents for palladium

Reagent	Acidity and Medium	λ_{max} (nm)	$10^{-4}\varepsilon$ (l mol^{-1} cm^{-1})	Ref.
5-Cl-PADAB	0.01–2.4 M HCl	572	6.5	[1]
5-Cl-PADAT	0.001–0.3 M HCl	580	6.9	[2]
2.4-TADAT	0.5–3.5 M HClO$_4$	590	5.7	[3]
DMTAA	0.9–3.5 M HClO$_4$	648	6.7	[4]
BTASTP	0.64–3.2 M HNO$_3$	690	6.3	[5]
BTASCP	0.32–3.2 M HNO$_3$	688	5.85	[5]
BTASTA	0.96–2.56 M HNO$_3$	695	6.08	[5]
BTADMTA	0.32–3.2 M H$_2$SO$_4$	718	6.65	[6]
TEADAT[a]	pH1.42 (0.25 M NaCl)	536	5.2	[7]
BTAMB	pH2.0–6.0	695	4.96	[8]
Phen, Cadion A, Peregal O	pH8.2–10.5 (Na$_2$B$_4$O$_7$–HCl)	490	8.01	[9]
5-NO$_2$-PADAT	0.18–4.6 M H$_2$SO$_4$	592	12.5	Present method

[a] TEADAT: 3-(5'-tetrazolylazo)-2, 6-diaminotoluene.

5-NO$_2$-PADAT reacted with palladium (II) in relatively strong acidic medium at room temperature to form a 1:1 chelate. The absorption maximum is at 592 nm and the molar absorptivity is 1.25×10^5 l mol^{-1} cm^{-1}. Compared with other typical reagents for the determination of palladium shown in Table 1, 5-NO$_2$-PADAT is the most sensitive. Relatively large amounts of other metal ions, including noble metal ions, do not react.

A simple, rapid spectrophotometric method for determination of palladium with high sensitivity and good selectivity is proposed, and was used to determine palladium in industrial samples with satisfactory results.

2. Experimental

2.1. Reagents

The following reagents were used.

Pd standard solution. 0.1000 g of pure palladium (99.99%) was dissolved in 50 ml of aqua regia. 1 ml of 20% sodium chloride was added, and the solution was heated until it was nearly dry. 2 ml of hydrochloric acid was added and the mixture was evaporated almost to dryness, repeating three times. The residues were dissolved in 1 M hydrochloric acid, transferred to a 100 ml volumetric flask and diluted to volume with 1 M hydrochloric acid. The concentration of this solution was 1.000

mg ml^{-1}, and it was diluted with water to contain 10.0 μg ml^{-1} Pd as required.

5-NO$_2$-PADAT solution, 1.0×10^{-3} M in ethyl alcohol.

Sulphuric acid (1:1).

0.25 M sodium acetate–0.25 M acetic acid buffer solution was used for pH adjustment.

All chemicals used were of analytical-reagent grade, and all solutions were prepared with redistilled water.

2.2. Apparatus

Absorbances and absorption spectra were recorded with a Model 722 (Shanghai Analytical Instrument Factory) and a Hitachi Model U-2000 spectrophotometer with 1 cm cells respectively. The pH measurements were made with a Model pHS-3E pH meter (Jiangsu Electroanalytical Instrument Factory). Elemental analyses were done with a PE Model PE-2400 analyzer. A Mattson Model PK-6000 infrared spectrophotometer and a Bruker Model AC-80 NMR spectrometer were used for recording IR and NMR spectra.

2.3. Synthesis of 5-NO$_2$-PADAT

Preparations of 5-nitro-2-amino-pyridine and its diazotate were described in Refs. [10,11].

Preparation of 5-NO$_2$-PADAT. Dissolve 5.7 g (0.03 mol) of diazotate of 5-NO$_2$-2-amino-pyridine

in 81 ml of aqueous ethanol solution (1:1), and cool the solution to 0°C. Dissolve 3.8 g of 2,4-diamino-toluene in 30 ml of ethanol, and add 7.8 ml of hydrochloric acid solution (1:3). Add this solution dropwise to the diazotized solution with vigorous stirring. Stir for 2–3 h, continue stirring for 2 h at room temperature, and then let the mixture stand overnight. Filter off the precipitate, wash with ethanol and recrystallize from ethanol. Purple lustrous flakes were obtained (m.p. 238.3°C), and the yield was about 40%. The structure has been verified by elemental analysis, IR and ^{1}H NMR. Elemental analysis: $C_{12}H_{12}O_2N_6$ requires 52.93% C, 4.44% H, 30.87% N; found 53.06% C, 4.37% H, 29.80% N. IR(KBr): νas(NH$_2$) 3503 cm^{-1}, νs(NH$_2$) 3400 cm^{-1}, νas(CH$_3$) 2918 cm^{-1}, νs(CH$_3$) 2860 cm^{-1}, νas(NO$_2$) δNH νC–C νN=N 1640, 1588, 1498, 1408 cm^{-1}, νs(NO$_2$) 1334 cm^{-1}, δC–N 1292 cm^{-1}. ^{1}H NMR (solvent: DMSO): δCH$_3$ 2.05 ppm, δNH$_2$ 3.53 ppm, δH$_3$ 5.92 ppm, δH$_6$ 7.30 ppm, δH$_3$, 7.73, 7.85 ppm, δH$_4$, 8.39, 8.42, 8.50, 8.53 ppm, δH$_6$, 9.20, 9.23 ppm.

was soluble in various organic solvents, e.g. ethanol dioxane, tributylphosphate, DMSO and DMF. The dissociation equilibrium of the reagent was studied by a spectrophotometric method as described in Ref. [12]. Four species of this reagent (H_3L^{3+}, H_2L^{2+}, HL^+ and L) were involved in the acid-dissociation behaviour. These four forms are related by the following equilibrium.

The absorbance curves of these four forms as a function of [H$^+$] (H$_0$ or pH) are plotted in Fig. 1.

The dissociation constants were determined by finding the centers of these curves for selected wavelengths. The mean values were pK_{a_1} = -5.35 ± 0.05, $pK_{a_2} = 0.05 \pm 0.05$, $pK_{a_3} = 6.10 \pm 0.05$. The pK_{a_1} value is assigned to the deprotonation of the nitrogen atom of the pyridyl ring; pK_{a_2} and pK_{a_3} correspond to the deprotonation of the 4 and 2-amine groups respectively.

3.2. Absorption spectra

The absorption spectra of 5-NO$_2$-PADAT and its palladium chelate were recorded and are

	$H_3L^{3+} \overset{pK_{a_1}}{\underset{H^+}{\rightleftharpoons}}$	$H_2L^{2+} \overset{pK_{a_2}}{\underset{H^+}{\rightleftharpoons}}$	$HL^+ \overset{pK_{a_3}}{\underset{H^+}{\rightleftharpoons}}$	L
λ_{max} (nm)	445	420	438	534
isosbestic point (nm)	(429)	(423)	(467)	
ε (l mol^{-1} cm^{-1})	5.36×10^4	5.48×10^4	5.54×10^4	3.41×10^4

2.4. General procedure

Transfer an aliquot of solution containing up to 9 μg of Pd (II) to a 10 ml volumetric flask. Add 1 ml of H$_2$SO$_4$ (1:1) solution and 0.5 ml of 1.0×10^{-3} M 5-NO$_2$-PADAT solution. Dilute to volume with water and mix well. After 10 min record the absorbance at 592 nm in a 1 cm cell against a reagent blank.

3. Results and discussion

3.1. Properties of the reagent

The reagent was sparingly soluble in water, but

shown in Fig 2. The absorption maximum of the reagent lies at 421 nm and the chelate has two absorption peaks, at 552 and 592 nm. The latter was chosen for measurements as its sensitivity is higher, and the absorbance of the reagent itself is smaller at 592 nm.

3.3. Effect of acid medium and its concentration

The colour reaction could be performed in sulphuric acid, hydrochloric acid or perchloric acid medium. The absorbance was at an equal maximum in 0.18–4.6 M H$_2$SO$_4$, 0.06–1.5 M HCl and 0.06–3.6 M HClO$_4$. Subsequent determinations were therefore carried out in 0.9 M sulphuric acid.
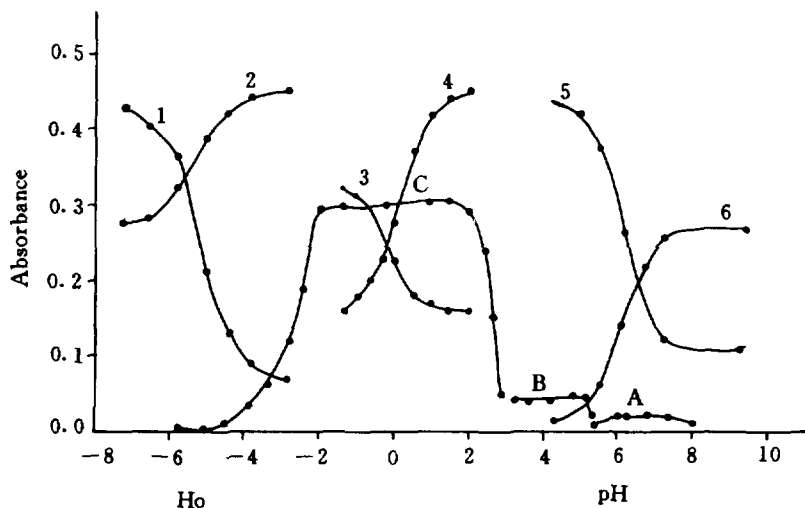
Fig. 1. Absorbance vs. pH curves for 5-NO₂-PADAT and its palladium complexes, 1 cm cell, 8.0×10^{-6} M reagent, at (1) 445 nm, (2) 420 nm, (3) 400 nm, (4) 438 nm, (5) 438 nm, (6) 534 nm. Complex [Pd (II)] = 3.48×10^{-6} M with a large excess of reagent, at (A) 664 nm, (B) 507 nm, (C) 592 nm.

3.4. Effect of the reagent concentration

The absorbances of a series of solutions containing 4.0 μg of palladium and various amounts of 1.0×10^{-3} M 5-NO₂-PADAT solution were measured. It was found that 0.1 ml of 1.0×10^{-3} M 5-NO₂-PADAT solution sufficed

to complex 4.0 μg of Pd; with higher reagent concentrations the absorbance was essentially constant. Therefore 0.5 ml of the reagent solution was used. The time for the absorbance to reach a stable value was only 5 min at room temperature and the absorbance was stable for at least 72 h.
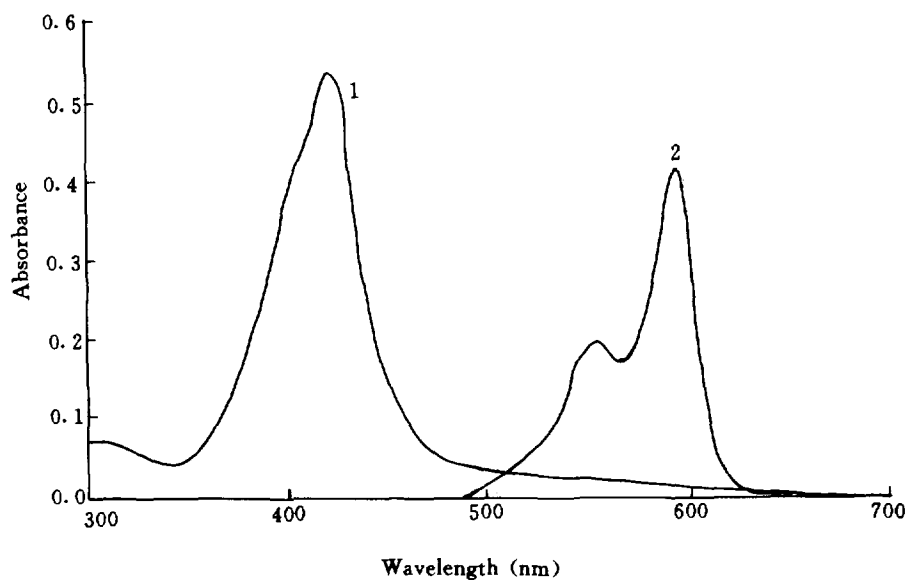

Fig. 2. Absorption spectra of 5-NO₂-PADAT and its palladium chelate, 1 cm cell: (1) 5-NO₂-PADAT (1.0×10^{-5} M) vs. H₂O; (2) Pd(II) chelate (3.48×10^{-6} M) vs. reagent blank.

Table 2
Tolerance limits for the determination of palladium[a]

Ion added	Amount tolerated (mg)
NaCl	300
KNO$_3$, KBr, Li$_2$SO$_4$	100
Sn(IV), Cd(II), Zn(II)	20
Fe(III)	16
Al(III)	14
Mg(II), Ca(II)	10
Sb(V)	8
Cu(II)	7
Ni(II)	6
Mn(II)	3
Co(II), Bi(III), As(III)	2
Hg(II)	1
Cr(III)	0.3
V(V)	0.2
Ti(III), Ge(IV), Au(III), Rh(III), Ir(III), Ru(III), Pt(IV), Os(III)	0.1
Ag(I)	0.08
Pb(II)	0.06
Mo(VI)	0.04

[a] The solution contained 4.0 μg of Pd(II).

3.5. Composition of the chelate

The composition of the chelate was determined by the continuous variation and molar ratio methods. Both indicated that a 1:1 palladium reagent chelate was formed.

3.6. Calibration graph

The calibration graph obtained by the general procedure showed good linearity over the range 0–0.9 μg ml^{-1} palladium. The linear regression equation was $A = 1.158x + 0.011$ (x: μg ml^{-1}),

and the correlation coefficient was 0.9998. The apparent molar absorptivity was 1.25×10^5 l mol^{-1} cm^{-1}, and the Sandell sensitivity was 8.51×10^{-4} μg cm^{-2}.

3.7. Effect of diverse ions

Numerous cations and anions were examined by applying the method to a fixed amount of palladium in the presence of increasing amounts of the ion being studied. The tolerance limit was taken as the amount that caused an error of $\pm 5\%$ in the absorbance. For the determination of 4.0 μg of palladium by this method, the foreign ions can be tolerated at the levels given in Table 2. It was shown that cations and anions examined, including all other noble metal ions, do not interfere in the determination of palladium.

3.8. The probable mechanism of the reaction

Reactions of palladium with 5-NO$_2$-PADAT at different acidities were investigated by the spectrophotometric method, and the results are shown in Fig. 1. At pH 6–8 the major species of the reagent is L, it reacts with Pd(II) to form chelate A ($\lambda_{max} = 664$ nm); at pH 3.2–5.2 the major species of the reagent is HL$^+$, it reacts with Pd(II) to form chelate B ($\lambda_{max} = 507$ nm); at H$_0 = -2$–0 the major species of the reagent is H$_2$L^{2+}, it forms chelate C ($\lambda_{max} = 592$ nm) with Pd(II). At pH 0–2 the majority species of the reagent is HL$^+$, it reacts with Pd(II) to form chelate B, which could easily change into chelate C by protonation of the β-nitrogen of the azo groups.

Table 3
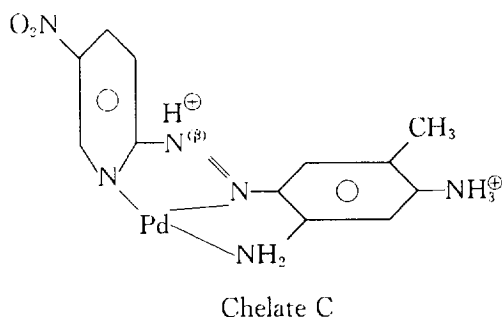Results for the determination of palladium in the industrial sample

Sample	2,4-TADAT method		Proposed method	
	$\bar{X}$ (%)[a]	RSD (%)	$\bar{X}$ (%)[a]	RSD (%)
Molecular sieve[b]	0.204	0.7	0.206	0.4
Ni-alloy[c]	0.0925	1.0	0.0889	0.9

[a] Mean of nine determinations.
[b] Na$_2$O·Al$_2$O$_3$·2SiO$_2$ containing a trace of Pd.
[c] Major composition (%): Ni, 85; Cu, 10; Fe, 3; Co, 1.

Therefore, in the range $H_0 = -2$–pH 2, 5-NO$_2$-PADAT reacts with Pd(II) to form chelate C despite the two different major species of the reagent, this was used in the analysis. The structures of chelates A–C are
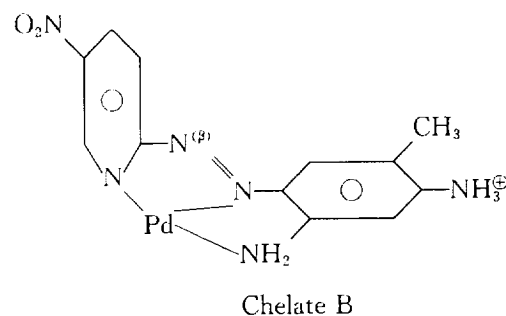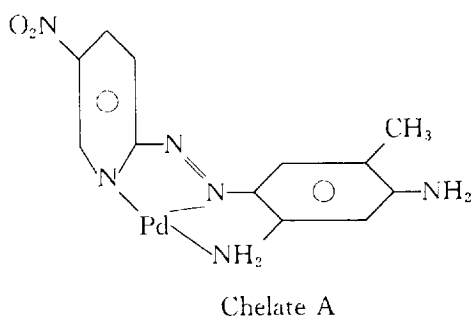
general procedure. The results obtained are consistent with those obtained by the 2,4-TADAT spectrophotometric method [3] (Table 3).

Chelate A

Chelate B

Chelate C

3.9. Applications

The proposed method has been applied to the determination of palladium in nickel alloys and molecular sieves. The procedure was as follows. Dissolve an accurately weighed sample in 20 ml of aqua regia and evaporate the solution to 10 ml. Add 0.5 ml of 20% sodium chloride, and evaporate the mixture until nearly dry. Add 2 ml of hydrochloric acid and heat the solution almost to dryness, repeating 2–3 times. Dissolve the residues in 1 M hydrochloric acid, and filter. Transfer the filtrate to a 100 ml volumetric flask, dilute to volume with 1 M hydrochloric acid and mix well. Take an appropriate aliquot of the sample solution and determine palladium by the

References

[1] S. Shibata, Y. Ishiguro and R. Nakashima, Anal. Chim. Acta, 64 (1973) 305.

[2] G. Zhang, C. Li, B. Liu and Y. Jin, Huaxue Xuebao, 43 (1985) 888.

[3] G. Zhang, Y. Hu and G. Xu, Fenxi Huaxue, 15 (1987) 986; Chem. Abstr., 108 (1988) 231068t.

[4] G. Zhang and Q. Han, Huaxue Shiji, 13 (1991) 119; Chem. Abstr. 115 (1991) 173701a.

[5] F. Zhang, B. Wu, H. Liu and C. Wu, Microchem. J., 48 (1993) 104.

[6] P. Liu, H. Liu and C. Wu, Talanta, 38 (1991) 1143.

[7] O. Hernandez, A.I. Jimenez, F. Jimenez, J.J. Arias and J. Havel, Talanta, 41 (1994) 775.

[8] T. Katami, T. Hayakawa, M. Furukawa and S. Shibata, Bunseki Kagaku, 33 (1984) 676.

[9] Y. Zhu and Y. Li, Anal. Lett., 26 (1993) 309.

[10] W.T. Caldwell and E.C. Kronfeld, J. Am. Chem. Soc., 64 (1942) 1695.

[11] H. Zhang, W. Mu and J. Cheng, Huaxue Shiji, 14 (1992) 279.

[12] G. Zhang. H. Yang and Q. Mu, Huaxue Shiji, 13 (1991) 29; Chem. Abstr., 115 (1991) 114402f.

Ion-selective electrode for salicylate assay in blood serum

Takashi Katsu*, Yuki Mori

Faculty of Pharmaceutical Sciences, Okayama University, Tsushima, Okayama 700, Japan

Abstract

A salicylate-selective membrane electrode made with heptyl-4-trifluoroacetylbenzoate as a neutral carrier was successfully applied for the determination of salicylate in blood serum. This procedure is advantageous because the free concentration of the drug in serum can be determined without sample preparation. The free salicylate concentrations determined by the ion-selective electrode compared to those obtained by conventional colorimetry gave a linear correlation coefficient 0.997 in the salicylate concentration range 0.1–2.5 mM.

1. Introduction

Ion-selective electrodes have become important and useful in chemical and medical analyses [1–3]. We are interested in applying these electrodes to therapeutic drug monitoring in clinical analysis. Such monitoring is fundamental to pharmacotherapy, as it can be used to adjust the doses of drugs with similar therapeutic and toxic concentration ranges [4]. So far, a lithium ion-selective electrode has been successfully applied for monitoring blood concentration of lithium carbonate, which is administered to patients with manic disorders [5], and currently this electrode is widely used in clinical laboratories because of its easy handling. In addition to this electrode, we introduced new ion-selective electrodes to monitor the blood levels of the antiepileptic and antiarrhythmic drugs bro-

mide [6] and procainamide [7] respectively. As an extension of these studies, we applied a salicylate-selective electrode to drug monitoring in blood serum. Although various salicylate electrodes have been developed and applied to pharmaceutical and clinical analyses [2,8,9], the direct determination of salicylate in blood serum in situ has not yet succeeded owing to the low sensitivity of the electrodes under physiological conditions [9,10]. We were particularly interested in constructing a new salicylate-selective electrode using a carbonate ionophore [11]. This ionophore, of course, had originally been developed to make a carbonate ion-selective electrode [11], but was also found to be suitable for constructing a certain specific carboxylate electrode such as a benzoate electrode [12]. In the present study, we applied this ionophore for the construction of a salicylate electrode, which was especially effective for determining free salicylate concentration in blood serum.

* Corresponding author. Tel.: + 81 86 251 7955; fax: + 81 86 255 7456

2. Experimental

2.1. Reagents

The sources of the reagents were as follows: carbonate ionophore I (ETH 6010, heptyl-4-trifluoroacetylbenzoate), methyltridodecylammonium chloride (MTDACl) and o-nitrophenyl octyl ether (NPOE) from Fluka (Buchs, Switzerland); poly(vinyl chloride) (PVC; degree of polymerization 1020) from Nacalai Tesque (Kyoto, Japan); sodium salicylate from Kanto Kagaku (Tokyo, Japan); acetylsalicylic acid (aspirin) from Wako (Osaka, Japan). All other chemicals used were of analytical-reagent grade.

2.2. Electrode system

The salicylate-selective electrode was based on a PVC membrane [11,12] and its components were 1.7 mg of carbonate ionophore I, 1.2 mg of MTDACl (40 mol% relative to the ionophore), 30 mg of NPOE and 30 mg of PVC. The materials were dissolved in tetrahydrofuran and poured into a flat Petri dish (30 mm diameter) from which the solvent was allowed to evaporate at room temperature. The resulting membrane was cut out and stuck to a PVC tube (4 mm o.d., 3 mm i.d.) using tetrahydrofuran as the adhesive. The PVC tube was filled with an internal solution of 1 mM sodium salicylate and 10 mM NaCl, and the sensor membrane was conditioned overnight. The electrochemical cell arrangement was: Ag, AgCl | internal solution| sensor membrane | sample solution| 1 M lithium acetate (salt bridge) | 10 mM KCl | Ag, AgCl. The electromotive force (e.m.f.) between the silver/silver chloride electrodes was measured using a voltmeter of high input impedance made with a field-effect transistor operational amplifier (LF356; National Semiconductor, Sunnyvale, CA; input resistance $> 10^{12}\Omega$) and recorded. The selectivity coefficients of the electrode were evaluated by the fixed-interference method [13] using the respective sodium salts. The detection limit was defined as the intersection point of the extrapolated linear regions of the calibration graph [13].

A typical procedure for determining salicylate in serum was as follows. The electrodes were placed in 100 μl of serum under constant stirring with a stirring bar. This electrode system, including the reference electrode [14], is compact. Therefore, volumes as low as 100 μl can be assayed. Serum samples containing salicylate were prepared by adding sodium salicylate to human serum. All measurements were performed at a constant temperature of 25°C.

2.3. Colorimetry

Salicylate concentrations in sera were also determined by a colorimetric procedure based on the color formed when salicylate complexes with ferric ions [15]. The procedure is summarized as follows. The serum samples were ultrafiltrated through Centricon-30 (Amicon, Beverly, MA; molecular weight cut-off $> 30,000$) to remove salicylate bound to serum protein. The filtrate (100 μl) was pipetted into a test tube (10 ml) containing 1.2 ml of 24.8 mM ferric nitrate and 62 mM nitric acid, to produce a violet color. The absorbance at 540 nm was determined using a Shimadzu UV-2100 spectrophotometer.

3. Results and discussion

3.1. Response characteristics in blood serum

The clinical range of salicylate in serum required for anti-inflammatory therapy is 150–300 μg ml^{-1} (1.1–2.2 mM) [4,16]. Thus, we examined the response of the electrode to salicylate in serum to confirm whether the present method is applicable to this concentration range. A calibration graph was obtained by measuring a known amount of sodium salicylate added to a serum sample and plotting the concentration against the corresponding e.m.f. value. As is shown in Fig. 1 (curve a), the calibration graph of the electrode covered the clinical concentration range. However, the electrode exhibited a super-Nernstian response with a slope of -80 mV per concentration decade (in the range 1–10 mM). As will be discussed later, this abnormal electrode response

can be attributed to the binding of salicylate in proteins in the serum samples. The detection limit for salicylate in serum was 0.3 mM. The response time of the electrode (90% final signal) was below 10 s when the concentration of salicylate was changed from 0.5 to 2 mM. We also examined the response of the electrode without the ionophore and containing only the ion-exchanger MTDACl [17]. The detection limit for salicylate in serum became significantly higher (0.6 mM), showing that the salicylate electrode based on the lipophilic quaternary ammonium salt alone responded weakly to salicylate, as has been suggested previously [9,10]. Thus, the use of the carbonate ionophore was effective for determining salicylate concentration in serum.

We constructed a calibration graph after the serum sample was ultrafiltrated through Centri-con-30 (Fig. 1, curve b). The electrode exhibited a near-Nernstian response in the range 0.2–10 mM salicylate with a slope of −55 mV per concentration decade. The lower limit of detection for salicylate was remarkably improved to 0.04 mM. As salicylate binds serum protein such as albu-

min, [4,18], the free concentration of salicylate remarkably decreased in the presence of serum protein, and thus the calibration graph from the serum sample (curve a) shifted to a higher concentration of salicylate than that from the deproteinized sample (curve b). The deviation from the Nernstian response observed in blood serum can be explained by the concentration dependence of salicylate binding on serum [4]. That is to say, in the lower concentration range of salicylate most of the drug bound to serum proteins, while in the higher concentration region the portion of the drug bound to proteins decreased, thus generating a steep slope. The percentage of salicylate bound to protein can be easily estimated by comparing these two calibration graphs (curves a and b), as the concentration of free salicylate can be determined by the curve b calibration graph and the total salicylate (the sum of the concentrations of the free salicylate and that bound to protein) can be estimated from the curve a calibration graph. For example, when 1 and 5 mM salicylate were added to the serum, 79% and 54% of the salicylate bound to serum protein respectively.

3.2. Application to drug monitoring

For therapeutic drug monitoring, determining the free concentration of a drug is claimed to be physiologically more relevant than determining the total concentation of drug [4,9,16]. Thus, this method is very useful as the electrode is responsive only to free concentration. Although the free concentration of salicylate can be determined using the calibration graph shown in Fig. 1 (curve b), we were particularly interested in obtaining the calibration graph from a much simpler solution. We found that the calibration graph (Fig. 1, curve c), generated from physiological saline containing 0.15 M NaCl and 5 mM 4-(2-hydroxyethyl)-2-piperazineethanesulfonic acid–NaOH (pH 7.4) afforded similar results to the deproteinized serum sample (curve b) on a higher concentration range. Although the detection limit measured in the physiological saline (0.01 mM) was significantly lower than that in the deproteinized serum sample, the improved detection limit appeared to be mainly attributable to removing the interference
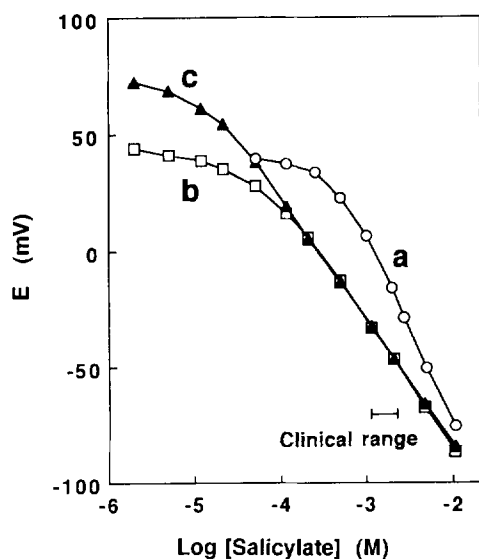

Fig. 1. Comparison of the response of the electrode to salicylate in (a) serum, (b) deproteinized serum, and (c) physiological saline containing 0.15 M NaCl and 5 mM 4-(2-hydroxyethyl)-2-piperazineethanesulfonic acid–NaOH (pH 7.4). The clinical concentration range required for anti-inflammatory therapy is also shown.

Table 1
Selectivity coefficients, $\log k_{i,j}^{Pot}$ [a]

Interfering ion (j)	Concentration (M)	$\log k_{i,j}^{Pot}$
Cl^-	0.5	−4.4
HCO_3^-	0.05	−2.4
CH_3COO^-	0.5	−3.9
Acetyl salicylate	0.0005	−0.6

[a] i = salicylate and j = interfering ion

of bicarbonate, as the serum samples contained a high concentration of bicarbonate (28 mM) [19] and the electrode responded to this significantly. However, the difference in the curves b and c of the calibration graphs was confined to the lower concentration range of salicylate. Thus the calibration graph shown in curve c can be used, except when the salicylate concentration range is extremely low. This agreement of the calibration graphs is useful as the free salicylate concentration can be estimated by comparing the e.m.f. readings measured in serum with the curve c calibraion graph. The total concentration of salicylate can also be evaluated using the curve a calibration graph. However, in this case, the calibration graph should be generated from an individual patient, since the protein content, such as that of albumin, significantly differs among individuals [4].

In Table 1, the selectivity coefficients of the electrode are summarized, together with the concentrations of interfering ions used. The electrode was sufficiently selective against the chloride ions present in serum at high concentration (103 mM) [19], whereas there was slight interference from bicarbonate ions due to the rather lower selectivity than that of chloride ions. This electrode did not respond strongly to acetyl salicylic acid (aspirin), which is the parent drug of salicylate medicines. Thus, the electrode avoided serious interference by this drug although aspirin is rapidly deacetylated in the body to produce pharmacologically active salicylate [4,18].

We compared the free concentrations of salicylate in serum samples, determined by potentiometry using the calibration graph (Fig. 1, curve c), with those determined by colorimetry [15]. As
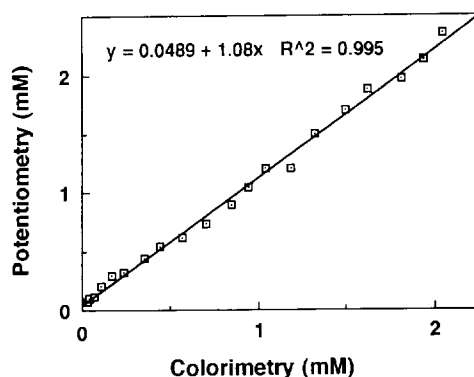

Fig. 2. Correlation of the free salicylate concentrations in 20 serum samples determined by potentiometry using a salicylate-selective electrode and by colorimetry.

shown in Fig. 2, the correlation was good in the salicylate concentration range 0.1–2.5 mM. The colorimetric method requires deproteinization to estimate the free salicylate concentrations in serum samples, whereas the potentiometric method does not. Thus, the present method is much simpler, more rapid and economical. Free salicylate concentrations in whole blood can also be monitored, as the procedure is independent of sample color or turbidity. This new method will markedly reduce the workload involved in therapeutic drug monitoring for salicylate in the clinical setting.

Acknowledgements

References

[1] A. Lewenstam, M. Maj-Zurawska and A. Hulanicki, Electroanalysis, 3 (1991) 727.
[2] V.V. Cosofret and R.P. Buck, Crit. Rev. Anal. Chem., 24 (1993) 1.
[3] J. Wang, Anal. Chem., 67 (1995) 487R.
[4] T. Iga and Y. Saito (eds.), TDM No Jissai (Practice in TDM), Yakugyo Jiho Sha, Tokyo, 1993.
[5] R.L. Bertholf, M.G. Savory, K.H. Winborne, J.C. Hundley, G.M. Plummer and J. Savory, Clin. Chem., 34 (1988) 1500.

[6] T. Katsu, K. Furuno, S. Yamashita, H. Kawasaki, Y. Gomita, Y. Ohtsuka and S. Ohtahara, Clin. Chim. Acta, 234 (1995) 157.

[7] T. Katsu, K. Furuno, S. Yamashita and Y. Gomita, Anal. Chim. Acta, 312 (1995) 35.

[8] S.S.M. Hassan and M.A. Hamada, Analyst, 113 (1988) 1709.

[9] N.A. Chaniotakis, S.B. Park and M.E. Meyerhoff, Anal. Chem., 61 (1989) 566.

[10] Q. Chang and M.E. Meyerhoff, Anal. Chim. Acta, 186 (1986) 81.

[11] C. Behringer, B. Lehmann, J.-P. Haug, K. Seiler, W.E. Morf, K. Hartman and W. Simon, Anal. Chim. Acta, 233 (1990) 41.

[12] T. Katsu and N. Hanada, Anal. Chim. Acta, (1996) in press.

[13] G.G. Guilbault, Ion-Sel. Electrode Rev., 1 (1979) 139.

[14] T. Katsu, H. Kobayashi and Y. Fujita, Biochim. Biophys. Acta, 860 (1986) 608.

[15] J. Svirbely, in L.A. Kaplan and A.J. Pesce (Eds.), Clinical Chemistry: Theory, Analysis, and Correlation, C.V. Mosby, St. Louis, MO, 1984, p. 1382.

[16] J. Koch-Weser, N. Engl. J. Med., 287 (1972) 227.

[17] T. Katsu and T. Kayamoto, Anal. Chim. Acta, 265 (1992) 1.

[18] W.G. Clark, D.C. Brater and A.R. Johnson, Goth's Medical Pharmacology, 13th Edn., Mosby-Year Book, St. Louis, MO, 1992, p. 356.

[19] L.I. Kleinman and J.M. Lorenz, in L.A. Kaplan and A.J. Pesce (Eds.), Clinical Chemistry: Theory, Analysis, and Correlation, C.V. Mosby, St. Louis, MO, 1984, p. 363.

Separation and preconcentration of ultratrace lead in biological organisms and its determination by graphite furnace atomic absorption spectrometry

Youwen Tang*, Bingren Chen, Shengjun Mo

Department of Chemistry, South China Normal University, Guangzhou 510631, People's Republic of China

Abstract

A biological organism (chitosan) was utilized to preconcentrate lead ions from tap water. This preconcentration was achieved by mixing 0.8 ml of chitosan slurry with 10–50 ml of lead-containing solution and subsequently separating by centrifugation. The chitosan paste was then dissolved in 1 ml of 0.2% nitric acid and analysed by graphite furnace atomic absorption spectrometry. The extraction efficiency can approach 100% in the pH range 4–10. The amount of chitosan used was not critical. The effect of some impurities was also investigated. If six samples were prepared simultaneously, the time needed to preconcentrate each sample was less than 3 min. Two different modes of standard addition (the standard lead solutions being added before and after preconcentration) were used for analysis of tap water samples, and the results obtained by the two modes were found to be quite consistent.

Keywords: Separation; Preconcentration; Lead; Biological organisms; Graphite furnace atomic absorption spectrometry

1. Introduction

Graphite furnace atomic absorption spectrometry (GFAAS) is one of the most common techniques used for ultratrace analysis because of its advantages such as high sensitivity, low detection limits and low sample volume requirement. However, use of atomic absorption spectrometry to directly determine some ultratrace components is often hindered by the following two factors: (1) the analyte concentrations are at or below the limits of detection; and (2) the matrix interferes with the determination. It is therefore essential to preconcentrate the samples prior to analysis.

Solvent extraction, ion exchange, coprecipitation and electrodeposition are useful techniques often used for preconcentration. However, these approaches may be time-consuming, have limited specificity for a particular class of ion and, in addition, their procedures may be complex. For this reason, attempts have been made to explore better techniques for preconcentration of specific ions.

---

* Corresponding author.

In general, the structures of biological organisms differ, and there are different functional groups on their surfaces. As a result, many biological organisms have the ability to adsorb (or absorb) selectively the analyte of interest without preconcentrating the matrix. Green et al. [1] reported that gold complexes can be quantitatively separated from solutions by a pure algae strain. Holcombe and co-workers have also demonstrated that unicellular green algae can be used successfully to quantitatively separate trace copper, nickel and cobalt from river and sea-water samples [2,3] and cadmium from river samples [4]. The advantages of using algae as a preconcentrator over other preconcentration techniques are convenience, minimum time requirement, a low blank and a high preconcentration factor.

In this research, we have investigated the possibility of using another bio-organism (chitosan) as a preconcentrator. Chitosan ((1,4)-2-amino-2-deoxy-β-D-glucosamine) is a amine polysaccharide, the deacetylated derivative of chitin. Chitin is a type of macromolecule and occurs widely in nature. Chitosan contains two kinds of functional groups, an amino group and a hydroxy group. It can be dissolved in acid solution and separated out in basic solution. Eiden and Tewell [5] have demonstrated the interaction of lead with chitosan. Their result suggested that the uptake of Pb^{2+} on chitosan is a Langmuir-type adsorption. But there is a paucity of data on how chitosan can quantitatively adsorb metal ions at very low concentrations, and how chitosan is used as a preconcentrator for ultratrace analysis. The objective of the present work was to study the ability of chitosan to preconcentrate lead ions at the parts per billion level from 10–50 ml water samples, as well as the conditions under which the preconcentration proceeds. The techniques have been used successfully to determine ultratrace lead in tap water.

2. Experimental

2.1. Materials

The preparation of chitosan has been described previously [6]. The chitosan used for this experi-

ment contained 83% water. Dry chitosan contained 9% amine groups.

2.2. Preparation of chitosan slurry

Before use, 0.5 g of chitosan was added to 10 ml of 0.3% nitric acid. After the polysaccharide was dissolved, seven drops of 1 mol L^{-1} sodium hydroxide were added to the polysaccharide solution. The chitosan sediments separated out, then the mixture was centrifuged and the supernatant was decanted and discarded. The chitosan biomass was subsequently washed with deionized water and centrifuged again. After discarding the washing solution, 10 ml of deionized water was added to the sediments. The mixture was then agitated and the chitosan slurry was ready for use.

2.3. Procedures

The sample was prepared by adding 0.8 ml (containing 6.8 mg dry polysaccharide) of chitosan slurry to 10 ml of a solution containing lead. The pH of each solution was adjusted by dropwise addition of nitric acid or sodium hydroxide solution. The mixture was agitated for 5 min, and then centrifuged. After the supernatant was decanted, 1 ml of 0.2% nitric acid was added to the chitosan paste, and the mixture was agitated to dissolve the biomass for determination later.

Due to the high volatility of lead, 0.5 μg of Pd was used as a matrix modifier, so as to be able to increase the thermal pre-treatment up to 900°C without loss of Pb. In this way, interfering biological matrix could be completely removed before atomisation.

Three replicates were carried out for each experiment. When a significant blank signal was detected, the blank value was subtracted from the corresponding sample signal. Typical blank values will be given later in the paper.

Table 1
Furnace operating conditions

Step no.	Temperature (°C)	Ramp time (s)	Hold time (s)	Argon flow (l min^{-1})	Read[a]
1	100	10	20	3	
2	900	10	30	3	
3	1600	0	5	0	*
4	2600	1	3	3	

[a] The absorbance to be recorded. The * indicates that the record begins in step number 3.

2.4. Apparatus

All experiments were conducted with a Perkin-Elmer 2380 atomic absorption spectrometer equipped with a HGA-400 graphite furnace atomiser. The operation conditions and temperature programmes are listed in Table 1. The Pb hollow-cathode lamp was operated at 4 mA. The spectral band pass and the wavelength of the monochromator were set to 0.7 nm and 283.3 nm respectively. The data were recorded with a Perkin-Elmer R100A recorder as peak heights.

3. Results and discussion

3.1. Effect of pH on Pb adsorption

To investigate the effect of pH on the adsorption of very low concentrations of lead, 10 ml of 10 ng ml^{-1} lead solution at various pH values was mixed with 0.8 ml of chitosan slurry. After 5 min of agitation, the mixture was centrifuged and the supernatant liquid decanted. The chitosan paste was then mixed with 1 ml of 0.2% nitric acid and 5 mg l^{-1} Pd solution to yield a Pb solution which was 10 times more concentrated than the initial solution (assuming 100% efficiency). Solutions thus obtained were subsequently analysed by GFAAS. Experiments showed that after the sample was preconcentrated by chitosan, the pH values of supernatant changed considerably. The pH value of acid samples was increased while that of basic samples was decreased. Table 2 indicates the effect of chitosan on the pH of samples.

Fig. 1 demonstrates the effect of pH on Pb adsorption by chitosan. It can be seen from this figure that the pH range for optimum Pb adsorp-

tion is wide. When the pH value of the samples was changed from 4.03 to 10.10, the recovery approached 100%. This result is better than that achieved with the use of algae to preconcentrate lead [7]. Mahan et al. [7] have reported that recoveries of 6 mg of Stichococcus bacillars, Chlorella Pyrenoidosa and Chlamydomonas reinhariti used to preconcentrate 0.5 μg lead in 25 ml samples were 80%, 40% and 75% respectively. It is obvious that the efficiency of Pb uptake by chitosan is much higher than that by algae.

3.2. Effect of chitosan mass on lead adsorption

In order to investigate the effect of chitosan mass on Pb adsorption, 0.2, 0.4, 0.6, 0.8, 1.0 and 1.2 ml chitosan slurry were added to 10 ml of sample solutions containing 0.1 μg Pb. After 5 min of agitation and centrifugation, all solutions were made up to 1 ml final volume with 0.2% HNO$_3$ and analyzed. Experiments indicated that when less chitosan was used, the efficiency of Pb adsorption was increased. However, when 0.6 ml of chitosan slurry was used, the recovery was almost 100%.

3.3. Effect of preconcentration factor on Pb adsorption

The aim of using chitosan to preconcentrate lead is to reduce the interference of the matrix in the original sample, and to increase the analyte concentration, so as to improve the analytical sensitivity and accuracy. As a result, the effect of sample volume on preconcentration should be determined, i.e. whether the ratio of initial to final sample volume can affect the extraction efficiency of chitosan for lead. Experiments were conducted

Table 2
Effect of Chitosan on the pH of samples

| pH of samples before preconcentration | 3.00 | 4.03 | 5.16 | 6.35 | 8.95 | 10.10 | 10.64 | 11.62 |
| pH of supernatant after centrifugation | 4.50 | 6.20 | 8.00 | 8.82 | 9.23 | 9.91 | 10.30 | 11.40 |

using 0.8 ml of chitosan slurry to preconcentrate 0.1 μg Pb^{2+} in different volumes. The final solution volume for analysis was 1 ml. The result of the experiment is shown in Table 3.

Table 3 shows that when 0.8 ml of chitosan is used, increasing the sample volume up to 25 ml has no effect on the recovery of lead, but increasing the initial volume to 50 ml makes lead recovery unfavorable.

3.4. Effect of impurities and matrix

Several ions which could affect Pb adsorption by chitosan (by competitive binding at the chitosan adsorption sites) were also considered. The effect of interfering ions on preconcentration was studied with 0.8 ml of chitosan slurry being added to 10 ml of sample containing interfering ions and 0.1 μg Pb^{2+}. The inorganic interfering ions were all added in the form of nitrates. 100 μg ml^{-1} Ca^{2+}, 100 μg ml^{-1} Mg^{2+}, 1 mg ml^{-1} Na^- and 1.0 μg ml^{-1} Fe^{3+} do not interfere with the preconcentration of lead, but 10 μg ml^{-1} Fe^{3+} is sufficient to reduce the recovery to 75%. Environ-

mental samples are often polluted by organisms and surfactants. For this reason, experiments to determine the effect of sodium citrate and surfactants on Pb adsorption were performed. 0.01% dodecyl sodium sulfate and sodium citrate decreased the recovery of Pb to 56% and 58% respectively. However, when 0.1% cetyltrimethyl ammonium bromide was added, the recovery was still 100%. Results indicate that the hydrophobic group does not affect the extraction efficiency of chitosan; however, anions of hydrophilic groups complexing Pb^{2+} decrease the extraction efficiency of chitosan for Pb.

3.5. Effects of the preconcentration and centrifugation times on extraction efficiency

A good approach for preconcentration should be simple and quick. To evaluate the dependence of extraction efficiency on the preconcentration and centrifugation times, 0.8 ml of chitosan slurry was aded to 10 ml of solution containing 0.1 μg Pb. After the sample was agitated for 1 min, the extraction efficiency of chitosan for lead was 77%, and after 2 min of agitation it was 83%. After the mixture was agitated for 3 min the recovery reached 100%.

The mixture could be separated completely after only 5 min centrifugation. The centrifugation available for this study allowed preparation of up to six samples simultaneously. Thus, if six samples
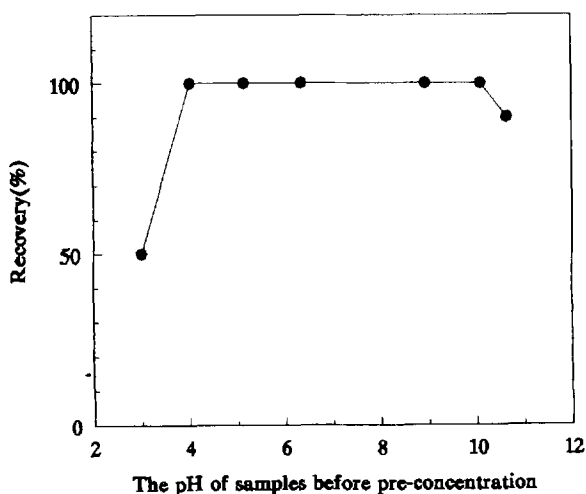

Fig. 1. The effect of pH on adsorption of lead by chitosan.

Table 3
Dependence of Pb adsorption of chitosan on sample volume

Initial sample volume (ml)	Final volume (ml)	Concentration factor	Recovery of Pb (%)
10	1	10	100 ± 2^a
25	1	25	100 ± 2^a
50	1	50	97 ± 3^a

[a]Standard deviation.

were prepared each time, the time spent to pre-concentrate one sample was less than 3 min. However, with most preconcentration techniques, the time required to preconcentrate one sample is 10–30 min. A minimum time requirement is one of the major advantages for using chitosan as a preconcentrator over other preconcentration techniques.

3.6. Preconcentration of ultratrace lead in tap water

To verify the capability of chitosan to precon-centrate lead in environmental samples, 0.8 ml of chitosan slurry was used to preconcentrate 10 ml of a tap water sample. The final volume of solution for analysis was 1.0 ml. A blank solution was analyzed with the same procedures. The blank value was subtracted from the corresponding tap water sample signal. The typical lead concentration of a blank solution was 1.5 ± 0.3 ng ml^{-1}. The blank lead value does not come from the chitosan; it most probably comes from impurities existing in the chemical reagents, e.g. sodium hydroxide and nitric acid. Because the matrix may also be concentrated and may interfere with the determination of Pb, two different standard addition approaches were used for analysis of the tap water samples. In the first approach, 0, 0.05, 0.10 and 0.15 μg of lead standard solution were added to 10 ml of four tap water samples. After the samples were preconcentrated by chitosan, 1 ml of

final solution was used for determination. The average value of three replicates determined for Pb in tap water was 7.6 ng ml^{-1}, and the standard deviation was 0.5 ng ml^{-1}. In the second approach, 0.8 ml of four chitosan slurrys was added to 10 ml of four tap water samples. After the samples were preconcentrated and the mixtures were centrifuged, 0, 0.05, 0.10 and 0.15 μg of lead standard solution were added to the four sediments. The final volumes of all solutions were made up of 1 ml in 0.2% HNO$_3$ and analyzed. The value determined for Pb with the second approach and its standard deviation were 7.5 ng ml^{-1} and 0.6 ng ml^{-1} respectively, which are in good agreement with that obtained by the first approach. These results suggest that chitosan can be effectively used to quantitatively preconcentrate ultratrace lead in environmental samples.

References

[1] B. Green, M. Hosea, R. Mcpherson, M. Henzl, M.D. Alexander and D. Darnall, Environ. Sci. Technol., 20 (1987) 627.
[2] S. Mo and J.A. Holcombe, Anal. Chem., 62 (1990) 1994.
[3] S. Mo and J.A. Holcombe, Talanta, 38 (1991) 503.
[4] V. Majidi and J.A. Holcombe, J. Anal. At. Spectrom., 4 (1989) 439.
[5] C.A. Eiden and C.A. Tewell, J. Appl. Polym. Sci., 25 (1981) 1587.
[6] B. Chen, Chem. J. Chin. Univ., 13 (1992) 1008.
[7] C.A. Mahan, V.M. Majidi and J.A. Holcombe, Anal. Chem., 61 (1989) 624.

Simultaneous high performance liquid chromatographic determination of vanadium, nickel, iron and copper in crude petroleum oils using bis(acetylpivalylmethane)ethylenediimine as a complexing reagent

M.Y. Khuhawar*, S.N. Lanjwani

Institute of Chemistry, University of Sindh, Jamshoro, Sindh, Pakistan

Abstract

A method is described for the simultaneous high performance liquid chromatographic (HPLC) determination of copper, iron, nickel and vanadium, based on complexation of analytes by bis(acetylpivalylmethane)ethylenediimine (H_2APM_2en) followed by solvent extraction and HPLC separation on a reversed-phase. C-18. 5 μm column with UV detection at 260 nm. The method has been applied to the determination of metals in crude petroleum oils collected from the South Indus Basin oil fields. The results obtained are compared with those obtained by flame atomic absorption spectrometry.

Keywords: HPLC; Metal determination; Petroleum oils

1. Introduction

Heavy crude petroleum oils contain vanadium, nickel, iron and copper as organically bound metals, mostly as metalloporphyrins and metallo-non-porphyrins [1,2]. Their determination is of considerable importance, because the metal complexes may poison and foul catalysts or cause undesirable side reactions in refinery operations, such as fluid cracking and hydrodesulfurization

[3]. A number of analytical methods have been used for the determination of metal ions in crude petroleum oils, including atomic absorption spectrometry (AAS) [4], inductively-coupled plasma atomic emission spectroscopy (ICP-AES) [5], radioisotope X-ray fluorescence [6], neutron activation [7], gas chromatography (GC) [8] and liquid chromatography [9]. Zeng and Uden [10,11] have reported high temperature GC with microwave-induced plasma atomic emission spectroscopy for the determination of vanadyl, nickel and iron porphyrins in crude oils. In the present work bis(acetylpivalylmethane)ethylenediimine [N,N'-

---

* Corresponding author.

ethylenebis(5,5-dimethyl-4-oxohexane-2-imine)] (H_2APM_2en) (Fig. 1) has been used to complex the metals of interest which are subsequently extracted, separated and determined by HPLC in crude petroleum oils.

Belcher et al. [12] have used H_2APM_2en for GC determination of copper and nickel in metal alloys and water samples. Dilli and Patsalides [8] have applied the reagent for the GC determination of vanadium in crude oils. Recently the reagent has also been used for the HPLC determination of copper and nickel in metal alloys and water samples [13].

2. Experimental

2.1. Solvent extraction

An aliquot of solution (1–5 ml) containing 0–100 μg of vanadium, nickel, iron and copper was transferred to a well-stoppered test tube and sulphur dioxide was passed for 30 s. Sodium acetate–acetic acid buffer (2 ml, 1 M) pH 6 was added and the contents were heated gently to near dryness. H_2APM_2en solution (1% w/v in methanol, 5 ml) was added and the contents were heated for 15–20 min. During heating the volume of the solution was reduced to about 1 ml. Water (2 ml) and chloroform (2 ml) were added and the contents were shaken well. The layers were allowed to separate and exactly 1 ml of the chloroform layer was transferred to a sample vial. The solvent was evaporated and the residue dissolved in methanol (0.5 ml). The methanolic solution (5 μl) was injected onto a Microsorb C-18, 5 μm column (150 × 4.6 mm i.d.) and complexes were eluted with methanol: acetonitrile: water (60:20:20 v/v/v) at a flow rate of 1 ml min^{-1}. Detection was achieved using a UV monitor fixed at 260 nm.

2.2. Analysis of metals in crude petroleum oils

The crude petroleum oil samples were collected from the Leghari, Halipota, Dabhi, Golarchi and Tando Alam oil fields located in the South Indus Basin near Hyderabad and Badin, Sindh, Pakistan. The samples were collected directly from the source, when oil was being pumped out of the wells. 20–100 g of sample was transferred to a beaker and sulphuric acid (95–98%; 400 ml) was added. The contents were heated on a hotplate until white fumes of sulphur trioxide were evolved. The mixture was allowed to partially cool, 400 ml of nitric acid (65%) was added slowly and the contents were heated gently. Perchloric acid (72%) (200 ml) was added dropwise to maintain vigorous oxidation with excessive evolution of brown fumes of nitrogen oxides. The clear solution was heated to near dryness. The residue was dissolved in water and the volume was adjusted to 25 ml. A 2–12 ml aliquot of the solution was taken, the pH was adjusted to 6 and the extraction procedure was followed as above. A blank was also prepared simultaneously.

The reagent H_2APM_2en was synthesized as previously reported [12].

2.3. Apparatus

A Hitachi 655A liquid chromatograph connected to a variable wavelength monitor, Rheodyne 7125 injector and Hitachi D2500 Chromato-integrator were used.

A Microsorb C-18, 5 μm (150 × 4.6 mm i.d.) column (Rainin Instruments, USA) was used.

A varian Spectra AA-20 atomic absorption spectrometer with an air–acetylene flame atomizer was used for the determination of copper, nickel and iron using the conditions recommended by the manufacturer.
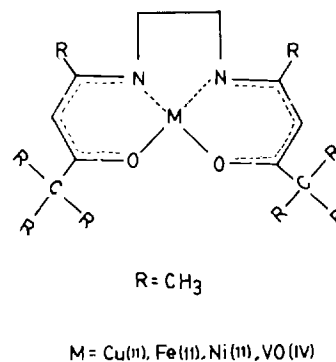

R = CH₃

M = Cu(II), Fe(III), Ni(II), VO(IV)

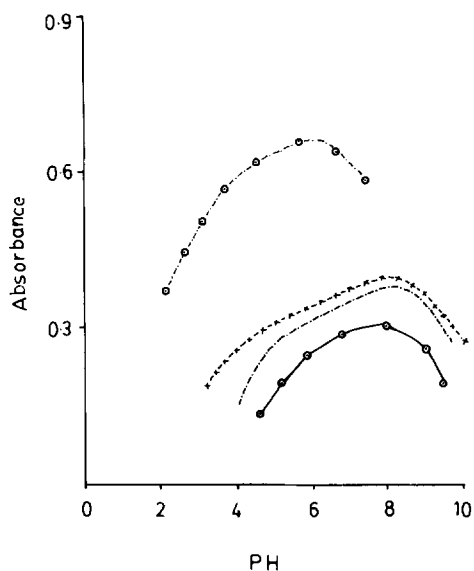Fig. 1. Structural diagram of metal chelates.

Fig. 2. Effect of pH on the extraction of (1) iron(II) (100 μg), (2) nickel(II) (200 μg), (3) copper(II) (200 μg) and (4) vanadium(IV) (200 μg) with H_2APM_2en in chloroform (5 ml).

3. Results and discussion

The derivatization of copper(II), nickel(II), oxovanadium(IV) and iron(II) in the aqueous phase with the reagent H_2APM_2en was investigated spectrophotometrically. The maximum absorbances were measured at 548 nm, ($\epsilon 428$), 570 nm ($\epsilon = 441$), 440 nm ($\epsilon = 1920$) and 456 nm, ($\epsilon = 377$) for copper(II), nickel(II), iron(II) and oxovanadium(IV) respectively. The optimal pH for the extraction of iron(II) was 6. The extraction of copper(II), nickel(II) and oxovanadium(IV) occured at pH 5–9 with a maximum at 7.5–8 (Fig. 2) [12]. However, at pH 7.5–8, a significant decrease in the extraction of iron(II) was observed. At pH 6 the derivatization and extraction of iron(II) and copper(II) was rapid, but they were slow for nickel(II) and heating times of 15–20 min were sufficient for quantitative transfer from aqueous to organic phase. Some difficulties were encountered in extraction of vanadyl from aqueous solution [8,9,14]. Thus, after reduction of vanadium(VI) to vanadium(IV) with sulphurous acid, the solution was heated to near dryness in the presence of acetate buffer at pH 6. The derivatization was carried out in methanol. Using these

conditions it was possible to extract copper(II), nickel(II), iron(II) and oxovanadium(II) as metal chelates simultaneously.

4. Conclusion

The complexes were easily separated using a reversed-phase HPLC column and isocratically eluting with a ternary mixture of methanol: acetonitrile: water (60:20:20 v/v/v) (Fig. 3). Linear calibrations were obtained by plotting average peak height ($n = 3$) against concentration with 0–100 μg sample in an aliquot of water. The coefficient of correlation (τ) was observed to be 0.994, 0.988, 0.994 and 0.995 for copper, nickel, iron and vanadium respectively. The detection limit was measured at least three times the background noise and was 1 μg per aliquot for each of the metal ions. Finally, the method was applied to the determination of metal ions in crude
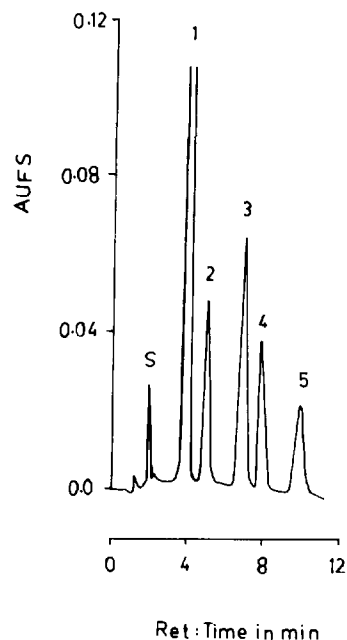

Fig. 3. HPLC separation of (S) solvent (1) reagent, (2)oxo-vanadium(IV) (60 μg ml^{-1}), (3) iron(II) (60 μg ml^{-1}), (4) nickel (II) (60 μg ml^{-1}) and (5) copper(II) (60 μg ml^{-1}) complexes of H_2APM_2en. Eluent: methanol: acetonitrile: water (60:20:20 v/v/v). Flow rate: 1 ml min^{-1}. Detection: UV at 260 nm.

Table 1
Analyses of metal ions in crude petroleum oils

Sample	Metal concentrations found by HPLC[a] (ng g^{-1})($n = 3$)				Metal concentrations found by flame AAS (ng g^{-1})		
	Vanadium	Copper	Iron	Nickel	Copper	Iron	Nickel
Tando alum	200(4.2)	87(5.1)	130(6.8)	80(3.7)	100(2.9)	136(1.4)	68(4.6)
Halipota	210(7.0)	80(4.8)	148(5.7)	100(4.6)	73(1.5)	138(2.6)	110(2.2)
Laghari	230(2.5)	96(4.4)	168(4.9)	110(6.5)	100(4.9)	180(5.2)	106(1.6)
Mazari	216(6.0)	70(3.7)	120(4.7)	88(3.9)	62(3.2)	128(3.8)	80(6.6)
Dabhi	186(3.7)	86(4.3)	138(3.9)	120(5.0)	80(1.9)	146(2.2)	130(3.8)

[a] RSDs (%) are given in parentheses.

petroleum oils. The results shown in Table 1 indicate RSDs in the range 2.4–7% ($n = 3$) and compare reasonably with AAS results: RSDs in the range 1.4–6.6% ($n = 3$).

References

[1] R.H. Fish and J.J. Komlenic, Anal. Chem., 56 (1984) 510.
[2] R.H. Fish, J.J. Komlenic and B.K. Wines, Anal. Chem., 56 (1984) 2452.
[3] J.F. Branthaver, in R.H. Filby and J.F. Branthaver (Eds.), Metal Complexes in Fossil Fuels, ACS Symp. Ser. 344, American Chemical Society, Washington, DC, 1987, Chapter 12.
[4] F.J. Langmyhr and U. Aadalen, Anal. Chim. Acta, 115 (1980) 365.
[5] J.L. Fabee and M.L. Ruschak, Anal. Chem., 57 (1985) 1853.
[6] M. Alvarez, J. Alvarado, A.R. Cristiano, L.M. Marco and M.M. Perez, J. Radioanal. Nucl. Chem., 144 (1990) 327.
[7] Z. Ding, Z. Chai, J. Fu, C. Sheng, Q. Lin and D. Wu, Hijishu, 13 (1990) 203.
[8] S. Dilli and E. Patsalides, Anal. Chim. Acta, 128 (1981) 109.
[9] M.Y. Khuhawar, S.N. Lanjwani and G.Q. Khaskhali, J. Chromatogr. A, 689 (1995) 39.
[10] Y. Zeng and P.C. Uden, J. High Resolut. Chromatogr., 17 (1994) 223.
[11] Y. Zeng and P.C. Uden, J. High Resolut. Chromatogr., 17 (1994) 217.
[12] R. Belcher, A. Khalique and W.I. Stephen, Anal. Chim. Acta, 100 (1978) 503.
[13] M.Y. Khuhawar and A.I. Soomro, Talanta, 39 (1992) 609.
[14] S. Dilli, A.M. Maitra and E. Patsalide, Inorg. Chem., 21 (1982) 2832.

Thermometric titrations of amines with nitrosyl perchlorate in acetonitrile solvent

Turgut Gündüz*, Esma Kiliç, Orhan Çakirer

Department of Chemistry, Faculty of Science, University of Ankara, Ankara, Turkey

Received 8 May 1995; revised 3 October 1995; revised 11 December 1995 accepted 11 December 1995

Abstract

Thirteen aliphatic and four aromatic amines, namely diethylamine, triethylamine, *n*-propylamine, di-*n*-propylamine, tri-*n*-butylamine, isopropylamine, di-isopropylamine, *n*-butylamine, di-*n*-butylamine, tri-*n*-butylamine, isobutylamine, *sec*-butylamine, *tert*-butylamine, aniline, N,N-dimethylaniline, 2-nitroaniline and 4-nitroaniline were titrated thermometrically with nitrosyl perchlorate in acetonitrile solvent. All the aliphatic amines gave very well-shaped thermometric titration curves. The calculated recovery values of the amines were very good. In comparison, the aromatic amines, aniline and N,N-dimethylaniline gave rather well-shaped titration curves, but the recovery values were fairly low. 2-Nitro- and 4-nitro anilines gave no thermometric response at all. The heats of reaction of the amines with nitrosyl perchlorate are rather high. However, the average heat of reaction of the aromatic amines is approximately two-thirds that of the average heat of the aliphatic amines. To support this method all the amines were also titrated potentiometrically and very similar results to those obtained with the thermometric method are seen. The nitrosyl ion is a Lewis acid, strong enough to titrate quantitatively aliphatic amines in acetonitrile solvent, but not strong enough to titrate aromatic amines at the required level in the same solvent.

Keywords: Aliphatic amines; Aromatic amines; Nitrosyl perchlorate; Thermometry

1. Introduction

A number of methods such as potentiometry, conductimetry, spectrophotometry and thermometry can be used for the titration of diverse chemical compounds in non-aqueous media. Among these however, thermometry, in some respects, has definite advantages over the other methods [1–6]. These advantages briefly are as follows: (i) low electrical conductivity of non-

aqueous media does not interfere; (ii) precipitation, which occurs during some titrations, does not affect this method; (iii) end points are generally very sharp; (iv) there is no electrode poisoning; and (v) the equipment can be set up in a medium equipped laboratory.

Furthermore, in contrast to other methods, thermometry can be applied to (i) redox titration; (ii) acid–base titration; (iii) complexometry and; (iv) volumetric precipitation. As is well known, these are the basic and major analytical reactions on which titrimetry is based [7–20].

* Corresponding author. Fax: + 90 312 2232395.

In the present work, due to the above mentioned advantages of thermometry, we have tried to titrate amines, in particular 13 aliphatic and four aromatic amines, namely diethylamine, triethylamine, n-propylamine, di-n-propylamine, tri-n-propylamine, isopropylamine, di-isopropylamine, n-butylamine, di-n-butylamine, tri-n-butylamine, isobutylamine, sec-butylamine, tert-butylamine, aniline, N,N-dimethylaniline, 2-nitroaniline and 4-nitroaniline. All the aliphatic amines gave very well-shaped titrations curves and from these, we have calculated the mean recovery values of the amines and have been found excellent results. Whereas the aromatic amines, aniline and N,N-dimethylaniline gave rather well-shaped titration curves, the mean recovery values calculated from these curves were fairly low. On the other hand, 2- and 4-nitroanilines did not give useful titration curve.

The heats of reaction of the aliphatic amines were calculated from the initial slopes (up to the 30% neutralization) of the titration curves of the amines. As is seen from Table 1 the reactions are rather exothermic. However, the heats of reaction of the aromatic amines are very low in comparison to the heats of reaction of the aliphatic amines.

There are many examples of the titration of amines with Brönsted acids [1–3,7,16–18], but unfortunately, titrations with Lewis acids are very limited due to the difficulties of finding appropriate Lewis acids and solvents [1,3,4,21–23].

2. Experimental

2.1. Apparatus

Thermometric titration is a titration performed in an adiabatic system, the temperature of which is plotted against the volume of titrant used. In order to meet the requirements of this definition, a small fume-cupboard was insulated carefully with polystyrene foam sheets. A small window was cut in the sheets to allow the operator to look at the titration assembly and use it properly. The assembly consisted of (i) a small Dewar flask with a capacity of 30 cm^3; (ii) a tin-tipped semi-mi-

croburette with a reservoir; (iii) a Beckmann and two accurate mercury thermometers; and (iv) a magnetic stirrer. The Dewar flask was placed in a 250 cm^3 beaker and the walls of the Dewar flask was insulated from the walls of the beaker with the foam polystyrene sheets. The bottom of the beaker was also insulated with the polystyrene sheets. The mouth of the Dewar flask was covered with a thick foam stopper with two holes, shaped from thick polystyrene. A Beckmann thermometer and a tin-tipped semi-microburette were pushed through the polystyrene into the Dewar flask. On top of the reservoir of the semi-microburette U-tubing filled with anhydrous calcium chloride was placed to prevent moisture entering. The Beckmann thermometer was immersed to a fixed depth of solution in each titration and temperature changes of 0.001°C were read. The volume of the titrant solution was read to 0.01 cm^3. Except for the graduated parts and the tap, the semi-microburette was also insulated with blown polystyrene to minimize heat exchanges during the titration. Two mercury thermometers were used to measure the ambient temperature of the assembly and to measure the temperature of the titrant in the reservoir. Both thermometers read the temperature to 0.01°C. The entire set-up has been schematically reported in our early work, which deals with the thermometric titration of urea with antimony pentachloride [24].

All the titrations were carried out at 20 ± 1°C in an insulated fume-cupboard. Under these conditions, the heat capacity of the reaction cell was determined by the method given in Refs. [1] and [18] and was found to be 30.1 J °C^{-1}.

The amine solution used for the determination of the percentage purity (recovery value) and the heat of reaction was kept in the insulated fume-cupboard for at least 2 h to allow it to reach thermal equilibrium with the titrant. However, for the determination of the percentage purity only, half an hour was sufficient, because in such cases thermal equilibrium was not necessary between titrand and titrant [2,8]. The volume of the amine solution taken into the Dewar flask was 15.0 cm^3 and this was magnetically stirred during the addition of titrant. The titrant was added in 0.25 cm^3 quanities. After each addition of titrant at least

one minute was allowed to elapse before measurements were made, to allow the solution to reach thermal equilibrium, and the temperature rise was read by the Beckmann thermometer. The temperature rise after each addition of the titrant was rather large to read with accuracy by the Beckmann thermometer. The overall time needed to complete a titration of an amine solution to obtain its percentage purity (recovery value) only is 45 min. Of this two-thirds of the time is spent waiting for thermal equilibrium and the remaining time is spent on the actual titration.

2.2. Chemicals

Nitrosyl perchlorate was prepared and purified as described in Ref. [25]. The main reaction taking place in the preparation of the compound are as follows:

$$NaNO_2 + HNO_3 \rightarrow NO + NO_2$$

$$NO + NO_2 + 2HClO_4 \rightarrow 2\ NOClO_4 + H_2O$$
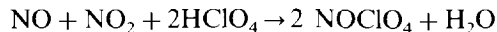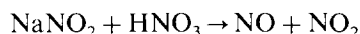
The white crystals formed in the reaction medium were filtered, washed and dried for 24 h under high vacuum. The compound obtained in this way decomposed at 108°C, and as described in the reference method is pure enough. So, it was accepted as the primary standard and was used to prepare a 0.050 M solution.

Acetonitrile and triethylamine (both 99% purity) were purchased from Merck and used after purification [26]. n-Propylamine, tert-butylamine, n-butylamine and sec-butylamine (all 98% purity) and di-n-propylamine, isopropylamine, di-n-butylamine, tri-n-butylamine, diethylamine, di-isopropylamine, tri-n-propylamine and isobutylamine (all 99% purity) were puchased from BDH and used without further purification.

Aniline (pure) was purchased from Riedel de Haen and used after purification [26]. N,N-dimethylaniline (98% purity) was purchased from Merck and used without further purification. 2-Nitroaniline (99% purity) was purchased from Fluka and used without further purification. 4-Nitroaniline was purchased from Riedel de Haen and used after purification twice [26].

3. Results and discussion

Thirteen aliphatic and four aromatic amines were titrated thermometrically with nitrosyl perchlorate in acetonitrile solvent. As examples the titration curves of the four amines are given in Fig. 1. Each amine was titrated four times and the titration curves were drawn. From such titration curves the recovery values were calculated and from the recovery values a mean recovery value and relative standard deviation were found. These are given in Table 1. In the calculation of the recovery values, the amines present were accepted to be standards.

In order to choose an appropriate solvent for this work, we tested a number of dipolar aprotic solvents such as nitrobenzene, dimethylsulfoxide, acetone, acetonitrile and found acetonitrile most appropriate. The dipolar aprotic solvents were tested because of the polar characters of the titrant and titrands and, in addition to this, the titrant has a definite ionic character. Acetonitrile
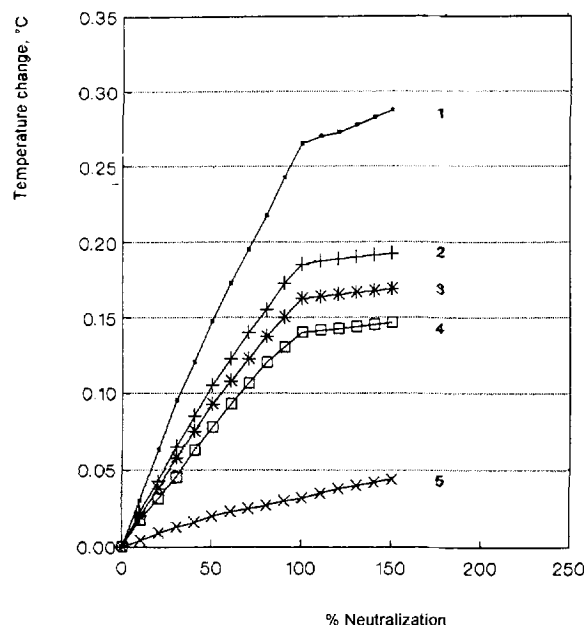

Fig. 1. Thermometric titration curves of some aliphatic amine (approx. 0.005 M) with nitrosyl perchlorate (0.050 M) in acetonitrile solvent, at 20 ± 1°C. (1) n-Butylamine, (2) isobutylamine, (3) sec-butylamine, (4) tri-n-butylamine, (5) a blank titration curve.

Table 1

The mean recovery values and the heats of reaction of the aliphatic and aromatic amines (approx. 0.005 M) titrated thermometrically with nitrosyl perchlorate (0.005 M) in acetonitrile solvent at $20 \pm 1°C$

Amine	No. of tests	Mean recovery value (%)	Rel. std. dev. (%)	Mean $-\Delta H_R$ (kJ mol^{-1})	Std. dev. (kJ mol^{-1})
Diethylamine	4	98.37	0.72	87.8	7.3
Triethylamine	4	99.31	0.39	72.6	2.3
n-Propylamine	4	99.72	0.40	74.5	5.5
Di-n-propylamine	4	99.14	0.48	76.4	2.7
Di-isopropylamine	4	98.95	0.76	73.3	5.2
Isopropylamine	4	98.81	0.18	79.4	1.6
Tri-n-propylamine	4	98.89	0.56	76.3	3.8
n-Butylamine	4	100.76	0.55	79.5	3.0
Di-n-butylamine	4	98.00	0.57	87.3	1.7
Isobutylamine	4	98.00	0.58	78.1	4.6
Sec-butylamine	4	98.65	0.08	74.1	4.8
Tri-n-butylamine	4	99.19	0.92	70.0	7.7
Tert-butylamine	4	99.15	0.97	74.6	4.8
Anioline	4	97.68	0.32	53.8	6.8
N,N-Diethylaniline	4	95.38	0.93	57.1	6.5
2-Nitroaniline	4	–	–	–	..
4-Nitroaniline	4	–	..	..	–

readily dissolved all the reactants and products. No precipitate was observed during the titrations.

The concentration of the amines was prepared to be approximately 0.005 M and the concentration of the titrant was exactly 0.050 M. These were the best concentrations fixed by the experiments. The titrations were performed discontinuously and the amount of the titrant added at a time was 0.25 cm³. The amount of amine solution taken from the stock solution was 15.0 cm³.

In order to check the validity of this method, we have also titrated all the amines named above with a potentiometric method in the same solvent with nitrosyl perchlorate and have obtained very similar results to those obtained with thermometric method [27].

The heat of reaction of an amine was calculated from its corrected titration curves. To do this, four corrected titration curves were drawn for each amine and from the initial slopes of these curves four heats of reaction were calculated for each amine. The average of these was taken as the heat of reaction of that amine. The heats of the amines are also collected in Table 1 together with the standard deviations. As is easily discerned from Table 1, the average heat of reaction (55.4

kJ mol⁻¹) of the aromatic amines is approximately two-thirds that of the average heat of reaction heat (77.2 kJ mol⁻¹) of the aliphatic amines. The direct and corrected titration curves of isobutylamine are given in Fig. 2, as an example.

In the calculation of the heats of reaction H_R, we have used the following relation [1,7,18,28]:

$$\frac{\Delta T}{\Delta V} = \frac{\Delta H_R \cdot M}{c \cdot d \cdot V + C'}$$

where $\Delta T/\Delta V$ is the initial slope of the corrected titration curve; M is the molarity of the titrant; c is the specific heat of the solvent; d is the density of the solvent; V is the volume of the reaction mixture in the Dewar flask at the end-point; and, C' is the heat capacities of the Dewar flask, stirrer, etc.

$\Delta T/\Delta V$, as a rule, is calculated from the initial slope (up to the 30% neutralization) of the corrected titration curve. In this region, the reaction between titrant and titrand is considered to be complete (mass action law) and the other effects such as mixing heat, dilution heat, stirring heat, etc. are nearly negligible.

For example, by using the following data ΔH_R for isobutylamine is found to be 82.8 kJ mol^{-1}: $\Delta T/\Delta V = 0.07$; $V = 16.45$ cm^3; $C' = 30.1$ J °C^{-1}; $d = 0.782$ g cm^{-3}; $c = 2.26$ J g^{-1} °C^{-1}; and $M = 0.050$ mol dm^{-3}.

As is easily discerned from the Table 1, the mean recovery values of aliphatic amines are good, but the mean recovery values of the aromatic amines are not good. The higher mean recovery value of aniline than that of N,N-dimethylaniline indicates that some steric hindrance prevents the nitrosyl ion in the case of N,N-dimethylaniline from reaching (hyperconjugation). On the other hand 2-nitro and 4-nitro anilines did not give any significant titration curves due to the strong electron withdrawing character of the nitro group. Such electron withdrawing effect of the nitro group depletes the amine group electronically by means of the phenyl group.

The reaction between an amine and nitrosyl acid is in the 1/1 mole ratio.

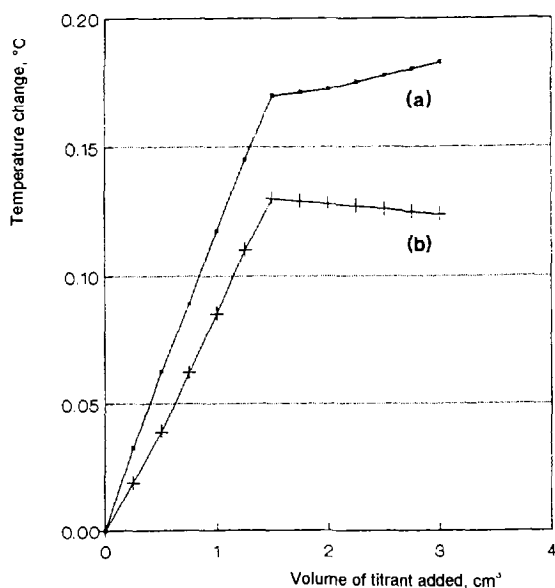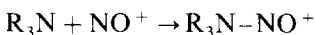$$R_3N + NO^+ \rightarrow R_3N-NO^+$$

Fig. 2. Direct (a) and corrected (b) thermometric titration curves of the isobutylamine (approx. 0.005 M) with nitrosyl perchlorate (0.050 M) in acetonitrile solvent at 20 ± 1°C.

(R stands for an alkyl, aryl or hydrogen group)

In order to support the reaction between an amine and nitrosyl ion, hydrochlorides of amines were also prepared and titrated with the nitrosyl ion under the same conditions as for the free amines, but no useful titration curves were observed. This clearly indicates that the reaction between an amine and nitrosyl ion is as shown above. A blank test for each amine was also performed under the same conditions and no significant mixing heat, dilution heat, stirring heat and heat exchange were observed taking into account Fig. 1 curve (5). The smooth increase of the titration curves from the beginning is also a good indication that the effects of these factors are not important in fixing end-points in such titrations. However, these effects have been taken into account in drawing corrected curves and in calculation of the heats of reaction of the compounds.

4. Conclusions

Common aliphatic amines can be titrated thermometrically with the nitrosyl ion in acetonitrile solvent, but aromatic amines under the same conditions cannot be titrated. The nitrosyl ion acts as a Lewis acid and is strong enough to titrate the aliphatic amines quantitatively, but it is not strong enough to titrate aromatic amines. The reaction between an aliphatic amine and nitrosyl ion is a typical Lewis acid–base reaction. The average heat of reaction in such cases is 77 kJ mol^{-1}.

Thermometric titrations can be accomplished by simple equipment in a medium equipped laboratory.

References

[1] H.J. Keily and D.N. Hume, Anal. Chem., 36 (1964) 543.

[2] L.S. Bark and S.M. Bark, Thermometric Titrimetry, Pergamon Press, Oxford, 1969, Chapter 7.

[3] H.J.V. Tyrell and A.E. Beezer, Thermometric Titrimetry, Chapman and Hall, London, 1968, Chapter 5.

[4] J. Kucharsky and L. Safarik, Titrations in Non-Aqeous Solvents, Elsevier, Amsterdam, 1965.

[5] J. Barthel, Thermometric Titrations, Wiley, New York, 1975, Chapter 5.

[6] L.D. Hansen R.M. Izaat and J.J. Christensen, in J. Jordan (Ed.) Applications of Thermometric Titrimetry to Analytical Chemistry, Treatise on Titrimetry. Vol. II, Marcel Dekker, New York, 1974.

[7] E.J. Forman and D.N. Hume, Talanta, 11 (1964) 129.

[8] J. Barthel, F. Becker and N.G. Schmahl, Z. Physik. Chem. Neue Folge, 29 (1961) 58.

[9] H.W. Linde, L.B. Rogers and D.N. Hume, Anal. Chem., 25 (1953) 404.

[10] I.M. Kolthoff and V.R. Stenger, Volumetrik Analysis, Vol. 1, Interscience Publishers, New York, 1941.

[11] E.J. Greenhow, Chem. Rev., 77 (1977) 835.

[12] J. Jordan, J.K. Grime and D.H. Waugh. Anal. Chem., 48 (1976) 427.

[13] S.I. Ajiboye and L.S. Bark, J. Thermal Anal., 35 (1989) 1739.

[14] S.I. Ajiboye and L.S. Bark, J. Thermal Anal., 39 (1989) 1495.

[15] J.O. Hill and S. Korce, Thermochim. Acta, 148 (1989) 341.

[16] J.M. Estela, M. Far and V. Cerda, Thermochim. Acta, 153 (1989) 143.

[17] G.A. Vaughan and J.J. Swithenbank, Analyst, 92 (1967) 364.

[18] E.J. Forman and D.N. Hume, J. Phys. Chem., 63 (1959) 1949.

[19] A. Izquierdo, J. Carrasco, R. Arenos, Thermochim. Acta, 113 (1987) 257.

[20] J.A. Hatcher, J.A. Lynch and E.T. Lane, Microchem. J., 47 (1993) 127.

[21] T. Gündüz, N. Gündüz, E. Kiliç, A. Kenar, G. Çetinel, Analyst, 111 (1986) 1099.

[22] T. Gündüz, N. Gündüz, E. Kiliç, A. Kenar, Analyst, 111 (1986) 1103.

[23] T. Gündüz, E. Kiliç, O. Atakol and A. Kenar, Analyst, 112 (1987) 1735.

[24] T. Gündüz, E. Kiliç and O. Çakirer, Talanta, 42 (1995) 1757–1759.

[25] G. Brauer, Handbuch der Preparativen Anorganischen Chemie, Ferdinant Enke Verlag, Stuttgart, 1954.
K. Cruse, B. Drobny, G. Huck and H. Möller, Z. Chem. 259 (1949) 154.

[26] D.D. Perrin, W.L.F. Armerago and R.D. Perrin, Purification of Laboratory Chemicals, Pergamon Press, Oxford, 1966.

[27] T. Gündüz, E. Kiliç and O. Çakirer, unpublished work, 1993.

[28] H.J. Keily and D.N. Hume, Anal. Chem., 28 (1956) 1294.

Alcohol biosensor based on alcohol dehydrogenase and Meldola Blue immobilized into a carbon paste electrode

S. García Mullor[a], M. Sánchez-Cabezudo[a], A.J. Miranda Ordieres[b], B. López Ruiz[a],*

[a]Secc. Dptal. Química Analítica, Facultad de Farmacia, Universidad Complutense, 28040 Madrid, Spain
[b]Departamento de Química Física y Analítica, Universidad de Oviedo, 33071 Oviedo, Asturias, Spain

Abstract

A yeast alcohol dehydrogenase amperometric carbon paste-based biosensor, with Meldola Blue as a mediator and a dialysis membrane with a very small molecular weight cut-off for protection, is described. The influence of membrane pore size on the stability and overall kinetics of the biosensor is shown using cyclic voltammetry and stationary potential measurements. The operating potential is +50 mV vs. Ag/AgCl, KCl sat. reference electrode. Application of this device to the determination of ethanol in alcoholic beverages was achieved successfully. In these kinds of samples and at this working potential no interferences were found.

Keywords: Biosensor; Alcohol; Alcohol dehydrogenase; Meldola Blue

1. Introduction

The determination of all kinds of alcoholic compounds, particularly ethanol, in a variety of samples is important. The determination of ethanol is particularly relevant to the food industry, especially in alcoholic beverages such as beer, wines, and spirits.

Biosensors, devices involving immobilized biological material connected to an appropriate detector system, have been successfully used in several clinical, industrial, environmental, and food determinations Ref. [1–5].

In the case of ethanol, a number of enzyme-based electrochemical devices have been developed. There are two appropriate enzymes for this purpose: alcohol oxidase (AOD) Ref. [6–8] and alcohol dehydrogenase (ADH) Ref [9,10]. ADH has been used less frequently than AOD because this enzyme depends on NADH, the co-enzyme, for enzymatic activity, and consequently co-immobilization of both enzyme and co-enzyme is needed. In addition, this co-enzyme requires an overpotential of about 1 V for oxidation, and at this potential a number of other substances, present in food samples, are also oxidized and interfere in the measurement.

---

* Corresponding author. Fax: +34 1 394 1754.

There is a way of improving the electron-transfer kinetics; this consists of the use of a substance with electrocatalytic properties (redox mediator) for oxidation of NADH. Biosensors based on ferrocene Ref. [11,12], quinones Ref. [13,14], viologen derivatives Ref [15], tetrathiofulvalene Ref. [16], phenoxazines Ref. [17], ruthenium Ref. [18], osmium polymers Ref. [19,20], several organic dyes Ref. [21–26], etc., have been reported. Water-insoluble mediators are preferred because of the facility of retaining in carbon paste. However, water-insoluble mediators are not always the best electrocatalysts. When water-soluble mediators are used they must be prevented from dissolving into the contact solution, and the electrode is frequently covered with different types of polymeric film. The preparation of these films takes time and the stability of the resulting biosensor is usually unacceptable.

The amperometric alcohol biosensor described in this paper consists of a modified carbon paste electrode (MCPE) into which the enzyme ADH, the co-enzyme NAD⁻, and a water-soluble mediator, Meldola Blue (MB) have been incorporated. To retain all of these substances in the paste for a reasonably long time, a dialysis membrane with a molecular weight cut-off (MWCO) of 500 Da has been used in this work.

MB has been chosen because of its convenient oxidation of NADH via a catalytic effect which permits the use of an applied potential of about 0.0 V. Using this potential most electrochemical interferences are eliminated. The replacement of the polymeric film by a dialysis membrane presents two advantages: (1) very simple and fast electrode fabrication; (2) high stability over time (stable response for about a month).

2. Experimental

2.1. Apparatus

Cyclic voltammetry and amperometric measurements were performed using a Polarecord E 506 Metrohm and a triangular wave generator VA-Scanner E 612 Metrohm connected to an X–Y recorder. All the experiments were carried out in a

20 ml electrochemical cell using a platinum wire auxiliary electrode. a silver/silver chloride/saturated potassium chloride reference electrode, and the modified carbon paste working electrode.

2.2. Reagents

All solutions were prepared with distilled water. The enzyme ADH (EC 1.1.1.1) from baker's yeast, and β-nicotinamide adenine dinucleotide, in its oxidized form of NAD⁻ and reduced form NADH, were purchased from Sigma Chemical Co. MB was from Aldrich. The cellulose ester dialysis membranes, with MWCO 2000 and 500, were obtained from Spectra/Por. Graphite powder and paraffin oil were obtained from Fluka. All other reagents were of analytical-reagent grade. The buffer used was a 0.10 M phosphate buffer, pH 7.5.

2.3. Electrode preparation

The carbon paste was prepared by hand-mixing the graphite powder together with ADH (4%), NAD⁺ (8%) and/or MB (2%) in a mortar for about 15 min until a uniform paste was obtained. Then 30 μl paraffin oil was added for each 100 mg of paste, and mixed for another 15 min. The electrode was constructed using a 1.0 ml plastic syringe with a copper rod inside, with a diameter equal to the inner diameter of the syringe. The modified carbon paste was tightly packed into the syringe. The copper rod serves as electrical contact. The surface of the electrode was polished by rubbing gently on a sheet of white paper, to produce a flat, shiny surface. Finally, the electrode was covered with the dialysis membrane with the aid of an O-ring. Electrodes were stored at 4°C in phosphate buffer, pH 7.5, when not in use.
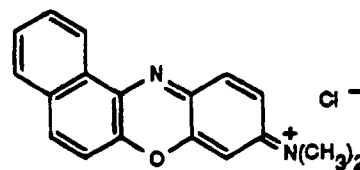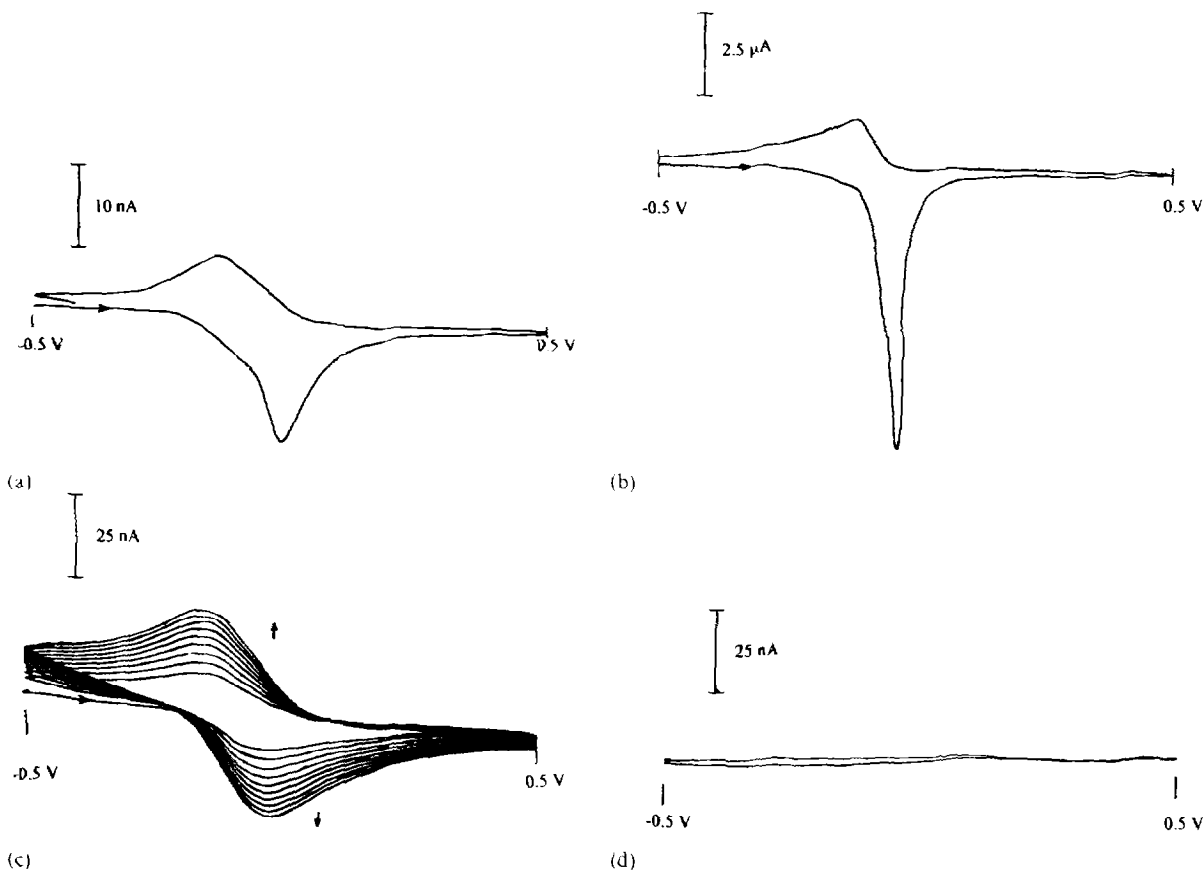

Scheme 1

Fig. 1. Cyclic voltammograms of 1.0×10^{-3} M MB in phosphate buffer solution: (a) unmodified carbon paste electrode; (b) glassy carbon electrode; (c) unmodified carbon paste electrode covered with a MWCO 2000 dialysis membrane; (d) unmodified carbon paste electrode covered with a MWCO 500 dialysis membrane.

3. Results and discussion

3.1. Cyclic voltammetry

Cyclic voltammetry was used to ascertain the electrochemical properties of the proposed sensor as well as the stability of the amperometric response to ethanol.

First of all, when continuous cyclic voltammograms of the MCPE modified with 3% MB were recorded, both anodic and cathodic currents decreased in each cycle. This confirmed the tendency of the MB to enter the solution because of its high solubility in water. After this, three different cyclic voltammograms for 1×10^{-3} M MB in buffer solutions were recorded and are shown in Fig. 1. Voltammogram (a) corresponds to an MB

solution using an unmodified CPE without membrane; MB reaches the electrode and shows quasi-reversible electrochemical behaviour with $\Delta E = 125$ mV. In addition, the shape of the anodic peak indicates that the reduced form is adsorbed on the electrode surface, probably due to the lower water solubility of this form. This peak changes its shape, showing the same aspect as the cathodic peak, when the concentration of MB is about 1×10^{-5} M. When a glassy carbon surface is used, a sharper peak is also present (Fig. 1(b)), confirming the different solubilities of the reduced and oxidized MB forms, and the electron transfer rate is significantly faster ($\Delta E = 78$ mV). When the CPE is covered with the MWCO 2000 dialysis membrane (Fig. 1(c)), MB also reaches the electrode surface and, from a reversibility point of

view, exhibits an electrochemical behaviour similar to its behaviour without the membrane ($\Delta E =$ 125 mV). However, the sharp anodic peak disappears and peak currents, both anodic and cathodic, increase with consecutive cyclic scans. In contrast, when the CPE was covered with the MWCO 500 dialysis membrane, no signal was observed (Fig. 1(d)). This means that the MB cannot reach the electrode surface, i.e. MB cannot pass through this membrane, confirming that this membrane can retain MB in the carbon paste electrode.

In the second set of experiments, MB was incorporated into the carbon paste (3% w/w) and the electrode was covered with the MWCO 2000 dialysis membrane. The MB exhibited a similar behaviour inside the paste to that in the solution, independent of the pore size of the membrane. The electron transfer rate seems slightly slower when MB is inside the paste; this must be due to the difficulty of diffusion in an oily medium. When MB is in solution, as well as when MB is inside the carbon paste, it always reaches the electrode surface by diffusion, as was shown by the straight line obtained when i_a was plotted vs. the square root of the potential scan rate.

The electrocatalytic oxidation of NADH in the presence of MB has been previously reported Ref. [20]. The cyclic voltammogram corresponds to that of the biosensor with a MWCO 500 membrane, in phosphate buffer, and shows a quasi-reversible behaviour similar to that shown by the MB in solution when a CPE was used. In the first scan $\Delta E = 195$ mV and $i_c/i_a = 3.36$, but in the last scan $\Delta E = 292.5$ mV and $i_c/i_a = 1.34$. Therefore the complete operation of the biosensor, including both enzymatic and electrochemical reactions, can be illustrated as shown below:

The electrochemical reaction $MBH \rightleftharpoons MB^+ + H^+ 2e^-$ that takes place at the electrode surface is reversible and closes the cycles of all these reac-
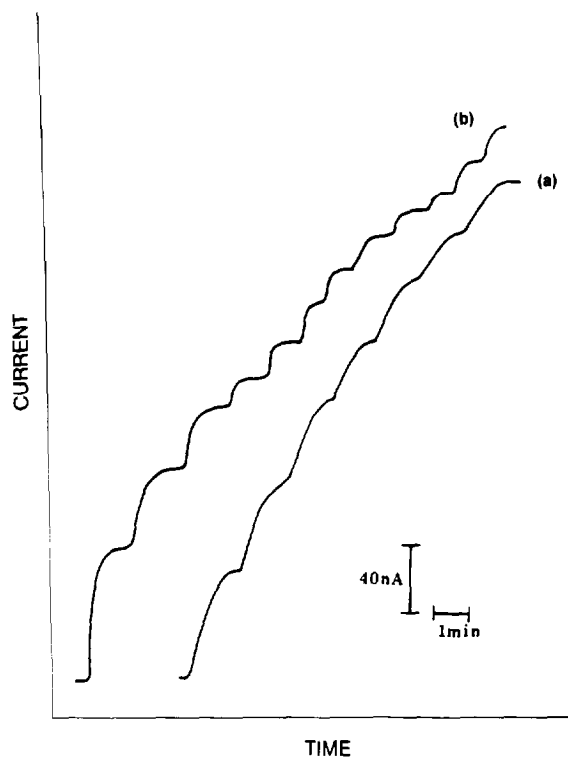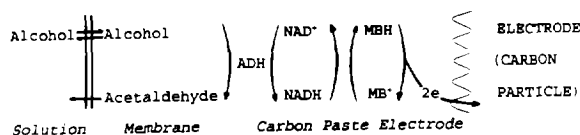

Fig. 2. Amperometric response for successive additions of 1.0 mM ethanol solution: (a) biosensor covered with a MWCO 500 dialysis membrane; (b) biosensor covered with a MWCO 2000 dialysis membrane.

tions. Therefore, the changes in anodic current produced by this biosensor are proportional to the alcohol concentration changes in the sample.

3.2. Stationary potential measurements

Fig. 2 shows the response of the biosensor at a constant potential of 0.05 V vs. Ag/AgCl KCl sat., immersed in a stirred phosphate buffer solution and when successive additions of ethanol were made. The biosensor response when covered with the MWCO 2000 membrane is slightly faster than when MWCO 500 membrane was used, probably due to the difficulty of MB crossing the membrane, but the increase in the current becomes lower and lower with successive additions, perhaps because of the loss of mediator facilitated by the stirring of the solution.

Fig. 3. Calibration graph for ethanol in a phosphate buffer solution, using the proposed biosensor: (a) covered with a MWCO 2000 dialysis membrane: (b) covered with a MWCO 500 dialysis membrane.
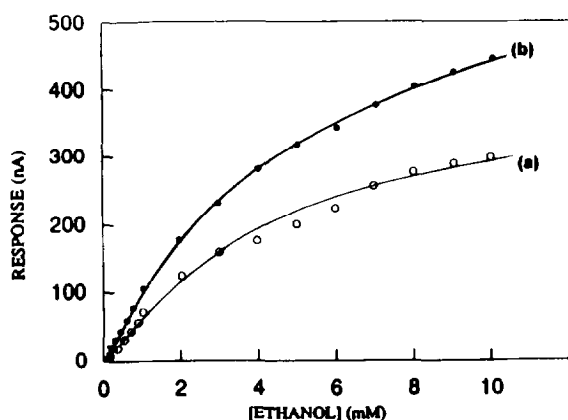
Calibration graphs were performed for each step of the biosensor preparation. In the first step only the enzyme was incorporated into the paste, and the co-enzyme and MB were in the solution to which the alcohol sample was added. In the second step, when enzyme and co-enzyme were added to the paste, the results were the same. However, the response of the biosensor was the highest, up to twice the response in all the other experiments described above, which proves that in order to obtain a rapid global reaction, physical contact between enzyme, co-enzyme and mediator is needed. The linear range was also the largest, 0.1–20 mM, showing a higher detection limit of 20 mM and a lower detection limit of 0.1 mM. In this case, as Fig. 3 shows, the smaller the pore size of the membrane, the larger the response. This could be due, as was indicated above, to the loss of the mediator.

3.3. Analysis of alcoholic beverages

The performance of the biosensor was tested by applying it to the determination of the ethanol concentration of different beverages: whisky, gin anis (aniseed liqueur) and wine have been analysed using the proposed biosensor.

The only sample treatment required was an appropriate dilution, (1:20000) for the wine and (1:50000) for the others, with phosphate buffer solution to fit the analyte concentration within the linear range of the calibration curve. The high dilution used presents an additional advantage because the greater the dilution, the lower the interferences that are detected.

The quantification method chosen was standard addition, because when the calibration curve method was employed the reproducibility of the results obtained on different days was lower. These samples were also analysed following the *Official Method of the European Community* (1985), consisting of a distillation. Table 1 summarizes the concentrations found and the recoveries obtained by the biosensor. As can be seen, the results show excellent agreement with the label of the beverage and with the results obtained by the *Official Method*.

4. Conclusions

The approach reported here consists of a physical immobilization of the enzyme, co-enzyme and mediator, without chemical reaction and without successive steps for each molecule. The dialysis membrane proposed is of such small pore size that all the molecules remain in the paste for an ex-

Table 1
Results for alcohol determinaiton in alcoholic beverages

Beverage	Label indicated alcohol content (%)	Experimentally obtained alcohol content (%) ($N = 5$)	RSD (%)	Recovery (%) ($N = 5$)
Whisky	40	38.0 ± 0.5	1.3	96.5 ± 1.4
Gin	40	34.6 ± 1.3	3.8	108.0 ± 13.5
Anis	36.5	37.9 ± 1.4	3.7	95.0 ± 17.0
Wine	12	12.7 ± 3.0	23.6	104.0 ± 3.5

tended period of time even when they are hydro-soluble. In addition, the preparation of the biosensor is very simple, and requires only a short time. The only requirement for reliable sensor response is the polishing of the surface before each determination. Therefore, the main advantages of this device are due to the presence of the dialysis membrane which permits easy preparation and provides a long period of stability of the biosensor. It also presents similar higher and lower limits of determination and linear range to those of previous alcohol biosensors. The analytical application of this biosensor in the ethanol determination of real samples has been demonstrated and offers an interesting alternative to other determinations of ethanol, with applications in clinical, biotechnological and agricultural analysis.

Acknowledgements

References

[1] L. Gorton, G. Bremle, E. Csöregi, G. Jönsson-Pettersson and B. Persson, Anal. Chim. Acta, 249 (1991) 43.

[2] L. Gorton, E. Csöregi, E. Dominguez, J. Emnéus, G. Jönsson-Pettersson, G. Marko-Varga and B. Persson, Anal. Chim. Acta, 250 (1991) 203.

[3] E. Pariente, L. Hernandez and E. Lorenzo, Bioelectrochem. Bioenerg., 27 (1992) 73.

[4] M.H. Smit and G.A. Rechnitz, Anal. Chem., 64 (1992) 245.

[5] J. Czaban, Anal. Chem., 57 (1985) 345A.

[6] E.L. Gulberg, A.S. Attiyat and G.D. Christian, J. Autom. Chem., 2 (1980) 189.

[7] M. Mason, Am. J. Enol. Vitic., 34 (1983) 173.

[8] G.G. Guilbault, B. Danielsson, C.F. Mandenius and K. Mosbash, Anal. Chem., 55 (1983) 1582.

[9] E. Dominguez, H.L. Lan, Y. Okamoto, P.D. Hale, T.A. Skotheim, L. Gorton and B. Hahn-Hagerdal, Biosens. Bioelectron., 8 (1993) 229.

[10] Q. Chi and S. Dong, Anal. Chim. Acta, 285 (1994) 125.

[11] J. Wang, L. Wu, Z. Lu, R. Li and J. Sanchez, Anal. Chim. Acta, 228 (1990) 251.

[12] L. Gorton, H.l. Karan, P.D. Hale, T. Inagaki, Y. Okamoto and T.A. Skotheim, Anal. Chim. Acta, 228 (1990) 23.

[13] C. Ueda, D.C.S. Tse and T. Kuwana, Anal. Chem., 54 (1982) 850.

[14] T. Ikeda, T. Shibata and M. Senda, J. Electroanal. Chem., 261 (1989) 351.

[15] P. Hale, L. Boguslavsky, H. Karan, H. Lan, H. Lee, Y. Okamoto and T. Skotheim, Anal. Chim. Acta, 248 (1991) 155.

[16] H. Gunashingham and C. Tan, Analyst, 115 (1990) 35.

[17] G. Bremle, B. Persson and L. Gorton, Electroanalysis, 3 (1991) 77.

[18] N. Morris, M. Cardosi, B. Birch and A.P. Turner, Electroanalysis, 4 (1992) 1.

[19] E. Rohde, E. Dempsey, M.R. Smyth and J.G. Vos, Anal. Chim. Acta, 278 (1993) 5.

[20] J.T. Ohara, R. Rajagopalan and A. Heller, Anal. Chem., 65 (1993) 3512.

[21] R. Ghosh and J.R. Quayle, Anal. Biochem., 99 (1979) 112.

[22] S. Yabuki, F. Mizutani and M. Asai, Biosens. Bioelectron., 6 (1991) 311.

[23] J. Kulys, H.E. Hansen, T. Bush-Rasmussen, J. Wang and M. Ozsoz, Anal. Chim. Acta, 288 (1994) 193.

[24] S.D. Sprules, J.P. Hart, S.A. Wring and R. Pittson, Analyst, 119 (1994) 253.

[25] M.A.T. Gilmartin, J.P. Hart and B.J. Birch, Analyst, 119 (1994) 243.

[26] G. Jönsson-Petersson and L. Gorton, Biosensors, 1 (1985) 237.

Poly(o-aminophenol)-modified bienzyme carbon paste electrode for the detection of uric acid[1]

E. Miland[a,2], A.J. Miranda Ordieres[a], P. Tuñón Blanco[a,*], M.R. Smyth[b], C. Ó Fágáin[c]

[a]Departamento de Química-Física y Analítica, Universidad de Oviedo, 33006 Oviedo, Asturias, Spain
[b]School of Chemical Sciences, Dublin City University, Dublin 9, Ireland
[c]School of Biological Sciences, Dublin City University, Dublin 9, Ireland

Abstract

A reagentless uric acid selective biosensor constructed by immobilising uricase and horseradish peroxidase (HRP) in carbon paste without the addition of an electron transfer mediator is described. The response of the electrode is based on the enzymatic reduction of hydrogen peroxide in the presence of uric acid. Uricase and HRP were dispersed in the carbon paste and the optimum paste mixture was determined. Poly(o-aminophenol) was electropolymerised at the working surface area of the electrode acting as a conducting polymer layer. Cyclic voltammetry was used to characterise the permselective characteristics of the polymer layer. At an applied potential of 50 mV vs. Ag/AgCl, a linear response was obtained up to 1×10^{-4} M, with a limit of detection of 3×10^{-6} M. The sensor had a response time of 37 s, a calibration precision of 2.2% ($n = 4$) and an estimated sample frequency of 20 h^{-1}. Responses to the analyte of interest were pH dependent. The sensor was incorporated into a flow injection system for the qualification of uric acid in human serum. Results compared favourably with a standard spectrophotometric method.

Keywords: Aminophenol(poly)-modified electrode; Enzyme electrode; Uric acid

1. Introduction

The detection, identification and quantification of uric acid (2,6,8-trihydroxypurine) in human physiological fluids is of great importance in the diagnosis and therapy of patients suffering from a range of disorders associated with altered purine metabolism, most notably gout and hyperuricaemia [1]. Other medical conditions, such as leukaemia and pneumonia, have been associated with enhanced urate levels. A number of detection methods based on the reduction properties [2] of the molecule have been employed. A more selective approach is the use of uric oxidase which specifically catalyses the oxidation of urate resulting in the production of allantoin (Eq. (1)).

$$\text{uric acid} + O_2 + 2H_2O \rightarrow \text{allantoin} + H_2O_2 + CO_2 \tag{1}$$
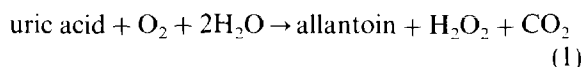
Allantoin, and its enzymatically reduced product, allantoic acid, account for 70–80% of the organic nitrogen in the xylem of nitrogen-fixing soybean plants and other species of tropical grain legumes [3]. Dilena et al. [4] utilised UV spectrophotometry to detect enzymatic degradation of uric acid by exploiting the chromophore existing at the C(4)=C(5) bond. Uric acid has been shown to rapidly adsorb onto carbon paste electrode surfaces [5–7]; this phenomenon has led to the development of a controlled adsorption process for its selective determination in flowing streams.

Various types of electrochemical enzyme sensors have been reported for urate determination [8–10]. The first amperometric method for its quantitative determination in biological fluids was reported by Nanjo and Guilbault based on the consumption of dissolved oxygen [11]. Janchen et al. carried out similar studies in the presence of oxygen [12]. Coulometry, using a porous carbon felt electrode, has also been applied to its determination in human urine. The compound of interest was electrolysed with nearly 100% current efficiency at the carbon surface. Hydrogen peroxide however, is not electroactive at this surface [13,14].

As previously stated, uricase specifically catalyses the oxidation of uric acid. The disappearance of oxygen, H_2O_2 or CO_2 production [15] may be exploited for urate sensing. In the first situation, dissolved O_2 may also be consumed by compounds such as ascorbic acid and thiol-containing substances [16]. Moreover, ascorbate and thiols may also react with peroxide produced by the uricase-catalysed reaction of uric acid. Electrochemical enzyme sensors have been developed based on the amperometric determination of enzymatically liberated H_2O_2 from the uricase reaction (Eq. (1)) [17–20]. These systems exploit the anodic electroactivity of peroxide. Unfortunately, its oxidation has been reported to require relatively high applied potentials (> 0.4 V) and is therefore susceptible to interferences from readily oxidizible molecules. The elimination of interfer-

ences was achieved by Kulys and colleagues when horseradish peroxidase (HRP) served as a catalyst for the reaction between H_2O_2 and hexacyanoferrate(II) followed by reduction of the resulting hexacyanoferrate(III) at 0 V vs. Ag/AgCl [21]. Tatsuma and Watanabe observed that with a uric acid oxidase/HRP bi-layer modified electrode, anodic current (at an applied potential of + 0.5 V) results primarily from urate oxidation and is only partially due to peroxide oxidation [19]. Operating at a lower potential of + 150 mV, coupled with a HRP mediator system, significantly reduces the magnitude of urate oxidation. Its detection in peroxidase-containing systems can be adversely affected, as oxidised urate can donate electrons to peroxidase, thus reducing its capacity to detect enzymatically generated H_2O_2 [22].

The feasibility of using HRP for the amperometric biosensing of organic peroxides is known [23]. In 1979, there was a report of an electron transfer between carbon black and the active sites of HRP without the addition of a mediator [24]. Peroxidases other than HRP such as cytochrom c peroxidase [25] and a fungal peroxidase from *Arthromyces ramosus* [26] have been applied in this fashion. Gorton has reviewed the increasing number of reports on mediatorless mode electrodes where charge transfer between the electrode and enzyme occurs only if the enzyme is in intimate contact with the conducting surface [27]. Peroxidase and glucose oxidase have been co-immobilized on graphite to provide a reagentless glucose sensor even though the nature of electron transfer was unclear [28]; Wollenberger et al. have suggested the possible role of surface functionalities in electron mediation [29].

In this paper, we describe the development of a novel reagentless bienzyme sensor for the indirect amperometric detection of uric acid via the bio-catalytic production of hydrogen peroxide. The co-immobilisation of uricase and HRP in carbon paste, coupled with the electropolymerisation of *o*-aminophenol at the surface of the electrode, has proven to be an interesting alternative to conventional methods for the preparation of biosensors. Such modified surfaces are of interest from an analytical viewpoint in that they may be used to enhance analyte permeability while reducing inter-

ference effects. The sensor was also examined for its applicability to urate quantification in human serum.

2. Experimental

2.1. Reagents

Horseradish peroxidase (HRP, E.C. 1.11.1.7, type VI A), uric acid, uricase (uric acid oxidase, E.C. 1.7.3.3) and cellulose membrane dialysis tubing (12 000 Da cutoff) were purchased from Sigma. Hydrogen peroxide was obtained from Aldrich. o-Aminophenol was purchased from Fluka Chemika.

Standard urate solutions were made up daily by dissolving uric acid in a stoichiometric excess of NaOH, made up in background electrolyte, 0.1 M phosphate buffer. Standards were then wrapped in aluminium foil to prevent thermal and photodegradation. Carbon paste was prepared by mixing 1.8 ml of paraffin oil (Uvasol, Merck) with 5 g of spectroscopic grade graphite powder (Ultra Carbon, Dicoex, Bilbao). All other reagents (sulphuric acid, sodium hydroxide) were of analytical grade. Serum samples obtained from Bio-Quim Laboratories (Oviedo), were diluted as deemed appropriate with background solution.

2.2. Apparatus

Cyclic voltammetry and amperometry were performed using a Metrohm E612 VA scanner in conjunction with an E641 VA detector, connected to a Linseis LY1600 x–y recorder plotter to record voltammograms. A Linseis L6012B revorder was used for recording amperometric measurements. Static measurements were carried out in a Metrohm glass cell, incorporating a conventional three-electrode system. The working electrode was a piston-type carbon paste electrode with a Teflon body and stainless steel contact. The active surface was a disk with a geometric area of 7.1 mm^2. Potentials were measured and referred to a silver/silver chloride/saturated potassium chloride reference electrode. A platinum wire served as an auxillary electrode. The test solution

(20 ml) was magnetically agitated (500 rev min^{-1}) when necessary. The rate of agitation was measured using an electronic speed meter (Heidolph 2001).

Flow injection amperometric measurements were carried out using a twelve cylinder Spetec Perimax 12 Peristaltic pump and a six-port rotary valve (Rheodyne 7125) as carrier propulsion and injection systems, respectively. Analysis was carried out in a home-made thin-layer flow cell (Kissinger design) [30], equipped with a working electrode of geometric proportions as described previously. A down stream compartment connected to the thin layer cell outlet contained the reference electrode incorporating a low resistance liquid junction and a stainless steel waste tube acting as a counter electrode.

The kinetic parameters k_m and V_{max} for the bienzyme electrodes were calculated using an Enzfitter programme.

2.3. Electrode preparation

Uricase, HRP and ferrocene (used in preliminary trials) were added to unmodified carbon paste and mixed thoroughly for 30 min. The resulting mixture was packed into the well of the working electrode to a depth of approximately 2 mm and the surface then smoothed on a sheet of white paper. Easily renewable surfaces are highly desirable as HRP undergoes inactivation upon exposure to increasing concentrations of peroxide [29].

Electropolymerisation of the monomer (o-aminophenol) at the working surface area of the electrode was carried out in 0.1 M acetic acid, pH 5.0, in the potential range 0–0.7 V for 10 min at a scan rate of 50 mV s^{-1}. The acetic acid medium was previously purged with helium to remove moleclar oxygen. The quality of the electropolymerised layer was verified by carrying out a cyclic scan in the aforementioned voltage range. The electrode was then rinsed for a short time in phosphate buffer. In both static and flow systems, the assembled cell was equilibrated with the supporting electrolyte (not purged with helium as molecular oxygen acts as a natural co-factor for uricase, thus depleting H_2O_2 production) while

applying a working potential. Signals were recorded after the transient signal decayed.

3. Results and discussion
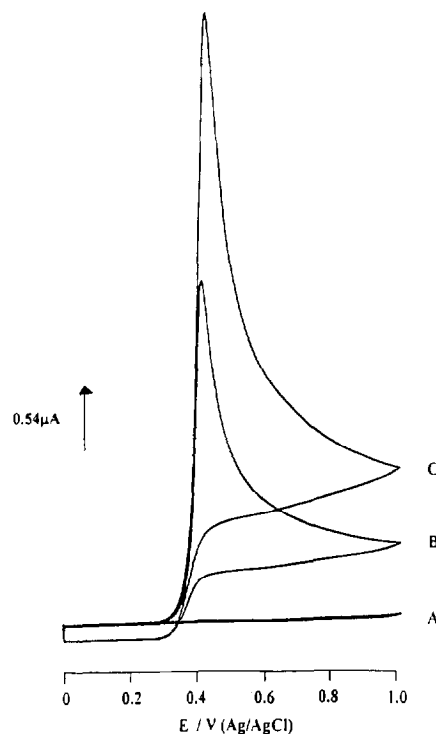
3.1. Cyclic voltammetry

Cyclic voltammetry was performed on bare and polymer-modified electrodes to examine their permselective and electrocatalytic properties. Fig. 1(a) and 1(b) depict the electro-oxidation of uric acid to allantoin on bare and polymer-coated surfaces, respectively. Oxidation-type reactions of reduced biomolecules such as urate involve anodic processes, the magnitude of this current being proportional to increasing analyte concentration. This particular process occurs at both electrodes, at an almost identical potential (+ 0.4 V), the anodic current reduced approximately 50% at the poly(o-aminophenol)-modified electrode. This is expected as such membrane-covered electrodes generally yield signals of smaller magnitude due to the imposition of an additional diffusion barrier. The ratio between the current at the latter electrode and that of the bare electrode is a measure of coating permeability.

The permeability properties of poly(o-aminophenol) acting as a conducting polymer were compared to those of a cellulose dialysis membrane (12 000 Da cut-off) by amperometry. An optimised loading of enzyme was used (see later) in the carbon paste.

The polymer-modified electrode has a higher maximum enzymatic reaction rate, $V_{max} = 3.17 \times 10^{-1}$, compared to that of the cellulose membrane covered electrode, $V_{max} = 1.91 \times 10^{-1}$. The apparent Michaelis constant, K_m, of the latter electrode was 1.99×10^{-3}, which was slightly higher than that of the polymerised sensor ($K_m = 1.92 \times 10^{-3}$). The higher K_m value would suggest mass transfer limitations between the bienzyme layer and the analyte solution (Fig. 2).

Hydrolysis of membrane films has been reported to increase porosity [31]. A similar idea was investigated in the case of poly(o-aminophenol). On storage in 0.1 M phosphate buffer, pH 7.5, amperometric responses to standard additions

of uric acid increased by approximately 150% after 2 h. The enzymatic production of peroxide due to uricase catalysis may in some way alter the

(a)
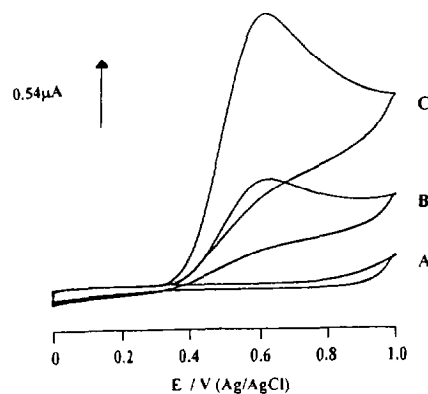
(b).

Fig. 1. Cyclic voltammetric behaviour of uric acid at (a) unmodified carbon paste electrode (no enzyme present) (b) poly(o-aminophenol)-modified electrode. (A) 0.1 M phosphate buffer, pH 6.5; (B) 0.5 mM uric acid; (C) 1.0 mM uric acid. Conditions: sensitivity, 5 μA; scan range, 0 to + 1.0 V; scan rate, 50 m V s^{-1}.

Fig. 2. Dependence of current (nA) on uric acid additions in 0.1 M phosphate, pH 6.5. Poly(o-aminophenol)-modified carbon paste electrode (■); cellulose membrane covered carbon paste electrode (●); applied potential +0.05 V.
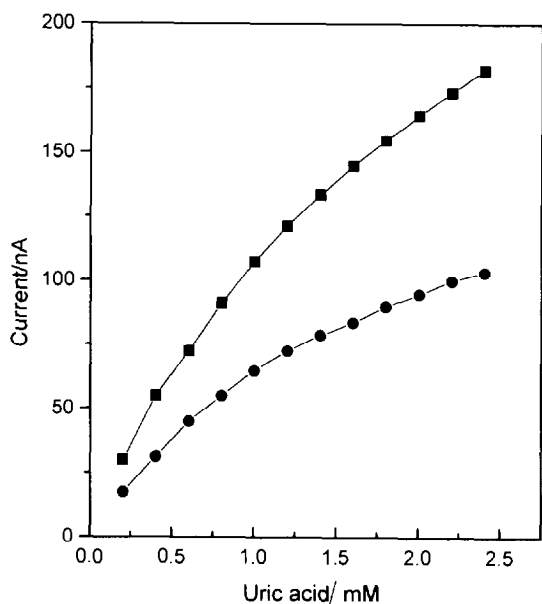
selectivity properties of the polymer, causing an increase in film permeability with time. Such "increases" in signals remained for 24 h followed by a return to initial signal intensities; this phenomenon is probably due to a number of complex processes.

The effect of increasing the concentration of monomer during the electropolymerisation process was explored. An increasing concentration resulted in more intense signals to injections of uric acid standards, in stirred solutions. This phenomenon was also observed when the sensor was applied to a flowing stream set-up. Faster response times were recorded (24s for $t_{95\%}$ of signal) for a polymer layer built in a 5×10^{-4} M concentration of o-aminophenol as opposed to 39s for a 10-fold increase in monomer concentration (flow rate, 1 ml min^{-1}). Operation at a higher flow rate of 2 ml min^{-1} resulted in a reduction of 42% in estimated response times. These results indicate a rapid replenishment of the solution from the surface, i.e. lack of analyte trapping. Another explanation for this is that the faster the sample plug passes the electrode, the smaller the fraction of

consumed sample in the enzyme layer at the electrode surface (kinetic limitations) [28]. Fast sensor response times are an important prerequisite in flow injection applications, however a reduction in signal intensity usually results.

The polymer film was formed at the CPE surface by electrodeposition. This layer is required only for retaining the enzyme composition in the carbon paste [33]. Polymerisation of o-aminophenol continues until the surface is completely covered, which is signalled by the current decreasing to a minimum as the monomer cannot penetrate this film [34]. The dispersion of the flow at 0.85 and 2.48 ml min^{-1} was evaluated from measurements of 5×10^{-5} M uric acid. The dispersion factors, $D = (i_{\text{steady state}}/i_{\text{peak max}})$ [32] of the flow system was 1.0 for a flow rate of 0.85 ml min^{-1} and 1.15 for 2.48 ml min^{-1}.

3.2. Optimization of uric acid sensor design

A study was undertaken to examine the necessity for an electron transfer mediator [27]. Carbon paste electrodes containing 5% w/w ferrocene and 10% w/w enzyme (uricase + HRP), exhibited slow responses and small amperometric signals to uric acid additions. Removal of ferrocene from the electrode alleviated this problem. On addition of uric acid standards to the test solutions incorporating ferrocene-modified electrodes, peaks in current were followed by slow gradual decreases to the original baseline level due to the diffusion of ferricinium ions to the bulk solution. Coating the electrode surface with a cation-exchange membrane such as Nafion would prevent such a diffusional effect [35]. Non-ferrocene containing electrodes did not exhibit this behaviour.

An investigation was performed to find the optimum ratio of the amounts of HRP and uricase used in the reaction mixture for immobilisation. The amount of immobilised enzyme utilised in all preliminary investigations did not exceed 15% w/w. Greater percentages did not improve the response characteristics of the sensor. Different paste mixtures were prepared with one enzyme maintained at a fixed % (w/w) value while the proportion of the other was varied. Fig. 3 illustrates the responses to urate for various paste

compositions. A gradual increase with relative increases in % uricase was noted. Response times reduced with increasing proportions of uricase up to a certain point, after which they were stable. Electrodes modified with 3% (w/w) HRP gave rise to the greatest sensitivity; higher percentages gave no further improvement. The relationship that exists between the sensitivity of an electrode and the immobilised activity depends primarily on the affinity of the oxidase (uricase) for its specific substrate (uric acid) [36]. In bienzyme systems, it is appropriate that a higher auxillary enzyme activity be maintained compared with that of the detecting activity, in order to enzymatically oxidise as much intermediate metabolite in the microenvironment as possible into substances that can be detected by an electrochemical transducer. In addition, it appears unnecessary to load higher activity if no improvement in sensitivity is attained. Thus a paste mixture of 7% w/w uricase and 3% w/w HRP was subsequently used.

Our method for preparing the carbon paste/ paraffin oil mixture was similar to that of Cai et al. [7]. The procedure for incorporating HRP and

Fig. 3. Effect of enzyme loading on the sensitivity of the biosensor. (■) Uricase fixed at 7% w/w (●); HRP fixed at 3% w/w. Measurements were performed in 20 ml of 0.1 M phosphate buffer, pH 6.5 on addition of 3 × 10⁻⁴ M uric acid.

uricase into the carbon paste was based on that of Wollenberger et al. [29] and Domínguéz-Sanchez et al. [37]. It may be true that higher response currents are obtained in response to substrate additions when enzymes are added to graphite prior to adding paraffin oil [38]. As is well known, dry graphites have very high capacitive currents (one of the original reasons for producing paste electrodes was to lower the residual current). Mixing graphite with any solvent always decreases electron transfer rates as the hydrocarbon chain of the mulling agent lengthens [39]. It has been reported however that carbon paste electrodes incorporating paraffin oil as the mulling agent as opposed to such materials as silicone oil, bromonaphthalene and nujol (mineral oil), have the widest useful potential range [40].

3.3. Hydrodynamic studies

Even though amperometric signals are characteristic of membrane diffusion processes, it is important to ensure that current signals are due to enzymatically generated H₂O₂ and not due to direct electron transfer of uric acid at the working surface of the electrode. Hydrodynamic voltammograms (Fig. 4) were constructed for four electrode designs over the voltage range −0.1 to +0.35 V. Stepwise potential increases (50 mV) were applied and the resulting steady state currents were recorded and plotted versus applied potential (mV). At potentials more negative than −0.2 V, a rapid loss of activity was observed due to the irreversible reduction of HRP [41]. Reduction processes (cathodic current) were apparent for all electrode types, with the exception of the unmodified one (no enzyme present). Moreover, the respective electrodes containing uricase and peroxidase only, exhibited relatively weak cathodic currents in the presence of urate. However, reduction current was significantly enhanced with the bienzyme electrode. An operating potential of 50 mV was selected for further amperometric studies. Voltammograms for all electrode types show a sharp anodic rise in anodic current over the potential range 250-650 mV (full results not shown in Fig. 4). Direct oxidation of uric acid occurs at potentials above 0.25 V, peaking at
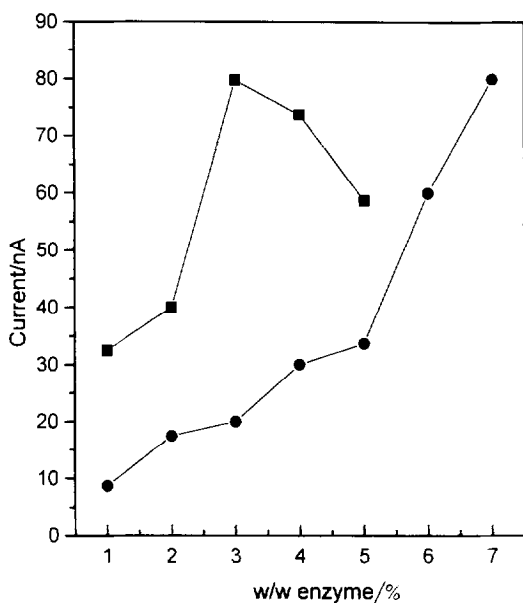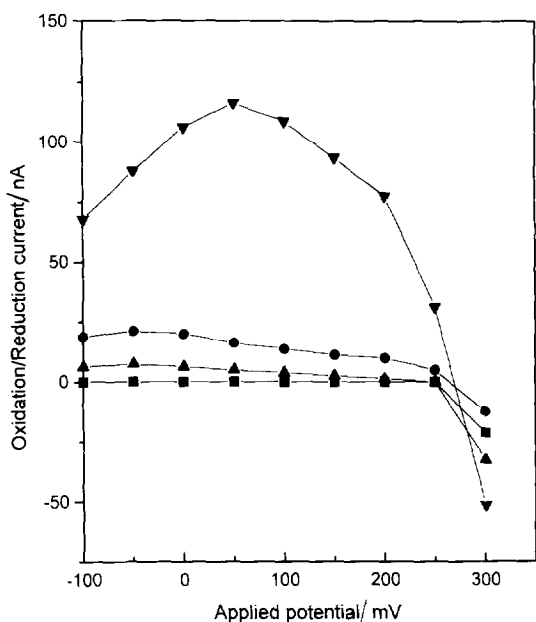
Fig. 4. Hydrodynamic voltammograms recorded in a stirred 0.1 M solution of phosphate buffer (pH 6.5 at 25°C) containing 4×10^{-4} M uric acid. All electrodes were poly(o-aminophenol)-modified. (■) 100% w/w carbon paste; (▲) 7% w/w uricase; (●) 3% w/w HRP; (▼) 7% w/w uricase and 3% w/w HRP.

approximately 0.5 V [19] (for a 100% w/w carbon paste electrode, no enzyme present). The magnitude of this oxidation current was greater when uricase was added to the paste (93% w/w and 7% w/w uricase). At this potential, a great deal of noise due to background currents and potential interference from other electroactive compounds was observed. It was previously attempted to elucidate this oxidation current by cyclic voltammetry; however, no cathodic return [42] was observed, similar to the findings of Jawad et al., therefore the oxidation process was considered irreversible. It appears that the urate oxidation wave masks the reduction (of uric acid) process observed. From the data obtained it was estimated that the reduction current at 50 mV was approximately 1% of the corresponding oxidation process at 650 mV.

As no mediator is incorporated into the carbon paste mixture, the existence of a naturally occurring mediator for the peroxidase reaction was investigated. An electrode modified with 3% w/w

HRP was used. Poly(o-aminophenol) and uric acid were considered as possible mediators to the reaction. Various configurations of the HRP electrode were designed for experiments: (A) CPE with poly(o-aminophenol) deposited at surface: (B) electrode similar to the latter except 5×10^{-3} M uric acid in solution (in voltammetric cell); (C) CPE with cellulose acetate membrane (12 000 Da cut-off) at working surface area with 5×10^{-3} M o-aminophenol in test solution.

The poly(o-aminophenol)-modified electrode (A) was compared to a cellulose membrane electrode employing (C) uric acid as a test mediator in solution. The latter electrode displayed a significantly higher affinity for H_2O_2 ($K_m = 2.83 \times 10^{-3}$ M) compared to that of the former ($K_m = 2.45 \times 10^{-5}$ M). The rate of reaction also increases in the presence of urate. In the case of monomer-modified electrodes, the affinity of peroxidase for hydrogen peroxide appears not to have been enhanced in the presence of uric acid. This would indicate that poly(o-aminophenol) does not act as mediator to the reaction, even though p- and o-aminophenol have been reported as being excellent electron donors to oxidised HRP. This was further illustrated when H_2O_2 was injected into a solution containing the monomer (cellulose membrane electrode, 12 000 Da). The resulting current was anodic in nature. A relatively small reduction current was produced from an electrode containing uricase and peroxidase (poly(o-aminophenol) at surface) on injecting urate relative to responses from the optimum design electrode. These data would seem to suggest that the electrocatalytic reduction of H_2O_2 by HRP immobilised on carbon paste takes place without electron-mediating substances suggesting that peroxidase is capable of performing electron transfer to the electrode.

The response of the biosensor is pH dependent (Fig. 5). The pH range studied was 5.0–9.0. Greater sensitivity was achieved at lower pH values; a best fit approximation suggests an optimum pH of 6.6. However, a "compromised" pH value of 7.5 was chosen in order to mimic the macroenvironment of physiological fluids and to promote the long term stability of the sensor. Noisy baselines were recorded when using background solutions in the pH range 5.0–7.0. As variation in the

ionic strength of the electrolyte solution is thought not to have an effect on sensitivity [20], it was not investigated. The pH of a working medium is a factor that affects the response of a biosensor when the enzymes' activity is controlled by ionising groups. It is important to determine the best pH range in order to make the electrode compatible with the matirx of interest. The reported optimum pH of uricase is in the range 8.5–9.2 [14,42,43]. However, the pH of most physiological fluids lies below this range. Keedy and Vagdama [20] reported a low pH dependence for a uricase electrode in solution. More significantly, pH response profiles were found to change when using different background solutions. Peroxidase has been utilised satisfactorily in the pH range 7.0–8.0 [44].

3.4. Calibration characteristics in static systems

Fig. 6 shows the typical amperometric responses recorded as a function of uric acid concentration. Responses were found to be linear up to 1×10^{-4} M urate with a detection limit of 3.14×10^{-6} M and a correlation coefficient of 0.9996. The reproducibility expressed in terms of

Fig. 6. Calibration plot for the amperometric determination of uric acid in a static system. Applied potential = + 0.05 V vs. Ag/AgCl. Carbon paste modified with 3% w/w HRP and 7% w/w uricase and coated with poly(*o*-aminophenol). Also shown are the typical responses in the 10^{-5}–10^{-4} M range.

relative standard deviation was 2.2% ($n = 4$) for a concentration of 2×10^{-5} M uric acid. The sensor had a response time ($t_{98\%}$) of 37s. The sensor response was found to be stable for 2 days while stored in background electrolyte at room temperature.

3.5. Interference studies

A prerequisite of quantifying an important analyte in physiological fluids is a high degree of selectivity. The sensor response should be specific for that analyte and not involve other electroactive substances in the sample. A range of naturally
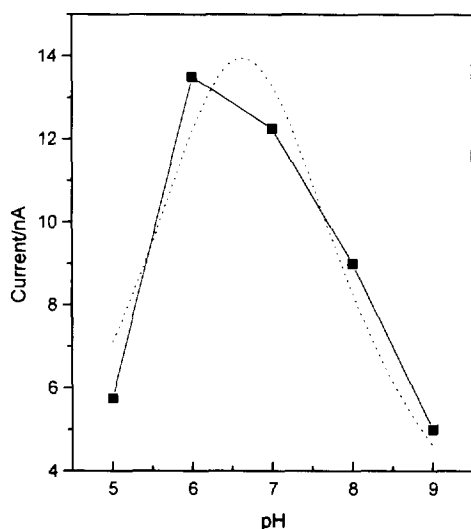

Fig. 5. Effect of pH on the amperometric response of the poly(*o*-aminophenol)-modified carbon paste biosensor. Applied potential = + 0.05 V. Readings carried out in 0.1 M phosphate. (■) Experimental data; (---) Best fit curve.
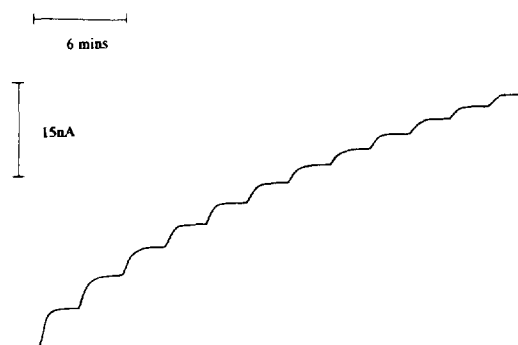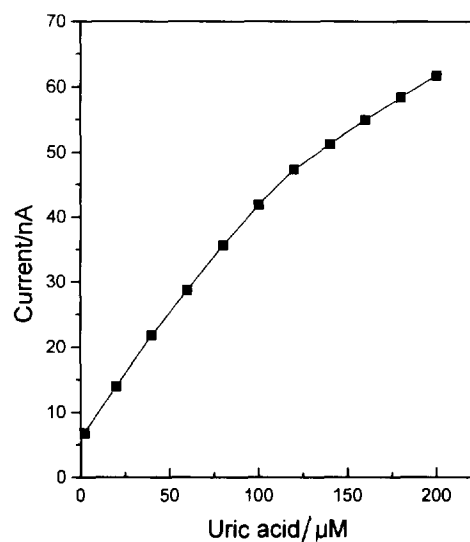
occurring substances in blood were then examined for their potential interference effects. Results were compared with a standard urate response acting as a control (5×10^{-4} M). Alternate uric acid injections were made in a cell containing 0.1 M phosphate buffer and another cell containing a known concentration of the test compound made up in background solution. Ascorbic acid gave approximately 2 and 15% increases in signal for mean (2.8×10^{-4} M) and upper (3.41×10^{-4} M) levels found in blood respectively. The presence of bilirubin [45] was found to have a detrimental effect on urate signals. A concentration of 1.7×10^{-4} M resulted in decreases of 35% in signal intensity. As bilirubin is too big to pass through the polymer layer, it is possible that some form of interaction occurs with uric acid at the working surface area of the electrode, resulting in a diminished current. As the bilirubin level tested is high and anticipated physiological levels would be significantly lower, it was hoped that this fact coupled with dilution of serum samples would minimise this effect.

Fig. 8. Flow injection amperometric responses to uric acid standards. Conditions: carrier stream was 0.1 M phosphate buffer, pH 7.5; flow rate = 1 ml min^{-1}; sample loop volume was 500 μl; applied potential was +0.05 V vs. Ag/AgCl. (A) 2×10^{-5} M; (B) 4×10^{-5} M; (C) 6×10^{-5} M; (D) 8×10^{-5} M; (E) 1×10^{-4} M; (F) 2×10^{-4} M; (G) 4×10^{-4} M; (H) 6×10^{-4} M; (I) 8×10^{-4} M.

3.6. Application of sensor in a flow injection system

The bienzyme electrode was then investigated as the working electrode in a flow injection system. Preliminary results suggested that the detection of uric acid is feasible over a wide range of experimental conditions. The applied working potential was fixed at 50 mV vs. Ag/AgCl. The carrier stream was 0.1 M phosphate buffer, pH 7.5. Carrier solutions were not degassed by purging with helium prior to operation. Somewhat noisy baselines and high background cur-
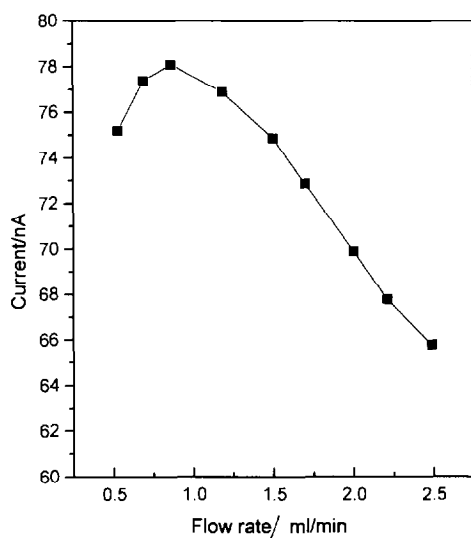

Fig. 7. Variation of the electrode response with flow rate. Applied potential = +0.05 V vs. Ag/AgCl. Uric acid concentration = 5×10^{-5} M.
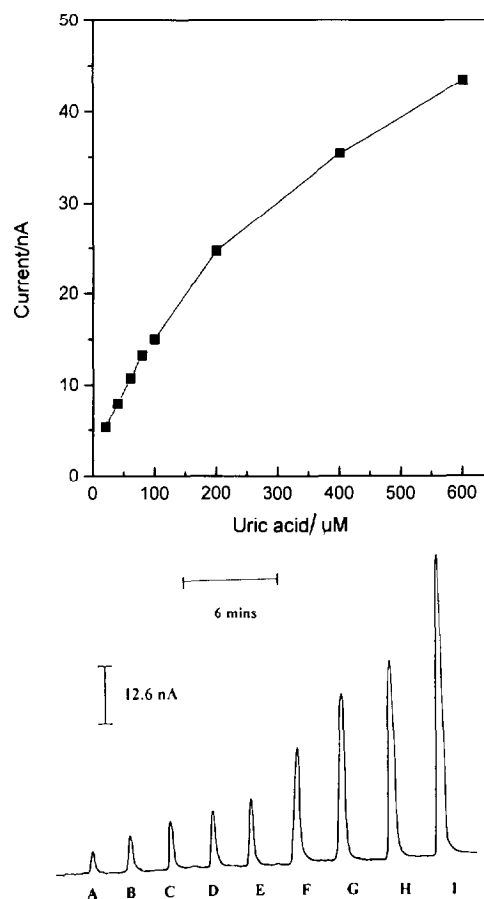
Table 1
Determination of uric acid in real samples with poly(*o*-aminophenol) uricase/HRP modified carbon paste electrode

Serum sample	U.A.[a] concentration determined by UV at 293 nm (mg L^{-1})	U.A. concentration determined by sensor (mg L^{-1})	Results (%)
1	5.3	4.9	93
2	4.6	4.1	90
3	5.5	5.2	95
4	6.2	5.6	91
5	3.9	3.7	95

Experimental conditions as described in text.
[a]U.A., Uric acid.

rents were found with carrier streams in the pH range 5.0–7.0. As with analysis in quiescent solution, peak currents were marginally higher at pH values below 7; for a 2×10^{-4} M urate standard, an increase of 33% in signal was observed (using a carrier stream, pH 6.0) relative to injecting the same standard into a carrier stream of pH 7.5. Analysis in stirred solution showed a relative increase of 19.35%.

The effect of varying the flow rate of the carrier stream was then examined (Fig. 7). Three electrodes were examined in the flow system with a relative standard deviation of less than 6.0%. The highest sensitivity for 5×10^{-5} M injections of urate was obtained at a flow rate of 0.85 ml min^{-1} with appreciable decreases in signal intensity at higher flow rates. Moreover, operation at high flow rates resulted in distorted baselines. Decreasing the sample loop volume from 500 to 300 μl resulted in a decrease in sensitivity, a narrowing of the linear dynamic range and lower detection limits. Use of the smaller loop resulted in slight memory effects. Longer washing times at the expense of sample frequency could alleviate this problem; however, employing the larger sample loop eliminated this problem. The most suitable monomer concentration for poly(*o*-amino-phenol) coating of the electrode surface was found to be 5×10^{-3} M, even though a concentration ten times less than this improved response times and more rapid returns to baseline levels.

The calibration characteristics of the electrode in flowing streams were then examined. Fig. 8 shows typical signals for uric acid standards. The calibration plot provided a linear response up to 2×10^{-4} M with a slope, intercept and correlation coefficient of 2.13×10^4 nA mol^{-1} l, 0.71 nA and 0.9996 ($n = 6$), respectively. No linear ranges existed at higher concentrations. The L.O.D. was calculated at 6.8×10^{-6} M. Increasing the flow rate from 0.85 to 2.0 ml min^{-1} reduced the detection limit to 8.1×10^{-6} M and slightly reduced the dynamic range. A series of 6 repetitive injections of 1×10^{-4} M urate yielded a relative standard deviation of 2.0%. The maximum allowable sample frequency was estimated as being 20 h^{-1}. The electrode, incorporated into the flow system, was found to be more stable than in stirred solution. This phenomenon is probably due to the continuous flow of the carrier stream washing unreacted urate from the carbon paste of the working electrode.

The influence of allopurinol on uric acid amperometric signals was examined. The drug inhibits xanthine oxidase, in that its oxidised form (oxypurinol) binds tightly to the reduced form of the enzyme. The oxidase catalytically converts hypoxanthine to uric acid and hydrogen peroxide [46]. Allopurinol is used in the treatment of chronic gout and hyperuricaemia (symptoms associated with enhanced urate levels). A high concentration of the oxidase inhibitor (1×10^{-3} M) was added to the carrier stream. No adverse effects such as background current, baseline drift or signal noise were observed. Repeated injections of uric acid (1×10^{-4} M) were carried out in the presence and absence of the drug. A reduction in current signal of 10.5% was noted. Two possibilities may account for this: oxidation of allopurinol thus interfering with the oxidase catalytic mechanism and/or blockage or interaction at the working electrode surface. Again, it was hoped that dilution of samples could reduce such a problem.

3.7. Analysis of serum samples

Serum samples containing different concentrations of uric acid were then analysed using the optimum design sensor (Table 1). Samples were diluted 1:10 with carrier solution and the pH adjusted to 7.5 (when required). Diluted samples were then injected directly into the flow system and the concentration of uric acid present estimated from a calibration plot. Results were in reasonable agreement with those determined by UV spectrophotometry. Repeated exposure of the electrode to diluted serum had no adverse effect on amperometric signal size.

4. Conclusion

In this study, a novel reagentless sensor based on the co-immobilisation of HRP and uricase in a carbon paste for the detection of uric acid has been described. The electrode works at a very favourable potential and has a short response time. The composition of the carbon paste may go some way in explaining the nature of the response where heterogeneous electron transfer occurs between HRP and the electrode, however, the precise nature of this mechanism remains unclear [29].

Conducting polymer coatings can be electrodeposited at the working area of electrodes with great precision. We have noted that poly(o-aminophenol) is stable for a considerable length of time when stored in background electrolyte at room temperature. Physical characteristics such as film thickness can be easily controlled thus regulating the rate of analyte diffusion through the immobilised layer [47].

The advantage of this polymer is that it appears to have effectively protected the electrode from interferences and fouling. To our knowledge, analysis of unspiked human serum compared as well as, if not better, than other previously reported enzyme/electrode based methods for the detection of uric acid in a complex physiological matrix. Note here that in our interference studies the concentrations of potential interferents tested were much higher than

anticipated physiological levels. Moreover, serum samples were simply diluted with background electrolyte rather than extraction which is time consuming and restricts the sampling frequency.

References

[1] G.G. Guilbault, Analytical uses of immobilised enzymes, Marcel Dekker, New York, 1984.

[2] C.P. Price and P.R. James, Anal. Clin. Biochem., 25 (1967) 484.

[3] P.H.S. Reynolds, M.J. Boland, D.G. Blevins, D.P. Randall and K.R. Schubert, Trends Biochem Sci., (1982) 366.

[4] B.A. Dilena, M.J. Peak, H.L. Pardue and J.W. Skorg, Clin. Chem., 32 (1986) 486.

[5] E. Gonzalez, Anal. Chim. Acta, 242 (1991) 267.

[6] J. Wang and B.A. Freiha, Bioelectrochem. & Bioenerg., 12 (1984) 225.

[7] X. Cai, K. Kalcher, C. Neuhold and B. Ogorevc, Talanta, 41 (1994) 407.

[8] T. Kawashima, K. Tomida, N. Tominaga, T. Kobayashi and H. Onishi, Chem. Lett., (1984) 653.

[9] L. Jin, J. Ye, W. Tong and Y. Fang, Mikrochim. Acta, 112 (1993) 71.

[10] H. Iwai and S. Akihama, Chem. Pharm. Bull., 34 (1986) 3471.

[11] M. Nanjo and G.G. Guilbault, Anal. Chem., 46 (1974) 1769.

[12] M. Janchen, G. Walzel, B. Neef, B. Wolf, F. Scheller, M. Kuhn, D. Pfeiffer, W. Sojka and W. Jaross, Biomed. Biochim. Acta, 9 (1983) 1055.

[13] S. Uchiyama, T. Obokata and S. Suzuki, Anal. Chim. Acta, 225 (1989) 425.

[14] S. Uchiyama, F. Umesato and S. Suzuki, Anal. Chim. Acta. 230 (1990) 195.

[15] T. Kawashima, A. Arima, N. Hatakeyma, N. Tominaga and M. Ando, Nippon Kagaku Kaishi, 10 (1980) 1542.

[16] M.A.T. Gilmartin, J.P. Hart and B.J. Birch, Analyst, 119 (1994) 243.

[17] N. Kageyama, Clin. Chim. Acta, 31 (1971) 421.

[18] R. Haeckel, Clin. Chem. Acta, 24 (1978) 1846.

[19] T. Tatsuma and T. Watanabe, Anal. Chim. Acta, 242 (1991) 85.

[20] F.H. Keedy and P. Vagdama, Biosens. Bioelectron., 6 (1991) 491.

[21] J.J. Kulys, V.S.A. Laurinavicius, M.V. Pesliakiene and U.V. Gureviciene, Anal. Chim. Acta, 141 (1983) 13.

[22] K.G. Paul, P.D. Boyer, H. Lardy and L. Myrback (Eds.), The Enzymes, Academic Press, New York, 1963, p. 227.

[23] J. Wang, B. Freiha, N. Naser, E. Gonzalez-Romero, U. Wollenberger, M. Ozsoz and O. Evans, Anal. Chim. Acta, 254 (1991) 81.

[24] A.I. Yaropolov, V. Malovik, S.D. Varfolomeev and I.V. Berezin, Dokl. Akad. Nauk SSSR, 249 (1979) 1399.

[25] R.M. Paddock and E.F. Bowden, J. Electroanal. Chem., 260 (1989) 487.

[26] J. Kulys and R.D. Schmid, Bioelectrochem. Bioenerg., 24 (1990) 305.

[27] L. Gorton, Electroanalysis, 7 (1995) 23.

[28] G. Jönsson-Pettersson, Electroanalysis, 3 (1991) 741.

[29] U. Wollenberger, J. Wang, M. Ozsoz, E. Gonzalez-Romero and F. Scheller, Bioelectrochem. Bioenerg., 26 (1991) 287.

[30] G. Farsang, T. Dankhazi, J. Loranth and I. Daruhazi, Talanta, 35 (1988) 855.

[31] J. Wang and L. Hutchins, Anal. Chem., 57 (1985) 1536.

[32] J. Ruzicka and E.H. Hansen, Flow Injection Analysis, Wiley, New York, 1981.

[33] R.J. Geise, J.M. Adams, N.J. Barone and A.M. Yacynych, Biosens. Bioelectron., 6 (1991) 151.

[34] A. Ivaska, Electroanalysis, 3 (1991) 247.

[35] D.J. Harrison, R.B.F. Turner and H.P. Baltes, Anal. Chem., 60 (1988) 2002.

[36] E.M. D'Urso and P.R. Coulet, Anal. Chim. Acta. 281 (1993) 535.

[37] P. Domínguéz-Sanchez, A.J. Miranda-Ordieres, A. Costa-Garcia and P. Tuñón-Blanco. Electroanalysis, 3 (1991) 281.

[38] L. Gorton, G. Jönsson-Petersson, E. Csöregi, K. Johansson, E. Dominguez and G. Marko-Varga, Analyst, in press.

[39] M.E. Rice, Z. Galus and R.N. Adams, J. Electroanal. Chem., 143 (1983) 89.

[40] E.D. Kinsley and D.J. Curran, Anal. Chim. Acta, 206 (1988) 385.

[41] P. Domínguéz-Sanchez, C.K. O'Sullivan, A.J. Miranda-Ordieres and P. Tuñón-Blanco, Anal. Chim. Acta, 291 (1994) 349.

[42] M.A. Jawad, J. Dorie and N. El Murr, J. Food Sci., 56 (1991) 594.

[43] M.A.T. Gilmartin and J.P. Hart, Analyst, 119 (1994) 833.

[44] O. Ryan, M.R. Smyth and C. Ó Fágáin, Enz. Microb. Tech., 16 (1994) 501.

[45] J. Wang and M. Ozsoz, Electroanalysis, 2 (1990) 647.

[46] E. Watanabe, K. Ando, I. Karube, H. Matsuoka and S. Suzuki, J. Food Sci., 48 (1983) 496.

[47] M. Alvarez Icaza and V. Bilitewski, Anal. Chem., 65 (1993) 525a.

Hydrogen chromate PVC matrix membrane sensor for potentiometric determination of chromium(III) and chromium(VI) ions

Saad S.M. Hassan[a,*], M.N. Abbas[b], G.A.E. Moustafa[b]

[a]Department of Chemistry, Faculty of Science, Ain Shams University, Cairo, Egypt
[b]National Research Center, Dokki, Cairo, Egypt

Abstract

A novel potentiometric Cr^{6+} PVC matrix membrane sensor incorporating nickel tris(1,10-bathophenanthroline) hydrogen chromate as an electroactive material and 2-nitrophenyl phenyl ether as solvent mediator is described. In a phosphate buffer solution of pH 5, the sensor displays a rapid and linear response for Cr^{6-} over the concentration range 2×10^{-2}–8×10^{-6} M with an anionic slope of 55.5 ± 0.2 mV decade^{-1} and a detection limit of the order of 0.4 μg ml^{-1}. The sensor is used for sequential determination of Cr^{6+} and Cr^{3+} by direct monitoring of Cr^{6+} followed by oxidation of Cr^{3+} and measurement of the total chromium. The average recoveries of Cr^{3+} and Cr^{6+} at concentration levels of 0.5–50 μg ml^{-1} are $98.1 \pm 0.4\%$ and $99.1 \pm 0.4\%$ respectively. Redox and precipitation titrations involving Cr^{6+} as a titrant are monitored with the sensor. Cr^{3+} and/or Cr^{6+} in wastewaters of some industries (e.g., leather tanning, electroplating, aluminum painting) and the chromium contents of some alloys and refractory bricks are assessed. The results agree fairly well with data obtained using the standard diphenylcarbazide spectrophotometric method.

Keywords: Chromium(III); Chromium(VI); PVC matrix membrane sensor; Potentiometric determination

1. Introduction

Determination of chromium has received considerable attention because of the highly toxic nature of Cr^{6+} and the useful biological activity of Cr^{3+} [1]. Both forms of chromium enter the environment from various sources as the effluent

discharge of tanning industries, electroplating, oxidative dyeing, chemical industries, steel works and cooling water towers. Techniques and approaches in current use for the separate and sequential determination of both forms of chromium include spectrophotometry [2–4], spectrofluorimetry [5], atomic absorption spectrometry [6,7], differential pulse polarography [8], differential pulse voltammetry [9], ion chromatog-

* Corresponding author.

raphy [10], X-ray fluorescence [11] and gas chromatography [12,13]. Most of these methods involve several manipulation steps and require sophisticated instruments.

Direct potentiometric methods for determining chromium, however, are simpler, much faster and less expensive. Potentiometric sensors for Cr^{6-} based on the use of the chromate salts of quaternary phosphonium [14,15], quaternary ammonium [16–20], crystal violet [21] and barium [22,23] as electroactive materials dispersed in lipophilic solvents [18,21] and poly(vinyl chloride) [14–17,19] and silicon rubber [22] membranes have been suggested. A solid-state Cr^{3+} chalcogenide membrane sensor has also been described [24]. Many of these sensors, however, are not sensitive enough to permit measurement of chromium at concentration levels of $< 10^{-3}$ or 10^{-4} M [18,19,21,22], display poor selectivity in the presence of various common cations and anions (e.g. F^-, SO_4^{2-}, I^-, S^{2-}, Cu^{2+}, Ni^{2+}, Pb^{2+}, Fe^{2+}, Ba^{2+}, Ca^{2+}, Mg^{2+}) [16,22,23], exhibit non-Nernstian response [15,22] and have long response times.

The present work describes the preparation and potentiometric characterization of a novel Cr^{6+} PVC sensor based on the use of nickel tris-(bathophenanthroline) hydrogen chromate ion-pair complex as electroactive material and 2-nitrophenyl phenyl ether as a plasticizer. The sensitivity, stability and selectivity of the sensor are significantly better than many of those previously advocated. The sensor has been used satisfactorily for sequential determination of Cr^{3+}/Cr^{6+} in various industrial materials and for the monitoring of some redox and precipitation titrations involving Cr^{6+}.

2. Experimental

2.1. Apparatus

All potentiometric measurements were performed at $25 \pm 1°C$ using an Orion Model SA 720 digital pH/millivoltmeter with a nickel tris(1,10-bathophenanthroline) hydrogen chromate PVC matrix membrane sensor in conjunction with a double-junction Ag/AgCl reference electrode (Orion 90-02) containing 10% (w/v) potassium chloride in the outer compartment. A combination Ross glass pH electrode (Orion 81-02) was used for all pH measurements.

Spectrophotometric measurements were made at 540 nm with a Shimadzu UV-240 recording spectrophotometer using 10 mm matched fused silica cuvettes.

2.2. Reagents and materials

All chemicals were of analytical-reagent grade and deionized doubly-distilled water was used throughout. Bathophenanthroline monohydrate (phen) was obtained from Merck. Ni(II) sulphate, potassium dichromate, potassium chromate, diphenylcarbazide, tetrahydrofuran (THF) and poly(vinyl chloride) (PVC) powder were obtained from Aldrich. 2-Nitrophenyl phenyl ether (NPPE) was purchased from Kodak. A stock 10^{-1} M chromium(VI) standard solution was prepared by dissolving 1.94 g of K_2CrO_4 in 100 ml of deionized bidistilled water. Chromium(VI) solutions (10^{-2}–10^{-6} M) were prepared by serial dilutions. Phosphate buffer (7×10^{-2} M) pH5 was freshly prepared.

2.3. Nickel tris(1,10-bathophenanthroline) hydrogen chromate membrane sensor

A 10 ml aliquot of 10^{-2} M chromate solution was mixed with a 5 ml aliquot of 10^{-2} M Ni(II) tris(1,10-bathophenanthroline) solution. After stirring for 5 min, a yellow hydrogen chromate ion-pair complex was precipitated, filtred off on a Whatman filter paper No. 42, washed with cold water, dried at room temperature for 24 h and ground to a fine powder. A 10 mg portion of Ni(II) tris(1,10-bathophenanthroline) hydrogen chromate ion pair was thoroughly mixed in a glass Petri dish (5 cm diameter), with 0.35 ml NPPE, 0.19 g PVC and 5 ml THF. The petri dish was covered with a filter paper and left to stand overnight to allow slow evaporation of the solvent at room temperature. A PVC master membrane (≈ 0.1 mm thick) was obtained and used for the preparation of the sensor as previously described [25,26].

2.4. Determination of Cr^{6+} and Cr^{3+}

The hydrogen chromate PVC sensor was immersed in conjunction with a double junction Ag/AgCl reference electrode into a 9.0 ml phosphate buffer solution pH 5. After potential stabilization to ±0.2 mV, a 1.0 ml aliquot of 10^{-3}–10^{-5} M $K_2Cr_2O_7$ solution (≡ 52–0.52 μg ml^{-1} Cr^{6+}) was added. The potential reading was plotted as a function of the logarithm of Cr^{6+} concentration and the plot was used for subsequent measurement of unknown Cr^{6+} samples.

2.5. Determination of Cr^{3+}

A 10 ml aliquot of Cr^{3+} test solution containing 10–50 μg ml^{-1} Cr^{3+} was transferred to a 50 ml beaker, followed by addition of a 2–3 ml aliquot of 2×10^{-2} M $KMnO_4$ and 2 ml of 9 M H_2SO_4. The test solution was heated on a boiling water bath for 10 min. More $KMnO_4$ was added dropwise when the pink colour disappeared. A few drops of 2.5% w/v sodium azide were slowly added dropwise until complete decolourization. The solution was transferred to a 25 ml standard flask, diluted with deionized doubly-distilled water to the mark and shaken. A 1.0 ml aliquot of this test solution was transferred to a 50 ml beaker containing 9.0 ml stirred phosphate buffer (pH 5) and the chromium sensor. The chromium content was measured as described above.

Chromium(VI) and chromium(III) in synthetic mixtures and in industrial wastewaters were sequentially determined using the above procedures successively after appropriate sample dilutions.

2.6. Determination of chromium in alloys

A 0.5 g portion of chromium-containing steel (12–29% w/w Cr) was transferred to a 100 ml beaker and dissolved in 10 ml of 16 M HNO_3 and 15 ml of 70% $HClO_4$. The solution was evaporated until dense fumes of $HClO_4$ were produced and boiled gently for 5 min to oxidise the chromium. The beaker and contents were cooled rapidly and the solution was diluted by addition of 20 ml of deionized distilled water. The solution

was transferred quantitatively to a 500 ml volumetric flask and diluted to the mark with deionized distilled water. The chromium was potentiometrically determined as described above.

2.7. Determination of chromium in refractory bricks

A 0.2–0.3 g sample of the fine powder of the brick sample was transferred to a nickel crucible followed by addition of 0.3 g sodium peroxide and 5 g of potassium pyrosulphate. The mixture was fused at 800°C in a muffle furnace for 30 min. The residue was dissolved in ≈ 400 ml of 8 M hydrochloric acid solution and boiled to a final volume of 100 ml. The solution was transferred to a 500 ml volumetric flask and made up to the mark with doubly-distilled deionized water. The Cr^{6+} content was measured as previously described.

3. Results and discussion

3.1. Sensor characteristics

The potentiometric response characteristics of a Cr^{6+} sensor based on the use of nickel tris-(bathophenanthroline) hydrogen chromate ion-pair complex as a novel electroactive material and 2-nitrophenyl phenyl ether as a plasticizer in a PVC matrix were evaluated according to IUPAC recommendations [27] and the results are given in Table 1. In a phosphate buffer of pH 5, the sensor exhibits a linear and stable response for Cr^{6+} over the concentration range 2×10^{-2}–8×10^{-6} M with an anionic slope of 55.5 ± 0.2 mV decade^{-1} (Fig. 1), the lower limit of detection being 8×10^{-6} M(≡ 0.4 μg ml^{-1} Cr^{6+}). Although other buffer solutions of pH 5 (e.g. acetate) can be successfully used, a response graph with a lower limit of detection is obtained with the phosphate buffer solution. It should be mentioned that addition of aqueous Cr^{6+} test solution to 0.1 M phosphate buffer pH 5 does not cause a pH change of more than 0.15 pH units (≈ 9 mV) for final Cr^{6+} concentrations of 10^{-3}–10^{-6} M.

Table I

Response characteristics of a nickel tris(bathophenanthroline) hydrogen chromate PVC matrix membrane sensor

Parameter	Cr^{6+} sensor[a]
Slope (mV decade^{-1})	-55.5 ± 0.3
Intercept (mV)	-91.1 ± 0.3
Correlation coefficient (r)	0.997
Lower detection limit (M)	8×10^{-6}
Lower limit of linear range (M)	2×10^{-5}
Response time for $[Cr^{6+}]$ change from 1×10^{-4} to 1×10^{-3} M (s)	20 ± 2
Working acidity range (pH)	4–6

[a] Average of five measurements.

The time required for the sensor to reach 95% of the steady potential response at pH 5, after successive immersion in a series of Cr^{6+} solutions, each having a 10-fold difference in concentration from the last, ranges from 20 s for $[Cr^{6-}] \geq 10^{-4}$ M to 30 s for lower concentrations. The standard deviation of the sensor potential readings over a period of 10 min is ± 0.2 mV. The sensor exhibits a day-to-day reproducibility of about ± 1 mV for the same solutions over a period of 6 weeks after preparation. The useful lifetime of the sensor is 6 weeks, during which the potential slope is reproducible to within ± 2 mV per concentration decade.

Chromium(VI) is present in aqueous solutions as chromate, dichromate, hydrogen chromate, chromic acid, hydrogen dichromate, trichromate and tetrachromate [28]. The last three ions have been detected only in strongly acidic solutions. Within the pH range 4–5.5, however, the monovalent hydrogen chromate anion is the predominant species. The pH of aqueous 10^{-2}–10^{-4} M Cr^{6+} solutions was changed by the addition of very small volumes of dilute NaOH or H_2SO_4 solutions and the potential of the solutions was monitored. The results reveal that the sensor response is relatively independent of the pH variation over the pH range 4–6. As the pH value increases up to 8, the starting potential of the chromium solutions is shifted towards more positive values. This corresponds to the decrease in the measurable concentration of $HCrO_4^-$. The calibration slope declines to < 30 mV decade^{-1} which is almost equivalent to the Nernstian slope for a doubly-charged anion. This behaviour can
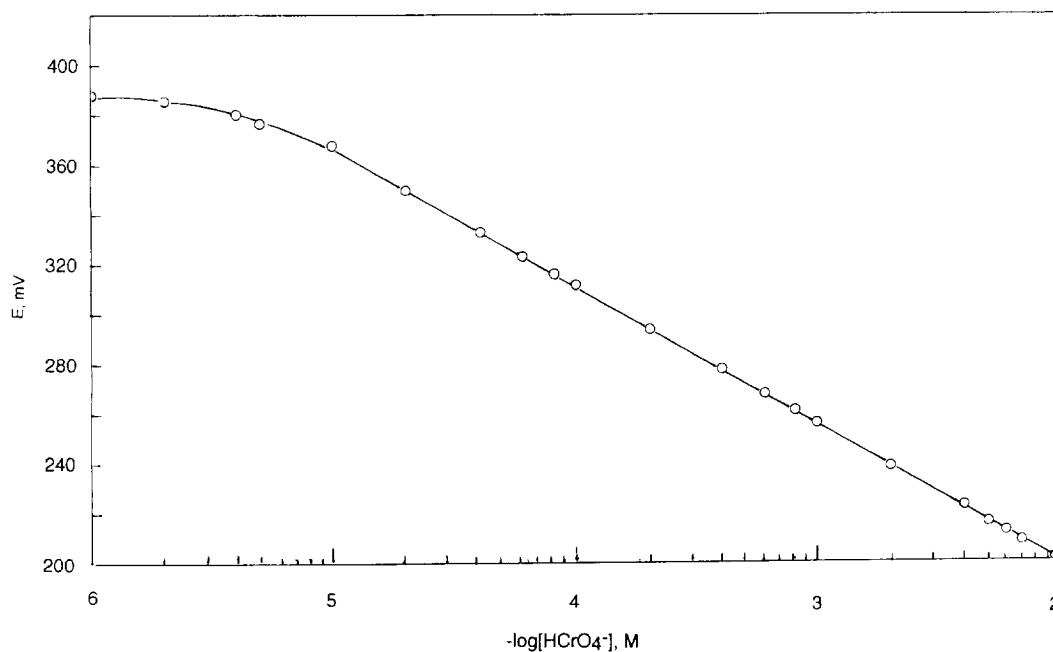

Fig. 1. Potential response of nickel tris(bathophenanthroline) hydrogen chromate PVC matrix membrane to different concentrations of Cr^{6+} in 0.1 M phosphate buffer solutions of pH 5.

Table 2

Potentiometric selectivity coefficients of a nickel tris-(bathophenanthroline) hydrogen chromate PVC matrix membrane sensor

Interferent (B)	$K^{pot}_{Cr,B}$	Interferent (B)	$K^{pot}_{Cr,B}$
Mn^{2+}	1.1×10^{-2}	F^-	1.1×10^{-3}
Mg^{2+}	1.0×10^{-2}	Cl^-	2.0×10^{-3}
Cu^{2+}	1.3×10^{-2}	Br^-	3.6×10^{-3}
Co^{2+}	1.2×10^{-2}	I^-	14.6
Ni^{2+}	1.1×10^{-2}	SO_3^{2-}	1.1×10^{-3}
Fe^{2+}	0.9×10^{-2}	SO_4^{2-}	1.76×10^{-3}
Pb^{2+}	1.2×10^{-2}	SCN^-	41.4
Zn^{2+}	1.4×10^{-2}	CN^-	1.4×10^{-3}
Cr^{3+}	7.0×10^{-2}	CH_3COO^-	2.4×10^{-3}
Al^{3+}	0.6×10^{-2}	NO_3^-	1.14
Hg^{2+}	26.5	ClO_4^-	87.2×10^2

be explained by the increased influence of OH^- and formation of the divalent $Cr_2O_7^{2-}$ anions. All subsequent measurements were performed in a phosphate buffer of pH 5.

The influence of some 22 different cations and anions on the hydrogen chromate sensor was investigated. The selectivity coefficients were determined by the separate solution method [27,29], at pH 5, using 10^{-3} M test solutions. Table 2 reveals no interferences by the cations—Mn^{2+}, Mg^{2+}, Cu^{2+}, Ni^{2+}, Fe^{2+}, Pb^{2+}, Zn^{2+}, Cr^{3+}, and Al^{3+}—and serious interference by Hg^{2+}. Addition of EDTA significantly reduces the effect of almost all cations. The sensor displays a good selectivity for $HCrO_4^-$ over many anions. However, anions which are more lipophilic than $HCrO_4^-$ interfere, as is expected for most ion-exchange-type membranes. The interference effect of the ions is in good agreement with the Hofmeister pattern [30] of selectivity sequence:

$$SCN^- > I^- > NO_3^- > HCrO_4^- > Br^- > CH_3COO^- > Cl^- > F^- \equiv SO_4^{2-}$$
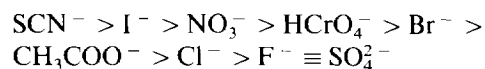
Direct determination of $HCrO_4^- - Cr^{6+}$ in the presence of high concentrations (> 10-fold excess) of ClO_4^-, SCN^- and NO_3^- anions gives unacceptable results. A successful approach for determining $HCrO_4^- - Cr^{6+}$ in mixtures containing these interfering anions was achieved by treating

the sample test solutions with ascorbic acid to convert chromate $-Cr^{6+}$ into Cr^{3+} cation, followed by passing the solutions through an anion exchange column (Cl^- form) to retain all the interfering anions. Chromium(III) cations in the effluent were then oxidized to chromate–Cr^{6-} and monitored with the hydrogen chromate sensor. Typical determination of 1.0 mg of Cr^{6+} mixed with 1.0 mg each of ClO_4^-, SCN^-, and NO_3^- in a final volume of 100 ml following this procedure shows an average recovery of 98.1% Cr^{6+} and a mean standard deviation of 0.8% ($n = 5$).

3.2. Analytical applications

Analytical usefulness of the Cr^{6+} sensor was examined for direct determination of various concentrations of Cr^{6+} (0.5–50 μg ml^{-1}) using the standard addition (spiking) technique. Results of an average recovery of 99.5% and a mean standard deviation of 0.6% are obtained ($n = 10$). The sensor also proved useful for quantification of Cr^{6+} after prior oxidation with MnO_4^- followed by removal of the excess oxidant with sodium azide [31]. Table 3 presents results obtained for sequential determination of synthetic mixtures containing various proportions of Cr^{6+} and Cr^{3+}. Practically, Cr^{6+} is directly measured with

Table 3

Sequential potentiometric determination of Cr^{3+}/Cr^{6+} in some synthetic binary mixtures using a nickel tris-(bathophenanthroline) hydrogen chromate PVC matrix membrane sensor

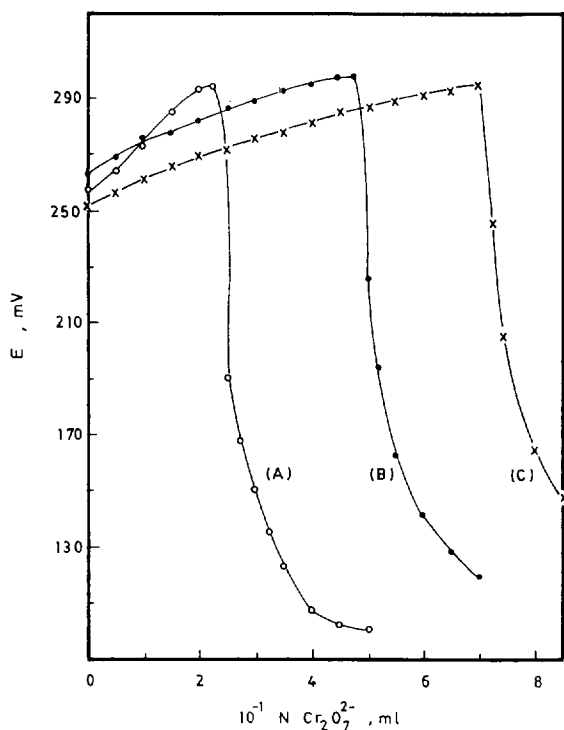| Added (μg ml^{-1})		Recovery[a] (%)	
Cr^{3+}	Cr^{6+}	Cr^{3+}	Cr^{6+}
8.0	–	98.4 ± 0.5	–
8.0	2.0	98.7 ± 0.3	99.1 ± 0.2
8.0	4.0	97.9 ± 0.3	98.7 ± 0.4
8.0	6.0	98.1 ± 0.4	99.4 ± 0.4
8.0	8.0	97.8 ± 0.5	98.9 ± 0.3
6.0	8.0	98.2 ± 0.4	99.3 ± 0.4
4.0	8.0	97.6 ± 0.4	98.5 ± 0.5
2.0	8.0	97.8 ± 0.3	98.7 ± 0.5
–	8.0	–	99.8 ± 0.3

[a] Average of three measurements.

Fig. 2. Typical potentiometric titration curves for (A) 2.5, (B) 5.0, and (C) 7.5 ml of 0.1 N iron(II) with standard 0.1 N $K_2Cr_2O_7$ using a nickel tris(bathophenanthroline) hydrogen chromate PVC matrix membrane sensor.

the sensor and, after oxidation of Cr^{3+}, the total chromium is sequentially determined and Cr^{3+} is obtained by difference. Average recoveries of 99.1% (standard deviation 0.4%) and 98.1% (standard deviation 0.4%) are obtained for Cr^{6+} and Cr^{3+} in their mixtures respectively.

The chromium sensor was utilized as an indicator electrode in conjunction with a Ag/AgCl reference electrode for titrimetric determination of high concentrations of Cr^{6+} ($> 10^{-3}$ M). The sensor was also used for following some redox and precipitation titrations. Fig. 2 shows typical potentiometric titration curves of Fe^{2+} with $Cr_2O_7^{2-}$. One (± 0.01) mole of $Cr_2O_7^{2-}$ is reproducibly consumed per 6 moles of Fe^{2+}. The shape of the titration curves is typical to those obtained in some other redox titrations using ion selective electrodes [32]. The inflection break at the equivalence point is -160 mV. Fig. 3 depicts a typical potentiometric precipitation titration curve of

Tl^+ with CrO_4^{2-}. A sharp inflection break of ≈ 60 mV is obtained at a 2:1 thallium:chromate stoichiometric reaction, the relative standard deviation being 0.3% ($n = 10$). Many other inorganic and organic species can be similarly determined by monitoring their reaction with Cr^{6+}.

The use of a Cr^{6+} sensor for the determination of chromium in some environmental samples was also examined. Hexavalent and trivalent chromium ions, in grab and composite wastewater samples collected from some industries (e.g. leather tanning, electroplating and aluminum painting), were determined. The chromium contents of some industrial materials (e.g. refractory bricks and alloys) were similarly assessed after appropriate dissolution of the test sample. The results (Tables 4 and 5) were compared with data obtained using the standard diphenylcarbazide spectrophotometric method [31]. A close agreement within 0.1–0.7% is obtained, indicating the
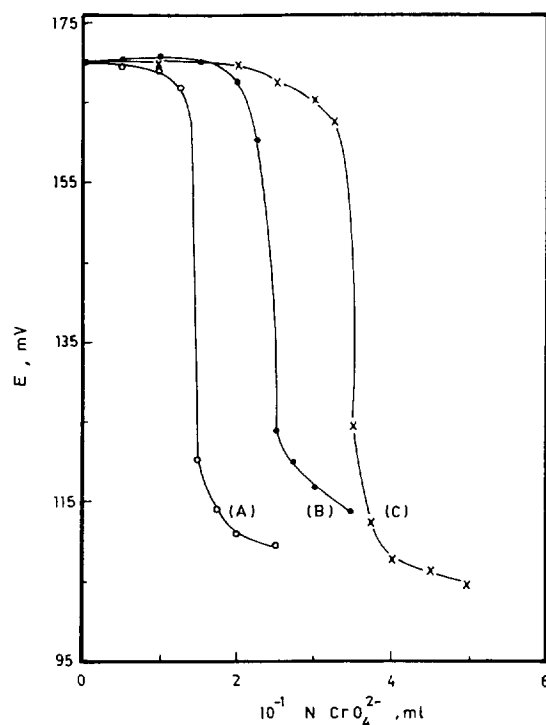

Fig. 3. Typical potentiometric titration curves for (A) 1.5, (B) 2.5, and (C) 3.5 ml of 0.1 N thallium(I) with standard 0.1 N K_2CrO_4 using a nickel tris(bathophenanthroline) hydrogen chromate PVC matrix membrane sensor.

Table 4
Determination of chromium in some industrial wastewaters using spectrophotometry and potentiometry with a nickel tris-(bathophenanthroline) hydrogen chromate PVC matrix membrane sensor

Wastewater source	Cr^{3+} found[a] (mg l^{-1})		Cr^{6+} found[a] (mg l^{-1})	
	Potentiometry	Spectrophotometry	Potentiometry	Spectrophotometry
Leather tanning	2.4 ± 0.1	2.2 ± 0.1		..
	1.6 ± 0.1	1.5 ± 0.1	..	–
	96.0 ± 0.2	92.5 ± 0.3	–	
Electroplating	.	...	86.1 ± 0.3	88.1 ± 0.4
	–	–	124.5 ± 0.4	125.0 ± 0.3
	–	–	100.6 ± 0.5	101.2 ± 0.5
Aluminum painting	5.3 ± 0.2	5.1 ± 0.2	11.8 ± 0.2	12.0 ± 0.3
	8.7 ± 0.2	8.5 ± 0.2	15.2 ± 0.1	15.0 ± 0.2
	7.4 ± 0.2	7.3 ± 0.2	14.5 ± 0.2	15.0 ± 0.2

[a] Average of three measurements.

efficiency, accuracy and applicability of the proposed potentiometric sensor for determining Cr^{6+} and Cr^{3+} in various matrices and in coloured and turbid solutions. The proposed potentiometric sensor also has some significant advantages over many of those previously described [15,16,18,19,21–23], as it offers a lower limit of detection (8×10^{-6} M), covers a wider range of concentrations (2×10^{-2}–8×10^{-6} M), displays a faster response (20–30s) and exhibits reasonable selectivity in the presence of many common interfering ions.

Table 5
Determination of chromium in some refractory bricks and alloys using spectrophotometry and potentiometry with a nickel tris(bathophenanthroline) hydrogen chromate PVC matrix membrane sensor

Sample	Chromium found[a] (%w/w)	
	Potentiometry	Spectrophotometry
Refractory brick (1)	1.1 ± 0.1	1.1 ± 0.1
Refractory brick (2)	4.9 ± 0.2	4.8 ± 0.3
Refractory brick (3)	2.7 ± 0.1	2.6 ± 0.1
Chrome–steel alloy	28.0 ± 0.3	27.6 ± 0.2
Chrome–Ni–steel alloy	22.9 ± 0.2	23.3 ± 0.3
Chrome–Mo–V alloy	11.6 ± 0.1	11.7 ± 0.2

[a] Average of three measurements.

References

[1] S.A. Katz and H. Salem, J. Appl. Toxicol., 13 (1993) 217.
[2] J.C. de Andrade, J.C. Rocha and N. Baccan, Analyst, 109 (1984) 645.
[3] J.C. de Andrade, J.C. Rocha and N. Baccan, Analyst, 110 (1985) 197.
[4] M.J. Arrabal, P.V. Gonzales, C.C. Gamez, A.S. Misiego and A.M. de la Peña, Analyst, 119 (1994) 1537.
[5] V. Kabasakalis, Anal. Lett., 26 (1993) 2269.
[6] K.S. Subramanian, Anal. Chem., 60 (1988) 11.
[7] R.M. Milačič and J. Štupar, Analyst, 119 (1994) 627.
[8] C. Harzdorf and G. Janser, Anal. Chim. Acta, 165 (1984) 201.
[9] J. Golimowski, P. Valenta and H.W. Nuernberg, Fresenius' Z. Anal. Chem., 322 (1985) 315.
[10] C.H. Ngoc and A.R. Timerbaev, Zavod. Lab., 56 (1990) 19; Anal. Abstr., (1991) 10D86.
[11] N.I. Shcherbinina, G.R. Ishmiyarova, I.E. Nikitina, G.V. Myasoedova, L.A. Polosukhina, I.I. Uralov, A.D. Simonva and E.Y. Daniova, Zh. Anal. Khim., 45 (1990) 766; Anal. Abstr., (1991) 3H74.
[12] H. Schaller and R. Neeb, Fresenius' Z. Anal. Chem., 327 (1987) 170.
[13] H. Tanaka, T. Nakano and Y. Kanazawa, Bunseki Kagaku, 32 (1983) 740.
[14] A.M. Tsygankov, V.V. Kuznetsov, N.P. Tarasova, G.A. Yagodin, A.F. Zhukov and Yu. I. Urusov, Zh. Anal. Khim., 41 (1986) 2228; Anal. Abstr., (1987) 10H79.
[15] K. Wang and R. Yu, Fenxi Huaxue, 14 (1986) 599; Anal. Abstr., 49 (1987) 5J121.
[16] D. Guo, C. Ji, P. He and H. Gao, Anal. Proc. (London), 24 (1987) 343.
[17] D. Feng and Ch. Chen, Huaxue Xuebao, 41 (1983) 371; Anal. Abstr., (1984) 6J145.

[18] P.C. Gritzapis, C.E. Efstathiou and T.P. Hadjiioannou, Anal. Chim. Acta, 171 (1985) 165.

[19] T. Limori, M. Sugawara and T. Kambara, Denki Kagaku Oyobi Kogyo Butsuri Kagaku, 47 (1979) 549; Anal. Abstr. (1981) 2J131.

[20] Yu. I. Urusov, V.V. Sergievskii, A.F. Zhukov and A.V. Gordievskii, Zh. Anal. Khim., 34 (1979) 156.

[21] E. Hopirtean, C. Lifeanu and F. Kormos, Rev. Chim. (Bucharest), 28 (1977) 378.

[22] U.O. Lukkari, E.J. Hakoila and H.K. Lukkari, Acta Chem. Fenn., 45 (1972) 182.

[23] E.J. Hakoila, U.O. Lukkari and H.K. Lukkari, Acta Chem. Fenn., 46 (1973) 174B.

[24] Matsushita Electric Ind. Co. Ltd., Br. Pat. 1,330,443 (2.3.72); Anal. Abstr., 26 (1974) 2467.

[25] T.S. Ma and S.S.M. Hassan, Organic Analysis Using Ion Selective Electrodes, Academic Press, London, 1982.

[26] S.S.M. Hassan and S.A.M. Marzouk, Talanta, 41 (1994) 891.

[27] IUPAC Analytical Chemistry Division, Commission on Analytical Nomenclature, Pure Appl. Chem., 66 (1994) 2527.

[28] R.K. Tandon, P.T. Crisp, J. Ellis and R.S. Baker, Talanta, 31 (1984) 227.

[29] S.S.M. Hassan and M.A. Hammada, Analyst, 113 (1988) 1709.

[30] F. Hofmeister, Arch. Exp. Pathol. Pharmakol., 14 (1888) 247.

[31] Z. Marczenko, Separation and Spectrophotometric Determination of Elements, Ellis Horwood, Chichester, 1986.

[32] A. Campiglio, Analyst, 118 (1993) 545.

Book reviews

Kirk-Othmer Encyclopedia of Chemical Technology, 4th edn., edited by J.I. Kroschwitz and M. Howe-Grant (Vol. 13, Helium Group to Hypnotics), Wiley, New York, 1995, xxviii + 1100 pp., £195.00. ISBN 0-471-52682-7.

Volume 13 of this encyclopedia continues and concludes with topics beginning with the letter 'H'. Twenty-nine entries are covered and in-depth treatments ranges from 155 pages devoted to Hormones to 10 pages devoted to Hydrogen-Ion Activity.

The first topic covers the Helium Group (helium, neon, argon, krypton, xenon and radon) and includes details of physical properties, quantum-mechanical effects, production, economic aspects and uses of the gases. A small separate entry covers compounds from this group—especially xenon compounds. The other element included in this volume is Hydrogen and although emphasis is placed on technological details I was surprised to see no mention of hydrogen bonding. Hydrogen Chloride, Hydrogen Peroxide and Hydrogen Energy are also dealt with as separate entries. The element holmium is included with the Lanthanides in another volume.

The section on Hormones is extensive and has sub-entries entitled: Survey, Anterior pituitary hormones, Anterior pituitary-like hormones, Posterior pituitary hormones, Human growth hormone, Brain oligopeptides, Sex hormones and Estrogens and antiestrogens. Two other bio-related topics in this volume include: Histamine and Histamine Antagonists plus Hypnotics, Sedatives, Anticonvulsants and Anxiolytics.

Obvious technological entries include: High Performance Fibers, High Pressure Technology, High Temperature Alloys, Hollow-Fiber Membranes, Holography, Hydraulic Fluids and Hydrothermal Processing. The latter section contains rare editorial omissions as there are no numbers associated with references to Tables and Figures.

Other entries include, Hemicellulose, Herbicides, Hydantoin, Hydrazine, Hydrides, Hydroboration, Hydrocarbons and some Hydroxy compounds.

As with all the other volumes in the fourth edition of this encyclopedia the range of topics covered and the depth of treatment given make this an essential work for inclusion in all good science libraries.

P.J. Cox

A Practical Approach to Chiral Separations by Liquid Chromatography, edited by G. Subramanmian, VCH, Weinheim, 1994, xvi + 405 pp., £72.00. ISBN 3-527-28288-2.

Methodologies for chiral separation continue to offer considerable challenges in the fields of chromatography and capillary electrophoresis. In the course of twelve chapters, this book with contributions from internationally recognised experts seeks to provide a broad framework spanning an introduction to the topic, through legislatory outlines and their implications to the "nuts and bolts" of the practical chromatographic application and its industrial uses. Separate chapters cover the use of the main recognised chemical classes of selective chiral stationary phases, without inclusion of an excessive amount of theory, yet providing sufficient theoretical background for a proper appreciation of the methodologies.

Book reviews

Kirk-Othmer Encyclopedia of Chemical Technology, 4th edn., edited by J.I. Kroschwitz and M. Howe-Grant (Vol. 13, Helium Group to Hypnotics), Wiley, New York, 1995, xxviii + 1100 pp., £195.00. ISBN 0-471-52682-7.

Volume 13 of this encyclopedia continues and concludes with topics beginning with the letter 'H'. Twenty-nine entries are covered and in-depth treatments ranges from 155 pages devoted to Hormones to 10 pages devoted to Hydrogen-Ion Activity.

The first topic covers the Helium Group (helium, neon, argon, krypton, xenon and radon) and includes details of physical properties, quantum-mechanical effects, production, economic aspects and uses of the gases. A small separate entry covers compounds from this group—especially xenon compounds. The other element included in this volume is Hydrogen and although emphasis is placed on technological details I was surprised to see no mention of hydrogen bonding. Hydrogen Chloride, Hydrogen Peroxide and Hydrogen Energy are also dealt with as separate entries. The element holmium is included with the Lanthanides in another volume.

The section on Hormones is extensive and has sub-entries entitled: Survey, Anterior pituitary hormones, Anterior pituitary-like hormones, Posterior pituitary hormones, Human growth hormone, Brain oligopeptides, Sex hormones and Estrogens and antiestrogens. Two other bio-related topics in this volume include: Histamine and Histamine Antagonists plus Hypnotics, Sedatives, Anticonvulsants and Anxiolytics.

Obvious technological entries include: High Performance Fibers, High Pressure Technology,

High Temperature Alloys, Hollow-Fiber Membranes, Holography, Hydraulic Fluids and Hydrothermal Processing. The latter section contains rare editorial omissions as there are no numbers associated with references to Tables and Figures.

Other entries include, Hemicellulose, Herbicides, Hydantoin, Hydrazine, Hydrides, Hydroboration, Hydrocarbons and some Hydroxy compounds.

As with all the other volumes in the fourth edition of this encyclopedia the range of topics covered and the depth of treatment given make this an essential work for inclusion in all good science libraries.

P.J. Cox

A Practical Approach to Chiral Separations by Liquid Chromatography, edited by G. Subramanmian, VCH, Weinheim, 1994, xvi + 405 pp., £72.00. ISBN 3-527-28288-2.

Methodologies for chiral separation continue to offer considerable challenges in the fields of chromatography and capillary electrophoresis. In the course of twelve chapters, this book with contributions from internationally recognised experts seeks to provide a broad framework spanning an introduction to the topic, through legislatory outlines and their implications to the "nuts and bolts" of the practical chromatographic application and its industrial uses. Separate chapters cover the use of the main recognised chemical classes of selective chiral stationary phases, without inclusion of an excessive amount of theory, yet providing sufficient theoretical background for a proper appreciation of the methodologies.

In some contrast the inclusion of a chapter on theoretical modelling techniques as an aid to understanding separation mechanisms, although an esoteric approach to many practical chromatographers, is a welcome deviation from the norm.

The book succeeds as a broadly aimed text which will provide a primer for the novice as well as a more in-depth discussion for the more experienced chromatographer seeking to extend his understanding of chiral methodologies. Regrettably the pace of rapid development in the field and the time taken in coming to publication is reflected in the useful, but dated references to each chapter (no references post 1991). In spite of this drawback, the book is to be recommended as an addition to the library of any aspiring analytical scientist.

D.G. Durham

Practical Guide to Infrared Microspectroscopy, edited by H.J. Humecki, Dekker, New York, 1995, x + 472 pp., US$150.00. ISBN 0-8247-9449-4

The strength of this book, as with others in the series, is its scope. There are chapters on forensic science (paint and fibres), pharmaceuticals, art, earth sciences and electronics; there are practical guides to sample handling and there are chapters on the application of theory to achieve optimisation. Each has been contributed by an experienced practitioner in the field and the extensive references at the end of each chapter would, alone, make it a useful source book.

However, it is badly and irritatingly flawed by the presence of typographical and grammatical errors. For example, spectra should be the plural of spectrum but it is not always so here. Also, there are three different definitions of the equation for the least resolvable separation (LRS) in three separate chapters and the book is also let down by an inadequate index.

Although the need to use other techniques is stressed throughout, the fact that infrared microspectroscopy is always operator intensive, and therefore relatively expensive, is not considered.

Nevertheless this book is a practical and stimulating guide to the technique. The fact that this is so, despite its flaws, is a measure of its usefulness to the practising infrared microscopist.

M. Underhill

Pharmacoepidemiology, by B.L. Strom, Wiley, Chichester, 1994. xviii + 741 pp., £75.00. ISBN 0-471-94058-5.

This substantial revision of the first edition (17 of the 41 chapters are totally new) reflects the rapid progress and growth in the field of pharmacoepidemiology. Although predominantly American, the book derives an international dimension from its 59 authors, with 38 from the United States, nine from Canada, five from the United Kingdom, three from Sweden, two from Australia and one each from the Netherlands and France.

The book is divided into five parts. In the introduction (Part I) the editor defines the subject and describes the historical background, purpose and potential. Epidemiologic study designs, including sample size considerations, are clearly and concisely presented. Reasons for performing pharmacoepidemiology studies and a consideration of risk tolerance complete a helpful introduction on the basic principles of the subject.

In providing various perspectives on pharmacoepidemiology, Part II indicates some of the organisations and professions for whom this book will be relevant. Views are expressed from a university department of epidemiology and preventive medicine, the pharmaceutical industry, a regulatory agency and the US courtroom.

The meat of the book lies within Parts III and IV which deal respectively with the systems available and with selected special applications and methodologic issues. The advantages and limitations of spontaneous reporting systems in the United States, Sweden, France and the UK are presented, as are those for intensive hospital-based cohort studies, such as the Boston Collaborative Drug Surveillance Program. These systems have influenced the US Joint Commission on Accreditation of Health Care Organisations to

In some contrast the inclusion of a chapter on theoretical modelling techniques as an aid to understanding separation mechanisms, although an esoteric approach to many practical chromatographers, is a welcome deviation from the norm.

The book succeeds as a broadly aimed text which will provide a primer for the novice as well as a more in-depth discussion for the more experienced chromatographer seeking to extend his understanding of chiral methodologies. Regrettably the pace of rapid development in the field and the time taken in coming to publication is reflected in the useful, but dated references to each chapter (no references post 1991). In spite of this drawback, the book is to be recommended as an addition to the library of any aspiring analytical scientist.

D.G. Durham

Practical Guide to Infrared Microspectroscopy, edited by H.J. Humecki, Dekker, New York, 1995, x + 472 pp., US$150.00. ISBN 0-8247-9449-4

The strength of this book, as with others in the series, is its scope. There are chapters on forensic science (paint and fibres), pharmaceuticals, art, earth sciences and electronics; there are practical guides to sample handling and there are chapters on the application of theory to achieve optimisation. Each has been contributed by an experienced practitioner in the field and the extensive references at the end of each chapter would, alone, make it a useful source book.

However, it is badly and irritatingly flawed by the presence of typographical and grammatical errors. For example, spectra should be the plural of spectrum but it is not always so here. Also, there are three different definitions of the equation for the least resolvable separation (LRS) in three separate chapters and the book is also let down by an inadequate index.

Although the need to use other techniques is stressed throughout, the fact that infrared microspectroscopy is always operator intensive, and therefore relatively expensive, is not considered.

Nevertheless this book is a practical and stimulating guide to the technique. The fact that this is so, despite its flaws, is a measure of its usefulness to the practising infrared microscopist.

M. Underhill

Pharmacoepidemiology, by B.L. Strom, Wiley, Chichester, 1994. xviii + 741 pp., £75.00. ISBN 0-471-94058-5.

This substantial revision of the first edition (17 of the 41 chapters are totally new) reflects the rapid progress and growth in the field of pharmacoepidemiology. Although predominantly American, the book derives an international dimension from its 59 authors, with 38 from the United States, nine from Canada, five from the United Kingdom, three from Sweden, two from Australia and one each from the Netherlands and France.

The book is divided into five parts. In the introduction (Part I) the editor defines the subject and describes the historical background, purpose and potential. Epidemiologic study designs, including sample size considerations, are clearly and concisely presented. Reasons for performing pharmacoepidemiology studies and a consideration of risk tolerance complete a helpful introduction on the basic principles of the subject.

In providing various perspectives on pharmacoepidemiology, Part II indicates some of the organisations and professions for whom this book will be relevant. Views are expressed from a university department of epidemiology and preventive medicine, the pharmaceutical industry, a regulatory agency and the US courtroom.

The meat of the book lies within Parts III and IV which deal respectively with the systems available and with selected special applications and methodologic issues. The advantages and limitations of spontaneous reporting systems in the United States, Sweden, France and the UK are presented, as are those for intensive hospital-based cohort studies, such as the Boston Collaborative Drug Surveillance Program. These systems have influenced the US Joint Commission on Accreditation of Health Care Organisations to

In some contrast the inclusion of a chapter on theoretical modelling techniques as an aid to understanding separation mechanisms, although an esoteric approach to many practical chromatographers, is a welcome deviation from the norm.

The book succeeds as a broadly aimed text which will provide a primer for the novice as well as a more in-depth discussion for the more experienced chromatographer seeking to extend his understanding of chiral methodologies. Regrettably the pace of rapid development in the field and the time taken in coming to publication is reflected in the useful, but dated references to each chapter (no references post 1991). In spite of this drawback, the book is to be recommended as an addition to the library of any aspiring analytical scientist.

D.G. Durham

Practical Guide to Infrared Microspectroscopy, edited by H.J. Humecki, Dekker, New York, 1995, x + 472 pp., US$150.00. ISBN 0-8247-9449-4

The strength of this book, as with others in the series, is its scope. There are chapters on forensic science (paint and fibres), pharmaceuticals, art, earth sciences and electronics; there are practical guides to sample handling and there are chapters on the application of theory to achieve optimisation. Each has been contributed by an experienced practitioner in the field and the extensive references at the end of each chapter would, alone, make it a useful source book.

However, it is badly and irritatingly flawed by the presence of typographical and grammatical errors. For example, spectra should be the plural of spectrum but it is not always so here. Also, there are three different definitions of the equation for the least resolvable separation (LRS) in three separate chapters and the book is also let down by an inadequate index.

Although the need to use other techniques is stressed throughout, the fact that infrared microspectroscopy is always operator intensive, and therefore relatively expensive, is not considered.

Nevertheless this book is a practical and stimulating guide to the technique. The fact that this is so, despite its flaws, is a measure of its usefulness to the practising infrared microscopist.

M. Underhill

Pharmacoepidemiology, by B.L. Strom, Wiley, Chichester, 1994. xviii + 741 pp., £75.00. ISBN 0-471-94058-5.

This substantial revision of the first edition (17 of the 41 chapters are totally new) reflects the rapid progress and growth in the field of pharmacoepidemiology. Although predominantly American, the book derives an international dimension from its 59 authors, with 38 from the United States, nine from Canada, five from the United Kingdom, three from Sweden, two from Australia and one each from the Netherlands and France.

The book is divided into five parts. In the introduction (Part I) the editor defines the subject and describes the historical background, purpose and potential. Epidemiologic study designs, including sample size considerations, are clearly and concisely presented. Reasons for performing pharmacoepidemiology studies and a consideration of risk tolerance complete a helpful introduction on the basic principles of the subject.

In providing various perspectives on pharmacoepidemiology, Part II indicates some of the organisations and professions for whom this book will be relevant. Views are expressed from a university department of epidemiology and preventive medicine, the pharmaceutical industry, a regulatory agency and the US courtroom.

The meat of the book lies within Parts III and IV which deal respectively with the systems available and with selected special applications and methodologic issues. The advantages and limitations of spontaneous reporting systems in the United States, Sweden, France and the UK are presented, as are those for intensive hospital-based cohort studies, such as the Boston Collaborative Drug Surveillance Program. These systems have influenced the US Joint Commission on Accreditation of Health Care Organisations to

require all hospitals to develop the capability to document and evaluate adverse drug reactions that occur in their patients.

Specific chapters are then devoted to particular systems utilising data from health maintenance organisations and other sources in North America (e.g., Puget Sound, Kaiser Permanente, Harvard, Medicaid and Saskatchewan). The record linkage approach to pharmacoepidemiology is illustrated by separate chapters on the Netherlands (where the experience of NARD and the WHO Drug Utilisation Research Group and the organisation of community pharmacies combine forces to provide unique pharmacoepidemiological opportunities) and the Tayside Medicines Monitoring Unit (MEMO) in Scotland. A number of American inpatient databases are examined, some of which are already capable of linkage to outpatient databases. Further chapters on the Clincial Pharmacy Surveillance Network (Buffalo), case-control surveillance and other approaches are rounded off with valuable advice on how to choose among the available alternatives.

Part IV will be of greatest interest to those readers with some background and experience in pharmacoepidemiology or those with specialised interests within the field. Less common applications of pharmacoepidemiology which are covered include premarketing studies and studies on beneficial drug effects. A review of the current status of descriptive epidemiologic approaches to the study of the processes of drug utilisation is usefully complemented by a chapter on evaluating and improving physicial prescribing. Important methodological issues, for example, determining causation from case reports, bias and confounding, validity of data and novel approaches to study design and statistical analysis are essential reading. Chapters on therapeutic drug monitoring, pharmacoeconomics, quality of life measurements, N-of-1 randomised clinical trials and meta-analysis examine the potential contribution and some of the current limitations of these methodologies in pharmacoepidemiological research.

Part V looks to the future, outlining the ever increasing importance attached to the subject from a number of perspectives, all of which point to the need for more trained personnel and more research. The appendices provide sample size tables and a glossary.

This comprehensive book succeeds admirably in its goal of serving both as an introduction to pharmacoepidemiology and as an excellent reference source for those with some background in the subject.

J.A. Cromarty

Quality Assurance in Analytical Chemistry, by W. Funk, V. Dammann and G. Donnevert, VCH, Weinheim, 1995, xxii + 239 pp., DM 125.00. ISBN 3-527-28668-3.

This volume should be a timely addition to the libraries of the many analytical laboratories in the UK currently progressing towards ISO 9000 and other accreditation standards. It should also be welcomed by analysts tasked with maintaining and improving established quality systems.

The book presents a four phase model of analytical quality assurance, but before doing so dedicates sixteen pages to symbols and definitions relating to the subject. With so many symbols, terms and acronyms relating to quality assurance appearing in modern scientific literature, it is refreshing to find a large number so clearly explained and accessible in one volume. The four phases are each very thoroughly dealt with by a separate chapter. Phase I is concerned with establishing a new analytical procedure and deals with, amongst many others, such matters as calibration, precision, accuracy and testing for linearity. This chapter contains some information (e.g., the conditions and limitations of the use of internal standards) which should be common knowledge to most analytical chemists. However, the mathematics involved are, at times, daunting and some understanding of statistics is essential. The first phase is concluded by an excellent summary of the information which should be included in the documentation of a fundamental analytical process. Phase II is concerned with preparative quality assurance, intended to be performed before the first routine use of a process, and to be primarily

require all hospitals to develop the capability to document and evaluate adverse drug reactions that occur in their patients.

Specific chapters are then devoted to particular systems utilising data from health maintenance organisations and other sources in North America (e.g., Puget Sound, Kaiser Permanente, Harvard, Medicaid and Saskatchewan). The record linkage approach to pharmacoepidemiology is illustrated by separate chapters on the Netherlands (where the experience of NARD and the WHO Drug Utilisation Research Group and the organisation of community pharmacies combine forces to provide unique pharmacoepidemiological opportunities) and the Tayside Medicines Monitoring Unit (MEMO) in Scotland. A number of American inpatient databases are examined, some of which are already capable of linkage to outpatient databases. Further chapters on the Clincial Pharmacy Surveillance Network (Buffalo), case-control surveillance and other approaches are rounded off with valuable advice on how to choose among the available alternatives.

Part IV will be of greatest interest to those readers with some background and experience in pharmacoepidemiology or those with specialised interests within the field. Less common applications of pharmacoepidemiology which are covered include premarketing studies and studies on beneficial drug effects. A review of the current status of descriptive epidemiologic approaches to the study of the processes of drug utilisation is usefully complemented by a chapter on evaluating and improving physicial prescribing. Important methodological issues, for example, determining causation from case reports, bias and confounding, validity of data and novel approaches to study design and statistical analysis are essential reading. Chapters on therapeutic drug monitoring, pharmacoeconomics, quality of life measurements, N-of-1 randomised clinical trials and meta-analysis examine the potential contribution and some of the current limitations of these methodologies in pharmacoepidemiological research.

Part V looks to the future, outlining the ever increasing importance attached to the subject from a number of perspectives, all of which point to the need for more trained personnel and more research. The appendices provide sample size tables and a glossary.

This comprehensive book succeeds admirably in its goal of serving both as an introduction to pharmacoepidemiology and as an excellent reference source for those with some background in the subject.

J.A. Cromarty

Quality Assurance in Analytical Chemistry, by W. Funk, V. Dammann and G. Donnevert, VCH, Weinheim, 1995, xxii + 239 pp., DM 125.00. ISBN 3-527-28668-3.

This volume should be a timely addition to the libraries of the many analytical laboratories in the UK currently progressing towards ISO 9000 and other accreditation standards. It should also be welcomed by analysts tasked with maintaining and improving established quality systems.

The book presents a four phase model of analytical quality assurance, but before doing so dedicates sixteen pages to symbols and definitions relating to the subject. With so many symbols, terms and acronyms relating to quality assurance appearing in modern scientific literature, it is refreshing to find a large number so clearly explained and accessible in one volume. The four phases are each very thoroughly dealt with by a separate chapter. Phase I is concerned with establishing a new analytical procedure and deals with, amongst many others, such matters as calibration, precision, accuracy and testing for linearity. This chapter contains some information (e.g., the conditions and limitations of the use of internal standards) which should be common knowledge to most analytical chemists. However, the mathematics involved are, at times, daunting and some understanding of statistics is essential. The first phase is concluded by an excellent summary of the information which should be included in the documentation of a fundamental analytical process. Phase II is concerned with preparative quality assurance, intended to be performed before the first routine use of a process, and to be primarily

of concern to personnel who will be carrying out the routine analyses. Here the more practical requirements of an analytical process are considered, starting with the determination of the quality required and ending with the preparation of quality control charts for the routine use to follow. Topics covered in this chapter include specificity, costs and external quality requirements (e.g., law, international agreements, etc.) but the greater part is devoted to the subject of control samples and the principles of quality control charting. Shewhart charts, R-charts and cusum charts are all dealt with in depth. Phases III and IV are concerned respectively with routine quality assurance and external analytical quality assurance and will be of particular interest to those establishing quality systems in accordance with an accreditation standard, whether with new or established methodology. Phase II deals with issues ranging from laboratory environment and management, outfitting equipment, materials and personnel, to the reporting of analytical results, problem solving and, in some depth, corrective measures and systematic trouble shooting. Phase IV deals with audits and interlaboratory tests and concludes with recommendations for the organisation of external quality assurance. A total of 154 references are given and appendices of sample calculations and statistical tablets are also included.

This work was first produced in Germany in 1992 and, according to the preface "···was quickly accepted by analysts as a textbook on analytical quality assurance and analytical quality control." The English edition is a revised and updated version of the original. There is little doubt that this very competent translation will be as well received in the UK as the original was in Germany.

S.R. Reddick

Neutron Spectroscopy, by Yu. A. Izyumov and N.A. Chernoplekov, Plenum, New York, 1994. xiv + 373 pp. US$89.50. ISBN 0-306-11033-4.

Covering the more theoretical and physical aspects of the subject, Neutron Spectroscopy is aimed primarily at the solid state physicist rather than the chemical community. This means the title should be read in its narrower sense, covering the very traditional areas of neutron scattering established in the infancy of the subject and pursued with vigour ever since. Concentrating as it does on magnetic and fundamental excitations, the chemical relevance of much of the material is limited.

That nonwithstanding, the text is a clear and comprehensive account of the fundamental aspects of neutron spectroscopy and while the applications covered are restricted to physical rather than chemical systems, the principles thus established are of more general applicability.

The book opens with a detailed account of basic neutron scattering theory applied in this area, augmented by valuable and comprehensively worked examples putting the theory into practice. The theory is accounted clearly and covers the main aspects of the microscopic mechanisms of the dynamics of materials and how neutrons can be used to elucidate these.

Subsequent chapters cover, again from a mostly theoretical standpoint, magnetic excitations and phase transitions, structural phase transitions, along with phonons and critical scattering. These are illustrated by brief reviews of some of the pertinent experimental data. Most of this again reflects the fact that these were the main subjects in the earliest days of neutron spectroscopy, with many of the classic early works referred to. A brief account of experimental techniques is given, and the work concludes with the most chemically relevant section, on metal hydrides.

In conclusion, a solid theoretical and physical text, with its strengths lying firmly in these areas. The weakness for this reader was the lack of experimental detail, especially the lack of account of the recent dramatic advances in neutron instrumentation and techniques. There are also better texts covering the wide use of neutrons in a range of chemically more relevant materials whatever the technical merits of this particular work.

C.C. Wilson

of concern to personnel who will be carrying out the routine analyses. Here the more practical requirements of an analytical process are considered, starting with the determination of the quality required and ending with the preparation of quality control charts for the routine use to follow. Topics covered in this chapter include specificity, costs and external quality requirements (e.g., law, international agreements, etc.) but the greater part is devoted to the subject of control samples and the principles of quality control charting. Shewhart charts, R-charts and cusum charts are all dealt with in depth. Phases III and IV are concerned respectively with routine quality assurance and external analytical quality assurance and will be of particular interest to those establishing quality systems in accordance with an accreditation standard, whether with new or established methodology. Phase II deals with issues ranging from laboratory environment and management, outfitting equipment, materials and personnel, to the reporting of analytical results, problem solving and, in some depth, corrective measures and systematic trouble shooting. Phase IV deals with audits and interlaboratory tests and concludes with recommendations for the organisation of external quality assurance. A total of 154 references are given and appendices of sample calculations and statistical tablets are also included.

This work was first produced in Germany in 1992 and, according to the preface "···was quickly accepted by analysts as a textbook on analytical quality assurance and analytical quality control." The English edition is a revised and updated version of the original. There is little doubt that this very competent translation will be as well received in the UK as the original was in Germany.

S.R. Reddick

Neutron Spectroscopy, by Yu. A. Izyumov and N.A. Chernoplekov, Plenum, New York, 1994. xiv + 373 pp. US$89.50. ISBN 0-306-11033-4.

Covering the more theoretical and physical aspects of the subject, Neutron Spectroscopy is aimed primarily at the solid state physicist rather than the chemical community. This means the title should be read in its narrower sense, covering the very traditional areas of neutron scattering established in the infancy of the subject and pursued with vigour ever since. Concentrating as it does on magnetic and fundamental excitations, the chemical relevance of much of the material is limited.

That nonwithstanding, the text is a clear and comprehensive account of the fundamental aspects of neutron spectroscopy and while the applications covered are restricted to physical rather than chemical systems, the principles thus established are of more general applicability.

The book opens with a detailed account of basic neutron scattering theory applied in this area, augmented by valuable and comprehensively worked examples putting the theory into practice. The theory is accounted clearly and covers the main aspects of the microscopic mechanisms of the dynamics of materials and how neutrons can be used to elucidate these.

Subsequent chapters cover, again from a mostly theoretical standpoint, magnetic excitations and phase transitions, structural phase transitions, along with phonons and critical scattering. These are illustrated by brief reviews of some of the pertinent experimental data. Most of this again reflects the fact that these were the main subjects in the earliest days of neutron spectroscopy, with many of the classic early works referred to. A brief account of experimental techniques is given, and the work concludes with the most chemically relevant section, on metal hydrides.

In conclusion, a solid theoretical and physical text, with its strengths lying firmly in these areas. The weakness for this reader was the lack of experimental detail, especially the lack of account of the recent dramatic advances in neutron instrumentation and techniques. There are also better texts covering the wide use of neutrons in a range of chemically more relevant materials whatever the technical merits of this particular work.

C.C. Wilson

Selectivity enhancements for the determination of thorium by flow-injection analysis through the formation of the Th-DTPA-HQS fluorescent ternary complex[1]

Liwen Ye, Charles A. Lucy*

Department of Chemistry, The University of Calgary, 2500 University Drive, N.W. Calgary, Alta., T2N 1N4, Canada

Abstract

Addition of diethylenetriaminepentaacetic acid (DTPA) to the fluorescent binary complex of thorium and 8-hydroxyquinoline-5-sulfonic acid (HQS) forms the Th-DTPA-HQS fluorescent ternary complex. The formation of this ternary complex enhances the selectivity for the determination of thorium. Excesses of DTPA and HQS are used as reagents in flow-injection analysis to detect thorium. The excess DTPA effectively masks potentially interfering ions by preventing the formation of fluorescent binary metal-HQS complexes. The presence of lanthanides and transition metals does not interfere with the thorium detection with this method (the ratio of molar intensity for metals to molar intensity for thorium is $< 0.3\%$ with the exception of lutetium, for which molar intensity ratio is 1.34%). The detection limit for thorium is 12 ng ml^{-1}.

Keywords: Selectivity enhancements; Thorium determination; Flow-injection analysis; Th-DTPA-HQS fluorescent ternary complex formation

1. Introduction

Determination of trace concentrations of thorium is important in nuclear technology and environmental chemistry. Several analytical techniques have been employed for the detection of thorium. Radiochemical neutron activation analysis [1-3], inductively coupled plasma [4], mass spectrometry [5], and inductively-coupled plasma mass spectrometry (ICP-MS) [6] are very sensitive methods for the determination of Th^{4+}. However, they require expensive and specialized instrumentation. Electroanalytical techniques [7-10] have been employed to determine thorium, but they lack satisfactory selectivity as the presence of lanthanides and transition metals interferes with the determination of thorium. UV-visible spectrophotometry has been widely used for the determination of thorium.

* Corresponding author. Fax: +403 289 9488; e-mail: lucy@acs.ucalgary.ca

The chromogenic ligands of Arsenazo III [11–17], Semimethylthymol Blue [18], *m*-carboxychlorophosphonazo [19], 1-(2-pyridylazo)-2-naphthol (PAN) [14], and DBF–Arsenazo [20] complex with Th^{4+} to form UV–visible absorbing complexes. The sensitivity of chromogenic ligands is typically 20–50 ng ml^{-1} [11–13] and with the exception of DBF–Arsenazo for which the claimed detection limit is 2 ng ml^{-1} [20], the sensitivity of the chromogenic ligand methods for Th^{4+} is not better than the other techniques mentioned. Furthermore, lanthanides and uranium also form complexes with these chromogenic ligands, and interfere with the detection of thorium. Therefore a chromatographic separation or sample pretreatment is generally required when thorium is determined in the presence of other metal ions [11,12,20].

Fluorescence can also be used to determine thorium. The reagent 8-hydroxyquinoline-5-sulfonic acid (HQS) forms a fluorescent binary complex with Th^{4+} [12]. "Binary" complex refers to the complexation of a metal by a single type of ligand. The complexation equilibrium can be expressed as

$$Th^{4+} + nHQS^{2-} \rightleftharpoons Th(HQS)_n^{(4-2n)} \qquad (1)$$
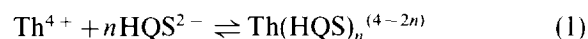
However, other metals, such as Mg^{2+}, Ca^{2+}, Cd^{2+}, Zn^{2+}, La^{3+} and Lu^{3+}, also form strongly fluorescent complexes with HQS [21]. Thus, like the UV–visible spectrophotometric methods discussed above, these metals interfere with the determination of thorium.

Addition of the strong chelating agent diethylenetriaminepentaacetic acid (DTPA) to the Th–HQS binary complex system can prevent the other metals from forming interfering fluorescent complexes. The manner in which DTPA does this is explained as follows. DTPA forms very strong binary complexes with metals.

$$M^{n-} + DTPA^{5-} \rightleftharpoons M(DTPA)^{(n-5)} \qquad (2)$$
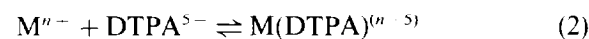
Thus in a solution containing excess DTPA and HQS, metals will be present as DTPA complexes. Thorium is a multi-coordination site center metal ion. In certain media, the thorium is potentially of 10-coordination [22]. DTPA is an octadentate chelating ligand. After complexing with DTPA,

thorium still has two coordination sites available. These two "unsaturated" coordination sites further complex with the second ligand, HQS in this case.

$$Th(DTPA)^- + HQS^{2-} \rightleftharpoons [Th(DTPA)HQS]^{3-} \qquad (3)$$
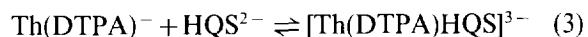
This complex, which consists of one central ion and two types of chelating ligand is called a "ternary complex". The ternary complex of Th–DTPA–HQS can be classified as a "coordination-unsaturated" or "inner sphere" ternary complex. The formation of "coordination-unsaturated" [23] or "inner sphere" [24] ternary complexes provides great selectivity. The formation of the ternary complex depends on the coordination number of the metal, the dentation of the first type of ligand and the dentation of the second type of ligand. In fluorescence analysis, there is the additional criterion that the metal must form a fluorescent complex. In the case of the DTPA/HQS reagent, only thorium fulfills all of these criteria. DTPA effectively masks other metal ions, preventing the formation of fluorescent binary metal–HQS complexes.

Flow-injection analysis (FIA) is a simple and efficient instrumental technique. In FIA the analyte merges with one or more reagents to yield a product which is monitored by a detector. In this work, the fluorescent ternary complex of Th–HQS–DTPA is proposed to be an indicator for sensitive and selective determination of thorium. A simple FIA system using a DTPA and HQS mixture as reagent will be demonstrated. The optimum conditions for the system and the application to detection of thorium will be discussed.

2. Experimental

2.1. Apparatus

Fig. 1 shows a schematic of the FIA manifold used in this work. The FIA system consisted of a solvent delivery pump (Pump 1 in Fig. 1) (Model 625, Waters Associates, Milford, MA), a sampling valve (Model 9125, Rheodyne, Berkeley, CA) fit with a 50 μl loop and a fluorimetric detector (Model 470, Waters; $\lambda_{ex} = 360$ nm; $\lambda_{em} = 500$ nm).

The output signal from the fluorimetric detector was digitized at 2 Hz with a CHROM-1AT (Keithley MetraByte) data acquisition board enhanced for faster data acquisition, and analyzed using LabCalc (Galactic) on a 486-based microcomputer. The pump and injector were fit with PEEK tubing. A 15 cm column packed with 5 μm C_{18} particles was positioned between the pump and injector to provide sufficient back pressure for optimal pumping. The reagent was delivered by constant pressure pumping (Pump 2 in Fig. 1) through application of nitrogen pressure (40 psi) to a cylinder containing the reagent [25,26]. Low pressure tubing and fittings (Alltech Associate, Deerfield, IL) connected the reagent delivery system to the effluent stream. The carrier stream from the delivery pump (1.0 ml min^{-1}) merged with the reagent (0.3 ml min^{-1}) at the mixing tee (316 stainless steel, 90° ports), flowed through the reaction coil, 510 cm of tightly spiraled 0.50 mm i.d. knitted Teflon tubing (RXN 1000 Coil, Waters; 1000 μl volume), and then directly to the detector.

2.2. Reagents and standards

All reagent solutions were prepared by dissolving analytical or ACS grade reagents in distilled deionized water (Nanopure Water System, Barnsted). No special treatment was required throughout the solution preparation. The reagents HQS (Janssen Chimica) and DTPA (Janssen Chimica) were dissolved in deionized water to prepare the stock solutions. The 1 M stock buffer solution was prepared by dissolving 2-amino-2-methyl-1-propanol (AMP) (J.T. Baker Inc.) in deionized water and adjusting the pH to 11.0 by adding nitric acid.
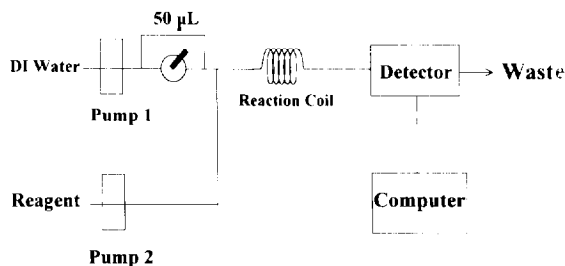

Fig. 1. Schematic diagram for the FIA manifold used for Th^{4+} determination. See text for details.

The 1 mM stock Th^{4+} solution was prepared by diluting 1000 μg ml^{-1} thorium ICP standard solution in 5% HNO_3 (Johnson Matthey, Ward Hill, MA). (**Caution: thorium nitrate is corrosive, irritates skin and eyes, and is radioactive. Care required when handling.**) The other stock metal solutions were prepared using analytical grade salts. Lower concentrations were achieved by dilution in volumetric Nalgene-ware. All solutions were stored in Nalgene plastic bottles.

2.3. Procedures

In studies of sensitivity and interference, various concentrations of Th^{4+} and different metal ions were injected into the sampling valve and delivered by deionized water carrier stream (1 ml min^{-1}), merged with the reagent (1 mM HQS, 5 mM DTPA, and 100 mM AMP, pH = 11.02), allowed to react in the reaction coil and then passed through the detector. The fluorescent intensity was measured by the area of the peak.

For the rest of the experiments (e.g. pH effect and effect of HQS concentration, etc.), the specific solution, which contained certain concentrations of reagents and was adjusted to a certain pH value, was prepared in a volumetric flask. The solutions were then allowed to sit for a time period sufficient to ensure that the reaction goes to completion. This solution, which was the product of reagents, was injected into the sampling valve and carried to the detector by the deionized water stream. The effluent was detected by the fluorescent the detector and resultant peak areas were used for quantification.

3. Results and discussion

3.1. Optimizing conditions for fluorescent ternary complex of Th-DTPA-HQS

3.1.1. pH effect

Fig. 2 shows the effect of pH on both thorium (binary Th-HQS complex) and thorium-DTPA (ternary Th-HQS-DTPA complex) fluorescent response. The optimal pH for the Th-HQS complex is at pH 4 (Fig. 2 (curve a)) while the optimal
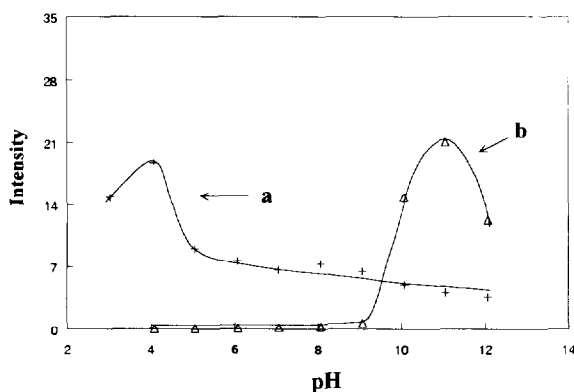
Fig. 2. pH effect for Th–HQS binary complex and Th–DTPA–HQS ternary complex. (a) Th–HQS binary complex. (b) Th–DTPA–HQS ternary complex. Experimental conditions: (a) 1×10^{-5} M Th^{4+}, 1×10^{-4} M HQS adjusted to various pH values; (b) 1×10^{-5} M Th^{4+}, 1×10^{-4} M HQS and DTPA at different pH values.

pH for the Th–DTPA–HQS ternary complex is around pH 11 (Fig. 2 (curve b)). Addition of DTPA shifts the optimal pH value to high pH by preventing formation of thorium hydroxides. The fluorescent intensity of the ternary complex is slightly higher (12%) than that of the binary complex when both optimal values are compared.

From Fig. 2, it could be concluded that the ternary complex of thorium does not significantly enhance the sensitivity for determination of Th^{4+}. However, when HQS is used as a reactant in a FIA system, some metal ions (e.g. Mg^{2+}, Ca^{2+}, Cd^{2+}, etc.) present as the matrix of the sample in the system form strongly fluorescent complexes with HQS [21]. These fluorescent complexes interfere with the determination of thorium. The addition of DTPA to the reagent results in the formation of DTPA complexes with these matrix metals, leaving the HQS isolated from these metals whereas Th–DTPA further complexes with HQS and forms the fluorescent ternary complex.

Based on the results shown in Fig. 2, the reagents are buffered to pH 11 in the rest of the experiments.

3.1.2. Concentration of DTPA

To study the effect of the concentration of DTPA on the fluorescent response, Th^{4+} and HQS concentrations were fixed at 1×10^{-5} M

and 1×10^{-4} M respectively, and the concentration of DTPA was varied from 5×10^{-6} M to 1×10^{-2} M. All the solutions were buffered at pH 11.0 using 10 mM AMP.

Fig. 3 shows that the fluorescent intensity remains constant after the concentration of DTPA reaches 1×10^{-5} M, which is the same concentration as that of Th^{4+}. DTPA is an octadentate ligand while Th^{4+} is a 10-coordination ion. The Th–DTPA complex should be present at 1:1 ratio. The results in Fig. 3 confirm that the ratio of Th^{4+}: DTPA is 1:1 in the Th–DTPA–HQS ternary complex. In Fig. 3, the intensity is almost constant (actually, it increases slightly) with increasing concentration of DTPA even up to a thousand-fold excess of DTPA. Thus addition of excess DTPA does not suppress the signal for the ternary complex. This is significant as the excess DTPA suppresses the background fluorescence from metal impurities in the reagent and samples. In a later section, we will discuss the role of excess DTPA in the selectivity of Th^{4+} determination.

3.1.3. Concentration of HQS

To determine the optimal concentration of HQS, Th^{4+} and DTPA concentrations were fixed at 1×10^{-5} M and 2×10^{-5} M respectively and the concentration of HQS was varied from 5×10^{-6} M to 5×10^{-4} M. All solutions were buffered at pH 11.0 with 10 mM AMP. The
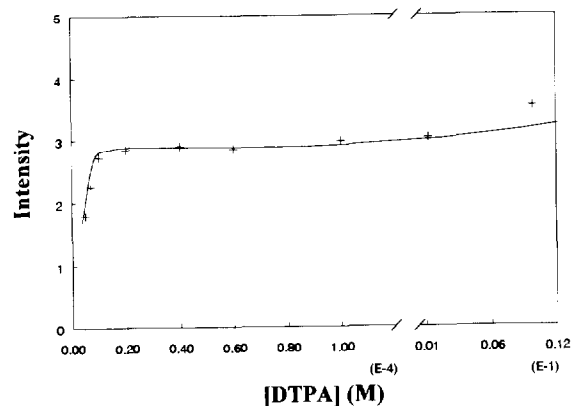

Fig. 3. Concentration effect of DTPA. Experimental conditions: 1×10^{-5} M Th^{4+}, 1×10^{-4} M HQS, 10 mM AMP (pH 11.0) at DTPA concentrations from 5×10^{-6} M to 1×10^{-2} M.
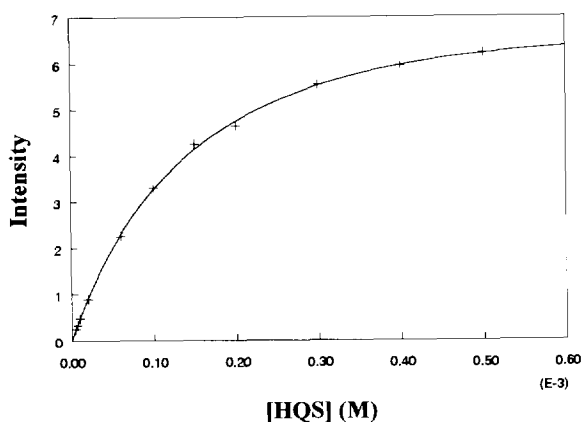
Fig. 4. Concentration effect of HQS: (+) experimental data; (———) theoretical regression curve. Experimental conditions: 1×10^{-5} M Th^{4+}, 2×10^{-5} M DTPA, 10 mM AMP (pH 11.0) at different concentrations of HQS from 5×10^{-6} M to 5×10^{-4} M.

results are shown in Fig. 4. DTPA forms a much more stable complex with Th^{4+} than HQS does [27,28]. Thus DTPA will preferentially complex Th^{4+}, leaving only two coordination sites free for HQS complexation. In the presence of excess DTPA, the equilibrium governing the fluorescent intensity is expressed by Eq. (3). The stability constant for the formation of the ternary complex is

$$K_f = \frac{[Th(DTPA)(HQS)^{3-}]}{[Th(DTPA^-)]\alpha_{HQS^{2-}}[HQS]} \qquad (4)$$

The fluorescent intensity is proportional to the concentration of Th–DTPA–HQS complex. At pH 11, $\alpha_{HQS^{2-}}$ is 0.9974 based on literature stability constants [27]. A nonlinear fit (Slide Write plus, Advanced Graphics Software, Inc.) of the data in Fig. 4 yields a formation constant of $5.7 \pm 0.6 \times 10^3$ ($r^2 = 0.9995$). In Fig. 4, the solid line is a theoretical regression based on Eqs. (3) and (4). As the formation constant of the ternary complex is not large, the reagent HQS should be kept in large excess to insure optimal fluorescent intensity for the ternary complex.

To summarize the optimal conditions. the reagent should be adjusted to pH 11 and the concentrations of DTPA and HQS should be kept in large excess relative to the concentrations of the Th^{4+} sample. Thus, 1 mM of HQS and 5 mM of

DTPA in 100 mM AMP (pH 11.0) was employed as the reagent for the determination of thorium.

3.2. Application of thorium fluorescent ternary complex

3.2.1. Detection of Th^{4+}

The reagent mixture of DTPA and HQS merged with the distilled deionized water carrier stream into which Th^{4+} was injected. The complexation took place in the 1000 μl reaction coil and the ternary complex product flowed through the sample cell of the fluorescent detector. Concentrations of Th^{4+} ($0-1 \times 10^{-5}$ M) were injected into the sampling valve with a 50 μl sample loop. Distilled deionized water was tested as a blank sample. The response peak for blank sample had a peak area equivalent to the response peak area for 5×10^{-8} M Th^{4-} since the change in back pressure varied the flow rate of reagent at the moment of injection. Peak areas are used when the calibration curve is calculated. Linear response was observed for injection of 5×10^{-8} M (2.5 pmole)–1×10^{-5} M (500 pmole) Th^{4+} (slope: $1.911 \pm 0.065 \times 10^6$; intercept: 0.00483 ± 0.251; $r^2 = 0.9910$). The estimated detection limit is 12 ng ml^{-1}.

3.2.2. Interference of other metal ions

Some alkaline earth ions, transition metal ions and lanthanide ions can form fluorescent binary complexes with HQS [21]. Like the Lu–Hexadentate–HQS ligands for selective detection of Lu^{3+} [29], Th–DTPA–HQS has high selectivity for determination of Th^{4+}. The stronger chelating ligand DTPA competes with HQS and strips those metal ions from HQS to form more stable metal–DTPA complexes. These metal ions are fully complexed by the octadentate DTPA, and so no further complexation by HQS can occur. Thus DTPA masks the fluorescent response from these metal–HQS complexes.

To test the selectivity of the Th^{4-} reagent, 1×10^{-4} M concentrations of a number of metal ions were injected into the FIA manifold. The intensities were recorded and the interfering indexes were calculated based on the ratio of molar intensity of the metal vs. the molar intensity observed for Th^{4-}.

Table 1
Interfering indexes of metal ions with DTPA–HQS reagent[a]

Metal ion	Interfering index[b] (%)	Metal ion	Interfering index[b] (%)
Mg^{2+}	0.069	Zn^{2+}	0.0013
Ca^{2+}	0.016	Pb^{2+}	0.014
Sr^{2+}	0.022	Fe^{3+}	−0.0001
Ba^{2+}	0.045	La^{3+}	0.162
Mn^{2+}	0.034	Er^{3+}	0.0043
Co^{2+}	−0.00003	Gd^{3+}	0.086
Ni^{2+}	0.016	Lu^{3+}	1.34
Cu^{2+}	0.049	UO_2^{2+}	−0.23
Cd^{2+}	−0.0006	Th^{4+}	100

[a] Experimental conditions: 1×10^{-4} M of each metal was injected using a 50 μl sampling valve, reagent was 1 mM HQS, 5 mM DTPA, 100 mM AMP (pH 11.02).
[b] As defined by Eq. (5).

Interfering index

$$= \frac{\text{Molar intensity of metal ion}}{\text{Molar intensity of } Th^{4+}} \times 100(\%) \qquad (5)$$

Table 1 presents the metals tested along with the observed interfering indexes.

From the experimental results, the DTPA–HQS reagent system has high selectivity for Th^{4+}. Of the metals tested only Lu^{3+} (interfering index 1.34%) interferes significantly with Th^{4+} detection. All other metals display interfering indexes of < 0.3%. Therefore, the DTPA-HQS reagent is a potent FIA reagent system for the detection of Th^{4+} in complex matrices.

4. Conclusion

The DTPA–HQS reagent system can be used to sensitively and selectively determine Th^{4+} ion using FIA through the formation of the Th–DTPA–HQS ternary complex. The dynamic range for determination of Th^{4+} is from 5×10^{-8} M (2.5 pmole) to 1×10^{-5} M (500 pmole) Th^{4+}. The presence of transition metals and lanthanides does not interfere in the determination of Th^{4+}.

Acknowledgment

References

[1] L. Benedik and A.R. Byrne, J. Radioanal. Nucl. Chem., 189 (1995) 325.
[2] K.H. Theimer and V. Krivan, Anal. Chem., 62 (1990) 2722.
[3] C.A. Huh and M.P. Bacon, Anal. Chem., 57 (1985) 2138.
[4] A. Marco, Analyst, 114 (1989) 319.
[5] L.W. Green, N.L. Elliot and T.H. Longhurst, Anal. Chem., 55 (1983) 2394.
[6] K. Takeda, T. Yamaguchi, H. Akiyama and T. Masuda, Analyst, 116 (1991) 501.
[7] G.-A. Mazzocchin, S. Daniele and L.M. Moretto, Talanta, 37 (1990) 317.
[8] Z. Zhao, X. Cai, P. Li and H. Yaung, Talanta, 33 (1986) 623.
[9] J. Wang and J. Zadeii, Anal. Chim. Acta, 188 (1986) 187.
[10] C.L. Sharma and R.S. Arya, Talanta, 26 (1979) 577.
[11] P.E. Jackson, J. Carnevale, H. Fuping and P.R. Haddad, J. Chromatogr., 671 (1994) 181.
[12] J.L.P. Pavon, C.G. Pinto, E.R. Garcia and B.M. Cordero, Anal. Chim. Acta, 264 (1992) 291.
[13] J.L.P. Pavon, C.G. Pinto, B.M. Cordero and J.H. Mendez, Anal. Chem., 62 (1990) 2405.
[14] B.M. Cordero and J.L.P. Pavon, Anal. Chim. Acta, 234 (1990) 239.
[15] J.L.P. Pavon, B.M. Cordero, J.H. Mendez and R.M.I. Agudo, Anal. Chem., 61 (1989) 1789.
[16] V. Hamilton, W. Dalespall, B.F. Smith and E.J. Peterson, J. Chromatogr., 469 (1989) 369.
[17] Y.K. Kvaratskheli, Y.V. Demin, G.R. Kukushkin, R.P. Antonova and A.E. Doroshevich, J. Anal. Chem. USSR, 44 (1989) 1126.
[18] M.A.H. Hafez, I.M.M. Kenawy and M.A.M. Ramadan, Anal. Lett., 27 (1994) 1383.
[19] C-G. Hsu, X-M. Lian and J-M. Pan, Talanta, 38 (1991) 1051.
[20] X-X. Zhang, M-S. Wang and J-K. Cheng, Anal. Chim. Acta, 237 (1990) 311.
[21] K. Soroka, R.S. Vithanage, D.A. Phillips, B. Walker and P.K. Dasgupta, Anal. Chem., 59 (1987) 629.
[22] K.W. Bagnall, The Actinide Elements, Elsevier, Amsterdam, 1972, p. 221.
[23] T.S. West, Natl. Bur. Stand. (U.S.), Monogr., 100 (1967).
[24] L. Sommer, G. Ackermann, D.B. Thorburn and S.B. Savvin, Pure Appl. Chem., 62 (1990 2147.
[25] L. Fossey and F.F. Cantwell, Anal. Chem., 55 (1983) 1882.

[26] L. Fossey and F.F. Cantwell, Anal. Chem., 57 (1985) 922.

[27] R.M. Smith and A.E. Martell, Critical Stability Constants, Vol. 2, Plenum Press, New York, 1975.

[28] R.M. Smith and A.E. Martell, Critical Stability Constants, Vol. 1, Plenum Press, New York, 1975.

[29] C.A. Lucy and L. Ye, Anal. Chem., 67 (1995) 79.

Photometric determination of anionic surfactants with a flow-injection analyzer that includes a chromatomembrane cell for sample preconcentration by liquid–liquid solvent extraction[1]

L.N. Moskvin[a], J. Simon[b,*], P. Löffler[b], N.V. Michailova[a], D.N. Nicolaevna[a]

[a]*Department of Chemistry, State University of St. Petersburg, Stavy Petergof, St. Petersburg 198904, Russia*
[b]*Department of Chemistry, Free University of Berlin, Fabeckstrasse 34/36, D-14195 Berlin, Germany*

Abstract

Chromatomembrane cells proved to be applicable to flow-injection analysis whenever computer-operated manifolds for liquid–liquid or liquid–gas extraction procedures were required. Proceeding in accordance with the Methylene Blue method the determination of anionic surfactants was studied by applying the chromatomembrane cell for preconcentration and extraction of the ion-pair complex being formed. Spectrophotometric detection at 650 nm was made possible by using a flowthrough cell within a range of 0.02–5.0 mg dodecylsulfate per liter of water. The absorbance was found to respond proportionally to the product of preconcentration time and surfactant concentration, its slope factor being calculated with $\pm 3\%$ standard deviation. A mechanism for the preconcentration cycle inside the cell is suggested.

1. Introduction

The determination of anionic surfactants in wastewater by measurement of the Methylene Blue index (MBAS) according to ISO 7875-1 is a common practice. The method includes ion-pair extraction which unfortunately creates difficulties whenever automation is required [1–3]. The batch process [4] has the disadvantage of low distribu-

tion coefficients which restrict the detection limit to 0.05 mg l^{-1} under optimal conditions. Del Valle et al. [5] reported that the sensitivity can be improved to meet the requirements of environmental monitoring by using time-based continous sampling followed by flow-injection spectrophotometric determination.

Until now the performance of flow-injection (FI) liquid–liquid extraction systems has been limited by inadequate approaches to the problem of phase separation [6] at the end of the procedure. Eventually, Liu and Dasgupta [7] decided in favour of a technique which made phase separation unecessary. The amount of analyte extracted into the organic phase is calculated from its absorbance and the length of the organic segments passing a UV/Vis detector at the outflow of the extraction coil. The system is based on dual-wavelength spectrophotometric measurements and works with automated data processing.

An alternative approach to extraction procedures arises from the applicaton of chromatomembrane cells in FI systems. The novel extraction module consists of a rectangular block of biporous PTFE. Polar liquids fill the macropores whereas the micropores remain available only for non-polar liquids or gases. The capillary pres-
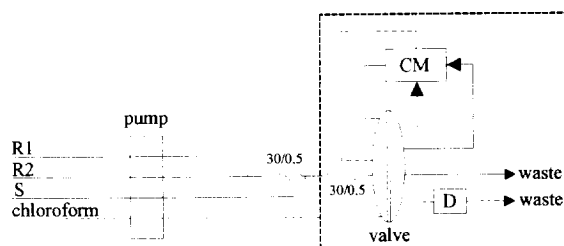

Fig. 1. Schematic flow diagram for the determination of dodecylsulfate. Broken line: automated extraction module (Fig. 2).

sure of polar liquids prevents their penetration into the macropores. We recently reported [8,9] on the special construction of a chromatomembrane cell which allows the two phases to flow independently through the unit and come into contact over an interfacial area of about 0.7 m^2 cm^{-3} biporous PTFE. Taking into account the very small volumes of the contacting phases it is easy to understand that the analyte transfer through the expanded boundary cannot be restricted kinetically. The pressures under which both phases are supplied into the cell have to comply with the physico-chemical requirements [9] and should be controlled to ensure stable operating conditions.
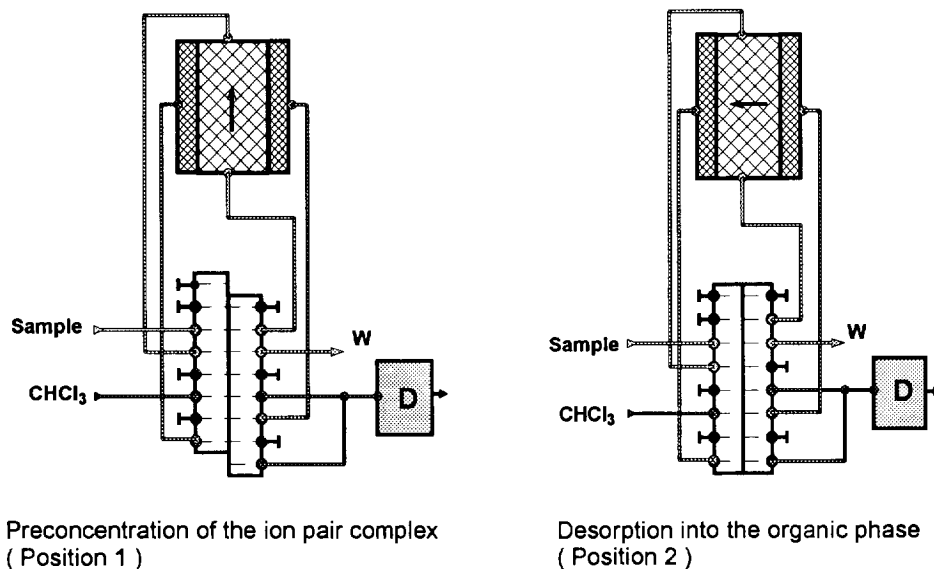

Preconcentration of the ion pair complex
(Position 1)

Desorption into the organic phase
(Position 2)

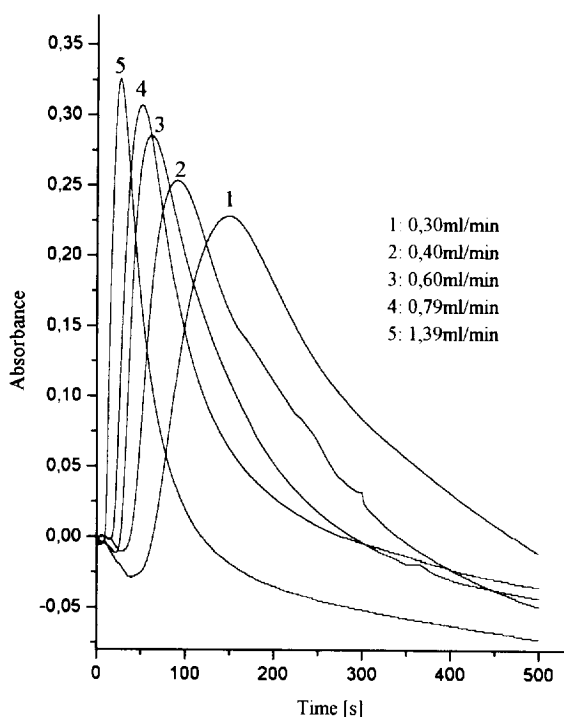Fig. 2. Automated preconcentration and extraction by means of an 8-channel, 16-port multifunctional valve.

Fig. 3. Dependence of the absorbance of the ion-pair complex on the flow rate of the organic phase ($t_p = 60$ s; $c_w = 5$ μg ml^{-1}).

In the case of applying the "stop-flow-mode" the chromatomembrane cell is suitable for preconcentration procedures as well. An efficiently working manifold, however, will be designed by integrating this novel device into flow systems for automated analysis [10]. In general the choice of the method for detecting the analyte is an open one, even online delivery to an additional separation device such as GC or HPLC is possible.

In this paper a new automated FI system is introduced which demonstrates the advantages of the application of chromatomembrane cells to the critical step of ion-pair extraction intended for the Methylene Blue method. For meeting the requirements of environmental monitoring the sophistication of the procedure will increase as soon as the chromatomembrane cells are produced commercially (i.e. a second cell could be introduced further on for backwashing the chloroform phase from the matrix components).

2. Experimental

The ion-pair complex between dodecylsulfate and Methylene Blue (MB) was formed in acetate buffer at pH 4.7. The samples (S) containing different amounts of sodium dodecylsulfate dissolved in water had to be mixed for that purpose with equal portions of MB (R1: 1.25×10^{-4} mol l^{-1}; carefully purified before use, i.e. the aqueous MB solution was washed with CHCl$_3$ to remove components soluble in organic solvents) and sodium acetate buffer (R2: 0.1 mol l^{-1}). After merging the three conduits the ion pairs were formed. Throughout the period while the aqueous phase passed the reaction coil (Fig. 1) its outflow was delivered to a chromatomembrane cell (size $3.0 \times 0.5 \times 1.0$ cm^3; free volume of each phase about 0.2 ml; macropores 200 μm i.d.; micropores 0.3 μm i.d.) which was used for the preconcentration of the ion-pair complex and its subsequent extraction with chloroform.

An FI spectrophotometric system suitable for automated dodecylsulfate determination was realized by means of a combination of an FIAS 300 instrument and a UV/Vis spectrometer Lambda 2S (Perkin Elmer GmbH, Bodenseewerk, Germany). The FIAS 300 FI tool was equipped with an 8-channel, 16-port multifunctional valve [11] to perform computer-aided preconcentration procedures. The maximum absorbance of the ion-pair complex dissolved in chloroform is 650 nm.

The radial mixing of the three components R1, R2 and S (each flowing at 0.45 ml min^{-1}) was achieved with the use of a standard chemifold (Fig. 1: short coils of 30 cm length are provided for ion-pair formation). The aqueous phase containing the ion-pair complex passed the chromatomembrane cell with a flow rate of 1.35 ml min^{-1} (position 1 shown in Fig. 2). While the ion-pair is preconcentrating in the water/chloro-

Table 1

Absorbance dependence on the volume of aqueous phase: $c_w \cdot V_{aq.sol.} = 2.25$ μg dodecylsulfate; $c_w \cdot t_p = $ const.

Absorbance	0.479	0.428	0.451	0.467
V (aq.sol.) (ml)	1.35	2.7	5.4	13.5

Table 2
Absorbance dependence on the preconcentration time: $c_w = 5$ μg ml^{-1}; $R = 0.99917$

Absorbance	0.057	0.193	0.294	0.431	0.505	0.624	0.746	0.871	0.976
Time (s)	15	30	45	60	75	90	105	120	135

form phase boundary inside the cell the surplus of MB remains in the flowing aqueous phase. A definite period of time later (preconcentration time) the aqueous phase was stopped and the organic phase started to flow. The ion-pair complex now being extracted by chloroform passed a flow through cell ($d = 10$ mm; $v = 18$ μl) for detection by means of the spectrometer (position 2 shown in Fig. 2).

Given that both the preconcentration time (1 min) and the content of dodecylsulfate (5 μg ml^{-1}), need to be kept constant we optimized the measurement of absorbance by varying the flow rate of the organic phase. Fig. 3 shows the result. We decided that 0.60 ml min^{-1} was the optimum flow rate to be used in all further investigations. Taking into account a capacity of about 0.2 ml for chloroform inside the chromatomembrane cell it should be emphasized that the ion-pair complex is always finally dispersed in a volume of 3 ml organic phase.

Reasonable values of absorbance can be obtained by varying the preconcentration time. The more a sample had been diluted the longer the preconcentration time which had to be chosen. Table 1 shows that the detected absorbance is always at the same level as long as the product of concentration and volume having passed through the chromatomembrane cell remains constant. The corresponding mass of dodecylsulfate is 2.25 μg in all cases but it had to be diluted in different volumes of water which had to pass during the preconcentration time. Incidentally, this agrees with all observations we noticed from other applications of the chromatomembrane cell.

3. Results and discussion

In principle two different approaches exist, for working with the FI system just described. On the

one hand a standard solution containing 5 μg ml^{-1} dodecylsulfate was used to form the ion-pair complex which had to flow with the aqueous phase through the chromatomembrane cell for preconcentration inside. The quantity of the ion-pair complex later extracted by chloroform depends on the preconcentration time (t_p), i.e. the period for which the aqueous phase has flowed through the cell. The absorbance shows a linear response to the preconcentration time (Table 2).

On the other hand a normal calibration graph will be obtained in the case where the preconcentration time remains fixed and the concentration of dodecylsulfate varies (Table 3). Because of the fact that the detected quantity of dodecylsulfate (m) equals the product of its concentration in the aqueous phase (c_w) × flow rate of the aqueous phase (v_w) × preconcentration time (t_p) it is easier to standardize the x-axis in terms of m. If the original concentration is required it can be calculated from the formula

$$c_w = \frac{m}{v_w \cdot t_p}$$

It is worth mentioning that there is now the possibility of setting the parameters in the way required to obtain values of absorbance in the range of best confidence. Referring to the concentration of dodecylsulfate in the original sample the FIA system proved to be reliable in the range 0.02–5.0 mg l^{-1}. The slope factor of the calibration plot was calculated with a standard deviation of $\pm$ 3%. Corresponding to the preconcentration time the volume of the aqueous samples varied in the range 0.2–2.2 ml. Probably the limit of detection will decrease with prolonged preconcentration time. This is of interest for further investigation.

The results are altogether satisfying even though some notes seem to be necessary to explain the mechanism of the preconcentration cycle

Table 3
Calibration for dodecylsulfate: t_p = const.; R = 0.9983

Absorbance	0.105	0.240	0.314	0.447	0.664	0.932
m (dodecylsulfate) (μg)	0.562	1.125	1.688	2.25	3.375	4.5

inside the chromatomembrane cell. The procedures established up to now to determine anionic surfactants using the MB method suffer from the small-scale distribution coefficient of the ion-pair complex between water and chloroform. Often this is the reason for decreased confidence in results.

The chromatographic behaviour of the ion-pair complex inside the chromatomembrane cell was investigated under the condition of a stationary chloroform phase. A simple strategy was found: the micropores of the cell were filled with pure chloroform and then the inlet and outlet for the non-polar phase were shut. The ion-pair complex

Fig. 4. Preconcentration and extraction cycle inside the chromatomembrane cell.

in stoichiometric composition dissolved in water was pumped through the macropores of the cell. We measured the retention volume which was observed to be 350 times larger than the free volume of the cell in the case of a 1×10^{-5} mol l^{-1} aqueous solution. However, as this concentration increased the retention volume decreased correspondingly. In other words the concentration is inversely proportional to the retention volume observed.

This is comprehensible if it is assumed that the ion-pair complex is adsorbed at the interface boundary between the two liquids. The quantity of adsorbed complex can expand greatly because of the fact that the concentration area inside the cell extends over about 0.7 m^2 cm^{-3} biporous PTFE. The break point will not occur until the interface boundary has been saturated. Then the ion-pair complex will be able to leave the cell with the flowing aqueous phase.

Returning to the normal mode of operation with the chromatomembrane cell we understand that the extraction procedure requires a bigger volume of chloroform because it has to remove the entire quantity of ion-pair complex adsorbed at the phase boundary. As mentioned above the extraction volume of chloroform amounts to 3 ml in all cases.

Fig. 4 expresses our model of the preconcentration cycle in detail. The ion-pair complex completely adsorbs at the phase boundary as long as the aqueous phase flows through the cell. In the meantime the surplus of MB is flushed away with the water. The extraction procedure with chloroform must start before the phase boundary has been saturated. The volume of the organic phase required to desorb all ion pairs from the phase boundary depends on the extent of the contact area inside the chromatomembrane cell. As soon as the extraction procedure has finished the pre-
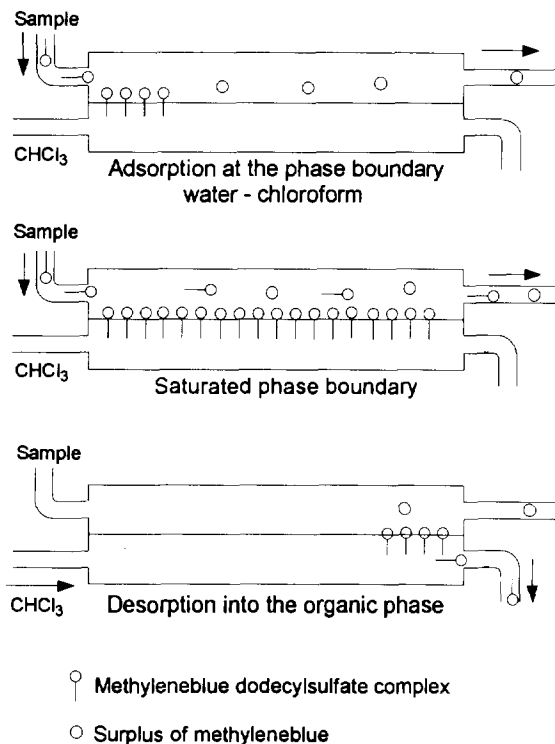
concentration cycle can start again. The mechanism suggested above is able to explain the strong retention volumes observed in spite of the knowledge that the distribution coefficient only amounts to five. In summary the chromatograpic process can be classified as liquid adsorption–liquid chromatography.

4. Conclusions

The application of chromatomembrane cells has been made possible by developing a computer-operated procedure to determine anionic surfactants corresponding to the MB method. Moreover, the distinguishing features of the process are good recovery and remarkable accuracy. Even though the current stage of development does not meet the recommendation of the European Committee for Standardization (ISO 7875-1) in all details further adjustments of the procedure reported here should be easily attainable. Wastewater samples normally contain Cl⁻ and NO_3^- which interfere by forming ion pairs with MB. To avoid excessive results for the MBAS in this case a backwashing step with aqueous buffer solution is provided. For this purpose a second chromatomembrane cell should be included in the FI analyzer. Otherwise a correction on the basis of adjusted calibration procedures has to be proved according to the paper of Burkhardt et al. [12].

References

[1] X. Qian and Y. Chen, Anal. Chem. (China), 17 (1989) 77–79.
[2] F. Caneto, Q. Rios and M.D. Lugue de Castro, Anal. Chem., 60 (1988) 2354–2357.
[3] S. Motomizu, M. Oshima and T. Kuroda, Analyst, 113 (1988) 747–753.
[4] J. Kawase, A. Nakae and M. Yamanaka, Anal. Chem., 51 (1979) 1640.
[5] M. del Valle, J. Alonso and J. Bartroli, Analyst, 113 (1988) 1677.
[6] K. Backstrom, L.G. Danielsson and L. Nord, Anal. Chim. Acta, 187 (1986) 255.
[7] H. Liu and P.K. Dasgupta, Anal. Chim. Acta, 288 (1994) 237–245.
[8] L.N. Moskvin, J. Chromatogr. A, 669 (1994) 81–87.
[9] L.N. Moskvin and J. Simon, Talanta, 41 (1994) 1765–1769.
[10] P. Löffler, J. Simon, A. Katruzov and L.N. Moskvin, Fresenius, J. Anal. Chem., 352 (1995) 613–614.
[11] Z.L. Fang, J. Ruzicka and E.H. Hansen, Anal. Chem. Acta, 164 (1984)23.
[12] M.R. Burkhardt, P.J. Cinotto, G.W. Frahm, M.T. Woodworth and J.W. Pritt, U.S. Geological Survey, Open-File Report 95-189, Denver, CO, 1995.

ELSEVIER

Talanta

Chemical speciation by flow-injection analysis.
A review[1]

Luigi Campanella[a], Krystyna Pyrzyńska[b], Marek Trojanowicz[c],*

[a]Department of Chemistry, University of Rome "La Sapienza", P.le Aldo Moro.5, 00185 Rome, Italy
[b]Department of Chemistry, University of Warsaw, Pastura 1, 02-093 Warsaw, Poland
[c]Institute of Nuclear Chemistry and Technology, Ul. Dorodna 16, 03-195 Warsaw, Poland

Abstract

Speciation of elements in natural matrices, especially of trace metals, is one of the predominant development trends of modern inorganic analysis. The main part of the conventional speciation procedures is a suitable combination of separation and chemical conversion steps, for which the most appropriate methodology seems to be the use of flow-injection. A shorter time of performance of these operations in flow-injection manifolds is advantageous in terms of avoiding the shift of chemical equilibria during the speciation measurement. Numerous other advantages are also pointed out in this review based on 58 references. Among flow-injection analysis methods published so far for speciation the determination of different oxidation states predominates, while a much smaller number of papers have been published on the determination of the degree of complexation or the determination of organometallic compounds.

Keywords: Flow-injection analysis; Natural matrices; Speciation; Trace metals

1. Introduction

Most commonly in the chemical literature "speciation" is used to mean the analytical determination of the concentrations of various chemical species containing a given element in a particular material, although it is often also used to mean the existence of a given element in a particular matrix in various chemical forms. One can also find the term "speciation analysis", meaning the determination of the concentrations of the individual physicochemical forms of the element in a sample that together constitute its total concentration. The first meaning is used most frequently and this is the one adopted in this paper.

---

* Corresponding author. E-mail: mtrojano@post office. newisham.utas.edu.au

The importance of knowing that a given element occurs in different physicochemical forms in various natural matrices, not only for macrocomponents but also for trace elements, has been widely recognized in the last 20 years in environmental science, biology and medicine. This is evident from the hundreds of original research papers published in scientific journals and several books published in recent years [1–6]. Various chemical forms of binding of the element of interest exhibit different reactivity, toxicity and bioavailability. The most difficult problem encountered in speciation is to develop a procedure which does not disturb the chemical equilibria between forms of the element existing in a given matrix. It might then be concluded that the most satisfactory procedure should be based on the determination of the total amount of all elements in a given material followed by the computer-aided calculation of the concentrations of particular species based on ionic and redox equilibrium constants. It is obvious, however, that the success of such a procedure is limited by difficulties in taking into consideration all kinetic factors, adsorption proceses, polymerization reactions and heterogeneous processes. The number of available stability constants is also limited; hence in practice the procedures of analytical determination of particular species predominate with the use of different detection methods, separation operations and chemical conversion into detectable species.

Flow-injection analysis (FIA), intensively developed over the past 20 years, offers several valuable advantages for speciation of both macro- and microelements. Its main feature is a shorter analysis time than in conventional, manual procedures, because in many cases the condition of not disturbing the equilibria in analyzed samples is much better fulfilled. Also of very great importance is a reduced human participation in time-consuming operations such as sample conditioning, reagent manipulation and calibration of the measuring system. Very advantageous is the possibility of using on-line preconcentration techniques and non-chromatographic separations such as ion-exchange, dialysis, solvent or solid-phase extraction.

Early works on speciation using FIA were reviewed by Luque de Castro [7,8]; however, the last few years have brought significant progres in this field. Amongst the numerous ways to determine the distribution of elements in natural matrices the FIA speciation studies have focused on three areas: simultaneous determination of species in different oxidation states, determination of the complexation degree of metallic elements or determination of the content of a given complex compound. There were also some attempts to use FIA for the speciation of organometallic species, although FIA cannot by any means compete with chromatographic techniques.

2. General remarks on speciation using FIA

The literature concerning chemical speciation employing FIA methods provides a large variety of designs of the measuring systems utilizing various detectors as well as different examples of off-line and especially on-line sample manipulation. A relatively simple task is to design a set-up with several detectors, mostly two, where each of them can selectively produce the analytical signal corresponding to the concentration of a particular chemical form of a given element. They can be arranged in series, if in at least one of them a substantial dispersion of the sample segment does not occur, or in parallel with sample splitting between the two branches of the manifold. Simultaneous injection with two combined valves to various branches of the FIA manifold is also used.

Most often, however, single detector manifolds are employed, which usually require much greater creativity to design the whole measuring system successfully. The least complicated systems are developed when off-line sample pretreatment is involved. Such systems utilize the advantages of the flow-injection methodology to a limited extent. In most FIA systems designed for speciation, the determination of various species by the same detector is achieved through various methods of on-line sample manipulation. For each sample injection a single analytical signal is most often produced in the detector; however, the simple
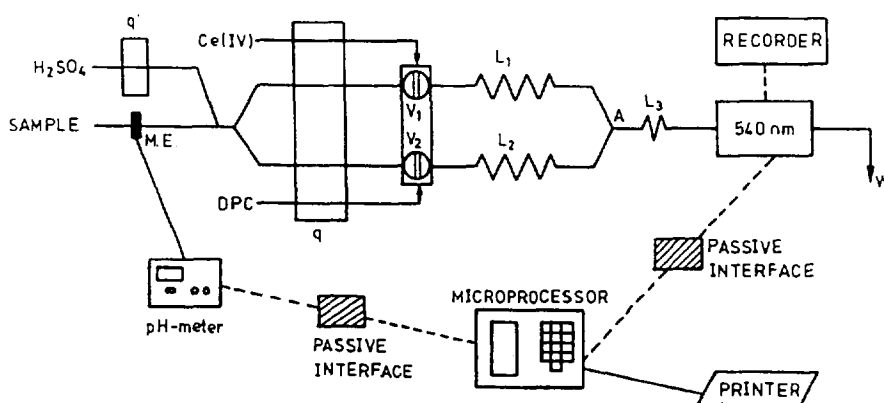
Fig. 1. Manifold of the reversed FIA system used for speciation of chromium with pH measurements of aspirated sample [12]: q,q', peristaltic pumps; V_1, V_2, injection valves; L_1, L_2, reaction coils; M.E., pH glass microelectrode.

changing of reagent solutions in the manifold between successive injections or the simple and fast rearrangement of the manifold allows one to obtain a signal corresponding to different chemical forms of the element. Among methods of on-line chemical conversion the most frequently used are reduction and oxidation, selective sorption on appropriate sorbents or total retention followed by fractional elution as well as volatization. Kinetic discrimination is seldom utilized for this purpose, i.e. differences in the reaction rates among various sepecies. The change of reagents in the manifold for the determination of various forms is arranged by the use of selecting valves or by designing reversed FIA systems with injection of reagent into the stream of continuously aspirated sample.

Different pretreatment of various aliquots of the same sample is managed in the manifold with the splitting of the sample zone between different branches of the FIA manifold. This different pretreatment, followed by merging sample segments into a single stream approaching the detector, allows one to obtain, for instance, two independent analytical signals for one injected sample solution. Two signals for one injected sample can also be obtained for simultaneous injection with two combined valves into separate parts of the FIA manifold. The most common configuration, where two signals are obtained for different species, is a FIA set-up with selective on-line retention of one form or with retention of the total amount and then selective consecutive elution.

More detailed discussion of FIA manifolds used for speciation is given below together with presentation of their chemical applications. Although the presentation of FIA systems for speciation is the main aim of this review, we have decided to present all collected information not according to technical arrangements of FIA set-ups, but rather according to the nature of the chemical problems solved in this way. We hope that such a means of presentation may be more interesting for a larger circle of analysts than just those interested mainly in developing flow analytical methods.

3. Speciation of different oxidation states

The largest number of FIA systems have been developed for the speciation of different oxidation states of the target element. Two basically different concepts of measurement can be distinguished. In two consecutive measurements with some changes to the manifold, with different off-line sample modification or in a more complex manifold, firstly the total content of a given element is determined and then the content of particular species. In another type of FIA system the selective determination of each form of different oxidation state is carried out.

The first of these two options is usually simpler to be developed. Most often it has been used for the speciation of chromium, iron and arsenic,
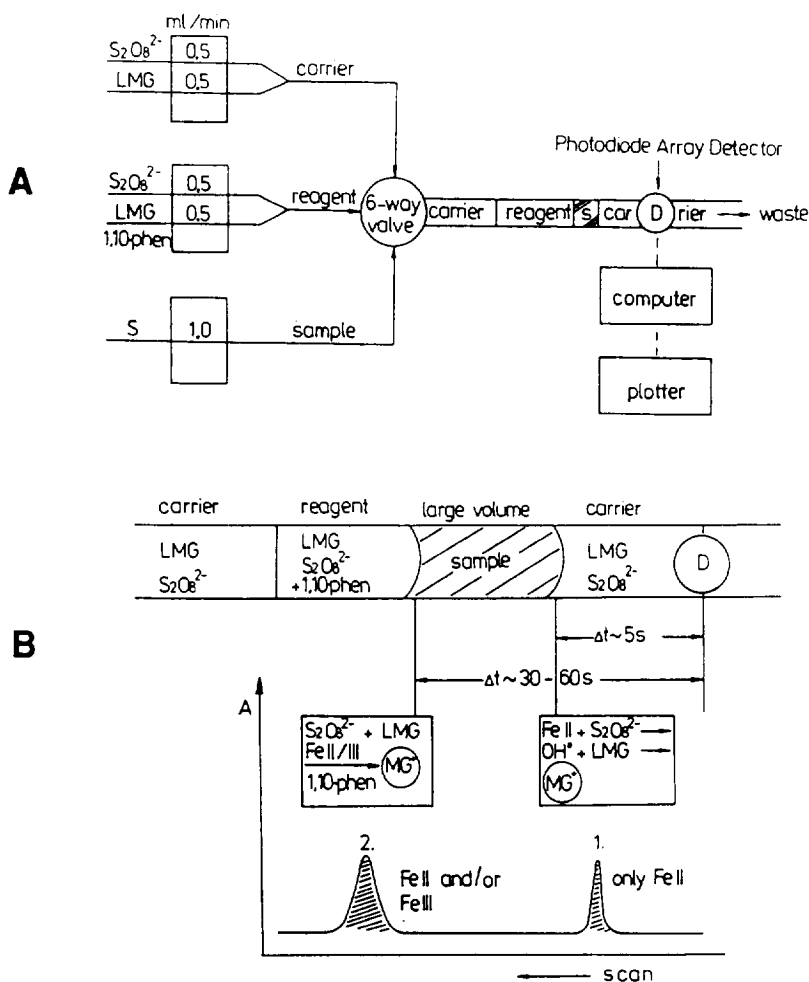
Fig. 2. Manifold of the FIA system used (A) and schematic diagram of the sample/reagent sequencing (B) in speciation of iron utilizing kinetic discrimination of analytes in the reaction between Leucomalachite Green (LMG) and $S_2O_8^{2-}$ with 1,10-phenanthroline (1,10-phen) as activator [17].

although FIA systems for the speciation of other elements have also been reported.

In the speciation of chromium, besides determining the total content of Cr(III) and Cr(VI), Cr(VI) content is separately determined using spectrophotometric determination with diphenylcarbazide and AAS detection. In the least complicated manifold a series arrangement of the spectrophotometric and AAS detectors was applied [9]. Several systems were developed with a spectrophotometric detector only and on-line oxidation of Cr(III) to Cr(VI) in order to determine total chromium content [10–13]. In several sys-

tems reversed FIA measurements were employed with continuous sample aspiration and injection of reagents[11,12]. Especially worthy of mention is the system shown in Fig. 1, in which continuous monitoring of pH is performed [12]. The sample segment is split into two streams, where Cr(VI) and total chromium are measured, whereas knowledge of the pH value allows the calculation of the content of hydroxylated complexes of Cr(III) and protonated and polymerized forms of Cr(VI). Other configurations were developed with the use of double-beam detection with two spectrophotometric flow cells, which gave the most

reproducible results [13]. In determinations with AAS detection, the on-line sorption of the Cr(VI) complex with sodium diethyldithiocarbamate on C18 was adopted, whereas total chromium was determined after oxidation of Cr(III) with peroxydisulphate [14].

A FIA system with spectrophotometric and AAS detectors in series was also reported for the speciation of iron, where determination of Fe(II) was based on reaction with 1,10-phenanthroline [9]. This reaction was also utilized in three other FIA systems with spectrophotometric detection only [15–17]. In order to determine total iron, Fe(III) was on-line reduced on a column with Jones reductor [15]; alternatively a complex of Fe(III) with 1,10-phenanthroline was reduced photochemically [16]. A unique system for iron speciation was also developed with the use of kinetic discrimination (Fig. 2) [17]. It was based on different kinetic–catalytic behaviours of Fe(II) and Fe(III) in the redox reaction between Leuco-malachite Green and peroxodisulphate with and without the presence of 1,10-phenanthroline acting as activator.

Differences in on-line sample pretreatment were utilized in the design of FIA systems for the speciation of As(III) and As(V) with spectrophotometric [18] and AAS [19,20] detection. Sequential detection of $AsO_2^- - AsO_4^{3-}$ mixtures was based on the formation of heteropolyacids with MoO_4^{2-} [18]. When sample in the manifold merges with iodate solution, it oxidizes arsenite and the obtained signal corresponds to the sum of both arsenic anions. When sample is not oxidized it gives a signal corresponding to arsenate alone. Using hydride generation AAS for detection total arsenic was determined using arsine generation in 6 M HCl, whereas As(III) alone can be determined by generation of arsine in citrate buffer at pH 3 [19]. A more sophisticated AAS procedure was also used, which was based on the generation of arsine in a FIA system and its subsequent trapping in a graphite furnace coated with appropriate absorbers [20]. The arsine was transferred to the graphite furnace through an electronically-activated arm. As(III) was determined using addition of NaOH to a water carrier stream, while potassium iodide was used when total arsenic had to be determined.

Various chlorine-containing species can be determined in flow-injection systems with spectrophotometric detection. In the speciation of low concentrations of chlorite and chlorate ions chlorite was selectively determined by using its reaction with iodide at pH 2, which liberates iodine, while in 6 M HCl both species produce iodine, which is then measured spectrophotometrically [21]. Differentiation of residual free and combined chlorine was based on different reactions of the two species with 2,4-dinitrophenyldiazonium ion depending on the acidity in a reversed flow-injection system [22]. Iodide can be directly determined over a wide concentration range using potentiometry with an ion-selective membrane electrode, whereas iodine can be determined after on-line reduction to iodide with sodium metabisulphite [23].

Total phosphorus and orthophosphate were determined in wastewater in the FIA systm with two detectors [24]. Orthophosphate was determined as molybdovanadophosphoric acid using a spectrophotometric method and the solution from the flow cell of the spectrophotometer was directly introduced into an inductively-coupled plasma. In another reported system with spectrophotometric detection orthophosphate was determined as the sum of orthophosphate and pyrophosphate after on-line separation and preconcentration of both analytes on an inert support modified with a diorganotin extractant [25]. The sum of both anions was determined after preliminary hydrolysis of pyrophosphate to orthophosphate by use of inorganic pyrophosphatase dissolved in solution.

The speciation of inorganic selenium was carried out in FIA systems with cathodic stripping voltammetric detection with a mercury film on a glassy carbon electrode [26], with anodic stripping voltammetry at a gold electrode [27], and with hydride generation AAS detection [28], which allows Se(IV) detection. In all three cases the sum of Se(IV) and Se(VI) was determined after reduction of Se(VI) to Se(IV), carried off-line chemically [26,27] or on-line in a microwave unit [28]. In the system with anodic stripping voltammetry the on-line removal of the interfering cations on a Chelex-100 column was employed [27].

More complex and more difficult to design are FIA speciation systems with selective determina-
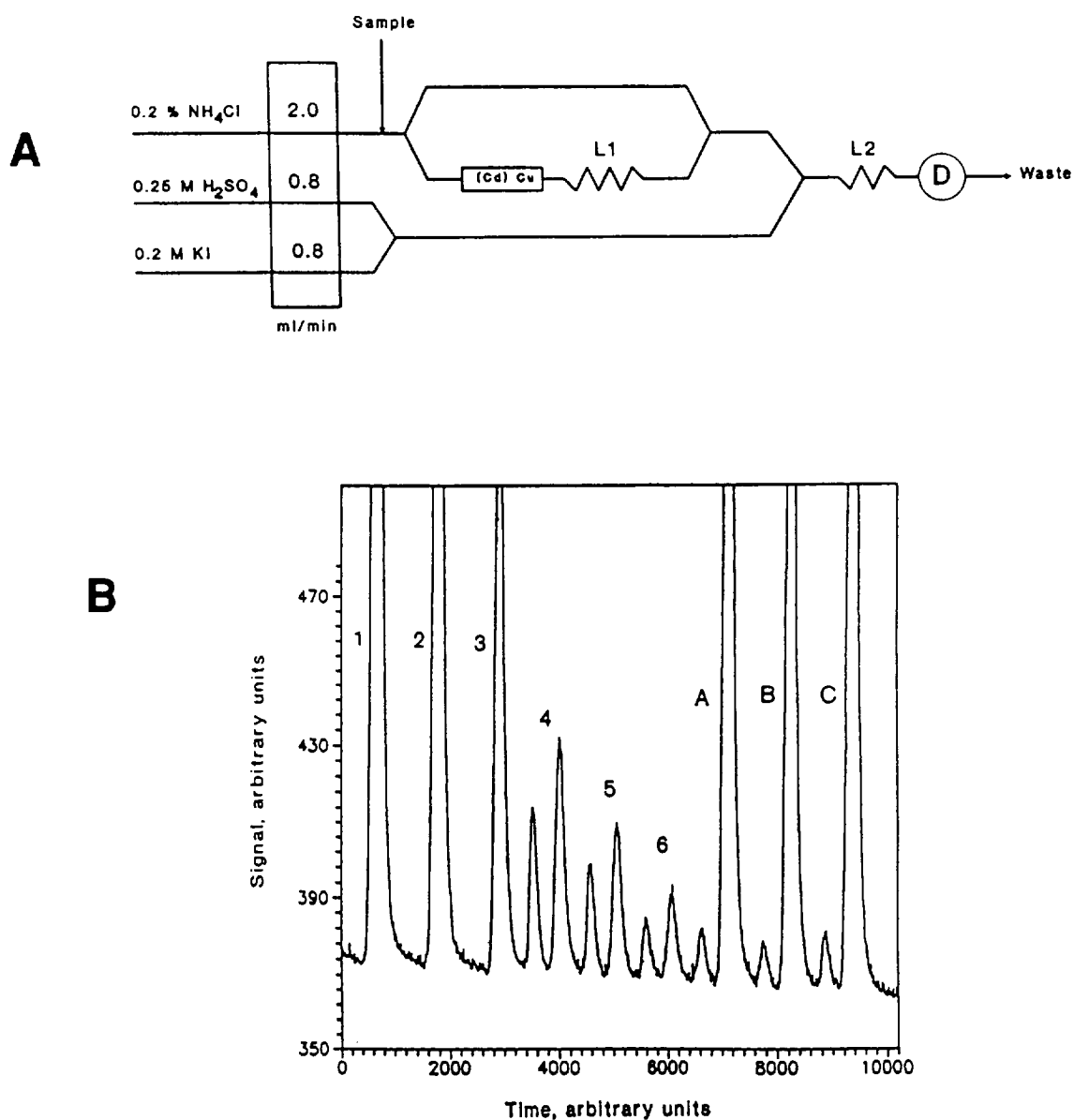
Fig. 3. Manifold of the FIA system used (A) and display of experimental data obtained (B) for simultaneous determination of nitrite and nitrate with indirect biamperometric detection [33]: L_1, L_2, reaction coils; (Cd)Cu, copperized cadmium microcolumn; 1–3, nitrate standard solutions; 4–6, nitrite standard solutions; A–C, natural water samples.

tion of each individual form of the element of interest. In this type of FIA system for speciation several papers reported manifolds for nitrate and nitrite, but also for chromium and iron speciation. Nitrogen in most samples does not occur as nitrate and nitrite only, hence the methods for their determination are included in this type of FIA system, although in most FIA speciation systems both these analytes are determined both together and separately. Simultaneous FIA determination of nitrate and nitrite was carried out with spectrophotometric [29–32], amperometric [33], AAS [34] and chemiluminescence [35] detection. In the measuring set-up with a dual absorbance monitor
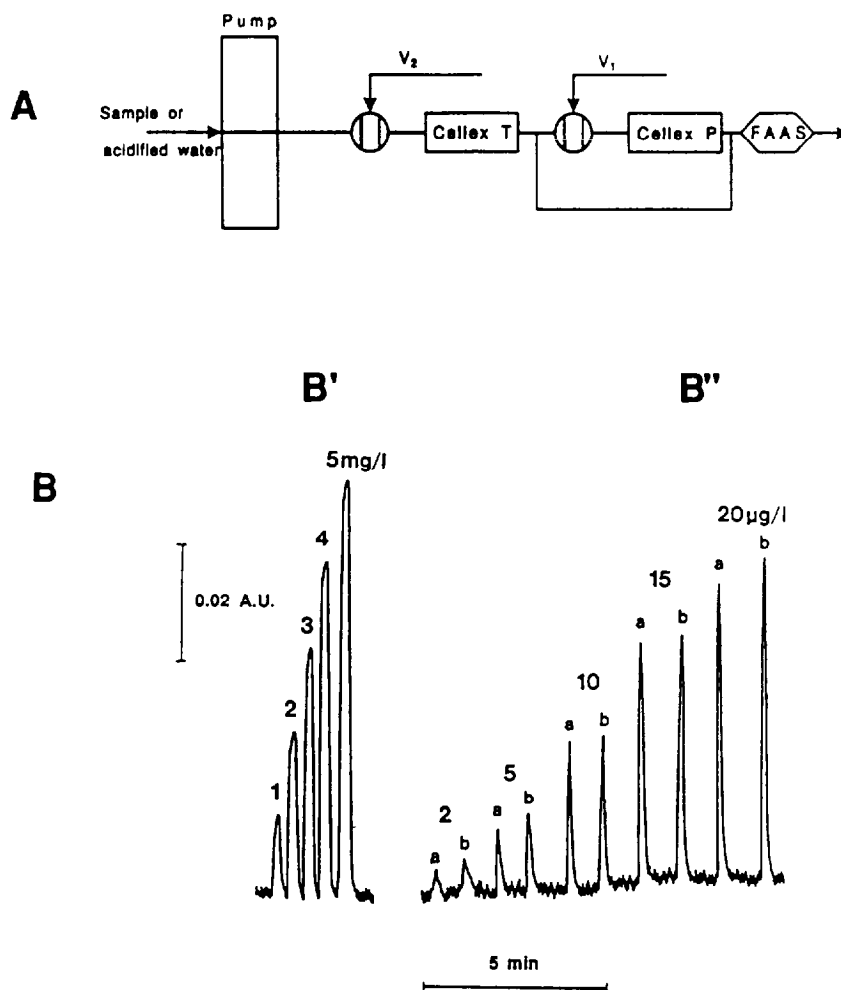
Fig. 4. Manifold of the FIA system with AAS detection and on-line preconcentration on cellulose sorbents used for speciation of chromium (A) and comparison of recordings (B) obtained with (B′) conventional aspiration and (B″) with FI AAS system with preconcentration of (a) Cr(III) and (b) Cr(VI). In B″: aspirated sample volume, 100 ml; flow rate, 5.0 ml min⁻¹ [38].

connected to a dual-channel recorder both species were determined using common methods, where nitrite is diazotized and product is transformed into a coloured azo dye. The injected sample is split between two branches of the manifold and in one of them nitrate is on-line reduced to nitrite [29]. Two separate signals are measured for nitrate and the sum of nitrite and nitrate. The same method in FIA systems with single detector and two injection valves was used by other authors [30,31]. For the on-line reduction of nitrate to nitrite copperized metallic cadmium micro-columns are most often used [29–31,33]; however,

photo-induced reduction with UV radiation in the presence of complexones was also reported [32]. In the system with indirect biamperometric detection the analytical signal is observed when nitrite oxidizes iodide to iodine and the reversible couple is formed [33]. The injected sample is split in a FIA manifold into two segments (Fig. 3). One of them is transported through a reducing mini-column and a delay loop. For each injected sample two peaks are obtained, the first of which corresponds to nitrite and the second to the sum of nitrite and nitrate. Sequential determinations of nitrate and nitrite with AAS detection were based

on continuous liquid–liquid extraction [32]. Nitrate reacts with bis(2,9-dimethyl-1,10-phenanthrolinato) copper(I) to form an ion pair which is extracted into 4-methyl-2-pentanone in a flow-injection manifold. In one aliquot of sample nitrite is oxidized by Ce(IV), so that total nitrate is determined. In another, nitrite is converted to nitrogen with sulfamic acid, so that only original nitrate is determined. By measuring the AAS signal of copper in the organic phase, both species can be determined. Nitrite and nitrate were also determined in the reversed FIA system with chemiluminescence detection in the gas phase and transfer reduced NO to the gas phase through a PTFE membrane [35]. NO produced by injection of Ti(III) solution corresponds to the sum of nitrate and nitrite, whereas injection of iodide results in reduction of nitrite only. Detection is based on chemiluminescence from the reaction of NO with ozone. A reversed system with continuous sample aspiration and sequential injection of appropriate reagents was also used in the selective determination of nitrite with the formation of azo dye and ammonia using the Nessler method [36].

The speciation of chromium in FIA systems, where for each injected sample signals corresponding to Cr(III) and Cr(VI) were obtained, was reported with inductively-coupled plasma–atomic emission spectrometry, (ICP–AES) [37] and AAS [38] detection. In the first-mentioned system a microcolumn of activated alumina was used in the FIA manifold to separate and preconcentrate Cr(VI) from Cr(III). After detection of Cr(III), ammonia solution was injected to elute Cr(VI) from the column. In the system with AAS detection two columns with different functionalized cellulose sorbents were used for selective sorption of Cr(III) and Cr(VI) from continuously aspirated sample (Fig. 4) [38]. Sequential elution with appropriate solutions provides two peaks corresponding to Cr(III) and Cr(VI) contents in the sample.

Several different FIA methods were developed for iron speciation, where individual signals were obtained for Fe(II) and Fe(III). In the system with two spectrophotometric detectors and simultaneous sample introduction by two coupled injection valves, iron(II) was determined with

1,10-phenanthroline, whereas iron(III) was determined with thiocyanate [39]. In the system with AAS detection a packed bed reactor with Dowex 1 anion exchange resin was used to retain chloride complexes of Fe(III), whereas Fe(II) species passed through the reactor to the detector [40]. This was followed by the separate elution of Fe(III) to the detector by change of carrier solution. On-line solid-phase extraction was also employed in two other FIA systems for iron speciation with spectrophotometric [41] and AAS [42] detection. In the first system Fe(II) was preconcentrated on a C18 column with immobilized ferrozine and then eluted with methanol. Determination of Fe(III) required on-line reduction with ascorbic acid [41]. In the second one injected sample was mixed with ferrozine solution and while Fe(III) is directly carried to the flame AAS
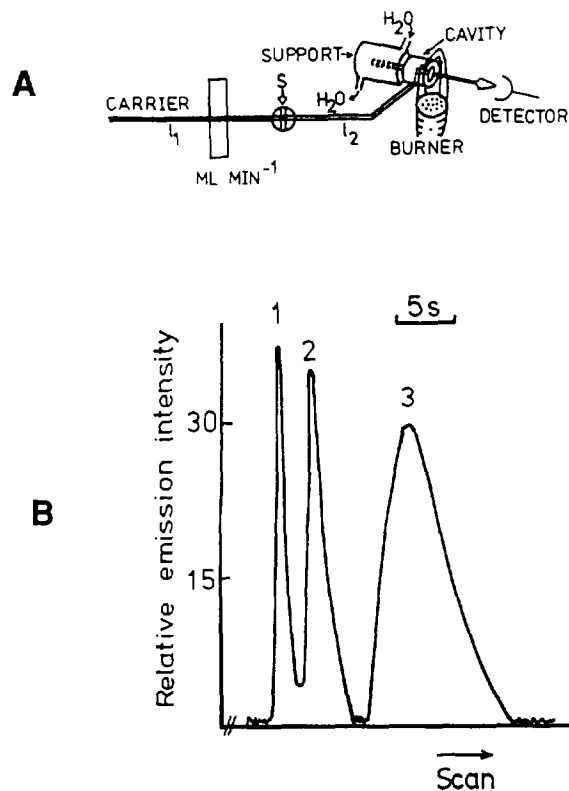

Fig. 5. Schematic diagram of the FIA system with molecular emission detection (A) used for speciation of sulphur anions and response from a mixture of sulphur anions (B): 1, sulphide; 2, sulphite; 3, sulphate [44].

detector, Fe(II)–ferrozine complex is temporarily retained on a C18 column and is then subsequently eluted with methanol.

Speciation of vanadium was carried out using flame AAS with an on-line procedure for the preconcentration of V(V) using silica-bonded ion-exchange resin [43]. While V(V) retention took place, the unretained V(IV) passed to an AAS detector, which was followed by elution of V(V) species with a plug of sodium hydroxide solution.

Simultaneous flow-injection determination of sulphite, sulphide and sulphate was reported in a system with a molecular emission cavity detector, which was based on the sequential appearance of S_2 emission peaks corresponding to these species (Fig. 5) [44]. In the system with an atomic absorption spectrometer operated in the emission mode a 3 μl sample was injected and detection limits for sulphur anions were in the range 0.06–0.15 ng for injected samples.

A list of the applications of flow-injection methodology to the speciation of different oxidation states of 10 elements is shown in Table 1. With a few exceptions optical methods of detection are mostly used, mainly molecular absorptive spectrophotometry in the visible range and AAS. The majority of practical applications concern natural waters, often spiked with analytes. Numerous developed methods exhibit a sufficiently low detection limit to find practical applications for natural samples. It seems that from the point of view of environmental analysis speciation procedures should also be developed for elements such as antimony, manganese, thallium and tellurium, as well as simpler methods for the speciation of oxidation states of sulphur. Especially desirable seems to be the development of simple speciation methods for medical applications [45].

4. Speciation of complexes

In most natural matrices elements occur only in a small fraction of cases as simple, hydrated cations and are mostly present in ion pairs or complex compounds with inorganic and organic ligands. In natural waters only a few percent of non-complexed cations of Al, Pb and Cr(III) can

be found, and above 80% only e.g. potassium or calcium [46].

Although it seems to be a simpler task than determination of different oxidation states, determination of the degree of complexation in FIA systems has been reported in a much smaller number of papers.

The possibility of speciation was investigated for a model mixture of Cu(II) with EDTA in a simple FIA system with AAS detection and a microcolumn containing chelating resin with salicylate-complexing groups [47]. Three different fractions of complexed species of Cd, Cu and Zn were determined in a FIA system with AAS detection and two microcolumns with Chelex-100 and strongly basic anion exchange resin (Fig. 6) [48]. Metal species such as hydrated free ions, labile metal complexes and possibly metals loosely associated with colloidal matter were retained on Chelex-100. The strongly basic anion exchanger retained negatively charged organic matter such as humic material. The third, unretained fraction includes metals strongly associated with very large colloidal matter that do not dissociate in any of the columns used.

Two different FIA methods with spectrophotometric [49] and fluorimetric [50] detection were developed for the speciation of aluminum complexes. In a set-up with spectrophotometric detection the determination was based on Pyrocatechol Violet chelation. The incorporation of on-line preconcentration on a cation-exchange column allows measurements of the concentrations of non-labile monomeric forms of Al, whereas total reactive aluminum and total monomeric Al were differentiated by off-line sample pretreatment [49]. The fluorimetric detection was based on the formation of an Al–salicylaldehyde picolinohydrazone fluorescent complex retained on C18 sorbent packed in the flow-cell located in a conventional spectrofluorimeter [50]. Three forms of Al (acid reactive, total monomeric Al, and non-labile monomeric Al) can be determined in a similar way, as was described for the system with spectrophotometric detection [49]. Two other forms, acid-soluble and labile monomeric Al, can be evaluated by difference by injecting three sample aliquots into the continuous system and the use of

Table 1
Speciation of different oxidation states using flow-injection analysis

| Element	Species	Detection method	Analysed real samples	Reference
As	As(III), As(V)	Spectrophotometry	Spiked natural waters	18
		HG–AAS	Natural waters	19
		HG–ET–AAS	Natural waters	20
Cl	Chlorite, chlorate	Spectrophotometry	--	21
	Residual chlorine, free and combined	Spectrophotometry	Spiked natural waters	22
Cr	Cr(III), Cr(VI)	Spectrophotometry	Leather treatment effluent	10
		Spectrophotometry	--	11, 12, 13
		AAS	Waters	14, 38
		AAS + spectrophotometry	Corrosion test seawater	9
		ICP–AES	Reference waters	37
Fe	Fe(II), Fe(III)	Spectrophotometry		15, 17, 39
		Spectrophotometry	Catalysts	16
		Spectrophotometry	Reference seawater	41
		AAS	–	40, 42
		AAS + spectrophotometry	Mineral process liquids	9
I	Iodide, iodine	Potenetiometry	Pharmaceutical preparations	23
N	Nitrate, nitrite	Spectrophotometry	–	29, 31
		Spectrophotometry	Natural waters	30, 32
		Amperometry	Natural waters	33
		AAS	Foodstuffs	34
		Chemiluminescence	River waters, wastewater	35
	Ammonia, nitrite	Spectrophotometry	Natural waters	36
P	Phosphate, total phosphorus	ICP–AES + spectrophotometry	Wastewater	24
	Ortho-, pyrophosphate	Spectrophotometry	River water	25
S	Sulphide, sulphite, sulphate	Molecular emission		44
Se	Se(IV), Se(VI)	Cathodic stripping voltammetry	Spiked natural waters	26
		Anodic stripping voltammetry	Spiked natural waters, lyophilised pig kidney	27
		HG–AAS	Reference waters	28
V	V(IV), V(V)	AAS	Yeast cells	43
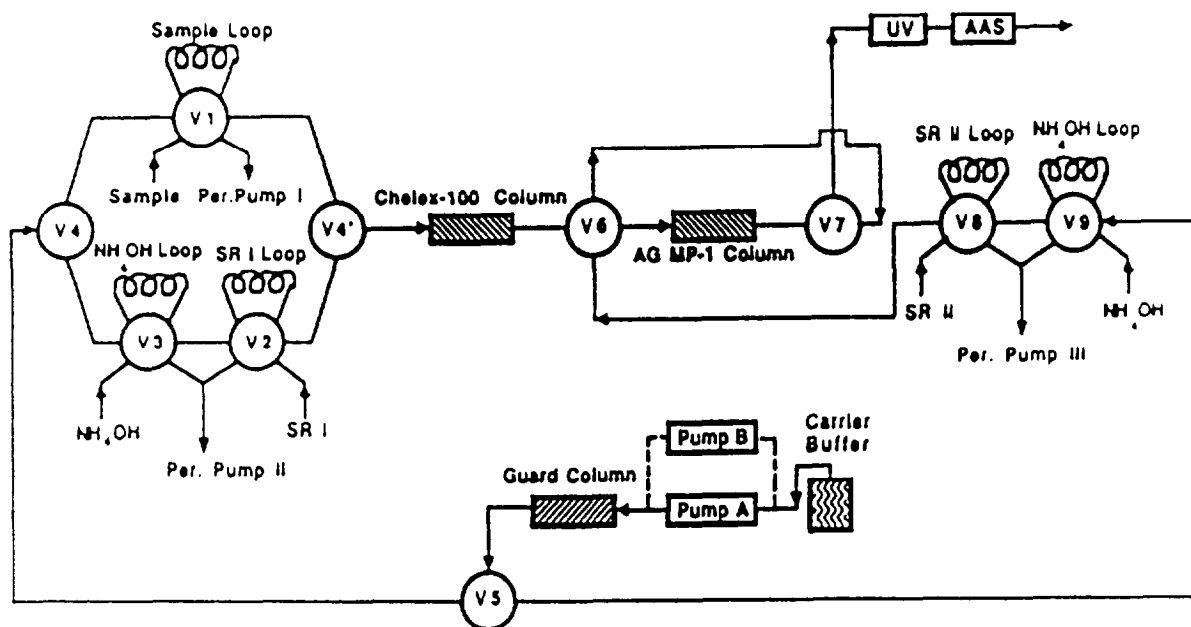
Fig. 6. Schematic diagram of the FIA system with AAS detection used for speciation of cadmium, copper and zinc employing on-line sorption on Chelex-100 and anion-exchange AG MP-1 columns [48].

an on-line ion-exchange microcolumn. The authors provide interesting results of the application of the developed methods to various natural waters, where practically no presence of non-labile monomeric aluminum was found.

5. Speciation of organometallic compounds

Organometallic compounds with covalent metal–carbon bonds have essentially different chemical properties than coordination complexes or hydrated metal cations. They are much more volatile and lipophilic and usually exhibit stronger toxicity, although the degree of toxicity is strictly related to the nature of the monitoring biosystem [51]. The known exceptions are organometallic compounds of arsenic, which are less toxic than inorganic arsenic compounds.

In all developed FIA systems for speciation of organometallic compounds atomic spectroscopy detectors were employed. Speciation of arsenic was carried out in a commercial set-up for hydride generation AAS [52]. By carrying out hydride generation in selected acidic media the

determination of As(III) alone, of the sum of mono- and dimethylated arsenic (with different sensitivities, which can be used for their differentiation), and of all these species together with As(V) is possible. The conditions of hydride generation are adjusted in the FIA system by changing the reagent solutions.

Sequential determination of inorganic mercury and methylmercury in a system with cold vapour–atomic fluorescence spectrometry detection on separation and preconcentration of methylmercury using a microcolumn of sulphydryl cotton of relatively high affinity for methylmercury has been described [53]. Inorganic mercury is not retained on the column and passed to the detector. The retained methylmercury is eluted with hydrochloric acid.

For FIA speciation of organolead compounds two approaches have been reported, so far, with flame AAS detection. In a simpler system oriented towards speciation in natural waters, both inorganic lead and alkyl-lead species were separated and preconcentrated on-line on cationic cellulose sorbent Cellex P with phosphonic acid functional groups [54]. Elution first with nitric acid and then

Table 2
Speciation of complexes using flow-injection analysis

Element	Complexing ligand	Detection method	Analysed real samples	Reference
Al	Not specified	Spectrophotometry	Fresh water	49
	Citrate, oxalate, acetylacetone	Fluorimetry	River, mineral and tap waters	50
Cd	Not specified	AAS	River water	48
Cu	EDTA	AAS		47
	Acetate, glycine, iminodiacetate, NTA, EDTA	AAS	River water	48
Zn	Not specified	AAS	River water	48

Table 3
Speciation of organometallic compounds using flow-injection analysis

Element	Determined species	Detection method	Analysed real samples	Reference
As	As(III), As(V), monomethylarsonic and dimethylarsinic acids	Hydride generation AAS	–	52
Hg	Hg(II), methylmercury	Cold vapour atomic fluorescence spectroscopy	Spiked tap and river waters	53
Pb	Pb(II), tetraethyl-lead	AAS	Spiked tap and surface waters	54
	Total lead, tetraethyl-lead, tetramethyl-lead	AAS	Gasoline	56

with ethanol allows one to obtain two signals corresponding to the sum of inorganic lead and di- and trialkyl-lead compounds and to tetraethyl-lead respectively. A more complex procedure was developed for FIA determination of total lead and speciation of tetraethyl- and tetramethyl-lead in gasoline [56]. In this case it was necessary to use on-line emulsification of the samples , which was achieved by injection of the sample into a stream of commercial emulsogen solution. For both speciation and determination of total lead, demetallation by means of iodine solution in petroleum spirit was also employed. As before and after

demetallation the two tetraalkyl-lead species exhibit different senstivities of AAS response, this difference was utilized for the speciation.

6. Conclusions

Among over 5000 papers published, so far, on various aspects of FIA [56], only about 50, to our knowledge, were devoted to speciation. Not many of them consider and indicate the advantages which FIA offers in comparison to manual procedures. Practical applications are focused mainly

on various natural waters, as speciation in other matrices is much more difficult, primarily in terms of preserving concentrations of all forms existing in a given material during sample pretreatment.

In our opinion the development of procedures for the determination of the total amount of an element of interest and of its speciation will be one of the development trends in FIA in the near future. It should also be mentioned that FIA can also be successfully applied to the facilitation of sample pretreatment prior to speciation analysis performed by much more powerful techniques such as capillary gas chromatography coupled with microwave-induced plasma emission spectrometry, which was used for speciation of organotin compounds [57] and mercury [58] in natural waters.

Acknowledgements

References

[1] M. Bernhard, F.E. Brinckman and P.J. Sadler (Eds.), The Importance of Chemical Speciation in Environmental Processes, Springer, Berlin, 1986.

[2] G.G. Leppard (Ed.), Trace Element Speciation in Surface Waters and its Ecological Implications, Plenum, New York, 1983.

[3] J.R. Kramer and H.E. Allen (Eds.), Metal Speciation. Theory, Analysis and Application, Lewis Publishers, Chelsea, MI, 1988.

[4] G.E. Batley, Trace Element Speciation: Analytical Methods and Problems, CRC Press, Boca Raton, FL, 1989.

[5] J.A.C. Broekaert, S. Gücer and F. Adams (Eds.), Metal Speciation in the Environment, Springer, Berlin, 1990.

[6] A.M. Ure and C.M. Davidson (Eds.), Chemical Speciation in the Environment, Blackie, London, 1995.

[7] M.D. Luque de Castro, Talanta, 33 (1986) 45.

[8] M.D. Luque de Castro, Mikrochim. Acta, 109 (1992) 165.

[9] T.P. Lynch, N.J. Kernoghan and J. N. Wilson, Analyst, 109 (1984) 839.

[10] J.C. Andrade, J.C. Rocha and N. Baccan, Analyst, 110 (1985) 197.

[11] J. Ruz, A. Rios, M.D. Luque de Castro and M. Valcarcel, Fresenius' Z. Anal. Chem., 322 (1985) 499.

[12] J. Ruz, A. Torres, A. Rios, M.D. Luque de Castro and M. Valcarcel, J. Autom. Chem., 8 (1986) 70.

[13] J. Ruz, A. Rios, M.D. Luque de Castro and M. Valcarcel, Anal. Chim. Acta, 186 (1986) 139.

[14] M. Sperling, X. Yin and B. Weltz, Analyst, 117 (1992) 629.

[15] A.T. Faizullah and A. Townshend, Anal. Chim. Acta, 167 (1985) 225.

[16] R.-M. Liu, D.-J. Liu and A.-L. Sun, Analyst, 117 (1992) 1767.

[17] H. Müller and V. Müller, Anal. Chim. Acta, 230 (1990) 113.

[18] P. Linares M.D. Luque de Castro and M. Valcarcel, Anal. Chem., 58 (1986) 120.

[19] R. Torralba, M. Bonilla, A. Palacios and C. Camara, Analusis, 22 (1994) 478.

[20] M. Burguera and J.L. Burguera, J. Anal. At. Spectrom., 8 (1993) 229.

[21] D.G. Themelis, D.W. Wood and G. Gordon, Anal. Chim. Acta, 225 (1989) 437.

[22] A. Chaurasia and K.K. Verma, Fresenius' J. Anal. Chem., 351 (1995) 335.

[23] D.E. Davey, D.E. Mulcahy and G.R. O'Connel, Talanta, 37 (1990) 313.

[24] J.L. Manzoori, A. Miyuzaki and H. Tao, Analyst, 115 (1990) 1055.

[25] B.Ya. Spivakov, T.A. Maryutina, L.K. Shpigun, V.M. Shkinev, Yu.A. Zolotov, E. Ruseva and I. Havezov, Talanta, 9 (1990) 889.

[26] D.W. Bryce, A. Izquierdo and M.D. Luque de Castro, Fresenius' J. Anal. Chem., 351 (1995) 433.

[27] D.W. Bryce, A. Izquierdo and M.D. Luque de Castro, Anal. Chim. Acta, 308 (1995) 96.

[28] L. Pitts, P.J. Worsfold and S.J. Hill, Analyst, 119 (1994) 2785.

[29] L. Anderson, Anal. Chim. Acta, 110 (1979) 123.

[30] J.F. Van Staden, Anal. Chim. Acta, 138 (1982) 403.

[31] M. Novic, S. Tezak, B. Pihlar and V. Hudnik, Fresenius' J. Anal. Chem., 350 (1994) 653.

[32] S. Motomizu and M. Sanda, Anal. Chim. Acta, 308 (1995) 406.

[33] M. Trojanowicz, W. Matuszewski, B. Szostek and J. Michalowski, Anal. Chim. Acta, 261 (1992) 391.

[34] M. Silva, M. Gallego and M. Valcarcel, Anal. Chim. Acta, 179 (1986) 341.

[35] T. Aoki and M. Wakabayashi, Anal. Chim. Acta, 308 (1995) 308.

[36] F. Canete, A. Rios, M.D. Luque de Castro and M. Valcarcel, Analyst, 113 (1988) 739.

[37] A.G. Cox, I.G. Cook and C.W. McLeod, Analyst, 110 (1985) 331.

[38] A.M. Naghmush, K. Pyrzyñska and M. Trojanowicz, Anal. Chim. Acta, 288 (1994) 247.

[39] T.P. Lynch, N.J. Kernoghan and J.N. Wilson, Analyst, 109 (1984) 843.

[40] G.E. Pacey and B.P. Bubnis, Int. Lab., September (1984) 30.

[41] S. Blain and P. Treguer, Anal. Chim. Acta, 308 (1995) 425.

[42] S. Krekler, W. Frenzel and G. Schultze, Anal. Chim. Acta, 296 (1994) 115.

[43] B. Patel, S.J. Haswell and R. Grzeskowiak, J. Anal. At. Spectrom., 4 (1989) 195.

[44] J.L. Burguera and M. Burguera, Anal. Chim. Acta, 157 (1984) 177.

[45] R. Cornelis, F. Borguet and J. De Kimpe, Anal. Chim. Acta, 283 (1993) 183.

[46] C. Steinberg, Water Res., 14 (1980) 1239.

[47] E.B. Milosavljevic, J. Ruzicka and E.H. Hansen, Anal. Chim. Acta, 169 (1985) 321.

[48] Y. Liu and J.D. Ingle, Jr., Anal. Chem., 61 (1989) 525.

[49] M.J. Quintela, M. Gallego and M. Valcarcel, Analyst, 118 (1993) 1199.

[50] P. Canizares and M.D. Luque de Castro, Anal. Chim. Acta, 295 (1994) 59.

[51] P.J. Craig (Ed.), Organometallic Compounds in the Environment. Principles and Reactions, Longman, Harlow, UK, 1986.

[52] T.R. Rude and H. Puchelt, Fresenius' J. Anal. Chem., 350 (1994) 44.

[53] W. Jian and C.W. McLeod, Talanta, 39 (1992) 1537.

[54] A.M. Naghmush, K. Pyrzyñska and M. Trojanowicz, Talanta, 42 (1995).

[55] R. Borja, M.de la Guardia, A. Salvador, J.L. Burguera and M. Burguera, Fresenius' J. Anal. Chem., 338 (1990) 9.

[56] E.H. Hansen, Anal. Chim. Acta, 308 (1995) 3.

[57] J. Szpunar-Lobinska, M. Ceulemans, R. Lobinski and F.C. Adams, Anal. Chim. Acta, 278 (1993) 99.

[58] H. Emteborg, D.C. Baxter and W. Frech, Analyst, 118 (1993) 1007.

Head-space flow injection for the on-line determination of iodide in urine samples with chemiluminescence detection[1]

J.L. Burguera* , M.R. Brunetto, Y. Contreras*, M. Burguera, M. Gallignani, P. Carrero

IVAIQUIM (Venezuelan Andean Institute for Chemical Research), Faculty of Sciences, University of Los Andes, P.O. Box 542, Mérida, 5101-A, Venezuela

Abstract

A simple head-space (HS) flow injection (FI) system with chemiluminescence (CL) detection for the determination of iodide as iodine in urine is presented. The iodide is converted to iodine by potassium dichromate under stirring in the closed HS vial, and the iodine is released from urine by thermostatting and is carried in a nitrogen flow through an iodide trapping solution. The concomitant introduction of aliquots of iodine, luminol and cobalt(II) solutions by means of a time-based injector into an FI system allowed its mixing in a flow-through cell in front of the detector. The emission intensity at 425 nm was recorded as a function of time. The salting-out of the standard solutions affected the gas–liquid distribution coefficient of iodine in the HS vial. The typical analytical working graphs obtained under the optimized experimental conditions were rectilinear from 0 to 5 mg l^{-1} iodine, achieving a precision of 2.3 and a relative standard deviation of 1.8 for ten replicate analyses of 50 and 200 μg l^{-1} iodine. However, a second-order process becomes significant at higher iodine concentrations (from 10 to 40 mg l^{-1}). The detection limit of the method is 10 μg l^{-1} (80 ng) iodine when 8 ml samples are taken. Data for the iodide content of 10 urine samples were in good agreement with those obtained by a conventional catalytic method, and recoveries varied between 101 and 103% for urine samples spiked with different amounts of iodide. The analysis of one sample takes less than 20 min. In the present study the iodide levels found for 100 subjects were 86.8 ± 19.0 (61–125) μg l^{-1}, which is lower than the WHO's optimal level (150–300 μg per day).

Keywords: Chemiluminescence detection; Head-space flow injection; Iodide; Urine

1. Introduction

Iodine is an essential microconstituent in the human body, which contains an average of 14 mg of the element, concentrated mostly in the thyroid gland [1]. About 1 mg of iodine per week is needed by the body to ensure normal levels for the synthesis of the thyroid hormones thyroxin

---

and triiodothyronine [2]. An urinary iodine excretion below 40 g per day (80 μg I^- per day) is indicative of iodine deficiency in man, if renal clearance is normal [5], whereas a daily excretion of less than 60 μg I^- per day is indicative of the existence of endemic goiter in a community [6].

Of the many methods available for the determination of iodine, the most commonly used are colorimetry [7–10], neutron activation analysis (NAA) and those adapted from the serum-protein-bound iodine [11,12]. While colorimetric methods are time-consuming and require sample handling [13], NAA has an excellent intrinsic sensitivity for iodine; however, low levels of this element in biological materials cannot be easily measured by conventional reactor-flux instruments because of interferences from the high activities of thermal neutron activation products of Na, K, Mn, Br, and Cl which are generally present in large amounts [14]. The analytical sensitivity and sampling throughput has usually been improved either by the automation of catalytic [15], pneumatoamperometric [16] and colorimetric procedures [17] or by using stopped-flow and flow injection (FI) techniques [18–22]. On the other hand, iodine has also been determined by monitoring the chemiluminescence (CL) emissions from the iodine–luminol [23,24] and iodine–hydrogen peroxide–sodium hypochlorite systems [25]. However, the most important limitations are that several metal ions and other species may enhance the same reactions [26–29] so that separation or masking is required for real samples. This disadvantage can be eliminated by using head-space (HS) techniques [30,31]. These make use of the equilibrium between the volatile components of a liquid or solid sample and the surrounding gas phase in a sealed vessel, and aliquots of the gas being removed by an inert gas, usually for GC analysis. Thus the HS technique is a very convenient way to separate volatile analytes from the bulk of the matrix. This work presents an on-line HS-FI system for the sensitive and accurate determination of iodide in urine by a CL reaction. The iodine is generated in the HS device and carried in a nitrogen flow to a vial, where it is trapped in a KI solution, followed by the determination of iodine in the concentrate. The reproducible and sequential introduction of aliquots of

the iodine, cobalt(II) and luminol solutions into a FI system by means of time-based introduction device [32] allowed the generation of CL in front of the detector. The Co(II)-catalyzed reaction of iodine with luminol has been selected for its simplicity, sensitivity and speed [33–35].

2. Experimental

2.1. Apparatus

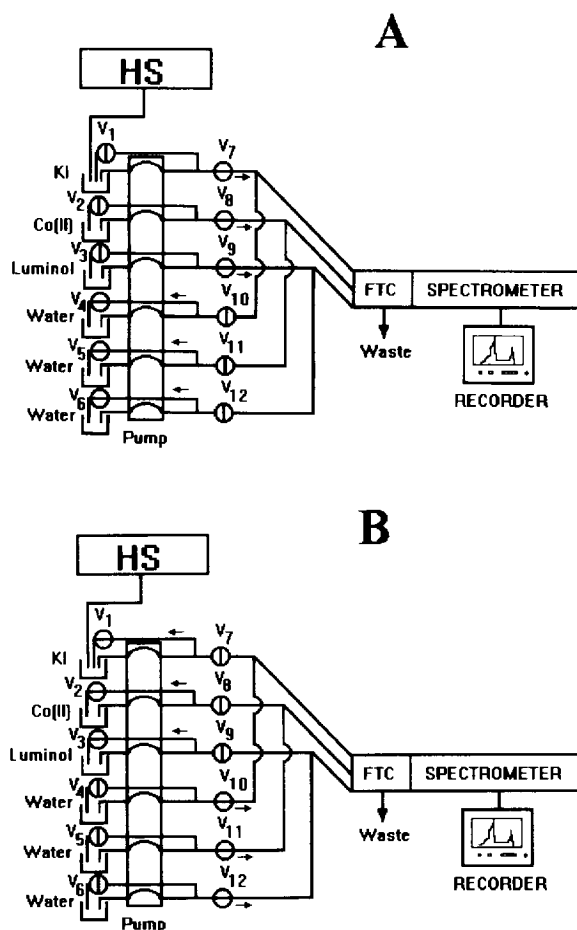A schematic diagram of the HS-FI-spectrophotometric system is given in Fig. 1. The outlet of a

Fig.1. Schematic diagram of the HS-FI-spectrometric system used for the determination of iodide in urine. (A) Injecting mode of the FI system; (B) washing mode of the FI system. FTC, flow through cell.
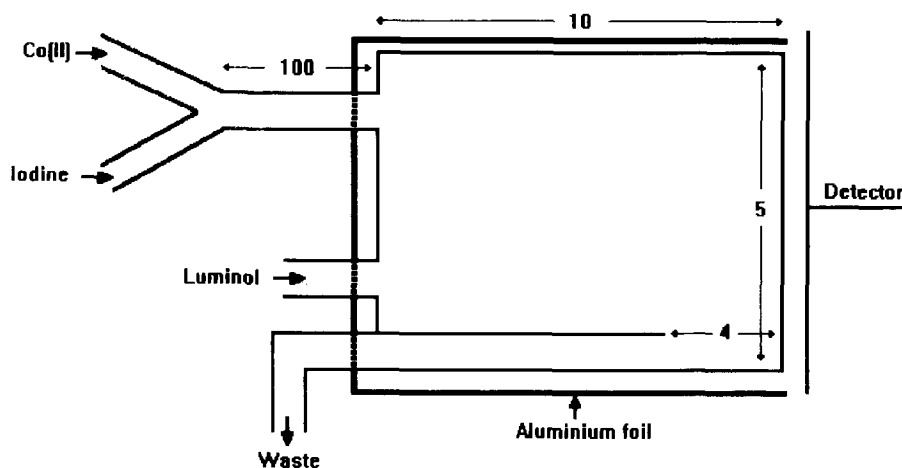
Fig. 2. Flow-through cell used for CL measurements. Dimensions are in millimeters.

semiautomatic Perkin-Elmer HS sampler model HS-40 is connected through a capillary column (0.53 mm i.d.) with a vial which contains the iodine trapping solution of potassium iodide. Determinations were performed in a Varian 634 spectrophotometer operated in the visible mode with a glass home-made flow-through cell shown in Fig. 2. The system also included a seven-channel variable-speed Ismatec IPC persitaltic pump with Tygon pump tubes, a home-made time-based injector [32] controlled by a Gralab 900 timer which permitted the dispensing of electronically controlled pulses to the solenoid valve, and a Cole-Parmer 156 recorder operated with a chart speed of 2 cm min^{-1}. PTFE tubing of 0.8 mm i.d. was used throughout unless otherwise stated.

2.2. Reagents

Unless stated otherwise, all solutions were prepared from analytical-reagent-grade chemicals. Deionized, distilled water was used throughout. A stock iodide solution (250 mg l^{-1}) was prepared by dissolving 0.0300 g of potassium iodide in 100 ml of a salted solution containing 10 g l^{-1} and 5 g l^{-1} of NaCl and KCL, respectively. Working solutions of iodide were prepared by suitable dilution with the same salted solution. For iodine trapping purposes, a 0.2% (w/v) potassium iodide solution was prepared by dissolving 200 g of KI in 800 ml of water. A stock luminol solution

$(2 \times 10^{-3}$ mol l$^{-1})$ was prepared by dissolving 0.0123 g of luminol (B.D.H.) in 50 ml of 0.1 mol l^{-1} sodium carbonate buffer, pH 12.0. Stock cobalt(II) solution (0.1 mol l^{-1}) was prepared by dissolving 2.911 g of Co(NO$_3$)$_2 \cdot$6H$_2$O in 100 ml of water; working solutions were prepared daily by appropriate dilution with water. A stock potassium dichromate solution (0.01 mol l^{-1}) was prepared by dissolving 0.2942 g of K$_2$Cr$_2$O$_7$ in 1.0 mol l^{-1} of hydrochloric acid.

2.3. Procedure

The operating HS-FI-CL conditions were optimized and are given below. The optimization of these experimental conditions for the determination of iodide was carried out by means of the univariate method, with the aim of finding a suitable compromise between peak height, sample throughput, reproducibility and sample volume used per analysis. An 8 ml amount of potassium iodide solution (for calibration purposes) or a urine sample, and 1 ml of 0.01 mol l^{-1} potassium dichromate solution were placed in the HS sample vial. After an agitation time of 1.5 min, a selected thermostatting temperature of 140°C was applied for 15 min. During sample thermostatting, the HS system was in the "standby" position, and a carrier stream of nitrogen at a pressure of 24 psi flowed through the tube which connected the HS with the iodine trapping vial. At the end of the

thermostatting time, when the HS was in the "pressurization" position, the HS sampling needle descended, pierced the septum cap of the sample vial and entered the HS vial. The sample vial was pressurized with nitrogen at 45 psi during 0.2 min. At the end of the pressurization time, the flow of nitrogen was stopped, and the vapor from the HS vial passed for 2.5 min into a vial containing 3 ml of 0.1% (w/v) potassium iodide, where the trapping of iodine took place. Thereafter, the solenoid valve of the time based device was activated to open the valves V_4, V_5, V_6, V_7, V_8 and V_9 and to close the valves V_1, V_2, V_3, V_{10}, V_{11}, and V_{12} (Fig. 1A) for 3 s. In this way, the iodine, 1×10^{-5} mol 1^{-1} Co(II) and 1×10^{-3} mol 1^{-1} luminol solutions were pumped at pumping rates of 6.0 ml min^{-1}, 4.4 ml min^{-1} and 7.0 ml min^{-1}, which allowed the injection of 0.30 ml, 0.22 ml and 0.36 ml of each solution, respectively. The injected volumes of iodine and cobalt(II) solutions were premixed 10 cm before their entrance into the flow-through cell, and thereafter mixed in front of the detector with the injected volume of luminol solution, while the streams of water flowed within their respective closed-flow circuits. The emission intensity was recorded as a function of time over 10 s at 425 nm. The solenoid valve was then operated in the reverse mode for 30 s (washing position) to flush the reagents out from the flow-through cell with water (Fig. 1B). The alternation of both solenoid positions allowed the repetitive and reproducible introduction of sample–reagent mixture plugs into the carrier stream. A calibration curve was obtained by using the emission readings for each standard concentration. The iodide concentration of each sample was determined as iodine by reference to this analytical curve. The water streams were pumped continuously at 4.4 ml min^{-1} during the washing process to ensure a stable baseline.

3. Results and discussion

3.1. Preliminary observations

It was found that when luminol is oxidized by iodine in the presence of Co(II), the emission is of

such short duration that the mixing time becomes critical; consequently, seriously distorted emission with low sensitivity was obtained using a conventional 0.5 ml flow-through cell with a 10 ml optical path, which made meaningful studies impossible. Therefore, in this study the emission profile was obtained by employing a home-made flow-through cell (Fig. 2), which allowed the mixing of sample and reagents in front of the detector. Also, the stability of trace iodine in the trapping vial was of vital importance if the full analytical potential of this sensitive method for iodine is to be realized. Therefore, the glass vial was silanized and protected from light [36] during trapping, and the injections of aliquots of the iodine solution were made within 20 min of the sample absorption measurement.

### 3.2. HS experimental conditions

The choice of a septum for sealing the HS vial was important for obtaining reproducible analyses. Butyl rubber septa adsorb iodine, which made their use unsuccessful because of low reproducibility. On the other hand, PTFE coated with silicone rubber septa showed no affinity for iodine, which made their use preferable.

The sensitivity of the analysis improved as the volume of sample in the HS vial increased (Fig. 3a). A 5 ml sample volume provided adequate sensitivity. Although larger sample volumes than 5 ml did not make a great difference with regard to sensitivity, in order to achieve the minimum detection limit a volume of 8 ml was needed. As the volume of the liquid becomes particularly significant, it affects the ratio of liquid to gas in the HS vial [37]; therefore, less volatile iodine is likely to be found in the gas phase and low distribution coefficients (see below) [38] are obtained. These results are in close agreement with those previously reported by Ettre and Kolb [38], which concluded that in the case of samples with low distribution coefficients (less than 10), the sample volume has a significant influence on the "sensitivity" of the HS analysis.
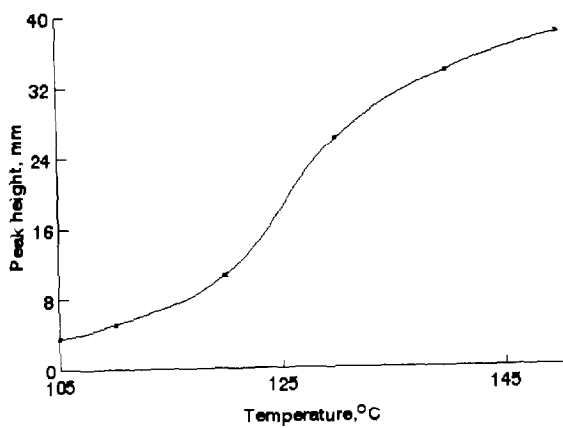
An acidified potassium dichromate solution was used to oxidize iodide to iodine. This oxidant has some advantages over others, e.g. it is obtainable
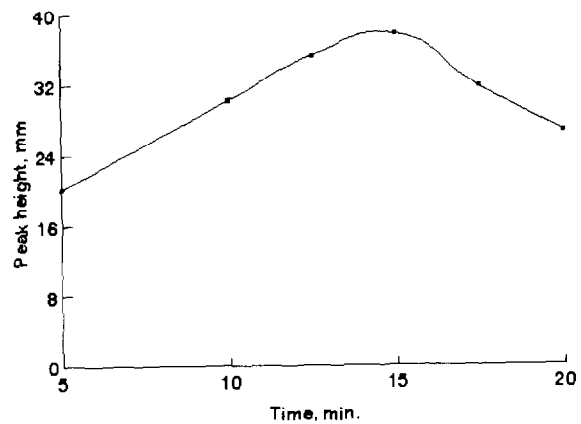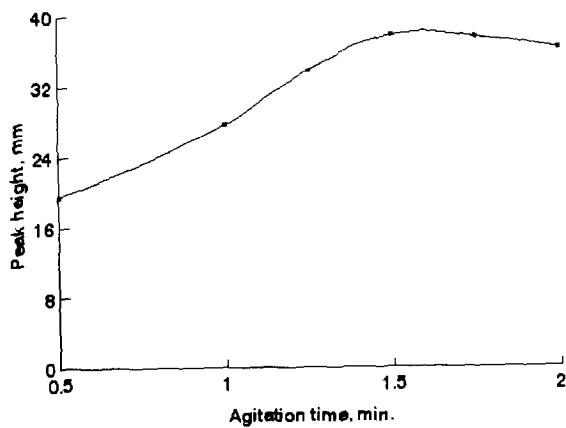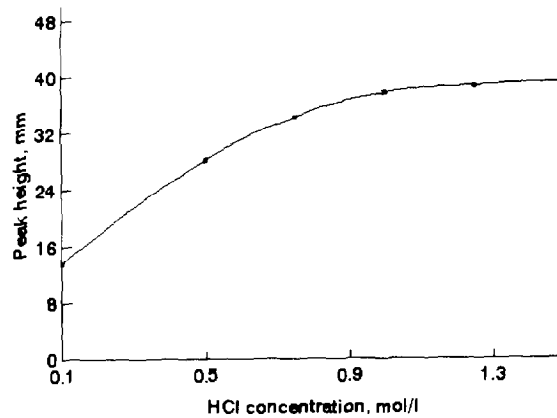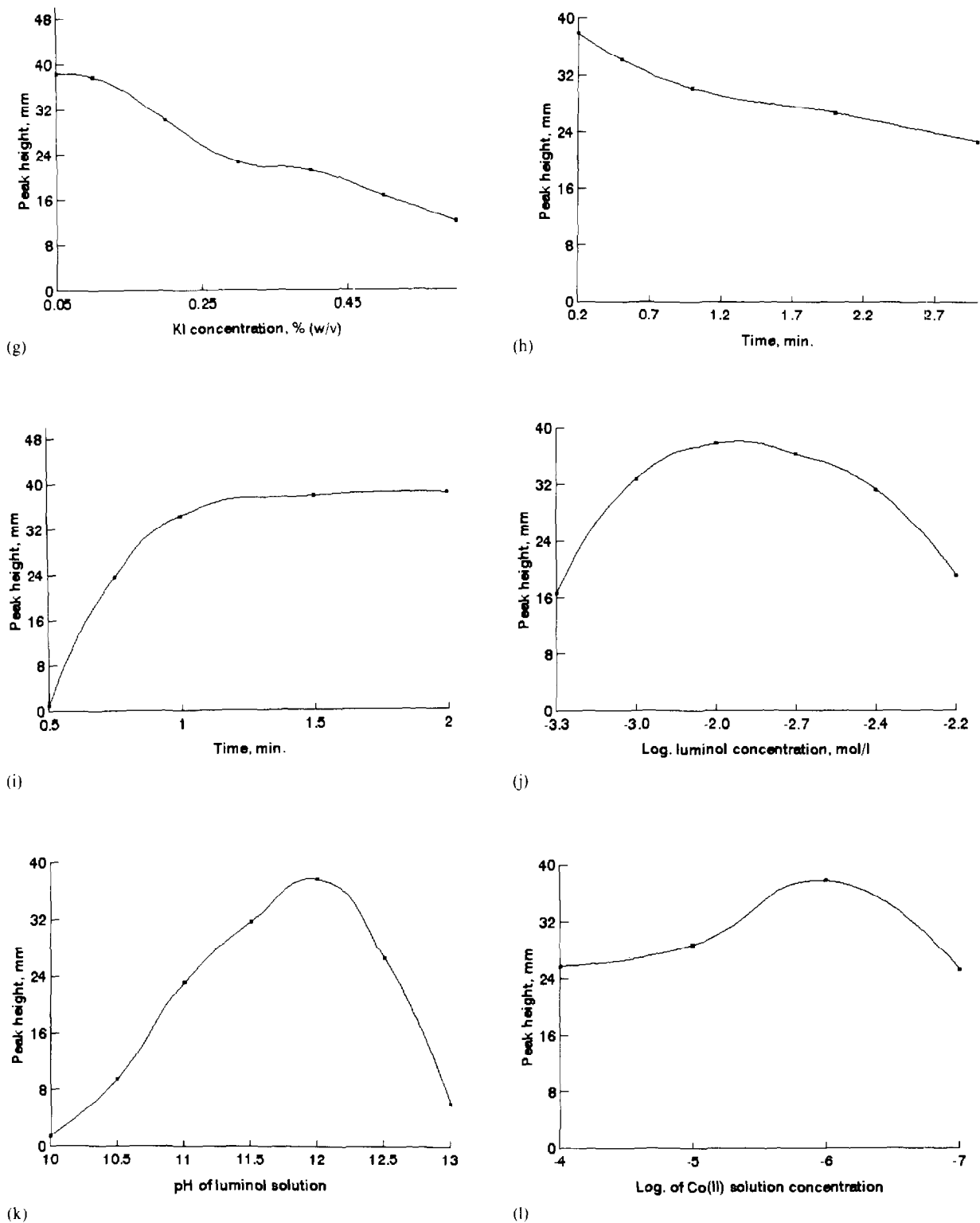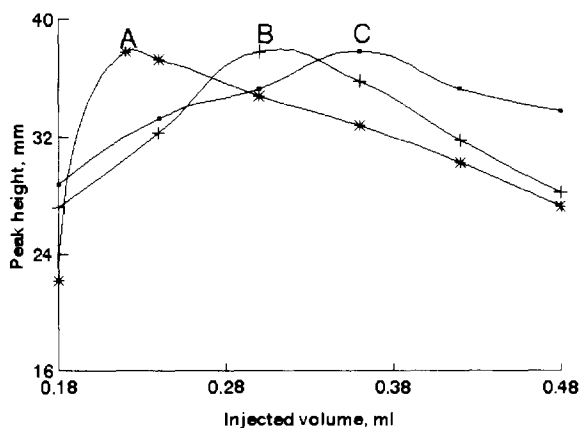
Fig. 3 (a)–(f).

(g)

(h)

(i)

(j)

(k)

(l)
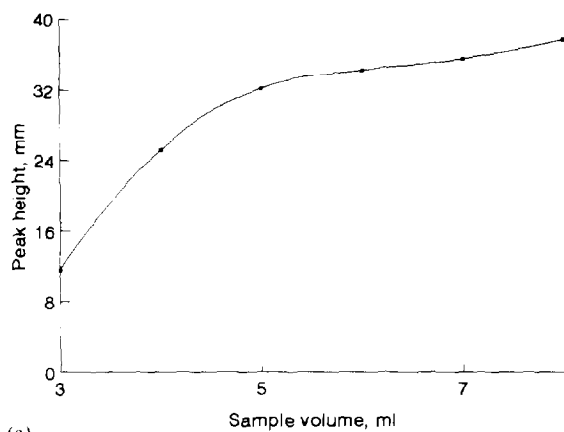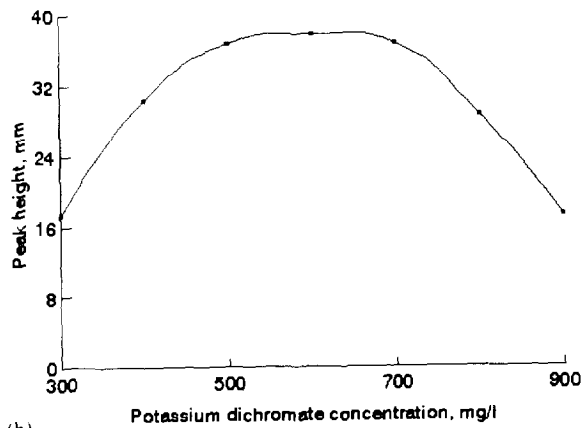
Fig. 3 (g)–(l).

Fig. 3. Effects of (a) sample volume, (b) potassium dichromate concentration in the HS vial, (c) HS vial thermostatting temperature, (d) HS vial thermostatting time, (e) sample–potassium dichromate solution agitation time in the HS vial, (f) hydrochloric acid concentration in the iodine trapping vial, (g) potassium iodide concentration in the iodine trapping vial, (h) HS vial pressurization time, (i) HS injection time, (j) luminol concentration, (k) pH, (l) cobalt(II) concentration, and (m) cobalt(II) (curve A), iodine (curve B) and luminol (curve C) solution volumes injected into the FI system on the CL signal (3 mg l^{-1} iodine; other conditions are as specified in Table 3.)

in a state of high purity, being used as a primary standard, the solution does not change on standing, and it has an appropriate standard oxidation–reduction potential for the generation of iodine from iodide [39]. The effect of the oxidant concentration on the CL emission intensity was examined in the 300–900 mg l^{-1} range. Fig. 3b shows that better sensitivity was observed with a potassium dichromate concentration of 600 mg l^{-1}. There was little difference when the acidity of the oxidant solution was kept between 0.5 and 2.0 mol l^{-1} of hydrochloric acid.

Higher thermostatting temperatures of the sample increased the sensitivity of the analysis (Fig. 3c). This effect is likely to be due to an enhanced concentration of iodine in the gas phase owing to a higher partition coefficient of this volatile compound [37]. However, temperatures above 150°C were avoided due to the risk of degrading the sample, bursting the container or losing the analyte due to chemical interaction with the vial septum [40] and to a larger variation of the CL

signal. Besides, higher sample temperatures may lead to more water vapor purged on to the trapping adsorbent media with a reduction in the sensitivity and precision of measurements [41]. The CL signal increased with an increase of the thermostatting temperature up to 15 min; thereafter the emission intensity markedly decreased (Fig. 3d). Taking into account the sensitivity, sampling frequency and the error, the HS was thermostatted at a temperature of 150°C for 15 min.

The stirring of the sample with the potassium dichromate solution in the HS vial is necessary to prevent the entrapment of the volatile analyte within the matrix through homogenization during the extraction procedure. Fig. 3e shows that the iodine reached an equilibrium in 1.5 min.

3.3. Iodine trapping conditions

It is usual to dissolve iodine in a solution of potassium iodide for the preparation of standard iodine solutions [39]. Therefore, in this work an acidified potassium iodide solution was used as an efficient medium for trapping the iodine resulting from the vapor generated in the HS vial. It is generally assumed that in this process a complex compound, KI_3, is formed, but this is not very stable, for the solution behaves as thought it were a solution of iodine [39]. As long as the pH of the solution is below 8 it has little or no effect on the iodine–iodide system. Above this level, however, iodine reacts with hydroxyl ions to form hypoiodite which, being unstable, is converted to iodate [39]. Therefore, the acidity of the potassium iodide trapping solution must be maintained between certain limits. Hydrochloric acid concentrations higher than 1.0 mol l^{-1} maintained the iodide solution at the optimum pH range for the absorbance of iodine (Fig. 3f). Fig. 3g shows the effect of the iodide trapping solution concentration on the CL response. As the iodide concentration increased beyond 0.1% (w/v), a decrease in the CL peak height was observed due to the formation of the triiodide ion, I_3^- [23]. Although this ion increases the solubility of iodine and keeps the iodine from volatilizing, it does not react with luminol to generate CL.

The iodine trapping efficiency in the iodine trapping vial is compound-dependent and involves a knowledge of other factors also, including the vapor pressure of the compound, the HS sample vial pressure (carrier gas pressure) and the interaction between the analyte and the adsorbent solution. A sample pressurization of 45 psi during 0.2 min provided an adequate analyte vapor stream from the HS vial to the trapping adsorbent vial (Fig. 3h). The injection time was varied from 0.5 to 2 min (Fig. 3i). Sufficient sample quantity was delivered after 1.5 min with maximal absorbance efficiency in the KI solution.

3.4. CL experimental conditions

The CL peak height would be expected to vary according to certain parameters which affect the emission intensity, e.g. luminol, catalyst and oxidant concentration and pH of the luminol solution.

The effect of varying the luminol concentration is shown in Fig. 3j. The emission was most intense at a 1.6×10^{-3} mol l^{-1} luminol concentration in the solution injected in the FI system (Fig. 1). Characteristically there is a decrease in efficiency at higher luminol concentrations, which may be due to luminol (or its aminophthalate oxidation products) acting as an organic complex to reduce the "availability" of the metal ion for catalysis [35].

The effect of pH (10.5–13) on the intensity was investigated. CL was produced only in the alkaline environment. Higher intensity was observed at pH 12.0 (Fig. 3k). The buffer was prepared from sodium hydrogen carbonate, and a glass electrode was employed to measure the pH after the reaction has taken place, to ensure the buffer capacity was sufficient. The intensity maximum occurred at a relatively high pH value, as other investigators have reported a maximal quantum yield in the 10–11.5 interval [33,35,41]. This behaviour may be most likely attributed to the particular pattern of mixing in the flow cell [42] or to a particular catalyst [35]. The effect of the catalyst concentration on the CL intensity in the luminol oxidation by iodine was also investigated (Fig. 3l). The emission intensity was dependent on

Co(II) concentration. The final emission intensity chosen was 10^{-5} mol l^{-1} of Co(II).

3.5. FI experimental conditions

In the FI system used, a peristaltic pump was the driving force for the sample, luminol, catalyst and washing solutions. Therefore the volume of the sample and reagents to be injected depended on the pumping rate of each solution and on the time of solenoid activation during the injection (Fig. 1A). The flow rate of these solutions and therefore their mixed volumes in the flow-through cell were different. The pumping rate of each solution was varied between 2.0 and 8.0 ml min^{-1} and the time of the solenoid activation during the injection was varied between 1 and 14 s. In either case, the CL emission increased on increasing the injected volume, and thereafter a slight decrease was observed (Fig. 3m). Higher signals were observed with pumping rates of 6.0 ml min^{-1}, 4.4 ml min^{-1} and 7.0 ml min^{-1} of iodine, cobalt(II) and luminol solutions, which allowed the injection of 0.30 ml, 0.22 ml and 0.36 ml of each solution, respectively, for a solenoid activation time of 3 s.

3.6. Matrix matching of the standard solutions

It is known that matrix components in the liquid phase affects the HS behaviour of volatile substances [43]. To evaluate the effect of the sample matrix on HS analysis, a study was performed in which the recovery of the analyte from a pooled urine sample with "known" amounts of iodide and spiked with different amounts of this analyte was compared with those achieved from iodide solutions prepared in different matrixes and water. Because sodium, potassium and chloride are major components of urine [44], different samples were prepared with and without sodium chloride and potassium chloride addition. Table 1 shows that for samples prepared with 10 g l^{-1} NaCl and 5 g l^{-1} KCl the recovery was close to 100%. Also, the recovery of iodine added as iodide to urine was good and varied between 94 and 99%. It should be noted, however, that recovery problems were observed in two cases: the samples with high salt content (150 g l^{-1} NaCl and 70 g

Table 1
Recovery studies in different matrixes

Matrix	Iodide concentration (mg l^{-1})		Recovery (%)
	Spiked	Found	
Urine	1.5	1.56	99
	2.5	2.48	96
	4.0	3.90	94
Water	1.5	1.17	78
	2.5	1.93	77
	5.0	3.80	76
10 g NaCl + 5 g l^{-1} KCl	1.5	1.55	103
	2.5	2.55	102
	5.0	5.05	101
150 g l^{-1} NaCl + 70 g l^{-1} KCl	1.5	2.22	148
	2.5	3.73	149
	5.0	7.50	150

[a] 70 μg l^{-1} I^{-} endogenous content.

l^{-1} KCl) and solutions prepared in water. While in the high salt content sample the recovery was high (about 150%), in the solution prepared with water the recovery was generally poor, frequently less than 78%. This salting-out effect of high concentrations of NaCl and KCl may be due to the fact that inorganic salts are known to enhance the vaporization of volatile substances [43–47]. Whereas, the addition of physiological amounts of salt to the aqueous samples provided an adequate salting-out effect to produce good recovery values. In our case, the salting-out effect does not affect the results obtained for the determination of iodide in urine samples because the physiological levels of sodium, potassium and chloride in urine are about 3.85 g l^{-1} (from 0.9 to 5.0 g l^{-1}), 2.28 g l^{-1} (from 0.9 to 3.9 g l^{-1}) and 7.0 g l^{-1} (from 3.8 to 9.0 g l^{-1}), respectively [45,48,49].

Table 2 shows the regression equations of the CL signal as a function of iodine concentration obtained from standard iodide solutions prepared with and without salt addition and from iodide-spiked urine samples. These data were obtained by running calibration curves using the method of standard additions with overlapping ranges. Each calibration set included five data points and was run at least three times. It was found that regardless of the solution used for the iodide standard

preparation, the response was first order for the concentration range 0–5 g l^{-1} iodine, and second order for the range 10–40 g l^{-1} I$_2$. The occurrence of these first- and second-order processes are in agreement with results previously published by Seitz and Hercules [23,35]. Comparison of the slopes of the calibration graphs, obtained by preparing standard solutions in different media, further confirmed that there is a salting-out effect on sensitivity. When pure water and too high a concentration salting-out solutions were used, the response of the analyte was affected by the composition of the matrix. However, there was virtually no effect of the matrix on preparing standard solutions with a physiological salt content. As a consequence, the linear portion of the 0–5 g l^{-1} iodine curve served as a calibration graph for standard and working solutions prepared in solutions containing 10 g l^{-1} and 5 g l^{-1} NaCl and KCl, respectively.

As the concentration of the analyte in the gas phase is proportional to the concentration of the undissociated part of the analyte in solution, salting out by adding inorganic salts to an aqueous solution can produce an increase in sensitivity of over one-hundredfold in favorable cases. The liquid and gas phase concentrations are related to each other by the partition coefficient K (defined

Table 2
Regression equations of the CL signal obtained in different matrixes

Matrix	Regression line[a]	r	Iodine concentration range (mg l^{-1})
Water	$E_{CL} = -0.051 + 15.92\ X$	0.9990	0–5
	$E_{CL} = -10.843 + 3.745\ X$	0.9997	10–40
10 g l^{-1} NaCl + 5g l^{-1} KCl	$E_{CL} = 0.010 + 12.60\ X$	0.9997	0–5
	$E_{CL} = -10.513 + 3.021\ X$	0.9998	10–40
150 g l^{-1} NaCl + 70 g l^{-1} KCl	$E_{CL} = 0.038 + 7.940\ X$	0.9995	0–5
	$E_{CL} = -4.998 + 1.528\ X$	0.9990	10–40
Urine	$E_{CL} = 2.450 + 12.10\ X$	0.9986	0–5
	$E_{CL} = -8.500 + 3.069\ X$	0.9998	10–40

[a] E_{CL} and X indicate the CL emission intensity (peak height in millimeters) and analyte concentration in milligrams per litre, respectively. From 0 to 5 mg l^{-1} iodine (1mm represents 1 mV) and from 10 to 40 mg l^{-1} iodine (1 mm represents 10 mV), the recorder was operated at 1 mV and 10 mV full scale, respectively. The experimental conditions were as specified in Table 3.

as C_s/C_G where C_s and C_G are the equilibrium concentrations of the analyte in the sample and in the gas phase of the HS vial, respectively) [47,50,51]. The partition coefficient is matrix-de-pendent and is unknown for most analyses; it must therefore be accounted for by calibrating the sampling system. In our particular case, K for solutions prepared in water, 10 g l^{-1} NaCl + 5 g

Table 3
Optimized operating conditions for the determination of urine by HS-FL-CL

Step	Parameter	Value
Chemical	Co(II) concentration	1×10^{-5} mol l^{-1}
	pH luminol solution	12.0
	Luminol concentration	1.6×10^{-3} mol l^{-1}
	KI sorbent solution concentration	0.1% (w/v)
	NaCl concentration in the HS vial	10 g l^{-1}
	KCl concentration in the HS vial	5 g l^{-1}
	$K_2Cr_2O_7$ concentration in the HS vial (in 1 mol l^{-1} HCL)	560 mg l^{-1}
HS	Urine sample volume	8 ml
	Thermostatting time	15 min
	Thermostat temperature	150 °C
	Pressurization time	3 min
	Agitation time	1.5 min
	Injection time	2.5 min
	Carrier gas pressure	24 psi
	High pressure valve	45 psi
	Volume of $K_2Cr_2O_7$ solution	1 ml
FI	Sample injection volume	0.30 ml
	Luminol solution injection volume	0.36 ml
	Cobalt (II) solution injection volume	0.22 ml
	Peristaltic pump flow rate	6.4 ml min^{-1}
	Time of injection	3 s
Spectrophotometry	Wavelength	425 nm
	Slit width	2.0 nm

1^{-1} KCl and 150 g 1^{-1} NaCl + 7 g 1^{-1} KCl solutions was 2.1, 2.6 and 4.1, respectively. Thus, the addition of salt to aqueous solutions containing iodide augmented K, so that sensitivity is reduced (Table 2). The magnitude of this effect depends on the amount of salt added and K of the compound [47]. According to our results, as $K < 10$, the ratio of the volumes of the two phases is particularly significant [47]. Therefore, this further confirms that an adequate addition of NaCl and KCl salts is important in order to minimize matrix effects.

3.7. Analytical figures of merit

On the basis of the above results, calibration graphs were prepared from 0 to 5 mg 1^{-1} for iodine determination using the HS-FI-spectrometric optimum conditions given in Table 3. The precision of this procedure was estimated by measuring the CL signal (peak height) from ten replicate analyses of 50 g 1^{-1} and 200 g 1^{-1} iodine solutions by the recommended procedure; the corresponding relative standard deviations were 2.3% and 1.8%, respectively. The detection limit for iodine, defined as three times the standard deviation of the peak height signals, was 10 g 1^{-1} I_2.

The accuracy of the proposed procedure was further tested by determining the iodide content in 12 urine samples of different "healthy" subjects by the iodine-catalyzed cerate–arsenite method with spectrometric detection [52] and the proposed procedure. Good agreement was obtained for all samples, which is an indication of satisfactory accuracy of the proposed method. By applying Student's t test and the F test [53] to the results (for a confidence limit of 95%), it was found that there were no statistically significant differences between the means of both populations.

From the experimental point of view, the HS sampling technique is very simple, and combined with the FI system provides precise and accurate results for the determination of iodide in urine. Also, the CL reaction used provided adequate sensitivity for the determination of low analyte contents in the samples under study and permitted sequential measurements with a low carry-over.

References

[1] E.I. Underwood, Trace Elements in Human and Animal Nutrition, 4th edn., Academic Press, New York, 1977, pp. 271–301.

[2] G. Pethes, The Need for Trace Element Analysis in the Animal Sciences, 1, in Elemental Analysis of Biological Materials, Tech. Rep. Ser. No. 197, International Atomic Energy Agency, Vienna, 1980, Chapter 1.

[3] H. Willgerdt, B. Stach and E. Keller, Z. Klin. Med., 46 (1991) 965.

[4] M.Z. Mocan, H. Mocan, H. Kizilkaya and S. Tokel, Tr. Elem. Med., 9 (1992) 59.

[5] D.A. Koutras, Activation Analysis in the Study of Mineral Metabolism in Man, International Atomic Energy Agency, Vienna, 1968.

[6] J.B. Stanbury, H. Hermans, B.S. Hetzel, B.A. Pretell and N. Querido, WHO Chron., 28 (1974) 220.

[7] E.B. Sandell and I.M. Kolthoff, Microchim. Acta, 1 (1937) 9.

[8] R. Malvano, G. Buzzigoli, M. Scarlrttini, G. Cenderelli, G. Gandolfi and P. Grosso, Anal. Chim. Acta, 61 (1972) 201.

[9] P.J. Garry, D.W. Lashley and G.M. Owen, Clin. Chem., 19 (1973) 950.

[10] M. Dermelj, Z. Slejkovec, A.R. Byrne, B. Kenda, T. Cerk and B. Gorenc, Microchim. Acta, 1 (1991) 151.

[11] J. Benotti, N. Benotti, S. Pino and H. Gardyna, Clin. Chem., 11, (1965) 932.

[12] J.T. Dunn, H.E. Crutchfield, R. Gutekunst and A.D. Dunn, Thyroid, 3 (1993) 119.

[13] F. de Venanzi, A.G. Briceño and M.J. Carucci, Interciencia, 15 (1990) 30.

[14] R.R. Rao and A. Chatt, Anal. Chem., 63 (1991) 1298.

[15] W. May, D. Wu, C. Eastman, P. Bourdoux and G. Maberly, Anal. Chem., 36 (1990) 865.

[16] A. Trojánek and P. Papoff, Anal. Chim. Acta, 247 (1991) 73.

[17] P.J. Garry, D.W. Lashley and G.M. Owen, Clin. Chem., 19 (1973) 950.

[18] D.E. Davey, D.E. Mulcahy and G.R. O'Connell, Talanta, 37 (1990) 313.

[19] M.C. Gutiérrez, A. Gómez-Hens and D. Pérez-Bendito, Analyst, 114 (1989) 89.

[20] S. Ventura, M. Silva and D. Pérez-Bendito, Anal. Chim. Acta, 266 (1992) 301.

[21] J. Moller and B. Winter, Fresenius' Z. Anal. Chem., 320 (1985) 451.

[22] J. Atienza, M.A. Herrero, A. Maquieira and R. Puchades, Crit. Rev. Anal. Chem., 22 (1991) 331.

[23] W.R. Seitz and D.M. Hercules, J. Am. Chem. Soc., 96 (1974) 4094.

[24] W.M. Hardy, W.R. Seitz and D.M. Hercules, Talanta, 24 (1977) 297.

[25] J.L. Burguera and M. Burguera, Quim. Anal., 78B (1982) 307.

[26] U. Isacsson and W. Wettermark, Anal. Chim. Acta, 83 (1976) 227.

[27] S.D. Hoyt and J.D. Ingle, Jr., Anal. Chim. Acta, 87 (1976) 163.

[28] J.L. Burguera, M. Burguera and A. Townshend, Anal. Chim. Acta, 127 (1981) 199.

[29] J.L. Burguera and A. Townshend, Talanta, 28 (1981) 731.

[30] G. Charalambous (Ed.), Analysis of Food and Beverages: Headspace Techniques, Academic Press, New York, 1978.

[31] B. Kolb (Ed.), Applied Headspace Gas Chromatography, John Wiley, Chichester, 1992.

[32] P. Carrero, J.L. Burguera, M. Burguera and C. Rivas, Talanta, 40 (1993) 1967.

[33] J.L. Burguera, A. Townshend and S. Greenfield, Anal. Chim. Acta, 114 (1980) 209.

[34] W.R. Seitz, Crit. Rev. Anal. Chem., 13 (1981) 1.

[35] W.R. Seitz and D.M. Hercules, in M.J. Cormier, D.M. Hercules and J. Lee (Eds.), Chemiluminescence and Bioluminescence, Plenum Press, New York, 1973, pp. 427–449.

[36] G. Ham, R. Belcher, L.J. Kricka and T.J.N. Carter, Anal. Lett., 12 (1979) 535.

[37] Z. Penton, J. High Resolut. Chromatogr. (HRC), 15 (1992) 834.

[38] L.S. Ettre and B. Kolb, Chromatography, 32 (1991) 5.

[39] R. Belcher, A.J. Nutten and A.M.G. MacDonald, Quantitative Inorganic Analysis, 3rd. edn., Butterworth, London, 1970.

[40] L. Ghaoui, J. Chromatogr., 642 (1993) 389.

[41] S.M. Abeel, A.K. Vickers and D.D. Decker, J. Chromatogr. Sci., 32 (1994) 328.

[42] J.L. Burguera and A. Townshend, Talanta, 28 (1981) 1981.

[43] J.L. Burguera and M. Burguera, Acta Cient. Venez., 34 (1983) 79.

[44] T. Shinohara, Anal. Chim. Acta, 276 (1993) 247.

[45] P.L. Altman and D.S. Dittmer, Blood and Other Body Fluids, Federation of American Societies for Experimental Biology, Bethesda, Maryland, USA, 1971, p. 363.

[46] T.C. Voice and B. Kolb, J. Chromatrogr. Sci., 32 (1994) 306.

[47] Z. Penton, J. High Resolut. Chromatogr., 15 (1992) 834.

[48] A. Rodriguez R., Medi-Data: Valores Normales, 3rd. edn., Rodram Corporation, Mexico, 1990, p. 22.

[49] Ciba-Geigy, Tablas Científicas, 6th. edn., Ciba-Geigy, Basel, Switzerland, 1971, p. 558.

[50] B. Kolb, Headspace Gas Chromatography, Bodenseewerk Perkin-Elmer GmbH, Uberlingen, Germany, 1992.

[51] C.F. Poole and S.A. Schuette, Contemporary Practice of Chromatography, Elsevier, Amsterdam, 1984, Chapter 7, pp. 429–581.

[52] H. Hoch and C.G. Lewallen, Clin. Chem., 15 (1969) 204.

[53] C. Liteanu and I. Rica, Statistical Theory and Methodology of Trace Analysis, Wiley, New York, 1980, pp. 33–51.

ELSEVIER

Talanta

Monitoring CP-93,393 reaction mixtures by flow-injection analysis–mass spectrometry [1]

S.T. Colgan *, T.R. Sharp, P.D. Hammen, R.H. Reed, G.J. Horan, P.W. Gwiazda

Pfizer Central Research, Groton, CT 06340, USA

Received 29 September 1995; revised 7 November 1995

Abstract

CP-93,393 is a drug candidate at Pfizer. Flow-injection analysis–mass spectrometry (FIA–MS) was used to monitor reaction completion for CP-93,393 reaction mixtures. FIA–MS provides essentially instantaneous results, is relatively simple to operate, and is a universal system that can be used to monitor any reaction as long as the product has a molecular weight that differs from the molecular weights of the reactants. The mass spectrometer for these studies employed atmospheric pressure chemical ionization. Samples were introduced into the mass spectrometer with a flowing stream of solvent.

Keywords: CP-93,393; Flow-injection analysis; Mass spectrometry

1. Introduction

In-process control (IPC) assays are used in chemical and pharmaceutical production plants to assess the progress and completeness of chemical reactions. When a reaction has reached a predetermined level of completion, the reaction can be stopped and the product is either isolated or the next step of the reaction can be started. Reaction completion is usually determined by measuring the disappearance of a starting material.

An ideal IPC assay has the attributes summarized below. One of the most important features

of an IPC is that it provides meaningful data in a timely fashion to the process chemist controlling the reaction. For example, if a reaction is complete in 2 h, but the data from the IPC is unavailable for several hours, the product can be over-reacted, potentially producing unwanted side products. At the very least the time of the plant personnel is wasted, and the equipment in the production facility is unnecessarily occupied. Another highly desirable feature of an IPC is that the methodology is universal in nature and can provide quantitative data for all steps of a chemical synthesis. A methodology that could be used to monitor reaction completion of many different chemical syntheses (producing different final products) would be even more valuable. Other desirable attributes of IPC methodologies are that they are simple to operate and maintain, are

---

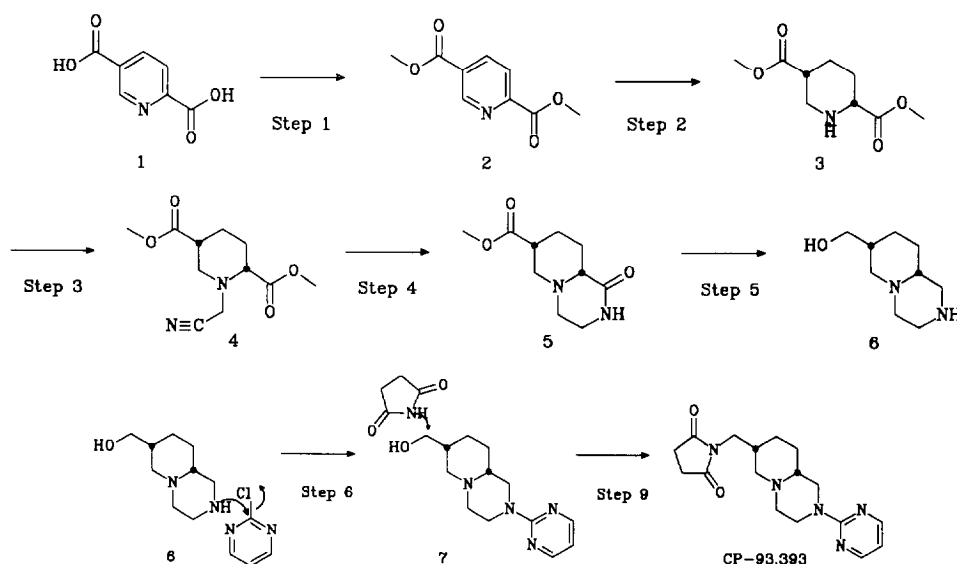* Corresponding author. Fax: (+ 1)860 441 5423.

Fig. 1. Synthetic pathway of CP-93,393.

rugged, with a minimum amount of down-time, and are inexpensive in terms of both purchasing and maintainance.

Methodologies that have been traditionally developed to monitor reaction completion include high performance liquid chromatography (HPLC), gas chromatography (GC), and thin layer chromatography (TLC). Recently, near-infrared spectroscopy (NIR) has been applied to monitor reaction completion [1]. All of the above techniques, however, have drawbacks for use in monitoring reaction completion. HPLC, GC, and TLC require time for equilibration and running samples. Universal chromatographic systems can be developed for a complete synthesis but these usually involve gradient elution (HPLC) or temperature programming (GC) to elute and resolve all process intermediates. Thus for universal chromatographic systems, excessive times are often required to re-equilibrate the system between injections. HPLC is further limited to samples that have a chromophore, electrophore, or fluorophore. GC is limited to samples that are volatile and stable at elevated temperatures. TLC is inexpensive, but has limited peak capacity, resolution,

and sensitivity. In addition, the time required to equilibrate a TLC development chamber can be excessive and/or difficult to determine. Use of NIR for monitoring reaction completion has been limited because it measures bulk properties and is non-specific in nature. Additional problems are encountered with non-homogeneous (slurry-type) reaction mixtures.

Although mass spectrometry may be the ideal technique to monitor reaction completion, the prohibitive cost of a mass spectrometer in the past has discouraged its use for this purpose. Currently, several suppliers offer bench-top mass spectrometers that cost, on average, approximately $200 000. The resonable cost of these units, combined with the availablity of several soft ionization techniques, should significantly increase the use of mass spectrometry for reaction completion monitoring.

This paper describes the use of flow-injection analysis–mass spectrometry (FIA–MS) to determine reaction completion of CP-93,393 reaction mixtures. FIA–MS has previously been used for the determination of arsenic and chloroform [2]. The synthetic pathway used to produce CP-93,393 is shown in Fig. 1.

2. Experimental

Before FIA–MS was evaluated for CP-93,393 reaction mixtures, conventional methodologies were evaluated. For steps 1 and 2, an ion-pairing, reversed-phase LC system was developed. Conventional reversed-phase approaches failed to retain the very polar isocinchomeronic acid (compound 1). Disappearance of compounds 3-6 could not be monitored by LC because all of these compounds lack a chromophore, fluorophore or electrophore. Gas chromatographic conditions were successfully developed for compounds 3-5, but all GC experiments attempted for compound 6 were hampered by tailing and irreproducible peak areas. Compound 7, which contained a chromophore, could be monitored by conventional reversed-phase LC.

Samples were introduced into the mass spectrometer with a flowing stream of solvent, pumped through an atmospheric pressure chemical ionization (APCI) liquid chromatography-mass spectrometry (LC–MS) interface. A schematic diagram of the APCI interface is shown in Fig. 2. Flow-injection analyses often involve on-line mixing of reagent and sample solutions. For FIA–MS, the reagent is simply the carrier solvent; a separately pumped reagent solution is not needed. When the sample enters the APCI ion source it is nebulized with nitrogen. A corona discharge needle promotes ionization, and the reactions that occur in the ion source involve charge transfer among the ionized solvent molecules and the analytes. The ionized analytes enter the high-vacuum mass analyzer region through a small orifice. Skimmers and focusing lenses remove unionized species [3].
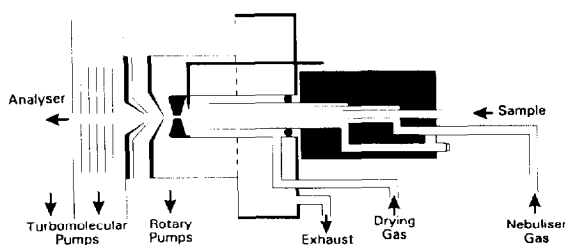

Fig. 2. Schematic diagram of the APCILC MS interface (courtesy of Fisons Instruments).
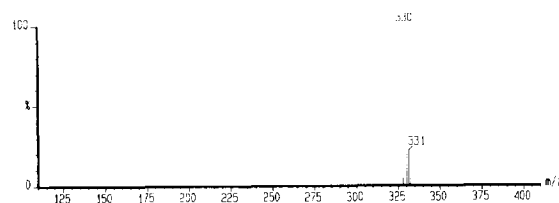

Fig. 3. APCI mass spectrum of CP-93,393.

Experiments have been done using either a Fisons Instruments Trio 2000 single quadrupole mass spectrometer or a Fisons Instruments Quattro triple quadrupole instrument. Both use identical APCI LC–MS interfaces. A Hewlett-Packard 1050 quaternary HPLC system was used to mix and deliver solvents. The autoinjector provided reproducible injections of samples into the flowing solvent stream. An in-line UV–vis detector recorded responses for UV-active components when appropriate. For these studies, the solvent used as a carrier and to dissolve samples was a 50/50 (v/v) mixture of acetonitrile and an aqueous 0.05 M ammonium acetate solution. The ammonium acetate promoted ionization of compound 1. The flow rate was 0.5 ml min^{-1} and the sample injection volume was 1 μl.

3. Results and discussion

The synthetic pathway used to produce CP-93,393 is shown in Fig. 1. Production steps 7 and 8 have been ommitted from the scheme, as they are non-synthetic, i.e. they comprise an optical resolution and a salt change.

The APCI mass spectrum of CP-93,393 is shown in Fig. 3. The abundant protonated molecular ion at m/z 330, combined with negligible fragmentation, is indicative of an ideal candidate for the application of FIA–MS to monitor reaction completion using APCI ionization. Although a small amount of fragmentation is acceptable, if the product has a fragment with the same m/z value as the protonated molecular ion of its precursor, successful application of this technique becomes more difficult. For the same reason, FIA–MS cannot be used to determine enantiomeric purity or the completeness of a reaction

Compound 1 (isocinchomeronic acid) r.m.m. 167 daltons

Compound 3, r.m.m. 201 daltons

Compound 2, r.m.m. 195 daltons

Compound 4, r.m.m. 240 daltons

Compound 5, r.m.m. 212 daltons

Compound 6. r.m.m. 170 daltons

Compound 7, r.m.m. 248 daltons
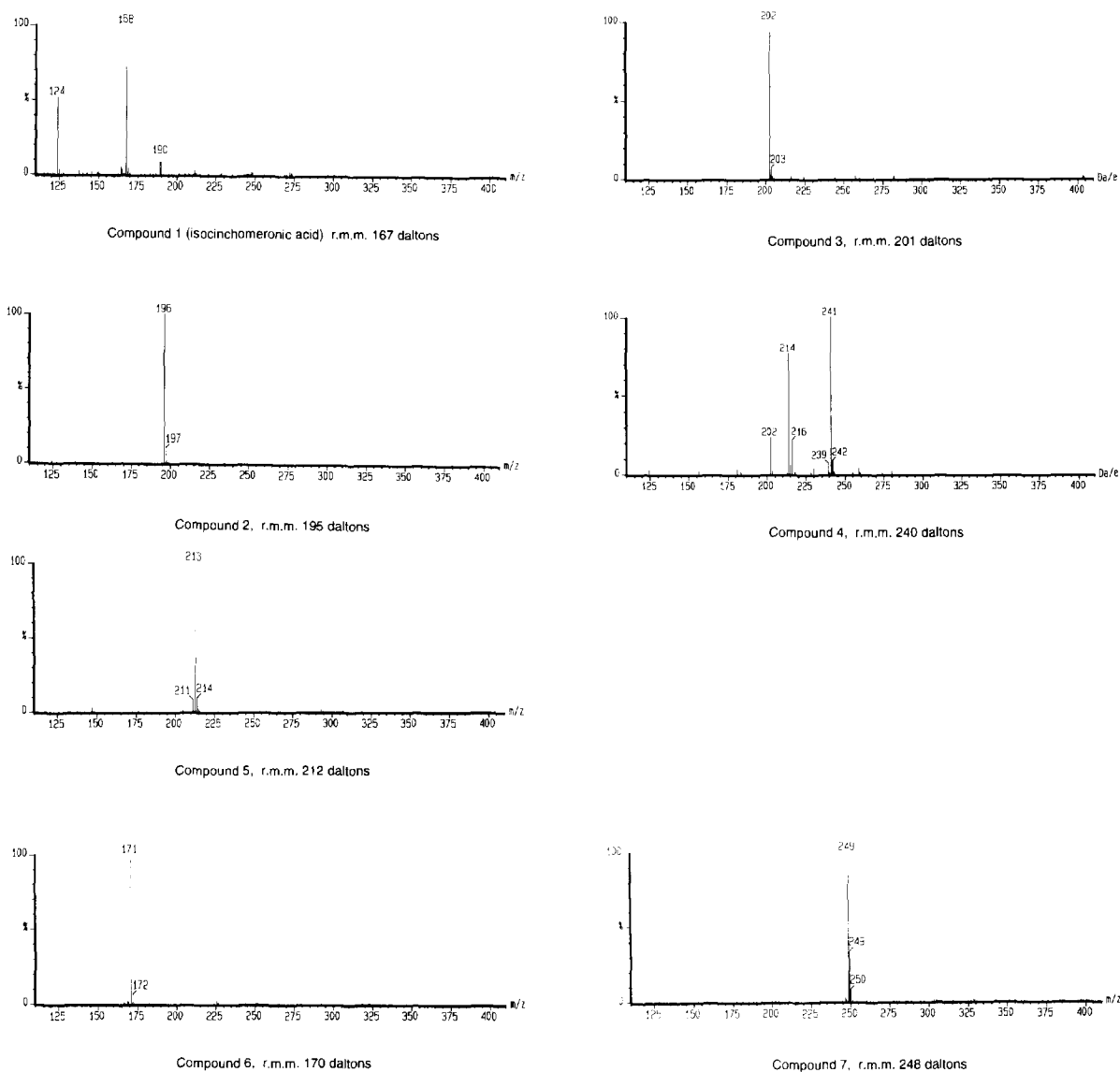
Fig. 4. APCI mass spectra of compounds 1–7.

wherein the reactant and product have the same relative molecular masses.

The mass spectra of compounds 1–7 are shown in Fig. 4. With the exception of compound 4, the mass spectrum of each intermediate shows an abundant protonated molecular ion with minimal fragmentation. With compound 4, however, a fragment of significant abundance at m/z 202 appears, and is consistent with the protonated molecular ion of compound 3, its synthetic pre-

cursor. Under these conditions, it would be difficult to deconvolute the percentage of the ion at m/z 202 that originated from residual (unreacted) compound 3. This could be accomplished through a standard addition approach, or by identifying conditions that would minimize fragmentation of compound 4. Careful selection of the mass spectrometer lens parameters and adjustment of the solvent flow rate into the LC–MS interface has minimized this interference for the

Fig. 5. Mass spectra of 1% (top) and 5% (bottom) spikes of compound 6 in compound 7.

present. Use of softer ionization approaches such as electrospray may eliminate this interference. Attempts using this latter possibility have not yet been explored.

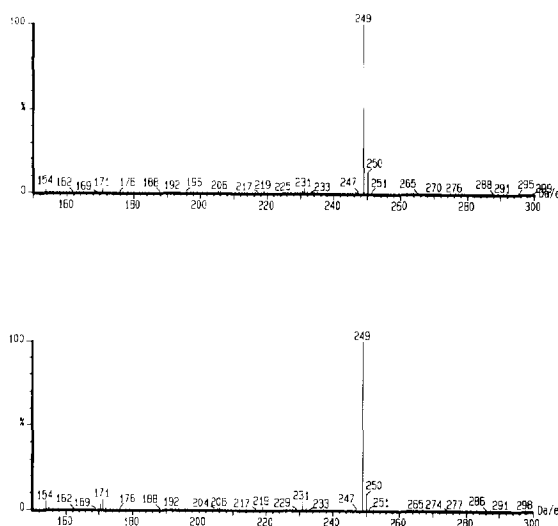To demonstrate the feasibility of this technique, synthetic reaction mixtures of step 6 were prepared. These samples contained the product (compound 7) and 1, 2 and 5% spikes of compound 6 (relative to compound 7). Traditional methodologies were previously unsatisfactory for monitoring this step. Fig. 5 illustrates the mass spectra of mixtures containing 1% and 5% spikes of compound 6 with respect to compound 7. The peak at m/z 171 corresponds to the residual starting material. These spectra represent a reaction mixture near completion; a reaction mixture at an earlier time frame would have a mass spectrum contain-

ing a larger peak at m/z 171 relative to m/z 249, the protonated molecular ion of compound 7, the product.

Quantitative data for 1%, 2% and 5% spikes of compound 6 are shown in Table 1. Target levels of residual starting material are typically 1–2%. If the level of starting material is below the target level, the reaction can be stopped. The data in Table 1 illustrate that 1% and 2% levels of compound 6 are readily distinguishable and that the precision of the method is adequate to serve as a limits test. Another point worth noting is that at the two higher concentrations, the response of compound 6 is slightly lower when present as a mixed standard with compound 7. This quenching may be attributed to a number of sources including the relative proton affinity of each species in the ion source. For quantitative purposes, quenching can be accommodated by matrix matching wherein the standard of the minor component is prepared in a solution containing the reaction product. The slightly higher response of compound 6 in the presence of compound 7 at the 1% level may be attributable to trace levels of compound 6 in the standard of compound 7 used to prepare the solution.

Responses of the mass spectrometer to six replicate injections of a 2% spike of compound 6 in the presence of compound 7 using specific ion monitoring at m/z 249 (product) and 171 (reactant) are illustrated in Fig. 6. The bottom trace in Fig. 6 was generated by digitally smoothing the m/z 171 selected ion trace using a moving average smoothing function — a feature of the mass spectrometer data system. The data listed in Table 1 were obtained after smoothing. The peaks at m/z 249 are off-scale and could not be used for quantita-

Table 1
Quantitative data of compound 6

Concentration (mg ml^{-1}) of compound 6	Relative concentration (%)	Peak area (% RSD^a) of compound 6	Peak area (% RSD^a) of compound 6^b
0.05	1	51 000 (14)	58 000 (15)
0.10	2	115 000 (9)	112 000 (7)
0.25	5	279 000 (7)	255 000 (5)

^{a} % RSD = percent relative standard deviation, $n = 6$.
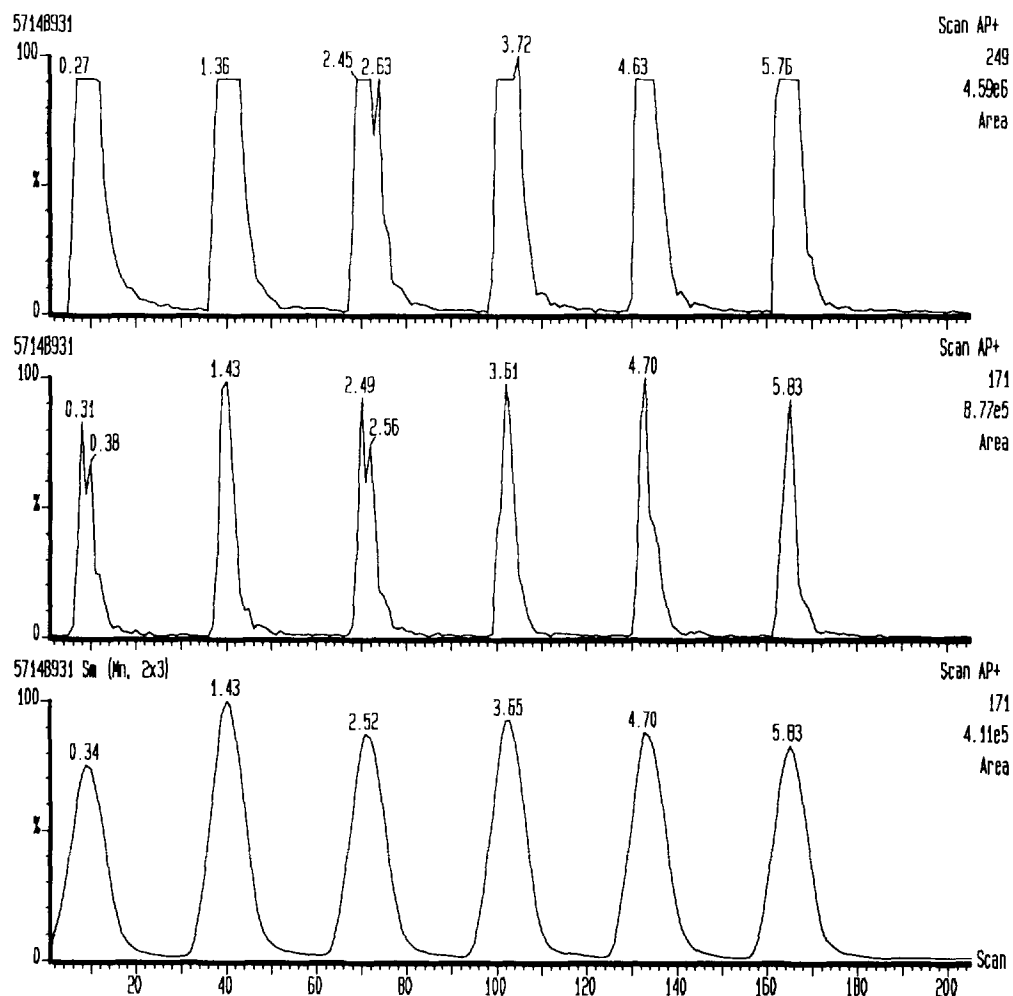^{b} These solutions contanied compound 7, the product of the reaction.

Fig. 6. Response of the mass spectrometer to six replicate injections of a 2% spike of compound 6 in the presence of compound 7 using specific ion monitoring at m/z 249 (product, top) and 171 (reactant, middle). The bottom trace was generated by smoothing the m/z 171 (middle) trace. The numbers at the apex of each peak represent the time in minutes.

tive purposes. These are typical data and illustrate the reproducibility obtainable with this technique.

4. Conclusions

The feasibility of using FIA–MS for monitoring reaction completion has been demonstrated using the CP-93,393 synthetic pathway as a test case. Re-examination of the introduction reveals that FIA–MS does indeed have most of the desirable attributes of the methodology targeted for use in an IPC laboratory. One injection per minute is

clearly achievable (Fig. 6) and quantitative data can be provided in a matter of minutes. No time is needed for re-equilibration of the chromatographic system. Although the monitoring of residual levels of compound 3 with this technique may be difficult, all other synthetic steps in the CP-93,393 synthesis are amenable to FIA–MS analysis and this technique can be considered to be a universal system, albeit with a few exceptions. In addition, preliminary work on other drug candidates has indicated that FIA–MS will be widely applicable. Since most of the bench-top mass spectrometers use Windows-based PC controls,

with a minimum amount of training, IPC laboratories staffed with trained personnel should easily be able to adopt and use FIA–MS to monitor reaction completion.

In terms of ruggedness, a mass spectrometer will potentially have more problems than traditional methodologies used to monitor reaction completion. These instruments require periodic maintenance and must be operated by trained personnel. The vacuum pumps associated with mass spectrometers also require periodic maintenance. If there is a problem with these instruments, a mass spectrometer may require a longer down-time before it is operational again.

The cost of a bench-top mass spectrometer is roughly 3–4 times that of an LC system. If a single FIA–MS system can replace several LC and/or GC systems, this approach becomes competitive economically. In addition, the expense associated with developing chromatographic systems is saved.

Application of FIA–MS to the monitoring of reaction completion has several distinct advantages over traditional methodologies. It is anticipated that this technique will be adopted by IPC laboratories to complement existing equipment and that its use will increase as the cost of mass spectrometers decreases and the skill of IPC personnel increases.

References

[1] P.K. Aldridge, D.H. Burns, J.J. Kelly and J.B. Callis, Proc. Control. Qual., 4 (1993) 155.

[2] J.S. Canham and G.E. Pacey, Anal. Chim. Acta, 214 (1988) 385.

[3] E.C. Huang, T. Wachs, J.J. Conboy and J.D. Henion, Anal. Chem., 62 (1990) 713A.

Fluorimetric flow-injection analysis of total amounts of aldehydes in auto exhaust gas and thermal degradation emission gas with cyclohexane-1,3-dione[1]

Tadao Sakai[a,*], Hideki Nagasawa[a], Harumitsu Nishikawa[b]

[a]Department of Applied Chemistry, Aichi Institute of Technology, Yachigusa, Yakusa-cho, Toyota 470-03, Japan
[b]Gifu Prefectural Health and Environmental Research Center, Yabuta-minami, Gifu 500, Japan

Abstract

A simple flow-injection (FI) spectrofluorimetric method for the assay of total volatile aldehydes in auto exhaust gas and emission gas from thermal degradation was developed. Aldehydes, such as formaldehyde, acetaldehyde, propionaldehyde and n-butyraldehyde, reacted with cyclohexane-1,3-dione (CHD) to form more strongly fluorescent compounds. A two-channel flow system was assembled. Distilled water and 0.02% CHD were delivered at 0.75 ml min^{-1}. The optimum conditions were pH 5 (2.2 M CH_3COONH_4–CH_3COOH buffer solution), reaction temperature 70°C, reaction coil length 0.5 mm i.d. × 7 m, cooling coil length 2 m, sample size 60 μl, excitation and emission wavelengths, 376 nm and 452 nm. Aldehydes in sample gas (10 l) were collected by passing the gas at a flow rate of 0.5 l min^{-1} through two impingers connected in series. 10 ml of methanol was used as an absorbent and diluted sample solution was injected into the carrier stream. The calibration graph was linear in the range 100–1000 ppb. The detection limit was 30 ppb and a sampling frequency of 30 h^{-1} was attained. Relative standard deviation for 10 standard formaldehyde solutions (500 ppb) was 1.5%. This rapid and simple FI method was applied to the determination of the total amount of aldehydes, calculated as formaldehyde, in auto exhaust gas and emission gas from the thermal degradation of polymers.

The method is useful for monitoring aldehyde emissions and investigating the removal effect of aldehydes from various sources.

Keywords: Fluorimetric flow-injection analysis; Aldehydes; Auto exhaust gas; Emission gas; Cyclohexane-1,3-dione

1. Introduction

Aldehydes are present in the exhaust gases of-gasoline-powered vehicles and emission gases from thermal degradation of polymers and other organic compounds. Along with hydrocarbons, aldehydes are important air pollutants, in that they influence human health and plant growth [1].

Formaldehyde in particular is a well-known eye irritant and suspected carcinogen and inhibits active sites of protein. Acetaldehyde also shows a strong chemical activity. Methods for determining trace amounts of formaldehyde in atmospheric air and beverages have been reported [2–6]. Some of the methods mentioned in the literature have been developed as continuous flow-injection (FI) methods for rapid or selective determination of formaldehyde. High performance liquid chromatographic (HPLC) separation of aliphatic aldehydes such as formaldehyde, acetaldehyde, propionaldehyde and heptylaldehyde, has also been proposed [7] and the present authors have reported capillary gas chromatography (GC) with a flame thermionic detector for the selective determination of aldehydes in exhaust gas [8]. Although each aldehyde can be successfully analysed by FI, HPLC and GC, these methods have some drawbacks, i.e. a long reaction time, tedious sample pre-treatment and complicated derivatization.

Although Suzuki [7] has reported that aliphatic aldehydes react with cyclohexane-1,3-dione (CHD) to form fluorecent products, the reaction was time-consuming and tedious.

In this study, different analytical conditions with CHD were optimized for the rapid FI injection determination of volatile aldehydes in several kinds of gases, although individual aldehydes cannot be determined. Moreover, this system is simply and easily assembled.

2. Experimental

2.1. Apparatus

A combined sampling device (Model HS-6, Kimoto Electric, Osaka) was used for sampling gases including aldehydes. The volume of the impinger used was 30 ml and the flow rate was 0.5 l min⁻¹.

A Hitachi Model F-2000 spectrofluorimeter (Tokyo) was used for recording fluorescence spectra and measuring their intensity.

A Taiyo Mini 80 thermostat was used for controlling the derivatization temperature.

2.2. Reagents

2.2.1. CHD

20 g of ammonium acetate and 0.25 g of CHD (Tokyo Kasei Kogyo, Tokyo) were dissolved in 200 ml of distilled water containing 10 ml of acetic acid.

2.2.2. Formaldehyde standard solution

2.86 g of formaldehyde (35% Katayama Kagaku, Osaka) was dissolved in 100 ml of methanol to produce a 1% (w/v) methanolic solution. The stock solution was standardized by titrimetry [9].

2.2.3. Other aldehyde standard solutions

1 g of acetaldehyde (Merck, 99.5%), propionaldehyde or n-butyraldehyde was dissolved in 100 ml of methanol to prepare 1% solution. The stock solution was diluted to an appropriate concentration as required.

2.3. General procedure (batchwise method)

Mix 0.1–0.4 ml of 0.0001% of the standard aldehyde solution and 1 ml of 0.25% CHD in a 10 ml calibrated flask and dilute to the mark with distilled water. Allow to react for 30 min at 50°C in the thermostatted bath. After cooling, measure the relative fluorescence intensity at excitation and emission wavelengths of 375 nm and 452 nm respectively.
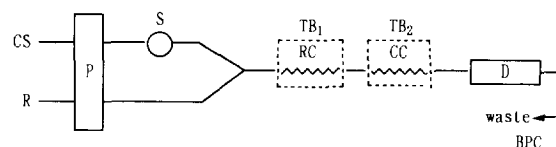
Fig. 1. Flow-injection manifold for aldehyde determination: CS, carrier solution (H₂O); R, 0.02% CHD solution; P, double-plunger micro-pump; S, sample injection (60 μl); RC, reaction coil (0.5 mm × 7 m); CC, cooling coil (0.5 mm i.d. × 2 m); TB, thermostatted bath; TB₁, 70°C; TB₂, 10°C; D, detector (fluorescence spectrophotometer); BPC, back pressure coil (0.25 mm i.d. × 2 m); flow rate 0.75 ml min⁻¹; excitation wavelength, 376 nm; emission wavelength, 452 nm.

2.4. FI procedure

The manifold of the FI system used is shown in Fig. 1. A double plunger micro-pump (Sanuki Kogyo Model DM2U-1026, Tokyo) is used to pump the solutions. Distilled water (carrier) and the reagent solution of 0.02% CHD in ammonium acetate–acetic acid buffer (pH 5) are delivered at a flow rate of 0.75 ml min⁻¹. The samples (60 μl), containing up to 1 ppm aldehyde, are injected into the carrier stream by means of a six-way injection valve to which a volume control loop is attached. The sample and reagent are mixed in a 7 m reaction coil placed in the thermostatted bath (70°C). After cooling the mixture (cooling coil, 2 m long), the relative fluorescence intensity of products is monitored by a spectrofluorimetric detector (Soma Optics Model S-3350, Tokyo) with a micro-flow cell (15 μl). A Sekonic SS-250F flat-bed recorder (Tokyo) is used. The PTFE tubing is 0.5 mm i.d. except for the back-pressure coil which is 0.25 mm i.d. (2 m long).

2.5. Collection of sample gases

The auto exhaust gas and emission gas from thermal degradation of polymer (polybutyl-methacrylate) were collected by drawing the gas through 10 ml of absorbent solution (methanol) in two impingers at a rate of 0.5 l min⁻¹ for 20 min. The solution in the first impinger was diluted 10–1000 fold with distilled water before injection.

3. Results and discussion

3.1. Fluorescence spectra

Aldehydes, such as formaldehyde, acetaldehyde, propionaldehyde and *n*-butyraldehyde, reacted with CHD to form the decahydroacridine-1,8-dione derivatives in the presence of ammonium acetate.

The reaction is as follows:

dione derivatives in the presence of ammonium acetate. The reaction is as follows
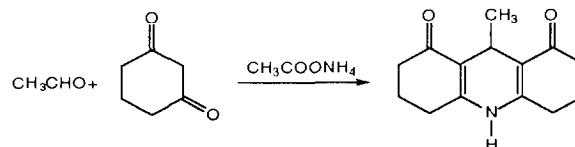
The derivatives gave strong fluorescence. The excitation wavelength was 376 nm and the emission wavelength was 452 nm.

3.2. Batchwise study

The reaction rate between each aldehyde and CHD was very slow and at room temperature the derivatives were not produced.

The effect of reaction temperature was investigated to accelerate the rate for 0.02 ppm of each aldehyde. As shown in Fig. 2, fluorescent derivatives did not form below 40°C. However, the relative fluorescence intensity was enhanced with increasing temperature. In the range 60–70°C, a considerable intensity enhancement was observed. Although higher temperature was favorable for sensitivity, the intensity of the background level
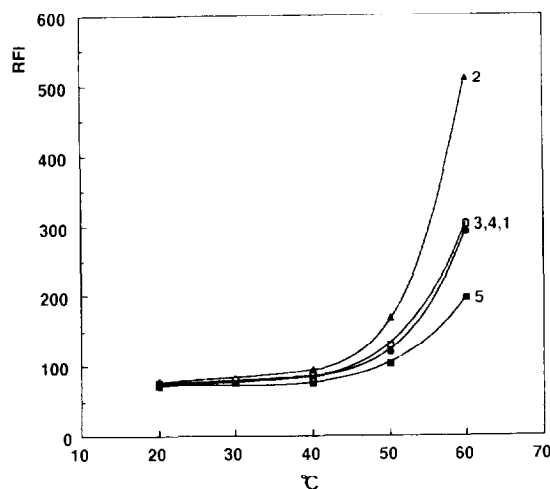
Fig. 2. Effect of reaction temperature in the batchwise method: aldehydes, 0.02 ppm; reagent, 0.025% CHD; buffer, 2.2 M CH₃COONH₄–CH₃COOH (pH 5); reaction time, 30 min; cooling temperature, 10°C; cooling time, 5 min; excitation wavelength, 376 nm; emission wavelength, 452 nm. (1) Formaldehyde; (2) acetaldehyde; (3) propionaldehyde; (4) *n*-butyraldehyde; (5) blank.

Fig. 3. Effect of pH in the batchwise method: aldehydes, 0.02 ppm; reagent, 0.025% CHD; reaction temperature, 50°C; reaction time, 30 min; cooling temperature, 10 °C; cooling time, 5 min; excitation wavelength, 376 nm; emission wavelength, 452 nm. (1) Formaldehyde; (2) acetaldehyde; (3) propionaldehyde; (4) n-butyraldehyde; (5) blank.

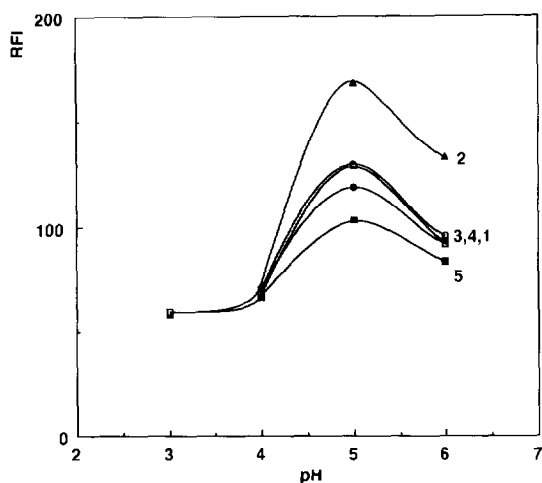increased and also it was difficult to maintain a constant higher temperature. In the batchwise work, 50°C was chosen and the reaction time was fixed at 30 min. The effect of pH on the formation of derivatives was investigated in the range pH 3–6. The result is shown in Fig. 3. The derivatives were not formed below pH 4. At pH 5, the strongest fluorescence intensity was obtained, while at pH 6, the intensity decreased. It is assumed that an excess of electrons from the deprotonation of the ring nitrogen proton would inhibit fluorescence intensity. The effect of CHD concentration was investigated in the range 0.005–0.05%. Although the fluorescence intensity increased with increasing reagent concentration, the background level became excessively large. In this work, 0.025% CHD was used.

3.3. FI study

Although the conditions for the assay of volatile aldehydes by the batchwise method were determined, the method lacked reproducibility and rapidity and the background level was excessively large.

In unstable reaction systems such as this, the introduction of a FI method is favorable. Therefore, in order to determine total aldehydes more rapidly and simply than with the batchwise method, the FI system with spectrofluorimetric detection, as shown in Fig. 1, was investigated.

3.4. Effect of reagent concentration

The effect of the CHD concentration on fluorescence was studied for 1 ppm formaldehyde. A 2.2 M CH_3COONH_4–CH_3COOH solution buffered at pH 5 was used for preparing the reagent solution. The concentration of CHD was varied from 0.005 to 0.025%. The peak height increased with increasing reagent concentration. However, in this work, 0.02% CHD was used to obtain an appropriate peak signal and to maintain a lower background intensity.

3.5. Effect of temperature on the formation of fluorescence derivatives

Although 50°C was chosen in the batchwise method because of the ease of controlling temperature, the formation of derivatives was incomplete at 50–60°C in the FI system. Above 70°C, strong signals were obtained. For sensitive determination of aldehydes, 75°C was preferable. However 70°C was chosen to obtain constant peak heights. Because slight variations in temperature gave a larger error, reproducibility became poorer above 70°C.

3.6. Effect of flow rate and injection volume

The flow rate of the reagent solution was varied from 0.5 to 1 ml min^{-1} (Fig. 4). When the flow rate increased, the peak height decreased because the reaction rate was low and the formation of fluorescence derivatives at the faster flow rate was insufficient. A flow rate of 0.75 ml min^{-1} was used.

The injection volume was varied in the range 20–100 μl. A larger volume was suitable for greater sensitivity. However, a volume of 60 μl was used for rapid determination.

3.7. Effect of the reaction coil and cooling coil lengths

The effect of the length of the reaction coil was examined. The coil length was varied within the range 1–7 m. With lengths greater than 4 m, the peak height greatly increased. For good sensitivity without sacrificing sampling frequency, a 7 m reaction coil length was used. After reaction at 70°C, it was necessary to cool the mixture in the cooling bath to obtain reproducible signals. The effect of the length of the cooling coil was studied in the range 1–3 m. In general, an increase in coil length gives a lower peak height because of dispersion, but in this case the peak height increased slightly with increase in length. It is assumed that the reaction rate was low. Accordingly, a 2 m cooling coil was used.

3.8. Calibration graphs

Fig. 5 shows calibration graphs for aldehyde determinations in the range 100–400 ppb at 70°C, but the linearities were good up to 1000 ppb aldehydes when 60 μl portions of the standard solutions were injected. The slopes for both

Fig. 5. Calibration graphs for aldehyde derivatives with CHD: sample size, 60 μl; reagent, 0.02% CHD; buffer, 2.2 M CH_3COONH_4–CH_3COOH (pH 5); reaction temperature, 70°C; reaction coil, 0.5 mm i.d. $\times$ 7 m; cooling temperature, 10°C; cooling coil, 0.5 mm i.d. $\times$ 2 m; flow rate, 0.75 ml min^{-1}; excitation wavelength, 376 nm; emission wavelength, 452 nm. (1) Formaldehyde; (2) acetaldehyde; (3) propionaldehyde; (4) n-butyraldehyde.

formaldehyde and acetaldehyde were large compared to those of propionladehyde and n-butyraldehyde. Since formaldehyde is a representative compound for the aldehydes and the sensitivity was best in its calibration graphs, the amount of aldehydes in the gases was calculated as formaldehyde in this study. Fig. 6 shows the flow signals for formaldehyde standard solution and diluted sample solutions in duplicate. The relative standard deviation was 1.5% for 10 runs with 500 ppb formaldehyde solution. The sample frequency was 30 samples h^{-1} in the proposed manifold. Although the FI method does not have a separating function for each aldehyde, it is acceptable for determining the total amount of these volatile aldehydes.

3.9. Determination of total aldehydes in auto exhaust gas and emission gas from thermal degradation

In previous reports [5–8], trace amounts of formaldehyde in atmospheric air and beverages and of aliphatic aldehydes such as formaldehyde,
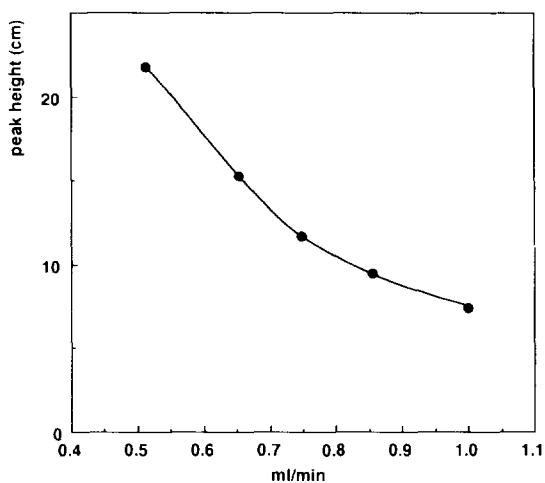

Fig. 4. Effect of flow rate in the FI method: formaldehyde, 1 ppm; sample size, 60 μl; reagent, 0.02% CHD; buffer, 2.2 M CH_3COONH_4–CH_3COOH (pH 5); reaction temperature, 70°C; raction coil, 0.5 mm i.d. $\times$ 7 m; cooling temperature, 10°C; cooling coil, 0.5 mm i.d. $\times$ 2 m; excitation wavelength, 376 nm; emission wavelength, 452 nm.
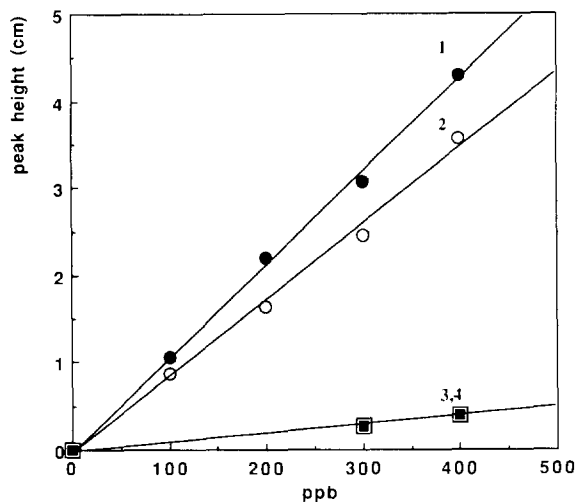
acetaldehyde and butyraldehyde have been determined sensitively and selectively. These methods are useful only for formaldehyde determination, however, and lack rapidity. In studies of atmospheric pollutants, however, it is very important to determine and monitor the total amount of volatile aldehydes, which are important environmental pollutants, as well as hydrocarbons, exhausted in air. The proposed FI method was applied to the determination of the total amount of volatile aldehydes in several kinds of gases exhausted under different combustion conditions. Up to 10 equivalents of ketones such as acetone and 2-butanone did not interfere with the determination of 1 ppm formaldehyde. The results obtained are shown in Table 1. The collection efficiency of the sample gas in the first impinger was 99.8%. In the case of the thermal degradation emission gas of polybutylmethacrylate (PBM), it

Table 1
Analytical results of total aldehydes calculated as formaldehyde in various gas samples

Samples	Found[a]	RSD (%)
Auto exhaust A	4.4 ppm	1.23
Auto exhaust B	10.5 ppm	1.74
Emission gas from thermal degradation of PBM[b]		
100°C	N.D.	
300°C	350 ppm	0.77
500°C	716 ppm	2.22
700°C	332 ppm	2.86

[a] Average of 3 determinations
[b] Polybutylmethacrylate.
N.D., not detected.

was found that the amount of aldehydes evolved peaked at 500°C. Also, it was possible to monitor the amount of aldehydes evolved at different engine speeds. Consequently, it is possible to apply the FI method for evaluating an engine function and for investigating thermal degradation conditions of polymers and other organic compounds.

Fig. 6. Flow signals for formaldehyde standard and sample solutions: sample size, 60 μl; reagent, 0.02% CHD; buffer, 2.2 M CH_3COONH_4–CH_3COOH (pH 5); reaction temperature, 70°C; reaction coil, 0.5 mm i.d. × 7 m; cooling temperature, 10°C; cooling coil, 0.5 mm i.d. × 2 m; flow rate, 0.75 ml min^{-1}; excitation wavelength, 376 nm; emission wavelength, 452 nm. 1 Formaldehyde: (1) 0.2 ppm; (2) 0.4 ppm; (3) 0.6 ppm; (4) 0.8 ppm; (5) 1 ppm. (S_1) Auto exhaust A; (S_2) auto exhaust B; (S_3) emission gas from PBM at 300°C; (S_4) 500°C; (S_5) 700°C.

4. Conclusion

Volatile aldehydes, such as formaldehyde and acetaldehyde, are exhausted from gasoline-powered vehicles and produced by thermal degradation of various polymers and thereby become important air pollutants. It is very important to monitor and decrease the amounts of these exhaust gases to preserve our atmospheric environment. Although this system does not have a separating function for the analysis of each aldehyde, the FI method proposed here can be applicable for the rapid and reproducible determination of total volatile aldehydes.

References

[1] J.A. Swenberg, W.D. Kerns, R.J. Michell, E.J. Gralla and K.L. Pavkov. Cancer Res., 40 (1980) 3398.
[2] S. Steinberg and I.R. Kaplan, Int. J. Anal. Chem., 18 (1984) 253.

[3] M. Koga, M. Murata, M. Maeda and M. Takagi, Bunseki Kagaku, 43 (1994) 1027.

[4] R. Goebel, A. Krug and R. Kellner, Fresenius' J. Anal. Chem., 347 (1993) 491.

[5] H. Tsuchiya, S. Ohtani, K. Yamada, M. Akagiri, N. Takagi and M. Sato, Analyst, 119 (1994) 1413.

[6] Y. Maeda, X. Hu, S. Itou, M. Kitano, N. Takenaka, H. Bandow and M. Munemori, Analyst, 119 (1994) 2237.

[7] Y. Suzuki, Bunseki Kagaku, 34 (1984) 314.

[8] H. Nishikawa, T. Hayakawa and T. Sakai, Bunseki Kagaku, 36 (1986) 381.

[9] Japan Pharmaceutical Society (Eds.), Eisei Shiken-hou Chuukai, (Standard Methods of Analysis for Hygienic Chemists - with commentary), Kinbara Publishing, Tokyo, 1990.

Determination of ultra-trace amounts of arsenic(III) by flow-injection hydride generation atomic absorption spectrometry with on-line preconcentration by coprecipitation with lanthanum hydroxide or hafnium hydroxide[1]

Steffen Nielsen, Jens J. Sloth, Elo H. Hansen*

Chemistry Department A, Technical University of Denmark, Building 207, DK-2800 Lyngby, Denmark

Abstract

A time-based flow-injection (FI) procedure for the determination of ultra-trace amounts of inorganic arsenic(III) is described, which combines hydride generation atomic absorption spectrometry (HG-AAS) with on-line preconcentration of the analyte by inorganic coprecipitation–dissolution in a filterless knotted Microline reactor. The sample and coprecipitating agent are mixed on-line and merged with an ammonium buffer solution, which promotes a controllable and quantitative collection of the generated hydroxide on the inner walls of the knotted reactor incorporated into the FI–HG-AAS system. Subsequently the precipitate is eluted with 1 mol l^{-1} hydrochloric acid, allowing ensuing determination of the analyte via hydride generation. The preconcentration of As(III) was tested by coprecipitation with two different inorganic coprecipitating agents namely La(III) and Hf(IV). It was shown that As(III) is more effectively collected by lanthanum hydroxide than by hafnium hydroxide, the sensitivity achieved by the former being ≈ 25% better. With optimal experimental conditions and with a sample consumption of 6.7 ml per assay, an enrichment factor of 32 was obtained at a sample frequency of 33 samples h^{-1}. The limit of detection (3σ) was 0.003 $\mu g\ l^{-1}$ and the precision (relative standard deviation) was 1.0% ($n = 11$) at the 0.1 $\mu g\ l^{-1}$ level.

Keywords: On-line preconcentration by coprecipitation–dissolution; Coprecipitation with hydroxides of lanthanum and hafnium; On-line addition of the coprecipitant; Flow-injection hydride generation atomic spectrometry; Arsenic(III) assay

1. Introduction

* Corresponding author. Fax: +45 45 88 31 36; e-mail: ehh@kemi.dtu.dk

In 1994, Tao and Hansen [1] for the first time introduced a procedure for on-line flow-injection (FI) preconcentration, in which ultra-trace amounts of the analyte (Se(IV)) were coprecipitated with an inorganic coprecipitant, i.e.

La(OH)₃. The preconcentration procedure combined on-line coprecipitation–dissolution in a knotted Microline reactor and hydride generation (HG) of the dissolved concentrate, the detection being achieved by AAS (quartz tube). The elegant aspect of this procedure is that the inorganic precipitate is easily dissolved in dilute acid (1 mol l⁻¹ HCl), which is also the required medium for the ensuing hydride generation reaction. With such an approach an ordinary FI–HG-AAS system without preconcentration is readily extendable to a time-based FI–HG-AAS system with on-line preconcentration. In their procedure, Tao and Hansen added the coprecipitating agent off-line by spiking each sample before the samples were introduced into the FI system. Recently, this procedure has been improved by facilitating on-line mixing of sample and coprecipitating agent [2]. As was shown, the results with on-line addition of the coprecipitant yielded similar results to those with off-line addition. However, the more automated FI system is obviously preferable as the sample manipulations are significantly reduced. As knowledge of how to optimally control and exploit the method of on-line preconcentration by coprecipitation–dissolution is still insufficient, the present methodological study is therefore devoted to obtaining a better understanding of the processes involved, thereby allowing identification of the significant operational parameters and devising means for their optimization. For the very same reasons, aqueous standards were applied throughout the experimental work.

The optimization procedure is illustrated for the determination of ultra-trace amounts of As(III) by coprecipitation with two different agents, namely La(III) and Hf(IV). According to the literature [3,4] these copre-cipitants are interesting as they have both been shown to coprecipitate As(III) quantitatively in batch methods. Further, the hydroxides of these coprecipitants, La(OH)₃ and Hf(OH)₄, are readily dissolved in dilute acid.

2. Experimental

2.1. Apparatus

A Perkin-Elmer Model 2100 atomic absorption spectrometer was used in combination with a Perkin-Elmer Model FIAS-400 flow-injection unit (equipped with two individually controlled peristaltic pumps and a five-port FI valve), with hydride generation accessories (the gas–liquid separator used in the chemifold was a Perkin-Elmer W-configuration unit). An arsenic hollow cathode lamp (S. & J. Juniper, Harlow, UK) was used at a wavelength of 193.7 nm with a spectral bandpass of 0.7 nm, and was operated at 9 mA. The temperature of the quartz atomizer cell was set at 900 °C. Special care was taken to make the conduit between the outlet of the gas–liquid separator and the quartz atomizer cell as short as possible (≈ 6 cm). The filterless knotted reactor precipitate collectors were made from 0.5 mm i.d., 1.8 mm o.d. Microline tubing (cross-linked ethyl vinyl acetate) by tying interlaced knots (the optimal length of the knotted reactor, L_{KR}, was 200 cm). The knots were made with approximately 5 mm diameter loops. All the other reaction coils, connections and conduits in the FI manifold (Fig. 2) consisted of 0.5 mm i.d. PTFE (polytetrafluoroethylene) tubing. The output signals were processed with a time constant of 0.5 s in the peak-height mode and recordings from the graphics screen were printed out by an Epson Model FX-850 printer. The actuation times of the injector valve and the two pumps were programmed with the use of the FI software of the Model 2100 atomic absorption spectrometer.

2.2. Reagents and standard solutions

All the reagents were of analytical-reagent grade, and distilled water was used throughout. Sodium tetrahydroborate solution (1.50% (m/v) in 0.05 mol l⁻¹ sodium hydroxide) was prepared fresh daily. Lanthanum nitrate solution (0.50% (m/v)) was made by dissolving 0.6662 g of lanthanum nitrate hexahydrate in 100 ml of distilled water. Hf(IV) solution (1.00%) was prepared by dissolution of 1.4869 g of HfOCl₂ in 100 ml of
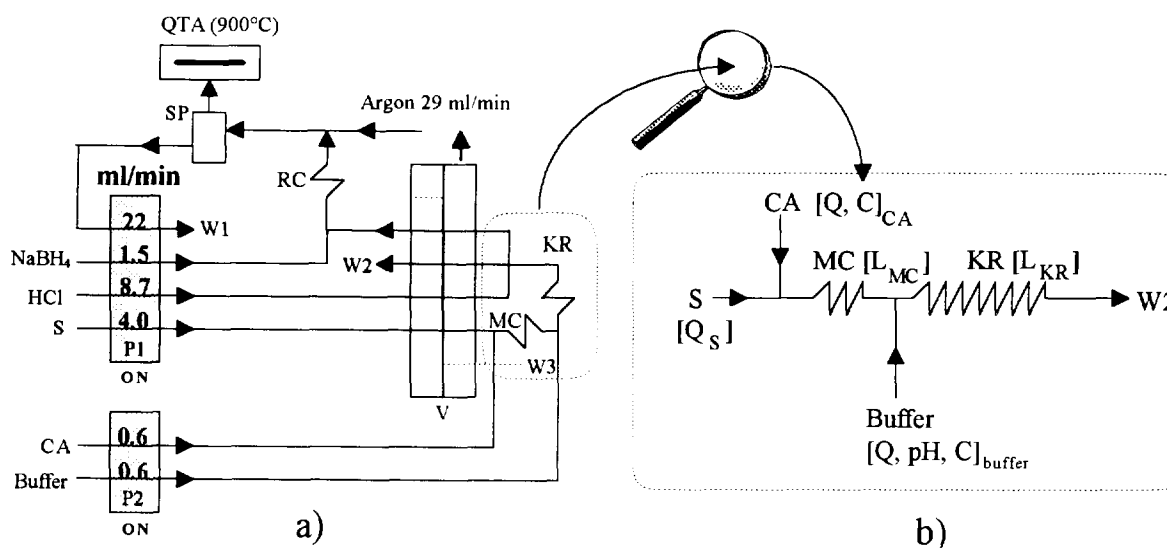
Fig. 1. (a) Schematic diagram of the time-based FI–HG-AAS system for on-line coprecipitation–dissolution as shown in the loading (precipitating) stage. The pumping rates depicted are the eventually optimzed values; S, sample solution; CA, coprecipitation agent; QTA, quartz cell; Ar, argon; MC, mixing coil; RC, reaction coil; KR, filterless knotted reactor; SP, gas–liquid separator; P1 and P2, peristaltic pumps; V, valve; W, waste. (b) Identification of the operational parameters which influence the coprecipitation procedure. Q, C and L refer to flow rates, concentrations and lengths, respectively.

distilled water. The buffer solution, made freshly every day, was in all instances 0.3 mol l^{-1} ammonium chloride adjusted to the appropriate pH by addition of 0.3 mol l^{-1} ammonia. Standard solutions of As(III) for calibration were prepared by three-stage aqueous dilutions of a 1000 mg l^{-1} stock solution, which was made by dissolving 1.724 g of NaAsO$_2$ in 25 ml of 20% (w/v) potassium hydroxide, followed by neutralization with 20% (v/v) sulphuric acid using phenolpthalein as indicator, finally making the sample solution up to 1000 ml with 1% (v/v) sulphuric acid.

All glassware was soaked for at least 24 h in 1 M nitric acid, and finally rinsed in distilled water before use.

2.3. Operational procedure

The time-based FI–HG-AAS system with on-line addition of the coprecipitant, La(III), is shown in Figs. 1 and 2, depicting the optimized experimental parameters. In the precipitation procedure (Fig. 1a), the sample (S), hydrochloric acid and sodium tetrahydroborate solutions were introduced by pump 1, and the buffer and coprecip-

itating agent (CA; either La(III) or Hf(IV)) were delivered via pump 2. During the precipitation sequence both pumps were activated for a period of 100 s. The sample and coprecipitant were premixed in the mixing coil (MC) of length (L_{MC}) of 6 cm, and subsequently merged with the buffer solution at the entrance to the knotted reactor (KR) which had a length (L_{KR}) of 200 cm. The precipitate, which was formed instantaneously after the merging point of the KR, was collected on the inner walls of the KR. The effluent emerging from the reactor was discarded. Simultaneously, the acid was pumped through the by-pass of the rotor of the valve and directed into the hydride generation system. During this stage, the baseline for the final readout was established.

At the end of the precipitation period pump 2 was stopped, and the valve was actuated automatically from the fill mode to the inject mode for a period of 10 s (dissolution–hydride-generation procedure; Fig. 2a), by which the acid was introduced directly into the KR where the precipitate adhering to the inner walls of the reactor was dissolved. This concentrated plug zone was directed from the KR to the hydride generating
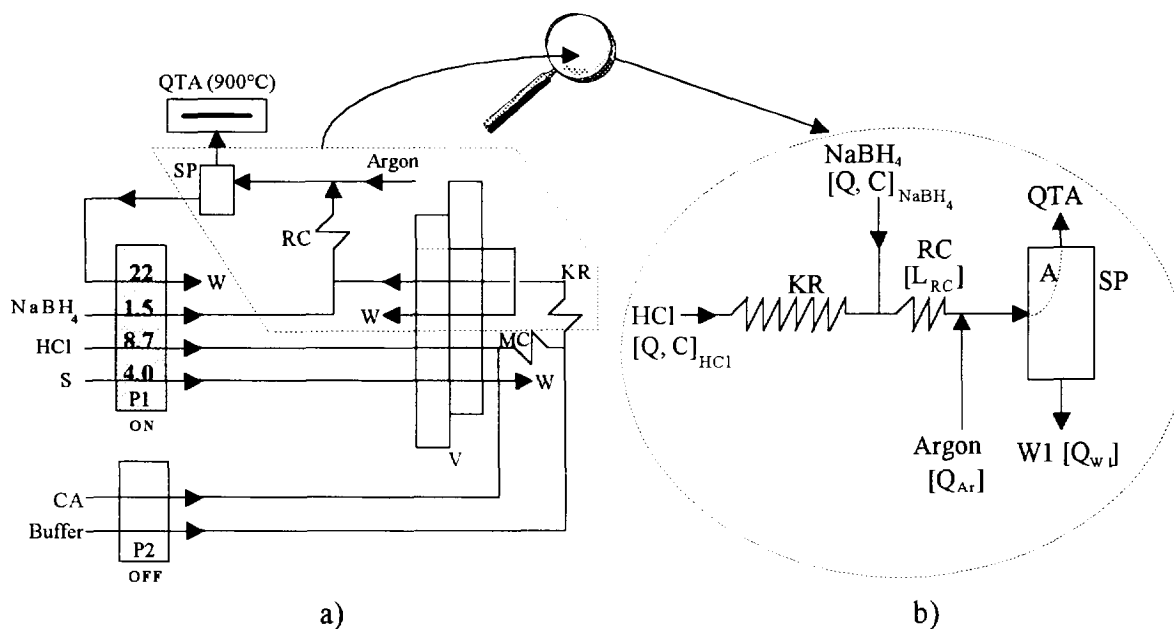
Fig. 2. (a) Schematic diagram of the time-based FI–HG-AAS system as shown in the dissolution–hydride generation stage. (b) Identification of the operational parameters which influence the dissolution–hydride generation procedure. For explanation of symbols and abbreviations. see Fig. 1.

system, where the analyte was merged with a reducing solution of sodium tetrahydroborate. After passing through a reaction coil (RC) of length $L_{RC} = 60$ cm, the gas–liquid mixture was guided into the gas–liquid separator (SP) in which the arsine and the evolved hydrogen were separated from the liquid phase and swept into the atomizer cell by a steady argon carrier flow. The absorption signal was then recorded. The waste from the gas–liquid separator, which included unreacted sodium tetrahydroborate, acid and some argon, was removed by aspiration. The elution stage lasted for 10 s. During this interval the sample solution was interchanged so that the remainder of the previous sample in the sample pump tube could be effectively washed out and the next sample kept ready for precipitation.

3. Results and discussion

3.1. Basis of the optimization procedure

The interpretation of the peaks recorded by the AAS instrument formed the basis for an effective optimization of the FI preconcentration procedure, as the peaks reflect the effect and efficiency of the preconcentration technique incorporated into the FI system, that is, the coprecipitation–dissolution process, and, following elution, the chemical and/or physical modifications of the analyte in the concentrate into a detectable species via hydride generation and subsequent gas–liquid separation. However, in order to exploit a method completely and thereby reach the limit of detection of the detector concerned, the optimization procedure must be performed most systematically. Thus the optimization was controlled by estimating the gradient of every single peak, that is, the ratio between the area (I) and the absorbance (A) of the signals was evaluated. As the maximum effect of preconcentration was desired, resulting in maximum peak areas, the FI procedure was optimized so as to obtain the lowest I/A ratios. To achieve this end it was imperative that the final

optimization of the FI procedure was completely controllable and reproducible.

Since the coprecipitation and dissolution/hydride generation processes are completely separate and individual, they will also be treated as such in the following, where the optimization procedure will be described by firstly setting the present investigation into context with current knowledge, and secondly by identifying and detailing the individual parameters/factors important to the two individual processes and the overall operation. The optimization procedure is thus based on a factorial approach, where the response function was the minimization of the I/A ratio.

3.2. Introduction to the procedure of coprecipitation

First of all, as the time available for the coprecipitation process under dynamic conditions is limited, typically from a few seconds to a few tenths of a second, this process must happen extremely fast to allow a quantitative recovery of the analyte. Furthermore, this requires a close and compatible interaction between the precipitate collector and the precipitate generated, i.e. the character of the precipitate. From previous work [2] the authors achieved some very important experiences with on-line coprecipitation in KRs, the geometrical design of which leads to the generation of a strong secondary flow pattern, which promotes quantitative coprecipitation although the KR is filterless. Thus, the material of the KR is a very important factor. In order to achieve quantitative coprecipitation of the analyte, the KR has to be tightly knotted, the material of its construction must have a high affinity to the precipitate formed, and the inorganic precipitate must in turn be gelatinous to facilitate the entrapment of the analyte species. Unfortunately, the number of commerically accessible tubular polymer materials with a high hydrophilic character and suitable dimensions (preferably of an inner diameter (i.d.) of about 0.5–0.7 mm [5]) is rather restricted. However, in the experimental work with on-line coprecipitation of Se(IV), where the coprecipitant and sample were mixed on-line, the results strongly indicated that the collection of the

analyte in $La(OH)_3$ in a knotted Microline reactor $(i.d._{KR} = 0.50$ mm) was quantitative below a sample flow rate of $Q_S = 6.4$ ml min^{-1} [2], although the hydrophilic character of Microline (vinyl acetate) is not particularly high. Since no better material appears to be available, this material was also selected for use herein to make the KRs.

Another important factor, as identified previously [2], is the total flow rate through the KR. Hence, it is not sufficient to optimize the capacity of the KR. This is due to the fact that if the flow rate through the KR is too high the efficiency of adherence of the precipitate on the inner walls of the KR decreases condsiderably, and with that the enrichment factor (EF) and the concentration efficiency fator (CE) decrease too [2]. With this experience in mind a sample flow rate of $Q_S = 4.0$ ml min^{-1} seemed to be a rational choice. Further, it is essential that the developed FI procedure should possess practical applicability, and therefore the preconcentration period (T_c) was limited to $T_c = 100$ s, which in turn determined the obtainable value of EF. Thus, at $T_c = 100$ s and with a subsequent elution period (T_E) of 10 s, which is sufficient for cleaning the system between each analytical cycle, the sampling frequency (f) became 33 h^{-1}.

From a practical point of view the FI procedure should be able to handle samples in acidic media, since environmental samples are typically preserved by addition of acid to a pH level of ≈ 3. Therefore all aqueous standards were prepared at a pH of 3.

3.3. Optimization of the experimental parameters for the on-line preconcentration by coprecipitation of As(III) with La(III)

The experimental parameters which have an influence on the coprecipitation process are identified in the inset of Fig. 1, (part b, where brackets refer to the individual parameters), and comprising the concentration of the coprecipation agent La(III) (C_{CA}), the pumping rate of this constituent (Q_{CA}), the characteristics of the buffer (pH, C_0 and $Q)_{Buffer}$, and the lengths of the mixing coil (L_{MC}) and KR (L_{KR}). To achieve an effective preconcentration procedure and to exploit the

capacity of the KR, these parameters must be optimized very carefully, because the process of coprecipitation is very sensitive under the dynamic conditions prevailing, and because the residence time of the coprecipitation media in KR is only of the order of a few seconds. Consequently, every single liquid element must be accounted for during the process of coprecipitation.

As AS(III) is to be determined at ultra-trace levels through coprecipitation under weakly alkaline conditions by mixing the sample with large excesses of La(III) and ammonium buffer, it is preferential if the flow rates of these constituents (Q_{CA} and Q_B) can be kept as low as possible in order to avoid excessive dilution of the sample and to limit the flow rate through the KR. Experimentally it was found that conditions were optimal for Q_{CA} and $Q_B \approx 0.5$–0.6 ml min^{-1}.

Since the sample and the coprecipitant are mixed on-line prior to entering the KR, it might be expected that it is necessary to utilize a certain pathlength in order to effect this, but, as was also verified in previous work [2], the shortest possible length of MC (here corresponding to 6 cm) was, in fact, sufficient. This is not surprising considering that the ratio of the flow rates of the coprecipitant and the sample was 1/8.

Using $Q_{CA} = Q_B = 0.5$ ml min^{-1} and a sample flow rate Q_S of 4.0 ml min^{-1}, the residence time (T_{KR}) of the coprecipitating media in a KR of L_{KR} 200 cm and i.d.$_{KR}$ 0.5 mm will be ≈ 4.7 s. Considering this very short residence time, the effects of the pH value of the buffer (the concentration of which was fixed at $C_{OB} = 0.3$ M in order to maintain a high buffering capacity) and the La(III) concentration (C_{CA}) were closely investigated. The results are shown in Fig. 3.

As can be seen, optimal conditions for preconcentrating As(III) by collecting the analyte in the generated lanthanum hydroxide are found in a fairly narrow pH interval, i.e. $9.50 < pH_B < 9.70$, while the concentration of the coprecipitating agent should be in the range $90 < C_{CA} < 180$ ppm. This clearly demonstrates that the process or mechanism of coprecipitation is critical under the dynamic conditions, particularly the pH_B value, which for off-line applications has been found to be optimal over a much wider range, i.e. 9–11 [3].

As is apparent from Fig. 3, the efficiency of collection decreases at higher concentrations of La(III) and/or higher values of pH_B. A reasonable explanation might be that large particles are formed under these conditions, whereby the efficiency of adherence to the inner walls of KR is reduced as larger particles are dislodged and carried to waste (W2, Fig. 2) [1]. Thus, it is essential that the inorganic precipitate is generated in the form of small, curdy particles which willingly adhere to hydrophilic Microline tube. During the following investigations $pH_B = 9.60$ and $C_{CA} = 100$ ppm were used.

The optimization of the capacity of the KR is very important. Its i.d. must necessarily be small, i.e. i.d.$_{KR} \approx 0.50$–0.70 mm, in order to allow for the creation of a strong secondary flow pattern within it. Settling for an i.d. of 0.5 mm, the optimal capacity was therefore determined by optimizing the length of the reactor, L_{KR}.

For $L_{KR} < 175$ cm, the collecting capacity of KR was found to increase almost linearly, while at lengths exceeding 175 cm it remained practically constant (Fig. 4). These results contain some very interesting information about the coprecipitation process. Thus, by depicting the normalized absorbances (A/A_{AV}) for a given length of KR, where A_{AV} (here $A = 0.229$) is the average value of
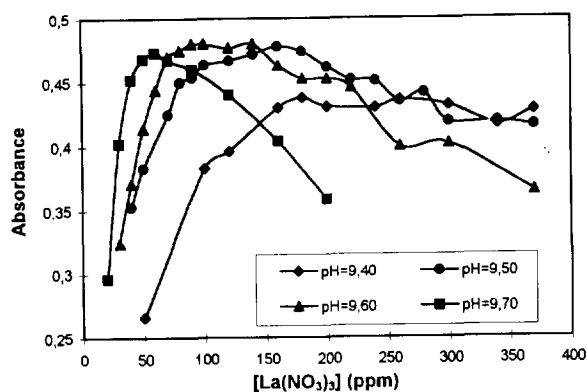

Fig. 3. The influence of the La(III) concentration on the efficiency of the coprecipitation process at different pH values as measured by the recorded output signals. All measurements were made on As(III) standards at a concentration of 0.50 μg l^{-1} at a sample loading time (T_C) of 100 s and for $L_{KR} = 200$ cm. Operational conditions are otherwise as given in Figs. 1 and 2.
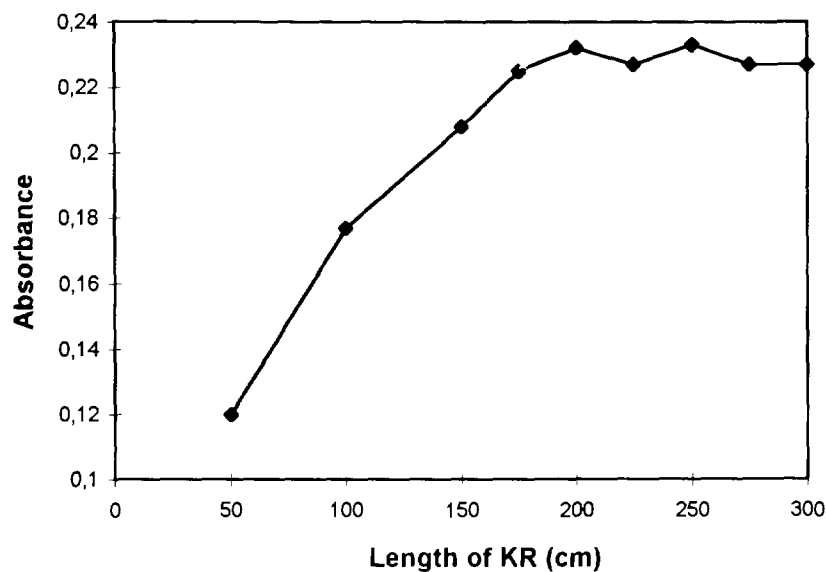
Fig. 4. Effect of the length of the KR on the recorded output signal as determined for a 0.20 μg l^{-1} As(III) standard. $T_C = 100$ s and $L_{KR} = 200$ cm. Operational conditions are otherwise as given in Figs. 1 and 2.

the absorbances obtained for $L_{KR} \geq 175$ cm, an indication for the concentration distribution of the analyte within the KR at the end of the coprecipitation period can be obtained, provided that it can be assumed that the composition of the precipitate is generated uniformly throughout any cross-section of the KR–an assumption which seems reasonable according to the flow pattern in the KR, and becuse the coprecipitation takes place on-line. Such a concentration distribution curve is shown in Fig. 5 for a reactor of length 200 cm (other experimental parameters are shown in the Figure legend). The highest A/A_{AV} value (concentration) was obtained at a length of ≈ 50 cm, and in fact 57% of all the precipitate is collected within this part of the reactor, while only a minor fraction is contained in that part of the reactor which exceeds 100 cm. This observation strongly indicates that the length of MC (6 cm) is sufficient for mixing sample and coprecipitant on-line, and that the coprecipitation process takes place very quickly. Furthermore, as the signals are constant for $L_{KR} \geq 175$ cm, the coprecipitation is obviously quantitative for a reactor of 200 cm. Consequently, the affinity between the Microline reactor and the precipitate La(OH)$_3$ is adequate. To keep the KR as short as possible,

and thereby avoid unneccesary back pressure during the period of coprecipitation and in the moment of dissolution, $L_{KR} = 200$ cm was selected. Back pressure in the FI system might possibly cause fluctuations resulting in non-reproducible results, but with the conditions used no such problems were encountered, which confirms that lanthanum hydroxide is readily dissolved in 1 M HCl.

The last parameter of the coprecipitation sequence to be optimized was the sample loading period (T_C). Obviously, for increasing values of T_C the amount of precipitate increased: thus it was found that the preconcentration effect increased almost linearly up to $T_C = 150$ s, which indicates that the collection is quantitative. However, long sample loading times will—for a fixed value of the sample flow rate, which, as stipulated earlier, for practical reasons was fixed at 4.0 ml min^{-1}—lead to lower sampling rates. A T_C value of 100 s was therefore adopted, although only two-thirds of the capacity of the reactor was thus exploited.

The time that the coprecipitating media takes to reach equilibrium, T_{Eq}, may be found by extrapolating the curve for absorbance (A) vs. T_C to $A = 0$ or by calculating the line of regression.
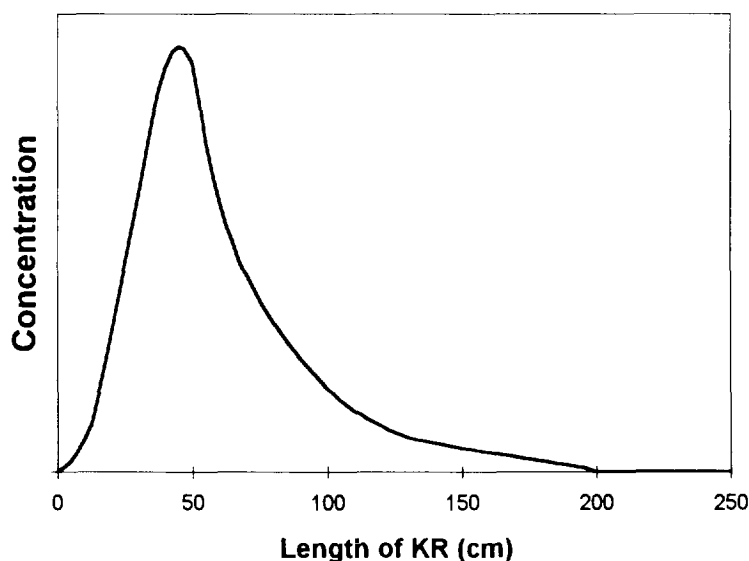
Fig. 5. Calculated concentration distribution of the analyte (As(III)) in a KR of 200 cm at the end of the coprecipitation period, using an As(III) concentration of 0.20 µg l⁻¹. Operational conditions are otherwise as given in Fig. 4.

Using the latter approach T_{Eq} was determined to be -2.4 s. Of course, a negative value of T_{Eq} is impossible, but this value again emphasises that the coprecipitation happens very quickly and virtually instantaneoulsy.

3.4. Optimization of the experimental parameters for the on-line dissolution of the precipitate in the KR and hydride generation of As(III)

To achieve a high sensitivity via the ensuing hydride generation procedure, the precipitate in the KR must be dissolved immediately to obtain a plug zone of concentrate. Thus the approach of dissolution–hydride generation will be virtually identical to the common FI–HG-AAS system without preconcentration. Therefore the flow rate, Q_{HCl}, and the concentration of the acid, C_{HCl}, are very important factors. Apart from the fact that the geometrical design of the KR promotes the conditions for achieving an effective preconcentration, it also, via the inherent secondary flow pattern, facilitates effective dissolution. Consequently, the degree of dispersion and the extent of inhomogeniety of the concentrate formed by the dissolution process are both limited, which in turn

promotes the conditions for achieving low I/A values via effective hydride generation and strict control of the FI processing of the concentrate from the KR to the quartz tube atomizer.

The parameters which are of importance for the dissolution–hydride generation procedure are identified in Fig. 2b. Optimization of this part of the assay sequence is well described elsewhere [5,6], and therefore only a few comments will be linked to the hydride generation part of the procedure.

As it was found previously [1] that 1 M HCl readily dissolved the La(III) precipitate quickly and effectively, even if elevated flow rates were used (around 8–9 ml min⁻¹), this medium was also used herein. Higher concentrations did not have any significant effect. However, the efficiency of the hydride generation is very much dependent on the concentration of the sodium tetrahydroborate. Thus it was found that the optimal concentration of this constituent was 1.50% (m/v). Pumped at a rate of 1.50 ml min⁻¹, this means that the concentration of sodium tetrahydroborate in the final reaction medium is 0.22% (m/v) while that of HCl is 0.085 M. These conditions caused a vigorous evolution of hydrogen in the RC. The evolved hydrogen therefore undoubtedly

contributes considerably to the stripping of the analyte from the RC to the gas–liquid separator (SP), which explains why a rather low optimal flow rate of argon, $Q_{Ar} = 29$ ml min^{-1}, sufficed. In spite of the relatively large pressure fluctuations generated by the discontinuous release of hydrogen, the gas segmentation actually does limit the dispersion of the concentrate in the RC, which, for the same reasons as for the KR, is knotted. The length of RC was optimized to $L_{RC} = 60$ cm (i.d.$_{RC} = 0.50$ mm), which indicates that the hydride generation happens immediately. By prolonging the reaction time, i.e. $L_{RC} > 60$ cm, the signals obtained were very reproducible, indicating that the analyte is transported smoothly from the RC to the quartz-tube atomizer via the gas–liquid separator. However, to achieve maximum signals, it is extremely important to control the flow rate of the liquid withdrawal from the gas–liquid separator, Q_{W1}. By varying this parameter, it was noticed that the signals dropped significantly, i.e. up to 10–15%, if $Q_{W1} > Q_{W1,opt.}$ (≈ 22 ml min^{-1} with the ultimately optimized flow rates). This shows that unless the waste flow of W1 (Q_{W1}) is very conscientiously adjusted, there is a possibility of considerable loss of analyte into the waste.

3.5. The influence of sample flow rate on the performance of the FI–HG–AAS system

As mentioned earlier, the collection efficiency gradually decreased at higher sample flow rates which was the reason why it was fixed at 4.0 ml min^{-1}. However, if the sample flow rate was varied at levels below 4.0 ml min^{-1} while keeping the total amount of analyte introduced constant, virtually identical calibration curves were obtained. Thus, when comparing two calibration runs where the aspirated sample volume (V_S) of As(III) in both cases was 6.7 ml, but where the sampling time (T_C) and the sample flow rate (Q_S) in the first instance were 100 s and 4.0 ml min^{-1} respectively and 200 s and 2.0 ml min^{-1} in the second one, the linear slopes of the two calibration graphs deviated by less than 10% from each other (the slope being highest for the lower flow rate). If the difference in the two calibration runs

is beyond the experimental error, it does, however, show that it is a reasonable assumption to consider the coprecipitation quantitative up to a sample flow rate of 4.0 ml min^{-1} and with T_C equal to 100 s. The characteristics of performance under these conditions are given in Table 1.

As mentioned above, the ratio between the area (I) and the absorbance (A) of the individually recorded peak signals was a guiding parameter in the optimization procedure. Since the area reflects the effect of the coprecipitation, it is not surprising that it remained practically constant for aspiration of identical amounts of As(III), but as the optimization progressed the absorbances increased, i.e. the I/A ratio decreased progressively. By calibration at $(T_C, Q_S) = (100$ s, 4.0 ml min$^{-1})$, the average value of the I/A ratio, $(I/A)_{AV}$, in the concentration range of As(III) 0.05–0.30 μg l^{-1}, approached a value of around 1.91, which seemed to be the optimal efficiency obtainable. By comparison, calibration at $(T_C, Q_S) = (200$ s, 2.0 ml min$^{-1})$ yielded an $(I/A)_{AV}$ value of 1.93. Thus, these results show that (1) La(OH)$_3$ effectively collects As(III) on the inner walls of a knotted Microline reactor under the dynamic conditions prevailing, and (2) the dissolution of La(OH)$_3$ is effective and so is the hydride generation reaction. Apparently the concentration distribution of the analyte in the KR (Fig. 5) promotes appropriate conditions for dissolution of the coprecipitate.

In the concentration range investigated (i.e. 0–0.20 ppb As(III)), the presence of As(V) did not influence the signal provided that the concentration was below 0.20 ppb. Whether higher concentrations of this species can be tolerated in the coprecipitation reaction with La(III) or Hf(IV) can only be estimated by optimising the dissolution–hydride generation conditions to eliminate, if possible, the differences in kinetic behaviours of As(III) and As(V).

3.6. Evaluation of the preconcentration effect

To estimate the effect of the preconcentration obtained the same FI–HG-AAS system was used to determine As(III) without preconcentration. The optimal parameters obtained by optimizing the elution/hydride generation procedure with

Table 1

Characteristics for the FI–HG-AAS system with on-line coprecipitation–dissolution

Parameter	Analyte		
	Se(IV)[a]	As(III)[a]	As(III)[b]
Sample flow rate (ml min^{-1})	4.8	4.0	4.0
$\{C_{CA}$ (ppm)/pH$\}_{optimal}$	210/9.10	100/9.60	100/9.10
Calibration range (μg l^{-1})	0.01–0.30	0.005–0.30	0.005–0.40
Regression equation in calibration range	0.510 C+0.005	1.170 C+0.017	0.906 C+0.017
(6 standards, $n = 3$, C_i in μg l^{-1})	($r = 1.000$)	($r = 0.998$)	($r = 0.996$)
(I/A)$_{Average}$ (analyte concentration range 0.05–0.40 ppb)	N.D[c]	1.91	2.11
Sample volume per assay (ml) (loading time, 100 s)	7.9	6.7	6.7
Sampling frequency, f (samples h^{-1})	33	33	33
Relative standard deviation ($n = 11$, 0.10 μg l^{-1}) (%)	0.5	1.0	0.3
Limit of detection (3σ) (μg l^{-1})	0.006	0.003	0.003
Enrichment factor (EF)	30	32	25
Concentration efficiency (CE = EF f/60)	16.5	17.4	13.5

[a] Coprecipitation with La(OH)$_3$.
[b] Coprecipitation with Hf(OH)$_4$.
[c] Not determined.

La(III) were reused except that the argon flow rate had to be readjusted. A sample volume of 100 μl was employed, which in turn required an optimal argon flow rate of 43 ml min^{-1}. Consequently, the elution/hydride generation procedures with and without preconcentration were almost identical, which again indicates that the dissolution of La(OH)$_3$ is very effective. With a calibration series comprising As(III) standards in the range 2.0–10.0 μg l^{-1}, the (I/A)$_{AV}$ value was found to be approximately 2.28, that is somewhat higher than the value found for the optimized system with on-line preconcentration (1.91). The characteristics of performance are given in Table 2.

3.7. On-line preconcentration of As(III) by coprecipitation–dissolution with Hf(IV) as coprecipitant

As mentioned earlier, Hf(IV) has proved to be an effective coprecipitating agent for As(III) in batch procedures, and therefore it would be highly interesting to estimate its potential capacity on the FI–HG-AAS approach (also because this

element, in fact, is named after the capital of Denmark). To compare the efficiencies of La(III) and Hf(IV), the coprecipitation procedure with the use of Hf(IV) was optimized according to the same principles as described above for La(III). Thus, in the FI preconcentration procedure for collection of As(III) in Hf(OH)$_4$ the parameters of the elution/hydride generation procedure as employed for La(III) were reused. The results obtained are given in Table 1, to which the following comments should be added.

Table 2

Characteristics for the FI–HG-AAS system without preconcentration

Sample volume, V_s (μl)	100
Calibration range (μg l^{-1})	0.50–10.0
Regression equation in calibration range (7 standards, $n = 3$, C_{As} in μg l^{-1})	0.037 C+0.006 ($r = 0.999$)
Sampling frequency, f (samples h^{-1})	120
Relative standard deviation ($n = 11$; 5 μg l^{-1}) (%)	0.4
Limit of detection (3σ) (μg l^{-1})	0.081

By comparison with the results attained by using La(III), the investigation with Hf(IV) yielded a surprising outcome as optimal results could be achieved within wider ranges of the values of the critical parameters. Thus, similar responses were found for $9.10 \le pH_B \le 9.40$ and $180 \le C_{Hf(IV)} \le 300$ ppm. Therefore the coprecipitation of As(III) seemed, in fact, to be more robust using Hf(IV) rather than La(III) under the dynamic conditions in the FI system.

During the ensuing investigations pH_B was fixed at 9.10 and [Hf(IV)] at 220 ppm. Analogous to the results obtained by La(III) similar indications can be drawn. Thus the concentration distribution of the analyte achieved using Hf(IV) was almost identical to the distribution in Fig. 5. By varying T_C the results obtained indicate that the coprecipitation of As(III) is quantitative or almost quantitative until $T_C = 175$ s using the optimal length of the KR, $L_{KR} = 200$ cm, whereby only $\approx 60\%$ of the capacity of collection of the KR is exploited at $T_C = 100$ s. The results obtained by varying T_C are interesting. Thus while the collection efficiency of La(III) decreased slightly for $T_C \ge 50$ s, it remained constant in the range $75 \le T_C \le 175$ s for Hf(IV), which indicates that the coprecipitation is quantitative or almost quantitative during that part of the coprecipitating period.

Two calibrations were performed by coprecipitation with Hf(IV) using equal amounts of As(III), where the aspirated sample volume (V_S) was 6.7 ml and (T_C, Q_S) was (100 s, 4.0 ml min^{-1}) and (200 s, 2.0 ml min^{-1}). Contrary to the observation made for collection of As(III) in La(OH)$_3$, the highest sample flow rate for Hf(IV) exhibited the steepest slope of the calibration curve ($\approx 5\%$ higher than for the lower flow rate), although the integrated signals were of the same order of magnitude, i.e. the effect of preconcentration was identical. This indicates that the efficiency of dissolution is reduced by preconcentrating equal sample volumes at increasing T_C. By calibration at (T_C, Q_S) of (100 s, 4.0 ml min^{-1}) and (200 s, 2.0 ml min^{-1}) the $(I/A)_{AV}$ values were 2.11 and 2.29 respectively, in the concentration range of As(III) 0.05–0.40 μg l^{-1}. This effect will be explained in the following section. The characteristics of performance for Hf(IV) are given in Table 1 at calibration conditions of $(T_C, Q_S) = (100$ s, 4.0 ml min^{-1}).

3.8. Comparing the efficiency of La(OH)₃ and Hf(OH)₄ as collecting agents for coprecipitating As(III) in a knotted Microline reactor.

By comparing the results of the calibration curves that were achieved using La(III) and Hf(IV), the difference in the collection efficiencies of As(III) in the two hydroxides can be estimated because the conditions of the elution/hydride generation procedures were identical for the two calibrations. The comparison is described for the conditions $(T_C, Q_S) = (100$ s, 4.0 ml min^{-1}).

By collecting As(III) the effect and efficiency of preconcentration obtained are highest using La(OH)$_3$, as the integrated signals are higher and the I/A ratios are lower than by using Hf(OH)$_4$. The efficiency ratio of Hf(OH)$_4$ to La(OH)$_3$ was $= 77.4\%$, as calculated from the respective slopes. Consequently, As(III) is more effectively collected in La(OH)$_3$ than Hf(OH)$_4$ using a knotted Microline reactor.

As both La(III) and Hf(IV) coprecipitate As(III) instantaneously, the explanation for the less effective collection of As(III) by Hf(IV) could be ascribed to a less effective adherence of the coprecipitate and/or collection of the analyte in Hf(OH)$_4$. These possibilities were evaluated by a simple experiment, where As(III) was coprecipitated in the batch mode with the two agents. It was observed that the precipitates of both La(OH)$_3$ and Hf(OH)$_4$ were generated very fast but, while La(III) formed small, fine hydroxide particles, the precipitate of Hf(OH)$_4$ appeared very bulky. Such a precipitate might reduce the efficiency of adherence to the inner walls of the knotted reactor and/or promote the dislodgement of particles from it. Furthermore, the efficiency of adsorption of the analyte on the precipitate might be reduced as the very bulky precipitate of Hf(OH)$_4$ limits the surface area of the precipitate on which the analyte can be adsorbed.

Thus the formation of a bulky precipitate of Hf(OH)$_4$ explains why the efficiency of the FI procedure decreased when longer sampling periods (T_C) were employed. This caused the genera-
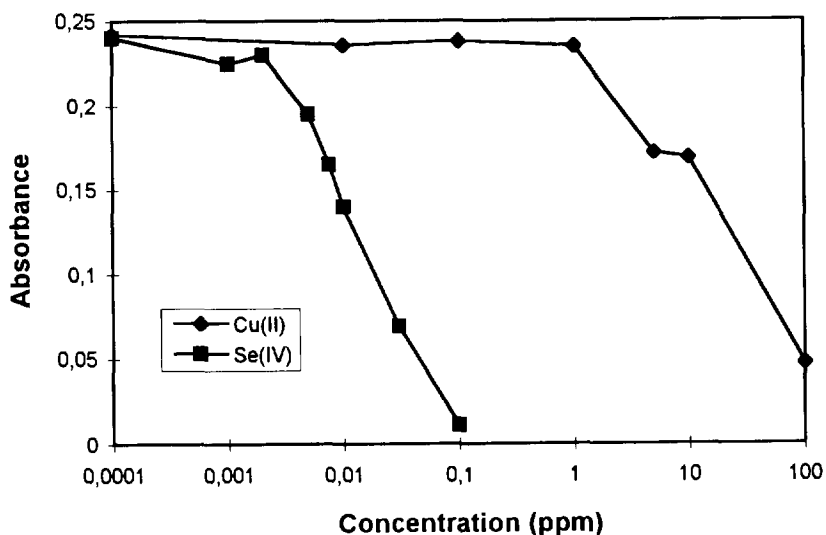
Fig. 6. The influence on the recorded output signal of a 0.20 μg l^{-1} aspirated As(III) sample at increasing concentrations of Cu(II) and Se(IV). Operational conditions are otherwise as given in Figs. 1 and 2.

tion of a disproportionately large amount of Hf(OH)$_4$, i.e. the ratio of analyte/precipitate decreased with increasing T_C although identical sample volumes were aspirated. This deteriorated the ensuing dissolution process which in turn led to broadening of the recorded peak signals. Hence, a suitable coprecitating agent should possess the ability to form small, gelatinous particles, which willingly adhere to the hydrophilic Microline tube and easily dissolve. From a thermodynamic point of view, the chance of obtaining many, smaller particles at the expense of fewer larger ones is much higher when the mixing occurs fast and abruptly, and this is quite feasible in a FI system. This is also probably the explanation why the optimal operational conditions under the dynamic conditions of FIA are different from those of batch assays, and also why it is by no means a trivial exercise to transform a batch assay into a FI procedure [1].

3.9. Investigations of interferences

If the FI–HG-AAS system with on-line preconcentration is to have any practical utility, e.g. for assays of natural water samples, it is essential that it can tolerate the presence of pertinent ions and at the concentration levels at which they may be found in such samples. In this work, which by no means was intended to be a thorough investigation of interferences, the work was therefore centered on two representative interferents, i.e. Cu(II) and Se(IV). The former is known to generally interfere in the hydride generation reaction [7], while the latter has been shown to be coprecipitated with La(OH)$_3$. To investigate the extent of these two interferences, 0.20 μg l^{-1} As(III) samples were spiked with increasing levels of these two constituents. The results are shown in Fig. 6.

It appears that concentrations of Cu(II) up to 1 ppm, i.e. at 5000 times excess, could be tolerated without any interference, yet at higher concentrations the recorded As(III) signal decreased. Thus, at a Cu(II) level of 10 ppm, the signal was reduced $\approx$ 30% compared to the signal without addition of Cu(II). In comparison, Tao and Hansen [1] found that by preconcentration of Se(IV), using a similar FI system but with off-line addition of the coprecipitating agent to the sample, the signal for a Se(IV) sample of 0.50 μg l^{-1} was reduced by 36% at a Cu(II) level of 0.50 ppm. Consequently, the determination of As(III) is much more tolerable of Cu(II). In determinations of 10 μg l^{-1} As(III) samples with the FI–HG-AAS system without preconcentration and by spiking samples off-line with Cu(II) at a level of

40 ppm it was found that the signals were only reduced by 19%. This strongly indicated that the decreasing signals for Cu(II) concentrations above 1 ppm are mainly due to the fact that the conditions of the coprecipitation process are impaired in the presence of Cu(II).

As for the investigation concerning Se(IV), it is seen from Fig. 6 that the interference of Se(IV) is much stronger than that exhibited by Cu(II). Already, at a Se(IV) concentration of 5 μg l^{-1} the signal for the 0.20 μg l^{-1} As(III) sample is reduced by 15%. For comparison, Tao and Hansen found that for the determination of Se(IV), at a level of 0.50 μg l^{-1}, the signal was reduced by less than 5% at an As(III) concentration of 50 μg l^{-1} [1]. Again, the interfering effect of Se(IV) in the determination of As(III) is probably due to the fact that the conditions of the coprecipitation process are impaired by the presence of Se(IV). Yet, the Cu(II) as well as the Se(IV) interference are non-signal yielding interferences, and therefore they can readily be compensated for by applying the standard-addition approach, which under any circumstances would be the option of choice when assaying natural samples.
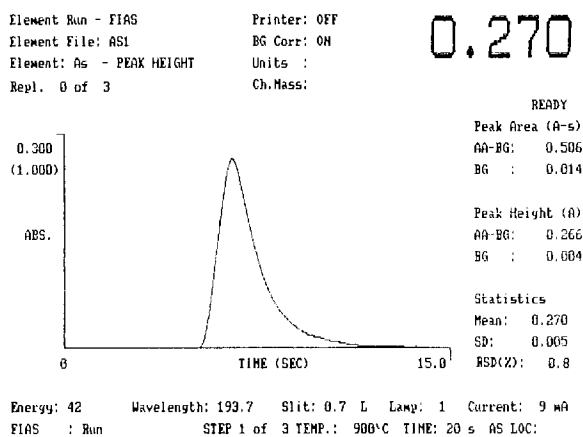
Fig. 7. Typical peak readout for a 0.20 μg l^{-1} aspirated As(III) sample as obtained by the Fl–HG-ASS system depicted in Figs. 1 and 2. Note that the area under the peak up to the peak maximum (which is reached 1.4 s after initiation of the peak) corresponds to approximately 30% of the total area, while the remaining 70% is 'distributed' over the remaining 5–6 s.

3.10. The gas–liquid separator

As each of the experimental parameters was systematically optimized, whereby it was possible to identify any limiting factors of the FI procedure with the incorporated quartz-tube atomizer, it became of interest to investigate if the technical conditions could somehow be improved.

Attention was especially focused on the gas–liquid separator. As detailed in Section 2, the separator used herein was the one commercially available from Perkin-Elmer; the so-called W model, which has a 'dead volume' of 3 ml. Recently an alternative gas–liquid separator has been developed by Fang [6] and such a unit was placed at the disposal of the authors at his proposal. This separator, which has a dead volume of 4.5 ml, proved unfortunately to have an inferior performance, which clearly shows that in order to develop an improved gas–liquid separator—at least for measuring analyte concentrations below 1 μg l^{-1}—attention must be focused on minimizing its dead volume.

The following observations indicate that the sensitivity can indeed be improved by minimizing the dead volume of the Perkin-Elmer W model separator. The dissolution of the precipitate in the knotted reactor happened instantaneously, which was readily visible by the ensuing 1–2 s of vigorous gas liberation/foaming in the gas–liquid separator. With the dimensions selected, the hydride generation reaction itself was completed within ≈ 1 s, and from the readout on the monitor it was evident that the essential part of the signal (the peak height maximum) was available after ≈ 1.4 s, while the time required to record all of the signal peak was about 6.5 s (Fig. 7). These feats indicate that an essential part of the gas concentrate became delayed by approximately 2–3 s by the passage of the gas–liquid separator or, more specifically, that the argon stream and the hydrogen developed caused a pronounce dilution of the concentrate in this unit. To minimize this effect it would be very interesting to test a Perkin-Elmer W model with a dead volume of less than 3 ml.

4. Conclusion

With the results obtained in previous work [1,2], and the work reported in this paper, it is apparent that the FI approach for preconcentration of trace levels of elements by on-line coprecipitation–dissolution in inorganic media offers itself as an attractive and effective option.

The coprecipitation process is very sensitive under the dynamic conditions prevailing, especially regarding the optimal value of the pH of the buffer used and the concentration of the coprecipitating agent. This is amply demonstrated in the difference of the optimal values of these two parameters for the preconcentration of As(III) and Se(IV), although the very same coprecipitating agent, La(III), was used in the two cases (Table 1).

Although the coprecipitation process proceeds extremely fast using either La(III) or Hf(IV), it was found that La(OH)$_3$ collected As(III) more effectively than Hf(OH)$_4$ using a knotted Microline reactor. This is probably due to the fact that the precipitate of Hf(OH)$_4$ was generated as bulky particles, which impaired both the conditions for the on-line coprecipitation process and also the ensuing on-line dissolution of the precipitate. This, in turn, proved that an ideal precipitating agent should give rise to the formation of small, gelatinous particles, which promote conditions for willing adherence to the hydrophilic Microline tube and subsequently give rise to ready dissolution.

From the experience gained by on-line preconcentration of As(III) and Se(IV) via coprecipitation–dissolution in inorganic media it is expected that subjecting other hydride-forming elements to a similar procedure should not pose any serious problems. Further, as the FI procedure presented herein seems to have reached completion, it should in the future be of great interest to investigate the possiblities to include on-line speciation of As, Sb, Se and Te. Whether the on-line reduction should be incorporated in the period of preconcentration or in the period of elution remains to be answered. In this context it must be borne in mind that the threshold of tolerance of the coprecipitation process towards interfering species was low. Therefore the on-line reduction of the analyte might preferably be executed during the period of elution, which requires that the on-line preconcentration and the sensitivity of the analyte species measured are identical. Similar considerations must be made for achieving a selective determination of the analyte at the lowest oxidation state, as the same method of hydride generation is to be used.

Presently, work is in progress along these lines, with As, Se and Sb as analytical species.

References

[1] G.H. Tao and E.H. Hansen, Analyst, 119 (1994) 333.
[2] S. Nielsen, J.J. Sloth and E.H. Hansen, Analyst, 121 (1996) 31.
[3] O. Kujirai, M. Kohri, K. Yamada and H. Okochi, Anal. Sci. 6 (1990) 379.
[4] J. Ueda and S. Kagaya, Bull. Chem. Soc. Jpn., 65 (1992) 1496.
[5] Z.L. Fang, Flow Injection Separation and Preconcentration, VCH, Weinheim, 1993.
[6] Z.L. Fang, Flow Injection Atomic Absorption Spectrometry, Wiley, Chichester, UK, 1995.
[7] B. Welz and M. Melcher, Analyst, 109 (1984) 569.

Non-linearity with metal–metal indicator complex reactions in flow-injection analysis [1]

J.F. van Staden *, D. Malan

Department of Chemistry, University of Pretoria, Pretoria 0002, South Africa

Received 13 August 1995; revised 21 November 1995; accepted 21 November 1995

Abstract

The linearity of the standard calibration curve in a flow-injection system involving a calcium–cresolphthalein complexone reaction was improved by replacing the organic base, 2-amino-2-methylpropan-1-ol, with the weak inorganic acid–conjugate base, boric acid–borate system as buffer. This was done after a theoretical study done on the relationship between the amount of coloured complex, $Ca_2(CPC)^{2-}$, as major chromophore formed and the total amount of calcium added at different pH values, and employing the knowledge obtained via proton side-reactions. It was shown that a linear calibration curve between 150 and 1000 mg l^{-1} of standard Ca^{2+} solutions was obtained with a buffer solution containing 0.05 mol l^{-1} boric acid, 0.05 mol l^{-1} KCl and 35 g l^{-1} sodium acetate at a pH of 8.5.

Keywords: Calcium–cresolphthalein complexone reaction; Flow-injection; Non-linearity; Standard calibration curve

1. Introduction

Non-linear calibration curves are sometimes obtained in flow-injection systems. These curves are either non-linear over the whole concentration range or only linear over a limited concentration range and furthermore tend to flatten when an element is determined over a wide concentration range. This has an influence on the accuracy and precision of results obtained. Although this is not such a big problem with modern technology involving computers and chemometrics, many routine laboratories do not have these facilities or access to these facilities and therefore have problems in reporting the correct results. There are two main factors that may contribute to this phenomenon, i.e. the physical and chemical parameters involved in the optimisation of a flow-injection system. Physical parameters such as sample volume, line length, tube diameter, etc. are usually easily optimised in order to obtain linear calibration curves in the working concentration range of a specific element. With chemical parame-

---

* Corresponding author. Fax: (+ 27)12-432863.

[1] Presented at the Seventh International Conference on Flow Injection Analysis (ICFIA '95), held in Seattle, WA, USA, August 13–17, 1995.

ters, the reaction involved governs the optimisation process and therefore optimisation in this regard is not always such an easy process.

In flow-injection systems where spectrophotometry is used as the detection method, the intensity measured at a certain wavelength of the coloured complex formed is directly proportional to the amount of the metal ion present in a sample if only one complex is formed [1]. The reaction must however fulfill all the requirements needed for flow-injection spectrophotometry. Although the reaction may not reach completion in the flow-injection system, each standard and sample is treated in exactly the same way due to the hydrodynamic nature of the system. This normally results in a linear calibration curve.

Complexation reactions between metals and ligands often result in the formation of more than one product [2–8]. An in-depth discussion on this phenomenon formed the subject of many papers from a number of authors including a recent valuable detailed publication by Budesinsky [8] on the optimal acidity of complexes by solution of polynomials and by iteration. If a metal ion M with analytical concentration (total metal ion concentration) C_M reacts with a ligand L to form a number of complexes as illustrated above, the mass balance (material balance) [3,6,7] on the metal ion is given by

$$C_M = [M] + [ML] + [ML_2] + [ML_3] + \cdots + [ML_n]$$
$$= [M] + \beta_1[M][L] + \beta_2[M][L]^2 + \beta_3[M][L]^3$$
$$+ \cdots + \beta_n[M][L]^n$$

where n is the maximum coordination number of the complexes, [ ] are the concentrations of the different substances, K_1, K_2, $K_3 \cdots K_n$ are the formation constants for each step in the overall reaction process, and β_n is the overall formation constant with $\beta_1 = K_1$, $\beta_2 = K_1 K_2$, $\beta_3 = K_1 K_2 K_3$, etc.

The extent to which a complexation reaction proceeds to form any of these complexes is determined by the experimental conditions and the formation constants for each step in the overall reaction process. In order to quantify the concentration of each complex in solution, the degree of formation [6] (complex formation fractions), α, is given by the general equation

$$\alpha_n = \alpha_{ML_n} = \frac{[ML_n]}{C_M} = \frac{\beta_n[M][L]^n}{C_M} = \beta_n[L]^n \alpha_0$$

where $n = 0, 1, 2, 3, \ldots$ and

$$\alpha_0 = \alpha_M = \frac{[M]}{C_M} = (1 + \beta_1[L] + \beta_2[L]^2 + \beta_3[L]^3 + \cdots$$
$$+ \beta_n[L]^n)^{-1}$$

The α values represent the ratios of the concentrations of the individual metal-containing species to the analytical concentration of the metal C_M. It can however be seen from the expressions that the α values are functions of the equilibrium constants and the free (i.e. not bound to M) ligand concentration. Hence it is possible to plot a series of component distribution curves [6] ($n + 1$ of them) of α_n vs. [L]. The α_n function is used as an atlas of metal–ligand equilibria in aqueous solution to show at a glance the relative proportions of each of the species in solution [9]. In order to visualize how these quantities of different complexes vary with the addition of a ligand to a metal, it is useful to employ graphs, called logarithmic concentration diagrams, having log concentration along the vertical y axis vs. log [L] or pL along the horizontal x axis. It is further possible to construct a complexometric titration curve by transforming the results in a logarithmic concentration diagram into a titration curve, where a metal ion is titrated with a ligand. The pattern obtained with this titration curve resembles the calibration curve actually obtained when the intensity of a coloured complex product at a certain wavelength is measured in a flow-injection spectrophotometric system. It is clear from this information that due to the formation of a number of complexes the calibration curve is only linear over a limited concentration range and that a non-linear calibration curve is obtained when extended to a full concentration range.

It is possible to extend the linearity of the calibration curve to the full concentration range by manipulation of the reaction conditions through side-reactions [2,4,5,7] of the ligands or metal ions in the complexes. When another metal ion, N, or proton, H^+, is added to the complex, ML_n, there is a competition between the other metal, N, or proton H^+, for the ligand, L, and the ligand, L, is 'withdrawn' from the complex,

ML_n. The dissociation of ML_n is enhanced and the concentrations of these complexes are decreased by the amount bound in the side-reaction complexes. To evaluate the extent of the side-reaction quantitatively in order to control the side-reaction, a side-reaction coefficient (α) is introduced which for the addition of a proton is given by

$$\alpha_{L(H)} = \frac{[L']}{[L]}$$

$$= \frac{[L] + [HL] + [H_2L] + [H_3L] + \cdots + [H_mL]}{[L]}$$

$$= 1 + \beta_1^{H^+}[H^+] + \beta_2^{H^+}[H^+]^2 + \beta_3^{H^+}[H^+]^3$$

$$+ \ldots + \beta_m^{H^+}[H^+]^m$$

where $[L']$ is the conditional free ligand concentration.

This clearly shows that the side-reaction coefficient is only dependent on the concentration of the proton added and if this is carefully controlled then the dissociation of the original complex can be controlled.

The complexometric reaction between calcium as metal ion and cresolphthalein complexone (CPC) as metallochromic indicator was chosen as a scale model to illustrate this concept. In flow-injection analysis the standard curve is non-linear when calcium is determined over a wide concentration range measuring the calcium–CPC complex. At high calcium concentrations the calibration curve tended to flatten. The reasons for the non-linearity of the standard curve have been investigated and this paper gives an account of the results obtained. This paper also describes conditions used with side-reactions to extend the linearity of the calibration curve and the results obtained in this regard.

2. Experimental

2.1. Reagents and solutions

All reagents were prepared from analytical-reagent grade chemicals unless specified otherwise. Doubly-distilled, deionised water was used throughout. All solutions were degassed before

measurements with a vacuum pump system. The main solutions were prepared as follows.

2.2. Standard calcium solution

A calcium stock solution was prepared by dissolving 24.9800 g of analytical-reagent grade calcium carbonate carefully in approximately 0.5 mol l^{-1} hydrochloric acid which was added dropwise until all of the calcium had just dissolved. The solution was boiled for a few minutes in order to remove carbon dioxide. The calcium solution was then neutralised with approximately 0.1 mol l^{-1} sodium hydroxide solution, adjusting the pH to ≈ 9, whereafter it was diluted to 1 l with distilled water in order to obtain a stock solution containing 10 g l^{-1} of calcium. Standard working solutions containing 1, 4, 8, 15, 40, 100, 150, 250, 500, 750 and 1000 mg l^{-1} of calcium were prepared by suitable dilution of the stock solution.

2.3. CPC reagent

The solution was prepared by dissolving 50 mg of CPC, obtained from BDH, and 1.0 g of quinolin-8-ol in distilled water to which a few drops of concentrated hydrochloric acid were added. The pH of the solution was adjusted to ≈ 4 with sodium hydroxide, whereafter it was quantitatively diluted to 2 l with distilled water.

2.4. Base solution

Four buffer solutions were prepared by taking 50 ml of stock solution containing 0.1 mol l^{-1} boric acid and 0.1 mol l^{-1} KCl for each buffer solution and adding amounts of sodium acetate to

Table 1
Buffer solutions: experimental design

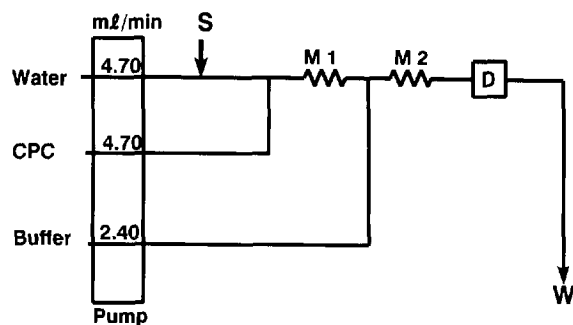| Buffer	pH	[Sodium acetate] (g l^{-1})
A	8.5	35
B	8.5	10
C	9.5	35
D	9.5	10

Fig. 1. A schematic diagram of the flow system used. S, sample; M, mixing coil; D, detector; W, waste; M1 = 30 cm; M2 = 405 cm; tube i.d. = 0.76 mm.

each as indicated in Table 1. The pH of each buffer solution was adjusted with 0.1 mol l^{-1} NaOH to the pH values given in Table 1. The final buffer solutions were each quantitatively diluted to 100 ml with distilled water.

2.5. Instrumentation

A schematic diagram of the flow system used is outlined in Fig. 1. The manifold consisted of Tygon tubing (0.76 mm i.d.) cut to the required lengths and wound around glass tubes with an o.d. of 10 mm. The following equipment also formed part of the flow-injection analysis (FIA) system: a Gilson minipuls peristaltic pump (operating at 10 rev min^{-1}) was used to supply the different streams and a VICI Valco 10-port multifunctional valve was used for injection of 25 μl samples. A Unicam 8625 UV/Vis spectrophotometer equipped with a 10 mm Hellma-type flow-through cell (volume: 80 μl) was used as the detector. The whole FIA system was controlled from a computer with a FLowTEK program [10] and the signal output of the detector was fed to the same program for data processing.

3. Results and discussion

CPC is a metallochromic indicator that has been used successfully for a long period for the determination of metal ions such as calcium, strontium and barium. The indicator was originally introduced by Anderegg et al. [1,11] as a complexometric reagent for the determination of calcium in complexometric titrations with EDTA. Under these circumstances there is a reasonably well-defined colour change with a small change in metal ion concentration at the endpoint of the titration. The value of CPC as an indicator for the direct spectrophotometric determination of the alkaline earth metals was soon realised [12] and it was adapted for the colorimetric estimation of calcium in serum [13]. Many variants of the method have been used. Most continuous-flow analytical procedures involve the use of a procedure similar to that used by Kessler and Wolfman [14] for the determination of calcium with CPC and diethylamine—sodium acetate as a base component. The absorbance of the calcium–CPC complex is measured at 580 nm and pH 12.0. Working at this pH and wavelength gave less interference from magnesium. Gitelman [15] improved this method by introducing quinolin-8-ol to eliminate interference from magnesium and by measuring the absorbance of the complex at 570 nm. Some methods also incorporated cyanide as stabiliser and to complex other potentially interfering metals. Moorehead and Biggs [16] modified this method by replacing the toxic and volatile diethylamine (pK_a 11.0) with the more stable 2-amino-2-methylpropan-1-ol (AMP) (pK_a 9.6) as a base solution. The CPC reagent is almost colourless at pH 10, but highly coloured at pH 12; therefore, the blank was reduced and the sensitivity increased. Moorehead and Biggs reported that as the interference from magnesium was eliminated by using quinolin-8-ol, it was not necessary to work at higher pH. Basson and van Staden [17] found that AMP as a base gave a sufficiently stable solution for the FI determination of calcium in animal feeds, which obviates the use of toxic potassium cyanide as stabiliser. An organic base is used to provide the necessary alkaline conditions, inorganic alkalis tending to cause high blanks [18].

Although the sensitivity of the method was excellent, a major problem was the narrow linear range of the calibration curve. CPC does not only

function as a metallochromic indicator, but also at the same time acts as an acid–base indicator. A fully protonated CPC indicator in acidic conditions can be represented as $H_6(CPC)$. $H_6(CPC)$ is deprotonated under alkaline conditions to various ionic forms of CPC. The actual amount and x values of each ionic form at different pH values can be calculated from the pK_a values for the dissociation of CPC given by Anderegg et al. [2,11] and these are outlined in a x distribution diagram of x vs. pH in a simple graphical form in Fig. 2. The spectrophotometric method for the determination of free calcium is based on the reaction between the metallochromic CPC indicator and calcium using the correct pH conditions. However, with CPC indicator, the equilibrium situation is rather involved, and the choice of the best experimental conditions is not quite simple. CPC forms $Ca(CPC)^{4-}$, $CaH(CPC)^{3-}$ and $Ca_2(CPC)^{2-}$ complexes with Ca^{2+} (or Mg^{2+}). A weak absorbing complex $H_2(CPC)^{4-}$ is also formed [11]. The concentration of these species is a function of pH, metal ion concentration and ionic surroundings. The colour formation is enhanced by bivalent metals and an increase in pH. A graphical presentation [2] of the equilibrium, based on the values of the stability constants determined by Anderegg et al. [11], offers a guide to choosing the most favourable conditions. Corns and Ludman [19] postulated the type of equilibrium involved as

Fig. 2. An x distribution diagram of x vs. pH for the different ionic forms of CPC.

$$Ca^{2+} + H_2(CPC)^{4-} \rightleftharpoons CaH_2(CPC)^{2-}$$
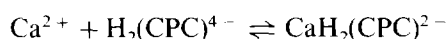
with the ionisation of the complex so formed:

$$CaH_2(CPC)^{2-} \rightleftharpoons CaH(CPC)^{3-} + H^+$$
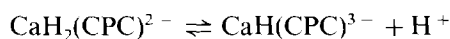
According to these authors further reaction could then occur between this complex and a second calcium ion

$$Ca^{2+} + CaH(CPC)^{3-} \rightleftharpoons Ca_2H(CPC)^-$$
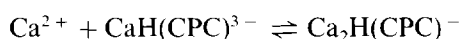
with subsequent ionisation to

$$Ca_2H(CPC)^- \rightleftharpoons Ca_2(CPC)^{2-} + H^+$$
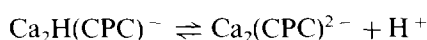
Anderegg et al. [11] postulated that the formation of the coloured complex only occurred on binding of the second calcium ion, in the same way that full colour development of phenolphthalein only occurs on ionisation of the second phenolic hydrogen atom, and formation of a quinoid structure. However, the $H(CPC)^{5-}$ ion is pale pink in colour [11], which implies that the $CaH(CPC)^{3-}$ ion may also be coloured, although the $Ca_2(CPC)^{2-}$ ion would be exected to be the major chromophore.

Corns and Ludman [19] studied the reasons for the non-linearity of the standard curve for the CPC reaction. They found that calcium forms both 1:1 and 2:1 complexes with CPC; at low calcium concentrations the 1:1 complex predominates and caused non-linearity. At high concentrations the CPC concentration becomes limiting, resulting in flattening of the calibration curve. Cowley et al. [20] improved the linearity of the calibration curve to a certain extent in the physiological range 20–200 mg l^{-1} with the addition of sodium acetate to the AMP buffer solution. The option was investigated for FIA with the addition of various amounts of sodium acetate (15–35 g l^{-1}) to various amounts of AMP (15–35 g l^{-1}) in different combinations using the FI system in Fig. 1, but with the pH of the CPC indicator solution at 1.5 as previously described. Calibration curves in the range 0–1000 mg l^{-1} of standard free calcium solutions were recorded and the final pH measured. The following conclusions were drawn from the results obtained. Addition of various amounts of sodium acetate to the buffer stream had only a minor effect on the calibration curve if
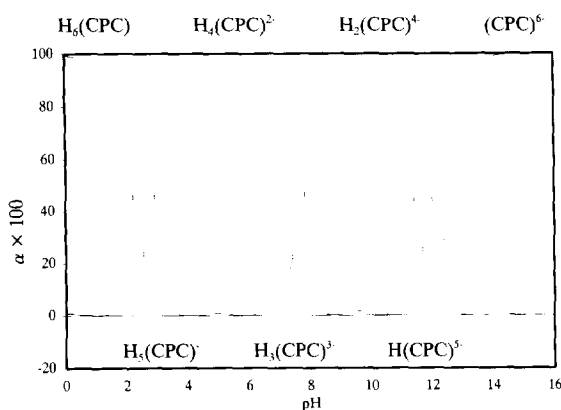
the addition was done to a buffer with a high concentration of AMP. However, with smaller amounts of AMP in the buffer the amount of sodium acetate added had an influence on the calibration curve. The disappointment was that all efforts tried did not give a linear calibration curve. It seemed that the acetate anion as ligand was a minor role player in the reaction and that it was not possible to use manipulation of reaction conditions through the side-reaction of acetate as ligand in order to get a linear calibration curve. It was, however, observed that the final pH of the different experiments above varied considerably for the different solutions, depending on reaction conditions. It followed from the results that pH played a bigger role in the linearisation of the calibration curve than the acetate anion.

A theoretical study was done on the relationship between the amount of coloured complex $Ca_2(CPC)^{2-}$, as major chromophore formed and the total amount of calcium added at different pH values. Calculations were done using a Lotus-123 spreadsheet. The overall constants, $\log \beta_{11} = 7.8$, $\log \beta_{21} = 12.8$, the conditional formation constants corresponding to the proton side-reaction, $\log K_{1H} = 11.6$, $\log K_{2H} = 7.6$, and the pK_a values of the CPC indicator ($pK_{a_1} = 2.2$, $pK_{a_2} = 2.9$, $pK_{a_3} = 7.0$, $pK_{a_4} = 7.8$, $pK_{a_5} = 11.4$ and $pK_{a_6} = 12.0$) given by Bishop [4] were used. The results for number of pH values are outlined in Fig. 3. It is clear from the results that the best chance for linearity was at a pH of 8–9. Although a beautiful titration curve was obtained at a pH of 10, linearity over a wide range was not possible. The results also showed that the possibility of linearity decreased drastically with an increase in pH above 11 and that the flattening of the calibration curve as experienced by various authors came into operation.

The method was then modified by replacing the organic base, AMP (pK_a 9.6) with the weak inorganic acid–conjugated base, boric acid–borate system as buffer. Boric acid with the lower pK_a value of 9.23 was chosen as it tended to keep the pH value of the buffer to 9 easier than AMP. This was nearer to the linear goal as illustrated in Fig. 3. Various concentrations and buffer systems of the boric acid–borate buffer without the addition

of sodium acetate were studied, but without success. Results were not repeatable which showed that the formation of the major chromophore was not consistent. This was confirmed by the instability of the final pH measured in the FI system. The preparation of the CPC reagent solution was changed to the preparation described in Section 2 where the pH of the final CPC reagent solution was changed from 1.5 to 4. This resulted in a more stable final pH measured in the FI system. The calibration curve was, however, still not linear.

A factorial experiment was used to investigate the influence of the amount of sodium acetate added and the pH of the buffer solutions at the same time. The following four buffer solutions were prepared by taking 50 ml of stock solution containing 0.1 mol l^{-1} boric acid and 0.1 mol l^{-1} KCl for each buffer solution and adding amounts of 0.1 mol l^{-1} NaOH and 250 g l^{-1} sodium acetate as indicated in Table 2. The final buffer solutions were each quantitatively diluted to 100 ml with distilled water.

The calibration curves obtained using these buffer solutions in the FI system are given in Fig. 4. It is clear from these results that both the proton and acetate ligand side-reations as well as interaction between the two had an influence on the linearity of the calibration curve. An amount of 35 g l^{-1} (14 ml of 250 g l^{-1} sodium acetate added) gave a sufficient side-reaction with the calcium to decompose the major chromophore to such an extent that the calibration curve A became linear. The proton side-reaction at pH 8.5 was sufficient to enhance this tendency. The final pH of the FI system was measured as 8.1. It is, however, also clear from the response that the sensitivity of the method decreased due to the decomposition of the major chromophore under the influence of proton and ligand side-reactions. The reaction capability of the $H_2(CPC)^{4-}$ species at pH 8.5 is also not fully utilised as seen from the α distribution diagram in Fig. 2. Enlargement of calibration curve A (in Fig. 4) showed that the calibration curve is actually linear between 150 mg l^{-1} and 1000 mg l^{-1} of standard Ca^{2+} solutions as illustrated in Fig. 5. It is possible to increase the sensitivity of the method by increas-
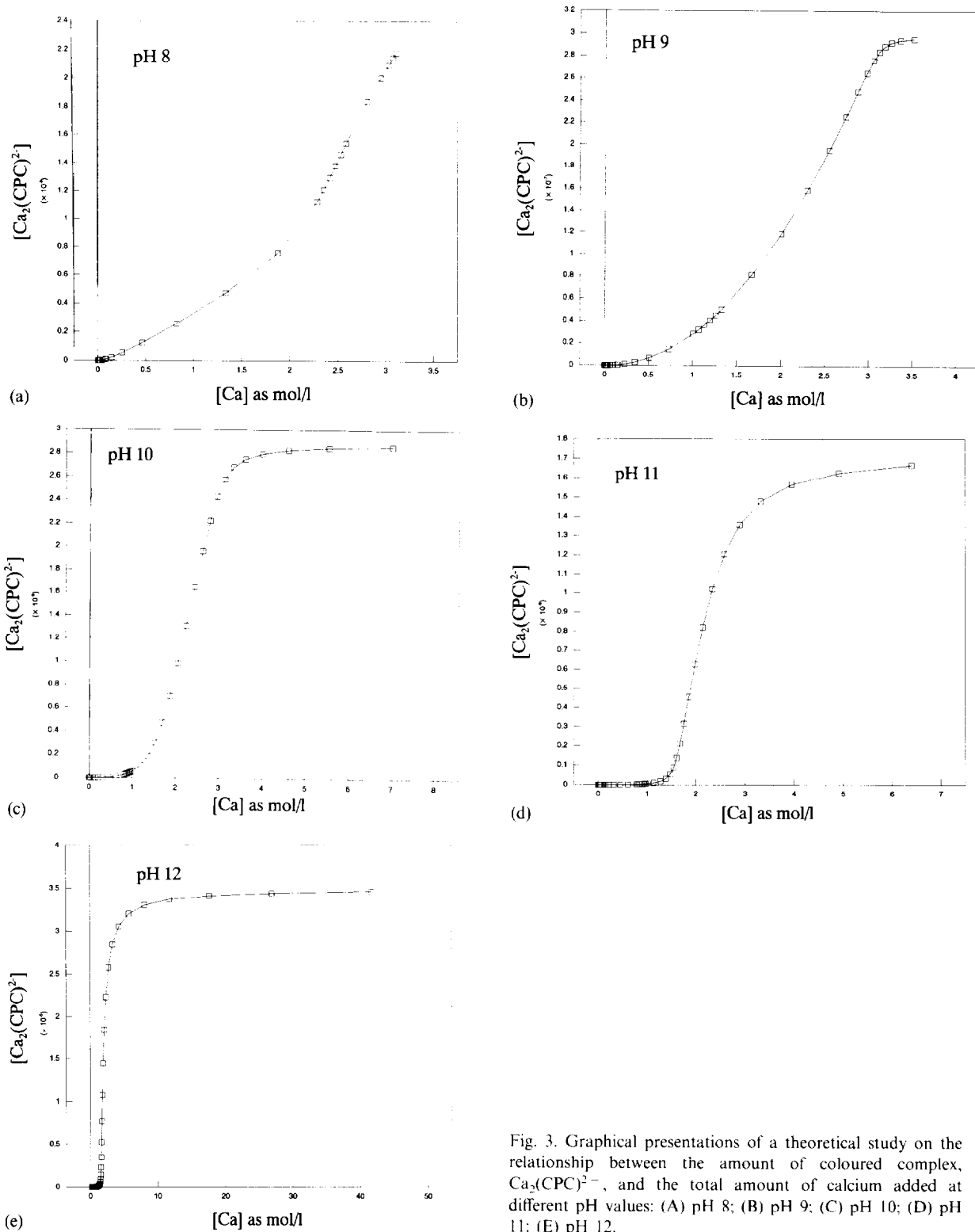
Fig. 3. Graphical presentations of a theoretical study on the relationship between the amount of coloured complex, $Ca_2(CPC)^{2-}$, and the total amount of calcium added at different pH values: (A) pH 8; (B) pH 9; (C) pH 10; (D) pH 11; (E) pH 12.

Table 2
Preparation of buffer solutions

Buffer	pH	Volume NaOH (ml)	Volume sodium acetate (ml)
A	8.5	10.1	14
B	8.5	10.1	4
C	9.5	34.6	14
D	9.5	34.6	4

ing the concentration of CPC in the CPC reagent solution.

4. Conclusion

The linearity of the standard calibration curve in a FI system involving a calcium–CPC reaction was improved by replacing the organic base AMP with the weak inorganic acid–conjugate base, boric acid–borate system as buffer. This was done after a theoretical study done on the relationship between the amount of coloured complex, $Ca_2(CPC)^{2-}$, as major chromophore formed and the total amount of calcium added at different pH values and employing the knowledge obtained via proton side-reactions. It was shown that a linear calibration curve between 150 and 1000 mg l^{-1} of standard Ca^{2+} solutions was obtained with a buffer solution containing 0.05 mol l^{-1} boric acid, 0.05 mol l^{-1} KCl and 35 g l^{-1} sodium acetate at a pH of 8.5.

Fig. 5. Enlargement of calibration curve A in Fig. 4.
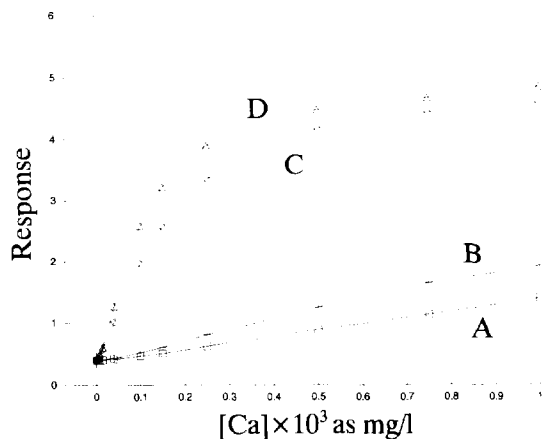
Fig. 4. Calibration curves of four different buffer solutions evaluated in the FIA system.
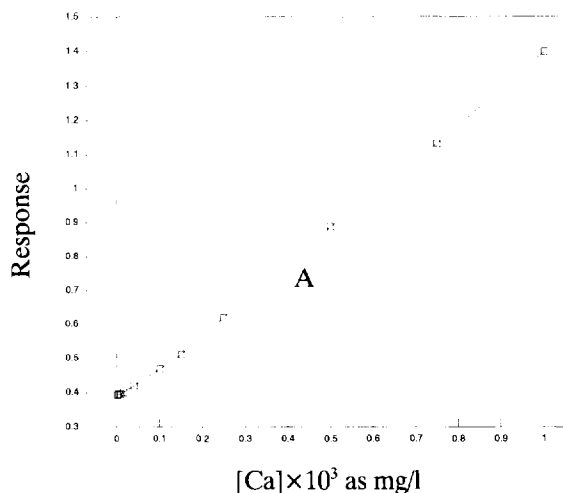
References

[1] J. Ruzicka and E.H. Hansen, Flow Injection Analysis, 2nd edn., John Wiley, New York, 1988.

[2] A. Ringbom, Complexation in Analytical Chemistry, Interscience Publishers, New York, 1963.

[3] W.B. Gunther, Chemical Equilibrium, Plenum Press, New York, 1975.

[4] E. Bishop, Indicators, Pergamon Press, Oxford, 1972.

[5] O. Budevsky, Foundations of Chemical Analysis, John Wiley, New York, 1979.

[6] F.R. Hartley, C. Burgess and R.M. Alcock, Solution Equilibria, Ellis-Horwood, Chichester, UK, 1980.

[7] H. Freiser, Concepts and Solutions in Analytical Chemistry. A Spreadsheet Approach, CRC Press, Boca Raton, FL, 1992.

[8] B.W. Budesinsky, Talanta, 42 (1995) 423.

[9] J. Kragten, Atlas of Metal–Ligand Equilibria in Aqueous Solution, Ellis-Horwood, Chichester, UK, 1978.

[10] G.D. Marshall and J.F. van Staden, Anal. Instrum., 20 (1992) 79.

[11] G. Anderegg, H. Flaschka, R. Sallman and G. Schwarzenback, Helv. Chim. Acta, 37 (1954) 113.

[12] F.H. Pollard and J.V. Martin, Analyst, 81 (1956) 348.

[13] J. Stern and W.H.P. Lewis, Clin. Chim. Acta, 2 (1957) 576.

[14] G. Kessler and M. Wolfman, Clin. Chem., 10 (1964) 686.

[15] H.J. Gitelman, Anal. Biochem., 18 (1967) 521.

[16] W.R. Moorehead and H.G. Biggs, Clin. Chem., 20 (1974) 1458.

[17] W.D. Basson and J.F. van Staden, Analyst., 103 (1978) 296.

[18] H. Diehl, Anal. Chem., 39 (1967) 30A.

[19] C.M. Corns and C.J. Ludman, Ann. Clin. Biochem., 24 (1987) 345.

[20] D.M. Cowley, B.M. Mottram, N.B. Haling and T.J. Sinton, Clin. Chem., 32 (1986) 894.

Enhanced surfactant determination by ion-pair formation using flow-injection analysis and dynamic surface tension detection[1]

Toby E. Young, Robert E. Synovec*

Department of Chemistry, Box 351700, University of Washington, Seattle, WA 98195, USA

Abstract

Chemical analysis of surface active species (surfactants) is of interest for many applications, such as in process monitoring, biomedical applications, environmental monitoring and surface science investigations. Recently, we reported a dynamic surface tension detector (DSTD) based upon optically probing the size of a repeating drop resulting from constant flow of an aqueous solvent out of the end of a capillary. Presence of a surfactant in a growing drop reduces the surface tension at the air–solvent interface, causing the drop to detach at a smaller volume, which is detected. The DSTD has a kinetic dependence, and with increasing flow rate the sensitivity decreases due to diffusional and adsorption effects. We report that for the sodium salt of dodecylsulfate (DS), the DSTD performs significantly better with a stainless steel (S.S.) capillary dropper than with a fused silica dropper because the S.S. dropper exhibits a smaller adsorption effect as a function of time. Flow-injection analysis with the DSTD of DS was found to enhance sensitivity 50-fold by in-situ reaction with the ion-pair reagent tetrabutylammonium hydroxide (TBA) in water, even though the TBA alone was not very surface active. The TBA–DS system serves as a model for a selective detection method in which surface activity is exploited and enhanced. The detection limit for DS, as TBA–DS, was 400 ppb. Additionally, weakly surface active species such as TBA could be analyzed "indirectly" by ion-pair formation with DS. The enhanced sensitivity is due to increased packing of the ion-pairs at the air–aqueous solvent interface. The flow rate dependence on the sensitivity of detecting the TBA–DS ion-pair was examined. Two limiting conditions were observed as a function of ion-pair concentration: sensitivity decreases linearly with inverse flow rate at high flow rates and approaches a steady state at slower flow rates.

Keywords: Surfactants; Ion-pair formation; Flow-injection analysis; Dynamic surface tension detection

1. Introduction

The rapid detection of surfactants in a liquid stream traditionally relied upon methods common to the detection of other classes of chemical compounds. Conductively [1], evaporative light scattering [2], and refractive index [3] (RI) detection have been used but do not provide the selectivity and chemical information often desired. UV/Vis [4] absorbance and fluorescence [5] detection are popular and can be extended to surfactants which do not possess a chromophore by derivatization.

For the detection of charged surfactants, a common approach to supplying a chromophore is through the addition of an ion-pairing agent which possesses a chromophore [6–9]. This approach has been used in chromatography [1,10–12] as well as in flow-injection analysis (FIA) [13,14]. While all of these approaches work, they fail to take advantage, as a detection mechanism, of the very physical property of surfactants which characterize them as a class of compounds, namely, an ability to alter the surface tension of a liquid. The dynamic surface tension detector (DSTD) however, does take advantage of this property and is able to selectively detect only those species in a matrix which alter the surface tension of a solvent–air interface in a dynamic, repeating fashion. The original report relating the experimental DSTD work to FIA and liquid chromatography demonstrated excellent sensitivity and selectively for surfactants, with a time dependence [15]. We then improved the limit of detection by incorporating a true-volume-based detection mechanism, as applicable in this work [16].

Surface tension measurements of liquids have long been of interest to researchers and numerous methods such as the Wilhelmy plate [17,18] and drop weight method [19–23] exist for their quantification. These methods, however, are employed under static conditions making their use in a real-time laboratory or process analyzer impractical. The DSTD differs in that it measures bulk surface tension in a dynamic mode. Based on the drop volume method which has been developed as a standard method in surface and interfacial studies [24–30], the DSTD works by forming a repeating drop at the tip of a capillary under a constant volumetric flow rate, and monitoring the change in drop volume when a surfactant is present. The presence of a surfactant in the drop will cause the surface tension to lower and consequently the drop will detach at a smaller final volume relative to the solvent drop volume.

In our present work, we were interested in being able to enhance the DSTD signal through two separate avenues. First, we investigated the question of how sensitivity would change if a material other than fused silica were used as the capillary. In this case, we compared stainless steel (S.S.) to fused silica tubing. Second, to what degree was the DSTD signal enhanced through the formation of an ion-pair with the surfactant analyte and detecting the ion-pair versus the analyte itself?

The material from which the capillary is constructed affects the DSTD response. Previously, fused silica capillaries had been used with much success but their relatively short lifetime became an ongoing issue, particularly in the context of using the DSTD as an analytical instrument. According to Hool and Schuchardt [31], the orifice dimensions of a capillary are very critical in droplet formation and subsequent detachment, with the surface area available to the drop for wetting a major point of consideration. More exactly, the outside diameter (o.d.) of a capillary in comparison with its inside diameter (i.d.) determines the "effective" diameter of the capillary. Machining the capillary o.d. as close as possible to the i.d. was found to minimize the front facial surface area and give superior performance. An investigation into the performance of a S.S. capillary was undertaken with its results being compared with that of the fused silica.

The primary focus of this paper is to report our observations that the DSTD response to ionic surfactants could be enhanced through the formation of an ion-pair between an analyte and an appropriate ion-pairing agent prior to detection. Obviously, the ability to increase the sensitivity of the DSTD would be quite advantageous and with that in mind several experiments were designed and carried out in order to more fully understand the enhancement effect. Answers to two specific questions were sought. First and foremost, to what degree was the DSTD sensitivity actually enhanced through ion-pair formation? Second, what ratio of ion pairing agent to analyte is needed to optimize the enhancement? Meyers [32] indicates that the packing density of adsorbed surfactants is altered when ion-pairs are formed and that the altered packing increases the efficiency of surface tension lowering. Efficiency is defined as the bulk concentration necessary to reduce the surface tension by a given amount. Higher efficiency manifests itself as an increase in

the surface binding constant [32,33], K_2, of the surfactant or the ion-pair in Eq. (2), which increases $S(t)$ and consequently $\Delta r_{1,2}$ via Eq. (4), as described in the Theory section. The model system used in this study consisted of sodium dodecyl sulfate (SDS) and tetrabutylammonium hydroxide (TBA). The end goal of this work is to apply the advantageous ion-pairing effect to the rapid analysis of surfactants using the DSTD.

Also of interest was how the DSTD signal varied with drop time (inversely proportional to flow rate) and analyte concentration. Delahay and Fike [34] examined through computer simulations the kinetics of the adsorption of a hypothetical analyte on an expanding mercury sphere. Their results with regard to how the surface layer concentration depends upon initial concentration and growth rate were compared with our observations on the behavior for the DSTD. They state that the kinetics are strongly dictated by the quantity C^0/α, where C^0 is the bulk analyte concentration and α is the parameter defining a Langmuir isotherm. By solving the boundary value problem, Delahay and Fike plotted the ratio Γ_t/Γ_e of the surface concentration Γ_t at time t to the equilibrium surface concentration Γ_e. Increasing the C^0/α ratio resulted in lowering the time required to reach equilibrium, where equilibrium is defined by a constant Γ_t/Γ_e value. Furthermore, the equilibrium surface layer concentration increases with the bulk concentration. Instead of Γ_t/Γ_e, we rely on the change in drop volume, or drop radius, Δr, as an indicator for surface coverage since, as will be shown, Δr is proportional to the relative change in surface tension, $\Delta \gamma / \gamma$, and $\Delta \gamma / \gamma$ is proportional to analyte surface coverage, Γ_t/Γ_e. Increasing the surface layer concentration results in a lowering of the surface tension which on the DSTD is seen by a decrease in Δr. When the surface layer concentration has reached a maximum, Δr should become constant.

2. Theory

A complete derivation of the theory describing the operation of the optical-based DSTD has been published previously [15,16]. The main results are

given here to provide adequate background information. The DSTD probes a length dimension of a continuously growing drop surrounded by air, and the measured data provide a direct relation of changes in drop volume to changes in surface tension. From a fundamental point of view, changes in surface tension, $\Delta \gamma_{1,2}$, relative to some baseline surface tension, as caused by the presence of a surface-active species, manifests itself as a change in drop volume, $\Delta V_{1,2}$, relative to some baseline volume, V_1. Mathematically,

$$\frac{\Delta \gamma_{1,2}}{\gamma_1} = \frac{\Delta V_{1,2}}{V_1} \tag{1}$$

where the bulk solvent is labeled with a subscript 1, the analyte with a subscript 2, and a mixture of the two with the subscript 1,2.

We will now consider the signal, $S(t)$, of the optical-based DSTD as a function of time, t. A change in surface tension, and thus $S(t)$, comes from three contributions: (1) relative change in surface tension; (2) relative degree of surface activity of the analyte; and (3) transport of the surface-active species to the air–liquid interface. $S(t)$ was derived [15] from a combination of the treatment of surface tension of a two-phase system [35] and the classical drop weight method of surface tension as reported by Adamson [21] and, in terms of Eq. (1) is given by

$$S(t) = \frac{\Delta V_{1,2}}{V_1}(t)$$

$$= C_2 \left(\frac{t_1}{t_{eq}}\right) \frac{M_1}{10^6 M_2} \beta K_2 \left(\frac{\gamma_2}{\gamma_1} - 1\right) \tag{2}$$

where t_1 is the baseline drop time interval for the solvent, C_2 is the concentration of the analyte near the surface as observed at the detector, t_{eq} is defined as the time required for the solution to reach equilibrium under static conditions, M_1 and M_2 are the molecular masses of the solvent and analyte respectively, K_2 is a thermodynamic constant determining the surface binding constant for the analyte, β describes the relative geometry of the analyte, and γ_1 and γ_2 are the coefficients of surface tension for the solvent and analyte respectively.

As with RI detection, the DSTD requires an absolute change in the probed physical property, in this case surface tension, and this is given by the $(\gamma_2/\gamma_1 - 1)$ term. Selectivity and enhanced sensitivity for surfactants depends upon their ability to form and maintain a concentrated surface layer, and this is defined by the βK_2 term. Lastly, the basis of the time-dependent response comes from analyte transport to the surface by diffusion and convection. In previous work [15] the concentration of an analyte at the drop surface over time is given by the linear approximation

$$C_2(t) = \left(\frac{t_1}{t_{eq}}\right) C_2 \qquad (3)$$

where the equilibrium signal is defined when $t_1 = t_{eq}$, thus making $C_2(t) = C_2$. Eq. (3) describes the transport of an analyte to the surface, relating the determination of surface tension by static and dynamic methods, and is strictly valid only when $t_1 \ll t_{eq}$.

While Eq. (2) describes the various physical mechanisms involved in producing a response, the detection of a surface-active species comes through actually measuring the physical change in a repeating drop volume. In practice, however, the change in drop radius, $\Delta r_{1,2}$, is actually measured and further analysis can show that $S(t)$ in Eq. (2) is approximately equal to three times the relative change in drop radius as a function of time [16]:

$$S(t) = \frac{\Delta \gamma_{1,2}}{\gamma_1}(t) = \frac{\Delta V_{1,2}}{V_1}(t)$$

$$= 3\left(\frac{\Delta r_{1,2}}{r_1}\right)(t) \qquad (4)$$

The last term gives the instrumental-based limit-of-detection (LOD) when $\Delta r_{1,2}$ is taken as three times the standard deviation of successive drops. Currently, the smallest change in drop radius detectable is 0.5 μm. The DSTD is designed to detect small changes in drop radius with optimal operation in the range of 120 μm change in drop radius, or 10% of the baseline drop radius. Since the $\Delta r_{1,2}$ measurement is recorded just prior to detachment of a given drop (maximum drop vol-

ume), then the time dependence of Eq. (4) can take on the additional meaning of the recording time of successive drops in a FIA experiment. Then, it is understood that the time dependence for a drop growth is involved as well.

3. Experimental

The experimental apparatus is shown in Fig. 1. Degassed water was used as the primary carrier solvent for all FIA analyses and was purchased as 100% HPLC-grade (J.T. Baker, Phillipsburg, NJ). An Isco SFC-500 Micro Flow Syringe Pump was used throughout (ISCO, Lincoln, NE). Analytes consisted of reagent-grade SDS and the quaternary amine TBA and were used without further purification (Aldrich Chemical Co., Milwaukee, WI).

Analytes were introduced into the system using an injection valve (Rheodyne 7125, Cotati, CA) fitted with either a 20 μl or 85 μl injection loop (sample loop in Fig. 1), depending on the experiment conducted. An ion-pairing agent was mixed with analyte either in volumetric glassware or combined using a precision microliter pipette (Rainin, Pipetman, Woburn, CA) before injection; alternatively, the ion-pairing agent could be introduced into the carrier solvent as an additive via a second injection valve (ion-pair reagent loop in Fig. 1) located immediately upstream from the sample loop. In-situ mixing of 20 μl injected
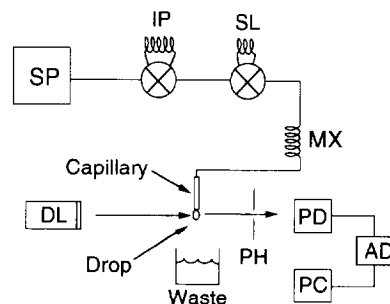

Fig. 1. Schematic of the DSTD: DL, diode laser with attached focusing lens; PH, 0.25 in pin hole aperture; PD, photodiode; AD, data acquisition board; PC, personal computer; SP, syringe pump; IP, 1 ml ion-pair reagent loop; SL, sample loop, 20 or 85 μl; MX, 70 μl mixing coil.

analyte solution with the ion-pairing agent in this manner occurs in a 70 μl mixing coil. When this latter approach is desired, a 1 ml loop is placed on the ion-pair reagent valve (Valco C10U. Houston, TX) allowing for 5 min of temporary change to the carrier solvent at 200 μl min^{-1}. All tubing consisted of 1/16 in o.d. × 0.007 in i.d. poly(etheretherketone) (PEEK) tubing (Upchurch, Oak Harbor, WA).

For analyte detection purposes, liquid would flow into a capillary from which drops approximately 8 μl in volume would form at the capillary tip. Capillaries of two different materials were studied. The fused silica capillaries had dimensions of 0.33 mm o.d. × 0.20 mm i.d. with the ends flush and manually polished before use with sandpaper containing 1 μm aluminum oxide particles to minimize surface roughness. Because the o.d. of the capillary is smaller than conventional 1/16 in i.d. chromatography fittings, it was first inserted into a piece of 0.010 in PEEK tubing and then secured with epoxy. This piece of PEEK tubing could then be coupled to the carrier solvent line with the fittings used.

S.S. capillaries were also examined. To prepare these, a 5 cm length of 1/16 in o.d. × 0.007 in i.d. S.S. tubing was cut with one end tapered to a cone such that the o.d. was approximately 50% larger than the i.d. at the tip. The capillary assembly was mounted using a clamp on a vertical post and connected to an X–Y–Z stage micrometer (Newport, 460 X–Y–Z, Fountain Valley, CA).

A photodiode placed behind the capillary and in-line with the diode laser is interfaced to an amplifier/voltage offset box and then to a personal computer (Delphi 80486-33, Seattle, WA) via a data acquisition board. A chart recorder is also connected to provide immediate hard copy output. Raw data were collected at a rate of 20 data points per second with each data point the average of 200 A/D reads. Processed data consisted of a measure of the final radius growth of the drop, represented as an intensity voltage, which could then be converted to $S(t)$ using Eq. (4) and the detector calibration curve. To obtain a calibration curve, the X–Y–Z translational stage upon which the capillary is mounted is used to
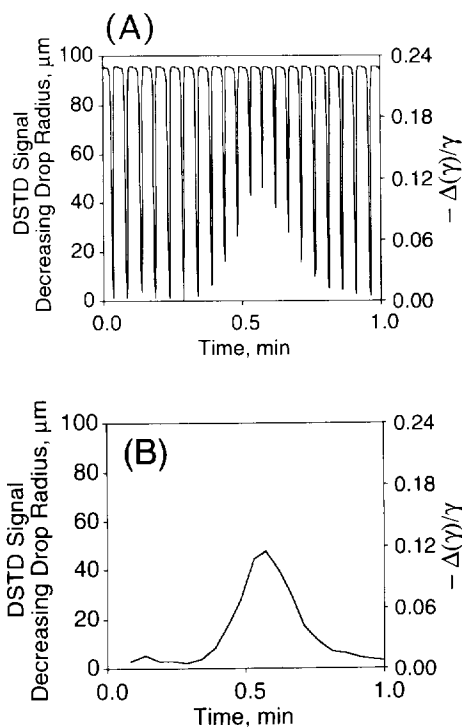
Fig. 2. (A) Raw data for FIA analysis of 500 ppm SDS as seen by the DSTD. Baseline drop growth is indicated by a 0 μm change in drop radius. Detection of the analyte is seen as a decrease in the final drop radius, or an increase in observed light intensity. The $\Delta\gamma/\gamma$ scale was calculated using Eq. (4) with $r_1 = 1240$ μm. (B) Raw data are processed such that only the data point corresponding to maximum drop growth is kept with the collection of these points forming the FIAgram. The data are offset vertically from zero for clarity.

position the drop in the laser beam path and relate change in drop radius, Δr, to an intensity voltage. As a drop grows at the tip of the capillary, it will significantly block out light from the diode laser. When a surfactant is present in a drop, the surface tension decreases, forcing the drop to detach at a smaller final volume, or smaller final radius, relative to a baseline solvent response. Detection of an analyte is seen as a decrease in final drop radius, or, as an increase in laser light intensity.

The raw signal, as collected by the computer before processing, is shown in Fig. 2A for a 500 ppm SDS sample. Two separate scales are used on

the dependent axes; the decrease in drop radius, $\Delta r_{1,2}$, is given on the left side with the relative change in surface tension, $\Delta\gamma/\gamma$, on the right. The conversion between $\Delta r_{1,2}$ and $\Delta\gamma/\gamma$ is given by Eq. (4). Baseline drop growth is indicated by a 0 μm decrease in drop radius, offset to about 4 μm in fig. 2A for clarity. To convert from a voltage as given by the detector to a $\Delta\gamma/\gamma$ value, the following steps are done. The maximum Δr occurs at the point of drop detachment. The numerical value of the maximum Δr is found by converting the intensity voltage at the detachment point to Δr with the detector calibration curve. The $\Delta\gamma/\gamma$ value is then calculated using Eq. (4), where Δr is divided by the baseline drop radius, r, and then multiplied by three. The final processed data consist of the data points at maximum Δr which form the FIA response curve, as shown in fig. 2B. The baseline drop radius is found by counting the number of drops formed over a given period of time at a given flow rate and then dividing this number into the flow rate to get the volume per drop. Assuming a spherical drop, its radius is found through the formula for volume of a sphere.

At a flow rate of 60 μl min^{-1} and below, the drop volume remains constant at 8 μl for both capillary materials tested but then steadily decreases with increasing flow rate. Table 1 shows how the baseline drop radius changes with flow rate using the S.S. capillary, where baseline response is for pure water. At a flow rate of 250 μl min^{-1}, for example, baseline drop radius decreases by 18 μm, a 1.5% change. The slight decrease in baseline radius with increasing flow

Table 1
Change in baseline drop radius with flow rate. The maximum baseline drop radius is 1240 μm, an 8 μl drop

Flow rate (μl min^{-1})	Drop radius (μm)	Percent decrease in drop radius
30	1240	0.0
60	1240	0.0
120	1237	0.2
200	1228	1.0
250	1222	1.5
300	1214	2.1
350	1204	3.0

rate was insignificant in the calculations reported in this paper.

For those experiments in which an ion-pairing agent is used, the contribution of the ion-pairing agent to the total DSTD signal needs to be subtracted if the ion-pairing effect on the analyte response is to be accurately determined. If the ion-pairing agent itself is surface active, then its presence will cause the baseline drop radius r_1 to decrease which would need to be taken into account when using Eq. (4). TBA, however, is only weakly surface active with a 500 ppm sample producing a Δr value of only 20 μm out of a total drop radius of 1240 μm. With SDS as the ion-pairing agent, however, a 500 ppm sample causes the drop radius to lower by approximately 70 μm.

4. Results and discussion

4.1. Flow rate and capillary material dependence

To investigate the performance of the S.S. capillary and compare it with the fused silica at constant drop volume, the change in drop radius, Δr, as a function of flow rate for an analyte mixture of SDS and ion-pairing agent TBA was examined. The results are shown in Fig. 3. The change in drop radius is actually negative (decreasing final drop volume) but for clarity the absolute value of Δr is plotted. For the fused silica capillary, the response to an injected analyte concentration of 50 ppm SDS mixed with 250 ppm TBA was measured over a flow rate range of 20-200 μl min^{-1}. For the S.S. capillary, 15 ppm SDS with 250 ppm TBA was measured over a range 30-400 μl min^{-1}. The injected volume of 85 μl was large enough to ensure that the concentration at the peak maximum remained undiluted. The flow rate dependence of the DSTD for both capillaries can be divided into two regions. At lower flow rates Δr for each data set is approximately the same and remains constant while approaching 60 μl min^{-1}. Then, the data sets branch off such that at any given flow rate, Δr for the S.S. capillary always remains greater than that for fused silica. Since Δr for each capillary is not the same over the flow rate range examined this
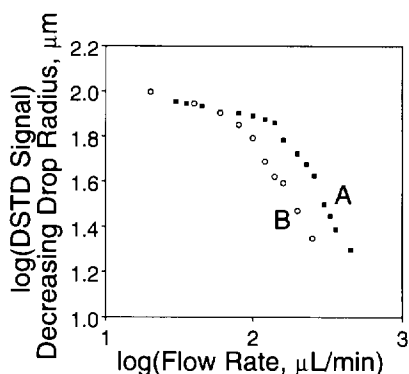
Fig. 3. A comparison of a fused silica and a S.S. capillary as a function of volumetric flow rate. (A) The response is for 85 μl of 15 ppm SDS, in 250 ppm TBA, injected concentration using the S.S. capillary. (B) The response is for 85 μl of 50 ppm SDS, in 250 ppm TBA, using the fused silica capillary. At flow rates below 60 μl min^{-1}, the DSTD response is essentially identical with either capillary but, due to difference in analyte concentrations, the DSTD signal with S.S. is 3.3 times more sensitive. Above a 100 μl min^{-1} flow rate the advantage for S.S. is six-fold.

implies that the capillary material does play a role in determining DSTD sensitivity and that perhaps the response can be maximized by choosing an appropriate material in which to construct the capillary.

The difference in sensitivity for the two capillaries will now be quantified (Fig. 3). While in the lower flow rate region, Δr for each capillary is approximately the same, the SDS analyte concentration at the detector with the S.S. capillary is 3.3 times less when compared to fused silica (15 ppm vs. 50 ppm). In other words, at flow rates below 60 μl min^{-1} a 3.3-fold increase in sensitivity is observed through the use of the S.S. capillary. At higher flow rates, however, sensitivity increases even further over the fused silica capillary. Looking at a flow rate of 200 μl min^{-1}, for instance, the change in drop radius is approximately 1.8 times larger with S.S. than with fused silica; coupling this with the 3.3.-fold difference in analyte concentration gives nearly a six-fold increase in sensitivity for the S.S. capillary. By switching to a S.S. capillary a two-pronged advantage is obtained. First, the S.S. capillary allowed for analysis of analytes at lower concentrations than previously obtained [15,16]. Second, the ability to

work at higher flow rates and still maintain the same signal is possible. Essentially, the flow rate dependence curve for fused silica has been shifted toward higher flow rates with the use of S.S., pointing towards a difference in the kinetic dependence of these materials with the surface tension measurement.

To better understand the behavior of the DSTD with the S.S. capillary, a series of flow rate curves were obtained at varying analyte concentrations. Fig. 4 depicts Δr vs. drop time (inversely proportional to flow rate) for a series of SDS–TBA mixtures, with the TBA concentration kept constant at 250 ppm. The curves were collected utilizing the S.S. capillary. In the shorter drop time regime—higher flow rate—the slope increases with the concentration of SDS injected and is described by Eqs. (2) and (3). The DSTD signal appears to reach a plateau when the surface layer concentration has reached a maximum for the drop time allowed and additional analyte cannot effect a change in surface tension. Also, the time required to reach equilibrium shifts towards lower drop times as the concentration of SDS increases; moreover, the equilibrium Δr value of each curve also increases with SDS concentra-
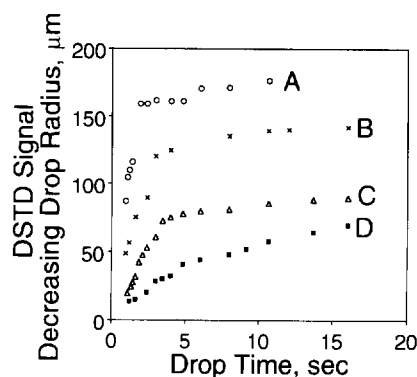
Fig. 4. DSTD signal as a function of drop time, obtained by changing flow rate for different SDS concentrations injected. Curves A, B, C, and D are for injected concentrations of 50, 25, 15 and 10 ppm SDS respectively. All samples were 85 μl in volume and contained 250 ppm TBA. The time required to reach equilibrium, as defined by approaching a constant Δr value, shifts towards shorter drop times with increasing SDS concentration. The DSTD signal linearly decreases with decreasing drop time in the kinetically-limited short drop time regime.
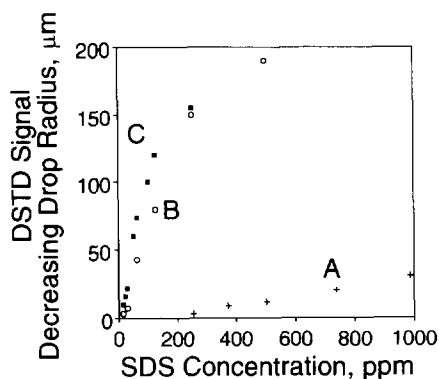
Fig. 5. DSTD response as a function of SDS concentration at different TBA concentrations. Curve A is for SDS without TBA present. Curve B has the TBA concentration held equal to the SDS concentration. Curve C has the TBA concentration at 10 ppt. TBA and SDS were mixed prior to injection with an injected volume of 85 μl. The flow rate was 60 μl min^{-1}. Enhancement of the DSTD signal through ion-pair formation is seen by comparing the data set with only SDS present with the other two data sets for SDS which also contain TBA. No signal advantage is obtained by increasing the TBA concentration beyond that of SDS.

tion. Consistent with the results of Delahay and Fike [34], the time required to reach equilibrium decreases with increasing bulk SDS concentration. For example, equilibrium for 15 ppm SDS is reached with a drop time of approximately 4 s: raising the concentration to 50 ppm SDS lowers the equilibrium drop time even further to 2 s.

4.2. Ion-pair formation

We have observed that the DSTD response to ionic surfactants could be enhanced through the formation of ion-pairs between the analyte and an appropriate ion-pairing agent prior to detection. The model system used in this study consisted of the analyte SDS and the ion-pairing agent TBA. Two questions were of interest. To what degree was the DSTD signal actually enhanced through ion-pair formation? Secondly, what ratio of ion-pairing agent to analyte is needed to optimize the enhancement?

To answer the first question, three calibration curves with SDS as the analyte and TBA acting as the ion-pairing agent are shown in Fig. 5. The curve of lowest slope, labeled (A), is of SDS

without TBA present. The second curve, labeled (B), has the TBA concentration always kept equal to the SDS concentration. Lastly, the third curve, labeled (C), has the TBA concentration at 10 ppt, much larger than the SDS concentration range. A sample volume of 85 μl was used throughout with the SDS and TBA mixed prior to injection. Looking at Fig. 5 it becomes obvious that TBA greatly enhances the response for SDS while TBA itself exhibits a very small response. Taking the ratio of the slope of curve B to the slope of curve A, a 50-fold enhancement is seen.

The second question of what ratio of ion-pairing agent to analyte is needed to optimize the enhancement is answered in part with Fig. 5. The calibration curves where TBA is present but in different concentrations nearly match one another (Fig. 5, curves B and C). It should also be noted that at no point did the concentration of ion-pairing agent fall below the concentration of the analyte. These two facts led us to conclude that to maximize the sensitivity for SDS detection, the concentration of the ion-pairing agent must be at least equal to the maximum concentration of the analyte intended to be analyzed and that increasing the ion-pair concentration beyond the analyte concentration provides no additional enhancement. If such an advantage did exist, then the
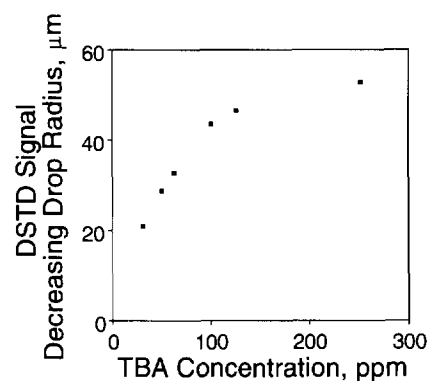

Fig. 6. DSTD response to TBA with 100 ppm SDS present. Injection volume was 85 μl with a flow rate of 60 μl min^{-1}. Up to 100 ppm TBA, enough SDS is present to completely ion-pair the TBA. Above 100 ppm TBA, the SDS becomes a limiting reagent and the DSTD response quickly levels off. TBA itself is weakly surface active, with very little inherent response.
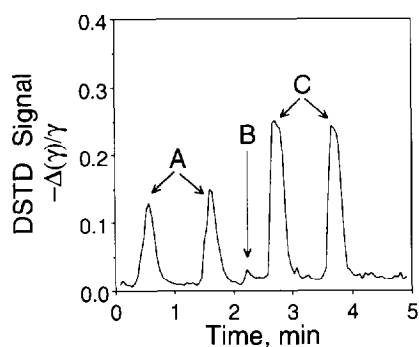
Fig. 7. FIA and DSTD detection of SDS via in-situ ion-pair formation with TBA. (A) Duplicate injections of 500 ppm SDS in water. (B) Injection of 500 ppm of the ion-pairing agent TBA into carrier solvent. This was done via the ion-pair reagent injection valve containing a 1 ml sample loop, thus providing approximately 5 min of altered background. (C) Duplicate injections of 20 ppm SDS mixed in situ with TBA. Flow rate was 200 μl min^{-1} with an analyte sample volume of 20 μl. The ion-pairing agent and analyte were combined in a 70 μl mixing coil prior to detection. Listed concentrations are the amounts injected.

curve with 10 ppt TBA should have yielded a more sensitive response than when TBA was kept equal to the SDS concentration.

Fig. 6 is a calibration curve for TBA with a constant SDS concentration of 100 ppm. TBA is not surface active enough to provide much of a response but in the presence of 100 ppm SDS, the signal is observed by an indirect detection mechanism, since the baseline signal (SDS alone) is subtracted. What should be noticed in Fig. 6 is that up to approximately 100 ppm TBA, the SDS concentration is always in excess, allowing all available TBA to be ion-paired and the signal maximized. Beyond the 100 ppm mark, however, SDS is a limiting reagent and some TBA will not be ion-paired causing the DSTD signal to level off. Beyond a concentration of 100 ppm TBA, it is predicted that Δr should become constant since the maximum number of ion-pairs have formed. The point at which Δr does level off is approximately where the TBA and SDS concentrations are equal, in this case 100 ppm. In fact, looking at Fig. 6, it is observed that the calibration curve does level off sharply past the 100 ppm TBA mark. We conclude that DSTD signal enhancement through ion-pair formation only occurs up

to the point where the ion-pairing agent and analyte are present in equal amounts for the SDS-TBA system. Increasing the ion-pairing agent concentration beyond the analyte concentration does not provide any additional advantage, though at the same time it does not harm the analysis either.

4.3. FIA of surfactants through in-situ ion-pair formation

The end goal of this work is to apply the advantageous ion-pairing effect to the rapid analysis of surfactants using FIA and the DSTD. To this end, it was concluded that the ion-pairing agent would need to be present in the carrier solvent and the ion-pairs formed in situ for real-time analysis to occur. The in-situ formation was facilitated with a mixing coil placed between the sample loop injection valve and the capillary (see Fig. 1). By introduction of an ion-pairing agent such as TBA into the carrier solvent upstream from where analytes are injected, the requisite ion-pairs can form before entering the detector.

Fig. 7 depicts the data from the FIA experiment. First, 20 μl of 500 ppm SDS was injected in duplicate into a pure water carrier solvent (200 μl min^{-1}) and the detector response recorded. The signal plotted in this case is the true DSTD re-

Fig. 8. Detection of TBA via in-situ ion-pair formation with SDS. Flow rates and volumes injected are the same as in Fig. 7 except SDS becomes the ion-pairing agent and TBA the analyte. (A) Injection of 500 ppm TBA into carrier solvent water. (B) Injection of 500 ppm SDS into the carrier solvent. (C) Reset capillary position. (D) Duplicate injections of 25 ppm TBA mixed in situ with SDS.

sponse, that is, the relative change in surface tension, $\Delta\gamma/\gamma$, as defined in Eq. (4) and converted as in Fig. 2AB. Once th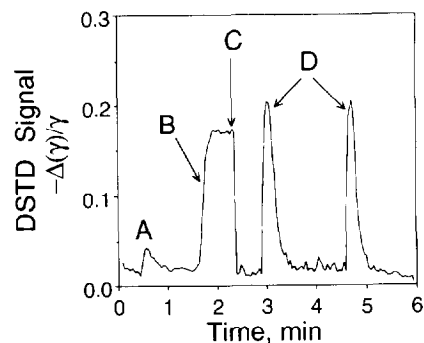e signal returned to baseline after the second injection, 500 ppm TBA was injected into the carrier solvent from the ion-pair reagent loop and the new, slightly altered, baseline was allowed to equilibrate. As stated previously, TBA itself is only slightly surface active and as such the change in baseline is not significant in the data conversion to $\Delta\gamma/\gamma$. With the TBA present in the carrier solvent, a 20 μl sample of 20 ppm SDS was injected, allowed to mix with the TBA in the mixing coil and the response recorded. As is evident, even with a 25-fold less concentrated sample the relative change in surface tension of SDS is approximately twice as great when TBA is present than when TBA is absent. In short, this means a 50-fold increase in sensitivity for SDS is possible through the formation of an ion-pair with TBA prior to detection by the DSTD. The LOD for SDS as a DS–TBA ion pair, where DS is the dodecyl sulfate ion, was determined to be 400 ppb (LOD $= 3 \times$ standard deviation of the baseline noise). Note that these analyses were conducted at a flow rate of 200 μl min^{-1} which, prior to the use of the S.S. capillary and the ion-pairing agents, was not possible.

Fig. 8 is the role reversal of the chemical species used in Fig. 7. TBA is the analyte and SDS acts as the ion-pairing agent present in the carrier solvent. This situation has an added importance in that it shows how non- or weakly-surface active molecules, such as TBA, can be detected with the DSTD by having an appropriate ion-pairing agent present in the carrier solvent. The relative change in surface tension, $\Delta\gamma/\gamma$, for the TBA–DS complex is roughly four-fold greater than that for TBA alone while the TBA–DS concentration was 20-fold lower, meaning the overall sensitivity has been increased 80-fold. The 1 ml plug of 500 ppm SDS injected into the carrier solvent yields a constant DSTD response as seen in Fig. 8 at about the 2 min mark. To keep the two subsequent injections on scale, the baseline light intensity was readjusted. To do this, the position of the capillary was moved further into the path of the laser beam by an amount equal to the decrease in baseline drop radius caused by the SDS.

5. Conclusion

We found that the DSTD is a more sensitive detector by switching from a fused silica capillary to one made of S.S. This allowed for operation of the DSTD at significantly higher flow rates than previous with a six-fold increase in sensitivity. Furthermore, the detection of SDS was enhanced 50-fold by the formation of an ion-pair between SDS and the quaternary amine TBA giving a final LOD of 400 ppb. The methodology reported here should be ideally suited for process analysis and biomedical applications. For purposes of environmental monitoring, however, the LOD for this method would have to be lowered further [36]. The formation of drops for the purposes of analytical measurements is not restricted to the detection of surfactants. Dasgupta et al. has recently shown that a droplet formed at the end of a capillary is capable of acting as a sampling device for gas soluble analytes such as NH_3, SO_2 and NO_2 [37,38]. Also, the feasibility of using a fiber drop analyzer (FDA) for viscosity, spectral absorbance and RI measurements has been recently reported in the literature [39]. Future work will tend towards applying the DSTD as a detector in liquid chromatography and developing FIA methodologies for analyzing mixtures of surfactants where the ion-pairing agent is present in the carrier solvent so that the enhancement effects can be realized.

Acknowledgment

References

[1] M. Shahbaz, J. Wangsa and N. Danielson, Anal. Chem., 64 (1992) 583.

[2] G.R. Bear, J. Chromatogr., 459 (1988) 91.

[3] D.C. Cullum (Ed.), Introduction to Surfactant Analysis, Blackie, London, 1994.

[4] M. Kudoh and K. Tsuji. J. Chromatogr., 294 (1984) 456.

[5] F. Smedes, J.C. Kraak, C.F. Werkhoven-Goewie, V.A.T. Brinkman and R.W. Frei, J. Chromatogr., 247 (1982) 123.

[6] B.A. Bidlingmeyer, J. Chromatogr. Sci., 18 (1980) 525.

[7] B.A. Bidlingmeyer and F.W. Warren, Anal. Chem., 54 (1982) 2351.

[8] A.B. Few and H.R. Ottewell, J. Colloid. Sci., 11 (1956) 34.

[9] G.V. Scott, Anal. Chem., 40 (1968) 768.

[10] S. Eksborg and G. Schill, Anal. Chem., 45 (1973) 2092.

[11] S. Eksborg, P. Lagerstrom, R. Moden and G. Schill, J. Chromatogr., 83 (1973) 99.

[12] H. Daood, P. Biacs, M. Dakar and F. Hajdu, J. Chromatogr. Sci., 32 (1994) 481.

[13] C.C. Lindgren and P.K. Dasgupta, Talanta, 39 (1992) 101.

[14] K. Yamamoto and S. Motomizu, Anal. Chim. Acta, 246 (1991) 333.

[15] L.R. Lima III, D.R. Dunphy and R.E. Synovec, Anal. Chem., 66 (1994) 1209.

[16] L.R. Lima III and R.E. Synovec, J. Chromatogr., 691 (1995) 195.

[17] H. Zhou, Xheijing Daxue Xuebao Ziran Kevueban, 26 (1992) 139.

[18] D. Bergink-Martens, C. Bisperik, H. Bos, A. Prins and A. Zuidberg, Colloids Surfaces, 65 (1992) 191.

[19] H. Ewart and E. Kenneth, J. Chem. Educ., 69 (1992) 814.

[20] G. Parsons, G. Buckton and S. Chatham, Int. J. Pharm., 82 (1992) 145.

[21] A. Adamson, Physical Chemistry of Surfaces, John Wiley, New York, 1982, pp. 20-22.

[22] J. Beck, A. Lefebvre and T. Koblish, J. Propul. Power, 7 (1991) 207.

[23] C. Sun and Q. Deng, Huaxue Tongbao, 9 (1992) 50.

[24] T. Lohnstein, Z. Phys. Chem., 84 (1913) 410.

[25] C.C. Addison, J. Chem. Soc., 570 (1946) 579.

[26] P. Joos and E. Rillaerts, J. Colloid Interface Sci., 79 (1981) 96.

[27] R. Miller and K.-H. Schano, Colloid Polym. Sci., 264 (1986) 277.

[28] S.R. Babu, J. Colloid Interface Sci., 115 (1987) 551.

[29] R. Miller and K.-H. Schano, Tenside Deterg., 27 (1990) 238.

[30] M. Paulsson and P. Dejmek, J. Colloid Interface Sci., 150 (1992) 394.

[31] K. Hool and B. Schuchardt, Meas. Sci. Technol., 3 (1992) 451.

[32] D. Meyers, Surfaces, Interfaces and Colloids. Principals and Applications, VCH. New York, 1991.

[33] R. Miller, P. Joos and V.B. Fainerman, Adv. Colloid Interface Sci., 49 (1994) 249.

[34] P. Delahay and C.T. Fike, J. Am. Chem. Soc., 80 (1958) 2628.

[35] K.A. Connors and J.L. Wright, Anal. Chem., 61 (1989) 194.

[36] R.D. Swisher, Surfactant Biodegradation, Marcel Dekker, Inc., New York, 1987.

[37] S. Liu and P.K. Dasgupta, Anal. Chem., 67 (1995) 2042.

[38] A.A. Cardoso and P.K. Dasgupta, Anal. Chem., 67 (1995) 2562.

[39] N.D. McMillan, E. O'Mangain, J. Walsh, L. Breen, D.G.E. McMillan, M.J. Power, J.P. O'Dea, S.M. Kinsella, M.P. Kelly, C. Mamil and D. Orr, Opt. Eng., 33 (1994) 3871.

Gas chromatographic sensing on an optical fiber by mode-filtered light detection[1]

Carsten A. Bruckner, Robert E. Synovec*

Department of Chemistry, Box 351700, University of Washington, Seattle, WA 98195, USA

Abstract

A chemical sensor for gas phase measurements is reported which combines the principles of chemical separation and fiber optic detection. The analyzer incorporates an annular column chromatographic sensor, constructed by inserting a polymer-clad optical fiber into a silica capillary. Light from a helium–neon laser is launched down the fiber, producing a steady intensity distribution within the fiber, but a low background of scattered light. When sample vapor is introduced to the sensor, and an analyte-rich volume interacts with the polymer cladding, chromatographic retention is observed *simultaneously* with a change in the local refractive index of the cladding. An increase in cladding refractive index (RI) causes light to be coupled out of the fiber, with detection at a right-angle to the annular column length to provide optimum S/N ratio. This detection mechanism is called mode-filtered light detection. We report a gas chromatographic separation on a 3.1 m annular column (320 μm i.d. silica tube, 228 μm o.d. fiber with a 12 μm fluorinated silicone clad) of methane, benzene, butanone and chlorobenzene in 6 min. The annular column length was reduced to 22 cm to function as a sensor, with selected organic vapors exhibiting unique retention times and detection selectivity. The detection selectivity is determined by the analyte RI and the partition coefficient into the cladding. The calculated limit of detection (LOD) for benzene vapor is 0.03% by volume in nitrogen, and several chlorinated species had LOD values less than 1%. For binary mixtures of organic vapors, the detected response appears to be the linear combination of the two organic standards, suggesting that the annular column may be useful as a general approach for designing chemical sensors that incorporate separation and optical detection principles simultaneously.

Keywords: Chemical sensor; Chemical separation; Fiber optic; Gas chromatography; Mode-filtered light detection

1. Introduction

There is continued interest in the development of fiber optic-based chemical analyzers for use in on-line monitoring systems for process analysis, as well as in environmental and clinical applications. Optical methods for gas sensing have several advantages over conventional chemical

methods, which include the possibility of fast, remote, selective, nondestructive, and safe detection [1]. Much of the work in this field is aimed towards taking advantage of optical fibers as the intrinsic sensing element. Fiber optics are able to act as sensors because their light-carrying ability is dependent on the physical nature of the fiber core and the surrounding cladding. If the core or cladding is altered by analyte interaction, the modulation of the guided light can be used for analyte detection. A large portion of the fiber optic sensors in the literature are evanescent wave sensors [1–6]. Evanescent wave sensors rely on the analyte modulation of the evanescent field, which is that portion of the guided wave power distribution residing outside the fiber core. An absorbing species will interact with the evanescent field, and the transmitted light at the fiber exit will show a decrease in intensity for the wavelengths absorbed. Many evanescent field sensors are commonly used for liquid phase detection [2–4]. Sensitivity improves with increased analyte/evanescent field interaction, which is why lengths of exposed fiber up to several meters have been used [2]. Fewer examples exist for evanescent field detection in the gas phase [1,5,6]. The sparseness is mainly due to the gas medium being a thousand-fold more dilute, making trace component detection that much more difficult. Efforts have been made to improve sensitivity by tapering the exposed fiber section [13], or by preconcentrating analytes into the polymeric cladding [5].

An alternative mode of detection involves monitoring the refractive index (RI) of the cladding. The number of paths, or modes, that light can propagate along an optical fiber are constrained by the relative RIs of the core and cladding. Changes in RI of the cladding after the allowable modes of propagation, and thus the transmission properties of the fiber. If analyte partitioning changes the cladding RI, the change in transmitted light allows for analyte detection. In a conventional sensing configuration, changes in the intensity of transmitted light are monitored [7–11]. As with evanescent wave detection, a drawback of this detection method is that small changes in a large background need to be discerned. We have been investigating the use of

optical fibers with the RI detection mechanism as intrinsic sensors in small volume systems, for which extended lengths of exposed fiber are unsuited [12,13]. Our work takes advantage of the idea that, instead of monitoring transmitted light, it is better to collect the mode-filtered light that is scattered normal to the fiber axis. The background is substantially lower than transmitted intensity measurements, and the S/N advantage allows a shorter length of fiber to be used as the sensing element.

Detecting from the side of the fiber can give the fiber additional selectivity [12,13]. By inserting a fiber into a transparent capillary tube, we have produced a configuration which provides chromatographic information as well as detection

A

B
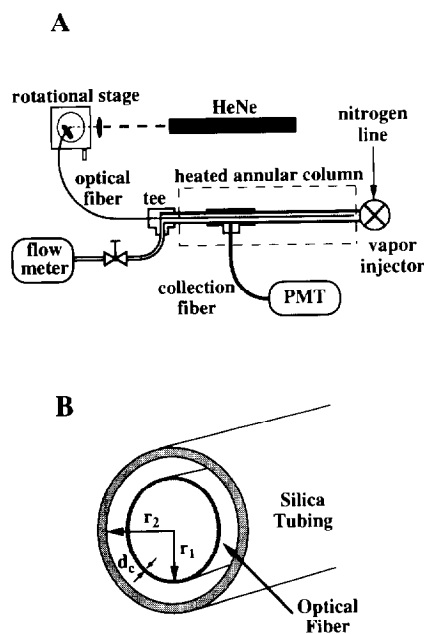
Fig. 1. (A) Schematic of annular column sensor: HeNe laser light focused with 5× lens and launched at an angle of 25° into an optical fiber; this fiber goes into the capillary tube to form the annular column; headspace vapor is introduced to the column via the vapor injector; gas flow controlled with a needle valve; a second optical fiber carries light scattered from the annular column to a PMT. (B) Close-up of annular column: an optical fiber is inserted in a fused silica capillary tube, and gas samples flow in the channel between the fiber and the tube. Separation efficiency is improved by reducing the cladding thickness, d_c, and the distance between the fiber and the tube, $r_2 - r_1$.

(Fig. 1A). The fiber cladding functions as the stationary phase, allowing components in a sample to migrate at different rates down the length of what we term an "annular column" (Fig. 1B). After a certain degree of separation has been achieved, the components pass the detection section of the fiber. The light that is mode-filtered and scattered at this point passes through the capillary tube and is monitored (Fig. 1A). This technique has been applied by us to speciate organics, primarily in aqueous phase samples [12,13]. This paper presents the rationale for mode-filtered light detection, and expands upon the application of the annular column sensor to gas phase analysis. First, we briefly describe the theory of mode-filtered light detection in the context of gas phase measurements. Second, the first report of a gas chromatographic separation on an annular column is presented. Third, the reproducibility of the gas sensor is considered. Finally, the simultaneous separation and detection of gas phase samples are reported, and a two component mixture deconvoluted using vapor standards.

2. Theory

Consider the two cases of measuring the change in transmitted beam intensity as shown in Fig. 2, along with a third case to be discussed shortly. With an incident beam intensity I_0 coupled into a fiber optic at a wavelength of negligible absorbance, conservation of energy requires that I_0 will be either transmitted as I_T, or mode-filtered as I_F due to the natural mode-filtering processes in the fiber optic as a result of the numerical aperture (NA) condition and scattering centers. This relationship is simply

$$I_0 = I_T + I_F \tag{1}$$

where I_T is the transmitted beam background, and I_F is the mode-filtered light background. The mode-filtered light signal, ΔI_F, due to an induced change in the local NA along the fiber optic, is equivalent for both measurements shown in Fig. 2, transferring from I_T to I_F, as I_0 remains constant:

A

B
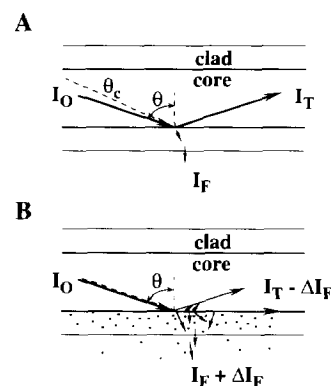
Fig. 2. Mode-filtered light detection mechanism: light propagates in a fiber if the critical angle θ_c is less than the propagated angle θ. (A) A small fraction of light is filtered out of the side, I_F. (B) A partitioning analyte with a RI greater than the cladding RI increases θ_c, resulting in $\theta_c \geqslant \theta$. Under this condition more light is filtered out. Monitoring mode-filtered light, I_F, has an S/N advantage over the traditional method of monitoring transmitted light, I_T. See text for details.

$$I_0 = (I_T - \Delta I_F) + (I_F + \Delta I_F) \tag{2}$$

The noise in the transmission measurement is proportional to I_T, while in the direct mode-filtered light measurement, the noise is proportional to I_F, assuming one is not shot-noise-limited in either case. If the ratio of the backgrounds is given as β, the ratio of noise levels is

$$\beta = I_T/I_F \tag{3}$$

Thus, the S/N ratio of the direct mode-filtered light measurement relative to the conventional transmission measurement at the end of the fiber is equal to β, since the signal is ΔI_F for both. As β values are around 10–100, there is a S/N advantage in measuring mode-filtered light directly.

While Eqs. (1–3) were derived with the entire fiber length in mind, a third case also warrants consideration. If one directly measures the mode-filtered light over a small fraction of the fiber surface area, ϕI_F, it follows from Eqs. (1) and (2) that both I_F and ΔI_F will be reduced by the same fraction, ϕ. Thus the S/N ratio for the case of measuring ϕI_F should be equivalent to the second case, measuring all of I_F, and will also be β times better than the conventional transmission mea-

surement case. Again, this assumes that one is not shot-noise-limited. Use of a typical helium–neon or diode laser of 5 mW is generally sufficient to avoid a shot-noise-limited measurement. Now, the small area measurement, while providing optimum S/N ratio, also affords unique advantages to small volume chemical analysis which we are taking advantage of in our design by monitoring light in only a narrow section of the annular column (Fig. 1A).

The critical angle θ_c is defined as the minimum angle at which a light ray will be totally internally reflected at the core–clad interface (see Fig. 2). Light can propagate in a fiber for extended distances only if the rays reflect at angles of $\theta > \theta_c$. Since θ_c is dependent on the relative RIs of the core and cladding through the equation

$$\sin \theta_c = n_{clad}/n_{core} \tag{4}$$

where n is the RI of the core or clad, changes in n_{clad} will affect the critical angle. Analyte partitioning into the cladding may change n_{clad}, and the resulting critical angle change results in the mode-filtered light signal ΔI_F. For a small concentration of extracted analyte

$$\Delta I_F = \alpha \Delta \theta_c \tag{5}$$

where α is a proportionality constant that takes into account the light collection efficiency and the conversion of the light flux to the detected current [12]. The change in critical angle (Fig. 2) is quantitatively related to experimental conditions, as given by

$$\Delta \theta_c = (n_{clad}/n_{core})\{(n - n_{clad})/NA\}K_d C_{v,m} \tag{6}$$

where n is the RI of the interacting chemical species, and NA is the numerical aperture of the fiber optic. The partition coefficient K_d describes the relative chemical affinity of a given chemical species between the solvent phase and the fiber clad, i.e. the relative concentration of a given species between these two phases. Essentially, K_d describes the enrichment one observes for the analyte concentration in the cladding over the initial concentration in the bulk solvent, given as $C_{v,m}$, with units of volume fraction. Thus, the mode-filtered light signal to the first order is given by Eqs. (5) and (6) and is linear with respect to

analyte RI, analyte concentration and K_d [12]. This paper presents data for analytes with appreciable sensitivity. Sensor response to analytes like pentane, which due to a low K_d value have a negligible sensitivity, are not shown, but the added selectivity for analytes with large K_d value should be recognized.

3. Experimental

The feasibility of performing chromatography with an annular column was demonstrated with a 3.1 m section of 228 μm o.d fiber with a 12 μm fluorinated silicone cladding (removable jacket, fiber type HCR-H200B, Ensign-Bickford, Avon, CT) inserted into an equal length of 320 μm i.d. undeactivated silica tubing (Polymicro Technologies, Phoenix, AZ). Attached to the end of the column was a pressure restrictor, 20 cm of 50 μm i.d. silica tubing (Polymicro Technologies). The column was run at 120°C and 20 psi in a Hewlett-Packard 5890 gas chromatograph with splite injection and flame ionization detection.

The remainder of the data was collected using a set-up incorporating optical detection (Fig. 1). The annular column consisted of the same optical fiber, inserted into a 530 μm i.d. fused silica capillary (J&W Scientific, Folsom, CA). Helium–neon laser light at 633 nm was focused with a 5 × objective into 3.5 m of the polymer clad fiber, the last 20 cm of which was inserted into the capillary tube for exposure to vapor. Focusing the light into the fiber ensured that the limiting source of noise was due to intensity fluctuations of the laser and not shot noise. Care was taken to prevent damaging the fiber, as faults in the fiber could scatter light, which would interfere with light that scattered as a result of analyte partitioning. The fiber was sealed to the tee end of the column (Fig. 1A) by gently clamping a ferrule down onto a piece of 0.010 in. i.d. PEEK tubing through which the fiber was inserted. A micropositionable fiber chuck mounted on a rotational stage (Newport, Fountain Valley, CA) was used to control the angles at which light was coupled into the optical fiber. Light propagating near the critical angle θ_c is more susceptible to mode filter-

ing upon perturbation of the cladding. The optimum S/N ratio was obtained when light was launched at 25° normal to the fiber face, so that condition was used. This launch angle is just within the acceptance angle of 26°, resulting in a large portion of the light propagating close to the critical angle. Nitrogen as the carrier gas was introduced at 20 psi at the opposite end of the column, with a flow of 0.4 ml min^{-1}, measured at the column outlet. Since the sensitivity of the device is dependent on analyte affinity with the cladding (K_d, Eqs. (5) and (6)), which in gas phase studies can be varied with temperature, a temperature-controlled heating strip was placed along the annular column, and both were wrapped in fiberglass insulation. The signal was recorded by measuring the light emitted from the side of the fiber through the capillary tube (polyimide coating removed) with a photomultiplier tube (PMT; type 1P28, Hamamatsu). The elevated temperatures prevented the use of the PMT next to the column, so 1 m of a 500 μm diameter core optical fiber from the PMT was butted perpendicular to the column with a tee, 7 cm from the column exit, to collect the mode-filtered light. The proximity of the collection and emission fibers allowed light from no more than a 1.5 mm length of the emission fiber to be monitored, despite the large 60° acceptance angle of the collection fiber. A power supply operated the PMT at 700 V, and the signal was sent to a chart recorder or computer via a current-to-voltage converter (model 3A14, Pacific Instruments, Concord, CA). Figs. 4–6 represent the signal after a 3 s moving average was applied to the raw data.

Sample vapor was injected with a 300 μl injection loop using a 10-port electrically actuated valve with computer control (model EQ36, Valco, Houston, TX). An in-house system continuously fed headspace samples through the injection loop from organic liquids slowly purged at ambient temperature with nitrogen. Injected vapor concentrations were estimated by comparing the partial pressures of the samples to the total pressure in the purging vessel.

4. Results and discussion

An optical fiber inserted in a capillary tube allows the fiber cladding to function as a stationary phase, providing a gas chromatographic separation in the annular column. As shown in Fig. 3, the annular column separates compounds based on their relative affinities to the fiber cladding. Earlier experiments without the inserted fiber showed no measurable retention of these compounds on the capillary wall at this temperature. As can be seen, the later eluting compounds are broadened considerably relative to methane. This phenomenon is not unexpected, given the thickness of the stationary phase. The polymer cladding is 12 μm thick, much thicker than traditional GC stationary phases, which are of the order of 1 μm or less. As a result, the large resistance to mass transfer in the stationary phase slows the exchange rate of analytes between the stationary and mobile phases. In subsequent experiments, the inserted fiber provided detection as well as chromatographic modulation of compounds (Fig. 1A). The emphasis for these experiments was not on the optimization of the chromatography per se, but instead on the development of the sensing aspect of the annular column. As a result, the column length was shortened to both simplify column preparation and reduce run times.

Reproducibility of the gas phase sensor was then considered. Fig. 4 shows multiple headspace injections of benzene at 90°C, which provides a measure of the system reproducibility. These data
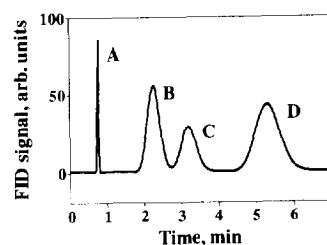
Fig. 3. Separation of methane (A), benzene (B), butanone (C), and chlorobenzene (D) on a 3.1 m annular column with flame ionization detection, run at 120°C. This Figure highlights the chromatographic ability of the annular column configuration. Band broadening of peaks is the result of the thick 12 μm cladding.

C.A. Bruckner, R.E. Synovec / Talanta 43 (1996) 901–907
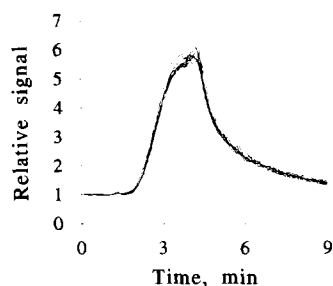
Fig. 4. Annular column sensor response to seven benzene headspace injections, at 5% (v/v) in nitrogen at 20 psi. Responses normalized by dividing analyte response into background response. Intergrated area precision is 4.3% RSD.

Fig. 5. The annular column sensor provides selective temporal information for various species. Shown are responses to separate vapor injections of 23% (v/v) methylene chloride (M), 11% chloroform (C), and 4% trichloroethylene (T).

were corrected for light source intensity drifts by dividing the analyte response into the background response. The benzene concentration is 5% (v/v) in nitrogen, so the limit of detection is 0.03% (3σ) for the given run conditions. The relative standard deviation of the integrated response was 4.3%, which includes sample introduction error. The thickness of the cladding required a lengthened period of analyte exposure to the fiber before the sensor response equilibrated. The data therefore bear a stronger resemblance to steady-state sensor experiments than to chromatographic data. Note the low amount of background light relative to the analyte signal, which was collected by monitoring the filtered light emitted from a small section of the exposed fiber. It is this feature of mode-filtered light detection that makes it possible for the sensor to monitor its chromatographic capability. The traditional fiber optic detection mechanism, monitoring the transmitted light, is not sufficiently sensitive to measure analyte partitioning on such a small surface area, due to the high background. For transmission-type measurements, an extended length of exposed fiber is required to increase the analyte signal relative to the background. However, transmission-type measurements integrate the sensor response along the entire length of the fiber, which inhibits their use as chromatographic sensors. Operating the system at lower temperatures increased the partitioning into the cladding, which improved the detector sensitivity (Eq. (6)). However, at temperatures approaching ambient, the sensor response

became erratic. This behavior may result from hardening of the cladding at lower temperatures, or from vapor condensation on the fiber surface, which would scatter light unpredictably. The chosen operating temperature was therefore a compromise between detection sensitivity and sensor reliability.

The separation and detection of analytes by the same device is demonstrated in Figs. 5 and 6. Fig. 5 shows the superposition of three chlorinated compounds, and highlights the temporal selectivity of the sensor. Detection limits are based on calculated injection concentrations of 23% methylene chloride (v/v), 11% chloroform, and 4% trichloroethylene. Detection limits at three times the baseline noise level for methylene chloride, chloroform, and trichloroethylene are there-
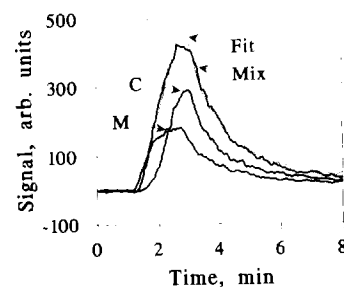
Fig. 6. Sensor response to headspace of a 1:1 mixture of methylene chloride (M) and chloroform (C). Pure headspace injections of the two components were fit to this mixture, and the best fit using classical least-squares (CLS) also predicted a 1:1 mixture. Pure component responses are scaled so their sum is the best fit line. CLS required all the baselines to be centered at zero.

fore 0.5% (v/v), 0.2%, and 0.06% respectively. The varying detection limits of these compounds result from differing degrees of cladding preconcentration (K_d, Eq. (6), combined with the magnitude of the RI difference between the compounds and the cladding ($n - n_{clad}$, Eq. (6)). These detection limits highlight the fact that, for analytes with RIs different from the cladding RI, the annular column sensor is generally more sensitive to compounds with higher boiling points, which tend to preconcentrate in the non-polar cladding to a greater extent. This is because analyte boiling point is often correlated with the size of the non-polar group on the analyte. Fig. 6 shows how well the sensor responds to the headspace of a 1:1 mixture of methylene chloride and chloroform, relative to the sensor's response to the pure components. Since the components in the mixture are not fully resolved in a chromatographic sense, quantitation of the mixture required fitting the pure component responses to the mixture response using classical least-squares. The best fit mixture is also shown in Fig. 6 as a superimposed line on the actual response. The best fit also predicts a 1:1 concentration of the two components, implying that the signals are additive. Note that good quantitation does not require complete component resolution as long as the individual responses are distinct and reproducible [14].

5. Conclusion

It has been demonstrated that the annular column fiber sensor configuration can provide chromatographic information in addition to just sensitive detection. This additional information endows the annular column sensor with more selectivity in the identification of analytes. Detecting mode-filtered light directly from the side of the fiber holds promise for obtaining improved detectability. Future developments of the annular column sensor include the replacement of the fiber cladding with different coatings more suited to analyte partitioning. Reducing the thickness of the cladding will shorten the response time of the sensor and improve the chromatographic efficiency. The modified surface layer must still allow the fiber to conduct light efficiently, and it must be robust enough for extended use.

Acknowledgment

References

[1] H. Tai, H. Tanaka and T. Yoshino, Opt. Lett., 12 (1987) 437.

[2] J. Bürke, J.P. Conzan and H.J. Ache, Fresenius' Z. Anal. Chem., 342 (1992) 394.

[3] M.D. DeGrandpre and L.W. Burgess, Anal. Chem., 60 (1988) 2582.

[4] B.D. Gupta, C.D. Singh and A. Sharma, Opt. Eng., 33 (1994) 1864.

[5] B. Mizaikoff, K. Taga and R. Kellner, Vibr. Spectrosc., 8 (1995) 103.

[6] A. Messica, A. Greenstein, A. Katzir, U. Schiess and M. Tacke, Opt. Lett., 19 (1994) 1167.

[7] F.K. Kawahara, R.A. Fiutem, H.S. Silvus, F.M. Newman and J.H. Frazar, Anal. Chim. Acta, 151 (1983) 315.

[8] S.M. Klainer, J.R. Thomas, D.K. Dandge, C.A. Frank, M.S. Butler, H. Arman and K. Goswami, SPIE J., 1434 (1991) 119.

[9] K. Goswami, S.M. Klainer, D.K. Dandge and J.R. Thomas, in R.P. Buck, W.E. Hatfield, M. Umaña and E.F. Bowden (Eds.), Biosensor Technology, M. Dekker, New York, 1990, pp. 299–310.

[10] J.F. Giuliani and N.L. Jarvis, Sens. Actuat., 6 (1984) 107.

[11] J.F. Giuliani and N.L. Jarvis, J. Chem. Phys., 82 (1985) 1021.

[12] R.E. Synovec, A.W. Sulya, L.W. Burgess, M.D. Foster and C.A. Bruckner, Anal. Chem., 67 (1995) 473.

[13] R.E. Synovec, C.A. Bruckner, L.W. Burgess and M.D. Foster, SPIE J., 2293 (1994) 167.

[14] T.J. Bahowick and R.E. Synovec, Anal. Chem., 67 (1995) 631.

Electroinjection analysis. The introduction of a new variant of flow-injection analysis and comparison with electrophoretically-mediated microanalysis[1]

V.P. Andreev*, A.G. Kamenev, N.S. Popov

Institute for Analytical Instrumentation, Russian Academy of Sciences, 26 pr. Rigsky, 198103 St. Petersburg, Russian Federation

Abstract

A new method of mixing sample and reagent due to the difference in their electrophoretic mobilities is introduced. Unlike electrophoretically-mediated microanalysis, sample and reagent are injected from the opposite ends of a capillary tube. This method is compared with electrophoretically-mediated microanalysis. Experiments are performed showing the possibilities of this new method.

1. Introduction

Improvement of sample and reagent mixing without an increase in the product dispersion is very important for the maximization of flow-injection analysis (FIA) sensitivity, especially in the case of rapid kinetic analysis. Mathematical modeling of FIA with a fast second-order reaction [1] showed that if sample and reagent were initially premixed then a shorter reaction tube will minimize product dispersion and maximize sensitivity of the analysis. Longer reaction tubes cause expansion of the product dispersion due to the non-uniform flow profile.

The imperfections of sample and reagent mixing in the mixing tees has been shown [2] and a much better way to mix sample and reagent with the help of a coaxial jet mixer was proposed [3].

A new method of sample and reagent mixing called electrophoretically-mediated microanalysis (EMMA) was proposed and developed [4–7]. In the EMMA method, sample and reagent are mixed in the capillary electrophoretic system due to the difference in their electrophoretic mobilities.

The objective of this paper is to present another variant of sample and reagent mixing based on the same idea as EMMA and to introduce a new

---

* Corresponding author.

variant of FIA. We have called this technique electroinjection analysis (EIA), and have compared its properties with EMMA.

2. Idea of the method

In both methods (EMMA and EIA) mixing of sample and reagent takes place in the capillary with the longitudinal electric field applied. In fact both methods were realized with the help of capillary electrophoresis systems built in the laboratory. Mixing of sample and reagent in both methods is due to the difference in their electrophoretic mobilities. However, in EMMA, sample and reagent are injected from the same end of the capillary while in our method sample and reagent are injected from opposite ends of the capillary. The principles of both methods are presented in Fig. 1. In EMMA the slower reactant is injected first followed by injection of the faster one. As the faster one passes through the slower one, they will react and the product is then detected photometrically. In our method both reactants are injected simultaneously from opposite

Fig. 1. Principles of the methods of EIA and EMMA.

ends of the capillary. They meet in the capillary, pass through one another and react. As can be seen from Fig. 1, in EMMA there is some critical minimum length needed to mix sample and reagent. This is determined by w_{min}, which is equal to sample length, and by the difference in the electrophoretic mobilities of the reactants:

$$l_{mix} = t_{mix} \cdot \mu_s E = \frac{w_{min}}{\Delta\mu_{ep} E} \cdot \mu_s E = \frac{w_{min}}{\Delta\mu_{ep}} (\mu_{ep.s} + \mu_{osm})$$

where l_{mix} is the mixing length, t_{mix} is the mixing time, $\mu_s = \mu_{ep.s} + \mu_{osm}$ is the sample mobility, $\Delta\mu_{ep} = \mu_{ep.s} - \mu_{ep.r}$ is the difference in electrophoretic mobilities of sample and reagent, μ_{osm} is the electroosmotic mobility and E is the electric field strength. So, the smaller the difference in electrophoretic mobilities of the reactants the longer the mixing tube must be. According to EIA one can mix sample and reagent in very short tubes. In fact tube length is limited only by the sum of the initial sample and reagent lengths. When comparing EIA and EMMA, the question of analytical capabilities naturally arises. What are the possible samples and reagents for both methods? Are there any restrictions? In both cases, the capillary must be filled with some liquid with non-zero conductivity. In both cases, at least one of the reactants must be charged. In both cases, total velocity of the reactant is equal to the sum of its electrophoretic velocity and the electroosmotic velocity of the liquid in the capillary. Due to the presence of electroosmotic flow during EIA one can mix not only oppositely charged reactants but also neutral and charged reactants. Even reactants with the same charge can be mixed if one of them has low molecular weight and the other has high molecular weight.

Let us assume that the zeta potential of the capillary wall is negative ($\zeta < 0$), then the eletroosmotic flow is in the same direction as the electric field. In order to mix positive sample ions ($z_s > 0$) with negative reagent ions ($z_r < 0$) having total velocities equal to

$$v_s = (|\mu_{ep.s}| + |\mu_{osm}|)E \qquad (1)$$

$$v_r = (|\mu_{ep.r}| - |\mu_{osm}|)E \qquad (2)$$

then one must satisfy the condition $v_r > 0$, i.e.
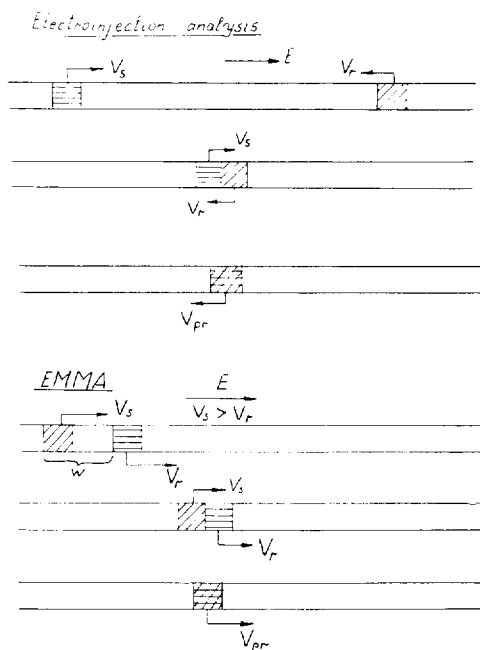
$$|\mu_{ep.r}| > |\mu_{osm}| \tag{3}$$

and this condition is quite natural for low molecular weight reactants. The same condition must be fulfilled if one of the reactants is neutral ($z_s = 0$) and the other is negatively charged ($z_r < 0$), then the first one is carried by the electoosmotic flow

$$v_s = |\mu_{osm}|E \tag{4}$$

and the second one must have an electrophoretic mobility larger than the electroosmotic mobility. If both reactants are negatively charged ($z_s < 0$, $z_r < 0$) then:

$$v_s = (|\mu_{osm}| - |\mu_{ep.s}|)E \tag{5}$$

$$v_r = (|\mu_{ep.r}| - |\mu_{osm}|)E \tag{6}$$

and in order to mix reactants one must have:

$$|\mu_{ep.s}| < |\mu_{osm}| \tag{7}$$

$$|\mu_{ep.r}| > |\mu_{osm}| \tag{8}$$

Condition (7) is natural for high molecular weight reactants while condition (8) is natural for low molecular weight reactants. Sample and reagent are quite interchangeable, so one can mix with the help of EIA not only high molecular weight samples and low molecular weight reagents, but also low molecular weight samples and high molecular weight reagents. The rule is simple: the reactant that is injected in the direction opposite to the direction of the electroosmotic flow must have a high eletrophoretic mobility.

If the zeta potential of the capillary wall is positive then the same conditions must be fulfilled, but the signs of the charges of the reactants must be reversed and so positively charged reactants can be mixed if one of them has a low molecular weight and the other has a high molecular weight. If the zeta potential of the capillary wall is equal to zero then the reactants must have opposite charges in order to be mixed.

When using EMMA one can easily mix reactants with electrophoretic mobilities having the same sign as μ_{osm}. However, if the sign of electrophoretic mobility of one of the reactants is different from the sign of electroosmotic mobility, then the electrophoretic mobility must be smaller than the electroosmotic mobility of the liquid in

the capillary, and this is natural for high molecular weight reactants. This is probably the reason why EMMA was proposed and realized for biochemical reactions. EIA can be used for low molecular weight objects as well.

As can be seen, both EIA and EMMA have some limitations so far as the values and signs of the electrophoretic mobilities of the reactants are concerned. However, virtually any pair of reactants can be mixed either by EIA or EMMA, except in the case where both reactants have zero charge. In fact, these are not conflicting methods at all. They can be combined, as is shown in the following section of the paper, or realized with the same instrument — a capillary electrophoresis system with two samplers, designed so as to be capable of injecting reactants from both ends of the capillary simultaneously. However, in the case where electrophoretic mobilities of the reactants have values that permit the use of either method, it seems that EIA has some advantages over EMMA. Firstly, the possibility to use very short capillaries for EIA, and consequently to use lower electric fields, was previously mentioned. Secondly, in EMMA cross contamination of sample and reagent is possible at the introduction end of the capillary. During EIA this is impossible because sample and reagent are injected through opposite ends of the capillary. Thirdly, in the case of sorption of the reactants on the capillary wall during EMMA, there might be chemical interaction between moving and sorbed ions which might lead to the tailing of the product peak. However, in EIA, sample and reagent move in different paths and such interaction is impossible. Finally, during EMMA reactants are injected one after another, in comparison to EIA where they can be injected simultaneously electrokinetically. This seems to be an advantage not only in so far as the time of analysis is concerned. This simple type of injection seems to be the optimal one at least for the fast chemical reactions with neutral product. Let us assume the ideal situation where the reaction rate is much higher than the rate of electrophoretic transport, concentrations of both reactants are equal, and neutral product is produced. Then this situation may be described by the simplistic model presented in Fig. 2. Ideally an
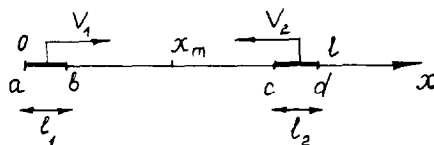
Fig. 2. Simplistic model of sample and reagent mixing in EIA.

infinitely thin product zone will be formed when point b meets point c at the same place where point a meets point d. Coordinates of these points are determined by the following simple equations:

$$x_{ad}/v_1 = (l - x_{ad})/v_2 \tag{9}$$

$$(x_{bc} - l_1)/v_1 = (l - l_2 - x_{bc})/v_2 \tag{10}$$

where l is the length of the capillary, v_1 and v_2 are the velocities of reactant transport and l_1 and l_2 are the initial lengths of the reactant zones. Then from $x_{ad} = x_{bc}$, it follows that the simple condition

$$l_2/l_1 = v_2/v_1 = (\mu_{ep2} + \mu_{osm})/(\mu_{ep1} + \mu_{osm}) \tag{11}$$

can easily be satisfied if the reactants are injected electrokinetically and simultaneously by simply putting the ends of the capillary to the sample and reagent bottles and applying a high voltage to them.

3. Experimental

Preliminary experiments to demonstrate the experimental realization of EIA were performed with the help of a capillary electrophoretic system made in the laboratory. The system is presented in Fig. 3. The main difference from the usual capillary electrophoresis system is that we have included two samplers and the potential to inject reactants from both ends of the capillary simultaneously. The inner diameter of the quartz capillary was 100 μm. The potential difference applied to the capillary in most of the experiments was 15 kV. Most of the capillary, with the exception of the sample and reagent zones, was filled with distilled water. As a result very low electrical current was observed (it was never larger than 10 μA), and thus no problems with Joule heating occurred. Fig. 4 presents the typical peak for the well-known analytical reaction between Fe^{3+} ions and sulfosalicylic acid. The sample, standard
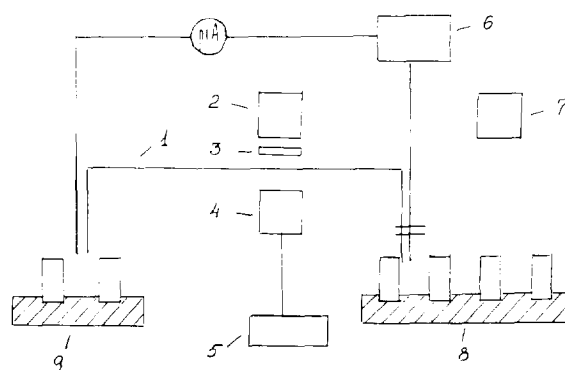
Fig. 3. Capillary electrophoresis system used for EIA experiments: (1) quartz capillary; (2) lamp; (3) filter; (4) photodetector; (5) analog recorder; (6) power source; (7) air pump; (8,9) samplers.

aqueous solution of Fe^{3+} ions, and the reagent, 0.5% solution of sulfosalicylic acid, were electrokinetically injected simultaneously through opposite ends of the capillary. The injection time was 40 s. Approximately 10 min after the injection the product peak was detected photometrically at $\lambda = 430$ nm. The experiments were performed for sample concentrations varying from 10^{-5} g
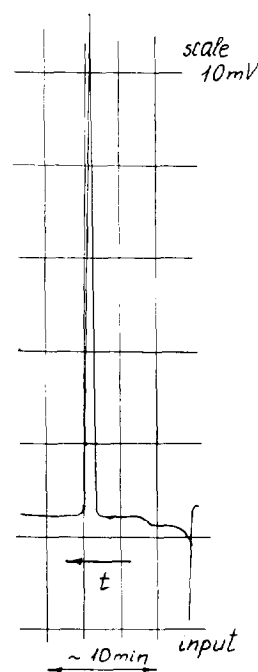
Fig. 4. Typical peak of the product of the analytical reaction of determination of Fe^{3+} with the aid of sulfosalicylic acid.
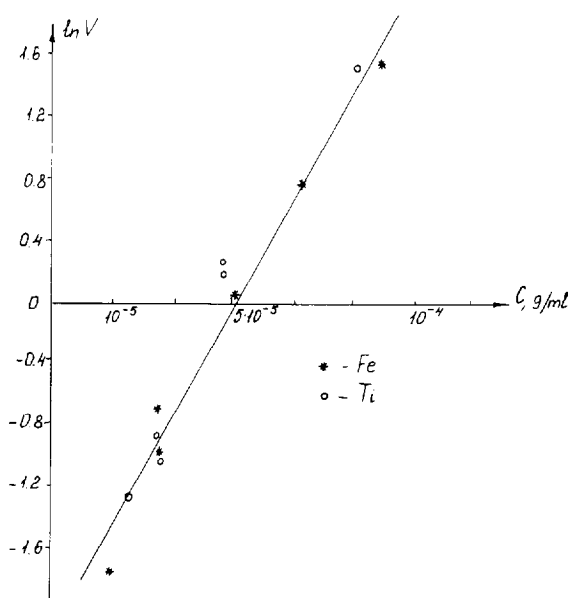
Fig. 5. Logarithm of the detector output vs. sample concentration for determination of Fe^{3+} and Ti^{4+}: (∗) Fe^{3+}; (○) Ti^{4+}.

ml^{-1}–10^{-4} g ml^{-1} and the resulting calibration curve (dependence of the logarithmic detector output vs. concentration) was practically linear (see Fig. 5).

The analytical reaction in the determination of Ti^{4+} ions using hydrogen peroxide and sulfuric acid was also realized. Actually, it was a combination of EIA and EMMA because two reactants, Ti^{4+} and hydrogen peroxide, were sequentially injected from one end of the capillary and sulfuric acid was injected from the opposite end of the capillary. The product of the reaction was detected photometrically at $\lambda = 580$ nm. A series of three injections is presented in Fig. 6. The same range of sample concentrations as in the case of the determination of Fe^{3+} ions was studied. Results of the experiments are presented in Fig. 5. The detection limit for both reactions appeared to be nearly the same and equal to 10^{-5} g ml^{-1} with the signal-to-noise ratio equal to 3. This detection limit is rather close to the detection limit reported in Ref. [7] for EMMA of ethanol and could be significantly improved by well-known methods used to enhance the sensitivity of absorbance detectors, such as using z-cells [8] or multireflec-

tion cells [9].

Of course the results presented are preliminary ones and much more experimental work must be done. The objective of presenting these experimental results is to show the possibility of the experimental realization of EIA and the possibility of combining EIA and EMMA. Either of these methods or their combination can be realized with the help of a simple capillary electrophoretic system designed in such a way as to be capable of injecting reactants from both ends of the capillary simultaneously.

4. Conclusion

The new EIA method shares the advantages of EMMA: minimal volumes of analyte and reagent (nanoliters), minimal dispersion of the product and the possibility to separate analyte from the matrix components due to the intrinsic separative capacity of electrophoresis. EIA and EMMA can be combined to realize chemical reactions with several reagents. There are also some advantages of EIA when compared with EMMA, among them the possibility to prevent cross contamination of sample and reagent since they are injected from opposite ends of the capillary. EIA has a lot
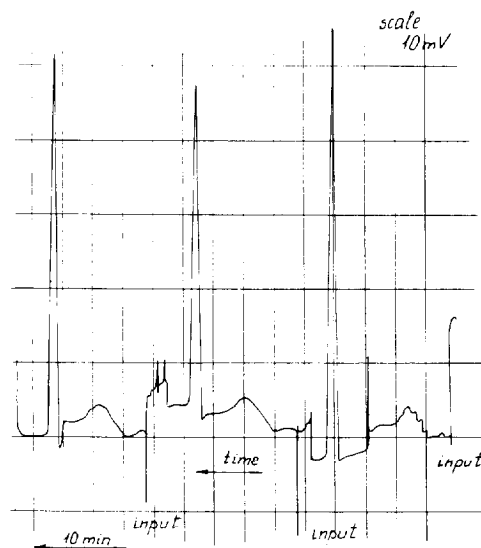
Fig. 6. Series of three experiments for the determination of Ti^{4+} with the aid of hydrogen peroxide and sulfuric acid.

of potential as far as micromachining is concerned, because to realize EIA on a microchip one need not have moving parts for sample injection, or even an injection cross that was used in the microchip variant of CE [10]. The simplest EIA could be realized on a microchip with just the help of one microgroove with a micro reservoir at each end.

References

[1] V.P. Andreev and T.V. Kondratieva. Talanta, 41 (1994) 1755.

[2] G.D. Clark, J.M. Hungerford and G.D. Christian, Anal. Chem., 61 (1989) 973.

[3] I.D. Scampavia, G. Blankenstein, J. Ruzicka and G.D. Christian, Anal. Chem., 67 (1995) 2743.

[4] J. Bao and F.E. Regnier, J. Chromatogr., 608 (1992) 217.

[5] B.J. Harmon, D.H. Patterson and F.E. Regnier, Anal. Chem., 65 (1993) 2655.

[6] B.J. Harmon, I. Leesong and F.E. Regnier, Anal. Chem., 66 (1994) 3797.

[7] B.J. Harmon, D.H. Patterson and F.E. Regnier, J. Chromatogr., 657 (1993) 429.

[8] S.E. Moring, R.T. Reel and R.E.J. van Soest, Anal. Chem., 65 (1993) 3454.

[9] T. Wang, J.H. Aiken, C.W. Huie and R.A. Hartwick, Anal. Chem., 63 (1991) 1372.

[10] D.J. Harrison, A. Manz, Z. Fan, H. Ludu and H.M. Vidmar, Anal. Chem., 64 (1992) 1926.

Field-portable flow-injection analysers for monitoring of air and water pollution [1]

Peter W. Alexander[a],* Lucy T. Di Benedetto[a], Telis Dimitrakopoulos[a],
D. Brynn Hibbert[b], J. Catherine Ngila[b], Margaret Sequeira[b], Damien Shiels[b]

[a]*Department of Physical Sciences, University of Tasmania, P.O. Box 1214, Launceston, Tas 7250, Australia*
[b]*Department of Analytical Chemistry, University of New South Wales, Sydney N.S.W. 2052, Australia*

Abstract

There has been a rapid growth in the development of field-portable analytical instrumentation capable of in-situ and real-time feedback of data from remote sites. Advances have been made in applications for many technologies aided by developments in electronics, computing and telecommunications systems. This report presents a brief review of these developments and particularly of portable flow-injection systems applied in both the liquid and gas phase modes of operation with potentiometric sensors and gas sensors of the tin-oxide semiconductor types.

Keywords: Air pollution; Portable flow-injection systems; Water pollution

1. Introduction

The aim of this paper is to present a range of applications of portable monitors for the analysis of various aqueous and gas samples. For the analysis of aqueous samples, a multi-cell consisting of potentiometric sensors has been investigated in the flow-injection mode. Multiple sensors have been employed in flowthrough cells in which the cells-in-series concept has been applied to measure various anions with improved sensitivity over conventional single-cell systems. A portable multi-sensor monitor has also been developed using tin-oxide semiconductor sensors to monitor various gases and vapours.

The emergence of monitoring portability is contingent on recent advances in the development of chemical sensors, biosensors, gas sensors and disposable test strip sensors. Combinations of sensors with electronic transducers allows conversion of molecular or ion recognition response into an electrical signal which is then used to determine the analyte concentration. Chemical sensors have the potential to form the basis of low-cost, long-term monitoring devices as shown in Table 1 which lists the types of sensor configurations re-

Table 1
Components required for construction of sensors

Recognition elements	Sensing layers	Electronic transducers	Detection methods
Complexing agents	PVC	Electrodes	Electrochemical
Ionophores	Gels	Transistors	Optical
Antibiotics	Cellulose	Optical fibres	Thermal
Ion exchangers	Epoxy	Photodiodes	Mass changes
Antigens	Graphite	Thermistors	Conductivity
Antibodies	Nafion	Semiconductors	Impedance
Enzymes	Solid state crystals	Piezoelectric crystals	Frequency
	Glasses	Surface acoustic wave devices	

ported previously [1,2]. In addition, there are now available many options based on miniature versions of conventional laboratory instruments, such as gas chromatography [3].

The ideal type of monitor is one which has automated sample introduction and calibration, self-cleaning capabilities, in-built algorithms for sample analysis, and provides data storage, data plotting and telecommunications options. Table 1 indicates the various components used in sensor configurations to produce portable monitors. The possibilities for remote site monitoring depend on the weight and power requirements of the monitor, as listed in Table 2. Classifications may be arbitrarily assigned as being fixed-site, transportable, portable, submersible, or hand-held analysers. The monitor types developed particularly of portable operation and applications are summarised in Table 2. Power consumption is a most important parameter to be considered.

1.1. Transportables

Advances have occurred with regard to development of transportable instruments in many areas including mass spectrometry, gas chromatography, ion mobility spectrometry, infrared and UV spectroscopy, X-ray fluorescence and laser radar spectroscopy. A review has recently been published [3] on these techniques which remain highly costly. However, the relatively low

cost person-portable and hand-held types of monitors have undergone remarkable advances in the last 10 years due to the improvements in sensor design and miniaturised electronics and computing mentioned above. The main advances have been made in molecular and ion analysers, and gas and vapour analysers. These are applicable in many of the areas of technology mentioned below.

1.2. Chemical ion sensors

Relatively low cost portable monitoring techniques have been produced and are based on flow-injection analysis, electrochemistry, chemical sensors, gas sensors, biosensors, and filed test kits. Portable devices have been developed for a range of applications such as medical, automotive, industrial, food processing and production, domestic water production, mining, forensic and legislative, oceanographic and environmental areas, particularly for monitoring of water quality and air pollution. Reviews mentioned above on flow-injection techniques for water monitoring and air pollution monitoring have been published [1–3].

Many application areas are in environmental chemistry. User-friendly, field-portable instruments of low cost are now available so that on-the-spot testing can be performed at suspected sites of pollution and also for other quality assur-

Table 2
Classification of remote-site and portable monitors

Type	Weight	Applications
Fixed-site	> 100 kg	Bench top instruments in remote-site housing
Transportable	> 10 kg	Mobility in cars, boats, aircraft
Portable	< 10 kg	Man-portable in backpacks or shoulder packs
Hand-held	< 0.5 kg	Pocket-sized instruments
Submersible	Variable	Designed according to depth requirements

ance tests which may need to be carried out at sites remote from chemical laboratories [4]. The advent of portable notebook computers interfaced to appropriate electronic data acquisition systems has made this possible. Data loggers are alternatives to using notebook computers for long-term operation in remote sites. Communication systems have also decreased in price to such an extent that it has become feasible for field operation with direct transmission of data back to central laboratory computers by use of cellular telephones which can be operated at acceptable costs. The use of portable chemical monitors has therefore taken on a new dimension whereby many non-technical personnel can have access to such systems for monitoring and surveillance purposes. Table 3 shows the types of species detectable with low-cost ion sensors applicable in portable flow-injection analysis (FIA) monitors [5–7] and in ion chromatography [8] in place of the large conventional ion-selective electrodes.

The portability is based on low-cost miniature flowthrough cells containing potentiometric metallic electrode sensors which can be coated with polymer membranes for ion selectivity. The design of a single cell is shown in Fig. 2. The metallic copper electrode responded to various anionic and cationic species shown in Table 3.

1.3. Multi-sensor arrays in FIA

Combinations of these cells in a single FIA system have been used for improved sensitivity in

potentiometric detection of chloride and cyanide [10–12], and have been applied in portable FIA systems [13] with up to three ion sensors for potassium, sodium and nitrate [14]. A four-sensor cell has been reported [15] with ion-selective membrane electrodes for potassium, calcium, nitrate, and chloride, as well as screen printing technology for batch fabrication of integrated chemical sensor arrays [16] for potassium, ammonium, calcium and pH.

1.4. Test kits, disposable test strips and submersible probes

Portable field kits based on colorimetric analysers [17] are available for a wide range of pollutants and nutrients. These require reagent solutions specific for the analyte, and a field-portable photometer equipped with a data-logging facility. Metal cations, inorganic anions and some types of organic and bio-pollutants can be determined. Up to 120 preprogrammed calibrations are possible. Immunoassays and enzyme assays have also been reported based on colour-forming reagents. Pesticides and coliform testing are examples of applications.

Field-portable and submersible electrochemical probes and other electrochemical methods such as anodic stripping voltammetry for trace toxic metals have been described. Test kits are also available based on submersible electrochemical probes for dissolved oxygen, pH, chloride, conductivity, and temperature. Hand-held pH meters, conductivity, and oxidation–reduction potentials have become commonly used, and compact ion

Table 3
Chemical species detected with metallic copper electrode sensors [5–8]

Amino acids	Carbohydrates	Organic acids
Oxidising agents	Organic complexes	Enzyme and substrate
Metallic cations	Reducing sugars	Inorganic anions
Organic amines	Carboxylic acids	Fatty acid
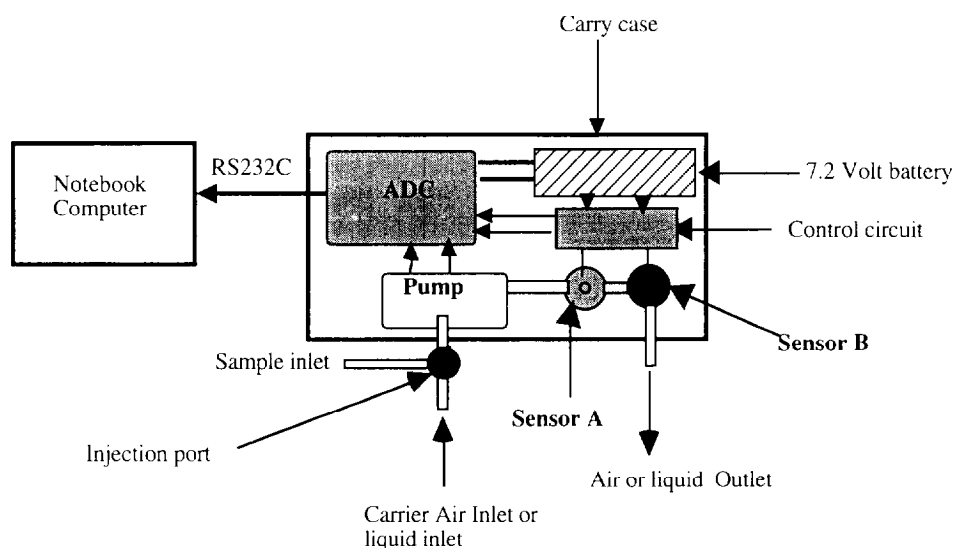
Fig. 1. Block diagram of the portable monitor showing the general purpose design for either liquids or gases, depending on the pump and sensors used.

meters based on planar membrane ion-selective electrodes are available for pH, nitrate, chloride, calcium, potassium and sodium. Portable digital voltammeters have been produced for anodic stripping determinations of trace metals.

Disposable test strip methods have also become available based on the early work on blood glucose sensors [18]. Reflectance spectroscopy has been used with test strips coated with immobilised reagents which react to produce a colour change [18]. Reflectance meters are available as small as pocket size for a wide range of analytes including glucose, ammonium ions, ascorbic acid, copper, iron, lead, phosphate, and sulfite. Amperometric methods and anodic stripping voltammetry have also been used as portable methods for test strip sensors. The amperometric blood glucose test strip analyser has been developed [19] in the shape and size of a ball-point pen, and has become highly successful. Hand-held anodic stripping voltammeters have been produced [20] based on disposable test strips containing the electrode sensors for copper and lead in water samples. These developments are proving of immense value in many fields of technology, allowing for rapid tests to be performed in the field.

1.5. Gas sensors

Gas sensors have been developed for many applications, and a number of types of sensor are available [21]. Portable and hand-held monitors are available for many toxic gases including carbon monoxide, sulfur dioxide, nitrogen oxides, hydrogen sulfide, and volatile organic compounds. The sensors are of numerous types including electrochemical, tin-oxide semiconductors, piezoelectric, surface acoustic wave, infrared, photoionization, and thermal conductivity devices [21].

In the present paper, we review developments of portable analysers and report on new flow-injection monitors for liquids which can also be operated in the gas phase mode. The portable liquid FIA systems developed are based on both single-cell and multi-cell potentiometric sensors applied for the detection of potassium, chloride, nitrate and cyanide. For gas analysis, methods for detection of various gases such as carbon monoxide and total hydrocarbons from car exhaust, and volatile alcohols such as ethanol in beverages, are also reported using tin-oxide semiconductor gas sensors in portable monitors. Diamond [22] has published a review on electrochemical sensor arrays for the analysis of aqueous samples based on

potentiometric, amperometric and voltammetric modes as well as recent advances of gas analysis based on the development of the electronic nose.

2. Experimental

2.1. Design of the portable liquid monitors

The data presented in this paper were recorded using portable FIA instrumentation previously developed [13,14]. Both the liquid and gas analysers were designed in a similar way, as shown in Fig. 1. The electronic circuit, pump and flowthrough sensor cells were constructed in a carry case. For liquid analysis, cells containing ion-selective electrodes (ISEs) were used with a two-channel peristaltic pump (Alitea, OEM-S2) to introduce liquid samples into the flow cell. Flow rates could be varied in the range of 1–8 ml min^{-1}. Manual injections were performed using a Rheodyne-type 5020 rotary injection valve with replaceable sample loops varying in volume from 20–200 μl.

Numerous types of flow cells have been designed and employed for the analysis of liquids. Two types of flowthrough cells were employed in this study. Firstly, a flowthrough perspex block using wire indicator electrodes (< 0.5 mm id) has

Fig. 3. Top and side views of a flow cell housing a planar design liquid-polymer-membrane-based potassium ISE.

been employed with our portable flow-injection monitor which has been described previously [9], and combinations of these cells have been made for studying multi-sensor response [14]. A six-cell system has also been constructed containing six-sensor electrodes and six-reference electrodes and has also been described previously [11] and is shown in Fig. 2. The total volume of the flowthrough cell was approximately 120 μl, the flow rates used were typically 1–2 ml min^{-1} and the carrier stream was seawater. The second flow cell design employed a commercial potassium planar-type ISE obtained from Horiba Ltd. (Japan) that was assembled in a flowthrough cell for flow-injection analysis, as shown in Fig. 3. The potassium planar ISE employed was a liquid-polymer-membrane-based electrode, and the cell volume was approximately 500 μl. Much higher flow rates of up to 6.8 ml min^{-1} were used with this cell due to the larger dead volume and the carrier stream employed was 10 mM lithium acetate.

2.2. Gas analyser design

The hand-held monitor was designed and constructed in-house and is the subject of a provi-

Fig. 2. Multi-sensor potentiometric cell for flow-injection analysis with up to six metallic sensor electrodes (S1...) and six Ag/AgCl reference electrodes (R1...), constructed of perspex, length 120 mm, width 50 mm, internal flow path 1.0 mm diameter.
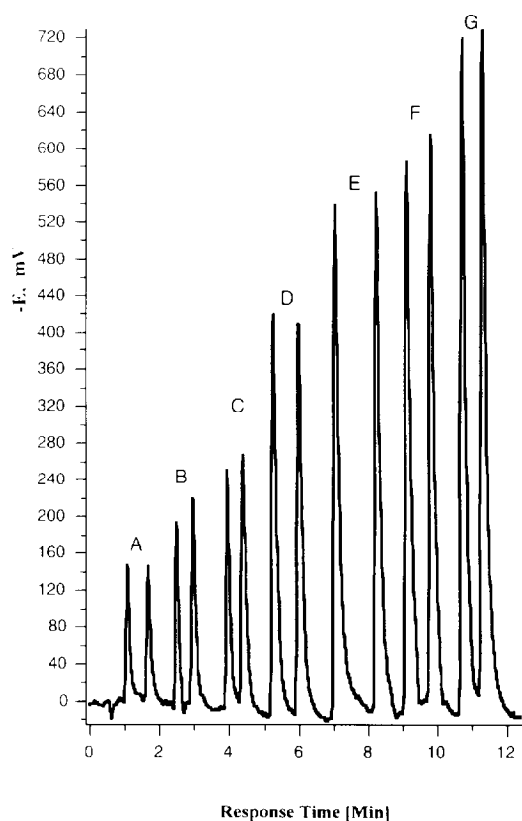
Fig. 4. Peak height response observed for cyanide using six metallic copper electrodes: (A) 5 ppm; (B) 10 ppm; (C) 20 ppm; (D) 40 ppm; (E) 60 ppm; (F) 80 ppm; (G) 100 ppm cyanide in FIA mode.

sional patent [27]. The analyser was fitted with two Taguchi-type sensors (TGS812 and TGS824) obtained from Figaro Inc. (Osaka, Japan) and built into a flowthrough compartment. The gases were pumped through the compartment using a diaphragm pump at a flow rate of 1 l min^{-1}. The sensors and pump were controlled by an electrical

circuit described previously and operated with a rechargeable Ni–Cd battery pack of 7.2 V and 1.4 A h output.

The data from both the liquid and gas analysers were acquired using an eight-channel, 12-bit analog-to-digital converter (ADC) with a serial output at 9600 baud rate with RS-232C serial output to a notebook computer (Macintosh Powerbook 150). The ADC, the pump and the control circuit were powered with a 7.2 V rechargeable Ni–Cd battery pack. The total weight of the system was about 2 kg.

The acquired data from either the liquid or gas analyses were displayed in real time millivolt readings plotted as a function of time using a data acquisition program titled Satod$^\copyright$ (Ver. 1.37) and were saved as text files. The software package IGOR PRO (AD Instruments, Sydney, N.S.W.) was used for data analysis and graphical representation of the data.

3. Results and discussion

3.1. Results for the flow-injection potentiometric analysers

As an example, the portable system described in Section 2 has been successfully used for ISE analysis [13,14] with both conventional ISEs in flowthrough cells and with a three-sensor array of planar electrodes. The FIA output for a cyanide six-cell monitor with metallic copper sensor electrodes is shown in Fig. 4, illustrating the well-defined peaks obtained with a response slope of -370 mV decade^{-1} change in concentration.

Table 4
Single and multi-cell response characteristics for several anions and cations

Ion	Sensor	No. of cells	Slope (mV decade^{-1})	Det. limit (ppm)	Interferences
Cyanide	Copper	6	-370	0.04	S^{2-}, I^-SCN
Chloride	Ag/AgCl	6	-360	0.01	S^{2-}, I^-SCN^-, CN^-
Nitrate	Polypyrroledoped	3	-153	0.02	S^{2-}, ClO_4^-, $Cr_2O_7^{2-}$
Potassium	Valinomycin	1	51	0.02	Na^+, Ca^{2+}, Mg^{2+}
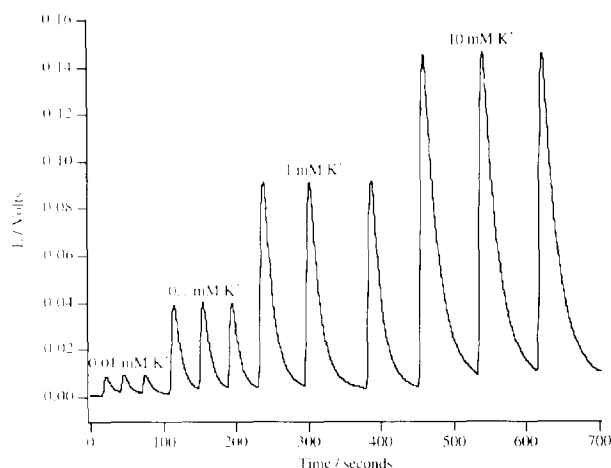
Fig. 5. FIA peaks for the planar-designed potassium ISE in the flow-injection mode. The carrier was 0.01 M lithium acetate, the flow rate was 6.8 ml min^{-1} and the injection volume was 100 μl.

The data show the very high peaks obtained by use of the cells-in-series approach with an array of sensor electrodes. Various other sensor arrays have been employed in FIA techniques as mentioned above. Batch injection analysis (BIA) has been introduced by Wang and Chen [23] and by Diamond et al. [24]. Wang et al. [25] have also developed a remote sensor electrode for potentiometric stripping analysis.

Similar results have been obtained with chloride and nitrate using six-cell and three-cell systems respectively, as reported recently [26]. Table 4 summarises the data obtained for these cells. Clearly, the electrode responses for cyanide, chloride and nitrate were enhanced in a multi-cell arrangement and improved sensitivity and detection limits were observed.

With a new approach, a planar electrode for potassium has been successfully employed for FIA. The data show excellent peak formation, as shown in Fig. 5, giving a response slope of 50.7 mV decade^{-1} using a 0.01 M lithium acetate background in FIA mode. In this case the injection volume was 100 μl. The observed slow return to baseline for the higher potassium ion concentration was the result of the dispersion of the injected sample zone, due to the relatively large surface area of the electrode used in this arrange-

ment. The calibration data are shown in Table 4. The possibility of using the planar design in a serial array of sensor electrodes has been recently reported [14]. Thus, many possible combinations of sensor electrodes should be possible with the portable monitoring system reported here.

3.2. Results for gas sensors

Tin-oxide semiconductor sensors are widely used in gas vapour monitors [21]. These devices are limited by lack of selectivity, sensitivity, and reproducibility. However, recent developments have led to much improved performance in hand-held monitors employing the Figaro-type gas sensors [27,28]. Fig. 6 shows some data for the response of hydrocarbons using a portable gas sensor device recently developed [27] with dual semiconductor sensors. The peak heights recorded in Fig. 6 are dependent on the concentration of total hydrocarbons in a sample, and vary linearly with the log concentration of hydrocarbons with only a limited working range.

3.3. Monitoring car exhaust emissions

Carbon monoxide (CO) and total hydrocarbons (THC) can be monitored using the dual tin-oxide
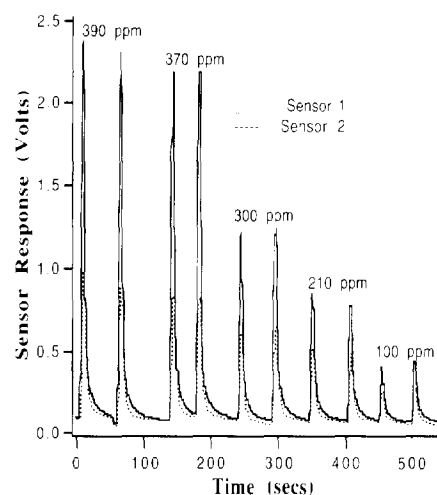
Fig. 6. Peaks recorded with the portable gas analyser for various concentrations of a C1–C6 hydrocarbon mixture. The sensors used were: sensor 1, TGS824; sensor 2, TGS812.
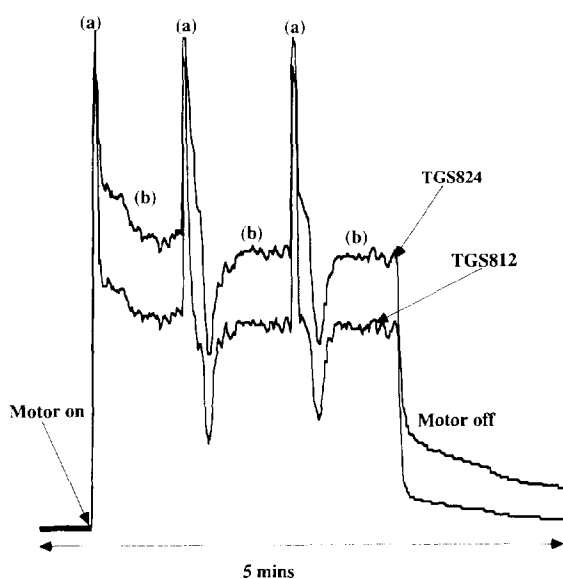
Fig. 7. The response of two types of Figaro gas sensor in the portable monitor observed for the following conditions: (a) peaks during the acceleration of the motor; (b) during idling of a 1983 Toyota Corolla.

semiconductor gas sensors [27], and clearly show that the Figaro-type sensors respond well to CO and hydrocarbons and could be used for continuous on-the-spot measurements for pollutants released in the atmosphere. These results show that the tin-oxide type of sensor is useful in a flowthrough configuration for monitoring air quality in situations where these gases occur due to pollution from automobile engines and other sources.

Continuous monitoring was also possible with the hand-held monitor using the dual tin-oxide semiconductor gas sensors. Fig. 7 shows the car exhaust profile of an 1983 Toyota Corolla. The initial peak response shows a burst of car exhaust expelled upon starting the motor, then decaying as it idles and the second and third peak responses were the result of acceleration. Turning the motor off resulted in a decrease in the response shown in Fig. 7 back to ambient readings.

A comparison between exhaust emissions from a 1987 Toyota Celica and a 1983 Toyota Corolla was performed with the same hand-held monitor described above. The car exhaust profiles for the

Celica and the Corolla are given in Fig. 8, the former being fitted with a catalytic converter to reduce emissions. These profiles show the calculated CO and THC concentrations expelled from these cars. Clearly Figs. 8A and 8B show that the CO and THC concentrations are the lowest when idling (plateau region), but acceleration caused a peak response for both cars. Fig. 8 shows that both the CO and THC levels are much higher for the Corolla than for the Celica when idling, but the THC levels are similar for both cars when accelerating. The performance of the hand-held monitor therefore offers a simple, low-cost method for real-time monitoring of car emissions by government authorities and hence a means to help reduce the pollution problem from vehicular exhausts.
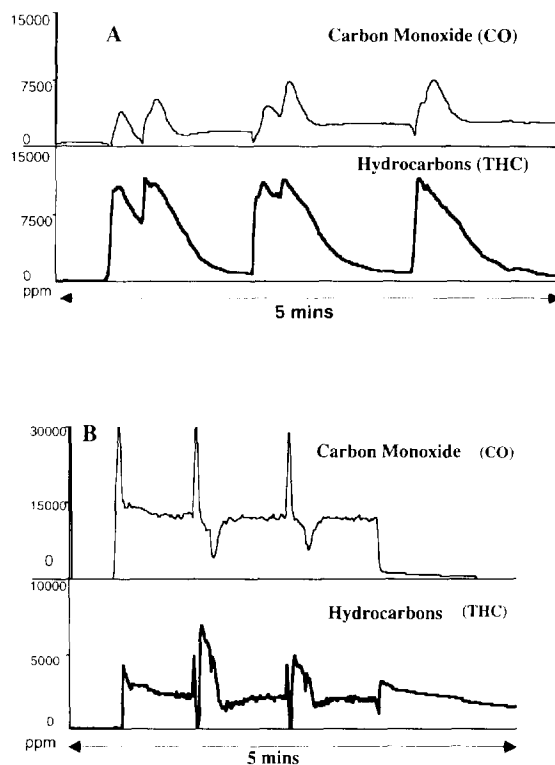
Fig. 8. The car exhaust emissions calculated for carbon monoxide and total hydrocarbon observed for (A) 1987 Toyota Celica and (B) 1983 Toyota Corolla from the data recorded in Fig. 7.
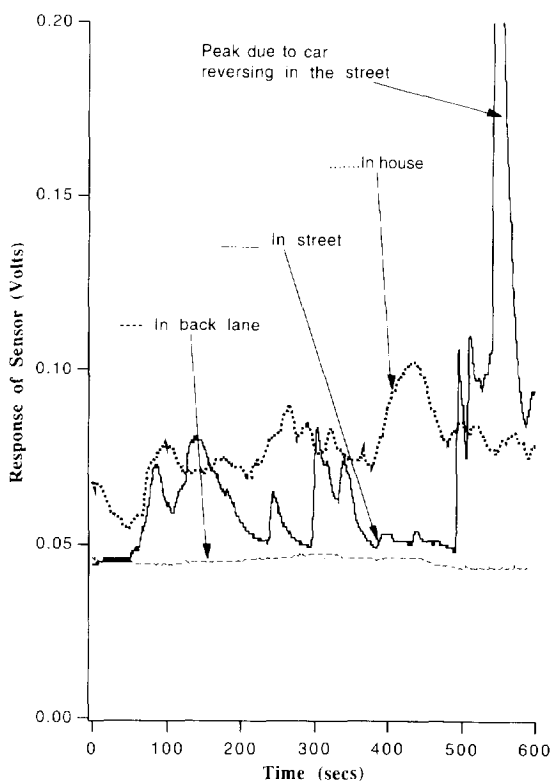
Fig. 9. Monitoring of response of a single gas sensor (TGS812) to hydrocarbon emissions for vehicles travelling over a speed hump situated on a busy road close to an apartment building.

3.4. Air pollution in residential homes

The hand-held monitor was used for testing hydrocarbons from car exhausts in homes situated near traffic speed humps on a busy road. The data in Fig. 9 show the problem in a particular house, indicating consecutive measurements recorded over 10 min periods while traffic flowed across the speed hump on the road outside the house. A single sensor, the TGS812, sensitive to total hydrocarbon emissions, was used to detect pollution problems inside the house. The data shown in Fig. 9 were for a single sensor showing voltage readings using the TGS812 sensor in comparison with the baseline readings in the back lane.

The sensor was independently calibrated for total hydrocarbons and carbon monoxide, as described previously [27]. The calibration plot for

this sensor towards total hydrocarbons is shown in Fig. 6. The single sensor used here is most sensitive to hydrocarbons and much less sensitive to carbon monoxide [27]. The traffic speed hump was situated on the road about 30 m from the front of the house. Measurements were made in the street next to the hump, in the house with the front windows open, and in the back lane which was about 130 m from the road and protected by trees and plants from the traffic emissions. The readings in each location were taken consecutively, since only one monitor was available. The data show a flat baseline reading for the back lane. In the street, peaks were observed each time a vehicle slowed down and then accelerated over the hump. The readings inside the house were higher than in the street and indicate peaks as vehicles passed over the traffic hump outside. The evidence is clear that the vehicular emission gases
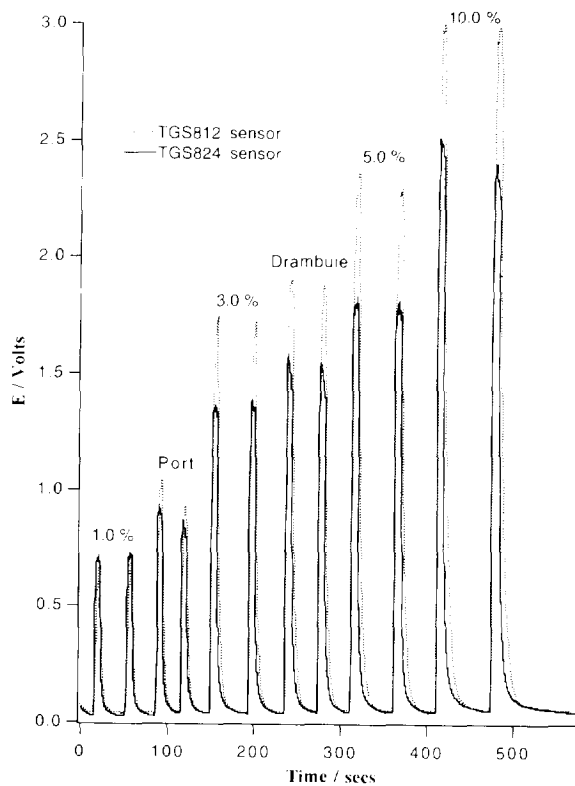
Fig. 10. Peaks for ethanol standards and various diluted alcoholic beverages recorded using two different Figaro-type gas sensors in the portable monitor.

are being trapped inside the house, and showed increases due to the traffic hump. This type of measurement is therefore valuable for rapid testing of pollution problems in urban areas.

3.5. Determination of ethanol in alcoholic beverages

The response characteristics of the dual-sensor monitor have also been used to evaluate alcohol levels in beverages. The detection method was based on the head space analysis of vapour above aqueous samples containing ethanol reported previously [29]. Relative standard deviations of better than 5% were obtained with the Figaro-type sensors, depending on the ethanol concentration, as shown in Fig. 10. The port and Drambuie samples were analysed after a 10-fold dilution and these samples were bracketed by the ethanol standard solutions as shown in Fig. 10. The accuracy of this method gave a correlation coefficient of 0.9999 in comparison with gas chromatographic analysis [29].

4. Conclusions

The use of these mobile sensor devices is a radical departure from traditional methods of chemical analysis involving sampling and transport of the samples back to laboratories for chemical and biochemical testing. Examples of tests for safety and quality control in food technology, mining, chemical industries, environmental, and medical areas are numerous, and further rapid development of portable sensing technology can be expected.

Acknowledgements

References

[1] W.P. Carey, Trends Anal. Chem., 13 (1994) 210–218.
[2] K.N. Andrew, N.J. Blundell, D. Price and P.J. Worsfold, Anal. Chem., 66 (1994) 916A–922A.
[3] H.L.C. Meuzelaar (Ed.), Trends Anal. Chem., 13 (1994) 252–294.
[4] P.W. Alexander, Proc. RACI Symp. Field-Portable Monitoring in the Environment, ICI House, Melbourne, October 1994.
[5] P.W. Alexander, M. Trojanowicz and P.R. Haddad, Anal. Lett., 17(4A) (1984) 309–320.
[6] P.W. Alexander, M. Trojanowicz and P.R. Haddad, J. Chromatogr., 295 (1984) 397–402.
[7] P.W. Alexander, M. Trojanowicz and P.R. Haddad, Anal. Chem., 56 (1984) 2417–2423.
[8] P.R. Haddad and P.W. Alexander, in P. Jandik and R.M. Cassidy (Eds.), Advances in Ion Chromatography, Vol. 2, Century International, Medfield, MA, 1990, pp. 45–71.
[9] P.W. Alexander, B. Glod and P.R. Haddad, J. Chromatogr., 589 (1992) 203–207.
[10] P.W. Alexander and D.B. Hibbert, Australian Pat., (to Unisearch Ltd.), No. P17728, April 1988.
[11] D. Shiels, P.W. Alexander and D.B. Hibbert, Proc. 11th Australian Anal. Chem. Symp., Hobart, Tas., July 1991, p. 121.
[12] D.B. Hibbert, P.W. Alexander, S. Rachmawati and S.A. Caruana, Anal. Chem., 62 (1990) 1015–1019.
[13] T. Dimitrakopoulos, P.W. Alexander, D.B. Hibbert, L. Cherkson and J. Morgan, Electroanalysis, 7 (1995) 1118–1120.
[14] T. Dimitrakopoulos, P.W. Alexander and D.B. Hibbert, Electroanalysis, in press.
[15] T.J. Cardwell, R.W. Cattrall, P.C. Hauser and I.C. Hamilton, Anal. Chim. Acta, 214 (1988) 359.
[16] H.D. Goldberg, R.B. Brown, D.P. Liu and M.E. Meyerhoff, Sens. Actuat. B, 21 (1994) 171–183.
[17] F.I. Ormaza-Gonzales and A.P. Villalba-Flor, Water Res., 28 (1994) 2223–2228.
[18] B. Walter, Anal. Chem., 55 (1983) 499A–517A.
[19] M.J. Green and P.I. Hilditch, Anal. Proc., 28 (1991) 374.
[20] B. Fleet, H. Gunasingham, R.R. Delangin, B. Narayanan and T.F. Tang, Sitest Pty. Ltd., P.O. Box 467, Warners Bay, NSW 2282, Australia, 1995.
[21] J.W. Gardner, P.N. Bartlett, P.T. Moseley, D.E. Williams and J.O.W. Norris (Eds.), Techniques and Mechanisms in Gas Sensing, Adam Hilger, Bristol, UK, 1991.
[22] D. Diamond, Electroanalysis, 5 (1993) 795.
[23] J. Wang and L. Chen, Analyst, 119 (1994) 1345.
[24] D. Diamond, J. Lu, Q. Chen and J. Wang, Anal. Chim. Acta, 281 (1993) 629.
[25] J. Wang, N. Foster, S. Armalis, D. Larson, A. Zirino and K. Olsen, Anal. Chim. Acta, 310 (1995) 223.
[26] J.C. Ngila, D.B. Hibbert and P.W. Alexander, Proc.

13th Australian Anal. Chem. Symp., Darwin, N.T., July 1995, p. AS 45-1.

[27] P.W. Alexander, D.B. Hibbert, L. Cherkson and J. Morgan, A Portable Monitor for Automobile Exhaust Emissions, Australian Provisional Pat., February 1993.

[28] R. Ryan, S. Wadell, K. Bowles, P.W. Alexander, L.

Cherkson, J. Morgan and D.B. Hibbert, Proc. 6th Int. Working Party on Stored-product Protection, Canberra, A.C.T., April 1994.

[29] L. Di Benedetto, P.W. Alexander and D.B. Hibbert, Anal. Chim. Acta, 321 (1996) 61–67.

Potentiometric and voltammetric detection using a two-channel fountain cell[1]

M. Wasberg*, K. Stenlund, A. Ivaska

Åbo Akademi, Laboratory of Analytical Chemistry, Biskopsgatan 8, FIN-20500 Åbo, Finland

Abstract

The design and use of a two-channel fountain cell in potentiometric and voltammetric detection is described. The two flows produced two distinct sectors inside the thin layer region and one of the sectors was used as the internal electrolyte of a reference electrode built into the cell body and the other as the indicator/counter electrode section. The behavior of the flowthrough $Ag/AgCl$ reference electrode was first investigated and found satisfactory and it was then employed as the reference electrode in the subsequent experiments. Continuous and flow-injection measurements were made using the Fe^{III}/Fe^{II} redox couple in potentiometry and the reduction of Fe^{III} in voltammetry.

Keywords: Iron; Potentiometric detection; Two-channel fountain cell; Voltammetric detection

1. Introduction

Electrochemical detection in flowing systems has been done using flow cells of various designs and two very widely used types are *wall-jet* and *thin layer* cells [1–4]. In the former the incoming electrolyte is directed perpendicularly towards the working electrode and in the latter the electrolyte is passed through a thin layer created using a spacer in which the working electrode is placed. The so-called fountain cell was developed for use in optical measurements [5] and is basically a combination of the wall-jet and the thin layer electrode. In the fountain cell the incoming electrolyte is directed perpendicularly towards one of the walls which confines a circular thin layer region so as to create a radial flow from the entrance orifice towards a circular "well" of larger volume at the perimeter of the thin layer. The geometry and properties of the fountain cell are such that the incoming flow spreads out equally in all directions from the center, and if the cell is equipped with two or three entrance orifices close to the center of the thin layer, the flows will establish themselves in very well-defined parts of this region. Depending on the ratio of the flow rates in a two-channel flow cell the sectors occupied by the two flows will vary, so that the flow with higher flow rate will occupy a larger sector of

---

* Corresponding author. Fax: (+358) 21-2-654-479; e-mail: mwasberg@ra. abo. fi
[1] Presented at the Seventh International Conference on Flow Injection Analysis (ICFIA '95), held in Seattle, WA, USA, August 13–17. 1995.

the circular thin layer area than the flow with the lower flow rate. There is also a thin layer cell commercially available with radial flow pattern which is intended for chromatographic detection [6]. This cell, which is made for amperometric measurements, is only a single-channel two-electrode cell for small currents and is thus not intended for general use. It is, however, of the fountain cell type and needs to be mentioned here.

The fountain cell has been evaluated in a perfusion study of living cells in which it was connected to a flow-injection system and a fluorescence microscope was used as detector [7]. It is the aim of this work to investigate the possibilities of the fountain cell as an electrochemical detector using voltammetric and potentiometric methods of detection. The special properties of this detector, which include the possiblility of using multiple flows as well as the radial flow pattern [7] in the thin layer region, make it attractive for this purpose. Its ability to let two or more independent flows meet in the detector region [8] should allow differential measurements to be made in a novel way and the circular symmetry of the thin layer region allows convenient placement of working/indicator, counter and reference electrodes. The use of two flows was examined in this work. One of the flows contained a reference electrolyte solution which together with the built-in Ag/AgCl electrode comprised a reference electrode in one half of the thin layer region. This part of the cell is referred to as the "in-cell" reference electrode. The other flow contained the components to be detected and passed by a working/indicator electrode and a counter electrode. This section of the cell is referred to as the "detection side".

2. Experimental

All chemicals used were of analytical grade and the solutions were prepared by using distilled, deionized water (MilliQ). Teflon tubing was used to transport electrolytes and PVC tubing was used in the peristaltic pump. Before use the block containing the electrodes was ground by hand with emery papers of successively finer grit ending

with size 1000 after which it was polished first with coarse and later with fine alumina powder. The electrodes were polished with alumina before each deposition of Ag/AgCl. The in-cell reference electrode was prepared by oxidizing the silver disk electrode (3 mm diameter) galvanostatically in a solution containing 1 mol dm^{-3} KCl for 12 min at a current of 100 μA to produce a very smooth layer of AgCl. The counter electrode for AgCl deposition was of circular shape and made of 0.5 mm diameter platinum wire. After deposition of AgCl and before assembling the cell the electrode was stored in the same solution at open circuit. When not in use the cell was filled with 1 mol dm^{-3} KCl, by pumping this solution through both channels, or opened and the electrode block placed in the same solution. All KCl solutions used were saturated with AgCl. The potentiometric measurements were made with a pH meter (Metrohm 691) equipped with an analog recorder output. The resolution of this output was 1 mV and the signal was recorded using a 12 bit A/D converter (ADC1000, Pico Instruments) connected to the parallel port of an IBM AT-compatible computer. Voltammetric and amperometric measurements were made using computer-interfaced laboratory-built instrumentation. Solution flow through the cell was achieved by a peristaltic pump or by means of hydrostatic pressure. The peristaltic pump (Desaga STA) enabled the use of variable pumping speeds and by using 0.8 mm i.d. PVC tubing in the pump flow rates from 0.004 to 0.04 ml s^{-1} were obtained. In some measurements hydrostatic pressure from a height of 30–40 cm was used. Selection of different flows and flow injection was made using a computer-controlled eight-channel valve (Pharmacia MV8), the use of which has been described earlier [9].

3. Results and discussion

3.1. Flow cell details and investigation of flow pattern

The cell which is sketched in Fig. 1 was made of Plexiglass and consisted of three parts: a cell top

B, center "flow introduction block" A and an electrode block E at the bottom. The blocks were held together by four corner-positioned 6 mm diameter screws fitting into threads in the electrode block. The cell top and the flow introduction block were sealed by a gasket D when the cell was in use and with a similar 0.25 mm thick gasket/spacer the center block and electrode block were sealed and separated so as to create a thin layer region of spacer thickness between the blocks. This thin layer region was circular in shape (diameter 20 mm) and extended from the center of the cell where the inlet orifices were positioned out to the inner perimeter of the well indicated in A. The position of the thin layer region is also indicated by a dashed circle on the electrode block marked E in Fig. 1. The volume of the thin layer region was thus $\approx 80\ \mu l$ using the 0.25 mm thick spacer. In detail the cell thus consisted of the followng parts:
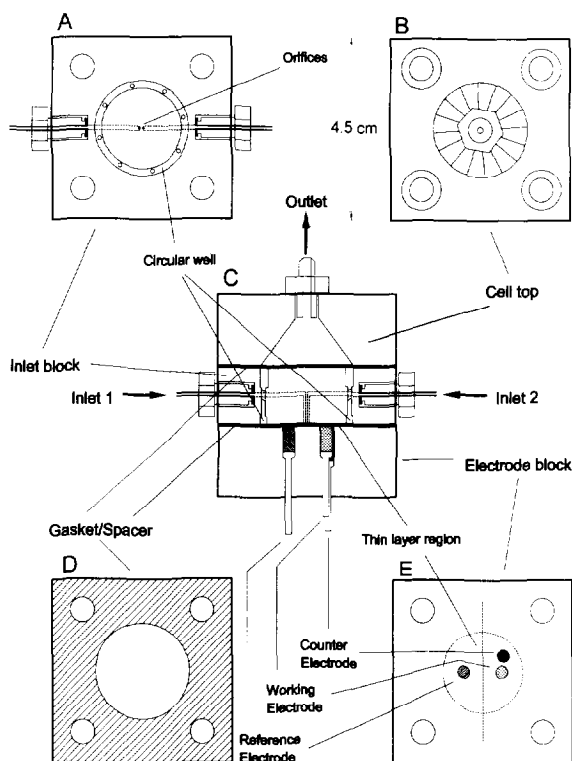
Fig. 1. Sketch of the fountain cell in assembled form from the side (C) and separated into parts: (A), inlet block; (B), cell top; (D), gasket/spacer; (E), electrode block.

- an electrode block at the bottom (E in Fig. 1) into which the electrodes were molded using a polyester resin. The electrodes were placed in holes drilled in the proper positions all the way through the bottom of a cylindrical molding cavity machined in the center of the electrode block. The width of the cavity was somewhat larger than the diameter of the circular well (see part A in Fig. 1). The reference electrode consisted of a silver cylinder (99.98% purity), 3 mm diameter and 5 mm in length, and the working/ indicator electrode consisted of a gold cylinder (99.98% purity) of the same size. Both these electrodes were soldered to brass holders which protruded through the positioning holes. The counter electrode was made of glassy carbon and had the same shape and size as the other electrodes. This electrode was fixed to the brass holder by pressing it by force into an oval hole at the top of the brass holder. The brass gave way to accept the electrode and no electrical contact problems were encountered when using the counter electrode.

- a central flow introduction block (A in Fig. 1) where the two electrolyte flows entered the cell. The flows first passed through 1 mm diameter channels which narrowed to 0.5 mm at a 90° turning point. A circular "well" with a width of 3 mm and a depth of 4 mm was milled in the block (see Fig. 1) to disrupt the thin layer region and to reduce flow velocity. A similar, somewhat deeper well, was milled from the opposite side of the block and the two wells were connected by eight 1.6 mm diameter holes. The Teflon tubing for electrolyte flow (0.5 mm i.d.) was widended at the contact point with the flow introduction block to produce a flange which was pressed to the cell body by means of hollow nuts made of plastic.

- the cell top (B in Fig. 1) which is used to collect the electrolyte from the well has a collection chamber shaped like a cone which narrows at the upper end and connects to a fitting for the outlet tube.

A series of experiments were made in order to make sure that the two incoming flows really
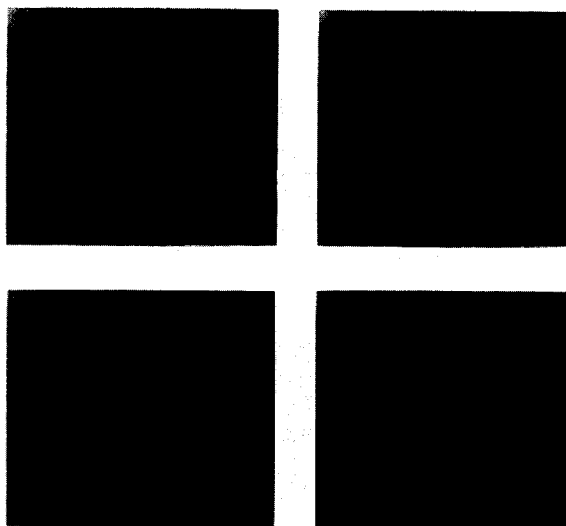
Fig. 2. Effect of flow rate ratio on flow profiles in the fountain cell. Two dyed solutions were used and at equal rates the flows each occupied half of the cell (A). Photographs B-D show the results of using various unequal flow rates.

behaved as expected, i.e. that they occupied two well-defined sectors of the circular thin layer region. Especially, it was of importance that the thin layer region was divided into two equal parts at equal flow rates, so that the electrodes were exposed correctly to the incoming flows. Photographs showing the thin layer region occupied by two differently-dyed solution flows at four different flow rate ratios are displayed in Fig. 2.

To design and construct a two-channel fountain cell was somewhat more demanding than to make a thin layer or wall-jet cell. However, once the acrylic parts were machined and the electrodes molded in place and polished a remarkable well behaved cell was obtained. The two flows, i.e. the in-cell reference electrode electrolyte flow and the analyte flow, stayed well separated and even when the reference electrode side was contaminated by mistake e.g. by a ferric/ferrous solution, it recovered quite rapidly. The fast recovery may have been due to the very smooth finish of the AgCl layer obtained in the electrolytic deposition. The pores of the AgCl layer could not therefore have been very deep and the contaminants were washed rapidly away. The reproducibility and stability of the flow patterns in Fig. 2 are also remarkable,

even when the flows were propelled by peristaltic pump. Especially, the border region displayed a sharp change between the solutions indicating little or no mixing of the flows. This fact is a prerequisite for a multiple channel fountain cell and one of the reasons why it works in electrochemical measurements. All potentiometric measurements are inherently differential measurements, involving measurement of the difference of potentials of two half cells which are in contact through a liquid junction. In a two-channel fountain cell this liquid junction consists of the sharp dividing line(s) between the two flows, but here no glass frits or asbestos fibres are needed to separate the electrodes.

The effective dead volume of the cell used was also small. Using a 0.25 mm spacer the dead volume was only ≈ 80 μl, not counting the in-cell reference electrode side. By decreasing the spacer thickness it should be possible to decrease the volume further. Being a thin layer cell the thin layer area is quite large and can accommodate a number of electrodes, a fact which could be useful for detectors equipped with multiple sensors.

In the initial experiments with the cell, silicon tubing was used in the peristaltic pump and this introduced problems in the form of gas bubbles appearing in this section. Once created these bubbles were transported into the cell and often clung to the walls of the cell in the thin-layer region. The tendency of the bubbles to do this might have been due to the properties of the polyester polymer which was used to mold the electrode in place. After changing to PVC tubing the problems with the bubbles were essentially eliminated. It is also likely that an improvement in the sensitivity to bubble retainment could be achieved by designing the input channels so that the flow is upwards, and it is our aim to do this in the next generation of fountain cells.

3.2. Stability of in-cell reference electrode and potentiometric measurements with the Fe^{III}/Fe^{II} couple

One of the basic ideas of this investigation was to use one half of the thin layer region of the fountain cell as a reference electrode. Thus, all

potentials measured would be made with reference to this in-cell reference electrode and the quality of all potential measurements would rely on the stability and reproducibility of its potential. The reference electrode part of the cell was comprised of the left-hand side of the thin layer region indicated by a dashed circle on part E of Fig. 1. In order to determine the potential behaviour of this in-cell reference electrode an SCE (saturated calomel electrode) was placed in a beaker (containing electrolyte up to a level of ≈ 2 cm) into which the cell outlet tube was also placed, and the potential difference between these two electrodes was recorded under different conditions. The solution level in the beaker was kept constant by pumping out excess electrolyte by means of and aspiration pump. During these measurements both channels of the fountain cell were fed with the reference electrode solution, i.e. 1 mol dm^{-3} KCl.

In Fig. 3 potential data are shown for a long time stability experiment extending over 4 days. The potential of the in-cell Ag/AgCl reference electrode vs. the SCE was recorded for a flow of a 1 mol dm^{-3} KCl solution (saturated with AgCl). The flow rate was 0.02 ml s^{-1} and a freshly prepared Ag/AgCl electrode was used. In the beginning there is a rather sharp 4 mV increase in the potential difference which takes place during
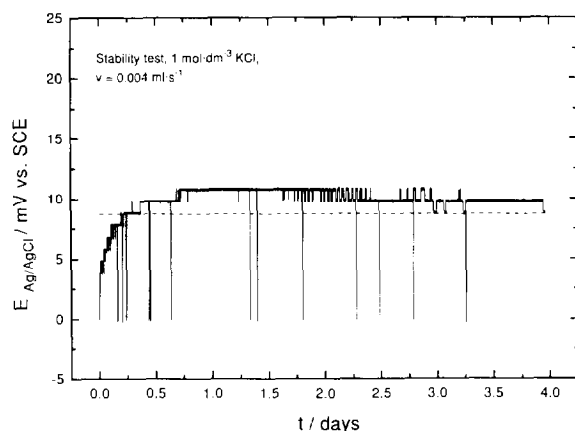
Fig. 3. Data from potential stability experiment for an in-cell Ag/AgCl reference electrode in which the potential was measured against an SCE placed in the outlet stream. The measurement started with a freshly made Ag/AgCl surface.
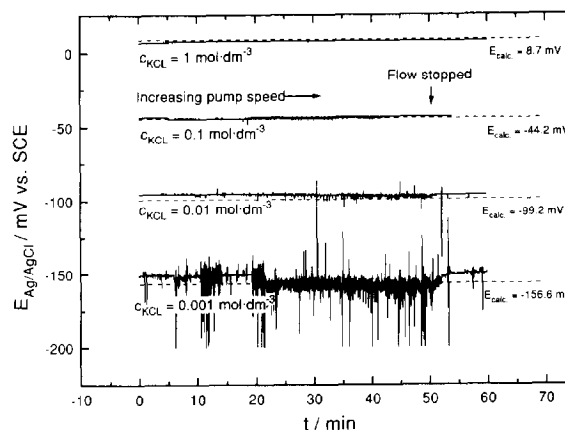
Fig. 4. Potential of in-cell Ag/AgCl electrode measured against an SCE for KCl solutions of different concentrations and different flow rates. The flow rate was initially 0.004 ml s^{-1} and finally 0.04 ml s^{-1}. The flow rate was increased in ten steps every 5 min and the pump was stopped at $t = 50$ min.

the first 6 h and after this the variation is of the order of ± 1 mV. During the last 1.5 days the potential difference is stable at 9 mV. The spikes seen in the curve occurred while filling up the KCl container, during which the pump was also stopped. The broken line at 8.7 mV indicates the potential value obtained from theory and the tabulated chloride ion activity coefficient [10] for the concentration used.

Another shorter stability test was made using different pumping speeds and different KCl concentrations and the results are summarized in Fig. 4. During the measurements the pumping speed was increased in ten steps from 0.004 to 0.04 ml s^{-1} and the pump was stopped at $t = 50$ min. For the 1 mol dm^{-3} KCl solution stable potential readings were obtained ≈ 1 mV below the calculated value. No effect of flow rate could be detected and the signal was fairly free of noise. This is also the case for the flow of 0.1 mol dm^{-3} KCl, except that the noise level has increased somewhat. For the 0.01 and 0.001 mol dm^{-3} solutions the noise level increased further and a flow rate dependence could also be seen. For the 0.01 mol dm^{-3} solution a difference of ≈ 10 mV is obtained between slow flow rate and flow at full pumping speed.

In order to investigate the behavior of the fountain cell in potentiometric detection, using

the in-cell reference electrode, the potential of the Au indicator electrode was measured in solutions containing Fe^{II} and Fe^{III} in different concentration ratios. Two solutions flows were thus used: one of 1 mol dm^{-3} KCl (saturated with AgCl) for the reference electrode and the other one containing the iron species. The flows were produced by the peristaltic pump and in this case the solution flow was changed manually after stopping the pump. In the measurement solution flow the concentration of Fe^{III} was kept constant at 0.2 mol dm^{-3} and the concentration of Fe^{II} was varied: 0.2, 0.02, 0.002, 2×10^{-4} and 2×10^{-5} mol dm^{-3}. The measurement solutions were passed through the cell in succession in two duplicate measurements starting with the 0.2 mol dm^{-3} Fe^{II} solution. Data from this experiment are shown in Fig. 5.

A series of potentiometric flow-injection experiments were also done. The carrier used was a solution of 0.1 mol dm^{-3} NaOH containing 0.2 mol dm^{-3} $Fe(CN)_6^{3-}$ and 2×10^{-5} mol dm^{-3} $Fe(CN)_6^{4-}$. The solutions injected were of the same salts with $c_{Fe(III)} = 0.2$ mol dm^{-3}, $c_{Fe(II)} = 2 \times 10^{-3}$ mol dm^{-3} Fe^{II} and $c_{Fe(III)} = 0.2$ mol dm^{-3}, $c_{Fe(II)} = 0.2$ mol dm^{-3} Fe^{II}. The two solutions were injected using the peristaltic pump at a flow rate of 0.02 ml s^{-1} and the eight-channel computer-controlled valve. The valve and flows were
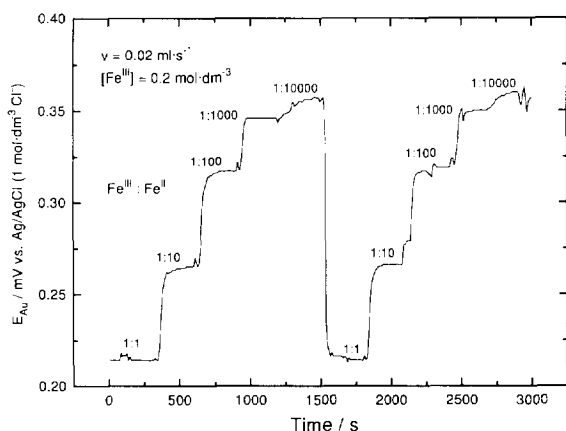
Fig. 5. Potential of Au electrode measured against in-cell Ag/AgCl reference electrode (1 mol dm^{-1} KCl, sat. AgCl) for 0.1 mol dm^{-1} NaOH solutions having different concentration ratios of $K_4Fe^{II}(CN)_6$ and $K_3Fe^{III}(CN)_6$.
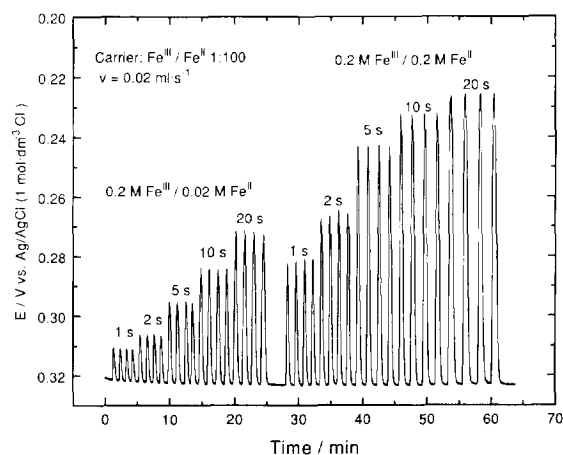
Fig. 6. Data from potentiometric flow-injection experiment with varying injection times using an in-cell reference electrode and two different Fe^{III}/Fe^{II} solutions. Carrier solution: 0.1 mol dm^{-3} NaOH with $c_{Fe(III)} = 0.2$ mol dm^{-3} and $c_{FF(II)} = 0.0002$ mol dm^{-3}. The solutions injected were also prepared in a base electrolyte of 0.1 mol dm^{-3} NaOH and are described in the Fig.

set up so that the carrier occupied one of the channels and the solutions to be injected the adjacent channels. The injection time was then the time for which the valve was kept in the position at the adjacent channels. The injection volume was thus varied by varying the time of injection. Results obtained with injection times from 1 to 20 s are shown in Fig. 6. In order to investigate the reproducibility of the FIA (flow-injection analysis) 20 peaks were recorded and the trace is shown in Fig. 7. The r.s.d. was 0.7%.

The in-cell reference electrode shows a stability which is adequate for FIA, i.e. after the initial 5–6 mV change the potential was stable. The pH meter used had a recorder output with a resolution of 1 mV, which made the measurement of smaller changes in potential by computer impossible. However, it can be concluded from the data in Fig. 3 that once the potential has stabilized the long-term change in potential is at the most 1 mV, and this is certainly adequate for most analytical measurements, especially those involving FIA in which the background signal is recorded immediately before injection.

The flow rate of the reference electrode solution had little effect on the potential as long as c_{KCl}

was 10 mmol dm^{-3} or higher. For this concentration there is a difference in potential of only about 2 mV between stationary solution and flowing solution at maximum pump speed (0.04 ml s^{-1}). For the 1 mmol dm^{-3} KCl solution the same difference is 9 mV. The reason for the change in measured cell potential as the flow rate and ion strength are varied is the streaming potential, the value of which is also higher the more dilute the electrolyte is and the higher the flow rate is. There was also a noticeable increase in the noise level at lower concentrations and the data in Fig. 4 clearly show that the noise successively increases as the concentration decreases. One reason for the noise increase is the streaming potential itself which fluctuates as the flow pulsates with the frequency of the pump rollers. Potential data were acquired once a second and this rate was too low compared to the roller frequency to enable us to distinguish any signals due to flow pulsation. This was checked by Fourier analysis of the signals at different pumping speeds. The potential signal could thus have been sampled at any point on the pump pulsation cycle, which also varied during the experiment. The electrical properties of the KCl electrolyte change with dilution and the decreased conductivity (higher impedance) in the medium between the two electrodes used makes the measurement more susceptible to noise pickup
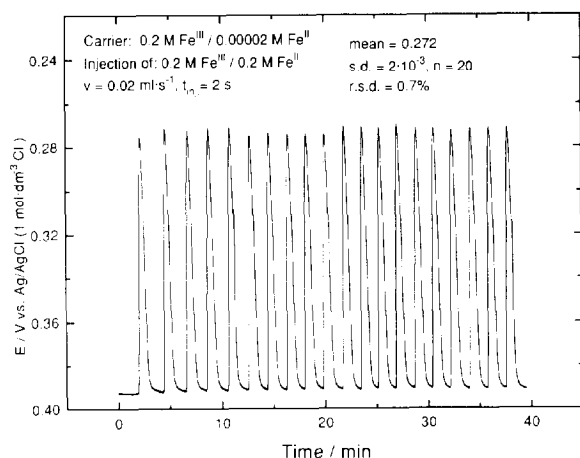
Fig. 7. Measurement of peak height repeatability in potentiometric flow-injection experiment. An r.s.d. of 0.7% was obtained for 20 injections of 40 μl.

from the surroundings. Although most of the noise at $c_{KCl} = 1$ mmol dm^{-3} is due to pumping a clearly increased noise level was observed for the static electrolyte too.

The ferric/ferrous redox system was chosen for the potentiometric evaluation because of the simplicity of the indicator electrode arrangement and because it is widely used as a test system. However, there were some drawbacks to this choice, e.g. no data on the activity coefficients for ferric and ferrous hexacyanides were found for the electrolyte used and this in turn made the calcuation of the potential responses inexact. Also, the electrode potential response to changes in solution redox potential could sometimes be slow, especially if one of the redox components were present in low concentration. However, reproducible peaks were obtained for the solutions used in FIA. It must be kept in mind that variations in injection volume in this case depend on the precision with which the multichannel valve is manipulated. For shorter injection times a larger relative variation is obtained. A special source of variation is the peristaltic flow pulsation which also has a larger influence for shorter injection times. The r.s.d. of 0.7% obtained for an injection time of 2 s must be considered satisfactory considering the simplicity of the injection system used.

3.3. Voltammetric detection of Fe^{III} on gold electrode

The fountain cell was equipped with two electrodes (gold and glassy carbon) on the detection side and these, together with the in-cell reference electrode, comprise a three-electrode electrochemical cell suitable for voltammetric and amperometric measurements. The glassy carbon electrode was placed downstream with respect to the gold electrode and for this reason the gold electrode was chosen as working electrode and the glassy carbon as counter electrode. In this configuration the reaction products produced at the counter electrode could not end up on the working electrode.

The behavior of the cell in the reduction of Fe^{III} in 0.1 mol dm^{-3} NaOH was studied in a cyclic voltammetric experiment. The cyclic voltam-
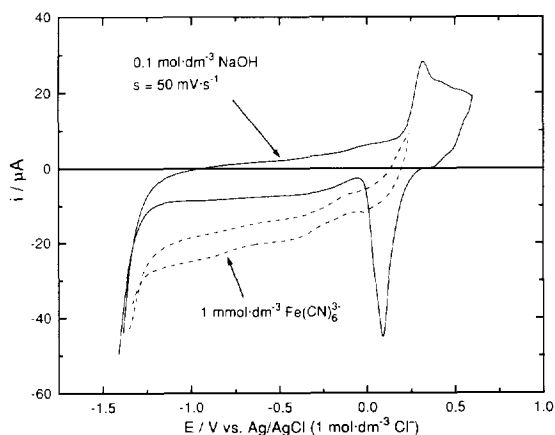
Fig. 8. Cyclic voltammetric curves at a scan rate of 50 mV s^{-1} obtained using the fountain cell equipped with a gold working electrode. The solid line is for the supporting electrolyte (0.1 mol dm^{-3} NaOH) showing surface oxidation and reduction peaks typical for gold. The broken line is for a solution of 1 mmol dm^{-3} K$_3$Fe(CN)$_6$ in supporting electrolyte.

mograms recorded in the fountain cell, both for the supporting electrolyte (solid line) and for 1 mmol dm^{-3} K$_3$Fe(CN)$_6$ (broken line), are shown in Fig. 8. The scan rate was 50 mV s^{-1} and the solution flow of 0.02 ml s^{-1} was hydrostatically produced in order to avoid limiting current oscillations due to the pulsating flow caused by the peristaltic pump. Oxidation of the gold surface in pure electrolyte gives rise to a peak at 0.32 V and the reduction of the layer produced gives a corresponding reduction peak at 0.09 V. Below a potential of about −1.25 V reduction of the electrolyte starts to take place to a significant degree. When the 1 mmol dm^{-3} ferric solution was introduced a reduction current was obtained in the cyclic voltammetric scan (broken line) at potentials on the negative side of the oxide reduction peak.

FIA with amperometric detection was investigated by selecting a potential of −0.75 V and injecting ferric solutions of different concentrations into a carrier consisting of 0.1 mol dm^{-3} NaOH supporting electrolyte. Data for five different concentrations are shown in Fig. 9. The flow rate was 0.02 ml s^{-1}. With the intention of determining the repeatability of the amperometric FIA 18 injections of 40 μl of 2 mmol dm^{-3} fe^{III} were recorded and the results are shown in Fig. 10. An r.s.d. of 1.3% was obtained.
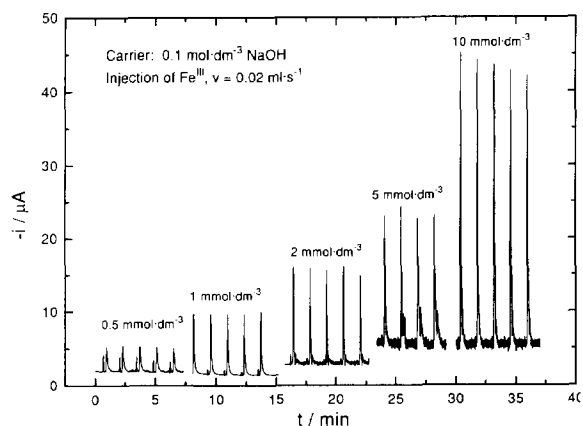
Fig. 9. FIA peaks obtained for the amperometric reduction of different concentrations of Fe(CN)$_6^{3-}$ in 0.1 mol dm^{-3} NaOH. The flow rate was 0.02 ml s^{-1} and the flow was produced by hydrostatic pressure. Potential: −0.5 V.

Reduction of Fe(CN)$_6^{3-}$ was chosen for the experiments on voltammetric detection because of its well-known character and because the reaction product (Fe^{II}) is soluble in the electrolyte phase, an aspect which is of importance in avoiding surface fouling and changes on solid electrodes. In Fig. 8 the typical surface processes of a gold electrode are shown with clear, sharp oxidation and reduction peaks. The steep changes in current for these peaks are an indication of negligible iR drop in the cell, a result which indicates good
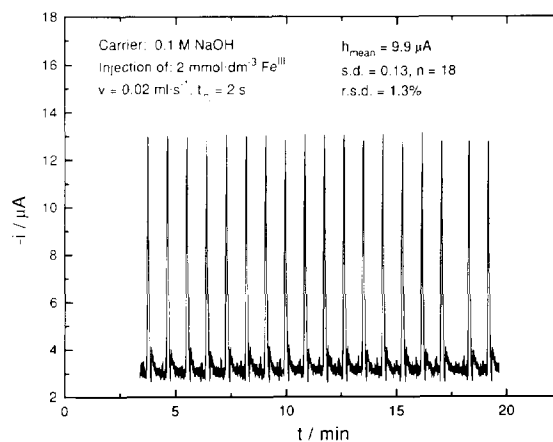
Fig. 10. Amperometric FIA repeatability measurement. An r.s.d. of 1.3% was obtained for a ferric ion concentration of 2 mmol dm^{-3} and an injection volume of 40 μl.

potential control despite the thin layer configuration. The contact area between the reference electrode "internal" electrolyte and the cell supporting electrolyte is large in the fountain cell and extends over the whole width of the thin layer section. This is in contrast to conventional cells in which the potential of the electrolyte is measured at only one point, at the tip of the reference electrode. In some flow detectors this point may even be outside the cell. The good potential control apparent here may be due to the special design of this cell with its in-cell reference electrode, but conclusive evidence will be pursued in a separate study. As 1 mmol dm^{-3} Fe(CN)$_6^{3-}$ is introduced on the detection side (Fig. 8, broken line) a reduction current appears due to reduction of this ion. This process starts immediately the oxide layer is removed, even when it is only partially removed. This is analogous to the case with oxidation of Fe^{III} on the same electrode in which the oxide film also inhibits the bulk process [11].

The injection of different concentrations of Fe(CN)$_6^{3-}$ produced the peaks shown in Fig. 9, and in this case the lower concentrations produced more reproducible peaks. Especially at the highest concentration of 10 mmol dm^{-3} Fe^{III} a continuous decrease in peak height is observed as the injections are repeated. It is not clear what the reason for this behavior is. However, a concentration of 10 mmol dm^{-3} is rather high and at this level the concentration of electroactive contaminants present in the reagents may be high enough

to produce surface compounds affecting the state and properties of the solid working electrode. The r.s.d. for amperometric detection of 2 mmol dm^{-3} Fe^{III} was higher than for the potentiometric detection (1.3% compared to 0.7%). This must in part be due to the linear concentration dependence of the amperometric signal compared with the logarithmic dependence for the potentiometric signal. Mass transport phenomena are also more important in amperometry than in potentiometry, which in turn makes the stability of the signal from the former more dependent on flow variations.

References

[1] K. Stulik and V. Packova, Crit. Rev. Anal. Chem., 14 (1984) 297–351.

[2] P. Bersier and J. Bersier, Crit. Rev. Anal. Chem. 16 (1985) 297–351.

[3] F. Hawkridge, in P. Kissinger and W. Heinemann (Eds), Laboratory Techniques in Electroanalytical Chemistry, M. Dekker, New York 1984, pp. 337–366.

[4] P. Kissinger, Ref. [3], pp. 611–636.

[5] K. Scudder, C. Pollema and J. Ruzicka, Anal. Chem., 64 (1992) 2657–2660.

[6] BAS Europe Newsflash, December 1994, p. 2.

[7] C. Pollema and J. Ruzicka, Analyst, 118 (1993) 1235–1240.

[8] J. Ruzicka, analyst, 119 (1994) 1925–1934.

[9] M. Wasberg and A. Ivaska, Anal. Chim. Acta, 179 (1986) 433–438.

[10] W. M. Latimer, Oxidation Potentials, 2nd edn., Prentice-Hall, New York, 1952.

[11] F. Baumann and I. Shain, Anal. Chem., 29 (1957) 303–306.

Flow-injection analysis systems with immobilized enzymes. Improvement of applicability by integration of coupled reactions, separation steps and background correction[1]

Hanns-Ludwig Schmidt*, Thomas Becker, Isa Ogbomo, Wolfgang Schuhmann

Lehrstuhl für Allgemeine Chemie und Biochemie, Technische Universität München, Vöttingerstr. 40, D-85350 Freising-Weihenstephan, Germany

Abstract

The specificity of enzymes is often not sufficient to simultaneously determine two parent substrates in a given matrix. Approaches to enhance the selectivity by applying the principle of an array arrangement to flow-injection analysis (FIA) systems based on several immobilized isoenzymes are successful. Immobilized enzymes and detectors in FIA systems often suffer from interferences from impurities of the matrix. Examples are given which prove that this problem can be overcome by an integrated preseparation of the analyte (pervaporation, electrodialysis) or by correction of the matrix signal based on background subtraction using computerized data accumulation and processing.

Keywords: Flow-injection analysis; Bioprocess control; Fuzzy logic; Sample pretreatment; Enzyme selectivity

1. Introduction

Routine food quality analysis and on-line fermentation control demand specific, fast and reliable substrate determination. In this context the simultaneous determination of two or more substances is often needed. In principle this can either be performed by enzymatic analysis or by means of an efficient separation method (GC or HPLC). However, in the case of very similar substrates the specificity of available enzymes may not be sufficient, or the separation system needed must be very sophisticated. Both alternatives may be laborious and time-consuming, and hence slow and not suitable for on-line application. Flow-injection analysis (FIA) with integrated immobilized enzymes, supplemented by fast and continuous modules for clean-up and preseparation of analytes, or with integrated background correction, may combine the advantages of enzymatic analysis and efficient separation. In addition, for the

---

determination of very similar substrates with non-specific enzymes it should be possible to combine the response of different FIA lines in the manner of an array for the enhancement of specificity. The present contribution will demonstrate the advantages and limits of this principle using various examples, most of which are based on commercially available enzymes.

2. Results and discussion

2.1. FIA systems with integrated clean-up or separation modules

The continuous monitoring of a given amino acid out of a mixture in a FIA system with an oxidase or dehydrogenase can easily be performed, providing a specific enzyme is available. Sometimes the problem is restricted to the task of determining a given amino acid in the presence of a limited amount of a few others. The corresponding analysis system should also imply a certain versatility in that it could be used for the determination of different amino acids. In this respect, we have connected a continuously working electrodialysis module to a FIA system [1], schematically shown in Fig. 1, in which amino acids are determined by the unspecific amino acid oxidase reaction and the monitoring of the enzymatically formed H_2O_2 is by means of an amperometric electrode. The buffer in the central chamber of the electrodialysis unit was adjusted to the pH value
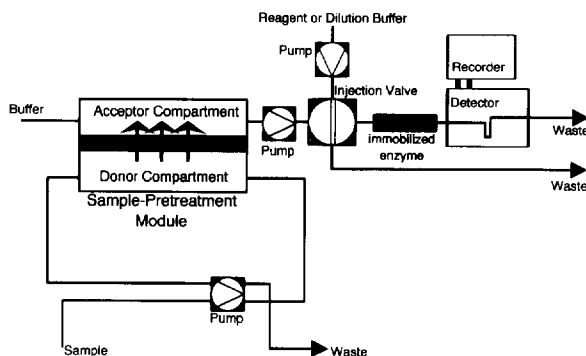
Fig. 1. FIA system with integrated sample-pretreatment module.

of the isoelectric point of the amino acid to be monitored, with the expectation that this one would pass the chamber, while other amino acids were eliminated by migration in the electric field. In practice, with complex mixtures of amino acids, it turned out that this separation procedure was not sufficient to quantitatively remove interfering amino acids. The analytical error was dependent on the type and concentration of the foreign amino acids. However, as proved for the analysis of arginine in the millimolar-range, satisfactory results were obtained when not more than three foreign amino acids were present and their total concentration did not exceed that of the analyte in question by a factor of four. Therefore, the device will be of advantage for the continous monitoring of a given amino acid in the presence of impurities of others. Its selectivity may be changed by shifting the pH value of the carrier buffer in the central chamber of the electrodialysis unit to that of the isoelectric point of the amino acid in question.

In the case of monitoring volatile analytes we proved that it would be advantageous to separate the analyte from the sample liquid through a pervaporation module [2], and use the secondary circuit of this device as the input to the enzyme-based FIA system, generally with an integrated dehydrogenase and NADH monitoring system [3] (for principal FIA set-up see Fig. 1). With this arrangement enzyme and detector are protected from interfering impurities, and hence show prolonged lifetime and reduced noise respectively. In addition, the substrate concentration in the secondary circuit can be adjusted to the linear detection range of the biosensor either by varying the relative flows of the primary and secondary liquid streams or the temperature of the donor chamber in the pervaporation module. This principle worked very well in the case of routine assay of ethanol in beer or with the monitoring of acetic acid in a fermentation broth [4]. The related reaction pathways are shown in Scheme 1.

It is useful to vary the relative concentrations of mixtures of homologue substrates and hence to support the selectivity of the enzymes. An extraordinary challenge for the application of the pervaporation principle was the analysis of diacetyl

Ethanol + NAD$^+$	Alcohol dehydrogenase $\underset{\longleftarrow}{\longrightarrow}$	Acetaldehyde + NADH + H$^+$
Acetate + ATP	Acetate kinase $\underset{\longleftarrow}{\longrightarrow}$	Acetylphosphate + ADP
Phosphoenolpyruvate + ADP	Pyruvate kinase $\underset{\longleftarrow}{\longrightarrow}$	Pyruvate + ATP
Pyruvate + NADH + H$^+$	Lactate dehydrogenase $\underset{\longleftarrow}{\longrightarrow}$	Lactate + NAD$^+$
Diacetyl + 2 NADH + 2 H$^+$	Diacetylreductase $\underset{\longleftarrow}{\longrightarrow}$	Butanediol + 2 NAD$^+$
Pentanedione + 2 NADH + 2 H$^+$	Diacetylreductase $\underset{\longleftarrow}{\longrightarrow}$	Pentanediol + 2 NAD$^+$
Acetoin + NADH + H$^+$	Diacetylreductase $\underset{\longleftarrow}{\longrightarrow}$	Butanediol + NAD$^+$

Scheme 1.

(butane-2,3-dion) in beer [5] (see Scheme 1). This compound seriously impairs the flavour of beer, and the control of its reduction to acetoin and butanediol in the course of the maturation process of beer is of great importance. At the beginning of the process beer contains approximately 0.01 ppm of this compound, and in addition about the same concentration of pentanedione-1,2 and 20 times more acetoin (butane-2-ol-3-on). There is no enzyme available which is specific for diacetyl, all dehydrogenases in question having similar affinities to pentanedione-1,2 and acetoin. We could, by pervaporation, attain a shift of the relative concentrations of the three substrates, in that the excess of acetoin was drastically reduced. However, we have still obtained an integral response which could only be corrected using acetoin concentrations independently determined by GC. Hence, in this case, because of the extreme ratio of the competing substrates, the integrated pervaporation could not completely compensate for inadequate specificity of the enzyme.

2.2. FIA systems with coupled enzyme reactions

A mixture of similar substrates is often analyzed in an enzyme-based FIA system by a common indicator enzyme reaction supported by a suitable auxiliary reaction. For example, the determination of maltose or sucrose and glucose is possible by means of the glucose oxidase reaction before and after hydrolysis of the disaccharides

with a glucosidase (integral measurement). Xylose can be measured with the unspecific glucose dehydrogenase reaction using NAD$^+$ as oxidant; however, in the presence of glucose this substrate has to be eliminated by means of the (specific) glucokinase reaction (differential measurement). The reaction sequence is shown in Scheme 2.

The differential principle has been used as a reference method in a study of the applicability of two unspecific enzymes (glucose oxidase, glucose dehydrogenase) for the parallel determination of xylose and glucose in mixtures [6]. In a FIA system (Fig. 2) the two substrates either passed only the dehydrogenase "channel" (immobilized enzyme) or a subsequent oxidase and dehydrogenase "channel". The activity of the immobilized oxidase was chosen such that the substrates were only partially converted. The two fluorimetrically obtained NADH signals for the mixture in the two "channels" allowed calculation of the individual concentrations of the two compounds using a partial least-squares algorithm. Encouraging results were obtained providing the enzymes had slightly different affinities for the substrates and the ratio of xylose/glucose was not below the value of 25. The same principle, although with the use of four "channels", namely two with individual dehydrogenases and two with subsequent oxidases/dehydrogenases, was used for the monitoring of mixtures of the three lipophilic amino acids valine, leucine and isoleucine. Only slight affinity differences existed for these sub-

$$Xylonic\ acid + NADH + H^+$$

$$\Big\uparrow\Big\downarrow \quad \substack{+NAD^+ \\ Glucose\ dehydrogenase\ (unspecific)}$$

Xylose + Glucose + ATP $\xrightarrow[\;\;\;\;\;\;\;\;\;\;]{Glucokinase\ (specific)}$ Xylose + Glucose-6-phosphate + ADP

$$\Big\uparrow\Big\downarrow \quad \substack{Glucose\ oxidase\ (unspecific) \\ +O_2}$$

$$Xylonic\ acid + H_2O_2$$

1. Dehydrogenase reaction only

Xylose + Glucose + 2 NAD$^+$ $\xrightarrow[\;\;\;\;\;\;\;]{Glucose\ dehydrogenase}$ Xylonic acid + Gluconic acid + 2 NADH + 2 H$^+$

2. Sequential oxidation by oxidase and dehydrogenase

Xylose + Glucose + 2 O$_2$ $\xrightarrow[(partial\ conversion)]{Glucose\ oxidase}$ Xylonic acid + Gluconic acid + 2 H$_2$O$_2$

Xylose + Glucose + 2 NAD$^+$ $\xrightarrow[\;\;\;\;\;\;\;]{Glucose\ dehydrogenase}$ Xylonic acid + Gluconic acid + 2 NADH + 2 H$^+$

Scheme 2.

strates with the oxidases or dehydrogenases available. It turned out, that by a mathematical treatment of the NADH signals in the different FIA lines ("channels") not only one individual amino acid out of the three could be identified, but also a quantitative analysis of all of them was possible, when they occurred in the millimolar-range in comparable concentrations [6]. In any of the following systems the so-called "nested-loop" injection of the sample into a plug of NAD$^+$ carrier was used instead of a continous flow of NAD$^+$-containing buffer, in order to save this expensive coenzyme [7] (Fig. 3). The determination of glucose and fructose in different technical syrups was
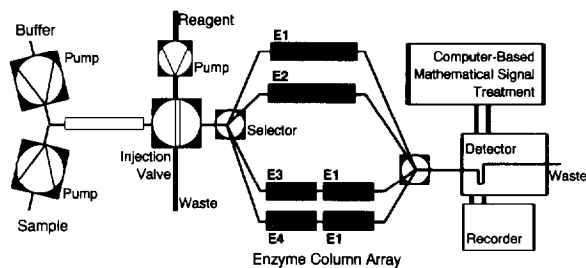
Fig. 2. FIA system with integrated enzyme-column array and mathematical signal treatment.

performed as a reference with a classical FIA system using specific enzymes, namely glucose dehydrogenase/NAD$^+$ for glucose and mannit dehydrogenase/NADH for fructose [8] (Scheme 3). The inconvenience of this system was that in one case the production, and in the other the consumption, of NADH had to be determined. Therefore, we conceived a new alternative in which we used just one dehydrogenase and the formation of NADH only. We determined glucose before and after equilibration of the two isomers with hexose isomerase, and from the two values and the known equilibrium constant the fructose concentration could be calculated. The results found for both carbohydrates were in excellent agreement with those measured by the classical FIA method and by an independent HPLC analysis. We believe that this principle will be of general importance.

2.3. Mathematical background corrections

Photometric or fluorimetric NADH determinations in untreated real samples often suffer interferences from unknown background signals of variable intensity. In classical enzymatic analysis a correction for this background is made by using a
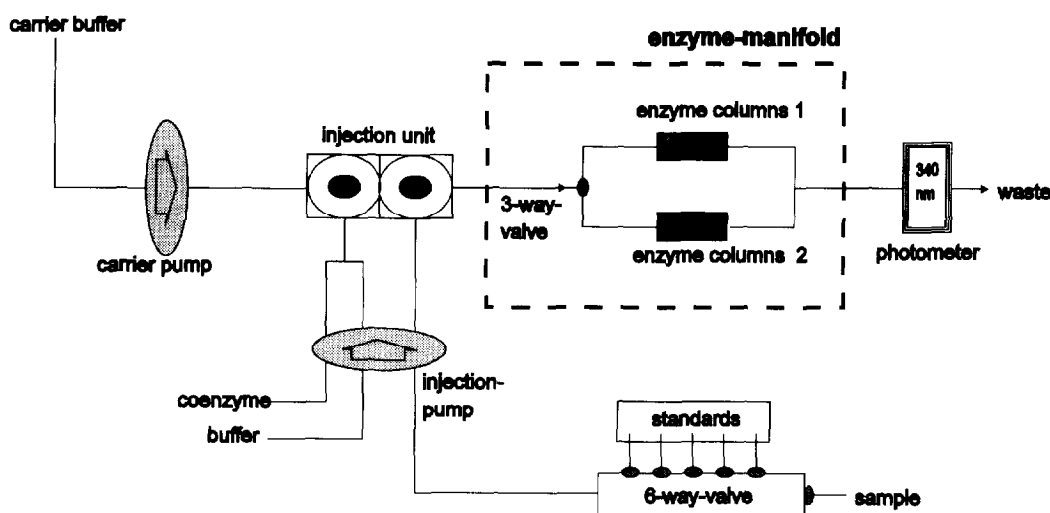
Fig. 3. Schematic representation of a FIA system with nested-loop injection, variable enzyme manifold and mathematical signal treatment.

"reference cuvette" for compensation. The analog procedure in FIA would be the individual injection of a sample with and without NAD$^+$ and the storage and subtraction of the signals, preferably in the form of the whole absorption peaks, leading to a corrected signal peak. This procedure will be successful in cases where the absolute response for the signal background is relatively low and the signal-to-noise ratio is high. In order to meet this condition we developed a FIA system which worked with very small injection volumes on the basis of a special conformation of the injection valves used. Thus, the absolute response for interfering compounds was low. An additional effect was the enhancement of the stability and lifetime of the immobilized enzyme.

One application dealt with the on-line parallel determination of D- and L-lactate in the course of a 100 h fermentation with a mixed culture of *lactobacilli* for the acidification of beer [8]. The results were in excellent accordance with those obtained by classical off-line analysis. An additional drawback occurred when ethanol was determined in untreated beer. The first results obtained were not satisfactory, probably because the samples contained—in addition to impurities

interfering with the measurement—ingredients which seemed to partially inhibit the enzyme. Correct results could be obtained only after a five fold dilution of the samples. As this would cause an additional treatment and hence would imply errors, we have conceived, based on parameters typical for an ideal shape of the response curve (NADH absorption peak observed for ethanol in water), a program for the correction of "realistic" curves using fuzzy logic [8]. With the use of this program correct and reproducible ethanol values were obtained even after injection of undiluted samples of beer. Again, we are convinced that these principles of mathematical background and matrix compensation are of general value and importance for future developments.

3. Conclusions

The versatility, selectivity and reliability of FIA systems with integrated immobilized enzymes can readily be enhanced by the integration of physical sample pretreatment modules, the combination of (not necessarily specific) enzyme reactions and by mathematical treatment of the response signals. In cases where neither specific

$$\text{Glucose} + \text{NAD}^+ \xrightleftharpoons[\text{Glucose dehydrogenase}]{} \text{Gluconolactone} + \text{NADH} + \text{H}^+$$

$$\text{Fructose} + \text{NADH} + \text{H}^+ \xrightleftharpoons[\text{Mannit dehydrogenase}]{} \text{Mannit} + \text{NAD}^+$$

$$\text{Glucose} + \text{Fructose} + \text{NAD}^+ \xrightleftharpoons[\text{Glucose dehydrogenase}]{} \text{Gluconolactone} + \text{Fructose} + \text{NADH} + \text{H}^+$$

$$\Big\updownarrow \text{ Hexose isomerase}$$

$$\text{Glucose} + \text{Fructose} + \text{NAD}^+ \xrightleftharpoons[\text{Glucose dehydrogenase}]{} \text{Gluconolactone} + \text{Fructose} + \text{NADH} + \text{H}^+$$
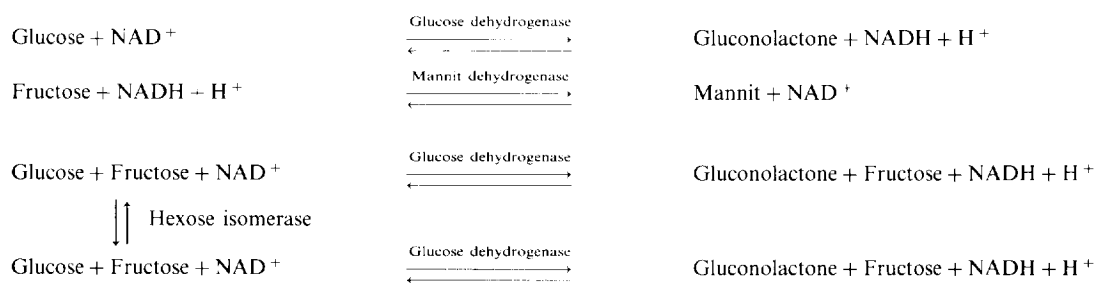
Scheme 3.

enzymes are available nor satisfactory auxiliary procedures can be provided, classical off-line and discontinuous separation methods have to be applied for the analysis of mixtures of similar substrates or the elimination of matrix interferences.

Acknowledgements

References

[1] J.C. Cooper, J. Danzer and H.-L. Schmidt, Anal. Chim. Acta, 282 (1993) 369.

[2] I. Ogbomo, U. Prinzing and H.-L. Schmidt, J. Biotechnol., 14 (1990) 63.

[3] I. Ogbomo, A. Steffi, W. Schuhmann, U. Prinzing and H.-L. Schmidt, J. Biotechnol., 31 (1993) 317.

[4] U. Prinzing, PhD Thesis, TU München, 1991.

[5] I. Ogbomo and H.-L. Schmidt, to be published.

[6] U. Englbrecht and H.-L. Schmidt, J. Chem. Tech. Biotechnol., 63 (1995) 68–74.

[7] T. Becker, W. Schuhmann, R. Betken, H.-L. Schmidt, M. B. Leible and A. Albrecht, J. Chem. Tech., Biotechnol., 58 (1993) 183.

[8] T. Becker, Ph.D. Thesis, TU München, 1995

Potentiometric flow-injection determination of trace hydrogen peroxide based on its induced reaction in iron(III)–iron(II) potential buffer containing bromide and molybdenum(VI)[1]

Hiroki Ohura[a], Toshihiko Imato[b,*], Sumio Yamasaki[a], Nobuhiko Ishibashi[†]

[a] *Department of Industrial Chemistry, Faculty of Engineering, Kyushu Sangyo University, Matsugadai, Higashi-ku, Fukuoka 813, Japan*

[b] *Department of Chemical Science and Technology, Faculty of Engineering, Kyushu University, Hakozaki, Higashi-ku, Fukuoka 812-81, Japan*

Abstract

A rapid and highly sensitive potentiometric flow-injection method for the determination of trace hydrogen peroxide was developed by use of an Fe(III)–Fe(II) potential buffer solution containing bromide and Mo(VI). The analytical method was based on a linear relationship between a concentration of hydrogen peroxide and a largely transient potential change of an oxidation–reduction potential electrode due to bromine generated by the reaction of hydrogen peroxide with the potential buffer solution. The oxidation of bromide to bromine by hydrogen peroxide occurred very rapidly with the assistance of Mo(VI) when Fe(II) existed in the potential buffer solution. It was estimated by batchwise experiments that hydroxyl radical, OH·, was generated by the reaction of hydrogen peroxide with Fe(II) as an intermediate, and subsequently oxidized bromide to bromine. In a flow system, analytical sensitivities to hydrogen peroxide obtained by the detection of the transient change of potential were enhanced about 75 fold compared with those obtained by using the potential change caused by the reaction of hydrogen peroxide with the potential buffer solution without bromide and Mo(VI). Sensitivities increased with decreasing concentration of the Fe(III)–Fe(II) buffer in the reagent solution. The detection limit ($S/N = 3$) of 4×10^{-7} M (13.6 ppb) was achieved by using the 1×10^{-4} M Fe(III)–Fe(II) buffer containing 0.4 M NaBr, 1.0 M H_2SO_4 and 0.5% $(NH_4)_6Mo_7O_{24}$. Analytical throughput was ≈ 40 h^{-1} and the RSD ($n = 6$) was 0.6% for measurement of 4×10^{-6} M hydrogen peroxide. The proposed method was applied to the determination of hydrogen peroxide in real rainwater samples, and was found to provide a good recovery for H_2O_2 added to rainwater samples.

---

* Corresponding author. Fax: (+81) 92-651-5606; e-mail: imatorcc @ mbox.nc.kyushu-u.ac.jp

† Deceased.

1. Introduction

Hydrogen peroxide in the atmosphere is known to be formed by a reaction of two HO_2 radicals, which are produced in photochemical oxidation processes of hydrocarbon compounds [1]. The amount of hydrogen peroxide existing in photochemical smog is said to be increased in summer due to an increase in the intensity of ultraviolet light. Sulfur oxides (SOx) and nitrogen oxides (NOx) which are discharged at industrial areas, are major causes of acid rain as they are oxidized to sulfate ion and nitrate ion by hydrogen peroxide in the atmosphere. The oxidation process of these oxides in the liquid phase is different from that in the gas phase. In the liquid phase, hydrogen peroxide is said to be a dominant source of oxidant for SOx and NOx [2]. Therefore, hydrogen peroxide in rainwater also plays a part in the formation processes of acid rain, so that the development of an analytical method for hydrogen peroxide is important in atmospheric environmental analysis.

An analytical method for trace hydrogen peroxide in rainwater is required to be highly sensitive and accurate. Furthermore, since trace hydrogen peroxide is unstable and is rapidly decomposed by many substances, a rapid analytical method which can be operated in a substantially closed system, is desirable for measuring hydrogen peroxide. Flow-injection analysis (FIA) [3] has been shown to be a versatile and valuable tool that can analyze many samples automatically and quickly and is therefore suitable for analyzing unstable analytes such as hydrogen peroxide in rainwater. There have been many reports on the determination of hydrogen peroxide using FIA. Spectrophotometric [4–7], fluorophotometric [10–13] and chemiluminescence methods [14–19] using peroxidase, and a spectrophotometric method using titanium(IV)–2-((5-bromopyridyl)azo)-5-(N-propyl-N-sulfopropylamino) phenol (Ti–PAPS) reagent [8,9] have been reported and applied to rainwater samples [7–9,12,13,18,19]. An ultra-highly sensitive flow analysis that detected a concentration as low as 10^{-11} M by applying a sensitized chemi-

luminescence method [20,21] has also been reported. Electrochemical methods based on amperometry for determination of hydrogen peroxide have been reported where a preoxidase immobilized column or oxidation reaction of iodide were employed [22–25]. However, few reports on the potentiometric determination of trace hydrogen peroxide have appeared [26].

Recently, we have reported on the potentiometric FIA of redox components utilizing reactions with potential buffer solutions consisting of a redox pair such as Fe(III)–Fe(II), $Fe(CN)_6^{3-}$–$Fe(CN)_6^{4-}$ and Ce(IV)–Ce(III) [27–30]. In a previous paper [29], a highly sensitive potentiometric method for determination of various oxidizing components such as bromate ion, chlorite ion, Cr(VI) and hydrogen peroxide has been proposed by detecting the largely transient potential change of an oxidation–reduction potential (ORP) electrode which appears for a short period after mixing a sample with a Fe(III)–Fe(II) potential buffer containing bromide. Our method has been applied to the determination of Cr(VI) in seawater and sufficient sensitivity was obtained to meet the Japan standards level for Cr(VI) in effluent water (≈ 500 ppb) [30]. In this method, bromine generated by the reaction of Cr(VI) with bromide was proved to cause the large potential change by spectrophotometric studies of the reaction. Furthermore, from the spectrophotometric studies, it was clarified that Fe(II) induced the oxidation of bromide and Cr(V) generated as an intermediate during the reaction of Cr(VI) with Fe(II) oxidized bromide to bromine.

In this paper, the potentiometric analytical method for hydrogen peroxide, reported in Ref. [29], was examined in detail to improve the sensitivity, and was applied to rainwater. Furthermore, in order to elucidate the reaction mechanism involved in the present method, bromine generated by the reaction of hydrogen peroxide with the Fe(III)–Fe(II) potential buffer containing bromide was determined by batchwise experiments.

2. Experimental

2.1. Reagents and solutions

Standard aqueous solutions of hydrogen peroxide were prepared by diluting analytical grade hydrogen peroxide (purity 30%); (Katayama Ltd.) with deionized water. Stock solutions (0.1 M) of Fe(III) and Fe(II) in 0.1 M H_2SO_4 were prepared according to the procedure described previously [29]. The stock solution (2%) of Mo(VI) was prepared by dissolving ammonium molybdate (Katayama) with hot deionized water. An Fe(III)–Fe(II) potential buffer solution containing 0.4 M NaBr, 0.5% Mo(VI) and 1.0 M H_2SO_4 (Solution A) was prepared by mixing the above stock solutions mentioned above. An Fe(III)–Fe(II) buffer solution without bromide and Mo(VI) (Solution B) was prepared in the same manner as solution A. Solutions A and B were used as the reagent solutions of the flow system as well as for the batchwise experiments.

2.2 Procedure for flow-injection determination of hydrogen peroxide

A schematic diagram of the flow-injection system is given in Fig. 1a. The flow-injection apparatus consisted of a peristaltic pump, a sample injection valve, a flowthrough ORP electrode detector, which consists of a gold-plated ORP electrode and a silver/silver chloride reference electrode, a potentiometer and a recorder as described previously [29]. PTFE tubing of 0.5 mm i.d. was used for the manifold.

Solution A was pumped through the reagent channel (R.S.) at a flow rate of 1 ml min^{-1}, while water was pumped through the carrier channel (C.S.) at the same flow rate. The reagent and carrier channels are maintained at 25°C. The sample solution (200 μl) was injected into the carrier stream and merged with the reagent stream at confluence point C. Hydrogen peroxide in the sample reacted with the components in the reagent stream in the 100 cm long reaction coil (R.C.). The mean residence time of the sample zone in the R.C. was about 6 s. The change of potential of the ORP electrode detector (D) was measured with the potentiometer and its signal was recorded as a peak.

2.3. Procedure for batchwise experiment and determination of bromine generated by the reaction of hydrogen peroxide with the reagent solution

The relationship between the potential change of the ORP electrode and the reaction time was examined by the same batchwise experiments as described previously [29]. 10 ml of a H_2O_2 sample solution was added quickly to 10 ml of solution A or solution B in which the ORP electrode and the reference electrode used for the detector were immersed. The potential change of the ORP electrode was measured as a function of time and recorded.

A schematic diagram of the experimental apparatus for determinations of free bromine generated by the reaction of hydrogen peroxide with the reagent solutions used for the flow system is given in Fig. 2. Solution A (45 ml) was placed in a reaction vessel (a) at 25°C and bubbled vigorously
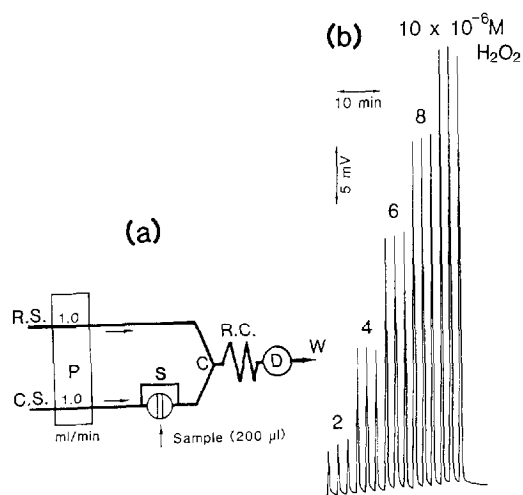
Fig. 1. Schematic FIA diagram for H_2O_2 (a) and calibration peaks (b). R.S., reagent stream (solution A); C.S., carrier stream (H_2O); R.C., reaction coil (100 cm × 0.5 mm i.d.); P, peristaltic pump; S, sample injector (200 μl); C, confluence point; D, flowthrough type ORP electrode detector; W, waste. The temperature of R.S. and C.S. was maintained at 25°C.
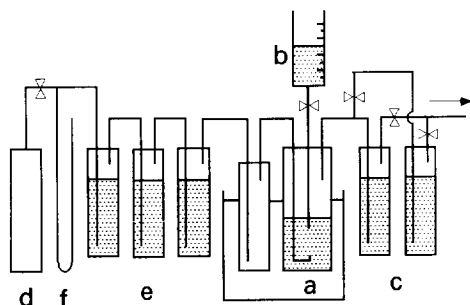
Fig. 2. Schematic diagram of the experimental apparatus for determination of bromine evolved by the reaction between H_2O_2 and reagent solution: (a) reaction vessel, solution A (45 ml); (b) syringe, H_2O_2 solution (5 ml); (c) KI solution (100 ml); (d) N_2 gas bomb; (e) gas scrubber; (f) manometer.

with N_2 carrier gas. 5 ml of H_2O_2 solution (b) was quickly added to solution A. The total volume of the mixed solution in the vessel was 50 ml. The reaction was allowed to take place for 30 s and then free bromine generated in vessel (a) was transferred by N_2 gas to a vessel (c) filled with a KI solution (100 ml), pH 7.4–7.6. Bromine was absorbed by the KI solution and iodine oxidized by bromine was determined spectrophotometrically at a wavelentgh of 352 nm ($\varepsilon = 2.76 \times 10^4$).

3. Results and discussion

3.1. Potential change of ORP electrode for reaction of hydrogen peroxide with reagent solutions in batch system

The reaction between H_2O_2 and Fe(II) in sulfuric acid solution is expressed as follows:

$$H_2O_2 + 2Fe^{2+} + 2H^+ \rightarrow 2Fe^{3+} + 2H_2O \qquad (1)$$
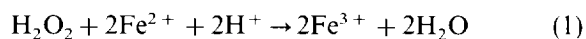
Fig. 3 shows the potential response of the ORP electrode arising from the reaction between H_2O_2 and solution A or B in the batchwise experiment. Curve (a) shows the potential change when a 1×10^{-4} M H_2O_2 solution was added to solution B. The response potential increased gradually with time and finally reached a constant equilibrium potential after reaction for 1 min. The observed potential change between the initial potential and the equilibrium potential agreed well with the value (10.38 mV) calculated from the

Nernst equation based on reaction (1). When the 1×10^{-4} M H_2O_2 solution was added to solution B containing 0.5% Mo(VI), the potential quickly increased from the same initial potential to the same equilibrium potential as those for the above solution. However, the time for the potential to reach the equilibrium potential was as short as 15 s. This means that Mo(VI) acts as a catalyst of reaction (1). Curve (b) shows the response potential change when solution B containing bromide was used. The potential increased quickly within 6 s, decreased gradually with time after passing through a maximum, and finally reached a constant equilibrium potential which is almost the same as that of curve (a). The potential change of the maximum point at a reaction time of 6 s, was ≈ 5 times larger than that of curve (a) at the same time. This mountain-shaped transient potential may be due to bromine generated as an intermediate by the reaction between hydrogen peroxide, bromide and Fe(II) in sulfuric acid solution. That is, the electrode reaction seems to be shifted from the standard potential of the Fe(III)–Fe(II) couple (0.77 V vs. NHE) to that of the Br_2–Br^- couple (1.06 V vs. NHE). Curve (c) shows the
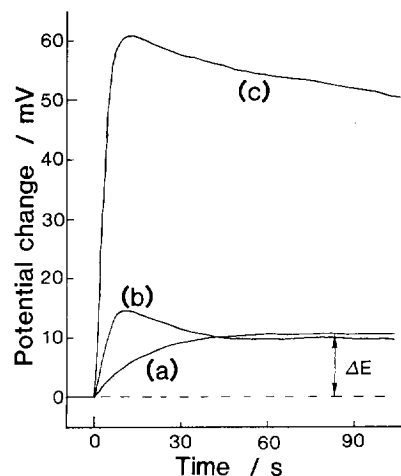
Fig. 3. Potential change of the ORP electrode by addition of the H_2O_2 solution to the Fe(III)–Fe(II) buffer solution: (a) 1×10^{-4} M H_2O_2 solution + solution B; (b) 1×10^{-4} M H_2O_2 solution + solution B containing 0.4 M NaBr; (c) 5×10^{-5} M H_2O_2 solution + solution A. ΔE is the potential difference between the initial potential and the equilibrium potential of the ORP electrode after addition of the H_2O_2 solution to the Fe(III)–Fe(II) buffer solution.
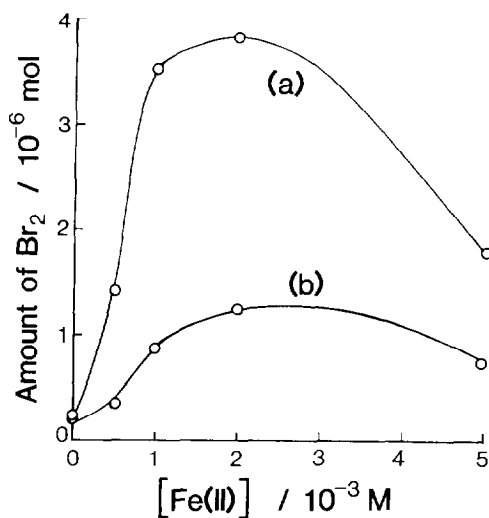
Fig. 4. Amount of bromine generated by the reaction between H_2O_2 and bromide solution containing Fe(II) and Mo(VII) or ethanol: (a) 5 ml of 2×10^{-3} M H_2O_2 was added to 45 ml of the solution A; (b) 5 ml of H_2O_2 was added to 45 ml of solution A containing 20 (v v%) ethanol. The reaction time is 30 s.

response potential when solution A was used. In this case, in spite of the lower concentration of H_2O_2, half of the concentration in curves (a) and (b), the potential change is steep and its maximum potential is much larger than that of curve (b). This indicates that the reaction rate for generation of bromine is accelerated by the addition of Mo(VI) to the reagent solution if the potential maximum comes from bromine. Sensitivity (mV/ mM^{-1}), based on the potential change normalized by the concentration of H_2O_2 at the maximum of the curve (c), was $\approx 1.2 \times 10^3$ and was enhanced by ≈ 40 fold compared to the transient potential change at the same time for curve (a). The potential change at the maximum was almost proportional to the H_2O_2 concentration down to 1×10^{-5} M. The decrease in the potential with increasing reaction time after passing through the maximum may be due to consumption of bromine. The potential change was increased $\approx$ 1.2 times when the concentration of Fe(III)– Fe(II) in solution A was decreased from 1×10^{-3} M to 1×10^{-4} M, keeping the concentrations of Mo(VI) and bromide the same. This may be due to a decrease in the reduction rate of bromine by

Fe(II). Therefore, a highly sensitive determination of hydrogen peroxide is expected if the potential change around the maximum obtained by lowering the concentration of Fe(III)–Fe(II) in solution A can be detected by a flow-injection system which is capable of using a transient reaction.

3.2. Reaction mechanism of transient potential change by reaction between hydrogen peroxide and reagent solutions containing bromide, Fe(II) and Mo(VI)

In order to elucidate the large potential change described above, the elementary reactions which possibly occur between H_2O_2, Br^-, Fe(II) and Mo(VI) in an acidic solution were examined experimentally and theoretically. Reaction (2) is expected to occur spontaneously, judging from the following facts:

(1) From the results of the batchwise experiments, the large transient potential change, believed to be due to bromine generation, was observed when solution A was used.

(2) The value of the Gibbs' free energy of the reaction between H_2O_2 and bromide in the acidic solution is negative [31]:

$$H_2O_2 + 2Br^- + 2H^+ \rightarrow Br_2 + 2H_2O$$

$$\Delta G = -32.5 \text{ kcal mol}^{-1} \qquad (2)$$

This suggests that the amount of bromine generated by reaction (2) is dependent on the concentration of bromide, but it was not true experimentally for solution A containing different concentrations of bromide. Therefore, the effect of the concentration of Fe(II) on the amount of bromine generated by the reaction of hydrogen peroxide with solution A was examined using the apparatus shown in Fig. 2. In this apparatus, the residence time of bromine generated in the reaction vessel is very short, and bromine is transported quickly to vessel (c) filled with the KI solution. The reaction time in the vessel was set at 30 s, because the time at the maximum of the transient potential described above was very short. The results are shown in Fig. 4. As can be seen from curve (a), the amount of bromine generated was very small when the reagent solution

contained bromide and Mo(VI) without Fe(II), but the amount of bromine increased markedly with increasing concentration of Fe(II) up to 2 × 10^{-3} M in the reagent solution. Therefore, this indicates that the presence of Fe(II) in the reagent solution contributes greatly to the generation of bromine. This may be because Fe(II) induces the oxidation of bromide in a similar manner to when bromide is oxidized by Cr(V) in the presence of Fe(II) as reported previously [30]. The decrease in the amount of bromine with increasing concentration of Fe(II) above 2 × 10^{-3} M may be due to the consumption of bromine by reaction with Fe(II).

Kolthoff and Medalia [32] reported that the rate equation of reaction (1) can be expressed by a first-order reaction with respect to H_2O_2 and Fe(II) and measured the rate constant for the reaction. They pointed out that reaction (3), where hydroxyl radical (OH·) is produced as an intermediate, is a rate-limiting step of reaction (1). This radical is known to oxidize organic compounds such as alcohols, acetone, acetic acid, etc. Curve (b) in Fig. 4 shows the case where solution A containing 20% (v/v) ethanol was used. The amount of bromine is less than one-third that of curve (a). This result suggests that the hydroxyl radical generated as an intermediate of reaction (1) reacts with bromide to generate bromine as expressed by reaction (4). The lower amount of bromine in the presence of ethanol may be because hydroxyl radical reacts preferably with ethanol than with bromide. It is possible to believe that this side-reaction of hydroxy radical

with ethanol suppressed the reaction with bromide. Therefore, the generation of bromine by addition of H_2O_2 to the solution containing Br$^-$ and Fe(II) in sulfuric acid can be explained by considering the elementary reactions (3)–(5). The contribution of reaction (2) to the generation of bromine seems to be very small, as can be seen from Fig. 4 at the concentration of Fe(II) = 0.

$$H_2O_2 + Fe^{2+} + H^+ \rightarrow Fe^{3+} + OH· + H_2O \quad (3)$$

$$OH· + Br^- + H^+ \rightarrow 1/2Br_2 + H_2O \quad (4)$$

$$OH· + Fe^{2+} + H^+ \rightarrow Fe^{3+} + H_2O \quad (5)$$
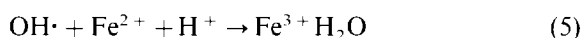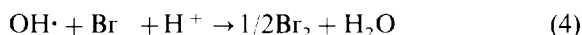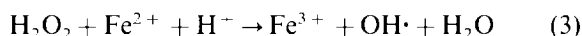
H_2O_2 reacts with Fe^{2+} to produce hydroxyl radical and the hydroxyl radical produced simultaneously oxidizes Br$^-$ and Fe^{2+}. The abrupt potential increase shown in Figs. 3b and 3c can be explained by the bromine generated from the elementary reaction above. The presence of Mo(VI) in the solution may accelerate reactions (3) and (4). The overall reaction of H_2O_2 with the solution containing Br$^-$ and Fe^{2+} is expressed by reaction (6) (sum of reactions (3) and (4))

$$H_2O_2 + Fe^{2+} + Br^- + 2H^+$$
$$\rightarrow 1/2Br_2 + Fe^{3+} + 2H_2O \quad (6)$$
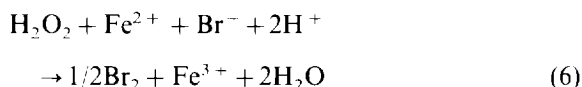
As shown in Figs. 3b and 3c, the potential decreases after passing through the maximum. This decrease in the potential can be explained by consumption of bromine:

$$1/2Br_2 + Fe^{2+} \rightarrow Fe^{3+} + Br^- \quad (7)$$
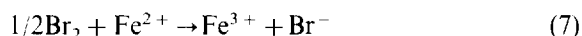
Reaction (1) is the sum of the elementary reactions (3) and (5). The reactions of H_2O_2 with solutions A and B are expressed by the same overall reaction (1), but the former reaction consists of the elementary reactions (3), (4) and (7), while the latter reaction consists of reactions (3) and (5). That is, the presence of bromide in solution A may act as an homogeneous catalyst for the formation and reduction of bromine.

3.3. Flow-injection analysis of trace hydrogen peroxide

The flow system utilizing the detection of the large transient potential change described in the

Table 1
Effect of concentrations of Fe(III)–Fe(II) buffer in solutions A and B on sensitivity (the flow system is the same as that of Fig. 1a)

Fe(III)–Fe(II) concentration[a]	Sensitivity (mV mM^{-1})		Enhancement factor[b]
	Solution A	Solution B	
1 × 10^{-2}	5.6 × 10^2	10	56
1 × 10^{-3}	2.5 × 10^3	42	60
1 × 10^{-4}	3.3 × 10^3	44	75

[a] Both Fe(III) and Fe(II) are dissolved in the same concentration in the buffer.
[b] Defined as the ratio sensitivity obtained by solution A to that obtained by solution B.

Table 2
Recovery of H_2O_2 added to rainwater (samples A and B were collected at Kyushu Sangyo University and the pHs were 4.22 and 4.17 respectively)

Sample (Date)	H_2O_2 added ($\times 10^{-6}$ M)	H_2O_2 found ($\times 10^{-6}$ M)	Recovery (%)
A	0	0	
(30/10/93)	2.50	2.41	96.4
	5.00	4.79	95.8
	7.50	7.41	98.8
B	0	0	
(8/11/93)	2.50	2.58	103.5
	5.00	5.20	104.1
	7.50	7.41	98.8

previous section was designed as shown in Fig. 1a. The concentration of the potential buffer solution and the reaction time were important factors for the sensitive determination of H_2O_2 based on the detection of the transient potential change. The sensitivity to hydrogen peroxide increased with increasing concentrations of sulfuric acid and sodium bromide in the potential buffer solution, and became almost constant at about 0.5–1.0 M sulfuric acid and ≈ 0.4 M sodium bromide. Since the reaction time which gave the maximum potential was 6 s from the batchwise experiments shown in Fig. 3c, a 100 cm long reaction coil and a pumping rate of 1 ml min^{-1} for the carrier and reagent streams were set for the flow system to maintain the reaction time at 6 s. The calibration peaks for the standard H_2O_2 sample are shown in Fig. 1b. The relative standard deviation (RSD) for peak heights was 0.6% for determinations of six samples of 4×10^{-6} M hydrogen peroxide. A sampling rate of 40 H^{-1} was possible with the present manifold. The detection limit at a signal-to-noise ratio of 3 was 4×10^{-7} M (13.6 ppb). In this case, sensitivity, peak heights normalized by concentrations of H_2O_2, was 3.3×10^3 mV/ mM^{-1} and was 75 times larger than that using the reagent solution without bromide and Mo(VI) i.e. solution B. The sensitivity was also dependent on the concentration of Fe(III)–Fe(II) in solution A. The sensitivities to H_2O_2 obtained for solution A at different Fe(III)–Fe(II) concentrations are

listed in Table 1 together with those for solution B. The sensitivity increases with decreasing concentration of Fe(III)–Fe(II) for the solutions A and B in the same way as for the batchwise experiments. The enhancement factor, defined as the sensitivity ratio, for solutions A and B increased slightly with decreasing concentration of Fe(III)–Fe(II). The sensitivities obtained for solution A with the flow system were about twice those obtained for the same solution with the batch system. The lower sensitivity with the batch experiment may be due to escape of the generated bromine into the atmosphere because of the open system [29].

The effects of several coexisting ions for the determination of hydrogen peroxide were examined. Coexisting 100 fold amounts of Cl^-, SO_4^{2-}, NO_3^-, Na^+, K^-, Mg^{2+}, Ca^{2+} and NH_4^+ which are usually contained in rainwater were tolerated for the determination of 4×10^{-6} M hydrogen peroxide.

3.4. Application to hydrogen peroxide in rainwater

It is generally said that hydrogen peroxide content in rainwater is greatly influenced by the season of the year. For example, Matsubara et al. [9] have reported that the concentration of hydrogen peroxide in rainwater was $(7-9) \times 10^{-6}$ M in summer and $(0.5-1.5) \times 10^{-6}$ M in winter in the Kanto district of Japan. These results were obtained with theri FIA method using the Ti–PPAS reagent. Our proposed method was applied to two rainwater samples collected at our university in November. The results are shown in Table 2. Hydrogen peroxide in two samples could not be detected either by our proposed method or by the method of Matsubara et al., using the Ti–PPAS reagent. This means that H_2O_2 in the rainwater sample must be less than 13.6 ppb, the detection limit of our method, or 1.36 ppb ($S/N = 2$), that of the method of Matsubara et al. Our method was than applied to the rainwater sample to which a known amount of the standard H_2O_2 solution was added. The proposed method provided a a good recovery within 95–104% for samples containing hydrogen peroxide at the 10^{-6} M level.

4. Conclusion

In conclusion, the proposed flow-injection analysis method for hydrogen peroxide was improved in sensitivity compared to the previous method [29] and applied to the determination of hydrogen peroxide in a rainwater sample. It was realized that hydroxyl radical, OH·, produced by the induced reaction of hydrogen peroxide with Fe(II), contributes to the generation of bromine which causes the large transient potential. The proposed method could be useful for the determination of concentrated hydrogen peroxide in the bleaching process of dyeing.

References

[1] O. Tsuruta, Modern Chemistry, 8 (1990) 16 (in Japanese).

[2] K. Murano, Rainwater and Fog Acid, Syoukabou, Tokyo, Japan, 1993, p. 48 (in Japanese).

[3] J. Ruzicaka and E.H. Hansen, Flow Injection Analysis, Wiley, New York, 1981.

[4] L. Gorton and L. Ogren, Anal. Chim. Acta, 130, (1981) 45.

[5] T. Yamane, Bunseki Kagaku, 33 (1984) E203.

[6] M.M. Fishman, Anal. Chem., 53 (1980) 185R.

[7] B.C. Mandsen and M.S. Kromis, Anal. Chem., 56 (1984) 2849.

[8] C. Matsubara, K. Sakai and K. Takamura, Nihon Kagaku Kaishi, 5 (1991) 430.

[9] C. Matsubara, T. Sato, Y. Sato and K. Takamura, Bunseki Kagaku, 42 (1993) 773.

[10] Y. Hayashi, K. Zaitsu and Y. Ohukura, Anal Sci., 1 (1985) 65.

[11] E.L. Wehry, Anal. Chem., 52 (1980) 75R.

[12] A.L. Lazrus, G.L. Kok, S.N. Gitlin, J.A. Lind and S.E. Mclaren, Anal. Chem., 57 (1985) 917.

[13] N. Beltz, W. Jaeschke, G.L. Kok, S.N. Gitlin, A.L. Larzus, S.E. McLaren, D. Shakespeare and V.A. Mohnen, J. Atmos. Chem., 5 (1987) 311.

[14] D.T. Bostich and D.H. Hercules, Anal. Chem., 47 (1975) 447.

[15] D.C. Williams III, G.F. Huff and W.R. Scitz, Anal. Chem., 48 (1976) 1003.

[16] G. Rule and W.R. Seitz, Clin Chem., 25 (1979) 1635.

[17] B. Olsson, Anal. Chim. Acta, 136 (1982) 113.

[18] K. Yoshizumi, K. Aoki, I. Nouchi, T. Okita, T. Kobayashi, S. Kamakura and M. Tajima, Atmos. Environ., 18 (1985) 395.

[19] P. Van Zoonen, D.A. Kamminga, C. Gooijer, N.H. Velthorst and R.W. Frei, Anal. Chim. Acta, 174 (1985) 151.

[20] G.L. Koh, Atmos. Environ., 14 (1980) 656.

[21] M. Ishi and R. Shirai, Bunseki Kagaku, 41 (1992) 125.

[22] E.L. Gulberg, J. Autom. Chem. 2 (1980) 189.

[23] T. Cho, S. Yoshida and S. Hirose, Bunseki Kagaku, 32 (1983) 6.

[24] H. Lundback, Anal. Chim. Acta, 145 (1983) 189.

[25] M.A. Abdalla and H.A. Al-Swaidan, Anal. Lett., 22 (1989) 1729.

[26] K.G. Boto and L.F.G. Williams, Anal. Chim. Acta, 85 (1976) 179.

[27] H. Ohura, T. Imato, S. Yamasaki and N. Ishibashi, J. Flow Injection Anal., 8 (1991) 2.

[28] H. Ohura, T. Imato, S. Yamasaki and N. Ishibashi, Bunseki Kagaku, 40 (1991) 93.

[29] N. Ishibashi, T. Imato, S. Yamasaki and H. Ohura, Anal. Chim. Acta, 261 (1992) 405.

[30] H. Ohura, T. Imato, S. Yamasaki and N. Ishibashi, Bunseki Kagaku, 43 (1994) 31.

[31] W.M. Latimer, Oxidation Potentials, 2nd edn., Prentice-Hall, Englewood Cliffs, NJ, 1952, p. 38.

[32] I.M. Kolthoff and A.I. Medalla, J. Am. Chem. Soc., 71 (1949) 3784.

Determination of primary aromatic amine in quality control of X-ray contrast media by flow-injection analysis[1]

Gro Johansen[a,*], Kjersti Grini[a], Karina Langseth-Manrique[a],
Kåre Helge Karstensenb[b]

[a]Nycomed Imaging AS, P.O. Box 4220, Torshov, N-0401 Oslo, Norway
[b]SINTEF, P.O. Box 124, N-0314 Oslo, Norway

Abstract

An automated flow-injection method for determination of primary aromatic amines based on the Bratton–Marshall reaction is described. This method is used for analysis quality control of three different X-ray contrast media (Omnipaque[®], Imagopaque[®] and Visipaque[®] which are viscous solutions. In flow-injection analysis, such samples cause refractive index effects and low, broad peaks due to prolonged residence time. hese interferences are minimized by the use of a carrier solution (7 w/v % NaCl in 1 M HCl) with same refractive index as the samples, careful pH adjustment, use of knotted coils, and a specially designed detector. Validation of the method in the concentration range 4–40 μg ml^{-1} (injected samples) shows a repeatability ($n = 6$) and day-to-day reproducibility ($n = 9$) of 0.4–9.2 and 2.3–17.5% RSD respectively. The accuracy is 81(near the lower limit of detection)–101%, with a limit of detection of 1 μg ml^{-1}. Linearity was shown in the concentration range tested. The method is well suited for in-process analysis, release control and stability testing of both drug substance and drug product. The cost of analysis is reduced compared to the manual method.

Keywords: Aromatic amine; Flow-injection analysis; Quality control; X-ray contrast media

1. Introduction

Nycomed Imaging AS, acknowledged as a world leader in contrast agents for X-ray, magnetic reso-

nance imaging (MRI) and ultrasound techniques, develop, manufacture, and promote contrast agents within these modalities. The company is, in common with other pharmaceutical companies, interested in reduction of production time and costs; here we include analytical costs. Thus, simple, rapid and precise analytical methods are continuously developed and flow-injection analysis (FIA) is one of the promising techniques evaluated.

* Corresponding author. Fax: (+ 47) 22-89-1200; e-mail: gro.johansen@nycomed.telemax.no
[1] Presented at the Seventh International Conference on Flow Injection Analysis (ICFIA '95), held in Seattle, WA, USA, August 13–17, 1995.

Omnipaque®, Imagopaque® and Visipaque® are non-ionic, iodinated X-ray contrast media supplied as ready-for-use aqueous injection solutions with different iodine concentrations. A primary aromatic amine—5-amino-N,N'-bis(2,3-dihydroxypropyl)-2,4,6-triiodo-1,3-benzenedicarboxamide (Cpd 5400)—is an intermediate in the chemical manufacturing process of these contrast media and hence is a possible impurity in the products. The primary aromatic amine concentration is controlled in-process, for release and during stability studies of both drug substance and drug product. The current analytical method is a manual, time-consuming spectrophotometric technique based on the Bratton–Marshall [1] reaction. The number of papers on FIA determination of primary aromatic amines [2–7] published, and the fact that the samples are aqueous with a well-defined sample matrix, made FIA an attractive technique.

This paper presents an FIA method developed for the quantification of Cpd 5400 in the contrast media. As these media are concentrated and viscous samples, refractive index (RI) effects [8] and broad peaks with prolonged retention time [9] were expected. Optimisation steps are thus presented, as well as validation results.

2. Experimental

2.1. Reagents

Sodium chloride, sodium nitrite and hydrochloric acid of p.a. grade were prepared in degassed deionized water to the concentrations given in Fig. 1. The carrier solution consisted of 7% w/v NaCl in 1 M HCl. Solutions of 0.1% w/v N-(1-naphthyl)-ethylenediamine-dihydrochloride (NEDD) (Merck, Darmstadt), and 0.6 mM NaNO$_2$ were freshly prepared. 5-Amino-N,N'- bis(2,3-dihydroxypropyl)-2,4,6-triiodo-1,3-benzenedicarboxamide (Cpd 5400), the X-ray contrast media drug substances (iohexol, iopentol, and iodixanol), and the corresponding drug products (Omnipaque®, Imagopaque®, and Visipaque®) were all manufactured by Nycomed Imaging AS.

2.2. Instruments

Two commercial FIA systems were used for development, optimization and validation of the method: a Tecator 5010 Flow-Injection Analyzer equipped with Tecator 5017 Sampler, Tecator 5023 Spectrophotometer and Tecator V100 Injector (Tecator AB, Sweden), and a Lachat QuickChem AE Ion Analyzer (Lachat Instruments, Milwaukee, WI) equipped with a spectrophotometric detector designed by Lachat for samples with high matrix concentration. The analytical manifold designed for this analysis, reagents, flow rates and detection wavelength are shown in Fig. 1.

2.3. Procedure

Six calibration aqueous standards (4, 8, 12, 20, 40, and 50 μg Cpd 5400 ml^{-1}) were prepared by first diluting the standard stock solution (1000 μg Cpd 5400 ml^{-1}) with carrier solution to 100 μg Cpd 5400 ml^{-1} and then by taking aliquots (1.0–12.0 ml) of the latter, further diluted to 25.0 ml with carrier solution. Samples of drug substance (1.22 g weighed accurately) were dissolved in 10 ml of water. Concentrated HCl was added (3.0 ml), and the mixture was then diluted to 20.0 ml with water. Drug product samples were prepared by adding 3.0 ml HCl, and diluting to a concentration equivalent to 60 g drug substance ml^{-1}. Samples for the validation were prepared by spiking the X-ray drug substances with various amounts of Cpd 5400 prior to dilution with water. Final concentrations are given in Table 1.
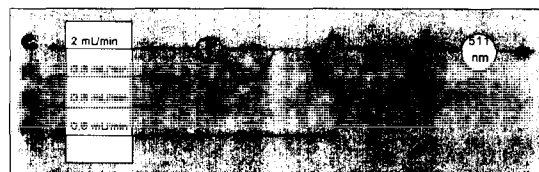
Fig. 1. Flow-injection manifold for primary aromatic amine analysis: I, injector, 40 μl loop; C$_1$, reaction coil knotted, 40 cm × 0.8 mm; C$_2$, reaction coil, knotted, 200 cm × 0.8 mm; C$_3$, reaction coil, knotted, 50 cm × 0.8 mm; C, carrier, 7% w/v NaCl in 1 M HCl; R$_1$, 1 M HCl; R$_2$, 0.6 mM NaNO$_2$; R$_3$, 0.1% w/v NEDD.

Table 1
Validation data for FIA method for determination of primary aromatic amine (Cpd. 5400) in X-ray contrast media. Samples of spiked drug substance

Added Cpd 5400 (μg g^{-1})	Accuracy (% recovery)	Linearity[a]	Precision		Sensitivity	
			Repeatability (%RSD) ($N = 6$)	Reproducibility (%RSD) ($N = 12$)	LOD (μg g^{-1})	LOQ (μg g^{-1})
Iohexol (51.4–308)	98.2–100	$r = 0.998$ $n = 0.96$	0.4–1.8	2.4–3.0	20	65
Iopentol (51.3–513)	97.0–97.3	$r = 0.998$ $n = 0.98$	0.7–2.5	2.3–4.0	27	90
Iodixanol (51.3–819)	81.3–101.2	$r = 0.9997$ $n = 0.99$	1.1–9.2	2.8–17.5	24	81

[a] r = regression coefficient; n = factor of curvature, in $Y = a + bx^n$; zero within 95% confidence limits for all methods.

Standards and sample solutions are injected into the manifold. The concentration of the samples is calculated by using peak area and standard curve.

3. Results and discussion

3.1. Manual method

The manual procedure for determination of primary aromatic amines is based on the Bratton–Marshall reaction. The amine is diazotized with nitrous acid giving a diazonium ion which is coupled to NEDD. The reaction product, an azo dye, is measured spectrophotometrically at 495 nm. This procedure involves a cumbersome reaction, which requires low temperature (ice bath) for stabilization of the diazonium ion, and addition of nitrous acid at an exact given time interval. Excess nitrous acid must be removed by adding sulphamic acid, with subsequent debubbling of the nitrogen formed, as nitrous acid decomposes the chromogen and azo dye. The produced azo dye must be measured within a specific time interval.

3.2. FIA method

The FIA method is based on a paper presented by Koupparis and Anagnostopoulou [2]. With a

combination of low nitrous acid concentration and the advantageous kinetic nature of FIA, they were able to eliminate the removal of excess nitrous acid. The method was fast, sensitive, linear and worked well with aqueous solutions of Cpd 5400.

3.3. Optimisation

To optimize the system for Cpd 5400, a 2^4 factorial design with reaction time (flow rates), acid, nitrite, and NEDD concentrations as variables was performed. It was shown that the main effects were caused by the reaction time and the acid and nitrate concentrations. Further univariate optimisation of reaction time (flow rates, reaction coil dimensions), concentration of HCl and nitrous acid, and wavelength, resulted in the manifold described in Fig. 1.

To make analysis as simple and fast as possible, injection of undiluted samples would be advantageous. However, the contrast media are highly concentrated, and have high viscosities (22–27 cP). Fig. 2 shows injection of undiluted Visipaque[R] (320 mg I ml^{-1}) and aqueous standard (4 Cpd 5400 μg ml^{-1}). Here, two major effects of FIA of viscous and concentrated samples are demonstrated. Firstly, an RI effect occurs when the sample matrix of samples with low analyte concentration is more concentrated than the car-

rier, and vice versa. The RI effect, characterized by a positive and a negative peak, is superimposed upon the analytical signal, making determination of low analyte concentrations impossible. Secondly, the sample viscosity causes prolonged residence time in the coils resulting in lower and broader peaks (Fig. 2).

With a combination of several simple steps, these problems were minimized: sample dilution and reduction of injection volume is the easiest way to eliminate problems caused by concentrated sample matrix. However, the low analyte concentration prevents dilution of the samples by more than 5–10 fold. Thus, to minimize the RI effect, a carrier with the same RI as the diluted samples was introduced. It consisted of a high concentration of an inert compound—7% w/v NaCl in 1 m HCl. Aqueous standards were also diluted with the carrier. Finally, to make the method more rugged, a detector designed by Lachat to minimize RI effects was used. In this detector, the light aperture is reduced in size and placed slightly off center, the surface area of the photodiode is increased, and the flow cell has a flat, highly polished surface.

Injection of analyte-free sample in the manifold results in a negative peak. This peak, which is another effect of sample viscosity, is superimposed upon the analytical signal, causing an analytical error. This is explained by a slow, pH-dependent reaction between NEDD and nitrous acid which causes an absorbing background. The reaction time available for this reaction is short (coil 3, Fig. 1). When a viscous sample is injected, the background absorption is

Fig. 2. Maximized FIA signals of undiluted Visipaque® 320 mg I ml⁻¹ (a), and aqueous standard 4μg Cpd 5400 ml⁻¹ (b).

lower compared to normal conditions. This is caused by incomplete mixing and hindered molecular transport, and the result is a negative peak. The diazotation of the amine is not hindered by the sample viscosity, because the reaction time is longer (coil 2, Fig. 1), nor is the fast coupling reaction with NEDD in coil 3.

The samples were adjusted with acid to compensate for this loss of background absorption. The amount of acid added was chosen carefully, since the diazotation reaction is also pH-dependent. The accuracies and the linearity given in Table 1 show that the amount of acid added is just sufficient to compensate for the loss of background absorption. For further minimization of sample viscosity effects, knotted coils were used to optimize mixing. Under these conditions, the use of peak area instead of peak height was adequate to compensate for the broader sample peaks compared to aqueous standard peaks.

Fig. 3 shows FIA signals obtained when the physical interferences were minimized.

3.4. Validation

Linearity and accuracy (given as the recovery of added amounts of Cpd 5400) were tested at six and three concentration levels respectively. Precision was tested at three levels: as repeatability with six sample replicates, and as reproducibility over three days with a total of 12 sample replicates. The specificity was studied by analyzing blank samples of the injection solutions without drug substance addition: i.e. excipients only. Lower limit of detection (LOD) and lower limit of quantitation (LOQ) were determined by use of the variation around the calibration curve ($S_{y,x}$), and its slope (b): ($3xS_{y,x})/b$ and ($10xS_{y,x})/b$ respectively. The validation results are shown in Table 1. The linearity is given as absorbance versus added amount of Cpd 5400 in the concentration range from the LOQ—corresponding to 4–40 μg Cpd 5400 ml⁻¹ in injected samples. The detection limit is approximately 1 μg ml⁻¹. As the chemistry is specific for primary aromatic amines, and no
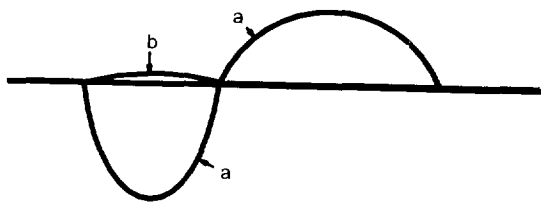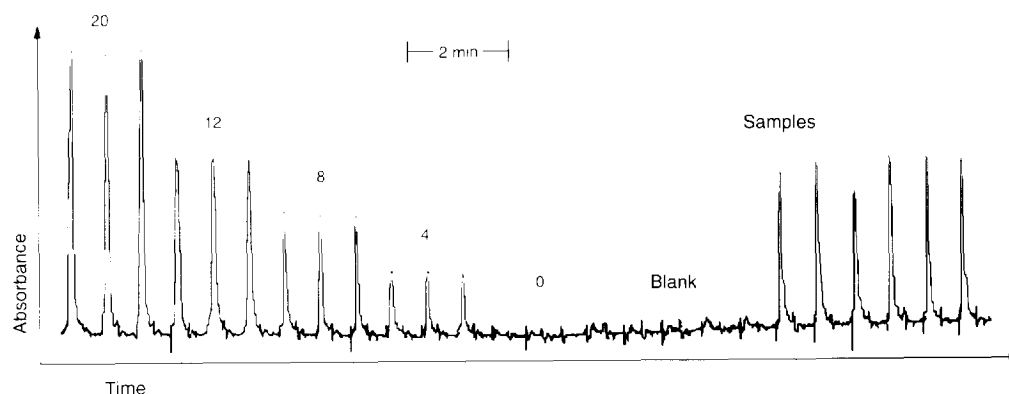
Fig. 3. FIA signals of calibration standards (4. 8. 12, 20 μg Cpd 5400 ml⁻¹). blank samples and samples of Visipaque* 320 mg I ml⁻¹.

matrix interferences were observed when analyzing blank samples, the method is selective for primary amine in X-ray contrast media.

viscous samples, each application has to be "tailored".

4. Conclusions

FIA is an excellent tool for automation of the Bratton–Marshall reaction. The method described in this paper is well suited for the analysis of Cpd 5400 in in-process control, for product release and instability testing. The validation results are equal to, or better than, the current manual method. Because the FIA method is so simple and fast, the analytical costs can be reduced significantly, depending on the amount of samples analyzed in a series. The method is currently being evaluated for other applications.

FIA can be used for the analysis of concentrated, moderately viscous samples, but to overcome the physical interferences caused by highly

References

[1] A.C. Bratton and E.K. Marshall, J. Biochem., 128 (1939) 537–550.

[2] M.A. Koupparis and P.I. Anagnostopoulou, Anal. Chim. Acta, 204 (1988) 271–283.

[3] A.G. Fogg, N.K. Bsebu and M.A. Abdulla, Analyst, 107 (1982) 1462–1465.

[4] K.K. Verma and K.K. Stewart, Anal. Chim. Acta, 214 (1988) 207–216.

[5] A.M. Alweheid, Analyst, 115 (1990) 1419 1422.

[6] J.S. Esteve Romero, G. Ramis Ramos, R. Forteza Coll and V. Cerda Martin, Anal. Chim. Acta, 242 (1991) 143–146.

[7] M.C. Mahedro and J.J. Aaron, Anal. Chim. Acta, 269 (1992) 193 198.

[8] G. Ham, Anal. Proc., February (1981) 67 70.

[9] D. Betteridge, W.C. Cheng, E.L. Dagless, P. David and T.B. Godd, Analyst, 108 (1983) 17 32.

Flow-injection determination of trace hydrogen peroxide or glucose utilizing an amperometric biosensor based on glucose oxidase bound to a reticulated vitreous carbon electrode[1]

Masoud Khayyami[a,*], Gillis Johansson[b], Dario Kriz[a], Bin Xie[a],
Per-Olof Larsson[a], Bengt Danielsson[a]

[a]*Pure and Applied Biochemistry, Chemical Center, Lund University, P.O. Box 124, S-221 00 Lund, Sweden*
[b]*Analytical Chemistry, Chemical Center, Lund University, P.O. Box 124, S-221 00 Lund, Sweden*

Abstract

An electron transfer mediator, 8-dimethylamino-2,3-benzophenoxazine (Meldola Blue), dissolved in the carrier solution in a flow-injection system, was found to reduce the oxidation potential for hydrogen peroxide from 600–1200 mV without mediator to -100 mV vs. Ag/AgCl with the mediator present. The very low background current of reticulated vitreous carbon (RVC) at this potential makes it possible to detect very low levels of hydrogen peroxide or glucose. Glucose oxidase was covalently coupled with carbodiimide to RVC, and the RVC was formed into a column inserted in a flow-injection system. The calibration curve was linear from 30 nM to 10 μM glucose with 5 μM mediator. At higher mediator concentrations, the linear range was extended to 1000 μM, but with a much higher background current. The sample throughput was about 60 h^{-1}. The current response decreased to 50% of the original response after 20 days. The coulometric yield was high because the sample was pumped through the pores of the RVC. It was 16% and 55% at a flow rate of 1 ml min^{-1} at mediator concentrations of 5 and 50 μM respectively.

1. Introduction

A great number of biosensors for glucose determination have been described in the literature over the last two decades [1–3]. The major goal has been to develop sensors for determining glucose in blood. Some work has also been devoted

---

* Corresponding author. Fax: (+46)46-46-10-46-11.

[1] Presented at the Seventh International Conference on Flow Injection Analysis (ICFIA '95), held in Seattle, WA, USA, August 13–17, 1995.

to determination of glucose in biotechnological processes. Very little emphasis has been put on developing glucose sensors for the submicromolar range.

Hydrogen peroxide is a reaction product in a number of enzymatic reactions used in substrate determinations. It can be determined spectrophotometrically using peroxidase-catalyzed color reactions of the Trinder type [4]. It can also be determined electrochemically by oxidation at about + 1200 mV vs. SCE on glassy carbon [5] or at lower potentials on platinum or by using chemically-modified electrodes, e.g. + 400 mV at palladium sputtered on carbon [6]. With catalysts such as peroxidases on the electrode surface reduction starts at + 600 mV and reaches a constant value at − 200 mV [7]. A number of soluble or immobilized mediators have been used for lowering the necessary electrode potentials for detection of hydrogen peroxide produced by oxidases. Mediators

for glucose determination include N-methylphenazinium salts [8] and Meldola Blue. Both mediator and enzymes were incorporated into carbon paste electrodes [9].

The superior electrochemical properties of reticulated vitreous carbon (RVC) [10] have prompted a study of this material for use as a sensor at very low concentration levels. Previously glucose oxidase has been coupled covalently to RVC and the production of hydrogen peroxide was determined by oxidation at + 900 mV vs. SCE [11].

In this paper we report on the use of a soluble electron transfer mediator, Meldola Blue, which can detect hydrogen peroxide or glucose down to − 100 mV vs. Ag/AgCl. Glucose oxidase was used in this study because this enzyme is very stable and has been comprehensively studied previously. It is thus a good model system although the use of other oxidases may provide even higher sensitivity from a practical point of view. The ability to select a potential at which the background currents are extremely low should be of great importance in making sensors for low substrate levels.

2. Experimental

2.1. Chemicals

Glucose oxidase (GOx) type S-X (*Aspergillus niger*), Meldola Blue, 8-dimethylamino-2,3-benzophenoxazine and 1-cyclohexyl-3-(2-morpholinoethyl)-carbodiimide metho-p-toluenesulfonate were obtained from Sigma. The RVC, porosity grade 100-S (pore size nominally 0.25 mm), was from Energy Research and Generation Inc. (Oakland, CA).

The potentiostat (model MA 5410, Chemel AB, Lund, Sweden) was set at a voltage of − 100 mV vs. Ag/AgCl. The carrier buffer was 0.1 M sodium phosphate, pH 7.0, containing 1.9 mg Meldola Blue 1^{-1} (5.0 μM). Meldola Blue is unstable at higher pH, the half-life time at pH 7.0 is 100 h [12], and new buffer solutions were therefore prepared every day. The peristaltic pump was from Alitea AB (model C-4v). Sample injection was through a 100 μl loop.

Fig. 1. Cell configuration for determination of glucose or hydrogen peroxide.

Table 1

Peak currents at various applied voltages (vs. Ag/AgCl) observed when injecting 100 μl of 1 μM glucose samples into a phosphate buffer, pH 7.0, containing 5 μM Meldola Blue. Flow rate 1 ml min^{-1}

Applied voltage	(mV)	−150	−100	−50	0	50	100	150
Peak current	(nA)	270	230	230	230	250	250	280

2.2. Preparation of the column

RVC cylinders (1.5 × 0.5 cm^2) were cut (using eye and dust inhalation protection devices) from a block of material and left in 6 M HCl for 1 h. They were washed with distilled water until the solution reached pH 5, and then left in dry methanol for 2 h. Finally, the cylinders were dried in an oven at 110°C overnight. A cylinder was fixed in a glass tube as shown in Fig. 1 with a counter electrode of the same material. The reference electrode was mounted downstream, which should be acceptable due to the low currents.

2.3. Immobilization

A 0.05 M acetate buffer (pH 5.1) containing carbodiimide (40 mg ml^{-1}) was pumped through the system at a flow rate of 0.2 ml min^{-1} for 150 min in order to activate the RVC surface. Then acetate buffer was circulated under an ice bath at a flow rate of 1.2 ml min^{-1} for 30 min. For immobilization of GOx, an enzyme solution (60 mg per 10 ml) in buffer was circulated in the column under an ice bath at a flow rate of 0.2 ml min^{-1} for 3 h. The final rinsing procedure consisted of pumping a cold phosphate buffer (0.1 M, pH 7.5) for 5 min.

3. Results and discussion

The RVC material is porous and can be shaped in the form of a column permitting a liquid to be pumped through, thus giving efficient mass transfer to the surface. The surface area will be very large but the background current will still be low because of the favourable properties of RVC. A large surface area is necessary in order to immobilize a sufficient amount of enzyme but it is also necessary to obtain a high coulometric yield. The

electrode was made in the form of a cylinder and inserted into a flow-injection system.

3.1. Reaction properties

Injection of 10 μM glucose samples produced oxidation peaks which were almost independent of the applied voltage, see Table 1. The redox potential of adsorbed Meldola Blue is −175 mV at pH 7.0 [12]. The applied voltage should therefore be sufficient to keep the mediator in the oxidized form. The potential was set to −100 mV for all subsequent experiments.

The mediator concentration has a pronounced effect on both the background current (Table 2) and the response factor and linearity of the calibration curve, Fig. 2. The lowest background was obtained with a mediator concentration of only 5 μM. The current at 10 μM glucose for example was much lower than that at the higher mediator concentrations; compare the current scale in the inset of Fig. 2 with that of the main graph. A low mediator concentration decreased the linear range (not shown in Fig. 2) because the amount present in the sample zone becomes less than that of the hydrogen peroxide or glucose. The coulometric yield at a flow rate of 1 ml min^{-1} was 16, 45 and 55% at mediator concentrations of 5, 20 and 50 μM respectively.

The current due to glucose oxidation at −100 mV in the presence of mediator decreased when the flow rate increased, see Fig. 3. For compari-

Table 2

Observed background currents of the enzyme-covered RVC electrode in a phosphate buffer, pH 7.0, containing various concentrations of mediator. Applied voltage, −100 mV vs. Ag/AgCl; flow rate, 1 ml min^{-1}

Mediator concentration	(nM)	5	20	50
Background current	(nA)	10	200	6000
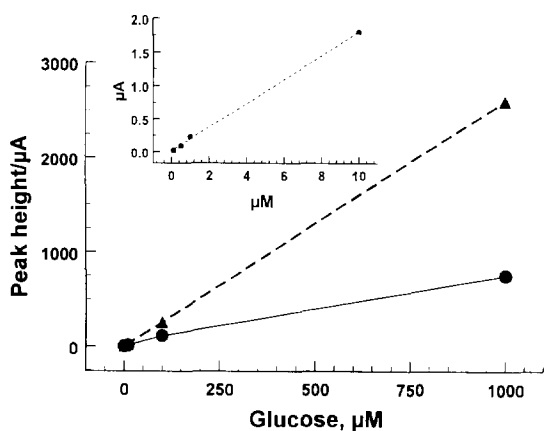
Fig. 2. Influence of mediator concentration on the response to glucose injections (100 μl) with various concentrations of Meldola Blue: (▲) 50 μM; (●) 20 μM. The inset shows the low range response with 5 μM mediator. Phosphate buffer containing mediator, pH 7.0; applied potential, – 100 mV; flow rate, 1 ml min⁻¹.

son, Fig. 3 also gives the currents for hydrogen peroxide oxidation at + 600 mV in the absence of mediator. This is the potential where the oxidation of hydrogen peroxide begins. The curves for hydrogen peroxide and glucose follow each other closely, indicating that similar rate-limiting steps are involved. The fast decrease in response with flow rate is due to a reduced residence time at the RVC electrode giving more time for the reactions.
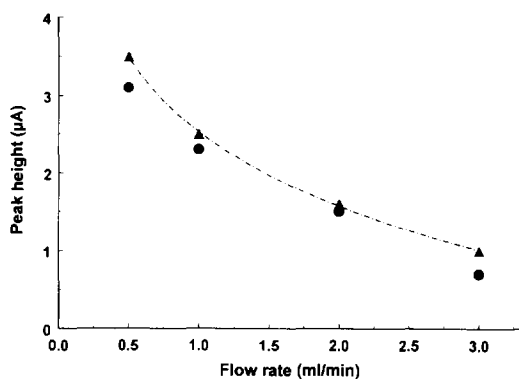
Fig. 3. Response variation with flow rate for injections (100 μl) of 10 μM glucose (●). Phosphate buffer, pH 7.0, containing 5 μM Meldola Blue; applied potential, – 100 mV vs. Ag/AgCl. The Figure also shows the response to hydrogen peroxide at + 600 mV in a buffer without any added mediator (▲).
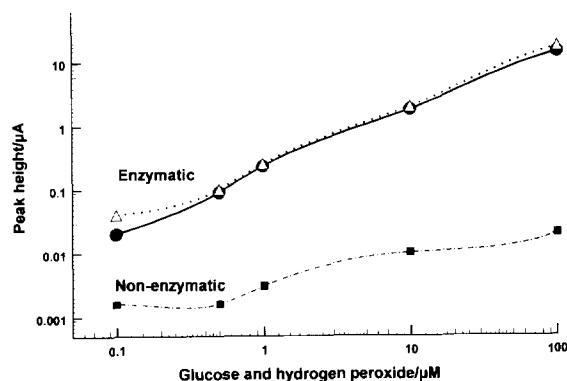
Fig. 4. Peak currents for hydrogen peroxide (△) and glucose (●) injections (100 μl) with a carrier of phosphate buffer, pH 7.0, containing 5 μM Meldola Blue. The non-enzymatic oxidation of glucose (■) is also shown. Flow rate, 1.0 ml min⁻¹; applied potential, – 100 mV vs. Ag/AgCl.

Diffusion within the pores also plays an important role in the mass transfer because less substrate reaches the pore walls at shorter residence times.

Kulys et al. [9] suggest that Meldola Blue (MB) shuttles electrons from the redox center of glucose oxidase (GOx) to the graphite surface according to the following scheme (corrected by us):

glucose + GOx(FAD)

$\rightarrow$ GOx(FADH₂) + gluconolactone　　　　(1)

GOx(FADH₂) + MB⁺

$\rightarrow$ GOx(FAD) + MBH + H⁺　　　　(2)

MBH $\rightarrow$ MB⁺ + H⁺ + 2e⁻　　　　(3)
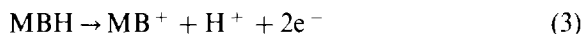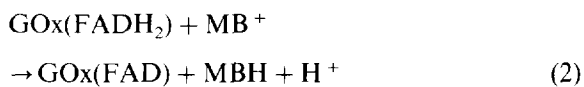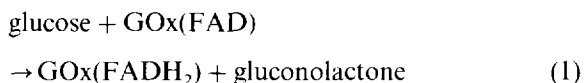
In our studies, we observed that the response to hydrogen peroxide closely followed that of glucose. The following observations have to be accounted for in a complete description of the reaction mechanism. Hydrogen peroxide injections into a system with an RVC electrode without enzyme but with mediator produced only negligible responses at – 100 mV. This proves that the enzyme is necessary for the hydrogen peroxide reaction. A mixture of equal concentrations of mediator and hydrogen peroxide (5 μM) was put in a spectrophotometer cuvette and monitored at 568 nm. The absorbance decreased linearly with time from 0.81 to 0.75 AU in 15 min and continued to decrease after 2 h. Oxygen will react with

the reduced mediator until it is finally colorless and no quantitative data can be drawn from the experiment. The mean residence time in the flow system is 28 s at 1 ml min^{-1}, i.e. the direct reaction between mediator and hydrogen peroxide is far too slow to explain the observation that hydrogen peroxide produces peaks at -100 mV. The peak heights for glucose injections decreased substantially when the carrier was deoxygenated. Although the oxygen was not completely removed the experiment nonetheless proves that oxygen is important. This indicates that the glucose first reacts with oxygen to produce hydrogen peroxide which is then oxidized enzymatically. This path does not exclude a parallel reaction according to Eq. (2). The mediator is reduced and reoxidized electrochemically. The reaction scheme will then be

$$\text{glucose} + O_2 \xrightarrow{\text{GOx}} H_2O_2 + \text{gluconolactone} \quad (4)$$

$$H_2O_2 + MB^+ \xrightarrow{\text{GOx}} MBH + O_2 + H^+ \quad (5)$$
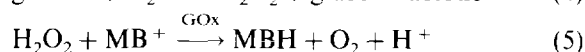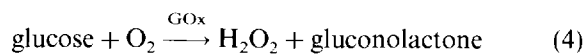
followed by Eq. (3). The proposed scheme is tentative and has to be supported by a mechanistic study.

Fig. 4 shows calibration curves for three decades. The current reached a plateau at 100 μM and did not increase when the glucose or hydrogen peroxide concentration was increased to 1

or 10 mM (not shown). The plateau is due to small amounts of mediator in comparison with the concentrations of glucose or hydrogen peroxide. The two curves are almost identical (even at 1 and 10 mM) which indicates that Eq. (5) is the rate-limiting step. Thus the rate is highly dependent on the mediator concentration (see Fig. 2).

The current observed with glucose as a sample decreased only slightly over the pH range 6–8. Hydrogen peroxide generated by the enzymatic reaction of glucose is produced at the pore walls within the diffusion layer. It reacts with the enzyme and mediator which are also present within the diffusion layer. The mediator is regenerated electrochemically and immediately available for a new oxidation cycle. The fact that the calibration curves for glucose fall very close to those for hydrogen peroxide demonstrates that very little hydrogen peroxide is lost to the bulk solution during glucose oxidation.

A blank electrode without enzyme was also prepared and its response to various levels of glucose is shown in Fig. 4. The oxidation current is concentration dependent and 1–3 orders of magnitude lower than the currents in the presence of enzyme. It is, however, much higher than the background current obtained in the absence of glucose. A possible explanation for this non-enzymatic reaction is a direct oxidation of some of the six tautomers of glucose. The aldehyde, and possibly also the gem-diol, which are present at 0.0024% and 0.0077% respectively (27°C) [13], could be oxidized by the mediator or directly at the electrode.

The electrode stability can be seen in Fig. 5. It can be seen that the response remains almost constant initially because the enzyme is in excess and some deactivation can occur without affecting the results. Subsequently, enzyme or electrode degradation reduces the response.
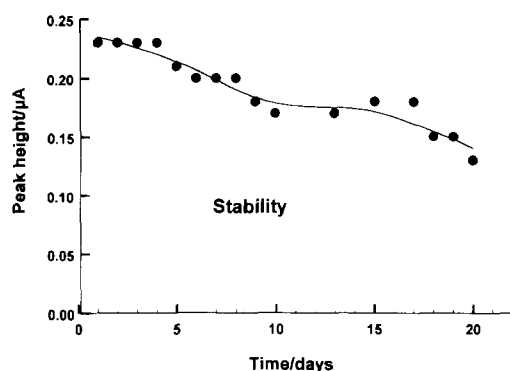
Fig. 5. Stability tests made by injecting 100 μl of 1 μM glucose. Phosphate buffer, pH 7.0, containing 5 μM Meldola Blue; applied potential, -100 mV; flow rate, 1 ml min^{-1}.

4. Conclusions

The low level calibration curve is linear up to about 10 μM and the detection limit is at present around 30 nM glucose but could perhaps be

lowered with further optimization. The electrode performs well in a flow-injection system and a throughput of 60 samples h^{-1} was readily obtained. The detection system is very attractive for low level measurements. The porous electrode material results in a high coulometric yield combined with a low inherent background current. Another advantage is the possibility of covalently immobilizing enzymes directly onto the RVC electrode.

Acknowledgements

References

[1] F. Scheller and F. Schubert, Biosensors, Elsevier, Amsterdam, 1992.

[2] P.N. Bartlett, P. Tebbutt and R.G. Whitaker, Prog. React. Kinet., 16 (1991) 55.

[3] B. Xie, M. Khayyami, T. Nwosu, P.-O. Larsson and B. Danielsson, Analyst, 118 (1993) 845.

[4] P. Trinder, Ann. Clin. Biochem., 6 (1969) 24.

[5] H. Lundbäck and G. Johansson, Anal. Chim. Acta, 155 (1983) 47.

[6] L. Gorton, Anal. Chim. Acta, 178 (1985) 247.

[7] L. Gorton, G. Jönsson-Pettersson, E. Csöregi, K. Johansson, E. Dominguez and G. Marko-Varga, Analyst, 117 (1992) 1235.

[8] G. Jönsson and L. Gorton, Biosensors, 1 (1985) 355.

[9] J. Kulys, H.E. Hansen, T. Buch-Rasmussen, J. Wang and M. Ozsoz, Anal. Chim. Acta, 288 (1994) 193.

[10] J. Wang, Electrochim. Acta, 26 (1981).

[11] H.J. Wieck, G.H. Heider, Jr. and A. Yacynych, Anal. Chim. Acta, 158 (1984) 137.

[12] L. Gorton, A. Torstensson, H. Jaegfeldt and G. Johansson, J. Electroanal. Chem., 161 (1984) 103.

[13] S.R. Maple and A. Allerhand, J. Am. Chem. Soc., 109 (1987) 3168.

Flow-injection systems for determination of trace manganese in various salts by catalytic photometric detection[1]

Takeshi Yamane*, Kazuo Koshino

Department of Chemistry, Faculty of Education, Yamanashi University, Takeda-4, Kofu 400, Japan

Received 13 November 1995; revised 11 December 1995; accepted 11 December 1995

Abstract

Two flow-injection analysis (FIA) systems for the determination of trace manganese in salts are presented using highly sensitive catalytic detection based on the oxidation of 3,4-dihydroxybenzoic acid by hydrogen peroxide. Two different approaches, the use of a large sample volume injection in a usual FIA mode (system A) and on-line coupling of a cation-exchange separation column with detection in a continuous flow system (system B), have proved very effective for eliminating the blank peak problem and thus affording direct injection of a sample solution containing a large concentration of salt. The limits of determinations are 0.04 ppm and 0.01 ppm for systems A and B respectively, when a 5 g sample is used for preparing the 100 ml sample solution. The proposed FIA systems were satisfactorily applied to the determination of manganese at 0.03–1.59 ppm in solar salts (salts made by exposing brine to the sun) with good precision.

Keywords: Catalytic photometric detection; Flow-injection systems; Manganese

1. Introduction

The determination of some metals, e.g. calcium, magnesium, iron, manganese, vanadium, etc., in sodium chloride is of considerable interest particularly in the chemical industry for quality checks of salts as raw materials and for monitoring such metals during the electrolysis process. A photometric method [1] with oxidation of mangan-

ese(II) to permanganate, and atomic absorption spectrometry (AAS) [2–4] have been used for this purpose. The former lacks the necessary sensitivity for most solar salts (made by exposing brine to the sun) and the latter requires the time-consuming and laborious separation and/or preconcentration of manganese from the matrix salt since AAS is subject to interference from a large background absorption by the matrix.

Flow-injection analysis (FIA) with catalytic photometric detection has proved to be a powerful method for rapid, simple and reproducible determination of trace metals. Recently, a FIA method has been reported with catalytic detection

* Corresponding author. Fax: (+81) 552-20-8183.

based on the malachite Green–periodate reaction for trace manganese in salts [5]. However, off-line batch procedures for preseparation of manganese using a minicolumn packed with chelating resin (Dowex A-1) were still needed, because the method suffered severely from a refractive index problem which occurred when the sample solution containing salt was injected into the carrier stream. In addition, the indicator reaction used required a long reaction time to achieve high sensitivity, which resulted in a long analysis time. Therefore, this method does not make use of the characteristic advantages of FIA, namely simplicity and rapidity. A blank peak effect is one of the great problems in FIA for determining trace constituents and is due to refractive index perturbation which occurs when samples containing a large excess of salts are injected into the carrier stream. One of the authors [6] has proposed a simple way to eliminate this blank peak effect based on the provision of a non-dispersed zone for analytical measurements in the sample plug. Ion-exchange separation, coupled directly with detection in a continuous flow system, described previously for determining manganese in river water [7], seems to be another possible way to remove the matrix effect. In the present work, we have studied these two approaches in the FIA determination of trace manganese in salts in order to allow direct injection of sample solutions into the FIA system. Manganese-catalysed oxidation of 3,4-dihydroxybenzoic acid (DHBA) by hydrogen peroxide [8] has also been examined as a means for detecting trace manganese especially if the catalytic reaction rate detection can be used to eliminate the blank peak effect, even in the presence of large amounts of sodium chloride.

2. Experimental

2.1. Solutions

All reagents were of analytical-reagent grade, unless otherwise noted.

The DHBA solution was prepared by dissolving 2.00 g of reagent in 30 ml of ethanol and diluting to 100 ml with water. Before use, 20 ml of this

solution was diluted to 50 ml with water and the resulting solution was mixed with a 1.5% hydrogen peroxide solution in a 1:1 ratio.

Sodium carbonate solution (1.0 M) was prepared by dissolving the reagent in water.

The eluent was prepared by mixing 0.15 M sodium tartrate, 0.0045 M tartaric acid and 0.3 M sodium chloride.

2.2. Apparatus and general procedure

Fig. 1 shows a schematic diagram of the manifold used. In the determination by FIA without on-line separation (system A), the cation-exchange column (SC) should be omitted in accordance with replacing eluent (C) by distilled water as carrier. All components in contact with solution (tubing, valves, and connectors) were made of Teflon, Daiflon, ceramics or glass. The separation column (SC) was prepared by slurry packing the strong cation-exchange resin (Hitachi Custom Resin No. 2611, 15.5 μm) into a borosilicate glass column (4 mm i.d., 7 cm long). A Tokyo Rikakikai Model LP-1000 pump (metal-free type) and a Sanuki Kogyo Model DM2M-1024 pump were used. The sample solution was injected into the carrier stream (or eluent stream) with a six-way valve with a 5 m sample loop (0.5 mm i.d.), and the absorbance was measured at 480 nm with a Jasco model UVIDEC-100VI spectrophotometric detector. The peak height or the height of
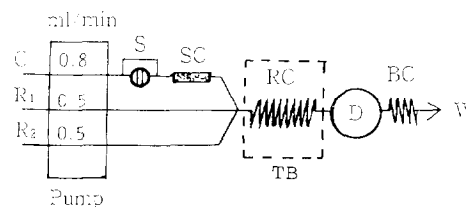
Fig. 1. Flow-injection manifold for determination of manganese in salts: C, carrier (water for a large sample volume injection; 0.15 M sodium tartrate–0.0045 M tartaric acid–0.3 M sodium chloride as eluent in the case of introducing SC); R₁, indicator mixture (2.6 × 10⁻² M DHBA and 0.75% hydrogen peroxide); R₂, 1.0 M sodium carbonate solution; S, sample injection with loop (0.5 mm i.d., 5 m long); SC, separation column (cation-exchange resin, 4 mm i.d., 7 cm long); RC, reaction coil (0.5 mm i.d., 5 m long); D, spectrophotometric detection at 480 nm; BC, back-pressure coil; TB, temperature-controlled bath (40°C); W, waste.

signal response from the baseline is rectilinearly related to the manganese concentration. The calibration graphs were made with standard manganese solution to which sodium chloride was added in the same concentration as in the sample solution.

2.3. Sample preparation

2.3.1. For soluble manganese

A salt sample (2–3 g for normal solar salt) was accurately weighed and dissolved in $\approx$ 60 ml water. The resultant solution was filtered through a membrane filter (0.45 μm) and then diluted to 100 ml with water. The sample weight can be increased within 5 g of the upper limit so that the manganese level determined in the sample solution by peak height measurements should fall into linear ranges of 2–12 ppb for system A and 0.5–15 ppb for system B.

2.3.2. For total manganese

The salt sample was dissolved in $\approx$ 5 ml of water together with 3.6 ml of 2.0 M hydrochloric acid and 3 ml of 1.5% hydrogen peroxide solution by heating for 5–10 min on a hotplate. After cooling, the resultant solution was treated as for soluble manganese.

3. Results and discussion

3.1. Catalytic determination of manganese in a continuous flow system

Manganese-catalyzed oxidation of DHBA by hydrogen peroxide was successfully used in the sensitive determination of manganese. Basically, the reaction conditions and the FIA manifold were almost the same as those described previously [7, 8]. A minor modification was made to the present study such that a mixed solution of DHBA and hydrogen peroxide was used as the indicator mixture to simplify the flow system. The increase in absorbance at 480 nm, recorded as the peak shape signal in this FIA system, due to the catalyzed reaction is the measure of the manganese concentration.
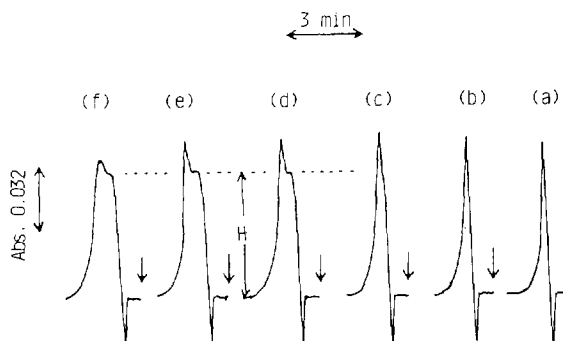
Fig. 2. Dependence of the shape of signal response on the sample loop length for injection of a sample solution containing a mixture of 4.0 ppb manganese and 0.85 M sodium chloride. Sample loop length: (a) 1 m; (b) 2 m; (c) 3 m; (d) 4 m; (e) 5 m; (f) 6 m.

3.2. FIA system with large sample volume injection (system A)

The concept for eliminating the blank peak effect presented by one of the authors can be realized by the use of a larger sample injection. Fig. 2 shows the dependence of the shape of the signal response on the sample loop length when the sample solution containing 4.0 ppb manganese plus 0.85 M sodium chloride was injected. In the signal response, a plateau on the upper side of the ascending signal was observed with a sample loop longer than 300 cm, although a blank peak appears as a set of sharp negative and positive peaks. The increase in the sample loop length from 3 m to 6 m did not show any effect on the height of this plateau from the baseline at constant manganese concentration. This shows that there is a portion of the sample plug which is unaffected by the carrier stream. By using a 5 m sample loop, the effect of sodium chloride concentration on the sample solution was studied for the catalytic detection of 8.0 ppb manganese. As shown in Fig. 3, the height of the plateau initially increased with increasing sodium chloride concentration and then reached an almost constant value in the range 0.51–1.3 M. An initial increase in the height may be attributed to a rate-enhancing effect of sodium chloride on the manganese-catalyzed reaction as described later. Based on these results it is clear that the real signal of manganese

can be recognized and measured at this plateau portion of the overall signal response even in the presence of excessive sodium chloride. It is noted that there was found to be a slight drop in the signal response for blank solution (no manganese) from the baseline level when the sodium chloride concentration was increased too much (> 0.86 M). The reason is not clear. Although this seems to be the limitation of catalytic detection in the media containing a higher concentration of salt, it is evident that the blank peak has little effect on the trace manganese determination using the large sample volume injection.

Calibration graphs obtained by plotting the height of the plateau (H in Fig. 2) against the manganese concentration were rectilinear in the range 2–15 ppb manganese both in the presence and absence of 0.85 M sodium chloride, although the graph became steeper in the presence of sodium chloride, as shown in Fig. 4. The increased slope of the graph is probably due to the rate-enhancing effect of sodium chloride on the catalytic reaction, as was observed in another catalytic reaction [9]. This increased slope, however, was found to be almost unchanged by increasing the sodium chloride concentration from 0.51 to 1.5 M. Although manganese in concentrations as low as 0.2 ppb can of course be detected, the limit of determination was defined here as the lowest concentration of linear response, thus

Fig. 4. Calibration graphs for system A with a 5 m sample loop for (a) manganese standard solution and (b) manganese standard solution containing 0.85 M sodium chloride.

taken as 2 ppb. This value corresponds to 0.04 ppm based on a solid sample if a 5 g sample is used for preparing the 100 ml sample solution. The relative standard deviation for 8.0 ppb manganese was 0.9% ($n = 5$). An injection rate of 20 h^{-1} is estimated.

3.3. FIA system with on-line cation-exchange separation (system B)

In order to achieve the separation and/or preconcentration of manganese from a sodium chloride matrix, a strong cation-exchange column with tartrate solution as eluent was introduced and coupled on-line with the catalytic detection system. The elution conditions entail some modifications to the procedure proposed earlier [7], because the sample solution in the present study contains large amounts of sodium chloride which cause a lowering of the distribution coefficient of manganese [10] and may impair the separation efficiency. Different ratios of the concentrations of tartaric acid, tartrate and sodium chloride in the eluent were examined for obtaining a baseline separation of the manganese peak from the sodium chloride matrix. An eluent of 0.15 M tartrate, 0.0045 M tartaric acid and 0.3 M sodium chloride (pH 5.1) was found to be best to provide good resolution of manganese from a large blank peak which appeared at void volume as a set of negative and positive peaks. Typical signal traces

Fig. 3. Dependence of peak height (H) on sodium chloride concentration in sample solution containing 8.0 ppb manganese with use of a 5 m sample loop.

for manganese are shown in Fig. 5. It is notable that repetitive sample injections can be performed because the eluent works as carrier solution and also regenerates and washes the column. In this FIA system it is evident that the blank peak effect on the signal response from trace manganese by the catalytic reaction can no longer exist. The peak height increased on decreasing the flow rate of the carrier solution; an increase in the peak height by about 1.3 times was observed when the flow rate was decreased from 0.8 to 0.4 ml min⁻¹ keeping the flow rate of other solutions constant at 0.5 ml min⁻¹. This should be attributed to an increase in the residence time, and hence the reaction time, at a constant reaction coil length.

Fig. 6 shows the dependence of peak height on the concentration of sodium chloride added for the sample solution of 10 ppb manganese. The peak height gradually decreased with increasing sodium chloride concentration despite the well-resolved peak shape which remained. A similar peak height dependence was also observed in the case of cation-exchange separation of magnesium and calcium [11]. A decrease in the peak height at higher sodium concentration suggests that there is a limitation on improving the limit of determination by taking a larger sample weight for preparation of the sample solution. An attempt to improve sensitivity was made by on-line preconcentration using the same separation column from the solution prepared with a limited lower sodium

Fig. 6. Effect of sodium chloride concentration on peak height for 10 ppb manganese solution in the FIA system with separation column (system B).

chloride concentration. The peak height for 10 ppb manganese increased linearly with increase in the sample loop length up to 8 m even in the presence of 0.85 M sodium chloride. This indicates that the sensitivity of manganese determination can be improved by using a large sample volume. However, the use of a sample loop longer than 8 m resulted in a tendency towards deviation from the linear relationship and poorer peak resolution, probably due to partial elution (leakage) of manganese. Therefore, a 0.85 M sample solution and an 8 m sample loop were considered the limits for achieving sensitive determination of manganese in salt.

Calibration graphs were rectilinear for manganese in the range 0–15 ppb in the presence of 0.85 M sodium chloride. The slopes of the graphs have a tendency to gradually decrease with increasing sodium chloride concentration above 0.51 M; for instance, equations of the calibration graph in the presence of 0.51 M and 0.68 M sodium chloride are $Y = 1.17X$ with a correlation coefficient of 0.999 and $Y = 1.07X$ with a correlation coefficient of 0.998 (Y, peak height in cm; X, manganese concentration in ppb) respectively. Thus it is recommended to prepare the calibration graph using the same concentration of sodium chloride as in the sample solution. For the sample injection with a 5 m sample loop, the relative standard deviation for 7.0 ppb manganese is 1.4% ($n = 5$) and the limit of determination (defined as

Fig. 5. Typical signal traces for manganese in solar salt for the FIA system with separation column (system B).

five times the limit of detection) is 0.5 ppb, which corresponds to 0.01 ppm based on a solid sample when a 100 ml sample solution is prepared by dissolving 5 g of sample. This limit of determination is lowered to one-quarter that of the FIA system A. The sensitivity of this FIA method is sufficient for analysis of most solar salts to judge from the manganese contents reported in the literature [3–5]. An analysis rate of 8 h^{-1} is estimated.

3.4. Interference study

The effect of foreign ions on the determination of 5.0 ppb manganese with the two FIA systems A and B was studied. No significant interference was observed in either FIA system with the following ions (μg ml^{-1}): Ni(II) (10), Cu(II) (10), Pb(II) (20), Fe(III) (0.5), Al(III) (10), V(V) (10), Cr(III) (0.3), Mg(II) (20), Ca(II) (20), Cd(II) (5), Mo(VI) (5), F$^-$ (100), Br$^-$ (100), I$^-$ (20), H$_2$PO$_4^-$ (100). Cobalt showed a positive interference at the same level as manganese in FIA system A. The concentrations of ions mentioned above in most salt samples are usually lower than the levels examined in this study. It is noted that FIA system B is recommended for use when samples are suspected to contain metal ions in high concentration, because metals with a rela-

tively stronger tendency to form complexes with tartrate [10], such as copper, iron, cobalt, cadmium, nickel, lead, and zinc, should be easily separated by elution before manganese. Experiments showed that these ions did not affect manganese determination in system B at 50 ppm levels. In addition calcium and magnesium, which form relatively weaker complexes with tartrate, did not show any effect even at 100 ppm.

3.5. Analysis of salt samples

Manganese was determined in solar salts using the present FIA systems; the preparation of the sample solution was, in principle, based on the method described in the literature. Soluble and total manganese are defined here as manganese determined in the sample solutions prepared by treatment with distilled water, and with a mixture of hydrochloric acid and hydrogen peroxide respectively. The results obtained with the two FIA systems are summarized in Table 1, and show good agreement with each other. Such agreement for soluble manganese indicates that FIA system A has good selectivity and is applicable to the usual solar salts. Satisfactory precision, less than 3% relative standard deviation, was obtained with the exception of the results for the Australian sample 2 which were close to the limit of determination. It is a characteristic advantage of FIA system B that the determination of total manganese can be made conveniently because the sample solution containing hydrochloric acid and hydrogen peroxide can be directly injected without any perturbation of the catalytic reaction detection.

Table 1
Analysis of solar salts by the proposed FIA systems

Sample	Manganese determined in sample (ppm)[a]		
	Soluble Mn		Total Mn
	FIA (A)	FIA (B)	FIA (B)
Mexican	0.31 (3.0)[b]	0.30 (3.3)[b]	0.40 (2.5)[b]
Australian			
(1)	0.47 (2.1)	0.49 (2.3)	0.98 (1.2)
(2)	0.04$_4$ (10)		0.03$_5$ (11)
(3)	0.51 (2.5)	0.53 (2.1)	0.84 (1.7)
(4)	0.85 (0.9)	0.84 (1.1)	1.59 (0.9)

[a] Sample solutions were prepared by dissolving 2–3 g of solid salt in 100 ml of solution. A 5 m sample loop was used.
[b] Parentheses denote the relative standard deviations for 3–5 determinations.

4. Conclusions

Two approaches to FIA, the use of a large sample volume injection and the introduction of on-line cation exchange separation, both coupled with catalytic detection by the DHBA–hydrogen peroxide reaction, have proved to be very effective to determine trace manganese in the presence of excessive levels of salts by eliminating the blank

peak refractive index problem, consequently allowing the direct injection of sample solutions. The main advantage of the present FIA systems over conventional photometric and AAS methods is that the analysis is achieved in a continuous and nearly closed system without instrumental and operational complexity. A short analysis time of 3–7 min is an additional important merit of the FIA systems. Moreover, the present FIA systems provide 2–10 times higher sensitivity than that of AAS. It can be said that FIA system B is more applicable than system A to a wide variety of salt samples as the former is superior to the latter with respect to the limit of determination and the tolerance level of co-existing metal ions. However, system A enables more rapid and simpler analysis than system B. The difference in the optimal salt concentration in the sample solution between the two systems is not so significant.

Acknowledgement

References

[1] H. Inoue, Bunseki Kagaku, 10 (1961) 124.
[2] The Salt Science Research Foundation and The Society of Sea Water Science, Japan, Analysis of Salt and Measurements of its Physical Properties, The Society of Sea Water Science, Japan, Tokyo, 1992, p. 195.
[3] Y. Akama, T. Nakai and B. Kawamura, Bulletin of the Society of Sea Water Science, Japan, 34 (1980) 196.
[4] K. Uesugi, M. Yamaguchi and Y. Ishihara, Bull. Sea Water Sci. Jpn., 36 (1983) 387.
[5] S. Kawakubo, M. Iwatsuki and T. Fukasawa, Bull. Sea Water Sci. Jpn., 43 (1989) 48.
[6] T. Yamane and M. Saito, Talanta, 39 (1992) 215.
[7] T. Yamane, Anal. Sci., 2 (1986) 191.
[8] T. Yamane and Y. Nozawa, Bunseki Kagaku, 33 (1984) 652.
[9] M. Dubravcic, Analyst, 80 (1955) 146, 295.
[10] F.W.E. Stretlow and T.N. van der Walt, Anal. Chem., 54 (1982) 457.
[11] T. Yamane, T. Morimoto, M. Yamasaka and E. Goto, Bull. Sea Water Sci. Jpn., 48 (1994) 165.

Flow-injection spectrophotometric determination of ascorbic acid in pharmaceutical products with the Prussian Blue reaction [1]

Joaquim A. Nóbrega *, Gisele S. Lopes

Grupo de Química Analítica, Departamento de Química, Universidade Federal de São Carlos, Caixa Postal 676, CEP 13565-905, São Carlos, SP, Brazil

Abstract

A lot of modern analytical strategies for exploiting chemistries have been developed by using flow-injection analysis. However, even after 20 years of flow-injection evolution, there still are new quantitative procedures being established using old qualitative assays. The formation of Prussian Blue is a classical test to detect Fe^{2+} using hexacyanoferrate(III) as a precipitating reagent. This reaction was evaluated for spectrophotometric determination of ascorbic acid employing Fe^{3+} and hexacyanoferrate(III) as chromogenic reagents. An excess of the complexing anion avoids the formation of precipitate and forms a deep blue solution when Fe^{3+} is reduced to Fe^{2+} by ascorbic acid. The maximum absorbance of the colored complex occurs at 700 nm and the molar absorptivity is 3.0×10^4 l mol^{-1} cm^{-1}. Under flow-injection conditions the Prussian Blue reaction was employed with an intermittent flow of an oxalate alkaline solution for removing the colored product adsorbed on tube and flow-cell walls. Reference solutions containing 5.0×10^{-6}–1.0×10^{-4} M of ascorbic acid were employed to obtain the analytical curve ($r = 0.9999$). For all solutions the relative standard deviation was lower than 1.0% ($n = 10$). Results obtained for ascorbic acid determination in pharmaceutical products (Cewin, Redoxon and Cebion) are in good agreement with those obtained by using a flow-injection procedure involving the reaction between triiodide and ascorbic acid. The sampling frequency is 140 h^{-1} and only 430 μl of reagents is consumed in each determination.

Keywords: Ascorbic acid; Flow-injection analysis; Iron; Pharmaceuticals; Prussian Blue reaction

1. Introduction

Ascorbic acid (Vitamin C) is essential for the development and regeneration of muscles, bones, teeth and skin. Vitamin C has also been used for the treatment of the common cold, mental illness, infertility, cancer and AIDS [1]. Many analytical methodologies have been proposed for the deter-

* Corresponding author. Fax: +55 162 74 8350; e-mail: djan@power.ufscar.br
[1] Presented at the Seventh International Conference on Flow Injection Analysis (ICFIA '95), held in Seattle, WA, USA, August 13–17, 1995.

mination of ascorbic acid taking into account its chemical role. Redox processes are generally involved in these determinations and it is possible to minimize air oxidation by using techniques such as flow injection (FI). The FI systems proposed are mainly based on electroanalytical detectors due to inherent redox chemistry of the analyte and reagents. Optical FI methods also involve redox reactions with ascorbic acid in which a colored compound is formed or decomposed. Thus, the formation of ferroin complex from the reduction of Fe(III)–phenanthroline [2] and a method using chloramine T in the presence of starch–KI solution [3] were adapted to flow systems. Descolorimetry was also employed by reduction of cerium(IV) [4] and by reduction of triiodide [5]. This last paper involves the on-line formation of iodine and the measurement of the inverse peaks caused by the excess of triiodide at 350 nm or the triiodide/starch complex at 580 nm.

The objective of the present work was to adapt the Prussian Blue reaction for the determination of ascorbic acid. The formation of Prussian Blue is a classical qualitative test to detect Fe(II) using hexacyanoferrate(III) as reagent [6]. The first step is the oxidation of iron(II):

$$Fe^{2+} + [Fe(CN)_6]^{3-} \rightarrow Fe^{3+} + [Fe(CN)_6]^{4-} \qquad (1)$$
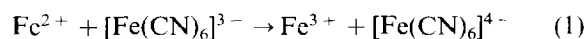
The second step is the formation of hexacyanoferrate(II) ferric complex (Prussian Blue):

$$4Fe^{3+} + 3[Fe(CN)_6]^{4-} \rightarrow Fe_4[Fe(CN)_6]_{3(s)} \qquad (2)$$
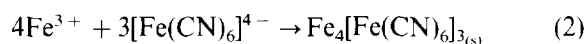
The complex formed is highly insoluble ($K_s = 3.0 \times 10^{-41}$; Ref. [7]). Employing an excess of the complexing anion and Fe(III) as colorimetric reagents, a deep blue soluble compound is formed when Fe(III) is reduced to Fe(II) by ascorbic acid:

$$2Fe^{3+} + C_6H_8O_6 \rightarrow 2Fe^{2+} + C_6H_6O_6 + 2H^+ \qquad (3)$$
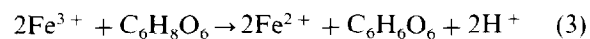
The excess of hexacyanoferrate(III) avoids the occurrence of precipitation [6]. The procedure was successfully applied for the determination of ascorbic acid in pharmaceutical products.

2. Experimental

2.1. Apparatus

An eight-channel Ismatec peristaltic pump (model 7618-40, Switzerland) fitted with Tygon pump tubing was used for propulsion of fluids. The manifolds were constructed with polyethylene tubing (0.8 mm i.d.). Sample injection was done by using a laboratory-constructed three-piece manual commutator [8] made of Perspex, with two side bars and a sliding central bar which is moved for sampling and injection.

The UV-visible absorption spectra were obtained with a diode array spectrophotometer (Hewlett-Packard, model 8452A, USA) using a quartz cuvette with an optical path of 1.0 cm. All flow measurements were carried out using a Femto spectrophotometer (model 435, Brazil) with a glass flow-cell (optical path 1.0 cm). This equipment was connected to a two-channel strip-chart recorder (Cole–Parmer model 12020000, USA).

2.2. Reagents, analytical solutions and sample preparation

All reagents were of analytical-reagent grade and all solutions were prepared using distilled-deionized water.

Reference solutions containing from 5.0×10^{-6} to 1.0×10^{-4} M ascorbic acid were prepared immediately before use by dilution of a 1.0×10^{-2} M stock solution in a 0.014 M nitric acid medium with deaerated water, because ascorbic acid oxidation is slower in acidic medium. The effect of acidity on sensitivity was evaluated using 0.014 and 0.14 M nitric acid solutions.

The Fe(III) reagent was prepared by dissolving iron(III) nitrate salt in 0.014 M nitric acid in the following concentrations: 1.0×10^{-4}, 5.0×10^{-3}, 1.0×10^{-3}, and 1.0×10^{-2} M, for the evaluation of the effect of Fe(III) concentration on sensitivity. The hexacyanoferrate(III) solutions (5.0×10^{-2} and 5.0×10^{-3} M) were prepared by dissolving the potassium salt in water.

A complexing solution containing 0.5% w/v oxalic acid in 0.1 M sodium hydroxide was em-

ployed for removing the blue complex adsorbed on the tube and flow-cell walls.

The triiodide procedure was implemented by using solutions containing 8.0×10^{-2} M potassium iodide and 5.0×10^{-5} potassium iodate. A 1.0×10^{-3} M sulfuric acid solution was employed as carrier.

Three solutions of pharmaceutical products (Cewin, Redoxon, and Cebion) were prepared by dissolving suitable amounts of the commercial liquid samples in 0.014 M nitric acid solution and diluting the resulting solution to adjust the concentration to that required by the experimental conditions adopted. A solid product (Supradyn) was also analysed after grinding and dissolution in 0.014 M nitric acid solution.

2.3. Procedure

Fig. 1 shows a schematic flow diagram in which chromogenic reagents (R_1: 1.0×10^{-3} M Fe^{3+} and R_2: 5.0×10^{-3} M $[Fe(CN)_6]^{3-}$) were introduced by confluence and the carrier stream is a 0.014 M nitric acid solution. As can be seen in Fig. 1, during the sampling state, i.e. while the sample loop is filled, the intermittent flow of alkaline oxalate solution is introduced and the
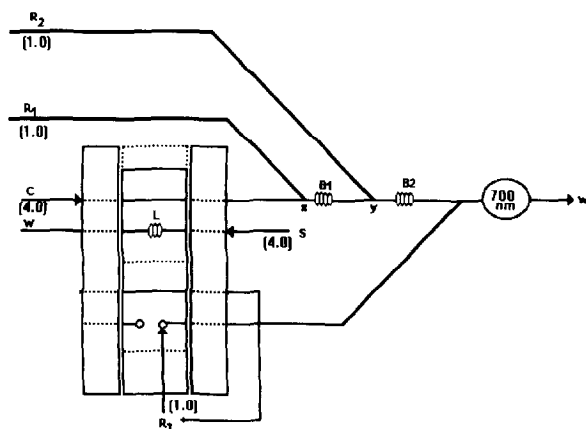
Fig. 1. Flow diagram with colorimetric reagents (R_1 and R_2) introduced by confluence (x and y points). B_1 and B_2 are reactors of 150 and 100 cm respectively. L is a sample loop of 100 cm. C, carrier stream; W, waste; S, sample or reference solution. R_3 is an intermittent flow of an alkaline oxalate solution. Numbers between parentheses represent the flow rates.
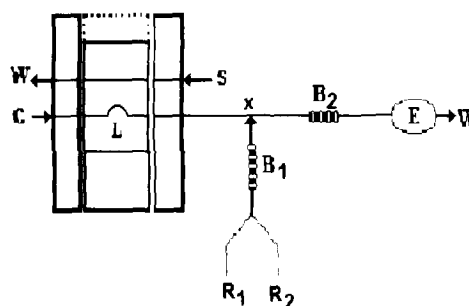
Fig. 2. Flow diagram adapted from Hernández-Méndez et al. [5]. C is a 1.0×10^{-3} M sulfuric acid solution flowing at 3.0 ml min^{-1}, R_1 is a potassium iodide solution and R_2 is a potassium iodate solution, both flowing at 1.5 ml min^{-1}. B_1 and B_2 are reactors of 300 and 150 cm respectively. E, spectrophotometer; W, waste; S, sample or reference solution. L is a sample loop of 100 cm.

adsorbed complex on the flow-cell walls is removed. After commutation, ascorbic acid solution is injected and the alkaline oxalate solution remained recycled. The blue compound formed was measured at a wavelength of 700 nm.

For comparison of results the triiodide procedure proposed by Hernández-Méndez et al. [5] was adapted. Iodine is generated in the flow system (Fig. 2) as triiodide ion by reaction between iodide and iodate in a long reactor (B_1) and a steady spectrophotometric signal is measured at 350 nm. After injecting ascorbic acid, the excess of triiodide is measured by inverse peaks that reflect consumption of triiodide by the redox reaction between ascorbate and triiodide.

3. Results and discussion

Considering that the Prussian Blue reaction had been employed only in qualitative tests, a first experiment was made to obtain the UV–visible absorption spectrum of this compound. Fig. 3a shows the absorption spectrum for chromogenic reagents, i.e., Fe(III) mixed with hexacyanoferrate(III), and a strong absorption band can be observed in the UV region and a weaker band with wavelength peak at 420 nm, which is related to the formation of the brown complex hexacyanoferrate(III) ferric [6]. After adding ascorbic

(a)

(b)
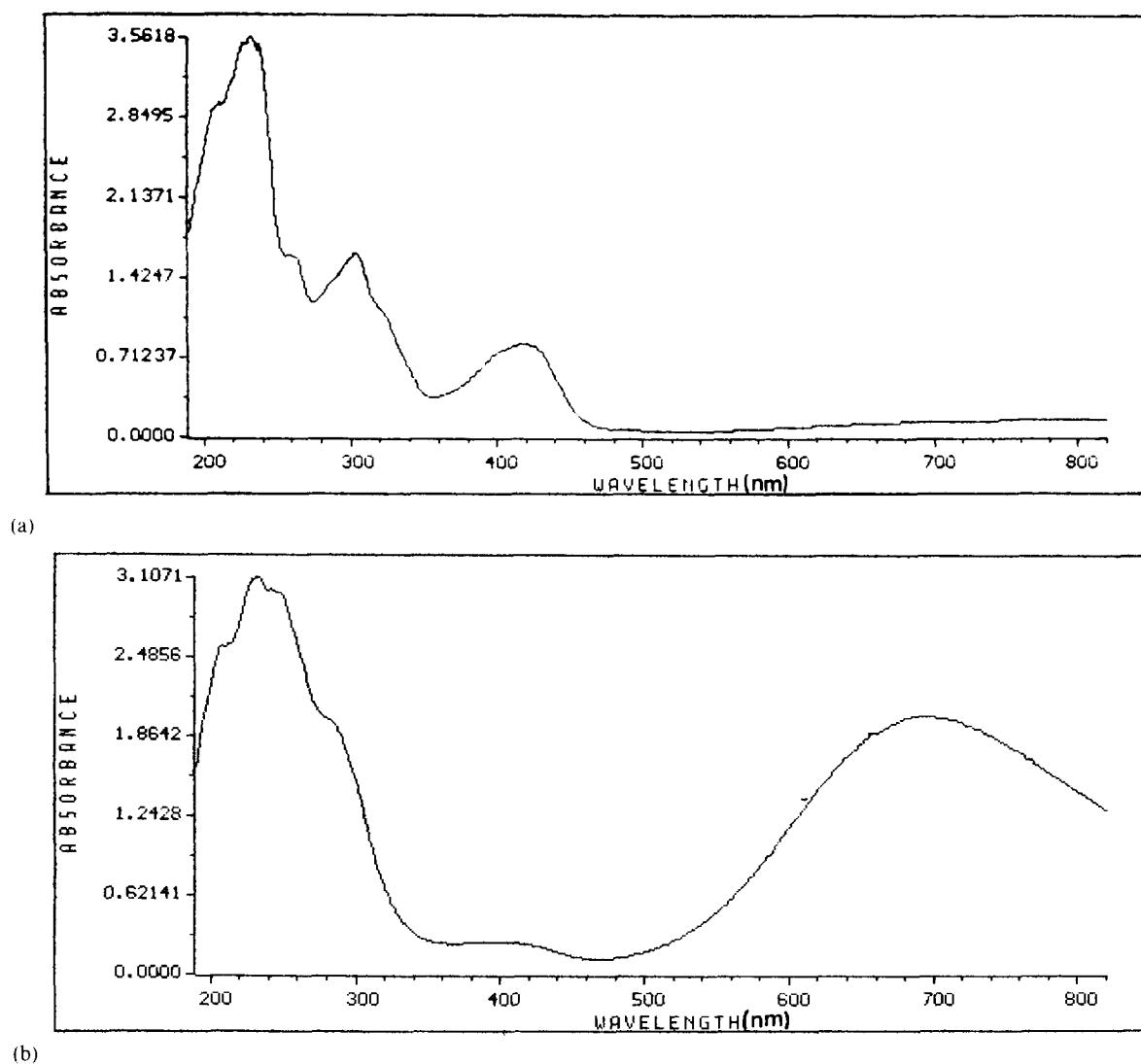
Fig. 3. UV–visible absorption spectra. (a) Chromatogenic reagents: Fe(III) plus hexacyanoferrate(III). (b) Chromatogenic reagents as for (a) plus ascorbic acid.

acid to this mixture, the absorption spectrum changed as can be seen in Fig. 3b due to the formation of Prussian Blue ($Fe_4[Fe(CN)_6]_3$), with an absorbance peak at 700 nm. The experimentally determined molar absorptivity of the complex compound formed is 3.0×10^4 l mol^{-1} cm^{-1}. Taking into account this value of molar absorptivity, it can be estimated [9] that if the minimum absorbance to be measured is 0.010 and the optical path is 1.0 cm, the lowest concentration of ascorbic acid that can be spectrophotomet-

rically determined is approximately 3×10^{-7} M.

The first flow diagram projected involved the transport of the injected solution of ascorbic acid by a carrier stream and the introduction of chromogenic reagents at confluence points, such as that shown in Fig. 1. After less than 1 h of measurements, the extension tubes and the glass flow-cell walls were strongly impregnated by the blue compound and a gradual increment in the baseline was observed. This problem was aggravated when relatively concentrated ascorbic acid

solutions were introduced, e.g. after injecting a 1.0×10^{-4} M solution the absorbance of the baseline was increased by 10%. Thus, accumulation of the blue complex on the tube and flow-cell walls should be avoided. The hexacyanoferrate(III) ferric complex is soluble in an alkaline oxalate solution [6] and this solution was evaluated to circumvent complex adsorption. When this solution was introduced as a confluent reagent, the formation of the blue complex did not occur. This effect can be explained by considering the complexing capacity of oxalate for both iron redox forms and the fact that oxalate concentration was higher than hexacyanoferrate(III) concentration. In subsequent experiments, oxalate solution was introduced as an intermittent flow after the measurement of the signal maximum (Fig. 1). It was observed that the sensitivity was critically dependent on the location of the confluence point. When the intermittent flow was introduced immediately after the injection point a strong decrease in sensitivity was observed and this can be explained by considering the merging caused by dispersion between the rear zone of the oxalate solution and the front zone of the sample. To avoid this deleterious effect, the penetration between oxalate and sample zones should be minimized, and this can be attained by changing the location of the confluence point. An increase in sensitivity was experimentally observed by increasing the reactor length between the sample injection point and the oxalate introduction point. Best sensitivity was achieved when the confluence point was put 10

Table 1
Ascorbic acid concentrations in pharmaceutical products and standard deviations ($n = 5$) as determined by the proposed procedure and the triiodide procedure [5]

Sample	Proposed procedure (% w/v)	Triiodide procedure (% w v)
Cewin	21.8 ± 0.10	22.6 ± 0.20
Redoxon	22.4 ± 0.10	21.6 ± 0.20
Cebion	23.4 ± 0.20	24.2 ± 0.10

cm before the flow cell. Using this flow diagram, sensitivity was not affected and baseline stability was accomplished. It should be mentioned that desorption processes of the blue complex adsorbed on the B_2 reactor caused loss of precision in experiments with concentrated ascorbic acid solutions. However, for ascorbic acid concentrations in the range 10^{-4}–10^{-5} mol l^{-1} this effect did not happen.

The effect of Fe(III) concentration was also evaluated. In the proposed methodology, Fe(III) concentration should be higher than ascorbic acid concentration. Additionally, the sensitivity and reproducibility should not be negatively affected. Low concentrations of Fe(III), such as 1.0×10^{-4} M, caused a strong decrease in sensitivity. However, higher concentrations of Fe(III), such as 5.0×10^{-3} M, caused a loss of linearity, probably due to bad reproducibility caused by desorption processes, which are more critical when the formation of the blue compound is increased. Considering the compromise between sensitivity and linearity, all further measurements were made employing a 1.0×10^{-3} M Fe(III) solution. Taking into account these same effects, hexacyanoferrate(III) concentration was fixed at 5.0×10^{-3} M, which is five-fold higher than the Fe(III) concentration, to avoid the precipitation of the blue compound formed [6].

The acidity effect was evaluated by changing the composition of the carrier stream. When 0.14 M nitric acid was used as carrier the sensitivity decreased, and this effect can be related to higher protonation of ascorbic acid in this medium, since the reducing agent is the ascorbate anion [10]. Best results were attained by using a solution containing 0.14 M nitric acid as carrier stream. This is also suitable for sample preparation because ascorbic acid oxidation is slow in acid medium.

Using the established conditions, the sampling frequency is 140 h^{-1} and the relative standard deviation was 0.65% for a solution containing 6.0×10^{-5} M ascorbic acid ($n = 10$). This compound was determined in three samples of pharmaceutical products (Table 1). Results obtained by the proposed procedure are in good agreement with those established us-

ing a previously proposed procedure [5] and with label values. For Supradyn, which is a polyvitaminic compound, positive errors were observed in ascorbic acid determination and this can be explained by considering the presence of Vitamin E which is also a reducing agent [11] and acted as interferent. Some preliminary results obtained for determining ascorbic acid in natural and artificial tropical fruit juices also showed positive errors, probably caused by citric acid. These interference effects are being critically assessed for evaluating other samples that could be analyzed by the Prussian Blue procedure.

Acknowledgements

References

[1] M.B. Davies, J. Austin and D.A. Partridge, Vitamin C: Its Chemistry and Biochemistry, The Royal Society of Chemistry, Cambridge, 1991.

[2] S.M. Sultan, A.M. Abdennabi and F.E.O. Suliman, Talanta, 41 (1994) 125.

[3] M. Valcárcel, F. Lázaro, A. Ríos and M.D. Luque de Castro, Analyst, 111 (1986) 163.

[4] S.M. Sultan, Talanta, 40 (1993) 593.

[5] J. Hernández-Méndez, A. Alonso Mateos, M.J. Almendral Parral and C. García de María, Anal. Chim. Acta, 184 (1986) 243.

[6] A.I. Vogel, Textbook of Macro and Semimicro Qualitative Inorganic Analysis, 5th edn., Longman, London, 1979.

[7] Ju. Lurie, Handbook of Analytical Chemistry, Mir Publishers, Moscow, 1975.

[8] H. Bergamin-Filho, E.A.G. Zagatto, F.J. Krug and B.F. Reis, Anal. Chim. Acta, 101 (1978) 17.

[9] Z. Marczenko, Separation and Spectrophotometric Determination of Elements, 2nd edn., Ellis-Horwood, Chichester, UK, 1986.

[10] L.J.A. Martins and J. Barbosa da Costa, J. Chem. Educ., 65 (1988) 176.

[11] A.A. Schilt, Analytical Applications of 1,10-Phenanthroline and Related Compounds, 1st edn., Pergamon Press, Oxford, 1969.

Lead preconcentration onto C-18 minicolumn in continuous flow and its determination in biological and vegetable samples by flame atomic absorption spectrometry[1]

Rosimar Lima, Katia Christina Leandro, Ricardo Erthal Santelli*

Geochemistry Department, Federal Fluminense University, Niteroi, Rio de Janeiro 24020-007, Brazil

Abstract

A procedure for the preconcentration and determination of lead in vegetable and biological samples was developed in the continuous mode coupled to a flame atomic absorption spectrometer. Lead is quantitatively preconcentrated in acetic buffer as its diethyldithiocarbamate chelate onto a C-18 minicolumn, placed in the loop of a proportional injector, eluted by a stream of methyl isobutyl ketone and introduced directly into the nebuliser. A detection limit of $3 \ \mu g \ l^{-1}$ is obtained using a time-based technique for 2 min preconcentration and an RSD of 3.8% was readily achieved for three measurements of $25 \ \mu g \ Pb \ l^{-1}$. The sample throughput is $24 \ h^{-1}$. Using preconcentration times of 10 min an enrichment factor of 189 can be obtained. The continuous flow system was used for some reference sample analysis and the obtained results reveal that the methodology can be easily applied for vegetable and biological sample analysis.

Keywords: Biological samples; Flame atomic absorption spectrometry; Lead; Preconcentration; Vegetable samples

1. Introduction

Solid phase extraction (SPE) has long been used in chromatography for separations and, more recently, in continuous flow analysis for both separation and preconcentration. Since its introduction in analytical chemistry several years ago [1], modified silica with hydrocarbon chains has been employed for trace metal preconcentra-

tion, after on-line chelation with a suitable reagent. Rapid extraction is generally ensured because the coating is very thin (typically in the range $10–100 \ \mu m$) and therefore the sample flow rate can be higher. As the neutral forms of analytes are more efficiently extracted by non-ionic polymeric coatings, the pH of the aqueous sample must be adjusted to prevent analyte ionization [2]. SPE has a number of attractive features compared with the traditional extraction technique. It is fairly simple, inexpensive, can be used in the field, needs relatively little toxic solvents, and can be easily automated [2]. Notwithstanding these ad-

---

* Corresponding author.

vantages, for trace metal analysis in flow systems it was used primarily for water samples and its application to other matrices has not been widely reported.

Lead, even at very low concentrations, is a well-known toxic element for animals and humans. For humans, the main lead sources are water and food, and therefore rapid and sensitive methods must be accessible for its determination in these samples [3].

The advantage of continuous automatic techniques such as flow analysis are particularly attractive when extensive manipulation is involved in a given determination, as is the case in preconcentration procedures [4,5]. Flow systems have also been successfully proposed for metal preconcentration, employing several techniques, e.g. solvent extraction [6], precipitation–dissolution [7], activated carbon [5,8], activated alumina [9], ion-exchange [10], cellulose sorbent [11] and fullerenes [12,13]. Regarding lead determination, bonded silica was used for the establishment of several analytical methods. Ruzicka and Arndal [14] were the first to explore the analytical potential of C-18 for lead preconcentration in the continuous mode employing two flow systems. In the first flow system a fixed volume of 4.0 ml of sample solution containing 1 mg l^{-1} lead was introduced, giving a preconcentration factor of 5.6 with a detection limit of only 0.1 mg l^{-1}. In another flow system based on sample time loading a preconcentration factor of 60 was obtained using a 40 ml sample volume. In this way a detection limit of 0.01 mg l^{-1} was attained. Fang et al. [15] proposed a flow system coupled to a graphite furnace atomic absorption spectrometer (GFAAS) using a microcolumn containing only 15 μl of sorbent. A preconcentration factor of 26 was obtained using 2.1 ml of sample solution and the methodology was tested in spiked sea water. Similarly, Porta et al. [16], employing a C-18 microcolumn, obtained recoveries of 92 ± 10% for lead from spiked sea water, but a double elution was necessary to obtain these results. In other studies, Sperling et al. [17] and Welz et al. [18], improving lead preconcentration from real sea water, obtained an enhancement factor of 20. In another paper, the research group of Welz et al. [19] obtained a

preconcentration factor of 64 using a microcolumn containing 9 μl of C-18 connected to a GFAAS. Berndt et al. [20], using high-performance flow atomic spectrometry, obtained a detection improvement of 48 times when coupling a C-18 minicolumn for the analysis of drinking water. All of these workers used diethyldithiocarbamates as chelating reagents.

The aim of this work was the development of a preconcentration flow system methodology for lead determination by flame atomic absorption spectrometry for vegetable and biological sample analysis. Diethylammonium N,N-diethyldithiocarbamate (DDTC) was selected as the lead chelation agent in acetic medium and C-18 as the solid phase extractor.

2. Experimental

2.1. Apparatus

A Perkin-Elmer 3100 atomic absorption spectrometer equipped with a hollow cathode lead lamp and a deuterium background corrector was used. The instrument was set at a wavelength of 217 nm and the air–acetylene flame was adjusted according to the manufacturer's recommendations. An Ismatec MP-13R peristaltic pump was used with Tygon tubes for the propelling system. A proportional injector–commutator made of PTFE was operated for selecting both the preconcentration and elution steps. The sorption minicolumn was made by packing a PTFE tube (3 cm long × 2 mm i.d.) with about 100 mg of C-18 and small glass wool beads at the ends to prevent material losses. This minicolumn was initially flushed with methanol and subsequently with methyl isobutyl ketone before use. After each elution cycle it was ready for re-use without further treatment. The transient signals were measured with a single pen record (RB-201, Equipamentos Cientificos do Brasil).

2.2. Reagents

Analytical-reagent grade reagents were always used as well as distilled, deionized water.

A 1000 μg ml^{-1} lead stock solution was prepared by dissolving 1.598 g of lead nitrate in water containing 30 ml of 65% HNO$_3$ and making up the volume to 1000 ml. The lead calibration solutions, containing 10% v/v of the buffer solution, were prepared daily by appropriate dilution of the stock solution.

Diethylammonium N,N-diethyldithiocarbamate was prepared daily at a concentration of 0.1% w/v.

Acetic acid buffer solution, pH 4.6, was prepared by adding 60 ml of glacial acetic acid to 800 ml of water, adjusting the pH to 4.6 with 57% ammonium hydroxide and making up the volume to 1000 ml with water.

Modified silica C-18 from commercially available Sep-Pak cartridges (Waters) was used to prepare the minicolumn.

Methyl isobutyl ketone and acetylene (atomic absorption grade) were also used.

2.3. Flow system

A flow system was built to perform the lead preconcentration and determination steps, as shown in Fig. 1. In the preconcentration step, the sample (S) merges with the reagent stream (R) and the lead–diethyldithiocarbamate complex formed in the reaction coil (RC) is retained by the C-18 while it passes through the minicolumn. At the same time, methyl isobutyl ketone (MIBK) fills the loop (L) and water (C) flows through the atomic absorption nebulizer (AAS). By switching the commutator (I), a small volume (20 μl) of
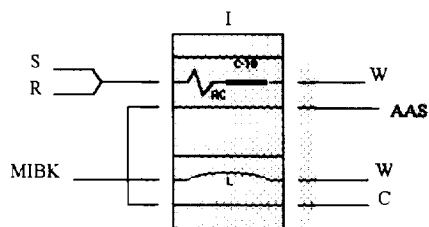
Fig. 1. Flow system for preconcentration and determination of lead. S, sample solution in acetic acid buffer (4.0 ml min^{-1}); R, reagent (0.27 ml min^{-1}); L, loop of MIBK (380 μl); C, carrier (water, 3.0 ml min^{-1}); RC, reactor coil (200 cm); C-18, minicolumn; W, waste; AAS, flame atomic absorption spectrometer.

water washes the minicolumn and water (C) displaces the MIBK from the loop (L) and flows through the C-18 minicolumn. The lead complex goes through the AAS nebulizer producing a transient signal. Peak height was always used as the measurement parameter.

3. Results and discussion

3.1. Chemical and flow optimizations

The system depicted in Fig. 1 was studied in relation to chemical and flow variables (univariate method) in order to obtain the best analytical conditions. The sample pH was tested within the range 2.8–8.1. Best results were obtained at pH 4.6 in acetic acid buffer medium. The reagent concentration was investigated between 0.0001 and 0.2% (w/v), and the highest signals were found at concentrations higher than 0.01%. In order to prevent some interferences due to the presence of other metallic species the reagent concentration was chosen to be 0.1%. The sample flow rate was studied in the range 2–7.5 ml min^{-1}. Flow rates of $\leqslant$ 4 ml min^{-1} revealed maximum absorbance signals, but analyte losses were observed at flow rates higher than 4 ml min^{-1}, owing to short residence times which entail incomplete retention. Therefore, this parameter was adjusted to 4 ml min^{-1} for future optimization. The reagent flow rate was tested in the range 0.07–0.6 ml min^{-1}. For flow rates lower than 0.27 ml min^{-1} incomplete retention was observed due to the lack of the reagent. With flow rates higher than 0.27 ml min^{-1} the system shows higher and reproducible signals. We do not recommend higher flow rates due to the possibility of reducing the sample flow rate and lowering the sample throughput. Therefore a reagent flow rate of 0.27 ml min^{-1} was selected. The carrier flow rate was adjusted to 3 ml min^{-1} to give better nebulization of the organic phase. The reactor coil length was investigated in the range 14–250 cm and the best complex formation was observed with a 200 cm coil length. A reactor coil length < 200 cm did not ensure sufficient residence time which is required for lead complexation by di-
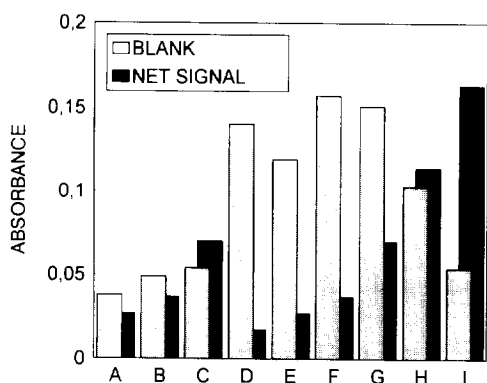
Fig. 2. Selection of the eluent. Blank and net absorbance signals obtained when eluting the lead chelate after a preconcentration time of 2 min (8.0 ml sample volume) for 100 μg Pb^{2-} l^{-1}: A, methanol; B, butanol; C, ethanol; D, dichloroethane; E, N,N-dimethylformamide; F, acetylacetone; G, methyl ethyl ketone; H, carbon tetrachloride; I, methyl isobutyl ketone.

ethyldithiocarbamate. With a reaction coil length of > 200 cm the absorbance signals remained higher and constant. A study for the choice of the best eluent was done using several organic solvents. Methanol, butanol, ethanol, dichloroethane, N,N-dimethylformamide, acetylacetone, methyl ethyl ketone, carbon tetrachloride and methyl isobutyl ketone were assayed. The results can be seen in Fig. 2. Water-miscible solvents give bad results, probably because they mix with the water carrier. For the immiscible organic solvents studied (with the exception of MIBK) the blank signals were so high that these solvents were useless for this purpose. Best conditions were obtained with MIBK (low blank with high analytical signals). Also, the minimum volume of MIBK necessary to displace the complex from the C-18 minicolumn was evaluated to be within the range 250–500 μl. The highest absorbance signal was obtained with 380 μl of MIBK which gives better recoveries without any peak carryover. In order to use a less toxic organic solvent 380 μl of MIBK was chosen for the lead complex elution.

3.2. Interference study

The effect of the concomitants was studied with analytical lead solutions prepared with and with-

out each interferent species. Co(II), Ni(II) and Cr(VI) did not interfere up to an interferent/analyte ratio of 100. Cu(II) did not affect the lead signal if the interferent/analyte ratio was not higher than 10. These ratios are never obtained with real samples such as those analyzed in this work.

Interference studies were also done using real samples. For this test, two vegetable samples (almond leaves) and one biological sample (fish tissue) were prepared. The almond leaves were collected from two different areas: an urban area with heavy traffic and a rural area. The leaves were washed with water, dried at air temperature and ground using a knife grinder. The fish tissue was lyophilized and ground using the same knife grinder. These samples were homogenized and stored in plastic bottles inside a dessicator. With solutions of these samples, prepared as described in Section 3.3, addition curves were constructed using the flow system depicted in Fig. 1. The ratios of the slopes of the addition curves and the analytical curves (aqueous standards) varied from 0.994 to 1.01, showing that trace metals present at their normal concentration levels in these samples do not influence the lead signals, and corroborating the fact that there is no influence from these matrices in the lead preconcentration and determination steps.

3.3. Sample preparation

The samples used for the interference study and the reference sample materials analyzed with the developed methodology were decomposed by wet ashing with acid treatment, based on the study of Icbinoki and Yamazaki [21]. Before analysis all samples were dried at 120°C for 24 h. The weighed samples (the weights depend on the lead content) were placed in a Pyrex beaker and after the addition of 15 ml of 65% nitric acid, the covered beaker was allowed to stand for one night. Then, the samples were heated slowly on a hotplate until they became transparent (colorless or pale yellow). Then 5 ml of 72% perchloric acid was added and the heating was continued until the liquor became colorless (until complete wet ashing of the organic mater). The solution was

then heated almost to dryness. After cooling, the residue was extracted with the buffer solution, filtered, and the volume made up with water, maintaining the 10% v/v buffer solution concentration. These samples were analyzed immediately after dissolution. A blank solution was prepared for each sample batch dissolution and was used to prepare the analytical lead solutions for calibrations.

During the sample preparation step it was noted that if any organic matter remains, a big interference occurs because lead remains bonded to the original organic matter and therefore is not able to react with the diethyldithiocarbamate. However, the minicolumn is also able to retain neutral organic matter, competing with the Pb–DDTC complex in the sorption processes. This results in a very small recovery of lead from the samples. Therefore, the implementation of a sample preparation step involving $HClO_4$ was needed and according to Gorsuch [22] this treatment is the best way to oxidise all traces of organic matter from real samples.

3.4. Analytical features

Using the flow system of Fig. 1, lead can be determined in the range 20–100 $\mu g\ l^{-1}$ with time-based sampling for only 2 min, equivalent to a sample volume of 8 ml (sample flow rate of 4.0 ml min^{-1}). The calibration equations are typically $A = -0.001 + 3.005 \times 10^{-3}$ [Pb($\mu g\ l^{-1}$)] with $r^2 = 0.998$. The detection limit calculated as three times the standard deviation of the peak absorbance was 3 μg Pb l^{-1}. The RSD at the 25 μg l^{-1} level was 3.8% for all three measurements. The sample throughput was 24 h^{-1}. Fig. 3 shows some typical peaks obtained using the flow system and a manual flame AAS signal. The flame transparency in the working wavelength region is uniquely responsible for the blank signal.

An enrichment factor of 60, calculated as the ratio between the slopes of the calibration graphs obtained by this flow method and the manual direct aspirations, was readily achieved. By using a 10 min preconcentration time, enrichment factors as high as 189 can be obtained, which ensure the lowering of the detection limit by a factor of
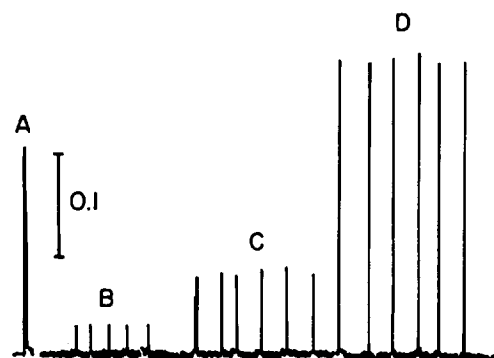
Fig. 3. Typical absorbance signals (FIA peaks) obtained with the flow system in Fig. 1 using a preconcentration time of 2 min (8.0 ml of sample volume loading): A, signal obtained when aqueous solution containing 4 μg Pb^{2+} ml^{-1} was introduced into the FAAS using direct aspiration; B, blank; C, 20 μg Pb^{2+} l^{-1}; D, 100 μg Pb^{2+} l^{-1}.

three. These values are bigger than those obtained by comparing only volumes of sample and eluent (≈ 20) due to the faster complex elution and due to the very low dispersion of the organic phase (380 μl of MIBK pumped at 3.0 ml min^{-1} by a water stream crossing only 25 cm × 0.5 mm i.d. tubing to get ahead of the AAS nebulizer).

3.5. Determination of trace amounts of lead in vegetable and biological samples

The developed methodology was used for lead determination in almond leaves, fish tissue and for some reference sample analysis. For this purpose, each sample was mineralized in duplicate as described in Section 3.3 together with similar blanks which allowed for the contribution of the lead present in the reagents for the digestion procedure. Each dissolved sample was analyzed in triplicate (except for the fish flesh sample). These

Table 1
Results obtained for lead determination in the analysis of almond leaves and fish tissue. Results in $\mu g\ g^{-1}$ for dry samples

Sample	Analytical curve	Standard addition
Almond leaves 1	1.72 ± 0.03	1.61 ± 0.03
Almond leaves 2	1.15 ± 0.02	1.18 ± 0.02
Fish tissue	3.45 ± 0.06	3.22 ± 0.06

Table 2
Results obtained for the analysis of reference sample materials. Results in $\mu g\ g^{-1}$ for dry sample

Reference sample	Obtained values	Certified values
Citrus leaves (NIST)	$13.2 \pm 0.3\ (n = 3)$	13.3
Fish tissue MA-B-3/TM (IAEA)	$4.74 \pm 0.03\ (n = 3)$	4.62 $(3.85–5.13)^a$
Copepoda MA-A-1/TM (IAEA)	$2.1 \pm 0.1\ (n = 3)$	2.1 $(1.8–2.4)^a$
Fish flesh MA-A-2/TM (IAEA)	$0.80 \pm 0.02\ (n = 2)$	0.58 $(0.51–0.65)^a$

^{a} Confidence interval.

results can be seen in Table 1 and Table 2. The results found for the almond leaf samples and for the fish tissue, when compared with the standard addition methods, are consistent and acceptable in all instances. The two samples of almond leaves (collected at different sites) had the same lead content, probably due to the fact that this species is not a good pathfinder for lead (not recommended for biogeochemistry prospecting) or owing to a large lead scattering. However, the results obtained for the reference samples agreed very well with the certified values, corroborating the fact that the developed methodology can be applied for lead preconcentration and determination in vegetable and biological analysis. The concomitants did not influence the analytical signal due to their very low concentrations in the real samples analyzed.

Our methodology, when compared to another published previously, shows some similarities and differences. In the work of Peña et al. [8] the performance of the activated carbon minicolumn was similar to that in this work. The analytical range was extended but the detection limit was worst than that obtained by us, assuming the same preconcentration time. Peña et al. found similarities when they compared their results with results obtained by C-18 sorbent extraction. Naghmush et al. [11], using different cellulose

sorbents, detected some interferences due to the presence of Fe(III), Cu(II), Ca, Mg, K and Na. Their method was applied successfully for water samples and showed very low detection limits $(0.17\ \mu g\ l^{-1})$ when employing 50 ml of sample (six times more than that used in this work). Yebra Biurrum et al. [10] found a similar detection limit $(3.1\ \mu g\ l^{-1})$ using only 2 ml sample volume when employing a new chelating resin (containing polyaminophosphonic acid as chelating group) synthesized by their research group.

4. Conclusion

In conclusion, the developed methodology can be easily applied for vegetable and biological sample analysis for lead determination with good selectivity, reproducibility and accuracy. Our methodology is also comparable with techniques such as GFAAS, especially in terms of time and detection limit, and is advantageous for laboratories seeking cheaper analysis methods.

Acknowledgments

References

[1] C.F. Poole and S.A. Schuvette, J. High Resolut. Chromatogr., 6 (1983) 526.
[2] Z. Zhang, M.J. Yang and J. Pawliszyn, Anal. Chem., 66 (1994) 844A.
[3] D. Rodríguez, P. Fernández, C. Pérez-Conde, A. Gutiérrez and C. Cámara, Fresenius' J. Anal. Chem., 349 (1994) 442.
[4] M. Valcárcel and M.D. Luque de Castro, Non-Chromatographic Continuous Separation Techniques, Royal Society of Chemistry, Cambridge, 1991.
[5] R.E. Santelli, M. Gallego and M. Valcárcel, Talanta, 41 (1994) 817.
[6] E.A. Novikov, L.K. Shpigun and Y.A. Zolotov, Anal. Chim. Acta, 230 (1990) 157.

[7] R.E. Santelli, M. Gallego and M. Valcárcel, Anal. Chem., 61 (1989) 1427.

[8] Y.P. de Peña, M. Gallego and M. Valcárcel, Talanta, 42 (1995) 211.

[9] M.C. Pannain and R.E. Santelli, Talanta, (1996) in press.

[10] M.C. Yebra-Biurrum, A. Bermejo Barrera, M.P. Bermejo-Barrera and M.C. Barciela-Alonso, Anal. Chim. Acta, 303 (1995) 341.

[11] A.M. Naghmush, K. Pyrzynska and M. Trojanowicz, Talanta, 42 (1995) 851.

[12] M. Gallego, Y.P. de Peña and M. Valcárcel, 66 (1994) 4074.

[13] Y.P. de Peña, M. Gallego and M. Valcárcel, Anal. Chem., submitted.

[14] J. Ruzicka and A. Arndal, Anal. Chim. Acta, 216 (1989) 243.

[15] Z. Fang, M. Sperling and B. Welz, J. Anal. At. Spectrom., 5 (1990) 639.

[16] V. Porta, O. Abollino, E. Mentasti and C. Sarzanini, J. Anal. At. Spectrom., 6 (1991) 119.

[17] M. Sperling, X. Yin and B. Welz, J. Anal. At. Spectrom., 6 (1991) 295.

[18] B. Welz, X. Yin and M. Sperling, Anal. Chim. Acta, 261 (1992) 477.

[19] B. Welz, M. Sperling and X. Sun, Fresenius' J. Anal. Chem., 346 (1993) 550.

[20] H. Berndt, A. Müller and G. Schaldach, Fresenius' J. Anal. Chem., 346 (1993) 711.

[21] S. Icbinoki and M. Yamazaki, Anal. Chem., 57 (1985) 2219.

[22] T.T. Gorsuch, The destruction of organic matter, Pergamon Press, Oxford, 1970.

Evaluation of a glassy carbon electrode modified by a bilayer lipid membrane with incorporated DNA

C.G. Siontorou[a], A.-M. Oliveira Brett[b], D.P. Nikolelis[a],*

[a]*Laboratory of Analytical Chemistry, Department of Chemistry, University of Athens, Panepistimiopolis-Kouponia, 15771-Athens, Greece*
[b]*Universidade de Coimbra, Departamento de Quimica, P-3049 Coimbra Codex, Portugal*

Abstract

The objective of the present work was the evaluation and characterization of a glassy carbon (GC) electrode modified by a bilayer lipid membrane (BLM) with incorporated single-stranded deoxyribonucleic acid (ss DNA). Various procedures were developed and tested for the incorporation of ss DNA at the electrode modified by the lipidic membrane:

1. formation of self-assembled BLMs over ss DNA adsorbed on the electrode surface;
2. direct adsorption of ss DNA into a BLM modified GC electrode;
3. formation of a BLM with incorporated ss DNA at the electrode surface using the monolayer folding technique.

Differential pulse voltammetry (i.e. oxidation of guanine and adenine residues) was used to monitor the incorporation of ss DNA at the GC electrode modified by the BLM. The results have shown that the lipid membrane enhances the stability of ss DNA during a "medium-exchange" of the electrode and prohibits its diffusion from the electrode surface. The third scheme was proven to be the most appropriate as both electrode modification by the BLM and DNA adsorption occur in one stage and much faster (as no BLM thinning process is required) as compared to the former two techniques; furthermore, maximized loading of DNA in BLMs is achieved which reduces by ca. 10-fold the DNA amounts that can be detected electrochemically. Conventional planar "free-suspended" and self-assembled metal supported BLMs were used to monitor in situ the incorporation of ss DNA in these membranes. The results have shown that the adsorption of ss DNA at lipid membranes (as a medium for DNA incorporation on an electrode surface) can occur much faster, using milder conditions and smaller amounts of DNA than by previously described techniques.

Keywords: Bilayer lipid membranes; Chemically modified electrode; DNA; Glassy carbon electrode

1. Introduction

A growing interest has recently arisen in the development of DNA sensors which are expected

* Corresponding author.

eventually to replace conventional methods in gene diagnoses using nucleic acid hybridization techniques for infectious diseases. DNA biosensors that are being developed presently are based largely on piezoelectric, electrochemical, or opti-

cal transducers. Brabec and Palecek have pioneered the electrochemistry of nucleic acids and their adsorption/oxidation at different types of carbon electrodes [1] and this type of transduction scheme has gained popularity with substantial achievements in the field of biosensing. Such achievements include sequence-specific gene detection with DNA modified electrodes [2,3], selective detection of cystic fibrosis using modified carbon electrodes to which DNA was covalently bound [4,5] and differential pulse voltammetric determination of traces (picomole range) of RNA in the presence of DNA and nucleic acid components [6]; the detection limit was recently improved to the femtomole range by using constant current potentiometric analysis at carbon paste electrodes; this may open doors for investigating structural transitions and interactions of RNA [7]. A number of studies have been reported in the literature concerning the adsorption of single-stranded DNA (ss DNA) at bare (unmodified) carbon electrodes [2,8]. This type of DNA adsorption results in the use of long adsorption times (more than 30 min) under vigorous conditions (i.e. high temperatures [2] or potentials [8]), whereas great concerns have arisen on the stability of adsorbed DNA during "medium-exchange" experiments.

The goal of our work is to investigate the use of lipid membranes either for the modification of carbon electrodes for improved incorporation of DNA or as transducers to monitor directly DNA hybridization, since lipids are known to associate with DNA with high affinity [9] and therefore create a biosensor for rapid nucleic acid detection. The work herein reports the evaluation and characterization of a glassy carbon (GC) electrode modified by a bilayer lipid membrane (BLM) with incorporated ss DNA. Several procedures were used in the present studies to modify the glassy carbon electrode with lipid membranes for ss DNA incorporation. Results from direct ss DNA adsorption from solution on a GC modified electrode and the stability of adsorbed DNA during a medium-exchange of the electrode are described herein. Examples of the use of BLM systems to monitor directly the incorporation of ss DNA in membranes are provided.

2. Experimental

2.1. Materials and apparatus

The lipid used throughout this study was egg phosphatidylcholine (egg PC; lyophilized, Avanti Biochemicals, Birmingham, AL, USA). Gramicidin D was supplied from Sigma Chemical Co. (St. Louis, MO, USA). Calf thymus DNA (sodium salt, type I) was also obtained from Sigma Chemical Co. and was used without further purification. Silver wires (diameters 0.5 and 1.0 mm) were obtained from Aldrich Chemical Co., Inc. (Milwaukee, WI, USA). All other reagents were of analytical-reagent grade. Water was purified using a Milli-Q cartridge filtration system (Millipore, El Paso, TX, USA) and had a minimum resistivity of 18 MΩ cm.

Single-stranded DNA (ss DNA) was prepared by the following procedure. An accurately weighed sample of approximately 3 mg of calf thymus DNA was treated with 0.5 ml of pure perchloric acid and stirred to dissolve for 10 min. A volume of 0.5 ml of 9 M NaOH was then added to neutralize the solution, followed by the addition of 0.1 M KCl electrolyte solution such that the final volume was 10 ml and the pH value 5.5. The resulting solution of ss DNA was scanned from 220 to 300 nm (using a Hitachi U-2000 spectrophotometer) and the absorbance at 260 nm was found to be 0.219, whereas the absorbance of a solution containing 3 mg native DNA (not denatured) was found to be 0.040. These data can not be used to calculate the concentration of ss DNA in solution; however, they indicate that denaturation has occurred [10].

The differential pulse voltammograms were recorded using a μAutolab potentiostat/galvanostat running with model GPES version 3 software, from Eco-Chemie, The Netherlands. The potential range studied was from +0.025 to +1.4 V vs. SCE, and the differential pulse voltammetry conditions were pulse amplitude, 50 mV; pulse width, 70 ms; interval time, 400 ms; and scan rate, 5 mV s^{-1}. A one-compartment cell contained a GC electrode (Tokai, GC, area 0.07 cm^2), a platinum gauze counter electrode and a SCE reference

electrode. The working electrode was polished with diamond paste down to 1 μm particle size on a polishing table before use and thoroughly cleaned; it was repolished as necessary, and always between adsorption experiments.

The equipment for the formation of conventional planar "free-suspended" solventless BLMs have been described in detail elsewhere [11]. BLMs were formed in an aperture of 0.32 mm diameter in a Saran-Wrap (PVDC; DowBrands, L. P., Indianapolis, IN, USA) partition of thickness ca. 10 μm that separated two identical Plexiglas chambers (each with volume of 10 ml and an air/water interface of 3 cm^2) and were supported in a 0.1 M KCl electrolyte solution. A two-electrode configuration was used throughout the experiments using self-assembled BLMs (s-BLMs) and consisted of a sensing electrode (i.e. silver wire of 0.5 or 1.0 mm diameter with a s-BLM) and a Ag/AgCl electrode acting as a reference. A 25 mV dc voltage was applied across the membrane between two Ag/AgCl reference electrodes when using the former technique of free-suspended BLMs, whereas a 25 mV dc potential was applied between the sensing and reference electrode when using the metal-supported s-BLMs (above and beyond the open circuit potential of this electrode system). A digital electrometer (Model 614, Keithley Instruments, Cleveland, OH, USA) was used to measure the ionic current through the BLMs and as a current-to-voltage converter. The electrochemical cell and electronic equipment were isolated in a grounded Faraday cage.

2.2. Procedures

A stock solution of PC (2.5 mg ml^{-1}) in n-hexane was used for the preparation of a dilute PC solution (0.2 mg ml^{-1}) in the same organic solvent on a daily basis; this stock lipid solution was stored in a nitrogen atmosphere at $-4°C$. Planar free-suspended BLMs were prepared by the application of a 10 μl volume of dilute lipid solution onto the electrolyte surface in the one cell compartment, and then over a period of a few seconds, the water level in one solution compartment was brought below the aperture

and then raised again with a disposable syringe [11]. When the ion current stabilized (over a period of about 5 min), the ss DNA solution was injected in one solution compartment using continuous gentle stirring. s-BLMs were constructed according to established techniques [12,13]. The stock PC solution (2.5 mg ml^{-1}) was used for the formation of metal supported s-BLMs. A lipid layer was deposited onto a nascent metallic surface cut with a scalpel just before or while immersing the metal wire into the lipid solution. The wire coated with the lipid solution was subsequently immersed into a 0.1 M KCl aqueous solution, and the ionic current was stabilized over a period of 25 or 40 min for diameters of silver wire of 0.5 or 1.0 mm, respectively. Ionic current stabilization was followed by injection of ss DNA solution while stirring continuously. All experiments were done at $25 \pm 1°C$.

3. Results and discussion

3.1. Characterization of BLM structure and the stability of lipid membranes on the solid electrodes

The Langmuir-Blodgett technique has previously been used to deposit a controlled number of lipid layers on glassy carbon electrodes [14,15]. However, the method of formation of stabilized metal supported s-BLMs as reported by Tien et al. [12,13] was chosen from various techniques owing to the simplicity and low cost of BLM preparation. The diameter of the wires that were used was found to play an important role in the time for BLM stabilization, and on the magnitude and noise of the background ion current. An increase in the diameter of the silver wires from 0.5 to 1.0 mm resulted in a decrease in the time for BLM stabilization from 40 to 25 min, respectively; furthermore, this increase resulted in an increase in the background ion currents and decrease in the noise levels. The impedance of BLM assemblies on metals is directly related to the noise levels and the stabilization time due to the packing effects of the BLMs, which depend on the diameter and the

degree of surface roughness of the wire used to support BLMs [13,16,17]. Any BLMs used for electroanalytical experimentation must be characterized to demonstrate the existence of the BLM structure. Specific capacitance is often used as the primary criterion for membrane characterization (i.e. to estimate the apparent thickness of the lipid bilayer and whether there is any solvent retained in the hydrocarbon region of the BLMs) [11]. The electrical capacitance of s-BLMs was measured as previously described [11] over time until a steady-state value was obtained. The steady-state value of membrane specific capacitance was found 4 mF cm^{-2} (for silver wire of 0.5 mm diameter) which is in agreement with previous reports [13,17]; however, this value can not be used to estimate the hydrocarbon thickness of the s-BLM, since the actual area of the bilayer is not known.

Chemical characterization of the bimolecular thickness of s-BLMs can be derived from the addition of gramicidin as this peptide transports monovalent cations through the membrane by the formation of ion-channels and the conductance increases many fold [11]. Gramicidin does not induce conductance alterations if the membrane is thicker than one bilayer [18,19]. The ion selectivity of BLMs containing gramicidin D for the transport of monovalent ions is greatest for ammonium and potassium ions relative to sodium and lithium [19]. Experiments using s-BLMs were done using 0.1 M NaCl as the electrolyte solution which provided a background ion current value of ca. 100 pA, whereas in the presence of 4 μM gramicidin the ion current increased to 166 nA. Similar experiments using KCl as the electrolyte have provided larger ion current increases. The bilayer structure of the lipid film on the glassy carbon electrodes was also verified by using gramicidin and 0.1 M KCl as the electrolyte; the ion current values were ca. 100 nA in the absence of gramicidin and increased to 1 μA in the presence of 1 μM gramicidin.

Cholesterol has been used extensively in lipid mixtures to prepare metal supported BLMs and it acts as a stabilizing agent [20]. The use of cholesterol to stabilize BLMs on solid electrodes was found to be unnecessary in our experiments as the lipid membranes prepared herein were stable for

long periods of time (routinely over 48 h) and were not prone to collapse in response to a mechanical or electrical shock. This is an advantage as compared to planar free-suspended BLMs which are normally stable for periods of time of ca. 6 h and suffer from mechanical or electrical instability [11].

3.2. BLM formation over ss DNA adsorbed on the electrode surface

The glassy carbon electrode was modified with ss DNA adsorbed at + 1.4 V [8]. The electrode with adsorbed ss DNA was then immersed in a solution containing PC (2.5 mg ml^{-1}) in n-hexane and the lipid layer was thinned into a bilayer by subsequent immersion in 0.1 M KCl for ca. 30 min. It was assumed that the ss DNA that was adsorbed on the electrode surface was covered by this bilayer. By scanning from 0.025 to 1.4 V, peaks corresponding to guanine and adenine were observed (Fig. 1).

These peaks continued to appear and were not reduced in magnitude when the BLM modified electrode with incorporated ss DNA was transferred to another 0.1 M KCl supporting electrolyte solution (medium-exchange procedure). These results show that the lipid membrane can strongly hold DNA molecules on the electrode
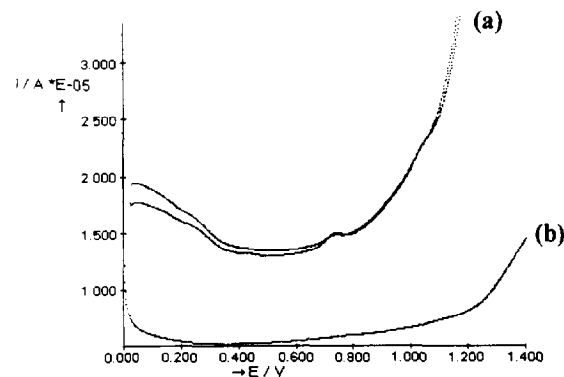
Fig. 1. Differential pulse voltammograms obtained in 0.1 M KCl supporting electrolyte: (a) two successive scans of a glassy carbon electrode modified by a lipid membrane on which ss DNA was adsorbed prior to BLM formation; (b) glassy carbon electrode without ss DNA.
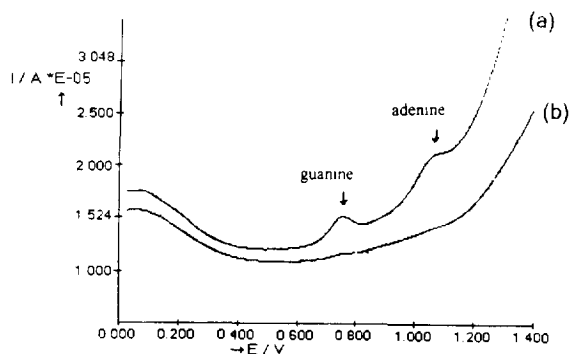
Fig. 2. Differential pulse voltammograms obtained in 0.1 M KCl supporting electrolyte plus 27 μg ml^{-1} ss DNA: (a) glassy carbon electrode modified by a BLM, formed on the electrode surface in 0.1 M KCl solution prior to DNA addition to the electrolyte solution: (b) clean glassy carbon electrode.

surface [9,21] during medium-exchange procedures. Previous voltammetric studies of ss DNA adsorption at a GC electrode have shown that there is significant loss of DNA during medium-exchange of the electrode in a solution not containing ss DNA [8]. Recent studies have reported that electrochemical treatment of carbon electrodes may improve ss DNA adsorption [7].

3.3. Direct adsorption of ss DNA into a BLM modified GC electrode

The GC electrode was immersed in a solution containing PC (2.5 mg ml^{-1}) in n-hexane and the lipid layer was thinned into a bilayer by subsequent immersion in 0.1 M KCl for ca. 30 min. Small aliquots of ss DNA (6.5, 12, 14, 20, 25 and 27 μg ml^{-1}) were added to the KCl solution and the potential was scanned from 0.025 to 1.4 V. The results are shown in Fig. 2. Note that the solutions were gently stirred for 20 s after DNA addition and prior to potential scanning; this time was found to be sufficient to obtain maximized signal magnitude which is in agreement with the time of DNA incorporation obtained when using s-BLMs (vide infra).

The guanine (1.46 μA) and adenine (0.97 μA) peaks observed in Fig. 2(a) exhibit the direct

adsorption of ss DNA at the BLM modified GC electrode; no peaks were observed using a bare electrode dipped in a 0.1 M KCl solution containing 27 μg ml^{-1} ss DNA (Fig. 2(b)). The peak magnitude was decreased with a decrease of ss DNA concentration in solution, i.e. a peak magnitude of ca. 97 nA was observed when using a solution of ss DNA with a concentration of 6.5 μg ml^{-1}. These peaks continued to appear and were not reduced in magnitude during medium-exchange procedure.

3.4. Incorporation of ss DNA into BLM at a GC electrode using the monolayer folding technique

The monolayer folding technique [11] was used in order to maximise DNA loading in BLMs while the latter are deposited on the GC electrode. This was attempted in order to use smaller amounts of ss DNA for electrode modification than those previously described (vide supra) or reported [8]. ss DNA solution was co-deposited with the lipid film on the electrolyte surface and a subsequent film casting on the GC electrode surface was followed. The results have provided a detectable guanine peak of 125 nA using 0.6 μg of ss DNA; smaller amounts of ss DNA did not provide a measurable signal. Present research is focused on estimating the surface coverage of the electrode with lipid films containing DNA using scanning electron microscopy, and exploiting the stability of lipid modified GC electrodes with incorporated DNA.

3.5. Incorporation of ss DNA in free-suspended BLMs

Measurements of ion conductivity changes (i.e. recordings of ion current vs. time) through conventional free-suspended BLMs [11] were used to monitor in situ ss DNA incorporation in lipid membranes and therefore to estimate the time required for association of ss DNA with lipid membranes. The use of liposomes as agents for DNA transfer was previouly described [9] and recent research using vesicles has been focused on exploiting DNA–lipid interactions [21]. However, no studies have been reported in the literature to

date to study these interactions using lipid membranes with a bilayer structure. Various volumes of the solution containing ss DNA were injected into the electrolyte solution after BLM formation and current stabilization. Fig. 3 shows a typical recording obtained after ss DNA injection in bulk electrolyte solution. A minimum volume of 4 μl of ss DNA solution (270 μg ml^{-1}) was required to induce increases in ion current values larger than the background (residual) ion current values; the concentration of ss DNA in bulk solution was 0.108 μg ml^{-1} and the ion current increased by 15.8 pA. The ion current increase was correlated to ss DNA concentration in bulk solution by the equation: ΔI (pA) = 277.5 C (μg ml^{-1}) – 14.6 (r^2 = 0.9995). Concentrations of ss DNA in bulk solution larger than ca. 0.27 μg ml^{-1} caused membrane rupturing. Control experiments involving the use of double-stranded DNA (ds DNA) were performed as well to demonstrate that the ion current increases were due to ss DNA/membrane interactions. It is therefore presumed that no alteration of the DNA conformation from ss to ds occurs in BLMs. These results suggest the potential of BLMs to act as a medium for DNA hybridization and offer a route to monitor this phenomenon.

The results in Fig. 3 show that the incorporation of ss DNA in BLMs occurs within 1.3 to 2.5 min. These data also indicate that for all ss DNA concentrations that were tested, it takes about the same delay time for the current increases to be observed. The relative invariable delay time
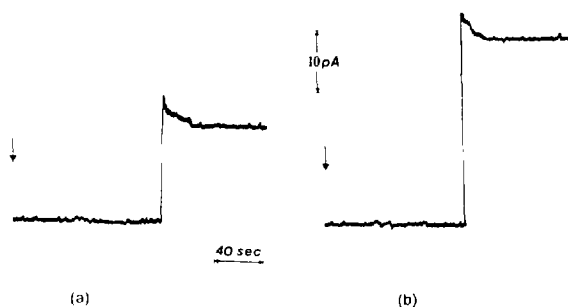
Fig. 4. Typical recordings obtained with s-BLMs. The ss DNA concentration in the bulk electrolyte solution was (a) 54 ng ml^{-1} and (b) 148 ng ml^{-1}. The arrow shows the injection of ss DNA in solution.

(much longer than mixing or diffusion times) does not appear to be related to ss DNA concentration, and suggests a mechanism of response in pertinent analogy to the function of a protein in BLMs. The electrochemical results indicate that a critical concentration of ss DNA exists beyond which increases of ion conductivity occur. These increases were noticed either in response to stepwise increases of DNA in the bulk solution or injections of DNA to a bulk solution containing no DNA (the regression equations correlating ion current to DNA concentration practically coincided). There were no discernible threshold transients observed during our experiments, suggesting that critical events due to changes of the surface potential of the BLMs were absent [22]. The results presented herein indicate that ss DNA spans the membrane to form a conductive pore. It is also possible that the increases of ion current values are likely to be due to concurrent DNA–lipid interactions which tend to disrupt the continuum of lipid interactions on one side of a BLM. However, the present results indicate that the incorporation of ss DNA in BLMs can be studied in situ by monitoring ion permeability changes and that the time required for the incorporation is less that 2.5 min.

3.6. Incorporation of ss DNA in BLMs

Stabilized s-BLMs on metal electrodes were used to monitor ss DNA incorporation in BLMs. Fig.

Fig. 3. Typical recordings obtained with planar free-suspended BLMs. The ss DNA concentration in the bulk electrolyte solution was (a) 108 ng ml^{-1} and (b) 162 ng ml^{-1}. The arrow shows the injection of ss DNA in solution.

4 shows the typical recordings obtained with increases in ss DNA concentration in the bulk solution. The required time for ss DNA incorporation in membranes is of the order of ca. 10 s (for all concentrations of DNA). This time is less than that obtained using free-suspended BLMs (vide supra); note that the reproducibility of the required time for DNA incorporation in s-BLMs is of the order of ± 14%. The shorter time delay for DNA incorporation can be correlated to the structure of s-BLMs. One side of the metal supported BLMs is in contact with the aqueous electrolyte solution, whereas the second monolayer touches the metal surface with some regions (depending on the metal roughness) covered with the electrolyte solution. Any ion rearrangement at these regions will occur more rapidly than in a homogeneous membrane such as those with a planar bilayer structure as a direct result of packing effects. An increase in ss DNA concentration in the bulk electrolyte solution results in increased ion current values obtained with s-BLMs (Fig. 5). The minimum detectable ion current increase (as set by the signal to noise ratio of 3) is ca. 10 nA, which is caused by an amount of ss DNA in bulk solution of about 30 ng ml^{-1}. This amount is far smaller that those previously used to incorporate ss DNA on metal electrodes [8], a substantial advantage of the present method. Reproducibility of the response was found to be of the order of ± 4 to 7% ($N = 5$, 95% confidence limit).
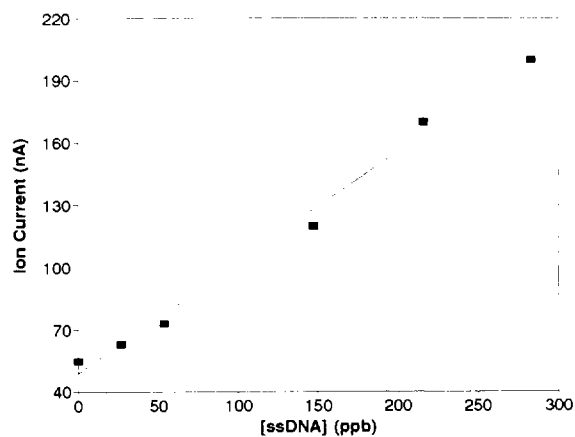
Fig. 5. Ion current dependence on ss DNA concentration in the bulk electrolyte solution using s-BLMs.

4. Conclusions

Various procedures were developed for the incorporation of ss DNA at a GC electrode modified by BLMs. Results using differential pulse voltammetry (i.e. oxidation of guanine and adenine residues) have shown that the lipid membrane enhances the stability of ss DNA towards a medium-exchange transfer of the electrode and prohibits diffusion of ss DNA from the electrode surface. The monolayer folding technique is preferred to the dip-casting methods for electrode modification by BLMs for DNA incorporation. Both phenomena can be achieved by the former technique in one stage, without a BLM thinning process which results in a substantially reduced time for electrode modification with incorporated DNA. Furthermore, maximized loading of DNA in BLMs can be achieved with the monolayer folding technique which reduces by ca. 10-fold the DNA amounts that can be detected electrochemically. Conventional planar BLMs and s-BLM systems results have shown that the adsorption of ss DNA at lipid membranes acting as a medium to incorporate ss DNA on an electrode surface can occur much faster using milder conditions and smaller amounts of ss DNA than by previously established protocols. Present research is focused on the potential of the GC electrode modified by BLM and/or using stabilized systems of BLMs for DNA hybridization and preparation of DNA sensors.

References

[1] E. Palecek, in G. Milazzo (Ed.) Topics in Bioelectrochemistry and Bioenergetics, Vol. 5, Wiley, London, 1983, p. 65.

[2] K. Hashimoto, K. Ito and Y. Ishimori, Anal. Chim. Acta, 286 (1994) 219.

[3] K. Hashimoto, K. Ito and Y. Ishimori, Anal. Chem., 66 (1994) 3830.

[4] K.M. Millan and S.R. Mikkelsen, Anal. Chem., 65 (1993) 2317.

[5] K.M. Millan, A. Saraullo and S.R. Mikkelsen, Anal. Chem., 66 (1994) 2943.

[6] E. Palecek and M. Fojta, Anal. Chem., 66 (1994) 1566.

[7] J. Wang, X. Cai, J. Wang, C. Jonsson and E. Palecek, Anal. Chem., 67 (1995) 4065.

[8] C.M.A. Brett, A.M. Oliveira Brett and S.H.P. Serrano, J. Electroanal. Chem., 366 (1994) 225.

[9] J.G. Smith, R.L. Walzem and J.B. German, Biochim. Biophys. Acta, 1154 (1993) 327.

[10] V. Brabec, Bioelectrochem. Bioenerg., 8 (1981) 437.

[11] D.P. Nikolelis and U.J. Krull, Talanta, 39 (1992) 1045.

[12] H. Ti Tien and Z. Salamon, Bioelectrochem. Bioenerg., 22 (1989) 211.

[13] M. Zviman and H. Ti Tien, Biosens. Bioelectron., 6 (1991) 37.

[14] M. Sugawara, K. Kojima, H. Sazawa and Y. Umezawa, Anal. Chem., 59 (1987) 2842.

[15] S. Nagase, M. Kataoka, R. Naganawa, R. Komatsu, K. Odashima and Y. Umezawa, Anal. Chem., 62 (1990) 1252.

[16] T. Hianik, J. Dlugopolsky and M. Gyepessova, Bioelectrochem. Bioenerg., 31 (1993) 99.

[17] T. Hianik, V.I. Passechnik, D.F. Sargent, J. Dlugopolsky and L. Sokolikova, Bioelectrochem. Bioenerg., 37 (1995) 61.

[18] M.C. Goodall, Arch. Biochem. Biophys., 147 (1971) 129.

[19] P. Yeagle, The Structure of Biological Membranes, CRC Press, Boca Raton, FL, 1992, Chapters 15 and 16.

[20] M. Rehak, M. Snejdarkova and M. Otto, Electroanalysis, 5 (1993) 691.

[21] J. Gustafsson, G. Arvidson, G. Karlsson and M. Almgren, Biochim. Biophys. Acta, 1235 (1995) 305.

[22] D.P. Nikolelis, M.G. Tzanelis and U.J. Krull, Anal. Chim. Acta, 281 (1993) 569.

Calcium-selective electrode based on a calix[4]arene tetraphosphine oxide

Tom McKittrick[a], Dermot Diamond[a,*], Debbie J. Marrs[b], Paul O'Hagan[b], M. Anthony McKervey[b]

[a]*School of Chemical Sciences, Dublin City University, Dublin 9, Ireland*
[b]*School of Chemistry, Queen's University, Belfast BT9 5AG, UK*

Abstract

A new ligand capable of producing calcium-selective electrodes with excellent characteristics is presented. The ligand (1) is a calix[4]arene bearing phosphine oxide ligating groups on the lower rim and this is the first report that such ligands can discriminate in favour of calcium ions against magnesium ions and the alkali metal ions. This calcium selectivity is in complete contrast to the behaviour of the well-known calix[4]arene tetraester derivatives (such as 2) which are selective for sodium against other alkali metal ions and group II ions. Electrodes based on PVC membranes incorporating ligand 1 display almost nernstian slopes and excellent selectivity against common interferents, including magnesium (log $K_{Ca,Mg}^{pot}$). The electrodes have demonstrated effective lifetimes of at least 7 weeks (duration of the study) and very fast response times.

Keywords: Calcium-selective electrode; Calix[4]arene; PVC membrane; Tetraphosphine oxide

1. Introduction

A new series of calixarene derivatives with lower rim phosphine oxide ligating groups have recently been synthesised and shown to exhibit interesting metal complexation behaviour with certain lanthanides and actinides [1]. In this study, selective extraction was demonstrated even under very highly acidic conditions (e.g. 4 M HNO_3) and in the presence of a large excess of sodium. We recently reported the properties of a Eu^{3+}-se-

lective PVC membrane electrode based on ligand 1 which showed excellent selectivity against a wide range of common ions [2]. The lack of response to alkali metal ions was particularly interesting given the well documented selective complexation of sodium ions by tetraester calixarene derivatives such as 2 [3]. During screening experiments for determining the characteristics of the Eu^{3+}-selective electrode based on 1, a relatively large response to Ca^{2+} was noted. This prompted us to investigate the possibility of making a calcium-selective sensor based on ligand 1.

In this paper, we report on a calcium(II)-selective electrode incorporating 1 as the sensing

---

* Corresponding author.
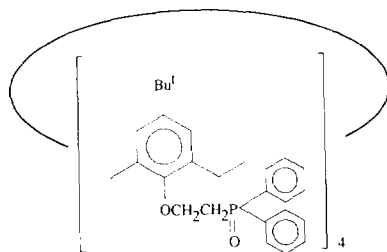
Ligand 1
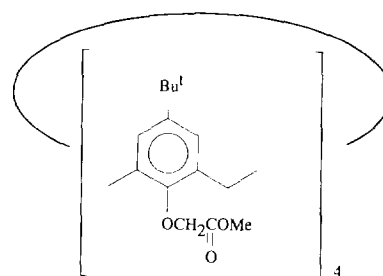
Ligand 2

ionophore in a PVC membrane. The results are compared to those of an electrode based on the tetramethylester calix[4]arene (2).

2. Experimental

All membrane components except the ligands were obtained from Fluka and used as received. Other reagents including metal chlorides were purum grade obtained from Reidel-de-Haen. Ligands 1 [1] and 2[4] were synthesised as described previously. PVC membranes were prepared by a standard procedure [5] using the following composition: ligand, 10.0 mg; potassium tetrakis p-chlorophenylborate (KTpClPB), 1.0 mg; nitrophenyloctylether (2-NPOE), 1.0 g; PVC, 500 mg. The membrane components were dissolved in tetrahydrofuran (THF) and the resulting solution poured into a glass mould. Upon evaporation (overnight), transparent PVC membranes about 0.2 mm thick were obtained from which electrode membranes were cut using a cork borer. The membranes were clipped into the tip of an electrode body which was then filled with 0.1 M $CaCl_2$ as internal reference electrolyte. Cell potentials were measured relative to a calomel electrode using a Hewlett Packard μV meter (Model 34401A). Transient responses were captured using an MIO-6 I/O card and virtual instrument software developed in-house using LabView (ver 3.0).

Calibration solutions were prepared by serial dilution of 0.1 M $CaCl_2$ stock solution to 10^{-6} M

with deionised water. All activity values were calculated using the Davies equation. Selectivity coefficients were estimated by the separate solutions method at 0.1 M concentrations of primary and interfering ions. Injection experiments were carried out in an electrolyte that was 10^{-2} M LiCl and 10^{-4} M $CaCl_2$. This involved injecting 250 μl aliquots of a 0.1 M solution of a metal ion chloride into a stirred 50 ml portion of the background electrolyte to give an approximate six-fold concentration excess of the injected ion over the initial calcium concentration. The high background of LiCl ensured that the ionic strength remained relatively unchanged. LiCl was chosen as ionic strength adjuster following initial screening experiments which demonstrated no response by the electrode to lithium ions. Electrodes were conditioned in 0.1 M $CaCl_2$ solution between experiments. In each case, the initial injection was followed by two 250 μl injections of 0.1 M $CaCl_2$ to investigate whether the presence of the interfering ion had any effect on the calcium response. These injections cause approximate six-fold and two-fold increases in the calcium ion activity, which in turn should generate electrode responses of the order of $+20$ mV and 5–6 mV respectively. It should be stressed that these injection experiments are used as quick screening experiments, and not precision measurements, as the change in potential depends on the electrode slope, the exact amount of electrolyte added and the initial concentrations of the ions. Nevertheless, they do provide convincing evidence of selectivity and a useful indication of the dynamic respone behaviour of the sensors.
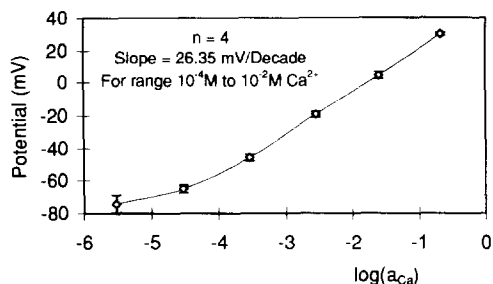
Fig. 1. Typical calibration curve obtained with $CaCl_2$ solutions. The solid line is the average of $n = 4$ measurements with one electrode, with the standard deviations are shown as error bars. The slope is 26.35 mV decade^{-1} measured over the activity range 10^{-4}–10^{-2} M $CaCl_2$ (no correction for residual junction potential).

3. Results and discussion

The electrodes generated very stable potentials with little drift. Fig. 1 shows a typical calibration curve, with the electrode slope being 26.3 mV decade^{-1} (0.1 M to 10^{-4} M Ca Cl_2). In order to assess the electrode lifetime, the slope over the above range was measured each week over a period of 6 weeks, while the electrode was in continual use (Fig. 2). After a small initial decline in slope, the electrode continued to function in a reproducible manner for the rest of the assessment period, and in no case did the slope fall below 22 mV decade^{-1} ($n = 5$ electrodes).

Selectivity was investigated by the separate solutions method and by injection experiments. The calculated selectivity coefficients for electrodes based on both ligands are summarised in Table 1. Clearly, there is a striking change in the selectivity, with the tetraester (2) being very selective for sodium against all ions tested, and the tetraphosphine oxide (1) being very selective for calcium ions against all other ions tested. In order to

Table 1
Selectivity coefficients for the tetraphosphine oxide (1) and tetraester (2) calix[4]arenes measured by the separate solutions method with 0.01 M chlorides of the metals

Ligand	Log K_{ij}^{Pot}	
	1	2 [3]
Na^+	−2.2	0.0
K^+	−2.7	−2.7
NH_4^+	−2.0	−3.5
Li^+	−1.6	−2.9
Mg^{2+}	−2.6	−3.7
Ca^{2+}	0.0	−3.5

verify the selectivity, injection experiments were performed as described in the experimental section (Fig. 3). The results clearly demonstrate the almost total lack of response to the interfering ions injected, despite an approximate six-fold excess of the injected ion over that of the initial calcium concentration. Furthermore, in every case, there was little or no apparent effect on the subsequent injection of two similar aliquots of calcium, which led to responses which were effectively nernstian within the limits of reproducibility of the experiment.

Fig. 2. Effect of continual use on an electrode slope.
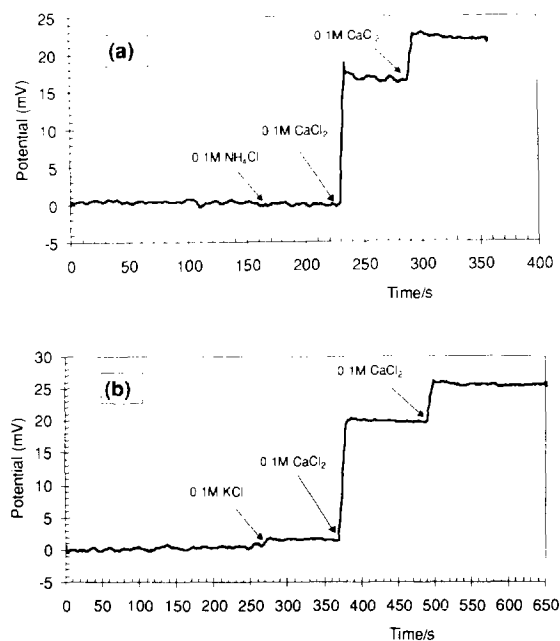
Fig. 3 (a and b)
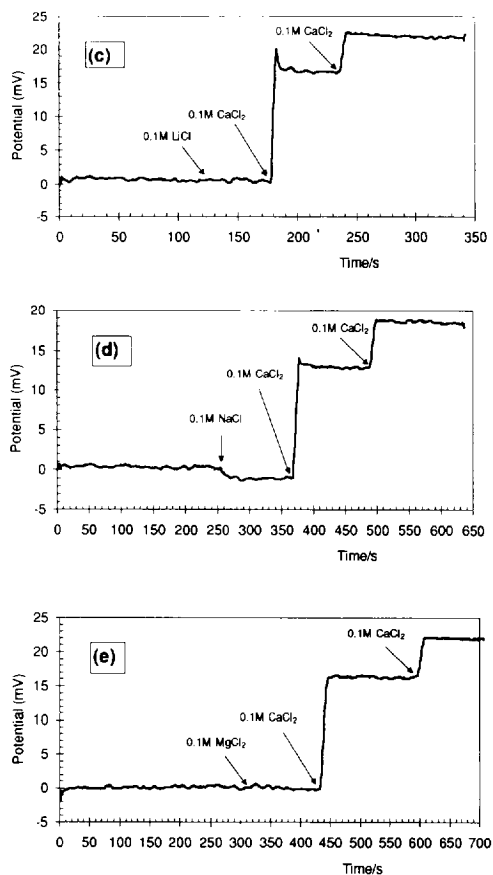
Fig. 3. Transient responses to injection of 250 μl aliquots of various metal chlorides followed by two further injections of 250 μl aliquots of 0.1 M CaCl₂. Injection points indicated by arrows.

Previously, calcium-selective electrodes have been fabricated with varying degrees of success using a number of different ligand types, including lipophilic diamide derivatives [6], macrocyclic polyethers [7] and a polymerisable benzo-15-crown-5 [8]. A water hardness electrode (which

responds to both Ca^{2+} and Mg^{2+}) has also been reported [9]. However, to our knowledge, this is the first report of a selective electrode for calcium based on phosphine oxide ligating groups and, as such, offers the possibility of a new series of calcium-selective ligands based on the well-known ease of modification of the calixarene building block.

Physicochemical measurements and modelling experiments based on energy minimisation calculations are underway to probe the structural basis for the affinity between the phosphine oxide ligand and the calcium ion.

References

[1] J.F. Malone, D.J. Mars, M.A. McKervey, P. O'Hagan, N. Thompson, A. Walker, F. Arnaud-Neu, O. Mauprivez, M.-J. Schwing-Weill, J.-F. Dozol, H. Rouquette and N. Simon, J. Chem. Soc., Chem. Commun., (1995) 2151.

[2] T. Grady, S. Maskula, D. Diamond, D.J. Mars, M. McKervey and P. O'Hagan, Anal. Proc. Commun., 32 (1995) 471.

[3] A. Cadogan, D. Diamond, M.R. Smyth, M. Deasy, M.A. McKervey and S.J. Harris, Analyst, 114 (1989) 1551.

[4] M.A. McKervey, E.M. Seward, G. Ferguson, B. Ruhl and S.J. Harris, J. Chem. Soc., Chem Commun., (1985) 388.

[5] J. Lu, Q. Chen, D. Diamond and J. Wang, Analyst, 118 (1993) 1131.

[6] K. Toth, E. Lindner, M. Horvath, J. Jeney, I. Bitter, B. Agai and L. Toke, Electroanalysis, 5 (1993) 781.

[7] L. Cazaux, P. Tisnes, C. Picard, C. D'Silva and G. Williams, Analyst, 119 (1994) 2315.

[8] T. Nakumura, C. Hayashi and K. Izutsu, Anal. Chim. Acta, 292 (1994) 305.

[9] A. Rondinini, P.R. Mussini, A. Vertova, A. Bortoluzzi, L. Bono and P. Longhi, Sens. Actuat., B23 (1995) 27.

Short communication

Laser-induced breakdown spectroscopy of silicate, vanadate and sulfide rocks

J.M. Vadillo, J.J. Laserna*

Department of Analytical Chemistry, Faculty of Sciences, University of Málaga, 29071-Málaga, Spain

Abstract

Laser-induced breakdown spectroscopy (LIBS) in air at atmospheric pressure has been used to study four geological samples belonging to different structural families. Atomic emission spectra of vanadinite, pyrite, garnet and a type of quartz (compostela's quartz) are shown. The 532 nm line of a Nd:YAG laser at an irradiance of 18×10^{11} W cm^{-2} was used. The precise focus of the beam allowed microanalysis of a 0.02 mm^2 surface area working in single-laser shot mode. The use of an intensified gateable charge-coupled-device (CCD) detector permitted time-resolved studies. The spectral lines have been assigned to transitions in the neutral charge state of the corresponding atom of the material under investigation. The behavior of different transitions with time delay are shown. In experiments, minor components contained in several minerals have been detected. This fact has been used to demonstrate the applicability of the technique to characterize and identify similar minerals.

Keywords: Geochemical analysis; Laser-induced breakdown spectroscopy; Laser-induced plasmas; LIBS

1. Introduction

The effect of a short pulse of laser radiation focused on a sample produces an irradiance sufficient to vaporize a small spot of a solid on the surface, resulting in a high-temperature and electron-density plasma that can be spectrally analyzed by optical emission spectroscopy. This technique is called laser-induced breakdown spectroscopy (LIBS) [1].

The physics of laser/surface interaction is a well-known process. The surface reflects some of the energy and the remaining part is absorbed by the surface. Due to the short laser pulse duration, there is not enough time for thermal diffusion into the surface material outside the focal spot. This fact explains the quick heating of the surface, resulting in a rapid vaporization. The vapor moves outward from the surface and by a multi-photon absorption process; some of the material is ionized creating an appreciable ionic population. When a sufficient density of ions and electrons is created, an inverse Bremstrahlung process

---

* Corresponding author.

causes the incident laser light to be absorbed minimizing the laser light reaching the sample surface. The electrons are heated causing an increase in temperature, and rapid energy transference and electron–ion collisions which result in neutral species. Subsequent spectral analysis has been successfully used for elemental analysis in solids [2], gases [3], liquids [4] and aerosols [5]. Applications of LIBS for the analysis of solids include the detection of contaminants on electronic microcircuits [6], on-line process control [7] and analysis of noble and alloyed jewelry metals [8]. The advantages of improving the technique by working under high vacuum have been also described [9].

LIBS allows direct analysis of a wide range of solids, including minerals and rocks and shows great capabilities to perform routinely non-destructive identification of microscopic inclusions in their material hosts [10]. The simple requirements in sample-preparing-and-handling provide several advantages with respect to other widely used techniques including electron and ion microprobes [11]. LIBS can be used to identify, map out the distribution and determine the quantity of elemental constituents of the sample. The main advantage is the possibility of simultaneous multi-element analysis over a wide spectral range without pre-treatment or transport of the sample to the excitation source (inductively coupled plasma atomic emission spectrometry (ICP-AES)). Although the coupling of laser ablation to ICP-AES or ICP-MS (inductively coupled plasma mass spectrometry) systems is becoming a powerful tool in geochemical analysis, it can be said that LIBS is the right choice when the number of elements to be found is large or the composition of the sample is unknown [12].

The high performance of charge-coupled-device (CCD) detectors in terms of spectral range, quantum efficiency, integration time and gating, allows resolution of the complex spectra of geological samples better than using scanning spectrometers with photomultipliers tubes detectors [13]. Furthermore, because of the two-dimensional character of the CCD detector, spatial and spectral information can be achieved simultaneously. When combined with intensifier devices, extremely

low light levels can be recorded without increasing acquisition times.

In this paper, time-resolved LIBS is used to obtain the spectra of minerals from different families including sulfides, vanadates and silicates. No sample preparation is required. In addition, time-resolved LIBS is used to improve the signal-to-noise ratio (SNR) as well as to reduce the Stark effect and continuum background often found in LIBS spectra. Examples are shown to demonstrate the capability to conduct geological taxonomy and to analyze a field sample.

2. Experimental

2.1. Apparatus

The experimental setup for time-resolved LIBS is shown schematically in Fig. 1. The second harmonic of a pulsed Nd:YAG laser ($\lambda = 532$ nm, pulse width 5 ns, 170 mJ pulse^{-1}, Continuum, Surelite SLI-20) was used to irradiate the samples. The beam was focused at normal incidence onto the sample surface with a glass planoconvex lens with a focal length of 100 mm and f-number of 4. The spot area was 0.012 mm^2, which resulted in an irradiance of 18×10^{11} W cm^{-2}.

A 1:1 image of the plasma was focused using a planoconvex quartz lens with focal length of 100
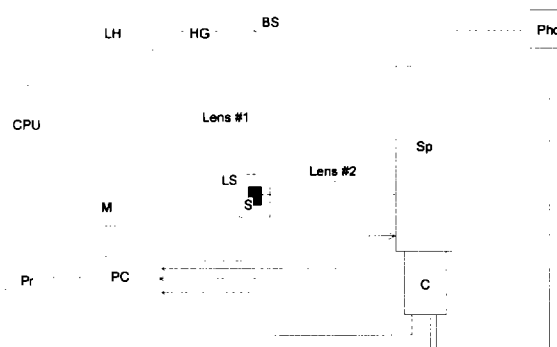
Fig. 1. Schematic setup used in this paper. LH, laser head; CPU, cooling power unit; HG, second harmonic generator; BS, beam splitter; Phd, trigger photodiode; Sp, spectrograph; C, CCD detector; LS, linear stage; S, sample; PC, personal computer; M, monitor; Pr, printer; Lens #1, glass lens; Lens #2, quartz lens.
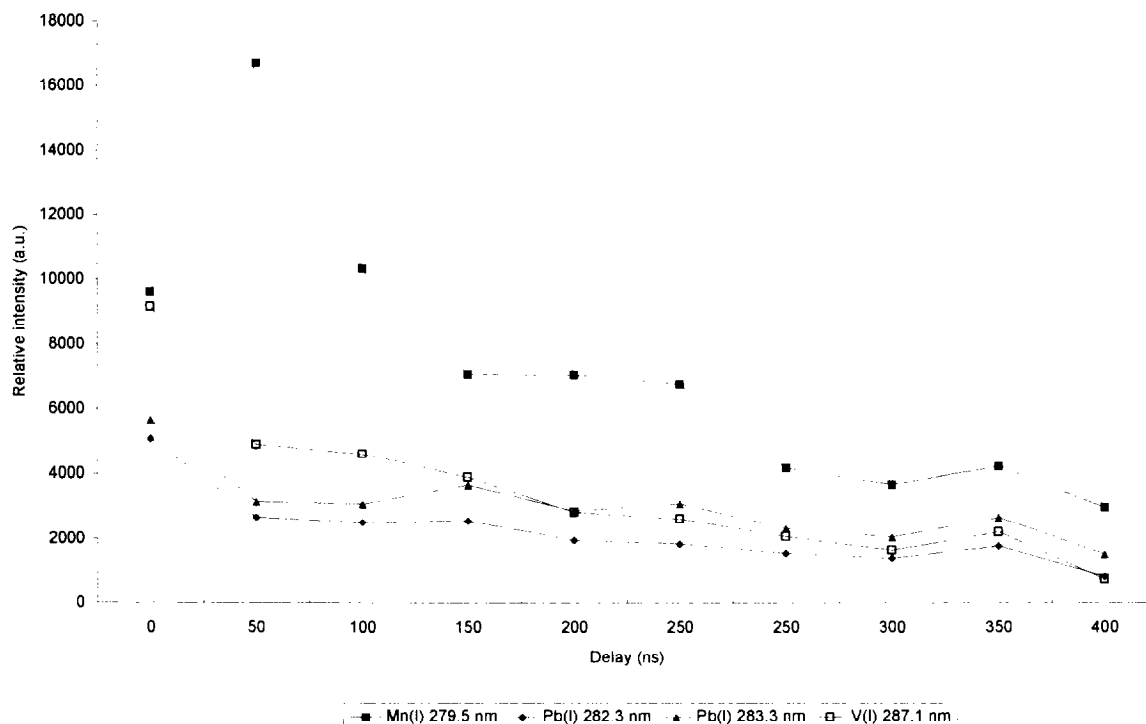
Fig. 2. Variation of peak intensity as a function of time delay. Sample: vanadinite; wavelength: 291 nm; gate width: 100 ns; laser energy: 170 mJ; MCP gain: 700 V.

mm and f-number of 4 into the entrance slit of a 0.5 m focal-length Czerny–Turner spectrograph (Chromex, 500 IS). Light was dispersed using a 2400 grooves mm^{-1} holographic grating (250 nm blaze). The entrance slit width was 10–200 μm, and the height was 10 mm. The spectrograph was computer controlled using specific software (Chromex Host Control Software 2.21).

The dispersed plasma light is detected using a solid-state two-dimensional CCD (Stanford Computer Optics, 4 Quik 05). The CCD consists of 752(h) × 582(v) elements. The photoactive area is 6 × 4.5 mm^2. The device is equipped with an S 20 Q photocatode (spectral response from 180 to 820 nm) and an intensifier system (microchannel plate, MCP). The intensifier system allows a high photonic gain, better than 10^6 electrons/photon. Extremely high system responses are achieved (50–500 000 ASA) with a 12 bit dynamic range. Operation of the detector was controlled by 4 Spec 1.20 Software. Shutter and delay times can be selected in 50 ns steps. A fast photodiode was used as the external trigger for exact synchroniza-

tion of the incident laser pulse and opening of the camera shutter.

The experimental conditions were optimized in order to obtain the best SNR. A gate width of 100 ns was used in all experiments, while the time delay was varied when required. The MCP gain was fixed in 700 V when single-shot experiments were run. When different shots were accumulated in order to improve the SNR, the gain was reduced.

Video image capture, processing and display were made using a PC-compatible monochrome frame grabber (Data Translation, DT2855). As images are captured, they can be displayed with 768 × 512 square pixels resolution and 256 gray levels. This number of pixels and gray levels produced a high-definition display with continuous tones to match real images. Later on, they can be output for real-time images processing and pseudo-color display into a VESA-ISA Local Bus PC specially equipped for fast capture and processing images.
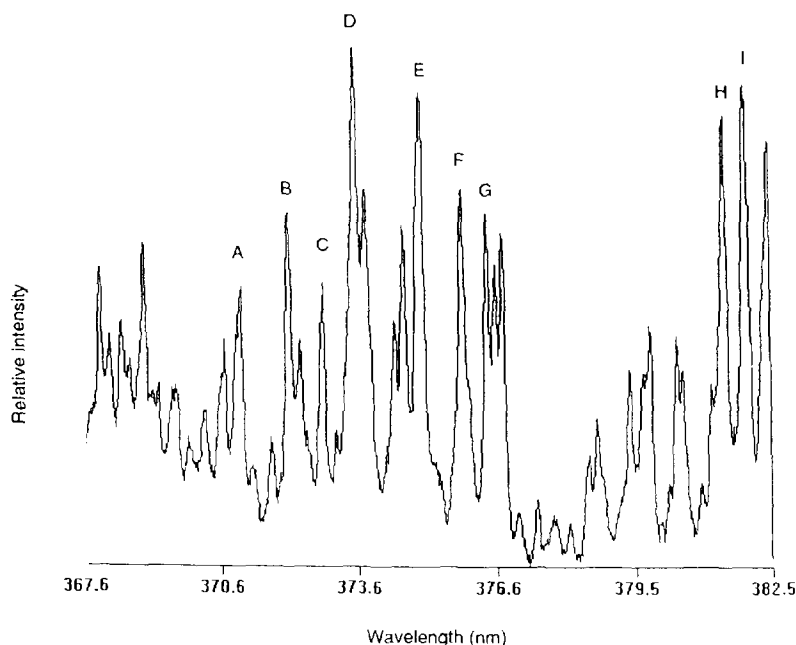
Fig. 3. Pyrite single-shot LIBS spectrum. Time delay: 500 ns. Other conditions as in Fig. 2.

2.2. Samples

Samples were directly taken from the field and analyzed without other treatment than washing the surface with deionized water to remove dust and mud. Four mineral species were analyzed: garnet, vanadinite, compostela's quartz and pyrite. Details on chemical structures and atomic cells implants will be discussed in the results and discussion section.

Table 1
Designations of peaks labeled in Fig. 4. All signals correspond to Fe[(I)] transitions

Line	Wavelength (nm)	Upper energy level (cm^{-1})
A	370.9	34329
B	372.0	26875
C	372.7	34547
D	373.5	33695
E	374.9	34040
F	375.8	34329
G	376.4	34547
H	381.6	38175
I	382.0	33096

3. Results and discussion

3.1. Time-resolved analysis

Spectral analysis of geological samples obtained using LIBS involves complex spectra in the presence of a noisy background with many overlapped peaks due to band broadening (Stark effect). Spectral lines corresponding to high populated energy levels are the result of the elevated plasma temperature. Spectra can be drastically simplified and the SNR greatly improved by delaying observation of the plasma. Time-resolved LIBS is useful since three benefits are achieved. First, there is a considerable decrease of the continuum emission due to Bremstrahlung radiation occurring immediately after plasma formation. Second, it is possible to avoid spectral interferences between species that emit at different times during plasma decay allowing characterization of different species. Third, spectral resolution improves because the Stark effect contribution is minimized.

The temporal behavior of different atomic species of the plasma is illustrated in Fig. 2. As

shown, the 279.5 nm transition corresponding to Mn[(1)] shows a different temporal behavior reaching its maximum intensity at 50 ns of delay while the rest of the lines decay immediately after plasma formation.

3.2. Spectral analysis

Fig. 3 shows a pyrite (FeS$_2$) emission spectrum. The selected window does not allow the observation of sulfur lines and only Fe[(1)] lines are plotted. Although the laser is a powerful mean of inducing plasmas and it is able to produce ionization states as high as other continuum plasma sources (ICP, microwave-induced plasma and other), these are often not visible. The explanation must be found in the pulsed nature of the laser-induced plasma that determines many secondary processes of recombination (with oxygen mainly involved). These processes reduce the lifetime of many ionic lines in the spectrum and can be minimized working under vacuum conditions. Table 1 summarizes the results and spectroscopical parameters of the most relevant lines [14].

In order to show the applicability of the method in the determination of mineral species, LIBS spectra of compostela's quartz and garnet were obtained. Fig. 4 shows line emission of quartz (top) and garnet (bottom). Both minerals contain the same silicate matrix with differences due to their three-dimensional structure. Garnet involves a large group of nesosilicates with many isostructural minerals. The general formula is $A_3B_2(SiO_4)_3$, where A refers to large divalent cations, mainly Mg^{2+}, Fe^{2+} and Mn^{2-}, and B alludes to trivalent cations a few smaller in size, Al^{3+}, Fe^{3+} and Cr^{3+}. On the other hand, compostela's quartz is a very typical quartz variety from northern Spain, characterized by a light-red color due to iron insertions. Cr^{2+}, Mn^{2+} and Mg^{2+} can also be found [15]. Large similarities in spectral behavior of both samples are expected and only the analysis of insertions in the atomic cell can be fruitful to discriminate the samples. As Fe, Cr, Mn and Mg insertions can be found in both garnet and quartz, the presence of Al emission lines in the garnet spectrum provides information required to discriminate the minerals. For
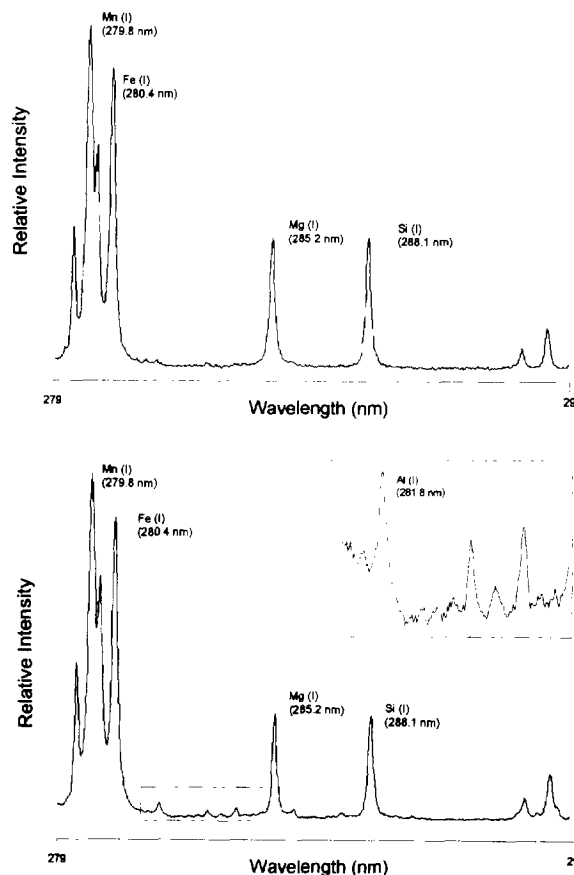
Fig. 4. Comparison of LIBS spectra of Compostela's quartz (top) and garnet (bottom). Time delay: 500 ns; accumulated shots: 10; MCP gain: 600 V. Other conditions as in Fig. 2.

this purpose, experimental data were obtained by accumulating ten shots in order to avoid surface interferences and to improve the SNR. Fig. 4 shows lines corresponding to Fe[(1)], Mn[(1)], Mg[(1)] and Si[(1)] in both garnet and quartz as expected. However, a detailed comparison reveals an aluminum line at 281.8 nm in garnet, which is not found in the LIBS spectrum of compostela's quartz.

4. Conclusions

In the present paper, the laser-induced plasma emission phenomenon described can be used to detect and identify atomic constituents on the

surface of inorganic minerals. Analysis can be performed quickly in air at atmospheric pressure with a comparatively simple experimental setup. Furthermore, the laser plasma light is collected and directed to the detection system using a lens or a fiber optic cable which allows direct field measurements from samples located in difficult sites.

Enhancement of spectral lines with respect to the plasma continuum has been achieved by time-resolved spectroscopy. The quick decay of continuum emission in the first 100 ns suggests that laser-induced plasma emission of neutrals is the dominant process. The development of similar experiments under vacuum conditions would be useful to enhance the lifetimes of the ionic lines. The applicability of the method has been illustrated in the characterization of two very similar mineral species. In a second study, quantitative results will be reported.

Acknowledgements

References

[1] D.A. Cremers, L.J. Radziemski and T.R. Loree, Appl. Spectrosc., 38 (1984) 721.

[2] L.M. Cabalin, N. Calvo, L. Ayala and J.J. Laserna, Quim. Anal., 12 (1993) 113.

[3] J.B. Morris, B.E. Forch and A.W. Miziolek, Appl. Spectrosc., 44 (1990) 1040.

[4] J.R. Wachter and D.A. Cremers, Appl. Spectrosc., 41 (1987) 1042.

[5] K.C. Ng, N.L. Ayala, J.B. Simeonsson and J.D. Winefordner, Anal. Chim. Acta., 269 (1992) 123.

[6] D.K. Ottesen, Appl. Spectrosc., 46 (1992) 593.

[7] C.J. Lorenzen, C. Carlhoff, U. Hahn and M. Jogwich, J. Anal. At. Spectrom., 7 (1992) 1029.

[8] J.J. Laserna, N. Calvo and L.M. Cabalin, Anal. Chim. Acta., 289 (1993) 113.

[9] T.L. Thiem, R.H. Salter, J.A. Gardner, Y.I. Lee and J. Sneddon, Appl. Spectrosc., 48 (1994) 58.

[10] T.P. Mernagh and A.G. Trudu, Chem. Geol., 103 (1993) 113.

[11] L. Moenke-Blankenburg, Laser Microanalysis, Wiley, New York, 1989, Chapter 11.

[12] L. Moenke-Blankenburg and D. Günther, Chem. Geol., 95 (1992) 85.

[13] R. Montes, in J.J. Laserna and D. Pérez Bendito (Eds.) Temas Avanzados de Análisis Químico, Edinford, Málaga, 1994, Chapter 3.

[14] J. Reader, C.H. Corliss, W.L. Wiese and G.A. Martin, Wavelengths and Transition Probabilities for Atoms and Atomic Ions. NSRDS-NBS 68, US Government Printing Office, Washington, DC, 1980.

[15] C.S. Hurlbut, Jr. and C. Klein, Manual de Mineralogía, 3rd ed., Reverté, Barcelona, 1988.

Selectivity enhancement for glutamate with a Nafion/glutamate oxidase biosensor

Shengtian Pan[a], Mark A. Arnold*

Department of Chemistry, University of Iowa, Iowa City, IA 52242, USA

Abstract

Response properties and selectivity are reported for glutamate biosensors constructed with a film of Nafion between the platinum anode and a layer of immobilized glutamate oxidase. The effects of enzyme loading, sample pH and temperature are established. Operation at pH 7.8 and 37°C results in linearity up to 800 μM and a limit of detection of 0.3 μM. Nafion enhances selectivity for glutamate over test species that include ascorbic acid, uric acid and acetaminophen. Selectivity enhancement was greater over the anionic interferences because of electrostatic repulsion and the extent of this enhancement depends on the thickness of the Nafion layer. Even under ideal conditions, some interfering signal is observed when glutamate levels are ten-times less than ascorbate.

Keywords: Glutamate; Nafion/glutamate oxidase biosensor; Selectivity enhancement

1. Introduction

Numerous reports have described work to develop a functioning biosensor for glutamate [1–5]. Typically, glutamate oxidase is immobilized at the surface of an anodic electrode and the enzymatic generation of hydrogen peroxide is monitored amperometrically. The two major applications for such glutamate biosensors are as monitors for bioreactors [6] and as real-time sensors during neurochemical experiments [7]. In both cases, selectivity for glutamate over easily oxidized endogenous species is critical for acceptable accuracy.

Ascorbate represents a major potential interference, especially in neurochemical systems where high and varying levels of ascorbate can be present. Ascorbate interference is caused by direct oxidation at the electrode surface. One strategy to enhance sensor selectivity is to add a layer of Nafion which electrostatically repels anions, such as ascorbate, while freely passing hydrogen peroxide. This strategy has been used effectively with electrochemical sensors for dopamine [8,9] and blood glucose [10,11]. In both cases, Nafion coated electrodes provide sufficient selectivity enhancement for accurate measurement under conditions where the analyte concentration is greater than or equal to that of ascorbate. In some neuro-

---

* Corresponding author.

[a] Present address: College of Engineering, University of California, Riverside, CA 92521, USA.

chemical situations, however, glutamate levels can be orders of magnitude lower than ascorbate levels, which places further demands on sensor selectivity.

In this paper, Nafion is evaluated as a means to enhance selectivity of glutamate measurements performed with the glutamate oxidase based biosensor. Selectivity for glutamate over ascorbate is characterized with and without a thin layer of Nafion positioned between the immobilized enzyme and a platinum anode. Although the response to ascorbate is attenuated significantly in the presence of the Nafion layer, this response is not completely eliminated. Even with the Nafion layer, measurement inaccuracies can be substantial depending on the relative concentrations of glutamate and ascorbate. As a result, the utility of this glutamate biosensor in neurochemical experiments will be restricted to situations where the relative amounts of ascorbate and glutamate permit accurate measurements. Besides our characterization of the Nafion membrane, the effects of enzyme loading, pH and temperature are evaluated, and conditions for the optimal glutamate response are identified.

2. Experimental

2.1. Apparatus

Amperometric measurements were made with a Model DCV-5 Voltammetry Controller from Bioanalytical Systems, (West Laffayette, IN, USA) and recorded on a Sargent-Welch Model XKR strip chart recorder. All pH measurements were made with a Ross-type combination pH electrode (Orion Model H4100-12) in conjunction with a Model ϕ72 meter. Solution temperatures were controlled with VWR model 1140 water bath (Polyscience Corp., Niles, IL, USA).

2.2. Reagents and supplies

Platinum electrodes were disk shaped with a diameter of 1.6 mm (MF-2013). These electrodes were purchased, along with the silver–silver chloride reference electrodes (MF-2020), from

Bioanalytical Systems. Glutamate oxidase (8 U mg^{-1}) was generously donated from Hitoshi Kusakabe from Yamasa Shoyu Co. Ltd. (Choshi, Chiba 288, Japan). Nafion was purchased from Aldrich Chemical Co. (Milwaukee, WI, USA) as a 5% (w/w) suspension of the perfluorinated ion-exchange powder in a mixture of low molecular weight aliphatic alcohols and 10% water. L-Glutamic acid (monosodium salt, 99–100%), bovine serum albumin (BSA, 98–99%) and glutaraldehyde (Grade II, 25% aqueous solution) were obtained from Sigma Chemical Co. (St. Louis, MO, USA). Concentrated hydrogen peroxide (30%) was purchased from Fisher (Chicago, IL, USA) and was standardized periodically by titration with sodium thiosulfate. All other chemicals were obtained from common suppliers as reagent grade materials.

All solutions were prepared with distilled–deionized water by passing the house distilled water through a three-house Milli-Q water purification unit. The working buffer had a pH of 7.4 and contained the following salt concentrations: 50 mM NaCl, 10 mM KH$_2$PO$_4$ and 40 mM Na$_2$HPO$_4$. Solutions of L-glutamate were prepared by dissolving L-glutamic acid (dried at 104°C for 2 h) in working buffer.

2.3. Procedures

2.3.1. Electrode preparation

Platinum electrodes were polished sequentially with 3, 1 and 0.3 μm aluminum oxide lapping films and washed in a sequence of acetone, distilled–deionized water, nitric acid (1:1) and distilled–deionized water in an ultrasonic cleaner. Polished electrodes were electrochemically pretreated in 0.5 M sulfuric acid by cycling the applied voltage between −0.4 to 1.3 V versus Ag/AgCl at a scan rate of 50 mV s^{-1} for 10 min.

Nafion layers were constructed by placing a 10 μL aliquot of a 1% Nafion suspension on the surface of a treated platinum electrode. Films were formed by allowing the solvent to evaporate at room temperature for 20 min. Different film thicknesses were generated by either using a different concentration of Nafion or applying a different volume.

Glutamate oxidase was immobilized by crosslinking with BSA and glutaraldehyde. First the platinum electrode was polished, washed and electrochemicaly pretreated. A Nafion film was prepared by placing one 10 μL aliquot and, subsequently, four individual 3 μL aliquots of 1% Nafion on the surface of the platinum electrode. In each case, the previous layer was allowed to dry before the next aliquot was administered. An enzyme solution was prepared by dissolving 0.5 mg of glutamate oxidase in 5 μL phosphate buffer (pH 6.86). This glutamate oxidase solution was mixed well with 2.5 μL of 10% (w/w) BSA and 1.25 μL of 2.5% glutaraldehyde. A 2 μL aliquot of this final mixture was placed on the Nafion film. Approximately 0.91 units of glutamate oxidase were immobilized on a surface area of 0.2 mm^2. After drying at room temperature for 30 min, the electrode was washed thoroughly with phosphate buffer to remove any unretained enzyme. Different enzyme loadings were obtained by adjusting the concentration of the glutamate oxidase stock solution.

2.3.2. Sensor response measurements

Sensor responses were measured by recording anodic currents as a function of time. Unless stated otherwise, the working electrode potential was maintained at 0.65 V versus a Ag/AgCl reference electrode. Data for the response curves were collected by first immersing the sensing tip in a blank solution of working buffer to determine the background current. Microliter additions of a glutamate standard were then added sequentially and the corresponding steady-state currents were noted. In most cases, the sample solution was stirred with a magnetic stir bar. Stirring was stopped, however, to reduce noise when solutions with low glutamate concentrations were measured. Response times were measured as the time required to achieve 95% of the final steady-state response after a step change in glutamate concentration.

3. Results and discussion

Response properties for the glutamate biosen-

sor have been measured as a function of enzyme loading, solution pH and operating temperature. In addition, the effect of Nafion on electrode selectivity has been established with particular interest in the effect of Nafion layer thickness.

3.1. Operational parameters

The amount of glutamate oxidase required to saturate the sensing tip was determined by comparing the response curves obtained from a series of sensors constructed with different amounts of immobilized glutamate oxidase. The results are presented in Fig. 1. As the amount of immobilized glutamate oxidase approaches 0.91 units, the sensor response becomes independent of the amount of enzyme. Below this saturation point, however, the response is strongly affected by the amount of glutamate oxidase. The slope of the calibration curve increases with increasing glutamate oxidase concentrations, until a saturating amount is reached. Unless noted otherwise 0.91 units of glutamate oxidase were used for the construction of all subsequent sensors.
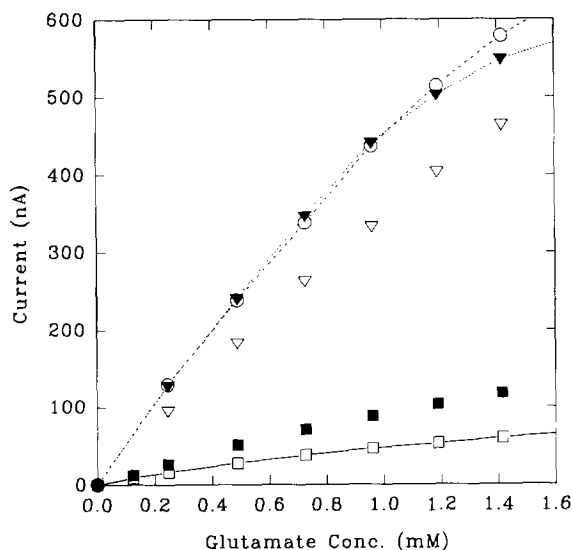
Fig. 1. Sensor response curves with enzyme loadings (U per membrane) of 0.001 (open squares); 0.01 (closed squares); 0.23 (open triangles); 0.91 (closed triangles); and 1.37 (circles).
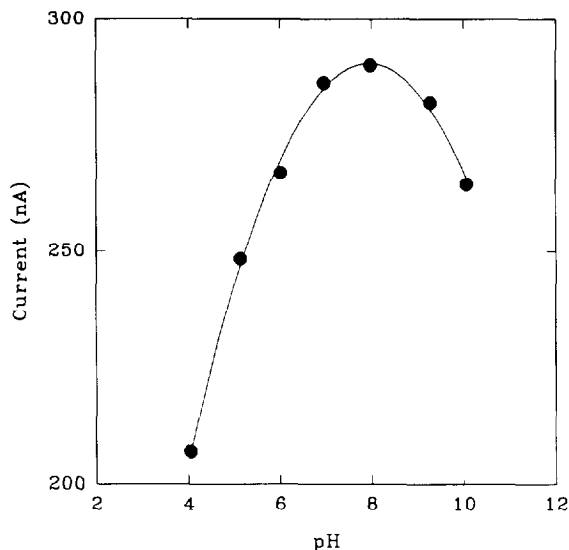
Fig. 2. pH profile for response to glutamate.

The magnitude of the sensor response depends strongly on solution pH. The sensor response was monitored at different solution pH values for a step in glutamate concentration from zero to 0.7844 mM at room temperature. Fig. 2 shows how the response depends on solution pH. The maximum response is obtained at pH 8.0 and over 95% of this maximum response is obtained over the pH range from 6.5 to 9.5. This pH profile is similar to that reported for the free enzyme [12] where the optimum pH is 7–8.

Temperature also strongly influences the sensor response as expected because of the well known effects of temperature on reaction kinetics, enzyme activity and mass transport [13]. The effect of temperature was evaluated by measuring the sensor response to 0.37 mM glutamate over a temperature range from 5.6 to 63.0°C. Enzyme loading was reduced in this experiment to 0.23 U at the electrode surface in order to amplify the temperture effects. The magnitude of the response increases dramatically as the temperature increases from 5.6 to 48°C. The temperature coefficient over this range is approximately 8.5 nA °C^{-1}. A maximum response is observed at 48°C and the response drops at a rate of 2.8 nA °C^{-1} as the temperature increases beyond 48°C. Glutamate oxidase is a thermally stable enzyme [14]

which accounts for large responses at temperatures above 40°C. Thermal degradation of the enzyme does become a factor, however, above 48°C.

Ideal sensor response properties are obtained with at least 0.91 units of immobilized enzyme operating at pH 8.0 and 48°C. More importantly, these results demonstrate that the sensor can operate well over a wide range of pH and temperature values. Finally, the influences of pH and temperature are sufficiently strong that precautions to control these parameters are required for accurate measurements.

3.2. Nafion and selectivity

As expected, easily oxidized species, such as ascorbic acid, uric acid and acetaminophen, are positive interferences when biosensors are prepared without Nafion. The magnitude of this type of interference is illustrated by comparing the sensor responses in solutions containing only 0.369 mM glutamate and those containing 0.369 mM glutamate plus 0.369 mM of the interfering compound. Direct oxidation of the added compound increases the measured current which results in systematic errors corresponding to apparent glutamate levels of 191.9, 186.5 and 197.0%, the actual values in the presence of ascorbic acid, uric acid and acetaminophen, respectively.

Such interfering responses are reduced in the presence of Nafion and the extent of this reduction depends on the thickness of the Nafion layer.

Table 1
Ascorbate oxidation with different Nafion layer thicknesses

Thickness (μm)	Electrode response (μA)[a]	
	$E_{app} = 0.4V$[b]	$E_{app} = 0.6V$[b]
0	0.98 (100%)	1.08 (100%)
2.2	0.12 (12%)	0.48 (44%)
4.5	0.085 (8.7%)	0.22 (20%)
6.7	0.021 (2.1%)	0.06 (5.6%)
9.0	0.012 (1.2%)	0.03 (2.8%)
11	0.004 (0.4%)	0.014 (1.3%)

[a]Per cent response with no Nafion given in parenthesis.
[b]Measured relative to Ag/AgCl.

Table 1 summarizes steady-state currents measured for 1.0 mM ascorbate solutions with different Nafion layer thicknesses for two applied potentials (0.4 and 0.6 V versus Ag/AgCl). At both potentials, the response drops significantly as the Nafion layer thickness grows from 0 to 11 μm. At 11 μm, the relative response decreased to 0.4 and 1.3% of the original values at applied potentials of 0.4 and 0.6 V, respectively.

Nafion also reduces the electrode response to hydrogen peroxide. The Nafion layer adds an additional diffusion barrier which lowers the flux of hydrogen peroxide to the electrode surface, thereby lowering the monitored current. Of course the extent of signal reduction is greater for ascorbate and the other anionic species, because both electrostatic repulsion and diffusion barrier effects are combined to reduce responses from these interferences. Relative to no Nafion, a 6.7 μm layer of Nafion results in a 35% reduction in the steady-state current for hydrogen peroxide. Under the same conditions, nearly 95% of the response to ascorbate is removed. Without Nafion, currents for ascorbate are approximately 41% of those for the same concentration of hydrogen peroxide. This percentage drops to less than 3% when the Nafion layer thickness reaches 6.7 μm. No further reduction in the relative response to ascorbate was obtained with thicker layers. It is important to stress that some response was observed for ascorbate at all Nafion layer thicknesses which suggests absolute selectivity for hydrogen peroxide is not possible with this approach.

By altering the response to hydrogen peroxide, the Nafion layer also affects the response to glutamate. Without Nafion, the mean response (± 95% confidence interval) for 10 consecutive measurements of 0.5 mM glutamate was 446 (± 10) nA and the corresponding response time was 7 (± 1.5) s. With a 5 μm thick Nafion film, the mean current and response time are 195 (± 10) nA and 14 (± 1) s, respectively, for seven consecutive measurements at the same glutamate concentration. Nafion causes a 2.3-fold decrease in magnitude of response and 2-fold increase in response time. Still, linear calibration curves are achieved with Nafion. Example curves are presented in Fig. 3 over wide and narrow ranges of glutamate
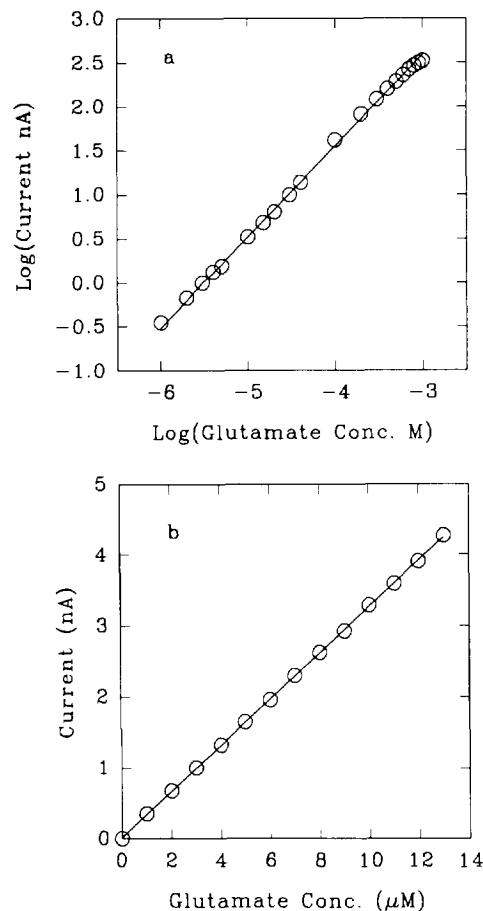
Fig. 3. Calibration lines for glutamate showing (a) log-log plot for a wide dynamic range and (b) normal plot for the micromolar concentration range.

concentrations. Fig. 3a illustrates linearity over a wide range of glutamate levels. Regression analysis of these data reveal a slope of 1.022 (± 0.008), a y-intercept of 5.64 (± 0.03) and a correlation coefficient of 99.90% for this log-log plot. Fig. 3b presents a calibration line for 1 to 13 μM glutamate. Regression analysis indicates a slope of 0.3253 (± 0.0009) nA μM^{-1}, a y-intercept of 0.018 (± 0.013) nA and a correlation coefficient of 99.99%. The calculated limit of detection (S N = 3) from Fig. 3b is 0.3 μM and the response times are approximately 14 s at all concentrations. Data for both curves were collected at 37°C.

Selectivity for glutamate over anionic species is enhanced with the Nafion layer. No differences in sensor response were observed when the electrode was exposed to solutions of 0.369 mM glutamate and 0.369 mM glutamate plus 0.369 mM ascorbate or urate. This lack of response is strikingly different than that noted above in the absence of the Nafion film. Some effect of ascorbate was observed, however, when the ascorbate concentration was 10 times greater than glutamate. In this experiment, the sensor tip was immersed in an air saturated solution composed of 0.369 mM glutamate and no ascorbate. After the steady-state current was noted, solid ascorbic acid was added to give a final ascorbate concentration of 3 mM. The average relative difference in the response caused by the addition of ascorbic acid was 2.08% for six repeated trials. Ascorbate was added in this way to minimize the production of hydrogen peroxide via anaerobic oxidation [15]. The Nafion layer was much less effective in reducing interference from acetaminophen. The electrode response increased by 29.9% when comparing the responses to solutions with 0.369 mM glutamate alone and 0.369 mM glutamate plus 0.369 mM acetaminophen. Although the interfernce by acetaminophen is sizable with the Nafion layer, the magnitude of interference is reduced considerably compared to sensors without Nafion (see above for specific values). Enhancement in selectivity over the neutral acetaminophen is presumably caused by differential diffusion barrier effects by Nafion between acetaminophen and hydrogen peroxide.

4. Conclusion

Selectivity for glutamate can be enhanced by incorporating a thin layer of Nafion between the electrode surface and the immobilized layer of glutamate oxidase. The extent of selectivity enhancement depends on the thickness of the Nafion film. Even with the maximum thickness, however, response to interferences cannot be completely eliminated. Inaccurate measurements can result from oxidizable anionic species, such as ascorbate, when the glutamate concentration is ten-

times less than the interfering species. As a result, this electrode configuration does not provide the selectivity needed for many neurochemical experiments where ascorbate levels are known to be two orders of magnitude greater than glutamate. Under such demanding conditions, alternative selectivity enhancement strategies, such as Wilson's dual enzyme system [7] or our hydrogen peroxide gas-sensing scheme [15], are needed to ensure accuracy. Nevertheless, the Nafion/glutamate oxidase system described here offers the key advantages of being easy to construct and simple to operate, which makes it a viable alternative when the selectivity demands permit.

References

[1] A.-J. Wang and M.A. Arnold, Anal. Chem., 64 (1992) 1051.
[2] S. Kar and M.A. Arnold, Anal. Chem., 64 (1992) 2438.
[3] T. Yao, N. Kobayashi and T. Wasa. Anal. Chim. Acta, 231 (1990) 121.
[4] B.A. Dremel, R.D. Schmid and O.S. Wolfbeis, Anal. Chim. Acta, 248 (1991) 351.
[5] P.N. Bartlett and R.G. Whitaker, Biosensors, 3 (1987/88) 359.
[6] C.Y. Chen and Y.C. Su, Anal. Chim. Acta, 243 (1991) 9.
[7] Y. Hu, K.M. Mitchell, F.N. Albahadily, E.K. Michaelis and G.S. Wilson, Brain Research, 659 (1994) 117.
[8] G. Nagy, G.A. Gerhardt, A.F. Oke, M.E. Rice and R.N. Adams. J. Electroanal. Chem., 188 (1985) 85.
[9] J. Wang and P. Tuzhi, Anal. Chem., 58 (1986) 3257.
[10] K. Hajizdeh, H.B. Halsall and W.R. Heineman, Talanta, 38 (1991) 37.
[11] Y. Zhang, Y. Huand and G.S. Wilson, Anal. Chem., 66 (1994) 1183.
[12] S. Kuriyama and G.A. Rechnitz, Anal. Chim. Acta, 131 (1981) 92.
[13] M.D. Trrevan, Immobilized Enzymes. An Introduction and Applications in Biotechnology, John Wiley & Sons, Chichester, 1980, Chapter 2.
[14] A. Bohmer, A. Muller, M. Passarge et al., Eur. Biochem., 182 (1989) 327.
[15] S. Pan and M.A. Arnold, Anal. Chim. Acta, 283 (1993) 663.

Adaptation of microthermal probes for the determination of biochemical species

Volodymyr Lysenko[a,b], Georges Delhomme[c], Alexey Soldatkin[a,d], Vitaly Strikha[b],
André Dittmar[c], Nicole Jaffrezic-Renault[a], Claude Martelet[a,*]

[a]Laboratoire de Physicochimie des Interfaces, UMR CNRS 5621, Ecole Centrale de Lyon BP 163, 69131 Ecully Cedex, France
[b]Semiconductor Department, Kiev University, Vladimirskaya St. 64, Kiev 252017, Ukraine
[c]Laboratoire de Thermorégulation, URA CNRS 1341, Faculté de Médicine Université Lyon 1, 8 Av. Rockefeller,
69373 Lyon Cedex 08, France
[d]Institute of Molecular Biology and Genetics, National Academy of Science of the Ukraine, 150 Zabolotny St.,
Kiev 252143, Ukraine

Received 6 September 1995; accepted 7 December 1995

Abstract

A glucose sensitive enzymatic thermal sensor based on a pair of commercial microthermal probes was fabricated by cross-linking of the corresponding enzymes (glucose oxidase and catalase) with bovine serum albumin onto the chip surfaces. The characteristics of this sensor were optimised by testing it in different conditions. To find the maximal sensitivity, the calibration curves of this sensor were measured in different buffer solutions with and without the addition of H_2O_2 to the analysed samples at various rates of sample flow stream. Different buffer solutions and hydrogen peroxide concentraions were used to realise the principles of a chemical and biochemical amplification of the biosensor response. It was shown that the level of the biosensor response and its dynamic range increase if hydrogen peroxide is added to the analysed samples and depend on the type of buffer solutions tested and the rate of the sample flow stream.

Keywords: Biosensor dynamic range; Biosensor sensitivity; Chemical and biochemical amplification; Enzyme thermal sensor; Glucose

1. Introduction

Thermal biosensors based on either thermocouples or thermopiles [1–5] have been applied successfully in biochemical analysis. The recent developments in this field were mainly focused on miniaturisation and multi-analytes capabilities offered by the micromachining and microelectronics technologies. Another approach in the design of new low-cost biosensors is to use a commercial probe and to modify it in order to obtain new properties. By this way it is possible to combine the well stated advantages of the original sensor with the new properties of the modified one to obtain a simple multisensor with the reliability of

* Corresponding author.
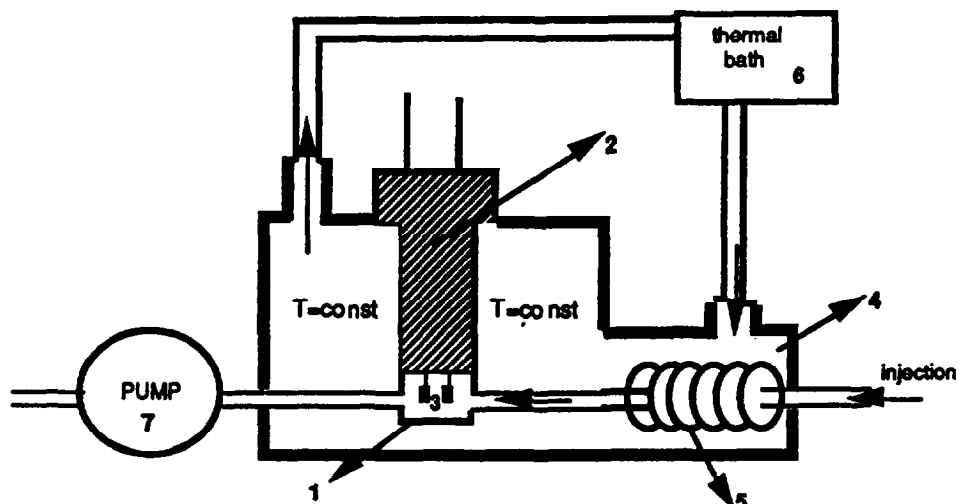
Fig. 1. Experimental set-up. 1, glass reaction cell; 2, plexiglas homemade cork with a pair of thermistors; 3, thermistors; 4, heat exchanger; 5, metallic tube to be used to heat the solution injected into the reaction cell; 6, thermostatic bath; 7, peristaltic pump.

a commercial transducer and the simplicity of a single type of signal treatment.

With this aim, in the present work, we have modified classical microprobes used for minimally invasive measurement of temperature, thermal conductivity and tissue blood flow [6,7] with enzymatic membranes. Consequently it has been possible to add biochemical sensing capabilities to a probe previously designed for the physical measurement of physiological parameters. Before using these two types of microprobes simultaneously it was necessary to optimise the measurement conditions of the enzymatically modified classical thermal probe, by altering the buffer type and increasing the sensitivity by the addition of specific chemical reagents.

2. Experimental

2.1. Materials

Glucose oxidase (EC 1.1.3.4) from *Aspergillus niger* with an activity of 180 U mg^{-1}, catalase (EC 1.11.1.6) from bovine liver with an activity of 13 000 U mg^{-1} and bovine serum albumin (BSA) were purchased from Sigma. A 25% aqueous solu-

tion of glutaraldehyde (GA) was obtained from Merck. All other reagents were of purum analytical grade. Bidistilled or deionized water was used throughout for the preparation of samples, buffer and other solutions.

2.2. Enzyme immobilisation

Glucose oxidase and catalase were immobilised using a modified procedure described earlier [8]. Solutions of glucose oxidase, catalase and BSA (10% w/w) were prepared in a 10 mM phosphate buffer (KH$_2$PO$_4$-NaOH), pH 7.4. Prior to their deposition on the sensor chip these solutions were mixed in defined proportions and then glycerol and GA were added. The mixture composition used was 5% glucose oxidase, 1% catalase, 5% BSA, 10% glycerol and 2.5% GA. As a differential experimental set-up was used, a drop of the enzyme-containing mixture was deposited on the sensitive area of one of the thermistors, whilst a mixture containing 11% BSA, 10% glycerol and 2.5% GA was deposited on the reference thermistor. The membranes were dried for 15–20 min at room temperature. Before use the membranes were soaked in a 10 mM phosphate buffer, pH 7.4, for at least 15–20 min to equilibrate the membrane system.
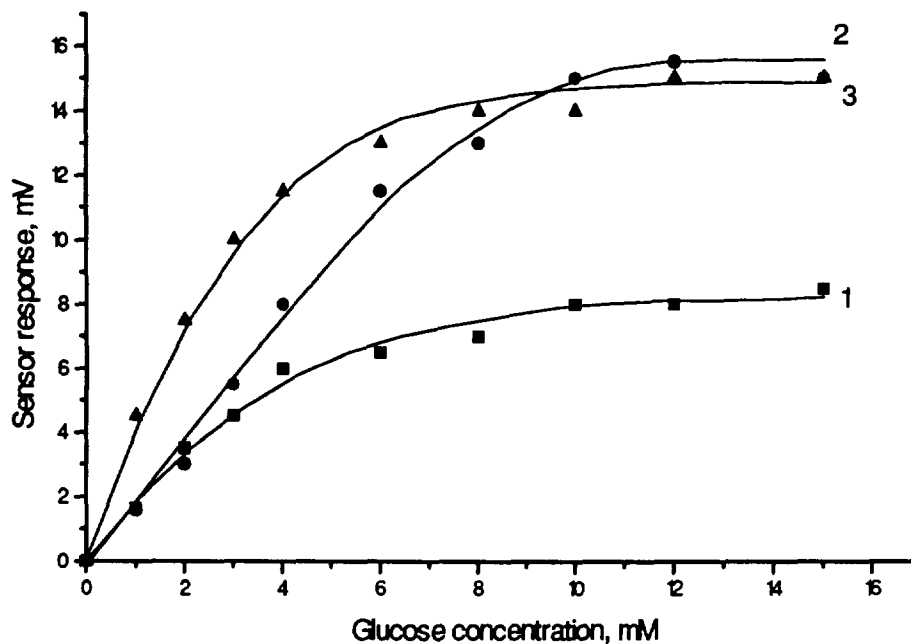
Fig. 2. Calibration curves of the glucose sensor in different buffer solutions: curve 1, 100 mM phosphate buffer, pH 7.4; curve 2, 100 mM TRIS buffer, pH 7.4; curve 3, 100 mM HEPES buffer, pH 7.4.

2.3. Apparatus

Two matched thermistors "Betatherm" 10 K3MCD2 (10 000 Ω at 25°C, temperature coefficient of -4% °C^{-1} (25°C)) connected to a Wheatstone bridge have been used. These thermistors were fabricated using microtechnology techniques by ASLEC (France). The active parts of the thermistors were covered by a polyimide layer for an efficient electrical insulation. The biomembrane containing the enzymes was applied to the surface of one of the thermistors and the membrane without enzyme was applied to the surface of the other thermistor. As a result of the enzyme reaction the temperature increases near the enzyme thermistor surface whilst the temperature near the other thermistor does not change. The temperature difference between the two thermistors leads to the thermistor resistance difference being converted into the voltage signal by means of an electrical scheme. This signal is directly proportional to the concentration of the substrate in the buffer solution. After amplification, the differential signal of the two thermistors

was registered with a recorder.

The pair of thermistors was placed within a thermostated glass cell (volume of 80 ml) (Fig. 1). Buffer solution was constantly pumped through the cell at flow rate of 0.80 ml min^{-1} by means of a homemade peristaltic pump. The temperature of the solution inside the cell and the solution flowing into the cell was held at 28°C by means of thermostated bath. Temperature oscillations of the cell solution were 5×10^{-3}°C; thus the thermistor differential reduced the noise of the temperature changes to 10^{-4}°C for oscillations of low frequencies (period $= 1$ mn) and 10^{-5}°C for oscillations of high frequencies (period < 1 min). The measurements were carried out using a potentiometric recorder at a sensitivity of 5×10^{-3}°C for a full-scale deflection in the 50 mV range. Glucose solutions at different concentrations were injected through the cell, and the measurements were carried out in a steady-state situation. The total time required for a determination depends on the cell geometry and the flow rate; for the experimental conditions used it usually takes 2–3 min.
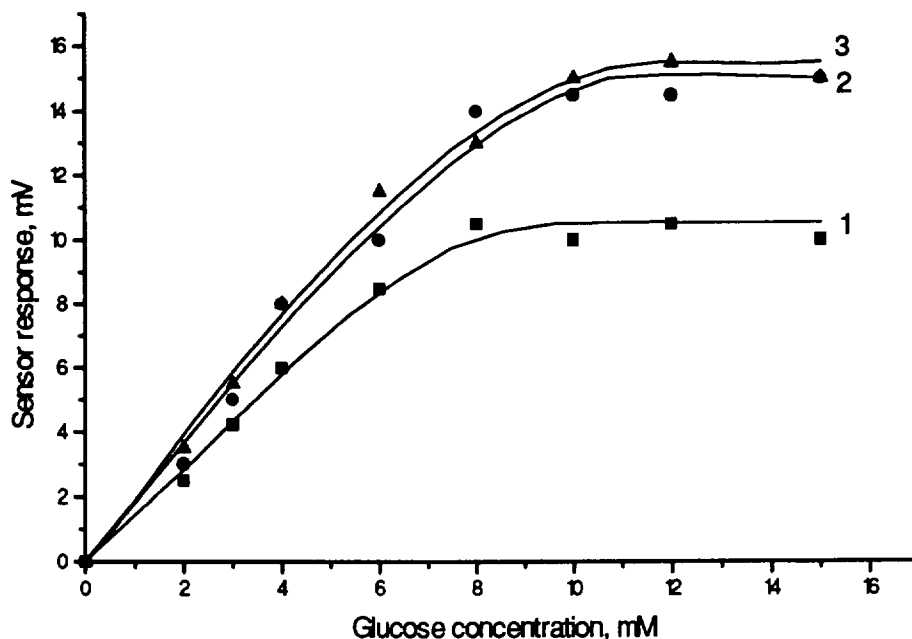
Fig. 3. Calibration curves of the glucose biosensor in TRIS buffer, pH 7.4, at different concentrations of buffer: curve 1, 20 mM; curve 2, 50 mM; curve 3, 100 mM.

3. Results and discussion

When glucose is injected into the cell, the following reactions occur close to the thermistor covered by the membrane containing the enzymes glucose oxidase and catalase:

$$\beta\text{-D-glucose} + O_2 \xrightarrow{\text{GOD}} \text{D-glucono-}\delta\text{-lactone} + H_2O_2 \ (79 \text{ kJ mol}^{-1}) \tag{1}$$
$$\downarrow$$
$$\text{D-gluconate} + H^+$$

$$H^- + \text{buffer} \rightleftharpoons \text{buffer} - H \ (X \text{ kJ mol}^{-1}) \tag{2}$$

$$\overset{\text{Catalase}}{H_2O_2 \longrightarrow H_2O + 1/2O_2} \ (100 \text{ kJ mol}^{-1}) \tag{3}$$
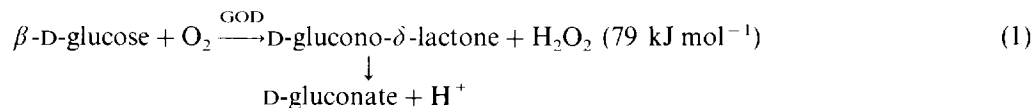
Glucose oxidase oxidises glucose with a heat production of about 80 kJ mol^{-1}. The differential pair of glucose sensitive thermistors can register this heat production, which is proportional to the concentration of glucose in the sample; nevertheless the sensitivity of such a process can be not very high. There is a possibility of increasing the total amount of heat produced in the actual oxidation of glucose by using the heat produced in the second and third reactions (buffer protonation (2) and hydrogen peroxide decomposition by

catalase (3)) and, thus, realising an effective chemical and biochemical amplification of the biosensor response to the glucose concentration.

For effective chemical amplification of the biosensor responses different types of buffer solutions were used. As can be seen in Fig. 2, the biosensor responses depend on the type of buffer, and the calibration curves show different shapes and various dynamic ranges. The biosensor response is higher in HEPES (N-(2-hydroxy-ethylpiperazine-N'-(2-ethane – sulphonic acid)) and TRIS (tris(hydroxymethyl(aminomethane)) buffers compared to the one obtained in a phosphate buffer (pH for each buffer solution was the same and was equal to 7.4). Comparison of the calibration curves of the biosensor obtained in HEPES and TRIS buffers shows that the sensor
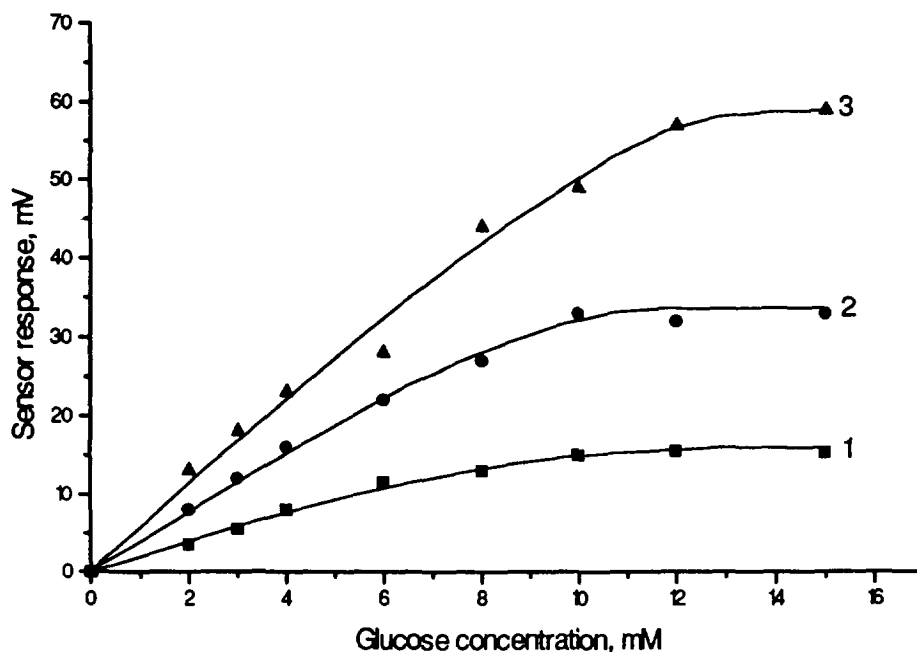
Fig. 4. Calibration curves of the glucose biosensor in 100 mM TRIS buffer, pH 7.4, at different concentrations of hydrogen peroxide: curve 1, 0 mM; curve 2, 1 mM; curve 3, 3 mM.

response in HEPES buffer is higher in the range from 2 to 8 mM glucose concentration, but a larger linear dynamic range of the glucose sensor is obtained in TRIS buffer. Further, TRIS buffer was chosen and the dependence of the glucose biosensor response on the buffer concentrations was studied. These results are presented in Fig. 3. As one can see, a buffer concentration of 20 mM is not sufficient for a complete binding of all the protons generated by reaction (1). In 50 and 100 mM buffer solutions the sensor response is higher and almost the same; thus a buffer concentration of 50 mM is sufficient to obtain a maximum signal. But the effect obtained by changing from phosphate buffer to TRIS or HEPES buffer cannot be explained only by the higher protonization enthalpy of these buffers. It is probable that the buffer effects of an enzyme conformation more favourable to the molecular recognition occur, inducing a better enzymatic turn-over. So it is well known that HEPES constitutes a good tissue culture medium; the growing ability of the cells is related to their metabolism which is governed mainly by enzymatic reactions. On the other

hand, phosphate based buffers present poor long term stability and such polluted aged buffers could induce enzyme inhibition.

The possibility of biochemical amplification of the biosensor response by the use of reaction (3) was studied. The results are presented in Fig. 4. Hydrogen peroxide was added in the solutions of buffer and glucose. Catalase decomposes H_2O_2 and therefore the concentration of oxygen increases in the cell solution. From Fig. 4 it is seen that increasing the concentration of hydrogen peroxide only up to 1 mM induces a significant increase in the sensor response value and the sensor linear range; such low H_2O_2 concentrations do not affect the enzyme activity. This effect of biochemical amplification by using the catalase reaction was investigated earlier and reported by Tran-Minh and Vallin [9]. But in our case the combination of chemical and biochemical amplification of the sensor responses is much more efficient.

All the results presented were obtained with a flow rate of 0.8 ml min^{-1} in the cell. Therefore in further experiments the influence of the flow rate in the cell on the sensor characteristics was stud-
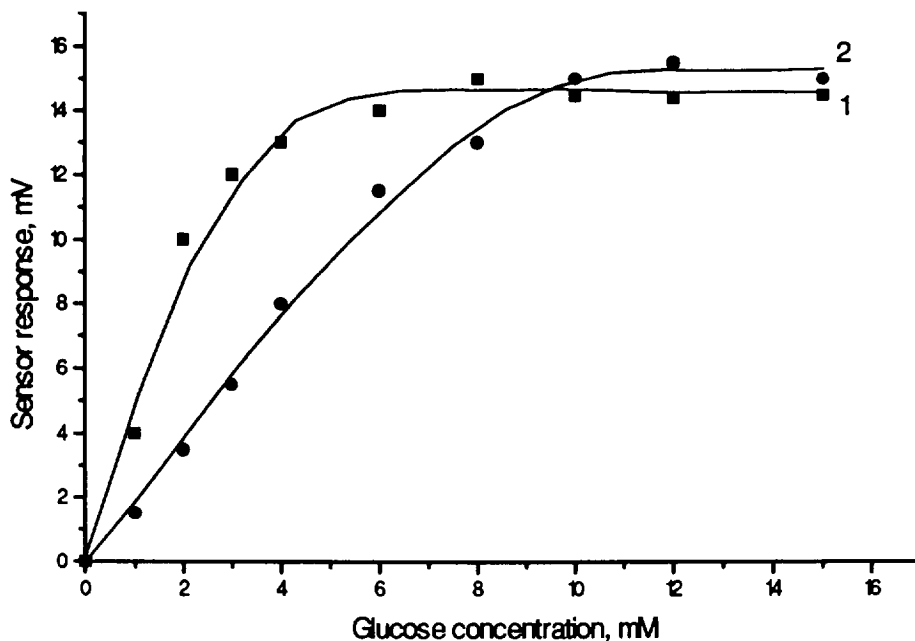
Fig. 5. Calibration curves of the glucose biosensor in 100 mM TRIS buffer, pH 7.4 with different sample flow rates in the cell: curve 1, 0.08 ml min^{-1}; curve 2, 0.8 ml min^{-1}.

ied. It was shown (Fig. 5) that when the flow rate in the cell decreases from 0.8 to 0.08 ml min^{-1} the sensor demonstrates a more narrow linear dynamic range. This effect can be explained by the differences between the diffusion rates for glucose and oxygen in the enzyme membrane. For high glucose concentrations nearly the same maximum sensor response corresponding to the maximum rate of the enzymatic reaction V_m is reached. At low flow rates the reaction is limited by oxygen diffusion which is not at a sufficient concentration near the enzymatic membrane; thus a low value of the Michaelis constant K_m is observed. K_m values correspond approximately to the substrate concentration giving the $V_m/2$ rate and reach about 1.5 mM. For higher flow rates the renewal of oxygen is sufficient and a value for K_m of around 4 mM is observed, which is closer to the values (4.5 mM) usually given for the immobilized GOD/catalase system [10].

4. Conclusions

A glucose sensitive enzymatic thermal sensor based on a pair of commercial microthermal probes was prepared by cross-linking the corresponding enzymes (glucose oxidase and catalase) with bovine serum albumin on the sensor surfaces. Characteristics of the obtained sensor were tested in different conditions. To find the maximal sensitivity, the calibration curves of this sensor were measured in different buffer solutions, with and without the addition of H_2O_2 to the samples at various sample flow rates in the cell. Different buffer solutions and hydrogen peroxide concentrations were used to realise the principles of a chemical and biochemical amplification of the biosensor response. It was shown that the value of the biosensor response and its dynamic range increase in the presence of hydrogen peroxide and depend on the type of buffer solutions tested and the rate of the sample flow stream.

In the future such a sensor could be integrated into multimicrosensing devices for the simultaneous measurements of physical and chemical parameters.

References

[1] B. Xie. B. Danielsson and F. Winquist. Sensors and Actuators, B15 (1993) 443.
[2] B. Xie. U. Hedberg. M. Mecklenburg and B. Danielsson, Sensors and Actuators, B15 (1993) 141.
[3] B. Xie. M. Mecklenburg. B. Danielsson, O. Ohman and F. Winquist. Anal. Chim. Acta, 299 (1994) 165.
[4] B. Xie, M. Mecklenburg, B. Danielsson et al., Analyst, 120 (1995) 155.
[5] P. Battaillard, E. Steffgen, S. Haemmerli, A. Manz and H.M. Widmer, Biosensors and Bioelectronics, 8 (1993) 89.
[6] G. Delhomme, A. Dittmar, W.H. Newman, H.F. Bowman and M. Jouvet. Sensors and Actuators, 6 (1992) 87.
[7] G. Delhomme. W.H. Newman, B. Roussel et al., IEEE Trans. BME. 41 (1994) 656.
[8] A.A. Shul'ga, A.C. Sandrovsky, V.I. Strikha et al., Sensors and Actuators, B10 (1992) 41.
[9] C. Tran-Minh and D. Vallin. Anal. Chem., 50 (1978) 1874.
[10] G. Coutouly, Génie Enzymatique. une Introduction, Masson. Paris, 1991. p. 162.

Moclobemide-selective membrane electrode and its pharmaceutical applications

Raluca-Ioana Stefan[a], George-Emil Baiulescu[a], Hassan Y. Aboul-Enein[b,*]

[a]Depatment of Analytical Chemistry, Faculty of Chemistry, University of Bucharest, Blvd. Republicii # 13, 70346, Bucharest-3, Romania

[b]Bioanalytical and Drug Development Laboratory, Biological and Medical Research Department (MBC-03), King Faisal Specialist Hospital and Research Centre, P.O. Box 3354, Riyadh 11211, Saudi Arabia

Abstract

A liquid membrane electrode prepared with moclobemide–dipicrylamine ion-pair complex, dissolved in nitrobenzene as solvent, was studied for analytical performance. The linear response covers the range 10^{-3}–10^{-6} M moclobemide solution, with a slope of 50.7 mV decade^{-1} (pH range 3.5–8). The detection limit is 3×10^{-7} M. The electrode shows stability, good reproducibility and fast response. The selectivity of the electrode is good. There are two important interfering ions: mianserin and thiamine (Vitamin B_1). The compression excipients (such as Mg^{2+}, starch, talcum powder) do not interfere. These characteristics of the electrode enabled it to be used for the determination of moclobemide in drugs and as an active substance, via indirect and direct potentiometric methods. Via an indirect potentiometric method moclobemide, as an active substance, can be determined with an average recovery of 99.96% and a relative standard deviation of 0.85%, and this method can also be used for its determination in drugs with a relative standard deviation of < 2%. The electrode is useful for the determination of the dissolution rate of moclobemide tablets. The physical processes are numerically simulated by typical equations. The apparent first-order rate constants for disintegration and dissolution were calculated.

Keywords: Moclobemide-selective membrane sensor; Pharmaceutical analysis; Potentiometric methods; Dissolution rate; Content uniformity

1. Introduction

The development of ion-selective membrane electrodes has been quickly followed by applications not only in inorganic analysis but also in the pharmaceutical field [1–4]. From the analytical point of view they represent a favorable means for

determining various ions owing to their ability to monitor selectively and continuously the activity of a particular ion in a solution. They can be used in kinetic studies [5], resolution of reaction mechanisms, biochemical and biomedical research, and flow-injection analysis.

Moclobemide (MB), p-chloro-N-(2-morpholinoethyl)benzamide, is widely used in the treatment of depression.

* Corresponding author.
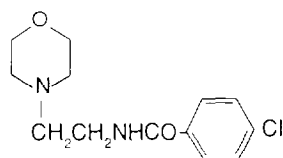
Moclobemide

The pharmacokinetics of moclobemide were studied [6–8]. The structure of moclobemide was confirmed by Wonters et al. [9]. The official standard method for the assay of moclobemide is based on non-aqueous titration [10]. In this paper, a method for the determination of moclobemide in pharmaceutical preparations is proposed. The method is fast and shows good reproducibility.

2. Experimental

2.1. Electrode design

The membrane electrode, based on a moclobemide–dipicrylamine (DPA) ion-pair complex, was prepared by impregnating the support material (a graphite rod) as described elsewhere [11] with a solution of 10^{-3} M ion-pair complex in nitrobenzene and attaching it to the end of a Teflon tube. When not in use, the electrode was kept in a 10^{-3} M MB^+DPA^- solution.

2.2. Apparatus

A Cole Parmer pH/mV meter was used for all direct potentiometric measurements. The electrode was used in conjunction with a Radiometer K401 calomel electrode. The titration curves were obtained by using an automatic titration assembly consisting of an ABU 12 autoburette, a TTT2 titrator, and a SBR 2c recorder (Radiometer, Copenhagen, Denmark). The pH measurements were performed with a Radiometer G202 B glass electrode in combination with a Radiometer K401 calomel electrode. The dissolution test was performed in a basket-stirrer USP-type apparatus [10].

2.3. Reagents and materials

Moclobemide and its pharmaceutical preparations were supplied by the Institute of Chemical and Pharmaceutical Research, Bucharest. Other materials and the reagents DPA and nitrobenzene (NB) were obtained from Fluka (Buchs, Switzerland).

Solutions of moclobemide were prepared by serial dilution while keeping the pH constant (citrate buffer pH 4.5, 71.9 ml of 0.1 M sodium citrate solution and 29.1 ml of 0.1 M HCl solution). A solution of DPA (10^{-2} M) was prepared by dissolving 0.4390 g DPA and diluting it in 100 ml of 5% Na_2CO_3 solution. The standard solution of sodium tetraphenylborate (NaTPB), of concentration 5×10^{-2} M, was prepared by dissolving 17.1220 g of the compound in distilled water and diluting it to 1 l, which dilution factor was determined using a chloroquine diphosphate standard substance.

2.4. Recommended procedures

2.4.1. Direct potentiometry

Standard solutions of 10^{-2}–10^{-6} M of pH 4.5 (citrate buffer) were prepared by serial dilutions of a 10^{-2} M solution of moclobemide. The electrode was placed in the stirred standard solutions and graphs of E (mV) vs. pMB were plotted. The unknown concentration is determined from the calibration graph.

2.4.2. Potentiometric titration

The electrode was placed in the sample solution (30–40 ml, concentration approximately 10^{-2} M, containing 2 ml of 5 M HCl solution) and the solution was titrated with 5×10^{-2} M NaTPB. The end point corresponds to the maximum slope on the E (mV) vs. volume of titrant curve (1 ml of 5×10^{-2} M NaTPB is equivalent to 13.4 mg of moclobemide).

2.4.3. Content uniformity assay of moclobemide tablets

One tablet was placed in each of 10 separate 100 ml beakers and dissolved by shaking with about 30–40 ml distilled water, in the presence of

2 ml of 5 M HCl solution. The solutions were titrated potentiometrically, as described above.

2.4.4. Dissolution test

The test was carried out according to the USP XXII method [10], with the use of the equipment described elsewhere [12]. One tablet was placed in the basket, and the dissolution medium (250 ml of 0.1 M HCl) was maintained at $37.0 \pm 0.5°C$. The basket was rotated at 50 rev min^{-1}. For the potentiometric determination, after an appropriate time interval (1 min) the potential values are recorded, and the amount of moclobemide is calculated from the calibration graph. In order to investigate all the important physical processes during the dissolution period, the release profiles were numerically simulated by typical equations [13].

3. Results and discussion

3.1. Electrode response

The equation of the calibration graph is $E = E° + 50.7 \times \log[MB]$ with a correlation coefficient of 0.9997.

The response characteristics of the electrode are shown in Table 1. The stability of the electrode response was checked over a period of 8 months. The response time of the electrode depends on the

E(mV) vs SCE
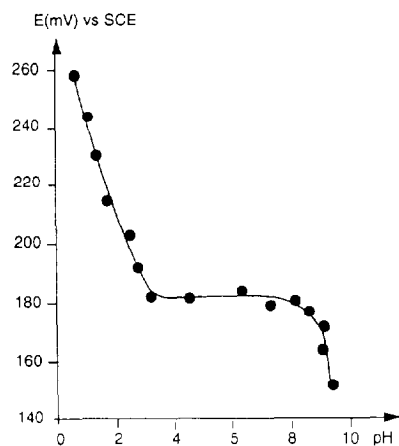
Fig. 1. Effect of pH on the response of the moclobemide electrode (10^{-3} M moclobemide solution).

Table 1

Response characteristics for moclobemide-selective electrode (all values are the average of 20 determinations; all measurements made at 25°C)

Parameter	Response
Slope (mV pMB^{-1})	50.7 ± 0.8
Intercept, $E°$ (mV)	329.91 ± 2.12
Linear range (M)	10^{-3}–10^{-6}
Detection limit (M)	3×10^{-7}

concentration of moclobemide (less than 1 min for 10^{-3}–10^{-4} M moclobemide solutions and 1–2 min for 10^{-5}–10^{-6} M moclobemide solutions). The electrode response displayed good stability and reproducibility over the test, as shown by the relative standard deviation values.

3.2. Effect of pH on the response of the electrode

The effect of pH on the response of the potential readings of the moclobemide was checked by recording the emf of a cell which contained 10^{-3} M moclobemide solution at various pH values, which were obtained by the addition of very small volumes of HCl and/or NaOH solution (10^{-1} M or 1 M of each). The E (mV) vs. pH graph presented in Fig. 1 shows the pH independence in the range 3.5–8.

At higher pH values, free base precipitates in the test solutions and consequently the concentration of unprotonated species gradually increases. As a result, lower emf readings are recorded. At low values, the concentration of protonated species gradually increases and the emf is a function of pH.

3.3. Selectivity of the electrode

Moclobemide has to be determined in pharmaceutical dosage forms which contain various inorganic and organic substances. The effect of some of these matrices on the response of the electrodes was studied by the mixed solution method. The concentrations of interfering ions and moclobemide were 10^{-2} M and 10^{-4} M respectively.

The selectivity coefficients, presented in Table 2, indicated that the response of the proposed mem-

Table 2

Selectivity coefficients for the moclobemide-selective membrane electrode (all values are the average of 20 determinations; all measurements made at 25°C)

Interfering species	K_{MB, J^z}^{pot}
Ephedrine	2.12×10^{-1}
Pyridoxine (Vitamin B_6)	4.19×10^{-1}
Polyvinylpyrolidone	1.80×10^{-1}
Mg^{2+}	1.05×10^{-3}
Thiamine (Vitamin B_1)	8.10×10^{-1}
Mianserin	1.04

brane electrode is highly affected by mianserin and thiamine (vitamin B1). Excipients such as Mg^{2+}, starch and talcum powder do not interfere.

3.4. Analytical applications

The electrode proved to be useful for the assay of the moclobemide content of pharmaceutical formulations using the potentiometric titration method. The results obtained are given in Table 3. As can be seen, a high precision was obtained (RSD < 2%).

Table 3

Determination of moclobemide with a moclobemide-selective membrane electrode

Product	Sample	Recovery (% of nominal value)[a]	RSD (%)[b]
Moclobemide	1	100.00	0.85
raw material	2	99.69	
	3	99.89	
Moclobemide A[c]	1	99.21	1.05
100 mg per tablet	2	98.20	
	3	98.76	
Moclobemide B[c]	1	99.98	1.03
100 mg per tablet	2	99.41	
	3	99.58	

[a] All values are the average of four determinations.
[b] RSD (%) refers to all 12 determinations.
[c] Moclobemide A represents a batch obtained with high pressure pastillation.
[d] Moclobemide B represents a batch of talcum powder-coated tablets obtained with low pressure pastillation.
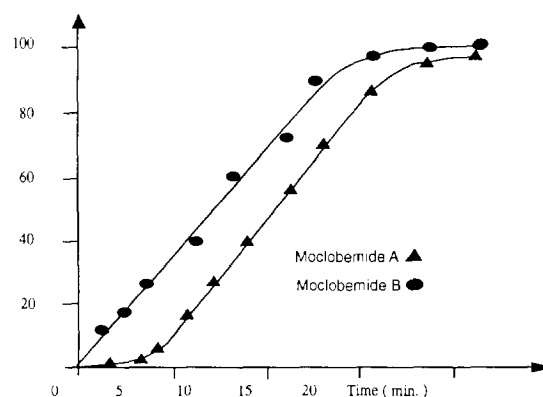
Fig. 2. Dissolution profiles of moclobemide A and moclobemide B. All values are the average of six determinations.

The results obtained by potentiometric titration of moclobemide raw material and moclobemide A and moclobemide B tablets were in good accordance with those obtained by potentiometric titration in non-aqueous media [10] with 0.1 N $HClO_4$: 99.20%, 99.25% and 99.40% respectively.

The desirability of an in-vitro test that adequately reflects the physiological availability of solid dosage forms of drugs is now recognized. The measurement of a parameter that is related to the rate of dissolution of a solid has been suggested as a more realistic variable and this has led to numerous papers describing different methods and equipment for monitoring dissolution tests [13–15].

The dissolution test was performed with a basket-stirrer USP-type apparatus operated at 50 rev min^{-1} in 250 ml of 0.1 M hydrochloric acid (simulated gastric fluid) by the direct potentiometric moclobemide membrane electrode method. The simulated gastric fluid was kept at $37.0 \pm 0.5°C$. The equation of the new calibration graph is $E = 24.37 + 79\,016.2 \times c$ with a correlation coefficient of 0.9078 (c is the moclobemide concentration in mole l^{-1}).

Fig. 2 shows the dissolution profiles of moclobemide tablets. Taking into account the S shape of the curves, there are some possibilities for the simulation of physical processes involved in the dissolution steps. The release of the active principle of the uncoated tablets (moclobemide A)

in simulated gastric fluids follows the Langenbucher model [16] (for high pressure pastillation, 6 kgf cm^{-2}) i.e. the dissolution process involves two main steps: an initial step of about 3 min during which there is a disintegration process followed by a rapid process of active principle dissolution. The Fick–Higuchi model is followed for talcum powder-coated tablets (moclobemide B) (low pressure pastillation, 3 kgf cm^{-2}): i.e. the dissolution process involves a rapid release of the active principle. All other simulation possibilities tested were found to be inadequate for the moclobemide tablets. A graphical method was proposed for the disintegration–dissolution analysis of cumulative percent dissolved vs. time data [5]. With the aid of this method, we can determine the pharmacokinetics of moclobemide tablets. The apparent first-order rate constants for disintegration (k_d) and dissolution (k_s) respectively were: $k_d = 0.156$ min^{-1}, $k_s = 0.394$ min^{-1} for moclobemide A and $k_d = 0.778$ min^{-1}, $k_s = 0.940$ min^{-1}, for moclobemide B. In both cases, the dissolution process is more rapid than the disintegration process. There are no degradation products detected in the in-vitro test. The differences between the dissolution and disintegration rates are due to the different values of pressure utilized for manufacturing the tablets. The compression excipients do not interfere.

4. Conclusions

The moclobemide-selective membrane electrode, based on the MB$^+$DPA$^-$ ion-pair complex, exhibits useful analytical characteristics for the determination of moclobemide in pharmaceutical formulations. This is due to its good and reproducible response characteristics. These character-istics enable the electrode to be used in the quantitative analysis and determination of the dissolution profiles of moclobemide in its pharmaceutical formulations. The advantage of the electrode technique for carrying out such a test is that the selective electrode can monitor continuously the concentration of the active ingredient in the standardized dissolution cells.

References

[1] V.V. Cosofret and R.P. Buck, Pharmaceutical Applications of Membrane Sensors. CRC Press Inc., Boca Raton, FL, 1992.

[2] Z.R. Zhang and V.V. Cosofret, Sel. Electr. Rev., 12 (1990) 35.

[3] V.V. Cosofret and R.P. Buck, Anal. Chim. Acta 174 (1984) 299.

[4] V.V. Cosofret and R.P. Buck, Crit. Rev. Anal. Chem., 24 (1993) 1.

[5] A.E. Yazigi, J. Pharm. Sci., 70 (1981) 535.

[6] O. Svein, Th. W. Guentert, T. Lorno and G. Hermodsson, J. Pharm. Pharmacol., 44 (1992) 413.

[7] Z. Gorka and W. Zajaczkowski, Pol. J. Pharmacol. Pharm., 43 (1991) 177.

[8] C.H. Ghiter, E. Nilsson, B. Muehlbawer, K.H. Antonin and P.R. Bieck, J. Neural Transm. Gen. Sect., 89 (1992) 129.

[9] J. Wonters, F. Moureau, B. Norberg, G. Evrard and F. Durant, Bull. Soc. Chim. Belg., 102 (1993) 329.

[10] The United States Pharmacopoeia XXII, US Pharmacopoeia Convention Inc., Rockville, MD, 1990.

[11] V.V. Cosofret, Rev. Roum. Chim., 23 (1978) 1489.

[12] A.A. Bunaciu, M.S. Ionescu, R.I. Stefan, I. Ioan and H.Y. Aboul-Enein, Anal. Lett., 27 (1994) 1647.

[13] A.A. Bunaciu, Pittsburgh Conference and Exposition Abstract Book, New Orleans, LA, 1992. Paper No. 638.

[14] J. Cooper and J.E. Rees, J. Pharm. Sci., 61 (1972) 1511.

[15] K. Heilmann, Therapeutic Systems, Rate-Controlled Drug Delivery: Concept and Development, 2nd revised edn., Georg Thieme Verlag, Stuttgart, 1984, p. 24.

[16] F. Langenbucher, J. Pharm. Pharmacol., 24 (1972) 979.

Talanta

Amperometric determination of lactate dehydrogenase based on a carbon fiber microcylinder electrode modified covalently with Toluidine Blue O by acylation

H.X. Ju *, L. Dong, H.Y. Chen

Department of Chemistry, Nanjing University, Nanjing 210093, People's Republic of China

Abstract

A method has been developed for the modification of a carbon fiber microcylinder electrode with acylation. The stability and surface coverage of the Toluidine Blue O-modified microelectrode were studied by cyclic voltammetry. The modified electrode showed significant activity for the electrocatalytic oxidation of NADH in pH 6.8–7.8 solution. The catalytic current increased linearly with increasing concentration of NADH from 4.0×10^{-5} to 1.5×10^{-3} M. A simple amperometric determination based on electrochemical detection of NADH produced from the enzymatic reaction of lactate with NAD^+ under the catalysic effect of lactate dehydrogenase (LDH) is reported. The experimental factors which had primary influence on the analytical performance were studied. The sensor had a linear response over a range of LDH concentrations from 5.0 U l^{-1} to 200 U l^{-1} at -0.2 V vs. SCE under optimum conditions. A satisfactory result was obtained for the determination of LDH in clinical blood samples.

Keywords: Acylation; Amperometric determination; Carbon fiber microcylinder electrode; Lactate dehydrogenase; Toluidine Blue O

1. Introduction

Many current works in the analytical field are devoted to chemically-modified electrodes and biosensors [1,2]. Some mediators have been fixed on the electrode surface by adsorption, electrochemical polymerization or polymer coating to efficiently facilitate electron transfer and to determine some biomolecules [1–4]. The irreversible adsorption of commercial dyes on a

graphite electrode is a simple method for preparing modified electrodes [2,5]. In order to increase the stability of the modifying layer, Persson and co-workers [2,6,7] synthesized derivatives of Toluidine Blue O by introducing several aromatic rings to enhance π-electron overlapping with the carbonaceous surface. However, at a microelectrode modified by irreversible adsorption, no matter what the mediator is, even if it has a few aromatic rings, the stability of the modified microelectrode is very poor because of the high mass transport rate of

* Corresponding author.

the microelectrode [8,9], which makes the mediator, and its product, diffuse rapidly away from the surface during the process of electrochemical reaction. Thus, the catalytic efficiency declines greatly.

The application of carbon fiber microelectrodes (CFMEs) for electrochemical determinations has attracted great interest [8,9–13]. The preparation of modified CFMEs is usually done by using noble metal deposition [12], polymer coating [13,14] or covalent modification [15]. On the surface of a carbon electrode, the process of covalent modification is usually done by acylation [16–18]. Hajizadeh et al. [18] have used a crosslinking agent — triisocyanate — to fix thionin on a graphite electrode by acylation. The method has also been used to immobilize enzyme at a CFME by using carbodiimide [19,20]. However, to our knowledge, there has been no report until now of covalent modification by direct amidation with thionyl chloride at a CFME. In this work, Toluidine Blue O (TBO) was covalently bonded to the surface of a CFME for the first time. The stability of TBO-modified CFME is very good. The modified electrode can effectively catalyze the oxidation of NADH at a carbon fiber microelectrode.

The coenzyme NAD⁻ and its reduced form NADH are used by over 250 dehydrogenases, and play a major role in many biological redox reactions. The direct electrochemical determination of NADH, particularly in a small system, is very important in clinical medicine. The electrochemical oxidation of NADH, whose normal formal potential is −0.56 V vs. SCE at pH 7.0 and 25°C, has been extensively studied at various modified electrodes [2,5,6,18,21–28]. Willner and Riklin [27] developed the amperometric sensors for NADH and malic acid by covalently linking pyrroloquinolinequione (PQQ) or PQQ and malic enzyme with 1-ethyl-3[3-(dimethylamino)propyl]-carbodiimide (EDC) and N-hydroxysulfosuceinimide sodium salt at a self-assembled cyteamine monolayer-modified Au electrode. Katz et al. [28] used cystamine and cysteamine to functionalize both Au and Pt electrodes and to covalently link PQQ with EDC; the modified electrodes can also catalyze the oxidation of NADH. However, little study of the direct electrochemical determination of NADH at

a CFME has been reported. The electrocatalytic oxidation of NADH at a TBO- (and its derivatives) modified graphite electrode has been presented by Persson and co-workers previously [2,6]. However, if the TBO-modified carbon fiber microelectrode was prepared with their method, its stability was very poor [29]. Moreover, the determination of lactate dehydrogenase (LDH) with a TBO-modified CFME has never been studied. Here we report on the use of a TBO-modified microelectrode in biosensors for the monitoring of LDH based on the determination of NADH. The results will be very significant for the monitoring of enzyme in a small clinical system and the development of microbiosensors.

2. Experimental

2.1. Materials and reagents

TBO (B.S. grade) was obtained from the Chroma Chemical Reagent Company (UK), the reduced form of nicotinamide–adenine dinucleotide (NADH, >95%) and LDH (EC 1.1.1.27, Type XI, from rabbit muscle, 700 U mg⁻¹) were from Sigma (USA). These reagents were directly used as received without further purification. The reagents used for making up 0.2 M pH 2–12 phosphate buffer solutions, thionyl chloride (SOCl₂), and other reagents, obtained from chemical companies in The People's Republic of China, were of analytical-reagent grade. Pyridine was redistilled with P₂O₅ (8 g per 100 ml) and was stored over a 4 Å molecular sieve activated at 550°C. Water used in the experiment was doubly-quartz-distilled. Carbon fibers (PAN-type) with 6–7 μm diameter were obtained from the Shanghai Synthetic Fiber Research Institute. Epon 812 epoxy resin (New York, USA) was used to seal the electrodes.

2.2. Preparation of TBO-modified CFME

The method of fabrication of the CFME was similar to that given in a previous paper [9]. Briefly, a single carbon fiber was sealed in a glass capillary tube with epoxy resin. First, a CFME of

length 6-10 mm was washed thoroughly with acetone and distilled water in an ultrasonic bath, and pretreated electrochemically in 1.0 M H_2SO_4 solution with a triangular-wave potential sweep from -1.0 V to $+2.0$ V at a scan rate of 200 mV s^{-1} for 50 min. Next, the treated electrode was washed with doubly-distilled water and dried in air, and immersed in $SOCl_2$ for 30 min. Then the electrode was rinsed with tetrahydrofuran (THF) to remove $SOCl_2$ remaining on its surface, and dipped in anhydrous pyridine solution containing 1.0×10^{-3} M TBO for 15 min. During this process pyridine, as proton acceptor, deprotonated the oxidized TBO and gradually converted it into the imino form which reacted with the $-COCl$ group on the electrode surface. Finally, the modified electrode was rinsed with phosphate buffer (pH 7.0) and stored in the same buffer solution.

2.3. Procedures

Electrochemical measurements were carried out with a Model BAS-100B Electrochemical Analyzer with a PA-1 Preamplifier (Bioanalytical Systems (BAS), West Lafayette, IN) to amplify current and filter out noise and an FPG-310 Color Plotter (Fujitsu Company, Japan) to record the voltammograms. A type 501 thermostat (Shanghai, People's Republic of China) was used to control the experimental temperature at $20 \pm 0.1°C$.

A three-electrode configuration with a saturated calomel electrode (SCE) as reference, Pt wire as counter and the above-modified electrode as working electrode was employed. After deaerating with pure N_2 for 10 min, the electrochemical measurements were carried out under a nitrogen atmosphere.

3. Results and discussion

3.1. Cyclic voltammogram of TBO-modified CFME

The cyclic voltammograms of the TBO-covalently-modified electrode in pH 7.0 buffer solution at a scan rate of 100 mV s^{-1} showed a couple of cathodic and anodic peaks (Fig. 1). Their peak

potentials were at -276 mV and -228 mV ($E^{o'} = -252$ mV, $\Delta E_p = 48$ mV) respectively. The peak potentials shifted slightly in a positive direction in comparison with those of soluble TBO at a bare carbon fiber microelectrode [29] and the change in the normal formal potential was about 29 mV. The small change was similar to that resulting from acylation found in the literature [16,30], indicating that TBO on the electrode surface had been acylated.

At the beginning of the cyclic voltammetric sweep of the TBO-covalently-modified electrode, the cathodic and anodic peak currents decreased rapidly, then dropped gradually to a constant value and remained at this value for a very long time (see Fig. 1). Furthermore, no change in peak current appeared after the modified microelectrode had been dipped in pH 7.0 buffer solution for several weeks, indicating that the stability of the TBO-covalently-modified CFME was very good. However, the half life of TBO adsorbed on the CFME is only 55 min [29]. The better stability indicated that TBO was firmly fixed on the surface of the carbon fiber by a covalent bond. The decrease in peak current at the beginning of the sweep was due to the desorption of some adsorbed TBO. Because the differences in peak potentials of acylated TBO and adsorbed TBO,
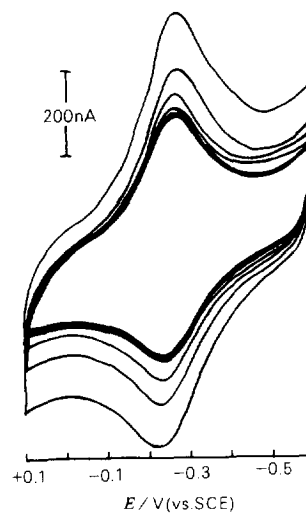
Fig. 1. Cyclic voltammograms of TBO-modified microelectrode in pH 7.0 phosphate buffer solution at 100 mV s^{-1}.

about 25 mV for the cathodic and 32 mV for the anodic peak, were small, only a single pair of peaks occurred, as shown in Fig. 1.

The reactions in the process of TBO covalent modification can be described as follows. First of all, a lot of carboxyl groups were formed on the surface of the carbon fiber during electrochemical pretreatment [15,20], they were then acylated by the reaction between –COOH and $SOCl_2$ to form –COCl groups under the usual conditions. Finally, these –COCl groups were amidated with TBO in the presence of excess organic base pyridine, as a proton acceptor, which removed the positive charge of TBO and converted it to the imino form, to form the amido link and to covalently bond TBO to the surface of the carbon fiber. Thus, this method of preparing a modified carbon fiber electrode can greatly enhance the stability.

3.2. Surface concentration of TBO at modified microelectrode

The surface concentration Γ of TBO can be calculated according to $\Gamma = Q/nFA = S/nFAv$, where Q is the charge consumed during complete reduction of TBO, S is the peak area of the cyclic voltammogram, and the other symbols have their usual meanings. At a microcylinder electrode with a geometric area A of 2.0×10^{-3} cm^{-2}, the surface concentration Γ_{exp} was 3.4×10^{-10} mol cm^{-2} ($n = 2$), which was determined from the steady cyclic voltammogram at 100 mV s^{-1} in pH 7.0 buffer solution.

Given that the horizontal section area of methylene blue, which is of similar structure to TBO, is 0.75 nm^2 [31], the theoretical mono-layer adsorbance Γ_{theory} of MB at an electrode is 2.2×10^{-10} mol cm^{-2}. Comparing $\Gamma_{exp,TBO}$ with $\Gamma_{theory,MB}$, TBO fixed on a carbon fiber surface was a monolayer due to the roughness of the pretreated carbon fiber surface, and almost the whole electrode surface was activated by electrochemical oxidation and acylation.
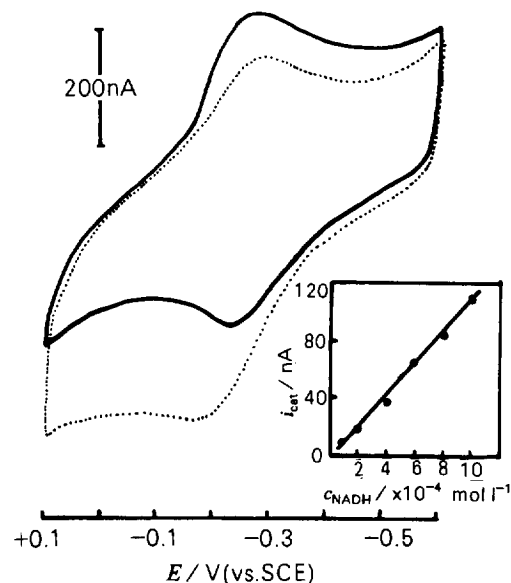
Fig. 2. Cyclic voltammograms of TBO-modified electrode in pH 7.0 buffer solution ( ) and pH 7.0 buffer including 1.0×10^{-3} M NADH ( ); inset: relation between catalytic peak current and concentration of NADH at $v = 100$ mV s^{-1}.

3.3. Electrocatalytic oxidation of NADH at TBO-modified carbon fiber electrode

This work showed that the TBO-modified electrode was able to catalyze the oxidation of NADH in pH 7.0 phosphate buffer solution via an electron transfer reaction between acylated TBO and NADH at the heterogeneous boundary layer. The experimental results are shown in Fig. 2. When the buffer solution included 1.0×10^{-3} M NADH, the anodic peak current of the cyclic voltammogram increased, the cathodic peak current decreased, and the anodic peak potential shifted in a positive direction by about 60 mV, which is very characteristic of an electrocatalytic oxidation process. The shift resulted from the catalytic reaction between acylated TBO and NADH, which possibly changed the ratio of surface concentrations of oxidized and reduced forms of TBO and the electron transfer rate between the electrode and the TBO at the same potential. The catalytic mechanism can be expressed as follows:

$$TBO_{red} - 2e \rightleftarrows TBO_{ox}$$

$$NADH + TBO_{ox} \rightarrow TBO_{red} + NAD^+$$
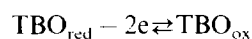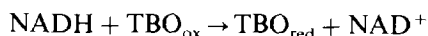
The catalytic current i_{cat} ($= i_2 - i_1$, where i_1 and i_2 are the anodic peak currents of the modified electrode in buffer without and with NADH respectively) of NADH increased linearly with increasing concentration of NADH from 4.0×10^{-5} to 1.5×10^{-3} M (inset to Fig. 2) with a correlation coefficient of 0.992 and a relative standard deviation of 1.5% for six determinations with 1.0×10^{-3} M NADH.

3.4. Effects of experimental conditions on catalytic peak current

Fig. 3 shows the dependence of catalytic peak current on scan rate. At a high scan rate the catalytic peak current was proportional to $v^{1/2}$; however, at a lower scan rate the plots deviated from linearity. The catalytic current curve (broken line in Fig. 2) tended to a sigmoidal shape with the decrease of the scan rate. These are the characteristics of diffusion mass transport at a microelectrode. Considering that the peak potential was independent of v, the electrode process was controlled by the diffusion of NADH in solution [13,32]. Thus, the interfacial chemical reaction rate between bonded TBO and NADH was large, and the electrode process is similar to
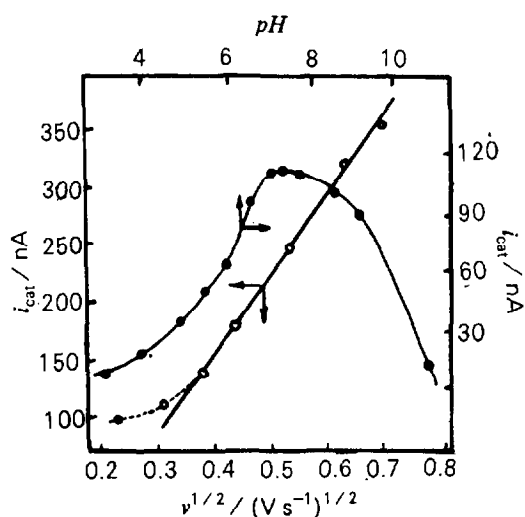
Fig. 4. Scheme of electrochemical response for LDH at a TBO-modified electrode.

the direct electrochemical oxidation of NADH at the electrode.

The catalytic peak current also depended greatly on the pH of the solution (Fig. 3). When the pH was low, the catalytic current was very small, and it increased with increase of pH. However, when the pH was >7.8, the current decreased with increase in pH. This phenomenon is similar to those described in Refs. [2] and [18], which resulted from both decomposition of NADH in acid solution and the rate of reaction between the TBO and NADH. With increasing pH the reaction rate and catalytic current decreased [2]. However, when the pH was <7, because the experiment was carried out after NADH was added to background for about 1 min in order to stir and deaerate, part of the NADH would decompose, which resulted in the decrease of the catalytic peak current. NADH is stable in neutral and basic pH solutions and the concentration of NADH did not change with time. Therefore, the catalytic peak current was a maximum between pH 6.8 and 7.8. A pH of 7.0 was used for the subsequent work [18].

3.5. Response of the modified microelectrode to LDH

When the pH 7.0 phosphate buffer solution included 1.0×10^{-3} M NAD^+, or 1.0×10^{-3} M NAD^+ and L-lactate, both the anodic and cathodic peak currents of the cyclic voltammogram of the TBO-modified microelectrode did not change. This result indicated that NAD^+ and L-lactate did not interfere with the electrode process of the TBO electrode. However, when the solution of 1×10^{-3} M NAD^+ and lactate included 100 U l⁻¹ LDH, the cyclic voltammogram of the TBO-modified electrode showed the same change as in Fig. 2, indicating that LDH cata-

Fig. 3. Plots of catalytic peak current vs. $v^{1/2}$ at pH 7.0 (○) and vs. pH of solution at 100 mV s⁻¹ (●).

lyzed the oxidation of lactate with a simultaneous reduction of NAD^+ to produce NADH. The formed NADH diffused to the electrode surface and catalyzed the electrode reaction of TBO. With increasing LDH concentration, the catalytic peak current increased, which is the basis for the determination of LDH. The overall reaction process can be seen in Fig. 4.

3.6. Effect of experimental conditions on the amperometric response to LDH

In amperometric measurements, the potential dependence of LDH response (hydrodynamic voltammogram) in the range $-0.6-+0.1$ V indicated that the amperometric response of the modified electrode to LDH started at -0.35 V. With the positive shift of applied potential, the response rose sharply up to -0.2 V, and then exhibited almost a constant value. An applied potential of -0.2 V was chosen for subsequent work.

The effect of pH on the LDH response was very obvious. In the pH range 4–6.8, the amperometric response to LDH increased with increasing pH. The response remained constant at pH 6.8–8.5, and then decreased when pH was >8.5. A wider pH range of stable response to LDH than to NADH occurs because the reaction of lactate and NAD^+ under the catalysis of LDH is a process of releasing H^+, and therefore a high pH is advantageous to the positive reaction. However, too high a pH would result in both the decomposition of NAD^+ and the decrease of the reaction rate between NADH and mediator. Therefore, the amperometric determination was performed at pH 8.0.

NAD^+ concentration also affected the response of the modified electrode to LDH. At various LDH concentrations, all responses increased with increasing NAD^+ concentration, and remained constant when the NAD^+ concentration was larger than 1.0×10^{-3} M, which was selected as an optimum condition. In order to quicken the catalytic reaction of LDH, an excess lactate concentration of 5.0×10^{-3} M was selected.

3.7. Application of TBO-modified electrode in the measurement of LDH

Fig. 5 shows a typical trace of the steady state current–time response of the TBO-modified electrode at -0.2 V with successive injections of LDH (in 50 U l^{-1} steps). With the injection of LDH the response increased, and the time to reach constant response was very short (<10 s). The calibration plots of amperometric response vs. the concentration of LDH (inset to Fig. 5) showed a linear relationship. The linear response range was from 5.0–200 U l^{-1} with a correlation coefficient of 0.990. The relative standard deviation of results was 3.2% for five successive determinations at 100 U l^{-1}.

After a clinical human blood serum sample of 200 μl was injected into 1.8 ml pH 8.0 buffer solution including 1.1×10^{-3} M NAD^+ and 5.5×10^{-5} M lactate for 30 s, the amperometric response of the TBO-modified microelectrode was used to assay the LDH content without any interference. The average value of three determinations with an interval of 8 h was 23 U l^{-1} (SD = 0.5) in the diluted solution. Thus, the content of LDH in the human blood serum sample was 230 U l^{-1}. The result was close to the value of 225 U l^{-1} obtained by spectrophotometry (LDH–L method) at 340 nm wavelength. The advantages of the biosensor are that it has a
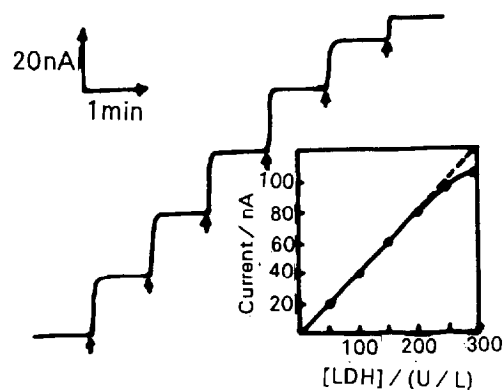
Fig. 5. Amperometric response to successive addition of 50 U l^{-1} LDH in pH 8.0 buffer including 1.0×10^{-3} M NADH and 5.0×10^{-3} M lactate with an interval of 1 min at -0.2 V. Inset: calibration curve of LDH at TBO-modified carbon fiber electrode.

shorter response time to LDH, it can detect LDH by a direct electrochemical method in a smaller system and it could potentially be used for in vivo and clinical analysis.

Acknowledgement

References

[1] P.N. Bartlett and J.M. Cooper, J. Electroanal. Chem., 362 (1993) 1.

[2] B. Persson and L. Gorton, J. Electroanal. Chem., 292 (1990) 115.

[3] R. Santucci, M. Brunori, L. Campanella and G. Tranchida, Bioelectrochim. Bioenerg., 29 (1992) 177.

[4] M. Marchesiello and E.M. Genies, Electrochim. Acta, 37 (1992) 1987.

[5] L. Gorton, A. Torstensson, H. Jaegfeldt and G. Johansson, J. Electroanal. Chem., 161 (1984) 103.

[6] B. Persson, J. Electroanal. Chem., 287 (1990) 61.

[7] L.I. Boguslavsky, L. Geng, I. Kovalev, S.K. Sahni, Z. Xu, T.A. Skotheim, V. Laurinavichius, B. Persson and L. Gorton, Biosens. Bioelectron., 10 (1995) 693.

[8] R.M. Wightman and D.O. Wipf, in A.J. Bard (Ed.), Electroanalytical Chemistry, Vol. 15, M. Dekker, New York, 1989, pp. 267–353.

[9] H.X. Ju, H.Y. Chen and H. Gao, J. Electroanal. Chem., 361 (1993) 251.

[10] J. Wang and Q. Chen, Anal. Chem., 66 (1994) 1007.

[11] E.N. Navera, M. Suzuki, E. Tamiya, T. Takeuchi and I. Karube, Electroanalysis, 5 (1993) 17.

[12] J. Wang and L. Angnes, Anal. Chem., 64 (1992) 456.

[13] H.X. Ju, Y.G. Xun and H.Y. Chen, J. Electroanal. Chem., 380 (1995) 283.

[14] L.I. Netchiporouk, A.A. Shul'ga, N. Jaffrezic-Renault, C. Martelet, R. Olier and R. Cespuglio, Anal. Chim. Acta, 303 (1995) 275.

[15] P. Pantano and W.G. Kuhr, Anal. Chem., 63 (1991) 1413.

[16] J.C. Lennox and R.W. Murray, J. Electroanal. Chem., 78 (1977) 395.

[17] W.J. Albery and A.R. Hillman, Ann. Rep. Prog. Chem., Sect. C, 78 (1981) 277.

[18] K. Hajizadeh, H.T. Tang, H.B. Halsal and W.R. Heineman, Anal. Lett., 24 (1991) 1453.

[19] P. Pantano, T.H. Morton and W.G. Kuhr, J. Am. Chem. Soc., 113 (1991) 1832.

[20] E. Csöregi, L. Gorton and G. Marko-Varga, Anal. Chim. Acta, 273 (1993) 59.

[21] Z. Samec and P.J. Elving, J. Electroanal. Chem., 144 (1983) 217.

[22] C.J. McNeil, J.A. Spoors, D. Cocco, J.M. Cooper and J.V. Bannister, Anal. Chem., 61 (1989) 25.

[23] P.C. Pandey, Anal. Biochem., 221 (1994) 392.

[24] C. Cai, H. Ju and H. Chen, Anal. Chim. Acta, 310 (1995) 145.

[25] M. Vreeke, R. Maidan and A. Heller, Anal. Chem., 64 (1992) 3084.

[26] A.S.N. Murthy and Anita, Bioelectrochem. Bioenerg., 33 (1994) 71.

[27] I. Willner and A. Riklin, Anal. Chem., 66 (1994) 1535.

[28] E. Katz, T. Lötzbeyer, D.D. Schlereth, W. Schuhmann and H.-L. Schmidt, J. Electroanal. Chem., 373 (1994) 189.

[29] H.X. Ju and H.Y. Chen, Acta Chim. Sin., 52 (1994) 1118 (in Chinese).

[30] J.F. Evans, T. Kuwana, M.T. Henne and G.P. Royer, J. Electroanal. Chem., 80 (1977) 409.

[31] V. Svetličić, J. Clavilier, V. Žutić and J. Chevalet, J. Electroanal. Chem., 312 (1991) 205.

[32] K. Aoki, K. Tokuda and H. Matsuda, J. Electroanal. Chem., 199 (1986) 69.

Review

Basic aspects and applications of tristimulus colorimetry

K.M.M. Krishna Prasad*, S. Raheem, P. Vijayalekshmi, C. Kamala Sastri

Physical Chemistry Research Laboratories, School of Chemistry, Andhra University, Visakhapatnam 530003, Andhra Pradesh, India

Abstract

A detailed account of the specification of colour using the 1931 Commission International de L'Eclairage tristimulus coordinates and subsequent colour spaces for the measurement of small differences in colour is provided along with a review of the application of quantitative parameters for the evaluation of colour changes of acid–base and complexometric indicators. The development of screened indicators to improve the quality of colour changes at the equivalence point is discussed. Various computer programs proposed to calculate the different parameters by different algorithms are reviewed.

Keywords: Colour specification; Computer programs; Indicators; Tristimulus colorimetry

1. Introduction

Colour is what we see [1]. The sensation that results when one looks at a coloured object depends upon the nature of the surrounding field and the nature of the field to which the observer has been previously exposed. Therefore, the fundamental specification of colour must consider it as an inherent property of an object and must be based on objective measurements [2]. This specification of colour enables one to define it in terms of a set of physical operations. Consequently, the set of physical operations carried out to arrive at a physical quantity is considered as the definition of colour [3].

The visual stimulation that results when one looks at a coloured surface depends upon the character of the light by which the surface is illuminated. If a source of light is radiating energy confined within a narrow band of wavelengths such as the violet region of the spectrum, the surface will reflect only violet light. In other words, if a source is illuminated by light of substantially a single wavelength it will reflect light of this wavelength, except in the case of materials that exhibit fluorescence. Even though it is known that green paint reflects green light more effectively than light of other wavelengths, it is possible to make the green paint take on any hue of the spectrum, if suitably illuminated. However, when light of daylight quality, which is a mixture of all the components of the visible spectrum in

---

* Corresponding author.

nearly equal proportions, falls upon the surface of the green paint, blue–greenish light is reflected into the eye of the observer. In the case of an individual colour, the wavelength of the spectral region with which that particular colour is most closely identified, when illuminated by daylight, is known as its dominant wavelength [4]. However, in the case of purple it is impossible to find a single region of the spectrum that simulates this colour and the observed dominant wavelength (from the spectral reflectance curve) is that of the green colour which is complementary to purple, where the complement of a colour is the colour that produces a neutral grey in an additive mixture of the two colours.

Extensive investigations have been carried out to study the distrubution of energy (E_0) in daylight [5] by dispersing it into a spectrum by means of a prism. Each spectral region is then isolated and the amount of energy present in each region is determined from the reading of a sensitive temperature-measuring device, the surface of which has been blackened so as to convert the light energy into heat. From these studies a filter has been prepared which, when used with a tungsten lamp operated at the proper temperature, provides a source that is a close approximation to the average daylight (which is considered as a mixture of sunlight and blue light from the sky on a clear day). A source having this distribution of energy was adopted as an international standard of illumination at a meeting of the International Commission of Illumination (Commission International de L'Eclairage; CIE) in 1931 [6]. This standard source is usually denoted I.C.I. illuminant C. Two other standards, designated illuminant A and illuminant B, were also adopted at the same meeting. Illuminant A represents a source having an energy distrubution similar to that of a gas-filled tungsten lamp, whereas illuminant B is an approximate representation of mean noon sunlight. Illuminant B is slightly yellower than illuminant C and has an energy distribution intermediate between those of illuminants A and C. The characteristics of these three standard illuminants are given below [7,8].

1.1. Illuminant A

Illuminant A is a tungsten lamp operated at a temperature of 2800 K.

1.2. Illuminant B

Illuminant B utilises a lamp having the spectral quality of illuminant A in combination with a filter. The filter consists of 1 cm thick layers of each of the solutions B_1 and B_2. These solutions are in a double cell constructed of optical glass. The composition of each solution is as follows.

Solution B_1: copper sulphate ($CuSO_4 \cdot 5H_2O$), 2.452 g; mannite [$C_6H_8(OH)_6$], 2.452 g; pyridine (C_2H_5N), 30.00 ml, distilled water to make up to 1000.0 ml.

Solution B_2: cobalt ammonium sulphate [$CoSO_4(NH_4)_2SO_4 \cdot 6H_2O$], 21.71 g; copper sulphate ($CuSO_4 \cdot 5H_2O$), 16.11 g; sulphuric acid (density 1.835 g cm^{-3}), 10.00 ml, distilled water to make up to 1000.0 ml.

1.3. Illuminant C

Illuminant C consists of a source having the spectral quality of illuminant A in combination with a filter. An identical cell is used but the solutions C_1 and C_2 have the following compositions.

Solution C_1: copper sulphate ($CuSO_4 \cdot 5H_2O$), 3.412 g; mannite [$C_6H_8(OH)_6$], 3.412 g; pyridine (C_2H_5N), 30.00 ml, distilled water to make up to 1000.0 ml.

Solution C_2: cobalt ammonium sulphate [$CoSO_4(NH_4)_2SO_4 \cdot 6H_2O$], 30.580 g; copper sulphate ($CuSO_4 \cdot 5H_2O$), 22.520 g; sulphuric acid (density 1.835 g cm^{-3}), 10.00 ml, distilled water to make up to 1000.0 ml.

The spectral energy distributions of the three standard illuminants A, B and C, as adopted by the C.I.E., are taken from the consolidated study of Judd [3,4].

The question to be considered now is how light with a known distribution of energy will stimulate the eye of an observer. Even though no two observers respond in the same manner to a stimulus, the differences are very small except in the

case of observers with colour blindness [9]. Normally, an observer exposed to light of a known spectral quality cannot describe the sensation that it produces in absolute terms but only in terms of reference to some other visual sensation. Such a reply is not a description of the sensation but it does provide information that another stimulus evokes the same sensation. The analogy suggests the possibility of evaluating a colour in terms of certain standard or primary stimuli. However, it is already known that the sensation of any colour stimulus on the observer's eye can be duplicated by mixing light from three primary sources in the correct proportions. This can be achieved with the help of an optical instrument containing a suitable photometric field of view [6]. The light whose colour is to be matched is introduced into one half of the field and the light from the three sources is introduced in controlled amounts into the other half. By manipulation of the controls. a setting can be found where an exact colour match between the two halves of the field is obtained. For any given colour there is one setting for each of these controls that will produce a match. By calibrating the controls, the amount of each primary can be recorded. The unknown colour can then be specified by three numbers X, Y and Z. These numbers are known as the tristimulus values and each number represents the amount of one of the primary stimuli. The tristimulus values for any colour can then be obtained by the experimental work of an observer on a properly designated optical instrument [5]. When the same experiment is carried out by another observer for the same colour, the tristimulus values obtained are slightly different from the values reported by the earlier observer even though neither of the observers can be classed as colour blind. The two specifications may differ slightly because of the individual characteristic nature of the observers in obtaining the exact colour match by mixing the three primaries. This has led to the comparison of inter-laboratory experimental data of different groups of observers. However, the combination of the basic colour mixture data from a large group of carefully selected observers and spectrophotometric data resulted in a method to compute the average tristimulus values for any test sample.

Since the readings obtained with a spectrophotometer are independent of the peculiarities of an observer's eye, this procedure provides a basis for the specification of colour in terms of the average chromatic properties of an internationally accepted group of observers.

Initially, it is essential to determine the chromaticity values of radiation of different wavelengths with standard observers using a simple optical instrument (colorimeter). One half of the photometric field of the colorimeter is illuminated by a measured quantity of light of approximately a single wavelength, for example 400 nm. Then the observer determines the amount of each of the three primaries required to colour-match both halves of the field. These amounts of the primaries are the tristimulus values for this quantity of light of this wavelength [6]. The wavelength of light is then changed to 410 nm. Again a colour match is made and the tristimulus values are recorded. This process is continued until the entire visible spectrum has been examined. Experiments of this sort were carried out by a number of researchers and the results obtained by them were summarized and published in a convenient form by the Colorimetry Committee of the Optical Society of America [2]. After the publication of these data, it became feasible to base tristimulus specifications on spectrophotometric data. In this way the uncertainties associated with the colorimeter can be avoided and the spectrophotometer can be used to determine the tristimulus values. However, Wright [10] and Guild [11] independently redetermined the fundamental data employing a number of carefully selected observers. The primaries employed in the experimental study of Wright [10] are spectrum colours and their wavelengths are 650, 530 and 460 nm. However, Guild [11] chose red, blue and green primaries in his investigations. When the results of these two investigators were reduced to a comparable basis, it was discovered that their data were in extraordinary good agreement with each other and also in good agreement with Optical Society of American data [2]. In 1931, the CIE undertook the task of bringing out an international standard procedure for the evaluation of tristimulus values for the pure spectrum colours. The tristimulus values that were adapted

by the CIE using good experimental techniques and a number of observers for various spectrum colours are presented at intervals of 10 nm [2].

The tristimulus values ($\bar{x}$, $\bar{y}$, $\bar{z}$) of the pure spectrum colours indicate the amount of each of the primaries that is required to colour-match a unit quantity of radiant energy of the various wavelengths. The value of $\bar{x}$ represents the amount of a primary which is a reddish purple of higher saturation than any obtainable colour having this hue. The value of $\bar{y}$ represents the amount of a green primary considerably more saturated than the spectrum colour whose wavelength is 520 nm. The value of $\bar{z}$ represents the amount of blue primary that is considerably more saturated than the spectrum colour whose wavelength is 477 nm.

The tristimulus values of the spectrum colours at different wavelengths, with 10 nm intervals, that were adapted by the International Commission on Illumination are presented in Table 1. This provides the necessary data for evaluating a stimulus that is equivalent to the given sample when the latter is illuminated by light having the spectral quality of illuminant C and is viewed by the standard observer.

2. Determination of tristimulus values

The tristimulus values of a test sample can be determined by adopting two equivalent procedures which are denoted "weighted ordinate method" and "selected ordinate method".

2.1. Tristimulus values obtained by the weighted ordinate method

The tristimulus values of the test sample can be determined by multiplying the transmittance at a particular wavelength by the product of the energy and tristimulus value of that wavelength followed by the summation of these values corresponding to each primary. Once the spectrum of the sample whose chromaticity values are to be determined is available, the procedure tends to be the multiplication of the transmittance at a particular wavelength by the $E_0\bar{x}$, $E_0\bar{y}$ and $E_0\bar{z}$ values at that wavelength and the same procedure is also

repeated at other wavelengths. The summation of the product values for each of the three primaries results in three chromaticity values (X, Y, Z) for that colour and can be represented mathematically as follows [12]:

$$X = \sum_{380\ \text{nm}}^{700\ \text{nm}} E_0 \bar{x} T \Delta\lambda \tag{1}$$

$$Y = \sum_{380\ \text{nm}}^{700\ \text{nm}} E_0 \bar{y} T \Delta\lambda \tag{2}$$

$$Z = \sum_{380\ \text{nm}}^{700\ \text{nm}} E_0 \bar{z} T \Delta\lambda \tag{3}$$

Table 1
Tristimulus values of pure spectrum colours

Wavelength (nm)	$\bar{x}$	$\bar{y}$	$\bar{z}$
400	0.0143	0.0004	0.0679
410	0.0435	0.0012	0.2074
420	0.1344	0.0040	0.6456
430	0.2839	0.0116	1.3856
440	0.3483	0.0230	1.7471
450	0.3362	0.0380	1.7721
460	0.2908	0.0600	1.6692
470	0.1954	0.0910	1.2876
480	0.0956	0.1390	0.8130
490	0.0320	0.2080	0.4652
500	0.0049	0.3230	0.2720
510	0.0093	0.5030	0.1582
520	0.0633	0.7100	0.0782
530	0.1655	0.8620	0.0422
540	0.2904	0.9540	0.0203
550	0.4334	0.9950	0.0087
560	0.5954	0.9950	0.0039
570	0.7621	0.9520	0.0021
580	0.9163	0.8700	0.0071
590	1.0263	0.7570	0.0011
600	1.0622	0.6310	0.0008
610	1.0026	0.5030	0.0003
620	0.8544	0.3810	0.0002
630	0.6424	0.2650	0.0000
640	0.4479	0.1750	0.0000
650	0.2835	0.1070	0.0000
660	0.1649	0.0610	0.0000
670	0.0874	0.0320	0.0000
680	0.0468	0.0170	0.0000
690	0.0227	0.0082	0.0000
700	0.0114	0.0041	0.0000

2.2. Tristimulus values obtained by the selected ordinate method

In the weighted ordinate method a summation is made of the values of $E_0\bar{x}T$, $E_0\bar{y}T$ and $E_0\bar{z}T$ at wavelengths equally spaced throughout the visible region, i.e. $\Delta\lambda$ is constant. However, in the selected ordinate method, the wavelength intervals are unequal and are chosen so as to give constant $E_0x\Delta\lambda$, $E_0y\Delta\lambda$ and $E_0z\Delta\lambda$ values. The integration process in this procedure is effected by making a summation of transmittance values at median wavelengths of each of these wavelength intervals. The three sums are multiplied by factors which are proportional to the constants, $E_0x\Delta\lambda$, $E_0y\Delta\lambda$ and $E_0z\Delta\lambda$. The values of the wavelengths at which the transmittance values are measured are known as selected ordinates. The mode of calculation using 100, 30 and 10 selected ordinate methods has been described by Hardy [2]. The values of the ordinates (median wavelenghts) for the three standard illuminants A, B and C are tabulated [2]. In addition, the factor values used to multiply the summation of the transmittance values to obtain tristimulus values are mentioned. The selected ordinate method reduces the process of determining the tristimulus values to mere addition of transmittance values, whereas the weighted ordinate method involves many multiplications followed by summation.

In the present investigation the weighted ordinate method is adopted for the evaluation of chromaticity coordinates.

2.3. Chromaticity diagram

In order to understand the relationship between the various colours a graphical representation of the tristimulus values has been proposed. It was found that this would require a three-dimensional coordinate system which is not practicable. Therefore the coordinates denoted by trichromatic coefficients as

$$x = \frac{X}{X + Y + Z} \tag{4}$$

$$y = \frac{Y}{X + Y + Z} \tag{5}$$
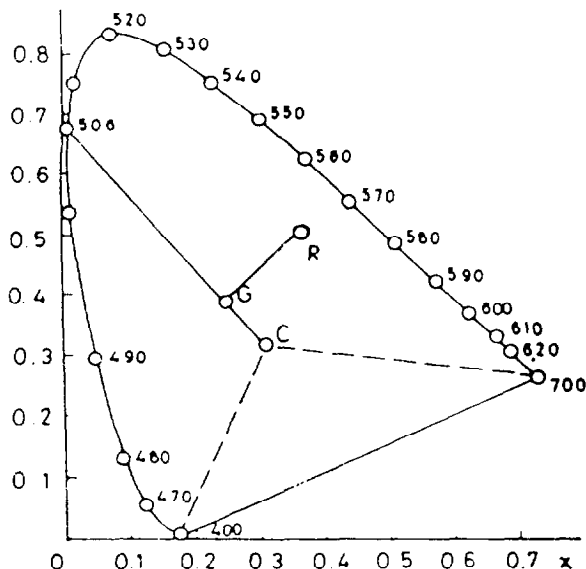
Fig. 1. Chromaticity diagram showing that the green (G) may be regarded as a mixture of illuminant (C) and a spectrum colour having a wavelength of 506 nm and (R) is the colour point of a red colourant.

and

$$z = \frac{Z}{X + Y + Z} \tag{6}$$

are used for convenient representation of chromaticity in a two-dimensional diagram as shown in Fig. 1. Among the coordinates z is dependent on x and y and so only x and y need to be considered for the description of the sample colour. However, the trichromatic coefficients (coordinates), used to denote true colour points on the chromaticity diagram are

$$x = \frac{\sum E_0\bar{x}T\Delta\lambda}{\sum E_0\bar{x}T\Delta\lambda + \sum E_0\bar{y}T\Delta\lambda + \sum E_0\bar{z}T\Delta\lambda} \tag{7}$$

$$y = \frac{\sum E_0\bar{y}T\Delta\lambda}{\sum E_0\bar{x}T\Delta\lambda + \sum E_0\bar{y}T\Delta\lambda + \sum E_0\bar{z}T\Delta\lambda} \tag{8}$$

$$z = \frac{\sum E_0\bar{z}T\Delta\lambda}{\sum E_0\bar{x}T\Delta\lambda + \sum E_0\bar{y}T\Delta\lambda + \sum E_0\bar{z}T\Delta\lambda} \tag{9}$$

The curve (Fig. 1) represents the locus of all the spectrum colours and the points on this curve are

trichromatic coefficients which are calculated from the trichromatic values of pure spectrum colours. The trichromatic coefficients for standard illuminant C are $x = 0.3101$ and $y = 0.3163$ (Fig. 1).

A chromaticity diagram is of immense value especially when more than one colour exists in the form of a mixture. If R and G represent red and green on the chromaticity diagram, then the point corresponding to an additive mixture of these two colours will always lie on the line joining R and G, regardless of the proportion in which these colours are mixed.

All real colours lie within the area enclosed by the solid line, since every real colour can be considered to be a mixture of its spectral components in various proportions. All the real colours lying both within the solid line and above the broken lines in Fig. 1 can be considered as a mixture of standard illuminant C and spectrum light of a certain wavelength. Consequently the colour point G can be treated as a mixture of standard illuminant C and spectrum light having a wavelength of 506 nm. This wavelength is known as the dominant wavelength. Since the green lies on a line which terminates as a pure spectrum colour at one end and at the illuminant point at the other end, the sample is not so pure a green as the corresponding spectrum colour. The ratio of the distances of the sample point and the pure spectrum point from the illuminant point is denoted as the purity of the sample. The numerical procedure proposed by Judd [13] for the calculation of the dominant wavelength is adopted in the present investigation.

As the three-dimensional coordinate system of representation of chromaticity is reduced to a two-dimensional system, the colour space is non-uniform. Judd [14] suggested the possibility of constructing chromaticity diagrams in which approximately equal distances separate points representing all pairs of equally bright colours which are just noticeably different under certain specified conditions of observation. Methods for the transformation of CIE coordinates into other coordinate systems were pursued by MacAdam [15,16]. Breckenridge and Schaub [17] proposed a coordinate system called the rectangular uniform

chromaticity scale (RUCS) in which the first quadrant contains only greens, the second blues, the third purples and the fourth reds and yellows. General transformation equations for changing coefficients into RUCS (U, V) coordinates are given by

$$U = 0.075 - \frac{0.832(x + y - 1)}{1.0x - 7.05336y - 1.64023} \qquad (10)$$

$$V = \frac{3.6970x - 5.07713y - 1.36896}{1.0x - 7.05336y - 1.64023} - 0.5 \qquad (11)$$

The reverse transformation equation, i.e. conversion of RUCS coordinates into CIE coordinates, was also proposed by these authors.

Measurement of the colour difference represented by two points on the chromaticity diagram is not feasible because equal distances between two points do not represent the same amount of colour difference at different locations in the chromaticity diagram. MacAdam [18] studied this factor and represented the experimental results in the form of 25 ellipses in the chromaticity diagram. In each for these ellipses every line from the centre to any point on the periphery of the ellipse represents approximately 100 chromaticity steps just noticeable by the eye of an observer. The determination of a unit standard deviation for colour matching (ΔS), was suggested by MacAdam [19] using the emperical relation

$$\Delta S = [g_{11}(\Delta x)^2 + 2g_{12}(\Delta x)(\Delta y) + g_{22}(\Delta y)^2]^{1/2} \qquad (12)$$

in which g_{11}, $2g_{12}$ and g_{22} were determined from the contour diagrams and Δx and Δy indicated the numerical differences between the coordinates of two neighbouring colour points whose colour difference is being measured.

The CIE recommended a colour space denoted as CIE Lu^*v^* to promote uniformity of practice in the evaluation of colour differences [20]. This colour space is produced by plotting the quantities L, u^*, v^* in rectangular coordinates and which were defined as

$$L = 116(Y/Y_n)^{1/3} - 16 \qquad (13)$$

$$u^* = 13L(u - u_0) \qquad (14)$$

$$v^* = 13L(v - v_0) \qquad (15)$$

where the values of u, v, u_0 and v_0 were given as

$$u = \frac{4X}{X + 15Y + 3Z} \quad \text{and} \quad v = \frac{9Y}{X + 15Y + 3Z} \quad (16)$$

$$u_0 = \frac{4X_n}{X_n + 15Y_n + 3Z_n} \quad \text{and}$$

$$v_0 = \frac{9Y_n}{X_n + 15Y_n + 3Z_n} \quad (17)$$

In the expressions for u_0 and v_0, the values of X_n, Y_n and Z_n are tristimulus values of the standard illuminant C ($X_n = 98$, $Y_n = 100$ and $Z_n = 118$) and the coordinates (u, v) are the simplified transformation to the perceptually more uniform chromaticity spacing (PMUCS) as recommended by CIE [5,21]. The total colour difference ΔE^*(CIE Lu^*v^*) between two colours, each given in terms of L, u^*, v^*, is calculated from

$$\Delta E^* \text{CIE}(Lu^*v^*) = [(\Delta L)^2 + (\Delta u^*)^2 + (\Delta v^*)^2]^{1/2} \quad (18)$$

Another uniform colour space (CIE La^*b^* 1976) [22,23] recommended by the *CIE Colorimentry Committee Working Program on Colour Differences* is produced by plotting the quantities L, a^*, b^* in rectangular coordinates which are defined as

$$L = 116(Y/Y_n)^{1/3} - 16 \quad (13)$$

$$a^* = 500[(X/X_n)^{1/3} - (Y/Y_n)^{1/3}] \quad (19)$$

$$b^* = 200[(Y/Y_n)^{1/3} - (Z/Z_n)^{1/3}] \quad (20)$$

The total colour difference ΔE^* CIE La^*b between two colours each given in terms of L, a^*, b^* is calculated from

$$\Delta E^* \text{CIE}(La^*b^*) = [(\Delta L)^2 + (\Delta a^*)^2 + (\Delta b^*)^2]^{1/2} \quad (21)$$

Richter [24] suggested a new uniform colour space LABHNU 1977 whose coordinates were obtained from the expressions:

$$L = 116(Y/Y_n)^{1/3} - 16 \quad (13)$$

$$A^* = 500(A' - A'_n)Y^{1/3} \quad (22)$$

$$B^* = 500(B' - B'_n)Y^{1/3} \quad (23)$$

where

$$A' = 1/4(x/y + 1/6)^{1/3} \quad (24)$$

and

$$B' = -1/12(z/y + 1/6)^{1/3} \quad (25)$$

2.4. Complementary tristimulus colorimetry

The procedure described for specifying colours by tristimulus colorimetry is applicable for characterisation of additive colours only. However, in the case of chemical indicators, subtractive colours are involved. Moreover, the concentration of the indicator and the presence of other colorants influences the final colour of a solution in a complicated way. This difficulty arises because the intensity of the light leaving the titration vessel is related to the concentration in an exponential manner in accordance with Beer's law. Consequently, the simple treatment of additive colours is no longer applicable to evaluating the quality of colour change of indicators.

In view of the above, Reilley et al. [25] resorted to the application of complementary tristimulus colorimetry for the characterisation of the color quality of indicator transitions. The "complementary tristimulus coordinates" (Q_x, Q_y, Q_z) are calculated by following essentially the same procedure adopted in the case of tristimulus coefficients (coordinates), but the transmittance value is replaced by the absorbance value (A) in these calculations. The complementary tristimulus coordinates can be represented as

$$Q_x = \frac{\sum E_0 \bar{x} A \Delta\lambda}{\sum E_0 \bar{x} A \Delta\lambda + \sum E_0 \bar{y} A \Delta\lambda + \sum E_0 \bar{z} A \Delta\lambda} \quad (26)$$

$$Q_y = \frac{\sum E_0 \bar{y} A \Delta\lambda}{\sum E_0 \bar{x} A \Delta\lambda + \sum E_0 \bar{y} A \Delta\lambda + \sum E_0 \bar{z} A \Delta\lambda} \quad (27)$$

$$Q_z = \frac{\sum E_0 \bar{z} A \Delta\lambda}{\sum E_0 \bar{x} A \Delta\lambda + \sum E_0 \bar{y} A \Delta\lambda + \sum E_0 \bar{z} A \Delta\lambda} \quad (28)$$

The relationship between the tristimulus coordinates and the complementary tristimulus coordinates is derived and presented as follows:

$$P_r = G_r - J(Q_r - G_r) - J^2(Q_r - G_r + Q_r^d) \quad (29)$$

where P_r (where $r = 1, 2$ and 3 implies x, y and z) is the true colour point and Q_r is the complementary colour point, G_r is the illuminant point, Q_r^d is a measure of the dichromatistic tendency of the colour system and J is the optical concentration which is a product of the concentration (c) and the total absorptivity of the colour system (E).

The complementary colour point Q_r specifies the colour of a subtractive colour system in a concentration-independent way, whereas the true colour point is concentration-dependent and moves from the grey point to the periphery of the chromaticity diagram as the concentration increases. Since the complementary colour point is related to the light absorbed by the solution, this point will be located in the chromaticity diagram at a place corresponding to the complementary colour of the true colour point. However, the coordinates of the illuminant point (grey light) are the same and are independent of the colour system.

Eq. (29) was further simplified by introducing two other quantities, namely V_r and W_r, which are sufficient to describe a dilute colour system fully and are given by

$$V_r = Q_r - G_r \tag{30}$$

$$W_r = V_r - Q_r^d \tag{31}$$

The expression for the true colour point in terms of these quantities can be written as

$$P_r = G_r - JV_r - J^2 W_r \tag{32}$$

This equation is used as a unified basis for the interpretation and calculation of colour phenomena, such as designation of colour change, quality of the end points and screening of the indicators.

2.5. Determination of quality of colour change

The overall quality of colour change of an indicator at the end point is a composite function of two factors, namely (1) the chemistry of reaction which governs the colour change and (2) the colour phenomena in the solution and their relation to the observing eye. The latter problem is much more complex because it involves physiological and psychological parameters.

In order to solve this problem Reilley et al. [25] took advantage of the numerical characterisation of the colour of the indicator by complementary tristimulus colorimetry to evaluate the quality of colour change of the indicator. Since any colorant has fixed complementary tristimulus coordinates on the chromaticity diagram, the distance between the two points of the titrant solution before and after the end point is considered as a quantitative measure of the quality of colour change of the indicator used in this titration. The longer the distance between the two points, the better will be the quality of colour change at the end point. However, the distance alone is not adequate, as the location of the points in the diagram is also important. Besides these two factors, the greyness should also be considered.

Let $Q_{r,b}$ and $Q_{r,a}$ represent the complementary colour coordinates of an indicator before and after the end point. The quality of the colour change at the end point is considered to be good if the distance between the points is considerable. Also, if the line traverses through the grey point and extends beyond it, the quality of colour change is better still, because a grey (colourless) region appears during the transition of the indicator from one colour to another at the end point and provides a better memory factor.

For a set of indicators the quality of their colour change at the end point can be compared on a quantitative basis from the measured value of the distance between complementary colour coordinates before and after the colour change of the respective indicators. Such comparison is worthwhile only when all the corresponding lines joining the $Q_{r,b}$ and $Q_{r,a}$ coordinates of the set of indicators are lying in the same location of the chromaticity diagram. Only when the length, location and direction of the line joining $Q_{r,b}$ and $Q_{r,a}$ are the same for two different indicators is the quality of colour change for these two indicators considered to be equal. Therefore, the point to be made in the study of chromatic differences is that equal distances do not represent the same quality of colour change at different locations in the chromaticity diagram.

Bhuchar et al. [26] studied this factor and utilised the RUCS coordinates (U, V) in accor-

dance with the transformation recommended by Breckenridge and Schaub [17] (Eqs. (10) and (11)), to calculate a parameter called the specific colour discrimination (SCD), which is defined as the average number of colour discrimination steps for an acid–base indicator for one pH unit. It can be obtained from the relationship

$$SCD = \frac{1}{3} \times 1000 \frac{[(U_2 - U_1)^2 + (V_2 - V_1)^2]^{1/2}}{pH_2 - pH_1} \quad (33)$$

in which (U_1, V_1) and (U_2, V_2) are the RUCS coordinates at the pH values pH_1 and pH_2. This relationship can be expressed in a simplified way as

$$SCD = \frac{1}{3} \times 1000 \times \frac{\Delta\sigma}{\Delta pH} \quad (34)$$

The parameter SCD is correlated with the unit standard deviation for colour matching (ΔS) values of MacAdam [19] ellipses (Eq. (12)), using the data of several phthalein and sulphonephthalein indicators, (phenolphthalein, cresolphthalein, thymolphthalein, Phenol Red, Cresol Red, Thymol Blue and Congo Red), by plotting SCD vs. ΔS. The slopes of the straight lines obtained for all the studied indicators are found to be unity, indicating a correlation between these two parameters. Therefore the numerical value of SCD at the pH of maximum colour change (pH_{mcc}) is taken as the quantitative measure of the quality of colour change. The half bandwidth of the SCD vs. pH peak is inversely proportional to the rapidity of the colour change. This study of Bhuchar et al. [26] enabled comparison of the quality of colour change of a series of acid–base indicators and the rapidity of colour change at the end point. Bhuchar and Agarwal [27] synthesised two sulphamphthalein indicators, namely phenol sulphamphthalein and o-cresol sulphamphthalein, to evaluate the colour change in terms of SCD, which is determined from RUCS coordinates and PMUCS coordinates (Eq. (16)), in order to compare this parameter with the CIE La^*b^* 1976 parameter. From the results, it was concluded that ΔE^* CIE La^*b^* (Eq. (21)) appears to have the same significance as ΔS, the unit standard deviation for colour matching (Eq. (12)). It is further stated that CIE La^*b^* recommendations

are preferred over the RUCS or PMUCS modes of calculation. No matter how the numerical values of the pH of maximum colour change, the half bandwidth of the change of SCD in pH units and the SCD value would hold true. The graphs drawn between a^* and b^* (Eqs. (19), (20)) are presented to clearly visualise the transition of the indicators, since the origin in this plot is the illuminant point (grey).

Cacho et al. [28] proposed another parameter, based on the optical concentration J, to evaluate the equality of colour change of indicators in aqueous medium. The progress of optical concentration values of acid–base indicators, such as o-cresolphthalein, thymolphthalein, phenolphthalein, phenol red, crespol red, thymol blue and congo red, with change of pH is shown by plotting $\Delta J/\Delta pH$ vs. pH. From the value of $\Delta J/\Delta pH$ at the pH of the maximum colour change, the quality scale of these indicators in the alkaline region is proposed in descending order as cresolphthalein > thymolphthalein > cresol red > thymol blue > phenol red > congo red > phenolphthalein. This order of quality of colour change is the same as the one proposed by Bhuchar et al. [26], indicating that the behaviour of the parameter $\Delta J/\Delta pH$ is similar to that of SCD. A similar parameter has been utilised for evaluation of colour changes of complexometric indicators in the titration of calcium with EDTA [28].

Martinez Calatayud et al. [29] ignored this parameter because in most cases two peaks are obtained in the graphs $\Delta J/\Delta pH$ vs. pH, causing gross errors in calculating the pH of maximum colour change. It is also concluded that the total colour difference ΔE^* is the most uniform parameter because of its linear behaviour with respect to the standard deviation of colour matching (ΔS). Fernandez and Guzman Chozas [30] stated that the total colour difference ΔE^* CIE La^*b^* and the parameters of SCD are adequate for describing a colour change because the CIE La^*b^* parameters are linearly related to the LABHNU parameters.

Kotrly and Vytras [31] proposed a method for the calculation of the optimum concentration of an indicator in a particular titration by plotting

the parameter $\Delta\text{pH}/\Delta E^*$ (index of colour change perceptibility) against log C/C_0, where C is the indicator concentration used for the calculation of the particular chromaticity transition and C_0 is the experimental value of the indicator concentration. The value of the concentration C at the minimum of this curve is taken as the optimum concentration of the indicator in the titration. Reilley and Smith [32] proposed an expression for the determination of the equilibrium constant of the indicator $\text{p}K_a$ using complementary tristimulus coordinates, which is expressed as

$$\text{p}K_a = \text{pH} - \log \frac{(Q_r)_\text{A} J_\text{A} - Q_r J}{Q_r J - (Q_r)_\text{B} J_\text{B}}$$

where Q_r is the complementary colour point, and $(Q_r)_\text{A}$ and $(Q_r)_\text{B}$ are the chromaticity coordinates of the indicator at the pH mentioned in the above equation in acidic and base media respectively. Flaschka [33] also reported a similar equation for the determination of $\text{p}K_a$ which includes the optical concentration (J) term also.

2.6. Specification of colour changes of complexometric indicators

The parameters described for specifying the colours and colour differences in accordance with tristimulus colorimentry are determined at different C_L/C_M (ratio of the concentrations of ligand to metal ion) values for the evaluation of quality of colour change of indicators, in order to give an objective basis for indicator selection in complexometric titrations.

The 1931 CIE parameters (x, y), the RUCS coordinates (U, V), the dominant wavelength (λ_d) and the purity (p_e) were used to evaluate the quality of colour change of indicators such as xylenol orange, methyl thymol blue, pyrocatechol violet, pyrogallol red and bromopyrogallol red, in the titration of lead (II) with ethylene diaminetetraacetic acid (EDTA) by Kotrly and Vytras [34]. Methyl thymol blue is recommended as the most suitable indicator for this titration, since its colour transition curve passes very close to the grey point. A study with the involvement of the CIE Lu^*v^* parameters also supported the same conclusion [35]. However, a study by Martinez

Calatayud et al. [36] on the specification of colour changes of these indicators with the help of coordinates (x, y), RUCS coordinates (U, V), PMUCS coordinates (u, v), CIE La^*b^* and $\Delta J/\Delta(C_\text{L}/C_\text{M})$ vs. C_L/C_M revealed that bromopyrogallol red is the most suitable indicator, followed by methyl thymol blue. However, Arsenazo III is reported to be superior in terms of its colour change over all the other indicators studied in this titration, as the plot of $\Delta E^*/\Delta(C_\text{L}/C_\text{M})$ vs. C_L/C_M exhibited a higher peak for this indicator [37]. The quality of this indicator is assessed in the complexometric titration of calcium(II), bismuth(III), iron(III) and lanthanum(III) by specifying the colour changes with the coordinates (x, y), CIE La^*b^* parameters and the plot a^* vs. b^*. Arsenazo II and sulphosalicylic acid acid indicators are recommended over salicylic acid and potassium thiocyanate in the titration of iron(III) with EDTA from a study of the trichromatic parameters (x, y), (U, V) and CIE La^*b^* [38].

The quality of colour change of indicators such as Arsenazo III, calcein, calcon, eriochrome blue black B, methyl thymol blue, murexide, phthalein complexone and thymolphthalein complexone in the titration of calcium(II) with EDTA is specified from the parameters (x, y), (Q_x, Q_y), colour concentration (J), dominant wavelength (λ_d) and purity of the colour (p_e) determined at different values of C_L/C_M near the end point and from a plot of $\Delta J/\Delta(C_\text{L}/C_\text{M})$ vs. C_L/C_M [39]. The following order of indicator quality of colour change has been mentioned: thymolphthalein complexone > phthalein complexone > Arsenazo III > calcon = murexide > calcein > methyl thymol blue = eriochrome blue black B. However, arsenazo (2-(4-arsonophyl)-(azo-7-(antipyril)azo-1,8-dihydroxy-3,6-naphthalene disulphonic acid) is considered a superior indicator in this titration because the trajectory of the (x, y) curve is almost perpendicular to the major axis of the MacAdam ellipse situated in that region [40]. A sharp peak observed in the plot of $\Delta E^*/\Delta(C_\text{L}/C_\text{M})$ vs. C_L/C_M for this indicator further confirmed its superior quality of colour change.

Vytras et al. [41] studied the trichromatic parameters, namely (x, y), (Q_x, Q_y), PMUCS (u, v), the colour concentration (J), dominant wave-

length (λ_d), purity of the colour (p_e) and CIE Lu^*v^* parameters for the specification of colour changes of the metallochromic indicators eriochrome blue SE, eriochrome red B, naphthylazoxine 6S, SNAZOXS (disodium salt of 8-hydroxy-7-[(4-sulphonaphthyl) azo]-5-quinoline sulphonic acid) and zincon[2-(2-(α-(2-hydroxy-5-sulphonphenyl azo) benzylidene) hydrazino) benzoic acid] in the titration zinc(II) with EDTA and claimed that zincon gives the best colour quality of transition, since the colour change is from blue to orange–yellow and passes close to the point of achromatic colour. Cacho et al. [28] determined the values of the optical concentration (J) via the titration of copper(II) with EDTA using indicators such as PAN(1-(pyridyl(-2′-azo-2-naphthol))), MeTDAN(2-(5-methyl-1,3,4-thiadiazolyl azo-1)-2-naphthol), murexide, MeTDAΔMF(2-(5-methyl-1,3,4-thiadiazolylazo-6)-3,4-dimethyl phenol) and TeADMF(5-(1,2,3,4-tetrazolylazo-6)-2,4-dimethyl phenol), and the order of the quality of colour change is ascertained from a plot of $\Delta J/\Delta(C_L/C_M)$ vs. C_L/C_M. However, Martinez Calatayud et al. [29] in their critical search for an ideal chromatic parameter stated that the colour concentration (J) showed a non-uniform behaviour and hence it is not recommended for the measurement of quality of colour change. The parameter ΔE^* is preferred in this regard, as it is more uniform against the standard deviation of colour matching, ΔS.

Cacho et al. [42] used arsenazo [2-(2-arseno phenyl) azo-7-(4-azo-1,8-dihydroxy-3,6 naphthalein disulphonic acid] as metallochromic indicator in the titration of calcium(II) with EDTA and its colour quality was studied using CIE chromaticity diagrams.

Cacho et al. [43] investigated the performance of five metallochromic indicators in the determination of barium using tristimulus chromaticity theory and concluded that metolphthalein and thymolphthalein complexone were the most suitable out of the indcators studied. Further to this, Cacho et al. [44] carried out a comparative study of metallochromic indicators for the titrimetric determination of magnesium with EDTA and observed that eriochrome black T and antipyrl-o-arsenazo I were the most suitable indicators for this titration.

The quality of colour changes at the end point in the complexometric titration of bismuth (III) with EDTA, using the indicators hematoxylin, PAN [1-(2-pyridyl azo)-naphthol-2], PAR [4-(2-pyridyl azo)-resorcinol], xylenol orange and thoron, was studied by means of the 1931 CIE trichromatic system, using SCD and colour difference (ΔE^*) and hematoxylin was recommended as the most suitable indicator for this titration [45]. Krishna Prasad and Raheem [46] applied trichromatic colorimetry for the specification of colour changes of metallochromic indicators, namely PAR, eriochrome black T, bromopyrogallol red, solochrome blue black B, pyrocatechol violet and PAN, in the complexometric titration of cadmium(II) to assess the quality of colour change at the equivalence point using the CIE La^*b^* 1976 system and the value of the SCD parameter. Prasad and Raheem [47] measured the quality of colour change of the complexometric indicators eriochrome black T, bromopyrogallol red, solochrome blue black B, pyrocatechol violet, methyl thymol blue, chromeazurol S and solochrome dark blue in the titration of magnesium(II) with EDTA with the help of tristimulus colorimetry. Studies on the specification of colour changes of the complexometric indicators in the titration of metal ions, namely copper(II) [48], nickel(II) [49] and cobalt(II) [50], with EDTA were carried out recently.

2.7. Specification of colour changes of acid–base indicators in aqueous medium

Fortune and Mellon [51] carried out a spectrophotometric study of a number of neutralisation indicators and specified the colour of the indicators before and after the equivalence point with the help of trichromatic evaluation. These authors also mentioned the trichromatic values of the mixed indicators, namely methyl red and bromocresol green. Kotrly et al. [52] characterised the specification of colour changes of the indicators phenolphthalein, phenol red, thymol blue, bromothymol blue, methyl red and congo red with the help of the CIE colorimetric system. The colour quality of the studied indicators was specified by a curve on the chromaticity diagram.

The authors tabulated the true colour coordinates, dominant wavelength, purity of colour and RUCS coordinates at different pH values for all the studied indicators. Vytras and Kotrly [53] developed procedures for the calculation of all absorbance curves for the colour transition of an acid–base indicator when three consecutive dissociation equilibria are involved. ALGOL computer programs were developed by these authors to calculate the true colour coordinates from the absorbance values. The evaluation of the dominant wavelength and the excitation purity was also discussed. The mathematical treatment of the colour transitions of acid–base indicators has been applied to compute the colour changes of bromothymol blue and phenol red. Bhuchar and co-workers [26,27] proposed a quantitative measure of the quality of colour change, namely specific colour discrimination, to evaluate the colour changes of phthalein and sulphonephthalein indicators, phenolphthalein, cresolphthalein, thymol phthalein, phenol red, cresol red, thymol blue and congo red. Barbosa et al. [54] carried out a comparative study of some hydroxyanthraquinones, namely alizarin, alizarin S, quinalizarin and quinizarin with bromocresol green and methyl orange as reference indicators. The numerical values of the chromaticity coordinates, complementary chromaticity coordinates, pK_a values, pH of maximum colour change and the quality of colour change indicated that these hydroxyanthraquinones have a colour change quality similar to that of bromocresol green. The semicarbazones and thiosemicarbazones derived from 1,2-naphthoquinone, namely 1,2-naphthoquinone-2-semicarbazone (NQS), and its 4-sulphonic derivatives (NQS4S) and 1,2-naphthaquinone-2-thiosemicarbazone 4-sulphonic acid (NQT4S)], are reported as acid–base indicators by the evaluation of their transition limits via tristimulus chromaticity coordinates [55]. In this study the true colour coordinates, the PMUCS coordinates, RUCS and CIE $La*b*$ 1976 parameters are evaluated for the specification of the colour changes of these acid–base indicators and it is stated that NQS4S exhibit similar sharpness to that shown by methyl red. Fernandez and Guzman Chozas [30] utilised a new colour space denoted as LABHNU 1977 [24] with

the object of attaining uniformity for the CIE $Lu*v*$ and CIE $La*b*$ 1976 systems. These authors studied the specification of the colour change of the indicators pyridine-2-aldehyde-p-nitrophenyl hydrazone and 6-methylpyridine-2-aldehyde-p-nitrophenyl hydrazone with the help of the LABHNU colour space and observed that the $\Delta E*$ values evaluated by this method linearly relate to those obtained by the application of the CIE $La*b*$ colour space. Gulati et al. [56] studied the colour transition of 2-(2′-lepidylazo-)-1-naphthol-4-ammoniumsulphonate as an acid–base indicator with the help of the true colour coordinates and RUCS coordinates along with the SCD parameter and found that the sensitivity of the indicator is comparable to that of thymol blue. Bhaskare et al. [57] studied the use of the azo dye α-(2-hydroxy-4-sulpho-phenylazo)-p-(nitrobenzyl cyanide) as an acid–base indicator by evaluating the sensitivity of the indicator in terms of the indicator in terms of specific colour discrimination steps and the half bandwidth of the change of specific colour discrimination in pH units. Kotoucek and Lemr [58] carried out investigations for satisfactory functioning of celestine blue as an acid–base indicator for visual titrations of strong and moderately strong protolytes. On the basis of the tristimulus coordinates the CIE $La*b*$ 1976 parameters were calculated with the help of the TRICHROM program on an EC 1033 computer. Kotoucek and Lemr [59] studied the characterisation of the colour change of some acid–base indicators of the phenoxazine dye group and disodium 2,8-dihydroxy 1,4-naphthaquinone-3,6 disulphonate using tristimulus chromaticity coordinates, CIE $La*b*$ parameter, dominant wavelength and purity of colour. Dissociation constants of indicators were calculated from the values of trichromatic complementary coordinates and are compared with the published values.

2.8. Specification of colour changes of indicators in non-aqueous acid–base titrimetry

Non-aqueous acid–base titrimetry has gained considerable importance for the ease with which the quantitative analysis of pharmaceutically im-

portant compounds can be carried out in non-aqueous media. A number of non-aqueous titrimetric procedures have been developed in this way involving visual indicators.

The use of 1,4-dihydroxy anthraquinone as an acid–base indicator in isopropyl alcohol medium is studied by the evaluation of colour change limits via complementary chromaticity coordinates at different pH values in the titration of benzoic acid and veronal with 0.1 M tetrabutyl ammonium hydroxide [60]. The dissociation constants pK_1 and pK_2 are evaluated in accordance with the method of Reilley etal. [25] and it was shown that these values coincide with those determined by the standard methods. This new indicator is used in the titration of aromatic acids, aliphatic acids, amino acids, aromatic heterocycles and phenols in isopropyl alcohol with tetra butyl ammonium hydroxide with a relative error of less than 0.8%. Barbosa et al. [61] studied a series of commercial indicators—cresol red, thymol blue, bromophenol blue, bromocresol green, bromocresol purple, bromothymol blue, methyl orange, methyl red and neutral red—in order to establish them over the whole useful pH range in propan-2-ol medium. These authors evaluated the complementary chromaticity coordinates, specific colour discrimination, pH of maximum colour change, half band width of specific colour discrimination peak, pK_{in} and optimum indicator concentration together with the CIE $La*b*$ 1976 parameters. To illustrate the usefulness of the work, a mixture of picric acid and benzoic acid was titrated with tetrabutyl ammonium hydroxide using thymol blue as indicator and also a relationship between pK_{in} in aqueous and propan-2-ol medium was proposed. Barbosa et al. [62] carried out similar studies with 2-methyl propan-2-ol medium to establish the above-mentioned commercial indicators over the whole useful pH range. The chromatic parameters, the chromaticity coordinates, complementary chromaticity coordinates, optical concentration, specific colour discrimination, pH of maximum colour change, half bandwidth, $\Delta E*$ value of CIE $La*b*$ 1976, and CIE $Lu*v*$, together with the optimum indicator concentration, are evaluated utilising the indicator transition in the titration of trichloroacetic acid

with tetrabutyl ammonium hydroxide. A linear relationship between pK_{in} values in 2-methyl propan-2-ol and in aqueous medium is also proposed. Mixtures of dithio uracil and 2,4-dichlorophenol were titrated with tetrabutyl ammonium hydroxide using methyl red and thymo blue as indicators. Barbosa et al. [63] studied a series of acid–base indicators, namely p-naphthol benzein, neutral red, tropaeolin 00, quinalidine red, brilliant green, malachite green and bromocresol green, in acetonitrile medium and determined the chromaticity coordinates, pK_a values, transition pH ranges, pH of maximum colour change, optimum concentration for titration and quality of colour change for each of these studied indicators together with the effect of ionic strength on their properties. These authors recommended neutral red or a mixture of bromocresol green and tropaeolin 00 as indicators in the titration of a binary mixture of tetramethyl guanidine and pyridine. The indicator transition ranges at zero ionic strength are presented for all the studied indicators. These authors further reported that the studied indicators provided very sharp end points in titrations of bases with the dissociation constants of the order of 10^{-10} or lower. Bosch and Roses [64] proposed 1,2-naphthoquinone-2-thiosemicarbazone as an acid–base indicator for use in isopropyl and t-butyl alcohol media and evaluated the quality of colour change by determining the parameters specific colour discrimination, pH of maximum colour change, half bandwidth of specific colour discrimination peak, true and complementary colour coordinates together with the parameters of CIE $La*b*$ 1976, and CIE $Lu*v*$. This indicator is found to yield results of very good accuracy and precision in titrations of trichloroacetic, dichloro acetic and chloro acetic acids. Martinez Calatayud et al. [65] carried out studies using tristimulus colorimetry theory on several recommended indicators (crystal violet, methyl violet, tropaeolin 00, bromocresol purple and malachite green) for the titration of metformine with perchloric acid and in acetic acid medium and found that crystal violet and methyl violet were most suitable. With the help of CIE $La*b*$ 1976 parameters these authors were able to develop screened indicators of crystal violet and methyl violet by mixing them with appropriate

inert colorants such as neozapan yellow and thymol blue. Barboza et al. [66] extended their studies on the chromatic characterisation of several commercial indicators (metanil yellow, quinalidine red, 4'-dimethyl aminobenzal rhodamine, tropaeolin 00, brilliant green, crystal violet, malachite green, p-naphtholbenzein, nile blue and sudan red) in anhydrous acetic acid medium and evaluated the chromatic parameters in the titration of either urea or sodium acetate in anhydrous acetic acid medium with perchloric acid. The colour sequence of these indicators, described with the widely-used chromaticity coordinates, complementary chromaticity coordinates, the specific colour discrimination parameter and the parameters CIE $La*b*$ 1976, and CIE $Lu*v*$, enabled these authors to determine the formation constants of the indicators and also the optimum concentration of the indicator. These authors also determined the indicator transition range, in terms of pC_{HClO_4} of indicators in acetic acid medium. An objective study on the comparison of the colour changes of the indicators crystal violet and methyl violet in acetic acid medium for the determination of a number of pharmaceutically important compounds revealed that the trichromatic parameters and the transition curves of both these indicators coincide with each other, indicating that these two dyes are identical in their behaviour [67]. Barbosa et al. [68] carried out investigations to determine the optimum concentrations of the indicators crystal violet, alizarin-9-imine and quinalizarin-9-imine in anhydrous acetic medium with the help of tristimulus coordinates and observed that the first two are good indicators. Barbosa et al. [69] further carried out a comparative study of colour change quality of the indicators crystal violet, p-naphthol benzein, tropaeolin 00, malachite green and nile blue in acetic medium. Barbosa and Bosch [70] carried out similar studies with N,N-dimethyl formamide medium to test the properties of the indicators thymol blue, bromocresol green, bromothymol blue, meta cresol purple, phenol red and azoviolet with the help of the chromatic parameters, complementary colour coordinates, specific colour discrimination parameter and the parameters of the CIE $La*b*$

and CIE $Lu*v*$. It is also stated that a binary mixture of 2,6-dihydroxy benzoic and benzoic acids was titrated in the presence of azoviolet with an error of less than 2%.

2.9. Screening

A screened indicator is an indicator which changes from one colour to its complementary colour through greyness at the equivalence point of the titration. Such a screened indicator is obtained by mixing the indicator with one or more inert dyes in a definite proportion. Reilley and co-workers [25,32] and Flaschka [33] derived an expression for the volume of the inert dye solutions which should be added to 1 ml of the indicator solution, so that the resulting mixture, the screened indicator, exhibits greyness at the end point.

Since the coordinates of the grey point (0,0) in the chromaticity diagram with V_r coordinates $(V_r = Q_r - G_r)$, a mixture of "i" colorants will exhibit greyness if

$$\sum_{i=0}^{i} V_{ri} \cdot J_i = 0$$

If two inert dyes are used to achieve this condition, the above equation can be written as

$$V_{r,e} \cdot J_e m_e + V_{r,b} \cdot J_b \cdot m_b + V_{r,v} \cdot J_v \cdot m_v = 0$$

where $V_{r,e}$ represents the coordinates of the pure indicator at the equivalence point and $V_{r,b}$ and $V_{r,v}$ are the coordinates of the two inert dyes, J is the optical concentration, "m" represents the volume of solution, and the subscripts e, b and v correspond to the indicator, a blue inert dye and a violet inert dye respectively. Since $V_{r,e}$ (calculated from the coordinates of the limiting forms of the indicator), $V_{r,b}$, $V_{r,v}$ and the corresponding J values are known, the volumes m_b and m_v to be added to 1 ml of the dye can be calculated by solving the simultaneous equations which result on incorporating $r = 1$, 2, since $V_{1,e}$ is $V_{x,e}$ and $V_{2,e}$ is $V_{y,e}$. Flaschka [33], following the procedure described, prepared a screened acid-base indicator of methyl orange with the inert colorants blue CI 671 and violet CI 697 and the colour coordinates of this mixture at the equiva-

lence point are found to be the same as those of the illuminant point. Reilley and Smith [32] reported the screening of methyl red with kiton yellow and brilliant blue and they preferred inert colorants whose V_r points are located near the periphery of the chromaticity diagram. Bosch et al. [71] studied the colour changes of different screened indicators and reported that all the screened indicators which can be prepared from the same pure indicator and different screening dyes show colour changes that, when plotted on the complementary chromaticity diagram, are on the same straight line. These authors calculated the slope of this straight line from the colour parameters of the pure indicator and consequently determined the parameters relating to the colour changes of all the possible screened indicators prepared from this pure indicator. These authors employed a parameter known as relative greyness (g), which is a measure of the amount of grey proportion in a colour and is given by the expression

$$g = \frac{G_r(Q_r^0 - Q_r)}{Q_r^0(Q_r - G_r)}$$

where Q_r, G_r and Q_r^0 correspond to the complementary "r" coordinate of the colour, the illuminant and the pure spectrum colour of that wavelength respectively, for the comparison of the quality of colour change of the screened indicators prepared from the same or different indicators.

These authors equalised the relative greyness equations of both the limiting forms of the screened indicator to obtain the conditions for best colour change. By applying these theoretical considerations, two screened indicators, mixtures of NQT4S–sandolan turquoise EAS–picric acid and NQT–sandolan turquoise EAS–picric acid, are proposed. It is shown that these two indicators exhibit a colour change between the complementary colours through colourlessness with the same amount of relative greyness for both the limiting forms of the indicators.

The method of caluclation of the composition of screened indicators, as described by Reilley and Smith [32], has been applied for the screening of eriochrome blue SE in the titration of

zinc(II) and SNAZOXS in the titration of copper(II) with EDTA [72]. Eriochrome blue SE is screened with methyl blue and alizarin pure blue to obtain an achromatic hue at the end point. Martinez Calatayud and Pascual Marti [38] reported methylene blue as an inert colorant to screen sulphosalicylic acid indicator in the titration of iron(III) with EDTA to improve the quality of colour change which is measured from the $\Delta J/\Delta(C_L/C_M)$ vs. C_L/C_M plot. In the titration of lead(II) with EDTA, two screened indicators in powder form with the following compositions were proposed [73]:

(1) Eriochrome black T–methyl red (7.4 + 1)– NaCl (1 + 100)
(2) Bromopyrogallol red–naphthol green B–thymol blue (2.5 + 21 + 1)–NaCl (1 + 100)

From the values of percent standard deviation of the result, it has been shown that the screening of the indicator improved the accuracy of the determination. The (a^*, b^*) curves of both the screened indicators pass through the origin, indicating occurrence of achromatic colour at the end point. Cacho et al. [74] proposed five screened indicators to improve the quality of colour change for the complexometric titration of calcium(II) with EDTA, using tristimulus colorimentry. The studied indicators are calcon–tartrazine–orange-II   (6.8 + 1 + 4.6), thymolphthalein   complexone–orange-II–tartrazine (14.22 + 1.22 + 1), Arsenazo III–renazol brilliant blue–tartrazine (25.2 + 8.9 + 1), phthaein complexone–tartrazine–renazol brilliant blue (2.47 + 1 + 1.1) and methylthymol blue–orange II-tartrazine (13 + 2.9 + 1).

Bhuchar and Das [75] screened phenol red, an acid–base indicator, with methylene blue and compared the quality of the colour change with that of another screened indicator, phenol red screened with copper oxalato complex, with the help of the SCD parameter and concluded that the former screened indicator is superior in its quality of colour change.

Vytras et al. [76] proposed the screening of the acid–base indicators phenol red, bromothymol blue and methyl red by mixing with appropriate inert colorants as mentioned below:

Indicator	Inert colorants
Phenol red	Methylene blue – picric acid
Phenol red	Methylene blue – tartrazine
Methyl red	Methylene blue – picric acid
Methyl red	Methylene blue – tartrazine
Bromothymol blue	Phenosafranine – orange II
Bromothymol blue	Phenosafranine – Eg acid orange GG

Vytras and Kotrly [53] determined the tristimulus coordinates of the screened indicators phenol red (with methylene blue and tartrazine) and bromothymol blue (with phenosafranine and orange II) at different pH values using a computer program for the simulation of absorbance curves. Zahradnicek [77] recommended screened indicators such as ethyl orange–nile blue A and phenol red–methylene blue for improving the sharpness of colour change at the end point in acid–base titrations. The stability of the mixed indicator is demonstrated by the position of the complementary colour points in the chromaticity diagram [78]. Zahradnicek and Subert [79] reported that the colour transition curve of the screened indicator methyl orange–methylene blue passes through the grey point whereas that of the screened indicator dimethyl yellow–nile blue A deviates slightly from the grey point, possibly due to slight decomposition in the latter case. These indicators are used in the determination of medical substances.

Martinez Calatayud et al. [65] proposed screened indicators in acetic acid medium for the titration of metformine with perchloric acid. The screened indicators crystal violet–neozapan yellow and methyl violet–thymol blue exhibited very low values of percent relative standard deviation in comparison with the unscreened indicators, indicating the higher accuracy of the screened indicators. It has also been shown that (a^*, b^*) graphs of both the screened indicators have curves passing through the origin. Barbosa et al. [80] proposed three efficient indicators consisting of malachite

green and a screening dye for use in anhydrous acetic acid media utilising the concepts of tristimulus colorimetry. Krishna Prasad and Raheem [81] proposed the following screened indicators for acid–base titrations and reported a single colour transition curve for screened indicators formed by mixing with different inert colorants:

Methyl red + methylene blue (3:1)
Methyl red + indigo carmine (3:2)
Methyl red + malachide green (2.5:2)
Ethyl red + methylene blue (6:1)
Ethyl red + indigo carmine (3:2)
Dimethyl yellow + methylene blue (3:1)
Dimethyl yellow + indigo carmine (2:1)

Lemr and Kotoucek [82] have written a computer program for the peparation of screened indicators for acid–base titrations. These authors [83] prepared six screened acid–base indicators and their colour characteristics are studied with the help of the 1931 CIE parameters.

2.10. Other applications of tristimulus colorimetry

Reilley and Smith [32] developed mathematical equations for the analysis of binary and ternary mixtures of dyes with the help of complementary chromaticity coordinates. Flaschka [84] simplified the procedure by reducing the number of wavelengths at which the absorbances are measured for calculating the complementary coordinates and proposed a mathematical procedure for the determination of the concentrations of individual components in binary and ternary mixtures. This procedure is further improved by adopting a least-squares approach for solving this problem and it is claimed that this method is superior compared to the earlier methods [85]. With the help of complementary tristimulus colorimetry, a mixture consisting of plutonium in four different oxidation states ($+3$, $+4$, $+5$, $+6$) is analysed by representing the data points of the individual pure components as the vertices of a pyramid and the data points corresponding to a mixture of these four components lie within the pyramid [86].

Reilley et al. [25] determined the stability constant of the complex formed between copper ion and (7-4(sulpho-1-naphthyl azo)-8-hydroxy quinoline-5-sulphonic acid) using the complementary tristimulus coordinates by drawing a plot of

Q_xJ vs. Q_yJ at different ratios of ligand to metal ion concentrations. The pH range of existence of mixed complex formed between copper(II), aluminium(III) and tartrate ion is determined with the help of complementary tristimulus colorimetry [87]. Trichromatic colorimetry has recently been applied to the determination of the colour of transition metal complexes [88]. The chromaticity coordinates of the transition metal compounds $Cr(NO_3)_3$, $CrCl_3$, $Cr_2(SO_4)_3$, $COCl_2$, $NiCl_2$ and $CuSO_4$ in aqueous solutions are determined at varying concentrations and it is stated that the trichromatic parameters link colour properties of a substance with those of spectroscopic origin, which depend on d electrons, crystal field symmetry and the nature of the bond. Tawa and Hirose [89] applied simplified tristimulus colorimetry for the determination of primary and secondary amines in the presence of tertiary amines by enabling their complexes with copper(II) ion to be extracted into chloroform. The unreacted copper(II) is estimated because of its catalytic effect on the reaction between hydrogen peroxide and pyrocatechol by determining the pseudo-first order rate constants with the help of simplified tristimulus colorimetry. Tawa and Hirose [90] determined mixtures of aniline and its derivatives by a differential reaction using a mixture of potassium hexacyanoferrate(III) and potassium dichromate as oxidant. Necessary rate proportionality constraints for application of the differential rate method are determined by simplified complementary tristimulus colorimetry and from the slope of the straight line portion of the plots of concentration of semiquinone vs. time. Application of simplified tristimulus colorimetry has been proposed by Tawa and Hirose [91], in a method aimed at determining uric acid in serum without the removal of proteins. The method requires calculations of absorbance at 290 nm as a function of time by simplified tristimulus colorimetry and computation of initial and final absorbances based on the kinetics of first order reactions and using multiple linear regression analysis. The chemical detector system uses uricase catalysis for the conversion of uric acid to allantoin.

Simplified complementary tristimulus colorimetry [92] has been applied for the identification of

the reactive species involved in the oxidation of oxalate ion with permanganate and catalytic decomposition of hydrogen peroxide by mixed catalysts (sodium tungstate and copper(II)). The expression derived for the mole fraction of the light-absorbing species in terms of complementary tristimulus coordinates is utilised for the calculation of the pseudo-first order rate constant of the oxidation reaction of the sulphonephthalein dyes, cresol red and cresol purple, by potassium periodate. It has also been shown that the presence of the coloured impurity, bromocresol green, has no effect on the value of the pseudo-first order rate constant determined by this procedure. This study has been applied for the determination of the rate constants of consecutive irreversible first-order reactions and is illustrated by the assay of xanthine oxidase which catalyses the oxidation of hypoxanthine to uric acid [93].

The tristimulus coordinates are utilised for the quantitative analysis of dyes [94] and the identification of drugs [95] by high performance liquid chromatography.

2.11. Computer program for tristimulus calculations

Because of the numerous multiplications and additions involved in obtaining tristimulus values and the associated parameters, the necessity of the development of computer programs was appreciated even in the early stages of application of tristimulus colorimetry for the measurement of quality of colour change of indicators.

In 1960 Reilley and Smith [32] developed an analogue computer by considering various computer circuits available for multiplying and summing operations. The algorithm adapted for this analogue tristimulus computer for the calculation of chromaticity coordinates is the weighted ordinate method at the selected wavelengths.

Vytras and Kotrly [52], considering the relationship between the absorbance value and the equilibrium system of an acid-base indicator, wrote programs in ALGOL to simulate the absorbance curve of a given indicator at a given pH. From the simulated absorbance curve, the chromaticity coordinates can be calculated by another

program, which is also written in ALGOL. The genreal program developed by these authors is capable of calculating the chromaticity coordinates of an indicator at different values of delta (the fraction of the indicator in the unprotonated form) by taking the individual dissociation constants as input data. This simulation program has been applied to evaluate the results for the colour changes of the indicator phenolphthalein, the screened indicator phenol red in combination with tartrazine and methylene blue, and another screened indicator bromothymol blue in combination with orange II and phenosafranine.

Martinez Calatayud et al. [96] proposed a computer program for the determination of the chromaticity coordinates, the RUCS coordinates, the CIE La*b* 1976 parameters and the values of the optical concentrations. An output consisting of all these parameters for 34 different indicator solutions has been presented.

Bosch et al. [71] developed the computer program COLOR on a Hewlett-Packard series 200 microcomputer system for the computation of tristimulus values, tristimulus coordinates, complementary tristimulus coordinates, RUCS coordinates, CIE La*b* 1976 and CIE Lu*v* paramaters, total colour difference and the index of greyness. This program is capable of displaying a graphical output (on screen, printer or plotter) of all the chromaticity bidimensional systems evaluated in this program. Other facilities included in this program are calculation of the dissociation constant of the indicator from complementary chromaticity coordinates, computation of the optimum indicator concentration, graphical output of ΔE^* vs. pH and SCD vs. pH curve. Two other programs, GRIS 1 and GRIS 2, are capable of calculating the chromaticity coordinates of the screened indicators which are screened with one and two inert colorants respectively.

Roses [97] reported the program SUPER COLOR written in BASIC for the evaluation of the colour changes of indicators, which has the capabilities of COLOR, GRIS 1 and GRIS 2 as well as simulating the colour change of an indicator.

The chromaticity parameters on the indicators methyl orange, bromocresol green and 1,2-naphthaquinone-2-thiosemicarbazone-4-sulphonic acid have been determined by the application of the SUPER COLOR program.

Cacho et al. [28] proposed a program RI-CANER, written in BASIC, for the evaluation of the chromaticity parameters and colour concentration. Recently, another program for the determination of tristimulus coordinates was proposed [88].

Kotrly and Vytras [98] carried out a comparative study of the results obtained by the weighted ordinate method and the selected ordinate method (10 and 30 selected ordinates) and concluded that the former procedure is more reliable at $\Delta\lambda = 10$ nm. These authors claimed that there is a higher propability of introducing gross personal error whilst reading the transmittance values from the graphs at 90 different non-integral wavelengths while adapting the 30 selected ordinate method and so discarded the application of this selected ordinate method.

Zahradnicek and Subert [99] also concluded that the selected ordinate method is inferior in terms of accuracy to the weighted ordinate method. Kotrly and Vytras [98] preferred the weighted ordinate method for the evaluation of chromaticity coordinates not only for the accuracy of the results obtained but also for ease of development of the computer program. However, a computer program has been written for the selected ordinate method algorithm using the Lagrange interpolation technique for reading the absorbance at the non-integral wavelengths [100].

References

[1] F.W. Billmeyer, Jr., in H.F. Mark, D.F. Othmer, C.G. Overbergh and G.T. Seaborg (Eds.), Kirk. Othmer Encyclopedia of Chemical Technology, Vol. 6, John Wiley, New York, 1979, p. 523.

[2] A.C. Hardy, Handbood of Colorimetry, The Technology Press, Massachusetts Institute of Technology, Cambridge, MA, 1936.

[3] D.B. Judd, Measurement and specification of colour, in M.G. Mellon (Ed.), Analytical Absorption Spectroscopy, 2nd edn., John Wiley, New York, 1953.

[4] D.B. Judd, J. Opt. Soc. Am., 23 (1993) 259.

[5] CIE, Proc. 15th Session, Vienna, 1963, Vol. A.P. 35 (recommendation No. 1), p. 80 (Committee report), p. 108 (report on Committee session at Vienna).

[6] CIE, Proc. 8th Session, Cambridge, UK, 1931, pp. 19-29 (recommendations 1-5).

[7] CIE, Proc. Stockholm, 1971, No. 15 (E-1.3.1) (colorimetry report).

[8] R. Davis and K.S. Gibson, Misc. Publ. 114, Natl. Bureau of Standards, Washington, DC, 1931.

[9] CIE, Proc. 11th Session, Paris, 1948, p. 241 (colorimetry).

[10] W.D. Wright, Trans. Opt. Soc., 29 (1927) 225.

[11] J. Guild, Philos. Trans. R. Soc. London, Ser. A, 230 (1931) 149.

[12] F.W. Billmeyer, Jr. and M. Saltzman, Principles of Color Technology, 2nd edn., John Wiley, New York, 1981.

[13] D.B. Judd, J. Opt. Soc. Am., 21 (1931) 729.

[14] D.B. Judd, J. Opt. Soc. Am., 25 (1935) 24.

[15] D.L. MacAdam, J. Opt. Soc. Am., 27 (1937) 294.

[16] D.L. MacAdam, J. Opt. Soc. Am., 32 (1942) 2.

[17] F.C. Breckenridge and W.R. Schaub, J. Opt. Soc. Am., 29 (1939) 370.

[18] D.L. MacAdam, J. Opt. Soc. Am., 32 (1942) 247.

[19] D.L. MacAdam, J. Opt. Soc. Am., 33 (1943) 18.

[20] CIE Colorimetry Committee—Working Program on Color Difference, J. Opt. Soc. Am., 64 (1974) 896.

[21] CIE Proc., Session 14, Brussels, A (1959) 37.

[22] H. Pauli, J. Opt. Soc. Am., 66 (1976) 866.

[23] R.G. Kehni, J. Opt. Soc. Am., 66 (1976) 497.

[24] K. Richter, Color Res. Appl., 5 (1980) 25.

[25] C.N. Reilley, H.A. Flaschka, S. Laurent and B. Laurent, Anal. Chem., 32 (1960) 1218.

[26] V.M. Bhuchar, V.P. Kukreja and S.R. Das, Anal. Chem., 43 (1971) 1847.

[27] V.M. Bhuchar, and A.K. Agarwal, Analyst, 107 (1982) 1439.

[28] J. Cacho, C. Nerin, L. Ruberte and E. Rivas, Anal. Chem., 54 (1982) 1446.

[29] J. Martinez Calatayud, M.C. Pascual Marti and P. Campins Falco, Anal. Chem., 58 (1986) 200.

[30] A.M.C. Fernandez and M. Guzman Chozas, Talanta, 34 (1987) 673.

[31] S. Kotrly and K. Vytras, in E. Wannien (Ed.), Essays on Analytical Chemistry, Pergamon Press, Oxford, 1977, pp. 259-280.

[32] C.N. Reilley and E.M. Smith, Anal. Chem., 32 (1960) 1233.

[33] H. Flaschka, Talanta, 8 (1961) 342.

[34] S. Kotrly and K. Vytras, Vyso Skola Chem. Technol., Pardubice, I/19 (1969) 21 (Chem. Abstr., 74, 150861y).

[35] K. Vytras, S. Kotrly and J. Vytrasova, Collect. Czech. Chem. Commun., 40 (1975) 3815.

[36] J. Martinez Calatayud, M.C. Pascual Marti and S. Sagrado Vives, Analusis, 13 (1985) 87.

[37] J. Martinez Calatayud, M.C. Pascual Marti and S. Sagrado Vives, Quim. Anal., 65 (1986) 83.

[38] J. Martinez Calatayud and M.C. Pascual Marti, Analusis, 12 (1984) 409.

[39] J. Cacho, A. Garnica and C. Nerin, Anal. Chim. Acta, 162 (1983) 113.

[40] J. Cacho Palomar, A. Lopez-Molinero and M. Ibanez, Mikrochim. Acta, 73 (1986) 73.

[41] K. Vytras, J. Vytrasova and S. Kotrly, Talanta, 22 (1975) 529.

[42] J. Cacho, A.L. Molinero and E. Pinilla, Collect. Czech. Chem. Commun., 51 (1986) 2712.

[43] J. Cacho, A. Lopez-Molinero and A. Guitart, Microchem. J., 36 (1987) 339.

[44] J. Cacho, A. Lopez-Molinero and J. Enrique Castells, Analyst, 112 (1987) 1723.

[45] K.M.M. Krishna Prasad and S. Raheem, Talanta, 38 (1991) 763.

[46] K.M.M. Krishna Prasad and S. Raheem, Anal. Chim. Acta, 264 (1992) 137.

[47] K.M.M. Krishna Prasad and S. Raheem, Analusis, 20 (1992) 401.

[48] K.M.M. Krishna Prasad and S. Raheem, Mikrochim. Acta, 112 (1993) 63.

[49] S. Raheem and K.M.M. Krishna Prasad Talanta, 40 (1993) 1809.

[50] S. Raheem, Ph.D. Thesis, Andhra University, 1992.

[51] W.B. Fortune and M.G. Mellon, J. Am. Chem. Soc., 60 (1938) 2607.

[52] S. Kotrly, K. Vytras, J. Oharek and E. Vondruskova, Vyso. Skola Chem. Technol., Pardubice, I/22 (1970) 19 (Chem. Abstr., 75, 14558 y).

[53] K. Vytras, S. Kotrly, Vyso. Skola Chem. Technol., Pardubice, 26 (1971) 3 (Chem. Abstr., 77, 28445 n).

[54] J. Barbosa, E. Bosch and R. Carrera, Talanta, 32 (1985) 1077.

[55] A. Izquierdo, E. Bosch and V. Rodrigo, Talanta, 29 (1982) 1125.

[56] A. Gulati, B.S. Garg and R.P. Singh, Indian J. Chem., 20A (1981) 1048.

[57] C.K. Bhaskare, S.V. Kulkarni and V.A. Jadhav, J. Shivaji Univ. Sci., 16 (1976) 61 (Chem. Abstr., 89, 139748f).

[58] M. Kotoucek and K. Lemr, Acta Univ. Palacki Olomuc. Fac. Rerum. Nat., 85 (1986) 135 (Chem. Abstr., 107, 50938k).

[59] M. Kotoucek and K. Lemr, Acta Univ. Palacki Olomuc, Fac. Rerum. Nat., 85 (1986) 167 (Chem. Abstr., 107, 50939m).

[60] J. Barbosa, J. Sanchez and E. Bosch, Talanta, 31 (1984) 279.

[61] J. Barbosa, E. Bosch and F. Suarez, Analyst, 110 (1985) 1473.

[62] J. Barbosa, E. Bosch and M. Roses, Analyst, 112 (1987) 179.

[63] J. Barbosa, M. Roses and V. Sanz-Nebot. Talanta, 35 (1988) 1013.

[64] E. Bosch and M. Roses, Talanta, 35 (1988) 419.

[65] J. Martinez Calatayud, M.C. Pascual Marti and P. Campins Falco, Analyst, 110 (1985) 981.

[66] J. Barbosa, D. Barron and E. Bosch, Analyst, 112 (1987) 1717.

[67] M. Zahradnicek, S. Stefek and M. Blesova, Acta Fac. Pharm. Univ. Comenianae, 14 (1967) 167 (Chem. Abstr. 70 6561a).

[68] J. Barbosa, E. Bosch, R. Carrera and G. Rauret, Mikrochim. Acta, (1987) 13.

[69] J. Barbosa, B. Barron and E. Bosch, Analusis, 16 (1988) 458.

[70] J. Barbosa and C.M. Bosch, Talanta, 38 (1991) 1297.

[71] E. Bosch, E. Casassas, A. Izquierdo and M. Roses, Anal. Chem., 56 (1984) 1422.

[72] K. Vytras, S. Kotrly, J. Vytrasova and S. Zielina, Collect. Czech. Chem. Commun., 41 (1976) 2846.

[73] J. Martinez Calatayud, M.C. Pascual Marti and S. Sagrado Vives, Analyst, 110 (1985) 837.

[74] J. Cacho, C. Nerin and M.J. Torres, Microchem. J., 41 (1990) 227.

[75] V.M. Bhuchar and S.R. Das, J. Opt. Soc. Am., 54 (1964) 817.

[76] K. Vytras, S. Kotrly, E. Vondruskova and B. Vorac, Collect. Czech. Chem. Commun., 35 (1970) 3379.

[77] M. Zahradnicek, Cesk. Farm., 16 (1967) 59 (Chem. Abstr., 67, 96465n).

[78] M. Zahradnicek, M. Blesova and J. Subert, Cesk. Farm., 16 (1967) 334 (Chem. Abstr., 8, 35527h).

[79] M. Zahradnicek and J. Subert, Acta Fac. Pharm. Univ. Comenianae, 16 (1968) 85 (Chem. Abstr., 72, 27989C).

[80] J. Barbosa, E. Bosch, J.L. Cortina and M. Roses, Mikrochim. Acta, Part III, (1991) 89.

[81] K.M.M. Krishna Prasad and S. Raheem, Asian J. Chem., 4 (1992) 726.

[82] K. Lemr and M. Kotoucek, Acta. Univ. Palacki. Olomuc. Fac. Rerum. Nat., 91 (1988) 119.

[83] K. Lemr and M. Kotoucek, Collect. Czech. Chem. Commun., 54 (1989) 346.

[84] H. Flaschka, Talanta, 7 (1960) 90.

[85] H. Flaschka, Talanta, 8 (1961) 8.

[86] G.L. Silver, Talanta, 14 (1967) 637.

[87] H. Flaschka, J. Butcher and R. Speights, Talanta, 8 (1961) 400.

[88] A. Bartecki and T. Tlaczala, Spectrosc. Lett., 23 (1990) 727.

[89] R. Tawa and S. Hirose, Chem. Pharm. Bull., 27 (1980) 2515.

[90] R. Tawa and S. Hirose, Chem. Pharm. Bull., 28 (1980) 2136.

[91] R. Tawa and S. Hirose, Chem. Pharm. Bull., 28 (1980) 3381.

[92] R. Tawa and S. Hirose, Talanta, 26 (1979) 237.

[93] R. Tawa and S. Hirose, Talanta, 27 (1980) 759.

[94] P.C. White and T. Calterick, Analyst, 115 (1990) 919.

[95] S. Yoshida, K. Manabe, M. Kito and S. Hirose, Microchem. J., 43 (1991) 94.

[96] J. Martinez Calatayud, M.C. Pascual Marti and S. Sagrado Vives, Afinidad, 43 (1986) 143.

[97] M. Roses, Anal. Chim. Acta, 204 (1988) 311.

[98] S. Kotrly and K. Vytras, Talanta, 18 (1971) 253.

[99] M. Zahradnicek and J. Subert, Acta Fac. Pharm. Univ. Comenianae, 19 (1970) 53 (Chem. Abstr., 74, 150685u).

[100] S. Raheem, M. Phil. Dissertation, Andhra University, 1986.

Review

Microwave-assisted sample preparation in analytical chemistry

Frank E. Smith*, Edward A. Arsenault

Department of Chemistry and Biochemistry, Laurentian University, Sudbury, Ontario, P3E 2C6, Canada

Abstract

The speed and efficiency of instrumentation for chemical analysis has improved dramatically over the past twenty years. Until recently, however, methods of sample preparation had not changed to keep pace, so this had become the slowest step in analytical chemistry methodology. The widespread adoption of domestic microwave ovens during the past twenty-five years has eventually led to their usage in chemical laboratories. Microwave technology has now advanced to the point where it is revolutionizing chemical sample preparation and chemical synthesis. Since the first application of a microwave oven for sample preparation in 1975, many microwave-assisted dissolution methods have been developed— these are applicable to virtually any kind of sample type. This review attempts to summarize all the microwave-assisted dissolution and digestion methods reported up to and including 1994. In addition, some very recent developments in continuous-flow automated dissolution systems are discussed, as is the emergence of databases and software packages related to the application of microwave technology to sample dissolution.

There are 344 references.

Keywords: Analytical chemistry; Microwave-assisted sample preparation

1. Introduction

Microwave-assisted sample preparation techniques are becoming widely used in analytical laboratories all over the world. This review is an attempt to describe the most significant advances made, and to summarize the available literature up to the beginning of 1995. For the convenience of readers, methods have been divided according to sample type (e.g. geological, environmental, etc.). This inevitably leads to overlap, as some samples fall within more than one category, but it also makes for faster information retrieval. This review includes microwave techniques applied to atmospheric pressure dissolutions, fusions, Kjeldahl determinations and ashing procedures but focuses on the major application of microwave heating in this field, which is high-pressure dissolutions in sealed vessels/systems, where the elevated temperatures attained lead to faster sample breakdown and analyte dissolution.

* Corresponding author. Tel: (705) 675 1151 ext. 2101. Fax: (705) 675 4844. e-mail: fsmith@nickel.laurentian.ca

Microwave ovens have been used in chemical laboratories for the sintering of ceramic mixtures [316], moisture analysis [311] and the wet ashing of biological and geological materials [31,32,81] for many years. The pressure dissolution of geological specimens in Parr bombs heated in water baths has also been exploited for a long time [11]. However, it is only within the last decade that the two techniques have been combined to provide rapid pressure dissolutions of analytical samples prior to AA or ICP analysis (10,132,148,270,319–321].

It is interesting to review briefly the circumstances which have led up to the development and adoption of this new pressure-dissolution technique. Since many of the first studies were carried out by researchers from the minerals sector, it is appropriate to trace the story from this perspective–however, the very significant contributions of researchers in other fields, notably Abu-Samra [31,32], Brown [81] and Kingston and Jassie [270] and all their co-workers must be acknowledged.

Efficient exploitation of minerals in the earth's crust requires extensive knowledge of the detailed geology, mineralogy and geochemistry of the various deposits, as well as a comprehensive understanding of the behavior of the various ores and minerals at different stages of the mining, milling, smelting and refining processes. Analytical chemistry is fundamental to the acquisition of this knowledge. Over the past decade, the mining and smelting industry has come under increasing pressure on two main fronts–economic and enviromental. On the economic front, inflation along with weak metal prices, increasing competition and lower quality ore bodies have forced companies to improve efficiency and productivity. At the same time, society has become increasingly concerned with the environmental effects of the industry. This has led to a demand for more stringent controls on emissions and effluents, and for the monitoring and revegetation of previously devasted areas. These influences have in turn made efficient management more and more dependent on reliable chemical analysis at all stages of the mining and smelting process. Analytical chemistry has never had a more important role to play. Similar trends are evident in other indus-

tries, and the signs are that the role of analytical chemistry will become even more crucial in the future. These pressures have favored the trend for analytical chemistry instrumentation to become more and more sophisticated. Improved instruments with the capability to detect ever-smaller quantities of more and more elements and compounds, more rapidly than before, are constantly being developed and usually incorporate powerful computational capabilities. However, many of these advanced techniques require the sample to be in solution form prior to analysis and yet few innovations had been made to sample dissolution methods. Conventional wet ashing dissolution techniques are very slow, and involve heating samples in various acids or mixtures of acids in an oven or on a hot plate for extended periods of time. Often the sample–acid mixture must be brought down to dryness, cooled, and then re-reheated with more acid in order to ensure dissolution. Also, these techniques are susceptible to loss of volatile analytes and cross-contamination. Other problems often associated with conventional sample preparation techniques include, tedium, danger due to the use of strong oxidizers, incomplete digestion and the need for large amounts of reagents, constant supervision and special fume hoods. For those samples containing intractable matrices such as refractory minerals, closed vessels such as steel-jacketed Teflon™ PTFE bombs or glass Carius tubes heated in a conventional oven have traditionally been used– again, lengthy heating times are required. Thus sample preparation became the slow step in the analytical process, providing the impetus for the development of fast and reliable alternative methods to those traditionally employed.

In 1975 Abu-Samra and his co-workers reported the use of microwave ovens for the purpose of wet ashing biological samples prior to elemental analysis [31,32]. These authors used a domestic microwave oven equipped with a spray fume scrubber to wet ash a range of biological samples. The only previously recorded laboratory uses of microwave ovens were for the drying of wet cake and paste in an inorganic chemical manufacturing plant [311] and for the sintering of silica and alumina mixtures [316]. The inspiration

for pressure-dissolution studies came from a US Bureau of Mines report [16], which described how a rapid dissolution of some mineral samples had been achieved by using a microwave oven to heat samples and an acid mixture contained in polycarbonate bottles. When this experiment was repeated [10], the method showed great potential, but the vessels proved unsuitable for more rigorous conditions—the vessels needed to be transparent to microwave radiation, chemically inert and resistant to acid attack, able to withstand high temperatures and pressures, and yet be reasonably cheap. Vessels should also be small enough to allow up to a dozen inside the oven at the same time, yet be readily sealed and opened to enable routine use by laboratory staff. A range of commerically available Teflon™ bottles was tried, but these deformed or burst during the heating process. Some test vessels were machined out of solid Teflon™ blocks, but it was found that the screw threads in the cap deformed during the heating, allowing the cap to explode off. Finally, a vessel was constructed from 4 cm diameter Teflon™–PFA tubing and end caps and this proved successful. Arrangements were then made with the manufacturer [337] to make vessels from the tubing. These were marketed and eventually became the vessel of choice for microwave experimentation. The identification and development of this more suitable vessel was a very important step forward and led to the development of a variety of digestion protocols [10,20,132,270,319–321], and also to a range of organic and organometallic syntheses [315,322–326], all extremely fast compared to the traditional methods they were intended to replace. Since then, both oven and vessel design have improved markedly. Dramatic reductions in sample preparation times, containment of volatiles and sample type versatility are evident advantages for closed vessel dissolutions when compared to classical wet digestion methods. Closed vessels result in the development of high temperatures and pressures which make dissolutions much more vigorous and rapid; hence the greater speed of the technique. The increased acceptance of the microwave pressure-dissolution technique is reflected by the dramatic rise in the number of publications appearing over the past

few years. These report dissolution methods involving geological, botanical, zoological, environmental, food, sludge, coal and ash, metallic material and synthetic material samples. Other papers focus on drying, on-line/flow-injection/continuous-flow systems, extraction/desorptions, distillations, total nitrogen determinations (Kjeldahl), reviews, general reports and databases, automated/robotic systems, oven modifications, special dissolution techniques and equipment, safety and moisture content determinations.

In many analytical laboratories, the microwave pressure-dissolution technique is already the method of choice for sample preparation. The new protocols reported have been, in most instances, verified exhaustively against standard reference materials. Microwave pressure-dissolution must now be considered an accepted technique. Other microwave-assisted processes for sample preparation are being constantly developed and put into practice. This is an extraordinarily dynamic and rapidly changing area of chemistry.

2. Microwave-assisted dissolution procedures

2.1. Geological samples

Geological materials often contain immutable matrices resistant to acid attack. Many of these matrices consist of refractory minerals (e.g. chromite) with high melting points or other compounds which may require several hours of heating in acids, or a fusion process, for satisfactory dissolution. The introduction of microwave-assisted pressure dissolution techniques has been a major advance in geochemical analysis. Since the introduction of this new technique [10], many other reports have been published involving the use of microwave energy for the dissolution of geological samples [1–30,129]. Table 1 is a summary of these references (see also Table 5 on environmental samples).

Some researchers used modified ovens [7,13,16,22,28] for their dissolutions. The most common modification involved systems for purging the oven's cavity of fumes to a fume hood either with compressed air, CO_2 gas or fan forced

Table 1
Geological samples

Sample(s)	Digestion mode and special information/equipment	Required reagents	Analyte	Method of analysis	Ref.
Bastnaesite ore: containing limonite, baryte and quartz	Closed 150 mL Teflon™ vessels compared with open-air methods	HCl, HF–HCl, HCl–H_2O_2	Ce, Eu, Gd, La, Nd, Pr, Sm, Y	ICP-ES	1
Ores	Domestic oven; open corundum crucibles; 70% electrical saving compared to muffle furnace/alkali fusion	NaOH	U, Th		2
V–Ti–Fe ore	Closed Teflon™ vessels; compared to classical methods	HCl–HF	Si, Al, Ca, Co, Cu, Fe, Mg, Mn, Ni, Ti, V	ICP, AAS	3
Geological	PTFE beakers surrounded by solid MgO inside tightly sealed PTFE containers	HNO_3–HF–$HClO_4$, MgO	(1) Ba, Be, Ca, Ce, Co, Cu, Fe, La, Mn, Ni, Sr, Ti, Vi, Zr (2) K, Li, Na	(1) ICP–AES (2) FAAS	4
Cu concentrates	The heating process and digestion system are discussed; compared with international standard methods	HNO_3–HCl	As, Ag, Hg, Pb, Sb, Zn	AAS	5
Geological: Cu/Ni sulfide–enriched	CEM MDS–81 oven; closed 150 mL Savillex Teflon™–PFA vessels; compared with two other classical methods; three-step dissolution	HNO_3–HCl then HF, EDTA, H_3BO_3	Major, minor and trace elements, oxides	ICP–ES	6
Thirty-three standard reference materials of rock, soil and sediment, and 18 standard reference materials of ores and minerals	Modified domestic oven with a turntable placed inside a fume hood purged with compressed air via tubing; closed 250 mL polycarbonate vessels and threads wrapped with Teflon™ tape inside a polyethylene food container sealed with a top to hold 12 vessels; all metal parts covered with plastic tape; safety discussed; 100 samples/day prepared; refractory minerals such as quartz, chromite, corundum, rutile and zircon are only paritally dissolved; all elements except Cr, P, Mg and Ti can be completely recovered; two-step dissolution	HNO_3, then HCl–HF, then H_3BO_3	Ag, Al, As, Au, B, Ba, Be, Bi, Fe, Ca, Cd, Ce, Co, Cr, Cu, Ga, Ge, In, K, La, Li, Mg, Mo, Mn, Na, Nb, Ni, P, Pb, Sc, Si, Sn, Sr, Ti, Tl, V, W, Y, Yb, Zn, Zr	ICP–OES, dc arc spectrography	7

Table 1 (continued)
Geological samples

Sample(s)	Digestion mode and special information/equipment	Required reagents	Analyte	Method of analysis	Ref.
Powdered carbonate rock samples, i.e. GFSs: 400 (dolomite), 401 and 402 (limestones) and 403 (limestones–dolomite blend); NIST SRM 88a (dolomite)	CEM MDS-81D oven; (1) open 120 mL Teflon™–PFA vessels with ethanoic acid on a hot plate then (2) closed with pressure release valves in microwave; heating process discussed; compared with two other author's work (classical methods) and certified values	(1) ethanoic acid, then (2) HF–HNO_3, then H_3BO_3 in microwave oven again	SiO_2, Al_2O_3, Fe_2O_3, CaO, MgO, Na_2O, K_2O	AAS	8
NBS SRMs: 613 & 615 glass wafers, 278 obsidian rock and 603 K-feldspar; US geological survery whole rock standards: BCR-1 basalt, GSP-1 granodiorite, G-2 granite and zircon	CEM MDS-81 oven; closed 60 mL Savillex Teflon™ vessels surrounded by a 300 mL Teflon™ jar; discussion of the action of microwaves with sample–acid mixture	HNO_3–HF–$HClO_4$, HCl	Pb and some isotopes of Pb and U	Isotope dilution technique	9
Sulfide minerals: feeds, tailings and concentrates (Ni, Cu, pyrrhotite)	Toshiba model ER-800BTC domestic oven; closed 150 mL Savillex Teflon™–PFA vessels; compared with classical open beaker method; incomplete digestion for some samples especially high silica ones such as tailings; eight-fold reduction in digestion time	K–chlorate–HF–HNO_3 mixture	Cu, Ni	AAS	10
G-2 granite and MESS-1 marine sediment, silicate and quartz standard reference materials	Panasonic model NE-7970C domestic oven; lab.-designed, 1/2 in. thick walls and base, Lorran 20 mL Teflon™–TFE bombs (Lorran Int., Porters Lake, Nova Scotia, Can., B0J 2S0) which do not require annealing, machined from molded, stress-relieved Teflon™–TFE rods; with pressure release seals (250 psi); vessels are hand-tightened; domestic microwave pressure cooker with a pressure indicating stem used to contain leaking fumes; compared with same vessels in boiling water	Aqua regia HF, then boric acid upon dilution	SiO_2, Al_2O_3, Cr, Zn	GF-AAS	11

Table 1 (continued)
Geological samples

Sample(s)	Digestion mode and special information/equipment	Required reagents	Analyte	Method of analysis	Ref.
Standard rock sample andesite JA-1	A Koizumisango NDR-0500 oven; closed 23 mL PTFE Parr 4781 bomb with a pressure release mechanism (Teflon™ screw, max. pressure 100 Kg cm^{-2})	HNO$_3$ or aqua regia, then HF, then H$_3$BO$_3$ for Si determination	Fe, K, Mg, Mn, Na, Si	AAS	12
Ga and Ge ores: goethite, jarosite, hematite and some secondary Cu minerals; Zn processing waste: sphalerite, gypsum, quartz and anglesite	Modified Sears Kenmore Model 88861 domestic oven with an exhaust duct vented to a fume hood: closed Savillex 50 mL Teflon™ vessels; inhibition of volatile chlorides being formed; 20 samples/h; two-step dissolution; discussion of volatilization: GaCl$_3$ and (201°C) GeCl$_4$ (84°C)	HF–HNO$_3$, then H$_3$BO$_3$ HNO$_3$	Ga, Ge	nitrous oxide–acetylene FAAS or EAAS	13
Geological: Au and Ag bearing ores	microwave dissolution compared to fire assay technique		Au, Ag		14
Two fractions of Au and Pt group bearing rocks i.e. metallic and non-metallic parts	A dry chlorination method and wet microwave dissolution method	HF HNO$_3$–HCl	Platinum group elements and Au	ICP-MS	15
Slag, feldspar and Ni–Cu alloy	Modified conventional oven; fumes expelled to a fume hood using a CO$_2$ gas flow through pre-drilled holes; turntable used: two-stage dissolution; close polycarbonate bottles; in agreement with certified values (rel. std. dev. was 1%);	HF–HClO$_4$–HNO$_3$, then boric acid	Al, Ca, Cu, Fe, K, Mg, Mn, Na, Ni, Si	AAS, ICP-OES, XRS	16
Geological and metallurgical materials	Recommendations for the development of methods: in Russian with only the title translated				17
Minerals	Closed vessels; manual and robotic control; in Russian with only the title translated				18
Na$_2$SO$_4$, Cu–Pb–Zn ores	Microwave heating as an alternative in gravimetry; also Na$_2$O$_2$–ZnO fusion using microwave energy		S	Gravimetry	19

Table 1 (continued)
Geological samples

Sample(s)	Digestion mode and special information/equipment	Required reagents	Analyte	Method of analysis	Ref.
(1) Ores (2) blister Cu	Closed Teflon™–PFA vessels; advantages over conventional methods; new technology such as lined vessels, temperature and pressure probes, and flow-through systems	HNO_3–HCl	(1) As, Cu, Se, Zn (2) Ni	(1) ZE–FAAS (2) AAS	20, 21
A U-rich sandstone (DL-la), a granite (BOE), a river sediment (SRM 1645) and a nearshore, marine sediment (RIID)	Modified Hitachi MR-6750 domestic oven inside a fume hood; closed Teflon™ bombs in a sealed box which is flushed with compressed air; how to digest obdurate minerals using Parr bombs	HNO_3–HCl HF	U, Th, some isotopes (^{238}U, ^{234}U, ^{232}Th, ^{230}Th)	Radio-chemical separation and alphaspectrometry	22
Free silica in a K–feldspar matrix, quartz, respirable dust samples	Closed vessels; procedure for determining the quantity of free silica in respirable dust samples, quartz recovery was 97%	Pyrophosphoric acid	Free silica		23
Fe ores and slags; representative CRMs; Fe, C and low-alloy steels	Commercial lab. oven; selection of acid mixtures and vessels; study of variables; establishment of operating procedures				24
Au-bearing ores	PATENT: pulsed microwave energy technique where the Au-bearing ore is exposed to pulses for 1–30 s with 10 s–2 min intervals between pulses for a total treatment of about 1 h; then leached by cyanidation to recover Au; Pb and Zn can be recovered as well	Cyanide	Au, Pb, Zn		25
Stone cutting waste	Closed PTFE vessels; filtered then residue ashed in a clay crucible at 1000°C; weight of fired material $\times 400 = \%$ SiC	HCl HF	SiC	Gravimetric	26
NBS: 278 obsidian rock, 688 basalt rock, 1633 and 1633a coal fly ash, 1645 river sediment and 1646 estuarine sediment	CEM MDS-81 commercial oven; closed 120 mL PTFE vessels; compared with high-temperature $Li_2B_4O_7$ fusion and PTFE bomb method using HF, HNO_3 or $HClO_4$	HF, HNO_3 or $HClO_4$, or HF–aqua regia	Al, Ba, Ca, Co, Cr, Cu, Fe, K, Mg, Mn, Na, Ni, Sc, Si, Ti, V, Zr	ICP-ES	27

Table 1 (continued)
Geological samples

Sample(s)	Digestion mode and special information/equipment	Required reagents	Analyte	Method of analysis	Ref.
Buddingtonite	Domestic oven modified by fitting tubing through the ventilation holes for cavity purging with compressed air and all exposed interior metal parts covered with plastic tape; 12 closed polycarbonate vessels capped with polypropylene screw caps inside a PE food container; ammonium determinations compared with those from Kjeldahl method; safety discussed	HF HCl	Ammonium K, Na	IC, potentiometric-measurements using an ammonia-specific electrode	28
US Geological Survey diabase W-1 and basalt BCR-1; NBS SRM 1632, 1632a and 1635 coals, 1633 and 1633a fly ash, 1645 sediment; IAEA SRM SL-1 sediment, polymers	Domestic Sears Kenmore oven; open Teflon™ or polycarbonate beakers inside a Pyrex vacuum desiccator	aqua regia–HF	Al, As, Ba, Be, Ca, Co, Cr, Cu, Fe, K, Li, Mg Mn, Na, Ni, P, Pb, Si, Sr, Ti, V, Zn	ICP-AES	29
Geological	Field instrumentation for a microwave digestion method followed by portable AAS		Metals, semi- and volatile organics	AAS, XRF for higher levels or inorganics	30

air. Most of the microwave dissolutions were performed using sealed vessels but some studies involved the use of pressure release mechanisms [8,11,12] and pressure and/or temperature monitors [11,20,21]. Three of these papers discussed the use of specialty dissolution vessels [11,20,21] while only two discussed the safety aspects of using closed vessels and microwave energy [7,28]. Some of the closed vessel dissolutions made use of containers which enclosed the vessels to prevent leaked fumes from destroying oven cavities [7,9,11,22,28]. Two dissolution methods used open vessels such as corundum crucibles [2] and Teflon™ or polycarbonate beakers [29]. Fusion procedures using microwave ovens are being developed [19] and a handbook describing them is to be published early in 1996 [332].

Despite the widespread use of certified reference materials, comparisons were also made with other non-microwave-assisted techniques to test the reliability, accuracy and precision of microwave methods [1–3,5,6,8,10,11,14,15,19,27, 129]. Discussions of the practicality of the technique for automation and robotics [18], flow-through systems [20,21] and field instrumentation for microwave digestions followed by portable AAS [30] have been reported. One report describes a pulsed microwave energy technique, followed by cyanide leaching, to recover Au, Pb and Zn [25].

By judicial adjustment of the various parameters (choice of acid mixture, power setting, time of irradiation) it has been found possible to dissolve most geological samples using the microwave-assisted pressure-dissolution technique. Precision and accuracy are generally as good as or better than those attained through conventional dissolution protocols.

2.2 Biological samples

It has become increasingly apparent that trace elements play an important role in biological systems, sometimes as nutrients and sometimes as toxins. There are even reports that they are responsible for causing diseases, such as urolithiasis [33]. One of the major problems in the determination of trace metals in biological materials is the dissolution 'of organic matter. The numerous problems associated with the destruction of organic matter have been described by Gorsuch [314]. When dealing with botanical and food samples, similar problems are encountered—the paragraphs that follow should be taken to include samples of these types as well.

The high pressure generated using closed vessels raises the boiling point of the acid(s) used and substantially increases the dissolution rate of these organic matrices. For example, nitric acid normally boils at 120°C, but at 5 atm in a closed container, it boils at 176°C when heated by microwaves [270]. This is 56°C above its normal boiling point and this results in an increase of its oxidation potential and speeds up its reactions. Under classical hot-plate conditions, the organic matrices of biological samples would remain intact due to the low boiling point of nitric acid. Under these circumstances, reagents such as perchloric acid would have to be used for the complete destruction of the organic matter.

The closed vessel microwave approach makes it possible to avoid the use of perchloric acid which is potentially explosive when in contact with easily oxidized inorganic or organic materials, expecially at elevated temperatures. Great care should be taken when heating percholoric acid under pressure, even by itself—one report [270] has shown that closed vessels heated with only 5 mL of perchloric acid remain pressurized even after cooling with liquid nitrogen. Instead of vaporizing and condensing like other acids, perchloric acid generates chlorine gas via an irreversible decomposition reaction when high temperatures are reached. The chlorine gas is not easily frozen and maintains a high pressure within the vessels. Despite the hazard, some authors do report the use of perchloric acid mixtures under pressure for

decomposition of biological samples (see Tables 2, 3, and 4).

Fortunately, pressure dissolutions involving other acid mixtures can usually be substituted with acceptable results. However, even when other acids are used, the considerable change in internal pressure generated by the production of CO_2 and NO_2 as the organic matrices are decomposed must be anticipated and controlled to prevent vessel rupture, microwave oven damage and possible personal injury. As a safety precaution, vessels with some kind of pressure release mechanism are recommended. Biological, botanical and food samples are primarily composed of three basic constituents: carbohydrates, proteins and lipids. Carbohydrates are the first constituent to decompose at approximately 140°C. Next, proteins decompose at about 150°C, followed by the lipids at around 160°C [193,270]. At each of these temperatures, significant increases in pressure are recorded with virtually no increase in temperature. Thus, for safety reasons and for determining the most efficient temperature for decomposition, the analyst should have some knowledge of the constituents of a sample matrix.

Abu-Samra et al. [31,32] were the first to report the use of a microwave oven for sample dissolution, vide supra. They used a nitric–perchloric acid mixture to oxidize biological samples in open 125 mL Erlenmeyer flasks using a domestic microwave oven. Since then, numerous articles have been published involving the use of microwave energy for the dissolution of biological samples [31–93,121,122,125]. Table 2 summarizes these reports. (See also Table 3 on botanical samples and Table 4 on food samples). Some reports describe interesting oven modifications [31–33,41,87,122]. Small holes can be drilled through an oven's side and liner in order to accommodate an exhaust port to remove fumes to a scrubber [31,32]. A water-jet aspirator can be used to remove fumes to a fume scrubber [87,122]. The cavity of an oven can also be sprayed with a silicone spray as a form of protection [87]. Two dissolution systems involved the use of focused microwaves in order to increase efficiency and to decrease digestion time [36,65].

Table 2
Biological samples

Sample(s)	Digestion mode and special information/equipment	Required reagents	Analyte	Method of analysis	Ref.
NBS CRMs: 1577a bovine Liver and 1571 orchard leaves, hair, fingernail and *Drosophila*	Modified domestic oven; open 125 mL flasks; fume scrubber using solid CaO, $CaCO_3$, liquid NaOH and water spray trap materials were tried; water aspirator, vacuum cleaner and a drum fan also tried for oven venting; Plexiglas box to protect oven from fumes	HNO_3-$HClO_4$	As, Co, Cr, Cu, Pb, Se, Ni, Zn	AAS, NAA	31, 32
Urinary calculi	Sharp (Model R6950 E) domestic oven; 50 mL flasks covered with small beakers all inside a dessicator connected to a fume scrubber using NaOH; no loss of any elements; excellent agreement with hot-plate method	HNO_3–$HClO_4$	Al, Ca, Cu, Fe, K, Li, Mg, Mo, Mn, Na, P, Pb, S, Sr, Zn	ICP-AES, XRD	33
NBS CRM 1577a bovine liver	CEM MDS-81D oven; closed 60 mL Teflon™–PFA with high-pressure release valves compared to open glass 30 mL beakers; powered fixed-torque capping station; fumes vented to a fume hood via a flexible duct; drying	HNO_3–H_2O_2	Fe	AAS	34
NIES CRMs: #5 human hair, #1 pepperbrush, #6 mussel, #7 tea leaves; NIST SRM 1566 oyster tissue	Mitsubishi RO-2500 domestic oven; closed PFA Tuf-Tainer vials in PTFE vessels enclosed in a jacket of polypropylene to protect oven from the fumes	HCl–$HClO_4$–HNO_3–HF, NAOH in the outer PTFE vessel	Al, Cu, Fe, Mn, Zn	ICAP	35
NIST SRM 1577a bovine liver	Special continuous power output, focused microwave system (via a waveguide); close stainless steel jacketed 28 mL tetrafluoro-metoxil–PTFE vessels (m.p. 350–380°C) in a ceramic vessel liner; rupture discs; fluid cooling system for pre- and post-digesting cooling of vessels; internal and external antennas provide coupling of microwave energy between a magnetron and the sample and acid(s)	HNO_3, can also use H_2SO_4 due to the higher melting point of the TFM–PTFE polymer vessel	residual C	Microcoulo-meter, Knobloch apparatus, elemental analyzer	36
BCR CRMs: 186 pig kidney, 184 bovine muscle, 062 olive leaves, 060 and 061 aquatic plants; NRCC CRMs: DORM-1 and DOLT-1 fish tissues and TORT-1 lobster hepatopancreas; NIST SRMs: 2670 freeze-dried urine and 1572 citrus leaves	Panasonic (Model NN-8507/8557) domestic oven with a rotating antenna for homogeneous microwave distribution; used closed PTFE Parr 478 bombs and results in agreement with certified values	HNO_3–HCl, then NaOH for pH adjustment, $NaClO_4$ and buffer	Ni	ICP-AES	37
NBS: oyster tissue and bovine liver; SRMs: 1643a and 1643b water samples	Domestic oven; 23 mL Parr Teflon™ bombs (maximum pressure 1200 psi); 30 s dissolutions	HNO_3	Cd, Cu, Fe, Pb, Zn	AAS	38

Table 2 (continued)
Biological samples

Sample(s)	Digestion mode and special information/equipment	Required reagents	Analyte	Method of analysis	Ref.
NBS SRM 1577 bovine liver; NIES CRM # 6 mussel, # 1 pepperbush and # 7 tea leaves	Mitsubishi R0-2500 domestic oven; capped 7 mL Tuf-Tainer PFA vials inside closed 50 mL Teflon™–PFA vessel all enclosed inside a polypropylene jacket; can digest 500 mg samples	HNO_3–HCl– $HClO_3$–HF mixture	Ca, Cu, Fe, K, Mg, Mn, Na, Zn	AAS	39
Fish muscle, IAEA MA-M-2/TM lyophilized muscle tissue	Prolabo Microdigest 300 oven; borosilicate glass flasks; 5 min, two-step dissolutions; optimum amount of HF required for best recovery was found to be 1 mL for a 1 g sample	HNO_3, or HNO_3–H_2SO_4 or HNO_3– H_2SO_4–H_2O_2	Hg	CV-AAS	40
Serum, NIST SRM 1577a bovine liver	Modified domestic oven with a plastic turntable and fumes directed to a fume hood; closed 50 mL PTFE centrifuge tubes; annealing method for vessels (200°C for 96 h)	HNO_3–H_2SO_4, then H_2O_2	As, Se	HG-AAS	41
Human plasma, NIST CRMs: 1572 citrus leaves, 1567a wheat flour	CEM MDS-81D oven; closed 120 mL PFA Teflon™ vessels with pressure release valves, collection vessel, tubing and powered fixed-torque capping station; multi-stage dissolutions	HNO_3–HCl	B	ICAP	42
Mussel, tobacco, peat, pine bark, ryegrass, apple, rice, vine leaves, cotton, hay, lettuce, flour, skim milk powder—spiked, BCR # 61, BCR # 60, pepperbush, NIST SRM 1548 and SRM 1573a, baby food	Moulinex 430 commercial oven and a Milestone microwave system (MLS-1200 MEGA); four digestion procedures using 25 mL Parr bombs (max. pressure 8×10^6 Pa) and MRD 1000/6/100/110 Teflon™ vessels (max. pressure 11×10^6 Pa)	HNO_3, HF, H_2O_2, $HClO_4$ and mixtures of these depending on the sample type	B, Cu, Fe, Mn, P, Pb, Zn	ICP-ES, FAAS, GF-AAS, ET-AAS	43
Hemodialysis water			Al	DPP, GF-AAS	44
Pig liver	Closed vessels	HNO_3–H_2O_2	Fe, Mn, Se	FAAS, HG-AFS	45
Biological, food, botanical	Open vessels				46
Pig liver	Closed PTFE vessels; cooled in an ice bath	HNO_3–H_2O_2	Mn, Fe	FAAS	47
CRMs: 1577a bovine liver, 1572 citrus leaves, 1575 pine needles, NIST 1648 urban particulate and 1576a flour, BCR CRMs: 186 pig kidney, 184 bovine muscle, 62 olea europae, 60 lagarosiphoumajur, 150 milk powder, 141 soil and 185 sediment	Semi-closed 3 mL Teflon™ tubes sealed only by Teflon™ tape mounted on a tray inside a Sterilite box, which was covered inside with a transparent plastic film; two-step dissolution	HNO_3–H_2O_2, then aqua regia–HF, boric acid	Cu, Cd, Fe, Mn, Pb	Ze-GF-AAS	48
Biological and some SRMs	Closed Teflon™ vessels		Ni	ETA-AAS, ICP-AES	49

Table 2 (continued)
Biological samples

Sample(s)	Digestion mode and special information/equipment	Required reagents	Analyte	Method of analysis	Ref.
Human vertebrae, NIST SRMs: 1577 bovine liver and 1573 tomato leaves	All Teflon™ coated microwave digestion system		Ba, Bi, Cd, Co, Cs, Cu, Mo, Mn, Pb, Sr, Th, Tl, U, Zn	ICP-MS	50
Biological, and 5 NBS standard reference materials	Compared with conventional procedures		Al, Ca, Cu, Fe, K, Mg, Mn, Na, P, Sr, Zn	ICP-AES	51
Feces, urine	Sharp R-9280 oven; open crucibles; testing of the chelating effect of 1,2-dimethyl-3-hydroxy-pyrid-4-one for Fe overloaded rates	HNO₃	Fe	GF-AAS	52
Human semen, NIST 1577a bovine liver	Compared with conventional method		Cd, Cu, Cr, Pb, Zn	GF-AAS	53
Biological, NIST SRMs: 1570 spinach, 1571 orchard leaves, 1572 citrus leaves, 1573 tomato leaves, 1575 pine needles and 1577a bovine liver; BCR 63 milk powder; IAEA H4 animal muscle	Amana RS 560A domestic oven with rotating antenna for homogeneous microwave distribution; closed 60 mL Teflon™ vessels (Model 561R2, Savillex Corp., Minnetonka, MI, USA); safety vessels of 7.5 mL of vegetable oil/100 mL sample for excess microwave absorption; essentially the same accuracy and precision with only slightly higher detection limits as compared to the regular oven Teflon™ bomb method	HNO₃ with 9ppm Y as an internal standard	As, Ba, Br, Ca, Cr, Cu, Fe, K, Mn, Mo, Ni, Pb, Rb, Se, Sr, Ti, V, Zn	PIXE	54
Marine organisms, RMs: soils, sediments, wheat flour, citrus leaves, copepod homogenate, fish flesh homogenate, mussel tissue, olive leaves	Programmable Milestone MLS 1200 microwave oven; closed 120 mL PTFE bombs with pressure release valves (100 psi) and reflux system; recovery 104% and precision 1%	HNO₃–HCl, then H₂O₂, and HNO₃ for reflux system	As, B, Ba, Cd, Co, Cr, Cu, Fe, Hg, Mn, Ni, Pb, Sb, Se, Sr, Zn	ICP-AES, GF-AAS	55
SRMs: oyster tissue, bovine liver, milk powder, flour	Radarange domestic oven with a rotating antenna placed in a fume hood; lidded plastic box inside; closed 60 mL Teflon™–PFA vessels, three-step dissolution	HNO₃	Hg	CV-AAS	56
SRMs: cod muscle, muscle tissue, orchard leaves, fish flesh, lobster hepatopancreas, bovine liver and muscle, bread, milk powder and spruce needles; red cabbage, blood, urine, cooking oil, human breast milk	Buchi MLS 1200 domestic oven and a CEM MDS 81D oven; with PMD (Pressurized Microwave Digestion) quartz vessels with Teflon™ caps (by Paar, Graz, Austria); vessels have cooling unit, a piston indicating pressure and a sensor that shuts off power to the oven when 85 bar is attained until pressure is reduced; cooling unit; 10 samples at a time	HNO₃–HClO₄–H₂SO₄	As, Cd, Co, Cu, Ni, Pb	HG-AAS, DPASV	57
Biological	Teflon™ autoclaves		Twenty-four trace elements	ICP-AES, ET-AAS	58

Table 2 (continued)
Biological samples

Sample(s)	Digestion mode and special information/equipment	Required reagents	Analyte	Method of analysis	Ref.
SRMs: oyster tissue, rice flour, wheat flour, bovine liver, human urine	Modified CEM MDS 81 oven (a 360° reversing turntable, 12-position carousel, variable speed exhaust fan to remove fumes to a fume hood via a PVC hose mounted at the back wall of the cavity and a flexible and a rigid stainless stell waveguide attenuator cutoff grounded and mounted at the cavity wall to proved access for temperature and pressure lines); closed 60 mL Teflon™–PFA vessels (Savillex) with temperature (thermocouple) and pressure (transducer) probes; annealation of vessels; computer monitored system; reaction control techniques and safety precautions	HNO_3, H_2SO_4, HCl	Power absorption tests		59
CRMs: bovine liver, pine needles			Trace elements		60
SRMs: feces, citrus leaves, wheat flour and mixed diet	CEM MDS-81D oven with a rotating turntable and variable-speed exhaust fan; closed 120 mL Teflon™–PFA vessels (CEM Corp.); compared with traditional HNO_3–$HClO_4$ method	HNO_3–HCl. with and without HF, $HClO_4$ or H_2O_2	Ca, Cu, Fe, K, Mg, Mn, P, Zn	ICP-ES	61
NBS bovine liver; several hundred fish tissue samples (liver, muscle and kidney), plant, soil and plasma samples	Domestic oven; closed 60 mL Savillex Teflon™–PFA vessels (Savillex) placed inside a wide-mouth plastic container closed with a screw cap	HNO_3–H_2SO_4	Ca, Cd, Cr, Cu, Fe, Pb, Zn and l in Plasma	FAAS	62
Bone and teeth	Moulinex (Model Micro-chef FM 2515) domestic oven; closed 23 mL Parr 4781 Teflon™ bombs; cleaning of vessels; the first time that Ba and Cd levels in teeth have been reported	HNO_3	(1) Ce, Fe, K, Mg, Na, Zn (2) Ba, Cd, Pb	(1) AAS (2) GF-AAS	63
NRCC lobster hepatopancreas, marine biological reference material TORT-1	Commercial CEM MDS-81 oven: (1) closed 120 mL Teflon™–PFA vessels with pressure release valves; (2) closed 23 mL Parr Teflon™ bombs and (3) closed 100 mL Berghof PTFE vessels with rupture foil; 11 mL sample cups and an all PTFE microsampling device	HNO_3–H_2O_2	As, Cd. Co, Cr, Cu, Fe, Mn, Mo, Ni, Pb, Se, Sr, V, Zn	FAAS, ZE-GF-AAS, carbon analyzer, CO_2 Coulometer	64
Alfalfa, hevea leaves, mixed feed, tuna fish, SRMs: mussel and fish flesh homogenate, animal muscle, milk powder, bovine liver and wheat flour	Automated focused microwave Prolabo A-300 digestion system equipped with two pumps for the addition of reagents; digestion and extraction using 150 mL Kjeldahl flask topped with a 50 mL reservoir and vertical condenser; compared with conventional method	HNO_3, $HClO_4$	Se	ET-AAS	65
Biological NBS and CBR samples			As, Na, Ca, Cd, Cu, Fe, K, Mg, Mn, Pb, Zn	FP-ICP	66

Table 2 (continued)
Biological samples

Sample(s)	Digestion mode and special information/equipment	Required reagents	Analyte	Method of analysis	Ref.
Freeze-dried mussel, tea leaves, lotus-seed flour, SRMs: tea leaves and mussel	Closed PTFE vessels	HNO_3, $HClO_4$, HF, H_2O_2; mixtures	Multi-elements	ICP-AES	67
Haemodialysis water	Commercially available CEM MDS-81D oven; comparison of closed 7 mL Parr-type PTFE bombs and closed Teflon™–PFA vessels with pressure release valves	HNO_3–H_2O_2	Al	GF-AAS, DPP	68
NIST SRMs: liver and oyster; IAEA-CRM: human animal muscle	Panasonic NE-6660C conventional oven with a rotating turntable; closed 23 mL Teflon™ PFA Parr bombs	HNO_3, H_2O_2	Al, As, Ba, Ca, Cd, Ce, Cr, Cs, Cu, Fe, La, Li, Mg, Mn, Ni, Rb, Sb, Se, Sr, Mo, Tl, V, Y, Zn	ICP-MS	69
Eight octocoral species	Panasonic NE-7660/6660 domestic oven with a rotary tray; drying of samples; closed 200 mL thick-walled Pyrex glass test tubes with screw caps; compared with conventional sample drying and dissolution	HNO_3	Cd, Cu, Ni, Pb, Zn, total organic C	GF-AAS	70
Three NIST SRM bovine livers and one of orchard leaves and IAEA animal muscle	CEM MDS-81D oven; closed Teflon™ Parr bombs and 120 mL Teflon™ vessels with pressure release valves; two-step dissolution; problem in determining Al due to the detection limits of the methods	HNO_3	Al, B, Ca, Co, Cr, Cu, Fe, K, Mg, Mn, Na, Ni, P, Pb, S, Zn	ICP-AES, NAA	71
Human bone	CEM MDS-81D oven; closed 7 mL machined, and PTFE vessels with pressure release valves	HNO_3–H_2O_2	Al	DPP, GF-AAS	72
NIST SRM 1577a bovine liver; BCR CRMs: milk powders 150 and 151, olive leaves 62, sewage sludge 146, bovine muscle 184; SRMs: 1575 pine needles and 1566 oyster tissue; fiish muscle, pig kidney, peas, kale, lettuce	Domestic oven; closed 25 mL PTFE vessels (max. pressure 10 bar, supplied by Valtech Plastics, Thirsk); study of the stabilizing effects of Ru and Pd modifiers for retaining volatile analyte species during the charring step and for removal of interfering matrices; Ru better and retains volatiles 200–500°C higher than normal	HNO_3	Ag, Cd, Cu, Fe, Ga, Hg, Mn, Pb, Sb, Se	ZE-GF-AAS, ET-AAS, FANES	73
NIES CRMs: No. 6 mussel and fish tissue	Delonghi MW-155 domestic oven; closed PTFE vessels in a lidded plastic box to protect the oven from fumes	HNO_3–H_2SO_4, then H_2O_2; Na_2SO_3, KIO_3, H_2O_2	Se	DPP compared with HG-AAS	74
CBR CRM 278 mussel tissure, fish	Moulinex FM-460 oven; closed PTFE Parr bombs (model 4782); 90 s dissolution	HNO_3	Hg	CV-AAS, HG-AAS	75
Mussel products, NIST SRM 1556a oyster tissue; CBR CRM 278 mussel tissue	Bauknecht (Model MWT-732) domestic oven; closed 120 mL PTFE vessels compared with dry mineralization; moisture determination (drying) compared with conventional method	HNO_3–H_2O_2	As	GF-AAS	76

Table 2 (continued)
Biological samples

Sample(s)	Digestion mode and special information/equipment	Required reagents	Analyte	Method of analysis	Ref.
NIST SRMs: bovine liver 1577a and citrus leaves 1572; breakfast cereal mix	Prolabo Microdigest A-300 digestion apparatus (Rhone Poulenc, Prolabo Division Paris, France); oven vessels; programs for sample type; compared with hot plate method	$HNO_3-H_2O_2$ and sometimes H_2SO_4 as well; no need for $HClO_4$	Ca, Cu, Fe, K, Mg, Mn, Na, Zn	FAAS	77
NBSs: oyster tissue 1566, bovine liver 1577, spinach 1570, citrus leaves 1572, tomato leaves 1573, pine needles 1575, what flour 1567, rice flour 1568; apple leaves	CEM MDS-81 oven; closed 100 mL volumetric flasks	HNO_3, then H_2O_2	Ba, Ca, Cr, Cu, Fe, K, Mg, Mn, Na, Ni, P, S, Zn	ICAP-ES	78
NBS SRM 1577a bovine liver	CEM microwave digestion system; closed 60 or 120 mL PFA–Teflon™ vessels by Savillex; temperature measurement via a fibreoptic thermometer and pressure via a pressure sensor; vessels cooled in a dry ice–ethanol bath; residual organic species in a nitric acid digest identified which are destroyed if perchloric acid used (atmospheric pressure)	HNO_3 alone or with $HClO_4$	Residual organic species, Cu, Zn	UV/vis spectrophoto-meter, voltammetry, HPLC	79
Femur and parietal (skull) bones from 48 female rats, food	Domestic oven; open 125 mL flasks; rats given various concentrations of Pb in their drinking water	HNO_3	Pb	FAAS	80
Archaeological bone (ancient skeletal remains)	Open 25 mL conical flasks; samples cleaned ultrasonically	HNO_3 followed by $HClO_4$	Sr	FAAS	81
Pig liver	Closed 30 mL PTFE vessels; vessels cooled in an ice bath	$HNO_3-H_2O_2$	Mn, Fe	FAAS	82
Bone and brain tissue	1 h predigestion at 200°C then 6 min with HNO_3 in closed PFA vessels; improvement in detection limits for Al; digestion time, blank levels of Al (10 to 1 ppb) and amount of acid required (reduced 70%) were decreased	HNO_3	Al	GF-AAS	83
NRCC: (1) lobster hepatopancreas (TORT-1) and (2) marine sediment (MESS-1)	CEM MDS-81 commercial oven; closed 120 mL Teflon™–PFA vessels (CEM) with and without pressure release valves (75–85 psi); pressure measurements via a CEM PM pressure transducer attached to one of the digestion vessels with a pressure sensor designed to open if internal pressure within the line reached 100 psi; capping station; all vessels annealed; one or two stage dissolutions and subsequent evaporation on a hot plate (1) compared with hot-plate method (2); safety discussed	(1) HNO_3-HClO_4 or (2) HNO_3-HClO_4- HF	(1) As, Cd, Co, Cr, Cu, Fe, Mn, Ni, Pb, Se, Zn (2) same as above; total carbon in TORT-1	FAAS, GF-AAS, ICP-AES, total carbon analyzer, ICP-MS, ASV (using two-stage digests)	84

Table 2 (continued)
Biological samples

Sample(s)	Digestion mode and special information/equipment	Required reagents	Analyte	Method of analysis	Ref.
NBS SRM 1577 bovine liver	Domestic Philips AKB 100 oven; open conical flasks heated to near dryness; criteria for sample preparation and suitability of sample solution for ICP analysis discussed; compared with conventional extraction with HNO_3, solubilization in tetramethylammonium hydroxide, digestion with H_2O_2 and $HClO_4$, digestion in Teflon™-lined steel bombs, low-temperature ashing and muffle furnace ashing; safety discussed	HNO_3–$HClO_4$	Cd, Cu, Fe, Mn, Pb, Zn	ICAP-AES	85
Human blood	Domestic oven; stable tracer ^{58}Fe technique for iron utilization studies in man; open 250 mL Erlenmeyer flasks heated to dryness then dissolved with HCl, buffered with Na citrate, reduced with hydroquinone and complexed with 1, 10-phenanthroline	HNO_3–$HClO_4$	^{58}Fe	NAA, UV/vis spectrophotometer for complexed Fe	86
(1) Human teeth (2) Swordfish and Tunafish	Modified domestic oven with its cavity sprayed with silicon, a Pyrex jar used as an interior cavity and a Nalgene #6140 aspirator used to remove fumes from the cavity to a fume trap and a KOH scrubber; (1) 30 open ASV cells (Pyrex 20 × 85 test tubes) taken to dryness (2) open 125 mL Erlenmeyer flasks with a small funnel; blank Pb levels lowered from 9 ng (hot plate) to 5 ng	(1) HNO_3–$HClO_4$–H_2SO_4 (2) HNO_3–H_2SO_4	(1) Pb (2) Hg	(1) ASV (2) CV-AAS	87
Human blood (plasma and red cells)	Domestic oven, open 125 mL flasks; measurement of the extent of ^{70}Zn enrichment in plasma samples in man	HNO_3–H_2O_2	^{68}Zn and ^{70}Zn	NAA	88
NIST SRMs: 1577 bovine liver, 1566 oyster tissue, 1571 orchard leaves, 1570 spinach, 1572 citrus leaves, 1549 non-fat milk powder; IAEA: H-4 animal muscle, A-11 milk powder, V-10 hay, H-9 mixed human diet, total diet samples; NIES CRM-3 chlorella; RM-127 potato powder, RM-8 wheat flour, RM-115 animal muscle, RM-121 milk powder; whole egg and milk powder, wheat gluten, bovine muscle powder, corn bran, durum wheat flour; USDIET-I and II; DBW-9a and -11a swedish diets	Domestic Admiral oven; closed Parr bomb equipped with pressure release valves; cooled in a refrigerator; safety discussed	HNO_3	I	PNAA	89

Table 2 (continued)
Biological samples

Sample(s)	Digestion mode and special information/equipment	Required reagents	Analyte	Method of analysis	Ref.
NIST 1577a bovine liver		HNO_3	Se	ZE-AAS	90
Human head hair of 53 gas station workers and an equal number of controls	Domestic Philips AKB 100 oven; microwave dissolution (NaOH scrubber) in open test tubes before flow-injection/ASS Pb determination; hair washed first with EtOH and water; effects of washing, sample digestion of procedures, head sampling site, hair color, age, smoking habits and duration of exposure to Pb discussed; Pb content of gas station workers almost three times higher than normal controls	HNO_3–$HClO_4$	Pb	FI-AAS	91
NBS SRM 1577 bovine liver; NIES CRMs: #6 mussel, #1 pepperbush, #7 tea leaves	Domestic Mitsubishi RO – 2500; closed 7 mL Teflon™–PFA vessels	HNO_3–$HClO_4$–HCl–HF	Ca, Cu, Fe, K, Mg, Mn, Na, Zn	FAAS	92
Protein samples	Evaluation of microwave-assisted protein hydrolysis protocol	HCl	Amino acids		341
Protein samples	Comparison of the recovery of amino acids after vapor phase hydrolysis of proteins in a Pico Tag apparatus and a microwave hydrolysis system	HCl	Amino acids		342
Biological tissue containing seleno-amino acids	Direct detection of seleno-amino acids following microwave-assisted hydrolysis	HCl	Seleno-amino acids	Anion exchange electrochemical detection	344
Non-defatted lobster hepatopancreas tissue LUTS-1		HNO_3–H_2O_2	Seven trace elements, Hg	ICP-MS	93

Three papers discussed vessel annealation methods [41,59,84] which is important for decreased vessel porosity and increased strength. Gil et al. report the first simultaneous determinations of both barium and cadmium levels in teeth—they used a domestic oven and 23 mL Parr Teflon™ bombs [63]. Closed vessels were sometimes cooled using an ice bath [82], a refrigerator [89] or a dry ice–ethanol bath [79]. This allowed for the opening of vessels sooner than normal due to reduced vapor pressures. Safety concerns when using closed vessels were discussed in only three papers [59,85,89]. Open vessels were used less often but can provide complete dissolutions fairly quickly depending on the sample type [31–33,40,46,48,52,65,77, 80,81,85–88,91,122].

Sometimes special equipment was required and installed, such as fume scrubbers [31–33,87,91,122], vessels with pressure release mechanisms [34,36,42,55,64,71,72,84,89] and pressure and temperature monitors [57,59,79,84]. Other equipment included containers which enclose dissolution vessels to protect the microwave oven's cavity from leaking fumes [35,39,56,74,87], dissolution vessel cooling systems [36,57] and automatic capping modules [84,201]. One particularly noteworthy report [36] describes the design, construction and testing of a special vessel which incorporates a microwave source inside a stain-

Table 3
Botanical samples

Sample(s)	Digestion mode and special information/equipment	Required reagents	Analyte	Method of analysis	Ref.
Oilseed rape stems, maize, wheat, barley	Teflon™-lined microwave bombs (Scientific & Medical Products, Manchester, UK; max. pressure 7.6×10^5 Pa and 180°C); compared with conventional method	NaOH, then HCl for pH adjustment; extracted with ethyl acetate	Total phenolic acids	Extraction	94
Barley straw, carnations, oak leaves, pine needles and rye grass	Microwave dissolution compared to classical method		Four major and six trace elements	ICP, ICP-MS	95
Standard reference materials; plant materials	Commercial lab. microwave–acid digestion system; closed Teflon™–PFA vessels with pressure release valves; compared with a dry ashing procedure; did not result in complete mineralization of samples although good results were obtained for the metals studied	HNO_3–HCl	Ca, Cu, Fe, Mg, Mn, Zn	FAAS	96
Plant material and standard reference materials	Open vessels; effects of acidic digestion mixtures upon dissolution; reaction vessels and power levels; procedure optimized	Various acids			97
Algae, seagrasses, fresh water and terrestrial plants, spermatophyta leaves, wood, rhizomes, roots and bark, NBS SRMs: pine needles and citrus leaves, *Pinus radiata* leaves	Modified Sanyo EM-840 domestic oven placed inside a fume hood; 50 mL Nalgene FEP (fluorinated ethylene propylene) Teflon™ vessels buried to half their height in a Pyrex container and sand; a glass water vacuum pump attached to Teflon™ tubing to vent off fumes from the container; instrument availability, purchase price, operating costs, acid volume and number of samples per hour compared to classical methods; safety aspects	HNO_3–$HClO_4$	Ca, K, Mg, P, S	ICP-ES	98
Plant tissues—BCRs: #279, #62 and #60; IAEA V-10 hay; halophyte *Aster tripolium*	CEM MDS-81D oven; closed 120 mL Teflon™–PFA vessels with pressure release valves (max. pressure 120 psi)	HNO_3–HCl, or HNO_3 alone	Ca, Cd, Cu, Fe, K, Mg, Mn, Na, Pb, Zn	FAAS, GF-AAS	99
NIST SRM citrus leaves #1572; agricultural crops: ryegrass, alfalfa, stargrass, bahiagrass, leucaena	CEM MDS-81D oven; 13 different power levels and times of exposure; closed 120 mL Teflon™–PFA vessels (exhaust ports in the centre of the lids) with pressure rupture release discs; compared with dry ashing and H_2SO_4–H_2O_2 wet digestion; diagrams of microwave vessels and system	HNO_3–HCl	Ca, Cu, Fe, K, Mg, Mn, P, Zn	ICP	100

Table 3 (continued)
Botanical samples

Sample(s)	Digestion mode and special information/equipment	Required reagents	Analyte	Method of analysis	Ref.
NIST SRMs: 1572 citrus leaves, 1575 pine needles, 1573 tomato leaves and 1567 wheat flour	CEM MDS – 81D oven; semi-closed 120 mL Teflon™ vessels with an exhaust port which allow the addition of H_2O_2 and HCl without removing the screw cap lids; Teflon™ coated oven cavity; compared with an open and closed (bomb) microwave method; three-step dissolution; 36–48 samples person/day	HNO_3, then H_2O_2, then HCl	Al, Ca, Fe, K, Mg, Mn, Na, P, S	ICP-AES	101
High organic content sample: sweet bay	CEM MDS-81D oven; semi-closed 120 mL Teflon™–PFA vessels covered with a predigestion reflux condenser or a cold finger assembly cooled using chilled heptane for preventing excessive pressure when samples are later digested under pressure; entering and leaving temperatures of coolant heptane measured by a Technosyn temperature probe; pressure monitoring via an external transducer (Sensym SX150DN); diagrams of both condenser and finger assemblies	HNO_3, heptane (chilled in a cardice with a CO_2-methanol slurry)	Mn	FAAS	102
Plant materials: six different reference materials	Closed Teflon™ · PFA vessels; method is dependent on the sample type and elements to be determined	HNO_3–HCl, or HNO_3– HF-H_2O_2	Al, Ca, Cr, Cu, Fe, K, Mg, Mn, Si, Ti, Zn	FAAS, DCP-AES	103
Plant tissue and CRMs	A dissolution method was developed without the use of H_2SO_4 and/or $HClO_4$ which create various molecular species which overlap with several important isotopes	HNO_3	Cr, Ni and other elements	ICP-MS	104
Plant material, reference materials: NIES rice flour 10c; IAEA V-10 hay and NBS wheat flour	CEM MDS-81D oven; closed 120 mL Teflon™–PFA vessels; four-step dissolution; precision and accuracy good enough for the application to long-term tracer studies with stable isotopes of Mo	HNO_3 then perhydrol, spiked solution (^{97}Mo-enriched aqua regia)	Mo and Mo isotopes	ID-MS	105
NBS SRM plant samples: citrus leaves and peach leaves; $(NH_4)_2SO_4$	CEM MDS – 81D oven; closed 120 mL Teflon™–PFA vessels with pressure venting system; special cap with two ports for pressure and temperature (fibre-optic-fluoroptic thermometry system) monitoring; fumes vented to a fume hood via PVC piping; capping machine; comparison with wet ash digestion	HNO_3–HCl, and HNO_3 H_2O_2	S	ICP	106

Table 3 (continued)
Botanical samples

Sample(s)	Digestion mode and special information/equipment	Required reagents	Analyte	Method of analysis	Ref.
Plant materials: citrus leaf standard, peach and tomato leaves: $(NH_4)_2B_4O_7 \cdot H_2O$	CEM MDS – 81D oven; closed vessels compared with dry ash digestion	HNO_3, then H_2O_2	B, S	ICP-ES	107
Wood and wood-based materials (plywood and particleboards)	Non-destructive method based on measuring microwave attenuation		Moisture		108
Plants, food	Comparison with other decomposition techniques such as acid-oven, pressure, plasma and UV dissolutions	Mineral acids	Heavy metals		109
Plants and biological fluids	Open 125 mL vessels	$HNO_3 - HClO_4$	Se	INAA	110
Eight peat samples	CEM MDS-81 commercial oven; four closed 60 mL Savillex PTFE–PFA vessels, two to a set of Nalgene 16-500 polypropylene bottles with loosely closed lids; sample heated with HNO_3 on a hot plate at 130°C then inside nalgene bottles in a microwave oven with $HClO_4$, cooled, then again in the oven with HF, then brought to dryness on a hot plate, compared with conventional hot-plate and dry ashing methods; caution advised; new method requires only 2 h compared to 30 h on a hot-plate with 45 mL of acid	HNO_3 then $HClO_4$ then HF (the greater the silicate content, the greater the amount of HF used)	Al, Ca, Cu, Fe, K, Li, Mg, Mn, Na, Zu	FAAS	111
NBS SRM 1571 orchard leaves	Open vessels; digests analyzed using a CRA and Woodriff furnace; acid fumes exhausted to a fume hood	HNO_3, $HClO_4$ and a few drops of HF	Cr, Cu, Pb, Zn	CRA and Woodriff furnace GF-AASs	112

less steel jacketed vessel lined with TFM–PTFE™. Inside the vessel, a steel waveguide focuses the microwave energy directly onto the sample. Operating temperatures of up to 350°C are attainable.

Much of the research has included results from standard reference materials for verification purposes. In addition, much of the development work was carried out in paralled with a more traditional method, and the results of the two methods compared [33,51,53,61,65,70,76,77,84,85,121,122]. In addition, there are reports of studies on biological materials involving drying [34,70,76], automation [65], a Kjeldahl apparatus/technique [249] and reflux/extraction systems [55,65]. The use of

microwave-transparent, inert, closed vessels for sample dissolution appears to be the method of choice for the destruction of organic matter. Loss of analyte by volatilization or adsorption onto the walls of the vessel is negligible despite the generation of the high pressures and temperatures associated with the technique. In most instances, the high pressures and temperatures result in complete dissolution of the organic matter which often remains after dissolution by conventional techniques. There are some reports of the use of microwave ovens for protein hydrolysis (particularly vapor phase) prior to amino acid analysis [341–344]. In view of the long reaction times required for conventional protein hydrolysis, this

Table 4
Food samples

Sample(s)	Digestion mode and special information/equipment	Required reagents	Analyte	Method of analysis	Ref.
Brine shrimp (adult *Artemia* sp.)	Modified Penney RE-705TC domestic oven; open polyethylene and polypropylene cups and vials inside a closed polypropylene or pyrex container attached to a water aspirator and KOH scrubber for time removal. No loss of volatile trace elements	HNO_3	Cu, Cd, Fe	HG-AAS	113
Meat, oatmeal	Domestic oven; moisture determination by weighing samples before and after treatment, error < 0.01%		Moisture	None	114
Food	Domestic oven; closed 50 mL PTFE vessels cooled afterwards at −25°	HNO_3–H_2O_2	Ca, Cu, Fe, Mg, Mn, Zn	ICP-AES	115
SRM IAEA A-11 full-cream milk powder; soyabean flour, chocolate cream, milk chocolate, peanut butter, sunflower oil, linseed	(1) MWS 700 (Bacuknecht) and (2) Prolabo Microdigest 300M domestic ovens; (1) closed 50 mL low-pressure PTFE vessels with pressure release blast discs (1 MPa) connected to an acid container via PTFE tubing — a three-step dissolution; compared with: (1) high-pressure 23 mL polyimide bombs with PTFE sample vessels; (2) open quartz Kjeldahl flasks with a Vigreux colomn—three or four-step dissolution; (3) cool plasma ashing with microwave excitation and wet pressure digestion with conductive heat in an autoclave (Tolg); reproducibility, completion of digestion, contamination problems and loss of analytes discussed	HNO_3 then after the second stage of dissolution H_2O_2, or HNO_3–H_2SO_4, or HNO_3 alone	(1) Cu, Fe, Zu (2) Ni and other low concentration elements (3) Hg, Se	(1) FAAS (2) GF-AAS (3)HG-AAS	116
Food	PATENT: food material that had been sterilized and/or bleached is irradiated (1000–3000 MHz) to decompose H_2O_2 residues	H_2O_2			117
Grapefruit juice	Domestic General Electric JET 212 oven; closed 60 mL Teflon™–FEP bottles; advantages and possibility of automation discussed	Aqua regia	B, Ba, Ca, Cu, Fe, K, Li, Mg, Mn, Na, P, Rb, Sn, Sr, Zn	ICP-AES	119
Brine shrimp	Penny RE-705TC domestic oven modified with a water aspirator and KOH scrubber; open polyethylene autosampler cups; compared with dry ashing, hot block and high-pressure techniques	HNO_3	Cd, Cu, Fe	GF-AAS	120

Table 4 (continued)
Food samples

Sample(s)	Digestion mode and special information/equipment	Required reagents	Analyte	Method of analysis	Ref.
Shellfish, SRM lobster hepatopancreas	Closed vessels; compared with wet and dry ash procedures		Cd, Cr, Cu, Pb, Zn	FAAS	121
Roasted soyabean flour (kinakao), cabbage, seaweed, hog liver, NBS SRM 1566 oyster tissue	Domestic Toshiba ER-500 oven modified using a water-jet aspirator to draw fumes to an NaOH scrubber, open Erlenmeyer flasks; compared with conventional wet digestion method	HNO_3–H_2SO_4	As, Cd, Cu, Mn, Pb, Zn	AAS, GF-AAS	122
Food: rice, maize and red beans	Domestic oven Model WBL-823 (Jinan Quanli); four covered 30 mL PTFE vessels; Fe(III) later complexed	$HClO_4$–HNO_3	Fe	Adsorption chronopotentiometric determination	123
Wheat flour, mixed diet, pig liver	Closed 44 mL custom PTFE vessels; vessels cooled in a −25°C refrigerator	HNO_3–H_2O_2	Ca, Cu, Fe, Mg, Mn, Zn	ICP-AES	124
Food	Comparative study of conventional and microwave-assisted protein hydrolysis protocols	HCL	Amino acids		343
Thirty-two different fish species; CRM 278 mussel tissue	Domestic Moulinex FM-460 oven; closed Parr 4782 vessels	HNO_3 with a few micrograms of VO_5 as catalyst	Pb	ET-AAS	125

would appear to be an area where microwave-assisted techniques will become very important.

2.3. Botanical samples

Elemental analysis of botanical tissues is an essential requirement of soil fertility programs, nutrient budget and cycling investigations, environmental monitoring and elemental uptake studies. Botanical samples have the same dissolution problems encountered for biological samples described about–the destruction of organic matrices comprising carbohydrates, proteins and lipids.

Many articles have been published describing the use of microwaves for the dissolution of botanical samples [31,32,35,37,39,42,43,46,48,50,54, 55,57,60–62,65,67,71,73,77,78,89,92,94–112,147]. Tables 2, 3 and 5 contain these references, detailing the use of microwaves to various botanical samples.

Oven modifications included the use of forced air to purge fumes to fume scrubbers [31, 32] and the use of a glass water vacuum pump attached to Teflon™ tubing to vent fumes [98]. Many of the closed vessels used were equipped with some form of pressure release mechanism [45,55,71,89,96,99,100,106] such as pressure release valves, rupture discs and exhaust ports. One type of closed vessel was equipped with a cooling unit [57] while others were simply cooled in a refrigerator [89] before opening. Internal vessel temperature measurements were monitored via fibre-optic fluoroptic thermometry [106]. Pressure measurements were made via a real-time monitor [106], one with a piston which protrudes as the pressure increases [57] and one with an external transducer [102]. Often, the vessels were enclosed in containers such as a plexiglas box [31,32], polypropylene jackets [35,39], a Pyrex vacuum desiccator [98] and polyethylene bottles [111] to protect the oven's cavity. The reliability, precision

and accuracy of the technique has been tested by comparison with conventional techniques [61,65,77,94–96,98,100,101,106,107,109,111]. Safety however, has only been discussed in three papers [89,98,111]. Reports of particular interest involved a focused microwave system with the possibility of automation [65], special reflux systems [55,65] including one using either a condenser or a cold finger assembly cooled with microwave-transparent heptane [102] and a non-destructive method for determining moisture [108].

2.4. Food samples

Food samples present the same general problems as discussed for biological samples. Foods which are higher in lipids generally require higher dissolution temperatures and/or other acid mixtures than foods comprised mostly of proteins. High-protein foods generally require higher dissolution temperature and/or other acid mixtures than high carbohydrate foods.

Although the use of nitric acid alone for the treatment of food samples commonly results in the incomplete digestion of organic material, the method appears to provide reproducible results [79,270]. No significant traces of carbohydrates, proteins and lipids were detected chromatographically after using this method. Only a few organic molecules remained intact and they have been identified. For example, chromatographically separated liver digestate sequestered only o-, m- and p-nitrobenzoic acids. These are assumed to be of aromatic amino acid origin through their nitration and subsequent oxidation from the original protein.

Many articles have been published concerning the use of microwaves for the dissolution of foods [43,46,48,54–57,59,61,65,67,73,75,77,78, 80,87,89,94,100,101,109,113–125,145]. Two papers do not involve dissolution techniques but rather moisture determination by drying [114] and a patent for the decomposition of peroxide residues [117]. Tables 2, 3, 4 and 5 contain these references, detailing the use of microwaves to various food samples. Of particular interest, one technique used vanadium pentoxide as a dissolu-

tion catalyst [125]. Some reports describe oven modifications: several of these involved the use of a water aspirator and scrubber for fume removal and disposal [87,113,118,120,122]. The interior of one microwave oven was coated with a silicone spray to protect the cavity from corrosive fumes [87]. One oven was modified by making use of a flexible and rigid stainless steel waveguid attenuator cutoff, grounded and mounted at the cavity wall, with a 360° reversing turntable, a variable speed exhaust for removal of fumes via a PVC hose mounted at the back of the cavity, and a 12-position carousel, all with computer control [59]. Containers used to enclose dissolution vessels were a lidded plastic box [56] and a closed polypropylene or Pyrex™ container [113], all of which were later vented off in a fume hood. Refluxing and/or extractions have also been reported [55,57,59, 61,65,77,78,100,101,116]. Dissolutions, refluxing and extractions could also be performed using a focused, automated microwave system [65]. One method describes a microwave-assisted procedure for the hydrolysis of food protein prior to amino acid analysis [343].

Specialty vessels described included pressurized microwave digestion quartz vessels with cooling units [57], Teflon™-lined microwave bombs [94] and custom-made 44 mL PTFE vessels [124]. A method for vessel annealation was presented only once [59]. Safety aspects of using closed vessels under pressure were discussed only twice [59,89]. Some vessels were equipped with pressure release mechanisms such as pressure release valves [55,89] and discs [100,116]. The pressure was monitored via transducer probes and the temperature via a thermocouple [59]. The pressure was also measured using quartz vessels equipped with pistons monitored by sensors which shut off the oven power at 85 bar, until the pressure had dropped [57]. A refrigerator was used to cool dissolution vessels [89] in order to shorten sample preparation time. Open vessels were used less often to perform food dissolutions [46,48,65,77,80,87,113,118,120,122, 123].

Comparisons were sometimes made with other conventional techniques for validation and re-

producibility of microwave-assisted dissolutions [61,65,77,94,100,101,109,116,120–122].

2.5. Environmental samples

Many environmental samples are sediments. Sediments are highly variable and complex matrices, considered to be the ultimate sink of heavy metals released into the environment [143] and also reserviors for other environmental pollutants such as organochlorine insecticides [237]. The relative ease with which metals are released from, or bound to sediments is poorly understood. With increasing environmental and health regulations, the demand for environmental analysis and the range of sample types has grown enormously over the past decade. Environmental samples may be inorganic, organic or biological in nature, or a mixture of all three. Circumstances may dictate that rapid results are needed—this category therefore includes a very wide variety of sample types and analytical methods, but microwave-assisted pressure dissolution is gaining wide acceptance as the method of choice for sample preparation in this field [7,11,22,23,27,29,38,48,55,62,84,98,118,126–152]. Table 5 lists the applications of microwave techniques to various environmental samples (see also Tables 1, 3, and 6). Three reports describe the purging of oven cavities for fume removal either with compressed air [7,22] or via a glass water vacuum pump [98].

Safety measures and cautionary notes when using closed vessels were expressed in only four papers [7,98,128,132]. However, some of these vessels were equipped with pressure release mechanisms such as valves [55,84,118,141, 144,147] and seals [11,136]. Techniques of annealing vessels were presented in two papers [84,151]. One author monitored pressure via a stem which protruded from a domestic microwave pressure cooker enclosing the dissolution vessels [11] while three others used pressure transducers [84,118,136]. Containers used to enclose dissolution vessels in case of fume leakage were polyethylene containers [7,128], a domestic microwave oven pressure cooker [11], a sealed box [22] and Pyrex™ vacuum desiccators

[29,98]. Special dissolution vessels are described such as one-half inch thick 20 mL Teflon™–TFE bombs which do not require annealing [11], fluorinated ethylene propylene–Teflon™ vessels [98] and double-walled, lined Teflon™–PFA vessels [142]. One author mentioned that double-walled 200 psi dissolution vessels are now available which may be useful for better recoveries of Sb when digesting soils [138]. Only five researchers used open vessels to perform dissolutions [29,48,98,130,143].

Comparisons were made with conventional techniques for the validation of elemental recoveries in terms of precision and accuracy [11,27, 84,98,126,128,129,133,137–142,147,150,151]. Mention has been made of possible automation and advanced computer control [137], the use of a uranium salt for the neutralization of the electrical charges within oven cavities [142], software for finding the best dissolution method [144] and a reflux apparatus [55].

2.6. Sludge samples

Perhaps the most important type of sludge is that which comes from the treatment of sewage. This sludge is produced in large quantities all over the world and is often deposited at specific sites. Although there are appreciable benefits in the application of this sludge to farmland [154,313], there is also the risk of toxic elements and bacteria accumulating in the soil due to improperly treated sewage. This accumulation can lead to the contamination of soils, ground water, lakes and streams etc. and eventually to contamination of the food chain, e.g. fish, crops and livestock.

A few articles have been published involving the use of microwave techniques for the dissolution of sludge samples [73,137–141,152–155]. Table 6 summarizes these reports (see also Table 2 and 5). All the articles involve the dissolution of sludges with the exception of one article which discussed a microwave oven/electronic balance system for the determination of total solids content [153]. Three articles concern the loss of antimony when sludge samples

Table 5
Environmental samples

Sample(s)	Digestion mode and special information/equipment	Required reagents	Analyte	Method of analysis	Ref.
Lake sediments and mine tailings along with CRMs	CEM oven, Savillex vessels. Acid mixture digestion. Pressure limited to reduce loss of volatiles—improved recovery of As and Se compared to hot-plate digestion	HCl HNO₃ HF	As, Se	HG-AAS	118
Standard reference sediment and soil; suitable for anthropogenically contaminated soils and sediments	Compared with hot-plate digestion method; faster, more routine and less subject to technician error	HNO₃	Ag, As, Ba, Cd, Cr, Cu, Hg, Ni, Pb, Se, Tl, Zn		126
Four reference soils from the CCRMP: SO-1, SO-2, SO-3 and SO-4; mineral soil and clay samples	Commercial oven; closed 60 mL Savillex Teflon™–PFA vessels; freezer used to cool vessels; addition of boric acid prevents loss of Si	HNO₃–HF, then H₃BO₃	Al, Ca, Fe, K, Mg, Mn, Na, Si, Ti	ICP-AES	127
Three reference soils and nine other randomly selected soils	Sears Kenmore (Model 87751) oven; closed 60 mL Savillex Teflon™–PFA (fully fluorinated alkoxy-side chain) vessels inside a 4 L polyethylene container; effect of power level; compared to an open vessel method with HNO₃–HF-HClO₄; safety	HNO₃–HF	Cu, Zn	AAS	128
Venezuelan red mud, NBS SRMs; phosphate rock and flint clay	National Panasonic (Model NE6660) domestic oven; closed 100 mL PTFE vessels; polyethylene and polycarbonate vessels tried as well; compared with conventional and soild sampling techniques	HNO₃–HF–HCl (9:5:6 best), then H₃BO₃	Ag, Au, Cd, Cr, Pb	GF-AAS	129
Aqueous heat transfer agent of power stations	Elektronika SP-01 oven; open glass beakers, porcelain, PTFE and PET vessels; shapes of and effect of vessel material investigated (glass, porcelain, PTFE and PE)	Mineral acids, NaOH for Si	Fe, Cu, Ni, Pb, Si, Zn		130
SRMs: pond sediment, soil-1, soil 83401 and other silicate samples	Domestic oven; closed PTFE vessels; vessels cooled in a refrigerator; combination of HNO₃ and H₂O₂ greatly increases reaction rate and accelerates digestion process of organic matrices	HNO₃–HF H₂O₂	Ba, Ca, Cr, Cu, Fe, Mg, Mn, Sr, Zn		131
Soils	A procedure developed using closed vessels to minimize loss of As	Various acid mixtures	As		132
Aged (<80 years) Zn-contaminated soils from a location subject to airborne contamination from a smelter site	Evaluation of the technique for routine lab. use, compared with block digester and hot-plate techniques; significantly more complete metal release, greater metal concentration values and replication uniformity with microwave digestion method		Zn		133

Table 5 (continued)
Environmental samples

Sample(s)	Digestion mode and special information/equipment	Required reagents	Analyte	Method of analysis	Ref.
Enviromental CRMs	Testing and evaluation of the suitability of microwave methods		Trace elements and recovery of volatiles such as As, Hg, and Se		134
NBS 1646 estuarine sediment	Evaluation for replacing EPA method 3050 digestion; as the duration of the microwave 3050 simulation increased, it tended to recover higher amounts for most elements but incomplete recoveries for the NBS 1646 sample			ICP-OES	135
Soils, NIST SRM sediments 1646 and 2704	CEM MDS-81D oven; (1) closed 120 mL Teflon™-PFA vessels with pressure release valves, one has a pressure transducer attached through the lid; compared with conventional method (2) in platinum crucibles	(1) HNO_3 or by (2) HF-$HClO_4$	Cd	GF-AAS	136
Soils, sludges, sediments and oils	Closed vessel methods compared with conventional dissolution methods; automation and computer control of microwave dissolution procedures				137
NIST SRM 2704 river sediment, sludges, soils and solid wastes	Closed Teflon™ vessels; a correlation between the loss of Sb due to oxidation and subsequent absorption onto reactive silicate surfaces when using HNO_3 alone; recommendation that Sb should be excluded from recoverable metals using this EPA accepted method; solutions to the problem; mention of a commerically available, double-walled dissolution vessels (max. pressure 200 psi)	HNO_3 and HNO_3–HCl	Twenty-two elements, Sb	FAAS, GF-AAS, ICP	138
Sediments, soils, sludges and solid wastes	Reasons for Sb loss and remedies; an update of the obove reference (same authors)	HNO_3 or HNO_3-HCl	Sb		139
Sediments, soils, sludges and solid wastes	Reasons for Sb loss (a solubility problem) and remedies; a reply to comments made by the above authors	HNO_3 or HNO_3–HCl	Sb		140
Thirty samples from salt marshes, aquatic sediments, suspended matter, arable land, grassland and woodlands, sludges, CBR CRMs: 141 soil-calcareous loam, 142 soil-light sandy, 143 sewage sludge-soil and 145 sewage sludge; IAEA CRMs: SL-1 lake sediment and SOIL 7 soil	CEM MDS-81D oven; extraction of metals from soils using closed 120 mL Teflon™-PFA vessels with pressure release valves; compared with the conventional reflux method by three independent labs, with the conclusion that the recoveries are equal to or slightly higher using the microwave technique; three step dissolution	Aqua regia	Cd, Cr, Cu, Fe, Mn, Pb, Zn	AAS, ZE-GR-AAS, ICP-AES	141

Table 5 (continued)
Environmental samples

Sample(s)	Digestion mode and special information/equipment	Required reagents	Analyte	Method of analysis	Ref.
BCSS-1 and PACS-1 marine sediments, NIST SRM 1633a coal fly ash, an internal quality control dust, MESS-1	CEM MDS – 81D oven; closed double-walled, lined Teflon™–PFA vessels; a vial with some radioactive U salt for oven electrical charge neutralization; compared with the conventional hot-plate method; advantages and disadvantages of using different acid mixtures are discussed; disadvantages of using boric acid; method could be useful for continuous flow microwave digestion	Aqua regia, or aqua regia–HF, or HNO_3, then sometimes H_3BO_3	Al, As, B, Ba, Be, Bi, Ca, Cd, Co, Cr, Cu, Fe. Mg, Mo, Mn. Ni, Pb, Se, Ti, V, Zn	ICP-AES, NAA	142
NBS SRMs: 1645 river sediment and 1646 estuarine sediment, and other polluted sediments	Samsung (Model Re-705TC) domestic oven; open 250 mL polyethylene centrifuge bottles for the sequential extraction of elements into: (1) exchangeable; (2) carbonate bound; (3) Fe–Mn oxide bound; (4) organic bound and; (5) residual binding fractions	(1) $MgCl_2$, Tween 80 surfactant (2) Na acetate, acetic aci (3) NH_2OH – HCl, acetic acid (4) $HNO_3 H_2O_2$ (5) aqua regia, HF, H_3BO_3	Ca, Cr, Fe, Mn, Pb, Zn	FAAS	143
NBS 2740 Buffalo river sediment	CEM MDS-81D oven; closed PTFE vessels with pressure release valves; 18 different digestion methods subjected to SIRIUS (PCA) and PROMETHEE (multi-criteria decision making method) method rankings; use of GAIA for the display and evaluation of PROMETHEE results: two methods, both using HF, HNO_3 and HCl. were found to be best	HNO_3, HCl, HF. H_2O_2 – mixtures of two or three, or acetic acid. then H_3BO_3	Co, Cu, Mn, Pb, Zn	ZE-F-AAS, ZE-GF-AAS	144
Soils, sediments and foods, six standard reference materials	Closed PTFE vessels; all results in good agreement with the certified values	(1) HNO_3–H_2O_2 (2) HNO_3–H_2O_2–HF, H_3BO_3	Multi-elements	ICP-AES	145
Soils, solid wates and oils, NBS SRMs representative of oils and soils	Draft method of digestion to solublilize those elements most likely to be made environmentally available; compared with SW-846 Method 3050	HNO_3	Those elements made environmentally available	ICPS, GF-AAS	146
Twenty-two soils including marine and river clay, peat and reclaimed moorland soil, IAEA soil 5	CEM MDS-81 commercial oven; closed 120 mL Teflon™ vessels with pressure release valves; compared with open digestions with HNO_3, HCl or a HNO_3–H_2SO_4 potassium peroxodisulfate and a closed digestion in a Teflon™ bomb with HNO_3; closed systems the best	HNO_3–HCl	organic and inorganic Hg	CV-AAS, NAA	147

Table 5 (continued)
Environmental samples

Sample(s)	Digestion mode and special information/equipment	Required reagents	Analyte	Method of analysis	Ref.
SO-1 regosolic C horizon soil, SO-2 podzolic B horizon soil, SO-3 calcareous C horizon soil and SO-4 black chernozemic A horizon soil	Domestic Toshiba model ER 855BTC oven: closed 150 mL Teflon™-PFA vessels, four-step dissolution; safety precautions: compared with CANMET values of each soil type	HNO_3, then HNO_3-$HClO_4$-H_2SO_4	As	FAAS	132
Industrial wastewater	Detection limits were 1.9 ppb for Ni and 0.40 ppb for Cr		Cr, Ni	GF-AAS	149
Airborne particulates	Compared with conventional extraction and digestion with HNO_3	HNO_3-$HClO_4$	Cd, Cu, Pb, Zn	DPASV	150
NRCC MESS-1 and BCSS-1 marine sediments	Closed Teflon™-PFA vessels: annealing of vessels; results comparable or superior to those obtained using conventional methods: significant precision improvements especially for those elements with poor conventional precision	HNO_3-HCl	Environmentally significant elements	ICP-AES GF-AAS	151

were digested using closed vessels [138,139,140]. One report of the use of automated procedure is of particular interest [137].

Some comparisons of dissolution efficiency were made with conventional techniques [137–141].

2.7. Coal and ash samples

Using conventional procedures, coals and other samples such as ashes, require heating periods of about 12 h for total dissolution. Microwave procedures have reduced this heating period to a matter of a few minutes [27,29,142,157,160–162,167–169]. Besides being useful in performing dissolutions, microwaves have found use in moisture content determinations [156,158,163,165,166], desulfurization [164] and in the determination of the unburnt carbon content of coals [159]. Table 7 lists and summarizes these references (see also Tables 1 and 5). In one report concerning coal fly ash, a uranium salt was used for the neutralization of the electrical charges within an oven cavity [142]. A technique for the determination of unburnt car-

bon based on microwave attenuation and phase shift differences [159], and a mositure determination technique based on input and output 10 GHz microwave energy differences [163] have been patented. Moisture has been determined using a microwave meter while the sample was being simultaneously heated and weighed [165,166], and from projecting final weights from a weight loss curve after a fraction of the time required for complete drying [156].

Many microwave-assisted determinations were compared with the results from conventional methods [27,142,158,161,162,166,167,169].

2.8. Metallic samples

The determination of metal purity and the elemental composition of alloys is of utmost importance in the metallurgical industry. Companies have the responsibility of providing metals and alloys of particular elemental composition as specified by their customers. Samples are often analyzed as solids following fire assay or directly from metal castings using XRF and

Table 6
Sludge samples

Sample(s)	Digestion mode and special information equipment	Required reagents	Analyte	Method of analysis	Ref.
Sludge and waste water samples	Closed vessels; 110 mL liquid and 1 g soil samples; sample preparation and processing time was reduced by 5–50 times with ashing done at 180°C using HNO₃; microwave unit has a Teflon™-coated inner chamber equipped with a 2.8 m³ min⁻¹ aspirator exhaust system and a Teflon™ carousel 12-sample holder	HNO₃ or HNO₃, HNIO₃ mixtures to avoid the use of HClO₄	Concentration and isolation of various metals for subsequent analysis		152
Dewatered activated sludge	Microwave oven electronic balance system		Determination of total solid content		153
BCR 144, 145 and 146 sewage sludge standards; sewage sludges	CEM MDS-81 oven; six closed 120 mL PTFE vessels in a carousel	HF aqua regia, or aqua regia alone, then boric acid	Al, As, Be, Ca, Cd, Co, Cr, Cu, Fe, K, Mg, Mn, Mo, Na Ni, Pb, Sb, Sc, Se, Sn, Ti, Tl, V, W, Zn, Zr	ICP-AES, FAAS	154
Sewage sludges and CRM sludge samples	Closed vessels	HNO₃ and 2-ethyl-hexan-1-ol	Cd, Cu, Fe, Mn, Pb, Zn	FAAS	155

OES. Solution samples may be prepared for analysis by fusion followed by wet ashing or by straight wet ashing techniques. However, these sample preparation methods are time consuming and labor intensive and often result in incomplete elemental digestions. An example is the problem of completely digesting Al in steels without having spectroscopic interference from salt matrices (from fusions) [176]. Other problems include the hydrolyzation of refractory elements (e.g. Ta and W) when hydrofluoric acid is not used, the low solubility of fluoride salts of Y [172], Pb, Ca, U and Th, and the loss of volatile fluorides of Si, As and Se [270].

Microwave techniques are often well suited for the dissolution of metallic samples. For example, hydrofluoric acid can be used in closed vessel dissolutions to digest silicate matrices and to stop the hydrolyzation of refractory elements without the loss of volatile fluorides. After cooling, boric acid can be added to complex unreacted hydrofluoric acid. This allows for the use of conventional glassware, acts as a matrix

modifier for AAS and more importantly redissolves precipitated fluorides [270]. The solid sample itself may absorb microwave radiation, creating a heated surface on which the acid(s) can react. Microwave muffle furnaces are now commerically available [332] based on oven linings made out of the highly efficient microwave absorber silicon carbide. This microwave absorber rapidly heats up the oven's cavity to ashing or fusion temperatures. Other solid samples may reflect microwaves, creating high sample–acid interface microwave densities. This can result in very rapid heating of the acid(s) used and create turbulence and sample agitation both of which sweep sample surfaces clean of acid-resistant coatings, exposing fresh, unexposed sample surfaces which are open to acid attack.

Under some circumstances, the use of microwave energy in the presence of metallic materials is not recommended. Specifically, interaction of certain metals with microwave energy can result in uncontrolled sparking and electrical arcing, possibly leading to electrical

Table 7
Coal and ash samples

Sample(s)	Digestion mode and special information/equipment	Required reagents	Analyte	Method of analysis	Ref.
8-Mesh coal	Open vessels; final weight predicted by projecting the weight loss curve to its end point after a fraction of the time required for complete drying		Determination of water content		156
Certified coal reference standard AR-1800, NBS 1632a; petroleum coke samples	Domestic oven; closed, modified Pyrex glass test tubes; microwave treatment the most efficient method for V extraction	HNO_3–HF	V	GF-AAS, XRF	157
Coal, esp. sub-bituminous western coal (USA)	Open vessels; no coal degradation; compared to conventional methods		Moisture content		158
Fly ash	PATENT: generation and transmission of microwaves through fly ash; receiver of a microwave signal passed through the sample, and a means to determine the attenuation and phase shift differences of the transmitted signal to produce a measure of the unburnt C content; can be used to control a coal-fired boiler		C	Attenuation phase shift differences of the signal	159
Particulates, ashes and oil fuels	Closed vessel; wet and dry digestion of waste samples before elemental analysis; effect of preparation conditions: acid matrix, heating time and pressure	Different acid matrices	Fifteen toxic or hazardous elements	ICP-AES	160
Coal ash samples	Alternative to the $Li_2B_4O_7$ fusion process; requires the use of HCl for P determination	HNO_3–HF–HCl	P and others		161
Coals and coke containing 43–88.8% fixed C	Proportional relationship was observed between time for complete digestion and fixed C content for both acid mixtures; compared with PTFE bomb method	HNO_3–H_2SO_4 or HNO_3–$HClO_4$	Cu, Mn, Ni, Pb and Zn	AAS	162
Crude lignite	PATENT: 10 GHz microwaves passed through brown coal; sieved (<2 mm) coal is sampled by means of compressed air into a quartz tube inclined 15° to the microwave source; measure the difference between input and output energies as it passes through the sample	None	Water content	Microwave meter	163

Table 7 (continued)
Coal and ash samples

Sample(s)	Digestion mode and special information/equipment	Required reagents	Analyte	Method of analysis	Ref.
Bitumite coal	Samples irradiated at 2.45 GHz for various lengths of time to determine the coal desulfurization effect			[57]Moessbauer measurements	164
Coals with a moisture content between 0–15%	Use of a microwave meter to determine the moisture content in coals; use 1.5 kg samples; determination error was 0.8%		Moisture content	A microwave meter	165
Coals	A measuring device was developed for a rapid moisture determination in samples which are continuously weighed when heated by microwaves; integrated gas sensors prevent samples from overheating; thus preventing gas evolution; comparable to the drying cabinet method (DIN 59718)		Moisture analysis	Moisture is monitored by a computer in response to weight changes	166
Alpha Resources reference standards: AR-1800, 1803 and 2777 coals; NBS SRM 1632a coal; Venezuelan coal samples	Domestic National Panasonic NE-6660; closed 200 mL thick-walled Pyrex glass test tubes; compared with conventional method; decomposition efficiencies compared; effects of acid mixtures, heating power and time settings investigated to optimize dissolution	HNO_3–$HClO_4$	Fe, Ni, V	ETA-AAS	167
Coal fly ash	Closed PTFE vessels; four different decomposition procedures investigated; microwave decomposition with HNO_3–HF–$HClO_4$ was applicable for all the elements and gave results in agreement with the certified values	HNO_3–HF–$HClO_4$	As, Cd, Pb, Sb, Se, Tl	Stabilized temp. platform furnance technique with ZE-AAS, NAA for As, Sb, Se	168
Twenty-two coals	Six closed autoclavable 25 mL polypropylene bottles (Cat. # 2006-0004) placed in a sealed plastic container; later centrifuged or filtered; P complexed; compared with the Australian standard method (dry oxidation procedure); safety discussed; two step dissolution	HCl HF then boric acid	P	UV-vis spectrophotometer	169

component and magnetron damage. This can be a problem and is a safey hazard when performing closed vessel dissolutions. Several metallic materials, especially iron-based alloys, spark when subjected to microwave energy. This sparking can ignite the hydrogen gas generated

from the dissolution of metals [270,176]. Fernando et al. recommend that dissolution vessels be sealed under an inert atmosphere to eliminate the presence of oxygen in the gas volume generated when digesting metals [176]. Matthes et al. were the first to use a microwave oven for the dissolution of metals [16]. Since then, several articles have been published outlining microwave dissolution procedures for metallic materials [16,17,20,21,24,170–178,189,190]. Table 8 summarizes these reports (see also Tables 1 and 9). Closed vessels were almost exclusively used to digest metallic materials [16,20,21,172,175–177] as opposed to open vessels which were used only once [173]. None of the closed vessels were equipped with any sort of pressure release mechanism, and safety was discussed in only two papers [174,176]. Comparisons of results were made with those obtained using conventional techniques [170,171,174–177].

2.9. Synthetic material samples

Microwave-assisted dissolution techniques show their versatility through their application to a variety of synthetic materials. Reports have been made concerning the dissolution of polymers [29], $(NH_4)_2SO_4$ [106] and $(NH_4)_2B_4O_7\cdot4H_2O$ [107], activated carbon [188] and other inorganic samples [184], inks [182], resins [188] and other organic materials [184], oils [137,146,160,179], wear metals in lubricating oils [190], carbon fibre–epoxy materials [180], automotive [181] and petroleum industry catalysts [192] and glass samples [191]. In addition, a number of patents have been issued concerning microwave techniques and devices for the dissolution of radioactive and medical wastes [183], ZnO-based samples [185], man-made wastes [186] and spent nuclear fuels [189]. Microwave techniques have also been used for moisture determinations of asphalt [187], plywoods and particleboards [108]. Table 9 summarizes these reports and lists the references (see also Tables 1, 3, 5 and 7). Microwave dissolution efficiencies were sometimes compared with conventional efficiencies in terms of elemental recoveries [106,107,137,146,182,192].

2.10. Mixed samples

Some articles describe research involving the microwave dissolution of more than one sample type. For this reason, these articles have been grouped together into a separate category—Table 10.

Geological [193,201], specifically diabase, oil shales and rocks [194], basalt [194,200], minerals [194,199], ores [194,198], refractory samples [199] and obsidian rock [200] have been digested. Dissoluton methods have been described involving biological samples [196,197,199,201], carbohydrates, proteins and lipids [193], oyster tissue and animal materials [194], bovine liver [194,200], lobster hepatopancreas [195] and marine tissue [202]. Botanical samples [193], orchard leaves [194], tomato leaves and pine needles [194,200], peat [195] and dry plant leaves [197] have been digested. Food samples [197], spinach and vegetable samples [194] and flour [203], and environmental samples such as sediments [194,200,202], soils [194,196], muds [195,203] and dusts [204] have been digested. Sludges [198,200] and coals/ashes [194,197,200,204] have been digested. Metallic materials [193] such as alloys [194], automobile shredder wastes [198], steels [201] and metals on filter media [204] as well as other synthetic materials such as glass [193], polymers like polypropylene [194,203], butyl rubber[194], polyethylene, and polyurethane [203], catalysts, industrial pipe deposits and scales [194], petroleum, heavy oil fertilizers and activated carbon [197], medical and toxic wates [198], gas [200], fibreglass and paper [203], air sampling filters, powdered lead-based, powdered and liquid paints and paint scrapings [204] have all been digested using microwave-assisted techniques.

3. Microwave-assisted sample drying

A common problem associated with the process of assaying in analytical laboratories is obtaining precise and reproducible methods of sample drying. Drying is defined as the removal

Table 8
Metallic samples

Sample(s)	Digestion mode and special information equipment	Required reagents	Analyte	Method of analysis	Ref.
Steel reference samples	Effects of temperature of digestion and Si level in samples are described; compared with conventional dissolution techniques		Si	AAS, ICP	170
Metal alloy samples (e.g. steel samples containing <0.5% W, Ti and Nb, or Cu)	Comparison of pressurized sample preparation devices (High pressure Asher and Pressurized Microwave Decomposition Device)	(1) HNO_3–HCl or (2) HNO_3–HCl–H_2SO_4–H_3PO_4	(1) Cr, Cu, Mn, Ni, P, S, V (2) Nb, Ti, W	ICP	171
NBS 899 (Tracealloy C); Ni-based superalloys (Ni–Cr–Al–Y)	Whirlpool (Model MW-8750) domestic oven; 12 closed 250 mL polycarbonate, flat bottomed centrifuge bottles with polypropylene screw caps placed inside a polycarbonate container; wind-up mechanical carousel	HNO_3, HCl, HF and mixtures of them, H_3BO_3	(2000 ppm). Al, Co, Cr, Hf, Mo, Ni, Ta, Ti, W	ICP-OES	172
Czechoslovakian, British and German ferrochromium and ferromanganese CRMs: CSAN 4-2-01, 4-2-02, 4-2-03, 4-2-04, 4-3-01, 4-3-02, BCS 203 2, 204 1, 208 1, 280; BAM ECRM 530-1, 533-1	Philips M 704 domestic oven; open PTFE beakers; found that only H_2SO_4 and H_3PO_4 were required for dissolution (including Si), and so HF is not needed	HNO_3, HCl, H_2SO_4, H_3PO_2, and various mixtures of them	Al, Co, Cr, Cu, Mo, Mn, Ni, Si, Ti, V	ICP-AES FAAS	173
Inorganic samples: e.g. Cr_3C_2–Ni–Cr and Ni alloy samples	CEM MDS 81D oven; closed PTFE 4782 Parr bombs with a pressure-indicating screw which protrudes from the cap; advantages and disadvantages are given; compared with other methods; diagram of bomb; safety precautions	Various acid mixtures depending on the sample type and or required elemental analysis	Various elements	Can be applied to various instrumentation	174
Tool steels, SKD 61 and 11, MBH 34C and 37B	Closed vessels; compared with hot plate method	HNO_3 HCl–HF	Various elements	ICP-AES	175
NBS SRM 365 electrolytic iron and 179 (steel with a nominal Si content of 3%); BCS 452 (a mild steel) and 317 (3.49% Si); Spex Hi Pure iron (for calibration blank)	Domestic Sears Kenmore oven; closed 60 mL Savillex Teflon™ vessels; use of a carousel; caution advised for metallic materials (should be present in an inert atmosphere to prevent ignition); compared with Parr bomb method	HNO_3 HCl–HF	As, Al, Cr, Cu, Mo, Mn, P, Ni, Si, Sn, Ti, V	DCP-ES	176
Twenty-four high-alloy steel CRMs: NBS 892, 890, 346, 168, 73B, 161, 343, 133A, 160B and 101F; BAM 228-1, 278-1, 328-1, CrNiSiMn1, 277-1 and CrMnMoNiTi1; IRSID 204-1; BCS 339, 211 1, 342, 340, 338 & 341; JK 8F	CEM commercial oven; closed Teflon™-PFA vessels; all steels completely dissolved except NBS 892 which required more HNO_3 and reheating under pressure in the oven followed by fuming on a hot plate with H_2SO_4–H_3PO_4; compared with two hot-plate fuming and a fusion procedure and dissolution with H_2SO_4 then H_2O_2 (hot plate)	HNO_3 HCl–HF	Cr	Titration with dichromite solution	177
BCS 346 (Ni-based alloy)	System found to have a detection limit of 1.3 ng		As	Continuous flow HG-AAS	178

of volatiles from a sample [207]. It should result in identical sample compositions despite differences in starting volatile content and sample history. Usually, the major volatile component required to be removed from a sample is water. Different sample types absorb varying amounts of water and therefore must be dried to an equilibrium weight. When a plot of weight loss versus time reaches a plateau, equilibrium weight has been achieved. Many samples are hygroscopic and must be kept in a moisture-free environment after drying, such as that provided by a desiccator. Variation in water content is one of the most common sources of non-reproducible sample weights. This can result in lower assay precision and accuracy, and possibly give biased analytical data. In order to eliminate, or at least minimize the problem, samples are usually dried before weighing. Classical or conventional methods of drying include the use of convection ovens, vacuum ovens and desiccators. All three methods are effective and can result in samples with reproducible composition. However, some samples may contain different temperature-dependent volatile components or degrees of hydration. This can lead to varying equilibrium weights and should be of concern to the analyst. Generally, the least aggressive method yielding reproducible and stable sample composition is the recommended pretreatment. The least aggressive method minimizes the risk of chemical alteration of the sample.

Microwave-assisted drying provides a rapid and simple alternative to conventional methods of drying. Specialty microwave ovens are now commerically available for this purpose [331–333,335,339]. Since solvent molecules are directly heated by the microwave radiation, they can be volatilized without heating the container they are in. This reduces the cooling time required in a desiccator before accurate weight measurements can be made. (Heat from sample containers can cause inaccurate and fluctuating balance readings due to rising warm air). In concert with drying samples, moisture determinations can be made. Table 11 summarizes the use of microwave methods for

the drying of a variety of sample types [205–212].

4. Continuous flow digestion systems and on-line applications

The microwave-assisted pressure dissolutions described in previous sections of this review have been essentially batch processes, with separate digestions for each sample. Several continuous flow systems have been described [213–224,340], and some are now available as commerical packages [331–334,337]. The development of these flow-through and stopped-flow (or "discrete-flow" [331]) microwave pressure dissolution systems which may be connected to flow-injection manifolds for a variety of instruments is a further step towards total automation. These systems are of particular interest in the determination of toxic and volatile elements such as mercury. Table 12 contains summaries of these on-line systems. They generally involve the introduction of the sample in the form of a slurry via an autosampler. Slurries are usually made by the pretreatment of samples with an appropriate acid or acid mixture while being stirred in an open vessel. The slurry is then aspirated into the closed system by a peristaltic pump to the microwave oven. The slurry is digested as it passes through a coil made out of a microwave-transparent material located inside the oven's cavity. After the pressure dissolution stage, some sytems have incorporated filters, cooling steps and gas trap chambers to condense and to remove gas vapors generated from the dissolution step. Finally, the digestate may be injected into a carrier stream via an injection valve where it is carried to the appropriate instrument for analysis, or collected in an autosampler tray. These systems have great potential for handling situations with a high throughput of relatively easy-to-treat samples, but operators should be prepared for breakdowns and malfunctions—even the commerical models are only just out of the development stage. Within a few years,

Table 9
Synthetic materials

Sample(s)	Digestion mode and special information/equipment	Required reagents	Analyte	Method of analysis	Ref.
Cold rolling oil (of emulsion type used in mills during manufacture of steel and stainless steel sheets — usually called "coolant")	Open 200 mL beakers; samples (coolant) were digested using one of several organic acids whereby the surfactants are not destroyed but the Fe fines are dissolved; all organic acids successful except succinic acid	NaOH, oxalic acid, maleic acid, citric acid, DL-malic acid, succinic acid, CCl_4 or $HCCl_3$	Determination of non-ionic surfactants (82–98% recovery)	HPLC	179
Ciba-Geigy T800/924, T800/922 and T800/914 carbon fibre–epoxy materials	Domestic oven; closed Parr 4782 bombs; determination of fibre volume fraction (volume of resin holding fibres together)	HNO_3			180
Monolithic ceramic automotive catalysts	CEM MDS-81D oven; closed 120 mL PFA-Teflon™ vessels with pressure release valves (120 psi)	HCl–HF, or HNO_3–HCl–HF, then $HClO_4$ on a hot plate or H_3BO_3	Ba, Ca, Ce, Fe, La, Mn, Ni, P, Pb, Pd, Pt, Rh, S, Zn	ICP-MS, WD-XRF	181
Inks: polyamide, nitrocellulose and aqueous acrylic-based ink samples, packaging inks	CEM MDS-81D or a Floyd RMS-15 OPCM oven; closed 120 mL PFA-Teflon™ vessels (CEM); compared with open vessel hot plate method	HNO_3	Ag, As, Ba, Cd, Co, Cr, Cu, Hg, Ni, Pb, Sb, Se, Sr	ICP-AES, CV-AAS, GF-AAS, PIXE, NAA	182
Radioactive waste liquids and medical diagnostic wastes (e.g. containing ^{125}I)	PATENT: a microwave oven connected to a microwave source via a waveguide tube and an insulator; used for concentrating waste materials				183
Inorganic and organic materials	Closed vessels with an excess pressure security system for dissolving materials with volatile components; written in German, only the summary is translated	HCl, HF, HNO_3, KOH			184
ZnO-based samples	PATENT: closed vessels; analysis of ZnO-based devices	HF–HCL or HF–HNO_3			185
Man-made wastes	PATENT: open vessels; recovery of Hg from crushed wastes (such as Hg battery); heated by microwaves to 100–700°, then gas carried off by flowing air and collected in a condenser at −5°C	None	Hg		186
Hot-mix asphalt concentrate	Use of 12.4–18.0 GHz sweep of radiation to detect moisture by measurement of dielectric constant and the loss factor	None	Moisture		187
Activated C and resin	Teflon™ bottles	Acid mixtures	Au, Ag and base metals	ICP-AES and others	188
Spent nuclear fuel	PATENT: a device consisting of a microwave heater under a barrel containing a sample basket which is connected via a pipe to a solvent dispenser, for the dissolution of spent nuclear fuel				189

Table 9 (continued)
Synthetic materials

Sample(s)	Digestion mode and special information/equipment	Required reagents	Analyte	Method of analysis	Ref.
Wear metals in lubricating oil (engine oil) and NBS lubricating oil	Closed vessels		Al, Cu, Fe, Ni, Pb	FAAS	190
Glass samples		$HF-HNO_3-HCl$ then B_3BO_3	Non-radioactive elements	ICP-AES, AAS	191
Three types of heterogeneous petroleum industry catalysts (Ketjen, Catal and Laterite)	Domestic Balay Bahm-100 oven, closed 125 mL vessels; compared with conventional techniques	HNO_3-isoamyl alcohol then H_3PO_4, also aqua regia	Co, Fe, Mo, Ni	FAAS, XRF	192

reliability problems should have been dealt with, and the instruments should be adaptable to the more rigorous digestion conditions required for difficult samples.

5. Solvent extraction and desorption systems

Several conventional techniques are available for the extraction and/or desorption of analytes from particulate matter. Although these techniques are widely accepted, each has inherent limitations and problems. Solvent extraction methods, such as Soxhlet extraction, tend to be inefficient and can lead to the generation of chemical artifacts due to the harsh sample treatment. The shake flask method is tedious and is also inefficient in that it is primarily superficial in function and requires several large amounts of solvent(s). Thermal desorption procedures are superficial in function as well since they make use of infrared radiation (IR) to heat a sample. This frequency of radiation is considered to be surface heating radiation since it only penetrates matter to a depth of less than one micron. Particles become non-uniformly heated through this mechanism since the interiors can only be heated by conduction. Another problem is that chemical artifact generation is possible using IR since energies lie in the range of 0.3 to 30 kcal mol^{-1}, which lies very close to the 30 to 225 kcal mol^{-1} energy range required for bond dissociation (microwave radiation at 2.45 GHz has an energy of about 0.23 cal mol^{-1}).

Microwave extractions are proving to be efficient and are even suitable for the extraction of labile components from various complex matrices. Particles are heated uniformly by microwaves since they are able to penetrate them to a depth of several thousand microns. Also, the degradative effects of high temperatures can be avoided by adjusting power levels, exposure times and number of repeats of irradiation. It has been demonstrated that the high temperatures which can be generated using microwave energy are not required in order to facilitate rapid desorption from matrices [238].

Table 13 summarizes microwave extraction and desorption techniques [229–242]. Patents have been issued for an extraction system which may be automated [239] and for a microwave vacuum oven which can quickly extract volatiles without causing overheating [241]. Microwave extraction/desorption techniques have also been compared to steam distillation [232–234], Soxhlet [235,237,238,242], chloroform fumigation [236], reflux [237,240], polytron [237] and shake flask methods [238].

6. Microwave Kjeldahl systems

Distillation has been used to separate volatile chemical components since about AD 100 when the method was used to separate ethanol for the production of brandy [243]. The technique is still widely used today in a variety of industries and for a range of separations. Whereas conven-

Table 10
Mixed samples

Sample(s)	Digestion mode and special information equipment	Required reagents	Analyte	Method of analysis	Ref.
Biological (three carbohydrates: soluble starch, amylopectin-amylose and glucose, two proteins: SRM 926 and one lipid: tristearin C-18 fatty acid ester), botanical, geological, metallic and glass materials	Closed Teflon™–PFA; real-time temperature and pressure monitors; discussion of the reproducibility of decomposition conditions; reasons for different decomposition temperatures; discussion of automation practicality	HNO_3	Volatile elements such as P, Se, Te and V	Multi-element techniques such as ICP, XRF and ICP-MS	193
US Geological Survey diabase W-1 and Basalt BCR-1; IAEA lake sediment SL-1; NBS: 1632, 1633 and 1633a fly ash, 1571 orchard leaves, 1570 spinach, 1566 oyster tissue, 1645 sediment, 1577 bovine liver, 1573 tomato leaves, 1575 pine needles; three polypropylene standards prepared in the lab, doped with Al, Ca, Si and Ti charcoals, oil shales, soils, minerals, ores, rocks, sediments, butyl rubber, catalysts, alloys, industrial pipe deposites and scales, vegetable and animal materials	Domestic Sears Kenmore oven; open but covered Teflon™ or polycarbonate beaker inside a Pyrex desiccator partially evacuated which is later vented inside a fume hood, then boric acid added and heated in a water bath; important not to let the sample go to dryness due to loss of Si as SiF_4; coals and polymers were ashed first in a muffle furnace (chromite or titanium minerals in coals may not be completely dissolved); useful for coal desulfurization (inorganic); Cr, Mg and Ti results low probably due to incomplete dissolution of chromite and Mg–Ti minerals in the rock samples	Aqua regia HF then boric acid to neutralize the HF by forming tetrafluoro-boric acid	Al, As, Ba, Be, Ca, Co, Cr, Cu, Fe, K, Li, Mg, Mn, Na, Ni, P, Pb, Si, Sr, Ti, V, Zn	ICP-ES, XRF for polymers	194
(1) Lobster hepatopancreas (2) Fluvial and marine muds; peat	Closed vessels	HNO_3	(1) As, Cd, Co, Cr, Cu, Fe, Mn, Ni, Pb, Se, Zn (2) Hg	(1) CV-AAS (2) AAS	195
Biological, soil, sediment	Closed PTFE vessels	HNO_3, H_2O_2 or HNO_3–H_2O_2–HF, boric acid	Multi-elements	ICP-AES	196
Biological, dry plant leaves, coal, petroleum, heavy oil, fertilizers, food and activated C samples	PATENT: (wet sample decomposition apparatus) microwave heating container; microwave controller; gas collector having a gas discharge opening for removal of liberated gases		N and metals	The appropriate analyzer	197
Medical, automobile shredder and toxic wastes, ores and sludges	PATENT: microwaves focused with a concave microwave guide in an anaerobic atmosphere; breaks down complex molecules; can be a continuous or batch process		Simpler molecules, or elements		198

Table 10 (continued)
Mixed samples

Sample(s)	Digestion mode and special information equipment	Required reagents	Analyte	Method of analysis	Ref.
Biological, mineral, refractory samples	Modified domestic oven: safety testing			ICP-AES, FAAS	199
SRMs: coal fly ash, sediment, basalt and obsidian rock, tomato leaves, pine needles, bovine liver, bituminous coals, gas, coking and steam coal, sludges	CEM MDS 81 microwave oven: closed 125 mL PTFE vessels; good recoveries of Cr from samples containing chromite; aqua regia–HF mixture the best	HNO_3–HF–HCl mixtures, then boric acid	Twenty-five elements, volatiles like As, Cd, Cr, Pb, Sb, Si, Se and Tl	ICAP-AES, GF-AAS	200
Biological and geological standard reference materials	Closed PTFE-vessels; automatic capping and gas exhaust modules		Trace elements	ICP-MS	201
Marine tissue, geological sediments and steel	Closed polycarbonate vessels: pass nitrogen gas or air to evacuate oven				202
Mud, flour, fibreglass, paper, polyethylene, polypropylene and polyurethane	Features, advantages and applications of a microwave oven for dissolutions; compared with conventional methods				203
SRMs: 1633a coal fly ash and 1579 powdered lead-based paint; NIST SRM 2676b metals on filter media; air sampling filters, dusts and ashes, paint scrapings, powdered and liquid paints (cellulose and isophthalic acid polyester-based industrial), mixed metal dust/ash internal QC sample	CEM Model MDS 81D microwave digestion system; closed vessels; method does not decompose the polymers in paints allowing for their removal, thus reducing possible matrix effects	HF–aqua regia, HNO_3 for paints	Ag, Al, As, B, Ba, Be, Ca, Cd, Co, Cr, Cu, Fe, Mg, Mn, Mo, Ni, P, Pb, Sb, S, Sn, Ti, V, W, Zn	ICP-AES, NAA	204

tional distillation techniques rely on conduction for heating, microwave heating results from direct interaction of the energy with the sample. This allows energy transfer to the entire sample as opposed to this taking place via convection currents as with conductive heating. This advantage makes microwave heating an excellent candidate for replacing distillations and reflux procedures limited by long heating periods. For example, a major limitation of Kjeldahl procedures is the extended period of digestion needed for complete nitrogen recovery—this is commonly from 3–6 h. Microwave heating can re-

duce this time to a matter of several minutes since the sulfuric acid used in the Kjeldahl method is a strong microwave absorber. Microwave heating can raise a Kjeldahl digestion mixture to 360°C in 2 min and to 400°C in 4 min, compared to the same temperatures in 15 and 45 min respectively, using a block digestor [270]. Once the optimum temperature is attained, the microwave power can be stopped, ending heating and stopping the temperature from rising due to the absence of an external hot mass. Research has shown that microwave Kjeldahl digestions can be as much as 20 times

Table 11
Microwave-assisted drying of various sample types

Sample(s)	Digestion mode and special information/equipment	Required reagents	Analyte	Method of analysis	Ref.
Rice leaves	DRYING: Sharp R-4K53 commercial oven: comparison of classical methods with microwave oven techniques for determination of dry weight and N concentration	None	None		205
Water samples	DRYING: open vessels; drying of water samples: compared to the standard method	None	Total solids		206
Non-fat milk powder (SRM 1549), bituminous coal (SRM 1632b), clays, copper ore, wheat flour (SRM 1567a), rice flour (SRM 1568a), buffalo river sediment (SRM 2704), $Na_2HPO_4·7H_2O$ and $CuSO_4·5H_2O$ (for loss of hydrated water)	DRYING: CEM AVC-80 drying oven equipped with a top loading electronic balance stem and a pan protruding through the oven cavity floor; a Thermopad if needed: compared with conventional oven and thermal drying techniques	None	Moisture	Electronic balance	207
Treated and untreated wastewaters, mixed liquor suspended solids, recycle solids and primary, thickened and dewatered sludges	DRYING: household microwave oven used to dry the samples: open vessels; comparable to conventional oven technique		Determination of suspended and total solids		208
Various wastewater treatment sludges	DRYING: open vessels; drying of samples; comparable to conventional oven technique: decreases drying time by 96%		Determination of suspended and total solids		209
Precipitates: $AgCl_2$, $BaSO_4$ and $CaC_2O_4·H_2O$	DRYING: open crucibles for thermogravimetric determinations; Mettler AE200 analytical balance: water molecules directly heated leaving the crucible relatively cool: allows for faster weighing: compared with conventional drying; water of hydration of the oxalate is not lost		Drying of precipitates	Mettler AE200 analytical balance	210
$BaSO_4$ precipitate	DRYING: open sintered glass filter crucible: compared with a traditional technique		Drying of precipitates	Analytical balance	211
Various samples of different geometry and size	DRYING: measurements of moisture profiles compared with convective drying; several methods for determining local moisture profiles are presented and discussed	None	Moisture profiles		212

faster and yet show comparable accuracy and precision to that of a conventional digestion.

Table 14 summarizes microwave Kjeldahl methods for the determination of total nitrogen content [243–251]. Alvarado et al. used a domestic microwave oven and a commerical laboratory Kjeldahl apparatus and compared the results obtained from both [249]. All other researchers used specialty microwave Kjeldahl systems. Comparisons were made with conventional techniques in terms of recoveries and time required [243 247,249,250]. Two patents have been issued for microwave Kjeldahl apparatuses [245,251].

7. Databases and software packages

A wide range of different microwave-assisted dissolution protocols have been developed to treat the enormous variety of samples requiring dissolution prior to chemical analysis. Many of these methods are becoming standardized and are replacing some of the conventional standard methods. Currently, the development, testing and certification of new standard methods is slowed down by the lack of skilled manpower to perform these tasks, so there is a delay in making this new technology readily available to all potential users. As the number of methods increases, so does the task of making these methods available to analysts. To help remedy this situation, new standard methods are now being encapsulated in database formats capable of electronic inter-laboratory transfer. As well, software has been developed to create, format and transfer protocols for microwave-assisted dissolutions.

With ready access to a database of validated methods, an analyst may be able to find an appropriate dissolution method by entering relevant information about the sample, analyte(s), instrumentation etc. (i.e. analytical descriptors). Once a method has been selected by the software, which best matches the analytical descriptors, the database can yield not only details of the required procedure, but also other imporant

information such as safety advice and recommendations based on research experience. Systems like these have the capability of "learning" additional procedures as other new and successful methods are developed.

Table 15 summarizes four published software systems for microwave dissolution databases [225–228]. Of special interest, Walter et al. discuss a database/software system capable of retrieving dissolution parameters and controlling sample preparation and dissolution through automation [227]. Feinberg et al. have prepared a database of nearly 780 different outlines of microwave dissolution procedures [228].

8. Reviews

Numerous reviews have been published these are summarized in Table 16 [252–282]. These reviews discuss microwave techniques, equipment, applications, theoretical microwave principles and mechanisms, various dissolutions, drying and moisture determinations, history, advantages, safety guidelines, economy, automation and robotics, sample preparation characteristics, prediction of dissolution parameters and data handling.

9. General reports

A number of general reports have been published. These are summarized in Table 17 [283–294]. These papers are more specific and focused than the reviews. One report compared microwave bomb methods with EPA method 3050 [284] and another described a specialty microwave digestion system (Q Wave-1000). New areas of microwave technology application were discussed in another report [293]. One publication discusses non-microwave-assisted methods of acid pressure decompositions, but was included in this review [294] since much of the information presented is relevant to microwave pressure dissolutions, such as advantages, problems, PTFE vessel material characteristics and decomposition efficiencies.

Table 12
Continuous-flow digestions and on-line applications

Sample(s)	Digestion mode and special information equipment	Required reagents	Analyte	Method of analysis	Ref.
Whole blood	FLOW-INJECTION: modified Panasonic (Model NE-7660 6660) domestic oven with a coiled Pyrex tube is used for dissolutions; peristaltic pump; Solvaflex tubing	Triton X-100 (anti-clogging agent), HNO_3, HCl	Cu, Fe, Zn	AAS	213
Biological	FLOW-INJECTION: a review with 41 references about the use of microwave ovens for the decomposition of biological samples and its combination with flow-injection AAS			FI-AAS	214
Solid samples such as a slurry, e.g. sewage sludge, CRM 144 and 146	ON-LINE DIGESTION: closed flow-injection analysis system; slurries passed through a PTFE coil located in a domestic Balay Bahm 100 microwave oven for digestion, then injected into a carrier stream and transported to an AAS flame using a peristaltic pump; 12 samples h	HNO_3	Pb	FAAS	215
Sewage sludge, two ECB reference samples	Direct introduction of slurries from batch digestions using a single-channel manifold; influence of flow-injection parameters on the sensitivity and accuracy of the procedure was established		Cu, Mn, Pb	FI-AAS	216
Hg compounds used to determine Hg recovery, lake, river and rain water, urine samples: (Lanonorm metals 1 and 2, control urine for metals, lyphochek urine metals level II, seronorm trace elements urine and toxic metals in freeze-dried urine - NIST SRM 2670)	ON-LINE SAMPLE PRE-TREATMENT: flow-injection system; Prolabo Maxidigest MX 350 oven with a TX 31 Maxidigest programmer; focused microwave digestor; PTFE reaction coil; peristaltic pump; filters; antifoaming agents for urine analysis; CEM MDS-81D oven for off-line digestions	HCl, $KBrO_3$, $NaBH_4$, KBr, $K_2S_2O_8$, $KMnO_4$, H_2SO_4, HNO_3, $K_2Cr_2O_7$, NaOH	Hg	AAS, HG-AAS, FI-CV-AAS compatible for Hg	217
Biological and environmental samples	ON-LINE SAMPLE PRE-TREATMENT: flow-injection system; Prolabo Maxidigest MX 350 oven; focused microwave digestor; PTFE reaction coil; peristaltic pump	HCl, $KBrO_3$, $NaBH_4$, KBr, $(NH_4)_2S_2O_8$, HNO_3, CH_3COOH, H_2SO_4, NaOH	As, Bi, Hg, Pb, Sb, Se, Sn, Te	HG-AAS, CV-AAS, AAS	218
Urine and environmental waters	ON-LINE DIGESTION: for flow-injection manifold; testing for the determination of the most successful oxidation mixtures; optimization of chemical reagents and analytical conditions; 13 30 samples h	$K_2S_2O_8$, NaOH, KBr, HCl, $KBrO_3$, $(NH_4)_2S_2O_8$, HNO_3, CH_3COOH, H_2SO_4, Tartaric acid	As, Bi, Hg, Pb, Sn	CV-AAS, HG-AAS	219

Table 12 (continued)
Continuous-flow digestions and on-line applications

Sample(s)	Digestion mode and special information equipment	Required reagents	Analyte	Method of analysis	Ref.
Bovine whole blood, human whole blood and concentrated blood, recoveries of five Hg compounds	ON-LINE: Prolabo Maxidigest MX 350 oven with a TX3 1 Maxidigest programmer; focused microwave digestor; 10 m × 0.9 mm long PFA digestion coil knitted around a PTFE backbone tube, then coiled again to be water cooled; system maintenance discussed; compared with off-line autoclave digestion using open PTFE vessels, various reagents added at different stages of the system	Triton X-100, $NaBH_4$, NaOH, HCl, Dow Corning DB 110A: Si anti foaming agent, KBr, $KBrO_3$, $KMnO_4$, HNO_3, $HClO_4$, $K_2S_2O_8$	Hg	FI-CV-AAS	220
Artichoke, dietary products, sewage sludge, certified tomato leaves and sewage sludge samples	ON-LINE DIGESTION: Balay Bahm 100 domestic oven; using 100 cm of 0.8 mm Teflon™ digestion coil; peristaltic pump for sample transport; ice water cooling bath then injection into an AAS	HNO_3 H_2O_2	Cu, Mn	AAS	221
	FLOW-INJECTION: a patent for an apparatus including a continuous-flow digestion system				222
Bovine liver (SRM 1577), orchard leaves (SRM 1571), other botanical standards (e.g. MOE V85-1)	STOPPED-FLOW DIGESTION SYSTEM: slightly modified domestic Toshiba (model EXP-1690C) oven; Teflon™–PFA tube serves as a sample container and a digestion vessel; closed-vessel approach minimizes the risk of sample cross contamination; compared with hot-plate digestion method	HCl, HNO_3 or aqua regia or HNO_3-H_2O_2	Al, Ba, Cd, Cu, Fe, Mg, Mn, Zn	ICP-OES	223
CRMs: mussel, chlorella, sargasso, pepperbrush, bovine liver (SRM 1577a)	Continuous-flow microwave digestion on-line with AAS; samples introduced as slurries with 5% HNO_3; comparison of flow-injection with direct determination results—no loss in sensitivity	HNO_3	Fe, Ca, Mg, Zn	AAS	340
Horse kidney reference material, bituminous coal (NIST 1632b), Hershey's cocoa powder, pine needles (SRM 1575), bovine liver (SRM 1577a), oyster tissue (SRM 1577a)	ON-LINE SAMPLE PRE-TREATMENT: stopped-flow-injection system; CEM MDS-81 oven; glass reaction vessel inside microwave cavity attached to PTFE tubing; pressure transducer, compared with microwave and hot-plate-ash methods; certain degree of maintenance required	Triton X-100 HNO_3	Fe, Ca, Cd, Mg, Zn	FAAS, ICP-AES	224

10. Automation and robotics

The simplicity and efficacy of microwave dissolution techniques easily lends itself to the ad-vantages of automation and robotics. Systems have been developed which are capable of weighing-out samples, adding acids, capping and uncapping vessels, carrying out microwave disso-

Table 13
Microwave extraction and desorption systems

Sample(s)	Digestion mode and special information/equipment	Required reagents	Analyte	Method of analysis	Ref.
Lean lateritic Ni ores leached with H_2SO_4	EXTRACTION: separation extraction process for immiscible liquids; gravity separation of mixed liquids is accelerated by microwave irradiation by heating over 10°C in 15–20 s; compared with conventional gravity separation; suitable for Ni extraction from ores leached with H_2SO_4	H_2SO_4, alamine (C_{8-14} primary alkyl amine) 20, isodecanol 10 and kerosine 70. vol.%.	Ni		229
	EXTRACTION: design, operational safety and applicatons of a microwave digester system with rotor technology; pressure extraction (yields of 99% for pesticides), accuracy and recovery rates presented	Solvents	Various elements, pesticides		230
Hedera helix L. leaves	EXTRACTION METHOD: National Panasonic (Model NE 1330) domestic oven; all but the summary written in French	MeOH	Hedera-saponin C and alpha-hederin	HPLC	231
Lippia sidoides leaves	EXTRACTION: essential oil extracted by a current of air as sample heated for 5 min was identical when compared to steam distillation		Essential oils		232
Lemon	EXTRACTION: of aroma compounds compared to steam distillation		Aroma compounds	GC	233
Plant	EXTRACTION: of essential oils (1 min) compared to steam distillation (2 h)		Essential oils		234
Plants: raw and processed broad bean, cottonseed meal	EXTRACTION: of antinutritive compounds compared to the Soxhlet extraction technique; microwave extraction found to be more effective with respect to yields and protection of compounds; method suitable for the rapid extraction of large sample series		Various anti-nutritive compounds: (pyrimidine-glu-cosides and gossypol)		235
Soils, sand, silt and clay	EXTRACTION: domestic Sharp (Model R-6740) oven; for C and N, microwave biocide potential compared with chloroform fumigation method; microwave method not as effective as $CHCl_3$ fumigation for microbial biomass estimates in soils due to inactivation of enzymes normally active during the 24 h of fumigation	Water	C, N	Extraction with 0.5 M K_2SO_4 and ninhydrin method for N, oxidation diffusion for C	236

Table 13 (continued)
Microwave extraction and desorption systems

Sample(s)	Digestion mode and special information equipment	Required reagents	Analyte	Method of analysis	Ref.
Sediments	EXTRACTION: domestic Kenmore (Model 85962) oven; extraction of pesticides using open 5 mL Reacti-Vials; microwave extraction (30 s × 5 repeats) compared with other conventional techniques such as Sohxlet (8 h of Soxhlet extraction), polytron and reflux—better recoveries; evaluation of sediment moisture, microwave effects, extraction time and solvent, pesticide concentration and type	Various solvents and solvent mixtures	Pesicides	GC	237
Yeast, lupine, maize, soya bean, baby food, walnut, meat flour, Fava bean, cottonseed and soils	EXTRACTION: domestic Toshiba ER 638 ETD type oven; closed screw-cap vials; compared with Soxhlet and shake-flask method; almost 100 times faster than traditional methods; more efficient than Soxhlet extraction for polar compounds with water-containing solvents; recoveries of non-polar compounds were only slightly less with a non-polar water-free solvent; higher recoveries for sensitive molecules due to lower temperatures and shorter extraction times	MeOH H$_2$O. or methanol or hexane	Crude fat. vicine, convicine, gossypol, pesticides	HPLC, chrom- atographic column	238
Food	EXTRACTION: a patent for an analytical apparatus for drying of a preweighed sample, reweighing to determine volatile loss, followed by solvent extraction, and final measurement of residual solids, may be automated		Fats, oils . . .		239
Aromatized products: candies, chewing gum, coffee	EXTRACTION: of aromatic fraction (essential oils); compared with conventional methods such as refluxing, simultaneous distillation solvent extraction, hydrodistillation		Aromatics	GC- MS	240

lutions, diluting digestates, transferring vessels, and even cleaning and reusing the vessels. Once such a system is operational, the only things the analyst has to do is supply and place the representative sample(s) in locations recognized by the system and then initiate the controlling pro-

Table 13 (continued)
Microwave extraction and desorption systems

Sample(s)	Digestion mode and special information/equipment	Required reagents	Analyte	Method of analysis	Ref.
Various samples	EXTRACTION: a patent for a microwave vacuum oven; quickly removes volatile material from samples without overheating them; oven has a vacuum chamber for receiving samples in a closed vessel and a vacuum source for expelling volatiles; object is to accelerate removal of volatiles, eliminate weight determinations and reduce problems from overheating	None	Determination of volatile material content		241
Organic compounds, coconut charcoal	DESORPTION: use of a microwave desorption apparatus for releasing compounds from the surface of particulate matter collected on a filter; low MW species recovery more efficient than the Soxhlet extraction; > 130 Watts required to desorb high MW compounds; microwave basics; both polar and non-polar species may be desorbed	Cyclo-hexane, water, standards containing polycyclic aromatic hydro-carbons, pesticides and PCBs in acetone	Isolation of chemical components	GC-MS	242

gram. Automation and robotics not only work around the clock they also free analysts of often tedious and potentially dangerous work, allowing them to perform other, more intellectually challenging tasks. Table 18 summarizes primarily the application and functioning of these systems. One of these automated systems has been patented [298].

11. Other relevant articles

The few articles remaining are quite specific and do not readily fit into any of the other categories. They include a discussion of a vessel cooling technique [303], special equipment [304], microwave oven modifications [305], fundamental relationships and prediction methods [306], safety [307], temperature control [308],

temperature measurement [309] and super-heating effects [310]. These are summarized in Table 19.

12. General considerations

12.1. Safety

Great care should be taken when using the pressure-digestion methods outlined above. This is particularly true when new protocols are being developed. Many of the references given describe methods in which oxidizing and reducing agents which react to form gaseous products are heated together in sealed vessels. There are few reports of accidents in the literature, but most of those involved in development work have encountered explosions.

Table 14
Microwave Kjeldahl systems

Sample(s)	Digestion mode and special information/equipment	Required reagents	Analyte	Method of analysis	Ref.
Limonene (Citrus oil)	KJELDAHL METHOD: open 1 L Pyrex boiling flask for distillation connected to a collection apparatus outside oven; compared with steam distillation	$CuSO_4-H_2SO_4-K_2SO_4$, then $(NH_4)_2SO_4$	Total N	Modified Kjeldahl method	243
Seven soils, wheat leaf, corn grain, rice straw	KJELDAHL METHOD: CEM MDS-81D oven; (1) closed Teflon™-PFA vessels; and; (2) 50 mL Kimax or Pyrex Erlenmeyer flasks for microwave Kjeldahl method; compared with conventional method	(1) HCl, HF, H_3BO_4 (2) H_2SO_4, K_2SO_4	Total N	Modified Kjeldahl method	244
Succinimide oil C 5935	KJELDAHL METHOD: a patent; a receiver with retention capacity extended by a cylindrical neck and a microwave cavity whose height is almost the same as the receiver; new microwave oven compared with using an IR and conventional microwave ovens	H_2SO_4–Kjeldahl catalyst	Total N in 1 h	Modified Kjeldahl method	245
Food: milk, wheat flour, powdered egg, casein, meat and grass hay	KJELDAHL METHOD: collaborative study involving 11 labs. as an alternative Kjeldahl method	$H_2SO_4-H_2O_2$ and no catalyst	N	Modified Kjeldahl method	246
Eight A1 horizons of italian soils	KJELDAHL METHOD: CEM MDS-81D oven; closed Teflon™ vessels; compared with three other conventional methods	$HF-HCl$, then H_3BO_3, then H_2O_2	Total N	Micro-Kjeldahl apparatus	247
Food	KJELDAHL METHOD: Maxidigest MX-350 focused microwave digester; a prototype application of an expert system for a fully automated, open vessel, focused microwave digestion system; based on selection of reagents, reagent volume, digestion time, average power and analytical method	Reagents are provided by the expert system based on the input of analysis criteria	Strictly adapted to the Kjeldahl N determination in food samples	KJELTEC 1026 (PERSTORP)	248
Amino acids: Val. Ser, Leu, Phe, Tyr, Trp, Cys, cassaba and gamelte leaves, fractional corn germ, ocumo, white broad beans, precooked corn flour, milk powder and whey, squid and octopus flour, canned ham	KJELDAHL METHOD: National Panasonic (Model NE-6660) domestic oven; closed 200 mL thick-walled Pyrex glass test tubes fitted with polypropylene screw caps on a Petri dish inside a sealed 2 L plastic jar; Labconco micro-Kjeldahl apparatus, Model 60/300 coupled to a Pregel-Parnas-Wagner distillation unit, Model 7051-G10	H_2SO_4 K_2SO_4 HgO	Total N	Kjeldahl method	249

Table 14 (continued)
Microwave Kjeldahl systems

Sample(s)	Digestion mode and special information equipment	Required reagents	Analyte	Method of analysis	Ref.
Meat	KJELDAHL METHOD: Prolabo Maxidigest oven; three-step 11 minute digestion program; 19 minute digest for tryptophan; compared with conventional hot-plate method using Cu as a catalyst		Total N	Kjeldahl method	250
Organic samples	KJELDAHL METHOD: a patent for a microwave-based apparatus; reactive vessel extends via a hollow tubular body outside the oven; air cooled; scrubber for digestion gas evolution removal		Total N	Modified Kjeldahl method	251

Oven modifications should be carried out with caution, since leaked microwave radiation poses a health hazard. An excellent summary of this aspect is given by Kingston and Jassie [270].

12.2. Economy and efficiency

The conversion of electrical energy into microwave energy by a magnetron is an inefficient process [263]. However, since a microwave oven heats internally yet does not become heated itself, and may not heat the vessel containing the sample, microwave ovens are more economical than conventional electric ovens for some applications [263,317,318].

12.3. Superheating

The effect of pressure on the boiling point of a solvent is well known and widely understood, but it has recently been reported that many organic solvents, when heated in a microwave oven at atmospheric pressure, may boil at temperatures 13–26°C above their normal boiling points [327]. The explanation for this probably lies in the fact that conventional boiling occurs via heat transfer from the walls of a vessel, where there are large numbers of nucleation sites. In microwave heating however, heat transfer takes place far from the walls, where the number of nucleation sites around which bubbles may readily form is very limited, leading to superheating effects.

12.4. Specific "microwave" or athermal effects

A few reports have appeared which suggest that, in certain instances, reactions carried out by microwave heating give different products from those carried out by conventional heating [328, 329]. This question is of great concern to the food industry, in view of the widespread use of domestic microwave ovens, and so Unilever and Nestlé sponsored a special meeting on this issue during the summer of 1993, in Switzerland [338]. It was generally agreed that all the anomalous results reported could be explained on the basis of localized superheating effects at different hotspots in the reaction mixtures, and that there were no athermal effects. This conclusion is not surprising in view of the energy considerations. Microwave radiation is of low energy, about 1 J mol^{-1} of photons. When this is compared to bond energies (H-bonds approxi-

Table 15
Databases and software packages for microwave dissolution systems

Sample(s)	Digestion mode and special information equipment	Required reagents	Analyte	Method of analysis	Ref.
All sample types depending on whether such a sample type exists in the database; however new samples and their dissolution procedures may be invented and stored	HYBRID EXPERT-DATABASE SYSTEM 1: provides advice on the microwave preparation of samples elemental analysis: furnishes information on the dissolution of samples; based on a microcomputer and commercially available software	Varies with sample type. Information available within software package	Specified by user	Specified by user	225
All sample types depending on whether such a sample type and standard method for dissolution exists in the database: however new samples and their dissolution procedures may be invented and stored	EXPERT-DATABASE SYSTEM 2: provides advice on the microwave preparation of samples for elemental analysis; furnishes information on the dissolution of samples; standard methods encapsulated in a database format which can be transferred among laboratories, generation of microwave procedure files; applicable to automated and robotic (Zymate Lab Automation System) systems/procedures	Varies with sample type. Information available within software package	Specified by user	Specified by user	226
All sample types depending on whether such a sample type and standard method for dissolution exists in the database; however new samples and their dissolution procedures may be invented and stored	DATABASE: Automated (Zymate Lab Automation System) intelligent control of microwave sample preparation; three integrated components: (1) database to assist in selecting new procedure parameters; (2) retrieving parameters for establishing procedures, and; (3) control of sample preparation and dissolution	Varies with sample type Information available within software package	Specified by user	Specified by user	227
All sample types depending on whether such a sample type and standard method for dissolution exists in the database; however new samples and their dissolution procedures may be invented and stored	DATABASE: nearly 780 different outlines of open-vessel focused microwave digestions using the Microdigest A300 system stored in a database which define guidelines and propose reference digestion procedures; procedures were analyzed statistically according to selection of and combination of reagents, reagent volume, digestion time, average power and analytical method used	Alone or combined pairs of reagents: H_2SO_4, boric acid, HCl, HF, HNO_3 and H_2O_2	Specified by user	Specified by user	228

Table 16
Reviews covering microwave applications

Sample types	Review details	Ref.
Various sample types	REVIEW: 69 references covering the application of microwave techniques in analytical chemistry with respect to sample dissolution, moisture determination, AES and chromatography	252
Various sample types	REVIEW: 37 references dealing with application of microwave ovens for drying, dissolution of samples, acceleration of reactions and preparation of new materials in the laboratory	253
Various sample types	REVIEW: 54 references dealing with applications of microwaves and their application for sample dissolution	254
Various sample types	REVIEW: Eight-references covering the history and applications of microwave heating for acid digestion of samples; commercial application	255
Various sample types	REVIEW: 40 references concerning the applications of microwave heating for dissolution and decomposition of organic and inorganic materials for elemental and isotopic analysis; principles, advantages and instrumental equipment discussed	256
Various sample types	REVIEW: 38 references dealing with the techniques of microwave heating and their uses covering four sections: mechanism of sample decomposition, general applications, areas of attention and conclusion	257
Various sample types	REVIEW: 19 references covering the theoretical concepts, equipment and their applications in microwave heating for acid dissolution, two mechanisms discussed: ionic conduction and dipole rotation	258
Various sample types	REVIEW: 17 references concerned with the working principle, equipment and applications of microwave digestion	259
Various sample types	REVIEW: without references discussing the advantages of high-pressure degradation compared with conventional high-pressure methods; requirements for vessel materials employed	260
Various sample types	REVIEW: 14 references covering theory, instruments (AAS and ICP-AES), applications, methods and advantages of microwave digestion extraction technique	261
Various sample types: plant leaves, nickel alloy, silicate material, coal flyash, organics, geological (Fe ore, dolomite), copper nickel ore, wool, aluminum, bronze	REVIEW: 28 references giving options for the use of domestic microwave ovens and PTFE vessels for sample dissolution; various lab. practices and examples of successful dissolution recipes; safety; vessel and microwave oven limits and specifications; Kjeldahl determinations	262
Inorganic materials	REVIEW: 36 references concerning densifying and strengthening ceramic components; economy of using microwave ovens; dielectric measurements; rates of heating; equipment; reaction kinetic enhancement	263
Blood, ores, food, cement, quartz, silicate fibres	REVIEW: six references covering the principles of microwave energy and instrumentations and advantages of microwave decomposition	264
Animal, plant, ore and alloy samples	REVIEW: 25 references outlining the characteristics of microwave heating; acids and vessels used	265
Samples with complex biological matrices	REVIEW: ten references describing microwave-assisted high-temperature and pressure wet ashing systems for sample preparation of complex biological matrices; automated control of pressure and temperature	266
Many sample types	REVIEW: 72 references relating to the digestion mechanism; open and closed vessel systems; efficiency; commercial microwave digestion systems; applications	267
Biological, food, plant, blood, geological, soil, sediment, environmental materials, waste water, sewage sludge, coal, oil, metallic materials, fly ashes and other samples	REVIEW: 181 references covering the applications of microwave dissolution	268

Table 16 (continued)
Reviews covering microwave applications

Sample types	Review details	Ref.
Various samples	REVIEW: 51 references discussing the characteristics of sample preparation, factors affecting microwave absorption, equipment and uses for the technique	269
Geological (phosphate rock, tin ore, sulfide ore, Au ore, Ni an Cu ores, feeds, concentrates and tails, Pb or Ag fire assay beads and chromite), metallic, botanical, biological (blood), pharmaceutical (vitamins, aztreonam), metallurgical (NBS 121C steel, Cu slag, superalloys, NBS 127 Pb–Sn solder and TiO_2); and food samples	REVIEW: a book covering dissolution methods, monitoring and prediction of digestion parameters, guidelines for developing dissolution methods, Kjeldahl N determination, manual and remote operation of microwave systems, remote operation for dissolutions in highly radioactive environments, robotic systems and safey guidelines, theoretical concepts of microwave heating and equipment design; flow-injection-ICP	270
Organic and geological	REVIEW: 39 references outlining microwave oven systems and dissolution techniques	271
Metal contaminated soils	REVIEW: 50 references covering the benefits, ovens, soil digestion methods, organic bound metals and engineering applications	272
Food and feeds	REVIEW: no listed references discussing the interest in microwaves for rapid analysis of agrofood products and preparation for analysis	273
Food	REVIEW: no listed references discussing the interest in microwaves for mineralization of food products; discussion of recently developed automated systems	274
Paper	REVIEW: two references describing the advances in paper moisture measurement by microwave loss	275
Biological, geological, and other samples	REVIEW: 21 references covering the working principle of microwave sample dissolution; applications to sample dissolution	276
Minerals, rocks, ceramics and other related materials	REVIEW: direct heating of minerals showing how they heat; explanation as to why based on the mineral's chemical composition and physical properties	277
Samples amenable to ICP-AES analysis	REVIEW: ten references concerning advances in plasma emission transport processes (for ICP-AES) with an emphasis on direct injection nebulization techniques	278
	REVIEW: without references discussing the advantages of using microwaves during the high-pressure degradation for trace analysis; compared to conventional high-pressure methods; special requirements and materials employed; MWS 1200 system described	279
Soil and plant material	REVIEW: 11 references; development and application of new equipment for sample preparation, robotics, instrument control and data handling, for soil testing and plant analysis	280
MACSP: two sediments, three biological tissues and three seawater CRMs	REVIEW: 21 references; an overview of the Marine Analytical Chemical Standards Program (MACSP) including rapid dissolution techniques using microwave heating	281
	REVIEW: 14 references concerned with the theory, instruments, applications, methods and advantages of microwave techniques for dissolution	282

mately 20 kJ mol⁻¹, the C–H bond energy about 350 kJ mol⁻¹), it seems unlikely that microwave energy could preferentially rupture any chemical bonds.

12.5. Radioisotope studies—microwave syntheses of radioactively labelled compounds for tracer studies in medicine

The isotope of carbon, ¹¹C, which is a positron emitter, has a half-life of just 20 min. This means that if ¹¹C-labelled compounds are used in PET studies, at the end of the testing period, residual radiation will quickly decay, reducing the risk of radiation damage to the patient. But, as the half-life is so short, speedy synthesis of labelled compounds is essential. This is an area where microwave synetheses can be used very effectively [330].

12.6. Lined reaction vessels

The latest reaction vessels available for digestions or syntheses incorporate a Teflon™–PFA liner, cover and rupture membrane enclosed in a casing and cap of Ultem™–polyetherimide. These are safe at pressures of up to 200 psig (1380 kPa) and temperatures up to 250°C. Special vessels that can operate at up to 600 psig (4140 kPa), or even 1600 psig (11 040 kPa) are also available. The vessels are also available fitted with ports to accommodate temperature and pressure probes [331–335].

12.7. Temperature probes

Temperature is a crucial factor in all chemical reactions and digestions, but some difficulties arise if conventional thermocouples are used in the reaction mixture inside the microwave cavity—the microwave radiation may interact directly with the probe. This problem has been resolved by the use of fibre optic probes. Several types are used, depending on the manufacturer [331–334].

12.8. Digestion systems with both temperature and pressure monitors and settings

Four systems are now commercially available which incorporate simultaneous pressure and temperature monitoring [331–334]. The reaction/digestion may be pre-set to run at either a given temperature, or a given pressure. The temperature or pressure may be programmed to vary in a step-wise fashion over a pre-determined time period. The systems are microprocessor-controlled, and printouts of reaction conditions may be obtained.

13. Conclusions

Though only relatively recently developed, the microwave-assisted dissolution technique is rapidly becoming the method of choice for the routine handling of large numbers of analytical samples. Although the approach does not so far provide a universal sample preparation technique, it does offer certain advantages over conventional dissolution techniques. For example, the rate-determining step for sample throughput is usually sample preparation. Microwave-assisted dissolution techniques offer a reasonably economical solution to this problem. As the result of saving time, these techniques are generally more economical in the long run as well, through savings due to reduced labor costs. Also, these techniques often require smaller amounts of sometimes expensive reagents, can contain corrosive fumes thereby preventing contamination and loss of volatile elements, require less supervision, are simpler and more efficient, and have proven to be reliable. Another major advantage of the speed with which microwave-assisted dissolutions occur, is that this can lead to rapid availability of results. Modern process control often requires constant monitoring of analytical parameters—these are sometimes available via on-line XRF analyses, but often AAS or ICP results are needed, so that a rapid sample dissolution method becomes a necessity for efficient plant operation.

Table 17
General reports concerning microwave applications

Sample(s)	Digestion mode and special information/equipment	Required reagents	Analyte	Method of analysis	Ref.
Foods, biological, botanical, man-made oils, environmental, sludge, geological, coal, metallic and ash samples	GENERAL REPORT: general guidelines for microwave sample preparation; advantages and disadvantages of classical and microwave dissolution techniques, extractions; Kjeldahl analysis; safety	Depends on the sample type	Whatever is required by the analyst	Appropriate for determination	283
	GENERAL REPORT: comparison of high-pressure microwavable bomb method with EPA method 3050			AAS, ICP-ES	284
	GENERAL REPORT: Proceedings of an International Conference on Millimeter and Submillimeter Waves and Applications				285
	GENERAL REPORT: Microwave dissolution: development of a new sample preparation technique				286
Various samples	GENERAL REPORT: comparison of the use of polycarbonate and Teflon™ vessels; discussion of sample types not amenable to microwave-assisted digestion; compared with Na_2O_2 fusion method				287
Various samples	GENERAL REPORT: reviews (11 references) a selection of the available techniques and the results obtained from the analysis of several types of samples				288
Ceramics, dried fish tissue, Fe oxide, minerals, foods, lipstick, paint, paper pulp, peanut butter, oils, alumina catalyst, alloys, coca, fly ash, silicon glue, sediment, solid waste, paints: practically all types	GENERAL REPORT: describes the Q Wave-1000 microwave digestion system (Questron Corp.): power readout, microwave-transparent internal temperature and pressure probes, automatic load adjustment, computer integration and on-line applications directory, efficiency, safety mechanisms and full graphics	Depends on the sample type		AAS, ICP, ICP-MS	289
SRMs: serpentite, limestone, dolomite, andesite, hawaiian basalt, granite, marine mud, cody shale and nepheline syenite	GENERAL REPORT: CEM MDS-81D oven: critically evaluates results obtained from using closed 120 mL PTFE–PFA vessels, compared with alkali fusions using a muffle furnace and open Teflon™ PTFE beakers on a hot plate ($HClO_4$–HF)	HF–HNO_3–HCl_4	Seven mineral oxides and nine other elements by ICP-AES, 38 elements by ICP-MS	ICP-AES, ICP-MS	290

Table 17 (continued)
General reports concerning microwave applications

Sample(s)	Digestion mode and special information equipment	Required reagents	Analyte	Method of analysis	Ref.
Non-specific	GENERAL REPORT: a focus outlining the problems with conventional techniques and the advantages of using microwave dissolution techniques	None	None	None	291
Non-specific	GENERAL REPORT: a focus outlining NBS-CEM Corporation's developments in microwave dissolution technology and techniques: closed vessels, replacing conventional methods, pressure and temperature measurements, microwave muffle furnace	Various acids and acid mixtures	Non-specific	Non-specific	292
Synthetic polymers, inorganic and organic acids, water and organic solvents	GENERAL REPORT: discussion of new areas of microwave technology application in labs. and process engineering; material properties and absorption coefficients given	None	None		293
Inorganic and organic samples	GENERAL REPORT: non-microwave methods of acid pressure decompositions in trace element analysis; advantages of pressure decompositions, problems, PTFE vessel material, safety, pressure casings, heating systems, decomposition efficiency and conditions and sample types discussed	Various acids and acid mixtures	Whatever is required by the analyst	Whatever is suitable for the determination	294

Techniques involving microwaves are not without faults albeit they can be minimized. One disadvantage when compared with the use of open digestion vessels is that dissolution variables such as sample weight and type, acid volume, microwave power, microwave distribution homogeneity and duration of exposure must be collectively acknowledged and controlled with all due respect to the possible explosive nature of the method. However, such control itself is advantageous since dissolution conditions are accurately reproduced without surpassing vessel limitations. As well, analyte accuracy and precision limits within batches of samples should be reduced due to this reproducibility.

Microwave-assisted dissolutions, though relatively rapid, do themselves have one disconcertingly slow step. This is the necessary delay in opening closed vessels with high internal pressures. These must be cooled to room temperature in order for this pressure to be reduced to a safe level. Several methods of shortening cooling times have been investigated such as internal vessel cooling systems, refrigeration or use of a freezer, cooling in ice, water or some other cold material such as liquid nitrogen. However, the time required for cooling of vessels by whatever method is only a minor inconvenience when considering how much time can be saved in performing dissolutions. For example, it takes 24 h

Table 18
Automation and robotics for microwave systems

Sample(s)	Digestion mode and special information equipment	Method of analysis	Ref.
	AUTOMATION: microwave systems with remote control		295
Various sample types	AUTOMATION: focused microwave source to decrease dissolution time; open vessels; compared with classical techniques		296
	AUTOMATION: Microdigest A 300 using open and closed sytems	AAS, ICP	297
Mineral, organic or organometallic compounds	AUTOMATION: a patent, for an oven capable of receiving sample containers, means of placing samples at a fixed place inside its cavity, means of transporting samples to and from the oven and an automated command module; application selects the method, temperature and duration of exposure depending on the sample type		298
Organic and inorganic samples	AUTOMATION: Microdigest A301 system; description and applications		299
Titanium dioxide	AUTOMATION: CEM MDS-81D oven; 140 mL Milestone 140-10 digestion vessels equipped with pressure regulating valves; robotic system weighs out samples, adds acids, torques on caps, carries out microwave dissolution, dilutes and transfers the solutions to beakers and cleans the digestion vessels; 60 samples/16.5 h; reliability; software written in MODULA-2; sample identification data and operating parameters; closed 140 mL vessels with pressure regulating valves	ICP-AES	300
Environmental	AUTOMATION: integrated system of independent computer programs to encapsulate and transfer standard methods which involve automated equipment		301
Refractory tantalum metal powder	ROBOTICS: a robotic system in a quality control laboratory environment for trace element analysis for the control of a manufacturing process; closed Teflon™ vessels. After cooling the digestate is diluted robotically. Better precision and accuracy for some volatile elements using the robotic system	DCP	302

for the complete dissolution of wool using classical methods whereas only eight minutes are required using microwave digestion [227]. This is 180 times faster!

The usefulness of microwaves in analytical chemistry is increasingly evident. From a meager start in the 70s represented by only seven references, publication has increased to 132 references in the 80s and to 166 references in only the first four years of the 90s! This review has not only shown that microwaves can be used in the dissolution of a wide variety of sample types but also in other analytical areas as well. Microwave energy has proven to be useful in shortening drying, extraction, Kjeldahl determination, ashing and fu-

sion times as well as in increasing efficiency. Microwave techniques are also exceptionally applicable to continuous flow and on-line systems due to their simplicity and ease of use. These systems are now commerically available although essentially still in the prototype stage, but within the next year or so they will most likely replace the closed-vessel methods described above in high-throughput situations.

Acknowledgements

Table 19
Other relevant articles

Report details	Ref.
VESSEL COOLING TECHNIQUE: CEM MDS-81D oven: closed or open 120 mL Teflon™ vessels; during, pre- and post-digestion cooling technique of vessels using microwave transparent liquid N_2, speeds up cooling times, lowers internal pressures; pressure release mechanism and transducer	303
SPECIAL EQUIPMENT: modified domestic oven; magnetic stirring device, fibre optic and fluoroptic thermometer, discussion of microwave heating mechanisms	304
MICROWAVE OVEN MODIFICATIONS: modified commercial oven; cavity lined with polypropylene, a polypropylene turntable, incorporation of inlet and outlet ports and the use of an external system to purge the oven's cavity	305
Understanding and identification of the fundamental relationships for controlling interactions between microwave energy and sample–acid solutions; to develop methods for predicting digestion conditions accomplished by measuring parameters required to calculate microwave power absorption and temperature	306
SAFETY: concerned with routine acid digestions or microwave heating of liquids in sealed vessels which do not have designed safety mechanisms for pressure relief; acid attack of equipment	307
TEMPERATURE CONTROL: inlet and outlet ports for circulating chilled water through Tygon tubing connected to a 50 mL jacketed reaction vessel or to a small reflux condenser; an independent thermistor temperature probe (0–100°C); used to maintain solutions at constant temperatures	308
TEMPERATURE MEASUREMENT: a miniature gas thermometer using a pressure transducer indicates the temperature of samples heated by microwaves without undesired effects of traditional probes; serves as the basis of a safety device that prevents the accumulation of flammable vapor when organic molecules are irradiated	309
SUPERHEATING EFFECTS: liquid surface is at the normal b.p. whereas the bulk contains substantial localized superheating with these areas slightly above the b.p. (several degrees)	310

Appendix

Abbreviations used in text

Instrumentation

AA	Atomic adsorption
AAS	Atomic obsorption spectroscopy/metry
ASV	Anodic stripping voltammetry
CRA	Carbon rod atomizer
CV-AAS	Cold vapor-AAS
DCP-AES	Directly coupled plasma-AES
DPASV	Differential pulse anodic stripping voltammetry
DPP	Differential pulse polarography
ETA-AAS	Electrothermal atomization-AAS
ET-AAS	Electrothermal AAS
FAAS	Flame atomic absorption spectroscopy
FANES	Furnace atomic non-thermal excitation spectroscopy
FP-ICP	Flame photometry-ICP
FI-AAS	Flow injection-AAS
FI-CV-AAS	Flow-injection-CV-AAS
GC	Gas chromatography
GC–MS	Gas chromatography–mass spectroscopy
GF	Graphite furnace
HG-AAS	Hydride generation-AAS
HG-AFS	HG-atomic fluorescence spectroscopy
HPLC	High performance liquid chromatography
IC	Ion chromatography
ICAP	Inductively coupled argon plasma
ICP-AES	Inductively coupled plasma-atomic emission spectroscopy
ICP-ES	ICP-emission spectroscopy
ICP-MS	ICP-mass spectroscopy
ICP-OES	ICP-optical emission spectroscopy
ID-MS	Isotope dilution-mass spectroscopy
INAA	Instrumental neutron activation analysis
NAA	Neutron activation analysis
OES	Optical emission spectroscopy
PET	Positron emission tomography
PNNA	Preconcentration NAA
PIXE	Particle induced X-ray emission

WD-XRF	Wavelength dispersive XRF		Teflon™ PFA	A copolymer—fluoroalky backbone has perfluoroalkoxy side chains [337]
XRF	X-ray fluorescence			
XRS	X-ray spectroscopy			
XRD	X-ray diffraction		TFM–PTFE	Tetrafluorometoxil–polytetrafluoroethylene [36]
ZE-GF-AAS	Zeeman effect-HG-AAS			

Standards

BAM ECRM	Bundensanstalt für Material-forschung und-prufurg (BAM) Euronorm CRM
BCR	Community Bureau of Reference (BCR, Belgium)
BCS CRM	British Chemical Standard CRM
CBR	Community Bureau of Reference
CCRMP	Canadian Reference Materials Project
CRM	Certified Reference Material
CSAN CRM	Czechoslovakian Analytical Normal CRM
DWB	N/A
ECB	European Community Bureau
GFS	G. Frederick Smith Chemical Company
IAEA	International Atomic Energy Agency
IRSID	N/A
MBH	N/A
MOE	Ontario Ministry of the Environment
NBS	National Bureau of Standards
NIES	National Institute for Environmental Studies (Japan)
NIST	National Institute of Standards and Technology
NRCC	National Research Council of Canada
RM	Reference Material
SKD	N/A
SRM	Standard Reference Material

Vessel materials

PFA	Perfluoroalkoxy [337]
PTFE	Polytetrafluoroethylene (Teflon™) [337]

References

[1] T. Paukert, Chem. Listy, 86 (1992) 143.
[2] Z. Zhang and J. Cai, Fenxi Huaxue, 18 (1990) 1078.
[3] B. Li, Z. Yu and K. Han, Guangpuxue Yu Guangpu Fenxi, 11 (1991) 60.
[4] F. Luo, C. Lang and M. Wang, Lihua Jianyan, Huaxue Fence, 27 (1991) 230.
[5] H. Ma, S. Wu, Y. Chen, C. Chen and H. Hu, Yankuang Ceshi, 12 (1993) 28.
[6] J.L. Bouvier and G.E.M. Hall, Pap. -Geol. Surv. Can., 87-1A (1987) 458.
[7] P.J. Lamothe, T.L. Fries and J.J. Consul, Anal. Chem., 58 (1986) 1881.
[8] A.J. Kemp and C.J. Brown, Analyst, 115 (1990) 1197.
[9] L.B. Fischer, Anal. Chem. 58 (1986) 261.
[10] F. Smith, B. Cousins, J. Bozic and W. Flora, Anal. Chim. Acta, 177 (1985) 243.
[11] R.T.T. Rantala and D.H. Loring, Anal. Chim. Acta, 220 (1989) 263.
[12] T. Suzuki and M. Sensui, Anal. Chim. Acta, 245 (1991) 43.
[13] R.A. Davidson, D.D. Harbuck and D.D. Hammargren, At. Spectrosc. 11 (1990) 7.
[14] J. Ching, B. Schmidt and A. Mojica, Precious Met., 17th (1993) 131.
[15] B.J. Perry, R.R. Barefoot, J.C. Van Loon, A.J. Naldrett and D.V. Speller, Spec. Publ. Chem. Soc., 124 (1993) 91.
[16] S.A. Matthes, R.F. Farrell and A.J. Mackie, Tech. Prog. Rep—U.S. Bur. Mines, TPR 120, 9 (12 pp), 1983.
[17] S.A. Mettes, Probopodgot. v Mikrovoln. Pechakh: Teoriya i Prakt., M., (1991) 58.
[18] D.M Labrek, Probopodgot. v Mikrovoln. Pechakh: Teoriya i Prakt., M., (1991) 269.
[19] W. Xu, M. Zou, J. Zhao and Z. Li, Fenxi Huaxue, 20 (1992) 1291.
[20] F.E. Smith, B.G. Cousins and J.Y. Maillet, Educ. Chem., 24 (1987) 13.
[21] J. Bozic and F.E. Smith, Ores and concentrates —special considerations, in C. Riddle (Ed.), Handbook on the Analysis of Geological Materials, Marcel Dekker Inc., 1993, Chapter 6.
[22] W.R. Alexander and T.M. Shimmield, J. Radioanal. Nucl. Chem., 145 (1990) 301.
[23] Y. Shinohara, Ind. Health, 31 (1993) 91.
[24] M.G. Del Monet Tamba, M.T. Dorado Lopez and A. Gomez Coedo, Prog. Anal. Chem. Iron Steel Ind., (1992) 293.

[25] J.P. Beeby, Patent, PCT Int. Appl. WO 92 18, 249, 1992.

[26] W.T. Westbrook, Am. Ceram. Soc. Bull, 66 (1987) 1759.

[27] M. Bettinelli, U. Baroni and N. Pastorilli, J. Anal. At. Spectrom., 2 (1987) 485.

[28] P.R. Klock and P. J. Lamothe, Talanta, 33 (1986) 495.

[29] R.A. Nadkarni, Anal. Chem., 56 (1984) 2233.

[30] R.A. Jenkins, M.P. Maskarinec, W.H. Griest, F.F. Dyer, R. L. Moody and M.V. Buchanan, Report, 1988, ORNL TM-10542; Order No. DE88015357, 107 pp., Available from Energy Res. Abstr. 13 (1988) Abstr. No. 49176.

[31] A. Abu-Samra, J.S. Morris and S.R. Koirtyohann, Anal. Chem., 47 (1975) 1475.

[32] A. Abu-Samra, J.S. Morris and S.R. Koirtyohann, Trace Subs. Environ. Health 9 (1975) 297.

[33] M.A.E. Wandt and M.A.B. Pougnet, Analyst, 111 (1986) 1249.

[34] D.B. Van Wyck, R.B. Schifman, J.C. Stivelman, J. Ruiz and D. Martin, Clin. Chem., 34 (1988) 1128.

[35] I. Hirofumi, U. Tetsuo, O. Kyoko, I Chuzo and N. Genkicki, Anal. Sci., 6 (1990) 385.

[36] H. Matusiewicz, Anal. Chem., 66 (1994) 751.

[36] E. Vereda Alonso, A. Garcia de Torres, J. M. Cano Pavon, Analyst, 117 (1992) 1157.

[38] R.A. Stripp and D.C. Bogen, J. Anal. Toxicol., 13 (1989) 57.

[39] I. Kojima, T. Uchida and C. Iida, Anal. Sci., 4 (1988) 211.

[40] G. Schnitzer, C. Pellerin and C. Clouet, Lab. Pract., 37 (1988) 63.

[41] D. Mayer, S. Haubenwallner, W. Kosmus and W. Beyer, Anal. Chim. Acta, 268 (1992) 315.

[42] A.A. Ferrando, N.R. Green, K.W. Barnes and B. Woodward Biol. Trace Elem. Res., 37 (1993) 17.

[43] M.D. Mingorance, M.L. Perez-Vazquez and M. Lachica, J. Anal. At. Spectrom., 8 (1993) 853.

[44] J.E. Tahan and R.A. Romero, Libro Men.— Encuentro Nac. Electroquim., 5th (1992) 99.

[45] L. Xu, J. Zhu, L. Zhang and C. Qiu, Lihua Jianyan, Huaxue Fence, 24 (1988) 278.

[46] R.T. Uait, Probopodgot, v Mikrovoln. Pechakh: Teoriya i Prakt., M., (1991) 80.

[47] L. Xu, J. Zhu and L. Zhang, Fenxi Huaxue, 15 (1987) 1053.

[48] D. Chakraborti, M. Burguera and J.L. Burguera, Fresenius' J. Anal. Chem., 347 (1993) 233.

[49] E. Vereda Alonso, A. Garcia de Torres, J. M. Cano Pavon, Mikrochim. Acta, 110 (1993) 41.

[50] K. Shiraishi and J.F. McInroy, Biomed. Res. Trace Elem. 2 (1991) 289.

[51] M.A.B. Pougnet and M.A.E. Wandt, ChemSA, 12 (1986) 16.

[52] S. Venkataram and Y.E. Rahman, Br. J. Haematol. 75 (1990) 274.

[53] J. Alvarado, R. Moreno and A.R. Cristiano, J. Trace Elem. Electrolytes Health Dis. 5 (1991) 173.

[54] T. Pinheiro, H. Duflou and W. Maenhaut, Biol. Trace Elem. Res., 26 27 (1990) 589.

[55] M. Achilli, R. Barban, B. Zucchi and W. Martinotti, Water, Air, Soil Pollut., 57–58 (1991) 495.

[56] G. Vermeir, C. Vandecasteele and R. Dams, Anal. Chim. Acta, 220 (1989) 257.

[57] P. Schramel and S. Hasse, Fresenius' J. Anal. Chem., 346 (1993) 794.

[58] E.M. Sedykh, I.N. Petrovskaya, H.E. Matusiewich, N.P. Starshinova, L.N. Bannykh, V.A. Orlova, N.M. Kuz'min, Zh. Anal. Khim., 46 (1991) 292.

[59] H.M. Kingston and L.B. Jassie, Anal. Chem., 58 (1986) 2534.

[60] V. Hudnik and S. Kozak-Legisa, Vestn. Slov. Kem. Drus., 39 (1992) 25.

[61] G.M. Schelkoph and D.B. Milne, Anal. Chem., 60 (1988) 2060.

[62] P. Aysola, P. Anderson and C.H. Langford, Anal. Chem., 59 (1987) 1582.

[63] F. Gil, M.L. Perez, A. Facio, E. Villanueva, R. Tojo and A. Gil, Clin. Chim. Acta, 221 (1993) 23.

[64] H. Matusiewicz, R.E. Sturgeon, and S.S. Berman, J. Anal. At. Spectrom., 4 (1989) 323.

[65] P. Hocquellet and M. P. Candillier, Analyst, 116 (1991) 505.

[66] M. Lachica, Analusis, 18 (1990) 331.

[67] X. Zeng, Q. Li, C. Liu, Y. Sun, X. Chen and Q. Guan, Fenxi Huaxue, 19 (1991) 605.

[68] R.A. Romero, J.E. Tahan and A.J. Moronta, Anal. Chim. Acta, 257 (1992) 147.

[69] J.K. Friel, S. Craig, S.E. Jackson and H.P. Longerich, Analyst, 115 (1990) 115 269.

[70] R. Jaffe, C.A. Fernandez and J. Alvarado, Talanta, 39 (1992) 113.

[71] E. Andrasi, A. Dozsa, L. Bezur, L. Ernyei and Z. Molnar, Fresenius' J. Anal. Chem., 345 (1993) 340.

[72] R.A. Romero, J.E. Tahan and J.A. Navarro, Anal. Sci, 7 (1991) 829.

[73] D. Littlejohn, J.N. Egila, R.M. Gosland, U.K. Kunwar, C. Smith and X. Shan, Anal. Chim. Acta., 250 (1991) 71.

[74] W.G. Lan, M.K. Wong and Y.M. Sin, Talanta 41 (1994) 53.

[75] M. Navarro, M.C. Lopez, H. Lopez and M. Sanchez, Anal. Chim. Acta, 257 (1992) 155.

[76] N. Ybanez, M.L. Cervera, R. Montoro and M. De la Gauardia, J. Anal. At. Spectrom., 6 (1991) 379.

[77] P.J. Oles and W.M. Graham, J. Assoc. Off. Anal. Chem., 74 (1991) 812.

[78] T.R. White, Jr., G.E. Douthit and E. Garnett, J. Assoc. Off. Anal. Chem., 68 (1985) 766.

[79] K.W. Pratt, H.M. Kingston, W.A. MacCrehan and W.F. Koch, Anal. Chem., 60 (1988) 2024.

[80] J.E. Denton, G.D. Potter and J.A. Santolucito, Environ. Res., 23 (1980) 264.

[81] A.B. Brown and H. Keyzer, Contrib. Geol., 16 (1978) 85.

[82] L. Xu, J. Zhu and L. Zhang, Fenxi Huaxue, 15 (1987) 1063.

[83] E.M. Skelly and F.T. Di Stefano, Appl. Spectrosc., 42 (1988) 1302.

[84] S. Nakashima, R.E. Sturgeon, S.N. Willie and S.S. Berman, Analyst, 113 (1988) 159.

[85] J.L.M. de Boer and M.J. Maessen, Spectrochimica Acta, 38 (1983) 739.

[86] J.J. Carni, W.D. James, S.R. Koirtyohann and E. R. Morris, Anal. Chem., 52 (1980) 216.

[87] P. Barrett, L.J. Davidowski, Jr., K.W. Penaro and T.R. Copeland, Anal. Chem., 50 (1978) 1021.

[88] M. Janghorbani, B.T.G. Ting, N.W. Istfan and V.R. Young, Am. J. Clin. Nutr., 34 (1981) 581.

[89] R.R. Rao and A. Chatt, Anal. Chem., 63 (1991) 1298.

[90] C.K. Martin, J.C. Williams J. Anal. At. Spectrom., 4 (1989) 691.

[91] J.L. Burguera, M. Burguera, C.E. Rondon, C. Rivas, J. A. Burguera and O.M. Alarcon, J. Trace Elem. Electrolytes Health Dis., 1 (1987) 21.

[92] I. Kojima, T. Uchida and C. Iida, Anal. Sci., 4 (1988) 211.

[93] J.W. McLaren, K.W.M. Siu, J.W. Lam, S.N. Willie, P.S. Maxwell, A. Palepu, M. Koether and S.S. Berman, Fresenius' J. Anal. Chem., 337 (1990) 721.

[94] G.J. Provan, L. Scobbie and A. Chesson, J. Sci. Food Agric., 64 (1994) 63.

[95] J.L. Imbert, Analusis, 18 (1990) i15.

[96] W. Van Delft, H.J. Horstman, H. Lammers and G. Vos, Colloq. Atomspektrom. Spurenanal., 5th (1989) 603.

[97] D. Wang, M. Zou, S. Xie, L. Liu, H. Zhang, W. Wang and Q. Jin, Fenxi Huaxue, 18 (1990) 482.

[98] M.-A. Mateo and S. Sabate, Anal. Chim. Acta, 279 (1993) 273.

[99] J. Nieuwenhuize and C.H. Poley-Vos, At. Spectrosc. 10 (1989) 148.

[100] J.E. Rechcigl and G.G. Payne, Commun. Soil Sci Anal., 21 (1990) 2209.

[101] Y.P. Kalra, D.G. Maynard and F.G. Radford, Can. J. For. Res., 19 (1989) 981.

[102] H.J. Reid, S. Greenfield, T.E. Edmonds and R. M. Kapdi, Analyst, 118 (1993) 1299.

[103] L.H.J. Lajunen, J. Piispanen and E. Saari, At. Spectrosc., 13 (1992) 127.

[104] S. Yamasaki, A. Tsumura and D. Cai. Appl. Plasma Source Mass Spectrom., 22nd (1990) (pub. 1991), 110.

[105] M. Saumer, E. Gantner, J. Reinhardt and H.J. Ache, Fresenius' J. Anal. Chem., 344 (1992) 109.

[106] C.R. Finch, H.D. Pennington, C.G. Lyons and S.E. Littau, Commun. Soil Sci. Plant Anal., 21 (1990) 583.

[107] H.D. Pennington, C.R. Finch, C.G. Lyons and S.E. Littau, HortScience, 26 (1991) 1496.

[108] V. Bozek, I. Moudry and M. Novotny, Drevo, 43 (1988) 2.

[109] L. Dunemann, Colloq. Atomspektrom. Spurenanal., 5th (1989) 593.

[110] J.S. Morris, H. Anderson and M. Cordis, Trans, Am. Nucl. Soc., 34 (1980) 174.

[111] C.S.E. Papp and L.B. Fischer, Analyst, 112 (1987) 337.

[112] J.A. Kraowski and T.R. Copeland, Anal. Chem., 51 (1979) 1843.

[113] R. Blust, A. Van der Linden and W. Decleir, At. Spectrosc. 6 (1985) 163.

[114] L.V. Dracheva and M.Y. Kabanova, Pishch. Prom-st., 6 (1989) 60.

[115] L. Xu and W. Sen, Yingyang Xuebao, 11 (1989) 65.

[116] L. Dunemann and M. Meinerling, Fresenius' J. Anal. Chem., 342 (1992) 714.

[117] R. Ishigaki, Patent, Kokai Tokkyo Koho JP 62, 111, 674, 1987.

[118] N. Elwaer and N. Belzile, Int. J. Environ. Anal. Chem., 61 (1995) 189.

[119] S. Nikdel and C.M. Temelli, Microchem J., 36 (1987) 240.

[120] R. Blust, A. Van der Linden, E. Verheyen and W. Decleir, J. Anal. At. Spectrom., 3 (1988) 387.

[121] H.T. McCarthy and P.C. Ellis, J. Assoc. Off. Anal. Chem. 74 (1991) 566.

[122] R. Demura, S. Tsukada and I. Yamamoto, Eisei Kagaku, 31 (1985) 405.

[123] J. Wenrui and J. Wang. Anal. Chim. Acta. 245 (1991) 77.

[124] L. Xu and W. Shen, Fresenius' Z. Anal. Chem., 332 (1988) 45.

[125] C. Cabrera, M.L. Lorenzo, C. Gallego and M.C. Lopez, Anal. Chim. Acta. 246 (1991) 375.

[126] A.D. Hewitt and C.M. Reynolds, At. Spectrosc. 11 (1990) 187.

[127] C.J. Warren, B. Xing and M.J. Dudas, Can. J. Soil Sci., 70 (1990) 617.

[128] B. Kratochvil and S. Mamba, Can. J. Chem. 68 (1990) 360.

[129] J. Alvarado and A. Petrola, J. Anal. At. Spectrom., 4 (1989) 411.

[130] L.V. Dracheva, Zavod. Lab., 56 (1990) 10.

[131] L. Xu and W. Shen, Fresenius' Z. Anal. Chem., 333 (1989) 108.

[132] J. Huang, D. Goltz and F. Smith, Talanta, 35 (1988) 907.

[133] C.M. Reynolds, Report, 1992 21 pp., available from Gov. Rep. Announce. Index (US) 93 (1993), Abstr. No. 319, 037.

[134] P. Quevauviller, J.L. Imberta and M. Olle, Mikrochim. Acta, 112 (1993) 147.

[135] W.R. Kammin and M.J. Brandt, Spectroscopy, 4 (1989) 49.

[136] G.S.R. Krishnamurti, P.M. Huang, K.C.J. Van Rees, L.M. Kozak and H.P.W. Rostad, Commun. Soil Sci. Plant Anal., 25 (1994) 615.

[137] M. Kingston and P.J. Walter, Spectroscopy 7 (1992) 20.

[138] A.D. Hewitt and J.H. Cragin, Environ. Sci. Technol. 25 (1991) 985.

[139] J.R. Wakakuwa and D.E. Kimbrough, Environ. Sci. Technol., 26 (1992) 1849.

[140] A.D. Hewitt and J.H. Cragin. Environ Sci. Technol. 26 (1992) 1848.

[141] J. Nieuwenhuize, C.H. Poley-Vos, A.H. Van den Akker and W. Van Delft, Analyst, 166 (1991) 347.

[142] A.M. Paudyn and R.G. Smith, Can J. Appl. Spectrosc., 37 (1992) 94.

[143] K.I. Mahan, T.A. Foferaro, T.L. Garza, R.M. Martinez, G.A. Maroney, M.R. Trivisonno and E.M. Willging, Anal. Chem., 59 (1987) 983.

[144] S. Kokot, G. King, H.R. Keller and D.L. Massart, Anal. Chim. Acta., 259 (1992) 267.

[145] L. Xu, W. Shen and J. Zhu, J. Environ. Sci., 1 (1989) 69.

[146] D.A. Binstock, P.M. Grohse, A. Gaskill, Jr., K.K. Luk, P.L. Swift, H.M. Kingston and C. Sellers, ASTM Spec. Tech. Publ., 1062 (1990) 259.

[147] W. Van Delft and G. Vos, Anal. Chim. Acta., 209 (1988) 147.

[148] J. Labrecque. Proc. 17th Canadian Mineral Analysts Conference. Val D'or, Quebec, Canada, September 1985.

[149] C. Huang, I.L. Huang, C.Y. Kuo, L.W. Shiu, R.C. Kao and M.S. Kuo. Huan Ching Pao Hu (Taipei), 11 (1988) 1.

[150] H.T. Tsai, J.R. Lu and C.N. Shaio, Hua Hsueh, 46 (1988) 239.

[151] C.G. Millward and P.D. Kluckner, J. Anal. At. Spectrom., 4 (1989) 709.

[152] E. Boffelli, Inquinamento, 30 (1988) 96.

[153] J.B. Reeves and S.B. Shank, Toxic Hazard. Wastes, Proc. Mid-Atl. Ind. Waste Conf., 18th, 1986, p. 369.

[154] M. Bettinelli and U. Baroni, Int. J. Environ. Anal. Chem., 43 (1991) 33.

[155] A. Morales, F. Pomares, M. De la Guardia and A. Salvador, J. Anal. At. Spectrom. 4 (1989) 329.

[156] J.S. Summer and W.D. Morrow, Proc. Conf.—Int. Coal Test. Conf., 4th, 1984, 34.

[157] J. Alvarado, M. Alvarez, A.R. Cristiano and L.M. Marco, Fuel, 69 (1990) 128.

[158] M.L. Jacobs, Proc. Conf.—Int. Coal Test. Conf., 4th, (1984) 29.

[159] N.G. Cutmore, Patent, Can., CA 1,322,222, 1993.

[160] D.A. Binstock, P.M. Grohse, P.L. Swift, A. Gaskill, Jr., T.R. Copeland and P.H. Friedman, ASTM Spec. Tech. Publ., 1990, 1062, 312.

[161] M.W. Osborne and E.L. Curry. Proc. Conf.— Int. Coal Test. Conf., 6 (1987) 16.

[162] K. Igarashi, R. Nakashima and T. Naya. Bunseki Kagaku, 40 (1991) T71.

[163] M. Weber and W. Praxmarer, Patent, Ger. (East) DD 203,398, 1983, 13 pp.

[164] S. Weng and J. Wang, Chin. Sci. Bull., 37 (1992) 1603.

[165] E. Chrusciel, M. Kopec and B. Turek, Arch. Min. Sci., 35 (1990) 247.

[166] C. Bachmann, Aufbereit.—Tech., 30 (1989) 77.

[167] J. Alvarado, L.E. Leon, F. Lopez and C. Lima, J. Anal. At. Spectrom., 3 (1988) 135.

[168] M. Bettinelli, U. Baroni and N. Pastorilli, J. Anal. At. Spectrom., 3 (1988) 1005.

[169] K.W. Riley, H.N.S. Schafer and H. Orban, Analyst, 115 (1990) 1405.

[170] M.T. Dorado Lopez, M.A. Palaios Vida and A. Gomez Coedo, Congr. Nac. Cienc. Technol. Metal, 7th, 1990, 3, 205.

[171] P. Halmos, E. Gegus and J. Borszeki, Magy. Kem. Foly., 99 (1993) 420.

[172] P.A. Vozzella and D.A. Condit, Anal. Chem., 60 (1988) 2497.

[173] I. Hlavacek and I. Hlavackova, J. Anal. At. Spectrom., 6 (1991) 535.

[174] B.D. Zehr and M.A. Fedorchak, Am. Lab., 23 (1991) 40, 42.

[175] T.Y. Chang, F.J. Isieh and C. Lee, MRL Bull. Res. Dev., 4 (1990) 5.

[176] L.A. Fernando, W.D. Heavner and C.C. Gabrielli, Anal. Chem., 58 (1986), 511.

[177] B. Berglund and C. Wichardt, Anal. Chim. Acta., 236 (1990) 399.

[178] P.G. Riby, S.J. Haswell and R. Grzeskowiak, J. Anal. At. Spectrom., 4 (1989) 181.

[179] K. Karube, Y. Iwasaki, R. Matsushita, S. Koizumi and W. Ishibashi, Anal. Sci., 7 (1991) 113.

[180] P. Green, J. Mater, Sci, Lett., 10 (1991) 1162.

[181] J.A. Brown, Jr., F.W. Kunz and R.K. Belitz, J. Anal, At. Spectrom., 6 (1991) 393.

[182] T.N. Donvito, T.S. Turan and J.R. Wilson, Tappi J., 75 (1992) 163.

[183] K. Matsumoto, Patent, Jpn., Kokai Tokkyo Koho JP 60,140,194, 1985, 4 pp.

[184] O. Buresch, W. Hoenle, U. Haid and H.G. Von Schnering, Fresenius' Z. Anal. Chem., 328 (1987) 82.

[185] M. Hidaka, Patent, Jpn. Kokai Tokkyo Koho JP 04, 122,836, 1992 5 pp.

[186] T. Fujii. Patent Jpn. Kokai Tokkyo Koho JP 61, 60, 840, 1986, 5 pp.

[187] I. L. Al-Quadi, J. Test Eval., 20 (1992) 43.

[188] G.M. Russell, Rep.—MINTEK, 1986 M289.

[189] T. Morimoto, S. Shirakawa and J. Izumi, Patent, Jpn. Kokai Tokkyo Koho Jp 61,202,194, [86, 202, 194], 1986, 3 pp.

[190] W.T. Muse, Report, 1990, CRDEC-TR-167; Order No. AD-A223070, 14 pp., Available from Gov. Rep. Announce, Index (US) 90 (1990) Abstr. No. 050,713.

[191] C.J. Coleman, N.E. Bibler and R.A. Dewberry, Proc. Symp. Waste Management., 2 (1990) 651.

[192] R.A. Morales, C.A. Salvador and M.C. De la Guardia, Anal. Chim. Acta., 235 (1990) 405.

[193] H.M. Kingston and L.B. Jassie, J. Res. Natl. Bur. Stand. (US) 93 (1988) 269.

[194] R.A. Nadkarni, Anal. Chem., 56 (1984) 2233.

[195] E. Palacios, Tec. Lab., 15 (1993) 18.

[196] L. Xu, W. Shen and J. Zhu, Fenxi Huaxue, 18 (1990) 597.

[197] K. Kawasaki and Y. Katsuno, Patent, US 4,347,216, 1982.

[198] P.W. Roszel, Patent, Can Pat. Appl., CA 2,026,103, 1992.

[199] E.V. Williams, Proc. Chem. Conf., 40th (1987) 47.

[200] M. Bettinelli, U. Baroni and N. Pastoreli, Anal. Chim. Acta., 225 (1989) 159.

[201] T. Noeltner, P. Maisenbacher and H. Puchelt, Spectroscopy, 5 (1990) 49.

[202] J.P. Batchelor, Chem. N.Z., 52 (1988) 33.

[203] E. Palacios, Quim. Ind., 36 (1990) 649.

[204] A.M. Paudyn and R.G. Smith, J. Anal. At. Spectrom., 5 (1990) 523.

[205] S. Peng, M.R.C. Laza, F.V. Garcia and K.G. Cassman, J. Plant Nutr., 17 (1994) 209.

[206] L.K. Wang, D. Barris, P. Milne and M. Mulloy, Gov. Rep. Announce. Index (US), 83 (1983) 779.

[207] E.S. Beary, Anal. Chem., 60 (1988) 742.

[208] D.J. Lumley and A. Kuhlin, Vatten, 43 (1987) 89.

[209] J. Verink, G. Hesse and H. Rueffer, Vom Wasser, 57 (1981) 75.

[210] R.Q. Thompson and M. Ghadiali, J. Chem. Educ., 70 (1993) 170.

[211] F. Jiang and R. Jiang, Yankuang Ceshi, 12 (1993) 135.

[212] A. Stammer and E.U. Schluender, Chem. Eng. Process., 32 (1993) 339.

[213] M. Burguera, J.L. Burguera and O.M. Alarcon, Anal. Chim. Acta., 179 (1986) 351.

[214] M. De la Guardia, A. Salvador, J.L. Burguera and M. Burguera, J. Flow Injection Anal., 5 (1988) 121.

[215] V. Carbonell, M. De la Guardia, A. Salvador, J.L. Burguera and M. Burguera, Anal. Chim. Acta, 238 (1990) 417.

[216] R. Martinez-Avila, V. Carbonell, M. De la Guardia and A. Salvador, J. Assoc. Off. Anal. Chem. 73 (1990) 389.

[217] B. Welz, D. Tsalev and M. Sperling, Anal. Chim. Acta., 261 (1992) 91.

[218] D.L. Tsalev, M. Sperling and B. Welz, Analyst, 117 (1992) 1728.

[219] D.L. Tsalev, M. Sperling and B. Welz, Analyst, 117 (1992) 1735.

[220] T. Guo and J. Baasner, Talanta, 40 (1993) 1927.

[221] M. De la Guardia, V. Carbonell, A. Morales-Rubio and A. Salvador, Talanta 40 (1993) 1609.

[222] G.R. Beecher, D.L. Kemper and J.E. Jordan, Patent, U.S. US 5,192,984, 1993, 25 pp.

[223] V. Karanassios, F.H. Liu, B. Liu and E.D. Salin, J. Anal. At. Spectrom. 6 (1992) 457.

[224] T.J. Gluodenis, Jr. and J.F. Tyson, J. Anal. At. Spectrom., 8 (1993) 697.

[225] F.A. Settle, Jr., B.I. Diamondstone, H.M. Kingston and M.A. Pleva, J. Chem. Inf. Comput. Sci., 29 (1989) 11.

[226] F.A. Settle, Jr., P.J. Walter, H.M. Kingston, M.A. Pleva, T. Snider and W. Boute, J. Chem Inf. Comput. Sci., 32 (1992) 349.

[227] P.J. Walter, H.M. Kingston, F.A. Settle, M.A. Pleva, W. Boute and J. Christo, Adv. Lab. Autom. Rob., 7 (1991) 405.

[228] M.H. Feinberg, Analusis, 19 (1991) 47.

[229] H. Lowenhaupt and M. Hollenbeck, Patent, Eur. Pat. Appl., EP 183,501, 1986, 18 pp.

[230] W. Lautenschlaeger and J. Dorfer, Labor Praxis, 16 (1992) 509.

[231] R. Elias, A.M. Diaz Lanza, E. Vidal-Ollivier, C. Maillard, F. Crespin, G. Balansard and G. Boudon, J. Pharm. Belg., 46 (1991) 177.

[232] A.A. Craveiro, F.J.A. Matos, J.W. Alencar and M.M. Plumel, Flavour Fragrance J., 4 (1989) 43.

[233] J.R.J. Pare, J.M.R. Belanger, A. Belanger and N. Ramarathnam, Dev. Food Sci., 29 (1992) 141.

[234] G.J. Collin, D. Lord, J. Allaire and D. Gagnon, Parfums Cosmet., Aromes 97 (1991) 105.

[235] K. Ganzler and A. Salgo, Z. Lebensm.-Unters. Forsch., 184 (1987) 274.

[236] C.A. Monz, D.E. Reuss and E.T. Elliott, Agric., Ecosyst. Environ., 34 (1991) 55.

[237] F.I. Onuska and K.A. Terry, Chromatographie, 36 (1993) 191.

[238] K. Ganzler, A Salgo and K. Valko, J. Chromatogr., 371 (1986) 299.

[239] M.J. Collins, Patent, US, US 4,554,132, 1985.

[240] B. Rocca, C. Arzouyan, J. Estienne and S. Cucce, Ann Falsif. Expert. Chim. Toxicol., 85 (1992) 347.

[241] R.G. Harris, Patent US US 4,606,650, 1986 7 pp.

[242] D.A. Lane and S.W.D. Jenkins, Polynucl. Aromat. Hydrocarbons: Chem., Charact. Carcinog., Int. Symp., 9th 1984 (Pub. 1986), 437.

[243] B.F. Armstrong and E.D. Neas, Sep. Sci. Technol., 25 (1990) 2007.

[244] X.T. He, R.L. Mulvaney and W.L. Banwart, Soil Sci. Soc. Am. J., 54 (1990) 1625.

[245] R. Commarmot, D. Didenot and J.F. Gardais, Patent Fr., Demande FR 2,560, 529, 1985 20 pp.

[246] C.L. Suard, M.H. Feinberg, J. Ireland-Ripert and R.M. Mourel, Analusis, 21 (1993) 287.

[247] L.V. Antisari and P. Sequi, Soil Sci. Soc. Am. J., 52 (1988) 1020.

[248] M. Feinberg, C. Suard and J. Ireland-Ripert, Chemom. Intell. Lab. Syst., 22 (1994) 37.

[249] J. Alvarado, M. Marquez and L.E. Leon, Anal. Lett., 21 (1988) 357.

[250] A. Bermond and C.J. Ducauze, Analusis, 19 (1991) 64.

[251] E.D. Neas and T.S. Floyd, Patent, Eur. Pat. Appl., EP 249,500, 1987 12 pp.

[252] Q. Jin, Fenxi Huaxue, 16 (1988) 668.

[253] M.A.B. Pougnet, ChemSA, 15 (1989) 284.

[254] A. Sinquin, T. Gorner and E. Dellacherie, Analusis, 21 (1993) 1.

[255] I. Kojima, Bunseki, 4 (1990) 291.

[256] Z. Sulcek, J. Novak and J. Vyskocil, Chem. Listy, 83 (1989) 388.

[257] R. Wu and M. Ding, Fenxi Shiyanshi, 10 (1991) 51.

[258] B. Li, Guangpuaxue, Yu Guangpu Fenxi, 12 (1992) 103.

[259] D. Dan, Huaxue Tongbao, 10 (1989) 46.

[260] W. Lautenschlaeger, Labor Praxis, 12 (1988) 1348.

[261] C.M. Chen, Shih Yu, 25 (1989) 17.

[262] G.M. Kimber and S. Kotot, Trends Anal. Chem. 9 (1990) 203.

[263] D.M.P. Mingos and D.R. Baghurst, Br. Ceram. Trans. J. 91 (1992) 124.

[264] H.M. Kuss, CLB Chem. Labor Biotech., 42 (1991) 11.

[265] I. Kojima, Bunseki, 1 (1992) 14.

[266] L. Dunemann, GIT Fachz. Lab., 37 (1993) 854.

[267] H. Matusiewicz and R.E. Sturgeon, Prog. Anal. Spectrosc., 12 (1989) 21.

[268] H.M. Kuss, Fresenius' J. Anal. Chem., 343 (1992) 788.

[269] I.V. Kubrakova and N.M. Kuz'min, Zavod. Lab., 58 (1992) 1.

[270] H.M. Kingston and L.B. Jassie (Eds.), Introduction to Microwave Sample Preparation, ASC Professional Reference Book, American Chemical Society, Washington, DC, 1988.

[271] A. Landgraf, Labor Praxis, 13 (1989) 996.

[272] C.M. Reynolds, Eng. Aspects Met.-Waste Manage., (1992) 49.

[273] J.F. Soulabaille, Analusis, 18 (1990) i14.

[274] D. Mathe, Analusis, 18 (1990) i19.

[275] J.G. Anderson, IFAC Proc. Ser., 8 (1984) (Instrum. Autom. Pap. Rubber, Plast. Polym. Ind.), 63.

[276] C. Lang, M. Wang and F. Luo, Lihua Jianyan, Huaxue Fence 25 (1989) 315.

[277] Microwaves and Minerals, Industrial Mineral Background Paper #14. Atomic Energy of Canada Ltd. Research Company, Chalk River, Ontario and Voss Associates Engineering Ltd., Victoria, British Columbia, 1990.

[278] M.E. Tatro, Spectroscopy, 1 (1986) 18.

[279] W. Lautenschlaeger, Labor Praxis, 12 (1988) 1348.

[280] R.C. Munter, Commun. Soil Sci. Plant Anal. 21 (1990) 1831.

[281] R.E. Sturgeon and S.S. Berman, Stud. Environ. Sci., 24 (1988) (Chem. Prot. Environ. 1987) 333.

[282] C.M. Chen, Shih Yu, 25 (1989) 17.

[283] L.B. Gilman, General Guidelines for Microwave Sample Preparation, (CEM Corporation, P.O. Box 200, Matthews, NC 28106), 1988.

[284] W.R. Kammin and M.J. Brandt, Spectroscopy, 4 (1989) 22.

[285] Proc. International Conference on Millimeter and Submillimeter Waves and Applications, San Diego, California, USA, 1994, 628 pp.

[286] L.B. Jassie, Ph.D. Thesis (American Univ., Washington, DC, USA), 1989, 252 pp.

[287] G.M. Russel, ChemSA, 16 (1990) 116.

[288] G.J. DeMenna and W.J. Edison, ASTM Spec. Tech. Publ., 944 (1987) (Chem. Anal. Met.), 45.

[289] A. Grillo and M. Moses, Am. Lab., 24 (1992) 58.

[290] M. Totland, I Jarvis and K.E. Jarvis, Chem. Geol., 95 (1992) 35.

[291] S.A. Borman, Anal. Chem., 60 (1988) 715A.

[292] S.A. Borman, Anal. Chem., 58 (1986) 1424A.

[293] W. Lautenschlaeger, Labor Praxis, 14 (1990) 376.

[294] E. Jackwerth and S. Gomiscek, Pure Appl. Chem., 56 (1984) 479.

[295] E.F. Sterken, T.S. Floyd and O.P. Manchester, Probopodgot. v Mikrovoln. Pechakh: Teoriya 1 Prakt., M.,(1991) 248.

[296] D. Didenot, Spectra 2000 [Deux Mille], 146 (1990) 44.

[297] D. Mathe, Analusis, 19 (1991) i21.

[298] R. Commarmot, D. Didenot and J.F. Gardais, Patent, Fr., Demande FR 2,560,686, 1985, 32 pp.

[299] D. Mathe, Analusis, 19 (1991) M20.

[300] J.D. Norris, B. Preston and L.M. Ross, Analyst, 117 (1992) 3.

[301] H.M. Kingston, P.J. Walter, F.A. Settle, Jr. and M.A. Pleva, Proc. Int. Symp. Lab. Autom. Rob., 1991 (Pub. 1992), 619.

[302] M.R. Saati, Adv. Lab. Autom. Rob., 6 (1990) 521.

[303] H.J. Reid, S. Greenfield and T.E. Edmonds, Analyst, 118 (1993) 443.

[304] K.D. Raner, C.R. Strauss, F. Vyskoc and L. Mokbel, J. Org. Chem., 58 (1993) 950.

[305] M.A.B. Pougnet, Rev. Sci. Instrum., 64 (1993) 529.

[306] H.M. Kingston and L.B. Jassie, Mater. Res. Soc. Symp. Proc., 124 (1988) 121.

[307] L. Gilman and W. Grooms, Anal. Chem., 60 (1988) 1624.

[308] M. Pagnotta, A. Nolan and L. Kim, J. Chem. Ed., 69 (1992) 599.

[309] G. Bond, R.B. Moyes, S.D. Pollington and D.A. Whan, Meas. Sci. Technol., 2 (1991) 571.

[310] G. Bond, R.B. Moyes, S.D. Pollington and D.A. Whan, Chem. Ind., 18 (1992) 686.

[311] J.A. Hesek and R.C. Wilson, Anal. Chem. 46 (1974) 1160.

[312] R.F. Farrell, S.A. Matthes and A.J. Mackie, Rep. Invest.—U.S. Bur. Mines 1980, RI 8480.

[313] R.M. Sterrit and J.N. Lester, Sci. Total Environ., 16 (1980) 55.

[314] T.T. Gorsuch, The Destruction of Organic Matter, Pergamon, New York, 1970.

[315] F.E. Smith, Microwaves in the laboratory—recent advances, Keynote Presentation, Proc. 2nd ANIAC International Conference, Kuala Lumpur, Malaysia, November 1993.

[316] A.J. Berteaud and J.C. Badot, J. Microwave Power, 11 (1976) 315.

[317] L.M. Sheppard, Amer. Ceram. Soc. Bull., 67 (1988) 1656.

[318] S. Das and T.R. Curlee. Amer. Ceram. Soc. Bull., 66 (1987) 1093.

[319] F.E. Smith, B. Cousins, J. Bozic and W. Flora, Proc. IUPAC Symposium on Analytical Chemistry in the Exploration, Mining and Processing of Materials, Pretoria, South Africa, 1985.

[320] J. Bozic, W. Flora, F. Smith and B. Cousins, Proc. 68th Canadian Chemical Conference, Kingston, Ontario, Canada, 1985.

[321] F.E. Smith, B. Cousins, J. Bozic and W. Flora, Proc. 17th Annual Canadian Mineral Analysts Conference, Val d'Or, Québec, Canada, September 1985.

[322] R.N. Gedye, F.E. Smith, K.C. Westaway, H. Ali, L. Baldisera, L. Laberge, and J. Rousell, Tetrahedron Lett. 27 (1986) 279.

[323] R.N. Gedye, F.E. Smith, K.C. Westaway, Can J. Chem. 66 (1988) 17.

[324] R.J. Gedye, F.E. Smith, K.C. Westaway, Educ. Chem., 25 (1988) 55.

[325] R.J. Giguere, T.L. Bray, S.M. Duncan and G. Majetich, Tetrahedron Lett. 27 (1986) 4945.

[326] R.J. Giguere, A.M. Naman, B.O. Lopez, A. Arepally and D.E. Ramos, Tetrahedron Lett. 28 (1987) 6553.

[327] D.R. Baghurst and D.M.P. Mingos, J. Chem. Soc., Chem. Comm., (1992) 674.

[328] J. Berlan, P. Giboreau, S. Lefeuvre and C. Marchand, Tetrahedron Lett. 32 (1991) 2363.

[329] J. Berlan, K. Cann-Pailler, J.L. Imbert and R. Tessier, French Patent 9114720, 28.11.1991.

[330] J.O. Thorell, Ph.D Diss., Karolinska Hospital and Inst. Stockholm, Sweden. 1993.

[331] Questron Corporation, P.O. Box 2387, Princeton, NJ 08543, USA.

[332] CEM Corporation, P.O. Box 200, Matthews, NC 28106, USA.

[333] Floyd Associated Inc., Lake Wyle, SC, USA.

[334] MILESTONE s.r.l., via Fatebenefratelli 1/5, 24010 Sorisole, Bergamo, Italy.

[335] Parr Instrument Company, 211 Fifty-Third St., Moline, Illinois 61265 USA.

[336] Dr. Chris Strauss, CSIRO Division of Chemicals and Polymers Private Bag 10, Clayton, Victoria 3168, Australia.

[337] The Savillex Corporation, 6133 Baker Rd., Minnetonka, Minnesota 55345, USA.

[338] R. Gedye, Proc. 29th Microwave Power Symposium, Chicago, USA, July 1994.

[339] Prolabo, 12 rue Pelée, 75011, Paris, CEDEX 11, France.

[340] S.J. Haswell and D. Barclay, Analyst, 117 (1992) 117.

[341] A. Peter, G. Laus and G. Van Binst, Peptide Research, 6 (1993) 1.

[342] E. Tatar, M. Khalifa, G. Zaray and I. Molnar-Perl, J. Chromatogr. A., 672 (1994) 109.

[343] E. Marconi, G. Panfili, L. Bruschi, V. Vivanti and L. Pizzoferrato, Proc. 3rd Int. Conf. on Amino Acids, August 1993, Vienna, Austria.

[344] S. Cavalli and N. Cardellicchio, J. Chromatogr. A., 706 (1995) 429.

A new method for the determination of residual piperazine in pharmaceuticals by capillary gas chromatography

K.N. Ramachandran*, G.S. Kumar

Shriram Institute for Industrial Research, 14, 15, Sadararmangala Industrial Area, Whitefield Road, Bangalore 560 048, India

Abstract

A new selective open tubular capillary gas chromatographic method is developed for the determination of trace amounts of piperazine. Piperazine is extracted from pharmaceuticals into cyclohexane and is partitioned with water. The aqueous solution is then injected into a 5% crosslinked Ph–Me silicone column programmed at 50–180 °C for 10 min. Piperazine is eluted after 3.18 min under isothermal conditions. The lower limit of determination is 0.4 ppm. This method has been successfully applied for the assay of piperazine in pharmaceutical formulations and its trace determination in fluoroquinolone drugs such as norfloxacin and ciprofloxacin. The method is reproducible and the standard and relative standard deviation for 10 repeated injections of 2 μg piperazine are 0.7 and ±2.1% respectively.

1. Introduction

Piperazine is one of the most potent drugs used as anthelmintics. It is also one of the raw materials used in the synthesis of fluoroquinolone drugs such as norfloxacin, ciprofloxacin, etc. [1]. The pharmocological significance of piperazine has led to the development of several methods for its determination in pharmaceutical formulations. Nonaqueous titration [2] and gravimetric methods [3] are the most popular. In addition several colorimetric methods [4–20] have been reported for

its determination. However, these methods are not applicable for the determination of residual piperazine in fluoroquinolone drugs. A survey of the literature failed to indicate a suitable method for the trace analysis of this compound. Methods such as high performance liquid chromatography (HPLC) and potentiometry, reported for the determination of norfloxacin or ciprofloxacin, cannot be used for piperazine. This necessitates the development of a suitable method for the determination of residual piperazine in pharmaceutical formulations and their standards.

In this paper a new, sensitive and selective capillary gas chromatographic method is pro-

---

*Corresponding author. Fax: (+80) 845-2734.

posed for the determination of piperazine. Piperazine is extracted into water and injected into a pre-conditioned column of 5% Ph–Me silicone. The column is programmed at 50–180°C for 10 min. The lower limit of determination is 0.4 ppm. This method has been applied for the determination of residual piperazine in norfloxacin, ciprofloxacin, etc. The results have been compared with those from other established methods and found to be satisfactory.

2. Experimental

2.1. Reagents

All reagents used were of AnalaR grade and solvents were supplied by Merck. Piperazine was obtained from Aldrich. Doubly–distilled deionised water was used.

2.2. Equipment

A Hewlett Packard Series II 5890 gas chromatograph with a flame ionization detector and a 30 m × 0.3 mm i.d fused silica column coated with a 3.0 μm film of 5% cross linked Ph–Me silicone was used. The carrier gas was nitrogen, at a flow rate of 1 ml min^{-1}, measured with a bubbler flow meter at a column temperature of 50°C. The injector and detector temperatures were kept at 200°C and 225°C respectively. The column temperature was programmed at 50°C for 5 min, then
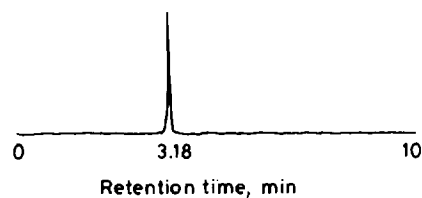
Concentration of piperazine is 0.4 ppm

Fig. 1. Chromatogram of piperazine.

increased by 15°C min^{-1} to 180°C and held at that temperature for 10 min. The injection volume was 1 μl on the column. Standard and sample solutions were injected in five replicates. Data analyses were performed on a HP 3395 integrator system. Calibrated glassware was used for all volumetric purposes. Millipore 0.45 μm filters were used for filtration of samples.

2.3. Analytical standard preparation

Stock solution (1000 ppm): 100 mg of anhydrous piperazine was accurately weighed in to a 100 ml calibrated volumetric flask and made up to the mark with distilled water.

Working standard: working standards were prepared by appropriate dilution of the stock solution.

2.4. Procedures

2.4.1. Preparation of calibration graph

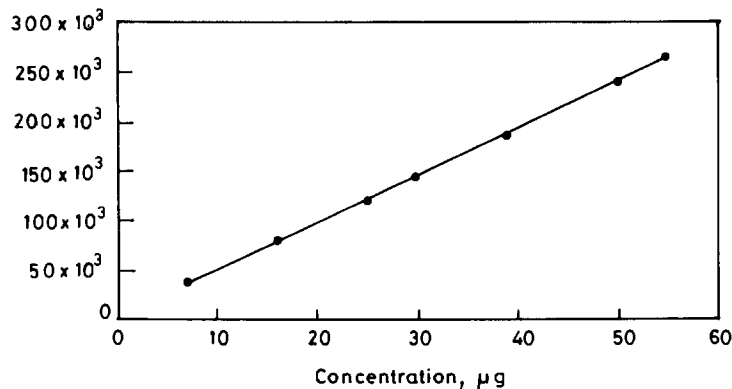1 μl of an aliquot of standard piperazine solution (0.4–10 ppm) was injected into a pre-condi-

Fig. 2. Calibration graph for piperazine.

Table 1
Retention times of solvents and piperazine

Compound	Retention time (min)	Compound	Retention time (min)
Piperazine	3.21	DMF	21.3
Methanol	2.21	Benzyl alcohol	27.5
Ethanol	2.73	Ethyl acetate	5.6
Acetone	3.15	DMSO	23.4
Diethyl ether	2.85	Carbon tetrachloride	6.95
Isooctane	3.17	Benzene	7.6
Dochloromethane	3.69	Hexane	4.41
Chloroform	4.95		

tioned column programmed at 50–180°C under programmed conditions. Instrumental and integrator parameters such as attenuation, range and chart speed were set at their optimum values. A calibration graph of peak area vs. concentration was prepared.

2.4.2. Determination of piperazine in norfloxacin and ciprofloxacin

1 g of norfloxacin was transferred into a 25 ml separatory funnel along with 10 ml (2 × 5 ml) of cyclohexane. The mixture was shaken thoroughly for 10 min and filtered under suction with a 0.45 μm filter. The cyclohexane filtrate was partitioned with 10 ml water in another separatory funnel for 10 min. The organic phase was discarded and the aqueous phase was thermostatted at 45°C for 10 min. 1 μl of this solution was injected on to the column as described above.

Table 2
Percentage recovery/extraction efficiency of piperazine from real samples

Sample	Piperazine added (μg)	Piperazine found (μg)	% Recovery
Norfloxacin USP	-	3.5 ($\pm$0.4)	-
	5	8.4 ($\pm$0.1)	98.8
	10	13.4 ($\pm$0.2)	98.8
Ciprofloxacin HCl	–	2.6 ($\pm$0.2)	–
	5	7.5 ($\pm$0.3)	98.1
	10	12.4 ($\pm$0.1)	98.4

2.4.3. Determination of piperazine in piperazine citrate

1 mg of piperazine citrate was taken in a 100 ml volumetric flask and diluted to 100 ml. 1 μl aliquots of the sample were injected on to the column as described above.

3. Results and discussion

A composite chromatogram showing the retention time of piperazine is given in Fig. 1. Under optimum conditions piperazine was eluted as a singlet. The mean peak area and retention time are 77 214 (AU) and 3.18 min respectively. The attenuation and range of the instrument were set according to the concentration of the sample. The lower limit of detection is the concentration which would give a peak height equal to three times the baseline noise. This value for piperazine was 0.4 mg. A monovariant calibration graph was made with the integrator for assay. A linear relationship between the peak area and concentration is shown in Fig. 2. The slope, intercept of the best fit line and coefficient of correlation are 5.876, −0.0063 and 1.000 respectively.

The compatibility of various solvents for extraction of piperazine from fluoroquinolone drugs was studied. Although piperazine is highly soluble in water, water is not the preferred solvent since most of the pharmaceuticals used in the present study were also soluble in water. The performance of the column is affected in such cases. Among several solvents studied such as acetone, ethanol, methanol, isooctane, dichloromethane, chloro-

Table 3
Comparison between the results obtained from the proposed method and the USP method[a]

Sample	Piperazine added (μg)	Piperazine found (μg)	
		Proposed method	USP method
Norfloxacin USP	-	4.1	16.3
	5	8.0	16.3
	10	13.9	16.5
	25	29.0	21.5
Ciprofloxacin HCl	–	1.8	24.2
	5	6.4	24.4
	10	11.2	24.5
	25	26.1	29.8

[a]Means of three replicate analyses are given.

form and cyclohexane, cyclohexane was found to be the best for extraction of piperazine. After the extraction of piperazine into cyclohexane, piperazine was partitioned into the aqueous phase prior to injection. Retention times of piperazine and general solvents are given in Table 1.

The efficiency of the extraction procedure was studied by replicate injections of extracted piperazine on to the column. The results are given in Table 2.

3.1. Effect of temperature

The effect of temperature on elution of piperazine was studied. A column temperature of 50°C was sufficient for piperazine elution. Injector and-detector temperatures of 200 and 225°C were found to be the most suitable for the precise determination of piperazine. An increase in tem-

perature does not have any adverse effect on performance. While analysing pharmaceutical materials such as norfloxacin and ciprofloxacin, the column temperatue was raised to 180°C. This helps to avoid the interference of non-volatile residues and enables reproducible performance of the column. Under optimum conditions the column was programmed at 50°C for 5 min, then increased at 15°C min^{-1} to 180°C and held at that temperature for 10 min.

3.2. Linearity and precision studies

Solutions for the linearity studies were prepared by suitable dilution of the stock. Reproducibility was assessed by performing 10 replicate injections of a solution containing 2 μg of piperazine. The mean, standard and relative standard deviations were 1.974 μg, 0.041 μg and ± 2.1% respectively.

Table 4
Results of analysis[a]

Sample No.	Norfloxacin USP (μg)		Ciprofloxacin USP (μg)		Piperazine citrate (%)	
	I[b]	II[c]	I[b]	II[c]	I[b]	II[c]
1	4.1	3.9	1.8	1.5	96.85	96.9
2	3.7	3.55	1.6	1.42	96.1	96.0
3	3.2	3.21	1.65	1.42	96.3	96.3

[a]Means of three replicate analyses are given; analyses were carried out after extraction by the proposed method.
[b]Proposed method.
[c]USP method after extraction.

3.3. Applications

The proposed method has been successfully applied for the determination of residual piperazine in norfloxacin and ciprofloxacin and their reference standards (Table 3). Piperazine was also estimated by the potentiometric titration method of the USP [2]. The values obtained by the USP procedure were very high, due to interferences. Hence piperazine was extracted as proposed here and analysed. Results of analyses are given in Table 4.

3.3.1. Piperazine in reference materials

The proposed method has been applied for the determination of trace impurities of piperazine in reference materials of norfloxacin and ciprofloxacin. About 1 mg of these substances was dissolved in 100 ml of water, filtered through a 0.45 μm filter, injected on to a pre-programmed column and analysed as described earlier.

4. Conclusion

The capillary gas chromotographic method described above is novel, selective and sensitive to trace levels. The method has been successfully applied for the determination of residual piperazine in norfloxacin and ciprofloxacin and for the assay of piperazine samples. The method is reproducible and free from interferences such as amino compounds and ammonia. The method is superior to non-aqueous titration and gravimetric methods.

Acknowledgement

References

[1] Y.M. Dessouky, Analyst, 99 (1974) 482.
[2] United States Pharmacopoeia, USP 23, NF 18 (Asian edn.), USP Convention Inc., Rockville, MD, 1995, p. 1233.
[3] British Pharmacopoeia, Vol. 2, Pharmaceutical Press, London, 1988.
[4] K. Helrich, Official Methods of Analysis, Association of Official Analytical Chemists, Inc., Va, USA, 1995, p. 533.
[5] M. Masse, Pharm. Acta Helv., 33 (1958) 80.
[6] R.E. Pandratz, J. Pharm Sci., 50 (1961) 175.
[7] P.D. Sirsat, Indian J. Pharm., 37 (1975) 101.
[8] V. Dasgupta, Am. J. Pharm., 33 (1976) 283.
[9] G.R. Rao, G. Kanji Lal, and K.R. Mohan, Analyst, 103 (1978) 993.
[10] S. Hanana and A. Tang, J. Pharm. Sci., 62 (1973) 2027.
[11] A.S Abou-Ouf, A. Taha and M.B. Saidom, J. Pharm. Sci., 62 (1973) 1700.
[12] J.W. Cavett, and J.P. Heotis, J. Assoc. Off. Agric. Chem., 41 (1958) 323.
[13] S.H. Parlmulter, J. Assoc. Off. Agric. Chem., 41 (1958) 506.
[14] M.F. Loucks, and L. Nauer, J. Assoc. Off. Anal. Chem., 50 (1967) 268.
[15] H. Wachsmuth and L.V. Koeckhoven, J. Pharm. Belg., 17 (1962) 220.
[16] T.R. Baggi, J. Assoc. Off. Anal. Chem., 57 (1974) 1144.
[17] R.S. Mulliken and W.B. Persson, Molecular Complexes, Wiley Interscience, New York, 1969.
[18] A. Townshend, Proc. Soc. Anal Chem., 10 (1973) 39; 13 (1976) 64.
[19] U. Muralikrishna, Indian J. Pharm. Sci., 45 (1983) 28.
[20] U. Muralikrishna, and N. Someswar Rao, Analyst, 109 (1984) 1277.

Amperometric flow-injection method for the assay of L-ascorbic acid based on the photochemical reduction of Methylene Blue

Luis E. León*

Departamento de Química, Universidad Simón Bolívar, Apartado 89000, Caracas 1080-A, Venezuela

Abstract

Ascorbic acid (AA) is determined by amperometric detection based on the photochemical reduction of Methylene Blue (MB^+) in 0.1 M phthalate buffer at pH 3.8. In this medium, MB^+ using flow-injection analysis. The carrier stream is 1 mM MB^+ is reduced quasi-reversibly at a glassy carbon electrode at -0.34 V vs. Ag/AgCl, while AA is oxidized irreversibly at about 0.3 V. The reactor is irradiated with a 500 W halogen lamp to facilitate the development of the photochemical reaction. A laboratory-built wall-jet electrode system was used. The Leucomethylene Blue formed in the reaction is detected at $+0.050$ V. At 2.2 ml min^{-1} and using a sample loop of 43 μl, the method allows the determination of AA in the range $5.0-90.0$ μg ml^{-1}, with a relative standard deviation of $1.3-4.8\%$, a detection limit of 1.9 μg ml^{-1} and a sampling frequency of $45-50$ h^{-1}.

Keywords: Amperometry; L-Ascorbic acid; Flow injection; Methylene Blue; Photochemical reduction

1. Introduction

The determination of ascorbic acid (AA) has received great attention in analytical chemistry due to its wide use in soft drinks, human and animal food, and drugs. It is also important clinically to determine its concentration in blood, urine and some tissues [1]. Numerous conventional methods have been described for the determination of AA [2,3]. Several flow-injection (FI) methods with electrochemical detection have also been proposed for its determination [4,8]. Strohl

and Curran [4] used a reticulated glassy carbon electrode to carry out the coulometric and amperometric determination of AA, achieving detection limits of a few nanograms. Almuaibed and Townshend [5] used a miniamperometric detector for individual and simultaneous determination of uric acid and AA. Fogg et al., [6] used a sessile mercury drop electrode for determination of AA and dopamine without deoxygenation. Two amperometric methods using immobilized enzyme (ascorbic acid oxidase) reactors have also been proposed [7,8].

The electrochemical characterization of Methylene Blue (MB +) in aqueous solution has been reported [9–11] and it is known that MB^+ is re-

---
* Corresponding author. Fax: +58 2 9063961; e-mail: lleon@usb.ve

duced to Leucomethylene Blue (LMB) by a reversible two-electron process [12].

In a previous paper [13], AA was determined indirectly by spectrophotometry at 666 nm based on the photobleaching of MB^+ in a FI system. Samples of AA were injected into a buffered MB^+ carrier stream. The peaks recorded were of decreasing absorbance owing to the reduction of MB^+ with AA. Although the method was shown to be very simple and accurate, it only allowed determination of AA in the range 0.18–6.12 μg ml^{-1}. In this paper, luminous light is again used for determination of AA by photobleaching of MB^+ in a FI system. The determination is based on the measurement of the current due to the oxidation of LMB formed during the photobleaching process. The present method allows direct, amperometric determination of AA in the range 5.0–90.0 μg ml^{-1}. This is a more acceptable linear range to work in particularly for the kind of samples being considered.

2. Experimental

2.1. Reagents

All reagents used were of analytical-reagent grade purity. AA and 2,6-dichloroindophenol were purchased from Merck and MB^+ was purchased from Aldrich (basic blue 9, C.l. 52015).
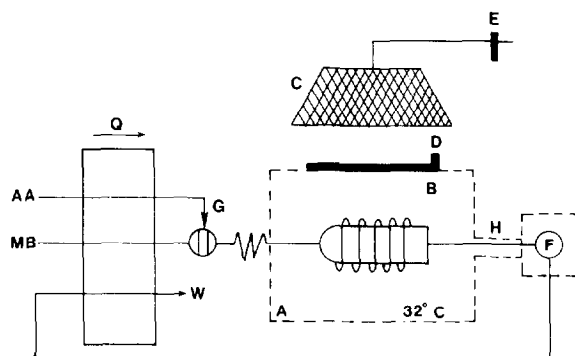
Fig. 1. Schematic diagram of the FI configuration used: A, thermostated water bath; B, reactor; C, tungsten lamp; D, mechanical shutter; E, light intensity regulator; F, detector; G, injection valve; H, light-tight protection; W, waste; Q, peristaltic pump; AA, ascorbic acid; MB, Methylene Blue.
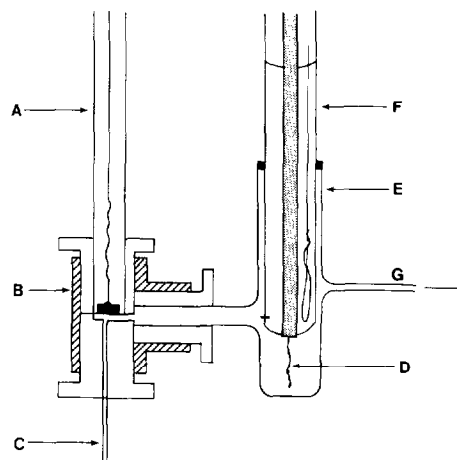

Fig. 2. Laboratory-built electrochemical flow cell: A, working electrode; B, Teflon body; C, Teflon tubing (inlet); D, auxiliary electrode; E, glass holder; F, reference electrode; G, glass tubing (outlet).

2.2. Manifold

Fig. 1 shows the scheme of the FI configuration used. The sample is injected into a MB^+ carrier stream (0.1 M phthalate buffer at pH 3.8) by means of an Omnifit 1106 sample injection valve (G). The reactor B (Teflon, 150 cm long, 0.5 mm i.d.) is irradiated with a 500 W halogen lamp (C) to facilitate the development of the photochemical reaction. The reactor is wrapped around a Pyrex test tube and placed in a thermostatically-controlled water bath (A) 5 cm below the water level and 15 cm from the radiation source. The tubing connecting the reactor and the electrochemical detector (F) was protected from light with black PVC tubing of 1 mm i.d. Flow rates were maintained using a Gilson Minipuls 3 peristaltic pump (Q).

2.3. Apparatus

A three-electrode potentiostat (Tacussel PGS201T) with electrochemistry software (Tacussel ELCOM201) was used for the cyclic voltammetry experiments. Amperometric measurements were made by means of a PAR 173 potentiostat/galvanostat equipped with a Houston Instruments Omnigraphic 2000 X–Y recorder [14]. Fig. 2 shows the laboratory-built electrochemical flow

cell. It was equipped with a glassy carbon electrode (0.071 cm²) (A), a platinum wire auxillary electrode (D), and a 3 M KCl. Ag/AgCl reference electrode (F).

2.4. Procedure

Samples and standards were examined using the flow system shown in Fig. 1. Samples of vitamin C tablets were dissolved in 50 ml 0.1 M HClO₄. The final solution was filtered and diluted to volume with 0.1 M HClO₄. Dilute samples were prepared by appropriate dilution in 0.1 M phthalate buffer. The final pH was 3.8. The resulting solutions were protected from light during all experiments and kept in a refrigerator prior to use.

3. Results and discussion

Fig. 3 illustrates the cyclic voltammogram of 1 mM MB⁺ (curve A) and 1 mM AA (curve B) in 0.1 M potassium hydrogen phthalate at 5 mV s⁻¹. MB⁺ is reduced at a glassy carbon electrode at − 0.34 V giving LMB, which is oxidized at − 0.27 V, while AA is oxidized irreversibly at about + 0.3 V. The LMB formed in the reaction between MB⁺ and AA can be detected at + 0.050 V.

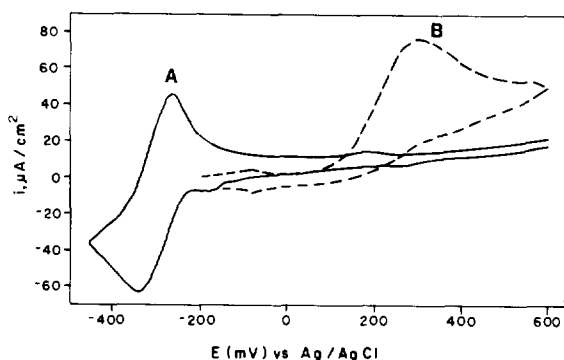Fig. 3. Cyclic voltammograms of 1 mM MB (A) and 1 mM AA (B) in 0.1 M potassium hydrogen phthalate, 0.1 M KCl, 10 μM TX; pH 3.8; scan rate, 5 mVs⁻¹.
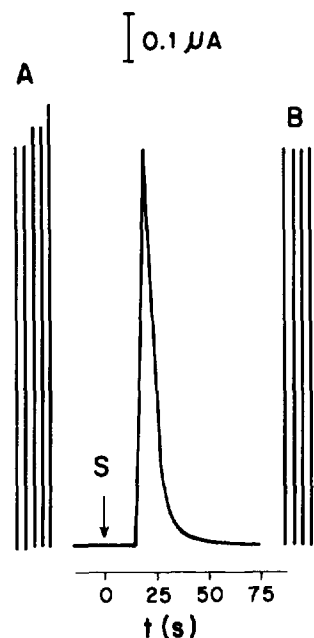

Fig. 4. Amperometric response to 30.0 μg ml⁻¹ of AA. A, without TX; B, after adding TX.

3.1. FI variables

The reactor was irradiated with a 500 W halogen lamp to facilitate the developement of the photochemical reaction. The variation of the FI peak with light intensity was similar to previous results [13]. It increases almost linearly up to 90% of applied power, after which the peak height becomes independent of intensity. All the experiments were done at 90% of maximum power. The signal increases linearly with pumping rate between 1.0 and 3.0 ml min⁻¹. The experiments were done at 2.2 ml min⁻¹ with a loop of 43 μl. These conditions give a residence time of 20 s and a sampling rate of 45–50 h⁻¹. The increase in the signal with the temperature was not significant. However, the heat produced by the lamp increases the water temperature up to 32°C; therefore, this temperature was chosen for further experiments. Fig. 4 shows the response of the detector when a sample of 30.0 μg ml⁻¹ of AA is injected in the FI system. Fig. 4A shows the poor reproducibility of the signal after each injection. This effect can be suppressed if each injection is made after

Table 1
Determination of AA in vitamin C tablets

Sample[a]	AA content[b]	Amperometry[c]	AOAC[c]	F-test	t-test
A	1000	997.0 (0.87)	997.2 (0.29)	9.00	−0.05
B	500	498.3 (0.92)	497.4 (0.31)	8.84	0.42
C	500	498.6 (0.89)	498.8 (0.39)	5.19	−0.09
D	500	497.1 (0.61)	496.2 (0.47)	1.69	0.19
E	500	498.2 (0.96)	498.9 (0.34)	7.91	−0.11

[a] All samples gave on dilution a white suspension of starch, which is used as a "vehicle" in these preparations. They also contain fructose (A–D) and artificial fruit flavor compounds (E). In addition, sample A contains sodium carbonate. A, Redoxon[R] (effervescent), Merck, S.A.; B. Lilly Co. of Venezuela; C. Roche Products, S.A.; D, Roche Products, S.A. (generic); E, Cebión[R] (chewable), Merck, S.A.

[b] In milligrams per tablet

[c] Average of five determinations: milligrams per tablet; (RSD)

reaching the baseline, but this takes at least 2 min. This behavior was suppressed by adding Triton X-100 (TX) to the carrier solution [12]. The result is illustrated in Fig. 4B. It seems that LMB, which is less soluble than MB +, tends to be adsorbed on the FI manifold. Furthermore, LMB tends to form compact and conductive layers with MB$^+$ which is already adsorbed on the electrode. The presence of TX seems to decrease the adsorption phenomena of LMB, thus decreasing the time needed to reach the baseline after each injection. The influence of TX concentration on the signals was not studied.

3.2. Determination of standard AA samples

The standard solutions of AA injected yielded a linear peak current–AA concentration response in the range 5.0–90.0 μg ml^{-1} which obeyed the equation

$$i_p = 0.03194c - 0.1207 \ (r = 0.999)$$

where i_p is the peak current (μA) and c is the concentration of AA (μg ml^{-1}). The precision of the method expressed as the relative standard deviation for $n = 9$ was 4.8% and 1.3% for 5.0 and 90.0 μg ml^{-1} of AA respectively. The detection limit was 1.9 μg ml^{-1} (three times the baseline noise).

A study of potential interferents that may be present in most vitamin C tablets [13] was performed with samples containing 10.0 μg ml^{-1} of AA and 100-fold amounts of the following compounds: glucose, fructose, sacchrose, sodium tartrate, citric acid, sodium benzoate and maleic acid. There is no major interference from these species. Sodium benzoate may give the strongest interference. However, benzoate is oxidized at about +0.150 V. Potential interference by this compound could be reduced by detecting LMB at more negative potentials, e.g. 0.0 or −0.050 V.

Table 1 lists five commercial AA samples. All samples gave a white suspension on dilution. This was found to be particles of starch, which is used as a "vehicle" in these preparations. Other general constituents of these drugs are fructose and citric acid. In addition, sample A contains sodium carbonate and sample E contains articificial flavor compounds. The method was not applied to assay AA in biological fluids; further studies with these kinds of samples may require additional information on matrix composition.

3.3. Analysis of vitamin C tablets

Table 1 lists the results obtained on application of the proposed method to vitamin C tablets. These results are compared with those obtained by the AOAC standard method [15]. Column five shows the results obtained on application of the F test. There are no significant differences between the standard deviations of both methods since the critical value of F for a

two-tailed test at the 5% level of probability is 9.605. Column six shows the respective results obtained on application of the t test. Since the critical value of t ($P = 0.05$) is about 2.31, it may be concluded that both methods give similar results [16].

The conventional, titration method employs simpler, economical materials, and it is probably the method of choice for the analysis of few samples. However, the proposed method can be readily implemented on a very simple configuration and it is the best choice for the analysis of large amounts of samples. There is a further advantage of the FI system: the carrier solution once prepared can stand for a long period of time without losing its titer. In the titration method, solutions of 2,6-dichloroindophenol must be filtered and then kept out of direct sunlight and stored in a refrigerator; furthermore, their titer must be checked regularly [15].

The results indicate that the proposed method can be implemented on a very simple FI configuration with the typical advantages of continuous analysis over the conventional, time-consuming, titration method. The method described is adequate for measurements of AA in purified materials, specifically vitamin C tablets. However, compared to other amperometric determinations, the proposed method effectively lowers the applied potential and the presence of other reducing agents with ascorbic acid may not interfere in the electrode reaction. Also, the inherent selectivity of

the photobleaching process increases the potential of the method.

References

[1] F. Lázaro, A. Ríos, M.D. Luque de Castro and M. Valcárcel, Analyst, 111 (1986) 163.

[2] F. Lázaro, A. Ríos, M.D. Luque de Castro and M. Valcárcel, Analyst, 111 (1986) 167.

[3] S.M. Sultan, A.M. Abdennabi and F.E.O. Suliman, Talanta, 41 (1994) 125.

[4] A.N. Strohl and D.J. Curran, Anal. Chem., 51 (1979) 1045.

[5] A.M. Almuaibed and A. Townshend, Talanta, 39 (1992) 1459.

[6] G. Fogg, A.M. Summan and M.A. Fernandez-Arciniega, Analyst, 110 (1985) 341.

[7] C.W. Bradberry and R.N. Adams, Anal. Chem., 55 (1983) 2439.

[8] G.M. Greenway and P. Ongomo, Analyst, 115 (1990) 1297.

[9] V. Svetlicic, J. Tomaic, V. Zutic and J. Chevalet, J. Electroanal. Chem., 146 (1983) 71.

[10] V. Svetlicic, V. Zutic, J. Clavilier and J. Chevalet, J. Electroanal. Chem., 195 (1985) 307.

[11] V. Zutic, V. Svetlicic, J. Clavilier and J. Chevalet, J. Electroanal. Chem., 183 (1987) 219.

[12] R. Rodriguez-Amaro, E. Muñoz, J.J. Ruiz, J.L. Avila and L. Camacho, J. Electroanal. Chem., 358 (1993) 127.

[13] L.E. León and J. Catapano, Anal. Lett., 26 (1993) 1741.

[14] A. Flores, L.E. León and A. Calvo, Anal. Lett., 17 (1984) 1913.

[15] K. Helrich (Ed.), AOAC Official Methods of Analysis, AOAC, Washington, DC, USA, 1990, p. 1058.

[16] J.C. Miller and J.N. Miller, Statistics for Analytical Chemistry, John Wiley, New York, 1984, pp. 53–59.

Talanta

Use of 4-chloro-7-nitrobenzofurazane as a derivative reagent for the determination of amino acids by cathodic stripping square wave voltammetry in biological fluids

Oscar Nieto*, Pedro Hernández, Lucas Hernández

Department of Analytical Chemistry and Instrumental Analysis, Universidad Autónoma de Madrid, E-28049 Madrid, Spain

Abstract

The rapid and simple reaction of 4-chloro-7-nitrobenzofurazane with amino acids allows the determination of amino acids in urine using cathodic stripping square wave voltammetry. The obtained compounds are adsorbed on a hanging mercury drop electrode for determination by voltammetric methods using phosphate buffer at pH 2.0 as supporting electrolyte. The proposed method allows determination with an error of $\leq 5.68\%$. A limit of detection (3σ) of 3.64 nM (0.766 ng ml^{-1}) and a limit of determination (10σ) of 12.12 nM (2.55 ng ml^{-1}) are obtained for arginine determination. The proposed method has been applied to the determination of amino acids in urine.

Keywords: Amino acid determination; 7-Chloro-4-nitrobenzofurazane; Square wave voltammetry

1. Introduction

The problem of the determination of amino acids for applications in the fields of medicine, biology, etc., can be solved with the use of voltammetric techniques. Several methods for determination of amino acids using electrochemical techniques have been proposed, depending on the concentration level and on the selectivity. For instance, a sample containing amino acids is decomposed by dry ashing and the amount of NH_3, formed as a product of reaction, is determined using a selective electrode for NH_3 [1]. Several proposed methods are based on potentiometric or conductimetric titration, either of the amino acid [2–4] or its basic nitrogen in non-aqueous media [5]. These methods are very common in the determination of arginine in the presence of aztreonam [6,7].

Amino acids are able to form complexes with cupric ions [8] as well as charge-rate complexes with p-benzoquinone [9]. These properties have been applied to the colorimetric determination of amino acids in urine.

The direct determination of amino acids by voltammetric techniques is usually performed with metallic electrodes such as Cu [10] and Au [11]. The amino acids are determined either by amperometric metal–amino acid complexation or by electrocatalytic oxidation to form metallic ox-

* Corresponding author. Tel.: (+32) 14-571-252; fax: (+32) 14-584-273; e-mail: palmeiro@davinci.irmm.jrc.be

ides in the presence of the amino acid. Hui and Huber [12] used a nickel oxide working electrode for the direct determination of the amino acid by flow-injection analysis. A high oxidation state of Ni, maintaining the potential at $+0.49$ V versus SCE, is involved in the reaction mechanism. The disadvantages of these methods are the lack of sensitivity and selectivity.

The determination of amino acids by voltammetric techniques is possible via a derivatization reaction. Nussbaum et al. [13] derivatized the amino acids with naphthalene-2,3-dicarboxyaldehyde to give cyanobenzo (f) isoindole-amino acid. Using cyclic voltammetry, an anodic peak appears due to the oxidation of the indole group. In this way, the problem of the quenching effect, produced in the determination of these compounds by fluorescence, is avoided [14]. Li et al. [15] determined the amino acids by cyclic voltammetry and differential pulse polarography in borax and acetaldehyde buffer. A Schiff's base is formed and the determination is carried out by the reduction of the imido group. Moreira et al. [16] derivatized the amino acids with phenylisothiocyanate to form phenylthioidantoin amino acids. The determination was carried out by differential pulse cathodic stripping voltammetry in the presence of Cu(II) salts.

There are many publications concerning methods of determination of amino acids using biosensors. These biosensors are based either on the response of different kinds of electrodes to the decomposition of amino acids to L-aminoacidoxidase [17–19] or on measurement of the difference of potential generated by two biosensors [20]. In the case of arginine, either electrodes with immobilized arginase and urease using Tris–EDTA buffer as supporting electrolyte [21] or electrodes with immobilized *Streptococcus faecium* bacteria, selective for arginine [22], have been used.

The derivative reagents which are used for determination of amino acids are common to every type of amino acid and, as a result, each derivatized amino acid exhibits the same response at the detector. Therefore, separation methods must be used for the determination of each of the amino acids. The separation technique most often used is high performance liquid chromatography

(HPLC). The direct determination of the amino acid by HPLC with electrochemical detection is carried out with metallic working electrodes such as Cu [10,23,24], Pt [25], or Ni using an alkaline eluent in the case of arginine and other compounds with a guanidine group [26]. In all cases, the detection is performed throughout the electrocatalytic oxidation of the metallic electrode in the presence of the amino acid.

In most of the methods proposed for the determination of amino acids by HPLC, a derivatization reaction is carried out. Typical reagents for the derivatization reaction are 4-fluoro-7-nitrobenzooxadiazole [27–30], o-phthalaldehyde/2-mercaptoethanol [31–34], ninhydrin [34], o-phthalaldehyde-t-butylthiol [35], phenylisothiocyanate [31,36,37] naphthalene-2,3-dicarboxyaldehyde [38, 39], perinaphthindantrione [40] or Sanger's reagent (2,4-dinitrofluorobenzene) [41], using electrochemical detection or other methods. There are few methods for determining amino acids by gas chromatography [42].

Another separation method frequently used for amino acid determinations is capillary electrophoresis with fluorimetric detection [43–47]. Olefirowicz and Ewing [47] added 3,4-dihydroxybenzylamine to the buffer for the indirect determination of amino acids by capillary electrophoresis with electrochemical detection.

In this work the use of 4-chloro-7-nitrobenzofurazane (CNBD) as derivative reagent in the determination of amino acids by voltammetric methods has been proposed. CNBD is a nonfluorescent reagent introduced by Ghosh and Whitehouse [48] in 1968. This reagent is converted into a highly fluorescent compound on reacting with compounds containing thiol and amine groups. Glycine reacts rapidly with this reagent in methanol or in aqueous solutions in the presence of potassium acetate. Cysteine methyl ester and glutathione react in aqueous solutions of phosphate buffer at pH 7.0.

Fager et al. [49] used CNBD as a derivative reagent for the determination of amino acids. The procedure for the derivatization reaction is described in Ref. [50]. The characteristic fluorescence of the NBD–amines is best observed in solvents with low polarity at an excitation wave-

length in the visible range (464 nm). Therefore, the use of quartz cells is not necessary for quantitative determination. The nitro and benzofurazane groups are electroactive and both electrochemical reaction mechanisms are widely known [51,52]. Imai and co-workers [27–30] used this derivative reagent for the determination of amino acids by chromatographic techniques with electrochemical detection [27–29] and others, but they did not study in detail the mechanism of reaction of both electroactive groups.

The study of the electrochemical behaviour as well as the optimization of the experimental parameters for the quantitative determination of NBD–amino acids is discussed in this paper. The aim of this study is to improve the sensitivity of analytical techniques with the use of electrochemical methods. In addition, the electrochemical techniques allow selective determinations and can be applied to complex matrices such as urine.

2. Experimental

2.1. Reagents

A standard solution of arginine (clorohydrate) from Sigma (St. Louis, MO) at a concentration of 1.00×10^{-2} M dissolved in water was used without further purification and preserved at 4°C. A standard solution of CNBD from Fluka at a concentration of 1.00×10^{-2} M dissolved in methanol was used without further purification, preserved at 4°C and protected from light. C_{18} Sep-Pak cartridges (Millipore) were used for the separation of amino acids from the urine. Amberlite IR-120 cationic resin from Carlo Erba was used for the separation of the amino acid mixture. Tridistilled metallic mercury was used. All the reagents used were of analytical grade quality, and the water was deionized using a Milliro-Milli Q system (Waters).

2.2. Apparatus

A PAR Model 384B potentiostat with a PAR Model 303A polarographic stand, equipped with a hanging mercury drop electrode, a Ag/AgCl/KCl (3 M) reference electrode and a platinum counter electrode was used. A PAR Model 305 magnetic stirrer is coupled to the polarographic stand.

A Bioanalytical System BAS-100 potentiostat equipped with a mercury pool working electrode, a saturated calomel reference electrode and a platinum counter electrode was used. The reference electrode and the counter electrode were isolated from the working solution with agar/electrolyte plug bridges. They were used for the coulometric experiments.

A Hewlett-Packard 5890 Series II gas chromatograph, equipped with a 5971A mass spectrometric detector, was used for identification of the reaction products.

2.3. Procedure

The conditions used for the reaction of amino acids with CNBD are the following: to a test tube are added 2 ml of methanol, 100 μl of a saturated solution of sodium acetate in methanol, 20 μl of a solution of 1.00×10^{-2} M CNBD and 5 μl of a solution of 10^{-2} M arginine in water. The mixture is heated in a water bath at 75°C for 20 min.

First, an aliquot of the above-mentioned solution is added to the supporting electrolyte. The pH is adjusted, if necessary, with a suitable amount of NaOH or $HClO_4$. A purge of nitrogen is applied for 5 min at the beginning of the work and for 1 min between each measurement. Each measurement is performed with a new mercury drop. The square wave voltammograms are recorded with the following parameters: square wave frequency, $f = 50$ Hz; scan increment, $\Delta E = 2$ mV; square wave amplitude, $a = 20$ mV. In the study of each parameter, in order to establish the most suitable conditions, the other parameters were kept as the values detailed above.

The studies of the influence of pH and accumulation potential were carried out using the following buffers: 0.04 M phosphate buffer in the pH ranges 2.0–3.0, 6.0–8.0 and 11.0–12.0; 0.04 M acetate buffer in the range pH 4.0–5.0; and 0.04 M borate buffer in the range pH 9.0–10.0. The equilibration time after accumulation was 5 s and the rest of the instrumental conditions were as mentioned above.

The coulometric study was carried out as follows. The reaction of CNBD with arginine is performed, using a ratio of [CNBD]:[Arg] = 8:1, under the experimental conditions for the derivatization reaction described above. The products of the reaction are dissolved in 0.04 M phosphoric acid at pH 2.0 and the NBD–Arg is extracted in ethyl acetate. Once the solvent has been removed with a stream of nitrogen in a water bath at 50°C, 10.0 ml of 0.08 M phosphoric acid at pH 2.0 is added and the final concentration of NBD–Arg was 1.0×10^{-4} M. The applied potential on the working electrode was -300 mV vs. SCE.

The procedure for separation of interferences, in order to achieve easy sample manipulation, is as follows. The original urine sample was collected 24 h before use and stored at 4°C in order to precipitate proteins. Then, the solutions were centrifuged at 2500 rev min^{-1} for 3 min. The supernatants were adjusted at pH 2.0 and passed over a C_{18} Sep-Pak cartridge previously activated by passing the following solvents through the cartridge: ethanol, ethyl acetate, 0.1 M ammonium acetate and water. The hydrophobic compounds are adsorbed on the silica but the amino acids remain in the solution. Afterwards, the amino acids are separated in a cationic resin IR-120 column (30 mm × 5.2 mm i.d.) previously equilibrated with 1.0 M HCl. The elution is carried out with solutions of 0.04 M citrate buffer at different pH values: 2.00, 2.50, 2.65, 2.80, 3.20, 4.00 and 4.90 with a flow rate of 0.5 ml min^{-1}. An aliquot of each collected fraction is added to a mixture of sodium acetate, CNBD and methanol and then the derivatization reaction is carried out as described above. The product is diluted in 0.08 M phosphate buffer at pH 2.0. Then the voltammograms are recorded under the most suitable conditions as determined from the calibration curve.

3. Results and discussion

Fig. 1 shows the square wave voltammogram of CNBD in 0.04 M phosphate buffer at pH 7.0 (voltammogram a). The peak at -380 mV (peak I) is due to the electrochemical reduction of the

nitro group and the peak at -1094 mV (peak III) is due to the electrochemical reduction of the benzofurazane (benzo-2-oxa-1,3-diazole) group. The voltammogram of CNBD which has reacted with arginine (voltammogram b) shows a decrease in current of the peak due to the reduction of the nitro group and the appearance of a new peak at -496 mV (peak II) which corresponds to the compound NBD–Arg.

When an accumulation potential is applied for 60 s there is no variation in the voltammogram of CNBD without amino acid (Fig. 2, voltammogram a). However, when CNBD has reacted with arginine, the current of the peak at -496 mV increases (Fig. 2, voltammogram b) after the application of an accumulation potential for 60 s. This indicates that the NBD–Arg complex is adsorbed on the surface of the mercury electrode and that peak I, due to CNBD, does not interfere with peak II.

In the voltammograms corresponding to both solutions, another peak appears at -650 mV. The origin of this peak has not been identified. The peak current is bigger in the voltammogram of CNBD with Arg than in the voltammogram with solely CNBD. When CNBD and Arg are present
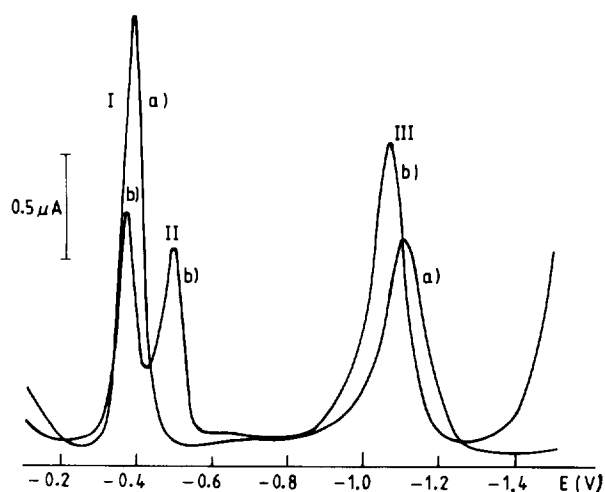

Fig. 1. Square wave voltammograms of CNBD (a) and NBD–Arg in a [CNBD]:[Arg] ratio of 4:1 (b) without applying an accumulation step. Conditions: supporting electrolyte, 0.04 M phosphate buffer at pH 7.0: SW amplitude, 20 mV: SW frequency, 50 Hz: scan increment, 2 mV.
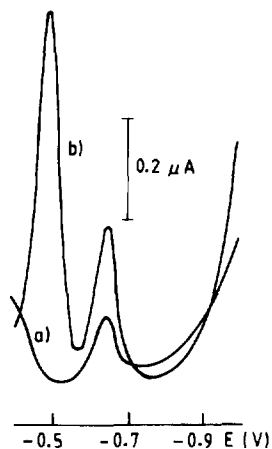
Fig. 2. Square wave voltammograms of CNBD (a) and NBD–Arg in a [CNBD]:[Arg] ratio of 4:1 (b) after the application of an accumulation potential of − 100 mV for 60 s. Other conditions, as in Fig. 1.

in the solution at pH 7.0 and have not reacted, this adsorption peak is already observed. In fact, the efficiency of the reaction is not quantitative under the given experimental conditions ([CNBD]:[Arg] = 4:1). Otherwise, there is no interference with this peak when arginine has reacted quantitatively with CNBD under the most suitable experimental conditions for the determination (a ratio of [CNBD]:[Arg] = 8:1 and the supporting electrolyte at pH 2.0 as detailed below).

It should be noted that no further purification is necessary after the derivatization reaction has been carried out.

A study of the accumulation potential at each value of pH studied was carried out. Fig. 3 shows a three-dimensional plot of the peak current, i_{pII}, vs. pH and vs. accumulation potential, E_{ac}. The optimum peak current is obtained at pH 2.0 ($i_{\mathrm{p}} = 2.90$ μA), when the applied accumulation potential is − 100 mV. Another maximum value is obtained at pH 8.0 when the applied accumulation potential is − 410 mV ($i_{\mathrm{p}} = 2.25$ μA). However, at basic pH the stability of the compound is low and the measurements are not reproducible.

There is a linear relationship between peak potential and pH according to the equation:

$$E_{\mathrm{p}}(\mathrm{mV}) = -154 - 51.4 \ \mathrm{pH}$$

A study of pH was also carried out by cyclic voltammetry, using a scan rate of $v = 100$ mV s^{-1}. The best accumulation potential obtained at each pH by square wave voltammetry was applied previously for 60 s, and the equilibration time was 5 s. The peak potential shifts with pH according to the equation:

$$E_{\mathrm{p}}(\mathrm{mV}) = -162 - 51.5 \ \mathrm{pH}$$

which value of the slope is very similar to the one obtained by square wave voltammetry. The value of the slope in both experiments suggests that the same number of electrons and protons are involved in the electrochemical reaction.

The most suitable supporting electrolyte is 0.08 M phosphate buffer at pH 2.0.

The study of the derivative reagent:amino acid ratio was carried out by preparing several solutions with the same amino acid concentration and varying the proportion of derivative reagent. The results obtained are shown in Fig. 4 where i_{p} vs. ratio of derivative reagent:amino acid, expressed as mol CNBD: mol Arg, is represented. The maximum value of i_{p} is obtained for a proportion of 8:1 and for higher ratios of CNBD to Arg the peak current does not increase. Hence, a CNBD to Arg ratio of 8:1 was used as the optimum for
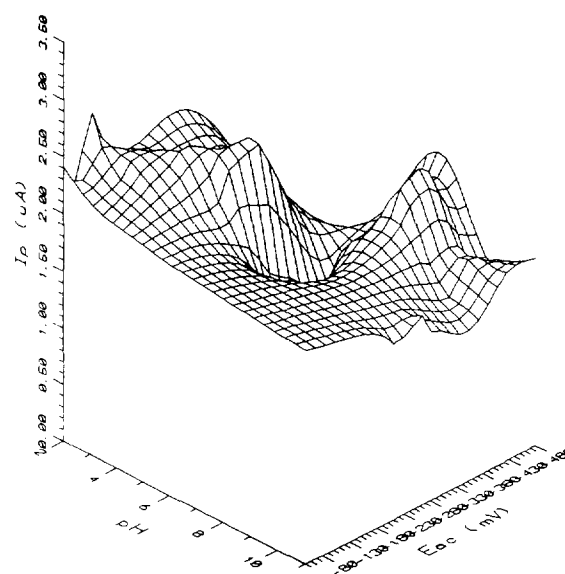

Fig. 3. Variation of i_{p} with pH and accumulation potential. Accumulation time, 60 s. Other conditions, as in Fig. 1.
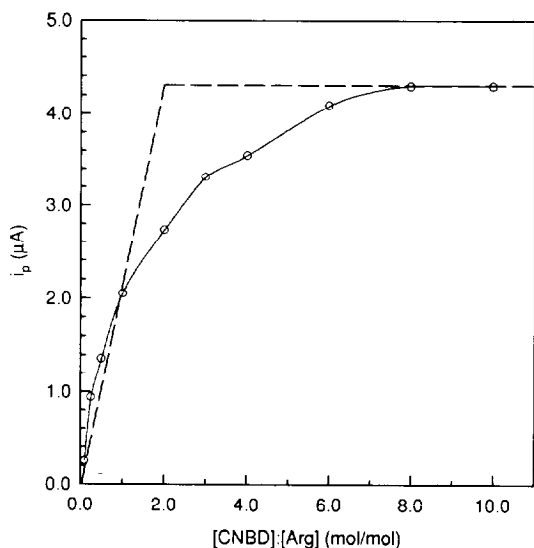
Fig. 4. Variation of i_p with molar ratio of [CNBD]:[Arg]. Supporting electrolyte. 0.04 M phosphate buffer at pH 2.0: accumulation time, 60 s at − 100 mV; other conditions, as in Fig. 1.

the final experiments. By mass spectrometry, the estimated stoichiometry for the compound NBD–Arg is 2:1, assuming that the molecular weight of the molecular ion is 499. From the results plotted in Fig. 4, a formation constant of $K_f = (1.4 + 0.4)10^{11}$ M^{-2} [53] has been evaluated.

The variation of the accumulation time was performed with different concentrations of arginine, maintaining the ratio of Arg to CNBD at 1:4 (mol/mol). The results are shown in Fig. 5. At high NBD–Arg concentrations the adsorption is rapid, decreasing i_p values are observed while the accumulation time increases once a maximum value has been reached. A maximum value for i_p for smaller concentrations of amino acid is observed and once the maximum i_p has been reached, i_p decreases for longer accumulation times. Therefore the same tendency is maintained but in a less pronounced way. From these results. an accumulation time of 120 s for the final studies has been chosen.

With the study of the influence of square wave frequency on the electrochemical response, several kinetic aspects, as well as the optimization of this parameter for the analytical application, can be deduced. The variation of i_p with square wave

frequency has a linear relationship according to the equation:

$$i_p(\mu A) = 0.77 + 4.26 \times 10^{-2} f(Hz) \quad r^2 = 0.995$$

These data show that the process of electrochemical reduction of the nitrobenzene group in NBD–Arg is regulated by a diffusion-controlled adsorption [54–57]. A square wave frequency of 120 Hz was chosen as optimum for the final experiments.

The variation of E_p with the logarithm of the square wave frequency is adjusted to a linear equation:

$$E_p(mV) = -192.8 - 46.9 \log f(Hz) \quad r^2 = 0.996$$

From the value of the slope, which corresponds to the expression $\Delta E_p / \Delta \log f = - RT/Fn\alpha$ [54], the charge rate coefficient can be evaluated. From a coulometric experiment performed using the conditions described in Section 2, the total charge exchanged on the electrode surface was 0.77 C, after blank subtraction, for 10.0 ml of a solution of 1.0×10^{-4} M NBD–Arg. We have taken into account that the electroactive group studied (peak II, Fig. 1) is due to the reduction of nitrobenzene
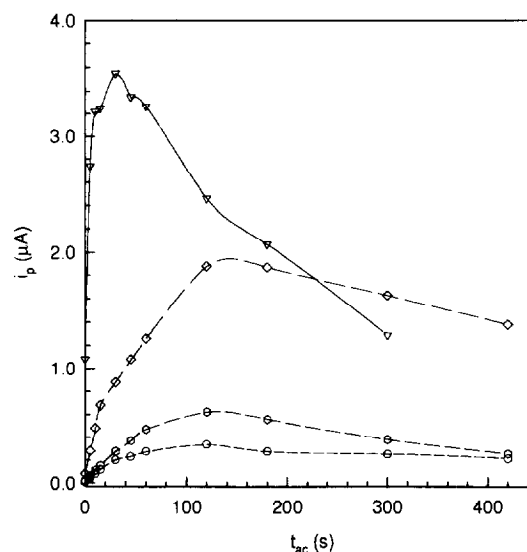

Fig. 5. Variation of i_p with accumulation time. Supporting electrolyte, 0.04 M phosphate buffer at pH 2.0; accumulation potential − 100 mV for 60 s; other conditions as in Fig. 1. Concentrations of NBD–Arg: ($\bigtriangledown$) 2.5×10^{-6} M; ($\Diamond$) 5.0×10^{-7} M; ($\bigcirc$) 2.5×10^{-7} M; ($\bigcirc$) 5.0×10^{-8} M.
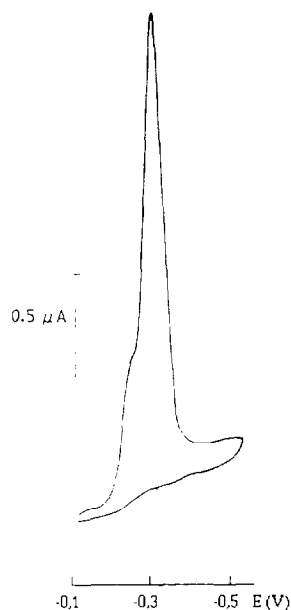
Fig. 6. Cyclic voltammogram of CNBD–Arg with a [CNBD]:[Arg] ratio of 4:1. Conditions: accumulation time. 60 s at 100 MV; supporting electrolyte. 0.04 M phosphate buffer at pH 2.0; scan rate. 100 mV s^{-1}.

group (Ph–NO$_2$ → Ph–NHOH), and that two NBD groups are bound to the molecule of arginine. Then, the number of electrons involved in the electrochemical process, $n = 4$, is obtained. Therefore, a charge rate transfer coefficient of $\alpha = 0.31$ is obtained.

These data can be confirmed by cyclic voltammetry. The voltammograms recorded (as shown in Fig. 6) have the characteristic shape of a totally irreversible electrochemical process and correspond to the electrochemical reduction of a nitrobenzene group. There is a shoulder at a potential more anodic than the peak of NBD–Arg and this is due to the excess of CNBD that has not reacted with arginine. The NBD–Arg complex is strongly adsorbed on the electrode surface and hence the CNBD peak (peak I) is overlapped by the NBD–Arg peak (peak II). The variation of i_p with scan rate is linear, according to the equation:

$$i_p(\mu A) = 1.45 \times 10^{-2} - 1.53 \times 10^{-2}v \quad r^2 = 0.987$$

where v is expressed in millivolts per second. The representation of peak current vs. scan rate indicates that it is a diffusion-controlled adsorption

process. The variation of the logarithm of peak current with peak potential obtained for each applied scan rate is linear, according to the equation:

$$\log(i_p) = -4.48 - 1.73 \times 10^{-2}E_p(mV)$$

$$r^2 = 0.979$$

where i_p is expressed in microamperes. The value of the slope, which corresponds to the expression $\Delta \log i_p/\Delta E_p = -\alpha nF/RT$ [57], allows one to evaluate the charge rate coefficient. A charge rate coefficient of $\alpha = 0.29$ is obtained by cyclic voltammetry, which is very close to the value obtained by square wave voltammetry.

Up to a square wave amplitude (SWa) of 50 mV, the peak current increases with the SWa, and for higher values of SWa the peak current remains constant. Hence. a SWa of 50 mV is applied for the final studies. Up to a SWa of 10 mV, the representation of i_p vs. SWa is adjusted to a straight line according to the equation:

$$i_p(\mu A) = 0.122 + 174.0 \, SWa(V) \quad r^2 = 0.990$$

The electrode surface concentration on the mercury drop can be calculated from the value of the slope of this equation [57]. The electrode area is 0.0278 cm^2 and hence a value of $\Gamma = 4.3 \, 10^{-9}$ mol cm^{-2} is obtained.

There is an increase in i_p with the scan increment range studied, from 1 to 10 mV; there is also an increase in half peak width from 65 to 155 mV with scan increment from 1 to 10 mV respectively as well. Therefore, with an agreement between selectivity and sensitivity in order to get the best optimization of the method, a scan increment of $\Delta E = 4$ mV is applied for the final studies.

Once all the parameters that can affect the determination of arginine with CNBD have been studied, the variation of the peak current with concentration of NBD–arginine is performed. The most suitable conditions obtained from the previous studies of the experimental parameters have been applied.

A series of arginine solutions of different concentrations reacted with the CNBD in a ratio of CNBD:Arg = 8:1 using the method described in Section 2. An aliquot of each reaction product is

added to a solution of 0.08 M phosphate buffer at pH 2.0 as the supporting electrolyte. An accumulation potential of -100 mV was applied for 120 s followed by an equilibration time of 2 s at -100 mV. The voltammograms were recorded with a square wave frequency of 120 Hz, a scan increment of 4 mV and a square wave amplitude of 50 mV.

A linear relationship between the peak current and the concentration of arginine in the concentration range 5.0–85.0 nM (1.05–17.9 ng ml^{-1} or arginine) is obtained according to the equations, adjusted by least-squares:

$$i_p(\mu A) = -0.0852 + 0.0256C$$

where C is the concentration of arginine expressed in nanomolar and

$$i_p(\mu A) = -0.0852 + 0.122C$$

where C is the concentration of arginine expressed in nanograms per milliliter. The correlation coefficient in both cases is $r^2 = 0.999$.

From the corresponding statistical study, the proposed method allows one to perform the determination of arginine with a relative error of $\leqslant$ 2.0% and a relative standard deviation of $\leqslant 5.7\%$. From the standard deviation of the blank, a limit of detection (3σ) of 3.64 nM (0.766 ng ml^{-1}) and a limit of determination (10σ) of 12.12 nM (2.55 ng ml^{-1}) are obtained.

Using the same experimental conditions for other NBD amino acid complexes, similar results are obtained, as expected. In fact, CNBD is not a specific reagent for arginine but it is for general use with primary and secondary amines. Different calibration plots for each amino acid, with small variations in sensitivity, are obtained. These variations depend on the stoichiometry of each NBD– amino acid and on the amount of NBD–amino acid adsorbed on the mercury electrode. Fig. 7 shows the corresponding standard additions of several NBD–amino acids in a 25 nM solution of NBD–Arg. Hence, the proposed method can be used as a general method for the determination of amino acids. It is necessary to apply a separation method for the determination of a single amino acid in urine samples following the method described above.

The quantification of the levels of amino acids in urine, once the separation method has been applied, can be performed using the calibration plot. The recovery in this procedure is $79 \pm 3\%$ for all samples. The recovery was monitored in each part of the separation method using both spectrophotometry with ninhydrin [58] and the proposed voltammetric method and similar results were obtained in all cases. The levels of amino acids found in urine samples taken from ten different individuals were in the range 3.5–4.8 nM.

The following list gives some representative values of individual amino acid concentrations (mM) found in urine. The pH values of the collected fractions are shown in parenthesis.

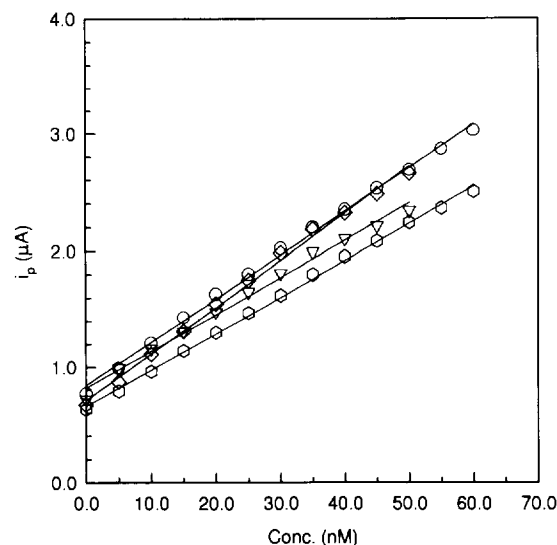| Arginine	0.02–0.04	(4.87)
Aspartic acid	0.05–0.08	(2.62)
Lysine	0.10–0.16	(4.53)
Glycine	1.20–1.60	(3.33)
Aspargine	0.03–0.06	(4.18)
Cysteine	0.08–0.12	(3.48)
Tryptophan	Absence	(3.23)
α-NH$_2$-butyric acid	Absence	(3.07)

Fig. 7. Standard additions of NBD–amino acids in 35.0 nM solutions of NBD–Arg. Conditions: supporting electrolyte, 0.08 M phosphate buffer at pH 2.0; accumulation potential, -100 mV for 120 s; SW amplitude, 50 mV; SW frequency, 120 Hz; scan increment, 4 mV. (○) NBD–Aspartic acid; (◇) NBD–lysine; (▽) NBD—aspargine; (○) NBD–serine.

Similar results have been obtained using spectrophotometry with ninhydrin as well. The relative standard deviations for the amino acid determinations are ≤ 6.2%. These values are in the range of normal levels of amino acids in urine for healthy humans [59].

Acknowledgements

References

[1] A. Nomura, Y. Morita and Y. Kogure, Kagaku Gijutsu Kenkyusho Hokoku, 79 (1984) 551–555.

[2] T. Gunduz, N. Gunduz, E. Kilic, F. Koshegu and S.G. Oztas, Analyst, 113 (1988) 715–719.

[3] T. Kashima, Y. Koide, A. Ito, K. Ohya and M. Kawamura, Kyoritsu Yakka Daigaku Nenpo, 30 (1985) 15–25.

[4] E. Athanasion-Malaki and M.A. Koupparis, Analyst, 112 (1987) 757–761.

[5] A. Pietrogrande, A. Guerrato, B. Bortoletti and G.D. Fini, Analyst, 109 (1984) 1541–1543.

[6] A.A.M. Wahbri, M.A. Abounassif, E.A. Gad-Kariem, M.A. Ibrahim and H.Y. Aboul-Enein, J. Assoc. Off. Anal. Chem., 71 (1988) 31–33.

[7] M.E. Mohamed, M.A. Abounassif, H.A. Al-Khamees, H. Kandil and H.Y. Aboul-Enein, J. Pharm. Belg., 43 (1988) 429–436.

[8] M.G. Wells, Clin. Chim. Acta, 25 (1969) 27–29.

[9] K. Lorentz and B. Flatter, Clin. Chem., 20 (1974) 1553–1555.

[10] P. Luo, F. Zhang and R.P. Baldwin, Anal. Chem., 63 (1991) 1702–1707.

[11] L.E. Welch, W.R. LaCourse, D.A. Mead, Jr., D.C. Johnson and T. Hu, Anal. Chem., 61 (1989) 555–559.

[12] B.S. Hui and C.O. Huber, Anal. Chim. Acta, 134 (1982) 211–218.

[13] M.A. Nussbaum, J.E. Przedwiecki, D.V. Staerk, S.M. Lunte and C.M. Riley, Anal. Chem., 64 (1992) 1259–1263.

[14] S.M. Lunte, T. Mohalbat, O.S. Wong and T. Kuwana, Anal. Biochem., 178 (1989) 202–207.

[15] P. Li, Z. Gao and C. Zhang, Anal. Chim. Acta, 236 (1990) 207–213.

[16] J.C. Moreira, R.D. Miller and A.G. Fogg, Electroanalysis, 3 (1991) 385–391.

[17] T. Nomura and G. Nakagawa, Bunseki Kagaku, 38 (1983) 29–33.

[18] D. Pfeiffer, U. Wollenberger, A. Makower, F. Scheller, L. Risinger and G. Johansson, Electroanalysis, 2 (1990) 517–523.

[19] T. Nomura, Y. Hikichi and G. Nakagawa, Bunseki Kagaku, 38 (1989) 596–600.

[20] S.G. Cha and E.M. Meyerhoff, Electroanalysis, 1 (1989) 205–211.

[21] P.D. Nikolelis and T.P. Hadjiioannou, Anal. Chim. Acta, 147 (1983) 33–39.

[22] C.A. Corcoran and R.K. Kobos, Anal. Lett., 16 (1983) 1291–1302.

[23] A. Ichimura, M. Nakatsuka, K. Ogura and T. Kitagawa, Nippon Kagaku Kaishi, 7 (1986) 987–992.

[24] K. Stulik, V. Pacakova, M. Weingart and M. Podolak, J. Chromatogr., 367 (1986) 311–321.

[25] J.A. Polta and D.C. Johnson, J. Liq. Chromatogr., 6 (1983) 1727–1743.

[26] W. Ding, H. Veening and R.M. Van Effen, J. chromatogr., 526 (1990) 355–366.

[27] H. Kotaniguchi, M. Kawakatsu, T. Toyo'oka and K. Imai, J. Chromatogr., 420 (1987) 141–145.

[28] K. Imai, Y. Watanabe and T. Toyo'oka, Chromatographia, 16 (1982) 214–215.

[29] H. Miyano, T. Toyo'oka and K. Imai, Anal. Chim. Acta, 170 (1985) 81.

[30] Y. Watanabe and K. Imai, J. Chromatogr., 309 (1984) 279.

[31] M.H. Joseph and P. Davies, J. Chromatogr., 277 (1983) 125–136.

[32] J.A. Hoskins, S.E. Holiday and F.F. Davies, J. Chromatogr., 375 (1986) 129–133.

[33] A. Pastoris, A. Sbaffi and L. Faniuolo, Chromatogram, 9 (1988) 3–5.

[34] D.A. Martens and W.T. Frankenberger, Jr., J. Liq. Chromatogr., 15 (1992) 423–439.

[35] D. Pallister, Curr. Sep., 8 (1987) 53–57.

[36] R.A. Sherwood, A.C. Titheradge and D.A. Richards, J. Chromatogr., 528 (1990) 293–303.

[37] T.J. Mahachi, R.M. Carlson and D.P. Poe, J. Chromatogr., 298 (1984) 279–288.

[38] M.D. Oates and J.W. Jorgeson, Anal. Chem., 61 (1989) 432–435.

[39] T. Uedea, R. Mitchell, F. Kitamura, T. Metcalf, T. Kuwana and A. Nakamoto, J. Chromatogr., 593 (1992) 265–274.

[40] W. Buchberger, Fresenius'Z. Anal. Chem., 318 (1984) 611.

[41] M. Chang, L. Chen, X. Ding, C.M. Selavka, I. Krull and K. Bratin, J. Chromatogr. Sci., 25 (1987) 460–467.

[42] K. Schneider, M. Neupert, G. Spiteller, H.V. Henning, D. Mathei and F. Scheler, J. Chromatogr., 345 (1985) 19–31.

[43] M. Albin, R. Weinberger, E. Sapp and S. Moring, Anal. Chem., 63 (1991) 417–422.

[44] N.A. Guzmán, J. Moschera, C.A. Bailey, K. Iqbal and A.W. Malick, J. Chromatogr., 598 (1992) 123–131.

[45] T. Uedea, R. Mitchell, F. Kitamura, T. Metcalf, T. Kuwana and A. Nakamoto, J. Chromatogr., 593 (1992) 265–274.

[46] W.G. Khur and S.E. Yeung, Anal. Chem., 60 (1988) 1832–1384.

[47] T.M. Olefirowicz and A.G. Ewing, J. Chromatogr., 499 (1990) 713–719.

[48] P.B. Ghosh and M.W. Whitehouse, Biochem. J. 108 (1968) 155–156.

[49] R.S. Fager, C.B. Kutina and E.W. Abrahamson, Anal. Biochem., 53 (1973) 290–294.

[50] Technical Bulletin, New Product News, Regis Chemical Co., 1011 North Franklin Street, Chicago, IL 60610, 1971.

[51] H. Lund and M.M. Baizer, Organic Electrochemistry, M. Dekker, New York, 3rd Edn., 1991, pp. 411–413.

[52] El-Jammal, J.C. Virè, O. Nieto Palmeiro and G.J. Patriarche, Electroanalysis, 4 (1992) 5764.

[53] D.R. Crow, Polarography of Metal Complexes, Academic Press, New York, 1969, pp. 56–84.

[54] M. Lovric, S. Komorsky-Lovric and R.W. Murray, Electrochim. Acta, 33 (1988) 739–744.

[55] J. Osteryoung and J.J. O'Dea, in A.J. Bard (Ed.), Electroanalytical Chemistry, Vol. 14, M. Dekker, New York, 1986, pp. 209–308.

[56] J.J. O'Dea, A. Ribes and J.G. Osteryoung, J. Electroanal. Chem., 345 (1993) 287–301.

[57] A.J. Bard and L.R. Faulker, Electrochemical Methods, John Wiley, New York, 1980, p. 224.

[58] C.H.W. Hirs (Ed.), Methods of Enzymology, Section 1 Vol. II, Academic Press, New York, 1967.

[59] L.A. Kaplan and A.J. Pesce, Quimica Clinica, Editorial Médica Panamericana S.A., Buenos Aires 4th edn., pp. 1003–1013.

Spectrophotometric determinations of some phenothiazine drugs

H.D. Revanasiddappa*, P.G. Ramappa

Department of Studies in Chemistry, University of Mysore, Manasagangotri, Mysore-570 006, India

Abstract

A rapid and sensitive spectrophotometric method has been developed for the quantitative determination of some phenothiazine derivatives as the pure substances and in different dosage forms. The method is based on the formation of red coloured products with 1% iodic acid in sulphuric or phosphoric acid medium. The reaction involves oxidation of the phenothiazine nucleus into a semiquinonoid radical. The optimum reaction conditions and other analytical parameters are evaluated. The influence of the substrates commonly employed as excipients with phenothiazine drugs has been studied. Statistical comparison of the results with those of an official method shows excellent agreement and indicates no significant difference in precision.

1. Introduction

Phenothiazine drugs are now widely used as tranquillizers, antihistaminics, antiemetics, analgesics and sedatives. In view of their importance considerable work has been done on their detection and quantification. Methods used for the determination of these drugs include titrimetry [1,2], spectrophotometry [3–8], fluorimetry [9], coulometry [10], gas liquid chromatography [11] and high performance liquid chromatography [12,13]. The official methods normally involve non-aqueous titrimetry or ultraviolet spectrophotometry [14–16]. The widespread use of these drugs has necessitated the development of a rapid, simple and precise method for their quality control.

In the present paper, a study of the spectrophotometric determination of seven phenothiazine drugs is described. The proposed method is based on interaction of phenothiazines with iodic acid in the presence of sulphuric or phosphoric acid medium to yield a red coloured product. The proposed method has been applied to the assay of these drugs in tablets, injection solutions, syrups and elixirs.

Experimental

2.1. Apparatus

Jasco model UVIDEC-610 and Elico model CL-27 spectrophotometers with 1 cm matched quartz cells were used for all absorbance measurements.

---

* Corresponding author. Fax: (+91)821-521-263 or 169;
e-mail: mul@nicfos.ernet.in

Table 1
Recovery of phenothiazines from various excipients by the proposed method

Phenothiazine	Amount present (mg)	Excipient (mg)						Recovery[a] (%)	RSD (%)
		Talc	Dextrose	Starch	Sodium alginate	Stearic acid	Gelatin		
PMH	120	300	300	300	100	100	50	98.8	1.30
IPH	100	200	200	300	150	50	50	97.6	1.40
TPH	80	400	300	250	150	80	75	96.8	1.44
PCPM	60	350	400	300	120	60	80	97.9	1.60
TPPM	120	350	400	250	80	100	60	98.6	1.10
FPH	130	400	300	350	130	110	90	99.5	1.80
TFPH	100	300	350	250	120	60	80	98.2	0.98

[a] Average recovery from six experiments.

2.2. Reagents

All chemicals were of analytical-reagent grade. 1% iodic acid was prepared in distilled water.

2.3. Standard solutions of phenothiazines

Aqueous solutions of promethazine hydrochloride (PMH; Rhone-Poulenc Ltd., India), isothipendyl hydrochloride (IPH; German Remedies Ltd., India), thioproperazine mesylate (TPPM; Rhone-Poulenc), trifluoperazine hydrochloride (TFPH; SKF Ltd., India), fluphenazine dihydrochloride (FPH; Sarabhai Chemicals, India), trifluopromazine hydrochloride (TPH; Sarabhai Chemicals) and prochlorperazine maleate (PCPM; Rhone-Poulenc) were prepared by dissolving the requisite amount of the samples in distilled water. Insoluble PCPM was dissolved by the addition of a few drops of dilute hydrochloric acid. Working solutions were prepared as required by dilution.

2.4. Standard procedure for the determination of phenothiazines

An aliquot of the sample solution containing 12.5–800 μg of PMH, 5–900 μg of IPH, 7.5–800 μg of TPH, 5–1000 μg of TPPM, 10–1000 μg of FPH, 2.5–625 μg of TFPH or 10–1250 μg of PCPM was transferred into a series of 25 ml standard flasks. The acid concentration was adjusted to 3 M for PMH, 1.5 M for IPH and TPPM, and 1 M for FPH and TFPH with orthophosphoric acid and to 1 M for TPH and PCPM with sulphuric acid. 2 ml of 1% iodic acid was added to each flask, the contents were diluted to the mark with distilled water and mixed well. The absorbance was measured at 515 nm for PMH, at 510 nm for IPH and TPPM, at 500 nm for TPH, FPH and TFPH and at 525 nm for PCPM against the corresponding reagent blank. A calibration graph was drawn or regression equation calculated.

2.5. Analysis of synthetic mixtures containing phenothiazines

Synthetic mixtures with the compositions given in Table 1 were prepared. A portion of the mixture containing about 25 mg of PMH, IPH, TPPM, TFPH, FPH, TPH and PCPM was accurately weighed. The phenothiazine was extracted from the mixture, filtered and washed with distilled water. The filtrate and washings were then combined in a 100 ml calibrated flask and the volume was made up with distilled water. An aliquot of this solution was treated as described in Section 2.4, the drug content was evaluated and the results are presented in Table 1.

2.6. Procedure for pharmaceutical formulations

A quantity of the sample (a mixture of 20 powdered tablets) equivalent to 25 mg of the drug

Table 2
Determination of phenothiazine drugs in commercial pharmaceutical preparations

Sample	Phenothiazine present	Label claim (mg)	Official methods [14,15]	Proposed method	Recovery[a] (%)
Tablets					
Phenergan	PMH	25.00	24.52	24.90	99.6
Siquil	TPH	10.00	9.98	9.98	99.8
Stemetil	PCPM	5.00	5.08	4.94	98.8
Majeptil	TPPM	5.00		4.96	99.2
Espazine	TFPH	1.00	–	0.99	99.8
		5.00	5.02	4.95	99.0
Injection solutions					
Phenergan	PMH	25.00	24.60	25.10	100.4
Siquil	TPH	10.00	10.01	10.10	101.0
Stemetil	PCPM	12.50	12.50	12.49	99.9
Anatensol	FPH	25.00	25.52	24.85	99.0
Espazine	TFPH	1.00	1.00	1.00	100.2
Syrup					
Selvigon (15 ml)	IPH	4.50	–	4.46	99.0
Elixir					
Phenergan	PMH	1.00	–	0.98	98.0

[a] Average of six determinations.

was weighed accurately and transferred into a 100 ml standard flask and the volume made up with distilled water and filtered. Appropriate aliquots of the drug solution were taken and the standard procedure was followed for the analysis of drug content.

For the analysis of injection solution, syrup and elixir, the requisite volume was transferred to a 100 ml calibrated flask and diluted to the mark with distilled water. The phenothiazine content in the diluted solution was determined as described above. The results of the analysis are given in Table 2.

3. Results and discussion

Phenothiazines undergo one-electron reversible oxidation in acid medium to form a red intermediate which is believed to be a radical cation [17]. This was confirmed by the ion-exchange technique. The red species was retained by cation-exchange resin but not retained on an anion-exchange resin column.

3.1. Effect of acids

The stability of the coloured species depends on the nature of the acid medium. The red species is unstable in hydrochloric acid medium, and does not give maximum colour intensity in acetic acid medium. The maximum colour development is obtained in the range 1.0–2.0, 3.0–5.0, 0.75–3.0, 0.5–2.5 and 0.5–3.0 M orthophosphoric acid for IPH, PMH, TPPM, FPH and TFPH respectively. The maximum absorbance is obtained immediately and remained constant for a period of 12, 15, 14, 12 and 13 min for IPH, PMH, TPPM, FPH and TFPH respectively. The maximum colour intensity is obtained in the range 0.5–2.0 and 0.5–2.5 M sulphuric acid for TPH and PCPM respectively. The maximum absorbance is obtained instantaneously and is stable for a period of 13 and 15 min for TPH and PCPM respectively. Attempts to increase the stability of the coloured species were not successful. The intensity and stability observed are in the order $H_3PO_4 > H_2SO_4 \gg HCl \ggg CH_3COOH$ for PMH, TPPM, FPH and TFPH; $H_3PO_4 > H_2SO_4 > HCl$

Table 3
Optical characteristics and precision data

Parameter	PMH	IPH	TPH	PCPM	TPPM	FPH	TFPH
Beer's law limit (μg ml^{-1})	0.5–32	0.2–36	0.3–32	0.4–50	0.2–40	0.4–40	0.5–25
Molar absorptivity ($\times 10^3$ l mol^{-1} cm^{-1})	5.13	3.7	3.9	4.7	5.7	6.16	6.6
Sandell's sensitivity (mg cm^{-2} per 0.001 abs. unit)	0.063	0.0875	0.099	0.1273	0.114	0.0835	0.072
Correlation coefficient (r) Regression equation (Y)[a]	0.99	0.995	0.999	0.99	0.995	0.999	0.9999
Slope (b)	0.01295	0.00749	0.0093	0.00693	0.00894	0.00966	0.0105
Intercept (a)	0.05803	0.0099	0.0116	−0.007	−0.0021	0.02358	0.0177
% Relative standard deviation	0.95	1.2	1.1	1.25	1.1	1.3	0.99

[a] $Y = a + bx$, where x is the concentration in μg ml^{-1}.

for IPH; and $H_2SO_4 \approx H_3PO_4 \gg HCl \ggg CH_3$-COOH for TPH and PCPM. The colour is not obtained in acetic acid medium for IPH. Hence, 1.5 M and 1.0 M H_3PO_4 for IPH, TPPM and FPH, TFPH and PMH respectively, 1.0 M H_2SO_4 concentrations for TPH and PCPM were maintained in subsequent studies.

3.2. Effect of iodic acid concentration

The effect of the concentration of iodic acid was studied by measuring the absorbances at the specified wavelengths in the standard procedures for solutions containing a fixed concentration of phenothiazine and varying amounts of iodic acid. The constant absorbance readings were obtained in the range 1.0–5.0, 0.5–5.0, 1.0–7.0, 1.5–7.0, 1.0–5.0, 1.0–7.0 and 1.5–8.0 ml of 1% iodic acid solution for PMH, IPH, TPH, PCPM, TPPM, FPH and TFPH respectively. A volume of 2 ml of 1% iodic acid in a total volume of 25 ml was used in all subsequent work.

The maximum colour intensity remained constant in the temperature range 3–35°C. The order of addition of reagents had no effect. Beer's law range, molar absorptivity, slope, intercept and correlation coefficients obtained by linear least-squares treatment of the results are presented in Table 3.

3.3. Effect of diverse ions

The extent of interference by common anions and substances was determined by measuring the absorbance of a solution containing 20 ppm of phenothiazines and various amounts of diverse ions. An error of ± 2.5% in the absorbance readings was considered tolerable. The substances tested and the tolerance limits found are presented in Table 4. The proposed method is free from interferences by various ions and concomitant substances.

To test the accuracy of the method, recovery experiments were performed on synthetic mixtures prepared in the laboratory. The usual tablet diluents and excipients were found not to interfere with the analysis by the proposed method (Table 1).

The proposed method was successfully applied to the analysis of phenothiazine drugs in various pharmaceutical preparations. The contents of the phenothiazine drug were calculated using the formula

$$\text{mg phenothiazines} = \frac{A_t \times D \times C}{A_s \times 1000}$$

where A_t and A_s are the absorbances of the test and standard solutions respectively, D is the dilution factor and C is the concentration of phenothiazines in μg ml^{-1}. The samples were also determined by the regression equation method. The results of the assay of the tablets, injection

Table 4
Effect of interfering ions and substances on the determination of 20 ppm of phenothiazines

Ions added	Tolerance limit[a] (ppm)						
	PMH	IPH	TPH	PCPM	TPPM	FPH	TFPH
Fluoride	880	440	450		620	920	1320
Nitrate	10	6	–		8	5	50
Chloride	88	18	50	1760	44	18	176
Bromide	20	.	.	67	65	8	60
Sulphate	.	1100	365	3600	3260	–	3610
Iodide	2	5	6	10	4	2	18
Oxalate	45	1238	50	260	990	14	248
Citrate	1300	1280	300	2500	2560	640	320
Phosphate	1600	800	400	2000	1600	1920	720
Acetate	1440	576	750	2160	864	720	720
Carbonate	1360	204	680	1350		1300	–
Tartrate	400	200	700	800	60	600	80
Sulphite	40	20	120	65		80	13
Dextrose	9000	10000	8000	7000	10000	4000	8000
Alginate	40	280	320	350	320	20	310
Gum acacia	200	40	180	240	200	80	120
Ascorbic acid	2	20	16	20	40	6	20
Barbitone	2300	1600	2000	2500	2500	800	1800

[a] Amount causing an error of less than 2.5%.

solutions and syrup presented in Table 2 compare favourably with the official methods of the British Pharmacopoeia and the United States Pharmacopoeia [14–16]. The proposed method, which is simple and rapid, offers the advantages of sensitivity and a wide range of determination without the need for extraction or heating. The assay method does not involve any critical reaction conditions or tedious sample preparation. The method is unaffected by slight variations in experimental conditions such as acidity, reagent concentration and temperature. The wide applicability of the new procedure for routine quality control is well established by the assay of the phenothiazines in pharmaceutical preparations.

References

[1] M.I. Walash, M. Rizk, A.M. Abou-Ouf and F. Belal, Analyst, 108 (1983) 626.

[2] N.V. Pathak, I.C. Shukla and S.R. Shukla, Talanta, 29 (1982) 58.

[3] M. Stan, V. Dorneanu and C. Ghimicescu, Talanta, 24 (1977) 140.

[4] A.M. Taha, N.A. El-Rabbat, M.E. El-Komnos and I.H. Refat, Analyst, 108 (1983) 1500.

[5] P.G. Ramappa, H. Sanke Gowda and A.N. Nayak, Michrochem. J., 28 (1983) 586.

[6] P.G. Ramappa, H. Sanke Gowda and A.N. Nayak, Analyst, 105 (1980) 663.

[7] C.S.P. Sastry, A.S.R. Prasad Tipirneni and M.V. Suryanarayana, J. Pharm. Biomed. Anal., 8 (1990) 287.

[8] S.L. Bhongade and A.V. Kasture, Talanta, 40 (1993) 1525.

[9] J.J. Mellinger and C.E. Keeler, Anal. Chem., 36 (1964) 1840.

[10] G. Patriarche, Mikrochim. Acta, 5 (1970) 950.

[11] L. Laiten, I. Bello and P. Gaspar, J. Chromatogr., 156 (1978) 327.

[12] L.F.S. Chagonda and J.S. Millership, Analyst, 113 (1988) 233.

[13] A.C. Mehta, Analyst, 106 (1981) 1119.

[14] British Pharmacopoeia, HMSO, London, 1993; pp. 290, 546, 552, 687. 1980; pp. 558, 657, 811, 830.

[15] United State Pharmacopoeia, XXI edn., Mack Publishing Co., Easton, PA, 1985, pp. 444, 892, 885, 1087.

[16] Pharmacopoeia of India, Ministry of Health and Fam
ily Welfare, Government of India, New Delhi, 1985, pp. 219, 420, 529.

[17] P.C. Dwivedi, K. Gurudath, S.N. Bhat and C.N.R. Rao, Spectrochim. Acta, Part A, 31 (1975) 129.

A conductance sensor for dissolved sulphur dioxide using a series piezoelectric crystal device

Yuanjin Xu, Changyin Lu[1], Kang Chen, Lihua Nie, Shouzhuo Yao*

Department of Chemistry and Chemical Engineering, Hunan University, Changsha 410082, People's Republic of China

Abstract

A new piezoelectric crystal impedance sensor for the determination of sulphur dioxide in aqueous solution is presented. It is realized using a series piezoelectric crystal device which is constructed by connecting an AT-cut piezoelectric crystal to a probe in series. The probe is filled with an internal electrolyte solution that is separated from sample solutions by a gas-permeable membrane. The present sensor exhibits a favourable frequency response to 1×10^{-7}–1×10^{-3} M sulphur dioxide. The detection limit is 1×10^{-8} M. The effects of the sensor preparation are considered. Dynamic range, reproducibility, response time and selectivity of the sensor are also discussed. The proposed sensor has been used successfully for lamp sulphur determinations in petroleum samples.

1. Introduction

By using selective absorbent coatings, piezoelectric crystal sensors have been developed into highly sensitive devices for the detection of traces of atmospheric pollutants [1]. For the detection of sulphur dioxide in air, several coated piezoelectric crystal sensors have been developed [2–4]. However, the coated piezoelectric crystal sensor cannot be used directly in the determination of sulphur dioxide in aqueous solution because it is very sensitive to interference from water vapour.

In order to overcome the water vapour response of the coated piezoelectric crystal sensor, we report a new piezoelectric crystal impedance sensor for dissolved sulphur dioxide. In contrast to the coated piezoelectric crystal sensor based on the mass effect of a piezoelectric crystal, this sensor is based on the high sensitivity to solution conductivity of the series piezoelectric crystal device [5, 6].

The series piezoelectric crystal, which is constructed by connecting an AT-cut piezoelectric crystal and a conductive electrode in series, possesses a high sensitivity to solution conductivity and a good frequency stability [5, 6]. The oscillation frequency, *F*, is expressed as

* Corresponding author.
[1] On leave from: Hengyang Medical College, Hunan 421001, People's Republic of China.

$$F = F_0 \left[1 + \frac{\pi F_0 C_m (2\pi F_0 C_s - YG)}{4\pi^2 F_0 C_s (C_0 + C_s) - 2\pi F_0 C_0 YG + G^2} \right. $$

$$\left. - \pi F_0 C_m R_m Y \right] \tag{1}$$

where F_0, C_m, R_m and C_0 are the resonance frequency, motional capacitance, motional resistance and static capacitance of the piezoelectric crystal respectively. G and C_s are the conductance and capacitance of solution respectively. $Y = \tan(\theta)$, where θ is the oscillator phase angle.

The sensitivity to conductivity, i.e. the slope of the plot of frequency F vs. conductivity χ, can be calculated by differentiating eq. (1) with respect to χ. The theoretical response sensitivity to conductivity with various cell constants is illustrated in Fig. 1 for typical values. It can be seen that the series piezoelectric crystal device still has a highly sensitive response even in solutions of rather high conductivity. Compared with the direct conductivity measurement method [7], the series piezoelectric crystal device can be used in samples which contain large amounts of unreacted foreign electrolytes. Hence, it can be used as a new type of practical sensor, just like the potentiometric pH sensor and fibre optical pH sensor, to develop gas sensors and enzyme sensors using additional membranes.
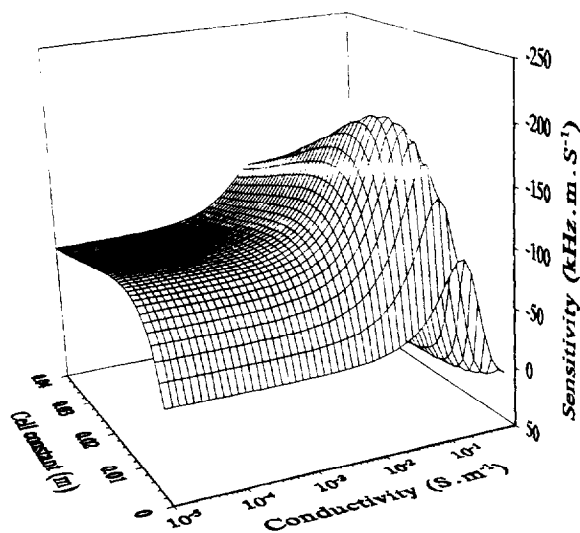
Fig. 1. Theoretical response sensitivity of the series piezoelectric crystal device to conductivity with various cell constants.
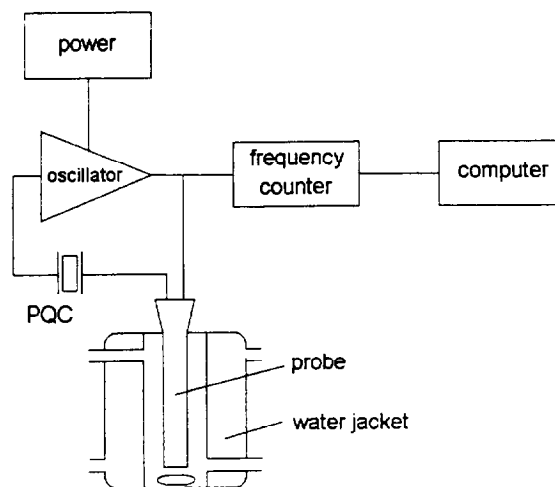

Fig. 2. Schematic diagram of the experimental system.

In this work, a novel impedance sensor for the determination of sulphur dioxide in aqueous solution was developed using a series piezoelectric crystal device. Unlike a potentiometric sensor [8–10], the proposed sensor requires neither a reference electrode nor a fragile internal glass pH electrode and thus it is simple to construct and easy to miniaturize. Compared with the sensor based on the conventional measurement of ionic conductivity with a mixed-bed ion exchanger used inside the sensing probe [11], the proposed sensor is very simple in design. Its high selectivity, utilizing an additional gas-permeable membrane, makes it suitable to be used directly in analytical determination of species in natural media. The use of the proposed sensor for lamp sulphur determination in petroleum samples was investigated. The accuracy of the sensor was also evaluated by comparing the results with those obtained by the conventional lamp sulphur determination method [12].

2. Experimental

2.1. Apparatus and reagents

The experimental apparatus was assembled as shown in Fig. 2. The IC-TTL oscillator was described previously [13]. The frequency output

from the oscillator was monitored by an Iwatsu Model SC7201 universal frequency counter and was recorded by a computer (Hewlett-Packard 300) which was interfaced to the frequency counter. The piezoelectric crystal was a 9 MHz AT-cut 12.5 mm disk with a gold electrode (6 mm in diameter) on both sides. The temperature of the test cell was thermostated at $25 \pm 0.1°C$ with a water jacket and a temperature controller. Teflon membranes with an average pore size of 0.02 μm were purchased commercially from Jiangsu Electroanalytical Instrument Co. An impedance analyzer (Hewlett-Packard 4192A) was used to measure the parameters of the sensor.

The probe is shown schematically in Fig. 3. The dimensions of the probe were about $15 \times 6 \times 0.3$ mm^3. Two finely ground platinum foils were used as electrodes. The thin layer between the electrodes was filled with an internal electrolyte solution (≈ 5 μl) which was separated from the sample solutions by two pieces of gas-permeable membrane mounted firmly on both sides of the probe. The cell constant of the probe was determined by measuring the conductance when the probe was filled with a standard KCl solution whose conductivity is accurately known.

The buffer solution used to acidify samples was made by adding 19 g Na_2SO_4 to about 800 ml of water in a 1 l volumetric flask, adding 5.3 ml of concentrated H_2SO_4 and diluting to the mark. The pH of the buffer was about 1.2. All other reagents used were of analytical grade. Doubly-distilled deionized water was used for all solutions.
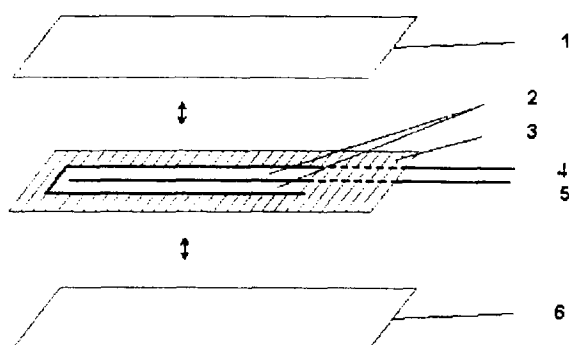

Fig. 3. Schematic diagram of the probe: (1). (6) gas-permeable membranes; (2) thin layer of internal electrolyte solution; (3) insulation substrate; (4,5) platinum electrodes.

2.2. Procedures

Sensor calibration was performed by immersing the probe in 3 ml of buffer solution and making an addition of $NaHSO_3$ standard solution.

Petroleum samples were burnt by the lamp combustion method [12]. The absorption solution contained 10.86 g $HgCl_2$, 5.9 g KCl, 0.06 g Na_2 EDTA, 3.42 g $NaH_2PO_4 \cdot H_2O$, 3.52 g Na_2HPO_4, and 20 ml glycerine per liter. Before acidifying the absorption solution, 0.5 g of sulfamic acid was added to destroy absorbed nitrogen oxides [9]. Then, the sulphur dioxide in the absorption solution was measured with the proposed sensor. For comparison, the sulphur in the petroleum samples was also determined by the conventional lamp combustion–titrimetric method [12].

3. Results and discussion

3.1. Theoretical background

When the probe is in contact with a sample, gaseous sulphur dioxide diffuses across the gas-permeable membrane until its partial pressure is equal on both sides. The sulphur dioxide that diffuses into the internal electrolyte solution will dissolve in water and come to equilibrium with bisulphite [10]:
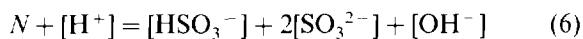
$$SO_2 + H_2O \rightleftharpoons HSO_3^- + 2H^- \qquad (2)$$
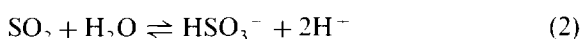
For the general case, the effect of sulphite must also be considered. The pertinent equilibrium equations are:

$$[SO_2] = K_p[H^+][HSO_3^-] \qquad (3)$$

$$[HSO_3^-] = K_1[H^+][SO_3^{2-}] \qquad (4)$$

$$[H^+][OH^-] = K_w \qquad (5)$$
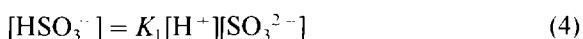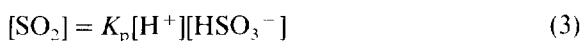
where $\log K_p = 1.9$ and $\log K_1 = 6.8$.

With N as the $NaHSO_3$ concentration of the internal electrolyte solution, the electroneutrality condition leads to the following relationship:

$$N + [H^+] = [HSO_3^-] + 2[SO_3^{2-}] + [OH^-] \qquad (6)$$
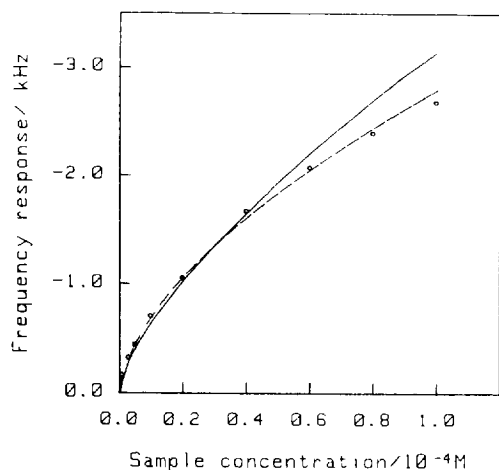
When the sample is acidified in an air-tight test cell:

Fig. 4. Frequency response of the sensor: (——) simulated; (○) experimental data; (– – –) regression results of experimental data. Cell constant, 0.0120 m. Internal electrolyte solutions: 5×10^{-4} M $NaHSO_3 + 1\%$ glycerine.

$$[SO_2] = K_p[H^+]_s[HSO_3^-]_s \qquad (7)$$

$$[SO_2] + [HSO_3^-]_s = C \qquad (8)$$

where C is the $NaHSO_3$ concentration of the sample solution. The subscript "s" denotes the sample solution phase.

From eqs. (3)–(8), the concentrations of $[H^+]$, $[HSO_3^-]$ and $[SO_3^{2-}]$ can be given as a function of C using a computer. The conductance, G, of the internal electrolyte solution can be calculated as

$$G = k\{\lambda_{H^+}[H^+] + \lambda_{OH^-}K_w/[H^+] + \lambda_{Na^+}N$$

$$+ \lambda_{HSO_3^-}[HSO_3^-] + \lambda_{SO_3^{2-}}[SO_3^{2-}]\} \qquad (9)$$

where k is the cell constant of the probe. The limiting molar ionic conductance, λ, used is (10^{-4} m^2 S mol^{-1}): H^+, 350; OH^-, 198; Na^+, 50.1; HSO_3^-, 50.0; SO_3^{2-}, 159.8.

From eqs. (1) and (9), the frequency response of the sensor as a function of sample concentration C can be calculated. The plot of this function and the experimental data are shown in Fig. 4. The correlation between the simulated curve and the experimental results is quite good in low concentration of sample.

3.2. Choice of buffer composition

The influence of the $NaHSO_3$ concentration in the internal electrolyte solution on the sensitivity was investigated. The frequency responses of the sensor filled with various concentrations of $NaHSO_3$ solution are shown in Fig. 5. It is evident that for the sensor filled with lower $NaHSO_3$ concentrations the sensitivity is higher for low sample concentrations. However, the sensor filled with high $NaHSO_3$ concentrations produces curves with a steady, continuous response for high sample concentrations. In the following experiments, the probe was filled with 5×10^{-4} M $NaHSO_3$ solution.

The influence of unreacted foreign electrolytes which exist in the internal electrolyte solution on the sensor sensitivity was also investigated. The sensitivity of the sensor with various concentrations of added foreign electrolyte, KCl, is shown in Fig. 6. When the KCl concentration is less than 1×10^{-3} M, the influence of the unreacted foreign electrolytes on the sensitivity is slight.

The osmotic effect is inherent in the design of the probes where a semi-permeable membrane separates two solutions, the sample and the internal electrolyte film [8]. If the total concentrations of dissolved species on the two sides of the mem-
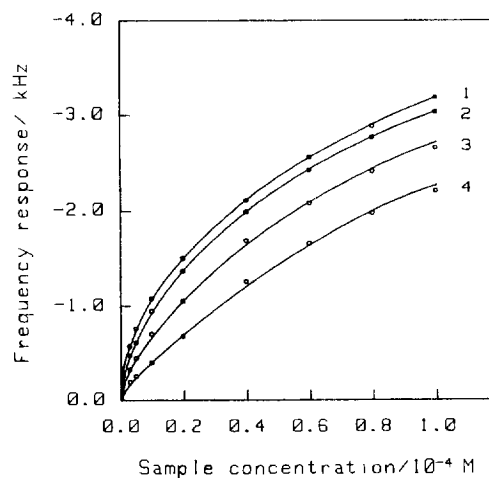

Fig. 5. Effect of $NaHSO_3$ concentration in internal electrolyte solution on sensor sensitivity. Cell constant, 0.0120 m. $NaHSO_3$ concentrations (M): (1), 0; (2), 1×10^{-4}; (3), 5×10^{-4}; (4), 1×10^{-3}.
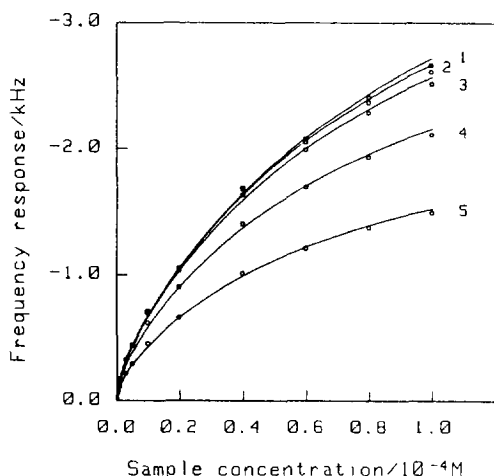
Fig. 6. Effect of foreign electrolyte concentration in internal electrolyte solution on sensor sensitivity. Cell constant, 0.0120 m. KCl concentrations (M): (1), 0; (2), 1×10^{-4}; (3), 5×10^{-4}; (4), 1×10^{-3}; (5), 3×10^{-3}.

brane are different, then an osmotic pressure difference results and water vapour diffuses across the membrane until the water activity is the same on each side. Transfer of water across the membrane results in dilution or concentration of the internal electrolyte solution, which causes the sensor response to drift. In contrast to a potentiometric sulphur dioxide sensor which responds to the concentration of H^+ of the internal solution, this sensor responds to the amount of ionic species exiting the internal solution. The osmotic effect of the sensor can be neglected for short term measurements. However, for long term applications and in storage the osmotic effect must be considered. To reduce the osmotic effect, some non-electrolyte can be added to the internal solution according to the concentrations of dissolved species of the sample solutions. In this work, the sensor is stored in a dilute solution of Na_2SO_3. Therefore, 1% glycerine is used in the internal electrolyte solution to reduce the osmotic effect and to inhibit the chain reaction mechanism by which free sulphur dioxide is oxidized [9].

3.3. Effect of cell constant

The cell constant of the probe, k, is an important parameter for design of a series piezoelectric

crystal impedance sensor. Various values of k result in quite different sensitivities to the solution conductivity (χ), and alter the solution capacitance (C_s) of the probe since $G = k\chi$ and $C_s = k\varepsilon + C_p$, where ε is the dielectric constant of the solution and C_p is the parasitic capacitance between the leading wires of the probe. As k increases, the sensitivity to conductivity increases; meanwhile, the solution capacitance also increases which reduces the sensitivity of the sensor's frequency response to solution conductance. The frequency response sensitivity of the sensor is determined by these two opposing factors. As shown in Fig. 7, the sensitivity of the sensor reaches a maximum around $k = 0.01$ m and decreases significantly when k is 0.0247 m. In this experiment, the cell constant of the probe is 0.0120 m.

3.4. Response properties

The sensor filled with 5×10^{-4} M $NaHSO_3 +$ 1% glycerine solution exhibits a favourable response to 1×10^{-7}–1×10^{-3} M sulphur dioxide, with a detection limit of 1×10^{-8} M. For 13 calibration samples in the range 1×10^{-7}–1×10^{-4} M sulphur dioxide the regression equation is given by
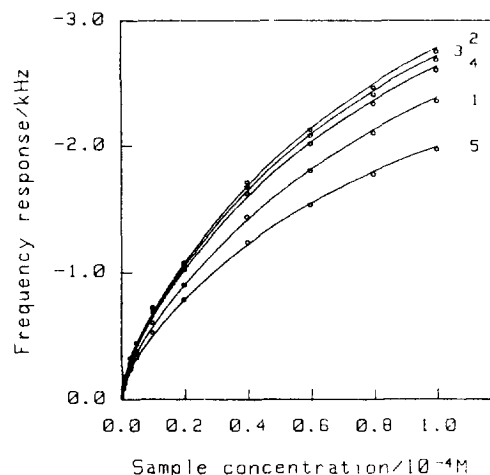

Fig. 7. Effect of the cell constant on sensitivity. Internal electrolyte solutions: 5×10^{-4} M $NaHSO_3 +$ 1% glycerine; cell constants (m): (1), 0.0043; (2), 0.0094; (3), 0.0120; (4), 0.0154; (5), 0.0247.

Table 1
Interferences in the sensor detection of sulphur dioxide

Interferent	Interferent concentration (M)	Sulphur dioxide concentration (M)	
		Added	Found
CH_3COOH	1×10^{-5}	1×10^{-5}	1.02×10^{-5}
	5×10^{-5}	1×10^{-5}	1.08×10^{-5}
HF	1×10^{-5}	1×10^{-5}	1.03×10^{-5}
	5×10^{-5}	1×10^{-5}	1.13×10^{-5}
CO_2	1×10^{-4}	1×10^{-5}	1.03×10^{-5}

$$\Delta F = -720\,175C^{0.603} \tag{10}$$

where C is the concentration of the sample. As shown in Fig. 4, the curve tends to slope downwards at higher concentrations.

The recovery of sulphur dioxide added to 2×10^{-5} M sulphur dioxide samples was $98.6 \pm 4.2\%$ ($n = 5$).

The response time (to 95% of the steady state) of the sensor is ≈ 3.5 min for sulphur dioxide concentration change from 1×10^{-5} to 1×10^{-4} M.

To test the short time reproducibility of the sensor, the frequency response was measured when the sensor was exposed to repeated concentration step changes between 1×10^{-5} and 5×10^{-5} M for sulphur dioxide samples. For five concentration step changes, the standard deviations in frequency were 5.6 Hz and 8.3 Hz for 1×10^{-5} and 5×10^{-5} M sulphur dioxide, which correspond to standard deviations of sulphur dioxide concentration of 0.8% and 1.2% respectively.

The sensor was used for 4 weeks without replacing the internal electrolyte solution. There is no significant loss in sensitivity with the probe being kept in a dilute Na_2SO_3 solution when not in use.

3.5. Interferences

The samples were prepared in strongly acidic solutions and so interference from ammonium and volatile amines can be ignored. Several potential interferences were tested and the results are listed in Table 1. The probe used was filled with 5×10^{-4} M $NaHSO_3 + 1\%$ glycerine as internal electrolyte solution. The interference from dissolved carbon dioxide is negligible.

3.6. Sample analysis

The proposed sensor has been used to determine sulphur in petroleum samples. For comparison, the samples were also analyzed by the lamp combustion–titrimetric method [12]. The results are shown in Table 2. It can be seen that the results obtained from the proposed sensor agree well with those obtained by the titrimetric method.

3.7. Comparison with potentiometric sulphur dioxide sensor

As summarized in Table 3, the proposed sensor has advantages over conventional sulphur dioxide sensors in terms of high sensitivity and rapid response. In addition, the proposed sensor is simple to construct and easy to miniaturize as it requires neither the reference electrode and fragile glass pH electrode which are used in the potentiometric sulphur dioxide sensor nor the mixed-bed ion exchanger which is used in the conventional conductivity sensor. Compared with the coated piezoelectric crystal gas sensor, the proposed sensor can be applied to aqueous samples directly. The advantages of this sensor should make it an attractive alternative to the sensors currently in use.

Table 2
Determination of sulphur in petroleum samples

Sample	Sulphur (wt.%)[a]	
	Proposed sensor	Titrimetric method
1	0.038 ± 0.0019	0.039 ± 0.0015
2	0.059 ± 0.0021	0.062 ± 0.0023
3	0.033 ± 0.0020	0.032 ± 0.0017

[a] Mean $\pm$ standard deviation ($n = 3$).

Table 3
Comparison with potentiometric sulphur dioxide sensor

Sensor	Response range (M)	Response time[a] (s)	Reference electrode	Ref.
Proposed sensor	$1 \times 10^{-7} - 1 \times 10^{-3}$	210	NO	This work
Potentiometric sensor	$5 \times 10^{-6} - 1 \times 10^{-2}$	335 425	Ag/AgCl	8

[a] Sulphur dioxide concentration changes from 1×10^{-5} to 1×10^{-4} M.

Acknowledgment

References

[1] G.G. Guilbault, Ion-Sel. Electr. Rev., 2 (1980) 3.
[2] J. Hlavay and G.G. Guilbault, Anal. Chem., 49 (1977) 1890.
[3] J.J. McCallum, Analyst, 114 (1989) 1173.
[4] R. Pribil and E. Bilkova, Talanta, 39 (1992) 361.
[5] T. Nomura, K. Takada and T. Mitsui, Bunseki Kagaku, 41 (1992) 309.
[6] D.Z. Shen, Y.J. Xu, L.H. Nie and S.Z. Yao, Talanta, 41 (1994) 1993.
[7] C.N. Reilley, in P. Delahay (Ed.), New Instrumental Methods in Electrochemistry, Interscience, New York, 1954, p. 319.
[8] M. Riley, in A.K. Covington (Ed.), Ion-Selective Electrode Methodology, Vol. II, CRC Press, Boca Raton, FL, 1979, Chapter 1.
[9] J.A. Krueger, Anal. Chem., 46 (1974) 1338.
[10] J.W. Ross, J.H. Riseman and J.A. Krueger, Pure Appl. Chem., 36 (1973) 473.
[11] S. Bruckenstein and J.S. Symanski, J. Chem. Soc., Faraday Trans. 1, 82 (1986) 1150.
[12] National Standards of China, Petroleum Products Determination Method, Standard Press of China, Beijing, 1990, GB 380-77.
[13] S.Z. Yao and Z.H. Mo, Anal. Chim. Acta, 193 (1987) 97.

Extraction of ternary complexes of thorium(IV) with 3-phenyl-4-benzoyl-5-isoxazolone and neutral donors from nitric acid medium

P. Thakur[1], R. Veeraraghavan, P.K. Mohapatra, V.K. Manchanda*, K.C. Dash[1]

Radiochemistry Division, Bhabha Atomic Research Centre, Trombay, Bombay 400085, India

Abstract

The extraction behaviour of thorium(IV) from aqueous nitric acid employing 3-phenyl-4-benzoyl-5-isoxazolone (HPBI) in the presence of tri-n-octyl phosphine oxide (TOPO) as well as tri-n-butyl phosphate (TBP) in xylene medium was investigated. The extraction constant ($\log k_{ex}$) for the binary organic phase species Th(PBI)$_4$ was determined to be 8.26 which is by far the largest amongst the corresponding values known for other β-diketones. The overall extraction constant ($\log K$) for the ternary species Th(PBI)$_4$·TBP and Th(PBI)$_4$·2TOPO were estimated to be 14.96 and 20.96 respectively. An inverse correlation of the adduct formation constant ($\log K_s$) with the pK_a of the β-diketones, 2-thenoyltrifluoroacetone, 1-phenyl-3-methyl-4-benzoyl-5-pyrazolone and HPBI, was observed. The steric as well as the electronic effects of adduct formation have been discussed. Analytical application of HPBI for the separation of ^{234}Th radiotracer from natural uranium (99.3% ^{238}U) has been suggested.

Keywords: Extraction; HPBI; Thorium(IV)

1. Introduction

The extraction behaviour of metal ions using β-diketones has been studied extensively [1]. This class of ligands is fascinating because of their unique property of extracting metal ions over a wide range of acidities with the proper choice of substituents. Employing dioxouranium(VI) as a typical metal ion, it has been shown by Batzar et

al. [2] that the lower the pK_a value of the β-diketone, the higher is the two-phase equilibrium constant of the binary extraction system as well as that of the ternary (synergistic) extraction system. Actinide ions, due to their large coordination number, invariably form coordinatively unsaturated β-diketonates which partition as hydrates towards the organic phase. The substitution of the inner-sphere water molecules by a neutral donor leads to higher distribution ratio values due to the enhanced organophilicity of the ternary complex.

In view of its modest pK_a value, favourable partition coefficient towards the organic phase

---

* Corresponding author. Fax: (+91) 22-556-0750/0534.
[1] Present address: Department of Chemistry, Utkal University, Vani-Vihar, Bhubaneshwar 751004, India.

and easy commercial availability, 2-thenoyltri-fluoroacetone (HTTA; Fig. 1, **I**) is the most extensively used β-diketone for analytical applications. However, it has a few limitations such as slow kinetics, poor loading characteristics, photo-sensitive decomposition, hydrolysis under conditions of high pH (> 7.0) and above all its inability to extract metal ions from strong acidic and complexing media. Pyrazolones and isoxazolones, however, have been found to be particularly effective analytical extractants for actinide ions from strong acidic as well as complexing media [3,4] encountered at different stages of the nuclear fuel cycle. The much lower pK_a values of these ligands arise due to the participation of the heterocyclic ring in electron delocalization, imparting additional resonance stabilization. Some recent reports explain the better extractability of these ligands based on the O–O distance [5].

We have been investigating the extraction behaviour of actinide ions such as UO_2^{2+}, Pu^{4+}, Np^{4+}, Am^{3+} etc. with pyrazolones and isoxazolones [6–10]. It was observed that whereas neutral donors such as tri-n-butyl phosphate (TBP) and tri-n-octyl phosphine oxide (TOPO) significantly enhance the extraction of bivalent uranyl ion and trivalent americium ion by the chelating extractants, such enhancement was marginal for tetravalent plutonium. This was attributed to the relatively small ionic radius of Pu^{4+} which offers large steric hindrance to the coordination of the neutral oxo donor when it is surrounded by four β-diketone moieties. It is envisaged that the larger size of Th^{4+} would help in reducing the steric hindrance offered to the incoming organophilic oxo donor, thereby increasing the extractability of the metal ion significantly. TBP and TOPO have widely differing basicities and are well known extractants employed in the nuclear industry. 3-Phenyl-4-benzoyl-5-isoxazolone (HPBI; Fig. 1, **III**) is known to have a much lower pK_a value than either HTTA or 1-phenyl-3-methyl-4-benzoyl-5-pyrazolone (HPMBP; Fig. 1, **II**). Therefore it was of interest to investigate the extraction behaviour of Th(IV) using HPBI as the chelating extractant and TOPO and TBP as the auxiliary ligands. Xylene was employed as the organic diluent. An attempt has also been made to compare

the extraction constant data obtained in the present work with those for similar systems involving either **I** or **II** reported in the literature.
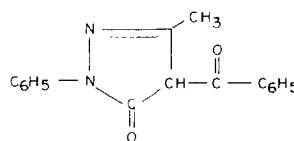
2. Experimental

2.1. Reagents

HPBI was prepared by the method reported in the literature [11] and recrystallized from benzene –hexane medium. The purity was checked by elemental analysis: %C = 72.50 (72.45); %H = 4.00 (4.15); and %N = 5.60 (5.28); m.p. = 146°C. The stock solution (2.00 × 10^{-2} M) was prepared by weighing the desired quantity of HPBI in xylene and was pre-equilibrated for 24 h using 1 M HClO$_4$. A stock solution of Th^{4+} (1.0 × 10^{-2} M) was prepared in 1 M nitric acid using the metal nitrate (Th(NO$_3$)$_4$·6H$_2$O) and was diluted to the desired concentration for the extraction studies.
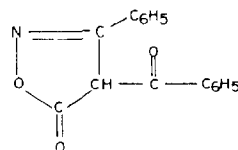
Arsenazo III solution was prepared by dissolving 25 mg of the reagent procured from Merck
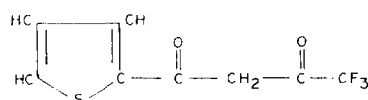
I   2-thenoyltrifluoroacetone (HTTA)

II   1-phenyl-3-methyl-4-benzoyl-5-pyrazolone (HPMBP)

III   3-phenyl-4-benzoyl-5-isoxazolone (HPBI)

Fig. 1. Structures of β-diketones.

Table 1

Conditions employed for the distribution experiments to determine the stoichiometries and extraction constants of binary and ternary systems

Variable parameter	Range of variation (M)	Other parameters
Binary extraction system Th(IV)–HPBI		
[HPBI]	2.25×10^{-3}–7.50×10^{-3}	$[H^+] = 0.5M$
[HNO$_3$]	2.85×10^{-1}–9.50×10^{-1}	$[HPBI] = 5.00 \times 10^{-3}$ M
		Ionic strength = 1.0 M[a]
Ternary extraction system Th(IV)–HPBI–S		
[HPBI][b]	1.00×10^{-3}–1.80×10^{-3}	$[TOPO] = 2.50 \times 10^{-4}$M
	1.20×10^{-3}–3.60×10^{-3}	$[TBP] = 1.00 \times 10^{-3}$ M
[TOPO][b]	2.50×10^{-4}–2.00×10^{-3}	$[HPBI] = 1.00 \times 10^{-3}$M
[TBP][b]	2.50×10^{-4}–1.25×10^{-3}	$[HPBI] = 1.50 \times 10^{-3}$M

[a] Ionic strength adjustment was done by the addition of suitable quantities of NaNO$_3$
[b] $[HNO_3] = 1.00$ M

(Germany) in 25 ml of distilled water. Analar grade TBP from BDH, proanalysi grade TOPO and extra pure grade xylene from E. Merck were used as received.

2.2. Procedure

2.2.1. Distribution studies

The aqueous phase (usually 1 ml) containing Th(IV) at the desired concentration of HNO$_3$ was equilibrated with the required organic phase (1 ml) containing the extractant. The equilibration was usually carried out for 1 h in a thermostated water bath at $25 \pm 0.1°C$. Subsequently the equilibration tubes were centrifuged, phases were separated and aliquots from the aqueous phase (200–500 μl) were assayed by spectrophotometry using a Beckmann DU-7 single beam spectrophotometer.

The equilibrium concentration of Th(IV) in the organic phase was determined by the difference between the initial and final Th concentrations in the aqueous phase. Occasionally the organic phase containing thorium was stripped by 10 M HNO$_3$ and the metal concentration was estimated by the above method. Excellent agreement ($\pm 2\%$) was observed between the Th concentrations determined by these two methods. Details of the experimental conditions employed for the present studies are listed in Table 1. The distribution ratio D was defined as the ratio of the

concentration of Th in the organic phase to that in the aqueous phase. The experiments were carried out in duplicate and the precision was found to be within $\pm 5\%$.

2.2.2. Estimation of Th

Thorium was assayed spectrophotometrically using Arsenazo III which forms a stable chelate compound with the former [12]. Fig. 2 shows the visible spectra of Arsenazo III and its complex with Th(IV). To arrive at the optimum HNO$_3$
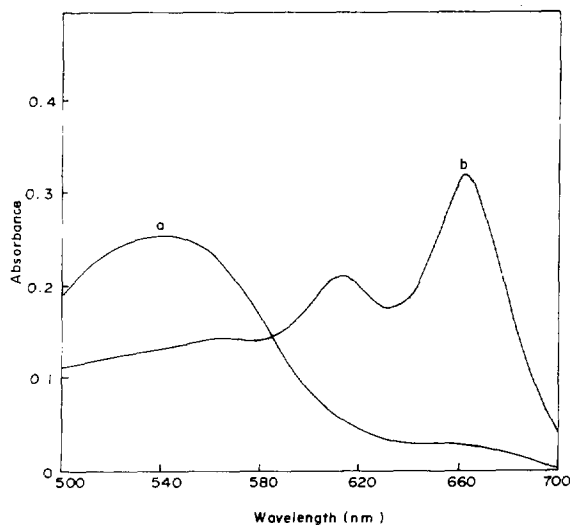

Fig. 2. Visible spectra of (a) 2.8×10^{-5}M Arsenazo III; (b) 3.2×10^{-6}M Th(IV) in 2.8×10^{-5}M Arsenazo III.

concentration for absorbance measurements, experiments were carried out in the acidity range 2.4–7.2 M. It was observed that the sensitivity of the measurement increases with acidity up to 4.8 M, remains constant in the range 4.8–6.5 M and decreases thereafter at higher acidity. All the measurements in the present studies were therfore carried out with 6 M HNO_3. Th(IV)–Arsenazo III complex was developed in 10 ml of solution containing 1 ml of 0.1% Arsenazo III solution and varying concentrations of thorium followed by the addition of 5 ml of 12 M HNO_3 and 1 ml of sulfamic acid (1 M). The absorbance of the solution against a suitable blank was measured at 660 nm. Beer's law was obeyed in the Th^{4+} concentration range 1.1×10^{-6} M–6.5×10^{-6} M. The molar extinction coefficient was determined to be 1.0×10^5 M^{-1} cm^{-1}.

3. Calculations

The extraction of Th(IV) by a β-diketone (HA) is represented by

$$Th^{4+} + 4HA_{(o)} \rightleftharpoons ThA_{4(o)} + 4H^+ \tag{1}$$
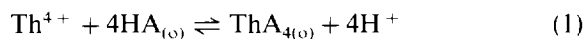
The subscript "o" refers to the species in the organic phase and those species without a subscript are in the aqueous phase. Charges of the species are omitted henceforth for the sake of simplicity. Applying the law of mass action, the extraction equilibrium constant (k_{ex}) can be expressed as

$$k_{ex} = \frac{[ThA_4]_o[H]^4}{[Th][HA]_o^4} \tag{2}$$

Neglecting the complexation by the isoxazolonate anion (A^-) in the aqueous phase [13], the distribution ratio for the binary extraction system Th(IV)–HA from nitric acid medium is given as

$$D_o = \frac{[ThA_4]_o}{[Th]\{1 + \sum \beta_i[NO_3]^i\}} \tag{3}$$

where β_i are the complex formation constants of Th^{4+} with nitrate ion in the aqueous phase ($\log \beta_1 = 0.1$; $\log \beta_2 = 0.8$) [14]. For the calculation of k_{ex}, the corrections for the aqueous com-

plexation of nitrate ion have been incorporated. On rearrangement Eq. (2) becomes:

$$\log k_{ex} = \log D_o + 4\log[H] - 4\log[HA]_o + \log(1 + X) \tag{4}$$

where $X = \sum \beta_i[NO_3]^i$. For a synergistic extraction system employing a neutral donor S the extraction equilibrium may be represented as

$$Th + 4HA_{(o)} + nS_{(o)} \overset{K}{\rightleftharpoons} ThA_4S_{n(o)} + 4H \tag{5}$$
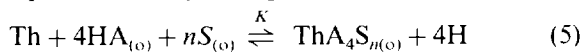
The overall extraction constant (K) is given as

$$K = \frac{[ThA_4S_n]_o[H]^4}{[Th][HA]_o^4[S]_o^n} \tag{6}$$

The distribution ratio for the synergistic extraction system (D) is given by

$$D = \frac{[ThA_4]_o + [ThA_4S]_o + [ThA_4S_2]_o + \cdots + [ThA_4S_n]_o}{[Th]\{1 + X\}} \tag{7}$$

From Eqs. (2), (6) and (7):

$$K = \frac{(D - D_o)[H]^4(1 + X)}{[HA]_o^4[S]_o^n} \tag{8}$$

Taking the logarithm:

$$\log K = \log(D - D_o) - 4\log[HA]_o - n\log[S]_o + 4\log[H] + \log[1 + X] \tag{9}$$

In the case where S = TOPO, K is referred to as K' for $n = 1$ and as K'' for $n = 2$. Determination of K' and K'' was done graphically by following the method reported earlier [7]. The organic phase adduct formation reaction is represented as

$$ThA_{4(o)} + nS_{(o)} \overset{K_S}{\rightleftharpoons} ThA_4S_{n(o)} \tag{10}$$

where K_S, the organic phase adduct formation constant, is given as

$$K_S = \frac{[ThA_4S_n]_o}{[ThA_4]_o[S]_o^n} \tag{11}$$

From Eqs. (2), (6) and (11):

$$K_S = K/k_{ex} \tag{12}$$

or

Table 2
Parameters of the equations for the best fit linear regression lines

Variable	Fixed parameter	Slope	Intercept	r^2
[PBI]	[H$^+$]	3.89 ± 0.08	9.37 ± 0.18	0.999
[H$^+$]	[PBI]	-3.78 ± 0.04	-1.55 ± 0.02	0.999
[TBP]	[PBI], [H$^+$]	0.97 ± 0.02	3.49 ± 0.07	0.999
[TOPO]	[PBI], [H$^+$]	1.29 ± 0.10	6.31 ± 0.41	0.991
[PBI]	[TBP], [H$^+$]	4.05 ± 0.10	10.41 ± 0.27	0.999
[PBI]	[TOPO], [H$^+$]	3.81 ± 0.15	11.74 ± 0.43	0.997

$$\log K_S = \log K - \log k_{ex} \qquad (13)$$

The interaction of TOPO with HNO$_3$ was considered to compute the concentration of the free ligand at equilibrium. It was unnecessary to follow this step in the case of TBP due to its lower basicity. Equilibrium constants for the acid uptake by TOPO are expressed as

$$H + NO_3 + TOPO \overset{K_H}{\rightleftharpoons} HNO_3.TOPO \qquad (14)$$

Total TOPO, [TOPO]$_t$, present in a distribution experiment is distributed as

$$[TOPO]_t = 2 \times [Th(NO_3)_4 \cdot 2TOPO]$$

$$+ [Th(PBI)_4 \cdot TOPO]$$

$$+ 2[Th(PBI)_4 \cdot 2TOPO]$$

$$+ [HNO_3 \cdot TOPO] + [TOPO]_f \qquad (15)$$

where [TOPO]$_f$ is the free concentration of TOPO at equilibrium. In the present experiments where the thorium concentration varies in the range $2.0 \times 10^{-5} - 2.8 \times 10^{-5}$ M and [TOPO]$_t$ varies in the range $2.5 \times 10^{-4} - 2.0 \times 10^{-3}$ M, TOPO bound to Th(IV) was found to be negligible (< 3%). However, TOPO bound with HNO$_3$ as HNO$_3 \cdot$TOPO is a large proportion of [TOPO]$_t$:

$$[TOPO]_f = \frac{[TOPO]_t}{1 + K_H} \qquad (16)$$

where K_H for TOPO is 8.9 [10]. [TOPO]$_f$ was employed throughout for the equilibrium constant data calculations as well as for the determination of the stoichiometry of the extracted species.

4. Results and discussion

4.1. Extraction of Th(IV) by HPBI alone

The variation of $\log D$ with $\log[HPBI]$ is linear with a slope of 3.89 ± 0.08 (Table 2) indicating that four moieties of the β-diketone are associated with the extracted species. The dependence of $\log D$ on log(hydrogen ion activity) is found to be -3.78 ± 0.04 (Table 2), thereby suggesting the validity of Eq. (4). These observations are consistent with the organic phase species Th(PBI)$_4$. Table 3 gives the extraction constant values obtained graphically as well as algebraically after incorporating nitrate complexation correction factors. The difference in the $\log k_{ex}$ values obtained by the two methods is due to the small variations in the observed slopes as compared to the expected values (Table 2), although it is within the statistical variation limit (95% confidence level). It is fascinating to note that the extraction constant for the Th(IV)–HPBI system is much larger than those for the Th(IV)–HPMBP [15] and Th(IV)–HTTA systems [16]. The $\log k_{ex}$ value obtained in the present work is larger than that reported by Jyothi and Rao [13], probably due to the use of diluents of different polarities in the two studies. The $\log k_{ex}$ values increase in the order Th(IV) < Np(IV) < Pu(IV) which follows their ionic potentials [6,8,9].

4.2. Synergistic extraction studies

Synergistic extraction of Th(IV) by HPBI and neutral donors has been carried out from 1 M HNO$_3$. Table 2 indicates the linear nature of the plots of $\log(D - D_o)$ vs. $\log[HPBI]$ at a fixed

Table 3
Extraction constants of Th(IV) in binary and ternary systems

Extraction constant (binary/ternary)	Variable	Graphical method	Algebraic method	Mean
$\log k_{ex}$	HPBI	7.95 ± 0.18	8.22 ± 0.04	
				8.26 ± 0.04
	H$^+$	8.37 ± 0.01	8.29 ± 0.04	
$\log K$ (TBP)	HPBI	15.06 ± 0.27	14.88 ± 0.04	
				14.96 ± 0.04
	TBP	14.93 ± 0.07	15.03 ± 0.02	
$\log K'$ (TOPO)	TOPO	16.82 ± 0.28	..	
$\log K''$ (TOPO)	TOPO	20.96 ± 0.47	–	

concentration of nitric acid as well as neutral oxo donor. Slope values of 3.81 ± 0.15 ([TOPO] = 2.5×10^{-4} M) and 4.05 ± 0.10 ([TBP] = 1.0×10^{-3} M) indicate that four HPBI moieties are attached to the ternary complexed species. The plots of $\log(D - D_o)$ vs. $\log[S]$ at fixed concentrations of HPBI and HNO$_3$ suggest that only one unit (slope = 0.97 ± 0.02) of the neutral donor is present in the ternary extracted complex of TBP. In the case of TOPO, apart from binary Th(PBI)$_4$ species, Th(PBI)$_4$·TOPO and Th(PBI)$_4$·2TOPO appeared to coexist (slope = 1.29 ± 0.10). A graphical method was therefore employed for computing the adduct formation constants [7]. Table 3 summarizes the extraction constant data obtained by graphical as well as algebraical methods after incorporating aqueous nitrate complexation correction.

It is clear from the data summarized in Table 4 that the equilibrium constant values for the formation of the adduct increase with increasing basicity. The $\log K_S$ values clearly show that TOPO is a more effective synergist than TBP. This observation is in line with our earlier report for trivalent, tetravalent and hexavalent metal ions [7,8,10].

Adduct formation constant data (Table 4) could be explained on the basis that the β-diketone with lower pK_a has less tendency to orient its electron cloud towards the ketonic oxygen atoms. This leads to a residual positive charge over the metal ion which is responsible for the greater interaction with the incoming neutral donor. Data in Table 4 suggest that the steric factors do not disturb the trend expected from the electronic effects.

The β-diketonate chelate is hydrated partially in the inner coordination sphere and more extensively in the outer coordination sphere [17]. The stronger M–L bond suggests greater polarizability of the donor electron cloud over the "O" atom, resulting in more extensive outer-sphere hydration (through H-bonding) and hence less partitioning towards the organic phase [18]. In the case of symmetrical complexes a greater number of water molecules can be accommodated in the secondary coordination shell, leading to lower distribution ratio values. In contrast, for sterically hindered complexes the number of water molecules associated in the secondary coordination shell is restricted due to the staggered geometry of the complex thereby rendering greater organophilicity.

It is interesting to note that the extracted species in the present work do not contain any nitrate ion as earlier reported by Irving and Edgington [16] for the HTTA extraction system. This is indicated by the slope analysis of plots of $\log D$ vs. both $\log[PBI]$ and $\log[H^+]$. It may be due to the better availability of the isoxazoloante anion (pK_a = 1.12) for complex formation, even at moderately high nitric acid concentrations, which eventually forms more organophilic ternary extractable species such as Th(PBI)$_4$·S.

4.3. Nature of the metal ion

We have reported earlier the extraction constants of Pu(IV) with HPMBP as well as HPBI [19]. It was observed that in spite of the significantly lower pK_a value of HPBI as compared to

Table 4
Comparison of the extraction constants of the Th(IV)–HPBI and Th(IV)–HTTA systems

β-Diketone	log k_{ex}	log K_S (TBP)	log K_S (TOPO)	Ref.
HPBI	8.26 ± 0.04	6.70 ± 0.04	8.56 ± 0.28[a]	Present work
			4.14 ± 0.55[a]	
HTTA	2.25	4.63	7.50	16

[a] In the case of TOPO, two adduct formation constants for Th(PBI)$_4$·TOPO and Th(PBI)$_4$·2TOPO respectively are reported

HPMBP, the k_{ex} value decreases slightly for the former (Fig. 3). This was attributed to the prominent role of steric factors in the case of HPBI (O–O distance 2.9 Å). Fig. 3 also shows the extraction constant data of Th(IV) with the three β-diketones which follow a linear inverse relation with the pK_a values of the ligands. This is similar to the trend reported earlier for the UO$_2$(VI)–β-diketone system [10]. In spite of the presence of four bulky PBI moieties around the Th(IV) ion, steric factors do not influence the trend expected on the basis of electronic effects. This is in sharp contrast to the behaviour of a similar extraction system involving Pu(IV), which can be explained on the basis of the larger size of Th(IV) (ionic radius = 1.05 Å) compared to Pu(IV) (0.96 Å) [20].
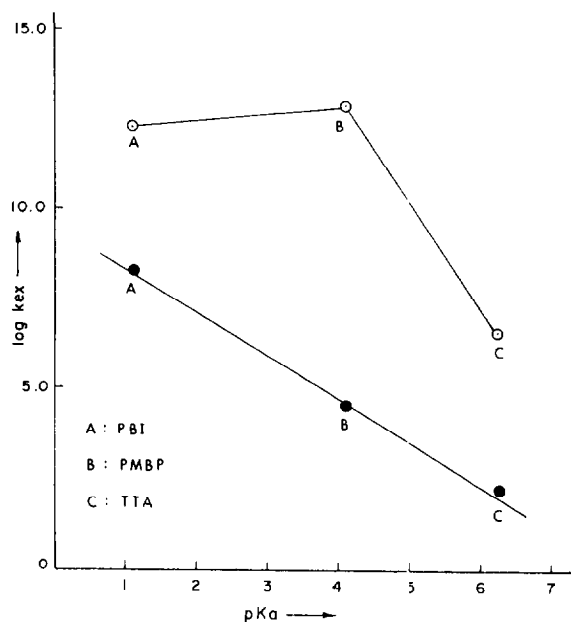

Fig. 3. Dependence of log k_{ex} on pK_a of β-diketones: (○), Pu(IV); (●), Th(IV).

In the Pu(IV) synergistic systems involving TOPO as the oxo donor, species of the type Pu(PBI)$_3$X·TOPO as well as Pu(PBI)$_3$X·2TOPO are co-extracted (where X = NO$_3^-$). It is interesting to note that in the present work with Th(IV), species of the type Th(PBI)$_4$·TOPO and Th(PBI)$_4$·2TOPO were predominant, indicating that there is no steric hindrance to the adduct formation. The adduct formation constant of Th(PBI)$_4$ with TOPO is larger by two orders of magnitude compared to the corresponding value for Pu(PBI)$_4$ [8,21].

4.4. Analytical significance

^{234}Th, the daughter product of naturally occurring ^{238}U, can be obtained from the latter when the two nuclides are in secular equilibrium. It is desirable to develop efficient methods for the chemical separation of trace concentrations of Th from kilogram quantities of U which enable the use of ^{234}Th as a radioactive tracer. The existing methods are based on the preferential extraction or adsorption of U(VI) as UO$_2$Cl$_4^{2-}$ using quarternary amines as liquid anion exchangers and Dowex 1X4 as the anion exchange resin material. In view of the presence of a large excess of U these methods have limitations for the recovery and purification of Th.

It is desirable to develop alternative methods based on the preferential transfer of trace concentrations of Th(IV) towards the organic phase leaving the bulk U in the raffinate. Due to the large difference in the extraction constants of HPBI with Th(IV) (log k_{ex} = 8.3) and UO$_2$(VI) (log k_{ex} = 1.4), this reagent offers promise for the recovery and purification of ^{234}Th from bulk ^{238}U. Preliminary experiments carried out in our

laboratory on depleted U solution using HPBI gave satisfactory results as revealed by α-spectrometry (^{233}U was used as a labelling tracer) and γ-spectrometry (γ peaks of ^{234}Th at 63 and 93 keV). Brief details of the analytical procedure are as follows.

30% Aliquat 336 in chloroform was saturated with uranium by contacting with a 8 M HCl solution of UO_3. The organic phase was stored for about 3 months to allow ^{234}Th ($t_{1/2} = 24.1$ days) activity to grow and attain secular equilibrium with ^{238}U ($t_{1/2} = 4.47 \times 10^9$ years). ^{234}Th thus produced was transferred to the aqueous phase by contacting the uranium-loaded organic phase with 8 M HCl. Th(IV) at the picomolar concentration level is associated with a millimolar concentration of uranium at this stage. The aqueous medium was subsequently changed to 0.5 M HNO_3. 0.01 M HPBI in xylene was used for the preferential extraction of Th(IV) followed by two cycles of scrubbing with 0.5 M HNO_3. A separation factor (D_{Th}/D_U) of approximately 2000 was achieved at every step. Th from the uranium-free organic phase was stripped by 8 M HNO_3 and the aqueous phase was freed from any dissolved ligand by contacting it twice with xylene.

5. Conclusions

Formation of adducts of the stoichiometry Th(PBI)$_4$·S and Th(PBI)$_4$·2S suggests the possibility of coordination numbers of nine and ten for Th^{4+} in these complexes. Adduct formation constants are noticeably larger (by about two log units) for the thorium (IV) ternary complexes as compared to the corresponding values for Pu(IV) complexes, conforming to the reduced role of steric factors in the case of Th^{4+}. Extraction constants of Th–HPBI are larger by about six log units and those of Th(IV) – HPBI–TBP by about eight log units than the corresponding values with HTTA. Consequently, thorium can be recovered from stronger acidic and complexing solutions. HPBI has been found to be a promising extractant

for the separation of ^{234}Th from natural uranium.

References

[1] A.K. De, S.M. Khopkar and R.A. Chalmers, in Solvent Extraction of Metals, Van Nostrand-Reinhold, London, 1970.
[2] K. Batzar, D.E. Goldberg and L.J. Newman, J. Inorg. Nucl. Chem., 29 (1967) 1511.
[3] W. Bacher and C. Keller, J. Inorg. Nucl. Chem., 35 (1973) 2945.
[4] A. Jyothi and G.N. Rao, Bull. Chem. Soc. Jpn., 61 (1988) 4492.
[5] S. Umetani, Y. Kawase, H. Takahara, Q.T.H. Le and M. Matsui, J. Chem. Soc., Chem. Commun., (1993) 78.
[6] V.K. Manchanda and P.K. Mohapatra, in M. Brown (Ed.), Transuranium Elements—A Half Century, ACS Books, Washington, DC, 1992, p. 331.
[7] P.K. Mohapatra and V.K. Manchanda, Radiochim. Acta, 57 (1992) 25.
[8] V.K. Manchanda and P.K. Mohapatra, Radiochim. Acta, 60 (1992) 185.
[9] P.K. Mohapatra and V.K. Manchanda, Radiochim. Acta, 61 (1993) 69.
[10] P.S. Mansingh, R. Veeraraghavan, P.K. Mohapatra, V.K. Manchanda and K.C. Dash, Radiochim. Acta, in press.
[11] F. Korte and K. Storiko, Chem. Ber., 4 (1959) 1961.
[12] S.B. Savvin, Talanta, 8 (1961) 673; 11 (1964) 1.
[13] A. Jyothi and G.N. Rao, Talanta, 37 (1990) 431.
[14] B.G. Oliver and A.R. Davis, J. Inorg. Nucl. Chem., 34 (1972) 2851.
[15] P.K. Mohapatra, V.K. Manchanda and R. Veeraraghavan, in preparation.
[16] H. Irving and D.N. Edgington, J. Inorg. Nucl. Chem., 20 (1961) 314.
[17] G.R. Choppin, in T. Sekine (Ed.), Solvent Extraction 1990. Elsevier, Amsterdam 1992, pp. 61–68.
[18] J. Narbutt, Solv. Extr. Ion Exch., 12 (1994) 1001.
[19] V.K. Manchanda and P.K. Mohapatra, Sep. Sci. Technol., 29 (1994) 1073.
[20] R.D. Shannon, Acta Crystallogr., Sect. A, 32 (1976) 1751.
[21] P.K. Mohapatra and V.K. Manchanda, in preparation.

The determination of lead, nickel and vanadium in Saudi Arabian crude oil by sequential injection analysis/inductively-coupled plasma mass spectrometry

Hassan M. Al-Swaidan

Chemistry Department, College of Science, King Saud University, P.O. Box 2455, Riyadh 11451, Saudi Arabia

Abstract

The coupling of sequential injection with inductively-coupled plasma mass spectrometry as an analytical tool for trace element detection is described. The technique is applied for determining the concentrations of lead, nickel and vanadium at part per billion levels in sample solutions of Saudi arabian crude oils. A microemulsion crude oil sampling procedure and a standard addition method using oil-soluble organo metallic salts of trace elements were used. A reference oil sample (NBS 1634b) was analyzed to obtain the accuracy and precision of the method. Results showed percentage recovery values of 98.2%, 95.7% and 101.4% and standard deviations of 2.9%, 1.5% and 2.0% for lead, nickel and vanadium respectively. The method is sensitive, requires only small sample volumes and is quick.

Keywords: Crude oil; Lead; Nickel; SIA/ICP-MS; Vanadium

1. Introduction

The determination of trace elements in petroleum is important in the oil industry because it provides information to the geologist about crude oil origins, migration and types. The determination of vanadium and nickel have been made for geological surveys. These elements are the source of environmental pollution, catalytic poisoning in the petroleum cracking process and corrosion of equipment, especially in the refinery. Crude oil containing lead as an organometallic compound is a very important source of pollutants especially if it is not replaced during the refining process of unleaded gasoline by methyl-tert-butylether (MTBE) [1].

Inductively-coupled plasma mass spectrometry (ICP-MS) exhibits high sensitivity and accuracy, with high sample throughput. ICP-MS also allows simultaneous multielement determination with rapid and easy operation for determination of trace metals in petroleum samples [2–4].

The direct dilution of petroleum-based materials with an organic solvent is an attractive sample preparation procedure because it is rapid and simple. The problems of carbon build-up on the mass spectrometer interface and excessive deterioration of the metal interface cones, which are associated with the direct analysis of organic solutions by ICP-MS, have been the major difficulties. The direct method of analysis causes instrumental errors and possible loss of volatile elements by

Table 1
FIA lab software method entries for Alitea MIS-1 sequential injection system

i.d.	Time (s)	Duration (s)	Pump 1	Pump 2	Valve 1	Valve 2
1	0.0	5	100		Home	0 on
2	5.0	2	−100		2	0 on
3	7.0	4	100	··	10	0 on
4	11.0	1	−100		2	0 on
5	12.0	5	100		Home	0 on

ICP-MS [5–7]. An acidified microemulsion technique simplifies the sample preparation procedure and the determination of trace metals in petroleum by ICP-MS [8,9].

A simple reduction of the organo matrix is accomplished by minimizing the use of organic solvents in the sample stream. The coupling [10] of flow injection (FI) to ICP-MS is an attractive approach for the analysis of solutions of high salt content. Advantages of the FI method over the conventional solution introduction method have been discussed in previous papers [11–14]. Sequential injection analysis (SIA) is based on a different approach, using a selector valve by which sample zone and reagent zones are sequentially injected into a channel [15], while in conventional FI the sample zone is injected into a flowing carrier stream and auxiliary reagents are merged with it on the way to the detector [16]. The benefits of the SIA technique include minimization of reagent consumption and waste disposal because flow is not continuous during the sequencing and measurement steps, and the handling of corrosive liquids in a closed system. The SIA technique requires only a single pump and a single valve in a single line system, and is capable of accommodating diverse reagents and sample concentrations by reconfiguration of the zone sequencing from a computer keyboard [17,18].

A previously investigated technique used an optimized acidified microemulsion as a sample pretreatment for the determination of trace elements in crude oil by ICP-MS [19]. We couple SIA with ICP-MS (SIA/ICP-MS) to optimize the accuracy and precision and increase the sensitivity of the analysis.

2. Experimental

2.1. Apparatus

A MIS-1 modular injection system (Alitea, USA) configured for SIA with a multiposition selection valve, reactor modules and a peristaltic pump was used as the sample introduction system. Teflon tubings used for the MIS were 30 cm of 0.8 mm i.d. for carrier solution, 15 cm for pump, 160 cm of 0.8 mm i.d. for holding coil, 5 cm of 0.5 mm i.d. connected to port 2 of sample, 10 cm of 0.8 mm id. for auxiliary waste (port 10) and 45 cm of 0.8 mm i.d. connected from port 1 directly to the concentric nebulizer into the ICP-MS system (all tubings were supplied by Upchurch Scientific, Inc.). The MIS is operated by Alitea's FIA lab software and an IBM-compatible PC and the operating instructions in the MIS manual are followed for SIA [20]. Table 1 includes FIA lab software method entries used for Alitea MIS-1 SIA. Flow rates are 60 μl s^{-1}. In step 1, 300 μl of carrier is pumped through the detector. Then 120 μl of sample is aspirated into the holding coil and then to waste, to wash the sampling tube with sample. Finally, 60 μl of sample is aspirated into the holding coil and is then propelled to the detector in step 5.

An Elan inductively-coupled plasma mass spectrometer model 250 with a standard addition program (Sciex) is used with a 15 BCO 12B computer (Matrix Electronic System Ltd.) and a plotter (Houston). A schematic diagram of the MIS-1 coupled to the ICP-MS instrument is given in Fig. 1 and the ICP-MS operating conditions are listed in Table 2. An Edmund Buhler vortex mixer model 25 was used for crude oil sample agitation.
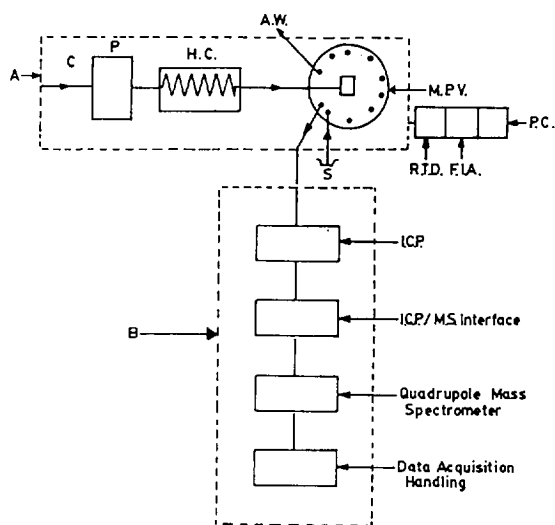
Fig. 1. Schematic diagram of (A) SI system coupled with (B) ICP-MS. C, carrier; P. pump; H.C., holding coil; A.W., auxiliary waste (port 10); S. sample (port 2); M.P.V., multiposition valve; R.T.D., R.T.D. A.D.A.-1100 interface card; F.I.A., Alitea F1B lab software; P.C., IBM-compatible PC.

2.2. Reagents

Chemicals used were of analytical-reagent-grade and include lead and nickel cyclohexane butyrate, bis[1-phenyl butanedionato-(1,3)] oxo vanadium (IV) (Eastman Organic Chemicals, Rochester, NY), indium oxide (Spex Industries, Inc., NJ) and analar nitric acid (sp.gr. 1.42, 69–71%, BDH Chemicals Ltd., Poole, UK). Tetralin (1,2,3,4 tetrahydronaphthalene, Fluka AG, Bucks, Switzerland) as a co-solvent and a nonionic surfactant Triton X-100 (BDH) as emulsifying agent were chosen.

Table 2
Elan ICP-MS instrumental parameters

RF incident power	1.2 kW	Resolution	Low
Plasma gas flow	13 l min^{-1}	Threshold	1
Auxiliary gas flow	1.4 l min^{-1}	Counting precision	0.1
Nebulizer gas pressure	40 psi	Measurement time	0.05 s
Measurement per peak	5	Sample flow	60 μl s^{-1}
Repeats per integration	5		

Table 3
General properties of Saudi Arabian crude oil samples

Test	Method	H	M	L
Gravity, API.				
°F	ASTM-D1289 [a]	28.03	30.4	33.7
C residue (wt.%)	ASTM-D189	6.75	5.87	3.58
S (wt.%)	ASTM-D129	2.79	2.59	1.81
Viscosity at 100°F, SUS [b]	ASTM-D445	118	71	49
Ash content (mg l^{-1})	ASTM-D482	96	55	34

[a] American Society for Testing Material.
[b] Suspended level type.

Deionized distilled water was obtained by a Corning Mega-pure water distillation apparatus model MP3.

Solutions of 40% (v/v) nitric acid were prepared by dilution of concentrated nitric acid. Stock solutions (100 ppm) of nickel, lead and vanadium were prepared by dissolving the weighed organometallic salts in 40% (v/v) nitric acid solution. Multi-element standard solutions of lead (2.5 ppm), nickel (25 ppm) and vanadium (50 ppm) were prepared by dilution from the stock solutions. A stock solution of indium oxide (100 ppm) was prepared by dissolving its weighed oxide in 1% (v/v) nitric acid solution.

2.3. Samples

Saudi Arabian heavy, medium and light crude oil samples supplied by Aramco (Saudi Arabia) were analyzed for lead, nickel and vanadium content. Some general properties of these samples are shown in Table 3. Standard Reference Material NBS1634b (Residual Fuel Oil, National Institute of Standards) was tested to determine the accuracy and precision of the method.

2.4. Procedure

Into three different stoppered glass bottles (200 ml), a 0.50 g aliquot of NBS oil sample was weighed. Portions of 1.5 ml of tetralin as a co-solvent, 0.5 ml of Triton X-100 as emulsifying agent, 5 ml of 40% (v/v) nitric acid solution and 0.5 ml
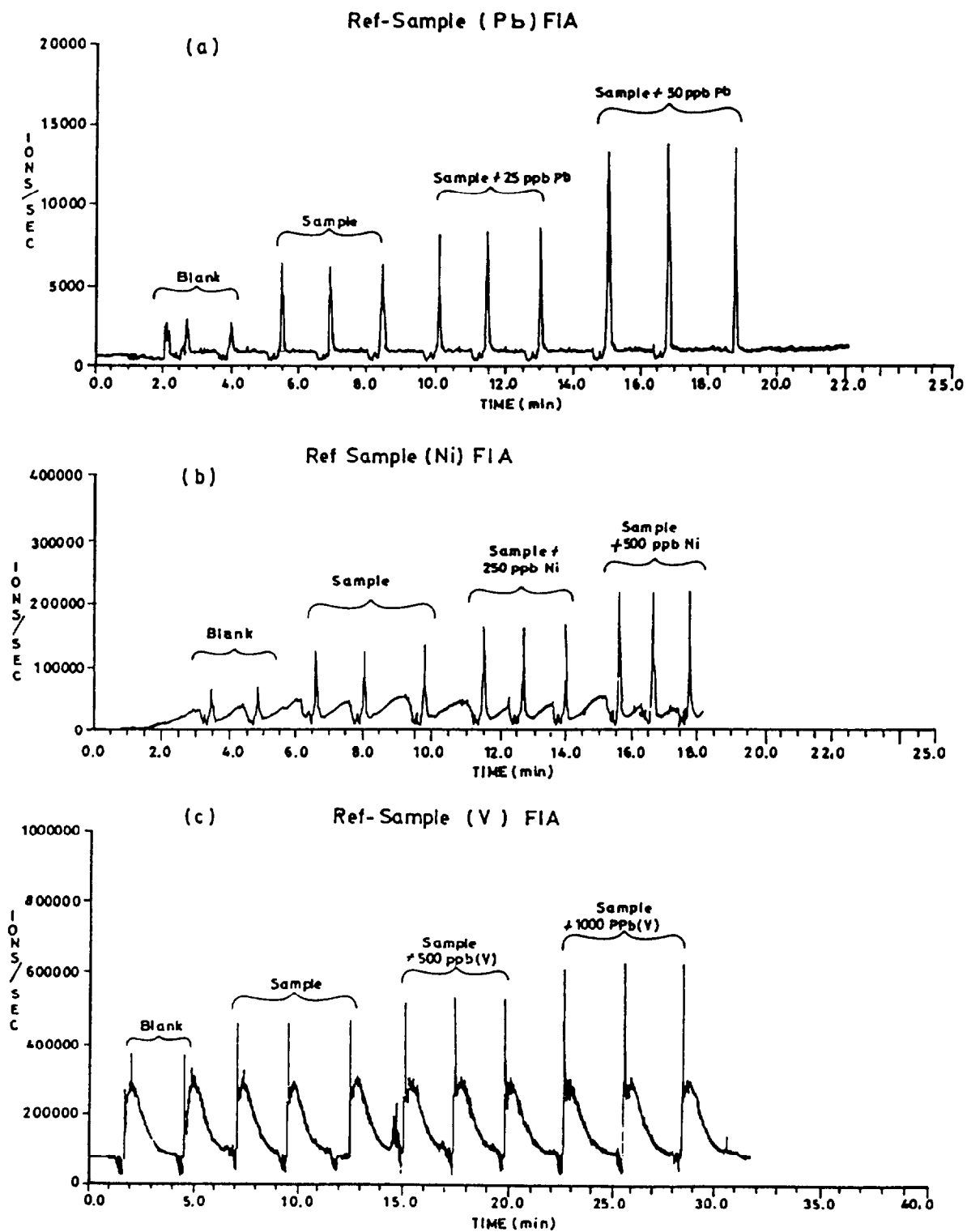
Ref-Sample (Pb) FIA

(a)

20000

I
O
N
S 15000
/
S
E
C

10000

5000

0

Blank

Sample

Sample + 25 ppb Pb

Sample + 50 ppb Pb

0.0   2.0   4.0   6.0   8.0   10.0   12.0   14.0   16.0   18.0   20.0   22.0   25.0
TIME (min)

Ref Sample (Ni) FI A

(b)

400000

I
O
N
S 300000
/
S
E
C

200000

100000

0

Blank

Sample

Sample + 250 ppb Ni

Sample + 500 ppb Ni

0.0   2.0   4.0   6.0   8.0   10.0   12.0   14.0   16.0   18.0   20.0   22.0   25.0
TIME (min)

(c)   **Ref-Sample (V) FIA**

1000000

800000

I
O
N
S 600000
/
S
E
C

400000

200000

0

Blank

Sample

Sample + 500 ppb(V)

Sample + 1000 PPb(V)

0.0   5.0   10.0   15.0   20.0   25.0   30.0   35.0   40.0
TIME (min)

Fig. 2. Typical peaks for (a) lead, (b) nickel and (c) vanadium in microemulsion solution of standard oil sample (NBS 1634b) using the SIA/ICP-MS technique.
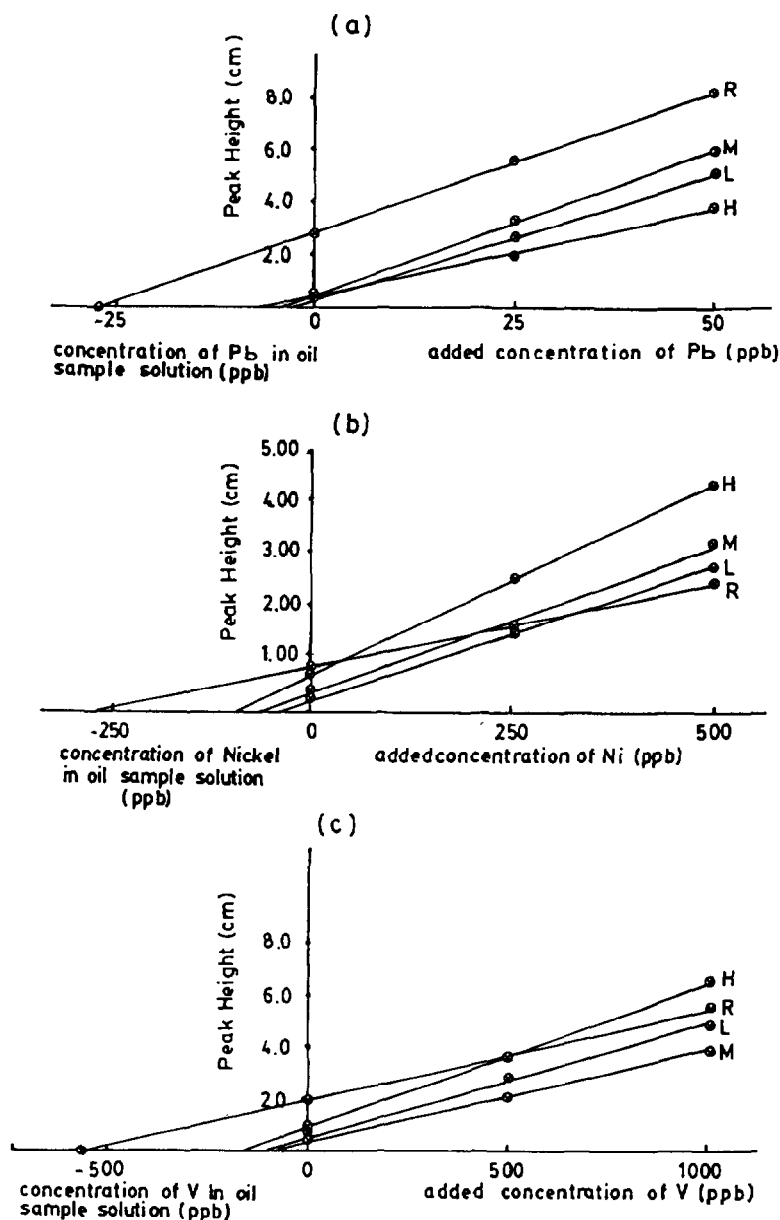
Fig. 3. Standard addition graphs obtained for (a) lead, (b) nickel and (c) vanadium in (acidified) microemulsion solution of oil samples using the SIA/ICP-MS technique (H, M, and L denote heavy, medium and light crude oil samples respectively and R denotes reference oil sample).

of 100 ppm indium solution were then added to each bottle. The multi-element standard solution (containing 2.5 μg g^{-1} Ni and 50 μg g^{-1} V) was used for spiking bottle Nos. 1, 2 and 3 with 0, 0.5 and 1 ml respectively. The bottles were then mechanically agitated with gradual addition of

deionized distilled water until 50 ml of homogeneous solution was obtained. A blank was prepared in a similar manner. These solutions were measured at 60 μl s^{-1} flow rates for Pb, Ni, and V contents using the proposed SIA/ICP-MS technique with the test and maintenance multiple ele-

Table 4
Recovery data for NBS 1634b sample by the SIA/ICP-MS method

Element	Concentration (μg g^{-1}) ± SD as % recovery		
	SIA/ICP-MS	Certified [21,22]	% Recovery
Pb	2.75 ± 0.08	2.80 ± (n.c.) [a]	98.2
Ni	26.8 ± 0.4	28 ± 2	95.7
V	56 ± 1	55 ± 1	101.4

[a] n.c. = not certified.

ments programs (Sciex). Replicates of the sample were analyzed to obtain the accuracy and precision of the method. The procedure was applied similarly for the determination of Pb, Ni and V in the different crude oil samples.

3. Results and discussion

SIA/ICP-MS will reduce the organic matrix by minimizing the use of organic solvents in the sample stream. The previous optimized acidified microemulsion procedure was chosen for crude oil sampling [19]. The sequential injection system easily introduces the sample by connecting the Teflon tube out of the multi-position valve directly to the concentric nebulizer of the ICP-MS instrument, as shown in Fig. 1. Plasma extinguishing problems

due to carbon build-up on the torch walls were solved by using an acidified microemulsion as the sample pretreatment technique.

The peaks of different solutions are plotted for Pb, Ni and V concentrations. Typical peaks of Standard Reference samples (NBS) solution obtained for Pb, Ni and V are shown in Fig. 2. Peak heights in centimeters for the sample only and for the sample with added concentrations of elements are constructed as standard addition graphs. These standard addition graphs of Pb, Ni and V for heavy, medium, light and NBS oil samples appear in Fig. 3. The NBS sample is analyzed three times for Pb, Ni and V concentrations and compared to standard values [21,22]. Recovery values calculated are 98.2% for Pb, 96% for Ni and 101.5% for V. Recovery data for NBS 16346 oil samples are listed in Table 4.

Calculations for different sample contents resulted in concentration ranges of 0.30–0.81 μg g^{-1} for Pb, 3.13–9.4 μg g^{-1} for Ni and 8.8–13.8 μg g^{-1} for V in the different analyzed Saudi oil samples. Each sample is analyzed 3–5 times to obtain the standard deviation values which are found to be less than 4% for all the analyzed elements. Table 5 includes concentrations, standard deviations and correlation coefficients for Pb, Ni and V in crude oil samples and a compari-

Table 5
Concentration (μg g^{-1}) and statistical data for Pb, Ni and V in crude oil samples by the SIA/ICP-MS method

Element	Crude oil sample	Concentration ± SD	Correlation coefficient
Pb	H	0.81 ± 0.02	0.995
	M	0.44 ± 0.01	0.997
	L	0.30 ± 0.01	0.998
Ni	H	9.4 ± 0.2	0.994
	M	6.9 ± 0.1	0.996
	L	3.13 ± 0.05	0.997
V	H	13.8 ± 0.3	0.995
	M	8.8 ± 0.2	0.996
	L	11.3 ± 0.2	0.997

Table 6
Concentration ± SD (μg g^{-1}) of Pb, Ni and V in Saudi Arabian crude oil samples obtained by proposed and other published methods

Element	Crude oil samples	Acidified microemulsion SIA/ICP-MS	Continuous aqueous microemulsion ICP-MS [3,9]
Pb	H	0.81 ± 0.02	0.780 ± 0.2
	M	0.44 ± 0.01	0.130 ± 0.003
	L	0.30 ± 0.01	0.17 ± 0.02
Ni	H	9.4 ± 0.2	8.3 ± 0.1
	M	6.9 ± 0.1	5.5 ± 0.2
	L	3.13 ± 0.05	2.09 ± 0.05
V	H	13.8 ± 0.3	25.5 ± 0.8
	M	8.8 ± 0.2	14.5 ± 0.4
	L	11.3 ± 0.2	13.4 ± 0.4

son made between the results obtained by the proposed method and other published methods is shown in Table 6 for the same sample.

It is found that concentrations of Pb and Ni obtained by the proposed SIA/ICP-MS method are higher than those found with the continuous ICP-MS method. Vanadium concentrations are lower with the SIA/ICP-MS method. This may be due to its high background signal (as shown in Fig. 2), especially in crude oil samples where solution concentrations are low.

4. Conclusions

The interfacing of sequential injection and inductively-coupled plasma mass spectrometry provides a new automated technique for trace elements analysis which is easy to handle, requires only small sample volumes and is sensitive. The results are reproducible and this technique can be used for the determination of other trace elements in crude oil samples.

Acknowledgments

References

[1] V. Valkovic, Trace Elements in Petroleum, The Publishing Co., Tulsa, OK, 1978.
[2] G.M. Heiftje, Anal. Chim. Acta, 216 (1989) 1.
[3] H.M. Al-Swaidan, Anal. Lett., 27 (1994) 145.
[4] H.M. Al-Swaidan, Sci. Total Environ., 145 (1994) 157.
[5] R.C. Hutton, J. Anal. At. Spectrom., 1 (1986) 259.
[6] D. Hauster, Spectrochim. Acta, 42B (1987) 63.
[7] D.R. Wiederin, R.S. Houk, R.K. Winge and A.P. D'Silva, Anal. Chem., 62 (1990) 1155.
[8] C.J. Lord, Anal. Chem., 63 (1991) 1594.
[9] H.M. Al-Swaidan, At. Spectrosc., 14 (1993) 170.
[10] H.M. Al-Swaidan, N. Lacy and G.D. Christian, Anal. Lett., 22 (1989) 2653.
[11] R.C. Hutton and A.N. Eton, J. Anal. At. Spectrom., 3 (1988) 547.
[12] J.R. Dean, L. Ebdon, H.M. Crews and R.C. Massey, J. Anal. At. Spectrom., 3 (1988) 349.
[13] J.J. Thompson and R.S. Houk, Anal. Chem., 58 (1986) 2541.
[14] R.S. Houk and J.J. Thompson, Biomed. Mass Spectrom., 10 (1983) 107.
[15] T. Gubeli, G.D. Christian and J. Ruzicka, Anal. Chem., 63 (1991) 2407.
[16] J. Ruzicka and E.H. Hansen, Flow Injection Analysis, 2nd edn., Wiley, New York, 1988.
[17] J. Ruzicka and G.D. Marshal, Anal. Chim. Acta, 237 (1990) 329.
[18] J. Ruzicka, G.D. Marshal and G.D. Christian, Anal. Chem., 62 (1990) 1861.
[19] H.M. Al-Swaidan, 2nd Int. Conf. Chemistry in Industry, Manama, Bahrain, 24–26 October, 1994, Vol. 2, p. 1371.
[20] Alitea MIS-1 Modular Injection System Manual for Sequential Injection Analysis Experiments, Alitea, USA, 1993.
[21] National Bureau of Standards, Certificate of Analysis, Standard Reference Material 1634 b, Trace Elements in Fuel Oils, National Bureau of Standards, Gaithersburg, MD, 1986.
[22] R.C. Paule and J. Mandel, J. Res. Nat. Bur. Stand., 87 (1982) 377.

Determination of copper by electrothermal AAS after electrodeposition on a graphite disk electrode

J. Komárek[a],*, P. Stavinoha[a], S. Gomišček[b], L. Sommer[a]

[a]*Department of Analytical Chemistry, Masaryk University, Kotlářská 2, 61137 Brno, Czech Republic*
[b]*Department of Chemistry and Chemical Technology, University of Ljubljana, Murnikova 6, 61001 Ljubljana, Slovenia*

Abstract

The electrodeposition of copper on a graphite electrode at a constant potential with subsequent atomization in the graphite atomizer HGA-400 has been studied. A special graphite disk electrode is suitable for electrochemical enrichment at $E = -0.7$ V vs. SCE and the determination of copper by electrothermal-atomic absorption spectrometry (ET-AAS) if atomized at 2300°C. In this way copper was determined in potable water and free Cu^{2+} could be distinguished from that bound in chelate speciations after using a suitable deposition potential of the working electrode. This approach seems to be an alternative to the commonly used anodic stripping voltammetry (ASV) for the preconcentration and determination of free metal ions.

1. Introduction

Previous separation and preconcentration techniques are frequently used in connection with AAS as a means of removing interferences and increasing sensitivity. The electrochemical deposition of minor concentrations of metals on suitable electrodes is one of the methods used prior to determination by electrothermal AAS. Wires from refractory metals especially tungsten [1–3], graphite [4,5] or a hanging mercury-drop [6,7] were suitable for electrodeposition. The atomization resulted from electrically heated tungsten wire being placed in the tube [1,2] or after shifting into a CRA-90 graphite atomizer [3]. Common graphite electrodes were pulverized prior to sampling in the graphite tube [4] or the electrode was part of the atomizer [8]. An electrode disk, properly cut and covered by the metal deposit was also inserted into the atomizer [9] or the electrode in a suitable form which was tightly led into the atomizer [5]. Recently a special graphite disk electrode was developed as a probe to be inserted into the atomizer without touching the wall of the tube. The electrodeposition of the metal took place on the disk, which was situated on a thin stem [10].

* Corresponding author.

Although metals can also be conveniently analyzed by anodic stripping voltammetry (ASV) [11,12], there are a number of elements, notably cobalt, nickel, manganese and chromium for which the deposition is irreversible. In the presence of other metals, intermetallic compounds may be formed and their redissolution by ASV is difficult [11]. Moreover, a broadened stripping peak or two peaks may be observed, the first one due to the voltammetric oxidation of metal, and the second one due to the adsorption in the presence of species in environmental samples [13]. ET-AAS may serve as a selective element detector of electrochemically deposited metals on the electrode and the electrothermal atomization simply replaces the ASV stripping step.

In this paper the electrodeposition of copper under a controlled potential was studied as a model on a graphite disk electrode in connection with the subsequent determination by ET-AAS and in the presence of complexing agents.

2. Experimental

2.1. Chemicals

Cu^{2+} standard solution containing 0.993 g l^{-1} Cu^{2+} was prepared by dissolving metallic copper (99.96%) in 10 ml of concentrated HNO_3 and diluting to 1:1 with bidistilled water. The solution was standardized by EDTA titration on murexide indicator.

Ethylenediaminetetraacetic acid disodium salt (EDTA) p.a., nitrilotriacetic acid (NTA) p.a. and dinitrilocyclohexylentetraacetic acid (DCTA) p.a. were obtained from Lachema Brno and N-(2-hydroxyethyl)ethylenediamine N',N,N''' triacetic acid trisodium salt hydrate (HEDTA) p.a. was obtained from Fluka-Chemika.

All other chemicals were of analytical grade purity.

2.2. Instruments

An AA spectrometer (Perkin-Elmer 3030) with a graphite atomizer HGA-400, a copper hollow cathode lamp Intensitron heated for 20 mA (324.8

nm) and a mercury electrodeless discharge lamp operated at 5 W (253.7 nm) were used. The atomization followed in argon.

A Radelkis OH 405 potentiostate for the metal deposition and an analogous precision potentiometer OP-205 for deposition potential adjustment on the developed disk graphite electrode were used. The potential was measured against a SCE, platinum served as the counter electrode, and electrodeposition followed during vigorous stirring of the solution containing the metal ion (50 ml). The electrolysis was carried out in the system with a single or four working electrodes. The single electrode was inserted into the graphite rod (5 mm diameter with the hole 3 mm in diameter). The contact to the potentiostate was connected to the upper part of the rod. In the four-electrode arrangement the four graphite disk electrodes were inserted into holes of 3 mm diameter in a graphite cube of size 30 × 30 × 10 mm located in a quadrangle position. The connection to the potentiostate was led from the upper part of the cube. The platinum electrode was isolated in the middle and the electrolysis took place on the four electrodes simultaneously. The arrangement with the four electrodes was used for practical application.

The graphite disk electrode was prepared from graphite rods (3 mm diameter, SU Elektrokarbon Topolčany and RW III Ringsdorffwerke Bonn) and the final disk was turned to 0.6 mm thickness, ground by a fine emery paper and polished by a dense filter paper. The resulting thickness of the disk was 0.5 mm (Fig. 1).

The prepared electrode was double ignited in a graphite tube at 2300°C for 6 s in argon; the stem of the electrode was protected by a tightly wound Teflon strip (10 × 40 mm) and the electrode was fixed up into the graphite contact of the electrolyzer. After the electrodeposition the electrode was rinsed with bidistilled water, the Teflon strip was removed and the electrode was rinsed with water and inserted by the use of an applicator into the enlarged sampling hole in the atomizer tube (3.5 mm diameter) horizontally through the orifice in the contact. The insertion of the electrode into the atomizer was realized by a graphite applicator of diameter 5 mm and length 11 cm

with an orifice of diameter 3 mm and depth of 10 mm (Fig. 1). The graphite applicator with the electrode was then slid into a glass tube in a holder. The correct positioning of the disk electrode in the graphite tube was indicated by a non-selective absorbance of 0.004–0.008.

The drying of the disk and stem of the electrode took 15 s at 160°C with a 5 s ramp, the pyrolysis stage took 15 s at 600°C with the same ramp and the atomization of copper took 5 s at 2300°C with no flow of argon and temperature-controlled maximal power heating. The cleaning of tubes followed at 2300°C for 3 s.

A scanning electron microscope (Philips SEM 500) was used for preparing photographs of the electrode surfaces.

The sensitivity of the determination corresponds to the slope of the calibration plots and the relative standard deviation (RSD) is calculated from six measurements.

2.3. Determination of copper in potable water

A 50 ml volume of the water sample, acidified with concentrated HNO_3 to pH 2, was electrolyzed for 1–5 min at $E = -0.7$ V (against SCE) and the copper was determined by ET-AAS under the conditions given above. The results were evaluated by the method of standard additions (1–10 μg l^{-1} Cu^{2+}). The RSD was 5.4–6.4% ($n = 6$) for 1,5–8 μg l^{-1} Cu. The results
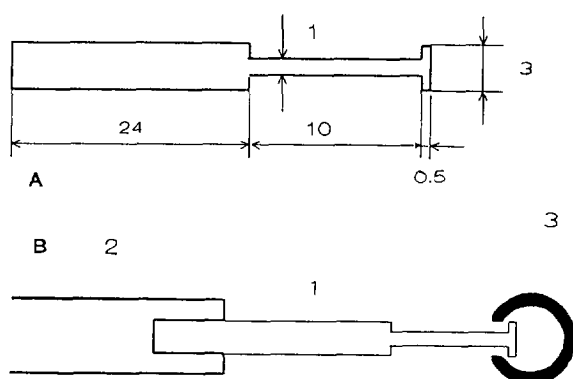

Fig. 1. Graphite disk electrode (A, data in mm) and its applicator for the atomizer HGA-400 (B). 1, Electrode; 2, holder; 3, tube.

were in good agreement with those observed by ASV.

3. Results and discussion

3.1. Conditions for electrodeposition

According to experimental $i = f(E)$ plots, the limiting current for copper was observed from $E = -0.15$ V for solutions containing 5 mg l^{-1} Cu^{2+} in 0.01 mol l^{-1} HNO$_3$, 0.005 mol l^{-1} H$_2$SO$_4$ or 0.01 mol l^{-1} HCl. The results of the ET-AAS for the amount of copper deposited on the disk electrode from solutions with 10 μg l^{-1} Cu^{2+} during a 2 min period continuously increased for the interval of $E = (-0.2$ V$)-(-1.2$ V$)$ with some delay at $(-0.6$ V$)-(-0.8$ V$)$. A potential $E = -0.7$ V vs. SCE was found to be optimal.

3.2. Effect of the electrode material

Cu^{2+} was sorbed in part from the solution on the graphite electrode surface even in a currentless state in an open electric circuit and could not be removed by rinsing with water. Comparing electrodes from graphite SU and RW III, the interaction of Cu^{2+} with the surface in diluted HNO$_3$ and HCl is considerably lower for graphite RW III and does not depend on the number of firings when less than ten. At pH 2 the sorption was independent of the acids used (HCl, HNO$_3$, H$_2$SO$_4$).

The dependence of the absorbance of the sorbed copper against the Cu^{2+} concentration in solution for various dipping times is shown in Fig. 2. The sorption of Cu^{2+} is not sufficiently reproducible and the RSD is often worse than 30%. The copper amounts deposited after an electrolysis of 2 min is by the order larger than that which was spontaneously sorbed. Thus, this copper does not influence expressly the determination of copper, especially during longer electrolysis times.

Burning of the electrodes from the periphery to the centre of the electrode disk was observed by the scanning microscope. Graphite RW III was more resistant to firing and was used for further measurements.
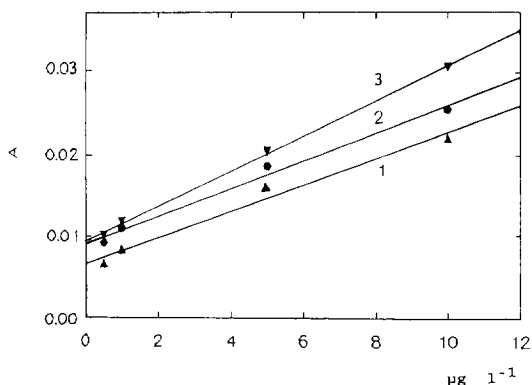
Fig. 2. Relationship between the absorbance of the sorbed copper against Cu^{2+} concentration in solution for various dipping times (RW III graphite). Curve 1, 10 s; curve 2, 2 min; curve 3, 10 min (0.005 mol l^{-1} H_2SO_4). Each point of the plot corresponds to the average of 16 measurements.

3.3. Selected conditions for ET atomization

The pyrolysis plot showed a constant course until a temperature of 1200°C was reached. The pyrolysis temperature used for the measurements was 600°C. Since the graphite disk electrode contained largely metallic copper deposits, this pyrolysis step partially corresponds to the completion of drying. Temperatures higher than 2300°C caused faster burning-off of the disk which negatively influenced the precision of the determination. The disk endured 10–11 firings without damage and the need for polishing. For larger numbers of firings the surface of the electrode increased and thus the amount of copper; consequently polishing with a dense filter paper is necessary after ten firings. After 40–50 firings polishing was unsuccessful and the RSD of the determination increases to more than 10% (for $A = 0.2$). High temperature gradients of heating led to a slight split of the absorbance signals (Fig. 3). Uniform peaks were obtained for temperature gradients of 3 s but the precision decreased. Thus, atomization by temperature-controlled maximum power heating was only used. The reason for peak splitting during fast heating may be caused by expansion of the gases but also by the temperature decrease at the increased sampling orifice. The sensitivity of the determination expressed with the slope of calibration plots $A = f(Cu, \mu g$

l^{-1}) was 0.012, 0.023, 0.048 and 0.072 $(\mu g \, l^{-1})^{-1}$ for electrodeposition times of 1, 2, 4 and 6 min, respectively.

3.4. Co-deposition of copper with mercury

Copper was deposited from solutions containing Cu^{2+} in the presence of 2.5×10^{-5} mol l^{-1} Hg^{2+}. Selected working parameters on the HGA-400 were 110°C (drying), 800°C (pyrolysis) and 2300°C (atomization) in this case. At 550°C two forms of mercury indicated by the absorbance minimum for mercury at 253.7 nm, i.e. free mercury atoms and the decomposition of the copper amalgam at this temperature. The signal for copper at 324.8 nm increases by 39% after the complete decomposition of the amalgam at 800°C in comparison to the results for copper without amalgamation. The RSD for copper was 2.2% in the presence of mercury. Reproducible signals were, however, obtained only during three firings on the disk electrode without polishing. The disadvantage of such procedure is the toxicity of released mercury vapors.

3.5. Effect of acids and NaCl

The electrodeposition of copper was studied from solutions containing HCl, H_2SO_4 or HNO_3 only and with a pH of 1–2 (adjusted with H_2SO_4 or HNO_3) (Fig. 4). The decrease of signal with the decrease of acid concentration could arise from
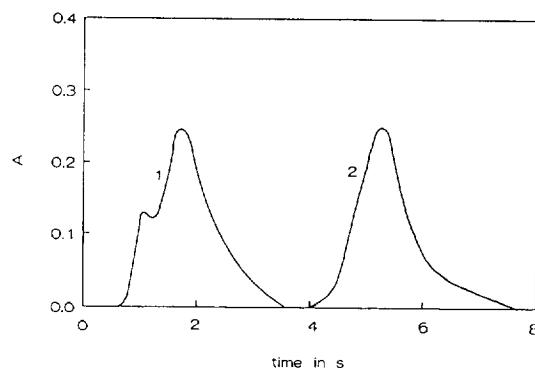

Fig. 3. Absorbance signals of copper after electrodeposition on the graphite disk electrode. peak 1, $t_R = 0$ s; peak 2, $t_R = 3$ s (10 $\mu g \, l^{-1}$ Cu^{2+}, 0.01 mol l^{-1} HNO_3).
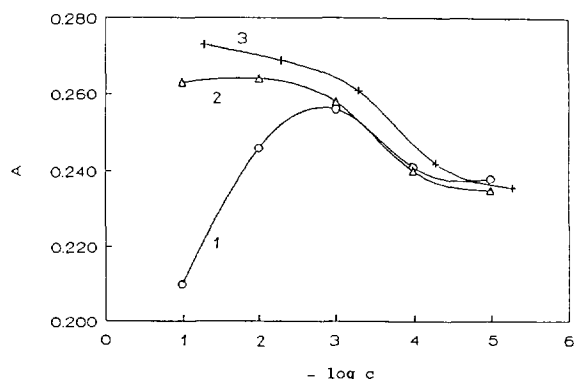
Fig. 4. Relationship between the copper absorbance on the logarithm of the acid concentration (in mol l^{-1}). Curve 1, HCl; curve 2, HNO_3; curve 3, H_2SO_4 (10 μg l^{-1} Cu^{2+}, $E = -0.7$ V).

the lower conductivity of solution. An increased concentration of hydrochloric acid interferes due to the formation of chlorine at the counter electrode.

If 10 μg l^{-1} Cu^{2+} solution was electrolyzed in 0.005 mol l^{-1} H_2SO_4 the amount of copper deposited decreased if more than 0.1 g l^{-1} of NaCl was present. This decrease reaches 36% with 0.4 g l^{-1} NaCl. The effect of more than 0.1 g l^{-1} NaCl is however negligible if the counter electrode was protected from the electrolyte by a glass tube with an agar sintered disk. The electrode separation eliminates the effect of chlorine formed by the oxidation of chlorides on the counter electrode.

3.6. Deposition of copper from solutions containing complexing reagents

For the determination of free Cu^{2+} in the presence of copper complexed in various stable chelates a suitable deposition potential must be selected, if free metal is deposited and no metal chelate decomposition takes place, or if the reagent is not reduced on the negatively charged electrode. As followed from studies of polarization plots in the system, $E = -0.19$ V against SCE was suitable in the presence of most of the studied chelating ligands. Thus, Cu–EDTA begins to decompose electrolytically at $E = -0.23$ V against SCE.

The concentration of free Cu^{2+} in solution was evaluated from calibration plots prepared under the same conditions, pH, potential and electrolysis time for Cu^{2+} solutions without ligand. The experimental results were compared with those calculated according to the modified SQUAD [14,15] program from the corresponding stability, protonation constants of the Cu–chelates or ligands and the stability constants of particular Cu–hydroxocomplexes [16] (cf. Table 1). The differences between the determined and calculated concentration of free copper in the presence of chelons such as EDTA, NTA, HEDTA and DCTA were no larger than 25%. Thus, such a way is suitable for the determination of free Cu^{2+} in the presence of metals bound in Cu–chelates.

Table 1
Concentration of free Cu^{2+} in solutions containing ligands under various conditions

Reagent	c_L (total) mol l^{-1}	c_{cu} (total) mol l^{-1}	pH[a]	c_{cu} (calculated) mol l^{-1}	c_{cu} (determined[b]) mol l^{-1}	Δ %[c]
NTA	1×10^{-3}	1×10^{-3}	6	1×10^{-6}	1.3×10^{-6}	+23
	2×10^{-3}	1×10^{-3}	4	9×10^{-7}	7.2×10^{-7}	−25
HEDTA	1×10^{-3}	1×10^{-3}	4	5×10^{-7}	4.6×10^{-7}	−7
EDTA	1×10^{-3}	1×10^{-3}	4	5×10^{-7}	6.6×10^{-7}	+24
	2×10^{-3}	1×10^{-3}	2	7×10^{-7}	8.6×10^{-7}	+18
DCTA	2×10^{-3}	1×10^{-3}	2	3×10^{-7}	3.0×10^{-7}	0

[a] $I = 0.1$ mol l^{-1} (adjusted by $NaNO_3$).
[b] determined by ET-AAS after preliminary electrodeposition.
[c] Δ % corresponds to the percentage difference between experimental and calculated values.

Acknowledgements

References

[1] W. Lund and B.V. Larsen, Anal. Chim. Acta, 72 (1974) 57.

[2] W. Lund and B.V. Larsen, Anal. Chim. Acta, 70 (1974) 299.

[3] E.J. Czobik and J.P. Matoušek, Spectrochim. Acta, 35 B (1980) 741.

[4] Y. Thomassen, B.V. Larsen, F.J. Langmyhr and W. Lund, Anal. chim. Acta, 83 (1976) 103.

[5] M. Veber, S. Gomišček and V. Streško, Anal. Chim. Acta, 193 (1987) 157.

[6] C. Fairless and A.J. Bard, Anal. Chem., 45 (1973) 2289.

[7] F.O. Jensen, J. Doležal, F.J. Langmyhr, Anal. Chim. Acta, 72 (1974) 245.

[8] J.P. Matoušek, Prog. Anal. Atom. Spectrosc., 4 (1981) 247.

[9] M. Veber and S. Gomišček, Proc. 6th Yug. Conference on Pure and Applied Spectroscopy, Bled, 1976, Vol. 1., p. 238.

[10] J. Komárek, M. Veber and S. Gomišček, Analytiktreffen 1990, Neubrandenburg 5-9 November, (Abstracts p. 112).

[11] F. Vydra, K. Štulik and E. Juláková, Electrochemical Stripping Analysis, Ellis Horwood, Chichester, 1976.

[12] G.E. Batley and T.M. Florence, J. Electroanal. Chem., 55 (1974) 23.

[13] G.E. Batley, Anal. Chim. Acta, 189 (1986) 371.

[14] L. Jančář and J. Havel, Scripta Fac. Sci. Nat. Univ. Purk. Brun., 14 (1984) 73.

[15] L. Jančář, R. Šulová, I. Jančářová and V. Kubáň, The Third Chemometrics Conference, Brno, 11–15 July 1993, (Abstracts p. 114).

[16] S. Kotrlý and L. Šůcha, Handbook of Chemical Equilibria in Analytical Chemistry, Ellis Horwood, Chichester, 1985.

Variable-angle synchronous fluorescence spectrometry and rank annihilation methods for mixture resolution

F. García Sánchez*, M. Cedazo, J. Lovillo, A. Navas Díaz

Departamento de Química Analítica, Facultad de Ciencias, Universidad de Málaga, 29071-Málaga, Spain

Abstract

The potential of variable angle synchronous spectroscopy (VASS) for fluorescent mixtures resolution was assessed and compared with the rank annihilation method (RAM). For this purpose, a set of excitation–emission matrices from three standard cyclodextrin fluorescence-enhanced solutions of the pesticides aminocarb, carbendazim and coumatetralyl and a mixture of them was obtained. Careful selection of the spectral routes to be scanned provides analyte signals that are free of interferences. Application of the rank annihilation method to excitation–emission matrices (EEMs) obtained by conventional scanning spectrofluorimetry gives quantitative results that show poor precision and accuracy when compared to those of VASS. The recoveries from ternary mixtures by VASS are within 99–104% and by RAM within 84–130%.

1. Introduction

Although spectrofluorimetry has great sensitivity and moderate selectivity as an analytical technique, these performances in multicomponent analysis fall considerably because overlapping spectra give rise to energy-transfer processes and inner filter effects that produce spurious analyte signals. At present there are two fundamental ways to avoid this problem: modifications in analytical sampling and signal processing by mathematical algorithms after the raw data are obtained.

Simultaneous multicomponent analysis can be performed by mathematical treatment of the data such as realized by principal components regression (PCR), partial least squares regression (PLS), rank annihilation method (RAM), etc. Alternatively it is possible to act over experimental data acquisition in such a way that the contribution to the analytical signal from interfering components can be eliminated, or at least minimized. Variable angle scanning spectrometry [1–3] gives a useful approach to data acquisition for the simultaneous

---

* Corresponding author.

analysis of fluorescent multicomponent samples because of the reduction of the interferences associated with the design of the technique.

Mixture resolution by fluorescence spectrometry performed by mathematical procedures normally gives good results, when there are no strongly overlapped spectral profiles that would facilitate energy transfer processes between donor molecules (emission spectra) and acceptor molecules (excitation spectra). This effect produces quenching of donor and enhancement of acceptor that changes the spectral profiles of the mixtures compared with those of the standard solutions. This aspect is not a problem in VASS in which the selected routes can circumvent spectral zones subject to these energy transfer processes. The results obtained in this paper can be interpreted in this context.

Three different types of synchronous scanning have been developed: constant wavelengths (CW), constant energy (CE) and variable angle (VA). CE and CW scans maintain a constant separation (in cm^{-1} and nm, respectively) between excitation and emission beams [4]. An alternative approach, denoted variable-angle synchronous scanning (VASS) varies the separation in a controlled way. The continuous variation of the wavelength separation between the monochromators can be achieved either mechanically, by varying the scan speeds of the two monochromators, or digitally, by processing the stored data. Because mechanical control of the monochromator's speed only produces linear scan paths [5] and the generation of VASS from stored data [6] is very time consuming, a commercial digital instrument has been modified [7] to generate the variable-angle synchronous scan directly from the spectrofluorimeter output. This permits the VASS scan to be obtained in a few minutes by following a path previously selected by inspecting the contour lines.

The reduced peak-half-widths is often cited as the most important attribute of synchronous techniques for the resolution in multicomponent analysis. Recently, the theory of variable-angle synchronous spectrofluorimetry has been described in detail [8] and it has been deduced that the resolution in synchronous techniques is more

related to the maximal peak intensity than with minimal peak width. Thus, the true advantage of VASS with respect to CWS is not the band narrowing effect but the capacity to go throughout maximal intensity peaks (circumvents overlapping spectral areas). This confirms the superior advantage of VASS in multicomponent analysis against CE, CW or derivative synchronous techniques due to the added flexibility in the choice of a scan path nearest to maxima.

Synchronous scanning methods have potential for multicomponent analysis that has not been fully realized, particularly for the automatization of sampling data. We report the simultaneous analysis of the agrochemicals aminocarb, carbendazim and coumatetralyl by VASS. The studied compounds display a low fluorescence quantum yield which is enhanced by using one of the almost universal features of cyclodextrin complexes such as fluorescence enhancement [9–11] by the inclusion of an organic fluorophore in the cyclodextrin (CD) cavity.

The technique of rank annihilation, described by Ho et al. [12] utilizes the excitation–emission matrix M, to determine quantitatively the concentration of a component in the presence of a mixture. The excitation–emission matrix of a standard solution of each analyte yields a series of standard reference matrices S_1, S_2, etc. Then, successive fractions β of S are subtracted from the mixture matrix M. When the fraction of S subtracted from M equals the amount of S originally present in M, the rank of the resulting difference matrix $M - \beta S$ is one less than the rank of M and the nth eigenvalue of the difference matrix goes to a minimum. The concentration of the analyte in the mixture is then given by β times the concentration of the analyte in the standard solution used to measure S. These operations are accomplished by performing a singular value decomposition (SVD) of the difference matrix:

$$v = \mathrm{svd}(M - \beta^* S)$$

and adjusting the scalar fraction β until the nth singular value $v(n)$ is a minimum.

In this paper we try to evaluate the performances of a technique based on the more precise acquisition of the signal from the sample (VASS)

so as to compare it with the results obtained by a chemometric technique (RAM) based on signal processing. The critical comparison of the results obtained by both methods is also an objective of this paper.

2. Experimental

Fluorescence spectra were obtained with a Perkin-Elmer LS-5 luminescence spectrophotometer equipped with a xenon lamp (9.9 W) pulsed at line frequency. The spectrometer was interfaced to an IBM-PC/AT computer via the RS232C serial interface. The software package FLUOROPACK [7] controlled the instrument, data acquisition and data processing. The software used for the data analysis was PC-MATLAB (MAt-Works Inc., Sherborn, MA, USA).

The solvents used were pro analysis (Merck). Water was distilled and deionized. The pesticide carbendazim (99%) was purchased from Riedel-de Haen; aminocarb (99%) and coumatetralyl (96%) were supplied by Dr. Ehrenstorfer (Augsburg, Germany); β-cyclodextrin was kindly supplied by Amaizo, Co. (USA).

The stock standard solutions of aminocarb, and coumatetralyl 1 g L^{-1} and carbendazim 0.25 g L^{-1} were prepared by dissolving the pesticide in methanol, and were stored in the dark at 4°C. Working solutions of coumatetralyl and carbendazim were prepared weekly and that of aminocarb each two days, by dilution with methanol. β-cyclodextrin was purified by recrystallization once from boiling water and 10^{-2} M aqueous solutions were prepared. A buffer solution of pH 4.5 was prepared from 0.2 M acetic acid/sodium acetate.

2.1. Sample preparation

Aliquots of sample solution to give a final concentration between 1.5–4.0 μg mL^{-1} of aminocarb, 6.7–300 ng mL^{-1} of coumatetralyl and 2.3–5 μg mL^{-1} of carbendazim were placed in a 10 mL standard flask. The contents were slowly evaporated to dryness by a nitrogen stream, and after adding 1 mL of pH 4.5 acetate

buffer, the volume was adjusted to 10 mL with 10^{-2} M β-cyclodextrin solution. The solution was sonicated for 20 min and the variable angle scanning spectra (VASS) was scanned. Finally, fluorescence intensity was measured in the VASS plots at 235/390 nm, 310/380 nm and 290/335 nm, respectively, and plotted against the concentration of each pesticide.

3. Results and discussion

Separate experiments were conducted to study the behavior of aminocarb, carbendazim and coumatetralyl in water and β-cyclodextrin solutions. In Table 1 the excitation and emission wavelengths and relative fluorescence intensities (RFI) in these media are presented. An emission enhancement in cyclodextrin media compared to water is observed. The weaker complexes produce faint emission signals. The formation constants of the β-CD complexes ([aminocarb] = 2 μg mL^{-1}, [coumatetralyl] = [carbendazim] = 1 μg mL^{-1}), obtained by the Benessi–Hildebrand methods [13] were 267 L mol^{-1}, 21 L mol^{-1} and 669 L mol^{-1} for the β-CD–aminocarb, –carbendazim and – coumatetralyl complexes, respectively. The maximum RFI is achieved in 10^{-2} M solutions of β-CD, a slight modification in this concentration has little effect on fluorescence intensity. Ethanol has also a little effect on the fluorescence; low proportions of this solvent are admitted but absence gives maximum sensitivity. A pH of 4.5 is adequate for sensitivity because it permits greater emission signals to be obtained.

Table 1
Excitation and emission wavelength and relative fluorescence intensity (RFI) for aminocarb, carbendazim and coumatetralyl in water and β-CD.

Compound	λ_{exc} (nm)	λ_{em} (nm)	RFI
Aminocarb (water)	237	383	185
Aminocarb (β-CD)	238	382	472
Carbendazim (water)	281	307	138
Carbendazim (β-CD)	210	307	264
	279		199
Coumatetralyl (water)	311	387	74
Coumatetralyl (β-CD)	311	387	785
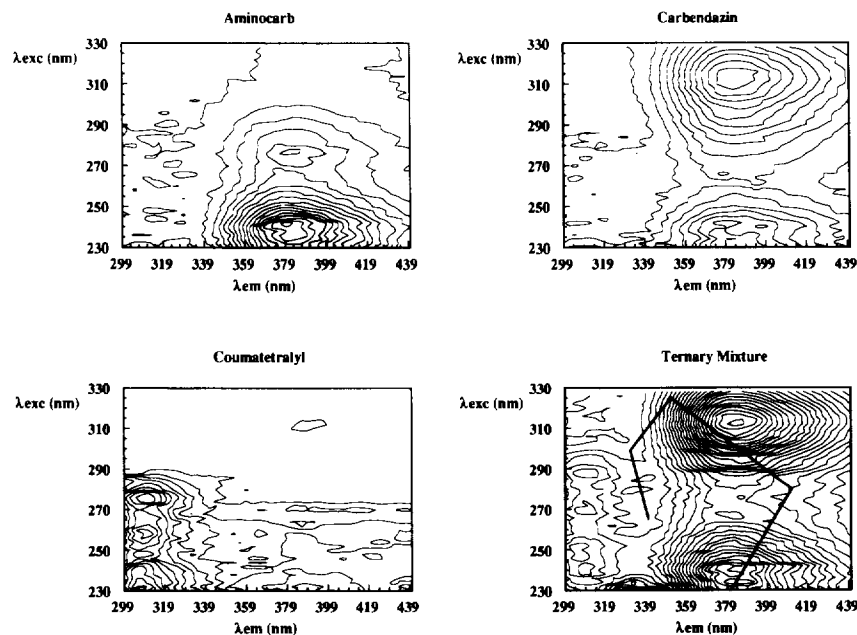
Fig. 1. Contour plots of aminocarb (3 µg mL⁻¹), carbendazim (5 µg mL⁻¹), coumatetralyl (0.5 µg mL⁻¹), and a mixture of them (approximately isoemissive, same concentrations as standards) showing the selected VASS route.

An EEM of the mixture (Fig. 1) was obtained and maxima of analytes were identified. The excitation and emission maxima pairs for β-CD complexes with aminocarb, coumatetralyl and carbendazim are 238–375 nm, 315–387 nm and 280–307 nm, respectively. This type of mixture cannot be resolved either by conventional fluorimetry (there are no excitation–emission pairs for selective excitation) nor synchronous scanning fluorimetry because the almost complete overlap of the spectral shapes impedes the detection of an interference-free signal. Moreover, using VASS, we can find those regions with minimum overlap and reduced cross interference between analytes.

The variable-angle scanning route was carefully determined by trial and error to traverse those parts of the three-dimensional (3-D) spectral zones with the least overlap. The scan was selected to transverse those parts of the 3-D data matrix with the least overlap and the nearest of the maximum peaks. In spite of the fact that losses in sensitivity occur because no maximum peaks are traversed, interference-free signals of the three components may be obtained from the

chosen routes that scan the three-dimensional zones by skirting the slopes of the peak and avoiding the areas of interference between the three compounds. Fig. 2 shows a 3-D variable angle scanning spectrum for a ternary mixture.

The superior advantage of VASS in multicomponent analysis against CE, CW or derivative synchronous technique is due to the added flexibility in the choice of a scan path nearest to
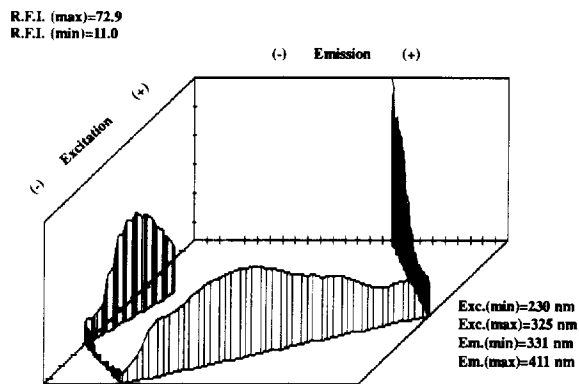
R.F.I. (max)=72.9
R.F.I. (min)=11.0

Fig. 2. Three-dimensional VASS of a ternary mixture (concentrations as in Fig. 1).
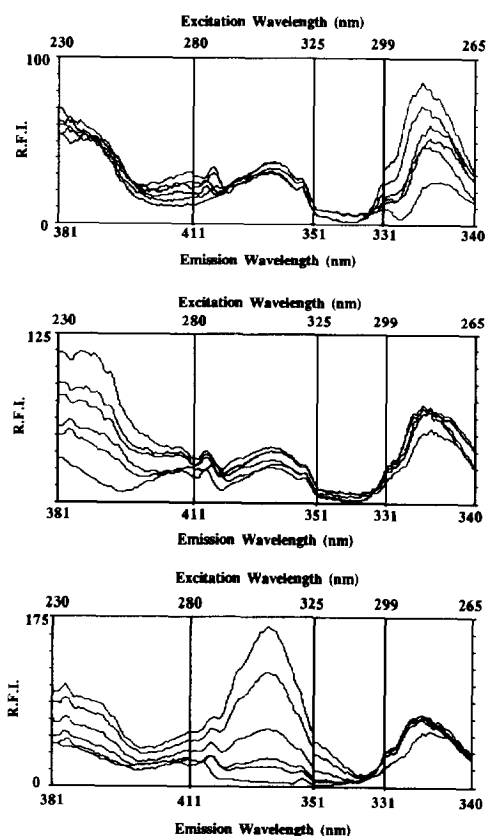
Fig. 3. Two-dimensional projection of several ternary mixtures. (A) [aminocarb] = 1 μg mL⁻¹; [coumatetralyl] = 0.05 μg mL⁻¹; [carbendazim] = 0, 1.5, 3 and 5 μg mL⁻¹. (B) [coumatetralyl] = 0.05 μg mL⁻¹; [carbendazim] = 5 μg mL⁻¹; [aminocarb] = 0, 1 > 1.5, 2.5, 3 and 5 μg mL⁻¹. (C) [carbendazim] = 5 μg mL⁻¹; [aminocarb] = 1 μg mL⁻¹; [coumatetralyl] = 0, 0.025, 0.05, 0.1, 0.2 and 0.3 μg mL⁻¹.

maxima. So, as expected the generation of VASS by following rigid routes, or by introducing a circular, elliptical or other function into the software routine, did not improve the method. The 2-D profiles of the optimized routes were less pronounced when rigid geometric functions were introduced.

Several 3-D variable angle spectra of a three-component mixture of the pesticides are shown in Fig. 3 to illustrate the potential utility of this technique for mixture analysis. The software program produces and displays the required data in 4–5 min. The fact that both monochromators of the spectrofluorimeter cannot be set to difficult

Table 2
Analytical parameters

Compound	Linear dynamic range (mg L⁻¹)	Limit of detection (ng mL⁻¹)	RSD (%)
Aminocarb	0.29–5.0	89	4.32
Carbendazim	0.18–5.0	55	8.99
Coumatetralyl	0.06–0.3	17	4.78

RSD, relative standard deviation.

scan speeds does not matter because the program signals override and differentially vary the excitation and emission monochromator drive motors of the spectrofluorimeter by pulsing their power input.

Once the VASS spectra were obtained, fluorescence intensity readings at the maximum of VASS spectra and setting of the excitation and emission monochromators at the adequate wavelengths were performed.

Linear calibration graphs were obtained by plotting the fluorescence intensity against standard concentrations of aminocarb, carbendazim and coumatetralyl. Table 2 gives the linear dynamic range, detection limits and precision of the method. The accuracy was evaluated through a interferences study; the effect of some pesticides (fenitrotion, chlorpiryfos, dicofol and tetradifon) on the determination of a synthetic sample of composition 2 μg mL⁻¹ aminocarb, 2 μg mL⁻¹ carbendazim and 0.12 μg mL⁻¹ coumatetralyl was evaluated. Various volumes of stock solutions of the different potential interferents were added to the standard solution in order to obtain different interferent-to-analyte ratios in the final solution. The results obtained are given in Table 3. Acceptable recoveries of coumatetralyl are obtained. Recoveries are low and high for

Table 3
Recoveries in the ternary mixture by VASS

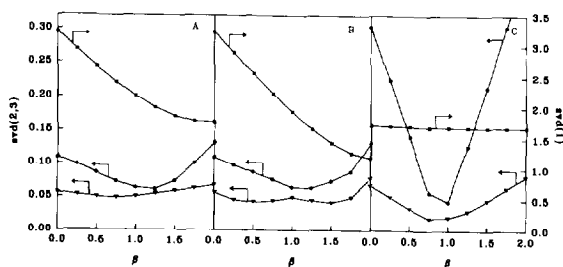| Compound	Taken (mg L⁻¹)	Found (mg L⁻¹)	Recovery (%)	RSD (%)
Aminocarb	2.0	1.99	99.5	4.56
Carbendazim	2.0	2.067	103.8	8.25
Coumatetralyl	0.11	0.115	106	3.09

Fig. 4. First (■), second (●), and third (▽) singular values as a function of β. (A) Aminocarb, 3 mg L^{-1}; (B) Carbendazim, 5 mg L^{-1}; (C) Coumatetralyl, 0.3 mg L^{-1}.

aminocarb and carbendazim, respectively, when the interferent is twice or higher than the analyte concentration.

To apply the RAM method to the three-component mixture under study, we used four data sets, each composed of an EEM of the single standard component and a mixture of the three standards. The EEM were smoothed and blank-subtracted to remove scattered light. The resulting 48 × 48 matrices were then analyzed. Although blank substraction does not totally eliminate high scattered light, the regions of analytical interest are situated far away from the scatter emission; thus, this event will not affect the estimated concentrations of the analytes.

Performing a singular value decomposition of the difference matrix $(M - \beta S)$ and adjusting the scalar fraction β until the nth singular value $v(n)$ is a minimum, we can obtain the optimum β value that multiplied by the standard matrix S (or the concentration of standard equivalent) gives the concentration of each standard in the mixture.

Fig. 4 shows the plot of the logarithm of the singular values (v) against the β parameter, showing the minimum value that gives the correct β value. It must be stressed that adequate selection of the svd values is critical to obtain good results.

The results of the rank annihilation method are summarized in Table 4. It can be observed from Table 3 that the recovery values are closest to 100% in the case of VASS indicating that interferences are avoided, while RAM suffers the interference of the other components in the mixture to a considerable extent. This result can be assigned to the incapacity of RAM, a method that uses all the

spectral data to calculate the individual concentrations in the mixture, to eliminate the interferences arising from energy transfer or inner filter effects.

Finally, it must be pointed out that chromatographic resolution of this type of mixtures with severe spectral overlap, may be better and faster provided that no degradation of the products, during the chromatographic elution occurs. Moreover, in this case the use of cyclodextrin may be troublesome in the chromatographic elution.

4. Conclusions

Cyclodextrin-enhanced fluorescence determination of the pesticides aminocarb, carbendazim and coumatetralyl was performed by VASS and RAM. Fluorescence spectral distribution show great overlap that precludes the direct determination of this type of mixture. VAS shows better analytical performances than RAM due to the resolution of mixtures of overlapping fluorescence compounds.

Acknowledgements

Table 4
Recoveries of three ternary mixtures by RAM

Mixture	Compound	Taken (mg L^{-1})	Found (mg L^{-1})	Recovery (%)
1	Aminocarb	3	3.084	102.8
	Carbendazim	5	5.4	108
	Coumatetralyl	0.3	0.253	84.49
2	Aminocarb	1.5	1.569	104
	Carbendazim	2.5	2.33	93.16
	Coumatetralyl	0.15	0.178	118.72
3	Aminocarb	1.5	1.908	127.2
	Carbendazim	2.5	2.55	102
	Coumatetralyl	0.3	0.39	130

References

[1] F. García Sánchez, A.L. Ramos Rubio, V. Cerdá and M.T. Oms, Anal. Chim. Acta, 228 (1990) 293.

[2] M.T. Oms, R. Forteza, V. Cerdá, F. García Sánchez and A.L. Ramos, Int. J. Environ. Anal. Chem., 42 (1990) 1.

[3] F. García Sánchez, A. Fernández Gutiérrez and C. Cruces Blanco, Anal. Chim. Acta, 306 (1995) 313.

[4] T.T. Ndou and I.M. Warner, Chem. Rev., 91 (1991) 493.

[5] J.N. Miller, Analyst, 109 (1984) 191.

[6] B.J. Clark, A.F. Fell, K.T. Milne, D.M.G. Pattie and M.H. Williams, Anal. Chim. Acta, 70 (1985) 35.

[7] F. García Sánchez, A.L. Ramos Rubio, V. Cerdá and M.T. Oms, Talanta, 35 (1988) 335.

[8] S.E. Cabaniss, Anal. Chem., 63 (1991) 1323.

[9] S. Scypinski and L.J. Cline Love, Anal. Chem., 56 (1984) 322.

[10] I.M. Warner and L.B. McGown, Anal. Chem., 64 (1992) 343R.

[11] F. García Sánchez, A. Navas Díaz and L. Sánchez Feria, Anal. Lett., 27 (1994) 2171.

[12] C.-N. Ho, G.D. Christian and E.R. Davidson, Anal. Chem., 50 (1978) 1108.

[13] A. Benessi and J.H. Hildebrand, J. Am. Chem. Soc., 71 (1949) 2703.

Spectrofluorimetric determination of iron(III) with 2-pyridinecarbaldhyde-5-nitro-pyridylhydrazone in the presence of hexadecyltrimethylammonium bromide surfactant

Ki-Won Cha*, Chan-Il Park

Department of Chemistry, Inha University, Incheon 402-751, South Korea

Abstract

2-pyridinecarbaldehyde-5-nitro-pyridylhydrazone (2PC-5NPH) was synthesized and its application in the spectrofluorimetric determination of Fe(III) ions in the presence of surfactants was examined. An emission peak of 2PC-5NPH, which increased remarkably by the addition of Fe(III), occurs at 420 nm upon excitation at 300 nm, and allows for the sensitive, selective determination of the ferric ion in the 0.20–1.45 μg ml^{-1} range. The detection limit is 0.028 μg ml^{-1} in the presence of hexadecyltrimethylammonium bromide (CTMAB).

Keywords: Hexadecyltrimethylammonium bromide surfactant; Iron(III); 2-Pryidinecarbaldehyde-5-nitro-pyridylhydrazone; Spectrofluorimetric determination

1. Introduction

Because of the ever-increasing interest in the determination of trace elements in industrial, biological and environmental materials at low concentrations, there is a need for the development of more sensitive analytical methods. The spectrophotometric method involving the use of organic reagents is one of the inexpensive and reliable methods.

Fluorescence complexes of iron have received a great deal of attention. Few spectrofluorimetric methods for the determination of iron have been reported and most of them are based on the fluorescence quenching of indicators, owing to the inherent strong paramagnetism of iron cation [1]. Mori et al. [2] recently proposed a sensitive and convenient fluorimetric procedure for the determination of iron using o-hydroxyhydroquinonephthalein as the fluorgenic reagent in the presence of Brij-58.

Hydrazones, in particular, nitrogen-containing heterocyclic hydrazones have attracted much attention as analytical reagents, because of high sensitivity and selectivity, easy synthesis and good yield. Their applications have been reviewed by Katyal and Dutt [3] and later by Jain and Singh [4].

* Corresponding author. Fax: (82) 82 872 2520.

In recent years, surfactants have become of great interest because they provide a reaction medium in which the sensitivity and selectivity of numerous reactions are improved. For example, the metal complexes formed in micellar media are generally more stable than those formed in the absence of micelles [5,6]. Most prior work has focussed on spectrophotometric determinations, but surfactants are now also being applied successfully in fluorimetry [7–12], giving even higher sensitivity and lower detection limits. This first of such applications was the determination of aluminium with lumogallion in the presecnce of the non-ionic surfactant polyethylene glycol monolauryl ether. Recently, Sanz Medel [13] and Garcia Alonso [14,15] and Hinze et al. [16], have reviewed the topic of micellar media in fluorimetric analysis.
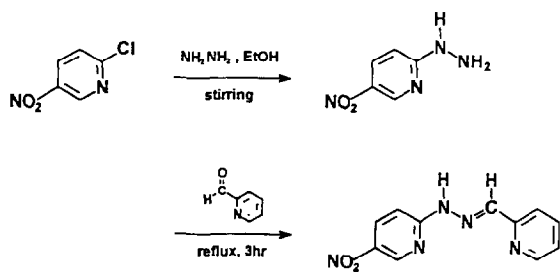
In this work, a new hydrazone, in which a nitro group was introduced in the 5-position of the pyridine ring moiety of 2-pyridinecarbaldehyde-pyridylhydrazone (2PC-5NPH), was synthesized and applied as a reagent for the determination of micro amounts of Fe(III). In addition, a study of the effect of surfactants on the fluorescence phenomena of the Fe(III)–2PC-5NPH complex was conducted.

The described, developed fluroscence method for ferric ion is sensitive, simple and very selective.

2. Experimental

2.1. Synthesis of 5-nitro-2-pyridylhydrazine

2PC-5NPH was synthesized according to Scheme 1 as follows: 1.58 g of 2-chloro-5-nitro-

pyridine was dissolved in 100 ml ethanol (0.01 M) at room temperature. To this solution was added dropwise, a solution of hydrazine monohydrate (7.5 g) with stirring. The mixture was stirred for an additional 60 min at room temperature, allowed to stand overnight in a refrigerator, filtered and dried at 50°C under reduced pressure to yield a red precipitate, which was used without purification in the next step, the synthesis of 2PC-5-NPH.

2.2. Synthesis of 2-pyridinecarbaldehyde-5-nitro-pyrdylhydrazone

2PC-5-NPH was synthesized by refluxing equimolar amounts of 2-pyridinecarbaldehyde and 5-nitro-2-pyridylhydrazine in ethanol–water (4:1, V/V) for 3 h. The product, a yellow crystal, was recrystallized from ethanol and dried at 110°C for 10 h under reduced pressure.

2.3. Reagent

Analytical-reagent grade chemicals and distilled, deionized water were used throughout. A iron(III) stock solution $(1 \times 10^{-3}$ M) was prepared by dissolving appropriate amounts of analytical grade $FeCl_3$ in doubly distilled water and this was standardized with EDTA [17]. Working solution were prepared by suitable dilutions of the stock solution with deionized water. The hexamethylenetetramine (HTM) was dissolved in deionized water.

Surfactant solutions were prepared by dissolving suitable amounts of surfactants in deionized water with gentle heating.

2.4. Apparatus

All fluorescence measurements were made with a Shimadzu RF-5000 spectrofluorophotometer using 1 cm quartz cells. The band passes were set at 5 nm for both the excitation and emission monochromators.

A Hitachi IR 435 infrared spectrophotometer, NOVA-310 pH meter and Yamato model MP-1 melting point apparatus were used. The surface tension of the soluble solutions were measured at 25°C $\pm$ 0.1 with a Fisher tensiometer equipped with a glass plate.

Scheme 1. Synthesis of 2PC-5NPH.

Table 1
Data of melting point, yields and infrared sprctra of synthesised hydrazone

Hydrazone	M.P. (°C)	Yield (%)	IR spectra (cm^{-1})		
			$\nu_{C=N}$	$\nu_{C=N}$	ν_{N-H}
5N-2PH	200	92.5	–	1420	1290
2PC-5NPH	236	71.8	1600	1423	1292

2.5. General procedure for the detemination of Fe(III) in the presence of surfactant

A 5 ml sample solution containing 1×10^{-4} M Fe(III) was placed in a 50 ml calibrated flask; 5.0 ml of 1×10^{-3} M 2PC-5NPH in methanol, 2.5 ml of 0.5 M hexamethylenetetramine and 10 ml of 1.0×10^{-3} M surfactant solution were added, then the contents were diluted to the mark with methanol and mixed thoroughly.

With excitation at 300 nm, fluorescence spectra and the fluorescence intensity at 420 nm were measured.

3. Results and discussion

3.1. Identification of the hydrazones

2PC-5NPH is yellowish solid which is slightly soluble in water but can be easily dissolved in methanol. Identification of the synthesized hydrazones was carried out by infrared (IR) spectra. IR spectra (potassium bromide pellet) of the synthesized hydrazones were measured in order to confirm their structures.

The spectra exhibited absorption peaks assigned to the stretching vibration of an azomethine bond ($-N=C<$) around 1600 cm^{-1}. The melting point, yield and IR spectral data of the synthesized hydrazones are summarized in Table 1.

3.2. Study of Fe(III)-2PC-5NPH complex

The 2PC-5NPH ligand reacted with Fe(III) to yield a yellow colored solution at pH 7.0. Fig. 1
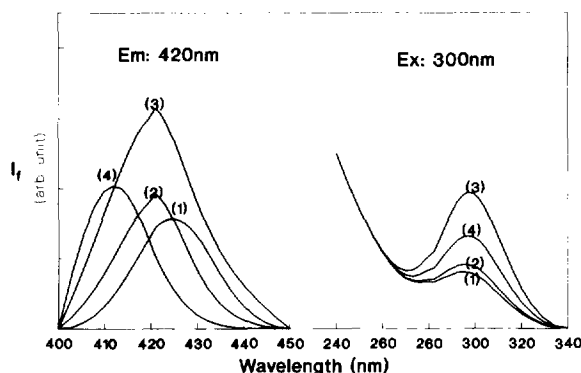

Fig. 1. Excitation (Ex) and emission (Em) spectra of 2PC-5NPH and its Fe(III) complex in 35% water and 65% methanol medium. (1) absence of Fe(III); (2) 2.6×10^{-7} M Fe(III); (3) 5.0×10^{-5} M Fe(III); (4) 1.0×10^{-4} M Fe(III): 1.0×10^{-4} M 2PC-5NPH.

shows the excitation and emission spectra of the reagent and its complex with Fe(III) at pH 7.0. The excitation and emission peak of the ligand were found to be 300 nm and 425 nm, respectively. As shown in Fig. 1, a remarkable increase in fluorescence intensity and absorbance of the ligand at each wavelength was observed in the presence of Fe(III). The excitation peak of the 2PC-5NPH in the precence of Fe(III) is also at 300 nm, but the emission peak shifts from 425 to 410–420 nm.

The pH effect on the fluorescence intensity of the Fe(III)-2PC-5NPH complex at 420 nm was made in the pH range 4.0–11.2 (Fig. 2). The
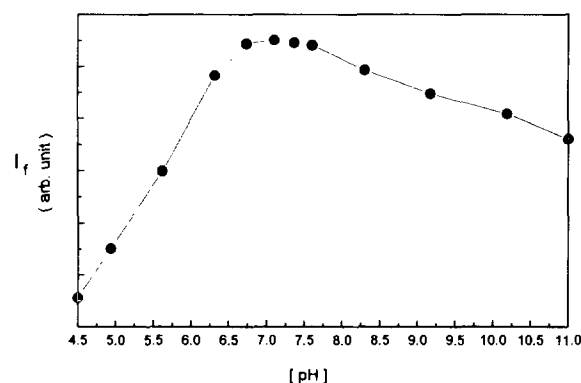

Fig. 2. Effect of pH on the fluorescence intensity of Fe(III)-2PC-5NPH in 35% water and 65% methanol medium. 2.0×10^{-5} M Fe(III): 1.0×10^{-4} M 2PC-5NPH.
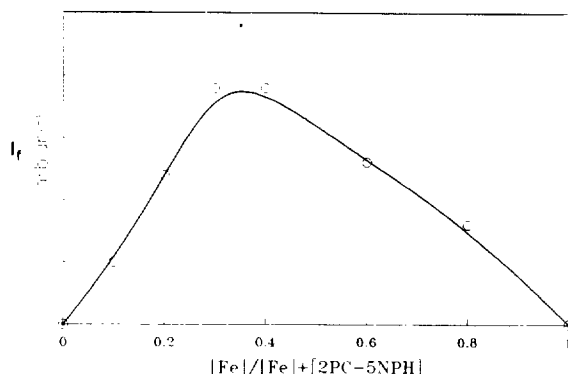
Fig. 3. Plot of the continuous variation method for formation of the Fe(III)–2PC-5NPH complex in 35% water and 65% methanol medium. [Fe^{3+}] and [2PC-5NPH]: 1.0 × 10^{-4} M.

results indicate that maximum fluorescence intensity was obtained at pH 7.0. Thus, pH 7.0 was selected as the optimum pH in further investigations. The solution pH was adjusted with hexamethylenetetramine solution and hydrochloric acid or sodium hydroxide.

In order to study the composition of Fe(III) and 2PC-5NPH, the mole ratio of Fe(III) and 2PC-5NPH in the Fe(III)-2PC-5NPH complex was determined using the continuous variation method.

The fluorescence intensity of each solution containing a different volume fraction of Fe(III) and 2PC-5NPH at the same concentration was measured. The results (Fig. 3) indicate that the mole ratio of Fe(III) and 2PC-5NPH in the complex was 1:2.

The composition of 2PC-5NPH and Fe(III) can be considered with the formation of the Fe(2PC-5NPH)$_2$ complex as follows:

$$Fe^{3+} + 2HL = FeL_2^- + 2H^+ \ (HL = 2PC\text{-}5NPH)$$
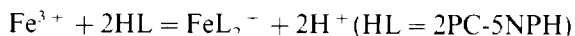
3.3. Effect of surfactant on the fluorescence intensity of the Fe(III)–2PC-5NPH complex

The effects of various surfactants were studied. As shown in Table 2 and Fig. 4, a remarkable increase of the absorbance and fluorescence intensity of the Fe(III)–2PC-5NPH complex was observed in the solution of cationic and non-ionic surfactants. The order of increase in absorbance and fluorescence intensity was hexadecyltrimethy-

Table 2
Fluorescent characteristics of Fe(III)–2PC-5NPH in the different surfactants

Surfactant	Concentration (M)	Fluorescence intensity λ_{em} (420 nm)	EF Em
None		21.8	1.0
CTMAB	1.0 × 10^{-4}	89.4	4.1
CPC	1.0 × 10^{-4}	32.7	1.5
DTMAB	1.0 × 10^{-4}	53.1	2.4
Triton X-100	1.0 × 10^{-4}	46.5	2.1
SDS	1.0 × 10^{-4}	20.6	0.9

Fe(III):1.8 × 10^{-5}; 2PC-5NPH: 1.0 × 10^{-4} M.
EF, enhancement factor.

lammonium bromide (CTMAB) > dodecyltrimethylammonium bromide (DTMAB) > Triton X-100 > cetylpridinium chloride (CPC). However, in a solution of the anionic surfactant, sodium dodecyl sulphate (SDS), a somewhat diminished fluorescence was observed.

3.4. Effect of CTMAB concentration

The greatest fluorescence intensity for the Fe(III)–2PC-5NPH complex was observed in the CTMAB surfactant. The influence of the CTMAB concentration on the fluorescence intensity of Fe(III)–2PC-5NPH complex is shown in Fig. 5.

The maximum fluorescence intensity of Fe(III)–2PC-5NPH was obtained at a CTMAB concentration of 2.0 × 10^{-4} M. Hence, 2.0 × 10^{-4}
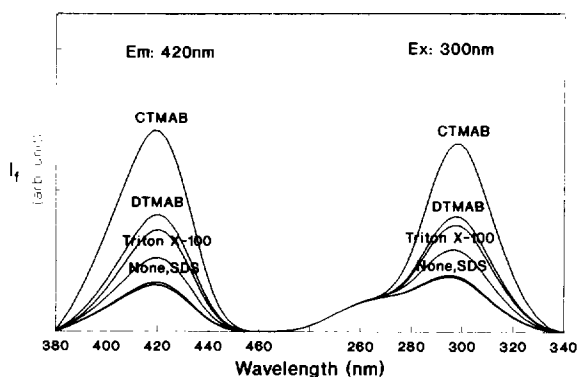

Fig. 4. Surfactant effects on the excitation and emission spectra of the Fe(III)–2PC-5NPH complex at pH 7.0. 1.8 × 10^{-5} M Fe(III); 1.0 × 10^{-4} 2PC-5NPH; 1 × 10^{-4} M surfactant.
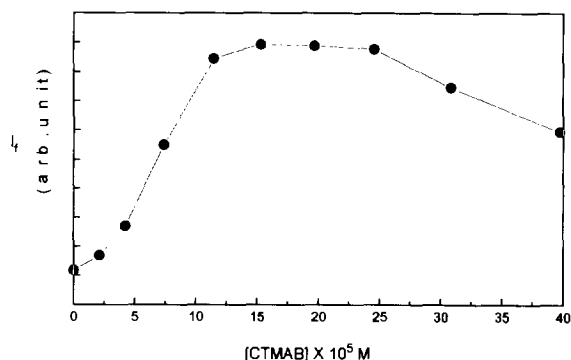
Fig. 5. CTMAB concentration effects on fluorescence intensity of Fe(III)–2PC-5NPH complex at pH 7.0. 1.8×10^{-5} M Fe(III); 1.0×10^{-4} M 2PC-5NPH.

M CTMAB was chosen as the optimum concentration in further studies.

The critical micellar concentration (CMC) of CTMAB in the water medium was determined as 5×10^{-4} M. When CTMAB was dissolved in the water above the CMC, the molecules of CTMAB exist mainly as a micelle state. The phenomenon of the increase of fluorescence intensity below 2×10^{-4} M can be considered as the solubility increase of Fe(III)–2PC–5NPH by the surfactant, but in a concentration higher than 2×10^{-4} M CTMAB, the bromide ion liberated from CTMAB reduced the fluorescence intensity of the complex.

The mole ratio of the Fe(III)–2PC-5NPH complex was also determined in the presence of 1×10^{-3} M CTMAB using the continuous variation method.

The mole ratio of Fe(III) and 2PC-5NPH in the presence of CTMAB was also 1:2.

3.5. Calibration curve

The conditions for determining Fe(III) with 2PC-5NPH were optimized. The most suitable concentration of 2PC-5NPH was found to be 1.0×10^{-4} M (for 1.0 μg ml^{-1} iron).

A linear relationship between fluorescence intensity and Fe(III) concentration was obtained in the 0.20–1.45 μg ml^{-1} range (Fig. 6). The calibration equation, obtained by the least-squares method, is: $Y = 1.496x - 0.04$ ($r = 0.997$, $n = 7$),
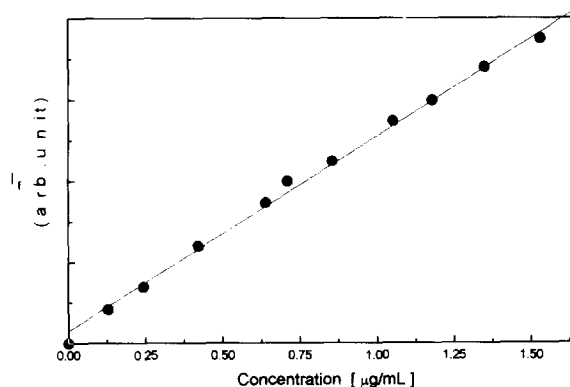

Fig. 6. Calibration curve of Fe(III)–2PC-5NPH at pH 7.0 using optimized procedure.

where Y is the relative fluorescence intensity, and x the concentration of Fe(III) in μg ml^{-1}. The detection limit ($S/N = 2$) was 0.028 μg ml^{-1} and the relative standard deviation at the 0.3 μg ml^{-1} iron level was 2.9% ($n = 7$).

3.6. Effect of foreign ions

The influence of common cations and anions on the determination of 1.0 μg ml^{-1} of Fe(III) was examined. The results are summarized in Table 3. The tolerated amounts of each ion were calcul-

Table 3
Effect of interfering ions on the determination of iron(III) (1 μg ml^{-1})

Interfering ion	Tolerated amount (μg ml^{-1})
Fe(II)	0.3
Cu(II)	0.1
Cd(II)	1.0
Pb(II)	10
Sn(II)	25
Al(III)	1.0
Pt(II)	4.0
Au(III)	10
Zr(IV)	3.0
Cr(II)	15
Pd(II)	0.5
Y(III)	15
Sc(III)	4.0
Oxalate	
Citrate	15
EDTA	

Condition: 2PC-5NPH: 1×10^{-4} M, CTMAB: 2×10^{-4} M.

ated as the concentration values which resulted in less than 5% deviation in the fluorescence intensity.

4. Conclusion

2PC-5NPH is a new fluorimetric reagent for the determination of Fe(III). The method described is very sensitive and selective for the direct determination of iron(III) over the range 0.20–1.45 μg ml^{-1} Fe(III). It was found that the fluorescence intensity of the Fe(III)–2PC-5NPH complex in the presence CTMAB was strongly enhanced. The excitation and emission peak of Fe(III)–2PC-5NPH are 300 nm and 420 nm, respectively, in both the presence and absence of CTMAB. The detection limit of the method is 0.028 μg ml^{-1}.

References

[1] A. Fernandez-Gutierrez and A. Munoz de la Pena. in S.G. Schulman (Ed.), Molecular Luminescence Spectroscopy; Methods and Applications, Part I, Wiley, New York, 1985, Chap. 4.

[2] I. Mori, Y. Fujita, K. Ikuta, Y. Nakahashi, K. Kato and N. Niwa, Anal. Lett., 22 (1989) 1969.

[3] M. Katyal and Y. Dutt, Talanta, 22 (1975) 151.

[4] P. Jain, R.P. Singh, Talanta, 29 (1982) 77.

[5] M. Falcon, J. Guiteras, A. Izquierdo and M.D. Prat, Talanta, 40 (1993) 17.

[6] M.P. San Andres, M.L. Marina and S. Vera, Talanta, 41 (1994) 179.

[7] W.L Hinze, K.L Mittal (Ed.), Solution Chemistry of Surfactants, Vol. 1, Plenum Press, New York, 1979, pp. 79–127.

[8] Gui-Fa Yan, Guo-Rong Shi and Yi-Ming Liu, Anal. Chim. Acta, 264 (1992) 121.

[9] J.J. Santana and J.D. Winefordner, Talanta, 39 (1992) 195.

[10] Ying-Xin Fan and Yong-Xi Zheng, Anal. Chim. Acta, 281 (1993) 359.

[11] J. Hernandez Garcia and J.J. Santana Rodriguez, Anal. Chim. Acta, 290 (1994) 146.

[12] S.M.Z. Al-Kindy and M.H. Abdel-Kader, Anal. Chim. Acta, 285 (1994) 329.

[13] N. Ishibashi and K. Kina, Anal. Lett., 5 (1972) 637.

[14] A. Sanz Medel and J.I. Garcia Alonso, Anal. Chim. Acta, 165 (1984) 159.

[15] A. Sanz Medel and J.I. Garcia Alonso, Anal. Chem., 57 (1985) 1681.

[16] W.L. Hinze, H.N. Singh, Y. Baba and N.G. Harvey, Trends Anal. Chem., 3 (1984) 193.

[17] A.I. Vogel, A Text Book of Quantitative Inorganic Analysis, 4th Edn., Longmans, London, 1978.

HPLC–Electrochemical detection with graphite–poly(tetrafluoroethylene) electrode Determination of the fungicides thiram and disulfiram

C. Fernández, A.J. Reviejo, L.M. Polo, J.M. Pingarrón*

Department of Analytical Chemistry, Faculty of Chemistry, Complutense University of Madrid, 28040 Madrid, Spain

Abstract

The suitability of composite graphite–poly(tetrafluoroethylene) (Teflon) electrodes as amperometric indicator electrodes in HPLC detection is demonstrated. The determination of the fungicides thiram and disulfiram in the presence of ziram has been chosen as an analytical problem. The optimization of working conditions, such as the choice of the organic solvent used in the mobile phase as well as its percentage, the potential applied to the composite electrode, and the time elapsed between mixing the carbamates and the injection, has been accomplished by using the wall-jet flow-cell configuration. The effect of the acetonitrile percentage used in the mobile phase on the retention of thiram, disulfiram, ziram and phenol was evaluated. Resolution up to the baseline can be achieved with 45% acetonitrile. The sensitivity of the determination of thiram and disulfiram in the presence of a constant concentration of ziram is slightly better when using a wall-jet cell; however, the background current is higher, as well as the baseline noise and the time necessary to achieve stabilization of the baseline before the injection. Lower limits of detection for both fungicides, as well as a better repeatability, were obtained when using a thin-layer flow cell configuration. As an application, the determination of thiram in spiked apple samples, at a level of 0.5 mg thiram kg^{-1} apple, has been carried out with a mean recovery of 97 $\pm$ 3% for a significance level of 0.05.

Keywords: Composite electrodes; Disulfiram; Graphite–Teflon; HPLC; Thiram

1. Introduction

The use of composite matrices, consisting of at least one conductor phase mixed with at least one insulator phase, for the fabrication of high performance indicator electrodes in flowing systems such as flow-injection analysis (FIA) and liquid chromatography (LC) is an area of increasing practical interest in modern electroanalysis. The main objective is, obviously, to improve the performance of conventional electrode materials such as glassy carbon (GC), essentially with regard to sensitivity and fouling of the electrode surface, which involves tedious chemical or electrochemical pretreatment of such a surface. An outstanding approach to achieve this is the use of carbon paste electrodes whose use in LC detection has

---

* Corresponding author.

been reviewed by Baldwin and Thomsen [1]. Nevertheless, some authors [2–4] have claimed that these electrodes show a lack of long-term stability in flowing streams mainly because of swelling phenomena. Several interesting strategies have been proposed to improve the mechanical stability of carbon electrode matrices, including the use of conductive carbon cement [5], or of several insulator materials such as Kel-F [6], epoxy [7], solid parafin [8], and Teflon (poly(tetrafluoroethylene)) [9].

Regarding Teflon–graphite electrodes, although Shah and Honigberg demonstrated in 1983 that these electrodes are useful for the electrochemical detection of phenolic compounds, separated by liquid chromatography [10], surprisingly, no further work on the use of this composite material for electrochemical detection (ED) in flowing systems was made until very recently, when our group reported flow-injection methods with amperometric detection based on the electrochemical oxidation of the N,N-dialkyldithiocarbamate fungicides thiram (tetramethylthiuram disulfide) and disulfiram (tetraethylthiuram disulfide) on these electrodes [11]. We showed that usual FIA methodologies used with conventional electrodes can also be applied to graphite–Teflon composite electrodes, which offer very advantageous properties from a practical point of view, in particular their compatibility with non-aqueous solvents and the very easy regeneration of the electrode when necessary.

In this paper, graphite–Teflon electrodes have been used as electrochemical detectors in HPLC. Because of the strong interference that the presence of thiram caused on the disulfiram amperometric signal, as well as the interference from other species previously tested [11] such as the fungicide zinc N,N-dimethyldithiocarbamate (ziram) and phenol, we have chosen the determination of both thiram and disulfiram in the presence of ziram as an analytical problem for evaluating graphite–Teflon composite electrodes as amperometric indicator electrodes in HPLC detection.

2. Experimental

2.1. Apparatus

Chromatographic separations were carried out using a Waters Model 510 (Millipore) solvent-delivery pump connected to a 10 cm × 0.46 cm i.d. C_{18} column packed with Lichrosorb RP18 with a particle size of 5 μm (Technokroma). Samples were injected by means of a Valco (Metrohm) injection valve with a sample loop of 10 μl. The column was thermostatted at 25°C.

Electrochemical detection was accomplished by using a Metrohm 656 detector provided with a Metrohm EA-1096 wall-jet cell. Detection with a thin-layer configuration was carried out with a Model MP-1305 EG&G PARC LC thin-layer cell. Electrode potentials were controlled by means of an Eco Chemie Autolab PSTAT 10 potentiostat equipped with the module ECD and using the software package GPES 3.1.

A P-Selecta Ultrasons ultrasonic bath, a P-Selecta Meditronic centrifuge, a W-2000 Heidolph rotary vacuum evaporator, and a Waring blender with glass container were also used.

2.2. Electrodes

Graphite–40% Teflon pellets were fabricated as described in a previous paper [9]. When working with the wall-jet cell, 3.0 mm diameter disk portions of the pellets were bored, and each disk was press-fitted into a Teflon holder. Electrical contact was made through a stainless-steel screw. A Metrohm Model 6.0727.000 Ag/AgCl/3 M KCl reference electrode and Metrohm Model 6.0333.010 gold counter electrode were also used.

When working with the thin-layer configuration, a cell body similar to that of the MP-1305 commercial cell was made from Teflon, leaving a 3.0 mm diameter hole in place of the conventional glassy carbon disk. This hole was partially refilled with carbon paste (Metrohm 6.2801.00) in order to allow electrical contact and finally, the 3.0 mm diameter graphite–40% Teflon disk was press-fitted into the cavity. The reference electrode used was an EG&G PARC Model P/N 219054 Ag/AgCl electrode.

2.3. Reagents and solutions

Thiram, disulfiram, ziram and phenol (Aldrich) stock solutions (2500 μg ml^{-1} in the case of thiram, disulfiram and phenol, and 750 μg ml^{-1} in the case of ziram) in acetonitrile (Panreac) were prepared weekly by weighing. More dilute standards were obtained by suitable dilution with acetonitrile. All stock solutions were stored at 4°C in the refrigerator.

The mobile phases used were mixtures of acetonitrile and 0.01 M phosphate buffer pH 7.4, and they were filtered through Whatman nylon membrane filters (0.45 μm pore size). All chemicals were of analytical-reagent grade, and the water used was obtained from a Millipore Milli-Q purification system.

2.4. Procedures

The graphite–Teflon electrode was polished daily for 5 s on a 150 grit SiC paper. No chemical or electrochemical regeneration of the electrode surface was then necessary during the whole working day.

Calibration graphs for both thiram and disulfiram were constructed with and without the presence of ziram as interference. They were obtained by injecting 10 μl aliquots of the appropriate stock solution of a mixture of the three herbicides in pure acetonitrile into the mobile phase (55:45 v/v mixture of 0.01 M phosphate buffer pH 7.4 and acetonitrile) at a flow rate of 2.0 ml min^{-1} (pressure = 1400 p.s.i.). Injections were carried out immediately after the preparation of the mixture solution of ziram, thiram and disulfiram, in that order. The oxidation signals were recorded at + 1.0 V vs. Ag/AgCl.

2.5. Determination of thiram in spiked apple samples

About 50 g of cut apple sample was weighed accurately and transferred to a blender. Then 50 μl of a 500 μg ml^{-1} thiram stock solution and 125 ml of chloroform were added. The mixture was homogenized at 18 500 rev min^{-1} for 1 min and transferred into six 35 ml centrifuge tubes.

The blender was rinsed several times with water and the rinsings were added to the tubes. After centrifugation at 4000 rev min^{-1} for 10 min, the organic phase was filtered through a Buchner funnel fitted with a No. 4 glass frit (10–16 μm diameter), transferred to a 250 ml vessel of the rotary vacuum evaporator, and evaporated to dryness at room temperature. The residues were dissolved in 4.5 ml of acetonitrile with the aid of ultrasonic stirring, filtered through nylon membrane filters of 0.2 μm pore size (Lida), and collected in a 5 ml volumetric flask, diluting to the mark with acetonitrile. A 10 μl portion of this solution was injected into the HPLC column, and chromatographed at a flow rate of 2 ml min^{-1}. The determination of thiram was carried out using a calibration graph, in the range 5.0–25.0 μg ml^{-1}, obtained by adding aliquots of fungicide stock solution to a blank apple sample subjected to the above treatment.

3. Results and discussion

The optimization of working conditions, such as the choice of the organic solvent used in the mobile phase as well as its percentage, the potential to be applied to the composite electrode, and the time elapsed between mixing the carbamates and the injection, was accomplished by using the wall-jet flow-cell configuration. The composite electrode composition, i.e. a mixture of graphite–40% Teflon, as well as the aqueous component of the mobile phase (phosphate buffer pH 7.4), were the same as those used in previous works [9,11].

3.1. Choice of the mobile phase

Prior to the coupling of the chromatographic column to the system, some assays were carried out in order to estimate the amperometric response of a graphite–40% Teflon electrode to the decrease in the polarity of 0.01 mol l^{-1} phosphate buffer (pH 7.4) carrier solution, due to the addition of different methanol or acetonitrile ratios. In order to do this, 60 μg ml^{-1} aliquots of thiram solutions prepared in the same medium as the carrier were injected into the flowing system with

no chromatographic column. The flow rate was 2.0 ml min^{-1}, and the applied potential + 1.0 V [11].

As the organic solvent percentage increased, a sharp decrease in the peak current as well as an increase in the background current were observed. The amperometric signal decreased by 80% if 25% methanol was used in the mobile phase, and by 95% if 50% was employed. If 75% methanol was used, the analytical signal was lower than the baseline noise.

When using acetonitrile, the signal decrease was somewhat lower. If the mobile phase contained 25% acetonitrile, i_p was 70% lower than in 0.01 M phosphate buffer medium, but the noise level and the background current were lower than when using methanol. For 75% acetonitrile, precipitation of phosphate was observed. Taking into account these results, acetonitrile was chosen as mobile phase modifier.

In previous work [11], amperometric flow-injection measurements of thiram and disulfiram in aqueous carrier solutions, using graphite–Teflon composite electrodes, were made by applying a potential of + 1.0 V to the electrodes. Nevertheless, in order to ascertain if the use of an acetonitrile:phosphate buffer mixture as mobile phase could affect this potential value for amperometric detection, the peak current values measured at different applied electrode potentials within the
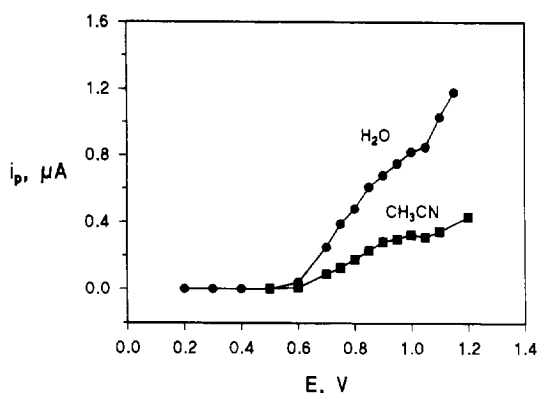

Fig. 1. Influence of the applied potential on the thiram peak current for a graphite–40% Teflon composite electrode. Carrier: (●) 0.01 M phosphate buffer (pH 7.4); (■) 40:60 v/v acetonitrile: 0.01 M phosphate buffer (pH 7.4). Flow rate 2.0 ml min^{-1}.

range 0.50–1.20 V were examined. Fig. 1 shows data obtained from 10 μl injections of 180 μg ml^{-1} thiram in a medium consisting of 40:60 v/v mixture of acetonitrile and 0.01 M phosphate buffer pH 7.4, used as mobile phase. Data obtained in 0.01 M phosphate buffer with no acetonitrile added are also displayed for comparison purposes. As can be seen, the shape of these plots is similar in both cases showing well-defined plateau zones between + 0.90 and + 1.1 V, and consequently, the same potential value of + 1.0 V was chosen to be applied to the graphite–Teflon electrode in subsequent experiments.

A very important aspect of the practical use of graphite–Teflon composite electrodes is to show how this material improves the performance of conventional electrodes, in particular of GC electrodes, in flowing conditions. Fig. 2 shows successive injections of 2.25 μg disulfiram, using the same carrier solution mentioned above, at both graphite–Teflon (A) and glassy carbon (B) amperometric indicator electrodes. As can be clearly seen, successive responses are highly reproducible when using the composite electrodes, whereas dramatic fouling of the electrode surface, leading to disappearance of the disulfiram peak, becomes evident in the case with a GC electrode. Furthermore, the magnitude of the peak current is very much larger at the graphite–Teflon electrode. Another important difference is the time needed to attain a stable baseline. As can also be observed in Fig. 2, a constant background current is reached after approximately 400 s in the case of the composite electrode, whereas at least 1500 s is needed when GC is used. All these practical aspects confirm the potentiality of graphite–Teflon composite electrodes as suitable indicator electrodes in flowing systems.

3.2. Separation of thiram, disulfiram, ziram and phenol

The effect of the acetonitrile percentage used in the mobile phase on the retention characteristics of thiram, disulfiram, ziram and phenol was evaluated. The respective capacity factors, when 0.6 μg of each substance was injected individually in mobile phases of different acetonitrile:phosphate
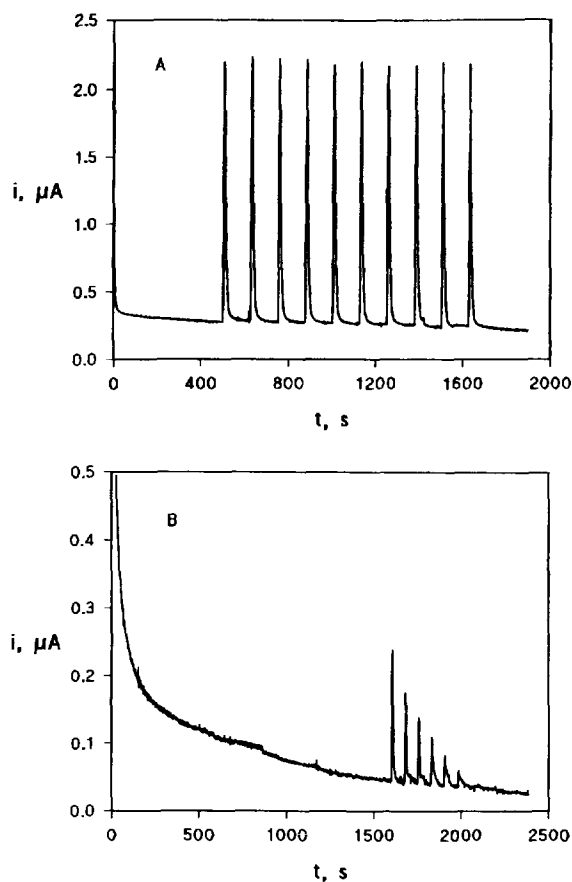
Fig. 2. Successive injection of 2.25 μg disulfiram in a 40:60 v/v mixture of acetonitrile and 0.1 M phosphate buffer pH 7.4 using (A) a graphite–40% Teflon electrode, (B) a GC electrode, as amperometric detector. Flow rate: 2.0 ml min⁻¹.

buffer ratios, are shown in Table 1. As can be deduced, ziram does not interact with the column, and its retention time practically coincides with the value of t_0 calculated from the quality control data of the column. However, no baseline perturbation at t_0 was detected when pure acetonitrile was injected and, consequently, the determination of ziram would also be possible. The k' values in Table 1 were calculated by taking the ziram retention time as t_0.

When acetonitrile percentages of 40% or lower were used, disulfiram exhibited retention times higher than 30 min and, therefore, its signal became broader and the analysis time increased considerably. However, as expected, when the acetonitrile content in the mobile phase increased,

the peak areas for both thiram and disulfiram decreased remarkably due to a lowering of the diffusion coefficient with changing ionic strength and viscosity of the medium. Resolution up to the baseline of the three fungicides can be achieved when an acetonitrile percentage of 45% is used.

When a solution containing a binary mixture of thiram and disulfiram was chromatographed, two peaks were obtained if the injection was made immediately after preparing the mixture. However, if a few minutes elapsed before the injection, a third peak appeared, probably corresponding to N,N-diethyl-N',N'-dimethylthiuram disulfide, with an intermediate retention ($k' = 6.9$ for 50% acetonitrile in the mobile phase). This effect has been described previously in the literature [12]. Fig. 3 shows chromatograms corresponding to a mixture of 60 μg ml⁻¹ thiram and 60 μg ml⁻¹ disulfiram when the injection (10 μl) was accomplished just after the preparation of the mixture, and after different elapsed times. As the time elapsed between preparation of the mixture and injection increased, the peak areas for thiram and disulfiram decreased and that of the compound with an intermediate retention increased up to approximately 90 min.

The above-mentioned third peak was not observed if a mixture of thiram and ziram was chromatographed, even though the injection was carried out 90 min after the preparation of the binary mixture solution. On the contrary, if a mixture of ziram with disulfiram was analysed, four peaks appeared in the chromatogram regis-

Table 1
Capacity factors for thiram, disulfiram, ziram and phenol in acetonitrile:phosphate buffer mobile phases. 0.6 μg of each substance injected. Flow rate: 2.0 ml min⁻¹

Fungicide	Mobile phase Acetonitrile: 0.01 M phosphate buffer (pH 7.4)			
	40:60	45:55	50:50	60:40
Ziram	0	0	0	0
Phenol	2.0	1.3	1.1	0.9
Thiram	7.0	4.2	3.0	2.0
Disulfiram	32.3	28.6	15.9	7.9

C. *Fernández et al. / Talanta 43 (1996) 1341–1348*
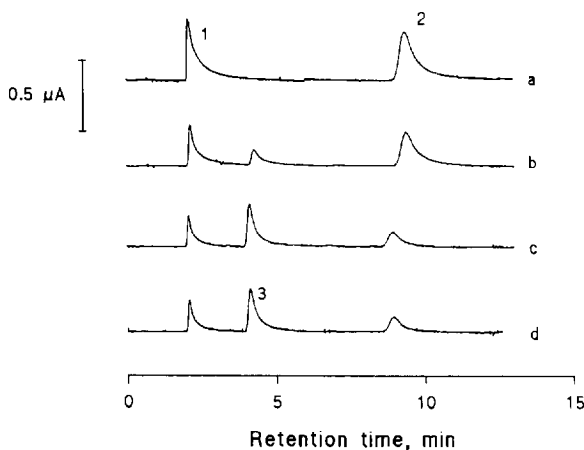

Fig. 3. HPLC-ED response for injections of a mixture of 60 μg ml^{-1} thiram (1) and 60 μg ml^{-1} disulfiram (2), when the injection was accomplished immediately after preparing the mixture (a), and 15 (b), 90 (c), and 180 min (d) later; (3) N,N-diethyl-N',N'-dimethylthiuram disulphide. Mobile phase. 50:50 v/v acetonitrile: 0.01 M phosphate buffer (pH 7.4); flow rate. 2.0 ml min^{-1}; E_{app} = + 1.0 V; volume injected, 10 μl.

Fig. 5. HPLC-ED response for a sample containing 30 μg ml^{-1} ziram (1), 30 μg ml^{-1} phenol (2), 30 μg ml^{-1} thiram (3), and 60 μg ml^{-1} disulfiram (4) injected immediately after preparing the mixture. Mobile phase, 38:62 v/v acetonitrile:0.01 M phosphate buffer (pH 7.4). Flow rate: 1.5 ml min^{-1} from (a) to (b), and 5.0 ml min^{-1} after (b).

tered some minutes after the injection, with capacity factors of 0, 3.0, 6.4 and 15.7, when 50% acetonitrile in the mobile phase was used (Fig. 4). The retention time of the second eluate was coincident with the retention time of thiram under the same conditions, and so it can be deduced that ziram, thiram, disulfiram and the aforementioned N,N-diethyl-N',N'-dimethylthiuram disulfide co-
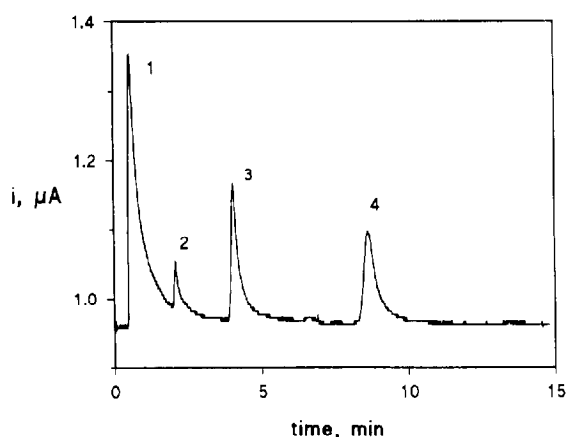
existed in solution.

Resolution up to the baseline of the peaks corresponding to the above-mentioned four compounds can be achieved with 45% of acetonitrile in the mobile phase and a flow rate of 2.0 ml min^{-1}. Consequently, these working conditions were chosen for all subsequent studies (calibration graphs and determination of thiram in apple samples), except those in which phenol was involved. However, if phenol was also present in the test solution, its peak overlapped with that of ziram, although this did not prevent the determination of thiram and disulfiram. If a complete separation of all these compounds was desired, a lower acetonitrile percentage had to be used, as well as a modification of the flow rate when running the chromatogram in order to avoid an excessive retention of disulfiram. This increase in the flow rate produced a baseline drift, as would happen if this problem was solved by using a mobile phase gradient. Fig. 5 shows a chromatogram obtained from a mixture containing ziram, phenol and thiram, each of them at 30 μg ml^{-1} level, and 60 μg ml^{-1} disulfiram using 38% acetonitrile in the mobile phase, and a flow rate of 1.5 ml min^{-1} between the points marked (a) and (b) in the chromatogram, and a flow rate of 5.0 ml min^{-1}

Fig. 4. Chromatogram obtained for a mixture of 60 μg ml^{-1} ziram (1) and 60 μg ml^{-1} disulfiram (4) injected 90 min after preparing the mixture, (2) thiram, and (3) N,N-diethyl-N',N'-dimethylthiuram disulphide. Conditions as in Fig. 3.
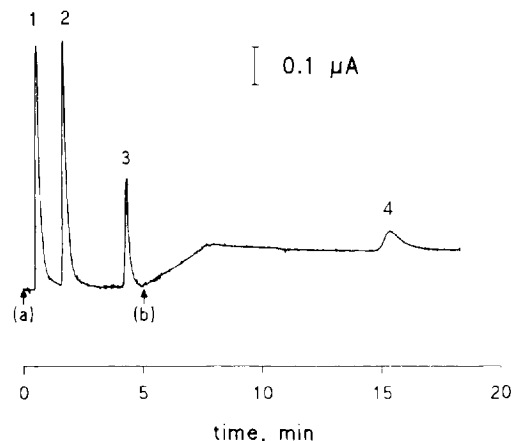
Table 2
Analytical characteristics of the calibration graphs for thiram and disulfiram in the presence of ziram, obtained by HPLC with amperometric detection at a graphite- Teflon composite electrode; E_{app} = +1.0 V; 45% acetonitrile in the mobile phase; flow rate, 2.0 ml min⁻¹; volume injected, 10 μl

Fungicide	Flow-cell configuration	Range of linearity (mg l⁻¹)	Correlation coefficient	Slope (μA s mg⁻¹)	Intercept (μA s)	RSD (%)	Determination limit (mg l⁻¹)	Detection limit (mg l⁻¹)
Thiram	Wall-jet	2 10	0.998	0.212 ± 0.008	−0.039 ± 0.05	5.3	1.2	0.4
		10- 100	0.9990	0.24 ± 0.03	−0.7 ± 0.9			
	Thin-layer	1–10	0.993	0.20 ± 0.02	0.01 ± 0.06	3.5	0.49	0.14
		10–100	0.9998	0.1343 ± 0.0002	0.4 ± 0.2			
Disulfiram	Wall-jet	6 10	0.99997	0.19 ± 0.02	0.0 ± 0.1	6.4	3.4	1.0
		10- 100	0.9992	0.16 ± 0.01	0.3 ± 0.6			
	Thin-layers	4- 10	0.9990	0.13 ± 0.01	0.01 ± 0.09	4.9	2.3	0.7
		10- 100	0.9998	0.123 ± 0.003	0.1 ± 0.2			

from (b). A 10 μl aliquot was injected immediately after the preparation of the mixture.

3.3. Calibration graphs. Comparison of wall-jet and thin-layer flow-cell configurations

Calibration graphs for both thiram and disulfiram in the presence of a constant concentration of ziram (45 and 4.5 μg ml⁻¹ for the upper and lower concentration ranges considered respectively) were constructed. For comparison purposes, both wall-jet and thin-layer flow-cell configurations were employed to obtain these calibration graphs. Ranges of linearity appear in Table 2. Sensitivity is always slightly better when using the wall-jet cell. However, background current is higher, as well as baseline noise and the time necessary to achieve stabilization of the baseline before the injection (35–40 min in the case of a wall-jet cell configuration vs. 10 min with a thin layer cell).

The analytical characteristics calculated from the respective calibration graphs are listed in Table 2. Relative standard deviations were calculated from 10 different solutions containing 2.0 μg ml⁻¹ thiram, 6.0 μg ml⁻¹ disulfiram and 4.5 μg ml⁻¹ ziram in the case of the wall-jet configuration, and 1.0 μg ml⁻¹ thiram, 4.0 μg ml⁻¹ disulfiram and 4.5 μg ml⁻¹ ziram for the thin-

layer configuration. The limits of determination and detection were calculated according to the 10 × standard deviation and the 3s criteria respectively, where s is the standard deviation of the signals from the above-mentioned solutions. As can be deduced, lower limits of determination and detection were obtained, as well as a better repeatability, for both thiram and disulfiram when using a thin-layer flow-cell configuration.

3.4. Determination of thiram in spiked apple samples

As an application of the HPLC with amperometric detection method using the graphite–PTFE composite electrode, the determination of thiram in spiked apple samples, at a level of 0.5 mg thiram kg⁻¹ apple, was carried out by applying the procedure described in Section 2. Thiram is widely used as an active fungicide, having been found in apples, and the amounts allowed in agricultural applications are 0.03–0.01 g kg⁻¹ [13]. In the European Union regulations tolerances for dithiocarbamates are drafted as 2–7 mg kg⁻¹ (expressed as carbon disulfide). The proposed procedure was first applied to a blank apple sample to which no thiram was added. The signals obtained when an aliquot of the blank sample extract was injected (1), as well as those corre-

sponding to succesive additions of 5 μg ml⁻¹ thiram to different aliquots of this extract (2–6). are shown in Fig. 6. The slope and intercept of the calibration plot constructed in this way were 0.120 ± 0.006 μA s 1 mg⁻¹ and 0.1 ± 0.1 μA s respectively ($r = 0.9995$). As can be observed, a chromatographic peak due to an unknown endogenous compound present in the apple appeared before the peak of thiram. This endogenous peak did not interfere with the thiram analytical signal, thus allowing thiram determination under the chosen working conditions.

For three determinations of apple samples spiked with thiram at a concentration level of 0.5 μg g⁻¹ (which implies a final thiram concentration in the analytical solution of 5.0 μg ml⁻¹). an experimental mean concentration of 4.8 ± 0.2 μg ml⁻¹ (0.48 ± 0.02 μg g⁻¹) was obtained with a mean recovery of 97 ± 3% for a significance level of 0.05. This recovery is better than that obtained by other authors in the same type of sample and at the same pesticide concentration level, using different HPLC with UV detection methodologies [14–16], indicating that the method proposed here is suitable for the determination of thiram in apple samples.
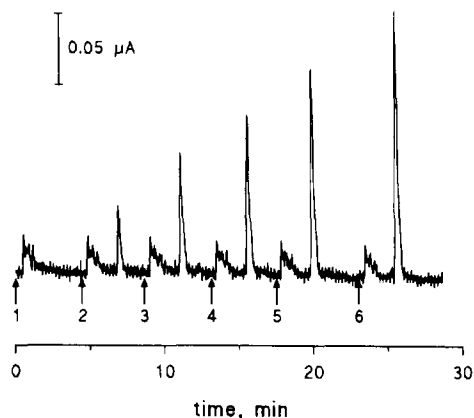

Fig. 6. HPLC–ED response with a graphite–Teflon electrode for an apple sample extract: (1) blank sample extract; (2)–(6) successive additions of 5 μg ml⁻¹ thiram to different aliquots of this extract. Mobile phase. 45:55 v/v acetonitrile: 0.01 M phosphate buffer (pH 7.4); flow rate, 2.0 ml min⁻¹; $E_{app} = +$ 1.0 V; volume injected, 10 μl.

4. Conclusions

All the aforementioned results demonstrate the suitability of graphite–Teflon composite electrodes for use as electrochemical detection systems in HPLC. The methodologies employed with conventional electrodes can also be used with these consolidated segregated composites which offer very advantageous practical properties, such as their compatibility with non-aqueous solvents, resistance to fouling, and the very easy regeneration of the electrode surface when necessary.

Acknowledgements

References

[1] R.P. Baldwin and K.N. Thomsen, Talanta, 38 (1991) 1.
[2] J.A. Cox, R.K. Jaworski and P.J. Kulesza, Electroanalysis, 3 (1991) 869.
[3] K. Stulik, V. Pacakova and B. Starkova, J. Chromatogr., 213 (1981) 41.
[4] A. Amine and J.M. Kauffmann, Bioelectrochem. Bioenerg., 34 (1994) 123.
[5] H. Huang and W.T. Kok, Anal. Chim. Acta, 273 (1993) 245.
[6] D.E. Tallman and S.L. Petersen, Electroanalysis, 2 (1990) 499.
[7] J. Wang, Anal. Chem., 53 (1981) 2280.
[8] C. Petit and J.M. Kauffmann, Anal. Proc., 32 (1995) 11.
[9] C. Fernández, A.J. Reviejo and J.M. Pingarrón, Anal. Chim. Acta, 305 (1995) 192.
[10] M.H. Shah and I.L. Honigberg, Anal. Lett. 16 (1983) 1149.
[11] C. Fernández, A.J. Reviejo and J.M. Pingarrón, Anal. Chim. Acta, 314 (1995) 13.
[12] R.M. Smith, R.L. Morarji and W.G. Salt, Analyst, 106 (1981) 129.
[13] E. Brandšteterová, L. Lehotay, O. Liška and J. Garaj, J. Chromatogr., 354 (1986) 375.
[14] K.H. Gustafsson and R.A. Thompson, J. Agric. Food Chem., 29 (1981) 729.
[15] K.H. Gustafsson and R.A. Thompson, J. Agric. Food Chem., 31 (1983) 463.
[16] R.A. Baumann, E. Dijkman, E.A. Hogendoorn and P. Van Zoonen, Rijksuniversiteit. Gent. 56 (1991) 941.

Synchronous fluorimetric determination of salicylic acid and diflunisal in human serum using partial least-squares calibration

A. Muñoz de la Peña*, M.D. Moreno, I. Durán-Merás, F. Salinas

Department of Analytical Chemistry, University of Extremadura, 06071 Badajoz, Spain

Abstract

The simultaneous determination of salicylic acid and diflunisal in human serum has been accomplished by synchronous fluorimetry, in combination with partial least-squares multivariate calibration. The total luminescence information of the analytes has been used to optimize the spectral data set for the calibration, by analysis of the three-dimensional excitation–emission matrices. The synchronous spectrum, maintaining a constant difference of $\Delta\lambda = 128$ nm between the emission and excitation wavelengths, has been selected as optimum to perform the determination. The method is based on the fluorescence of these compounds in chloroform containing 1% (v/v) acetic acid. Serum samples are treated with trichloroacetic acid to remove the proteins, and both analytes are extracted into chloroform–1% (v/v) acetic acid prior to the determination. For concentrations ranging from 60–240 μg ml^{-1} of each drug, analytical recoveries range from 96% to 103% for salicylic acid and from 97% to 105% for diflunisal.

Keywords: Diflunisal; Partial least-squares; Salicylic acid; Synchronous Fluorimetry

1. Introduction

Diflunisal [2-hydroxy-5-(2,4-difluorophenyl) benzoic acid] is a ring-substituted salicylic acid derivative with analgesic and anti-inflammatory properties which make the drug useful for the treatment of osteoarthritis [1]. A comparison of the pharmacological profile of diflunisal with those of some well-known anti-inflammatory agents, such as aspirin, ibuprofen and indomethacin, showed that diflunisal is more potent and less toxic than these drugs [2].

Two reports [3,4] have appeared demonstrating that diflunisal significantly interferes with salicylate measurements in most methods used in the routine analysis of this drug: photometry, fluorimetry and fluorescence polarimetry. This interference is a problem if the salicylate concentration determined by these methods is used for therapeutic monitoring, or in emergency toxicology screening of salicylate [3].

To analyze mixtures of salicylic acid and diflunisal in serum samples, gas chromatography [5] or high performance liquid chromatography [6] have been used.

Recently, a non-chromatographic method has been proposed for the simultaneous determination

---

* Corresponding author.

of diflunisal and salicylic acid in human serum by second-derivative synchronous fluorimetry [7].

Multivariate statistical methods, such as principal component regression (PCR) and partial least-squares (PLS), have been applied in the analysis of mixtures, using mainly infrared or UV/visible absorption spectroscopy. Only a small number of methods have been described in which fluorescence data are used for multicomponent analysis, by multivariate calibration methods [8]. Lindberg et al. [9] applied PLS calibration, for the first time, to emission fluorescence data, analyzing mixtures of humic acid and ligninsulfonate. Martens and co-workers [10–12] quantified three botanical components, pericarp, aleurone and endosperm, in several wheat varieties, to analyse the cereal composition, by applying PLS calibration. To perform the determination, a combination of several emission scans, recorded at different excitation wavelengths, characteristics of each of the mixture components, was used as the spectral data set.

Jones et al. [13] reported the use of excitation, emission and synchronous spectra for the determination of acyclovir and guanine, applying several multivariate calibration methods. In addition, they investigated the utilization of second-derivative synchronous spectra in the multivariate calibration methods. They found that the use of synchronous spectral data was the best choice for the determination of acyclovir, whereas the use of second-derivative synchronous spectra was the best choice for the determination of guanine.

Sánchez Peña et al. [14] applied PLS to the analysis of binary mixtures of sulfonamides by photochemically-induced fluorimetry. Recently [15], we reported on the optimization of the spectral data set for the resolution of ternary mixtures of salicylic acid and two of its main urinary metabolites, salicyluric acid and gentisic acid. The excitation spectrum was found to be the best spectral data set to determine salicylic and salicyluric acids, while the emission spectrum was the optimum for gentisic acid determination by PLS or PCR methods. Later on [16], the PLS method was applied to the determination of the three compounds in urine samples, using a data set composed of the excitation plus the emission spectra as the analytical signal.

In the present study, a method is reported for the simultaneous determination of salicylic acid and diflunisal in serum samples, by combination of synchronous fluorimetry and PLS multivariate calibration.

2. Experimental

2.1. Reagents

Stock solutions of salicylic acid (Merck) and diflunisal (Sigma), containing 500 μg ml^{-1}, were prepared in chloroform containing 1% (v/v) acetic acid. Working standard solutions were prepared by appropriate dilution. A 160 g l^{-1} solution of trichloroacetic acid in chloroform and a 0.5 M buffer solution of glycine/sodium hydroxide pH 9.4 were also used.

2.2. Apparatus

Fluorescence measurements were made on an SLM Aminco Bowman Series 2 luminescence instrument, equipped with a 150 W continuous xenon lamp, interfaced with a PC 386 microcomputer. Data acquisition and data analysis were performed with the use of AB2 software version 1.40, running under OS/2 2.0. The excitation and emission slits were both maintained at 8 nm. The scan rate of the monochromators was maintained at 4 nm s^{-1} for recording conventional spectra, and at 30 nm s^{-1} for the acquisition of three-dimensional excitation–emission spectra. All measurements were performed in 10 mm quartz cells, at 20°C, by use of a thermostatic cell holder and a Selecta model Frigiterm thermostatic bath.

2.3. Software

The GRAMS-386 Level I version 2.0 software package, with the PLS plus version 2.1G application software [17], was used for the statistical treatment of the data and the application of the PLS multivariate calibration method. The digitized spectra acquired with the Series 2 luminescence instrument were converted to ASCII XY format with the converter included in the AB2

software, and imported to the GRAMS-386 program through the included ASCII XY converter. A converter program running in BASIC, developed by us, was used to transform the bidimensional files, in ASCII XY format, to the software package SURFER for Windows [18], to obtain the three-dimensional excitation–emission matrices presented as contour plots. The contour plots in the two dimensions of excitation and emission are generated by linking points of equal fluorescence intensity to form the contour map.

2.4. Optimization of the procedure

In the literature, several methods have been proposed for determining salicylic acid or diflunisal in biological samples. Some of the procedures described for the determination of salicylic acid in biological fluids used a preliminary step of extraction in chloroform in acid medium and re-extraction of salicylic acid to aqueous solution in basic medium [15,19–21]. We performed several experiments to examine if this method was appropriate for the determination of salicylic acid and diflunisal in mixtures. Aliquots of serum were spiked with different quantities of salicylic acid or diflunisal and extraction with chloroform in hydrochloric acid medium was performed. An aliquot of the organic phase was taken and glycine/NaOH buffer solution pH 9.4 was used for the re-extraction. The fluorescence of the aqueous phase was measured. The obtained recoveries for salicylic acid were always higher than 95%; however, the recoveries found for diflunisal were between 80% and 90%. In consequence, this method was not adequate for the determination of both drugs in mixtures.

An alternative procedure, recently described in the literature [7], was investigated. The method used trichloroacetic acid to remove proteins, and extraction of salicylic acid and diflunisal into chloroform–1% (v/v) acetic acid solution prior to instrumental determination. Chloroform containing 1% (v/v) acetic acid has also been previously reported as a solvent mixture for the fluorimetric determination of salicylic acid in the presence of aspirin [22]. Using this approach, the recoveries were satisfactory for both drugs.

2.5. Procedure

Place 0.4 ml of serum containing 25–250 μg ml^{-1} of salicylic acid and 25–250 μg ml^{-1} of diflunisal into a test tube. Add 0.12 ml of trichloroacetic acid solution in chloroform and 1.6 ml of the chloroform–1% v/v acetic acid solution. Sonicate for 5 min and centrifuge for 3 min at 1500g. Take a 0.3 ml aliquot of the organic layer and dilute to 6 ml with chloroform–1% v/v acetic acid solution, for the measurements. Record the synchronous fluorescence spectra, maintaining a constant difference $\Delta\lambda = \lambda_{em} - \lambda_{ex} = 128$ nm, in the excitation range 231–364 nm. Use the synchronous spectra as the analytical signal to make the calibration. Perform the PLS-1 calibration with a calibration set of 16 samples following a two-factor, four-level design, in the final concentration ranges varying from 0.25–2.5 μg ml^{-1} and 0.25–2.5 μg ml^{-1} for salicylic acid and diflunisal respectively. Apply the optimized calibration matrix, calculated by application of the PLS-1 method, to analyze the synchronous spectra of the problem samples, and determine the concentrations of salicylic acid and diflunisal in the serum samples.

3. Results and discussion

3.1. Optimization of chemical variables

The excitation and emission spectra of both analytes were recorded in a solution of chloroform–1% (v/v) acetic acid. In this solvent mixture, salicylic acid shows an excitation maximum at 312 nm and an emission maximum at 444 nm, while diflunisal shows two excitation maxima, at 262 nm and 324 nm, and two emission maxima, at 402 nm and 448 nm.

Serum samples were treated as described in Section 2.5, and the fluorescence intensity was measured at the corresponding excitation and emission maxima of salicylic acid and diflunisal respectively. In both cases, recoveries higher than 95% were obtained and, in consequence, this procedure was selected for the analysis.

3.2. Contour plots

When using fluorescence data for calibration, two variables, the excitation and emission wavelengths, are available for optimization. When using fluorescence data, the prior optimization of the spectral data set, before the application of a multivariate calibration procedure, has been previously suggested and exploited [13,15,16].

The selection of the optimum spectral data set to perform the determination is best examined by collecting the total luminescence spectrum of each of the analytes, in the form of an excitation–emission matrix (EEM). The EEMs were collected by scanning the emission spectra, between 300 and 540 nm, at increments of the excitation wavelength of 4 nm, between 200 and 440 nm, and displayed as contour plots. Fig. 1 shows the contour plots corresponding to salicylic acid and diflunisal in chloroform–1% (v/v) acetic acid solution. The spectral data sets selected are represented in the contour plots as solid lines slicing the data matrix. To make the selection of the corresponding scanning conditions to obtain the
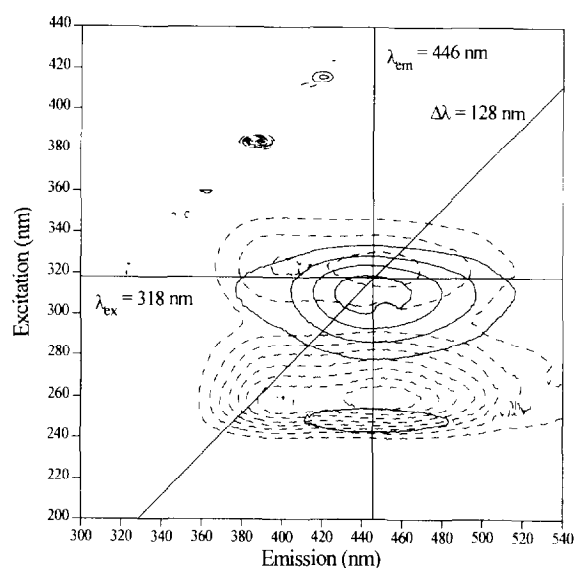

Fig. 1. Contour plots of the total fluorescence spectra of (—) salicylic acid and (- - -) diflunisal in chloroform–1% v:v acetic acid. The selected paths for scanning the excitation $(\lambda_{em} = 466$ nm), emission $(\lambda_{ex} = 318$ nm) and synchronous $(\Delta\lambda = 128$ nm) spectra are shown by the solid lines slicing the data matrix. [DF] = 0.62 μg ml^{-1}, [SA] = 0.62 μg ml^{-1}.

corresponding spectra, we considered the longer wavelength maxima of both compounds. They were selected, as compromise values, to pass as clse as possible to the maxima of the components of the mixture. Taking into account that the excitation maxima of salycilic acid and diflunisal are located at 312 and 324 nm respectively, the emission spectrum was recorded at 318 nm. Similarly, as the corresponding emission maxima are located at 444 nm and 448 nm, the excitation spectrum was recorded at an emission wavelength of 446 nm. For the selection of the optimum $\Delta\lambda$ value in the synchronous spectra for the resolution of the mixture, the following considerations were taken into account. The optimum $\Delta\lambda$ value for the individual determination of salycilic acid, without losing sensitivity, would be $\Delta\lambda = \lambda_{em\,(max)} - \lambda_{ex\,(max)} = 444 - 312$ nm = 132 nm. Similarly, for diflunisal determination: $\Delta\lambda = 448 - 324$ nm = 124 nm. The $\Delta\lambda$ value chosen (128 nm) is intermediate between 132 nm and 124 nm. This selection agrees very well with the optimum value $\Delta\lambda = 130$ nm chosen by other authors for the simultaneous determination of salycilic acid and diflunisal by second-derivative synchronous fluorescence spectroscopy [7]. The corresponding excitation, emission and synchronous spectra are presented in Fig. 2.

3.3. Matrix of calibration and selection of the spectral zones for the analysis by PLS

The three different data sets selected—the excitation spectra, the emission spectra and the synchronous spectra—were evaluated to perform the determination. Because full-spectrum methods, such as PLS, can use many wavelengths it seems that wavelength selection is unnecessary, and all available wavelengths are often used. However, measurements from spectral wavelengths that are non-informative in a model degrade performance. Correlation plots that search for wavelength ranges exhibiting good selectivity and sensitivity, for the analytes of interest, over the calibration set, were used for the wavelength range selections. The spectral regions between 228 and 366 nm for excitation, between 340 and 540 nm for emission and between $\lambda_{ex}/\lambda_{em} = 231/359$ and 364/492 nm
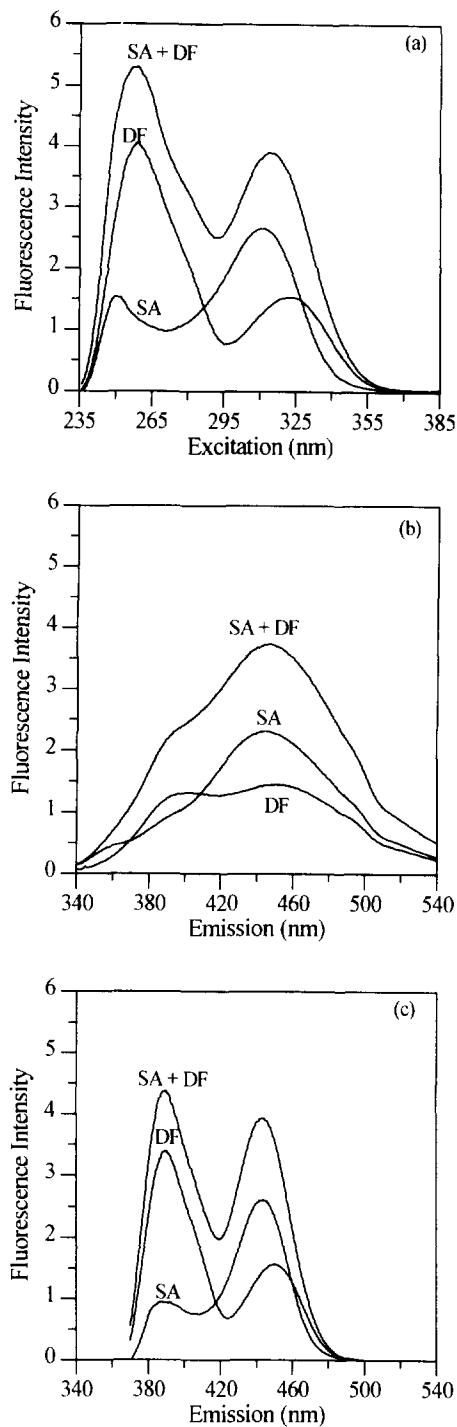
Fig. 2. (a) Excitation (λ_{em} = 466 nm), (b) emission (λ_{ex} = 318 nm) and (c) synchronous ($\Delta\lambda$ = 128 nm) spectral data sets for the determination of SA and DF using PLS-1 multivariate calibration. [DF] = 0.62 μg ml^{-1}, [SA] = 0.62 μg ml^{-1}.

for the synchronous path were selected for the analysis, because these are the zones with the maximum spectral information from the mixture components. This implies working with 139, 201 and 134 experimental points per spectra, as the spectra were digitized each nanometer.

Recent studies of multivariate calibration techniques for the multicomponent resolution of UV/visible data [23–25] or fluorescence data [14–16] revealed no significant difference between the predictions made by PCR and PLS. However, if one considers its theoretical advantages and optimal performance over a wide range of conditions, PLS is considered to be the method of choice [26]. The PLS-1 algorithm, that performs the PLS analysis one component at a time, has been selected to perform the determination.

A two-factor, four-level design with a calibration set of 16 samples was used to statistically maximize the information content in the spectra. The calibration set for the application of the PLS-1 calibration method is represented in Fig. 3. Each concentration was varied between 0.25 and 2.5 μg ml^{-1}, through the calibration matrix, and the run order of the experiments was randomized to avoid overfitting of the data by modeling spectrometer drift.

3.4. Selection of the optimum number of factors

An appropriate choice of the number of principal components, or factors, is necessary for a correct performance of PLS. The number of factors should account as much as possible for the experimental data without resulting in overfitting, and several criteria have been recommended for selecting the optimum number [27]. To perform that selection in the PLS-1 algorithm, cross-validation, leaving out one sample at a time, was used. The predicted concentrations were compared with the known concentrations of the compounds in each calibration sample, and the predicted error sum of squares (PRESS) was calculated [28]. The PRESS was calculated in the same manner each time a new factor was added to the PLS-1 model.

To select the optimum number of factors, the criterion proposed by Haaland and Thomas [28]
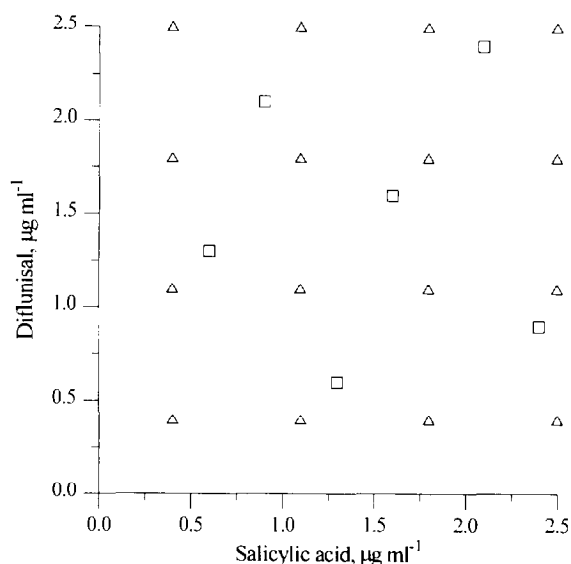
Fig. 3. Mixture design for the two-component mixtures used in the data set (△), for the PLS-1 calibration method. and composition of the synthetic mixtures assayed (□), for the evaluation of the predictive ability of the method.

was used. The model selected is that with the fewest number of factors such that PRESS for that model is not significantly greater than PRESS from the mode which yielded the minimum PRESS. The significance level is attributed by using an F test ($x = 0.25$). The optimum number of factors was two for salicylic acid and diflunisal determination, with the three spectral data sets employed.

3.5. Statistical parameters

Known concentrtions of all tested samples included in the calibration matrix were compared with the predicted concentrations, by cross-valida-

tion, for the three spectral data sets employed. The values of the root mean squared error, RMSE (RSD) [29], which is an estimate of the absolute error of prediction, by cross-validation, for each component in the calibration matrix, are summarized in Table 1. The correlation coefficients, R, obtained when plots of actual versus predicted concentrations were constructed, are also included in Table 1. In addition, to evaluate the predictive ability of the method, for each compound, PLS-1 was applied to the three spectral data sets of a series of problem mixtures, selected in the same concentration ranges as those used in the calibration set (Fig. 3). The prediction set of samples was run at the same time as the calibration set of samples. To quantify the predictive performance, the standard error of prediction (SEP) [29] and the relative error of prediction (REP) were calculated. The REP is the standard error of prediction, expressed as a percentage of the mean of the true concentrations on the prediction set [23].

In Table 2, the SEP and REP values obtained for salicylic acid and diflunisal prediction, by the three data sets used, are summarized. In accordance with the statistical data obtained by the internal cross-validation, the values found for the SEP and REP show that slightly better results for the prediction of salicylic acid and diflunisal were obtained when using the synchronous spectral data set as analytical signal and, in consequence, this spectral data set was selected for the application of the method to serum samples.

3.6. Application of the method to serum samples

For the application of the method, pooled serum samples were spiked with different quanti-

Table 1
Statistical parameters of the PLS-1 method. using the three spectral data sets

Component	Excitation spectrum		Emission spectrum		Synchronous spectrum	
	RMSE (RSD)[a]	R	RMSE (RSD)[a]	R	RMSE (RSD)[a]	R
Salicylic acid	0.030 (2)	0.9992	0.041 (2)	0.9986	0.028 (2)	0.9993
Diflunisal	0.039 (2)	0.9987	0.040 (2)	0.9987	0.038 (2)	0.9988

[a] Values in parentheses correspond to the number of factors used in prediction.

Table 2
SEP and REP (%) values for salicylic acid and diflunisal determination using the excitation, emission and synchronous spectral dat by PLS-1 calibration

Compound	Excitation spectrum		Emission spectrum		Synchronous spectrum	
	SEP	REP (%)	SEP	REP (%)	SEP	REP (%)
Salicylic acid	0.044	3.0	0.050	3.4	0.036	2.4
Diflunisal	0.056	3.8	0.059	4.0	0.047	3.2

ties of salicylic acid and diflunisal, in such a form that their concentrations were in the range 25–250 μg ml^{-1}. The selected concentrations for the binary mixtures are typical for salicylic acid and diflunisal levels in serum during the first 24 h from a typical subject following an oral dose of 650 mg of aspirin [30] and 500 mg of diflunisal [31].

The proposed method was then applied as described in Section 2.5. The percentage recoveries found by application of the PLS-1 calibration method are shown in Table 3. Three spectra of three different samples at the same concentration were used for each concentration level included in the Table. Analytical recoveries range from 95% to 103% for salicylic acid and from 97% to 105% for diflunisal. for concentrations ranging from 60 to 240 μg ml^{-1}.

The method is an alternative to that proposed

by Konstantianos and Ioannou [7], for the determination of salicylic acid and diflunisal in serum samples, by second-derivative synchronous fluorimetry. In that method, diflunisal is directly monitored by measuring the second-derivative synchronous fluourimetric signal from the maximum of excitation at 248 nm, to the minimum at 272 nm, where the contribution of the salicylic acid is negligible. However, no specific signal for salicylic acid is found in the second-derivative synchronous spectrum, and the signal from the minimum at 314 nm to the maximum at 334 nm is used to obtain the contributions of both analytes. In consequence, salicylic acid concentration is calculated by difference. In our case. the PLS calibration simplifies the method, allowing the determination of both analytes using the whole synchronous spectrum as the analytical signal, instead of measuring at a single wavelength.

Table 3
Recovery of salicylic acid (SA) and diflunisal (DF) in serum samples by combination of synchronous fluorimetry and PLS calibration

Serum concentration (μg ml^{-1})		Concentration found[a] (μg ml^{-1})		Recovery ± SD (%)	
SA	DF	SA	DF	SA	DF
60	130	59	126	98 ± 1	97 ± 3
90	210	86	220	96 ± 1	105 ± 2
130	60	134	62	103 ± 2	103 ± 2
160	160	163	165	102 ± 1	103 ± 1
210	240	216	250	103 ± 2	104 ± 3
240	90	237	88	99 ± 2	98 ± 2

[a] Average of three measurements.

4. Conclusions

The results obtained in this work allow us to conclude that the two components of the binary mixture are accurately determined by synchronous fluorimetry in combination with PLS calibration.

The total luminescence information contained in the three-dimensional excitation–emission matrices allows the selection of the most suitable spectral data set to perform the multivariate calibration. The narrowing of the emission band produced by the synchronous scanning slightly improved the resolution of the overlapping spectra of the analytes investigated.

The investigation of the combination of the different fluorimetric techniques [32]—conventional synchronous, variable-angle synchronous and constant-energy synchronous fluorimetry with PLS calibration—seems interesting for broader applications in drug analysis as a rapid alternative to chromatography.

Acknowledgements

References

[1] K.T. Tempero, V.J. Cirillo and S.L. Steelman, Br. J. Clin. Pharmacol., 4 (1977)315.

[2] J. Hannah, W.V. Ruyle, H. Jones, A.R. Matzuk, K.W. Kelly, B.E. Witzel, W.J. Holtz, R.A. Houser, T.Y. Shen and L.H. Sarett, J. Med. Chem., 21 (1978) 1093.

[3] C.L. Keegan, Clin. Chem., 31 (1985) 1922.

[4] R.W. Dalrymple and F.M. Stearns, Clin. Chem., 32 (1986) 230.

[5] D.J. Tocco, G.O. Breault, A.G. Zacchei, S.L. Steelman and C.V. Perrier, Drug Metab. Dispos., 3 (1975) 453.

[6] J.H. Moller, L. Dalgaard and S.H. Hansen, J. Chromatogr., 420 (1987) 99.

[7] D.G. Konstantianos and P.C. Ioannou, Eur. J. Pharm. Sci., 1 (1994) 209.

[8] L. Nørgaard, Talanta, 42 (1995) 1305.

[9] W. Lindberg, J.A. Persson and S. Wold, Anal. Chem., 55 (1983) 643.

[10] S.Aa. Jensen, L. Munck and H. Martens, Cereal Chem., 59 (1982) 477.

[11] S.Aa. Jensen and H. Martens, Cereal Chem., 60 (1983) 172.

[12] B. Pedersen and H. Martens, Multivariate calibration of fluorescence data, in L. Munck (Ed.), Fluorescence Analysis in Foods, Longman, Essex, 1989, Chapter 13.

[13] R. Jones, T.J. Coomber, J.P. McCormick, A.F. Fell and B.J. Clark, Anal. Proc., 25 (1988) 381.

[14] M. Sánchez Peña, A. Muñoz de la Peña, F. Salinas López, M.C. Mahedero and J.J. Aaron, Analyst, 119 (1994) 1177.

[15] A. Muñoz de la Peña, I. Durán-Merás, M.D. Moreno, F. Salinas and M. Martínez Galera, Fresenius' J. Anal. Chem., 351 (1995) 571.

[16] A. Muñoz de la Peña, I. Durán-Merás, M.D. Moreno, F. Salinas and M. Martínez Galera, Fresenius' J. Anal. Chem., 353 (1995) 221.

[17] GRAMS-386 Software Package, Version 2.0, and Add-on Application PLS plus version 2.1G, Galactic Industries, Salem, NH, 1993.

[18] SURFER for Windows Software Package, Version 5.0, Golden Software, Golden, Colorado, 1993.

[19] E.B. Truitt, Jr., A.M. Morgan and J.M. Little, J. Am. Pharm. Assoc. Sci. Ed., 44 (1955) 142.

[20] J.W. Putney, Jr. and J.F. Borzelleca, Arch. Int. Pharmacodlyn. Ther., 188 (1970) 119.

[21] A. Muñoz de la Peña, F. Salinas and I. Durán-Merás, Anal. Chem., 60 (1988) 2493.

[22] S.A. Winfield and A.T. Rhys Williams, J. Pharm. Biomed. Anal., 2 (1984) 561.

[23] I. Durán-Merás, A. Muñoz de la Peña, A. Espinosa-Mansilla and F. Salinas, Analyst, 118 (1993) 807.

[24] P. MacLaurin, P.J. Worsfold, M. Crane and P. Norman, Anal. Proc., 29 (1992) 65.

[25] P. MacLaurin, P.J. Worsfold, P. Norman and M. Crane, Anal. Proc., 118 (1993) 617.

[26] E.V. Thomas and D.M. Haaland, Anal. Chem., 62 (1990) 1091.

[27] H. Martens and T.Naes, Multivariate Calibration, John Wiley, New York, 1989.

[28] D.M. Haaland and E.V. Thomas, Anal. Chem., 60 (1988) 1193.

[29] E.V. Thomas, Anal. Chem., 66 (1994) 795A.

[30] E.N. Amick and W.D. Mason, Anal. Lett. 12 (1979) 629.

[31] J.W.A. Van Loenhout, H.C.J. Ketelaars, F.W.J. Gribnan, C.A.M. Van Ginneken and Y. Tan, J. Chromatogr., 182 (1980) 487.

[32] J.N. Miller, Analyst, 109 (1984) 191.

Talanta

Characterization of the ionization and spectral properties of mercapto-carboxylic acids
Correlation with substituents and structural features

M. Carla Aragoni, Massimiliano Arca, Guido Crisponi*, Franco Cristiani, Francesco Isaia, Valeria M. Nurchi

Dipartimento di Chimica e Tecnologie Inorganiche e Metallorganiche, Via Ospedale 72, 09124 Cagliari, Italy

Abstract

The ionization constants in aqueous solutions of meso- and DL-dimercaptosuccinic acid and of monomethyl and dimethyl meso-succinates were carefully determined by potentiometric and spectrophotometric methods as a result of the increasing interest in these molecules as heavy metal chelators. In order to explain the influence of various substituents on ionization and ^{13}C NMR properties, the study was extended to the related oxygen derivatives of succinic acid and to simpler ethanoic derivatives. With the Swain–Lupton dual substituent treatment it was possible to clarify the influence of substituents on both spectral and equilibrium parameters. The differences in pK due to conformation are also discussed.

Keywords: Ionization constants; Mercapto-carboxylic acids; Potentiometric measurements

1. Introduction

meso-Dimercapto succinic acid (DMSA) has been proposed as a very powerful ligand for the treatment of heavy metal poisoning [1–4]. A number of studies have appeared concerning both the in-vivo behaviour of this drug [5,6] and the chemical characterization of its metal complexes and related solution equilibria [7–15]. The involvement of both carboxylic and sulfhydryl bonding is well established, although some disagreement on the bonding schemes as well as the numerical values of equilibrium constants exists. The aim of the present work is to contribute to the knowledge of DMSA equilibria via a thorough study on the ionizations of DMSA and related molecules, to explain how their acid behaviour and consequently their binding properties towards metal ions [16,17], can be affected by substituents and conformations. In order to obtain reliable results accurate potentiometric and spectrophotometric measurements were used. Table 1 shows all compounds and nomenclature used in the paper.

* Corresponding author.

Table 1
Name, formula and index number of all compounds used (**0**, formic acid; **1**, acetic acid; **2**, glycolic acid; **3**, mercaptoacetic acid (thioglycolic acid); **4**, oxalic acid; **5**, ethylmercaptane; **6**, mercaptoethanol; **7**, 1,2-ethanedithiol; **8**, mercaptoacetic acid (thioglycolic acid); **9**, methylmercapto acetate; **10**, succinic acid; **11**, malic acid; **12**, DL-tartaric acid; **13**, meso-tartaric acid; **14**, mercapto succinic acid; **15**, DL-dimercapto succinic acid; **16**, meso-dimercapto succinic acid; **17**, monomethyl succinate; **18**, meso-monomethyl dimercapto succinate; **19**, meso-dimethyl dimercapto succinate)

0	1	2	3	4	5	6	7	8ᵃ	9
$COOH$	$COOH$	$COOH$	$COOH$	$COOH$	CH_3	CH_2OH	CH_2SH	$COOH$	$COOCH_3$
—	—	—	—	—	—	—	—	—	—
H	CH_3	CH_2OH	CH_2SH	$COOH$	CH_2SH	CH_2SH	CH_2SH	CH_2SH	CH_2SH

10	11	12	13	14	15	16	17	18	19
$COOH$	$COOH$	$COOH$	$COOH$	$COOH$	$COOH$	$COOH$	$COOH$	$COOH$	$COOCH_3$
—	—	—	—	—	—	—	—	—	—
CH_2	$CHOH$	$CHOH$	$CHOH$	$CHSH$	$CHSH$	$CHSH$	CH_2	$CHSH$	$CHSH$
—	—	—	—	—	—	—	—	—	—
CH_2	CH_2	$CHOH$	$CHOH$	CH_2	$CHSH$	$CHSH$	CH_2	$CHSH$	$CHSH$
—	—	—	—	—	—	—	—	—	—
$COOH$	$COOH$	$COOH$	$COOH$	$COOH$	$COOH$	$COOH$	$COOCH_3$	$COOCH_3$	$COOCH_3$
		DL	meso		DL	meso		meso	

ᵃ Mercaptoacetic acid is considered twice, as a substituted carboxylic acid and as a substituted thiol.

2. Experimental

2.1. Materials and methods

The compounds were all Aldrich products, with the exception of DL-tartaric and meso-tartaric acids which were purchased from Fluka, and DL-mercapto succinic acid, monomethyl and dimethyl dimercapto succinates which were synthesized by us according to Gerecke et al. [18]. The commercial compounds were used without further purification; the others were checked by ^{13}C NMR, IR spectra and elemental analysis with a CHN-S Fisons instrument. The following elemental analysis results were obtained:

Compound	15	18	19
Calculated (%)	C 26.4, H 3.3, S 35.2	C 30.6, H 4.1, S 32.7	C 34.3, H 4.8, S 30.5
Found (%)	C 26.7, H 3.4, S 35.1	C 30.5, H 4.3, S 32.0	C 33.9, H 4.9, S 30.8

Solutions of reagents were always freshly prepared by dissolving a weighed amount of reagent in freshly bidistilled water saturated with argon, in view of their aptitude for decomposition, and stored in a refrigerator. Taking into account the possibility of decomposition, the solutions were degassed with argon during the experimental work and periodically tested by recording UV spectra in solutions with a fixed addition of 0.1 M KOH.

2.2. IR

The IR spectra were recorded with a Perkin-Elmer 983 instrument in the range 4000–200 cm^{-1} using KBr pellets for solid compounds and CsI disks for neat liquids.

2.3. Potentiometric studies

Titrations were performed on a Dosimat 655 Metrohm automatic titrator connected to a Metrohm 654 pH meter, in a thermostatted glass cell equipped with a magnetic stirring system, a Metrohm glass electrode for highly alkaline solutions, a thermometric probe, a microburet delivery tube, an inlet–outlet ar-

gon tube and a salt bridge connected to the reference cell. This was filled with 0.1 M KCl solution, in which a saturated calomel electrode was dipped. The solutions (25 cm^3, at an ionic strength of 0.1 M KCl) were titrated at 25°C with carbonate-free 0.1 M KOH whose titre was controlled daily.

The electrode was calibrated for hydrogen ion concentration by titration with HCl; the resulting potentiometric data were analyzed with the Gran [19] procedure using our GRANPLOT program. The ionization constants were calculated with the PSEQUAD [20] program operating on the experimental data (ml, $log[H^+]$), as in Fig. 1A for dimethyl dimercapto succinate.

2.4. Spectrophotometric measurements

Absorption spectra were recorded on a Hewlett-Packard 8452 diode array spectrophotometer; a flow cell joined to a titration vessel with a peristaltic pump was used; the whole apparatus was thermostatted at 25°C and kept under an argon atmosphere. In order to make reliable spectrophotometric determinations of the ionization constants, 15–20 spectra (such as those presented in Fig. 1B for dimethyl dimercapto succinate) were collected at pH values in the range ±2 pH units around the pK value to be determined, by titrating the solutions with 0.1 M KOH (at an ionic strength of 0.1 M KCl). The spectra were then recorded by transferring the solution to the flow cell at a fixed time interval after each KOH addition. The concentrations of the acid solutions were chosen on the basis of their absorptivities estimated from previous measurements.

2.5. NMR measurements

Natural abundance ^{13}C NMR spectra were recorded on a Varian VXR-300 spectrometer at 75.43 MHz using 10 mm diameter tubes. The ^{13}C spectra were ^1H-decoupled by means of square
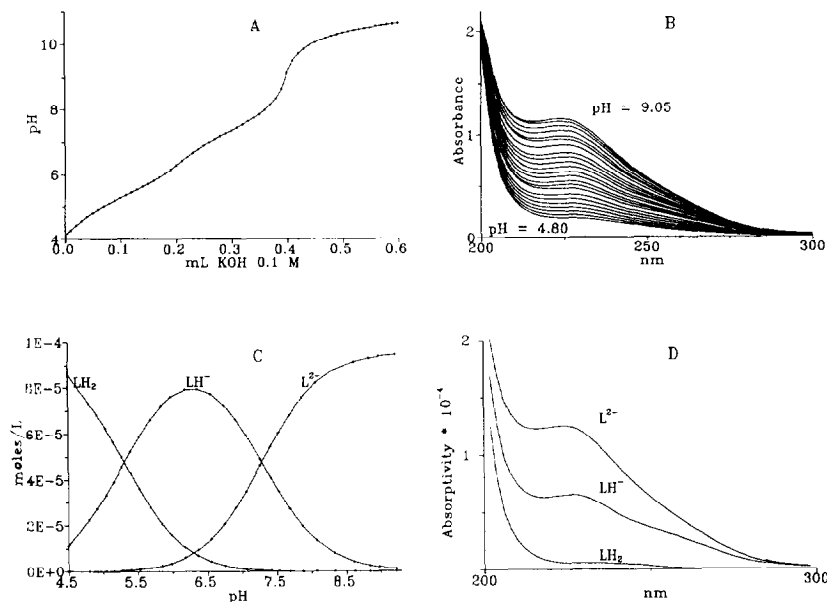
Fig. 1. Experimental data and calculated results for dimethyl dimercapto succinate (19): (A) potentiometric titration of 25 ml of 1×10^{-3} M 19 with 0.1 M KOH (points are experimental data, solid line is calculated); (B) UV spectra of 1×10^{-4} M solution of 19 at different H^+ concentrations; (C) distribution plots of a 1×10^{-4} M solution of 19 using the pK values in Table 2; (D) absorptivity spectra of the variously protonated forms of 19 obtained by SPECFIT least-squares calculations.

wave modulation of the decoupler carrier centered on the proton field. The carbon chemical shifts were measured at 21°C in $CDCl_3$ solutions ($\delta = 77.0$). The substances were first dissolved in the smallest possible amount of CD_3OD whenever their dissolution in pure $CDCl_3$ was not possible.

2.6. Calculation of ionization constants from spectrophotometric data

Matrix A of absorbance data for each substance collected at N_W wavelengths on N_S solutions of different pH was analyzed by the SPECFIT program [21]. SPECFIT performs evolving factor analysis which allows one to calculate the concentration profiles and spectra of all absorbing species without using the law of mass action or defining the stoichiometric composition of the species. As a second step, constants and spectra of all absorbing species can be calculated with the usual least-squares analysis; the results of such calculations on the experimental data for 19 are shown in Figs. 1C and 1D.

Matrix A was also analyzed with our SPECPEAK program [22] which performs a decomposition of spectra into the component gaussian peaks. The peak heights thus calculated give a further evaluation of ionization constants and of the reliability of the data.

3. Results and discussion

Before analyzing 14, 15, 16, 18 and 19 as chelating molecules, we carried out a preliminary study of their acid behaviour. In order to evaluate how structure and substituents affect acidity, the broader set of molecules presented in Table 1 was examined. Besides the above-mentioned compounds, the basic compound 10 and the analogous hydroxy compounds 11, 12, 13 and 17 were chosen to obtain a deeper insight into the effects of substituent on both chemical and spectral features. The simpler bifunctional 0–9 compounds were also considered, both to observe the influence of each substituent in a simpler structure and to compare the trends.

Table 2
Measured values of ionization constants (pK_{C1}, pK_{C2} refer to first and second ionization of COOH; pK_{S1}, pK_{S2} refer to first and second ionization of SH), ^{13}C NMR chemical shifts in ppm (δ_{C1}, δ_{C2} refer to the two COOH groups and δ_2 and δ_3 to carbon atoms in the chain) and IR frequencies in cm^{-1} of SH and CO stretchings (ν_{SH} and ν_{CO}).

Compound	pK_{C1}	pK_{C2}	pK_{S1}	pK_{S2}	δ_{C1}	δ_2	δ_3	δ_{C2}	ν_{SH}	ν_{CO}
0	3.57[a]									1709[c]
1	4.56[a]				178.0	21.0				1715[c]
2	3.62				174.0[b]	60.0[b]				1709[c]
3	3.44		9.96		176.7	26.1			2569	1711
4	1.00	3.38			160.1			160.1		1742[c]
5			10.12			18.9	18.3		2561	
6			9.40			64.0	28.0		2556	
7			8.71	9.77		28.0	28.0		2551	
8					176.7	26.1			2569	1711
9			7.99		170.7	25.6			2561	1738
10	4.00	5.24			174.9	28.8	28.8	174.9		1727–1691
11	3.24	4.68			175.0	67.0	39.0	172.0		1738–1693
12	2.82	3.97			173.4	71.9	71.9	173.4		1744
13	2.97	4.49			172.8	72.8	72.8	172.8		1733
14	3.12	4.52	10.24		174.8	36.0	39.5	173.1	2564–2548	1693
15	1.93	3.99	9.50	12.32	173.1	45.6	45.6	173.1	2558–2544	1728–1677
16	2.71	3.43	9.65	12.05	172.6	44.6	44.6	172.6	2563–2537	1693
17	4.27				178.2	28.9	28.6	172.6		1728–1693
18	2.8		7.15	9.98	174.5	44.7	44.5	171.0	2559–2542	1730–1702
19			5.23	7.32	171.2	44.8	44.8	171.2	2551	1721

[a] Ref. [26].
[b] Aldrich Library of NMR Spectra.
[c] The Aldrich Library of Infrared Spectra.

The pK values of the carboxylic groups were measured potentiometrically; those of the sulfhydrylic groups were measured potentiometrically and spectrophotometrically. The ^{13}C NMR and IR spectra of all these molecules were recorded to assess their strong dependence on substituents and for their prospective use in characterizing metal complexes. The collected data are summarized in Table 2. Values from the literature are specified.

In order to overcome the uncertainty inherent in potentiometry at a high pH, we resolved to resort to spectral measurements. Despite the scepticism of Rivera-Laos [23] on the reliability of the UV results of Egorova [1], it is possible to make correct measurements of ionization constants with this technique when operating in a controlled atmosphere. In a preliminary survey of these systems, large spectral variations in the 200–300 nm spectral range due to ionization of the SH groups were observed, while UV spectra appear completely insensitive to COOH deprotonation. The

pK values of ionization constants for SH, obtained both by SPECFIT and graphically from peak heights obtained by SPECPEAK, are in perfect agreement with potentiometric results.

The spectrophotometrically determined values of pK_{S2} for compounds 15 and 16 present uncertainties due to: (i) large amounts of base which alter in an assessable amount the ionic strength of the solution; (ii) changes in substances due to oxidation at high pH values. The pK values for compounds 18 and 19 are new. In fact only the values in 50% (v/v) water/methanol are reported in the dissertation of Rivera-Laos [23]. We easily prepared $\approx 10^{-3}$ M solutions of 18 and 19 in water by dissolving correct amounts of compounds in an ultrasonic bath, while Rivera-Laos reported that 18 and 19 were not water-soluble. Our results in water are ≈ 0.9 pK units lower than those in water/methanol, but they exhibit an analogous trend. The NMR and IR data agree perfectly with the previous results [23].

The ionization constants of DMSA, as studied by a large number of workers with pH metric measurements, present a large variability, above all in the first ionization at acidic pH and in the last ionization at high pH values. Our data for DMSA are comparable with those of Harris et al. [14] at the same temperature and ionic strength, and with those of Kiss et al. [15] considering that pK_1 increases and pK_2 and pK_3 decrease on increasing the ionic strength as pointed out by Vukicevic et al. [13]. The data published by Lenz and Martell [8] present a much higher pK_1 and a lower pK_3, while pK_2 is almost equal to our value. The data obtained at 20°C present a lower dispersion and as expected they are higher than those at 25°C.

Our results for **15** are comparable with those of Egorova and co-workers [1–4] at 20°C, the differences being similar to those for **16**.

As far as the last deprotonation is concerned, our comment is similar to that of Jones et al. [9] who state that "..the value 11.82 indicates the second sulfhydryl group only deprotonates at very high pH and thus is beyond the scope of the glass electrode. In view of this an estimated value of 12 is assumed". This was also confirmed by Harris et al. [14].

The ^{13}C NMR chemical shifts in $CDCl_3$ of all the compounds present typical values for the carboxylic group between 170 and 180 ppm, with the exception of compound **4** which has a 160.1 ppm shift; the values for the carbon atoms in the chain range from 10–80 ppm according to the substituent groups.

The IR bands for C=O stretching fall in the typical 1677–1744 cm^{-1} range, which is indicative of hydrogen bond association in related compounds. **10, 15, 17** and **18** show a splitting of ν_{CO}: it is reasonable to explain the presence of these two peaks as due to steric effects, as already proposed by Duncanson [24] for some derivatives of succinic acid. The values of ν_{SH} vibrations confirm that all the molecules carrying this group are involved in self-association; in the case of **14, 15, 16** and **18** a splitting of this band is also detectable.

In order to explain the numerical values of ionization constants as a function of structure and

substituents we analyzed first the trend of simple linear bicarboxylic acids as a function of the bonds between the two carboxylic groups; the data at 25°C and 0.1 μ reported in Fig. 2 are taken from Refs. [25–28]. Despite some disagreement among literature data, the trends are highly significant. The trend of the first ionization depends on inductive factors, which cause an increase in acidity with respect to unsubstituted monocarboxylic acids. This inductive effect vanishes almost completely for succininc acid (three bonds). The joint influence of inductive and resonance effects can rationalise the more complex trend of the second ionization: in this case a constant value is reached only for glutaric acid. It should be remarked that the limiting pK_1 and pK_2 values are respectively lower and higher than those obtained for linear carboxylic acids ≈ 4.6 at the same temperature and ionic strength. Furthermore, we wish to explain how the substituents in the basic structures of succinic acid affect the ionization of both carboxylic and proximal SH groups. To do this the next two sets of compounds were examined by Swain–Lupton (SL) dual substituent analysis [29,30] in the form $Y = Y_0 + r_1\mathscr{F} + r_2\mathscr{R}$. In set 1, which included compounds **0, 1, 2, 3** and **4**, we studied the influence of CH_3, CH_2OH, CH_2SH, COOH and COO$^-$ on COOH ionization, while in set 2 (**5, 6, 7, 8** and **9**) the effect of CH_3, CH_2OH, CH_2SH, COO$^-$ and COOCH$_3$ (which can be considered as COOH) on SH ion-
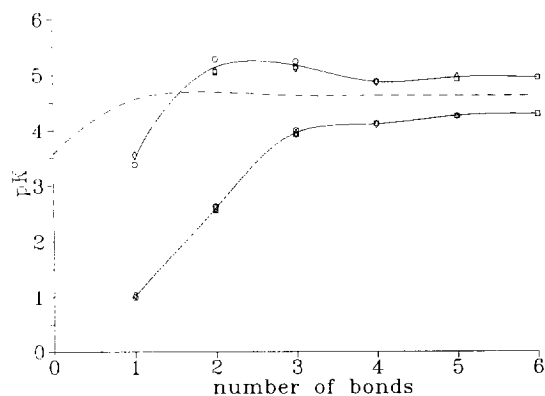

Fig. 2. pK_1 (lower curve) and pK_2 (upper curve) for bicarboxylic acids of different length vs. the number of bonds between the two COOH groups; the broken line represents the values for linear monocarboxylic acids.

Table 3
Results of the Swain–Lupton dual substituent analysis

Parameter	Case	Y_0	r_1	r_2	S.E.	Corr. coeff.
pK_{COOH}	a	3.559	−5.368	−6.296	0.152	0.9967
	b	3.553	−5.382	−6.170	0.150	0.9952
pK_{SH}	a	9.672	−4.346	−2.191	0.243	0.9895
	b	9.558	−4.357	−1.772	0.407	0.9420
δ_{COOH}		176.2	−42.14	−14.60	2.367	0.9861
δ_{CH_2X}		18.6		−61.46	1.921	0.9949
δ_{CH_2X}		20.3	−10.09	−64.32	1.717	0.9966
pK_1	c	4.244	−3.242	−0.527	0.313	0.9217
	d	4.124	−3.344	−0.671	0.294	0.9225
pK_2		5.426	−3.156	−0.625	0.272	0.9255
$p\beta_2$		9.551	−6.499	−1.296	0.274	0.9805
δ_{CHX}		34.0		−53.37	3.835	0.9693
δ_{CHX}		31.7	16.96	−47.46	3.659	0.9757
δ_{CHXCHY}		29.1	25.79	−51.11	1.203	0.9973

[a] Without $\mathscr{F}$ and $\mathscr{R}$ for CH_2SH.
[b] With $\mathscr{F}$ and $\mathscr{R}$ for CH_2SH.
[c] Calculated on **10–18** compounds.
[d] Calculated on **10–16**.

ization was examined. In these sets bivariate regression parameters were calculated by using $\mathscr{F}$ and $\mathscr{R}$ taken from Ref. [30]. Although no value for the CH_2SH group was available, $\mathscr{F} = 0.05$ and $\mathscr{R} = -0.05$ were estimated from the values for CH_2SMe in Table IV of Ref. [30]. The pK values of compounds **3** and **7** can thus be taken into account. The SL analysis performed on set 1 and set 2 data both with and without $\mathscr{F}$ and $\mathscr{R}$ for CH_2SH (cases b and a) gave almost similar
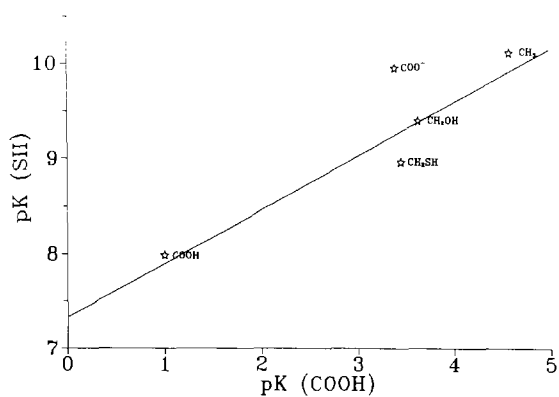
results, thus substantiating the above estimates. The values reported in Table 3 show a dependence of pK_{COOH} and pK_{SH} on both inductive and resonance factors.

The pK for COO^- is an outlier in the plot of pK_{SH} vs. pK_{COOH} for analogous substituents (see Fig. 3). This can be clearly explained by the different contributions of resonance in determining the ionization of the carboxylic group. The
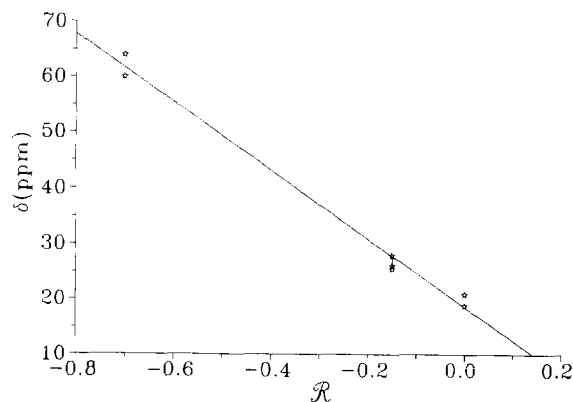

Fig. 3. pK_{SH} for set 1 compounds vs. pK_{COOH} for analogous compounds in set 2.

Fig. 4. Regression line of ^{13}C NMR chemical shifts of CH_2X carbon atoms in sets 1 and 2 vs. corresponding values of resonance SL parameters.
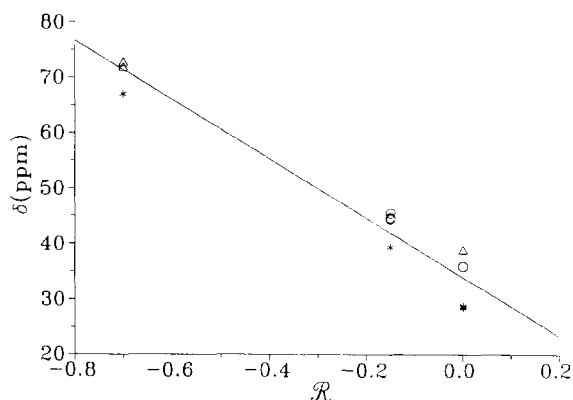
Fig. 5. Regression line of ^{13}C NMR chemical shifts of CHX CHY carbon atoms in set 3 vs. corresponding values of resonance SL parameters, where (*), ($\triangle$) and ($\bigcirc$) refer to Y–H, OH and SH respectively.

Fig. 6. Trends of pK_{SH} vs. number of methylated carboxylic groups. ($\bigcirc$) and ($\star$) refer to pK_{s1} and pK_{s2} respectively.

values of ^{13}C NMR chemical shifts of carboxylic groups can be analyzed in the same way. In this case a greater influence of the inductive effect is observed even if lack of data variability lowers the quality of the results. The ^{13}C NMR chemical shifts of carbon atoms close to COOH and SH groups of both sets 1 and 2 were treated together on the basis of SL parameters for the X substituent on CH_2X. In this way a clear influence of the effects of resonance is shown. A linear regression on the resonance parameters alone (see Fig. 4) does not give a significant variation in either standard error (S.E.) or correlation coefficient with respect to the bivariate regression, and this implies that chemical shifts for these molecules do not depend on inductive effects.

For the succinic acid derivatives (set 3) we calculated the SL parameters as the sum of the tabulated parameters for X and Y in the central part of COOH–CHX–CHY–COOH; this is a simplified assumption which does not take into account the distances of X and Y from the ionizable COOH group. As expected on the basis of SL parameters for COOH and $COOCH_3$, there is no appreciable difference between the results of cases c (which includes compounds **17** and **18**) and d. A very strong dominance of the field effect is evident here, unlike in set 1. A very similar behaviour is shown by the second ionization constant. A strong increase in correlation coefficient
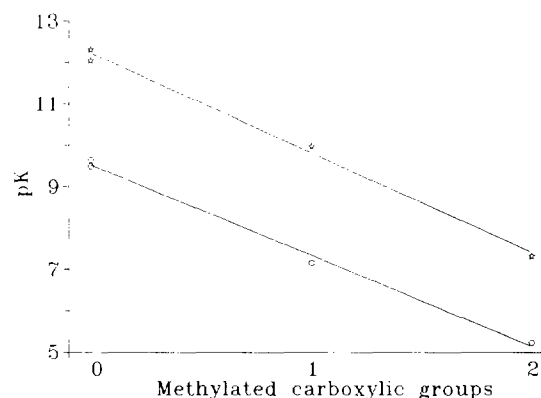
is evident when the $p\beta_2$ values are used instead of pK_2. This is probably because of some averaging of distance contributions. Also, in this case the chemical shifts depend strongly on the resonance parameter, but a second-order dependence on the substituent Y is evident, as clearly shown in Fig. 5. If a bivariate regression of the resonance parameter of X and the field parameter of Y is made, the S.E. and correlation coefficients are improved.

Regarding the deprotonations of the SH groups, each methylation of the carboxylic groups increases the acidity of both SH groups by about two pH units, as shown in Fig. 6. This can be ascribed to a large extent to the difference in electrical charge in the ionizable molecules. The results of the SL analysis show that this treatment
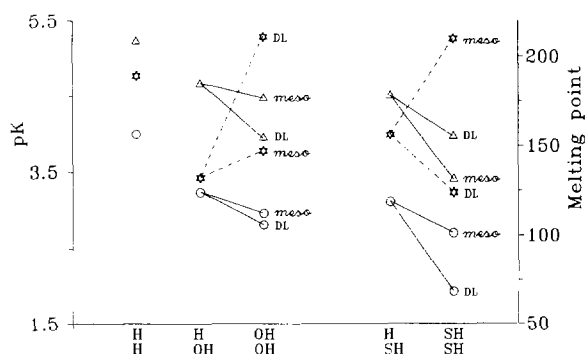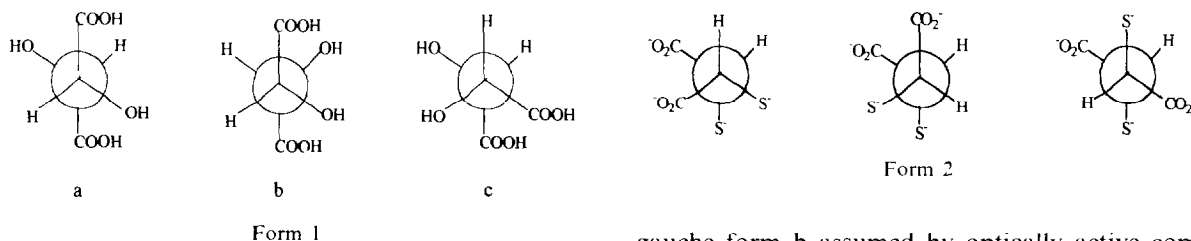

Fig. 7. pK_1 ($\bigcirc$), pK_2 ($\triangle$) and the melting point ($\star$) are reported vs. the X (upper) and Y (lower) substituents in the COOH–CHX–CHY–COOH molecules.

Form 1

Form 2

can thoroughly rationalize both the ionization and spectral features of sets 1 and 2 relating to simpler structures. In the third set, relating to the succinic acid derivatives, only the spectral parameters are explained satisfactorily, and the pK values are explained only in general terms. Intrinsically, an SL treatment cannot take into account those structural effects arising from conformation differences which largely affect acid behaviour. These marked differences between meso and DL forms are clearly depicted in Fig. 7, and are furthermore substantiated by the large variability of some solid-state properties, such as the frequencies and shapes of the v_{CO} band and, above all, the melting points.

The differences in acid behaviour between meso and optically active forms of tartaric acids were clearly discussed by Pettit and Swash [31] who stated that "...Provided that the interactions between the groups are purely steric in origin, the most stable conformation is the centrosymmetric anti conformer (see form a in the above scheme), in which all the similar groups are fully staggered about the central C–C axis. This conformation can only be adopted by meso form; the optically active forms necessarily contain sterically unfavourable gauche interactions (form b)". If in solution, as in the solid state, meso-tartaric acid assumes the conformation c to maximize hydrogen bonding, than the repulsion between the charged carboxylated groups is particularly unfavourable and this explains the pK_2 value of the meso form being higher than that of DL forms. The difference in the first deprotonation is smaller because the electrostatic repulsion in form c is eliminated. The intramolecular hydrogen bonding with SH groups is negligible in the case of the mercapto-succinic acids and therefore the meso compound 16 assumes the centrosymmetric anti conformation a, which is more stable than the

gauche form b assumed by optically active compounds. These latter considerations allow one to explain the fact that the pK_2 value of 16 is lower than those of both DL-mercapto succinic and meso-tartaric acids.

The very low pK_1 value of DL-mercapto succinic acid cannot be easily explained by the above arguments, and we should resort to some sort of hydrogen bonding stabilization of the fully protonated form of 15.

These considerations are basically in accordance with those on chelating properties of DMSA made by Arnold et al. [10] who suggest that "chelation is not present in the 1:1 complex of DMSA, despite the adjacent sulfhydryl groups, because of the resultant unfavourable proximity of the two deprotonated carboxylate groups which would result in this case".

References

[1] L.G. Egorova, Zh. Obshch. Khim., 42 (1972) 2240.
[2] L.G. Egorova, I.E. Okonishnikova, V.L. Niremburg and I.Y. Postovskii, Khim. Farm. Zh., 6 (1972) 14.
[3] L.G. Egorova and V.L. Niremburg. Zh. Obshch. Khim., 43 (1973) 1396.
[4] L.G. Egorova and V.L. Niremburg. Zh. Obshch. Khim., 43 (1973) 1548.
[5] H.V. Aposhian, M.M. Mershon, F.B. Brinkley. Chin-An Hsu and B.E. Hackley, Life Sci., 31 (1982) 2149.
[6] H.V. Aposhian, Ann. Rev. Pharmacol. Toxicol., 23 (1983) 193.
[7] A. Agren and G. Schwarzenbach. Helv. Chim. Acta, 38 (1955) 1920.
[8] G.R. Lenz and A.E. Martell, Inorg. Chem., 4 (1965) 378.
[9] D.C. Jones, G.L. Smith, P.M. May and D.R. Williams, Inorg. Chim. Acta, 93 (1984) 93.
[10] A.P. Arnold, A.J. Canty, R.S. Reid and D.L. Rabenstein, Can. J. Chem., 63 (1985) 2430.
[11] M. Rivera, H.V. Aposhian and Q. Fernando, J. Inorg. Biochem., 37 (1989) 283.
[12] R.J. O'Connor, E.L. McGown, K. Dill and S.F. Hallowell, Magn. Reson. Chem., 27 (1989) 669.

[13] N.S. Vukicevic, N.M. Vanlic-Razumenic and D.S. Veselinovic, Polyhedron, 8 (1989) 2809.

[14] W.R. Harris, Y. Chen, J. Stenback and B. Shah, J. Coord. Chem., 23 (1991) 173.

[15] T. Kiss, P. Buglyo, G. Micera, A. Dessi and D. Sanna, J. Chem. Soc., Dalton Trans., (1993) 1849.

[16] A.E. Martell and M. Calvin, Chemistry of the Metal Chelate Compounds, Prentice-Hall, Englewood Cliffs. NJ, 1952.

[17] H. Sigel, J. Inorg. Nucl. Chem., 37 (1975) 507.

[18] M. Gerecke, E.A.H. Friedheim and A. Brossi, Helv. Chim. Acta, 44 (1961) 955.

[19] G. Gran, Analyst, 77 (1952) 661.

[20] L. Zekany and I. Nagypal, in D.J. Leggett (Ed.), Computational Methods for the Determination of Formation Constants, Plenum Press, New York, 1985, Chapter 8.

[21] H. Gampp, M. Maeder, C.J. Meyer and A.D. Zuberbühler, Talanta, 32 (1985) 95.

[22] M.C. Aragoni, M. Arca, G. Crisponi and V.M. Nurchi, Anal. Chim. Acta, 316 (1995) 195.

[23] M.E. Rivera-Laos, Dissertation Abstract, University of Arizona, 1991.

[24] L.A. Duncanson, J. Chem. Soc., (1952) 1753.

[25] A.E. Martell and R.M. Smith, Critical Stability Constants, Vol. 3, Plenum Press, New York, 1977.

[26] R.M. Smith and A.E. Martell, Critical Stability Constants, Vol. 6, Plenum Press, New York, 1989.

[27] A. Vanni, G. Ostacoli and E. Roletto, Ann. Chim. Rome, 59 (1969) 847.

[28] M. Yasuda, K. Yamasaki and H. Ohtaki, Bull. Chem. Soc. Jpn., 33 (1960) 1067.

[29] C.G. Swain and E.C. Lupton, Jr., J. Am. Chem. Soc., 90 (1968) 4328.

[30] C. Hansch, A. Leo and R.W. Taft, Chem. Rev., 91 (1991) 165.

[31] L.D. Pettit and J.L.M. Swash, J. Chem. Soc., Dalton Trans., (1978) 286.

Talanta

ELSEVIER

Short communication

Anion-exchange enrichment of thallium and cadmium prior to their flame atomic absorption spectrometric determination in soils

E. Ivanova*, S. Tsakovski, G. Gentscheva, I. Havezov

Institute of General and Inorganic Chemistry, Bulgarian Academy of Sciences, BG-1113 Sofia, Bulgaria

1. Introduction

Thallium and cadmium are among the most toxic environmental pollutants. This makes their determination in soils and other environmental samples a problem of acute importance [1,2]. The reported natural cadmium content in cultivated Bulgarian soils is $0.1-0.5\ \mu g\ g^{-1}$ [3]. There are no official data for the thallium content but it is assumed to be of the same order.

Since standard reference materials for soils and related samples, especially ones with a certified thallium content, are hard to obtain, the accuracy of methods for trace pollutant determination in such materials is often checked by comparison with the results obtained by independent methods.

Conventional flame atomic absorption spectrometry (AAS) is still widely used despite developments with electrothermal AAS. There are less matrix interferences and related systematic errors with the flame technique. The major limitation of flame AAS is poor sensitivity in comparison with electrothermal AAS. Methods for improving the sensitivity of flame AAS using preconcentration and/or special sample introduction have been described [2]. For example, the use of a slotted quartz tube provides 2.6- and 2.3-fold increases in sensitivity for thallium and cadmium respectively [4]. This sample introduction technique cannot, however, be directly applied to soil digests since the matrix components present severely etch the quartz tube [4]. Therefore a preliminary separation of the analytes from the matrix soil components is necessary.

In our former work [5] the chlorocomplexes of Tl(III) were selectively sorbed on an anion-exchange resin from the soil digest in 0.1 M HCl. Since cadmium is also sorbed on anion exchangers from HCl solutions of relatively low acidity [6], it was of interest to study the possibilities for the simultaneous anion-exchange separation of Tl(III) and Cd(II) from the soil digest with a view to their subsequent flame AAS determination in the corresponding eluate.

* Corresponding author.

2. Experimental

Reagents of AR grade and redistilled water were used throughout. The stock solutions of the elements (1 mg ml^{-1}) were prepared from Merck titrisols. The flame atomic absorption spectrometer model SP 192 (Pye Unicam) equipped with a slotted quartz tube according to Ref. [4] was used. To prolong the lifetime of the quartz tube, it was coated prior to each run with a 1% (w/v) aqueous solution of LaCl$_3$ by aspirating for 3 min in the burner flame [5]. Calibration was performed by means of acidified aqueous standards comparable to the corresponding eluates of the analytes.

2.1. Procedures

2.1.1. Sample digestion

Grind the air-dried soil samples in an agate mortar to pass a 100-mesh sieve. Add 10 ml of aqua regia to 0.5 g of the soil sample in a glass beaker. Cover the beaker and allow to stand overnight. Heat the covered beaker on a water bath for 1 h at 90°C, then evaporate to a wet residue. Add 2 ml of concentrated HCl, dilute with water and filter into a 25 ml measuring flask. Add some drops of aqueous bromine to maintain thallium as Tl(III) and make up to volume with water. The final solution has an acidity of ≈ 1 M HCl.

2.1.2. Preconcentration of thallium and cadmium and separation from the matrix

Use a column of 5 mm i.d. the lower part of which (between the bottom and the outflow) is hydrophobised so that no liquid adheres to the column walls. Fill the column with the anion-exchange resin Dowex 1X8 (200–400 mesh, Cl$^-$ form) to a height of ≈ 10 mm (100 mg of resin). Pass the soil digest solution through the column at a rate of ≈ 0.5 ml min^{-1}. Wash the residual solution from the column with 0.5 ml of 1 M HCl. Pass five consecutive 0.5 ml aliquots of 2 M HNO$_3$. Collect the first 2.0 ml of the eluate and analyse for cadmium. Subsequently, pass three 0.5 ml aliquots of 2% (w/v) ascorbic acid and collect 1.0 ml of this eluate for thallium determination. The use of a new column filling for each run is

recommended since a layer of organic soil constituents settles on the top of the resin when the digest passes through the column. This layer cannot be removed from the resin and lowers the sorption efficiency in the subsequent runs. The effect is particularly manifested when soils rich in organic matter are analysed.

3. Results and discussion

The anion-exchange procedure [5] recently developed for thallium separation was modified in order to provide the simultaneous sorption of thallium and cadmium on the resin. The optimization experiments revealed that 1 M HCl was the suitable acid with the right chloride concentration for the simultaneous quantitative sorption of Tl(III) and Cd(II) as chlorocomplexes on the anion-exchange resin. Quantitative elution of Tl was achieved with 2% ascorbic acid [5] and that of Cd with 2 M HNO$_3$. The advantages of the batch technique used in Ref. [5] could not be utilized in the present work since different eluents were needed for the elution of thallium and cadmium from the resin and their use in a mixture did not yield quantitative recovery of the analytes. Therefore the column technique was employed. It was found that both the use of a very short layer (1 cm) of a fine-grained resin (200–400 mesh) and the addition of the eluents in small (0.5 ml) consecutive aliquots yielded extremely sharp elution curves of the analytes, which permitted the achievement of quantitative elution with minimum eluent volumes: 2.0 and 1.0 ml for cadmium and thallium respectively (see Fig. 1). It should be stressed that the elution of Cd should precede that of Tl, otherwise losses of Cd were registered due to its partial elution with Tl.

The behaviour of the major soil components accompanying the analytes in the aqua regia soil digest [Fe(III), Ca, Mg, Na, K and Al] during the anion-exchange enrichment was studied. That of Fe(III) was of particular interest, since, in contrast to alkali metals, alkaline earth metals and aluminium, the chlorocomplexes of Fe(III) were expected to be retained on the anion exchanger in 1 M HCl [6]. A model solution simulating the

aqua regia soil digest was used for this purpose. It contained 25 mg of Fe(III), 5 mg each of Ca, Mg, Al, Na and K, 1.0 μg of Tl (III) and 0.5 μg of Cd in 25 ml of 1 M HCl. The solution was passed through the separation procedure and elution was performed as described in Section 2. A subsequent 1.0 ml aliquot of the ascorbic acid solution was collected separately. In a second experiment the elution was performed in the following way: after washing out the column with 1 M HCl, alternating 0.5 ml aliquots of the solution of nitric acid and ascorbic acid were passed and a common 2.0 ml eluate for Cd and Tl was collected. A subsequent 1.0 ml aliquot of the nitric acid solution was collected separately. The concentrations of the elements in the washing solution and in the separate eluates were determined by flame AAS (pulse aspiration). The results obtained for Cd, Tl, Fe, and Mg are shown in Table 1. The concentrations of Ca, Na and K were at the same level as that of Mg. The concentration of Al was below the limit of detection.

It follows from the data presented in Table 1 that:

(i) Cd and Tl are quantitatively recovered from the simulated aqua regia soil digest by both elution procedures. Procedure 1 was preferred in the final version since it provided a higher extent of preconcentration for Tl;

(ii) the quantitative elution of Tl, especially in the case of alternating nitric and ascorbic acid solutions (procedure 2), is evidence for the successful course of the redox reaction between $TlCl_4^-$ and ascorbic acid under the dynamic conditions in the column, yielding the Tl(I) species
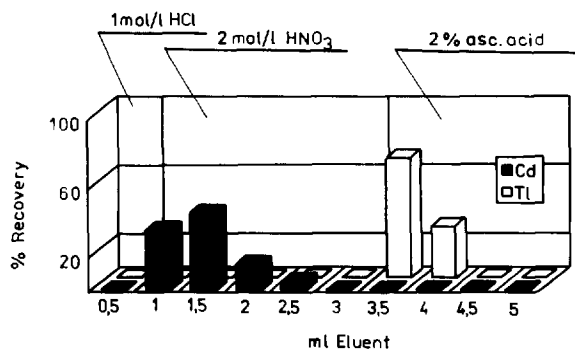

Fig. 1. Elution curves of cadmium and thallium.

Table 1
Recovered amounts of Cd, Tl, Fe and Mg in the separated eluates. Added to the model solution: 0.5 μg Cd, 1.0 μg Tl, 25 mg Fe(III) and 5 mg Mg

Solution	Volume	Element μg			
	(ml)	Cd	Tl	Fe	Mg
Elution procedure 1[a]					
1 M HCl	0.5	0	0	100	20
2 M HNO$_3$	2.0	0.5	0	5	0.5
2% ascorbic acid	1.0	0	1.0	0.5	0
2% ascorbic acid	1.0	0	0	0	0
Elution procedure 2[b]					
1 M HCl	0.5	0	0	100	20
2 M HNO$_3$ + 2% ascorbic acid	2.0	0.5	1.0	5	0.5
2 M HNO$_3$	1.0	0	0	0.5	0

[a] According to Section 2.
[b] A common eluate for Cd and Tl consisting of alternating aliquots of 2 M HNO$_3$ and 2% ascorbic acid.

which is not retained on the anion exchanger;

(iii) appreciable amounts of Fe(III) and other major soil components were detected only in the 1 M HCl washing solution, which implies that these were residues from the initial solution. Thus the negligible concentration of Fe(III) in the separate eluates can be related to insignificant sorption rather than to incomplete elution.

Table 2
Thallium and cadmium contents in Bulgarian cultivated soils digested with aqua regia. The average of five digestions is presented.

Soil sample	Thallium (μg g^{-1})		Cadmium (μg g^{-1})	
	Present work	Ref. [7]	Present work	Ref. [7]
Calcarous chernozem	0.68 $\pm$ 0.04	0.62	0.55 $\pm$ 0.03	0.49
Leached chernozem	0.49 $\pm$ 0.04	0.45	0.60 $\pm$ 0.03	0.56
Leached cinnamonic forest soil	0.52 $\pm$ 0.04	0.55	0.81 $\pm$ 0.03	0.77
Alluvial meadow soil	0.51 $\pm$ 0.04	0.50	0.70 $\pm$ 0.03	0.67
Grey forest soil	0.34 $\pm$ 0.04	0.38	0.35 $\pm$ 0.03	0.40

The method was applied to the determination of thallium and cadmium in some typical representatives of Bulgarian cultivated soils digested with aqua regia. The soil samples were taken from the top layer (0–20 cm) of several experimental fields of the Institute for Soil Research "N. Pushkarov", Sofia. The accuracy of the method was checked by comparing the results to those obtained by solvent extraction of the analytes from the aqua regia soil digest acidified with sulphuric acid, followed by flame AAS determination in the organic extract [7] (see Table 2).

The limits of detection of the flame AAS determination using the slotted quartz tube were 0.002 μg ml^{-1} amd 0.02 μg ml^{-1} for cadmium and thallium respectively. The limits of detection of the whole procedure were 0.01 μg g^{-1} and 0.04 μg g^{-1} for cadmium and thallium, respectively.

The relative deviation at the 0.5 μg/g^{-1} level was about 7%. The approach is amenable to flow-injection analysis.

References

[1] H. Gorbauch, H.H. Rump, G. Alter and C.H. Schmitt-Henco, Fresenius' Z. Anal. Chem., 317 (1984) 236.
[2] K. Robards and P. Worsford, Analyst, 116 (1991) 549.
[3] H. Tchuldgian, Heavy metal pollution of soils, in T. Boyadjiev (Ed.), Lectures on Soil Sciences, Project TCP/4502, FAO, Rome, 1989, p. 315.
[4] A. Brown, B.A. Milner and A. Taylor, Analyst, 110 (1985) 501.
[5] S. Tsakovski, E. Ivanova and I. Havezov, Talanta, 41 (1994) 721.
[6] O.G. Koch and G.A. Koch-Dedic, Handbuch der Spurenanalyse, Springer-Verlag, Berlin, 1974, p. 370.
[7] E. Ivanova, G. Gentscheva, M. Stoimenova and I. Havezov, Anal. Lab., 4 (1995) 14.

Urea solid-state biosensor suitable for continuous dialysis control

S. Zamponi[a], B. Lo Cicero[a], M. Mascini[a,*], L. Della Ciana[b], S. Sacco[b]

[a]Dipartimento de Sanita' Pubblica, Epidemiologia e Chimica Analitica Ambientale, Sezione di Chimica Analitica,
Via Gino Capponi 9, 50121 Firenze, Italy
[b]Sorin Biomedica, Saluggia 13040 Vercelli, Italy

Abstract

A solid state potentiometric biosensor for urea determination was assembled coupling a nonactin-based ISE without an internal solution with immobilized urease. The system proved to be useful for continuous monitoring of urea during dialysis treatment using the ultrafiltrate of blood as sample. A noticeable shift of potential occurred during the dialysis (probably due to continuous extraction of ionophore by the ultrafiltrate). Therefore a flow injection analysis assembly was necessary to control the shift of electrode potential.

Keywords: Dialysis; Solid-state biosensor; Urea

1. Introduction

The problem of monitoring the course of dialysis treatment in order to allow a personalized treatment (length and frequency) is still a challenge even though several suitable approaches have been recently published [1–8]. During dialysis treatment the concentration of urea in blood decreases from 50 mM to below 10 mM [9]. Nowadays no on-line monitoring of the dialysis performance is available and of course the treatment is rarely interrupted at the optimal point.

This paper reports the realization of a solid-state pontentiometric biosensor (a nonactin-based ion-selective electrode without an internal liquid solution coupled with immobilized urease) which is very practical and easy to change after every dialysis treatment and a procedure based on flow-injection analysis (FIA) which is proven to be necessary for continuous monitoring of the ultrafiltrate of blood. The FIA procedure permits the continuous control of the shift occurring at the potentiometric urea sensor which is probably due to a continuous extraction of the ionophore (nonactin) by the ultrafiltrate of lipophilic character.

We specifically refer to dialysis treatment where the ultrafiltration of blood realized in a suitable filter precedes the true dialysis process realized by a second filter where the dialysis liquid re-equilibrates the blood (Multimat system from Bellco,

* Corresponding author.

Italy). The ultrafiltrate of blood obtained in the first filter consists of a proteinaceous pale yellow liquid which contrains all low-molecular weight compounds and is wasted in the dialysis treatment. This liquid was considered the most suitable for continuous monitoring of urea because the urea concentration in this liquid corresponds perfectly to the blood concentration [10].

2. Experimental

2.1. Materials and apparatus

Urease (EC 3.5.1.5 from jack beans type VII, 400–800 U mg^{-1}) was obtained from Sigma. Nonactin was an ionophore from Fluka. All chemicals used were of analytical grade. All potentiometric measurements were made vs. the SCE with an Amel 336 potentiometer and an Amel 866 recording apparatus (Amel, Milan, Italy). A Rheodyne valve 7010 with pneumatic actuator 5701 (Rheodyne, Cotati, CA) and an air-controlled solenoid valve 7163 (Rheodyne) was used in conjunction with a Crouzet type TOP 948 programmable timer (Crouzet Componenti SpA, Milan, Italy) for automatic sampling. A flow cell of wall-jet type was obtained from Metrohm (cat. no. 656 (electrochemical detector); Metrohm, Herisau, Switzerland) where the urea sensor was adjusted instead of the working electrode. A Gilson (Gilson, Villiers-le-Bel, France) Minipuls peristaltic pump was used at a flow rate of 0.8 ml min^{-1} as the flowing apparatus.

2.2. Instrumentation

The sensor was obtained by immobilizing over a graphite electrode a layer of PVC–nonactin solution in tetrahydrofuran and over it a layer of urease immobilized with the use of bovine serum albumin and glutaraldehyde. The sensor has been used in a flow cell (preliminary experiments) or in a wall-jet provided with a sampling valve in the FIA procedure. The valve was actuated automatically with a pneumatic actuator and an electronic timer to obtain a peak every 4 min. The diagram of the instrumentation is presented in Fig. 1 with the scheme of the urea potentiometric sensor.

2.3. Procedures

2.3.1. Preparation of graphite electrode

Graphite powder (3.5 g) was thoroughly mixed with epoxy glue. As epoxy were mixed Araldite M (1 g), Araldite H 964 hardener (1 g) and Araldite Y960 (DY060) (0.5 g) as accelerator obtained from Fluka. After mixing the graphite with epoxy, it was introduced in a plastic syringe and to eliminate air bubbles pressure was applied with the piston of the syringe. The syringe was left for 24 h. The barrel of hardened graphite was then taken out of the syringe and cut into 5–10 mm long pieces. Each was fixed in a PVC tube with an external diameter of 7 mm and an internal diameter of 3.5 mm. A copper wire was glued from one side with the aid of conductive epoxy.
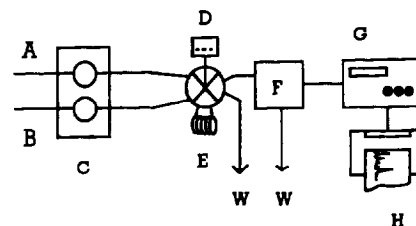
(a)
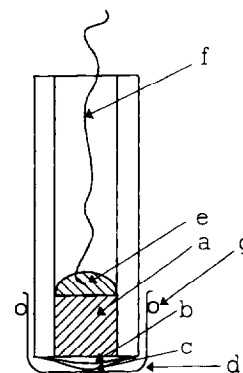
(b)

Fig. 1. (a) Scheme of FIA measurements: (A) phosphate buffer as carrier; (B) ultrafiltrate; (C) peristaltic pump; (D) timer; (E) sampling valve, 50 μl; (F) wall-jet cell; (G) potentiometer; (H) recorder; (W) waste. The sampling valve was operated by means of a pneumatic actuator controlled by a solenoid valve and a Crouzet timer. (b) Scheme of urea electrode: (a) graphite plug; (b) layer of nonactin in PVC; (c) layer of urease immobilized with BSA and glutaraldehyde; (d) cellulose acetate to retain membrane against the electrode surface; (e) conductive epoxy (silver-based); (f) copper wire; (g) O-ring.
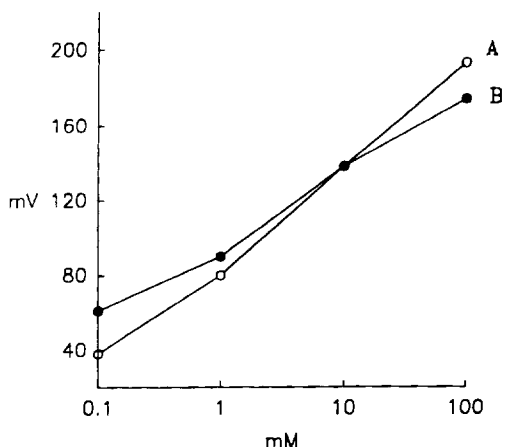
Fig. 2. Calibration curve of the solid-state sensor in a flow system for ammonium and urea in phosphate buffer (pH 7.0): (A) ammonium; (B) urea.

2.3.2. Immobilization of nonactin

5 mg of nonactin, 100 mg of PVC (high molecular weight), 200 mg of BBPA (bisbutylpentyladipate) and 1.5 ml of tetrahydrofuran were mixed and stirred in a closed flask (5 ml) for about 2 h, to allow complete solubilization of the compounds.
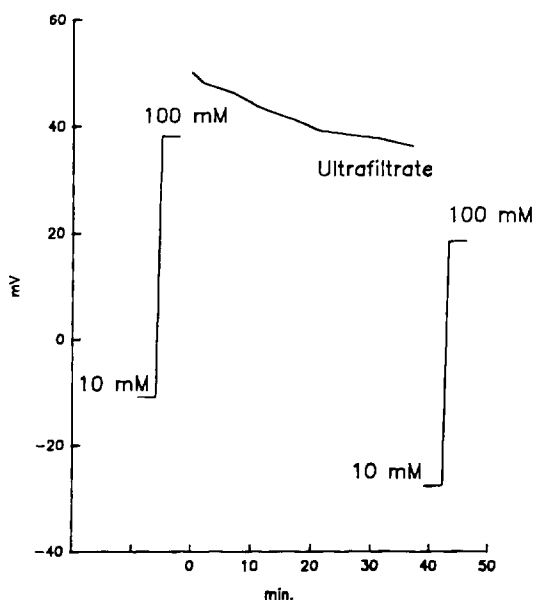

Fig. 3. Experiment with the ultrafiltrate. Two standard solutions, 10 and 100 mM, were prepared and flowed at the beginning and end of a 40 min experiment during when the ultrafiltrate (urea content 200 mM) flowed.

100 μl of this solution was layered over the graphite electrode (3.5 mm of graphite in a PVC tube with an external diameter of 7 mm). After 2–3 h the ammonia electrode was ready to be used [6].

2.3.3. Immobilization of urease

Over the nonactin-based layer was spread 2 mg of solid urease (type VII from Sigma), 10 μl of BSA (bovine serum albumin solution, 10 mg in 500 μl of phosphate buffer 0.02 M, pH 7.0) and 5 μl of glutaraldehyde solution (2.5%). The mixture was mixed carefully and allowed to dry for 1–2 h. Then the electrode was left in stirred glycine solution (0.5 M) for 30 min; during this period the free aldehyde groups react with the amino group of glycine [11]. The electrode was found to be stable for several months if kept dry in a refrigerator. When the sensor was fixed in the flow cell or in the wall-jet cell an additional membrane of cellulose acetate was mounted and fixed with an O-ring in order to protect all the layers and push them against the graphite sensor.

2.3.4. Ultrafiltrate samples

Samples were obtained by ultrafiltration of heparinized (50 U ml^{-1}) bovine blood (adjusted to
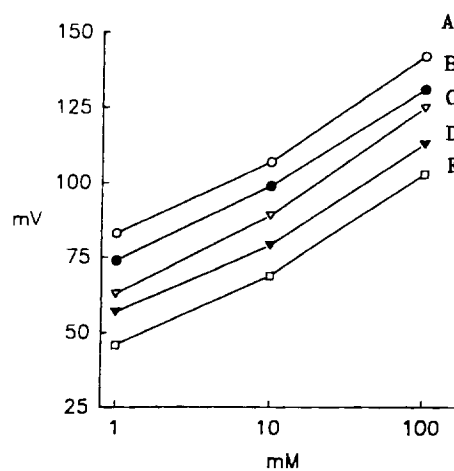

Fig. 4. Successive calibration curves obtained with a continuous flow of ultrafiltrate during a 5 h period. Each calibration curve was recoreded every hour. Curve A was measured at the start of the experiment, curve B after 1 h of continuous flow of ultrafiltrate, curve C after 2 h, etc. The slopes are reported in Table 1.

1376

S. Zamponi et al. Talanta 43 (1996) 1373 1377

Table 1
Voltages (mV) and slopes (mV) of the calibration curves recorded each hour at concentration values of 1, 10 and 100 mmol l [-1] (see Fig. 4)

Concentration (mM)	A		B		C		D		E	
	Voltage	Slope	Voltage	Slope	Voltage	Slope	Voltage	Slope	Voltage	Slope
1	83	24	74	25	63	26	57	22	46	23
10	107	35	99	32	89	36	79	34	69	34
100	142	–	131	–	125	–	113		103	–

40% v/v for hematocrit value), through a filter cartridge with a surface of 0.07 m² (Cod. 621) and with a surface area of 1.3 m² (Cod. N. BL627; commercially available from Sorin (Saluggia, Italy)). The hematocrit value was adjusted with phosphate buffer (sodium salts) in 0.1 M sodium chloride (about 250 ml of buffer per 1 l blood). The hematocrit value was adjusted to simulate human values in order to obtain similar flowing conditions in the filter cartridge. The concentration of urea in the ultrafiltrate was evaluated in the range 1–2 mmol l [-1].

3. Results and discussion

Fig. 2 shows the calibration curve obtained in the flow system with standard solutions of urea

and ammonium in buffer phosphate. Different solid-state sensors (more than 20 sensors were tried) show nerstian behavior in the range 1–100 mM; they have E_0 values which differ by up to ± 200 mV for unknown reasons and this value can shift from day to day. However, the potential value is very stable for several hours and permits easy determination in flow systems.

Fig. 3 reports the shift observed in an experiment where ultrafiltrate of constant urea concentration (obtained from heparinized bovine blood and adjusted to 40% v/v for the hematocrit value) flowed in the continuous mode. We can see how the signal shifted during the 40 min of continuous flow and that the signals obtained with two standard solutions (10 and 100 mM) of urea were shifted in the same period by about 25 mV.

Fig. 4 gives several calibration curves obtained in continuous flow in another experiment during a 5 h period, showing a continuous shift, while the slope was maintained almost constant. The slopes of the curves are given in Table 1.
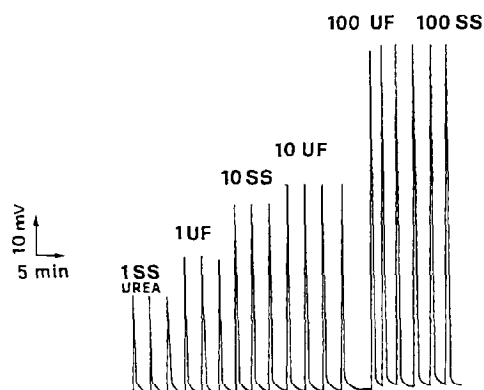

Fig. 5. Calibration curves of urea standard solutions (1, 10 and 100 mM of urea) realised in buffer (without potassium ion) (SS) and in ultrafiltrate (UF) recorded with the FIA procedure.
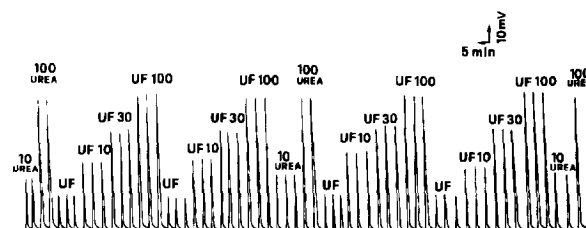

Fig. 6. Continuous recording over a 5 h period of calibration curves of standard solutions (SS) and ultrafiltrate spiked with a standard urea concentration (UF). UF 10, UF 30 and UF 100 are the signals obtained from ultrafiltrate spiked with 10, 30 and 100 mM urea respectively. 10 Urea and 100 Urea are the signals obtained with standard solutions of 10 urea and 100 nM respectively.

After assembling a FIA system (sampling valve 50 μl) we obtained the results reported in Fig. 5 with standard solutions in phosphate buffer and prepared in ulttrafiltrate. Fig. 6 shows results obtained over a long period (5 h) with consecutive injections of sampling probe standard solutions of urea, ultrafiltrate and ultrafiltrate with added urea in suitable concentrations (10, 30, 100 mmol l^{-1}), simulating the concentration values obtained during a real dialysis process. The baseline obtained in the last experiment is very stable and the sensitivity of the probe is not impaired by contact with the ultrafiltrate and the long duration of the experiment. Therefore we can conclude that this sensor preparation and this analytical procedure are very suitable for the continuous monitoring of urea in such applications.

In Figs. 5 and 6 it can be seen that in the low range of urea concentrations the peaks obtained in ultrafiltrate are higher than the same urea concentrations in buffer. This result was expected and is due to the well-known interference of potassium ions at the nonactin-based ammonium sensors. However, the low range of urea is the least important part of the calibration curve for clinical purposes.

The drift observed in the continuous flow experiment (Figs. 3 and 4) can be ascribed to the lipophilic nature of the ultrafiltrate which probably extracts the constituents of the PVC membrane (ionophore or softener) from it. This was reported with other ISEs with neutral carriers when in contact with blood or proteinaceous fluids [12]. However, the FIA procedure eliminates the problem, at least for up to 5 h. It is logical that the small period of contact between the ultrafiltrate and the sensor membrane permits one to obtain a very reproducible signal, but does not alter the composition and structure of the membrane. We think that this approach solves the problem of continuous monitoring of urea during the dialysis treatment with a cheap, disposable and easily fabricated sensor. For mass production the sensor can even be printed in a printing process (preliminary experiments in this laboratory proved it to be feasible) and therefore it can be considered to be a real disposable sensor.

References

[1] D. Martorell, E. Martínez-Fábregas, J. Bartroli, S. Alegret and C. Tran-Minh, Sens. Actuat. B, 15–16 (1993) 448.

[2] S. Alegret, J. Bartroli, C. Jiménez, E. Martínez-Fábregas, D. Martorell and F. Valdés-Pérezgasga, Sens. Actuat. B, 15–16 (1993) 453.

[3] P. Thavarungkun, H. Hakanson, O. Holst and B. Mattiasson, Biosens. Bioelectr., 6 (1991) 101.

[4] W. Sansen, P. Jacobs, A. Claes and M. Lamprechts, 2nd Workshop of Biomedical Engineering Action of the European Community on Chemical Sensors for In Vivo Monitoring, 12–15 November, 1989, Firenze, Italy.

[5] I. Karube, E. Tamiya, J.M. Dicks and M. Gatoh, Anal. Chim. Acta, 185 (1986) 195.

[6] G. Palleschi, M. Mascini, E. Martínez-Fábregas and S. Alegret, Anal. Lett., 21 (1988) 1115.

[7] P. Jacobs, J. Suls, W. Sansen and R. Hombrouckx, American Society For Artificial Internal Organs Journal, 39 (1993) M353.

[8] L. Garred, N. Amour, W. McCready and B. Canaud, American Society For Artificial Internal Organs Journal, J., 39 (1993) M337.

[9] P. Thavarungkul, H. Hakanson, O. Holst and B. Mattiasson, Biosens. Bioelectr., 6 (1991) 101.

[10] P. Smirthwaite, A. Fisher, I. Henderson, J. McGhee, N. Mokhtar, K. Simpson, A. Whitehead and J. Gaylor, American Society For Artificial Internal Organs Journal, 39 (1993) M342.

[11] M. Mascini and G.G. Guilbault, Anal. Chem., 49 (1977) 795.

[12] M. Mascini and G. Marrazza, Anal. Chim. Acta, 231 (1990) 125.

Measurement/data-processing method to improve the ruggedness of membrane-based sensors: Application to amperometric oxygen sensor

Sheldon Williams, Harry L. Pardue*, Christopher E. Uhegbu[1], Aaron M. Smith, Joanna Studley

Department of Chemistry, 1393 BRWN Bldg., Purdue University, West Lafayette, IN 47907-1393, USA

Abstract

This paper describes alternative measurement and data-processing approaches that can reduce effects of experimental variables on results obtained with a membrane-based sensor for oxygen. In the new approaches, the membrane-based sensor is first equilibrated with the sample solution, after which a polarizing voltage is applied and current vs. time data are recorded as the response decays toward a steady-state condition. Current vs. time data are then processed by a fixed-time option and an integration option designed to determine the charge corresponding to the total amount of oxygen inside the membrane when a polarizing voltage is applied. The current measured at a fixed time and the total charge varied linearly with oxygen concentration between 0.05 and 0.26 mmol l^{-1}. Pooled relative standard deviations ($N = 35$) for the measurement/data-processing step were near 0.4% for the new pre-equilibrium options compared to a value of 0.3% for the steady-state option. Dependencies of the pre-equilibrium options on membrane thickness and stirring rate in the most sensitive regions were at least two orders of magnitude smaller than for the steady-state option.

Keywords: Amperometric oxygen sensor; Data-processing method; Membrane-based sensors; Ruggedness

1. Introduction

Membrane-based devices are used for a variety of selective measurements in analytical chemistry [1–5]. One very popular membrane-based detector system is the so-called oxygen electrode which involves an amperometric electrode isolated from the sample solution by a membrane that is selective for small molecules, including oxygen [1,6]. Like most such devices, this one is usually used in the steady-state mode. It has been shown that results obtained with the "oxygen electrode" used in the steady-state mode are very sensitive to changes in stirring rates and properties of the membrane such as thickness and permeability [6–8]. Accordingly, to obtain reliable results by using

---

* Corresponding author.
[1] Present address: Diametrics Medical, Inc., 2658 Patton Road, Roseville, MN 55113, USA.

the steady-state mode, it is necessary to control variables within narrow tolerances.

A general approach to resolving such problems is to make measurements that depend on equilibrium conditions rather than rate processes. One such approach evaluated for the "oxygen electrode" is to first pre-equilibrate the solution inside the membrane with each sample solution with no polarizing voltage applied and then to apply the polarizing voltage and measure the initial rate of change of the resulting current [6,7]. An alternative approach is to use the same pre-equilibration procedure, then apply the polarization voltage, digitize and store current vs. time data, and use a curve-fitting procedure to extrapolate the transient data to the current at time zero [8].

The present study was undertaken to evaluate other data-processing approaches that can be used to extract the desired information from the transient data resulting from the pre-equilibration approach. The rationale for this extended study is based on the belated realization that if the rate of the mass transfer process to and across the membrane is slow relative to the rate of equilibration of the measurement process inside the membrane, then virtually all features of the measured signal will be related to the bulk concentration of analyte in the sample solution and independent of variables that affect the rates of mass transfer across the membrane. Two alternative data-processing approaches were used to test this hypothesis by using the membrane-based "oxygen electrode" as a model system.

The simpler of the two approaches is an analog of the conventional fixed-time kinetic option [9–12]; it involves measurement of the signal amplitude at a fixed point in time for each response. The more complex of the two approaches is a hybrid of the integration and predictive curve-fitting options [12–14]; it involves integration of the time-dependent current and use of curve-fitting methods to extrapolate the resulting charge vs. time data to the value of charge at $t = 0$ (Q_0) and as $t \to \infty$ (Q_∞). These extrapolated values are used to compute the total charge ($\Delta Q_\infty = Q_\infty - Q_0$) corresponding to electrolysis of all the analyte (oxygen) inside the membrane when a polarizing voltage is applied.

The latter option was complicated by the facts that current–time responses included charging currents near zero time and did not decay to zero at longer times but rather to finite steady-state values. Two approaches similar to those described earlier [15] were used to extract the charge corresponding to analyte inside the membrane when a polarizing voltage was applied. One option involved integration of the unmodified signal including the component approaching steady state and use of a model for simultaneous zero-order and first-order processes [16] to extract the desired component of the charge. The other approach involved subtraction of the steady-state current from all time-dependent currents before integration of the transient response; this is called the background-correction option herein.

2. Experimental

The same data reported in an earlier paper [8] were used for this study. Accordingly, an abbreviated procedure is presented here.

Samples were prepared by adding aliquots of an air-saturated solution (≈ 0.26 mmol l^{-1} oxygen) to a fixed volume of deaerated water. For linearity and reproducibility studies, five runs were made at each of eight different oxygen concentrations between 0 and 0.26 mmol l^{-1}. For studies of effects of variables, five runs were made at each of three different membrane thicknesses and four different stirring rates at a fixed oxygen concentration (0.26 mmol l^{-1}).

The "oxygen electrode" was equilibrated with each test solution by immersion in the solution for 30 s before the polarizing voltage was applied. When the polarizing voltage was applied, 250 data points were collected at intervals of 0.0006 s per point for the first 100 points and 0.027 s per point for the last 150 points.

For the fixed-time approach, current amplitude was measured at the same time after the polarizing voltage was applied for each sample. Fixed-time measurements were taken near the peak (0.17 s), on the steep part of the decay curve (1.2 s) and in the region approaching steady state where the

rate of change of signal was sufficiently small that timing errors would not have unusually large effects (3.92 s, the average of ten data points between 3.75 and 4.1 s). For the integration option without background subtraction, unmodified current vs. time data were integrated between 0.33 and 4.1 s and a model for simultaneous zero-order and first-order processes [16] was fit to the data to resolve the charges resulting from the transient and steady-state components. For the integration option with background subtraction, the average of the last ten data points (3.75–4.1 s) was subtracted from each signal value and the resulting data between 0.33 and 4.1 s were integrated. A first-order model [14] was then fit to charge vs. time data to extrapolate to $t = 0$ and $t \rightarrow \infty$.

3. Results and discussion

Unless stated otherwise, random uncertainties are reported at the level of one standard deviation based on five runs per sample.

3.1. Response curves

Fig. 1 shows typical plots of current vs. time without (plot a) and with (plot b) background correction. Zero time corresponds to the point at which the polarizing voltage was applied. The initial rise represents charging current and the gradual decrease after the peak is caused by depletion of oxygen inside the membrane at a rate faster than it is replaced by mass transfer across the membrane.

It is apparent from the plots that the currents did not reach true steady-state values during the 4 s measurement period. Accordingly, use of currents from the latter parts of these responses for background correction tend to overcompensate for the steady-state current.

Fig. 2 includes charge vs. time data without and with background correction. The open circles in the upper plot (without background correction) represent experimental data and the solid curve through the points represents a fit of a model for simultaneous zero- and first-order processes to the
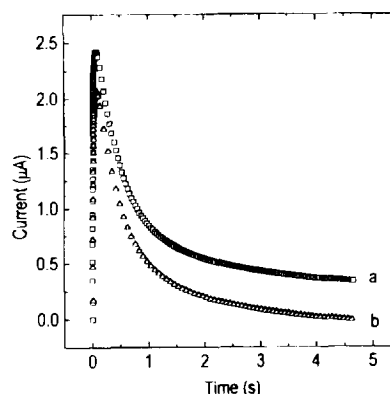

Fig. 1. Current vs. time response after pre-equilibrium with air-saturated solution (0.26 mmol l^{-1} O_2) without (a) and with (b) background correction.

data. The curvature reflects the decaying current after the polarizing voltage is applied and the nearly linear extension at longer times represents the approach to steady state. Clearly, the model for combined zero- and first-order processes fits the data very well. The lower plots (curves b and c) represent the first-order component of the charge vs. time data obtained by the fitting process. The open triangles represent the first-order component from the fit of the model for combined zero- and first-order processes to data without background correction and the open squares represent charge vs. time data obtained from background-corrected data (plot b in Fig. 1). The
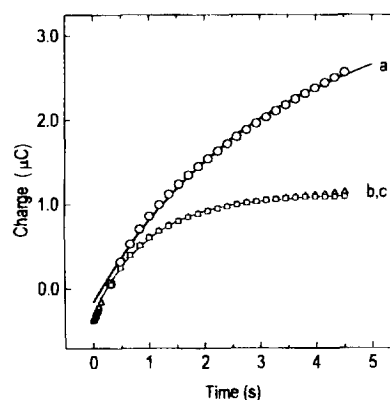

Fig. 2. Integrated response curve for air-saturated solution without (○, △) and with (□) background subtraction. Experimental data (○, □); fitted data (——). First-order component from model for combined zero- and first-order models (△).

Table 1
Linear least-squares results and pooled standard deviations for selected options

Option	Slope (SD) (NA mmol^{-1} l^{-1}/ NC mmol^{-1} l^{-1})[a]	Intercept slope (SD) (10^{-3} μmol l^{-1})	Estimated standard /slope (μmol l^{-1})	Correlation coefficient	Pooled RSD (%)[b]
Steady state [17]	0.714 (0.01)	−5.6 (2.5)	6.3	0.998	0.3[d]
Predicted I_0 [8]	28.6 (0.9)	24 (4.5)	0.015	0.98	2.7[e]
Fixed time[c]	0.92 (0.02)	6.9 (4.3)	0.012	0.988	0.4[f]
Integration					
with background correction	12.8 (0.31)	5.5 (4.0)	0.011	0.99	0.4[g]
without background correction	9.9 (0.24)	4.5 (3.8)	0.011	0.99	0.4[g,h]

[a] μA mmol^{-1} l^{-1} for current-based options; μC mmol^{-1} l^{-1} for charge-based options.
[b] Seven groups of five runs each. [c] Measured at 3.92 s.
[d] [h] Average signals: [d] 0.192 μA; [e] 2.55 μA; [f] 0.338 μA; [g] 1.38 μC; [h] 1.42 μC.

solid curve is a fit of a first-order model to the latter data. The darker area near zero time represents the higher data rate at shorter times. This is the difference between the change at $t = 0$ and $t \to \infty$ ($\Delta Q_x = Q_x - Q_0$) that is used to quantify oxygen concentration.

The negative values of extrapolated charges in Fig. 2 merit comment. Because the integration process was begun at 0.3 s, the apparent charge at that point is zero. Accordingly, extrapolation to $t = 0$ is expected to give negative values. It is the total difference between values at $t = 0$ and $t \to \infty$ that is used to quantify oxygen concentration.

3.2. Linearity

Each of the three data-processing options yielded linear plots of the measurement objective (current at fixed time or extrapolated charge) vs. concentration. Results for linear least-squares fits of measurement objectives vs. concentration are given in Table 1. In each case, intercepts and standard errors of the estimates are divided by slopes to normalize results to concentration units for easy comparison. Intercepts are similar for the two integration options and about five-fold smaller than for the fixed-time option. Standard errors of the estimates and correlation coefficients are about the same for all three options.

Fixed-time results were also obtained near the peak (0.17 s) and on the steep portion of the decay curve (1.2 s). In each case, calibration plots

were linear. Slopes for the three measurement times (0.17, 1.2 and 3.92 s) were 16.8, 3.5 and 0.92 μA mmol^{-1} l^{-1} respectively; intercepts were 0.02, −0.009 and 0.004 mmol l^{-1} respectively; standard errors of the estimates were 0.015, 0.009 and 0.01 μA respectively; and correlation coefficients were 0.964, 0.986 and 0.988 respectively. All statistics were slightly improved for the two measurements at longer times after the peak than at the peak.

If the time-dependent data behaved ideally, then we would expect the same results from both integration options. However, this is not the case; data without background correction do not follow combined zero-order/first-order behavior exactly and data with background correction do not follow first-order behavior exactly. Accordingly, identical results are not expected or obtained for the two integration options. This is reflected primarily by the different slopes in Table 1.

3.3. Imprecision

The uncertainty associated with sample preparation and handling is much larger than that associated with the measurement and data-processing steps. Because our primary focus was on features of different measurement/data-processing options, imprecision is reported here for repeat runs on air-saturated samples. For seven data sets of five runs each on air-saturated samples (0.26 mmol l^{-1} oxygen), pooled standard deviations for

the fixed-time option, and the integration option without and with background correction were 0.0012 μA, 0.0042 μC and 0.0044 μC respectively, corresponding to relative standard deviations (RSDs) of 0.34%, 0.30% and 0.31% respectively. For the same data sets, pooled RSDs for the steady-state option and the predicted signal at $t = 0$ [8] were 0.2% and 2.6% respectively. The imprecisions for the three options included in this study are only slightly degraded relative to the steady-state option and are almost 10-fold less than that for the extrapolation option described earlier [8].

3.4. Variable dependencies

The principal advantage expected for the options described herein is low sensitivity to changes in experimental variables. Results in Figs. 3A and 3B illustrate effects of membrane thickness and stirring rate on the three new options described herein along with results obtained with the conventional steady-state option. All results are normalized to the value at one extreme of the range of variables studied to facilitate comparisons. Whereas results obtained with each of the three pre-equilibrium options are virtually independent of both membrane thickness and stirring rate throughout the ranges examined, steady-state results decrease by about 50% when the membrane thickness is increased three-fold and increase by about 25% from no stirring to a moderate level of stirring.

These sensitivities to membrane thickness and stirring rate can be quantified by using error coefficients (ECs), defined as the change in concentration per unit change in the variable of interest. ECs for the different options computed as described earlier (Eq. (2) in Ref. [8]) are summarized in the first two data columns of Table 2.

Ratios of ECs for the steady-state option divided by values for the other options (EC_{ss}/EC_{opt}) are included as the last two columns in the Table. In the most sensitive regions, the pre-equilibrium options are all at least two orders of magnitude more rugged than the steady-state option. Improvement factors approach unity at greater membrane thicknesses and higher stirring rates.

4. Conclusions

With the exception of the procedure involving extrapolation of current to zero time, the precision of the pre-equilibrium procedures is similar to that of the steady-state approach. Accordingly, it is possible to exploit the improved ruggedness of the pre-equilibrium approaches described herein without sacrificing precision.

The different pre-equilibrium options evaluated in this and the previous study [8] have similar degrees of ruggedness for the conditions studied. However, it is important to note that there are some fundamental differences among them. The initial-rate option described earlier [6,7] and the
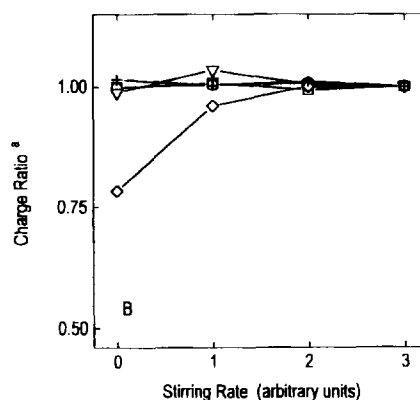
(a)
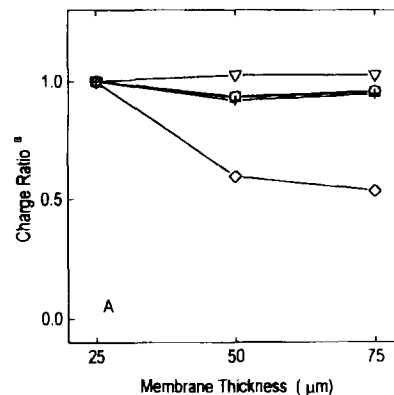
(b)

Fig. 3. Effects of membrane thickness (A) and stirring rate (B) on results from five different data-processing options. Options (both frames): steady state ($\Diamond$); fixed time (+); integrated signal without ($\bigcirc$) and with ($\square$) background subtraction; and extrapolated signal at zero time [18] (∇).

Table 2
ECs for different measurement/data-processing options

Option	ECs		Ratio of ECs[c]	
	Thickness[a] $(mmol\ l^{-1}\ \mu m^{-1})$	Stirring rate[b] $(mmol\ l^{-1}\ au^{-1})$	Thickness	Stirring rate
Steady state	−0.1	0.08	1.0	1.0
Integration				
without background correction	−0.00036	0.0009	280	90
with background correction	−0.0003	0.0008	330	96
Fixed time	−0.00005	−0.00015	2000	530

[a] 25–50 μm.
[b] 0–1 arbitrary units (au).
[c] Ratio of steady-state value to other values; reflects improved ruggedness.

fixed-time option reported herein both replace one group of kinetic processes with another, and consequently can be expected to depend on variables such as temperature that could affect these processes. The procedure involving extrapolation to the current at zero time [8] should, in principle, eliminate kinetic aspects of mass-transfer processes but is expected to depend upon variables that affect electrode kinetics. Moreover, that approach is complicated by the charging current when a polarizing voltage is applied and is subject to large uncertainties associated with extrapolated intercepts. Because the integration options produce a charge corresponding to the total amount of analyte in the fixed volume inside the membrane, they have the best chance of eliminating effects of all kinetic processes so long s the rate of the electrolysis process inside the membrane is sufficiently fast relative to the rates of mass transfer to and across the membrane. In this regard, this approach probably will be most effective with thick membranes and little or no stirring.

The principles illustrated here for the "oxygen electrode" should be applicable to other membrane-based "sensors" such as an amperometric sensor for carbon monoxide [5] and other gases [18]. These principles should also be applicable to other types of applications of membranes such as those cited earlier [1–4] as well as to separations or preconcentrations based on combinations of membranes with flow systems [19]. Furthermore,

whereas it was convenient to use a pre-equilibrium procedure in this example, this is just one option for the general concept. In the most general sense, the primary goal is to obtain an equilibrium-based result. If it is not feasible to establish an equilibrium condition experimentally, then another option is to extrapolate transient responses to equilibrium values [14]. For example, an alternative approach with the "oxygen electrode" would be to completely deplete the analyte inside the membrane and then to follow the approach to equilibrium as the concentration of oxygen inside the membrane approaches that in the sample solution. This would require an intermittent measurement approach that would minimize depletion of oxygen concentration inside the membrane.

Acknowledgment

References

[1] H.L. Hitchman, Measurement of Dissolved Oxygen, Wiley, New York, 1979.
[2] F.V. Bright, T.A. Betts and K.S. Litwiler, Anal. Chem., 62 (1990) 1065.

[3] S. Bruckenstein and J.S. Symanski, Anal. Chem., 58 (1986) 1766.

[4] R.G. Melcher, Anal. Chim. Acta., 214 (1988) 299.

[5] H.J. Vreman et al., Clin. Chem., 40 (1994) 1927.

[6] K.H. Mancy, D.A. Odom and C.N. Reilley, J. Electroanal. Chem., 4 (1962) 65.

[7] H.Y. Wang and X. Li, Biosensors, 4 (1989) 273.

[8] C.E. Uhegbu and H.L. Pardue, Anal. Chem., 64 (1992) 2378.

[9] H.A. Mottola, Kinetic Aspects of Analytical Chemistry, Wiley-Interscience, New York, 1988.

[10] D. Perez-Bendito and M. Silva, Kinetic Methods in Analytical Chemistry, Ellis-Horwood, Chichester, UK, 1988.

[11] J.S. Ingle and S.R. Crouch, Anal. Chem., 43 (1971) 697.

[12] M.D. Love and H.L. Pardue, Anal. Chim. Acta, 299 (1994) 195.

[13] L.C. Thomas and R.A. Othman, Talanta, 38 (1991) 773.

[14] G.E. Meiling and H.L. Pardue, Anal. Chem., 50 (1978) 1611.

[15] C.E. Uhegbu, K.B. Lim and H.L. Pardue, Anal. Chem., 65 (1993) 2443.

[16] W.E. Weiser and H.L. Pardue, Clin. Chem., 33 (1987) 237.

[17] C.E. Uhegbu and H.L. Pardue, Anal. Chim. Acta, 237 (1990) 413.

[18] Z. Cao, W.J. Buttner and J.R. Stetter, Electroanalysis, 4 (1992) 253.

[19] T. Aoki, J. Flow Inject. Anal., 11 (1994) 24.

Electrocatalytic modified electrode for remote monitoring of hydrazines

Joseph Wang*, Qiang Chen, Gemma Cepria[1]

Department of Chemistry and Biochemistry, New Mexico State University, Las Cruces, NM 88003, USA

Received 15 January 1996; accepted 5 February 1996

Abstract

A remote electrochemical sensor for field monitoring of hydrazine compounds is described. The new submersible probe relies on the coupling of an effective electrocatalytic modified electrode to a 50 ft long shielded cable. The catalytic surface, based on an electorpolymerized film of 3,4-dihydroxybenzaldehyde, offers low-potential detection of hydrazine compounds. Such catalytic activity results in high sensitivity and selectivity, and hence offers convenient measurements of micromolar hydrazine concentrations in untreated groundwater, river water or lake water samples. Coexisting sample constituents do not contrubute to the response. Operational conditions have been optimized to meet the spacific requirements of remote operation. The concept seems suited for the remote monitoring of other contaminants via the judicious choice of the surface modifier.

Keywords: 3,4-Dihydroxybenzaldehyde; Electrocatalytic modified electrode; Field monitoring; Hydrazines

1. Introduction

Because of the toxicological significance of hydrazine compounds, a reliable method is required for their environmental and industrial monitoring. Continuous measurement of hydrazines, affected in the natural media, is preferable, since it affords the option of an in-situ warning system and avoids the errors and delays inherent in laboratory-based analyses. Controlled-potential electrochemical techniques, particularly those relying on electrocatalytic modified electrodes, have been de-

veloped for the detection of hydrazine compounds [1-4]. The adaptation of these schemes for field measurements of hydrazines is thus a logical extension of their capabilities.

In this paper we describe a remote modified electode for in-situ monitoring of hydrazine contaminants. The new remote sensor (Fig. 1) couples the strong electrocatalytic action of electropolymerized films of 3,4-dihydroxybenzaldehyde (3,4-DHB) [5] towards hydrazine compounds [2] with the attractive features of our new remote electrode configuration [6,7]. Such a configuration was employed recently for stripping-based monitoring of toxic metals [6,7]. While such stripping work has relied on the use of a bare gold fiber electrode, the present sensor employs, for the first time, an

---

* Corresponding author.

[1] Permanent address: Faculty of Sciences, University of Zaragoza, 50.009 Zaragoza, Spain.
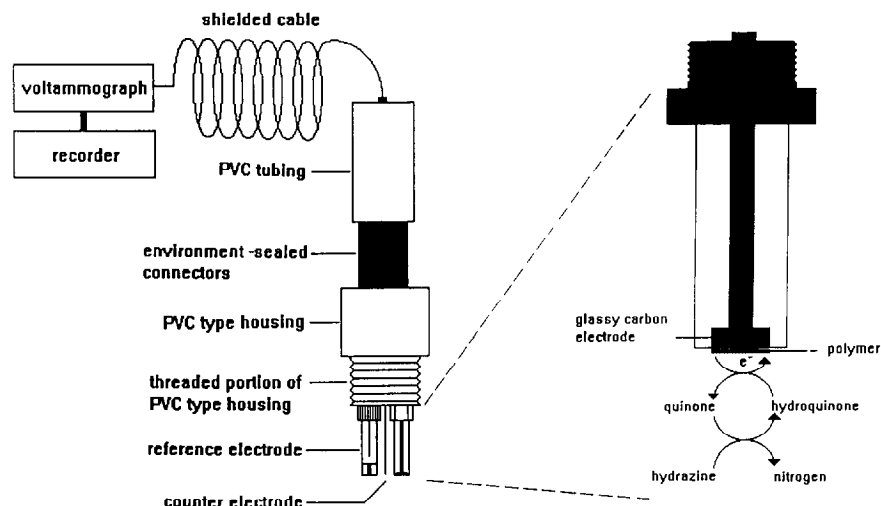
Fig. 1. Schematic diagram of the remote electrochemical sensor for monitoring hydrazines. The right-hand displays the electrocatalytic action of the polymer-modified working electrode.

electrocatalytic modified electrode for facilitating the detection of contaminants. The electrocatalytic considerations are thus coupled with the requirements for remote operation, including large instrument–sample distances, sealed electrical contacts, a rugged and compact electrode assembly and the ability for rapid maintenance. Although the new concept of remote modified electrodes is presented within the framework of hydrazine sensing, it could be extended to other relevant polllutants (via a judicious choice of the modifier). The challenges, obstacles and solutions for a submersible operation of catalytic electrodes in untreated water samples are explored below in connection with our novel remote electrode assembly.

2. Experimental

2.1. Apparatus

Chronoamperometric and voltammetric experiments were performed with the BAS Model CV-27 voltammetric analyzer (Bioanalytical Systems, West Lafayette, IN), in connection with a BAS X–Y–t recorder. Experiments were performed in a 40 ml plastic (PVC) beaker. A schematic diagram of the remote modified electrode is shown in

Fig. 1. The probe design is similar to that of our previously reported remote metal sensor [5,6], with the exception that a modified glassy carbon electrode (3 mm diameter, Model MF-2012) replaces the gold fiber. The working electrode is cut to a 2.5 cm length for compatibility with the PVC-based sensor tip. The electrode assembly, housed in a PVC housing tube, was connected to the 50 ft long shielded cable via a three-pin environmentally-sealed rubber connector. A Ag/AgCl electrode (BAS, Model RE-4) served as reference. Details of the probe design are given in Refs. [6] and [7].

2.2. Surface activation and modification

The glassy carbon was first polished with a 0.25 μm alumina slurry, and then thoroughly rinsed with double-distilled water. Subsequently, the surface was activated for 5 min in a 1 M NaOH solution, while holding the potential at + 1.2 V. The electrode was then treated for an additional 5 min by scanning the potential between − 0.2 and + 1.0 V while dipping in a phosphate buffer solution. The activated electrode was subsequently modified by immersion in a 1 mM 3,4 DBH/phosphate buffer solution while holding the potential at + 3.0 V for 3 min. Subsequently, the surface was rinsed with the buffer solution.

2.3. Reagents and procedure

All solutions were prepared with deionized water. Hydrazine sulfate was obtained from J.T. Baker (Phillipsburg, NJ), while 1,2-dimethylhydrazine dihydrochloride, methylhydrazine, and 3,4-DBH were purchased from Aldrich. **Caution: in view of their toxicity, special attention is required in the handling of hydrazine compounds.** The river water and lake water samples were collected from the Rio Grande river (at Las Cruces, NM) and Lake Ontario (at Rochester, NY). The groundwater sample was obtained at the Hanford Site (Richland, WA).

Chronoamperometric and cyclic-voltammetric experiments were conducted at room temperature, while placing the sample ≈ 50 ft from the voltammetric analyzer. The chronoamperometric experiments relied upon stepping the potential from open circuit to $+0.2$ V; the steady-state current (after ≈ 45 s) was used for the quantitation.

3. Results and discussion

The use of the 3,4-DHB-coated remote electrode for the mediated detection of hydrazine compounds in natural water samples is illustrated in Fig. 2b. This figure shows typical cyclic voltammograms for hydrazine (A), methylhydrazine (B) and dimethylhydrazine (C) in an untreated groundwater sample. The 3,4-DBH-modified electrode displays a well-behaved redox process ($E^0 = +0.15$ V) in the unspiked natural water sample (a). Such peaks are attributed to the redox reaction of the surface-confined quinone moiety. A similar response was observed in a phosphate buffer blank solution, indicating that none of the groundwater sample constituents is contributing to the response. A substantial increase of the anodic peak, characteristic of an electrocatalytic process, is observed upon addtion of the different hydrazine compounds. Consistent with a strong catalytic action, no current is observed upon scanning in the cathodic direction. As will be illustrated below, such a defined low-potential catalytic response greatly faciltates the direct monitoring of hydrazine compounds at large in-
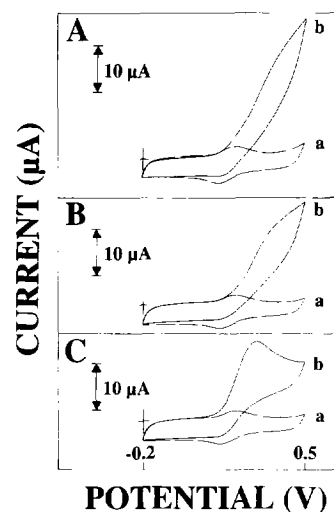

Fig. 2. Cyclic voltammograms for 1×10^{-3} M hydrazine (A;b), methylhydrazine (B;b) and dinethylhydrazine (C;b) in groundwater, along with the corresponding blank groundwater response (A–C;a). Scan rate: 100 mV s^{-1}.

strument/sample distances. The challenges of such measurements in untreated samples are explored below.

The quantitation of hydrazine compounds at the remote sensor is best carried out using the chronoamperometric operation mode. Fig. 3A displays chronoamperograms for successive 5×10^{-6} M increments in the hydrazine concentra-
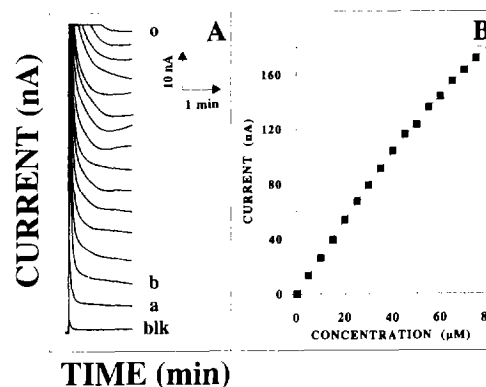

Fig. 3. (A) Chronoamperometric response of the remote electrode to successive 5×10^{-6} M increments in the hydrazine concentration (a–o). Also shown is the corresponding background response (blk) and the resulting calibration plot (B). Potential step to $+0.2$ V; phosphate buffer solution (0.05 M, pH 7.4).
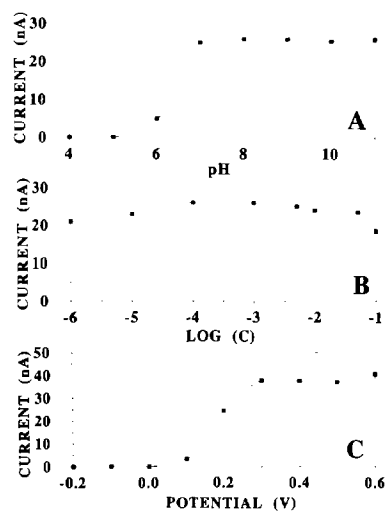
Fig. 4. Effect of the solution pH (A), buffer concentration (B), and measurement potential (C) upon the response to 8×10^{-6} M hydrazine. Other conditions as in Fig. 3.

tion (a–o). The remote electrode offers convenient quantitation of these micromolar concentrations. The current decays rapidly (20 s) to a steady-state value. The latter depends upon the analyte concentration over the entire (5–80 μM) concentration range examined. Linearity prevails over the 5–40 μM range (slope: 1.56 nA μM^{-1}; correlation coefficient: 0.998); a slight curvature is observed for higher levels.

The adaptation of modified electrodes for in-situ monitoring poses several challenges. Unlike laboratory-based sensing applications, where the solution conditions can be adjusted for optimal performance, submersible probes rely on the use of the natural conditions (i.e. untreated samples). Fig. 4 examines the influence of solution variables, relevant to field operation. The catalytic response is nearly independent of the pH over a broad range (between 7 and 11). A sharp decrease of the signal is observed in acidic solutions, with disappearance of the response below pH 5 (A). Such a profile reduces the applicability of the probe. Yet, as will be illustrated below, the probe operates well in numerous relevant natural water matrices (of sufficiently high pH, i.e. above 6). Programmable pH compensation, common with various water profilers, may be useful for addressing the pH dependence between 5 and 7. Field

calibrations, using the target sample [6], should also be useful for this task. Unlike its pH profile, the hydrazine sensor displays a very broad ionic-strength independence (B). Less than 20% signal changes are observed for buffer concentrations ranging from 10^{-6} to 10^{-1} M.

Fig. 4C displays the dependence of the hydrazine response upon the operating potential. The anodic detection of the hydroquinone form of the catalyst (i.e. the product of the catalytic reaction) starts at $+0.1$ V; the response rises sharply up to $+0.3$ V and levels off at higher potentials. Potential steps to $+0.2$ V were employed in all subsequent work, as a compromise between sensitivity and selectivity. Such an operational potential minimizes possible contributions from coexisting electroacitve constituents.

The remote modified electrode displays a remarkably stable response. The long-term stability, shown in Fig. 5, was monitored by measuring the chronoamperometric steady-state current for 1 $\times$ 10^{-5} M hydrazine (in a river water sample) over a 10 day period using the same electrode surface. The coated electrode functioned in a normal fashion throughout. While a slight (about 10%) decrease in the response was observed over the first 5 h, the catalytic activity remained constant thereafter. A relative standard deviation of 3.0% was calculated for this prolonged series of experiments. Another shorter (5 h) experiment, involving repetitive measurements of 5×10^{-6} M dimethylhydrazine in a river water sample, yielded a highly stable response (with a relative standard deviation of 3.7%; $n = 30$). Such behaviour is consistent with the high stability of redox-active
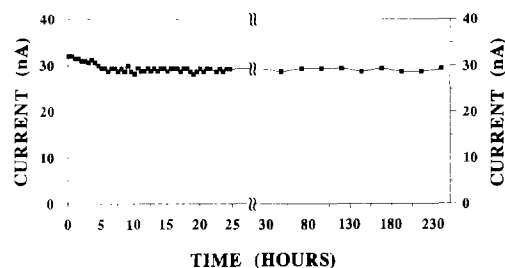

Fig. 5. Stability of the response of the remote electrode to 1×10^{-5} M hydrazine in an untreated river sample. Potential step to $+0.2$ V.
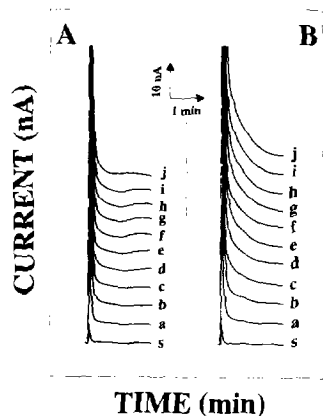
TIME (min)

Fig. 6. Chronoamperometric response to untreated groundwater (A) and lake water (B) samples containing increasing levels of hydrazine and dimethylhydrazine respectively, in 2×10^{-6} M steps (a–j). The corresponding sample response is also shown (s). Other conditions as in Fig. 5.

3,4-DHB electropolymerized films [5]. The electropreparation approach also assures good control of the surface coverage and thus reproducibility between different surfaces.

The performance of the sensor in untreated natural water samples is demonstrated in Fig. 6. This Figure demonstrates the chronoamperetric response of the submersible probe to groundwater (A) and lake water (B) samples with increasing levels of hydrazine and dimethylhydrazine respectively (a–j). This probe responds to these 2×10^{-6} M concentration changes. Detection limits of around 5×10^{-7} M can thus be estimated for both compounds ($S/N = 3$). Notice also the negligible response of the unspiked sample (amperogram s), indicating the absence of electroactive interferences (at low potential accrued form the catalytic action). A nearly linear response is observed for both compounds. Such response characteristics (including the sensitivity) are similar to those observed in "synthetic" samples (e.g. Fig. 2), reflecting the minimal matrix effects (including pH ones). Similar response characteristics were observed for all three hydrazine compounds in these lake water and groundwater samples (not shown).

4. Conclusion

In conclusion this paper demonstrates that hydrazine compounds can be monitored at large sample/instrument distances by coupling the surface modification technology with our recently developed submersible probe design. The remote monitoring capablility is coupled to a sensitive, selective and reversible response. While the new concept of a remote modified electrode is presented within the context of hydrazine detection, it could be extended to other relevant contaminants (via a judicious choice of the modifier). The rich and diverse chemistry—accrued from the deliberate tailoring of electrode surfaces—should greatly benefit the remote monitoring of pollutants, and environmental electrocatalytic in general. Work in this laboratory is thus progressing towards the development and testing of new remote probes based on electrocatalytic and preconcentration surfaces.

References

[1] J. Zagal, C. Fierro and R. Rozas, J. Electroanal. Chem., 119 (1981) 403.
[2] J. Wang and P. Pamidi, Electroanalysis. 8 (1996) 244.
[3] J. Zen and J. Tang, Anal. Chem., 208 (1995) 67.
[4] J. Wang and Z. Lu, Electroanalysis, 1 (1989) 517.
[5] F. Pariente, E. Lorenzo and H. Abruna, Anal. Chem., 66 (1994) 4337.
[6] J. Wang, D. Larson, N. Foster, S. Armalis, J. Lu, X. Rongrong, K. Olsen and A. Zirino, Anal. Chem., 67 (1995) 1481.
[7] J. Wang, N. Foster, A. Armalis, D. Larson, A. Zirino and K. Olsen, Anal. Chim. Acta, 310 (1995) 223.

Phase inversion cellulose acetate membranes for suppression of protein interferences in anodic stripping voltammetry 2[1]. Improvement of the membrane preparation procedure

Boy Hoyer*, Nina Jensen

Department of Chemistry, Aarhus University, Langelandsgade 140, 8000 Aarhus C, Denmark

Abstract

Phase inversion (PI) cellulose acetate membranes were cast on glassy carbon electrodes from a solution containing acetone as solvent and aqueous magnesium perchlorate as pore former. It is shown that a significant improvement of the reproducibility and permselective properties of the membrane is obtained by allowing complete evaporation of the solvent in a controlled humidity environment before the membrane is gelated. By using cadmium and lead as test analytes and differential pulse anodic stripping voltammetry as the detection method, it was found that the modification of the electrode greatly reduces the interference from albumin, lysozyme, gelatin and polyethylene glycol (MW 6000). The permselectivity of the PI membrane can be controlled by varying the amount of magnesium perchlorate in the casting solution and the relative humidity during the pre-gelation conditioning of the membrane.

Keywords: Anodic stripping voltammetry; Phase inversion cellulose acetate membranes; Protein interferences

1. Introduction

One of the most serious limitations of the applicability of electroanalytical methods is fouling of the electrode surface due to adsorption of macromolecular constituents of the sample [1]. Usually, the symptom of this interference is a gradual decrease in the response towards the analyte [2], which introduces accuracy risks and necessitates frequent regeneration of the electrodes. Recent

* Corresponding author.
[1] For Part 1 see Ref. [21].

research (reviewed in Refs. [3–5]) has shown that coating the electrode surface with a permselective membrane is one of the most promising strategies for suppressing or eliminating adsorption interferences. However, the design of such membranes is not trivial because a compromise must be sought between protection of the electrode and the inevitable loss of sensitivity caused by the diffusional resistance of the membrane. The protective membranes should be as thin as possible, and this favours an approach in which the membrane is cast in situ on the electrode surface because the membrane need not be mechanically self-supporting.

Cellulose acetate (CA) has proven to be one of the most useful materials for the preparation of protective membranes on electrodes. In particular, Wang and co-workers [6–9] have demonstrated that in-situ-formed CA membranes are useful for suppression of adsorption interferences and selective detection of low molecular weight species. In their work, the permselectivity of the CA coating is controlled by base hydrolysis. However, this approach also has disadvantages because the polymer backbone is partly broken down by the treatment, and poor stability and reproducibility of the resulting modified electrodes has been reported [10]. The phase inversion (PI) method for preparation of permselective CA membranes has been widely used for the manufacture of reverse osmosis, ultrafiltration and dialysis membranes for more than 30 years [11,12] but the potential of this technology for coating electrodes with protective membranes has only recently been explored by Kuhn and co-workers [13,14] and by us [15]. In the wet PI method, the permselectivity of the CA membrane is controlled by adding a pore former or swelling agent to the casting solution [12]. After evaporation of the solvent, the polymer is precipitated by immersion in a non-solvent gelation bath. The formation of the membrane structure takes place during this step, and anisotropic membranes with a dense skin layer and a more porous sublayer are generally obtained [12].

We have previously shown [15] that CA membranes prepared by the PI method give better protection against interference from albumin in anodic stripping voltammetry (ASV) than those prepared by the base hydrolysis method. Equally importantly, the permeability characteristics of the PI membranes are more reproducible. Most likely, these differences can be ascribed to the fact that the PI method does not involve any degra-dation of the membrane polymer. The PI membranes were cast from the "classical" four-component system of Loeb and Sourirajan [11] in which acetone serves as solvent for CA and aqueous magnesium perchlorate is the pore former.

In the present work, significant improvements in the preparation of the PI membranes are presented which increase the permselectivity further and reduce the variation in the properties of individual membrane preparations. Also, the study of the capability of the membranes to suppress adsorption interferences has been extended with more proteins as well as a surfactant. It is also shown that the permeability of the membrane can be controlled via the amount of pore former added to the casting solution and by varying the relative humidity during the pre-gelation drying step.

2. Experimental

2.1. Apparatus

Voltammetric measurements were performed with a programmable electrochemical analyser [16]. The electrochemical cell comprised a Metrohm 628-50 rotating disk electrode unit with a 3 mm diameter glassy carbon electrode. The reference electrode was a Radiometer K401 saturated calomel electrode (SCE), while the counter electrode was a glass-fitted platinum wire (1 cm long, 0.5 mm thick).

The constant humidity environment needed for the pre-gelation drying of the PI membranes was established in 500 ml soft plastic bottles in which the air was in equilibrium with an aqueous solution of lithium chloride. Each bottle contained the appropriate amount of the salt dissolved in 50 g of water. In this manner, a relative humidity from 13% to 100% (25°C) can be obtained [17]. For example, the 21% relative humidity environment was established by dissolving 30.4 g lithium chloride in 50 g of water. The electrode tip was inserted into the bottle through a hole cut in the side.

2.2. Reagents

Buffers and supporting electrolyte media were prepared from Merck Suprapur reagents and triply-distilled water, while other reagents were of analytical grade. The acetone was a special, dry grade (Merck, max. 0.01% (w/w) water). CA (39.8% acetyl content, MW 30 000) was obtained from Aldrich. Bovine albumin (fraction V, essentially globulin-free, lyophilized, MW 66 000) and

lysozyme (from chicken egg white, lyophilized, MW 15 000) were obtained from Sigma. A 0.1% (w/v) solution of the surface-active compounds was prepared daily. Unless stated otherwise, the composition of the casting solution for the PI membranes was: 20 g acetone, 0.250 ml 0.9 M Mg $(ClO_4)_2$ in water and 0.05 g CA. The concentration of CA in this solution is 0.25% (w/v). Note that magnesium perchlorate is extremely hydroscopic, and therefore the actual concentration of solutions prepared by weighing out and dissolving the salt is uncertain and must be measured. The standard method for the determination of hardness of water by titration with EDTA was used for this purpose.

2.3. Procedure for preparation of modified electrodes

Prior to coating, the glassy carbon electrode was polished with 0.25 μm diamond paste, rinsed with ethanol and dried with lens paper. Coating with CA was done by inverting the rotating disk electrode and applying 2.5 μl of the casting solution to the glassy carbon surface while the electrode was spinning at 1500 rev min $^{-1}$. When the acetone had evaporated, the electrode tip was placed in a bottle with controlled humidity for 10 min. The relative humidity was 21% unless stated otherwise. Hereafter, the electrode was quickly withdrawn from the bottle and immersed in an ice-water gelation bath (0°C) for 30 min. This transfer was done in less than 1 s. Unless stated otherwise, mercury was deposited on the glassy carbon/CA substrate by electrolysis for 10 min at -1 V vs. SCE in deaerated acetate buffer spiked with 2.5 × 10 $^{-5}$ M mercury(II). A conventional thin mercury film electrode (TMFE) was prepared in the same manner, but minus the polymer coating. In the following, a TMFE coated with CA by the PI process is abbreviated as PI-TMFE.

2.4. Procedure for differential pulse (DP) ASV measurements

All measurements were performed in 0.1 M acetate buffer spiked with 2.0 × 10 $^{-7}$ M Cd(II)

and 2.0 × 10 $^{-7}$ M Pb(II). Solutions were deaerated with argon for 5 min prior to DPASV measurements. The working electrode was rotated at 750 rev min $^{-1}$ during deposition, while stripping was carried out in a quiescent solution following a 15 s rest period. The stripping signals were recorded in differential pulse mode with the following instrumental settings: deposition potential, -1000 mV vs. SCE; deposition time, 2 min; scan range, -1000 to -50 mV vs. SCE; pulse height, 50 mV; pulse width, 20 ms; sampling time, 2 ms; pulse repetition time, 0.24 s; effective scan rate, 12.3 mV s $^{-1}$. Signals were smoothed with a seven-point Savitsky–Golay algorithm, and the background signal was corrected for by subtraction of an interpolated linear baseline. A freshly prepared electrode was preconditioned by performing two deposition/stripping cycles in the acetate buffer.

In the interference experiments, the surfactant concentration in the test solution was raised incrementally in the following sequence: 1, 2, 5, 10 and 20 ppm. Two stripping measurements were carried out after each addition. In this manner, the dependence of the DPASV peak current on the surfactant concentration could be studied, and the adsorption of surfactant onto the working electrode was closer to equilibrium.

3. Results and discussion

Several improvements in the preparation of the PI-TMFE have been introduced in the present study, including better control of the water content in the casting solution by use of dried acetone, application of the casting solution to the electrode whilst spinning, and pre-gelation drying of the coating in a controlled humidity environment. However, the experiments left no doubt that the last-mentioned improvement is by far the most important. When bulk membranes are produced by the wet PI process, it is common practice to allow a partial evaporation of the solvent prior to gelation [12], however, this drying step becomes a source of poor reproducibility with thin films because the zone in which the solvent is depleted extends throughout the polymer layer.

Table 1
Effect of surface-active compounds on the DPASV peak currents for cadmium and lead

Surfactant	Electrode type	Cd		Pb		n^b
		Mean change of peak current[a] (%)	Standard deviation of change of peak current (%)	Mean change of peak current[a] (%)	Standard deviation of change of peak current (%)	
None	PI-TMFE II	−8	2	−10	2	2
	PI-TMFE III	−9	3	−13	2	2
Albumin	TMFE[c]	−85	3	−75	3	5
	PI-TMFE I[c]	−26	12	−28	11	18
	PI-TMFE II	−7	2	−16	5	4
Lysozyme	TMFE	−80	8	−63	5	3
	PI-TMFE II	−37	4	−23	6	4
	PI-TMFE III	−8	4	−12	2	4
Gelatin	TMFE	−81	5	−52	8	3
	PI-TMFE III	−17	9	−11	6	4
PEG 6000	TMFE	−85	0.4	−38	0.6	3
	PI-TMFE III	−41	2	−9	0.1	2

[a] Change in DPASV peak current after addition of 20 ppm surfactant (see Section 2).
[b] No. of individual electrode preparations.
[c] Data from Ref. [15].

Moreover, the fraction of the solvent which evaporates prior to the gelation step depends on experimental parameters such as the duration of the drying step, temperature, and convection in the drying environment, which also lower the reproducibility. It is therefore preferable to allow complete evaporation of the solvent, and the number of components in the polymer film is reduced from four to three (CA/magnesium perchlorate/water) before it is immersed in the gelation bath. Equally importantly, the water content is also under control due to the constant humidity drying environment.

As can be seen from Table 1, the new scheme

for preparation of the PI-TMFE (type II) offers considerably better protection against the albumin interference than the previous method (type I) described in Ref. [15]. A t-test (assuming unequal variances of the populations) showed that the peak depression observed with the two electrode modifications is different at a 99.9% confidence level for cadmium as well as lead. Also, control experiments were carried out in which no surfactant was added, and the "natural" fall-off in the signals for the PI-TMFE II is no different to that observed when albumin is added (cf. Table 1). This means that the PI-TMFE II is insensitive to

Table 2
DPASV peak currents of cadmium and lead obtained with the PI-TMFE and the TMFE

Electrode type	Cd		Pb		n^a
	Mean peak current (μA)	Standard deviation of peak current (μA)	Mean peak current (μA)	Standard deviation of peak current (μA)	
TMFE[b]	5.7	1.9	10	1.1	10
PI-TMFE I[b]	2.4	1.1	4.5	1.7	26
PI-TMFE II	2.0	0.4	3.4	0.5	8
PI-TMFE III	1.6	0.3	2.4	0.6	8

[a] No. of individual electrode preparations.
[b] Data from Ref. [15].

the albumin interference within the concentration range tested. Furthermore, the variability of individual electrode preparations with respect to the suppression of the albumin interference is much smaller for the new electrode modification procedure. These improvements can be attributed to the introduction of the drying step as discussed above.

Next, the suppression of the interference from lysozyme was tested. This protein has a much lower molecular weight than albumin (15 000 and 66 000 respectively), and it therefore poses a greater challenge for the permselectivity of the PI membrane. Lysozyme also causes a dramatic decrease in the DPASV signals at the conventional TMFE (cf. Table 1). The PI-TMFE II offers a substantial reduction of the interference from lysozyme, but does not eliminate it. Therefore, a PI membrane with a denser skin layer (type III) was produced by lowering the concentration of magnesium perchlorate in the pore former from 0.9 to 0.7 M. In order to maintain a suitable mercury loading on the electrode, the concentration of mercury in the plating solution was tripled. In this manner, the interference from lysozyme could also be eliminated (cf. Table 1). The PI-TMFE III also offers good protection towards interference from gelatin, but some suppression of the cadmium peak remains. However, the interpretation of this result is complicated by the fact that gelatin is a product of the structural and chemical degradation of collagen and shows a wide molecular weight distribution [18], including a significant fraction with MW below 10 000.

Polyethylene glycol (PEG; MW 6000) caused suppression of the cadmium signal at the PI-TMFE III. Assuming that the permselectivity of the CA membranes is primarily based on molecular weight [8], it can therefore be concluded that the molecular weight cut-off of the PI-TMFE III is in the range 6000–14 000. This result must be viewed in relation to the requirements for protection of the electrode set by the sample type and the electroanalytical method applied. An important potential application of the PI membranes lies in clinical chemistry, and it is interesting to note that ultrafiltration of human serum samples with a 5 kDa filter was found to be necessary in order to obtain undistorted voltammograms of redox probes added to the serum [19]. With respect to clinical analysis it would therefore be desirable to achieve a somewhat lower molecular weight cut-off of the PI membranes. Work to this aim is currently in progress in our laboratory.

As shown in Table 2, the DPASV peak currents obtained with the conventional TMFE are reduced by factors of approximately three for the PI-TMFE II and four for the PI-TMFE III. This order is in agreement with the general rule that a decrease in the molecular weight cut-off of a size-exclusion membrane is accompanied by loss of sensitivity owing to the increased diffusional resistance. In comparison, a reduction of the sensitivity in ASV by a factor as high as 18 has been reported when bulk CA membranes are applied for protection of the electrode [20]. It has also been reported that the response of an amperometric detector was reduced between 10 and 20 times

when a base-hydrolyzed CA film was applied to the working electrode [8].

Voltammograms obtained with the conventional TMFE and the three types of PI-TMFE are shown in Fig. 1. The peak potentials for cadmium and lead were the same at the TMFE and the PI-TMFE I and II (− 715 and − 545 mV vs. SCE respectively), while the peak positions at the PI-TMFE III were 10–15 mV more positive for cadmium as well as for lead. The reason for this difference is not known. For all electrode types, the peak width at half wave height was close to 45 mV for both metals. The moderate effect of the coating on the DPASV peak characteristics (apart from the peak height) indicates that the polymer layer is a passive membrane without specific interaction with the analyte. Also, the shape and size of the background signal were not affected noticeably by the polymer coating (cf. Fig. 1). At the conventional TMFE, all surfactants tested shifted the peak potentials for cadmium and lead in the positive direction. Addition of 20 ppm surfactant was accompanied by the following shifts in peak potentials for cadmium and lead respectively: albumin, + 30 and + 20 mV; lysozyme, + 23 and + 11 mV; gelatin, + 19 and + 8 mV; PEG 6000, + 14 and + 4 mV. For the combinations of surfactant and PI-TMFE type listed in Table 1, the addition of 20 ppm surfactant caused peak shifts in only two cases, namely lysozyme/PI-TMFE-II (+ 4 and + 3 mV for cadmium and lead respectively) and PEG 6000/PI-TMFE III (+ 8 and + 3 mV). The addition of the surfactant also
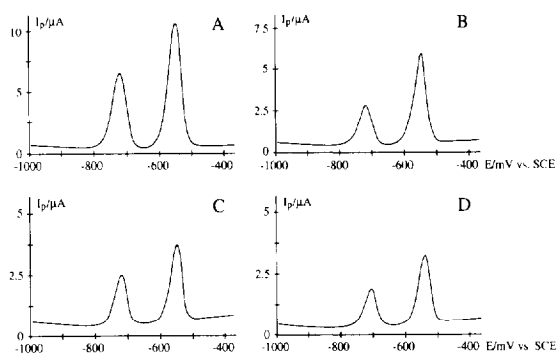

Fig. 1. DPASV signals of cadmium and lead obtained with (A) TMFE, (B) PI-TMFE I, (C) PI-TMFE II and (D) PI-TMFE III. The measurement conditions are given in Section 2.
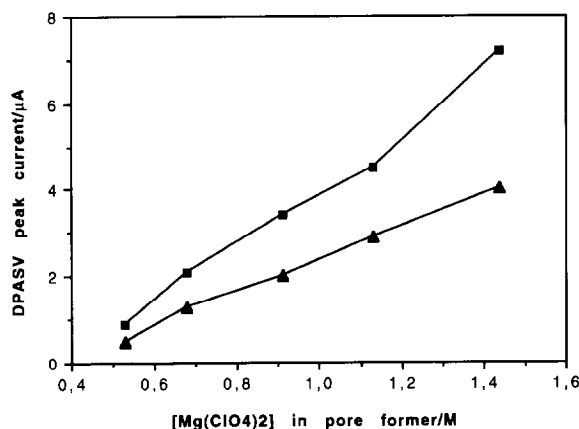

Fig. 2. Effect of the concentration of magnesium perchlorate in the pore former on the DPASV peak currents of cadmium (▲) and lead (■) obtained with the PI-TMFE. Apart from the parameter varied, the standard formulation of the casting solution was used (see Section 2). No surfactant has been added. Each point represents the average of not less than two electrode preparations.

caused significant signal suppression for both combinations (cf. Table 1), and the analyte signal which was most suppressed by the surfactant also exhibited the largest peak shift. These observations are not surprising because signal suppression and peak shift at the PI-TMFE both indicate that the surfactant has penetrated the membrane and caused interference at the electrode/electrolyte interface. However, it was also found that addition of albumin to the PI-TMFE I caused suppression of the cadmium and lead signals (cf. Table 1) without any concomitant peak shift.

As shown in Fig. 2, the DPASV peak currents for cadmium and lead depend strongly on the amount of magnesium perchlorate in the pore former. Since this salt is a powerful desiccant and the polymer coating is dried under constant humidity conditions, it is reasonable to assume that the molar quantities of magnesium perchlorate and water in the film are proportional at the moment when the electrode is immersed in the gelation bath. The porosity of the PI membrane can therefore be controlled via the amount of magnesium perchlorate in the casting solution. Fig. 3 shows the decrease in the DPASV peak current caused by albumin addition as a function of the magnesium perchlorate content in the pore former. The apparent increase in the sensitivity of

the PI-TMFE towards the albumin interference seen with the most dense PI membrane ([Mg(-$ClO_4)_2$] = 0.53 M) is an artifact related to insufficient mercury loading of the electrode. Control experiments, in which no albumin was added, showed decreases in the DPASV peak currents comparable to those given in Fig. 3. However, when the concentration of Hg(II) in the plating solution was tripled, the fall-off in the signals was similar to that obtained with 0.7 M and 0.9 M $Mg(ClO_4)_2$ as pore former (see Fig. 3). Apparently, the signal stability of the PI-TMFE deteriorates when the amount of mercury deposited becomes too low, and the increased diffusional resistance of PI membranes with dense skin layers should therefore be compensated for in the mercury deposition step.

As expected, some increase in the sensitivity of the PI-TMFE towards albumin is seen at the highest concentrations of $Mg(ClO_4)_2$ in the pore former (1.13 M and 1.44 M). Still, the extent of the albumin interference is much smaller than at the bare TMFE, while the DPASV peak currents for cadmium and lead obtained with the PI-TMFE (using 1.44 M $Mg(ClO_4)_2$ as pore former) are reduced by 28% and 21% respectively relative to those obtained with the TMFE. Thus,

Fig. 4. Effect of the relative humidity during the drying step on the DPASV peak current for cadmium (▲) and lead (■) obtained with the PI-TMFE. No surfactant has been added. Each point represents the average of not less than four electrode preparations.

it is also possible to produce PI membranes which only reduce the sensitivity moderately and yet offer good protection against interference from albumin.

The effects of the relative humidity in the pre-gelation drying step on the characteristics of the PI-TMFE are shown in Figs. 4 and 5. The DPASV peak current only displays minor variations when the relative humidity is 35% or higher
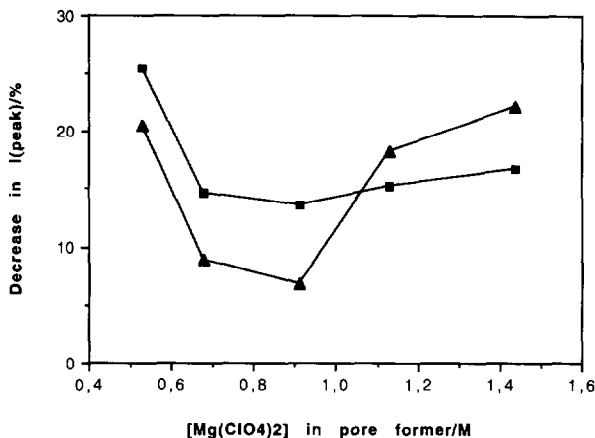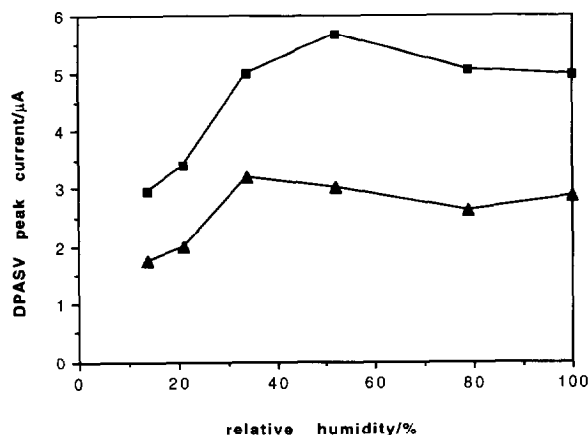

Fig. 3. Effect of the concentration of magnesium perchlorate in the pore former on the discriminative power of the PI-TMFE towards albumin: (▲) cadmium; (■) lead. Apart from the parameter varied, the standard formulation of the casting solution was used (see Section 2). The ordinate shows the decrease in the DPASV peak current after incremental addition of 20 ppm albumin. Each point represents the average of not less than two electrode preparations.
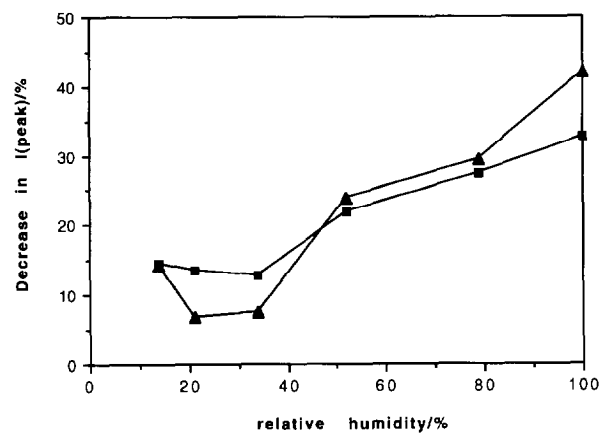

Fig. 5. Effect of the relative humidity during the drying step on the discriminative power of the PI-TMFE towards albumin: (▲) cadmium; (■) lead. The ordinate shows the decrease in the DPASV peak current after incremental addition of 20 ppm albumin. Each point represents the average of not less than four electrode preparations.

(cf. Fig. 4), whereas the peak depression caused by albumin increases monotonically with the relative humidity in this range. Consequently, the pre-gelation conditioning of the membrane should be done at a relative humidity of 35% or lower. The increase in the sensitivity of the electrode towards the albumin interference at the lowest humidity tested (13% relative humidity, cf. Fig. 5) is probably an artifact related to reduced signal stability owing to insufficient mercury deposition on the electrode as discussed above.

As previously mentioned [15], the spin-coated PI membranes have diffuse, concentric refraction rings, which is evidence of a non-uniform thickness of the polymer layer. The rings develop during the evaporation of the casting solvent. It is believed that further progress in the preparation of the PI membranes is linked to the achievement of a uniform polymer layer, which means that alternative coating methods must be found. At present, the feasibility of applying the casting solution to the electrode surface by electro-spraying is being explored.

There is no reason to expect that the attractive properties of PI membranes for suppression of electrode fouling should be limited to ASV. Protective membranes are an integral part of most electrochemical (e.g. amperometric) sensors for analysis of biological fluids owing to the complex nature of the matrix [4,5], and the PI process for preparation of CA membranes could also prove to be useful for such applications.

References

[1] B. Fleet and H. Gunasingham, Talanta, 39 (1992) 1449.
[2] P.L. Brezonik, P.A. Brauner and W. Stumm, Water Res., 10 (1976) 605.
[3] J. Wang, ACS Symp. Ser., 487 (1992) 125.
[4] S.A. Emr and A.M. Yacynych, Electroanalysis, 7 (1995) 913.
[5] P.H. Treloar, I.M. Christie and P.M. Vadgama, Biosens. Bioelectron., 10 (1995) 195.
[6] J. Wang and L.D. Hutchins-Kumar, Anal. Chem., 58 (1986) 402.
[7] J. Wang, M. Bonakdar and M.M. Pack, Anal. Chim. Acta, 192 (1987) 215.
[8] J. Wang and L.D. Hutchins, Anal. Chem., 57 (1985) 1536.
[9] L.D. Hutchins-Kumar, J. Wang and P. Tuzhi, Anal. Chem., 58 (1986) 1019.
[10] M.E.R. Dam, K.N. Thomsen, P.G. Pickup and K.H. Schrøder, Electroanalysis, 7 (1995) 70.
[11] S. Loeb, ACS Symp. Ser., 153 (1981) 1.
[12] R.E. Kesting, Synthetic Polymeric Membranes, 2nd edn., Wiley, New York, 1985, Chapter 7.
[13] L.S. Kuhn, S.G. Weber and K.Z. Ismail, Anal. Chem., 61 (1989) 303.
[14] L.S. Kuhn and S.G. Weber, Electroanalysis, 3 (1991) 941.
[15] B. Hoyer and N. Jensen, Talanta, 42 (1995) 767.
[16] K.N. Thomsen, H.J. Skov and L. Kryger, Anal. Chim. Acta, 219 (1989) 105.
[17] W.A. Roth and K.S. Scheel (Eds.), Landolt-Börnstein Physikalish-Chemische Tabellen (third supplementary volume), Springer-Verlag, Berlin, 1936, p. 2504.
[18] A. Veis, The Macromolecular Chemistry of Gelatin, Academic Press, New York, 1961, p. 84.
[19] J.M. Elbicki and S.G. Weber, Biosensors, 4 (1989) 251.
[20] J.H. Aldstadt and H.D. Dewald, Anal. Chem., 65 (1993) 922.
[21] B. Hoyer and N. Jensen, Talanta, 42 (1995) 767.

Talanta

Second-derivative constant-wavelength synchronous scan spectrofluorimetry for determination of benzo[b]fluoranthene, benzo[a]pyrene and indeno[1,2,3-cd]pyrene in drinking water

M.J. López de Alda Villaizán*, M.S. García Falcón, S. González Amigo, J. Simal Lozano, M.A. Lage Yusty

Department of Analytical Chemistry, Nutrition and Bromatology, Area of Nutrition and Bromatology, Faculty of Pharmacy, University of Santiago de Compostela, E-15706 Santiago de Compostela, La Coruña, Spain

Abstract

The use of derivative constant-wavelength synchronous scan fluorimetry is reported for the determination of three polycyclic aromatic hydrocarbon pollutants in drinking water (linearity range 0.4–4 μg l^{-1}). The limits of detection (LD) and quantification (LQ) (μg l^{-1}) are 0.01 and 0.07 for benzo[b]fluoranthene, 0.03 and 0.12 for benzo[a]pyrene and 0.19 and 0.57 for indeno[1,2,3-cd]pyrene in the presence of three other pollutants, benzo[k]fluoranthene, benzo[ghi]perylene and fluoranthene. The precision (RSD ≤ 10.6%) and recovery (≥ 85%) were satisfactory.

Keywords: Benzo[a]pyrene; Benzo[b]fluoranthene; Indeno[1,2,3-cd]pyrene; Synchronous scan spectro fluorimetry

1. Introduction

Polycyclic aromatic hydrocarbons (PAHs) are a group of essentially man-made organic compounds which are now widely distributed in the environment. Since some of these compounds, e.g. benzo[b]fluoranthene, benzo[a]pyrene and indeno[1,2,3-cd]pyrene, are known carcinogens [1], monitoring of their levels is considered necessary. However, owing largely to the complexity of the matrices in which they occur and the often low

concentrations to be measured, no standardized official method for the quantification of PAHs has yet been developed. For drinking water, the WHO nevertheless suggested a joint recommended limit of 200 ng l^{-1} for the six PAHs designated as indicators (benzo[b]fluoranthene, benzo[k]fluoranthene, benzo[ghi]perylene, benzo[a]pyrene, fluoranthene and indeno[1,2,3-cd]pyrene), and the same limit has been adopted as an official maximum allowable concentration by the European Union (EU), formerly the European Community (EC) [2], while EC-Council Directive 75/440/EEC on the quality required of surface waters destined

---

* Corresponding author.
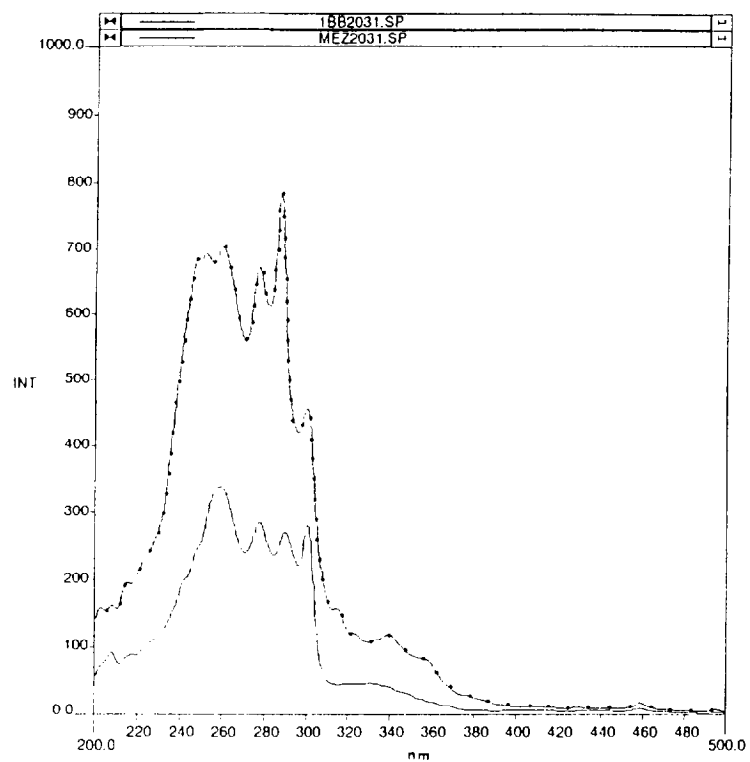
(A)
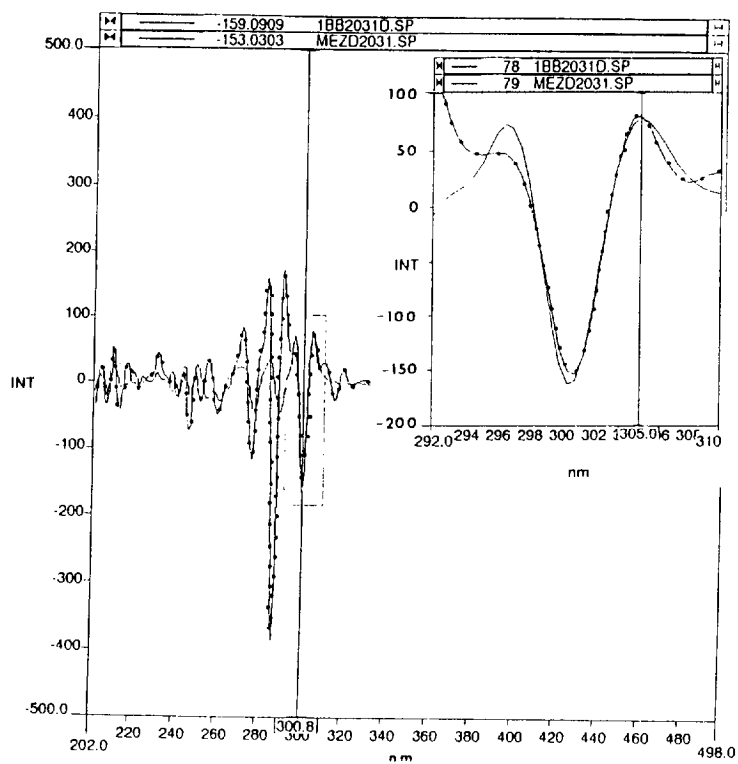
(B)

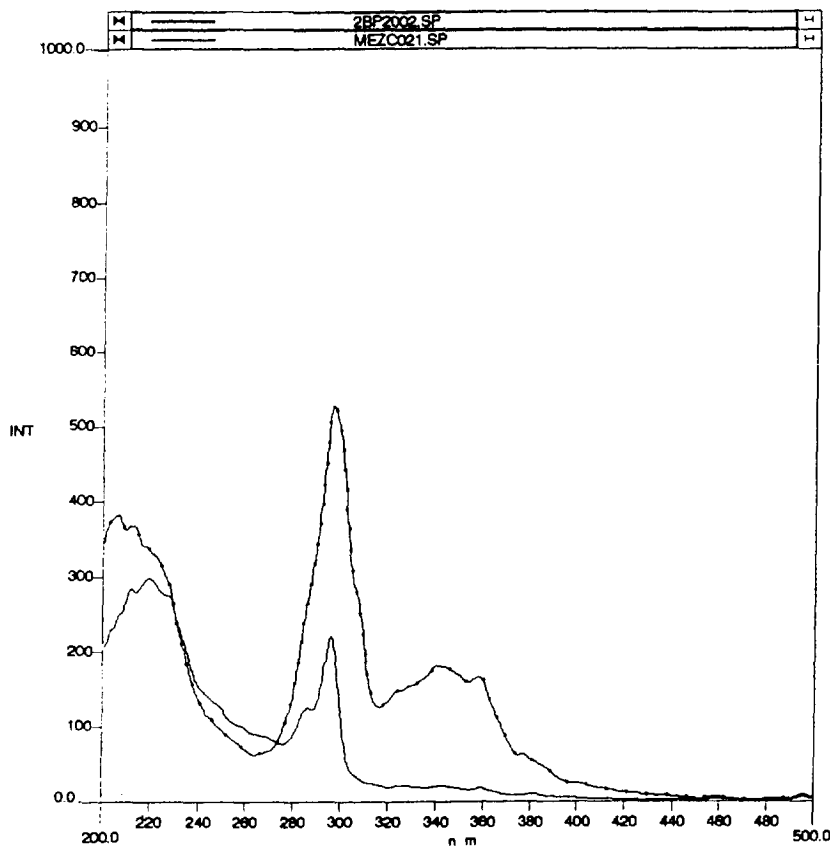Fig. 1. (A) Normal and (B) second-derivative synchronous fluorescence spectra of 2.0 μg l^{-1} solutions of benzo[b]fluoranthene in hexane (—) or hexane containing 0.2 μg l^{-1} of benzo[k]fluoranthene and 2.0 μg l^{-1} of each of the other PAHs (•), $\Delta\lambda = 160$ nm. Inset: magnification of boxed area.

for the production of drinking water [3] stipulates the same allowable maximum of 200 ng l^{-1} for class A1 and A2 waters and 1000 ng l^{-1} for class A3 waters.

There have been a number of different approaches to the quantification of PAHs. The EC proposed, as a reference method for surface waters destined for the production of drinking water [4], measurement of UV fluorescence after thin-layer chromatography in comparison with measurements of standard mixtures of the six indicator substances mentioned above, and for drinking water itself [2].

For surface water, tap water and wastewater, the American Society for Testing and Materials subsequently published a liquid chromatograpic (LC) method with UV and/or fluorescence detection [5], and for urban and industrial wastewaters

the US Environmental Protection Agency [6] later recommended a gas chromatographic–mass spectrometric (GC–MS) method. However, a number of authors [7–12] have proposed the use of synchronous spectrofluorimetry (first developed by Lloyd [13] in 1971), which offers several advantages over the others: analysis is rapid and so allows a high throughput of samples; the solvent consumption is limited to that required for the preparation of the sample; the detection and quantification limits are low; and the sensitivity is much better than that of UV–visible absorption methods. The selectivity of the technique is enhancable not only by the virtual absence of non-fluorescent interferents in the sample, but also by the simultaneous scanning of both the excitation and emission monochromators, which affords narrower bands than in conventional spec-

(A)

Fig. 2(A)
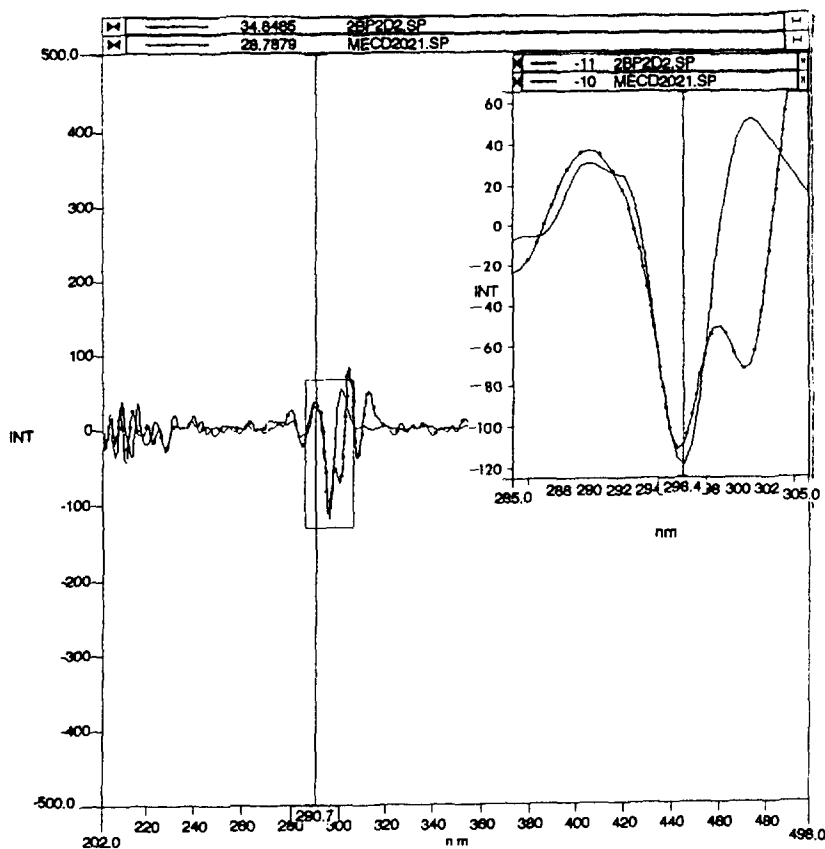
(B)

Fig. 2. (A) Normal and (B) second-derivative synchronous fluorescence spectra of 2.0 μg l^{-1} solutions of benzo[a]pyrene in hexane (—) or hexane containing 0.2 μg l^{-1} of benzo[k]fluoranthene and 2.0 μg l^{-1} of each of the other PAHs (•), $\Delta\lambda = 110$ nm. Inset: magnification of boxed area.

trofluorimetry and virtually eliminates interference from Rayleigh scattering [7,14–21]. As with other spectroscopic techniques, analysis of multi-component samples whose spectra have overlapping bands can be further improved by using the derivative modes [17,22].

Synchronous spectrofluorimetry has been adopted for the global determination of total amounts of the six named PAHs, officially designated as indicators of drinking water quality [23,24].

This paper describes a second-derivative constant-wavelength sychronous scan spectrofluorimetric method for the individual determination of the six carcinogenic PAHs, namely benzo[b]fluoranthene, benzo[a]pyrene and indeno[1,2,3-cd]pyrene in the presence of benzo[k]fluoranthene, benzo[ghi]perylene and fluoranthene.

2. Experimental

2.1. Materials

2.1.1. PAH standards

Benzo[a]pyrene and fluoranthene were obtained from Aldrich and benzo[b]fluoranthene, benzo[k]fluoranthene, benzo[ghi]perylene and indeno[1,2,3-cd]pyrene from Sugelabor. (Caution: all these compounds, except benzo[ghi]perylene, are suspected carcinogens and all are toxic; they

should be handled only in a hood, using safety glasses and other appropriate approved safety measures, to avoid contact with skin, eyes and clothing.) Solutions of benzo[b]fluoranthene, benzo[a]pyrene and indeno[1,2,3-cd]pyrene in hexane were prepared at concentrations of 0.4, 1.0, 2.0 and 4.0 μg l^{-1}. Four stock solutions containing the following mixtures (all in hexane) were likewise prepared: 0.04, 0.1, 0.2 and 0.4 μg l^{-1} benzo[k]fluoranthene + 10-fold masses (μg l^{-1}) of each of the other five indicator PAHs.

2.1.2. Extractant/solvent

n-Hexane for residue analysis (Merck) was used.

2.2. Apparatus

The spectrofluorimeter was a Perkin-Elmer LS-50 luminescence spectrometer equipped with a xenon

discharge lamp, Monk–Gillieson mono-chromators and 1 cm quartz cuvettes. For acquisition and processing of spectral data by Fluorescence Data Manager software, the instrument was serially interfaced (RS232C) to a PC.

2.3. Working conditions

For each of the above solutions, three scans with excitation – emission wavelength differences of 110, 160 or 185 nm were run at a scan rate of 240 nm min^{-1} between 200 and 500 nm (excitation slit width 2.5 nm and emission slit width 20 nm).

3. Results and discussion

The optimum excitation – emission wavelength difference for each PAH was obtained by scanning
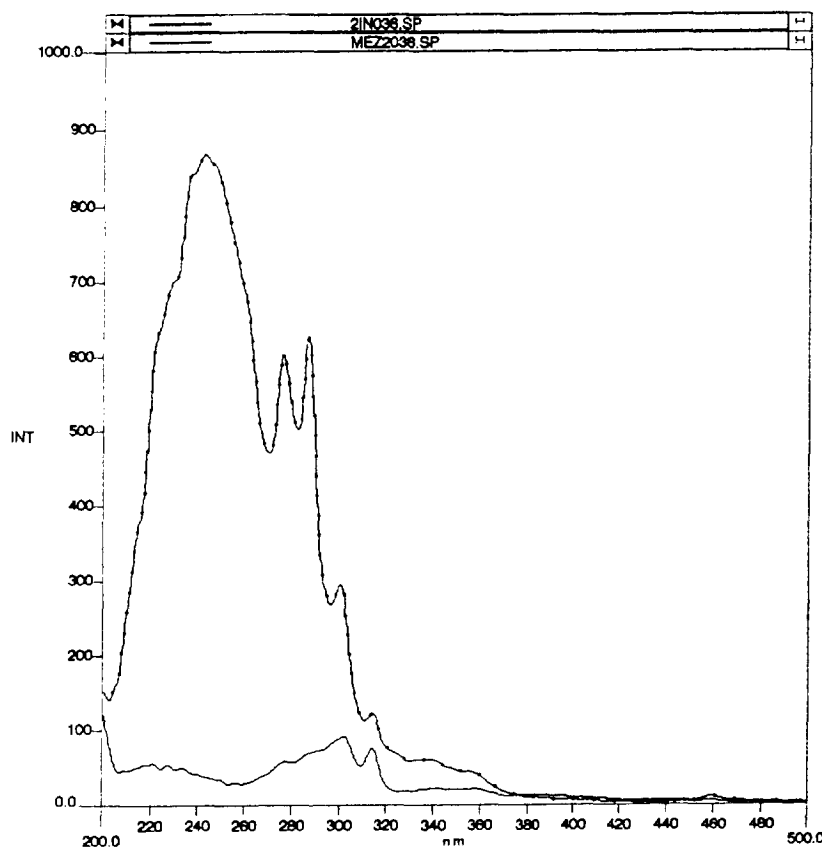
(A)

Fig. 3(A)
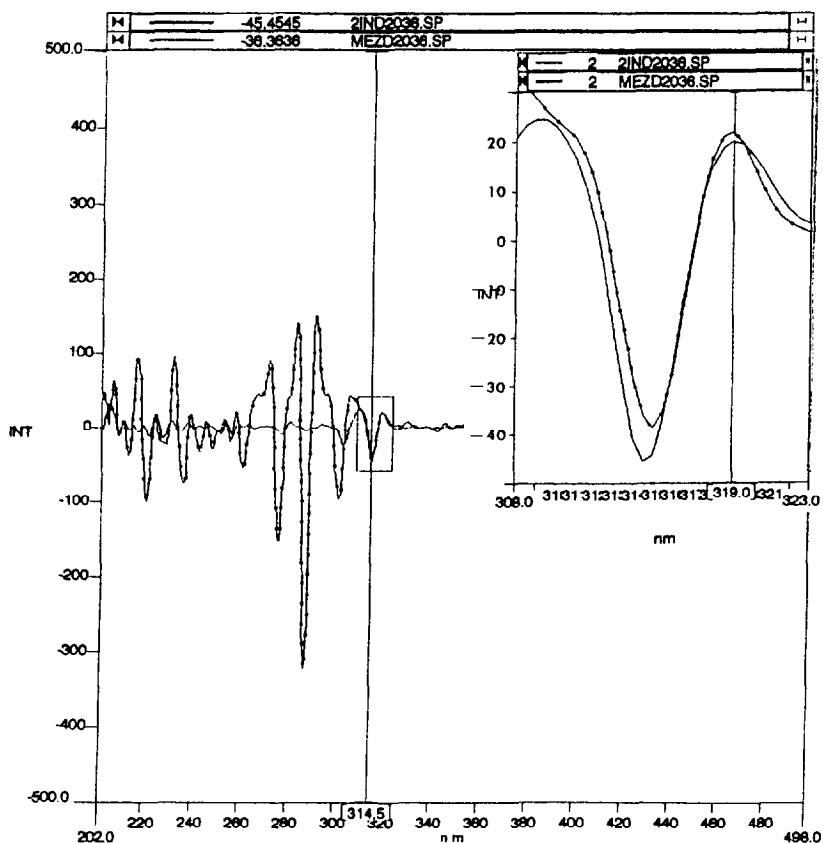
(B)

Fig. 3. (A) Normal and (B) second-derivative synchronous fluorescence spectra of 2.0 μg l^{-1} solutions of indeno[1,2,3-cd]pyrene in hexane (—) or hexane containing 0.2 μg l^{-1} of benzo[k]fluoranthene and 2.0 μg l^{-1} of each of the other PAHs (•), $\Delta\lambda$ = 185 nm. Inset: magnification of boxed area.

its solutions between 200 and 500 nm with the difference set at 10 nm (scan 1) and increasing this difference by 5 nm for each of 49 successive scans. Comparison of the scans with the narrowest, best defined bands with the corresponding spectra of mixtures with the other admixed five indicator PAHs showed overwhelming interference (Fig. 1(A)–3(A)). However, in the second-derivative spectra there were wavelength intervals allowing the detection and quantification of the target PAHs in the presence of the others, coincidence between the single- and multiple-PAH spectra at these wavelengths showing that the multiple-PAH peak was due solely to the target PAH (Fig. 1(B)–3(B), Table 1).

For quantification, the calibration lines listed in Table 2 were constructed by regressing the

peak-to-trough heights of these second-derivative peaks against the concentrations of the working solutions specified in the Experimental section. Following the recommendations of the American Chemical Society's Subcommittee on Environmental Analytical Chemistry [25], limits

Table 1
Scan number, wavelength intervals and chosen second-derivative peaks for the detection and quantification of each PAH

Compound	Scan No.	$\Delta\lambda$ (nm)	Chosen 2nd-derivative peak (nm)
Benzo[b]fluoranthene	31	160	300–305
Benzo[a]pyrene	21	110	290–296
Indeno[1,2,3-cd]pyrene	36	185	314–319

Table 2
Calibration lines, blank signals and limits of detection and quantification of the three PAHs.

Compound	Calibration line[a]: $I = Ax + B$		r	Blank mean[b]	Signal SD (%)	LD (μg 1^{-1})	LQ (μg 1^{-1})
	A	B					
Benzo[b]fluoranthene	118.48	3.95	0.9992	2.56	0.95	0.01	0.07
Benzo[a]pyrene	78.34	2.68	0.9991	2.45	0.95	0.03	0.12
Indeno[1,2,3-cd]pyrene	24.77	1.81	0.9967	2.55	1.34	0.19	0.57

[a] x = Concentration in μg 1^{-1}.
[b] Second-derivative signal.

of detection (LD) and quantitation (LQ) were calculated as the concentrations corresponding to the mean blank signal + three and ten standard deviations, respectively.

In previous experiments [23] using constant-wavelength synchronous scan fluorescence spectrometry, the suitability of hexane for analyses of this type (for which it is recommended by the EU [2]) was evaluated and it was found to have both excellent extractive capacity and spectrofluorimetric properties [26].

There were no signs of interference from the aqueous matrix in the determination of these PAHs (no significant differences were observed between the spectrum of hexane and that of hexane extracts of PAH-free water), and any signal distortion due to drift of background noise was automatically corrected by using the second-derivative method. The method precision and recovery were calculated by spiking six replicate distilled PAH-free water samples [23] with 0.2 μg 1^{-1} of benzo[k]fluoranthene and 2 μg 1^{-1} of each of the other PAHs (Table 3).

This technique is rapid, easy to apply and offers limits of detection and quantification which can-

Table 3
Precision and recoveries obtained for six replicate distilled PAH-free water samples each spiked with 0.2 μg 1^{-1} of benzo[k]fluoranthene and 2 μg 1^{-1} of each of the other PAHs

Compounds	Recovery (%)	Precision (RSD, %)
Benzo[a]pyrene	91.3	8.9
Benzo[b]fluoranthene	99.5	8.5
Indeno[1,2,3-cd]pyrene	85.0	10.6

not be matched by some chromatographic methods. For these reasons, it is ideally suited to the regular monitoring of PAH levels in large numbers of water samples.

4. Conclusions

The described technique allows the determination of three of the six carcinogenic polycyclic aromatic hydrocarbons whose presence in drinking water is officially recognized as indicative of pollution, namely benzo[b]fluoranthene, benzo[a]pyrene, and indeno[1,2,3-cd]pyrene, in the presence of the other three. For benzo[b]fluoranthene, a working emission – excitation wavelength difference of 160 nm affords limits of detection and quantification in hexane of 0.01 and 0.07 μg 1^{-1}, respectively, for the second-derivative peak at 300–305 nm. In the case of benzo[a]pyrene, a working emission – excitation wavelength difference of 110 nm affords limits of detection and quantification in hexane of 0.03 and 0.12 μg 1^{-1}, respectively, for the second derivative peak at 290–296 nm. However, for indeno[1,2,3-cd]pyrene, a working emission – excitation wavelength difference of 185 nm affords limits of detection and quantification in hexane of 0.19 and 0.57 μg 1^{-1}, respectively, for the second derivative peak at 314–319 nm.

(N.W. Spain) for the concession of bursaries to M.J. López de Alda V. and M.S. García F.

References

[1] Guias para la Calidad del Agua Potable, Vol. 1, Recomendaciones. Scientific Publication No. 481, Organización Panamericana de la Salud, Washington, DC, 1985.

[2] Council of the European Communities, Council Directive of 17 July 1980 Relating to the Quality of Water Intended for Human Consumption, Directive 80/778/EEC, Off. J. Eur. Commun., L 229 (1980) 11.

[3] Council of the European Communities, Council Directive of 16 June 1975 Concerning the Quality Required of Surface Water Intended for the Abstraction of Drinking Water in the Member States, Directive 75/440/CEE, Off. J. Eur. Commun., L 194 (1975) 26.

[4] Council of the European Communities, Council Directive of 9 October 1979 Concerning the Methods of Measurement and Frequencies of Sampling and Analysis of Surface Water Intended for the Abstraction of Drinking Water in the Member States, Directive 79/869/CEE, Off. J. Eur. Commun., L 271 (1979) 44.

[5] ASTM, Annual Book of ASTM Standards, 11th edn., American Society for Testing and Materials, Philadelphia, PA, 1989, Method D 4657-87.

[6] EPA, 40 CFR, Ch. 1 (7-1-89 Edition) Pt. 136, App. A. Meth. 625, Environmental Protection Agency, Washington, DC, 1989.

[7] T. Vo-Dinh, Anal. Chem., 50 (1978) 396.

[8] B. Santoni and C. Mandon, Analusis, 9 (1981) 259.

[9] A.F. Leigh, T.J. Bradley, H. Shigeki and J.D. Winefordner, Anal. Chem., 58 (1986) 1440.

[10] P.H. Baudot, M.L. Viriot, J.C. Andre, J.Y. Jezequez and M. Lafontaine, Analusis, 19 (1991) 85.

[11] C. Morel, O. Samhan, P. Litherathy, H. Al-Hashash, L. Molin, T. Saeed, K. Almatrouk, M. Martín-Bouyer, A. Saber, L. Paturel, J. Jarosz, M. Vial, E. Combet, C. Fachinger and J. Suptil, Fresenius' J. Anal. Chem., 339 (1991) 699.

[12] L. Qun, H.X. Zhi, X.J. Goh and C.G. Zhen, Anal. Chim. Acta, 256 (1992) 285.

[13] J.B.F. Lloyd, Nature Phys. Sci., 231 (1971) 64.

[14] T. Vo-Dinh, R.B. Gammage, A.R. Hawthorne and J.H. Thorngate, Environ. Sci. Technol., 12 (1978) 1297.

[15] E.L. Inman and J.D. Winefordner, Anal. Chem., 54 (1982) 2018.

[16] C.M. Byron and T.C. Werner, J. Chem. Educ., 68 (1991) 433.

[17] J. Zhang, J. Yang, Y. Ren and Y. Zhang, Anal. Chim. Acta, 279 (1993) 281.

[18] J.C. Andre, Ph. Baudot and M. Niclause, Clin. Chim. Acta, 76 (1977) 55.

[19] J.C. Andre, M. Bouchy, M. Niclause and Ph. Baudot, Anal. Chim. Acta, 92 (1977) 369.

[20] J.C. Andre, M. Bouchy and M.L. Viriot, Anal. Chim. Acta, 105 (1979) 297.

[21] E.L. Inman and J.D. Winefordner, Anal. Chim. Acta, 138 (1982) 245.

[22] M. Salgado, C. Bosch, F. Sánchez Rojas and J.M. Cano Pavón, Quím. Anal., 5 (1986) 374.

[23] M.J. López de Alda, S. Garcia, M.A. Lage and J. Simal, J. AOAC Int., 78 (1995) 402.

[24] M.J. López de Alda, J. Simal and M.A. Lage, Talanta, 42 (1995) 967.

[25] ACS Subcommittee on Environmental Analytical Chemistry, Anal. Chem., 52 (1980) 2241.

[26] M.J. López de Alda, E. Álvarez, S. García, M.A. Lage and J. Simal, Analusis, 22 (1994) 495.

Long-wavelength stopped-flow fluorimetric determination of lysozyme

B. Gala, A. Gómez-Hens, D. Pérez-Bendito*

Department of Analytical Chemistry, Faculty of Sciences, University of Córdoba, E-14004 Córdoba, Spain

Abstract

The use of Cresyl Violet and sodium dodecyl sulphate for the kinetic fluorimetric determination of lysozyme from dynamic fluorescence measurements at a long wavelength in the range near 600 nm was explored. The high initial rate of this system allows analytical measurements to be made within ca. 2 s after the reactants are mixed, by using the stopped-flow mixing technique, which makes the method applicable to automatic routine analysis. The calibration graph is linear over the range 0.5–40 μg ml^{-1} lysozyme hydrochloride and the detection limit of 0.19 μg ml^{-1}. The precision is less than 2% (relative standard deviation). The results obtained by applying the proposed method to the analysis of pharmaceutical samples with no pretreatment shown how readily it can be adapted for routine analyses. Analytical recoveries ranged between 94.0 and 104.0%.

Keywords: Cresyl Violet; Fluorimetry; Kinetic method; Lysozyme; Pharmaceuticals; Stopped-flow

1. Introduction

Long-wavelength fluorescent dyes in analytical applications have attracted considerable attention in recent years on account of their advantages over conventional fluorescent dyes, such as reduced background interferences and sample photodecomposition [1]. Among others, long-wavelength fluorescent dyes have been used as labels in immunoassay [2] and as reagents in chromatography [3] and capillary electrophoresis [4]. Diode lasers are frequently used as light sources in near-infrared fluorescence spectroscopy

because their high irradiance and very narrow bandwidth afford very low detection limits and good selectivity. However, most lasers only emit a few discrete wavelengths, so optimum excitation can only be achieved if the output matches the fluorophore excitation wavelengths. In addition, the current practical limit for a commercial diode laser is 660 nm [5].

In this work, the scope of the analytical application of long-wavelength fluorescence dyes was extended to the simple, fast kinetic determination of proteins in the presence of an anionic surfactant, sodium dodecyl sulphate (SDS). For this purpose, several azine dyes with fluorescent properties in the spectral region near 600 nm were tested and a kinetic fluorimetric method for

* Corresponding author.

lysozyme determination was developed. Experiments were carried out with a 450 W xenon arc lamp as the light source because the excitation wavelengths for these compounds are shorter than the above-stated limit for diode lasers (660 nm). The high initial rates obtained for these systems cannot be measured by using the batch technique, requiring the use of the stopped-flow mixing technique to obtain kinetic measurements. In addition, this technique facilitates automation through automatic mixing of sample and reagent solutions and kinetic data from the mixed solution can be acquired for immediate processing in order to obtain the analytical information.

Lysozyme is a proteolytic enzyme present in numerous pharmaceutical preparations of antibiotics such as tetracyclines, penicillins and aminoglycosides because it is claimed to enhance their antimicrobial activity when given concomitantly. This protein has been determined in pharmaceutical preparations by measuring the fluorescence intensity of 4-methylumbelliferone released by lysozyme from 4-methylumbelliferyl tetra-N-acetyl-β-chitotetraoside, which acts as the substrate [6]. Since the enzyme also appears to catalyse the hydrolysis of the substrate to the saccharide, without release of the fluorescent moiety, the sensitivity of the assay was increased by adding β-N-acetylhexaminidase, obtaining a rectilinear calibration graph from 10 to 70 μg ml^{-1} lysozyme. A chromatographic method using a similar substrate (4-methylumbelliferyl tri-N-acetyl-β-chitotrioside) has been described for the determination of lysozyme in food [7]. Other fluorimetric methods for lysozyme determination by using other substrates such as fluorescein isothiocyanate-labelled peptidoglycan [8] and fluorescamine-labelled peptidoglycan [9] have been described. Also, 4-nitrophenyl penta-N-acetyl-β-chitopentaoside has been proposed as substrate for the photometric determination of lysozyme [10], which liberates 4-nitrophenol. Turbidimetry has been also used for the determination of lysozyme involving *Micrococcus luteus* as substrate [11,12]. The method, with a rectilinear calibration graph from 0.5 to 15 μg ml^{-1} lysozyme, has recently been adapted to commercial analyser [13], but data on throughput have not been given.

The methods involving a lysozyme-substrate reaction require an incubation time close to 30 min at 37°C. However, the alternative method described in this paper avoids the use of a substrate and allows the fast and simple determination of lysozyme by using the stopped-flow mixing technique. Its usefulness was assessed by analysing various pharmaceutical samples.

2. Experimental

2.1. Instrumentation

A Model 8000C photon counting spectrofluorimeter from SLM-Aminco (Urbana, IL, USA), equipped with a 450 W xenon arc source and an R928 photomultiplier tube, was used. The instrument was furnished with an SLM-Aminco Milliflow stopped-flow reactor, a TWC computer and a Roland plotter. The stopped-flow module, fitted with an observation cell of 0.2 cm pathlength, was controlled by the associated electronics, the computer and a pneumatic syringe drive system. The solutions in the stopped-flow module were kept at a constant temperature of 20°C by circulating water from a thermostated tank.

2.2. Reagents

A 200 μg ml^{-1} stock aqueous solution of lysozyme hydrochloride (grade VI, Sigma) was prepared. Aqueous solutions of Cresyl Violet acetate (9.3 $\times$ 10^{-5} M, Sigma) and SDS (1.5 $\times$ 10^{-2} M, Merck) were also prepared. A 0.1 M borate buffer solution was made from boric acid and adjusted to pH 10.0 with sodium hydroxide.

2.3. Procedure

Two aqueous solutions (A and B) were used to fill the 2 ml drive syringes of the stopped-flow reactor. Solution A contained lysozyme hydrochloride at a final concentration between 3.6 $\times$ 10^{-8} and 2.9 $\times$ 10^{-6} M, borate buffer (1.7 $\times$ 10^{-2} M) and SDS (1.5 $\times$ 10^{-3} M). Solution B contained SDS (1.5 $\times$ 10^{-3} M), borate buffer (1.7 $\times$ 10^{-2} M) and Cresyl Violet acetate (1.4 $\times$

10^{-5} M). In each run, 0.04 ml of each solution was mixed at a flow-rate of 20 ml s^{-1} in the mixing chamber. The increase in the fluorescence intensity with time throughout the reaction was monitored at λ_{ex} 585 nm and λ_{em} 627 nm using the slow kinetic acquisition mode of the instrument. All measurements were carried out at 20°C. Fluorescence values were obtained for 10 s and processed by the computer, running a linear-regression program for application of the initial-rate method. The reaction rate was determined in ca. 2 s and each standard or sample was assayed in triplicate. The blank signal was found to be negligible at 20°C.

2.4. Determination of lysozyme in pharmaceutical samples

Analyses for lysozyme were carried out similarly to the above-described procedure. Each sample was analysed by weighing and powdering a tablet, transferring the powder into an appropriate volumetric flask (50 or 250 ml) and diluting to volume with distilled water. The suspension was shaken for 5 min in an ultrasonic bath (50 W) and then filtered. Finally, an aliquot of the filtrate was treated as described above.

3. Results and discussion

3.1. Spectral studies

Three fluorescent azine dyes [Cresyl Violet (λ_{ex} 585, λ_{em} 627 nm), Nile Blue (λ_{ex} 624, λ_{em} 675 nm) and Azure B (λ_{ex} 647, λ_{em} 673 nm)], were assayed for use as reagents for lysozyme. These compounds exhibit an intense fluorescence in aqueous solutions that is not affected by the presence of lysozyme, as shown in Fig. 1 for Cresyl Violet. However, SDS completely quenches the fluorescence of the dye at a concentration below the critical micelle concentration (c.m.c.). The c.m.c. for SDS in this system was measured with a stalagmometer, and found to be 1.7 × 10^{-3} M, which is approximately five times lower than that reported in pure aqueous solutions (8.1 × 10^{-3} M) [14]. Under these conditions, the presence of

lysozyme caused an increase in the fluorescence intensity (Fig. 1) proportional to the concentration of the protein (Fig. 2). These results were obtained at a pH lower than the isoelectric point of lysozyme (11.0).

On the other hand, the fluorescence of the dyes was not quenched but rather increased at an SDS concentration above its c.m.c. This can be attributed to the fact that the interaction between Cresyl Violet and SDS changes when micelles are formed and dye molecules are sheltered from non-radiative processes by the micellar environment. Under these conditions, the presence of lysozyme does not affect the fluorescence of these systems. Also, placing SDS with a non-ionic (Triton X-100) or cationic surfactant (cetyltrimethylammonium bromide) results in no difference between the sample and blank. Two other anionic surfactants assayed (Tergitol 7 and sodium dodecylbenzenesulphonate) provided poorer results than SDS.

A possible explanation for the behaviour of SDS in this system is the following: the surfactant
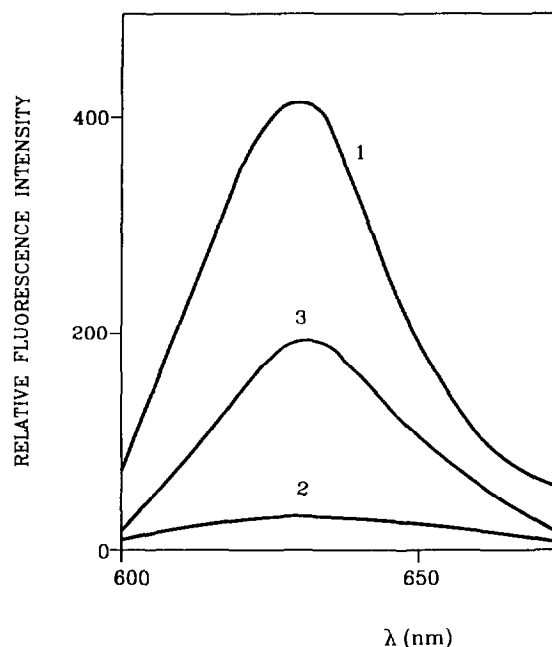

Fig. 1. Emission spectra for Cresyl Violet (1) in the absence and presence of lysozyme, (2) in the presence of SDS and (3) in the presence of SDS and lysozyme. [Cresyl Violet] = 1.4 × 10^{-5} M; [lysozyme] = 25 μg ml^{-1}; [SDS] = 1.5 × 10^{-3} M.
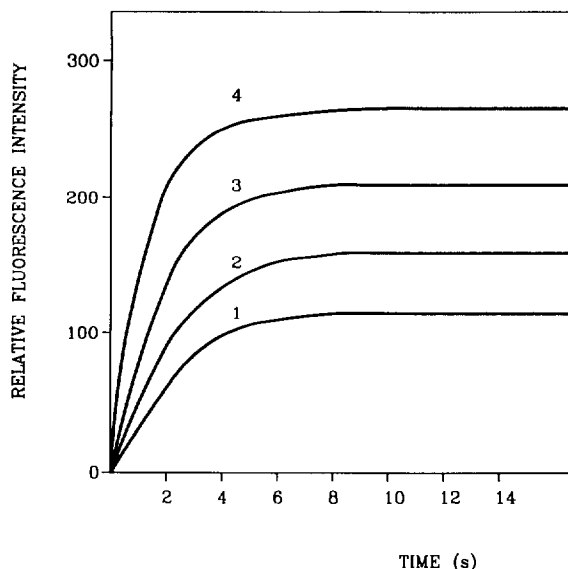
Fig. 2. Kinetic curves obtained for Cresyl Violet–SDS–lysozyme system at different lysozyme concentrations (1) 10, (2) 20, (3) 30 and (4) 40 μg ml^{-1}. [Cresyl Violet] = 1.4 × 10^{-5} M; [SDS] = 1.5 × 10^{-3} M.

monomers, which are negatively charged, interact with Cresyl Violet, which is positively charged, causing a change in the electronic distribution of this dye and a loss of fluorescence. Lysozyme, a bulky molecule with numerous positive charges, can partially react with SDS to release Cresyl Violet and restore the original fluorescence signal. The interaction between SDS and lysozyme can be ascribed to the fact that SDS is a protein denaturant [15].

The kinetic curves for these systems were obtained by using the stopped-flow mixing technique. Although the three dyes behaved similarly, the best initial rate values were obtained with Cresyl Violet. Thus, the initial rates obtained for 20 μg ml^{-1} lysozyme by using Cresyl Violet, Nile Blue and Azure B were 49, 3.5 and 2.8 s^{-1}, respectively. Fig. 2 shows the kinetic curve obtained using Cresyl Violet; as can be seen, the initial rate could be obtained within only 2 s.

3.2. Effect of reaction variables

Experimental variables were optimized using the univariate method. All reported concentra-

tions are initial concentrations in the syringes (twice the actual concentrations in the reaction mixture at time zero after mixing). Each kinetic result was the average of three measurements. The optimum values taken were those for which the relative standard deviation of the initial rate measurements was minimal, under conditions where the reaction order concerning the variable studied was zero or as close to it as possible.

One of the most critical variables of this system was the SDS concentration because, as noted above, no interaction between lysozyme and Cresyl Violet was observed in the absence of the surfactant or in the presence of a concentration above its c.m.c.; also, the fluorescence intensity of the dye was strongly dependent on the SDS concentration. Fig. 3 (A) shows the variation of the initial rate of the system with the concentration of SDS in the range 8 × 10^{-4}–3 × 10^{-3} M. As can be seen, the maximum initial rate was obtained near the c.m.c. of SDS and decreased above it. The blank signal was negligible up to the c.m.c. but increased above that level, so no difference between the sample and blank was observed at an SDS concentration close to 3 × 10^{-3} M.

The effect of pH was studied over the range 4.4–12.0 by using different amounts of sodium hydroxide and hydrochloride acid (Fig. 3(B)). The reaction rate of the system increased slightly up to pH 10.7, which is very close to the isoelectric point of lysozyme, and decreased sharply at higher pH values. Consequently, no interaction between lysozyme and SDS exists when the protein is negatively charged. pH 10 was chosen as optimal and a borate buffer was used to adjust it in the samples. The study of the effect of the buffer concentration showed that the initial rate was independent of this variable over the range 2 × 10^{-2}–4.5 × 10^{-2} M, outside which the initial rate was lower. Fig. 3(C) shows the effect of the Cresyl Violet concentration; as can be seen, the initial rate increased sharply up to a 1.2 × 10^{-5} M reagent concentration, remained constant from this concentration up to 1.7 × 10^{-5} M and decreased slightly beyond that point.

The initial rate of the system was found to be independent of the temperature in the range 15–35°C and to increase slightly above it, increasing
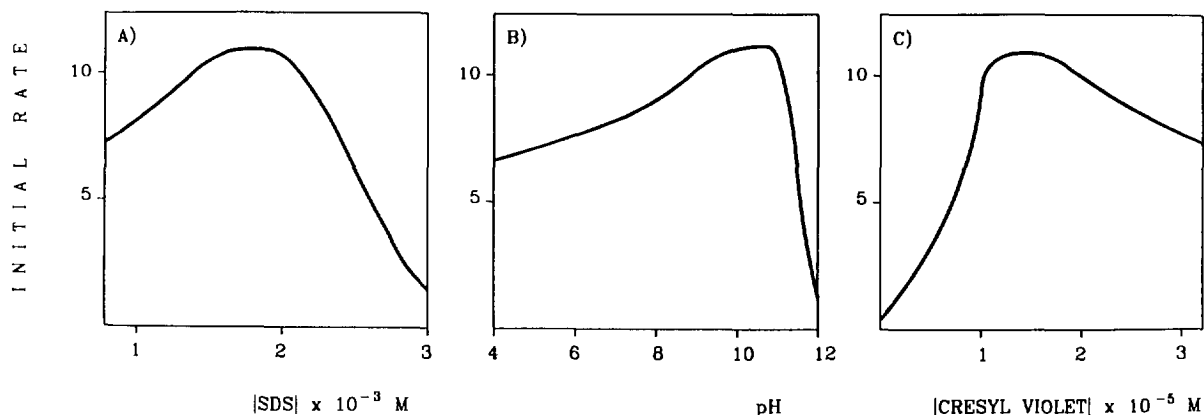
Fig. 3. Effects of (A) SDS concentration, (B) pH and (C) Cresyl Violet concentration on Cresyl Violet–SDS–lysozyme system. [lysozyme] = 20 μg ml^{-1}; [Cresyl Violet] = 1.4 $\times$ 10^{-5} M (A) and (B) and SDS 1.5 $\times$ 10^{-3} M in (B) and (C); 10^{-2} M borate buffer (pH 11.3) in (A) and (C).

also the blank signal. A temperature of 20°C was chosen to avoid working under high-temperature conditions where, in addition, the blank signal must be subtracted.

Based on the slopes of the fluorescence vs. time curves obtained for solutions containing different amounts of lysozyme, the reaction is first order with respect to the analyte. Under the working conditions used, the reagents exhibited a pseudo-zero-order dependence, so the following kinetic equation is proposed: $v = k$[lysozyme], where v is the reaction rate and k is the conditional rate constant.

3.3. Figures of merit of the proposed method

The fluorescence–time curves obtained for different amounts of lysozyme under the optimum conditions were processed by the initial-rate method. The calibration graph was linear over the concentration range 0.5–40.0 μg ml^{-1} and conformed to the equation $v = 2.56C + 1.25$, where v is the initial rate (s^{-1}) and C the lysozyme hydrochloride concentration (μg ml^{-1}). The Pearson correlation coefficient (r) was 0.998 ($n = 11$). The detection limit, calculated according to IUPAC recommendations [16], was 0.19 μg ml^{-1}. The blank standard deviation was determined by assaying 30 samples, each containing a very low analyte concentration (0.25 μg ml^{-1}), enough to yield an adequate signal. This procedure is usually

used to determine the detection limit when the blank does not give an appreciable signal. The sampling rate was 60 h^{-1}, calculated from the time taken to perform three replicate analyses including changeover in the stopped-flow module (about 30 s). The precision was studied at two concentrations of lysozyme hydrochloride, 5 and 25 μg ml^{-1}; the relative standard deviations obtained by measuring the initial rate ($n = 11$) were 1.2 and 1.8%, respectively.

Equilibrium measurements can also be carried out by using this approach. However, the detection limit obtained was 0.79 μg ml^{-1}, which was much higher than that obtained by kinetic methodology. Also, the relative standard deviations for 5 and 25 μg ml^{-1} lysozyme hydrochloride were higher (2.8 and 7.5%, respectively).

The selectivity of the proposed method was assessed by assaying several potentially interfering compounds that frequently accompany lysozyme in pharmaceutical preparations. A substance was considered not to interfere at a given concentration if the reaction rate obtained in its presence was within one standard deviation of the value obtained with the analyte alone. All the compounds assayed (tetracycline, ampicillin, tyrothricin, bacitracin, benzocaine, sodium cyclamate, saccharin and sucrose) were tolerated up to at least a 100-fold excess relative to the analyte. One of the most salient features of the proposed method is speed; since the time required

Table 1
Determination of lysozyme in pharmaceutical preparations

Sample[a]	Lysozyme hydrochloride content (mg)		Recovery		
	Certified	Found[b]	Added (μg/ml)	Found[b] (μg/ml)	Recovery (%)
1	40	38 ± 1	5	5 ± 1	94.0
			10	10 ± 1	96.0
			15	15 ± 2	99.3
2	25	24.9 ± 0.9	5	4.9 ± 0.8	98.0
			10	10.2 ± 0.7	102.0
			15	15 ± 1	102.6
3	20	19 ± 1	5	4.8 ± 0.9	96.0
			10	10 ± 1	99.0
			15	14.2 ± 0.3	94.6
4	10	10.2 ± 0.2	5	4.8 ± 0.8	96.0
			10	9.5 ± 0.7	95.0
			15	15 ± 1	99.3
5	5	5 ± 1	5	5 ± 1	104.0
			10	10.4 ± 0.7	104.0
			15	1 ± 1	103.3

[a] Trade names, manufacturers' names and compositions of samples: (1) Trofalgón, Madariaga, lysozyme hydrochloride (40 mg), cyanocobalamin (1 mg), excipient (cellulose); (2) Finegosán, Merck, lysozyme hydrochloride (25 mg) tetracycline hydrochloride (250 mg), excipient (lactose and others); (3) Espectral fuerte, Centrum, lysozyme hydrochloride (20 mg), ampicillin trihydrate (500 mg), excipient; (4) Bucometasona, Kalifarma, lysozyme hydrochloride (10 mg), tyrothricin (10 mg), triamcinolone acetonide (1 mg), cetrimonium bromide (10 mg), benzocaine (20 mg), sucrose (506.5 mg), saccharin (2.86 mg), sodium cyclamate (30 mg), excipient; (5) Lizipaina, Upsa Medica, lysozyme hydrochloride (5 mg), papain (2 mg), bacitracin (200 U.I.), saccharin (2 mg), sucrose (1372 mg), excipients.
[b] Means of six determinations ± SD.

to obtain analytical data is only ca. 2 s, the method is a useful, simple alternative to automatic routine procedures for the determination of lysozyme.

3.4. Applications

In order to validate the proposed stopped-flow method of lysozyme, it was applied to various pharmaceutical samples by direct analysis (with no sample pretreatment), using initial-rate measurements. The results obtained from the average of six determinations of six different tablets of each sample are summarized in Table 1. Recoveries were determined by adding three different amounts of lysozyme hydrochloride standard to each sample and subtracting the results obtained for similarly prepared pharmaceuticals to which no analyte was added. Table 1 lists the analytical recoveries obtained, which ranged from 94.0 to 104.0% (mean 98.9%).

4. Conclusions

The proposed method is the first reported application of kinetic methodology in conjunction with the stopped-flow mixing technique for the development of a rapid method for the determination of lysozyme by using initial rate measurements at long wavelengths. The results obtained show that the method can readily be adapted to automatic quality control of the analyte in pharmaceutical preparations. Therefore, it extends the scope of application of long-wavelength fluorescence dyes to fast kinetic determinations with improved analytical features relative to equilibrium measurements.

The method can be considered universal for protein determinations (a prior separation will be required for determining lysozyme in the presence of other proteins). However, when selectivity is not a limitation (e.g. in the quality control of

lysozyme in pharmacuetical formulations), the main aim is to develop a fast, simple, sensitive method of use for routine analyses. Despite the reliability of the methods previously described for lysozyme determination, which are based on its reaction with different substrates, they are time-consuming as they require a previous incubation step. However, the proposed stopped-flow method allows measurements to be made shortly after mixing and analytical data to be acquired in only a few seconds.

Acknowledgements

References

[1] G. Patonay and M.D. Antoine, Anal. Chem., 63 (1991) 321A.

[2] D.A. Palmer and J.N. Miller, Anal. Proc., 30 (1993) 144.

[3] A.J.G. Mank, H. Lingeman and C. Gooijer, Trends Anal. Chem., 11 (1992) 210.

[4] T. Higashijima, T. Fuchigami, T. Imasaka and N. Ishibashi, Anal. Chem., 64 (1992) 711.

[5] T. Imasaka and N. Ishibashi, Anal. Chem., 62 (1990) 363A.

[6] H. Fukuda, T. Tanimoto and T. Yamaha, Chem. Pharm. Bull., 33 (1985) 3375.

[7] T. Shibata, S. Tsuji, K. Kobayashi, Y. Asai, T. Honda, K. Noda, M. Iwaida, E. Mochizuki, O. Sugahara and Y. Ito, Jpn. J. Toxicol. Environ. Health, 38 (1992) 437.

[8] Y. Zhou, Yaowu Fenxi Zazhi, 8 (1988) 329.

[9] I. Moser, F. Pittner and P. Dworsky, J. Biochem. Biophys. Methods, 17 (1988) 249.

[10] F. Nanjo, K. Sakai and T. Usiu, J. Biochem., 104 (1988) 255.

[11] G. Gorin, S.F. Wang and L. Papapavlou, Anal. Biochem., 39 (1971) 113.

[12] M. Jaeckle, R. Amado and W. Schmidt-Lorenz, Mitt. Geb. Lebensmittelunters. Hyg., 80 (1989) 137.

[13] J.A. Navarro Gonzalvez, J.A. Manzanos Arnaiz, C. Garcia Benayas, I. Vidriales Vicente and J. Arenas, Clin. Chem., 39 (1993) 151.

[14] L.J. Cline Love, J.G. Habarta and J.G. Dorsey, Anal. Chem., 56 (1984) 1133A.

[15] X.D. Yang, Y.X. Ci and W.B. Chang, Anal. Chem., 66 (1994) 2590.

[16] G.L. Long and J.D. Winefordner, Anal. Chem., 55 (1983) 712A.

Development of pH measurement system for legal traceability of pH standard solutions

Satoshi Ito[a],*, Hiromitu Hachiya[a], Keiko Baba[a], Masayoshi Eto[a],
Yasukazu Asano[a], Hiroko Wada[b]

[a]*Applied R&D Department, DKK Corp., 4-13-14, Kichijoji Kitamachi, Musashino, Tokyo 180, Japan*
[b]*Department of Applied Chemistry, Nagoya Institute of Technology, Gokiso, Showa, Nagoya 466, Japan*

Abstract

The best reproducible technology of pH measurement for precise pH buffer solutions regulated by Japanese Industrial Standards (JIS) was studied. A pH meter was devised with a high resolution of ± 0.0001 pH. An 18-bit analog-to-digital converter is used, one-bit resolution corresponding to 0.0019 mV (ca. 0.000032 pH) against an input electrode potential ± 500 mV. Digital data were treated smoothly for some types of noise, a reproducibility of ± 0.0002 pH being obtained with a potentiometer. A flow cell was devised to attain temperature control within $\pm 0.03°C$ and air-tight measurement prevented contamination with carbon dioxide. Also, the flow cell has a structure such that potassium chloride (KCl) inner solution effused from a ceramic junction of the reference electrode designed so as not to touch the glass membrane. A combination pH electrode (a glass electrode and a reference electrode) was assembled to minimize the dead volume of sample solution. This highly sensitive pH measuring system, consisting of a pH meter, a flow cell, a combination pH electrode, a circulating water thermostat and a peristaltic pump, was used for the certification of pH standard solutions in Japanese metrological law. The performance of this system was within ± 0.0006 pH reproducibility and 20–30 min response time (5 min within ± 0.0002 pH) at a sample flow rate of 3 ml min^{-1}.

Keywords: Legal traceability; pH measurement; pH standard solutions

1. Introduction

The pH value is given by the electromotive force (e.m.f.) of a cell with a hydrogen gas electrode and a reference electrode [1]. The practical pH value of a sample solution is determined by adding the pH value of a standard buffer solution to the value of the difference between the e.m.f. of the former cell against the sample solution and the e.m.f. against the standard buffer solution divided by the Nernstian slope for monocations (59.16 mV at 25°C) (a single standard method). In another definition of pH value by use of the linear

---

relationship between pH and the e.m.f. of the former cell, the operational pH value of the sample solution is determined by the e.m.f. against two types of standard buffer solution and against the sample solution (a multi-standard method). For a practical scale of pH a series of standard buffer solutions were defined in the literatures [2–5].

One of the most important areas where accurate values of pH measurement are required is in environmental water pollution control. The pH value of industrial waste water is regulated between pH 6.5 and 8.5 by the Basic Environment Law in Japan [6]. Therefore, the correct calibration of pH meters is very important to monitor environmental pollution by the industrial waste water, referring to precise pH standard solutions. In metrological law, a series of standard buffer solutions are provided as certified reference materials (CRMs) that are traceable to reference materials (RMs) [7]. In 1983, the Japanese government defined a precise pH standard solution, the reproducibility of which is ± 0.002 pH, to maintain a clean environment in the presence of industrial waste water. Therefore, a practical pH measuring system for the purpose of referring the sample buffer solutions to the primary pH standard solution was required. The standards of reproducibility of pH buffer solutions in Japanese Industrial Standards (JIS) are within ± 0.002 pH. Therefore, the development of a pH meter with a measurement ability of ± 0.0001 pH unit resolution was required to determine pH values of buffer solutions correctly. For the purpose mentioned above, we have developed a high-performance pH measuring system for Japanese pH standard solutions using a flow system, and developed an airtight flow cell system which has good stability to temperature changes and pH changes in pH buffer solutions.

A cell consisting of a hydrogen gas electrode and a silver–silver chloride electrode was reported as a pH measuring cell [8,9]. However, electrode preparation just before use, such as platinum black plating of a platinum electrode and silver chloride plating of a silver electrode, is indispensable for reproducible measurements. Therefore, this method is not very practical. As the most

practical method, we studied a cell with a glass electrode and a silver–silver chloride reference electrode. In comparison with the hydrogen gas electrode, the glass electrode has a high impedance of the glass membrane and a long response time. In the reference electrode, an appropriate and constant outflow of KCl from the liquid junction should be supplied for a stable liquid junction potential. However, the KCl might change the original pH value of the sample soltution slightly when it reaches the glass electrode. During the measurement, the pH standard solution should be kept away from ambient air to prevent a change in pH value due to dissolved carbon dioxide.

However, up to now, no pH measurement system has a ± 0.0001 pH unit resolution. In this work, we constructed a precise pH measurement system by developing a flow cell system with a glass electrode and a reference electrode in response to a request from the National Chemical Laboratory for Industry and studied the effects of temperature control, sample flow rate, response time and reproducibility on pH.

2. Outline of certification system for pH standard solutions in Japan

Fig. 1 shows the scheme for the traceability of pH standard solutions regulated by the Japanese government in 1984. In this traceability system, the pH standard materials made into a stock standard solution and primary pH standard solutions are prepared from it at the National Chemical Laboratory for Industry. The Chemical Inspection and Testing Institute, Japan (CITI), was founded as the certifying organization to supply pH standard solutions for practical use. Secondary pH standard solutions are prepared there using chemicals of pH measurement grade and certified by using the primary standard solutions. After all the pH standard solutions for practical use have been inspected and certified by the secondary pH standard solutions, they are distributed to the users of pH meters.

3. Experimental

3.1. Apparatus and reagents

A DKK Model EL6157 combination glass electrode was used. A Yamato Model BH-51 thermostat was used for temperature control of the sample solution. An Alitea Model U4-XV peristaltic pump was used to send the sample solution into the flow cell. A Yokogawa Model LR4110 analog recorder and an IBM Model N27 personal computer with software written in Microsoft Visual Basic were used to record and collect the data.

Potassium tetraoxalate, potassium hydrogenphthalate, potassium dihydrogenphosphate, disodium hydrogenphosphate, sodium tetraborate decahydrate, sodium hydrogencarbonate and sodium carbonate were obtained from Kanto Kagaku (Tokyo, Japan), Wako Chemicals (Osaka, Japan) and Merck (Darmstadt, Germany). All chemicals were of pH measurement grade or analytical-reagent grade. Pure water obtained with a Milli-Q SP Reagent Water System was used throughout. A Model F10 porous ceramic used as the ceramic junction was purchased from Kyocera (Kyoto, Japan). Z-7 chelating resin was purchased from Miyosi Oil and Fat (Tokyo, Japan).

Fig. 1. Traceability scheme for pH standard solutions in Japan.

3.2. Preparation of pH standard solution

Six kinds of pH standard solution were prepared as follows. A 0.05 mol (kg H_2O)$^{-1}$ potassium tetroxalate dihydrate solution was prepared as a pH 1.679 standard solution at 25°C according to JIS K 0018 [10]. A 0.05 mol (kg H_2O)$^{-1}$ potassium hydrogenphthalate solution was prepared as a pH 4.008 standard solution at 25°C according to JIS K 0019 [11]. A 0.025 mol (kg H_2O)$^{-1}$ $KH_2PO_4 + 0.025$ mol (kg H_2O)$^{-1}$ Na_2HPO_4 solution was prepared as a pH 6.865 standard solution at 25°C according to JIS K 0020 [12]. A 0.008695 mol (kg H_2O)$^{-1}$ $KH_2PO_4 + 0.03043$ mol (kg H_2O)$^{-1}$ Na_2HPO_4 solution was prepared as a pH 7.415 standard solution at 25°C according to JIS K 0023 [13]. A 0.01 mol (kg H_2O)$^{-1}$ $Na_2B_4O_7 \cdot 2H_2O$ solution was prepared as a pH 9.180 standard solution at 25°C according to JIS K 0021 [14]. A 0.025 mol (kg H_2O)$^{-1}$ $NaHCO_3 + 0.025$ mol (kg H_2O)$^{-1}$ Na_2CO_3 solution was prepared as a pH 10.012 standard solution at 25°C according to JIS K 0022 [15]. The primary standard pH solutions were obtained from the National Chemical Laboratory for Industry.

3.3. Preparation of pH electrode

The pH electrode used is shown in Fig. 2. The Model EL6157 is a combination-type pH electrode with a long-term stable reference electrode, which can eliminate silver chloride complex ions in the potassium chloride (KCl) inner solution by the use of chelating resins [16]. To stabilize the liquid junction potential thoroughly, a remodelled Model EL6157 pH electrode was used. The chelating resin was changed from MX-8 to Z-7, which was more effective in adsorbing silver chloride complex ions dissolved from the silver–silver chloride inner electrode. The ceramic junction was changed from Model F11 to Model F10, with which the outflow rate of the KCl inner solution was about five times that with the Model F11. Furthermore, the numer of ceramic junctions was changed from one to two by adding one at the opposite side of the electrode body. The diameter of the glass membrane is 6 mm and that of
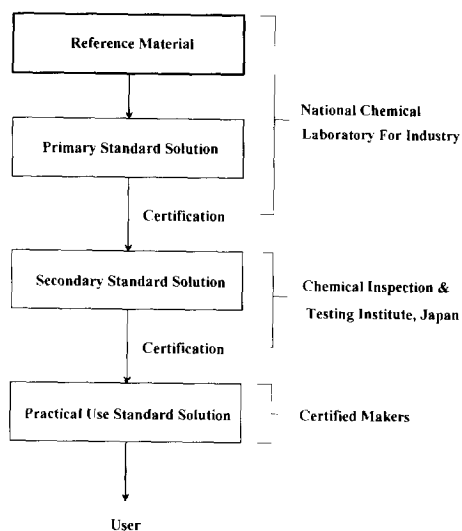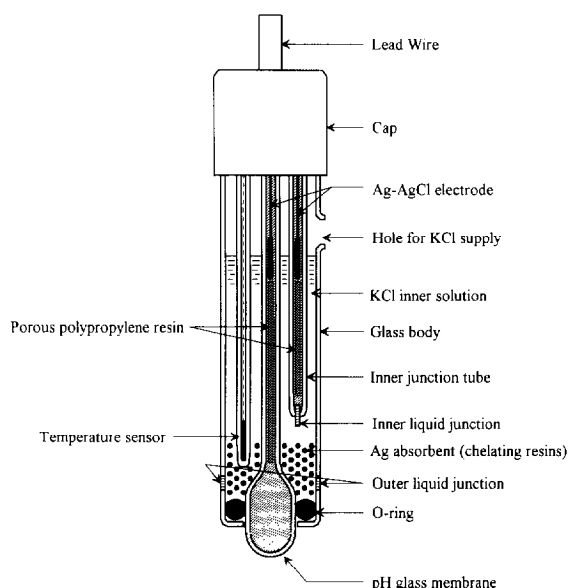
Fig. 2. Structure of stable pH combination electrode.

the electrode body with ceramic junctions is 12 mm.

3.4. Manufacture of pH flow cell

The pH flow cell developed is shown in Fig. 3. The flow cell consisted of an acrylic resin body and
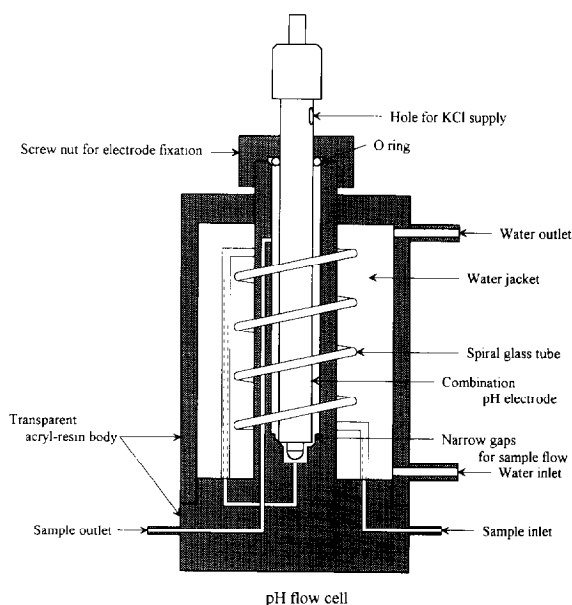

pH flow cell

Fig. 3. Structure of flow cell for pH.

a spiral glass tube to keep the temperature constant. The sample from the sample inlet was kept at a constant temperature (25°C) in the spiral glass tube, passing by way of the glass membrane and the ceramic liquid junction and being exhausted from the sample outlet. The length of the glass spiral tube was about 60 cm. The distance passed by the sample from the sample vessel to the glass membrane was about 1 m. The diameter throughout the sample route was 1 mm and the volume of the sample passage was about 0.8 ml. The dead volume around the glass membrane was about 0.6 ml. The flow cell has two narrow gaps, with a width of 2 mm and a depth of 0.5 mm, to separate the glass membrane from the liquid junction, because if KCl diffused from the liquid junction and contact with the glass membrane some errors would occur in pH measurements. The diameter of the flow cell was 66 mm and the height was 140 mm.

3.5. Development of high-resolution pH meter

A block diagram of the pH meter developed is shown in Fig. 4. The operational amplifier for conversion from the high-impedance e.m.f. of the glass membrane to the low-impedance output voltage was used as an analog amplifier. An analog-to-digital converter (ADC) of double integral type was used as an 18-bit ADC; 18 bits of the digital signal corresponded to $\pm$ 500 mV of e.m.f. The sampling time of the ADC was about 1 s. One-bit resolution was corresponded to 0.0019 mV. The e.m.f. was always referred to the reference voltage (0 and 500 mV). The pH meter has a function of two-point calibration operated by the 8-bit central processor unit (CPU) by means of operational software written in Intel PLM Compiler. The unknown pH(X) value was determined by the multi-standard method from two standard solutions of pH(X$_1$) and pH(X$_2$). Furthermore, as the pH(X) value was very close to the pH(X$_1$) value, the difference between these values was determined very precisely. The pH(X) value was calculated against E mV of the e.m.f. as shown in Eqs. (1), (2) and (3), where X_1 and E_1 correspond to the pH and the mV of the e.m.f. in the first-point calibration, respectively, and X_2 and E_2 to those of the e.m.f. in the second-point calibration, respectively.
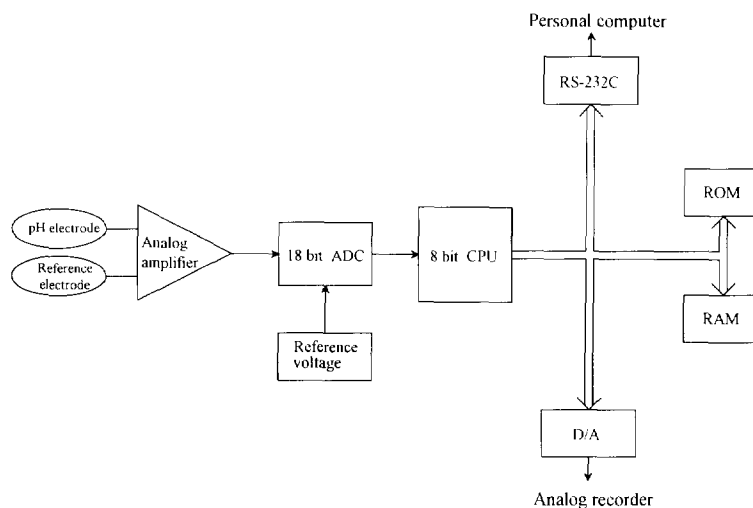
Fig. 4. Block diagram of precise pH meter.

$$X = [(X_2 - X_1)/(E_2 - E_1)](E - E_1) + X_1 \qquad (1)$$

When E_1 was changed to $E_1{}'$ by a repeated first-point calibration, the offset potential of the calibration curve was changed as follows:

$$X = [(X_2 - X_1)/(E_2 - E_1{}')](E - E_1{}') + X_1 \qquad (2)$$

Further, when E_2 was changed to $E_2{}'$ by a repeated second-point calibration, the offset potential and the sensitivity (electrode slope) of the calibration curve were changed as follows:

$$X = [(X_2 - X_1)/(E_2{}' - E_1{}')](E - E_1{}') + X_1 \qquad (3)$$

All measurements were made at 25°C. The data on the e.m.f. and pH were sent to the personal computer through the RS-232C interface, and at the same time were recorded on the analog recorder through the 14-bit digital-to-analog converter. All operations of calibration and the measurement were made through the personal computer.

3.6. pH-measuring flow system

Fig. 5 shows the pH-measuring flow system. The sample was sucked and carried into the flow cell by the peristaltic pump located downstream. Water was circulated at 2 l min^{-1} between the thermostat and the water-jacket of the flow cell and was maintained at 25 ± 0.03°C. The flow cell

body and the sample vessel were situated in an air-conditioned room. The relationship between the sample flow rate and the ambient tempreature was studied. The sample flow rate was examined between 0.5 and 6 ml min^{-1}. The characteristics of the thermal exchange in the flow cell were examined against the change in the ambient temperature. The sample vessel was purged with nitrogen to prevent contamination by atmospheric carbon dioxide. The e.m.f. of the pH electrode measured by the pH meter was recorded and collected by the analog recorder and the personal computer.

3.7. Verification procedure for pH standard solution

The procedure for verification of the prepared pH standard solution with the primary pH standard solution is as follows. First, the pH meter is calibrated by two kinds of primary pH standard solutions, the first-point calibration using one with same pH value and the second-point calibration with one with another pH value, which is usually different by several pH units. For example, if the prepared phosphate pH standard equimolal solution (pH 6.865) is verified, the first-point calibration of the pH meter is executed beforehand using the phosphate primary pH stan-
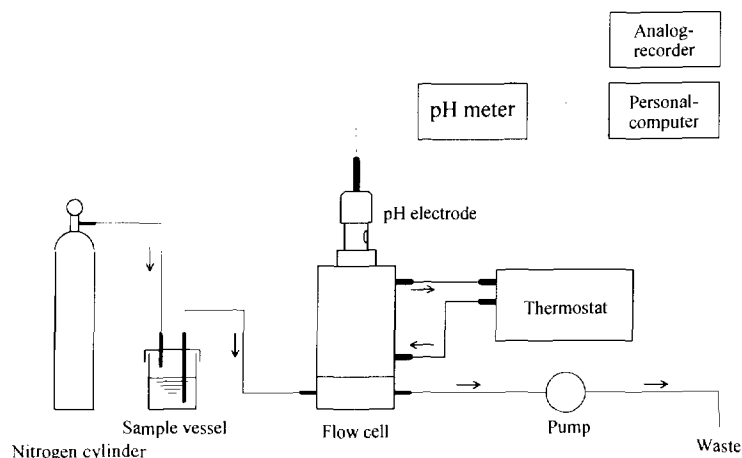
Fig. 5. Precise pH-measuring flow system for pH standard solutions.

dard equimolal solution (pH 6.865) and the second-point calibration is executed with the phthalate primary pH standard solution (pH 4.008). These calibrations were repeated several times until the measured value corresponded to the value of the standard solution within ± 0.0002 pH. Subsequently, a prepared pH standard solution was measured. When many samples were measured, the first-pont calibration was repeated after every few measurements and each set of data was corrected by interpolation from the difference between two of the first-point calibrations. The measurement was considered to have reached the final value when the e.m.f. remained constant within ± 0.0002 pH for 5 min.

4. Results and discussion

4.1. Effect of sample flow rate

Each pH standard solution has a temperature coefficient. Near 25°C, the temperature coefficients of the oxalate pH standard solution (pH 1.679), the phthalate pH standard solution (pH 4.008), the phosphate pH standard equimolal solution (pH 6.865), the phosphate pH standard solution (pH 7.413), the tetraborate pH standard solution (pH 9.180) and the carbonate pH standard solution (pH 10.012) are 0.001, 0.0012, — 0.0028, — 0.0028, — 0.0082 and — 0.0096 pH

$°C^{-1}$, respectively [2]. The calculated temperature values which give a 0.0001 pH error are 0.100, 0.083, — 0.036, — 0.036, — 0.012 and — 0.010°C, respectively. Therefore, the tempreature of the sample solution needed to be precisely controlled within ± 0.01°C.

The relationship between the sample flow rate and the ambient temperature is shown in Fig. 6. The water in the water-jacket of the flow cell was controlled at 25 ± 0.03°C. Lines 1, 2, 3, 4, 5, 6, 7 and 8 represent ambient temperatures of 26, 24, 27, 23, 28, 22, 29 and 21°C, respectively. When the sample flow rate was faster than 5 ml min^{-1},

Fig. 6. Relationship between flow rate and temperature of sample.

Fig. 7. Response time of pH flow system under different conditions.

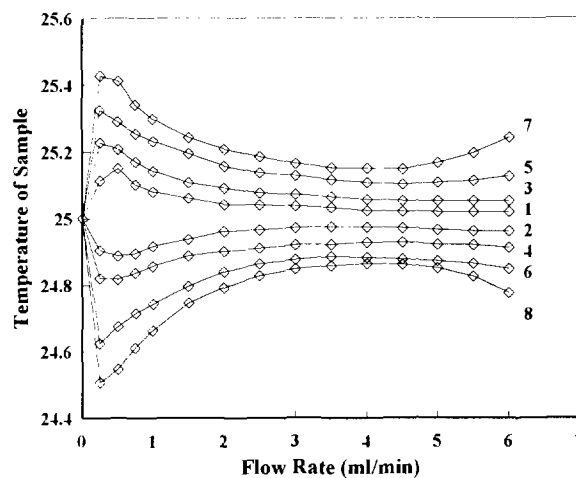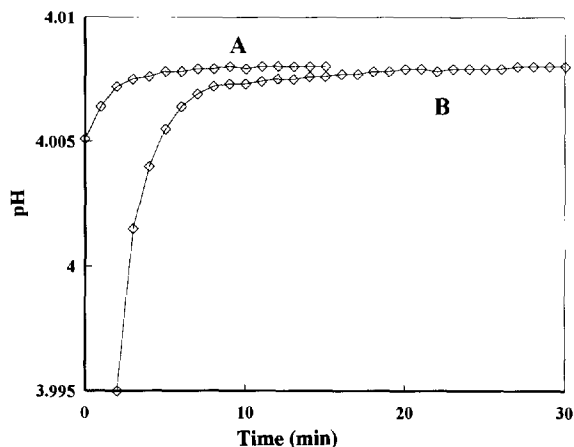the temperature control became worse owing to the inadequate temperature exchange capacity of the spiral glass tube. When the sample flow rate was lower than 2 ml min^{-1}, temperature control was lost because of the effect of the temperature change due to the flow cell body. The temperature of the sample remained constant in the flow rate range 2–5 ml min^{-1} when the ambient temperature was controlled at $25 \pm 1.5°C$ and the circulating water in the flow cell was controlled at $25 \pm 0.03°C$.

4.2. Response time

Fig. 7 shows the typical response time during measurement of the pH buffer solution using the present system. The response time was almost independent of the type of pH standard solution. The response time to the same type of pH standard solution is usually 10–15 min (A), e.g. from the secondary phthalate pH standard solution (pH 4.008) to the primary phthalate pH standard solution (pH 4.008). The response time in the case of the second-point calibration is usually 20–30 min (B), e.g. the primary oxalate pH standard solution (pH 1.679) to the primary phthalate pH standard solution (pH 4.008).

4.3. Reproducibility

In each of the six types of pH standard solution, after the pH system had been calibrated by the primary pH standard solution, the secondary pH standard solution was measured. Ten replicate measurements were made and the standard deviations of the final values were claculated. The standard deviations of the oxalate pH standard solution (pH 1.679), the phthalate pH standard solution (pH 4.008), the phosphate pH standard equimolal solution (pH 6,865), the phosphate pH standard solution (pH 7.413), the tetraborate pH standard solution (pH 9.180) and the carbonate pH standard solution (pH 10.012) were ± 0.0005, ± 0.0005, ± 0.0006, ± 0.0006, ± 0.0004 and ± 0.0004 pH, respectively. Although it seems that the phosphate standard solution is slightly inferior to the others, it can be concluded that overall reproducibility was ± 0.001 pH.

4.4. Other factors influencing precision

The pH standard solutions as CRMs are required to have a certified value of ± 0.002 pH. The specification of a pH meter to verify them inevitably requires a reproducibility of ± 0.001 pH. There are some factors to be considered with regard to precise pH measurement. First, temperature control is the most important. Not only the sample temperature but also the ambient temperature should be controlled precisely because the pH electrode is affected by the ambient temperature in the electrode cap. Second, the maintenance of a smooth KCl outflow and a clean liquid junction in the reference electrode is important, too. Third, the glass electrode should be renewed at least every 6 months because the response of the glass membrane gradually decreases with time. Fourth, small air bubbles on the surface of the glass membrane can affect the stability of the e.m.f. and also, the formation of air bubbles is not desirable for stable pH measurements because the dead volume from the sample vessel to the flow cell increases and a smooth KCl outflow might no longer apply. The formation of air bubbles on the glass membrane

can be effectively prevented by degassing the sample with an aspirator before measurements. In comparison with the classical cell of the hydrogen gas electrode and the silver–silver chloride electrode, the present pH measurement system seems to show improved reproducibility and response times in practical use.

5. Conclusion

We have constructed a precise pH measurement system for supporting the traceability of pH standard solutions in Japan, with the development of an improved pH meter, a pH glass electrode and a flow cell. This system was applied to the measurement of pH standard solutions regulated by JIS and a reproducibility (standard deviation) of ± 0.0006 pH was attained. We conclude that the present flow system for pH measurement is very useful for the certification of pH standard solutions in traceability systems.

Acknowledgements

References

[1] R.G. Bates, Determination of pH, Theory and Practice, Wiley, New York, 1964, pp. 1–33.

[2] R.A. Durst, Standard Reference Materials; Standardization of pH Measurements, NBS Special. Publication No. 260-53, National Bureau of Standards, Washington, DC, 1975.

[3] Echelle de pH des Solutions Aqueuses, OIML Recommandations Internationales R.I. No. 54, Sixth International Conference of Legal Metrology, USSR, June, 1980.

[4] Tentative Method for Determination of pH of Aqueous Solutions with the Glass Electrode, ASTM E 70–77, ASTM, Philadelphia, PA.

[5] A.K. Covington, R.G. Bates and R.A. Durst, Pure Appl. Chem., 57 (1985) 531.

[6] Six Environment Laws in Japan, 1994, pp. 3–8.

[7] Certification of Reference Materials—General and Statistical Principles, ISO Guide 35, ISO, Geneva, 2nd edn., 1989.

[8] H. Kitano and H. Uchiyama, Bull. NRLM, 32, No. 3 (1983) 119.

[9] S. Nakamura, N. Fudagawa and A. Kawase, Bunseki Kagaku, 28, No. 7 (1979) T39.

[10] Oxalate pH Standard Solution, JIS K 0018–1983, Japanese Standards Association, Tokyo, 1983.

[11] Phthalate pH Standard Solution, JIS K 0019–1983, Japanese Standards Association, Tokyo, 1983.

[12] Phosphate pH Standard Equimolal Solution, JIS K 0020–1983, Japanese Standards Association, Tokyo, 1983.

[13] Phosphate pH Standard Solution JIS K 0023–1983, Japanese Standards Association, Tokyo, 1983.

[14] Tetraborate pH Standard Solution, JIS K 0021–1983, Japanese Standards Association, Tokyo, 1983.

[15] Carbonate pH Standard Solution, JIS K 0022–1983, Japanese Standards Association, Tokyo, 1983.

[16] S. Ito, H. Hachiya, K. Baba, Y. Asano and H. Wada, Talanta, 42 (1995) 1685.

Room-temperature phosphorimetry studies of some addictive drugs following dansyl chloride labelling

Ai-Jun Tong*, Ying-Guang Wu, Long-Di Li

Department of Chemistry, Tsinghua University, Beijing 100084, China

Received 8 November 1995; revised 14 February 1996; accepted 16 February 1996

Abstract

A room-temperature phosphorimetric (RTP) method for the analysis of barbital, codeine, morphine and practolol after labelling with dansyl chloride (DNS-Cl) is described. The drug–DNS derivatives were obtained by refluxing with drug–ethyl acetate solutions and solid DNS-Cl in the presence of anhydrous potassium carbonate. The reaction conditions were investigated in detail. The fluorescence emission of drug–DNS derivatives shifted to longer wavelengths compared with that of DNS-Cl. The RTP phenomena observed for these derivatives by using a micellar stabilized room-temperature phosphorescence technique were examined and optimum conditions for their RTP emission were studied using an orthogonal array design. Derivative RTP spectra were obtained and successfully used to determine practolol by the established method without further separation.

Keywords: Addictive drugs; Dansyl chloride labelling; Room-temperature phosphorimetry

1. Introduction

Banned substances include narcotic and mental drugs and are sometimes abused by athletes to improve their physical performance in sport games and by drug addicts. On the other hand, some addictive drugs are very useful and essential in medical treatment. It is therefore very important to establish rapid, accurate and sensitive analytical methods for such drugs for the effective control of their illegal use in sport, for the confirmation of drug addicts, for their monitoring during drug rehabilitation programmes and for therapeutic drug monitoring.

Numerous methods have been established for addictive drug control. Gas chromatography (GC) [1], gas chromatography–mass spectrometry (GC–MS) [2], liquid chromatography (LC) [3] and radioimmunoassay [4] are some approved methods for drug screening. Alternative methods, including fluorimetric [5] and phosphorimetric [6,7] detection, chemiluminescence methods [8] and enzyme and fluorescence immunoassay [9,10], have also been developed.

Room-temperature phosphorimetry (RTP), especially the MS–RTP technique, is a recently developed method [11,12]. Phosphorescence emission usually appears at longer wavelengths than fluorescence, permitting selective detection in the presence of other fluorophores. The RTP tech-

---

* Corresponding author.

nique also has the advantages of simplicity, good sensitivity and the possibility of automation. Further, MS-RTP is a fluid system, which has prompted its widespread application to various samples. RTP determinations of trace organic components [13,14] and proteins [15], which show suitable phosphorescence emission, have been reported. Although there has been a report of RTP studies of amino acids with fluorescamine labelling [16], there has been little research work concerning phosphorescence labelling. The aim of this work was to apply the MS-RTP method to the determination of barbital, codeine, morphine and practolol with dansyl chloride (DNS-Cl) as a phosphorescence labelling reagent.

Dansyl chloride is a well known fluorescence labelling reagent, reacting with amino phenolic and active hydroxyl groups under suitable experimental conditions. The RTP properties and the possibility of using DNS-Cl as a phosphorescence probe for amino acids have been reported [17]. In this work, an MS-RTP method for the analysis of addictive drugs with DNS-Cl labelling was established. The labelling conditions were studied in detail and some factors which affect the RTP emission of the drug DNS derivatives were studied by an orthogonal array design. Derivative RTP spectra were used to determine the addictive drugs without further separation.

2. Experimental

2.1. Apparatus

RTP spectra and fluorescence spectra were measured with a Perkin-Elmer LS-50B luminescence spectrometer. When scanning phosphorescence spectra, the delay time and the gate time were set at 0.1 and 2.0 ms, respectively; the excitation and the emission slit widths were set at 15 and 20 nm respectively. When fluorescence spectra were recorded, both slit widths were set at 4 nm. Derivative spectra were obtained automatically on the instrument.

Phosphorescence lifetimes were obtained with phosphorescence short decay application of the instrument and the data were obtained automatically with an Enzfitter program.

2.2. Reagents and solutions

Barbital, codeine phosphate, morphine and practolol were reference chemicals, obtained from the National Laboratory of Narcotic Drugs, National Institute for the Control of Pharmaceutical and Biological Products (China). Stock solutions of 10^{-3} M of the above drugs in ethyl acetate were prepared. DNS-Cl (Fluka) product was purchased from Baitai Biochemicals (China) and was used as received. Sodium dodecyl sulphate (SDS) was obtained from Beijing Chemical Factory (China) and was recrystallized twice with hot ethanol before use. Other chemicals were of analytical-reagent grade.

Deionized water was redistilled in a sub-boiling quartz distillation system and was used throughout the experiments.

2.3. Labelling procedure

In a carefully dried 50 ml reaction vessel, 5 ml of 10^{-3} M drug in solution ethyl acetate, certain amounts of DNS-Cl solid and finely ground and dried K_2CO_3 were mixed. The reaction mixture was heated with an air bath with continuous stirring for slow refluxing of the ethyl acetate. The labelling time was about 20 min for morphine and practolol and 60 min for baribtal and codeine. After the solid had been separated, ethyl acetate solutions of drug–DNS derivatives were analysed immediately or placed in a refrigerator at 4°C to prevent thermal or light decomposition. A labelling blank was prepared at the same time by reaction with ethyl acetate solvent and DNS-Cl under the same experimental conditions.

2.4. MS-RTP measurements

A 0.5 ml volume of about 1.9×10^{-3} M drug–DNS derivative solution was transferred into a bottle placed in a thermostat. The solution was heated at 60°C to evaporate the solvent. The same amount of 0.2 M SDS solution was added and the mixture was shaken vigorously to dissolve the derivative.

A 0.4 ml volume of the above solution was transferred into a 10 ml colorimetric tube, then 2

ml of 0.2 M SDS solution, 2.5 ml of 0.1 M TlNO$_3$ solution (caution: thallium(I) salts are very toxic) and 2 ml of 0.1 M Na$_2$SO$_3$ solution were added. The mixture was diluted to a final volume of 8 ml with water, heated in a water bath at 30°C for 30 min and the phosphorescence spectrum was recorded. The RTP spectrum of a DNS-Cl blank was also recorded for comparison.

2.5. Quantitative analysis of practolol

A series of 1.0, 1.5, 2.0 and 3.0 ml of 1.57 × 10^{-3} M practolol–ethyl acetate solution were reacted with 3.0 mg of DNS-Cl in the presence of 200 mg of solid K$_2$CO$_3$, and 0.2 and 0.4 ml of the above practolol solutions were reacted with 1.6 and 1.8 mg of DNS-Cl, respectively, in the presence of 200 mg of solid K$_2$CO$_3$, then the reaction
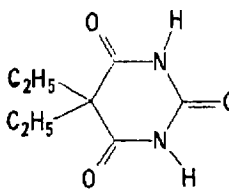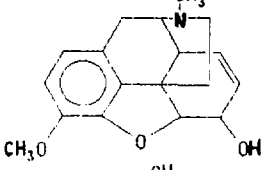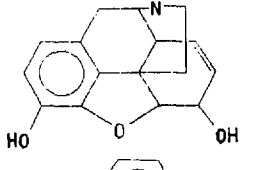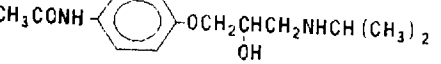
mixture was diluted to 10 ml with ethyl acetate. Two reaction blanks were prepared by reaction of 3.0 and 1.7 mg of DNS-Cl with 10 ml of ethyl acetate under the same labelling conditions as stated above. Certain amounts of the supernants were placed in colorimetric tubes and the RTP intensities were measured as stated above under the otpimum experimental conditions.

3. Results and discussion

3.1. Luminescence properties of barbital, codeine, morphine and practolol

The structures of the drugs studied and their luminescence properties are listed in Table 1. Except for practolol, the drugs show weak or

Table 1
Luminescence properties of the four addictive drugs studied (1.0 × 10^{-3} M ethyl acetate solution)

Drug	Structure	Fluorescence			RTP	
		λ_{ex} (nm)	λ_{em} (nm)	RFI[a]	SS–RTP[b]	MS–RTP
Barbital		272	390	41	None	None
Codeine		260, 284	340	275	None	None
Morphine		260, 271, 292	344	253	None	None
Practolol	CH$_3$CONH—⟨⟩—OCH$_2$CHCH$_2$NHCH(CH$_3$)$_2$ OH	—	—	—	None	None

[a] Relative fluorescence intensity.
[b] Filter paper substrate room-temperature phosphorescence, measured on a Hitachi model 850 type fluorescence spectrophotometer, fitted with a phosphorescence accessory and a laboratory-made sample holder; 1 M lead acetate, 1 M potassium iodide and 1 M thallium(I) nitrate were tested as heavy atoms.

stronger fluorescence emission, but no RTP emission was observed, so phosphorescence labelling is necessary for RTP studies of these drugs. Active groups (amino, phenolic and hydroxyl groups conjugated with double bonds) are present in these molecules, so derivatization with DNS-Cl is possible.

3.2. Derativatization conditions

The reaction of DNS-Cl with active groups (e.g. amino groups) and the hydrolysis of DNS-Cl could be expressed as shown in Scheme 1.

It is clear that a basic medium is preferred in the labelling reaction to neutralize the hydrochloric acid product. Further, the hydrolysis of DNS-Cl will also proceed in basic conditions. It is therefore important to control the acidity of the reaction mixture. Several systems have been developed for the derivatization of various compounds with DNS-Cl. In this work, four derivatization systems were tested, namely the $Na_2CO_3-NaHCO_3$ buffer system [18], Na_2CO_3 medium with benzene extraction [19], pyridine non-aqueous medium and ethyl acetate medium in the presence of solid K_2CO_3 [20]. Except for the last system, these labelling methods either gave no DNS-Cl derivatives or the labelling reproducibility was not satisfactory. Therefore, the last system was selected and its reaction conditions were investigated in detail.

First, the particle size, degree of drying and amount of K_2CO_3 greatly affect the labelling pro-

cedure. Only when finely ground, carefully dried K_2CO_3 was used with continuous stirring and its amount exceeded the amount of DNS-Cl by 40–60-fold could all four drugs be labelled successfully. This could be explained by phase-transfer catalysis of the labelling reaction. Adsorption–desorption equilibria for the drug and for DNS-Cl between the solid K_2CO_3 and the ethyl acetate solvent existed. Derivatization occured only when both the drug and DNS-Cl were adsorbed on K_2CO_3 to obtain a base medium. Hence the ability of phase transfer would be weak when the amount of K_2CO_3 was not sufficient or the agitation was not thorough. A larger particle size of K_2CO_3 resulted in a small specific surface area and thus a low phase-transfer ability. The degree of drying of K_2CO_3 also greatly affected the labelling reaction because of the hydrolysis of DNS-Cl. Dansyl acid is the main by product of the labelling reaction, and even small amounts of water will affect the derivatization. All vessels and chemicals should therefore be dried carefully before the labelling process. An air bath was used instead of a water bath in our investigations.

Second, the temperature of reaction, reaction time and amount of DNS-Cl also affect the labelling. A high temperature would induce thermal decomposition of the product and a low temperature would increase the labelling time. An adequate temperature was 80°C to allow ethyl acetate to reflux slowly. In spite of drying of all the vessels and chemicals, trace amounts of water still existed
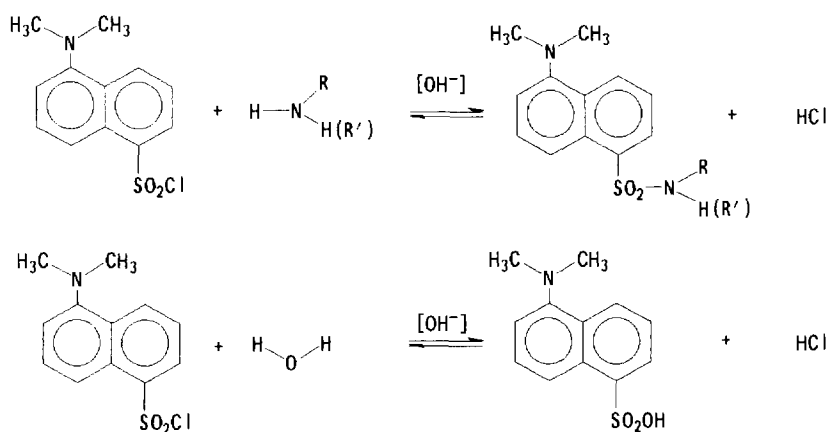
Scheme 1

and could not be neglected compared with the amounts of DNS-Cl and the drug. To prevent hydrolysis of DNS-Cl, the shorter the reaction time, the more complete is the derivatization. Our results showed that 20 min is needed for derivatization of the highly reactive drugs morphine and practolol and 60 min for the less reactive drugs barbital and codeine. Although an excess of DNS-Cl will be beneficial for quatitative derivatization of the drugs and decrease the effect of hydrolysis, an excess of drug instead of DNS-Cl is used to prevent separation in the subsequent RTP measurements. Solid DNS-Cl was used directly because of the restricted dissolution of DNS-Cl in ethyl acetate.

3.3. Fluorescence spectra of drug–DNS derivatives

Fluorescence spectra of the derivatives and DNS-Cl solutions in ethyl acetate were measured to confirm the labelling products. The results are summarized in Table 2. The emission wavelengths of the four derivatives were red shifted by 9–32 nm compared with that of DNS-Cl, indicating the formation of drug–DNS derivatives. It should be noted that the low-reactive codeine was successfully labelled under our experimental conditions, whereas its labelling was impossible in earlier study [18].

3.4. Room-temperature phosphorescence phenomena of drug–DNS derivatives

The RTP properties of the four drug–DNS derivatives were investigated using an MS–RTP

method. No RTP emission was obtained when the ethyl acetate solutions of the derivatives were treated with SDS micelles, $TlNO_3$ heavy atom perturber and Na_2SO_3 oxygen scavenger. It is considered that the existence of the organic solvent ethyl acetate would compete with the derivative for the protecting hydrophobic area and would increase the distance between the derivative and the heavy atom. These adverse effects of ethyl acetate resulted in no RTP emission. However, RTP emission was successfully observed for barbital–codeine– and practolol–DNS derivatives when the ethyl acetate was evaporated and the derivatives were redissolved in SDS micelles. RTP emission of morphine–DNS derivative was not observed under the same experimental conditions, and also no fluorescence of the SDS solution of its derivative after evaporation of the ethyl acetate was observed. The reason may be the thermal decomposition of morphine–DNS during the evaporation process or its poor solubility in SDS solution. Investigations of this aspect are in progress.

The RTP spectra and their first-derivative spectra of barbital–, codeine– and practolol–DNS are compared in Fig. 1. RTP determinations of the three drugs without separation of the reagent are possible using their first-derivative RTP intensities at fixed wavelengths at which the first-derivative RTP intensity of DNS-Cl was zero. The phosphorescence lifetimes for barbital–, codeine– and practolol–DNS are 0.543, 0.311 and 0.791 ms, respectively.

3.5. Optimum conditions for the RTP of drug–DNS derivatives

Developed by Cline-Love and Shaver [11], the MS–RTP method is one of the most important techniques for the RTP analysis of solutions. Several factors, such as concentrations and amounts of SDS, $TlNO_3$ and Na_2SO_3, deoxygenation time and temperature, are stated to be important factors which strongly affect the RTP intensities of phosphors. In this work, an orthogonal array design [21] was employed to evaluate the optimum values of these factors. Sixteen experiments were performed with a five-factor, four-level orthogonal array design (Table 3; the deoxygenation time

Table 2
Fluorescence properties of drug–DNS derivatives

Substance[a]	λ_{ex} (nm)	λ_{em} (nm)
DNS-Cl	328	496
Barbital–DNS	346	505
Codeine–DNS	328	505
Morphine–DNS	346	528
Practolol–DNS	346	525

[a] The concentration of DNS-CL was 2.0×10^{-5} M and the amounts of the drugs exceeded that of DNS-Cl 3–4-fold.

(1)

(2)

Fig. 1. RTP spectra (1) and first-derivative spectra (2) for drug—DNS derivatives and DNS-Cl. Ip = phosphorescence intensity; Idp = first-derivative phosphorescence intensity; B = barbital–DNS; C = codeine–DNS; P = practolol–DNS; D = DNS-Cl.

was fixed at 30 min). The results of these experiments were analysed by graphic interpretation. Thus, average RTP intensities for a certain factor at different levels were separately calculated; such average RTP intensities were taken as functions of the factors and the results were expressed as graphs. The following comments can be made.

The effects of SDS concentration are shown in Fig. 2. It can be seen that when the concentration of SDS was higher than 0.04 M, the RTP intensities of the three drug derivatives reached maxima. It is essential that the concentration of SDS be much higher than its critical micellar concentration (CMD) to give enough micelles to provide a protecting microenvironment for the RTP emission of phosphors. In subsequent experiments, 0.08 M SDS in the final solution was used.

Table 3
Orthogonal experimental design

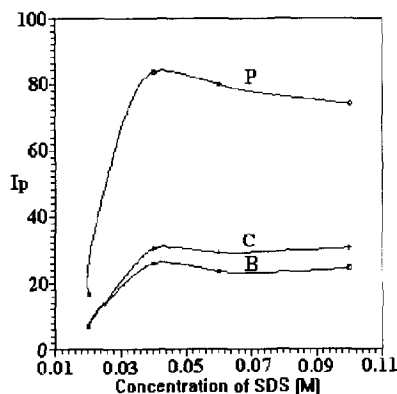| Level / Factor	Experimental No.															
	1	2	3	4	5	6	7	8	9	10	11	12	13	14	15	16
T (°C)	30	30	30	30	35	35	35	35	40	40	40	40	45	45	45	45
C (Na_2SO_3, M)	0.008	0.016	0.04	0.12	0.008	0.016	0.04	0.12	0.008	0.016	0.04	0.12	0.008	0.016	0.04	0.12
C ($TlNO_3$, M)	0.025	0.05	0.075	0.10	0.05	0.025	0.10	0.075	0.075	0.10	0.025	0.05	0.10	0.075	0.05	0.025
C (SDS, M)	0.02	0.04	0.06	0.10	0.06	0.10	0.02	0.04	0.10	0.06	0.04	0.02	0.04	0.02	0.10	0.06
t (min)	30	30	30	30	30	30	30	30	30	30	30	30	30	30	30	30

Fig. 2. Effects of SDS concentration on the RTP intensities of drug–DNS derivatives. Abbreviations as in Fig. 1.

Fig. 3. Effects of Tl/Na on the RTP intensities of drug–DNS derivatives. Tl/Na = molar ratio of Tl to the sum of Tl and Na; other abbreviations as in Fig. 1.

Thallium(I) nitrate is an external heavy atom perturber; it enhances the intersystem crossing from singlet to triplet and thus increases the phosphorescence emission. When the concentration of $TlNO_3$ was higher than 0.075 M in the measuring solution, the RTP intensities remained maxima. Another important factor is the concentration and amount of Na_2SO_3. Oxygen is a strong phosphorescence quenching agent, and its removal is always necessary in RTP measurements. Sodium sulphite is an effective oxygen scavenger [12], but its deoxygenation efficiency depends on the concentration of Na_2SO_3 and on the Tl/Na ratio (the molar ratio of Tl to the sum of Tl and Na) in the solution. The deoxygenation effect was not good when its concentration was too low or was too high for the replacement of the Tl^+ ions on the surface of the micelles by the Na^+ ions. Fig. 3 shows the effects of Tl/Na on the RTP intensities of the drug derivatives. Suitable molar ratios were 26% for barbital–DNS 30% for codeine–DNS and 29% for practolol–DNS.

The effects of temperature were also studied. The RTP intensities decreased as the temperature increased because of the increase in radiationless transitions at higher temperatures. In this study, 30°C was chosen as the measuring temperature for easy temperature control even in the hot summer season. On the other hand, it is an important advantage of the proposed method that strong
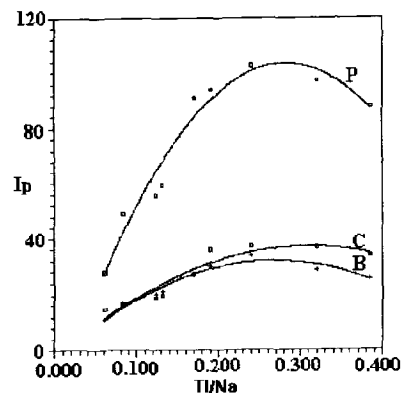
enough RTP intensities for the drug–DNS derivatives were obtained at such a high temperature.

3.6. Quantitative analysis

From Fig. 1, it can be seen that the phosphorescence emission of the drug–DNS derivatives was red-shifted by 14–26 nm compared with that of the DNS-Cl blank. If the wavelength at which the derivative RTP intensity of DNS-Cl was zero was chosen as the detection wavelength, the first-derivative RTP intensity at the wavelength was due only to the drug derivative. Hence the first-derivative spectra can be used for quantitation without prior separation of the excess reagent. Fig. 1(2) shows that all three drugs could be analysed using this method.

In this paper, quantitation of practolol was chosen as an example. A 2–20-fold excess of DNS-Cl was used and the reagent blanks were prepared correspondingly. Our results show that in the practolol concentration range 1.9×10^{-5}–2.8×10^{-4} M, the calibration graph was a straight line passing through the origin. The correlation coefficient was 0.993. The detection limit of practolol calculated as three times the standard deviation of the blank (five repeated labelling reactions and RTP detection experiments) divided by the slope of the calibration graph was 0.19 ppm.

Acknowledgements

References

[1] D.H. Cattin, R.C. Kammerer, C.K. Hatton, M.H. Sekera and J.L. Merdink, Clin. Chem., 33 (1987) 319.

[2] P. Jaxob, E.R. Lewis, B.A. Elias-Baker and R.T. Jones, J. Anal. Toxicol., 14 (1990) 353.

[3] C.E. Lau, F. Ma and J.L. Ealk, J. Chromatogr., 532 (1990) 95.

[4] H.N. Elsohly, M.A. Elsohly and D.F. Stanford, J. Anal. Toxicol., 14 (1990) 308.

[5] I. Jane and J.F. Taylor, J. Chromatogr., 109 (1975) 37.

[6] A.D. Campigli, J.J. Laserna, A. Berthod, and J.D. Winefordner, Anal. Chim. Acta, 244 (1991) 215.

[7] L.M. Cabalin, J.J. Laserna and A. Ruperez, Anal. Chim. Acta, 270 (1992) 239.

[8] R.W. Abbot, A. Townshend and R. Gill, Analyst, 112 (1987) 397.

[9] H.H. McCurdy, L.S. Callahan and R.D. Williams, J. Forensic Sci., 34 (1989) 858.

[10] D.L. Colbert, G. Gallacher, P. Ayling and G. Turner, Clin. Chim. Acta, 171 (1988) 37.

[11] L.J. Clin-Love and L.A. Shaver, Anal. Chem., 52 (1980) 154.

[12] M.E. Diaz Garcia and A. Sanz-Medel, Anal. Chem., 58 (1986) 1436.

[13] T. Vo-Dinh and J.R. Hooymann, Anal. Chem., 51 (1979) 1915.

[14] A.J. Tong, Y.G. Wu and L.D. Li, Anal. Chim. Acta, 322 (1996) 91.

[15] P. Sandor and J.M. Vanderkooi, Photochem. Photobiol., 49 (1989) 775.

[16] W.J. Long and S.Y. Su, Anal. Lett., 18 (1985) 543.

[17] L.D. Li and W.G. Huang, Anal. Chim. Acta, 312 (1995) 345.

[18] N. Parris and D. Gallelli, J. Liq. Chromatogr., 7 (1984) 917.

[19] F. Nachtmann, H. Spitzy and R.W. Frei, Anal. Chim. Acta, 76 (1975) 57.

[20] W. Dunges, G. Nanndorf and N. Seiler, J. Chromatogr. Sci., 12 (1974) 655.

[21] J.H. Qin, B. Deng and X.Q. Wang, Fenxi Shiyanshi, 4(10) (1985) 45.

An indirect method for the spectrofluorimetric determination of trace amounts of germanium after extraction as an ion association complex with rhodamine B in the presence of chromotropic acid

S. Nalini, T.V. Ramakrishna*

Department of Chemistry, Indian Institute of Technology, Madras 600036, India

Abstract

A highly sensitive and selective spectrofluorimetric method for the determination of 0.05–2.00 μg germanium is described. Germanium is treated with chromotropic acid at pH 2.5 and the resultant anionic complex is extracted as an ion pair with rhodamine B into toluene. Addition of butanol to the organic extract releases the fluorescent dye and facilitates its measurement at 570 nm after exciting at 540 nm. The method provides a detection limit of 0.003 μg ml^{-1} and is virtually free from interference from extraneous ions. The relative standard deviaiton is 2.9% for ten determinations of 1.0 μg germanium. The method has been applied to the determination of germanium in various ores, minerals and rock samples.

Keywords: Chromotropic acid; Germanium; Ion association complex; Rhodamine B; Spectrofluorimetry

1. Introduction

The determination of germanium by generation as its hydride and subsequent measurement by atomic absorption spectrometry [1–3] or direct current plasma atomic emission spectrometry [4,5] is potentially advantageous as the methods are rapid, require minimum sample pretreatment and are sensitive at the nanogram level. Unfortunately, the presence of heavy metals such as Fe, Pb, Cd, Zn and Cu proved troublesome as they

were found to affect the evolution of germane [3]. An added disadvantage of atomic absorption spectrometry is the loss of part of the germanium as volatile GeO, which affects the reproducibility [6]. Addition of certain amino acids, however, has been shown to improve the performance of the d.c. plasma technique [4,7]. The spectrophotometric method using phenylfluorone, although useful for determining concentrations of germanium as low as 0.01 μg ml^{-1} [8], lacks selectivity and hence necessitates prior separation of germanium either by distillation or extraction [9].

Spectrofluorimetric methods based on the reaction of germanium with resacetophenone [10],

---

* Corresponding author. Fax: (+91) 44-235-0509.

benzoin [11], quercetin [12], 3,7-dihydroxy flavone [13] and resarzon [14] have been reported. The reaction with 3,7-dihydroxy flavone is perhaps the most sensitive (detection limit 0.002 μg ml^{-1}) but, like other reactions, it is unselective and necessitates separation as a tetrachloride by extraction prior to determination. The quenching effect of Ge(IV) on the fluorescence intensity of *o*-chlorophenylfluorone has also been evaluated for its determination [15]. This method is slow and subject to a wide range of interferences.

The ability of germanium to react with hydroxy compounds to form anionic complexes is well known [16]. The reaction of germanium with chromotropic acid [17] appeared to offer analytical advantages as the resulting anionic complex was selectively extracted as an ion pair with rhodamine B into toluene. This finding, coupled with the fact that the addition of oxygen-containing solvents such as butanol resulted in complete dissociation of the ion association complex to release the fluorescent dye, suggested that the reaction could form the basis for the fluorimetric determination of germanium. This paper summarises the results of the evaluation of such a possibility. It was found that as little as 50 ng of germanium can be determined in the presence of many extraneous ions and the method can be applied directly to determination of germanium in minerals, rocks, and other geological materials.

2. Experimental

2.1. Apparatus

An Aminco Bowman spectrofluorimeter provided with a 250 VA xenon arc lamp was used for all fluorescence measurements. Slit widths of 5 mm for the excitation monochromator and 0.5 mm for the emission monochromator were employed for fluorescence measurements using a 1 cm quartz cell with polished sides and bottom. A standard 10 μg ml^{-1} quinine sulphate solution in 0.1 N H_2SO_4 was used to standardise the source intensity daily.

2.2. Reagents

2.2.1. Standard germanium(IV) solution (100 μg ml^{-1})

Dissolve 0.1441 g of germanium dioxide by heating gently with 20 ml of 2% NaOH. Transfer the solution to a 1 l standard flask and dilute to volume with distilled water. A suitable volume of this solution is diluted to obtain working standrds.

2.2.2. Glycine buffer (pH 2.5)

Dissolve 5 g of glycine and 3.896 g of NaCl in 666 ml of distilled water. Transfer the solution to a 1 l standard flask and dilute to volume with 0.1 N HCl.

Chromotropic acid (0.01%; aqueous solution), Rhodamine B (0.02%; aqueous solution), toluene and *n*-butanol (both analytical grade) were used.

2.3. Procedure

Transfer the sample solution (< 15 ml) containing up to 2 μg of Ge(IV) into a 60 ml separatory funnel. Add 1 ml each of 0.01% chromotropic acid, 0.02% rhodamine B and 3 ml glycine buffer. After a reaction time of 5 min, equilibrate the aqueous phase with 5 ml of toluene for 1 min. Allow the phases to separate and discard the aqueous phase. Wash the organic phase twice with 5 ml of glycine buffer and discard the washings. Mix 2.5 ml of the organic extract with 2.5 ml of butanol and measure the fluorescence intensity at 570 nm after exciting at 540 nm. Subtract the blank reading and establish the concentration of germanium by reference to a calibration graph prepared by applying the procedure to 0.05–2.00 μg of Ge(IV) in aqueous solution.

3. Spectral characteristics and reaction conditions

The excitation and emission spectra of the reagent blank and the ion associate in the presence of various concentrations of germanium are shown in Fig. 1. It is evident that the emission is a maximum at 570 nm and that there are three excitation maxima at 540 nm, 310 nm and 360 nm
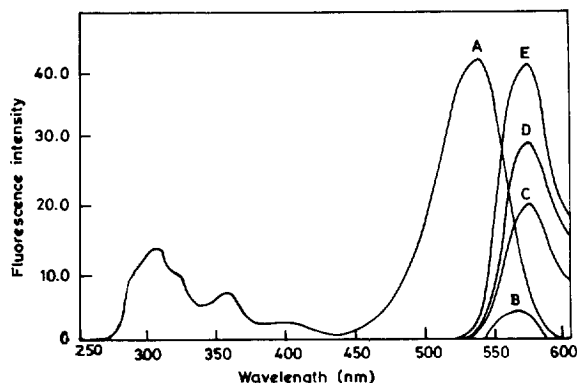
Fig. 1. Excitation (A) and emission (B-E) spectra. (A) 1.0 μg of Ge(IV), 1 ml, 0.01% chromotropic acid, pH 2.5, 1 ml, 0.02% Rhodamine B treated as in Section 2.3. (B) 0, (C) 0.5, (D) 0.75 and (E) 1.0 μg of Ge(IV), 1 ml, 0.01% chromotropic acid, 1 ml, 0.02% Rhodamine B, pH 2.5, treated as in Section 2.3.

(in order of decreasing prominence). As the fluorescence intensity was a maximum with excitation at 540 nm, it was decided to use this wavelength for excitation purposes.

Systematic study revealed that the fluorescence intensity is unaffected in the pH range 2.0–3.0. The influence of chromotropic acid and rhodamine B concentration is shown in Figs. 2 and 3 respectively. On the basis of these studies, 1 ml each of a 0.01% solution of chromotropic acid and a 0.02% solution of rhodamine B were chosen as optimal.
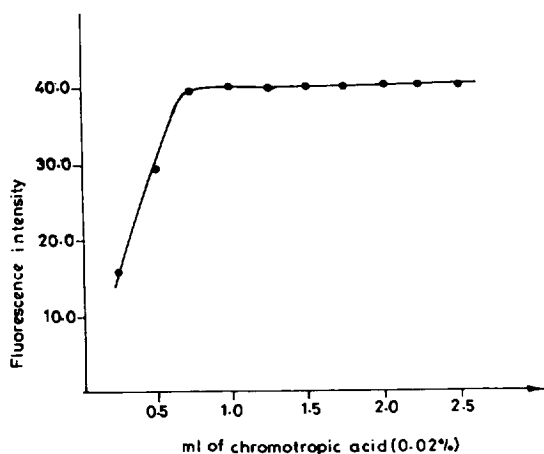

Fig. 2. Effect of chromotropic acid concentration: 1.0 μg of Ge(IV), 1.0 ml 0.02% Rhodamine B, 0.25-2.5 ml 0.02% chromotropic acid pH 2.5, treated as in Section 2.3.
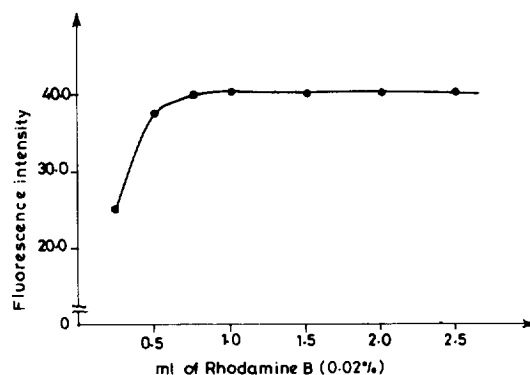

Fig. 3. Effect of Rhodamine B concentration: 1.0 μg of Ge(IV), 1 ml of 0.01% chromotropic acid, 0.25–2.5 ml of 0.02% Rhodamine B, treated as in Section 2.3.

The fluorescence intensity reached a maximum only when the ion pair was extracted after a reaction time of at least 5 min. Under the reaction conditions, a significant amount of the dye was found to coextract into toluene, which resulted in a high blank. However, washing the organic extract twice with the glycine buffer was found to be effective for stripping the free dye selectively from the toluene layer.

Of the solvents examined—benzene, toluene, cyclohexane, hexane, carbon tetrachloride and chloroform—extraction of the ion pair was quantitative only into benzene and toluene. 1 min equilibration was sufficient for complete extraction, which remained unaffected up to an aqueous volume of 20 ml. The addition of acetone, methanol, isobutyl methyl ketone and methyl ethyl ketone to the toluene layer was found to be as effective as the addition of butanol to break the ion pair and release the fluorescent dye. The fluorescence intensity of the liberated rhodamine B was stable for 4 h and varied linearly with germanium concentration in the range 0.05–2.00 μg in 20 ml of the aqueous phase.

The precision of the proposed method was checked by establishing the concentration of ten samples containing 1.0 μg Ge(IV). The mean recovery was found to be 97.1% with a relative standard deviation of 2.9%.

Both mole ratio and continuous variation methods indicated that the molar ratios of ger-

Table 1
Effect of foreign ions on the determination of 1.0 μg of Ge(IV)

Ions tested (1 mg)[a]	Remarks
AsO_4^{3-}, AsO_3^{3-}, Mg^{2+}, Ca^{2+}, Co^{2+}, Ni^{2+}, Cu^{2+}, Sb^{3+}, Zn^{2+}, Fe^{2+}, $Cr_2O_7^{2-}$, SeO_3^{2-}, TeO_3^{2-}, Bi^{3+}, Al^{3+}, SiO_3^{2-}, TiO^{2+}, Mn^{2+}, F^-, Pb^{2+}, Cd^{2+}, Hg^{2+}, Sn^{2+}, Sn^{4+}, Ba^{2+}, Mg^{2+}, Tl^+, Tl^{3+}, Ce^{4+}, VO_3^-, Cr^{3+}, WO_4^{2-}, PO_4^{3-}, In^{3+}, Li^+, Be^{2+}	No interference
BO_3^{3-} (400), MoO_4^{2-} (400)	Enhanced the fluorescence intensity
Fe^{3+}	Decreased the fluorescence intensity

[a] Tolerance limits (μg) are given in parentheses.

manium to chromotropic acid and germanium to rhodamine B were 1:1 and 1:2 respectively. This suggested that in the presence of excess chromotropic acid (CA) germanium forms $[GeO(CA)]^{2-}$, which then associates with two molecules of rhodamine B to extract as an ion pair into toluene.

3.1. Effect of diverse ions

A systematic study of the influence of 1 mg amounts of several ions in the determination of 1.0 μg germanium was carried out. Table 1 lists the effects of various ions on the analytical reaction.

Table 2
Determination of germanium in minerals and geological samples

Sample (wt./vol)	Amount present[a] (μg g^{-1})	Amount found (μg g^{-1})	
		Proposed method[b]	Phenylfluorone method
Anorthosite AN-G (80GOVI)[c] (46.3% SiO_2, 29.8% Al_2O_3, 3.1% Fe_2O_3, 15.9% CaO) (1.5 g 25 ml)	0.80	0.83 ± 0.01	0.83
Iron formation sample IF-G [c](84GOVI) (70.3% SiO_2, 55.8% Fe_2O_3, 1.5% CaO, 1.9% MgO) (1.0 g 25 ml)	24.00	23.62 ± 0.01	23.61
Granite AC-E (87GOVI)[c] (70.3% SiO_2, 14.7% Al_2O_3, 2.5% Fe_2O_3, 6.5% Na_2O, 4.5% K_2O) (2.0 g 25 ml)	2.30	2.30 ± 0.05	2.22
Basalt BE-N (80GOVI)[c] (38.2% SiO_2,10.1% Al_2O_3, 12.8% Fe_2O_3, 13.1% MgO) (2.0 g 25 ml)	1.20	1.22 ± 0.01	1.24
Galena (2.0 g 25 ml)	–	0.66 ± 0.01	0.58
Sphalerite (1.0 g 25 ml)	–	1.57 ± 0.01	1.57
Rhyolite (1.0 g 25 ml)	–	2.51 ± 0.05	2.53
Bauxite (1.0 g 25 ml)	–	2.13 ± 0.03	2.20

[a] Proposed values.
[b] Mean and standard deviation for three values.
[c] Geostandards reference materials.

The interference of Fe^{3+} was overcome by the addition of 1 ml of a 1% solution of ascorbic acid prior to the determination. Molybdate and borate, when present in excess of tolerance amounts, were overcome by the addition of 1 ml of 0.1% solution of fluoride.

4. Applications

The determination of the germanium content of a variety of geological and ore samples was carried out using the proposed method and the results are listed in Table 2.

Samples were brought into solution following the procedure described elsewhere [18]. Appropriate amounts of the samples (1.0–2.0 g) were initially heated for 10 min with 10 ml each of 16 N H_2SO_4 and concentrated HNO_3 in a platinum crucible. The contents were allowed to cool treated with 10 ml of HF and then heated to SO_3 fumes. The residue, after cooling, was treated with 10 ml of distilled water, heated to dissolve the soluble salts and made up to a known volume. The determination was completed by treating suitable aliquots with 1 ml each of a 0.1% solution of sodium fluoride and a 1.0% solution of ascorbic acid. The results, and those obtained by spectrophotometry using the phenylfluorone method after extractive separation of germanium as $GeCl_4$ [9], are given in Table 2. The data clearly show that the method is reliable for the determination of germanium in these samples.

5. Conclusion

The method described provides a simple, rapid and reliable means of determining trace amounts of germanium by spectrofluorimetry. Unlike most methods, including the one based on the reaction with morin [19] which required prior separation of germanium by extraction, the method evolved is virtually free from interferences as the deleterious effect of a few ions could be conveniently overcome by the addition of appropriate reagent solutions prior to determination. The application of the method to a variety of geological and mineral samples clearly demonstrates its usefulness for the determination of germanium at trace levels in complex matrices.

References

[1] X. Guo and R.R. Brooks, Anal. Chim. Acta, 228 (1990) 139.

[2] L. Halicz, Analyst, 110 (1985) 943.

[3] J.R. Castillo, R. Lanaja and J. Azanarez, Analyst, 107 (1982) 89.

[4] I.D. Brindle and X.C. Le, Anal. Chim. Acta, 229 (1990) 239.

[5] I.D. Brindle and C.M.C. Ponzoni, Analyst, 112 (1987) 1547.

[6] K. Sohrin, K. Isshiki and T. Kuwamoto, Talanta, 34 (1987) 341.

[7] I.D. Brindle, X.C. Le and X.F. Li, J. Anal. At. Spectrom., 4 (1989) 227.

[8] H.J. Cluley, Analyst, 76 (1951) 523.

[9] H. Onishi, Photometric Determination of Traces of Metals, Part IIA, 4th edn., John Wiley, New York, 1986, p. 607.

[10] N. Appala Raju and G. Rao, Nature, 174 (1954) 400.

[11] N. Appala Raju and G. Rao, Nature, 175 (1955) 167.

[12] X. Cheng, Z. Ma and Y. He, Fenxi Huaxue, 18 (1990) 680 (Anal. Abstr., 53 (1991) 8D44).

[13] A. Murata, N. Sugiyama and T. Suzuki, Bunseki Kagaku, 36 (1987) 27 (Anal. Abstr., 49 (1987) 5B101.

[14] A.M. Lukin, E.A. Serebryakova, Bozhelvol'nov and G.B. Zavarikhina, Trudy vses. nauchno-issled. Inst. Khim. Reakt, 30 (1967) 161 (Anal. Abstr., 15 (1968) 3263).

[15] M. Guo, J. Zhao, Y. He, Z. Zhao and F. Wang, Fenxi Shiyanshi, 9 (1990) 54 (Anal. Abstr., 54 (1992) 2E71.

[16] I.M. Kolthoff and P.J. Elving, Treatise on Analytical Chemistry, Part II, Sect. A, Vol. 2, John Wiley, New York, 1962, p. 218.

[17] F.S. Welcher, Organic Analytical Reagents, D. Van Nostrand, Princeton, NJ, 1948, p. 540.

[18] H. Shen, Z. Wang and G. Xu, Analyst, 112 (1987) 887.

[19] Y. Chen, G. Shanguan, N. Wang, Y. Chen, H. Wang and S. Zhang, Fenxi Huaxue, 20 (1992) 71 (Anal. Abstr., 54 (1992) 11H234).

Monitoring of molecular transformations in acid–base reactions by evolving factor analysis of Fourier transform infrared spectral data

Joaquim C.G. Esteves da Silva, Adélio A.S.C. Machado*, César J.S. Oliveira

LAQUIPAI, Chemistry Department, Faculdade de Ciências, P4050 Porto, Portugal

Received 26 September 1995; revised 5 February 1996; accepted 13 February 1996

Abstract

An evolving factor analysis procedure with concentration constraints (gradient concentration window) was applied to the analysis of data sets of aqueous Fourier transform infrared (FT-IR) spectra of carboxylic acids (acetic, malonic and succinic acids) collected in experiments with varying pH. Besides the calculation of the number of acid–base systems, this procedure allowed the calculation of the FT-IR spectra of the acid–base species present in equilibrium as well as the corresponding pK_a values.

Keywords: Acid–base properties; Aqueous FT-IR; Carboxylic acids; Evolving factor analysis

1. Introduction

The qualitative or quantitative analysis of species in aqueous solutions by Fourier transform infrared spectroscopy (FT-IR) with a suitable accessory, either a transmittance or an ATR-based cell, has received increased interest in recent years [1–14]. One of the most important aspects of FT-IR is that it allows the determination of the molecular status of the substances under examination [15–19]. Structural transformations can be easily investigated because a lot of information exists concerning infrared band assignment [19]. In contrast, quantitative aqueous FT-IR analysis

has been less frequently applied, probably because it usually implies complex situations involving one or more spectral sets, with each spectrum constituted of a large number of bands, some of which are often overlapping. Moreover, only in rare instances have chemometric techniques such as multivariate calibration and self-modeling curve resolution been applied to quantitative aqueous FT-IR analysis [4,20].

A previous study [13] showed the potential of FT-IR for the analysis of the molecular transformations that occur in acid–base aqueous reactions, when coupled to chemometric methods of principal component analysis (PCA) to treat sets of spectra obtained at variable pH. However, the spectral information was not fully explored and

* Corresponding author.

Table 1
Parameters of gaussian curves used as a basic set for the simulation of spectra

Species	Position	Width	Height
Sim1 (0.2 M monoprotic acid with $pK_a = 4.5$)			
Constant	1.50	1.0	0.3
	1.32	0.02	0.15
AH	1.20	0.02	0.3
A$^-$	1.56	0.02	0.5
	1.42	0.02	0.3
	1.35	0.015	0.2
Sim2 (0.2 M diprotic acid with $pK_{a1} = 2.8$ and $pK_{a2} = 4.5$)			
Constant	1.50	1.0	0.3
	1.40	0.03	0.09
AH$_2$	1.33	0.02	0.2
	1.30	0.02	0.15
	1.22	0.02	0.1
AH$^-$	1.55	0.015	0.5
	1.37	0.01	0.3
A^{2-}	1.55	0.015	1.0
	1.37	0.01	0.6
	1.26	0.01	0.1

only the number of components was calculated by PCA. Indeed, the IR spectra of the detected components contain the most useful information about the structural transformation induced by the experimental factor variation, in this case the pH, and thus deserve further exploration.

A procedure for the transformation of the abstract information obtained from the PCA of synchronous fluorescence (SyF) spectral data collected as a function of the pH was developed recently [21]. It is based on evolving factor analysis (EFA) with concentration constraints (EFA with a gradient concentration window, GCW) and allows the characterization (spectral data and acid–base properties) of the acid–base systems in the data set under analysis. Contrary to IR spectroscopy, little information exists about band assignment in SyF spectroscopy, due to both the restricted application of this technique and the more complex correlation of fluorescence spectra characteristics with molecular parameters. This limitation reduces the utility of the calculated SyF spectra in absolute terms, al-
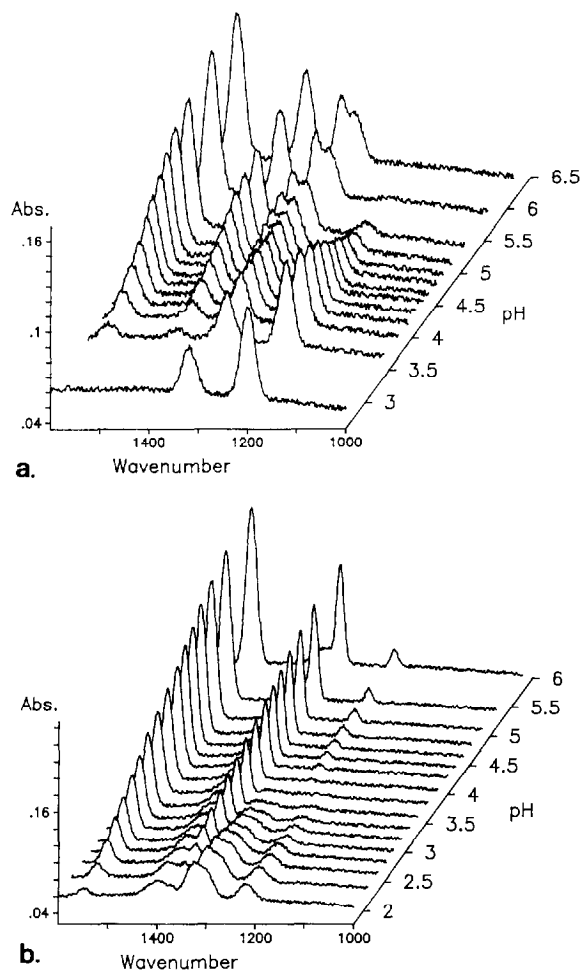
Fig. 1. Simulated FT-IR spectra as function of pH: (a) Sim1; (b) Sim2.

though they proved to be very adequate for comparative studies [21–24].

This paper reports further studies of the spectroscopic analysis of systems in chemical equilibrium, more precisely the application of EFA with a GCW to sets of FT-IR spectra of aqueous solutions of carboxylic acids, collected at varying pH. The objectives of the present study were: (i) to evaluate the application of relatively simple chemometric data analysis (PCA and EFA) to quantitative FT-IR; (ii) to study the application of EFA with a GCW for the analysis of aqueous FT-IR data, particularly for the calculation of the spectral data of the components of mixtures; and (iii) to develop in
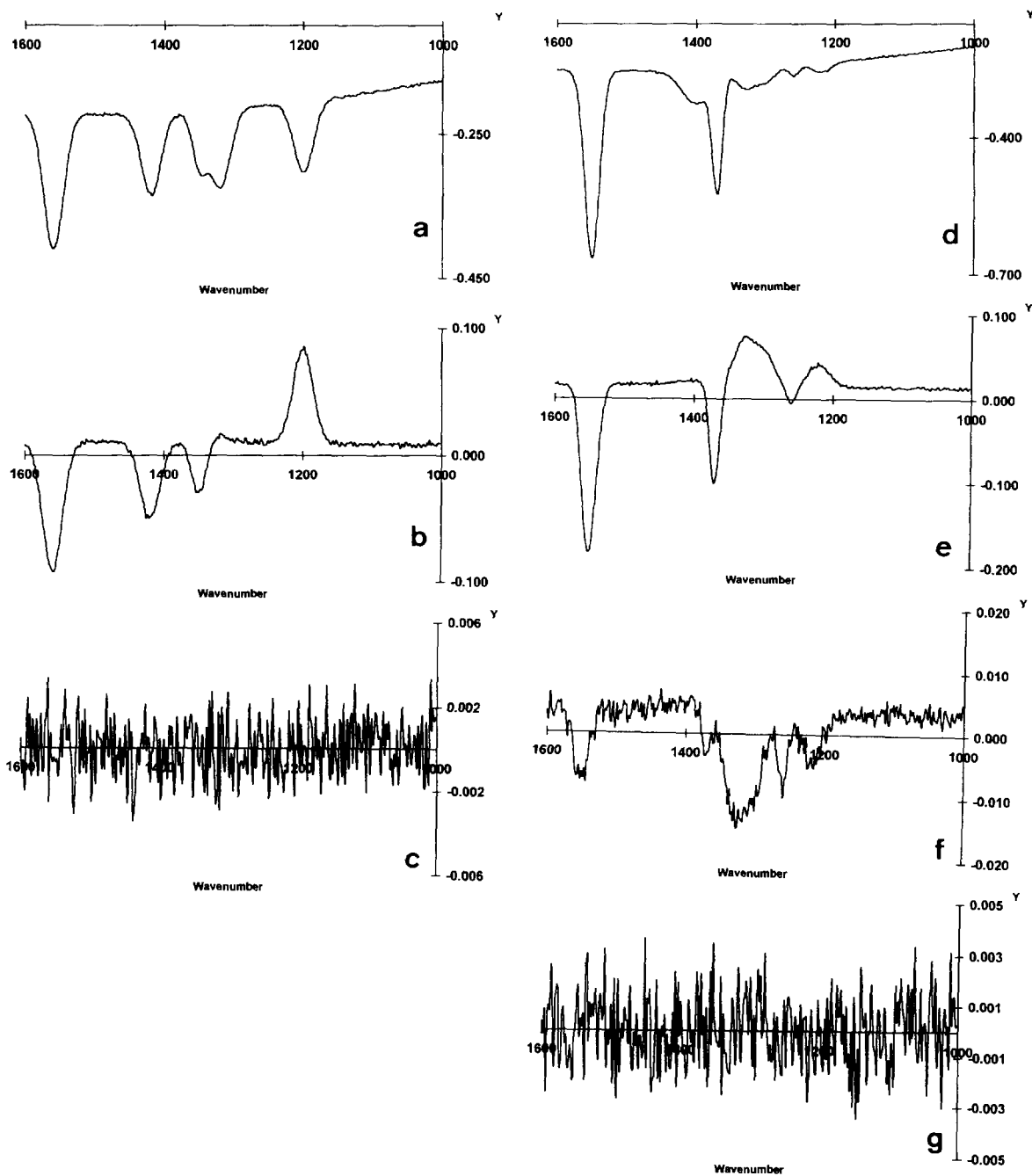
Fig. 2. Calculated FT-IR abstract spectra: (a)–(c) Sim1; (d)–(g) Sim2 data set.

more depth our previous study [13] of the FT-IR characterization of the protolysis of carboxylic acids in aqueous solutions. An improved experimental methodology was used, based on a flow

accessory (circle cell), to obtain better quality data as a consequence of reduced sample manipulation.

Three carboxylic acids were selected for the present study: a monoprotic acid (acetic acid); a

Table 2
Eigenvalues analysis of the simulated data sets[a]

i	EV	%V	RE	IE	XE	Ind
		Sim1 (pH: 2.6, 6.0]; 13 spectra)[b]				
1	19.253	98.664	0.00834	0.00231	0.00802	5.79×10^{-5}
2	0.2561	1.313	0.00115	0.00045	0.00106	9.53×10^{-6}
3	0.0005	0.003	0.00114	0.00055	0.00100	1.14×10^{-5}
4	0.0005	0.003	0.00112	0.00062	0.00093	1.38×10^{-5}
		Sim2 (pH: [1,8, 6.0]; 17 spectra)[b]				
1	26.2507	97.780	0.01089	0.00264	0.01056	4.25×10^{-5}
2	0.5782	2.154	0.00168	0.00058	0.00158	7.49×10^{-6}
3	0.0076	0.028	0.00114	0.00048	0.00103	5.81×10^{-6}
4	0.0006	0.002	0.00112	0.00054	0.00098	6.63×10^{-6}
5	0.0005	0.002	0.00111	0.00060	0.00092	7.68×10^{-6}

[a] i, number of eigenvalues; EV, eigenvalue; %V, percentage of variance of each EV; RE, real error; IE, imbedded error, XE, extracted error; Ind, factor indicator function.
[b] [...], pH interval; and number of spectra used in calculations.

diprotic acid with two well separated pK_a s values (malonic acid) and a diprotic acid with two very similar pK_a s values (succinic acid). Two simulated data sets were also generated to assess the data analysis procedure with respect to the information provided for interpretation of the calculated spectra of the components.

2. Experimental

2.1. Simulated FT-IR spectra

FT-IR spectra were simulated by adding gaussian curves according to two schemes (Table 1):

Table 3
Evolution of the SSR as a function of the number of iterations (n) of the secondary EFA

n	Sim1	Sim2	Acid		
			Acetic	Malonic	Succinic
1	0.14651	0.10339	0.86648	1.12506	0.80606
2	0.00473	0.01397	0.00183	0.00555	0.05043
3	0.00472	0.00593	0.00181	0.00423	0.03038
4	0.00472	0.00584	0.00181	0.00362	0.02117
10	0.00470	0.00584	0.00179	0.00282	0.00990
20	0.00470	0.00584	0.00179	0.00281	0.00910
30				0.00281	0.00907

Sim1, monoprotic acid; Sim2, diprotic acid. Different spectral characteristics were considered in the design of these sets: in Sim1, a monoprotic acid model, different sets of bands correspond to the acid and conjugated species; in Sim2, a diprotic acid model, besides different bands, the species AH^- and A^{2-} show two superimposed bands, at 1.55 and 1.37, although with different intensities. Moreover, both sets are constituted of some bands that do not vary with pH ("constant" in Table 1). These characteristics have been observed in experimental data sets, as discussed below.

2.2. Reagents

Analytical-grade reagents were used for the preparation of 0.2 M solutions of the acids in 1.0 M sodium chloride.

2.3. Experimental titrations

Potentiometric titrations with pH measurement were conducted with a PC-controlled system assembled from a Crison MicropH 2002 pHmeter, a Crison MicroBU 2030 microburette, an Ingold U262-S7/120 pH electrode and an Ingold 373-90-WTE-ISE-S7/105-120 reference electrode. The experiments were made under
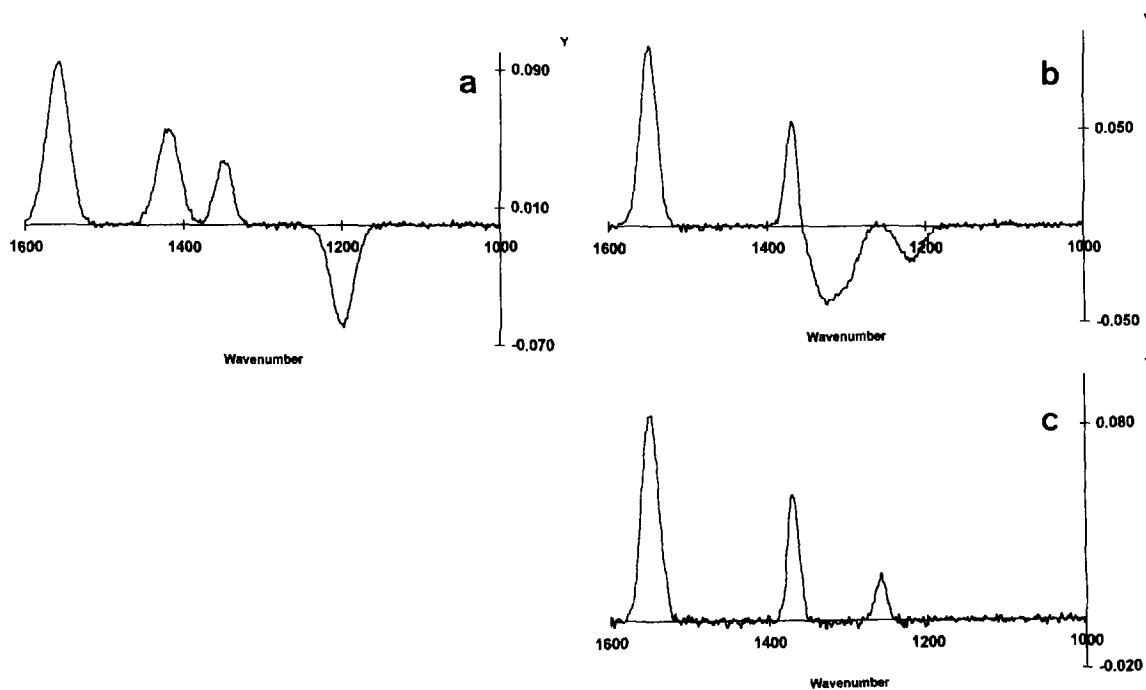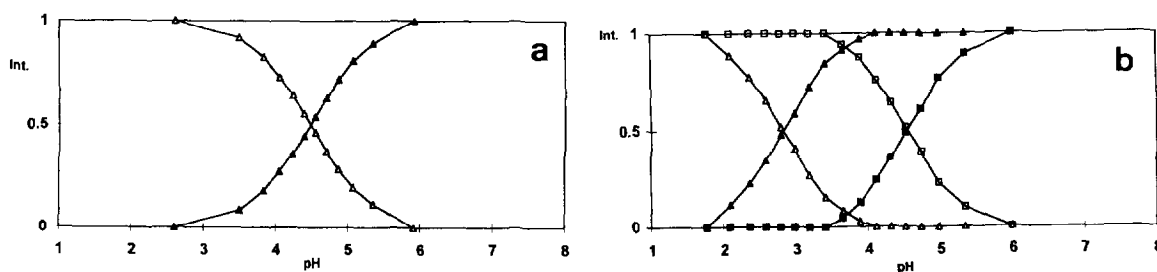
Fig. 3 (A)

Fig. 3 (B)

Fig. 3. EFA solution for the simulated data sets: (A) FT-IR spectra of the varying components (positive and negative bands correspond respectively, to the conjugated base and acid species); (B) acid–base distribution diagrams (triangles and squares represent the first and second acid–base systems respectively; filled and open symbols represent the conjugated base and acid species respectively).

nitrogen at $25.0 \pm 0.2°C$. The cell was calibrated by titrating 25.00 ml of 1.0 M sodium chloride with a standard solution of 0.1 M nitric acid (Titrisol Merck).

FT-IR spectra were recorded on a Nicolet Model 550 Magna operating in the mid-infrared range with a DTGS detector. The spectra were recorded in the 3000–800 cm^{-1} range with a 4 cm^{-1} resolution. 200 scans were accumulated.

A Spectra-Tech micro-flow circle cell with a ZnSe crystal was used as sampling accessory, with a Gilson Minipuls 2 peristaltic pump to force the displacement of the sample to the flow cell.

All the spectra were obtained using a solution of 1.0 M sodium chloride as background. Spectral data were stored on disk and converted to ASCII format with LABCALC software (Galactic

Industries Co., USA). In the data analysis, reduced spectra in the range 1600–1000 cm^{-1}, constituted of 312 points, were used.

2.4. Programs and data treatment

Titrations were simulated with a generic program for the simulation of potentiometric titrations in which the Newton–Raphson method is used for solving mass balance equations. At each pH value, the FT-IR spectrum was obtained by addition of the contributions of the acid and conjugated base species present. Simulated spectra were constituted of 312 points in the 1600–1000 cm^{-1} range.

For PCA and EFA, the covariance about the origin and the corresponding error functions [13,21,25] were used: RE, real error; IE, imbedded error; XE, extracted error; and Ind, factor indicator.

All software developed in this laboratory was written and compiled with Turbo Pascal 5.0 (Borland International, USA). An IBM AT-compatible computer with math coprocessor was used for calculations.

3. Theory

The calculation procedure for the EFA with a GCW has already been described previously [21] and only a brief summary will be given here.

3.1. PCA and EFA plots

The number of components (nc) is calculated by PCA [13,21,25] or its graphical representation as EFA plots (logarithm of the eigenvalues as a function of the number of spectra included in the calculations) [13,21,25,26] or from the analysis of the abstract spectra sets resulting from PCA. The first component corresponds to a constant spectrum and each of the others corresponds to an acid–base system. The number of components is equal to one, corresponding to a constant section of the spectral data (the constant component), plus the number of components that show no linear relation (the varying components).
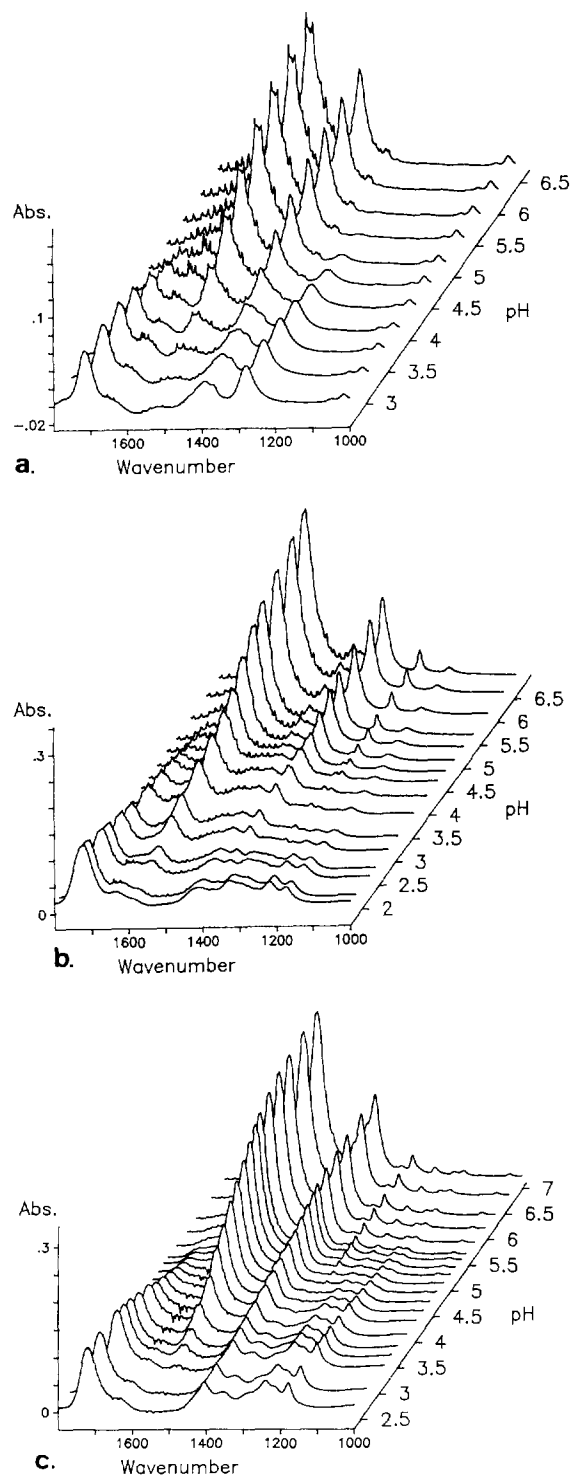

Fig. 4. Experimental FT-IR spectra as function of pH: (a) acetic acid; (b) malonic acid; (c) succinic acid.

The GCWs for the second to the nc components are determined from the analysis of the forward and backward EFA plots. Two discriminating matrices Ds and Dz (ns × nc, where ns is the number of spectra and nc is the number of components in the data matrix) with the GCW information are defined by a two-model design: model "S", the coefficients before the GCW are zero and those after the GCW are one; model "Z", the coefficients before the GCW are one and those after the GCW are zero; in both matrices, the elements of the first column are equal to one (this column corresponds to the constant component) and the value of the coefficient in the GCW is 0.5. The "S" model follows the increase in concentration of the conjugated base as the pH is raised and the "Z" model the corresponding decrease in concentration of the acid.

3.2. Evolving factor analysis (Secondary EFA)

The discriminating matrices Ds and Dz, defined above, are used as a first guess for the concentration matrix C (ns × nc). The calculation of the spectra of the components, or matrix S (nc × np), and their concentrations, consists of the following iterative procedure [21,26,27].

$$S = (C^T C)^{-1} C^T F \tag{1}$$

$$C = F S^T (S S^T)^{-1} \tag{2}$$

where F (ns × np) is the data matrix. The matrix C recalculated by this procedure is subjected to the following constraints:

$$\text{if} \quad D_{i,j} = 0 \text{ then } C_{i,j} = 0 \tag{3a}$$

$$D_{i,j} = 1 \text{ then } C_{i,j} = 1 \tag{3b}$$

$$C_{i,j} > 1 \text{ then } C_{i,j} = 1 \tag{3c}$$

$$C_{i,j} < 0 \text{ then } C_{i,j} = 0 \tag{3d}$$

with $i = 1...$nc and $j = 1...$ns. With the new C matrix, the procedure is repeated until convergence is achieved.

The quality of the iterative process is followed by the analysis of the sum of the squares of the residuals function (SSR):

$$\text{SSR} = \sum_{i=1,\text{ns}} \sum_{j=1,\text{np}} (F_{i,j} - F'_{i,j})^2 \tag{4}$$

where $F_{i,j}$ and $F'_{i,j}$ are the experimental and estimated data respectively.

Table 4
Eigenvalues analysis of the experimental data sets[a]

i	EV	%V	RE	IE	XE	Ind
Acetic acid (pH: [2.6, 7]; 11 spectra)						
1	3.9835	94.372	0.00873	0.00263	0.00832	8.73×10^{-5}
2	0.2369	5.612	0.00049	0.00021	0.00044	6.07×10^{-6}
3	0.0006	0.013	0.00022	0.00012	0.00019	3.51×10^{-6}
4	0.0001	0.002	0.00011	0.00006	0.00009	2.18×10^{-6}
Malonic acid (pH: [1.6, 7]; 18 spectra)						
1	17.420	92.222	0.01772	0.00443	0.01715	7.87×10^{-5}
2	1.2849	6.802	0.00649	0.00229	0.00607	3.31×10^{-5}
3	0.1835	0.972	0.00028	0.00012	0.00026	1.68×10^{-6}
4	0.0002	0.001	0.00022	0.00011	0.00019	1.50×10^{-6}
5	0.0001	0.001	0.00012	0.00007	0.00010	1.01×10^{-6}
Succinic acid (pH: [2.3, 8]; 20 spectra)						
1	20.393	94.998	0.01423	0.00335	0.01383	4.92×10^{-5}
2	1.0505	4.894	0.00215	0.00072	0.00203	8.42×10^{-6}
3	0.0212	0.099	0.00065	0.00027	0.00059	2.89×10^{-6}
4	0.0015	0.007	0.00033	0.00015	0.00029	1.68×10^{-6}
5	0.0003	0.001	0.00022	0.00012	0.00019	1.32×10^{-6}

[a] See footnotes in Table 2.

The two sets of spectra, as well as the concentration profiles calculated with models "S" and "Z", are analyzed as discussed in Ref. [21].

4. Results and discussion

4.1. Simulated data sets

Figs. 1(a) and 1(b) show the two simulated FT-IR spectra sets. Different variations and the

appearance and disappearance of bands are observed. The following procedure shows how the intrinsic underlying model of each data set can be calculated.

4.1.1. PCA, EFA plots and abstract spectra

The first objective in the spectral data analysis is the calculation of the number of components. In this study three methods were used: eigenvalues analysis, abstract spectra and EFA plots. Table 2 shows the results of the eigenvalues
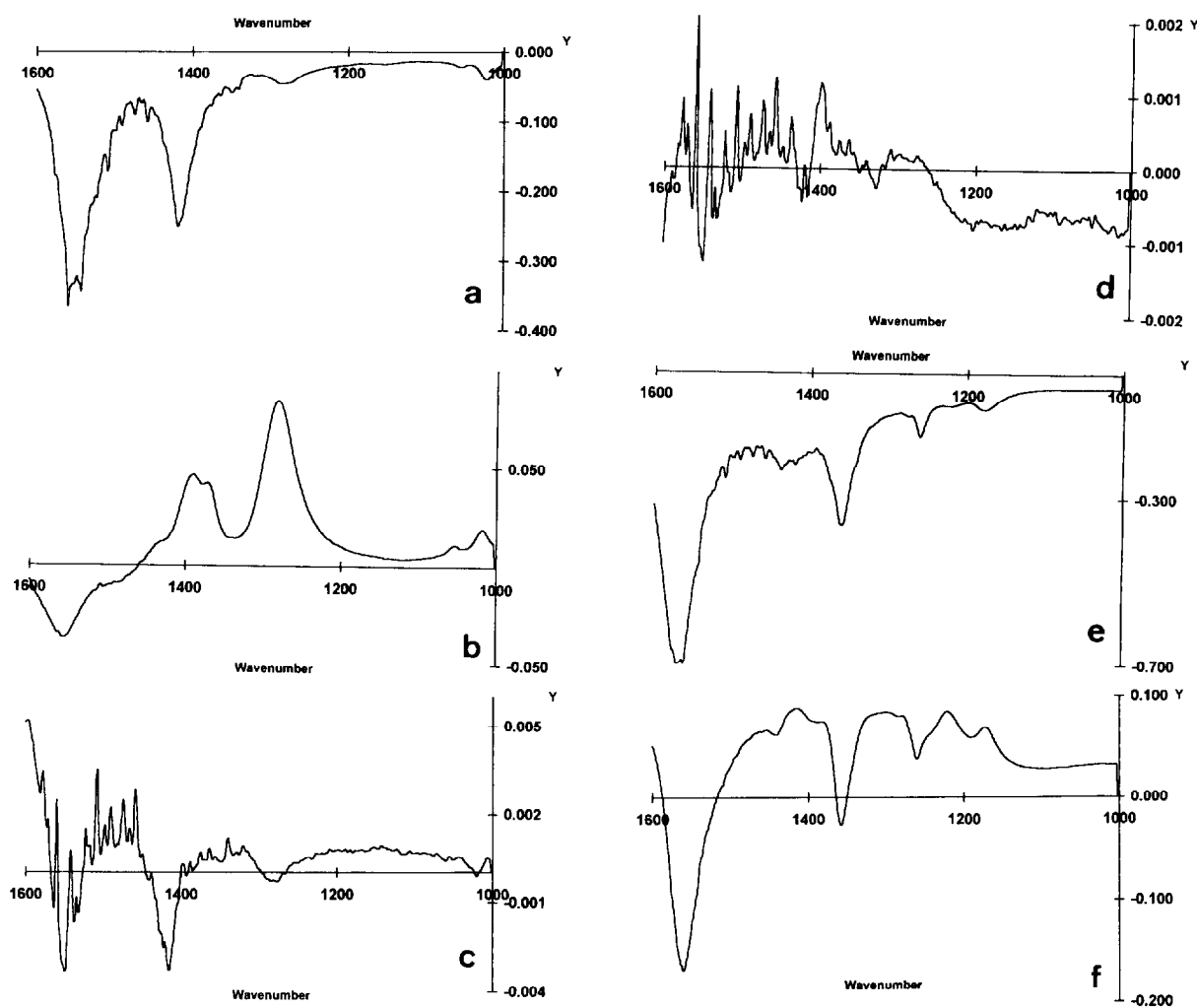

Fig. 5. Calculated FT-IR abstract spectra for (a–d) acetic acid and (e–i) malonic acid.
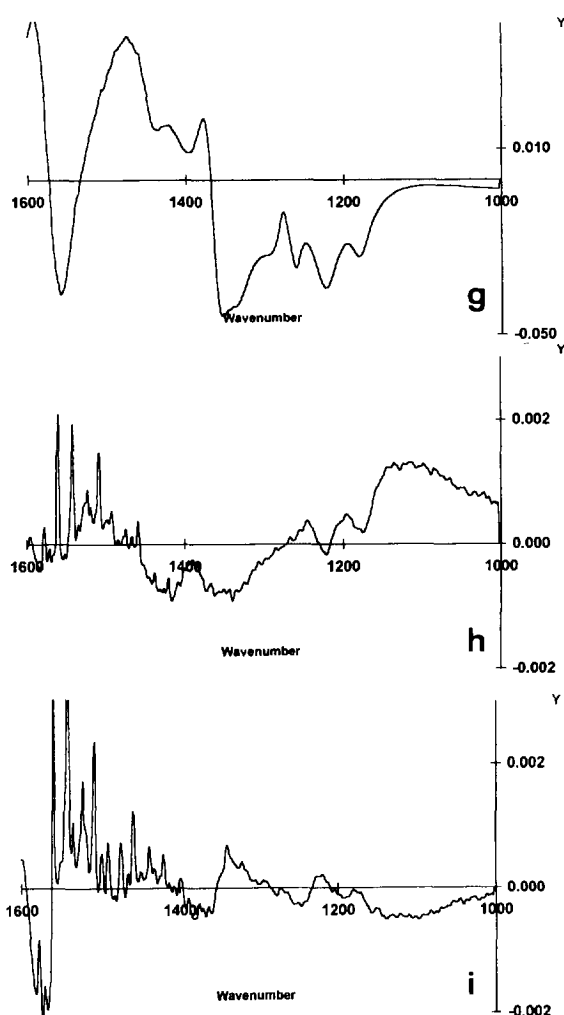
Fig. 5. (continued)

analysis and Fig. 2 shows the abstract spectra for the two simulated data sets. The shapes of the EFA plots are similar to those reported in Ref. [13].

From the values in Table 2, two and three components are found for the Sim1 and Sim2 data sets respectively, from the minima of the IE and Ind error functions and the stabilization of the RE and XE error functions. The EFA plots and the analysis of the abstract spectra of Fig. 2 gave the same information. Only the first two abstract spectra of Sim1 (Figs. 2(a) and 2(b)) and the first three abstract spectra of Sim2

(Figs. 2(d)–2(f)) contain signals. The next abstract spectra of both Sim1 (Fig. 2(c)) and Sim2 (Fig. 2(g)) contain only noise. The analysis of these noise spectra reveals that the random noise level is similar over the whole wavenumber range, as expected from the design of the simulations.

The number of components found for the two simulated data sets agrees with those expected [13]. Indeed, the number of components is equal to the number of acid–base systems plus one, corresponding to a constant background spectrum.

4.1.2. Secondary EFA

The information contained in the EFA plots was used to build the discrimination matrices [21] and the secondary EFA was performed. The iterative procedure converged quite rapidly (less than 20 iterations were required), as shown in Table 3.

The calculated spectra (using model "S") and concentration profiles for the varying components of the simulated data sets are shown in Fig. 3. The calculated spectrum for the constant component is not included because it contains no useful information about the bands that show variations upon change of pH.

The calculation spectrum for the Sim1 simulation (Fig. 3(A)a) is composed of three positive bands and one negative band. The positive bands correspond to the conjugated base (its concentration increases with pH) and the negative band to the acid. This result, as well as the positions and intensities of the bands, show perfect agreement with the data used to generate Sim1 (Table 1). The analysis of the calculated first spectrum of Sim2 (Fig. 3(A)b) allows the identification of both positive and negative bands, explained as for the corresponding spectrum of Sim1 (Fig. 3(A)a). In contrast, the calculated second spectrum of Sim2 (Fig. 3(A)c) shows only positive bands, namely those corresponding to the A^{2-} species, while the two bands of the AH^- species, which should be negative (similar to the positive bands of the first spectrum, Fig. 3(A)b), are not present. This is due to superposition of bands of AH^- and
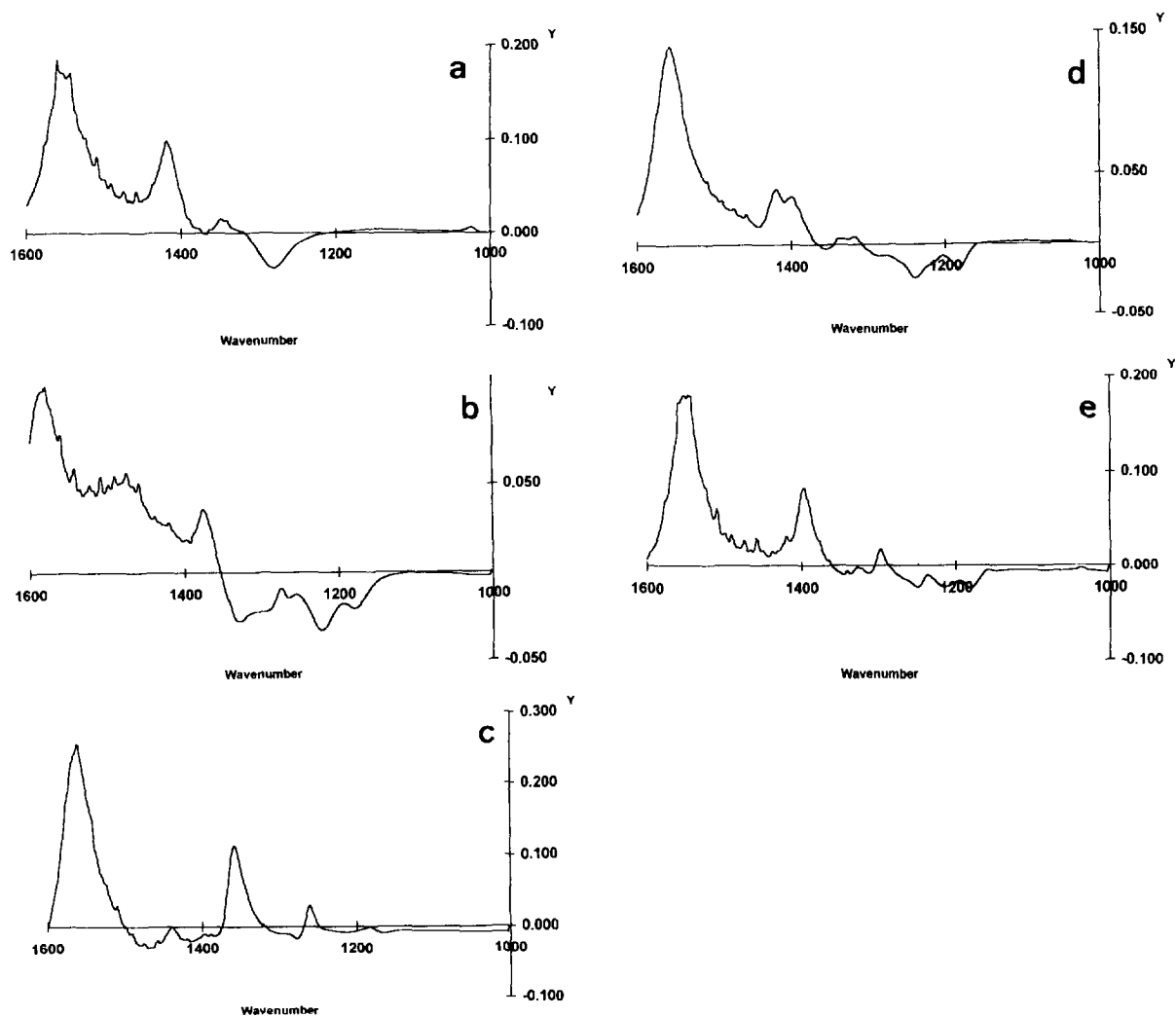
Fig. 6. Calculated FT-IR spectra of the varying components: (a) acetic acid; (b), (c) malonic acid; (d), (e) succinic acid. Positive and negative bands correspond to the conjugated base and acid species respectively.

A^2. Indeed, only the overall variation resulting from the two opposite variations (increase in the A^{2-} and decrease in the AH^- concentration) is recorded in the calculated spectrum.

The analysis of the spectra shown in Fig. 3(A), which correspond to the varying components, also reveals that the non-varying bands are not accounted for. This is expected, because these bands fall in the constant spectrum that corresponds to the first (constant) component. Indeed, the absence of contributions of non-varying bands is an important property of the

EFA, because it allows an easier identification of the spectral variations.

The analysis of the calculated concentration profiles, which correspond to the acid–base distribution diagrams, allows the calculation of the pK_a s values at the crossover points of the two curves corresponding to each acid–base system (at 50% ionization). Fig. 3(B)a,b shows that the calculated pK_a s values reproduce exactly those used to generate the simulated data, namely $pK_a = 4.5$ for Sim1 and $pK_{a1} = 2.8$ and $pK_{a2} = 4.5$ for Sim2.
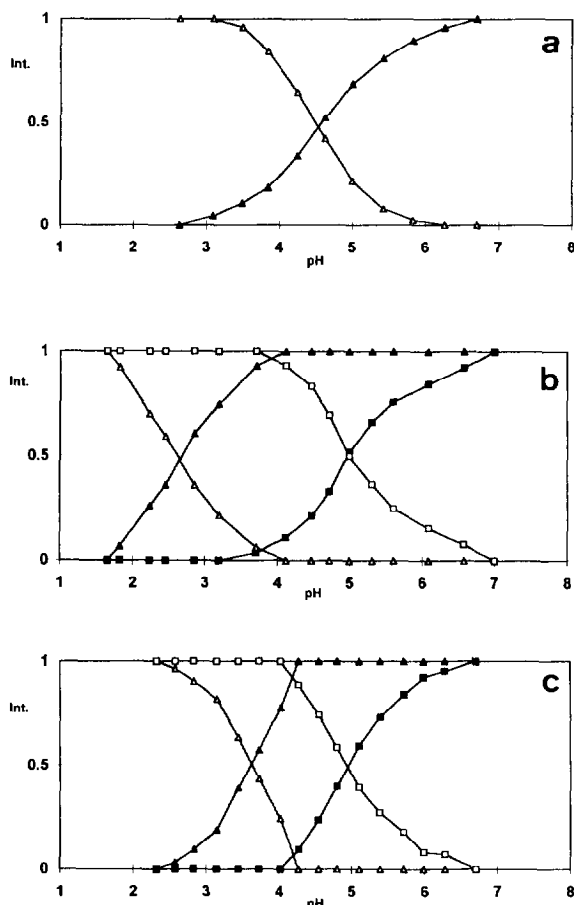
Fig. 7. Calculated acid–base distribution diagrams: (a) acetic acid; (b) malonic acid; (c) succinic acid. Triangles and squares represent the first and second acid–base systems respectively; filled and open symbols represent the conjugated base and acid species respectively.

In conclusion, the solution of the EFA with a GCW described rigorously the spectral variations of the two simulated data sets. The position and shape of the varying bands, as well as the type of variation with the changing factor, pH in the present case, were properly recovered. The concentration profiles of the species were also rigorously determined, which allowed the calculation of the pK_as values of the intrinsic acid–base systems.

4.2. Experimental data sets

Fig. 4 shows the FT-IR spectra of acetic, malonic and succinic acids as a function of pH in the 1800–1000 cm^{-1} range. Besides the existence of several bands displaying different variations with pH, a particularly high noise level is detectable around 1640 cm^{-1}. This is the position of the maximum of the FT-IR water spectrum and, because this noise causes variations in the data which are difficult to model, the 1800–1600 cm^{-1} wavenumber region was removed from all the spectra before data analysis.

4.2.1. PCA, EFA plots and abstract spectra

Table 4 shows typical results obtained from the eigenvalue analysis of the experimental data sets. The determination of the number of components is not as straightforward as that for the simulated data sets, particularly because the IE and Ind error functions show no minima. Nevertheless, from the analysis of the RE and XE error functions and from the variations of eigenvalue magnitude, the number of components is found to be two for acetic acid and three for the other two acids. Indeed, at these numbers of components, the RE and IE error functions stabilize their magnitudes and the eigenvalue that corresponds to the next component is much smaller than the previous one. These results are compatible with the EFA plots, as discussed previously [13], and with those found for the simulated data sets: the number of components in these data sets is also equal to the number of acid–base systems plus one.

The analysis of the abstract spectra, shown in Fig. 5 for acetic and malonic acids as examples, supports these conclusions about the number of components. Indeed, for the acetic acid only the first two abstract spectra (Figs. 5(a) and 5(b)) clearly contain signals, while the third and fourth (Figs. 5(c) and 5(d)) correspond to noise. For malonic acid, the first three abstract spectra (Figs. 5(e)–5(g)) contain information, but the following (Figs. 5(h) and 5(i)) correspond to noise. However, the type of noise present in the experimental sets is markedly different from that

Table 5
Characteristics of the calculated FT-IR spectra of the acid–base species calculated with model "S"[a]

Acid	N	Sp	Positive bands			Sp	Negative bands				
			1	2	3		1	2	3	4	5
Acetic	1	A⁻	1553	1419		AH	1280				
Malonic	1	AH⁻	1581	1480	1374	AH₂	1330	1299	1264	1220	1177
	2	A²⁻	1561	1357	1259	AH⁻	1470				
Succinic	1	AH⁻	1560	1420	1410	AH₂	1239	1180			
	2	A²⁻	1552	1397	1297	AH⁻	1248	1212	1179		

[a] Position of the bands in cm^{-1}; number of the acid-base systems; Sp, acid-base species.

in the simulated sets. Indeed, Figs. 5(c), 5(d), 5(h) and 5(i) reveal a higher level of noise in the 1600–1300 cm^{-1} range than for lower wavenumbers. This is due to the effect of the water band in these spectra.

4.2.2. Secondary EFA

The iterative procedure for the experimental data sets shows a pattern similar to that observed for the simulated data sets (see SRR function evolution as a function of the number of iterations in Table 3). The results of the secondary EFA, namely the spectra (calculated with model "S") and concentration profiles of the components, are shown in Figs. 6 and 7

Table 6
Comparison of the calculated pK_a s values with literature values[a]

Acid	Number of systems	pK_a	
		This work[b]	Literature
Acetic	1	4.5	4.55
Malonic	2	2.7	2.74
		5.0	5.11
Succinic	2	3.8	3.95
		5.0	5.05

[a] Literature values of 25°C and $I = 1.0$ M with the exception of acetic acid (20°C) and succiric acid ($I = 0.5$ M) [28,29]
[b] Precision of graphical estimate: ±0.1.

respectively. The main characteristics of the calculated FT-IR spectra are shown in Table 5.

The calculated spectra of the varying components show the following characteristics: (i) the existence of clear positive and negative bands (the positive are stronger than the negative) in the spectrum of the first varying component (which corresponds to the first acid–base system); and (ii) for malonic and succinic acids, the spectrum of the second varying component (second acid–base system) shows no clear negative bands. The existence of positive and negative bands is due to opposite concentration variations when the pH is increased, and consequent opposite variations for the bands corresponding to acid and conjugated base. The existence of closely spaced bands in narrow acid–base reaction, in the present case to the carboxylic and carboxylate groups. Constant bands, i.e. those corresponding to structures not involved in the reaction that is being monitored, are accounted for in the calculated constant component.

The calculated spectra of the AH (acetic acid) and AH₂ (malonic and succinic acids) acid species are composed of a main band in the range 1220–1280 cm^{-1}. This is due to the C–O stretching of the carboxylic structures, because its intensity decreases with the increase in pH for the three acids. Other neighboring bands, which are only clearly detected for malonic acid, are probably due to the C–O or C–C stretching vibrations.

The calculated spectra of the A⁻ (acetic acid) and A²⁻ (malonic and succinic acids) species

are composed of the following bands: a band in the range 1552–1561 cm^{-1} due to asymmetric COO$^-$ stretching; a band in the range 1357–1419 cm^{-1} due to symmetric COO$^-$ stretching; and, for the case of the diprotic acids, a third band in the range 1259–1297 cm^{-1}, which is probably due to $-CH_2-$ deformation. The comparison of these calculated infrared frequencies for the carboxylate stretchings with literature values, also obtained in aqueous solution [19], shows good agreement.

For the AH$^-$ species of malonic and succinic acids the analysis of the calculated spectra is complex and, as far as the authors know, there is no literature information available to allow a comparison.

The calculated concentration profiles shown in Fig. 7 are similar to those for the simulated data sets and allow the calculation of the pK_as values of the corresponding acid–base systems. These are presented in Table 6 together with literature values. An overall good agreement between calculated and literature values was found.

5. Conclusions

The results of the present study show that the application of EFA with a GCW to aqueous FT-IR spectroscopy can be a very useful technique because it provides data for elucidation of molecular transformations during chemical reactions and for calculation of equilibrium constants. Considering the vast amount of information contained in the literature about the assignment of IR bands and their correlation with molecular structure, the procedure is expected to be far-reaching for resolution of this type of problem.

The technique has the potential to be incorporated in software already available for instrument control. However, the analysis with EFA of FT-IR spectral sets collected during a chemical transformation requires specific constrictions (in the concentrations and/or spectra) adequate to the transformation that is being experimentally provoked.

References

[1] P.R. Griffiths and J.A. Haseth, Fourier Transform Infrared Spectrometry, Wiley, New York, 1986, Chapter 14.

[2] M. Clure, P.B. Roush, J.F. Williams and G.A. Lehmann, Am. Soc. Test. Mater., Spec. Tech. Publ., 934 (1987) 131.

[3] J.H. Hopkinson, C. Moustou, N. Reynolds and J.E. Newbery, Analyst, 112 (1987) 501.

[4] D.H. Haaland, Multivariate calibration methods applied to quantitative FT-IR analyses, in J.R. Ferraro and K. Krishnan (Eds.), Practical Fourier Transform Infrared Spectroscopy: Industrial and Laboratory Chemical Analysis, Academic Press, New York, 1990. Chapter 8.

[5] B.R. Singh and M.P. Fuller. Appl. Spectrosc., 45 (1991) 1017.

[6] N. Wellner and G. Zundel, J. Mol. Struct., 317 (1994) 249.

[7] A. Menikh and M. Fragata, J. Mol. Struct., 319 (1994) 101.

[8] A. Ahmed and H.A.T. Riahi, J. Mol. Struct., 319 (1994) 145.

[9] J.L. Kirsch, R.E. Zimmerman and L.G. Tensmeyer, Appl. Spectrosc., 48 (1994) 1150.

[10] F. Fu, D.B. DeOliveira, W.R. Trumble, H.K. Sarkar and B.R. Singh, Appl. Spectrosc., 48 (1994) 1432.

[11] G. Erik and R.J. Marie, Spectrochim. Acta, Part A. 50 (1994) 2137.

[12] J.M. Millot, N. Allam and M. Manfait, Anal. Chim. Acta. 295 (1994) 233.

[13] A.A.S.C. Machado and J.C.G. Esteves da Silva, Chemomet. Intell. Lab. Syst., 17 (1992) 249.

[14] P.R. Pike, P.A. Sworan and S.E. Cabaniss, Anal. Chim. Acta, 280 (1993) 253.

[15] K. Nakamoto, Y. Morimoto and A.E. Martell, J. Am. Chem. Soc., 84 (1962) 2081.

[16] K. Nakamoto, Y. Morimoto and A.E. Martell, J. Am. Chem. Soc., 85 (1963) 309.

[17] D.T. Sayer and J.T. Tackett, J. Am. Chem. Soc., 85 (1963) 314.

[18] M.K. Kim and A.E. Martell, J. Am. Chem. Soc., 85 (1963) 3080.

[19] K. Nakamoto, Infrared Spectra of Inorganic and Coordination Compounds, 2nd edn., Wiley, New York, 1970, pp. 220 224, 239–244.

[20] C.L. Putzig, M.A. Leugers, M.L. McKelvy, G.E. Mitchell, R.A. Nyquist, R.R. Papenfuss and L. Yurga, Anal. Chem., 66 (1994) 26R.

[21] A.A.S.C. Machado and J.C.G. Esteves da Silva, Chemomet. Intell. Lab. Syst., 19 (1993) 155.

[22] J.C.G. Esteves da Silva and A.A.S.C. Machado, Anal. Lett., 28 (1995) 2401.

[23] J.C.G. Esteves da Silva and A.A.S.C. Machado, Analyst, 120 (1995) 2553.

[24] J.C.G. Esteves da Silva, A.A.S.C. Machado and C.S.P.C.O. Silva, Anal. Chim. Acta, 318 (1996) 365.

[25] E.R. Malinowski and D.G. Howery, Factor Analysis in Chemistry, Wiley, New York, 1980.

[26] H. Gampp, M. Maeder, C.J. Meyer and A.D. Zuberbuhler, Talanta, 32 (1985) 1133.

[27] H. Gampp, M. Maeder, C.J. Meyer and A.D. Zuberbuhler, Talanta, 33 (1986) 943.

[28] L.G. Sillen and A.E. Martell, Stability Constants, The Chemical Society, London, 1964.

[29] L.G. Sillen and A.E. Martell, Stability Constants—Supplement No. 1, The Chemical Society, London, 1971.

Simultaneous determination of quinoline yellow and brilliant blue FCF in cosmetics by solid-phase spectrophotometry

L.F. Capitán-Vallvey, N. Navas Iglesias, I. de Orbe Payá, R. Avidad Castañeda*

Department of Analytical Chemistry, University of Granada, E-18071 Granada, Spain

Abstract

A method for the simultaneous determination of quinoline yellow (QY) and brilliant blue FCF (BB) in mixtures by solid-phase spectrophotometry has been developed. Both colorants were isolated in Sephadex DEAE A-25 gel showing maximum absorbances at 632 nm and 415 nm for BB and QY respectively. The applicable concentration ranges were between 25.0 and 500.0 μg l^{-1} for BB and between 50.0 and 750.0 μg l^{-1} for QY. The detection limits were 6.1 and 13.4 μg l^{-1} for BB and QY respectively. Application of the method to real samples (colognes, after shave lotions and shampoo gels) involves a previous extraction process of the colorants before their isolation on the gel.

Keywords: Cosmetics analysis; Quinoline yellow–brilliant blue FCF determination; Solid-phase spectrophotometry

1. Introduction

Quinoline yellow (CI 47005) and brilliant blue FCF (CI 42090) are two synthetic colorants widely used as additives in cosmetic products. In Spain, the use of quinoline yellow (QY) has been authorized provisionally without stating the maximum limit of concentration, while brilliant blue FCF (BB) can only be used up to 1% (w/w) in lipstick and up to 25 μg ml^{-1} in other cosmetics [1,2]. As the synthetic colorants can produce discomfort in susceptible individuals [3], quantitative analysis of these chemicals would be appreciated.

Traditionally, spectrophotometric methods have been used for these purpose if the sample only contains one colorant. When the sample contains two or more colorants (usually two or three), a previous separation step is needed. The separation can be carried out by thin layer chromatography (TLC) [4].

Electroanalytical techniques have been also proposed for the detection and determination of these compounds [5,6] and more recently derivative spectrophotometry and ratio spectra derivative [7] have also been suggested. However, the analysis of synthetic colorants in cosmetics is not very easy because the complex composition of most of the cosmetic products is often not pro-

* Corresponding author.

vided by the majority of manufacturers since they do not feel obliged to reveal what they consider as trade secrets.

We propose in this paper a sensitive method for the simultaneous determination of QY and BB either single or as a mixture in cosmetics by conventional and/or first-derivative spectrophotometry. In the case of real samples of shampoo gel a previous separation step of the colorants using methylene chloride is needed. Thus, the method is simple, sensitive, inexpensive and does not show the possible interferences caused by other additives usually present in cosmetics because of the previous extraction.

2. Experimental

2.1. Apparatus and software

A Perkin-Elmer Lambda-2 spectrophotometer (with 1 mm cell) connected to an IE 486 computer fitted with PECSS software and a Hewlett-Packard Laser III printer were used for all measurements. Statgraphics software package [8] was used for the statistical analysis of the calibration graphs. Smoothed and derivative spectra were calculated by the Savitzky and Golay method [9,10].

Further, we used a Crison 501 digital pH meter with a combined glass–saturated calomel electrode and an Agitaser 2000 rotating bottles agitator.

2.2. Reagents

All reagents were of analytical reagent grade. Reverse osmosis quality water was used throughout.

Quinoline yellow stock solution (10.0 mg l^{-1}) (Aldrich Chemical Company Inc.) was prepared by exact weighing of the standard product and dissolution in water. This solution remains stable for at least one month. Solutions of lower concentration were obtained by dilution with water.

Brilliant blue FCF stock solution (10.0 mg l^{-1}) (Aldrich Chemical Company Inc.) was prepared in water by exact weighing of the standard, and

working solutions were obtained by dilution with water. The stock solution was stable for at least one month.

Buffer solutions of pH 4.0 were prepared from 0.1 M sodium acetate solution (Merck) and 0.1 M acetic acid (Merck).

Sephadex DEAE A-25 anion exchanger (Pharmacia Fine Chemicals) in the chloride form and without pretreatment was used as solid support.

2.3. Absorbance measurements

The absorbance spectra of the colorant–gel systems packed in a 1 mm cell were recorded against the blank between 400 and 800 nm at 20.0 ± 0.5°C and stored in a disk file. These spectra were smoothed with 13 experimental points and the first-derivative of the QY spectrum was calculated and recorded using 4 nm intervals. If the sample contained only one of the colorants the absorbance measurements of the gel beads containing the colorant were carried out (in a 1 mm cell) at 415 nm and 800 nm in the absorption spectrum for QY and at 632 nm and 800 nm for BB. The latter measurement (800 nm) is the range where only the gel absorb radiation. The net absorbance for the colorant–gel systems was obtained from $A_n = A_\lambda - A_{800}$ where A_λ is the absorbance at 415 nm or at 632 nm [11]. If the sample contained QY and BB, the first-derivative spectrum was used to determine QY and the zero-order spectrum was used for the determination of BB and then the measurements were carried out at 453 nm for QY, applying the "zero crossing" technique [12,13], and at 632 nm for BB.

2.4. Extraction process

In the analysis of real samples, a extraction process of the colorants must be carried out before doing the absorbance measurements. Namely, the sample amount was shaken after mixing it with an appropriate volume of methylene chloride. In accordance with Holló and Wieg [14], if the proportion of ethanol/water in the sample is smaller than 80/20 (v/v) and the methylene chloride volume is equal or higher that

4/5 parts of the volume of the sample, two phases are formed. Otherwise, only one-phase ethanol/water/methylene chloride is obtained. Working at the proportion of ethanol/water/methylene chloride above suggested, the hydroalcoholic phase formed contains the colorants while the organic phase contains the other additives present in the commercial products.

2.5. Procedure

Standards containing between 25.0 and 500.0 μg l^{-1} of BB and between 50.0 and 750.0 μg l^{-1} of QY were prepared as follows: in a 100 ml calibrated flask, an appropriate volume of standard solution and 5.0 ml 0.1 M acetic/acetate buffer solution (pH 4.0) was placed and made to the mark with water. The mixture was transferred into a 250 ml glass bottle and 50 mg of Sephadex DEAE A-25 gel was then added. After mechanical shaking for 10 min the gel beads were collected by filtration under suction and packed into a 1 mm cell together with a small volume of solution (0.2 ml) with the aid of a pipette. Blank solution containing all the reagents except the analyte was prepared in the same way as the sample. The absorbances (at $^1D_{453}$ and $^0D_{632}$) were measured against a 1 mm cell of reference packed with gel equilibrated with blank solution and the net absorbance was obtained as described under Section 2.3.

2.6. Procedure for real samples

To 10.0 ml of eau de cologne or 5.0 ml of after shave lotion in a 100 ml calibrated flask, 5.0 ml of 0.1 M acetic/acetate buffer solution (pH 4.0) was added and the solution was made to the mark with water. This solution was then transferred into a 250 ml glass bottle and treated as described under Section 2.5.

To analyze shampoo gel the following procedure was carried out: 50 ml of ethanol was added to 1 g of shampoo gel in a 100 ml calibrated flask, and water was added to make the solution to the mark. This solution was then transferred into a 250 ml separatory funnel and 80 ml of methylene chloride were added. The mixture was shaken for

1 min and the hydroalcoholic phase (containing the colorants) was then transferred into a 100 ml calibrated flask. A volume of 5.0 ml of 0.1 M acetic/acetate buffer solution (pH 4.0) were then added and made to the mark with water. The resulting solution was transferred into a 250 ml glass bottle and then treated as described under section 2.5. Previous to the determination of the colorants in commercial cosmetic samples, identification by TLC [4] was carried out.

3. Results and discussion

3.1. Spectral characteristics

Fig. 1 shows the absorption spectra of BB and QY isolated in Sephadex DEAE A-25 gel. As can be seen the absorption spectrum of BB shows two absorption bands between 400 and 440 nm and between 502 and 694 nm, whereas QY only shows an absorption band between 400 and 460 nm. This fact allows the determination of BB in the presence of QY at $\lambda = 632$ nm using the absorption spectra of the mixture, but does not allow the determination of QY in the presence of BB because at $\lambda = 415$ nm the absorption spectra of both colorants overlap considerably hindering the
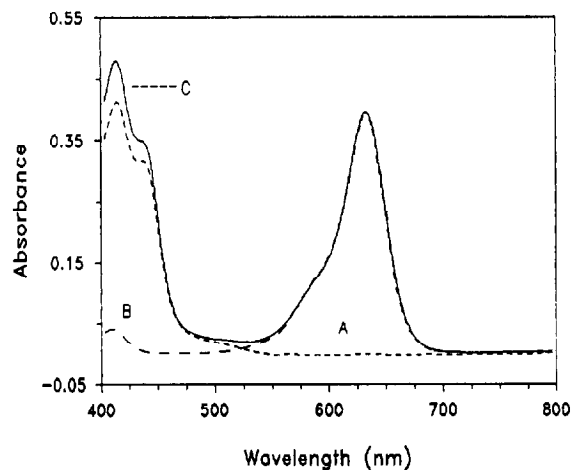

Fig. 1. Absorption spectra of (A) QY (500.0 μg l^{-1}); (B) BB (200.0 μg l^{-1}) and (C) a mixture of both compounds, in the same concentration levels, isolated in Sephadex DEAE A-25 gel in all cases.

Fig. 2. First-derivative absorption spectra of (A) QY (500.0 μg l^{-1}); (B) BB (200.0 μg l^{-1}) and (C) a mixture of both compounds, in the same concentration levels, isolated in Sephadex DEAE A-25 gel in all cases.
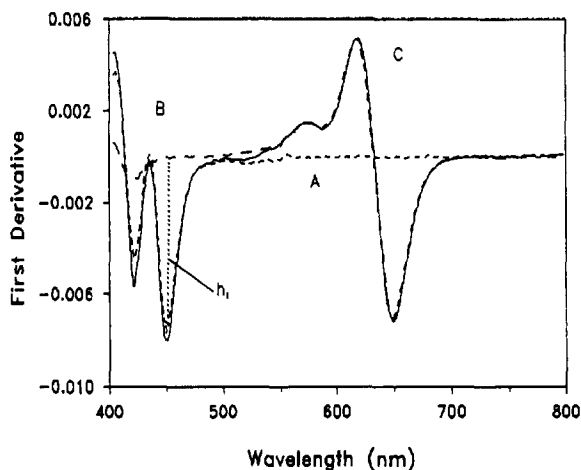

Fig. 3. Influence of the ethanol/water (v/v) proportion in the process. (A) BB (200.0 μg l^{-1}) and (B) QY (500.0 μg l^{-1}).

resolution of their mixtures by conventional spectrophotometry.

However, QY can be determined in the presence of BB using the first-derivative spectrum of the mixture of both chemicals and applying the above-mentioned "zero crossing" technique. It is assumed that the derivative of the spectral band is equivalent to the sum of the derivatives of its component bands. Therefore, the total derivative spectrum is only a function of the concentration of the other component when the first-derivative spectrum of one of the two components is zero. Fig. 2 shows that the height h_1 ($\lambda = 453$ nm) is only proportional to the QY concentration allowing its determination.

The two-phase extraction process allows not only the separation of the colorants but also avoids the interferences produced by other additives (fragrances, emulsifiers, etc.) usually present in cosmetic products. These additives show absorption bands in the same region as QY, which often hinders the use of conventional and derivative spectrophotometry for the determination of this colorant.

3.2. Experimental and instrumental parameters
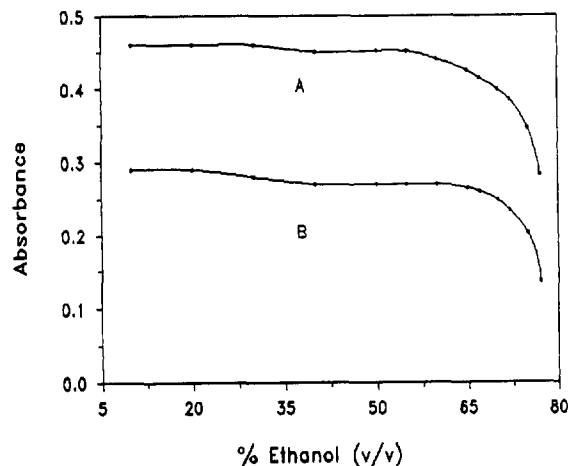
The absorbance measurements were practically

not affected by the experimental parameters, percentages of ethanol and/or amount of methylene chloride, but the extraction process was indeed affected by these parameters. Fig. 3 shows that for values of the percentage of ethanol/water higher that 70/30 (v/v) the absorbance of the system decreases noticeably. This fact can be attributed to the formation of one single-phase ethanol/water/methylene chloride as explained above. We

Table 1
Statistical calculations

Parameters[a]	BB	QY	
Signal measured	$^0D_{632}$	$^1D_{453}$	$^0D_{415}$
Intercept	$-5.89 \cdot 10^{-4}$	$-5.97 \cdot 10^{-4}$	$1.87 \cdot 10^{-2}$
Slope	$1.81 \cdot 10^{-3}$	$1.52 \cdot 10^{-5}$	$7.80 \cdot 10^{-4}$
P_{lof} (%)[b]	35.2	26.8	28.6
Linear dynamic range (μg l^{-1})	25.0–500.0	50.0–750.0	20.0–700.0
Detection limits (μg l^{-1})	6.1	13.4	5.8
Quantification limits (μg l^{-1})	20.3	44.5	16.2
Relative standard deviations (%)	1.8	2.2	1.9

[a] Data obtained for 100 ml sample volume.
[b] Probability level of the lack-of-fit test.

Table 2
Statistical calculations of BB (25.0–500.0 μg l^{-1}) and QY (50.0–750.0 μg l^{-1}) in mixtures

Compound determined	Other compound present	Concentration (μg l^{-1})	Slope (μg l^{-1})	Intercept
Brilliant	Quinoline	0.0	$1.81 \cdot 10^{-3}$	$-5.89 \cdot 10^{-4}$
blue FCF	yellow	50.0	$1.93 \cdot 10^{-3}$	$5.61 \cdot 10^{-4}$
		250.0	$1.91 \cdot 10^{-3}$	$4.75 \cdot 10^{-4}$
		750.0	$1.84 \cdot 10^{-3}$	$6.14 \cdot 10^{-4}$
Quinoline	Brilliant	0.0	$1.52 \cdot 10^{-5}$	$-5.97 \cdot 10^{-4}$
yellow	blue FCF	25.0	$1.54 \cdot 10^{-5}$	$1.40 \cdot 10^{-4}$
		200.0	$1.73 \cdot 10^{-5}$	$4.61 \cdot 10^{-4}$
		400.0	$1.53 \cdot 10^{-5}$	$2.61 \cdot 10^{-4}$

have selected 50/50 (v/v) ethanol/water as the working proportion. On the other hand, we found that the proportion CH_2Cl_2 (ethanol–water) must be 4/5 for the optimum extraction. One min was selected as a shaking time for the extraction process because we found that for times above 30 s the process was not influenced by this parameter.

In order to test the pH influence on the fixation of the colorants in the Sephadex DEAE A-25 gel different values of pH were studied using hydrochloric acid (1.0 M and 0.1 M) and sodium hydroxide (1.0 M and 0.1 M) solutions. At pH values lower than 2.9 the absorbance of the gel system (colorant–Sephadex DEAE A-25) decreases, probably due to the protonation of the sulfonic groups that hindered the fixation of QY and BB. For pH values between 2.9 and 10.0 the measurements of absorbance remained practically constant showing a maximum absorption at pH = 4.0. In this range of pH (between 2.9 and 10.0) the sulfonic groups remain unprotonated

Table 3
Determination of QY and BB in cosmetics

Cosmetic product	BB (μg l^{-1})[a] $^0D_{632}$	QY (μg l^{-1})[a] $^1D_{453}$	$^0D_{415}$	R.M.[a]
Cologne 1	306.0	653.0		
Cologne 2	np[b]	—	1725.0	1760.0
Shampoo gel	1943.0	30342.0		
After shave	8442.0	np		8400.0

[a] Data are the average of three independent determinations and are referred to the original real samples.
[b] Not present in this sample.

allowing fixation on the anionic gel. At pH values higher than 10.0 the OH$^-$ ions present in the solution compete with QY and BB reducing the absorbance of the solid phase. A pH 4.0 was selected as an optimum value for the fixation of the colorants on the Sephadex gel. Buffer solutions of acetate, monochloroacetate and hydrogen phthalate were tested for adjustment of the pH. Sodium acetate/acetic acid buffer solution (pH 4.0) was found to yield the best results.

Other experimental variables were the amount of gel (Sephadex) used, equilibration time, percentage of ethanol, ionic strength of the solution, scan speed, sample volume and speed of shaking. These variables could influence the fixation of the colorants on the solid support (Sephadex gel) and hence could affect the absorbance measurements. Ten min was selected as the equilibration time because longer times did not provided any improvement. The speed of shaking did not influence the results. We selected 80 rev min^{-1}. The ionic strength only influenced the results when the NaCl concentration was higher than 1.5 M.

The amount of solid support and sample volume of solution for the equilibration process with the Sephadex gel are however more critical. A mass of 50 mg was selected as the optimum amount of Sephadex gel because a large amount of the gel lowered the absorbance measurements. Consequently, only the amount required to fill the cell and facilitate handling (50 mg) was used in all the measurements. Increasing the sample volume of solution for equilibration with the Sephadex gel increases the sensitivity of the method. This effect can be assessed by measuring the absorbance of

Sephadex gel equilibrated with different volumes of solution containing the same concentration of colorants and proportional amounts of the other reagents. The experimental data show a linear dependence of the absorbance measurements on sample volume below 500 ml. However, we have taken a 100 ml sample volume because the sensitivity of the method in this case is high enough for the determination of the BB and QY in real samples.

3.3. Analytical parameters

The calibration graphs for standard samples treated according to the procedure above were linear for the concentration ranges between 50.0 and 750.0 μg l^{-1} for 100 ml of sample volume in the case of QY and between 25.0 and 500.0 μg l^{-1} for the same sample volume in the case of BB. The adjustment of these calibration graphs was carried out by the linear regression model. The lack-of-fit test [8], for three replicates, was applied to probe its linearity as suggested by the Analytical Methods Committee [15].

The repeatability of the method was determined as the relative standard deviation (RSD) for two series (one for QY and the other for BB) of ten independent determinations containing in the first, 500.0 μg l^{-1} of QY, and in the second, 300.0 μg l^{-1} of BB. In both cases 100 ml of sample volume were equilibrated with the solid support. The IUPAC detection limits [16,17] and the quantification limits [18] were also calculated in accordance with the equation:

$$L = \frac{ns_{b}}{m}$$

where L is the detection or quantification limit, s_{b} is the blank standard deviation, m is the slope of the calibration graph and $n = 3$ or $n = 10$ when the detection limit or quantification limit are calculated. These and other analytical parameters are summarized in Table 1.

4. Applications of the method

4.1. Synthetic mixtures

A recovery study was carried out in synthetic samples containing several amounts of BB and QY

in order to check the accuracy of the proposed method. Calibration graphs of one colorant with and without different amounts of the other colorant were constructed. The results obtained show that the slopes of these calibration graphs are similar and that the intercepts have no influence on the measurement of the analytical signals. The null hypothesis test (student's t-test, $p = 0.01$) was applied to the experimental data to prove these facts. We can conclude that the accuracy of the method is acceptable in all instances. The results obtained are summarized in Table 2.

4.2. Determination of QY and BB in real samples

Two colognes, one after shave lotion and one shampoo gel were selected as appropriate commercial products to apply the method in real samples. The cologne labeled 1 contains BB and QY, cologne, 2 only contains only QY, the shampoo gel contains QY and BB and the after shave lotion contains only BB. Samples were prepared and treated as described under Section 2.6. A previous identification by TLC of the colorants present in the samples was carried out.

For 100 ml sample volumes the average values found for three independent determinations agrees with the results obtained by the reference methods [19]. Table 3 shows the results obtained.

In conclusion, this method provides a practical application of first-derivative spectrophotometry in combination with solid-phase spectrophotometry to multi-component colorant analysis without the need of a previous separation.

References

[1] Publicaciones del Consejo General de Colegios Oficiales de Farmacéuticos. Cosmetología Teórico-Práctica, 3rd edn., 1985, 384.

[2] E. Bel Prieto and J.M. Suñe Arbussà, Ciencia Pharmaceutica, 2 (1992) 27.

[3] I. Suresh, Lecturer in Pharmacy, College of Pharmaceutical Sciences, Berhamzur, Orisa, Dec. 1990, 51.

[4] A. Senzel (Ed.), Newburger's Manual of Cosmetic Analysis, 2th edn., The Association of Official Analytical Chemist, Washington, 1977, 121.

[5] A.A. Barros, Analyst, 112 (1987) 1359.

[6] A.G. Fogg and D. Bhanot. Analyst, 112 (1987) 1319.

[7] J.J. Berzas Nevado, J. Rodríguez Flores and M.J. Villaseñor Llerena, Anal Lett., 27 (1994) 1009.

[8] Statgraphics V.6.0, Manugistics Inc. and Statistical Graphics Corporation, USA, 1992.

[9] A. Savitzky and M.J.E. Golay, Anal. Chem., 36 (1964) 1627.

[10] A. Savitzky, Y. Termonia and J. Deltour. Anal. Chem., 44 (1972) 1906.

[11] F. Capitán, L.F. Capitán-Vallvey. M.C. Valencia, J.M. Bosque, F. Molina and I. de Orbe, Analusis, 19 (1991) 177.

[12] B. Morelli, Analyst, 108 (1983) 870.

[13] B. Morelli, Analyst, 113 (1988) 1077.

[14] J. Holló and A. Wieg, Yearbook Inst. Agr. Chem. Technol. Univ. Tech. Sci., Budapest, Hungria, 1952 III and 1954 VII.

[15] Analytical Methods Committee, The Royal Society of Chemistry, Analyst, 119 (1994) 2363.

[16] IUPAC, Nomenclature, Pure Appl. Chem., 45 (1976) 105; Spectrochim. Acta, 33B (1978) 242.

[17] Analytical Method Committee, Analyst, 112 (1987) 199; 113 (1988) 1469.

[18] Guidelines for Data Acquisition and Data Quality Evaluation, Anal. Chem., 52 (1980) 2242.

[19] Official Methods of Analysis, J. Assoc. Off. Anal. Chem., 46 (1990) 1115.

Separation studies of molybdenum(VI) and rhenium(VII) using TPPO as an extractant

Santosh V. Vartak, Vijay M. Shinde*

Analytical Laboratory, Department of Chemistry. The Institute of Science, 15, Madam Cama Road, Bombay 400 032, India

Abstract

A simple, rapid and reproducible method for the extractive separation of molybdenum(VI) and rhenium(VII) is proposed using triphenylphosphine oxide (TPPO) dissolved in toluene as an extractant. The extractions are carried out from the hydrochloric and hydrobromic acid medium. The extraction of molybdenum is quantitative from 2.54–3.10 M hydrochloric acid and from 3.76–3.98 M hydrobromic acid, and that of rhenium is from 6.78 7.91 M hydrochloric acid. The probable nature of the extractable species is established using log distribution ratio–log concentration plots. The method permits mutual separation of molybdenum(VI) and rhenium(VII) and is applicable for the analysis of alloys and pharmaceutical sample. The detection limits for molybdenum(VI) and rhenium(VII) are 0.8 ppm and 4 ppm respectively.

1. Introduction

Molybdenum is an important trace element in nature, required by both plants and animals in very small amounts. It has a large number of applications in various fields. It is used in radios, thermocouples, anticathodes of X-ray tubes and in the production of special steels. Molybdenum is a major product of uranium fission. Rhenium is a trace metal and used largely in high temperature filaments and in petroleum refineries as a catalyst. A Re–Mo alloy is reported to be superconducting

at 10 K. In view of these applications both elements are required in pure form. In this communication we propose a simple method for extractive separation and determination of molybdenum(VI) and rhenium(VII), using triphenylphosphine oxide (TPPO) as an extractant.

Potassium ethyl xanthate [1], diethyldithio carbamate [2,3], 1-10 phenanthroline [4], mesityloxide [5], diisopropylether [6], bis(2-ethylhexyl)phosphate [7], bis(2-ethylhexyl)hydrogenphosphate [8], tributylphosphate [9,10], tris(2-ethylhexyl) phosphate [11], OOS-tripropylphosphorodithioate [12], cyanex 301 [13,14], and alamine 310 [15] are the reported extractants for molybdenum while

---

* Corresponding author.

Table 1
Optimum extraction conditions for molybdenum(VI) and rhenium(VII)

Metal ion	Halide concentration/ total volume	[TPPO]/diluent	Extraction period (s)	Stripping solution	Estimation procedure
Mo(VI), 20 μg	2.54–3.10 M HCl and 3.76–3.98 M HBr/10 ml	5 ml of 6% TPPO/toluene	60	2 × 5 ml water	Thiocyanate [28]
Re(VII), 100 μg	6.78–7.91 M HCl/10 ml	5 ml of 6% TPPO/tolune	120	2 × 5 ml water	Thiocyanate [29]

α-benzoin oxime [16], tri-n-octylamine [17,18], cyclohexanone [19], ethylxanthate [20], mesityl oxide [21], tributylphosphate [22,23], trioctylphosphine oxide [24] and aliquat 336 [25] are the reported extractants for rhenium. These methods, however, have limitations such as interference by other ions [1,3–5,7,12], longer extraction periods [2,5,13–16,22], use of salting out agents [5,10,19,21], multiple extraction [3,4,23], critical pH [8,18,25], higher acidic conditions [11,12], milligram amounts of metal used [9], visual comparison for determination [6] and highly acidic stripping agents [17]. The proposed method is free from all these drawbacks and has the following advantages.

1. Extraction occurs in a single step and recoveries of the elements are > 99.0%.
2. It provides mutual separation of molybdenum(VI) and rhenium(VII).
3. The method is applicable for the analysis of alloys and pharmaceutical samples.
4. The method is rapid, reproducible, accurate and free from interference due to commonly associated elements.

2. Experimental

2.1. Apparatus

The absorbance measurements were taken on a Shimadzu UV-VIS 160A spectrophotometer (Shimadzu Corporation, Japan).

2.2. Reagents and chemicals

The stock solutions of molybdenum(VI) and rhenium(VII) were prepared by dissolving 0.046 g of ammonium molybdate in 250 ml distilled water and 0.155 g of potassium perrhenate in 100 ml of distilled water (containing 5 ml of 6 N H_2SO_4), respectively. Solutions of lower concentrations were obtained by dilution and were standardised by standard methods [26,27]. TPPO (Fluka grade) dissolved in toluene was used for extraction and separation of molybdenum(VI) and rhenium(VII).

All other chemicals used were of analytical reagent grade.

2.3. General extraction procedure for molybdenum(VI) and rhenium(VII)

To an aliquot of a solution containing 20 μg of molybdenum(VI) and 100 μg of rhenium(VII), hydrochloric acid was added to obtain 2.54 M and 6.78 M solutions, respectively, in a total volume of 10 ml. The aqueous solution was then equilibrated for 60 s with 5 ml of 6% TPPO dissolved in toluene for molybdenum(VI). For rhenium(VII), the acqueous solution was equilibrated with 5 ml of 6% TPPO dissolved in toluene for 120 s. After stripping with 2 × 5 ml of water both of the elements were determined spectrophotometrically with the thiocyanate method [28,29] as follows. For rhenium(VII), 2 ml of concentrated hydrochloric acid, 1 ml of 20% potassium thiocyanate solution and 2 ml of 35% stannous chloride solution were mixed together and allowed to stand for 5 min. The absorbance at 430 nm was measured against a reagent blank prepared analogously. For molybdenum(VI), 2 ml of concentrated hydrochloric acid, 1 ml of 10% ferrous ammonium sulfate solution, 3 ml of 10% potassium thiocyanate solution and 3 ml of 10%
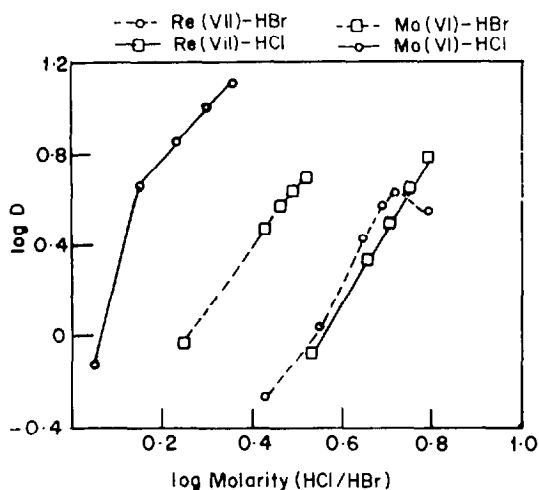
Fig. 1. Extraction of Mo(VI) and Re(VII) as a function of HCl and HBr concentration.

stannous chloride solution were mixed together and the absorbance was measured after 5 min at 465 nm against a reagent blank prepared analogously. The molybdenum and rhenium contents were computed from earlier drawn calibration plots. The optimum extraction conditions are given in Table 1.

3. Results and discussion

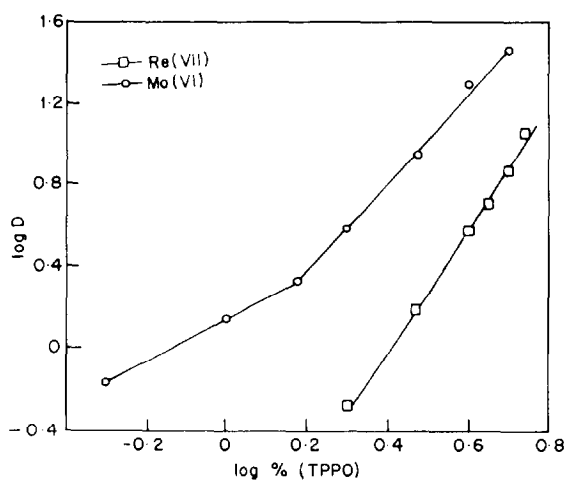In order to ascertain the optimum concentra-

Fig. 2. Extraction of Mo(VI) ane Re(VII) in HCl as a function of TPPO concentration.

tion of acid (HCl/HBr) and TPPO (using toluene as diluent) for the quantitative extraction of molybdenum(VI) and rhenium(VII), the extraction studies were carried out at various concentrations of hydrochloric acid (1.13–7.91 M) and hydrobromic acid (1.77–6.2 M) with different concentrations of TPPO (0.5–6.0%). The quantitative extraction of rhenium(VII) occurred with 5 ml of 6% TPPO dissolved in toluene at 6.78–7.91 M hydrochloric acid solution whereas from hydrobromic acid solution its extraction was incomplete. The quantitative extraction of molybdenum(VI) from 2.54–3.10 M hydrochloric acid and

Table 2
Effect of foreign ions

Ion	Tolerance limit (μg)	
	Molybdenum(VI) (20 μg)	Rhenium(VII) (100 μg)
Ca(II)	10000	10000
Pb(II)	10000	10000
Mg(II)	10000	10000
Zn(II)	10000	10000
Cd(II)	10000	10000
Fe(III)	8700	10000
Ni(II)	5000	5000
Co(II)	5000	5000
Ba(II)	6000	7000
Hg(II)	4000	3000
Cu(II)	4000	4000
Bi(III)	3000	2000
Sb(III)	None	None
Mn(II)	3000	3000
Al(III)	3000	2500
V(V)	2500	1000
Ce(IV)	2500	1000
Te(IV)	None	None
Ti(IV)	2800	2000
W(VI)	1500	500
Sn(II)	1000	800
Cr(VI)	1800	1500
Ascorbate	3000	2500
Thiosulfate	3000	3000
Tartarate	5000	3000
EDTA	1000	1500
Thiourea	2000	2000
Citrate	5000	4000
SO_4^{2-}	5000	3000
NO_3^-	3000	3000
NO_2^-	3000	3000
PO_4^{3-}	3000	3000

3.76–3.98 M hydrobromic acid was feasible with 5 ml of 6% TPPO in toulene.

The effect of various diluents such as toluene, xylene, benzene, chloroform and carbon tetrachloride on the extraction of both molybdenum(VI) and rhenium(VII) was investigated using the proposed method. A 6% solution of TPPO in toluene provided quantitative extraction of molybdenum and rhenium. The extraction, however, was incomplete with other diluents.

While prolonged shaking had no adverse effect on the extraction of molybdenum(VI) and rhenium(VII), a shaking period of 60 s for molybdenun(VI) and of 120 s for rhenium(VII) was adequate for the quantitative extraction.

3.1. Nature of extracted species

The nature of the extracted species was established using log–log plots of the distribution ratio versus TPPO concentration and hydrochloric acid concentration. The plot of the log of the distribution ratio versus the log of the hydrochloric acid concentration (at 6% TPPO in toluene) for molybdenum(VI) and rhenium(VII), gave slopes of 2.3 and 3.2, respectively. Similarly, a plot of the log

of the distribution ratio versus the log of the TPPO concentration at 2.54 M HCl for molybdenum(VI) and 6.78 M HCl for rhenium(VII), gave slopes of 2.1 and 3.3 for molybdenum(VI) and rhenium(VII), respectively. It indicates a metal to TPPO ratio of 1:3 for rhenium(VII). For molybdenum(VI), at lower TPPO concentration it was 1:1 and at higher TPPO concentration it was 1:2. Hence the probable extracted species were solvated salts of the type $MoO_2Cl_2 \cdot 2TPPO$ and $ReO_2Cl_3 \cdot 3TPPO$. TPPO, being more basic, supplanted the water molecules and rendered the species hydrophobic (Figs. 1 and 2).

3.2. Effect of foreign ions

To an aliquot of the solution containing a fixed amount of molybdenum (20 μg) and rhenium (100 μg), varying amounts of foreign ions were added to study their interference in the recommended procedure. The tolerance limit of the foreign ion was set at the amount required to cause $\pm 2\%$ error in the extraction and subsequent determination of molybdenum(VI) and rhenium(VII) by the proposed method. The results are reported in Table 2.

Table 3
Binary separations of molybdenum(VI) and rhenium(VII)

Composition of mixture	Recovery[a] of Mo(VI)/Re(VII) (%)	Relative error (%)	Recovery[a] of added ions (%)	Relative error (%)	Estimation procedure for added ions
Re(VII), 100 μg/ Mo(VI), 20 μg	MO(VI), 99.6	Mo(VI), 0.4	99.7	0.3	
Mn(II), 40 μg	Re(VII), 99.2	Re(VII), 0.8	99.2	0.8	Formaldoxime [31]
Re(VII), 100 μg Mo(VI), 20 μg	Mo(VI), 99.42	Mo(VI), 0.58	99.2	0.8	
Cu(II), 20 μg	Re(VII), 99.33	Re(VII), 0.67	99.2	0.8	PAR [30]
Re(VII), 100 μg Mo(VI), 20 μg	Mo(VI), 99.48	Mo(VI), 0.52	99.0	1.0	
Ti(IV), 50 μg	Re(VII), 99.37	Re(VII), 0.63	99.3	0.7	H_2O_2 [31]
Mo(VI), 20 μg U(VI), 50 μg	Mo(VI), 99.51	0.49	99.3	0.7	PAR [33]
Mo(VI), 20 μg V(V), 40 μg	Mo(VI), 99.42	0.58	99.51	0.49	PAR [32]
Mo(VI), 20 μg Re(VII), 100 μg	Mo(VI), 99.48	0.52	99.33	0.67	Thiocyanate [29]

[a] Average of triplicate analysis.

Table 4
Analysis of standard alloys and drug sample

Sample	Composition	Amount of Re/Mo expected	Amount of Re/Mo found[a]	Coefficient of variation, (%)
Alloys				
Mn–Mo steel	Mn, 1.61%; Cr, 0.09%;	1 mg Re	0.987 mg Re	0.86
BCS[b] 214/2	Mo, 0.26%; Ni, 0.15%;	0.26 mg Mo	0.256 mg Mo	0.78
	Cu, 0.21%; V, 0.01%;			
	+1 mg Re			
Ce–Zn–Zr	Zr. 0.56%; Mn, 0.006%;	1 mg Re	0.985 mg Re	1.21
BCS 307	Fe, 0.0021%; Zn, 2.08%;			
	Cu, 0.005%; Ni, 0.001%;			
	Total rare earths 2.84%;			
	+1 mg Re			
Nimonic 901	Ti, 2.95%; Al, 0.24%;	1.46 mg Mo	1.45 mg Mo	0.53
BCS 387	S, 0.003%; Cu, 0.032%;			
	C, 0.03%; Cr, 12.46%;			
	B, 0.016%; Pb, 0.008%;			
	Mn, 0.08%; Mo, 5.83%;			
	Co, 0.21%; P, 0.07%;			
	Ni, 41.9%; Fe, 36.0%;			
	Bi < 0.00003%;			
	Ag < 0.00002%			
Drug				
Rediplex	Folic acid IP, 5 mg;	3.18 mg Mo	3.153 Mo	0.31
(ESPI chemicals,	Vit. C, IP, 150 mg;			
India)	Vit. B6, IP, 3 mg;			
	Vit. B12, IP, 15 mg;			
	ferrous fumarate, IP, 308			
	mg;			
	cupric sulphate, USP, 0.2			
	mg;			
	molybdenum 3.18 mg			

[a] Average of triplicate analysis.
[b] British Chemical Standard.

3.3. Binary separation of molybdenum(VI) from rhenium(VII), copper(II), manganese(II), vanadium(V), titanium(IV) and uranium(VI)

Molybdenum(VI) and rhenium(VII) were separated by extracting molybdenum(VI) from 2.54 M hydrochloric acid solution with 5 ml of 6% TPPO dissolved in toulene. It was then stripped with water and determined by the thiocyanate method [28]. Rhenium (VII), under this condition, remained in the aqueous phase which was then determined by the thiocyanate method [29]. Copper (II), manganese(II), vanadium(V), titanium(IV) and uranium(VI) remained quantitatively in the aqueous phase at the optimum extraction conditions of molybdenum(VI) and were determined spectrophotometrically using 4-(2-pyridlazo)resorcinol [30], formaldoxime [31], 4-(2-pyridylazo) resorcinol [32], hydrogen peroxide [31] and 4-(2-pyridylazo) resorcinol [33]. The recoveries of molybdenum and that of the added ions were ≥ 99.0%. The results are reported in Table 3.

3.4. Binary separation of rhenium(VII) from molybdenum(VI), copper(II), manganese(II) and titanium(IV)

Separation of molybdenum(VI) and rhenium(VII) was discussed above. Rhenium(VII) was separated from titanium(IV) copper(II), and man-

ganese(II) as these ions remained quantitatively in the aqueous phase at the optimum extraction conditions of rhenium(VII). Copper(II), manganese(II) and titanium(IV) were then spectrophotometrically determined by 4-(2-pyridylazo)resorcinol [30], formaldoxime [31] and hydrogen peroxide [31], respectively. The results are reported in Table 3.

3.5. Analysis of alloys and pharmaceutical sample

A 100 mg alloy sample, Mn–Mo steel (BCS 214/2), was dissolved in aqua regia, followed by the addition of 5 ml perchloric acid. The solution was evaporated to dryness and diluted to 25 ml with distilled water after leaching up with distilled water. A mass of 25 mg of alloy Nimonic 901 (BCS 387) was dissolved in aqua regia, evaporated to dryness and diluted to 25 ml with distilled water. A mass of 100 mg of alloy Ce–Zn–Zr (BCS 307) was dissolved in concentrated hydrochloric acid and diluted to 25 ml with distilled water. Since we could not procure samples containing rhenium, a known quantity of rhenium was added to the standard alloy solutions BCS 214/2 and BCS 307. An aliquot from each alloy solution was than analysed by the proposed method. Rediplex tablet manufactured by ESPI chemicals, India, was dissolved in 10 ml of perchloric acid. The solution was evaporated to dryness and then the residue was leached up with distilled water, the solution was filtered and diluted to 100 ml with distilled water. An aliquot of Rediplex solution was then taken for the extraction and determination of molybdenum by the proposed method. The results are reported in Table 4.

References

[1] V. Yatirajam and R. Jaswaant. Talanta, 21 (1974) 439.
[2] W. Armin and B. Sixto, Anal. Chem., 47 (1975) 2.
[3] V. Bhaskara Sarma and M. Suryanarayana, Z. Anal. Chem., 240 (1968) 6.
[4] U. Dhingra and L.R. Kakkar, Analyst, 113 (1988) 675.
[5] V.M. Shinde and S.M. Khopkar, Indian J. Chem., 7 (1969) 504.
[6] G.S. Reddi and C.R.M. Rao, Anal. Chim. Acta., 244 (1991) 245.
[7] G.M. Vol'dman, A.N. Zelikman and I. Sh. Khutoreskaya, Izv. Vyssh. Ucheb. Zaved. Tsvet. Metall., 17 (1974) 97.
[8] N.R. Das, B. Nandi and S.N. Bhattacharya, Anal. Chim. Acta., 159 (1984) 255.
[9] G.M. Vol'dman. A.N. Zelikman and S.V. Shakhbazyan, Arm. Khim. Zh., 30 (1977) 33.
[10] S.C. Dhara and S.M. Khopkar, Indian J. Chem., 5 (1967) 12.
[11] A.D. Barve and V.M. Shinde, Indian J. Chem., 33A (1994) 1126.
[12] A.I. Busev and I.V. Radionova, Anal. Lett., 2 (1969) 9.
[13] P. Behera, R. Mishra and V. Chakravortty, J. Radioanal. Nucl. Chem., 173 (1993) 161.
[14] P. Behera, R. Mishra, I. Mohanti and V. Chandravortty, J. Radioanal. Nucl. Chem., 178 (1994) 179.
[15] P. Behera V. Chakravortty, Indian J. Chem., 32A (1993) 825.
[16] S. Khaira and L.R. Kakkar, Fresenius' Z. Anal. Chem., 335 (1989) 404.
[17] L. Karagozov and Kh. Vasilev, Hydrometallurgy, 4 (1979) 51.
[18] L.G. Anokhina and N.A. Agrinskaya, Trudy. Novocherk. Politekh. Inst., 289 (1974) 14.
[19] N. Iordanov, M. Pavlova and D. Boikova, Talanta, 23 (1976) 463.
[20] M. Elsie Donaldson and E. Mark, Talanta, 29 (1982) 663.
[21] V.M. Shinde and S.M. Khopkar, Anal. Chem., 43 (1971) 473.
[22] N. Iordanov and S. Mareva, C.r. Acad. Bulg. Sci., 19 (1966) 913.
[23] S.D. Karavaeva and A.K. Shokanov, Akad. Nauk. Kazak. SSR., 3 (1967) 92.
[24] N. Iordanov and M. Pavlova, Chemica. Analit., 17 (1972) 819.
[25] D.G. Baichler and C.H. Long, At. Absorpt. Newsl., 8 (1969) 56.
[26] A.I. Vogel, A Textbook of Quantitative Inorganic Analysis, 4th edn, Longman, London, 1978, p. 471.
[27] N. Howell Furman, (Ed.), Standard Methods of Chemical Analysis, 6th edn, Vol. 1, Van Nostrand Reinhold Co., p. 918.
[28] A.I. Vogel, A Textbool of Quantitative Inorganic Chemistry, 3rd edn, Longman, London, 1961, p. 903.
[29] E.B. Sandell, Colorimetric Determination of Traces of Metals, Interscience, New York, 1959, p. 757.
[30] O.A. Talaer, A.Kh. Akhmedov and A.S. Akhmedov, Zh. Anal. Khim., 24 (1969) 834.
[31] Z. Marczenko, Spectrophotometric Determination of Elements, Ellis Horwood, Chichester, 1976, p. 342, 556.
[32] J.S. Gaudh and V.M. Shinde, Sep. Sci. Tech., 30 (1995) 2573.
[33] M.B. Dalvi and S.M. Khopkar, Talanta, 25 (1978) 599.

High sensitivity flow-based analysis system using a semiconductor laser and thin long flow-through cell for the determination of total phosphorus in water

Takashi Korenaga*[1], Fusheng Sun[2]

Toyama National College of Technology, 13, Hongo-machi, Toyama 939, Japan

Received 11 September 1995; revised 26 February 1996; accepted 28 February 1996

Abstract

A highly sensitive detection system using a semiconductor laser (SCL) and a thin long flow-through cell (TLFCT) to match flow-based analysis, such as flow injection analysis (FIA), has been developed. The SCL was a GaAlAs semiconductor laser emitting at 780 nm (5 mW), and the TLFTC, which has a 100 mm thin long light path, was made of a poly(tetrafluoroethylene) (PTFE) rod. The sensitivity was essentially improved about 10-fold in comparison to usual FIA-spectrophotometry using a 10 mm conventional flow cell. When this detection system was applied to the determination of total phosphorus (P) in water by molybdenum-blue spectrophotometry, the relative standard deviation, detection limit and linear range were 1.0% ($n = 10$ at 20 μg P l^{-1}), 0.6 (3 σ) and 1.0–50 μg P l^{-1}, respectively, and the results for the samples were fairly consistent with those by the official method. It may also be possible to apply the present detection system to other flow-based analytical methods such as the liquid chromatography family.

Keywords: Eutrophication; Flow injection analysis; Semiconductor laser; Spectrophotometry; Thin long flow-through cell; Total phosphorus; Trace analysis; Water

1. Introduction

As a large number of samples must be analyzed daily and the concentrations of most components in the samples are usually low, more sensitive and rapid flow-based analytical methods are needed in many fields, such as environmental chemistry, clinical chemistry, etc. Many ways have been studied for solving this problem.

* Corresponding author. Fax: +(81) 886-56-7112.

[1] Present address: University of Tokushima, Faculty of Integrated Arts and Sciences, 1-1, Minami-josanjima-cho, Tokushima 770, Japan.

[2] Permanent address: Suzhou Institute of Urban Construction and Environmental Protection, Department of Environmental Protection, Postcode 215008, Suzhou, China.

According to the Lambert–Beer's law increasing the light path length is one of the ways to improve the sensitivity of spectrophotometry. However this would be difficult when the light path length is very long because the intensity of the transmitted light, emitted from an ordinary light source such as tungsten lamp, may become too low to be measured, and a large amount of sample solution is needed. One of the possible ways to solve this problem is to use a light source, which can emit light with very strong intensity, excellent monochromaticity and coherence, and a cell with a thin light path. Several attempts on this topic have been reported [1,2]. However, it was indicated that the multireflection–multipass system for the elongation of the light path length is effective only for gas samples not liquid as this system requires a rather large amount of sample, and the adjustment of optical configuration is difficult when a cell filled with liquid is inserted between the mirrors. Wei et al. have used a powerful light source, such as a xenon discharge lamp, a tungsten incandescent lamp and a helium–neon laser, and a long capillary cell for increasing the sensitivity for determination of phosphorus [1].

Although the sensitivity was improved from several hundred fold to thousand fold times higher than normal spectrophotometry, it was reported that the source light hits the wall of the long capillary cell and as a result, the apparent sensitivity deviates from the ideal Lambert–Beer's law. Another test using a total-reflection long capillary cell [2] also has some troubles because the solvent had a refractive index higher than that of the cell material, and the linear range of the calibration curve for the analyte was narrow. As a SCL has more advantages (see Section 3) than other conventional lasers [3,4], it could be more suitable as a light source to match the thin long light path cell for increasing the sensitivity.

Application of FIA to automatic analysis yields a fast, precise, accurate and extremely versatile system that is simple to operate. Although photometry is currently the most important detection technique in FIA, the design of

photometric cells has not received attention in working laboratories [5]. Only a few papers on the subject have been reported [6–8], and the detection limits for these designs were not good enough for the determination of lower concentrations of analytes in samples. A photometric detector having higher sensitivity for practical trace analysis by FIA has not been reported.

Improving the sensitivity for the determination of phosphorus is very important in environmental analysis as phosphorus is one of the major nutrients besides nitrogen. The heavy growth of algae in lake and stream waters is sometimes caused by phosphorus, and this results in the eutrophication of the water. This concentration of phosphorus is often less than that detectable by an ordinary spectrophotometry. In order to explain the mechanism of phosphorus circulation in environmental waters, the development of a continuously and highly sensitive method for detecting phosphorus should be indispensable. FIA was first used to determine phosphorus by Ruzicka and Hansen [9] and since then some other papers for the determination of phosphorus in water by FIA have been published [10–13]. Most of the methods described in these papers were based on the method of molybdophosphate blue (MPB), but the sensitivities of these methods were not very high and the detection limits were generally around 2–10 μg P l^{-1}. Some modifications have been made to improve the sensitivity of the determination of phosphorus by FIA [14,15], but they were rather complicated.

In the present paper, a highly sensitive detection system, which had a SCL and TLFTC, compatible with FIA for continuous trace analysis and its application in the determination of total phosphorus in water were reported. This new detection system was more sensitive than usual FIA with an ordinary photometric detector, and it was inexpensive and convenient to operate. It could be suitable for the continuous analysis of multiple components in samples, and for use in other flow-based techniques, such as liquid chromatograph and capillary electrophoresis [16,17].
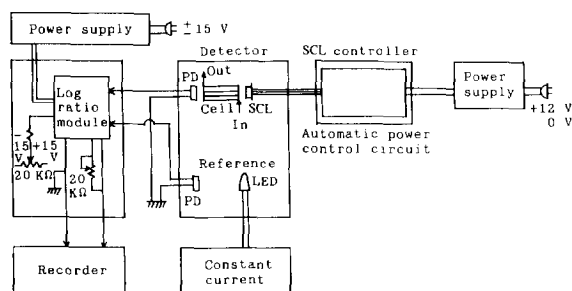
Fig. 1. High sensitivity detection system for FIA. SCL, semiconductor laser; LED, light emitting diode; PD, photo diode; In, inlet of TLFTC; Out, outlet of TLFTC.

2. Experimental

2.1. Reagents

All reagents were analytical reagent grade manufactured by Wako pure Chemical Industries Ltd, Osaka, Japan. Distilled water was used for all solutions and dilutions. Potassium dihydrogen phosphate was taken as a standard material for phosphorus, and it was dried for about 3 h at 110°C and then cooled to room temperature. It was used to prepare 50 mg P l^{-1} of stock standard solution with water. The oxidant, which was used for the oxidation of all phosphorus in samples to orthosphate, was prepared by dissolving 3 g of potassium persulfate in 1 liter of water. The developing reagent was composed of two parts, solutions A and B. Solution A was prepared by dissolving 6 g of ammonium molybdate tetrahydrate [$((NH_4)_6Mo_7O_{24}\cdot4H_2O)$] and 0.24 g of potassium antimonyl semihydrate tartrate $(K(SbO)C_4H_4O_6\cdot1/2H_2O)$ in about 300 ml of water, then adding 120 ml of 2 + 1 H_2SO_4 to the solution and diluting to 500 ml with water. Solu-
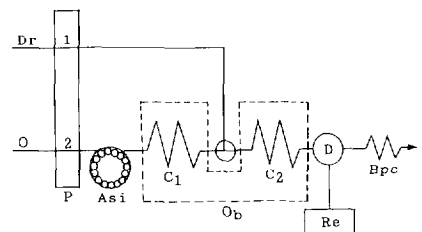

Fig. 2. Diagram of the FIA part. Dr, developing reagent; O, oxidant; P, pump (1, 2: 600 μl min^{-1}); Asi, automatic sample injector (300 μl); C$_1$ and C$_2$, coil (10 m × 1.0 mm i.d.); Ob, oil bath (140°C); D, detection system; Bpc, back pressure coil (3 m × 0.25 mm i.d.); Re, Recorder; W, Waste.

tion B was made by dissolving 7.2 g of L-ascorbic acid with water, and then diluting to 100 ml. Before delivering the developing reagent, solutions A and B were mixed by 5 + 1 and further diluted five times with water [18].

2.2. Apparatus

Fig. 1 shows the new detection system, which was essentially composed of three sections: semiconductor laser radiation, thin long light path absorption and logarithmic conversion-amplification and recording. A Model LN9805 K GaAlAs semiconductor laser (Semiconductor Selling Division, Matsushita Denshi Co. Ltd., Nagaokakyo, Kyoto, Japan) was used for the light source of the detector. The operation parameters of the laser are listed in Table 1. A light emitting diode (LED) (Model TLS143, Toshiba Co. Ltd., Japan) was used as a light source for the reference light beam of the detector. Two identical silicon photodiodes (PD) (Model S1087-01, Hamamatsu Photonics Co. Ltd., Japan) were arranged as receivers for the light beams of sample and reference, respec-

Table 1
Operation parameters of LN9805 K semiconductor laser

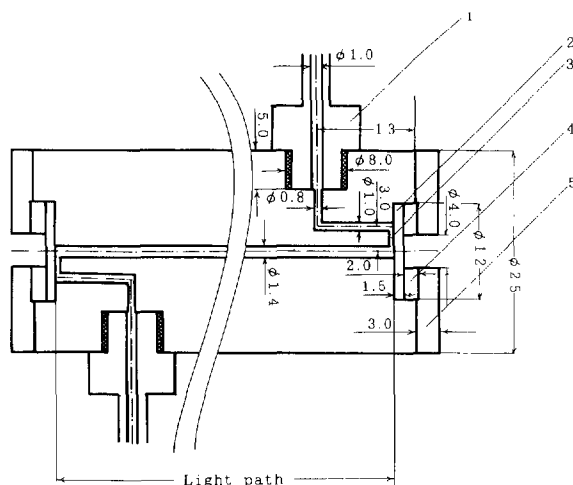| Threshold current (mA)	Output power (mV)	Wavelength (nm)	Far-filed patterns (°)		Monitor current (μA)
			$\theta_\parallel$	$\theta_\perp$	
29.5	5 (Po^a at 48.0 mA)	793	14.5	30.0	651 (Po = 2.5 mW)

^{a} Light output power.

Fig. 3. Schematic of TLFTC. 1, tube fitting; 2, quartz plate; 3, shallow gap; 4, PTFE spacer; 5, brass edge.

Fig. 4. Recording for peaks of phosphorus at 12 samples per hour analysis rate.

tively. A Model 757 N logarithmic ratio module and a Model LM308 three amplifying size differential OP amplifier (Analog Devices Co Ltd., USA), and a Model U-228 chart recorder ranged 0–10 V (Nihon Denshi Kagaku Co. Ltd., Tokyo, Japan) were used for the logarithmic conversion amplification and recordation, respectively.

A schematic diagram of the FIA is shown in Fig. 2. This part should be made of materials which are resistant to oxidation and reduction reagents, acids and bases. There were three reactions, the oxidation of total phosphorus to orthophosphate, the formation of MPA and the reduction of MPA to MPB, in the FIA system. Because the reactions were carried out at higher temperature (140°C) for increasing the reaction rate and improving the sensitivity, higher back pressure would exist. The double-plunger micropump, with a linear cam mechanism and short/fast reciprocation, can provide a continuous pulse-free flow. In addition, the micropump was sutable for operations against a higher than normal pressure, and for handling aggressive liquid [19]. Therefore, a pair of double-plunger micropumps (Model SR-3000, Sanuki Industry Co. Ltd., Japan) was used for pumping the reagents (600 μl min^{-1}). The standard solution of phosphorus or water sample (300 μl) were injected by an automatic injector (Model SJ-1700 ASI, Atto Co. Ltd., Japan). An oil bath (O_b, 140°C) was used,
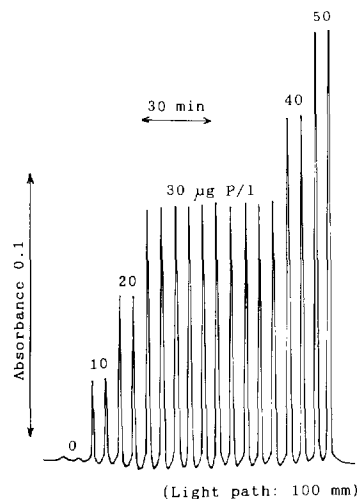
in which PTFE coils C_1 and C_2 (10 m × 1.0 mm i.d.) were immersed. C_1, C_2 and the path for the developing reagent were connected by a T-shaped PTFE connector. A PTFE back pressure coil (Bpc) (3 m × 0.25 mm i.d.) was put behind the TLFTC to decrease pulsations in the propelling system and prevent the formation of bubbles in the streams.

2.3. Design of TLFTC

Usually, the light path length of a commerically available flow-through cells for the application of photometry in FIA is 10 mm with 8 μl inner volume. In order to improve the detection sensitivity and decrease the reagent and sample consumption in the FIA laser spectrophotometry, the TLFTC was designed. The schematic of the TLFTC is shown in Fig. 3. It was made of PTFE rod, and the smoothness and linearity of the central thin and long hole (1.4 mm i.d.) must be very good to prevent the light emitted from the SCL from hitting the wall of the hole. TLFTCs with different lengths (10, 20, 50 and 100 mm) of light path were made for this study.

2.4. Detection system matching FIA

The reacted solution, leaving from coil C_2, flows into the TLFTC through the inlet hole

(9.7 mm × 1.0 mm i.d.) and shallow gap at one side of the TLFTC, and then flows out of the TLFTC through the other shallow gap and outlet hole (9.7 mm × 1.0 mm i.d.) at the other side of the TLFTC into the Bpc. The position of the SCL should be finely adjusted by moving the SCL so that the light beam emitted from the SCL can exactly pass the center of the thin long light path in the TLFTC, without hitting the wall of the thin long light path. The distance between the TLFTC and the SCL was not considered critical as the effect of the different distances (0–150 mm) on the absorbance for the determination of total phosphorus was not obvious. The light transmitted through the sample solution is received by the PD and converted to an electrical signal for the sample. The other light beam emitted from the LED is also received simultaneously by the other PD and converted to an electricial signal for the reference. Both of the signals are compared, logarithmically modulated and amplified in the logarithmic ratio module, and the final detection signal is recorded on the chart recorder.

2.5. Analytical procedure for determination of total phosphorus in water

The oxidation and developing reagents were pumped by a pair of double-plunger micropumps
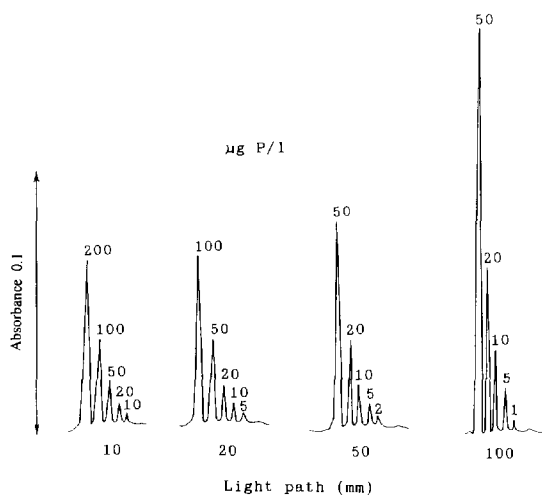

Fig. 5. Results of the determination for standard solution of phosphorus using different light path lengths of the TLFTC.

at a flow rate of 600 μl min^{-1}. The standard solution of phosphorus or sample (300 μl) were injected by the automatic injector at a rate of 12 samples per hour and merged into the stream of oxidation reagent, flowing into coil C_1. All of the phosphorus in the sample was oxidized to orthophosphate. The solution merged with the developing reagent in coil C_2, and was converted to MPA by reacting with ammonium molybdate and potassium antimonyl tartrate. Finally, the MPA was reduced to MPB by L-ascorbic acid in coil C_2, and the absorbance of the MPB solution flowing into the TLFTC was measured at 780 nm. The concentrations of phosphorus in the samples were calculated using a standard curve for phosphorus.

3. Results and discussion

3.1. Light source

A light source, that can emit intensive, coherent and monochromatic radiation is very important for spectrophotometry with a thin long light path cell. The He–Ne laser was used as the light source in long-capillary-cell absorption sectrophotometry because the laser can emit intensive light with good coherency and monochromaticity. The SCL has even more advantages than the He–Ne and other conventional lasers in conjunction with thin long light path spectrophotometry. The materials of the SCL are very sensitive to operation conditions, and the function of the SCL could be adjusted in many variables, such as temperature, pressure, radiation, different impurities and so on. The SCL has a very high conversion efficiency from electricity to light (theoretically it can reach 100%), quite large power output, very small dimension (several decimal μm are available) and excellent beam coherency and monochromaticity. It has a long life-time (10^5 h), low cost (one chip is about 10 US $) and wide range of wavelength (from near UV to IR). The GaAlAs has an alloplasm form, and it is very convenient for use as it can be continuously oscillated at room temperature [3,4,20]. Hereby, the GaAlAs was selected as the most suitable light source of the detector in thin long light path spectrophotometry and for

improving the sensitivity in FIA spectrophotometry.

The distance between the cell and the light source can be adjusted by moving the light source. Considering the light stability and the cheap price of LEDs, and the simplicity of light circuit system, the LED was selected as the light source of the reference light beam.

3.2. Concentration of oxidant and temperature of oxidation

The absorbencies for the determination of total phosphorus, using sodium triphosphate as a testing sample, were very similar using a range of concentrations of oxidant solution of 0.1–0.8% (w/v). Considering ecomony, 0.3% of oxidant solution was used in this study.

The oxidation of phosphorus to orthophosphate in the samples was not complete when the oxidation temperature was lower than 100°C. When the temperature was in a range of 120–160°C, the oxidation was complete and the results of the determination was almost identical. In the standard method of the Environmental Agency, Government of Japan, oxidation is carried out at 120°C, and the reaction time is 30 min [16]. In our work 13 min was sufficient when the reaction was carried out at 140°C in coil C_1 immersed in the O_b and the flow rate of the oxidant solution was 600 μl min^{-1}. Therefore, 140°C was used as the oxidation temperature.

3.3. Developing temperature

According to the standard method issued by the Environment Agency, Government of Japan, the developing temperature for phosphorus using a MPB method is 20–40°C (water bath), and the developing time is 15 min [18]. It was found that the sensitivity of the method for the determination of phosphorus was lower when developing was carried out at that temperature. Different temperatures from 20 to 160°C were tested and the sensitivity was highest when the temperature was in a range of 95–160°C and the flow rate of the developing reagent was 600 μl min^{-1}. With these considerations the temperature of the oxidation

for phosphorus was chosen to be 140°C and the coils C_1 and C_2 could be immersed in the same bath.

3.4. Analytical rate, precision and detection limit

Considering that the oxidation of phosphorus to orthophosphate in the coil C_1 took 13 min and a good separation between two peaks of neighboring samples (Fig. 4) was needed, the automatically continuous analysis rate for samples was set to 12 per hour. When 100 mm TLFTC was used, 10 measurements of 20 μg P l^{-1} standard solution gave an average absorbance of 0.0616 with a standard deviation (SD) of ± 0.0006. The relative standard deviation (RSD) and the detection limit (3 σ) were calculated to be 1.0% and 0.6 μg P l^{-1}, respectively.

3.5. Light path length of TLFTC and linear range for the determination of phosphorus

The effect of TLFTCs with different lengths (10, 20, 50 and 100 mm) of light path on the determination of phosphorus was tested, and the results are shown in Fig. 5. The sensitivity for the

Table 2
Recovery of phosphorus in some phosphorus compounds

Phosphorus compounds	Taken (mg P l^{-1})	Found (mg P l^{-1})	Recovery (%)
Sodium hypophosphite monohydrate	1.05	1.09	104
p-Nitrophenyl phosphate, disodium	1.02	1.03	101
Pyrophosphate acid	0.95	0.89	94
Polyphosphoric acid	0.99	0.89	90
Methaphosphoric acid	0.79	0.72	91
Penta sodium triphosphate	1.00	1.07	107
Adenosine 5'-monophosphate, sodium salt	1.02	1.03	101
Adenosine 5'-diphosphate, sodium salt	1.00	0.98	98

Table 3
Comparison of the results for the determination of phosphorus in wastewater and treated wastewater by present and official methods

Sample		Total phosphorus (mg P l^{-1})		Comparison with the official method	
		Present method	Official method	D (mg P l^{-1})	RD (%)
Wastewater	A	2.56	2.29	0.27	12
	B	0.30	0.29	0.01	3.4
	C	0.92	0.86	0.06	7.0
	D	1.04	0.99	0.05	5.1
	E	1.19	1.12	0.07	6.3
	F	1.68	1.50	0.18	12
	G	0.96	0.92	0.04	4.3
	H	1.76	1.55	0.21	14
Treated wastewater	A	0.03	0.02	0.01	5×10
	B	0.10	0.06	0.04	7×10
	C	0.05	0.02	0.03	2×10^2
	D	0.16	0.11	0.05	45
	E	0.22	0.24	-0.02	-8.3
	F	0.06	0.02	0.04	2×10^2
	G	0.07	0.06	0.01	2×10
	H	1.58	1.25	0.33	26
	I	0.06	0.06	0	0
	J	0.09	0.04	0.05	1×10^2
	K	0.03	0.04	-0.01	-3×10
	L	0.05	0.06	-0.01	-2×10
	M	1.09	0.96	0.13	14
	N	0.20	0.13	0.07	54
	O	0.04	0.04	0	0
	P	0.06	0.08	-0.02	-3×10
	Q	0.12	0.11	0.01	9.1
	R	0.15	0.12	0.03	25

determination of phosphorus by a 100 mm TLFTC was enhanced by about 10-fold when compared to usual FIA sectrophotometry using a 10 mm absorption cell. The longer the length of the TLFTC, the higher the detection sensitivity. The linear ranges for the determination of phosphorus, using 10, 20, 50 and 100 mm light path lengths, were 10–200, 5–100, 2–50 and 1–50 μg P l^{-1}, respectively.

3.6. Recovery of phosphorus in some phosphorus compounds and the determination of total phosphorus in water

The recoveries of phosphorus in some phosphorus compounds are listed in Table 2. From Table 2 it was known that the recoveries were between 94–107% when potassium dihydrogen phosphate was considered as the standard of phosphorus.

Some wastewater and treated wastewater were determined by this method and the official method. The results of the determination are shown in Table 3. The RDs, which were obtained by comparison with the results analyzed by the official method, for the concentrations of total phosphorus in the wastewater and treated wastewater, were 3.4–14 and -3×10–2×10^2%, respectively. Most of the results analyzed by the two methods showed little difference, except for a few results in the treated wastewater. The correlation between the results analyzed by both of the methods is shown in Fig. 6. It shows that the correlation was quite good.

Traces of total phosphorus in some natural waters, sea water, hot-spring water and snow, were determined to evaluate the applicability of the present method. The results are listed in Table
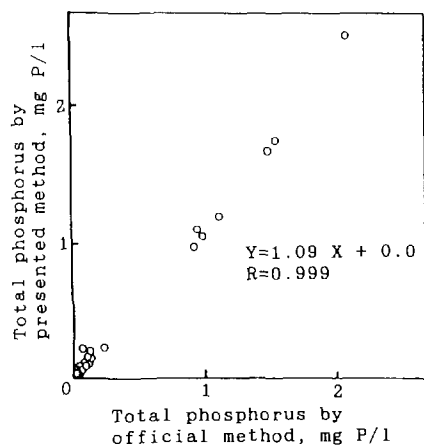
Fig. 6. Correlation between the results analyzed by the present and official methods.

technique was successfully applied to the automatically continuous monitoring of them in water.

The technique utilizes the merits of FIA, TLFTC and SCL, i.e. high speed, good reproducibility and automatically continuous analysis of FIA, thin long light path with low reagent and sample consumption, samples, high sensitivity of TLFTC, and excellent radiation intensity, monochromaticity and coherency of SCL. This technique could be used for the determination of other trace analytes in samples, and it may also be useful to other flow-based analytical techniques, such as liquid chromatograph, capillary electrophoresis, etc.

4. The RSD stated as above in these samples were in a range of − 7–12%. The results were similar except for the river water in which concentrations of total phosphorus were too low to be detected by the official method.

4. Conclusions

The application of laser spectrophotometry FIA with the new detection system, composed of the TLFTC and SCL, to the determination of total phosphorus and dissolved silica [21] in water have clearly illustrated that, by comparison with a normal 10 mm flow cell, the detection sensitivities were improved by about 10-fold. The analytical

Acknowledgements

Table 4
Results of the determination of total phorphorus in natural water

Sample		Total phosphorus (mg P l^{-1})		Comparison with official method	
		Present method	Official method	D (mg P l^{-1})	RD (%)
River water	1	0.004		–	–
	2	0.008	–	–	–
Water in mix zone of river and sea		0.042	0.031	0.011	3.5
Sea water		0.012	0.013	−0.001	−7.7
Hot-spring water		0.015	0.014	0.001	7.1
Snow	1	0.015	0.018	−0.003	−17
	2	0.019	0.017	0.002	12

References

[1] L. Wei, K. Fujiwara and K. Fuwa, Anal. Chem., 55 (1983) 951.

[2] K. Fuwa, L. Wei and K. Fujiwara, Anal. Chem., 56 (1984) 1640.

[3] T. Imasaka and N. Ishibashi, Anal. Chem., 62 (1990) 363 A.

[4] T. Imasaka, Anal. Sci., 9 (1993) 329.

[5] M. Valcarcel and M.D. Luque de Castro, in Flow-Injection Analysis: Principles and Applications, Ellis Horwood, Chichester, 1987, p. 153.

[6] D. Betteridge, W.C. Cheng, E.L. Dagless, P. David, T.B. Goad, D.R. Deans, D.A. Newton and T.B. Pierce, Analyst, 108 (1983) 17.

[7] D.J. Leggett, N.H. Chen and D.S. Mahadevappa, Anal. Chim. Acta, 128 (1981) 163.

[8] P.R. Freeman, I.D. Mackelve, B.T. Hart and T.J. Cardwell, Anal. Chim, Acta, 234 (1990) 409.

[9] J. Ruzicka and E.H. Hansen, Anal. Chim. Acta, 78 (1975) 145.

[10] Y. Hirai, N. Yoza and S. Ohashi, Bunseki Kagaku, 30 (1981) 465.

[11] T. Korenaga and K. Okada, Bunseki Kagaku, 33 (1984) 683.

[12] M. Aoyagi, Y. Yasumasa and A. Nishida, Anal. Chim. Acta, 214 (1988) 229.

[13] I.D. Mckelvie and B.T. Hart, Analyst, 114 (1989) 1459.

[14] M. Aoyagi, Y. Yasumasa and A. Nishida, Anal. Sci., 5 (1989) 235.

[15] S. Motomizu, H. Mikasa, M. Oshima and K. Toei, Bunseki Kagaku, 33 (1984) 116.

[16] A.T.J. Hank and E.S. Yeung, J. Chromatogr., A 708 (1995) 309.

[17] Q.B. Li and E.S. Yeung, Appl. Spectrosc., 49 (1995) 1528.

[18] Notification No. 140 of the Environment Agency, Japan, 1982.

[19] T. Korenaga, X.J. Zhou, T. Moriwake and S. Shinoda, Japan J. Toxicol. Environ. Health, 40 (1994) 122.

[20] I.V. Baiborodina, L.Z. Kriksunova and O.N. Litvinenko, in Handbook of Laser Technique, Mechanic Industry, Beijing, 1986, pp. 159–176.

[21] T. Korenaga and F. Sun, Anal. Chim. Acta, 318 (1996) 195.

Effect of alkyl substituents in hydrophobic 8-Quinolinol on the extraction of gallium(III) and applications to the separation of gallium(III) from aluminum(III)

Kousaburo Ohashi[a,*], Riyoichi Iwata[a], Shunsuke Mochizuki[a], Hisanori Imura[a], Kazuhisa Hiratani[b], Hideki Sugihara[b]

[a]*Department of Chemistry, Faculty of Science, Ibaraki University, Mito 310, Japan*
[b]*National Institute of Materials and Chemical Research Institute, Tsukuba 305, Japan*

Abstract

The extraction of gallium(III) with newly prepared 5-alkyloxymethyl-8-quinolinol derivatives with alkyl substituent at the 2-position in 8-quinolinol moiety has been studied. The Ga(III)-5-octyloxymethyl-8-quinolinol (HO_8Q), Ga(III)-2-methyl-5-octyloxymethyl-8-quinolinol (HMO_8Q), Ga(III)-2-methyl-5-hexyloxymethyl-8-quinolinol (HMO_6Q), and Ga(III)-2-n-butyl-5-hexyloxymethyl-8-quinolinol ($HNBO_6Q$) complexes extracted in heptane from a perchloric acid medium were $Ga(O_8Q)_3$, $Ga(OH)(H_2O)(MO_8Q)_2$, $Ga(OH)(H_2O)(MO_6Q)_2$ and $Ga(OH)H_2O)(NBO_6Q)_2$, respectively. The 2-$tert$-butyl-5-hexyloxymethyl-8-quinolinol did not exhibit any reactivity toward gallium(III). The extraction constants for $Ga(O_8Q)_3$ ($K_{ex} = [Ga(O_8Q)_3]_{org} [H^+]^3/[Ga^{3+}][HO_8Q]_{org}^3$), $Ga(OH)(H_2O)(MO_8Q)_2$ ($K_{ex} = [Ga(OH)(H_2O)(MO_8Q)_2]_{org} [H^+]^3/[Ga^{3+}][HMO_8Q]_{org}^2$), $Ga(OH)(H_2O)_2(MO_6Q)_2$ and $Ga(OH)(H_2O)(NBO_6Q)_2$, which were extracted in heptane from an acidic solution, are $10^{3.21 \pm 0.12}$, $10^{-4.24 \pm 0.16}$, $10^{-3.84 \pm 0.16}$ and $10^{-4.07 \pm 0.07}$, respectively at $I = 0.1$ M and 25°C.

$HNBO_6Q$ exhibited very high selectivity toward gallium(III) in the presence of aluminum(III). Even in the presence of a 100 fold excess of aluminum(III) to gallium(III) (1.43×10^{-5} M), gallium(III) was completely extracted and the distribution ratio of aluminum(III) was found to be less than 2.0×10^{-3}.

Keywords: Alkyl substituents; Gallium(III) extraction; Hydrophobic 8-quinolinol

1. Introduction

Selective separation of rare metal ions has been an attractive subject in analytical chemistry and separation science. The molecular design for the highly selective chelating extractants has been extensively studied to establish the most selective separation system for metal ions.

Since 8-quinolinol provides many extractable and stable metal complexes, it has been one of typical extractants for practical purpose, despite

low selectivity [1,2]. A Kelex 100 extractant characterized by very large hydrophobicity has been known to provide high extractability for gallium(III) from a strongly alkaline solution [3,4], and for palladium(II) from a strongly acidic solution [5].

The present authors have reported that the alkylated 8-quinolinol derivatives such as 5-octyloxymethyl-8-quinolinol (HO_8Q) and 2-methyl-5-octyloxymethyl-8-quinoinol (HMO_8Q) behave as highly selective extractants for molybdenum(VI) from a strongly acidic solution [6,7]. HO_8Q and HMO_8Q gave extractable 1:2 molybdenum(VI) complexes. The extraction constant for HO_8Q was about three orders of magnitude larger than that for HMO_8Q. Such a different extraction behavior between HO_8Q and HMO_8Q was explained by the steric hindrance of the methyl group at the 2-position.

The lack of reactivity of 2-methyl-8-quinolinol with alluminum(III) has been ascribed to the difficulty in forming an extractable Al(III)-2-methyl-8-quinolinol complex due to the steric hindrance of methyl group [2]. The substitution at the 2-position of 8-quinolinol does not remarkably affect the pK_{a1} and pK_{a2} values, but it seriously decreases the stability constants of metal ions such as copper(II), nickel(II) and zinc(II) [8]. A systematic study on the extraction behaviors of metal ions with 2-methyl-8-quinolinol has been done by Motojima and Hashitani [2]. However, a few extraction constants have been determined [9–11]. In this study, the extraction behavior of gallium(III) with alkylated 8-quinolinol was investigated to get detailed information concerning the steric effect of the alkyl substituents in the hydrophobic 8-quinolinol moiety on the extractability and selectivity for the metal ion.

2. Experimental

2.1. Reagents

2.1.1. Synthesis of 2-butyl-5-hexyloxymethyl-8-quinolinol ($HNBO_6Q$) and 2-tert-butyl-5-hexyloxymethyl-8-quinolinol ($HTBO_6Q$)

A 2.6 g quantity of 5-hexyloxymethyl-8-quinolinol (HO_6Q) dried under vacuum at 100°C was dissolved in 20 ml of dry ethylether and the solution cooled to 0°C under a dry nitrogen atmosphere. Next 32 ml of n-butyl lithium (51 mmol) was dropped into a stirred reaction flask containing HO_6Q in ethylether and kept below 0°C. The solution was allowed to stand for 4 h at 0°C. The reaction product was hydrolyzed by dropping water into the reaction flask, the ethylether was separated, and the solvent was evaporated to obtain a yellowish oil. The crude product was purified by chromatography on silica gel. Hydrochloric acid was added to the purified, oily $HNBO_6Q$ in methylene chloride. The yellow crystalline product of $HNBO_6Q \cdot 2HCl$ was recrystallized from methylene chloride (yield, 33%). Analysis calculated for $C_{20}H_{29}NO_2 \cdot 2HCl_2$: C, 61.85; N, 3.61; H, 8.05% and found: C, 61.64; N, 3.63; H, 8.34%. ^{1}H-NMR (300 MHz $CDCl_3$): 0.85(t, 3H), 0.97(t, 3H), 1.25(m, 6H), 1.41(m, 2H), 1.58(m, 2H), 1.81(m, 2H), 2.97(t, 2H), 3.47(t, 2H), 4.79(s, 2H), 7.06(d, 1H), 7.26(d, 1H), 7.34(d, 1H), 8.39(d, 1H). Precise mass calculated: 315.22 for $C_{20}H_{29}NO_2$ and found: 315.22.

In a similar manner, $HTBO_6Q$ was synthesized from HO_6Q and tert-butyl lithium and purified by chromatography on silica gel. The product was oily (yield, 26%). ^{1}H-NMR (300 MHz, $CDCl_3$): 0.85(t, 3H), 1.25(m, 6H), 1.51(s, 9H), 1.62(m, 2H), 3.47(t, 2H), 4.71(s, 2H), 7.07(d, 1H), 7.34(d, 1H), 7.61(d, 1H), 8.43(d, 1H). Precise mass calculated:315.22 for $C_{20}H_{29}NO_2$ and found: 315.22.

The extractants, (HO_8Q) [12] and (HMO_8Q) [7] were synthesized by our previous method. In addition, HO_6Q and HMO_6Q were synthesized by a similar manner to HO_8Q and HMO_8Q, respectively.

The structures of the 8-quinolinols are shown in Fig. 1.

A heptane solution of HO_8Q was prepared by dissolving weighed amounts of HO_8Q into heptane just before use. A HMO_8Q heptane solution was prepared by shaking weighed amounts of $HMO_8Q \cdot HCl$ with a mixture of heptane and a dilute aqueous ammonia solution. A gallium(III) perchlorate stock solution was prepared by replacing the chlordie ion of a spectroscopic stan-

dard gallium(III) chloride solution with perchlorate ion. Heptane was purified by distillation before use. All other chemicals were of reagent grade and used without further purification.

The ionic strength was kept at 0.1 M or 0.5 M $(1\ M = 1\ mol\ dm^{-3})$ by addition of sodium perchlorate or sodium chloride. The pH of an aqueous phase containing gallium(III) was adjusted with perchloric acid or sodium hydroxide solutions.

2.2. Apparatus

An inductively coupled plasma atomic emission spectrophotometer (ICP-AES, Nippon Jurrell Ash ICAP-575) was used for the determination of gallium(III) in aqueous solutions. The pH measurements were made by a Radiometer PHM93 pH meter. A mechanical shaker (Iwaki) was used

Fig. 1. Structures of 8-quinolinol derivatives.

5-octyloxymethyl-8-quinolinol
(HOsQ)

2-methyl-5-octyloxymethyl-8-quinolinol
(HMOsQ)

5-hexyloxymethyl-8-quinolinol
(HOsQ)

5-hexyloxymethyl-2-methyl-8-quinolinol
(HMOsQ)

2-n-butyl-5-hexyloxymethyl-8-quinolinol
(HNBOsQ)

2-tert-butyl-5-hexyloxymethyl-8-quinolinol
(HTBOsQ)

to equilibrate the extraction vials. All the experiments were carried out at 25°C in a thermostated room.

## 2.3. Extraction equilibrium

An aqueous gallium(III) solution $(1.01 \times 10^{-5}-1.01 \times 10^{-3}\ M)$ was placed in a 50 ml extraction vial fitted with a plastic cap. To the solution, an equal volume of organic solvent containing $1.01 \times 10^{-3}-1.01 \times 10^{-2}\ M$ of extractant was added and shaken for 12 h. After centrifugation, the gallium(III) concentration in the aqueous phase was determined by ICP-AES. To determine the gallium(III) concentration in the organic phase, the $Ga(III)$-HMO_8Q and $Ga(III)$-HO_8Q complexes were stripped with 1 M hydrochloric acid and the resulting aqueous solution analyzed by ICP-AES. The distribution ratio $(D = [Ga(III)]_{org}/[Ga(III)]_{aq})$ was calculated from the gallium(III) concentration in both phases, where the subscripts of org and aq represent the organic phase and the aqueous phase, respectively.

3. Results and discussion

3.1. Extraction of Ga(III) with HO_8Q from a perchloric acid and hydrochloric acid medium

A shaking time of 12 h was found to be sufficient to establish the extraction equilibrium of gallium(III) with $1.00 \times 10^{-3}\ M\ HO_8Q$ at pH 2.04. Under the given extraction conditions $(1.00 \times 10^{-2}\ M\ HO_8Q$, pH 1.10), the distribution ratio was independent of the initial gallium(III) concentration $(1.01 \times 10^{-5}-1.01 \times 10^{-3}\ M)$, suggesting that the extracted $Ga(III)$-HO_8Q complex is a mononuclear species. Also no aggregation of the 8-quinolinol derivatives themselves in heptane was separately ascertained by studying the distribution equilibrium [14]. Assuming that the extracted $Ga(III)$-HO_8Q complex is $Ga(O_8Q)_3$, the extraction equilibrium is provided as follows:

$$Ga^{3+} + 3HO_8Q_{org} \overset{K_{ex}}{\rightleftharpoons} Ga(O_8Q)_{3,\ org} + 3H^+ \qquad (1)$$
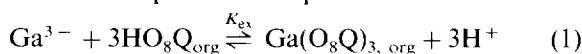
The extraction constant K_{ex} is expressed by Eq. (2):
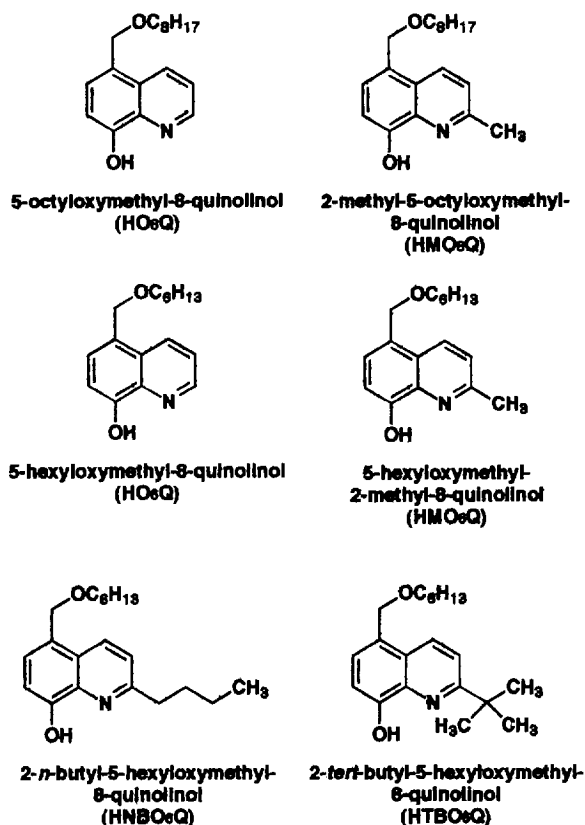
$$K_{ex} = \frac{[Ga(O_8Q)_3]_{org}[H^-]^3}{[Ga^{3+}][HO_8Q]_{org}^3} \qquad (2)$$

Under the acidic experimental conditions, the predominant species of gallium(III) in an aqueous phase is $Ga(H_2O)_6^{3+}$ and negligibly small amounts of $Ga(OH)(H_2O)_5^{2-}$ and $Ga(OH)_2(H_2O)_4^+$ occur. The fraction of the hydrolyzed species of gallium(III) was calculated using the following reported hydrolysis constants: $K_{h1} = 8.91 \times 10^{-4}$ ($K_{h1} = [Ga(OH)(H_2O)_5^{2+}][H^+]/[Ga(H_2O)_6^{2+}]$), $K_{h2} = 2.51 \times 10^{-7}$ ($K_{h2} = [Ga(OH)_2(H_2O)_4^+[H^+]^2/[Ga(H_2O)_6^{3+}]$) at $I = 0.1$ M and 25°C. The presence of dinuclear species can be neglected in lower gallium(III) concentration (1.08×10^{-4} M) [13]. For the calculation of the equilibrium constants, the hydrogen ion concentration was determined by using the measured pH value ($= -\log A_{H^+}$) and the activity coefficient ($\gamma = 0.83$) of the hydrogen ion at $= 0.1$ M.

If the concentrations of Ga(III)-HO_8Q complexes such as $Ga(O_8Q)_3$, $Ga(O_8Q)_2(H_2O)_2^+$, and $Ga(O_8Q)(H_2O)_4^{2+}$ in the aqueous phase are negligibly low compared with that of gallium(III), the distribution ratio of gallium(III) is represented by equation (3):

$$D = \frac{[Ga(O_8Q)_3]_{org}}{[Ga^{3+}](1 + K_{h1}[H^+]^{-1} + K_{h2}[H^+]^{-2})} \qquad (3)$$

From Eqs. (2) and (3), Eq. (4) is derived.

$$\log D + \log(1 + K_{h1}[H^-]^{-1} + K_{h2}[H^+]^{-2})$$
$$= -3 \log[H^+] + 3 \log[HO_8Q]_{org} + \log K_{ex} \qquad (4)$$

Based on calculations using literature, pK_{a1}, pK_{a2} and the distribution constant of HO_8Q between heptane and an aqueous solution at pH 1–2, the equilibrium HO_8Q concentration in an aqueous phase is negligibly low [14]. Therefore, the HO_8Q concentration in the organic phase is approximately equal to the initial HO_8Q concentration.

The plots of $\log D + \log(1 + K_{h1}[H^+]^{-1} + K_{h2}[H^+]^{-2}) + 3 \log[H^+]$ versus $\log[HO_8Q]_{org}$ provided a straight line with a slope of 3.2. This indicates that three molecules of HO_8Q are participating in the extraction of gallium(III).

The relationship between $\log D + \log(1 + K_{h1}[H^+]^{-1} + K_{h2}[H^+]^{-2}) - 3 \log[HO_8Q]_{org}$ and $-\log[H^+]$ gave a straight line with a slope of 2.9, implying that the extraction reaction accompanies the release of three hydrogen ions from HO_8Q molecules into the aqueous phase during the extraction reaction.

From these results, it was concluded that the molar ratio of gallium(III) to HO_8Q in the extracted Ga(III)-HO_8Q complex is 1:3 ($Ga(O_8Q)_3$). The log K_{ex} value was determined to be 3.21 ± 0.12 at $I = 0.1$ M and 25°C (Table 1). It was also ascertained that the extractability of gallium(III) with HO_8Q was independent of the chloride ion concentration (0.01–0.1 M) at $I = 0.1$ M(H, Na)(Cl, ClO_4).

3.2. Extraction of Ga(III) with HMO_8Q, HMO_6Q and $HNBO_6Q$ from perchloric acid and hydrochloric acid medium

The extraction equilibrium of gallium(III) (1.0×10^{-4} M) with HMO_8Q (1.0×10^{-2} M) at pH 1.1 was achieved by shaking for 50 h. The extracted Ga(III)-HMO_8Q complex is a mononuclear species as in the Ga(III)-HO_8Q case, as determined by the independence of the distribution ratio on the gallium(III) concentration (2.02×10^{-5}–1.01×10^{-3} M). The plots of log D versus $\log[HMO_8Q]_{org}$ at pH 3.1 gave a straight line with a slope of 2.2 (Fig. 2), suggesting that two molecules of HMO_8Q are included in the extracted gallium(III) complex. As mentioned above, three molecules of HO_8Q are included in the extracted gallium(III) complex. This difference may be ascribed to the steric hindrance of the methyl group at the 2-position of 8-quinolinol moiety. The steric hindrance of methyl group prevents the third molecule of HMO_8Q from coordinating to gallium(III). If the extracted Ga(III)-HMO_8Q complex is assumed to be $Ga(OH)(H_2O)(MO_8Q)_2$, the extraction equilibrium is represented by Eq. (5):

$$Ga^{3+} + 2HMO_8Q_{org}$$
$$+ 2H_2O \overset{K_{ex}}{\rightleftharpoons} Ga(OH)(H_2O)(MO_8Q)_{2, org} + 3H^+$$
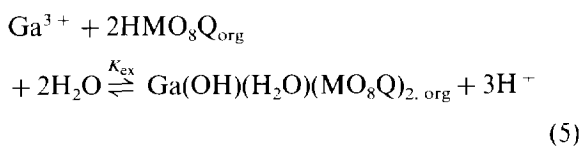
$$(5)$$

Table 1
Extraction constants of Ga(III) with 8-quinolinol derivatives in the acidic region

Extractant	log K_{ex}	Extracted complex	Solvent
HO$_8$Q	3.21 ± 0.12[a] (0.1 M (H, Na)ClO$_4$)	Ga(O$_x$Q)$_3$	Heptane
HMO$_8$Q	−4.24 ± 0.16[a] (0.1 M (H, Na)ClO$_4$)	Ga(OH)(H$_2$O)(MO$_8$Q)$_2$	Heptane
	1.30 ± 0.02[a] (0.5 M (H, Na)Cl)	Ga(Cl)(H$_2$O)(MO$_8$Q)$_2$	Heptane
HMO$_6$Q	−3.84 0.16[a] (0.1 M (H, Na)ClO$_4$)	Ga(OH)(H$_2$O)(MO$_6$Q)$_2$	Heptane
HNBO$_6$Q	−4.07 ± 0.07[a] (0.1 M (H, Na)ClO$_4$)	Ga(OH)(H$_2$O)(NBO$_6$Q)$_2$	Heptane
8-Quinolinol (HQ)	3.72[b] (0.1 M (H, K)ClO$_4$)	GaQ$_3$	Chloroform
Kelex 100[d] (HR)	3.26[c] (1 M(H, Na)NO$_3$)	GaR$_3$	Toluene

[a] This work.
[b] From Ref. [1].
[c] From Ref. [16].
[d] 7-(1-vinyl-3,3,5,5,-tetramethylhexyl)-8-quinolinol

The extraction constant K_{ex} is represented as follows:

$$K_{ex} = \frac{[Ga(OH)(H_2O)(MO_8Q)_2]_{org}\,[H^+]^3}{[Ga^{3+}][HMO_8Q]_{org}^2} \quad (6)$$

As discussed above, under the experimental conditions (pH 2.2–3.1), gallium(III) exists as

Fig. 2. Effects of the extractant (HA) concentration in heptane on the distribution ratio of Ga(III). Ga(III) 1.43 × 10^{-5} M; ■, HMO$_8$Q (−log[H$^+$] = 3.0); ●, MO$_6$Q (−log[H$^+$] = 2.9); ○, HNBO$_6$Q (−log[H$^+$] = 2.8).

Ga(H$_2$O)$_6^{3+}$, Ga(OH)(H$_2$O)$_5^{2+}$ and Ga(OH)$_2$(H$_2$O)$_4^+$ in an aqueous solution. Accordingly, the distribution ratio of gallium(III), D is shown by Eq. (7):

$$D = \frac{[Ga(OH)(H_2O)(MO_8Q)_2]_{org}}{[Ga^{3+}](1 + K_{h1}[H^+]^{-1} + K_{h2}[H^+]^{-2})} \quad (7)$$
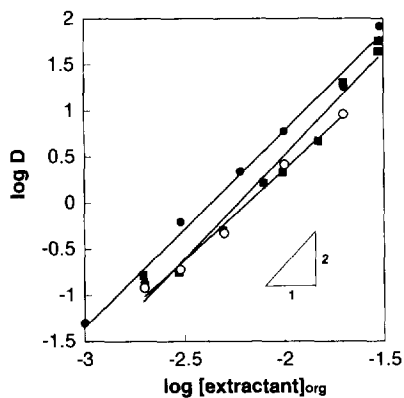
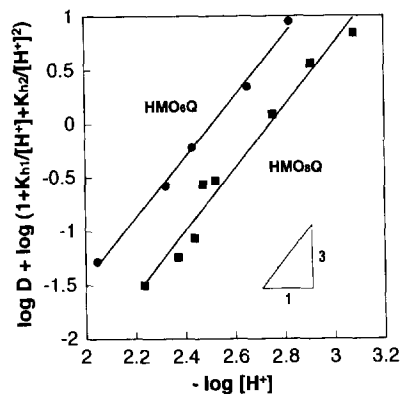From eqs. (6) and (7), the following equation is derived:

Fig. 3. Effects of the hydrogen ion concentration on the distribution ratio of Ga(III) with 0.01 M HMO$_8$Q and HMO$_6$Q in heptane. Ga(III): 1.43 × 10^{-5} M.

$$\log D + \log(1 + K_{h1}[H^+]^{-1} + K_{h2}[H^+]^{-2})$$

$$= -3\log[H^+] + 2\log[HMO_8Q]_{org} + \log K_{ex} \quad (8)$$

As shown in Fig. 3, the plots of $\log D + \log(1 + K_{h1}[H^+]^{-1} + K_{h2}[H^+]^{-2})$ versus $-\log[H^+]$ gave a straight line with the slope of 2.9. The result was consistent with the above assumption that three hydrogen ions participate in the gallium(III) extraction. The same results were obtained for the extraction of gallium(III) with HMO_6Q and $HNBO_6Q$. However, gallium(III) was not extracted with $HTBO_6Q$ at all. The $\log K_{ex}$ values of -4.24 ± 0.16 (HMO_8Q), -3.84 ± 0.16 (HMO_6Q), and -4.07 ± 0.07 ($HNBO_6Q$) were obtained at $I = 0.1$ M and 25°C (Table 1).

As mentioned above, the extractability of HO_8Q toward gallium(III) was independent of the chloride ion concentration. However, since the extraction of gallium(III) with HMO_8Q takes place at lower pH region in the presence of chloride ion than in the absence of chloride ion, the composition of the $Ga(III)-HMO_8Q$ complex extracted in the presence of chloride ion was studied. The independence of the distribution ratio of gallium(III) ion concentration suggests the extraction of the mononuclear gallium(III) complex. If we assume $Ga(Cl)(H_2O)(MO_8Q)_2$ as the extracted species, the extraction reaction can be shown by equation (9):

$$Ga^{3+} + 2HMO_8Q_{org}$$

$$+ Cl^- \overset{K_{ex}}{\rightleftharpoons} Ga(Cl)(H_2O)(MO_8Q)_{2org} + 2H^+ \quad (9)$$

Eq. (10) represents the extraction constant.

$$K_{ex} = \frac{D(1 + K_{h1}[H^+]^{-1} + K_{h2}[H^+]^{-2} + \beta_1[Cl^-])}{[H^+]^2 \quad [HMO_8Q]_{org}^2 [Cl^-]} \quad (10)$$

where β_1 is the formation constant of $GaCl^{2+}$ ($\beta_1 = 10^{-2}$ at 20°C) [15]. At constant hydrogen ion and chloride ion concentrations, the plots of $\log D$ versus $\log[HMO_8Q]_{org}$ are expected to give a straight line with a slope of two. The plots of $\log D$ versus $\log[HMO_8Q]_{org}$ gave a straight line with a slope of 2.0 and the relationship between $\log D + \log(1 + K_{h1}[H^+]^{-1} + K_{h2}[H^+]^{-2} + \beta_1[Cl^-])$ and $-\log[H^+]$ yielded a straight line with a slope
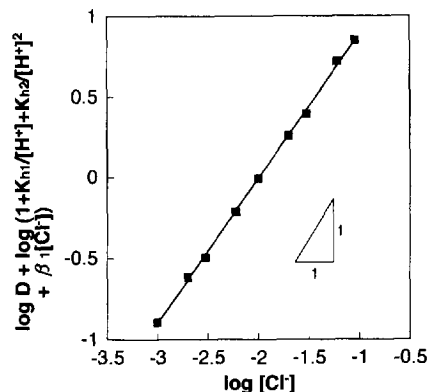

Fig. 4. Effect of chloride ion concentration on the distribution ratio of 1.43×10^{-5} M Ga(III) with 0.01 M HMO_8Q. $-\log[H^+] = 2.0$; $I = 0.1$ M (H, Na)(ClO$_4$, Cl).

of 2.0. As shown in Fig. 4, we found a linear relationship with a slope of 0.9 between $\log D + \log(1 + K_{h1}[H^+]^{-1} + K_{h2}[H^+]^{-2} + \beta_1[Cl^-])$ and $\log[Cl^-]$, indicating that one chloride ion was included in the gallium(III) complex in the course of the gallium(III) extraction.

These results support the above assumption that the extracted species should be $Ga(Cl)(H_2O)(MO_8Q)_2$. The K_{ex} value was $10^{1.30 \pm 0.02}$ at $I = 0.1$ M and 25°C (Table 1). The larger extraction constant for $Ga(Cl)(H_2O)(MO_8Q)_2$ than that for $Ga(OH)(H_2O)(MO_8Q)_2$ can be ascribed to the higher hydrophobicity of Cl^- than that of OH^-.

The structures of the extracted Ga(III)-8-quinolinol [1], $Ga(III)-HO_8Q$ and Ga(III)-Kelex 100 [16] complexes are expected to show octahedal coordination. $Ga(III)-Cl-HMO_8Q$ and $Ga(III)-OH-HMO_8Q$ (HMO_6Q, $HNBO_6Q$) complexes extracted into heptane may have a octahedral configuration, although the five coordinated structure cannot be ruled out since 2-methyl-8-quinolinol (HMQ) exhibits a five coordinated $Ga(Cl)(MQ)_2$ in solid. This structure was crystallographically characterized [17].

The facts that Ga(III) is extracted with Kelex 100 and HO_8Q as 1:3 Ga(III) complexes indicates that the steric hindrance of bulky alkyl group at the 7-position in 8-quinolinol moiety is not essential. On the other hand, the steric hindrance of alkyl group at the 2-position of HMO_8Q should be critical for small metal ions such as gallium(III).

Table 2
The distribution ratio (D) of Ga(III) in the presence of Al(III)

HA	[Al(III)]/[Ga(III)]	D	
		Al(III)	Ga(III)
HO$_6$Q	1	3.6×10^{-1}	2.5×10^2
	10	3.3×10^{-2}	2.5×10^2
	100	3.4×10^{-2}	1.0×10^3
HMO$_6$Q	1	3.0×10^{-2}	2.6
	10	3.8×10^{-3}	3.5
	100	1.0×10^{-4}	4.0
HNBO$_6$Q	1	4.6×10^{-2}	2.0×10^2
	10	5.5×10^{-3}	5.0×10^2
	100	1.4×10^{-3}	1.0×10^3

[Ga(III)] = 1.43×10^{-5} M; [HA]$_{org}$ = 0.01 M; pH = 2.84–2.99.

3.3. Separation of gallium(III) from aluminum(III)

Table 2 shows the distribution ratio of gallium(III) (1.43×10^{-5} M) and aluminum(III) (1.43×10^{-5}–1.43×10^{-3} M) with HO$_6$Q, HMO$_6$Q and HNBO$_6$Q (0.01 M) at pH 2.84–2.99. The distribution ratio of gallium(III) with HO$_6$Q in the presence of aluminum(III) (1.43×10^{-5} M–1.43×10^{-3} M) was more than 2.0×10^2. On the other hand, the distribution ratio of aluminum(III) was about 3.7×10^{-1} in the solution containing equal amounts of gallium(III) and aluminum(III). In the case of 10–100 fold excess of aluminum(III) to gallium(III), the distribution ratio of aluminum(III) was approximately 1.0×10^{-3}. Based on these results, HO$_6$Q seems not to be a highly selective extractant toward gallium(III). Although the distribution ratio of aluminum(III) with HMO$_6$Q was lower than that with HO$_6$Q, gallium(III) was not completely extracted. HNBO$_6$Q exhibited very high selectivity for gallium(III) in the presence of large amounts of aluminum(III). The distribution ratio of alumium(III) decreased with increasing aluminum(III) concentrations. The bulkiness of the alkyl group at the 2-position of hydrophobic 8-quinoli-

nol derivatives may play an important role in the selective separation of gallium(III) from aluminum(III). HNBO$_6$Q can be powerful extractants for practical use in analytical chemistry and hydrometalurgy due to the high selectivity and low solubility of these compounds in acidic aqueous solutions.

References

[1] J. Stary, Anal. Chim. Acta, 28 (1963) 132.
[2] K. Motojima and H. Hashitani, Bunseki Kagaku, 9 (1960) 151.
[3] A. Leveque and J. Helgorsky, Proc. International Solvent Extraction Conference, 1977, p. 439.
[4] T. Sato, T. Nakamura, M. Yabuta and H. Oishi, Chem. Lett., (1982) 591.
[5] F. Ma and H. Freiser, Inorg. Chem., 23 (1984) 2344.
[6] K. Ohashi, M. Inose, K. Nakamura and K. Yamamoto, Anal. Sci., 2 (1986) 439.
[7] E. Purnamawaty, T. Amimoto, H. Imura and K. Ohashi, Anal. Sci., 10 (1994) 749.
[8] H. Irving and H.S. Rossotti, J. Chem. Soc., (1954) 2910.
[9] F. Chow, Q. Fernando and H. Freiser, Anal. Chem., 37 (1965) 361.
[10] N.P. Rudenko and A.I. Sevastyanov, Zh. Neorg. Khim., 13 (1968) 184.
[11] A.I. Sevastyanov and N.P. Rudenko, Radiokhimiya, 11 (1969) 251.
[12] K. Ohashi, S. Nakata, M. Katsume, K. Nakamura and K. Yamamoto, Anal. Sci., 1 (1985) 467.
[13] C.F. Baes Jr. and R.E. Measmer, The Hydrolysis of Cations, J. Wiley & Sons, New York, 1976.
[14] H. Imura, M. Watanabe and K. Oshashi, Ibaraki University, Mito, unpublished data, 1991.
[15] D.F.C. Morris and B.D. Andrews, Electrochim. Acta, 12 (1967) 41.
[16] K. Inoue, D. Nakayama, J. Jpn. Inst. Met., 52 (1988) 567.
[17] M. Shiro and Q. Fernado, Anal. Chem., 43 (1971) 1222.

Application of partial least-squares regression to the resolution of highly correlated spectra. Simultaneous spectrofluorimetric determination of Al^{3+}, Ga^{3+} and In^{3+}

M. Blanco*, J. Coello, F. González, H. Iturriaga, S. Maspoch, A.R. Puigdomènech

Departament de Química, Unitat de Química Analítica, Universitat Autònoma de Barcelona, E-08193 Bellaterra, Barcelona, Spain

Abstract

The simultaneous spectrofluorimetric determination of mixtures of aluminium, gallium and indium as their 8-hydroxyquinoline complexes following extraction into chloroform is studied. The high collinearity of the spectra hindered their resolution by multiple linear regression (MLR) methodology; therefore, experimental data were processed by partial least-squares regression (PLSR) methodology. A previous step in the study of three-dimensional fluorescence spectrum is possible to select the best information to quantify this system with high collinearity. Finally the optimal conditions for quantitation, the best data preprocessing procedure and the most suitable spectral mode for calibration were established. Using an external set allowed the three analytes to be determined simultaneously at concentrations below 1 μg ml^{-1} with errors less than 10% for aluminium and indium, and 15% for gallium.

1. Introduction

Spectrofluorimetry is a highly useful interesting analytical technique on account of its increased sensitivity and selectivity. The development of fairly selective spectrofluorimetric methods is facilitated by the fact that only a small fraction of chemical species is naturally fluorescent, and by their discriminating capabilities, which afford appropriate selection of the excitation and/or emission wavelength. In the presence of several fluorescent analytes, wavelength selection is constrained by the width of both the absorption and emission bands; this restricts the number of available specific wavelengths for each analyte.

This severe constraint on mixture resolution has been addressed in various ways including the use of synchronous fluorescence spectra and derivative spectra (of both the fluorescence and the synchronous type [1,2]), which decrease bandwidth and hence increase selectivity. The excitation, emission and synchronous paths, in combination with differentiation techniques [3], and the use of a combination of excitation and

* Corresponding author.

emission spectra by partial least squares [4], are also used for the multivariate resolution of mixtures. Phase-resolved [5] and time-resolved spectrofluorimetry [6], which rely on differences in the fluorescence lifetime between mixture components, are effective in many cases but entail using sophisticated, expensive equipment.

Greater information can be obtained from a three-dimensional spectrum where fluorescence intensities are a function of both the excitation and the emission wavelength [7,8]. Three-dimensional spectra can be used to draw a contour map with the excitation and emission wavelengths represented on two axes and contour lines connecting points of identical fluorescence intensity. The selectivity can be increased by using from the fluorescence intensities three-dimensional matrix a vector of fluorescence intensities corresponding to excitation and emission wavelengths pairs. The selection of the different vectors to assay mixture quantitation has been made by visual inspection of the contour maps of the three complexes, selecting those with the bigger differentiation.

The growing use of computers in the laboratory has fostered the development and application of mathematical algorithms for processing the vast amounts of information provided by modern analytical instruments. Multivariate calibration techniques improve on the selectivity of analytical methods and avoid the need for preliminary separations in many instances [8–10].

In this work, the potential use of the fluorescence three-dimensional matrix information in combination with linear partial least-squares regression for the resolution of ternary mixtures of species with highly correlated absorption and emission spectra was assessed. The application is demonstrated with the oxinates of aluminium, galium and indium in chloroform (oxine or 8-hydroxyquinoline is a widely used extractant for the determination of metal ions [11] which forms complexes that are both fluorescent and UV-absorbing). Resolutions of binary mixtures of the above-mentioned metals [1,8] have been reported; while using multiple linear regression poses few problems—not even with strongly overlapped spectra—tertiary mixtures result in serious errors.

2. Experimental

2.1. Reagents

A 0.01 M 8-hydroxyquinoline solution (Merck) was prepared in water-saturated chloroform (Fluka). A 1 M acetic acid/sodium acetate buffer was also used. Stock analyte solutions of Al^{3+}, Ga^{3+} and In^{3+} containing 1 g l of each ion (Merck) were made in 1 M HCl in order to avoid hydrolysis of the metal ions. The solutions were standardized by back titration with ethylenediaminetetraacetic acid (EDTA) and Zn(II) using Eriochrome Black-T as indicator. Working-strength solutions were obtained from the stocks by appropriate dilution with double-distilled water.

2.2. Apparatus

Spectrofluorimetric measurements were made on a Perkin-Elmer LS 50 instrument furnished with a xenon flash tube, Monk-Gillieson monochromators and 10×10 mm quartz cells. The instrument was connected to an Epson PC AX-2 computer via an RS232-C interface. Its bundled software allows instrumental control, parameter selection, and recording and processing of spectra. All fluorescence measurements were made at a scan rate of 200 nm min^{-1} and 0.5 nm resolution by using excitation and emission windows of 15 and 10 nm, respectively. All spectra were averaged in groups of three as they were recorded.

A Cenco rotary agitator and a Radiometer 29 pH meter furnished with an Ingold U 455-57 glass electrode were also used.

2.3. Software

Experimental data were processed with FL Data Manager® (FLDM), a software package designed for instrumental control and handling of fluorescence spectra recorded on Perkin-Elmer spectrofluorimeters.

Contour plots were constructed with the program SigmaPlot v. 2.0, from Jandel Corp. (Erkrath, Germany). Partial least-squares regres-

sion (PLSR) calibration was done with Unscrambler v. 3.54, from Camo (Norway).

A multicomponent analysis program (MC) developed by the authors in Microsoft QuickBasic v. 4.5 was used for multiple linear regression (MLR) of the sample spectrum on those for the pure components. The program calculated the concentration of the mixture components and their confidence intervals, and also provided information about the regression quality from an analysis of the residuals between real and calculated spectra.

Derivative spectra were obtained with the program FDSG, also developed by the authors, which uses the Savitsky–Golay algorithm and allows the user to chose window size (from 3 to 21 points) and the resolution with which the spectra to be derived are input (0.5–4 nm at 0.5 nm intervals).

In order to compare the quality of the results obtained with the different calibration models used, the relative standard deviations for the error of prediction (RSEP) for each analyte in the sample set were calculated.

$$RSEP(\%) = \sqrt{\frac{\sum\limits_{1}^{n} (c_{found} - c_{added})^2}{\sum\limits_{1}^{n} c_{added}^2}}$$

where c_{found} is the concentration calculated, c_{added} is the concentration present in the mixture and n is the number of samples.

2.4. Extraction and recording of spectra for the metal–oxine complexes

The optimum conditions for extraction of the metal oxinates were determined by using aluminum solutions. The conditions thus established were also used for the other two ions.

The extraction tubes were loaded with 5 ml of a slightly acid solution containing one or more of the metal ions and 10 ml of oxine in chloroform, and placed in a rotary agitator at 50 rev min^{-1} for 10 min. Then, 5 ml of the buffer solution at pH 4.7 was added and further agitation was applied for 10 min. The extraction tubes were next centrifuged at 2000 rev min^{-1} for 5 min and

allowed to stand at about 25°C for 10 min in order to equilibrate both phases. Finally, the phases were separated and the spectrum for the organic one was recorded against a blank prepared using the same procedure.

Standard spectra were recorded for five solutions of each metal ion. The above-described procedure was employed to extract the complexes with oxine. Oxinate spectra were recorded in triplicate. The UV absorption spectra for the previous solutions were standardized and then averaged at a concentration of 3, 8 and 12 μg ml^{-1} for aluminium, gallium and indium, respectively (Fig. 1) so as to obtain a maximum value of absorption as similar as possible for the three complexes. Standard fluorescence spectra were recorded similarly; however, they were stadardized at 12.5 ng ml^{-1} for aluminium, 0.1 μg ml^{-1} for gallium and 0.25 μg ml^{-1} for Indium (Fig. 2) in order to obtain as similar as possible fluorescence spectra. These standard spectra were used for multiple linear regression calculations. Single (rather than triplicate) mixed spectra for the metal ions were recorded by using the same procedure.
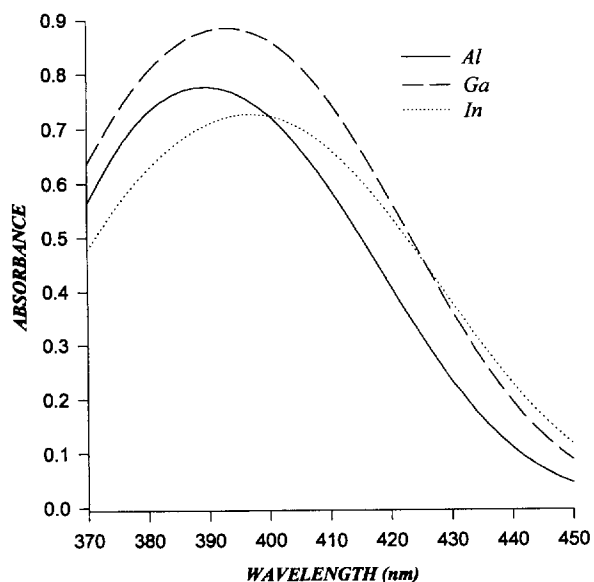

Fig. 1. UV absorption spectra of aluminium (3 μg ml^{-1}), gallium (8 μg ml^{-1}) and indium (12 μg ml^{-1}) oxinates at the wavelength range 300–430 nm.
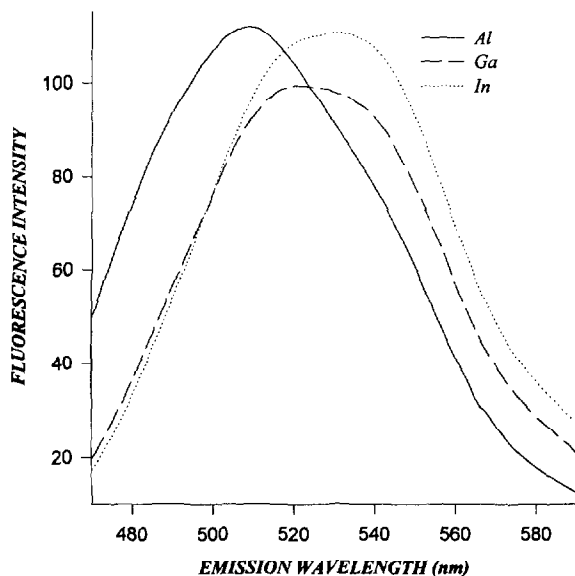
Fig. 2. Standard fluorescence spectra of aluminium (12.5 ng ml^{-1}), gallium (0.1 $\mu g\ ml^{-1}$) and indium (0.25 $\mu g\ ml^{-1}$) oxinates obtained at $\lambda_{ex} = 394$ and λ_{em} from 470 to 590 nm.

3. Results and discussion

3.1. Multiple linear regression

3.1.1. UV absorption spectra

In previous work we studied the simultaneous spectrophotometric determination of aluminium, iron, copper, titanium and nickel in binary, ternary and quaternary mixtures by extracting their oxine complexes into chloroform and using MLR [12] for calibration. Application of the same procedure to mixtures of aluminium, gallium and indium provided the results given in Table 1. As can be seen, binary mixtures were resolved with good precision; however, ternary mixtures could not be resolved at all (quantitation errors exceeded 100% for indium). This can be ascribed to the highly overlapped and virtually identical profile of the absorption spectra for the three complexes (Fig. 1), with the absorption maximum at 390, 394 and 398 nm for aluminium, gallium and indium, respectively. Such strong overlap resulted in high spectral collinearity, which is one of the constraints to MLR application [13]. The

2.5. Contour map

The contour map was drawn from solutions of the metal complexes prepared by applying the above-described procedure to three solutions containing 80 ng ml^{-1} Al^{3+}, 0.59 $\mu g\ ml^{-1}$ Ga^{3+} and 1.92 $\mu g\ ml^{-1}$ In^{3+}. Their emission spectra were recorded between 440 and 620 nm at excitation wavelengths over the range 350–450 nm at 4 nm intervals. The emission spectra obtained at the different excitation wavelengths were used to construct an excitation–emission matrix for each ion, from which the contour map was obtained with the aid of the program SigmaPlot v. 2.0. Fig. 3 shows the contour map for the aluminium oxinate, with its fluorescence maximum at $\lambda_{ex} = 394$ nm and $\lambda_{em} = 508$ nm. The contour maps for the other two ions were very similar with the same λ_{ex} and only differed appreciably in the position of the emission maximum (508, 522 and 531.5 nm for the aluminium, gallium and indium complex, respectively).
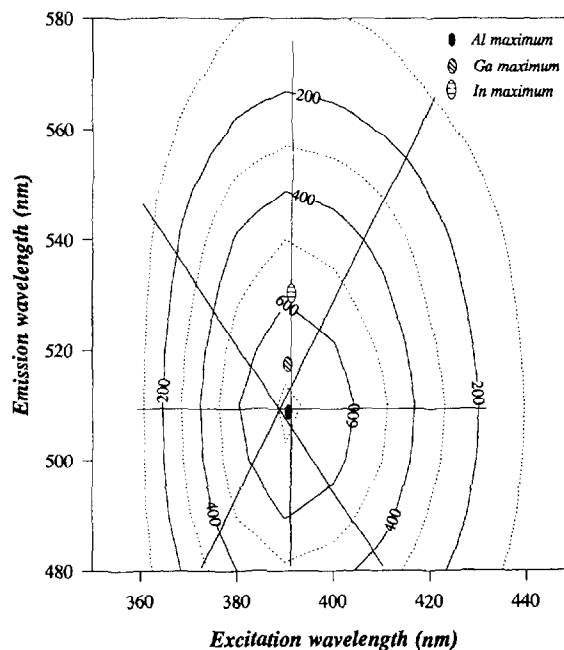

Fig. 3. Fluorescence contour map of aluminium oxinate and the fluorescence maximums of aluminium, gallium and indium oxinates.

Table 1

Quantitation of aluminium, gallium and indium in mixtures by MLR from absorbance or first-derivative spectra recorded over the range 390–430 nm, and fluorescence spectra obtained at $\lambda_{ex} = 390$ and λ_{em} from 470 to 590 nm

| Mixture | n | Concentration ranges (mg l⁻¹) | | | RSEP (%) | | | | | |
| | | | | | Absorbance | | | First-derivative | | |
		Al	Ga	In	Al	Ga	In	Al	Ga	In
Al–Ga	3	1–3	2.5–8	·	3.0	1.0	–	3.8	4.1	–
Al–In	3	1–3	·	3.5–11.5	2.8	–	2.3	4.0	–	4.8
Ga–In	3	–	2.5–8	3.8–11.5	–	2.5	3.7	–	8.8	9.1
Al–Ga–In	3	2	2.5–5.5	2–4.5	23	40	134	25	43	149
					Fluorescence			First-derivative		
		Al(μg l⁻¹)	Ga	In	Al	Ga	In	Al	Ga	In
Al–Ga–In	26	25–83	0.09–0.3	0.25–0.7	12	45	15	9	60	38

n, number of samples.

spectral correlation coefficient is one measure of spectral collinearity; as can be seen in Table 2, the coefficient for our absorption spectra was always greater than 0.99. From the results in Table 1 it follows that RSEP values for the first-derivative spectra were much poorer because derivation raised the spectral resolution but also decreased signals and increased spectral noise.

3.1.2. Fluorescence spectra

The lower collinearity between fluorescence spectra (Table 2), with emission maxima at 508, 522 and 531 for aluminium, gallium and indium, respectively (Fig. 2), encouraged us to attempt their resolution by MLR from standard spectra for pure solutions of each metal ion by using the wavelength of maximum absorption for the aluminium complex as the excitation wavelength for the three ions.

Table 2

Correlation coefficients for spectra

	Al–Ga	Al–In	Ga–In
Absorbance[a]	0.9973	0.9905	0.9979
Fluorescence[b]	0.9895	0.9877	0.9998
Fluorescence[c]	0.9598	0.9372	0.9973

[a] Wavelength range 390–430 nm.
[b] $\lambda_{ex} = 390$ nm; $\lambda_{em} = 470$–590 nm.
[c] $\lambda_{ex} = 394$ nm; $\lambda_{em} = 470$–590 nm.

An overall 26 solutions containing the three metal ions at concentrations over the previous ranges were prepared and quantified from their emission and first-derivative spectra. Table 1 shows the prediction errors obtained. As can be seen, RSEP values were much lower than those resulting from the absorbance spectrum but were still too high for gallium and indium. Such errors were even higher for first-derivative spectra as the likely result of the increased spectral noise (Fig. 4). In order to minimize the effect of noise on the quantitation, spectra were derived by using the Savitsky–Golay algorithm as implemented in the program FDSG, with optimization of both the number of points included in the window and the resolution with which the spectra to be derived were input. Very large window sizes resulted in exceedingly diminished signals and the loss of spectral information. The best signal-to-noise ratio for the intended purpose was obtained with a 7-point window and 2 nm resolution; even so, the errors were too large.

The high collinearity between the emission spectra hindered resolution of the mixtures; this prompted us to explore the potential use of the fluorescence three-dimensional matrix information in combination with MLR [8] in order to select a wavelength set with a lower correlation that might improve on the previous results. The excitation–
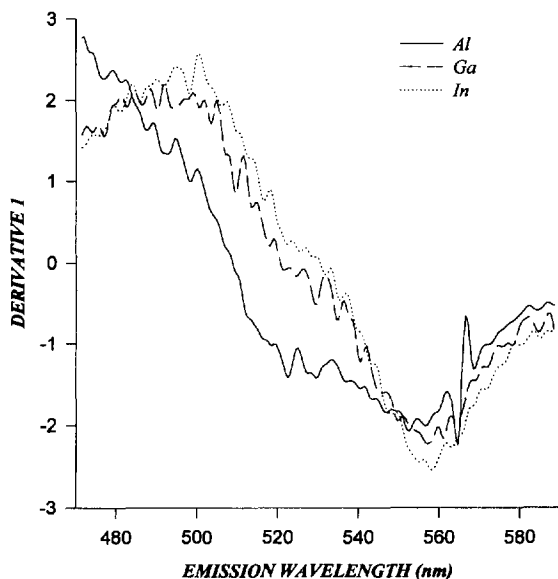
Fig. 4. Non-smoothed first-derivative fluorescence spectra of standard fluorescence spectra showed at Fig. 2.

emission matrix contained abundant information (9000 fluorescence data points for each sample), which allowed a subset of excitation-emission wavelength pairs to be selected for calibration and sample quantitation. Such points formed vectors in the contour plot that was chosen in such a way as to maximize the differences between the analytes. The following vectors were tested (Fig. 4).

(a) Recording the emission spectrum from 450 to 600 nm using $\lambda_{ex} = 394$ nm.

(b) Recording the excitation spectrum from 360 to 430 nm using the maximum emission wavelength for each complex as its λ_{em}.

(c) Recording the fluorescence intensity at various excitation-emission wavelength pairs over the ranges 360-430 nm (λ_{ex}) and 450-600 nm (λ_{em}) conforming to the equations $\lambda_{em} = 1.8 \ \lambda_{ex}$ and $\lambda_{em} = -1.25 \ \lambda_{em} + 995$.

(d) Combinations of the previous three.

The best quantitation results (maximum discrimination between the three analytes) were obtained with the model defined by the vector including $\lambda_{ex} = 394$ nm and λ_{em} between 450 and 600 nm. However, as can be seen from Table 1, the results were not significantly better: while lower, spectral collinearity was still too high—especially between the gallium and indium spectra (Table 2).

The fluorescence spectra obtained under these conditions were used in all the subsequent calculations.

3.2. Partial least-squares regression

Since none of the vectors tested decreased spectral collinearity for the system studied to an appreciable extent—prediction errors were thus relatively high—, we assayed PLSR calibration, which minimizes collinearity between the variables and is less markedly affected by noise [13].

3.2.1. Construction of the calibration matrix

The fluorescence spectra for 40 binary and ternary mixtures of the three metal ions at concentrations over the ranges 0-83 ng ml^{-1} aluminium, 0-0.30 μg ml^{-1} gallium and 0-0.76 μg ml^{-1} indium were recorded. Of the 40 mixtures, 24 were used to construct the calibration matrix and 16 as the external validation set to determine the predictive capacity of the method.

One key to the correct performance of PLSR is an appropriate choice of the number of principal components, which should account as much as possible for the experimental data without resulting in overfitting [13]. There are various recommended criteria for selecting the optimum number of principal components [14]. We used the cross-validation method and as many cancellation groups as objects were included in the calibration matrix, as well as the number of principal components minimizing the validation variance as the optimum number of principal components.

A preliminary model was constructed from fluorescence data for the previous samples over the wavelength range studied (450-600 nm). Then, the output parameters provided by the software were used to determine the objects and variables that were either outliers or contributed no significant information to the model. Such objects and variables were discarded and a calibration matrix consisting of 21 mixtures (three objects were removed to be detected like outliers, and data were recorded at 2 nm intervals over the wavelength range 470-550 nm) was constructed.
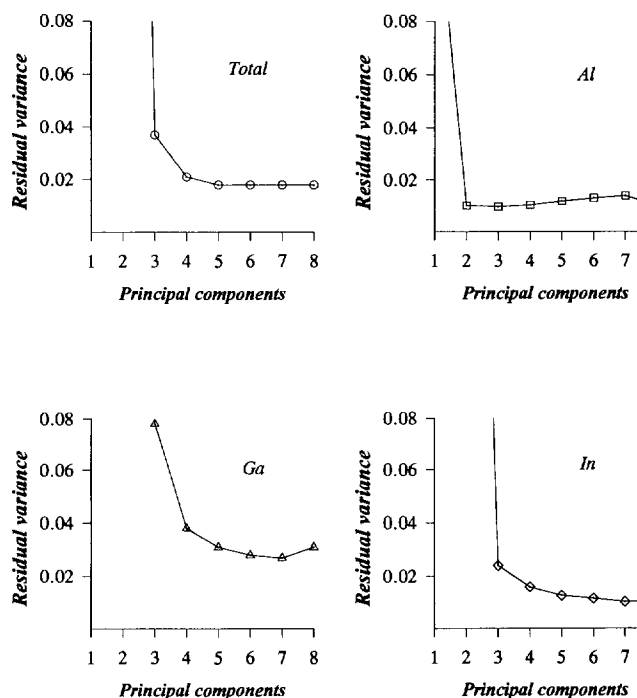
Fig. 5. Overall residual validation variance (total and for each ion) calculated with PLS2.

We assessed two data pretreatment procedures (mean-centring and autoscaling), and two PLSR calibration modes, namely PLS2, which uses all the analytes to be determined, and PLS1, which constructs the calibration model for each of the analytes. All these variants were implemented in two spectral modes: fluorescence and first derivative. The model with the maximum predictive capacity was determined from the overall error of prediction for each analyte in the validation samples.

A plot of the residual validation variance for each analyte and the overall residual validation variance against the number of principal components (Fig. 5) revealed the minimum value for the latter—the criterion used to determine the number of PCs to be included in the model—to be provided by five PCs with PLS2. On the other hand, the PLS1 calibration mode led to a different number of PCs for each ion (three for aluminium and seven for gallium and indium), also shown in Fig. 5. However, the predictive capacity was similar for the two modes.

Table 3 shows the prediction errors obtained for each analyte by applying the four models to the 16 external validation samples. The highest predictive value was that of the PLS2 model with autoscaled fluorescence intensity data (the RSEP was 7% for aluminium and indium and 15% for gallium). The errors for the three ions were substantially lower relative to the previous treatments.

The errors obtained for the three analytes with first-derivative spectra were greater than the previous ones—particularly those for gallium and in-

Table 3
Overall validation (in %) errors obtained with PLS2

	Al	Ga	In
Fluorescence			
mean-centring	7.1	16.4	8.6
autoscaling	6.8	14.9	7.5
First-derivative			
mean centring	9.1	42.3	20.5
autoscaling	8.3	44.8	22.6

Table 4
Concentrations of the three metal ions calculated by PLS2 from autoscaled fluorescence data for the validation samples, and overall prediction errors

[Al] (ng ml^{-1})		[Ga] (μg ml^{-1})		[In] (μg ml^{-1})	
Added	Found	Added	Found	Added	Found
53	51	0.20	0.22	0.51	0.46
27	30	0.10	0.12	0.76	0.71
80	70	0.10	0.12	0.25	0.22
27	24	0.20	0.18	0.51	0.52
50	49	0.12	0.15	0.61	0.55
66	67	0.24	0.24	0.30	0.30
33	30	0.12	0.17	0.38	0.29
50	52	0.18	0.19	0.61	0.61
66	64	0.18	0.20	0.46	0.44
0	1	0.12	0.12	0.78	0.78
50	50	0.15	0.12	0.61	0.63
66	66	0.12	0.16	0.30	0.23
33	39	0.09	0.08	0.53	0.55
33	33	0.15	0.16	0.61	0.57
33	30	0.21	0.19	0.69	0.70
83	86	0.12	0.13	0.30	0.29
Prediction error (%)					
6.8		14.9		7.5	

dium—since derivation increased spectral resolution but diminished signals, decreased the sensitivity to gallium and indium relative to aluminium, and increased noise.

In order to better illustrate the quality of the results obtained and the real significance of the RSEP values given in the previous tables, Table 4 shows the individual results for the 16 samples included in the external validation set. As can be seen, the resolution quality was highly satisfactory for all the mixtures.

4. Conclusion

Spectral collinearity is a major constraint to the simultaneous quantitation of several analytes using a multivariate calibration technique. The large amount of information supplied by spectrofluorimetry, which encompasses a three-dimensional space composed of λ_{ex}, λ_{em} and fluorescence intensity, allows an appropriate data

set to be used to reduce collinearity. Even so, high collinearity can prevent correct resolution of a mixture (e.g. the proposed mixture) by multiple linear regression. In such an event, applying partial least-squares regression to data for the best of several high correlated vectors can minimize collinearity problems and enable correct resolution of the mixtures. In this respect, we should emphasize the good resolution achieved for the mixture studied in this work despite the low concentration levels involved.

Acknowledgements

References

[1] F. García Sánchez, M. Hernández López and J.C. Márquez Gómez, Spectrochim. Acta, 43A (1987) 101.

[2] M. Salgado, C. Bosch, F. Sánchez Rojas and J.M. Cano Pavón, Quim. Anal., 5 (1986) 374.

[3] R. Jones, T.J. Coomber, J.P. McCormick, A.F. Fell and B.J. Clarck, Anal. Proc., 25 (1988) 381.

[4] A. Muñoz de la Peña, I. Durán-Merás, M.D. Moreno, F. Salinas and M. Martinez Galera, Fresenius' J. Anal. Chem., 351 (1995) 571.

[5] L.B. McGown and F.V. Bright, Crit. Rev. Anal. Chem., 18 (1987) 245.

[6] E. Soini and J.A. Lövgren, Crit. Rev. Anal. Chem., 18 (1987) 105.

[7] F. García Sánchez. A.L. Ramos Rubio, V. Cerdà and M.T. Oms, Anal. Chim. Acta, 228 (1990) 293.

[8] M.T. Oms, R. Forteza, V. Cerdà, S. Maspoch, J. Coello and M. Blanco, Anal. Chim. Acta, 233 (1990) 159.

[9] M. Blanco, J. Coello, F. González, H. Iturriaga and S. Maspoch, Anal. Chim. Acta, 226 (1989) 271.

[10] W. Lindberg, J.A. Persson and S. Wold, Anal. Chem., 55 (1983) 643.

[11] A. Fernández-Gutierrez and A. Muñoz de la Peña, in S.G. Shulman (Ed.), Molecular Luminescence Spectroscopy: Methods and Applications: Part 1, Wiley-Interscience, New York, 1985, Chapter 4, pp. 371–546.

[12] M. Blanco, J. Coello, F. González, H. Iturriaga and S. Maspoch, Anal. Chim. Acta, 230 (1990) 221.

[13] H. Martens and T. Naes, Multivariate Calibration, John Wiley, New York, 1989.

[14] J.E. Jackson, User's Guide to Principal Components, John Wiley, New York, Chapter 2, 1991.

Calcium carbonate solubility: a reappraisal of scale formation and inhibition

Jean-Yves Gal[a,*], Jean-Claude Bollinger[b], Henri Tolosa[c], Nathalie Gache[a]

[a]*Laboratoire de Chimie Analytique, Université de Montpellier-II, Sciences & Techniques du Languedoc, 34095 Montpellier, France*
[b]*Laboratoire de Chimie Analytique, Sciences de l'Eau & de l'Environnement, Faculté des Sciences, 87060 Limoges, France*
[c]*Service Physico-Chimie, Laboratoire Central des Industries Electriques, 92266 Fontenay-aux-Roses, France*

## Abstract

Considerable disparity exists in the published thermodynamic data for selected species in the $Ca^{2+}/CO_2/H_2O$ system near 25°C and 1 atm pressure. Some authors doubt the significance of $CaCO_3^0(aq)$ complexes although there is experimental evidence of their occurrence. Evaluation of all the published experimental and estimated data for aqueous calcium carbonate species confirms that the consistent set of constants given by Plummer and Busenberg in 1982 is the best available, and suggests a formation constant $\log \beta = 3.22$ for $CaCO_3^0(aq)$. This value was confirmed by additional experimental data and calculations using a specially developed computer program. The solubility s and solubility product K_s are critically evaluated for each solid polymorph (amorphous $CaCO_3$, ikaite, vaterite, aragonite and calcite) using a hydrated ion pair model and we give coherent explanations for the calcium carbonate precipitation/dissolution process and the existence of supersaturated waters. The practical cases of scale formation and its inhibition by phosphonate-type compounds are discussed and explained with the same model, taking into account the $CaCO_3^0(aq)$ species.

Keywords: Calcium carbonate; Scale formation; Scale inhibition; Phosphonates

1. Introduction

In a previous paper [1], we presented a model for the precipitation of an insoluble ionic compound MX by the initial formation of a partially hydrated uncharged soluble complex species MX_h^0 whose limiting solubility s depends on its degree of hydration. We can therefore write:
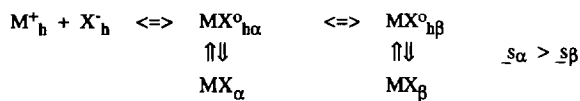
$$M_h^+ + X_h^- \Leftrightarrow MX_h^0 \Leftrightarrow MX\downarrow$$
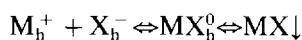
* Corresponding author. Fax: (33) 67.63.35.96.

$$\beta = |MX_h^0|/|M_h^+||X_h^-| \quad \text{and} \quad K_s = |M_h^+||X_h^-|$$

where $|\ |$ stands for activity. At equilibrium, $|MX_h^0| = s$, therefore $\beta = s/K_s$.

The more hydrated forms are more soluble and give higher K_s values. The more stable crystalline forms are generally those with lower solubility product K_s values, and therefore lower limiting solubility s values.

Since the value for the formation constant β probably does not depend significantly on the

$$M^+_h + X^-_h \iff MX^o_{h\alpha} \iff MX^o_{h\beta}$$
$$\Updownarrow \qquad\qquad \Updownarrow \qquad\qquad \underline{s}\alpha > \underline{s}\beta$$
$$MX_\alpha \qquad\qquad MX_\beta$$

Scheme 1.

hydration degree of the MX^0 species, if we know β and K_s, it is easy to evaluate the value of s according to the simple relationship

$$\log s = \log K_s + \log \beta$$

The value of K_s depends on the experimental method used, precipitation giving higher values than redissolution. This can be easily explained if we assume that the hydrated forms are first produced during precipitation and progressively evolve towards less hydrated forms. The kinetics of such processes are very important because if equilibrium is reached rapidly, the most insoluble compound should precipitate immediately.

When a compound has several different solid forms, it is assumed that these correspond to solutions of different hydrated forms of the same uncharged ion pair complex. It is probably correctly written as Scheme 1.

According to this scheme, it is possible to proceed from MX_α to MX_β by a redissolution–precipitation process since a $MX^0_{h\alpha}$-saturated solution is also saturated in $MX^0_{h\beta}$. This temporary formation of two different compounds makes it difficult to determine the corresponding solubility products.

However, in the case of redissolution of MX_β, MX_α should not precipitate because $s_\alpha > s_\beta$. MX_α supersaturation cannot therefore occur, and

only $K_{s\beta}$ can be determined by a study of MX_β dissolution.

Scheme 1 enables us to understand both why the more soluble forms generally precipitate first, and how, if we do not immediately dry out the first crystals obtained, solid phases can evolve towards the most thermodynamically stable species.

The formation of calcium carbonate scale is a subject of great practical interest because of its consequences for industrial or drinking water supplies. Various solid polymorphs can be obtained by varying temperature and other experimental conditions, and researchers now have a good knowledge of the influence of temperature on calcium carbonate solubility products (Table 1).

In the present paper, we reconsider this well-known calco-carbonic equilibrium for, although a large body of literature exists on this subject, the situation is still somewhat confusing because no clear link has been made between the studies carried out in various fields (explanation of the phenomena in hydrogeology and soil chemistry; tap water treatment and scale formation; acid rain effects; physiological equilibria during breathing or photosynthesis, etc.). We attempt here, in light of a new analysis of its thermodynamic aspects, to explain the calcium carbonate precipitation/redissolution process, focusing on the usefulness of the $\beta = s/K_s$ relationship. We clearly show the importance of the various hydrated forms of the soluble $CaCO^0_3(aq)$ complex on calcium carbonate precipitation, and use them to explain the behaviour of phosphonate-type scale inhibitors.

Table 1
Solubility products for the various forms of calcium carbonate

Form	Structure	$-\log K_s$ (at 25°C)	Temperature law (T in K; t in °C)	Reference
amorphous	–	6.40	$-\log K_s = 6.1987 + 0.005336t + 0.0001096t^2$	21
ikaite	monoclinic	6.62	$-\log K_s = 1696/T + 0.9336$	9
vaterite	hexagonal	7.91	$-\log K_s = +172.1295 + 0.077993T - 3074.688/T - 71.595 \log T$	20
aragonite	orthorhombic	8.34	$-\log K_s = +171.9773 + 0.077993T - 2903.293/T - 71.595 \log T$	20
calcite	rhomboedric	8.48	$-\log K_s = +171.9065 + 0.077993T - 2839.319/T - 71.595 \log T$	20

2. The association constant for the calcium/carbonate ion pair

The existence of the $CaCO_3^0(aq)$ ion pair in solution was first reported by Greenwald [2] in 1941. Based on calcite solubility measurements, he gave the value $\log \beta = 3.0$ for the $CaCO_3^0(aq)$ formation constant at 25°C. In 1960, Garrels et al. [3] used this ion pair concept for calcium carbonate solubility in seawater, but in 1961 these same authors [4] privileged the part of $MgCO_3^0$ and of $NaCO_3^-$ in their discussion. Thereafter, even the concept of such a $CaCO_3^0$ species was almost systematically ignored, although one year later they gave [5] the value $\log \beta = 3.2$. However, no recent papers dealing with calcium carbonate dissolution kinetics, and only some concerning scale formation [6–9], take $CaCO_3^0(aq)$ into consideration.

These papers by Garrels and his co-authors [3–5] were poorly interpreted by other researchers, and several unfortunate events have contributed to a failure of the $CaCO_3^0(aq)$ concept. In 1968, Nakayama [10] carried out a series of experiments (whose data will be discussed below) giving $\log \beta = 4.48$, but his work was criticized in 1970 by Lafon [11] who, based on the results of Nakayama [10] and Grezes and Basset [12], gave the value $\log \beta = 3.1$. In 1968, Langmuir [13] had already concluded that Garrels' value was overestimated, and in 1974 criticized [14] Lafon's procedure and minimized the importance of $CaCO_3^0(aq)$ compared to $CaHCO_3^+$. The same year, however, Langmuir contributed significantly to the determination of the formation constants for $CaCO_3^0(aq)$ and $CaHCO_3^+$ between 0°C and 50°C in a second paper [15]. These values (with $\log \beta = 3.20$ at 25°C) are, in fact, in good agreement with those of Garrels et al. [5] and Lafon [11].

In 1976, while Larson [16] proposed a value of $\log \beta = 3.22$ similar to those above, Martynova et al. [17–19] proposed a value, $\log \beta = 4.45$, similar to that of Nakayama, and Avnimelech et al. [6] used $\log \beta = 4.48$ without indicating their source.

In 1982, Plummer and Busenberg [20] published values now used as the reference values between

0°C and 90°C, with $\log \beta = 3.22$ at 25°C. These authors did not limit themselves to computer calculations using calcite redissolution data under various CO_2 partial pressures, but obtained, independently, the formation constants for the $CaCO_3^0$ (aq) and $CaHCO_3^+$ species by measuring the pH at equilibrium in various $K_2CO_3/CaCl_2$ mixtures in the absence of precipitate. Using these values, Brecevic and Nielsen determined the solubility products for the amorphous [21] and hexahydrated (or ikaite) [22] forms of calcium carbonate.

In 1983, the whole subject of formation constants versus temperature for the various (soluble and insoluble) polymorphs of calcium carbonate was studied again by Le Guyader et al. [23,24] who carried out calculations starting from solubility measurements at different pH values, and proposed a value, $\log \beta = 4.31$, again similar to that of Nakayama.

During on-going studies in the field of water treatment, Le Guyader et al. [7] attempted unsuccessfully to improve the classic Legrand–Poirier plots [25], their values being too discordant with those of Plummer and Busenberg. Although the $\beta = s/K_s$ relationship was reported in their first paper [23], it appears that, having used not only calcite redissolution, these authors may have obtained reproducible supersaturated solutions. By choosing $-\log K_s = 8.48$ for their calculations (like Plummer and Busenberg [20]), all experimental errors made in the s measurements are probably found in their β values. It is somewhat surprising that only Le Guyader et al. and Lafon explicitly take into consideration the need to determine a constant solubility value s, if equilibrium is in fact obtained.

If we use Plummer and Busenberg's $\log \beta$ and $\log K_s$ values at 25°C for calcite, the $CaCO_3^0$ (aq) limiting solubility is 5.5×10^{-6} mol L^{-1}. The calcium balance at equilibrium would therefore be only slightly, if ever, affected by the existence of this species.

We will show here that this is not the case, however, in natural systems or in cooling towers or heat exchangers when there is supersaturation. Scale formation kinetics can be better explained if the presence of hydrated $CaCO_3^0$ species in the solution is taken into consideration. It is re-

grettable that such a large body of contradictory results have delayed our knowledge of such an economically important compound whose correct formation constant ($\log \beta = 3.15$ at 25°C) was given as early as 1976 by Smith and Martell [26].

3. Comparison of the various sets of constants

We used the experimental data of Nakayama [10] for numerous long-term calcite redissolution studies under controlled carbon dioxide partial pressures at 25°C. These data include values for CO_2 partial pressure, total dissolved calcium concentration (determined by atomic absorption), pH and pCa, and calculated values for $\log \beta$ and $CaCO_3^0$ concentrations. It is regrettable that Nakayama chose to rely on ion selective electrode data for $pCa = -\log|Ca^{2+}|$, in spite of their imprecision under his experimental conditions. He was immediately criticized for this since only 28 mV corresponds to a ten-fold variation in calcium ion activity. Although it is possible to draw an even curve from the measured pH and total calcium concentration values (which seem to indicate that all solutions are in the same state of equilibrium) the $CaCO_3^0(aq)$ solubilities calculated by Nakayama are not constant. This, we believe, explains his $\log \beta$ values.

Knowing the P_{CO_2} values and the necessary thermodynamic constants, we were able to calculate the total calcium concentrations $[Ca^{2+}]_t$ and pH values. In Figs. 1 and 2 Nakayama's experimental data are compared to our values calculated using data in Table 2 where $\log \beta_1$ is the $CaHCO_3^+$ formation constant and

$$[Ca^{2+}]_t = [Ca^{2+}] + [CaHCO_3^+] + [CaCO_3^0]$$
$$+ [CaOH^+] + [Ca(OH)_2^0]$$

where [ ] stands for concentration. The equilibrium constants for carbon dioxide solubility and acidities are those used by Plummer and Busenberg [20]. For $CaOH^+$ we used $\log \beta = 1.30$ [27], and for $Ca(OH)_2^0$ we estimated $\log \beta = 0.12$ from thermodynamic data and retained $-\log K_s = 5.19$ [26]. Activity coefficients were calculated according to Davies [28].
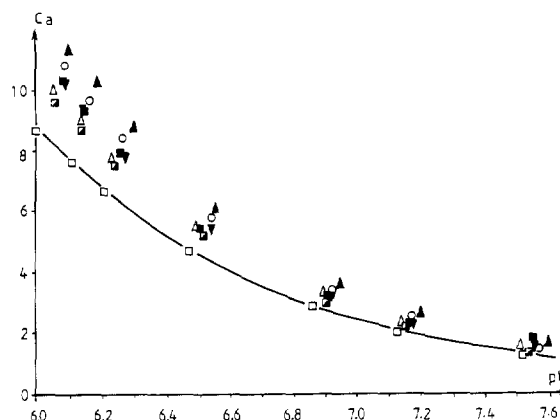

Fig. 1. Total calcium concentration (10^{-3} mol L^{-1}) versus pH: comparison of Nakayama's experimental results [10] □ and values calculated using constants taken from ▼, Smith and Martell [26]; ■, Lafon [11]; ○, Avnimelech and Raveh [6]; ▲, Nakayama [10]; △, Martynova et al. [17–19]; and ▨, Reardon and Langmuir [15].

The best agreement was obtained with the sets of constants from Plummer and Busenberg [20] and Le Guyader et al. [23]. This seems to validate previous studies minimizing the effect of $CaCO_3^0$ formation on calcocarbonic equilibria. Plummer and Busenberg's data give a $CaCO_3^0(aq)$ limiting solubility $s = 5.5 \times 10^{-6}$ mol L^{-1}, and those of Le Guyader et al. give $s = 6.8 \times 10^{-5}$ mol L^{-1}. This gives a more than ten-fold variation, without any modification of the total calcium solubility value, as calculated at the calcite solubility equilibrium. Solubility data alone therefore do not
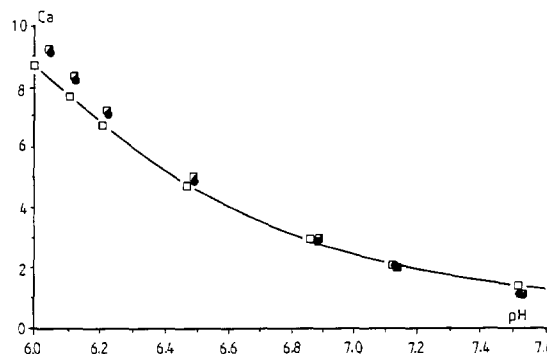

Fig. 2. Total calcium concentration (10^{-3} mol L^{-1}) versus pH; comparison of Nakayama's experimental results [10] □ and values calculated using constants taken from ▨, Le Guyader et al. [23] and ●, Plummer and Busenberg [20].

Table 2

Various thermodynamic constant sets for calcite at 25°C. (K_s = solubility product; β_1 = CaHCO$_3^+$ formation constant; β = CaCO$_3^0$ (aq) formation constant; s = calculated limiting solubility.)

Reference	$-\log K_s$	$\log \beta_1$	$\log \beta$	$-\log s$
Smith and Martell [26]	8.35	1	3.15	5.20
Lafon [11]	8.40	1.26	3.1	5.30
Avnimelech and Raveh [6]	8.35	1.24	4.48	3.87
Nakayama [10]	8.31	1.25	4.48	3.83
Martynova et al. [17–19]	8.44	1.26	4.45	3.99
Reardon and Langmuir [15]	8.42	1.01	3.20	5.22
Plummer and Busenberg [20]	8.48	1.11	3.22	5.26
Le Guyader et al. [23]	8.48	1.14	4.31	4.17

enable us to choose the best CaCO$_3^0$(aq) formation constant.
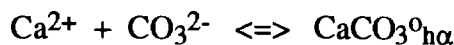
4. Supersaturated solutions

Because of its economical importance, calcium carbonate precipitation has been the subject of many studies. Heterogeneous reaction causes scaling on walls, notably of heating or cooling exchangers. Homogeneous kinetics involve precipitation in the bulk solution and have recently been better explained. By studying supersaturated solutions at various temperatures, sometimes with added inhibitors, Sawada [8], and more recently Clarkson [9], demonstrated that the ionic activity product

$$IAP = |Ca^{2+}||CO_3^{2-}|$$

remains stable for a certain length of time (which depends on temperature), equalling successively the solubility products of the amor-

phous, vaterite, aragonite and, finally, calcite forms. This clearly indicates that calcite formation involves the temorary formation of all of the other, more soluble, forms of calcium carbonate. This can be presented by Scheme 2 to which we have added, according to Clarkson [9], the hexahydrate CaCO$_3$·6H$_2$O, which is only obtained at low temperature or in the presence of inhibitors, and was characterized only recently in natural systems (in 1963 by Pauly [29] who named it ikaite, i.e. "from the Ika fjord").
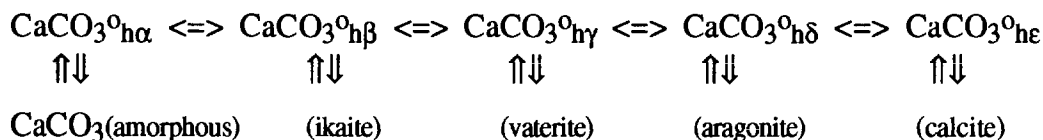
If we assume that $\log \beta$ at a given temperature is similar for all hydrated calcium carbonate species, it is possible to estimate the total CaCO$_3^0$(aq) concentration, depending on the nature of the polymorph at equilibrium. Values were calculated (Table 3) using $\log \beta$ data given by both Plummer and Busenberg [20] (3.22) and Le Guyader et al. [23] (4.31). It is clear that Le Guyader et al. overestimated the CaCO$_3^0$(aq) limiting solubility. Since the total calcium con-

$$Ca^{2+} + CO_3^{2-} \Leftrightarrow CaCO_3{}^0{}_{h\alpha}$$

or (according to the pH)

$$Ca^{2+} + HCO_3^- + H_2O \Leftrightarrow CaCO_3{}^0{}_{h\alpha} + H_3O^+$$

and hereafter

$$CaCO_3{}^0{}_{h\alpha} \Leftrightarrow CaCO_3{}^0{}_{h\beta} \Leftrightarrow CaCO_3{}^0{}_{h\gamma} \Leftrightarrow CaCO_3{}^0{}_{h\delta} \Leftrightarrow CaCO_3{}^0{}_{h\epsilon}$$

$$\Updownarrow \qquad \Updownarrow \qquad \Updownarrow \qquad \Updownarrow \qquad \Updownarrow$$

CaCO$_3$(amorphous)	(ikaite)	(vaterite)	(aragonite)	(calcite)

Scheme 2

Table 3

Limiting solubility (in 10^{-3} mol L^{-1}) at 25°C for each CaCO$_3$ polymorph, calculated from the CaCO$_3^0$(aq) formation constants given by Plummer and Busenberg [20], and by Le Guyader et al. [23].

Solid form	Ref. [20]	Ref. [23]
amorphous	0.66	8.13
ikaite	0.40	4.90
vaterite	0.02	0.25
aragonite	0.008	0.093
calcite	0.005	0.068

centration in solution during scale formation is usually about several millimoles per litre, it would not be possible to obtain the calculated values for the well-known transition through the amorphous form. Using the Plummer and Busenberg value, however, we arrive at a plausible CaCO$_3^0$(aq) concentration, which cannot be disregarded, of around one millimole at the beginning of precipitation.

In order to confirm these calculations, we measured the critical precipitation pH, as reported by Venderbosch and Overman [30] according to Feitler [31]. The pH of a sample was measured during continuous, slow addition of a sodium hydroxide solution until saturation was reached and the

solution became cloudy. The pH decreased rapidly during calcium carbonate precipitation and finally stabilized. The maximum pH value is the critical pH (pH$_c$), and the equilibrium value is the saturation pH (pH$_s$). We have developed a computer model that uses analytical data for a water sample to simulate the titration curve and enables us to directly determinate pH$_c$ and pH$_s$ values. We will show in a forthcoming paper that this computer program could be applied to nuclear power plants cooling tower management. It takes into consideration all of the complexes that can be formed, as well as the variations in ionic strength caused by reactions and dilution. Comparison of experimental and calculated titration curves can reveal the presence of a precipitation inhibitor. The software can also predict the pH$_c$ value at any temperature.

In this computer program, we used the Plummer and Busenberg value [20] for the CaCO$_3^0$ (aq) formation constant. In order to validate our choice, we used artificial solutions containing 2×10^{-3} mol L^{-1} NaHCO$_3$, 4×10^{-3} mol L^{-1} CaCl$_2$ and 2×10^{-4} mol L^{-1} HCl. With a Tacussel-Radiometer titration unit 'Titrimax TT100-TT200' equipped with its electroburette EBX-2, we titrated a 100 mL sample with 10^{-2} mol L^{-1} NaOH at a 0.38 mL min^{-1} addition rate. The pH was measured with
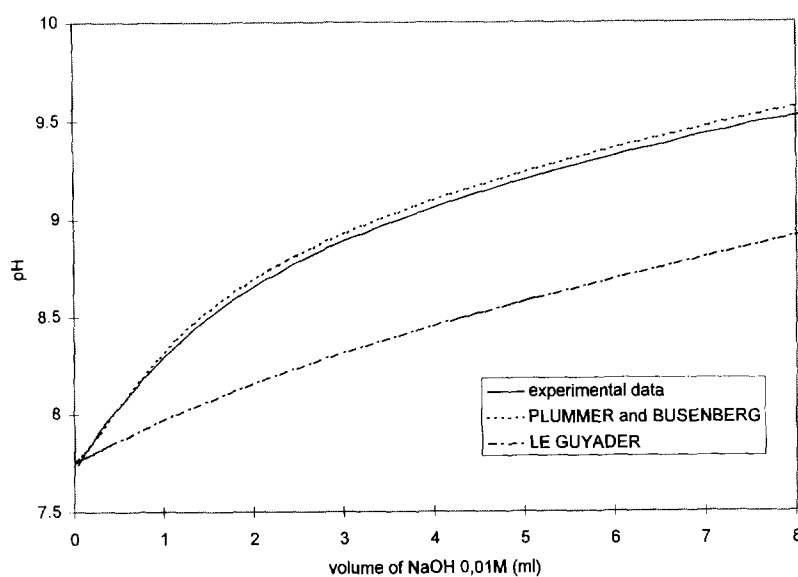

Fig. 3. pH variation during the addition of 10^{-2} mol L^{-1} NaOH solution to 100 mL of a solution containing 2×10^{-3} mol L^{-1} NaHCO$_3$, 4×10^{-3} mol L^{-1} CaCl$_2$ and 2×10^{-4} mol L^{-1} HCl. Comparison of experimental and calculated values.
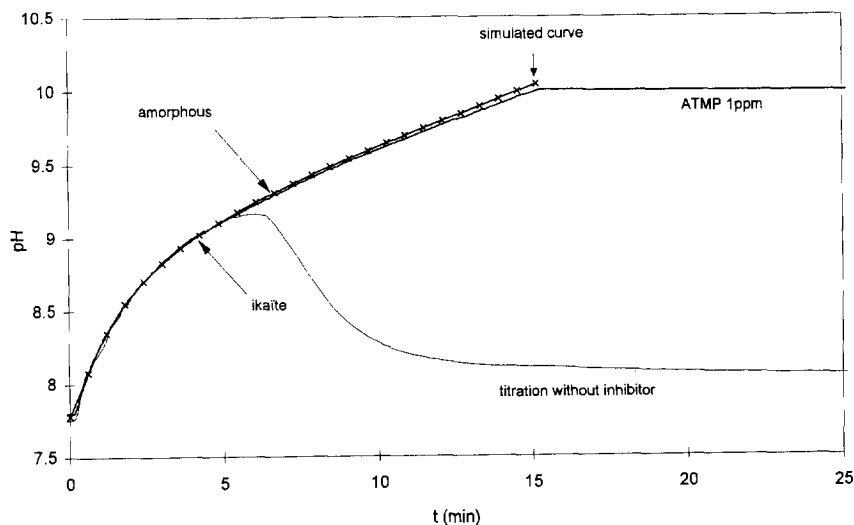
Fig. 4. pH as a function of time during and after the addition of 5×10^{-2} mol L^{-1} NaOH to 100 mL of a solution containing 4×10^{-3} mol L^{-1} NaHCO$_3$, 4×10^{-3} mol L^{-1} CaCl$_2$ and 5×10^{-4} mol L^{-1} HCl, without inhibitor and with 1 ppm ATMP. Total duration of NaOH addition, 15 min. Experimental curves and calculated data. The theoretical precipitation limits for ikaite and amorphous CaCO$_3$ are indicated by arrows.

a Hamilton combination glass electrode of the 'Flushtrode' type, in a thermostated cell at 25°C. The titration curves were simulated with our computer program. Data before precipitation (Fig. 3) gives evidence of a very good correlation between the experimental and simulated curves. When we used the value 4.31 instead of 3.22 for the CaCO$_3^0$ formation constant, there was a pH deviation of ca. 0.75 units.

Plummer and Busenberg's data [20] for the CaCO$_3^0$(aq) and CaHCO$_3^+$ formation constants, respectively

$$\log \beta = -1228.732 - 0.299444T + 35\,512.75/T$$
$$+ 485.818 \log T$$

$$\log \beta_1 = 1209.120 + 0.31294T - 34\,765.05/T$$
$$- 478.782 \log T$$

(where T is the temperature in kelvin) are therefore the most acceptable.

Studies were also carried out with other mixtures, halting NaOH addition when the solution became cloudy. We used artificial solutions containing 4×10^{-3} mol L^{-1} NaHCO$_3$, 4×10^{-3} mol L^{-1} CaCl$_2$ and 5×10^{-4} mol L^{-1} HCl. A 100 mL sample was titrated with 5×10^{-2} mol L^{-1} NaOH

at a 0.33 mL min^{-1} addition rate. Experiments were also done with the addition of 1 ppm (3.3×10^{-6} mol L^{-1}) of aminotris-(methylenephosphonic acid) (ATMP). Fig. 4 shows typical experimental titration curves obtained with and without this scale inhibitor and, for comparison, simulated curves assuming a supersaturated medium. Initial solutions were already supersaturated with respect to vaterite, aragonite and calcite, and the theoretical saturation thresholds for ikaite and amorphous calcium carbonate are indicated on the curves.

At 25°C, there is a divergence between simulated and experimental curves without ATMP inhibitor near the ikaite precipitation point (for 2.10 mL of added NaOH). With inhibitor and under our operating conditions, a pH of ≈ 10 is obtained without any turbidity, a point that will be discussed more thoroughly below. Since NaOH addition is stopped at a volume of 5 mL, only the slight pH decrease indicates that precipitation continues very slowly, as opposed to what occurred in the preceding case.

Without inhibitor and even at ambient temperature, calcium carbonate precipitation seems to be initiated by the ikaite polymorph, which thereafter changes into vaterite. For temperatures over 30°C,
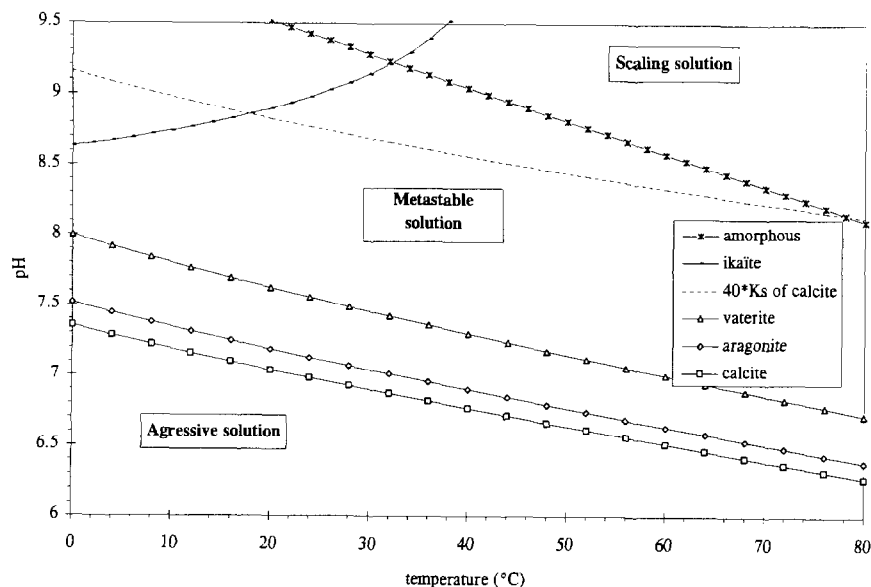
Fig. 5. The effect of temperature on the precipitation pH of the various $CaCO_3$ polymorphs, as calculated for a water sample with analytical data given in Table 4.

ikaite becomes more soluble than the amorphous form because its solubility increases with temperature (in spite of its increase in instability).

Fig. 5 gives the precipitation thresholds for calcium carbonate polymorphs in the case of a water sample from the Seine River; the analytical results are given in Table 4. (Our results for amorphous

Table 4
Analytical results for a typical French water sample (see Fig. 5). Location: Seine river, at Nogent-sur-Seine; Date: 15 December, 1994; Sampling temperature: 13.5°C.

Species	Concentration	
	mg L^{-1}	mol L^{-1}
soluble SiO_2	6	10^{-4}
Ca^{2+}	111	2.77×10^{-3}
Mg^{2+}	4.0	1.65×10^{-4}
Na^+	6.1	2.65×10^{-4}
K^+	2.0	5.12×10^{-5}
Cl^-	15	4.23×10^{-4}
SO_4^{2-}	20	2.08×10^{-4}
NO_3^-	26	4.19×10^{-4}
pH^a	8.5	
carbonate alkalinity[a]	0.3 meq L^{-1}	
total alkalinity[a]	4.86 meq L^{-1}	

[a] Measured at the laboratory temperature, i.e. 25°C.

calcium carbonate are only approximate at $T >$ 55°C due to the lack of data in Ref. [21].)

Fig. 5 also gives the threshold corresponding to 40 times the calcite solubility product. This value is often considered in water treatment as a maximum value for IAP, in order to avoid scaling phenomena. A calcite supersaturation index can therefore be defined as

$$\Omega = IAP/K_s$$

This value of 40 was originally proposed by Legrand et al. [25] without any theoretical justification, Legrand and Leroy [32] have since tentatively explained this figure by calculating the energy needed for bringing together the Ca^{2+} and CO_3^{2-} ions, but without taking into consideration $CaCO_3^0$ hydrated forms or the dissociation equilibrium of HCO_3^- into CO_3^{2-}. This limiting value of 40 has frequently been questioned. Roques and co-workers [33–36], for example, has repeatedly obtained solutions with $\Omega = 80$ to 100 during heterogeneous scale formation studies at various temperatures. At 25°C, however, the beginning of precipitation corresponds to $\Omega = 72$ for ikaite, and to $\Omega = 120$ for the amorphous form. Fig. 5 enables us to better understand what occurs in drinking water supplies: at

about 10 to 20°C there is only a slight difference between the ikaite solubility limit and the value $\Omega = 40$; for hot water, however, the amorphous form solubility is nearer this limit.

We believe this limiting saturation index value of $\Omega = 40$, as proposed by Legrand and Poirier, is well adapted to both temperature ranges of drinking waters uses, which explains its practical interest. Between 30 and 70°C it is possible to greatly exceed this value (see Fig. 5), because of the Ω value between 90 and 100 for the amorphous form. But it must be remembered that at various temperatures, this limiting value corresponds to different initially precipitating polymorphs.

Several remarks should be made at this point in our discussion.

- Pelouze [37] is erroneously given credit for the discovery of $CaCO_3 \cdot 6H_2O$. He operated at room temperature with a lime milk left in contact with the ambient atmosphere, and described only the existence of a series of hydrates. In the industrial world, only one paper [38] describes ikaite formation sometime during the winter at a water treatment plant located in northern England. We observed [39] a similar phenomenon at the Salindres Rhône-Poulenc plant near Alès, France, in 1991.

- Scheme 2 clearly shows that calcite solubility data obtained from a redissolution process are the most reliable because there is no chance of supersaturation. A thorough literature survey produced a coherent set of data whose differences come mainly from the nature of the ionic strength correction used. On the other hand, all values coming from saturated solution precipitation processes are slightly higher.

- Slack [38] explained spontaneous ikaite formation by the presence of phosphate derivatives in treated water. Starting from the same principle, Clarkson [9] obtained ikaite at ambient temperature in the presence of sodium tripolyphosphate $Na_5P_3O_{10} \cdot 6H_2O$.

- Isolating and drying the first crystals formed without added inhibitor led Tarits et al. [40] to mixtures where vaterite could be the main form.

- Although more recently obtained, and in the absence of inhibitor, we have not retained the ikaite solubility product given by Brecevic and Nielsen [22] because these authors described rhomboedric crystals whereas ikaite has always been characterized as monoclinic.

5. The role of $CaCO_3^0$ in scale formation

In an attempt to analyse scaling phenomena, taking into account formation equilibria for all of the $CaCO_3^0$ hydrated forms in solution, we see (Table 3) that saturated solutions, when near to the formation equilibria for ikaite and amorphous solid calcium carbonate, should contain high concentrations of the soluble form playing the role of the precursor. Since this concentration is approximately 10^{-3} mol L^{-1}, we are in the range sufficient for a relatively rapid solid formation rate.

If, on the other hand, we have a weakly saturated medium whose IAP is only slightly higher than the calcite solubility product, the $CaCO_3^0$ (aq) concentration in the solution is approximately 10^{-5} mol L^{-1}, and it is conceivable that, under such conditions, calcite crystal formation and growth takes place very slowly if there is successive $CaCO_3^0$(aq) element addition.

If this is, indeed, the case, we can understand why there are natural waters containing microcrystalline calcite and whose IAP is nearly ten times the calcite solubility product, without any rapid evolution towards the equilibrium state. The growth of existing seeds depends on their en- counter with species that, in the present case, are only present at concentrations of less than 10^{-4} mol L^{-1}.

But how can we explain this rapid transition from the initially precipitating to anhydrous crystalline forms, when we have supersaturated solutions? A series of successive equilibria are established beyond hydrated calcium carbonate clusters for dissolution/dehydration of the various $CaCO_3^0$ soluble species. Their respective concentrations cannot exceed the limiting values given in Table 3 but, as opposed to the case of slightly saturated solutions, their precursors are in a restricted space at the precipitate/solution interface, and any consumed species is restored through equilibria displacements starting from the redissolution of the precipitated form.
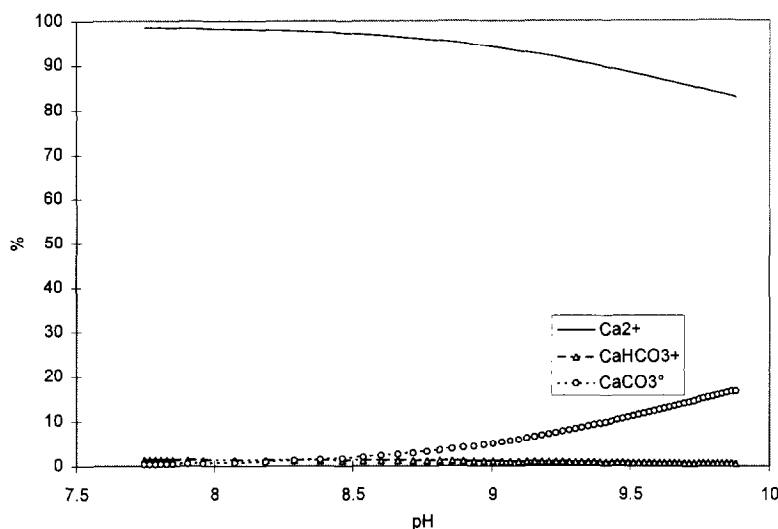
Fig. 6. Calcium soluble species distribution as a function of pH for the experiment with 1 ppm ATMP as given in Fig. 4.

For heterogeneous kinetic studies, IAP values in the bulk solution do not necessarily correspond to a transition through solid hydrated forms. Koutsoukos et al. [41], for instance, studied scale formation on various metallic walls and observed that, at 80°C, vaterite settles and progressively converts into calcite. Walls might take part in the $CaCO_3^0(aq)$ dehydration equilibria, giving out the necessary energy and contributing to a rapid renewal of the polymorphs that have been converted into vaterite and calcite crystals. Again, in the present case, the wall/solution interface would be a privileged place for the seed-growth kinetics by weakly concentrated species in solution.

Further remarks are as follows.

● The pH of natural waters is generally lower than 8.5, except during periods of high photosynthetic activity [42]. The $|HCO_3^-|/|CO_3^{2-}|$ ratio is therefore usually higher than 100. Taking into account the known values for the $CaHCO_3^+$ and $CaCO_3^0$ formation constants, it becomes evident that $CaCO_3^0(aq)$ is, in fact, often the least abundant species. Classical calculations are, however, somewhat cumbersome when using only the solubility product concept, because we must choose between different K_s values depending on the advancement of the precipitation reactions. It is of interest to introduce the concept of the ratio

$$|CaCO_3^0|/|Ca^{2+}| = \beta \times |CO_3^{2-}|$$

Indeed, it is useless to seek possible precipitation of a given calcium carbonate polymorph if we are not already in the $CaCO_3^0(aq)$ formation range. On the other hand, the higher the pH, the greater the $CaCO_3^0(aq)$ form contribution, although its percentage never, in fact, reaches 20% of total calcium in solution (Fig. 6).

● Because of a typographical error, it was thought [36] that House et al. [43] had introduced the $CaCO_3^0(aq)$ concept during their kinetic studies for $CaCO_3$ crystallization. In fact, they considered that the percentage of $CaCO_3^0$ is small enough to be neglected [44].

6. The action of scale formation inhibitors

Many authors have studied the inhibitory effect of common species such as magnesium cations or orthophosphate anions. Recently, other molecules such as sodium tripolyphosphate [9,45], ethane 1-hydroxy 1,1'-diphosphonic acid (EHDP) [41] and amino tris(methylene phosphonic acid) (ATMP) [46,47] have also been studied. Since, at pH > 6.5 to 7, the electrokinetic potential for calcite suspensions is positive [48], many authors have explained this inhibitory effect by electrostatic or adsorption phenomena, and adsorption

isotherm determination studies are in agreement with such assumptions [48–50].

From a practical point of view, polyphosphates and polyphosphonates are of major interest due to their presently increasing use as precipitating sequestrant additives in washing powders. Taking into account their very low concentrations in all applications (10^{-7} to 10^{-5} mol L^{-1}), it is evident that in spite of their complexing behaviour against Ca^{2+} cations [46,51,52], it is not by a masking effect [52] that they prevent scale formation. Nevertheless, it is not really evident that at such low concentrations they can act as crystal nuclei poisons.

Experiments by Clarkson et al. [9] with supersaturated solutions containing sodium tripoly-phosphate showed that, for concentrations of about 10^{-5} mol L^{-1}, both the amorphous and the hexahydrate forms are stabilized. These authors also showed an increase in tripolyphosphate consumption when the mixtures progress towards calcite precipitation.

During our studies with ATMP (as with 4×10^{-6} mol L^{-1} sodium tripolyphosphate) no turbidity was observed in spite of the fact that we were well beyond the respective precipitation thresholds for ikaite and amorphous forms. This enables us to reject the assumption that solid/solution interaction is the only process involved. Instead of conceiving only absorption phenomena which imply calcite existence, as soon as the critical pH is reached, we believe that the inhibitor/Ca^{2+} complexes might associate with the pre-cursors of crystalline solid species, which are present in the solution in the same concentration range. Because of their sizes and charges, these complexes will form to the detriment of crystalline growth and so will maintain $CaCO_3^0$(aq) dehydration equilibria beyond calcite solubility limits.

Operating with various polyphosphonates, Black et al. [53] totally changed the appearance of barite crystals. Instead of adsorption, they too suggested a reaction between $BaSO_4$ and the inhibitors giving rise to mixed crystals. Without clearly formulating a reaction in solution as we do here, these authors assume morphological changes in the solution order at the crystal interface.

Dalas and Koutsoukos [41] fixed EHDP onto metallic walls and thereby showed the inhibitory effect on direct formation of vaterite (and thereafter calcite) that would be obtained without such a surface treatment. While discussing their inhibitory effectiveness, Roques has also described [33] the morphological crystal changes when polyacrylates are added.

These results are in good agreement with our assumption of a solution reaction between the inhibitor and $CaCO_3^0$(aq). If inhibitors react only with $CaCO_3$ solid forms, their effects at a given concentration should be a function of the mass of seeds added to trigger crystallization, but this has never been described in the literature. On the other hand, the blending of inhibitors into the crystal lattice of the solids obtained corresponds well to Clarkson's observation [9] of a tripoly-phosphate consumption during evolution towards calcite precipitation.

In our studies, the precipitation of even the amorphous species is disturbed by the presence of inhibitor. We assume that this is due to the fact that our $CaCO_3^0$(aq)/inhibitor ratio was lower than the value in Clarkson's studies. In our case with ATMP, we calculate IAP to be 0.79×10^{-6} at pH 10 while Clarkson obtained at the mixing point pH = 11.3 and IAP = 1.38×10^{-6} (as estimated by us). Moreover, a crude mixing of both Ca^{2+} and CO_3^{2-} reactants cannot be compared with our operating conditions where a mixture is progressively raised to its precipitation pH.

Finally, we consider that calcium carbonate precipitation and its evolution towards calcite formation can be delayed using inhibitor agents if seed formation itself is altered by the presence of species associated with $CaCO_3^0$(aq). Such a model could explain why these compounds are effective at such low concentrations. Our model can also provide explanations for the mechanisms of the recently described preparation of hollow porous aragonite shells, as obtained in oil/water/surfactant microemulsions [54].

7. Conclusion

In the present paper we have given more evidence of the existence of the well-known

$CaCO_3^0$ (aq) species. Through a critical review of published data, we validate the value log $\beta = 3.22$ at 25°C, as given by Plummer and Busenberg [20], with NaOH titrations of sodium hydrogenocarbonate and calcium chloride mixtures. Always using the $\beta = s/K_s$ relationship, and assuming that β depends only slightly on the dissolved $CaCO_3^0$ species hydration state, we were able to estimate that the $CaCO_3^0$(aq) concentration should be ca. 10^{-3} mol L^{-1} in saturated solutions, a value that cannot be considered to be insignificant, particularly when calculating the calcium carbonate IAP value in a cooling tower.

Since up until now the various $CaCO_3^0$(aq) species have only rarely been taken into consideration in studies of scale formation prediction and kinetics, we would like to underline the importance of such a concept. Our model suggests the existence in solution of various $CaCO_3^0$ hydrated forms whose solubilities decrease with the number of hydration water molecules. Under such conditions, it is easier to understand the progressive change of precipitated forms towards calcite, the most insoluble crystalline species. Since these dehydration reactions are endothermic [55], we can also better explain why, when in contact with hot walls, there is a more rapid evolution towards aragonite or calcite. Finally, and without neglecting other experimental approaches concerning the part played by the inhibitor, we suggest that the assumption of an interaction between inhibitor and hydrated $CaCO_3^0$ forms can aid in our understanding of this well studied but controversial subject.

Acknowledgement

References

[1] J.C. Bollinger, B. Bourg, J.Y. Gal and P. Rouyer, Talanta, 39 (1992) 959.

[2] I. Greenwald, J. Biol. Chem., 141 (1941) 789.

[3] R.M. Garrels, M.E. Thompson and R. Siever, Am. J. Sci., 258 (1960) 402.

[4] R.M. Garrels, M.E. Thompson and R. Siever, Am. J. Sci., 259 (1961) 24.

[5] R.M. Garrels and M.E. Thompson, Am. J. Sci., 260 (1962) 57.

[6] Y. Avnimelech and A. Raveh, J. Environ. Qual., 11 (1982) 69.

[7] A. Marchand, G. Dorange and M. Le Guyader, Trib. Cebedeau, 38 (1985) 9.

[8] T. Ogino, T. Suzuki and K. Sawada, Geochim. Cosmochim. Acta, 51 (1987) 2757.

[9] J.R. Clarkson, T.J. Price and C.J. Adams, J. Chem. Soc., Faraday Trans., 88 (1992) 243.

[10] F.S. Nakayama, Soil Sci., 106 (1968) 429.

[11] G.M. Lafon, Geochim. Cosmochim. Acta, 34 (1970) 935.

[12] G. Grezes and M. Basset, C.R. Acad. Sci. Paris, 260 (1965) 869.

[13] D. Langmuir, Geochim. Cosmochim. Acta, 32 (1968) 835.

[14] R.L. Jacobson and D. Langmuir, Geochim. Cosmochim. Acta, 38 (1974) 301.

[15] E.J. Reardon and D. Langmuir, Am. J. Sci., 274 (1974) 599.

[16] T.E. Larson, F.W. Sollo, Jr. and F.F. McGurk, Res. Rep. Univ. Ill. Urbana-Champaign, Water Res. Cent., 108 (1976) 57 p.

[17] O.I. Martynova, L.G. Vasina and S.A. Pozdnyakova, Dokl. Akad. Nauk SSSR, 201 (1971) 1110.

[18] O.I. Martynova, L.G. Vasina and S.A. Pozdnyakova, Dokl. Akad. Nauk SSSR, 202 (1972) 1337.

[19] O.I. Martynova, L.G. Vasina and S.A. Pozdnyakova, Desalination, 15 (1974) 259.

[20] L.N. Plummer and E. Busenberg, Geochim. Cosmochim. Acta, 46 (1982) 1011.

[21] L. Brecevic and A.E. Nielsen, J. Cryst. Growth, 98 (1989) 504.

[22] L. Brecevic and A.E. Nielsen, Acta Chem. Scand., 47 (1993) 668.

[23] M. Le Guyader, G. Dorange, A. Marchland and H. Hanoun, Bull. Soc. Chim. Fr. Part I, (1983) 203.

[24] G. Dorange, A. Marchand and M. Le Guyader, Rev. Sci. Eau, 3 (1990) 261.

[25] L. Legrand, G. Poirier and P. Leroy, Les Equilibres Carboniques et l'Equilibre Calcocarbonique dans les Eaux Naturelles, Eyrolles, Paris, 1983.

[26] R.M. Smith and A.E. Martell, Critical Stability Constants, Vol. 4: Inorganic Complexes, Plenum Press, New York, 1976.

[27] E. Högfeldt, Stability Constants of Metal–Ion Complexes, Part A: Inorganic Ligands, Pergamon Press, Oxford, 1982.

[28] C.W. Davies, Ion Association, Butterworths, London, 1962.

[29] H. Pauly, Arctic, 16 (1963) 263.

[30] H.W. Venderbosch and L.J. Overman, Kema Sci. Tech. Rep., 4 (1986) 119.

[31] H. Feitler, Mater. Prot. Performance, 11 (1972) 31.

[32] L. Legrand and P. Leroy, Prévention de la Corrosion et de l'Entartrage dans les Réseaux de Distribution d'Eau, CIFEC, Neuilly-sur-Seine, 1995.

[33] H. Roques, Fondements Théoriques du Traitement Chimique des Eaux, Vol. 1 and 2, Lavoisier, Paris, 1990.

[34] H. Roques, C. Hort and M. Rola, Traitement Antitartre des Eaux par des Procédés Physiques et Electrochimiques, Applications Industrielles, Journées d'Etude ENSEE, Grenoble, 1993, p. 13.

[35] L. Dedieu, C. Hort, A. Martin-Dominguez, M. Rola and H. Roques, Trib. Eau, 571 (1994) 3.

[36] C. Hort, Thèse de Doctorat, Université de Toulouse, 1994.

[37] J. Pelouze, Ann. Chim. Phys., 48 (1831) 301.

[38] J.G. Slack, Water Res., 14 (1979) 799.

[39] V. Riou, Rapport Stage 3° année, I.S.I.M., Université de Montpellier-II, 1991.

[40] C. Tarits, P. Leroy, R. Letolle and P. Blanc, C. R. Acad. Sci. Paris, Ser. II, 311 (1990) 1297.

[41] E. Dalas and P.G. Koutsoukos, Desalination, 78 (1990) 403.

[42] J.Y. Gal, C.R. Acad. Sci. Paris, Ser. III, 312 (1991) 269.

[43] G.E. Cassford, W.A. House and A.D. Pethybridge, J. Chem. Soc., Faraday Trans., 79 (1983) 1617.

[44] W. Davison and W.A. House, Water Res., 22 (1988) 577.

[45] A.M. Kavanagh, T. Rayment and T.J. Price, J. Chem. Soc., Faraday Trans., 86 (1990) 965.

[46] K. Sawada, T. Araki and T. Suzuki, Inorg. Chem., 26 (1987) 1199.

[47] A. Khalil, C. Colin, C. Gabrielli, M. Keddam and R. Rosset, C. R. Acad. Sci. Paris, Ser. II, 316 (1993) 19.

[48] A.G. Xyla, E.K. Giannimaras and P.G. Koutsoukos, Colloids Surf., 53 (1991) 241.

[49] T. Ogino, N. Tsunashima, T. Suzuki, M. Sakaguchi and K. Sawada, Nippon Kagaku Kaishi, (1988) 899.

[50] A.G. Xyla, J. Mikroyannidis and P.G. Koutsoukos, J. Colloid Interface Sci., 153 (1992) 537.

[51] R.K. Samakaev, N.M. Dyatlova and L.T. Dytyuk, Russ. J. Inorg. Chem., 29 (1984) 1819.

[52] Les Séries de Phosphonates Dequest 2000/Dequest 2010. Agents Multifonctionnels de Contrôle des Ions Métalliques dans les Solutions Aqueuses, Bulletin Technique n° 53-46, Monsanto Europe, Bruxelles, 1988.

[53] S.N. Black, L.A. Bromley, D. Cottier, R.J. Davey, B. Dobbs and J.E. Rout, J. Chem. Soc., Faraday Trans., 87 (1991) 3409.

[54] D. Walsh and S. Mann, Nature, 377 (1995) 320.

[55] Y. Kojima, A. Kawanobe, T. Yasue and Y. Arai, J. Ceram. Soc. Jpn., 101 (1993) 1145.

Medium effect on acidity constants of some heterocyclic nitrogen azomethines

M.A. El-Taher*, A.A. Gabr

Department of Chemistry, Faculty of Science, Aswan, Egypt

Received 15 December 1995; revised 8 March 1996; accepted 15 March 1996

Abstract

The effects of different organic solvent–water mixtures on the acidity constants of some azomethines derived from 3-amino-1,2,4-triazol; 2-amino-1,3-pyrimidine and also 2-amino-4-methyl-1,3-pyrimidine have been examined. Two pK_a values for the o-OH derivatives were determined; one is assigned to the deprotonation of the nitrogen azomethine group and the other one is ascribed to the ionization of the OH group. The p-OH derivatives give one pK_a due to the ionization of the OH group. On the other hand, it was observed that with the increase in the amount of organic solvent in the medium, the pK_a of the compound studied is decreased. This behaviour can be accounted for in terms of the high stabilization of both the non-protonated and ionic forms of these compounds by dispersion forces rather than by hydrogen bonding. Also, the effects of medium polarizability on the pK_a values and thus on the spectra of the charge transfer band observed have been discussed.

Keywords: Heterocyclic nitrogen imines; pK_a

1. Introduction

The knowledge of pK_a is considered to be of interest for organic and inorganic compounds because it has a significant role in many chemical reactions. Therefore, numerous works [1–8] have been devoted to the determination of pK_a values of the Schiff bases. Despite this, information concerning the effect of the medium on the ionization process has not been fully reported.

The aim of the present work has been to study the effect of the medium on the ionization constants of some azomethines derived from 3-

amino-1,2,4-triazol; 2-amino-1,3-pyrimidine and thus 2-amino-4-methyl-1,3-pyrimidine. A number of organic solvents of various polarities and basicities as well as of different tendencies to donate or to accept hydrogen bonds have been investigated in the present work. The azomethine derivatives under examination are

(I–III): X = o-OH(a); p-OH(b).

---
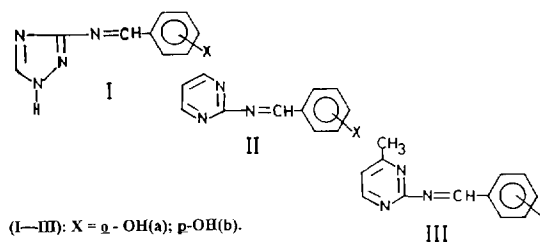
* Corresponding author.

2. Experimental

2.1. Materials and solutions

Heterocyclic azomethines under investigation were prepared as described earlier [9]. The structures of the different synthesized compounds were confirmed by micro-chemical analysis and no impurities were detected by IR spectroscopy.

All the chemcials used in this study were obtained, as high purity materials, from Fluka. They were used without further purification. The solvents used were methanol, ethanol, acetone and dimethylformamide (DMF). They were purchased from Merck, Uvasol grade.

The concentration of the solutions prepared could not be higher than approximately 1×10^2 mol dm^{-3} because of the low solubility of some of the compounds used.

2.2. Buffer solutions [10]

The modified universal buffer solutions of pH values 1.70–11.90 were prepared in aqueous media containing varying proportions of the organic solvents used in this work. The pH values of these solutions were checked using a MV-87 digital Pracitronic pH meter, accurate to ± 0.01 pH units at 25°C.

Because of the presence of organic solvent in the aqueous media of different pH values, the acidity, basicity, dielectric constant and ion activities of these partially aqueous solutions are altered compared to those of the pure aqueous ones. The measured pH values of the former solutions must be corrected according to the following equation [11]:

$$pH^* = pH(R) - \delta$$

where pH*, is the corrected reading and pH(R), is the meter reading obtained in a partially aqueous media, the pH meter is standardized using standard aqueous buffer solutions. The values of δ, of the aqueous buffer solutions containing varying amounts of the organic solvents were determined following Douheret [11].

The electronic absorption spectra of the freshly prepared dilute solutions were recorded on a Shimadzu UV-Visible Recording Spectrophotometer UV-240, using 1.0 cm matched silica cells, at 25°C.

Infrared spectra were recorded in the region 4000–200 cm^{-1} on a Pye Unicam SP 100 Infrared Recording Spectrophotometer, using the KBr disc technique.

3. Results and discussion

The electronic absorption spectra of the compounds under investigation in pure aqueous buffer solutions and also in those containing different proportions of the orgainic solvents, namely, methanol, ethanol, acetone or DMF were recorded (Fig. 1, as a representative example).

Generally, the charge transfer (CT) band observed in the absorption spectra of all the compounds studied shows a decrease in its intensity and meanwhile exhibits also a slight red shift in its λ_{max} as the pH of the medium is increased. On further increase in the pH values (≥ 7.30), this band exhibits splitting. This behaviour is attributed to the possible existence of such compounds in the NH/OH tautomeric equilibrium [6]. The first split at the shorter wavelength is ascribed to the CT transition within the enol form (non-ionized form), while the second one at the longer wavelength is due to the CT within the keto form (ionized form). Thus, in solutions of low pH values, these compounds exist mainly in the enol form, while they occur as keto form in the alkaline solutions. On the other hand, we can deduce that the CT interaction occurring within the solute molecule of these compounds is easier under the basic conditions relative to that under neutral or acidic ones. This is owing to the high mesomeric interaction of the OH group belonging to these compounds in the alkaline media, which increases the charge density on the keto tautomer resulting in easier CT interaction. A clear isosbestic point at different positions confirms the existence of such compounds in keto⇔enol tautomeric equilibrium.

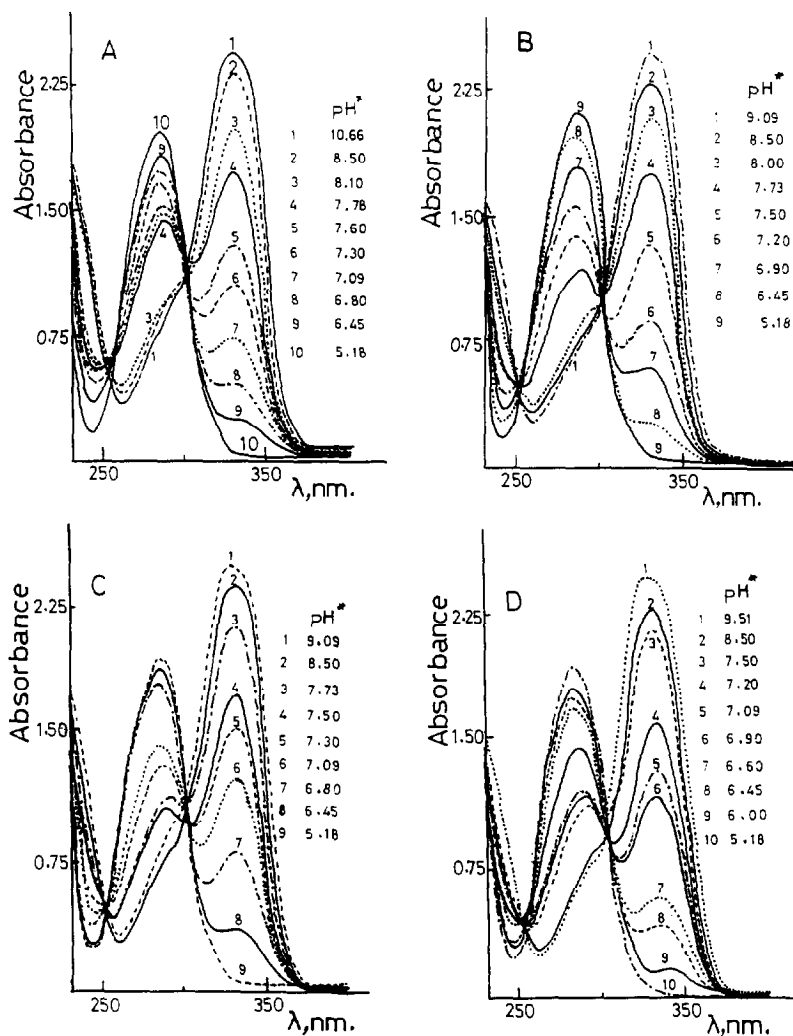Fig. 1. Absorption spectra of 1×10^{-4} mol dm^{-3} of compound III$_b$, in solutions containing different wt% ethanol: A, 0.0%; B, 10%; C, 30%; D, 50%.

The recorded visible absorption spectra of the compounds (I–III)$_{a,b}$, in pure aqueous buffer solutions and also in those containing different proportions of organic solvents, were used in the determination of the acidity constant (pK_a) of these compounds. The absorbance–pH curves (Fig. 2), are typical dissociation curves supporting the acid–base equilibrium. The mean pK_a values were determined from the above curves using the spectrophotometric methods, namely,

the half-wave height, limiting absorbance [12] and modified colleter methods [13]. The limit of accuracy of the pK_a values was checked using the least-squares method. The results obtained are listed in Tables 1–4.

3.1. Effect of molecular structure on pK_a

The pK_a values of both the pyrimidine and triazol rings cannot be determined since the de-
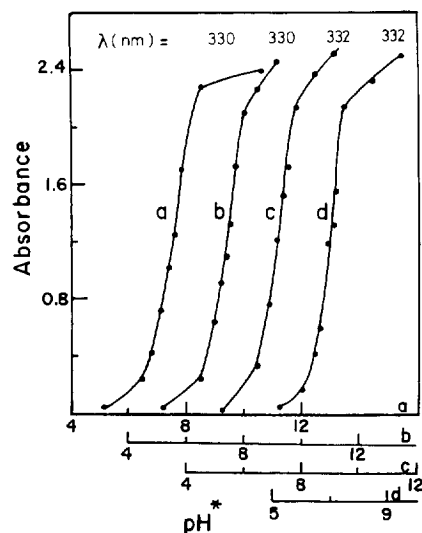
Fig. 2. Absorbance–pH* curves for compound III$_b$, in universal buffer solutions containing different percentages of ethanol, by wt% ethanol: a, 0.0%; b, 10%; c, 30%; d, 50%.

protonation of the pyrimidine and the triazol rings does not show any order in the absorbance of the CT band and other bands. This makes the

evaluation of pK_a values inaccurate. Also, the inability to determine pK_a values of the deprotonation of the azomethine group in the p-OH derivatives is mainly attributed to the effect of the ionization of the OH group belonging to these compounds on the absorbance of the C=N bond, which probably takes place at a pH near the value of pK_a of the deprotonation of azomethine group.

In all the media studied, the absorption spectra of the compounds (I–III)$_{a,b}$, are characterized by a clear isosbestic points denoting the existence of an acid–base equilibrium.

$$H^+A \Leftrightarrow A + H^+ \quad o - OH \text{ derivatives}$$

$$HA \Leftrightarrow A^- + H^+ \quad o - OH \text{ and } p - OH \text{ derivatives}$$
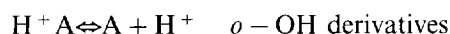
The results listed in Tables 1–3, refer to a chemical equilibria occurring between the different species of the o-OH compounds (I$_a$, II$_a$ and III$_a$). Equilibrium between the protonated

Table 1
Mean pK_a and λ_{max} values for 1×10^{-4} mol dm^{-3} of compound I$_a$ in organic solvent–water mixtures. at 25°C

% (W/W) of organic solvent	dielectric constant of the medium, at 25°C	pK_{a1}	λ_{max} (nm)		pK_{a2}	λ_{max} (nm)	
			Protonated form	Non-protonated form		Non-ionic form	Ionic form
0.0	78.50	7.99 ± 0.02	330	382	10.39 ± 0.02	330	382
				methanol			
10	75.81	7.90 ± 0.03	340	385	10.35 ± 0.01	340	385
30	69.60	6.71 ± 0.08	341	386	10.21 ± 0.03	341	386
50	62.00	6.20 ± 0.05	341	390	10.10 ± 0.01	341	390
				ethanol			
10	76.25	7.21 ± 0.03	340	380	10.30 ± 0.02	340	380
30	70.73	6.52 ± 0.03	340	387	10.20 ± 0.05	340	387
50	63.27	6.30 ± 0.06	341	390	10.03 ± 0.06	341	390
				acetone			
10	76.66	7.20 ± 0.01	340	385	10.25 ± 0.03	340	385
30	71.99	6.35 ± 0.01	340	390	10.15 ± 0.05	340	390
50	65.31	6.15 ± 0.08	341	392	9.90 ± 0.05	341	392
				DMF			
10	77.39	6.80 ± 0.09	342	390	10.15 ± 0.05	342	390
30	74.49	6.30 ± 0.01	343	392	10.10 ± 0.01	343	392
50	70.24	6.20 ± 0.02	345	394	9.41 ± 0.04	345	394

Table 2
Mean pK_a and λ_{max} values for 1×10^{-4} mol dm^{-3} of compound II_a in organic solvent–water mixtures, at 25°C

% (W/W) of organic solvent	Dielectric constant of the medium, at 25°C	pK_{a1}	λ_{max} (nm)		pK_{a2}	λ_{max} (nm)	
			Protonated form	Non-protonated form		Non-ionic form	Ionic form
0.0	78.50	8.10 ± 0.03	305	380	10.63 ± 0.08	305	380
				methanol			
10	75.81	7.93 ± 0.05	305	380	10.53 ± 0.05	305	380
30	69.60	7.81 ± 0.08	305	383	10.21 ± 0.01	305	383
50	62.00	7.72 ± 0.01	306	387	10.05 ± 0.01	306	387
				ethanol			
10	76.25	7.80 ± 0.07	300	380	10.41 ± 0.07	300	380
30	70.73	7.72 ± 0.07	302	385	10.10 ± 0.03	302	385
50	63.27	7.60 ± 0.05	304	388	9.91 ± 0.01	304	388
				acetone			
10	76.66	7.77 ± 0.01	305	380	10.11 ± 0.05	305	380
30	71.99	7.65 ± 0.03	308	386	9.51 ± 0.08	308	386
50	65.31	7.60 ± 0.01	312	390	9.35 ± 0.09	312	390
				DMF			
10	77.39	7.75 ± 0.01	305	380	10.05 ± 0.03	305	380
30	74.49	7.50 ± 0.02	305	390	9.41 ± 0.06	305	390
50	70.24	7.15 ± 0.08	306	400	9.00 ± 0.01	306	400

and neutral forms, and another one between the neutral and the ionic forms are shown below:
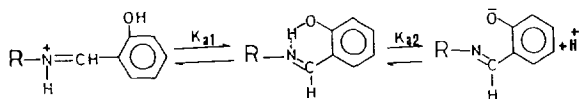
According to the above representative scheme, it is noticed that the o-OH compounds give two pK_a values. pK_1, can be assigned to the deprotonation of the nitrogen azomethine group and pK_2, is ascribed to the ionization of the phenolic OH group. On the other hand, the p-OH derivatives have one pK_a, mainly due to the ionization of the phenolic OH group. In addition, the pK_a value of the o-OH group is higher than that of the p-OH group. This is most likely due to the strong intramolecular hydrogen bonding between the o-OH group and the nitrogen azomethine group, as represented above. This will result in an increase in the stability of the o-OH group, so its ionization is difficult, i.e. a high pK_a value of the molecule is observed [5–8].

3.2. Effect of medium on pK_a

Careful examination of the pK_a values of the compounds studied in different organic solvent–water media shows that the pK_a values of all the compounds are largely dependent on both the proportion and nature of organic co-solvent used. The ionization and deprotonation constant values for all the compounds studied and for the o-OH compounds, respectively, decrease by increasing the percentage of organic co-solvent in the medium.

The acidity constant in aqueous medium (K_n), may be related to that in partially aqueous medium (K_m), by means of Eqs. 1 and 2 [14],

$$K_n = K_m \gamma_{H^+} \gamma_A / \gamma_{H^+A} \tag{1}$$

$$K_n = K_m \gamma_{H^+} \gamma_{A^-} / \gamma_{HA} \tag{2}$$

where γ is the activity coefficient of the subscripted species in a partially aqueous medium relative to that in a pure one. It is known that the electrostatic effect of the solvents will operate only

Table 3
Mean pK_a an λ_{max} values for 1×10^{-4} mol dm^{-3} of compound III$_a$ in organic solvent–water mixtures, at 25°C

% (W/W) of organic solvent	Dielectric constant of the medium, at 25°C	pK_{a1}	λ_{max} (nm)		pK_{a2}	λ_{max} (nm)	
			Protonated form	Non-protonated form		Non-ionic form	Ionic form
0.0	78.50	8.61 ± 0.05	284	380	9.65 ± 0.04	284	380
				methanol			
10	75.81	8.61 ± 0.01	285	380	9.60 ± 0.03	285	380
30	69.60	7.90 ± 0.06	286	381	9.35 ± 0.03	286	381
50	62.00	7.82 ± 0.08	290	383	9.32 ± 0.01	290	383
				ethanol			
10	76.24	8.20 ± 0.09	285	380	9.51 ± 0.05	285	380
30	70.73	7.80 ± 0.09	288	382	9.34 ± 0.01	288	382
50	63.27	7.61 ± 0.07	290	384	9.30 ± 0.01	290	384
				acetone			
10	76.66	7.82 ± 0.05	308	380	9.36 ± 0.03	308	380
30	71.99	7.40 ± 0.03	308	380	9.31 ± 0.05	308	380
50	65.31	6.81 ± 0.01	310	382	8.90 ± 0.08	310	382
				DMF			
10	77.39	7.60 ± 0.08	285	380	9.50 ± 0.01	285	380
30	74.49	7.31 ± 0.01	288	383	9.30 ± 0.01	288	383
50	70.24	6.40 ± 0.05	290	385	8.70 ± 0.02	290	385

on the activity coefficients of any charged species [14]. In the case of deprotonation of the o-OH compounds studied, the electrostatic effect on the activity coefficient of the proton (H$^+$) exceeds that on the acid (H$^-$A). Consequently the electrostatic effect is expected to exhibit a relatively high influence on the deprotonation constant of these compounds. So, regarding the ionization of the compounds studied, the magnitude of this effect on the proton (H$^+$) and free base (A$^-$) increases compared to that on the neutral compound (HA). Thus, the deprotonation and ionization constants (K_{a_1} and K_{a_2}) of these compounds are expected to increase with the increase in the percentage of organic solvent in the medium. These are in accordance with the results given in Tables 1–4.

Furthermore, it was previously indicated that the ionization constants of the acids are affected by solvent properties such as the dielectric constant, acidic and basic strengths [15–17]. Also, stabilization of the different species existing in equilibrium through hydrogen bonding, proton–solvent interaction and dispersion forces originating from interactions between the solvent and solute molecules, plays a significant role in the

ionization constants of acids. Accordingly, the observed decrease in the pK_a values of all the compounds under investigation, as the percentage of the organic solvent in the medium is increased, can be attributed mainly to the high stabilization of both the non-protonated and ionic forms of these compounds by dispersion forces rather than by hydrogen bonding. This stabilization may be due to the high effective density of dispersion centres of the solvents under study relative to that of water [18]. This behaviour is ascribed also to the high stabilization of the proton by its interaction with organic solvent–water mixtures rather than with water molecules alone [14]. Consequently, the activity coefficients of both the non-protonated and ionic forms and of the proton decrease by increasing the percentage of the organic co-solvent in the medium. This will result in an increase in the ionization constant (low pK_a) of these compounds.

In the different media studied, an increase in the pK_a values of the compounds under investigation is observed in the presence of the same percentage of organic co-solvent in the medium according to the following sequence:

Table 4
Mean pK_a and λ_{max} values for 1×10^{-4} mol dm^{-3} of compounds I$_b$–III$_b$ in organic solvent–water mixtures, at 25°C

% (W/W) of organic solvent	Dielectric constant of the medium, at 25°C	Compound I$_b$			Compound II$_b$			Compound III$_b$		
		pK_a	λ_{max} (nm)		pK_a	λ_{max} (nm)		pK_a	λ_{max} (nm)	
			Non-ionic form	Ionic form		Non-ionic form	Ionic form		Non-ionic form	Ionic form
0.0	78.50	8.08 ± 0.03	315	354	7.59 ± 0.01	283	330	7.61 ± 0.01	285	330
				methanol						
10	75.81	7.91 ± 0.02	315	355	7.50 ± 0.02	285	330	7.45 ± 0.04	285	330
30	69.60	7.60 ± 0.05	317	355	7.35 ± 0.05	285	333	7.36 ± 0.05	286	332
50	62.00	7.41 ± 0.05	318	356	7.20 ± 0.03	286	335	7.30 ± 0.01	288	332
				ethanol						
10	76.25	7.80 ± 0.06	315	355	7.40 ± 0.03	285	330	7.43 ± 0.01	285	330
30	70.73	7.25 ± 0.01	316	356	7.25 ± 0.01	286	335	7.20 ± 0.01	286	333
50	63.27	7.20 ± 0.02	317	357	7.00 ± 0.03	288	336	7.05 ± 0.06	288	336
				acetone						
10	76.66	7.55 ± 0.09	315	355	7.35 ± 0.03	308	330	7.25 ± 0.08	303	330
30	71.99	7.10 ± 0.05	317	356	7.20 ± 0.02	310	335	7.00 ± 0.05	308	335
50	65.31	7.00 ± 0.06	320	356	6.90 ± 0.01	312	335	6.91 ± 0.05	310	335
				DMF						
10	77.39	6.90 ± 0.05	315	365	7.30 ± 0.01	285	332	7.30 ± 0.01	385	330
30	74.49	6.85 ± 0.01	318	370	6.91 ± 0.01	286	335	6.90 ± 0.02	385	335
50	70.24	6.50 ± 0.09	320	375	6.51 ± 0.05	288	337	6.75 ± 0.01	386	338

DMF < acetone < ethanol < methanol

This behaviour is expected to occur as a result of the decrease in the medium polarizability on going from DMF–water mixtures to methanol–water mixtures within the above sequence [18]. This strongly confirms the fact that the high stabilization of both the non-protonated and ionic forms by dispersion forces and that of the proton by its interaction with solvents, are the very important factors responsible for the decrease in the pK_a values of the compounds studied as the percentage of organic solvent in the medium is increased. The low pK_a values observed in the case of DMF compared to that in alcohol or acetone under the same conditions, is attributed to the high basicity of DMF i.e. solvent with strong hydrogen bond acceptor (from the protonated compounds). The reduced pK_a values exhibited in DMF can be ascribed also to the strong dispersion interaction of the free base with DMF relative to that occurring with other solvents [16].

In the context of the present work it is also worth mentioning that the CT absorption band of the compounds under investigation shows a slightly red shift with increase in the percentage of solvent in the medium. This is attributed mainly to the increase of the free negative charge on the oxygen atom of the Schiff base by increasing the percentage of solvent in the medium [3]. This is due to the weak tendency of the solvent molecules to form donor hydrogen bonds with the oxygen atom relative to water molecules. This in turn will reflect itself in the increase of the intramolecular charge transfer within the molecule and thus a lower excitation energy is required. In addition, the visible band influenced by intramolecular CT within the solute molecule shows also a red shift in the DMF medium relative to that in alcoholic media. This can perhaps be ascribed to the protonation of the nitrogen atom of the heterocyclic

ring by alcohol molecules, whereas alcohol acts as a proton donor solvent (donor hydrogen bond). Such protonation will result in blocking of the n-electrons of the nitrogen atom; thereafter, the electron charge transfer through the solute molecule is not easy. Accordingly, high excitation energy is required and a blue shift is observed in the alcoholic media. When DMF acts as a hydrogen bond acceptor, therefore, a red shift of the CT band is observed through it [7].

References

[1] D. Heinert and A.E. Martell, J. Am. Chem. Soc., 85 (1966) 183.
[2] G.O. Dudek and E.P. Dudek, J. Am. Chem. Soc., 88 (1966) 2407.
[3] H.S. El-Kashef, R.A. El-Hamide, M.R. Mahmoud and M.M. Hamed, Can. J. Chem., 59 (1981) 731.
[4] M.R. Mahmoud, A.M. Awad and A.M. Shaker, Spectrochim. Acta, 41A (1985) 10, 1177.
[5] F.A. Adam, M.A. El-Taher and M.R. Mahmoud, Chem. Scr. 29 (1989) 161.
[6] M.T. El-Haty, A.E. Mohamed, F.A. Adam and A.A. Gabr, Spectrochim. Acta, 46A, (1990) 12, 1743.
[7] A.A. Gbar, Spectrochim. Acta, 46A (1990) 12, 1751.
[8] M.A. El-Taher and A.A. Gabr, Pakist. J. Scient. Res., 37 (1994) 4.
[9] K.N. Campbell, A.H. Sommers and B.K. Campbell, J. Am. Chem. Soc., 66 (1944) 82.
[10] H.T.S. Britton, Hydrogen Ions, 4th Edn., Vol. 1, Van Nostrand Comp., New York, 1956.
[11] G. Douheret, Bull. Soc. Chim. Fr., (1967) 1412.
[12] R.M. Issa, H. Sadek and I.I. Izzat, Z. Phys. Chem. N.F., 74 (1971) 17.
[13] J.C. Colleter, Ann. Chem. Paris, 5 (1960) 415.
[14] R.G. Bates, in J.F. Coetzee and C.D. Ritchie (Eds.), Solute–Solvent Interactions, Marcel Dekker, New York, London, 1969, pp. 64, 78, 221.
[15] G. Charlot and B. Tremillon, Chemical Reactions in Solvents, Pergaman Press, 1969, pp. 55, 306.
[16] H. Strehlow, Z. Phys. Chem., 24 (1960) 240.
[17] C.E. Newall and A.M. Easthan, Can. J. Chem., 39 (1961) 1752.
[18] M. Alfenaar and G.L. Deligny, Rec. Trav. Chim., 86 (1967) 292.

Flow-injection photometric determination of sub-nanogram amounts of cobalt by its catalysis of the oxidative coupling of 3-methyl-2-benzothiazolinone hydrazone with N,N-dimethylaniline in a micellar medium[1]

Zhu-Yue Yu[a], Norio Teshima[a], Shigenori Nakano[b], Takuji Kawashima[a],*

[a]Laboratory of Analytical Chemistry, Department of Chemistry, University of Tsukuba, Tsukuba 305, Japan
[b]Chemical Institute, Faculty of Education, Tottori University, Koyama cho, Tottori 680, Japan

Abstract

A catalytic flow-injection photometric method was developed for the determination of levels of cobalt as low as 10^{-10} mol 1^{-1}. The method is based on the catalytic action of cobalt(II) on the oxidative coupling of 3-methyl-2-benzothiazolinone hydrazone with N,N-dimethylaniline to form a colored dye ($\lambda_{max} = 590$ nm) in the presence of hydrogen peroxide. The extremely activating effect was obtained in the presence of 1,2-dihydroxybenzene-3,5-disulfonate (Tiron) and sodium hydrogencarbonate as activators. Furthermore, the sensitivity of the method was enhanced by adding sodium dodecylsulfate as a surfactant. Linear calibration graphs were obtained over the range 0.04–0.2 ng ml^{-1} and 0.1–0.5 ng ml^{-1} cobalt(II), respectively, at a sampling rate of 30 per hour. The detection limit (signal/noise = 3) was 5 pg ml^{-1} and the relative standard deviations for 0.1 and 0.04 ng ml^{-1} cobalt ($n = 10$) were 1.0 and 2.3%, respectively. The method was applied to the determination of cobalt in pepperbush.

Keywords: Catalytic flow-injection photometric method; Cobalt determination

1. Introduction

* Corresponding author. Fax: (81) 298-53-6503; e-mail: kawasima@staff.chem.tsukuba.ac.jp

Many metal ion-catalyzed reactions are utilized for the kinetic-based determinations of species [1,2]. These catalyzed reactions are known to be affected by various chemical substances, particularly the activator and sufactant. Hence, the

effects of activators and surfactants on catalyzed reactions have been increasingly exploited in the last few years to improve the features of kinetic-catalytic methods [1–3].

Since kinetic-based methods are time dependent, they need care in the mixing of reactants at regular time intervals to obtain reproducible results. The flow-injection analysis lends reproducibility to both reagent addition and reaction times; the flow-injection technique is a suitable means of extending the applicability of kinetic-based methods to routine analysis [4].

The demand for highly sensitive methods for determining ultratrace amounts of cobalt has increased in industrial and environmental analysis. Indeed, a number of kinetic-catalytic methods have been reported using batch and flow-injection mode with various monitoring systems such as photometric [5–9], chemiluminescent [10–12] and thermometric [13] detections.

The oxidative coupling of 3-methyl-2-benzothiazolinone hydrazone (MBTH) with N,N-dimethylaniline (DMA) to form a colored dye ($\lambda_{max} = 590$ nm) in the presence of hydrogen peroxide has already been employed as an indicator reaction for the catalytic determinations of copper(II) [14–16], chromium(III) [17] and manganese(II) [18,19]. It was found that cobalt(II) also acts as a catalyst on this coupling reaction. This paper describes a highly sensitive catalytic flow-injection method for the photometric determination of cobalt(II) by using this indicator reaction. The catalytic activity of cobalt(II) can be effectively enhanced by disodium 1,2-dihydroxybenzene-3,5-disulfonate (Tiron) together with sodium hydrogencarbonate as activators. In addition, the sensitivity of the proposed method can be improved by adding sodium dodecylsulfate (SDS) as a surfactant. The method can be successfully applied to the determination of cobalt in pepperbush (National Institute for Environmental Studies (NIES) certified reference material No. 1) in the presence of triethylenetetramine (trien) as a masking agent for copper.

2. Experimental

2.1. Apparatus

Fig. 1 provides a schematic diagram of the flow-injection manifold used in this study. The flow lines was connected up with Teflon tubing (0.5 mm i.d.) and three-way connectors. Reagents and carrier streams were propelled by two double plunger-type pumps (Sanuki Kogyo, DM2M-1026). Samples were injected using a six-way valve (Gasukuro Kogyo, MPV-6) into the carrier stream. Absorbances were measured at 590 nm with a Soma Kogaku S-3250 spectrophotometer fitted with a flow-through cell (8 μl volume, 10 mm path length) and recorded with a Hitachi model 561-1003 recorder. Two circulating thermostated baths (Taiyo Kagaku Co., C-630) were used to control the reaction temperature and to stabilize the base line. The pH of the solution was measured with a Horiba F-8AT pH meter.

2.2. Reagents

All reagents used were of analytical reagent grade. Water, purified with a Millipore Milli-Q PLUS system, was used to prepare the solutions.

A 100 ng ml^{-1} cobalt(II) stock solution was prepared by diluting a 1000 μg l^{-1} cobalt(II) standard solution for atomic absorption spectrometry (Kanto Chemicals) in 0.01 mol l^{-1} hydrochloric acid. Working cobalt(II) solutions of appropriate concentrations were prepared daily in
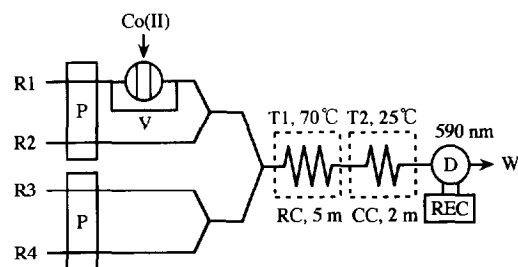

Fig. 1. Flow system for the catalytic determination of cobalt. R1, carrier solution; R2, $H_2O_2 +$ Tiron $+$ NaHCO$_3$; R3, DMA; R4, MBTH $+$ SDS $+$ tris; P, pump; V, six-way valve; RC, reaction coil; CC, cooling coil; T1, T2, thermostated baths; D, spectrophotometric detector; REC, recorder; W, waste.

the same acid. A stock solution of 0.05 mol 1^{-1} MBTH was prepared by dissolving 2.7 g of the monohydrochloride (Tokyo Kasei Co.) in water and diluting to 250 ml. A stock solution of 0.1 mol 1^{-1} DMA was prepared by dissolving 3.0 g of the compound (Wako Junyaku Co.) in 0.1 mol 1^{-1} hydrochloric acid and diluting to 250 ml with the same acid. A hydrogen peroxide stock solution of 4 mol 1^{-1} was prepared from the commercial reagent (30%, Wako Junyaku Co.). Stock solutions of 0.8 mol 1^{-1} tris(hydroxymethyl) aminomethane (tris) (Wako Junyaku Co.), 0.1 mol 1^{-1} sodium hydrogencarbonate (Kanto Chemicals), 0.1 mol 1^{-1} Tiron (Dojindo Lab.), 0.2 mol 1^{-1} SDS (Tokyo Kasei Co.) and 1.0×10^{-2} mol 1^{-1} trien (Wako Junyaku Co.) were also prepared in water. More diluted solutions were prepared from these stock solutions.

2.3. Sample decompostion

An aliquot of 200 mg of dried pepperbush (NIES certified reference material No. 1) is weighed into a Teflon vessel. Five milliliters of concentrated nitric and 1 ml of perchloric acids are added into the vessel. After fastening the cap tightly, the vessel is heated in the oven at 90°C for 2 h and 130°C for 2 h for decomposition. After cooling and removing the cap of the vessel, the sample is transferred to a 100 ml volumetric flask and the volume is adjusted with water. More dilute sample solutions for the measurements are diluted with 0.01 mol 1^{-1} hydrochloric acid [20].

2.4. Procedure

As shown in Fig. 1, the carrier solution of 1×10^{-2} mol 1^{-1} hydrochloric acid (R1), a mixture of 0.6 mol 1^{-1} hydrogen peroxide, 6.0×10^{-2} mol 1^{-1} Tiron and 7.0×10^{-2} mol 1^{-1} sodium hydrogencarbonate (R2), 3.0×10^{-2} mol 1^{-1} DMA (R3), a mixture of 2.0×10^{-2} mol 1^{-1} SDS and 2.5×10^{-3} mol 1^{-1} MBTH containing 8.0×10^{-2} mol 1^{-1} tris buffer (R4) were pumped at a flow rate of 1.0 ml min^{-1}. A 160 μl sample solution was injected into the carrier stream. The color development proceeded in the reaction coil of 5 m length at 70°C, and then the colored

solution was passed through the cooling coil of 2 m length at 25°C and then the flow-through cell. The absorbance of the dye produced was monitored continuously at 590 nm.

3. Results and discussion

In the presence of hydrogen peroxide, MBTH reacts with DMA to produce a blue-violet indamine dye, which has an absorption maximum at 590 nm. The rate of color-forming reaction is catalytically accelerated by cobalt(II). The cobalt(II)-catalyzed reaction possibly involves the oxidation of cobalt(II) to cobalt(III); the coloration is catalyzed by trace amounts of cobalt as a result of the regeneration of cobalt(III) by hydrogen peroxide. In the present system, the synergistic activating effect of Tiron and hydrogencarbonate and the micellar enhancing effect of SDS on the catalyzed reaction were observed.

3.1. Effect of reaction variables

The sensitivity of kinetic-catalytic methods can be augmented by an activator. It has been defined as a substance which does not catalyze the indicator reaction but increases its rate in the presence of a catalyst. The use of activators in catalytic methods also permits an improvement in their selectivity [1,2]. Tiron is known as an activator for cobalt(II)-catalyzed reactions [7]. It was found that Tiron and hydrogencarbonate when present together greatly enhanced the catalytic activity of cobalt(II) in this reaction. Fig. 2 shows the effects of Tiron and sodium hydrogencarbonate concentrations on the catalysis of cobalt(II) at a concentration of 2 ng ml^{-1} cobalt(II). The peak heights increased with increasing Tiron or sodium hydrogencarbonate concentration. The peak height ratio between the presence of 6.0×10^{-2} mol 1^{-1} Tiron and its absence was 59. By the same way, the peak height ratio between the presence of 7.0×10^{-2} mol 1^{-1} sodium hydrogencarbonate and its absence was 56. On the other hand, the catalytic activity of cobalt(II) was strongly enhanced by using Tiron together with hydrogencar-
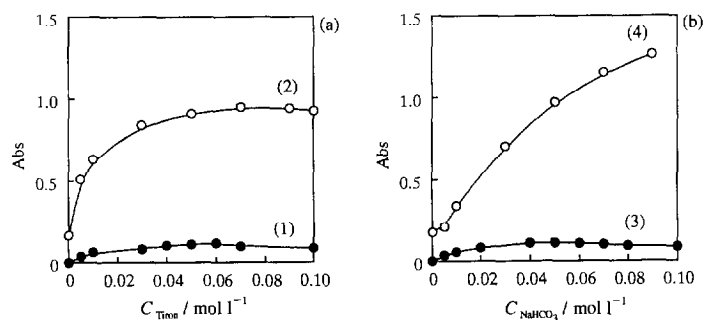
Fig. 2. Effects of Tiron (a) and sodium hydrogencarbonate (b) concentrations on the cobalt(II)-catalyzed reaction. (1) Tiron only; (2) in the presence of 5.0×10^{-2} mol 1^{-1} NaHCO$_3$; (3) NaHCO$_3$ only; (4) in the presence of 6.0×10^{-2} mol 1^{-1} Tiron. Other conditions as in the text.

bonate. In the presence of a 5.0×10^{-2} mol 1^{-1} hydrogencarbonate, the peak heights increased with increasing Tiron concentration up to 6.0×10^{-2} mol 1^{-1}, above which they remained almost contant (Fig. 2(a)); a Tiron concentraton of 6.0×10^{-2} mol 1^{-1} was used for the procedure. In the case of sodium hydrogencarbonate with 6.0×10^{-2} mol 1^{-1} Tiron, an increase in the hydrogencarbonate concentration substantially increased the peak heights (Fig. 2(b)). However, bubbles were observed at higher concentrations. A sodium hydrogencarbonate concentration of 7.0×10^{-2} mol 1^{-1} was thus selected. The peak height ratio between the presence of 6.0×10^{-2} mol 1^{-1} Tiron with 7.0×10^{-2} mol 1^{-1} sodium hydrogencarbonate and the absence of activators was above 1000; a synergistic effect of the two activators was observed in this catalyzed reaction.

One of the possibilities for further increasing the sensitivity of kinetic-catalytic methods is the application of micellar medium [3]. Surfactants form micelles at the concentration above the critical micellar concentration (CMC). Micelles can control reaction pathways, change reaction mechanisms, and alter the physico-chemical properties of solubilized compounds. The effects of cationic (cetylpyridinium chloride, 1-laurylpyridinium chloride, zephiramine), nonionic (brij 35, tween 80, tween 20) and anionic (sodium dodecylbenzensulfonate (SDBS), sodium dodecylsulfate (SDS)) surfactants on the cobalt(II)-catalyzed reaction were tested at their concentrations of 1.0% w/v by injecting 0.2 and 0.4 ng ml^{-1} cobalt(II) solutions.

The results are shown in Table 1. When cationic surfactants were added, precipitates were produced; the measurements of absorbance were impossible. In the case of nonionic surfactants, the absorbances increased slightly. On the other hand, significantly higher abosrbances were obtained in the presence of anionic surfactants. Thus SDS was chosen as a surfactant. The effect of the SDS concentration was examined over the range 0–4.0×10^{-2} mol 1^{-1}. The peak heights increased with increasing SDS concentration up to 2.0×10^{-2} mol 1^{-1} almost corresponding to the CMC, above which constant peak heights were obtained. A concentration of 2.0×10^{-2} mol 1^{-1} SDS was

Table 1
Effect of surfactant on the absorbance

Surfactant[a]	Absorbance	
	$C_{Co(II)}$ 0.2 ng ml^{-1}	$C_{Co(II)}$ 0.4 ng ml^{-1}
No surfactant	0.013	0.027
(SDBS)[b]	0.102	0.189
(SDS)[b]	0.110	0.210
Brij 35[c]	0.037	0.071
Tween 80[c]	0.035	0.070
Tween 20[c]	0.040	0.076
Cetylpyridinium chloride[d]	–	–
1-Laufylpyridinium chloride[d]	–	–
Zephiramine[d]	–	–

[a] The concentrations of all surfactants used were 1 w/v%.
[b] Anionic surfactant.
[c] Nonionic surfactant.
[d] Cationic surfactant.
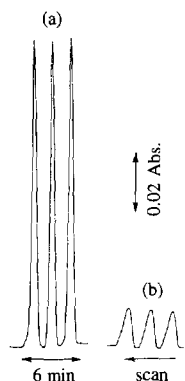
Fig. 3. Peak profiles in the presence (a) and absence (b) of SDS. $C_{Co(II)}$, 0.2 ng ml^{-1}. Other conditions as in the text.

chosen for the procedure. The peak height ratio between the presence of 2.0 ± 10^{-2} mol l^{-1} SDS and its absence was about 8 as shown in Fig. 3. In the presence of surfactant, sensitivity can be augmented as a result of the increased effective concentration of reagents on the micellar surface [3].

The effect of the reaction temperature on the peak height was examined over the range 30–80°C at a fixed cobalt(II) concentration of 0.2 ng ml^{-1}. The peak heights increased with increasing temperature up to 70°C and became constant above 70°C. The reaction temperature was therefore fixed at 70°C. The length of the reaction coil was varied in the range 1–15 m. The peak heights increased with increasing coil length; a 5 m reaction coil was chosen, taking into account reproducibility and sampling rate. The effect of pH on the peak height was examined over the pH range 6–9 by using tris buffer solutions. Since a maximum signal was obtained at a pH around 8, the catalyzed reaction was carried out at pH 8.

The effect of concentration of the reactants on the catalyzed reaction was examined at a concentration of 0.2 ng ml^{-1} of cobalt(II). The peak heights increased with MBTH concentration up to 2.0×10^{-3} mol l^{-1}, above which they changed little. Therefore, a 2.5×10^{-3} mol l^{-1} MBTH was selected as the recommended concentration for the sake of solubility of the reagent. The peak heights increased with DMA concentration up to 3.0×10^{-2} mol l^{-1} and decreased thereafter, possibly owing to the liberation of DMA in a weakly

alkaline solution. A 3.0×10^{-2} mol l^{-1} DMA concentration was chosen for the procedure. The effect of hydrogen peroxide concentration was examined over the range 0–0.8 mol l^{-1}. The peak heights increased up to a hydrogen peroxide concentration of 0.5 mol l^{-1}, above which almost constant peak heights were obtained. A hydrogen peroxide concentration of 0.6 mol l^{-1} was therefore selected for the procedure.

3.2. Analytical characteristics

Fig. 4 shows typical flow signals for cobalt(II) using the present flow system under the optimum conditions. By changing the sensitivity of the detector, linear plots were obtained for two concentration ranges 0.04–0.2 ng ml^{-1} and 0.1–0.5 ng ml^{-1}, respectively. The limit of detection for the proposed method is 5 pg ml^{-1} (signal/noise = 3). The reproducibility was satisfactory with the relative standard deviations of 1.0 and 2.3% for ten determinations of 0.1 and 0.04 ng ml^{-1} cobalt(II), respectively, and the sampling rate was 30 h^{-1}.

3.3. Interferences

The selectivity of the present method was assessed by studying the effect of foreign ions on the determination of 0.2 ng ml^{-1} cobalt(II). The results are summarized in Table 2. A relative error of less than $\pm 5\%$ was considered to be tolerable.
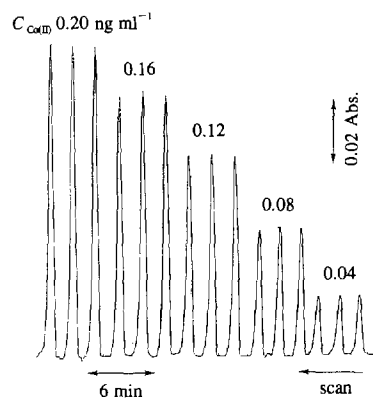

Fig. 4. Typical flow signals for cobalt(II). Conditions as in the text.

Table 2
Effect of foreign ions and compounds on the determination of 0.2 ng ml^{-1} of cobalt(II)

Tolerance ratio[a] [ion] or [compound]/[Co(II)]	Ion and compound added
10000	Na(I), Zn(II), Pb(II), Mo(VI), F$^-$, Cl$^-$, PO$_4^{3-}$, ClO$_4^-$, ClO$_3^-$, oxalate, tartrate, citrate
5000	K(I), Mg(II), SO$_4^{2-}$
2000	Sb(III), Ti(IV), I$^-$
1000	Al(III)
500	Ca(II), Ba(II), Cd(II), Se(IV), As(III)
200	Cr(III), Sr(II)
100	Sn(II), Ni(II)
50	Mn(II)
7	Fe(II, III)
0.2	Cu(II)

[a] A ± 5% error was considered to be tolerable.

Up to a 10 000-fold excess for most foreign ions, and a 5000-fold excess of potassium(I), magnesium(II) and sulfate did not interfere. Iron(II, III) showed positive interferences when present in seven-fold excess. A serious negative interference was observed from copper(II), although it is not fully understood at present why the copper(II) ion showed negative interference in the present method. Detailed results will be reported elsewhere. Masking with trien has been tried to eliminate its interference [21]. Fig. 5 shows the effect of trien concentration in the presence and absense
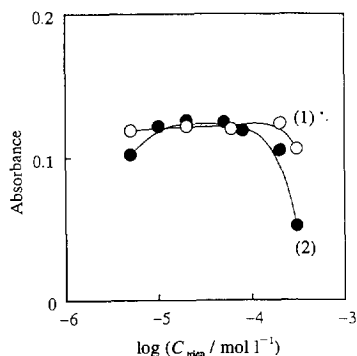
Fig. 5. Effect of trien concentration in the absence (1) and presence (2) of copper(II). (1) $C_{Co(II)}$, 0.2 ng ml^{-1}; (2) $C_{Co(II)}$, 0.2 ng ml^{-1} + $C_{Cu(II)}$, 0.2 ng ml^{-1}. Other conditions as in the text.

Table 3
Determination of cobalt in pepperbush[a]

Cobalt found[b] (μg g^{-1})	
Calibration method	Standard addition method
16.90[c]	16.14[c]
19.13[d]	23.24[d]

[a] The certified value is 23 ± 3 μg g^{-1}.
[b] Average value for three determinations: relative standard deviations were less than 2.3%.
[c] In the absence of trien.
[d] In the presence of trien.

of copper(II). The concentration of trien up to 2.0×10^{-4} mol l^{-1} did not affect the catalyzed reaction and the interference of copper(II) was effectively eliminated over the range of 5.0–8.0×10^{-5} mol l^{-1} trien. A trien concentration of 5.0×10^{-5} mol l^{-1} was therefore selected for the proposed method.

3.4. Application

The proposed method was applied to the determination of cobalt in the reference pepperbush. Analytical results were obtained by the calibration and standard addition methods. The results are shown in Table 3. Since copper(II) in pepperbush interfered in the determination of cobalt in the absence of trien, the contents of cobalt in the pepperbush were lower than the certified value as is seen in Table 3. In the presence of trien, the analytical results of cobalt obtained by the standard addition method were in good agreement with the certificate value.

4. Conclusions

The proposed flow-injection photometric method is one of the highly sensitive kinetic-catalytic methods for the determination of cobalt. In this system, extremely high catalytic activity of cobalt (II) was obtained with a synergistic activating effect of Tiron and sodium hydrogencarbonate. Moreover, the sensitivity was enhanced by the micellar effect of SDS as an anionic surfactant. Samples can be analyzed at a rate of 30 h^{-1} with

relative standard deviations of below 2.3%. The serious interference of copper(II) can be eliminated with trien. The method was applied to the analysis of pepperbush with satisfactory results.

References

[1] D. Perez-Bendito and M. Silva, Kinetic Methods in Analytical Chemistry, Ellis Horwood, Chichester, 1988.
[2] T. Kawashima and S. Nakano, Anal. Chim. Acta, 261 (1992) 167.
[3] D. Perez-Bendito and S. Rubio, Trends Anal. Chem., 12 (1993) 9.
[4] J. Ruzicka and E.H. Hansen, Flow Injection Analysis, 2nd edn., John Wiley & Sons, New York, 1988.
[5] M. Otto, J. Rentsch and G. Werner, Anal. Chim. Acta, 147 (1983) 267.
[6] T. Yamane, Mikrochim. Acta (Wien), 1 (1984) 425.
[7] T. Kawashima, T. Minami, A. Ata, M. Kamada and S. Nakano, J. Flow Injection Anal., 2 (1985) 40.
[8] T. Deguchi, A. Higashi and I. Sanemasa, Bull. Chem. Soc. Jpn., 59 (1986) 295.
[9] K. Isshiki and E. Nakayama, Talanta, 34 (1987) 277.
[10] M. Yamane, T. Komatus, S. Nakahara and S. Suzuki, Anal. Chim. Acta, 155 (1983) 259.
[11] C.M. Sakamoto Arnold and K.S. Johnson, Anal. Chem., 59 (1987) 1789.
[12] H. Sakai, T. Fujiwara, M. Yamamoto and T. Kumamaru, Anal. Chim. Acta, 221 (1989) 249.
[13] M.T. Oms, R. Fortez and V. Cerda, Anal. Chim. Acta, 258 (1992) 177.
[14] F. Holz, Fresenius' Z. Anal. Chem., 313 (1984) 29.
[15] S. Nakano, H. Ihara, M. Tanaka and T. Kawashima, Mikrochim. Acta (Wien), 1 (1985) 455.
[16] S. Satoh, N. Iwamura, N. Teshima, S. Nakano and T. Kawashima, J. Flow Injection Anal., 10 (1993) 245.
[17] S. Nakano, S. Hinokuma and T. Kawashima, Chem. Lett., (1983) 357.
[18] S. Nakano, A. Ohta and T. Kawashima, Mikrochim. Acta (Wien), II (1985) 273.
[19] Y. Miyata, T. Hirano, S. Nakano and T. Kawashima, Anal. Sci., 7 (1991) 97.
[20] J. Vanloon, Selected Methods of Trace Metal Analysis, John Wiley & Sons, New York, 1985, p. 92.
[21] S. Nakano, M. Odzu, M. Tanaka and T. Kawashima, Mikrochim. Acta (Wien), 1 (1983) 403.

A comparative study of the degradation of different starches using thermal analysis

Poonam Aggarwal, David Dollimore*

The Department of Chemistry and Pharmacy, The University of Toledo, Toledo. OH 43606, USA

Abstract

Four starches obtained from different sources were treated to thermal analysis and their mechanisms of degradation were deciphered using a rising temperature method of evaluation. A comparison of the solid state reactivity between the four starches was made, using a method known as the $\alpha_s-\alpha_r$ method. By this method, it was possible to differentiate between four starches of completely different plant origin. Potato starch and rice starch were found to have the highest reactivity.

Keywords: Starch degradation; Thermal analysis

1. Introduction

Starch is arguably one of the most actively investigated biopolymers [1]. The structure of starch, consisting of amylose and amylopectin units has been well characterized [2]. Amylose, the linear constituent of starch consists of α-D-glucopyranose units linked by α-(1,4)α glycosidic linkages only, while in amylopectins, there are α-(1,6)α glycosidic linkages as well, which lead to branching [3–6]. There is considerable interest in the thermal decomposition of starch, as thermal treatment of dry starch usually leads exclusively to its depolymerization if the temperature does not exceed 300°C [7]. The products of pyrolyzed starch, known as dextrins, are commerically used as industrial gums [8].

However, the ratio of amylose to amylopectin is dependent on the source from which the starch is extracted. Watson has reported the percent amylose content in starches obtained from various sources [9]. There have been several reports of studies of the degradation pattern of starch from different origins analyzed by differential thermal analysis (DTA), in the literature [10–14]. Greenwood and Muirhead have demonstrated that compounds such as alumina and sodium chloride used as reference materials, in which the starch samples were mixed, affected the thermal degradation curves of starches [15] and suggested that the acquisition of data on starches should be carried out in the absence of these materials. Nevertheless no significant differences in the thermograms were noticed between starches from different origin. In order to address this problem, we

* Corresponding author. Fax: (+1) 419 537 4033.

decided to develop a general thermal analysis technique for the comparative analysis of starches. In an attempt to compare the solid state reactivity of different starches, four starches originating from different plants were treated to thermal analysis. The starches used for the study were rice, potato, corn and wheat starch. All four starches degrade to carbon in an atmosphere of flowing nitrogen. In this study the kinetic pathway followed by these four different starches was compared, by introducing the α_s–α_r method to determine the solid state reactivity of these starches on a comparitive basis, without recourse to Arrhenius parameters.

2. Experimental

The thermal analysis equipment used in this study was a simultaneous TG–DTA (thermogravimetry–differential thermal analysis) unit from TA instruments, model number 2960, in which the TG and DTA signals are simultaneously obtained on the same sample being thermally treated. The gas flow rate was monitored with the help of an electronic flow meter. In all of the experiments a steady flow rate of 100 ml min^{-1} was maintained. Rising temperature experiments were conducted in which the heating rate was 10°C min^{-1} while considering all of the four starches. For each experiment a sample size of 5–7 mg of starch was used. Variation in sample size did not show any significant difference in either the percent weight loss or the temperature range at which the degradation could be observed. The samples were held in alumina crucibles, with empty alumina crucibles used for the reference holders, and the samples were used undiluted as suggested by Greenwood [7]. The presence of alumina crucibles did not have any effect on the degradation sequence, as was evidenced by the experiments in which the data was replicated using platinum crucibles. The starch samples were obtained from the Sigma Chemical Company. There was no residue after ignition in air for all of the four starches studied and they were all unmodified. All the starches were heated in an atmosphere of dry nitrogen from ambient to 500°C on the TG unit.

The α_s–α_r method is used here to determine the solid state reactivity of different starches on a comparative basis. In this method, the reactivity of the four starches was compared from their TG data (but any other thermal analysis data would suffice). The data obtained from the TG of rice starch was used as the reference, called α_r and the other three were designated α_s. Here both α_r and α_s refers to the fraction decomposed in a single stage decomposition. The solid state reactivity was then assessed from the plots of the extent of the reaction of the samples against that of the reference, calculated from experiments conducted under identical conditions of temperature, gas flow and heating rates.

3. Results and discussion

Solid state reactivity of the four different starches was studied and compared using the α_s–α_r method of evaluation. The reactivities of the starches was compared by noting the extent of decomposition, alpha (α) or the fraction decomposed [16]. α is determined by the following equation:

$$\alpha = \frac{w_i - w}{w_i - w_f}$$

where w is the % weight of substance; w_i is the % weight of substance at the initial time and w_f is the % weight of substance at the final time.

The TG plot of rice starch was used as the reference material, though any of the four could be selected and $\alpha_{\text{reference}}$ (α_r) was calculated from that. The other three were called α_{sample} (α_s). As can be seen from Fig. 1, the reactivity of potato starch is greater than rice used as a reference, while wheat and corn starch have lower reactivity. A plot of temperature against time and a derivative plot of the same was used also to compare the starches (Fig. 2). In all of the four cases, a plot of time against temperature appeared as a straight line, and this should indicate that there is no perturbation due to the reaction temperature of the sample, with the slope indicative of the heating rate employed. However differences in heat capacity due to the applied heating rate and due
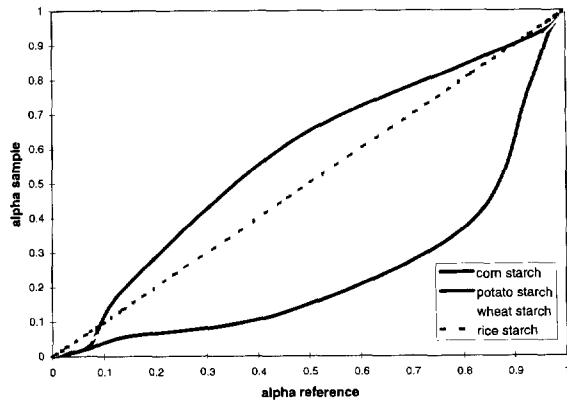
Fig. 1. α_s–α_r plot of the starches with α_r as rice starch.

to the reaction being either exothermic or endothermic, may lead to the presence of a perturbation. In this case the perturbation is hardly noticed since probably only small perturbations are involved within a narrow temperature range. A derivative plot of time–temperature dT/dt plotted against time is clearly explicit with regard to this minute perturbation and gives much the same information as to whether an exothermic or an endothermic event is occurring (Fig. 2). Once the rate of 10°C min^{-1} has been established, the derivative plot indicates a background variation of less than 0.1°C; however in the region of the decomposition of the starch, the perturbation rises to 0.6°C.
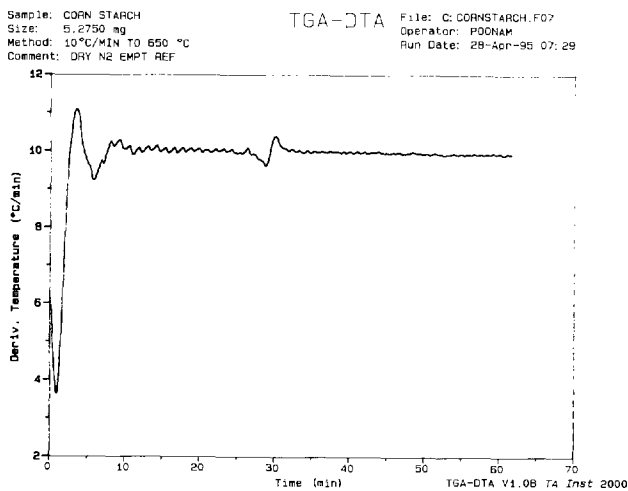
Fig. 2. Derivative time–temperature plot of corn starch from TGA data.
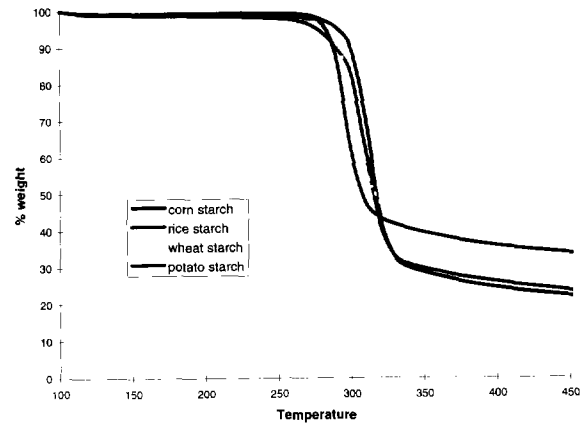
Fig. 3. TG plots of the four starches in an atmosphere of dry nitrogen.

The fact that initially the perturbation dropped the heating rate below the programmed 10°C min^{-1} would indicate the occurrence of an endothermic degradation. This can also be used to give an indication of the actual heating rate of the sample under investigation. In all the cases, the conventional heating rate of 10°C min^{-1} was used but a slight variation does occur, probably due to the difference in heat capacities between the individual samples.

Starches were treated to thermal analysis in the TG unit under an atmosphere of dry nitrogen, where they undergo depolymerization and finally conversion to carbon, as can be seen from the TG plots (Fig. 3); the degradation process commences
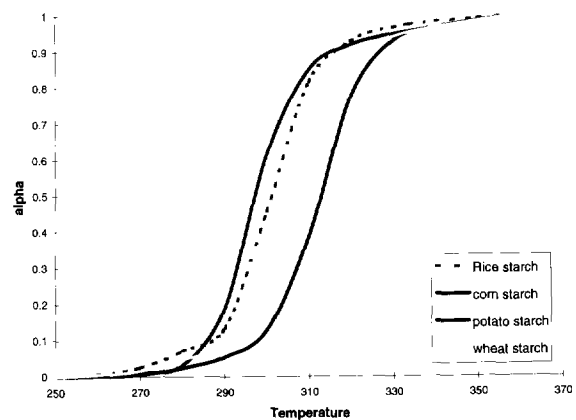

Fig. 4. α plot of starches against temperature.

Table 1
Order of reactivity of different starches when α_r is 0.05 and 0.5

Entry number	At $\alpha_r = 0.05$ α_s/α_r	At $\alpha_r = 0.5$ α_s/α_r	Starch (α_s)
1	0.4	0.29	corn
2	0.6	0.78	wheat
3	0.9	1.27	potato

at 250°C and by 400°C there is complete weight loss in all of the four cases. The plot of the alpha values for each starch against temperature (Fig. 4) also shows the reactivity of potato and rice starch to be higher than that for wheat and corn starch. From Table 1 it can be seen that at a low α_r value (0.05) the order of the reaction is rice > potato > wheat > corn starch, while at $\alpha_r = 0.5$, the reaction is in the order, potato > rice > wheat > corn starch.

4. Conclusions

In this study a new method is utilized to provide a comparative method of assessing solid state reactivity which avoids the complexities involved in quoting the Arrhenius parameters and the reaction rate mechanism. The reactivity of rice and potato starch in the solid state was found to be higher than wheat and corn starch. This study demonstrates the applicability of the $\alpha_s–\alpha_r$ method to differentiate between the rates of degradation of starch from disparate sources. The differences in solid state reactivities between the starches are subtle by conventional TG–DTA methods. However, the use of the $\alpha_s–\alpha_r$ method

reveals a distinct difference in the reactivities of these starches. We believe that this method illustrates an example for the comparison of similar materials and can be applied to other samples.

References

[1] H.F. Mark and N.G. Gaylord, in Encyclopedia of Polymer Science and Technology, Vol. 12, Wiley Interscience, New York, 1985, p. 787.

[2] K.H. Meyer, M. Wertheim and P. Bernfeld, Helv. Chim. Acta., 23 (1940) 865.

[3] W. Pigman (Ed.), The Carbohydrates, Chemistry, Biochemistry, Physiology, Academic Press Inc., New York, 1957, p. 21.

[4] H.O. Bouveng and B. Lindberg, Adv. Carbohydr. Chem. 15 (1960), 53.

[5] R.D. Guthrie and J. Honeyman, An Introduction to the Chemistry of Carbohydrates, 2nd edn., Clarendon Press, Oxford, 1964.

[6] A.H. Nissan, G.K. Hunger and S.S. Sternstein, in Encyclopedia of Polymer Science and Technology, Vol. 3, Wiley Interscience, New York, 1970, p. 131.

[7] P. Tomasik, M. Palaasinki and S. Wiejak, Adv. Carbohydr. Chem. Biochem., 47 (1989) 279.

[8] C.T. Greenwood, Adv. Carbohydr. Chem. Biochem., 22 (1967) 483.

[9] S.A. Whatson, in R.L. Whistler and E.F. Paschall, (Eds.), Starch Chemistry and Technology, Vol. II, Academic Press Inc., New York, 1967, p. 1.

[10] D. Costa and G. Costa, Chim. Ind. (Milan), 33 (1951) 71.

[11] A.T. Perkins and H.L. Mitchell, Trans. Kansas Acad. Sci., 60 (1957) 437.

[12] H. Morita, Anal. Chem., 28 (1956) 64.

[13] H. Morita, Anal. Chem., 29 (1957) 1095.

[14] M.C.P. Varma, J. Appl. Chem. (London), (1958) 8, 12, 117.

[15] C.T. Greenwood and H.E. Muirhead, Staerke., 20 (1968) 102.

[16] P.K. Heda, D. Dollimore, K.S. Alexander, D. Chen, E. Law and P. Bicknell, Thermochim. Acta., 255 (1995) 255.

Continuous flow system for the evaluation of the extrinsic coagulation pathway

J.M. Fernández-Romero, M.D. Luque de Castro*

Department of Analytical Chemistry, Faculty of Sciences, University of Córdoba, E-14004 Córdoba, Spain

Abstract

A simple and reliable method for the evaluation of the extrinsic coagulation pathway is presented. The method is based on the monitoring of the last step of the coagulation pathway in which the human plasma is clotted by the presence of the coagulations factors (prothrombin, factor V, factor X, calcium and phospholipids) in an excess of thromboplastin. It has been developed using a flow injection system involving the merging-zones and stopped-flow modes. The clotting reaction rate is monitored photometrically at 340 nm. The linear range expressed as a percentage of total clottable activity was found to be between 10 and 100%, with a relative standard deviation between 0.9 and 2.8%. The usefulness of the method was tested by determining the fibrin clotting capacity in human plasma from healthy and sick individuals with excellent agreement with the conventional clotting method (automated coagulation laboratory–nephelometric method).

Keywords: Extrinsic coagulation factors; Flow injection; Haemostasy; Plasma

1. Introduction

The wide range of clinical parameters involved in the coagulation and fibrinolysis processes makes the global evaluation of the haemostasy in the clinical laboratory difficult. The analytical procedures have been focused on the elucidation of the different steps involved. Specific tests for the estimation of the primary haemostasy, plasmatic coagulation and fibrinolysis have been developed so far.
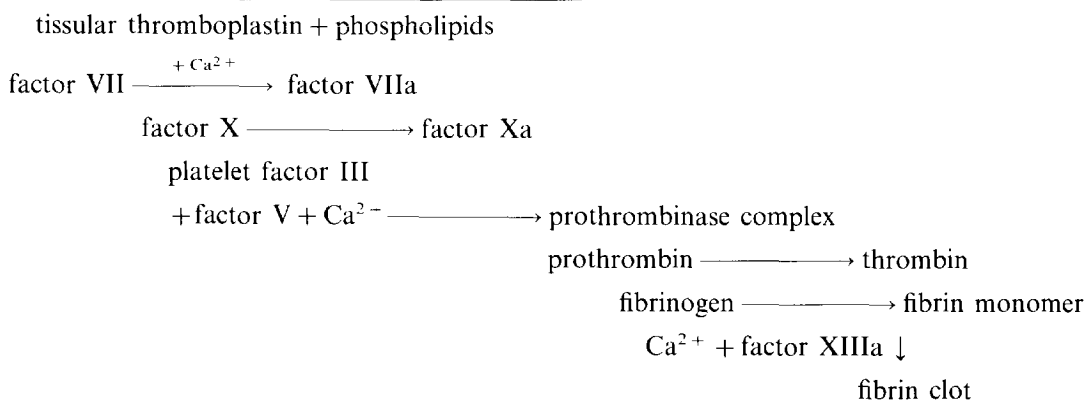
The procedures used in the clinical laboratory are mainly based on the capacity of the human plasma to in vitro clotting, induced by the presence or absence of different coagulation factors. The methods thus developed require two steps: the first is a preparative stage in which the blood sample is treated with anticoagulant substances in order to avoid the spontaneous coagulation. In a second step the plasma obtained is recalcified and mixed with the reagent containing additional coagulation factors required for the clotting step. The correlation between the clotting time and the endogenous coagulation factors is used for the diagnosis of haemostasy diseases and for the evaluation of the anticoagulant therapy.

* Corresponding author. E-mail: qa1meobj@lucano.es

The fibrin clot formed is usually monitored by the physico-chemical changes it produces in the medium (e.g. changes in the physical state, viscosity, conductivity, colour).

A number of chronometric methods with different degrees of automation and based on the above-commented changes have been described in the literature (clotting [1–4], agglutination [5–7] and precipitation [8,9]). The development of new chromogenic and fluorimetric substrates has increased the use of optical techniques with this aim in the last decade, so photometric [10–15], tur-

the sequential injection technique and a robotic method for the detemination of factor XIII have been proposed [47,48].

An automated method for the evaluation of the extrinsic coagulation pathway in human plasma is reported here. The method is an adaptation of the manual prothrombin time test to a flow injection (FI) approach. This method is used as screening of the total prothrombinase complex formed, including prothrombin, factor V, factor X_a, Ca^{2+} and phospholipids, according to the following sequence:

$$\text{tissular thromboplastin} + \text{phospholipids}$$

$$\text{factor VII} \xrightarrow{+ Ca^{2+}} \text{factor VIIa}$$

$$\text{factor X} \longrightarrow \text{factor Xa}$$

$$\text{platelet factor III}$$

$$+ \text{factor V} + Ca^{2-} \longrightarrow \text{prothrombinase complex}$$

$$\text{prothrombin} \longrightarrow \text{thrombin}$$

$$\text{fibrinogen} \longrightarrow \text{fibrin monomer}$$

$$Ca^{2+} + \text{factor XIIIa} \downarrow$$

$$\text{fibrin clot}$$

bidimetric or nephelometric [16–18] and fluorimetric [19–22] methods have been developed. Also a growing adaptation of these methods to commonplace clinical analysers has been implemented in the last few years [23–28].

The protein nature of the most abundant coagulation factors involved in the haemostasy process allowed the development of a large number of immunoassays based on the synthesis of new radioactive or enzymatic labels (radioimmunoassay [29], enzyme linked immunosorbent assay [30–33]). Immunoassay separation techniques such as immunoblotting [34], electroimmunodiffusion [35] or radioimmunodiffusion [36]) have also been used. In this area, application of other chromatographic or non-chromatographic separation techniques such as isoelectrofocusing [37], gel electrophoresis [38], affinity chromatography [39], molecular exclusion chromatography [40], high performance liquid chromatography [41–44] and gas chromatography [45,46] has been reported.

Recently, a continuous flow method based on

According to the literature [24,49] this method can be used to evaluate the extrinsic coagulation pathway. The approach designed for implementation of the method is based on the merging-zones and stopped-flow modes and the clotting reaction rate is monitored photometrically at 340 nm.

2. Materials and methods

2.1. Apparatus

A Unicam 8625 UV/VIS spectrophotometer furnished with a Hellma 176.052QS flow cell (25 μl inner volume) and equipped with a Perkin-Elmer R-100 recorder and a Neslab Exacal EX-110 recirculating thermostat was used. A Gilson Minipuls-2, four-channel peristaltic pump with a rate selector, a laboratory-made dual injection valve built using two Rheodyne 5041 injection valves and PTFE tubing of 0.5 mm i.d. were also used. A Zennitt data PC system connected via an RS-232 interface to the detector was used for

absorbance-time data acquisition, processing and delivery.

2.2. Reagents and standards

The buffer used was an aqueous solution containing 10 mmol 1^{-1} 5,5-diethylbarbituric acid sodium salt (Merck No. 500538) adjusted to pH 7.3 with hydrochloric acid. A carrier solution containing 100 mmol 1^{-1} sodium chloride (Merck No. 10.6404) and 20 mmol 1^{-1} calcium chloride (Merck No. 2382) was prepared in the above-mentioned buffer. Calcium thromboplastin (Sigma T-7280) was diluted to the appropriate extent in the carrier solution.

Coagulation control level I (Sigma C-7916) containing standardized human plasma diluted as required in the carrier solution was used for quality control of the coagulation testing according to the literature [50].

2.3. Samples

Venous blood with 129 mmol 1^{-1} trisodium citrate (1 ml per 9 ml of blood) as anticoagulant was collected with clean venipuncture and minimal stasis from healthy and sick individuals. Plasma samples were kept separate, snap frozen in small aliquots and stored at −50°C until assay (after thawing at 37°C for five minutes).
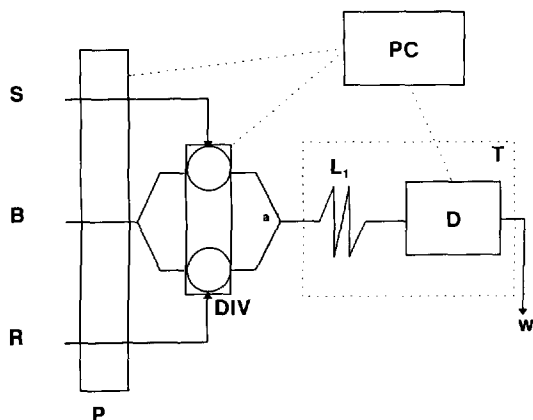
Fig. 1. Merging-zones/stopped-flow manifold. S, denotes sample; B, buffer; R, reagent; P, peristaltic pump; DIV, dual injection valve; a, merging point; L_1 open reactor; D, detector; T, thermostat; PC, personal computer; and w, waste. The boxed zone was thermostated.
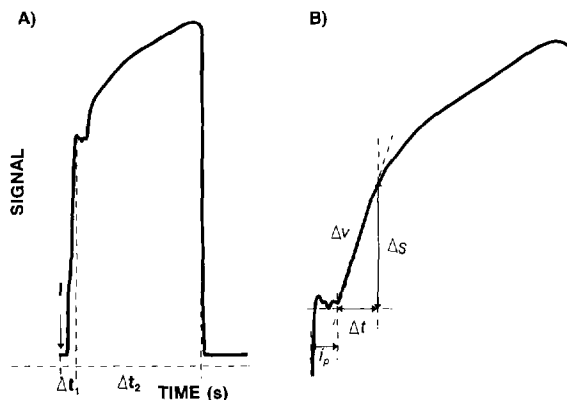

Fig. 2. (A) Typical absorbance–time recordings. 1, denotes injection, Δt_1, delay time and Δt_2, stop time. (B) Detail of the coagulation curve. i_p, ΔS, and Δt denote induction period, increment of signal and time, respectively.

2.4. Flow injection manifold and procedure

The symmetrical merging-zones and stopped-flow manifold shown in Fig. 1 was used in order to minimize the reagent and sample consumption. It consists of a peristaltic pump (P) which propels the carrier (B) stream through two channels. A dual-injection valve (DIV) inserts both the calcium thromboplastin and sample solutions simultaneously into the buffer streams. Both plugs are merged at point a and then driven through the reactor L_1. When the reaction plug reaches the flow cell the peristaltic pump is halted. The clotting process is monitored during the stop time. Finally, the pump functioning is re-started and the clotting plug is wasted. A PC synchronizes the pumping periods with the injection time.

2.5. Types of measurements

Fig. 2 depicts the typical absorbance–time recordings obtained. The signal shows two parts (Fig. 2(a)). The first one, developed during Δt_1, is due to the absorption of the reaction ingredients at the selected wavelength and the second (developed in the Δt_2 interval) corresponds to the coagulation process. The latter can also be divided into two parts (see Fig. 2(B)): the first one corresponds to the induction period independent of the coagulation step, probably due to the initial adherency of the plug on the wall of the flow cell. The second part corresponds to the formation of the clot.

Table 1
Optimization of the variables

Type	Variables	Range studied	Optimum value
Instrumental	Wavelength (nm)	200–800	340
Physical	Temperature (°C)	20–60	50
FI	Flow rate (ml min^{-1})	0.6–2.0	1.6
	Sample volume (μl)	10–100	50
	Reagent volume (μl)	10–100	50
	Reactor length (cm)	10–100	15
	Delay time (s)	10–20	14
	Stop time (s)	30–120	90
Chemical	[5,5-Diethylbarbituric acid] (mmol l^{-1})	0–100	10
		0–20	15
	[Sodium chloride] (mmol l^{-1})	0–40	20
	[Calcium chloride] (mmol l^{-1})	6.0–8.0	7.3
	pH	1–10	5
	Reagent dilution	1–10	5
	Sample dilution		

The signal acquired, provides a way to establish a relationship between the initial coagulation rate and the total clotting activity in the sample. According to the common procedure followed for the estimation of the prothrombin time, by using the automated coagulation laboratory (ACL)-nephelometric method, it is also feasible to establish a relationship between the total clotting activity and the prothrombin time commonly used in the literature [49].

The measurement of the initial reaction rate was made along the linear-rising portion of the kinetic curve by using the equation $V = (A_2 - A_1)/(t_2 - t_1)$ where A_2 and A_1 are the absorbances over the linear portion of the curve defined by times t_2 and t_1, respectively.

3. Results and discussion

3.1. Study of the variables

The optimization of the process was aimed at enabling the calcium thromboplastin/sample mixture to reach the detection system as soon as possible, thus allowing a more complete monitoring of the overall process. The variables influencing the system were studied by the univariate method. Table 1 shows the ranges in which the variables were studied and the optimal values found.

3.1.1. Physical variables

The increase in temperatue had a favourable effect on the analytical signal, due to an increase in the coagulation reaction rate, up to 50°C; above this value the change was insignificant. The induction period decreased when the temperature increased above 35°C.

3.1.2. Chemical variables

The influence of the buffer concentration (5,5-diethylbarbituric acid sodium salt) on the analytical signal in the range studied was insignificant. A concentration of 10 mmol l^{-1}, enough to keep the working pH constant at 7.3, was adopted for further experiments. The carrier–buffer solution has a sodium chloride concentration of 14.54 mmol l^{-1} in order to acheive an ionic strength simialr to that of plasma.

The effect of dilution on both the calcium thromboplastin reagent and plasma solution were studied in order to minimize reagent and sample consumption. A dilution factor of five caused an acceptable clotting response with low reagent and

Table 2
Features of the method

Equation[a]	Linear range[b]	r^2	Relative standard deviation %[c]			Sampling frequency (h^{-1})
			Low	Medium	High	
ln $Y = 7.213 - 0.522$ ln X	10–100	0.9985	2.8	1.1	0.8	50

[a] Y denotes total clotting activity in %, X denotes the coagulation reaction rate.
[b] measured in % of total clotting activity.
[c] Value for 20, 50 and 80% of total clotting activity.

sample consumption. The carrier solution had a calcium concentration of 20 mM in order to avoid the dispersion of the calcium from the thromboplastin solution introduced into the dynamic system.

3.1.3. Hydrodynamic variables

High flow rates increased the analytical signal by reducing the plug dispersion along the system as the residence time of the plug was shorter, but in turn they made less precise delay time measurements. A flow rate of 1.6 ml min^{-1} was chosen as a compromise between both effects. Injection volumes of 50 μl for both calcium thromboplastin and sample provided the highest analytical signal. A length of 15 cm for reactor L$_1$ was selected as the minimum length that provided efficient mixing of the two plugs. Higher length increased the dispersion and decreased the analytical signal, i.e. a length of 60 cm caused a decrease in the peak height of 20%. Shorter reactors are not sufficient to connect the merging point a and the flow cell.

The time variables of the stopped-flow mode provided an optimal analytical signal for a delay time of 14 s for which the centre of the reacting plug was at the detector; the signal increased with the stop time but levelled off at 90 s. A plateau was obtained for longer times, which showed the stabilization of the clotting process.

3.2. Features of the method

The calibratin graph was obtained using the optimum values of the variables studied above. The human plasma calibration control was diluted to an appropriate extent in order to obtain a prothrombin activity between 5 and 100%, cal-

culated according to the conventional procedure [49]. Ten standard solutions were injected in triplicte into the FI manifold. The typical exponential relationship between the percentage of prothrombin activity and the coagulation rate obtained was represented by the following equation:

$$Y = 1357X^{-0.5422} \quad (r^2 = 0.9690)$$

where Y is the percentage of prothrombin activity and X is the reaction rate. Nevertheless, the data fit the equation below better

$$\ln Y = 7.213 - 0.5422 \ln X \quad (r^2 = 0.9985)$$

which represents the behaviour of the biochemical system between 10 and 100% of prothrombin activity; it was used in order to establish both the precision and applicability of the method.

A relationship can also be established between the coagulation reaction rate and the prothrombin time parameter (commonly use in clinical analysis), according to the mathematical expression:

$$Z = 1.403X^{-4.096} \quad (r^2 = 0.9747)$$

where Z is the prothrombin time and X is the reaction rate.

The precision afforded by the method was studied at three levels of prothrombin activity (20, 50 and 80%). Eleven samples of each level were injected in triplicate into the dynamic manifold. The repeatability, expressed as the percentage relative standard deviation, was better than 2.8% in all instances (see Table 2).

The sampling frequency was estimated at 50 per hour, due to the time required for the development of the clotting process.

3.3. Application to real samples

The performance of the method was tested by applying it to the determination of the total clotting activity in plasma, using twenty-five samples (from healthy and sick individuals) from a hospital. The samples were classified according to the procedence in normal plasma or plasma with anticoagulant therapy (courmarin or heparin treatment).

The results were compared with those obtained by using the ACL–nephelometric method [24] as shown in Fig. 3. The correlation equation and coefficient are as follows:

$$Y = 0.974X + 1.106 \quad (r = 0.9980)$$

where Y is the FI method and X is the ACL method. As can be seen, an excellent correlation exists between the proposed and the conventional method.

4. Conclusions

An automatic method based on flow injection has been used for the evaluation of the haemostasy process. This is the first time that a continuous flow system has been proposed to implement this assay.
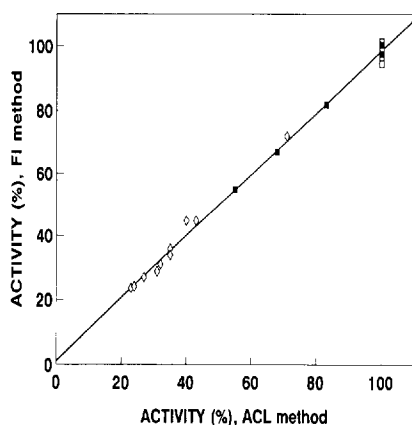
Fig. 3. Correlation between the proposed method (FI) and the ACL–nephelometric method. Normal plasma samples (□) plasma (ten samples with similar concentration) after treatment with coumarin (■) or heparin (△).

The simplicity, repeatability and sensitivity of the method make it a valid alternative to the commercial methods for the determination of the prothrombin activity in plasma.

The sample throughput achieved by the FI approach surpasses that of the existing methods for this parameter. The results obtained by applying the continuous method to plasma samples agree well with those provided by the conventional method widely used in clinical laboratories.

The approach is a useful tool for the estimation of the extrinsic coagulation pathway (prothrombin, factor V, factor X_a, Ca^{2-} and phospholipid). It could be the basis for the development of new approaches in this area of clinical analysis.

Acknowledgements

References

[1] P.V. Nash and T.D. Bjornsson, Anal. Biochem., 138 (2) (1984) 319–323.
[2] M. Enomoto, I. Tanimizu and M. Sakuragawa, Thromb. Res., 57 (5) (1990) 729–736.
[3] M. Poggio, A. Tripodi, G. Mariani and P.M. Mannucci, Thromb. Haemostasis., 65 (2) (1991) 160–162.
[4] P. Han, K.P. Fung and U. Rahdakrishnan, Thromb. Haemostasis., 65 (4) (1991) 360–363.
[5] S. Halvorsen, O.H. Skjoensberg, R. Ruyter and H.C. Goldal. Thromb. Res., 57 (4) (1990) 489–497.
[6] D. Prisco, R. Pannicca, M. Costanzo and R. Abbate, Thromb. Res., 59 (1) (1990) 207–212.
[7] S. Halvorsen, O.H. Skjoensberg and H.C. Goldal, Thromb. Res., 61 (3) (1991) 341–348.
[8] P. Desvignes and P. Bonnet, Clin. Chim. Acta., 110 (1) (1981) 9–17.
[9] U. Funke, G. Toepfer, M. Shulze, A. Seifert, G. Friedel, K. Eckardt, M. Stepanauskas and H. Thrum, Z. Klin. Med., 45 (8) (1990) 683–686.
[10] K. Asai and M. Asai, Clin. Chim. Acta, 144 (2–3) (1984) 163–171.

[11] P. Leprince, B. Rogister and G. Moonen, Anal. Biochem., 177 (2) (1989) 341–346.

[12] W.L. Chandler, G. Schemer and J.R. Stratton, J. Lab. Clin. Med., 113 (3) (1989) 362–371.

[13] A. Hijikata-Okunomiya, Thromb. Res., 57 (5) (1990) 705–715.

[14] H. Vinazzer and K. Stocker, Thromb. Res., 61 (3) (1991) 235–241.

[15] H. Groetsch, G. Berscheid, M. Hropot and R. Ben-Youssef, Thromb. Res., 64 (2) (1991) 285–290.

[16] M. Macart, A. Koffi, G. Henocque, J.F. Mathieu and J.C. Guilbaud, Clin. Chem., 35 (2) (1989) 211–214.

[17] J.V. Wieding, G. Eisinger and H. Koestering, J. Clin. Chem. Clin. Biochem., 27 (2) (1989) 57–63.

[18] G.S. Retzinger, B.C. Cook, R.E. Smith and M.C. McGinnis, Anal. Biochem., 195 (1) (1991) 18–23.

[19] L. Lorand, K.N. Parameswaran, P.T. Velasco, L.K.H. Hsu and G.E. Siefring, Anal. Biochem., 131 (2) (1983) 419–425.

[20] P.R. Reczek, A.S. Martel, M. Lorenzi-Anderson, L. Hills and P.R. Jensen, Thromb. Res., 37 (3) (1986) 431–436.

[21] D.M. Monroe, G.B. Sherrill and H.R. Roberts, Anal. Biochem., 172 (2) (1988) 427–435.

[22] S. Morikawa, S. Tanigushi, M. Fujiwara, K. Kumada, T. Ishida, K. Horlike and M. Nozaki, Thromb. Res., 55 (4) (1989) 427–438.

[23] G.E. Siefring, D.K. Riabov and J.A. Wehrly, Clin. Chem., 29 (4) (1983) 614–617.

[24] C. Rousseaux, F. Truchaud, C. Pioda, D. Lemecier and A. Truchaud, Spectra Biol., 6 (4) (1988) 53–56.

[25] J.J.M.L. Hoffmann and M.A.L. Verhappen, Clin. Chem., 34 (10) (1988) 2135–2140.

[26] H. Ihara, M. Ohtsuka, Y. Aoki and T. Aoki, Clin. Chem., 34 (12) (1988) 2582–2583.

[27] H.J. Siemens and T. Wagner, Lab. Med., 12 (4) (1989) 125–128

[28] Z. Jelic-Ivanovic and N. Pevcevic, Clin. Chem., 36 (4) (1990) 698–699.

[29] G. Stehle, J. Harenberg, H. Schmidt-Gayk and R.J. Zimmermann, Clin. Chem. Clin. Biochem., 21 (2) (1983) 91–95.

[30] G. Rock, Thromb. Res., 57 (5) (1990) 183–188.

[31] M. Tanaka, M. Minesaki and K. Kato, Clin. Chem., 103 (3) (1980) 287–295.

[32] G.J. Doellgast, Anal. Biochem., 167 (1) (1987) 97–105.

[33] G. Elgue, B. Pasche, M. Blomback and P. Olsson, Thromb. Haemostasis, 63 (3) (1990) 435–438.

[34] B. Laemmle, M. Berretini and J.H. Griffin, Anal. Biochem., 156 (1) (1986) 118–125.

[35] T. Eller, B. Pohl, P. Zuerrlein and F. Keller, Haemostaseologie, 11 (1) (1991) 33–38.

[36] Commitalo Italiano per la standarizzazione dei metodi in ematologia a laboratorio. Fibrinogen assay: a collaborative study of six different methods. Clin. Chem., 37 (5) (1991) 714–719.

[37] H. Yoshida, M. Ono, T. Manabe and T. Okuyama, Seibutsu Butsuri Kagaku, 33 (3) (1989) 119–124.

[38] A. Gurusinghe, P.A. Ryan and P.A. Davis, Electrophoresis, 7 (2) (1986) 96–98.

[39] C. Kyuas, A. Haeberli, P. Walder and P.W. Straub, Thromb. Haemostasis, 63 (3) (1990) 439–444.

[40] B.G. Belen' kii, E.S. Gankina, J.J. Kever, I.O. Kostyuk, A.E. Saminkskii and N.A. Illarionova, Bioorg. Khim., 13 (7) (1987) 894–897.

[41] S.J. Lucas and A. Henschen, J. Chromatogr., 369 (2) (1986) 357–364.

[42] W. Schroeder, M. Dumas and U. Klein, J. Chromatogr., 512 (1990) 213–218.

[43] H. Salari and G.K. Eigendorf, J. Chromatogr. Biomed. Appl., 527 (2) (1990) 303–314.

[44] M.L. Blank, E.A. Cress, V. Fitzgerald and F. Snyder, J. Chromatogr., 508 (2) (1990) 382–385.

[45] A.L. Fisher, M. Morris and J.D. Gilbert, Biol. Mass. Spectrom., 20 (7) (1991) 408–414.

[46] M. Balazy, P. Braquet and N.G. Bazan, Anal. Biochem., 196 (1) (1991) 1–10.

[47] M. Guzmán, C. Pollema, J. Ruzicka and G. Christian, Talanta, 40 (1) (1993) 81–87.

[48] M. Guzmán and B.J. Compton, Talanta, 40 (12) (1993) 1943–1950.

[49] A.J. Quick, Hemorrhagic Diseases and Thrombosis, 2nd edn., Lea and Febiger, Philadelphia, 1966.

[50] M.S. Sirridge, Laboratory Evaluation of Hemostasis, Lea and Febiger, Philadelphia, 1967.

Analysis of lead and tin in strong brine and high iron systems using the microsampling technique

T.S. Wai, H. Darus, N. Mohamed*

School of Chemical Sciences, Universiti Sains Malaysia, 11800 Penang, Malaysia

Abstract

The development of hydrometallurgical techniques such as the iron(III) chloride–sodium chloride system for the recovery of metals from scrap materials necessitates the analyses of these metals in a high salt medium during the recovery studies. An alternative method for the analysis of lead and tin in strong brine and high iron systems by flame atomic absorption spectrometry is a microsampling technique in combination with in situ standard addition. Relative standard deviations of 1.2% and 2.2% were obtained for the analysis of lead and tin respectively. The accuracy for the method is also satisfactory with recoveries ranging from 90% to 102%. The microsampling technique is rapid and simple, requires small volumes of sample and offers no clogging problems during the atomic absorption analyses.

Keywords: Lead and tin analysis; Microsampling technique

1. Introduction

The dissolution of scrap materials from which metals of interest are to be recovered is one of the basic steps in the recycling especially that of solid scrap materials. One of the most common solvent systems used in the dissolution of metal alloys is a mixture of concentrated acids. For example, a standard procedure in the dissolution of solder is by heating the alloy in a mixture of concentrated hydrochloric and nitric acids. A mixture of fluoroboric acid and hydrogen peroxide has also been used to dissolve a lead alloy containing tin and

antimony [1]. The use of hydrometallurgical processing for the recovery of metals from scrap materials offers another alternative. Kolodziej and Adamski [2] have suggested the ferric chloride hydrometallurgical process which uses acid solutions of ferrous chloride to recover silver from electronic scrap materials. Langer et al. [3] have tried the cupric chloride process for the recovery of copper from scrap materials. McDonald et al. have used cupric bromide in the recovery of copper from copper sulfide and ore concentrates [4]. An attempt has been made to use ferric chloride in a solution of sodium chloride of high concentration as a leaching reagent for solder in order to recover the tin and lead (T.S. Wai and H. Darus,

---

* Corresponding author. Fax: (60) 4-657-4854.

unpublished results). This mixture is a non-acidic solvent consisting of a mixture of iron(III) chloride–sodium chloride, which is less corrosive compared to acids. Because of the presence of a high concentration of iron(III) and sodium chloride, the analysis of lead and tin in the mixture needs further studies.

The presence of these ions may cause problems during the analysis of lead and tin using atomic absorption spectroscopy involved in the recovery studies. Many studies have been reported on the analysis of lead and tin but studies on the effects of the analysis of both elements in concentrated salt medium have been rather limited [5–10]. The interference effect of cations is usually overcome by using solvent extraction techniques or ion exchange methods. Even though the interfering elements are eliminated by these methods, these methods are tedious and problems such as the loss of the analyte during the extraction process or passage through the ion exchange column cannot be avoided. An alternative method is presented here for the analysis of lead and tin in strong brine and high iron systems by flame atomic absorption spectrometry using a microsampling technique in combination with in situ standard addition. In the microsampling technique, small volumes (< 500 µL) of solution were pipetted into a Teflon sampling cone and directly nebulized by a conventional capillary pneumatic nebulizer in a premixed flame. The transient recorder responses that result have similar precision and sensitivity to that obtained with normal larger (1–5 mL) samples by atomic absorption studies [11–13]. This sample introduction technique was found to be less susceptible to system clogging than normal steady state aspiration techniques since less sample is aspirated per analysis. The method of standard additions is used to ascertain

the elemental concentration in order to overcome sample matrix effects. Standard additions were performed on-the-spot in the Teflon sampling cone.

2. Experimental

2.1. Apparatus

A GBC Scientific Equipment Pty Ltd. (Australia) Model 903 atomic absorption spectrometer equipped with a standard nebulizer, 10 cm burner head, hollow cathode lamps and Pantos model Unicorder U-228 strip chart recorder was used for the analysis of lead. Background correction using a deuterium lamp was employed.

An IL 357 atomic absorption spectrometer equipped with a standard nebulizer, 5 cm burner head and hollow cathode lamps was used for the analysis of tin. The instrument parameters are given in Table 1.

Microliter pipettes (fixed and variable volume) were used. A Teflon sampling cone was constructed as shown in Fig. 1 with a capacity of 5 µL up to 2 mL with a 45° taper.

2.2. Reagents

All reagents were of analytical grade. All water used was deionized and distilled.

- Standard lead solutions: (1000 µg mL^{-1} Pb): a mass of 1.5985 g of analytical grade Pb(NO$_3$)$_2$ (Riedel de-Hahn) was dissolved in distilled, deionized water; 10 mL concentrated nitric acid

Table 1
Instrument parameters

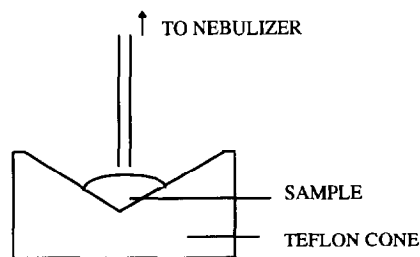| Element	Wavelength	Slit Width	Current	Flame
Pb	217.0 nm	1.0 nm	5.0 mA	Air–acetylene
Sn	235.5 nm	160 nm	6.0 mA	NO$_2$–acetylene

Fig. 1. Teflon sampling cone.

Table 2
Determination of lead in a synthetic tin–lead alloy

Sample	Concentration of Pb spike (ppm)	Concentration of Pb determined (ppm)	Percentage recovery (%)
P1	2.50	2.25	90.0
P2	2.50	2.45	98.0
P3	2.50	2.55	102.0
P4	5.00	5.20	104.0

was added and the solution was diluted to 1 liter.

● Standard tin solutions: (1000 μg mL^{-1} Sn): a mass of 1.000 g tin (99.99%) (Datuk Keramat Smelting, Pulau Pinang) was dissolved in aqua regia (HCl:HNO$_3$; 10:2), and diluted to 1 liter.

● Standard iron solutions: (1000 μg mL^{-1} Fe): ammonium iron(II) sulfate, $(NH_4)_2$ $Fe(SO_4)_2 \cdot$ (6H$_2$O), from E. Merck (Damstadt, Germany) was dissolved in 1 liter of water.

● Lead Standard 948206: Orion Research Incorp., Cambridge, Massachusetts, USA (lead as lead perchlorate, certified traceable to National Bureau of Standards SRM 928).

● Tin–lead alloy wire (60/40).

● Concentrated nitric acid (65%) from Riedel de Hahn.

● Concentrated hydrochloric acid (36%) from Ajax Chemical.

● Sodium chloride from R. M. Chemical, R & M Marketing, Essex, UK.

● Disodium salt of ethylenediaminetetraacetic acid (EDTA).

● Sodium fluoride from Fluka.

● Hexamine from BDH.

● Xylenol orange from BDH.

2.3. Procedure

2.3.1 Synthetic tin–lead alloy solution

Synthetic tin–lead alloy solutions with a 60:40 tin to lead ratio were prepared using standard tin and lead solutions. These solutions also contained 100 ppm iron(II) and 2.0 M sodium chloride to simulate samples resulting from the dissolution of the tin–lead alloy by ferric chloride hydrometallurgy.

2.3.2. Standard lead 948206

The original lead standard solution contained 0.1000 ± 0.005 mol L^{-1} lead (in the form of lead perchlorate). This is equivalent to 20720 μg mL^{-1} of lead. For the purpose of analysis, this stock solution was diluted to a range between 0 and 10 ppm.

2.3.3. Pure tin–lead alloy

The pure tin–lead alloy used in these studies is in the shape of a wire (diameter 1.2 mm, gauge 18 S.W.G.). The wires were cut with a pair of pliers to a length of 1.0 ± 0.2 cm. One alloy sample was dissolved in a mixture of 10 mL of concentrated hydrochloric acid and 2 mL of concentrated nitric acid, heated slowly on a hot plate, cooled and later filtered through some glass wool to get rid of the insoluble impurities. Another alloy sample was dissolved using ferric chloride hydrometallurgical dissolution (T.S. Wai and H. Darus, unpublished results).

2.3.4. Microsampling technique

Sample (100 μL) was pipetted into the Teflon cone using a micropipette. Water (100 μL) was added to the sample in the cone. The sample was then introduced by manually inserting the end of the plastic nebulizer tubing into the cone. A transient recorder signal resulted immediately. The concentration was estimated by comparison with the steady state signal of the appropriate standard solutions. The concentration was evaluated by the method of standard additions which was in situ in the Teflon cone. The volume of the standard added was 100 μL of an appropriate standard. At least three replicates were carried out for each sample.

2.3.5. Direct measurement

The standard solutions and the samples were aspirated directly into the flame. The concentrations of tin and lead in the samples were calculated by means of a calibration curve. These results were then compared to those obtained by the method of in situ standard additions using the microsampling technique.

Table 3
Determination of lead in standard lead samples

Sample	Concentration of Pb (certified value, ppm)	Concentration of Pb (ppm)		Percentage recovery (%)	
		DM	SA	DM	SA
LS1	20720	20800	18400	100.4	88.8
LS2	20720	18800	20000	90.7	96.5

DM, direct measurement.
SA, standard addition using the microsampling technique.
LS1 in distilled water.
LS2 in 2.0 M NaCl solution.

2.3.6. Titration method

Several solutions, 0.2 M standard EDTA solution, 0.01 M $Pb(NO_3)_2$ standard solution, 30% aqueous hexamine solution and a 0.2% xylenol orange solution were prepared. About 0.4 g of sample was weighted accurately. It was then dissolved in 10 mL concentrated hydrochloric acid and 2 mL of concentrated nitric acid with gradual heating. The mixture was then brought to the boil for 5 min. A volume of 25 mL of a 0.2 M standard EDTA solution was added and the mixture was again brought to the boil for another minute. A clear solution was obtained. This was then diluted to 250 mL with distilled water in a volumetric flask. Aliquots (25 mL) of the sample were pipetted into three separate conical flasks. Hexamine solution (15 mL), 110 mL of distilled water and four drops of xylenol orange were added to each of the conical flasks. Each mixture was then titrated with standard lead (II) nitrate solution until the color change from yellow to reddish purple was observed. Sodium fluoride (2 g) was then added to the mixture. The color of the solution then turned yellow as a result of EDTA being released from the tin(IV)–EDTA complex. This solution was then titrated until a purple color, which was stable for at least a minute, was observed.

2.3.7. Precision and accuracy of the microsampling technique

The precision and accuracy of the microsampling technique with in situ standard addition for the analysis of lead and tin in various media were evaluated.

Three samples of the synthetic tin–lead alloy solution were each spiked with 2.5 ppm of lead. The concentration of lead in these samples were then obtained by using the microsampling technique. The recoveries for the 2.5 ppm spike were then calculated.

Two solutions of the lead standard 948206 were prepared. One solution, LS1, was diluted from the stock solution with distilled water. The other, LS2, was prepared containing 2.0 M NaCl, 100 ppm iron and 100 ppm tin. The concentration of lead was determined using the microsampling technique and the direct measurement method.

A comparison between the three methods, that is, the method of standard addition using the microsampling technique, the direct measurement method and the titrimetric method was made for two alloy samples. One sample, PS1, was dissolved in a mixture of concentrated hydrochloric acid and concentrated nitric acid. The other sample, PS2, was dissolved in a mixture of $FeCl_3$–NaCl (T.S. Wai and H. Darus, unpublished results).

3. Results and discussion

3.1. Accuracy of the determination of lead using the microsampling technique

The recovery percentage for the 2.5 ppm lead spike on three samples of synthetic tin–lead alloy solutions was calculated. The recovery percentage ranged from 90.0% to 102.0%. Another sample which was spiked with 5.0 ppm lead gave a recov-

Table 4
Comparison between the three methods for the determination of lead and tin

Sample	Sample weight (g)	Weight determined (g)				Percentage (%)					
		A		B		A		B		C	
		Pb	Sn	Pb	Sn	Pb	Sn	Pb	Sn	Pb	Sn
PS1	1.0045	0.4906	0.5600	0.4746	0.5500	48.84	55.75	47.25	54.75	48.03	51.97
PS2	0.2314	0.1150	0.1330	0.1150	0.1250	49.70	54.02	49.70	54.02	49.92	50.52

A, standard addition using the microsampling technique.
B, direct measurement.
C, titrimetric method.
Note: for the titrimetric method, a different sample was used.

ery of 104.0%. The results are shown in Table 2. This showed that the microsampling technique gave accurate results for the determination of lead in samples containing 2.0 M NaCl and 100 ppm iron.

Two samples of standard lead, LS1 and LS2, were analyzed for lead using the microsampling technique and the direct measurement method.

Table 5
Precision data for the three methods in the determination of tin and lead

Method	Standard addition using the microsampling technique	Direct measurement method	Titrimetric method
Pb			
Mean (%)	49.27	48.48	48.98
Standard deviation	0.6	1.7	1.3
Relative standard deviation (%)	1.2	3.5	2.7
Sn			
Mean (%)	54.88	54.38	51.24
Standard deviation	1.2	0.5	1.0
Relative standard deviation (%)	2.2	0.9	2.0

Recoveries for the lead are shown in Table 3.

3.2. Comparison between the three methods for the determination of tin and lead

The results show good agreement for the determination of tin and lead between the three methods as shown in Tables 4 and 5. The relative standard deviation for the determination of lead using the microsampling technique, 1.2%, was the lowest among that obtained for the three methods whilst that for the titrimetric method is the highest, 2.7%. However, the relative standard deviation for the determination of tin using the microsampling technique was the highest.

4. Conclusion

The precision for the microsampling technique is satisfactory (a relative standard deviation of 1.2% for the analysis of lead and about 2.2% for the analysis of tin). The accuracy for the method is also satisfactory with recoveries of 90% to 102%. Therefore, with respect to the precision and accuracy of the microsampling technique together with its advantages, such as it being rapid and simple, requires small volumes of sample and has no clogging problems during the atomic absorption analysis, this technique was found to be suitable for the determination of the lead and tin in solder samples or solder dissolved using the iron(III) chloride hydrometallurgical process.

Acknowledgements

References

[1] T.M. Quarrell, R.J.W. Powell and H.J. Cluley, Analyst, 98 (1973) 443.

[2] B. Kolodziej and Z. Adamski, Hydrometallurgy, 12 (1984) 117.

[3] S.H. Langer, M.A. Nametz, T.D. Kaun and J.H. Anderson, in Chloride Hydrometallurgy Proceedings, Benelux Metallurgie, Brussels, 1977. p. 134.

[4] G.W. McDonald, H. Darus and S.H. Langer, Hydrometallurgy, 24 (1990) 291.

[5] D.G. Biechler, Anal. Chem., 37 (1965) 1054.

[6] N.G. Sellers, Anal. Chem., 44 (1972) 410.

[7] R.M. Dagnall, T.S. West and P. Young, Anal. Chem., 38 (1966) 358.

[8] M.E. Hofton and D.P. Hubbard, Anal. Chim. Acta, 52 (1970) 425.

[9] J. Ramirez-Munoz, Anal. Chem., 42 (1962) 517.

[10] O.K. Galle, Appl. Spectrosc., 25 (1971) 664.

[11] H.T. Delves, Analyst, 95 (1970) 431.

[12] H. Berndt and E. Jackwerth, Spectrochim. Acta, Part B, 30 (1975) 169.

[13] R.C. Fry, S.J. Northway and M.B. Denton, Anal. Chem., 50 (1978) 1719.

The separation and isolation of gold by selective extraction and transport through a polyurethane ether-type membrane

R.D. Oleschuk, A. Chow*

Department of Chemistry, University of Manitoba, Winnipeg, Manitoba R3T 2N2, Canada

Received 1 December 1995; revised 6 March 1996; accepted 7 March 1996

Abstract

The separation and isolation of gold(III) by selective extraction and transport through a ether-type polyurethane membrane was studied. Gold was found to be extracted into the membrane in strongly acidic solutions of HCl and HBr as the $HAuBr_4$ and $HAuCl_4$ complexes. Once extracted, the $HAuCl_4$ and $HAuBr_4$ complexes diffuse through the membrane and are recovered quantitatively in a receiving cell solution. This phenomenon was studied for the separation of a variety of binary metal solutions as well as for the separation of gold from a solution of gold ore. The preconcentration of gold was also achieved by adjusting the starting and receiving cell solution volumes.

Keywords: Gold; Isolation; Polyurethane ether-type membrane; Selective extraction; Separation; Transport

1. Introduction

In polyurethane chemistry the term "membrane" has been applied to two separate physical entities: a non-porous polymer film as used in this investigation, and foam-like films that are porous, allowing solution to percolate through them. The non-porous membranes suffer from the disadvantage of possessing a lower surface area. However, they prevent the two solutions on either side of the membrane from coming in contact with one another, ensuring the complete separation of the two phases on either side of the membrane.

Polyurethane foams were first shown by Bowen [1] to extract metals selectively from aqueous solution. Since then polyurethane foams have been extensively investigated for the sorption of both metals and organics from solution. Several reviews of the subject have been published [2–6].

When performing extractions with "foam-like" sorbents, it is often necessary to perform an additional extraction step to obtain the isolated species from the foam. Also, once the foam is saturated with a species, it is no longer an efficient sorbent. These two problems can be overcome by using polyurethane in the form of a membrane. Since the species is only in the membrane for a short period of time and is then isolated on the other side, it eliminates the additional extraction

---

* Corresponding author. Fax: (204) 275-0905.

step required when using the foam. The membrane can also become saturated like the foam, but will continue to perform the separation as the saturated species is transported through the membrane.

It has previously been shown that cobalt thiocyanate [7] complexes, as well as iron [8,9] and gallium [9] chloride complexes, can be extracted and transported through polyurethane membranes. The extent and rate of transport are dependent on the temperature, the affinity of the complex for the membrane and the amount of extracting species present in solution. The amount of extractable species in solution is then dependent on the individual stability constants of the metal complexes, and the relative concentrations of the complexing species present in solution. For gallium and iron the extracting species were shown to be $GaCl_4^-$ and FeX_4^- (where $X = Cl$, Br) respectively. Gold(III) is a softer acid than Ga(III) and Fe(III) in a Pearson [10] sense, so it prefers to form complexes with the larger halides at lower halide concentrations. Gold(III) forms halide complexes with chlorine, bromine and iodine. The iodide complex is less stable than the chloride and bromide, and extremely difficult to prepare in pure form [11]. The gold(III) halide complexes are analogous to those of iron(III) and gallium(III), all of which possess the formula MX_4^-.

Several researchers [12–15] have investigated the extraction of gold by polyurethane foams from aqueous media. Gold was observed to be extractable using an unloaded polyurethane ether-type foam from extremely acidic aqueous media (> 1 M HCl). The extraction was found to be due to the presence of the $AuCl_4^-$ complex formed at high HCl concentrations.

In this paper, gold is shown to be quantitatively and selectively extracted, transported and recovered, either alone or in the presence of other metals in solution. The effects of using both the chloride ($AuCl_4^-$) and bromide ($AuBr_4^-$) complexes on the transport process were investigated. The investigation into the extraction, the transport and the elution of gold from the membrane was undertaken to determine the viability of the separation as well as to obtain a better understanding of the overall extraction and transport processes.

2. Experimental

All gold analyses were performed with a Varian SpectrAA-20 atomic absorption spectrometer equipped with an Instrumentation Laboratory Visimax™ hollow cathode lamp and a Varian Mark VI burner head coupled with an air–acetylene flame. The wavelength observed was 242.8 nm with a slit width of 1.0 nm and a lamp current of 4 mA. All chemicals used were of reagent grade.

A Varian Liberty 200 ICP emission spectrometer was used for the multi-element determinations made when performing the separation of gold from gold ore. Inter-element correction was used when overlapping emission lines were present.

Stock gold solutions were prepared using $NaAuCl_4$ supplied by Johnson-Matthey. Concentrated hydrochloric acid was supplied by Fisher Scientific and concentrated hydrobromic acid from Anachemia. All water used was purified by a Barnsted Nanopure™ II system using reverse osmosis-treated feedstock. The membranes used were of the polyurethane ether-type (XPR625-FS) in two different thicknesses (0.025 mm and 0.050 mm) which were provided by Stevens Elastomerics/Urethane Products Northampton, MA, USA.

The apparatus used for membrane testing was a modified Donnan Dialysis Cell consisting of two separate cells (a starting and receiving cell). The starting cell was a Nalgene™ 125 mL PETG (polyethylene terephthalate copolyester) media bottle (cat # 2015–0125) with a 2 cm hole drilled into the screw cap. A small notch was also cut at the side of the drilled hole to prevent air bubbles being trapped at the membrane solution interface. The receiving cell consisted of a 100 mL beaker that was cut to an appropriate height for the solution volumes used. The screw caps on the media bottles allowed a quick, easy way of fastening the membrane to the bottle with an air- and water-tight seal. Experiments performed at temperatures other than ambient, used starting cells with a small hole drilled in them to prevent any

pressure build up. Membranes were cut into 5 cm × 5 cm squares and placed on the top of the open media bottle holding the sample. The screw cap was placed on the bottle and carefully tightened, yielding a membrane with an active surface area of 5.3 cm². The media bottle was then inverted and immersed in the solution held by the receiving cell. Each unit was wrapped in Parafilm™ to minimize evaporation. For each experiment a number of units were prepared and stopped after various time increments to obtain a separation profile and establish reproducibility. After the cells were stopped by removing the starting cell from the receiving cell, each cell was individually weighed and the pH measured to determine any solution losses due to evaporation or leakage through the membrane. The volume of solution in each of the cells was calculated using solution density.

All gold solutions were prepared from a 500 mg L⁻¹ standard prepared by dissolving NaAuCl₄ in water. The gold ore used in the gold ore separations is from the Kirkland Lake Mine in eastern Ontario, Canada. Gold ore solutions were prepared by first digesting the ore in aqua regia for a period of one week. The nitric acid portion of the mixture was then evaporated off while adding aliquots of concentrated HCl. The acid content of the mixture was lowered by then boling this solution while adding aliquots of deionised water. The solution was then filtered using Whatman™ No.42 filter paper to remove the silicates not dissolved in the acid. Gold standard (8 mL of 500 mg L⁻¹ gold) was added to the gold ore solution in a 250 mL volumetric flask to allow easier quantitation of the gold by both AA and ICP analysis. Finally the solution was made to 2.0 M HBr to facilitate the separation.

3. Results and discussion

3.1. Extraction and transport of HAuCl₄ and HAuBr₄

Gold in the presence of suitable HCl and HBr concentrations forms either the $AuCl_4^-$ or $AuBr_4^-$ complexes [16–18] respectively. We investigated

the use of both these complexes for the extraction and transport of gold from one cell into another. An experiment with a starting cell solution of 2.0 M HCl and 16 mg L⁻¹ gold combined with 0.5 M KCl in the receiving cell was performed with the result shown in Fig. 1. The amount of gold in the starting cell is shown to decrease to the point where it is quantitatively extracted into the membrane after 50 h. Conversely, we see the appearance of gold in the receiving cell after just 2 h, which increases to the point where quantitative recovery of the gold (> 97%) is achieved after 50 h. This experiment was also performed with 2.0 M HBr/16 mg L⁻¹ gold in the starting cell combined with 0.5 M KBr in the receiving cell. These conditions were chosen to allow direct comparison between the two gold halide complexes. The results of this experiment are also shown in Fig. 1. The quantitative extraction of gold under these conditions takes place in under 20 h, while the quantitative recovery of the gold in the receiving cell occurs in approximately 40 h. The difference in extraction and transport rates of these two complexes can be explained by the relative hydrophobicity of each of the complexes. The $AuBr_4^-$
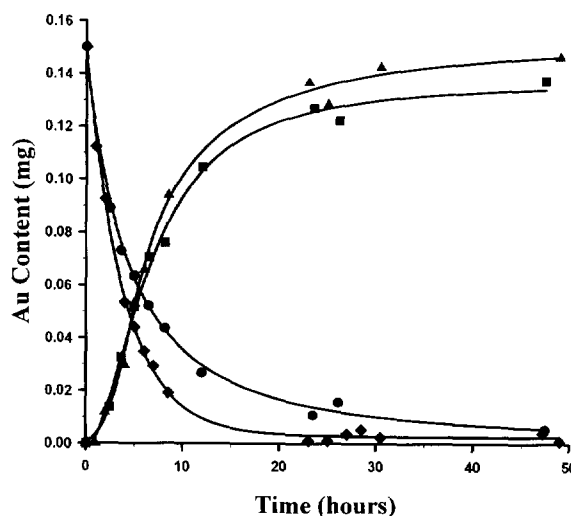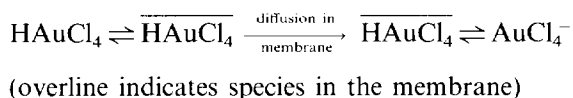

Fig. 1. Extraction and transport of HAuCl₄ and HAuBr₄ through a polyurethane membrane. The starting cell contains 10 mL of 15 mg L⁻¹ gold in 2.0 M HCl or HBr. The receiving cell contains 0.5 M KCl or KBr. ●, starting cell, HAuCl₄; ■, receiving cell, HAuCl₄; ◆, starting cell, HAuBr₄; ▲, receiving cell, HAuBr₄.

complex, possessing the larger bromide ligands, is more hydrophobic than the chloride analogue. Thus, the bromide complex will be more readily extracted into the hydrophobic membrane material. One would also expect that the stability constants of the gold complexes would play a factor in the extraction rate as shown by Oleschuk and Chow [8] for iron halide complexes. Pan and Wood [16,17] have performed detailed laser Raman studies on gold(III) chloride and bromide complexes in the concentration ranges in which we are working and found that the overwhelmingly predominant species present under these conditions were the $AuCl_4^-$ and $AuBr_4^-$ complexes. This explains the reason for the extraction into the membrane material but not the transport and recovery of the gold in the receiving cell solution.

Transport in the membrane material after extraction appears to follow Fick's law of diffusion and is concentration independent. The gold complex diffused through the membrane to the membrane/receiving cell interface and is then eluted into the receiving cell solution.

$$HAuCl_4 \rightleftharpoons \overline{HAuCl_4} \xrightarrow[\text{membrane}]{\text{diffusion in}} \overline{HAuCl_4} \rightleftharpoons AuCl_4^-$$

(overline indicates species in the membrane)

The conditions used in the receiving cell (0.5 M KCl and 0.5 M KBr respectively) favour the formation of the $AuCl_4^-$ and $AuBr_4^-$ complexes. This phenomena has been verified by UV/vis spectra of the receiving cell solutions. Both starting and receiving cell solutions possessed identical spectra with λ_{max} at 374 nm and 314 nm for the $AuBr_4^-$ and $AuCl_4^-$ complexes respectively.

The quantitative recovery of the gold in the receiving cell is attributable to the pH of the receiving cell solution. The pH of the receiving cell solution favours the formation of the non-protonated gold complexes (i.e. $AuCl_4^-$ and $AuBr_4^-$). The protonated neutral species are the only complexes that are extractable into the membrane material. Therefore, the protonated gold complexes diffuse through the membrane material and elute into the receiving cell solution where they form either the $AuCl_4^-$ or $AuBr_4^-$ non-protonated complexes depending on the salt used.
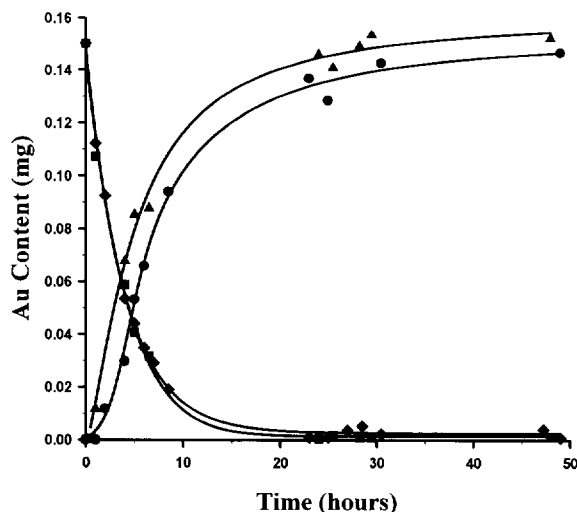

Fig. 2. Extraction and transport of $HAuBr_4$ using two different membrane thickness. The starting cell contains 10 mL of 15 mg L^{-1} gold in 2.0 M HBr. The receiving cell contains 0.5 M KBr. ▲, starting cell using a 0.025 mm thick membrane; ◆, receiving cell using a 0.025 mm thick membrane; ■, starting cell using a 0.05 mm thick membrane; ●, receiving cell using a 0.05 mm thick membrane.

These non-protonated gold halide complexes are not extracted by the membrane leaving the gold trapped in the receiving cell solution where it is quantitatively recovered.

3.2. Membrane thickness

To determine the effect of membrane thickness on the rate of transport, two different thicknesses of 0.025 mm and 0.05 mm were used. The solution conditions consisted of 2.0 M HBr/15 mg L^{-1} gold in the starting cell and 0.5 M KBr in the receiving cell. As expected the time required for the transport of the gold from the starting to receiving cells was faster for the thinner membrane. A transport profile for each thickness is shown in Fig. 2. The quantitative recovery of the gold in the receiving cell required approximately 20 h for the 0.025 mm membrane compared to approximately 40 h for the 0.05 mm membrane. The flux is inversely proportional to the membrane thickness and is in accordance with Fick's law of diffusion.

$$J_i = D_i \Delta c_i / x_i$$

where J is the flux of the penetrant (Au Br$_4^-$), D is the diffusivity constant of the membrane, Δc is the concentration difference within the membrane and x is the membrane thickness.

The time required for the complete extraction of the gold from solution into the membrane was the same for both thicknesses demonstrating that the rate limiting step of the overall process is the diffusion of the gold through the membrane material after it has been extracted. The increased rate of transport with the thinner membrane demonstrates that if an even thinner membrane was used, faster transport times could be obtained although this might lead to some mechanical problems such as leakage, because of the fragile nature of extremely thin films.

3.3. Effect of temperature

Experiments were carried out at four different temperatures (4, 22, 37 and 50°C) with starting cell conditions being 2.0 M HBr/16 mg L^{-1} gold and receiving cells containing 0.5 M KBr. Results depicting the sorption of the gold into the membrane material at different temperatures are shown in Fig. 3. With an increase in temperature an increase in the rate of sorption of the gold species into the
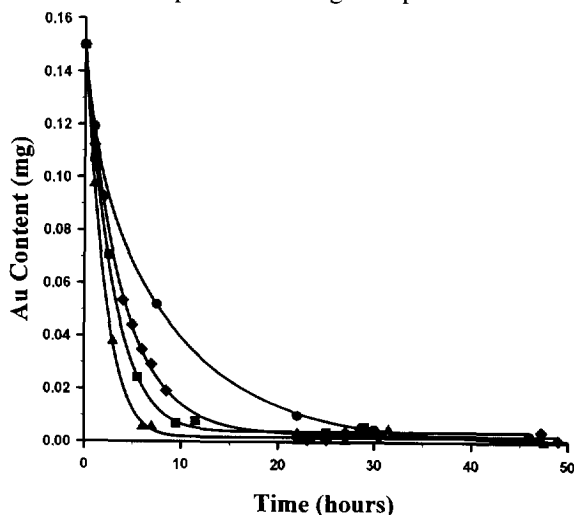
Fig. 3. Extraction of gold into a polyurethane membrane at 5, 22, 37 and 50°C. The starting cell contains 10 mL of 15 mg L^{-1} gold in 2.0 M HBr. The receiving cell contains 0.5 M KBr. ●, starting cell 5°C; ◆, starting cell 22°C; ■, starting cell 37°C; ▲, starting cell 50°C.
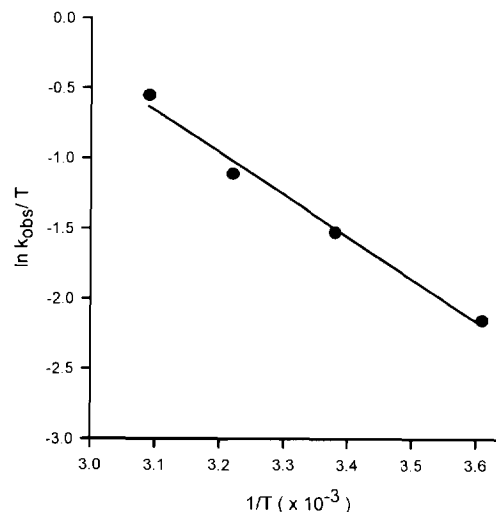
Fig. 4. Arrhenius plot of the gold extraction into a polyurethane membrane. The starting cell contains 10 mL of 15 mg L^{-1} gold Au in 2.0 M HBr. The receiving cell contains 0.5 M KBr.

membrane was observed. An increase in the rate of diffusion in the membrane material and rate of recovery for gold in the receiving cell was apparent. At 5°C the complete extraction of the gold species required approximately 30 h compared to 50°C where it required under 10 h. Conversely, the recovery of gold in the receiving cell at 50°C required 11 h while at 5°C the recovery of the gold was not complete even after 200 h.

The energy of activation was calculated to be 25 KJ mol^{-1} using an Arrhenius plot, as shown in Fig. 4. This value is consistent with values found for the sorption and transport of aqueous salt [19], acetic acid solution [20] and iron halides [8]. It was assumed that the gold remained in the AuBr$_4^-$ complex even though Pan and Wood [16] have shown that at higher temperatures the AuBr$_4^-$ starts to transform to the linear AuBr$_2^-$; the amount of this complex present was shown to be negligible. The linearity of the Arrhenius plot confirms that there is minimal transformation to AuBr$_2^-$.

The harsh acid and temperature conditions did not appear to alter the performance of the membrane material but changed the physical appearance of the membrane from clear and translucent to slightly opaque. After the experiment has been stopped and the membranes dried, they returned to their initial physical appearance. The change in

physical appearance is probably due to the swelling of the membrane from the absorption of water. The effects of the high acidity on the membrane were not apparent; polyether-type polyurethane is quite resistant to hydrolysis owing to the stability of the ether linkages incorporated in this polymer compared to the polyester polyurethane analogue.

3.4. Metal separations

The ability of gold to be transported under certain solution conditions using a polyether-type polyurethane membrane provides evidence that gold can be separated from other species using this process. Gold will preferentially form the extractable $HAuCl_4$ and $HAuBr_4$ complexes over other metals because of their higher stability constants. The separation of several binary metal systems has been achieved using this phenomenon. For example, in Fig. 5, data is shown for the separation of gold from a 2.0 M HBr solution containing 16 mg L^{-1} gold and 16 mg l^{-1} nickel. The receiving cell solution is 0.5 M KBr. The same transport profile is achieved for
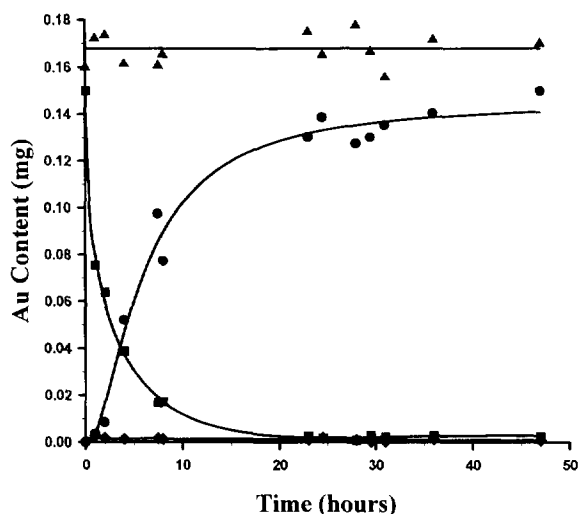
Fig. 5. Separation of gold and nickel using a polyurethane membrane. The starting cell contains 15 mg L^{-1} gold and 15 mg L^{-1} nickel in 2.0 M HBr. The receiving cell contains 0.5 M KBr. ■, gold content in starting cell; ●, gold content in receiving cell; ▲, nickel content in starting cell; ◆, nickel content in receiving cell.
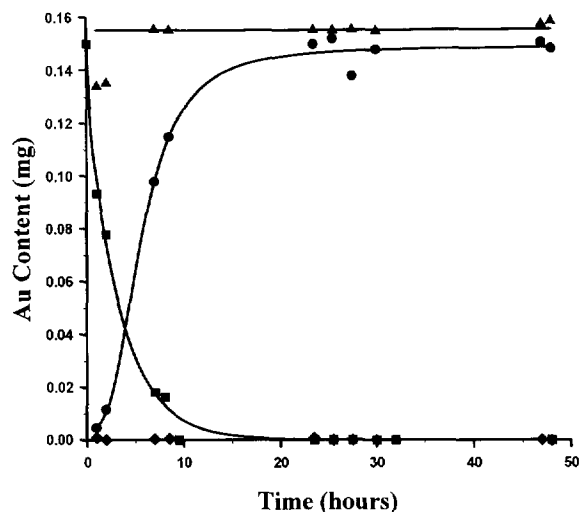
Fig. 6. Separation of gold and iron using a polyurethane membrane. The starting cell contains 15 mg L^{-1} gold and 15 mg L^{-1} iron in 2.0 M HBr. The receiving cell contains 0.5 M KBr. ■, gold content in starting cell; ●, gold content in receiving cell; ▲, iron content in starting cell; ◆, iron content in receiving cell.

gold as was demonstrated in previous figures. However, the nickel is neither extracted into nor transported through the membrane material. The extraction and transport of nickel would be evident by the decrease or increase of the nickel concentration of either the starting or receiving cells respectively. The basis of this separation is that gold forms the extractable $HAuBr_4$ at 2.0 M HBr concentrations, while the nickel does not form an extractable complex and thus remains in the starting cell. Therefore the gold is able to pass into the receiving cell where it is quantitatively recovered. This type of separation would be possible for all metals not able to form extractable complexes with the bromide ion.

There are some metals that are able to form extractable complexes with the bromide ion. It has previously been shown [8] that iron can be quantitatively transported and recovered using an analogous process. At HBr concentrations of 5.0 M, iron is present in the $HFeBr_4$ complex which is extractable into the polyurethane membrane material. A separation experiment involving gold and iron was performed with the results shown in Fig. 6. The experiment was performed with a starting

cell solution of 16 mg L⁻¹ gold and 16 mg L⁻¹ iron in 2.0 M HBr and 0.5 M KBr in the receiving cell. The extraction and transport of the gold follows the same extraction/transport profile as previously shown; however the iron is neither extracted nor transported through the membrane material. The lack of iron extraction can be explained by the iron bromide stability constants. At HBr concentrations of 2.0 M there is essentially no iron present as the FeBr₄⁻ complex; thus none of the iron is extracted and ultimately transported through the membrane material. The iron remains in the starting cell while the gold is transported through the membrane and quantitatively recovered in the receiving cell.

Several separations involving binary metal mixtures of gold and another metal have been successfully performed. These mixtures all involve gold with either nickel, zinc, iron, cadmium, tin or cobalt. In each case the extraction, transport and recovery of the gold species appears to be unaffected by the presence of the other metal in solution. The shape of the separation profiles are all virtually identical.

Although only separations using HBr to form the HAuBr₄ complex have been shown in this paper, several binary metal separations have been performed using hydrochloric acid (to form the HAuCl₄ complex) in place of hydrobromic acid and potassium chloride in place of potassium bromide. These separations were successful but were slightly slower than those for the bromide analogue. The lower rate of extraction can again be atrributed to the lower hydrophobicity of the chloride complex, HAuCl₄, relative to the bromide complex, HAuBr₄.

3.5. Preconcentration of gold

It is often valuable to concentrate as well as separate one species from another. Using a polyurethane ether-type membrane we attempted to concentrate gold by adjusting the solution volumes on either side of the membrane. Fig. 7 shows a separation and preconcentration experiment involving 30 mL of 5 mg L⁻¹ gold in 2.0 M HBr in the starting cell with 10 ml of 0.5 M KBr in the receiving cell. With these solution volumes

the quantitative transport and recovery of gold in the starting cell should produce a 15 mg L⁻¹ concentration of gold in the receiving cell, or a concentration factor of three. The concentration factor is defined as the ratio of the initial concentration to the final concentration of the particular element of interest.

This experiment clearly shows that gold can be transported and concentrated using the polyether-type polyurethane membrane material. The larger starting solution volume showed that the diffusion of the species through solution was hindering the extraction process to a significant degree. To minimize the effect of the larger solution volume the starting cell was stirred. This lead to a greatly increased rate of extraction and transport of the gold species. In all of the experiments performed in this paper the active surface area of the membrane has been kept at 5.3 cm² for the sake of comparison. If this area was increased the rate of extraction and consequently the overall concentration factor may be increased.

3.6. Separation of gold from gold ore

The ability of gold to be transported in the presence of other metals has already been shown in a previous section. Under these conditions the
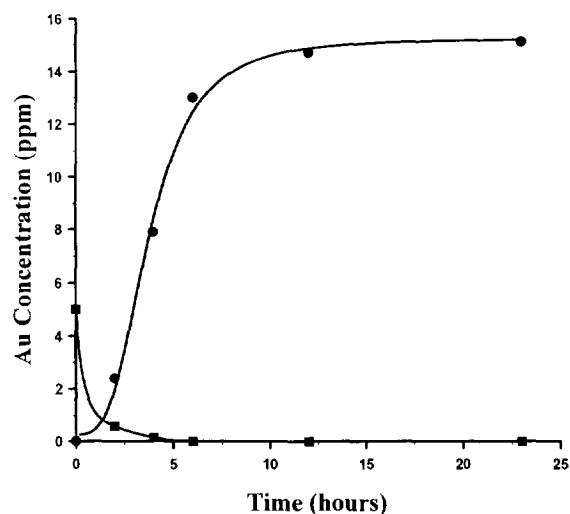

Fig. 7. Preconcentration of gold using a polyether-type polyurethane membrane. ■, gold concentration in starting cell; ●, gold concentration in receiving cell.

Table 1
Separation of gold from gold ore

Time (h)	Cell	Metal content (mg)					
		Au[a]	Mn	Fe	Zn	Cu	Co
0	starting	0.168	0.125	5.59	0.006	0.007	0.001
	receiving	–	–	–	–		–
1	starting	0.163	0.164	6.35	0.007	0.007	0.002
	receiving	0.002	0	0	0	0	0
2	starting	0.109	0.115	5.9	0.005	0.007	0.002
	receiving	0.010	0	0	0.001	0	0
5	starting	0.049	0.136	5.4	0.005	0.007	0.001
	receiving	0.066	0	0	0.002	0.001	0
7	starting	0.029	0.137	5.42	0.005	0.006	0.002
	receving	0.094	0	0	0.002	0	0
9.5	starting	0.013	0.139	5.42	0.006	0.007	0.002
	receiving	0.121	0	0	0.002	0	0
26	starting	0.004	0.137	5.36	0.004	0.006	0.001
	receiving	0.149	0	0.004	0.004	0.008	0
29	starting	0.004	0.139	5.41	0.004	0.006	0.001
	receiving	0.153	0	0.002	0.005	0.005	0.001
34	starting	0.004	0.138	5.40	0.004	0.006	0.001
	receiving	0.135	0	0.003	0.004	0.002	0
48	starting	0.005	0.134	5.30	0.004	0.006	0.001
	receiving	0.155	0	0.003	0.005	0.003	0

[a] The gold ore solution was spiked with gold standard to 16.0 mg L⁻¹ prior to the experiment; this results in 0.168 mg of gold in each starting cell.

selective transport of gold could be achieved resulting in the quantitative separation of gold. Those separations were of relatively simple systems of a binary metal mixture. To demonstrate the ability of a polyurethane ether-type membrane to separate gold from a much more complicated medium we attempted the separation of gold from a gold ore solution. The gold ore solution was prepared as described in the experimental section. The gold ore solutions were spiked with gold standard because the small amounts of gold in the ore (fire assay 3.06 oz per ton) would be difficult to analyse and quantitate. The top cell consisted of 10 mL of gold ore solution while the bottom cell contained 30 mL of 0.5 M KBr. This experiment was performed at room temperature, carried out over a period of 48 h and was unstirred. The results of the separation are presented in Table 1. The table lists the amount of each metal in both the top and bottom cells as determined by ICP and AA analysis. The metals analysed were chosen by performing an initial scan of several metals

suspected of being in the gold ore. If a metal was present in detectable concentrations it was further analysed for in each of the cells. The gold ore from the Kirkland Lake Mine is known to possess a large concentration of pyrite. This is demonstrated by the very large iron concentrations in the samples.

Examining the metal content of the starting cells we see that the gold content of the top cell decreases as it is extracted into the membrane until it is almost quantitatively extracted after 26 h. The amounts of the other metals in the starting cells do not change drastically over a 48 h period. This indicates that very little of the other metals are being extracted and transported into the receiving cell.

The analysis of the receiving cell once again shows the trend of the gold being transported through the membrane material and into the receiving cell solution. The initial gold content of zero at the start of the experiment gradually increases to 0.155 mg, a 92.3% recovery of the

initial gold in the starting cell after 48 h. Conversely, the analysis for the other metals in the receiving cells showed that there were no detectable amounts of either cobalt or manganese in any of the cells. Also the analysis of iron, zinc and copper showed that only microgram quantities of these metals were present in the receiving cell solution after 48 h. The small amounts of copper and zinc present approached the detection limits of the instrument and the concentrations of each in the receiving cell is not significant. The results of the gold ore separation again shows that there does not appear to be a competing ion effect between the other metals and gold even though some of those metals are present in much higher concentrations than gold. The rate of extraction and transport of the gold complexes is unchanged regardless of the concentrations of the other species in solution.

By performing the separation of gold from gold ore we are not suggesting that this technique be used for this purpose as there are techniques already developed that are far more efficient for this process. We are suggesting however, that polyurethane ether-type membranes may be used for the separation of gold from complex matrices possessing a large number of species.

4. Conclusion

A polyether-type polyurethane membrane can quantitatively transport gold from hydorochloric and hydrobromic acid solutions to KCl and KBr solutions, respectively. The transport process involves the extraction of the gold species, diffusion through the membrane material, and finally the quantitative elution of the gold species from the membrane. The extraction of the gold species is due to the two protonated gold halide complexes $HAuBr_4$ and $HAuCl_4$, that predominate in high concentrations of either HCl or HBr. The diffusion through the membrane follows a Fickian diffusion model. The elution from the membrane is caused by the formation of the $AuCl_4^-$ and $AuBr_4^-$ complexes that are not extractable into the membrane.

The transport process is aided by the use of a thinner membrane and an increase in temperature. Also, with an increase in the surface area of the membrane we can expect that the overall rate of extraction and capacity of the membrane will be increased significantly where it may be used in a practical setting. The rate limiting step for the transport and recovery of the gold is the diffusion through the membrane. From an Arrhenius plot the energy of activation was shown to be 25 kJ mol^{-1}.

In this investigation all of the cells, with the exception of the preconcentration experiments, were unstirred. This allowed the direct comparison of experiments with no error associated with different rates of stirring. With the addition of stirring we see a fourfold increase in the rate of extraction into the membrane, but this does not allow direct comparison of separate experiments because of the lack of the ability for precise control of individual stirring rates. The method is inexpensive and inherently simple compared to other techniques available and so these methods may provide a useful alternative to other separation processes. Quantitative recovery of gold from the membrane into the receiving cell solution indicates that there is no permanent sorption of the complex, and further that there is no reduction of the complex to metal by the polymer.

The separation of gold from a number of other metals in binary metal systems shows that a polyurethane ether-type membrane can be used to separate gold from metals that do not form extractable complexes in the presence of either HBr or HCl. Even in cases where a metal can form extractable complexes in the presence of either of these acids (i.e. iron), the membrane can still effectively separate the two metals based on the stability constants of those metal halide complexes.

Gold ore has large amounts of other metals besides gold which are not extracted and transported through the membrane into the receiving cell solution. The separation of gold from a gold ore solution demonstrates the ability of the membrane to separate gold from very complex matrices.

Acknowledgements

References

[1] H.J.M. Bowen, J. Chem. Soc. A, (1970) 1082.

[2] Z.B. Alfassi and C.M. Wai, Preconcentration Techniques for Trace Elements, CRC Press, Boca Raton, FL, 1985, p. 364.

[3] T. Braun, J.D. Navratil and A.B. Farag, Polyurethane Foam Sorbents in Separation Science, CRC Press, Boca Raton, FL, 1985.

[4] T. Braun, Fresenius' Z. Anal. Chem., 333 (1989) 1985.

[5] G.J. Moody and J.D.R. Thomas, Chromatographic Separation and Extraction with Foamed Plastics and Rubbers, Marcel Dekker, New York, 1982.

[6] T. Braun and A.B. Farag, Anal. Chim. Acta, 99 (1978) 1.

[7] R.F. Hamon, Studies on the Sorption of Cobalt Thiocyanate by Polyurethane. Ph.D. Thesis, University of Manitoba, Canada, 1981, p. 423.

[8] R. Oleschuk and A. Chow, Talanta, 42 (1995) 957.

[9] H.D. Gesser, G.A. Horsfall, K.M. Gough and B. Krawchuk, Nature, 268 (1977) 323.

[10] R.G. Pearson, J. Chem. Educ., 45 (1968) 581.

[11] R.J. Puddephatt, The Chemistry of Gold, Elsevier, New York, 1978.

[12] A.S. Khan and A. Chow, Talanta, 33 (1986) 182.

[13] T. Braun and A.B. Farag, Anal. Chim. Acta, 153 (1983) 319.

[14] S. Sukiman, Radiochem. Radioanal. Lett., 18 (1974) 129.

[15] P. Schiller, G.B. Cook, Anal. Chim. Acta, 54 (1971) 364.

[16] P. Pan and S. Wood, Geochim. Cosmochim. Acta, 55 (1991) 2365.

[17] P. Pan and S. Wood, J. Solution Chem., 22 (1993) 163.

[18] N. Bjerrum, Bull. Soc. Chim. Belg., 57 (1948) 432.

[19] S. Harogoppad and T. Aminabhavi, Polymer, 31 (1990) 2346.

[20] S. Harogoppad and T. Aminabhavi and R. Balundgi, J. Appl. Polym. Sci., 42 (1991) 1297.

Determination of fat-soluble vitamins in yogurt by HPLC with electrochemical detection

M.M. Delgado Zamarreño*, A. Sanchez Perez, M. Sanchez Rodriguez, M.C. Gomez Perez, J. Hernandez Mendez

Departmento de Quimica Analítica, Nutrición y Bromatología, Facultad de Ciencias Químicas, Universidad de Salamanca, 37008 Salamanca, Spain

Abstract

A method employing HPLC with electrochemical detection for the rapid and simultaneous determination of vitamins A, D_3 and E is described. The method uses a C-18 reverse phase column and 2.5 mM HAcO–NaAcO in methanol–water (99:1, v/v) solution as the mobile phase. The compounds are quantified using amperometric detection with a glassy carbon electrode at a potential of + 1300 mV (vs. Ag/AgCl) and the results are compared with those obtained using UV detection at a wavelength of 280 nm.

The method was successfully applied to the analysis of vitamins A, D_3 and E in yogurt samples. After saponification, fat-soluble vitamins were extracted and the methanolic solution of the extracts was injected directly into the chromatographic system, avoiding the clean-up step which is necessary when no electrochemical detection is used. Good recovery percentages were obtained.

Keywords: Electrochemical detection; High performance liquid chromatography; Vitamins A, D_3 and E; Yogurt

1. Introduction

In recent years, a great deal of research has been devoted to developing sensitive, selective, rapid and reliable methods for the analysis of fat-soluble vitamins in foods [1] because deficiencies of these vitamins cause serious nutritional diseases. The analysis of vitamins A, D_3 and E in milk is of major importance because dairy foods play a vital role in human nutrition.

Over the past few years, the consumption of yogurt has increased largely because of the nutritional and therapeutic advantages involved; it facilitates the assimilation of proteins, lactose and lipids and promotes a balanced intestinal flora [2]. Methods have been described for the analysis of fat [3], inorganic acids [4], lactose [5,6] carbohydrates [7], preservatives [8–10], ascorbic and dehydroascorbic [11] acid and α-dicarbonyl com-

* Corresponding author.

pounds [12], although currently there are no methods for the determination of liposoluble vitamins in yogurt samples.

Despite this, many research works have determined liposoluble vitamins in samples of milk and dairy products using liquid chromatography [13–28]. In some of these studies, the vitamins were extracted directly from the sample [13–18] and different extract cleaning steps were performed before quantification [19–28]. In most determinations, the classic method is used; this involves alkaline hydrolysis of the sample, followed by extraction of the vitamins from the unsaponifiable material and, finally, their injection into the chromatographic system.

In a previous paper [29] a method for the simultaneous determination of vitamins A, D_3 and E in milk samples, without the need for any clean-up step for the detection of vitamin D_3, was proposed. Recently [30] a directly-coupled sample treatment–HPLC method for on-line automatic determination of liposoluble vitamins in milk has been developed.

In this work, we report on an HPLC method with electrochemical detection for the analysis of vitamins A, D_3 and E in yogurt samples, studying extraction of the vitamins, with and without previous alkaline hydrolysis, from the fat material, for later injection into the chromatographic system.
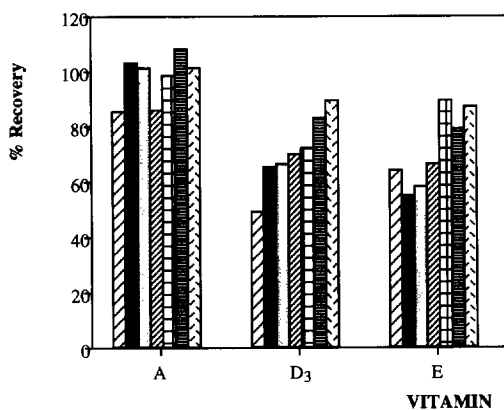
Fig. 1. Recoveries of clean-up step: C18 cartridges; solvents used in the standard solutions are shown in the Figure .
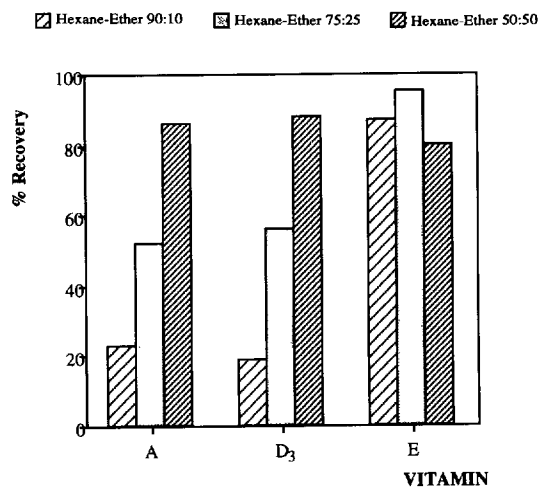

Fig. 2. Recoveries of clean-up step: Silica cartridges; solvents used in elution are shown in the Figure.

2. Experimental

2.1. Apparatus

2.1.1. Liquid chromatograph

An SP 8800 Spectra-Physics ternary pump equipped with a Rheodyne valve with an injection loop of 10 μl was used. The detectors were a UV Spectra-Physics SP 8450 and an electrochemical EG & G PAR model 400. Peak areas were measured by an SP 4290 Spectra-Physics integrator.

2.1.2. Chromatographic columns

An RP18 15 mm × 3.2 mm, 7 μm precolumn (Brownlee Labs) and an OD-224 RP18 220 mm × 4.6 mm, 5 μm column (Brownlee Labs) were used. Sep-Pak C18 and Silica cartridges (Millipore) and a Büchi RE 121 rotavapor with Büchi 461 water bath were also used.

2.2. Reagents

2.2.1. Chemicals

The following chemicals were used: all-trans-retinol, vitamin A (Sigma); cholecalciferol, vitamin D_3 (Fluka); α-tocopherol, vitamin E (Aldrich); potassium hydroxide, acetic acid and sodium acetate (A.R. grade; Panreac). Water was purified in an Elga-Stat water purification system.

Table 1
Determination of liposoluble vitamins in different yogurt samples with the direct extraction method. Results from three replicate analyses

Sample No.	Vitamin A (μg per 100 g)	Recovery (%)	Vitamin E (μg per 100 g)	Recovery (%)
1	0.99	89	0.86	85
2	0.017	98	0.03	101
3	0.87	78	0.015	100
4	0.46	101	0.065	97
5	0.75	95	0.01	81

2.2.2. Mobile phase

A solution of 2.5 mM acetic acid–sodium acetate in methanol–water (99:1, v/v) was used.

2.2.3. Alcoholic potassium hydroxide solution

50 ml ethanol and 15 ml of aqueous KOH 80% (w/v) solution were used.

2.2.4. Solvents

Hexane, chloroform, ethanol, ether, acetonitrile and LC-grade methanol (Carlo Erba) were used.

2.2.5. Samples

Commercial yogurt was used for the samples.

2.3. Procedures

2.3.1. Liquid chromatography

The HPLC operating conditions were optimized in a previous study [29]. The mobile phase used, degassed with helium, was a 2.5 mM acetic acid–sodium acetate buffer as supporting electrolyte in a methanol–water solution (99:1, v/v). The flow rate was set at 1.0 ml min^{-1}. Standards of vitamins or extracts from the samples dissolved in methanol were injected through the Rheodyne valve. Before use, the glassy carbon electrode was treated electrochemically, polarizing at -600 mV for 10 min and $+1400$ mV for 30 min in the flow stream. The detection potential for the vitamins was $+1300$ mV (vs. Ag/AgCl). The UV detection wavelength chosen was 280 nm, a compromise wavelength for the detection of the three vitamins. The results obtained with both detection methods were similar. The different parts of Section 3 show

the results corresponding to amperometric detection with the exception of Table 4, which shows those corresponding to both types of detection.

2.3.2. Analysis without hydrolysis

Yogurt samples (40 g) were treated with 40 ml of extractant mixture (hexane–chloroform, 2:1, v/v). This was stirred at 1000 rev min^{-1} for 2 h and protected from light. Following this, it was centrifuged at 4000 rev min^{-1} and the organic phase separated. This was evaporated in a rotavapor at 50°C and the residue was treated with 6 ml of methanol. Then, a clean-up step was performed, using C18 cartridges previously treated with 2 ml of the same solvent and adjusted to a final volume of 10 ml. This was then injected into the chromatographic system.

2.3.3. Analysis with alkaline hydrolysis

Samples (20 g of yogurt) were saponified overnight at room temperature with an alcoholic solution of potassium hydroxide plus ascorbic acid to avoid oxidation. The vitamins were extracted with hexane, the solvent was evaporated off, the residue was dissolved in 5 ml of methanol and was then injected into the HPLC system after filtration (0.45 μm pore size) without any clean-up step.

3. Results and discussion

3.1. Extraction of vitamins

In the analysis of fat-soluble vitamins, different

Table 2
Influence of KOH concentration. Results from three replicate analyses

Yogurt sample	Vitamin A $10^6 \times$ area		Vitamin E $10^6 \times$ area	
	KOH 60%	KOH 80%	KOH 60%	KOH 80%
1	3.83	3.20	3.89	3.25
2	2.36	3.11	2.63	3.98
3	3.44	4.09	3.55	4.76
4	2.91	3.15	2.95	3.10
5	2.22	2.93	1.89	2.56
6	2.25	4.64	1.34	3.31
7	3.25	3.98	2.49	3.76

steps are necessary: saponification, extraction and clean-up of the samples before injection into the HPLC system. To avoid the saponification step, direct extraction of the vitamins from the yogurt samples was attempted. The samples (40 g) were treated with 40 ml of different solvents and extractant mixtures: hexane, methanol, hexane–chloroform–ethanol (6.0: 3.5: 0.5, v/v/v), hexane–chloroform (2:1, v/v) and chloroform–hexane (2:1, v/v), with constant stirring in the dark for 2 h.

According to Elton-Bolt and Stacey [31], the ideal extractant mixture for extracting different liposoluble vitamins in cod-liver oil samples is hexane–chloroform–ethanol (6.0: 3.5: 0.5, v/v/v). However, in our case, the best results were obtained with a hexane–chloroform (2:1, v/v) mixture. Accordingly, this was used in all later analyses.

After centrifugation, the organic phase was removed by evaporation in a rotavapor under vacuum at 50°C and the residue, a few milliliters, was dissolved in 6 ml of methanol and passed through a cartridge to clean the extracts before they were injected into the chromatographic system.

3.2. Cleaning of extracts

A clean-up step is necessary prior to injecting the extracts into the chromatographic system to eliminate possible interferents. Accordingly, a study was carried out on the clean-up step with

standard solutions containing the three vitamins, applying the described procedure. To do so, the extracts dissolved in different solvents were passed through a C18 cartridge, to retain impurities but not the vitamins being studied. Different solvents were tested: acetonitrile, methanol and mixtures of both of these. The best recoveries for all vitamins were obtained with 100% methanol, as can be seen in Fig. 1. The solutions thus obtained were injected directly into the chromatographic system.

A further study was carried out using Silica cartridges, previously diluting the extracts in hexane instead of methanol. In this way, the vitamins
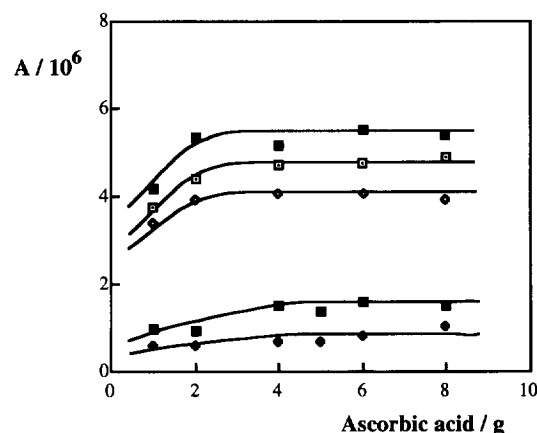

Fig. 3. Influence of ascorbic acid. Standard: (□) vitamin A; (◆) vitamin D_3; (▣) vitamin E. Yogurt sample: (◇) vitamin A; (■) vitamin E.
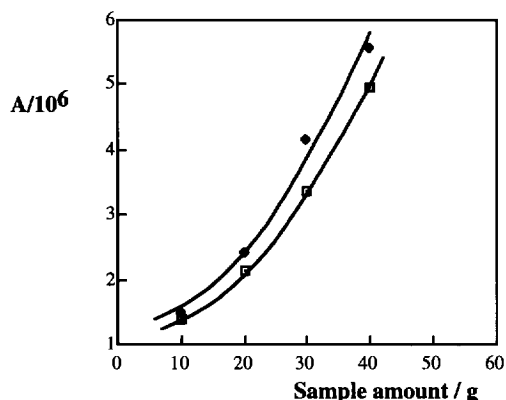
Fig. 4. Influence of amount of yogurt sample on analytical signal: (□) vitamin A; (◆) vitamin E.

were retained in the cartridge but not the interfering substances. Later, the vitamins were eluted with different hexane–ether mixtures. The best results were obtained with a hexane–ether mixture of 50:50 (v/v) (Fig. 2). The solution eluted was brought to dryness and the residue dissolved in 5 ml of methanol for injection into the chromatographic system. This step was necessary because direct injection of the eluate interferes in the quantitative evaluation of vitamin A since this elutes very early on, close to the chromatographic peak corresponding to the injection.

Although the recovery values obtained are similar using both types of cartridge, the C18 cartridge was chosen for work because it avoids the evaporation step with hexane–ether and later dilution in methanol, thus simplifying the process.

3.3. Analysis of vitamins in yogurt samples: Without hydrolysis

After optimization of the vitamin extraction steps and the extract clean-up procedure, different samples of yogurt were analyzed using the procedure without hydrolysis. Vitamin levels were measured in unspiked samples and in samples spiked with standard solutions to evaluate the contents and the recovery of the method respectively. Good recoveries were obtained for vitamins A and E (Table 1). In all cases, the amounts obtained were smaller than the contents found in the tables listing the food composition for these vita-

mins [32]. Vitamin D_3 did not appear in any of the samples of yogurt analyszed with this method. The conclusion drawn was that in yogurt samples it is necessary to saponify and extract the vitamins before injection into the HPLC system.

3.4. Analysis of vitamins in yogurt samples: With hydrolysis

In view of the poor results obtained in the determination of vitamins in yogurt using direct extraction of the vitamins, the method most commonly used for analyzing liposoluble vitamins in foods was used; this consists of alkaline hydrolysis of the fatty material and later extraction of the unsaponifiable material containing the liposoluble vitamins.

Among the variables that may affect sample treatment and quantification of the vitamins are the concentration of KOH, the amount of ascorbic acid added, the amount of sample to be treated, and the injection volume. In order to
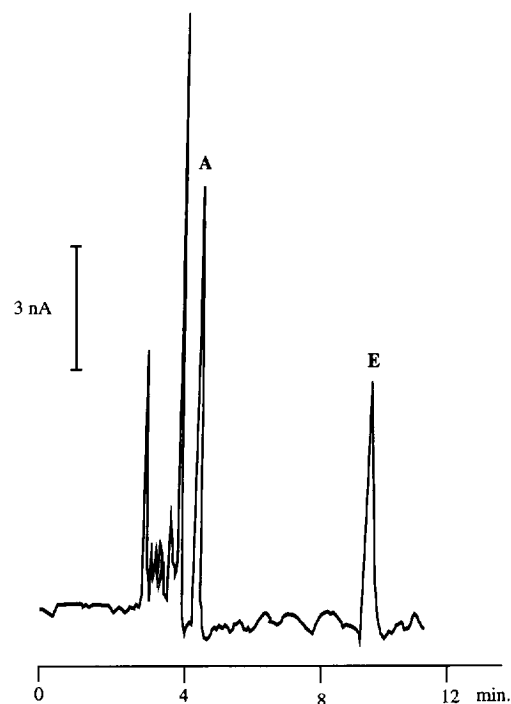

Fig. 5. Chromatogram obtained after application of the proposed method to a yogurt sample according to the scheme in the text.

Table 3
Determination of liposoluble vitamins in different yogurt samples with alkaline hydrolysis

Yogurt sample	Vitamin A			Vitamin E		
	Amperometry (μg per 100 g)	UV (μg per 100 g)	Recovery (%)	Amperometry (mg per 100 g)	UV (mg per 100 g)	Recovery (%)
1 ($n = 8$)	23 ± 3	25 ± 3	95 ± 9	0.073 ± 0.05	0.061 ± 0.06	98 ± 4
2 ($n = 5$)	23 ± 1	23 ± 1	89 ± 4	0.057 ± 0.06	0.059 ± 0.06	93 ± 10
3 ($n = 8$)	22 ± 2	22 ± 2	91 ± 6	0.064 ± 0.05	0.058 ± 0.04	100 ± 5
4 ($n = 5$)	26 ± 2	27 ± 2	88 ± 5	0.063 ± 0.03	0.058 ± 0.02	86 ± 3
5 ($n = 6$)	31 ± 3	28 ± 1	91 ± 5	0.087 ± 0.03	0.077 ± 0.04	103 ± 5

study the effects of these parameters on the determination of the vitamins, they were studied in the procedure involving hydrolysis.

3.4.1. Alcoholic potassium hydroxide solution

In samples of milk and other milk products, an alcoholic potassium hydroxide solution containing 15 ml of KOH at a concentration of 60% (w/v) and 50 ml of ethanol is generally used [29]. Since yogurt samples have different textures and it is possible that total hydrolysis of the fatty matter might not be completed, two assays were performed with KOH at 60% and at 80% following the indicated procedure with a view to checking whether there were any variations in the later evolution of the analytical signal. Table 2 shows that the best results are obtained with 80% KOH since hydrolysis is more complete.

3.4.2. Ascorbic acid

Ascorbic acid is added to the samples to be hydrolyzed as an antioxidant to protect the liposoluble vitamins, mainly vitamin E, in the alkaline medium in which hydrolysis is carried out. In order to check that the amount of ascorbic acid added is sufficient for complete protection of the vitamins, the above-described procedure was implemented both in standard solutions (containing the three vitamins under study) and in yogurt samples, in each case varying the amount of ascorbic acid added from 1–8 g. The data obtained are shown in Fig. 3. A working amount of 6 g of ascorbic acid per 40 g of yogurt was chosen—i.e. a ratio of 3/20—because the analyti-

cal signals obtained were thus reproducible and more sensitive than when lower amounts of ascorbic acid were used.
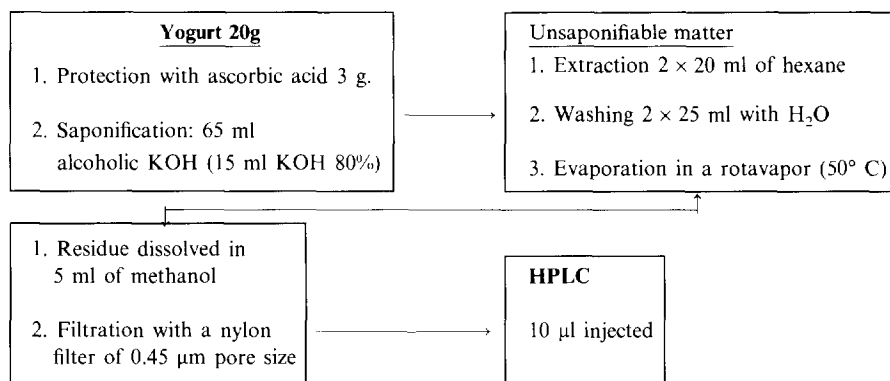
3.4.3. Sample amount

The vitamins in samples of yogurt are present at low concentrations, around the microgram per 100 g range. Although electrochemical and spectrophotometric determinations are sensitive, a minimum sample amount must be analyzed if vitamin detection is to be successful. However, the amount of sample cannot be increased too much because although with the sample preparation procedure and separation one is trying to achieve a situation in which the vitamins will be free of substances that might prevent their determination, they may be accompanied by components that gradually cause contamination of the C18 stationary phase to be used in the determination. Amounts of yogurt between 10 and 50 g were employed and the above-described method was applied, adding the corresponding amount of ascorbic acid to each sample but always maintaining the 3/20 ratio as the most suitable.

From the data thus obtained (Fig. 4) it can be deduced that 20 g of sample is sufficient for the determination of the vitamins. Larger amounts are not suitable because the extracts contain more interfering substances.

3.4.4. Analysis of Vitamins A and E

The method proposed for determination of liposoluble vitamins in yogurt samples is the following:

Yogurt 20g
1. Protection with ascorbic acid 3 g.
2. Saponification: 65 ml alcoholic KOH (15 ml KOH 80%)

→

Unsaponifiable matter
1. Extraction 2 × 20 ml of hexane
2. Washing 2 × 25 ml with H_2O
3. Evaporation in a rotavapor (50° C)

1. Residue dissolved in 5 ml of methanol
2. Filtration with a nylon filter of 0.45 μm pore size

→

HPLC
10 μl injected

Sponification of the samples with alcoholic potassium hydroxide was carried out at room temperature overnight. After extraction of the vitamins with hexane, the solvent was evaporated and the residue was dissolved in methanol and injected directly after filtration (0.45 μm filter) without the clean-up step (Fig. 5).

For the yogurt samples, the recovery percentages found were between 86% and 103% (Table 3). The amounts found for each vitamin in the different samples are summarized in Table 3. The day-to-day precision obtained (Table 4) was less than 10% in the five commercial brands of yogurt analyzed.

The result obtained in the analysis of vitamins A and E in the different samples analyzed are consistent with the contents specified by the manufacturers for those vitamins in yogurt samples, as can be seen in the tables relating to the composition of foods [32]. The day-to-day precisions obtained for the different samples of yogurt are shown in Table 4; as can be seen, the data are quite acceptable for this type of analysis.

3.4.5. Analysis of Vitamin D_3

Because of the low content of vitamin D_3 in yogurt, this vitamin is not detected using the proposed method. However, in yogurt enriched with this vitamin according to the specifications of the manufacturers it was possible to detect vitamin D_3 (Fig. 6) by modifying the procedure slightly and dissolving the extract with 2 ml of methanol instead of 5 ml and injecting 30 μl instead of 10 μl into the chromatograph. In this way, a larger amount of vitamin D_3 is injected into the system and it can be evaluated, although only in the case of enriched samples. Six samples of an enriched yogurt were analyzed; the vitamin D_3 content proved to be 0.09 ± 0.02 μg per g. The recovery of the method was $91 \pm 5\%$.

Table 4
Day-to-day precision, RSD (%), $n = 10$

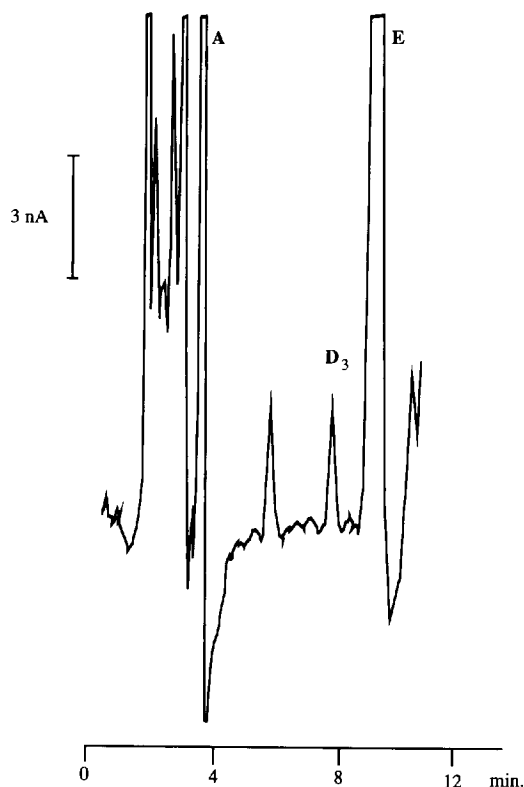| Yogurt sample	Amperometric detection		UV detection	
	Vitamin A	Vitamin E	Vitamin A	Vitamin E
1	8.33	5.55	8.00	4.92
2	4.35	8.62	4.35	5.17
3	5.00	4.68	9.09	3.51
4	3.85	1.59	8.00	1.69
5	6.45	3.45	3.57	3.90

Fig. 6. Chromatogram obtained after application of the modified method to a yogurt sample enriched with vitamin D_3.

4. Conclusion

A method is described for the determination of vitamins A, D_3 and E in samples of yogurt. The results obtained in the cases of vitamins A and E are very acceptable for the different samples analyzed. It was only possible to determine vitamin D_3 in yogurts enriched with this vitamin.

Acknowledgement

References

[1] P.J. Van Niekerk, in R. Macrae (Ed.), HPLC in Food Analysis, 2nd edn., Academic Press, London, 1988, pp. 133–184.

[2] A.Y. Tamime and R.K. Robinson, Yoghurt Science and Technology, Pergamon Press, Oxford, 1985, Chapter 1, pp. 1–6.

[3] P. Casado Cimiano, Métodos de Análisis Lactológicos, ILE (Industrias Lácteas Españolas), Madrid, 1982.

[4] R.T. Marsill, H. Ostapenko and R.E. Simmons, J. Food Sci., 46 (1981) 52–57.

[5] E. Lechener, Rev. Inst. Laticinios Candido Tastes, 36 (1981) 3–6.

[6] J.M. Beebe and R.K. Gilpin, Anal. Chim. Acta, 146 (1983) 255–259.

[7] M.L. Richmond and D.L. Barfuss, J. Dairy Sci., 65 (1982) 1394–1400.

[8] P. Toppino, R. Volpato, G. Amelotti and G. Contarini, Sci. Tec. Latt-Casearia, 41 (1990) 137–152.

[9] F. Olea Serrano and I. Sánchez López, J. Liq. Chromatogr., 14 (1991) 709–711.

[10] F. Ramos and M.I.N. Da Silveira, Port. Fram., 39 (1989) 90–94.

[11] N. Bilic, J. Chromatogr., 543 (1991) 367–374.

[12] M. Yamaguchi, J. Ishida, X.-X. Zhu, M. Nakamura and T. Yoshitake, J. Liq. Chromatogr., 17 (1994) 203–211.

[13] R.S. Mills, J. Assoc. Off. Anal. Chem., 68 (1985) 56–58.

[14] S.F. O'Keefe and P.A. Murphy, J. Chromatogr., 445 (1988) 305–309.

[15] A. Takeuchi, T. Okano and N. Tsugama, J. Micronutr. Anal., 4 (1988) 193–208.

[16] W.O. Landen, J. Assoc. Off. Anal. Chem., 68 (1985) 183–187.

[17] W.O. Landen, D.M. Hines, T.W. Hamill, J.I. Martin, E.R. Young, R.R. Eitenmiller and A.M. Soliman, J. Assoc. Off. Anal. Chem., 68 (1985) 509–511.

[18] M.L. Grace and R.A. Bernhard, J. Dairy Sci., 67 (1984) 1646–1654.

[19] E.J. De Vries and B. Borjse, J. Assoc. Off. Anal. Chem., 65 (1982) 1228–1233.

[20] D.C. Sertl and B.E. Molitor, J. Assoc. Off. Anal. Chem., 68 (1985) 177–182.

[21] H. Johnsson and H. Hessel, Int. J. Vitam. Nutr. Res., 57 (1987) 357–365.

[22] V.K. Agarwal, J. Assoc. Off. Anal. Chem., 71 (1988) 19–22.

[23] C.J. Lammi-Keefe, J. Pediatr. Gastrenterol. Nutr., 5 (1986) 934–937.

[24] W. Knifel, F. Ulbert and U. Winkler-Macheiner, Dtsch. Lebensm-Rundsch., 83 (1987) 137–139 (Chem. Abstr., 107 (1987) 95416c).

[25] S.L. Reynolds and H. Judd, Jr., Analyst, 109 (1984) 489–492.

[26] A.F. Wickroski and L.A. McLean, J. Assoc. Off. Anal. Chem., 67 (1984) 62–65.

[27] J. Ballester, E. Cortes, M. Moya and M.J. Campello, Clin. Chem., 33 (1987) 796–799.

[28] H. Johnsson, B. Halen, H. Hessel and A. Nyman, Int. J. Vitam. Nutr. Res., 59 (1989) 262–268.

[29] M.M. Delgado Zamarreño, A. Sanchez Perez, C. Gomez Perez and J. Hernandez Mendez, J. Chromatogr., 623 (1992) 69–74.

[30] M.M. Delgado Zamarreño, A. Sanchez Perez, M.C. Gomez Perez and J. Hernandez Mendez, J. Chromatogr.,

694 (1995) 399–406.

[31] R.R. Elton-Bolt and C.I. Stacey, Anal. Chim. Acta, 127 (1981) 213–218.

[32] B. Holland, I.D. Unwin and D.H. Buss, The Composition of Foods (Milk Products and Eggs), 4th edn., Royal Society of Chemistry, London, 1989, p. 75.

Sulphate determination after its reduction to hydrogen sulphide and volatile separation by molecular absorption spectrometry

A. Lopez Molinero*, R. Batlle, A. Villareal, J.R. Castillo

Department of Analytical Chemistry, Faculty of Sciences, University of Zaragoza, 50009 Zaragoza, Spain

Abstract

A rapid spectrophotometric method for sulphate determination in a discontinuous mode is described. The method is based on sulphate reduction to hydrogen sulphide followed by its volatilization and absorption in an alkaline solution. The reduction is obtained when a sulphate sample is heated to 287 °C for 15 min, with a mixture of $Fe°/KI$ and phosphoric acid. The resulting gas is swept by nitrogen flow into a 0.1 M sodium hydroxide solution and the absorbance of the sulphide ions is measured directly at 230 nm. The proposed method enabled us to determine 50–700 μg of total sulphate with a relative standard deviation of the order of 5%. The method has been applied for the determination of sulphates in liquid (mineral waters) and solid (gypsiferous soils) samples.

Keywords: Absorption spectrophotometry; Reduction; Sulphate determination; Volatilization

1. Introduction

There is great interest in developing new and practical methods for sulphate determination. Recently, methods have been reported in the literature which include analytical techniques such as UV–Vis molecular spectrophotometry and turbidimetry [1–3], atomic spectroscopy [4], isotopic dilution [5], X-ray difraction [6], electroanalysis [7], sensors [8,9], ion chromatography [10] or capillary ion electrophoresis [11]. The vast majority of these papers are concerned with procedures involving an important level of automatization [12].

The reduction of sulphate to hydrogen sulphide and its subsequent determination can be considered to be among the most interesting methods for sulphate determination. Ajwa and Tabatabai [13] compared some methods for sulphate determination in soils and arrived at the conclusion that the Methylene Blue colorimetric method after the reduction of SO_4^{2-} to hydrogen sulphide can be considered to be among the most accurate methods. Certain reagents have been proposed for this reduction. Steinbergs et al. [14] used magnesium for the determination of total sulphur in soil and plant material. Metallic iron has also been used. Two classical reduction mixtures have been

---

* Corresponding author.

proposed: one by Johnson and Arkley [15] composed of hydriodic acid–hypophosphorous acid–formic acid; and a second, which is similar, composed of hydriodic acid and red phosphorus proposed by Lorant and Kopetz [16]. More recently, Norwitz [16] used a mixture of hydriodic, hypophosphorous and hydrochloric acids.

In these methods the reduction step is followed by colorimetric determinations of H_2S, after its previous absorption. For this purpose an alkaline zinc acetate solution is normally used. Then, in an acid medium, sulphide reacts to yield Methylene Blue [17,18]. This is the basis of a large number of analytical procedures. Other determinations have been proposed. Norwitz [16] measured the brownish–yellow colour of the lead sulphide obtained in an ammomia collecting solution. This methodology gives excellent analytical values but is time-consuming. This seriously restricts its possibilities as a practical method.

The purpose of this paper is to develop an alternative procedure for sulphate determination based on its reduction to hydrogen sulphide. It uses common reductant reagents, takes a short reaction time and produces a high level of analytical performance.

The proposed methodology simplifies and systematizes the experimental procedure for treating samples (heating/reducing and collecting of gaseous products). The measuring step is also simplified by direct reading of sulphide absorbance in alkaline solution. It is applicable not only to liquid but also to solid samples.

2. Experimental

2.1. Apparatus

A Hewlett Packard 8452A diode array spectrophotometer equipped with 10 mm quartz cells and interfaced to a Vectra CS data station was used for absorbance measurements. A Sartorius Research R 200D balance, with a readability of 0.01 mg, was used for solid sample weights.

2.2. Hydrogen sulphide generation and collection assembly

The system for generation and collection of the hydrogen sulphide is shown in Fig. 1. It consists of a reaction flask which is placed inside a metallic cup. Its inlet tube is connected to a tank of nitrogen by rigid nylon tubing. This gas acts as a carrier gas and its pressure and flow are controlled. The outlet tube of the vessel is connected to a calibrated flask by rigid nylon tubes. The flask contains the collecting solution which is cooled by dipping it into a cold ice/water bath.

A homogeneous and reproducible manner for heating the reagents during reduction/distillation was obtained by placing the reaction vessel in a brass hot cup. The cup was then heated with a cylindrical electric heater (heater jacket; Bas-Can; 125 W). The electric heating conditions were controlled by an autotransformer to 110 V and 0.5 A. The preheating time was 20 min and the temperature was then maintained constant at 287 ± 3 °C.

2.3. Reaction flask

A schematic diagram of the home-made reaction flask, made from glass, used by us in this method is shown in Fig. 2. It consists of two pieces (head and vessel) which can easily be adapted for operation.
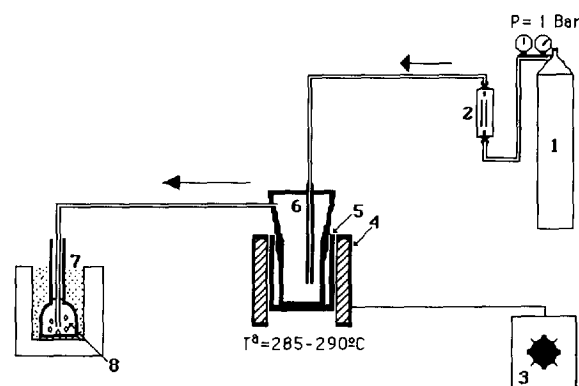

Fig. 1. Experimental assembly: (1) nitrogen/air supply; (2) flow regulator; (3) autotransformer AT25021IC E.BOAR; (4) cylindrical electric heater; (5) brass cup; (6) reaction flask; (7) ice/water bath (0 °C); (8) recovery solution.
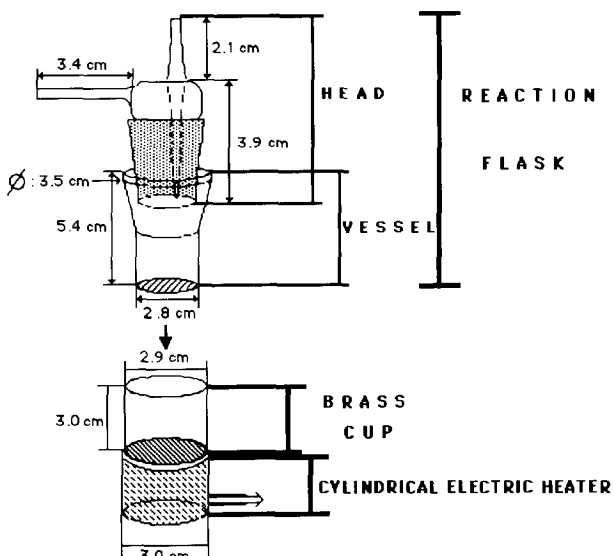
Fig. 2. Reaction flask and electrical heater system: reaction flask composed of two components (head and vessel) and the heater system composed of the brass cup surrounded by a cylindrical electric heater or heater jacket.

2.4. Reagents

All chemicals used were of analytical grade. Deionized water, quality Milli Q, was used in all dilutions.

2.4.1. Standard potassium sulphate solution (5000 μg ml^{-1} sulphates)

Dissolve 0.900 g of potassium sulphate (previously dried to 120 °C) in water and dilute to 100 ml in a calibrated flask. 1 ml of solution = 1.667 mg of sulphur. Sodium sulphate and calcium sulphate solutions were prepared in a similar manner.

2.4.2. Standard sulphide solution (1000 μg ml^{-1})

Dissolve 0.7506 g of sodium sulphide in water and dilute to 100 ml in a calibrated flask. The concentration was standardized by iodometric back-titration. Working standard sulphide solution had to be used within 30 min of standardization, as the concentration of sulphide

decreased after this time owing to oxidation by air.

2.4.3. Reducing mixture

2.4.3.1. Fe^0 suspension in vaseline oil (40 g l^{-1}).
Prepared by adding 2.000 g of iron powder to 50 ml of vaseline oil in a 100 ml beaker.

2.4.3.2. Potassium iodide solution (25 g l^{-1}).
Dissolve 2.5 g of KI in 100 ml of water. Concentrated phosphoric acid (85%) and O.I.M. sodium hydroxide were used.

2.5. Procedure for hydrogen sulphide generation

Samples are placed in the glass reaction vessel and are heated at a constant temperature of 287 ± 3 °C for 15 min. If the sample is liquid, take a suitable volume of solution (of the order of 0.1–1 ml), if solid the correct weight of sample (of the order of 2–5 mg), and wash with a few microlitres of distilled water. In both cases the solvent is evaporated. When dry, add 10 μl of KI solution and evaporate the solvent (this takes no more than a few seconds). Add 0.3 ml of phosphoric acid and 0.5 ml of Fe^0/vaseline oil suspension. After stoppering the vessel, the N_2 carrier gas (at a steady flow of 70 ml min^{-1} at 1 bar pressure) is channelled through it and bubbled into a 0.1 M NaOH solution. In this way the distilled hydrogen sulphide is absorbed. The alkaline collecting solution is maintained at 0 °C for 15 min.

2.6. Determination

Hydrogen sulphide in the collecting solution is determined spectrophotometrically by measuring the solution absorbance at 230 nm. The calibration graph was prepared by treating 50 μl of standard sulphate solution (containing between 50 and 700 μg of sulphate, as sodium sulphate) and the distilled gas was collected in a 10 ml calibrated flask. A reagent blank was run throughout the entire procedure.

3. Results and discussion

3.1. Optimization of the reduction reaction

From the value of the standard potential for the SO_4^{2-}/S^{2-} couple ($E° = 0.15$ V) it can be deduced that many other couples with lower $E°$ could be used as reductant agents. However, this reaction has important limitations. In the analytical literature this reduction has only been reported with strong reductants such as metallic iron, Mg^0 [14,19] and mixtures based on hydriodic acid/hypophosphite. We have studied other reductants such as Zn^0, Devarda alloy, and $NaBH_4$, but the best results were obtained by working in acid medium (orthophosphoric acid) with a mixture of KI/Fe^0, the Fe^0 being iron powder suspended in vaseline oil. In this way the reduction can be described by the following reactions:

$$SO_4^{2-} + 8H^+ + 12I^- \rightleftharpoons S^{2-} + 4I_3^- + 4H_2O$$
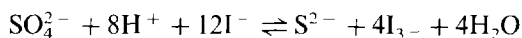
in organic phase (vaseline oil):

$$I_2 + Fe^0 \rightleftharpoons 2I^- + Fe^{2+}$$
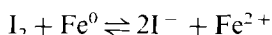
The conditions for the reduction reaction have been optimized by experimenting with the composition of the reductant ($KI/Fe^0/$vaseline oil), the acid medium and also the heating procedure.

The amount of KI added must be as small as possible, because higher quantities produce an undesirable deposition of I_2 in tubes. 2.5×10^{-4} g (10 μl of 25 g l^{-1} KI solution) was found to be best.

The vaseline oil, as an organic phase, has proved to be an optimum medium for extracting the iodine vapour, with high thermal stability during the heating step. The amount of vaseline oil is not as important as the amount of KI but an excess should be avoided in order to diminish the organic vapour distillation. Therefore 0.5 ml was chosen as the minimum volume that covers the bottom of the flask.

Iron powder has proved to be the critical reagent. It must be added in excess to ensure complete reduction. 20 mg was found to be required for the reduction of up to 1.0 mg of sulphate.

Various acids (HCl, $HClO_4$, H_3PO_4, HAc) were tested to find the best one for providing the acidic medium necessary for the reaction conditions. In this sense phosphoric acid was the best reagent. The experimental results obtained in its optimization are collected in Fig. 3. The sulphide absorbance in the collecting solution increased with increasing acid volume up to 0.3 ml, above which it decreased. Therefore 0.3 ml of concentrated phosphoric acid was chosen. If standard potassium sulphates are used, they must be previously treated with NaOH solution and then the optimum volume of acidic medium increases to 0.4 ml.

3.2. Heating and heating system

The effect of heat on reduction and distillation is very clear. The procedure is accelerated at a higher temperature. The most effective and reproducible way of heating the reaction vessel was by using an electrical power-regulator system. It consists of a cylindrical electrical heater (heater jacket) wrapped around a metallic cup made of brass. Details of the set-up are given in Fig. 1. The electrical system employed was calibrated. The power dissipated by the electrical heater jacket was varied and the temperature attained at the reaction vessel wall, and also the time taken, were measured. A thermopar, type J, connected to an electrical source type N.R-1-17 (also calibrated by a multimeter HP type 3458A) was utilized. In conclusion, it can be said that working with the power regulator at 0.455 A and 110 V, an opti-
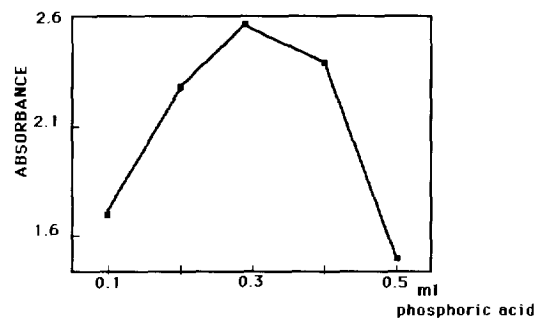

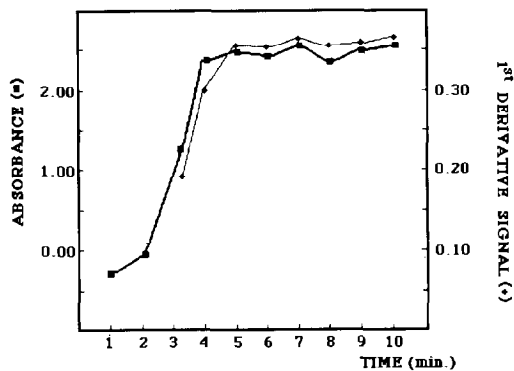Fig. 3. Effect of acidity on absorbance. For reduction of 900 μg of sulphates.

Fig. 4. Evolution of sulphide absorbance in the collecting solution (——) and variation of the first derivative signal of the collecting solution (—) as a function of heating time, when 700 μg of sulphate (as sodium sulphate) is reduced.

mum temperature of 287 ± 3 °C was obtained after 20 min of stabilization. The temperature was then maintained constant throughout the procedure.

3.3. The reaction heating time

When the glass reaction vessel is placed in the thermally stabilized hot cup, it attains the optimum temperature in only a few seconds. Working at 287 ± 3 °C, the heating time needed for the reduction/distillation of SO_4^{2-} was studied. 700 μg of SO_4^{2-} (as sodium sulphate) was taken and the reduction procedure given above was run. The set-up (Fig. 1) was connected to the HP diode array spectrophotometer flow cell which was filled with 0.1 M NaOH solution. The molecular absorption spectrum of the collecting solution and its first derivative spectrum were recorded every 60 s throughout the procedure. The variation of the absorbance at 230 nm (the absorption maximum wavelength of the sulphide ions in aqueous solution) with time is shown in Fig. 4. It can be observed that after 5 min the absorbance is a maximum and is stabilized. This is also seen when the variation of the first derivative spectrum signal with time was utilized. In spite of previous results we work with a heating time of 15 min, i.e. we propose an extra heating time above that determined experimentally as a security interval to ensure total sulphate reduction and also as a way of increasing the reproducibility of the procedure.

3.4. Flow of inert gas

An optimum flow of nitrogen gas of 70 ml min^{-1} at 1 bar pressure was regulated. Nitrogen can be replaced by air. In this case sensitivity is reduced, but by no more than 10%.

3.5. Recovery solution

Certain experiments were carried out using cooled ammonia solution or sodium hydroxide solution at different concentrations for hydrogen sulphide absorption. The results were more reproducible with cooled sodium hydroxide solution at 0.1 M. Under that condition (pH 13) the ratio of the species $H_2S:HS^-:S^{2-}$ is $5 \times 10^{-5}\%:50\%:50\%$ respectively.

3.6. Distilled gas identification

The chemical composition of the gaseous product of the reaction was confirmed by two tests:

(i) the characteristic yellow colour of the cadmium sulphide precipitate;

(ii) the absorption spectum of the sodium hydroxide alkaline collecting solution which after sulphate reduction is similar to the positive sulphide spectrum in alkaline solution. This is shown in Fig. 5.

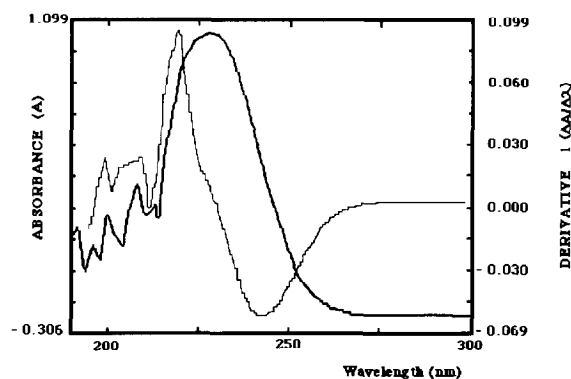This confirms hydrogen sulphide generation.

Fig. 5. Absorption spectrum for hydrogen sulphide dissolved in 0.1 M sodium hydroxide solution (——) and first derivative spectrum (—).

3.7. Spectrophotometric measurement

After sulphide absorption several colorimetric methods of sulphide determination were tested. We investigated Norwitz's spectrophotometric method [16] based on ammonia/lead citrate solution, also the Methylene Blue method [17] and the Boedeker reaction [20]. These three methods are time-consuming and can be considered very laborious. However, the sulphide ions in NaOH alkaline solution present an absorption spectrum with the absorbance maximum at 230 nm that makes a simple method for its determination possible by direct absorbance measurements at 230 nm. Also the first derivative spectrum can be used as an alternative measurement if over-heating at the reduction step produces volatilization of the organic vaseline oil which has an absorbance maximum at 195 nm.

3.8. Performance of the method: calibration graph

Calibration graphs were prepared by evaporating to dryness amounts of standard sodium sulphate solution and utilizing the reduction/distillation procedure. If potassium sulphate solution is used instead of sodium sulphate the same procedure is followed except that the experiment is performed by treating amounts of the solution with a few drops of 0.1 M sodium hydroxide solution and evaporating the solution to dryness. A reagent blank experiment without sodium or potassium sulphate is performed using the same procedure as previously. The calibration graph was linear between 50 and 700 μg of SO_4^{2-}, with a correlation coefficient of 0.999 ($n = 8$). The corresponding regression equation was:

$$A = 0.068 + 2.6 \times 10^{-3}(SO_4^{2-})$$

where the amount of sulphate (SO_4^{2-}) is expressed in micrograms and the absorbance (A) is measured at 230 nm against the reagent blank solution. The relative standard deviation for the determination of 400 μg sulphate is 5.7% ($n = 10$). The theoretical detection limit (signal/noise = 3) was 3.9 μg of sulphates. The time required to process a liquid sample was 15 min.

3.9. Interferences: effect of metals associated with sulphates

The effects of sodium, potassium and calcium, which are associated with SO_4^{2-}, have been studied. An experiment was performed with the same weight of sulphate ion (3 mg) but with three different metal salts. The degree of interference produced by the cation associates on the reduction reaction was evaluated by two parameters:

(i) the sensitivity value derived from the absorbance signal/mg ion sulphate ratio;

(ii) the time required to finish the reaction.

The results are summarized as follows:

Sulphate as sodium salt: shows a sensitivity value of 1.11. This is the highest. Therefore it can be said that this is the most sensitive salt and also the fastest to reduce.

Sulphate as potassium salt: shows a sensitivity value of 0.474. The whole reaction took more than 15 min.

Sulphate as calcium salt: shows a sensitivity value of 0.439. Its sensitivity is similar to that of potassium but lower. It takes of the of 60 min to be reduced.

3.10. Other interferences

The presence of nitrate was studied because it is a very common anion associated with sulphate in real samples and has an oxidizing effect. It was checked that the presence of nitrate at the same level as sulphate does not affect the reduction efficiency, i.e. 200 μg of nitrate did not cause reduction in the recovery of 200 μg of sulphate. However, it was noted that the addition of an excess of 0.5 ml of 6 M HNO_3 (190 mg of nitrate) drastically reduced the recovery of sulphate.

3.11. Elimination of interferences

From Section 3.9 the marked effect of potassium and calcium on sensitivity can be seen. Certain experiments were carried out in order to eliminate their influence.

It was found that the addition of NaOH solution to potassium sulphate restores the signal to the same level as that of sodium sulphate but the

Table 1

Comparison of sulphate contents of mineral water as determined by the proposed and reference methods [19]

Parameter	Reference method	Proposed method
Volume of sample (ml)	10	3
No. of determinations	5	6
Sulphate found (mg l^{-1})[a]	127.7	129.2
%Relative standard deviation	1.7	4.1

[a] Results are the average of determinations.

time required was still 15 min. The elimination of the calcium effect was attempted with sodium hydroxide and certain ligands. The addition of EDTA tetrasodium salt produced the best results and restored the signal of sulphate. In this case solid calcium sulphate and EDTA tetrasodium salt were dissolved in the minimum amount of water, according to a ratio of the order of grams sulphates/grams EDTA = 1/1. The solution was then evaporated and submitted to the reduction procedure, which required 60 min.

In contrast, the interference of nitrate was prevented by adding a sufficient quantity of Fe^0 in vaseline oil suspension (about 20 mg of Fe^0 for every 5 mg of nitrate added) to the reaction flask.

3.12. Application of the method

The proposed method was applied to the determination of sulphate in mineral water and also in solid gypsiferous soils. These two types of sample were not certified but their contents were compared with those obtained using reference methods.

The results for the determination of sulphates in mineral water samples are collected in Table 1 and were compared with a nephelometric method [17]. As can be seen, they were similar and the precision of the proposed method is poorer than that of the reference method. How-

ever, the one-tailed F-test for the comparison of precision shows that the standard deviation of the proposed method is not significantly greater than that of the reference method. Also, a statistical t-test was applied to test the means of these two determinations. So, for nine degrees of freedom the critical value of $|t|$ ($P = 0.05$) is 2.26 and since the experimental value of $|t|$ is 0.21, there were no significant differences between the two methods. The sulphate contents in gypsiferous soil samples were determined using the following procedure: solid samples were homogenized and ground to < 150 μm; between 2 and 5 mg of powdered sample was weighed into the reaction vessel; a similar weight of EDTA tetrasodium salt was also added to the reaction vessel and both sample and ligand were dissolved in a small amount of deionized water. The solution was then analyzed according to the procedure described above. The same samples were analysed by the colorimetric reference method [21]. This method is based on the displacement of chromate ions from sparingly soluble barium chromate by sulphate ions. The chromium is then determined from the colour of the chromate ions. The results are collected in Table 2. As can be seen the results were almost identical with an important, but not significant, difference in precision. In this case a paired t-test was applied to compare the difference between the three pairs of results given by the two methods. The critical value of $|t|$ ($P = 0.05$) for two degrees of freedom is 4.30 and since the experimental value of $|t|$ (1.02) is less than this, it can be said that no significant differences were found between the means of the two methods.

Acknowledgements

Table 2
Comparison of sulphate contents[a] in gypsiferous soils as determined by the proposed and reference methods [19]

Soil sample	Reference method		Proposed method	
	Sample taken (mg)	Sulphate content (% (w/w), n)	Sample taken (mg)	Sulphate content (% (w/w), n)
1	500	53.0 ± 0.6, n = 3	2.5	52.6 ± 0.2, n = 3
2	500	31.6 ± 0.5, n = 3	4.5	32 ± 2, n = 4
3	500	23.9 ± 0.5, n = 3	5.0	20 ± 4, n = 3

[a] Results are expressed as the average of n different determinations ± the standard deviation.

References

[1] O.M. Guimaraes, J.F. De Andrade, E.A. Neves and G.O. Chierice, Anal. Lett., 26 (1993) 2491.

[2] A. Sakuragawa, S. Nakayama and T. Okutani, Anal. Sci., 10 (1994) 77.

[3] Z. Zhi, A. Rios and M. Valcarcel, Quim. Anal., 13 (1994) 121.

[4] D.L. Miles and J.M. Cook, Anal. Chim. Acta, 141 (1982) 207.

[5] E. Karltun, Commun. Soil Sci. Plant Anal., 25 (1994) 207.

[6] S. Okuyama, T. Mitsui and Y. Fujimura, Bunseki Kagaku, 43 (1994) 383.

[7] J. Kalous, D. Brazdova and K.Vytras, Anal. Chim. Acta, 283 (1993) 645.

[8] A. Ishihara and S. Asakura, Sens. Actuat. B13 (1993) 248.

[9] A.L. Smirnova, V.N. Tarasevitch and E.M. Rakhman'ko, Sens. Actuat. B19 (1994) 392.

[10] S.I. Wada, Y. Kakuto, R. Itoi and T. Kai, Commun. Soil Sci. Plant Anal., 25 (1994) 1947.

[11] S.A. Oehle, R.D. Blanchard, C.L. Stumpf and D.L. Wulfeck, J. Chromatogr. A, 680 (1994) 645.

[12] J.S. Cosano, M.D. Luque de Castro and M. Valcarcel, J. Autom. Chem., 15 (1993) 141.

[13] H.A. Ajwa and M.A. Tabatabai, Commun. Soil Sci. Plant Anal., 24 (1993) 1817.

[14] A. Steinbergs, O. Iismaa, J.R. Freney and N.J. Barrow, Anal. Chim. Acta, 27 (1962) 158.

[15] C.M. Johnson and T.H. Arkley, Anal. Chem., 26 (1954) 1525.

[16] G. Norwitz, Analyst, 96 (1971) 494.

[17] Z. Marczenko, Separation and Spectrophotometric Determination of Elements, Ellis-Horwood, Chichester, UK, 1986.

[18] D.D. Siemer, Anal. Chem., 52 (1980) 1971.

[19] W. Schoniger, Mikrochim. Acta, (1954) 74.

[20] W. Moser, R.A. Chalmers and A.G. Fogg, J. Inorg. Nucl. Chem., 27 (1965) 831.

[21] S. Utsumi, S. Tanaka and A. Isozaki, Bunseki Kagaku, 32 (1983) 63.

Preparation, characterization and metal sorption studies of a Chrome-Azurol-S-loaded anion-exchange resin

Zenovia Molodovan*, Luminiţa Vlădescu

Faculty of Chemistry, University of Bucharest, 13, Bv. Republicii, Sector 3, 70346 Bucharest, Romania

Abstract

Chrome Azurol S (CS) was imobilized on an strongly basic anion-exchange resin (Dowex 2×4, in Cl^- form) by batch equilibration. The modified resin was stable in acetate buffer solution and in 0.1 M HCl and H_2SO_4, but it was readily degraded with 2–6 M HCl and HNO_3. Retention of Ba(II), Sr(II), Ca(II), Mg(II), Al(III), Cr(III), Zn(II), Fe(III), Ti(IV), Mn(II), Co(II), Ni(II), Cu(II), Cd(II) and Pb(II) was studied using the batch equilibration method. The uptake and recovery yields were determined by using inductively-coupled plasma atomic emission spectroscopy (for Mg, Al, Cr, Ti, Fe, Mn, Ni, Zn, Cu, Cd and Pb) and atomic absorption spectrophotometry (for Ba, Sr, Ca and Co). The optimum pH value was established for performing a selective separation of Al(III) from the other metal ions. The sorption capacities of the CS-loaded resing for Al(III), Cr(III), Mg(II) (at pH 6), Fe(III) (at pH 5) and Ti(IV) (at pH 4) were 14, 2.9, 0.3, 3 and 3.9 μmoles g^{-1} respectively. On this basis a method for separating Al(III) from other cations was established.

Keywords: Anion-exchange resin; Chrome Azurol S; Metal sorption

1. Introduction

Many complexing agents have been employed for the separation of metal ions on anion-exchange resins. These reagents, which have chelating groups, have been introduced into the resins by simple loading and the modified resins have been used for the selective recovery or preconcentration of metal ions [1]. Torre and Marina [2] discussed the potential of anionic chelating agents loaded on anion-exchange resins in a thorough review. Chrome Azurol S (CS) has been used as a chromogenic agent in determinations of some metal ions using complexometric titrations or spectrophotometry [3,4].

The purpose of the present work is to explore the possibility of separating some metal ions from mixtures by use of a common anion-exchange resin loaded with CS. The sorption behaviour of Ba(II), Sr(II), Ca(II), Mg(II), Al(III), Cr(III), Zn(II), Fe(III), Ti(IV), Mn(II), Co(II), Ni(II), Cu(II), Cd(II) and Pb(II) on the chelating-agent-

* Corresponding author.

loaded resin was investigated at different pH values. The separations are based on the different affinities of these metal ions for the chelating resin as a function of pH. The proposed method was applied to the determination of Al(III) in a certified reference material sample of zinc.

2. Experimental

2.1. Apparatus

A Spectroflame (Spectro Analytical Instruments, Germany) Model P inductively-coupled plasma atomic emission spectrometer was used for determination of Mg(II), Al(III), Cr(III), Ti(IV), Fe(III), Mn(II), Ni(II), Zn(II), Cu(II), Cd(II), Pb(II), Sn(II), Sb(III) and Zr(IV). A Pye-Unicam atomic absorption spectrophotometer Model SP 192 equipped with an air–acetylene flame burner and a deuterium continuum source background corrector was used for determination of Ba(II), Sr(II), Ca(II) and Co(II). An Orion EA 920 pH meter equipped with a combined glass-calomel electrode was used for all pH measurements. A Specord M40 UV–Vis spectrophotometer was used for spectrophotometric determinations.

2.2. Reagents

All the reagents were of analytical-reagent grade.

The chloride form of the strongly basic anion-exchange resin Dowex 2 × 4 was used for the preparation of the chelating-agent-loaded resin. The exchange capacity of the resin was found to be 3.98 meq g^{-1} of air-dried resin.

The ligand employed was Chrome Azurol S (3'-sulfo-2',6'-dichloro-3,3'-dimethyl-4-hydroxy-fuchsone-5,5'-dicarboxylic acid sodium salt) produced by Merck (Darmstadt, Germany).

Working solutions of cations (10^{-3} M) were prepared by diluting Merck atomic absorption standard metal ion solutions with distilled water. Buffer solutions of pH 1–6 were prepared using a mixture of hydrochloric acid and potassium chloride (pH 1–2), tartrate buffer (pH 3) and acetate buffer (pH 4–6).

2.3. Procedure

2.3.1. Preparation of CS-loaded resin

The batch method was used for retention of CS on the resin. Thus, a weighed amount (≈ 100 mg) of dry resin (chloride form) was treated with 10 ml of reagent solution of known concentration and shaken with a mechanical shaker. Then, the loaded resin bed was filtered off in a fritted-glass funnel and washed with distilled water to remove the excess reagent. The supernatant solution and the rinsing water were collected in a 25 ml volumetric flask. The amount of CS in the supernatant solution was determined spectrophotometrically at 435 nm.

2.3.2. Procedure for the sorption of metal ions as a function of pH

Weighed amounts (100 mg) of chelating resin (0.04 mmoles CS per gram of dry resin) were equilibrated with aliquots (10 ml) of buffer solutions (pH 1–6) by shaking the mixtures with a mechanical shaker for about 1 h. Then, to these mixtures, aliquots (4 ml) of 10^{-3} M solutions of each of Ba(II), Sr(II), Ca(II), Mg(II), Al(III), Cr(III), Zn(II), Co(II), Ni(II), Cu(II), Cd(II), Pb(II) and Mn(II) and 1 ml of 10^{-3} M solutions of Fe(III) and Ti(IV) were added and shaken for 2 h. After this treatment, the resin was filtered off in a fritted-glass funnel, washed with distilled water and the excess of metal ion remaining in solution was recovered in a 25 ml volumetric flask. An appropriate volume of each filtrate was used for the determination of the metal ion.

3. Results and discussion

3.1. Retention of CS on anionic resin

The amount of CS loaded on the chelating resin was determined by the batch method. The sorption capacity was found to be 0.32 mmoles CS per gram of dry resin. In order to investigate the stability of the CS-loaded resin in the presence of other anions the most common acid solutions (HCl, HNO$_3$ and H$_2$SO$_4$) were used (Fig. 1). The effects of the anions in the sequence NO$_3^-$ > Cl$^-$

$> SO_4^{2-}$ are quite similar to their affinities for anion-exchange resin Dowex 2 × 4. It was observed that the chelating agent was quantitatively held by the resin in the presence of 0.1 M acid solutions. Some CS was still retained on the resin even in 1 M HCl or H_2SO_4 due to the π–π interaction between the benzene ring of CS and the divinylbenzene moiety of the resin matrix. The sorption of the chelating agent molecule by its chelating groups, such as the hydroxyl group, has to be taken into consideration.

3.2. Sorption of metal ions on CS resin

In order to determine the optimum conditions of the sorption of metal ions by the loaded resin, the optimum pH ranges were investigated by the batch method.

3.2.1. Sorption of Al(III)

The sorption behaviour of Al(III) on CS resin as a function of pH is shown in Fig. 2. The sorption of Al(III) increases with pH. After the sorption of Al(III), the colour of the resin changed from orange to brown. It was observed that the retention of Al(III) was complete at pH 6. The reacting ratio of Al(III) to CS was found to be approximately 1:3 under the conditions used, as shown in Fig. 3, which corresponds to the ratio in the reaction of Al(III) with CS in solution.
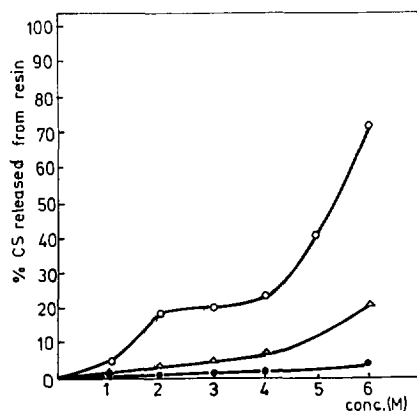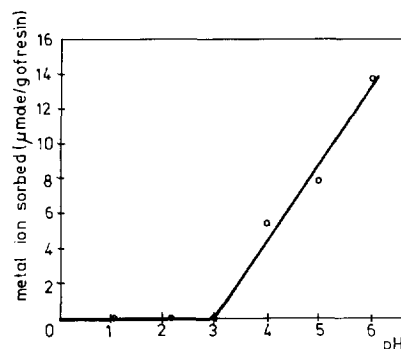

Fig. 2. Retention of Al(III) as a function of pH. Resin taken: 0.1 g (0.04 mmoles CS per gram of resin); volume of solution: 14 ml; concentration of Al(III): 8 ppm.

The desorption of Al(III) from the chelating resin is complete with 0.2 M HCl. The variation of the sorption of Al(III) on CS resin with pH is in good agreement with the variation of the absorbance of the metal–ligand complex in solution as a function of pH (Table 1).

3.2.2. Sorption of Fe(III) and Ti(IV)

Fe(III) and Ti(IV) also form complexes in solution. The absorbance values of these metal–ligand complexes as a function of pH are shown in Table 1. The Fe(III)–CS complex was found to show maximum absorbance at pH 6 while the Ti(IV)–CS complex presents maximum absorbance at pH 5. Owing to their tendency to hydrolyse, tests with
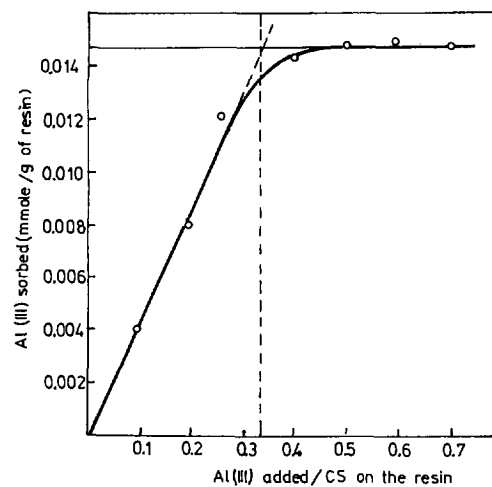

Fig. 1. Release of CS from the chelating resin in the presence of (●) H_2SO_4; (△) HCl; (○) HNO_3.

Fig. 3. Binding ratio of Al(III) to CS loaded on the resin (0.04 mmoles CS per gram of resin).

Table 1
Variation of absorbance of cation–CS complexes as a function of pH

pH	Absorbances of CS complexes[a] with		
	Al(III) $(\lambda = 560$ nm)	Fe(III) $(\lambda = 580$ nm)	Ti(IV) $(\lambda = 600$ nm)
1	0.01	0.15	0.03
2	0.03	0.30	0.08
3	0.28	0.40	0.17
4	0.96	0.50	0.24
5	1.19	0.60	0.30
6	1.26	0.62	0.29

[a] 2 ml CS $(10^{-3}$ M) + 0.5 ml metal ion $(10^{-3}$ M) + 10 ml buffer solution (pH 1–6), diluted to 25 ml with distilled water in a calibrated flask.

small amounts of Fe(III) and Ti(IV) (5 ppm) were made. The results indicated that the sorption capacities of the loaded resin for Fe(III) and Ti(IV) increase with pH and reach a maximum of 3 μmoles g^{-1} for Fe(III) at about pH 5 and 3.9 μmoles g^{-1} for Ti(IV) at pH 4 (Fig. 4). Fe(III) at pH 6 and Ti(IV) at pH 5–6 are not retained because of their hydrolysation. It was also found that Fe(III) in the presence of 5%
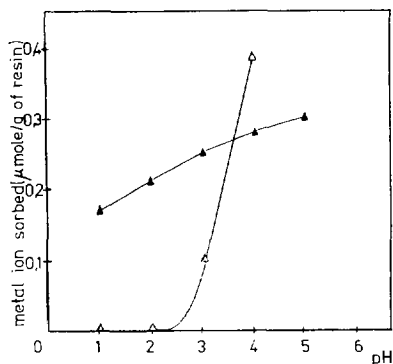

Fig. 4. Retention of Fe(III) and Ti(IV) as a function of pH: (▲) Fe(III); (△) Ti(IV). Resin taken: 0.1 g (0.04 mmoles CS per gram of resin); concentration of Fe(III) and Ti(IV) solutions: 5 ppm.

$NH_2OH \cdot HCl$ solution is not retained by the CS-loaded resin because Fe(III) is reduced to Fe(II), which does not form a complex with CS.

3.2.3. Sorption of other metal ions

The sorption characteristics of the complexing resin for Ba(II), Sr(II), Ca(II), Mg(II), Co(II), Cr(III), Ni(II), Zn(II), Mn(II), Cu(II), Cd(II) and Pb(II) were also studied in the same pH range. Small retentions of Mg(II) and Cr(III) were observed at pH 6 (0.3 μmoles g^{-1} for Mg(II) and 2.9 μmoles g^{-1} for Cr(III)). The other metal ions were not retained by the chelating resin in the pH range 1–6.

The effect of possible interferents encountered in real samples has been tested: the retention of Sn(II), Sb(III) and Zr(IV) being investigated. We used 1 ppm solutions of Sn(II), Sb(III) and Zr(IV), to prevent the precipitation of their hydrolysed ions, particularly at pH 3–6. It was observed that these metal ions could be tolerated up to a level of 1 ppm.

4. Application

The results of the present study have been applied to the determination of Al(III) in a zinc sample supplied by The Institute of Rare and Nonferrous Metals (Bucharest). 2 g of zinc was completely dissolved in a minimum volume of concentrated hydrochloric acid (about 10 ml) by heating on a water bath. The solution was evaporated to a very small volume. To this a small volume of water was added. The solution was cooled, filtered and diluted to 50 ml in a calibrated flask. An aliquot (15 ml) of the sample was adjusted to pH 6 with 0.1 M NaOH and added to a mixture of 0.1 g of loaded resin and 10 ml of acetate buffer (pH 6). The mixture was shaken for about 3 h. The supernatant solution had been eliminated and the resin was then washed with distilled water. The retained Al(III) was then eluted with 25 ml of 0.2 M HCl and determined in the supernatant solution by inductively-coupled plasma atomic emission spectrometry (ICP-AES). The results are given in Table 2. These results are in good agreement

Table 2
Determination of Al(III) in a zinc sample

Sample	Composition (μg g^{-1})	Concentration of Al(III) (μg g^{-1})	
		Certified value	Found[a]
Zinc	Cd, 3.75; Cr, 0.20; Cu, 2.50; Fe, 14.75; Mg, 0.025; Mn, 0.65; Ni, 27.25; P, 0.032; Pb, 33.75; Sb, 0.025; Si, 163.75; Sn, 0.025; Ti, 0.105; Zr, 0.025	35 ± 3	33 ± 2

[a] Mean of three determinations.

with the certified values. It was observed that under optimum experimental conditions the sorption of Al(III) was quantitative and the interferences caused by low concentrations of metal ions such as Cr(III), Ti(IV) and Fe(III) were negligible.

5. Conclusion

The proposed method is able to separate and concentrate Al(III) using the reaction of Al(III) with CS supported on the anion-exchange resin. The method described above can be used for separation of an element from complex mixtures. Also, the value of the direct determination of the element from complex mixtures. Also, the value of the direct determination of the element can be controlled by introduction of an intermediary stage: preconcentration, followed by its proper determination.

Acknowledgements

References

[1] M.L. Marina, V. Gonzales and A.D. Rodriguez, Microchem. J., 33 (1986) 275.
[2] M. Torre and M.L. Marina, Crit. Rev. Anal. Chem., 24 (1994) 327.
[3] S.M. Malat and H. Hrachovcova, Collect. Czech. Chem. Commun, 29 (1964) 484.
[4] P. Pakalus, Anal. Chim. Acta, 32 (1965) 57.

A series expansion of the extended Debye–Hückel equation and application to linear prediction of stability constants

J.J. Baeza Baeza, G. Ramis-Ramos*

Departament de Química Analítica, Facultat de Química, Universitat de València, 46100 Burjassot, València, Spain

Abstract

The Debye–Hückel semiempirical extended equation is frequently used to calculate activity coefficients of chemical species and equilibrium constants at ionic strengths different from those used in their experimental evaluation. A series expansion of the extended Debye–Hückel equation is proposed here and checked with experimental data taken from the literature. The expansion is linear in the ionic parameters and yields a geometrical series which converges rapidly and that enables the accurate calculation of interpolated and extrapolated activity coefficients and equilibrium constants by simple and multiple linear regression without previous knowledge of the ionic parameters.

Keywords: Activity coefficients; Debye–Hückel equation; Ionic strength; Stability constants

1. Introduction

In the experimental evaluation of equilibrium constants an inert electrolyte is used to maintain a given ionic strength, I. Consequently, experimental values of the constants are found in the literature at only a few (frequently large) values of I. However, accurate values of equilibrium constants at low and variable ionic strengths are of great interest in calculations related to speciation and transport modelling of nutrients and pollutants in water resources, in physiological fluid studies and in other fields [1,2].

To calculate an equilibrium constant at any I value, the activity coefficients of the species involved must be evaluated. These can be calculated by the extended form of the semiempirical Debye–Hückel equation [1,3–7]:

$$\log \gamma_i = -A z_i^2 \frac{\sqrt{I}}{1 + B a_i \sqrt{I}} + c_i I \tag{1}$$

where γ_i and z_i are the activity coefficient and the charge of species i respectively, and the parameters A, B, a_i and c_i depend on the composition of the medium and on the temperature. The ionic parameters, a_i and c_i, also depend on the nature of the i species. Frequently, the term in c_i is neglected [8] and empirical values of a_i are used [3,9]. According to the Bates–Guggenheim con-

---

* Corresponding author.

vention $Ba_i = 1.5$ for Cl^-, and this has also been extended to other ions [10]. Additional polynomial terms have been proposed, e.g. a term in $I^{3/2}$ [4].

Other more complex algorithms which relate activity coefficients to I have been developed [6,7,11–14]. The specific interaction theory (SIT) [11] relies on the Debye–Hückel equation and takes into account short-range interaction forces that are specific to each solute. The Pitzer algorithm [12] allows the accurate prediction of the properties of mixtures when the properties of the pure components are accurately known. However, this algorithm uses a great number of empirical parameters, many of which are not known. A recent study has shown that the Pitzer algorithm is very useful to fit data over wide I ranges and in mixtures of electrolytes; however, with a single electrolyte and at low ionic strengths it does not show remarkable superiority to other similar models [6].

The empirical nature of I and the ionic parameters, and the systematic errors which affect extrapolation to low values of I, have been the subject of controversy [15,16]. However, the Debye–Hückel expression is widely used [17,18]. Unfortunately, this equation and the algorithms cited above are non-linear in the ionic parameters. These should be already known or simultaneously obtained with the constants by non-linear iterative procedures. In this work, a series expansion of the extended Debye–Hückel equation is proposed and checked using literature data. The series expansion converges rapidly and is linear in the ionic parameters, which enables the accurate calculation of interpolated and extrapolated activity coefficients and equilibrium constants by single and multiple linear regression. Previous knowledge of the ionic parameters is not required.

2. Theory

2.1. A linear series expansion of the Debye–Hückel equation

The extended Debye–Hückel equation (Eq.(1)) is non-linear in a_i, but as shown next linearization

can be achieved by a series expansion. For this purpose, the non-linear term can be written as a sum of a linear term with an arbitrary constant, α, and an error, ε, giving:

$$\frac{\sqrt{I}}{1 + Ba_i\sqrt{I}} = \frac{\sqrt{I}}{1 + \alpha\sqrt{I}} + \varepsilon = F + \varepsilon \qquad (2)$$

where F is a function of I. Rearranging we have:

$$\varepsilon = F\frac{\sqrt{I}}{1 + Ba_i\sqrt{I}}(\alpha - Ba_i) \qquad (3)$$

By substituting the value of ε given by Eq. (3) into Eq. (2), we have:

$$\frac{\sqrt{I}}{1 + Ba_i\sqrt{I}} = F + F\frac{\sqrt{I}}{1 + Ba_i\sqrt{I}}(\alpha - Ba_i) \qquad (4)$$

and:

$$\frac{\sqrt{I}}{1 + Ba_i\sqrt{I}} = F + F(F + \varepsilon)(\alpha - Ba_i) \qquad (5)$$

If the process is repeated, the following geometrical series results:

$$\frac{\sqrt{I}}{1 + Ba_i\sqrt{I}} = \sum_{j=o}^{N} F^{j+1}(\alpha - Ba_i)^j \qquad (6)$$

where N is the number of terms of the series. The series reason is:

$$R = F(\alpha - Ba_i) \qquad (7)$$

The series converges in all cases when α is larger than Ba_i; further, the convergence is quicker the closer to zero is the reason, i.e. as Ba_i is closer to α. Similarly, a Taylor development [19] of the Debye–Hückel equation leads to the same series. Further, if $\alpha = 0$, the series proposed by Datta and Grzybowsky [20] results.

2.2. Evaluation of activity coefficients and ionic parameters

The equations obtained by taking only one or two terms of the series, i.e. by making $N = 1$ and $N = 2$ in Eq. (6) and substituting into Eq. (1), are given in Table 1 (Eqs. (8–11)). If at least two experimental points at two values of I are available, Eq. (8) can be used to obtain A and c_i. With three or more points simple linear regression can be used. Similarly, Eq. (9) can be used to evaluate

Table 1
Equations obtained from Eqs. (6) (upper part) and (14) (lower part) by making $N = 1$ and $N = 2$

N	Equation		Evaluated parameters	Min. no. data[a]
1	$\log \gamma_i = -Az_i^2 F + c_i I$	(8)	A, c_i	2
2	$\log \gamma_i = -Az_i^2 F - Az_i^2(\alpha - Ba_i)F^2 + c_i I$	(9)	A, Ba_i, c_i	3
1	$\log \gamma_i = +Az_i^2 F = c_i I$	(10)	c_i	1
2	$\log \gamma_i + Az_i^2 F = -Az_i^2(\alpha - Ba_i)F^2 + c_i I$	(11)	Ba_i, c_i	2
1	$\log K_c = \log K_0 + Q_1 F + CI$	(18)	$\log K_0$, Q_1, C	3
2	$\log K_c = \log K_0 + Q_1 F + Q_2 F^2 + CI$	(19)	$\log K_0$, Q_1, Q_2, C	4
1	$\log K_c - Q_1 F = \log K_0 + CI$	(20)	$\log K_0$, C	2
2	$\log K_c - Q_1 F = \log K_0 + Q_2 F^2 + CI$	(21)	$\log K_0$, Q_2, C	3

[a] Minimum number of points required to calculate the parameters; with more points, linear regression should be applied.

A, Ba_i and c_i using data at three values of I. With more than three data sets multiple linear regression can be applied.

Eqs. (8) and (9) can also be conveniently written as indicated by Eqs. (10) and (11) in Table 1. Eq. (10) is useful to obtain c_i from a single experimental point and a literature value of A. Similarly, Eq. (11) can be used to evalute Ba_i and c_i using a known value A and points measured at two values of I. With more data, the parameters can be obtained by simple linear fitting. It should be noted that F is a function of I; therefore, the regression straight lines obtained with Eqs. (8) and (11) and the regression plane given by Eq. (9) are curves on the $\log \gamma_i$ vs. I plane.

2.3. Evaluation of equilibrium constants

An equilibrium reaction in which n species are involved can be expressed as

$$\sum_{i=1}^{n} q_i[A_i] = 0 \qquad (12)$$

where q_i and $[A_i]$ are the stoichiometric coefficients, positive for reactants and negative for products, and molar concentrations respectively. The equilibrium constant at zero ionic strength, K_0, is

$$K_0 = \prod_{i=1}^{n} (A_i)^{q_i} = \prod_{i=1}^{n} [A_i]^{q_i} \prod_{i=1}^{n} \gamma_i^{q_i} = K_c K_\gamma \qquad (13)$$

where (A_i) is the activity of the i species, and K_c is

the concentration constant at any I. Taking logarithms and using Eq. (6):

$$\log K_c = \log K_0 + CI + \sum_{j=1}^{N} Q_j F^j \qquad (14)$$

where N is the number of terms of the series which are taken. The other symbols are:

$$C = \sum_{i=1}^{N} (-c_i q_i) \qquad (15)$$

$$Q_j = A \sum_{i=1}^{N} q_i z_i^2 (\alpha - Ba_i)^{j-1} \qquad (16)$$

It should be observed that Q_1 does not depend on the ionic parameters:

$$Q_1 = A \sum_{i=1}^{N} (-z_i^2 q_i) \qquad (17)$$

Eq. (14) can be used to evaluate $\log K_0$, C and Q_j, and to interpolate and extrapolate $\log K_c$ values using experimental data obtained at a few values of I. Thus, by making $N = 1$ in Eq. (6) and substituting in Eq. (14), Eq. (18) of Table 1 results. If data at three values of I are known, Eq. (18) can be used to obtain $\log K_0$, Q_1 and C. If more data are available, the parameters can be evaluated by multiple linear regression. Similarly, Eq. (19), which is obtained by making $N = 2$, can be used to evaluate $\log K_0$, Q_1, Q_2 and C if data at four or more values of I are available.

If A is known, Q_1 can be calculated from the reaction stoichiometry. Then, Eqs. (18) and (19)

can also be conveniently written as indicated in Eqs. (20) and (21) of Table 1. Data at only two values of I are enough to obtain log K_0 and C using Eq. (20). If more than two data points are available, log K_0 and C can be obtained by simple linear regression. Data points at three or more values of I and multiple linear regression are required with Eq. (21).

3. Results and discussion

3.1. Convergence of the series

The convergence of the series was checked at several values of the difference $(\alpha - Ba_i)$ and I. It should be remembered that no error is produced, even with $N = 1$, when $\alpha = Ba_i$. Fig. 1 shows the relative error obtained at increasing values of N when the logarithm of the activity coefficient of a hypothetical monovalent cation of $Ba_i = 3$ was predicted with $\alpha = 2$ at several I values. Convergence was quicker at lower values of I; however, the series converged rapidly in all cases, with errors below 1% when $N \geq 4$. Fig. 2 shows the error obtained at different I values when α was varied with $N = 2$ and $Ba_i = 2$. The error increased quickly as α moved away from Ba_i, and was also higher at larger values of I.

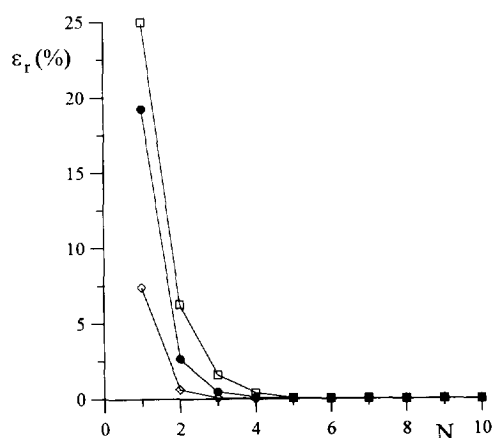Fig. 1. Relative error (percent) of the predicted logarithm of the activity coefficient of a hypothetical ion of $Ba_i = 3$ at increasing values of N. Series calculated with $\alpha = 2$ and $I = 1$ (□), 0.1 (●) and 0.01 M (◇).
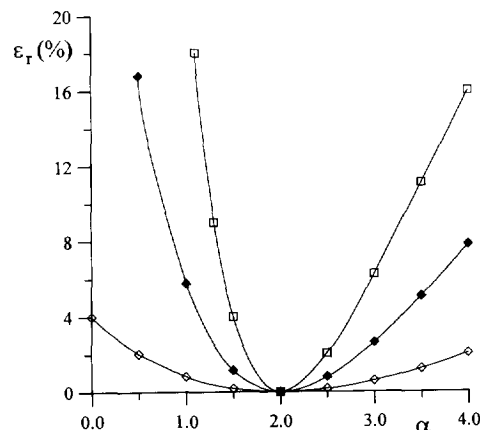

Fig. 2. Relative error (percent) of the predicted logarithm of the activity coefficient of a hypothetical ion when α is moved away from $\alpha = Ba_i = 2$ with $N = 2$ and $I = 1$ (□), 0.1 (◆) and 0.01 M (◇).

3.2. Fitting of experimental data

Data of the activity coefficient of proton (Table A1) and of several equilibrium constants (Tables A2, A3 and Table 5) at different values of I were taken from the literature. Eqs. (8–11) and (18–21) were used to fit the data using $\alpha = 1$.

First, the data series of Table A1 were used to obtain the regression curves with Eqs. (8–11). The average of the absolute deviations between experimental and fitted values of the logarithm of the activity coefficient of proton, log γ_H, are given in Table 2. The best fittings corresponded to Eqs. (9) and (11), where $N = 2$. A lower value of r was obtained with Eq. (8), and the lowest r corresponded to Eq. (10) in which the parameter A was maintained constant and only c_i was allowed to be fitted. The 25°C data series and the regression curves obtained with Eqs. (8) and (9) are plotted in Fig. 3. It can be observed that Eq. (9) accurately predicted all the data, and that Eq. (8) was somewhat less accurate.

Eqs. (18–21) were used to fit both pK_w data and the logarithms of the stability constants of the complexes $FeCl^{2+}$ and $FeSCN^{2+}$ at increasing I values. The data given in Tables A2 and A3 were used in the fittings. The averages of the absolute deviations between fitted and experimental values are shown in Tables 3 and 4. In both

Table 2
Mean of the absolute values of the residues of linearly fitted γ_H (r given between parentheses) using the data of Table A1[a]

Equation	10°C	25°C	37°C	45°C
8	0.011 (0.98)	0.010 (0.990)	0.008 (0.990)	0.008 (0.990)
9	0.0021 (0.9995)	0.0016 (0.9997)	0.0008 (0.9999)	0.0013 (0.9997)
10	0.03 (0.89)	0.03 (0.87)	0.03 (0.86)	0.03 (0.84)
11	0.004 (0.9990)	0.0021 (0.9994)	0.0009 (0.9999)	0.0015 (0.9996)
A[b]	0.498	0.510	0.523	0.537

[a] Data at temperatures other than 25°C were also taken from Ref. [4].
[b] Used to calculate the Az_i^2F term in Eqs. (10) and (11) (data taken from Ref. [4]).

cases, the deviations between experimental and fitted values were small. The best fittings were obtained with Eqs. (19) and (21), where $N = 2$, and the poorest with Eq. (20), in which $N = 1$ and only two parameters were fitted.

Next, Eq. (18) and only three experimental pK_w values taken at $I = 0.10$, 0.50 and 3.01 M were used to predict the data at intermediate values of I. The average relative error was 0.02, 0.03 and 0.07% for the LiCl, NaCl and KCl series respectively. When Eq. (20) and only two experimental points were used, i.e. $I = 0.10$ and 3.10 M, the average relative error increased to 0.03, 0.14 and 0.3% respectively. The LiCl series and the regression curve predicted by Eq. (20) are shown in Fig. 4. The curves predicted by the Pitzer, SIT and Debye–Hückel algorithms using $pK_{w,0} = 14.00$ and the ionic parameters given by Elizalde and

Fig. 3. γ_H data series of Table A1 at 25°C and regression curves obtained with Eqs. (8) (broken line) and (9) (solid line) using all the data.

Aparicio [14] are also shown in the Figure. Predictions made with these algorithms were much less accurate.

3.3. Linear extrapolation to zero ionic strength

Eqs. (18–21) and all the data given in Table A3 were used to calculate the logarithms of the stability constants of $FeCl^{2+}$ and $FeSCN^{2+}$ at $I = 0$. As shown in Table 4, Eq. (20) gave the most accurate results, and Eq. (19) lead to absurd values. The large and very large deviations in relation to the expected values were due to the presence of maxima and minima in the regression functions which caused dramatic effects in some cases when extrapolation was used to evaluate data located at large distances from the experimental values. However, the deviations found were always small when these equations were used to interpolate data.

The capability of Eq. (20) to reliably extrapolate data to $I = 0$ is also shown in Tables 5 and 6.

Table 3
Mean of the absolute values of the residues of linearly fitted pK_w values using the data of Table A2[a]

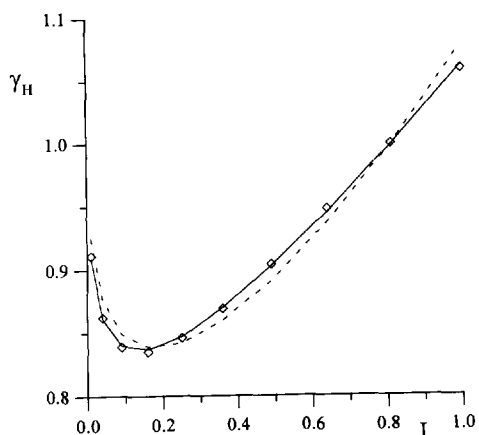| Equation	LiCl	NaCl	KCl
18	0.0018	0.0012	0.005
19	0.0017	0.0011	0.0024
20	0.0018	0.007*	0.019*
21	0.0018	0.002	0.0021

[a] For Eqs. (20) and (21), $Q_1 = -1.018$, $r > 0.999$, except for the two cases indicated with asterisks which gave $r = 0.996$ and 0.98.

Table 4

Mean of the absolute values of the residues, d (r given between parentheses), values predicted to $I = 0$, log K_0, and deviation from the literature value, ε, for the logarithm of the stability constants of FeCl^{2+} and FeSCN^{2-} [a]

Equation	FeCl^{2+}			FeSCN^{2+}		
	d (r)	log K_0	ε	d (r)	log K_0	ε
18	0.033 (0.9992)	5.29	3.91	0.0003 (0.99999)	2.62	0.47
19	0.021 (0.9997)	−22.9	−24.3	0.00007 (1.0000)	2.70	−0.39
20	0.09 (0.995)	1.18	−0.20	0.022 (0.911)	3.20	0.11
21	0.031 (0.9992)	3.15	1.77	0.0008 (0.9999)	2.95	0.14

[a] Data of Table A3; for Eqs. (20) and (21), $Q_1 = -3.054$.

In Table 5, this equation with $\alpha = 1$ and data taken at two values of I were used to extrapolate the logarithm of the protonation constant of ammonia to $I = 0$. Taking into account that the extrapolated values were obtained using only two points at very large ionic strengths, the differences from the literature value could be considered to be small. In the upper part of Table 6, the ionic product of water at $I = 0$, p$K_{w,0}$, was calculated using only two points at increasing values of I. The predicted p$K_{w,0}$ value was always in the vicinity of the expected value, 14.00 [11], even when two very close points at high I values were used. In the lower part of the Table, several points located within two rather different I ranges were used. Both low and high I ranges also lead to

Fig. 4. pK_w data series of Table A2 for LiCl: curve predicted by Eq. (20) using only the data at $I = 0.10$ and 3.01 M (solid line), and curves calculated by the Pitzer (dashed line), SIT (dotted line) and Debye–Hückel (dot-dashed line) algorithms using log K_0 and the ionic parameters given in Ref. [14].

p$K_{w,0}$ values close to 14.00.

3.4. Influence of α

The results given above were further improved by optimising α. The correlation coefficient r, was used to steer the optimisation process. The optimum value of α can be obtained by any non-linear optimization procedure; however, owing to the few data points used a simple direct search procedure was applied in this work. Thus, for the activity coefficient of proton at 10°C using Eq. (20), r improved from 0.89 to 0.997 when α increased from 1 to its optimum value which was 2.47. Also pK_w data of the LiCl and NaCl series at $I = 0.5$, 1.0 and 1.5 M were fitted using Eq. (20) with different values of α. As shown in Fig. 5, r further approached one by optimising α. Optimum values of α were found in the vicinity of 1.0 and 1.3 for the LiCl and the NaCl series respectively. The absolute differences between extrapolated p$K_{w,0}$ values and 14.00 are also plotted in
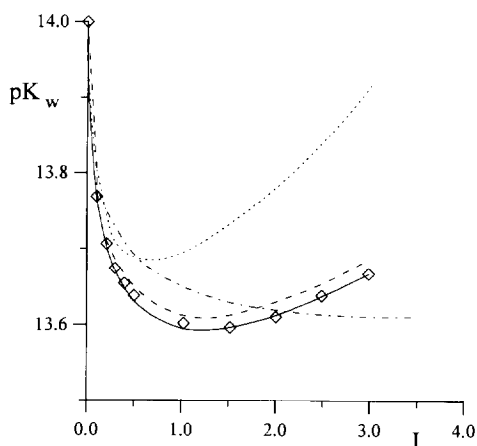
Table 5

Literature log K_c data and predicted log K_0 values using Eq. (20) for the protonation of ammonia [a]

Electrolyte	log K_c (I)	log K_c (I)	log K_0	ε [b]
LiCl	9.84 (4.53)	9.63 (2.82)	9.280	0.020
KCl	9.87 (3.35)	9.60 (1.86)	9.263	0.003
KBr	10.0 (4.20)	9.57 (1.85)	9.232	−0.028

[a] Log K_c data taken from Ref. [21] at the I values indicated between parentheses.

[b] Deviation from log K_0 value given in Ref. [21]; Eq. (20) used with $Q_1 = 0$.

Table 6

Logarithm of the ionic product of water at $I = 0$, $pK_{w,0}$, obtained with Eq. (20)[a]

LiCl	NaCl	KCl
14.008 (0.10-0.20)	14.005 (0.11-0.21)	14.002 (0.11-0.21)
13.997 (0.30-0.40)	14.015 (0.21-0.51)	14.020 (0.21-0.51)
14.008 (0.50-1.01)	14.030 (0.51-1.01)	14.040 (0.51-1.01)
14.006 (1.51-2.01)	14.035 (1.01-2.01)	14.064 (1.01-2.01)
14.002 (0.10-0.50)	14.014 (0.11-1.01)	14.019 (0.11-1.01)
14.006 (1.01-3.01)	14.036 (0.51-3.01)	14.090 (1.01-3.01)

[a] Points taken from Table A2 at the I ranges given between parentheses; upper part: only two points at increasing I values were used; lower part: the available four or five points within the indicated I range were used; $Q_1 = -1.018$.

the Figure. The minimum difference was produced at the same values of α that gave the best fittings. Analogous conclusions were obtained by modifying α in the evaluation of the protonation constant of ammonia to $I = 0$ (results not shown).

Finally, we have compared the results obtained with Eqs. (8-11) and (18-21), using an optimum value of α, with the results given by the equation of Datta and Grzybowsky [20] in which $\alpha = 0$. In all cases, Eqs. (8-11) and (18-21) gave better linearity and more accurate results. Further, when the parameter A or Q_1 was assumed to be known, i.e. taken from the literature, the Datta and Grzybowsky equation lead to much worse results.

4. Conclusions

It has been shown that the proposed series converges quickly, and that excellent fittings can be obtained using only one or two terms of the series. If experimental data at two or more values of I are available, the ionic parameters and the logarithms of the activity coefficients can be simultaneously evaluated by linear regression. Thus, the systematic errors associated with the use of previously known values of the ionic parameters are avoided, and iterative procedures are not required.

Eqs. (10) and (20) gave the worst fittings; however, they can be used to interpolate activity coefficients and equilibrium constants using

points measured at only one and two different values of I respectively, whereas more experimental points are required with the other equations. In the fittings, and provided that more experimental data than those strictly required by the equations are used, obtaining a correlation coefficient close to one means that the data are accurate and that they adequately follow the Debye-Hückel extended equation.

Finally, Eqs. (9), (11), (19) and (21), which include the term $N = 2$ of the series, are not recommended for obtaining extrapolated values. In some circumstances, deviations can be larger
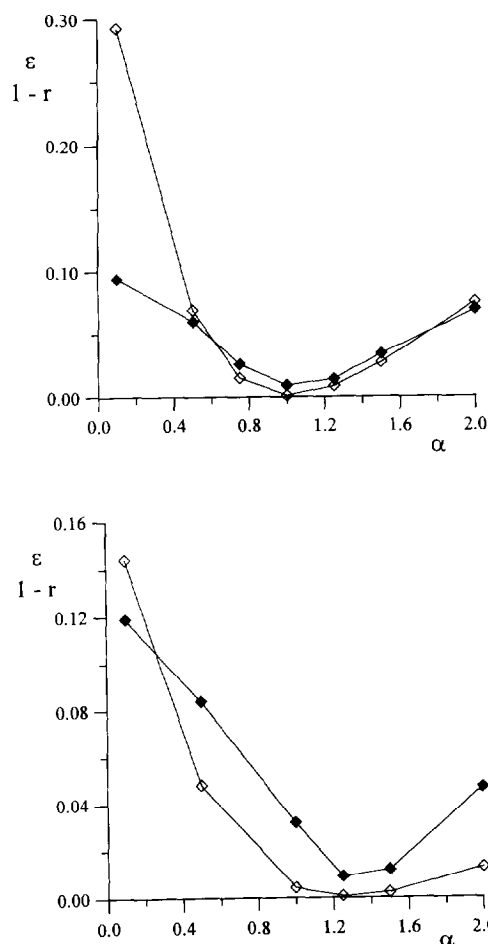

Fig. 5. Correlation coefficient as 1-r (◆) and $\varepsilon = |pK_{w,0} - 14.00|$ (◇) at increasing values of α; $pK_{w,0}$ values obtained with Eq. (20) using only three pK_w values ($I = 0.5$, 1.0 and 1.5 M) taken from Table A2 for LiCl (upper part) and NaCl (lower part).

Appendix

Table A1

Activity coefficient of proton at 25°C and several I values
(from Ref. [4])[a]

I	0.01	0.04	0.09	0.16	0.25	0.36	0.49	0.64	0.81	1.00
γ_H	0.911	0.862	0.839	0.835	0.846	0.869	0.904	0.948	1.00	1.06

[a] The data are recommended average values calculated from data taken in a number of different ionic media using the following model: $\log \gamma_H = -[0.5\sqrt{I}/(1 + 1.5\sqrt{I})] + CI + DI^{3/2}$, where C and D are constants.

Table A2

pK_w values at several I values and at 25°C in the presence of different electrolytes (from Ref. [18])

LiCl		NaCl		KCl	
I	pK_w	I	pK_w	I	pK_w
0.10	13.770	0.11	13.783	0.11	13.789
0.20	13.708	0.21	13.745	0.21	13.759
0.30	13.676	0.51	13.711	0.51	13.738
0.40	13.655	1.01	13.728	1.01	13.772
0.50	13.638	2.01	13.843	1.51	13.827
1.01	13.602	3.01	13.981	2.01	13.890
1.51	13.598			3.01	14.023
2.01	13.613			3.51	14.082
2.51	13.641				
3.01	13.672				

Table A3

Logarithms of the stability constants of the complexes $FeCl^{2+}$ (in $HClO_4$ at 25°C) and $FeSCN^{2+}$ (in KNO_3, temperature not given) at several I values (from Ref. [21])

$FeCl^{2+}$		$FeSCN^{2+}$	
I	$\log K_c$	I	$\log K_c$
0	1.38[a]	0	3.09[a]
2	0.53	0.4	2.11
3	0.76	0.5	2.08
4	1.10	1.0	2.00
5	1.50	1.5	1.97
7	2.46	2.0	1.96
8	3.13		

[a] $\log K_0$ (taken also from Ref. [21]).

than expected owing to the presence of maxima and minima in the regression function. To evaluate extrapolated $\log \gamma$ and $\log K$ values, Eqs. (10) and (20) respectively, are recommended. Systematic errors will be reduced by using experimental data as close as possible to the predicted value.

References

[1] M.C. Ortiz, J. López Palacios and L.A. Sarabia, Quim. Anal., 8 (1987) 33.
[2] E.A. Jenne (Ed.), Chemical Modelling in Aqueous Systems, American Chemical Society, Washington, D.C., 1979.
[3] P.W. Linder and K. Murray, Talanta, 29 (1982) 377.
[4] S. Capone, A. De Robertis, C. De Stefano, S. Sammartano and R. Scarcella, Talanta, 34 (1987) 593.
[5] G. Anderegg and S. Kholeif, Talanta, 41 (1994) 1507.
[6] S. Fiol, I. Brandariz and M. Sastre de Vicente, Talanta, 42 (1995) 797.
[7] R. Cazallas, M.J. Citores, N. Etxebarria, L.A. Fernández and J.M. Madariaga, Talanta, 41 (1994) 1637.
[8] G.H. Nancollas and M.B. Thomson, Pure Appl. Chem., 54 (1982) 2675.
[9] J. Kielland, J. Am. Chem. Soc., 59 (1937) 1675.
[10] L. Šucha and S.T. Kotrly, Solution Equilibria in Analytical Chemistry, Van Nostrand Reinhold, London, 1972.
[11] G. Scatchard, J. Am. Chem. Soc., 13 (1961) 2636.
[12] K.S. Pitzer, J. Phys. Chem., 77 (1973) 2300.
[13] G.E. Jackson and L.F. Seymour, Talanta, 42 (1995) 9.
[14] M.P. Elizalde and J.L. Aparicio, Talanta, 42 (1995) 395.

[15] B.W. Darvell and V.W.H. Leung, Chem. Br., 27 (1991) 29.

[16] C.B. Monk, Chem. Br., 29 (1993) 1034.

[17] G. Anderegg, Talanta, 40 (1993) 243.

[18] H.S. Harned and B.B. Owen, The Physical Chemistry of Electrolyte Solutions, 3rd edn., Van Nostrand Reinhold, New York, 1957.

[19] W. Cheney and D. Kincaid, Numerical Mathematics and Computing, 2nd edn., Brooks/Cole, Monterey, CA, 1985, Chapter 1.

[20] S.P. Datta and A.K. Grzybowsky, Trans. Faraday Soc., (1959) 1179.

[21] L.G. Sillén and A.E. Martell, Stability Constants, Supplement No. 1, The Chemical Society, London, 1971.

Short communication

Spectrophotometric determination of the theophylline in plasma by the apparent content curves method

M.J. Llobat-Estellés*, R.M. Marín-Saez, M.D. San-Martín Ciges

Department of Analytical Chemistry, Faculty of Chemistry, University of Valencia, Avda. Dr. Moliner 50, 46100-Burjassot, Valencia, Spain

Abstract

A direct spectrophotometric procedure for the determination of theophylline in plasma is proposed. This procedure is based on the apparent content curves method and it is not necessary to know the nature and contents of interferent substances. Bias errors introduced by plasma and metabolites are avoided. The results obtained are in agreement with those provided by an immunofluoroassay used as a reference method.

Keywords: Apparent content curves method; Plasma; Spectrophotometry; Theophylline

1. Introduction

Theophylline is a bronchodilator drug generally used in the treatment of bronchial asthma and neonatal apnea. For this purpose, plasma levels of theophylline of 10–20 μg ml^{-1} must be obtained because higher values produce undesirable secondary effects and lower values do not induce therapeutic effects. Also, differences in the individual elimination of theophylline make it necessary to monitor the plasma levels of patients treated with theophylline.

To determine theophylline in plasma, several methods have been proposed [1–3], most of them

being based on techniques such as UV–visible spectrophotometry [4–9], chromatography [2,10–14] or immunological tests [15–19]. Spectrophotometric methods are widely used but absorption measurements have low selectivity and therefore the proposed procedures include experimental steps designed to minimize the influence of the different constituents of the plasma.

In this paper, we propose the application of a mathematical model that permits the determination of an analyte in the presence of unknown interferences. This method is based on the apparent content curves approach [20–22] and it has been satisfactorily applied to the spectrophotometric determination of theophylline in pharmaceuticals [23].

* Corresponding author.

For application of this method, only the absorbance values of the sample at three wavelengths and the response coefficients of the analyte at the same wavelengths are needed. Additivity is also assumed.

2. Theoretical

Apparent content curves can be obtained, as described in previous papers [20–22], by plotting F_i values versus λ_i, F_i being calculated as

$$F_i = \left[\frac{S_T}{\alpha_A}\right]_i$$

where S_T is the analytical signal of a multicomponent sample at wavelength i and α_A is the response coefficient of the analyte at the same wavelength.

Considering that

$$(S_T)_i = (\alpha_A)_i\, C_A + \left(\sum_k^n \alpha_K\, C_K\right)_i$$

α_A and α_K being the response coefficients of the analyte (A) and each of the interferents (K) and C_A and C_K their corresponding contents, the expression for F_i becomes

$$F_i = \left[\frac{\alpha_A\, C_A + \sum_i^n \alpha_K\, C_K}{\alpha_A}\right]_i = C_A + \left[\frac{\sum_i^n \alpha_K\, C_K}{\alpha_A}\right]_i$$

$$= C_A + \Delta C_A$$

Hence, in the absence of interferent substances, the curves are straight lines with zero slopes and y-intercepts equal to C_A. However, the presence of interferences leads to different shapes for these curves, depending of the nature and contents of the interferences.

In this way, the apparent content curves show the presence of interferences, and further, they indicate the maximum contents of analyte possible (minimum of the curve in each case). In addition, the apparent content curves constitute the basis of an analytical procedure that, after identifying the total interferent present, called "apparent interferent", allows the determination of an analyte without the need for standard solu-

tions of real interferences in the sample and without the need to resort to any separation method.

For the identification of the total interferent, a computational program is used. The program looks for three signals that represent, at three established wavelengths, the spectrophotometric behaviour of the interferent present [22]. For this, the signals must obey a series of fixed conditions that imply

$$\frac{W_1}{[(\alpha)_1\, C_1]_1} = \frac{W_2}{[(\alpha)_1\, C_1]_2} = \frac{W_3}{[(\alpha)_1\, C_1]_3}$$

W_1, W_2, W_3 being the signals found and α_1 and C_1 the unknown response coefficients at the three working wavelengths and the concentration of the interferent respectively.

Once the "nature" of the interferent present has been established, determination of the analyte is carried out by the program [20–22] using F values for the sample and F^P values for the total interferent, defined as:

$$F^P_i = \frac{W_i}{\alpha_i}$$

Taking these values into account, C_A can be calculated from the expression

$$C_A = F_1 - F^P_1\left(\frac{F_1 - F_2}{F^P_1 - F^P_2}\right)$$

where $(F_1 - F_2)/(F^P_1 - F^P_2)$ is a correction factor (theoretical dilution of the signals found) that allows an interferent effect of suitable value to be obtained.

3. Experimental

3.1. Apparatus and reagents

A Perkin-Elmer Lambda 16 UV spectrophotometer was used.

The solvents propan-2-ol and dichloromethane were obtained from Panreac. An $H_2PO_4^-$ – HPO_4^{2-} HPO_4^{2-} of pH 7.4 was prepared. Stock solutions of theophylline, 1,3-dimethyluric acid, 3-methylxanthine, caffeine and 1,7-dimethylxanthine (Sigma) in suitable solvents were used to develop the experimental procedure.

1591

3.2. General procedure

For the determination of theophylline in plasma two solutions are prepared. For the first, to 0.5 ml of plasma add 0.25 ml of $(NH_4)_2SO_4$
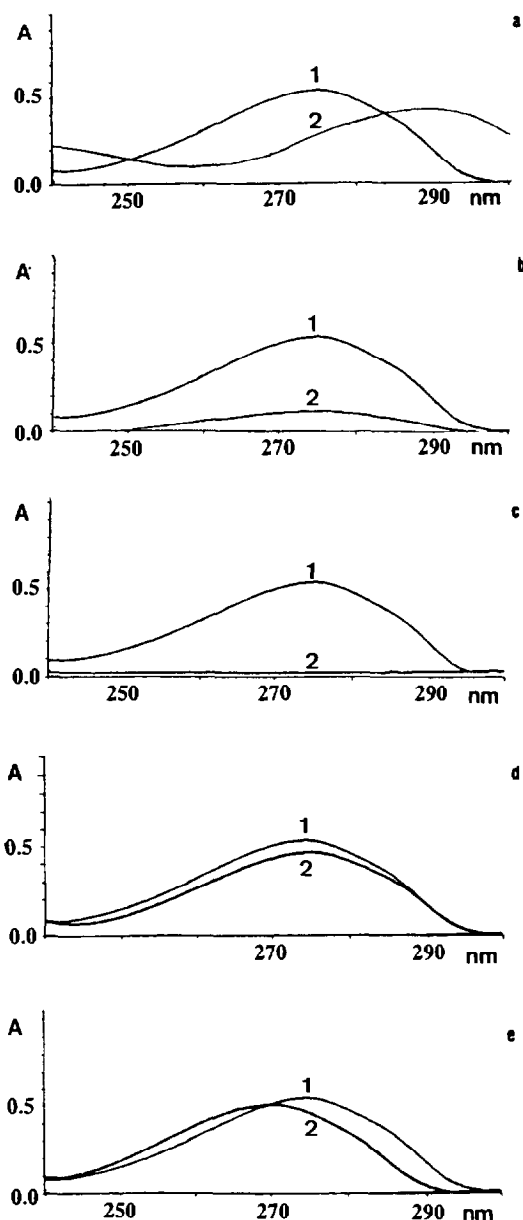

Fig. 1. Absorption spectra in dichloromethane–propan-2-ol of theophylline and its metabolites: (1) 10 ppm of theophylline; (2) 10 ppm of (a) 1,3-dimethyluric acid, (b) 3-methylxanthine, (c) 1-methyluric acid, (d) caffeine and (e) 1,7-dimethylxanthine.

Table 1
Calibration curves for theophylline in the presence of metabolites

Metabolite	y-Intercept	Slope
None	-0.003 ± 0.01	0.0457 ± 0.0007
1,3-Dimethyluric acid	0.02 ± 0.01	0.0437 ± 0.0006
3-Methylxanthine	0.02 ± 0.02	0.044 ± 0.001
1-Methyluric acid	0.003 ± 0.004	0.0447 ± 0.0003
Caffeine	0.185 ± 0.006	0.0459 ± 0.0004
1,7-Dimethylxanthine	0.168 ± 0.003	0.043 ± 0.002

(saturated solution), distilled water to 1 ml and 2.5 ml of dichloro-methane–propan-2-ol (19:1), shake the mixture for 5 min and centrifuge at 1000 rpm. For the second solution, proceed in the same way but use a standard solution of theophylline instead of distilled water.

Absorbance values at 264, 268 and 272 nm of the organic layers of both solutions are obtained using dichloromethane–propan-2-ol (19:1) as a blank. From these values, calibration graphs for standard additions at the three working wavelengths are estimated and F_i values are obtained as the ratio of y-intercept to slope in each case. Once the F_i values and the response coefficients (slopes of the calibration graphs) have been obtained, the program calculates the content of theophylline in the sample.

4. Results and discussion

4.1. Study of the extraction procedure

Extraction of theophylline was carried out with dichloromethane–propan-2-ol (19:1) [2]. In this medium, the absorption spectra of theophylline showed a broad band with a maximum at 274 nm (Fig. 1). The responses were linear over the dynamic range of concentration studied (2–10 ppm), the equation of the straight line obtained being $A = 0.0004 + 0.544C$ ($r = 0.9994$).

After extraction of theophylline from an aqueous solution, the spectra obtained were identical, the recoveries obtained being 94.5% and 85.2% for ratios of volume of aqueous layer to organic layer of 2:10 and 2:5, respectively.

In the presence of plasma and using a ratio of volumes of 2:5, a calibration graph for theophylline was obtained with the equation $A = 0.089 + 0.0337C$ ($r = 0.998$), whereas in the ab-
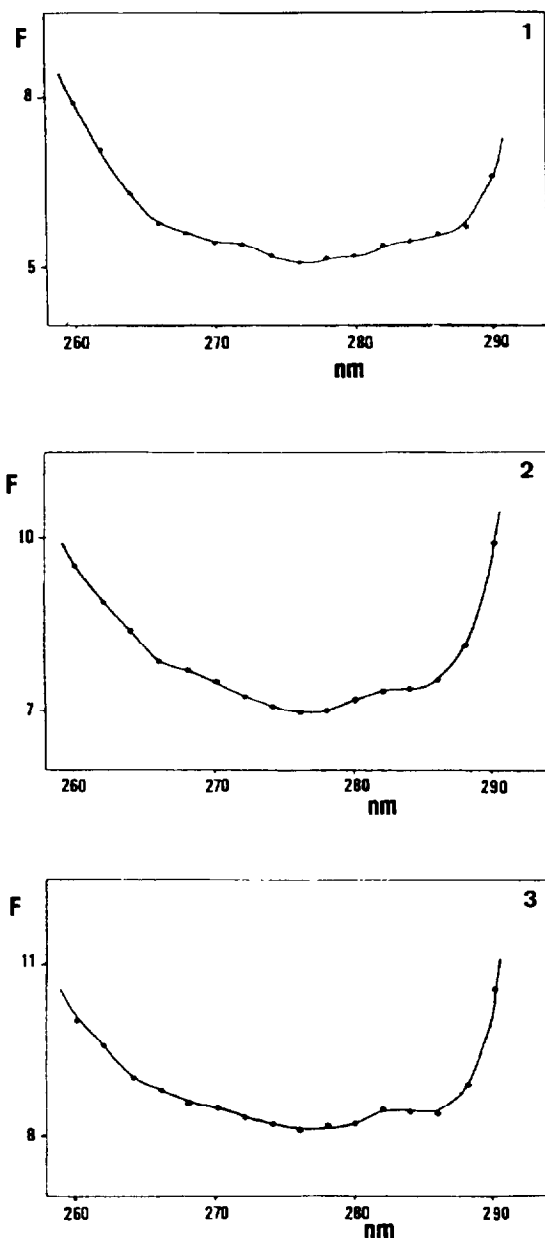
Table 2

Theoretical and experimental contents of theophylline obtained by applying the proposed procedure and reference method

Sample Composition		Theophylline content (ppm)	
		Proposed method	Reference method
1	5 ppm theophylline 10 ppm 1,3-dimethyluric acid 5 ppm 3-methylxanthine 5 ppm 1-methyluric acid 5 ppm caffeine 3 ppm 1,7-dimethylxanthine	5.4 ± 0.7	5.6
2	15 ppm theophylline 20 ppm 1,3-dimethyluric acid 10 ppm 3-methylxanthine 3 ppm 1-methyluric acid 2 ppm caffeine 5 ppm 1,7-dimethylxanthine	14.9 ± 0.7	15.4
3	25 ppm theophylline 8 ppm 1,3-dimethyluric acid 4 ppm 3-methylxanthine 4 ppm 1-methyluric acid 3 ppm caffeine 2 ppm 1,7-dimethylxanthine	25.3 ± 0.7	24.9

Fig. 2. Apparent content curves for three different synthetic samples containing real plasma and various concentrations of theophylline and metabolites. Compositions of samples are given in Table 2. (1) Sample 1; (2) sample 2; (3) sample 3.

sence of plasma the equation found was $A = -0.003 + 0.0457C$ ($r = 0.9997$). Therefore, a constant error (y-intercept $\neq 0$) and a proportional error (different slopes) are introduced by the constituents of plasma.

Finally, the potential interference introduced by the principal metabolites of theophylline was studied. As can be seen in Fig. 1, the spectrophotometric behaviours of substances such as 1,3-dimethyluric acid, 3-methylxanthine, 1-methyluric acid, caffeine and 1,7-dimethyxanthine are similar to that of theophylline and so they constitute potential interferences.

The influence of such substances on the absorption spectra of the extracts was studied in the following way. A series of solutions containing various concentrations of theophylline and a fixed concentration of one of the interferents tested was prepared. These solutions were extracted and the absorption spectra of the extracts were obtained. The responses at 274 nm were plotted against

theophylline content and the equations of the straight lines and standard deviation values obtained are given in Table 1.

From these values, it can be concluded that the differences between the y-intercepts obtained are statistically significant and so a constant error for a probability level of 95% can be confirmed. However, the differences between the slopes obtained are not significant and so proportional error cannot be deduced.

In conclusion, the determination of theophylline in extracts of plasma must be carried out using experimental procedures that avoid or minimize proportional errors introduced by plasma and, therefore, constant errors introduced by plasma and metabolites.

4.2. Determination of theophylline

To verify the proposed procedure experimentally, three synthetic samples were prepared as follows. To 45 ml of plasma, various amounts of theophylline and metabolites (1,3-dimethyluric acid, 3-methylxanthine, 1-methyluric acid, caffeine and 1,7-dimethylxanthine) were added to give a total volume of 50 ml. Each sample was analysed in triplicate using the general procedure described above.

Apparent content curves for the organic layers corresponding to each sample are shown in Fig. 2. As can be seen, in all cases the lower values are clearly above the theoretical contents given in Table 2. The results obtained by application of proposed procedure agree with those provided by an immunological test used as a reference method (Table 2).

Table 3
Experimental contents of theophylline obtained by applying the proposed procedure and the reference method samples from patients

Sample	Theophylline content (ppm)	
	Proposed method	Reference method
1	10.0	10.4
2	15.0	15.9

Finally, the proposed procedure was applied to samples from patients treated with theophylline. As can be seen (Table 3), the results obtained agree with those provided by the reference method.

5. Conclusions

The determination of theophylline in plasma can be carried out using the apparent content curves method. The proposed procedure is simple, and constant and proportional bias errors introduced by other constituents of the matrix plasma are avoided.

References

[1] J. Hu, Y. Wang and Q. Kong, Yaown Fenxi Zazhi, 8 (1988) 217.
[2] D.S. Sitar, K.M. Piafsky, R.E. Rangno and R.I. Ogilvie, Clin. Chem., 21 (1975) 1774.
[3] J. Moncrieff, J. Chromatogr., Biomed. Appl., 106 (1991) 177.
[4] D.N. Bailey, J. Anal. Toxicol., 2 (1978) 94.
[5] H.A. Schwertner, J.E. Wallace and K. Blum, Clin. Chem., 24 (1978) 360.
[6] D.-R. Liang, Y.-P. Qin, M.-Z. Liang, Y. Huang and J.-Z. Zeng, Huaxi Yike Daxue Xuebao, 18 (1987) 256.
[7] S.L. Waren, Ann. Allergy, 38 (1977) 198.
[8] D.C. Hohnadel, T.H. Grove and P.J. Alonzo, J. Anal. Toxicol., 2 (1978) 141.
[9] S. Ogihara, M. Hyodo and T. Kudo, Igaku no Ayumi, 115 (1980) 19.
[10] M.J. Cooper, B.L. Mirkin and M.W. Anders, J. Chromatogr., 143 (1977) 324.
[11] R. Desiraju, E.T. Sugita and R.L. Maycock, J. Chromatogr. Sci., 15 (1977) 563.
[12] M. Wenk, B. Eggs and F. Follath, J. Chromatogr., 276 (1983) 341.
[13] M.A. Evenson and B.L. Warren, Clin. Chem., 22 (1976) 851.
[14] R.F. Adams, F.L. Vandemark and G.J. Schmidt, Clin. Chem., 22 (1976) 1903.

[15] C.E. Cook, C.R. Tallent, E.N. Amerson, M.W. Myers, J.A. Kelpler, G.F. Taylor and H.D. Christensen, J. Pharmacol. Exp. Ther., 199 (1976) 679.

[16] A.L. Nesse and L.F. Soyka, Clin. Pharmacol. Ther., 21 (1977) 633.

[17] K.E. Opheim, V. Ainardi and V.A. Raisys, Clin. Chem., 29 (1983) 1698.

[18] R.B. Volcich, G.M. Schier, I.E. Gan, A.R.I.S. Seralyser and T.D. Abbott, Clin. Chem., 30 (1984) 1721.

[19] R.H. Dodge, Clin. Chem., 31 (1985) 496.

[20] M. Llobat-Estellés, R. Marin-Saez and M.D. San-Martín Ciges, Fresenius' J. Anal. Chem., 342 (1992) 538.

[21] A.R. Maurí-Aucejo, M. Llobat-Estellés, R. Marín-Saez, M.D. San-Martín Ciges and C. Alvarez Alonso, Fresenius' J. Anal. Chem., 346 (1993) 888.

[22] M. Llobat-Estellés, A.R. Maurí-Aucejo, R. Marín-Saez, M.D. San-Martín Ciges and A. Cerdán-Vidal, Anal. Chim. Acta, 282 (1993) 671.

[23] R. Marín-Saez, M. Llobat-Estelles, M.D. San-Martín Ciges and A.R. Maurí-Aucego, Anal. Lett., 26 (1993) 641.

Prussian-Blue-based amperometric biosensors in flow-injection analysis

Arkady A. Karyakin[1], Elena E. Karyakina[1], Lo Gorton*

Department of Analytical Chemistry, University of Lund, P. O. B 124, S-221 00 Lund, Sweden

Abstract

Optimisation of the electrodeposition of Prussian Blue onto mirrored glassy carbon electrodes yielded a modified electrode practically insensitive to oxygen reduction. At the same time the electrode activity towards hydrogen peroxide reduction was extremely high. This allowed the detection of hydrogen peroxide by electroreduction over a wide potential range. Flow-injection investigations of this electrode inserted into a flowthrough electrochemical cell of the confined wall-jet type showed that the response for hydrogen peroxide is limited by diffusion. Glucose and alcohol biosensors were made by immobilisation of glucose oxidase and alcohol oxidase respectively, within a Nafion layer, onto the top of the Prussian-Blue-modified electrodes. By increasing the density of Nafion and decreasing the measuring potential the glucose biosensor was made completely insensitive to both ascorbate and acetominophes.

1. Introduction

Accurate, rapid, and automatic analysis is required nowadays for clinical and industrial laboratories. Flow-injection analysis (FIA) with an enzyme electrode as the sensing element in the detector seems to accomplish this function. Operation of amperometric biosensors requires a con

jugation between the enzyme and electrochemical reactions. First generation biosensors are based on direct electrochemical detection of either the substrate or the product of the enzyme reaction. In the case of hydrogen-peroxide-producing oxidases the substrate and product refer to molecular oxygen and hydrogen peroxide respectively. Amperometric detection of these substances is usually done at platinum or platinised electrodes [1]. Electrochemical detection of hydrogen peroxide in the presence of oxygen is usually accomplished by its oxidation at anodic potentials ($> +0.6$ V, Ag/AgCl). However, all biological fluids contain a

---

* Corresponding author.
[1] Permanent address: Chemical Department, M.V. Lomonosov Moscow State University, 119899 Moscow, Russia.

series of various reductants, e.g. ascorbate, bilirubin, etc., which are easily co-oxidised at similar potentials, producing an additional current response, and this makes quantitation of the hydrogen peroxide produced and hence the enzyme substrate concentration impossible. A lot of effort has therefore been made to drastically decrease the necessary applied potential for following oxidase-based reactions. One way is to exchange the enzyme's natural reoxidation reagent (molecular oxygen) for an artificial electron acceptor [2,3]. Another is to decrease the overpotential for electrochemical conversion of hydrogen peroxide. Covering carbon electrodes with a layer of finely dispersed noble metals has proven highly catalytically efficient for both electrochemical oxidation and reduction of hydrogen peroxide [4]. However, the selectivity for hydrogen peroxide varies greatly with the metal chosen and the type of deposition [5]. Enzyme electrodes for detection of hydrogen peroxide could also be made by immobilisation of peroxidase at carbon electrodes either using a mediator or in a mediatorless approach [4,6,7]. In spite of the high enzyme activity towards hydrogen peroxide reduction the enzyme electrodes, at least in the mediatorless approach, are only seldom reported to have similar current densities as the electrodes based on noble metals [8]. The main reason for this is that not all of the immobilised peroxidase molecules are in direct electron transfer contact with the electrode [8].

Two of the current authors [9,10] and others [11] have previously reported that highly sensitive first generation amperometric-oxidase-based biosensors can be developed on the basis of Prussian-Blue-modified electrodes. One of the advantages of the first generation biosensors is that the oxidase can use its own "natural" reoxidation reagent, i.e. molecular oxygen. An absence of artificial mediators avoids the problem of competition between different electron acceptors. Prussian Blue was found to be a better electrocatalyst of hydrogen peroxide reduction than specially pretreated platinum and hydrogen peroxide could be selectively detected at the Prussian-Blue-modified electrode in the presence of molecular oxygen by both electrooxidation and electroreduction, even though at potentials below 100 mV a

slight electrocatalytic effect was also noticed for the reduction of oxygen [9,10]. This also made possible detection of hydrogen peroxide within "the optimal potential range for enzyme based amperometric biosensors" i.e. between approximately -200 and $+150$ mV (Ag/AgCl, pH 7) [4,7]. Prussian Blue is also a comparatively cheap and stable electrocatalyst compared with an enzyme (peroxidase), making it an attractive material for possible mass production of the base electrode material for biosensors.

A glucose amperometric biosensor can be constructed through immobilisation of glucose oxidase in a layer of Nafion cast directly onto the Prussian-Blue-modified electrode [4,7]. The use of an unconventional medium (Nafion, a perfluorinated polyelectrolyte) for the immobilisation of the enzyme resulted in a prolonged stability of the enzyme in this matrix. Moreover, the selectivity of the enzyme electrode was increased because the Nafion membrane also served as a barrier for negatively charged possible interfering compounds (e.g. ascorbate [12,13], paracetamol [14] etc.). The response of this biosensor exhibited a linear dependence on the analyte concentration in the range between 1×10^{-6} and 5×10^{-3} M glucose. The cathodic current density after addition of 1×10^{-6} M glucose was equal to 0.18 μA cm^{-2} [10].

The use of a further optimised method for the depostion of Prussian Blue on glassy carbon electrodes to obtain an improved selectivity for hydrogen peroxide reduction with regard to simultaneous reduction of oxygen is reported here. The electrodes were also used in biosensor configurations covered with membranes of high Nafion content and with immobilised glucose oxidase or the less stable alcohol oxidase. The applicability of these electrodes in the flow-injection mode is shown.

2. Experimental

2.1. Materials

All inorganic salts and glucose were obtained at the highest purity. Absolute ethanol was prepared

by distillation of sodium alcoholate and used immediately. Nafion (5% solution in 90% low chain aliphatic alcohols) was obtained from Aldrich (Steinheim, Germany). Glucose oxidase (EC 1.1.3.4) from *Asperigillus niger* (VII-S, 180 IU mg^{-1}) was produced by Sigma (St. Louis, MO). Alcohol oxidase (EC 1.1.3.13) from *Hansenula sp.* (Sigma) had an initial activity of 30 IU mg^{-1}.

2.2. Deposition of Prussian Blue

Glassy carbon disk electrodes (1.5 mm diameter) were used as working electrodes. Prior to use, the glassy carbon electrodes were mechanically polished with aluminium powder (Al_2O_3, 1 μm) until a mirror finish was observed. A three-compartment electrochemical cell containing a platinum net auxiliary electrode and an Ag/AgCl reference electrode in 1 M KCl was used for the deposition of Prussian Blue. The three electrodes were connected to an electrochemical analyser (bioanalytical Systems, West Lafayette, IN, model BAS-100W). The cell construction allowed deaeration of the working electrode space. Electrodeposition of Prussian Blue at the surface of the polished glassy carbon electrodes was done by immersing the electrode in a deaerated solution containing 1M KCl and 3mM HCl initially and also containing 1 mM $K_3[Fe(CN)_6]$ and 1mM $FeCl_3$ and applying a constant potential of 0.4 V for 30 or 100 s. After deposition the Prussian Blue films were activated in 0.1 M KCl by cycling the applied potential in a range between -0.05 and 0.35 V at a sweep rate of 50 mV s^{-1}. The total coverage of Prussian Blue at the electrode surface was between 2-3 and 4-5 nmol cm^{-2} after 30 s and 100 s of deposition respectively, if a transfer of four electrons per unit cell is assumed [15].

2.3. Preparation of enzyme membranes

Enzyme-containing Nafion membranes were prepared according to our recently reported method from enzyme suspensions in 90% ethanol and 10% water [16]. To this aim the lyophilised enzyme samples were dissolved in water to a final concentration for alcohol oxidase of 80 mg ml^{-1}

and for glucose oxidase of 40 mg ml^{-1}. It was shown that such concentrations caused no enzyme inactivation. Finally, the enzyme suspension was made by addition of ethanol or a water-ethanol mixture to the enzyme solution. An "enzyme-polyelectrolyte complex" was made by mixing the enzyme suspension with the Nafion solution. Enzyme-containing Nafion membranes were prepared by syringing 10 μl of the enzyme-polyelectrolyte complex to the surface of the Prussian-Blue-modified electrode and allowing the solvent to evaporate at room temperature. After deposition the enzyme-Nafion membranes were thoroughly washed with water. When not in use the electrode was stored dry in a refrigerator at 4°C.

Three different types of glucose electrodes were made using a slight variation in the immobilisation of glucose oxidase. Type I refers to the sensing electrode with a simple membrane made from the enzyme-polyelectrolyte complex with a Nafion content of 0.25%. The type II electrode was made in a similar way, but by first syringing 5 μl of glucose oxidase suspension in ethanol onto the electrode surface prior to deposition of the same enzyme-polyelectrolyte complex as above. To prepare the type III electrode the same procedure as for type I was followed except that a more concentrated (0.5%) Nafion solution was used to prepare the enzyme-polyelectrolyte complex. The total amount of immobilised glucose oxidase was almost equal for electrodes of types I and III. Alcohol oxidase was immobilised on the top of a Prussian Blue layer from an enzyme-polyelectrolyte complex with a Nafion content of 1%.

2.4. Flow-injection set-up

The flow-injection system consisted of a peristaltic pump (Gilson, Villier-le-bel, France, model Minipuls 2), A pneumatically-operated valve (Cheminert, Valco Instruments, Houston, TX, type SVA) equipped with a 50 μl injection loop, and a flowthrough amperometric cell of the confined wall-jet type [17] under three-electrode potentiostat control (Zäta Electronic, Lund, Sweden). The output of the potentiostat was connected to a strip chart recorder (Kipp & Zonen,

Delft, The Netherlands). The inlet section of the cell contained the Ag/AgCl reference electrode in a circular chamber filled with 0.1 M KCl from an external syringe. This chamber contacted the working electrode space by means of four holes (0.3 mm i.d.) concentrically surrounding the inlet (0.5 mm i.d.). The auxiliary electrode was a platinum wire encircling the outlet chamber. Glassy carbon disk electrodes (as above) were used as working electrodes. The distance between the nozzle and the working electrode was about 2 mm. The flow rates used were between 0.7 and 0.8 ml min^{-1}. A dispersion coeficient of about 1.5 was reached by injection of 50 μl of the sample. All connections in the system were made with Teflon tubing (0.5 mm i.d.). Before use all solutions were degassed to prevent microbubbles appearing in the system.

3. Results and discussion

3.1. Optimisation of Prussian Blue deposition

As already mentioned, Prussian Blue has been found to be a very efficient catalyst of hydrogen peroxide electroreduction [9,10]. However, according to the procedure followed in Refs. [9,10] it was also shown to be active for electroreduction of oxygen at potentials more negative than 100 mV. Hence there was a limited potential range where one can use Prussian-Blue-modified electrodes for the determination of hydrogen peroxide in the presence of oxygen.

The development of oxidase-based biosensors requires the electrocatalyst to be practically insensitive to oxygen and to operate at potentials from -100 mV to 100 mV (Ag/AgCl/1 M KCl). In the given potential range there is also only a minor influence of reductants on the biosensor response. It was therefore concluded to reconsider the optimisation of the deposition of Prussian Blue to obtain a catalyst even more selective for hydrogen peroxide.

As indicated in Ref. [15] the activity of Prussian-Blue-modified electrodes for the electroreduction of molecular oxygen is dependent on the conditions in which they are prepared. Thus it seemed as though

the selectivity of the catalyst layer could be controlled by the procedure of its deposition. Indeed, if molecular oxygen was not electrocatalytically reduced at the modified electrode, one could find a potential region where ascorbate, paracetamol, etc. were not oxidised and thus the response would be only to hydrogen peroxide.

Here, in contrast to the previous procedure [9,10], the electrodeposition of Prussian Blue was performed at a constant potential, where only ferric chloride was reduced. Furthermore, the initial concentrations of $K_3[Fe(CN)_6]$, KCl, HCl, and Fe^{3+} have been changed and $FeCl_3$ was used instead of $Fe(No_3)_3$. Through thorough optimisation of both the potential and the time of deposition polycrystal films were obtained with an extremely high redox activity. Fig. 1 presents a cyclic voltammogram of a Prussian-Blue-modified electrode registered in 0.1 M KCl. As seen in the case of a thin film (2 nmol cm^{-2}) the peak separation at a sweep rate of 20 mV s^{-1} was lower than 15 mV, indicating an almost electrochemically-reversible behaviour [18].

Fig. 2 illustrates the steady-state voltammograms of hydrogen peroxide and molecular oxygen reduction at the resulting electrode. To stabilise the thin layer of the electrocatalyst, the modified electrode was covered with 1% Nafion by dip-coating. The solid electrolyte was found to affect neither the redox nor the electrocatalytic properties of the deposited Prussian Blue (data not shown). In Fig.
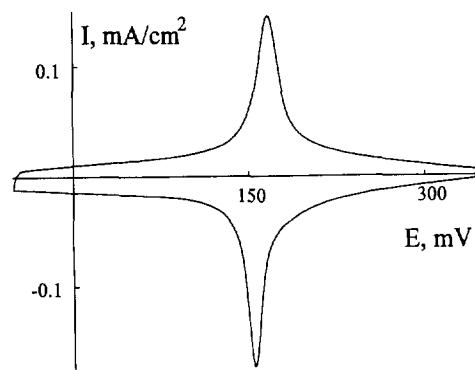

Fig. 1. Cyclic voltammogram of Prussian-Blue-modified electrode (coverage: 2 nmol cm^{-2}) registered in 0.1 M KCl at a sweep rate of 20 mV s^{-1}.
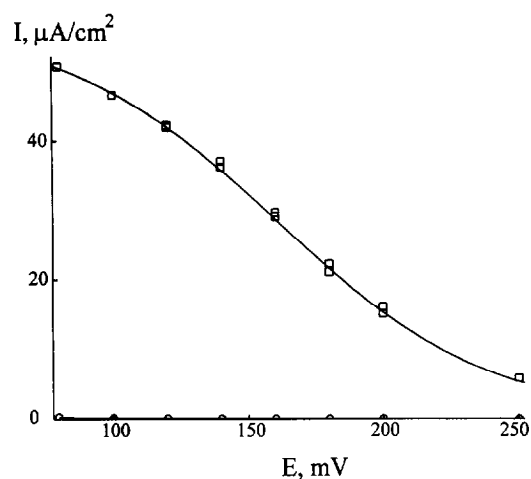
I, μA/cm^2

Fig. 2. Steady-state voltammograms of reduction of oxygen from air-saturated solution (○) and 0.2 mM hydrogen peroxide (□) at (1%) Nafion-covered Prussian-Blue-modified electrode (2 nmol cm^{-2}) registered in 0.1 M KCl, with stirring.

2 it is seen that the current of oxygen reduction over the entire potential range was negligible and was even lower than that of O_2 reduction at a bare glassy carbon electrode (data not shown). In contrast, the modified electrode was still extremely active for hydrogen peroxide electroreduction. The half wave potential of H_2O_2 reduction (Fig. 2) coincided with the formal potential of Prussian Blue found from the cyclic voltammograms, evaluated as the mean of the anodic and cathodic peak potentials [18] (Fig. 1), indicating a very fast reaction between hydrogen peroxide and the catalyst.

One of the most useful tools for hydrodynamic voltammetric studies is the wall-jet electrode, where a jet of solution issued from a circular nozzle is allowed to impinge normally on a working disk electrode. A counter electrode is set at an appropriate position remote from the wall jet. The equation for the limiting diffusion controlled current, I_d, at the wall-jet electrode was evaluated in Ref. [19]:

$$I_d = 1.38nFC_0 D^{2/3} v^{-5/12} V^{3/4} a^{-1/2} R^{3/4}$$

where C_0 and D are the concentration and diffusion coefficient of the depolariser respectively, v is the kinematic viscosity, V is the volume flow rate of the solution, a is the diameter of the nozzle and

R is the electrode radius. From the point of view of analytical chemistry it is essential that the limiting current is proportional to the concentration of the electroactive species.

It is interesting to compare the wall-jet electrode with the most common electrochemical hydrodynamic tool, the rotating disk electrode, as the limiting current depends on the diffusion coefficient of the depolariser similarly for both systems [18]. For a disk electrode with a diameter of 3 mm (i.e. a larger one than used in this report) inserted in the current wall-jet system (having an outlet nozzle of 0.5 mm i.d. and a flow rate of 1 ml min^{-1}), the registered limiting diffusion-controlled current would be of the same order as that obtained for a corresponding rotating electrode at a rotation velocity of 240 rev min^{-1}. The kinematic viscosity is assumed to be equal to 0.01 cm^2 s^{-1} [18]. For wall-jet electrodes with a diameter less than 3 mm (as is the case in this paper) the dependence of the limiting current on the electrode radius is different from that predicted by the given equation. However, from the data presented in Ref. [18] it was possible to estimate the current that is expected for the 1.5 mm i.d. disk electrode used in this study with the present set-up (flow rate of 1 ml min^{-1} and with the 0.5 mm nozzle) and to conclude that it would correspond to a rotating electrode with a speed of between 900 and 1000 rev min^{-1}. Considering the thickness of the diffusion layer [18,20] instead of the limiting current, similar correlations could be obtained.

One of the main advantages of the flow-injection technique as an analytical tool is the possibility of using small sample volumes. Indeed a 50 μl sample is sufficient to reach a value of dispersion of 1.5 [21]. This means that the peak height reaches between 60 and 70% of the steady-state current response obtained through a continuous flow of the analyte.

Uncovered Prussian-Blue-modified electrodes were applied to the flow-injection technique as sensors for hydrogen peroxide. The thicker film (4.5 nmol cm^{-2} obtained after 100 s of deposition) showed the most stable response. Calibration curves for determination of hydrogen peroxide with this electrode showed a linear dependence of the peak current on hydrogen per-

oxide concentration in the range between 1μM and 0.2 mM. At millimolar and higher concentrations of hydrogen peroxide a slow inactivation of the electrocatalyst was noticed. The linear dependence of the current response on analyte concentration, together with the arguments above, indicate that under the present conditions the sensor response is very fast and should be virtually limited by diffusion of hydrogen peroxide. Replotting the calibration curve in logarithmic coordinates resulted in a straight line with a slope equal to 1.0, indicating the same limiting step over the entire range. Since the diffusion layer in the wall-jet system is thin, the activity of the electrocatalyst for the hydrogen peroxide reduction was extremely high. This conclusion supports the use of the optimised Prussian-Blue-modified electrodes for construction of corresponding biosensors to be used in the flow-injection mode where there is a need for a fast responding sensor and where the detection of the enzyme product should not be the limiting step.

3.2. Flow-injection glucose analysis

Glucose oxidase was immobilised on the surface of the Prussian-Blue-modified electrode in a Nafion layer as described in Section 2. We have recently reported [16] on the beneficial properties of the sensor when the enzyme is immobilised in Nafion using a high concentration of ethanol: the remaining initial activity of the enzyme, an increased long-term stability, and increased reproducibility between similarly-prepared electrodes. The concentration of Nafion in the enzyme–polyelectrolyte complex was varied so that for types I and II it was 0.25% and for type III 0.5%. The calibration curves were recorded independently at two potentials: 0 mV and −50 mV (Ag/AgCl/0.1 M KCl).

Typical FI peaks registered for the response of an electrode of type III to glucose injections are shown in Fig. 3. A stable response with sufficiently high reproducibility was observed after continuous injections (RSD < 0.5%, $n = 5$, glucose concentration 0.5 mM). It is seen that the time for one analysis was 30–40 s, depending on the glucose concentration. Calibration curves for glucose
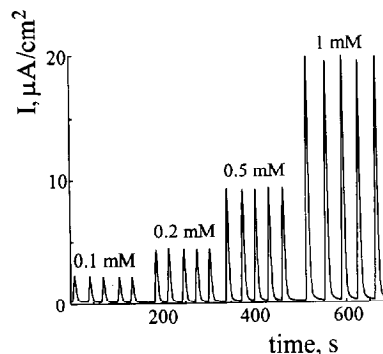

Fig. 3. Typical response of the flow-injection glucose analysis obtained for an electrode of type III: carrier, 0.02 M phosphate buffer, pH 5.5 with 0.1 M KCl (flow rate 0.7 ml min^{-1}); applied potential, 0 mV (Ag/AgCl/0.1 M KCl).

obtained in the FI system for electrodes of types I and III are shown in Fig. 5. There is a certain concentration range where the dependence of the response on glucose concentration gives a straight line in logarithmic coordinates, with a slope of unity. However, the injection of samples with a low analyte concentration gave well recognisable responses for type III electrodes and, to some extent, also for type I electrodes (see Fig. 4), independent of the glucose content. At the same time the injection of free buffer solution caused no response from the system. No real explanation for this behaviour can be given at this time but it may be caused by a local change in pH at the electrode–polyelectrolyte interface.
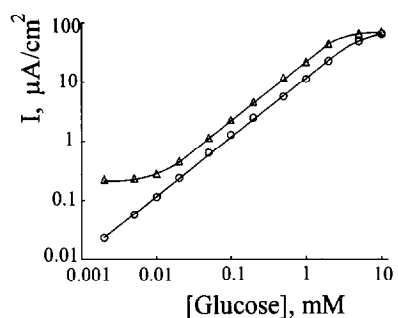

Fig. 4. Calibration curves for glucose in the flow-injection system: (○), electrode type I; (△), electrode type III; applied potentials were 0 mV and −50 mV (Ag/AgCl/0.1 M KCl) respectively; carrier, 0.02 M phosphate buffer, pH 5.5 with 0.1 M KCl (flow rate 0.7 ml min^{-1}).
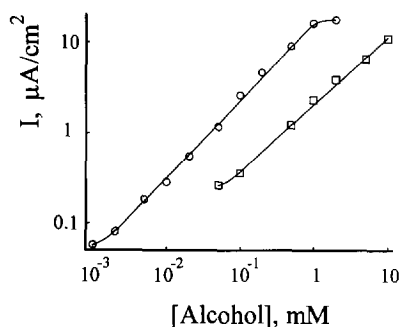
Fig. 5. Calibration curves for methanol (○) and ethanol (□) in the flow-injection system; applied potential, 0 mV (Ag/AgCl/0.1 M KCl); carrier, 0.02 M phosphate buffer, pH 7.5 with 0.1 M KCl (flow rate 0.8 ml min^{-1}).

Table 1 summarises some properties of the three types of glucose sensors studied in the flow-injection system. It is seen that an increase in both membrane density (type III) and the amount of immobilised enzyme (type II) caused a shift in the detection limit to higher glucose concentrations. However, it should be pointed out that the detection limits for types II and III were taken as the lowest analyte concentration, where the response started to become dependent on the glucose content. Comparing the two calibration curves in Fig. 4, it is seen that the response of type III electrodes was higher than that of type I even though the linear range is more restricted for both low (<10 μM) and high concentrations (>2 mM).

One of the most important problems to solve for any practical application of amperometric biosensors is to minimise the effect of interfering substances possibly present in a real sample. For oxidase-based systems reductants are the most severe interferences and among these ascorbate [12,13] and acetaminophen [14] are two of the most powerful ones, having upper concentration limits in biological liquids of 0.1 and 0.2 mM respectively.

The interferences of ascorbate and acetaminophen were tested in the flow-injection system with the Prussian-Blue-based biosensor as the electrochemical detector. Since the response to glucose was a cathodic current, the influence of the reductants resulted in a decrease in the response to glucose. Table 1 summarises the influ-

ence of these reductants in their limiting concentrations on the glucose response of the different types of enzyme electrodes. For each sensor the corresponding concentration of glucose is shown, which will be completely masked by the presence of the respective reductant.

The comparative influence of acetaminophen was found to be low. A signficant effect was observed only in the case of electrodes of type I at a measuring potential of 0 mV (Ag/AgCl/0.1 M KCl). In all other cases the concentration of the analyte that could be masked by this interference was lower than its detection limit. Ascorbate was found to be a more powerful interfering compound. For the type I electrode the anodic response to 0.1 mM ascorbic acid was equal to the cathodic response to 0.5 mM glucose at 0 mV. However, when the measuring potential was shifted to −50 mV the response to 0.1 mM ascorbate was decreased by a factor of 10. Even the type I electrode is possibly suitable for analytical applications for the detection of glucose, for example in a complex matrix.

Nafion membranes have already been used to decrease the ascorbate interference [12,13]. Thus a further improvement in the biosensor properties can be made either by increasing the density of the Nafion layer or by increasing the content of the immobilised enzyme. The aim of the latter approach is to improve the response towards the analyte. The influence of the interferant will obviously be decreased because the response to ascorbate is independent of the activity of glucose oxidase. Indeed it is seen in Table 1 that enzyme electrodes of types II and III are less dependent on the presence of ascorbate. The type III biosensor operating at a measuring potential of −50 mV was completely independent of ascorbate. The masking effect after addition of 0.1 mM ascorbic acid was at the level of the detection limit for glucose at this electrode.

3.3. Flow-injection ethanol analysis

Alcohol oxidase is known to exhibit a low operation stability [22], the reason being that it is inactivated by hydrogen peroxide, which is the product of the enzyme-catalysed reaction. In spite

Table 1
Flow-injection analysis of glucose

Parameter	Electrode type					
	I		II		III	
	Measuring potential (mV)		Measuring potential (mV)		Measuring potential (mV)	
	0	−50	0	−50	0	−50
Detection limit (M)	2×10^{-6}	2×10^{-6}	5×10^{-6}	5×10^{-6}	1×10^{-5}	1×10^{-5}
Response to 0.1 mM glucose (μA cm^{-2})	1.3	1.3	2.5	2.5	2.1	2.2
Response to 0.5 mM glucose (μA cm^{-2})	5.7	5.8	10	10	11.5	11.7
Response to 1 mM glucose (μA cm^{-2})	11.5	11.5	23	21	21	22
Response to 5 mM glucose (μA cm^{-2})	49	51	46	42	66	64
Glucose concentration (M) which will be masked by 0.1 mM ascorbate	5×10^{-4}	5×10^{-5}	1.5×10^{-4}	1.5×10^{-5}	1×10^{-4}	1×10^{-5}
Glucose concentration (M) which will be masked by 0.2 mM acetaminophen	5×10^{-6}	–	–	–	–	–

of using a high density of the Nafion membrane (1% Nafion in the enzyme-polyelectrolyte complex) the response of the alcohol biosensor was continuously decreased. Experiments with a lower Nafion content used for making the enzyme-polyelectrolyte complex revealed a less stable response (data not shown). However, the rate of inactivation of the final enzyme electrode was relatively low. This made possible the recording of the calibration curves shown in Fig. 5. During such an investigation (≈ 6 h) the response was reduced by less than 10%, which was controlled by repeated measurements of injected samples, maintaining a constant concentration of methanol.

It is seen in Fig. 5 for both methanol and ethanol that within certain concentration ranges (for methanol between 5 μM and 1 mM, for ethanol between 0.1 and 10 mM), the response resulted in a straight line in logarithmic coordinates. The response to methanol is much higher than that to ethanol. One reason for this is that the product formed in the reaction of methanol

with alcohol oxidase is formaldehyde, which is a good substrate for alcohol oxidase, whereas the product formed in the oxidation of ethanol, acetaldehyde, is a poor substrate. Methanol is also a smaller molecule than ethanol with an expected higher diffusion rate within the Nafion layer. The detection limit (evaluated as three times the noise level) of the system for methanol was 1 μM whereas that for ethanol was much higher, 0.05 mM. However, the addition of ethanol, even in micromolar amounts, gave a stable response independent of the analyte concentration (not shown in Fig. 5), similar to what was obtained for glucose for electrodes of type III (see Fig. 4). Since the behaviour of the biosensor in the flow-injection system with a low alcohol content was not clear, it was decided to compare the responses towards different alcohols in the millimolar region. Table 2 summarises the effectiveness of analysis of the following five different alcohols: methanol, ethanol, *n*-propanol, *i*-propanol, and *i*-butanol. The relative response is decreased as the hydrophobicity of the alcohol is increased.

Table 2

Flow-injection analysis of alcohol. The relative response towards 1 mM concentrations of different alcohols

Alcohol	Relative response (%)
Methanol	100
Ethanol	14.5
n-Propanol	2.6
i-Propanol	1.4
i-Butanol	1.4

4. Conclusion

Through the optimisation of Prussian Blue electrodepostion an electrocatalyst was produced which was almost insensitive to dissolved oxygen at an applied potential close to 0 mV, resulting in improved possibilities for using Prussian-Blue-modified electrodes in biosensors compared with our previous reports [9,10]. At the same time the activity towards hydrogen peroxide reduction was extremely high. This allowed electrochemical detection of hydrogen peroxide over a wide potential range by its electrocatalytic reduction. Given the low applied potential at which these amperometric biosensors can operate it follows that they are less sensitive to interference by ascorbate. Prussian-Blue-modified electrodes also have potential for use in flow-injection systems due to the high rate of the catalytic reaction.

The method of enzyme immobilisation into Nafion films from enzyme suspensions in a water–ethanol mixture with a high ethanol content, which was shown to give good results in steady-state measurements [16], also gave good results in flow-injection systems. Even a labile enzyme such as alcohol oxidase could be partially stabilised using this method.

. In principal it is foreseen that other hydrogen-peroxide producing oxidases could be immobilised using similar procedures as outlined here for the development of Prussian-Blue-based biosensors and applied in flow-injection systems.

References

[1] G.G. Guilbault and G.J. Lubrano, Anal. Chim. Acta, 64 (1973) 439.

[2] P.N. Bartlett, P. Tebbutt and R.P. Whitaker, Prog. React. Kinet., 16 (1991) 55.

[3] A. Heller, J. Phys. Chem., 96 (1992) 3579.

[4] L. Gorton, E. Csöregi, E. Domínguez, J. Emnéus, G. Jönsson-Pettersson, G. Marko-Varga and B. Persson, Anal. Chim. Acta, 250 (1991) 203.

[5] J. Wang, L. Fang, D. Lopez and H. Tobias, Anal. Lett., 26 (1993) 1819.

[6] I.V. Berezin, V.A. Bogdanovskaya, S.D. Varfolomeev, M.R. Tarasevich and A.I. Yaropolov, Dokl. Akad. Nauk SSSR, 240 (1978) 615.

[7] L. Gorton, Electroanalysis, 7 (1995) 23.

[8] T. Ruzgas, L. Gorton, J. Emnéus and G. Marko-Varga, J. Electroanal. Chem., 391 (1995) 41.

[9] A.A. Karyakin, O.V. Gitelmacher and E.E. Karyakina, Anal. Lett., 27 (1994) 2861.

[10] A.A. Karyakin, O.V. Gitelmacher and E.E. Karyakina, Anal. Chem., 67 (1995) 2419.

[11] Q. Chi and S. Dong, Anal. Chim. Acta, 310 (1995) 429.

[12] W. Matuszewski, M. Trojanowicz and A. Lewenstam, Electroanalysis, 2 (1990) 607.

[13] E.N. Navera, M. Suzuki, E. Tamiya, T. Takeuchi and I. Karube, Electroanalysis, 5 (1993) 17.

[14] Y. Zhang, Y. Hu, G.S. Wilson, D. Moatti-Sirat, V. Poitout and G. Reach, Anal. Chem., 66 (1994) 1183.

[15] K. Itaya, N. Shoji and I. Uchida, J. Am. Chem. Soc., 106 (1984) 3423.

[16] A.A. Karyakin, E.E. Karyakina, L. Gorton, O.A. Bobrova, L.V. Lukachova, A.K. Gladilin and A.V. Levashov, Anal. Chem., in press.

[17] R. Appelqvist, G. Marko-Varga, L. Gorton, A. Torstensson and G. Johansson, Anal. Chim. Acta, 169 (1985) 237.

[18] A.J. Bard and L.R. Faulkner, Electrochemical Methods: Fundamentals and Applications, John Wiley, New York, 1980.

[19] J. Yamada and H. Matsuda, J. Electroanal. Chem., 44 (1973) 189.

[20] H. Gunasingham and B. Fleet, Anal. Chem., 55 (1983) 1409.

[21] J. Ruzicka and E.H. Hansen, Flow Injection Analysis,

John Wiley, New York, 1988.

[22] T.D. Gibson, I.J. Higgins and J.R. Woodward, Analyst, 117 (1992) 1293.

Electroluminescent method for determining hydrogen peroxide and peroxydisulphate ions in aqueous solution using TiO₂ film electrodes

S.K. Poznyak, A.I. Kulak

Institute of Physico-Chemical Problems, Belarusian State University, 220080 Minsk, Belarus

Abstract

An electrochemical optical sensor system with luminescence response was proposed for the continuous determination of hydrogen peroxide or peroxydisulphate concentration in aqueous solutions. The electroluminescence (EL) of TiO₂ film electrodes, which arises under conditions of the cathodic polarization as a result of the hole injection into the TiO₂ from high-energy $OH^{\cdot}$ or $SO_4^{-\cdot}$ radicals produced by the electroreduction of H_2O_2 or $S_2O_8^{2-}$ ions on the electrode surface, was used as the analytical signal. The EL response is linearly related, in a logarithmic scale, to the hydrogen peroxide or peroxydisulphate concentration ranging from 10^{-3} to 10^{-1} M H_2O_2 and from 5×10^{-4} to 1 M $Na_2S_2O_8$. It was shown that a substantial increase in the quantum efficiency of the EL and, as a consequence, in the sensitivity of the sensor system can be achieved by doping TiO₂ films with chromium. The potential dependence of the EL spectrum for TiO₂ electrodes in $S_2O_8^{2-}$ solutions differs essentially from that in H_2O_2 solutions which allows measurement of the concentration of $S_2O_8^{2-}$ ions when they coexist with H_2O_2 in solution.

Keywords: Electroluminescent method; Hydrogen peroxide determination; Peroxydisulphate ion determination; TiO₂ film electrodes

1. Introduction

The determination of hydrogen peroxide and peroxydisulphate ions is of practical importance in chemical, biological, clinical and other fields. This motivates the growing interest in developing novel types of sensors for these substances. Several methods for the determination of H_2O_2 and $S_2O_8^{2-}$ ions in aqueous and organic solutions, such as titrimetry [1,2], spectrophotometry [3–5],

chemiluminescence [6–9], polarography [10,11], amperometry [12–16] and others, have been reported. Based on the chemiluminescence method, chemical sensors with an optical response (so-called optrodes) have been developed for H_2O_2 detection [17,18]. These sensors allow use of fibre optics [18–20]. Electrochemical methods offer an alternative way of developing sensors for H_2O_2 and $S_2O_8^{2-}$. For example, various enzyme-modified electrodes have been proposed as a basis

for amperometric sensors sensitive to H_2O_2 [13–16]. Most chemical and electrochemical sensors for H_2O_2 detection are based on using complex organic molecules (enzymes) as reagents which can deteriorate sensor characteristics such as lifetime or response time.

In the present paper, we propose an electrochemical reagentless sensor system with optical response based on semiconductor electroluminescence. It is well known [21–23] that minority carrier injection into semiconductor electrodes from some redox species in solution can cause radiative recombination between electrons and holes. Since definite species in solution take part in this process, the luminescence response of a semiconductor electrode could be used as a signal allowing detection of these species. In the previous report [24], we have shown that the change in intensity of electrochemically generated luminescence of TiO_2 electrodes can be related to the H_2O_2 concentration in aqueous solutions. In the present paper, the results of studying electroluminescence (EL) processes on TiO_2 film electrodes in solutions containing H_2O_2 or $S_2O_8^{2-}$ ions are described in view of using them in analytical purposes. We demonstrate the possibility of the increase in EL response due to doping TiO_2 films with chromium. Moreover, we show that the distinctions in the EL behaviour of TiO_2 electrodes in an H_2O_2 solution and in a solution containing $S_2O_8^{2-}$ ions can be used to detect these ions when they occur simultaneously with H_2O_2 in solution.

2. Experimental

2.1. Electrode preparation

The TiO_2 film electrodes were fabricated by hydrolysis of a solution containing 1 wt.% $Ti(OC_4H_9)_4$ in tert-butanol. In this process chemically polished titanium plates were coated by a definite dose of this solution. After evaporation of the solvent in air at room temperature, the plates were heated at 200°C for 30 min in a humid atmosphere to complete the hydrolysis of $Ti(OC_4H_9)_4$. This procedure of film deposition

followed by heating was repeated three times to give a film thickness of ca. 100 nm estimated by the interference method. Finally the TiO_2 electrodes were heated at 700°C for 1 h in a purified argon atmosphere. According to electron diffraction and Raman spectroscopy data, the TiO_2 films obtained are polycrystalline (rutile modification). To produce chromium doped TiO_2 films, a definite amount of $CrCl_3 \times 6H_2O$ was added to 1% $Ti(OC_4H_9)_4$ solution in tert-butanol.

2.2. Experimental methods and reagents

Measurements were carried out in a standard three-electrode cell with a quartz window and a platinum counter-electrode at room temperature. All potentials were determined with respect to an Ag/AgCl reference electrode (+0.201 V versus NHE) and controlled by a conventional potentiostat with a programmer. Simultaneous measurements of EL intensity and current density as a function of potential were taken under a linear potential sweep, and EL response was monitored by a photomultiplier. The output of the photomultiplier was amplified by a sensitive high-resistance voltmeter and plotted on an $X-Y$ recorder. In some cases, we used a pulsed polarization of the working electrode. The potential was pulsed between 0 V (31.5 ms) and a more negative potential (12 ms) (see the inset of Fig. 2). Such polarization allowed us to prevent some irreversible changes of the electrode properties possible under forward bias. Moreover, a lock-in technique increased markedly the sensitivity and the signal-to-noise ratio of the detection system. To obtain electroluminescence spectra, the electrochemical cell was introduced inside the sample compartment of a Spex Fluorolog spectrofluorimeter. All spectra were corrected for the spectral sensitivity of a photomultiplier.

All solutions were prepared using chemicals of analytical reagent grade and doubly distilled water. The electrolyte in the cell was stirred with a magnetic stirrer during the measurements when it was necessary. The concentration unit, mol 1^{-1}, is abbreviated as M in the present paper.

3. Results and discussion

3.1. Dependence of sensor response on the electrode potential

In order to determine the range of operating potentials for an electroluminescence sensor system based on TiO_2 film electrodes, the electroluminescence intensity (I^{EL}) and the cathodic current density (i_c) were simultaneously recorded as a function of electrode potential (E) (Fig. 1). Electrochemically generated luminescence of titanium dioxide in H_2O_2 or $S_2O_8^{2-}$ solutions was previously reported [21,25–27] to arise under forward bias according to the following mechanism. Initially, H_2O_2 or $S_2O_8^{2-}$ ions are reduced by the
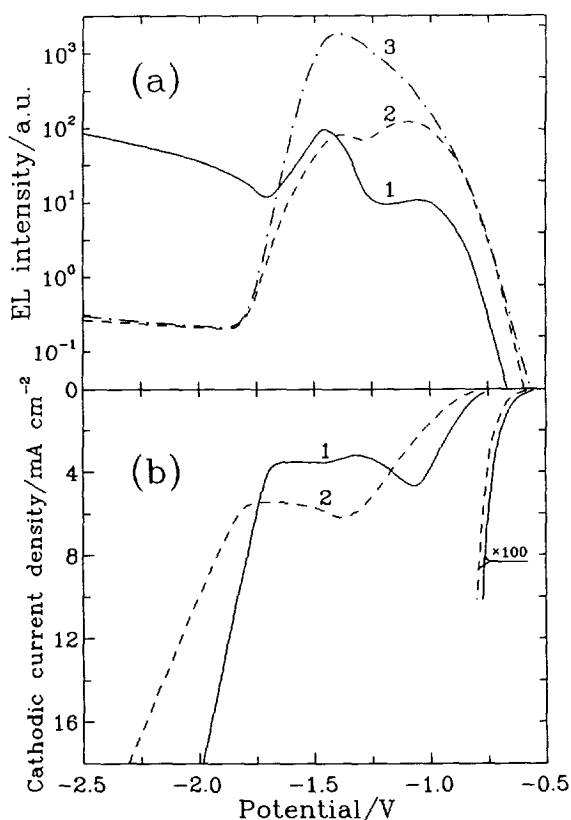
Fig. 1. Electroluminescence intensity versus potential (a) and cathodic current density versus potential (b) curves for un-doped (1,2) and chromium-doped (0.1 wt.% Cr) TiO_2 film electrodes (3) in 0.1 M H_2O_2 + 0.1 M NaOH (2,3) and in 0.1 M $Na_2S_2O_8$ + 0.1 M NaOH (1). Potential was swept from 0 V with a rate of 4 mV s^{-1}.

conduction band electrons producing OH˙ or SO_4^{-}˙ radicals. Then these radicals acting as very strong oxidants inject holes into the valence band or onto intra-band-gap surface states of TiO_2. As can be seen from Fig. 1, there is an exponential increase in the cathodic current, associated with the reduction of H_2O_2 or $S_2O_8^{2-}$ ions, at potentials more positive than the flat band potential of TiO_2 ($E_{fb} \sim -1.0$ V) as determined by capacitance measurements. The EL onset potential agrees sufficiently well with the onset potential of the cathodic current. At $E < E_{fb}$, the cathodic current is saturated due to the diffusion limitation and, at $E < -1.8$ V, increases again owing to the onset of the hydrogen evolution reaction.

The potential dependences of the EL intensity are more complex as compared to i_c–E relations (Fig. 1). Two peaks of EL intensity can be distinguished on the I^{EL}–E curves, with a more negative peak occurring in the potential region of the diffusion limited current. It is noted that when the EL response is used to detect H_2O_2 or $S_2O_8^{2-}$ ions, the TiO_2 electrode should not be polarized at very negative potentials ($E < -1.7 - -2.0$ V), since this results in irreversible changes of electroluminescence and other properties of the electrode which are caused by the cathodic reduction of TiO_2.

3.2. Effect of doping TiO_2 film

Since the sensitivity of the EL sensor system based on TiO_2 electrodes could be improved by increasing the quantum efficiency of the EL process, we attempted to do this by means of doping TiO_2 films with chromium. The choice of this dopant is justified by the previously reported conclusion [26,28] that the photoluminescence intensity is considerably enhanced by the introduction of chromium in monocrystals and polycrystalline samples of rutile. Figs. 1 and 2 show the effect of the chromium doping level on the EL response obtained under potentiodynamic and pulsed polarization of the TiO_2 electrodes. Increasing the chromium concentration in the oxide film enhances markedly the EL intensity over the wide potential range. Characteristically, this doping improves only the quantum efficiency of the EL
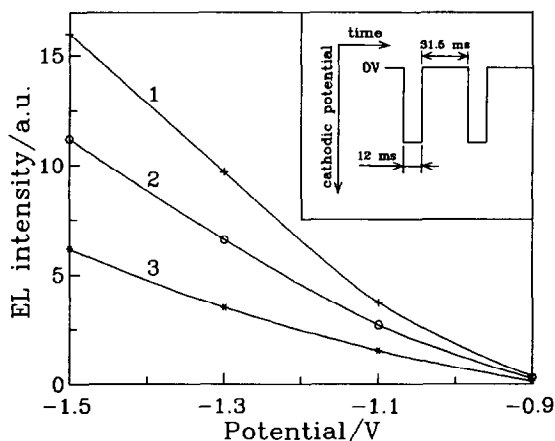
Fig. 2. Dependence of the EL intensity on potential obtained under pulsed polarization of undoped (3) and chromium-doped TiO$_2$ film electrodes with 0.02 wt.% Cr (2) and 0.1 wt.% Cr (1) in a solution containing 0.1 M H$_2$O$_2$ and 0.1 M NaOH. The inset shows the potential pulses used to generate electroluminescence.

process and does not change the electrocatalytic activity of TiO$_2$ electrodes. The effect of chromium doping on the EL response is likely to be associated with increasing the concentration of deep recombination centres lying near the band gap centre of TiO$_2$ which are characteristic of rutile [28].

3.3. Emission spectra

Fig. 3 shows typical EL spectra for TiO$_2$ film electrodes. It should be noted that chromium doping practically does not modify the EL spectra. In H$_2$O$_2$ solution, the only band is at 850 nm in the spectrum. This band has been observed more than once in the photoluminescence and electroluminescence spectra of monocrystals and polycrystalline sintered samples of rutile both in air and in solution [25–31]. We did not reveal a noticeable effect of potential (up to − 1.7 V) on the position of this band in the EL spectrum. At more negative potentials, we failed to measure the EL spectrum reliably in H$_2$O$_2$ solution because of the low intensity of the emitted light. The EL spectrum observed in S$_2$O$_8$$^{2-}$ solution at potentials of up to − 1.1 V is similar to that in H$_2$O$_2$ solution. However, at $E < − 1.2$ V, a band lo-

cated in the visible spectral range appears (Fig. 3). The reasons of this band appearance associated with the change of the EL mechanism were previously considered in detail [31] and will not be discussed in the present paper. Here, it is important to note that the marked dependence of the EL spectrum on potential in peroxydisulphate solutions can be used to measure the concentration of S$_2$O$_8$$^{2-}$ ions in the presence of H$_2$O$_2$ in solution as will be shown below.

3.4. Time dependence of sensor response

In order to estimate the response time characteristics of the EL sensor system under consideration, we studied the transient behaviour of the I^{EL} when a pulsed polarization was applied and switched off. The I^{EL} versus time curves are shown to depend essentially on the analyte (H$_2$O$_2$ or S$_2$O$_8$$^{2-}$ ions) concentration (C) in solution. In dilute solutions, after an initial sharp drop within several minutes, the I^{EL} reaches a steady-state value or decreases slowly in conformity with the i_c–τ dependence. These transients of I^{EL} and i_c are caused by the diffusion limitation on the analyte transport to the electrode surface. The experimental fact that stirring the solution increases markedly a steady-state value of I^{EL} confirms this conclusion. In more concentrated
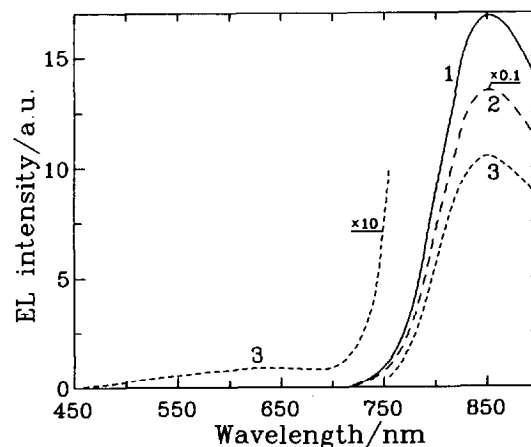

Fig. 3. Electroluminescence spectra for undoped TiO$_2$ film electrodes measured at − 1.0 V (1,2) and − 1.4 V (3) in 0.1 M H$_2$O$_2$ + 0.1 M NaOH (2) and in 0.1 M Na$_2$S$_2$O$_8$ + 0.1 M NaOH (1,3).
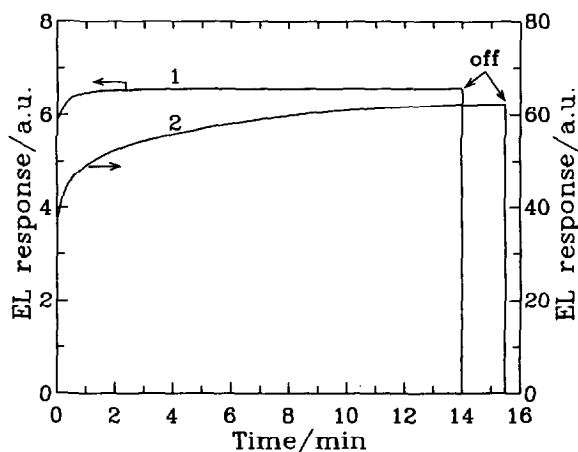
Fig. 4. Time dependence of the EL response for chromium-doped (0.1 wt.% Cr) TiO_2 film electrodes in 0.1 M $H_2O_2 + 0.2$ M KOH (2) and in 0.1 M $K_2S_2O_8 + 0.2$ M KOH (1) after starting the pulsed polarization (− 1.1 V); off denotes that the pulsed polarization has been switched off.

solutions ($C > 0.1$ M), the I^{EL} does not fall after starting the pulsed polarization and even somewhat increases before reaching a constant value. Fig. 4 represents typical transients of I^{EL} observed in alkaline solutions with 0.1 M H_2O_2 or
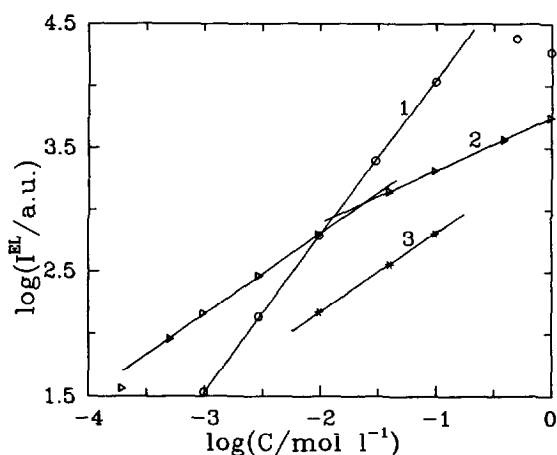
Fig. 5. Dependence of the steady-state EL response on the analyte concentration in a logarithmic scale for chromium-doped (0.1 wt.% Cr) TiO_2 film electrodes in H_2O_2 (1), $Na_2S_2O_8$ (2) and $Na_2S_2O_8 + 0.1$ M H_2O_2 (3) alkaline (0.1 M NaOH) solutions stirred with a magnetic stirrer. The potential was pulsed from 0 V to − 1.1 V (1,2) and −1.4 V (3). The EL emission was monitored at wavelengths longer than 700 nm (curves 1,2) and at wavelengths shorter than 700 nm (curve 3).

0.1 M $Na_2S_2O_8$ when a pulsed polarization was switched on and switched off. Characteristically, the EL rise time (10–15 min) in H_2O_2 solution is markedly longer than that (1–3 min) in $S_2O_8^{2-}$ solution. These transients may be tentatively associated with the activation of the electrode due to the electrochemical reaction. This assumption is confirmed by the fact that the EL rise time decreases considerably when applying the pulsed polarization repeatedly after reaching a steady-state value of I^{EL}. Thus, some limitation of the proposed sensor system which is associated with a relatively long rise time of the EL response can be partly overcome by preliminary training (the pulsed polarization during 15–20 min) of TiO_2 electrodes in solution just before the measurements. The EL decay time is much shorter than its rise time and lasts fractions of a second.

3.5. Relation between sensor response and analyte concentration

Fig. 5 shows the plots of steady-state EL intensity (measured on chromium-doped TiO_2 electrodes in stirring solutions) versus analyte (H_2O_2 or $S_2O_8^{2-}$ ions) concentration in a logarithmic scale. The log(I^{EL}) versus log C plot is linear in a rather wide range of H_2O_2 concentrations from 10^{-3} to 10^{-1} M. Above 10^{-1} M, there is a change in slope, the EL response levels off and even somewhat decreases at H_2O_2 concentrations above 0.5 M. Unlike the calibration plot for H_2O_2 solutions, the log(I^{EL}) versus log C curve obtained in peroxydisulphate solutions has a distinct bend at concentrations of ca. 2×10^{-2} M. Two linear parts can be distinguished on this curve, one from 5×10^{-4} to 10^{-2} M and another 5×10^{-2} to 1 M. Below 5×10^{-4} M $Na_2S_2O_8$, TiO_2 electrodes show a non-linear response in a logarithmic scale, but optical signals are still observed down to 10^{-4} M. As noted above, the characteristic dependence of the EL spectrum on potential in peroxydisulphate solutions gives the opportunity for the detection of $S_2O_8^{2-}$ ions on the background of H_2O_2. When monitored at wavelengths within the visible range of spectrum ($\lambda < 700$ nm) and at potentials negative to − 1.2 V, the EL response
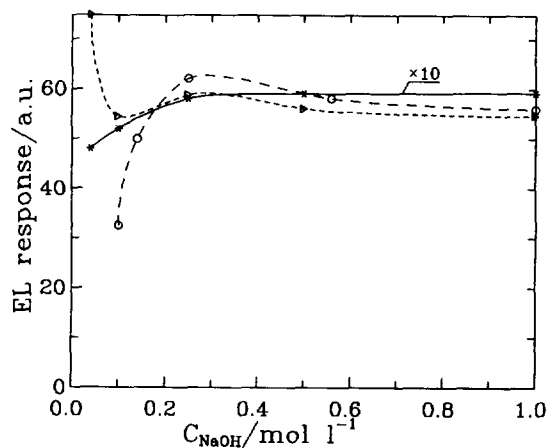
Fig. 6. Electroluminescence response versus NaOH concentration curves for chromium-doped (0.1 wt.% Cr) TiO_2 film electrodes in alkaline solutions containing 0.1 M H_2O_2 (·), 0.1 M H_2O_2 + 0.25 M Na_2SO_4 (△) and 0.1 M $Na_2S_2O_8$ (✳). The potential was pulsed between 0 V and – 1.1 V.

must reflect the contribution of the $S_2O_8{}^{2-}$ ions to the electroluminescence generation process. Fig. 5 shows the plot of $\log(I^{EL})$ versus $\log(C_{Na_2S_2O_8})$ obtained at $\lambda < 700$ nm and $E = -1.4$ V (pulsed polarization) in solutions containing 0.1 M H_2O_2 and various concentrations of $Na_2S_2O_8$. This plot is linear from 10^{-2} to 10^{-1} M peroxydisulphate indicating that the presence of H_2O_2 in solution does not noticeably influence the measurement of $S_2O_8{}^{2-}$ concentration under such conditions.

3.6. Effect of pH

The EL response of TiO_2 electrodes to H_2O_2 or $S_2O_8{}^{2-}$ species depends, to some extent, on the concentration of alkali in solution. The dependences of the EL intensity on the NaOH concentration in solutions containing 0.1 M H_2O_2 or 0.1 M $Na_2S_2O_8$ are shown in Fig. 6. The EL response varies markedly in the region of relatively low concentrations of alkali ($C_{NaOH} < 0.1$ M). Moreover, in H_2O_2 solutions without an indifferent supporting electrolyte, the response falls off with decreasing NaOH concentration due to a lowering of the conductivity of the solution. The addition of 0.25 M Na_2SO_4 as a supporting electrolyte to alkaline solutions of H_2O_2 results in the opposite

effect: the EL intensity increases with decreasing pH at $C_{NaOH} < 0.1$ M. At C_{NaOH} more than 0.1 M up to 1 M, the EL intensity is slightly affected by the alkali content in H_2O_2 and $S_2O_8{}^{2-}$ solutions (Fig. 6).

Thus, the experimental results obtained show that the EL emission occurring at the TiO_2-solution interface under negative polarization can be used to determine the H_2O_2 or peroxydisulphate content in aqueous solutions within a rather wide range of concentrations. It should be noted that titanium dioxide is a semiconductor with the wide band gap (approx. 3.02 eV) and the low location of the valence band edge in the energy scale [32]. This is an advantage in using TiO_2 as a basis for the sensor development, because TiO_2 electrodes are electrochemically stable and the hole injection into the TiO_2 valence band directly from the known oxidizing redox species, which are chemically stable in aqueous solution, is negligible [21,27]. The possibility of this hole injection in hydrogen peroxide or peroxydisulphate solutions appears due to the specific two-step mechanism of H_2O_2 or $S_2O_8{}^{2-}$ electroreduction producing active intermediates (radicals) with a large positive redox potential during the first step. This peculiarity gives reasons to hope for a high selectivity of the proposed sensor system based on TiO_2 electrodes with respect to hydrogen peroxide or peroxydisulphate ions. Further study concerning the sensor characteristics (e.g. selectivity, long-term stability) is currently being conducted and the results will be reported later.

Acknowledgements

References

[1] N.K. Murty, V. Satyanarayana and Y.P. Rao, Talanta, 24 (1977) 757.
[2] P.E.A. Boudeville, Anal. Chem., 55 (1983) 612.
[3] H. Afsar, R. Apak and I. Tor, Analyst, 115 (1990) 99.

[4] A.N. Baga, J.G.R. Alastair, N.B. Nazhat and A.S.-N. Rajiha, Anal. Chim. Acta, 204 (1988) 349.

[5] T. Nakano and A. Takahashi, Anal. Sci., 6 (1990) 823.

[6] K. Hool and T.A. Nieman. Anal. Chem., 60 (1988) 834.

[7] S. Sakura and H. Imai. Anal. Sci., 4 (1988) 9.

[8] T. Segawa, T. Kamidate and H. Watanabe, Anal. Sci., 6 (1990) 763.

[9] K. Yamashita, S. Yamazaki-Nishida, Y. Harima and A. Segawa, Anal. Chem., 63 (1991) 872.

[10] E. Nakoila, Talanta, 15 (1968) 55.

[11] D. Amin, Analyst, 106 (1981) 1217.

[12] M.A. Abdalla and H.M. Al-Swaidan. Anal. Lett., 22 (1989) 1729.

[13] M. Cosgrove, G.J. Moody and J.D.R. Thomas, Analyst, 113 (1988) 1811.

[14] T. Tatsuma, Y. Okawa and T. Watanabe. Anal. Chem., 61 (1989) 2352.

[15] U. Wollenberger, U. Bogdanovskaya, S. Bobrin, F. Scheller and M. Tarasevich, Anal. Lett., 23 (1990) 1795.

[16] T. Tatsuma and T. Watanabe, Anal. Chem., 63 (1991) 1580.

[17] H.E. Posch and O.S. Wolfbeis, Microchim. Acta, 1 (1989) 41.

[18] T.M. Freeman and W.R. Seitz, Anal. Chem., 50 (1978) 1242.

[19] W.R. Seitz. Anal. Chem., 56 (1984) 16A.

[20] A.J. Guthrie, R. Narayanaswamy and D.A. Russell, Trans. Instrum. Meas. Control., 9 (1987) 71.

[21] B. Pettinger, H.-R. Schoppel and H. Gerischer, Ber. Bunsenges. Phys. Chem., 80 (1976) 849.

[22] L.P. Bicelli, Surf. Technol., 26 (1985) 93.

[23] A.B. Ellis, in R.B. Hall and A.B. Ellis (Eds.), Chemical Structure of Interfaces, VCII, Deerfield Beach, FL, 1986, p. 245.

[24] S.K. Poznyak and A.I. Kulak, Sensors Actuators B, 22 (1994) 97.

[25] Y. Nakato, A. Tsumura and H. Tsubomura, J. Phys. Chem., 87 (1983) 2402.

[26] Y. Yakato, H. Ogawa, K. Morita and H. Tsubomura, J. Phys. Chem., 90 (1986) 6210.

[27] B. Smandek and H. Gerischer, Electrochim. Acta, 34 (1989) 1411.

[28] L. Grabner, S.E. Stokowski and W.S. Brower, Jr., Phys. Rev. B, 2 (1970) 590.

[29] G. Nogami, R. Shiratsuchi and S. Ohkubo. J. Electrochem. Soc., 138 (1991) 751.

[30] R.R. Addis, Jr., A.K. Ghosh and F.G. Wakim, Appl. Phys. Lett., 12 (1968) 397.

[31] S.K. Poznyak and A.I. Kulak, Dokl. AN Belarusi, 37 (1993) 53.

[32] H.O. Finklea, Stud. Phys. Theor. Chem., 55 (1988) (Semicond. Electrodes) 43.

Talanta

Short communication

Polyphenol oxidase–catechol: an electroenzymatic model system for characterizing the performance of matrices for biosensors

J.-L. Besombes, S. Cosnier*, P. Labbé

Laboratoire d'Electrochimie Organique et de Photochimie Rédox, URA CNRS 1210, Université Joseph Fourier Grenoble 1, BP 53, 301 rue de la Chimie, 38041 Grenoble Cedex 9, France

1. Introduction

Enzyme electrodes are analytical devices based on the combination of the high specificity of biocatalytic reactions with the electrochemical (mainly amperometric) transduction of the recognition event [1]. Analysis of enzyme electrode kinetics is of importance for designing a sensor or for optimization of parameters [2–6]. Since the overall sensor response depends on the enzymatic reaction and on the mass transfer processes, the enzyme layer permeability and the efficiency of the enzymatic reaction are two crucial biosensor parameters. Their determination can give valuable information for the optimization of the biosensor configuration as well as for the development of new strategies for enzyme immobilization [5,7].

For this purpose, we present in this paper the properties of an original electroenzymatic system

based on polyphenol oxidase (PPO) and catechol for evaluating the performance of host matrices used to fabricate enzyme electrodes. PPO and catechol constitute a versatile system since the substrate (catechol) and product (*ortho*-quinone) of the enzymatic reaction can be independently determined electrochemically. Furthermore, the thermal deactivation of immobilized PPO can give additional information about the substrate diffusion through the host matrix loaded with enzymes. The utilization of this simple system to obtain criteria for optimization of sensor performance is exemplified here for enzyme electrodes fabricated by polymer entrapment [8–10]. The model of the electrode material was a polypyrrole film obtained by electropolymerization of an amphiphilic monomer, the 12-(pyrrol-1-yl)dodecyltriethylammonium tetrafluoroborate (1) [11]. The influence of the amount of enzyme immobilized within this model of electrode material on the characteristics of the resulting enzyme electrodes is investigated via the PPO–catechol system.

---

* Corresponding author.

2. Experimental

2.1. Instrumentation

The electrochemical instrument consisted of a PAR model 362 potentiostat in conjunction with a Sefram TRP recorder. All experiments were carried out using an undivided thermostated three-electrode cell. The working electrode was a glassy carbon disk (5 mm diameter) polished with diamond paste. A saturated calomel electrode (SCE) and a platinum counter electrode were used. All measurements were carried out at 30°C.

2.2. Reagents

Polyphenol oxidase (EC 1.14.18.1, from mushroom, 123 units mg^{-1}) was purchased from Fluka and catechol was obtained from Aldrich. The synthesis of monomer 1 has been described previously [11]. Supporting electrolytes were 0.1 M LiClO$_4$ from Fluka and 0.1 M phosphate buffer (pH 6.5).

2.3. Enzyme electrode preparation

The poly 1–PPO electrodes were prepared as previously reported [8]. An aqueous dispersion of 1 (6 mM) and PPO solution (20 g l^{-1}) were mixed in water to produce several 3 mM aqueous dispersions of 1 containing 1.7, 3.3, 6.7 or 10 g l^{-1} enzyme. 30 μl portions of these mixtures were deposited at the surface of a glassy carbon electrode and dried under vacuum. The polymerization of the adsorbed monomer 1–enzyme film was carried out by controlled potential electrolysis for 30 min at +0.75 V vs. SCE in deaerated aqueous 0.1 M LiClO$_4$ solution. The irreversible inactivation of the immobilized enzyme was performed by immersion of poly 1–PPO electrode in a water-bath thermostated at 65°C for 15 min. Before electrochemical experiments, the electrode was potentiostated at −0.2 V or 0.7 V for 30 min to allow the background current to decay to a steady-state value.

3. Results and discussion

PPO catalyzes the oxidation of several monohydroxy and o-dihydroxybenzene derivatives to o-quinones involving molecular oxygen [12]. Therefore, the analytical capabilities of an amperometric PPO-based biosensor can be investigated by applying a potential of −0.2 V vs. SCE to detect the enzymatically-generated o-quinones.

In contrast, catechol can be detected amperometrically via its electrooxidation at 0.7 V and the immobilized PPO can be inactivated by thermal denaturation [13]. Thus depending on the applied potential (−0.2 or 0.7 V) and the reactive state of the enzyme (active or inactive), the immobilized PPO–catechol system can provide information about the biomaterial permeability as well as the enzymatic reaction and transduction efficiencies.

Fig. 1 illustrates the three configurations of this system used providing the following parameters: (A) the current density for the diffusion of the enzymatically-generated o-quinone; (B) the current density for the catechol diffusion through the active biomaterial; and (C) the current density for the catechol diffusion through the inactivated biomaterial. In order to keep this model simple, we assume that the diffusivity of catechol in the biomaterial is identical to that of o-quinone and that the supply of cosubstrate (O$_2$) for PPO is considered to be plentiful [14].

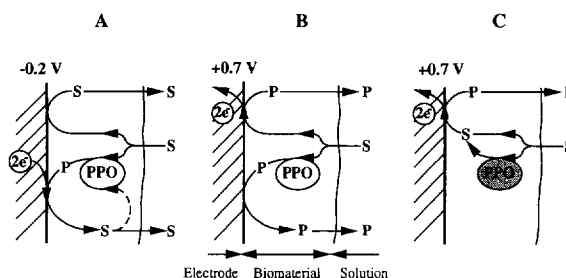Fig. 1. Schematic description of the three functioning configurations of the PPO–catechol electrochemical system: (A) bioelectrode potentiostated at −0.2 V; (B) and (C) bioelectrodes potentiostated at 0.7 V, PPO being inactivated in configuration (C). S and P denote respectively the catechol substrate and the 1,2-benzoquinone enzymatically or electrochemically produced.

The ability of this system for evaluating the characteristics of polymer matrices has been investigated in the case of functionalized polypyrrole. As previously reported [8,10], the polypyrrole enzyme electrodes were fabricated by adsorption on the electrode surface of a monomer 1-enzyme mixture followed by the electropolymerization of the adsorbed amphiphilic pyrroles. Following this procedure of biosensor construction, four poly 1-PPO electrodes were prepared with different amounts of enzyme (from 0.05–0.3 mg), the amount of monomer 1 remaining constant. The voltammograms of the resulting modified electrodes exhibit, in the anodic region, the reversible oxidation of the polypyrrole matrix ($E_{\frac{1}{2}}$ = 0.48 V, with an anodic and cathodic peak potential separation (ΔE_p) equal to 0.04 V, $v = 0.1$ V s^{-1}) typical of N-substituted polypyrroles [15]. The apparent surface coverage Γ_1 can be determined from the charge recorded under the polypyrrole oxidation wave, assuming one electron per three pyrrole units [15]. It appears that the four poly 1–PPO electrodes present similar apparent surface coverages ($\Gamma_1 = (3.8 \pm 0.2) \times 10^{-8}$ mol cm^{-2}), indicating a similar film thickness for the four enzyme electrodes. The steady-state current responses of these bioelectrodes to catechol were evaluated in "air-saturated" 0.1 M phosphate buffer (pH 7) stirred at 500 rev min^{-1} by holding the bioelectrodes at -0.2 V (Fig. 1A). All bioelectrodes present the same behavior. The response currents increase linearly with increasing substrate concentration, these linear parts being followed by a curvature for catechol concentrations higher than 400 μM (see for example Fig. 2). The comparison of the S_A bioelectrode sensitivities (S_A defined as the slope of the linear part of the calibration curve) indicates that the S_A sensitivity increases with increasing enzyme loading (Table 1).

The efficiency of the enzymatic reaction was investigated by potentiostating these bioelectrodes at 0.7 V in order to detect the catechol non-enzymatically-oxidized during its diffusion through the different biomaterials (Fig. 1B). All the different resulting calibration curves for catechol exhibit two linear parts indicating a low sensitivity for low catechol concentrations (up to 400–800 μM),
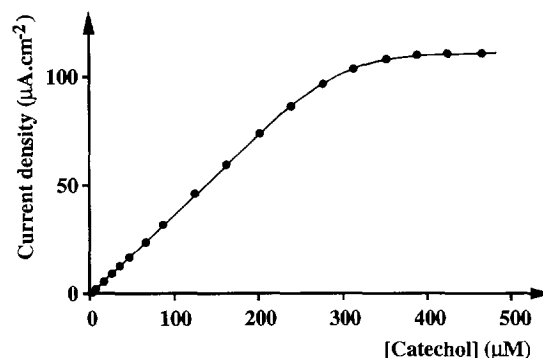

Fig. 2. Calibration curve for catechol obtained at a poly 1 PPO electrode (prepared with 0.3 mg PPO). Applied potential -0.2 V vs. SCE, air-saturated 0.1 M phosphate buffer (pH 6.5) kept under vigourous stirring at 30°C.

followed by a marked increase in sensitivity for higher substrate concentrations (Fig. 3). The first part of the calibration curves corresponds to the concentration range where the enzymatic reaction rate, and hence the enzymatic catechol consumption, increase linearly with substrate concentration. The strong increase in the electrode

Table 1
Comparison of biosensor sensitivities[a], percentages of catechol consumption and detected o-quinone versus the enzyme loading

Parameter	Amount of PPO deposited for biosensor construction (mg)			
	0.05	0.1	0.2	0.3
S_A[b] (mA M^{-1} cm^{-2})	20	61	139	345
S_B[c] (mA M^{-1} cm^{-2})	221	82	39	29
S_C[d] (mA M^{-1} cm^{-2})	441	361	320	344
$(S_C - S_B)/S_C^e$ (%)	46	77	88	92
$S_A/(S_C - S_B)^f$ (%)	11	22	50	110

[a] Each sensitivity value is reported as the mean of four independent measurements recorded with two bioelectrodes.
[b] S_A = biosensor sensitivity towards catechol at -0.2 V (Fig. 1A).
[c] S_B = biosensor sensitivity towards catechol at 0.7 V before enzyme saturation (Fig. 1B).
[d] S_C = biosensor sensitivity towards catechol at 0.7 after thermal denaturation of immobilized PPO (Fig. 1C).
[e] $(S_C - S_B)/S_C$ ratio represents the percentage of catechol consumed by the enzymatic reaction.
[f] $S_A/(S_C - S_B)$ ratio represents the percentage of enzymatically-generated o-quinone detected at the electrode surface.
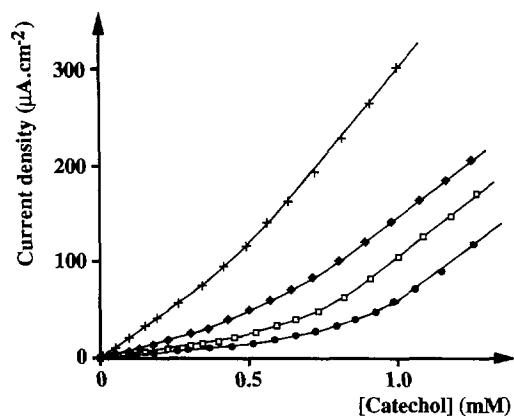
Fig. 3. Calibration curves for catechol obtained at poly 1–
PPO electrodes prepared with (+) 0.05, (♦) 0.1, (□) 0.2 and
(●) 0.3 mg of deposited PPO. Applied potential 0.7 V vs. SCE.
Other experimental conditions as in Fig. 2.

sensitivity observed in the second part of the calibration curves indicates that the saturation rate of the enzymatic reaction is reached. Thus, the electrode sensitivity should become independent of the enzymatic consumption of catechol, this latter being constant and independent of the catechol concentration. Effectively the catechol sensitivity of the bioelectrodes fabricated with 0.1, 0.2 and 0.3 mg PPO remains constant within experimental error $(203 \pm 5$ mA M^{-1} cm$^{-2})$ under catechol saturation conditions of the immobilized enzymes, suggesting a similar biofilm permeability. In contrast, the bioelectrode fabricated with 0.05 mg PPO exhibits a higher catechol sensitivity (360 mA M^{-1} cm^{-2}). This phenomenon can be related to the low enzyme loading, which induces an increase in the biomaterial permeability. It should be noted that the values of catechol concentration corresponding to the enzyme saturation increase with increasing enzyme loading. As expected, it is clear that the sensitivity of the amperometric electrode response to catechol before the enzyme saturation (S_B) decreases with increasing enzyme loading (Table 1). This result corroborates the relationship previously observed at -0.2 V between the S_A bioelectrode sensitivity and the enzyme loading.

In contrast, the thermal denaturation of the immobilized enzymes allows one to quantify at

0.7 V the catechol diffusion through the different biomaterials. Thus, the effect of the enzyme loading on the biomaterial permeability was investigated by comparison of catechol sensitivity (S_C) (Table 1). It appears that the increase in the amount of deposited enzyme induces a decrease in the biomaterial permeability. In particular, the bioelectrode fabricated with 0.05 mg PPO exhibits the highest S_C (411 mA M^{-1} cm^{-2}) while this sensitivity decreases down to 320 and 344 mA M^{-1} cm^{-2} for the bioelectrodes elaborated from 0.2 and 0.3 mg PPO respectively. This result is in good agreement with the variation of the catechol sensitivity of bioelectrodes previously observed at 0.7 V under substrate saturation conditions of the immobilized active enzymes.

In addition to this information, the PPO–catechol system allows one to calculate various parameters in order to evaluate the biomaterial performance. For instance, the comparison of sensitivities for the same bioelectrode measured at 0.7 V towards low concentrations of catechol after its diffusion through an enzymatically-active (S_B) or inactive (S_C) biomaterial allows one to estimate the percentage of catechol enzymatically oxidized during its permeation (Fig. 1B and 1C). This parameter could represent the efficiency of the enzymatic reaction and therefore illustrate the influence of the host matrix (permeability, denaturing microenvironment, etc.) on the enzymatic step as well as the influence of the amount of immobilized enzyme. Thus, the values of the percentate of enzymatically-oxidized catechol (defined as the ratio of sensitivities $(S_C - S_B)/S_C$) versus the enzyme loading are summarized in Table 1. As expected, this percentage increases unambiguously with increasing enzyme loading. The most efficient enzymatic conversion is obtained with the bioelectrode corresponding to 0.3 mg PPO since almost all the permeant (92%) is consumed.

The PPO–catechol system also allows us to examine the efficiency of the bioelectrochemical detection via a comparison of the amounts of o-quinone electrochemically detected and enzymatically generated. This is illustrated by the value of the $S_A/(S_C - S_B)$ ratio, S_A and $(S_C - S_B)$ being biosensor sensitivities corresponding to the

electroreduction of enzymatically-generated *o*-quinone (Fig. 1A) and the enzymatic disappearance of catechol respectively. It is clear that the efficiency of the bioelectrochemical detection increases with enzyme loading, reaching 110% for the bioelectrode fabricated with 0.3 mg PPO (Table 1). Furthermore, this value (110%) seems to indicate a signal amplification due to the well-known substrate recycling [16] (Fig. 1A). In contrast, the weak efficiency (11%) obtained with the bioelectrode fabricated with the lowest amount of PPO (0.05 mg) could indicate that much of the *o*-quinone diffused back to the solution and did not reach the electrode surface. This phenomenon could be correlated with the permeability increase previously observed for this biomaterial (Table 1), as well as with a weak efficiency of substrate recycling (Fig. 1A) due to the low enzyme loading.

In conclusion, the electroenzymatic system based on PPO and catechol constitutes a powerful means of obtaining an insight into the detailed processes that occur in amperometric enzyme-based sensors. It is expected that this system will be a useful model for comparing various types of host matrix used for bioelectrode fabrication.

Acknowledgements

The authors thank Dr. A. Deronzier for his interest in this work.

References

[1] A.P.F. Turner. I. Karube and G.S. Wilson (Eds.), Biosensors: Fundamentals and Applications, Oxford University Press, New York, 1987.

[2] L.D. Mell and J.T. Maloy, Anal. Chem., 47 (1975) 299.

[3] R.A. Kamin and G.S. Wilson, Anal. Chem., 52 (1980) 1198.

[4] P.N. Bartlett and R.G. Whitacker, J. Electroanal. Chem., 224 (1987) 27.

[5] T. Tatsuma and T. Watanabe, Anal. Chem., 64 (1992) 625.

[6] T. Ruzgas, L. Gorton, J. Emnéus and G. Marko-Varga, J. Electroanal. Chem., 391 (1995) 41.

[7] P. Gros and A. Bergel, J. Electroanal. Chem., 386 (1995) 65.

[8] S. Cosnier and C. Innocent, J. Electroanal. Chem., 328 (1992) 361.

[9] L. Coche-Guérente, S. Cosnier, C. Innocent, P. Mailley, J.-C. Moutet, R.M. Morelis, B. Leca and P.R. Coulet, Electroanalysis, 5 (1993) 647.

[10] L. Coche-Guérente, S. Cosnier, C. Innocent and P. Mailley, Anal. Chim. Acta, 311 (1995) 23.

[11] (a) L. Coche-Guérente, A. Deronzier, B. Galland, P. Labbé. J.-C. Moutet and G. Reverdy, J. Chem. Soc., Chem. Commun., (1991) 386.
(b) L. Coche-Guérente, A. Deronzier, B. Galland, J.-C. Moutet, P. Labbé, G. Reverdy, Y. Chevalier and J. Amhrar, Langmuir, 10 (1994) 602.

[12] J.L. Smith and R.C. Krueger, J. Biol. Chem., 237 (1962) 1121.

[13] S. Cosnier and C. Innocent, Bioelectrochem. Bioenerg., 31 (1993) 147.

[14] H.W. Duckworth and J.E. Coleman, J. Biol. Chem., 245 (1970) 1613.

[15] S. Cosnier, A. Deronzier and J.-F. Roland, J. Electroanal. Chem., 285 (1990) 133.

[16] P. Önnerfjord, J. Emméus, G. Marko-Varga, L. Gorton, F. Ortega and E. Dominguez, Biosens. Bioelectron., 10 (1995) 607 (and references cited therein).

Book reviews

Kirk-Othmer Encyclopedia of Chemical Technology, 4th edn., edited by J.I. Kroschwitz and M. Howe-Grant, Volume 14, Imaging Technology to Lanthanides, Wiley, New York, 1995, xxviii + 1116 pp., £195.00. ISBN 0-471-52683-5 (v.14).

Entries in the volumes of this edition of the encyclopedia are arranged in alphabetical order and with volume 14 the mid-point of the alphabet has been reached. With about 1000 + pages and about 30–40 entries per volume the coverage of topics is extensive. Some of the entries at first sight may not seem to be directly related to chemistry but closer inspection reveals that the topics are indeed of prime importance. For example, in this latest volume over 150 pages are devoted to information retrieval and information storage materials. In the former we are presented with an excellent survey of numerous modern chemical databases—some that I currently use and some which I did not know existed. Similarly in the latter, the various chemical processes involved in the production of both magnetic and optical devices for data storage are covered. A smaller entry related to these topics, Laboratory Information Management Systems, is included in this volume.

Topics related to medicinal and pharmaceutical chemistry include entries on Immunoassay, Immunotherapeutic Agents, Industrial Antimicrobial Agents and Insulin and Other Antidiabetic Agents. There is also information on Industrial Hygiene which covers hazard evaluation and control. Insect Control Technology is also well represented with 80 pages and 77 references.

Elements specifically dealt with in this volume include Indium, Iodine, Iron and the Lanthanides. Classes or groups of compounds include: Imines, Inclusion Compounds, Initiators, Inks, Inorganic High Polymers, Ionomers, Isocyanates, Ketenes, and Ketones. There are also separate entries for Indole, Isoprene and Itaconic Acid.

Techniques included are Infrared Technology and Raman Spectroscopy, Ion Exchange, Ion Implantation and Kinetic Measurements. Finally, there are entries on Insulation and Laminated Materials.

The usual high standard of supplied information is maintained with this volume of the encyclopedia. The editors are to be congratulated for their efforts in making these multi-authored volumes suitable for a wide range of readers.

P.J. Cox

Anticancer Drugs from Animals, Plants and Microorganisms, by G.R. Pettit, F.H. Pierson and C.L. Herald, Wiley, Chichester, 1994, xii + 670 pp., £78.00. ISBN 0-471-03657-9.

This book represents an update of the ongoing review by the authors of the expanding field of biosynthetic products with potential in cancer chemotherapy. The initial chapter briefly introduces the subject of cancer causing and related lethal viral diseases, with particular emphasis on the significance of HIV infection. This is followed by a chapter which seeks to illustrate the public

Book reviews

Kirk-Othmer Encyclopedia of Chemical Technology, 4th edn., edited by J.I. Kroschwitz and M. Howe-Grant, Volume 14, Imaging Technology to Lanthanides, Wiley, New York, 1995, xxviii + 1116 pp., £195.00. ISBN 0-471-52683-5 (v.14).

Entries in the volumes of this edition of the encyclopedia are arranged in alphabetical order and with volume 14 the mid-point of the alphabet has been reached. With about 1000 + pages and about 30–40 entries per volume the coverage of topics is extensive. Some of the entries at first sight may not seem to be directly related to chemistry but closer inspection reveals that the topics are indeed of prime importance. For example, in this latest volume over 150 pages are devoted to information retrieval and information storage materials. In the former we are presented with an excellent survey of numerous modern chemical databases—some that I currently use and some which I did not know existed. Similarly in the latter, the various chemical processes involved in the production of both magnetic and optical devices for data storage are covered. A smaller entry related to these topics, Laboratory Information Management Systems, is included in this volume.

Topics related to medicinal and pharmaceutical chemistry include entries on Immunoassay, Immunotherapeutic Agents, Industrial Antimicrobial Agents and Insulin and Other Antidiabetic Agents. There is also information on Industrial Hygiene which covers hazard evaluation and control. Insect Control Technology is also well represented with 80 pages and 77 references.

Elements specifically dealt with in this volume include Indium, Iodine, Iron and the Lanthanides. Classes or groups of compounds include: Imines, Inclusion Compounds, Initiators, Inks, Inorganic High Polymers, Ionomers, Isocyanates, Ketenes, and Ketones. There are also separate entries for Indole, Isoprene and Itaconic Acid.

Techniques included are Infrared Technology and Raman Spectroscopy, Ion Exchange, Ion Implantation and Kinetic Measurements. Finally, there are entries on Insulation and Laminated Materials.

The usual high standard of supplied information is maintained with this volume of the encyclopedia. The editors are to be congratulated for their efforts in making these multi-authored volumes suitable for a wide range of readers.

P.J. Cox

Anticancer Drugs from Animals, Plants and Microorganisms, by G.R. Pettit, F.H. Pierson and C.L. Herald, Wiley, Chichester, 1994, xii + 670 pp., £78.00. ISBN 0-471-03657-9.

This book represents an update of the ongoing review by the authors of the expanding field of biosynthetic products with potential in cancer chemotherapy. The initial chapter briefly introduces the subject of cancer causing and related lethal viral diseases, with particular emphasis on the significance of HIV infection. This is followed by a chapter which seeks to illustrate the public

health hazard of environmental exposure to a variety of carcinogens, examples of which are presented in five tables; synthetic carcinogens, carcinogenic antitumor drugs, environmental and other naturally occurring carcinogens together with the effects of irradiation and tumor promoters. The main review, in tabular form however, is contained in the following chapters which spans some 450 pages. These are subdivided into three sections and the first of these "Antineoplastic and/or cell growth inhibitory agents", is arranged in nine chapters on the basis of biological origin. The second and third sections survey "Marine animal" and "Marine plant biosynthetic products" respectively, in eight chapters which are organised on the basis of chemical class.

Typically details are given of name, structure, biological origin and biological activity together with an indication of the accumulated spectral data. This information has been meticulously cross referenced to over twelve hundred published papers. The bringing together of this data provides a fascinating resource both to the molecular biologist seeking compounds to probe novel mechanisms of molecular cellular interactions or to the biosynthetic, medicinal or synthetic organic chemist in a quest for novel methodological targets. The book therefore deserves a place on the library shelf of those researchers working in the development of new anticancer drugs and will provide a ready source of new inspiration as well as hours of pleasurable "browsing". It is perhaps to be regretted that this type of publication may perish in the future to be replaced by a less stylish electronic means of information dissemination.

D.G. Durham

Good Laboratory Practice Regulations, 2nd edn., edited by A. Weinberg, Dekker, New York, 1995, x + 294 pp., US$125.00. ISBN 0-8247-9377-3.

This is Volume 69 in the Drugs & Pharmaceutical Sciences Series of Textbooks and Monographs, and is a second edition of Volume 38 which was edited by Allen F. Hirsch. The Good

Laboratory Practices prescribe standards for the conduct of studies designed to establish the safety of products regulated by the US Food & Drug Administration. Study reports are submitted to the FDA in food and colour petitions, investigational new drug applications, new drug applications, biological product licence applications, and other requests for permission to market a product. If safety and efficacy are established adequately, marketing of the product is permitted. GLPs are part of the International Market Place. The US and other members of the 24 nation Organization for Economic Cooperation and Development (OECD) have been involved in extensive international consultation in efforts to bring industrial and environmental chemical programmes into harmony. This 2nd edition of Good Laboratory Practice Regulations addresses these topics as well as discussing all aspects of the FDA's GLP regulations and techniques for implementation. These topics are presented within the contexts of an historical perspective and current laboratory automation.

Chapter 1 gives an historical perspective of the FDA focusing on problems and solutions; proposed regulations from the FDA and EPA; and GLP revisions. Chapter 2 provides a general discussion of all aspects of the FDA's GLP regulations. Chapter 3 discusses the Environmental Protection Agency (EPA), foreign GLP regulations and the EPA Federal Insecticide, Fungicide and Rodenticide Act (FIFRA) GLPs. Chapter 4 explores the implementation of GLPs in a non-GLP analytical laboratory. Chapter 5 introduces economic behaviour as a means of evaluating and optimizing the use of automation and instrumentation technology in regulated laboratories. Chapter 6 addresses computer system validation and how it establishes the credibility of laboratory data and automated procedures. Chapter 7 presents a regulator's perspective of the laboratory inspection process. Chapter 8 presents summary commentary and ventures a forecast as to the future value and effectiveness of the GLPs as robotic laboratories become more common. An up-to-date bibliography provides useful references for GLPs.

health hazard of environmental exposure to a variety of carcinogens, examples of which are presented in five tables; synthetic carcinogens, carcinogenic antitumor drugs, environmental and other naturally occurring carcinogens together with the effects of irradiation and tumor promoters. The main review, in tabular form however, is contained in the following chapters which spans some 450 pages. These are subdivided into three sections and the first of these "Antineoplastic and/or cell growth inhibitory agents", is arranged in nine chapters on the basis of biological origin. The second and third sections survey "Marine animal" and "Marine plant biosynthetic products" respectively, in eight chapters which are organised on the basis of chemical class.

Typically details are given of name, structure, biological origin and biological activity together with an indication of the accumulated spectral data. This information has been meticulously cross referenced to over twelve hundred published papers. The bringing together of this data provides a fascinating resource both to the molecular biologist seeking compounds to probe novel mechanisms of molecular cellular interactions or to the biosynthetic, medicinal or synthetic organic chemist in a quest for novel methodological targets. The book therefore deserves a place on the library shelf of those researchers working in the development of new anticancer drugs and will provide a ready source of new inspiration as well as hours of pleasurable "browsing". It is perhaps to be regretted that this type of publication may perish in the future to be replaced by a less stylish electronic means of information dissemination.

D.G. Durham

Good Laboratory Practice Regulations, 2nd edn., edited by A. Weinberg, Dekker, New York, 1995, x + 294 pp., US$125.00. ISBN 0-8247-9377-3.

This is Volume 69 in the Drugs & Pharmaceutical Sciences Series of Textbooks and Monographs, and is a second edition of Volume 38 which was edited by Allen F. Hirsch. The Good

Laboratory Practices prescribe standards for the conduct of studies designed to establish the safety of products regulated by the US Food & Drug Administration. Study reports are submitted to the FDA in food and colour petitions, investigational new drug applications, new drug applications, biological product licence applications, and other requests for permission to market a product. If safety and efficacy are established adequately, marketing of the product is permitted. GLPs are part of the International Market Place. The US and other members of the 24 nation Organization for Economic Cooperation and Development (OECD) have been involved in extensive international consultation in efforts to bring industrial and environmental chemical programmes into harmony. This 2nd edition of Good Laboratory Practice Regulations addresses these topics as well as discussing all aspects of the FDA's GLP regulations and techniques for implementation. These topics are presented within the contexts of an historical perspective and current laboratory automation.

Chapter 1 gives an historical perspective of the FDA focusing on problems and solutions; proposed regulations from the FDA and EPA; and GLP revisions. Chapter 2 provides a general discussion of all aspects of the FDA's GLP regulations. Chapter 3 discusses the Environmental Protection Agency (EPA), foreign GLP regulations and the EPA Federal Insecticide, Fungicide and Rodenticide Act (FIFRA) GLPs. Chapter 4 explores the implementation of GLPs in a non-GLP analytical laboratory. Chapter 5 introduces economic behaviour as a means of evaluating and optimizing the use of automation and instrumentation technology in regulated laboratories. Chapter 6 addresses computer system validation and how it establishes the credibility of laboratory data and automated procedures. Chapter 7 presents a regulator's perspective of the laboratory inspection process. Chapter 8 presents summary commentary and ventures a forecast as to the future value and effectiveness of the GLPs as robotic laboratories become more common. An up-to-date bibliography provides useful references for GLPs.

This book is not an easy read. One maddening aspect is the overuse of TLAs and FLAs (three and four letter abbreviations), although without them the book would be much longer. Chapter 2, as well as being the longest by far, is also the most difficult to assimilate. This is due to the nature of the subject material itself and to the thoroughness of the author, and certainly not because of any deficiency in style. Indeed, in the subsection on Testing Facilities Operation, much useful advice is given for the preparation and revision of Standard Operating Procedures (SOPs). For example, "...it is always a good idea to solicit comments from those who use the SOP manual (the workers at the bench)...". The chapter of most interest to a reader new to the subject of GLP and to those persons tasked with implementing GLPs in their laboratories will be Chapter 4. It outlines reasons for adopting GLPs, how to develop a Quality System and what it should consist of, the need for the Quality Assurance Unit to maintain a sense of humour(!), helpful hints for writing SOPs, and the need for random audits. The chapter on computer systems validation is also highly relevant and direct, pulling no punches on the subjects of poor quality control in the computer software industry, and jargon-filled non-explanations of computer professionals.

There are very few typographical errors, although on two occasions "pH" is referred to as "Ph". Although written primarily from the American viewpoint, a general interpretation will serve practitioners in almost any country. Notwithstanding the comments above, this book deserves its place on the shelf of the Quality Assurance Manager in any laboratory.

D.F. Rendle

Chromatography for Inorganic Chemistry, by M. Lederer, Wiley, Chichester, 1994, vi + 221 pp., £17.95 (softback), £39.95 (hardback). ISBN 0-471-94286-3 (softback), 0-471-94285-5 (hardback).

This book is associated with a course of lectures given by the author to advanced students at a number of Universities in Switzerland and Israel, and does not therefore aim to cover the entire literature. The author also assumes a working knowledge of the principles of chromatography, and does not survey the analytical applications of chromatography since these are already covered in other more detailed texts. Nevertheless the book provides a wide coverage of the applications of chromatography in inorganic chemistry.

The book starts with an historical introduction; following chapters deal with solvent extraction, paper and thin-layer chromatography, electrophoresis, gel filtration, ion exchange, HPLC, ion and gas chromatography, and the separation of isotopes and optical isomers. Each chapter contains many examples of the applications of each technique, liberally illustrated with clear diagrams and tables of factural information. The final chapter deals in more detail with the chromatography and electrophoresis of specific elements, including condensed phosphates, sulphur compounds and selected transition metals, lanthanides and actinides.

As might be expected from a book connected with a lecture course, the text is written in a very personal style. The examples tend to be chosen from the author's own work which of course allows him to present them with authority. Citations are given which allows the student to follow up the work from the literature. Within these confines the book is very readable and pitched at the right level for its intended readership.

D.R. Russell

This book is not an easy read. One maddening aspect is the overuse of TLAs and FLAs (three and four letter abbreviations), although without them the book would be much longer. Chapter 2, as well as being the longest by far, is also the most difficult to assimilate. This is due to the nature of the subject material itself and to the thoroughness of the author, and certainly not because of any deficiency in style. Indeed, in the subsection on Testing Facilities Operation, much useful advice is given for the preparation and revision of Standard Operating Procedures (SOPs). For example, "...it is always a good idea to solicit comments from those who use the SOP manual (the workers at the bench)...". The chapter of most interest to a reader new to the subject of GLP and to those persons tasked with implementing GLPs in their laboratories will be Chapter 4. It outlines reasons for adopting GLPs, how to develop a Quality System and what it should consist of, the need for the Quality Assurance Unit to maintain a sense of humour(!), helpful hints for writing SOPs, and the need for random audits. The chapter on computer systems validation is also highly relevant and direct, pulling no punches on the subjects of poor quality control in the computer software industry, and jargon-filled non-explanations of computer professionals.

There are very few typographical errors, although on two occasions "pH" is referred to as "Ph". Although written primarily from the American viewpoint, a general interpretation will serve practitioners in almost any country. Notwithstanding the comments above, this book deserves its place on the shelf of the Quality Assurance Manager in any laboratory.

D.F. Rendle

Chromatography for Inorganic Chemistry, by M. Lederer, Wiley, Chichester, 1994, vi + 221 pp., £17.95 (softback), £39.95 (hardback). ISBN 0-471-94286-3 (softback), 0-471-94285-5 (hardback).

This book is associated with a course of lectures given by the author to advanced students at a number of Universities in Switzerland and Israel, and does not therefore aim to cover the entire literature. The author also assumes a working knowledge of the principles of chromatography, and does not survey the analytical applications of chromatography since these are already covered in other more detailed texts. Nevertheless the book provides a wide coverage of the applications of chromatography in inorganic chemistry.

The book starts with an historical introduction; following chapters deal with solvent extraction, paper and thin-layer chromatography, electrophoresis, gel filtration, ion exchange, HPLC, ion and gas chromatography, and the separation of isotopes and optical isomers. Each chapter contains many examples of the applications of each technique, liberally illustrated with clear diagrams and tables of factural information. The final chapter deals in more detail with the chromatography and electrophoresis of specific elements, including condensed phosphates, sulphur compounds and selected transition metals, lanthanides and actinides.

As might be expected from a book connected with a lecture course, the text is written in a very personal style. The examples tend to be chosen from the author's own work which of course allows him to present them with authority. Citations are given which allows the student to follow up the work from the literature. Within these confines the book is very readable and pitched at the right level for its intended readership.

D.R. Russell

Spectrophotometric determination of bio-active compounds with chloramine-T and gallocyanine

C.S.P. Sastry[a,*], K. Rama Srinivas[a], K.M.M. Krishna Prasad[b]

[a]Foods and Drugs Laboratories, Department of Organic Chemistry, Foods, Drugs and Water, Andhra University, Visakhapatnam-530 003, India
[b]Department of Physical and Nuclear Chemistry, Andhra University, Visakhapatnam-530 003, India

Abstract

A simple, sensitive and selective method for the spectrophotometric determination of drugs, viz., sulphamethoxazole, tetracycline HCl, amidopyrine, nifurtimox and isoniazid and biologically important amino acids, cysteine, aspartic acid and arginine based on their reactivity with chloramine-T (CAT) is proposed. The method involves the addition of excess CAT of a known concentration in the presence of 0.25 M HCl and the determination of the unreacted CAT by measurement of the decrease in the absorbance of the dye, gallocyanine (λ_{max}: 540 nm), the most suitable of several dyes that were tested. This method was applied to the determination of drug contents in pharmaceutical formulations and to the measurement of the aspartic acid content of some protein hydrolysates. The method is useful for the determination of the target compounds in microgram quantities from 0.4–5.6 μg mL^{-1} with the exceptions of arginine (1.0–8.0 μg mL^{-1}) and nifurtimox (0.8–5.6 μg mL^{-1}). Standard deviations were typically $\leqslant 0.5$ mg per dose (RSD 0.5–1.2%). No interferences were observed from common excipients in formulations, and detailed interference studies of other amino acids in the determination of cysteine, aspartic acid and arginine are reported. The validity of the method was tested against spectrophotometric and titrimetric reference methods. Recoveries were 99.8–102.1%.

Keywords: Chloromine-T; Gallocyanine; Spectrophotometry

1. Introduction

In recent years there has been a growing interest in the role of chloramine-T (CAT) as an analytical reagent in the determination of organic compounds [1]. CAT was developed for its disinfectant and antiseptic properties. As a result of the high yields of the products obtained in its reactions, it has been adopted for use in the determination of many orgainc compounds. CAT acts as a selective oxidizing agent in both acid and alkaline media [2,3]. When the reaction is stoichiometric and fast, the solution of CAT is useful in titrimetric determinations in which the end point is detected with either a visual indicator [4–6] or potentiometry [4]. In many instances, direct titration with CAT with a visual or poten-

---

* Corresponding author.

tiometric end point was not practicable, because the oxidation, though rapid, was not instantaneous and a back titration procedure was developed [7]. An excess of standard CAT is added to the analyte solution and is allowed to react for a given time. The excess CAT present in the acidic medium is determined by titrimetry [7,8]. However, titrimetric procedures are not suitable for the determination of compounds at microgram levels [4–8]. The aim of the present work is to provide a simple and sensitive spectrophotometric method for the determination of some typical bio-active compounds based on their reactivity with CAT.

Azine and oxazine dyes are well known for their high absorptivity, but they have not been utilized for estimating excess CAT in the indirect determinations of bio-active compounds. The present investigation proposes a selective and sensitive indirect spectrophotometric method for the determination of drugs, sulphamethoxazole (N'-(5-methylisoxazol-3-yl) sulphanilamide; SMX; CA: 723-46-6; antibacterial agent), tetracycline HCl (4-dimethylamino 1,4,4α,5,5α,6,11,12α-octahydro-3,6,10,12,12α-pentahydroxy-6-methyl-1,11,-dioxo (4S-(4α,4$\alpha\alpha$,5$\alpha\alpha$,6β, 12$\alpha\alpha$))-2-naphthacene carboxamide; TTC; CA: 60-54-8; antibacterial agent), amidopyrine (4-dimethylamine-2,3-dimethyl-1-phenyl-3-pyrazolin-5-one; AMP; CA: 58-15-1; antiinflammatory agent), nifurtimox (3-methyl-N-((5-nitro-2-furanyl) methylene)-1,1-dioxide-4-thiomorpholinamide; NIF; CA: 23256-30-6; antitrypanocide agent) and isoniazid (4-pyridinecarboxylic acid, hydrazide; INH; CA: 54-84-3; antitubercular agent) and the amino acids, cysteine (CYS, CA: 52-90-4), aspartic acid (ASP, CA: 617-45-8) and arginine (ARG, CA: 627-75-8) in pure form and also in pharmaceutical formulations for drugs and protein hydrolysates for aspartic acid. Any one of the bio-active compounds mentioned above is made to react with an excess of CAT and the excess unreacted CAT oxidizes the oxazine dye, gallocyanine (phenoxazine-5-ium,1-carboxy-(7-dimethylamino)-3,4-dihydroxy chloride; GC; C.I. No. 51030) to a colourless form, thereby causing a decrease in the absorbance of GC. A few visible spectrophotometric methods reported for the estimation of SMX [9–12], TTC

[13–17], AMP [18–21], INH [22–26], CYS [27–30], ASP [27,31,32], ARG [33–35] and NIF [36], suffer from one or other disadvantage such as low sensitivity, lack of selectivity and simplicity. The proposed method is superior over these reported methods for its simplicity, high sensitivity and rapidity of the determination.

2. Experimental

2.1. Apparatus

A Milton Roy spectronic 1201 UV-visible spectrophotometer (USA) with 1 cm matched quartz cells was used for all the absorbance measurements. An Elico model LI-120 digital pH meter (Hyderabad, India) was used for pH measurements.

2.2. Reagents

All chemicals were of analytical grade and all solutions were prepared in triply distilled water. An aqueous solution of gallocyanine (CA: 1562-85-2, E. Gurr & Co., High Wycombe, UK, 1 mg mL^{-1}) was prepared and was further diluted to 100 μg mL^{-1}. Aqueous solutions of chloramine-T (CA: 127-65-1, Loba, Bombay, India, 1 mg mL^{-1}) were prepared and standardized iodometrically [37]. This solution was further diluted to 200 μg mL^{-1}. A 5 M aqueous solution of hydrochloric acid (CA: 7647-01-01, E. Merck, Bombay, India) was also prepared.

2.3. Preparation of standard drug or amino acid solution

Aqueous solutions containing 1 mg mL^{-1} of pharmaceutical grade sample of each drug or analytical grade sample of amino acid were prepared separately by dissolving initially in either 10 mL of dimethyl formamide (NIF, from Bayer, Germany) or 0.1 M HCl (INH, from Loba, Bombay, India) or 0.1 M NaOH (SMX, from German Remedies, Bombay, India) or hot water (ASP, from Loba, Bombay, India) or water (AMP, from Ciba-Geigy, Bombay, India; TTC, from Hoechst,

Bombay, India; CYS, from Loba, Bombay, India; ARG, from Loba, Bombay, India), followed by dilution with distilled water. Stock solutions were further diluted stepwise with distilled water to give the working standard solutions.

2.4. Analysis of pure forms

To each of 25 mL graduated test tubes containing aliquots of the standard drug solution (SMX: 0.5–4.0 mL, 10 μg mL^{-1}; TTC, AMP, INH: 0.5–4.5 mL, 20 μg mL^{-1}; NIF: 0.5–3.5 mL, 40 μg mL^{-1}) or amino acid solution (CYS, ASP: 1.0–6.0 mL, 20 μg mL^{-1}; ARG: 0.5–4.0 mL, 50 μg mL^{-1}), 1.25 mL of 5 M HCl and 2.0 mL of CAT (200 μg mL^{-1}) were added and the solutions diluted to 15 mL. After 10 min (except NIF or ASP: 30 min; ARG: 55 min), 10 mL of GC was added and mixed thoroughly and the absorbances were measured after 5 min at 540 nm against distilled water. The blank solution was prepared in a similar manner omitting bio-active compound. The decrease in absorbance corresponding to consumed CAT, which reflects the drug or amino acid concentration, was obtained by subtracting the absorbance of the blank solution from that of the test solution. Calibration graphs were prepared by plotting the decrease in the absorbance of the dye (GC), against the amount of drug or amino acid. The amount of drug or amino acid in any sample was calculated from its calibration curve.

2.5. Analysis of formulations

Since NIF formulations were not available in the Indian market, we prepared these according to the literature method [38,39]. Tablet, injection or capsule powder equivalent to 100 mg of active ingredient was treated with 10 mL of DMF, 0.1 M HCl, 0.1 M NaOH or water as given under standard stock solution preparation and the isoluble portion, if any was filtered off. The filtrate was diluted to 100 mL with water to give nominally 1 g L^{-1} concentration. The stock solutions in each case were further diluted with distilled water to obtain working solutions and were analysed as described under the procedure for pure samples.

2.6. Analysis of aspartic acid in protein hydroysates

An accurately weighed model mixture of protein hydrolysate powder equivalent to 100 mg of ASP was treated with 10 mL of hot water as given under standard stock solution preparation. It was further diluted to 100 mL with water to give nominally 1 mg mL^{-1}. This solution was further diluted to the requisite concentration and was analysed as described under the procedure for pure samples.

3. Results and discussion

In the preliminary experiments several azine and oxazine dyes such as neutral violet (NV, CA: 3562-46-7), neutral red (NR, CA: 553-24-2), wool fast blue BL (WFB, CA: 6378-88-7), azocarmine-G (AG, CA: 25641-18-3), lissamine blue BF (LBBF, CA: 6448-97-1), gallocyanine (GC, CA: 1562-85-2), gallamine blue (GB, CA: 1563-02-6), solocrome prune AS (SPAS, CA: 6416-51-9) and cresyl fast violet acetate (CFVA, CA: 10510-54-0) were tested for reaction with CAT in acidic medium. These investigations revealed that gallocyanine, neutral violet, gallamine blue and solocrome prune AS exhibit a quantitative reaction as shown by a definitive decrease in absorbance for a specific concentration of CAT even within 1 min (Fig. 1). As the difference in absorbance was found to be higher in the case of gallocyanine than for the remaining three, further studies were carried out with gallocyanine.

The similarity in the nature of the spectra recorded with GC, GC–CAT and drug or amino acid–CAT–GC in 0.25 M HCl medium indicates that the products formed by the interaction of drug or amino acid–CAT and CAT–dye do not affect the accuracy of the determination.

The method involves two steps, namely reaction of the drug with an excess of CAT giving products involving oxidation and the estimation of excess CAT using a known excess of GC. The excess dye remaining, is then measured with a spectrophotometer at 540 nm. The effect of reagent concentration, acidity and waiting period
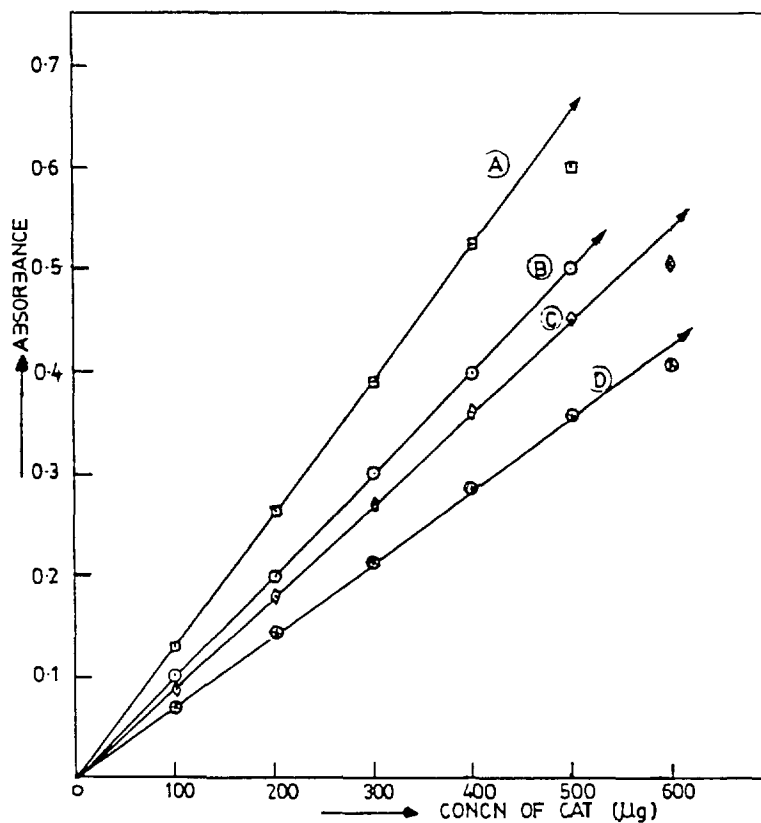
Fig. 1. Effect of CAT on dyes in HCl (0.25 M) medium—curve A: CAT–GC system, [GC] = 0.1188 × 10⁻³M; curve B: CAT–NV system; [NV] = 0.4822 × 10⁻⁷ M; curve C: CAT–GB system, [GB] = 0.1191 × 10⁻³ M; curve D: CAT–SPAS system, [SPAS] = 0.1140 × 10⁻³ M.

in each step with respect to maximum sensitivity, blank minimum, adherence to Beer's law, reproducibility and stability of final colour were studied by means of controlled experiments varying one parmeter at a time [40].

3.1. Effect of acidity

The studies on the variation of acid concentration indicated that a constant absorbance is obtained in 0.15 to 0.4 M HCl, 0.1 to 0.25 M H₂SO₄ or 0.25 to 0.45 M CH₃COOH at a CAT concentration of 400 μg. As the difference in absorbance between the sample and the blank was found to be highest for the HCl medium, subsequent studies were carried out in 0.25 M HCl.

3.2. Effect of CAT concentration

In order to ascertain the linear relationship between the concentration of added CAT and the corresponding decrease in the absorbance of the GC (1000 μg), experiments were carried out in 0.25 M HCl medium with varying amounts of CAT. As the decrease in absorbances was found to be linear up to 400 μg of CAT (Fig. 1), subsequent studies were carried out with 1000 μg of GC and 400 μg of CAT in 0.25 M HCl medium.

3.3. Waiting period

A time span of 5 to 20 min for the reaction between the compound and CAT in first step (except ASP or NIF (25 to 40 min) and ARG (50
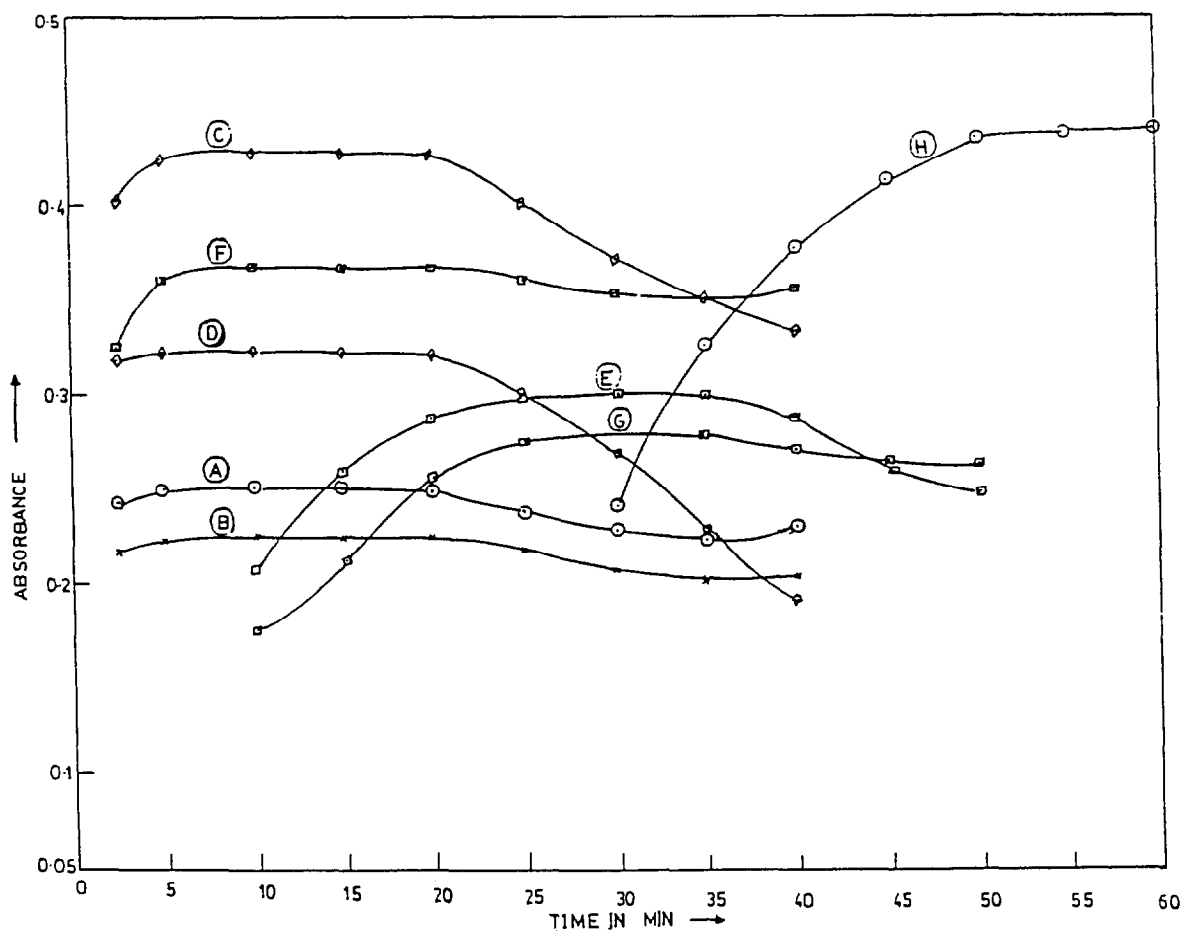
Fig. 2. Effect of oxidation time on drug/amino acid–CAT $(0.5680 \times 10^{-4}$ M)–GC $(0.1188 \times 10^{-3}$ M) systems. curve A: SMX–CAT–GC system, [SMX] = 3.1580×10^{-6} M; curve B: INH–CAT–GC system, [INH] = 1.1667×10^{-5} M; curve C: AMP–CAT–GC system, [AMP] = 1.3853×10^{-5} M; curve D: TTC–CAT–GC system, [TTC] = 6.6542×10^{-6} M; curve E: NIF–CAT–GC system, [NIF] = 1.3929×10^{-5} M; curve F: CYS–CAT–GC system, [CYS] = 1.6528×10^{-5} M; curve G: ASP–CAT–GC system, [ASP] = 1.2021×10^{-5} M; curve H: ARG–CAT–GC system, [ARG] = 3.7974×10^{-6} M.

to 60 min)) and 2 to 60 min between the CAT and GC in the second step, resulted in a constant and maximum difference in absorbance of the test and blank solutions (Fig. 2). Hence waiting periods of 10 min (30 min for ASP or NIF; 55 min for ARG) and 5 min were maintained in further studies of the first and second steps respectively. The above optimum conditions are incorporated in the procedure.

3.4. Analytical data

The optical characteristics such as Beer's law limits, molar absorptivity and percentage relative standard deviation for the method are given in

Table 1. Regression analysis using the method of least squares was made to evaluate the slope (b), intercept (a), correlation coefficient (r) and standard error of estimation (S_e) [41,42] for each system and the values are found to be in the following order—SMX: 0.300, 1.25×10^{-3}, 0.9999 and 1.65×10^{-3}; TTC: 0.100, 1.69×10^{-3}, 0.999 and 2.33×10^{-3}; AMP: 0.132, 0.05×10^{-3}, 0.9998 and 2.87×10^{-3}; NIF: 0.076, 1.43×10^{-3}, 0.9998 and 2.07×10^{-3}; INH: 0.139, -0.55×10^{-3}; 0.9999 and 2.45×10^{-3}; CYS: 0.182, -1.33×10^{-3}, 0.9999 and 1.62×10^{-3}; ASP: 0.174, 3.87×10^{-3}, 0.9997 and 2.82×10^{-3}; ARG: 0.050, 1.19×10^{-3}, 0.9999 and 1.45×10^{-3}.

Table 1
Optical characteristics, prescision and accuracy

Name of the bio-active compound	Test amount in μg	Parameters		
		Beer's law range (μg mL^{-1})	Molar Absorptivity (L mol^{-1} cm^{-1})	Relative standard deviation[a] (%)
Drugs:				
SMX	20	0.2–1.6	7.5984×10^4	0.78
TTC	80	0.4–4.8	4.9292×10^4	0.62
AMP	80	0.4–3.6	3.1762×10^4	0.45
NIF	100	0.8–5.6	2.1546×10^4	0.87
INH	40	0.4–3.6	1.8171×10^4	0.62
Amino acids:				
CYS	50	0.4–2.4	2.1780×10^4	0.62
ASP	40	0.4–2.4	2.2942×10^4	0.18
ARG	200	1.0–8.0	1.0533×10^4	0.63

[a] Average of six replicate samples.

3.5. Interferences

The commonly used excipients and additives in the formulations of drugs such as talc (up to 250-fold excess (w/w) compared to the drug), starch (200-fold), boric acid (150-fold), stearic acid (50-fold), cetyl alcohol (10-fold), glyceryl monostearate (30-fold), sodium lauryl sulphate (7-fold) and glycerin (10-fold) do not interfere with the determination of the mentioned drugs by the proposed method. The method was applied for the estimation of drugs in pharmaceutical formulations and the results were compared with the reference methods for SMX [12], TTC [17], AMP [19], NIF [36] and INH [43] by the application of F- and t-statistics and it is observed that the results of the proposed method compared with the reference method within the 95% confidence level.

The commonly existing amino acids in food proteins such as glycine (up to 13-fold molar excess compared to CYS or ASP); tyrosine (12-fold); alanine or leucine (11-fold); valine, isoleucine, glutamic acid, phenylalanine, tryptophan, proline or hydroxyproline (10-fold); serine, threonine, glutamine or histidine (9-fold); lysine or hydroxylysine (8-fold); and arginine (0.5-fold) do not interfere with the determination of ASP or CYS by the proposed method. However cystine or aspargine interferes in the proposed

method even if present in minor amounts. With the available information an attempt has been made to apply the present method in the determination of ASP in protein hydrolysates which do not contain CYS, cystine and aspargine. As β-lactoglobulin and chymotrypsinogen have compositions which satisfy the above conditions, model mixtures [44] of these two protein hydrolysates are prepared by mixing the amino acids as for the following compositions.

β-Lactoglobulin: alanine, 5.8 mg; arginine, 2.8 mg; aspartic acid, 11.3 mg; glutamic acid, 18.4 mg; glycine, 1.4 mg; histidine, 1.66 mg; leucine, 15.2 mg; iso-leucine, 7.3 mg; lysine, 11.2 mg; methionine, 3.12 mg; phenylalanine, 3.6 mg; proline, 5.0 mg; serine, 3.8 mg; threonine, 5.2 mg; tyrosine, 3.87 mg; and valine, 6.2 mg.

Chymotrypsinogen: alanine, 5.8 mg; arginine, 2.7 mg; aspartic acid, 10.9 mg; glutamic acid, 7.4 mg; glycine, 6.3 mg; histidine 1.16 mg; isoleucine, 4.9 mg; leucine, 8.9 mg; lysine, 7.7 mg; methionine, 1.11 mg; phenylalanine, 3.77 mg; proline, 3.8 mg; serine, 10.9 mg; threonine, 10.7 mg; tyrosine, 2.69 mg; and valine, 10.3 mg.

The results obtained in the proposed and reference [32] methods for ASP determination in protein hydrolysates are also presented in Table 2.

As an additional check of accuracy, recovery experiments were performed by adding a fixed amount of the compound (either drug or ASP) to

Table 2
Analysis of pharmaceutical formulations and protein hydrolysates by the proposed and reference methods

Name of the sample	Labelled amount (mg)	Amount found[a] (mg)		Particulars of reference method	% Recovery by proposed method[b]
		Proposed	Reference		
Pharmaceutical Formulations:					
SMX					
Tablets	800	800.0 ± 0.42	799.1 ± 0.32	Metol-N-bromo succinimide (Vis. spectrophotometric method) [12]	99.9 ± 0.45
TTC					
Tablets	250	249.3 ± 0.39	248.7 ± 0.28		100.8 ± 0.50
Capsules	250	249.6 ± 0.34	249.3 ± 0.32	Brucine-IO$_4^-$ (Vis. spectrophotometric method) [17]	100.1 ± 0.19
Injections	500	501.0 ± 0.46	499.9 ± 0.34		100.0 ± 0.42
AMP					
Tablets	125	124.5 ± 0.45	124.1 ± 0.32	3-Methyl-3-bebzothiazolinone hydrazone HCl-Fe[III] (Vis. spectrophotometric method) [19]	99.8 ± 0.40
NIF					
Tablets	50	49.9 ± 0.51	49.6 ± 0.48	3-Methyl-2-benzothiazolinone hydrazone HCl-Fe[III] (Vis. spectrophotometric method) [36]	100.3 ± 0.50
INH					
Tablets	50	49.9 ± 0.35	49.7 ± 0.34	Iodometry (Titrimetry) [43]	101.1 ± 0.81
Protein hydrolysates:					
ASP					
β-Lactoglobulin	11.3	11.45 ± 0.15	11.51 ± 0.13		102.1 ± 0.08
Chymotrypsinogen	10.9	11.11 ± 0.16	11.20 ± 0.14	Metol-NaOCl (Vis. spectrophotometric method) [32]	101.6 ± 0.10

[a] Average ± standard deviation of six determinations.
[b] Recovery of 10 mg (pharmaceutical formulations) or 11.3 mg (β-lactoglobulin) or 10.9 mg (chymotrypsinogen) added to the pre-analysed sample (average of three determinations).

a pre-analysed sample of either pharmaceutical formulation or model mixture of protein hydrolysate. The results are summarized in Table 2. The statistical parameters presented in Table 2 indicate that the proposed method does not differ significantly from the reference method of each compound.

3.6. Chemistry

CAT undergoes hydrolysis in aqueous acidic medium to give sodium hypochlorite followed by hypochlorous acid [45]. This reacts with the drug or amino acid to form the relevant oxidation products, probably a mixture, which appears to be reproducible under the specified experimental conditions. The remaining hypochlorous acid may

be responsible for the bleaching of the colour of the dye. As the bio-active compounds in the present study are structurally dissimilar (possess different basic moieties and functional groups), the reactivity of CAT on each bio-active compound depends upon the vulnerable positions for its participation in oxidation. Sometimes, the oxidation under specified experimental conditions yields different products in varied proportions. So, the consumption of CAT varies from bio-active compound to bio-active compound. The mole ratios in the reaction between CAT and individual bio-active compounds under the experimental conditions for this method have been found to be 7.5, 5.0, 3.0, 2.0, 2.0, 2.0, 2.5 and 1.0 for SMX, TTC, AMP, NIF, INH, CYS, ASP and ARG, respectively.

The bio-active compounds used in this study are representative of a larger class of bio-active compounds which react with CAT. The proposed method is advantageous when compared to many of the reported visible spectrophotometric methods in having higher absorptivities. This is a decisive advantage since the interference from the associated ingredients shall be generally far less at higher wavelengths than at lower wavelengths. The method is sensitive enough to permit the determination of as little as 0.4 μg mL^{-1} of the analytes except for NIF (0.8 μg mL^{-1}) and ARG (1.0 μg mL^{-1}). The present method is superior over many of the reported spectrophotometric procedures used for the analysis of these compounds for its high sensitivity with reasonable precision and accuracy, simplicity and applicability to the intact molecule directly.

References

[1] M.M. Campbell and G. Johnson, Chem. Rev. 78 (1978) 65.

[2] A.V.R. Murthy and V.S. Rao, Proc. Indian Acad. Sci., Sect. A, 35 (1952) 69.

[3] M.C. Agarwal and S.P. Mushran, Z. Naturforsch., Teil B, 27 (1972) 401.

[4] K.K. Verma and A. Gupta, Anal. Chem., 54 (1982) 249.

[5] K.K. Verma, Chem. Anal. (Warsaw), 25 (1980) 1035.

[6] N.V. Rao and C.K. Sastri, J. Indian Chem. Soc., 64 (1987) 131.

[7] D.S. Mahadevappa and H.M.K. Naidu, Talanta 20 (1973) 349.

[8] D.S. Mahadevappa and A.S. Ananda Murthy, Talanta, 17 (1970) 431.

[9] K.A. Sanyal and D. Laha, J. Assoc. Off. Anal. Chem., 66 (1983) 1447.

[10] J. Feng, S. Tong and X. Zhou, Yaowu Fenxi Zazhi, 13 (1993) 245.

[11] S. Raghuveer, I.R.K. Raju, D.K. Vasta and C.M.R. Srivastava, Indian Drugs, 30, (1993) 132.

[12] C.S.P. Sastry, B.G. Rao, B.S. Reddy and S.S.N. Murthy, Indian J. Chem. Soc., 58 (1981) 655.

[13] U. Saha, J. Assoc. Off. Anal. Chem., 72 (1989) 242.

[14] M.K. Emara, F.H. Askal and A.G. Saleh, Talanta, 38 (1991) 1219.

[15] M. Ayed, M. El-Sadek and S. Mastaffa, Anal. Lett., 19 (1986) 2169.

[16] D.D. Mishra, I. Islam and J.P. Sharma, Mikrochim. Acta, 3 (1986) 97.

[17] T.E. Divakar, M.K. Tummuru and C.S.P. Sastry, Indian Drugs, 22 (1984) 28.

[18] P. Zhang, Q. Zhu, Y. Zhang, Q. Liu and N. Shen, Fenxi Huaxue, 21 (1993) 1473.

[19] C.S.P. Sastry and A.R. Mohan Rao, Mikrochim. Acta, 1 (1989) 3.

[20] F.A. Ibrahim, M.S. Rizk and F. Belal, Analyst, 111, (1986) 1285.

[21] D.M. Shingbal, Indian J. Pharm., 37 (1975) 157.

[22] M.K. Emara, I.M. Abdel Mohamed, F.H. Askal and A.I. Darwish, Anal. Lett., 26 (1993) 2385.

[23] M.S. Mohrous, H.G. Daabees, Y.A. Baltagy and M.M. El-Semary, Egypt. J. Pharm. Sci., 33 (1992) 453.

[24] B. Prodromos Issopoulos, Acta Farm. Hung., 61 (1991) 198.

[25] M.I. Eugen'ev, I.I. Eugen'eva, N.G. Nikolaeva et al., Khim. Farm. Zh., 25 (1991) 80.

[26] A. El-Shanawany, L.A. El-Aziz, S. Lashini and M. Abou Kull, Zigazig J. Pharm. Sci., 1 (1992) 21.

[27] A.M. Dimas Zaia, J.W. Berreta, J.N. Santos and S.A. Endo, Anal. Chim. Acta., 277 (1993) 89.

[28] A. Berada, B.N. Tadros and Y.A. Gawargious, Mikrochim. Acta, 3 (1989) 143.

[29] C.S.P. Sastry, P. Satyanarayana and T.M. Murali, Analyst., 110 (1985) 189.

[30] C.S.P. Sastry, P. Satyanarayana, A.R. Mohana Rao, N.R.P. Singh and K. Hemalatha, Acta Cienc. Indica (Chem.), 41 (1988) 227.

[31] H. Stegeman and H.F. Griffin, J. Chromotogr., 3 (1960) 150.

[32] M.K. Tummuru, K.E. Rao and C.S.P. Sastry, Mikrochim. Acta, 2 (1984) 199.

[33] D. Vincent and P. Brygoo, Bull. Soc. Chim. Biol., 28 (1946) 43.

[34] A. Demenko and E. Mecarelli, Mikrochim Acta, 1 (1979) 135.

[35] S. Sakaguchi, J. Bio-Chem. (Japan), 37 (1950) 331.

[36] C.S.P. Sastry, K. Rama Rao, D. Murali Krishna, B.S. Sastry and B.S. Prasad, Talanta, 41 (1994) 1957.

[37] A.I. Vogel, Quantitative Inorganic Analysis, Clay, London, 1961, pp. 392, 396.

[38] H.A. Liberman and L. Lachman (Eds.), Pharmaceutical Dosage Forms: Tablets, Vol. 1, Dekker, New York, 1980.

[39] L. Lachman, H.A. Liberman and J.L. Kaing (Eds.), The Theory and Practice and Industrial Pharmacy, 2nd Edn., Henry Kimpton, London, 1976.

[40] D.L. Massart, B.G.M. Yandeginste, S.N. Deming, Y. Michotte and L. Kaufman, Chemometrics, A Text Book, Elsevier, Amsterdam, 1988, p. 293.

[41] M.D. Patergill and D.E. Sands, J. Chem. Educ., 58 (1979) 244.

[42] R.B. Davies, J.E. Thompson and H.L. Pardue, Clin. Chem., 24 (1978) 611.

[43] Ministry of Health and Finance Welfare, India, Pharmacopoeia of India, Vol. 1, 1985, p. 268.

[44] J.C. Lewis, N.S. Snell, D.I. Hirchmann and H. Fraenkelconrat, J. Biol. Chem., 186 (1950) 23.

[45] S.N. Banerjee, J. Indian Chem. Soc., 36 (1958) 449.

The electrochemical reduction of fullerenes, C_{60} and C_{70}

Guowang Diao, Liang Li, Zuxun Zhang*

Department of Chemistry and National Key Laboratory of Coordinational Chemistry, Nanjing University, Nanjing, 210093, People's Republic of China

Abstract

The hexaanion of fullerene, C_{60}^{6-}, was obtained in 1:5 (v/v) acetonitrile–toluene mixture with a mercury hemispherical ultramicroelectrode as a working electrode at a temperature of up to 30°C. The C_{70}^{6-} ion also can be observed under the same conditions. The differences between the redox potentials of C_{60} relative to C_{70} indicate that it is easier to add electrons to C_{70} and its anions compared to the counterparts of C_{60}. The results show that the mercury electrode is very suitable for investigation of the properties of the electrochemical reduction for the fullerenes, particularly C_{60}, at room temperature.

Keywords: Electrochemical reductions; Fullerenes

1. Introduction

Since 1990 the unusual properties of the fullerenes have caused a worldwide boom in the investigation of these systems. For example, according to the theoretical calculations, as this highly symmetrical C_{60} molecule (I_h, the Icosahedral point group symmetry) has three-fold degenerate LUMOs (the lowest unoccupied molecular orbitals) [1], it is expected that cyclic voltammetry of fullerenes would exhibit six one-electron reduction waves if sufficiently negative potentials are applied. In fact C_{60}^{6-} and C_{70}^{6-} have been generated and detected in solution by electrochemical reduction of fullerenes under special conditions. Xie et al. [2] generated and detected the C_{60}^{6-} and C_{70}^{6-} ions by electro-chemical reduction of

fullerenes in solution with a glass carbon electrode as a working electrode. They pointed out that the experimental temperature must be under 5°C in order to generate the C_{60}^{6-} ion by electrochemical reduction. Later C_{60}^{6-} was also obtained at lower temperatures by other scientists [3–7]. However, at room temperature, C_{60}^{6-} cannot be obtained in solution by the electrochemical method because of the limits of the solvent in the negative potential range.

As one would expect, the advantage of the large overpotential for hydrogen evolution makes mercury the material of choice for the cathodic process. It is expected that the sixth reduction wave of C_{60} can be observed at room temperature if a mercury electrode is selected as a working electrode. Therefore, the mercury hemispherical ultramicroelectrode served as a working electrode to investigate the behavior of the electrochemical reduction of fullerenes in this paper. The six re-

* Corresponding author.

duction waves of C_{60} have been obtained in 0.1 M Tetrabutylammonium hexafluorophosphate (TBAPF$_6$) acetonitrile–toluene (volume ratio, under 1:5) mixed solvent at a temperature of up to 30°C for the first time. Under the same conditions, the voltammograms of fullerene, C_{70}, with six reduction waves also can be observed. The results show that the reduction of C_{70} and its anions are easier than the counterparts of C_{60}.

2. Experimental

2.1. Reagents

The fullerenes were produced by a modified Krätschmer–Huffmam method [8]. From the mixture of products obtained by this technique C_{60} was extracted and purified respectively according to the references [9]. The purity was checked after separation by liquid chromatography [10]. C_{70} (> 98%) was purchased from China Yin-Han Fullerene High-Tech. Co. Ltd. (Wuhan University) and used as received. Acetonitrile (HPLC grade, Aldrich) was dried over 4Å molecular sieves for 24 h. Then under argon it was refluxed over P_2O_5 and distilled just before use. Toluene (HPLC grade, Sigma) was kept over $CaCl_2$ for a day. Then, under argon, it was refluxed over sodium for 10 h and distilled prior to use. The supporting electrolyte was TBAPF$_6$, obtained by metathesis tetrabutylammonium bromide (99%, Aldrich) with potassium hexafluorophosphate (98%, Aldrich) in water. It was recrystallized twice from a water–ethanol mixture and dried in a vacuum over at 60°C. The solution was prepared under schlenk systems in argon. All supporting electrolyte was used at a concentration of 0.1 M in toluene–acetonitrile (5:1 in volume).

2.2. Instrumentation

Electrochemical experiments were carried out using an air-tight three-electrode cell under an argon atmosphere. A platinum and a silver wire served as the counter and quasi reference electrode. The working electrode is a platinum ultra-micro-disk electrode (radius 10 μm) and mercury

hemispherical untramicroelectrode (Hg(Pt)) prepared by electroplating mercury onto the above platinum ultramicrodisk electrode [11]. Cyclic voltammetry (CV) and differential pulse voltammetry (DPV) were performed with a BAS-100B electrochemical analyzer equipped with a low current preamplifier and Faraday cage.

3. Results and discussion

From the background, shown in Fig. 1(a), a wider expansion of the available potential window down to − 3.4 V versus a ferrocenium/ferrocene (Fc$^+$/Fc) redox couple (all potential reported in this paper are relative to a Fc$^+$/Fc couple) on a mercury hemispherical ultramicroelectrode was observed at 21.3°C with the use of a mixed solvent system. Under our experimental conditions
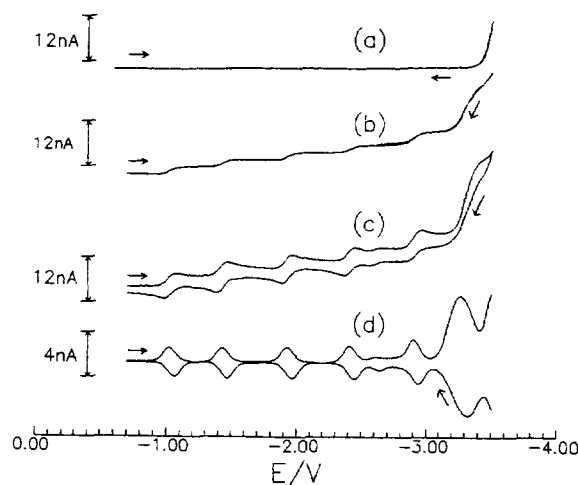

Fig. 1. (a) At 21.3°C, the cyclic voltammogram of the acetonitrile–toluene (1:5 in volume) solvent mixture containing 0.1 M TBAPF$_6$, in the absence of fullerenes, with a 5 mV s^{-1} scan rate, and the mercury hemispherical ultramicroelectrode as a working electrode. All potentials are relative to the Fc$^+$/Fc couple. (b) The cyclic voltammogram of 0.539 mM C_{60} in above system; scan rate is 5 mV s^{-1}; other experimental conditions are the same as those described in (a). (c) The cyclic voltammogram under the same conditions except for a scan rate of 1575 mV s^{-1}. (d) The differential pulse voltammogram of C_{60} (50 mV pulse, 30 ms pulse width, 300 ms period, 25 mV s^{-1} scan rate).
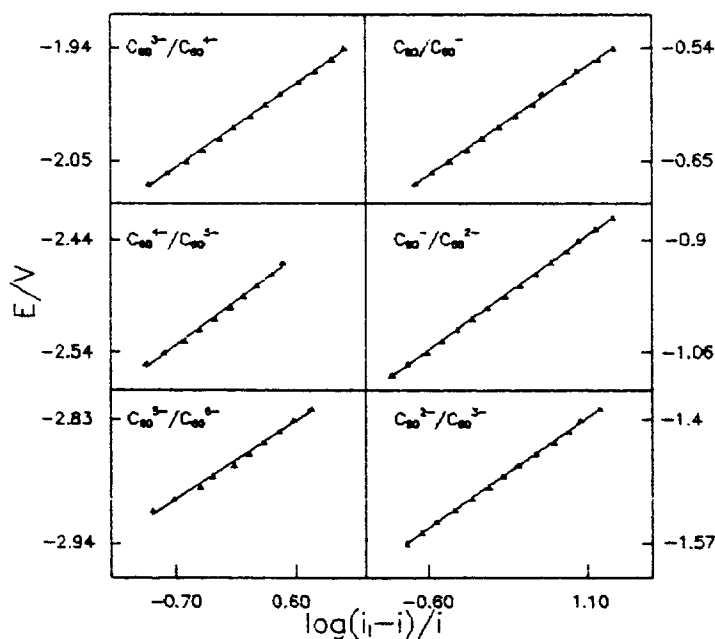
Fig. 2. The plots of E against log $(i_1 - i)/i$ according to Fig. 1(b).

the ferrocenium/ferrocene redox potential is 0.41 V relative to the silver quasi reference electrode. The use of a mercury electrode allowed the first observation of the six electron reductions of C_{60} at room temperature. At 21.3°C, the cylic voltammograms of a 0.539 mM solution of C_{60} in 5:1 (v/v) toluene–acetonitrile at the mercury hemispherical ultramicroelectrode are shown in Fig. 1(b) and (c). The differential pulse voltammogram is presented in Fig. 1(d). Six reduction processes are clearly resolved and are assigned to the generation of the $-1, -2, -3, -4, -5$, and -6 anions of C_{60}. According to Fig. 1(b) the plots of E versus log $(i_1 - i)/i$ for six redox couples of C_{60} are all straight lines (Fig. 2) with slopes of 57, 60, 58, 57, 61 and 54 mV, which show that the six one-electron electrochemical reduction procedures of C_{60} are performed. The values of the half potential, $E_{1/2}$, obtained from the intercepts of these lines are $-1.03, -1.44, -1.94, -2.42, -2.91$ and -3.28 V. The values of $E_{1/2}$ are close to those previously reported in literature [12]. The minor reduction wave at -2.65 V may be due to an electroactive impurity in the C_{60} starting material [13].

According to Fig. 1(d) the peak potential differences between the anodic and cathodic processes are 33, 33, 41, 41, 41 and 56 mV successively from the first to the sixth redox couple of C_{60}. The ratio of peak cathodic current and peak anodic current are 0.95, 0.87, 0.93, 1.05, 1.19 and 1.70 respectively. It is shown that first five reductions are more reversible than the sixth one.

Under the same conditions, similar results for the reduction of C_{70} were also obtained (Fig. 3). The values of the DPV peak potentials for the six waves of the cathodic proedure of C_{70} are $-1.00, -1.40, -1.84, -2.27$ and -3.16 V, which are similar to those reported in Ref. [2], but different from the values of C_{60}. According to Fig. 1(d), the values of the DPV peak potential for the six reduction waves of C_{60} are $-1.03, -1.44, -1.93, -2.41, -2.91$ and -3.27 V respectively. The differences between the redox potentials of C_{70} relative to C_{60} indicate that it is easier to add electrons to C_{70} and its ions compard to the C_{60} counterparts, especially for higher charged ions. The further investigation of the properties of electrochemical reduction of C_{70} is currently underway.
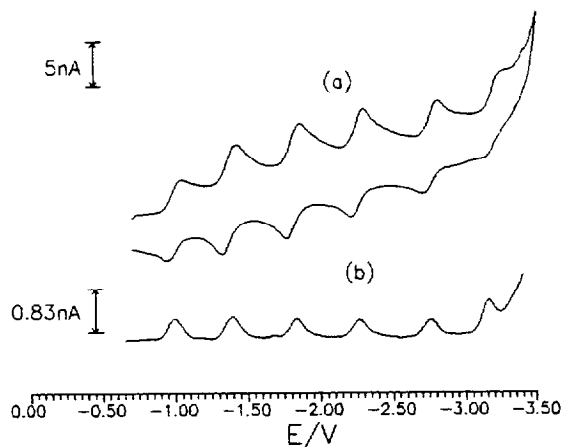
Fig. 3. (a) The cylic voltammogram for C_{70} recorded in 0.1 M TBAPF$_6$ acetonitrile–toluene (1:5 v/v) at 21.3°C on a mercury hemispherical ultromicro-electrode. Scan rate is 10 V s^{-1}. (b) The differential pulse voltammogram of C_{70} in the above system (50 mV pulse, 30 ms pulse width, 300 ms period, 25 mV s^{-1} scan rate).

Only four reduction waves of C_{60} on a platinum ultramicrodisk electrode are shown at 21.3°C (Fig. 4). This is due to the negative potential limits for the platinum electrode in the solution. However, for the mercury electrode the six reduction waves of C_{60} can be obtained (Fig. 5) even at
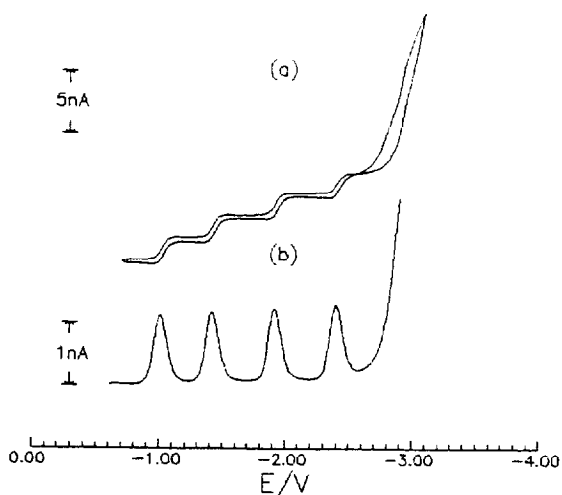
Fig. 4. (a) The cyclic voltammogram of C_{60} under the same conditions as those in Fig. 1 (c) except for the use of a platinum ultramicrodisk electrode as a working electrode and a 100 mV s^{-1} scan rate. (b) The DPV curve of C_{60} at the platinum ultramicrodisk electrode. Other experimental conditions are the same as those in Fig. 1(d).
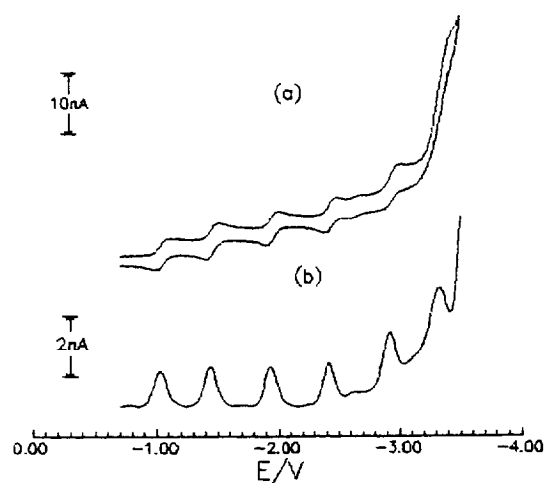
Fig. 5. (a) At 30°C, the cyclic voltammogram of C_{60} at the mercury hemispherical ultramicroelectrode (scan rate 1 V s^{-1}; other conditions are the same as those in Fig. 1(b). (b) The DPV curve of C_{60} (at 30°C; other conditions are the same as those described in Fig. 1(d)).

30°C. It is clear that the mercury electrode is suitable for studying the behavior of the electrochemical reduction of the fullerenes even at 30°C in our experimental conditions.

In conclusion, this paper presents the electrochemical formation of C_{60}^{6-} at room temperature by the use of a mercury hemispherical ultramicroelectrode. However, the current of the sixth reduction wave of C_{60} is significantly greater than that of the other five reduction waves. The reason may be a chemical follow-up process, which will return C_{60}^{6-} to C_{60}^{5-}. Normally spurious electrophilic impurities, such as trace water, trace oxygen, or even supporting electrolyte, trigger the chemical reaction of highly charged anions. The mechanism of the chemical reaction can not be confirmed at this stage. Our further investigation will focus on the mechanism of this process. In contrast, the current of the six reduction waves for C_{70}, are similar to each other, which indicate the stability of C_{70}^{6-} is better than C_{60}^{6-}. Xie et al. [2] have pointed out that the sixth reduction wave of C_{70} at 25°C can be obtained with the glass carbon electrode as the working electrode while the counterpart wave of C_{60} can not be obtained at this temperature. In this paper, with a mercury electrode as the work-

ing electrode, the six waves for both C_{60} and C_{70} were obtained at room temperature. In summary, the mercury electrode is very suitable for the study of the electrochemical properties of the fullerenes at room temperature.

Acknowledgements

References

[1] A.D. Haymet, Chem. Phys. Lett., 122 (1985) 421.

[2] Q. Xie, E. Pérez-Cordero and L. Echegoyen, J. Am. Chem. Soc., 114 (1992) 3978.

[3] Y. Ohsawa and T. Saji, J. Chem. Soc. Chem. Commum., 1992 781.

[4] F. Zhou, C. Jehoulet and A.J. Bard, J. Am. Chem. Soc., 114 (1992) 11004.

[5] K. Meerhloz, P. Tschuncky and J. Heinze, J. Electroanal. Chem., 347 (1993) 425.

[6] F. Paolucci, M. Marcacclo, S. Roffia, G. Orlandl, F. Zerbetto, M. Prato, M. Maggini and G. Scorrano, J. Am. Chem. Soc., 117 (1995) 6572.

[7] N. Li, W. Huo, Z. Gu, X. Zhou, Y. Xun and Y. Wu, Acta Phys.-Chim., 10 (1994) 399.

[8] W. Krätschmer, N. Sorg, D.R. Huffman, Surf. Sci., 156 (1985) 814.

[9] W.A. Scrivens, P.V. Bedworth and J.M. Tour, J. Am. Chem. Soc., 114 (1992) 7917.

[10] L. Isuacs, A. Wehrsing and F. Diederich, Helv. Chim. Acta, 76 (1993) 1231.

[11] K.R. Wehmeyer and R.M. Wightman, Anal. Chem., 57 (1985) 1989.

[12] F. Ariaa, Q. Xie, Y. Wu, Q. Lu, S.R. Wilson and L. Echegoyen, J. Am. Chem. Soc., 116 (1994) 6388.

[13] M.M. Khaled, R.T. Carlin, C. Trulove, Gareth R. Eatobn and S.S. Eaton, J. Am. Chem. Soc., 116 (1994) 3465.

Conductometric titration of thiosulfate using new-type conductivity cells

E. Forizs*, Cs. Muzsnay

Department of Chemistry, Babeş-Bolyai University, Cluj-Napoca, Romania

Abstract

The conductometric titration of thiosulfate with silver ions using non-conventional conductivity cells is described. For this purpose conductivity cells with different cell constants and electrode constructions, equipped with silver, amalgamated silver, stainless-steel and polished platinum electrodes were used. Two well-resolved break-points were observed at 1:1 and 2:1 silver/thiosulfate stoichiometries. Accurate conductometric determinations can be made, using the second break-points of the titration curves as equivalence points, in the range of thiosulfate concentrations 10^{-4}–10^{-2} M. Reverse titrations are less accurate.

Keywords: Conductivity cell; Thiosulfate; Titration

1. Introduction

The determination of sulfur-containing anions has generally been performed by argentometric or mercurimetric titration with potentiometric end-point detection, using sulfide-sensitive membrane electrodes, or mercury, silver, and carbon indicator electrodes [1–5]. The conductometric end-point detection of an argentometric titration of thiosulfate was not recommended by Kolthoff in his classical monograph [6], because during the titration irregular conductivity variations were observed. This is due to the use of conductivity cells equipped with platinized platinum electrodes. In titration systems where precipitates are formed, classical conductivity cells cannot be used. Using non-conventional conductivity cells proposed by the authors, considerable conductivity variations were observed in the course of titrations. For this purpose we studied the behavior of some new-type conductivity cells in argentometric titrations of thiosulfate equipped with silver, amalgamated silver, stainless-steel [7–10] and polished platinum electrodes. These cells were used with good results, giving particular curves in titrimetric determination of Cl^- and I^- ions [11]. In the course of the titrations the pH variations were also determined.
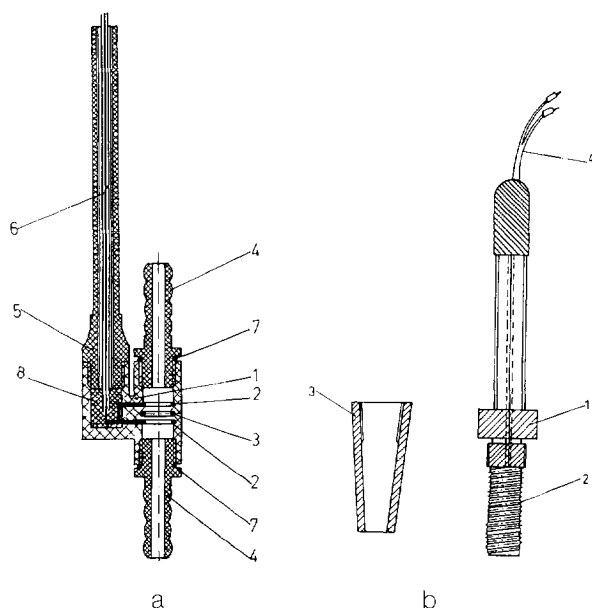
* Corresponding author.

Fig. 1. Conductivity cells for measurement with low-frequency alternating current. (a) Ring type: (1), cell body; (2,3), electrodes; (4), connection (for flow); (5), handle; (6), screened cable; (7), O-ring; (8), epoxy resin. (b) Spiral type: (1), cell body; (2), electrodes; (3), bell protection; (4), screened cable.
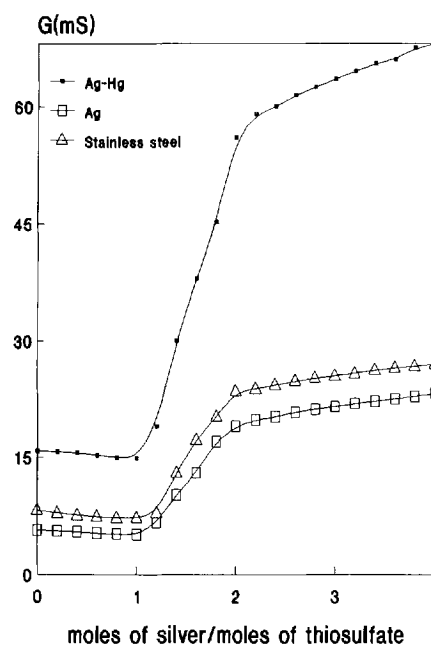

Fig. 2. Conductometric titration curves of 50 ml 5 mM $Na_2S_2O_3$ with 0.1 M $AgNO_3$ using conductivity cells equipped with amalgamated silver (Ag–Hg), silver (Ag) and stainless-steel electrodes.

2. Experimental

2.1. Apparatus

A Radelkis OK/102 type conductometer (Hungary) was used, equipped with two kinds of monoaxial dip-type conductivity cells. The laboratory-made cells employed in conductometric titrations had the following different electrode constructions.

Ring type. This type contains three stainless-steel rings in a polypropylene body (Fig. 1a).

Spiral type. This type was made of two silver, amalgamated silver or platinum wires of 0.4 mm diameter and different lengths ($l = 15$ mm, 10 mm) (Fig. 1b).

The amalgamation of the silver electrode was done with doubly-distilled mercury. Characteristic data for the conductivity cells are reported in Table 1.

A pH-100 Otopeni-type digital pH meter (Romania), equipped with a glass electrode and a saturated calomel electrode with a salt bridge (1 M sodium nitrate) was used for the determination of pH values in the course of titrations. The conductance and potential values were read at fixed time intervals of 60 s after each titrant portion was added.

50 ml thiosulfate samples of 10^{-2}–10^{-4} M concentration were titrated with 10^{-1}–10^{-2} M solutions of $AgNO_3$. The titrant was added in 0.5 or 0.1 ml portions with magnetic stirring.

Table 1
Characteristic data for the conductivity cells

Electrode feature	Cell constant (cm^{-1})
Polished platinum spiral, $l = 15$ mm	0.0625
Silver spiral $l = 15$mm	0.0753
$l = 10$mm	0.715
Amalgamated silver spiral, $l = 15$ mm	0.0713
Stainless-steel ring	0.132

All titrations were performed at room temperature $(23 \pm 2°C)$. During the titrations the temperature variations did not exceed $\pm 0.2°C$.

2.2. Reagents

All reagents (analytical grade) were purchased from Reactivul Chemical Co. (Bucharest, Romania). Silver nitrate solutions were standardized by

Table 2
Conductometric titration data of thiosulfate with silver nitrate at a 1:1 ratio of Ag/S_2O_3

Electrode materials	Taken (mg ml^{-1})	Found[a] (mg ml^{-1})	Relative error (%)
Ag	0.0249	0.2050	0.40
	0.2496	0.2474	−0.88
Ag–Hg	0.0243	0.0242	−0.41
	0.2494	0.2513	0.76
Pt	0.0249	0.0248	−0.40
	0.2496	0.2467	−1.16
Stainless-steel	0.2503	0.2480	−0.92

[a] Mean of three determinations.

Table 3
Conductometric titration data for thiosulfate with silver nitrate at a 2:1 ratio of Ag/S_2O_3

Electrode materials	Taken (mg ml^{-1})	Found[a] (mg ml^{-1})	Recovery (%)	RSD (%)
Ag	0.0249	0.0251	100.8	0.5
	0.2496	0.2519	100.9	0.3
	2.4913	2.5006	100.4	0.2
Ag–Hg	0.0243	0.0244	100.4	0.8
	0.2494	0.2506	100.5	0.7
	2.4901	2.4987	100.4	0.5
Pt	0.0249	0.0250	100.4	0.2
	0.2496	0.2521	101.0	0.3
	2.4960	2.5210	101.0	4.4
Stainless-steel	0.0245	0.0246	100.4	0.6
	0.2503	0.2522	100.8	0.4
	2.4963	2.5094	100.5	0.6

[a] Average of three determinations.

potentiometric titration with sodium chloride. Sodium thiosulfate solutions were standardized iodometrically in the usual way. 0.1 M stock solutions were used and diluted as required.

3. Results and discussion

Some examples of titration curves are shown in Fig. 2. Two distinct, sharp end-points were obtained at 1:1 and 2:1 silver/thiosulfate ratios. In the first part of the curves the conductance values decrease slightly, corresponding to the formation of thiosulfate complex ions $[Ag(S_2O_3)_x]^{1-2x}$; $x = 1-3$. These complex ions have lower mobilities than the noncomplexed thiosulfate ion.

The recoveries calculated from the first equivalence points are satisfactory only in solutions more dilute than 10^{-3} M. Some analytical results are reported in Table 2. Above concentrations of 10^{-3} M, the first equivalence point shows an error of about $+12\%$.
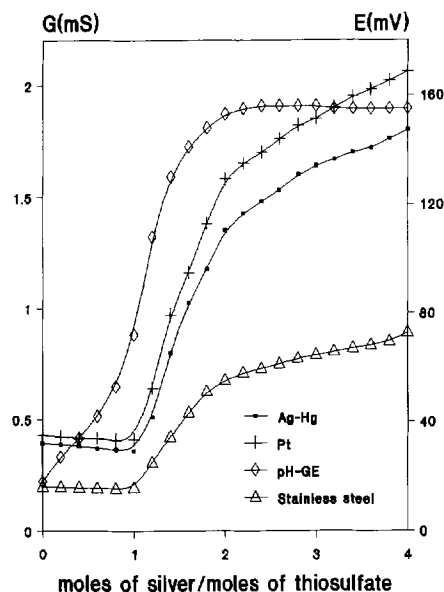

Fig. 3. Conductometric and potentiometric titrations of 50 ml 1 mM $Na_2S_2O_3$ with 0.1 M $AgNO_3$ using conductivity cells equipped with amalgamated silver (Ag–Hg), platinum (Pt), stainless-steel and glass (pH-GE) electrodes.
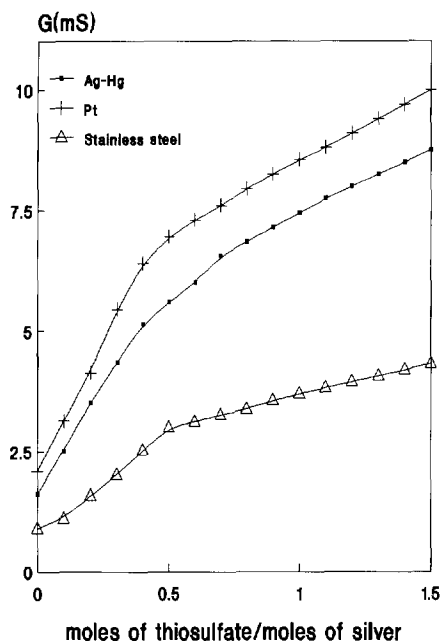
Fig. 4. Conductometric titration of 50 ml 1 mM AgNO₃ with 0.1 M Na₂S₂O₃ using conductivity cells equipped with amalgamated silver (Ag-Hg), platinum (Pt) and stainless-steel electrodes.

Following the addition of titrant after the 1:1 Ag/S₂O₃ ratio end-point, the curves show a very sharp increase of conductance values due to the formation of sulfuric acid. The formation of sulfuric acid proceeds on the basis of the following catalytic reaction [2]:

$$AgS_2O_3^- + Ag^+ + H_2O = Ag_2S + H_2SO_4$$
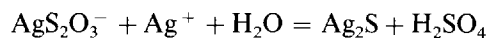
The catalytic effect can be attributed to the action of both Ag^+ and H_3O^+ ions.

At the 2:1 ratio of Ag/S₂O₃ end-point a well-resolved break-point is observed corresponding to the completion of the silver sulfide precipitation. An excess of titrant, increasing the concentration of silver nitrate in solution, increases the conductance values. Of the conductivity cells studied the amalgamated silver cells have the greatest sensitivity, followed by the silver cells;

the stainless-steel cells have the lowest sensitivity. The equivalence points obtained at room temperature coincide well with the theoretical ones (Table 3).

The acidity of solution increases in the course of titrations; after the 2:1 ratio of Ag/S₂O₃ end-point the pH of the solution remains practically constant (Fig. 3).

Three illustrative curves for the reverse titrations are shown in Fig. 4. The conductometric titration curves show increasing character from the start and present only one well-resolved break-point at the 1:2 S₂O₃/Ag ratio.

Some other species, e.g. halides, cyanides, thiocyanates and cyanates, may cause interference at about 10^{-5} M concentrations.

In this work we have come to the conclusion that it is possible to titrate thiosulfate ions with silver nitrate by means of a conductometric method using non-conventional conductivity cells. The recoveries listed in Table 3 in terms of amounts of thiosulfate taken and recovered are reasonably good, with an error of < 1%, with the exceptance of the conductivity cell equipped with platinum electrodes.

References

[1] J. Havas, Hung. Sci. Instrum., (1973) 35.
[2] G Piccardi, R. Udisti and P. Cellini-Legittimo, Microchim. Acta, Part III, (1989) 7.
[3] V.I. Berestetskii and F.M. Tulyupa, Zh. Anal. Khim., 44 (1989) 328.
[4] E. Schmidt and E. Pungor, Magy. Kem. Foly., 76 (1970) 307.
[5] E. Pungor, Anal. Chem., 39 (1967) 28A.
[6] I.M. Kolthoff, Konduktometrische Titrationen, Th. Steinkopff, Dresden, Germany, 1923.
[7] Cs. Muzsnay, Magy. Kem. Foly., 92 (1987) 23.
[8] Cs. Muzsnay and A. Szabo, Rom. Pat. 72123, 1979.
[9] Cs. Muzsnay, Stud. Univ. Babes-Bolyai, Ser. Chem., 22 (1977) 68.
[10] E. Hopîrtean, F. Mihălcioiu, E. Forizs and F. Kormos, Sens. Actuat. B, (1994) 317.
[11] Cs. Muzsnay and E. Forizas, Stud. Univ. Babes-Bolyai, Ser. Chem., 31 (1986) 55.

Spectrophotometric determination of acrivastine in urine and capsules

Heba H. Abdine*, Azza A. Gazy, Salah M. Blaih, Mohamed A. Korany

Pharmaceutical Analytical Chemistry Department, Faculty of Pharmacy, University of Alexandria, Alexandria, 21521, Egypt

Abstract

Three sensitive and accurate spectrophotometric methods are presented for the determination of the antihistaminic acrivastine (ACR) in capsules and urine. The first method utilizes the reaction of 2-nitrophenylhydrazine hydrochloride in presence of dicyclohexylcarbodiimide and pyridine. The violet colour of the resulting acid hydrazide is measured at 550 nm. The second method is based on alkaline oxidation of the drug with potassium permanganate and subsequent measurement of the formed manganate ion at 608 nm. The third method uses derivative spectrophotometry for the determination of ACR. The last method is extended to the in vitro determination of the drug in urine. All methods gave a relative standard deviation of less than 2%.

Keywords: Acrivastine; Derivative spectrophotometry; Urine

1. Introduction

Acrivastine (ACR), (*E,E*)-3-{6-[1-(4-methyl-phenyl)-3-(1-pyrrolidinyl)-1-propenyl]-2-pyridinyl}-2-propenoic acid, is a potent competitive histamine H_1-receptor antagonist. The drug lacks significant anticholinergic effects, and has a low potential to penetrate the central nervous system [1] owing to the presence of the polar acrylic acid side-chain in the molecule. The literature reveals only one paper concerning the determination of ACR and its metabolite in human plasma using GC–MS [2].

2-Nitrophenylhydrazine hydrochloride (2-NPH · HCl) has been used for the determination of a wide range of aliphatic and aromatic acids in aqueous ethanol in the presence of pyridine and recently this method has been used for the determination of several drugs [3,4]. Alkaline $KMnO_4$ is used for the oxidation of organic compounds containing different unsaturated centres [5]. The use of derivative spectrophotometry in the analysis of pharmaceutical matrices and biological samples is well established, especially its potential for the elimination of interfering substances such as additives, excipients and endogenous substances [6,7].

The aim of this work was the development of simple and sensitive analytical methods for the

---

* Corresponding author.

assay of ACR capsules, utilizing its reaction with 2-NPH·HCl in the presence of dicyclo-hexylcarbodiimide (DDC) and pyridine and also through oxidation with alkaline $KMnO_4$. Furthermore ACR was determined both in its dosage form and in urine by using first- and second-derivative spectrophotometric measurements.

2. Experimental

2.1. Apparatus

A Perkin-Elmer Model 550S UV–VIS double-beam spectrophotometer with 1 cm quartz cuvettes and a Hitachi Model 561 recorded were used. The following operating conditions were used: scan speed, 120 mm min^{-1}; chart speed, 60 mm min^{-1}; $D_1 = (dA/d\lambda)$; $D_2 = (d^2A/d\lambda^2)$; and scan range 400–250 mm. The minimum and maximum ordinate settings were selected to record the maximum amplitude of the most concentrated standard solution at not less than 80% of the recorder full-scale deflection (25 cm).

2.2. Materials

All materials used were of analytical grade. Acrivastine (ACR) authentic sample and Semprax capsules (Amriya for Pharmaceutical Industries under license from the Wellcome Foundation, London, labelled to contain 8 mg of ACR per capsule) were used.

2.3. Reagents and solutions

The following solutions were prepared: 1% (w/v) $KMnO_4$ in distilled water; 0.24 M 2-NPH·HCl solution, by dissolving 0.456 g of 2-NPH·HCl in 100 ml of ethanol; 0.25 M DCC solution by dissolving 0.516 g of DCC in 100 ml of ethanol; 5.6% (v/v) pyriding solution, by diluting 5.6 ml of pyridine with ethanol to 100 ml; and 10% ethanolic KOH solution, by dissolving 10 g of KOH in 5 ml of distilled water and diluting to 100 ml with ethanol.

2.4. Preparation of calibration graphs

2.4.1. 2-NPH·HCl method

Dissolve 50 mg of ACR in 100 ml of ethanol. Pipette aliquot volumes ranging from 0.5 to 1.0 ml (in 0.1 ml steps) into 10 ml volumetric flasks, to each add 1 ml each of the 2-NPH·HCl, pyridine and DCC solutions and stopper the flasks. Heat at 80°C for 10 min, then add 0.5 ml of 10% ethanolic KOH solution, heat the flasks for 5 min at 60°C, then cool to room temperature and dilute to volume with ethanol. Measure the absorbance against a reagent blank at 550 nm.

2.4.2. $KMnO_4$ method

Dissolve 25 mg of ACR in 100 ml of 0.1 M H_2SO_4. Pipette aliquot volumes ranging from 0.2 to 0.6 ml (in 0.1 ml steps) into 10 ml volumetric flasks, to each add 1 ml of 1 M NaOH and 0.3 ml of 1% $KMnO_4$ and mix. Dilute to 10 ml using distilled water. Measure the absorbance in 1 cm cells against a reagent blank at 608 nm.

2.4.3. Derivative spectrophotometric method

Dissolve 25 mg of ACR in 100 ml of 0.1 M NaOH. Pipette aliquot volumes ranging from 0.1 to 0.4 ml (in 0.1 ml steps) into 50 ml volumetric flasks and dilute to volume with 0.1 M NaOH solution. Record the D_1 and D_2 values at the recorded λ (Table 1).
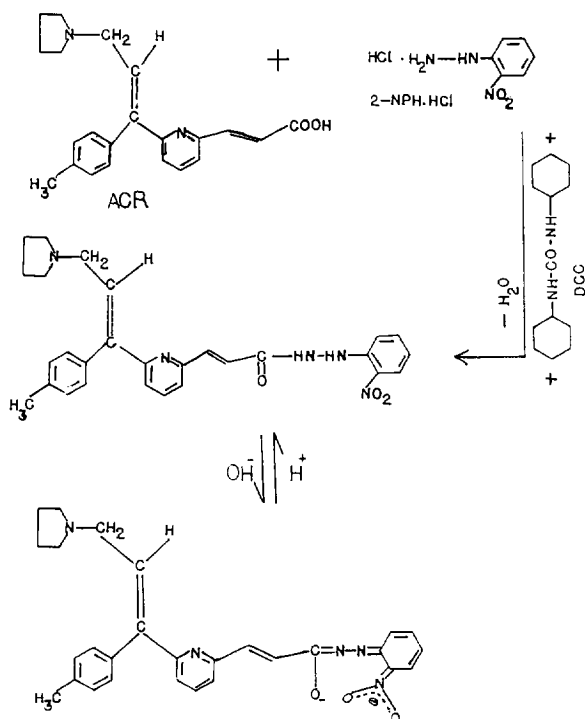
2.5. Procedure for capsules

2.5.1. 2-NPH·HCl method

Place an accurately weighed portion of the mixed contents of the capsules equivalent to 50 mg of ACR in a beaker, extract with ethanol, filter into a 100 ml volumetric flask and dilute to volume with ethanol. Proceed as descibed in Section 2.4.1.

2.5.2. $KMnO_4$ method

Place an accurately weighed portion of the mixed contents of the capsules equivalent to 25 mg of ACR in a beaker and extract with ca. 20 ml of chloroform. Filter into a 100 ml volumet-

Scheme 1.

2.5.3. Derivative method

Place an accurately weighed portion of the mixed contents of the capsules equivalent to 25 mg of ACR in a beaker, extract with 0.1 M NaOH, filter into a 100 ml volumetric flask and dilute to volume with 0.1 M NaOH. Proceed as described in Section 2.4.3.

2.6. In vitro determination of ACR in urine

Dissolve 25 mg of ACR in 100 ml of 0.1 M H_2SO_4. Transfer aliquot volumes ranging from 0.1 to 0.4 ml (in 0.1 ml steps) into sets of separating funnels each containing 2 ml of urine and extract with 5 ml of chloroform. Transfer the chloroform extracts into 50 ml volumetric flasks, evaporate to dryness, dissolve the residue in 0.1 M NaOH and dilute to volume with 0.1 M NaOH. Record the D_1 and D_2 values.

3. Results and discussion

3.1. 2-NPH · HCl method

Containing a carboxylic group, ACR reacts with 2-NPH · HCl in the presence of DCC and pyridine to form the corresponding acid hydrazide derivative. The reaction mechanism is illustrated in Scheme 1 [8].

The violet colour of the resulting acid hydrazide was measured at 550 nm. The experimental conditions were optimized to achieve

ric flask, dilute to volume with chloroform and mix. Transfer 0.2–0.6 ml (in 0.1 ml steps) into separate 10 ml volumetric flasks. Evaporate to dryness and dissolve the residue in 1 ml of 0.1 M H_2SO_4. Proceed as described in Section 2.4.2.

Table 1
Analytical parameters for the determination of ACR using the proposed spectrophotometric methods

Method	Concentration range (μg ml^{-1})	Wavelength, λ (nm)	Linear regression		Correlation coefficient, (r)	RSD[a] (%)	Apparent molar absorptivity, ϵ (l mol^{-1} cm^{-1})
			Intercept (a)	Slope (b)			
KMnO$_4$	5–15	608	0.032	0.0514	0.9989	1.5	17907.76
2-NPH · HCl	25–50	550	−0.012	0.0114	0.9993	1.3	3971.76
Derivative spectrophotometry:							
D_1	0.5–2.0	315	0.125	10.55	0.9993	1.2	
D_2	0.5–2.0	268	−0.25	12.65	0.9999	0.9	–

[a] Relative standard deviation ($n = 5$).

high sensitivity, a low blank reading and high colour stability, as described previously [3,4].

3.2. KMnO₄ method

Alkaline permanganate is a known reagent for the hydroxylation of alkenes. This process is thought to proceed via cyclic permanganic esters, and finally to lead to the formation of a 1,2-diol and other oxidation products [5]. Thus, ACR was oxidized, owing to the presence of unsaturated centres, by $KMnO_4$ in alkaline medium. Under the conditions used, the resulting green manganate ion (MnO_4^{2-}) was mea-

sured spectrophotometrically at its λ_{max} of 608 nm (Fig. 1).

The experimental conditions were studied and it was found that a $KMnO_4$ concentration of 30 μg per ml of the final assay solution was optimum (Fig. 2).

3.3. Derivative method

The zero-order, first-derivative and second-derivative spectra of ACR in 0.1 M NaOH are presented in Fig. 3. The two analyticl wavelengths of 315 nm (for D_1) and 268 nm (for D_2) were selected on the basis of reasonable sensitivity and reproducibility.

The sensitivity of the derivative methods allowed its application in the concentration range 0.5–2.0 μg ml^{-1}, whereas the direct A_{max} did not give satisfactory results in this concentration range. Linear plots of the measured derivatives values versus concentration in the range stated in Table 1 were obtained with negligible intercepts. Such a finding encourages the use of derivative methods for the assay of ACR in capsules (Table 2).

Regression analysis of the results obtained by the three methods using the method of least squares to calculate the slope (b), intercept (a) and correlation coefficient (r) are presented in Table 1. Replicate determinations at different concentration levels of the drug were carried out to test the precision and reproducibility of the proposed methods. The relative standard deviations were found to be less than 2% (Table 1).
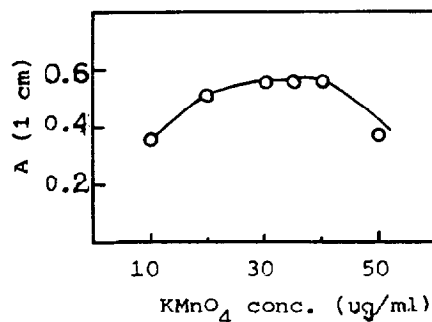

Fig. 1. Absorption spectra for the coloured reaction product of 12.5 μg ml^{-1} ACR with $KMnO_4$ solid line. Dashed line, reagent blank.

Fig. 2. Influence of $KMnO_4$ concentration on the colour intensity developed from 12.5 μg ml^{-1} ACR.
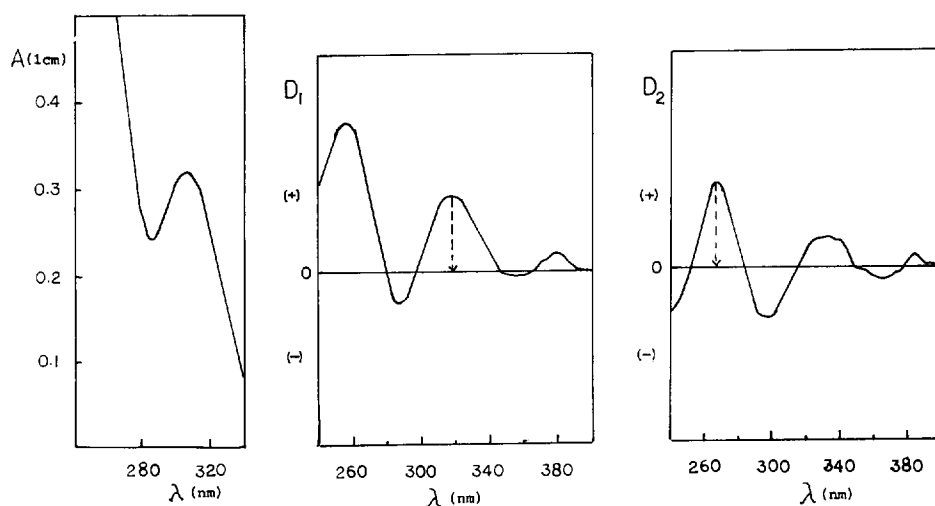
Fig. 3. (a) Zero-order (10 μg ml^{-1}) and (b) first-derivative and (c) second-derivative (2 μg ml^{-1}) spectra of ACR in 0.1 M NaOH.

The proposed methods were applied to the determination of ACR in capsules. The results obtained were both precise and accurate (Table 2).

3.4. In vitro determination of ACR in urine

It has been reported that 84% of the ACR dose was recovered in urine, predominantly in the unchanged form of the drug [9]. The above-described derivative spectrophotometric methods (D_1 and D_2) were used for the in vitro determination of ACR in urine. Direct measurements of

spiked urine gave a positive error. This error was corrected by prior extraction of the urine with chloroform. The results obtained (Table 3) indicated that the procedure was effective and reproducible.

In conclusion, the 2-NPH·HCl reaction is a specific method for the determination of the carboxylic group moiety of ACR. Hence the method may be utilized for stability studies of the drug. On the other hand, the $KMnO_4$ method is a general and simpler method for the determination of ACR through oxidation of the unsaturated centres of the drug. The derivative method was found to be more sensitive than the other two methods and was applied to the determination of ACR in urine.

Table 2
Determination of ACR in capsules using the proposed spectrophotometric methods

Method	Found[a] ± SD (%)	t[b]	F[b]
$KMnO_4$	100.1 ± 0.94	0.1970	2.09
2-NPH·HCl	100.0 ± 0.37	0.5981	3.086
Derivative spectrophotometry:			
D_1	100.14 ± 0.27	0.1960	5.796
D_2	100.1 ± 0.35	0.3029	3.449
A_{max} measurement[c]	100.2 ± 0.65		

[a] Average of five determinations.
[b] Theoretical values: $t = 2.26$ and $F = 6.26$ at $p = 0.05$.
[c] The proposed methods were compared with the conventional spectrophotometric method (A_{max}).

Table 3
Precision and recovery for the determination of ACR in spiked human urine

Added (μg ml^{-1})	Recovery (%)[a]	RSD (%)
0.5	98	1.0
1.0	99.7	0.3
1.5	100.7	0.2
2.0	101.3	0.1

[a] Mean of five experiments.

References

[1] R.N. Brogden and D. McTavish, Drugs, 41 (1991) 927.

[2] S.Y. Chang, F.R. Nelson, J.W.A. Findlay and L.C.E. Taylor, J. Chromatogr., Biomed Appl., 89 (1989) 288.

[3] M.A. Korany, M.H. Abdel-Hay, M.M. Bedair and A.A. Gazy, Talanta, 36 (1989) 1253.

[4] M.H. Abdel-Hay, M.A. Korany, M.M. Bedair and A.A. Gazy, Anal. lett., 23 (1990) 281.

[5] P. Sykes, A Guidebook to Mechanism in Organic Chemistry, Longman, London, 4th edn., 1978, p. 186.

[6] F.S. Rojas, C.B. Ojeda and J.M.C. Pavon, Talanta, 35 (1988) 753.

[7] M. Poulou and P. Macheras, Int. J. Pharm., 34 (1986) 29.

[8] R. Horikawa and T. Tanimura, Anal. Lett., 15 (A20) (1982) 1629.

[9] Wellcome Foundation, London Laboratories, personal communication.

Talanta

Derivative spectrophotometric determination of nickel using Br-PADAP

Sérgio L.C. Ferreira[a],*, A.C. Spinola Costa[a], Djane S. de Jesus[b]

[a]Instituto de Química, Universidade Federal da Bahia, Bahia, 40170-290, Brazil
[b]Centro Federal de Educação Technologica da Bahia, Bahia, 40300-010, Brazil

Abstract

A major problem with spectrophotometric methods for nickel is cobalt interference, because many of the reagents for nickel also react with cobalt. In this work, the interference of cobalt in the determination of nickel using 2-(5-bromo-2-pyridylaxo)-5-diethylaminophenol (Br-PADAP) was eliminated by the use of derivative spectrophotometry, using the zero-crossing method for evaluation of the derivative signal. Br-PADAP reacts with nickel(II) in the presence of Triton X-100 to form a red complex with absorption maxima at 530 and 562 nm. The reactions parameters and the conditions for the measurements of the first-derivative signal were studied and the results demonstrated that using the derivative technique, Br-PADAP can be used for nickel determination with a selectivity higher than that of ordinary spectrophotometry and with a limit of detection of 0.2 ng ml^{-1}. The pH should be in the range 5.0–6.0 using an acetate buffer. The determination of nickel in the presence of cobalt was performed with conventional and derivative procedures, and the results demonstrated that only the derivative method should be used and, of the methods used for evaluation of the derivative signal, the zero-crossing method is the best. The proposed procedure was used for nickel determination in steels standards. The results demonstrated that the procedure has satisfactory accuracy and precision. Cobalt interference can be also eliminated by using dual-wavelength spectroscopy.

Keywords: Br-PADAP; Cobalt interference; Derivative spectrophotometry; Nickel

1. Introduction

One of the major problems with spectrophotometric methods is cobalt interference during the determination of nickel, because many of the

reagents for nickel also react with cobalt. Normally [1,2] this interference is eliminated by procedures involving operations such as extraction, ion exchange and precipitation of nickel with dimethylglyoxime. In the present paper, we propose a procedure using 2-(5-bromo-2-pyridylazo)-5-diethylaminophenol (Br-PADAP) for nickel determination with derivative spectrophotometry to

* Corresponding author. Fax: (55) 71-237-4117 or (55) 71-235-5166.

increase of the selectivity. This method allowed the determination of nickel in the presence of cobalt without the need for chemical separation. The proposed method is simple, highly selective, reproducible and involves little reagent manipulation.

Br-PADAP is a good spectrophotometric reagent for nickel determination ($\varepsilon = 1.22 \times 10^5$ l mol^{-1} cm^{-1}), and has been used for nickel determination in aluminium alloys and nickel electroplating waste-water [3] and in our laboratory for the simultaneous determination of nickel and iron in copper-base alloys [4]. In both studies major cobalt interference was reported. Jarosz [5] used Br-PADAP as spectrophotometric reagent for nickel and separated it from cobalt using dimethylglyoxime.

Others procedures have been described for nickel determination by derivative techniques. Ishii et al. [6] used second-derivative spectrophotometry for the determination of micro-amounts of nickel with methylfurfural 1-phthalazinohydrazone as reagent. The procedure was proposed for nickel determination in the presence of cobalt, the cobalt interference being eliminated by formation of the cobalt(III) ammine complex or by extraction in the form of a thiocyanate complex. The surfactant Triton X-100 was used for solubilization of the reagent. Malinoswska and Kasiura [7] used 2-(2-thiazolylazo)-1-naphthol for nickel determination in the presence of several cations, the procedure being based on extraction of the resultant complex with chloroform. Murillo et al. [8] proposed the simultaneous determination of nickel and cobalt by first-derivative spectrophotometry using 1-hydroxy-2-carboxyanthraquinone as reagent; the derivative technique (zero-crossing method) allowed higher selectivity. Another procedure [9] was proposed for the simultaneous determination of nickel, zinc and copper by second-derivative spectrophotometry using 1-(2-pyridylazo)-2-naphthol as reagent. A procedure for the simultaneous determination of nickel and copper by third-derivative spectrophotometry using sodium cyanide [10] was proposed. These methods all have sensitivity lower than that with Br-PADAP.

2. Experimental

2.1. Reagents

All reagents were of analytical-reagent grade unless stated otherwise.

Nickel(II) solution (1000 μg ml^{-1}) was prepared by dissolving pure nickel (99.99%) in dilute nitric acid with heating and dilution to 1 l with demineralized water.

Br-PADAP solution (0.025%) was prepared by dissolving 0.0625 g of the compound (Aldrich) in 10 ml of ethanol and 100 ml of Triton X-100 solution (8%) and diluting to 250 ml with demineralized water.

Buffer solution (pH 5.25) was prepared by mixing 103.3 g of sodium acetate trihydrate and 14.1 ml of glacial acetic acid in 1 l of demineralized water.

Sodium thiosulfate solution (10%) was prepared by dissolution of 10.0 g of sodium thiosulfate pentahydrate in and dilution to 100 ml with demineralized water.

EGTA solution (0.001 M) was prepared by dissolving ethylene glycol-2-(2-aminoethyl)tetraacetic acid (Merck) in water.

2.2. Apparatus

Absorption spectra, first-derivative spectra and absorbences were measured with a Varian DMS-100 spectrophotometer and a Grafix FX-100 printer and a Perkin-Elmer Lambda 19 UV–VIS/NIR spectrometer with an Okidata Microline 320 printer, using a 1.0 cm cells.

A 300 Analyser pH meter was used to measure pH values.

2.3. Procedure

Transfer a portion of solution containing 1.00 μg of nickel(II) into a 25 ml standard flask and add 2.5 ml of acetate buffer (pH 5.25) and 1.0 ml of Br-PADAP solution. Mix and dilute to the mark with water. After 50 min, record the first-derivative spectrum from 800 to 400 nm against an appropriate blank at a scan speed of 400 nm min^{-1} and a slit width of 4 nm. Determine the
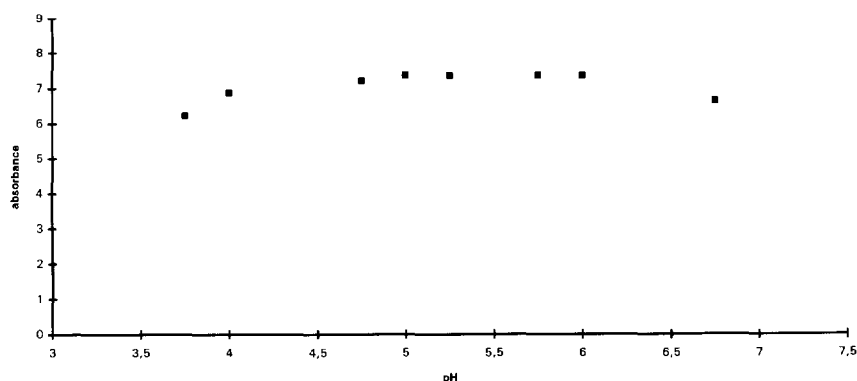
Fig. 1. Effect of pH on the Ni(II)-Br-PADAP system. Reference, reagent blank. [Ni(II)] = 0.08 μg ml^{-1}.

nickel content from the first-derivative spectrum by measuring first-derivative signal at 573 nm (zero-peak method) or at 563 nm (zero-crossing point for cobalt) and comparing the value obtained with an appropriate calibration curve. The wavelengths of the zero-peak and zero-crossing points quoted are those obtained in this work, and these values should be established independently for other instruments as part of the calibration procedure.

3. Results and discussion

3.1. Characteristics of the reagent and the complex

The reaction of Br-PADAP with nickel(II) cation in the presence of Triton X-100 forms a red complex with absorption maxima at 530 and 562 nm and a composition of 1:2 nickel(II)-Br-PADAP. The absorbance of the complex reaches a maximum 50 min after mixing the reagents and is stable for at least 24 h. The Br-PADAP reagent has an absorption maximum at 487 nm (at pH 5.25). It and its nickel(II) complex have low solubility in water but the reaction in the presence of Triton X-100 overcomes this inconvenience.

The order of addition of reagents was studied and the results demonstrated that it did not affect complex formation.

3.2. Effect of pH

The effect of pH on the nickel(II)-Br-PADAP system was studied and the results demonstrated that the derivative signal is maximum and constant in the pH range 5.0-6.0, as can be seen in Fig. 1. The effect of the buffer concentration on the nickel(II)-Br-PADAP complex was studied and the results demonstrated that it does not affect the derivative signal when the buffer is in the concentration range 0.10-0.40 M in acetate.

3.3. Effect of Triton X-100 surfactant on the nickel(II)-Br-PADAP system

Br-PADAP and its nickel(II) complex have low solubility in water, this is overcome by using Triton X-100 as surfactant [11]. The solubilization of 250 μg of reagent is obtained with 24 mg of Triton X-100 per 25 ml. Thus, 32 mg was selected as optimal. The study of the effect of the amount of Triton X-100 on the nickel(II)-Br-PADAP complex revealed that it does not affect the absorbance signal of the system when Triton X-100 is in the concentration range 1.0-1.6 mg ml^{-1}.

3.4. Conditions for measurement of first-derivative value

The effects of the scan speed and of the slit width (Δl) on the measurement of the first-derivative signal were examined. The results showed

that the scan speed had no effect. Hence a scan speed of 400 nm min^{-1} was chosen. It was also found that there was no significant difference in sensitivity at various Δl values, but an increase in slit width decreased the noise, hence a slit of 4 nm was selected for the measurements. The methods used for the quantitative evaluation of derivative signals were the peak-zero method and zero-crossing method [8,12,13].

3.5. Effect of interfering ions

Solutions containing 1.00 μg of nickel(II) and various proportions of several cations and anions were prepared and an ordinary procedure [4] was followed. The tolerance level for an ion was taken as the amount which caused a change of $\pm$ 2% in

Table 1
Nickel determination in the presence of various ions[a]

Ion	Excess[b]			Reagent used
	500:1	50:1	5:1	
Ca(II)	N	N	N	$CaCO_3/HCl$
Mg(II)	N	N	N	$MgCl_2\cdot6H_2O$
Ba(II)	N	N	N	$BaCl_2\cdot2H_2O$
Sr(II)	N	N	N	$Sr(NO_3)_2$
Al(III)	I	N	N	$Al_2(SO_4)_3$
V(V)	I	N	N	NH_4VO_3
Mo(VI)	N	N	N	$Na_2MoO_4\cdot2H_2O$
W(VI)	I	N	N	$Na_2WO_4\cdot2H_2O$
Cr(III)	I	N	N	$Cr(NO_3)_3\cdot9H_2O$
Mn(II)	I	N	N	$MnSO_4\cdot6H_2O$
Bi(III)	I	N	N	$Bi(NO_3)_3\cdot5H_2O/HCl$
Cd(II)	I	N	N	$Cd(Ac)\cdot2H_2O$
Pb(II)	I	N	N	$Pb(NO_3)_2$
Zn(II)	I	N	N	$ZnSO_4\cdot7H_2O$
Co(II)	I	I	I	$CoSO_4\cdot7H_2O$
Hg(II)[c]	N	N	N	HgO/HNO_3
Cu(II)[c]	N	N	N	$CuSO_4\cdot5H_2O$
Fe(III)[d]	I	N	N	$Fe_2(SO_4)_3/HCl$
Fe(II)	I	I	I	$Fe(III)+NH_2OH\cdot HCl$
NO_3^-	N	N	N	$NaNO_3$
Cl^-	N	N	N	$NaCl$
SO_4^{2-}	N	N	N	Na_2SO_4
CO_3^{2-}	I	N	N	Na_2CO_3
PO_4^{3-}	I	N	N	Na_3PO_4

[a] [Ni]: 1.00 μg per 25 ml.
[b] I = interferes; N = does not interfere.
[c] High amounts can be masked with thiosulfate [4].
[d] Masking with EGTA.

Table 2
Nickel determination in the presence of cobalt by conventional and derivative procedures

Co(II) present (μg)	Ni(II) present (μg)	Ni(II) found (μg)		
		Absolute method	Zero-peak method	Zero-crossing method
0.20[a]	1.00	1.10	0.98	0.99
1.00	1.00	2.20	0.96	0.99
1.00	2.00	3.13	1.89	1.95
6.00	2.00	6.34	1.89	1.93
5.00	1.00	4.81	0.87	0.99
7.00	1.00	6.05	0.82	0.99
10.00[b]	1.00	9.40	0.81	0.99
20.00	1.00	12.35	0.80	0.98
30.00	1.00	17.66	0.80	1.00
20.00	0.50	11.76	0.44	0.49
30.00	0.50	12.77	0.44	0.50

[a] 1.0 ml of Br-PADAP solution (0.025%).
[b] 2.0 ml of Br-PADAP solution (0.025%).

the absorbance. The results are listed in the Table 1 and demonstrate that the main interferents are cobalt(II), iron(II) and copper(II). The copper(II) interference can be easily eliminated with thiosulfate [4] and iron(III) with EGTA [3]. The iron(II) interference is substantial and cannot be eliminated with EGTA as masking agent or by first-derivative technique. The interference of the iron(III) cation is lower in the presence of chloride ion. The effect of ionic strength on the system is negligible for 0.1 M concentrations of sodium chloride and potassium nitrate.

3.6. Nickel determination in presence of cobalt by derivative spectroscopy

Cobalt is one of the main interferents in nickel determination. It reacts with Br-PADAP in the pH range adopted, forming a complex with absorption maxima at 589 and 570 nm and molar absorptivities of 8.30×10^4 and 7.87×10^4 l mol^{-1} cm^{-1}, respectively. Nickel determination in the presence of cobalt by the ordinary method shows results with positive errors, increasing with increase in the amount of cobalt. However, the derivative technique allows this determination when the zero-crossing method is used. Table 2

presents the results obtained during the determination of nickel in the presence of different amounts of cobalt.

The experiments described below also showed that nickel determination by the derivative procedure using the zero-crossing method is independent of the presence of cobalt at different concentrations.

Four calibration curves were prepared for standards having nickel concentrations in the range 10–200 ng ml^{-1} in the presence of 0, 1.0, 3.0 and 5.0 μg per 25 ml of cobalt. The first-derivative spectra were recorded and the heights were measured using the zero-peak and zero-crossing methods. The slope, intercept and correlation coefficient obtained are summarized in Table 3. The results demonstrated that nickel determination by the peak-zero method has a negative error, decreasing proportionally with increase in the amount of cobalt present. However, this can be avoided by using the zero-crossing method; the equations obtained revealed that nickel determination is independent of the presence of cobalt.

Fig. 2 shows the absorption spectrum of the nickel complex, the corresponding spectrum of the cobalt complex and total spectrum of a mixture of both complexes. All measurements were
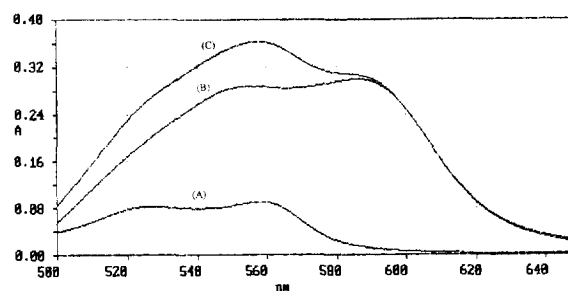
Fig. 2. Absorption spectra of (A) nickel complex, (B) cobalt complex and (C) mixture of nickel and cobalt complexes. Reference, reagent blank. [Ni(II)] = 0.04 μg ml^{-1}; [Co(II)] = 0.20 μg ml^{-1}. A = Absorbance.

recorded against a reagent blank. In it can be seen that nickel cannot be determinated with Br-PADAP in the presence of cobalt by ordinary spectrophotometry. Fig. 3 shows the first-derivative absorption spectra of the complexes of nickel and cobalt with Br-PADAP and a mixture of both complexes. It shows that the nickel determination must be performed using the zero-crossing method by measuring the derivative signal at 563 nm.

It can also be seen that cobalt can be determined in the presence of nickel by measuring the derivative signal at 616 nm, hence allowing the simultaneous determination of nickel and cobalt.

3.7. Nickel determination in presence of cobalt by dual-wavelength spectroscopy

The interference of cobalt in the determination of nickel using Br-PADAP can also be eliminated

Table 3
Statistical analysis of nickel determination in the presence of cobalt by first derivative spectrophotometry[a]

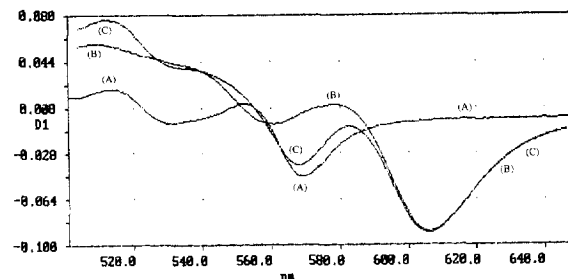| Co concentration (μg per 25 ml)	Cross-correlation equation	
	Zero-peak method	Zero-crossing method
0.0	H (cm) = 0.0886C$_{Ni}$ − 0.10 (r = 0.9998)	H (cm) = 0.0704C$_{Ni}$ + 0.01 (r = 0.9994)
1.0	H (cm) = 0.0884C$_{Ni}$ − 0.21 (r = 0.9998)	H (cm) = 0.0703C$_{Ni}$ + 0.02 (r = 0.9997)
3.0	H (cm) = 0.0867C$_{Ni}$ − 0.23 (r = 0.9997)	H (cm) = 0.0706C$_{Ni}$ + 0.02 (r = 0.9999)
5.0	H (cm) = 0.0853C$_{Ni}$ − 0.29 (r = 0.9995)	H (cm) = 0.0703C$_{Ni}$ + 0.01 (r = 1.0000)

[a] C$_{Ni}$ = 10–200 ng ml^{-1}.

Fig. 3. First-derivative absorption spectra of (A) nickel complex, (B) cobalt complex, and (C) mixture of nickel and cobalt complexes. Reference, reagent blank. [Ni(II)] = 0.04 μg ml^{-1}; [Co(II)] = 0.20 μg ml^{-1}. D$_1$-derivative signal × 10. ZP = zero-peak; ZC = zero crossing.

Table 4
Nickel determination in presence of cobalt by conventional and dual-wavelength spectrophotometry

Co(II) present (μg)	Ni(II) present (μg)	Ni(II) found (μg)	
		Ordinary spectrophotometry	Dual-wavelength spectrophotometry
0.20	1.00	1.10	0.99
1.00	1.00	2.20	1.00
3.00	1.00	3.82	0.99
5.00	1.00	4.81	0.99
5.00	2.00	6.52	2.01
5.00	0.50	6.15	0.45

Table 5
Analytical characteristics of the procedures

Analytical parameter	Ordinary spectrophotometry	Dual-wavelength spectrophotometry	Derivative spectrophotometry
Calibration sensitivity (S_C)	1.86 ml μg^{-1}	1.84 ml μg^{-1}	0.886 cm ml ng^{-1}
Analytical sensitivity (S_A)	0.81 ml ng^{-1}	0.71 ml ng^{-1}	11.42 ml ng^{-1}
Inverse of the analytical sensitivity ($1/S_A$)	1.24 ng ml^{-1}	1.41 ng ml^{-1}	0.09 ng ml^{-1}
Limit of detection (3σ)	1.8 ng ml^{-1}	2.0 ng ml^{-1}	0.2 ng ml^{-1}
Limit of quantification (3σ)	5.8 ng ml^{-1}	6.5 ng ml^{-1}	0.6 ng ml^{-1}
Linear dynamic range	5.8 ng ml^{-1}	6.5 ng ml^{-1}	0.6 ng ml^{-1}
	0.50 μg ml^{-1}	0.25 μg ml^{-1}	0.25 μg ml^{-1}
Relative standard deviation (%)	1.54%	1.22%	1.20%
Molar absorptivity		1.10×10^5 l mol^{-1} cm^{-1}	

by using dual-wavelength spectroscopy [12,13]. This can be performed by measuring the absorbances at 562 nm (absorption maximum for the nickel complex) and 596 nm, where the cobalt(II)–Br-PADAP complex has the same absorption as at 562 nm. Thus, the calibration curve for nickel determination is established by the relationship between the nickel concentration and the difference in the absorbances measure at 562 and 596 nm:

$$A_{562\ nm} - A_{596\ nm} = KC_{Ni}\ (\mu g/ml)$$

where A is the absorbance, K is the slope of the curve or calibration sensitivity and C is the nickel concentration.

Table 4 demonstrates the application of the technique to the determination of nickel in the presence of different amounts of cobalt.

3.8. Analytical characteristics

In the conventional spectrophotometric procedure, Beer's law was obeyed in the nickel concentration range 0–0.50 μg ml^{-1} and the graph passed through the origin with a molar absorptivity of 1.10×10^5 l mol^{-1} cm^{-1} at 562 nm. The calibration graph for the derivative method was linear from 0 to 250 ng ml^{-1} of nickel.

The slope of the analytical curve in the dual-wavelengh technique is normally lower than that obtained with conventional spectrophotometry; however, in the present case the slopes were virtually identical because the molar absorptivity of the nickel(II)–Br-PADAP complex is very low (5.42×10^2 l mol^{-1} cm^{-1}) at 596 nm.

The derivative technique has a higher sensitivity that the ordinary method, as can be seen from the calibration sensitivity, analytical sensitivity and

Table 6
Nickel determination in steels by different procedures

Standard	Ni certified (%)	Ni found[a]		
		First-derivative spectrophotometry	Dual-wavelength spectrophotometry	Ordinary spectrophotometry
German steel	0.220	0.23 ± 0.02	0.21 ± 0.01	1.98 ± 0.03
Steel IBP-50	0.33	0.33 ± 0.01	0.34 ± 0.01	0.56 ± 0.02

[a] At 95% confidence level

Table 7
Compositions of the standards analysed

Standard	Ni (%)	Mn (%)	Cr (%)	Co (%)	Mo (%)	Cu (%)	V (%)	W (%)
German steel[a]	0.220	0.205	4.231	2.730	0.953	—	1.981	11.92
Steel IBP-50	0.33	0.280	4.49	0.260	5.54	0.091	2.00	6.40

[a] CECA, MPI 234-1.

the inverse. The analytical sensitivity [14], calibration sensitivity [14], the limit of detection [15] and other analytical characteristics of the methods are summarized in Table 5.

3.9. Application

The derivative procedure and dual-wavelength spectroscopy were applied to the determination of nickel in steel standards. The results are presented in Table 6 and demonstrate that there is no significant difference between the certified value and the value found with the proposed procedures at the 95% confidence level. The compositions of standards analysed are given in Table 7.

Samples were prepared using hydrochloric acid, nitric acid and hydrofluoric acid. The iron(III) cation was extracted as the chloride complex using ethyl acetate as extraction solvent.

The great sensitivity of the derivative technique allowed the determination of nickel in sea water.

4. Conclusion

Br-PADAP is one of the most sensitive reagents for nickel determination by spectrophotometric

methods. The derivative technique allowed the selectivity during nickel determination using Br-PADAP to be increased. The results of analyses in comparison with certified values for two steel standards indicated that the proposed procedures have very good accuracy and precision.

References

[1] F.D. Snell, Photometric and Fluorometric Methods of Analysis–Metals, Part 1, Wiley, New York, 1978, pp. 879–930.
[2] Z. Marczenko, Spectrophotometric Determination of Elements, Ellis Horwood, Chichester, 1976.
[3] W. Fu-Sheng, Q. Pei-Hua, S. Nai-Kui and Y. Fang, Talanta, 28 (1981) 189.
[4] A.C.S. Costa, S.L.C. Ferreira and I.P. Lobo, Talanta, 40 (1993) 1267.
[5] M. Jarosz, Chem. Anal. (Warsaw), 31 (1986) 719.
[6] H. Ishii, T. Odashima and T. Imamura, Analyst, 107 (1982) 885.
[7] E. Malinowska and K. Kasiura, Chem. Anal. (Warsaw), 31 (1986) 797.

[8] J.A. Murillo, J.M. Lemus, A.M.L. Peña and F. Salinas, Analyst, 113 (1988) 1439.

[9] A.G. Melgarejo, A.G. Céspedes and J.M.C. Pavón, Analyst, 114 (1989) 109.

[10] W. Naixing, L. Weian and Q. Ping, Talanta, 40 (1993) 897.

[11] G.L. McIntire, CRC Crit. Rev. Anal. Chem., 21 (1990) 257.

[12] S. Kus and Z. Marczenko, Analyst, 112 (1987) 1503.

[13] H.-H. Perkampus, UV–VIS Spectroscopy and its Applications, Springer, Berlin, 1992, pp. 81–87.

[14] J. Medinilla, F. Ales and F.G. Sanchez, Talanta, 33 (1986) 329.

[15] D.A. Skoog and J.J. Leary, Principles of Instrumental Analysis, Saunders College Publishing, FL, 4nd edn., 1992, pp. 6–8.

Studies on the second reciprocal derivative constant-current stripping analysis

Xiangyuan Ruan[a,*], Yaling Su[a], Youming Zhou[a], Hsiangpin Chang[b], Dexiong Feng[c]

[a]*Department of Applied Chemistry, Dongguan Institute of Technology, Dongguan, Guangdong 511700, People's Republic of China*
[b]*Department of Chemistry, University of Texas, Austin, TX 787112, USA*
[c]*Department of Chemistry, Jinan University, Guangzhou 510632, People's Republic of China*

Abstract

Theoretical and experimental investigation have been made on a method called the second reciprocal derivative constant-current stripping analysis (SRD-CCSA). The SRD-CCSA is based on the measurement of the d^2t/dE^2 signal given by the curve of (d^2t/dE^2) versus the electrode potential (E). The d^2t/dE^2-E curve gives a maximum value (d^2t/dE^2)$_{max}$ and a maximum value (d^2t/dE^2)$_{min}$, which show as two peaks on the curve. Either of the heights of the peaks and the sum of absolute values of the two peaks are proportional to the bulk concentration of the analyte in solution, and they are much larger than (dt/dE)$_p$ in the first reciprocal derivative constant-current stripping analysis (FRD-CCSA). The ratio of peak–peak height in the SRD-CCSA to peak height in the FRD-CCSA is about 43n (where n represents the number of electrons transferred during the electrode process for the analyte). Potential difference (W_{pp}) between the two peaks is 48.2 mV n^{-1} at 25°C in the SRD-CCSA, which is noticeably smaller than the half-height width $W_{p/2}$, 65.5 mv n^{-1}, in the FRD-CCSA. The theory was verified with a home-made multireciprocal derivative measuring instrument. The experimental results were in good agreement with the theoretical ones.

1. Introduction

Studies on the theory and applications for chronopotentiometric stripping analysis (CPSA) or constant-current stripping analysis (CCSA) were very active [1–9]. The first reciprocal derivative constant-current stripping analysis (FRD-CCSA), once called reciprocal derivative constant-current stripping analysis (RD-CCSA)

[1] enhanced the sensitivity of CPSA or CCSA by about 13 n times and the resolution of the method was improved to 65.5 mV n^{-1}, represented by the half-height peak-width $W_{p/2}$. The theory of the FRD-CCSA was applied to chronopotential analysis (CPA) [3] and to adsorptive constant-current stripping analysis (ACCSA) [4] which is the same as adsorptive voltammetric stripping analysis (AVSA) during the preconcentration step, resulting in reciprocal chronopotentiometry analysis (FRD-CPA) and reciprocal derivative adsorptive

---

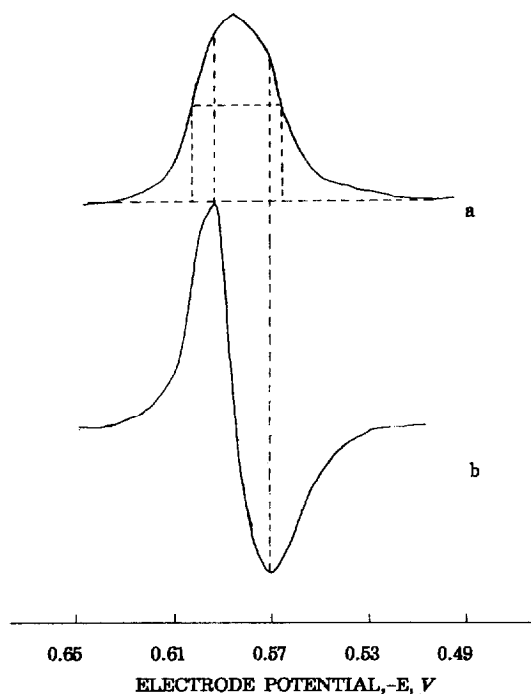* Corresponding author. Fax: (86) 769-226-2024.

Fig. 1. Comparison of schematic FRD-CCSA and SRD-CCSA signals for $n = 2$. (a) dt/dE versus E, (b) d^2t/dE^2 versus E. For definition of the symbols, see the text.
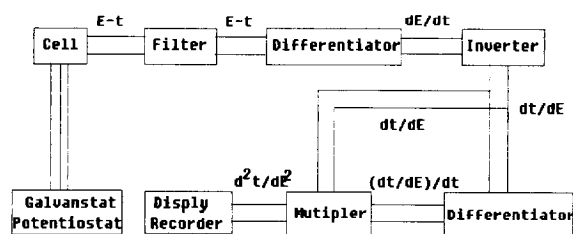
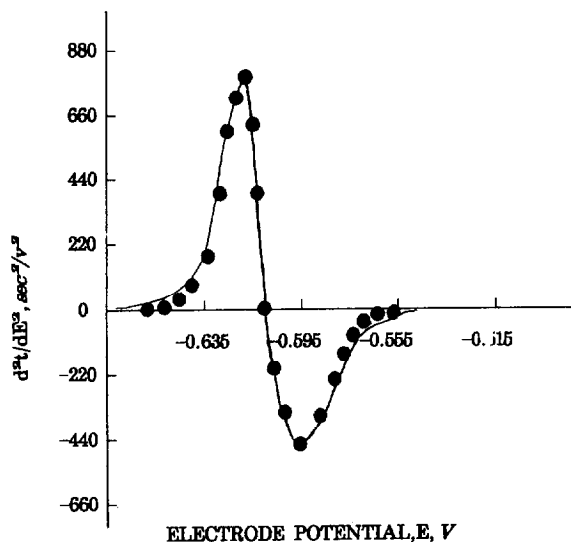

Fig. 2. Block diagram of the instrument set-up for SRD-CCSA.

Fig. 3. SRD-CCSA stripping curve: solid line, experimental curve; black dots, theoretical values calculated using Eq. (10). 4.0×10^{-7} mol 1^{-1} Cd^{2+}, $t_d = 60$ s, $i_s = 5$ μA.

constant-current stripping analysis (SRD-ACCSA). This make noticeable improvements in sensitivity and resolution for both of the methods.

In this paper we present a new thoery called the second reciprocal derivative constant-current stripping analysis (SRD-CCSA), i.e. deducing the $d^2t/dE^2–E$ curve and measuring $(d^2t/dE^2)_{pp}$ as the analyte signal instead of $(dt/dE)_p$ in FRD-CCSA. The $(d^2t/dE^2)_{pp}–E$ curve gives one maximum value $(d^2t/dE^2)_{max}$ and one minimum value $(d^2t/dE^2)_{min}$ (see Fig. 1b), which show as two peaks on the $d^2t/dE^2–E$ curve. Potential differ-

ence between the two peaks is noticeably smaller than the half-height peak-width $W_{p/2}$, 65.5 mv n^{-1}, at 25°C in FRD-CCSA. The sum of the absolute values of the two peak heights, or either of the two peak heights is proportional to the bulk concentration of the analyte in solution, and is much larger than $(dt/dE)_p$ in the FRD -CCSA. The theory was experimentally verified with a home-made multi-reciprocal derivative measuring instrument. The experimental results were in good agreement with the theoretical ones. This new approach to CCSA can enhance the sensitivity of the method by about 43 n times and its resolution is improved by about 25%, compared to those in FRD-CCSA.

2. Theory

2.1. Stripping curve of the SRD-CCSA

Equations describing the $E–t$ curve in the CCSA (or CPSA) and describing the $dt/dE–E$ curve in FRD-CCSA at the thin mercury-film electrode (TMFE) are as follows:

$$E = E' + RT \ln(t^{1/2}/\tau - t)/nF \text{ [10]} \tag{1}$$

$$dt/dE = nf[(2\tau + e^{-x})/(4\tau \, e^x + 1)1/2 - e^{-x}] \, [1]$$

$$\tag{2}$$

respectively, in which $f = F/RT$, and $x = 2nf(E - E')$ with

$$E' = E^o + RT \ln[2l/(\pi D_o)^{1/2}]/nF \tag{3}$$

where l is the thickness of the mercury film; τ is the transition time; D_o is the diffusion coefficient of the metal ion (M^{n+}) in solution; t is the stripping time for M^{n+}; and the other symbols have their normal electrochemical meanings. Differentiating Eq. (2) versus E and rearranging yields an equation describing the SRD-CCSA stripping curve, i.e. the d^2t/dE^2-E curve as follows:

$$d^2t/dE^2 = 2(nf)^2[e^{-x} - e^{-x}/(4\tau \, e^x + 1)^{1/2}$$
$$- 2\tau(2 \, e^x + 1)/(4\tau \, e^x + 1)^{3/2}] \tag{4}$$

Resolving Eq. (4) by numerical analysis and combining with Eq. (1), obtains a maximum value denoted by $(d^2t/dE^2)_{max}$

(a) INDIUM CONCENTRATION, $\times 10^{-8}$mol/l

(b) LEAD CONCENTRATION, $\times 10^{-7}$mol/l

(c) THALLIUM CONCENTRATION, $\times 10^{-8}$ mol/l
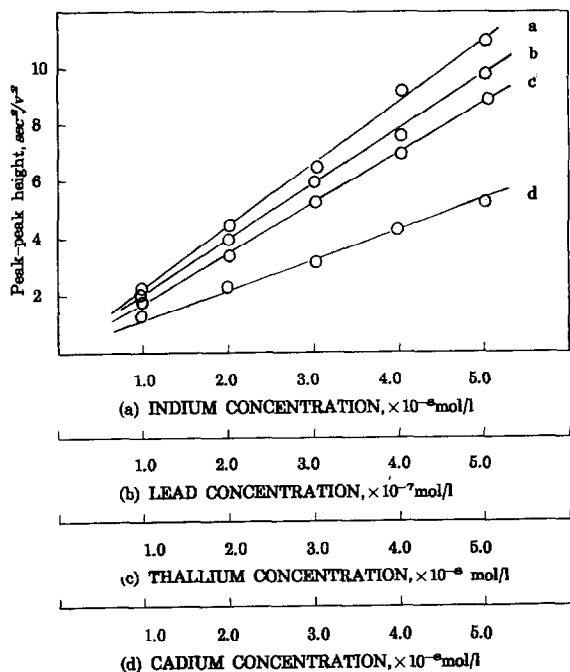
(d) CADIUM CONCENTRATION, $\times 10^{-8}$mol/l

Fig. 4. The dependence of $(d^2t/dE^2)_{pp}$ on C^0: curve a, $(d^2t/dE^2)_{pp}$ versus $[In^{3+}]$ curve b, $(d^2t/dE^2)_{pp}$ versus $[Pb^{2+}]$; curve c, $(d^2t/dE^2)_{pp}$ versus $[Tl^+]$; curve d, $(d^2t/dE^2)_{pp}$ versus $[Cd^{2+}]$. For other conditions see Fig. 3.
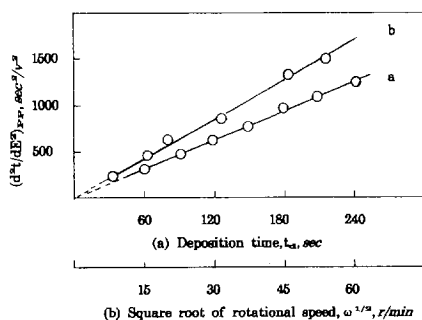
$$(d^2t/dE^2)_{max} = 0.2276(nf)^2\tau \tag{5}$$

at potential

$$E_{max} = E' - 0.805RT/nF - (RT \ln \tau)/2nF \tag{6}$$

and a minimum value denoted by $(d^2t/dE^2)_{min}$

$$(d^2t/dE^2)_{min} = -0.1520(nf)^2\tau \tag{7}$$

at potential

$$E_{min} = E' + 1.051RT/nF - (RT \ln \tau)/2nF \tag{8}$$

Eqs. (5) and (7) show that the d^2t/dE^2-E curve has two peaks, one of which is positive and the other negative. Either of the peak heights, are proportional to the transition time τ and to the bulk concentration of the analyte (C^0), considering that τ is proportional to C^0. By making the two extreme values absolute and then putting them together one obtains the height of the two peaks, denoted by $(d^2t/dE^2)_{pp}$: $(d^2t/dE^2)_{pp} = |(d^2t/dE^2)_{max}| + |(d^2t/dE^2)_{min}| = 0.3796(nf)^2\tau$

$$= 575.2n^2\tau \text{ (at 25°C)} \tag{9}$$

Substituting Eq. (9) into (4) yields

$$d^2t/dE^2 = 2(nf)2[e^{-x} - e^{-x}/(4k \, e^x + 1)^{1/2}$$
$$- 2\tau(2 \, e^x + 1)/(4k \, e^x + 1)^{2/3}] \tag{10}$$

in which $k = 1.9 \times 10^{-8}n^{-2}T^2(d^2t/dE^2)_{pp}$. Eq. (10), describing quantitively the relationship between the signal and the potential, is then called the stripping curve of SRD-CCSA.

2.2. Principle of the second reciprocal derivatization measurement

In principle,

$$d^2t/dE^2 = d(dt/dE)/dt \cdot dt/dE \tag{11}$$

If assuming $y = dt/dE$, then

$$d^2t/dE^2 = dy/dt \cdot y \tag{12}$$

Based on Eqs. (11) and (12), the principle of the second reciprocal derivatization measurement is as follows. Signal dt/dE from the derivative inverter described earlier [1] is first differentiated, yielding the signal $d(dt/dE)/dt$, then the signal $d(dt/dE)/dt$ is multiplied by the signal dt/dE, resulting in the signal d^2t/dE^2. It is very impor-

Fig. 5. The dependence of $(d^2t/dE^2)_{pp}$ on t_d and $\omega^{1/2}$: curve a, $(d^2t/dE^2)_{pp}$ versus t_d, 1.0×10^{-7} mol l^{-1} Cd^{2+}, $i_s = 5$ μA, $\omega = 2000$ rev min^{-1}; curve b, $(d^2t/dE^2)_{pp}$ versus $\omega^{1/2}$, 1.0×10^{-7} mol l^{-1} Cd^{2+}, $t_d = 55$ s, $i_s = 8$ μA.

tant to eliminate noises from 50 Hz city power and the electrolysis cell, for SRD-CCSA is very sensitive to both analytical signals and noises. Signals from the electrolysis cell are, therefore, first filtered by a high-frequency filter and a bandstop filter for 50 Hz city power, and then picked up by a computer. Other blank noises are eliminated by computer software. Sampling frequency of the computer should be carefully selected. A sawtooth-like curve might result if the sampling frequency is too high because if the sampling frequency is too high, the sign collected will be too small when compared with noises of about 6 mV irregularly from the instrument. On the other hand, an odd curve would emerge if the sampling frequency is too low for alot of signals will not be collected. Suitable sampling frequency for our instrument is in the range from 500 to 10 000 Hz. The operating principle of the instrument set-up for the SRD-CCSA is shown in Fig. 2.

2.3. Peak–peak width, resolution and specific potential

Combining Eq. (6) with eq. (8), the potential difference (W_{pp}) between the maximum and the minimum and the minimum vales of the stripping curve of SRD-CCSA is then obtained as follows:

$$W_{pp} = 1.876RT/nF = 48.2 \text{ mV n}^{-1} \quad (\text{at } 25°C) \tag{13}$$

Eq. (13) shows that the resolution of SRD-CCSA is much higher than that of linear sweep voltamme-

try, 173 mV n^{-1} [11], differential pulse polarography, 90.4 mV n^{-1} [12], semidifferential voltammetry, 54.4 mV n^{-1} [13], and the FRD-CCSA, 65.5 mV n^{-1} [1]. The resolution of SRD-CCSA and SRD-CCSA can be compared in Fig. 1.

Substituting Eq. (9) into (6) and (8), and rearranging the equations yields:

$$E^{M_{max}} = E_{max} + (RT \ln(d^2t/dE^2)_{pp})/2nF$$

$$= E' - (RT/nF)(1.309 - \ln(nF/RT)) \tag{14}$$

$$E^{M_{min}} = E_{min} + (RT \ln(d^2t/dE^2)_{pp})/2nF$$

$$= E' + (RT/nF)(0.567 + \ln(nF/RT)) \tag{15}$$

respectively. Apparently, E^M_{max} and E^M_{min} are functions of the standard potential (E^0) of the M^{n+}/M couple, the mercury film thickness (l), and the diffusion coefficient of the ion M^{n+} in solution, but independent of the signal $(d^2t/dE^2)_{pp}$, i.e. concentration (C^0) of the determined ion M^{n+} and other experimental conditions. E^M_{max} and E^M_{min}, therefore, can be used as parameters for qualitative identification. Eqs. (14) and (15) can be used to test if the measured signal $(d^2t/dE^2)_{pp}$ contains any noise or other signals from interfering ions, because $E_{max} + (RT\ln(d^2t/dE^2)_{pp})/2nF$ and $E_{min} + (RT\ln(d^2t/dE^2)_{pp})/2nF$ should be constants according to Eqs. (14) and (15).

2.4. Peak–peak height and factors affecting the peak–peak height

It is known that τ is proportional to the concentration (C_M) of metal M in a film of thickness l, i.e.

$$\tau = lC_M/\lambda \quad [10] \tag{16}$$

with

$$C_M = 0.62\omega^{1/2}D_0^{2/3}\mu^{-1/6}l^{-1}t_dC^0 \quad [1] \tag{17}$$

where $\lambda = i_s/nFA$, i_s is the stripping current (μA); A is the electrode area (cm^2); ω is the angular rotational velocity (s) during preconcentration; μ is the viscosity of the solution (cm^2 s^{-1}); t_d is the deposition time (s); and C^0 is the bulk concentration of the determined metal ion M^{n+} in solution. Dimensions of D_0 and l are cm^2 s^{-1} and cm, respectively.

Substituting Eq. (17) into (16), and then into (9) yields

$$(\mathrm{d}^2 t/\mathrm{d}E^2)_{pp}$$

$$= 3.058 \times 10^{15} n^3 T^{-2} A \omega^{1/2} D_0^{2/3} \mu^{-1/6} i_s^{-1} t_d C^0$$

$$= 3.44 \times 10^{10} n^3 A \omega^{1/2} D_0^{2/3} \mu^{-1/6} i_s^{-1} t_d C^0 \text{ (at 25°C)}$$

$$(18)$$

From Eq. (18), it can be seen that the peak–peak height of SRD-CCSA is proportional to the bulk concentration of the analyte in solution which is the basis for the quantitative application of SRD-CCSA. The peak–peak height is also proportional to the electrode area (A), deposition time (t_d), the square root of the angular rotational velocity of the working electrode during deposition, and it is a inverse function of the stripping current.

3. Experimental method

3.1. Apparatus

A laboratory-built multi-reciprocal derivative PSA/CCSA instrument equipped with a Compaq 386 computer and LQ 1600 typer were used. A thin mercury-film electrode deposited on a rotational glassy carbon electrode was used as the working electrode. Reference and counter electrodes were Ag/AgCl saturated with KCl and platinum respectively. A model DL-501 thermostat system was used to control the temperature of the solution.

3.2. Reagents

All the chemicals were analytical or guaranteed grade. Solutions were prepared with water triple-distilled in quartz. Cadmium and lead standard solutions were prepared from the nitrates and those of indium and thallium from the pure metals.

The supporting electrolyte, sodium nitrate (2.5 mol 1^{-1}) was pruified by catholic mercury-pool electrolysis for over 24 h and diluted to 0.25 mol 1^{-1} in use. Nitric acid was used to adjust the solution pH to about 4. The nitrogen used for deaeration was purified by passage through vanadium (ii) chloride solution.

3.3. Procedure

The disc rotational carbon electrode was first polished with alumina powder, then cleaned consecutively with nitric acid solution (1 + 1) and ammonia solution (1 + 1), 95% ethanol, and finally rinsed with triple-distilled water before use if the electrode had been used for about ten days, otherwise, the electrode only needed polishing with filter paper. The thin mercury-film electrode was prepared by depositing mercury from 2.0 × 10^{-4} mol 1^{-1} mercuric nitrate solution at $E_d = -1.0$ V. The predeposition of the analyte in the sample solution was done with a rotational velocity of $\omega = 2000$ rev min^{-1} or 209 s^{-1} and stripping was done in quiescent solution. Before deposition the solution was deaerated by the passage of nirtrogen for 15 min. After that a stream of nitrogen was passed over the surface of the solution to prevent oxygen from redissolving in the solution during the deposition and the stripping. All experiments were done at 25.0 ± 0.2°C.

4. Results and discussion

4.1. Validation of the SRD-CCSA stripping curve equation

A simulation method was used to validate the SRD-CCSA stripping curve equation, i.e. Eq. (10). $E_{\max}$ and $(\mathrm{d}^2 t/\mathrm{d}E^2)_{pp}$ values obtained from experimental stripping curves were first substituted into Eq. (14) to calculate the corresponding theoretical values of E'. Then the E' and $(\mathrm{d}^2 t/\mathrm{d}E^2)_{pp}$ values were substituted into Eq. (10) to calculate the $\mathrm{d}^2 t/\mathrm{d}E^2$ values at some potentials for the theoretical values. These were compared with the experimental curve. One of the results is depicted in Fig. 3. It can be seen from Fig. 3 that the theoretical values are in good agreement with the experimental curve in most regions, but slightly different at the beginning and the end, of the curve. This proved Eq. (10) to be correct, taking into consideration the capacitance effect

Table 1
Comparison between SRD-CCSA, FRD-CCSA and CPA signals

Element	τ (s)	y'_p (s V^{-1})	y''_{pp} (s² V^{-2})	y''_{pp}/τ (s V^{-1})			y''_{pp}/y'_p (s V^{-1})		
				Exptl	Thetl	RD (%)	Exptl	Thetl	RD (%)
Cd	0.98	25.4	2174.9	2219.3	2305.1	−3.7	85.6	86.6	−1.1
Pb	1.02	26.4	2251.8	2207.7	2305.1	−4.2	85.3	86.6	−1.5
Tl	1.06	13.8	587.3	554.1	576.3	−3.9	42.6	43.3	−0.2
In	1.01	36.2	4580.1	4534.8	5186.7	−12.6	126.5	29.9	−2.6

y''_{pp}, y'_p, Exptl, Thetl and RD represent $(d^2t/dE^2)_{pp}$, $(dt/dE)_p$, experimental, theoretical and relative derivation, respectively. $t_d = 100$ s, $i_s = 5$ μA, $\omega = 2000$ rev min^{-1} $[Cd^{2+}] = [Pb^{2+}] = [In^{3+}] = [Tl^+] = 7.2 \times 10^{-7}$ mol l^{-1}. The attenuations of SRD-CCSA for Cd, Pb, In and Tl are 1908, 190.8, 394.8 and 47.7, respectively, when the signals were measured with the instrument.

when the electrode potential changes quickly and negligibleness in theory at the extreme situations.

4.2. Factors affecting the peak–peak height $(d^2t/dE^2)_{pp}$

According to Eq. (18), there is a linear relation among $(d^2t/dE^2)_{pp}$ and the bulk concentration C^0 of the ion determined, the predeposition time t_d, the square root of electrode rotational speed, ω, during predeposition and the inverse value of the stripping current i_s. The dependence of the stripping peak–peak height $(d^2t/dE^2)_{pp}$ of the SRD-CCSA for Cd^{2+}, Pb^{2+}, In^{3+} and Tl^+ on $\omega^{1/2}$, i_s^{-1}, t_d and C^0 was studied independently one by one, while keeping the others constant. The plots of $(d^2t/dE^2)_{pp}$ versus C^0 for Cd, In, Tl and Pb are shown in Fig. 4, and versus t_d and $\omega^{1/2}$ shown in Fig. 5. The linear relations shown in Fig. 4 and Fig. 5 are in good agreement with the prediction
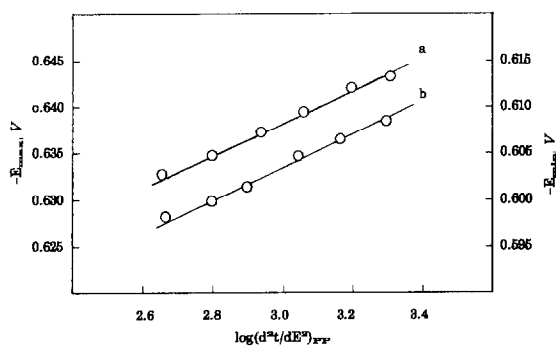

Fig. 6. The dependence of E_{max} and E_{min} on $(d^2t/dE^2)_{pp}$: curve a, E_{max} versus $(d^2t/dE^2)_{pp}$; curve b, E_{min} versus $(d^2t/dE^2)_{pp}$.

of Eq. (18). A non-linear relationship between $(d^2t/dE^2)_{pp}$ and i_s^{-1}, however, was observed in our experiment, although $(d^2t/dE^2)_{pp}$ increased with i_s^{-1}. This experimental phenomenon was discussed in an early paper [1].

4.3. Comparison of SRD-CCSA, FRD-CCSA and normal CPSA signals

To make a reliable comparison of SRD-CCSA with normal CPSA signals, the CPSA should be large enough to be measured precisely. The SRD-CCSA signal, however, will be over thousand volts, which is much too large for a normal integrated circuit. Even though those of the CPSA last only a second. Signals carried and exported by the laboratory-built instrument were, therefore, attenuated with five levels: 13.4, 47.7, 94.7, 190.8 and 399.7 times. The experimental results for Cd, Pb, In and Tl are listed in Table 1 and compared with the theoretical ones.

It can be seen from Table 1 that y''_{pp}/τ values for Cd^{2+}, Pb^{2+} and Tl^+ are close to those predicted from Eq. (9), but much smaller for In^{3+}, which may be caused by the lower reversibility of the In^{3+}/In couple.

The relation between FRD-CCSA and CPSA is as follows:

$$(dt/dE)_p = 0.343nf\tau = 13.35n \tau \text{ (at 25°C)} \quad (19)$$

Combining Eq. (9) with Eq. (19) yields:

$$(d^2t/dE^2)_{pp}/(dt/dE)_p = 43.3n \text{ (at 25°C)} \quad (20)$$

Table 2

E_{max} and E_{min} values at different peak–peak heights calculated according to Eq. (14) and (15)

	Cd^{2+}		Pb^{2+}		Tl^+		In^{3+}	
$-E_{max}$ (mV)	6302	6332	3615	3672	5087	5186	5647	5696
	6374	6403	3704	3744	5248	5306	5718	5747
$(d^2t/dE^2)_{pp}$	565	884	463	1031	315	588	499	1236
$(s^2 V^{-2})$	1460	2008	1591	2246	856	1372	2257	3798
$-E_{max}^{M*}$ (mv)	5895	5897	3221	3226	4358	4367	5381	5391
	5906	5915	3231	3238	4381	4379	5388	5394
$-E_{max}^{M}$ (mv)	5903		3229		4371		5389	
RD (%)	0.1		0.2		0.2		0.1	
$-E_{min}$ (mv)	6049	6081	3358	3417	4610	4665	5461	5512
	6112	6149	3446	3477	4726	4786	5535	5572
$-E_{min}^{M*}$ (mv)	5642	5646	2966	2971	3871	3846	5195	5207
	5654	5661	2973	2982	3959	3959	5205	5219
$-E_{min}^{M}$ (mv)	5651		2973		3859		5207	
RD (%)	0.1		0.2		0.2		0.1	

$(d^2t/dE^2)_{pp}/(dt/dE)_p$ values for Cd^{2+}, Pb^{2-}, In^{3+} and Tl^+ in Table 1 show that the experimental results are in good agreement with the theoretical ones, indicating that the sensitivity of the SRD-CCSA is enhanced by about 43.3n times, compared with that of the FRD-CCSA. It is also observed from Table 1 that the difference between the experimental values and the theoretical ones in $(d^2t/dE^2)_{pp}/(dt/dE)_p$ rises with an increase in electron number transmitted in the electrode process. The deviations may also come from the instrument.

4.4. Verification of the E_{max}, E_{min}, E_{max}^M and E_{min}^M equations

Plots of E_{max} against $\log(d^2t/dE^2)_{pp}$, and of E_{min} against $\log(d^2t/dE^2)_{pp}$ should give straight lines with a slope of $2.3RT/2nF$ according to Eqs. (6) and (8). From Fig. 6 we can see that the linear relations are very well demonstrated. The slopes

Table 3

Peak–peak width, W_{pp}, values (mV) for Cd^{2+}, Pb^{2+}, In^{3+} and Tl^+ calculated using Eq. (13)

	Cd^{2+}	Pb^{2+}	In^{3+}	Tl^+
Experimental values	25.3	18.4	47.9	25.9
Theoretical values	24.1	16.1	48.2	24.1
Relative error (%)	5.0	14.3	−0.6	7.6

of the lines for cadmium nitrate solution, however, are 17.8 mV for the E_{max}–$\log(d^2t/dE^2)_{pp}$ curve and 18.0 mV for the E_{min}–$\log(d^2t/dE^2)_{pp}$ curve, respectively, which are larger than the theoretical value of 14.8 mV. This may be due to the lower reversibility of the electrode process in the CCSA.

The element specific potentials for metal M, E_{max}^M and E_{min}^M, defined in Eqs. (14) and (15), respectively, are predicted to be constant, and are independent of the stripping signal, concentration of the determined ion and some experimental
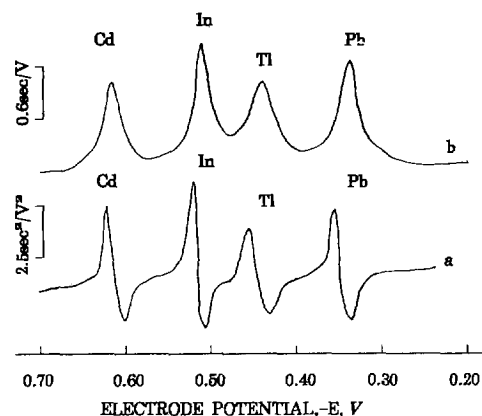

Fig. 7. Stripping curves of cadmium, indium, thallium and lead mixture: $[Cd^{2+}] = [Pb^{2+}] = 8 \times 10^{-8}$ mol l^{-1} $[Tl^+] = 1.2 \times 10^{-7}$ mol l^{-1}, $[In^{3+}] = 5.0 \times 10^{-8}$ mol l^{-1}, $t_d = 50$ s, $i_s = \mu A$, $\omega = 2000$ rev min^{-1}, $(d^2t/dE^2)_{pp}/13.4$.
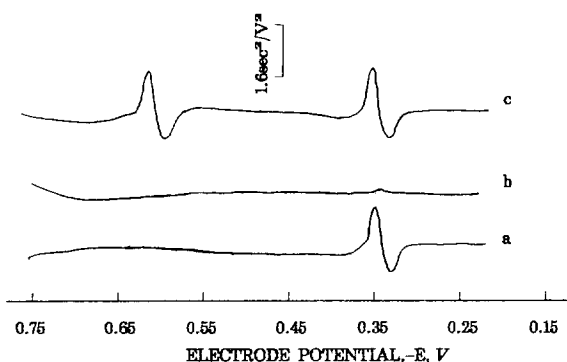
Fig. 8. Stripping curve for 1.0×10^{-10} mol l^{-1} Cadmium: curve a, SRD-CCSA curve for 0.25 mol l^{-1} NaNO$_3$ solution; curve b, FRD-CCSA curve for 0.25 mol l^{-1} NaNO$_3$ and 1.0×10^{-10} mol l^{-1} cadmium solution; curve c, SRD-CCSA curve for the same solution as in curve b.

variables such as t_d, ω and i_s. Results listed in Table 2 show that either E_{max} or E_{min} remains almost constant with a relative deviation of $\leqslant$ 0.2%, which indicates the accuracy of Eqs. (14) and (15).

4.5. Peak–peak width and resolution

Experimental peak–peak width (W_{pp}) values for Cd^{2+}, Pb^{2+}, In^{3+} and Tl$^-$ and their theoretical ones are listed in Table 3. In Table 3 we can see that the experimental values are close to the theoretical ones for the ions listed, although difference is observed in In. Taking into account the complexity of the electrode process and the errors from the responding and measuring signals in the instrument, Eq. (13) can be regarded to be correct.

Stripping curves given by both SRD-CCSA and FRD-CCSA for a mixture containing 10^{-8} mol l^{-1} levels of Cd^{2+}, Pb^{2+}, In^{3+} and Tl$^-$ are shown in Fig. 7. The peaks for these ions are more clearly separated from each other in SRD-CCSA than in FRD-CCSA, indicating very good resolution for SRD-CCSA.

4.6. Detection limit

Under the following experimental conditions: deaeration with high purified nitrogen for 30 min, predeposition with an electrode rotations velocity

of 2800 rev min^{-1} for 100 s at -1.0 V, a stripping current, i_s, 1 μA, the SRD-CCSA and FRD-CCSA signals for 1.0×10^{10} mol l^{-1} Cd^{2+} are shown in Fig. 8. Curve a is the stripping curve of SRD-CCSA obtained from a blank solution; a signal at a potential of -0.32 V was yielded by contaminating lead in the solution. Curve b, obtained by FRD-CCSA from the solution, shows no peak. Curve c obtained by SRD-CCSA from the same solution, however, shows a signal, 1.7 s^2 V^{-2} at a poential of -0.61 V for Cd^{2+} and another signal, 2.2 s^2 V^{-2}, at a potential of -0.32 V for contaminating Pb^{2+}. This detection limit shows that the sensitivity of the SRD-CCSA is very high.

5. Conclusions

From the description above it can be concluded that both the theory and the experimental results for SRD-CCSA show high sensitivity and excellent resolution. The theories describing the shape, and the change of the d^{2}t/dE^2–E curve are in agreement with the experimental results, proving that the theories presented in this paper are correct for SRD-CCSA, based on the d^{2}t/dE^2–E curve. It is believed that SRD-CCSA is one of the best methods, in terms of sensitivity and resolution for the determination of trace metal ions. The theory presented in this paper, by the way, could be applied to PSA, ACCSA, CPA etc. Applications of the theory are under way and the results will be given in later reports.

Acknowledgements

References

[1] X. Ruan and H. Chang, Talanta, 35 (1988) 861.
[2] X. Ruan and H. Chang, Talanta, 36 (1989) 1081.
[3] X. Ruan and H. Chang, Huaxue Xuebao, 49 (1991) 65.

[4] W. Jin and J. Wang, J. Electroanal. Chem., 306 (1991) 31.

[5] W. Jin, X. Zhao and Y. Liu, Anal. Lett., 25 (1992) 1741.

[6] L. Xiao and W. Jin, Talanta, 40 (1993) 1221.

[7] H. Huiliang, C. Hua, D. Jagner and L. Renman, Anal. Chim. Acta, 193 (1987) 61.

[8] H. Huiliang, D. Jagner and L. Renman, Anal. Chim. Acta, 202 (1987) 117.

[9] X. Ruan, J. Li, Y. Li and J. Deng, Chinese Chemical Letters, 3 (1992) 205.

[10] S.P. Perone and J. Brumfield, J. Electroanal. Chem., 13 (1967) 124.

[11] A.J. Bard and L.R. Faulkner, Electrochemical Methods, Wiley, New York, 1980 p. 195.

[12] A.J. Bard and L.R. Faulkner, Electrochemical Methods, Wiley, New York, 1980 p. 219.

[13] J. Mo, P. Cai, W. Huang and F. Yun, Huaxue Xuebao, 42 (1984) 556.

Effect of variables influencing $S_{1/2}$ in sequential injection analysis. Extrapolability of $S_{1/2}$ based results between SIA designs

A. Cladera*, E. Gómez, J.M. Estela, V. Cerdà

Departamento de Química, Universitat de les Illes Balears, E-07071 Palma de Mallorca, Spain

Abstract

The influence of variables including ionic strength, propulsion rate and instrumental design parameters on dispersion in a sequential injection analysis system was studied via $S_{1/2}$ and several other parameters related to the dispersion profile. The influence of such parameters on a real system was evaluated in the reaction of Fe(II) with o-phenanthroline by optimizing various instrumental designs using the simplex method and comparing the results.

Keywords: Sequential injection analysis (SIA); $S_{1/2}$

1. Introduction

Flow-through techniques in general and sequential injection analysis (SIA) in particular rely on the mutual dispersion of reactant segments being carried along a tube. Controlling dispersion in a given system is therefore very important with a view to its characterization and optimization. Ruzicka and Hansen [1] developed a dispersion coefficient for describing the dilution of a reagent plug on insertion into a flowing carrier stream:

$$D = \frac{C_0}{C} \tag{1}$$

* Corresponding author.

where C_0 is the initial concentration of reagent and C that after dispersion. While D is defined at any point of a system, use of D_{max} (the dispersion coefficient obtained when the maximum product concentration reaches the detector) is preferred.

As a rule, the type of dispersion a given system exhibits should be matched to the type of measurements it is intended to provide. Thus, direct meausurements (e.g. pH, conductivity, potentimetry) are best made at $D \simeq 1$ (minimum dispersion), whereas measurements of a chemical reaction can be carried out at intermediate D values (2–10); higher dispersion coefficients are usually reserved for cases involving high dilution.

Based on theoretical considerations for SIA, Gübeli et al. [2] proposed the parameter $S_{1/2}$, which denotes the injected volume that results in

$D_{max} = 2$, as the most convenient measure of dispersion in an SIA system irrespective of its symmetry and flow type. They also investigated the feasibility of using $S_{1/2}$ to extrapolate the results of a system to another of a different design.

It should be noted that the above considerations are based solely on physical dispersion in the system and take no account of the potential effects of chemical reactions and their kinetics. Also, the information provided by D and $S_{1/2}$ is always referred to a given point of the system rather than its dispersion profile, which can be of great significance regarding interpenetration of sample and reagent segments.

A literature scan revealed the absence of experimental work aimed at determining whether dispersion descriptors for a system can be used to extrapolate results to other systems. This paper reports a study of the effect of instrumental, physical and chemical variables on $S_{1/2}$ and the geometry of the dispersion profiles for sequential injection systems, which was undertaken to find out whether $S_{1/2}$ based results can be extrapolated to other systems.

2. Experimental

2.1. Reagents

The solutions used included methylene blue in 0.2 M $NaNO_3$, malachite green in 0.01 M acetic/acetate buffer at pH 4.5, and bromothymol blue in 0.01 M borax buffer at pH 9.2, all at variable concentrations. A 1.16×10^{-3} M o-phenanthroline solution in 1 M acetic/acetate buffer at pH 4.5, and another containing 2.1×10^{-5} M Fe(II) in 0.5% (w/v) hydroxylamine were also used.

2.2. Apparatus

The automatic SIA system used was designed by the authors and consisted of a PC compatible computer that actuated a Crison microBur 2030 titration autoburette, an electromechanically controlled 6-channel valve and a Hewlett-Packard HP 8452A diode array spectrophotometer. The instrumental design and control software used were

described in detail in a previous paper [3]. As can be seen in Fig. 1, the SIA manifold used was quite simple; the dimensions of the hold-up (A) and reaction (B) loops were altered as required to obtain various SIA systems exhibiting differential dispersion patterns. All connections were made from PTFE tubing with the dimensions stated in each case.

2.3. Procedure

2.3.1. Determination of $S_{1/2}$

$S_{1/2}$ for each system was determined from triplicate injections of increasing volumes of dye solution. The peak heights obtained were plotted against the injected volume and $S_{1/2}$ was calculated by interpolating the volume corresponding to one-half the absorbance of the undiluted dye.

2.3.2. Fe(II)/o-phenanthroline experiments

The design of the SIA systems studied was optimized using the reaction of Fe(II) with o-phenanthroline. In principle, the reaction involved four reactants, which were delivered via two channels by appropriate prior mixing of the compatible reactants. The experiments were carried out by aspirating preset volumes of o-phenanthroline and Fe(II) solutions, in this sequence, and subsequently propelling them to the detector via the reaction loop.
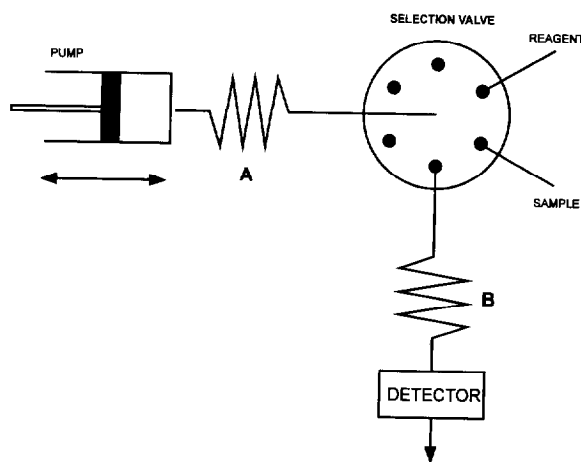

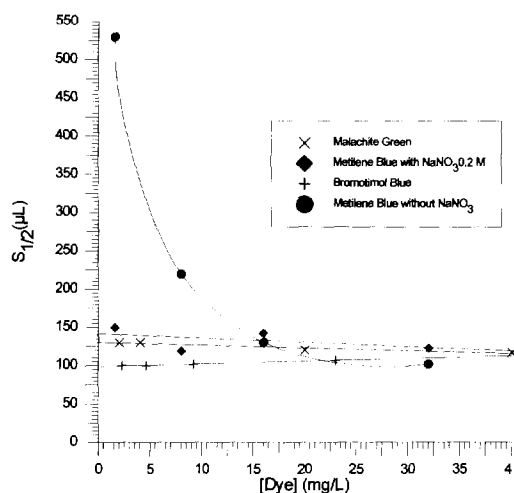Fig. 1. Basic SIA manifold used in the experiments. A, hold-up loop; B, reaction loop.

Fig. 2. Variation of $S_{1/2}$ with the type of dye and its concentration: ×, malachite green; ◆, methylene blue with 0.2 M $NaNO_3$; +, bromothymol blue; ●, methylene blue without $NaNO_3$. Hold-up loop i.d. = 1.5 mm; reaction loop i.d. = 0.5 mm; reaction loop length = 1 m; q = 3.6 mL min^{-1}.

3. Results and discussion

3.1. Influence of experimental parameters on $S_{1/2}$

3.1.1. Influence of the injected reactant

In preliminary experiments, we observed that the $S_{1/2}$ values calculated by injecting methylene blue in the system was dependent on the dye concentration. In order to investigate this phenomenon and the influence of the nature of the species used to calulate $S_{1/2}$, this value was determined for various concentrations of three different dyes, namely, bromothymol blue (BTB), malachite green (MG) and methylene blue (MB). BTB and MG, two acid–base indicators, were made in a buffered medium (0.1 M HAcO/NaAcO for MG and 0.01 M borax for BTB). As can be seen from the results (Fig. 2), both BTB and MG behaved very similarly: the dye concentration had virtually no effect on $S_{1/2}$. On the other hand, the MB concentration was found to strongly influence $S_{1/2}$, particularly at low levels (<10 mg L^{-1}). The experiments with MB were repeated by preparing solutions in a medium of controlled ionic strength (0.2 M $NaNO_3$), where the dye behaved identically with the other two (see Fig. 2). Experiments performed at a variable

ionic strength revealed the anomalous behaviour of MB to disappear at $NaNO_3$ concentrations above 0.04 M. This phenomenon is rather difficult to interpret, yet we believe it may have originated from adsorption of the dye onto the walls of the Teflon tubes, which may be hindered by the presence of an electrolyte or a higher dye concentration.

The most important consequence of the above-described results is that the correct determination of $S_{1/2}$ entails using controlled conditions as regards the dye, its concentration, the ionic strength, etc. in order to avoid a potential effect of the dye concentration on $S_{1/2}$ values.

Based on the results, we chose to use 23 mg L^{-1} BTB in subsequent experiments.

3.1.2. Influence of propulsion rate and flow reversals

In order to compare our experimental design with the previously reported flow injection analysis (FIA) and SIA systems, we have investigated the influence of the flow rate and the flow reversals on $S_{1/2}$. The influence of the flow rate during the time that the reactants are propelled to the detector on $S_{1/2}$ was studied by using a hold-up loop of 1.5 mm i.d. and a reaction loop of 1 m length × 0.5 mm i.d. The propulsion rate was varied between 3.5 and 19.0 mL min^{-1}. Unfortunately, the propulsion system available at the time these experiments were carried out did not allow the aspiration rate to be programmed, so the potential influence of this factor could not be investigated.

The experiments revealed that decreasing flow rates resulted in increasing $S_{1/2}$ values, the effect being more marked at low rates. It should be noted, however, that the $S_{1/2}$ values obtained at high flow rates hindered correct identification of the peak maximum since the peaks were too narrow at the maximum acquisition rate available (2.5 data/s). The results are consistent with those obtained with FIA systems [4] and can be explained on the grounds of the same theoretical considerations.

A unique feature of SIA systems is that mutual dispersion of the reactants is favoured by flow reversals in the system. In order to assess the

significance of the effect, a series of experiments was carried out in which the aspirated dye was followed by 100 μL of carrier and several 50 μL aspiration/propulsion cycles. The results showed the dispersion to increase markedly in the first few cycles and then more gradually in subsequent cycles, which is consistent with the previous observations of Gübeli et al. [2].

3.1.3. Dimensions of the reaction loop

The results obtained in the experiments aimed at determining the influence of the dimensions of the reaction loop on dispersion showed both the reactor length and its inner diameter have a strong effect: the greater the diameter and length were, the higher was $S_{1/2}$ as a result of the increased residence time and longer path travelled by the dye inside the system. These results are consistent with those for FIA systems.

It should be noted that two pieces of tubing of identical nominal inner diameter (0.5 mm) supplied by different manufacturer provided different results. The differential behaviour of the tubes cannot be exclusively ascribed to divergences between the nominal and actual diameters—in fact, the differences, as determined by measuring the capacity of both loops, were negligible. A more plausible explanation is that, because the tubes were from two different sources, they differed in their inner microstructure and therefore affected dispersion within differently. We also observed an anomalous behaviour from newly purchased tubing: the size and shape of the peaks obtained in the first few injections vary markedly until the tubing is "aged". This ageing process can be accelerated by passing dilute nitric acid for a few minutes. This effect, which is absent in FIA, must be considered in SIA, where the carrier flow is not maintained at a constant rate for a long time.

3.1.4. Influence of the diameter of the hold-up loop and the travelled path

In the experiments performed so far, a dye was aspirated and immediately propelled to the detector; consequently, the path it travelled inside the loop was the minimum required for aspiration. On the other hand, a chemical reaction entails aspirating at least two reactants (sample and reagent). As

a result, every aspirated substance except the last must travel a longer path along the hold-up loop, which will inevitably increase their dispersion.

In order to assess this effect, a series of experiments was carried out where a preset volume of dye solution was aspirated first, followed by a fixed volume of carrier (water). The $S_{1/2}$ values as a function of the aspriated carrier volume (0, 100, 200, 300 and 400 μL) at various diameters of the hold-up loop (0.56, 0.8, 1.0, 1.5 mm) was obtained. As expected, the path travelled inside the hold-up loop greatly affected the dye dispersion as a result of the longer distance travelled; however, the dispersion was scarcely affected by the inner diameter of the hold-up loop because the latter did not alter the residence time, which was only dependent on the aspirated volume. In fact, $S_{1/2}$ was found to depend virtually linearly on the aspirated carrier volume in every instance (R^2 ranged from 0.9781 to 0.9986).

It sould be noted that the path travelled by a substance cannot be altered at will as it is dictated by the chemical reaction involved and the aspirated reactant volumes in each case. Therefore, the dimensions of the reaction loop are much more influential than those of the hold-up loop—the latter need only be large enough to hold the aspirated reactants and prevent them from reaching the propulsion system (syringe) and contaminating the carrier.

3.2 Dispersion profile shape

The $S_{1/2}$ value for an SIA system is a measure of dispersion but provides no spatial information on diffusion profiles. To find out whether the shape of such profiles is indicative of the extent of mutual reactant dispersion in SIA systems, the way it is influenced by the most significant experimental variables was studied. For this purpose, a series of experimental assemblies was tested by injecting a dye volume equal to $S_{1/2}$ and comparing the shape of the peaks thus obtained, which were virtually the same height. In the assemblies tested we varied the reactor i.d. (0.5, 0.56, 0.8, 0.86, 1.0 and 1.5 mm), the reactor length (0, 1, 2 and 3 m) and the path travelled inside the hold-up loop (0, 100, 200, 300 and 400 μL).
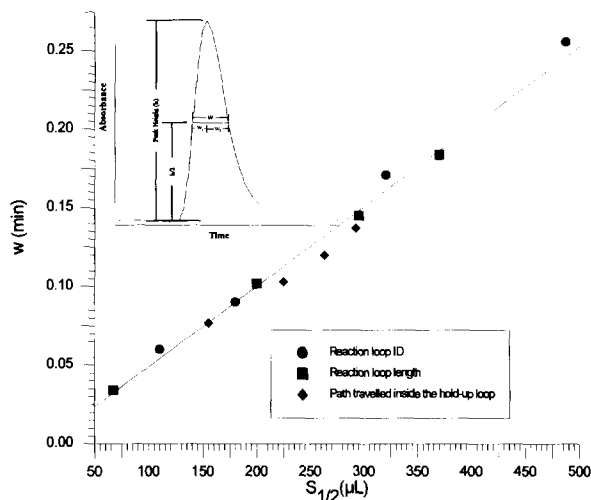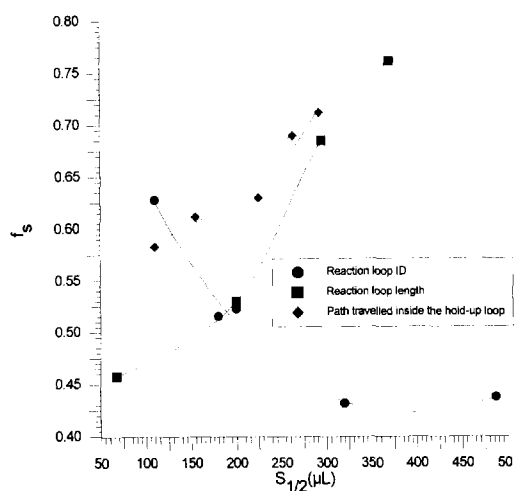
Fig. 3. Variation of peak width with $S_{1/2}$. Dye, BTB (23 mg L^{-1}); hold-up loop i.d. = 1.0 mm; $q = 3.6$ mL min^{-1}.

To summarize the results, two parameters related to peak shape were used, namely, the width at half-height (w) and a "symmetry factor" given by $f_s = w_1/w_2$ (the meanings of w, w_1 and w_2 are shown in Fig. 3). Figs. 3 and 4 show the variation of w and f_s, respectively, with $S_{1/2}$.

As can be seen from Fig. 3, whichever experimental variable is altered, peak width was linearly related to $S_{1/2}$ (the straight line thus obtained fitted the equation $w = 1.98 \cdot 10^{-3} + 5.1 \cdot 10^{-4}$

Fig. 4. Variation of peak symmetry with $S_{1/2}$. Dye, BTB (23 mg L^{-1}); hold-up loop i.d. = 1.0 mm; $q = 3.6$ mL min^{-1}.

$S_{1/2}$; $R^2 = 0.9858$), consistent with the expectations—in fact, the experimental design used ensured the same dispersion in every instance and hence a peak width proportional to the injected volume ($S_{1/2}$).

The situation of Fig. 4 is rather different. The symmetry of the dispersion profiles depends on both $S_{1/2}$ and the instrumental parameter fitted to obtain it. As can be seen in the figure, increasing $S_{1/2}$ by augmenting the reactor length or the path travelled along the delay coil also increased peak symmetry, probably as a result of the increased residence time, which is consistent with the theoretical predictions of Vanderslice et al. for FIA systems [5]. However, changes in symmetry with the reactor inner diameter followed the opposite trend, which in principle may have been the result of altering the tubing diameter resulting in an altered velocity profile within and hence in different dispersion mechanisms in each experiment.

As a rule, two systems having an identical $S_{1/2}$ value obtained from different combinations of instumental parameters may lead to dispersion profiles of the same width but different symmetry.

3.3. Optimization of systems involving a chemical reaction

In order to evaluate the effect of the parameters studied on a system involving a straightforward chemical reaction, four SIA systems for the determination of Fe(II) by its reaction with o-phenanthroline were assembled. They differed in the dimensions (length and inner diameter) of the reaction loop, which, as shown above, were the more influential of the parameters studied. The systems were designed in such a way that two had a very similar $S_{1/2}$ value—though obtained from different combinations of instrumental parameters—whereas the other two had a $S_{1/2}$ value below and above, respectively, the previous one.

The four systems were optimized using the simplex method with the aspirated sample and reagent volumes as optimization parameters (their concentrations and all other parameters were kept constant throughout). The simplex variant used was that of unidirectional advancement with contraction and interpolation [6], and the termination

Table 1
Characteristics of the systems optimized and optima obtained

System	Parameter			Optimum found			
	Reactor i.d. (mm)	Reactor length (m)	$S_{1/2}$ (μL)	$V_{reagent}$ (μL)	V_{sample} (μL)	F	No. iter.
A	0.86	0.59	264	295 ($1.12\ S_{1/2}$)	854 ($3.23\ S_{1/2}$)	152.3	21
B	0.56	2	250	255 ($1.02\ S_{1/2}$)	600 ($2.4\ S_{1/2}$)	164.3	16
C	0.5	1	110	256 ($2.3\ S_{1/2}$)	302 ($2.7\ S_{1/2}$)	172.2	20
D	0.86	1	487	291 ($0.60\ S_{1/2}$)	1078 ($2.21\ S_{1/2}$)	141.3	13

Reagent: 1.16×10^{-3} M o-phenanthroline in 1 M acetic/acetate buffer, pH 4.5.
Sample: 2.1×10^{-5} M Fe(II) in 0.5% (w/v) hydroxylamine.
$q = 3.6$ mL min^{-1}; hold-up loop i.d. $= 1.0$ mm.

criterion used was a difference less than 1% between the simplex vertices. The optimized object function was

$$F = \frac{h}{\exp\left(\dfrac{V_t}{V_{max}}\right)} \tag{2}$$

where h is peak height, V_t the total aspirated volume (sample and reagent) and V_{max} the maximum aspirable volume (4 mL in our case). This function was chosen in order to maximize simultaneously the analytical signal and the sample throughput (by minimizing the aspirated volume).

In principle, if the four systems had been equivalent, they should have exhibited similar optimal design parameters. Consequently, the differences between the optimum parameter values are measures of the degree of similarity between them.

Table 1 shows the experimental conditions used in each system and the position of its optima. Fig. 5 shows the dispersion profiles for the sample and reagent at each optimum, together with the analytical peak obtained in each case. The profiles were obtained by injecting two appropriate volumes of dye (23 mg L^{-1} BTB) and may not coincide fully with the actual profiles for the sample and reagent but are the best approximations one can obtain.

As can be seen, none of the four optima coincided. However, the two systems with the same

$S_{1/2}$ value were much more similar to each other than the rest regarding the position of their optima and the shape of their dispersion profiles.

4. Conclusions

From the results obtained in the study of the influence of experimental parameters, we can conclude that the FIA and SIA systems present similar behaviours as a consequence of their equivalent hydrodynamic foundation. However, SIA systems have a unique feature, the flow reversal, which modifies the interdispersion of the injected plugs.

The results obtained in this work allow one to draw several interesting conclusions about the design and optimization of SIA systems.

Thus, in studying the performance of a given system, one should bear in mind that dispersion profiles obtained by using a dye will possibly be somewhat different from the real profiles for the analytical reaction, even if the effect of the reaction and its kinetics are ignored. Consequently, such profiles can only be used as guidance.

Appropriate choice of various parameters allows one to obtain $S_{1/2}$ values over a relatively wide range for any SIA system. The choice must be consistent with the purpose of the work concerned. It should be noted, however, that similar
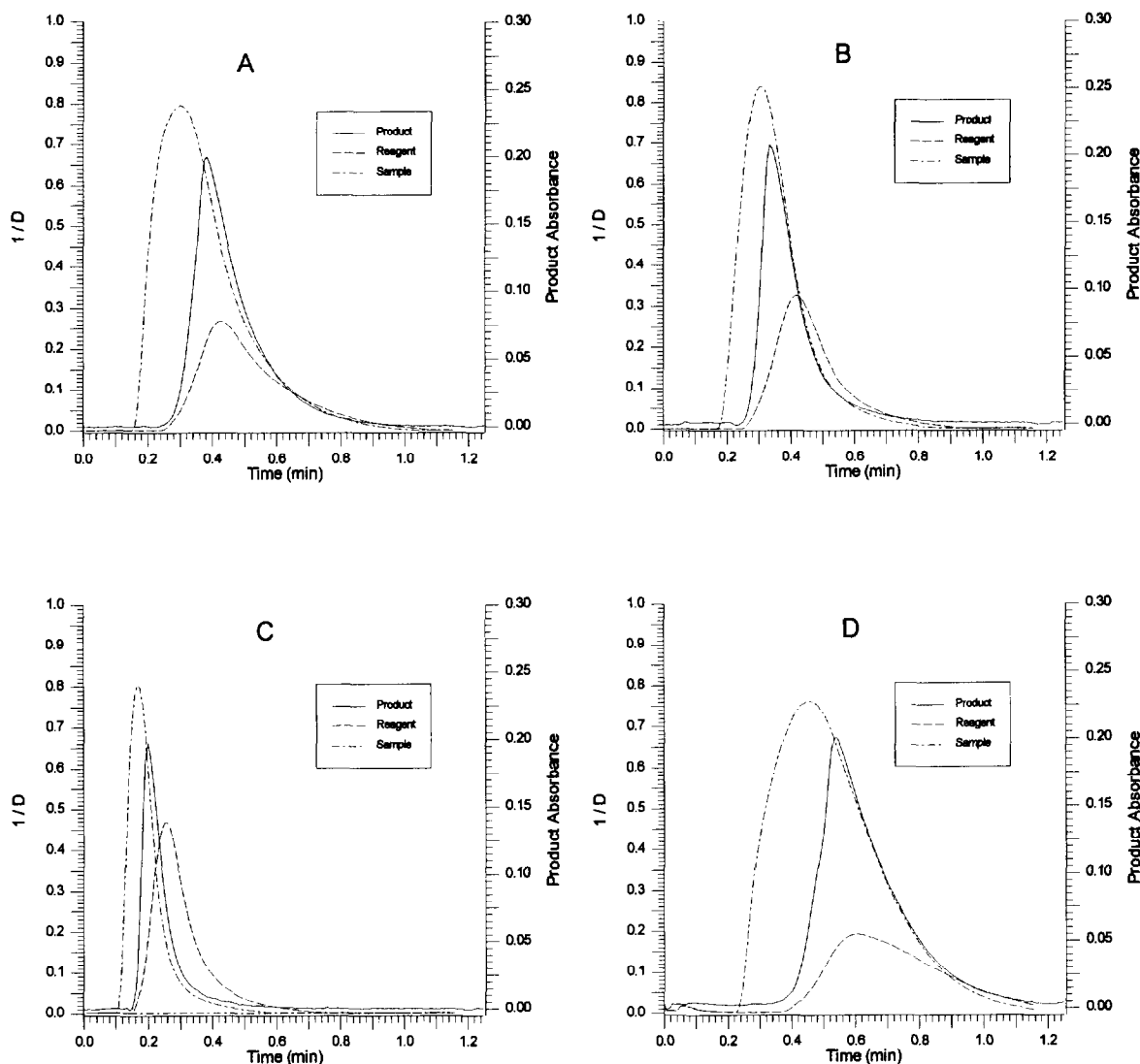
Fig. 5. Dispersion profiles and response obtained at the optima for the four systems studied. For conditions, see Table 1.

$S_{1/2}$ values obtained from different combinations of parameters can cause different dispersion profiles and therefore to a different extent of sample–reagent interdispersion. This can be almost critical depending on the particular chemical system involved.

The most influential parameters on SIA system design are the length and inner diameter of the reaction loop.

$S_{1/2}$ values seemingly do not allow for direct extrapolation of the results to different systems. While $S_{1/2}$ is a measure of dispersion in a given system, it provides no information on geometric factors (particularly symmetry). Therefore, while $S_{1/2}$ can be used as a guidance to choose a starting point, it seems each particular system must inevitably be optimized specifically.

Acknowledgements

References

[1] J. Ruzicka and E.H. Hansen, Anal. Chim. Acta, 78 (1975) 145.

[2] T. Gübeli, G.D. Christian and J. Ruzicka, Anal. Chem., 63 (1991) 2407.

[3] A. Cladera, C. Tomás, E. Gómez, J.M. Estela and V. Cerdà, Anal. Chim. Acta, 302 (1995) 297.

[4] J. Ruzicka and E.H. Hansen, Flow Injection Analysis, 2nd edn, John Wiley & Sons, New York, 1988.

[5] J.T. Vanderslice, A.G. Rosenfeld and G.A. Beecher, Anal. Chim. Acta, 179 (1986) 119.

[6] M.W. Routh, P.A. Swartz and M.B. Denton, Anal. Chem., 49 (1977) 1422.

Selective determination of cobalt using polyurethane foam and 2-(2-benzothiazolylazo)-2-p-cresol as a spectrophotometric reagent

Marcelo S. Carvalho[a],*, Izabel C.S. Fraga[b], Kátia C.M. Neto[a], Euclides Q. Silva Filho[a]

[a]Instituto de Engenharia Nuclear CNEN, P.O. Box 68550, Rio de Janeiro 21945–970, Brazil
[b]Departamento de Quimica, da Pontificia Universidade Católica do Rio de Janeiro, Rua Marques de São Vicente, 225 Gávea, Rio de Janeiro, Brazil

Abstract

The present work describes a selective, rapid and economical method for the determination of cobalt using the 2-(2-benzothiazolylazo)-p-cresol (BTAC) as a spectrophotometric reagent associated with a solid extraction on polyurethane foam. The BTAC reacts with Co(II) in the presence of Triton-X100 surfactant forming a green complex with maximum absorption at 615 nm. The reaction is used for cobalt determination within a pH range of 6.50–7.50, with an apparent molar absorptivity of 1.62×10^4 L mol^{-1} cm^{-1}. Beer's Law is obeyed for a concentration of at least 1.60 μg ml^{-1}. A selective procedure is proposed for cobalt determination in the presence of Fe(II), Hg(II), Zn(II) and Cu(II) up to milligram levels using masking agents. Polyurethane foam is used for the preconcentration and separation of cobalt from thiocyanate media and this procedure is applied to its determination in nickel salts and steel alloys.

Keywords: Cobalt determination; Spectrophotometric reagent

1. Introduction

Some highly sensitive reagents for the spectrophotometric determination of cobalt have been proposed, and their sensitivity, expressed in molar absorptivity, is as high as 6.0×10^3 M^{-1} cm^{-1} (4-bromodibenzoylmethane) [1], 1.00×10^4 M^{-1} cm^{-1} (3-hydroxy-propyl-1-phenylthiazine) [2], 9.80×10^4 M^{-1} cm^{-1} (5-Br-PADAP) [3], 11.60×10^4 M^{-1} cm^{-1} (5-Br-PADAB and TAMSMB) [4], and 1.20×10^3 M^{-1} cm^{-1} (2-nitroso-1-naphthol) [5]. Also, these reagents usually have low selectivity and interference occurs; especially when nickel, copper, mercury, molybdenum and iron are present in large quantities; therefore separation procedures are often required.

So far, cobalt has been separated from various interferents by solvent extraction from diethyldithiocarbamate using carbon tehrachloride at pH 10 [6] or from 4 M thiocyanate solution in

---

* Corresponding author. Fax: (+55) 21-5902692.

the presence of hydrochloric acid using methyl isobutyl ketone [7] with back extraction and spectrophotometric measurements. The anion exchange procedures for cobalt separation have been effectively used but metal elution frequently occurs at high (4–9 M) hydrochloric acid concentration [7]. Recently, a preconcentration method for cobalt determination has been proposed based on the adsorption of its ion associated complex with 2-nitroso-1-naphthol-3,6-disulphonate (nitroso R-salt) and tetradecyldimethylbenzylammonium iodide or chloride supported on naphthalene as a synthesized reagent [8,9]. The cobalt was measured by atomic absorption spectrometry or second derivative spectrophotometry, after solubilization of the loaded synthesized reagent in an appropriated volume of dimethilformamide.

Polyurethane foam (PUF) has been used as a solid organic sorbent for a wide variety of inorganic and organic compounds from different media [10–12]. The first detailed study on the separation and preconcentration of iron(III) and cobalt(II) in aqueous thiocyanate solutions was published by Braun and Farag in 1978 [11], and demonstrated that no more than five min was necessary to achieve quantitative (99%) extraction of cobalt from 0.2 M thiocyanate solutions in batch process. Hamon and Chow [13] published a systematic investigation of the extraction of cobalt from thiocyanate solution under a wide variety of conditions using cut cubes of PUF (1.3 cm edge), so that a volume of 150 mL of the cobalt–thiocyanate solution was equilibrated with 50 mg PUF by a batch squeezing extraction technique. This extraction was enhanced by high thiocyanate concentration and high ionic strength, between a pH range of 1.0–9.0, but it took a very long time to complete. PUF unloaded and loaded with 1-(2-pyridylazo)-2-naphthol has been shown to absorb quantitatively traces of cobalt, zinc and iron from acidic thiocyanate solutions and this formed the basis of subsequent cobalt determination by X-ray fluorescence [14,15] and neutron activation analysis [16] directly on the foam. The PUF thin layer spectrophotometry [17] was demonstrated as a technique; the colored complex was extracted and measured directly on the foam. Abbas et al. [18] presented a procedure for the microdetermination

of cobalt in water by direct PUF thin layer spectrophotometry based on the blue color of the cobalt–thiocyanate complex, which is quantitatively extracted from 1 M thiocyanate solutions, however the presence of Fe(III) and Mo(V) in large quantities cause interference.

The reagent 2-(2-benzothiazolylazo)-p-cresol (BTAC) was introduced by Gusev et al. [19] for the spectrophotometric determination of cadium, zinc and copper and layer by Fraga [20] as a spectrophotometric reagent for nickel determination in metal alloys.

This work describes the use of BTAC as a spectrophotometric reagent for cobalt, associated with solid extraction on PUF from thiocyanate medium to provide a selective, sensitive and rapid method for cobalt determination in the presence of large quantities of nickel, iron and molybdenum.

2. Experimental

2.1. Apparatus

Spectrophotometric measurements were made using a Micronal-B342II spectrophotometer with matched 1.00 cm quartz cells. A Porcyon-SA720 pH meter was used to measure the pH values of the solutions.

2.2. Reagents

All reagents were of analytical grade unless otherwise stated. BTAC (Pontifícia Universidade Católica-prepared [20]) solution (400 μg ml^{-1}) was prepared by dissolving the purified reagent in absolute ethanol (Merck). Standard cobalt(II) solution (1000 μg ml^{-1}) was prepared by dissolving cobalt(II) acetate in demineralized and double-distilled water, it was standardized by 4-(2-pyridylazo) resorcinol-EDTA complexometry. The buffer solution was prepared by mixing ammonium chloride solution with ammonium acetate solution in appropriate ratios and the pH was adjusted to 6.80.

Triton X-100 solution (5%) was prepared by dissolving 5.0 mL (Merck) in demineralized water and making to 100 mL. Potassium thiocyanate

solution (0.2 M) was prepared by dissolving the reagent (Carlo Erba) in demineralized water and adjusting to pH 3. The masking solution, containing thiocyanate, thiosulphate and tartarate (1%), was prepared by dissolving the sodium salts (P.A., Merck) in demineralized water.

A commercial, open cell, polyether-type PUF (Vulcan of Brazil—VCON 202, 42% resilience and 10–12 cells per linear cm) was pulverized and used as described previously [21].

2.3. General procedure

2.3.1. Spectrophotometric determination of cobalt (Procedure A)

A convenient aliquot of solution containing up to 16.00 μg of cobalt was transferred to a 10.00 mL standard flask; 1.00 mL of nitrate solution (1.0 M), 1.00 mL of masking solution, 1.00 mL of TRITON X-100 solution (5%), 1.00 mL of BTAC solution (200.00 μg mL^{-1}) and 2.00 mL of buffer solution (pH 6.80) were added. The standard flask was diluted to the mark with water and the absorbance at 615 nm measured against a blank prepared containing all the solutions except cobalt.

2.3.2. Separation of cobalt using PUF (Procedure B)

An aliquot of thiocyanate solution (0.2 M) at pH 3 [11,13], containing a convenient amount of cobalt was transferred to a stoppered flask; 100 mg of pulverized PUF was added and the volume was made up to 25.00 mL with the KSCN solution (0.2 M, pH 3). The system was then shaken mechanically (VKS-100 mechanical shaker, 100 counts per min) and the PUF was collected by vacuum filtration (filter paper $\phi = 2.0$ cm), washed with KSCN solution (0.2 M, pH 3), squeezed with a piston of Teflon and the cobalt was back extracted instantaneously with 10 mL of ethyl alcohol 80% solution [22]. The cobalt was measured as described in Procedure A, with a corresponding amount of alcohol added to the blank solution.

3. Results and discussion

3.1. Characteristics of the complex

The Co–BTAC complex has a low solubility in water, but when the reaction occurs in the presence of surfactant Triton X-100 it forms a green complex with maximum absorption at 615 nm in the pH range of 6.50 to 7.50. This complex is instantaneously formed, solubilized and it is stable for at least one hour. The stoichiometry was studied at pH 6.80 and a 1:3 (metal:ligand) molar ratio was achieved with the absorbance signal remaining unaltered up to 1:12, the molar absorptivity was $1.62 \pm 0.02 \pm 10^4$ L mol^{-1} cm^{-1}. The addition order of the reagents does not affect the complex formation.

3.2. Effect of pH

The effect of pH on the Co–BTAC system was studied and the results demonstrated that the absorbance signal is maximum and constant at the pH range 6.50–7.50 (Fig. 1). The general
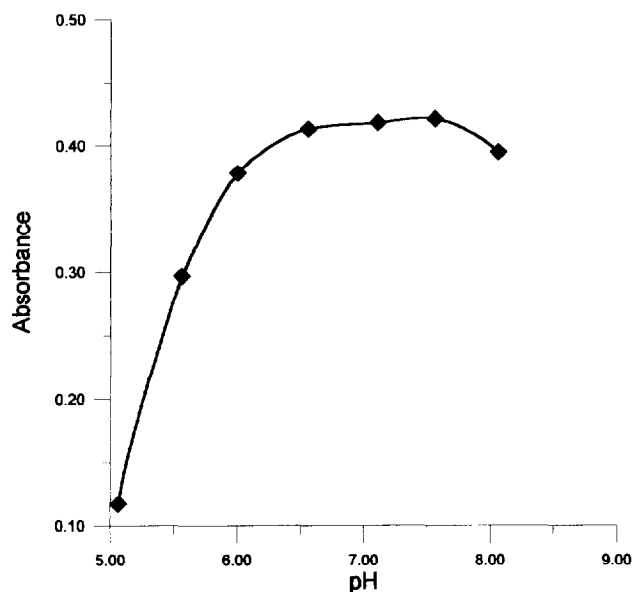

Fig. 1. Effect of pH on the system Co–BTAC in 0.5 M ammonium chloride–ammonium acetate buffer. [Co] = 1.34 × 10^{-3} M; $\lambda = 615$ nm; [BTAC] = 1.48 × 10^{-2} M; 0.50% Triton-X100 and 0.1 M NaNO$_3$.
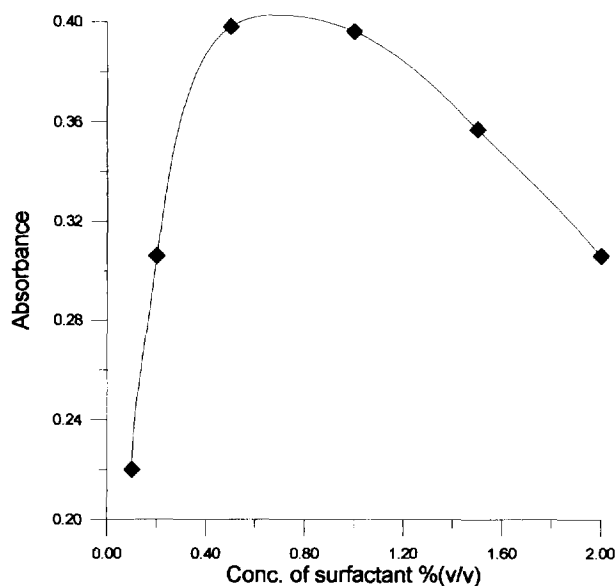
Fig. 2. Effect of surfactant Triton-X100 concentration on the system Co–BTAC in 0.5 M ammonium chloride–ammonium acetate buffer, pH 6.80. [Co] = 1.34 × 10⁻³ M; λ = 615 nm; [BTAC] = 1.48 × 10⁻² M; 0.1 M NaNO₃.

Procedure A was developed with an ammonium chloride–ammonium acetate solution adjusted to pH 6.80. The effect of the buffer concentration on the Co–BTAC system indicates that is does not affect the absorbance signal when the buffer analytical concentration varies up to 0.5 M.

3.3. Effect of Triton X-100 surfactant

The BTAC and its cobalt complex have a low solubility in water but they can be solubilized using Triton X-100. However, it was observed that the absorbance signal of the Co–BTAC system increases as the amount of surfactant is increased and a maximum signal is achieved between 0.4 and 1.0% (Fig. 2). Thus, 0.5% of Triton X-100 was selected as the optimal concentration in the general procedure.

3.4. Effect of interfering ions

The influences of some anions, cations and a number of complexing species that could be applied as selective masking agents were examined.

Solutions containing 10.00 µg of cobalt and various amounts of several cations and anions were prepared and measured under the optimum experimental conditions. The interference limit of an ion was arbitrarily established when a 2% change in the absorbance of the complex Co–BTAC was observed. Large amounts of thiocyanate (100 mg); chloride, fluoride, bromide, iodide, nitrate, acetate, thiosulphate and tartarate (10 mg); and sulphate and borate (5 mg) could be tolerated. Phosphate was tolerated at a low amount (0.01 mg) and EDTA interferes seriously. The metallic ions examined which did not interfere up to a 5 mg level are Cr(III), Mo(VI), Bi(III), Al(III), Fe(III) and Ga(III); and up to a 1 mg are Be(II), Mg(II), Mn(II), Sn(II) and Pb(II). However, up to 1 mg Fe(II), Hg(II), Zn(II), Cu(II) and Pd(II) could be masked with 1.00 mL of masking solution. Interference of Ni(II) was only eliminated by solid extraction on polyurethane foam (PUF).

3.5. Analytical characteristics of the method

The straight line calibration curve indicates that Beer's Law is obeyed up to a calculation of 1.60 µg mL⁻¹. The graph passes through the origin with the linear dynamic range between 0.08–1.06 µg mL⁻¹ and a coefficient of variation of 1.23%. The system Co–BTAC presents 273.5 mL µg⁻¹ as the analytical sensitivity [23], with 0.547 mL µg⁻¹ as the calibration sensitivity [23], 10 ng mL⁻¹ as the detection limit, and 80 ng mL⁻¹ as the limit of quantitation [24].

3.6. Solid extraction of cobalt using PUF as a separation procedure

Solid extraction of cobalt from 0.2 M thiocyanate solution at pH 3 was made in batch with 0.20 g of pulverized polyether-type PUF or in a column at a flow rate of 2.0 mL min⁻¹. Under this condition, the cobalt was completely extracted into the PUF while the nickel remained in solution. When the Fe(III) ion is reduced with ascorbic acid it is not extracted. Mo(V) is extracted only at low amounts and extraction is slow. To prevent Mo(V) interferences in the proposed procedure, 30% hydrogen peroxide (0.20

Table 1
Cobalt determination in the presence of nickel

μg Co taken	μg Ni taken	μg Co found	% Co recovery
10	–	9.9	98.9
10	–	9.9	99.0
10	10 000	10.1	101.1
1	5000	1.0	100.0

Table 3
Cobalt determination in nickel salts and standard steel alloys

Sample	% CO (95%)	Certified values (%)
$NiCl_2$	0.0075 ± 0.0005(5)	0.007[a]
$NiCl_2$	0.21 ± 0.006(5)	0.21[a]
$NiSO_4$	0.024 ± 0.001(4)	0.023[a]
M. Planck 234-1	2.725 ± 0.008(8)	2.73
F-50 (CNEN)	0.0445 ± 0.0001(20)	0.045
F-50 (CNEN)	0.0446[b]	0.045
IPT-AISI 136	0.259 ± 0.003(8)	0.26

[a] By ICP-AES.
[b] Standard addition.
(N), number of determinations.

mL) was added before the addition of the Triton solution during Procedure A. Cobalt extraction is swift and 10 min was sufficient to extract up to 73.00 μg cobolt with 60 mg of PUF, or 1.20 mmoles cobalt per gram PUF. Ten min was used for all of the extractions. The cobalt was quantitatively recovered (Table 1) after back extraction with 80% ethyl alcohol solution by batch procedures. Experiments using the column system required a very long time for complete cobalt elution because the polyether-type PUF used swells greatly in this medium [22].

3.7. Application

Procedure A was successfully applied to cobalt determination in waste water and the results, compared with inductively coupled plasma atomic emission spectrometry (ICP-AES) (Table 2), indicate that the proposed procedures provide very good accuracy and precision. For cobalt determination in nickel salts and standard steel alloys matrices a separation step was needed, then a solid extraction with PUF was applied as described in Procedure B. The standard steel alloys samples preparation were made using hydrofluoric and hydrochloric acids with 1.00 mL of 30% hydrogen peroxide. In all of the cases the samples were heated, evaporated to dryness, solu-

Table 2
Determination of cobalt in waste water

Sample	Co found (μg mL^{-1})	Co found by ICP-AES (μg mL^{-1})
A20-04	1.01 ± 0.03	1.06 ± 0.03
B20-01	1.28 ± 0.03	1.18 ± 0.05

bilized in 0.1 M hydrochloric acid solution and filtered, when necessary, before final dilution. Appropriate aliquots were taken and sufficient KSCN salt was added to make 0.2 M solutions; the pH was adjusted to 3 and ascorbic acid was used to reduce Fe(III). The results are presented in Table 3.

4. Conclusions

The solid extraction using PUF provides a simple, rapid, selective and economical method for preconcentration and separation of cobalt from samples containing large amounts of nickel, iron, and molybdenum into 0.2 M thiocyanate solution at pH 3. The back extraction with 80% ethyl alcohol solution was instantaneous and batch procedures may be recommended as more effective. This proposed cobalt separation procedure can be employed using another technique instead of spectrophotometry, and the PUF may be reused after washing with 80% ethyl alcohol solution and a large amount of distilled water [22]. The analytical appliation of the reagent BTAC is an original contribution for cobalt determination and the proposed method can be applied to the spectrophotometric determination of cobalt in matrices containing large amounts of nickel, iron and molybdenum.

Acknowledgements

References

[1] S.C. Sharma and M.P. Tyagi, Sci. Phy. Sci., 2 (1990) 7.

[2] D.N. Purohit and R. Bhatnagar, J. Sci. Res., 10 (1988) 7.

[3] Y. Sun and S. Qian, Yejin Fenxi, 7 (1987) 27.

[4] H. Wada, T. Ishizuki and G. Nakagaqa, Anal. Chim. Acta, 135 (1982) 333.

[5] E. Kiss, Anal. Chem. Acta, 66 (1973) 385.

[6] Atsushi Mizuike, Enrichment Techniques for Inorganic Trace Analysis, Springer-Verlag, New York, 1983.

[7] J. Starý, The Solvent Extraction of Metal Chelates. Pergamon Press, New York, 1964.

[8] M.A. Taher and B.K. Puri, Analyst, 120 (1995) 1589.

[9] B.K. Puri and S. Balani, Talanta, 42(3) (1995) 337.

[10] T. Braun, J.D. Navratil and A.B. Farag, Polyurethane Foam Sorbents in Separation Science, CRC Press, Florida, 1985.

[11] T. Braun and A.B. Farag, Anal. Chim. Acta, 89 (1978) 133.

[12] S. Palágyi, T. Braun, Separation and preconcentration of trace elements and inorganic species on solid polyurethane foam sorbents, in Z.B. Alfassi and C.M. Wai (Eds.), Preconcentration Techniques for Trace Elements, CRC Press, Boca Raton, 1992, p. 363.

[13] R.F. Hamon and A. Chow, Talanta, 31(11) (1984) 973.

[14] R.F. Hamon, A.S. Khan and A. Chow, Talanta, 29 (1982) 313.

[15] A. Chow, G. Yamashida and R.F. Hamon, Talanta, 28 (1981) 437.

[16] T. Braun, M.N. Abbas, A. Elek and B. Laslo, J. Radioanal. Chem., 67 (1981) 359.

[17] Y.A. Gawargious, M.N. Abbas, and H.N.A. Hassan, Anal. Lett., 21 (1988) 1477.

[18] M.N. Abbas, N.B. El-Assy, and Sh. A. Moniem, Anal. Lett., 22(6) (1989) 1555.

[19] S.I. Gusev, M.V. Zhvakina and A.I. Koshevnkova, Zh. Anal. Khim., 26 (1971) 1493.

[20] I.C. Serta Fraga, M.Sc. Dissertation, Pontifícia Univ. Católica, Rio de Janeiro, Brazil, 1989.

[21] M.S. Carvalho, J.A. Medeiros, A.W. Nóbrega, J.L. Mantovano and V.P.A. Rocha, Talanta, 42 (1995) 45.

[22] M.S. Carvalho, D.Sc. Thesis, Pontifícia Univ. Católica, Rio de Janeiro, Brazil, 1993.

[23] D.A. Skoog and J.J. Leary, Principles of Instrumental Analysis, Sounders College Publishing, London, 1992.

[24] J. Medinilla, F. Ales and F. Garcia Sanchez, Talanta, 33 (1986) 329.

Talanta

An electrostatic micro-collection interface for aerosol collection. Automated ion chromatographic analysis of aerosols

Shaorong Liu, Purnendu K. Dasgupta*

Department of Chemistry and Biochemistry, Texas Tech University, Lubbock, Texas 79409-1061, USA

Received 21 February 1996; revised 11 March 1996; accepted 11 March 1996

Abstract

A miniature aerosol collector based on electrostatic precipitation is described. The sampled aerosol is charged in the device by positive corona discharge and electrostatically collected. The device is operated as a collection interface for aerosol analysis, the collection surfaces can be washed in situ and the effluent subjected to chromatographic analysis on-line, all in a fully automated manner. At a sampling rate of 0.5 l min^{-1}, near unity collection efficiencies are obtained for aerosols of 1 μm and lower size, the size class of greatest environmental interest. Atmospheric aerosol constituents such as sulfate can be measured at the ng m^{-3} level. The disadvantage of the present system is that some artifact nitrate is generated (due to NO_x production in the corona) and reliable values of ambient nitrate aerosol cannot therefore be obtained.

Keywords: Aerosol collection; Automated ion chromatographic analysis; Electrostatic micro-collection interface

1. Introduction

Aerosols are ubiquitous in our environment. They affect visibility, climate, our health and quality of life. The exact role that atmospheric aerosols play depends on their chemical composition, size distribution, and concentration. A better understanding of the effects of aerosols requires a knowledge of all three of the above parameters. There are various techniques for aerosol collec-

tion and measurement; extant monographs describe these techniques [1,2]. For the measurement of aerosol particle size distribution and total mass concentration, many automated instruments are commercially available. However, at the present time, the measurement of the chemical composition of aerosols is usually carried out in discrete steps: first the sample is collected with filters, impactors or cyclones, and then analysis, usually preceded by a dissolution/extraction step, is carried out. Such multi-step methods are labor intensive and do not allow on-line analysis. A few automated schemes have been reported [3–10]. With the exception of the most recent papers

* Corresponding author. Fax: (806) 742-1289; e mail: VEPPD@ttacs.ttu.edu

[3–5], these are largely aimed toward a specific species such as aerosol H_2SO_4 and rely on some unique physicochemical property of that species. In recent years, significant efforts have been devoted to the mass spectrometric analysis of individual aerosol particles [11]; however, the cost and bulk of such instrumentation precludes their widespread use in the near future.

Collection of particles by electrical means is well known [12]. The velocity of a charged particle in an electric field can be much higher than its gravitational or inertial velocity. This is exploited in the industrial use of electrostatic precipitators for the removal of aerosols. The two basic steps involved are (a) to charge the particles and (b) to subject them to an electric field such that their electrostatic field induced migration will cause them to deposit on a collection surface. One characteristic of electrostatic precipitators is their high collection efficiencies (99–100%) over a wide range of particle sizes (approximately 0.05–5 μm) [12].

In this report, we describe a miniaturized electrostatic collector, similar in geometry to a wire-in-tube electrostatic precipitator [12], coupled to an ion chromatograph (IC). This arrangement permits the automated analysis of soluble components of atmospheric aerosols, with the exception of nitrogen oxyanions (because some NO_x is produced in the system). The relationships between the collection efficiency and the experimental parameters have been evaluated and are discussed.

2. Experimental

A schematic diagram of the overall experimental arrangement is shown in Fig. 1. It consists of three major parts, an aerosol generation system, an aerosol collection interface and an IC analysis system.

2.1. Aerosol generation system

Monodisperse aerosols were generated by a model 3450 Vibrating orifice aerosol generator equipped with a 20 μm diameter orifice (TSI, St. Paul, Minnesota, USA) by nebulizing sodium sul-

fate solutions of various concentration, and were used to test the performance of the micro-collection interface. A model 3054 aerosol neutralizer (TSI) was installed in the drying chamber of the aerosol generator to neutralize the electrostatic charge that exists on aerosol particles generated by solution nebulization. The neutralizer contains a 10 mCi krypton-85 radioactive source and is capable of charge neutralizing an aerosol flow up to 150 l min^{-1}. It was used throughout the experiment. In order to generate uniformly sized aerosol particles, we selected a flow rate and vibration frequency of 0.139 m min^{-1} and 68 kHz, respectively; this satisfies the condition, $3.5D_j < L < 7D_j$ (where D_j is the diameter of the orifice and L is the length of the liquid jet between vibrations; for the presently used combination, $L = 5.4D_j$), for the generation of uniform liquid droplets [13]. The sodium sulfate solutions were prepared in distilled and deionized water (NANOpure, Barnstead); the level of nonvolatile impurities in the solvent was negligible. After evaporation of the solvent in the drying chamber, the spherical equivalent diameter of the dry particles is given by
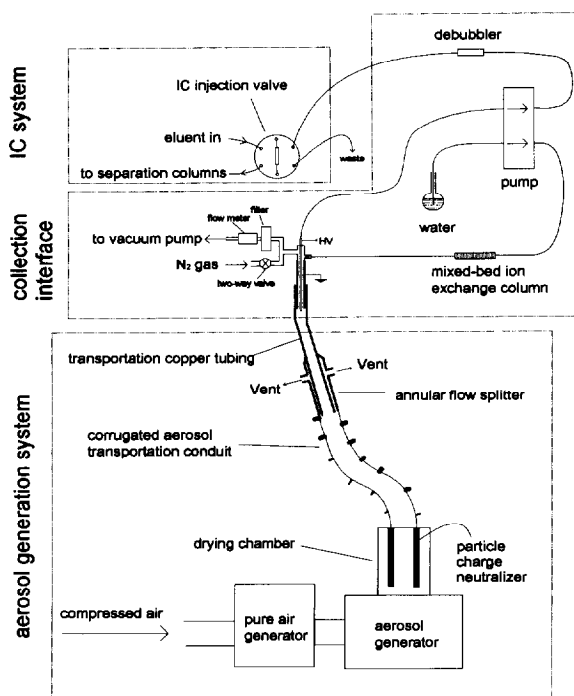

Fig. 1. Schematic diagram of the experimental arrangement.

$$d = d_i \cdot \sqrt[3]{\frac{C}{\rho}} \qquad (1)$$

where d_i is the diameter of the original droplet, C is the Na_2SO_4 concentration of the solution in g cm^{-3} and ρ is the density of solid Na_2SO_4.

A laser-based multichannel particle counter (model A2212-010115-1, Met-One, Grant's Pass, Oregon, USA) was used to measure the optical diameter of the particles. Although eq. (1) assumes spherical particles, aerosols of ionic salts produced by solution nebulization do not, of course, produce speherical particles. The diameters obtained from optical scattering experiments thus tend to be somewhat higher than the calculated spherical equivalent diameters. For a solution concentration of 15.6 μg cm^{-3} Na_2SO_4, a mass median diameter (MMD) of 1.26 ± 0.08 μm was obtained from the size distribution data generated by the laser particle counter. The aerosol formed by nebulizing sodium sulfate solution is probably in its most hydrated form: $Na_2SO_4 \cdot 10H_2O$ (molecular weight $= 322.19$ and $\rho = 1.464$). One thus calculates a particle diameter of 1.16 μm according to eq. (1), close to the results obtained with the optical instrument.

The dispersion and dilution air was provided by a model 737-14A pure air generator (AADCO, Clearwater, Florida, USA). These flow rates were set at 20 and 65 l min^{-1}, respectively. Under these conditions, the aerosol from the aerosol generator had a flow rate of about 85 l min^{-1}, which was much larger than the sampling flow rates (0.1–2 l min^{-1}) used in the present experiments. The aerosol flow was divided with a concentric annular flow splitter (Fig. 1). By adjusting the opening size of the split vents, the desired flow rate could be approximately obtained in the aerosol transportation tube (8 mm i.d. copper conduit). The collection device was directly inserted into the downstream end of the copper tube, the gap between the collection device body and the copper tube served as another vent.

2.2. Aerosol collection interface

The micro-collection interface in Fig. 1 is shown in greater detail in Fig. 2.
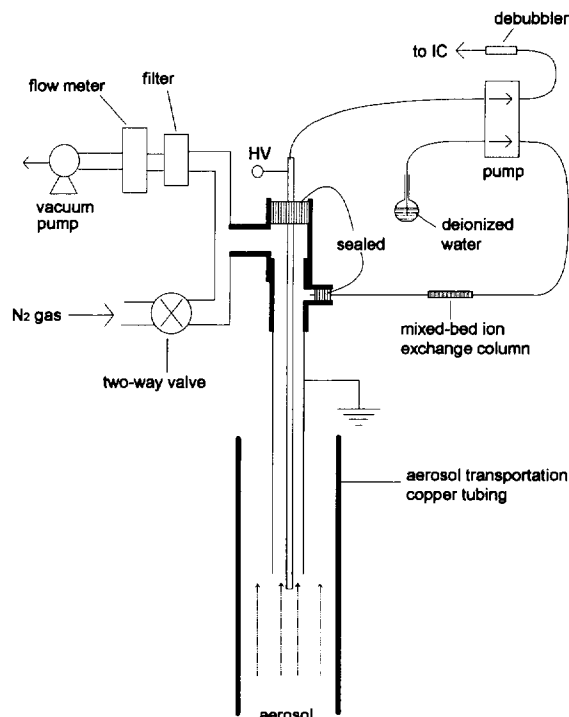

Fig. 2. Details of the collection interface.

The collection device consists of two concentric stainless steel tubes of about 30 mm × 2.7 mm i.d. × 3.4 mm o.d., and 80 mm × 0.2 mm i.d. × 0.4 mm o.d. These are referred to as the outer electrode and the center electrode, respectively. These tubes were fixed in position through two polypropylene tees (1/8" and 1/4", Ark-Plas Inc., Flippin, Arkansas, USA). The top end of the center electrode was extended through the tee and connected via a peristaltic pump to the preconcentration column of an IC system. The exposed part of this metal tube was connected to a high voltage power supply (Model PS350, Stanford Research Systems, Inc., Sunnyvale, California, USA). The outer electrode was electrically grounded. The bottom end of the center electrode protruded about 2 mm beyond the outer electrode end. This arrangement avoids arcing between the ends of the center and the outer electrodes. Such arcing must be avoided because it can occur before corona discharge begins. Arcing cause a current spike from which the high voltage power supply takes time to recover. Arcing could be eliminated

by making the center electrode protrude slightly below the outer electrode. The aerosol sample was aspirated into the collection chamber by a vacuum pump. The sampling flow rate was controlled by a mass flow controller (Model FC280, Tylan General, Torrance, California, USA) with an upstream filter to prevent aerosol intrusion. At any given sampling flow rate, an approximately isokinetic sampling condition [14] was obtained by adjusting the annular vent and thus the appropriate aerosol flow rate through the copper tube.

After the aerosol sample was collected for the desired period (typically 20 min), the collection surface was washed and the washings were preconcentrated on the IC system. Deionized water was delivered by a peristaltic pump. Before entering the annular aerosol collection area through the outer tube, the water was further deionized through a mixed-bed ion exchange resin (Dowex MR-3, Sigma) mini column. To ensure that all of the input liquid wash solution was aspirated back, the aspiration flow rate was set at nearly twice the input flow rate. Bubbles in the aspirated solution were removed before entering the IC preconcentration column by a debubbler. The debubbler was made by first cutting three rectangular openings (approximately 2 mm × 0.8 mm) on a segment of PTFE tube (approx. 30 mm × 1 mm i.d. × 1.4 mm o.d.) and then covering the openings by wrapping the tube with about 20 layers of stretched Teflon tape (plumber's tape). Without this debubbler, spikes and baseline shifts are observed in the chromatographic data output, complicating data interpretation. Typically, about 2 ml of deionized water was pumped through the system for complete washing. Before aerosol sampling was begun again, the system was cleaned and dried as follows. A two-way (on/off) valve was turned on and compressed nitrogen from a cylinder, regulated at 8 lb in^{-2}, was admitted into the annular space to blow away any lingering liquid and dry the whole system.

2.3. IC measurement system

The IC analysis system was based on a Dionex model DX-100 ion chromatograph equipped with a self-regenerating suppressor and a conductivity detector. The sampling loop of the IC injection valve was replaced with an AG 11 column (4 × 50 mm) for analyte preconcentration. An AS 11 column (4 × 250 mm) was used for separation. A 10 mM sodium hydroxide solution was used as the eluent at a rate of 1.0 ml min^{-1}.

2.4. Measurement of collection efficiency

The input aerosol concentration was measured by sampling the aerosol through a Millipore (type HA) membrane filter (0.45 μm pore size) at the same flow rate as that used by the collection interface, measuring the amount of sulfate in the aqueous extract of the filter by IC, and thus calculating the aerosol (sulfate) concentration. The ratio of the amount of sulfate collected by the collection device during the experiment to the amount of the sulfate aspirated through the collection device was considered the collection efficiency.

2.5. Experimental protocol

During the initilization step before each sampling/analysis cycle, the air and liquid pumps and the HV supply are switched off and compressed nitrogen is turned on for 60 s to clean and dry the system. The IC system is in the process of analyzing the sample from the previous cycle at this time. Sampling is conducted during the next step for a desired period (20 min is typical for ambient air experiments), with the sampling pump on and high voltage applied to the collector while the IC system continues its analysis of the sample from the previous cycle. In the final step, the collected sample is washed from the interface and loaded on to the IC preconcentration column. The sampling pump and the HV supply are turned off, the liquid pump is turned on and the IC injection valve is switched to the load mode. Washing/loading is conducted for 5 min to ensure that all the sample is loaded. The system then returns to the initialization step, with the IC valve simultaneously switching to the inject mode.

When a series of experimental runs were first commenced, the collection device was disconnected from the aerosol source tube to avoid any

residual water in the collection apparatus being blown into the aerosol source transportation conduit. The collection device was reconnected before step 2. There was no need to disconnect the collection device after the first measurement cycle.

Initially, the amounts of sulfate and nitrate were quantitated based on both peak area and peak height. Because there was no significant difference between these two approaches only peak heights were henceforth used.

3. Results and discussion

3.1. Dimension of the collection chamber

The dimension of the outer electrode for typical wire and tube geometry electrostatic precipitators is from approximately 15 cm i.d. × 2 m for small units, up to approximately 30 cm i.d. × 5 m for large units [15]. For the present experiments, this size was reduced to approximately 2.5 mm i.d. × 2.5 cm. With electrodes of this size, the collected aerosol could be washed off conveniently by pumping a modest amount of water through the annular space, because water covered the entire annular space as it flowed through this small gap. In principle, increasing the tube length will increase the particle collection efficiency. However, it is necessary that the center electrode be fixed concentrically in the system; this can be difficult when it is long, due to its flexibility. A stable corona discharge could not be generated if the center electrode was made significantly larger to improve rigidity. A center electrode that is too small is difficult to fix rigidly in position and exhibits high liquid flow resistance. This is problematic since it is the conduit through which the wash solution is aspirated.

3.2. Type of corona discharge

Generation of corona discharge inside the collection chamber results in charging of the particles and is important for high efficiency collection of the aerosol particles. Chemical composition of aerosols can vary as a function of size. If a collection device does not collect with a high,

preferably quantitative, efficiency, the analysis may be biased towards one end of the size spectrum.

Industrial electrostatic precipitators use negative corona discharge almost exclusively. This is reportedly because a negative corona is more stable when voltage on the center electrode was ramped; a spark discharge always preceded the establishment of a stable corona. The current spike associated with the discharge generally caused the high voltage power supply to shut itself off. This could be avoided by using the power supply in the constant current mode. A stable positive corona was obtained within a current range of about 6 to 70 μA. However, we could not obtain a stable negative corona. Even after the size of the collection electrode was increased to 4.4 mm i.d., only occasionally could we get a stable negative corona. Therefore, a positive corona was used throughout these experiments. A negative corona may nevertheless be feasible with the choice of alternative electrode materials.

We experimentally determined that a voltage of approximately 2.7 kV was the minimum required to generate a corona. Although this voltage varies with many experimental parameters, such as aerosol particle composition and concentration, gas phase composition, pressure, temperature, sampling flow rate, etc., no corona discharge was ever observed below 2.5 kV.

3.3. Collection efficiency as a function of high voltage on the center electrode

The collection efficiencies for two different aerosol sizes are shown in Fig. 3(a) as a function of the volgtage applied to the center electrode. Based on the current voltage curve (Fig. 3(b)), the voltage range can be divided into two parts, voltages lower than 2.5 kV where no corona discharge occurred and higher than about 2.8 kV where a stable corona was present. As can be seen from Fig. 3(a), before the presence of any corona discharge, the collection efficiency was low. Even before discharge occurs, the collection efficiency increased linearly with increasing voltage. Aerosol collection occurs in this regime because even in the absence of charging by a corona, there is

equilibrium Boltzmann charge on the particles [16]. Similar to the situation with an electrical aerosal analyzer [17], more particles deposit on the collection electrode as a higher voltage is applied. After corona discharge initially starts at approximately 2.5 kV, the current was not stable between 2.5 and 2.8 kV and increased very quickly with the voltage in this range as shown in Fig. 3(b). Above 2.5 kV, the collection efficiency, like the corona current, increased exponentially with the applied voltage. A stable corona and a stable current–voltage behavior was observed at applied voltages greater than 2.8 kV. Fig. 4 shows the collection efficiency as a function of corona current. It increased essentially linearly with the corona current until a corona current of about 20 μA.

Similar to the process that occurs during an electrical thunderstorm [18], NO_x was generated as corona discharge occurred. Fig. 5 shows the amount of nitrate detected as a function of the voltage applied and the corona current. The level of artifact nitrate formed in this manner is clearly related to the corona discharge. A linear relationship exists between the corona current and nitrate
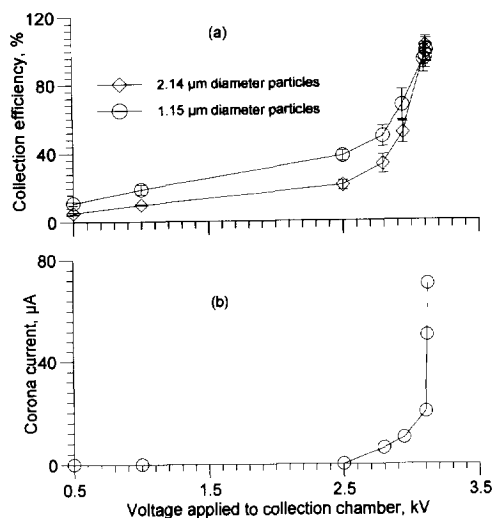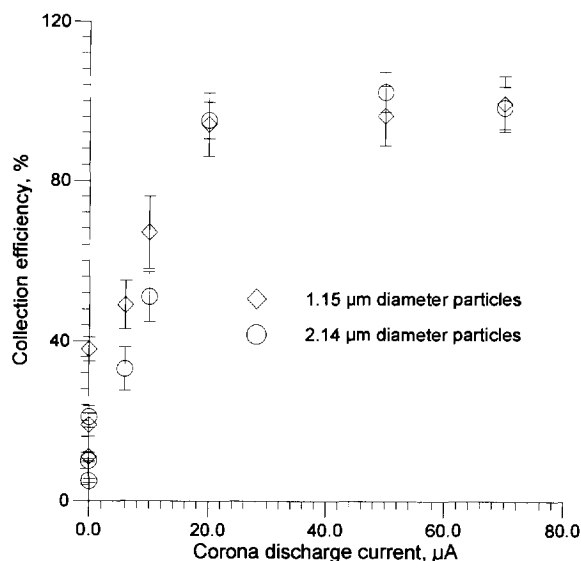

Fig. 4. Collection efficiency as a function of corona current.

amount collected (Fig. 5(b)). The nitrite levels found ranged from 5 to 10% of the nitrate concentrations. There is little doubt that the nitrate originates from the reaction of excited nitrogen and oxygen atoms in the corona followed by a reaction with water vapor. Substitution of cylinder nitrogen for air as the carrier gas virtually eliminated the occurrence of nitrate. Obviously, the present arrangement cannot be used to measure the levels of ambient aerosol nitrate.

Fig. 3. (a) Collection efficiency as a function of voltage on the center electrode: sampling flow rate: 500 ml min^{-1}; sampling time: 20 min, in this and all subsequent figures, as applicable. (b) Current–voltage curve of the collection device.
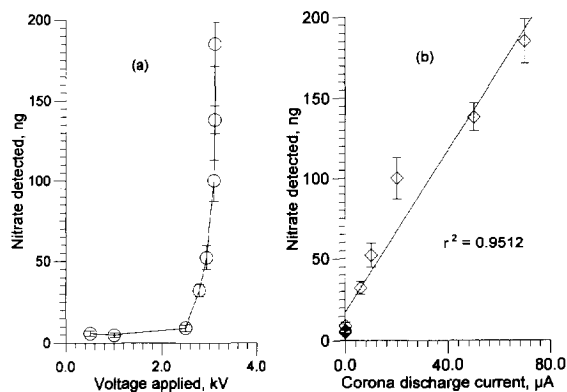

Fig. 5. (a) Nitrate detected as a function of voltage on the center electrode. (b) Nitrate detected as a function of corona current.
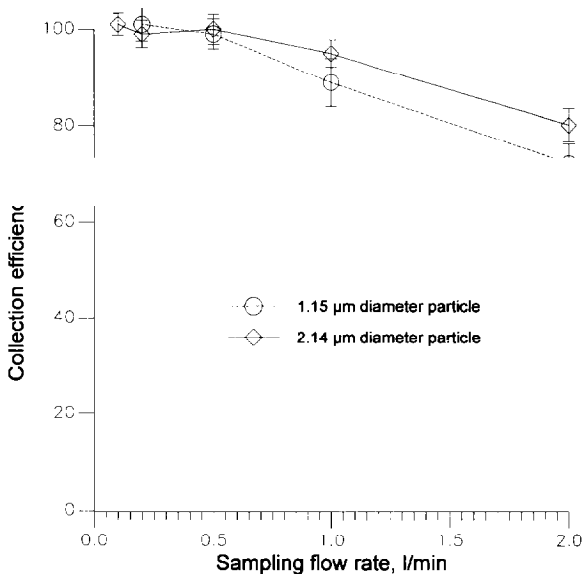
Fig. 6. Collection efficiency as a function of sampling flow rate. Corona current: 50 μA.

3.4. Collection efficiency as a function of sampling flow rate

Fig. 6 shows the collection efficiency as a function of sampling flow rate.

These experiments were conducted at sulfate levels (1.0–6.0 μg m^{-3}) that are typical of modest to high ambient sulfate concentrations. Almost quantitative collection was achieved at a flow rate of $\leqslant 0.5$ l min^{-1}. As the flow rate increased, the residence time of the particles inside the collection chamber decreased, and thence the collection efficiency decreased as well. An increase in the effective residence time in the collection area is expected to enhance the collection efficiency.

3.5. Collection of particulate sulfate as a function of sampling time

The collection of particulate sulfate increased linearly with the sampling time for both 2.14 μm and 1.15 μm diameter particles (Fig. 7). This is useful since measurement sensitivity can be improved by increasing the sampling time.

4. Conclusions

We have investigated a simple electrostatic aerosol collection device that is easily coupled to liquid phase analytical systems. Although the data here, particles of about 0.5 μm diameter have also been investigated, albeit in a less thorough manner. We could generate these smaller aerosols only in very low concetrations (about 100 ng m^{-3}); it therefore becomes tedious and time consuming to collect sufficient sample on the filter for IC analysis to determine the collection efficiency. The importance of filter blank corrections also becomes significant and becomes a significant source of error in computing collection efficiency. Preliminary data, however, indicated that collection efficiencies were $\geqslant 90\%$ at a flow rate of 0.5 min^{-1}. The error margin is such that this collection may have been quantitative. We believe therefore that this approach can be effectively used for the collection and analysis of ambient aerosols in the fine particle fraction ($\leqslant 2$ μm) which is generally the size class of importance both in regards to atmospheric visibility and human health effects. While
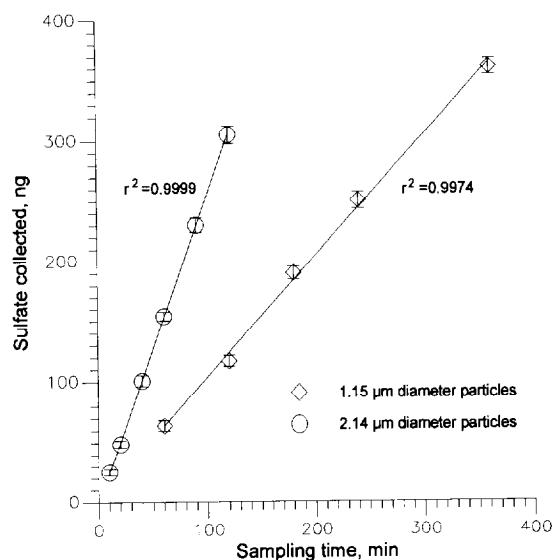

Fig. 7. Collection efficiency as a function of sampling time. Corona current: 50 μA; concentrations of the 1.15 μm and 2.14 μm diameter aerosols are 1.0 and 5.1 μg m^{-3}, respectively.

the generation of artifact nitrate is a disadvantage, the system can be readily used for the continuous collection and automated determination of slow or accidental release of hazardous substances that can be chromatographically determined. In the near future we expect to report on an electrical aerosol collection scheme from which nitrate production is eliminated.

Acknowledgements

References

[1] C.M. Murphy, Handbook of Particle Sampling & Analysis Methods, Verlag Chemie International Inc., Deerfield Beach, Florida, 1984.

[2] K. Willeke and P.A. Baron, (Eds.), Aerosol Measurement —Principles, Techniques and Applications, Van Nostrand Reinhold, New York, 1993.

[3] P.K. Simon and P.K. Dasgupta, Anal. Chem., 67 (1995) 71.

[4] P.K. Simon and P.K. Dasgupta, Environ, Sci. Technol., 29 (1995) 1534.

[5] A. Khylystov, G.P. Wyers and J. Slanina, Atmos. Environ., 29 (1995) 2229.

[6] K.G. Anlauf, P. Fellin, H.A. Wiebe, H.I. Schiff, R.S. Braman and R. Gilbert, Atmos. Environ., 19 (1985) 325.

[7] F. Lindqvist, Atmos. Environ., 19, (1985) 1671.

[8] D. Bardess, Z. Levin and E. Ganor, Atmos. Environ., 26A (1992) 675.

[9] M. Yamamoto and H. Kosaka, Anal. Chem., 66 (1994) 362.

[10] R.D. Cox, Anal. Chem., 52 (1980) 332.

[11] M.V. Johnston and A.S. Wexler, 67 (1995) 721A.

[12] T.T. Mercer, Aerosol Technology in Hazard Evaluation, Academic Press, New York, 1973, p. 146.

[13] J.M. Schneider and C.D. Hendricks, Rev. Instrum, 35 (1965) 1349.

[14] W.C. Hinds, Aerosol Technology, Wiley, New York, 1982, pp. 187–194.

[15] H.J. White, Industrial Electrostatic Precipitation, Addison-Wesley Publishing Company Inc., Reading, Massachusets, 1963, p. 39, also Chapter 4.

[16] K.T. Whitby and W.E. Clark, Tellus, 18 (1966) 573.

[17] R. Gunn, J. Colloid Sci., 10 (1955) 107.

[18] D.K. Brandvold, P. Martinez and R. Hipsch, Atmos. Environ., 30 (1996) 973.

Ionic medium effects on equilibrium constants
Part I. Proton, copper(II), cadmium(II), lead(II) and acetate activity coefficients in aqueous solution

L. Pezza[a], M. Molina[b], M. de Moraes[c], C.B. Melios[c,*], J.O. Tognolli[c]

[a]Departamento de Química Orgânica, Instituto de Química, UNESP, C.P. 355, 14.800-900 Araraquara, SP, Brazil
[b]Departamento de Química, Centro Tecnológico, Universidade Federal do Marahão, 65080-040 São Luis, MA, Brazil
[c]Departamento de Química Analítica, Instituto de Química, UNESP, C.P. 355, 14.800-900 Araraquara, SP, Brazil

Abstract

The molar single ion activity coefficients associated with hydrogen, copper(II), cadmium(II) and lead(II) ions were determined at 25°C and ionic strengths between 0.100 and 3.00 M (NaClO$_4$), whereas for acetate the ionic strengths were fixed between 0.300 and 2.00 M, held with the same inert electrolyte. The investigation was carried out potentiometrically by using proton-sensitive glass, copper, cadmium and lead ion-selective electrodes and a second-class Hg|Hg$_2$(CH$_3$COO)$_2$ electrode. It was found that the activity coefficients of these ions (y_i) can be assessed through the following empirical equations:

$$\log y_H = -0.542I^{0.5} + 0.451I; \log y_{Cu} = -1.249I^{0.5} + 0.912I; \log y_{Cd} = -0.829I^{0.5} + 0.448I^{1.5};$$

$$\log y_{Pb} = -0.404I^{0.5} + 0.117I^2; \text{ and } \log y_{Ac} = 0.0370I$$

Keywords: Ionic activity coefficients; Ionic medium effects

1. Introduction

Several complex systems of practical, biological, geological or general chemical interest comprise mixtures of electrolytes in aqueous solutions. One of the most important problems in the study of the equilibria involved in such systems is the knowledge of the individual activity coefficients of the species in the presence of a background electrolyte [1] and the derivation of equations relating the stability constants of these species and the ionic strength of the medium [2,3]. In such conditions, extra-thermodynamic considerations must be introduced to determine the individual activ-

* Corresponding author.

ity coefficient of an ionic or neutral substance, especially in the presence of an excess of inert electrolyte.

Following this reasoning, Uemasu and Umezawa [1] stressed that ion-selective electrodes (ISEs) provide activity values for individual ions rather than concentrations and, therefore, by using known concentrations, it is possible to evaluate ionic activity coefficients. They reported experimental and computational procedures to accomplish the aforementioned task for Cu(II) and Ca(II) ions at ionic strengths ranging from 0.010 to 3.00 M, held with different background electrolytes, in aqueous solution. Later, Capone et al. [4] determined the proton activity coefficients, also in aqueous solution, by using a proton-sensitive glass electrode, at 10, 25, 37 and 45 °C and $0.01 \leqslant I \leqslant 1.00$ M, in the presence of several background electrolytes.

Ochiai [5] also recognized that the activity and hence the activity coefficient of an individual ion can be measured, at least approximately, with an ion-selective electrode and suggested that traditional statements such as "activities or activity coefficients for individual ions cannot be measured because an individual ion cannot exist independently in a solution, and therefore the mean activity coefficient is the only meaningful parameter" may need revision, in spite of the fact that no solution containing only one kind of ion is possible.

In this paper, we propose a potentiometric method for evaluating the activity coefficients of hydrogen, copper(II), cadmium(II), lead(II) and acetate ions by using ion-selective electrodes in the presence of sodium perchlorate at 25 °C, adopting simple empirical equations relating these parameters with the ionic strength of the medium. In Part II, assuming that similar ions should display similar equilibrium parameters, simple equations are developed in order to calculate at least approximate values for equilibrium constants associated with some metal ion complexes, starting from the data obtained in this work.

2. List of main symbols

OAc   acetate ion

A_i	a function of λ_i and $[i]$ of the ions i involved in the system
d	a function of the λ_i values for the ions i involved in the system
E	electromotive force (emf) of the cell (mV)
$(E_i^{0'})_0$	limiting value of $(E_i^{0'})$ when $\log y_i = 0$ (mV)
E_j	liquid junction potential (mV)
h	molar hydrogen-ion concentration
i	a neutral substance or ion
I	ionic strength (M)
ISE	ion-selective electrode
p	for monovalent cations $p = 1$ and for bivalent cations $p = 2$
λ_i	actual equivalent conductance of i (ohm^{-1} cm^2 equiv^{-1})
λ_i^0	limiting equivalent conductance of i (ohm^{-1} cm^2 equiv^{-1})
M	molar or mol dm^{-3}
Me	metal ion
pa_{H}	$(-\log a_{\mathrm{H}^+})$
r	correlation coefficient of a linear regression
σ	standard error of estimate
T	temperature (°C)
[ ]	molar concentration

3. Experimental

3.1. Materials and solutions

All reagents were of analytical grade. Copper(II), cadmium(II) and lead(II) perchlorate were prepared from perchloric acid and the corresponding basic metallic carbonate. The products were recrystallized from ethanol and conveniently dried. Stock solutions were standardized complexometrically with EDTA. Stock solutions of sodium perchlorate were analysed by evaporating and drying to constant weight at 120 °C. Carbonate-free sodium hydroxide solutions were standardized potentiometrically with acid potassium phthalate and then stored in polyethylene bottles protected with soda-lime tubes. The perchloric acid solutions were standardized potentiometrically with standard sodium hydroxide solutions.

Chloride ions were not detected in these solutions. For the preparation of the solutions, distilled, deionized water and grade A glassware were used throughout.

3.2. Instruments

The emf values were read to the nearest 0.1 mV with a Metrohm 670 Titroprocessor. Metrohm ion-selective electrodes for hydrogen (EA 158), copper (6.0502.140), cadmium (6.0502.010) and lead (6.0502.170) ions and an Ag|AgCl double-junction reference electrode (6.0726.100) were used. A mercury(I) acetate electrode was prepared essentially as recomended by Larson and Mac-Dougall [6]. A thermostated titration cell (25.0 ± 0.1 °C) was employed. Volume measurements (± 0.001 ml) were made with Metrohm 665 automatic burettes. All experiments were performed in a thermostated room (25 ± 1 °C).

3.3. Potentiometric cells

The potentiometric cells used for the emf measurements in the study of the $i(ClO_4)_p$–$NaClO_4$ systems (where $i = H^+$, Cu^{2+}, Cd^{2+}, Pb^{2+}) were of the type

The x values were in the following ranges: $HClO_4$, $(1.00-6.00) \times 10^{-2}$ M; $Cu(ClO_4)_2$, $(0.200-6.00) \times 10^{-3}$ M, $pH = 3.005-3.204$; $Cd(ClO_4)_2$, $(0.200-6.00) \times 10^{-3}$ M, $pH = 3.505-3.693$; $Pb(ClO_4)_2$, $(0.200-6.00) \times 10^{-3}$ M, $pH = 2.608-2.966$; and NaOAc and HOAc, $(6.33-11.5) \times 10^{-2}$ M.

No flow of chloride ions from the reference electrode into the test solutions could be detected during the measurements. The glass electrode was stored in 0.1 M hydrochoric acid and washed thoroughly with water before use. The copper, cadmium and lead ISEs were polished with an abrasive strip for 1 min and then washed with water before use.
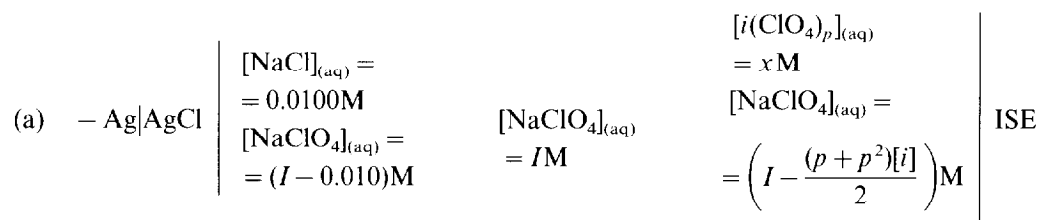
3.4. Convention

This work is based on several principles previously established by several workers [7-10]. The conventions adopted are as follows.
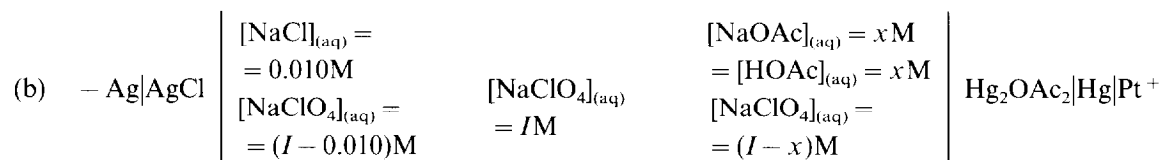
1. The emf of cells (a) and (b) may be defined by [8-10]

$$E = (E_i^{0'})_0 + S \log a_i + X_i[i] \tag{1}$$

where

(a)	$-$ Ag|AgCl	$[NaCl]_{(aq)} =$ $= 0.0100M$ $[NaClO_4]_{(aq)} =$ $= (I - 0.010)M$	$[NaClO_4]_{(aq)}$ $= IM$	$[i(ClO_4)_p]_{(aq)}$ $= xM$ $[NaClO_4]_{(aq)} =$ $= \left(I - \dfrac{(p + p^2)[i]}{2}\right)M$	ISE

The indicator electrode is the positive pole only in the case of glass and copper ISE. In the case of the $NaOAC$–$HOAc$–$NaClO_4$ system, the cell was of the type

(b)	$-$ Ag|AgCl	$[NaCl]_{(aq)} =$ $= 0.010M$ $[NaClO_4]_{(aq)} =$ $= (I - 0.010)M$	$[NaClO_4]_{(aq)}$ $= IM$	$[NaOAc]_{(aq)} = xM$ $= [HOAc]_{(aq)} = xM$ $[NaClO_4]_{(aq)} =$ $= (I - x)M$	Hg_2OAc_2|Hg|Pt$^+$

$E_i^{0'}$ = sum of all constant terms that contribute to the total measured emf (mV)

$a_i = y_i$ [i] = individual activity of an ion or a neutral substance i (mol dm^{-3})

[i] = molar concentration of an ion or a neutral substance i (mol dm^{-3})

y_i = molar activity coefficient of i

$(E_i^{0'})_0$ = limiting value of $E_i^{0'}$ when log $y_i = 0$ (mV)

S = experimental value obtained for the coefficient of the logarithmic term of the electrode potential (mV)

X_i = proportionality term between liquid junction potential (E_j) and [i] (mV mol^{-1} dm^3)

2. Within the considered concentration ranges, $HClO_4$, $NaClO_4$, $Cu(ClO_4)_2$, $Cd(ClO_4)_2$, $Pb(ClO_4)_2$ and NaOAc are strong electrolytes.

3. At constant T, maintaining constant and high enough I values, y_i will be constant [8].

4. The straight line obtained by plotting $E - S$ log [i] vs. [i] within a certain [i] range can be ex-trapolated for smaller [i] values (that is, $E_i^{0'}$ and X_i are valid, at least, for the entire 0–[i] range [8–10]).

5. For electrolyte (and non-electrolyte) mixtures, it is preferable to use empirical equations (with extra-thermodynamic but experimental and practical meaning) instead of theoretical equations [7].

3.5. Procedures

A 0.100 M $HClO_4$, $Me(ClO_4)_2$ or isomolar NaOAc–HOAc buffer solution, made up to the desired ionic strength value with $NaClO_4$, was added successively (in 0.3 ml increments) to a known volume of $NaClO_4$ solution of identical ionic strength in the potentiometric cell. After each addition, the emf of the cell was measured. In all cases equilibrium was easily reached (the criterion was to achieve constant emf values within ± 0.2 mV during 3 min, for $I \leqslant 1.0$ M and ± 0.1 mV during 1.5–2 min, when $I > 1.0$ M).

3.6. Calculation method

The emf of the cells (a) may be expressed by

Eq. (1). From this equation, we have

$$E = (E_i^{0'})_0 + S \log y_i + S \log [i] + X_i[i] \qquad (2)$$

If we consider (for each constant I value) that

$$E_i^{0'} = (E_i^{0'})_0 + S \log y_i = \text{constant} \qquad (3)$$

we obtain

$$E = E_i^{0'} + S \log [i] + X_i[i] \qquad (4)$$

From sufficient experimental $(E, [i])$ pairs of values, we can determine the $E_i^{0'}$, S and X_i parameters (corresponding to the fixed I value) using the multiple linear regression method. From the X_i value obtained we can find the $E_i^{0'}$ values corresponding to each experimental [i] value, calculated with Eq. (4), which will be used later.

The dependence of log y_i on ionic strength may be calculated by starting from the expression [7]

$$\phi_i = \log y_i = aI^{1/2} + bI + cI^{3/2} + \cdots \qquad (5)$$

where a, b, c, ... are empirical parameters.

From Eqs. (3) and (5), we obtain

$$E_i^{0'} = (E_i^{0'})_0 + S(aI^{1/2} + bI + cI^{3/2} + \cdots) \qquad (6)$$

By employing a suitable statistical program [11], and from sufficient $(E_i^{0'}, I)$ pairs, one can determine all parameters of Eq. (6) and, therefore, the mathematical relationship between y_i and I.

Similarly, for a cell of type (b), we have

$$E = (E_{OAc}^{0'})_0 - S \log a_{OAc} + X_{OAc} [OAc] \qquad (7)$$

$$E = (E_{OAc}^{0'})_0 - S \log y_{OAc} - S \log [OAc] + X_{OAc} [OAc] \qquad (8)$$

$$E_{OAc}^{0'} = (E_{OAc}^{0'})_0 - S \log y_{OAc} \qquad (9)$$

$$E = E_{OAc}^{0'} - S \log [OAc] + E_j \qquad (10)$$

$$E_{OAc}^{0'} = (E_{OAc}^{0'})_0 - S(aI^{1/2} + bI + cI^{3/2} + \ldots) \qquad (11)$$

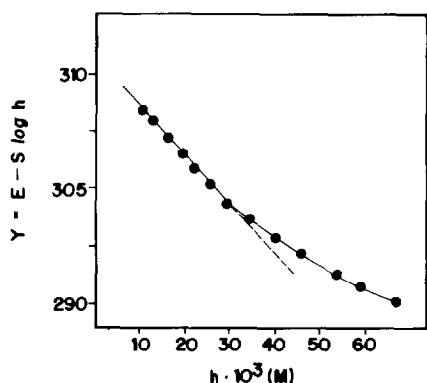The dependence between y_{OAc} and I may be obtained from Eq. (11).

Fig. 1. Y vs. h plot for the $HClO_4$–$NaClO_4$ system ($I = 0.100$ M). Only about one tenth of the experimental points, chosen at random, have been plotted.

4. Results and discussion

In the case of the hydrogen ion, Eq. (4) yields

$$Y = E - S \log h = E_H^{0'} + X_H h \qquad (12)$$

Y values can be obtained from the experimental E and S values. By plotting Y vs h, one obtains a set of points to which a straight line can be fitted (within a given h range), the intercept and slope of which are $E_H^{0'}$ and X_H, respectively. This linearity confirms that y_H remains constant at constant I.

At low h values, where $h \neq [HClO_4]$, the points move away from the straight line; at high h values

it is necessary to take care with the $h/[Na^+]$ ratio. According to Hartley et al. [12] substitution of ca. 5% of the inert electrolyte ions by other ions is possible without appreciable change in the activity coefficients of the latter. Beck and Nagypál [13] estimated this limit to be 20% if the total electrolyte concentration is kept at 3 M. On the other hand, we found a limit of 29%; this means that h cannot exceed 22.5% of the ionic strength of the medium. This fact can be easily observed at $I = 0.1$ M (Fig. 1). At higher I values, no deviation of the linear relationship is noted within the encompassed h range.

The data obtained for the X_H and S parameters are given in Table 1. The Henderson equation [17,18] for the $i(ClO_4)_p$–$NaClO_4$ systems may be simplified to

$$E_j = A_i \log\left(1 + \frac{[i]d}{I}\right) \qquad (13)$$

where A_i and d are functions of $[i]$ and/or λ_i involved in the system. For the ions studied in this work, and using λ_i^0 and data [18,19], we have the following $(A_i; d)$ values: H^+ ($-59.2; 2.55$), Cu^{2+} ($-14.9; -0.889$), Cd^{2+} ($15.7; -0.933$), Pb^{2+} ($9.92; -0.661$) and Ac^- ($59.2; -0.225$). On the other hand, from Eq. (13) and taking into account the X_H values determined for the $HClO_4$–$NaClO_4$ system from Eq. (4), we obtained

Table 1
y_H, pa_H, X_H and S data obtained for the $HClO_4$–$NaClO_4$ system ($h = 0.0100$ M, $T = 25.0 \pm 0.1$ °C)

I (M)	y_H	pa_H	X_H (mV mol^{-1} l)		S (mV per decade)	σ
			This work	Literature		
0.100	0.748	2.13	-441	-441 [14]; -430 [10]	58.1	0.052
0.300	0.689	2.16	-191	–	59.1	0.099
0.500	0.695	2.16	-102	-110 [10]	58.7	0.034
1.00	0.811	2.09	-61	-63 [15]; -75 [10]	59.0	0.027
1.20	0.886	2.05				
1.50	1.03	1.99	-43	–	59.3	0.055
1.60	1.09	1.96	–	–	–	
1.80	1.22	1.92	–	–		
2.00	1.37	1.86	-42	-28 [16]	59.3	0.028
2.40	1.75	1.76	–	–	–	
2.50	1.86	1.73	-23	–	59.3	0.042
3.00	2.60	1.59	-13	-16.5 [15]	59.1	0.087

Table 2

X_i, y_i and S data obtained for the $Me(ClO_4)_2$–$NaClO_4$ (Me^{2+} = Cu^{2+}, Cd^{2+}, Pb^{2+}) and $NaOAc$–$HOAc$–$NaClO_4$ systems ($T = 25.0 \pm 0.1°C$)

I (M)	X_i (mV mol^{-1} l)[a]				y_i				S (mV per decade)[b]			
	Cu^{2+}	Cd^{2+}	Pb^{2+}	OAc^-	Cu^{2+}	Cd^{2+}	Pb^{2+}	OAc^-	Cu^{2+}	Cd^{2+}	Pb^{2+}	OAc^-
0.100	58	−64	−29	–	0.497	0.665	0.747	–	31.7	29.6	26.9	–
0.300	19	−21	−10	−20	0.388	0.416	0.616	1.02	30.6	31.5	28.1	58.7
0.500	12	−13	−6	−12	0.374	0.373	0.554	1.04	29.4	28.5	27.6	63.3
1.00	6	−6	−3	−6	0.460	0.416	0.516	1.09	–	30.3	31.2	63.0
1.20	5	−5	−2	−5	0.532	0.479	0.532	1.11	28.1	–	–	–
1.50	4	−4	−2	−4	0.689	0.642	0.587	1.14	–	30.2	28.7	–
1.60	4	−4	−2	−4	0.757	0.721	0.614	1.15	29.2	–	–	61.7
1.80	3	−4	−2	−3	0.924	0.933	0.687	1.16	–	–	–	62.3
2.00	3	−3	−1	−3	1.14	1.24	0.788	1.18	27.6	30.0	26.9	61.8
2.40	2	−3	−1	–	1.79	2.41	1.12	–	29.7	–	–	–
2.50	2	−3	−1	–	2.02	2.88	1.24	–	–	28.9	27.0	–
3.00	2	−2	−1	–	3.74	7.80	2.26	–	29.8	30.1	28.5	–

[a] Calculated for the mean [i] value within the range employed (Eq. (13)).
[b] Calculated by linear regression from (E, log[i]) pairs. In all cases, r values higher than 0.999 were obtained.

$d = 2.28$ as a mean value. The difference between this value and that mentioned above (2.55) could be ascribed to the fact that for the application of the Henderson equation λ_i values should be used instead of λ_i^0 values. As far as the $Me(ClO_4)_2$–$NaClO_4$ and $NaOAc$–$HOAc$–$NaClO_4$ systems are concerned, the determination of liquid junction potentials from experimental data by using Eq. (4) was not possible because these values are of the order of magnitude of the experimental errors, as may be deduced from Table 2. Hence they were calculated through Eq. (13). These calculated values were used for $E_i^{0'}$ determination with Eq. (4), which provides also the X_i values ($X_i = E_j/[i]$).

In the computation of eq. (6) parameters, the following number of data were used: 112 ($E_H^{0'}$, I), 70 ($E_{Cu}^{0'}$, I), 88 ($E_{Cd}^{0'}$, I), 88 ($E_{Pb}^{0'}$, I) and 36 ($E_{OAc}^{0'}$, I). As a result, the following equations were obtained:

$$\phi_H = -0.542I^{1/2} + 0.451I \; (\sigma = 1.01) \tag{14}$$

$$\phi_{Cu} = -1.249I^{1/2} + 0.912I \; (\sigma = 0.63) \tag{15}$$

$$\phi_{Cd} = -0.829I^{1/2} + 0.448I^{3/2} \; (\sigma = 1.32) \tag{16}$$

$$\phi_{Pb} = -0.404I^{1/2} + 0.117I^2 \; (\sigma = 2.03) \tag{17}$$

$$\phi_{OAc} = -0.0370I \; (\sigma = 0.50) \tag{18}$$

The y_i values in Tables 1 and 2 were calculated with these equations. Among the various types of equations tested, none fit the experimental data as perfectly as these do. The coefficient of the first term of Eq. (14) is close to the theoretical A term of the Debye–Hückel equation, which is not the case for the Eqs. (15)–(18). The fitness of these equations to the ($E_i^{0'}$, I) points can be verified from plots shown in Fig. 2 and from statistical data given in connection with Eqs. (14)–(18).
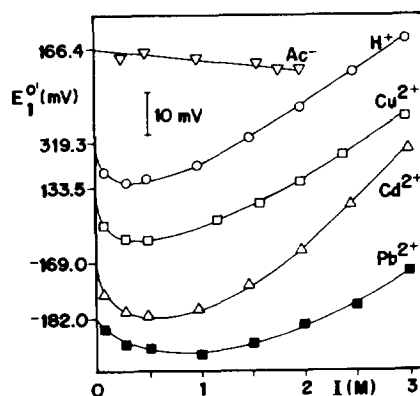

Fig. 2. $E_i^{0'}$ vs. I for the ions studied. The values on the ordinate correspond to ($E_i^{0'}$)$_0$. The symbol's height on the curves represents maximum and minimum experimentally determined $E_i^{0'}$ values.

The proton activity coefficients estimated in this work differ from those reported by Capone et al. [4] at 25 °C, up to $I = 1.00$ M, which is the highest ionic strength stated in their work. However, it is worth noting that they used in the calculations an extended Debye–Hückel expression whose first term comprises the ion size parameter ($\mathring{a}$). It is known that this parameter changes with the composition of the medium and, therefore, it does not convey a sufficiently accurate representation of ion size effect, mainly in electrolyte mixtures [7,14]. The large discrepancy found between the theoretical and experimentally determined A and B parameters for an extended Debye–Hückel equation, i.e.

$$\log y_i = \frac{-AI^{0.5}}{1 + BI^{0.5}} + CI \tag{19}$$

by Uemasu and Umezawa [1], in so far as Cu(II) and Ca(II) ions are involved, makes the above statement clearly apparent. Curves with characteristic minima for the H^+, Cu^{2+}, Cd^{2+} and Pb^{2+} ions were obtained. A straight line, however, fits the ($E^{0'}_{OAc}$, I) points, at least for the I range considered for the $NaOAc$–$HOAc$–$NaClO_4$ system. In the third column of Table 1 we have pa_H values for a 0.0100 M $HClO_4$ solution calculated within the studied I range. Of course, these results could not be obtained with electrodes simply calibrated with buffer solutions [10]. As can be seen, the salt effect is in general significant, suggesting that structural changes of the solvent together with ionic and ion–solvent (hydration) interactions should be taken into account for a realistic description of the systems considered. It is known [20,21] that the Na^+ ion has a weak ordering effect on the water structure, whereas the ClO_4^- ion acts as a powerful structure breaker. This suggests that the ClO_4^- ion should have a dominant role among the structural effects acting on water. The significant changes of the activity coefficients of the H^-, Cu^{2+}, Cd^{2+} and Pb^{2+} ions as the ionic strength increases could be ascribed, at least in part, to the structure-breaking effect fostered by the ClO_4^- anion. This is not the case,

however, for the activity coefficient behaviour of the OAc^- ion; in fact, this ion, a strong structure builder, seems to compensate for the effect of the ClO_4^- ion.

Acknowledgements

References

[1] I. Uemasu and Y. Umezawa, Anal. Chem., 55 (1983) 386.
[2] R.M. Smith, A.E. Martell and R.V. Motekaitis, Inorg. Chim. Acta, 99 (1985) 207.
[3] J.R. Duffield, F. Marsicano and D.R. Williams, Polyhedron, 10 (1991) 1105.
[4] S. Capone, A. De Robertis A, C. De Stefano, S. Sammartano and R. Scarcella, Talanta, 34 (1987) 593.
[5] E. Ochiai, J. Chem. Educ., 67 (1990) 489.
[6] W.D. Larson, F.H. MacDougall, J. Phys. Chem., 41 (1937) 493.
[7] J.E. Gordon, The Organic Chemistry of Electrolyte Solutions, Wiley, New York, 1975, pp. 36–41.
[8] G. Biedermann and L.G. Sillén, Ark. Kemi, 5 (1953) 425.
[9] H. Otahki and G. Biedermann, Bull. Chem. Soc. Jpn., 44 (1971) 1515.
[10] M. Molina, C. Melios, J.O. Tognolli, L.C. Luchiari and M. Jafelicci, Jr., J. Electroanal. Chem., 105 (1979) 237.
[11] Statistical Program STATGRAPHICS, version 2.7, SERIAL STG27 5-1C.
[12] F.R. Hartley, C. Burgess and R. Alcock, Solution Equilibria, Wiley, New York, 1980, pp. 23–24.
[13] M.T. Beck and I. Nagypál, Chemistry of Complex Equilibria, Wiley, New York, 1990, p. 17.
[14] F.J.C. Rossotti and H.S. Rossotti, The Determination of Stability Constants, McGraw-Hill, New York, 1961, pp. 17–37, 147–150.
[15] F.J.C. Rossotti and H.S. Rossotti, Acta Chem. Scand., 10 (1956) 957.
[16] O. Ginstrup, Acta Chem. Scand., 24 (1970) 875.
[17] P. Henderson, Z. Phys. Chem., 59 (1907) 118.
[18] G.T. Hefter, Anal. Chem., 54 (1982) 2518.
[19] R. Parsons, Handbook of Electrochemical Constants, Butterworths, London, 1959, pp. 82–90.
[20] R.W. Gurney, Ionic Processes in Solutions, McGraw-Hill, New York, 1953, p. 163.
[21] J. Steigman and J. Dobrow, J. Phys. Chem., 72 (1968) 3424.

Ionic medium effects on equilibrium constants
Part II[1]. Binary systems comprising some bivalent cations and monocarboxylates in aqueous solution

L. Pezza[a], M. Molina[b], C.B. Melios[a],*, M. de Moraes[a], J.O. Tognolli[a]

[a]Instituto de Química, UNESP, C.P. 355, 14800-900 Araraquara, SP, Brazil
[b]Departamento de Química, Centro Tecnológico, Universidade Federal do Maranhão, 65080-040 São Luis, MA, Brazil

Abstract

Simple equations were derived relating stoichiometric protonation constants of several monocarboxylates and formation constants associated with 1:1 complexes involving some bivalent cations and selected monocarboxylates, in aqueous sodium perchlorate media, at 25°C, as a function of ionic strength (I), allowing the interconversion of parameters from one ionic strength to another, up to $I = 3.00$ M. In addition, thermodynamic formation constants as well as activity coefficients of the species involved in the equilibria were estimated. The results show that the proposed calculation procedure is very consistent with critically selected experimental data.

Keywords: Activity coefficients; Formation constants; Medium effects

1. Introduction

The scarcity of quantitative studies dealing with weak interactions among ions in aqueous solution and the difficulty in distinguishing these interactions from those arising through ionic medium effects may be the reason for the lack of an adequate treatment concerning the ionic strength dependence of activity coefficients and hence equilibrium constants, including protonation of ligands and the thermodynamic stability of metal

ion complexes. The associated equilibria are of fundamental importance in any area where a knowledge of the chemical form of an element is a prime requirement, such as in "real life" systems (for example, ground-, sea- and wastewaters, blood plasma, urine, gastro-intestinal juices, food extracts) and in research including radioactive waste disposal, assessment of metal-dependent side effects of pharmaceuticals, the bioavailability of metal ions from foods and the use of metal complexes to suppress the activity of microorganisms [1–3].

In view mostly of the aforementioned requirements some progress has been attained regarding

---

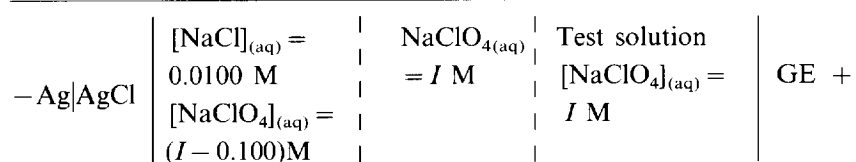* Corresponding author. Fax: (+ 55) 16-22-7932 or 5987.
[1] For Part I, see Ref. [12].

the search for procedures allowing the interconversion of equilibrium parameters from one ionic strength to another as well as the estimation of thermodynamic equilibrium constants (i.e. at zero ionic strength). The main approaches employed to reach this purpose have been; (a) use of extended Debye–Hückel equations [4–6]; (b) use of of the specific interaction theory of Brønsted [7]; (c) estimation by chemical trends and free energy relationships, using the library of equilibrium data which already exists in compilations [8]; (d) assessing the robustness of data and models through sensitivity analyses of the type used in modelling radioactive waste disposal sites [3].

It is worth noting that thermodynamic constants are important for setting up correlations aiming at a better understanding of fundamental factors influencing the coordination chemistry of metals and ligands in aqueous solution [5,9–11].

In the current absence of a comprehensive theory that can answer the fundamental questions concerning the dependence of equilibrium constants on ionic strength, it is of considerable interest to find equations (even empirical ones) that would allow equilibrium constants, measured at a given ionic strength, to be recalculated for any other ionic strength.

In a previous work from this laboratory [12] empirical equations relating the molar activity

with the corresponding ones critically selected from the literature [13]. The approach is presently restricted to binary systems comprising some bivalent cations and monocarboxylates (aliphatic and aromatic), in aqueous medium.

2. Experimental

Unless stated otherwise, experimental conditions, apparatus and conventions were the same as previously described [12].

3. Calculation methods

3.1. Protonation constants

Protonation constants (K_H) of acetic acid at different ionic strengths (0.300–3.00 M range) were determined by applying a potentiometric method [14,15]. Acetic acid solutions (0.01052–0.01071 M) made up to the desired ionic strength by adding sodium perchlorate (initial volume 35.00 ml) were titrated with sodium hydroxide solutions (0.0950–0.1000 M) the ionic strength of which were adjusted to a fixed value with sodium perchlorate. The titration vessel was the compartment shown in the right-hand side of the cell:

$-Ag|AgCl$	$[NaCl]_{(aq)} =$ 0.0100 M $[NaClO_4]_{(aq)} =$ $(I - 0.100)M$	$NaClO_{4(aq)}$ $= I$ M	Test solution $[NaClO_4]_{(aq)} =$ I M	GE +

coefficients of H^+, Cu^{2+}, Cd^{2+}, Pb^{2+} and CH_3COO^- (in aqueous solutions, at 25°C) to ionic strength were established. In the present work very simple equations have been derived, making feasible the interconversion of protonation and stability constants, in so far as changes in ionic strength are concerned; also, thermodynamic constants and activity coefficients associated with 1:1 complex species are estimated, via extrapolation of linear relationships. The predictive power of the developed procedure has been evaluated by comparing the calculated constants

3.2. Other equilibrium parameters

For the equilibrium $H^+ + A^- \rightleftharpoons HA$ corresponding to a given monocarboxylic acid, in aqueous solution, the thermodynamic protonation constant is defined as

$$^T K_H = \frac{[HA]}{[H][A]} \frac{y_{HA}}{y_H \cdot y_A} \tag{1}$$

where charges are omitted for simplicity.
From Eq. (1)

$$\log {}^T K_H = \log K_H + \log y_{HA} - \log y_H - \log y_A \tag{2}$$

Table 1

Protonation constants of acetic acid in aqueous solution as a function of ionic strength, adjusted with $NaClO_4$; $T = 25.0 \pm 0.1°C$

I(M)	log K_H	
	This work	Literature [13]
0.100	–	4.56 ± 0.03
0.300	4.54 ± 0.04	–
0.500	4.55 ± 0.01	4.50 ± 0.02
1.00	4.60 ± 0.02	4.58 ± 0.03
2.00	4.79 ± 0.04	4.80 ± 0.01
2.50	4.94 ± 0.01	–
3.00	5.06 ± 0.03	5.015 ± 0.005

and

$$Y = \log K_H - \phi_H - \phi_A = \log {}^T K_H - \phi_{HA} \qquad (3)$$

Given sufficient K_H, ϕ_H, ϕ_A and I values, $\log {}^T K_H$ and ϕ_{HA} can be estimated via linear relationships. Similarly, for the equilibrium $Me^{2+} + A^- \rightleftharpoons MeA^+$ of a divalent metallic cation with a monocarboxylate, the thermodynamic formation constant may be defined as

$$^T\beta_1 = \frac{[MeA]}{[Me][A]} \frac{y_{MeA}}{y_{Me} \cdot y_A} \qquad (4)$$

and

$$Y = \log \beta_1 - \phi_{Me} - \phi_A = \log {}^T\beta_1 - \phi_{MeA} \qquad (5)$$

where β_1 is a stoichiometric formation constant of MeA species. Starting from sufficient (Y, I) pairs, we can calculate $\log {}^T\beta_1$ and ϕ_{MeA} values, also via linear relationships, as will be shown later in this work.

4. Results and discussion

The determined protonation constants for acetic acid, along with critically selected corresponding data from the literature [13] are given in Table 1. These data, coupled with previously estimated parameters [12], ϕ_H and ϕ_{Ac}, allowed the calculation of the associated $\log {}^T K_H$ and ϕ_{HAc} values, via Eq. (3); for this particular case $\phi_A = \phi_{Ac}$ and $\phi_{HA} = \phi_{HAc}$. It was found that a straight line can be nicely fitted to the (Y, $I^{0.5}$) points, giving $\log {}^T K_H$ and ϕ_{HAc} as intercept and slope respectively. The values found are displayed in Table 2. Eq. (3) was also tested for 11 other monocarboxylic acids (aliphatic and aromatic, with and without additional functional groups) by assuming $\phi_{Ac} = \phi_A$. The results are shown in Table 2. Our study has been restricted to only 12 monocarboxylates due to the paucity of critically

Table 2

Estimates of $\log {}^T K_H$ and ϕ_{HA} for some monocarboxylic acids; aqueous solution, $T = 25°C$

Acid	I Range[a] (M)	n[b]	log $^T K_H$		$\phi_{HA}/I^{0.5}$	R^2	$10^3 \times \sigma$
			This work	Literature [13]			
Formic	0.1–3	5	3.78 ± 0.02	3.745 ± 0.007	0.232	0.9860	18
Acetic	0.1–3	7[c]	4.77 ± 0.01	4.757 ± 0.002	0.130	0.9930	7
Propionic	0.1–3	5	4.89 ± 0.01	4.874 ± 0.001	0.153	0.9871	11
Butyric	0.1–3	3	4.80 ± 0.01	4.819 ± 0.001	0.112	0.9993	3
Isobutyric	0.1–3	4	4.82 ± 0.02	4.849	0.120	0.9861	11
Lactic	0.1–2	4	3.89 ± 0.01	3.860 ± 0.002	0.190	0.9859	12
Glycolic	0.1–2	4	3.87 ± 0.01	3.832 ± 0.001	0.220	0.9945	9
Benzoic	0.1–1	3	4.20 ± 0.01	4.202 ± 0.003	0.147	0.9989	2
Furoic	0.1–2	3	3.18 ± 0.01	3.167 ± 0.007	0.144	0.9953	8
Pyruvic	0.1–2	4	2.49 ± 0.01	2.49 ± 0.1	0.291	0.9935	14
Phenylacetic	0.1–3	3	4.30 ± 0.01	4.310 ± 0.003	0.155	0.9996	3
Mandelic	0.1–3	3	3.45 ± 0.02	3.40 ± 0.01	0.272	0.995	18

[a] I adjusted with $NaClO_4$.

[b] Number of (log K_H, I) pairs used; taken from Ref. [13].

[c] Six values determined in this work (Table 1); the value at $I = 0.1$ was taken from Ref. [13].

　　　　　　　L. Pezza et al. / Talanta 43 (1996) 1697–1704

selected values from the literature [13]. Very good agreement is observed between literature and calculated $\log {}^{T}K_H$ values; this seems to be more than fortuitous, particularly when the chemical differences among the considered acids are taken into account. The results are somewhat surprising and very gratifying.

Regarding the $(\phi_{HA}/I^{0.5})$ data collected in Table 2, values within the range 0.112–0.155 were obtained for simple carboxylic acids, such as acetic, propionic, butyric, isobutyric, benzoic, furoic and phenylacetic. A higher set of data (i.e. between 0.190 and 0.291) is found for lactic, glycolic, pyruvic and mandelic acids; all these bear additional functional groups adjacent to the carboxyl. A high value (0.232) is provided by formic acid, which is apparently a simple monocarboxylate. However, its anomalous behaviour in aqueous solution is well known [16]. The behaviour of pyruvic acid will be discussed further in connection with its metal ion complexes.

In a similar fashion, Eq. (6) was used for the calculation of $\log {}^{T}\beta_1$ and ϕ_{MeA} associated with several Me(II)–monocarboxylate systems:

$$Y = \log \beta_1 - \phi_{Me} - \phi_{Ac} = \log {}^{T}\beta_1 - \phi_{MeA} \qquad (6)$$

By plotting Y vs. I, very good linear relationships are obtained for all systems considered in this work; some examples are given in Figs. 1–3. The calculated values for $\log {}^{T}\beta_1$ and (ϕ_{MeA}/I) are displayed in Table 3. Again, the set of formation constants used is limited by the paucity of reliable data for all bivalent cations other than Cu^{2+}, for which the gap is less pronounced. Within the restricted database available a very good agreement is generally found between the literature data and the corresponding values calculated via application of Eq. (6), in so far as $\log {}^{T}\beta_1$ values are concerned. As can be seen in Table 3 and Figs. 1–3, Eq. (6) was tested, for most of the considered systems, by putting the $\phi_{Me} = \phi_{Cu}$, ϕ_{Cd} or ϕ_{Pb}. The overall conclusion is that the effectiveness of the ion-selective electrodes in giving good estimates of y_{Me} follows the order Cu > Cd > Pb; it is noteworthy that this same order prevails with regard to the reliability of the aforementioned electrodes for analytical purposes [17].
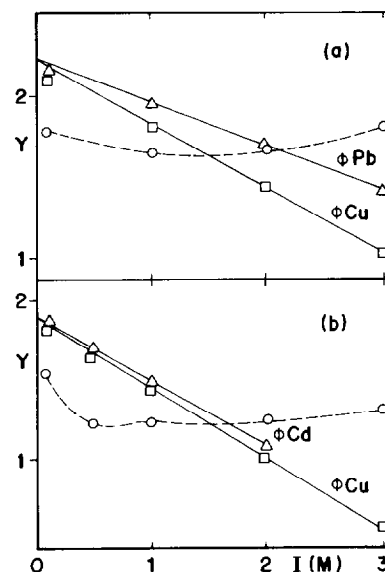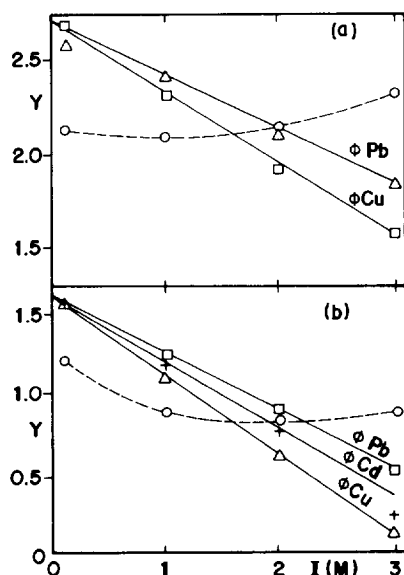

Fig. 1. Me^{2+}–acetate systems (a) Cu^{2+}; (b) Cd^{2+}. (○) $Y = \log \beta_1$; (□, △) $Y = \log \beta_1 - \phi_{Me} - \phi_{Ac}$. The ϕ_{Me} used for each correlation is indicated inside the Figure. The open circles are joined by a broken line just as a guide for the eye.

Most of the (ϕ_{MeA}/I) values found are within the range 0.3–0.4, the mean value being 0.38, except for the Hg^{2+}–monocarboxylate and Cu^{2+}–pyruvate complexes. The deviations for the Hg^{2+} complexes can be ascribed to an intrinsic behaviour of this cation as compared with the other ones considered in this work and/or to the greater uncertainty in the critically selected stoichiometric and thermodynamic stability constants for mercuric complexes, as shown in Table 3. It is known that the complexation of metal ions by pyruvate involves α-keto, diol (hydrated enol) and dimer species of this ligand [18–20]. The formation constants reported in the literature describe the net complexation; only a few papers give estimates for the individual complexation reactions, associated with each form of pyruvate in aqueous solution [19,20]. Furthermore, this feature seems to be characteristic for many α-keto-carboxylates [21–23]. Therefore, the uncertainty in the quoted formation constants for pyruvate complexes [13] is understandable and could explain, at least in part, why the ϕ_{MeA} for Cu^{2+}–pyruvate lie outside the observed range for most of the other systems encompassed in this work.

Assuming $\phi_{MeA} = 0.4\,I$ and taking into account that $\phi_{Ac} = 0.037\,I$ (see Ref. [12]), Eq. (6) can be rearranged as

$$\log \beta_1 \approx \log {}^T\beta_1 + \phi_{Me} - 0.36\,I \qquad (7)$$

Eq. (7) was tested in connection with systems for which β_1 is available at only one ionic strength in addition to an estimate for ${}^T\beta_1$. The results are shown in Table 4. In spite of the very few considered systems, it seems that Eq. (7) is able to predict stoichiometric constants from the corresponding thermodynamic ones and vice versa, at least for 1:1 Cu^{2+}–monocarboxylate complexes within about a tenth of a log unit. Such estimated values should have sufficient accuracy for most studies dealing with the modelling of environmental or physiological systems [8].

This work was based on the relatively small number of available critical protonation and stability constants for carboxylates and their Me^{2-} complexes [13]. The full test for the presently proposed calculation procedure requires the development of the largest possible database of reliable stability constants and associated protonation constants.

Fig. 2. Me^{2+}–acetate systems: (a) Pb^{2+}; (b) Zn^{2+}. (○) $Y = \log \beta_1$; (+, □, △) $Y = \log \beta_1 - \phi_{Me} - \phi_{Ac}$. The ϕ_{Me} used for each correlation is indicated inside the Figure. The open circles are joined by a broken line just as a guide for the eye.
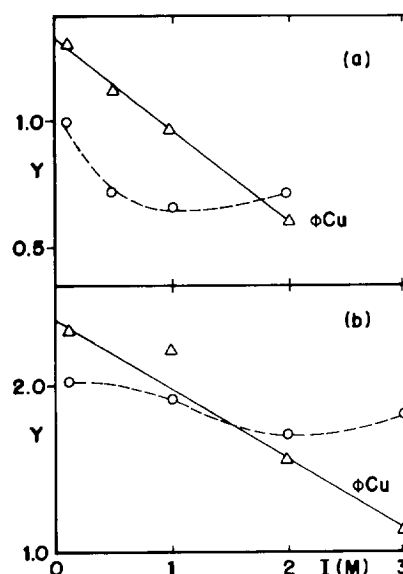

Fig. 3. Me^{2+}–monocarboxylate systems: (a) Ni^{2+}–acetate; (b) Zn^{2+}–glycolate. (○) $Y = \log \beta_1$; (△) $Y = \log \beta_1 - \phi_{Cu} - \phi_{Ac}$. The open circles are joined by a broken line just as a guide for the eye.

An inherent advantage of the proposed methodology is that through linear relationships, reliable estimates of thermodynamic constants can be obtained, via extrapolation. There are a number of techniques for estimating thermodynamic stability constants [24–26]; these are more commonly obtained by extrapolating stoichiometric constants, determined at several ionic strengths, to infinite dilution. Plots of $\log \beta_1$ (or $\log K_H$) against I, I^2, $I^{1/2}$, $I^{1/3}$, $I^{2/3}$, etc. are sometimes extrapolated by eye or by using complex functions such as the right-hand side of Eq. (8):

$$\log {}^T\beta_1 = \log \beta_1 - \frac{AZ_+ \cdot Z_- I^{0.5}}{1 + aBI^{0.5}} - CI \qquad (8)$$

against I or $I^{0.5}$, where a, A, B and C are constants, some or all of which may be treated as adjustable parameters [24,25]. None of these extrapolations are very reliable, except in a few favourable cases (see, e.g., Ref. [24]). The functions involving $\log \beta_1$ (or $\log K_H$) and ionic strength are markedly curved for most systems (i.e., of the type shown in Figs. 1–3, particularly Fig. 3a), making extrapolations to $I = 0$ rather uncertain. In fact is has been shown that the

Table 3

Estimates of log $^T\beta_1$ and ϕ_{MeA} for several Me^{2+}–Monocarboxylate complexes; aqueous solution, $T = 25°C$

Me^{2+}	Ligand	ϕ_{Me} used in Eq. (6)	I^a Range (M)	n^b	log $^T\beta_1$ This work	log $^T\beta_1$ Literature [13]	ϕ_{MeA}/I	R^2	$10^3 \times \sigma$
Cu	Formate	ϕ_{Cu}	0.1–3	3	1.99 ± 0.02	2.00 ± 0.02	0.377	0.9990	25
Cu	Formate	ϕ_{Cd}	0.1–3	3	1.93 ± 0.02	2.00 ± 0.02	0.467	0.9995	20
Cu	Acetate	ϕ_{Cu}	0.1–3	4	2.24 ± 0.03	2.21 ± 0.03	0.349	0.9980	23
Cu	Acetate	ϕ_{Pb}	1–3	3	2.25 ± 0.01	2.21 ± 0.03	0.280	0.9996	8
Cu	Propionate	ϕ_{Cu}	0.1–3	3	2.25 ± 0.01	2.22	0.355	0.9999	4
Cu	Glycolate	ϕ_{Cu}	1–3	3	2.96 ± 0.01	2.90 ± 0.02	0.380	1.0000	0
Cu	Methoxyacetate	ϕ_{Cu}	1–3	3	2.49 ± 0.01	–	0.385	0.9999	4
Cu	Pyruvate	ϕ_{Cu}	0.1–2	3	2.45 ± 0.03	$(2.2)^c$	0.653	0.9990	30
Cu	Pyruvate	ϕ_{Pb}	0.1–2	3	2.32 ± 0.01	$(2.2)^c$	0.468	0.9999	1
Co	Acetate	ϕ_{Cu}	0.5–2	3	1.30 ± 0.02	1.38 ± 0.09	0.384	0.9990	13
Co	Acetate	ϕ_{Cd}	0.1–2	3	1.35 ± 0.02	1.38 ± 0.09	0.406	0.9998	5
Ni	Acetate	ϕ_{Cu}	0.1–2	3	1.34 ± 0.01	1.43	0.368	0.9999	1
Ni	Acetate	ϕ_{Cd}	0.1–2	3	$1.29 + 0.01$	1.43	0.313	0.9994	15
Zn	Acetate	ϕ_{Cu}	0.1–3	4	1.60 ± 0.01	1.58 ± 0.01	0.455	0.9998	4
Zn	Acetate	ϕ_{Cd}	0.1–2	3	1.58 ± 0.01	1.58 ± 0.01	0.395	0.9999	4
Zn	Acetate	ϕ_{Pb}	1–3	3	1.60 ± 0.01	1.58 ± 0.01	0.350	0.9997	8
Zn	Glycolate	ϕ_{Cu}	0.1–3	3	2.37 ± 0.03	2.38	0.404	0.9980	35
Cd	Acetate	ϕ_{Cu}	0.1–3	5	1.94 ± 0.01	1.93	0.428	0.9998	4
Cd	Acetate	ϕ_{Cd}	0.1–3	4	1.91 ± 0.01	1.93	0.409	0.9997	8
Pb	Acetate	ϕ_{Cu}	1–3	3	2.70 ± 0.01	2.68	0.350	0.9997	8
Pb	Acetate	ϕ_{Pb}	1–3	3	2.71 ± 0.01	2.68	0.280	0.9996	8
Pb	Lactate	ϕ_{Cu}	0.1–3	3	2.70 ± 0.04	2.78	0.355	0.9970	29
Pb	Glycolate	ϕ_{Cd}	1–3	3	2.58 ± 0.02	–	0.450	0.9993	16
Hg	Formate	ϕ_{Cd}	1–3	3	3.48 ± 0.01	$(3.51 \pm 0.14)^c$	0.260	0.9995	8
Hg	Formate	ϕ_{Cu}	0.5–3	3	3.30 ± 0.01	$(3.51 \pm 0.14)^c$	0.120	0.9980	8
Hg	Acetate	ϕ_{Cd}	0.1–2	3	4.07 ± 0.01	$(4.29 \pm 0.12)^c$	0.161	0.9960	10
Hg	Acetate	ϕ_{Cu}	0.1–3	4	4.07 ± 0.01	$(4.29 \pm 0.12)^c$	0.173	0.9970	15
Hg	Propionate	ϕ_{Cd}	0.5–3	3	4.47 ± 0.01	$(4.38 \pm 0.14)^c$	0.367	0.9991	1
Hg	Butyrate	ϕ_{Cd}	0.1–1	3	4.11 ± 0.02	$(3.99 \pm 0.13)^c$	0.267	0.9990	5
Hg	Butyrate	ϕ_{Cu}	0.1–1	3	4.16 ± 0.01	$(3.99 \pm 0.13)^c$	0.316	0.9997	3

[a] I adjusted with $NaClO_4$.

[b] Number of (log β_1, I) pairs used; taken from Ref. [13].

[c] Doubtful value, according to Ref. [13].

deviation for values of $^T\beta_1$ obtained by using different extrapolation procedures may amount to several hundred percent [25,26]. Thermodynamic stability constants for two systems, namely Cu^{2+}–methoxyacetate and Pb^{2+}–glycolate, for which the corresponding values have not yet been assigned [13], were calculated in this work and are given in Table 3.

Another gratifying feature of our procedure is the fact that its good predictive power is not limited only to systems for which ϕ_{Me} parameters are available; thus, good estimates of thermody-

namic stability constants were also obtained for Co^{2+}, Ni^{2+}, Zn^{2+} and Hg^{2+} complexes. However, ϕ_A is available exclusively for acetate; in spite of this, protonation and formation constants in line with critically selected ones could be achieved for 13 monocarboxylates, other than acetate (Tables 2 and 3). This lends some support to the assumption made in the first part of this series [12], namely that similar ions should display closely related equilibrium parameters.

In some of the Y vs. I correlations it has been noted that one point moves away from the linear

relationship built upon the remaining points, e.g. the Y value corresponding to the Zn^{2+}–glycolate system, at $I = 1.00$ M (Fig. 3b). This suggests that the associated β_1 value might be in error and that the system probably deserves reinvestigation. Studies on systems comprising other metal ions and ligands are currently in progress in this laboratory.

5. List of symbols

A^-	monocarboxylate
Ac^-	acetate ion
HA	monocarboxylic acid
I	ionic strength (M)
M	molar or mol dm^{-3}
Me	metal ion
y_i	molar activity coeficient of an ion or a neutral substance, i

5.1. Greek letter

ϕ_i $\log y_i$

5.2. Other symbols

[]   molar concentration

Table 4
Estimates of $\log \beta_1$ for some Cu^{2+}–monocarboxylate complexes in aqueous solution. Application of Eq. (7). Parameters used: ϕ_{Cu}; $T = 25°C$.

Monocarboxylate	I(M)[a]	Literature values [13]		$\log \beta_1$ (Eq. 7)
		$\log \beta_1$	$\log {}^T\beta_1$	
Chloroacetate[b]	3.00	1.03	1.61	1.1
Phenylacetate	3.00	1.61	1.97	1.5
Butyrate	2.00	1.7 ± 0.2	2.14	1.5
Isobutyrate	0.10	1.75	2.17	1.8
Valerate	3.00	1.92	2.12	1.8

[a] I adjusted with $NaClO_4$.
[b] The reported value [13] for $I = 1.00$ M at 20°C is $\log \beta_1 = 0.91$. Assuming $\log {}^T\beta_1 = 1.61$ (actually the value for 25°C) and by using ϕ_{Cu} for $I = 1.00$ M (25°C), the calculated value from Eq. (7) is $\log \beta_1 = 0.9$.

References

[1] J.W. Patterson and R. Passino, Metals Speciation, Separation and Recovery, Vols. 1 and 2, Lewis Publishers Inc., Chelsea, MI, 1987 and 1990.
[2] J.R. Kramer and H.E. Allen, Metal Speciation: Theory, Analysis and Application, Lewis Publishers Inc., Chelsea, MI, 1991.
[3] J.R. Duffield, J.R. Johns, F. Marsicano and D.R. Williams, Polyhedron, 10 (1991) 1105, 1113, 1121 (and references cited therein).
[4] P.W. Linder and K. Murray, Talanta, 29 (1982) 377.
[5] B.S. Nakani and R.S. Hancock, J. Coord. Chem., 13 (1984) 143.
[6] A. De Robertis, C. De Stefano and S. Sammartano, J. Solution Chem., 19 (1990) 568 (and references cited therein).
[7] G. Biedermann and J. Glaser, Acta Chem. Scand., Ser. A, 40 (1986) 331.
[8] A.E. Martell, R.J. Motekaitis and R.M. Smith, Speciation of Metal Complexes and methods of predicting thermodynamics of metal–ligand reactions, in K.J. Ingolic and A.E. Martell (Eds.), Environmental Inorganic Chemistry, Verlag Chemie, Florida, 1985, pp. 89–115.
[9] R.D. Hancock and F. Marsicano, Inorg. Chem., 19 (1980) 2709.
[10] R.D. Hancock and A.E. Martell, Chem. Rev., 89 (1989) 1875.
[11] R.D. Hancock, Design of ligands with neutral oxygen donors. The basis of metal-ion size-based ligand selectivity, in A.F. Williams, C. Floriani and A.E. Merback (Eds.), Perspectives in Coordination Chemistry, VCH, New York, 1992, pp. 129–151.
[12] L. Pezza, M. Molina, M. de Moraes, C.B. Melios and J.O. Tognolli, Talanta, 43 (1996) 1689–1695.
[13] A.E. Martell and R.M. Smith, Critical Stability Constants, Vols. 3, 5 and 6, Plenum Press, New York, 1977, 1982, 1989.
[14] H.S. Rossotti, Talanta, 21 (1974) 809.
[15] M. Molina, C. Melios, J.O. Tognolli, L.C. Luchiari and M. Jafelicci, Jr., J. Electroanal. Chem., 105 (1979) 237.
[16] L.F. Fieser and M. Fieser, Quimica Orgânica, Editorial Grijalbo S.A., Mexico City, Mexico, 1960, pp. 203–205.
[17] A. Evans, Potentiometry and Ion Selective Electrodes, Wiley, London, 1987.
[18] N.V. Raghavan and D.L. Leussing, J. Indian Chem. Soc., 54 (1977) 68.

[19] D.L. Leussing and C.K. Stanfield, J. Am. Chem. Soc., 86 (1964) 2805.

[20] G.R. Choppin and R.E. Cannon, Inorg. Chem., 19 (1980) 1889.

[21] C.B. Melios, J.T.S. Campos, M.A.C. Mazzeu, L.L. Campos, M. Molina and J.O. Tognolli, Inorg. Chim. Acta, 139 (1987) 163.

[22] C.B. Melios, M. Ionashiro, H. Redigolo, M.H. Myano and M. Molina, Eur. J. Solid State Inorg. Chem., 28 (1991) 291.

[23] C.B. Melios, O.S. Siqueira, G. Llabres, H. Redigolo and M. Ionashiro, Proc. 29th Int. Conf. Coord. Chem., Lausanne, Switzerland, 1992, p. 126.

[24] F.J.C. Rossotti and H.S. Rossotti, The Determination of Stability Constants, McGraw-Hill, New York, 1961, pp. 28–35.

[25] F.R. Hartley, C. Burgess and R.M. Alcock, Solution Equilibria, Wiley, New York, 1980, pp. 24–26.

[26] M.T. Beck and I. Nagypal, Chemistry of Complex Equilibria, Wiley, New York, 1990, pp. 14–20.

Measurements of equilibrium water vapor pressures for the dehydration of magnesium, manganese and cobalt formate dihydrates by means of the transpiration method[1]

Yoshio Masuda[a,*], Makiko Hatakeyama[b]

[a]*Department of Environmental Science, Faculty of Science, Niigata University, Niigata 950-21, Japan*
[b]*Department of Chemistry, Faculty of Science, Niigata University, Niigata 950-21, Japan*

Abstract

The equilibrium water vapor pressures for the thermal dehydration of $Mg(HCO_2)_2 \cdot 2H_2O$, $Mn(HCO_2)_2 \cdot 2H_2O$ and $Co(HCO_2)_2 \cdot 2H_2O$ were measured by means of the transpiration method. These hydrates form isomorphous crystals with space group $P21/c$. In this structure, the water molecules lie in the planes parallel to the (100) planes. Thermodynamic data such as ΔG, ΔH and ΔS were derived from the values of the water vapor pressures. The relationship between these thermodynamic data and the crystal structures is discussed.

Keywords: Dehydration; Equilibrium water vapor pressure; Metal formate dihydrates; Transpiration method

1. Introduction

Crystalline hydrates cannot be distinguished from other solid reactants on chemical or structural criteria; however, the considerable interest which has been directed to the investigation of the dehydration of this group has made it convenient to discuss them as a single class. Generally, dehy-

drations are reversible reactions and the ease of water escape is influenced by the product phase, because such residual material tends to diminish the rate of diffusion of water from the reaction interface.

It is also known that the rate of thermal dehydration of hydrates is affected by the atmospheric water vapor pressure. Smith and Topley [1,2] found the phenomenon of an unusual variation in the dehydration rate with the atmospheric water vapor pressure. They reported that the rate constants for the dehydration of manganese oxalate dihydrate and copper sulfate pentahydrate vary unusually with the partial pressure of atmospheric water vapor. When the water vapor pres-

---

sure increases, the rate constant for the dehydration decreases sharply at first, passes through a minimum, increases more slowly and then decreases. This unusual phenomenon is known as the Smith–Topley effect. Garner and co-workers [3,4] carried out similar studies of copper sulfate pentahydrate and potassium ammonium chrome alum. A similar phenomenon has also been observed by Dollimore and co-workers [5,6] in the dehydration of calcium oxalate monohydrate and magnesium oxalate dihydrate. Recently, we have discovered similar phenomena in the dehydration of zinc, erbium and yttrium formate dihydrates [7–9].

Although the kinetics of the thermal dehydration of hydrates have been extensively studied by means of thermal analyses such as thermogravimetry (TG) and differential scanning calorimetry (DSC), the equilibrium water vapor pressures of the hydrates have been scarcely reported. It is very important to accumulate such fundamental thermodynamic quantities as the equilibrium water vapor pressure.

In this work, the equilibrium water vapor pressures for the dehydration of magnesium, manganese and cobalt formate dihydrates, which are known to form an isomorphous crystal structure with space group $P21/c$ [10,11], were measured by means of the transpiration method [12,13] using laboratory-made apparatus. The derived thermodynamic quantities such as the enthalpy changes, entropy changes and free energy changes for these thermal dehydrations were determined. It is of interest to discuss the relationship between the crystal structures and the thermodynamic quantities derived from the equilibrium water vapor pressures for the thermal dehydration of these hydrates.

2. Experimental

2.1. Reagents

Magnesium, manganese and cobalt formate dihydrates were purchased from Wako Pure Chemical Industries and recrystallized from a 10^{-4} M solution of formic acid. The crystals were air-

dried at room temperature. These samples were identified by means of TG and IR spectra. Each sample was pulverized in a mortar and pestle.

2.2. The transpiration apparatus

The equilibrium water vapor pressures for the dehydrations were measured using the laboratory-made apparatus shown in Fig. 1 [12,13]. Dry nitrogen at a known flow rate was passed through a loosely fitted plug of Pyrex glass wool into the saturation zone. This zone was about 80 mm in length in a 20 mm diameter Pyrex glass tube. The powdered sample (about 5 g) was piled in ridges to a depth of about 10 mm. A nitrogen stream saturated with the water vapor produced was discharged through another plug of Pyrex wool and a 20 mm length of 0.05 cm capillary. The exit gases were passed to absorbers made of magnesium perchlorate for analysis. The temperature of sample was determined with a chromel–alumel thermocouple fitted in the central thermocouple well shown in Fig. 1. The temperature of the furnace was controlled to ± 0.5 K with an EC-205 controller (Ohkura).

The equilibrium water vapor pressure, P_{H_2O}, was obtained in accordance with the equation

$$P_{H_2O} = \frac{n_{H_2O}}{n_{H_2O} + n_{N_2}} P(\text{a.p.})$$

where n_{H_2O} is the number of moles of water absorbed by the absorber in a given time interval, n_{N_2} is the number of moles of carrier nitrogen
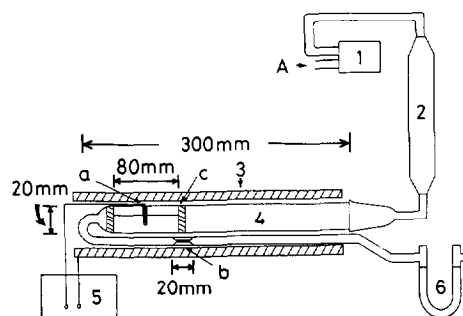

Fig. 1. Transpiration apparatus. 1, Flow control bulb; 2, dry column; 3, electric furnace; 4, reaction vessel; 5, temperature controller; 6, absorption vessel; a, thermocouple; b, capillary zone; c, glass wool.

flowing in a given time interval and P(a.p.) is atmospheric pressure (1 atm).

2.3. Thermal analyses

The TG and differential thermal analysis (DTA) curves were simultaneously recorded on a Rigaku TAS 200-TG–DTA system [14,15]. About 10 mg of sample were weighed into a platinum crucible and measured using α-alumina as a reference material. The enthalpy change for the dehydration was determined from the DSC curve recorded on a Rigaku TAS 200-DSC instrument [14]. The instrument was calibrated with the enthalpy change of the phase transition of potassium nitrate (400.9 K, $\Delta H = 5.4$ kJ mol^{-1}) and the enthalpy changes of melting gallium, indium, tin, lead and zinc (Ga, 309.94 K, $\Delta H = 5.59$ kJ mol^{-1}; In, 430 K, $\Delta H = 3.3$ kJ mol^{-1}; Sn, 505 K, $\Delta H = 7.07$ kJ mol^{-1}; Pb, 600.6 K, $\Delta H = 4.77$ kJ mol^{-1}; and Zn, 692.7 K, $\Delta H = 6.57$ kJ mol^{-1}) [16].

2.4. X-ray powder diffraction and Fourier transform (FT) IR spectrophotometry

The X-ray powder diffraction patterns were obtained with Rigaku Geigerflex RAD-γA and RAD-R diffractometers equipped with a high-temperature sample holder [17]. Cu Kα radiation, a nickel filter and a graphite monochromator were used in all measurements. The diffraction data were taken in steps of width 0.02°.

IR absorption spectra was measured from 400 to 4500 cm^{-1} in KBr discs with a Horiba FT-IR spectrophotometer.

3. Results and discussion

TG–DTA of the hydrates (Fig. 2) showed that the dehydration took place as a one-stage reaction:

$$M(HCO_2)_2 \cdot 2H_2O(s) \rightarrow M(HCO_2)_2(s) + 2H_2O (g)$$

Fig. 3 shows the relationship between the flow rate of nitrogen carrier gas and the values of the equilibrium water vapor pressure, P_{H_2O}, for the
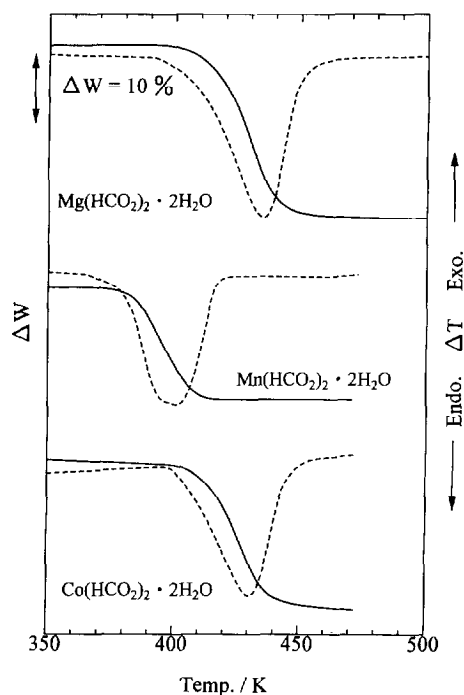
Fig. 2. TG (solid lines) and DTA (dotted lines) curves for the thermal dehydrations of magnesium, manganese and cobalt formate dihydrates.
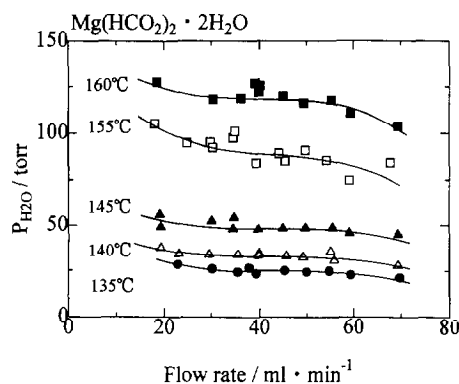
Fig. 3. Relationship between the flow rate of carrier gas and P_{H_2O}.

dehydration of magnesium formate dihydrate at various temperatures. When the flow rate increases, P_{H_2O} first decreases, passes through a constant value and then decreases. A similar tendency was observed for the other hydrates, and is explained as follows. At a slow flow rate, the water molecules produced appear to self-diffuse to

Table 1

P_{H_2O} for the dehydration of magnesium, manganese and cobalt formate dihydrates

Sample	Temperature (K)	P_{H_2O} (Torr)
$Mg(HCO_2)_2 \cdot 2H_2O$	408	24.7 ± 1.08
	413	33.6 ± 0.768
	418	48.2 ± 0.349
	428	86.8 ± 3.00
	433	121 ± 3.86
$Mn(HCO_2)_2 \cdot 2H_2O$	368	62.1 ± 2.99
	373	99.0 ± 4.24
	383	164 ± 5.45
	388	211 ± 6.45
$Co(HCO_2)_2 \cdot 2H_2O$	403	33.7 ± 1.90
	413	60.8 ± 0.693
	418	82.3 ± 4.25
	423	106 ± 1.30

the absorption tube, so P_{H_2O} shows an apparently high value, and at a higher flow rate the carrier gas cannot be saturated with the dissociated water molecules. An average of approximately constant values obtained during the medium flow rate region was adopted as the equilibrium water vapor pressure, P_{H_2O}, for the given temperature.

The P_{H_2O} values were determined for various temperatures around the peak temperatures of the

DTA curves of these dihydrates (Fig. 2), and the values are shown with the standard deviations in Table 1. The enthalpy changes, $\Delta H°$ were calculated from the equation on the basis of the temperature dependence of P_{H_2O}:

$$2 \ln\left(\frac{P_{H_2O}}{Torr}\right) = \frac{-\Delta H°}{RT} + \frac{\Delta S°}{R}$$

The free energy changes could also be obtained from the equation

$$\Delta G = -2RT \ln\left(\frac{P_{H_2O}}{Torr}\right)$$

and the values at 373 K, $\Delta G(373$ K) are shown in Table 2 together with the temperatures, T_i, at which weight loss of the dehydration is initiated, and the enthalpy change, $\Delta H(DSC)$, measured directly by means of DSC.

The values of $\Delta H°$ are larger than those of $\Delta H(DSC)$. The enthalpy change for the dehydration consists of a number of components, due to the energy for the dissociation of the coordinated water molecules, lattice energy, hydrogen-bond energy, etc. Although further analysis of the enthalpy change cannot be given at present because the crystal structures of dehydrated salts have not yet been clarified, the difference between $\Delta H°$ and $\Delta H(DSC)$ may be discussed as follows.

Table 2

Thermodynamic data derived from P_{H_2O}

Sample	$\Delta H°$ (kJ mol^{-1})	$\Delta H(DSC)$ (kJ mol^{-1})	$\Delta G(373$ K) (kJ mol^{-1})	$\Delta S°$ (J mol^{-1})	T_i (K)[a]
$Mg(HCO_2)_2 \cdot 2H_2O$	186 ± 2.74	149 ± 1.79	-3.90	509	392
$Mn(HCO_2)_2 \cdot 2H_2O$	140 ± 12.4	112 ± 1.58	-27.9	451	367
$Co(HCO_2)_2 \cdot 2H_2O$	163 ± 2.72	115 ± 2.72	-9.70	463	390

[a] Initiation temperature of thermal dehydration.

Table 3

Crystal data for magnesium, manganese and cobalt formate dihydrates

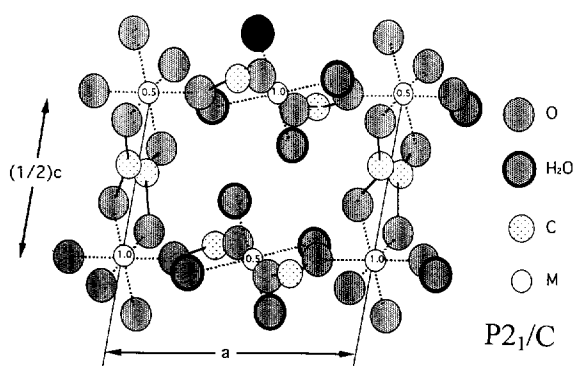| Sample	a(Å)	b(Å)	c(Å)	β(°)	r_{M2+}(Å)[a]	Interatomic distance (Å)	
						$M-H_2O(1)$	$M-H_2O(2)$
$Mg(HCO_2)_2 \cdot 2H_2O$	8.69	7.18	9.39	97.6	0.86	2.08	2.06
$Mn(HCO_2)_2 \cdot 2H_2O$	8.86	7.29	9.60	97.7	0.97	2.24	2.16
$Co(HCO_2)_2 \cdot 2H_2O$	8.63	7.06	9.21	96.0	0.79	2.07	2.06

[a] Ionic radius of metal ion.

Fig. 4. Projection of crystal structure of $M(HCO_2)_2 \cdot 2H_2O$ on the (010) plane.

Generally, the crystal structure of a hydrate must be broken by the dehydration and an amorphous dehydrated product may be formed immediately after the dehydration at the equilibrium state, and ΔH° seems to correspond to the reaction

$M(HCO_2)_2 \cdot 2H_2O(crystal)$

$\rightarrow M(HCO_2)_2(amorphous) + 2H_2O$ (g)
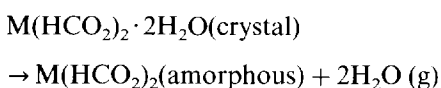
Crystalline anhydride products were obtained after the DSC measurement, so the value of $\Delta H(DSC)$ may correspond to the reaction

$M(HCO_2)_2 \cdot 2H_2O$ (crystal) $\rightarrow M(HCO_2)_2$ (crystal) + $2H_2O$ (g)
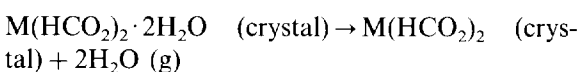
Therefore, the difference between ΔH° and $\Delta H(DSC)$ seems to be attributable to the enthalpy change for the exothermic crystallographic process:

$M(HCO_2)_2(amorphous) \rightarrow M(HCO_2)_2(crystal)$
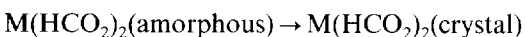
It is known that the title compounds have a isomorphous crystal structure. The lattice parameters of these hydrates are shown in Table 3. The crystals are monoclinic, with space group $P21/c$. The unit cell contains two kinds of metallic ions, which are not equivalent. One of them is coordinated by six carboxyl oxygen atoms and the other is coordinated by two carboxyl oxygen atoms and four oxygen atoms of water molecules. Both are in an octahedral form, with the water molecules lying on the plane parallel to the (100)

planes (Fig. 4). The kinetics of the dehydrations of these salts was described by a two-dimensional phase boundary reaction model [7,18].

The T_i, ΔH° and $\Delta G(373$ K) values are correlated to the thermal stability of these hydrates, and the stability may be related to the strength of the $M-OH_2$ coordination bond. If the strength of the $M-OH_2$ bond is assumed to depend on the electrostatic force between the metallic ion and the lone pair electrons of oxygen of the water molecule, the bond strength is dependent on the length of the $M-OH_2$ bond. It is noteworthy that a mutual correlation appears to be found among T_i, ΔH° and $\Delta G(373$ K) and the bond length of the $M-OH_2$ bond.

References

[1] M.L. Smith and B. Topley, Proc. R. Soc. London, Ser. A, 134 (1931) 224.

[2] B. Topley and M.L. Smith, J. Chem. Soc., (1935) 321.

[3] W.E. Garner and M.G. Tanner, J. Chem. Soc., (1930) 47.

[4] W.E. Garner and T.S. Jennings, Proc. R. Soc. London, Ser. A, 224 (1954) 460.

[5] D. Dollimore, T.E. Jones and P. Spooner, J. Chem. Soc. A, (1970) 2809.

[6] D. Dollimore, G.R. Heal and J. Mason, Thermochim. Acta, 24 (1978) 307.

[7] Y. Masuda and K. Nagagata, Thermochim. Acta, 155 (1989) 255.

[8] Y. Masuda and Y. Ito, J. Thermal Anal., 38 (1992) 1793.

[9] Y. Masuda, K. Hirata and Y. Ito, Thermochim. Acta, 203 (1992) 289.

[10] K. Osaki, Y. Nakai and T. Watanabe, J. Phys. Soc. Jpn., 18 (1963) 919.

[11] T. Ogata, T. Taga and K. Osaki, Bull. Chem. Soc. Jpn., 50 (1977) 1674.

[12] M. Taniguchi and T.R. Ingraham, Can. J. Chem., 42 (1964) 2467.

[13] S. Shimizu and M. Taniguchi, Nippon Kagaku Kaishi, (1977) 953.

[14] Y. Masuda, K. Nagaoka, H. Ogawa, O. Nakazato, Y. Yukawa and H. Miyamoto, J. Alloys Compd., in press.

[15] Y. Masuda and K. Iwata, J. Thermal Anal., 44 (1995) 1013.

[16] Chemical Society of Japan, Kagaku Binran Kisohen (Handbook of Chemistry) II, Maruzen, Tokyo, 3rd edn., 1984, pp. 267–271.

[17] Y. Masuda, A. Yahata and H. Ogawa, Inorg. Chem., 34 (1995) 3130.

[18] Y. Masuda and S. Shishido, Thermochim. Acta, 28 (1979) 377.

Modified spectrophotometric method for the determination of selenium in environmental and mineral mixtures using 2,3-diaminonaphthalene

K.N. Ramachandran*, G.S. Kumar

Shriram Institute for Industrial Research, 14 15 Sadarmangala Industrial Area, Whitefield Road, Bangalore, 560-048, India

Abstract

Reaction of selenium with 2,3-diaminonaphthalene was reinvestigated with bromide ion as a catalyst. In acid medium, selenium reacts with the above reagent to form a complex extractable with cyclohexane and with an absorption maximum at 378.5 nm. The molar absorptivity of the complex is 17.5×10^3 l mol^{-1} cm^{-1}. Beer's law is obeyed in the range 0.5–12 mg l^{-1}. The method is reproducible and the standard and relative standard deviation for seven replicate analyses of 2 mg l^{-1} of selenium are 0.05 absorbance units and 2.5%, respectively. The limit of detection is 0.012 mg l^{-1}. The method was optimized for the determination of selenium in water, soil, cereal and mineral mixtures and cattle feed and was compared with the reported 2,3-diaminonaphthalene method.

Keywords: Selenium; Spectrophotometry; 2,3-Diaminonaphthalene

1. Introduction

Selenium is a widely distributed metalloid with ubiquitous properties. As its toxicological and physiological importance has become more evident, there been increasing interest in the determination of this element [1–3]. The most commonly used methods are atomic absorption spectrometry (Hydride generation and electrothermal atomization), molecular fluorescence spectrometry, gas chromatography and spectrophotometry. Spectrophotometric methods are popular because of their simplicity and are based on piazselenol

complex formation between the reagent and selenium. The common reagents are o-diamines, 3,3-diaminobenzidine [4], dithizone, o-phenylenediamine [5], 2,3-diaminonaphthalene [6], 8-hydroxyquinoline [7,8], 6-amino-1-naphthol-3 sulphonic acid (J-acid) [9,10] and 2,3-diamino-1,4-dibromonaphthalene [11]. These are sensitive to pH, temperature and other physico-chemical parameters. Some of the colour development reactions are very slow and are susceptible to interferences from a large number of ions. 2,3-diaminonaphthalene is a widely used reagent for standardization and pharmaceutical testing owing to its lack of toxicity and ready availability [12]. Several modifications of this method has been

---

* Corresponding author.

published in recent years [12–15]. These methods require extraction, pH optimization and a long time (110 min) for colour development and cannot be applied to cattle feed or mineral mixtures.

In this work, the 2,3-diaminonaphthalene method [6] was modified and applied to the determination of selenium in the above samples. The reagent was modified by adding hydroxylammonium hydrochloride and potassium bromide and the analytical parameters were evaluated. The method was applied to the determination of selenium in water, soil, cereal and cattle feed samples and was compared with the reported method.

2. Experimental

2.1. Apparatus

A Hitachi Model 3021 double-beam UV–visible spectrophotometer with 10 mm matched silica cells was used for all spectral measurements. pH measurements were made with a Philips pH meter.

2.2. Reagents

All reagents were of AnalaR grade. Selenium-free water was prepared by sub-boiling of deionized water.

2.2.1. Selenium solutions

A stock standard solution of selenium was prepared from metallic selenium as reported [15]. Working standard solutions were prepared by appropriate dilution of the stock standard solution.

2.2.2. 2,3-diaminonaphthalene

(A) A 3×10^{-3} mol l^{-1} solution of the reagent was prepared by dissolving 100 mg of the reagent in water along with 500 mg of hydroxylammonium chloride by slow heating. This was diluted to 100 ml and stored in an amber-coloured bottle at 4 °C. The reagent was prepared 1 h before use.

(B) A 50 ml volume of the above solution was taken in an amber-coloured volumetric flask and 25 mg of potassium bromide were added. The

solution was shaken well and filtered. This reagent was used for the present investigation.

2.3. Procedure

2.3.1. Preparation of calibration graph

To an aliquot of solution containing 5–60 μg (1–10 ml) of selenium in a 25 ml boiling tube, 2 ml of reagent B were added and the pH was adjusted to 2 by dropwise addition of 1 mol l^{-1} HCl. The solution was then kept in a boiling water-bath for 5 min. The solution was allowed to cool and the piazselenol complex was extracted into 10 ml (5 × 2 ml) of cyclohexane. The cyclohexane layer was dried over anhydrous sodium sulphate. The absorbance of the solution was measured at 378.5 nm against a reagent blank.

2.3.2. Determination of selenium in water

To an aliquot of 100 ml of sample in a distillation flask, 1 g of potassium bromide and 10 ml of sulphuric acid were added and distilled as reported [6]. The distillate was collected in 5 ml of reagent B and analysed as above.

2.3.3. Selenium in soil samples

Depending on the available selenium concentration, 5 g of soil sample were place in a steam distillation flask with 200 ml of water and stirred thoroughly with a magnetic stirrer. A 5 ml volume of 10% sodium hydroxide solution was added and the mixture was concentrated to 50 ml by heating under vacuum. To this, 500 mg of potassium bromide were added after acidification with hydrochloric acid. The contents were distilled as reported [6] and the distillate was collected in 5 ml of reagent solution in a 100 ml impinger.

2.3.4. Determination of selenium in cereals and plant materials

A 5 g amount of cereal was placed in a 100 ml Kjeldahl flask and heated with selenium-free nitric acid for 20 min, 0.5 ml of perchloric acid was added and the mixture was heated gently with stirring in a fume-hood for 10 min. After cooling, 10 ml of water were added and the solution was heated for another 10 min. The contents were diluted to 50 ml after adding 10 ml of 0.1 mol l^{-1}

EDTA solution and analysed as recommended in Section 2.3.1.

2.3.5. Determination of selenium in mineral mixtures/cattle feed

For free selenium, 1 g of sample was taken in a flat-bottomed flask, 10 ml of water were added and the mixture was stirred at 50 °C for 10 min. The contents were filtered through a 0.45 μm filter under suction. The filtrate was acidified with HCl to pH 2 and analysed as above.

For total selenium to 1 g of the mineral mixture 10 ml nitric acid were added and digested for 10 min. To this 25 ml of water were added, filtered and the filtrate was analysed as recommended above.

3. Results and discussion

The absorption spectrum of the complex extracted with cyclohexane shows an absorbance maximum at 378.5 nm, whereas the reagent blank has negligible absorbance at this wavelength. The absorption was a linear function of concentration of selenium in the range 0.5–12 mg l^{-1}. The apparent molar absorptivity was 17.5×10^3 mol^{-1} cm^{-1}. The reproducibility of the method was assessed by calculation of the standard and relative standard deviations for a 2 mg l^{-1} solution of selenium, the values for seven replicate analyses being 0.05 absorbance units and 2.5%, respectively. The corresponding values for selenium using the reported method [6] were 0.092 absorbance units and 3.9%.

Under the optimum conditions, 6×10^{-3} mol l^{-1} of the reagent solution was sufficient for complete colour development. The effect of temperature on the colour development reaction was studied. The colour development requires 100–120 min at room temperature when the reagent mixture reported in the literature [6] is used. At higher temperature the reaction was not reproducible, probably owing to decomposition of the coloured complex. The optimum temperature range for complete colour development reaction was 80–100°C. The colour development reaction also depends on the pH of the solution. Maxi-

mum absorbance was obtained in the pH range 2 ± 0.3.

The effect of foreign ions on the determination of selenium was studied. The tolerance level for some of the investigation ions (in mg l^{-1}) are Ag$^+$, K$^+$, Ba^{2+} 5000; V^{5+}, Ca^{2+} 4800; Cu^{2+} 2500; Fe^{2+}, Fe^{3+}, 1200; Sb^{3+} 1000; Te^{4+} 800; Ce^{3+} 750; NO$_3^-$, NO$_2^-$, SO$_4^{2-}$ 1000; and Zn^{2+}, Bi^{3+}, Cd^{2+}, Sn^{2+} 250. Since most oxidants and reductants interfered, selenium was separated from the samples (soil, cereal and cattle feed) prior to its determination.

The presence of bromide ion enhances the colour development reaction and improves the precision of the method. The bromide ion helps the quantitative conversion of other forms of selenium to selenium(IV), which reacts with the dye in the bromide environment more rapidly and forms the complex. The role of bromide ion in the system is purely catalytic and even 5 ml of 2% bromide solution did not interfere in the reaction. Addition of bromide to the reagent makes it more stable at room temperature. It was found that in the presence of bromide ions at temperatures above 80°C the colour development reaction was fast and reproducible.

3.1. Application

The method was applied to the determination of selenium in several samples of water, cereals and mineral mixtures. The results (Table 1) were compared with those for the reported 2,3-diaminonaphthalene method [6]. The results obtained by the reported method [6] were high owing to interferences from other metal ions.

3.2. Comparison with another method

The proposed method has been compared with another reported method [6]. The current modification makes the reaction fast and enhances the reproducibility. Although the present method is less sensitive than J-acid methods, the modification is significant in view of its wide application. The proposed method will be useful for the accurate determination of selenium especially in complex mineral matrices.

Table 1
Application of the method[a]

Sample	Amount taken	Se added (mg l^{-1})	Se found (mg l^{-1})[b]		Recovery (%)	
			A	B	A	B
Water	5 ml	2	1.95	1.97	97.5	98.5
		4	3.81	3.95	95.3	98.7
		8	7.45	7.87	93.1	98.3
Cereal	2 g	0	2.1	1.6	N.A	N.A
			2.7	1.62		
			2.8	1.61		
Soil	5 g	0	5.1	3.9		
			5.9	3.85		
			6.3	3.88		
Mineral mixture	1 g	0	24.2	17.1		
			25.3	17.3		
			26.4	17.1		

[a] A = reported procedure [6]; B = present method.
[b] Means of three replicate analyses.

Acknowledgements

References

[1] A. Safavi and A. Akhami, Anal. Lett., 28 (1995) 1095.
[2] D.C. Adriano, Biogeochemistry of Trace Metals, Lewis, London, 1992.
[3] J. Tan and Y. Huang, J. Water Air Soil Pollut., 57–58 (1991) 59.
[4] D.B. Porcella, G.L. Bowie, J.G. Sanders and G.A. Cutter, J. Water Air Soil Pollution, 57–58 (1991) 3.
[5] A.D. Campbell and A.H. Yahaya, Anal. Chim. Acta, 119 (1980) 171.
[6] S.C. Lavale and M. Dave, J. Indian Chem. Soc., 66 (1989) 974.
[7] N.B. Lebed and R.P. Pantalar, Fresenius' Z. Anal. Chem., 41 (1986) 2224.
[8] A. Bhat and V.K. Gupta, J. Indian Chem. Soc., 59 (1982) 888.
[9] K.N. Ramachandran, R. Kaveeswar and V.K. Gupta, Talanta, 40 (1993) 781.
[10] R. Manish, K.N. Ramachandran and V.K. Gupta, Talanta, 41 (1994) 1623.
[11] K. Johansson, X. Luo and A. Olin, Talanta, 42 (1995) 1979.
[12] The United States Pharmacopeia, 23rd Revision, National Formulary 18, US Pharmacopeal Convention, Rockville, MD, 1995.
[13] G. Koble, K. Kalcher, K.J. Irgolic and R.J. Magee, Appl. Organomet.Chem., 7 (1993) 443.
[14] R.M. Olives, O.F.X. Donald, C. Camera and P. Quevauviller, Anal. Chim. Acta, 286 (1994) 357.
[15] X. Dauchy, A. Astruc and M. Astruc, Fresenius' Z. Anal. Chem., 348 (1994) 792.

Catalytic effect of some inorganic ligands on a ligand substitution reaction involving mercury(II) and its application as a differential kinetic method of analysis[1]

Shinkichi Yamada*, Fumihiro Umika, Motoshi Nakamura, Shigeru Nakamura

Laboratory of Analytical Chemistry, Faculty of Engineering, Shizuoka University, Johoku, Hamamatsu 432, Japan

Abstract

To design a sensitive and selective kinetic method for determining a catalyst, the kinetics of the ligand substitution reaction between the mercury(II)–4–(2-pyridylazo)resorcinol complex and 1,2-cyclohexanediamine-N,N,N',N'-tetraacetic acid together with the catalytic effect of some inorganic ligands on this reaction were studied. The rate constant for a catalyzed reaction path was found to be linearly correlated with the electron donor constant of the catalyst. From this correlation, the difference in reactivity between sulfite or thiosulfate and sulfate was established. Under the selected conditions, sulfite up to 1.5×10^{-6} M and thiosulfate up to 7×10^{-7} M could be determined with detection limits of 3×10^{-8} and 2×10^{-8} M in the presence of 10 000 and 25 000-fold molar amounts of sulfate, respectively. The tolerance level in the determination of 1×10^{-6} M of sulfite and 4×10^{-7} M of thiosulfate was studied for 15 inorganic anions and 44 metal ions.

Keywords: Differential kinetic analysis; Inorganic ligand catalysis; Ligand substitution reaction; Mercury(II)

1. Introduction

Ligand substitution reactions of a metal–chromogenic ligand complex (MR) with a polycarboxylic- or aminopolycarboxylic-type multidentate ligand (Y) can be written as

* Corresponding author.

[1] Presented at the 1995 International Chemical Congress of Pacific Basin Societies (PACIFICHEM '95) in the Symposium on Kinetic and Mechanistic Aspects of Analytical Chemistry, Honolulu, Hawaii, USA, December 17–22, 1995.

$$MR + Y \xrightarrow{k_f} MY + R \tag{1}$$

charges are omitted for simplicity, where k_f is the overall forward rate constant. This reaction system has been widely used in inorganic differential kinetic analysis [1–4]. It has been found that some reactions are catalytically accelerated by an additional ligand (A) and this catalytic effect provides a basis for the kinetic determination of the ligand carrying such a catalytic feature [5,6].

From mechanistic considerations concerning the formation constant of a mixed-ligand complex

[7,8], the catalytic effect of the additional ligand A on the substitution reaction (1) is found to be described by [9]

$$\log (k_f^A / k_f) = \alpha E(A) + \beta H(A) + \gamma E(A) \qquad (2)$$

where k_f^A is the overall rate constant for the catalyzed reaction path, E and H are the electron donor constant and basicity constant of catalyst A, respectively (their values are normalized to zero for A = H_2O and have been given for typical monodentate ligands [10] and some selected multidentate ligands [11] and α, β and γ are constants characteristic of the metal ion M; the values of α and β have been estimated from the stability of the metal complex [10] and that of γ from the reactivity of the metal ion and its complexes [9,12,13]).

For M = Hg^{2+}, which is a typical soft metal ion with negligibly small β and γ values compared with α, we have

$$\log (k_f^A / k_f) = \alpha E(A) = 5.8 E(A) \qquad (3)$$

With the value of $E(A)$, it has been demonstrated [9] that the catalytic effect of halide ions on the ligand substitution reaction of the mercury(II)-4-(2-pyridylazo)resorcinol (PAR; H_2R) complex with 1,2-cyclohexanediamine-N,N,N',N'-tetraacet-ic acid (CDTA; H_4Y) can be described by Eq. (3).

When the catalytic effect of an additional ligand other than halides on this ligand substitution reaction is assumed to be dscribed also by Eq. (3), some interesting differences in reactivity between related species are found. For example, the values of k_f^A for A = SO_3^{2-} and SO_4^{2-} are estimated to be $10^{14.0}$ and $10^{3.4}$ times larger than that of k_f, respectively. This marked acceleration effect of SO_3^{2-} and the large difference in reactivity between SO_3^{2-} and SO_4^{2-} provide an opportunity to design a sensitive and selective kinetic method for determining sulfite in the presence of sulfate with this reaction system.

In order to demonstrate this, we studied the kinetics of the substitution reaction between the Hg(II)-PAR complex and CDTA together with the catalytic effect of some inorganic ligands involving sulfate and sulfite.

2. Experimental

2.1. Reagents

All chemicals were of reagent grade. A solution of mercury(II) was prepared by dissolving the oxide in perchloric acid. The concentrations of mercury(II) and perchloric acid in the stock solution were 1.00×10^{-2} and 1 M, respectively. PAR and CDTA (Dojindo, Japan) were dissolved in 2.5 equivalents of sodium tetraborate and 2 equivalents of sodium hydroxide, respectively. The stock solutions used to study the effect of diverse ions were prepared by dissolving the corresponding sodium or potassium salt and the corresponding nitrate or perchlorate in distilled water for anions and metal ions, respectively. An equivalent amount of CDTA was added to the stock solution of sulfite in order to prevent possible air oxidation of sulfite catalyzed by trace amounts of heavy metal ions in the salt. This stock solution was freshly prepared just before use.

2.2. Measurements

Absorption spectra and absorbances were measured with a UV-3100 spectrophotometer (Shimadzu, Japan). Reactions were started by mixing the Hg(II)-PAR solution and CDTA solution with an MX-7 mixing device (Otsuka Electronics, Japan). The changes in absorbance at 500 nm were recorded as a function of reaction time. The temperature of the reaction solutions was maintained at $25.0 \pm 0.1°C$. The ionic strength (I) was maintained at 1 M with sodium perchlorate. The pH in the reaction solution was adjusted with borate buffer and was measured with a IM-20E digital ion meter (Toa Denpa, Japan) and a glass electrode.

3. Results and discussion

Among various chromogenic ligands [14,15] which form highly colored and water-soluble complexes with mercury(II) in weakly alkaline media, PAR was selected as R in Eq. (1). The mercury(II)-PAR complex was stable in the pres-

ence of a large excess (higher than 7×10^{-4} M) of PAR over the pH range 8.4–9.1. Employing CDTA, ethylenediamine-N,N,N',N'-tetraacetic acid (EDTA), glycol ether diamine-N,N,N',N'-tetraacetic acid (GEDTA) and diethylenetriamine-N,N,N',N'',N''-pentaacetic acid (DTPA) as Y in Eq. (1), the time necessary for complete substitution of the mercury(II)–PAR complex with ligand Y was studied at pH 9. This was found to be 15 min for 1×10^{-4} M CDTA, 30 s for 2×10^{-5} M EDTA and 1×10^{-4} M GEDTA and 20 s for 1×10^{-4} MDTPA. CDTA was therefore selected as the substitution ligand for the mercury(II)–PAR complex.

3.1. Substitution of mercury(II)–PAR complex with CDTA

Under the present experimental conditions in which $C_{Hg} = 1 \times 10^{-5}$ M, $C_{PAR} = (0.8-1) \times 10^{-3}$ M, $C_{CDTA} = (0.5-2) \times 10^{-4}$ M and pH = 8.4–9.1 (borate buffer), the reaction can be described as [5]

$$HgR_2{}^{2-} + HY^{3-} + H^+ \rightarrow HgY^{2-} + 2HR^-$$

$$(4)$$
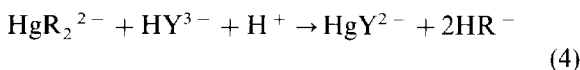
and the rate equation as

$$-d[HgR_2{}^{2-}]/dt = k_{0(H,R,Y)}[HgR_2{}^{2-}]$$ (5)

The conditional rate constant $k_{0(H,R,Y)}$ involving concentrations of hydrogen ion, PAR and CDTA was determined from the spectrophotometric first-order plot. The values of $k_{0(H,R,Y)}$ obtained at various $[H^-]$, $[HR^-]$ and $[HY^{3-}]$ were analyzed in the same manner as in Ref. [5]. $k_{0(H,R,Y)}$ was thus found to be expressed by

$$k_{0(H,R,Y)} = (k_1 + k_2[H^+])[HY^{3-}]/[HR^-]$$ (6)

with $k_1 = 2.6 \times 10^{-2}$ s^{-1} and $k_2 = 1.9 \times 10^7$ M^{-1} s^{-1}. Taking the differences in the concentration ranges of the reactants and in the ionic strength into consideration, these rate constants are in fairly good agreement with the values reported previously (1.9×10^{-2} s^{-1} and 2.4×10^7 M^{-1} s^{-1}, respectively [5]).

3.2. Catalytic effect of inorganic ligands

At $C_{Hg} = 1 \times 10^{-5}$ M, $C_{PAR} = 8 \times 10^{-4}$ M, $C_{CDTA} = 1 \times 10^{-4}$ M and pH = 8.9, reaction (4) was followed in the presence of Cl^-, Br^-, I^-, SCN^-, NH_3, NO_3^-, SO_4^{2-}, SO_3^{2-} and $S_2O_3^{2-}$, representing A in Eq. (2). Among these inorganic ligands, up to 1×10^{-2} M NO_3^- and SO_4^{2-} had no effect on the rate of the substitution reaction. Above this concentration, the reaction was decelerated, probably owing to the salt effect. The reaction was accelerated by the other ligands. The conditional rate constant $k_{0(A,H,R,Y)}$ was determined from the first-order plot in the presence of A and was found to be linearly correlated with the concentration of A, as shown in Fig. 1. The value of the intercept of this plot, which corresponds to the rate constant for the reaction path independent of A, was the same as that found in the absence of A at the same pH. Hence the following relationship was observed:

$$-d[HgR_2{}^{2-}]/dt = k_{0(A,H,R,Y)}[HgR_2{}^{2-}]$$

$$= \{k_{0(H,R,Y)} + k_{0(H,R,Y)}{}^A[A]\}[HgR_2{}^{2-}]$$ (7)

where $k_{0(H,R,Y)}$ and $k_{0(H,R,Y)}^A$ correspond to k_f and k_f^A in Eq. (2) at given concentrations of hydrogen ion, PAR, and CDTA. The value of k_f^A was determined from the slope of the linear plot of $k_{0(A,H,R,Y)}$ against [A].

The plot of $\log k_f^A$ against E(A) gives a straight line with a slope of 2.9 and an intercept of -2.6 (Fig. 2). Although the logarithmic value of k_f^A for
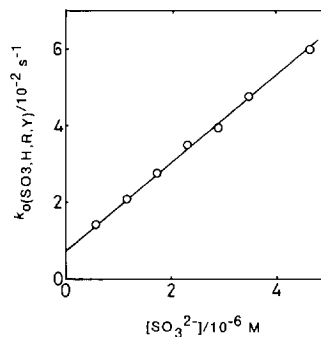

Fig. 1. Effect of sulfite concentration on $k_{0(SO_3,H,R,Y)}$. $C_{Hg} = 1 \times 10^{-5}$ M, $C_{PAR} = 8 \times 10^{-4}$ M, $C_{CDTA} = 1 \times 10^{-4}$ M, pH = 8.86 ± 0.02.
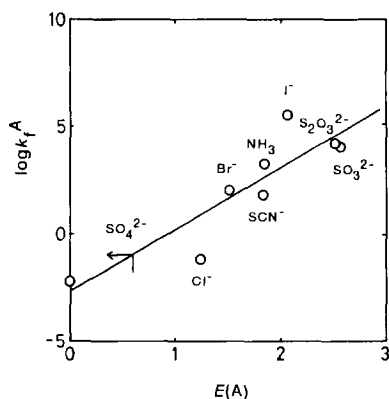
Fig. 2. Plot of $\log k_f^A$ against $E(A)$.

$A = H_2O(-2.2)$ is in agreement with that of the intercept of the straight line in Fig. 2, within experimental error, the present slope is considerably smaller than that predicted by Eq. (3). Although the reason for this discrepancy is not clear at present, the sufficient difference in reactivity between $SO_3{}^{2-}$ or $S_2O_3{}^{2-}$ and $SO_4{}^{2-}$ enabled us to design a kinetic method for the determination of $SO_3{}^{2-}$ or $S_2O_3{}^{2-}$ in the presence of a large amount of $SO_4{}^{2-}$.

3.3. Catalytic determination of sulfite and thiosulfate

Under the selected conditions in which $C_{Hg} = 1 \times 10^{-5}$ M, $C_{PAR} = 8 \times 10^{-4}$ M, $C_{CDTA} = 5 \times 10^{-4}$ M and pH = 8.4, the difference in absorbance at 4 and 20 s after the start of the reaction was plotted against the concentration of A. This calibration curve was linear up to 1.5×10^{-6} M $SO_3{}^{2-}$ or 7×10^{-7} M $S_2O_3{}^{2-}$. The detection limits, defined as 3σ of the intercept of the respective calibration curves, were 3×10^{-8} M for $SO_3{}^{2-}$ and 2×10^{-8} M for $S_2O_3{}^{2-}$. As shown in Table 1, the presence of 10 000-fold and 25 000-fold molar amounts of $SO_4{}^{2-}$ can be tolerated in the determination of 1×10^{-6} M $SO_3{}^{2-}$ and 4×10^{-7} M $S_2O_3{}^{2-}$, respectively.

3.4. Effect of diverse ions

The tolerance level of typical inorganic anions in the determination of 1×10^{-6} M $SO_3{}^{2-}$ or

4×10^{-7} M $S_2O_3{}^{2-}$ was studied and the results are summarized, together with the $E(A)$ values, in Table 1. The tolerance level was defined as the amount of an ion causing an error of not more than 5%. As expected, an anion with a smaller $E(A)$ value can be tolerated to a higher level. The results also show that, for anions having $E(A)$ values smaller than 1.8, the presence of 100-fold or greater molar amounts can be tolerated, except for bromide.

The tolerance levels of diverse metal ions were also studied and the results are summarized in Tables 2 and 3. Metal ions that caused positive errors due to complexation with PAR include Al(III), As(III), Be(II), Bi(III), Cd(II), Ce(III), Ce(IV), Cr(III), Cr(VI), Cu(II), In(III), La(III), Lu(III), Mn(II), Mn(VII), Sc(III), Se(IV), Sm(III), Ti(IV), Tl(I), Tl(III) and Y(III). Au(III) and Pd(II) caused negative errors due to complexation with PAR. Co(II), Fe(III), Ga(III), Ni(II), Zn(II) and Zr(IV) caused no errors in spite of the complexation with PAR. Ba(II), Ca(II), Ge(VI), Mg(II), Pb(II), Pt(II), Se(VI) and Sr(II) caused negative errors in spite of no reaction with PAR. Metal ions that caused no errors due to an absence of reaction with PAR (and probably also with CDTA) include As(V), K(I), Li(I), Mo(VI)

Table 1
Tolerance levels of diverse anions in the determination of 1×10^{-6} M sulfite or 4×10^{-7} M thiosulfate

Anion	$[\text{Anion}]/[\text{SO}_3{}^{2-}]$	$[\text{Anion}]/[\text{S}_2\text{O}_3{}^{2-}]$	$E(A)$
F^-	10000[a]	25000[a]	−0.27
$NO_3{}^-$	5000	25000[a]	0.29
$SO_4{}^{2-}$	10000[a]	25000[a]	0.59
CH_3COO^-	10000[a]	25000[a]	0.96
$HPO_4{}^{2-}$	5000	10000	
$HCO_3{}^-$	1000	2500	
Cl^-	100	250	1.24
Br^-	5	10	1.51
$N_3{}^-$	100	250	1.58
$NO_2{}^-$	2000	5000	1.73
SCN^-	1	2	1.83
NH_3	0.2	0.25	1.84
HS^-	0.04	0.1	
I^-	0.01	0.025	2.06
$S_2O_3{}^{2-}$	0.02		2.52
$SO_3{}^{2-}$		0.05	2.57

[a] Maximum ratio examined.

Table 2
Tolerance levels of divese metal ions in the determination of 1×10^{-6} M sulfite

$[Ion]/[SO_3^{2-}]$	Metal ion
1000[a]	As(V), K(I), Li(I)
100	Ag(I), Be(II), Cr(III), Cr(VI), Mo(VI), Se(IV), Se(VI), W(VI)
10	Al(III), Ba(II), Ca(II), Co(II), Fe(III), Ga(III), La(III), Mg(II), Ni(II), Pb(II), Sr(II), Tl(I), Zn(II), Zr(IV)
1	Ce(IV), Cu(II), Ge(IV), In(III), Pt(II), Tl(III)
0.1	As(III), Au(III), Bi(III), Cd(II), Ce(III), Lu(III), Mn(II), Mn(VII), Pd(II), Sc(III), Sm(III)
0.01	Ti(IV), Y(III)

[a] Maximum ratio examined.

and W(VI). Masking with 1×10^{-2} M fluoride did not result in any successful improvement in the tolerance levels given in Tables 2 and 3.

Sulfite and thiosulfate are metastable in aqueous solutions and oxidized to sulfate by atmospheric oxygen. Hence, it is essential to develop a method for determining sulfite and thiosulfate in the presence of as high sulfate levels as possible. A number of spectrophotometric

Table 3
Tolerance levels of diverse metal ions in the detemination of 4×10^{-7} M thiosulfate

$[Ion]/[S_2O_3^{2-}]$	Metal ion
1000[a]	As(V), K(I), Li(I), Mo(VI), Se(VI), W(VI)
100	Be(II), Cr(III), Cr(VI), Pb(II), Se(IV), Tl(I)
10	Al(III), Ba(II), Ca(II), Co(II), Fe(III), Ga(III), La(III), Mg(II), Ni(II), Sr(II), Zn(II), Zr(IV)
1	Ag(I), As(III), Cd(II), Ce(IV), Cu(II), Ge(IV), In(III), Mn(VII), Pd(II), Pt(II), Sc(III), Tl(III)
0.1	Au(III), Bi(III), Ce(III), Lu(III), Mn(II), Sm(III), Ti(IV), Y(III)

[a] Maximum ratio examined.

methods based on different principles for determining sulfite [16–26] and thiosulfate [20,24,25,27–33] at micromolar levels have been proposed. Compared with these, the present method provides the highest tolerance level of sulfate and the lowest detection limit for both anions without resort to chromatographic separation or chemical treatment.

Acknowledgements

References

[1] K.B. Yatsimirskii, Kinetic Methods in Chemical Analysis, Pergamon Press, Oxford, 1966.
[2] M. Kopanica and V. Stara, in G. Svehla (Ed.), Comprehensive Analytical Chemistry, Vol. 18, Kinetic Methods in Chemical Analysis, Elsevier, Amsterdam, 1983.
[3] D. Perez-Bendito, Analyst 109 (1984) 891.
[4] H.A. Mottola, in J.D. Winefordner and I.M. Kolthoff (Eds.), Chemical Ananysis, Vol. 96, Kinetic Aspects of Analytical Chemistry, Wiley, New York, 1988.
[5] S. Funahashi, M. Tabata and M. Tanaka, Anal. Chim. Acta, 57 (1971) 311.
[6] M. Tabata, S. Funahashi and M. Tanaka, Anal. Chim. Acta, 62 (1972) 289.
[7] M. Tanaka, J. Inorg. Nucl. Chem., 35 (1973) 965.
[8] M. Tanaka, J. Inorg. Nucl. Chem., 36 (1974) 151.
[9] S. Yamada, A. Murata and M. Tanaka, Mikrochim. Acta, III, (1988) 291.
[10] S. Yamada and M. Tanaka, J. Inorg. Nucl. Chem., 37 (1975) 587.
[11] S. Yamada, T. Kido and M. Tanaka, Inorg. Chem., 23 (1984) 2990.
[12] M. Tanaka and S. Yamada, J. Chem. Soc., Chem. Commun., (1976) 178.
[13] S. Yamada and M. Tanaka, Bull. Chem. Soc. Jpn., 58 (1985) 2234.
[14] F.D. Snell, Photometric and Fluorometric Methods of Analysis—Metals, Part 1, Wiley, New York, 1978.
[15] H. Onishi, in J.D. Winefordner and I.M. Kolthoff (Eds.), Chemical Analysis, Vol. 3, Part IIB, Photometric Determination of Traces of Metals, Wiley, New York, 1989.
[16] S.C. Pinillos, I.S. Vicente, J.S. Asensio and J.G. Bernal, Talanta, 42 (1995) 937.

[17] M.D. Luque de Castro and J.M. Fernandez-Romeo, Anal. Chim. Acta, 311 (1995) 281.

[18] A.M.G. Pieto, J.L.P. Pavon and B.M. Cordero, Analyst, 119 (1994) 2447.

[19] M.S. Abdel-Latif, Anal. Lett., 27 (1994) 2601.

[20] Y. Miura, M. Tsubamoto and T. Koh, Anal. Sci., 10 (1994) 595.

[21] T.A. Arowolo and M.S. Cresser, Analyst, 116 (1991) 1135.

[22] A. Safavi and A.A. Ensafi, Anal. Chim. Acta, 252 (1991) 121.

[23] P. Maclaurin, K.S. Parker, A. Townshend, P.J. Worsfold, N.W. Barnett and C. Crane, Anal. Chim. Acta, 238 (1990) 171.

[24] T. Koh, Y. Miura, M. Ishimori and N. Yamamuro, Anal. Sci., 5 (1989) 79.

[25] B. Badri, Analyst, 113 (1988) 351.

[26] T. Koh and Y. Miura, Anal. Sci., 3 (1987) 543.

[27] T.N. Shekhovtsova, A.A. Remizova, A.I. Chumakova, I.F. Dolmanova and Yu. I. Sokolov, Zh. Anal. Khim., 49 (1994) 676.

[28] T. Koh, N. Takahashi and K. Yokoyama, Anal. Sci., 10 (1994) 765.

[29] T. Koh, H. Wakabayashi and Y. Tonemura, Bull. Chem. Soc. Jpn., 67 (1994) 119.

[30] B. Demirata and H. Afsar, Anal. Sci., 8 (1992) 225.

[31] T. Koh, K. Kitami and Y. Yonemura, Anal. Sci., 7 (1991) 81.

[32] T. Koh, Y. Miura and M. Suzuki, Anal. Sci., 4 (1988) 267.

[33] Y. Miura and T. Koh, Anal. Chim. Acta, 173 (1985) 33.

Solvent extraction kinetics of rare earth elements

Jinzhang Gao*, Bo Peng, Haiyan Fan, Jingwan Kang

Department of Chemistry, Northwest Normal University, Lanzhou 730070, People's Republic of China

Abstract

The kinetics of solid–liquid extraction of rare earth elements (RE) (La, Ce, Sm, Dy and Yb) were studied with 1-(2-pyridylazo)-2-naphthol (PAN) at 60°C using paraffin wax as a diluent. The rate of extraction is first order with respect to metal ion and hydrogen ion in the aqueous phase and second order with respect to the extractant in the organic phase. The rate-determining step is the formation of an $[RE(PAN)_2]^+$ complex between RE^{3+} and PAN in the aqueous phase. The rate constant for the extraction was found to be about 10^{11} l mol^{-1} s^{-1}. The temperature dependence of extraction rate was determined and the activation parameters were calculated.

1. Introduction

Solid–liquid extraction using a molten diluent at high temperature as a new branch of extraction chemistry has various advantages. In this technique, organic substances which are solid at room temperature, such as naphthalene, biphenyl and paraffin waxes, are employed as diluents. The water-insoluble complex is readily extracted into the molten diluent at high temperature to achieve distribution equilibrium. Phase separation can be obtained by cooling the extraction system to room temperature. This procedure can efficiently avoid emulsion, a third phase and vaporization of solvent. Furthermore, rapid phase separation and high concentrations are also benefits for extraction work. Normally, liquid–liquid extractions are carried out at low temperatures and few data involving temperatures above 50°C have been reported. Previous papers [1–6] have reported systematic investigations of the solid–liquid extraction behavior of lanthanides with some organic reagents in the temperature range 55–85°C. It was found there are some differences in extraction mechanisms and thermodynamics between solid–liquid extraction and liquid–liquid extraction. All the organic reagents employed, such as TOPO, DBM, PMBP and PAN are very effective and efficient for the extraction of lanthanides because of their large partition coefficients between the aqueous phase and organic phase.

Solid–liquid extraction of rare earth elements with PAN was studied in previous work [5]. Information obtained on thermodynamics helps in understanding the extraction mechanism. However, further understanding of the extraction behavior

---

* Corresponding author.

and mechanism requires kinetic investigations of these high-temperature systems. This paper presents the results of a detailed study of the kinetics of the RE(III)–PAN–paraffin wax solid–liquid extraction system above 60°C (RE = rare earth element).

2. Experimental

2.1. Reagents

A 2×10^{-3} M 1-(2-pyridylazo)-2-naphthol (PAN) solution in acetone was prepared by dissolving the appropriate amount of PAN in acetone.

As buffer solutions, 0.1 M ammonium chloride and ammonia solutions were used.

Stock solutions of rare earth ions were prepared and the paraffin wax (m.p. 48–50°C) was purified according to Ref. [5]. Redistilled, deionized water was used throughout. All chemicals were of analytical-reagent grade.

2.2. Apparatus

A Model DF-101B magnetic stirrer (Zhejiang, China), a Model CS501 thermostat (Chongqing, China) with an accuracy ±0.1°C, a Model U-3400 spectrophotometer (Hitachi, Japan) and a Model PHS-10A digital acidity/ionometer (Xiaoshan, China) were used.

2.3. Procedure

A suitable amount of standard solution of RE(III) and buffer solution were placed in the extraction vessel with a water jacket (see the system in Ref. [5]). The volume of aqueous phase was kept to 10 ml with the ionic strength controlled at 0.1 with NaCl. A 1 g amount of paraffin wax was added to the vessel ($V_o:V_{aq} = 1.3:10$, where V_o is the volume of the organic phase and V_{aq} that of the aqueous phase). Water at the required temperature was introduced into the jacket with thermostatic control. After the wax had completely melted, 0.5 ml of 2×10^{-3} M PAN solution in acetone was added and magnetic
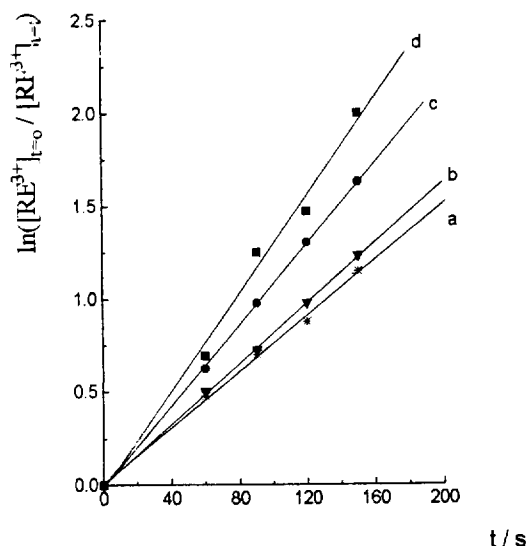
Fig. 1. Plot of $\ln([RE^{3+}]_{t=0}/[RE^{3+}]_{t=t})$ vs. time for Dy^{3+}–PAN–wax system. $[Dy^{3+}] = 2 \times 10^{-5}$ M, $[PAN]_o = 6.15 \times 10^{-4}$ M, $I = 0.1$ M (NaCl), $t = 60 \pm 0.1°C$, pH = (a) 8.60, (b) 7.93, (c) 7.83, (d) 7.65.

stirring was begun at a high speed, reaching a plateau region where a further increase in stirring speed had no effect on the rate of the extraction. The stirring was stopped after a period of time and the vessel was cooled to room temperature by circulation of cold water.
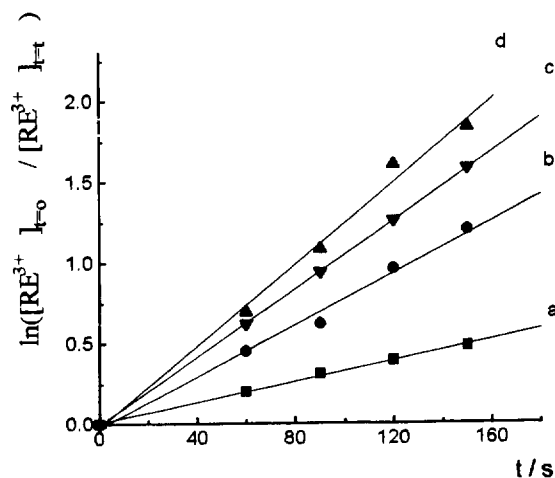

Fig. 2. Plot of $\ln([RE^{3+}]_{t=0}/[RE^{3+}]_{t=t})$ vs. time for Dy^{3+}–PAN–wax system. $[Dy^{3+}] = 2 \times 10^{-5}$ M, pH = 7.94, $I = 0.1$ M (NaCl), $t = 60 \pm 0.1°C$, $[PAN]_o = $ (a) 6.15×10^{-4} M, (b) 7.69×10^{-4} M, (c) 10.77×10^{-4} M, (d) 15.38×10^{-4} M.

After removal of the solid wax, the pH of the aqueous phase was measured and the amount of RE(III) determined as in Ref. [5]. The total recovery of RE(III) in both phases was calculated to be $100 \pm 2\%$.

3. Results and discussion

A preliminary series of experiments were performed to determine the effect on the rate of the extraction of varying the stirring speed. It was found that the rate of extraction increased rapidly at the high temperature of the experiments when the stirring speed was increased, up to a maximum value beyond which an increase in agitation had no significant effect on the rate of extraction. In all subsequent determinations, a stirring speed of 600 rpm within this "plateau region" was employed.

3.1. Reaction order with respect to the concentration of RE(III)

According to the general kinetic equation for the formation of metal chelates, the rate r of reaching extraction equilibrium is given by

$$r = -d[RE^{3+}]/dt = K[RE^{3+}]^a[HL]_o^b[H^+]^c \quad (1)$$

where K is the rate constant, RE^{3+} denotes rare earth ion Dy^{3+}, $[HL]_o$ denotes the PAN concentration the organic phase and a, b and c are the reaction orders of the reactants.

At constant pH and constant concentration of PAN in the organic phase, the above rate equation can be written as

$$r = -d[Dy^{3+}]/dt = k[Dy^{3+}]^a \quad (2)$$

where k is the observed rate constant. The reaction was assumed to be first order with respect to the concentration of Dy^{3+} ion in the aqueous phase, that is, $a = 1$, and we can integrate Eq. (2) and obtain

$$\ln([Dy^{3+}]_{t=0}/[Dy^{3+}]_{t=t}) = kt \quad (3)$$

where $[Dy^{3+}]_{t=0}$ and $[Dy^{3+}]_{t=t}$ are the concentrations of Dy^{3+} ion in the aqueous phase at time 0 and time t, respectively.
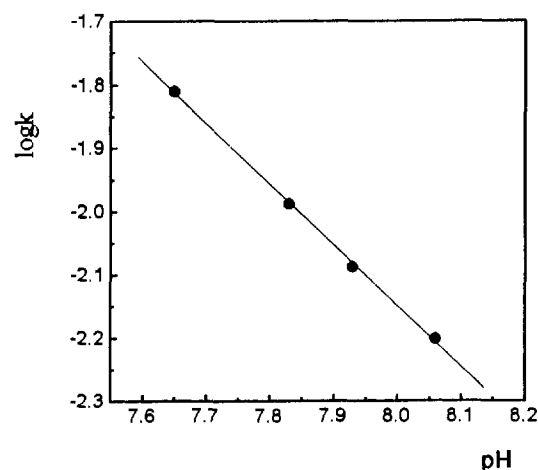

Fig. 3. Plot of $\log k$ vs. pH for Dy^{3+}–PAN–wax system. $[Dy^{3+}] = 2 \times 10^{-5}$ M, $[PAN]_o = 6.15 \times 10^{-4}$ M, $I = 0.1$ M (NaCl), $t = 60 \pm 0.1°C$, pH = (a) 8.60, (b) 7.93, (c) 7.83, (d) 7.65.

This assumption was validated when a plot of $\ln([Dy^{3+}]_{t=0}/[Dy^{3+}]_{t=t})$ vs. time was constructed and the points were found to lie on straight lines as shown in Figs. 1 and 2. Only the pH value is varied in Fig. 1 and only the concentration of PAN in the organic phase is varied in Fig. 2.
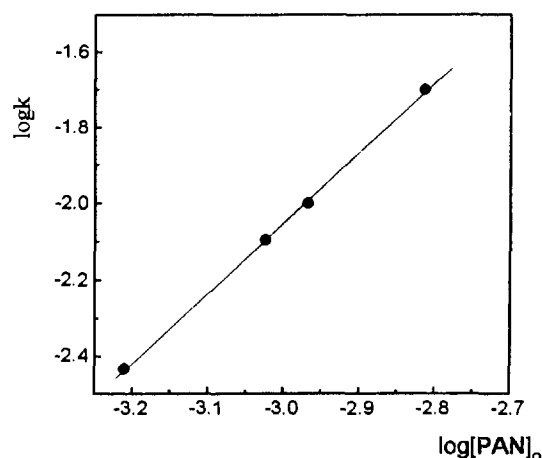

Fig. 4. Plot of $\log k$ vs. $\log[PAN]_o$ for Dy^{3+}–PAN–wax system. $[Dy^{3+}] = 2 \times 10^{-5}$ M, pH = 7.94, $I = 0.1$ M (NaCl), $t = 60 \pm 0.1°C$, $[PAN]_o = $ (a) 6.15×10^{-4} M, (b) 7.69×10^{-4} M, (c) 10.77×10^{-4} M, (d) 15.38×10^{-4} M.

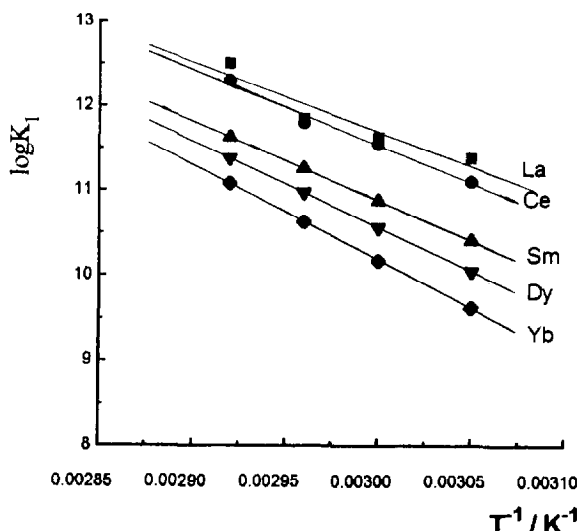Fig. 5. Plot of $\log K_1$ vs. $1/T$. $[PAN]_o = 6.15 \times 10^{-4}$ M, $I = 0.1$ M (NaCl), initial concentration of $RE^{3+} = 2 \times 10^{-5}$ M.

3.2. Reaction order with respect to hydrogen ion

Taking the above results with $a = 1$ into consideration, the following equation was obtained from Eqs. (1) and (2):

$$\log k = \log K + b \, \log[HL]_o c pH \tag{4}$$

In Fig. 3, the plot of $\log k$ vs. pH at a constant concentration of PAN in the organic phase is straight line with slope of 1, which indicates a first-order reaction with respect to the hydrogen ion.

3.3. Reaction order with respect to the concentration of PAN in the organic phase

In a similar fashion, a first-order reaction with respect to PAN was found according to the plot of $\log k$ vs. $[PAN]_o$ (Fig. 4).

3.4. Mechanisms of extraction reaction

Based on the data obtained above, the kinetic equation for the extraction can be rewritten as

$$r = -d[RE^{3+}]/dt = K[RE^{3+}][HL]_o^2[H^+] \tag{5}$$

Considering this rate equation and the major species in the extraction system, we suggest the

following steps in the extraction of RE(III) with PAN:

$$HL_o \rightleftharpoons HL_{aq}, \quad K_D = [HL]_o/[HL]_{aq} \tag{6}$$

$$H_2O \rightleftharpoons H^+ + OH^-, \quad K_{w,t} = [H^+][OH^-] \tag{7}$$

$$RE(OH)^{2+} \rightleftharpoons RE^{3+} + OH^-,$$

$$K_c = [OH^-][RE^{3+}]/[RE(OH)^{2+}] \tag{8}$$

$$RE^{3+} + 2HL_{aq} \xrightarrow{K_1} REL_2^+ + 2H^+ \tag{9}$$

$$REL_2^+ + Cl^- \rightleftharpoons REL_2Cl \tag{10}$$
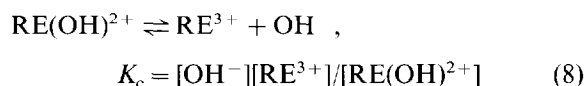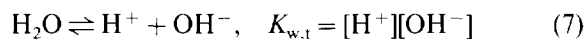
where K_D is the partition coefficient of PAN between two phases [6], $K_{w,t}$ is the dissociation constant of water at different temperatures [7,8], $1/K_c$ is the first-order stability constant of rare earth element hydroxide [8] and K_1 represents the rate constant of the path expressed by Eq. (9).

The first, second and third steps can be regarded as rapid equilibria, while the fourth is the rate-controlling step, with a first-order dependence with respect to RE^{3+} and second-order dependence with respect to PAN. The last step, however, is so fast that it can be neglected. In the given kinetic equation, a first-order dependence with respect to hydrogen ion is obtained, which means the RE^{3+} directly replaces the hydrogen ion in PAN before PAN dissociates. On the other hand, the presence of hydrated $RE(OH)^{2+}$ at the experimental acidity in the aqueous phase [9] and the dissociation of $RE(OH)^{2+}$ contribute to the first-order dependence with respect to hydrogen ion. Therefore, the above rate expression is equivalent to

$$-d[RE^{3+}]/dt = K_1[RE^{3+}][HL]_{aq}^2 \tag{11}$$

From Eqs. (6), (7), (8) and (11), we have

$$-d[RE^{3+}]/dt = K_1 K_c[RE^{3+}][H^+][HL]_o^2/K_{w,t}K_D^2 \tag{12}$$

This is the rate equation for the fourth step expressed by Eq. (9), which is rate controlling.

We can integrate Eq. (12) and obtain

$$\ln([RE^{3+}]_{t=0}/[RE^{3+}]_{t=t})$$

$$= (K_1 K_c[H^+][HL]_o^2/K_{w,t}K_D^2)t \tag{13}$$

Table 1
Rate constants and activation parameters

Temperature (K)	Parameter	La	Ce	Sm	Dy	Yb
328	K_1 ($\times 10^{11}$ M^{-1} s^{-1})	2.40	1.91	0.250	0.112	0.0420
	$\Delta_r^{\ddagger}H_m^{\ominus}$ (kJ mol^{-1})	154.732	168.328	177.796	192.500	211.720
	$\Delta_r^{\ddagger}G_m^{\ominus}$ (kJ mol^{-1})	9.132	9.754	15.30	17.542	20.164
	$\Delta_r^{\ddagger}S_m^{\ominus}$ (J K^{-1} mol^{-1})	443.90	453.72	495.42	533.42	584.01
333	K_1 ($\times 10^{11}$ M^{-1} s^{-1})	4.22	3.55	0.742	0.364	0.151
	$\Delta_r^{\ddagger}H_m^{\ominus}$ (kJ mol^{-1})	154.690	168.286	177.754	192.458	211.678
	$\Delta_r^{\ddagger}G_m^{\ominus}$ (kJ mol^{-1})	7.752	8.230	12.572	14.57	16.99
	$\Delta_r^{\ddagger}S_m^{\ominus}$ (J K^{-1} mol^{-1})	441.26	480.65	496.04	534.21	584.64
338	K_1 ($\times 10^{11}$ M^{-1} s^{-1})	7.08	6.03	1.78	0.93	0.42
	$\Delta_r^{\ddagger}H_m^{\ominus}$ (kJ mol^{-1})	154.649	168.245	177.713	192.417	211.637
	$\Delta_r^{\ddagger}G_m^{\ominus}$ (kJ mol^{-1})	6.454	6.905	10.33	12.16	14.39
	$\Delta_r^{\ddagger}S_m^{\ominus}$ (J K^{-1} mol^{-1})	438.43	477.44	495.20	533.21	583.57
343	K_1 ($\times 10^{11}$ M^{-1} s^{-1})	31.6	10.0	4.20	2.37	1.20
	$\Delta_r^{\ddagger}H_m^{\ominus}$ (kJ mol^{-1})	154.607	168.203	177.671	192.375	211.595
	$\Delta_r^{\ddagger}G_m^{\ominus}$ (kJ mol^{-1})	2.326	5.608	8.082	9.714	11.66
	$\Delta_r^{\ddagger}S_m^{\ominus}$ (J K^{-1} mol^{-1})	443.97	474.04	494.43	532.54	582.92
E_a (kJ mol^{-1})		157.459	171.055	180.523	195.227	214.447

The value of the rate constant K_1 in Eq. (12) at the experimental temperature can be calculated from the slope of the plot of $\ln([RE^{3-}]_{t=0}/[RE^{3+}]_{t=t})$ vs. time.

The temperature dependence of the rate constant K_1 of five rare earth ions (La, Ce, Sm, Dy and Yb) in the temperature range 55–70°C is shown in Fig. 5. The plots of $\log K_1$ vs. $1/T$ for the five ions are a series of straight lines. The activation energy E_a, activation enthalpy $\Delta_r^{\ddagger}H_m^{\ominus}$, activation free energy $\Delta_r^{\ddagger}G_m^{\ominus}$ and activation entropy $\Delta_r^{\ddagger}S_m^{\ominus}$ at different temperatures were calculated and the results are given in Table 1.

It can be seen from the data obtained that the activation enthalpy of the extraction increases from La to Yb. This is consistent with the degree of hydration of the rare earths from La to Yb due to the "lanthanide contraction". The hydrated $RE(OH)^{2+}$ prevents the formation of the extracted complex. Therefore, the rate constants decrease in the same order.

Acknowledgement

References

[1] Z.-L. Xu and L.-X. Dai, Fenxi Huaxue, 13 (1985) 784.
[2] J.-Z. Gao and G.R. Choppin, Solvent Extr. Ion Exch., 13 (1995) 495.
[3] J.-Z. Gao, G.-L. Hu, H.-Y. Fan and J.-W. Kang, Talanta, 41 (1994) 541.
[4] J.-Z. Gao, Z.-W. Pan, X.-Z. Du, J.-W. Kang and G.-B. Bai, Talanta, 40 (1993) 195.
[5] J.-Z. Gao, G.-L. Hu, J.-W. Kang and G.-B. Bai, Talanta, 40 (1993) 195.
[6] X.-Z. Du, J.-G. Hou, S. Zhao, J.-W. Kang and J.-Z. Gao, Analyst, 119 (1994) 1891.
[7] K.L. Cheng, K. Ueno and T. Lmamura, CRC Handbook of Organic Analytical Reagents (Chinese version), Geology Press, Beijing, 1985.
[8] R.C. Weast (Ed.), Handbook of Chemistry and Physics, CRC Press, Cleveland, OH, 61st edn., 1980–1981, p. D-168.
[9] Y.-J. Yin, Daxue Huaxue Shouce, Shandong Science Press, Jinan, 1985, pp. 318–321.

Re-examination of the structure of calcichrome (calcion) and its complexation with polyaromatic hydrocarbons in water

Bo-Long Poh*, Melati Khairuddean

School of Chemical Sciences, Universiti Sains Malaysia, 11800 Minden, Penang, Malaysia

Received 14 December 1995; revised 1 April 1996; accepted 5 April 1996

Abstract

A non-cyclic tetrameric structure has been suggested for calcichrome (calcion). This structure is consistent with its mass spectrum, proton NMR spectrum, elemental composition and complexing ability with polyaromatic hydrocarbons in water. The stability constants of the 1:1 complexes formed between calcichrome and seven polyaromatic hydrocarbons in water at room temperature have been measured.

Keywords: Calcichrome; Calcion; Complexation; Polyaromatic hydrocarbons

1. Introduction

Although calcichrome (also known as calcion) is used as a specific colorimetric reagent for the calcium ion, its structure is still controversial. Three structures have been suggested, the cyclic trimer 1 [1–3], the non-cyclic trimer 2 [4] and the dimer 3 [5,6]. Only structure 3 is consistent with the observed [5,7] elemental composition with a carbon to nitrogen ratio of 10:1 and the proton NMR spectrum indicating seven aromatic protons (one isolated and three pairs with the protons *meta* to each other) and three labile protons. However, structure 2 is the one that has found general acceptance in spite of a lack

of definitive analytical evidence (e.g. chemical suppliers assume this structure; see Scheme 1a).

Our interest in the structure of calcichrome arose when we observed that it formed strong complexes with polyaromatic hydrocarbons in water. The dimer 3, although consistent with the observed elemental composition and the proton NMR spectrum, could not account for this complexation ability because it has no hydrophobic cavity to enclose the polyaromatic hydrocarbons. We set out to establish the structure of calcichrome by examining its mass spectrum and re-examining its proton NMR spectrum. This paper suggests a non-cyclic tetrameric structure for calcichrome and reports the stability constants of the complexes formed between it and seven polyaromatic hydrocarbons in water.

---

* Corresponding author.

X = SO₃Na

1

X = SO₃Na

2

3 X = SO₃Na
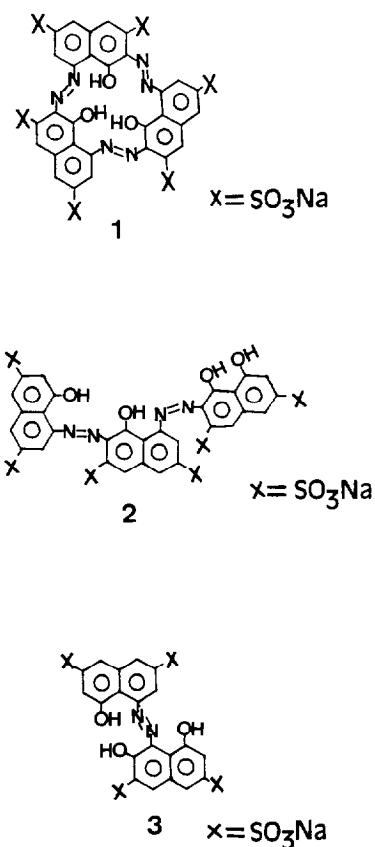
Scheme 1a

2. Experimental

2.1. Chemicals

Calcichrome and the polyaromatic hydrocarbons were commercial samples and were used without further purification. Elemental analysis of C, H and N in calcichrome agreed with the molecular formula $C_{40}H_{20}N_4O_{28}S_8Na_6 \cdot 28H_2O$.

2.2. Instrumentation

An AC300 300 MHz superconducting NMR spectrometer and a Hitachi U-2000 UV–visible spectrophotometer were used.

2.3. Determination of stability constants

Stability constants K of the complexes formed

between calcichrome and the polyaromatic hydrocarbons were obtained according to two methods described previously, solid–liquid extraction [8] and a transport method [9]. In the former method, 15 mg of each of the solid polyaromatic hydrocarbons were extracted with 5.80×10^{-4} M of calcichrome (5.80×10^{-3} M in the case of naphthalene). In the latter, the concentration of the polyaromatic hydrocarbons in the hexane phase was varied from 1.0×10^{-3} to 5.0×10^{-3} M and the concentration of calcichrome used was 5.80×10^{-4} M. All experiments were performed at least in duplicate.

3. Results and discussion

3.1. Structure of calcichrome

Calcichrome is assigned the non-cyclic tetrameric structure 4 on the basis of its mass spectrum, proton NMR spectrum and elemental composition. The laser desorption mass spectrum (positive-ion mode) of the acidic form of calcichrome (Na^+ replaced by H^+ from Dowex 50W-X8 hydrogen-form ion-exchange resin) in a dihydroxybenzoic acid matrix shows a peak at m/z 1358 (Fig. 1) which could be assigned to the $[M + 5H_2O + H]$ ion (inclusion of water molecules in the molecular ion was observed previously [10]). The observed peak at m/z 1358 rules out the possibility of structures **1**, **2** and **3** whose acidic forms have much lower m/z values (991, 981 and 651, respectively).
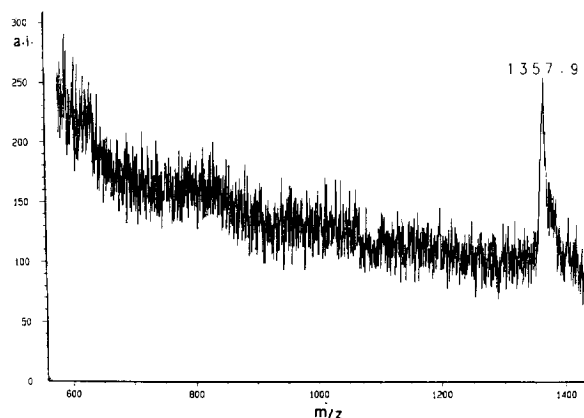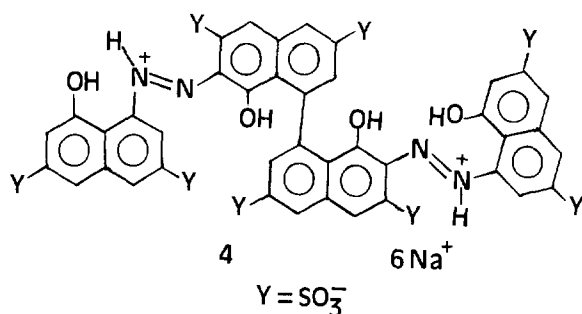

Fig. 1. Laser desorption mass spectrum (positive-ion mode) of calcichrome (with Na^+ replaced by H^+) in dihydroxybenzoic acid as matrix.

4   **6 Na⁺**

Y = SO₃⁻

Structure **4** is consistent with the observed 10 peaks of equal integration in the proton NMR spectrum of calcichrome in DMSO-d_6 (Fig. 2). There are seven kinds of aromatic protons (one isolated at 8.20 ppm and six *meta* to each other at 7.23, 7.33, 7.49, 7.61, 7.89 and 7.94 ppm with typical *meta* coupling constants of 1.1-1.5 Hz) and three kinds of labile protons at 11.79, 11.99 and 17.13 ppm (they disappear in D_2O solvent). We assign the 11.79 and 11.99 ppm peaks to the two kinds of phenolic protons and the 17.13 ppm peak to the diaza protons (previous workers [5,6] attributed all the three peaks to phenolic protons). Our assignment of the 17.13 peak to the diaza protons is supported by its disappearance when the proton NMR spectrum of a sample of calcichrome neutralized with two equaivalents of sodium hydroxide was recorded (Fig. 3). The other two phenolic proton peaks are still present and they are shifted downfield to 13.41 and 14.65

ppm. This downfield shift is consistent with better hydrogen bonding between the phenolic hydrogens and the diaza nitrogens when the latter are not protonated (a partial structure for protonated diaza nitrogens is shown as **5** and those for non-protonated diaza nitrogens with hydrogen bonding involving the phnolic hydrogens are shown as **6** and **7**).

5

6

7
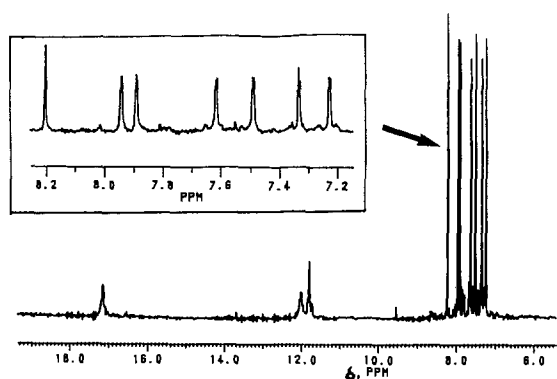
Fig. 2. 300 MHz proton NMR spectrum of calcichrome (0.1 g) in DMSO-d_6 (0.6 ml) at 25°C; solvent peak at 2.50 ppm (not shown) as internal reference. The inset is an expansion of the aromatic proton region.
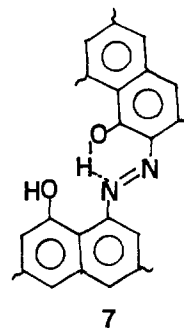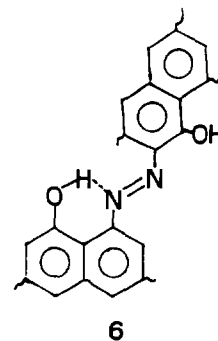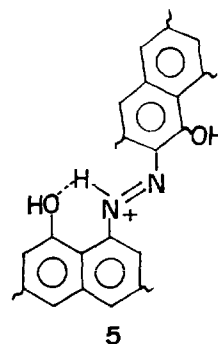
Structure **4** is also consistent with the reported elemental composition with a carbon to nitrogen ratio of 10:1 [5,7] and the formation of two products from the selective cleavage of the azo
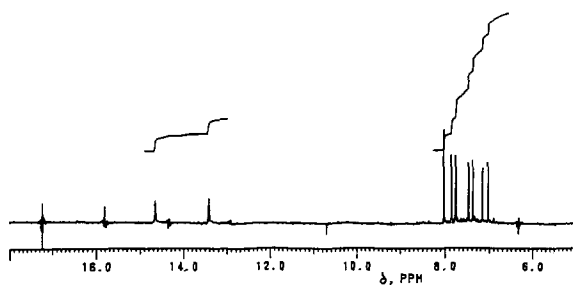
Fig. 3. 300 MHz proton NMR spectrum of calcichrome neutralized with two equivalents of NaOH (0.2 g) in DMSO-d_6 (0.6 ml) at 25°C; solvent peak at 2.50 ppm (not shown) as internal reference.

groups in calcichrome with tin(II) [6]. The two expected products from the azo cleavage reaction of structure **4** are **8** and **9** in a molar ratio of 2:1. The former, a smaller molecule, is expected to elute faster than the latter in column chromatography. It is expected to show four doublets with *meta* coupling constants in the proton NMR spectrum and the latter a singlet plus two doublets with *meta* coupling constants, in agreement with the reported results [6].

8   Y=SO₃Na

9   Y = SO₃Na
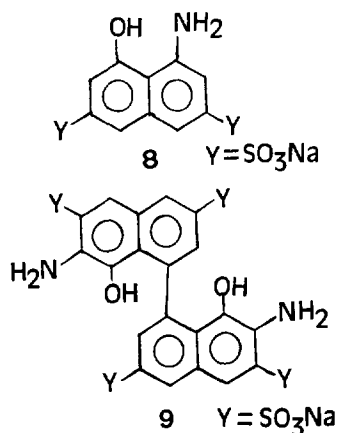
The formation of **4** could be explained in terms of a combination of two known mechanisms in diazonium ion reactions [11]. The first is the dimerization of two diazotized 1-amino-8-hydroxy-naphthalene-3,6-disulfonic acid (H-acid) with the loss of two nitrogen molecules. The second is the attack of two diazotized H-acid molecules on the two positions *ortho* to the two hydroxyl groups of the dimer.
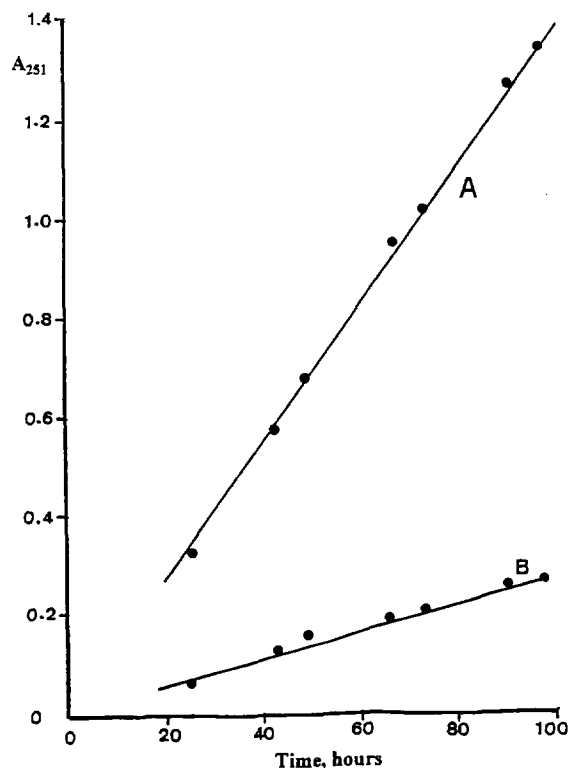

Fig. 4. Relationship between absorbance at 251 nm of anthracene in the receiving hexane phase and time. The initial concentration of anthracene in the source hexane phase is 1.0×10^{-3} M. (A) 5.80×10^{-4} M calcichrome in the aqueous phase and (B) no calcicrhrome in the aqueous phase.

3.2. Complexation with polyaromatic hydrocarbons

That calcichrome is able to complex with polyaromatic hydrocarbons in water is shown by (1) its ability to increase the solubility of the polyaromatic hydrocarbons in water (for example, 5.8×10^{-4} M calcichrome increases the solubility of chrysene 250-fold) and (2) its ability to increase the transport rate of polyaromatic hydrocarbons from one hexane phase to another through an intermediate aqueous phase (an example is shown in Fig. 4 for the transport of anthracene). The non-cyclic tetrameric structure **4** is able to complex with polyaromatic hydrocarbons because in its folded conformation, as indicated by CPK molecular models, the four naphthalene units enclose a

Table 1

Stability constants K of 1:1 complexes formed from polyaromatic hydrocarbons and calcichrome in water at room temperature

Hydrocarbon	K $(M^{-1})^a$	K $(M^{-1})^b$	K $(M^{-1})^c$	N^d
Naphthalene	$(1.0 \pm 0.1) \times 10^3$	$(1.1 \pm 0.6) \times 10^3$	4.5×10^2	2
Acenapthene	$(3.5 \pm 0.2) \times 10^3$	$(3.1 \pm 0.5) \times 10^3$	1.6×10^3	2.5
Fluorene	$(2.5 \pm 0.2) \times 10^4$	$(6.7 \pm 1.3) \times 10^3$	3.6×10^3	2.5
Anthracene	$(2.2 \pm 0.1) \times 10^4$	$(2.6 \pm 0.1) \times 10^3$	2.3×10^4	3
Phenanthrene	$(2.2 \pm 0.1) \times 10^4$	$(2.1 \pm 0.1) \times 10^4$	1.4×10^4	3
Pyrene	$(4.8 \pm 0.1) \times 10^4$	$(1.1 \pm 0.1) \times 10^5$	4.3×10^4	4
Chrysene	$(4.4 \pm 0.1) \times 10^4$	$(1.7 \pm 0.1) \times 10^5$	7.0×10^4	4

[a] Solid–liquid extraction method.
[b] Transport method.
[c] K values for cyclotetrachromotropylene as host [8].
[d] Number of aromatic rings in the guest molecule; a non-aromatic ring containing double bonds is counted as half [8].

hydrophobic cavity.

The stability constants K of the complexes formed were determined by two methods, solid–liquid extraction [8] and a transport method [9]. We have to make an assumption regarding the stoichiometry of the complexes since the usual mole ratio and Job plots to determine stoichiometry cannot be used in the solid–liquid extraction and transport methods. The solubility problem of the polyaromatic hydrocarbons in water also ruled out the use of electronic and NMR spectroscopic methods in our study. CPK molecular models indicate that the cavity size of the folded conformation of 4 is similar to that of cyclotetrachromotropylene, a cyclic tetramer formed from four naphthalene units [8,9]. Since the latter has been shown to form complexes of 1:1 stoichiometry [12–14], the same stoichiometry was assumed in this work. The K values (Table 1) are of the same order of magnitude as those of cyclotetrachromotropylene [8,9], indicating that calcichrome adopts a folded conformation in water and the size of its hydrophobic cavity is similar to that of cyclotetrachromotropylene. As with the latter host, log K increases linearly with increase in the number of aromatic rings in the guest molecule. For example, a plot of the log K values obtained from the transport method against the number of aromatic rings (N) in the guest molecules gives a straight line of slope 1.0 with a correlation coefficient of 0.978, close to the slope of 0.92 for cyclotetrachromotropylene as host [8].

Acknowledgements

References

[1] R.A. Close and T.S. West, Talanta, 5 (1960) 221.
[2] Z.J. Allan, J. Podstata and J. Jarkovsky, Collect. Czech. Chem. Commun., 34 (1969) 282.
[3] H. Einagaa and H. Ishii, Talanta, 28 (1981) 799.
[4] A.M. Lukin, K.A. Smirnova and G.B. Zavarikhina, Zh. Anal. Khim., 18 (1963) 444.
[5] C.V. Stead, J. Chem. Soc. C, (1970) 693.
[6] L.-K. Chau, M. Pruski and M.D. Poeter, Anal. Chim. Acta, 217 (1989) 31.
[7] A.E. Mendes-Bezarra and W.I. Stephen, Analyst, 94 (1969) 1117.
[8] B.-L. Poh and L.-S. Koay, Tetrahedron Lett., 31 (1990) 1911.
[9] B.-L. Poh, C.S. Lim and L.-S. Koay, Tetrahedron, 46 (1990) 6155.
[10] B.-L. Poh, L.Y. Chin and C.W. Lee, Tetrahedron Lett., 36 (1995) 3877.
[11] A.J. Dolenko and E. Buncel, in S. Patai (Ed.), The Chemistry of the Hydrazo, Azo and Azoxy groups, Part 2, Wiley, Chichester, 1975, chapter 17.
[12] B.-L. Poh, C.M. Tan and C.L. Loh, Tetrahedron, 49 (1993) 3849.
[13] B.-L. Poh, C.H. Lim, C.M. Tan and W.M. Wong, Tetrahedron, 49 (1993) 7259.
[14] B.-L. Poh and C.M. Tan, J. Inclus. Phenom. Mol. Recogn., 18 (1994) 93.

Peroxidase-catalysed luminol chemiluminescence method for the determination of glutathione

Tamio Kamidate *, Hiroto Watanabe

Faculty of Engineering, Hokkaido University, Kita-13, Nishi-8, Kita-ku, Sapporo, 060, Japan

Received 21 December 1995; revised 3 April 1996; accepted 5 April 1996
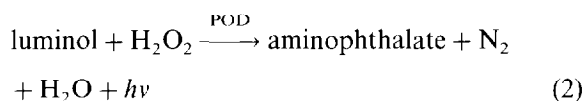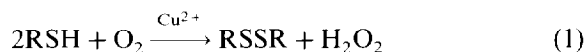
Abstract

A luminol chemiluminescence (CL) method was developed for the determination of glutathione (GSH). GSH was indirectly determined by measuring the amount of hydrogen peroxide formed during the Cu(II)-catalysed oxidation of GSH with oxygen. The amount of hydrogen peroxide formed was continuously measured using the *Arthromyces ramosus* peroxidase-catalysed luminol CL reaction. The CL intensities at maximum light emission were linearly correlated with the concentration of GSH over the range 7.5×10^{-7}–3.0×10^{-5} M. The detection limit for GSH was about 10 times better than that of the spectrophotometric method using Ellman reagent.

Keywords: Chemiluminescence; Glutathione; Luminol; Peroxidase

1. Introduction

Glutathione (GSH) plays an important physiological role in the protection of cellular constituents against oxidative damage in living cells. Many spectrophotometric and fluorometric methods have been developed for the determination of GSH [1,2]. Recently, chemiluminescence (CL) methods have attracted attention owing to their sensitivity. The lucigenin (Luc) CL reaction has been employed for the determination of GSH [3], but the detection limit was higher than that of the spectrophotometric methods using Ellman reagent [1].

The peroxidase (POD)-catalysed luminol CL provides a sound basis for the assay of hydrogen peroxide (H_2O_2) and enzymatically generated H_2O_2 [4]. In the Cu(II)-catalysed oxidation of aminothiols (RSH) such as cysteine with oxygen, H_2O_2 has also been shown to be produced as an intermediate from oxygen [5]. We previously applied the POD-catalysed luminol CL to the detection of H_2O_2 formed during the course of the Cu(II)-catalysed oxidation of cysteamine ($H_2NCH_2CH_2SH$) [6]. H_2O_2 was detected by simultaneously performing the reactions

$$2RSH + O_2 \xrightarrow{Cu^{2+}} RSSR + H_2O_2 \tag{1}$$

$$luminol + H_2O_2 \xrightarrow{POD} aminophthalate + N_2$$
$$+ H_2O + h\nu \tag{2}$$

* Corresponding author.

When *Arthromyces ramosus* peroxidase (ARP) was used as a catalyst for the luminol CL, a light emission–time profile followed the production rate of H_2O_2 in the catalytic oxidation of cysteamine. The purpose of the present study was to develop a highly sensitive CL method for GSH via the use of ARP-catalysed luminol CL coupled with Cu(II)-catalysed oxidation of GSH with oxygen.

2. Experimental

2.1. Materials

ARP was kindly supplied from Suntory. Luminol, GSH, L-cysteine and L-(+)-ascorbic acid were obtained from Kanto Chemical and were guaranteed-grade reagents. EDTA, 1,10-phenanthroline (Phen) and 2,2-dithiobis(5-nitropyridine) (DTNP) were purchased from Dojindo Laboratory. Reduced nicotinamide adenine dinucleotide (NADH) was obtained from Sigma Chemical. Copper(II) nitrate, ammonium iron(II) sulfate, citric acid, boric acid and tertiary sodium phosphate were obtained from Wako Pure Chemical Industries and were of guaranteed grade. All chemicals were used without further purification.

ARP solution was prepared with Carmody's buffer (pH 9.0), containing 6.9×10^{-2} M boric acid, 1.7×10^{-2} M citric acid and 6.6×10^{-2} M tertiary sodium phosphate [7]. The concentration of ARP was determined spectrophotometrically with an ε_{403} value of 1.02×10^5 l mol^{-1} cm^{-1} [8]. A 1.0×10^{-2} M stock solution of luminol was prepared by dissoloving the compound in 0.1 M NaOH solution. A 1.0×10^{-2} M stock solution of Cu(II), prepared from Cu(II) nitrate in 0.1 M hydrochloric acid, was standardized with EDTA. Working standard solutions of ARP, luminol and Cu(II) were prepared by serial dilution of the stock solutions with water and Carmody's buffer solution. A standard solution of GSH was made daily. All solutions were prepared with deionized water from a Millipore Milli-Q water purification system.

All of the reagent concentrations shown in the figures are initial concentrations.

2.2. Apparatus

All CL measurements were made using a luminometer constructed in this laboratory. A glass cuvette (20 mm × 22 mm i.d.) was placed on a magnetic stirrer in a dark-box. The light output was detected with a Hamamatsu Photonics R453 photomultiplier (PMT). The resultant photocurrent was measured with a TOA Electronics PM-18 type current meter and displayed on a chart recorder. A Cu(II) solution and a GSH solution were injected through Teflon tubing into the cuvette by using an injector (Iatron Laboratories, Dualpette type). Absorption spectra were measured with a Hitachi U-2000 spectrometer equipped with 1 cm quartz cells.

2.3. Cu(II)-catalysed oxidation of GSH with oxygen

The catalytic oxidation was carried out at pH 9.0 using the following conditions. A 2.5 cm³ portion of buffer solution was added to a glass cuvette. A 0.25 cm³ portion of 1.2×10^{-4} M Cu(II) solution and a 0.25 cm³ portion of 1.2×10^{-2} M GSH solution were simultaneously injected into the cuvette, and the catalytic oxidation was initiated. The entire solution, thus prepared, is referred to as the final solution. Oxygen was bubbled continuously at 45 cm³ min^{-1} during the reaction.

2.4. Preparation of calibration curve

The recommended procedure for the determination of GSH consisted of pipetting a 1.0 cm³ portion of a solution containing 1.0×10^{-4} M luminol and 5.0×10^{-7} M ARP into a glass cuvette on a magnetic stirrer in the luminometer. The whole solution was saturated with oxygen. Next, a 1.0 cm³ portion of 1.0×10^{-5} M Cu(II) solution and a 1.0 cm³ portion of GSH solution were simultaneously injected into the cuvette and the CL reaction was monitored. The pH of the reaction mixture was 11.0. Oxygen was bubbled continuously at 45 cm³ min^{-1} during the reaction. All measurements were made at 25°C. The maximum light emission was corrected for the light

emission of a blank containing no GSH. These background-corrected CL values are referred to as CL intensity.

2.5. Analytical procedure for GSH and H_2O_2

The concentration of GSH consumed and H_2O_2 formed during the catalytic oxidation were determined under the following conditions. A 0.1 cm^3 portion of the reaction mixture was pipetted into the cell containing 0.1 cm^3 of 1.0×10^{-3} M EDTA solution. The catalytic reaction was terminated with EDTA. Then, GSH was determined with DTNP by measuring the absorbance at 386 nm [1] and H_2O_2 with Fe(II)–Phen complex at 510 nm [9].

3. Results and discussion

3.1. Catalytic oxidation of GSH

The Cu(II)-catalysed oxidation of GSH was carried out according to the procedure:

$$2GSH + O_2 \xrightarrow{Cu^{2+}} GSSG + H_2O_2 \qquad (3)$$

The time course for GSH consumption and H_2O_2 formation are shown in Fig. 1. The concentrations of GSH and H_2O_2 on the vertical axis are those in the final solution. The concentration of H_2O_2 formed increased with increase in the reaction
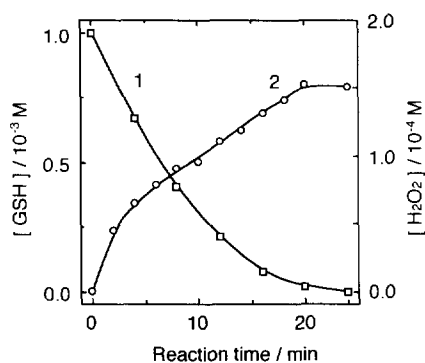

Fig. 1. Time course of GSH consumption and H_2O_2 formation during the catalytic oxidation. Curve 1, GSH consumption; curve 2, H_2O_2 formation. [GSH] = 1.2×10^{-2} M; [Cu(II)] = 1.2×10^{-4} M; pH = 9.0.
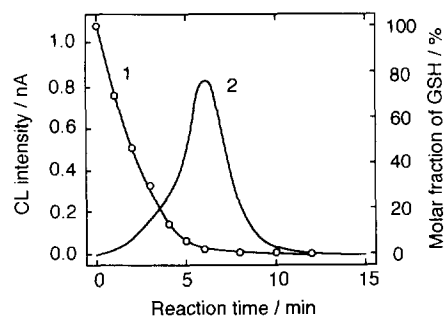

Fig. 2. CL response curve and time course of GSH consumption. Curve 1, time course of GSH consumption; curve 2, CL response curve. [GSH] = 5.0×10^{-4} M; [Cu(II)] = 1.0×10^{-5} M; [ARP] = 5.0×10^{-7} M; [luminol] = 1.0×10^{-4} M; pH = 9.0.

time. The amount of H_2O_2 formed was 1.5×10^{-4} M in the final solution. When GSH is converted quantitatively into H_2O_2, the reaction yield (mol%) should be 50% (reaction (3)), where the reaction yield is defined as the ratio of the amount of H_2O_2 formed to that of GSH used. However, the reaction yield of H_2O_2 was 30% after 25 min, as shown in Fig. 1. This is because part of the H_2O_2 formed was consumed as an oxidizing agent for the oxidation of GSH.

Next, we determined the amounts of GSH consumed during the reaction when coupled with the ARP-catalysed luminol CL reaction. The catalytic oxidation of GSH was performed at pH 9.0 according to the procedure in which 5.0×10^{-4} M GSH solution was used. The time course of GSH consumption is shown in Fig. 2 (curve 1). GSH was almost completely oxidized by 10 min after the start of the reaction.

PODs catalyse the oxidation of aminothiols such as cysteine through the POD cycle [10,11]. However, no reports have been found on ARP-catalysed oxidation of GSH. We then determined the concentration of GSH consumed during the catalytic oxidation by using ARP alone. The oxidation was carried out according to the same procedure as above, except that the buffer solution was employed in place of Cu(II) solution and luminol solution. After 10 min, nearly 2% of GSH was oxidized to GSSG. Therefore, GSH could be primarily oxidized by a Cu(II)-catalysed pathway (reaction (3)).

T. Kamidate, H. Watanabe / Talanta 43 (1996) 1733–1738

3.2. Light emission–time profile

We examined the CL measurement of H_2O_2 formed during the catalytic oxidation of GSH shown in Fig. 2 (curve 1). A typical CL response curve is shown in Fig. 2 (curve 2). The intensity of the light emission increased gradually with increase in the reaction time.

The time course of GSH consumption suggests that the maximum light emission may appear about 2 min after the start of the reaction. However, the maximum light emission appeared after 6 min, by which time GSH was almost completely oxidized. These results could be explained by the scheme proposed in Fig. 3. The numbers in parentheses show the effective oxidation level of iron in native ARP and ARP intermediates such as compounds I and II. Native ARP reacts with H_2O_2 produced by the catalytic oxidation of GSH and then catalyses the oxidation of luminol (LH$^-$) with the intermediates to form luminol radical (L$^-$) [12].

In the absence of GSH, the luminol radicals react with oxygen to yield endoperoxide (LO_2^{2-}). LO_2^{2-} then decomposes to yield an electronically

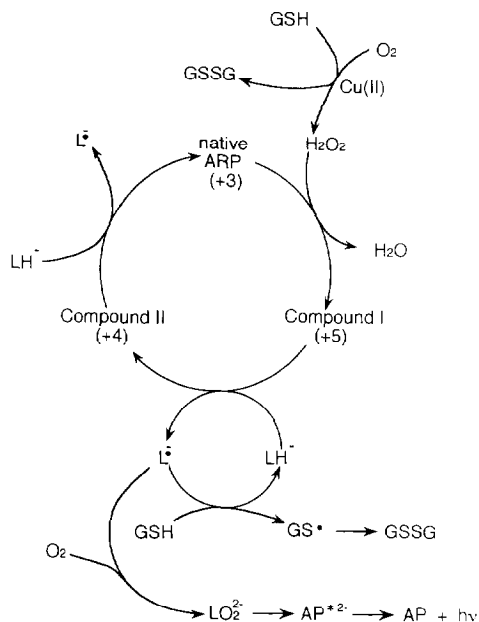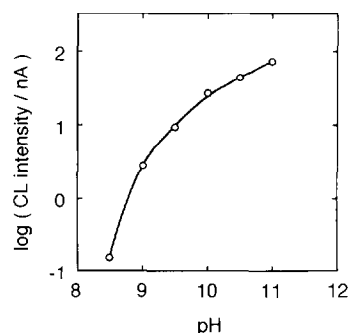Fig. 4. Effect of pH on the CL intensity. [GSH] = 1.0×10^{-5} M; [Cu(II)] = 1.0×10^{-5} M; [ARP] = 1.0×10^{-7} M; [luminol] = 1.0×10^{-4} M.

exited 3-aminophthalate dianion (AP^{*2-}), which returns to the ground state by emitting light. On the other hand, GSH acts effectively as a quenching agent for luminol radicals [13], thereby preventing the oxidation of luminol radicals to aminophthalate and subsequent light emission.

The appearance of the CL from the start of the reaction suggests that the formation rate of luminol radicals in ARP-induced luminol oxidation may be higher than the disappearance rate of luminol radical with GSH, although the rate constant of luminol radicals with GSH is still not available. However, the quenching reaction of luminol radicals with GSH may proceed simultaneously as long as GSH is present. Therefore, the maximum light emission could appear after almost complete consumption of GSH.

3.3. Optimum conditions for the determination of GSH

In the ARP-catalysed luminol CL coupled with Cu(II)-catalysed oxidation of GSH, the CL intensity was dependent on the concentration of GSH, although part of the H_2O_2 formed as a result of reaction (1) was consumed for further oxidation of GSH. We then optimized the conditions for the determination of GSH. In subsequent studies, the optimum conditions were determined by measuring the CL intensities so as to be maximum under the optimum conditions.

The effect of pH in the final solution was examined in the range 8.5–11.0. Fig. 4 shows that

Fig. 3. Scheme of ARP-catalysed luminol CL coupled with Cu(II)-catalysed oxidation of GSH with oxygen.

the CL intensity increased with increase in pH. This can probably be attributed to an increase in the rate of formation of H_2O_2 accompanying an increase in pH, since $pK_{a,SH}$ of GSH is 8.8 [14]. Hence a pH of 11.0 was chosen for the recommended procedure by considering the buffer capacity of Carmody's buffer solution [7].

The dependence on the ARP concentration was investigated in the range 5.0×10^{-8}–2.0×10^{-6} M. The optimization curve for ARP concentration is shown in Fig. 5. The CL intensity increased to the maximum value at 5.0×10^{-7} M, after which it decreased with increase in ARP concentration. Hence the optimum ARP concentration was chosen as 5.0×10^{-7} M.

The influence of luminol concentration was tested in the range 5.0×10^{-6}–2.0×10^{-4} M. The CL intensity exhibited a broad maximum at 1.0×10^{-4} M. The optimum luminol concentration was thus determined to be 1.0×10^{-4} M.

3.4. Analytical results and parameters

The calibration curve was prepared under the optimum conditions. Typical CL response curves are shown in Fig. 6. A logarithmic calibration curve for GSH is presented in Fig. 7. The calibration curve was linear over the range from the detection limit of 7.5×10^{-7} M to 3.0×10^{-5} M initial concentration of GSH with a slope of 0.82. The relative standard deviation for five successive experiments was 1.6% at 3.0×10^{-6} M GSH. The detection limit for GSH was defined as the con-
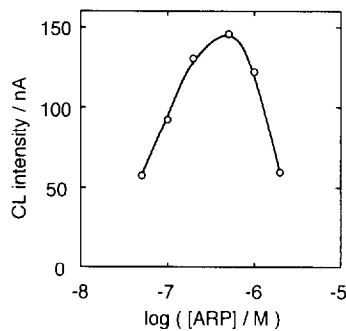

Fig. 6. Typical CL response curves. [GSH]: 1, 1×10^{-6}; 2, 6×10^{-6}; 3, 1×10^{-5}; 4, 5×10^{-5} M. [Cu(II)] = 1.0×10^{-5} M; [ARP] = 5.0×10^{-7} M; [luminol] = 1.0×10^{-4} M; pH = 11.0.

centration of GSH yielding an analytical signal greater than three times the CL intensity of the blank, which contained no GSH. The detection limit of the present method for GSH is about 10 and 20 times better than those of the spectrophotometric method with the use of Ellman reagent [1] and the Luc-CL method [3], respectively.

Next, we examined the effects of biological reductants such as ascorbic acid, NADH and cysteine on the CL intensity according to the recommended procedure in which the reductants

Fig. 5. Effect of ARP concentration on the CL intensity. [GSH] = 1.0×10^{-5} M; [Cu(II)] = 1.0×10^{-5} M; [luminol] = 1.0×10^{-4}; pH = 11.0.
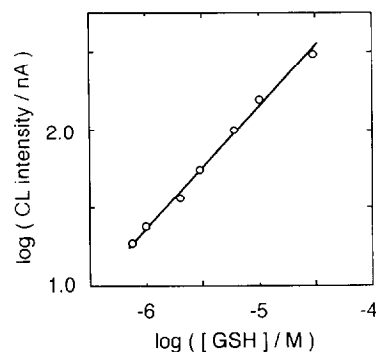

Fig. 7. Calibration curve for GSH. [Cu(II)] = 1.0×10^{-5} M; [ARP] = 5.0×10^{-7} M; [luminol] = 1.0×10^{-4}; pH = 11.0.

were added to a 3.0×10^{-6} M GSH solution. The tolerated concentration of each compound was taken as being the largest amount yielding an error of less than 5% in the CL intensity. The CL intensity decreased considerably in the presence of all of the reductants, even at a level equal to the concentration of GSH. This is because the reductants used act effectively as quenching agents for luminol radicals [13]. In the case of cysteine, the catalytic oxidation of GSH could also be influenced because Cu(II)-catalysed oxidation of cysteine could proceed simultaneously from the start of the reaction [15].

In conclusion, the ARP-catalysed luminol CL method provides excellent sensitivity for the determination of GSH. However, the method is not specific to sulfhydryl (–SH) compounds. Therefore, the proposed method could be applicable to the non-specific determination of aminothiols in analogy with the spectrophotometric method using Ellman reagent.

References

[1] A. Swaitditat and C.C. Tseu, Anal. Biochem., 45 (1972) 349.
[2] T. Toyooka and K. Imai, Anal. Chem., 56 (1984) 2461.
[3] W.L. Hinze, T.E. Riehl, H.N. Singh and Y. Baba, Anal. Chem., 56 (1984) 2180.
[4] T. Segawa, A. Kakizaki, T. Kamidate and H. Watanabe, Anal. Sci., 8 (1992) 785.
[5] J. Zwart, J.H.M.C. Van Wolput and D.C. Koningsberger, J. Mol. Catal., 12 (1981) 85.
[6] T. Kamidate, A. Katayama, H. Ichihashi and H. Watanabe, J Biolumin. Chemilumin., 9 (1994) 279.
[7] W.R. Carmody, J. Chem. Educ., 38 (1961) 559.
[8] B.B. Kim, V.V. Pisarev and A.M. Egorov, Anal. Biochem., 199 (1991) 1.
[9] H. Afsar, R. Apak and I. Tor, Analyst, 115 (1990) 99.
[10] B.E. Svensson, Biochem. J., 256 (1988) 757.
[11] H. Pichorner, A. Couperus, S.A.A. Korori and R. Ebermann, 31 (1992) 3371.
[12] H.P. Misra and P.M. Squatrito, Arch. Biochem. Biophys., 215 (1982) 59.
[13] J.K. Wong and M.L. Salin, Photochem. Photobiol., 33 (1981) 737.
[14] B.E. Svensson, Biochem. J., 253 (1988) 441.
[15] L. Ehrenberg, M. Harms-Ringdahl, I. Fedoresak and F. Granath, Acta Chem. Scand., 43 (1989) 177.

Investigation of equilibria in solution. Determination of equilibrium constants with the HYPERQUAD suite of programs

Peter Gans[a,*], Antonio Sabatini[b], Alberto Vacca[b]

[a]*School of Chemistry, University of Leeds, Leeds LS2 9JT, UK*
[b]*Dipartimento di Chimica, Università degli Studi di Firenze, Via Maragliano 77, 50144 Firenze and ISSECC, Consiglio Nazionale delle Ricerche, Via Nardi 39, 50132 Firenze, Italy*

Abstract

A new suite of 10 programs concerned with equilibrium constants and solution equilibria is described. The suite includes data preparation programs, pretreatment programs, equilibrium constant refinement and post-run analysis. Data preparation is facilitated by a customized data editor. The pretreatment programs include manual trial and error data fitting, speciation diagrams, end-point determination, absorbance error determination, spectral baseline corrections, factor analysis and determination of molar absorbance spectra. Equilibrium constants can be determined from potentiometric data and/or spectrophotometric data. A new data structure is also described in which information on the model and on experimental measurements are kept in separate files.

Keywords: Equilibrium constant; Potentiometry; Solutions; Spectrophotometry

1. Introduction

The determination of equilibrium constants is an important process for many branches of chemistry [1]. Developments in the field of computation of equilibrium constants from experimental data were reviewed a few years ago [2,3]. Since that time, many more programs have been published, mainly so as to be able to use microcomputers for the computations. In this paper, we concentrate on the elaboration of potentiometric and spectrophotometric data;

* Corresponding author.

the most commonly used programs for solution equilibrium constant determination are given in Table 1.

All of these programs use a least-squares approach, the principles of which have been expounded in detail [4]. Many programs follow what we may call a standard approach. In this, the sum of squares is minimized by means of the Gauss–Newton–Marquardt algorithm. The derivatives required by this algorithm were originally obtained numerically, but following Nagypal et al. [5] some programs used derivatives calculated analytically. The free concentrations are calculated by solving the non-linear simultaneous equa-

tions of mass balance using the Newton–Raphson method. Potentiometric data points are weighted by formula that allows for greater pH errors in the region of an end-point than elsewhere. For absorbance data points a relative weighting scheme is used.

Some noteworthy exceptions are as follows. Minimization using pit-mapping (LETAGROP [6,7] and ABLET [8] families), Davidon–Fletcher–Powell method (STEW [9]), direct search (EY608 [10]), the method of steepest descent (CFTSP [11]) orthogonal decomposition (CLINP [12], ELORMA [13], SIRKO [14]). MINUITS [15] used regression equations of the Padé type. In DHMINOPT [16] there are three minimization routines and if one using derivatives fails the Nelder–Mead simplex method is called automatically. Solution of the mass-balance equation using a bisection algorithm (CFTSP [11]) or "another procedure which iterates by systematically modified increments" (MAXIPOT-F [17]) or a projection method due to Bugaevsky (SIRKO [14]). There have been attempts to make corrections for activity variation (SCOGS2a [18], SPECA [19]) and to use extended Debye–Hückel theory (DCLET [8] and BSTAC [20], an augmented version of SUPERQUAD [21]). Refinement of stoichiometric indices is included as an option in POLET [22] and SQUAD84 [23]. ECORM [24] was a computer implementation of the old (pre-computer) graphical methods, as are KATCOM [25] and Sidrak and Aboul-Seoud's program [26].

PKAS [27] is notably original in many respects. As it treats only protonation/deprotonation reactions (cf TITRA [28], TITAN [29]), it is possible to apply procedures that cannot be applied in the more general case. Thus, there are only two mass-balance equations in the two unknowns [L] and [H], say. [L] is eliminated to leave a polynomial in [H] which is solved by Newton–Raphson iteration. The minimization involves some kind of direct search method which, unfortunately, was not specified in detail. The program is highly interactive and requires much input of chemical knowledge. Having said that, the authors claim that the program never crashes. BEST [30] also employs a direct search method described as fol-

lows: "perturb a small fraction of the basis set [of refinable parameters] by an increment, see the effect on the sum of squares [of residuals in pH] and repeat in an appropriate direction to affect further improvement". This sounds like something akin to a simplex minimization.

Perhaps the most interesting developments have been the two attempts to write programs that can handle *any* equilibrium data. SIRKO [14] has a universal response function and a system whereby analytical derivatives are generated for the Jacobian. MICMAC [31] requires the programming of a module (MOSP) specific to a particular type of experimental data, but because of this numerical derivatives must be employed in the Jacobian.

Our own work has had two fundamental motivations: to provide a robust program for the computation of equilibrium constants and to tackle the problem of model selection. Although MINIQUAD [32,33] was robust, and is still being used, Motekaitis and Martell [30] have articulated the criticism, of which we were only too well aware, that the function minimized did not involve experimentally observed quantities directly. This was put right in SUPERQUAD [21], which therefore had the significant advantage of providing a statistically sounder basis for model selection.

The problem of model selection arises with systems in which it is impossible, a priori, to state what chemical species will be present in appreciable concentrations in the reaction mixtures. In those cases there is a need for some criteria both to determine whether or not the computed equilibrium model is satisfactory in a chemical sense and to see if the calculated data points agree with those observed, within experimental error. We have discussed these criteria previously [21]. What emerges from the analysis is that the expectation value for the sample variance will be unity if, and only if, a weight matrix is used that is the inverse of the variance–covariance matrix of the experimental data [4].

Now, in order to help with the model selection process, it seems a good idea to make use of more than one kind of measurement simultaneously on the same set of reaction solutions. We therefore have developed HYPERQUAD, which can determine equilibrium constants from both potentio-

Table 1

Computer programs used for calculating equilibrium constants from potentiometric (V) and spectrophotometric (A) data

Program	Ref.	Data type[a]	Program	Ref.	Data type[a]
ABLET	[8]	A	MINIQUAD75	[33]	V
ACBA	[55]	V	MINISPEF	[67]	A
ACREF3AM	[56]	V	MINUITS	[15]	V
AP	[57]	V	MUCOMP	[68]	V
Asuero et al.	[58]	A	MUPROT	[69]	V
BEST	[30]	V	Nievergelt	[70]	A
BSTAC	[20]	V	NONLIN15	[71]	V, A
CFTSP	[11]	A	Papanastasiou and Zogas	[72]	V
CLINP	[12]	A	PHODEC	[73]	A
DALSFEK	[59]	V, A	PKAS	[27]	V
DCLET	[8]	A	POLET	[22]	V
DCMINOPT	[60]	A	PROTAF	[74]	V
DHMINOPT	[16]	V	PSEQUAD	[75]	V, A
ECORM	[24]	V	SCOGS2a	[18]	V
ELORMA	[13]	A	SCOGS2b	[76]	V
EQNMR	[61]	N	Sidrak and Aboul-Seoud	[26]	V
ESAB2M	[62]	V	SIRKO	[14]	G (C)
EY608	[10]	A	SPECA	[19]	A
HYPERQUAD	[34]	V, A	SPECFIT	[77]	A (E)
HYPNMR	[36]	N	SPFAC	[48]	A (E)
KATCOM	[25]	V	SQUAD	[78]	A
LETAGROP–SPEFO	[6]	A	SQUAD84	[23]	A
LETAGROP–VRID	[7]	V	STAR	[52]	A
LITRA	[63]	A	STBLTY	[79]	V
LOGMIN	[64]	V	STEW	[9]	V
MAXIPOT-F	[17]	V	SUPERQUAD	[21]	V
MICMAC	[31]	G (V, P, N)	TITAN	[29]	V
MINIGLASS	[65]	V	TITFIT	[80]	V
MINIMIX	[66]	A	TITRA	[28]	V
MINIQUAD	[32]	V	Wentworth et al.	[81]	A

[a] Additional data types used in calculations: E, ESR; C, Calorimetry; G, general; N, NMR; P, Polarography.

metric and spectrophotometric (absorbance) data. However, working simultaneously on different kinds of data makes it imperative that a full, rigorous weighting scheme is used. Only when this is so will it be possible to apply simple statistical tests for the goodness of fit, with an expectation value of unity for the sample variance. In order to implement this procedure we have developed a new means of estimating the error in a measure of absorbance.

We have previously outlined the main features used in the HYPERQUAD program [34]. Since that publication, we have developed a suite of inter-related programs which are directed towards data preparation, preliminary model exploration, simulation and preparation of speciation dia-

grams. Together these programs provide almost all the facilities which have previously been used on an ad hoc basis in the process of mode selection. The one exception is that we have not explicitly included an electrode calibration program. We assume that electrodes will be calibrated by means of a strong acid–strong base titration, which HYPERQUAD can handle. MAGEC [35] is a program designed for electrode calibration.

Another set of programs in the HYPERQUAD suite, HypNMR, is described elsewhere [36]. The principal program in that set can be used to determine equilibrium constants from NMR chemical shift data. It is assumed that the species in equilibrium are in rapid exchange on the NMR time-scale so that each value of chemical shift is

the concentration-weighted average of the shifts of the individual species.

2. The HYPERQUAD suite of programs

2.1. The data structure

It became clear very early on that the treatment of different kinds of experimental data logically required a well defined data structure. Previously all programs had used a single file for all the data. With a suite of programs, however, the data files serve as input to different procedures and must therefore be standardised. Conceptually there are four kinds of data file as follows.

(i) A model file. This file contains only the data relevant to a chemical model, viz. the names of the reagents, the equilibrium constants defined by initial value and stoichiometric coefficients, keys to indicate refinable quantities and whether or not a species absorbs light. In addition, our model file may hold the wavelengths at which measurements were made and any known molar absorbances. The model files are given the extension PAR.

(ii) Potentiometric data file. We have Instrument Potentiometric Data (extension IPD) and Program Potentiometric Data (extension PPD) files. The former are ASCII data files such as may be produced by an automatic titrator whilst the latter are suitable for HYPERQUAD. There is a facility in the data editor (HEDIT) for converting IPD to PPD. The PPD file contains the conditions (total amounts, burette concentrations, etc.) of a titration curve as well as the titration data (volume added, e.m.f. of pX measurement).

(iii) Spectrophotometric data. Instrument Absorbance Data (extension IAD) files are ASCII data files typically produced by a spectrophotometer, that is, they contain an absorbance spectrum. Three forms are at present acceptable: initial wavelength and increment, followed by absorbance values, wavelength and absorbance value pairs or the standard JCAMP-DX format [37,38]. A Base Absorbance Data (.BAD) file contains the concentrations, etc., used when the spectrum was recorded and it holds a complete spectrum in HYPERQUAD format. A Program

Absorbance Data file (extention PAD), on the other hand will contain absorbance data at wavelengths selected in the HydraSP program, and may hold data in the form of a spectrophotometric titration curve of batch data.

(iv) Output files. These are files produced during the computations. For example, HYPERQUAD produces a standard output file OUTPUT.RES which may be used in post-run processing of the results of a computation by means of the program HANDOUT.

The fact that the model files do not hold experimental data is a great advantage. For example, it means that one model file may be used with different data sets without the duplication that would have arisen with, say, SUPERQUAD [21]. Furthermore, the model file serves as input to the speciation program HYPHEN where experimental data are irrelevant. Other ways in which the data structure is advantageous are in the determination of end-points (program HENNA) where the model is irrelevant and in factor analysis (program HydraSP), where again the model is irrelevant.

2.2. Linking potentiometric and spectrophotometric data

Each titration curve or experimental spectrum is assigned a unique label. Absorbance Data files carry a second label which may or may not be the same as the label of a potentiometric data file. If this second "corresponding to" label is the same as one in the potentiometric data file then the concentrations, etc., are taken from that file. In this way, it is possible to process either potentiometric or spectrophotometric data on its own, or to process them together.

HYPERQUAD is distributed with a large number of specimen data files. Also, there is a set of template files which can be used for entering new data.

2.3. The HYPERQUAD data editor

The HYPERQUAD data editor HEDIT is designed to make data entry as chemist-friendly as possible. In fact, when this facility is used as

standard, users will not need to know how the data are actually stored in the data files. The data present in a model file (PAR), a potentiometric and/or spectrophotometric data file (PPD, BAD or PAD) are offered for editing in an intelligible form, i.e. reagents are identified by the names specified in the model file, quantities and concentrations are clearly labelled as such, and so forth.

There are two limitations at present to the type of data that may be handled in HEDIT. No more than two electrodes are allowed. Few people have made measurements using two electrodes, and no-one (at least to our knowledge) has yet made measurements using more. The maximum number of reagents is determined by screen resolution and is 12 at present. Otherwise, if the amount of data is more than can appear at one time on the screen there are screen-paging options. One great advantage of using HEDIT is that the user does not require any instructions on how to imput data to HYPERQUAD, although specifications are included in the documentation should anyone prefer to use a text editor.

In addition to being able to process Program data files, the data editor can convert Instrument data files to Program form. Also, if a BAD file corresponds to a single species in solution, this can be input into the model file in the form of a set of molar absorbances. For example, the spectrum of a metal ion could be recorded and transferred into the model file as just described. This is possible because the BAD file holds the concentration of the species which give rise to the spectrum, thus permitting the calculation of molar absorbance from the measurements.

2.4. The programs JOIN and SUPPER

JOIN is a utility·program that links the data from more than one titration curve into one data file. We have kept this as a separate program, rather than include the option in HEDIT, for this reason. The experimental data for any one titration will be stored in a file which is the primary record of the experimental data. Files containing data from more than one titration curve are secondary sources of data. SUPPER will take SUPERQUAD [21] data and convert it into PPD form.

2.5. The program Haber

This program is concerned with the estimation and treatment of errors in absorbance measurements. It is well known that errors in absorbance measurements may depend on the absorbance value. For example, when using a photomultiplier the signal error is often assumed to be proportional to the signal value. However, it is also clear that the magnitude of errors will depend on instrument settings. Therefore, we have devised a scheme whereby the error can be expressed as a simple empirical function that can be incorporated in a model file.

First it is necessary to collect a number of spectra obtained under identical conditions. This means that not only must the instrument conditions be the same but also the spectrum must not vary with time. We prefer to use solid samples such as doped glass filters for this purpose. Suppose n spectra have been obtained; we suggest $n = 9$ as a minimum. Then the abosrbance value is given by the mean of the n measurements and an estimate of the error at that absorbance value is given by the standard deviation of the n measurements:

$$\bar{A} = \frac{\sum_{j=1,n} A_j}{n}$$

$$s_A = \sqrt{\frac{\sum_{j=1,n} (A_j - \bar{A})^2}{n-1}}$$

The values of s_A are plotted on the screen as a function of $\bar{A}$ and the whole set of data is approximated by a simple four-parameter function. The first parameter specifies the function type, either quadratic or exponential. For a quadratic function we have $E = a + bA + cA^2$ and for the exponential function $E = a + be^{cA}$. The values of the parameters a, b and c may be adjusted interactively. It is possible to set one or more of these parameters to zero if that is required.

It may be noted that there is no attempt made to allow for the correlation that undoubtedly exists between the errors at different wavelengths in the same spectrum. Some evidence for this

correlation will be seen in the plots of s_A against $\bar{A}$ in the form of two values of s_A for some values of $\bar{A}$: there is one value when the absorbance curve has a positive slope and another when it has a negative slope. In any case one would normally choose an error function that passes through the middle of the data. We have taken the view that since the weights are only approximate, it is not worth correcting for correlation of errors.

The four parameters of the chosen error function are then entered into a model file. It is possible to have a different error function at each wavelength (thus allowing for the use of different detectors at different wavelengths) or that the error function is the same at all wavelengths.

In a HYPERQUAD calculation, the error at each absorbance value is calculated automatically from the error function in the model file and this is used to construct an approximate variance–covariance matrix for the absorbance measurements, from which the weights are derived. (see below)

2.6. The program HydrapH

This program takes as input a model file and a program Potentiometric Data file and is to be used for preliminary examintion of potentiometric data. The program offers 10 facilities. Six of these relate to presentation of the experimental data on the screen, i.e. e.m.f. or pH on the y-axis, volume, pH or a user-defined coordinate on the x-axis. Then there are species distrubution plots both as formation percentages relative to the total concentration of one reagent and as logarithms of concentration.

At least two programs have been already published concerning the simulation of titration curves, ESTA [39] and SCALPO [40]. We have included the interactive simulation of the titration curve(s) in HydrapH. In this, data in the model file may be amended in any way desired and either the calculated/observed titration curves are displayed or the difference (observed pH − calculated pH). It does not matter if the experimental readings are in mV or pH units. In parallel with the changes in the simulated titration curve there will also be changes in the speciation diagrams. Thus, it is possible to make a thorough prelimi-

nary analysis and ascertain both that the model is reasonable and that all the species postulated to be present and are in appreciable concentrations.

2.7. The program Henna

This is another program for the preliminary analysis of potentiometric data, concerned with end-point determination. The traditional methods used for end-point determination have limitations. Gran's method [41] fails for overlapping end-points [42]. First-derivative methods fail if the data are relatively sparse. For these reasons, we have developed a new algorithm in which the titration curve is fitted, by the method of least squares, by B-spline functions. A derivative of the B-spline function is used to determine the position of the end-point (maximum slope in the first derivative, zero in the second derivative, etc.). A similar procedure has been used to fit spectra [43]. For the purposes of the present application, the user needs to make only two choices: first the derivative required, the degree of the spline function being automatically chosen so that the derivative is a quadratic spline function, and second the number of B-spline pieces. These choices are made interactively. Optimal knot positions are determined automatically by repeated use of procedure called NEWNOT [44] and the observed/calculated titration curves are displayed along with the residuals and the desired derivative. After the user has indicated the approximate position of the end-point to be determined, its optimum position is calculated.

The only problem with this method arises when the number of data points in an interval between knots becomes equal to the degree of the spline function. In that case the calculated titration curve passes exactly through the observed data points, usually with wild oscillations. Since this does not normally happen near an end-point, it is not a serious problem for end-point determination.

2.8. The program HydraSP

This is the main program to be used for preliminary analysis of spectrophotometric data. It takes as input a model file and up to 28 spectra in the

form of BAD files. It offers five main facilities, as follows.

(i) Scaling and correction of data. Spectra can be scaled to equal concentration and path length in order to reveal isosbestic points. Scaling to equal areas can be used for the same purpose and will reveal isosbestic point in some circumstances where the simple scaling does not do so [45]. There is an offset facility which can be used to remove some baseline errors from the spectra. It works as follows. Assuming that the absorbance at the nth wavelength, λ_n, can be written as

$$A_{\lambda_n} = l \sum_j \varepsilon_{\lambda_n,j} c_j + B$$

where B is a constant baseline error, it follows that if the absorbance at one wavelength, λ_b, is subtracted from data at all wavelengths the Beer–Lambert law will still be obeyed but a constant baseline error will have been eliminated:

$$A_{\lambda_n} - A_{\lambda_b} = l \sum_j (\varepsilon_{\lambda_n,j} - \varepsilon_{\lambda_b,j}) c_j$$

The penalty for using this facility is that the molar absorbances are composite but if λ_b is chosen in a region where there is little absorbance this will be of little significance. Therefore, we recommend that spectra be recorded if at all possible with data near the true baseline. To make our procedure more robust we use a smoothed value for the absorbance to be subtracted.

(ii) Selection of wavelengths for HYPER-QUAD calculation. This is an interactive procedure so that the user can choose those wavelengths most suitable for the calculation. Now, in principle, data at one wavelength are sufficient for the purpose of calculating equilibrium constants. One would seek that wavelength which exhibits the maximum change in absorbance with changes in the experimental conditions. Choosing some points on either side of this will help to reduce the effect of noise in the spectroscopic data. However, if different species absorb in different parts of a spectrum, it may be very useful to include data from the different zones. We recommend that relatively few wavelengths are used for a HYPERQUAD calculation;

there is a separate facility for the calculation of the molar absorbances at all wavelengths.

(iii) Trial and error fitting. This is similar to the facility in HydrapH. It works at a single wavelength, which is first chosen interactively. The procedure works as follows. The species concentrations are calculated from the model and the experimental conditions. These concentrations (c_j above) are then used to determine the molar absorbances at the chosen wavelength, from the Beer–Lambert law by weighted linear least squares. The weights are chosen as $1/(\text{absorbance})^2$ so as to minimize the sum of relative errors (another weighting scheme may be used in HYPERQUAD).

(iv) Calculation and display of the molar absorbances at all wavelengths. This calculation proceeds in the same manner as in (iii), but at all wavelengths. The calculated spectra may be stored in ASCII form for plotting by another program, such as EXCEL or ORIGIN. This calculation is a particularly useful check on the validity of a chemical model. Indeed, one would be loath to accept any model for which the calculated spectra of the absorbing species were unreasonable, as, for example, when they had many negative values.

(v) Factor analysis. Factor analysis was first introduced in this field by Kankare [10]. Since then, Zuberbühler and co-workers have developed the concept of Evolving Factor Analysis (EFA) [46,47], which they also describe as model-free analysis of spectrometric data. A similar approach, called "self-modelling curve resolution in studies of spectrometric titrations", has also been published [48]. There is no doubt that factor analysis has the potential to be very useful in studies of equilibria, but in practice it is not easy to apply.

The basis of the application of factor analysis is the Beer–Lambert law, implying that the total absorbance at any wavelength is a linear combination of the absorbances due to a few factors. When the number of (multi-wavelength) observations exceeds the number of factors, it is possible to smooth the data by back transformation using the correct number of abstract factors, as was done in CLINP [12]. However, it is not generally appreciated that this process is based on the

method of least squares. Indeed, the eigenvalues calculated in factor analysis are nothing other than the Langrangian multipliers of a constrained least-squares problem. Therefore, the application of factor analysis in equilibrium studies can be seen as another application of the method of least-squares.

We have used singular value decomposition of the matrix of absorbance values, A, to derive the eigenvalues and eigenvectors of $A^T A$. This procedure eliminates the accumulation of errors inherent in the matrix multiplication. A variety of statistics are provided for 1, 2, ..., eigenvalue models as suggested by Malinowski and Howery [49]. With the aid of these statistics, it should be possible to deduce the number of light-absorbing species present in the equilibria.

The difficulty with factor analysis is that the relationship between the eigenvalues and the experimental errors is an implicit one. It is therefore difficult to establish criteria to determine if a small eigenvalue is effectively non-zero. Conny and Meglen [50] have made an analysis of the effects of experimental noise on the calculated eigenvalues, but their conclusions are not very precise.

As far as Target Factor Analysis is concerned, we see no value in this technique, given that it is possible to perform a full equilibrium analysis. The idea is as follows. Suppose that there are n species to be considered. Then the first n eigenvectors are the abstract factors. To convert them into molar absorbances, a large rotation matrix must be found. The rotation matrix has too many variables to be determined correctly, but some progress can be made by, for example, imposing the condition that molar absorbance must be positive. This will establish ranges for the molar absorbances. The technique was first described in 1974 [51].

By contrast, EFA may be useful as long as one remembers that one is dealing with abstract fators. A careful reading of the original papers [46,47] will reveal that key words such as "species" and "concentration profiles" are written in quotation marks, as here.

2.9. The program Hyphen

This program is different from the other programs in the HYPERQUAD suite in that it does not require experimental data. It can be used to simulate titration curves or to give species distribution diagrams for a wide variety of conditions. Thus, it is a speciation program limited to homogeneous equilibria in solution. There is a large literature referring to speciation programs which we feel is inappropriate to be discussed here. Suffice it to say that the core of the program is the solution of the equations of mass balance by the Newton–Raphson method. This is a sub-problem as far as HYPERQUAD is concerned, so we use the same routines in Hyphen as are used in HYPERQUAD. The model used for these calculations is in a PAR file, but the conditions are stored separately in scratch files that serve merely to allow one to start again where one left off before.

In addition, Hyphen has the facility to calculate the species' concentrations at a single data point defined by knowing, for each reagent, either the total concentration or the free concentration (e.g. pH).

2.10. The program HYPERQUAD

As far as potentiometric data are concerned, the algorithm used in the HYPERQUAD is virtually the same as in SUPERQUAD [21]. Thus the new mathematical features are concerned with the treatment of spectrophotometric data or with the simultaneous treatment of both potentiometric and spectrophotometric data. There are significant differences between the present version of HYPERQUAD and that described in a preliminary account [34]. These arose out of the need to apply a rigorous weighting scheme to the data. The following outline is presented in terms of a relatively simple system of potentiometric measurements using an electrode responding to the hydrogen ion and absorbance measurement at nl wavelengths; there are three reagents, M, L and H, and nk equilibrium constants.

The objective function is given in matrix notation simply as $U = r^T W r$, where r is a vector of residuals, $r = (y^{observed} - y^{calculated})$, $y^{observed}$ repre-

sents a measurment in mV, pH or absorbance and W is a matrix of weights. The residuals are ordered with potentiometric first and absorbance second. To minimize the objective function, we use the Gauss–Newton–Marquardt method summarized by the system of normal equations

$$(J^TWJ + \lambda D)\Delta p = J^TWr$$

where J is the Jacobian matrix and Δp is a vector of shifts to be applied to the parameters. D is taken as equal to the diagonal elements of J^TWJ and λ is the Marquardt parameter which may, of course, be zero. The method requires that the parameters be given initial values; these may be obtained with the aid of HydrapH or HydraSP.

The elements of the Jacobian relative to any unknown parameter p are obtained from the defining equations, the modified Nernst law (ionic charges are omitted for simplicity of notation):

$$E = E^0 + f\frac{RT}{nF}\ln[H]$$

$$\frac{\partial E}{\partial p} = \frac{\partial E}{\partial [H]}\frac{\partial [H]}{\partial p}$$

and the Beer–Lambert law:

$$A_\lambda = l\sum_{j=1,na}\varepsilon_{\lambda j}c_j$$

$$\frac{\partial A_\lambda}{\partial x} = l\sum_j\varepsilon_{\lambda j}\frac{\partial c_j}{\partial x}$$

$$= [M] + \sum p_k c_k$$

is the equation for reagent M; similar equations may be written for L and H. Moreover, the total concentration T_M is obtained from the initial amount n_M, burette concentration a_M, initial volume v_0 and added volume v. Thus the three mass-balance equations are

$$\frac{n_M + va_M}{v_0 + v} = [M] + \sum_{k=1,kn}p_k c_k$$

$$\frac{n_L + va_L}{v_0 + v} = [L] + \sum_{k=1,nk}q_k c_k$$

$$\frac{n_H + va_H}{v_0 + v} = [H] + \sum_{k=1,nk}r_k c_k$$

These are solved by the Newton–Raphson method and the normal equations matrix is used to derive $\partial[H]/\partial\beta_k$ as described earlier [34]. Other Jacobian elements such as $\partial E/\partial E^0$, $\partial E/\partial n$ and $\partial E/\partial a$ are easy to derive. When quantities such as E^0 are refined they are termed dangerous parameters. Now, with these equations the Jacobian for one data point can be constructed, as in the following example applicable to a system with one electrode, na absorbing species, nl wavelengths, nk equilibrium constants and nd dangerous parameters, denoted by $\alpha_1, ..., \alpha_{nd}$. Note that we further assume here that there is a molar absorbance for each species at every wavelength.

$$
\begin{array}{cccccccc}
0 & \cdots & 0 & 0 & \cdots & 0 & \cdots & 0 \\
\dfrac{\partial A_1}{\partial\varepsilon_{1,1}} & \cdots & \dfrac{\partial A_1}{\partial\varepsilon_{1,na}} & 0 & \cdots & 0 & \cdots & 0 \\
0 & \cdots & 0 & \dfrac{\partial A_2}{\partial\varepsilon_{2,1}} & \cdots & \dfrac{\partial A_2}{\partial\varepsilon2_{,na}} & \cdots & 0 \\
\vdots & \cdots & \vdots & \vdots & \cdots & \vdots & \ddots & \vdots \\
0 & \cdots & 0 & 0 & \cdots & 0 & \cdots & \dfrac{\partial A_{nl}}{\partial\varepsilon_{nl,1}}
\end{array}
$$

In addition, the system is subject to the constraint that the equations of mass balance are satisfied.

$$T_M = [M] + \sum_{k=1,nk}p_k\beta_k[M]^{p_k}[L]^{q_k}[H]^{r_k}$$

$$
\begin{array}{cccccccc}
\cdots & 0 & \dfrac{\partial E}{\partial\beta_1} & \cdots & \dfrac{\partial E}{\partial\beta_{nk}} & \dfrac{\partial E}{\partial\alpha_1} & \cdots & \dfrac{\partial E}{\partial\alpha_{nd}} \\
\cdots & 0 & \dfrac{\partial A_1}{\partial\beta_1} & \cdots & \dfrac{\partial A_1}{\partial\beta_{nk}} & \dfrac{\partial A_1}{\partial\alpha_1} & \cdots & \dfrac{\partial A_1}{\partial\alpha_{nd}} \\
\cdots & 0 & \dfrac{\partial A_2}{\partial\beta_1} & \cdots & \dfrac{\partial A_2}{\partial\beta nk} & \dfrac{\partial A_2}{\partial\alpha_1} & \cdots & \dfrac{\partial A_2}{\partial\alpha_{nd}} \\
\cdots & 0 & \vdots & \cdots & \vdots & \dfrac{\partial A_1}{\partial\alpha_1} & \cdots & \vdots \\
\cdots & \dfrac{\partial A_{nl}}{\partial\varepsilon_{nl,na}} & \dfrac{\partial A_{nl}}{\partial\beta_1} & \cdots & \dfrac{\partial A_{nl}}{\partial\beta_{nk}} & \dfrac{\partial A_{nl}}{\partial\alpha_1} & \cdots & \dfrac{\partial A_{nl}}{\partial\alpha_{nd}}
\end{array}
$$

At this point the normal equations matrix J^TWJ and right-hand side J^TWr can be built up by accumulation. To do this we use the factored weight matrix, $W = w^Tw$. First the Jacobian and residual are left-multiplied by the factor and then the normal equations are accumulated as

$(wJ)^T(wJ)$ and $(wJ)^Twr$. This process destroys the block-diagonal structure[1] that was previously described for the normal equations matrix [34]. The normal equations that result have the dimensions of $na \times nl + nk + nd$. It is obvious that the number of wavelengths, nl, should not be large, otherwise the normal equations become large and hence slow and difficult to solve.

Solution of the normal equations provides shifts for all the parametes. However, the shifts on the molar absorbances are not used. Instead, the equilibrium constants and dangerous parameters are updated with the shifts and the molar absorbances are calculated using the updated values by linear least-squares applied to the Beer–Lambert law. In this procedure we follow what appears to be standard practice going back to LETAGROP–SPEFO [6]. However, some authors have applied a non-negativity constraint to the molar absorbances (SPECA [19], STAR [52]). We have not done this because we believe that a negative molar absorbance is a good indicator that something is wrong with the chemistry.

To understand how a negative molar absorbance, $\varepsilon_{\lambda j}$, can arise we must write out the Beer-Lambert law in full:

$$A_\lambda = l \sum_{j=1,na} \varepsilon_{\lambda j} \beta_j [M]^{p_j} [L]^{q_j} [H]^{r_j}$$

Since the molar absorbance is multiplied by the equilibrium constant, this expression shows that we can expect the molar absorbances to be highly correlated with the equilibrium constants so that a small error in the latter can easily lead to a negative value in the former. Thus, negative molar absorbances indicate that the calculated equilibrium constants are in error.

The high correlation between molar absorbances and equilibrium constants is masked, but not eliminated, by the two-stage refinement process. It is a central problem in the determination of equilibrium constants from spectrophotometric data that can only be resolved by good experimental design. The calculation of all molar

---

[1] The normal equation will have the block-diagonal structure if a diagonal weight matrix is used, but no special provision is made for this eventuality.

absorbances with the aid of HydraSP may reveal negative values at wavelengths not used in a HYPERQUAD calculation, so that it would be good practice to calculate all molar absorbances as a check on the results of a calculation based on selected wavelengths.

2.11. Calculation of the free concentrations

The equations of mass balance can be written in the most general form as $(i = 1, nr)$

$$T_i = [X_i] + \sum_{k=1,nk} q_{ik} \beta_k \prod_{j=1,nr} [X_j]^{q_{jk}}$$

where $[X_i]$ represents the free concentration of the ith reagent. When the equilibrium constants, β, are "known", we have a system of nr non-linear simultaneous equations in nr unknown free concentrations. When these equations have been solved, the concentrations of all the species present in the equilibria will be "known". The solution of these equations is therefore required whenever we require the concentrations of the species, in HYPERQUAD, Hyphen, HydrapH and HydraSP. The calculation proceeds in two stages. First estimates must be made of all the free concentrations. Then these estimates are refined by Newton–Raphson iteration. Finally, the refinement must be terminated with a suitable criterion.

At the first point in a titration curve, or with batch data, we obtain first estimates by use of a modified Newton–Raphson technique with damping as suggested in the program ES4EC [53]. The modification is drastic: we set all off-diagonal elements of the Jacobian to zero, and improve each free concentration in turn. Subsequent points in a titration curve can utilise the last values calculated for the initial estimate. In the HYPERQUAD calculation some improvement in the initial estimate can be made on the second and subsequent iteration cycles. To illustrate this, consider the free hydrogen ion concentration at the jth point in a titration curve at the kth iteration cycle, $^k[H]_j$. A better estimate than $^k[H]_{j-1}$ (the concentration at the previous point in the titration curve) of this quantity is given by postulating that the slope relating to the free concentration is the same in the two iteration cycles, i.e. $^k[H]_j -$

$^k[\mathrm{H}]_{j-1} = {}^{k-1}[\mathrm{H}]_j - {}^{k-1}[\mathrm{H}]_{j-1}$. The time saved by improving the initial estimates of free concentrations is worthwhile as this calculation is the most time-consuming part of a HYPERQUAD calculation.

When it is known that the data points are equally spaced, as in Hyphen, the calculation can be speeded up by a simple extrapolation technique [54]. We have found that quadratic extrapolation works very well: $[\mathrm{X}]_i = [\mathrm{X}]_{i-3} - 3[\mathrm{X}]_{i-2} + 3[\mathrm{X}]_{i-1}$.

A serious problem can arise during a refinement if one or more of the equilibrium constants becomes negative. We allow this to happen as experience has shown that the "offending" constant may return to being positive later in the refinement. However, when an equilibrium constant is

tions are calculated to a relative precision of better than 1 part in 10^{15}.

2.12. Calculation of weights

In the "automatic" weighting scheme, the calculation of weights requires estimates of the errors on e.m.f., volume and absorbance. The last-named are derived from the empirical error function determined by the program HABER. Then, still assuming one electrode and nl wavelengths and assuming that the potentiometric and absorbnce data derive from a titration curve the variance–covariance matrix, M, for a single point is given by the "rigorous" method of least squares to be [4].

	E	A_1	A_2	$\cdots$	A_{nl}
E	$s_E^2 + \left(\dfrac{\partial E}{\partial v}\right)^2 s_v^2$	$\left(\dfrac{\partial E}{\partial v}\right)\left(\dfrac{\partial A_1}{\partial v}\right)s_v^2$	$\left(\dfrac{\partial E}{\partial v}\right)\left(\dfrac{\partial A_2}{\partial v}\right)s_v^2$	$\cdots$	$\left(\dfrac{\partial E}{\partial v}\right)\left(\dfrac{\partial A_{nl}}{\partial v}\right)s_v^2$
A_1		$s_{A_1}^2 + \left(\dfrac{\partial A_1}{\partial v}\right)^2 s_v^2$	$\left(\dfrac{\partial A_1}{\partial v}\right)\left(\dfrac{\partial A_2}{\partial v}\right)s_v^2$	$\cdots$	$\left(\dfrac{\partial A_1}{\partial v}\right)\left(\dfrac{\partial A_{nl}}{\partial v}\right)s_v^2$
A_2			$sA_2^2 + \left(\dfrac{\partial A_2}{\partial v}\right)^2 s_v^2$	$\cdots$	$\left(\dfrac{\partial A_2}{\partial v}\right)\left(\dfrac{\partial A_{nl}}{\partial v}\right)s_v^2$
$\vdots$	symmetrical			$\vdots$	$\vdots$
A_{nl}					$s_{A_{nl}}^2 + \left(\dfrac{\partial A_{nl}}{\partial v}\right)^2 s_v^2$

negative, there is no guarantee that all the free concentrations can be positive. (The condition is guaranteed by the existence of a unique free energy minimum at equilibrium when all the equilibrium constants are positive.) Now, we impose a non-negativity constraint on the free concentrations, as do most others, if for no other reason that we wish to take logarithms of free concentrations. Therefore, it can happen that the free concentration calculation may fail to converge. When this happens, we return to the main minimization routine and reduce the length of the shift vector for the equilibrium constants.

We attempt to satisfy the conditions of mass balance as nearly as is possible within machine accuracy. As double precision arithmetic is used throughout this means that the free concentra-

The parital derivatives $\partial E/\partial v$ and $\partial A/\partial v$ required for the above formula are estimated from the observed data by means of piece-wise fitting of a seven-point cubic polynomial (simpler estimates are used for the first and last three points). We note that in SIRKO [14] the derivatives are obtained from the calculated values by analytical differentiation, but the authors remark that the weight should then be recalculated at every refinement cycle. The weight matrix, W, would be the inverse of M, but it is not actually calculated. Instead we perform a Choleski factorisation, $M = m^T m$ and invert the lower-triangular factor, m, to obtain the weight matrix factor, w, such that $W = w^T w$. The lower triangle of this factored matrix is stored in a single-precision one-dimensional array in order to conserve computer mem-

ory. Other weighting schemes are available. Diagonal weights may be used if the automatic scheme requires too much memory. Diagonal weights would be invoked automatically with batch as opposed to titration data.

For spectrophotometric data the alternative function

$$U = \sum_k \left(\frac{\Delta A_k}{A_k^{obs}}\right)^2; \quad \Delta A_k = A_k^{calc} - A_k^{obs}$$

may be minimized by means of the use of another weighting scheme. To see how this comes about, we derive the ith unit-weighted least-squares normal equation in the usual manner [4] as

$$\sum_k \sum_j J_{ki} J_{kj} \Delta p_j = \sum_k J_{ki} \frac{\Delta A_k}{A_k^{obs}}$$

The elements of the Jacobian, J, are given by

$$J_{ki} = \frac{1}{A_k^{obs}} \frac{\partial A_k^{calc}}{\partial p_i}$$

where p_i is a refinable parameter. When this expression is substituted into the normal equation we obtain

$$\sum_k \sum_j \frac{\partial A_k^{calc}}{\partial p_i} \frac{\partial A_k^{calc}}{\partial p_j} \left(\frac{1}{A_k^{obs}}\right)^2 \Delta p_j$$

$$= \sum_k \frac{\partial A_k^{calc}}{\partial p_i} \left(\frac{1}{A_k^{obs}}\right)^2 \Delta A_k$$

Thus, setting the weights as $W_k = (1/A_k^{obs})^2$ and minimizing the sum of squared residuals is equivalent to minimizing the sum of squared relative residuals with unit weights. However, when this weighting scheme is used it is not possible to give an expectation value for U.

2.13. The program Handout

The HYPERQUAD program produces a standard file, OUTPUT.RES, which contains all the useful information that was generated during the equilibrium constant refinement(s). The program HANDOUT has four main functions. Two of these relate to viewing the results on screen or dumping selected items to a printer. The third allows the model file to be updated with the refined values for the equilibrium constants.

Lastly, there is a facility for drawing species distribution diagrams. These diagrams, which perforce relate to the experimental conditions, can be annotated by an interactive process involving the mouse, and the final diagram sent to a file. In that case, Hewlett-Packard (HP) Graphics Language is used so that the file may be dumped to an HP-compatible plotter or laser printer or imported into Word or WordPerfect as a picture.

2.14. Programming details

All programs were written in FORTRAN and compiled with MS FORTRAN 5.0 or 5.1 for an AT-style PC. They also appear to function correctly in a DOS window under Windows 95. They assume the presence of a Microsoft-compatible mouse, VGA graphics and a maths coprocessor. For HYPERQUAD there are no formal restrictions on the data. All arrays are dimensioned at run-time. This is achieved by first making a dummy pass through the data files to count all the quantities needed for the allocatable arrays. The arrays are then allocated and the data are read in. A similar system is used in HEDIT and most of the other programs. Thus, the only restriction on the data is imposed by the amount of memory available. It is our intention in the near future to recompile the programs with a 32-bit compiler; that will effectively remove all restrictions on data. Some restrictions may still remain that are imposed by what can be placed on the screen at the same time, but important screens, such as the one that shows the equilibrium constants, are already paged.

HYPERQUAD has been on beta release (mostly in Italy) for more than a year. All programs are fully documented. It has to be stated that we have encountered occasional difficulties with installation that we suspect are due to the use of non-standard mouse and keyboard routines (non-standard only in the sense that the routines are not in the compiler library).

3. Discussion

HYPERQUAD is different from all programs

that have been written before, in this field, in that it is not a single program but a suite of inter-related programs. This has been made possible by the developement of an associated data structure so that the HYPERQUAD programs access a common set of data files. By dividing the data conceptually into data relating to a model and data relating to experimental measurements of different kinds, it becomes possible to perform operations that were not possible before. For example, the model file can be used alone in the program Hyphen to simulate titration curves, that is, to find good experimental conditions, and then together with experimental data in the HYPERQUAD calculation. It is also possible that a model file which was designed for use with the program HypNMR [36] can be used in the simulation program Hyphen.

Within the suite there are many novelties. An important one is the idea of deriving an empirical function to relate the error on a spectrophotometric absorbance measurement to the absorbance value (program Haber). This function permits the construction of an approximate variance–covariance matrix for absorbances without the need to estimate the error on each absorbance measurement. That matrix is essential when it comes to determining the weights to be given to experimental observations in the least-squares calculation, particularly so when the observations may be of different kinds such as potentiometric and spectrophotometric.

Other new features are the creation of plot files in Hewlett-Packard Graphics Language for export to a plotter or laser printer, the use B-spline functions to locate end-points in potentiometric data, an offset procedure for coping with baseline errors in spectra and trial and error procedures for manual fitting of both potentiometric and absorbance data.

In summary, HYPERQUAD provides facilities, in one coherent package, for doing almost all processing of solution equilibrium data that has been done in the past, using standard data files and standard procedures for recalling data from files, for editing data and for saving data to files. The greatest novelty of the system is its comprehensive nature, with each program taking as input a standard model file and/or an experimental data file. The main difference between SUPERQUAD and HYPERQUAD is that the new program can handle spectrophotometric data in addition to potentiometric data.

4. Future developments

We do not believe that it is sensible for us to develop a program, such as SIRKO [14] or MIC-MAC [31], which claims to be able to handle any kind of data. Our experience has been that each kind of experimental data imposes certain requirements that are not present with the other. Thus, we are not attempting to integrate HypNMR [36] with HYPERQUAD because the NMR data usually consist of just single data points whereas HYPERQUAD is oriented towards data from titration curves. Likewise, we have a program PHAB already in an advanced stage of development as a separate entity. PHAB will deal with absorbance data at measured pH values so, unlike HYPERQUAD, the total hydrogen ion concentration is not known and the mass balance in protons is irrelevant. This imposes the need to calculate the free concentrations in a different way. The HYPERQUAD programs are highly modular so it is relatively easy to construct a new program for each substantially different kind of data. In addition, the user interface is standardized because it is based on a set of some 70 routines that constitute a HYPERQUAD subroutine library.

On the programming side, we must consider developing a Windows version of the software. The main advantages will be twofold. On the one hand we will be able to eliminate all restrictions on experimental data. At present the restrictions arise from the fact that we are limited to 640 k bytes of memory for program and data; that restriction disappears under Windows or with the use of a 32-bit compiler. The program which suffers most from this restriction is HydraSP, which can take a maximum of 57 344 data points (up to 28 spectra, each spectrum containing 2048 points). Second, there are restrictions imposed by what can be seen on the screen at any one time.

These restrictions can be removed by using automatically scrolling windows.

References

[1] R.J. Motekaitis and A.E. Martell, The Determination and Use of Stability Constants, VCH, New York, 1988.

[2] D.J. Leggett (Ed.), Computational Methods for the Determination of Formation Constants, Plenum Press, New York, 1985.

[3] M. Meloun, J. Havel and E. Högfeldt, Computation of Solution Equilibria, Ellis Horwood, Chichester, 1994.

[4] P. Gans, Data Fitting in the Chemical Sciences, Wiley, Chichester, 1992.

[5] I. Nagypal, I Páka and L. Zekany, Talanta, 25 (1978) 549.

[6] L.G. Sillén and B. Warnqvist, Ark. Kemi, 31 (1968) 377.

[7] L.G. Sillén, Acta Chem. Scand., 18 (1964) 1085.

[8] J. Havel and M. Meloun, in D.J. Leggett (Ed.), Computational Methods for the Determination of Formation Constants, Plenum Press, New York, 1985, p. 221.

[9] P. Gans and A. Vacca, Talanta, 21 (1974) 45.

[10] J.K. Kankare, Anal. Chem., 42 (1970) 1322.

[11] L. Lampugnani, L. Meites, P. Papoff and T. Rotunno, Anal. Chim. Acta, 1994 (1987) 77.

[12] A.A. Bugaevskii, Yu. V. Kholin and D.S. Konyaev, Russ. J. Inorg. Chem., 38 (1993) 328.

[13] H. Gampp, M. Maeder and A. Zuberbühler, Talanta, 27 (1980) 1037.

[14] V.I. Vetrogon, N.G. Lukyanenko, M.-J. Schwing-Weill and F. Arnaud-Neu, Talanta, 41 (1994) 2105.

[15] T. Michalowski, Talanta, 39 (1992) 1127.

[16] M. Meloun, M. Javúrek, and J. Militký, Mikrochim. Acta, 109 (1992) 221.

[17] F. Gaizer and I.I. Kiss, Talanta, 41 (1994) 419.

[18] J.P. Chandler, R.E. Thomson, H.O. Spivey and E.L.-F. Li, Anal. Chim. Acta, 162 (1984) 399.

[19] R. Cazallas, M.J. Citores, N. Etxebarria, L.A. Fernández and J.M. Madariaga, Talanta, 41 (1994) 1637.

[20] C. De Stefano, P. Mineo, C. Rigano and S. Sammartano, Ann. Chim., 83 (1993) 243.

[21] P. Gans, A. Sabatini and A. Vacca, J.Chem. Soc., Dalton Trans., (1985) 1195.

[22] J. Havel and M. Meloun, Talanta, 33 (1986) 525.

[23] M. Meloun, M. Javúrek and J. Havel., Talanta, 35 (1986) 513.

[24] E. Bottari, T. Coccitto, G. Curzio, M.R. Festa and R. Jasionowska, Ann. Chim., 78 (1988) 635.

[25] V. Gadiokov and Kh. Mikhailova, Comput. Chem., 13 (1989) 325.

[26] Y.L. Sidrak and A. Aboul-Seoud, J. Comput. Chem., 8 (1987) 575.

[27] R.J. Motekaitis and A.E. Martell, Can. J. Chem., 60 (1982) 3403.

[28] A. Johansson and S. Johansson, Analyst, 104 (1979) 601.

[29] W.E. Gordon, Anal. Chem., 54 (1982) 1595.

[30] R.J. Motekaitis and A.E. Martell, Can. J. Chem., 60 (1982) 168.

[31] A. Laouenen and E. Suet, Talanta, 32 (1985) 245.

[32] A. Sabatini, A. Vacca and P. Gans, Talanta, 21 (1974) 53.

[33] P. Gans, A. Sabatini and A. Vacca, Inorg. Chim. Acta., 18 (1976) 239.

[34] A. Sabatini, A. Vacca and P. Gans, Coord. Chem. Rev., 120 (1992) 389.

[35] P.M. May and D.R. Williams, in D.J. Leggett (Ed.), Computational Methods for Determination of Formation Constants, Plenum Press, New York, 1985, p. 37.

[36] C. Frassineti, S. Ghelli, P. Gans, A. Sabatini, M.S. Moruzzi and A. Vacca, Anal. Biochem., 231 (1995) 374.

[37] R.S. McDonald and P.A. Wilks, Appl. Spectrosc., 42 (1988) 151.

[38] J.G. Grasselli, Pure Appl. Chem., 63 (1991) 1782.

[39] P.M. May, R. Murray and D.R. Williams, Talanta, 32 (1985) 485.

[40] A. De Robertis, C. De Stefano, S. Sammartano and C. Rigano, Anal. Chim. Acta, 222 (1989) 385.

[41] G. Gran, Analyst, 77 (1952) 661.

[42] F.J.C. Rossotti, and H. Rossotti, J. Chem. Educ., 42 (1965) 375.

[43] P. Gans and J.B. Gill, Appl. Spectrosc., 38 (1984) 370.

[44] C. de Boor, A Practical Guide to Splines, Springer, New York, 1978.

[45] J.T. Bulmer and H.F. Shurvell, J. Phys. Chem., 77 (1973) 2085.

[46] H. Gampp, M. Maeder, C.J. Meyer and A. Zuberbühler, Talanta, 32 (1985) 1133.

[47] H. Gampp, M. Maeder, C.J. Meyer and A. Zuberbühler, Talanta, 33 (1986) 943.

[48] R. Tauler, E. Casassas and A. Izquierdo-Ridorsa, Anal. Chim. Acta, 248 (1991) 447.

[49] E.R. Malinowski and D.G. Howery, Factor Analysis in Chemistry, Robert E. Krieger, Malabar, FL, 1989.

[50] J.M. Conny and R.R. Meglen, Anal. Chem., 64 (1992) 2580.

[51] E.A. Sylvestre, W.H. Lawton and M.S. Maggio, Technometrics, 16 (1974) 353.

[52] J.L. Beltrán, R. Codony and M.D. Prat, Anal. Chim. Acta, 276 (1993) 441.

[53] A. De Robertis, C. De Stefano, C. Rigano and S. Sammartano, Anal. Chim. Acta, 191 (1986) 385.

[54] B.W. Darvell and V.W.-H. Leung, Talanta, 37 (1990) 413.

[55] G. Arena, E. Rizzarelli, S. Sammartano and C. Rigano, Talanta, 26 (1979) 1.

[56] M. Cromer-Morin, J.P. Scharff and R.P. Martin, Analusis, 10 (1982) 92.

[57] P. Decock and B. Sarker, Can. J. Chem., 65 (1987) 2798.

[58] A.G. Asuero, J.L. Jiminez-Trillo and M.J. Navas, Talanta, 33 (1986) 531.

[59] R.A. Alcock, F.R. Hartley and D.E. Rogers, J. Chem. Soc., Dalton Trans., 115 (1978).

[60] M. Meloun and J. Militký, Mikrochim. Acta, 112 (1993) 155.

[61] M.J. Hynes, J. Chem. Soc., Dalton Trans., 311 (1993).

[62] C. De Stefano, P. Princi, C. Rigano and S. Sammartano, Ann. Chim., 77 (1987) 643.

[63] S. Koch and G. Ackermann, Z. Chem., 29 (1989) 150.

[64] A. Poznajlo, J. Radioanal. Nucl. Chem., 134 (1989) 97.

[65] A. Izquierdo and J.L Beltrán, Anal. Chim. Acta, 181 (1986) 87.

[66] F. Gaizer and H.B. Silber, Acta Phys. Chem., 36 (1990) 28.

[67] F. Gaizer and A. Puskás, Talanta, 28 (1981) 925.

[68] M. Wozniac, J. Canonne and G. Nowogrocki, J. Chem. Soc., Dalton Trans., 2419 (1981).

[69] M. Wozniak and G. Nowogrocki, Talanta, 25 (1979) 633, 643.

[70] Y. Nievergelt, Analyst, 119 (1994) 145.

[71] P.D. Taylor, I.E.G. Morrison and R.C. Hider, Talanta, 35 (1988) 507.

[72] G. Papanastasiou and I. Zogas, Talanta, 42 (1995) 827.

[73] M.J. Collins, J. Chem. Educ., 63 (1986) 457.

[74] R. Fournaise and C. Pettifaux, Talanta, 34 (1987) 385.

[75] L. Zekany and I. Nagypal, in D.J. Leggett (Ed.), Computational Methods for the Determination of Formation Constants, Plenum Press, New York, 1985, p. 291.

[76] D.D. Perrin and H. Stunzi, in D.J. Leggett (Ed.), Computational Methods for the Determination of Formation Constants, Plenum Press, New York, 1985, p. 71.

[77] H. Gampp, M. Maeder, C.J. Mayer and A. Zuberbühler, Talanta, 32 (1985) 95, 257.

[78] D.J. Legget, in D.J. Leggett (Ed.), Computational Methods for the Determination of Formation Constants, Plenum Press, New York, 1985, p. 159.

[79] A. Avdeef, in D.J. Leggett (Ed.), Computational Methods for the Determination of Formation Constants, Plenum Press, New York, 1985, p. 355.

[80] A. Zuberbühler and T.A. Kaden, Talanta, 29 (1982) 201.

[81] W.E. Wentworth, W. Hirsch and E. Chen, J. Phys. Chem., 71 (1967) 218.

Simultaneous flow injection determination of iron(III) and vanadium(V) and of iron(III) and chromium(VI) based on redox reactions[1]

N. Teshima, K. Ayukawa, T. Kawashima*

Laboratory of Analytical Chemistry, Department of Chemistry, University of Tsukuba, Tsukuba 305, Japan

Abstract

A flow injection analysis (FIA) method is presented for the simultaneous determinations of iron(III)–vanadium(V) and of iron(III)–chromium(VI) using a single spectrophotometric detector. In the presence of 1,10-phenanthroline (phen), iron(III) is easily reduced by vanadium(IV) to iron(II), followed by the formation of a red iron(II)–phen complex ($\lambda_{max} = 510$ nm), which shows a positive FIA peak at 510 nm corresponding to the concentration of iron(III). On the other hand, in the presence of diphosphate the reductions of vanadium(V) and/or chromium(VI) with iron(II) occur easily because the presence of diphosphate causes an increase in the reducing power of iron(II). In this case iron(II) is consumed during the reaction and a negative FIA peak at 510 nm corresponding to the concentration of vanadium(V) and/or chromium(VI) is obtained. The proposed method makes it possible to obtain both positive (for iron(III)) and negative (for vanadium(V) or chromium(VI)) FIA peaks with a single injection.

Keywords: Chromium; Flow injection; Iron; Redox reactions; Simultaneous determination; Vanadium

1. Introduction

Redox potentials of metal ions vary upon the addition of a suitable ligand [1]. This phenomenon has the potential capacity for the development of new redox systems which are applicable to potentiometric titration [2–9]. By

---

* Corresponding author. Fax: + 81 298 536503; E-mail: kawasima@staff.chem.tsukuba.ac.jp
[1] Presented at the 1995 International Chemical Congress of Pacific Basin Societies (PACIFICHEM '95) in the Symposium on Kinetic and Mechanistic Aspects of Analytical Chemistry, Honolulu, Hawaii, USA, December 17–22, 1995.

using the ligand effect, we have developed methods for the potentiometric titration of chromium(VI) and copper(II) with iron(II) in the presence of diphosphate and/or neocuproin [10], and for vanadium(V) with iron(II) in the presence of ligands such as citrate, diphosphate and EDTA [11]. We also showed that a redox reaction of iron(III) with vanadium(IV) proceeds completely in the presence of 1,10-phenanthroline (phen) [12]. By using these redox systems, new types of spectrophotometric flow injection analysis (FIA) methods have been developed for the determination of chromium(VI) [13] and the simultaneous

determination of vanadium(IV) and vanadium(V) [14]. The aim of the present study was to develop simultaneous photometric FIA determinations of iron(III)–vanadium(V) and of iron(III)–chromium(VI) based on new redox systems in which phen and diphosphate participate. The present method is simple: it is possible to observe both positive (for iron(III)) and negative (for vanadium(V) or chromium(VI)) FIA peaks with a single injection of the sample solution with a single detector.

2. Experimental

2.1. Reagents

All reagents were of analytical-reagent grade and were used without further purification. The water used to prepare the solutions was purified with a Milli-Q PLUS water system (Millipore).

A stock solution of iron(III) (0.1 M) was prepared by dissolving 4.82 g of iron(III) ammonium sulfate dodecahydrate in 100 ml of 0.5 M sulfuric acid and was standardized with EDTA. Stock solutions of vanadium(V) and iron(II) were prepared as described previously [11]. A stock solution of vanadium(IV) (5×10^{-2} M) was prepared by dissolving vanadium oxide sulfate (vanadyl sulfate) n-hydrate in 100 ml of 5×10^{-2} M sulfuric acid. The concentration of vanadium(IV) solution was determined by a standard potassium permanganate titration. A stock solution of chromium(VI) was prepared by dissolving appropriate amounts of potassium dichromate (a primary standard) in 5×10^{-2} M sulfuric acid. Working solutions of metal ions were prepared by suitable dilution with 5×10^{-3} M sulfuric acid. Ligand solutions (0.1 M) of phen and diphosphate were prepared as described previously [14].

2.2. Apparatus

A schematic flow diagram for the simultaneous determinations of iron(III) and vanadium(V) and of iron(III) and chromium(VI) is shown in Fig. 1. Two double-plunger micro pumps (Sanuki Kogyo, DMX-2000) and two six-way injection valves (Sanuki Kogyo, SVM-6M2) were used to assemble

the system. The flow lines were made from Teflon tubing (0.5 mm i.d.). The absorbance change was measured at 510 nm with a spectrophotometer (Soma Kogaku, S-3250) equipped with a 10-mm micro flow cell (8 μl) and recorded on a recorder (Chino, EB 22005). The pH of the waste solution was continuously monitored with a Corning Model 12 pH/mV meter.

2.3. Procedure

In the flow system (Fig. 1), a carrier solution of 5×10^{-3} M sulfuric acid (C), 0.1 M acetate buffer solution in reservoir R_1, a mixed solution of vanadium(IV) (5×10^{-5} M) and iron(II) (5×10^{-5} M) in reservoir R_2 and 1×10^{-3} M phen solution in reservoir R_3 were pumped at a flow rate of 1.0 ml min^{-1}. A 400 μl volume of sample solution (iron(III)–vanadium(V) or iron(III)–chromium(VI)) and 100 μl of a mixture of diphosphate and acetate buffer solution were loaded into SL and RL, respectively. The sample solution and the diphosphate solution were injected into the carrier of sulfuric acid and acetate buffer streams simultaneously: the former and the latter were passed through a 0.1 m long coil (C_1) and a 1.5 m long delay coil (C_2), respectively. By monitoring the absorbance of the iron(II)–phen complex at 510 nm, both a positive peak for iron(III) and a negative peak for vanadium(V) or chromium(VI) were obtained with a single injection of the sample solution. All measurements were carried out at room temperature.
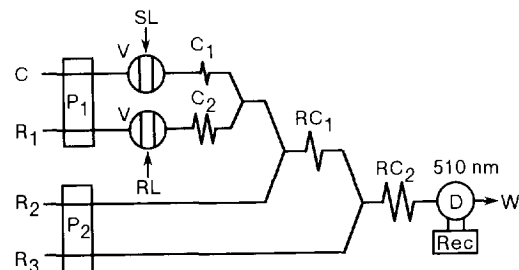

Fig. 1. Flow diagram of FIA for the simultaneous determination of iron(III) and vanadium(V) and of iron(III) and chromium(VI). P, pump; V, six-way injection valve; C_1, 0.1 m long coil; C_2, 1.5 m long delay coil; RC_1, reaction coil (0.2 m); RC_2, reaction coil (2 m); D, spectrophotometer (510 nm); Rec, recorder; W, waste. Other conditions as in the text.

3. Results and discussion

The conditional standard potential of the Fe(III)–Fe(II) system increases in the presence of phen because of the formation of the iron(II)–phen complex, i.e. log β_3 of the iron(II)–phen complex is higher than that of the iron(II)–phen complex [15]. Hence a redox reaction of iron(III) with vanadium(IV):

$$Fe^{3+} + VO^{2+} + H_2O \overset{K_{Fe-V}}{\rightleftharpoons} Fe^{2+}$$

$$+ VO_2^+ + 2H^- \tag{1}$$
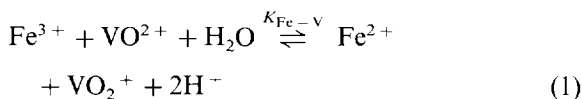
occurred completely in the presence of phen, producing the iron(II)–phen complex ($\lambda_{max} = 510$ nm), although the redox reaction would not take place without phen [12]. Iron(III) can thus be determined by measuring the absorbance of the iron(II)–phen complex which shows a positive FIA signal at 510 nm.

On the other hand, the presence of diphosphate causes a decrease in the potential of the Fe(III)–Fe(II) system. In other words, the reducing power of iron(II) increases owing to the presence of diphosphate. Thus, the reduction of vanadium(V) with iron(II):

$$Fe^{2+} + VO_2^+ + 2H^+ \overset{K_{V-Fe}}{\rightleftharpoons} Fe^{3+} + VO^{2+}$$

$$+ H_2O \tag{2}$$
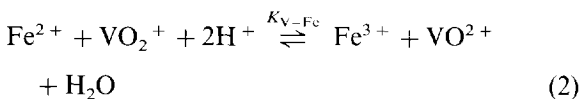
takes place easily [11]. The reduction of chromium(VI) to chromium(III) with iron(II):

$$6Fe^{2+} + Cr_2O_7^{2-} + 14H^+ \overset{K_{Cr-Fe}}{\rightleftharpoons} 6Fe^{3+} + 2Cr^{3+}$$

$$+ 7H_2O \tag{3}$$
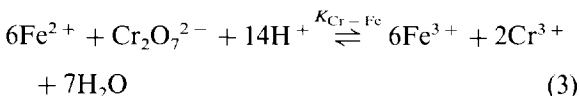
also occurred completely in the presence of diphosphate [10]. In these reduction reactions, the absorbance at 510 nm of the iron(II)–phen complex produced in the reaction coil RC_2 (Fig. 1) decreases with increase in the concentration of vanadium(V) and/or chromium(VI) because of the consumption of iron(II) with vanadium(V) and/or chromium(VI). Hence the determination of vanadium(V) and/or chromium(VI) is possible from the decrease in the absorbance of the complex at 510 nm.

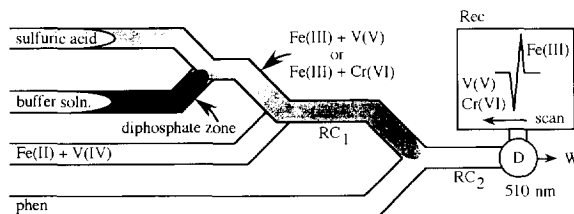In the FIA system shown in Fig. 1, the baseline absorbance is kept constant (about 0.14) as a

Fig. 2. Successive merging profile of the sample solution with reagent solutions.

result of the formation of the iron(II)–phen complex in RC_2 (2 m long). Fig. 2 shows a successive merging profile of the sample solution with reagent solutions. The phen stream merges into the front of a mixed sample zone and the reduction of iron(III) with vanadium(IV) proceeds in RC_2; a positive FIA peak for iron(III) appears. The diphosphate zone which passed through the delay coil (1.5 m long) merges into the rear of the sample zone, and the reduction of vanadium(V) and/or chromium(VI) with iron(II) proceeds in RC_1; the appearance of a negative FIA peak for vanadium(V) and/or chromium(VI) follows after the positive peak. By monitoring the absorbance of the iron(II)–phen complex at 510 nm, both positive (for iron(III)) and negative (for vanadium(V) or chromium(VI)) FIA peaks are thus obtained with a single injection of the sample solution.

3.1. Effect of variables

The optimum conditions for the simultaneous determination of iron(III) and vanadium(V) were studied by injecting an aliquot (400 μl) of a mixed sample solution of iron(III) and vanadium(V) (both the iron(III) and vanadium(V) concentrations were 2×10^{-5} M) into the FIA system shown in Fig. 1. Similarly, to establish the optimum conditions for the simultaneous determination of iron(III) and chromium(VI), an aliquot (400 μl) of a mixed sample solution of iron(III) and chromium(VI) (both the iron(III) and vanadium(V) concentrations were 2×10^{-5} M) was injected into the system. The concentrations of iron(II) (5×10^{-5} M) and vanadium(IV) (5×10^{-5} M) in R_2 were selected for the procedure based on the previous results [14].

The effect of pH on the peak height was examined over the range 3.4–5.5 and the results are shown in Fig. 3. In the simultaneous determination of iron(III)–vanadium(V) (Fig. 3(a)), the positive peak height for iron(III) was maximum and constant in the pH range 4.8–5.5, whereas the negative peak for vanadium(V) gradually decreased with increase in the pH of the solution up to 4.8, being kept constant in the pH range 4.8–5.5. A pH of around 5 was selected for the procedure because the heights of the positive and negative peaks were almost same at this pH. In the case of iron(III)–chromium(VI) (Fig. 3(b)), the positive peak height was maximum and constant in the pH range 4.2–5.5, while the magnitude of the negative peak for chromium(VI) was about three times larger than that of the positive peak for iron(III) at pH around 5. The result is attributable to the number of electrons that took part in the oxidation of iron(II) with chromium(VI). A pH of around 5 was also selected for the procedure.

The effect of the phen concentration was examined over the range 1×10^{-4}–1×10^{-2} M at a constant concentration of diphosphate (2×10^{-3} M). As shown in Fig. 4(a), both the positive and negative peaks for iron(III) and vanadium(V) rapidly increased with increasing phen concentration, and were almost constant at phen concentrations higher than 3×10^{-4} M. Similarly, in the case of iron(III)–chromium(VI) (Fig. 4(b)), both the peaks for iron(III) and chromium(VI) were
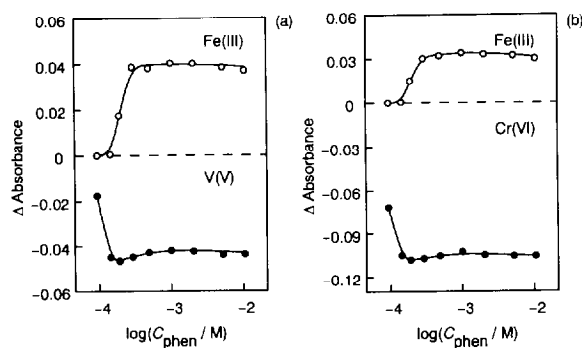

Fig. 4. Effect of phen concentration on the FIA peak heights for (a) iron(III) and vanadium(V) and (b) iron(III) and chromium(VI). The broken line denotes the baseline. Other conditions as in the text.

almost constant at phen concentrations higher than 3×10^{-4} M. The concentration of phen was selected as 1×10^{-3} M.

The effect of the diphosphate concentration loaded into RL was examined over the range 1×10^{-4}–1×10^{-2} M at a constant concentration of phen (1×10^{-3} M). In the case of iron(III)–vanadium(V), the positive peak height for iron(III) was maximum and constant over the concentration range examined, whereas the negative peak for vanadium(V) rapidly increased with increase in the diphosphate concentration, as shown in Fig. 5(a). In the case of iron(III)–chromium(VI) (Fig. 5(b)), the peak height for iron(III) was also independent of the diphosphate concentration, whereas the negative peak for
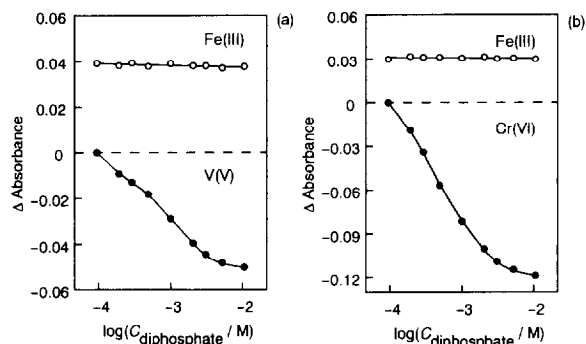

Fig. 3. Effect of pH on the FIA peak heights for (a) iron(III) and vanadium(V) and (b) iron(III) and chromium(VI). The broken line denotes the baseline. Other conditions as in the text.

Fig. 5. Effect of diphosphate concentration on the FIA peak heights for (a) iron(III) and vanadium(V) and (b) iron(III) and chromium(VI). The broken line denotes the baseline. Other conditions as in the text.

chromium(VI) rapidly increased with increase in the diphosphate concentration because the oxidation of iron(II) with chromium(VI) should be favored in the presence of diphosphate. A 2×10^{-3} M diphosphate concentration was selected.

The effect of RC_1 length was examined by varying the coil length. Almost constant peak heights for iron(III) and vanadium(V) were obtained over RC_1 lengths of 0.1–5 m. The negative peak for chromium(VI) increased with increase in the coil length of RC_1 up to 1 m because the oxidation of iron(II) with chromium(VI) should be favored with an increase in the coil length of RC_1. A 0.2 m length of RC_1 was used, taking into account the sample throughput.

The effect of RC_2 length was examined over the range 0.5–5 m. The positive peak for iron(III) gradually increased with increase in the RC_2 length up to 2 m, and remained constant at RC_2 lengths of 2–5 m, while the negative peak for vanadium(V) gradually decreased with increase in the RC_2 length. In the case of iron(III)–chromium(VI), both the positive and negative peaks for iron(III) and chromium(VI) exhibited curves similar to those for iron(III)–vanadium(V). A 2 m length of RC_2 was selected for the procedure because at least a 2 m length was needed to obtain a stable baseline.

3.2. Calibration graphs and simultaneous analysis of synthetic mixtures

Calibration graphs for iron(III), vanadium(V) and chromium(VI) were individually prepared; each sample solution was injected together with diphosphate solution into the flow system. The calibration graphs for iron(III) and vanadium(V) were linear over the range 1×10^{-6}–2×10^{-5} M, whereas the graph for chromium(VI) was slightly curved over the range 1×10^{-6}–2×10^{-5} M. The reproducibility of the method was satisfactory with relative standard deviations of 0.54, 0.82 and 0.47% for 10 determinations of 2×10^{-5} M iron(III), vanadium(V) and chromium(VI), respectively. The proposed method permits the analysis of 30 samples h^{-1} (60 peaks h^{-1}).

The simultaneous determinations of iron(III)–vanadium(V) and of iron(III)–chromium(VI)

Table 1
Simultaneous determination of iron(III) and vanadium(V) and of iron(III) and chromium(VI) in synthetic mixtures

Composite sample taken (10^{-6} M)		Found[a] (10^{-6} M)	
Fe(III)	V(V)	Fe(III)	V(V)
5.0	10.0	5.1	9.7
5.0	20.0	5.1	19.6
10.0	10.0	10.2	9.4
10.0	20.0	10.3	19.2
Fe(III)	Cr(VI)	Fe(III)	Cr(VI)
5.0	5.0	4.6	4.7
10.0	5.0	9.8	4.6
10.0	3.0	10.0	2.7
15.0	7.5	14.0	7.1

[a]Average values ($n = 3$).

were carried out on synthetic mixtures by using each calibration graph and the results are summarized in Table 1. Typical flow signals when equimolar mixed sample solutions of both ions were injected into the FIA system are shown in Fig. 6. The recovery and reproducibility of the method were satisfactory.

4. Conclusions

A simple and rapid flow injection procedure is proposed for the simultaneous determinations of iron(III) and vanadium(V) and of iron(III) and chromium(VI) by using the effect of ligands on the redox potential of the Fe(III)–Fe(II) system with a single spectrophotometric detector. The method can be successfully applied to the determination of iron(III)–vanadium(V) and iron(III)–chromium(VI) in synthetic mixtures.
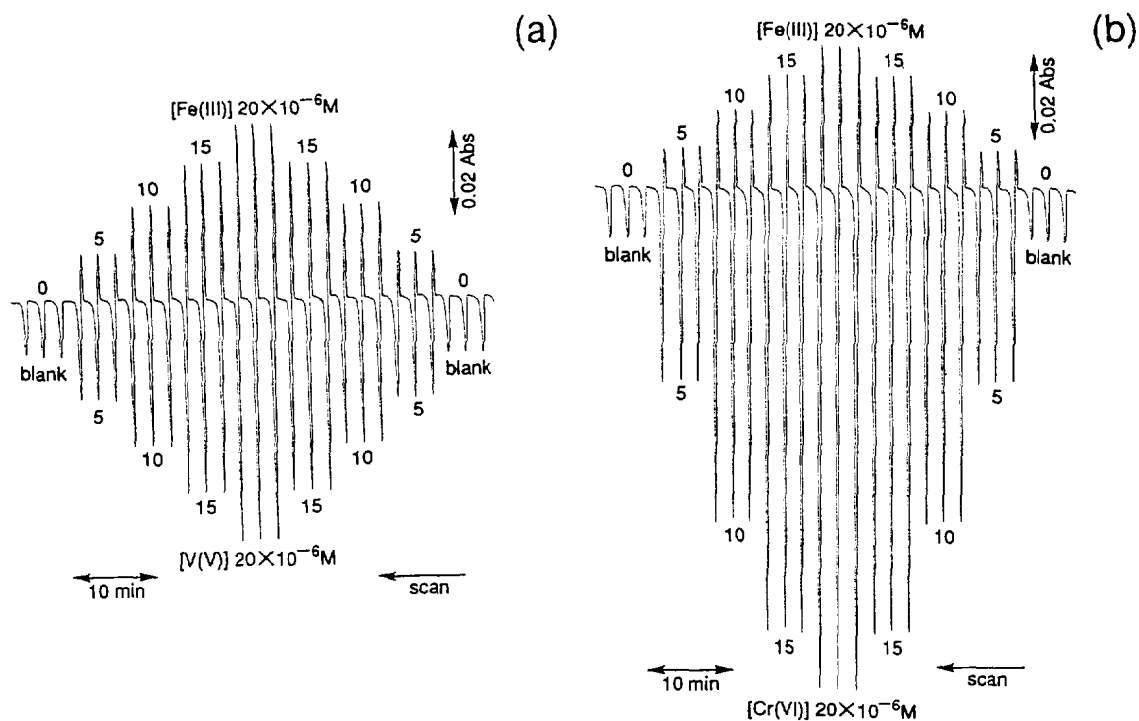
Fig. 6. Typical flow signals for (a) iron(III) and vanadium(V) and (b) iron(III) and chromium(VI). Conditions as in the text.

References

[1] E.P. Serjeant, Potentiometry and Potentiometric Titrations, Wiley, New York, 1984.

[2] R. Belcher and T.S. West, Anal. Chim. Acta, 5 (1951) 364.

[3] F. Vydra and R. Pribil, Talanta, 3 (1959) 103.

[4] F. Vydra and R. Pribil, Talanta, 5 (1960) 44.

[5] G.G. Rao and S.R. Sagi, Talanta, 9 (1962) 715.

[6] M. Tanaka and A. Ishida, Anal. Chim. Acta, 36 (1966) 515.

[7] N.K. Murthy and Y.P. Rao, Anal. Chim. Acta, 73 (1974) 413.

[8] N.K. Murthy and Y.P. Rao, Indian J. Chem., 14A (1976) 721.

[9] Y.P. Rao, G.V. Prasad and N.K. Murthy, Analyst, 112 (1987) 1777.

[10] H. Itabashi, K. Umetsu, K. Satoh and T. Kawashima, Anal. Sci., 6 (1990) 721.

[11] K. Umetsu, H. Itabashi, K. Satoh and T. Kawashima, Anal. Sci., 7 (1991) 115.

[12] N. Teshima, H. Itabashi and T. Kawashima, Chem. Lett., 1992 (1992) 2227.

[13] H. Itabashi, N. Teshima and T. Kawashima, Anal. Sci., 11 (1995) 693.

[14] N. Teshima, H. Itabashi and T. Kawashima, Anal. Sci., 10 (1994) 207.

[15] T.S. Lee, I.M. Kolthoff and D.L Leussing, J. Am. Chem. Soc., 70 (1948) 2348.

Chemiluminometric method for the determination of glycerol in wine by flow-injection analysis with co-immobilized glycerol dehydrogenase/NADH oxidase

Nobutoshi Kiba*, Naoki Azuma, Motohisa Furusawa

Department of Applied Chemistry and Biotechnology, Faculty of Engineering, Yamanashi University, Kofu 400, Japan

Abstract

A flow-injection method for the determination of glycerol in wine is described. Glycerol dehydrogenase and NADH oxidase were co-immobilized on poly (vinyl alcohol) beads and incorporated in a flow-injection system. The hydrogen peroxide produced was detected chemiluminometrically via a luminol–hexacyanoferrate (III) reaction. Wine was diluted 1000-fold with water and sample solution (50 μl) was injected into the carrier stream. The calibration graph was linear in the range 3×10^{-7}–3×10^{-4} M; the detection limit was 7×10^{-8} M and the sample throughout was 30 h^{-1} without carryover.

Keywords: Chemiluminescence; Enzyme reactor; Flow injection; Glycerol; Wine

1. Introduction

Glycerol, which is a by-product of alcohol fermentation, affects the sensory characteristics of wine, especially richness of taste.

Enzymatic flow-injection (FI) methods for specific determination of glycerol in wine have been developed using immobilized glycerol dehydrogenase (EC 1.1.1.6, GDH) [1,2]. In this system a basic buffer (pH 10.0) and a high concentration of NAD^+ (10 mM) were used to shift the reaction equilibrium towards dihydroxyacetone production, since the reaction is reversible and the equilibrium consant [3] of the reaction [Glycerol

$+ NAD^+ \rightleftharpoons$ dihydroxyacetone $+ NADH + H^+$] is 5×10^{-12}. Co-immobilized GDH/NADH oxidase reactor, which was prepared by covalently bonding to CNBr-activated Sepharose 4B, was used in a FI system for the determination of glycerol in wine with a Clark-type oxygen electrode [4]. In this system, a lower pH (9.2) and a lower concentration of NAD^+ (5 mM) were used because NADH oxidase (NAOD), which catalyzes the reaction in which NADH is oxidized by molecular oxygen to form hydrogen peroxide [$NADH + O_2 + H^+ \rightleftharpoons NAD^+ + H_2O_2$], serves as a trapping enzyme. In spite of much experimental effort, the method is not very sensitive; the lower limit of detection was 100 μM.

A chemiluminometric FI method has been proposed in which GDH and NAOD are separately

immobilized on controlled pore glass (CPG) and used in series under conditions of pH 9.0 and 5 mM NAD^+; the method is moderately sensitive, with a detection limit of 25 μM [5]. However, the method is unsuitable for use in routine analysis because CPG, used as a support for the enzymes, is unstable in alkaline solution [6]. An FI system [7] with co-immobilized glycerol kinase and glycerol-3'-phosphate oxidase and the chemiluminometric detection of H_2O_2 with luminol has been reported which provides a lower sensitivity than the amperometric FI methods with an immobilized GDH reactor [1,2]; the lower limit of detection was 138 μM.

FI methods with an immobilized enzyme reactor are subject to interference from polyphenols and dyes in wines because the compounds are adsorbed by the reactor and the accumulation of the compounds causes the inactivation of the enzyme [8,9]. Sensitive detections system permit the use of the method without the need for tedious sample pretreatment, except for dilution. This paper describes a chemiluminometric FI system for the sensitive determination of glycerol in wine with a co-immobilized GDH/NAOD reactor. A simple chemiluminometric FI system for the determination of glycerol can be achieved by coupling a co-immobilized GDH/NAOD reactor with a luminol chemiluminescence assay for the detection for H_2O_2, since the chemiluminometric reaction was carried out in media buffered at pH 10–11 [10,11]. In the present system, the enzymatic reactions and the chemiluminometic reaction were performed in the same buffered solution (0.1 M carbonate buffer pH 10.0). GDH and NAOD were co-immobilized on poly (vinyl alocohol) beads. GDH from Cellulomonas sp. [5] was used in this work and is much more stable than enzymes from Entrobacter aerogenes [1,2,4]. This method was applied to the determination of glycerol in wines without any pretreatment procedure, except for dilution.

2. Experimental

2.1. Reagents

GDH (from Cellulomonas sp., 56 U mg^{-1}) and

NAOD (EC number not assigned, from Bacillus stearothermophilus, 55 U mg^{-1}) [12] were obtained from Toyobo (Osaka, Japan) and Asahi Kasei (Tokyo, Japan) respectively. The activity for each enzyme was measured spectrophotometrically at 340 mm with glycerol or NADH as substrate at pH 10.0 at 38°C.

NAD^+ (free acid, 95%) and NADH (disodium salt, 99.5%) were purchases from Kohjin (Tokyo, Japan) and Boehringer Mannheim respectively. Glycerol was purchased from Sigma (St. Louis, MO). Poly (vinyl alcohol) beads (GS-520, 13 μm) were obtained from Showa Denko (Tokyo, Japan). All other chemicals, which were from Wako Pure Chemical (Tokyo, Japan), were of analytical-reagent grade.

A stock solution (1 mM) of glycerol was prepared by dissolving in water. Standards were prepared by diluting the stock solution with 5 mM ethanol solution. A potassium hexacyanoferrate (III) stock solution (200 mM) was prepared and diluted tenfold with water before use. Luminol solution (1.2 mM luminol in carbonate buffer (pH 10.0 comprising 0.3 M potassium carbonate/0.3 M potassium hydrogen carbonate) was prepared and allowed to stand for 2 days at room temperature to attain stability before use [11,13]. NAD^+ solution (1.5 mM NAD^+ in 0.01 M phosphate buffer (pH 7.0) was prepared daily.

2.2. Enzyme immobilization

The beads (2.0 g) were suspended in 30 ml of 30% chloromethyloxirane in 3 M NaOH. The suspension was incubated at 50°C for 1.5 h with shaking. The beads were allowed to react with concentrated aqueous ammonia (30 ml) at 40°C for 3 h. The attached amine amounted to 3.0 meq g^{-1} of dry beads. The aminated beads were packed into a stainless-steel column (4 cm × 4 mm i.d.) by the slurry-packing method. Glutaraldehyde (2% w/v) in 0.05 M phosphate buffer pH 7.0 was pumped through the column for 40 min at 0.2 ml min^{-1} and then the column was washed with deaerated water for 15 min at 0.6 ml min^{-1}. Enzyme solution (5 mg GDH (280 U) and 5 mg NAOD (275 U) in 10 ml of 0.1 M phosphate buffer pH 7.0) was circulated through the column

at 0.2 ml min⁻¹ for 6 h at 10°C. The time course
of the immobilization process for NAOD was
monitored by a spectrophotometer (Jasco Uvidec-
100-VI) with a flowthrough cell at 380 nm. The
immobilization yield was evaluated by the de-
crease in absorbance. NAOD was immobilized
with a 88% yield. The reactor was washed with
the NAD solution and stored in a refrigerator
when not in use.

For the purpose of comparison, an immobilized
GDH reactor was prepared in the same manner
by using an enzyme solution without NAOD.

2.3. Flow system and procedure

Fig. 1 shows a block diagram of the FI system
used in this work. The system consisted of four
piston pumps (Hitachi L-6000), an injector valve
(Sanuki SVI-6M2) equipped with a 50 μl loop, a
reactor, a water bath, a luminometer (Soma S-
3400) with a flowthrough cell (100 μl) connected
to a signal cleaner (SIC SC77) and a recorder
(TOA FBR-251A).

Wine was diluted 1000-fold with water and an

Fig. 2. FI manifold for the enzyme activity measurements: (A)
NAD⁺ solution (0.2 ml min⁻¹); (B) carbonate buffer (0.2 ml
min⁻¹); (C) 20 mM potassium hexacyanoferrate solution (0.2
ml min⁻¹); (D) 1.5 mM luminol (0.2 ml min⁻¹) in 0.3 M
carbonate buffer pH 10.0 (0.2 ml min⁻¹); (P1–P4) pumps; (S)
injector with a 50 μl loop; (E) immobilized enzyme reactor;
(WB) water bath; (V) three-way valve; (F) spectrofluorimeter
with a flowthrough cell; (M) mixing coil; (G) luminometer
with flowthrough cell; (SC) signal cleaner; (R) recorder; (W)
waste.

Fig. 1. Schematic diagram of chemiluminometric FI system
for the determination of glycerol with a co-immobilized glyc-
erol dehydrogenase/NADH oxidase reactor: (A) H₂O (0.2 ml
min⁻¹); (B) 1.5 mM NAD⁺ in 10 mM phosphate buffer pH
7.0 (0.2 ml min⁻¹); (C) 1.5 mM luminol in 0.3 M carbonate
buffer pH 10.0 (0.2 ml min⁻¹); (D) 20 mM potassium hexa-
cyanoferrate solution (0.2 ml min⁻¹); (P₁–P₄) pumps; (S)
injector with a 50 μl loop; (E) co-immobilized enzyme reactor
(4 cm × 4 mm i.d.); (WB) water bath thermostated at 30°C;
(M) mixing coil (60 cm × 0.5 mm i.d.); (G) luminometer with
a flowthrough cell (100 μl); (SC) signal cleaner; (R) recorder;
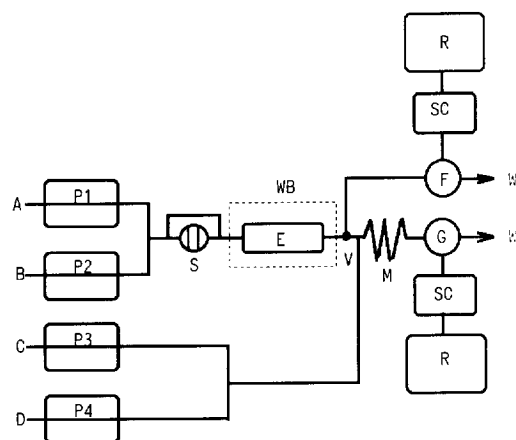(W) waste. All connecting tubing (0.5 mm i.d.) was made of
Teflon.

aliquot (50 μl) was injected into a carrier stream.
The results obtained by the present method were
compared with those obtained by use of an F-kit
(Boehringer Mannheim) with soluble enzymes,
glycerokinase (GK), pyruvate kinase (PK) and
lactate dehydrogenase (LDH), and co-factors,
ATP and NADH.

3. Results and discussion

3.1. Reactor performance

To establish the optimum conditions for the
co-immobilized GDH/NAOD reactor, the system
shown in Fig. 2 using a luminometer was used
and measurements were made to study the influ-
ence of pH, temperature and the NAD⁺ concen-
tration.

The effect of pH on the peak height was studied
in the range 9.0–11.0 using 0.2 M K₂CO₃/

KHCO$_3$ carbonate bufferes by injecting 100 μM glycerol (50 μl). The optimum pH for the enzymatic reactions was about 10.0. The peak height was not affected when the concentration of carbonate buffer (pH 10.0) was varied in the range 0.2–0.3 M; 0.3 M carbonate buffer was used in this system (Fig. 1). The effect of temperature on the peak height was examined in the range 30–45°C. The maximum peak height was obtained at 35°C. The reactor was kept at 30°C to prolong its lifetime. The effect of NAD$^+$ conentration on peak height was investigated in the range 0.1–5 mM by injecting 100 μM glycerol (Fig. 3). The maximum peak height was obtained between 1 and 3 mM NAD$^+$; the NAD$^+$ concentration in the reactor is between 0.5 mM and 1.5 mM. For GDH reaction at lower NAD$^+$ concentrations the equilibrium of the reaction is shifted to the left, but for NAOD reaction higher NAD$^+$ concentrations are undesirable for the production of H$_2$O$_2$. A 1.5 mM NAD$^+$ solution was used in this system; as shown in Fig. 1, as the solution was diluted three-fold with the luminol solution and

carrier stream, the concentration in the reactor is 0.5 mM. The result was compared with that of an immobilized GDH reactor. The dependence on NAD$^+$ concentration in an immobilized GDH reactor was studied in the range 0.1–5 mM using the system shown in Fig. 2 with a spectorfluorimeter (Jasco FP-210, with flowthrough cell (15 μl), $\lambda_{ex} = 340$ nm, $\lambda_{em} = 465$ nm) instead of the luminometer, by rotating the rotor of the three-way valve. The variation of peak height with the NAD$^+$ concentration is depected in Fig. 3; for NAD$^+$ below 4 mM, there was dependence of the concentration on the peak height. The results show that NAOD functions as a trapping enzyme in the co-immobilized GDH/NAOD reactor.

The influence of luminol concentration on the peak height was studied from 0.3 mM to 6 mM, using the system shown in Fig. 1. The peak height increased with an increase in the concentration. However, the inactivation of the reactor commenced at concentrations > 1.5 mM. As a compromise between sensitivity (peak height) and stability, a luminol solution of 1.2 mM was used; the luminol concentration in the reactor is 0.4 mM.

Under the conditions shown in Fig. 1, standard glycerol solution (100 μM) was injected into the system and the peak height was compared with the peak height for hydrogen peroxide. The conversion efficiency was 68%. The relative activities for glycerol (50 μM), 1, 2-propanediol (50 μM), 1, 2-butanediol (50 μM), 1, 2-ethanediol (50 μM) and ethanol (1 mM and 5 mM) were 100, 28, 20, 3, 4 and 5 respectively.

The operational stability of the reactor was evaluated over a period of 4 weeks. The reactor was used for 3 h per day (90 injections of 100 μM glycerol solution containing 3 mM ethanol) and then washed with the NAD$^+$ solution and stored in a refrigerator when not in use. The activity decreased slowly to 83% of the initial value after 4 weeks (2500 injections).

The influence of sulfite on the peak height for glycerol (50 μM) was measured in the range 5–50 μM. The presence of equimolar amounts of sodium sulfite depressed the peak height to 85% and the peak height was not influenced by the presence of < 15 μM sulfite; since normally the
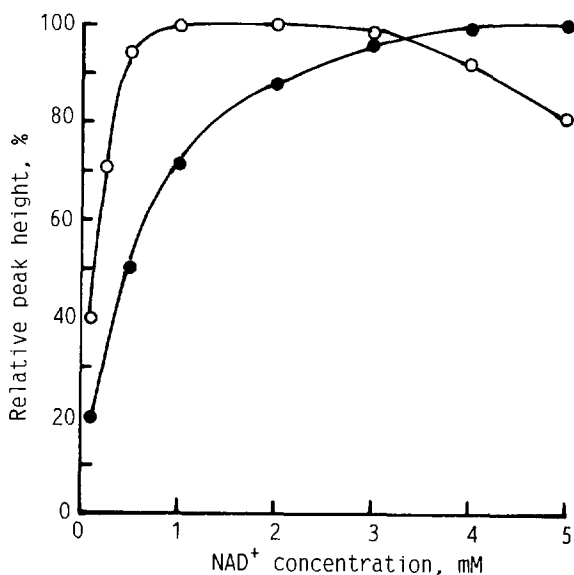

Fig. 3. Effect of NAD$^+$ concentration on the peak height: (○) = chemiluminescence detection, the peak height for 1 mM NAD$^+$ solution was taken as 100; (●) = fluoresence detection, the peak height for 5 mM NAD$^+$ solution was taken as 100. The results were obtained by using the system shown in Fig. 2.

concentration of glycerol in wine is not less than 10 times that of total sulfite [14], this method is not subject to interferenes from sulfites in wine. Under the same conditions, the peak height did not change with the presence of carbonates such as tartrate, citrate, lactate, succinate and acetate up to 1 mM.

The peak height was measured by changing the flow rates of the NAD^+ solution, the luminol solution and the carrier stream under the conditions shown in Fig. 1, keeping the flow rate ratio of the solutions at 1.0. The peak height decreased linearly on altering the total flow rate from 0.3 to 0.9 ml min^{-1}. Glycerol reacted in 92 and 44% yields at flow rates of 0.3 and 0.9 ml min^{-1}, respectively, and the half-peak width for the former was about twice that of the latter. A total flow rate of 0.6 ml min^{-1} (0.2 ml min^{-1} each) was selected, as a compromise between sensitivity (peak height) and sample throughout; at this flow rate the sample throughput was 30 h^{-1}.

3.2. Calibration

The plot of peak height against glycerol concentration was linear from 0.3–300 μM. Each standard solution contained 5 mM ethanol because in this reactor 1–5 mM ethanol concentrations were oxidized at a 5% relative activity of glycerol and normally wine contains 1.5–3 M (7–14%) ethanol; in this method wine was diluted 1000-fold with water. The least-squares calibration equation for glycerol was $Y = 0.9524X + 7.076$, where Y is log(peak height (cm)) and X is log(glycerol concentration (M)), with a linear correlation coefficient of $r = 0.9998$ (15 data points). The relative standard deviation (RSD) for seven replicate injections of 50 μM glycerol was 0.51%. The RSD ($n = 7$) for 50 μM glycerol in the system shown in Fig. 2 was 1.3% because of incomplete mixing of the luminol solution with the reactor eluent. The lower limit of detection (signal-to-noise ratio = 3) was 7×10^{-8} M.

3.3. Application

This system was used to determine the amount of glycerol in wine.

3.3.1. Precision and reproducibility

Red wine was repeatedly analyzed over a period of 3 weeks. The reactor was used for analyses of 90 samples per day and standards were measured at 30-sample intervals, in order to check the variation of the conversion efficiency. Since the conversion efficiency decreased linearly to 81% of the initial value after 3 weeks (1990 injections) because of the accumulation of polyphenols and dyes, the reactor was renewed every 10 days. This method gave precise and reproducible results; for red wine containing 73.4 mM glycerol (6.75 g 1^{-1}), the intra-day RSD was 0.67% and the outer-day RSD was 0.98%.

3.4. Comparison

The results ($n = 25$:13 red wines, 57.6–91.8 mM; 12 white wines, 45.8–57.3 mM) were compared with those obtained by use of an F-kit with soluble GK, PK and LDH. The calculated linear regression equation was $Y = 0.9997X + 1.126$ with a correlation coefficient of $r = 0.9988$ respectively. The present method gave slightly bigger values, because GDH oxidizes the diols present in wine.

4. Conclusion

The FI system with a co-immobilized GDH/ NAOD reactor and chemiluminescence detection is useful for the sensitive measurement of glycerol in wine without the need for any pretreatment procedure, except for dilution. Compared with the chemiluminometric FI method utilizing immobilized GDH and NAOD reactors [5] in series, the NAD^+ concentration is about three times lower and the sensitivity is 250 times higher. The co-immobilized GDH/NAOD reactor is stable enough to permit the measurment of more than 900 samples.

References

[1] K. Matsumoto, H. Matsubara, M. Hamada, T. Doi and Y. Osajima, Agric. Biol. Chem., 55 (1991) 1055.

[2] K. Matsumoto, H. Matsubara, M. Hamada and Y. Osajima, Nippon Shokuhin Kogyo Gakkai-Shi, 38 (1991) 699.

[3] R.M. Burton, in S.P. Colowick and N.O. Kaplan (Eds), Methods in Enzymology, Vol. 1, Academic Press, New York, 1955, p. 397.

[4] H. Ukeda, Y. Fujita, M. Sawamura and H. Kusunose, Anal. Sci., 10 (1994) 445.

[5] S. Kondruweit, B.A.A. Dremel and R.D. Schmid, Anal. Lett., 27 (1994) 1489.

[6] E.P. Plueddemann, Silica Coupling Agents, Plenum, New York, 1982, p. 227.

[7] R. Puchades, L. Lemieux and R.E. Simard, J. Food Sci., 56 (1991) 1097.

[8] N. Kiba, M. Oguchi and M. Furusawa, Talanta, 40 (1993) 1163.

[9] N. Kiba, J. Inagaki and M. Furusawa, Talanta, 42 (1996) 1751–1755.

[10] S.W. Lewis, D. Price and P.J. Worsfold, J. Biolumin. Chemilumin., 8 (1993) 183.

[11] M. Tabata, C. Fukunaga, M. Ohyabu and T. Murachi, J. Appl. Biochem., 6 (1994) 251.

[12] Y. Saeki, M. Nozaki and K. Matsumoto, J. Biochem., 98 (1985) 1433.

[13] Z.-H. Lan and H.A. Mottola, Anal. Chim. Acta, 293 (1994) 139.

[14] L.F. Burroughs and A.H. Sparks, J. Sci. Food Agric., 24 (1973) 187.

Adsorption–desorption and leaching of phenylurea herbicides on soils

Christine M. Fouqué-Brouard, Josette M. Fournier*

Centre Régional d'Etude des Produits Agropharmaceutiques (CREPA), 8 rue Becquerel, 49070 Beaucouzé, France

Abstract

Adsorption–desorption equilibria of phenylurea herbicides (chlortoluron, isoproturon, metobromuron, chloroxuron, difenoxuron) were determined in two different soils. Organic carbon content of the soils ranged from 1.1–5.6% and the clay fraction from 25–30%. Spiked aqueous suspensions of soils were centrifuged and urea derivative concentrations in the aqueous phase were determined using a HPLC–UV system. Adsorption isotherms conformed to the Freundlich equation. Freundlich K_f values indicated that organic carbon was the main factor affecting urea sorption in the studied soils. The R_f values calculated from the soil column displacement closely correlated with the adsorption K_f values. Results indicated that chloroxuron and difenoxuron were sorbed to a larger extent than the other three ureas on the two soils; as expected their mobilities through soil columns were very limited. The similarity between the molecular structures of chloroxuron and difenoxuron enables us to assume the phenoxy group to be the main structural feature in the adsorption phenomenon. The relationships between sorption, leaching and some characteristics of urea molecules such as water solubility and octanol–water partition coefficient were also examined.

Keywords: HPLC; Leaching; Phenylurea herbicides; Soil; Sorption

1. Introduction

Extensive information is required concerning the persistence and leaching of organic herbicide compounds which come into contact with soil. This is important for agronomic and environmental reasons. Persistence and leaching determine the possible contamination of groundwater. The behavior of pesticide residues in soils mainly depends on the amount of water moving through

the soil and to the extent to which pesticides are retained in soils, which in turn depends on the sorption properties of the soil. Soils are multicomponent mixtures [1,2]. Sorption of pesticides in soil systems has been extensively studied, but desorption is not yet fully understood [3–5]. Organic pesticides adsorb on both organic and inorganic surfaces depending on the chemical properties of the adsorbents and adsorbates involved [6]. Adsorption results in the binding of molecules in thin layers on the surface of solids and the binding forces vary from weak (van der Waals interac-

* Corresponding author.

Table 1
Physical and chemical characteristics of soils

Soil	% Clay	% Fine silt	% Coarse silt	% Fine sand	% Coarse sand	pH (water)	% OC
Grignon	24.9	21.5	47.2	5.4	1.0	7.7	1.1
Becon	30.1	28.0	12.1	8.7	21.1	5.8	5.6

tions) to very strong (specific adsorption of ions). Several investigators have shown that herbicidal efficiency and performance are related to the organic carbon content of soils [7,8]. Correlations between adsorption and soil organic carbon content are common [3,9]. Soil organic carbon is considered to be the most important adsorbing material for un-ionized pesticides.

The purpose of this analytical study was to obtain information on which structural groups of phenylurea are concerned in adsorption–desorption phenomena of two soils with different organic matter contents. After reaction of the soil with a solution of urea derivative of known composition at fixed temperature and pressure for a prescribed period of time, chemical analysis of the soil solution was performed to determine its urea composition using a HPLC-UV system. Ureas may be persistent herbicides and are frequently used in crop production.

Batch tests and soil column displacement studies were performed. The chosen ureas were isoproturon (N'-(4-isopropylphenyl)-N,N-dimethylurea), chlortoluron (N'-(3-chloro-4-methylphenyl)-N,N-dimethylurea), metobromuron (N'-(4-bromophenyl)-N-methoxy-N-methylurea), chloroxuron (N'-[4-(4-chlorophenoxy)phenyl]-N,N-dimethylurea), and difenoxuron (N'-[4-(4-methoxyphenoxy)phenyl]-N,N-dimethylurea). The adsorption–desorption processes determine the bioavailability and potential leaching of the ureas. A common parameter for modelling the transport of organic pesticides in soil is the adsorption coefficient K_{oc}, which is a measure of the partition of the chemical between the soil organic matter and the water phase. Adsorption of non-polar pesticides is mainly attributed to hydrophobic bonding. The octanol–water partition coefficient K_{ow} is widely used to predict the

behavior of organic pesticides in the environment [10–12].

2. Experimental

2.1. Herbicides and soils

Two soils (from Grignon (Yvelines, France) and Becon (Maine et Loire, France)) were chosen to provide different organic matter contents. Classical physical and chemical characteristics of these soils are given in Table 1 (data from Laboratory of Soils Analysis, Ancenis, Loire-Atlantique, France). The soils were air-dried and sieved through a 2 mm screen. They contained 3% and 10% w/w moisture respectively.

The herbicides were metobromuron, isoproturon, chlortoluron, chloroxuron and difenoxuron (Fig. 1). All herbicides had 97–100% purity (Dr. Ehrenstorfer, GmbH). Their water solubilities were 1300, 350, 330, 13 and 70 μmol l^{-} respectively [13,14]. The octanol–water partition coefficients (log K_{ow}) for metobromuron, isoproturon, chlortoluron and chloroxuron were 2.41, 2.25, 2.29 and 3.20 respectively [13]. In the case of difenoxuron, the octanol–water partition coeffi-
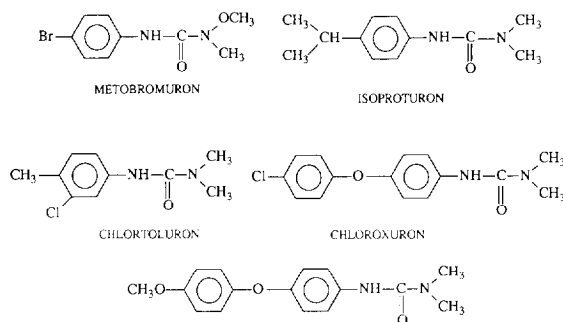

Fig. 1. Molecular structures of ureas.

Table 2
Retention times and wavelengths of maximum absorbance of the five urea derivatives

Derivative	Retention time (min)	λ (nm)
Metobromuron	13.10	244.2
Isoproturon	13.64	241.6
Chlortoluron	12.36	242.4
Chloroxuron	33.65	245.5
Difenoxuron	14.95	246.8

cient is calculated from the retention time obtained with reversed-phase HPLC [15].

2.2. Materials and methods

2.2.1. Materials

Methanol was HPLC-grade obtained from S.D.S. (Peypin, France). Water for HPLC was purified with a Seral System (Grosseron, St. Herblain, France).

2.2.2. Liquid Chromatograph System

HPLC analysis was performed with a Waters 600 liquid chromatograph equipped with a photodiode array detector (Waters 991) and an integrating system (NEC Powermate SX Plus and Waters 5200 Printer Plotter). The analysis were performed on a 25 cm × 4.6 mm i.d. Lichrospher RP-18 column and on a 1.4 cm × 4.6 mm i.d. Lichrosorb RP-18 pre-column. The injected volume was 25 μl (syringe, Model U6K, Hamilton), the flow rate was 1 ml min^{-1} and the eluent was a mixture of deionized water and methanol (40:60 v/v) (isocratic mode). The wavelength of maximum absorption for the five ureas ranged from 241–245 nm and retention times were between 12 and 15 min with the exception of that of chloroxuron which was 30 min (Table 2).

2.2.3. Preparation of standards

Standard stock solutions (2 × 10^{-3} M) were

prepared from the crystalline solids using methanol. Working standards were obtained by suitable dilutions of the stock solutions with methanol.

2.2.4. Linearity study

Standard concentrations ranging from 4 × 10^{-7} –2 × 10^{-4} M with internal standard (diuron at 10^{-4} M) were used to determine peak area response vs. concentration of urea derivative. The limit of detection was 2 × 10^{-7} M.

2.2.5. Reproducibility study

Two standard solutions were analyzed several times on the same day and on different days to determine the intra- and inter-day HPLC variations. The intra-assay % RSD based on 10 determinations done on the same day was 0.6%. The inter-assay % RSD based on 10 determinations done on five different days was 1%.

2.3. Sorption rate experiments

Batch sorption tests were performed in 50 ml flasks at 21 ± 1°C. 10 g of air-dried soil was equilibrated with 20 ml of a urea solution (40 μM urea in demineralized water pH 6.1) and methanol mixture (40:1 v/v). The samples were shaken with a mechanical shaker (Gyrotory Water Bath Shaker Model G76, New Brunswick Scientific Co., USA) at 20–22°C.

The rate of each phenylurea adsorption versus time was measured and used for evaluating the equilibration period for later K_f determinations. At different times (5, 20, 50 min, etc.), the suspension was centrifuged at 5000g for 15 min (Grignon soil) or 30 min (Becon soil). The difference in the centrifuging time is due to the different organic matter contents of the soil. The concentrations of nonsorbed solutes in a 450 μl aliquot of clear supernatant, with 50 μl of internal standard added, were determined by an HPLC procedure. Soil-sorbed amounts of urea derivatives were calculated as the difference between the initial urea concentration and the equilibrium concentration previously determined.

Table 3
Freundlich parameters of ureas in the soils (K_f and n are calculated with the Freundlich equation; C, μM; x/m, μmol g^{-1}; $K_f = 100$ K_f)

Parameter	Mean ± d[a] Metobromuron	Isoproturon	Chlortoluron	Chloroxuron	Difenoxuron
Grignon soil					
K_f	0.43 ± 0.08	0.52 ± 0.08	0.69 ± 0.07	0.72 ± 0.04	1.88 ± 0.21
n	0.71 ± 0.01	0.51 ± 0.01	0.56 ± 0.01	1.20 ± 0.05	0.62 ± 0.01
r	0.99	0.97	0.98	0.96	0.99
Becon soil					
K_f	2.07 ± 0.08	1.01 ± 0.03	1.49 ± 0.04	7.71 ± 0.14	2.70 ± 0.06
n	0.64 ± 0.03	0.66 ± 0.02	0.73 ± 0.03	0.90 ± 0.01	1.08 ± 0.03
r	0.99	0.99	0.98	0.99	0.97

[a] Absolute deviation.

For K_f determinations, the soil sample was stirred with 20 ml of a herbicide solution with different urea derivative concentrations (C_0, the initial concentration of urea, ranged from 4–200 μM). After the equilibration period (24 h), the suspension was centrifuged as described above. An aliquot of the liquid phase was analysed using the HPLC procedure. Urea derivative solutions without soil were prepared in the same way: no adsorption was observed on the walls of the flasks. Blank samples (soil with pure water) without urea derivative were also prepared in the same way: no peaks with the same retention times as urea derivatives were observed.

Adsorption isotherms parameters were calculated according to the Freundlich equation:

$$x/m = K_f \cdot C^n$$

where x/m is the rate of herbicide sorbed (per urea mass/soil mass), C is the herbicide concentration at equilibrium and K_f and n are empirical adsorption parameters calculated from experimental data using least-squares fitting. Each experiment was replicated twice with each soil and the reported results are the means of the two assays (Table 3).

Desorption studies were conducted on three herbicide solutions (20, 60 and 100 μM). After adsorption, according to the above experiment, and centrifugation, supernatant was replaced with a similar volume of demineralized water without

herbicide. Centrifuge tubes were shaken for 24 h at 21 × 1°C.

Desorption was achieved by removing all the supernatant from the centrifuged samples and then replacing it with demineralized water. This equilibration process was repeated five times. Each time an aliquot of the supernatant was analysed by HPLC. The amount of herbicide that remained on the soil was calculated as the difference between the initial amount and the desorbed amount.

2.4. Soil column displacement studies

Movement of the urea derivatives through saturated soil columns was estimated using the displacement technique: chromatography columns (1.5 cm i.d. × 30 cm) were packed with 10 g of soil and saturated with demineralized water. The flow rate was constant (3 ml h^{-1}). Then, a urea derivative solution (4 × 10^{-6} M) was injected into the column. Elution was stopped when the effluent concentration approached, or became identical to, the input concentration. At this stage, demineralized water was injected into the column to observe the desorption of urea derivatives. Column effluents were collected with an automatic fraction collector (Gilson Fraction Collector FC 203B) every 30 min. The concentration of urea deriva tive in the effluent was determined by the HPLC procedure.
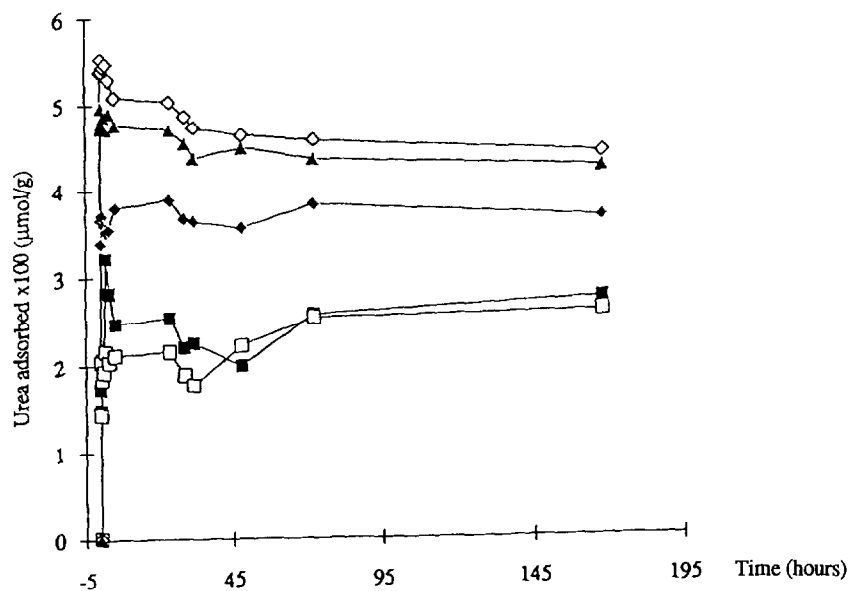
(a)
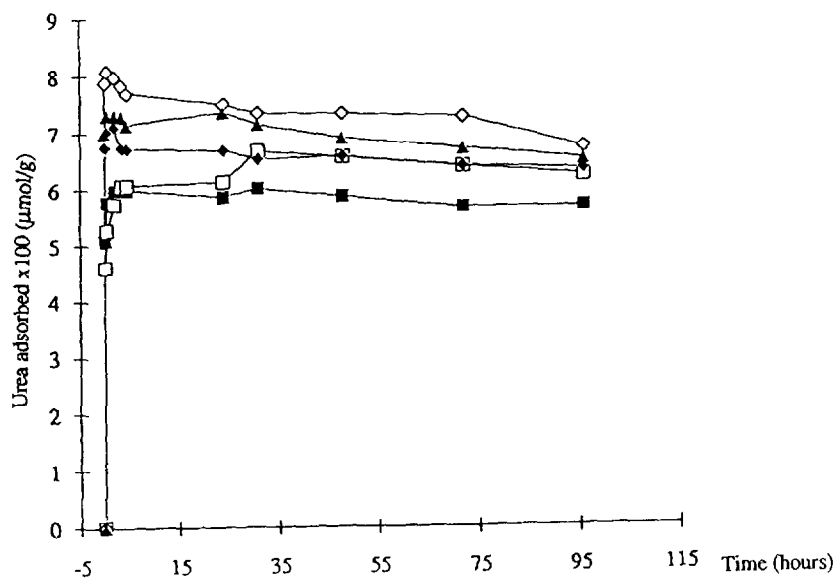
(b)

Fig. 2. Adsorption kinetic curves of urea derivatives on (a) Grignon and (b) Becon (soil): (■) metobromuron; (□) isoproturon; (▲) chlortoluron; (◇) chloroxuron; (◆) difenoxuron.

3. Results and discussion

3.1. Soil adsorption–desorption study

The equilibrium was attained practically within 8 h (Fig. 2). When equilibrium was reached more

chloroxuron than the other molecules was retained in the two soils. According to Gilchrist et al. [16], when a pesticide is mixed with soil it reacts with active sites that are available on the surfaces of the soil particles. Some are very reactive, so that they can hold pesticide molecules

strongly, while others are not reactive enough. The loosely bound pesticide molecules desorb.

With difenoxuron, chloroxuron and isoproturon, and Grignon soil, adsorption followed a rapid adsorption phase in which the amount of adsorbed urea increased rapidly. This first reaction phase is followed by some decrease before the attainment of a stationary state. Metobromuron and chlortoluron with Grignon soil, and all urea derivatives with Becon soil, did not show such a decrease. With atrazine the decreasing phase has been attributed to the diffusion of the molecules in the soil microporosities [16]. For the two soils significant amounts of chloroxuron and difenoxuron, compared to the other molecules, were retained in the soil. A greater amount of urea derivative was adsorbed by the Becon soil components than by the Grignon soil components.

Fig. 3 shows the adsorption isotherms of urea derivative in the Becon soil (Freundlich isotherms, $x/m = f(C)$). Adsorption isotherms in the Grignon soil are similar. The isotherms of metobromuron, isoproturon and chlortoluron are of the L-type according to the classification of Giles et al. [17] but the chloroxuron and difenoxuron isotherms are of the H-type. The H-type isotherms are usually interpreted as being due to a high relative affinity of the soil particles for the solutes, indicating a minor competition between solute and solvent molecules towards the adsorbing sites. The empirical Freundlich equation closely described the adsorption on the soil. The calculated parameters K_f and n, together with the coefficients r for the linear fit, are given in Table 3. Inspection of the data listed in this Table indicates that K_f follows the organic matter content in the soils. This trend agrees with the results of other studies which showed the part played by the organic matter in the adsorption processes [3,7,8,18]. With the exception of chloroxuron (Grignon) and difenoxuron (Becon), n values are less than unity, which is the result of decreasing adsorption as the adsorptive sites become occupied and this is in accordance with the results of Kozak and Weber [19] and Grover [20] for phenylurea herbicides.

For each urea, the x/m value was calculated with C equal to 20 μM from the Freundlich equations previously determined. The results were: 2.4×10^{-2} μmol g^{-1} for isoproturon, 3.5×10^{-2} μmol g^{-1} for metobromuron, 3.6×10^{-2} μmol g^{-1} for chlortoluron, 20.9×10^{-2} μmol g^{-1} for difenoxuron and 26.3×10^{-2} μmol g^{-1} for chlorxuron with the Grignon soil, and 7.3×10^{-2} μmol g^{-1} for isoproturon, 13.1×10^{-2} μmol g^{-1} for chlortoluron, 14.3×10^{-2} μmol g^{-1} for metobromuron, 69.5×10^{-2} μmol g^{-1} for difenoxuron and 114.8×10^{-2} μmol g^{-1} for chloroxuron with the Becon soil. These doses decrease in the order chloroxuron > difenoxuron > chlortoluron > me tobromuron > isoproturon for the Grignon soil and in the order chloroxuron > difenoxuron > metobromuron > chlortoluron > isoproturon for the Becon soil. The value of n for the adsorption of chloroxuron on the Grignon soil deviated from unity. This can be explained by the inversion of chloroxuron and difenoxuron according to the range of x/m values compared with the range of K_f values on the Grignon soil. The phenoxy group of chloroxuron and difenoxuron molecules is thought to be responsible for the increase in retention.
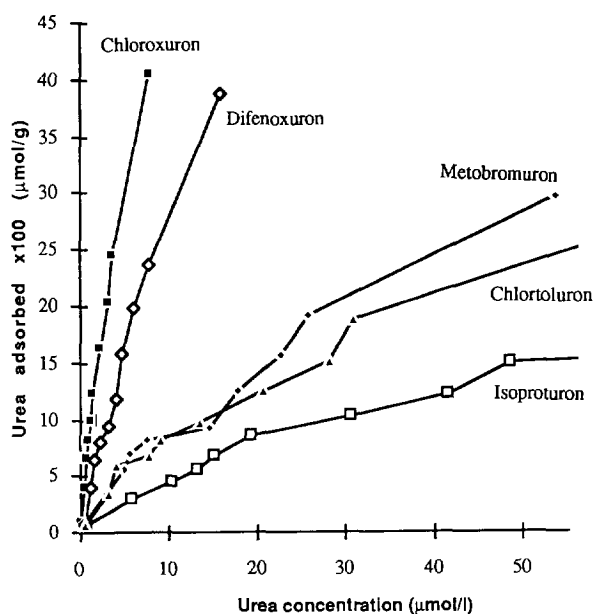

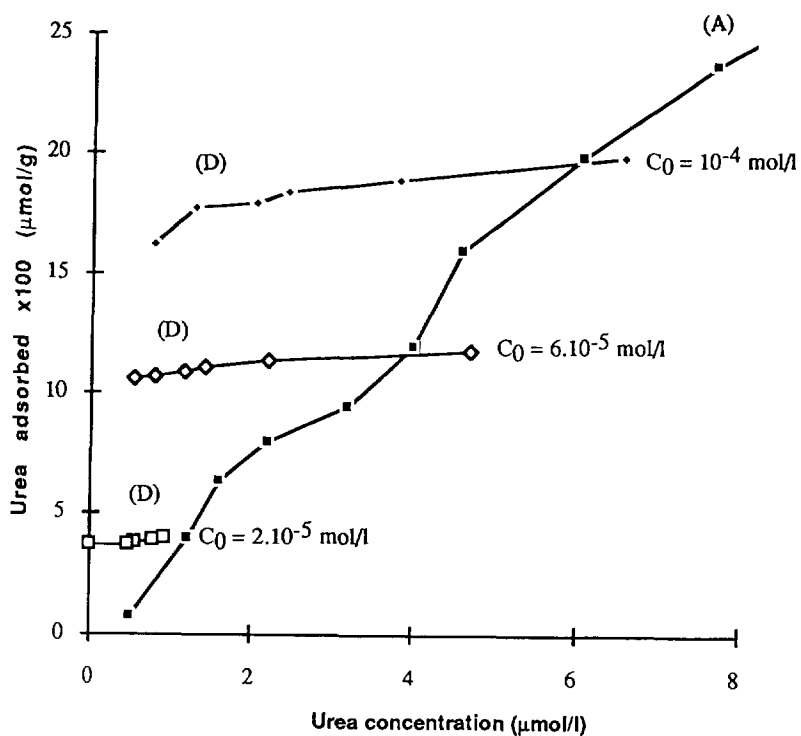Fig. 3. Urea adsorption isotherms on the Becon soil.

Fig. 4. Desorption and adsorption isotherms of difenoxuron on Becon soil.

An example of urea derivative desorption curves (D) is presented (difenoxuron desorption) together with the adsorption curve (A) in Fig. 4, where C_0 is the initial concentration of urea derivative. The humic compounds which are present in the Becon soil increased the percentage of non-desorbable urea as shown in Table 4. Metobromuron, chlortoluron and isoproturon desorptions are higher than those of chloroxuron and difenoxuron. Desorption isotherms show hysteresis for the two phenylphenoxyureas, indicating specific interactions.

3.2. Leaching

Figs. 5 and 6 show the curves of urea derivative mobilities through soil columns. The eluent volume needed for a urea to obtain 50% of the inlet concentration in the effluent $(C/C_0 = 0.5)$ was used as a direct estimation of its retardation factor. No tracer experiments were made in this study to estimate the residence time and dispersion of a non-adsorbate solute. The retardation factors obtained for ureas in Becon soil columns were greater than in Grignon soil columns. The organic matter content, which is higher in the Becon soil, could be responsible for the low urea mobilities through the Becon soil column. Because of the strong retention of chloroxuron in the soils, we were not able to determine its retardation factor; the adsorption process was so long that the value $C/C_0 = 0.5$ could not be reached even after 300 ml (Grignon) and 1500 ml (Becon). The retardation factor of an urea derivative correlates directly with its K_f value. Therefore chlorox uron and, in minor proportion, difenoxuron, in

Table 4
Percentage of urea remained adsorbed after five desorptions (C_{init}, initial urea concentration in μM; Q_0, dose of urea adsorbed before desorption in μmol g^{-1})

C_{init}	Metobromuron		Isoproturon		Chlortoluron		Chloroxuron		Difenoxuron	
	% urea	Q_0	% urea	Q_0	% urea	Q_0	% urea	Q_0	% urea	Q_0
Grignon soil										
2×10^{-5}	26	2.12	67	2.09	40	2.05	51	3.48	78	3.61
6×10^{-5}	16	5.10	39	4.10	21	5.07	82	10.62	73	9.35
10^{-4}	15	7.79	16	5.43	27	6.93	67	17.53	67	14.46
Becon soil										
2×10^{-5}	74	3.50	80	3.27	68	3.52	93	4.10	91	3.96
6×10^{-5}	75	9.42	61	8.49	54	10.61	79	12.33	92	11.91
10^{-4}	72	15.90	72	12.97	52	15.67	65	20.43	83	19.79

contact with a soil of high organic matter content might be less mobile in the soil profile than other urea derivatives. The close similarity in molecular structure and polarity of the two chemical compounds would suggest that other factors are involved in their different mobilities in soil. The most obvious cause could be their relative solubility in water. Chloroxuron is much less water soluble than difenoxuron. Since adsorption and leaching are often related to water solubility within a given herbicidal class, this may explain the reduced leachability of chloroxuron in comparison with other urea derivatives [21,22].

3.3. Relations with S_w and K_{ow}

Urea derivatives are adsorbed to a lesser extent in Grignon soil than in Becon soil. This difference may be attributed to the difference in soil characteristics since Becon soil has a higher organic matter content than Grignon soil. Because of the importance of the organic matter content in herbicide adsorption, especially with neutral molecules, the distribution coefficient K_f must be correlated with the organic matter content which is given by the relationship $K_{oc} = K_f/$%OC, where OC is the fraction of organic content in dry soil [3]. The solubilization in natural organic matter is due to a hydrophobic effect. Experimental and predicted thermodynamic data have shown that K_{oc} is closely correlated with

the octanol–water partition coefficient K_{ow} and the water solubility S_w [23] of the chemical product. Water solubility governs the retention of pesticides in soils. Chiou et al. [24] demonstrated that water solubility is the primary factor controlling the partition of nonionic organic solutes between soil organic matter and water.

Fig. 7 shows curves of log K_{ow} and log S_w versus log K_{oc}. Values of the sorption coefficient normalized by the organic carbon content of the soil (K_{oc}) are plotted on the horizontal scale, and solute water solubility (log S_w) and octanol–water partition coefficient (log K_{ow}) are plotted on separate vertical scales. As expected K_{oc} increases with the hydrophobic character of the molecules. As previously observed, binding is related not only to solubility parameters but also to the composition and molecular structure of both the soil and the associated molecules. The high binding of chloroxuron and difenoxuron could be attributed to the phenoxy group. The methoxy group of difenoxuron increases the electronic density on the aromatic ring. It may also be possible that the adsorption process involves charge transfers in the case of the difenoxuron molecule.

With the exception of chloroxuron, log K_{ow} correlates well with log K_{oc}. Therefore, the distribution of urea derivatives (except chloroxuron) can be viewed as partition (solubilization) between soil and water and distinguished from adsorption (surface condensation).
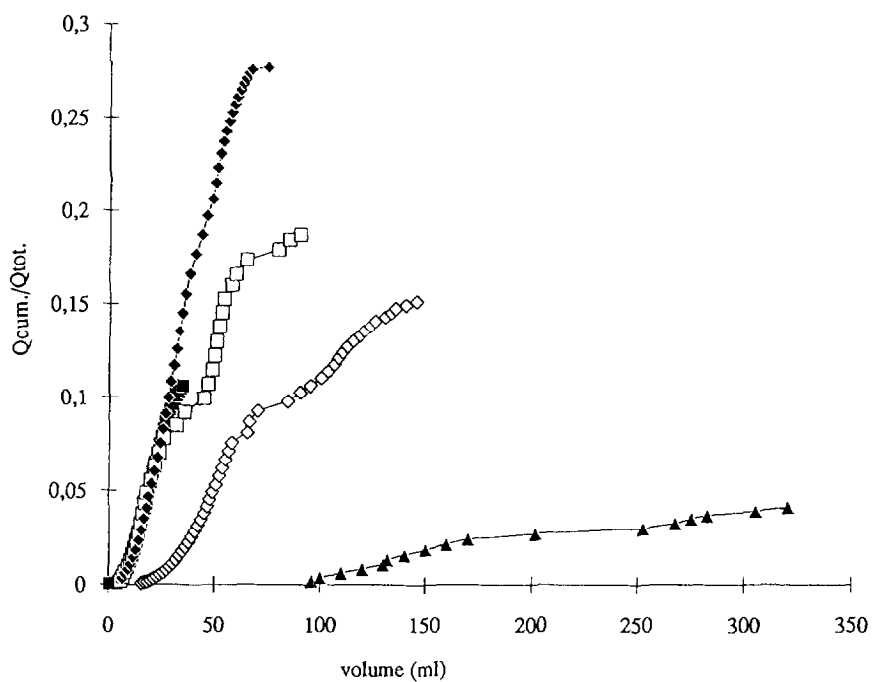
Fig. 5. Cumulative metobromuron (■); isoproturon (□); chlortoluron (◆); chloroxuron (▲); and difenoxuron (◇) leached in Grignon soil columns.
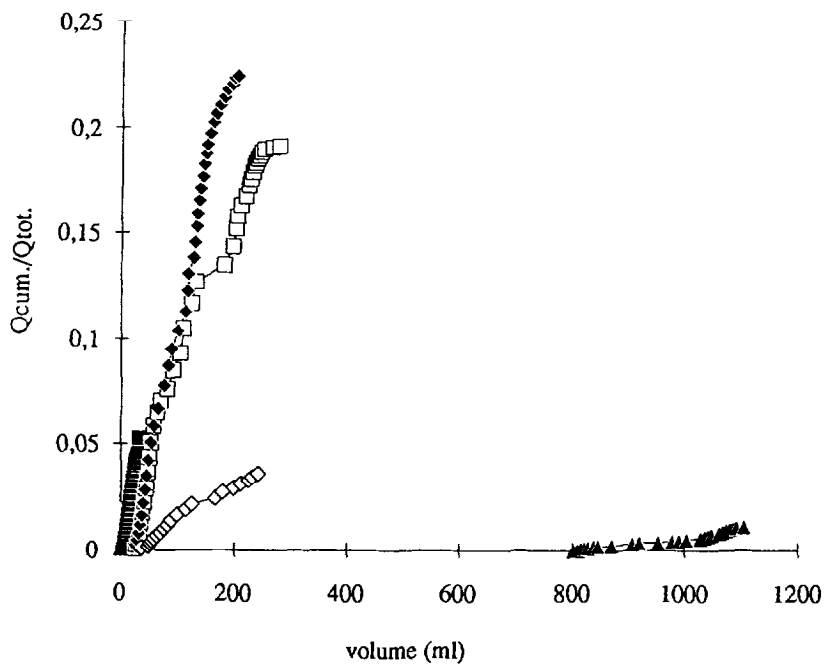

Fig. 6. Cumulative metobromuron (■); isoproturon (□); chlortoluron (◆); chloroxuron (▲); and difenoxuron (◇) leached in Becon soil columns.
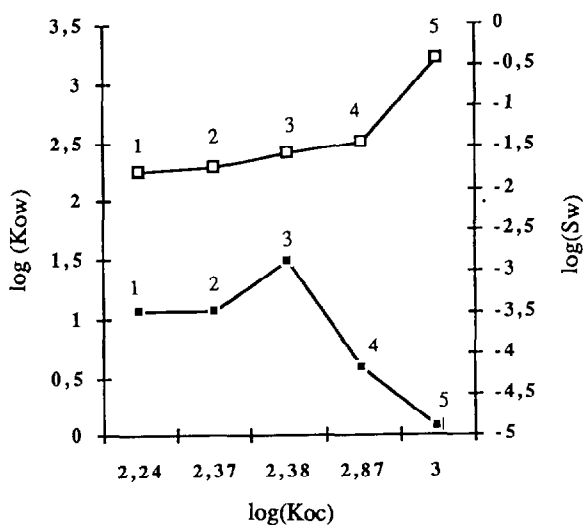
Fig. 7. Variations of log (K_{ow}) ($\square$) and log (S_w) (μM) ($\blacksquare$) versus log (K_{oc}): (1) isoproturon; (2) chlortoluron; (3) metobromuron; (4) difenoxuron; (5) chloroxuron.

4. Conclusion

An understanding of the sorption mechanism is fundamental for predicting the fate and distribution of many organic contaminants. Analytical data indicate that sorption of these urea derivatives by soils in the presence of water exhibits the characteristics of a partition process. With respect to pesticide–soil interactions the environmentally important distribution of urea derivatives between soil and water has been estimated by measuring K_f and R_f values. It is confirmed that organic matter content is an important soil component [25]. Results presented here show a relatively high soil sorption (and low soil mobility) for chloroxuron and difenoxuron compared to isoproturon, metobromuron and chlortoluron. Therefore, it seems that the adsorption in soils is conditioned by the phenoxy group. The combination of the three factors (structural feature, hydrophobicity and organic matter content of soil) is responsible for the K_f and R_f values of chloroxuron being significantly higher than the others. However, the adsorption mechanism on soil is probably more

complex than that usually accepted for neutral molecules and hydrophobic partitioning is only one of the processes involved.

References

[1] H.L. Bohn, B.L. McNeal and G.A. O'Connor, Soil Chemistry, John Wiley and Sons, New York, 1985.
[2] G. Sposito, The Chemistry of Soils, Oxford University Press, Oxford, 1989.
[3] J.W. Hamaker and J.M. Thompson, in C.A.J. Goring and J.W. Hamaker (Eds.), Organic Chemicals in the Soil environment, Dekker, New York, 1972, p. 49.
[4] W.C. Koskinen, G.A. O'Connor and H.H. Cheng, Soil Sci. Soc. Am., Proc., 43 (1979) 871.
[5] R. Calvet, Health Perspect., 83 (1989) 145.
[6] J.B. Weber, Adv. Chem. Ser., 111 (1971) 55.
[7] M. Hayes, Residue Rev., 32 (1970) 131.
[8] F. Stevenson, J. Environ., 1 (1972) 333.
[9] J.J. Hassett, W.L. Banward and R.A. Griffin, in C.W. Francis and S.I. Auerbach (Eds.), Environment and Solid Wastes, Butterworths, Boston, MA, 1983, p. 161.
[10] C.T. Chiou, L.J. Peters and V.H. Freed, Science, 206 (1979) 831.
[11] G.C. Briggs, J. Agric. Food Chem., 29 (1981) 1050.
[12] L.D. Pussemier, G. Szabo and R.A. Bulman, Chemistry, 21 (1990) 1199.
[13] H. Geissbühler, H. Martin and G. Voss, in P.C. Kearney and D.D. Kaufman (Eds.), Herbicides, Chemistry, Degradation and Mode of Action, Vol. 1, M. Dekker, New York, 1975 p. 209.
[14] The Agrochemicals Handbook, The Royal Society of Chemistry, Nottingham, UK, 1993.
[15] G. Briggs, Philos. Trans. R. Soc. London, 329 (1990) 375.
[16] G.F. Gilchrist, D.S. Gamble, H. Kodama and S.U. Khan, J. Agric. Food Chem., 41 (1993) 1748.
[17] C.H. Giles, T.H. MacEwan, S.N. Nakhwa and D. Smith, J. Chem. Soc., 111 (1960) 3973.
[18] E. Barriuso, U. Bauer and R. Calvet, J. Environ. Qual., 21 (1992) 259.
[19] J. Kozak and J.B. Weber, Weed Sci., 31 (1983) 368.
[20] R. Grover, Can. J. Soil Sci., 55 (1975) 127.
[21] T.M. Ward and R.P. Upchurch, J. Agric. Food Chem., 13 (1965) 334.
[22] G.W. Bailey, J.L. White and T. Rothberg, Soil Sci. Soc. Am., Proc., 32 (1968) 222.
[23] Y.-P. Chin and J.W. Weber, Environ. Sci. Technol., 23 (1989) 978.
[24] C.T. Chiou, P.E. Poeter and D.W. Schmedding, Environ. Sci. Technol., 17 (1983) 227.
[25] J.A. Smith, P.J. Witkowski and C.T. Chiou, Rev. Environ. Contamin. Toxicol., 103 (1988) 127.

Fiber optic sensor for laser-induced room-temperature phosphorescence detection of polycyclic aromatic compounds

A.D. Campiglia,[1] T. Vo-Dinh*

Advanced Monitoring Development Group, Health Sciences Research Division, Oak Ridge National Laboratory, Oak Ridge, TN 37831-6101, USA

Abstract

The development of a fiber optic sensor for the analysis of polycyclic aromatic compounds based on laser-induced room-temperature phosphorimetry is reported for the first time. A pulsed nitrogen laser was used to excite phosphorescence emission from compounds imbibed on filter-paper substrates. Thallium(I) acetate (0.1 M) was used to enhance phosphorescence emission from chrysene, 1,2-benzofluorene, 7,8-benzoquinoline, phenanthridine and 5,6-benzoquinoline. Lead(II) acetate (0.5 M) was employed for the determination of fluoranthene, which showed no phosphorescence signal on paper substrates pre-treated with thallium(I) acetate. Limits of detection at the ng/ml^{-1} level were estimated for all the compounds. An improvement in the limits of detection of the nitrogen heterocyclic compounds was obtained by using a low-background paper substrate. Satisfactory reproducibility of measurements was observed, varying from 6.1% (chrysene) to 11.9% (7,8-benzoquinoline). The linear behavior of the sensor response was also evaluated. Linear dynamic ranges extend over two and three orders of magnitude and show the potential of the device for the quantitative analysis of environmental pollutants.

Keywords: Fiber optic sensor; Laser-induced room-temperature phosphorescence detection; Polycyclic aromatic hydrocarbons

1. Introduction

The development of fiber optic sensors was initially conceived in the medical area [1]. Although a great deal of effort is still devoted to this field, more recent interests in optosensing technology have been directed toward environmental applications. The main reason for the fast development of environmental monitoring sensors is the continuous upgrading of legislation concerning ambient pollution. Such modifications include the addition of new pollutant targets, re-evaluation of limits of concentrations and an

---

* Corresponding author.
[1] Present address: Departamento de Quimica, Universidade de Brasilia, Brasilia, DF, CEP 70910-900, Brazil.

increase in the frequency and number of measurements required [2]. Special emphasis in environmental analysis has been put on monitoring polycyclic aromatic hydrocarbons (PAHs) throughout the ecosystem [3]. Some PAHs are well known to exhibit carcinogenic and/or mutagenic effects in humans [4]. In aquatic systems, the major sources of PAHs release are oil spills and leakage from waste sites and coking plants [5]. Depending on the compound and the water supply, PAH concentrations usually range from pg ml^{-1} in pure ground water samples to μg ml^{-1} in heavily contaminated sewage. Among the analytical techniques adapted for on-site aquatic analyses for PAHs, laser-induced fluorimetry with optical fibers has shown to be a selective and sensitive approach [6–12].

In this paper, we report for the first time the evaluation of a laser-induced room-temperature phosphorimetric (LI-RTP) sensor for the determination of polynuclear aromatic compounds (PACs). In addition to PAHs, the application of the LI-RTP sensor was extended to nitrogen heterocyclic compounds (NHCs) of industrial, environmental and biological importance. To the best of our knowledge, this is the first time that an LI-RTP sensor has been reported. Very few studies involving phosphorimetry and optosensing have been reported previously [13–17]. The advantage of coupling fiber optics into laser sources to measure phosphorescence emission at 77 K was demonstrated by Hieftje and co-workers [13,14]. Fiber optics have also been employed to detect RTP emission with commercial spectrofluorimeters [15–17]. Selective chemical sensors have been developed for ultratrace aluminum determination [15], quantitation of tetracyclines in urine and pharmaceutical preparations [16] and glucose determination in serum and beverage samples [17].

In this study, advantage was taken of the high coupling efficiency of laser excitation sources into fiber optics to develop a universal RTP sensor adaptable to different analytical situations involving phosphorescent compounds. Filter-paper was used as a solid substrate to induce phosphorescence emission [18] from several model polycyclic aromatic compounds (PACs), which include three PAHs (chrysene, 1,2-benzofluorene and fluo-

ranthene) and three NHCs (7,8-benzoquinoline, phenanthridine and 5,6-benzoquinoline). External heavy-atom perturbation [18,19] was employed to enhance RTP emission from the studied compounds. Limits of detection (LODs) at the ng ml^{-1} were obtained, showing satisfactory sensitivity for environmental analysis. The linearity of response of the RTP sensor was also evaluated, showing linear dynamic ranges (LDR) extended over about three orders of magnitude. Finally, we demonstrated the usefulness of a paper background reduction treatment [20] in improving the LODs obtained with the LI-RTP sensor.

Dimensions:
1: 24.9 cm x 5 cm x 11.4 cm
2: 5.5 cm x 2.7 cm x 3.4 cm
3: 24 cm x 8.5 cm x 12 cm
4: 9 cm x 4 cm x 12.5 cm
5: 10 cm x 7 cm x 5 cm
6: 43.5 cm x 17.5 cm x 42 cm
7: 5.5 cm x 4.7 cm x 5.5 cm
8: 28 cm x 16 cm x 12 cm
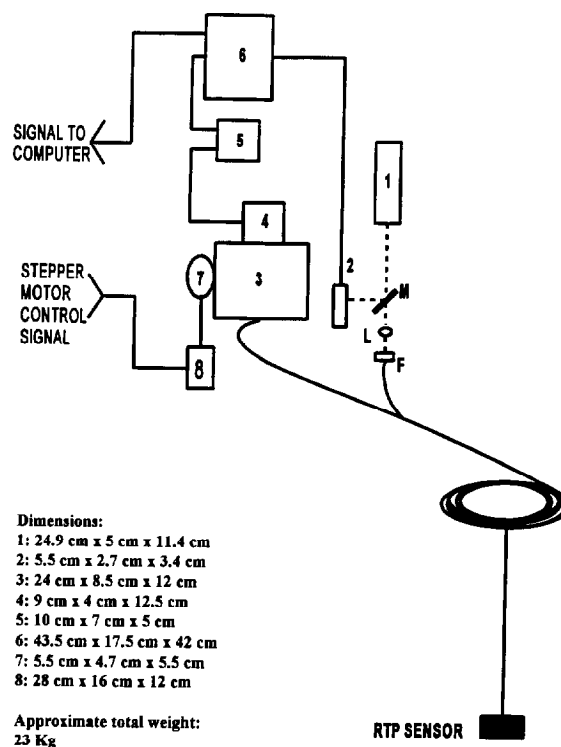
Approximate total weight:
23 Kg

RTP SENSOR

Fig. 1. Block diagram of the laser system employed with the LI-RTP sensor. 1 = Nitrogen laser; 2 = photodiode trigger; 3 = monochromator; 4 = PMT; 5 = preamplifier; 6 = boxcar; 7 = motor; 8 = motor control; L = lens; M = reflecting surface; F = fiber optic mount.
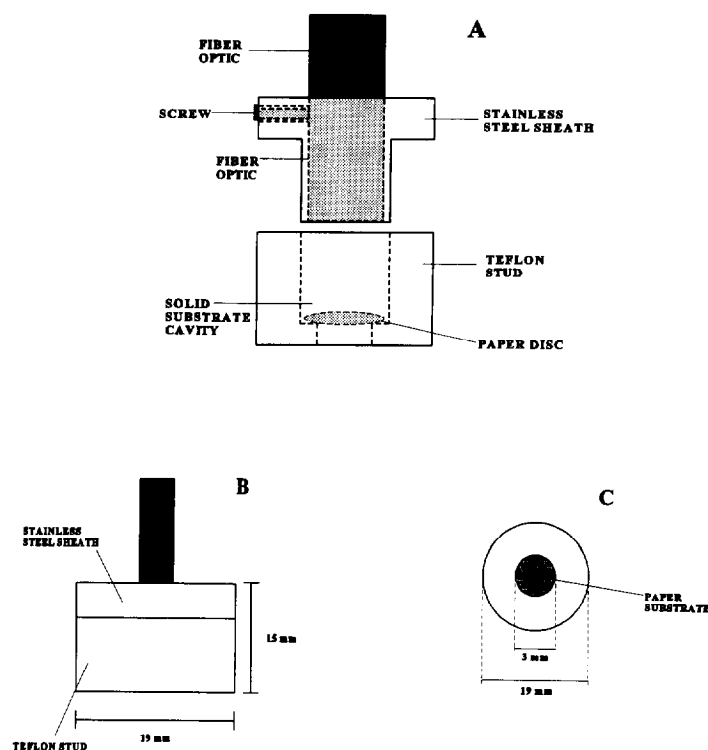
Fig. 2. Schematic diagram of the RTP sensor. (A) Cross-section; (B) side view; (C) bottom view showing the paper substrate in the sample cavity of the sensor.

2. Experimental

2.1. Instrumental

Fig. 1 shows a block diagram of the instrumental system employed. Excitation at 337 nm was performed by using a pulsed nitrogen laser (Laser Science VSL-337) with a typical pulse energy of 120 mJ. The repetition rate was 20 Hz and the pulse width 3 ns. The laser beam was focused on to one end of a bifurcated optical fiber with an $f/4$ convex lens, and directed to the surface of the solid substrate probe. The bifurcated fiber (Fiber Guide Industries, silica–silica glass, 150 cm length) consisted of a 600 μm central optical fiber surrounded by 18 optical fibers of 200 μm diameter (emission). The phosphorescence signal from the sample was transferred into a 10 cm focal-length monochromator (ISA Model DH-10). The output from the photomultiplier (Hamamatsu R928) was amplified by a laboratory-constructed

amplifier and fed into a gated boxcar averager (Stanford Research Systems RS250). For all measurements, the delay and gate time were 1 and 4 ms, respectively. The time constant of the boxcar was 1 s. A stepper motor was used to control the scanning of the monochromator. An analog-to-digital converter card (MetraByte DASH-16) was used for instrumental control, timing and data collection. The software employed to control the instrumental system was develped in our laboratory.

The RTP sensor is shown in Fig. 2. Basically, the device consists of two cylindrical parts (a stainless-steel sheath and a Teflon stud) easily attached by concentric incised threads. The fiber optic bundle passed through the center of the sheath and reached the sample compartment of the RTP sensor located between the two cylindrical parts. A hole (0.3 cm diameter) at the distal end of the Teflon stud allowed the entry of solution into the sample cavity. By dipping the sensor into the liquid sample, the paper substrate in the

sample cavity was imbibed with the solution. The sample collected by the filter-paper was then excited by the laser radiation from the fiber optic. By means of a screw in the sheath, the distance between the fiber optic and the surface of the solid substrate was kept constant during all measurements.

A commercial spectrofluorimeter (Perkin-Elmer LS 50B) was used to record the excitation spectra of the studied compounds. In all cases, the delay and gate time were 1 and 4 ms, respectively. The excitation and emission slits were 10 nm.

The ultraviolet (UV) irradiation treatment for paper background reduction was carried out in a Rayonet photochemical reactor (Southern N.E. Ultraviolet Co., Middletown, CT, USA) using five lamps with maximum wavelengths (λ_{max}) of emission at 254 nm and seven with λ_{max} at 300 nm.

2.2. Reagents

Whatman No. 40 filter-paper and distilled, deionized water were used throughout. All chemicals were of analytical-reagent grade and used without further purification. Chrysene, 1,2-benzofluorene, phenanthridine, fluoranthene, 7,8-benzoquinoline and 5,6-benzoquinoline were purchased from Aldrich at the highest purity available. Thallium(I) acetate and lead(II) acetate were obtained from Sigma. Methanol was acquired from J.T. Baker.

Stock solutions of PACs (10^{-3} M) were prepared in methanol–water (80:20, v/v). Working solutions were obtained by appropriate dilution with methanol–water (80:20, v/v). Thallium(I) acetate (0.1 M) and lead(II) acetate (0.5 M), both prepared in methanol–water (50:50, v/v), were used as phosphorescence enhancers.

2.3. Procedure

The background emission of the solid substrate was reduced by a combination of solvent extraction and irradiation treatment [20]. Strips of chromatography paper were extracted with water in a Soxhlet apparatus for 8 h and exposed to UV irradiation in a photochemical reactor for the same period of time.

Filter-paper was cut into 0.4 cm diameter circles with a hole puncher. The circular substrates were immersed in the heavy-atom salt solution for approximately 1 min, dried under an infrared (IR) heat lamp for 3 min and then stored in a desiccator to be used as solid substrate probe.

The paper substrate was placed in the sample cavity of the RTP sensor. Sample collection was performed by immersing the sensor in a vial with the analyte solution. Although no effort was made to optimize the exact immersion time of the RTP sensor in the sample solution, we observed that a period of 30 s–1 min was enough to obtain the maximum RTP signal from the studied compounds. Prior to RTP measurements, a drying step was carried out, keeping the solid substrate in the sample compartment of the sensor. The hole at the distal end of the Teflon stud allowed direct irradiation of the reverse side of the solid substrate by an IR lamp. In most cases, the signal intensities and spectra collection were performed after 5 min of IR irradiation.

3. Results and discussion

3.1. Heavy-atom effect

The performance of the RTP sensor was evaluated by testing six well known phosphorescent compounds previously examined by SSRTP [18]. The phosphorescence characteristics of 7,8-benzoquinoline, 5,6-benzoquinoline, phenanthridine, 1,2-benzofluorene, chrysene and fluoranthene have been studied on a wide variety of solid substrates and phosphorescence enhancers [18,21–25]. The combination of paper substrate and thallium(I) ions as phosphorescence enhancers has been shown to be particularly efficient in improving the RTP signal of these compounds.

Our preliminary studies, therefore, were performed on paper substrates pre-treated with a 0.1 M thallium(I) acetate (TlOAc) solution. With the exception of fluoranthene, all the PACs showed strong phosphorescence signals. The emisson wavelengths obtained with the LI-RTP sensor are given in Table 1. The excitation maxima of the compounds were acquired with a commercial

spectrofluorimeter. The emission characteristics of the PACs obtained with the LI-RTP sensor were in agreement with those obtained with the spectrofluorimeter, which shows the feasibility of the device for their identification in unknown samples. From the values in Table 1, it can be seen that the maximum excitation wavelengths (λ_{exc}) of 7,8-benzoquinoline, 5,6-benzoquinoline and phenanthridine are close to the emission wavelength of the nitrogen laser (337 nm). This proximity probably allows a certain degree of overlap between their maximum excitation bands and the laser line, which is necessary for RTP emission. In addition, the excitation spectra of the studied NHCs presented featureless bands in the wavelength range 300–400 nm. Although those bands were less intense than the maximum excitation bands, they certainly contributed to the high degree of excitation obtained with the nitrogen laser. A similar effect was observed for chrysene and 1,2-benzofluorene. Their maximum excitation bands were located below 300 nm (see Table 1), with obvious difficulties for overlapping with the

Table 1
Spectral characteristics of several PACs[a] obtained with a commercial spectrofluorimeter and a laser system with an LI-RTP sensor.

Compound[b]	λ_{exc}[c] (nm)	λ_{em}[d] (nm)
7,8-Benzoquinoline	303, *353*	*474*, 506
Phenanthridine	*315*, 355	470, *495*
5,6-Benzoquinoline	302, *355,*	*475,* 509
Chrysene	274	*515,* 550
1,2-Benzofluorene	270	505, *550*
Fluoranthene	284	No signal

[a] Whatman No. 40 filter-paper was used as a solid substrate and 0.1 M TlOAc was employed to enhance RTP emission.
[b] 10^{-4} M analyte solutions prepared in methanol–water (80:20 v/v) were used in all cases. Analyte concentrations giving phosphorescence signals between 15 and 20 times the background signal were employed.
[c] Maximum excitation wavelengths obtained with a commercial spectrofluorimeter. The peak with maximum intensity is in italics.
[d] Maximum emission wavelengths obtained with the LI-RTP sensor. Excitation wavelength = 337 nm. The peak with maximum intensity is in italics. A drying time of 5 min was employed.

laser line. However, these PAHs presented, at 337 nm, featureless absorption bands with approximately 20% of the maximum intensity observed at their λ_{exc}. Apparently, even when excited at a wavelength region of low absorption of energy, the high irradiance of the laser beam was sufficient to induce strong RTP emission from these compounds. On the other hand, fluorathene showed no RTP emission with the LI-RTP sensor. In the spectrofluorimeter, and still using 0.1 M TlOAc as phosphorescence enhancer, this compound showed a strong RTP signal with $\lambda_{exc}/\lambda_{em}$ at 284/555 nm. As a tentative means of shifting the λ_{exc} of fluoranthene towards 337 nm, and promote the necessary overlapping with the laser line to observe RTP emission with the fiber optic sensor, we employed a 0.5 M lead(II) acetate (Pb(OAc)$_2$) solution as a heavy-atom salt. This phosphorescence enhancer was chosen based on previous studies [24], which indicated strong phosphorescence emission from fluoranthene in the presence of lead(II) ions. As expected, the maximum excitation wavelength of the compound was observed at 365 nm, which is in agreement with the λ_{exc} previously reported [24]. As a consequence of the partial overlapping between its maximum excitation band and the laser line at 337 nm, we were able to detect fluoranthene's RTP emission with the LI-RTP sensor. Its maximum emission was observed at 545 nm.

3.2 Effect of drying time on the phosphorescence intensity and the precision of measurements obtained with the RTP sensor.

Previous studies [18,26–31] have shown that the presence of moisture and solvent molecules on the surface of the paper substrate might cause quenching of RTP signals. Either by competing with the analyte for bonding sites on the paper substrate, or by facilitating the transport of oxygen into the vicinity of the phosphor, the presence of water might also affect the reproducibility of measurements. To minimize its effect, a drying step prior to RTP detection is recommended. In addition, a flow of dry gas should be passed through the sample compartment of the instrument to avoid the presence of oxygen during
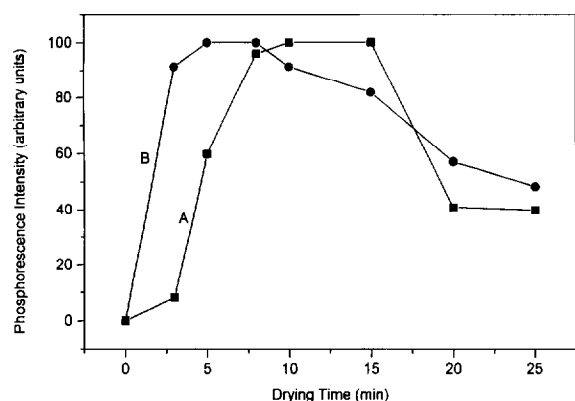
Fig. 3. Phosphorescence intensity as a function of drying time. Net RTP signals of (A) a 10^{-5} M solution of 7,8-benzoquinoline and (B) a 10^{-6} M solution of chrysene. In both cases, the analyte solutions were prepared in methanol–water (80:20 v/v) and 0.1 M TlOAc was used as a phosphorescence enhancer.

measurements. Interaction of triplet-state oxygen (the natural ground state of oxygen) with a molecule in the excited triplet state might cause radiationless deactivation of the excited molecule and production of excited singlet-state oxygen [18,22,32–34].

The drying conditions for the RTP detection of PACs have been studied previously [18,26–31]. When using filter-paper as a solid substrate, the usual procedure involves IR irradiation of the PAC solution spotted on the solid support. A similar procedure was therefore employed with the LI-RTP sensor. In our case, the IR radiation was directed towards the reverse side of the paper substrate probed by the fiber optic. Fig. 3 shows the net RTP intensities of 7,8-benzoquinoline and chrysene as a function of drying time. The drying temperature was adjusted to 60°C by varying the distance between the LI-RTP sensor and the IR lamp. The net signals plotted in the graphics were calculated from single measurements of three paper substrates impregnated with the blank and another three impregnated with the analyte solution. Chrysene emitted the maximum intensity after a drying time of 5 min. The RTP signal of 7,8-benzoquinoline reached its maxiumum value after 10 min of IR irradiation. The difference observed in the optimum drying times is not surprising, since it will depend on, among other parameters, the physico-chemical characteristics

of the phorphors [18,19]. In both cases, however, longer exposure to IR radiation caused intensity reductions. No changes in $\lambda_{exc}/\lambda_{em}$ were observed. Since our interest was focused on minimizing the drying time and therefore improving the sample throughout, we did not perform further studies to explain the observed reductions.

The reproducibility of measurements was evaluated after a drying time of 5 min. The relative standard deviations (RSDs) obtained with the RTP sensor are shown in Table 2. The RSD values were calculated with the equation RSD = $[(S_{A+B})^2 + S_B^2]^{1/2} \times 100/I_{A-B}$. Six measurements of analyte signals and respective blanks were used to evaluate the standard deviation of the analyte (S_{A+B}), the standard deviation of the blank (S_B) and the average of the analyte signal (I_{A-B}). All measurements were taken at the maximum emission wavelengths of the compounds. The best results were obtained for chrysene (6.1%). This is probably due to the drying time employed, which is within the optimum drying range of the compound (see Fig. 2). The phosphorescence intensity of 7,8-benzoquinoline after a drying time of 5 min, for example, was approximately 35% lower than its maximum intensity after 8 min of IR

Table 2
Precision of measurements obtained with the LI-RTP sensor[a]

Compound[b]	λ_{em}[c] (nm)	RSD[d] (%)
7,8-Benzoquinoline	474	11.9
Phenanthridine	495	7.9
5,6-Benzoquinoline	475	10.1
Chrysene	515	6.1
1,2-Benzofluorene	550	10.3
Fluoranthene	545	8.9

[a] Whatman No. 40 filter-paper was used as a solid substrate and 0.5 M Pb(OAc)$_2$ was employed to enhance the RTP emission of fluoranthene. All the other PACs were determined in the presence of 0.1 M TlOAc. A drying time of 5 min was used in all measurements.
[b] Methanol–water (80:20 v/v) solutions were employed in all cases. Analyte concentrations giving phosphorescence signals between 15 and 20 times the background signal.
[c] Maximum emission wavelengths at which measurements were perforemd. Excitation wavelength = 337 nm.
[d] RSD = relative standard deviation ($n = 6$). See text for definition.

Table 3
Analytical figures of merit for several PACs obtained with the LI-RTP sensor[a]

Compound[b]	λ_{em}[c] (nm)	LDR[d] ($\times 10^2$)	Slope[e] log–log	r[f]	LOD[g]	
					μM	ng ml^{-1}
7,8-Benzoquinoline	474	6.3	0.9987	0.95	1.0	185
Phenanthridine	495	4.5	0.9957	0.87	1.5	268
5,6-Benzoquinoline	475	7.2	0.9962	1.03	0.9	167
Chrysene	515	10.1	0.9985	0.96	0.04	10
1,2-Benzofluorene	550	11.8	0.9978	0.81	0.2	50
Fluoranthene	545	8.6	1.0000	0.98	0.05	10

[a] Whatman No. 40 filter-paper was used as a solid substrate and 0.5 M $Pb(OAc)_2$ was employed to enhace to RTP emission of fluoranthene. The RTP signals of all the other PACs were enhanced with 0.1 M TlOAc.
[b] Methanol–water (80:20 v/v) solutions used.
[c] Emission peaks with maximum intensity used for RTP measurements. Excitation wavelength = 337 nm.
[d] LDR = linear dynamic range; it was estimated by dividing the upper linear concentration by the limit of detection.
[e] Calculated from the plot of log I_p versus log (concnetration).
[f] r = Correlation coefficient of the linear plot.
[g] LOD = limit of detection; it was estimated as the concentration of analyte that yields a net RTP signal three times the standard deviation of the background.

irradiation. An improvement in the RSD value for this compound could have been obtained with a drying time of 8 min. A similar approach could have been used to improve the precision of measurements for all the PACs. In all cases, however, the RSD values obtained with the LI-RTP sensor were within the reproducibility range commonly observed with conventional instrumentation (5–15%) [18,19]. The effects of oxygen and humidity were probably minimized by the design of the LI-RTP sensor. The entry of oxygen in the sample cavity of the sensor is reduced to its diffusion through the filter-paper, since it can only occur by the hole at the distal end of the Teflon stud. In addition, the exposure of the dried substrate to atmospheric humidity is kept to a minimum. Considering the necessity for a short analysis time and simplicity of operation in field applications, and the satisfactory RSD values obtained, we performed all measurements in the absence of a flow of a dry gas and after a drying time of 5 min.

3.3. Analytical figures of merit (AFOM)

Table 3 shows the AFOM obtained with the LI-RTP sensor. Depending on the PAC, the linear dynamic ranges (LDR) of the calibration curves

extended over two to three orders of magnitude. In most cases, the slopes of the log–log plots and the correlation coefficients of the linear graphs were close to unity, showing the linearity of response of the sensing device. All the limits of detection (LODs) were estimated at the ng/ml^{-1} level, which is within the concentration range usually required for PAC determinations in contaminated samples [35,36]. By comparing the LODs reported in Table 3, it becomes clear that the values estimated for the NHCs are at least five times higher than those estimated for the PAHs. Although several experimental parameters can be optimized to improve the LODs in SSRTP analysis [37,38], we studied the effect of a paper treatment on background signal reduction [20,37–39]. Our choice was based on the position of the maximum emission peaks of the NHCs, which are in a wavelength region of higher background signal than the studied PAHs. The broad, featureless emission band of the paper substrate presents a plateau with maximum intensity between 470 and 500 nm. By applying a combination of water extraction and UV irradiation [20], we reduced the background emission of the paper substrate to approximately 85% of its original value. Table 4 shows the

Table 4

Effect of background reduction treatment of the analyte-to-background signal ratio and the LOD of some nitrogen heterocyclic compounds obtained with the LI-RTP sensor.

Compound[a]	S_A/S_B[b]		Treated paper: LOD[c] (ng ml^{-1})
	Untreated paper	Treated paper	
7,8-Benzoquinoline	4.4	15.3	53
Phenanthridine	2.0	17.4	38
5,6-Benzoquinoline	4.0	13.9	44

[a] Methanol–water (80–20 v/v) solutions were employed and 0.1 M TlOAc was used as a phosphorescence enhancer.
[b] Analyte-to-background signal ratio measured at the maximum emission wavelength of the analyte (see Table 3). Excitation wavelength = 337 nm.
[c] LODs obtained as those estimated in Table 3.

improvement obtained in the analyte-to-background signal ratios (S_A/S_B) for the NHCs. The LODs estimated on low-background filter-paper were from 3 to 7 times lower than those reported in Table 3. As expected, no modifications were observed to the $\lambda_{exc}/\lambda_{em}$ of the NHCs. The maximum peaks are in agreement with those reported in Table 1. Fig. 4 shows the RTP emission spectra of phenanthridine on a low-background paper substrate. Further
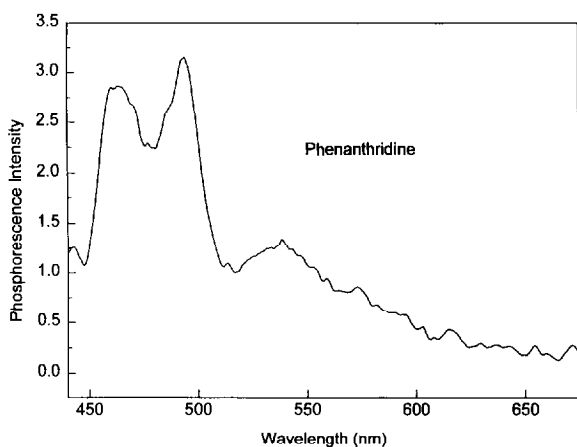
Fig. 4. Laser-induced RTP emission spectrum of a 10^{-5} M solution of phenanthridine (methanol–water (80:20 v/v)) obtained with the fiber optic sensor using a low-background paper substrate. TlOAc (0.1 M) was used to enhance phosphorescence emission. Laser excitation wavelength = 337 nm.

improvements in the LODs of the NHCs could have been obtained by drying each compound at its optimum drying time. In addition to low-background paper substrates, this possibility should be considered in the analysis of samples with PAC levels lower than ng ml^{-1}.

4. Conclusions

The LI-RTP sensor reported here has the potential to perform determinations of PACs in aquatic systems. The spectral characteristics obtained for six PACs and their AFOMs demonstrate the feasibility of the new sensor for qualitative and quantitative analyses of unknown samples.

The LI-RTP sensor presents several advantages over sensors based on laser-induced fluorimetry. Owing to the intrinsic characteristics of the phosphorescence phenomenon, a higher degree of selectivity should be expected from the LI-RTP device. The forbidden nature of the phosphorescence electronic transition [18,19] reduces the number of potential interferents in the analysis of complex mixtures. Furthermore, the long decay times of phosphorescence emissions (milliseconds to seconds) allow one to time discriminate against the interference from fluorescent concomitants, fluorescence background and other short-lived phenomena such as Raman effects and scattering. In the analysis of complex mixtures with several phosphorescent concomitants, the selectivity toward a target compound can be enhanced by selective external heavy-atom perturbation (SE-HAP) [24].

The proposed sensor also presents significant instrumental advantages. RTP emission usually occurs at longer wavelength regions than fluorescence, which allows the use of low-cost fiber optics for measurements beyond 450 nm. The measurements of triplet excited state lifetimes (microseconds to seconds) require less expensive instrumentation than fluorescence lifetimes, which are usually in the nanosecond range.

We believe that the RTP sensor is an attractive approach for field applications. The laser system is very simple to operate, relatively small and

requries minimum alignment. The design of the sensing device minimizes the contact of the analyte with quenching species such as oxygen and moisture, eliminating the need for the flow of dry gas usually employed with conventional instrumentation. By using appropriate heavy-atom salts, the λ_{exc} of compounds of interest can be shifted to overlap the excitation line of the nitrogen laser. As a consequence, a change in the excitation source might be avoided. Synchronous excitation techniques [40] can further improve the selectivity of RTP analysis. By spotting standard solutions on the paper substrates previously imbibed with the sample, on-site identification of compounds can be easily performed. Finally, by changing the paper substrate in the sample compartment, the LI-SSRTP sensor can be used for an infinite number of measurements. This represents a valuable feature for the analysis of a large number of environmental samples.

Acknowledgements

References

[1] S.G. Schulman (Ed.), Molecular Luminescence Spectroscopy, Methods and Applications, Part 2, Wiley, New York, 1988.

[2] S.M. Klainer, J.R. Thomas and J.C. Francis, Sensors Actuators B, 11 (1993) 81.

[3] T. Vo-Dinh (Ed.), Chemical Analysis of Polycyclic Aromatic Compounds, Wiley, New York, 1989.

[4] Grimer G. (Ed.), Environmental Carcinogens: Polycyclic Aromatic Hydrocarbons, CRC Press, Boca Raton, FL, 1983.

[5] M.J. Suess, Sci. Total Environ., 6 (1976) 239.

[6] J.P. Alarie and T. Vo-Dinh, Talanta, 38 (1991) 529.

[7] W.A. Chudyk, M.M. Carrabba and J.E. Kenny, Anal. Chem., 57 (1985) 1237.

[8] S.M. Inmam, P. Thibado, G.A. Theriault and S.H. Liberman, Anal. Chim. Acta, 239 (1990) 45.

[9] A. Miuone, B.W. Smith and J.D. Winefordner, Talanta, 37 (1990) 111.

[10] R. Niessner, U. Panne and H. Schroder, Anal. Chim. Acta, 225 (1991) 231.

[11] U. Panne and R. Niessner, Sensors Actuators B, 13–14 (1991) 288.

[12] A. Robbat, L. Tyng-Yun and B.M. Abraham, Anal. Chem., 64 (1992) 1477.

[13] R.T. Madison, M.K. Carroll and G.M. Hieftje, Appl. Spectrosc., 43 (1989) 422.

[14] M.K. Carroll and G.M. Hieftje, Appl. Spectrosc., 46 (1992) 126.

[15] R.P. Garcia, Y.M. Liu, M.E. Diaz-Garcia and A. Sanz-Medel, Anal. Chem., 61 (1991) 1759.

[16] F. Alvaro-Moreno, M.E. Diaz-Garcia and A. Sanz-Medel, Anal. Chim. Acta, 281 (1993) 637.

[17] M.J. Valencia-Gonzalez, Y.M. Liu, M.E. Diaz-Garcia and A. Sanz-Medel, Anal. Chim. Acta, 283 (1993) 439.

[18] T. Vo-Dinh, Room Temperature Phosphorescence for Chemical Analysis, Wiley, New York, 1984.

[19] R.J. Hurtubise, Phosphorimetry: Theory, Instrumentation and Applications, VCH, New York, 1990.

[20] A.D. Campiglia and C.G. De Lima, Anal. Chem., 59 (1987) 2822.

[22] T. Vo-Dinh and R.B. Gammage, Anal. Chem., 50 (1978) 2054.

[22] E. Lue-Yen Bower and J.D. Winefordner, Anal. Chim. Acta, 102 (1978) 1.

[23] C.D. Ford and R.J. Hurtubise, Anal. Chem., 51 (1979) 659.

[24] T. Vo-Dinh and J.R. Hooyman, Anal. Chem., 51 (1979) 1915.

[25] Y.S. Su and J.D. Winefordner, Microchem. J., 27 (1982) 151.

[26] E.M. Schulman and C. Walling, Science, 178 (1972) 53.

[27] E.M. Schulman and C. Walling, J. Phys. Chem., 77 (1973) 902.

[28] R.A. Painter, S.L. Wellons and J.D. Winefordner, Anal. Chem., 46 (1974) 736.

[29] S.L. Wellons, R.A. Painter, and J.D. Winefordner, Spectrochim. Acta, Part A, 30 (1974) 2133.

[30] E.M. Schulmam and R.T. Parker, J. Phys. Chem., 81 (1977) 1932.

[31] C.D. Ford and R.J. Hurtubise, Anal. Chem., 50 (1978) 610.

[32] R.T. Parker, R.S. Freelander and R.B. Dunlap, Anal. Chim. Acta, 12 (1980) 1.

[33] T. Vo-Dinh, G.L. Walden and J.D. Winefordner, Anal. Chem., 49 (1977) 1126.

[34] G.J. Niday and P.G. seybold, Anal. Chem., 50 (1978) 1577.

[35] G. Grimer (Ed.), Environmental Carcinogens: Polycyclic Aromatic Hydrocarbons, CRC Press, Boca Raton, FL, 1983.

[36] B.K. Afghan and A.S.Y. Chau (Eds.), Analysis of Trace Organics in the Aquatic Environment, CRC Press, Boca Raton, FL, 1990.

[37] S.M.C. Gioia and A.D. Campiglia, Anal. Chim. Acta, 287 (1994) 89.

[38] R.Q. Aucelio and A.D. Campiglia, Anal. Chim. Acta, 309 (1995) 345.

[39] J.F. de Ribamar Jr. and A.D. Campiglia, Microchem. J., 52 (1995) 101.

[40] T. Vo-Dinh and R.B. Gammage, Anal. Chem., 50 (1978) 2054.

Flow injection analysis of L-lactic acid using an enzyme–polyion complex-coated electrode as the detector

Fumio Mizutani*, Soichi Yabuki, Yoshiki Hirata

National Institute of Bioscience and Human-Technology, 1–1 Higashi, Tsukuba, Ibaraki 305, Japan

Abstract

The concentration of L-lactic acid was determined by a combination of flow injection analysis with amperometric enzyme sensor detection. The enzyme sensor was prepared by immobilizing lactate oxidase in a layer of polyion complex consisting of poly-L-lysine and poly(4-styrenesulfonate). The sensor-based system can be used for the determination of L-lactate concentration up to 6 mM with a sampling rate of 120 h^{-1}, and is stable for 8 weeks after 1000 L-lactate injections. The permselectivity of the polyion complex matrix is effective for reducing the response from electrochemical interferents such as L-ascorbic acid, uric acid and acetaminophen.

Keywords: Amperometric enzyme sensor; Flow injection analysis; Lactic acid

1. Introduction

The accurate, rapid and automatic determination of L-lactic acid is necessary in clinical and industrial food laboratories. Flow injection analyis (FIA) using an amperometric enzyme electrode as the detector can accomplish this function [1]. Previously, we have prepared amperometric biosensors by immobilizing enzymes (e.g. lactate oxidase (LOD)) into membranes consisting of poly-L-lysine–poly(4-styrenesulfonate) complex [2,3]. First, an aqueous solution containing an enzyme and the polycation was placed on a glassy carbon electrode, then an aqueous solution of the polyanion was added and dried. The resulting L-lactate-sensing electrode showed high performance characteristics such as rapid response (100% response, less than 5 s), a wide linear range (0.1 μM–0.3 mM), high stability (usable for at least 8 weeks) and high selectivity for the analyte. The high selectivity originated in the permselectivity of the polyion complex membrane; the membrane was very effective in restricting the transport of typical electrochemical interferents such as L-ascorbic acid (MW 176), uric acid (MW 168) and acetaminophen (MW 151), whereas that of the analyte (MW 90) was not restricted in the layer [2]. Hence the interferencial response could

* Corresponding author

be suppressed compared with the response for L-lactic acid.

These characteristics are particularly promising for the use of the enzyme electrode in an FIA system to determine L-lactic acid in biological and food samples. In an FIA system, the dynamic range for determining the analyte can be varied by the choice of the measuring conditions such as sample volume. The injection of a small volume of sample causes the lowering of the sample concentration in the flowing stream compared with the original concentration owing to the dispersion of the sample zone [4] which is effective for shifting the determinable concentration range towards higher levels. When the determinable range for L-lactic acid becomes as high as several millimolar, the system can be used for the assay of non-diluted sera; the concentration of L-lactic acid in normal sera is around 2 mM. This paper describes the determination of L-lactic acid in sera and food samples by an FIA system using an LOD–polyion complex-coated electrode detector.

2. Experimental

2.1. Materials

LOD (EC number not assigned; from *Pediococcus* sp., MW 80 000 [5]; 40 U mg^{-1}), peroxidase (EC 1.11.1.7, from horseradish, Type VI, 330 U mg^{-1}), uricase (EC 1.7.3.3, from *Candida utilis*, Type IV, 10 U mg^{-1}), poly-L-lysine hydrobromide (MW 90 000), and lithium L-lactate were obtained from Sigma. Poly(sodium 4-styrenesulfonate) (MW 70 000) was purchased from Aldrich. Human sera was obtained from Sigma and ICN. Other reagents were of analytical-reagent grade (Nacalai Tesque). Deionized, doubly distilled water was used throughout.

F-kits (Boehringer Mannheim) were used for the spectrophotometric measurement of L-lactic acid and L-ascorbic acid. The kit for L-lactic acid uses the enzyme pair of lactate dehydrogenase (EC 1.1.1.27) and glutamate–pyruvate transaminase (EC 2.6.1.2). The concentration of uric acid in serum samples was measured by using uricase

with the peroxidase–phenol–4-aminoantipyrine chromogenic system [6].

2.2. Enzyme electrode

A glassy carbon electrode (Model 11-1000, Bioanalytical Systems), 0.14 cm^2 in area, was polished with a 0.05 μm alumina slurry, rinsed with water and dried. On the electrode surface, 10 μl of 0.04 M potassium phosphate buffer (pH 7) containing LOD (10 μM) and poly-L-lysine (10 mM in the momomer unit), and the same buffer solution (6 μl) containing poly(4-styrenesulfonate) (20 mM in the monomer unit) were placed successively. The electrode was then allowed to dry at room temperature for 24 h.

2.3. Instrumentation and measuring procedure

The FIA system employed (Bioanalytical Systems) consisted of a PM-60 double-plunger pump, an LC-4C potentiostat and an FT-1 thermostat equipped with a flow-through cell and an injection valve. A single-line manifold for the FIA was made from 0.25 mm PTFE tubing with a distance of 60 cm between the injection valve and the flow-through cell. Such a long tube is considered to be effective in lowering the sample concentration at the flow-though cell due to the dispersion of a sample zone [7]. The flow-through cell consisted of the enzyme electrode, an Ag/AgCl reference electrode, a stainless-steel auxiliary electrode and a PTFE gasket (thickness 25 μm). A 5 μl sample loop was used for injecting sample solutions, unless stated otherwise.

A potassium phosphate buffer (0.1 M, pH 7.7), which was saturated with air, was used as a carrier solution. The flow rate was usually 0.5 ml min^{-1}. The pH of the buffer is close to the optimum pH of LOD [2,8]. The potential of the enzyme electrode was set at 1 V vs. Ag/AgCl. This potential was sufficient for the oxidation of the hydrogen peroxide produced through the LOD reaction on a carbon electrode [9,10]. The temperature of the flow-through cell was kept at 30.0 ± 0.5°C. When not in use, the flow-through cell with the enzyme electrode was left at room temperature.

3. Results and discussion

3.1. Effect of sample volume and flow rate

The electrode current increased after the addition of L-lactic acid to reach a peak and then returned the baseline. The relationship between the peak current and the L-lactate concentration was examined by using 5, 10, 20, 50 and 100µl sample loops. The use of a sample loop with a small volume was found to be useful for the determination of higher concentrations of L-lactic acid. Fig. 1 shows typical results obtained by using the 5 and 50 µl sample loops. The use of the 50 µl sample loop gave a calibration curve whose linear region extended only up to 0.5 mM. On the other hand, when the 5 µl sample loop was employed, a linear relationship was obtained up to 2.5 mM and a significant increase in the current was still observed with L-lactate concentrations between 2.5 and 6 mM. The determinable concentration range, up to 6 mM, enables us to apply non-diluted serum as the sample. Hence the 5 µl sample loop was used for subsequent examinations.

Fig. 2 shows the effect of the flow rate on the peak current for 1 mM L-lactic acid and the time for reversion to the baseline. Both the current response and the baseline reversion time decreased with increasing flow rate, first rapidly and then more gradually. The decrease of the current
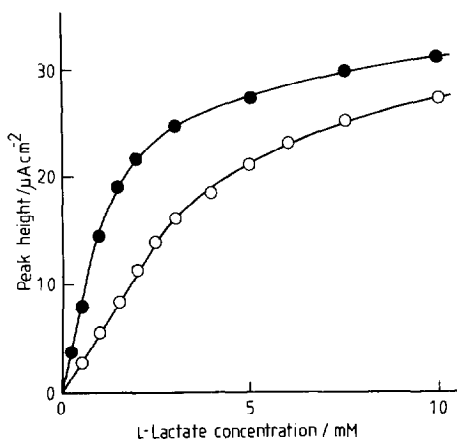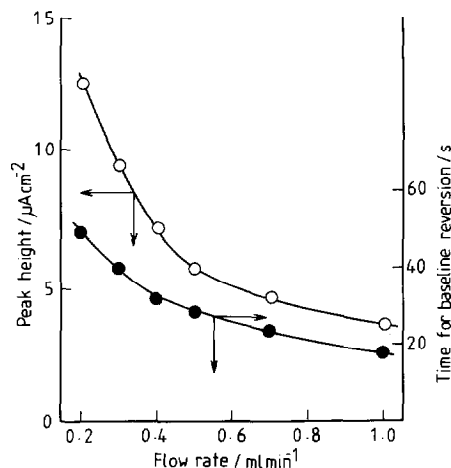

Fig. 2. Effect of flow rate on (○) the peak current for 1 mM L-lactic acid and (●) the baseline reversion time.

peak results from the increase in the dispersion of the sample in association with the increase in flow rate [4]. For subsequent measurements, the flow rate was set at 0.5 ml min⁻¹. In this condition, the travel time and the baseline reversion time were 10 and 30 s, respectively. These values agreed with those obtained from the semi-empirical model of Vanderslice et al. [7], where the detector response has been assumed to be very fast. The baseline reversion time provided a maximum sampling rate of ca. 120 h⁻¹.

Fig. 1. Calibration graphs for L-lactic acid obtained by using (○) 5 µl and (●) 50 µl sampling loops.
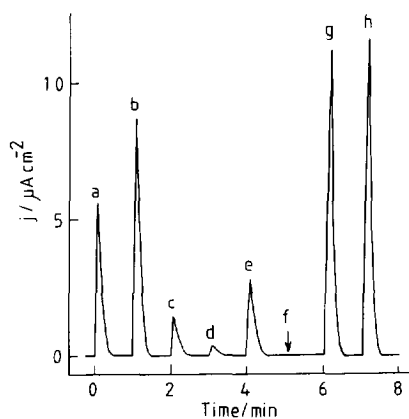

Fig. 3. Current–time curves for the addition of (a) 1 mM L-lactic acid, (b) 0.2 mM hydrogen peroxide, (c) 1 mM L-ascorbic acid, (d) 0.2 mM uric acid, (e) 1 mM acetaminophen, (f) 1 mM NADH, (g) 2 mM L-lactic acid and (h) a mixture of 2 mM L-lactic acid, 0.05 mM L-ascorbic acid and 0.2 mM uric acid.

Table 1
Comparison of results obtained for L-lactic acid in sera by different methods

Sample no.[a]	Proposed method		F-kit method
	L-Lactate concentration (mM)	RSD (%)	L-Lactate concentration (mM)
1	2.80	1.5	2.75
2	1.75	1.1	1.71
3	2.07	1.3	2.01

[a] The concentrations L-ascorbic acid and uric acid were determined to be 0.03 and 0.14 mM for the serum 1, 0.04 and 0.12 mM for the serum 2 and 0.04 and 0.18 mM for the serum 3.

The detection limit at the standard sample volume and flow rate was 20 μM (signal-to-noise ratio = 5). The relative standard deviation for 100 successive measurement of 2 mM L-lactic acid was 1.4%.

3.2. Response for L-lactic acid and interferents

Curves a–f in Fig. 3 show the current responses after the injection of L-lactic acid, hydrogen peroxide, L-ascorbic acid, uric acid, acetaminophen and NADH (the concentration was 0.2 mM for hydrogen peroxide and uric acid and 1 mM for the other species), respectively. The peak current for hydrogen peroxide was several times larger than that for the same concentration of L-lactic acid. The L-lactic acid introduced in the flow-through cell would be partially consumed on the solution side in the LOD–polyion complex membrane. This brings about a decrease in the concentration gradient of the hydrogen peroxide produced through the LOD reaction near the glassy carbon electrode, which results in a smaller response to the injection of L-lactic acid than in the case of hydrogen peroxide.

The injection of L-ascorbic acid, uric acid and acetaminophen brought about discernible current responses, indicating that these species interfere in the measurement of L-lactic acid, whereas NADH, having a much higher molecular weight (665), did not give a discernible response. However, the current response for each interferent was much smaller than that for L-lactic acid (and for hydro-

gen peroxide): the ratios of the response for the interferent to that for the same concentration of L-lactic acid were 0.25, 0.35 and 0.55 for L-ascorbic acid, uric acid and acetaminophen, respectively. The small ratio between the interferent and the analyte responses (or that between each electroactive species with a molecular weight higher than 150 and hydrogen peroxide (MW 34) suggests that the polyion complex layer shows permselectivity based on the solute size. The permselectivity of the polyion complex-based membranes has been proved as follows [2,3]. The ratios of anodic current response on the membrane-covered electrode to that on a bare glassy carbon electrode were measured for a variety of electroactive species whose molecular weights ranged from 30 (hydrazine) to 665 (NADH). The ratio was >0.5 for the electoactive species having molecular weights <100 and decreased sharply with molecular weights >100 (to 0.23 for hydroquinone (MW 110) and 0.03 for L-ascorbic acid).

The concentrations of L-lactic acid, L-ascorbic acid, uric acid and acetaminophen in normal sera are around 2, 0.05, 0.2 and 0 mM, respectively. Hence the current change caused by the interferents is expected to be 4% for measureing L-lactate concentration in the sera. Curves g and h in Fig. 3 show the current response for 2 mM L-lactic acid and for the mixture of 2 mM L-lactic acid, 0.05 mM L-ascorbic acid and 0.2 mM uric acid, respectively. The injection of the mixture actually gave a 4% excess peak current compared with the pure L-lactate solution, as shown in Fig. 3. Hence, the present system is expected to be useful for the assay of L-lactic acid in normal sera with an error of within a few per cent.

3.3. Determination of L-lactic acid in sera and sour milks

Table 1 gives the results for the determination of L-lactic acid in three kinds of normal sera. Each serum was used without dilution and was injected 10 times. The concentration was determined from the average value of the peak current for the 10 measurements. The relative standard deviation for each set of 10 measurements was within those obtained by the F-kit method.

Table 2
Comparison of results obtained for L-lactic acid in sour milks by different methods

Sample no.[a]	L-Lactate concentration	
	Proposed method	F-kit method
1	63.8	61.4
2	74.6	73.0
3	53.3	53.6
4	87.9	86.1
5	72.4	74.4
6	55.0	54.6
7	61.0	60.4
8	89.2	88.9
9	71.7	73.2
10	75.9	27.8

[a] The concentration of L-lactic acid in each sample was less than 1 mM.

The FIA system was also used for the determination of L-lactic acid in sour milks. Ten kinds of sour milks were used (each sample was diluted 50-fold with 0.1 M phosphate buffer (pH 7.7)) and the results were compared with those obtained with the F-kit method. The agreement was excellent (Table 2); the regression equation between the results obtained with the FIA (x in
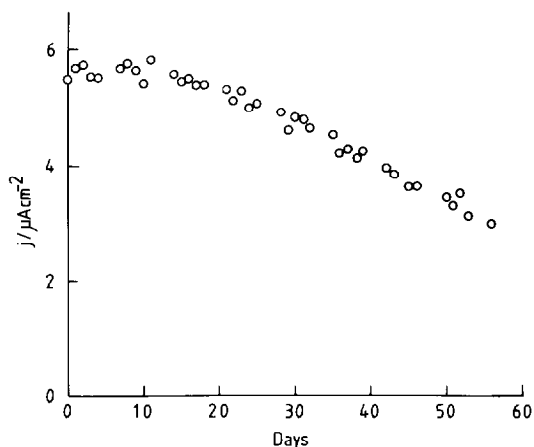

Fig. 4. Long-term stability of the enzyme electrode-based system. The electrode response for 1 mM L-lactic acid was measured 30 times a day. The average value for the 30 measurements is plotted against the number of days after the preparation of the enzyme electrode.

mM) and those with the F-kit method (y in mM) was $y = 0.975x + 1.078$ and the correlation coefficient was 0.991.

These results show that the present FIA system is useful for the simple and rapid determination of L-lactate concentration in non-diluted sera and (diluted) sour milks.

3.4. Stability of the sensor

The long-term stability of the enzyme electrode-based system was examined by determining 1 mM L-lactic acid 30 times a day on each day for 8 weeks. More than 1000 L-lactate injections were performed during this period. The system could be used even at the end of the eighth week. The average value for 20 measurements did not decrease for 3 weeks, as shown in Fig. 4. The current response gradually decrease after 3 weeks, but the current response on the 56th day was still more than 50% of the initial value. The relative standard deviation for the 30 measurements was within 1.5% on each day for the first 3 weeks, and increased slightly after 3 weeks to 2.5% on the 56th day. The present system thus showed a high stability.

High biocompatibility is another attractive feature of polyion complex membranes [11]. For example, the adhesion of platelets on a glass plate could be suppressed by coating the surface with a polyion complex [12]. The enzyme–polyion complex detector would therefore be useful for determining L-lactic acid in whole blood. Such an examination will be carried out in near future.

References

[1] B. Olson, H. Lundback, G. Johansson, F. Scheller and J. Nentwig, Anal. Chem., 58 (1986) 1046.
[2] F. Mizutani, S. Yabuki and Y. Hirata, Anal. Chim. Acta, 314 (1995) 233.
[3] F. Mizutani, S. Yabuki and Y. Hirata, Denki Kagaku, 63 (1995) 1100.
[4] A.U. Ramsing, J. Ruzicka and E.H. Hansen, Anal. Chim. Acta, 129 (1981) 1.
[5] Enzyme Catalog, Toyo Jozo, Tokyo, T-13, 1986.
[6] B.B. Bauminger, J. Clin. Pathol, 27 (1974) 1015.
[7] J.T. Vanderslice, K.K. Stewart, A.G. Rosenfeld and D.J. Higgs, Talanta, 28 (1981) 11.

[8] F. Mizutani, S. Yabuki and M. Asai, Anal. Chim. Acta, 245 (1991) 145.

[9] L. Gorton, Anal. Chim. Acta, 178 (1985) 247.

[10] F. Mizutani, S. Yabuki and T. Katsura, Anal. Chim. Acta, 274, (1993) 201.

[11] H.J. Bixler and A.S. Michaels, Encycl. Polym. Sci. Eng., 10 (1969) 765.

[12] K. Kataoka, T. Akaike, Y. Sakurai and T. Tsuruta, Macromol. Chem., 179 (1978) 1121.

Chelating ion-exchange resin membrane sensor for nickel(II) ions

G.N. Rao[a], Sandeep Srivastava[a], S.K. Srivastava[b,*], Manendra Singh[b]

[a]*Department of Chemistry, IIT, Hauz Khas, New Delhi-110016, India*
[b]*Department of Chemistry, University of Roorkee, Roorkee-247 667, India*

Abstract

A chelating ion-exchange resin (1-hydroxy-2-naphthaldoxime–formaldehyde polymer) containing nitrogen and oxygen donor atoms was prepared and characterized. The resin behaves as a selective chelating ion exchanger for some metal ions. The poly(vinyl chloride)-based membrane electrode of the resin shows a Nernstian response for Ni^{2+} over a wide concentration range (2.94×10^3–5.87×10^3 mg dm^{-3}) between pH 3.0 and 7.5. The electrode is found to possess adequate stability and specific selectivity with a response time of 10 s. The sensor can also be used in a partially non-aqueous medium having a 35% (v/v) non-aqueous content.

Keywords: Chelating ion-exchange resin; Membrane sensor; Nickel(II)

1. Introduction

Ion-exchange resins incorporating oxime and hydroxyoxime functional groups form an important class of polymeric ligands because of their strong chelating properties. The selectivity of a hydroxime resin prepared from substituted phenyl-acrylate polymer has been reported by Walsh et al. [1]. Resacetophenone oxime, after condensation with formaldehyde, forms a resin [2] which is highly selective to Cu(II) ions. A number of compounds having 2-hydroxyacryloximes [3] have been impregnated in polymeric matrices and these find extensive applications in the hydrometallurgy of Cu(II).

This class of compound, i.e. chelating ion-exchange resins, are found to possess specific selectivity for some metal ions and play an improtant role in separation processes. Recently we have reported the utility of salicylaldoxime–formaldehyde resin membranes for the estimation of zinc [4].

In this paper we report the electroanalytical applicability of a 1-hydroxy-2-naphthaldoxime–formaldehyde (HDF) resin membrane as a nickel ion sensor. The proposed sensor has very good selectivity for nickel over other cations.

Relatively few reports have appeared on the development of membrane sensors for nickel ions. Most of these involve an electroactive phase such as nickel–dimethylglyoxime complex [5,6], nickel phosphate [7] or nickel bis(2-ethylhexyl)phosphate [7,8]. Some liquid membrane electrodes in-

---

volving O,O'-diisobutyl dithiophosphatonickel(II) [9], nickel, 8-quinolinedithiocarboxylate [10], etc., in appropriate solvents, have also been tried for the estimation of nickel but most of these suffer from interference by metal ions which may be present as routine contaminants. The sensor reported in this paper can be prepared easily and exhibits much better selectivity for Ni^{2+} than that reported earlier.

Although the resin mentioned above shows a selective uptake of some metal ions in the sequence $Fe^{2+} > Pb^{2+} > Ni^{2+} > Zn^{2+} > Pd^{2+}$, the membrane selectivity does not necessarily follow the same pattern and is different to the pure material owing to the application of neutral binders, incorporated during fabrication. The presence of binding material affects the conductance of the membrane, which is an additional parameter of the sensor affecting the selectivity in comparison with the electroactive phase taken in the pure state.

2. Experimental

2.1. Reagents

All chemicals were of analytical-reagent grade. Solutions were prepared in doubly istilled water.

2.2. Synthesis and characterization of the resin

The procedure followed for the synthesis of the resin was similar to that followed for salicylaldoxime–formaldehyde and other compounds of the same series [11]. The procedure provides a product having optimum separation potential.

1-Hydroxy-2-naphthaldehyde (0.05 mol) was converted into the corresponding oxime using hydroxylammonium chloride and doubly distilled ethanol. 1-Hydroxy-2-naphthaldoxime was then mixed with formaldehyde in the molar ratio 1:4.2 and 3% (w/w) of 40% sodium hydroxide solution was added as a catalyst. The mixture was heated under reflux in an oil-bath at $115 \pm 1°C$ for 7 h. The resinous mass obtained was poured into a container and dried at $100 \pm 1°C$ for 10 h. The black granular resin obtained was powdered and sieved.

On the basis of elemental analysis (found, C 72.19, H 4.94, N 6.96; theoretical, C 72.00, H 5.00, N 7.00%) and infrared spectrometry the following structure of the repeating unit has been assigned to the product used as the electroactive phase:
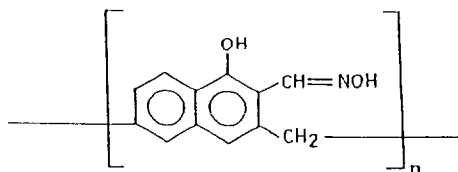
The number-average molecular weight of the resin as determined by vapour-phase osmometry in tetrahydrofuran (THF) at 30°C was 2625. Differential scanning calorimetric (DSC) scans of the resin showed a melting temperature of 120°C and a decomposition temperature of 280°C. Thermogravimetric analysis showed no mass loss in the region of 100°C, thereby indicating no moisture absorption. Major mass loss (31.5%) took place in the range 300–400°C and the breakdown of the polymer was observed at 500–600°C. The char yield obtained at 600°C was 12%.

2.3. Preparation of membranes

A heterogeneous membrane of this compound was prepared using PVC as binder material and a 1:1 mixture of the two was dissolved in THF. The resulting solution was stirred well and poured into a casting glass ring on a glass plate and the THF was evaporated at room temperature. A membrane sheet about 0.05 mm thick and 6 mm in diameter was cut away from inner edge and glued to one end of a Pyrex glass tube with Araldite. The process was optimized, after detailed preliminary investigations, so that the membrane generates reproducible potentials and the fabrication of membranes was carefully controlled to have batch-to-batch reproducibility.

2.4. Potential measurement

The membrane was equilibrated in 1.00 mol dm^{-3} nickel ammonium sulphate solution for 4 days, the time after which it generates repro-

ducible, noiseless and stable potentials when interposed between the test solution and an internal reference solution of 0.100 mol dm^{-3} concentration. Potentials were measured, as reported earlier [12], at 25 ± 1°C by direct potentiometry with the help of ceramic junction calomel electrodes and a saturated ammonium nitrate bridge. The measurement of potentials was made from low to high concentrations to avoid memory effects. The ionic strength of various solutions was maintained using NH_4NO_3 (10^{-3} mol dm^{-3}) and pH adjustments were made with dilute acid or hexamine. The standard deviation of about 20 measurements was 0.2 mV.

2.5. Evaluation of selectivity coefficient

The potentiometric selectivity of the membrane was evaluated in terms of selectivity coefficients obtained by a mixed solution (fixed interference) method (as recommended by IUPAC).

2.6. Conductance measurement

The conductance of the membranes (in different cationic forms) was measured by the modified method adopted by Lakshminarayanaiah et al. [13], which makes use of a mercury pool on both sides of the membrane to minimize polarization at the membrane interface. The membrane was cemented between two Pt electrodes with epoxy resin and kept in contact with electrolyte solution of 0.1 mol dm^{-3} concentration. The solution was then replaced by mercury previously equilibrated with the electrolyte solution of the same concentration and the conductance was measured by connecting the platinum electrodes to a conductance bridge.

3. Results and discussion

The static response time of the proposed membrane electrode is about 10 s over the entire working concentration range and the potentials remain constant for more than 3 min, after which a very slow divergence is observed. Under laboratory conditions, if the membrane is properly
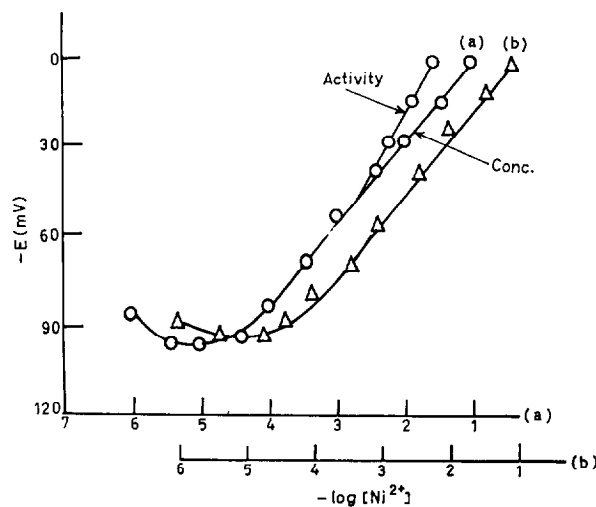

Fig. 1. Variation of membrane potential with (a) concentration/activity of nickel ions (taken as nickel ammonium sulphate) and (b) constant ionic strength.

stored in distilled water and if cross-contamination is avoided, it can be used for 2 months without observing any drift in potential. Thereafter it can be regenerated or else a new membrane can be fabricated and used.

The potential response of the membrane obtained with pure solutions is illustrated in Fig. 1(a). It is observed that the membrane electrode can measure Ni^{2+} ions in the range 2.35×10^3–5.87×10^3 mg dm^{-3} (4.00×10^{-5}–0.1 mol dm^{-3}) as per IUPAC recommendations and it also exhibits Nernstian behaviour (slope 28.50 mV per decade of concentration). Activity coefficients of solutions were obtained with the extended form of the Debye–Hückel equation and a potential vs. activity plot is also shown in Fig. 1(a). The working pH range of the sensor is 3.0–7.5 (Fig. 2). Fig. 1(b) depicts the potential vs. [Ni^{2+}] relationship obtained at constant ionic strength.

The performance of the proposed sensor system was also investigated in partially non-aqueous media using water–methanol and water–ethanol mixtures. The membrane works well in a partially non-aqueous medium up to a maximum of 35% (v/v) non-aqueous content (data not shown) without any change in the working concentration range or slope. However, at larger non-aqueous contents (> 35%) the slope and working concen-
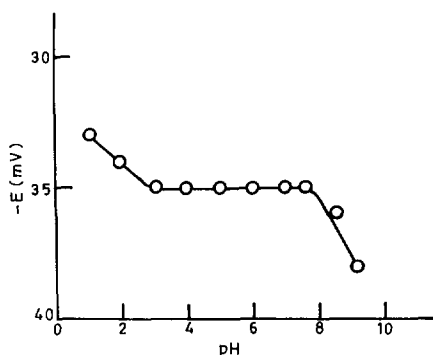
Fig. 2. Variation of membrane potential with pH.

tration range decrease appreciably. It was also possible to use the membrane as an indicator electrode for the potentiometric titration of nickel ions. Fig. 3 depicts the titration of 10 cm^3 of 1.00×10^{-4} mol dm^{-3} Ni^{2+} ions with 1.00×10^{-3} mol dm^{-3} EDTA solution. The necessary adjustment of pH was made before adding the titrant. A sharp inflection point and perfect stoichiometry are noteworthy features of this titration.

The performance of an electrode is judged by the selectivity for the determinand ion in presence of foreign ions. The selectivity pattern of membranes fabricated with the help of an inert binder is usually different to that of pure membrane material. Table 1 presents the conductance data for the membrane embedded with different cations (it is not possible to obtain conductance data for pure polymeric resin). The magnitude of the conductance (Table 1) amply justifies its application as an ion-selective electrode especially for
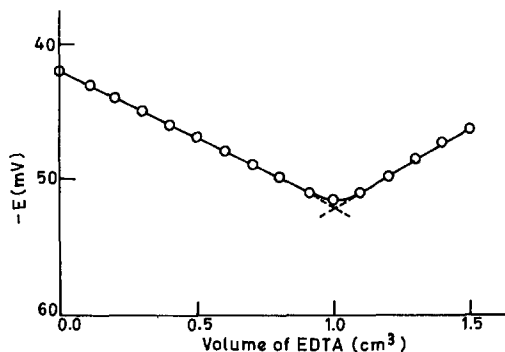
Table 1
Specific conductance of PVC-based 1-hydroxy-2-naphthaldoxime–formaldehyde polymer membranes in different cationic forms

Cation	Specific conductance (10^2 milli mhos cm^{-1})	Cation	Specific conductance (10^2 milli mhos cm^{-1})
Li$^+$	2.8	Ni^{2+}	5.8
Na$^-$	2.5	Mn^{2+}	3.6
K$^+$	2.8	Zn^{2+}	5.4
Ca^{2+}	3.8	Cd^{2+}	3.6
Sr^{2+}	4.8	Al^{3+}	3.8
Mg^{2+}	4.8	Fe^{3+}	4.2
Pb^{2+}	5.2		

the estimation of Ni^{2+}.

The selectivity coefficient values (Fig. 4) of a number of other ions in comparison with nickel were obtained at an interference level of 10^{-2} mol dm^{-3}. The membrane exhibits excellent selectivity for nickel ions and no interference is observed from normal interferents such as Zn^{2+}, Cd^{2+}, Co^{2+} and Pb^{2+}, even at this high concentration. Some monovalent cations register high selectivity coefficients and may cause some disturbance in the operation of this electrode at higher concentrations. To obtain a true assessment and tolerance limits of the sensor for the ions mentioned, above some mixed runs, i.e. monitoring of the
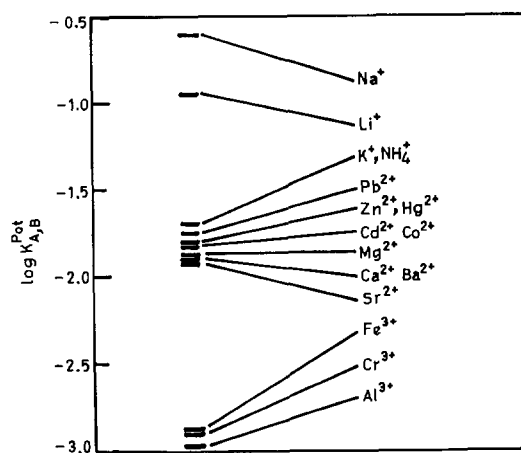

Fig. 3. Titration of 10 ml of 1.00×10^{-4} mol dm^{-3} Ni^{2+} ions with 1.00×10^{-3} mol dm^{-3} EDTA solution.

Fig. 4. Selectivity coefficients (log $K^{Pot}_{A,B}$) at 1.00×10^{-2} mol dm^{-3} concentration of interfering ions with respect to Ni^{2+} ions.
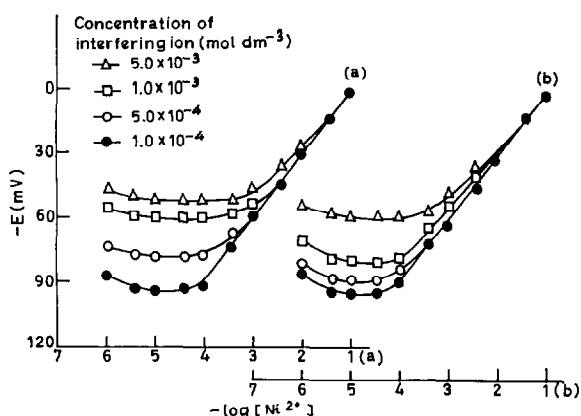
Fig. 5. Variation of membrane potential with concentration of interfering ions: (a) Na^+; (b) K^+.

sensor potential vs. concentration, were made with Ni^{2+} ions in contact with different concentrations of the interferents. The data (Fig. 5) reveal that Na^+ starts to interfere even at 10^{-4} mol dm^{-3} and the linearity range and the slope decrease, whereas with K^+ significant interference is only observed at 10^{-3} mol dm^{-3}. Other multivalent ions would normally not interfere unless present at very high concentrations, a situation which is hardly met.

The utility of the membrane electrode was also observed in solutions contaminated with proteinous matter and washings containing surfactants. Small amounts of these substances do not disturb the working of the membrane electrode. Potential vs. $[Ni^{2+}]$ plots obtained in the presence of 5.00×10^{-5} mol dm^{-3} of cationic (cetyltrimethylammonium bromide) and anionic (sodium dodecyl sulphate) surfactants (data not shown) correspond fairly well with the plot recorded with pure nickel ion solutions, but at higher concentrations, of which there is a slight possibility in actual practice, these can cause some disturbance of the working of electrode assembly.

4. Conclusion

Chelating ion-exchange resins provide a suitable matrix for the fabrication of membrane sensors. 1 - Hydroxy - 2 - naphthaldoxime – formaldehyde polymer membrane exhibits promising selectivity for Ni^{2+} ions and the proposed sensor can be used to estimate nickel over a wide concentration range.

Acknowledgements

References

[1] D.J. Walsh, P. Crosby and R.F. Dalton, Polymer, 24 (1983) 423.

[2] V. Sykora and F. Dubsky, Collect. Czech. Chem. Commun., 32 (1967) 3342.

[3] A. Warshawsky, Inst. Min. Metall. Trans., Sect. C, 101 (1974) 83.

[4] S.K. Srivastava, H. Vardhan, M. Singh, G.N. Rao and S. Srivasta, Anal. Proc., 32 (1995) 173.

[5] E. Pungor, K. Toth and J. Havas, Acta. Chim. Acad. Sci. Hung., 48 (1966) 17.

[6] E. Pungor, K. Toth and J. Havas, Microchim. Acta, (1966) 689.

[7] E.B. Buchann and J.L. Seago, Anal. Chem., 40 (1968) 517.

[8] S.P. Awasthi, V.T. Kulkarni and M. Sundaresan, J. Electrochem. Soc. India, 37 (1988) 309.

[9] E.A. Materova, V.V. Muckovikov and M.G. Grigorieva, Anal. Lett., 8 (1975) 167.

[10] O.A. Lebedera and E. Jansons, Latv. PSR Zinat. Akad. Vestis, Kim. Ser., 4 (1986) 423.

[11] S. Srivastava and G.N. Rao, Analyst, 115 (1990) 1607.

[12] S.K. Srivastava, V.K. Gupta and S. Jain, Analyst, 120 (1995) 495.

[13] N. Lakshminarayanaiah and V. Subrahmanayam, J. Phys. Chem., 72 (1968) 4314.

Determination of doxorubicin hydrochloride by visible spectrophotometry

Chilukuri S.P. Sastry*, Jana S.V.M. Lingeswara Rao

Foods and Drugs Laboratories, Department of Organic Chemistry, Foods, Drugs and Water, Andhra University, Visakhapatnam-530 003, India

Abstract

Four simple and sensitive visible spectrophotometric methods (A–D) have been described for the assay of doxorubicin hydrochloride either in pure form or in pharmaceutical formulations. Method A was developed based on oxidation of the drug with Fe(III) to produce Fe(II), which subsequently reacts with 1,10-*ortho*-phenanthroline to form a red colored complex (λ_{max}: 510 nm) at pH 4.6. Method B involves the reduction of Folin–Ciocalteu (F–C) reagent by the drug and the reduced species formed possesses a characteristic intense blue color (λ_{max}: 770 nm). In methods C and D, oxidation of the drug with periodate at specified experimental conditions yields formaldehyde and dialdehyde, which in turn react either with 3-methyl-2-benzothiazolinone hydrazone hydrochloride to form an intensely brilliant blue cationic dye (λ_{max}: 620–670 nm, method C) or by condensation with phenylhydrazine hydrochloride (PHH) to form orange-red colored product (λ_{max}: 510 nm, method D) in the presence of potassium ferricyanide. All of the variables have been optimized and the reaction mechanisms presented. The concentration measurements are reproducible within a relative standard deviation of 1.0%.

Keywords: Doxorubicin hydrochloride determination; Visible spectrophotometry

1. Introduction

Doxorubicin hydrochloride (DXH) is an anti-cancer agent, widely used in acute lymphocytic leukemia and various carcinomas. It is chemically known as (8S-*cis*)-5, 12-naphthacenedione, 10-((3-amino-2,3,6-trideoxy-L-lyxo-hexopyranosyl) oxy)-7,8,9,10-tetrahydro-6,8,11-trihydroxy-8-(hy-

_____
* Corresponding author.

droxyl acetyl)-1-methoxy hydrochloride and is official in the United States Pharmacopoeia [1]. Only a few methods, such as fluorimetry [2,3], voltametry [4], differential polarography [5], liquid chromatography [6,7], thin layer chromatography [8,9] and high pressure liquid chromatography [10–15] have been reported for its determination in biological fluids and in dosage forms. However, there is no report on visible spectrophotometry except a qualitative test with aerosol samples containing DXH [16]. Even

though the drug is colored, its aqueous solution possesses an λ_{max} value at 500 nm with a low ϵ_{max} value of 2.60×10^3. It is not sensitive enough to carry out estimations in microamounts. Hence there is a need for the development of sensitive methods for its determination by exploiting suitable chromogenic reagents for color development. The properties of the analytically important functional groups of DXH have not been exploited so far in the design of sensitive, accurate and flexible visible spectrophotometric methods for the determination of DXH in pharmaceutical formulations. So the authors have made some attempts in this direction and succeeded in developing four visible spectrophotometric methods by exploiting different structural features of the drug molecule.

Ferric ammonium sulphate or ferric chloride plays a prominent role in the colorimetric determination of organic compounds. Acting as an oxidant, ferric salt converts into ferrous salt and it can be detected easily by the usual reagent for divalent iron, *ortho*-phenanthroline (PTL) [17], bipyridyl or triazine [18], etc. Phosphomolybdotungstic acid, the well-known Folin–Ciocalteu reagent [19] was preferred by number of researchers for the determination of drugs containing phenolic or amino groups [20]. α-Ketols or α-amino-ols are oxidized by periodic acid, liberating formaldehyde as one of the products [21,22]. Sawicki et al. [23] suggested 3-methyl-2-benzothiazolinone hydrazone hydrochloride (MBTH) as a sensitive reagent for the determination of formaldehyde and other aldehydes. The Schryver reaction describes the estimation of formaldehyde with phenylhydrazine hydrochloride (PHH) in the presence of ferricyanide [24]. We have applied the above four reagents (Fe(III)/PTL, F–C, NaIO$_4$/MBTH and NaIO$_4$/PHH) for the determination of DXH in pure and pharmaceutical preparations.

2. Experimental

2.1. Instruments

A Systronics 106 digital spectrophotometer (Hyderabad) with 1 cm matched glass cells and an Elico LI-120 digital pH meter (Hyderabad) were used.

2.2. Reagents

All of the chemicals were of analytical reagent grade and all of the solutions were prepared with double-distilled water. Freshly prepared solutions were always used.

Fe(III) solution (2.0×10^{-2} M) was prepared by dissolving 0.96 g of ferric ammonium sulphate dodecahydrate (E. Merck) in 10 ml of concentrated HCl and made up to 100 ml with distilled water. F–C reagent (2.0 N), supplied by Loba Chemie Company was used directly for investigation.

Aqueous solutions of PTL (Burgoyene, 1.38×10^{-2} M), Na$_2$CO$_3$ (Sarabhai, 9.40×10^{-1} M), NaIO$_4$ (BDH, 9.35×10^{-3} M, for method C, and 4.0×10^{-2} M in 0.3 M HCl, for method D), MBTH (Fluka, 8.55×10^{-3} M), acetic acid (Qualigens, 3.5 M), PHH (Loba Chemie, 2.76×10^{-2} M) and potassium ferricyanide (Loba Chemie, 1.21×10^{-1} M) were prepared. A buffer solution was prepared by mixing equal volumes of 0.2 M acetic acid and 0.2 M sodium acetate and the pH of the solution was adjusted to 4.6.

2.3. Preparation of standard drug solution

A 1 mg ml^{-1} solution was prepared by dissolving 100 mg of pure DXH in 100 ml of distilled water and this stock solution was diluted stepwise with distilled water to obtain the working standard solutions of concentrations 20, 100 and 200 μg ml^{-1} for methods A and C, B, and D respectively.

2.4. Recommended procedures

2.4.1. Method A

Aliquots of 0.5–5.0 ml of the standard drug solution (20 μg ml^{-1}) were transferred into a series of 25 ml calibrated flasks and then solutions of 0.5 ml of Fe(III), 2.0 ml of PTL and 4.0 ml of pH 4.6 buffer were added to each flask successively. The flasks were heated on a boiling water bath for 30 min. The solutions were then cooled to the laboratory temperature and made up to the mark with distilled water. The absorbance values of the final colored solutions were measured at

510 nm within the stability period (1–60 min) against a reagent blank prepared in a similar manner but omitting the drug solution. The amount of drug was computed from a Beer–Lambert plot.

2.4.2. Method B

Aliquots (1.0–6.0 ml, 100 μg ml^{-1}) of the standard DXH solution were taken into a series of 25 ml calibrated tubes. Then 2.0 ml of F–C reagent and 9.0 ml of Na_2CO_3 solution were added successively and kept aside for 10 min at laboratory temperature. The solution was made up to the mark with distilled water and the absorbance of the solution was measured at 770 nm against a reagent blank prepared simultaneously within the stability period (5 min–5 h). The drug content was read from the calibration graph.

2.4.3. Method C

To a series of 25 ml standard flasks containing 0.5–4.0 ml of standard drug solution (20 μg ml^{-1}), 1.0 ml each of $NaIO_4$ (9.35 × 10^{-3} M) and acetic acid (3.5 M) were added. The total volume in each flask was brought to 10 ml with distilled water and kept in a boiling water bath for 15 min. After that 1.0 ml of MBTH solution was added and heated further for 1–2 min. It was later cooled and diluted to 25 ml with distilled water. The absorbance was measured at 620–670 nm against a reagent blank within the stability period (1–45 nm). The amount of DXH was computed from the Beer–Lambert plot.

2.4.4. Method D

Aliquots of the standard drug solution (0.5–2.5 ml, 200 μg ml^{-1}) were taken into a series of 25 ml calibrated flasks. Then 1.0 ml of $NaIO_4$ (4.0 × 10^{-2} M) was added and the solutions were allowed to stand for 30 min at room temperature. Later 1.5 ml of PHH solution and 1.0 ml of potassium ferricyanide solution were added successively and the solution was chilled in ice water for 5 min. Finally 5.0 ml of concentrated HCl was added and made up to the mark with methanol. The absorbance values were measured against a reagent blank at 510 nm within the stability period (1–15 min). The amount of DXH was computed from the calibration graph.

2.4.5. Analysis of pharmaceutical formulations for methods A and B

An accurately weighed amount of injection powder (vial) equivalent to 100 mg of DXH was dissolved in 100 ml of distilled water. This stock solution was further diluted to working standard solutions (20 μg ml^{-1}, for method A and 100 μg ml^{-1}, for method B) with the same solvent and was analyzed under the procedures described for pure samples.

2.4.6. Analysis of pharmaceutical formulations for methods C and D

An accurately weighed amount of injection powder equivalent to 100 mg of the drug was extracted with isopropyl alcohol (2 × 15 ml) and filtered. The combined filterate was evaporated to dryness and the residue was dissolved in 100 ml of distilled water to achieve a concentration of 1 mg ml^{-1}. This solution was further diluted stepwise with distilled water to working standard solutions (20 μg ml^{-1}, for method C and 200 μg ml^{-1}, for method D) and analysed under the procedures described for pure samples.

To compare the results obtained by the proposed procedures (A–D), an alternative or a reference procedure is necessary. A simple method has been developed as a reference method in our laboratory based on the earlier report [16] that the drug forms blue colored chromogen with NaOH.

2.4.7. Procedure for reference method

To each aliquot (0.5–4.0 ml, 50 μg ml^{-1}) of the aqueous solution of DXH (pure or formulation), 0.2 ml of 1.0 M NaOH was added and made up to 10 ml with methanol. The absorbance of the colored solution was measured at 560 nm during the stability period (1–15 min). The amount of the drug was computed from its Beer–Lambert plot.

3. Results and discussion

The optimum conditions for the development of the methods (A–D) were established by varying the parameters one at a time [25] and keeping others fixed, and observing the effect produced on the absorbance of the colored species.

In order to establish the experimental conditions in method A, DXH was allowed to react with Fe(III) in the presence of PTL. The effect of the reagent concentrations (Fe(III) and PTL), volume of buffer, temperature, time and order of addition of reagents were studied by means of control experiments. Optimization experiments reveals that the solutions of 0.5 ml of Fe(III) and 4.0 ml of buffer (pH 4.6) were necessary to attain the maximum color development. A volume of 2.0 ml of PTL solution and a heating time of 30 min on a boiling water bath were found to be optimal. The order of addition of the reagents has no effect on the absorbance of the colored species.

In order to establish the optimum volume of Na_2CO_3 solution in method B, the drug was allowed to react with F–C reagent in the presence of 10% Na_2CO_3 solution ranging from 1.0–14.0 ml. Constant absorbances were obtained with 8.0–10.0 ml; hence 9.0 ml was chosen. A volume of 2.0 ml of F–C reagent was found to be optimal. An increase in the volume of F–C reagent (> 2.0 ml) led to the precipitation. If the order of addition of the reagents (Na_2CO_3 and F–C), was reversed, the color was not noticed. Maximum color intensity was attained within 5 min after the addition of Na_2CO_3 solution and the colored product was stable for 5 h.

The influence of reagent concentrations ($NaIO_4$ and MBTH), temperature, volume of acid, heating time and order of addition of reagents with respect to maximum sensitivity, minimum blank, adherence to Beer's law and stability in method C were studied through control experiments. A volume range of 0.9–1.2 ml of $NaIO_4$ (9.35×10^{-3} M) was found to produce constant and reproducible absorbance values. So 1.0 ml of $NaIO_4$ was used in the procedure. A volume of 1.0 ml of acetic acid and 1.0 ml of MBTH were found to be necessary. A heating time of 15 min on a boiling water bath was required to produce maximum color development.

The influence of the concentration of $NaIO_4$ and the effect of oxidation time on color formation in method D has been optimized. The absorbances of the colored species remain constant within the volume range of 0.5–1.5 ml of $NaIO_4$ (4.0×10^{-2} M) and beyond the oxidation time of

30 min at room temperature. Hence 1.0 ml of $NaIO_4$ and an oxidation time of 30 min were selected for further work. A volume of 1.5 ml of PHH and 1.0 ml of potassium ferricyanide were found to be optimal. In the preparation of $NaIO_4$ solution, 0.3 M HCl was required. A minimum time of 5 min was found to be necessary for cooling in ice water prior to the addition of concentrated HCl. Maximum color intensity was attained within 2 min after the addition of methanol and the product was found to be stable up to 15 min after the attainment of maximum intensity.

The above optimum experimental conditions were incorporated in the recommended procedures for color development. Beer's law was found to be valid over the concentration ranges given in Table 1 at appropriate λ_{max} values (Fig. 1).

3.1. Reference method

The earlier report on the color test for DXH with NaOH in aerosol sample mentions the use of the solvent, dimethylsulphoxide (DMSO). However, in our systematic study of the effect of solvent (water, DMSO, dimethylformamide, methanol, acetic acid or 1,4-dioxane) in the DXH and NaOH reactions, methanol has been found to be superior when compared to other solvents with respect to maximum absorbance and stability. So in the reference method, the procedure mentioned above has been adopted. The sensitivity and precision data for this method is shown in Table 1.

3.2. Analytical data

The Beer's law limits, molar absorptivity, Sandell's sensitivity, detection limits [26], regression equation and correlation coefficients obtained by least squares treatment of these results are given in Table 1. The precision of each method was tested by analyzing six replicate samples containing 2.8, 16.0, 2.0 and 16.0 μg ml^{-1} of pure drug for methods A, B, C and D respectively. The percent standard deviation and the percent range of error at 95% confidence level of each method are given in Table 1.

Table 1
Optical and regression characteristics, precision and accuracy of the proposed and reference methods

Parameters	Methods				
	A	B	C	D	Reference
λ_{max} (nm)	510	770	620–670	510	560
Beer's law limits (μg ml^{-1})	0.4–4.0	4.0–24.0	0.4–3.2	2.0–20.0	2.5–20.0
Detection limits (μg ml^{-1})	0.034	0.22	0.086	0.42	0.18
Molar absorptivity (l mol^{-1} cm^{-1})	1.07×10^5	1.45×10^4	6.0×10^4	2.0×10^4	1.24×10^4
Sandell's sensitivity (μg g^{-2} 0.001 absorbance unit)	5.6×10^{-3}	4.0×10^{-2}	9.6×10^{-3}	2.8×10^{-2}	4.6×10^{-2}
Regression equation (Y)[a]					
Slope (b)	1.8×10^{-1}	2.4×10^{-2}	1.0×10^{-1}	2.0×10^{-2}	2.2×10^{-2}
Standard deviation on slope (s_b)	9.5×10^{-4}	1.51×10^{-4}	1.07×10^{-3}	3.74×10^{-4}	3.08×10^{-4}
Intercept (a)	3.1×10^{-3}	2.1×10^{-2}	-3.43×10^{-4}	3.43×10^{-2}	-5.3×10^{-3}
Standard deviation on intercept (s_a)	2.3×10^{-3}	2.36×10^{-3}	2.0×10^{-3}	4.96×10^{-3}	3.7×10^{-3}
Standard error of estimation (s_e)	2.97×10^{-3}	2.53×10^{-3}	2.52×10^{-3}	4.74×10^{-3}	4.4×10^{-3}
Correlation coefficient (r)	0.9999	0.9999	0.9997	0.9998	0.9995
Relative standard deviation (%)[b]	0.58	0.44	0.65	0.70	0.63
Percent range of error (95% confidence limit)	0.60	0.46	0.68	0.73	0.73

[a] $Y = a + bC$ where C is the concentration in μg ml^{-1} and Y is the absorbance units.
[b] Six replicate samples (concentrations of 2.8, 16, 2, 16 and 15 μg ml^{-1} of pure drug for methods A, B, C, D and reference respectively).

The interference studies in the determination of DXH in pharmaceutial formulation revealed that the normally existing excipients and additives like starch, lactose, talc, stearic acid, boric acid, gelatin, magnesium carbonate and sodium lauryl sulphate were found not to interfere even when present in excess (1–200 fold) in methods A and B. But in the case of methods C and D, substances possessing vicinal diols, α-amino-ol and α-ketol are expected to interfere since the above cited groups may undergo periodate oxidation leading to the formation of formaldehyde which proceeds the color reaction. In such cases, preliminary clean-up procedure with isopropyl alcohol is necessary to avoid interference due to the presence of starch and sugars like lactose prior to the estimation of DXH in formulations.

Commercial formulations (injections) containing DXH were successfully analyzed by the proposed methods. None of the excipients existing in DXH injections interfere in methods A and B even if water is directly used for solution preparation. However in methods C and D, the interfering excipients should be removed by selectively extracting DXH initially with isopropyl alcohol. The values obtained by the proposed and reference methods for injections were compared statistically by the t- and F-tests and found not to differ significantly. As an additional demonstration of accuracy, recovery experiments were performed by adding a fixed amount of the drug to the pre-analyzed formulations. These results are summarized in Table 2.

3.3. Chemistry of the colored species

In method A, the formation of the colored complex is due to the involvement of Fe(II) (formed through the oxidation of DXH with Fe(III)) and ortho-phenanthroline. The structure of this complex can be regarded as shown in Scheme 1, based on the previous reports [18,27].

The color formation by F–C reagent with DXH in method B may be explained in the following manner based on the analogy with the reports of the earlier workers [19,28]. The mixed acids in the F–C preparation involve the following chemical species: $3H_2O \cdot P_2O_5 \cdot 13WO_3 \cdot 5$

Table 2
Analysis of pharmaceutical formulations by the proposed and reference methods

Pharmaceutical formulations	Labelled amount (mg)	Amount found[a] (mg) Proposed methods				Reference method	% recovery by proposed methods[b]			
		A	B	C	D		A	B	C	D
Injection I₁	10	9.85 ± 0.019 $F = 1.17$ $t = 0.84$	9.91 ± 0.035 $F = 3.78$ $t = 1.65$	9.90 ± 0.028 $F = 2.4$ $t = 0.95$	9.89 ± 0.022 $F = 1.5$ $t = 0.72$	10.1 ± 0.018	98.7 ± 0.76	99.5 ± 0.81	98.9 ± 0.36	100.2 ± 1.2
Injection I₂	10	10.2 ± 0.071 $F = 3.9$ $t = 1.92$	9.95 ± 0.054 $F = 2.25$ $t = 1.60$	9.93 ± 0.02 $F = 3.24$ $t = 1.85$	10.3 ± 0.042 $F = 1.36$ $t = 0.73$	9.97 ± 0.036	99.2 ± 0.67	100.4 ± 0.70	98.8 ± 0.80	99.4 ± 0.73
Injection I₃	50	49.2 ± 0.084 $F = 1.1$ $t = 0.49$	49.7 ± 0.078 $F = 1.05$ $t = 0.60$	49.5 ± 0.10 $F = 1.56$ $t = 0.80$	50.2 ± 0.12 $F = 2.25$ $t = 1.27$	49.8 ± 0.08	100.5 ± 0.94	101.4 ± 0.87	99.4 ± 0.44	99.8 ± 0.95
Injection I₄	50	50.3 ± 0.075 $F = 1.15$ $t = 0.34$	49.6 ± 0.063 $F = 1.13$ $t = 0.47$	49.8 ± 0.09 $F = 1.65$ $t = 0.71$	49.4 ± 0.14 $F = 4.0$ $t = 2.1$	50.0 ± 0.07	98.9 ± 0.77	99.2 ± 0.57	99.6 ± 0.57	100.6 ± 0.61

[a] Average ± standard deviation ($n = 6$). The t- and F-values refer to comparison of the proposed method with the reference method; theoretical values at 95% confidence limit. $t = 2.57$, $F = 5.05$.

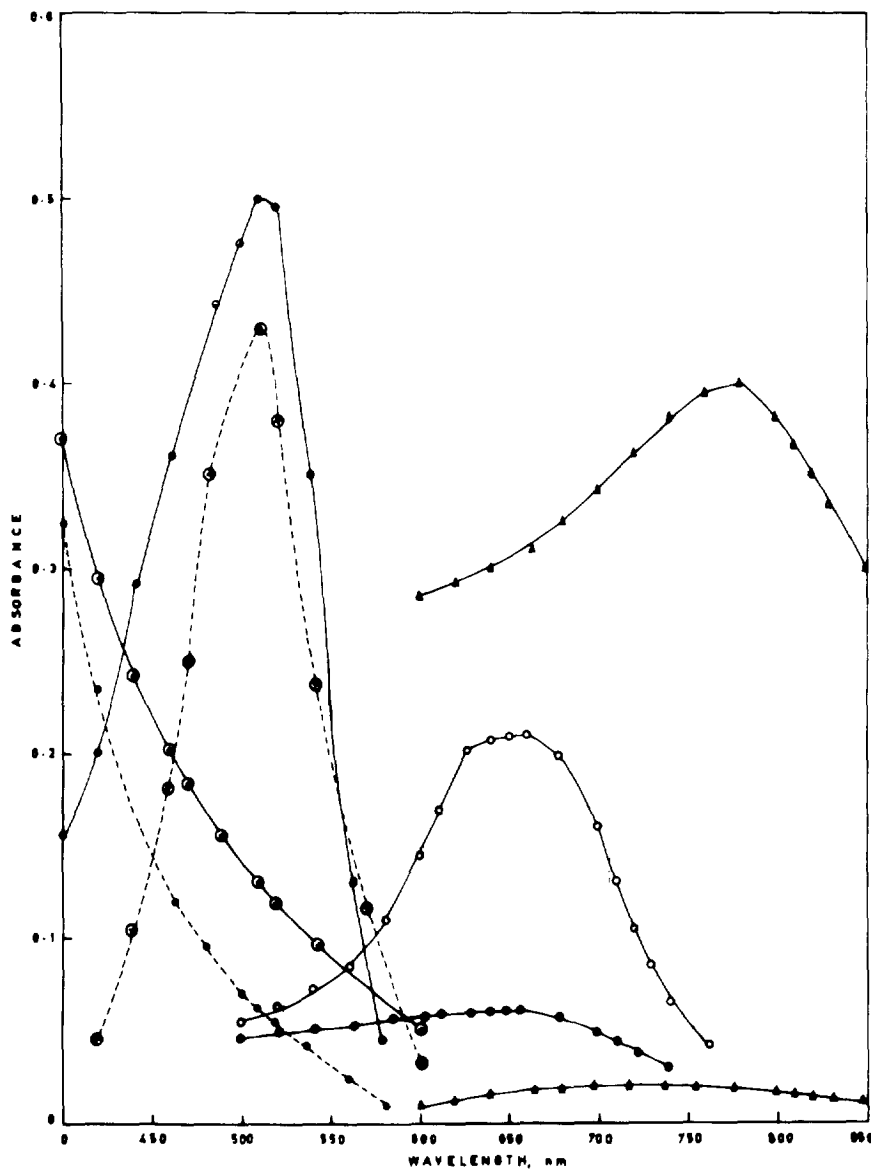[b] Recovery of 10 mg added to the pharmaceutical preparation (average of six determinations).

Fig. 1. Absorption spectra of DXH–Fe(III)–PTL system (············) against reagent blank (●───●) versus distilled water: DXH, 4.82 × 10⁻⁶ M; Fe(III), 4.0 × 10⁻⁴ M; PTL, 1.1 × 10⁻³ M; buffer (pH 4.6) solution, 4.0 ml. DXH–FC reagent system (△──△) against reagent blank (▲──▲) versus distilled water: DXH, 2.76 × 10⁻⁵ M; Na₂CO₃, 3.4 × 10⁻¹ M, F–C reagent (2.0 N), 2.0 ml. DXH-NaIO₄–MBTH system (········) against reagent blank (●──●) versus distilled water: DXH. 8.6 × 10⁻⁶ M; NaIO₄, 3.74 × 10⁻⁴ M; acetic acid, 1.4 × 10⁻¹ M; MBTH, 3.4 × 10⁻⁴ M. DXH-NaIO₄–PHH system (x──x) against reagent blank (x──x) versus distilled water: DXH 2.76 × 10⁻⁵ M; NaIO₄, 1.6 × 10⁻³ M; PHH, 1.65 × 10⁻² M; potassium ferricyanide, 4.84 × 10⁻³ M.

MoO₃·10H₂O and 3H₂O·P₂O₅·14WO₃·4MoO₃·10H₂O. DXH probably effects a reduction of 1, 2 or 3 oxygen atoms from tungstate and/or molybdate in F–C reagent (phosphomolybdotungstate),

thereby producing one or more of the possible reduced species which have a characteristic intense blue color.

As DXH contains α-ketol and α-amino-ol
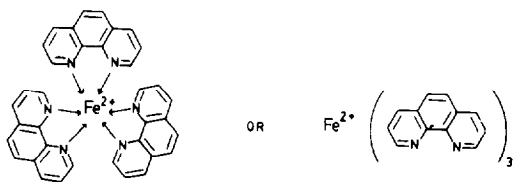
Scheme 1.

groups, sodium metaperiodate offers a wider scope for analytical determination. The above groups are attacked in the manner shown in Scheme 2. The two methods avoid the distillation or diffusion step and permit the determination of the liberated formaldehyde directly in the reaction medium colorimetrically either by oxidative coupling reaction with MBTH (method C) or by the

DXH

Method C :

Method D:

FORMAZAN DYE
Where R' = H (formaldehyde)
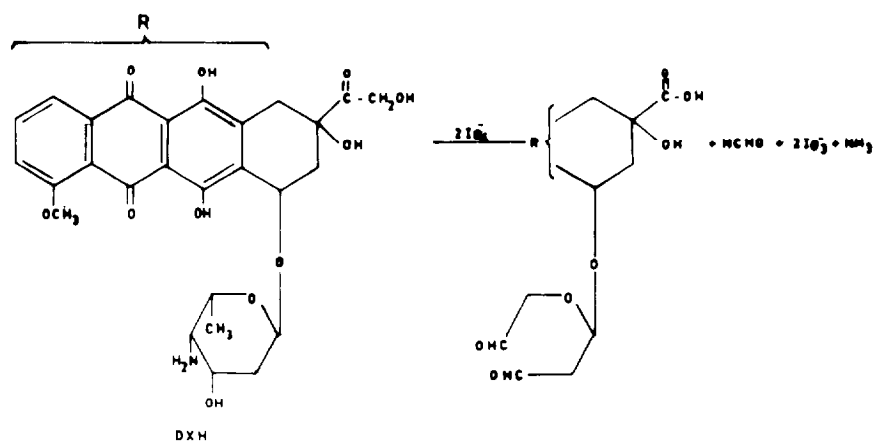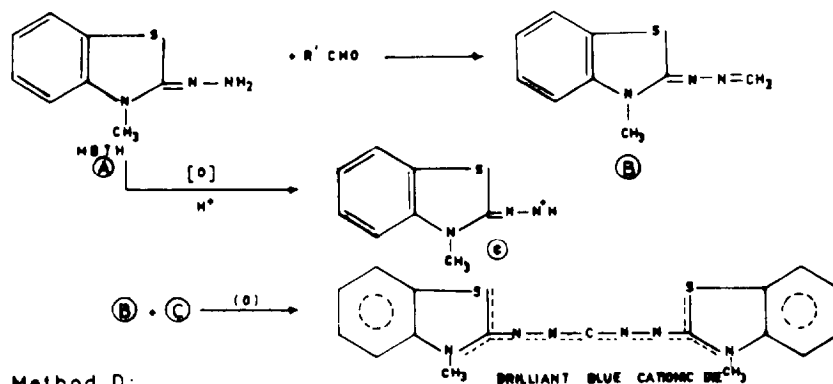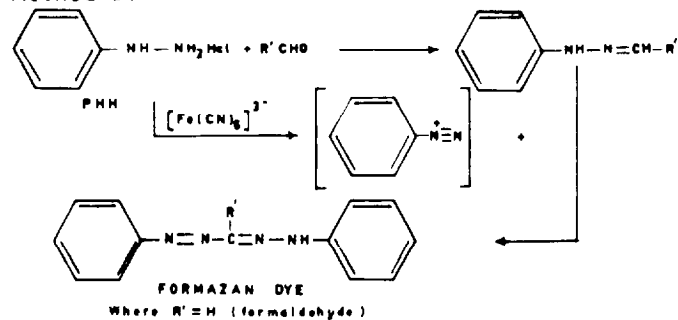
Scheme 2.

Schryver's reaction with PHH and ferricyanide [24] (method D). Both of the reactions are not specific and are essentially aldehyde group methods. However formaldehyde reacts rapidly when compared to the involvement of the other oxidation products (dialdehyde).

In method C, MBTH on oxidation with excess periodate, loses two electrons and one proton forming an electrophilic intermediate which in turn reacts with the aldehyde forming a brilliant blue cationic dye as already illustrated by Sawicki et al. [23]. This reaction is presented in Scheme 2. Method D was based on the reaction of aldehydes with PHH in the presence of potassium ferricyanide giving formazan dye (Scheme 2).

4. Conclusion

Methods A–D are applicable to the intact molecule of DXH (obviating the need for any preliminary treatment) and have the advantage of wider range. The sensitivity order of the procedures is $A > C > D > B >$ reference method and the order of λ_{max} values of the colored species is $B > C >$ reference method $> A = D$. Although the λ_{max} values of two methods (A and D) are somewhat less than that of the reference method, the molar absorptivities of all of the four proposed methods are considerably higher than that of reference method. Moreover, no visible spectrophotometric method has been reported so far. Thus all the proposed methods are simple, sensitive and useful for the determination of DXH in pure samples and pharmaceutical formulations. They provide a wide choice, depending upon the needs of the specific situation.

Acknowledgements

References

[1] United States Pharmacopoeia, XXII, Rockville, MD, USA, 1990, p. 478.
[2] A.A. Khabarov, Izobreteniya, 29 (1992) 240.
[3] N.M. Alykov, T.V. Nekrest 'Yanova and L.V. Yakovleva, Zh. Anal. Khim., 46(8) (1991) 1642.
[4] H.H.J.L. Ploegmakers, P.A. Moritz, P.J.M.M. Toll and W.J. Van Oort. J. Autom. Chem., 11(3) (1989) 106.
[5] L.A. Sternson and G. Thomas, Anal. Lett., 10(2) (1977) 99.
[6] V.E. Vander, H. Irth, U.R. Tjaden and G.J. Vander, Anal. Chim. Acta, 271(1) (1992) 69.
[7] H. Weenen, A.P.R.M. Osterop, P.S.E.J.M. Vander, J. Lankelma, V.W.J.F. Vander and H.M. Pinedo, J. Pharm. Sci., 75(12) (1986) 1201.
[8] K.K. Chan and C.D. Wong, J. Chromatogr., 343(9) (1979) 172.
[9] E. Watson and K.K. Chan, Cancer Treat. Rep., 60(11) (1976) 1611.
[10] D. Leca and F.R. Leca, Chromatographia, 35(7–8) (1993) 435.
[11] D.T. King and J.T. Stewart, J. Liq. Chromatogr., 16(11) (1993) 2309.
[12] J. De Jong, J.B. Vermorken and V.W.J.F. Vander, J. Pharm. Biomed. Anal., 10(4) (1992) 309.
[13] J. De Jong, C.N. Munnikrishna, W.S. Gueranol, A. Bast and V.W.J.F. Vander, J. Chromatogr., 574(2) (1992) 273.
[14] C.M. Riley, A.K. Ruyan and J. Graham-Pole, Anal. Lett., 20(1) (1987) 97.
[15] M.J. Sepaniak and E.S. Yeung, J. Chromatogr., 190(2) (1980) 377.
[16] G. Ziglio and V.G. Beltramelli., Ig. Mod., 83(1) (1985) 88.
[17] A. Besada, Anal. Lett., 20 (1987) 427.
[18] C.S.P. Sastry, D.G. Sankar, M.N. Reddy and M. Aruna, Indian J. Pharm. Sci., 50 (1988) 178.
[19] O. Folin and D. Ciocalteu, J. Biol. Chem., 73 (1927) 627.
[20] G. Ramana Rao, G. Kanjilal and K.R. Mohan, Analyst, 103 (1978) 993.
[21] W. Nicolet and J. Schinn, J. Am. Chem. Soc., 61 (1939) 1615.
[22] J. Bartos and M. Pesez, Colorimetric and Fluorimetric Analysis of Steroids, Academic Press, London, 1976, p.34.
[23] E. Sawicki, T.R. Hausen, T.W. Stanley and W. Elbert, Anal. Chem., 33 (1961) 93.
[24] M. Pesez and J. Bartos, Colorimetric and Fluorimetric Analysis Organic Compounds and Drugs, Marcel Dekker, New York, 1974, p. 504.
[25] D.L. Massart, B.G.M. Vandeginste, S.N. Deming, Y. Michotte and L. Kaufman, Chemometrics, a Text Book, Elsevier, Amsterdam, 1988, p. 293.
[26] IUPAC, Spectrochim. Acta, 33 (1978) 241.
[27] M.N. Reddy, D.G. Sankar, G.D. Rao and K. Sreedhar, The Eastern Pharmacist, XXXIV (401) (1991) 127.
[28] G.L. Peterson, Anal. Biochem., 100 (1979) 201.

Talanta

Separation study of mercury through an emulsion liquid membrane

Quanmin Li*, Qi Liu, Xianjun Wei

Department of Chemistry, Henan Normal University, Xinxiang 453002, People's Republic of China

Abstract

A study of the transport of Hg(II) ions through a tri-n-octylamine (TOA) – sorbital monooleate (Span 80) – toluene liquid membrane has been performed with varying concentrations of HCl, KCl, TOA, Span 80 and NaOH in the feed, membrane and stripping solutions. Maximum transport was observed with 0.01 M KCl, 2.5×10^{-2} M HCl, 1.5×10^{-2} M TOA, 3% (w/v) Span 80 and 0.05 M NaOH. With this system, mercury could be completely separated from Cu, Zn, Fe, Co, Ni, Pb, Mn and Cd. The transport mechanism of this metal ion through the membrane is based on the association of metal anions ($HgCl_4^{2-}$) with protonated TOA molecules at the feed-side interface, diffusion through the membrane, decomposition of the complex at the strip-solution-side membrane interface under alkaline conditions, and backdiffusion of TOA molecules. Transport with the membrane is dependent on the concentration gradient but in the surrounding solutions it is inversely related to the concentration gradient.

Keywords: Emulsion liquid membrane; Mercury; Separation

1. Introduction

Tri-n-octylamine (TOA) has been studied as a supported liquid membrane mobile carrier to separate Pd and Mo [1,2] and as an emulsion liquid membrane (ELM) mobile carrier to separate Au [3], but it has not been applied for the separation of mercury from other metal ions, and also no transport studies have been made

---

* Corresponding author.

using an ELM. TOA is an important extractant and can be combined with $HgCl_4^{2-}$ ions after its protonation [4].

In this paper, an ELM with TOA as mobile carrier is studied for the transport of mercury. Various parameters influencing the transport of mercury across the membrane have been optimized to separate mercury from Cu(II), Zn(II), Fe(II), Co(II), Ni(II), Pb(II), Mn(II) and Cd(II). Under the chosen conditions, Hg_2^{2+} will precipitate Hg_2Cl_2 and will therefore not be transported.

2. Experimental

2.1. Reagents

A standard (1 mg ml^{-1} solution of mercury was prepared from $HgCl_2$ (analytical grade) and distilled, deionized water. TOA (analytical grade) was obtained from Fluka. Sorbital monooleate (Span 80; chemical grade) was obtained from Tianda Experimental Factory (Tianjin, People's Republic of China). A 0.1 M solution of TOA and a 3% (w/v) solution of Span 80 in toluene were used in this work.

2.2. Apparatus

The following instruments were used: a motor-driven emulsifier (range 0–6000 rev min^{-1}); motor-driven stirrers (range 0–600 rev min^{-1}); and a model 722 spectrophotometer (Shanghai Analytical Instrument Factory, People's Republic of China).

2.3. Procedures

2.3.1. Preparation of ELM

20 ml portions of solutions of TOA and Span 80 in tolune were emulsified at a stripping speed of 2000 rev min^{-1}. Stripping solution was added at a rate of 20 ml min^{-1} until the volume ratio of organic membrane solution to stripping solution was 1:1. The solution was then stirred continuously for 15 min to obtain a stable white ELM.

2.3.2. Transport of metal ions

To 10 ml beakers containing metal ion feed solution was added 20 ml of ELM and the contents stirred at 200 rev min^{-1} for a given transfer time; the phases were allowed to separate, clear feed solution was pippetted into a 25 ml volumetic flask and analysed for the amount of cation remaining.

2.3.3. Determination of mercury [5]

5 ml of 3×10^{-4} M 2-[(5-bromor-2-pyridyl)azo]-5-diethylaminophenol (5-Br-PADAP) alcohol solution was added to 5 ml of 0.1 M $Na_2B_4O_7 \cdot 10H_2O$ buffer solution in a 25 ml vol-
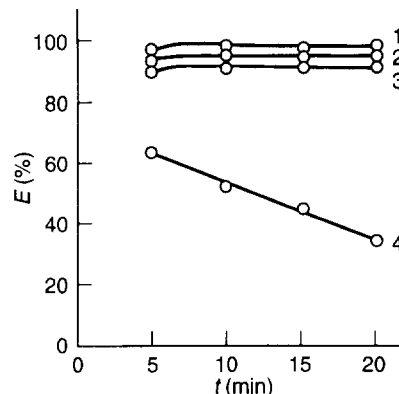

Fig. 1. The effect of HCl concentration in the feed on the percent extraction of Hg(II). Membrane phase: 1.5×10^{-2} M TOA + 3% (w/v) Span 80 + toluene. Stripping phase: 0.05 M NaOH. Feed phase: 100 μg ml^{-1} Hg(II) + 0.010 M KCl + HCl (M): (1) 2.5×10^{-2}; (2) 5.0×10^{-2}; (3)1.0×10^{-2}; (4) 5.0×10^{-3} ($HgCl_2^-$ precipitating HgO).

umetic flask containing mercury ions. After diluting to the mark the absorbance was read at 565 nm against the reagent blank.

In the separation experiment, the concentration of mercury as well as other cations was determined by inductively-coupled plasma atomic emission spectrometry (ICP-AES).

3. Results and discussion

3.1. The effect of hydrochloric acid concentration in the feed phase

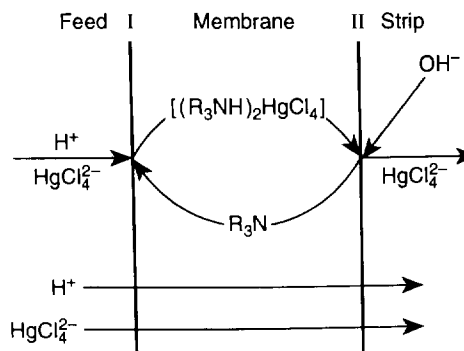The relationship between the concentration of

Fig. 2. Possible scheme for $HgCl_4^{2-}$ transport from HCl solution to NaOH solution through TOA Span 80–toluene liquid membrane.

Table 1
The effect of KCl concentration in the feed phase[a]

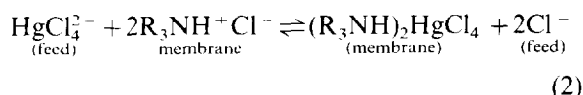| Conc. KCl (M)	0	0.005	0.010	0.050	0.100
Percent extraction	93.0	96.3	98.5	97.8	97.3

[a] Membrane phase: 1.5×10^{-2} M TOA – 3% (w v) Span 80. Feed phase: 0.025 M HCl + 100 μg ml^{-1} Hg(II). Stripping phase: 0.05 M NaOH. Transfer time: 10 min.

hydrochloric acid in the feed solution and extraction of mercury is shown in Fig. 1. An acid concentration of 2.5×10^{-2} M was found to be the best for mercury transport. The H$^+$ concentration in the feed solution was measured and it was found that with transport of mercury into the stripping phase, the H$^+$ concentration in the stripping phase decreased. This proved that H$^+$ transport into the stripping phase also occurs. In the presence of HCl and KCl in the feed phase, the transport process of mercury through an ELM is illustrated by the following reactions:
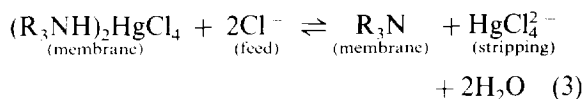
TOA (shown as R_3N) in the membrane phase reacts with hydrochloric acid in the feed:

$$\underset{\text{(membrane)}}{R_3N} + \underset{\text{(feed)}}{H^+ + Cl^-} \rightleftharpoons \underset{\text{(membrane)}}{R_3NH^+Cl^-} \qquad (1)$$
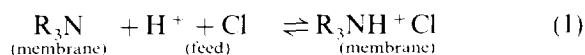
In the feed, $HgCl_4^{2-}$ exchanges with Cl^- of R_3NH^-Cl in the membrane phase:

Fig. 3. The effect of TOA concentration in the membrane phase on the percent extraction of Hg(II). Feed phase: 100 μg ml^{-1} Hg(II) + 0.010 M KCl + 0.025 M HCl. Stripping phase: 0.05 M NaOH. Membrane phase: 3% (w v) Span 80 – TOA: (1) 1.5×10^{-2} – 2.0×10^{-2}; (2) 1.0×10^{-2}; (3) 7.5×10^{-3}; (4) 5×10^{-3}.

$$\underset{\text{(feed)}}{HgCl_4^{2-}} + 2R_3NH^+Cl^- \rightleftharpoons \underset{\text{(membrane)}}{(R_3NH)_2HgCl_4} + \underset{\text{(feed)}}{2Cl^-} \qquad (2)$$

NaOH in the stripping phases reacts with $(R_3NH)_2HgCl_4^{2-}$ to strip mercury into the stripping phase:

$$\underset{\text{(membrane)}}{(R_3NH)_2HgCl_4} + \underset{\text{(feed)}}{2Cl^-} \rightleftharpoons \underset{\text{(membrane)}}{R_3N} + \underset{\text{(stripping)}}{HgCl_4^{2-}} + 2H_2O \qquad (3)$$

The expected mechanism of mercury transport in the present case is shown in Fig. 2. The transport of H$^+$ along a concentration gradient supplied the energy for the transport of mercury against a concentration gradient. It was discovered that the decrease of H$^+$ in the feed phase was more than that of mercury. This was due to the formation of $R_3NH^+Cl^-$-type species and transport into the stripping phase. At an HCl concentration in the feed of $> 2.5 \times 10^{-2}$ M, more $R_3NH^+Cl^-$ ions were transported into the stripping phase, the liquid membrane emulsified sparingly and thus the transport of mercury decreased. When the concentration of HCl was $< 5.0 \times 10^{-3}$ M, transport of mercury abruptly decreased with time. This is because less H$^+$ is available to protonate R_3N, and precipitation of Hg^{2+} as HgO blocks the transport of mercury. From Fig. 1, it is also found that the transport of mercury can be completed in 5 min, this is because extraction and back-extraction occur simultaneously, and the degree of dispersion of the ELM in the feed solution is high [6].

3.2. The effect of KCl concentration in the feed phase
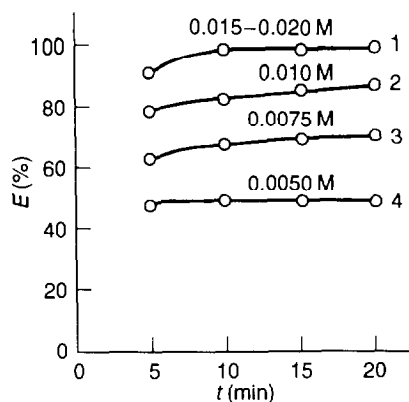
The influence of KCl concentration in the feed

Table 2
The effect of concentration of surfactant[a]

Conc. of Span 80 [%(w v)]	1	2	3	4	5
Percent extraction	93.1	95.0	98.5	97.0	96.0

[a] Membrane phase: 1.5×10^{-2} M TOA + Span 80. Feed phase: 0.025 M HCl + 100 μg ml^{-1} Hg(II) + 0.010 M KCl. Stripping phase: 0.05 M NaOH. Transfer time: 10 min.

solution upon the transport of mercury was also examined (see Table 1). Because KCl is a complexant for Hg^{2+} and a good salting-out agent [7], an increase in the KCl concentration increased the HgCl$_4^{2-}$ concentration and the stability of the membrane (preventing the membrane from emulsifying) and made separation easier. Therefore the extraction of mercury increased. We selected 0.01 M KCl in the experiment.

3.3. The effect of the concentration of TOA

The effect of the concentration of TOA (mobile carrier) in the organic phase on the extraction of mercury is shown in Fig. 3. The optimum concentration range of the carrier was 1.5×10^{-2}–2.0×10^{-2} M. In the experiment 1.5×10^{-2} M was selected for a rapid and complete transport of mercury.

3.4. The effect of the concentration of surfactant

Both the stability of the emulsion and the viscosity of the liquid membrane were altered by the proportion of surfactant in the organic phase. An increase in the concentration of Span 80 (surfactant) increased the stability of the emulsion; however, the extraction of mercury decreased. When the concentration of Span 80 was less than 2% (w/v), in the organic phase, the ELM was easy to break as the transfer time increased. A concentration of 3% (w/v) in the organic phase resulted in good extraction and stability (Table 2).

3.5. The effect of emulsion/feed volume ratio

Using 100 μg ml^{-1} mercury, 0.01 M KCl and 2.5×10^{-2} M HCl solution as the feed phase, 0.05 M NaOH solution as the stripping phase and 1.5×10^{-2} M TOA and 3% (w/v) Span 80 as the membrane phase, varying the emulsion/feed vol-
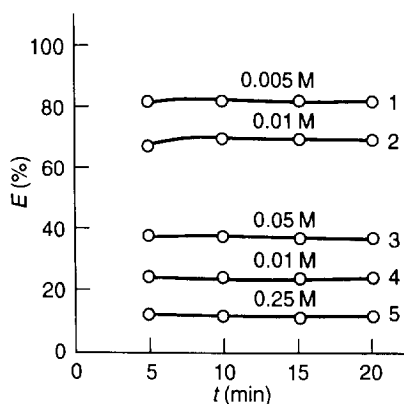

Fig. 4. The effect of KNO$_3$ concentration in the feed phase on the percent extraction of Hg(II). Membrane phase: 1.5×10^{-2} M TOA + 3% (w v) Span 80 + toluene. Stripping phase: 0.05 M NaOH. Feed phase: 2.5×10^{-2} M HCl + 100 μg ml^{-1} Hg(II) + KNO$_3$ (M): (1) 0.005; (2) 0.010; (3) 0.050; (4) 0.10; (5) 0.25.
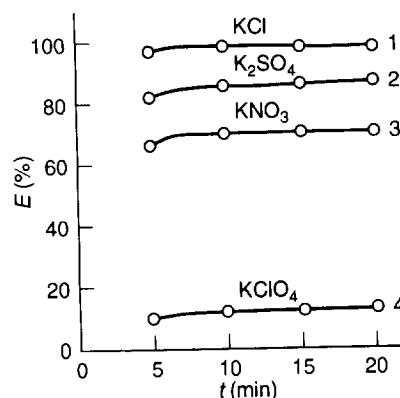

Fig. 5. The effect of different salts in the feed solution on the percent extraction of Hg(II): (1) 0.01 M KCl; (2) 0.02 M K$_2$SO$_4$; (3) 0.01 M KNO$_3$; (4) 0.01 M KClO$_4$.

Table 3
Percent extraction of Hg(II) with different salts in the feed[a]

Salt (0.010 M)	KCl	KBr	KI	KSCN
Percent extraction	98	100	100	100

[a] Membrane phase: 1.5×10^{-2} M TOA + 3% (w/v) Span 80. Feed phase: 0.025 M HCl + 100 μg ml^{-1} Hg(II). Stripping phase: 0.05 M NaOH. Transfer time: 10 min.

ume ratio from 1.75:10 to 2.5:10 to measure the extraction, the experimental result showed that the concentration of mercury in the feed solution decreased to less than 2 μg ml^{-1} after 10 min of transport. Therefore the extraction efficiency was > 98%. In the experiment, a 2:10 emulsion/feed volume ratio was selected and a 10-fold higher concentration of mercury was obtained.

3.6. The effect of concentration of NaOH in the stripping phase

The NaOH in the stripping phase functioned as a back-extractant. When the composition of emulsion was fixed, an increase in the hydroxyl ions resulted in faster decomposition of the mercury complex and removal of protons from the amine molecules, thus resulting in higher transport. However, it has been observed that above a concentration of 0.1 M NaOH, the transport decreased. This may be because the HgCl$_4^{2-}$

Table 4
The percent extraction of other cations in the presence of various salts at a concentration of 0.01 M[a]

Feed phase	Percent extraction							
	Fe	Mn	Cu	Zn	Co	Ni	Pb	Cd
KCl	0	0	0	0	0	0	0	0
KBr	0	0	[b]	0	0	0		21
KI	0	0		0	0	0		100
KSCN	0	0		70	50	4	0	5

[a] Membrane: 1.5×10^{-2} M TOA + 3% (w/v) Span 80. Feed phase: 0.025 M HCl. Stripping phase: 0.05 M NaOH. Initial amount of each ion: 100 μg ml^{-1}. Transfer time: 10 min.
[b] – means cation causes precipitation and no transport occurs.

precipitated HgO at higher NaOH concentrations and clogged the membrane. The maximum extraction was obtained in different feed solutions at 0.01–0.10 M NaOH. In the experiment, 0.05 M NaOH was selected.

3.7. The effect of other reagents in the feed phase

With a suitable acid concentration of the feed phase the concentration of KCl in the feed phase changed form 0.01 to 0.10 M and the extraction efficiency of mercury was always > 97%. If KCl was replaced by KNO$_3$, an increase in the concentration of KNO$_3$ obviously decreased the extraction of mercury (see Fig. 4), so the large NO$_3^-$ anion suppressed the transport of mercury. The regression equation of log E (logarithm of extraction of mercury) versus log C_{KNO_3} was log $E = 0.9139 - 0.4555$ log C_{KNO_3}; $r = -0.9983$.

KCl was replaced by KNO$_3$, K$_2$SO$_4$ and KClO$_4$ in turn and the results are shown in Fig. 5. ClO$_4^-$ is the biggest anion and so association with TOA resulted in a decrease in the transport of mercury. If 0.10 M KI, KBr and KSCN were added to the above systems respectively, the extraction efficiency of mercury reached 100% (Table 3). According to Ref. [8], Hg^{2+} can form a 1:4 complex with I$^-$, Br$^-$, SCN$^-$ and Cl$^-$; the logarithm of its accumulating stability constant (log β_4) is respectively 29.8, 21.0, 20.0 and 15.4. This shows that the more stable the anion complex, the less other anions interfere.

3.8. Separation of mercury from other metal ions

Under suitable conditions, transport of Cu, Zn, Fe, Co, Ni, Pb, Mn and Cd was studied in different feed solutions (shown in Table 4).

Results for the competitive transport of mercury and other common cations in mixed solution are shown in Table 5. (Note that the data of Table 5 come from ICP-AES measurements. All other data are from colorimetric measurements.) Selective transport of mercury was excellent in the KCl feed phase; under this condition the transport of Cu, Zn, Fe, Co, Ni, Pb, Mn and Cd was found to be negligible.

Table 5
Percent extraction of other cations from mixed solution[a]

Initial amount of each ion (μg ml^{-1})	Percent extraction								
	Hg	Mn	Cu	Zn	Co	Ni	Pb	Cd	Fe
50	99.3	0	0	0	0	1	0	1	1
100	98	2	0	2	0	1	2	2	1.5

[a] Membrane phase: 1.5×10^{-2} M TOA + 3% (w/v) Span 80. Feed phase: 0.025 M HCl + 0.01 M KCl. Stripping phase: 0.05 M NaOH. Transfer time: 10 min.

4. Conclusion

Extraction of mercury through a TOA-Span 80-toluene ELM was studied. The mechanism of transport of mercury was discussed and is presented in Fig. 2. The optimum conditions of transport have been found to be 0.01 M KCl and 2.5×10^{-2} HCl in the feed solution, 1.5×10^{-2} M TOA and 3% (w/v) Span 80 in the liquid membrane, and 0.05 M NaOH in the stripping solution. It is concluded that this method can be applied for the selective separation of mercury from a mixed solution of Cu, Zn, Fe, Co, Ni, Pb, Mn and Cd or as a preconcentrating step for measuring mercury. Small amounts of carriers are involved and the extraction efficiency is high.

References

[1] D.S. He, Sci. Technol. Membr., 9(4) (1989) 44.
[2] C. Malik and A. Li, Sep. Sci. Technol., 25(3) (1990) 263.
[3] Q.H. Cai, Z. Yan and H.J. Chao, Sci. Technol. Membr., 9(4) (1989) 33.
[4] Q.Z. Qin, J.J. Mao, Z.H. Jing and Z.R. Lu, Chemical Separation Method, Atomic Energy Press, Beijing, 1983, pp. 61,66.
[5] F. Liu, K.A. Li, J. Lu, Y.P. Shuen and S.Y. Tong, Ion-Exch. Adsorpt., 8(5) (1992) 400.
[6] T.L. Largman and S. Sifniades, Hydrometallurgy, 3 (1978) 153.
[7] F.G. Seeley, J. Chem. Eng. Data, 11 (1966) 424.
[8] W.B. Chang and K.A. Li, A Concise Handbook of Analytical Chemistry, Peking University Press, Peking, 1981.

Rapid procedure for the determination of gold at sub-ppm levels in geological samples by atomic absorption spectrometry

Arun Kumar Singh

Chemical Laboratory, Atomic Minerals Division. AMD Complex, Begumpet, Hyderabad-500 016, India

Abstract

A rapid and reliable procedure for the determination of gold in geological samples is reported that involves MnO_2 and HCl treatment of the samples followed by ethyl acetate extraction of gold and determination at the ppm and sub-ppm levels by flame atomic absorption spectrometry after evaporating off the organic solvent. The method was tested for the quantitative recovery of gold from the standard sample from the Kolar gold field and four other thoroughly analysed in-house standards from the Otha area, India. The procedure offers distinct improvements in speed of analysis and environmental safety. The higher RSD of the data is attributed ot the "nugget" effect.

Keywords: Atomic absorption spectrometry; Geological samples; Gold

1. Introduction

The continuing search of gold has led to improvements in analytical methodologies for its determination. Analytical procedures include the classical fire assay [1,2] and wet chemical treatment involving aqua regia, $HBr–Br_2$, $NaBr–H_2O_2$ and cyanide followed by separative preconcentration using anion exchange [3], solvent extraction [4,5], precipitation on tellurium and $Hg_2Cl_2–Hg$ or adsorption on activated charcoal [6] and polyurethane foam [7]. The gold content of samples has been determined using graphite furnace atomic absorption spectrometry (GFAAS) [8], flame atomic absorption spectrometry (FAAS) [9] and inductively coupled plasma

atomic emission spectrometry (ICP-AES).

Although GFAAS offers very high sensitivity, it suffers from poor precision. ICP-AES is less sensitive and not very selective. FAAS offers high selectivity and precision, although the determination limits are restricted to ppm and sub-ppm levels of gold in the solutions aspirated. Instrumental neutron activation analysis (INAA) also offers very high sensitivity. Using INAA, gold has been determined directly or after chemical pretreatment of the sample and its separation either by ion exchange or solvent extraction as the situation demands [10]. Although some bias has been reported between gold values determined by INAA and other techniques, this has been traced to variations in wet chemical methods of sample

treatment rather than to the efficiency of measurement by various instrumental techniques [11].

For a rapid appraisal of the gold potential of favourable areas, wet chemical procedures have found wider application. Work has been done on gold extraction by using $HCl-H_2O_2$ to leach the gold from manganese oxide ores [12] and subsequently using bleaching powder–HCl [13] and $KMnO_4$–HCl [14], which offers certain definite advantages. This prompted us to investigate other oxidizing solutions which could dissolve gold from geological samples quantitatively and rapidly.

Combinations of $NaClO_3$–HCl/$NaBiO_3$–HCl and MnO_2–HCl were investigated and this paper reports the results using MnO_2–HCl (1 M) for the wet chemical dissolution of gold (and palladium) from the sample matrix, followed by ethyl acetate extraction and final determination of gold using FAAS (242.8 nm) after evaporation of the organic solvent.

The procedure is simple, fast, quantitative. Since repeated evaporations of aqua regia solution to remove nitrates/nitrosyl compounds and bring it to only HCl medium are not required, the procedure is also environmentally safe.

2. Experimental

2.1. Instrumentation

All measurements were made using a Spectra AA-20 flame atomic absorption spectrometer, (Varian, Australia) with the operating parameters presented in Table 1.

Table 1
Flame AAS operating conditions

Wavelength	242.8 nm
Slit setting	1.0 nm
Lamp type	Au hollow cathode
Lamp current	4 mA
Background correction	Deuterium arc
Flame	Air acetylene
Flame condition	Lean

2.2. Chemicals

Reagents used included 1 M HCl (AnalaR), MnO_2 powder (AR grade) and ethyl acetate (AR grade).

A gold stock standard solution (100 μg ml^{-1}) was prepared by dissolving 1.0 g of $AuCl_3$ containing 25% Au (Johnson Matthey, London, UK) in 10% (v/v) HCl in a glass beaker on water-bath. The solution was cooled and transferred to a 250 ml volumetric flask and diluted to volume with 10% HCl. Working standard solutions were prepared by dilution of suitable aliquots with 10% HCl.

2.3. Procedure

A 10 g amount of gold-bearing sample (– 200 mesh) was taken and roasted at 650°C for 30 min in a porcelain dish and transferred into a 250 ml beaker, then 100 ml of 1 M HCl were added followed by 0.5 g of MnO_2. The solution was covered with a watch-glass and boiled for 1 h on a hot-plate. It was then cooled, filtered through a Whatman No.40 filter-paper (12.5 cm) and washed with 1 M HCl. The filtrate was concentrated to about 50 ml by boiling, cooled and extracted with 25 ml of ethyl acetate for 2 mn. The organic layer was collected in a separate extraction flask. The extraction was repeated three times with 25 ml of ethyl acetate each. The combined organic layer was scrubbed with about 20 ml of 1 M HCl to remove any extracted Fe and Mn. The organic extract was then cautiously evaporated in a beaker on a water-bath at 70°C. Aqua regia (2 ml) was added to the beaker and the mixture evaporated. The final solution was taken in 1 ml of aqua regia and made up to 10 ml with distilled water. At this stage 25% HCl can also be used, but the presence of HNO_3 keeps the gold in oxidized form. The gold absorbance was measured by FAAS (242.8 nm) using an air–acetylene flame with deuterium background correction. The gold content was determined by AAS after calibrating the instrument with suitable working standards.

Table 2
Results obtained by the proposed method and ICP-AES

Sample No[a]	Sample code	Reported value (aqua regia) (ppm)	MnO_2–HCl treatment and ethyl acetate extraction (ppm)[b]	ICP-AES (242.795 nm) (ppm[c])
1	KGF-1	22.0	23	–
2	M-1181	0.31	0.40	0.52
3	M-1182	23.7	23.0	21.0
4	M-1183	0.74	0.80	0.63

[a] Sample 1 from Kolar gold field. Mineralogy: quartz and native gold [16]. Samples 2–4 from Otha. Mineralogy: quartz, sericite and chlorite [15].
[b] Mean of five results. The RSD varies between 2 and 9%.
[c] Mean of four results.

3. Results and discussion

The MnO_2–HCl system was tested on a standard gold sample from the Kolar gold field, Karnataka, India, and three in-house standard samples from Otha, Himachal Pradesh, India, where gold has been found associated with uranium [15], the gold level ranging from 0.31 to 23.7 ppm. The standard samples were analysed by INAA and aqua regia–GFAAS. Table 2 shows the agreement in the values (means of five values). The high RSD values are attributed to the "nugget" effect. The results show that the MnO_2–HCl system is able to solublize gold quantitatively. Trace amounts of Fe and Mn which are co-extracted by ethyl acetate are removed after scrubbing with 1 M HCl. The standard addition method was applied to chlorite, biotite and schist samples from the Singhbhum Thrust Belt (Bihar) and the recovery was found to be more than 95% (Table 3). The gold in the same solution was also determined by ICP-AES (242.795 nm), as indicated in Table 2 (mean of four values). The higher concentration of gold is in excellent agreement with the FAAS values, provided the gold solution is free from the presence of manganese in high amounts.

It is true that a method based on aqua regia dissolution or dissolution by a similar oxidizing acid mixtures could lead to low results, being dependent on the sample matrix and the mineralogical association of the gold present. If gold particles are enclosed in quartz then dissolution

by an acid mixture, to which quartz is inert, will largely be a function of the extent to which grinding has liberated or exposed the gold to make it accessible to acid attack and the gold recovery may approach 100%, but will always be less than 100%.

The gold values obtained with the present method, however, show that the gold recovery is nearly quantitative when sample ground to −200 mesh is taken for treatment with MnO_2–HCl, and the quartz mineralogy of gold occurrence shows complete amenability.

The procedure is broadly applicable to a wide variety of geological samples, viz. carbonaceous, refractory, quartz, sericite, etc. This method obviates HF treatment of samples, which is critical especially for gold locked in a quartz matrix. Further, the results obtained by this method are well within the acceptable RSD limits of 2–9% (Table 2).

The MnO_2–HCl treatment also offers another advantage in that it dissolves out quantitatively and simultaneously palladium if present in the sample. Results for this aspect will be published elsewhere.

Acknowledgements

Table 3
Results for samples from Singhbhum Thrust Belt[a]

Sample	Au content in sample (ppm)	Au standard added (ppm)	Au recovered (ppm)[b]	Recovery (%)
M-4020	<0.1	12.2	11.6	95
M-4021	<0.1	12.2	11.8	96

[a] Mineralogy: chlorite, biotite, schist.
[b] Single value.

References

[1] A. Chow and F.E. Beamish, Talanta, 14 (1967) 219.

[2] F.E. Beamish and J.C. Van Loon, Analysis of Noble Metals: Overview and Selected Methods, Academic Press, New York, 1977. 327.

[3] F. Bea Barredo and C. Polo Polo, Anal. Chim. Acta, 94 (1977) 283.

[4] G.S. Chowdary and R.K Malhotra, presented at the 23rd Annual Convention of Chemists, Annamalai Nagar, India, 1985.

[5] A.R. Davidson, At. Spectrosc., 13 (1992) 199.

[6] F. Me, R. Sera, R. Enne, L. Trudu and E. Contiri, At. Spectrosc., 11 (1990) 128.

[7] Y.-X. Lu and X.-L. Wang, J. Geochem. Explor., 55 (1995) 49.

[8] A.L. Meier, J. Geol. Chem. Explor., 13 (1980) 77.

[9] R.A. Gurra-Lave and J.A. Jimenz-Prieto, At. Spectrosc., 12 (1991) 210.

[10] R.K. Iyer and K.R. Krishnamoorthy, J. Radioanal. Chem., 33 (1976) 243.

[11] G.E.M. Hall, J.E. Vaive, J.A. Coope and E.F. Weiland, J. Geochem. Explor., 34 (1989) 157.

[12] D.M. Afenya, Indian J. Technol., 24 (1986) 218.

[13] R.K. Tiwari and J.R. Gupta, At. Spectrosc., 14 (1993) 152.

[14] R.K. Tiwari and J.R. Gupta, At. Spectrosc., 15 (1995) 90.

[15] R.V. Singh, D.B. Sen, R.K. Talra and R. Singh, Curr. Sci., 60 (1992) 170.

[16] B.P. Radhakrishna and L.C. Curtis, Mineral Resources of India—3. Gold—The Indian Scene, Geological Society of India, Bangalore, 1991, 160.

Spectrophotometric methods for the determination of prazosin hydrochloride in tablets

K. Sreedhar[a], C.S.P. Sastry[b,*], M. Narayana Reddy[a], D.G. Sankar[a]

[a]Department of Pharmaceutical Sciences, Andhra University, Visakhapatnam-530 003, India
[b]Foods and Drugs Laboratories, School of Chemistry, Andhra University, Visakhapatnam-530 003, India

Abstract

Four simple and sensitive methods for the assay of prazosin hydrochloride (PRH) are developed. These methods are based on the formation of coloured species by treating it either with excess N-bromosuccinimide (NBS) and determining the unconsumed NBS with p-N-methyl aminophenol sulphate (metol)-sulphanilamide (SA) reagent (method A. λ_{max} 520 nm); with 3-methyl-2-benzothiazolinone hydrazone hydrochloride (MBTH) in the presence of ceric ammonium sulphate (CAS) (method B, λ_{max} 620 nm) or with acidic dyes such as orange-II (O-II) (method C, λ_{max} 490 nm) and alizarin violet 3B (AV-3B) (method D. λ_{max} 570 nm) under the specified experimental conditions. Regression analysis of Beer's law plot showed good correlation in the concentration range of 1.0–10.0, 2.5–25.0, 1.0–17.5 and 2.5–30.0 μg ml for methods A. B, C and D respectively.

Keywords: Prazosin hydrochloride; Spectrophotometry; Tablets

1. Introduction

Prazosin, 1-(4-amino-6,7-dimethoxy-2-quinazolinyl)-4-(2-furanylcarbonyl)piperazine, is a potent vasodilatory agent which has gained widespread acceptance in the management of hypertension [1] and also has been found to be value in the treatment of heart failure [2]. The drug and its formulations are official in the British Pharmacopoeia [3] and United States Pharmacopoeia [4]. Reported methods include titrimetric [5], UV spectrophotometric [6], fluorimetric [7], GLC [8], HPLC [9–11] and TLC [12]. As there is no visible-range spectrophotometric method for prazosin hydrochloride (PRH), sensitive and precise spec-

PRAZOSIN

Form 1

---
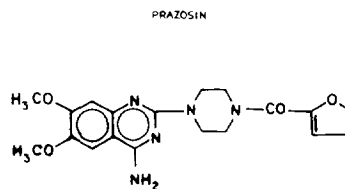
trophotometric methods would greatly aid in the determination of PRH in bulk samples and pharmaceutical formulations. This paper describes four visible-range spectrophotometric methods for PRH determination making use of its different structural features.

N-Bromosuccinimide (NBS) contains unstably bound bromine and is used for brominations and dehydrogenations of organic compounds. Sastry et al. [13] suggested a procedure for determining primary arylamines by treatment with p-N-methylaminophenol sulphate (metol) and NBS. Sawicki et al. [14] developed a procedure for determining aromatic amines and phenols by coupling with 3-methyl-2-benzothiazolinone hydrazone hydrochloride (MBTH) in the presence of an oxidant to form an intensely coloured oxidative coupling product. The acid dyes Orange II (O-II) and Alizarin Violet 3B (AV-3B) have been used for the determination of many drugs which are basic in nature [15]. We have applied these sensitive procedures to the determination of PRH in bulk samples and pharmaceutical formulations.

In method A of the present study, PRH was treated with standard NBS in excess. The NBS consumed, corresponding to PRH, was obtained by determining the excess NBS spectrophotometrically with metol and sulphanilamide (SA) and subtracting it from the NBS initially taken (i.e. blank − unconsumed). Method B involves the spectrophotometric determination of PRH with MBTH in the presence of cerium(IV) ammonium sulphate (CAS). Methods C and D are based on the formation of chloroform-soluble ion-association complexes with O-II and AV-3B. respectively.

2. Experimental

2.1. Apparatus

A Systronics (Hyderabad. India) Model 106 spectrophotometer with 1 cm matched glass cells was used for all absorbance measurements. An Elico (Hyderabad, India) Model LI-120 digital pH meter was used for pH measurements.

2.2. Reagents

All reagents were of analytical grade and all solutions were prepared in triply distilled water. Freshly prepared solutions were always used.

Aqueous solutions of NBS (Loba Chemie. India: 2.53×10^{-3} M), metol (Wilson Labs., India; 8.71×10^{-3} M), SA (IDPL Labs., India; 1.16×10^{-2} M, initially dissolved in the minimum quantity of dilute HCl and acetic acid (Wilson Labs., India, 3.5×10^{-1} M) were prepared for method A. Aqueous solutions of MBTH (Loba Chemie; 8.56×10^{-3} M) and CAS (Wilson Labs.; 1.58×10^{-2} M) in 0.72 M H_2SO_4 were prepared for method B. Aqueous solutions of O-II (Merck, India; 1.41×10^{-3} M) and hydrochloric acid (Merck; 0.1 M) were prepared for method C. A pH 4.4 phthalate buffer and an aqueous solution of AV-3B (Chroma, Germany; 6.079×10^{-3} M) were prepared for method D.

2.3. Standard drug solutions

An accurately weighed quantity of pure PRH equivalent to 50 mg was dissolved in and made to 50 ml with glacial acetic acid. This stock standard solution was further diluted stepwise with distilled water to obtain working standard solutions with concentrations of 100 and 50 μg ml^{-1}.

2.4. Analysis of bulk samples

2.4.1. Method A

Into a series of 25 ml volumetric flasks containing aliquots (0.5–5.0 ml) of PRH solution (50 μg ml^{-1}), 2.5 ml of NBS and 5.0 ml of acetic acid solutions were added successively and the total volume in each flask was made up to 15 ml with distilled water and kept aside for 25 min at room temperature. Then 1.5 ml of metol and 1.5 ml of SA solutions were added at 1 min intervals and the volume was made up to the mark with distilled water. The absorbances were measured against distilled water at 520 nm during the stability period of 10–30 min. A blank experiment was also carried out, omitting the drug. The decrease in the absorbance corresponding to PRH was obtained by subtracting the absorbance of the

drug solution from that of the blank. The amount of the drug was calculated from the calibration graph.

2.4.2. Method B

Into a series of 10 ml of volumetric flasks containing aliquots (0.25–2.5 ml) of PRH solution (100 μg ml^{-1}), 3.0 ml of MBTH solution was added, made up to 6 ml with distilled water and kept aside for 2 min at room temperature. Then 3.0 ml of CAS solution were added to each flask, kept aside for 20 min and diluted to mark with distilled water. The absorbances were measured within 15 min at 620 nm against a reagent blank prepared in a similar manner but omitting the drug. The drug concentration was read from a calibration graph prepared under identical conditions.

2.4.3. Method C

Aliquots of 0.2–3.5 ml of the standard solution of PRH (50 μg ml^{-1}) were transferred into a series of 125 ml separating funnels, then 2.0 ml of 0.1 M HCl and 1.0 ml of O-II solution were added to each funnel and the total volume of the aqueous layer in each funnel was brought to 10 ml with distilled water. A 10 ml portion of chloroform was added to each and the contents were shaken for 2 min. The absorbance of the separated chloroform layer was measured after 5 min at 490 nm against a reagent blank prepared simultaneously but omitting drug. The amount of PRH present was calculated from the calibration graph.

2.4.4. Method D

Aliquots of 0.2–3.0 ml of the standard solution of PRH (100 μg ml^{-1}) were transferred into a series of 125 ml separating funnels, then 5.0 ml of buffer solution (pH 4.4) and 2.0 ml of AV-3B solution were added to each funnel. The total volume of the aqueous layer in each funnel was brought to 10 ml with distilled water. A 10 ml portion of chloroform was added to each funnel and the contents were shaken for 2 min. The absorbance of the separated chloroform layer was measured after 5 min at 570 nm against a reagent blank prepared simultaneously but omitting drug. The amount of PRH present was calculated from the calibration graph.
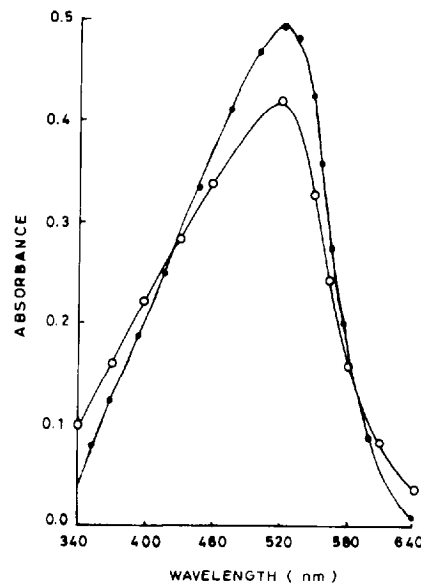
Fig. 1. Absorption spectra of PRH–NBS/metol–SA system (○) and NBS/metol–SA system (•). [PRH], 1.43 × 10^{-5} M; [NBS], 2.53 × 10^{-4} M; [metol], 5.22 × 10^{-4} M; [SA], 6.96 × 10^{-4} M; [CH$_3$COOH], 7.0 × 10^{-2} M.

2.5. Analysis of pharmaceutical formulations

Twenty tablets were accurately weighed and powdered and an amount of the tablet powder equivalent to 10 mg of PRH was treated with 8.0 ml of glacial acetic acid (warmed on a boiling water-bath for 5 min with occasional shaking). The solution was cooled to room temperature, filtered and made up to 10 ml with glacial acetic acid to give a solution of 1 mg ml^{-1}. This stock standard solution was further diluted stepwise with distilled water to obtain working standard solutions (for the above-mentioned methods) and were analysed by following the procedures in Section 2.4.

2.6. UV reference method

Twenty tablets were weighed and powdered. To a quantity of the powder containing the equivalent of 10 mg of PRH, 10 ml of glacial acetic acid were added and the mixture was warmed on a boiling water-bath. The solution obtained was cooled and filtered. To 1.0 ml of the filterate, sufficient distilled water was added to produce 200

ml. The absorbance of the solution was measured at λ_{max} of 248 nm. The content of the drug was calculated from the Beer–Lambert plot.

3. Results and discussion

The optimum conditions for the development of methods A–D were established by varying the parameters one at a time and keeping the others fixed and observing the effect produced on the absorbance of the coloured species.

3.1. Method A

The method involves two stages, namely oxidation with excess NBS and the determination of unreacted NBS using metol–SA reagent. Oxidation of PRH with 1.5–3.0 ml of NBS solution gave maximum and reproducible absorbance values. The effect of time and temperature of oxidation on the absorbance of the coloured species was studied by conducting the oxidation at different temperatures for different time intervals. Oxidation times ranging from 20–30 min at room temperature (28 ± 5 °C) gave constant and repro-
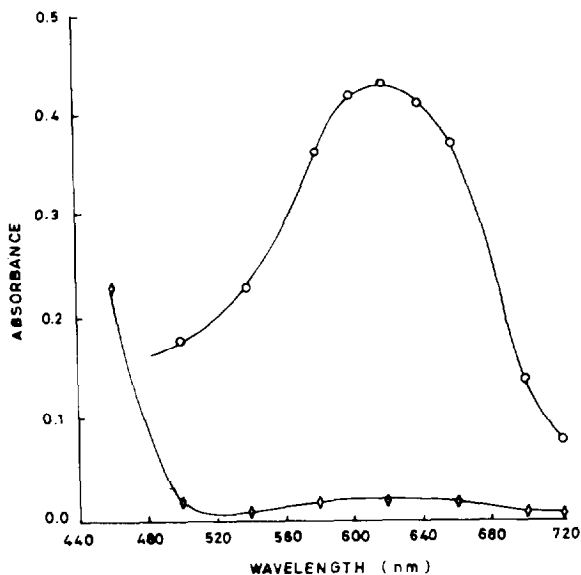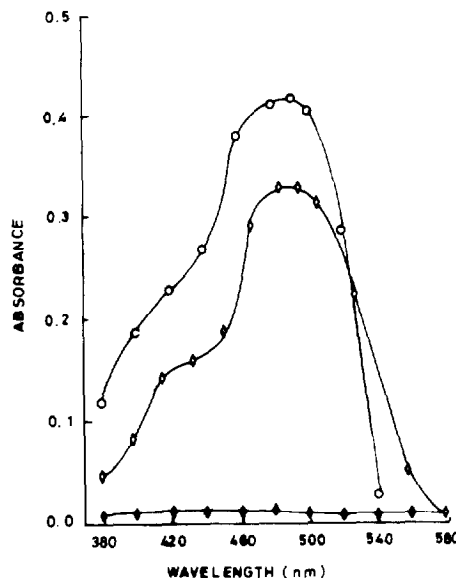

Fig. 3. Absorption spectra of PRH O-II system (○), its reagent blank (◆) and aqueous O-II dye in 0.1 M HCl (◇). [PRH], 2.38×10^{-5} M; [O-II], 1.41×10^{-4} M; [aqueous O-II], 1.38×10^{-5} M.

ducible absorbance values. Prolonging the oxidation time beyond 30 min and increasing the temperature gave erratic results. Maintaining the pH of the solution at 2.9 ± 0.2 was found to be the best for attaining the maximum sensitivity. This was achieved by the addition of 5.0 ml of 3.5×10^{-1} M acetic acid. Use of 1.0–2.0 ml of metol solution and 1.0–2.5 ml of SA solution afforded the maximum absorbance values. A waiting period of 1–3 min was necessary between the addition of metol and SA solutions for the generation of p-N-methylbenzoquinone monoimine (PMBQMI) by the action of NBS on metol. Prolonging the waiting period beyond 3 min resulted in low absorbance values, probably owing to the partial hydrolysis of the PMBQMI formed in situ to the quinone state. Among the water-miscible solvents examined, water was found to be the best for final dilution of the solution. Maximum colour intensity was attained within 10 min after the final dilution and remained stable for the next 20 min. The absorption spectrum of the coloured species is shown in Fig. 1.

Fig. 2. Absorption spectra of PRH MBTH system (○) and its reagent blank (◇). [PRH], 4.76×10^{-5} M; [MBTH], 2.56×10^{-3} M; [CAS], 4.74×10^{-3} M.

3.2. Method B

As the drug molecule possesses aromatic amino groups, the suitability of MBTH reagent for the determination was examined. The applicability of MBTH in conjunction with various oxidizing agents (potassium dichromate, sodium metaperiodate, chloramine-T, potassium hexacyanoferrate(III), iodine, iron(III) chloride and cerium(IV) ammonium sulphate (CAS)) for the determination of PRH was examined and CAS was found to be the best. The effects of reagent concentration (MBTH and CAS), temperature, H_2SO_4 strength in CAS solution, time and order of addition of reagents with respect to maximum sensitivity, minimum blank reading, adherence to Beer's law and stability of coloured species were studied through controlled experiments. For the colour development, 2.5–3.5 ml of MBTH solution, 2.5–3.5 ml of CAS solution and a temperature of $30 \pm 5°C$ were found to be optimum. An acid strength of 0.72 M H_2SO_4 was found to be optimum as a medium for the CAS solution. The order of addition drug, MBTH and CAS gives maximum sensitivity. Altering the order of addition (i.e. MBTH, CAS and drug or drug, CAS and MBTH) resulted in a loss of sensitivity. Maximum colour intensity was attained within 20 min after the addition of CAS solution. The coloured species was found to be stable for 20 min after the attainment of maximum colour intensity. The spectrum of the coloured species produced by the suggested procedure is shown to possess maximum absorbance at 620 nm (Fig. 2).

3.3. Method C

To establish the experimental conditions, the drug was allowed to react with O-II in dilute HCl ranging from 0.05 to 1.5 M and the complex was extracted into the chloroform layer. Constant absorbances were obtained with 0.08–0.12 M HCl, hence 0.1 M HCl was adopted. A 1.0 ml portion of O-II solution was found to be optimum. Shaking times of 1–4 min produced constant absorbance, hence a shaking time of 2 min was chosen.

3.4. Method D

In order to establish the optimum pH range, the drug was allowed to react with AV-3B in aqueous solution buffered to pH 4.0–5.0 and the complex formed was extracted into chloroform for measurement. Constant absorbances were obtained over the pH range 4.2–4.6 (phthalate buffer), hence a pH of 4.4 was adopted. A 2.0 ml portion of AV-3B solution was found to be optimum. Constant absorbance values were obtained for shaking periods between 1 and 4 min, hence a shaking time of 2 min was selected.

Chloroform was preferred among the water-immiscible solvents for the selective extraction of the drug-dye complexes in both methods C and D. A ratio of 1:1 aqueous to chloroform phases was required for efficient extraction of the coloured species. The absorption spectra of the coloured species are shown in Figs. 3 and 4.

The optical characteristics and data for methods A–D are presented in Table 1. The PRH values for tablet dosage forms with the proposed and reference methods are compared in Table 2 (the UV spectrophotometric method developed
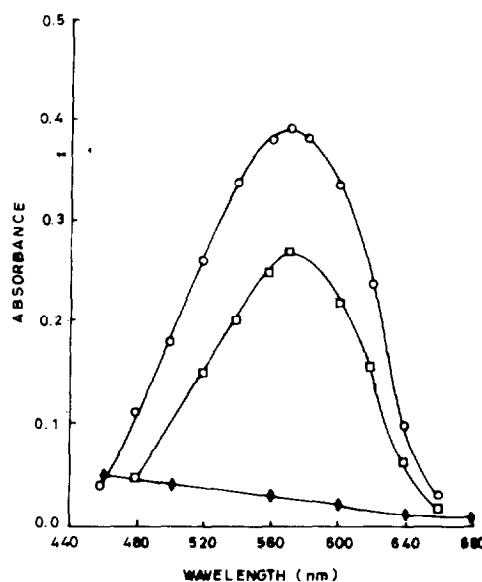

Fig. 4. Absorption spectra of PRH–AV-3B (○), its reagent blank (♦) and aqueous AV-3B dye in pH 4.4 buffer (□). [PRH], 3.57×10^{-5} M; [AV-3B], 1.21×10^{-3} M; [aqueous AV-3B], 2.45×10^{-4} M.

Table 1
Optical characteristics, precision and accuracy of the proposed methods A D for PRH

Parameter	A	B	C	D
λ_{max} (nm)	520	620	490	570
Beer's law limits (μg ml)	1.0–10.0	2.5–25.0	1.0–17.5	2.5–30.0
Molar absorptivity (1 mol^{-1} cm^{-1})	2.94×10^4	9.24×10^3	1.85×10^4	1.10×10^4
Sandell's sensitivity	0.0143	0.0455	0.0227	0.0385
(μg cm^{-2} per 0.001 absorbance unit)				
Optimum photometric range (μg ml^{-1})	2.0–8.0	5.0–20.0	3.0 15.0	5.0–25.0
Regression equation ($y = a + bC$):				
Slope(b)	0.070	0.022	0.0436	0.026
Intercept(a)	0.0025	0.005	0.005	0.005
Correlation coefficient (r)	0.9999	0.9998	0.9999	0.9998
RSD*^{a} (%)	0.64	1.95	0.91	0.73
Range of error (%) (confidence limits):				
0.05 level	± 0.53	± 1.60	± 0.77	± 0.61
0.01 level	± 0.79	± 2.40	± 1.14	± 0.90

^{a} Calculated from six determinations.

for the assay of PRH was used as a reference method for ascertaining the accuracy of the proposed methods). The results of the recovery experiments by the proposed methods are also given in Table 2.

The commonly used excipients and additives in PRH tablets such as talc (up to a 250-fold m m excess, compared with PRH), starch (200-fold), boric acid (150-fold), stearic acid (60-fold), sodium lauryl sulphate (10-fold) and propyl paraben (5-fold) did not interfere in any of the

Scheme 1.

methods. The results in Tables 1 and 2 show that the proposed methods can be applied for the analysis of pharmaceutical preparations with considerable precision, accuracy and sensitivity.

3.5. Chemistry of the coloured species

3.5.1. Method A

This method is based on the oxidation of PRH by NBS to form oxidation products (probably a mixture but reproducible under proposed experimental conditions), excess NBS being determined with metol–SA reagent. The coloured complex may be regarded as a charge-transfer type, shown in Scheme 1, presumed to take place by electron transfer from the highest occupied molecular orbital (π^*) of SA to the lowest empty molecular orbitals (π) of the two adjacent PMBQMI (formed in situ from metol and NBS) molecules as in the metol, iodine and INH reaction [16].
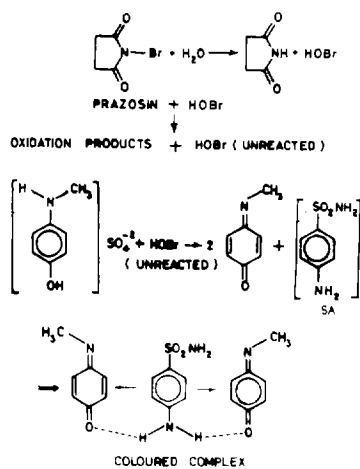
3.5.2. Method B

Under the reaction conditons, MBTH, on oxidation with CAS, loses two electrons and one proton to form an electrophilic intermediate, which is the active coupling species. One mole of this species undergoes electrophilic substitution to form a coloured product as shown in Scheme 2.
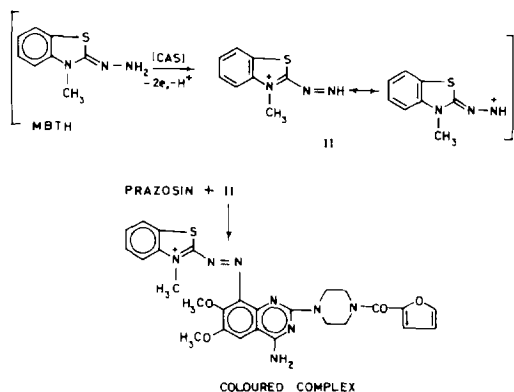
Table 2
Assay of PRH in pharmaceutical formulations

Formulation (tablets)	Labelled amount (mg)	Amount found by proposed methods (mg)[a]				Amount found by reference method[b] (mg)	Recovery by proposed (%)			
		A	B	C	D		A	B	C	D
I	1	0.94 ± 0.046 t = -0.25, F = 1.38	0.97 ± 0.042 t = 1.52, F = 1.65	1.98 ± 0.046 t = 0.74, F = 1.38	0.99 ± 0.068 t = 0.81, F = 1.59	0.95 ± 0.054	99.7	99.5	99.8	99.7
II	1	0.98 ± 0.054 t = 0.095, F = 1.11	0.99 ± 0.065 t = 1.01, F = 1.30	0.95 ± 0.042 t = 0.25, F = 1.84	0.96 ± 0.028 t = 0.60, F = 4.14	0.94 ± 0.057	99.8	99.8	99.3	99.6
III	2	1.99 ± 0.048 t = 1.63, F = 1.41	1.95 ± 0.065 t = 0.20, F = 1.30	1.96 ± 0.051 t = -0.46, F = 1.25	1.98 ± 0.046 t = -1.1, F = 1.53	1.94 ± 0.057	99.4	99.6	99.8	100.1
IV	2	1.95 ± 0.054 t = 0.25, F = 1.38	1.99 ± 0.049 t = 0.78, F = 1.13	2.00 ± 0.049 t = 1.04, F = 1.14	1.98 + 0.06 t = 0.47, F = 1.70	1.96 ± 0.046	99.6	99.5	99.7	99.8

[a] Average ± standard deviation of six determinations; the t- and F-values refer to comparison of the proposed method with the reference method. Theoretical values at 95% confidence limits; $t = 2.57$, $F = 5.05$.
[b] UV reference method.
[c] After adding three different amounts (0.5, 1.0 and 2.0 mg) of pure PRH to the pre-analysed pharmaceutical formulations.

Scheme 2.

3.5.3. Methods C and D

These two methods are based on the basic nature of the drug, which under specified experimental conditions forms ion-association complexes with certain acidic dyes (O-II and AV-3B) which are extractable into chloroform from the aqueous phase [17]. The stoichiometric ratio of PRH to O-II or AV-3B was determined with the slope ratio method and found to be 1:2.

3.5.4. Procedure for slope ratio method

Solutions of acid (for method C) or buffer (for method D) and dye (O-II for method C; AV-3B for method D) were taken in different 125 ml separating funnels and different concentrations of drug solutions were added such that on further addition of drug no dye to drug complex formation occurred. The complex was then extracted using chloroform. The maximum absorbance obtained in each case was termed A_{max} in that case. A linear graph was obtained when log q was

Scheme 3.

Scheme 4.
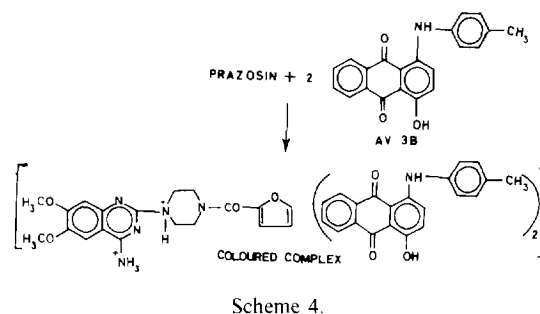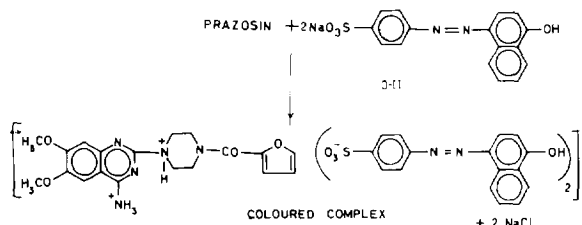
plotted against log r, where $q = A_{obs}/(A_{max} - A_{obs})$ and r is the concentration of the drug in mol l^{-1}. The slope dy/dx of the line gives the ratio of dye to drug in the complex.

The drug PRH (1 mol) and oppositely charged form of the dye (2 mol) behave as a single unit, being held together by electrostatic attraction. The structures are shown in Schemes 3 and 4.

4. Conclusions

The three proposed methods exploit different structural features (method A, unsaturation; method B, presence of amino groups in the quinazolinyl ring; methods C and D, basic property) of the PRH molecule. All the proposed methods have higher λ_{max} values and sensitivity. This is a decisive advantage since the interference from the associated ingredients will be less at higher wavelengths than at lower wavelengths. The sensitivity order of the procedures is A > C > D = B and the λ_{max} order of the coloured species is B > D > A > C. The proposed methods are simple, rapid and have reasonable precision and accuracy when compared with many of the reported methods. All the proposed methods are useful for the determination of PRH and provide a wide choice, depending on the needs of the specific situation.

References

[1] R.N. Brogden, R.C. Heel, T.M. Speight and G.S. Avery, Drugs, 14 (1977) 164.

[2] N.A. Awan, R.R. Miller, A.N. De Maria, K.S. Maxwell, A. Neumann and D.T. Mason, Circulation, 56 (1967) 346.

[3] British Pharmacopoeia, 1988 Vols. I and II, H.M. Stationery Office, London, 1988.

[4] United States Pharmacopeia, XXII Revision, US Pharmacopeial Convention, Rockville, MD, 1990.

[5] N. Kosta and K. Velasevic, Arh. Farm., 38 (1988) 3.

[6] B. Panzova, M. Ilievska, G. Trendovsica and B. Bogdanov, Int. J. Pharm., 70 (1991) 187.

[7] M.E. Mohamed and H.Y. Aboul-Enein, Pharmazie, 40 (1985) 358.

[8] T. Daldrup, F. Susanto and P. Michalke, Fresenius' Z. Anal. Chem., 308 (1981) 413.

[9] W.J. Bachman, J. Liq. Chromatogr., 9 (1986) 1033.

[10] D.J. Gisch, B. Feibush, B.T. Hunter and T.L. Ascah, Biochromatography, 4 (1989) 206, 210, 212.

[11] J.F. Bauer, S.K. Krogh, Z.L. Chang and C.F. Wong, J. Chromatogr., 648 (1993) 175.

[12] P. Lillsunde and T. Korte, J. Anal. Toxicol., 15 (1991) 71.

[13] C.S.P. Sastry, B.G. Rao, B.S. Reddy and S.S.N. Murthy, J. Indian Chem. Soc., 58 (1981) 655.

[14] E. Sawicki, T.W. Stanley, T.R. Hauser, W. Elbert and J.L. Noe, Anal. Chem., 33 (1961) 722.

[15] C.S.P. Sastry, T. Thirupathi Rao, A. Sailaja and T.A.S.R. Prasad, Indian J. Pharm. Sci., 54 (1992) 125.

[16] C.S.P. Sastry, B.S. Reddy and B.G. Rao, Indian J. Pharm. Sci., 43 (1981) 118.

[17] S.L. Bhongade and A.V. Kasture, Talanta, 40 (1993) 1525.

Sorption recovery of metal ions using silica gel modified with salicylaldoxime

A.R. Sarkar, P.K. Datta, M. Sarkar*

Department of Chemistry, University of Kalyani, Kalyani 741235, India

Abstract

Trace metals in water were preconcentrated with silica gel modified with salicylaldoxime and determined by AAS. Optimum conditions for the maximum recovery of metal ions, viz. Cu(II), Ni(II), Co(II), Zn(II) and Fe(III), for both batch and column methods were developed. The efficiency of the adsorbent with respect to different experimental conditions was established.

Keywords: Atomic absorption spectrometry; Metal ions; Salicylaldoxime; Silica gel; Sorption recovery

1. Introduction

Toxic metals have become an ecotoxicological hazard of prime interest and increasing significance, owing to their tendency to accumulate in vital organs in man and animals. Continuous exposure to even low doses of toxic metals is of concern because they cause, according to their degree of accumulation, progressively increasing toxic actions over long periods of the life span of an individual [1].

In densely populated and industrialized regions, alarming amounts of toxic metals are emitted from anthropogenic sources into soils and the aquatic environment. Among the various environmental chemicals, toxic metals are almost the only pollutant class without biodegradability. Instead,

they pass into the enviornment in a biogeochemical cycle with relative accumulations and different residence times in various types of ecosystems and with transformations to sometimes more or less toxic chemical species. Accurate and reliable to sometimes more or less toxic chemical species. Accurate and reliable methods must therefore be developed for their determination. Because of their extremely low concentrations, a preliminary concentration step is usually necessary prior to the determination of the metals.

Solvent extraction, although one of the most popular techniques for the separation of metals, has limited application in concentrating trace amount of ions present in large sample volumes. Among the different types of adsorbents reported, active carbon [2], ion-exchange resins [3], chelating agents supported on various substrates [2–3] and waste materials such as fly ash [9], rice husk

---

* Corresponding author.

ash [10] and waste Fe(III)/Cr(III) hydroxide [11] have beem applied for the removal or separation of metal ions. Kantipuly et al. [12] reviewed the application of chelating polymeric resins for the separation and concentration of trace metals from oceans, rivers and other natural systems. A review was presented by Terada [13] covering preconcentration by sorportion on activated carbon, porous polymers, C_{18}-bonded silica or glass beads, complex-forming adsorbents and natural polymers.

A survey of the literature on water analysis shows that silica gel can be used as a very successful adsorbing agent [14]. It does not swell or strain, has good mechanical strength and can undergo heat treatment. Moreover, chelating agents supported on silica gel as adsorbent are stable, easy to prepare and can be used selectively for the preconcentration of different metals. Preconcentration of metals with silica gel physically supporting sulphonated hydroxyazo dyes and sulphonaphthaleins [15] has been applied successfully to various samples of different origins. The use of chemically bonded silica gels [16–19] has also been reported. Recent progress in the preconcentration of metals using modified silica gel columns includes the use of surfactants as coating material on C_{18}-bonded silica [20], the formation of new stationary phases with a silica gel-bonded cationic polyelectrolyte with Ferron [21] as counter ion and ion-pair formation between a metal complex and a long-chain qaternary ammonium salt and subsequent sorption of this ion pair on the silica gel [22].

In the present investigation, Cu(II), Ni(II), Co(II), Zn(II) and Fe(III) in water were preconcentrated on silica gel loaded with salicylaldoxime and determined by AAS. Salicylaldoxime is widely applied in solvent extraction [23]. After being used successfully as a reagent for conductometric titration of some metal ions [24], it was chosen in the present study as a chelating agent for immobilization on silica gel. The substrate thus obtained can be used a number of times for the purpose of preconcentration of metals. Single-metal or multi-metal solutions can be preconcentrated from the same stock.

2. Experimental

All chemicals were of analytical-reagent grade. Silica gel H 4267 of particle size 60 μm, specific surface area 420 m^2 g^{-1} and pore size 120 Å was obtained from Sigma.

Stock solutions of Cu(II), Ni(II), Co(II), Zn(II) and Fe(III) (1mg ml^{-1}) were prepared by dissolving the respective metal salts in doubly distilled water. Multi-metal solutions (10–100 μg ml^{-1}) were prepared from the stock solutions. pH values were controlled using acetate buffer and phosphate buffer.

2.1. Apparatus

A Perkin-Elmer atomic absorption spectrometer was used for metal determinations and a Systronics pH meter was used to check the pH of the aqueous solutions. The column was a glass tube (160 × 6 mm i.d.) with a coarse sintered-glass disc and a tap at the bottom.

2.2. Synthesis of sorbent

First silica gel was refluxed with 6 M HCl for about 3 h to remove any contaminating metals such as iron. It was then washed with deionized water and dried under reduced pressure at 150°C. The dried silica gel was refluxed with salicylaldoxime in ethanol (10% w/w) at 70–80°C for 4 h. The solid thus obtained was filtered and dried under vacuum.

2.3. Procedure for adsorption experiment

The sorption of various metals was examined under both static and dynamic conditions. To determine the capacity and stability of the sorbent, the kinetics and pH of adsorption and the desorption behaviour, the static method was used. To determine the flow rate and sample volume in the column process, the dynamic method was used.

2.3.1. Static process

Volumes of 10 ml of each of the metal solutions (200 μg) and 10 ml of buffer solution were added

to 0.5 g of the adsorbent in a centrifuge tube and shaken in a mechanical shaker for 1 h at room temperature. The metal ion concentration in the supernatant was measured by AAS and the percentage retention of metal on the adsorbent was calculated.

2.3.2. Dynamic process

The chromatographic column was prepared by filling 10 g of the adsorbent, the bed length being about 10 cm.

A fixed volume of an aqueous solution of the metal ion was adjusted to a suitable pH and percolated through the column at a flow rate of 5 ml min $^{-1}$. After washing the column with about 20 ml of deionized water, an eluting solution of definite composition (4 M HNO_3) was passed through at a flow rate of 3 ml min $^{-1}$. The metal ion concentration in the eluate, after dilutions to the desired volume, was determined by AAS. Wet digestion of the samples with HNO_3 and H_2SO_4 was performed prior to estimating the concentration of metals by AAS following the methods of the APHA [25]. An air–acetylene flame was used with observation at 10 mm above the burner with the following wavelengths: Cu 324.8, Ni 232, Ca 240.7, Zn 213.9 and Fe 248.3 nm.

3. Results and discussion

3.1. Effect of pH

The adsorption behaviour of Cu(II), Ni(II), Co(II), Zn(II) and Fe(III) on the adsorbent at various pH values was investigated in the batch process. The results are shown in Fig. 1(A).

Cu(II) was adsobred quantitatively at pH 2.2 and for Ni(II), Co(II), Zn(II) and Fe(III) the maximum adsorption started at pH 3.5, 4.2, 5.5 and 7.3, respectively. A control measurement was done with untreated silica gel itself (Fig. 1(B)) and a remarkable difference in the retention of metal ions was observed between the adsorbent and the untreated silica gel. In all cases, except for Fe(III), quantitative retention occurred at much higher pH for the untreated silica gel compared with that for the adsorbent. Only for Fe(III) was the effect
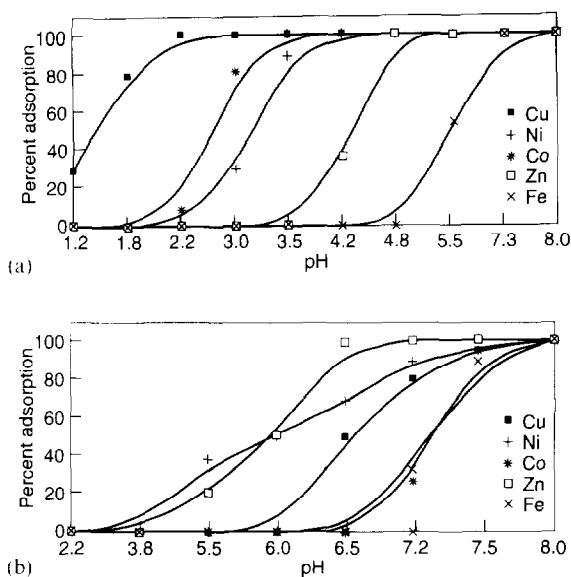

Fig. 1. Effect of pH on adsorption: (a) on salicylaldoxime-modified silica gel and (b) untreated silica gel.

of pH on both the untreated and treated silica gel similar.

From the results, the separation of Cu(II) from the rest of the metals is possible by varying only the pH of the solution. Similarly, Ni(II) and Co(II) can be separated from Zn(II) and Fe(III) and Zn(II) can be separated from Fe(III). However, Ni(II) and Co(II) cannot be separated from each other by this process and a modification is needed. The use of a surfactant or an organic modifier can be effective.

For a given ligand, the stability of complexes with dipositive metal ions follow the Irving–Williams order, which is considered to arise in part from a decrease in size across the series and in part from the ligand field effect. The observed
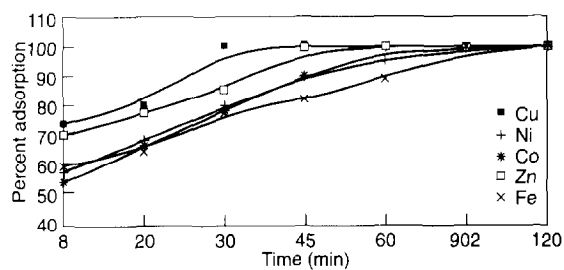

Fig. 2. Effect of time an adsorption.

Table 1
Sorption capacity of the adsorbent for different metal ions

Metal ion	Capacity (mmol g^{-1})
Cu(II)	0.08
Co(II)	0.06
Ni(II)	0.04
Zn(II)	0.04
Fe(III)	0.05

order of preferential adsorption of metal, i.e. Cu(II) > Ni(II) > Co(II) > Zn(II), is consistent with the Irving–Williams order of stability with the relative position of Fe(III) being ligand dependent, especially at the higher pH regions such as those examined here where hydrolysis may be substantiaal, and cannot be established with certainty.

3.2. Effect of shaking time

The effect of shaking time on the adsorption of the metals in the batch process is shown in Fig. 2. Compared with Cu(II), other metals needed a longer time to reach adsorptive equilibrium. The slower reaction kinetics seem to be due either to the slow rate of dissociation of their complexes if complexation is considered as the only mechanism during adsorption or due to their relatively small-size or ionic radii. The crystal field radii for these six-coordinate metals are reported to follow the order Co(II) > Fe(III) > Cu(II) > Ni(II) > Zn(II) [26], but the observed trend of adsorption, i.e. Cu(II) < Zn(II) < Co(II) < Ni(II) < Fe(III) [27], does not correspond to the relative sizes of the metal ions. It is in accordance with expectation that the characteristic lifetimes of water molecule exchange for these hexa-aquo ions. To retain all the metals, a shaking time of 2 h was allowed in the batch process.

3.3. Effect of flow rate

The effect of flow rate of the solutions through the column on the retention behaviour of the metals was studied over the range 1–10 ml min^{-1}. The adsorption of Cu(II) remains almost un-

changed regardless of any change in the flow rate. For Co(II), Ni(II), Zn(II) and Fe(II) no change in the percentage adsorption occurred up to flow rates of 7, 6.5, 8 and 9 ml min^{-1}, respectively. In subsequent experiments a flow rate of 5 ml min^{-1} was maintained for adsorption and 3 ml min^{-1} for elution.

3.4. Effect of volume of sample solution

By varying the volume of sample solution for a fixed amount of adsorbent and fixed amount of metal, no change in the percentage adsorption of metals was observed up to a volume of 1 l. As the present investigation was carried out with 25 ml of sample solution, a concentration factor of 40 was achieved and still higher concentration factors may be obtained by decreasing the elution volume.

3.5. Characteristics and effectiveness of the sorbent

To characterize the sorbent, the IR spectrum of the sorbent was measured first. The IR peaks obtained coincide with the peaks of the ligand (salicylaldoxime) itself, suggesting that the ligand was retained within the sorbent as such, without any structural change. In another experiment, ethanol was passed through the column packed with a weighed quantity of the sorbent to remove all the ligand from the sorbent. The absorption spectrum of the effluent was measured after suitable dilution. The effluent gave absorption peaks identical with those of an ethanolic solution of the ligand. Quantitative determination showed that the amount of ligand supported on the silica gel was 27 ± 2 mg g^{-1} of sorbent. The elemental analysis for C, H and N for the sorbent was again in conformity with the former data.

The adsorption capacity of the sorbent for each of the metals under study was measured by the batch method (Table 1). The adsorbent showed no change in its absorbability even when stored for 6 months. The process of adsorption and elution over the synthesized adsorbent was repeated several times and no decline in the percentage adsorption was found even after 10 such recy-

Table 2
Comparison of recoveries of metal ions

Metal	Initial concentration (ppb)	Recovery (%)		
		Solvent extraction [28]	Ion exchange [29]	Present method
Cu(II)	10	97	99	97
	20	98	100	99
Zn(II)	10	92	99	94
	20	93	99	96

clings. To judge the validity of the proposed method, a comparison of recoveries of the metal ions was made with other known methods and the results are given in Table 2. The results show that the present adsorbent can act as an effective adsorbent for preconcentration of the metals studied.

4. Conclusion

Preconcentration of the metals studied is possible by the use of silica gel modified with salicylaldoxime. The sorbent is easy to prepare and is stable and provides reproducibility and fast adsorbability. Separation of metals from a mixture is even possible. A large volume of water sample can be treated with a relatively small column and preconcentrated metals can be eluted in a small volume of eluent, resulting in a high concentration factor.

Further research will concentrate on the effects of various cations and anions, complexing ligands, background electrolytes, ionic strength, surfactants and alkali and alkaline earth metal ions on the preconcentration of metals. It is intended to develop a mathematical model to describe the metal preconcentration for the batch and column methods.

References

[1] L. Friberg, G.F. Nordberg and B. Vouk (Eds.), Handbook on the Toxicology of Metals, Elsevier, North–Holland Biomedical Press, Amsterdam, 1979.

[2] M.R. Matsumoto, A.S. Weber and J.H. Kyles, Chem. Eng. Commun., 1 (1989) 86.

[3] A. De Lucas, J. Zaroo and P. Canzizaras, Sep. Sci. Technol., (1992) 823.

[4] K. Brajter, E.O. Sleszynaska and M. Staskiewicz., Talanta, 35 (1988) 65.

[5] J. Chwastowska and E. Kosiarska, Talanta, 35 (1988) 439.

[6] N.N. Basargin, Z.S. Svanidze and Y.G. Rozouskü, Zavod. Lab., 59(2) (1993) 8.

[7] J. Jambor and T. Tavorek, Collect. Czech. Chem. Commun., 58 (1993) 1821.

[8] O. Abollino, C. Sarzanini, E. Mentasti and A. Liberatori, Spectrochim. Acta, Part A, 49 (1993) 1411.

[9] A.K. Singh, D.P. Singh and V.N. Singh. Environmentalist, 11 (1991) 217.

[10] T.K. Bansal and H.R. Sharma. Indian J. Environ. Protect., 12 (1992) 198.

[11] C. Namasivayam and K. Ranganatham, Indian J. Chem. Technol., 1 (1994) 351.

[12] C. Kantipuly, S. Katragadda, A. Chow and H.D. Gesser, Talanta, 37 (1990) 491.

[13] K. Terada, Pre-Conc. Tech. Trace Elem., CRC, Boca Raton, FL, (1992) 211.

[14] P. Janos, K. Stulik and V. Pacakova. Talanta, 38 (1991) 1445.

[15] R. Koejan, Analyst, 119 (1994) 1863.

[16] T.I. Tikhomirova, M.V. Lukyanova, V.J. Fedeeva, G.V. Kudryavtsev and B.P. Shpigun, Zh. Anal. Khim., 48 (1993) 73.

[17] H. Ince, S. Akman and U. Koklu, Fresenivs' J. Anal. Chem., 342 (1992) 560.

[18] M.B. Shabani, T. Akagi and A. Masuda, Anal. Chem., 64 (1992) 737.

[19] U. Pyell and G. Stork, Fresenivs' J. Anal. Chem., 342 (1992) 281.

[20] P. Janes, K. Stulik and V. Pacakova. Talanta, 39 (1992) 29.

[21] B.B. Prasad and S. Sundd. Bull. Chem. Soc. Jpn., 68 (1995) 559.

[22] P. Rychlovsky, J. Bily and E. Barakasova, Collect. Czech. Chem. Commun., 60 (1995) 76.

[23] A.K. De, S.M. Khopkar and R.A. Chalmers, Solvent Extraction of Metals, Van Nostrand Reinhold, New York, 1970.

[24] M. Sarkar, Analyst, 116 (1991) 53.

[25] APHA, AWWA and WPCF, Standard Methods for Examination of Water and Waste Water, APHA, Washington, 15th edn., 1980.

[26] R.D. Shannon, Acta Cryst., A32 (1976) 751.

[27] M. Eigen, Pure Appl. Chem., 6 (1963) 105.

[28] H. Armannson, Anal. Chim. Acta, 88 (1977) 89.

[29] H.M. Kingston, I.L. Bernes, T.J. Brady and T.C. Rains, Anal. Chem., 50 (1978) 2064.

Talanta

Study of coordination equilibria in systems of coexisting mononuclear and polynuclear complexes by an isosbestic point–spectrophotometric method

Jie Zhou*, Hong-Zong Yin, Xiang-Jin Qu, Yan-Hua Shun

Department of Basic Sciences, Shandong Agricultural University, Taian, Shandong, People's Republic of China

Abstract

This paper reports a method for determining the stability constants of complexes in a system of coexisting mononuclear and polynuclear complexes based on analysis of dual isosbestic points. First it is necessary to determine the dissociation degrees of either of the two complexes concerned in two directions, and then their stability constants. With this method, the conditional constant can be evaluated by appropriate treatment and selection of the proper equations for solutions. For demonstration purposes the scandium/Xylenol Orange system was used to test the model and satisfactory results were obtained.

Keywords: Coordination equilibria; Isosbestic point; Mononuclear complexes; Polynuclear complexes; Stability constants

1. Introduction

Systems of coexisting mononuclear and polynuclear complexes are found repeatedly in coordination chemistry, where the compositions of the complexes are usually MR and M_2R or MR_2 and M_2R_2 [1–4]. Because their equilibrium relation is quite complicated, methods previously reported for the determination of stability constants of complexes cannot be used for this type of coordination equilibrium. One of use [5] has developed a

method for the determination of the constants in the system of coexisting MR and M_2R complexes, although it is not suitable for the MR_2 and M_2R_2 model. New approaches are still required for this model. Making use of the characteristics of the isosbestic points of the absorption spectra found as system compositions vary, from which the dissociation degrees of MR_2 or M_2R_2 complexes in two directions can be obtained, we have developed a method to determine the stability constants of complexes in this case. The method is simple and reliable. It has been applied to the scandium/Xylenol Orange system, and satisfactory results are obtained.

* Corresponding author. Fax: (+91) 538 8226399.

2. Theory

Suppose the reactions between metal ion M and ligand R are as follows (the charges are omitted for simplicity):

$$M + 2R \rightleftharpoons MR_2 \tag{1}$$

$$MR_2 + M \rightleftharpoons M_2R_2 \tag{2}$$
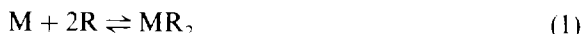
Their respective stability constants can be expressed as

$$K_1 = [MR_2]/[M][R]^2 \tag{3}$$

$$K_2 = [M_2R_2]/[MR_2][M] \tag{4}$$

From the mass balance equation, we obtain:

$$C_M = [M] + [MR_2] + 2[M_2R_2] \tag{5}$$

$$C_R = [R] + 2[MR_2] + 2[M_2R_2] \tag{6}$$

where C_M and C_R represent the total concentrations of the metal ion and ligand respectively. If there are three coloured species—R, MR_2 and M_2R_2—in the system. their absorption spectra are as shown in Fig. 1, which is usually obtained as
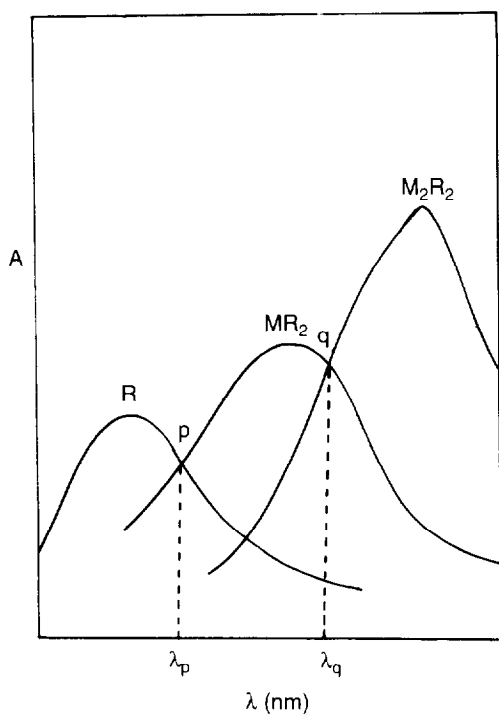

Fig. 1. Schematic diagram of the absorption spectra of R. MR_2. and M_2R_2.

C_M is gradually increased at fixed pH and C_R. If the two reactions take place strictly in this order, then MR_2 is first formed by reaction (1), and M_2R_2 is not formed by reaction (2) until R is fully consumed. In the first process, $[M_2R_2]$ is almost equal to zero. From Eq. (6), we obtain:

$$C_R = [R] + 2[MR_2] \tag{7}$$

The absorbance of the solution is expressed as

$$A = \varepsilon_R[R] + \varepsilon_{1.2}[MR_2] = (\varepsilon_{1.2} - 2\varepsilon_R)[MR_2] + \varepsilon_R C_R \tag{8}$$

In the second process, [R] is almost zero. According to Eq. (6), we obtain:

$$C_R = 2[MR_2] + 2[M_2R_2] \tag{9}$$

$$A = \varepsilon_{1.2}[MR_2] + \varepsilon_{2.2}[M_2R_2]$$
$$= (\varepsilon_{2.2} - \varepsilon_{1.2})[M_2R_2] + \varepsilon_{1.2}C_R/2 \tag{10}$$

From earlier discussions of the characteristics of isosbestic points [6,7]. we obtain $\varepsilon_{1.2} = 2\varepsilon_R$ at λ_p and $\varepsilon_{1.2} = \varepsilon_{2.2}$ at λ_q. According to Eq. (8) and (10) the absorbances of the solutions corresponding to the points p and q are expressed as

$$A_p = \varepsilon_R C_R \tag{11}$$

$$A_q = \varepsilon_{1.2} C_R/2 \tag{12}$$

In accordance with Eqs. (11) and (12), A_p and A_q are constant when C_R and the pH are fixed. Hence two isosbestic points p and q appear caused by the transformation of R into MR_2 and MR_2 into M_2R_2.

In practice, it is impossible for the two reactions to take place strictly in this order, as M_2R_2 can be formed before R is exhausted. Namely, reactions (1) and (2) overlap. In this case, the curves in the absorption spectra do not pass through the two isosbestic points but instead pass below them. Therefore, the absorbance of the solution is expressed as

$$A = \varepsilon_R[R] + \varepsilon_{1.2}[MR_2] + \varepsilon_{2.2}[M_2R_2]$$
$$= (\varepsilon_{1.2} - 2\varepsilon_R)[MR_2]$$
$$+ (\varepsilon_{2.2} - 2\varepsilon_R)[M_2R_2] + \varepsilon_R C_R$$
$$= (\varepsilon_R - 0.5\varepsilon_{1.2})[R]$$
$$+ (\varepsilon_{2.2} - \varepsilon_{1.2})[M_2R_2] + 0.5\varepsilon_{1.2}C_R \tag{13}$$

If the measuring wavelength selected is λ_p and $\varepsilon_{1,2} = 2\varepsilon_R$, then Eq. (13) can be written in the form

$$A_1 = (\varepsilon_{2,2} - 2\varepsilon_R)[M_2R_2] + \varepsilon_R C_R \qquad (14)$$

Substituting Eq. (11) into Eq. (14) yields:

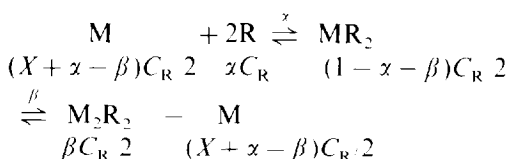$$[M_2R_2] = (A_p - A_1)C_R [2(A_p - A_0)] \qquad (15)$$

where A_0 is the saturation absorbance of M_2R_2 ($A_0 = 0.5\varepsilon_{2,2}C_R$) and is obtained by fixing C_R and increasing C_M to keep the absorbance of solutions constant. If λ_p is selected as the measuring wavelength, and $\varepsilon_{1,2} = \varepsilon_{2,2}$, Eq. (13) can be simplified to

$$A_2 = (\varepsilon_R - 0.5\varepsilon_{1,2})[R] + 0.5\varepsilon_{1,2}C_R \qquad (16)$$

Substituting Eq. (12) into Eq. (16) yields

$$[R] = (A_q - A_2)C_R (A_q - A_R) \qquad (17)$$

where A_R is the absorbance of pure reagent $R(A_R = \varepsilon_R C_R)$. If C_R is fixed and A_p, A_q, A_0 and A_R are held constant, then $[M_2R_2]$ and $[R]$ are only functions of A_1 and A_2 respectively according to Eqs. (15) and (16). In this case we can think of MR_2 being dissociated in two directions, the dissociation reactions being written as

$$M + 2R \underset{}{\overset{\alpha}{\rightleftharpoons}} MR_2$$
$$(X + \alpha - \beta)C_R 2 \quad \alpha C_R \quad (1 - \alpha - \beta)C_R 2$$
$$\overset{\beta}{\rightleftharpoons} M_2R_2 - M$$
$$\beta C_R 2 \quad (X + \alpha - \beta)C_R 2$$

where α and β represent the dissociation degrees of MR_2 in the left and right directions respectively at the equivalence point. $C_R/2$ represents the total concentration of MR_2, and the equilibrium concentrations of relevant species are as follows:

$$[MR_2] = (1 - \alpha - \beta)C_R 2 \qquad (18)$$

$$[M_2R_2] = \beta C_R 2 \qquad (19)$$

$$[R] = \alpha C_R \qquad (20)$$

$$[M] = (X + \alpha - \beta)C_R 2 \qquad (21)$$

In Eq. (21), $X = (2C_M - C_R) C_R$. Substituting Eqs. (18)–(21) into Eqs. (3) and (4), we obtain:

$$K_1 - (1 - \alpha - \beta) [(X + \alpha - \beta)(\alpha C_R)^2] \qquad (22)$$

$$K_2 = \beta [(x + \alpha - \beta)(1 - \alpha - \beta)C_R 2] \qquad (23)$$

Substituting Eqs. (19) and (20) into Eqs. (15) and (17) yields:

$$\alpha = (A_q - A_2)/(A_q - A_R) \qquad (24)$$

$$\beta = (A_p - A_1)/(A_p - A_0) \qquad (25)$$

According to the above discussion, A_p, A_q, A_R and A_0 are held constant at fixed C_R. A_1 and A_2 are measurable values and α and β can be evaluated from Eqs. (24) and (25) respectively. In addition, x is the given value in the experiment. Substituting these known values into Eqs. (22) and (23) gives K_1 and K_2.

3. Experimental

3.1. Apparatus

A Shimadzu UV-240 double-beam spectrophotometer and a pHs-2 acidimeter were used.

3.2. Reagents

A 1.98×10^{-4} M solution of Xylenol Orange (Xo) was prepared from commercial Xo which was purified by diethylamino ethyl–cellulose column chromatography [8] and its accurate concentration was determined by a spectrophotometric method [9]. A 1.00×10^{-2} M stock solution of scandium (III) was prepared from the pure oxide of scandium (Johnson Matthey). The working standard solutions were obtained by diluting the stock solution. HOAc/NaOAc buffer solution (pH 5.50) and 1 M potassium nitrate were prepared with analytical-reagent-grade chemicals.

3.3. Procedure

To each of a series of 25 ml calibrated flasks, add 2.5 ml of buffer solution, a known volume of Xo solution, a different volume of Sc solution and 2.5 ml of 1 M potassium nitrate. Dilute to the mark with distilled water and mix. Stand for 10 min and measure their absorption spectra or absorbance. Maintain the temperature of the solutions at $20 \pm 1°C$ throughout.

4. Results and discussion

Two different complexes were found in the determination of scandium using Xylenol Orange as colour reagent [4,10] when the pH or the mole ratio of the reactants was varied. Zou and Han [4] investigated their compositions in detail. They found $Sc(Xo)_2$ and $Sc_2(Xo)_2$ complexes at pH > 4.5 and thought that the formation of the two species depended on the mole ratio of the reactants. The results we obtained were the same as those in the literature [4]. However, their equilibrium relation has not been investigated in detail. Therefore, in this work the equilibria between 1:2 and 2:2 complexes and the reactants were studied.

4.1. Absorption spectra

When pH and C_{Xo} were fixed and C_{Sc} was gradually increased, a series of solutions resulted with absorption spectra as shown in Fig. 2, which shows that Sc(III) can form two complexes with Xo. Their maximum absorption wavelengths are 490 nm and 557 nm. In addition, two isosbestic points exist in Fig. 2. According to the literature [4], the compositions of the complexes with maxima at 490 nm and 557 nm are $Sc(Xo)_2$ (1:2) and $Sc_2(Xo)_2$ (2:2) respectively. In the presence of a large excess of Sc(III) with respect to the ligand, the 2:2 complexes predominate. With a large excess of the ligand, the 1:2 complexes predominate. The first isosbestic point p is at 456.5 nm and the second isosbestic point q is at 517.0 nm at pH 5.50.

4.2. Determination of stability constants

As discussed previously, in Fig. 2 all curves passing through point p correspond to reaction (1) and all curves passing through point q correspond to reaction (2). The curves passing through neither p nor q indicate that reactions (1) and (2) overlap. The experiments proved that the curves passed through neither p nor q in the C_{Sc}/C_{Xo} range 0.60–1.20. $Sc(Xo)_2$ complexes are thought to dissociate in two directions in this range. Their dissociation degrees α and β are obtained from
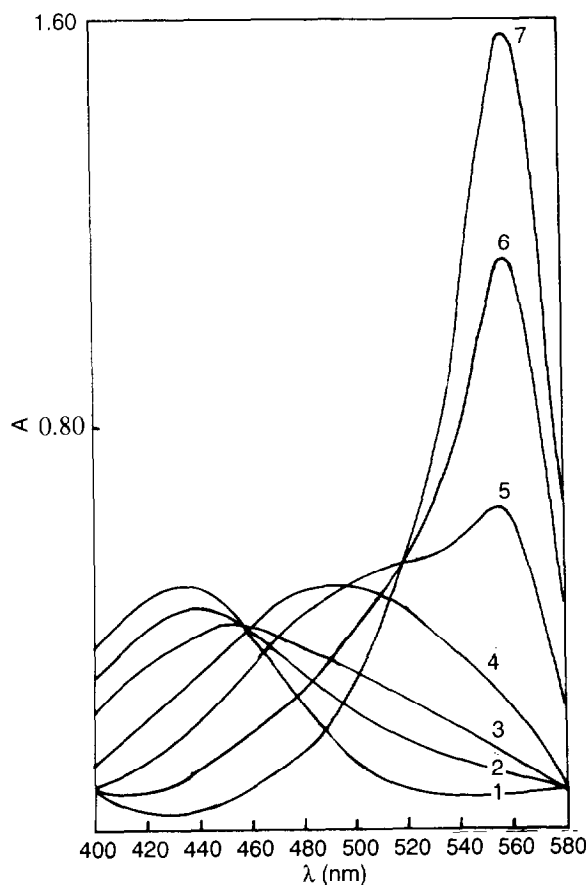

Fig. 2. Absorption spectra for the Sc–Xo system at different C_{Sc} values. $C_{Xo} = 2.00 \times 10^{-5}$ M, pH 5.50, 1 cm cells, distilled water as reference $C_{Sc}(\times 10^{-5}$ M): (1), 0.00; (2), 0.40; (3), 0.80; (4), 1.60; (5), 2.40; (6), 3.20; (7), 4.00.

curves passing through neither p nor q, such as curve 4 shown in Fig. 2. It should be explained that, according to the mechanism of complexation reactions and the above discussion, if the two species determined (R and M_2R_2) exist in the same solution, then the allowed C_M/C_R range is limited. The reason is simple, namely when $C_R > C_M/2$ the value of $[M_2R_2]$ tends towards zero and when $C_M > C_R$ the value of [R] tends towards zero. In addition, the C_M/C_R range relates to the absorption spectra of relevant species. Thus it is quite difficult to estimate it theoretically, and the range can only be found from the experiments approximately.

Table 1

Values of $\log K_1$, $\log K_2$ and associated parameters from the various solutions ($A_q = 0.518$, $A_p = 0.406$, $A_0 = 0.027$, $A_R = 0.074$)

x	A_1	A_2	$\chi(\%)$	$\beta(\%)$	$\log K_1$	$\log K_2$
0.60	0.390	0.430	19.82	4.22	10.81	3.87
0.70	0.385	0.437	18.24	5.54	10.84	3.94
0.80	0.381	0.448	15.77	6.60	10.94	3.98
0.90	0.375	0.456	13.96	8.18	11.02	4.04
1.00	0.369	0.461	12.84	9.76	11.06	4.09

A series of solutions were prepared at fixed C_{X_0} when C_{S_c} was gradually increased ($0.60 < C_{S_c}/C_{X_0} < 1.20$). We measured A_1 at 456.5 nm (λ_p) and A_2 at 517.0 nm (λ_q) with distilled water as reference. Substituting the values of A_1 and A_2 obtained into Eqs. (24) and (25), we could evaluate χ and β. K_1 and K_2 were then calculated from Eqs. (22) and (23) respectively. These results, and the values of the associated parameters, are listed in Table 1. The mean values of $\log K_1$ and $\log K_2$ are taken to be 10.93 and 3.98 respectively. The results given in Table 1 indicate that the method developed in this paper is comparatively reliable. However, the values of $\log K_1$ or $\log K_2$ determined increase somewhat with the ratio C_M/C_R. Such a regular increase cannot be ignored and demands further study.

Finally, it should be noted that, for a stepwise complexing system that consists of two complexes and a system of coexisting MR and M_2R complexes, two isosbestic points similar to those in this paper also appear in the absorption spectra as the system compositions vary. The stability constants of these complexes can be evaluated by a similar treatment and by selecting the appropriate equations for solutions. Thus this method is generally applicable and could be used for most systems of coexisting mononuclear and polynuclear complexes.

References

[1] H. Sato, Y. Yokoyama and K. Momoki, Anal. Chim. Acta, 99 (1978) 167.

[2] S. Murakami and T. Yoshino, Bull. Chem. Soc. Jpn., 54 (1981) 619.

[3] F.J. Langmyhr and P.E. Paus, Acta Chem. Scand., 20 (1966) 2456.

[4] S.F. Zou and B.Z. Han, Acta Chim. Sin., 47 (1989) 694.

[5] S.F. Zou, J. Zhou and W.A. Liang, Analyst, 119 (1993) 97.

[6] S. Kida, Bull Chem. Soc. Jpn., 29 (1956) 805.

[7] S.F. Zou and L.J. Dai, Acta Chim. Sin., 40 (1982) 33.

[8] H. Sato, Y. Yoshino and S. Harasawa, Talanta, 14 (1967) 1293.

[9] M. Murakami, T. Yoshino and S. Harasawa, Talanta, 14 (1967) 1293.

[10] S.S. Berman, G.R. Duval and D.S. Russel, Anal. Chem., 35 (1963) 1392.

Development of a nitrate ion-selective electrode based on an Urushi matrix membrane and its application to the direct measurement of nitrate-nitrogen in upland soils

Satoshi Ito[a,b,*], Keiko Baba[a], Yasukazu Asano[a], Hiroshi Takesako[c], Hiroko Wada[b]

[a]Applied R & D Department, DKK Corporation, 4-13-14, Kichijoji Kitamachi, Musashino, Tokyo 180, Japan
[b]Department of Applied Chemistry, Nagoya Institute of Technology, Gokiso, Showa, Nagoya 466, Japan
[c]Department of Agri-chemistry, Faculty of Agriculture, Meiji, Higashi mita 1-1-1, Tama-ku, Kawasaki 214, Japan

Abstract

A solid-state nitrate ion-selective electrode based on an Urushi matrix membrane was developed. Urushi, a natural oriental lacquer, has excellent mechanical strength and binding affinity for metal electrodes. Using the same technique for a dip-coating ion-selective electrode, an electrode was prepared by coating and hardening a sensing membrane on the metal base. The effects of the metal electrode on the electrode potential stability, the liquid-membrane components and the oven temperature for hardening of membrane were studied. The sensing membrane, consisting of 27.5 wt.% of o-nitrophenyl octyl ether, 27.5 wt.% of tri-n-octylmethylammonium nitrate and 45 wt.% of raw Urushi latex, was coated with a thickness of 0.5 mm on a silver disc which was plated with Ag/AgCl, then plated with copper and hardened in the oven at 80°C for 50 h. A semi-logarithmic calibration curve of potential versus nitrate ion concentration was obtained over the range 6–60 000 mg l^{-1} NO$_3^-$. The slope of the linear part of the curve was -56 mV per decade change in NO$_3^-$ concentration. Compared with a PVC matrix nitrate ion-selective electrode, the Urushi matrix nitrate ion-selective electrode was superior in terms of hardness and mechanical strength of the membrane, short response time and long life. The combination of an Urushi matrix nitrate ion-selective electrode with a porous PTFE junction reference electrode, air-tight structured KCl solution chamber and a temperature sensor was applied to field measurements of nitrate-nitrogen concentrations in upland soils. The values obtained for upland soils containing 30–50% of water were good agreement with those for soil solution.

Keywords: Ion-selective electrode; Nitrate; Soil; Urushi matrix membrane

1. Introduction

An ion-selective electrode is very useful as a detector in protable field analyses. The nitrate (NO$_3^-$) ion-selective electrode has been used to measure the environmental pollution of waste water, underground water, river water, etc. Nitrate ion measurement plays an important role in the

---

* Corresponding author. Fax: (81) 422-52-2042.

nutrition diagnosis of upland soils and plants. Nitrogen is one of the most important components together with phosphate and potassium in plants and crops. Althouth nitrogen fertilizer is applied to farm land as ammonium-nitrogen (NH_3-N), after nitrification it exists mainly as nitrate-nitrogen (NO_3-N) in soils. In recent years, as chemical fertilizers have become available at lower prices, serious problems have arisen with over-supply. In the measurement of vegetable crop soils, the solution obtained by centrifugation (i.e. soil solution) or by water extraction (i.e. 1:5 water extraction method) is analysed using an ion-selective electrode, ion chromatography or spectrophotometry [1-3]. However, farm land is extensive and variable and the nitrogen composition is uneven. Therefore, rapid and direct measurements in the field are requried instead of taking samples for laboratory measurement.

We examined the direct measurement of nitrate in upland soils in the field with a nitrate ion-selective electrode. We also studied a solid-state nitrate ion-selective electrode and developed a combination electrode for nitrate ion consisting of a solid NO_3 ion-selective electrode and a reference electrode. Phenanthrolinenickel(II) nitrate (Orion exchanger [4]), tridodecyl-hexadecylammonium nitrate (Corning exchanger [4]) and methyltricaprylylammonium nitrate [5,6] have been reported as nitrate liquid ion exchangers. Concerning liquid membrane electrodes, the coated wire electrode (CWE) and the PVC matrix electrode were introduced by Freiser [7], Moody and Thomas [8] and others. Zhang et al.'s method for vitamin B_1 with a PVC matrix membrane seems to be very useful and practical [9]. Compared with the lanthanum fluoride single-crystal membrane for a fluoride ion-selective electrode or the silver chloride/silver sulphide heterogeneous membrane for a chloride ion-selective electrode, the above liquid membrane electrode for a nitrate ion-selective electrode is inferior in mechanical strength and durability. Although this PVC matrix membrane is so soft that it can be readily used in water, it is unsuitable in contact with upland soils. To measure the membrane potential, one needs an inner so-

lution containing chloride (Cl^-) ion and nitrate (NO_3^-) ion, and an inner electrode such as a silver/silver chloride (Ag/AgCl) electrode. On the other hand, Hiiro and co-workers [10-18] reported an Urushi matrix membrane which had excellent durability and mechanical strength. We tried to adapt the Urushi matrix method to the nitrate ion membrane and improved the electro-chemical contact between the Urushi matrix membrane and the metal electrode. We studied hardening conditions so as not to damage the liquid membrane components by heating. We also studied metal electrodes and their surface treatment. We developed an Urushi matrix nitrate ion membrane that had hardness, mechanical strength, good electrode potential stability and good sensitivity.

We fabricated a combination of an Urushi matrix nitrate ion electrode with a reference electrode and a temperature sensor, and applied it to the direct measurement of upland soils with a portable potentiometer operated with dry batteries. As the reference electrode, a maintenance-free and a semi-solid porous PTFE junction reference electrode with an air-tight structured KCl solution chamber [19] was used. Upland soils usually contain 30-50 wt.% of water [20]. When a laboratory-use reference electrode with a ceramic junction is used directly in such upland soils, the potential of the reference electrode is unstable and inaccurate. The porous PTFE junction reference electrode, with a large junction area and large pore size, was found to give a stable liquid junction potential in contact with upland soils contained 30-50 wt.% of water. Furthermore, we developed an Urushi membrane tip which could be easily exchanged when the surface of the Urushi matrix membrane was damaged by small pieces of gravel in the soils.

2. Experimental

2.1. Apparatus and reagents

A DKK Model IOL-40 multi-channel ion meter was used for laboratory measurements, a DKK Model HPH-110 handy pH/mV meter for field

measurements and a DKK Model PK-5 electrical conductivity meter for measuring the impedance of the liquid membrane. A Sakuma Model 50B centrifuge was used to obtain the soil solution.

Several kinds of Urushi latex were obtained from Saito (Osaka, Japan). Tri-*n*-octylmethylammonium nitrate (TOMAN) and *o*-nitrophenyl octyl ether (*o*-NPOE) were obtained from Dojindo Laboratories (Kumamoto, Japan). Potassium nitrate, potassium chloride, potassium sulphate, potassium phosphate, hydrochloric acid, sulphuric acid, phosphoric acid, trimethanolamine, sodium hydroxide, boric acid and Devarda's alloy were obtained from Wako (Osaka, Japan). All chemicals were of analytical-reagent grade.

PTFE powder for moulding (M12, grain size ca. 20 μm) was purchased from Daikin Industries (Osaka, Japan). Pure water obtained with a Millipore Milli-Q SP system was used throughout.

2.2. Preparation of Urushi matrix membrane
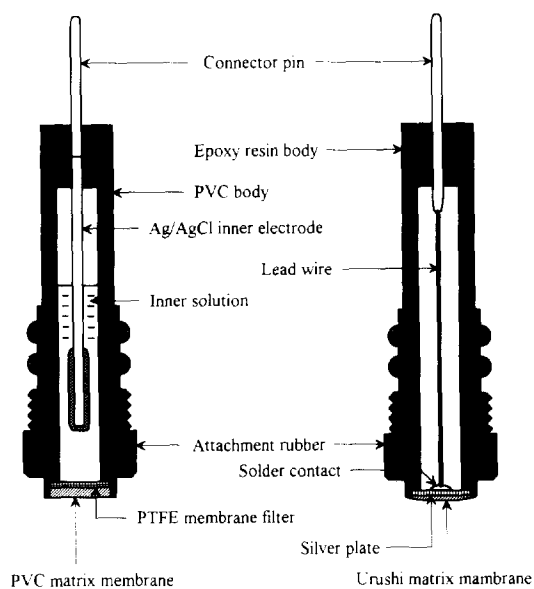
The structure of the Urushi matrix membrane

Fig. 1. Comparison of NO_3^- ion-selective electrode structure with PVC matrix and Urushi matrix.
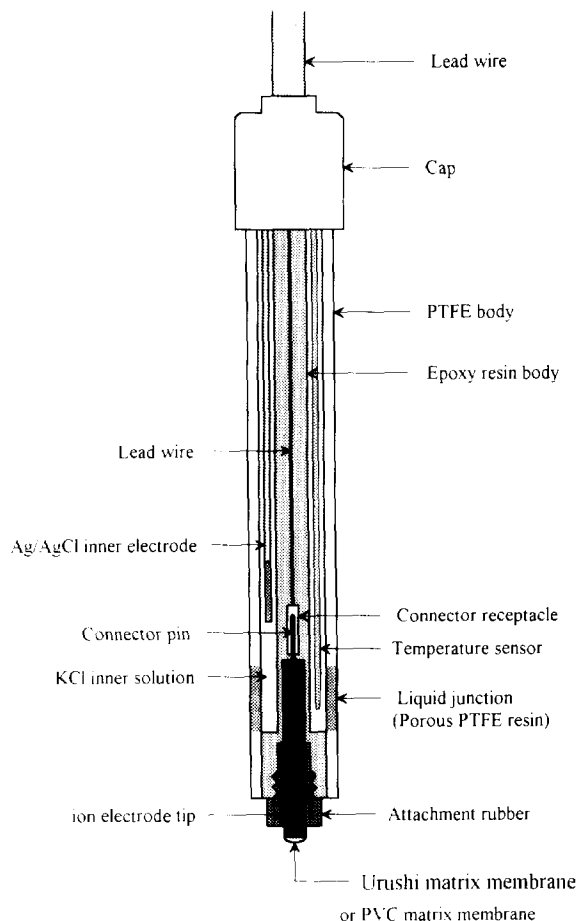

Fig. 2. Structure of combination nitrate ion electrode for direct analysis of upland soils.

tip is shown in Fig. 1. The three types of the metal disc, that is, the copper disc, the silver and that plated first with Ag/AgCl and then with copper, were examined. The electrode body tips were prepared by sticking a silver disc or a copper disc (6 mm in diameter, 1 mm in thickness) on one side of the epoxy resin body with an epoxy bond. The silver disc or the copper disc had a silver wire connected on the inside. The surface of the silver disc or the copper disc was flattened and polished with emery paper (No. 1200 grain size).

Some of the electrode body tips with silver disc were used as they were, others were plated as

Table 1
Membrane composition, contact metal. hardening conditions and characterists of Urushi matrix NO_3^- ion-selective electrode

No.	Composition			Contact metal	Hardening conditions			Characteristics		
	Urushi (%)	TOMAN (%)	o-NPOE (%)		Temperature (°C)	Time (h)	Slope (10 100 mg l^{-1} NO_3-N)	Impedance ($10^3\Omega$)	Stability (mV h^{-1})
I-1	46	36	18	Cu	30	1000	−55	500	6
II-1	54	23	23	Cu	80	50	−42	2000	3
II-2	45	32	23	Cu	80	50	−56	600	8
III-1	54	23	23	Ag AgCl	100	18	−30	5000	<1
III-2	45	32	23	Ag AgCl	100	18	−50	1500	<1
IV-1	45	32	23	Ag AgCl Cu	80	50	−56	500	<1
IV-2	45	27.5	27.5	Ag AgCl Cu	80	50	−56	800	<1
PVC matrix	19 (PVC)	1	80		30	12	−56	200	<1

follows before use. The silver disc was plated with Ag/AgCl in 0.1 M potassium chloride solution (2.5 × 10^{-5} A current, 0.5 h). Further, it was plated with copper in 0.1 M copper sulphate solution (2.5 × 10^{-5} A current, 1 h). The Urushi matrix membrane was prepared by the following procedure. Suitable amounts of Urushi, TOMAN and o-NPOE were mixed on a glass plate and the mixture (about 10 mg) was coated on the surface of the metal side of the electrode tip, and allowed to harden in an oven at 80°C for 50 h or at 100°C for 18 h.

2.3. Preparation of PVC matrix membrane

A PVC matrix membrane was prepared by the following procedure. PVC (0.19 g), TOMAN (0.01 g) and o-NPOE (0.8 g) were dissolved in 10 ml of tetrahydrofuran (THF). A drop of the THF solution was dropped on a PTFE membrane filter disc (0.45 μm pore size) that was left on the membrane side of the PVC electrode body, and the THF was allowed to evaporate in an oven at 30°C for 10 min. After the THF evaporation step had been repeated 15–20 times, about a 0.5 mm thickness of PVC matrix membrane was formed and left for 24 h in the room air.

After filling an inner solution (1 × 10^{-2} mol l^{-1} KCl, 1 × 10^{-2} mol l^{-1} KNO$_3$) and inserting an inner electrode (Ag/AgCl electrode), a PVC matrix electrode tip such as that shown in Fig 1 was fabricated.

2.4. Electrode assembly

A combination electrode body fabricated for laboratory and field measurements is shown in Fig. 2. This consisted of a reference electrode, a temperature sensor to compensate for the temperature effect of the NO_3^- ion electrode and a receptacle to connect with the NO_3^- ion electrode tip. An NO_3 ion electrode is attached to this body by the attachment rubber of the NO_3^- ion electrode tip. The reference electrode has an Ag/AgCl inner electrode and a porous PTFE junction. The saturated KCl solution and the KCl sludge are enclosed in it. The porous PTFE junction was made as follows. PTFE powder and uniform particles of KCl powder were placed in a mould, compressed and sintered at 350°C for 5 h in an oven. The PTFE with KCl powder was cut into the shape of the electrode body and the liquid junction part of it was washed with water to make it porous by dissolution of KCl in the PTFE junction.

2.5. Potential measurements

Potential measurements with the Urushi matrix membrane NO_3^- ion electrode and PVC matrix membrane NO_3^- ion electrode were made with the combination electrode shown in Fig. 2. The performance of the electrode was examined by measuring the e.m.f. of the following electrochemical cell:
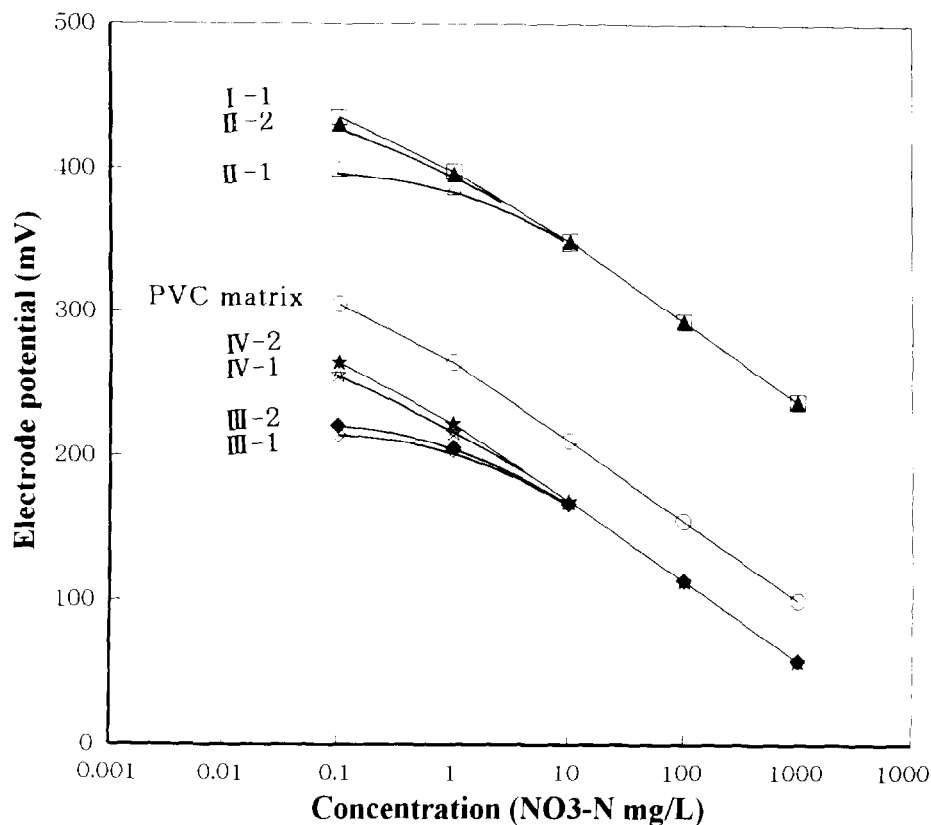
Fig. 3. Calibration curves for Urushi matrix and PVC matrix nitrate ion electrodes.

(i) Cu|Urushi matrix membrane|sample|sat. KCl|Ag/AgCl

(ii) Ag|Urushi matrix membrane|sample||sat. KCl|Ag/AgCl

(iii) Ag/AgCl/Cu|Urushi matrix membrane|sample||sat. KCl|Ag/AgCl

(iv) Ag/AgCl|inner solution|PVC matrix membrane|sample||sat. KCl|Ag/AgCl

In a laboratory measurement, the e.m.f. data from four electrodes were simultaneously fed to a personal computer from the potentiometer (Model IOL-40) through an RS-232C interface.

2.6. Calibration

Each membrane with the combination electrode was immersed in 0.1–1000 mg l^{-1} NO_3-N standard solution (10^{-3} mol l^{-1} = 14 mg l^{-1} NO_3-N), and calibration curves for each membrane were measured. To each NO_3-N standard solution 5×10^{-2} mol l^{-1} K_2SO_4 solution was added to adjust the ionic strength. The electrode potentials were recorded after their values had stabilized to within ± 0.1 mV min^{-1}. Potential–concentration curves were plotted as shown in Fig. 3.

2.7. Stability of electrode potential

The stability of the electrode potential was measured as follows. Each electrode was left in 10 mg l^{-1} standard solution for 5 days and the calibration curves for each electrode were measured once a day. After the electrodes had dried in room air, the stability of the electrode potential was measured again using the same procedure. The electrode potentials in 10 mg l^{-1} standard solution were plotted as a function of elapsed time.
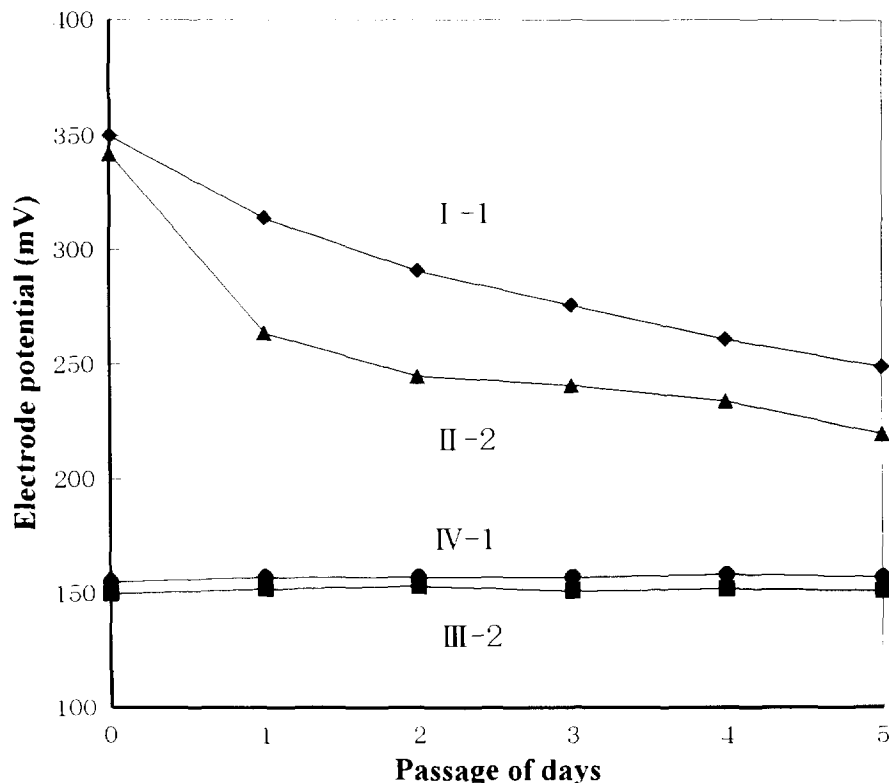
Fig. 4. Stability of Urushi matrix and PVC matrix nitrate ion electrode potentials.

2.8. Influence of pH

Each electrode was calibrated using standard solutions with pH varying from 1 to 12. The pH was adjusted by adding small volumes of H_2SO_4 or NaOH to the standard solution. The electrode potential were recorded after their values had stabilized, and were plotted as a function of pH and NO_3-N concentration.

2.9. Measurements of membrane impedance

The membrane impedance was measured with a Model PK-5 electrical conductivity meter (5 V a.c., 1 kHz) in 1 mol l⁻¹ KNO_3 solution using a platinum electrode at room temperature.

2.10. Influence of temperature

NO_3-N standard solutions from 1 to 1000 mg l⁻¹ were prepared in a water-bath at 5, 25, 45°C.

They were kept at a constant temperature to within ±0.1°C. The calibration curves for the electrode were measured in standard solution at 5°C and then at 25 and 45°C. The electrode potentials were recorded after their values had stabilized, and were plotted as a function of temperature and NO_3-N concentration.

2.11. Selectivity

Selectivity coefficients were determined by the mixed solution method, wherein the concentration of NO_3-N was fixed at 100 mg l⁻¹ and the concentration of an interfering ion was varied. The selectivity coefficients, $K_{A,B}^{pot}$, were calculated according to the equation $K_{A,B}^{pot} = C_A^{Z_B/Z_A}/C_B$, where C_A and C_B are the total concentration of NO_3-N and that of an interfering ion obtained graphically in the sample solution, respectively, and z_A and z_B are the charges of NO_3-N and the interfering ions, respectively.
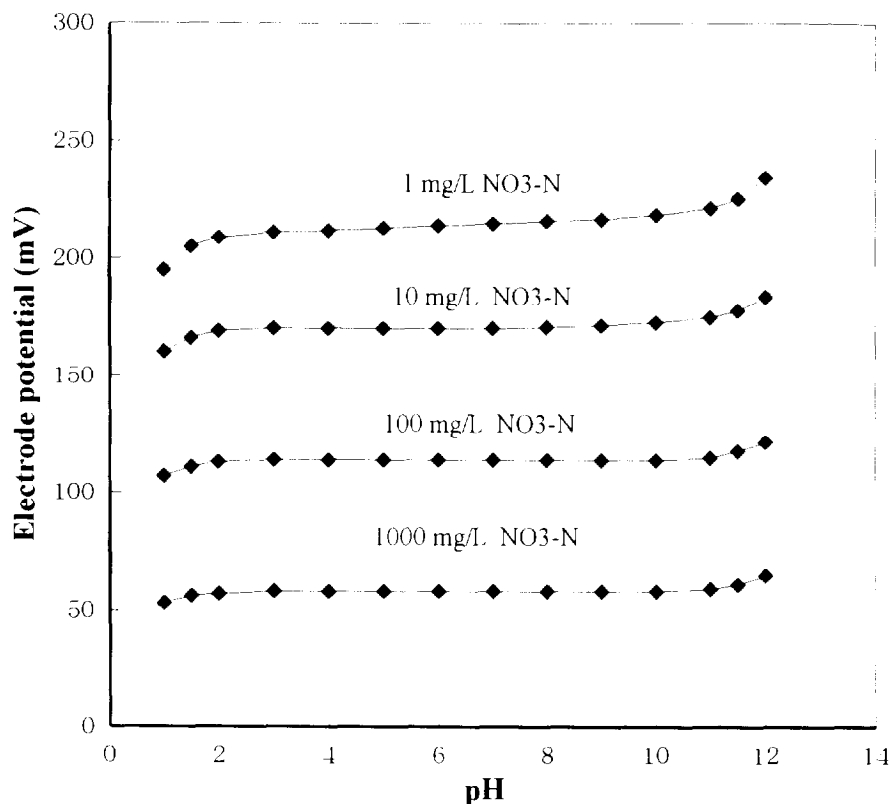
Fig. 5. Effect of pH on Urushi matrix nitrate ion electrode.

2.12. Durability of membrane in long-term storage

The Urushi matrix membrane electrode and the PVC matrix membrane electrode were stored in air and water, respectively, and the calibration curves were measured once a month. The change in the slope between 10 and 100 mg l⁻¹ NO₃-N standard solution was investigated. The durability on long-term storage is obtained from the change in air and that on long-term use from the change in the water.

2.13. Analysis of soil

Andosol that mostly occurs in the Kanto area in Japan was used as a sample soil. The sample solution was prepared by the following two methods, and was analysed by the manual method with an ion-selective electrode.

The water extraction solution [2] was used to compare the present Urushi matrix membrane electrode with the conventional PVC matrix membrane electrode. The air-dried soil (10 g) was dissolved in 50 ml of 5×10^{-2} mol l⁻¹ K_2SO_4 solution and the solution was filtered through a filter-paper (Toyo No. 6). The NO_3-N concentration in the 1:5 water extraction solution was measured with the Urushi matrix combination electrode and the PVC matrix combination electrode. The values obtained with the Urushi matrix combination electrode were compared with those obtained with the PVC matrix combination electrode.

The direct analysis of soil with the Urushi matrix combination electrode was compared with a manual analytical measurement of the soil solution. The soil (about 300 g, contained about 80 wt.% of water) that was collected from farm land was mixed in an airtight plastic bag and was left to
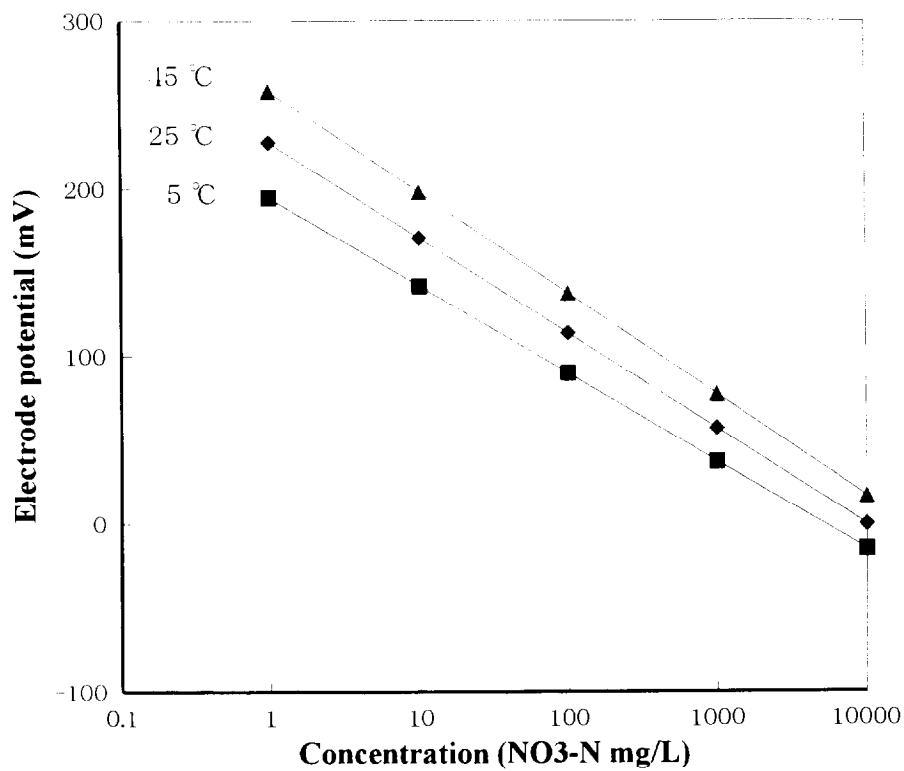
Fig. 6. Effect of temperature on Urushi matrix nitrate ion electrode.

homogenize for 3 days in an oven at 30°C. The Urushi matrix membrane electrode was inserted into the soil from the plastic bag. The e.m.f. became stable after 1–3 min by slightly pressing the soil against the Urushi matrix membrane and the porous PTFE junction of the reference electrode. The soil solution was obtained from the soil (100 g) by centrifugation (8900 rev min^{-1}, 60 min). A manual analytical measurement of the soil solution was made by the following procedure (Bremner method). The NO_3^- was converted into NH_3 gas by steam distillation with a catalyst (Devarda's alloy), and was trapped as NH_4^+ ion in absorbent solution (2% boric acid). The NH_4^+ ion solution was titrated with 0.1 mol l^{-1} Na_2CO_3 with methyl red and bromocresol green indicators, and the NO_3-N concentration in the soil solution was calculated. The values obtained by means of the Urushi matrix combination electrode were plotted against those obtained by the manual analytical method.

3. Results and discussion

3.1. Membrane material and characteristics

We examined four ways of hardening the Urushi matrix membrane as shown in Table 1. Method I is Hiiro et al.'s method, in which the membrane was hardened at room temperature in their originally manufactured oven with a rotating electrode holder able to provide 80–90% relative humidity at 30°C for 1000 h. We tried their method, but could not obtain sufficiently hard membrane. Also, the hardening time of 1000 h was considered to be too long.

The hardening time was reduced when the temperature increased. Without affecting the characteristics of the slope and impedance, we lowered the hardening conditions in method II to 80°C and 50 h. As shown in Table 1, the slope and impedance characteristics of membranes I and II-2 were good, but we found that there was a
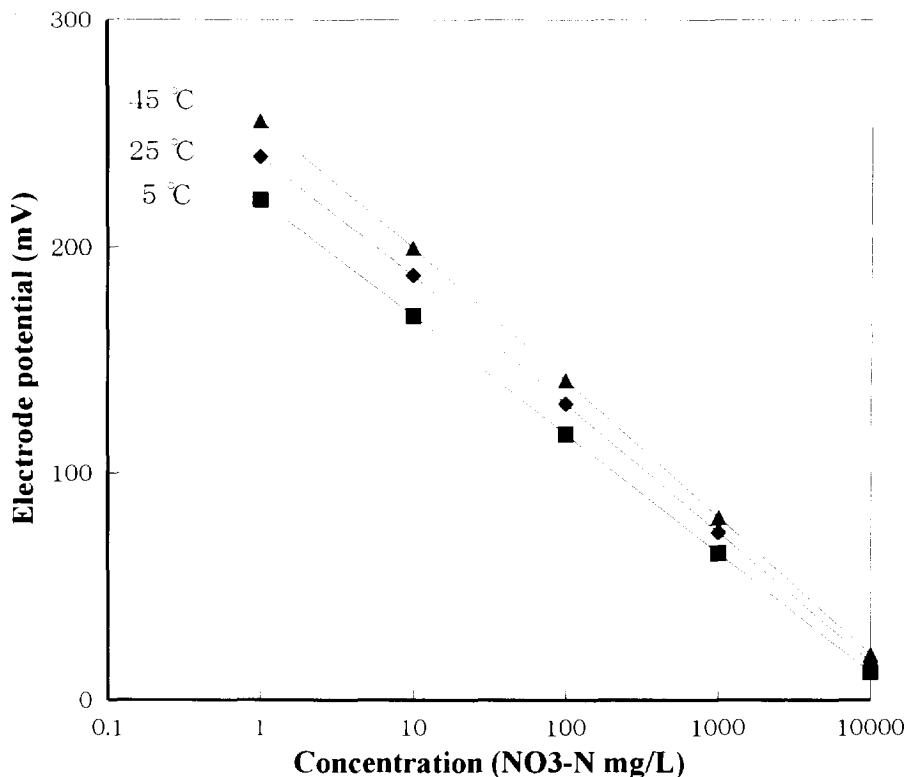
Fig. 7. Effect of temperature on PVC matrix nitrate ion electrode.

serious problem with the stability. As Fig. 4 shows, the e.m.f. of the electrode in a 100 mg l $^{-1}$ solution changed over several days. Although the e.m.f. change of the PVC matrix membrane electrode early in the measurement was within 1 mV h^{-1}, that of Urushi matrix membrane electrode was 3-8 mV h^{-1}.

We found that the surface of the copper disc had changed from metallic red to lusterless black when the Urushi matrix membrane of these electrodes was stripped off. We thought that the change in the e.m.f. occurred at the interface between the Urushi matrix membrane and the copper. Therefore, we tried to harden the Urushi matrix membrane on silver with plated Ag/AgCl (method III). As Hiiro et al. mentioned, we confirmed that the Urushi matrix membrane needed a copper catalyst for hardening. Although with conditions of 130°C and 8 h we were able to harden the Urushi matrix membrane on silver plated with Ag/AgCl, the membrane was too hard to respond

to the NO$_3$-N ion. After various examinations of the effect of lower temperatures on the response to the NO$_3$-N ion, we obtained good results at 100°C for 18 h.

The characteristics of the membrane III were good with regard to stability, but not impedance and slope. A hardening temperature of 100°C seemed to be too high.

We found that copper was indispensable for hardening as the Urushi matrix membrane silver plated with Ag/AgCl was superior in stability in the presence of copper. Furthermore, we tried to harden the Urushi matrix membrane on silver plated with Ag/AgCl and copper (method IV). The characteristics of membrane IV nearly equalled that of the PVC matrix membrane.

Table 1 shows the membrane composition, the contact metal, the hardening conditions and the characteristics of the Urushi matrix NO$_3^-$ ion electrode. For comparison, the membrane composition, the hardening conditions and the charac-

Table 2

Selectivity coefficients for the Urushi matrix NO_3 ion electrode and the PVC matrix NO_3^- ion electrode

Ion (j)	Selectivity coefficient ($K^{pot}_{NO_3,j}$)	
	Urushi matrix (IV-2) NO_3^- ion electrode	PVC matrix NO_3^- ion electrode
ClO_4	$> 10^3$	$> 10^3$
I^-	50	50
Br^-	1.5×10^{-1}	1.5×10^{-1}
HS	1×10^{-1}	1.5×10^{-1}
NO_2	5×10^{-2}	8×10^{-2}
CN	5×10^{-2}	7×10^{-2}
Cl^-	4×10^{-3}	8×10^{-3}
$RCOO$	1.5×10^{-3}	2.5×10^{-3}
HCO_3^-	1.5×10^{-3}	2×10^{-3}
SO_4^{2-}	$< 10^{-3}$	$< 10^{-3}$
$H_2PO_4^{2-}$	$< 10^{-3}$	$< 10^{-3}$
HPO_4^-	$< 10^{-3}$	$< 10^{-3}$
PO_4^{3-}	$< 10^{-3}$	$< 10^{-3}$

teristics of the PVC matrix NO_3 ion electrode are also shown in Table 1. In this case, PVC was used instead of Urushi and the contact metal was not used.

Fig. 3 shows the calibration curves for the Urushi matrix membrane electrode and the PVC matrix membrane electrode. The electrode potential of the PVC matrix membrane electrode is the e.m.f. when the inner solution is 1×10^{-2} mol l^{-1} KCl, 1×10^{-2} mol l^{-1} KNO_3, and can be changed by varying the composition of the inner solution. For the Urushi matrix membrane electrode, the electrode potential is changed with the

contact metal, which is copper or silver. The slope for 0.1–1 mg l^{-1} NO_3-N was -40 mV with the PVC matrix membrane electrode and was -35, -13, -38, -11, -15, -39 and -42 mV with the Urushi matrix membranes I-1, II-1, II-2, III-1, III-2, IV-1 and IV-2, respectively.

Fig. 4 shows the change in the electrode potential in 10 mg l^{-1} NO_3-N standard solution. Although the data for membranes I-1, II-2, III-2 and IV-1 are shown, the patterns of the changes between II-1 and II-2, between III-1 and III-2 and between IV-1 and IV-2 were almost the same. The pattern of the changes is obviously distinguished by the kind of contact metal (copper or silver). The change in electrode potential seems to be due to the potential change at the interface between the Urushi matrix membrane and the contact metal after the Urushi matrix membrane had gradually absorbed moisture. Therefore, after the 5-day measurement, and after the electrode had dried completely (for 1–2 weeks) in the room air, the same pattern of the potential change was repeated.

3.2. Effect of pH

The pH dependence of the Urushi matrix membrane electrode is shown in Fig. 5. It can be seen that the electrode is not influenced in the pH range 2–10. In the lower concentration range (1 mg l^{-1} NO_3-N), even between pH 2 and 10, a small increase in potential occurred. It would be preferable if the measurements were made at pH 7 with 0.05 mol l^{-1} phosphate buffer solution.

Table 3

Durability of the membrane on lont-term storage

Time (months)	Slope in 10–100 mg l^{-1} NO_3-N (mV)			
	Urushi matrix membrane		PVC matrix membrane	
	Storage in water	Storage in air	Storage in water	Storage in air
0	-56	-56	-56	-56
1	-55	-56	-54	-55
3	-53	-56	-50	-53
6	-50	-56	-40	-50
12	-45	-55	-20	-46
18	-30	-55	-15	-40

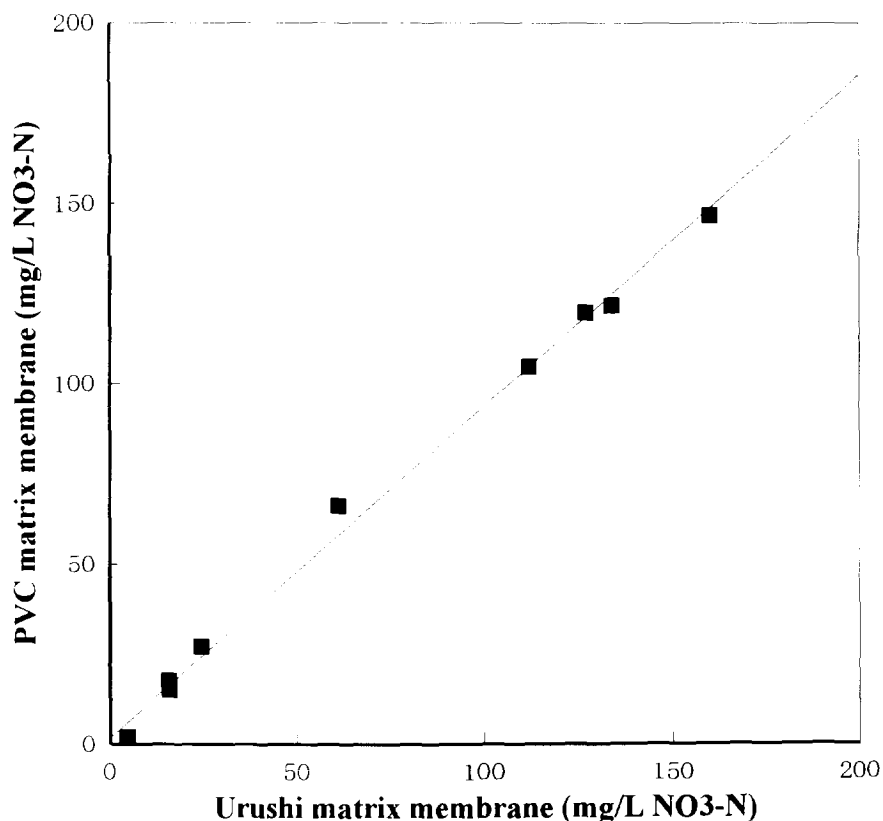S. Ito et al. Talanta 43 (1996) 1869–1881

1879

Fig. 8. Correlation between Urushi matrix electrode measurement and PVC matrix electrode measurement for the water extraction sample of soil.

3.3. Effect of temperature

The temperature dependences of the Urushi matrix membrane electrode and the PVC matrix membrane electrode are shown in Figs. 6 and 7, respectively. The isothermal point of the Urushi matrix membrane electrode is calculated as 10^7 mg l^{-1} NO_3-N; this is higher than the 5×10 mg l^{-1} NO_3-N for the PVC matrix membrane electrode. With increase from 10 to 100 and 1000 mg l^{-1} NO_3-N in the sample solution, the electrode potential of the Urushi matrix membrane electrode rises at 1.4, 1.2 and 1 mV °C^{-1} with increase in termperature, respectively (0.75, 0.6 and 0.4 mV °C^{-1} for the PVC matrix membrane electrode). For field measurements, the temperature compensation should be done electrically.

3.4. Effect of interfering compounds

The interference results are shown in Table 2. The selectivity coefficients followed those for most liquid ion-exchange membrane electrodes. There were no differences between the Urushi matrix membrane and PVC matrix membrane, essentially because the sensing membrane to NO_3^- ion was the same. Halide ions, especially Cl$^-$, mainly interfere with measurements with the NO_3^- ion electrode. In normal operation, interference from HCO_3^- and $RCOO^-$ should also be taken into account.

3.5. Durability of membrane
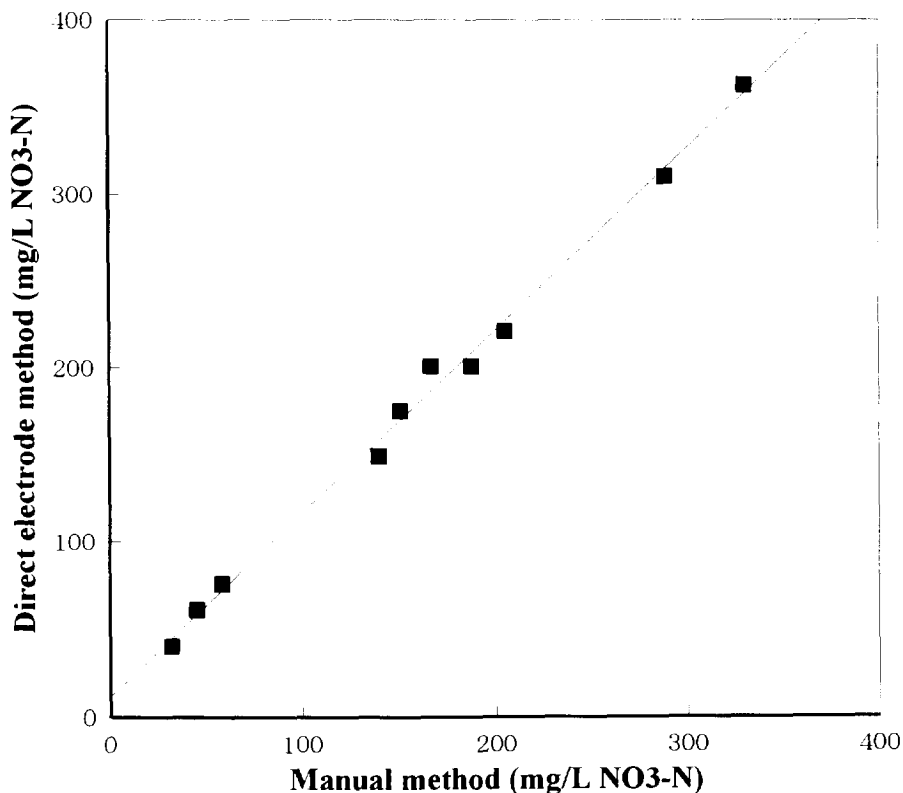
Table 3 shows the slope for 10–100 mg l^{-1}

Fig. 9. Correlation between direct measurement with Urushi matrix nitrate ion electrode and manual measurement by the Bremner method for the soil solution sample.

NO_3-N for the Urushi matrix membrane and PVC matrix membrane after long-term storage. The characteristics of the liquid membrane ion-selective electrode were gradually lost because a portion of the membrane components volatilized. The Urushi matrix membrane had kept its initial characteristics compared with those of the PVC membrane after 18 months in practical use.

3.6. Direct measurement of NO_3-N in upland soils

In the measurement of 1:5 water extraction solution, as Fig. 8 shows, the values with the Urushi matrix membrane electrode are good agreement with those with the PVC matrix membrane electrode ($r^2 = 0.996$, $y = 0.92x + 1.7$).

The correspondence between direct measurements on soils with the Urushi matrix combination electrode and the manual analytical measurement

of soil solution is shown in Fig. 9 ($r^2 = 0.994$, $y = 1.05x + 11$). Therefore, we conclude that the Urushi matrix NO_3^- ion electrode is able to measure NO_3^- ion in the soil solution when the electrode is directly inserted into the soils, without interference from small amounts of gravel.

The pH range of the upland soil used as vegetable crop soil was approximately 4–8. Although soils with pH 4 below exist (i.e. acid soils), these soils are not good for growing crops. For soils that need nutrition diagnosis, the Urushi matrix membrane electrode was able to measure NO_3^- ion directly without adding pH adjustment buffer solution. Concerning interferences, Milham et al. [3] suggested the use of a buffer solution to eliminate interfering ions such as Cl^-, HCO_3^- and $RCOO^-$ in soil analysis. Since buffer solution could not be used in the direct measurement of soils, the measured values for soils that included sea water were higher than the true values because of interference from Cl^-.

4. Conclusion

From studies of an Urushi matrix nitrate ion membrane and a contact metal, the Urushi matrix membrane electrode was shown to be equal to the PVC matrix membrane electrode with regard to detection range and selectivity. It was found that the Urushi matrix method is one of the most useful approaches for making a liquid membrane into the solid state. The Urushi matrix nitrate membrane had hardness and mechanical strength, and showed advantages of a short response time and a long lifetime. The combination of the Urushi matrix nitrate ion electrode with the porous PTFE junction reference electrode was able to measure NO_3-N directly in upland soils and was found to be very useful for the nutrition diagnosis of soils.

By making the liquid sensing membrane for an ion-selective electrode into the solid state, many practical applications can be expected in field measurements with ion-selective electrodes.

Acknowledgement

References

[1] M.A. Tabatabai and W.A. Dick. Ion Chromatographic Analysis of Environmental Pollutants, Vol. 2, Ann Arbor Science Publishers, Ann Arbor, MI, 1979, p. 361.

[2] Methods of Soil Nutrients Analysis. Yokendo, Japan, 1987. p. 4440.

[3] P.J. Milham, A.S. Awad, R.E. Paull and J.H. Bull, Analyst, 95 (1970) 751.

[4] H. Freiser, Ion-Selective Electrodes in Analytical Chemistry, Vol. 1, Plenum Press, New York, 1978, p. 294.

[5] C.J. Coetzee and H. Freiser, Anal. Chem., 40 (1968) 2071.

[6] C.J. Coetzee and H. Freiser, Anal. Chem., 41 (1969) 1128.

[7] H. Freiser, Ion-Selective Electrodes in Analytical Chemistry, Vol. 2, Plenum Press, New York, 1978, pp. 85–105.

[8] G.J. Moody and J.D.R. Thomas, Selective Ion Sensitive Electrodes, Merrow, Watford, 1971, pp. 57 128.

[9] G.H. Zhang, T. Imato, Y. Asano, T. Sonoda, H. Kobayashi and N. Ishibashi, Anal. Chem., 62 (1990) 1644.

[10] K. Hiiro, A. Kawahara and T. Tanaka, Nippon Kagaku Kaishi, 10 (1980) 1447.

[11] K. Hiiro, H. Mukai, A. Kawahara and S. Wakida, Annual Report of Kyoto University of Education, 79B (1991) 19.

[12] K. Hiiro, H. Mukai, A. Kawahara and T. Tanaka, Anal. Chim. Acta, 110 (1979) 321.

[13] S. Wakida, M. Yamane and K. Hiiro, Bunseki Kagaku, 38 (1989) 140.

[14] K. Hiiro, H. Mukai, T. Tanaka and A. Kawahara, Bunseki Kagaku, 25 (1976) 653.

[15] K. Hiiro, T. Tanaka, A. Kawahara and S. Wakida, Anal. Sci., 2 (1986) 145.

[16] K. Hiiro, A. Kawahara and T. Tanaka, Nippon Kagaku Kaishi, 10 (1980) 1447.

[17] K. Hiiro, S. Wakida, T. Tanaka, A. Kawahara and M. Yamane, Fresenius' Z. Anal. Chem., 326 (1987) 362.

[18] K. Hiiro, A. Kawahara and T. Tanaka, Bunseki Kagaku, 31 (1982) E33.

[19] S. Ito, F. Kobayashi, K. Baba, Y. Asano and H. Wada, Talanta, 43 (1996) 135 142.

[20] R.K. Schofield, Trans. 3rd Int. Congr. Soil Sci., 2 (1935) 37.

Simple solvent extraction technique for elimination of matrix interferences in the determination of methylmercury in environmental and biological samples by ethylation–gas chromatography–cold vapor atomic fluorescence spectrometry

Lian Liang[a,b,c,*], Milena Horvat[a], Elsa Cernichiari[b], Bob Gelein[b], Steven Balogh[d]

[a]*IAEA. Marine Environment Laboratory, 19 Avenue des Castellans, MC-98000 Monaco, Monaco*
[b]*Department of Environmental Medicine. University of Rochester, Rochester, NY 14642, USA*
[c]*CEBAM Analytical, Inc., 2419 11th Avenue, Portland. OR 97214, USA*
[d]*Metropolitan Council Environmental Services, 2400 Childs Road, St. Paul, MN 55106, USA*

Abstract

A solvent extraction technique involving no critical clean-up steps was developed for the determination of methylmercury (MeHg) in environmental and biological samples by aqueous phase ethylation, room temperature precollection, gas chromatographic separation and cold vapor atomic fluorescence spectrometric detection. Samples were first digested with KOH–methanol. then acidified prior to extraction with methylene chloride. MeHg was back-extracted from the solvent phase into water prior to aqueous phase ethylation. Recoveries close to 100% were obtained with RSDs less than 5% for all samples analyzed, making direct standardization possible. The detection limits were about 0.08 ng g^{-1} when analyzing 0.1 g of dry sea plant homogenate and 0.02 ng g when analyzing 0.5 g of wet sediment samples. Various certified reference materials and intercomparison samples, including sediments, sea plants and tissues, were analyzed, and the results were in good agreement with the certified values. The technique was applied to the determination of MeHg in both sea plants from the Atlantic and the red blood protein of dolphins from the Mediteranean Sea. in sediments from the Mediterranean Sea and Minnesota rivers and in soils from different origins. Concentrations of MeHg in dolphin red blood protein samples were as high as 300 ng g^{-1}.

Keywords: Cold vapor atomic fluorescence spectrometry; Ethylation; Gas chromatography; Matrix interferences; Methylmercury; Solvent extraction

1. Introduction

Methods based on aqueous phase ethylation with sodium tetraethyl borate [1] for the determi-

nation of methylmercury (MeHg) by gas chromatography-cold vapor atomic fluorescence spectrometry (GC-CVAFS) have significant advantages over other methods, and are now in wide use [2,3]. The primary advantage of the methods lie in the easy isolation of MeHg from the sample matrix by a simple purging of the volatile ethylation product, methylethylmercury. Tedious and involved critical clean-up steps [4] are thus unnessary. However, owing to severe matrix interferences with the ethylation reaction [2,5], only very small sample sizes can be used, hence only samples with relatively higher MeHg concentration can be analyzed, limiting the method's applicability to samples with low MeHg concentrations. To eliminate these interferences, a distillation technique was developed [6,7] which allows the application of the ethylation procedure for low MeHg concentrations in complex matrices. This method is now widely used. A number of valuable results have been obtained using this technique [8,9], which greatly promoted research on the biogeochemical cycle of mercury. However, we found that when high Hg^{2+} containing samples were distilled, a large amount of Hg^{2+} was transfered to the distillates. It has been found that owing to the presence of a large amount of Hg^{2+}, MeHg artifact may be formed during ethylation reactions in some cases [6]. Since distillation cannot isolate MeHg from Hg^{2+}, this problem cannot be eliminated by the technique. In addition, when samples containing large amounts of volatile compounds are distilled, volatile components transferred to the distillate interfere with the ethylation reaction and/or deposit on the GC column, suppressing the GC signal and preventing accurate determinations. Moreover, the distillation technique requires unusual equipment which most general laboratories do not have. To overcome these problems, a simple solvent extraction technique involving no critical clean-up steps was developed.

Some solvent extraction procedures have been developed for determining MeHg by GC-electron capture detection. As this detection method is not specific for mercury, very critical and tedious clean-up steps had to be used [4,10] to avoid chromatographic interferences. In the present work, the mercury-specific atomic fluorescence de-

tector was used, eliminating chromatographic interferences.

The solvent extraction demonstrated here serves simply to isolate MeHg from the major matrix in order to eliminate interferences with the ethylation reaction, resulting in a simplified technique. Recently, another solvent extraction technique was developed for the determination of organic mercury compounds by HPLC-AFS [11]. In that procedure, the mercury was first chelated with dithizone reagent and extracted into chloroform in the presence of citrate buffer. The solvent phase was separated from the slurry by filtration. The derivative of inorganic mercury in the solvent phase, dithizone-mercury complex, was destroyed with HNO_3, and entered the aqueous phase, while MeHg remained in the solvent phase, thus separated from the inorganic mercury. The organic compounds were finally back-extracted into the aqueous phase with sodium thiosulfate solution buffered with ammonium acetate. A recovery of 80% was reported. Compared with that procedure, the technique presented here has the advantages that no buffers or chelators were used, and only HCl and CH_2Cl_2 were employed for the extraction. Recoveries close to 100% were obtained, making direct standardization possible for all kinds of samples, ensuring the reliability of the method.

2. Experimental

2.1. Instrumentation, materials and reagents

The instrumentation, materials and reagents used have been detailed elsewhere [2,3]. In the analytical procedure, a Model 2500 CVAFS mercury dector from Tekran (Canada) was also used, and only Tenax traps [3] were used for precollection of ethylation derivatives.

2.2. Solvent extraction procedure

Depending on the MeHg concentration, an appropriate aliquot of sample (typically 0.05-0.2 g of dry sample, or 0.1-0.5 g of wet sample) was weighted into a Teflon vial or bottle. In this work,

30 ml Teflon FEP bottles (H-06327, Cole Parmer, USA) were used. Two ml of 25% KOH–methanol were added and the bottle was then capped tightly and heated in an oven at 75°C for 3 h for digestion. The digestate was allowed to cool to room temperature. A 6 ml volume of CH_2Cl_2 (GC60616-4, GC^2, Baxter Scientific Products, USA) were added to the digestate, and 1.5 ml of concentrated HCl were then added slowly. The mixture was capped and shaken for 10 min with a shaker. The mixture was poured into a Teflon FEP separating funnel (50 ml, H-06125-10, Cole Parmer) and, after the phases had separated, the lower solvent phase CH_2Cl_2 was collected in a 125 ml Teflon bottle. Another 6 ml of CH_2Cl_2 were added to the separating funnel, the slurry was washed and then separated and CH_2Cl_2 was collected in the 125 ml Teflon bottle. For small sample sizes, the slurry was washed once only. For larger sample sizes, the slurry was washed twice. Then approximately 80 ml of deionized water were added to the solvent phase in the 125 ml Teflon bottle. This bottle was placed in a water-bath at 80°C for solvent evaporation, i.e. back-extraction. Residual solvent remaining after the back-extraction was purged with nitrogen or other gases for 2 min. Prior to the ethylation reaction, the final volume was brought to a known amount unless the whole extract was to be analyzed. Depending on the concentration of MeHg, an appropriate aliquot was placed in the bubbler for the ethylation reaction, following the procedure described elsewhere [3]. For non-homogeneous samples, large sizes are required, and the volume of KOH–methanol solution is proportionally increased. However, after alkaline digestion, only part of the digestates is quantitatively taken for solvent extraction.

3. Results and discussion

3.1. Alkaline digestion and sample size

Alkaline digestion has been widely used for the release of mercury compounds from tissues. Over the past decade, many certified reference materials and intercomparison samples have been analyzed

directly after alkaline digestion by aqueous phase ethylation and GC–CVAFS, with recoveries close to 100% [5], indicating that mercury compounds are released completely by alkaline digestion. This is the basis of the technique described here. It was found that 2 ml of 25% KOH–Methanol were sufficient for digesting dry samples up to 0.5 g. The use of a considerably larger sample size is not necessary since the CVAFS is an extremely sensitive detector. In this technique, the MeHg was finally extracted from an acidified slurry of KCl and sample substances. A larger sample size requires more alkali–methanol and HCl, yielding more slurry and making the following steps (separating and washing) difficult, ultimately reducing the recovery. Therefore, larger sample sizes are not recommended. However, for non-homogeneous samples, it may be necessary to use larger sample sizes to improve the analytical accuracy. In this case, a sample as large as several grams can be used and more KOH–methanol should be added. After the alkaline digestion, however, only an appropriate aliquot of digestate should be taken for solvent extraction. After separation of the solvent phase, the slurry needs to be washed again with CH_2Cl_2 to achieve maximum recovery. For smaller samples sizes, we washed the slurry once. For larger sample sizes, however, and depending on the amount of slurry, two or more washings were required.

3.2. Effect of acidification on extraction recovery

In principle, MeHg can be extracted quantitatively from an acidic solution into an organic solvent. In this work, HCl was used for neutralization and acidification of the strongly alkaline digestate slurry. To optimize the acidification conditions, a series of aliquots (0.135–0.150 g) of certified reference sediment, IAEA 356, were digested with 2 ml of 25% KOH–methanol. Following the addition of 6 ml of CH_2Cl_2 to each of the cooled digestates, various volumes of concentrated HCl were added, and the slurries were shaken for either 20 s or 10 min. The results are shown in Fig. 1. When 0.5 ml of HCl was added, the pH of the slurry was > 12 and the recoveries were very low. When 1 ml of HCl was added, the
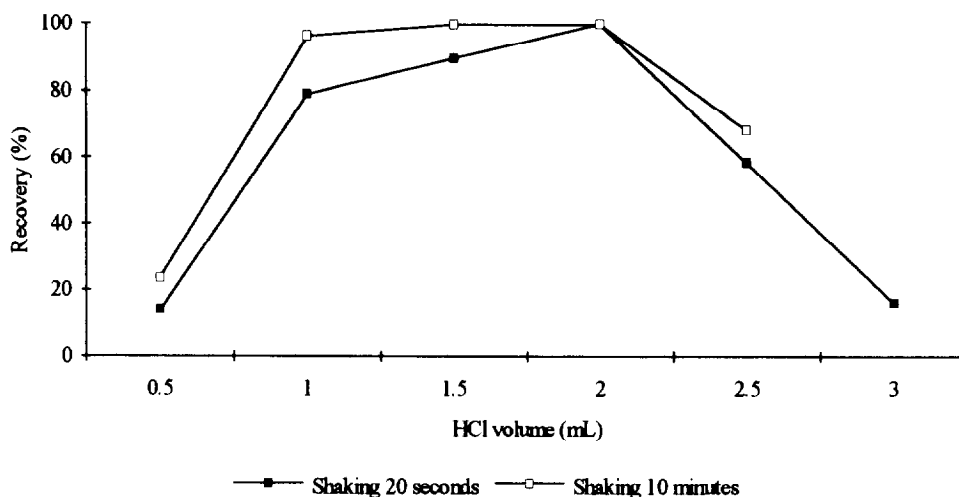
Fig. 1. Effect of acidification on the extraction recovery as a function of shaking time: (■) 20 s; ( ) 10 min.

pH was < 2 and 100% recovery was reached by shaking the slurry for 10 min, indicating that the recovery increased with increasing acidification. In addition, it was found that the amount of inorganic mercury (Hg^{2+}) transferred to the organic solvent decreased with increasing HCl volume. Sediment samples generally contain higher concentrations of Hg^{2-}, and the transfer of Hg^{2+} to the extract can make chromatography difficult. This should be taken into account in optimizing the extraction conditions. The optimum conditions should be those at which the recovery of MeHg is maximized, while Hg^{2+} transfer to the solvent phase is minimized. Thus, using more HCl should be suggested. However, when HCl volumes were increased further, a decrease in MeHg recovery was found. This is because an increased HCl concentration may decompose some of MeHg. Using the amount of HCl chosen in this work, most of Hg^{2+} was isolated with the other matrix, and no problem caused by Hg^{2-} transferred to the extract was observed, and therefore it was not necessary to increase the HCl volume here. With respect to shaking time, the two curves in Fig. 1 show that, at the same acidification, shaking for 10 min generally yields higher recoveries. In addition, no plateau was found on the 20 s shaking curve, suggesting that a longer shaking time should be used.

3.3. Effect of shaking time on extraction recovery

To optimize the shaking time further, a series of IAEA 356 digestates acidified with 1 or 2 ml of HCl were shaken for different times. The results are illustrated in Fig. 2. Considering the results shown in Figs. 1 and 2 in detail, we decided to use 1.5 ml of HCl for acidification and to shake for 10 min.

3.4. Effect of the ratio of CH_2Cl_2 to KOH methanol solution on the extraction recovery

In principle, as the ratio of CH_2Cl_2 to KOH–methanol solution increases, the amount of MeHg in the CH_2Cl_2 phase should also increase. We found that recoveries close to 100% can be reached at a ratio of 3:1. Thus, when using 2 ml of KOH–methanol, 6 ml of CH_2Cl_2 should be used.

3.5. Analytical performance

The analytical performance of the technique was evaluated by analysis of various certified reference materials and intercomparison samples with different concentration levels. The results are listed in Table 1. It can be seen that, except for LUTS-1, excellent agreement was obtained
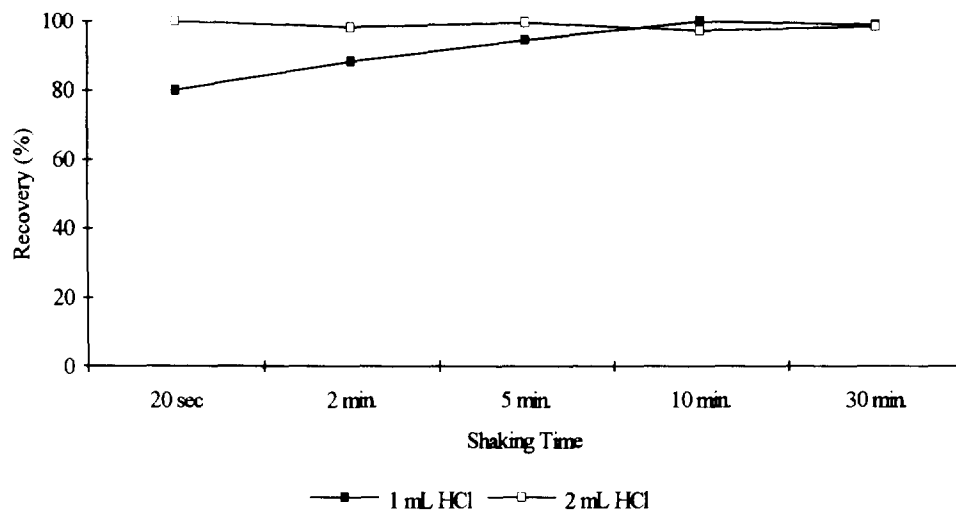
Fig. 2. Effect of shaking time on the extraction recovery as a function of acidification: (■) 1 ml of HCl; (□) 2 ml of HCl.

between the observed and certified values. For the material LUTS-1, the results are far from the certified value. We carefully analyzed it further by both direct ethylation of alkaline digestates and

Table 1
Results of determination of MeHg in CRMs and intercomparison samples by solvent extraction after alkaline digestion. ng g $^{-1}$ as Hg

Sample	MeHg concentration (ng g^{-1} as Hg)	
	Found	Certified
Sediments:		
IAEA 356	5.47 ± 0.14	5.46 ± 0.39
S 19 [BCR]	49.8 ± 1.3	Pending
Tissues:		
IAEA 142	45.2 ± 0.7	47.7 ± 4.3
LUTS-1 (fresh lobster hepatopancreas)	5.8 ± 0.1	9.4 ± 0.6
TORT-1	127 ± 6	128 ± 14
DOLT-2	699 ± 53	693 ± 53
DORM-1	728 ± 12	731 ± 60
Sea plant:		
IAEA 140 TM (sea plant homogenate)	0.82 ± 0.02	Pending
NIES No. 9 (Sargasso)	5.4 ± 0.4	5.7 ± 0.1^a

^{a}Information only [10].

distillation. The results of these three techniques were in good agreement. This suggests that the concentration of MeHg in this sample is not as stable as that in dry biological materials, and that it has changed after several years of storage. It is worth noting that, for the analysis of the sea plant sample, we tried to use distillation, but severe interference with the ethylation reaction was observed. Apparently, the problem stems from volatile compounds transferred to the distillate, making the analysis impossible. However, no analytical problem was encountered with solvent extraction. In this case, the technique was the only choice. The results listed in Table 1 were obtained against pure aqueous standards without correction for spike recovery. This is a significant advantage compared with other techniques [2,6,7,11]. where the results need to be corrected for spike recoveries.

3.6. Application of the technique

As mentioned above, the technique developed here showed significant advantages for the analysis of samples containing high concentrations of Hg^{2+}, such as sediments. In addition, for samples containing large amounts of organic volatile compounds which may pass to the distillate during

distillation, thus causing an interference with the ethylation reaction, the solvent extraction should be preferred. The analysis of sea plants mentioned above is one of these cases. Eggs and milks are also rich in organic volatile compounds, while low in MeHg concentration, for which the technique would be the best choice.

In addition, the analysis of whole blood and red blood protein can show severe interferences with the ethylation reaction. We carefully analyzed red blood protein samples of 13 dolphins from the Mediterranean Sea by the direct ethylation of alkaline digestates. Poor spike recoveries were obtained, and the observed precision was poor. However, recoveries close to 100% were obtained with excellent precision using the solvent extraction technique. A mean concentration of 207.6 $\pm$ 72.5 ng g^{-1} was found by solvent extraction, compared with 78.8 $\pm$ 43.6 ng g^{-1} by direct ethylation of alkaline digestate. Unfortunately, there are no blood samples certified for MeHg. We also used the technique for the analysis of sediment and soil samples from the Mediterranean Sea and Minnesota rivers and also other origins with satisfactory results. Some of them are typical high Hg^{2+}-containing and organic-rich samples. We also used the technique for the determination of MeHg in sludge samples with good results. These sludge samples were dried by centrifugation prior to alkaline digestion and solvent extraction.

Acknowledgements

References

[1] S. Rapsomanikis, O.F.X. Donard and J.H. Weber, Anal. Chem., 58 (1986) 35.
[2] N.S. Bloom, Can. J. Fish Aquat. Sci., 46 (1989) 1131.
[3] L. Liang, M. Horvat and N.S. Bloom, Talanta, 41 (1994) 371.
[4] G. Westoo, Acta Chem. Scand., 20 (1966) 2131.
[5] L. Liang, N.S. Bloom and M. Horvat, Clin. Chem., 40 (1994) 602.
[6] M. Horvat, N.S. Bloom and L. Liang, Anal. Chim. Acta, 282 (1993) 135.
[7] M. Horvat, L. Liang and N.S. Bloom, Anal. Chim. Acta, 281 (1993) 153.
[8] M. Horvat, V. Mandic, L. Liang, N.S. Bloom, S. Padberg, Y.-H. Lee, H. Hintelmann and J. Benoit, Appl. Organomet. Chem., 8 (1994) 533.
[9] N.S. Bloom, M. Horvat and C.J. Watras, Water Air Soil Pollut., 80 (1995) 1257.
[10] M. Horvat, Water Air Soil Pollut., 56 (1991) 95.
[11] H. Hintelmann and R.D. Wilken, Appl. Organomet. Chem., 8 (1994) 533.

Demonstration of an integrated capillary electrophoresis–laser-induced fluorescence fiber-optic sensor

Michael J. Sepaniak[a,*], Tuan Vo-Dinh[b,*], David L. Stokes[a,b], Victoria Tropina[a], Jason E. Dickens[a]

[a]*Department of Chemistry, University of Tennessee, Knoxville, TN 37996-1600, USA*
[b]*Advanced Monitoring Development Group, Health Sciences Division, Oak Ridge National Laboratory, Oak Ridge, TN 37831-6101, USA*

Abstract

A unique integrated separation-based fiber-optic sensor for remote analysis, that incorporates capillary electrophoresis (CE) directly at the fiber sensing terminus is described for the first time. Based on laser-induced fluorescence detection, the sensor offers the potential for high sensitivity. Although the broad-band nature of fluorescence spectra limits selectivity, the high separation power of CE provides a unique dimension of selectivity, while permitting a design of diminutive size. Previously reported fluorescence-based sensors that utilize a chemical reagent phase to impart selectivity tend to be inflexible (not readily adaptable to the detection of different species) and "one-measurement-only" sensors. Conversely, the CE-based fiber-optic sensor described here is both versatile and reusable. The analysis speed and the potential for remote control are further attributes which make the system amenable to remote sensing. A "single-fiber" optical detection arrangement and a "single-reservoir" CE system with the fiber-optic probing the outlet of the separation capillary are employed. A preliminary evaluation of the separation characteristics of this CE-based sensor is presented. Highlights include an observed separation efficiency of up to 3000 theoretical plates (8 cm separation capillary) and migration time reproducibility of less than 10% for frontal mode CE separations. The potential utility of the sensor for remote analysis is demonstrated with separations involving the CE analysis of charged fluorescent dyes, CE analysis of metal complexes based on in situ complexation and micellar electrokinetic capillary chromatographic analysis of neutral fluorescent compounds.

Keywords: Capillary electrophoresis; Integrated fiber-optic sensor; laser-induced fluorescence

---

* Corresponding authors. Fax: (423) 974-3454.

1. Introduction

A unique integrated separations-based fiber-optic sensor (SBFOS) for remote analysis, that incorporates capillary electrophoresis (CE) directly at the fiber terminus, is described for the first time. Fiber-optic-based sensors have been the focus of intensive research and development over the past two decades [1–6]. Since sensing applications involve in-situ measurements, the issue of selectivity is often critical. As a result, fiber-optic sensors have been demonstrated to yield selective detection in infrared [7], Raman [8,9] and surface-enhanced Raman spectroscopy [10–12] and various modes of spectroelectrochemistry [13]. Vibrational spectroscopic methods offer selectivity owing to the uniqueness of the spectra involved. Unfortunately, sensitivity is limited with those techniques. Although fluorescence-based detection is sensitive, spectral selectivity becomes more challenging owing to the broad-band nature of fluorescence spectra. However, fluorescence-based sensors that exhibit high selectivity have been developed by immobilizing at the fiber terminus substances such as permeability-selective polymer films [14–18] or chemically-selective affinity reagents (e.g. antibodies or enzymes) [19–24]. Such systems are generally inflexible and are not readily adaptable to the detection of different species. Furthermore, they tend to be "one-measurement-only" sensors. An extremely versatile element of selectivity that has not been adapted to fiber-optic sensing is that afforded by chemical separations. In particular, capillary electrokinetic separation techniques offer the attributes of high separation efficiency, speed, diminutive size, versatility and remote control, all of which are potentially important in the development of SBFOSs.

In the decade following the seminal paper describing modern CE [25], the prominence of the technique has grown dramatically. Most commonly, separations of ionic solutes are performed in modest length (25–75 cm), narrow bore (25–75 μm i.d.) capillaries filled with an aqueous running buffer solution. Electric fields of 100–500 V cm^{-1} transport solutes through the capillary based on electroosmotic flow (EOF) and electrophoretic migration [26,27]. Perhaps the most significant

advantage of the technique is the characteristic "plug-like" profile of EOF, which results in extraordinary efficiency (plate counts of 10^3–10^5 per cm of capillary are generally observed). Low-nl sample volume requirements and short analysis times are also relevant attractive features. As an electrokinetic phenomenon, CE has primarily been demonstrated to yield extremely efficient separations of charged solutes ranging from small inorganic ions to large proteins and oligonucleotides. However, neutral compounds have been separated via electrochromatographic modes of CE that involve adding micelles or cyclodextrins to the running buffer [28,29]. In fact, micellar electrokinetic capillary chromatography (MECC) has proven to be a valuable electrokinetic technique for separations of neutral compounds [28]. Another significant advantage of CE is the ease of such buffer modifications, thus affording tremendous flexibility for any single CE apparatus. In addition to the examples cited above, these buffer modifications include the use of zwitterionic substances, crown ethers, linear hydophilic polymers, organic modifiers, metal ions and complexing ligands [30]. In the light of the above factors, it is clear that CE has far-reaching applications and a wide range of selectivities. CE has been implemented in conjunction with electrochemical detection to probe the microenvironments of biological systems (e.g. single cells) using what have been termed "separations-based sensors" [31,32]. However, to our knowledge, separation technologies such as CE have not been incorporated as an element of selectivity in fiber-optic-based remote sensing.

The work reported here was undertaken to demonstrate the feasibility of integrating CE methodologies with fiber-optic sensing. Although capillary and fiber-optic dimensions are comparable, there are significant obstacles and complex considerations when integrating these technologies (see below). In this work, a "single-fiber" optical arrangement is employed [20–24]. The sensor is configured as a "single-reservoir" miniaturized CE system interfaced to a fiber-optic that monitors the outlet of the separation capillary. The relatively short separation capillary is simply filled with the buffer solution prior to measure-

ment. The sample acts as what is normally the injection-side reservoir and the performance of the sensor is evaluated in these studies using frontal electrokinetic modes of separation. The resulting linear sensor design should be well suited for many remote sensing applications.

We have demonstrated high sensitivity with fiber-optic sensors that employ laser-induced fluorescence (LIF) as the detection mode [20–24]. However, the work described in this paper was primarily focused on a preliminary evaluation of the separation (i.e. selectivity) characteristics of the SBFOS.

2. Experimental

2.1 Chemicals

The fluorescent dyes sodium fluorescein (E.M. Science, Cherry Hill, NJ, USA), Rhodamine 6G (Rhodamine 590) (Exiton, Dayton, OH, USA), and fluorescein isothiocyanate (FITC) (Sigma Chemical, St. Louis, MO, USA), were purchased at the highest commercially available purity and used as received. $MgSO_4$ and $CaSO_4$ (Baxter, Stone Mountain, GA, USA) were also used as received. The running buffer solution used was composed of 10 mM sodium phosphate, dibasic (J.T. Baker, Phillipsburg, NJ, USA) and 6 mM sodium tetraborate (Fisher Scientific, Fair Lawn, NJ, USA). Water used to prepare the buffer solution was purified with a Waters Milli-Q + filtration system. In general, the fluorescent dye solutions were approximately 0.1 mM in running buffer. A complexing agent, 8-hydroquinoline-5-sulfonic acid (HQS) (Sigma), was used for on-column (in situ) labeling of metal ions. For metal ion separations, the running buffer contained 2.5 mM HQS. Metal ion sample solutions were 0.5 mM $CaSO_4$ and 0.1 mM $MgSO_4$. A sample of Big Limestone Creek water was obtained from a site in Washington County, TN, and used in these studies without any modification. The methylamine and *n*-propylamine used for MECC work were obtained from Fisher and derivatized with 7-chloro-4-nitrobenzofurazan (NBD-C) from Aldrich Chemical (Milwaukee, WI, USA). If

derivatization was complete, sample solutions of the NBD-amines were 0.1–1 mM. The surfactant used for MECC separations, sodium dodecyl sulfate (SDS), was purchased at 99% purity from Sigma. Separation capillaries were obtained from Polymicro Technologies (Phoenix, AZ, USA) and rinsed with 0.1 M NaOH prior to use.

2.2. CE sensor

Fig. 1 depicts the general design of the sensor, which is composed of the following five essential components: (i) the separation capillary, (ii) the fiber-optic, (iii) a hydrostatic flow-restricting capillary, (iv) a low-volume, PEEK tee fitting and (v) the sample-side–detection-side electrode pair. Two such sensors were assembed for experiments performed at two separate sites, the University of Tennessee, Knoxville (UTK) and Oak Ridge National Laboratory (ORNL). The ORNL sensor was used for initial evaluations of the SBFOS involving CE separations of charged fluorescent dyes. The UTK sensor was used for all other SBFOS evaluations, involving CE separations of HQS–metal complexes and MECC separations of neutral fluorescently derivatized amines. Common to both sensors was the non-metallic PEEK tee (Upchurch, Model P712). The two opposing ports of the tee were used to position the fiber-optic on-axis efficiently with and very close to the end of the separation capillary. The third port (perpendicular to the separation/optical axis) allowed the flushing of the sensor. This side port also housed the restrictor capillary and detection-side electrode. Channels extending from each port to the central union of the tee were of diameter 0.020 in and length approximately 0.19 in. Other components of the sensor varied depending on the version involved (see below).

2.3 ORNL sensor

In addition to the tee and electrode pair, the SBFOS sensor assembled at ORNL was composed of the following: (i) separation capillary (8 cm × 50 μm i.d.), (ii) fiber-optic (General Fiber optics, Model 14-200, 1 m × 200 μm core diameter), and (iii) restrictor capillary (3 cm × 15 μm
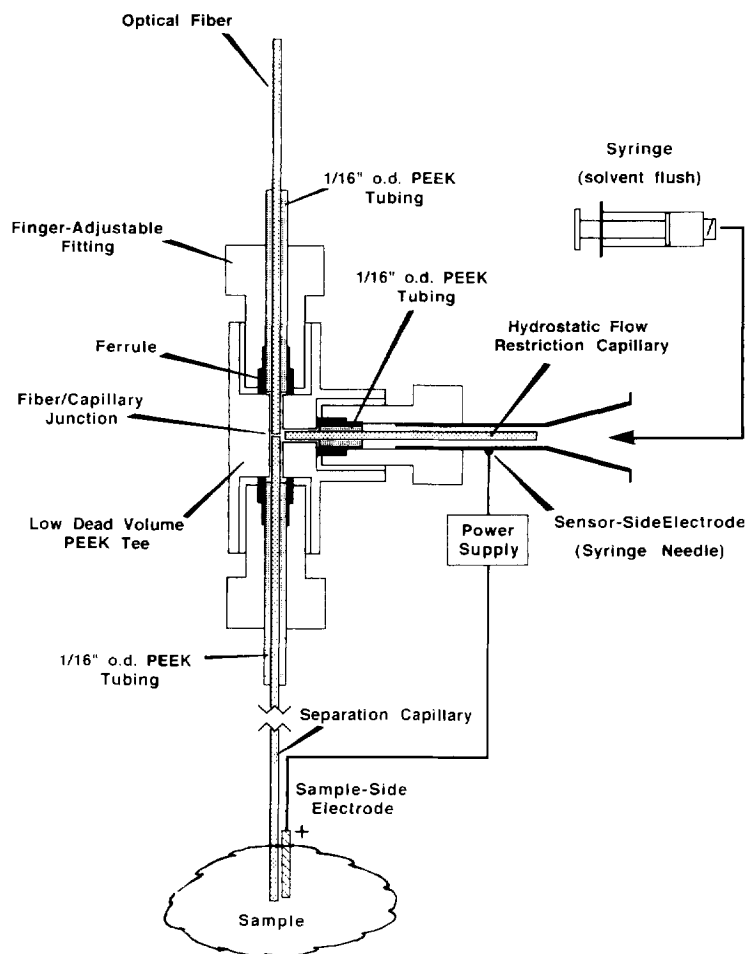
Fig. 1. Depiction of the SBFOS

i.d.). The separation capillary was affixed (5 min epoxy, Devcon) within the 0.020 in bore of a 3 cm segment of PEEK tubing (1/16 in o.d.). The PEEK tubing provided an air-tight coupling to a flangeless ferrule and facilitated connection to the tee with a threaded, finger-adjustable fitting. The capillary itself extended from the fitting assembly into the narrow bore at the center of the tee. The ends of the 1 m fiber-optic were polished with alumina lapping paper down to 0.3 μm grain. The fiber was affixed within PEEK tubing and connected to the tee in a manner similar to that used for the separation capillary.

The side port, used for flushing or filling the sensor, was furnished with a syringe needle which had been modified to accommodate the restrictor

capillary during electrophoresis. The syringe needle was carefully secured within the bore of the finger-adjustable threaded fitting without displacing the ferrule. The restrictor capillary was affixed within a short (4–5 mm) section of 1/16 in o.d. PEEK tubing, allowing an air-tight seal with the ferrule. This capillary was also arranged to extend into the narrow bore of the tee as shown in Fig. 1. The metal shaft of the syringe served as the detection-side electrode, and was therefore a source of gas formation during electrophoresis. However, the side port capillary provided a physical barrier against the introduction of gas bubbles into the tee. Residual liquid in the syringe needle fitting cone which engulfed the outside end of the restriction capillary allowed completion of

the electrical circuit even though the side port was left open to the atmosphere during electrophoresis. The sample-side electrode, electrically isolated from the CE sensor assembly, was set at positive bias voltages during separations using a Hipotronics 20 kV high-voltage power supply (Brewster, NY, USA).

2.4. UTK sensor

The SBFOS sensor used for studies at UTK was assembled as described above except that the restrictor capillary was 5 cm × 25 μm i.d. and the fiber-optic was a Polymicro Technologies Model FVP 100 with a 100 μm core diameter. Because the fiber-optic was smaller in diameter than the ORNL version, the end to be inserted into the SBFOS was affixed within the bore of a 10 cm section of 180 μm i.d., 400 μm o.d. capillary. The fiber tip, cement and encasing capillary were then collectively polished to a flush surface with lapping paper. Otherwise, assembly and application to electrical fields for the two sensors were identical.

2.5 SBFOS optics and instrumentation

The optics and instrumentation varied slightly between the two sites. Fig. 2 illustrates the optical arrangement used for SBFOS detection of fluorescent dyes at the ORNL site. The 457.9 nm line (10 mW) of an argon ion laser (Coherent, Innova-70) was the excitation source. The laser beam was directed through the hole of a plane mirror into a 50× objective lens (Newport, Model L50X), which focused the laser beam on to the fiber-optic of the SBFOS. Optimum coupling of the laser beam to the fiber was facilitated with an x, y, z fiber positioner. The fiber transmitted both the laser excitation and sample fluorescence signal to and from the sensor, while the plane mirror (with the hole) served as a pseudo beam splitter, oriented at 45° with respect to the excitation beam axis. The fluorescence signal from the SBFOS exited the fiber and was collimated by the objective lens. A majority of this collimated signal beam was reflected 90° off-axis towards a relay fiber-optic (600 μm core, Fiberguide Industries).

A 480 nm "cut-on" filter was inserted into the signal beam to reject the unwanted Rayleigh scatter. The detector was an uncooled photomultiplier tube (PMT) (RCA, Model IP-28) operated at 1000 V. Photocurrents from the PMT were amplified by a picoammeter (Keithley, Model 485) and electropherograms were directly recorded with a strip-chart recorder (Kipp and Zonen, Model BD 40).

The UTK sensor optical system was very similar to the ORNL system, except for replacement of the Coherent argon ion laser with an He–Cd laser (Omnichrome, Series 74, 325 nm, 20 mW) for the detection of HQS–metal complexes and an air-cooled argon ion laser (Cyonics, Model 2201, 488 nm, 10 mW) for the detection of NBD-amines. In addition, the relay fiber-optic was omitted (i.e. the collimated signal beam was focused directly on to the PMT). All lenses were quartz and 400 nm "cut-on" and 500 nm "cut-on" filters were used to reject Rayleigh scatter when using the He–Cd and argon ion lasers,
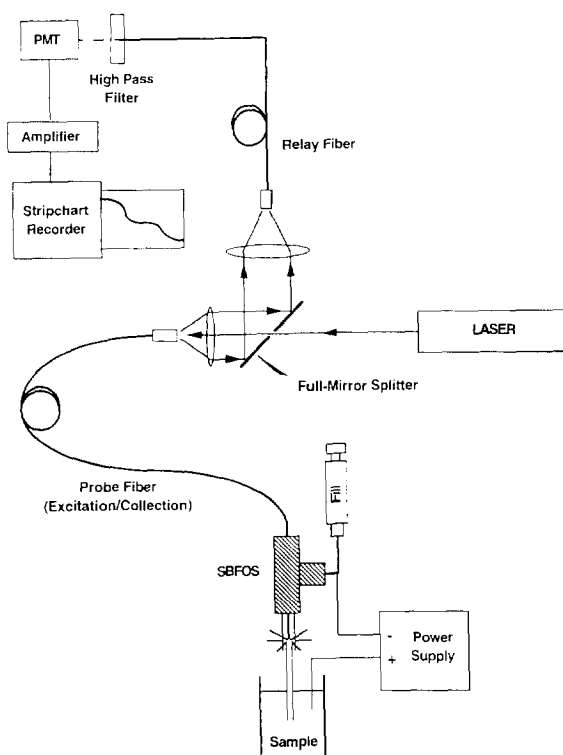

Fig. 2. Schematic diagram of the single fiber-based optical detection system.

respectively. Photocurrents from the PMT were amplified with a Pacific Precision Instruments (Concord, CA, USA), Model 126 photometer.

Conventional zonal and frontal CE separations were performed using a modular CE–LIF detection system that is described elsewhere [28]. The capillaries used for these conventional separations were typical in length (about 45 cm); however, the detection zone was positioned close to the inlet (about 8 cm) so as to mimic the sensor.

2.6 Sensor operation procedures

The first step in aligning the optics involved visually maximizing the coupling of the excitation beam on to the fiber (judged by monitoring the light intensity at the distal end of the fiber). Next, laser radiation was retro-passed into the system (i.e. made to impinge on the distal end of the fiber) and the lenses and mirror were adjusted to provide the proper alignment with the detector. Finally, the sensor was flushed with a fairly concentrated dye solution and signal levels were monitored as further positioning of the optical components was accomplished. Since this work focused on the separation characteristics of the SBFOS, little effort was made to fine tune the alignment or to use the best optical components.

Prior to each separation, the sensor was flushed with 0.1 M NaOH and then running buffer solution. Flushing steps were performed with an unmodified syringe needle (no restrictor capillary), taking care not to introduce gas bubbles into the system. In this case, the 16-gauge needle was inserted directly into the flangeless fitting ferrule, forming a snug fit. Subsequently, the flushing needle was replaced with the needle containing the restrictor capillary and the SBFOS was then submerged in the sample for initiation of the separation. Applied voltages with the SBFOS were relatively low (maximum of about 3 kV).

3. Results and discussion

Regardless of the selectivity and flexibility offered by CE, three major challenges must be addressed for its implementation in remote sens-

ing: (1) elimination (or acceptable reduction) of hydrostatic flow, (2) expulsion or elimination of electrolysis gases and (3) establishing suitable compromises between detectability and separation performance. In CE, elimination of gravity-driven hydrostatic flow is generally accomplished by the use of inlet and outlet buffer reservoirs at equal heights. As is demonstrated by the design depicted in Fig. 1, the SBFOS does not allow the luxury of level buffer reservoirs. If observed, a downward hydrostatic flow (away from the fiber-optic) in the separation capillary is expected to cause band dispersion [30]. Moreover, a relatively large applied field may be required to provide sufficient EOF to overcome the hydrostatic flow. Under these conditions, thermal dispersion of bands is also possible. The SBFOS described in this paper is designed to restrict gravity-driven hydrostatic flow by incorporating a narrow-bore capillary into the side port of the sensor (see Fig. 1), thereby relaxing inlet and outlet buffer reservoir position requirements. The relative positions of the ends of the separation capillary contribute less hydrostatic flow, making a vertical, linear capillary configuration feasible. It should be noted that incomplete dissipation of pressure applied during rinsing steps and/or pressure resulting from the build-up of electrolysis gases can also produce a detrimental hydrostatic flow with the SBFOS.

Owing to the small sample volumes associated with the use of CE, on-column detection is generally required to preserve the integrity of the separation. In this regard, the unique characteristics of lasers as excitation sources have rendered LIF detection extremely useful in CE [33–36]. Typical laboratory optical systems consist of extra-column lenses or fiber-optics for focusing and collecting excitation and signal radiation. It has recently been demonstrated by Taylor and Yeung [37,38] that the use of an excitation fiber-optic inserted into the end of a capillary for axial illumination yielded enhanced sensitivity. While such an arrangement demonstrates a potential for remote sensing, the apparent goal of that work was to utilize fiber-optic-based detection in CE, rather than incorporating CE as an element of selectivity in an optical configuration that is suitable for remote fiber-optic sensing.
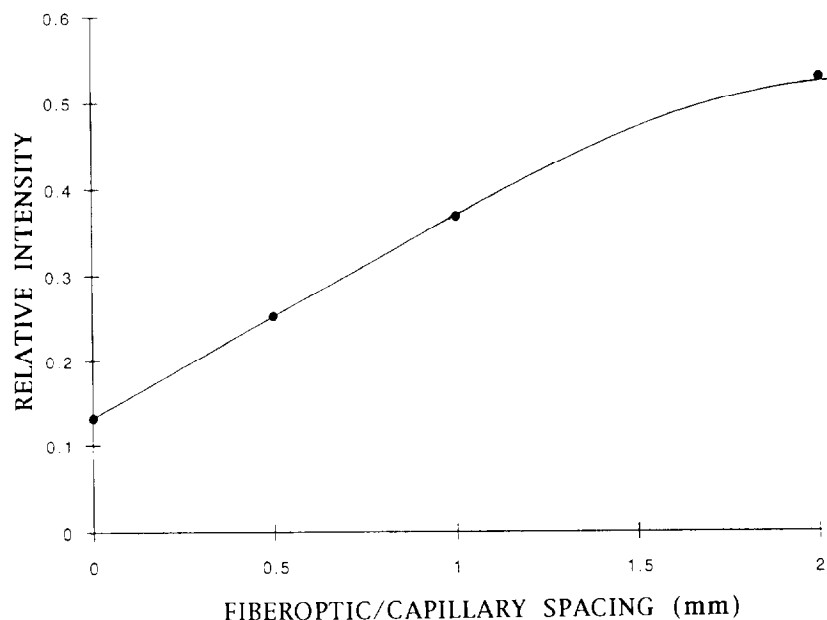
Fig. 3. Plot of relative fluorescence signal intensity versus fiber-optic–capillary spacing. The signal was generated by drawing a solution of fluorescein into the SBFOS via a syringe.

In this work, we utilized an optical arrangement for sensing applications that employs a single fiber for both excitation and signal collection (see Fig. 2) [19]. The streamline linear geometry should be well suited for remote analysis. Although a narrow diameter or tapered fiber could be inserted into the separation capillary, we opted for placing a larger, and hence more stable, fiber directly adjacent to the exit of the capillary. This resembles the approach that Huang et al. [39] employed in the positioning of electrodes for electrochemical detection in CE. Since a fiber will collect light most efficiently only to distance of a couple of fiber diameters from its end [19], this configuration probes the extremely small space between the fiber and capillary and a sub-mm segment at the capillary outlet. This assumes that internal reflection in the capillary is not significant. Benoit and Yappert [40] described a fiber-optic sensor that employs a capillary, functioning as a partially reflecting waveguide, to enhance sensitivity. If this waveguide effect were operative in our work, it would be expected consistently to broaden bandfronts, which was not observed in these studies (see below).

Although the effective detector volume and signal are dramatically increased as the fiber is backed away from the separation capillary, an extra-column dead volume is created and this also can dramatically broaden bandfronts. These effects are demonstrated in Figs. 3 and 4. The SBFOS was filled with a fluorescein solution and used to generate the plot of signal versus fiber–capillary spacing shown in Fig. 3. While the signals increased with increased spacing, the sharpness of bandfronts degraded. This is demon-
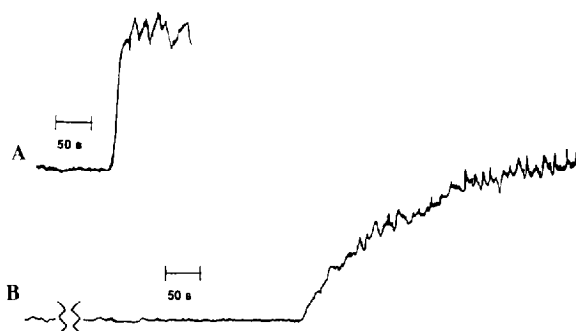

Fig. 4. CE bandfronts for Rhodamine 6G obtained using the SBFOS with capillary fiber-optic spacings of (A) 0 mm and (B) approximately 1 mm.

strated in Fig. 4 using the SBFOS to obtain the
frontal CE bandfronts of an injected Rhodamine
6G solution. Under the SBFOS conditions em-
ployed, a relatively sharp bandfront at a migra-
tion time of 110 s is observed when the fiber is
directly touching the capillary (Fig. 4(A). With a
spacing estimated to be 1.0 mm, the bandfront is
substantially broadened (i.e. the efficiency is very
poor) and the migration time is greater than 1000
s (Fig. 4(B). Clearly, the fiber–capillary spacing
must be negligible in order to maximize bandfront
sharpness. Unfortunately, excessive rinsing and
manipulation of the SBFOS described here occa-
sionally produced broad bandfronts, indicating
that an appreciable fiber–capillary spacing had
been created.

To achieve a positive band velocity (V_b) (i.e.
toward the fiber-optic) electrophoretic flow (V_{elec}),
one must overcome the opposing hydrostatic flow
(V_{hy}) as described by the equation

$$V_b = V_{hy} + V_{elec} = V_{hy} + (\mu_{eo} + \mu_{elec})E \qquad (1)$$

where E is the applied field and μ_{eo} and μ_{elec} are
electroosmotic and electrophoretic mobilities, re-
spectively. Under the conditions employed in this
work, cathodic EOF is directed toward the fiber-
optic. As the voltage and (hence E) is increased,
the V_b values increase and the migration times
decrease. However, since it is necessary to over-
come V_{hy}, the linear relationship between E and
V_b that is characteristic of CE is not observed in
this work (see below). To illustrate the effect of
V_{hy}, conventional zonal CE separations of Rho-
damine 6G (cation), FITC (neutral) and fluores-
cein (anion) were performed using a very short
effective capillary length (8 cm) with equal inlet
and outlet reservoir heights (no V_{hy} case) and with
the capillary outlet raised approximately 8 cm
(opposing V_{hy} case). The results are shown in Fig.
5. Independent experiments produced a V_{hy} of
roughly 1.2 cm min^{-1} for the conditions used to
generate Fig. 5(B) and, indeed, the V_b of FITC
decreases from 4.6 to 3.3 cm min^{-1} when compar-
ing Fig. 5(A) and (B). The adverse effect of a
hydrostatic flow on efficiency is also obvious in
Fig. 5. Using migration times from Fig. 5(A), the
experimental values of μ_{eo} (marked by FITC),
μ_{elec} (Rhodamine 6G) and μ_{elec} (fluorescein) are

A

0   80   160

B
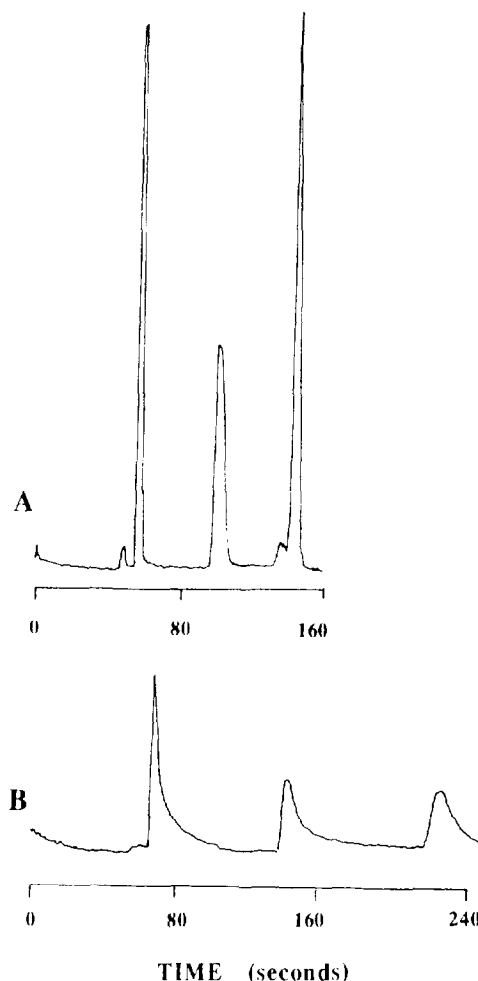
0   80   160   240

TIME   (seconds)

Fig. 5. Conventional zonal capillary electopherograms for
Rhodamine 6G, FITC and fluoresein (in order of elution).
Conditions 45 cm (8 cm to detection zone) × 75 μm i.d.
capillary, 220 V cm^{-1} applied field, phosphate–borate (pH 9)
running buffer, absorbance detection at 500 nm. Inlet and
outlet reservoir heights equal (A) and inlet raised 8 cm (B).

3.6×10^{-4}, 2.9×10^{-4} and -1.1×10^{-4} cm^2 V^{-1}
s^{-1}, respectively.

Despite the potential problems discussed above,
including band dispersion by Joule heating and
dead volume, some promising results were ob-
served in the CE separation of charged fluorescent
dyes. For example, an SBFOS separation of Rho-
damine 6G and fluorescein is shown in Fig. 6. The
peak-like shape of the fluorescein bandfront is
probably a result of photodegradation of that
solute. The efficiency of Rhodamine 6G is ap-

proximately 3000 plates. The equation $N = 16$ $(T_r/W)^2$ was used to determine the plate count (N), where the bandwidth (W) corresponds to the rise time of the bandfront between the baseline and the plateau. The retention time (T_r) corresponds to the elapsed time between the application of the voltage and the point of half-maximum intensity for the observed bandfront. The applied voltage is divided across the separation capillary, the restrictor capillary and the fiber–capillary junction. Since the last is not well defined, it is not possible to assign accurately a field to the separation or to calculate mobilities, as was possible with the separation shown in Fig. 5(A). The resolution (i.e. $\Delta T_r/W$) in this separation is approximately 7.

The effect of increasing the applied voltage on the performance of the SBFOS is demonstrated in Table 1, which also includes data on band velocity (and hence migration time) reproducibility (relative standard deviations for $n = 5$). When the voltage was increased to 3000 V, excessive currents were observed and the system eventually broke down (the current dropped to zero). Conversely, the system functioned at an applied voltage of 2500 V, yielding the data in the table. However, the current increase relative to the 1500 V case was considerably more than the expected 67%. This anomalous current effect, and the decrease in bandfront sharpness (the efficiency decreased about threefold), indicates excessive thermal load and a temperature increase in the system at the higher applied voltage. The lack of reproducibility in band velocity is probably due to a combination of heating effects and a lack of integrity in the conduction paths (i.e. the run-to-run currents exhibited a similar poor reproducibility).

The influence of V_{hy} on separations can also be seen in Table 1. As the applied voltage is increased from 1500 to 2500 V the resolution improves despite a decrease in efficiency. This unusual behavior is a result of the differences in $\mu_{eo} + \mu_{elec}$ for the two bands. The net mobility of the fluorescein anion is nearly four times smaller than that of the Rhodamine 6G cation. In the case of Rhodamine 6G, when the voltage is increased the band velocity nearly increases by the

expected 67%. Conversely, the impact of V_{hy} on V_b is much more signifcant for fluorescein and the increase in band velocity is much less than 67%. The net effect is a greater separation in the bandfronts of the two dyes at the higher applied voltage. Based on capillary diameter and length, the 3 cm × 15 μm i.d. restrictor capillary of the SBFOS used to generate the data in Table 1 should have reduced the hydrostatic flow fivefold in the 8 cm × 50 μm i.d. separation capillary. Future SBFOS designs will attempt to reduce V_{hy} further.

The frontal CE approach is instrumentally and operationally simple. Nevertheless, this mode of operation will influence both the detection and the separation characteristics of the SBFOS. With regard to the former, as each new front reaches the fiber-optic, the fluorescence background increases (i.e. the signal from the first component to elute contributes baseline noise that adversely affects the detectability and dynamic range for subsequent components). With regard to the separation characteristics, which are the focus of this paper, the running buffer in the capillary is displaced by sample solution as the separation proceeds. At some point, which is strongly influenced by the EOF, many CE systems will experience "reagent depletion" in the frontal mode of operation. For the simple case of natural fluorophores that can be separated based on differences in intrinsic mobility (e.g. see Fig. 6), there will not be a distinct point of reagent depletion. However, the EOF (and hence solute migration time) may be altered as the sample enters the sensor and this could complicate calibration. At times there may be advantages in reducing, eliminating or reversing the EOF via running buffer additives or capillary surface modification [28].

Most strategies for CE involve adding specific reagents to the running buffer to affect the separation or facilitate detection. In order for the SBFOS to be generally useful, it will be necessary to develop systems and protocols for which reliable analytical information is acquired before reagent depletion occurs. For example, a CE protocol we previously developed for the on-column labeling of metals with HQS was adapted in this work to the SBFOS [41]. HQS is a non-fluores-

Table 1
Effect of applied voltage on SBFOS separations of fluorescent dyes

Voltage (V)	Current (μA)	Rhodamine 6G bandfront		Fluorescein bandfront	
		V_b (cm min^{-1})	N	V_b (cm min^{-1})	R_s
1500	90	1.1 ($\pm$ 9%)	~3000	0.66 ($\pm$ 7%)	~7
2500	250	1.8 ($\pm$18%)	~1000	0.83 ($\pm$24%)	~9

cent, bidentated ligand that forms fluorescent complexes with a large number of metal ions. In addition to facilitating sensitive detection of the metals, the complexation conditions can be altered to adjust the effective mobility of a metal ion [41]. The SBFOS strategy involves first flushing the sensor with running buffer containing an appropriate concentration of HQS. When a field is applied, positively charged metals migrate quickly toward the fiber-optic (velocity greater than that of the sample solvent front which is driven largely by EOF) and negatively charged HQS will migrate slowly toward the fiber (velocity less than the solvent front). In essence, HQS rapidly meets the metals and, owing to the large formation constants involved, an equilibrium involving the various forms of complexed metal is established. This process reduces metal migration rates (due to the reduced charge of the complex relative to the free metal). The dynamics of these processes influence the sharpness and shape of the bandfronts, which migrate at rates characteristic of the metal.

Figs. 7–9 contain electropherograms illustrating separations of calcium and magnesium using in situ complexation with HQS and a frontal mode of operation. In Fig. 7(A), a conventional capillary frontal separation of the metals exhibits relative responses and mobilities similar to those observed in previous work involving zonal CE [41]. This separation was performed with HQS in both the running buffer and sample. Obviously, in remote analysis situations the sample will not contain running buffer reagents. When HQS is not present in the sample, the shapes of the bandfronts are altered (see Fig. 7(B)). The signal rises to a plateau, then drops back down to a lower plateau. This may be a result of a non-equi-

librium condition in the early stages of the separation (see above) or a manifestation of some stacking phenomena [42]. Nevertheless, the responses of the two metals are well separated and the overlay of the response of a sample with a twofold higher calcium concentration illustrates the potential of this approach for performing quantitative measurements. Signals fall to baseline values, indicating depletion of HQS in the system, at 350–400 s into the run. This is roughly the effective migration time of HQS.

Fig. 8 is an electropherogram of a calcium–magnesium sample (no HQS in the sample) obtained with the SBFOS that demonstrates its potential for remote sensing. The separation is considerably slower owing to a lower field and the presence of V_{hy}. This condition relaxes the non-equilibrium condition in the early stages of the
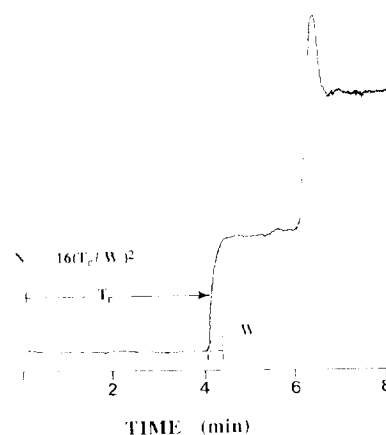

Fig. 6. Frontal capillary electropherogram of Rhodamine 6G and fluorescein (in order of elution) obtained using the SB-FOS. Conditions: 8.0 cm × 50 μm i.e. separation capillary and 3 cm × 15 μm i.d. restrictor capillary (ORNL sensor), applied voltage 1500 V, phosphate–borate (pH 9) running buffer, LIF detection using argon ion laser (see Experimental). The method for calculating efficiency as described in the text.
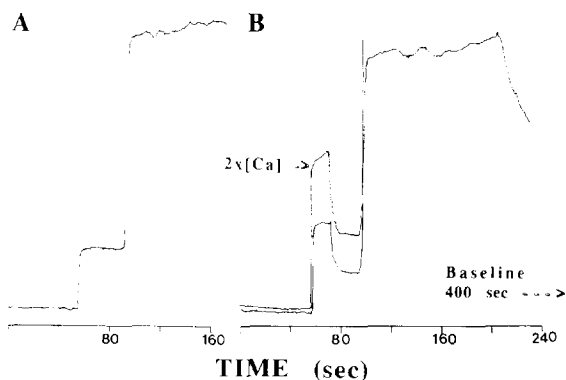
Fig. 7. Conventional frontal capillary electropherograms of calcium and magnesium (in order of elution) based on in situ HQS complexation with HQS in sample (A) and not in sample (B). Conditions: 40 cm (8 cm to detection zone) × 50 μm i.d. capillary, 190 V cm⁻¹ applied field. phosphate–borate (pH 8) running buffer with 2.5 mM HQS. LIF detection using He–Cd laser (see Experimental).

separation (see above) and may account for the absence of the dual plateau response seen in Fig. 7(B). The run was terminated before reagent depletion. Clearly, a shorter capillary could be used to reduce the analysis time. A duplicate run yielded similar results. Fig. 9 presents the results for the analysis of a ground water sample by using conventional frontal CE (Fig. 9(A) and the SBFOS (Fig. 9(B)), indicating the presence of calcium. Although calcium in this sample was not quantified and the sample was not analyzed by independent methods, the presence of a large concentration of calcium in a ground water source with the name Limestone Creek would not be surprising. The fact that the front in Fig. 9(B) occurs earlier than that for the SBFOS standard run shown in Fig. 8 may be due to changes in EOF due to differences in sample pH, or be simply a result of the poor migration time reproducibility of this design of SBFOS (see Table 1).

The MECC technique has greatly expanded the utility of CE and should be readily adaptable to the SBFOS. Neutral solutes are separated in MECC based on their distribution between the EOF-transported running buffer and an electrophoretically retarded micellar phase [28]. These solutes elute in a window that is created between the void time (t_0) and the effective retention time

of the micellar phase (t_m), which for the commonly employed SDS system occurs at about 3–4 times t_0. When the SBFOS is employed in this mode, reagent depletion should occur at about t_m (the negative micelles should migrate similarly to the HQS as described above). A MECC separation using the SBFOS is shown in Fig. 10. The baseline noise level is fairly high in these separations owing to an instability in the output of the laser employed. In Fig. 10(A) no SDS is present and the test solutes of NBD-methylamine and NBD-*n*-propylamine co-elute at t_0. When micelles are present (Fig. 10(B)), the solutes are easily separated before reagent depletion. Consistent with previous work [28], the signal is enhanced owing to the presence of the micelles. As was observed for SBFOS separations of the fluorescent dyes and HQS-metals, V_{hy} influences the separation of the NBD-amines. Normally, one would expect to observe less separation between these two NBD-amines [28], and experience reagent depletion at about 20–25 min (see above). However, the effect of V_{hy} is to decrease the observed migration rates, particularly for the more retained components (those with smaller V_{elec}), and delay reagent depletion. In a conventional (no V_{hy}) frontal MECC separation of
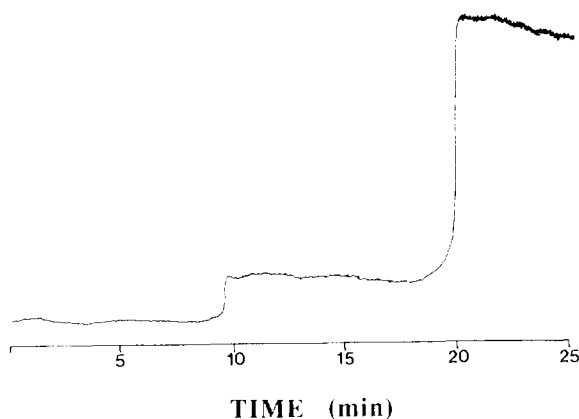

TIME (min)

Fig. 8. Frontal capillary electropherogram of calcium and magnesium (in order of elution) based on in situ complexation obtained using the SBFOS and no HQS in the sample. Conditions: 8.0 cm × 50 μm i.d. separation capillary and 5 cm × 25 μm i.d. restrictor capillary (UTK sensor), applied voltage 1500 V. phosphate–borate (pH 8) running buffer with 2.5 mM HQS. LIF detection using He–Cd laser (see Experimental).
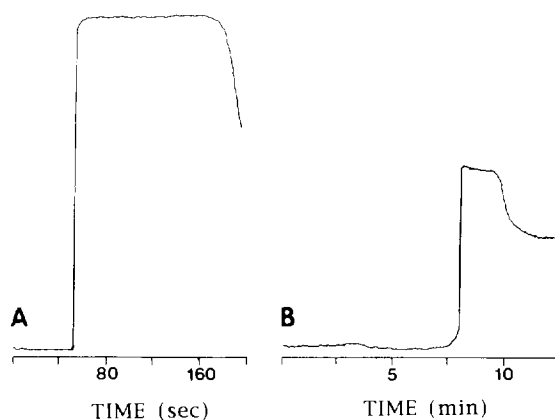
Fig. 9. Coventional (A) and SBFOS (B) frontal electropherograms of a sample of Big Limestone Creek water (Washington County, TN) showing a high apparent concentration of calcium. Conditions as in Figs 7 and 8.
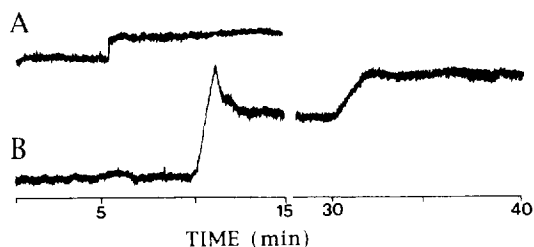

Fig. 10. Frontal CE (A) and MECC (B) electropherograms of NBD-methylamine and NBD-n-propylamine (in order of elution (in B)) obtained with the SBFOS. Conditions: phosphate borate (pH 9) running buffer with 50 mM SDS in (B) and no SDS in sample. LIF detection using air-cooled argon ion laser (see Experimental). Other conditions as in Fig. 8.

NBD-amines (not shown), reagent depletion was indeed observed at 3–4 times t_0.

Remote, in situ monitoring of chemicals offers many analytical advantages and challenges which are significant in the biomedical, environmental and industrial fields. Unfortunately, in situ measurements can be complicated and generally do not exhibit the analytical selectivity, sensitivity and reliability associated with conventional laboratory techniques. In this paper, we have described the design and fabrication and presented a preliminary evaluation of the performance of a fiber-optic sensor that utilizes CE techniques to impart a potentially versatile element of selectivity to the measurement process. In that regard, differ-

ent modes of operation are demonstrated under fairly realistic conditions. While improvements in the design, function and analytical reliability of the SBFOS are clearly needed, we feel that these preliminary results are sufficiently encouraging to warrant further research and development of the SBFOS.

Acknowledgements

References

[1] G. Boisde, F. Blanc, P. Mauchien and J.J. Perez, in O.S. Wolfbeis (Ed.), Fiber Optic Chemical Sensors and Biosensors, CRC Press, Boca Raton FL, 1991, Vol 2, pp. 135–49.

[2] S.M. Angel, M.N. Ridley, K. Langry, T.J. Kulp and M.L. Myrick, ACS Symp. Ser., 403 (Chem. Sens. Microinstrum.) (1989) 345.

[3] P.V. Lambeck, Proc. SPIE Int. Soc. Opt. Eng., 1511 (Fiber-Opt. Sens.: Eng. Appl.) (1991) 100.

[4] J.O.W. Norris, Analyst, 114 (1989) 1359.

[5] A.D. Kersey and A. Dandridge, IEEE Trans. Compon. Hybrids Manuf. Technol., 13 (1990) 137.

[6] C.M. Miller, S.C. Mettler and I.A. White, Opt. Eng. (N.Y.) 28 (1991) 363.

[7] B. Feldhaeuser, K. Meya and H.W. Siesler Proc. SPIE Int. Soc. Opt. Eng., 1145 (Int. Conf. Fourier Transform Spectrosc., 7th) (1989) 158.

[8] K.P.J. Williams, J. Raman Spectrosc, 21 (1990) 147.

[9] T. Iqbal, M.R. Shahriari, R. Ulbrich and G.H. Sigel Jr., Opt. Lett., 16 (1991) 1611.

[10] S. Dai, J.P. Young, G.M. Begun, J.E. Coffield and G. Mamantov, Mikrochim Acta, 108 (1992) 261.

[11] J.P. Alarie, D.L. Stokes, W.S. Sutherland, A.C. Edwards and T. Vo-Dinh, Appl. Spectrosc., 46 (1992) 1608.

[12] S.M. Angel, M.L. Myrick and F.P. Milanovich, in Frontiers in Bioprocessing 2, Proceedings, P. Todd, S.K. Sikdar and M. Bier (Eds.), American Chemical Society, Washington, DC, 1992, pp. 72–89.

[13] P.D. Beer, O., Kocian, R.J. Mortimer and C. Ridgway, Analyst 117 (1992) 1247.

[14] W.A. De Oliveria and R. Narayanaswamy, Talanta, 39 (1992) 1499.

[15] M. Lerchi, E. Bakker, B. Rusterholz and W. Simon. Anal. Chem., 64 (1992) 1534.

[16] M. Tabacco, Q. Zhou and B. Nelson, Proc. SPIE Int. Soc. Opt. Eng., 1587 (Chem., Biochem., Environ. Fiber Sens. 3) (1992) 271.

[17] U. Panne and R. Niessner, Proc. SPIE Int. Soc. Opt. Eng., 1587 (Chem., Biochem., Environ. Fiber Sens. 3) (1992) 21.

[18] P.F. Daley, B.W. Colston, Jr., S.B. Brown, K. Langry and F.P. Milanovich, Proc. SPIE Int. Soc. Opt. Eng., 1587 (Chem., Biochem., Environ. Fiber Sens. 3) (1992) 278.

[19] M.J. Sepaniak, B. Tromberg and T. Vo-Dinh, Prog. Anal. Spectrosc., 11 (1988) 481.

[20] B. Tromberg, M.J. Sepaniak, J.P. Alarie, T. Vo-Dinh and R. Santella, Anal. Chem., 60 (1988) 1901.

[21] J.P. Alarie, J. Bowyer, M. Sepaniak, A. Hoyt and T. Vo-Dinh, Anal. Chim. Acta, 236 (1990) 237.

[22] T. Vo-Dinh, J.P. Alarie, R. Johnson, M. Sepaniak and R. Santella, Clin. Chem., 37 (1991) 532.

[23] B. Tromberg, M. Sepaniak, T. Vo-Dinh and G. Griffin, Anal. Chem. 59 (1987) 1226.

[24] J. Bowyer, J.P. Alarie, M. Sepaniak, T. Vo-Dinh and R. Thompson, Analyst, 116 (1991) 117.

[25] J. Jorgenson and K. Lukas, Anal. Chem., 53 (1981) 1298.

[26] J. Jorgenson and K. Lukas, Science, 222 (1983) 266.

[27] C.L. Rice and R. Whitehead, J. Phys. Chem., 69 (1965) 4017.

[28] M. J. Sepaniak, D.F. Swaile, R.O. Cole and A.C. Powell, in Capillary Electrophoresis: Theory and Practice, P.D. Grossman and J.C. Colburn (Eds.), Academic Press, New York, 1992, pp. 159-189.

[29] M.J. Sepaniak, R.O. Cole and B.K. Clark, J. Liq. Chromatogr., 15 (1992) 1023.

[30] P.D. Grossman and J.C. Colburn (Eds.), Capillary Electrophoresis: Theory and Practice, Academic Press, New York, 1992.

[31] A.G. Ewing, R.A. Wallingford and T.M. Olefirowicz, Anal. Chem, 61 (1989) 292A.

[32] J.B. Chein, R.A. Wallingford and A.G. Ewing, J. Neurochem., 54 (1990) 633.

[33] M.A. Albin, P.D. Grossman and S.E. Moring, Anal. Chem., 65 (1993) 489A.

[34] J.Z. Zhang, D.Y. Chen, S. Wu, H.R. Harke and N.J. Dovichi, Clin. Chem. 37 (1991) 1492.

[35] T.T. Lee and E.S. Yeung, J. Chromatogr. 595 (1992) 319.

[36] Y. Cheng, R.D. Piccard and T. Vo-Dinh, Appl. Spectrosc., 44 (1990) 755.

[37] J.A. Taylor and E.A. Yeung, Anal. Chem. 65 (1993) 956.

[38] J.A. Taylor and E.A. Yeung, Anal. Chem., 64 (1992) 1741.

[39] X. Huang, R.N. Zare, S. Sloss and A.G. Ewing, Anal. Chem., 63 (1991) 189.

[40] V. Benoit and M.C. Yappert, Anal. Chem., 68 (1996) 183.

[41] D.F. Swaile and M.J. Sepaniak, Anal. Chem., 63 (1991) 179.

[42] M. Albin, P. Grossman and S. Moring, Anal. Chem., 65 (1993) 489A.

Screen-printed tyrosinase-containing electrodes for the biosensing of enzyme inhibitors

Joseph Wang[a,*], Valberes B. Nascimento[a,1], Stephen A. Kane[a,2], Kim Rogers[b], Malcom R. Smyth[c], Lucio Angnes[d]

[a]Department of Chemistry and Biochemistry, New Mexico State University, Las Cruces, NM 88003, USA
[b]U.S. Environmental Protection Agency, Exposure Research Program, 944 East Harmon Avenue, Las Vegas, NV 89119, USA
[c]School of Chemical Sciences, Dublin City University, Dublin 9, Ireland
[d]Departamento de Quimica, Universidade de Sao Paulo, Sao Paulo, SP 05508, Brazil

Abstract

Disposable amperometric inhibition biosensors have been microfabricated by screen printing a tyrosinase-containing carbon ink. The decrease in the substrate (catechol) steady-state current, caused by the addition of various pesticides and herbicides. offers convenient quantitation of micromolar levels of these pollutants. Unlike esterase-based disposable strips, the tyrosinase thick-film devices can be fabricated by incorporating the enzyme within the carbon ink. and do not require a prolonged incubation step in the presence of the inhibitor. The effect of experimental variables, such as the enzyme loading or substrate concentration. is assessed. Applicability to an untreated river water sample is illustrated. Such use of single-use devices for monitoring toxins addresses the problem of irreversible enzyme inhibition. and holds great promise for on-site field analysis.

Keywords: Biosensing; Electrodes; Enzyme inhibitors; Screen printing; Tyrosinase

1. Introduction

Electrochemical biosensors hold great promise for the task of on-site environmental monitoring [1,2]. One promising strategy is to employ enzyme electrodes for measuring various toxins, via the perturbation/inhibition of the biocatalytic activity [3]. Useful devices have thus been designed for monitoring organophosphate or carbamate pesticides [3,4], cyanide [5,6] or toxic metals [7,8]. Single-use inhibitor biosensors, based on modern microfabrication technology, are particularly attractive for field deployment due to their extremely low cost, compatibility with hand-held analyzers, and the irreversible nature of many enzyme inhibition processes. Screen-printed disposable sensors, based on a cross-linked cholin-

---

* Corresponding author.
[1] Permanent addresss: Departamento de Quimica, Universidade Federal Rural de Pernambuco, Recife, PE 52171-030, Brazil.
[2] Permanent address: School of Chemical Sciences, Dublin City University, Dublin 9, Ireland.

esterase layer, have been developed in recent years for the detection of various pesticides [9,10].

In this paper we describe the characterization and attractive performance of single-use inhibitor bisensor strips based on screen printing of tyrosinase-containing carbon inks. Tyrosinase is prone to inhibition by a wide range of water pollutants [11]. Such inhibition is known to occur through interaction with the active copper site [12]. We reported recently on the one-step preparation of tyrosinase screen-printed electrodes [13]. The remarkable tolerance of tyrosinase to the high-temperature firing conditions resulted in a greatly simplified fabrication protocol and convenient quantitation of its phenolic substrates. Similarly, in the following sections we report on the suitability of these thick-film strips for amperometric monitoring of inhibitors of tyrosinase.

2. Experimental

2.1. Apparatus

All voltammetric experiments were carried out using an EG&G PAR Model 264A voltammetric analyzer, in connection with a Houston Omniscribe strip-chart Y–t recorder. The experiments were performed at room temperature in a 10 ml electrochemical cell (BAS, Model VC-2). The working electrode strip, reference electrode (Ag/AgCl, Model RE-1, BAS) and platinum wire electrode joined the cell through holes in the Teflon cover.

2.2. Screen-printing fabrication

A semiautomatic screen printer machine (Model TF-100, MPM Inc., Franklin, MA) was used for fabricating the working electrode strips. The modified inks were prepared by thoroughly mixing for 1 h the appropriate amount of a commerical carbon ink (Product No. C10903D14, Gwent Electronic Materials Ltd., UK) with the enzyme. Typical preparations were 0.6% enzyme ink (w/w). A group of 10 electrodes were printed each time onto an alumina ceramic plate (1.33 in. × 4.00 in.) through a patterned stencil. This

allowed batches of 30 electrodes to be printed by using 1 g of ink mixed with 6 mg of enzyme. Each electrode consisted of a 1.0×30 mm^2 area. The film was cured at a temperature of 110°C for 2 h. Then a layer of insulator was screen printed onto part of the ink, leaving a defined 1.0×5 mm^2 working-electrode area.

2.3. Reagents

Chemicals were analytical-reagent grade and used as received. All solutions were prepared with doubly-distilled water. The enzyme used, tyrosinase, 4400 units mg^{-1} solid, was obtained from Sigma (t-7755, EC 1.14.18.1). The supporting electrolyte was a 0.05 M phosphate buffer solution (PBS) pH 7.4. Catechol (Sigma), sodium diethyldithiocarbamate (Aldrich), thiourea (Fisher), benzoic acid (Baker), 2,4-dichlorophenoxyacetic acid (Sigma), 4,6-dinitro-o-cresol (Sigma), warfarin (Sigma), pentachlorophenol (Aldrich), atrazine (Chem Service), sodium nitrate (Aldrich), sodium nitrite (Fisher), sodium azide (Sigma), sodium fluoride (Baker), cadmium (Aldrich), and lead (Aldrich) were used.

2.4. Procedure

The screen-printed electrodes were used without any further pretreatment. The amperometric experiments were performed at a potential of -0.2 V, using a stirring rate of 400 rev min^{-1}. The substrate addition (5×10^{-5} M catechol) was follwed by additions of the target inhibitor, using microliter aliquots of the corresponding solutions. All measurements were performed at room temperature.

3. Results and discussion

Fig. 1 displays the amperometric response of strips containing different tyrosinase loadings to 5×10^{-5} M catechol (S), followed by successive additions of 1×10^{-5} M of diethyldithiocarbamate (I). The sensor responds very rapidly to these substrate and pesticide additions, indicating that its biocatalytic and inhibition activities are

maintained (despite the 2 h curing at 110°C); steady-state currents are obtained within ≈ 1 min. Such fast responses are attributed to the absence of supportive/external membranes, which is inherent in the screen-printing fabrication process. A preincubation period is not required, in contrast to strips based on immobilized acetylcholinesterase [10]. Both the substrate and inhibitor responses increase upon increasing the enzyme loading in the ink. The resulting calibration plots (also shown) indicate that the inhibitor response is nearly proportional to the enzymatic activity. Note that the ratio of inhibition signal/substrate signal increases initially (from 0.14 to 0.26), upon raising the enzyme loading from 0.3% to 0.6% w/w, and then decreases slightly to 0.24 for the 1% loading. Such trends reflect the fraction of the enzyme inhibited at a given inhibitor concentration.

Fig. 2 displays calibration plots obtained with the 0.6% w/w tyrosinase-containing strip for submillimolar concentrations of the pesticide diethyldithiocarbamate (A), thiourea (breakdown product of dithiocarbamate pesticides; B) the antifungal agent benzoic acid (C), and the herbicides 2,4-dichlorophenoxyacetic acid (D) or 4,6-dinitro-o-cresol (E). The new strips offer convenient quantitation of these toxins. However, as expected for inhibition processes, such plots are not linear.
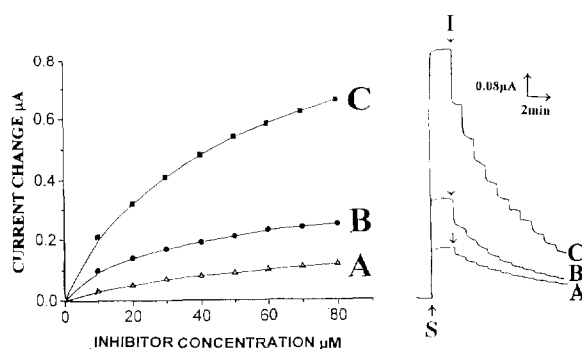

Fig. 1. Enzyme loading studies at various tyrosinase screen-printed electrodes. Enzyme loading: (A) 0.3; (B) 0.6; (C) 1.0% w w. Also shown (inset) are the respective current–time recordings. Catechol, 5×10^{-5} M, was used as substrate (S); sodium diethyldithiocarbamate, 10^{-5} M per step, was used as inhibitor (I). Applied potential, -0.2 V; electrolyte, phosphate buffer (0.05 M, pH 7.4); stirring rate, 400 rev min^{-1}.
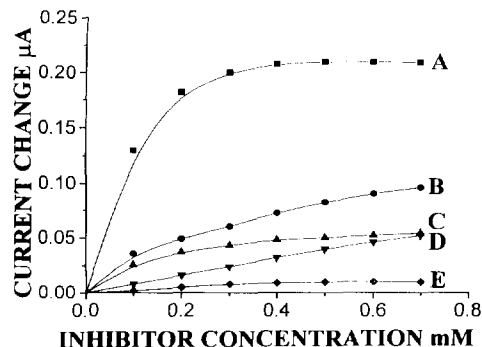

Fig. 2. Calibration plots obtained for inhibition at the 0.6% tyrosinase strip for: (A) sodium diethyldithiocarbamate; (B) thiourea; (C) benzoic acid; (D) 2,4-dichlorophenoxyacetic acid; (E) 4,6-dinitro-o-cresol. Other conditions are as given in Fig. 1.

A significant curvature is observed at high concentrations (reflecting saturation of the tyrosinase site). The quantitation of levels around the above such saturation is therefore limited. The trend in sensitivity: diethyldithiocarbamate > thiourea > benzoic acid > 2,4-dichlorophenoxyacetic acid > 4,6-dinitro-o-cresol, reflects the degree of inhibition. These profiles were used to estimate the apparent coefficients of inhibition, $I_{0.5}$, i.e. the concentrations corresponding to 50% of the inhibition signal, which were: 9.2×10^{-5} M (diethyldithiocarbamate), 1.0×10^{-4} M (benzoic acid) and 2.0×10^{-4} M (4,6-dinitro-o-cresol). The detection limits (S/N = 3) correspond to 2×10^{-6} M (diethyldithiocarbamate), 4×10^{-6} M (thiourea), 5×10^{-6} M (benzoic acid), 7×10^{-6} M (2,4-dichlorophenoxyacetic acid) and 9×10^{-6} M (2,4-dinitro-o-cresol). A lower sensitivity was observed for atrazine, pentachlorophenol or warfarin (not shown). No response was observed for similar additions of nitrate, nitrite or fluoride ions, sodium azide and lead or cadmium, over the concentration range 0.1–10 ppm, for each ion throughout that concentration range. The "tyrosinase-free" carbon strip, used as the control, was not responsive to any of the above 14 compounds.

Fig. 3 shows the influence of the substrate concentration upon the response of the screen-printed inhibitor biosensor. The diethyldithiocarbamate signal nearly doubles upon raising the catechol level from 2×10^{-5} to 5×10^{-5} M and
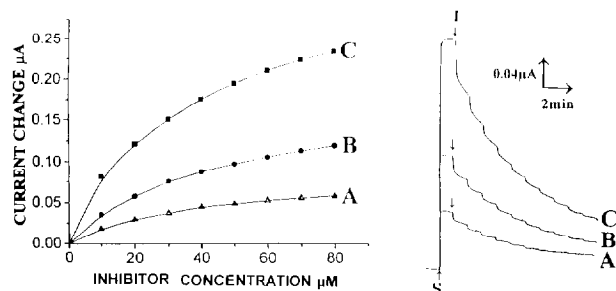
Fig. 3. Effect of substrate concentration on inhibition responses at 0.6% tyrosinase strip. Catechol concentration: (A) 2 × 10⁻⁵ M; (B) 5 × 10⁻⁵ M; (C) 1 × 10⁻⁴ M. Also shown (inset) are the corresponding current time recordings. Sodium diethyldithiocarbamate, 10⁻⁵ M per step, was used as inhibitor (I). Other conditions are as given in Fig. 2.

between 5×10^{-5} and 1×10^{-4} M. Note also the longer response times of the inhibitors signal at higher substrate concentrations. The shape of the resulting calibration plots is not greatly influenced by the catechol level. A potential of -0.2 V yielded the most favorable detection of the catechol substrate and the target inhibitors (not shown). As expected, such a low potential minimizes possible interference from coexisting constituents of relevant water samples. The data of Fig. 3 also indicate that the sensor is operating in the kinetic regime (with respect to the substrate reaction). It is thus essential to carefully control the substrate concentration.

Attempts to reuse the enzyme strips have been explored by repeating the calibration experiment (with intermittent water rinse). For thiourea the sensitivity decreased by 37% and by 54% for the second and third runs respectively (compared to the first run). Benzoic acid displayed 53% and 64% suppressions of the inhibitor response, while diethyldithiocarbamate yielded 67% and 79% losses of the initial signal (not shown). Such changes are expected for irreversible inhibition processes. (The catechol signal decreased in a similar fashion in the presence of the different inhibitors.) An irreversible inhibition was also reported for strips based on acetylcholinesterase [9]. The use of extremely

low cost single-use electrodes circumvents these inactivation effects. In contrast, conventional electrodes would require renewal of the enzyme layer.

The screen-printing process assures a good strip-to-strip reproducibility. For example, a relative standard deviation of 6.2% was calculated for the response for 1×10^{-5} M diethyldithiocarbamate at five different strips. Such reproducibility requires a uniform dispersion of the enzyme with the ink matrix. Manual mixing, for 60 min, was used to assure homogeneous dispersion of tyrosinase in the ink. It should be pointed out that in a few cases one or two strips from a 10-electrode lot would yield an unsatisfactory result. This can be readily detected prior to the inhibitor measurement from the magnitude of the substrate signal (this serves as a "built-in" quality test). The sensitivity of electrodes from different batches can differ by up to $\approx 30\%$ (requiring separate calibration for each batch). New strips displayed only 4% and 15% decreases in response after storage for 30 and 60 days respectively, in phosphate buffer at 5°C.

The environmental utility of the tyrosinase-based inhibitor biosensor is illustrated in Fig. 4. This shows the response for an untreated river water (Rio Grande) sample spiked with increasing
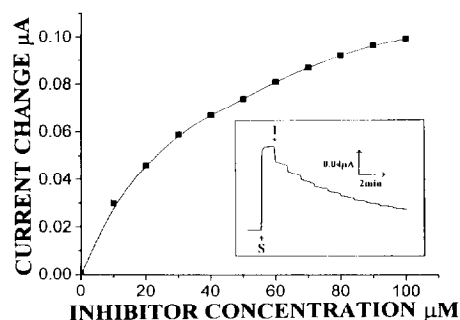

Fig. 4. Calibration plot obtained using a water sample from the Rio Grande river. No supporting electrolyte was used in this experiment. The inset shows the corresponding current–time recording. Catechol, 5×10^{-5} M, was used as substrate (S). Sodium diethyldithiocarbamate, 10^{-5} M per step, was used as inhibitor (I).

levels of diethyldithiocarbamate in 1×10^{-5} M steps. The strip responds rapidly to these micromolar concentration increments, despite the absence of deliberately added electrolyte. Similar to assays of "synthetic" samples, the response rises sharply with the inhibitor concentration at first (up to $\approx 4 \times 10^{-5}$ M), and then more slowly. However, caution is required when analyzing unknown samples due to the possible presence of mixtures of inhibitors.

In conclusion, the above experiments have demonstrated for the first time the utility of tyrosinase-based thick-film electrodes for monitoring enzyme inhibitors. The new strips offer convenient quantitation of micromolar concentrations of various water pollutants, and a nearly instantaneous response. A convenient one-step fabrication step is accomplished by incorporating the enzyme within the ink matrix. As is common for enzyme inhibition processes, such detection would not be specific in complex environmental samples. Such samples would thus benefit from designing arrays of several enzyme inhibition electrodes. Further improvements in the detectability are expected in connection with metallized carbon inks or bioamplification recycling reaction schemes. The coupling of the new disposable sensors with compact (hand-held) analyzers should facilitate the field testing of relevant enzyme inhibitors. Obviously, the same strips may also be useful for on-site environmental measurements of their phenolic substrates.

Acknowledgements

References

[1] K.R. Rogers, Biosens. Bioelectron. 10 (1995) 533.
[2] J. Wang. Electrochemical Sensors for Environmental Monitoring: A Review of Recent Methodology, U.S. EPA 540 R-95 507, Research Triangle Park, NC, 1995.
[3] J.L. Marty, D. Garcia and R. Rouillon, Trends Anal. Chem., 14 (1995) 329.
[4] A. Gunther and U. Bilitewski. Anal. Chim. Acta, 300 (1995) 117.
[5] M.H. Smit and A.E. Cass. Anal. Chem., 62 (1990) 2429.
[6] A. Amine. M. Alafandy, J.M. Kauffmann and M.N. Pekli, Anal. Chem., 67 (1995) 2822.
[7] I. Dolmoanova, T. Schekhovstova and V. Kutcheryaeva, Talanta, 34 (1987) 201.
[8] T. Shekhovtsova and S. Cherntskaya, Anal. Lett., 27 (1994) 2883.
[9] P. Skadal. Anal. Chim Acta, 269 (1992) 281.
[10] I. Hartley and J.P. Hart, Anal. Proc., 31 (1994) 333.
[11] J. Bescombes, S. Cosnier, P. Labbe and G. Reverdy, Anal. Chim. Acta, 311 (1995) 255.
[12] K. Lerch, Cell Biochem., 5 (1988) 125.
[13] J. Wang and Q. Chen, Anal. Lett., 28 (1995) 1131.

Ultraviolet spectrophotometric determination of copper in copper ores by flow-injection analysis

Amin T. Haj-Hussein*

Chemistry Department, Yarmouk University, Irbid, Jordan

Abstract

A flow-injection analysis (FIA) method for the ultraviolet spectrophotometric determination of copper in copper ores is described. The ore samples are dissolved in concentrated perchloric acid, the excess acid is neutralized with ammonia solution, and the resulting solution is used for the determination of copper. The UV-FIA system is based on the reaction of copper (II) ions with pyrophosphate and subsequent measurement of the absorbance of the dipyrophosphatocuprate (II) complex at 240 nm. The main factors which control the formation of this complex and the FIA variables influencing the system are discussed. The calibration graph is linear from 2 50 ppm copper. At a sampling rate of about 70 samples h $^{-1}$ with 50 μl sample injections, precision was about 1% relative standard deviation. Results obtained compare well with those obtained by atomic absorption spectrometry.

Keywords: Copper; Copper ores; Flow-injection analysis; Ultraviolet spectrophotometry

1. Introduction

The analysis of copper-containing materials has a vast literature. This is due to widespread interest in copper content in several branches of science (e.g. medicine, biology, industrial chemistry and geology). Copper is widely distributed in nature and is a major component of a wide range of minerals. It also occurs in smaller quantities in many metal ores. Geochemical prospecting and metallurgical analysis of copper made its determi-

nation in a great variety of samples necessary, and fast methods for continuous monitoring are still needed. Analyses for copper in copper ore samples can be performed by various methods including volumetry [1-5], gravimetry [6], electrogravimetry [6,7], potentiometry [7,8] spectrophotometry [9-11] and atomic absorption spectrometry (AAS) [11-14]. The analysis time for all these conventional methods is frequently significantly greater than that for automated methods. Moreover, reproducibility can seldom be matched by manual operations.

Because of the capabilities of flow-injection analysis (FIA), as developed by Ruzicka and

* Fax: (-962)-2-274-725.

Hansen [15], it is of interest to assess its value for copper ore analysis. The automatic nature of FIA ensures large throughputs and reduces the need for highly competent and well-organized analysts to perform the chemical analysis. Moreover, it offers great advantages such as flexibility, speed, high sampling rate and wide applicability in many fields.

In earlier work [16], it was found that Cu(II) ions react with pyrophosphate to form dipyrophosphatocuprate (II) complex, which exhibits a characteristic absorptivity in the ultraviolet region. The copper(II)-pyrophosphate system has been studied spectrophotometrically in the ultraviolet region for the determination of copper by Nebel and Boltz [17].

On the basis of these considerations, this work was undertaken to develop a method for the continuous ultraviolet spectrophotometric determination of copper in copper ores using FIA.

2. Experimental

2.1. Reagents

All chemicals used were of analytical reagent grade, unless otherwise specified; all solutions were prepared with deionized water.

2.1.1. Standard copper(II) solution

A stock solution of copper(II) (1000 ppm) was prepared by adding 1.5 ml of 60% perchloric acid to 0.1 g ($\pm$0.0001) of pure copper wire sample (99.9%; Merck). The mixture was heated gently under a fume hood until the sample was dissolved. After cooling, the solution was diluted to about 80 ml with water and ammonia solution (1 M) was added dropwise to neutralize the excess acid until the pH of the solution was about 5.0–5.5. The solution was made up to 100 ml with water. Working standards were prepared by diluting the stock solution with water.

2.1.2. Pyrophosphate reagent solution

These were 0.005–0.10 M sodium pyrophosphate (98% pure; Fluka) solutions at pH 5.0, 6.0. 8.0, 9.0, 10.0, 11.0 and 12.0. The pH of these

solutions were adjusted with perchloric acid or sodium hydroxide. All pH measurements were made using a Metrohm Herisau (Type E 520) pH meter.

2.1.3. Dissolution of copper ores

About 100 mg of sample (accurately weighed) was placed in a 25 ml volumetric flask and 1.5 ml of 60% perchloric acid and two small glass beads were added. A short-necked funnel was inserted into the neck of the flask. The mixture was heated gently under a fume hood until the sample was dissolved. After cooling for 3–4 min, about 50 ml of water was carefully added through the funnel. The contents were swirled and boiled for 5 min to expel hydrogen gas. On cooling, 1 M ammonia solution was added dropwise to neutralize the excess acid until the pH of the solution was about 5.0–5.5. The contents were digested for 5 min and the precipitate (mainly due to iron which is associated with copper ores) was allowed to settle. Finally the insoluble matter was filtered off and made up to 100 ml with water.

Sample solutions of five copper ores including native copper (Cu), bornite (Cu_5FeS_4), chalocite (Cu_2S), cuprite (Cu_2O) and malachite ($Cu_2CO_3(OH)_2$) were prepared. Working solutions were prepared by accurate dilution of each sample solution with water.

2.2. Apparatus

The flow diagram for the determination of copper is shown in Fig. 1. The FIA system was assembled from 0.51 mm Microline tubing. The manifold consists of two lines, the top one carrying the carrier into which the sample is injected and the lower carrying the reagent solution. Carrier and reagent solutions were delivered by an Ismatic peristaltic pump (Type MINI-S 860) operated with Tygon tubing. The sample is aspirated from the sample container into the injection valve using a Rheodyne four-way Teflon valve injector (Type 50). The injection sample is merged with the reagent stream in the reaction coil and then led to a flowthrough optical cell and finally to waste. A home-made confluence point with a mixing point was used to ensure rapid mixing of

the two streams in the 50 cm long coil. The absorbance was measured with a Varian DMS 100 UV–Visible spectrophotometer with a 10 mm micro flow-cell, 18 μl (Hellma type, Model QS178.12), and recorded with a Linear 1200 chart recorder.

2.3. FIA

The flow system illustrated in Fig. 1 is used. The sample solution (50 μl) injected into water (carrier stream flow rate, 0.6 ml min^{-1}) was merged into pyrophosphate (reagent stream flow rate, 0.6 ml min^{-1}) at point I in a confluence manner downstream. To ensure rapid mixing of the two streams, a "mixing point ii" is inserted immediately after the confluence point, forcing the combined stream through a 60° turn (during which the direction of flow is abruptly changed). After an injection, the valve was returned to the load position when the baseline was reached. The absorbance of the dipyrophosphatocuprate(II) complex is measured at 240 nm. The output of the ultraviolet spectrophotometer was registered on the chart recorder. When the baseline was reached, another slug of the sample could be injected. For calibration, a series of working standard solutions were injected. For calibration, a series of working standard solutions were injected before and after the sample runs. All solutions were analyzed in triplicate.
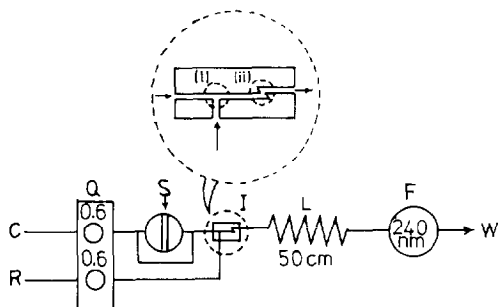

Fig. 1. Two-line manifold for the ultraviolet determination of copper. The i.d. of the Microline tubing was 0.51 mm from the injection valve to the detector. (C) carrier stream; (R) reagent stream; (Q) flow rate (ml min^{-1}); (S) sample injection; (I) confluence point (i) with mixing point (ii); (L) reaction coil; (F) flowthrough cell; (W) waste.
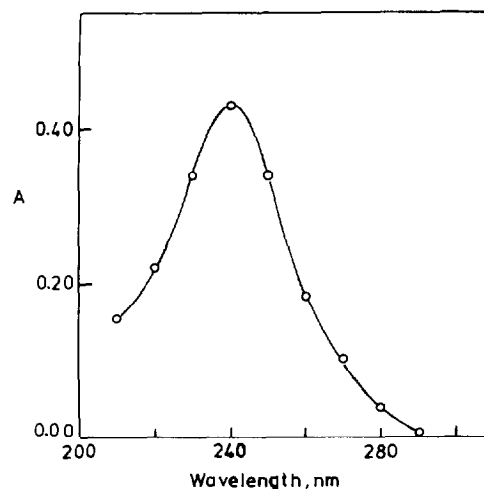
Fig. 2. Absorption spectrum for dipyrophosphatocuprate(II) ion at pH 9.0 with the manifold shown in Fig. 1. Carrier, water; concentration of pyrophosphate reagent; 0.05 M; concentration of Cu(II), 20 ppm; injection volume, 50 μl.

3. Results and discussion

Nitric acid in dilute and concentrated forms can be used for dissolution of copper ores. For sulfide ores, a strongly oxidizing solvent, aqua regia, or hot concentrated perchloric acid, which is a powerful oxidizing agent, can be used [11]. By using concentrated perchloric acid for dissolving sulfide copper ore samples, the process is simplified and accelerated. Moreover, liberation of sulfur and interferences of nitrite and nitrate ions, which absorb in the ultraviolet region, are avoided.

The FIA system used in this work allows rapid continuous analysis of copper by direct monitoring of the absorbance of the dipyrophosphato-cuprate(II) complex. Absorbance measurements were performed using the manifold shown in Fig. 1. The absorption spectrum for dipyrophos-phatocuprate(II) complex, obtained by injecting standard copper(II) solution (20 ppm) in the carrier stream and using 0.05 M pyrophosphate at pH 9.0 as reagent is shown in Fig. 2. The curve exhibits a band with maximum absorption at about 240 nm which was chosen as the optimum wavelength for studying the chemical variables and the FIA variables influencing the system.

3.1. Optimization of chemical variables

3.1.1. Pyrophosphate concentration

The effect of pyrophosphate concentration was determined using a concentration of 20 ppm of copper and a pH of 9.0. By injecting standard copper solution, the absorbance values at 240 nm were measured in the concentration range 0.005–0.100 M of pyrophosphate reagent solutions. Fig. 3 shows that the absorbance of the dipyrophosphatocuprate(II) complex formed is dependent on the pyrophosphate concentration. and a concentration of 0.025 M is necessary for the development of maximum absorbance. A large excess of pyrophosphate (0.05 M) is recommended to ensure sufficient reagent when larger amounts of copper are being measured.

3.1.2. pH

The effect of pH on the absorption spectra of solutions containing 10 ppm of copper and 0.05 M pyrophosphate was studied in the range 5.0–12.0. Fig. 4 shows that the maximum absorbance was obtained between pH 8.0 and 10.0. Therefore, a pH of 9.0 was recommended for attainment of maximum absorbance.

Fig. 4. Effect of pH on the determination of copper. Concentration of copper was 10 ppm; wavelength, 240 nm; other conditions as given in Fig. 2.

3.2. Optimization of FIA variables

3.2.1. Sample volume injection

As the sample volume increased from 25 to 100 μl, the signal increased by about 110% but tailing increased, thus lowering the sampling rate (90 to 30 samples h^{-1}). A 50 μl sample loop was selected for use.

3.2.2. Length of the reaction coil

Increasing the coil length lowered the peak height and increased the dispersion but improved the reproducibility, which was necessary to obtain a stable baseline. The coil lengths were optimized to give ample reaction time with minimum dispersion. A reactor length (L) of 50 cm and an i.d. of 0.51 mm were chosen for use.

3.2.3. Flow rate

The signal increased about 6% when the flow rate was changed from 0.74 to 1.6 ml min^{-1} but the residence time and dispersion were affected by the flow rate employed. Therefore, a flow rate of 1.2 ml min^{-1} (which is the sum of the flow rates of both lines of the two-line FIA system) was selected to achieve high sensitivity of the measure-
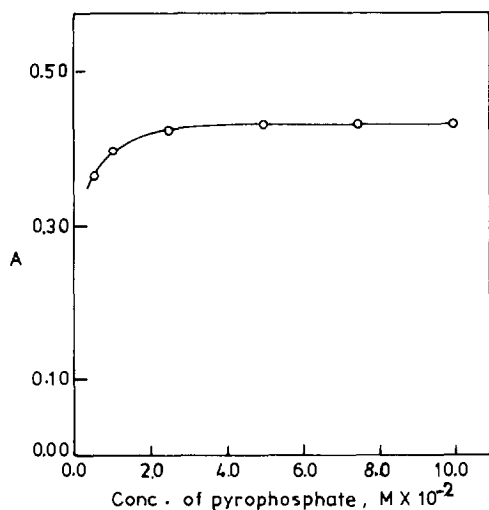

Fig. 3. Effect of pyrophosphate concentration on absorbance of dipyrophosphatocuprate(II) complex. Wavelength. 240 nm: other conditions as given in Fig. 2.
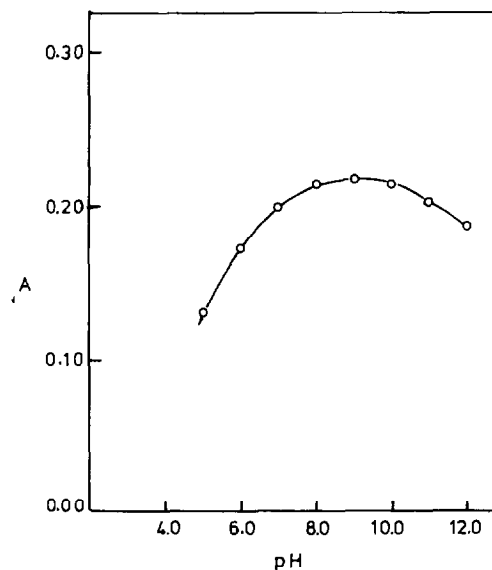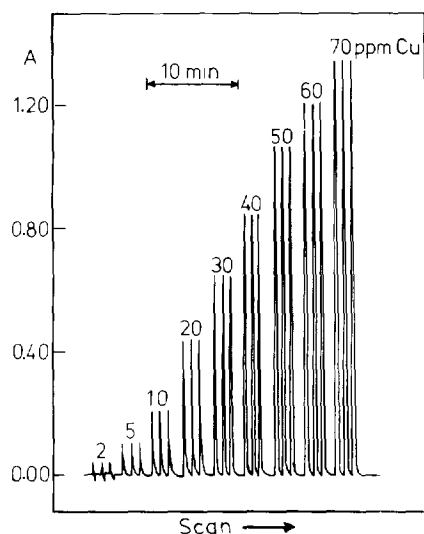
Fig. 5. Flow-injection signals for the ultraviolet determination of copper at a rate of approximately 70 samples h⁻¹ with the manifold shown in Fig. 1. Wavelength, 240 nm; other conditions as given in Fig. 2.

ments with a reasonable sampling rate. At this flow rate, the average sampling rate with 50 μl sample injections was around 70 samples h⁻¹.

3.3. Calibration

The flow system in Fig. 1 (reaction coil 50 cm long and 0.51 mm bore) was used for preparing the calibration graph. Standard copper solutions were injected from a sample loop of 25 cm of 0.51 mm bore Microline tubing (sample volume about 50 μl). Typical signals are shown in Fig. 5. The calibration graph is linear in the range 2–50 ppm copper. The limit of detection (3 SD) for copper was 0.3 ppm. For successive injections of a standard solution of copper (10 ppm), the precision of the method was found to be <1% RSD.

3.4. Interference study

In order to apply the automatic UV-FIA method for analysis of copper in copper ores, the interference effect of diverse ions which may be found in the common copper ores [18] were examined. The response produced by the standard solution containing 10 ppm of copper was compared with that produced by a similar copper

solution containing additions of various amounts of diverse ions. An error of less than 2.5% was considered to be tolerable. The following ions showed no interference at the concentrations (ppm) shown in parentheses: Ni^{2+} (100), Zn^{2+} (100), MoO_4^{2-} (100), Ca^{2+} (100), Mg^{2+} (100), Sn^{4+} (10) and AsO_4^{3-} (10). In contrast, Fe^{3+}, Pb^{2+} and Ag^- were found to cause serious interferences when their concentrations exceeded 1 ppm. In the determination of copper in copper ores, however, dissolving these ores in perchloric acid followed by addition of ammonia and filtration would remove Fe^{3+} as hydroxide. However, if Pb^{2+} and Ag^- are present in large amounts, they must be separated in some way. For trace amounts, the method of standard addition should ameliorate the problem somewhat.

3.5. Determination of copper in copper ores

The proposed method was applied to the determination of copper in native copper, sulfide copper ores (bornite and chalcocite), and oxidized copper ores (cuprite and malachite). The results (copper content, %) of the analyses are summarized in Table 1.

A measure of the reliability of the proposed method is given in Table 1 in which the results are

Table 1
Determination of copper in some copper ores by the proposed UV-FIA method and by AAS[a]

Sample[b]	Cu(II) content (%)	
	UV-FIA	AAS
Native copper	98.0	98.8
Bornite	30.8	29.8
Chalcocite	31.0	32.0
Cuprite	80.1	80.7
Malachite	55.8	54.2

[a] A Pye-Unicam SP9 atomic absorption spectrophotometer equipped with a copper hollow-cathode lamp was used. The wavelength was set at 324.8 nm and the operating conditions were adjusted following standard recommendations.
[b] Native copper (from new Tucson, AZ) was provided by the Geology Department, Yarmouk University. Bornite, chalcocite, cuprite and malachite were supplied by Dr. F. Krantz (Germany).

compared with those obtained using AAS by complete decomposition with nitric acid [11]. There is general agreement between the results of the two methods. It is also apparent that the results for copper were not affected by various elements in the ore samples.

References

[1] W.T. Elwell and I.R. Scholes, Analysis of Copper and its Alloys, Pergamon Press, Oxford, 1967.

[2] V.B. Khanna, B.M. Sood and A.K. Bhattacharyya, Indian J. Appl. Chem., 32 (1969) 11.

[3] B.P. Bhaduri and K.C. Jayaprakash, Indian J. Chem., 8 (1970) 1141.

[4] N.Kh. Lyapunova, Anal. Abstr., 30 (1976) 5B39.

[5] N.R. Desikan and M. Vijayakumar, Analyst, 110 (1985) 1399.

[6] A.I. Vogel, Quantitative Inorganic Analysis, Longmans, London, 1961.

[7] G. Rossi, Anal. Abstr., 39 (1980) 5B41.

[8] L. Peng, Anal. Abstr., 50 (1988) 10B43.

[9] G. Charlot, Colorimetric Determination of Elements, Elsevier, Amsterdam, 1964.

[10] Q. Yang, J. Nie, X. Zhang and Y. Wan, Anal. Abstr., 50 (1988) 3B43.

[11] R.E. Wainerdi and E. A. Uken, Modern Methods of Geochemical Analysis, Plenum Press, New York, 1971.

[12] M.E. Britske and I.V. Slabodenyuk, Anal. Abstr., 30 (1976) 5B42.

[13] S. Kazimierczyk, M. Michalewska and R. Jarosz, Anal. Abstr., 20 (1971) 3625.

[14] N.G. Kharmanova and Yu. F. Pogrebnyak, Anal. Abstr., 37 (1979) 3B8.

[15] J. Ruzicka and E.H. Hansen, Flow Injection Analysis, 2nd edn., Wiley, New York, 1988.

[16] R.P. Buck, S. Singhadeja and L.B. Rogers, Anal. Chem., 26 (1954) 1240.

[17] M.L. Nebel and D.F. Boltz, Anal. Chem., 36 (1964) 144.

[18] J.C. Bailar, Jr., H.J. Emeléus, Sir R. Nyholm and A.F. Trotman-Dickenson (Eds.), Comprehensive Inorganic Chemistry, Vol. 3, Pergamon Press, Oxford, 1973, p. 6.

Anodic stripping voltammetric determination of titanium(IV) using a carbon paste electrode modified with cetyltrimethylammonium bromide

Monika Stadlober, Kurt Kalcher*, Georg Raber, Christian Neuhold

Institut Für Analytische Chemie, Karl-Franzens Universität Graz, Universitätsplatz 1, A-8010 Graz, Austria

Abstract

A method is described for the voltammetric determination of titanium(IV) using a carbon paste electrode modified in situ with cetyltrimethylammonium bromide. The cationic micellar surfactant adsorbs onto the electrode particularly at negative potentials, simultaneously preconcentrating titanium(IV) as the oxalate complex with reduction to titanium(III). Anodic stripping voltammetry exploiting reoxidation can be used for the determination of trace levels of titanium(IV). Linearity between current and concentration exists between 5 and 160 $\mu g\ l^{-1}$ Ti(IV) (preconcentration time 2 min). The limit of detection (calculated as 3σ) is 0.1 $\mu g\ l^{-1}$, with a preconcentration time of 10 min.

Keywords: Anodic stripping voltammetry; Carbon paste electrodes; Cetyltrimethylammonium bromide; Titanium

1. Introduction

The determination of titanium(IV) by anodic stripping voltammetry is difficult, because at common potentials it cannot be reduced to the metallic state and deposited onto the electrode. Only the one-electron reduction of Ti(IV) to Ti(III), or the reverse oxidation, can be exploited by voltammetry [1]. Lingane and Kennedy [2] described the redox behaviour of titanium in strong mineral acids. At low hydrogen ion concentrations, the redox reaction is irreversible, because the Ti ions are solvated or even hydrolyzed. The reaction

becomes reversible on increasing the acidity of the supporting electrolyte, as higher acidity prevents formation of Ti(IV) hydroxo complexes, which are more difficult to reduce. By complexing titanium(IV) with organic acids such as oxalic acid, ethylenediaminetetraacetic acid (EDTA), citric acid, tartaric acid, salicylic acid, mandelic acid, and ascorbic acid, the electrode reaction becomes more reversible and can be better exploited for polarographic/voltammetric measurements [3–9].

Adsorptive stripping voltammetry with the use of complexing agents, which show excellent adsorption properties on the mercury electrode surface (Solochrome Violet RS, Cupferron, Pyrocatechol Violet, Beryllon III or 4-(2-pyridylazo)-resorcinol [10–15]), was often used to determine

* Corresponding author. Tel.: + 43 316 3805310; fax: − 43 316 384092.

trace levels of titanium. Another possibility is the exploitation of catalytic currents caused by chlorate or bromate during the reduction of titanium(IV) in the presence of oxalic acid, mandelic acid, or EDTA [16–20]. In this way differential pulse or square wave voltammetry or polarography combined with catalysis, which is mediation rather than catalysis, gives a further enhancement in sensitivity. The electrode process, however, is strongly irreversible; no reoxidation peak can be observed. Indirect polarographic methods are another approach for the determination of titanium [21].
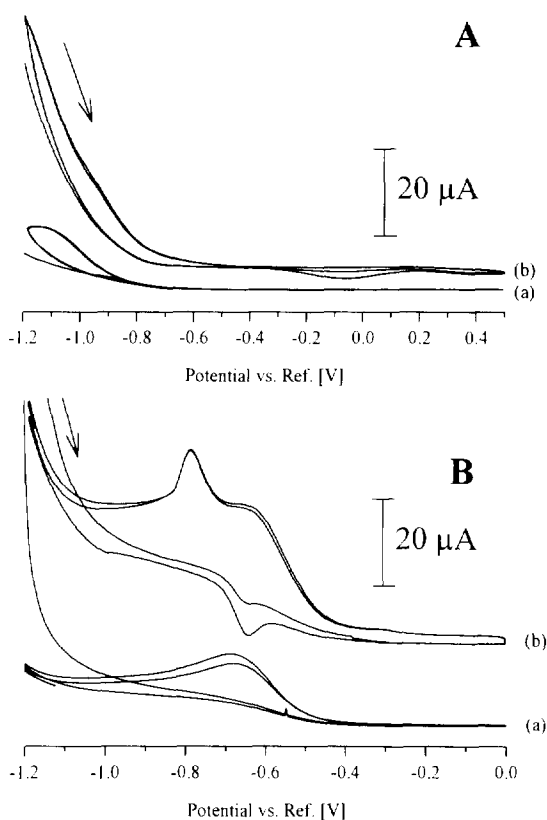

Fig. 1. Cyclic voltammograms of titanium(IV) at a plain (A) and a CTAB-modified (B) CPE. Equilibration time: 30 s; initial potential: − 1.2 V; final potential: (A) + 0.5 V, (B) 0 V; scan rate: 20 mV s⁻¹. (A) (a) 0, (b) 250 mg l⁻¹ titanium, supporting electrolyte 0.1 M KCl, 0.05 M acetate buffer, 0.01 M oxalic acid. (B) (a) 0, (b) 0.5 mg l⁻¹ titanium; supporting electrolyte 0.05 M acetate buffer, 0.01 M oxalic acid, 0.1 mM CTAB.

So far, no studies on the electrochemical determination of titanium with the use of carbon paste electrodes (CPEs) have been published. CPEs are very suitable for voltammetric and amperometric determinations because they are inexpensive, easy to handle and simple to modify [22,23]. With respect to the determination of titanium, in-situ modification with surfactants, in particular with cetyltrimethylammonium bromide (CTAB), is promising, since the anionic titanium species obtained by complexation can be preconcentrated on the electrode surface as lipophilic ion pairs.

CTAB is a cationic surfactant which belongs to the group of quaternary ammonium compounds. In suitable solvents it forms spherical micelles above the critical micellar concentration (CMC), which in water occurs at 0.9 mM (25°C). In the presence of electrolytes the CMC is lowered because of increased micellization from free ions. [24].

CTAB adsorbs onto the electrode surface by hydrophobic attraction and by electrostatic attraction at negative potentials. At concentrations lower than the CMC the surfactant acts as an ion-pairing agent, where monomers are adsorbed onto the electrode surface although only to a very small extent [25]. At concentrations higher than the CMC, strong adsorption of CTAB on the electrode surface is observed at negative potentials [25,26], which can lead to an extraordinary enhancement in the sensitivity of voltammetric measurements.

This paper describes a new and sensitive voltammetric method for the determination of titanium(IV) with CPEs by an adsorptive modification of the electrode with CTAB and accumulation of titanium (IV) as the oxalate complex.

2. Experimental

2.1. Apparatus

Voltammetric experiments were performed with a potentiostat Model 264A PAR (Princeton Applied Research) voltammetric analyzer in combination with an automatically controlled self-constructed cell compartment made of Plexiglass
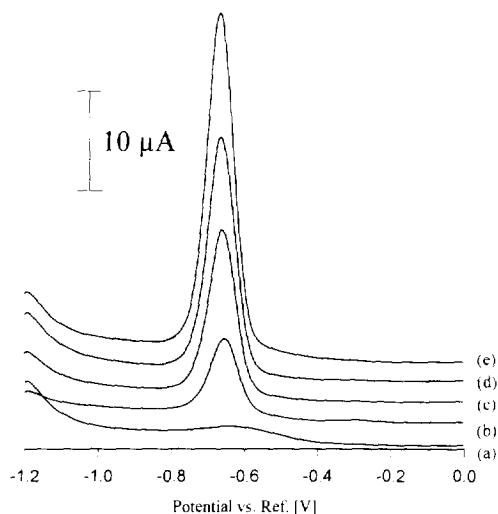
Fig. 2. DP voltammograms of Ti(IV) with a CPE modified in situ with CTAB. Supporting electrolyte 0.05 M acetate buffer, 0.01 M oxalic acid, 0.1 mM CTAB; 2 min deposition at − 1.2 V; Ti(IV) concentration: (a) 0; (b) 30; (c) 60; (d) 90; (e) 120 μg l⁻¹.

[27]. The cell consisted of a glass thermostatable titration vessel (20–60 ml; Metrohm 6.1418.220) with a platinum wire as counter electrode and saturated calomel electrode (SCE; Ingold 303-NS) as reference. The latter was in contact with the solution via a salt bridge (1 M KCl) with a Vicor frit to avoid contamination of the reference electrode. The solution in the cell could be stirred (≈ 300 rev min⁻¹) with a Teflon-coated stirring bar when required. The measuring solution was deaerated with highly pure argon or nitrogen (99.999%) for at least 5 min before voltammetric measurements; during the measurements argon was passed over the solution. The temperature of the solution was kept constant at 20°C with a thermostat (Haake R20).

Voltammetric curves were registered either on X–Y recorder (Compensograph X-Y 1929, Siemens) with manual evaluation by the tangent fit method, or transferred to a personal computer after A D conversion by an appropriate interface [28].

2.2. Working electrode

The body of the carbon paste electrode con-

sisted of a Teflon rod (outer diameter 10 mm) with a 3 mm deep centric hole (diameter 7 mm) for the carbon paste filling and a platinum wire through the center of the rod for electrical contact.

The carbon paste was prepared by thoroughly mixing 5 g of spectral carbon powder (RWB, Ringsdorff-Werke, Germany) with 1.6 ml of liquid paraffin oil (Uvasol, Merck), until a homogeneous consistency was achieved. The paste was packed into the electrodes and smoothed off with a PTFE plate.

2.3. Reagents

Deionized water was distilled twice in a quartz still and then purified by a cartridge deionization system (Nanopure, Barnstead). Oxalic acid, acetic acid and sodium acetate were of suprapure grade (Merck). All other chemicals were of analytical grade (p.a., Merck). CTAB was recrystallized from a 4:1 (v/v) acetone–methanol mixture prior to use. Stock solutions of titanium (1000 mg l⁻¹ Ti) were prepared by dissolving 0.6642 g of potassium titanyl oxalate (Ventron, Karlsruhe, Germany) in 100 ml of 0.1 M aqueous oxalic acid. Stock solutions of lower concentrations were freshly prepared by dilution. Stock solutions of salts used for investigations of their interference effects has concentrations of 1 or 10 g l⁻¹ with respect to the ion.

2.4. Procedure

2.4.1. Voltammetry

The supporting electrolyte for the voltammetric measurements consisted of 0.05 M acetate buffer and 0.01 M oxalic acid (pH 4.3). CTAB was added at a concentration of 1 × 10⁻⁴ M. Cyclic voltammograms (CVs) were recorded from − 1.2 to 0 V with a scan rate of 20 mV s⁻¹ and an equilibration time of 30 s, beginning in the anodic direction.

All quantitative measurements were performed in differential pulse (DP) mode. The initial potential was − 1.2 V, the final potential 0

V, the pulse height 50 mV, and the scan rate 10 mV s^{-1}. Prior to the differential pulse voltammetry (DPV) measurements the electrode was conditioned by applying a potential of -1.2 V for 15 min in the supporting electrolyte containing CTAB. Subsequently, titanium was added to the solution and preconcentrated onto the electrode surface with the initial potential applied.

2.4.2. Regeneration

Complete removal of residual titanium on the electrode was achieved by exposing the electrode to a separate solution containing 0.1 M sodium salicylate and 0.05 M acetate buffer (pH 4.7), applying a potential of -1.2 V for 1 min and scanning to -0.2 V. After this, the cleaning was completed by a 1 min exposure of the electrode to a stirred solution of 1 M potassium bromide without the application of a potential.

2.4.3. Analysis of a mineral sample (stone wool)

About 200 mg of the sample (Heralan, Heraklith, Austria) was fused with a five fold excess of NaKCO$_3$ in a platinum crucible for 20 min.
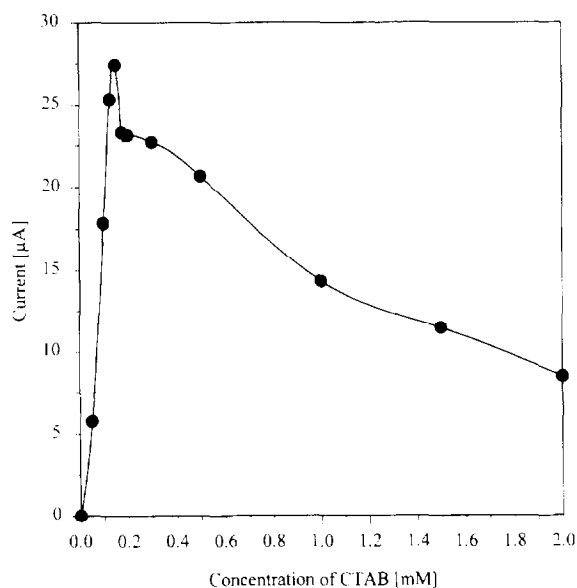

Fig. 3. Dependence of the peak current on the concentration of CTAB in the measurement solution. Supporting electrolyte 0.05 M acetate buffer, 0.01 M oxalic acid; 50 μg l^{-1} Ti(IV), 2 min deposition at -1.2 V.

Afterwards the reaction product was dissolved in 50 ml of hydrochloric acid (5 M). The resulting solution containing solid silicate was heated on a sand bath until most of the hydrochloric acid had evaporated. Then HCl (15 ml, 10 M) was added again and evaporated almost to dryness. This procedure was repeated twice. The residue was dissolved in hydrochloric acid (3 M), and the silicic acid was filtered off. The filtrate was diluted to a volume of 100 ml. For the voltammetric determination a 10 μl aliquot was added to 20 ml of supporting electrolyte.

3. Results and discussion

3.1. Choice of modifier

In order to determine Ti(IV) by voltammetry using CPEs, it is necessary to transform it into a complex, because otherwise highly acidic solutions must be used, yielding voltamograms of poor quality [2]. With CPEs it is hardly possible to employ such media, as the background currents at negative potentials are considerably high due to enhanced hydrogen evolution. Nevertheless, acidic solutions are required for a successful reduction of Ti(IV).

The titanyl cation TiO^{2+} forms a stable anionic complex with oxalic acid with a formation constant of 5×10^{10} l^2 mol^{-2} according to [29].

$$\text{TiO}^{2+} + 2(\text{C}_2\text{O}_4)^{2-} \rightleftharpoons [\text{TiO}(\text{C}_2\text{O}_4)_2]^{2-} \tag{1}$$
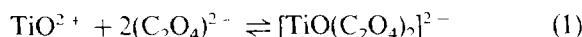
At a mercury electrode reduction occurs at about -0.3 V vs. SCE at pH 1.2 [3]

$$[\text{TiO}(\text{C}_2\text{O}_4)_2]^{2-} + 2\text{H}^-$$

$$+ e^- \rightleftharpoons [\text{Ti}(\text{C}_2\text{O}_4)_2] + \text{H}_2\text{O} \tag{2}$$
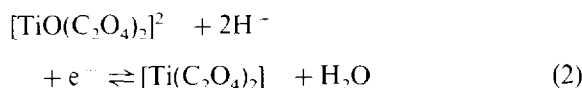
When using a CPE reduction of [TiO(Ox)$_2$]$^{2-}$ occurs at about -0.9 V (pH 4.3) as a weak signal superimposed on the hydrogen evolution current. This can be clearly seen in the cyclic voltammogram recorded with an unmodified electrode (Fig. 1A). The electrode reaction is rather irreversible, since reoxidation is anodically shifted to about -0.05 V. On lowering the pH the shift
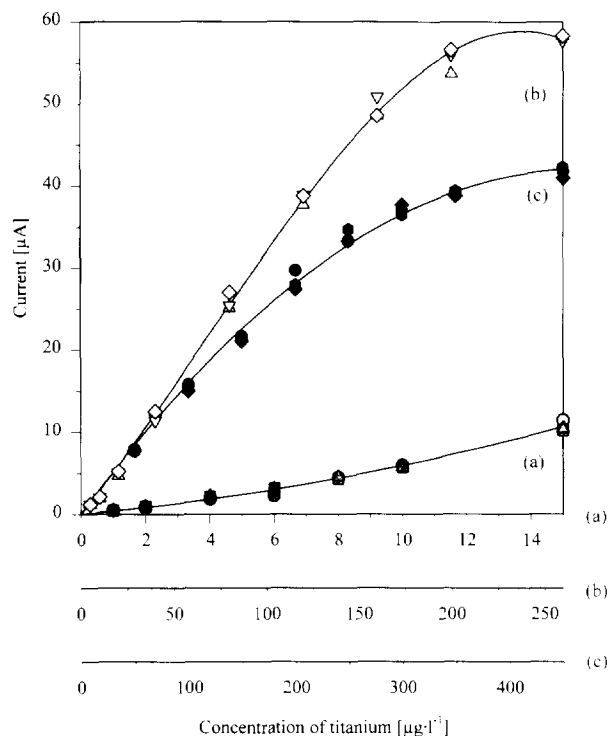
Fig. 4. Dependence of the DPV peak current on the titanium concentration. Supporting electrolyte 0.05 M acetate buffer, 0.01 M oxalic acid. 0.1 mM CTAB: deposition times: (a) 10; (b) 2; (c) 1 min.

becomes less, but the signal is still irreversible. Since the signals are always very small, the sensitivity is low and not suitable for trace analysis.

If CTAB is present in the solution at a concentration level higher than the CMC the titanium oxalate becomes preconcentrable at the electrode surface and yields a pronounced reduction and reoxidation signal of the redox couple $[TiO(Ox)_2]^{2-}$ $[Ti(Ox)_2]$ with a tremendous improvement in sensitivity (Fig. 1B).

The redox reaction without CTAB is strongly irreversible, whereas it becomes quasi-reversible in its presence. The reduction and reoxidation potentials occur at about -0.78 and -0.64 V vs. SCE respectively. The reduction signal shifts to more positive potentials compared to unmodified CPEs. This indicates that Ti(IV) is more easily reduced in the adsorbed form with cetyltrimethylammonium ions (CTA^-) than as a free complex in solution. However, the reoxidation potential shifts

to more negative values due to enhanced reversibility. Titanyl oxalate apparently shows a high affinity towards the postively charged CTA^+. Additionally it can be seen that the electrochemical response of titanium is overlapped by a broad wave caused by CTAB.

Other modifiers were investigated to determine their effect on the electrochemical behaviour of titanium. Anion exchangers, such as Amberlite LA2, Dowex 1 or Aliquat 336, yielded poor reproducibility and showed only low affinity towards titanyl oxalate.

Ion-pairing reagents other than CTAB, comprising lipophilic cations such as tetrabutylammonium bromide (TBAB), tetrabutylphosphonium bromide (TBPB), tetraphenylphosphonium chloride (TPPC), or tetraphenylammonium chloride (TPAC), were found to have an improving, albeit small, effect on the determination of titanium. This is due to the fact that the hydrophobic part of the counter ion is attracted by the lipophilic carbon paste, forming a monomolecular layer at the electrode surface, but interacts only slightly with titanyl oxalate. However, under open circuit conditions preconcentration of titanyl oxalate in the presence of the cationic surfactants is not effective.

The most sensitive and most reproducible results are obtained with an in-situ modification of the surface of the CPE with CTAB.

3.2. Preconcentration of titanium

Titanium as an oxalate complex can be preconcentrated onto the surface of CPEs in the presence of CTAB if a deposition potential more negative than -0.7 V is applied. If CTAB is used as a modifier in a separate solution under open circuit conditions titanium is also preconcentrable, but only to a much smaller extent requiring significantly higher Ti concentrations, probably due to washing out of accumulated species by medium exchange. Thus, application of a preconcentration potential for the determination of titanium at lower concentrations is essential.

The accumulation process can be explained analogously to reversed-phase ion-pair partitioning chromatography by two effects, i.e. in-situ

formation of an ion-exchanger at the electrode surface (A) and formation of ion pairs or micellar congregates in solution (B):

(A)

$$[CTA^-]_{x-mic,sol} \xrightarrow{-1.2\,V} [CTA^+]_{x-mic,surf} \qquad (3)$$

$$[CTA^-]_{x-mic,surf} + y[TiO(C_2O_4)_2]^{2-}{}_{sol}$$

$$\rightarrow \langle[CTA^-]_x\{[TiO(C_2O_4)_2]^{2-}\}_y\rangle_{surf} \qquad (4)$$

(B)

$$[CTA^+]_{x-mic,sol} + y[TiO(C_2O_4)_2]^{2-}{}_{sol}$$

$$\rightarrow \langle[CTA^+]_x\{[TiO(C_2O_4)_2]^{2-}\}_y\rangle_{sol} \qquad (5)$$

$$\langle[CTA^+]_x\{[TiO(C_2O_4)_2]^{2-}\}_y\rangle_{sol}$$

$$\xrightarrow{-1.2\,V} \langle[CTA^+]_x\{[TiO(C_2O_4)_2]^{2-}\}_y\rangle_{surf} \qquad (6)$$
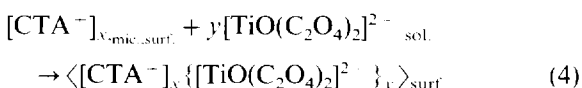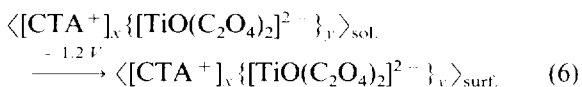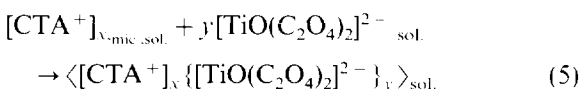
The subscripts "sol" and "surf" designate the bulk solution and the electrode surface respectively; "mic" indicates micelle.

When the concentration of CTAB in solution is above the CMC, mass transport and adsorption are probable via micelles rather that via individual surfactant ions [26]. At CTA$^-$ concentrations below the CMC only monomers are adsorbed on the electrode surface; therefore, the background current is low but the transport of the titanyl oxalate anions towards the electrode surface can be performed only with monomers, which is obviously not so effective.

The titanyl oxalate anion will be reduced simultaneously during the adsorption:

$$\langle[CTA^-]_x\{[TiO(C_2O_4)_2]^{2-}\}_y\rangle_{surf} + 2yH^+ + ye$$

$$\xrightarrow{-1.2\,V} \langle[CTA^+]_x\{[Ti(C_2O_4)_2]^-\}_y\rangle_{surf} + yH_2O \qquad (7)$$

3.3. Determination of titanium with CTAB and oxalate

When preconcentrating Ti in the presence of CTAB there is an overlap of the peak in the blank curve with the titanium signal. In principle DP voltammograms could be recorded in both directions yielding a response for titanium, but scanning in the anodic direction is more favorable. The analyte [TiO(Ox)$_2$]$^{2-}$ can be preconcentrated only at potentials significantly higher than -0.6
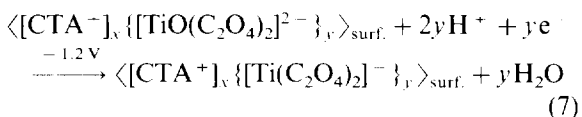
V, because the negative potential has a favorable effect on the adsorption of CTA$^+$ micelles. Simultaneously, reduction of [TiO(Ox)$_2$]$^{2-}$ occurs yielding [Ti(Ox)$_2$]$^-$, which is then immobilized by ion pairing. Therefore, the reoxidation signal recorded in the anodic scan is much more pronounced than the corresponding reduction peak. Another reason for exploiting the reoxidation signal is that its height can be evaluated much better, because of lower background currents and only a very small overlapping signal of the blank curve. Anodic DP voltammograms are shown in Fig. 2. As expected the peak currents increase with increasing negative deposition potentials. The titanium reoxidation current increases linearly from -0.7 V to -1.3 V. The more negative the applied deposition potential, the more effective is adsorption of the positively charged CTA$^+$ micelles, and thus the better is the transport of titanyl oxalate to the electrode surface. For practical reasons a deposition potential of -1.2 V was found to be optimal, although the reoxidation currents obtained with -1.3 V are even higher. However, the background also increases strongly, deteriorating the determination.

Optimization of the CTAB concentration in solution shows that only concentrations above the CMC are effective for preconcentrating titanium at low concentrations (Fig. 3). A maximum is obtained with a concentration of about 0.15 mM CTAB. When the CTAB concentration is increased further, the peak current decreases slowly, whereas the background current increases. Although peak currents have a maximum value at a concentration of 0.15 mM, best results in terms of reproducibility were obtained with only 0.1 mM CTAB.

Other parameters which greatly influence the analytical performance of the determination of titanium are the composition and the pH of the measurement solution. Many different supporting electrolytes, such as potassium bromide (0.1 M), potassium chloride (0.1 M) and hydrochloric acid (0.001 M), sulphuric acid (0.01 M), sodium oxalate (0.05 M), sodium salicylate (0.01 M), and acetate buffer (0.05 M) and oxalic acid (0.01 M), were examined to obtain optimal titanium reoxidation signals. Best performance was achieved

Table 1

Change in the peak current of the titanium reoxidation signal caused by anionic components. Solution for the measurement: 0.05 M acetate buffer, 0.01 M oxalic acid and 0.1 mM CTAB; titanium concentration: 100 μg l^{-1}; deposition time: 2 min; voltammetry: DPV; initial potential: -1.2 V; final potential: -0.0 V; scan rate: 10 mV s^{-1}

Interferent	Added as	Change of peak current ($\pm$ %) due to conc. of interferent (mg l^{-1})		
		0.5	5	50
AsO_2^-	$NaAsO_2$	± 0	± 0	-15
AsO_4^-	$NaHAsO_4$	± 0	± 0	-15
Br^-	KBr	± 0	± 0	Increasing background currents
Cl^-	NaCl	± 0	± 0	± 0
$Cr_2O_7^{2-}$	$K_2Cr_2O_7$	Decreasing	–	
F^-	NaF	-23	-58	-88
I^-	NaI	± 0	± 0	-32
MnO_4^-	$KMnO_4$	Decreasing		–
MoO_4^{2-}	$(NH_4)_6Mo_7O_{24}$	Overlapping	Overlapping	Overlapping
NO_3^-	$NaNO_3$	± 0	± 0	± 0
PO_4^{3-}	Na_3PO_4	± 0	± 0	± 0
SO_4^{2-}	Na_2SO_4	± 0	± 0	± 0
Salicylate $HOC_6H_4COO^-$	Na salicylate	± 0	-10 Decreasing	-65 Decreasing
VO_3^-	NH_4VO_3 in 0.3 M HNO_3	-30	-100	-100
WO_4^{2-}	Na_2WO_4	-21	-90	-100

with a solution containing acetate buffer (0.05 M) and oxalic acid (0.01 M) (pH 4.3).

When studying the influence of pH by addition of hydrochloric acid or sodium hydroxide to this solution the optimum was found at a value of 4.3. At pH 7 reoxidation could no longer be observed. This is also the case when decreasing the pH to 1.5. Also, the peak potential depends on the hydrogen ion concentration and decreases linearly with decreasing H$^+$ concentration with a slope of about 100 mV per pH unit. This suggests that two hydrogen ions are involved in the redox process according to Eq. (2).

The complete removal of accumulated titanium from the CTA$^+$-modified electrode surface requires further treatment of the electerode for repetitive use (regeneration). Various procedures including chemical and electrochemical treatment were investigated. The titanyl oxalate anions were not completely removed by exposing the electrode to a stirred aqueous solution of 1 M KBr; regeneration of the electrode surface via competitive ion exchange alone did not lead to complete regeneration of the surface. Therefore, it was nec-

essary to clean the electrode surface by electrochemical desorption of residual CTA$^+$-titanyl oxalate ion pairs. This was done in a stirred solution of 0.1 M sodium salicylate, as the latter is a very good counterion for CTAB [30]. The best method was found to be application of a potential of -1.2 V for 1 min and then scanning to -0.2 V. Ater this procedure the electrode was dipped into a stirred 1 M KBr solution for 1 min without the application of a potential.

The dependence of the reoxidation current on the deposition time gives a linear relation between current and time up to a period of 10 min. Longer times cause deviation from linearity due to the attainment of equilibrium conditions.

The dependence of the reoxidation current of titanium(IV) on the concentration, applying proper preconcentration times, is shown in Fig. 4. With a deposition time of 1 min a linear curve is obtained from 10–250 μg l^{-1} Ti(IV); with a 2 min deposition time linearity exists from 5–160 μg l^{-1}. When increasing the time of deposition up to 10 min, a linear range from 1–10 μg l^{-1} can be observed.

Table 2
Change in the peak current of the titanium reoxidation signal caused by cations; experimental parameters as in Table 1

Interferent	Added as	Change of peak current ($\pm$ %) due to conc. of interferent (mg l^{-1})		
		0.5	5	50
Ag^+	$AgNO_3$ in 0.5 M HNO$_3$	± 0	-25	-100
Al^{3+}	$AlCl_3$	-67	-100	-100
Cd^{2+}	$CdCl_2$	± 0	± 0	Overlapping
Co^{2+}	$CoCl_2$	± 0	-20	-100
Cr^{3+}	$CrCl_3$	± 0	-9	-31
Cu^{2+}	$CuCl_2$	-25	-42	-56
Fe^{3+}	$FeCl_3$ in 15% HCl	-14	-57	-97
Ga^{3+}	$Ga(NO_3)_3$	-38	-92	-100
Hg^{2+}	$Hg(NO_3)_2$ in dil. HNO$_3$	$+6$	-45	-54
In^{3+}	$In(NO_3)_3$	-22	-71	-100 Overlapping
Mn^{2+}	$MnCl_2$	± 0	± 0	-27
Ni^{2+}	$NiCl_2$	± 0	-37	-100
Pb^{2+}	$Pb(NO_3)_2$	Overlapping	Overlapping	Overlapping
Sb^{3+}	$SbCl_3$	± 0	± 0	-20
$Sb(V)$	$SbCl_5$ in 10 M HCl	± 0	-15	-100
$Sn(IV)$	$SnCl_4$ in HCl	-20	-63	Overlapping
Tl^{3+}	$TlCl_3$	± 0	-53	-100 Overlapping
UO_2^{2+}	$UO_2(acetate)_2$	-51	-86	-100 Overlapping
VO^{2+}	$VOSO_4$	-20	-90	-100
Zn^{2+}	$ZnSO_4$	± 0	-50	-100
ZrO^{2+}	$ZrOCl_2$	-30	-100	-100

The relative standard deviation is 4.0% for five repetitive measurements (50 μg l^{-1} Ti(IV), 2 min deposition time). The limit of detection (calculated as 3σ) of titanium is 0.46 μg l^{-1} with a deposition time of 2 min and 0.1 μg l^{-1} with 10 min.

3.4. Interferences

Interferences of many cations and anions with the reoxidation signal of titanium(III) were examined.

3.4.1. Anions

Common anions like nitrate, sulphate, phosphate, and chloride do not interfere even in a 500-fold mass excess with respect to titanium. The presence of a 500-fold excess of bromide results in slightly increasing background currents without changing the signal. The same excess of iodide leads to a diminution of the titanium signal by about 32%. This decrease is due to the fact that iodide is a very good counterion for CTAB micelles, because of its small hydrated ionic radius; competitive attraction between titanyl oxalate and iodide is the consequence. Fluoride already interferes at a five fold excess, owing to complexation of Ti(IV). Salicylate interferes by increasing the background current and decreasing the signal of titanium. This is obviously due to competitive concurrence for the ion exchanging groups. Vanadate and molybdate are complexed by oxalate forming ion pairs with CTAB; molybdate additionally yields an electrochemical response over-

lapping with the signal of titanium. Tungsten(VI) interferes severely, although no anionic complexes with oxalate are formed. Chromate and permanganate act as oxidizing agents for titanium(III), and therefore decrease its reoxidation currents.

3.4.2. Cations

Electroactive metal cations, which are reduced to the elemental state at a potential of -1.2 V, are accumulated onto the electrode surface. In the case where they do not form anionic oxalate complexes they interfere significantly at a 50-fold excess only, if the resulting electrochemical response overlaps with the reoxidation of Ti(III). At higher concentrations they show a decreasing effect on the titanium signal, if they are deposited on the electrode surface, because they reduce the available lipophilic surface area. Indium, thallium and copper form stable anionic oxalate complexes and give a reoxidation peak as well. Their preconcentration probably proceeds via direct electrolytic reduction as well as via the complex; they interfere at higher concentrations. Cobalt, nickel, zinc, aluminium, iron(III), uranium(VI), vanadium(IV), zirconium(IV), and gallium(III) are accumulated as anionic oxalate complexes, resulting in a decrease of the titanium reoxidation response. Chromium(III), manganese(II) and antimony(V) do not interfere severely up to a 50-fold excess because they do not form anionic oxalate complexes.

3.5. Sample

The proposed method was employed for the determination of titanium in a mineral sample (stone wool), where it is present as TiO_2. The sample, containing SiO_2, Al_2O_3, Fe_2O_3, CaO, MgO, Na_2O and TiO_2 and small amounts of other oxides, was digested with an equimolar mixture of sodium and potassium carbonate as described above. Control analyses were performed with inductively-coupled plasma mass spectrometry (ICP-MS). Table 3 shows the results. Although the electrochemical method shows higher relative standard deviations, the agreement between the different methods is satisfactory.

Table 3
Results of the determination of titanium in a mineral sample (stone wool)

Sample	Concentration of TiO_2 obtained by voltammetry (% ± standard deviation)	Concentration of TiO_2 obtained by ICP-MS (% ± standard deviation)
1	3.6 ± 0.2 (3)[a]	3.62 ± 0.03
2	3.7 ± 0.2 (3)[a]	3.72 ± 0.04
Mean value	3.6 ± 0.2	3.67 ± 0.04

[a]Number of replicate measurements.

References

[1] F. Vydra, K. Stulik and E. Julakova, Electrochemical Stripping Analysis, Wiley, New York, 1976.
[2] J.J. Lingane and J.H. Kennedy, Anal. Chim. Acta, 15 (1956) 295.
[3] R.L. Pecsok, J. Am. Chem. Soc., 73 (1950) 1304.
[4] R.L. Pecsok and E.F. Maverick, J. Am. Chem. Soc., 76 (1953) 358.
[5] J.B. Headridge and D.P. Hubbard, Anal. Chim. Acta, 36 (1966) 85.
[6] G. Mattock, J. Chem. Soc., 540 (1954) 989.
[7] G.M. Habashi, J. Electroanal. Chem., 8 (1964) 237.
[8] H. Li and C.M.G. Van den Berg, Anal. Chim. Acta, 221 (1989) 269.
[9] J. Musil, J. Dolezal and J. Vorlicek, J. Electroanal Chem., 24 (1970) 447.
[10] J. Wang and J.S. Mahmoud, J. Electroanal. Chem., 208 (1986) 383.
[11] A. Romanus, H. Mueller and D. Krisch, Fresenius, J. Anal. Chem., 340 (1991) 363.
[12] V. Gemmer-Colos and R. Neeb, Naturwissenschaften, 73 (1986) 498.
[13] D.V. Vukomanovic and G.W. VanLoon, Fresenius, J. Anal. Chem., 350 (1994) 352.
[14] J. Zhao, D. Sun, X. Wei and W. Jin, Anal. Chim. Acta, 306 (1995) 225.

[15] J. Zhou and R. Need, Fresenius, J. Anal. Chem., 338 (1990) 34.

[16] P.L. Buldini, D. Ferri and F. Zignani, Fresenius, J. Anal. Chem., 314 (1983) 660.

[17] D. Ferri and P.L Buldini, Analyst, 107 (1982) 1375.

[18] K. Yokoi and C.M.G. van den Berg, Anal. Chim. Acta, 245 (1991) 167.

[19] Y. Yamamoto, K. Hasebe and T. Kambara, Anal. Chem., 55 (1983) 1942.

[20] P.V.C. Rao and V.J. Koshy, Talanta, 41 (1994) 1911.

[21] Y. Castrillejo, R. Pardo, E. Barrado and P.S. Batanero, Electroanalysis, 1 (1989) 181.

[22] K. Kalcher, Electroanalysis, 2 (1990) 419.

[23] K. Kalcher, J.-M. Kauffmann, J. Wang, I. Svancara, K. Vytras, C. Neuhold and Z. Yang, Electroanalysis, 7 (1995) 5.

[24] C. Tanford, The Hydrophobic Effect: Formation of Micelles and Biological Membranes, Wiley, New York, 1980.

[25] C. Mousty and G. Mousset, New J. Chem., 16 (1992) 1063.

[26] S. Hu, Y. Yan and Z. Zhao, Anal. Chim. Acta, 248 (1991) 103.

[27] K. Kalcher, Fresenius, Z. Anal. Chem., 323 (1986) 238.

[28] K. Kalcher and C. Jorde, Comput. Chem., 10 (1986) 201.

[29] J. Stary, Anal. Chim. Acta, 28 (1963) 132.

[30] Z. Lin, J.J. Cai, L.E. Scriven and H.T. Davis, J. Phys. Chem., 98 (1994) 5984.

Supersonic Jet/Time-of-flight mass spectrometry of adenine using nanosecond and femtosecond lasers

Cheng-Huang Lin, Junichi Matsumoto, Satoshi Ohtake, Totaro Imasaka*

Department of Chemical Science and Technology, Faculty of Engineering, Kyushu University, Hakozaki, Fukuoka 812, Japan

Abstract

Mass spectra and ionization efficiencies of adenine were measured with nanosecond (15 ns) and femtosecond (500 fs) laser pulses at identical energy levels. A molecular ion is clearly observed in both spectra, but the efficiency is improved 10-fold when a femtosecond laser is used, indicating the distinct advantage of ultrashort laser pulses for multiphoton ionization of nucleobases in supersonic jet spectrometry.

Keywords: Adenine; Ionization efficiencies; Lasers; Mass spectra; Nucleobases

1. Introduction

A combination of laser-induced multiphoton ionization (MPI) and time-of-flight (TOF) mass spectrometry (MS) is an extremely useful technique in analytical spectroscopy [1,2]. The supersonic jet technique gives a narrow spectral feature in the ultraviolet and visible spectra and is, therefore, useful for the identification of molecules [3-5]. Such techniques have often been applied to polycyclic aromatic hydrocarbons (PAHs) [6,7] MPI/TOF-MS as well as fluorescence spectrome-

try have frequently been used for the detection of molecules. However, nucleobases have seldom been investigated with supersonic jet spectrometry. An examination of the literature reveals that only MPI/MS spectra of uracil, thymine [8], adenine, guanine [9], adenine–thymine and guanine–cytosine [10] have been reported. The reasons for this are obscure but are probably due to poor ionization efficiencies for nucleobases. Picosecond (and nanosecond) laser pulses have been used for efficient MPI in non-jet spectroscopy, e.g. for determination of PAHs with gas chromatographic detection [11]. Recently, femtosecond laser experiments have opened up a new field for examining rearrangements, fragmentations, and dissociations of small molecules when a su-

* Corresponding author. Fax: (+81)92-632-5209;
e-mail: imasatcm@mbox.nc.kyushu-u.ac.jp

(A) Nanosecond Laser System
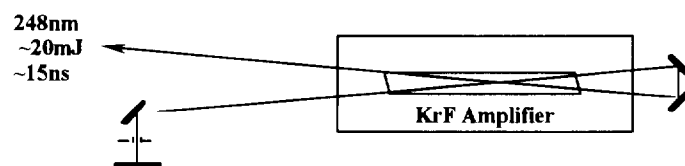
(B) Femtosecond Laser System
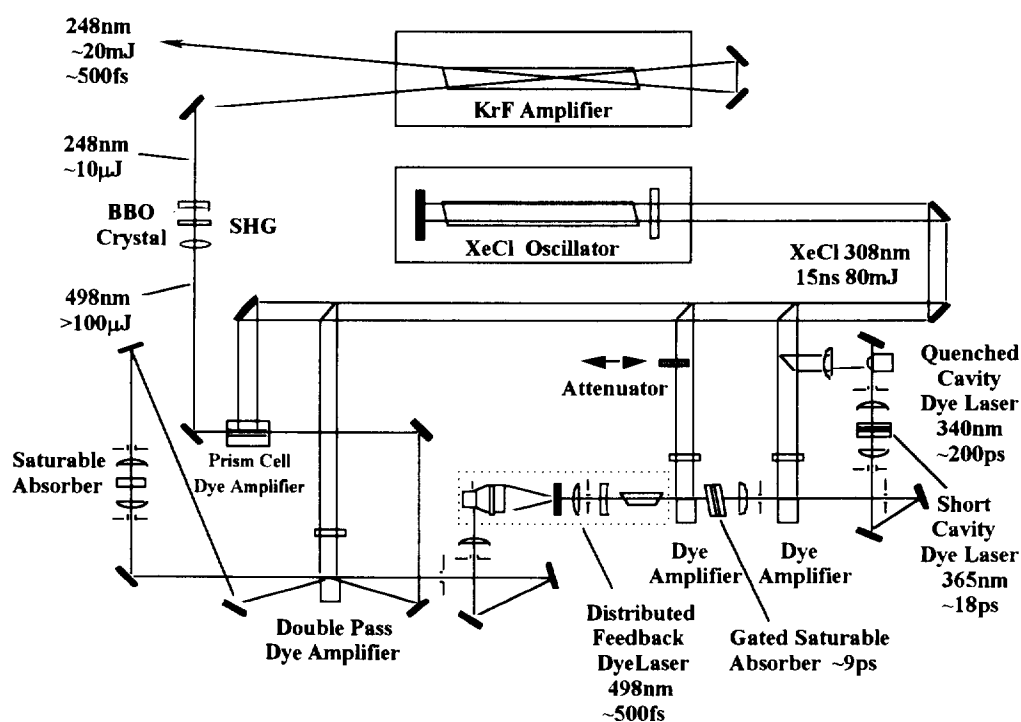
Fig. 1. Laser systems for generation of (A) 15 ns and (B) 500 fs pulses.

personic jet is used [12]. However, no quantitative evaluation of ultrashort laser pulses in analytical spectroscopy has been reported at the time of writing.

In this study, we report MPI/MS of the nucleobase adenine using an ultrashort pulse excimer laser. The mass spectra and ionization efficiencies obtained with nanosecond and femtosecond laser pulses are compared, in order to evaluate the advantages of femtosecond laser ionization in supersonic jet spectrometry.

2. Experimental

The experimental set-up comprises a nanosecond/femtosecond laser system and a supersonic jet/TOF mass spectrometer. The supersonic jet spectrometer used in this study has been reported in detail elsewhere [13,14]. The laser is commercially available from Lambda Physik and is only briefly described here. The laser system consists of a dye laser pumped by a XeCl excimer laser, and

a KrF excimer amplifier, as shown in Fig. 1. A quenched-cavity dye laser producing ≈ 200 ps pulses [15] is used as a pump source for a short-cavity dye laser to generate ≈ 9 ps pulses. After passing it through a gated-saturable absorber [16], the laser beam is then used to pump a distributed-feedback dye laser to generate ≈ 500 fs, 0.1 mJ pulses at 496 nm [17,18]. The laser beam is frequency-doubled to 248 nm by a β-BaB$_2$O$_4$ (BBO) crystal amplified to 20 mJ by a KrF amplifier. The peak laser power achieved is 40 GW. In contrast, the nanosecond laser pulse is generated by feedback of the amplified spontaneous emission (ASE) through the KrF discharge channel. It produces 15 ns, 10 mJ pulses at 248 nm. A mass spectrum was recorded using a digital oscilloscope (LeCroy 9360), and the signal was averaged 200 times. Adenine, which was used as a sample, was thermally vaporized by elevating the reservoir temperature to 300°C. The laser beam was focused into a supersonic jet using a quartz lens (1 m focal length) and the laser pulse energy was adjusted by passing it through a pinhole. Its value was monitored by a Joule Meter (Molectron, J3-05DW). Adenine was supplied by Kishida Chemicals (Osaka, Japan).

3. Results and discussion

The MPI/TOF mass spectrum was measured by changing the laser pulse energy from 0.02 to 1 mJ using the nanosecond/femtosecond laser. Fig. 2(A) shows the mass spectrum of adenine obtained using 15 ns (80 μJ) laser pulses. A signal peak at a flight time of 12.4 μs corresponds to a molecular ion of adenine (m/z 135), indicating a relatively soft ionization of the molecule. The mass spectrum for adenine has been reported by Li and Lubman [19], using a dye laser emitting at 222 nm, and showed a molecular ion and a fragment (m/z 108, M–HCN). The ionization potential of adenine is approximately 8.48 eV, and the laser wavelength used in this study (248 nm, 5.0 eV) is sufficiently short to allow two-photon ionization. When the laser pulse energy was increased to 1 mJ, the fragment signals (C1Hn, C2Hn. . . ; n = integer), which are negligibly small in Fig.

2(A), became stronger than the molecular ion signal. Fig. 2(B) shows the mass spectrum obtained using 500 fs (80 μJ) laser pulses. A strong mass peak corresponding to a molecular ion of adenine (flight time = 12.4 μs) is observed. The ionization efficiency is improved to 10-fold in comparison with the spectrum obtained using the nanosecond laser. This signal enhancement is slightly larger than the value obtained for thermally decomposed products of polystyrene (a six-fold increase), where softer ionization was also observed using femtosecond laser pulses [20]. The greater enhancement observed may be due to a faster relaxation rate, i.e. a shorter lifetime in the excited state for adenine in comparison with aromatic hydrocarbons, which result from the thermal decomposition products derived from polystyrene.

The ion signal in the mass spectrum increases with increase in the pulse energy in the experiments using both nanosecond and femtosecond lasers. However, the molecular ion is more efficiently dissociated to small fragments at higher pulse energies. Therefore, it is necessary to optimize the pulse energy to enhance ionization and to minimize photodissociation for sensitive detection of a molecular ion. The relationships between the ionization signals at m/z 135 and the laser
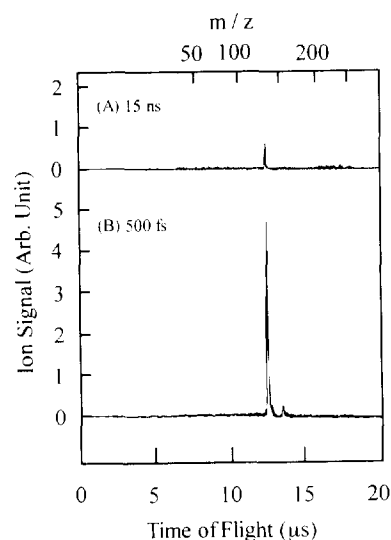

Fig. 2. Mass spectra for adenine, ionized at 248 nm and 80 μJ, using (A) 15 ns and (B) 500 fs laser pulses.
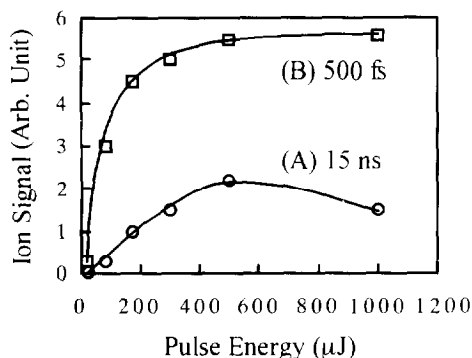
Fig. 3. Dependences of ion signal intensities at m/z 135 on laser pulse energy measured using (A) 15 ns and (B) 500 fs laser pulses. Many fragment peaks and signal peaks occurring from pump oil appear above 1.0 mJ, and so quantitative comparison is difficult above this pulse energy.

pulse energy are shown in Fig. 3. When a nanosecond laser is used, significant photodissociation occurs and the adenine signal decreases above 0.5 mJ. When a femtosecond laser is used, the ionization efficiency is always higher and increases to 1 mJ. This result implies that femtosecond MPI is desired for sensitive detection of a molecular ion.

In preliminary experiments, no signal could be observed for uracil. Two explanations are possible for low ionization efficiencies for nucleobases. First, the ionization potential of uracil might be sufficiently high that the molecule is not ionized using a conventional single-color UV laser. The order of ionization potentials for DNA and RNA bases is uracil (9.32–9.70 eV)>cytosine (8.87–9.43 eV)>thymine (8.68–8.94 eV)>adenine (8.26–8.91 eV)>guanine (7.77–8.30 eV) [21–24]. To overcome this problem, a far-UV laser and/or a two-color MPI scheme might be necessary [8]. The other possibility is that the fast relaxation of energy from the excited state, e.g. intramolecular radiationless transition or photodissociation, occurs before MPI. It is well known that the fluorescence quantum yields are much less for nucleobases, implying shorter lifetimes. Although the relaxation process is not fully understood for biological molecules such as nucleobases, the femtosecond laser may allow faster MPI than intramolecular energy relaxation because of the ultrashort pulse widths. The data presented herein

clearly show that the femtosecond laser is useful for inducing soft ionization of nucleobases and also for a significant improvement in ionization efficiency. The wavelength of the laser is, however, not adjusted to a specific transition, e.g. 0–0 transition. More efficient ionization could be accomplished using a tunable femtosecond laser.

Acknowledgments

References

[1] R. Tembreull and D.M. Lubman. Anal. Chem., 59 (1987) 1082.
[2] O.A. Mirgorodskaya, A.A. Shevchenko, I.V. Chernushevich, A.F. Dodonov and A.I. Miroshnikov, Anal. Chem., 66 (1994) 997.
[3] J.M. Hayes and G.J. Small, Anal. Chem., 5 (1983) 565A.
[4] D.H. Levy, Ann. Rev. Phys. Chem., 31 (1980) 187.
[5] R.E. Smalley, L. Wharton and D.H. Levy, Acc. Chem. Res., 10 (1977) 139.
[6] T. Imasaka, K. Tanaka and N. Ishibashi, Anal. Chem., 62 (1990) 374.
[7] T. Imasaka, M. Hozumi and N. Ishibashi, Anal. Chem., 64 (1992) 2206.
[8] B.B. Brady, L.A. Petcanu and D.H. Levy, Chem. Phys. Lett., 147 (1988) 538.
[9] R. Tembreull and D.M. Lubman, Anal. Chem., 59 (1987) 1082.
[10] A. Meffert, F. Moritz, M. Dey and J. Grotemeyer, Resonance Ionization Spectroscopy, (1994) 183.
[11] C.W. Wilkerson, Jr., S.M. Colby and J.P. Reilly, Anal. Chem., 61 (1989) 2669.
[12] M. Dantus, M.H.M. Janssen and A.H. Zewail, Chem. Phys. Lett., 181 (1991) 281.
[13] C.H. Lin, H. Fukii, T. Imasaka and N. Ishibashi, Anal. Chem., 63 (1991) 1433.
[14] C.H. Lin, M. Hozumi, T. Imasaka and N. Ishibashi, Analyst, 116 (1991) 1037.
[15] S. Szatmári and F.P. Schäfer, Appl. Phys. B, 33 (1984) 95.
[16] S. Saztmári, Opt. Quantum Electron., 21 (1989) 55.
[17] G. Almási and S. Saztmári, Opt. Commun., 88 (1992) 231.
[18] G. Szabó and Z. Bor, Appl. Phys. B, 47 (1988) 299.

[19] L. Li and D.M. Lubman, Int. J. Mass Spectrom. Ion Processes, 88 (1989) 197.

[20] J. Matsumoto, C.H. Lin and T. Imasaka, unpublished result, 1995.

[21] V.M. Orlov, A.N. Smirnov and Y.M. Varshavsky, Tetrahedron Lett., 48 (1976) 4377.

[22] N.S. Hush and A.S. Cheung, Chem. Lett., 34 (1975) 11.

[23] C. Lifshitz, E.D. Bergmann and B. Pullman, Tetrahedron Lett., 46 (1967) 4583.

[24] D. Dougherty and S.P. Mcglynn, J. Chem. Phys., 67 (1977) 1289.

Utility of quercetin for determination of some tertiary amine and quaternary ammonium salts

Fardous A. Mohamed, Abdel-Maaboud I. Mohamed, Horria A. Mohamed*, Samiha A. Hussein

Department of Pharmaceutical Analytical Chemistry, Faculty of Pharmacy, Assiut University, Assiut, Egypt

Abstract

A simple and sensitive spectrophotometric method for the assay of eight drugs containing quaternary ammonium or tertiary amine moieties is described. The method is based on the interaction of these drugs with quercetin after its oxidation with N-bromosuccinimide (as counter ion) to give highly colored ion-pairing complexes extractable with organic solvents. The absorbances of the colored complexes are measured in the range of 528–560 nm. Beer's law is obeyed for the studied drugs in the range 5–30 μg ml^{-1}. The method is successfully applied to the analysis of the studied drugs in commercial dosage forms.

Keywords: Ion pairing; Pharmaceuticals; Quercetin

1. Introduction

It is well known that a huge number of compounds belonging to different pharmaceutical classes contain either tertiary amine or quaternary ammonium moieties [1]. Accordingly, numerous spectrophotometric methods for their analysis have been reported [2–7]; few of them could be considered to be general for tertiary amines and many of these methods suffer from a lack of selectivity and simplicity.

Ion-pair formation methods provide a rapid and convenient technique for the measurement of tertiary amines and quaternary ammonium salts [8–11].

Quercetin is a naturally occurring flavonol which has been used before for the spectrophotometric and fluorimetric determination of metal ions [12].

In the present work, oxidized quercetin is used for extractive spectrophotometric determination of some tertiary amines and quaternary ammonium salts of different pharmacological classes, namely procaine · HCl and dibucaine · HCl (local anaesthetics), pheniramine maleate (antihistaminic), toclase citrate and oxeladine citrate (antitussives), butathamate citrate (sympathomimetic), oxyphenonium bromide (parasympatholytic) and cetylpyridinium chloride (antiseptic deter-

* Corresponding author.

Table 1
Absorption characteristics of studied drugs and summary of some statistical data

Drug	Conc. used for determinations (μg ml^{-1})	λ_{max} (nm)	ε_{max} (L mol^{-1} cm^{-1})	Linearity range (μg ml^{-1})	Limit of detection (μg ml^{-1})	Slope (SE)	Intercept (SE)	r^a
Butathamate citrate	200	530	6.10×10^3	5–50	3.7	0.0235 (0.0001)	−0.0045 (0.030)	0.9939
Dibucaine · HCl	150	528	1.54×10^4	2–30	1.0	0.0315 (0.0006)	0.0914 (0.011)	0.9994
Oxeladine citrate	200	530	6.74×10^3	5–50	2.8	0.0264 (0.0001)	−0.0631 (0.024)	0.9965
Pheniramine maleate	200	528	1.32×10^4	5–50	2.5	0.0191 (0.0007)	0.0802 (0.016)	0.9982
Procaine · HCl	200	535	8.70×10^3	5–50	1.6	0.0166 (0.0005)	0.0515 (0.009)	0.9979
Toclase citrate	150	529	1.72×10^4	2–30	1.2	0.0467 (0.0004)	0.0490 (0.019)	0.9914
Cetylpyridinium chloride	100	558	1.56×10^4	2–30	1.7	0.0384 (0.0003)	0.0525 (0.022)	0.9950
Oxyphenonium bromide	100	551	2.10×10^4	5–30	3.6	0.0273 (0.0001)	0.1079 (0.032)	0.9951

^{a} Correlation coefficient.

gent). The method is simple, sensitive and selective and can be applied to the analysis of pharmaceutical preparations. The proposed method has the additional advantage that primary and secondary amines do not interfere under the proposed reaction conditions.

2. Experimental

2.1. Instrument

A Uvidec-320 spectrophotometer (Jasco, Tokyo, Japan) was used.

2.2. Materials

The drugs listed in Table 1 are of pharmaceutical grade, obtained courtesy of the manufacturers, and were used as working standards without further treatment. The purities of the standards were checked according to some reported methods [1]. Pharmaceutical preparations were obtained locally. N-Bromosuccinimide (NBS) was obtained

from BDH (Poole, UK) and quercetin was from Merck (Darmstadt, Germany). All other chemicals and solvents used in this work were of analytical grade.

2.3. Reagents

2.3.1. NBS solution

NBS solution was 0.15% w/v in distilled water and was prepared fresh daily.

2.3.2. Quercetin solution

Quercetin solution was 0.2% w/v in ethanol.

2.3.3. Buffer solution

Teorell and Stenhagen buffer, pH 2.0–12.0, was used [13].

2.3.4. Standard drug solutions

Standard drug solutions were prepared by dissolving 50 mg of the studied drug (as a salt) in 100 ml of distilled water. Working standards covering the range 20–500 μg ml^{-1} were prepared by further dilution.

2.4. Preparation of samples

2.4.1. For tablets

Weigh and finely powder 20 tablets. Transfer an accurate weight of the powder equivalent to 50 mg of the drug into a 100 ml volumetric flask, shake thoroughly with about 75 ml of water for 10 min and then make up to volume with water. Filter and reject the first portion of filtrate. Dilute the prepared solution quantitatively with water to obtain the required concentration for analysis.

2.4.2. For injections

Mix well the contents of 10 ampoules. Dilute an accurately measured volume of the solution equivalent to 50 mg of drug quantitatively with water
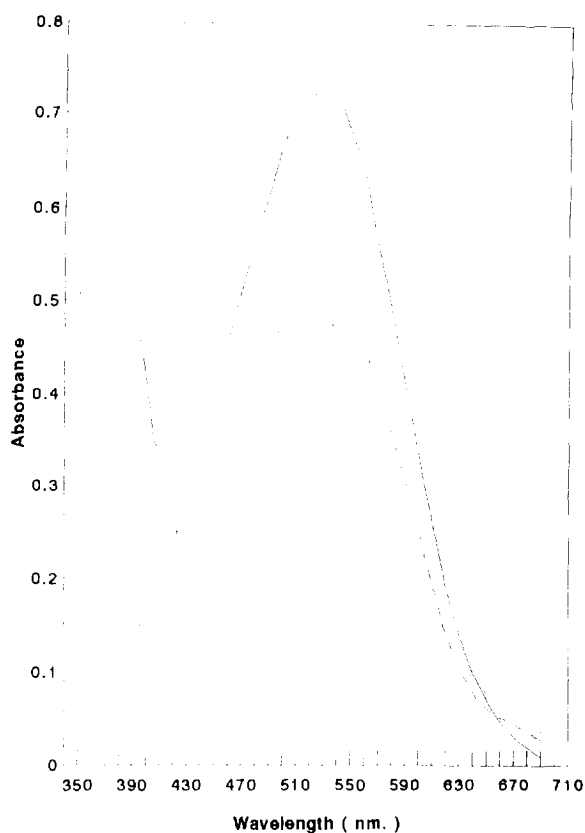
Table 2

Effect of pH variation on the absorption intensity of the ion-pair complex of dibucaine · HCl (12 μg ml^{-1}) with oxidized quercetin

pH	Absorbance[a] (at 528 nm)
2.0	0.068
2.5	0.091
3.0	0.121
3.5	0.187
4.0	0.278
4.5	0.466
5.0	0.468
5.5	0.467
6.0	0.407
6.5	0.370
7.0	0.146
8.0	0.022

[a] Average of four determinations.

to 100 ml. Dilute the resulting solution quantitatively with water to obtain the required concentration for analysis.

2.4.3. Recovery study

Transfer an accurately weighed amount of declared drug (25 mg) for each preparation to a 100 ml volumetric flask containing an accurately weighed quantity of the powdered tablets or an accurately measured volume of injection solution (equivalent to 25 mg of drug). Either dissolve the contents of the flask in water and treat as described in Section 2.4.1, or dilute quantitatively with water to obtain the required concentration as described in Section 2.4.2.

2.5. Determination

To 1 ml of either standard or sample drug solution in a 10 ml volumetric flask, add 1 ml of buffer solution pH 5.0 followed by 0.5 ml of quercetin solution and 1.0 ml of NBS solution. Mix well and extract with two 10 ml portions of dichloroethane. Combine the organic solvent extracts, filter over about 2 g of anhydrous sodium sulphate and reject the first 5 ml of filtrate. Measure the absorbance of the solution at the specified maximum (Table 1) against a blank treated similarly.

Fig. 1. Absorption spectra of ion-pair complexes from oxeladine citrate (—: 30 μg ml^{-1}), pheniramine maleate (...: 15 μg ml^{-1}) and oxyphenonium bromide (: 10 μg ml^{-1}) with quercetin NBS reagents.
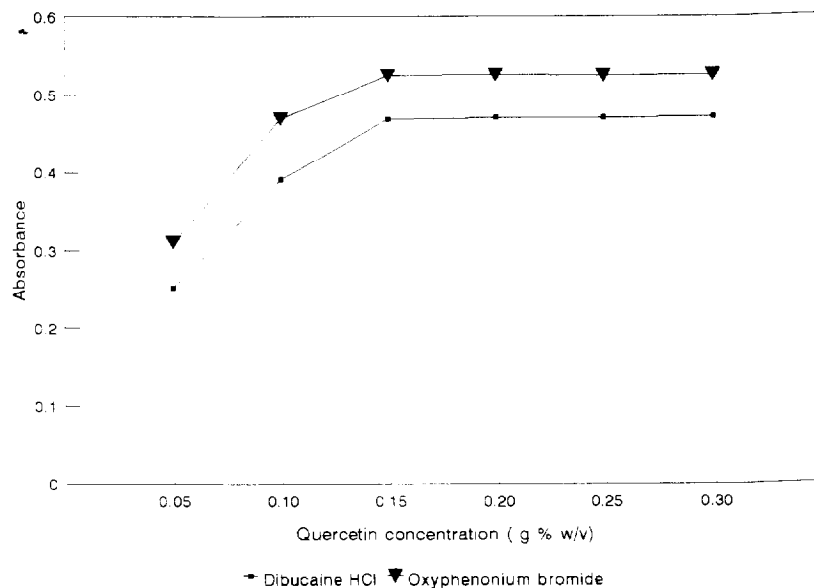
Fig. 2. Effect of quercetin concentration on the absorption intensity of the reaction products of (■) 12 μg dibucaine · HCl and (▼) 10 μg oxyphenonium bromide ml⁻¹.
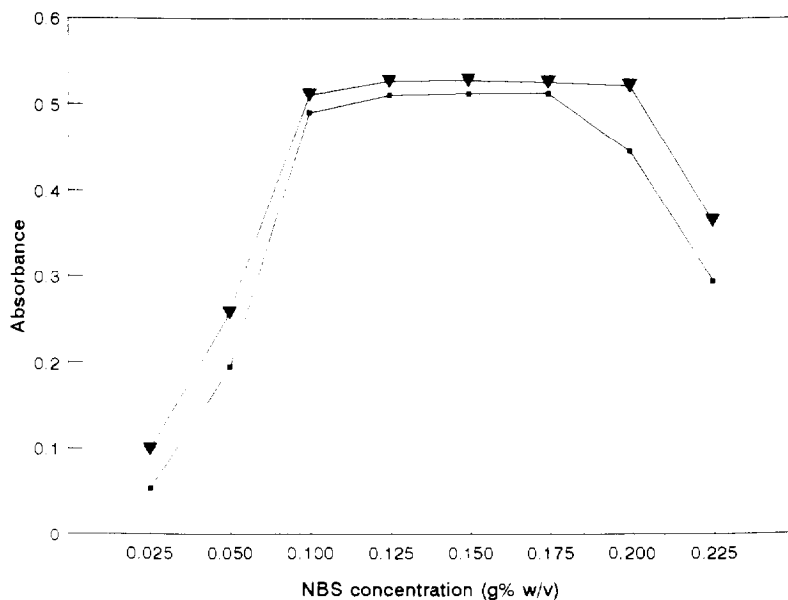

Fig. 3. Effect of NBS concentration on the absorption intensity of reaction products of (■) dibucaine · HCl (12 μg ml⁻¹) and (▼) oxyphenonium bromide (10 μg ml⁻¹).

3. Results and discussion

Preliminary investigations were carried out to test the reactivity of quercetin towards both tertiary amines and quaternary ammonium salts. Aqueous solutions of the tested compounds were

Table 3

Effect of solvents on the absorption intensity of reaction products of dibucaine · HCl (25 μg ml⁻¹)

Solvent	Wavelength (nm)	Absorbance[a]
Methylene chloride	325	0.617
	530	0.685
Dichloroethane	325	0.981
	528	0.874
Carbon tetrachloride	320	0.173
	518	0.066
Chloroform	325	0.674
	530	0.697
Benzene	328	0.632
	520	0.436

[a]Average of four determinations.

ity of the method, preoxidation of quercetin with NBS was carried out. Highly colored reddish-violet ion-pairing complexes absorbing in the wavelength range 528–558 nm were produced. These complexes were also extractable with chloroform and dichloroethane.

Fig. 1 shows the absorption spectra of oxeladine citrate, pheniramine maleate and oxyphenonium bromide association complexes with quercetin–NBS reagents as representative examples. The complexes have absorption maxima in the range 528–535 nm for the tertiary amines and 550–560 nm for the quaternary ammonium compounds. Spectral characteristics of the studied compounds are summarized in Table 1.
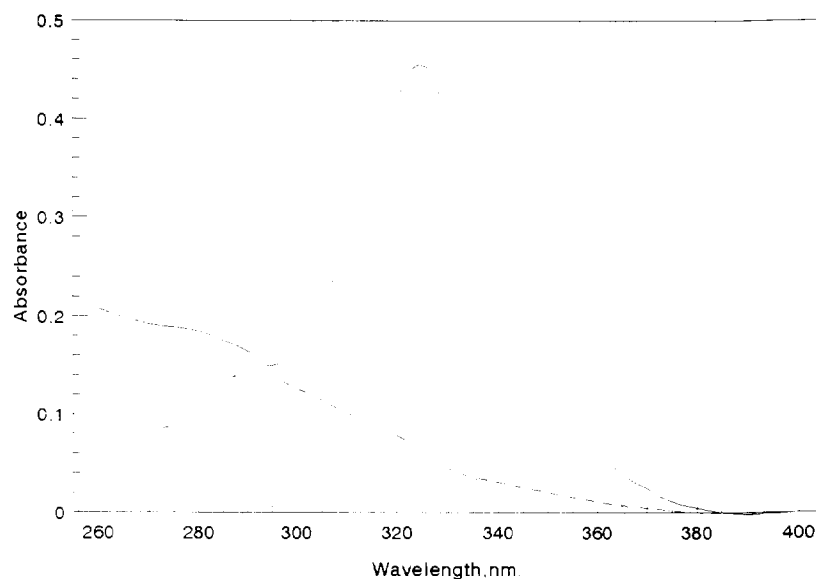
Fig. 4. Absorption spectra of aqueous solution of (—) dibucaine · HCl (20 μg ml⁻¹), (. . .) reaction mixture containing dibucaine · HCl (20 μg ml⁻¹) and (   ) blank after extraction with a 10 ml portion of dichloroethane (all measured against distilled water as a blank solution).

mixed with ethanolic quercetin solution. Intense yellow products were produced which were extractable with organic solvents such as chloroform and dichlorethane.

In order to increase the sensitivity and selectiv-

The reaction conditions, including pH, quercetin and NBS concentrations, extraction solvents, reaction and stability times and interferences, were investigated and optimized for all studied drugs.

3.1. Effect of pH

The effect of pH was studied by extracting the colored complexes formed with buffer of different pH values. Table 2 shows that a pH range of 4.5–5.5 is recommended. A buffer solution of pH 5.0 was selected for all subsequent work.

3.2. Effect of quercetin concentration

Several solutions of quercetin in the concentration range 0.05–0.25% w/v were prepared and tested with the studied drugs (0.5 ml portions were used). The obtained absorbances were

Wavelength, nm.
— Dibucaine HCl .... blank
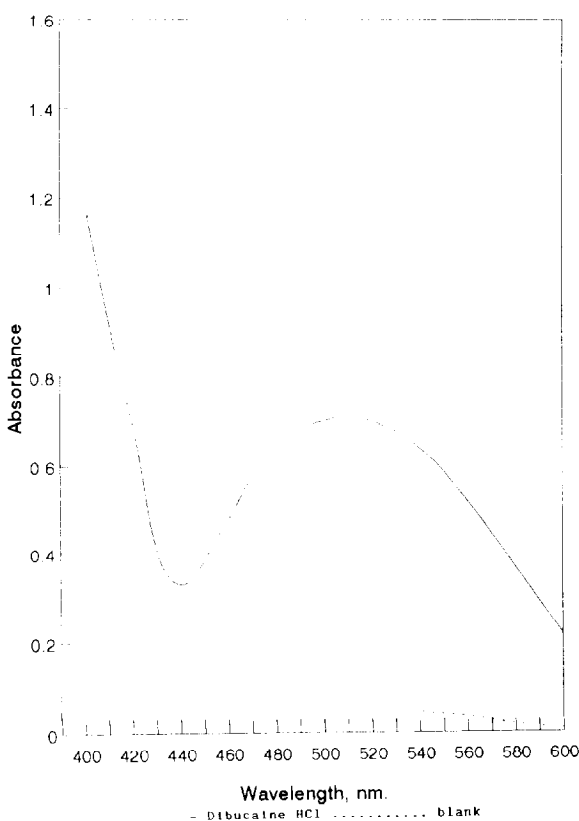
Fig. 5. Absorption spectra of (—) reaction mixture containing dibucaine · HCl (20 μg ml⁻¹) and (...) blank in dichloroethane after one extraction measured against pure dichloroethane.

plotted as a function of quercetin concentration. The highest color intensity was obtained using quercetin in concentrations ranging from 0.15 to 0.25% w/v (Fig. 2). Therefore 0.2% w/v quercetin solution was used for all subsequent work.

3.3. Effect of NBS concentration

In order to establish the optimal NBS concentration, aqueous solutions of NBS ranging from 0.025–0.2% w/v were added to quercetin solution and the reaction was carried out as usual. In each experiment 1 ml of NBS solution was used. Fig. 3 shows that 0.15% w/v NBS is the most suitable concentration for all the studied drugs. Concentrations greater than ≈ 0.175% w/v showed a marked decrease in absorption intensities, most probably due to the further oxidation of quercetin to other products [13].

3.4. Effect of solvents

Table 3 shows the effect of extraction with different organic solvents. The variations in the absorption intensity and wavelength of the ion-pairing complex from dibucaine · HCl were taken as being representative of the studied drugs. It is clear from the Table that the highest extraction efficiency is obtained using dichlorethane as extraction solvent. In addition, two extractions only (2 min shaking time) were found to be sufficient to achieve quantitative recovery of all the complexes in aqueous solution with good reproducibility and very small relative standard deviation (<2%). Figs. 4 and 5 show the absorption spectra of both experiment and blank (aqueous and organic phases) after one extraction for dibucaine · HCl, in addition to the spectrum of the pure drug.

Other solvents, such as methylene chloride and chloroform, can also be used. However, highly non-polar solvents such as carbon tetrachloride have very poor extractive efficiency for these dyes.

Table 4
Interferences from some common primary and secondary amines and related pharmaceutical compounds

Compound	Tested amount (μg ml⁻¹)[a]	Dibucaine · HCl (20 μg ml⁻¹) recovered[b]	
		μg	%
Methylamine · HCl	100	19.90	99.5
Ethanolamine · HCl	100	19.87	99.4
Morpholine	200	19.92	99.6
Piprazine citrate	100	20.20	101.0
Aniline · HCl	100	19.82	99.1
N-Methylaniline	100	20.10	100.5
Ethylenediamine · HCl	100	19.85	99.3
Aminophyline	100	19.84	99.2
Theophyline	100	19.88	99.4
Antazoline	50	19.96	99.8
Caffeine	100	19.85	99.3
Isoprenaline	50	19.88	99.4
Antipyrine	250	20.05	100.0
Adrenaline bitartrate	50	19.91	99.6

[a]Concentration in the final measured solution.
[b]Average of four determinations.

Table 5
Determination of some tertiary amine salts in commercial dosage forms using the proposed method and some reported methods[a]

Product	Ingredients	Nominal content (mg)	Found (%)	Added (mg)	Recovery (%)	Reported method (%)
Cosavil tablets	Pheniramine maleate Antipyrine salicylate Caffeine	11.25 250 15 per tablet	98.7 ± 0.8	15	99.2 ± 0.9	–
Avil tablets	Pheniramine maleate	75 per tablet	98.8 ± 0.8	75	99.6 ± 0.9	
Avil injections	Pheniramine maleate	45.5 per 2 ml	101 ± 1	50	100 ± 1	–
Procaine–adrenaline injections	Procaine · HCl Adrenaline bitartrate	40 per 2 ml 0.04 per 2 ml	99 ± 1 $t = 0.65$[b], $F = 1.62$	40	99.5 ± 0.9	99 ± 1[c]
Toclase tablets	Carbetapentane citrate	25 per tablet	99.5 ± 0.8 $t = 1.40$, $F = 2.64$	25	99 ± 1	99 ± 1[d]

[a]Average ± standard deviation of five determinations.
[b]Theoretical values of t and F at the 95% confidence limit are $t = 2.306$, $F = 6.39$.
[c]Ref. [15].
[d]Ref. [16].

3.5. Effect of time

The reaction between quercetin–NBS and tertiary amines or quaternary ammonium compounds is very rapid and the colored products can survive unchanged in aqueous solution before extraction for about 10 min without significant loss in intensity. However, at time > 10 min there may be a gradual decrease in the intensity of absorption in some cases.

Regarding the stability time of colored products after extraction with dichloroethane, it was noticed that absorbance was slightly increased in the first 5 min and then remained stable for at least 1 h.
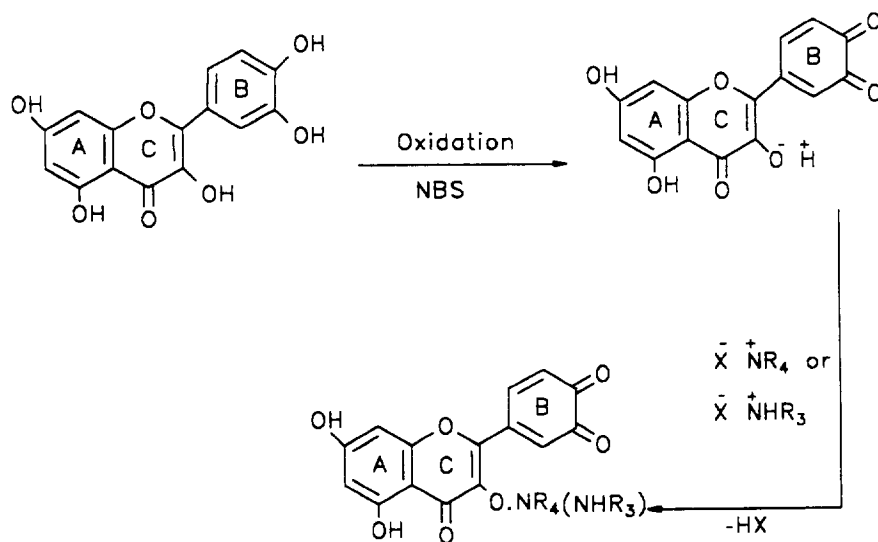
Scheme 1. Suggested mechanism for the formation of an ion-pair complex.

3.6. Interferences

Primary and secondary amines do not interfere with the determinations (Table 4), but other tertiary amines and quaternary ammonium salts will interfere and thus require prior separation from each other if present in mixtures.

The presence of traces of water in the organic solvent extracts may cause discrepancy in absorbance measurements and subsequent variation in results and so they must be removed by filtration over about 2 g of anhydrous sodium sulphate.

Regression analysis indicated excellent conformity with Beer's law over the concentration ranges listed in Table 1 for each drug. Separate determinations at different concentration levels for each drug gave coefficients of variation not exceeding 2%.

Some commercial dosage forms were successfully analyzed by the proposed method and reported methods. Recovery experiments were performed for each drug in its dosage form. The results are listed in Table 5 which indicated that common additives and excipients, in addition to other UV-absorbing constituents present in some dosage forms such as antipyrine salicylate and caffeine in cosavil tablets, did not interfere with the determinations. The results were compared with those obtained from other reported methods and were found to be in good agreement.

3.7. Reaction mechanism

Depending on the nature of quercetin and previous reports concerning its oxidation products [14] a suggestion for the reaction mechanism can be outlined (Scheme 1). Quercetin, being a flavonol, undergoes oxidation of the pyrocatechol moiety in ring B in the presence of mild oxidants to produce the highly colored o-quinone derivative. Ionization of the hydroxyl group of ring C most probably becomes easier leading to anion formation. The anion then interacts with protonated tertiary amine or quaternary ammonium moieties to form the colored ion-pair complexes.

4. Conclusion

The proposed method is simple, rapid, free from interferences, and selective for tertiary amine and quaternary ammonium salts, especially those of very low absorptivity in the UV range. The use of oxidized quercetin as analytical reagent provides a fairly higher extraction efficiency and sensitivity compared to other similar ion-pairing reagents. The method can be successfully used for

the routine analysis of tertiary amine and quaternary ammonium salts in pure forms and in different formulations.

References

[1] A.C. Moffat, J.V. Jackson, M.S. Moss and B. Widdop, Clark's Isolation and Identification of Drugs, 2nd edn., The Pharmaceutical Press, London, 1986.

[2] A.M. Taha, N.A.El-Rabbat and F. Abdel-Fattah, J. Pharm. Belg., 35 (1980) 437.

[3] M.A. Korany, A.M. Wahbi and I.I. Hewala, Arch. Pharm. Sci. Ed., 12 (1984) 26.

[4] S.A. Hussein, A.-M.I. Mohamed and H.Y. Hassan, Talanta, 36 (1989) 1147.

[5] A.I. Mohamed, H.Y. Hassan, H.A. Mohamed and S.A. Hussein, J. Pharm. Biomed. Anal., 9 (1990) 525.

[6] M.A. Korany, M.M. Bedair and A.El-Gindy, J. Pharm. Belg., 45 (1990) 252.

[7] Z.Y. Yao, Gongye Zazhi, 24 (1993) 223 (Anal. Abstr., 4G114 (1994)).

[8] S.K. Pant, B.K. Martin and C.L. Jain, Indian Drugs, 28 (1990) 105.

[9] B. Liebmann, D. Henk, H. Spahu Langguth and E. Mutschler, J. Chromatogr. Biomed. Appl., 110 (1991) 181.

[10] M. Forina, S. Lanteri, R. Boggia and E. Bertan, Quim. Anal., 12 (1993) 128.

[11] T. Perez-Ruiz, C. Martinez-Lozano, A. Sanz and C. Alonso, Talanta, 41 (1994) 1523.

[12] L. Pszonicki and W. Tkacs, Anal. Chim. Acta, 87 (1976) 177.

[13] M. Pesez and J. Bartos, Colorimetric and Fluorimetric Analysis of Organic Compounds and Drugs, M. Dekker, New York, 1974, pp. 623–632.

[14] J.B. Hanbone, T.J. Mabry and H. Mabry, The Flavonoids, Chapman and Hall, London, 1975, p. 311.

[15] A.I. Mohamed, H.Y. Hassan, H.A. Mohamed and S.A. Hussein, J. Pharm. Biomed. Anal., 9 (1991) 525.

[16] A.M. Taha, S.R. El-Shabouri and A.I. Rageh, Pharmazie, 37 (1982) 489.

Automatic determination of cobalt at the submicrogram per millilitre level using a flowthrough spectrophotometric sensor

E. Vereda Alonso, J.M. Cano Pavon, A. Rios, M. Valcarcel *

Department of Analytical Chemistry, Faculty of Sciences, University of Málaga, 29071 Málaga, Spain
Department of Analytical Chemistry, Faculty of Sciences, University of Córdoba, 14004 Córdoba, Spain

Abstract

A flowthrough spectrophotometric sensor for the determination of cobalt at the nanogram per millilitre level using pyridoxal 4-phenylthiosemicarbazone as reagent and integrated preconcentration and detection in the flow cell is proposed. The method is highly selective for cobalt(II); it features detection and determination limits of 0.02 and 0.06 μg ml^{-1} respectively, and a linear range of at least 0.04–18 μg ml^{-1}. The method is subject to very few interferences because the strongly acidic medium used prevents the formation of most complexes of the reagent with other metal ions. The method was applied to the determination of cobalt in pharmaceutical preparations.

Keywords: Cobalt; Flow injection; Flowthrough sensor; Pharmaceutical preparations; Spectrophotometry

1. Introduction

Several procedures for the flow-injection (FI) determination of cobalt, many of which use spectrophotometric or chemiluminescence detection, have been reported in the last few years. The spectrophotometric technique has been used in methods where cobalt acts as a catalyst for the oxidation of various coloured substances [1–5]. Differential kinetics have also been used for this purpose, particularly in the simultaneous determi-

nation of cobalt and nickel with salicylaldehyde thiosemicarbazone as reagent [6,7]. pH gradients have also been exploited for this purpose, in conjunction with 4-(2-pyridylazo) resorcinol [8]. However, the determination of cobalt usually involves gallic acid [9–11] or luminol [12,13], which are oxidized by hydrogen peroxide in the presence of the metal.

Both types of method are generally highly sensitive, with detection limits of a few nanograms or picograms per millilitre, which allows the determination of cobalt in biological samples and drinking waters. However, they are subject to a number of interferences which call for prior separations that normally make them time-consuming and unreliable.

---

* Corresponding author. Tel.: (+34)57-21-86-16; Fax: (+34)54-21-86-06.
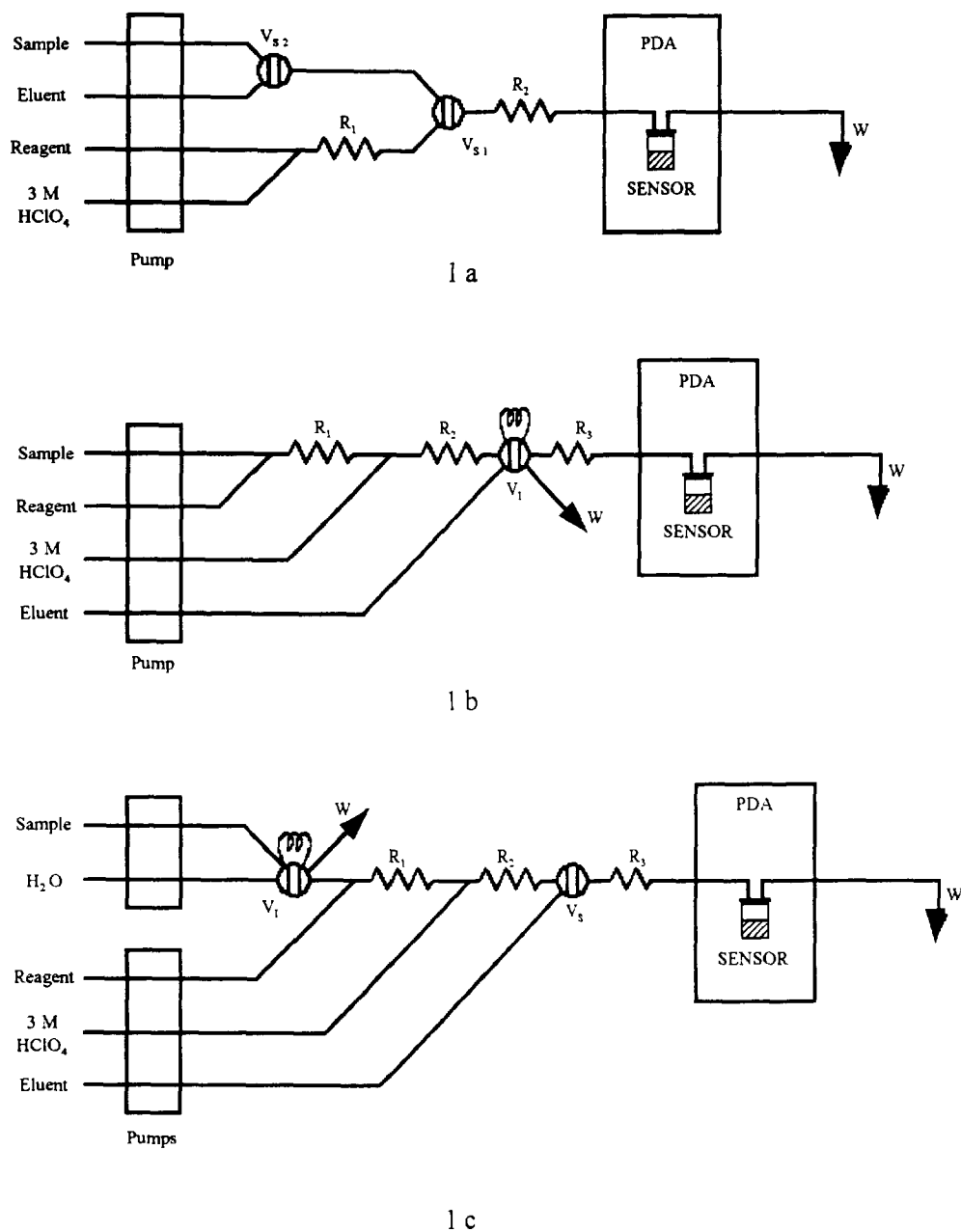
Fig. 1. Flow configurations tested for the determination of Co(II) with PPT: R_1, R_2, R_3, reactors; V_s, V_{s1}, V_{s2}, switching valves; V_1, injection valve; W, waste; PDA, photodiode-array detector.

Recently, a very selective method for the FI spectrophotometric determination of cobalt was developed. Based on the formation of a highly stable complex between cobalt and pyridoxal 4-phenyl-3-thiosemicarbazone (PPT) in a strongly acidic medium, the method is not very sensitive [14]. In this work, we improved its sensitivity and selectivity by using a flow manifold integrating preconcentration and detection in a sorbent material packed in a flow cell for the determination of

Table 1
Optimum values of FI variables

Sample flow rate (ml min⁻¹)	0.6
Reagent flow rate (ml min⁻¹)	0.4
3 M HClO₄ flow rate (ml min⁻¹)	0.6
Eluent flow rate (ml min⁻¹)	0.6
Length of reactor R_1 (cm)	116 (0.5 mm i.d.)
Length of reactor R_2 (cm)	150 (0.5 mm i.d.)
Length of reactor R_3 (cm)	35 (0.5 mm i.d.)
Injection loop volume (ml)	2.4 (in order to ensure approximately 30 s of constant absorbance before elution)

cobalt. This modified method provides better selectivity and sensitivity, with detection and determination limits of 0.02 and 0.06 μg ml⁻¹ respectively. The method relies on the recently developed flowthrough sensor technology [15,16] by which retention and detection are integrated in a FI system [17,18]. In this case, successive passage of the complex (previously formed in the flowing stream) and eluent through the flow cell and continuous photometric monitoring of the process provides the analytical information needed to determine the cobalt. The proposed method was used for the automatic on-line determination of this ion in vitamins contained in pharmaceutical preparations (it is present in the essential vitamin B_{12}) [19]. This vitamin takes part in a wide variety of metabolic processes involving factors that affect growth, homopoiesis and preservation of the intergrity of nerve cells.

2. Experimental

2.1. Reagents

All chemicals were of at least analytical-reagent grade, and bidistilled, deionized water was used throughout.

A stock solution of Co(II) was prepared from the nitrate (Merck P.A.) and standardized complexometrically. Standards of working strength were made by appropriate dilution as required.

A 0.05% solution of PPT was prepared by dissolving 0.05 g of the reagent in 30 ml of N,N-dimethylformamide (DMF) and diluting to 100 ml with water. The reagent was synthesized according to a procedure described elsewhere [20].

A 30% solution of perchloric acid in DMF–water (3/10, v/v) was used as eluent.

A 3 M perchloric acid solution was also used.

C_{18} in a Sep-Pak cartridge (Waters, Millipore Division), which demonstrated its resistance to the eluent, was used for retention–detection of cobalt in the flow cell.

2.2. Apparatus

A Hewlett-Packard 8452A diode-array detector interfaced to a Vectra ES/12 computer which delivered results through an HP Think-Jet printer was used. The flow manifold consisted of a Gilson Minipuls-3 peristaltic pump, a Rheodyne Type 50 six-port rotary valve and a Hellma OS 0.200 flow cell.

2.3. Manifold and procedure

Three different configurations were tested (Fig. 1). In the first configuration, the reagent was merged with 3 M HClO₄ to prevent the formation of complexes of other cations along reactor R_1; in this way, the reagent was retained first on the sorbent material (preconcentration step). When a preset volume of reagent had passed through the flow cell, V_{s1} was switched in order to introduce the sample. In this way, the reaction took place in the flow cell (reaction step) and the detector continuously monitored the absorbance increase (detection step). After the reaction was complete, V_{s2} was switched, thereby allowing the reaction product to be eluted from the sorbent material, which was thus made ready for a new sample.

In the second configuration, the sample was merged with the reagent along reactor R_1 and the

complex formed was merged with 3 M $HClO_4$ along reactor R_2, where a strongly acidic medium destroyed the complexes of other metal ions. The cobalt complex was retained on the sorbent material packed in the flow cell (preconcentration step) and the detector continuously monitored the signal increase up to a constant value. As the injection valve V_1 was switched to the "inject" position, the eluent passed through the flow cell to remove the retained complex and make the sorbent material ready for a new sample.

The third configuration was similar to the previous one but the sample was used to fill the injection loop instead of being continuously circulated as the carrier, thus reducing sample consumption.

3. Results and discussion

Cobalt forms a yellow 1:2 complex with PPT ($\lambda = 430$ nm, $\varepsilon = 1.35 \times 10^4$ 1 mol^{-1} cm^{-1}). The complex is stable in perchloric acid up to a concentration of 1.2 mol l$^-$ (12%) [14], conditions under which most of the complexes of PPT with other cations are not formed. This reaction can be carried out with the reagent or complex retained on a sorbent material. Thus in preliminary assays several sorbent materials were tested in order to find the most appropriate for this purpose. In an acid medium, the cobalt complex is in cationic form, so cationic exchange resins (Dowex, Amberlita, SP-Sephadex) were assayed; however, neither the reagent nor the complex was retained. Other sorbent materials, such as aluminium oxide, silicagel and C_{18}, were tested, but only the latter effectively retained both the reagent and the complex. The maximum absorption wavelength of the cobalt–PPT complex retained on C_{18} was 276 nm.

Of the buffered eluents tested, 30% perchloric acid in DMF–water proved to be the most efficient for removing the complex from the C_{18} without damaging it.

The next task was to select the most advantageous manifold among those shown in Fig. 1. The manifold depicted in Fig. 1a provided a poor response because the reagent was packed onto C_{18} phase before the passing of the sample, causing

the saturation of the C_{18} phase, so that subsequent passage of the sample through the sensor did not give a sensitive enough signal. The manifolds of Figs. 1b and 1c provided appropriate responses so that complex formed was passing directly through the sensor and the difference between blank and complex signals was better than the response provided by manifold 1a. Comparing manifolds 1b and 1c, the former was approximately 10 times more sensitive than the latter and so configuration 1b was finally selected.

3.1. Optimization of variables

The optimum reagent concentration was found to be 0.05% in DMF–water (3/10, v/v). The amount of DMF used was the minimum ensuring complete dissolution of the reagent, and DMF was also used in the eluent which also served as the carrier, in order to maximize peak height and ensure complete elution of the complex.

Based on the influence of the concentration of perchloric acid on the complex formation, 3 mol l^{-1} was found to be the optimum concentration as it produced the lowest standard deviation even though the peak height was somewhat greater with 1.5 mol l^{-1} perchloric acid. Obviously, once the different streams have merged, the acid concentration in the reaction plug will have been decreased by dilution.

The influence of the FI variables (stream flow rates, reactor lengths and injection volume) was studied and the optimum values found are summarized in Table 1.

Scans were performed in the kinetic mode at 276 nm for 150 s, in cycles of 2 s with an
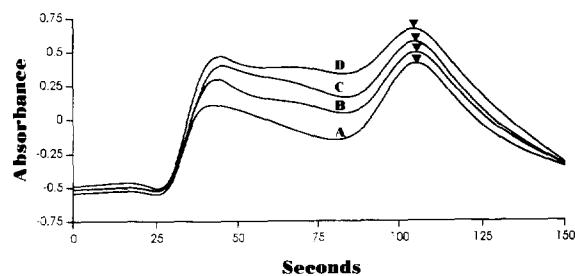

Fig. 2. FI peaks yielded by (A) blank, (B) 200, (C) 500 and (D) 800 ng ml^{-1}.

Table 2
Analytical figures of merit for the determination of cobalt by the proposed method

Linear range (μg ml^{-1})	Calibration equation[a]	Regression coefficient	RSD (%) ($n = 10$) (concentration, μg ml^{-1})
0.04–1	$y = 1.25 \times 10^{-4}x + 0.554$	0.994	± 3.2 (0.2)
1–18	$y = 2.80 \times 10^{-5}x + 0.663$	0.994	± 3.6 (2.0)

[a] y, Absorbance; x, cobalt concentration (μg ml^{-1}).

Table 3
Determination of cobalt in several synthetic samples using the proposed method

Sample No.	Concentration added (μg ml^{-1})	Concentration found $\pm$ standard deviation (μg ml^{-1}) ($n = 3$)
1	0.080	0.079 $\pm$ 0.001
2	0.20	0.19 $\pm$ 0.02
3	0.50	0.56 $\pm$ 0.05
4	1.00	0.96 $\pm$ 0.02
5	2.0	2.2 $\pm$ 0.1
6	5.0	5.1 $\pm$ 0.5

integrating time of 1.5 s. The maximum signal measured corresponded to the time at which the analyte started to be eluted. Fig. 2 shows typical recordings obtained and the point for analytical measurements (marked with arrowheads). Under these final experimental conditions, a sampling rate of 15 samples h^{-1} was reached.

3.2. Calibration curve and precision

In order to establish the optimal range for the determination of cobalt by the proposed method, several standard solutions of cobalt(II) were ina-jected into the flow system under the optimum experimental conditions. From the data obtained, two linear calibration curves were obtained from 0.04–1 μg ml^{-1} and from 1–18 μg ml^{-1} cobalt (Table 2).

The detection and determination limits, defined as the concentrations of analyte giving signals equivalent to three and ten times respectively the standard deviation of the blank plus the net blank intensity, were calculated to be 0.02 and 0.06 μg ml^{-1} respectively.

Various synthetic samples were readily resolved using pertinent calibration graphs (Table 3).

3.3. Interferences

The effect of various ions on the determination of cobalt by the proposed method was examined under the optimum working conditions. For this purpose, variable amounts of the ionic species tested were added to a 0.2 μg ml^{-1} solution of Co(II) up to a maximum interferent:cobalt ratio of 225:1 M/M; if any compound was found to interfere, the ratio was gradually lowered until the interference disappeared. The tolerated limits, defined as the interferent concentration (μg ml^{-1}) resulting in a deviation of less than $\pm 5\%$ in the analytical response, are shown in Table 4.

3.4. Application of the proposed method: determination of cobalt in pharmaceutical preparations

In a reaction flask 0.5–2 ml of vitamin ampoules and 3–6 ml of concentrated nitric acid were placed, and the mixture was refluxed until a colorless or pale yellow solution was obtained. Then, 0.5–1 ml of hydrogen peroxide was added and the mixture evaporated to a small volume by heating on a hot-plate to remove nitric acid. Next, the mixture was adjusted to pH 2 with NaOH solution and diluted to an appropriate volume (100 ml). Aliquots (10–20 ml) of this solution were determined using the recommended procedure. The standard-addition method was used and the results were obtained by extrapolation. Such results are given in Table 5 as the averages of three separate determinations. As can be seen, the cobalt concentrations determined by the proposed method are quite consistent with the specified values.

Table 4

Influence of foreign species on the determination of cobalt(II) by the proposed method

Foreign species	Tolerated ratio (M M)[a]
Pb(II), Ba(II), Ca(II), Be(II), Li(I), Sr(II), Na(I), K(I), Zr(IV), U(VI), W(VI), Ag(I), Fe(II), thiosulphate, sulphate, bromide, thiocyanate, oxalate, iodide, chloride, tartrate	>225
Bi(III), Tl(I), tetraborate	150
Ni(II), Cd(II), Zn(II), Mn(II), Hg(I), Cr(III), Sb(III), phosphate, nitrite, arsenate, citrate	100
V(V), Mo(VI), arsenite	50
Hg(II), Al(III), Cu(II), Fe(III)	25

[a] Maximum concentration tolerated for the interferent with respect to the analyte (μg ml^{-1} in each case).

Table 5

Determination of cobalt in vitamin B$_{12}$

Sample	Co content stated (μg ml^{-1})	Co added (μg ml^{-1})	Co found (μg ml^{-1})
Nervobion "5000"[a]	0.22		0.23 ± 0.03
		0.3	0.53
		0.6	0.86
B$_{12}$ Latino depot[b]	0.22		0.19 ± 0.01
		0.3	0.5
		0.6	0.78
Neuromade[c]	0.22		0.217 ± 0.006
		0.3	0.513
		0.6	0.826
Optovite[d]	0.35		0.35 ± 0.03
		0.3	0.7
		0.6	0.92
Neurodavur plus[e]	0.34		0.34 ± 0.02
		0.3	0.62
		0.6	0.93

[a–e] Composition of the pharmaceutical preparations:

[a] Nervobion "5000" (Merck). Vitamin B$_{12}$ (cyanocabalamin), equivalent to 0.2174 mg of cobalt, cocarboxylase (100 mg), pyridoxal-5-phosphate (100 mg), excipient (lidocaine) up to 2 ml.

[b] B$_{12}$ Latino depot (Syntex Latino, S.A.). Vitamin B$_{12}$ (cyanocobalamin), equivalent to 0.04348 mg of cobalt, excipient up to 1 ml.

[c] Neuromade fuerte (Knoll). Vitamin B$_{12}$ (cyanocobalamin), equivalent to 0.2174 mg of cobalt, pyridoxine CLH (100 mg), thiamine CLH (100 mg), lidocaine (6 mg), excipient up to 3 ml.

[d] Optovite B$_{12}$ (Normon, S.A.). Vitamin B$_{12}$ (cyanocobalamin), equivalent to 0.04348 mg of cobalt, excipient up to 2 ml.

[e] Neurodavur plus (Belmac, S.A.). Vitamin B$_{12}$ (hydroxycobalamin), equivalent to 0.2098 mg of cobalt, thiamine · HCl (50 mg), pyridoxine · HCl (50 mg), dexamethasone phosphate sodium (1.6 mg), lidocaine · HCl (12.5 mg), excipient up to 2.5 ml.

4. Conclusions

Automatic methods based on flowthrough sensors offer interesting assets such as simplicity, rapidity, low cost and flexibility. The proposed method exhibits selectivity (iron being the main interference, at a 25-fold level with respect to cobalt) and high sensitivity, with a detection limit of 0.02 μg ml^{-1}. It is more selective and simple than other continuous FI spectrophotometric

methods, because it requires neither separation nor masking of foreign species. The proposed method was successfully applied to the determination of cobalt in vitamins.

Acknowledgement

References

[1] T. Yamane, Nippon Kagaku Kaishi, 1 (1982) 93.
[2] T. Yamane, Anal. Chim. Acta. 130 (1981) 65
[3] T. Yamane, Mikrochim. Acta, Part I, (1984) 425.
[4] C. Maekoya, F. Mizuniwa, K. Usami and K. Osumi, Nippon Kagaku Kaishi, 7 (1983) 1023.
[5] T. Deguchi, A. Higashi and I. Sonemasa, Bull. Chem. Soc. Jpn., 59 (1986) 295.
[6] A. Fernández, M.D. Luque de Castro and M. Valcárcel, Anal. Chem., 56 (1984) 1146.
[7] A. Fernández, M.D. Luque de Castro and M. Valcárcel, Quim. Anal., 6 (187) 464.
[8] D. Betteridge and B. Fields, Anal. Chim. Acta, 132 (1981) 139.
[9] S. Nakahara, M. Yamada and S. Suzuki, Anal. Chim. Acta, 141 (1982) 255.
[10] M. Tamada, T. Komatsu, S. Nakahara and S. Suzuki, Anal. Chim. Acta, 155 (1983) 259.
[11] L.M. Sakamoto-Arnold and K.S. Johnson, Anal. Chem., 59 (1987) 1789.
[12] T. Komatsu, M. Ohira, M. Yamada and S. Suzuki, Bull. Chem. Soc. Jpn., 59 (1986) 1849.
[13] J.L. Burguera, A. Townshend and S. Greenfield, Anal. Chim. Acta, 114 (1980) 209.
[14] E. Cristofol de Alcaraz, F. Sánchez Rojas and J.M. Cano Pavón, Fresenius' J. Anal. Chem., 340 (1991) 175.
[15] M. Valcárcel and M.D. Luque de Castro, Analyst, 118 (1993) 593.
[16] M.D. Luque de Castro and M. Valcárcel, Trends Anal. Chem., 10 (1991) 114.
[17] F. Lázaro, M.D. Luque de Castro and M. Valcárcel, Anal. Chim. Acta, 214 (1988) 217.
[18] F. Lázaro, M.D. Luque de Castro and M. Valcárcel, Anal. Chim. Acta, 219 (1989) 231.
[19] E.J. Underwood, Trace Elements in Human and Animal Nutrition, 4th edn., Academic Press, New York, 1977.
[20] E. Cristofol de Alcaraz, F. Sánchez Rojas and J.M. Cano Pavón, Talanta, 38 (1991) 445.

Novel rapid decomposition and dissolution method for silicates using a mixed potassium metaborate/potassium carbonate flux

Nobutaka Yoshikuni*

Laboratory of Materials Science, Faculty of Engineering, Chiba University, Yayoi-cho, Inage-ku, Chiba 263, Japan

Received 16 January 1996; revised 15 April 1996; accepted 29 April 1996

Abstract

A novel method for the rapid dissolution of fused silicates in mineral acid is described. Fusion with 2.5 g of a $KBO_2-K_2CO_3$ (3:2, w/w) mixture in a platinum crucible at 1000°C will decompose 0.1 g of silicate samples such as basalt rock, glass sand and powdered glass in 10 min, and the cooled fusion cakes can be completely dissolved by 20 ml of 3 N mineral acids such as hydrochloric, nitric and sulfuric acids in less than 1 min at about 50°C. Fusion with 5.0 g of a $KBO_2-K_2CO_3$ (3:2, w/w) mixture can completely decompose 0.1 g of chrome refractory in 20 min and the cooled melt can be dissolved by 80 ml of 3 N hydrochloric or sulfuric acids in less than 30 s.

Keywords: Decomposition; Dissolution; Potassium carbonate; Potassium metaborate; Silicates

1. Introduction

The rapid preparation of silicate samples is very important for automatic and routine analysis of a large number of samples. Therefore, the rapidity of wet analyses of silicate samples such as rocks, sediments, soils, glasses, minerals, ores, refractories and silicon semiconductor materials can be enhanced by the use of fast and efficient methods of decomposition and/or dissolution. Two approaches are taken to this problem [1-3]: (i) fusion with one of, or various combinations of, boric acid, alkali metal carbonate, alkali metal borate, sodium hydroxide, sodium peroxide and

potassium superoxide; or (ii) wet decomposition with mixtures of hydrofluoric acid and various mineral acids. Powerful techniques for fusion decomposition of silicate samples have been established using boric acid-lithium carbonate [4-6], alkali metal metaborate [7], alkali metal tetraborate [8], alkali metal tetraborate-alkali metal carbonate [9,10] or other borate binary mixed flux systems. However, the use of these borate fusion fluxes is restricted within narrow limits because the dissolution time of the cooled fusion cakes is most frequently long, i.e. a few minutes to a few tens of minutes, at room temperature. Long-term storage and treatment of sodium peroxide [26] or potassium superoxide [27] is not easy. Wet methods use many acid binary mixed systems such as

* Corresponding author. Fax: + 81 472 51 7337.

hydrofluoric–hydrochloric [11], nitric [12], perchloric [13,14], sulfuric acids [15] or hydrofluoric–aqua regia [16–19] and others [20–22], but the acid systems often require a long time for complete decomposition of silicate samples. The decomposition times of the acid systems varied from a few tens of minutes in some instances to as much as a few hours. Moreover, high presences are required for dissolving refractory minerals such as zircon. Yoshikuni [23] reported a fusion method for decomposition and faster dissolution of silicate samples such as bauxite, ilmenite, magnetite, quartz and zircon sand.

From a literature survey, it is clear that no attempts have been made to use the potassium metaborate–potassium carbonate binary mixed system in the decomposition of silicate samples. This paper presents the easy decomposition of silicate samples using a potassium metaborate–potassium carbonate (3:2, w/w) mixed flux and the rapid dissolution, in less than 1 min, of the cooled fusion cake with a mineral acid such as hydrochloric, nitric or sulfuric acid at about 50°C. 2.5 g of a mixed flux of potassium metaborate–potassium carbonate (3:2, w/w) can fuse 100 g of silicate samples such as basalt rock, glass sand or powdered glass in a platinum crucible at about 1000°C in only 10 min.

2. Experimental

2.1. Apparatus

A Hitachi U-3210 spectrophotometer was used.

2.2. Reagents and samples

All reagents used were of analytical grade and distilled deionized water was used throughout. Potassium carbonate anhydrous, iron(III) sulfate *n*-hydrate and hydrogen peroxide (30%) were from Wako Pure Chemical Co. (Tokyo, Japan). Lithium metaborate anhydrous and 1,5-diphenylcarbazide were from Merck. Potassium metaborate anhydrous and sodium metaborate tetrahydrate were of the highest purity available from Kanto Chemical Co. Inc. Sodium metabo-

rate anhydrous was prepared by heating the tetrahydrate for 1 h in a platinum dish on a hot-plate. EDTA-2Na and Arsenazo III were from Dojindo Laboratories (Kumamoto, Japan).

2.3. Solutions

Fe(III) solution was prepared by dissolving iron(III) sulfate *n*-hydrate in 1 N sulfuric acid to form a solution with a concentration of 10 mg ml^{-1} Fe with respect to EDTA.

Chromium (Cr = 1.007 mg ml^{-1}) and zirconium (Zr = 0.995 mg ml^{-1}) standard solutions for atomic absorption spectrometry were from Merck.

2.4. Decomposition and dissolution of silicate samples

An accurately weighed (100 mg) silicate sample such as basalt rock, glass sand or powdered glass is placed in a platinum crucible and mixed with a binary flux of KBO_2–K_2CO_3 (1.5 g/1.0 g). The mixture is fused by heating strongly for 10 min in a muffle furnace at about 1000°C with a Bunsen burner to yield a clear melt. After a few minutes, the melt is rapidly (about 1 min) dissolved in 20 ml of 3 M hydrochloric or 3 N sulfuric acid at about 50°C with magnetic stirring. The sample solution is diluted to 50 ml with 3 N sulfuric acid or 3 M hydrochloric acid in a standard flask and chromium and zirconium in the total volume of, or an aliquot of, the sample solution are determined by a spectrophotometric method using 1,5-diphenylcarbazide or Arsenazo III.

2.5. Decomposition and dissolution of chrome refractory

The sample (100 mg, accurately weighed) of chrome refractory is placed in a platinum crucible and mixed with a binary flux of KBO_2–K_2CO_3 (3 g/2 g). The mixture is fused by heating strongly for about 20 min in a muffle furnace with the burner to yield a clear melt. After cooling the melt, the platinum crucible is inserted into a 100 ml tall beaker and about 80 ml of 3 N sulfuric acid is added to the beaker. The cooled fusion

cake can be rapidly dissolved with magnetic stirring at about 50°C. The sample soution is diluted to 100 ml with 3 N sulfuric acid in a standard flask. After further dilution, chromium in the aliquot is determined by spectrophotometry.

2.6. Determination of chromium [24]

Add about 3 ml of iron solution (Fe = 10 mg ml^{-1}) and 1.0 ml of 30% hydrogen peroxide to a sample solution containing 3–10 μg of chromium in a 100 ml beaker. The pH of the solution is then adjusted from 13.0 to 13.5 with 8 M sodium hydroxide solution and the beaker, after covering with a watch glass, is heated to boiling for 10 min on a hot-plate. The solution is filtered with a No. 5A filter paper and the pH of the filtrate solution is adjusted to 1.0 with sulfuric acid (1:1). Add 2 ml of 1,5-diphenylcarbazide (1% in acetone–water, 1:1) to the solution and dilute to 50 ml with 0.05 N sulfuric acid in a standard flask. After 5 min, measure the absorbance at 540 nm versus a blank.

2.7. Determination of zirconium [25]

Transfer an aliquot (5.0 ml) of the sample solution to a 25 ml standard flask and add 1 ml of 1% Arsenazo III aqueous solution to the flask. Dilute to the mark and adjust to 9 M hydrochloric acid using concentrated hydrochloric acid and water. Measure the absorbance at 665 nm versus a blank.

3. Results and discussion

A binary flux (2.5 g) of potassium metaborate–potassium carbonate (3:2, w/w) mixture can fuse 0.1 g of basalt rock, glass sand or powdered glass samples by heating strongly for 10 min in a muffle furnace at about 1000°C in a platinum crucible. After cooling to room temperature, the melt is rapidly dissolved in 20 ml of 3 M hydrochloric acid as well as nitric and sulfuric acids within a few tens of seconds (Table 1) because the glassy fusion cakes are full of cracks after cooling the material to a solid state, in contrast to the fusion

flux of lithium metaborate–lithium carbonate mixture. In addition, this dissolution mechanism is an exothermic reaction. Silicate samples with a large Cr_2O_3 content such as chrome refractory (100 mg) cannot be completely decomposed with 2.5 g of KBO_2–K_2CO_3 (3:2, w/w) in binary mixed fusion for 30 min. 100 mg of the chrome refractory can be completely decomposed with 5.0 g of KBO_2–K_2CO_3 (3:2, w/w) in fusion for 20 min, and the cooled fusion cake can be dissolved in less than 60 s with 80 ml of 3 N sufluric or 3 M hydrochloric acid (Table 2). The decomposition of silicate samples with a fusion flux such as Li_2CO_3, Na_2CO_3, K_2CO_3, $CaCO_3$, $Li_2B_4O_7$, $Li_2B_4O_7$–$LiBO_2$, Li_2CO_3–$Li_2B_4O_7$, Na_2CO_3–$Na_2B_4O_7$ or K_2CO_3–$K_2B_4O_7$ systems is an excellent method but chrome refractory cannot be completely decomposed. Using a binary flux of KBO_2–K_2CO_3 mixture, the dissolution of the mixture at a 3:2 ratio is faster than at a 2:1 ratio with 3 M hydrochloric acid. Therefore, the composition of the KBO_2–K_2CO_3 fusion system is very important for rapid dissolution with mineral acid at room temperature. With a 3:2(w/w)MBO_2–M_2CO_3 mixture, the speed of dissolution of the cooled cakes with mineral acid increases as follows:

$$KBO_2 - K_2CO_3 > NaBO_2 - Na_2CO_3$$

$$\gg LiBO_2 - Li_2CO_3$$
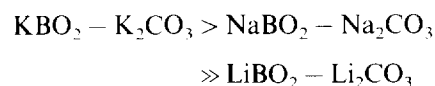
$NaBO_2 \cdot H_2O$ cannot be used because the monohydrate flux bubbles on heating.

100 mg of glass sand can be easily decomposed with a fusion of KBO_2–K_2CO_3 3:2 w/w (2.5 g), and the cooled fusion cake can be rapidly dissolved with 3 M hydrochloric acid. Before the determination of zirconium, the sample solution was diluted several times and therefore the borate matrix did not interfere. The recovery of zirconium is quantitative (Table 2). After decomposition and dissolution of silicate samples such as basalt rock, chrome refractory, glass sand or powdered glass, 1 ml of 30% hydrogen peroxide is added to an aliquot of the sample solution which is adjusted to pH 13.0–13.5 with sodium hydroxide solution. At pH 13.0–13.5 in the sample solution, silica and borate are precipitated as a

Table 1
Dissolution times and temperatures of various samples for fusion with 2.5 g of KBO_2 · K_2CO_3 3:2 w/w mixture[a]

Sample	Dissolution media (20 ml)	Dissolution time (min s)	Temperature (°C) Before dissolution	After dissolution
No sample	3 N H_2SO_4	0.32	21	39
(flux only)	3 M HCl	0.48	19	38
	3 M HNO_3	1.08	21	38
Quartz	3 N H_2SO_4	1.28	19	–
(100 mg powder)	3 N H_2SO_4	0.29	44	58
	3 M HCl	1.43	18	–
	3 M HCl	0.34	50	59
	3 M HNO_3	2.15	21	
	3 M HNO_3	0.27	51	65
Basalt rock	3 N H_2SO_4	1.57	21	
(100 mg)	3 N H_2SO_4	0.54	49	60
	3 N H_2SO_4	0.37	50	63
	3 M HCl	1.55	18	
	3 M HCl	0.44	50	59
Chrome	3 N H_2SO_4	1.30	21	–
refractory	3 N H_2SO_4	0.35	52	64
(50 mg)	3 M HCl	1.35	19	–
	3 M HCl	0.45	51	65
Glass sand	3 N H_2SO_4	1.27	21	
(100 mg powder)	3 N H_2SO_4	0.20	48	65
	3 M HCl	1.38	19	–
	3 M HCl	0.35	48	64
Special glass	3 N H_2SO_4	1.32	21	
(100 mg powder)	3 N H_2SO_4	0.22	52	65
	3 M HCl	1.38	18	
	3 M HCl	0.48	41	53

[a] Decomposition time: 10 min for all samples. [b] Samples: Basalt rock SRM 688, chrome refractory SRM 103a and glass sand SRM 81a were from NIST (Gaithersburg, MD). Quartz and special glass were from Asahi Glass Co (Tokyo, Japan).

transparent gel containing adsorbed chromium ion, and hence chromium cannot be measured in the filtrate. With the addition of 30 mg of iron(III) ion to an aliquot of the sample solution, the adsorption sites of the transparent gel can be completely saturated and the chromium can be quantitatively recovered in the filtrate. Chromium in an aliquot of the sample solution can be easily oxidized in alkaline solution (pH 13), and excess hydrogen peroxide can be completely decomposed with a catalyst of iron(III) ion on a hot-plate. At such elevated flux/sample ratios, problems from blanks might arise, but the interference of borate matrix in the determination of chromium was not examined. Before the determination of chromium, a large portion of the borate matrix was removed with the previously mentioned method of precipitation–filtration and then the borate matrix did not interfere. The values for chromium in samples of basalt rock, chrome refractory and glass sand determined with this procedure were in good agreement with the certified values (Table 2).

Table 2
Determination of chromium and zirconium in standard silicate samples[a]

Samples (Certified values)	Found		Found		Decomposition time (min)	Dissolution time (s) (dissolution media)
	Cr (μg g^{-1})	Recovery (%)	Zr (μg g^{-1})	Recovery (%)		
NIST SRM 688 Basalt rock (Cr = 332 μg g^{-1})	329	99.1 ($n = 6$) (RSD = 2.40%)	–		10	40 ± 10 (3N H$_2$SO$_4$, 20 ml)
NIST SRM 103a Chrome refractory (Cr = 2.19×10^5 μg g^{-1})	2.21×10^5	100.9 ($n = 7$) (RSD = 2.14%)	–		20	30 ± 5 (3N H$_2$SO$_4$, 80 ml)
NIST SRM 81a Glass sand (Cr = 31.5 μg g^{-1}, Zr = 250 ± 60 μg g^{-1})	30.6	97.1 ($n = 6$) (RSD = 8.28%)	257	102.8 ($n = 6$) (RSD = 9.28%)	10	40 ± 10 (3N H$_2$SO$_4$, 20 ml)[b] 35 ± 10 (3M HCl, 20 ml)[c]

[a] Samples taken = (100 + 15) mg. RSD: relative standard deviation. Fusion flux: KBO$_2$–K$_2$CO$_3$ (1.5 g 1.0 g) for basalt rock and glass sand: KBO$_2$–K$_2$CO$_3$ (3.0 g 2.0 g) for chrome refractory. Recovery: (determined value certified value) × 100.
[b] For the determination of chromium.
[c] For the determination of zirconium.

3.1. Application

Chromium in a powdered sample of a special glass plate from the Asahi Glass Company was spectrophotometrically determined with 1,5-diphenylcarbazide after decomposition and dissolution according to the above-mentioned procedures. The determined values of chromium in the glass plate samples were satisfactory with respect to the recommended values (Table 3).

4. Conclusions

The author has demonstrated a rapid dissolution method for the cooled cake of fused silicate samples such as basalt rock, glass sand, powdered glass and chrome refractory using potassium metaborate–potassium carbonate (KBO$_2$–K$_2$CO$_3$ = 3:2, w/w) binary mixed fusion flux and mineral acid dissolution systems at room temperature. The cooled cake can be instantaneously dis-

Table 3
Determination of chromium in a special glass from Asahi Glass Co. (Tokyo, Japan)[a]

Samples taken (mg)	Found		Decomposition time (min)	Dissolution time (s) (media)
	Cr (μg g^{-1})	Recovery (%)		
113.14	190	93.6	10	35 (3 N H$_2$SO$_4$ 20 ml)
95.53	221	108.8	10	40 (3 N H$_2$SO$_4$ 20 ml)
101.53	209	102.9	10	35 (3 N H$_2$SO$_4$ 20 ml)
101.65	189	93.1	10	50 (3 N H$_2$SO$_4$ 20 ml)
104.25	204	100.5	10	40 (3 N H$_2$SO$_4$ 20 ml)
116.31	205	101.0	15	30 (6 N H$_2$SO$_4$ 20 ml)

Average 203 (RSD = 5.93%)

[a] RSD: relative standard deviation. Fusion flux: KBO$_2$–K$_2$CO$_3$ (1.5 g 1.0 g). Recovery = [determined value recommended value] × 100.

solved with mineral acids such as 3–6 M hy-
drochloric acid and others because the dissolution
is exothermic.

Acknowledgement

The author thanks Asahi Glass Company
(Tokyo, Japan) for providing the special glass
plate samples.

References

[1] B. Bock. A Handbook of Decomposition Methods in Analytical Chemistry. International Textbook Company, Glasgow, UK, 1979.

[2] G.E.F. Hillebrand, G.E.F. Lundell, H.A. Bright and J.I. Hoffman, Applied Inorganic Analysis, 2nd edn., Wiley, New York.

[3] Z. Sulcek and P. Povondra, Methods of Decomposition in Inorganic Analysis, CRC Press, Boca Raton, FL, 1989.

[4] R.E. Santelli and R. De Csia dos Santos Araujo, Analyst, 117 (1992) 1519–1521.

[5] R. Kuroda, K. Oguma, K. Kitada and S. Kozuka, Talanta, 38 (1991) 1119–1123.

[6] R. Kuroda, K. Kitada, K. Oguma and T. Katayama, Fresenius' J. Anal. Chem., 338 (1990) 919–920.

[7] G.E.M. Hall and J.A. Plant, Chem. Geol., 95 (1992) 141–156.

[8] E. Bauer-Wolf, W. Wegscheider, S. Posch, G. Knapp, H. Kolmer and F. Panholzer, Talanta, 40 (1993) 9–15.

[9] M. Asif, S.J. Parry and H. Malik, Analyst, 117 (1992) 1351–1353.

[10] R. Boisvert, M. Bergeron and J. Turcotte, Anal. Chim. Acta, 246 (1991) 365–373.

[11] Z. Yu, H. Wang, C. Li and X. Wei, Yankuang Ceshi, 10 (1991) 9–12.

[12] E. Waidmann, M. Stoeppler and P. Heininger, Analyst, 117 (1992) 295–298.

[13] A.R. Fernando and J.A. Plambeck, Analyst, 117 (1992) 39–42.

[14] M.S. Rathi, P.P. Khanna and P.K. Mukherjee, Talanta, 38 (1991) 329–332.

[15] L. Fu, Y. Ren and L. Jianyan, Huaxue Fence, 28 (1992) 325–327.

[16] C. Garcia-Olalla and A.J. Aller, Anal. Chim. Acta, 252 (1991) 97–105.

[17] Z. Lukaszewski and W. Zembrzuski, Talanta, 39 (1992) 221–227.

[18] C.R.M. Rao, G.S. Reddi and T.A.S. Rao, Anal. Chim. Acta, 268 (1992) 357–359.

[19] M.A. Eid, J.A.C. Broekaert and P. Tschoepel, Fresenius' J. Anal. Chem., 342 (1992) 107–112.

[20] Z.H. Fan, L.X. Zhang and H.D. Zhou, Anal. Chim. Acta, 270 (1992) 267–269.

[21] P. Chattopadhyay, T.K. Sinha and T.S.B. Baul, Anal. Sci., 7 (1991) 931–933.

[22] J. Szpunar-Lobinska, Anal. Chim. Acta, 251 (1991) 275–280.

[23] N. Yoshikuni, Talanta, 36 (1989) 709–710.

[24] S. Hirano, Handbook of Applied Colorimetric Methods of Inorganic Analysis, Vol. 2, Kyoritsu, Tokyo, Japan, 1979.

[25] S. Hirano, Handbook of Applied Colorimetric Methods of Inorganic Analysis, Vol. 5, Kyoritsu, Tokyo, Japan, 1979.

[26] D.P.S. Rathore and P.K. Tarafder, Anal. Chim. Acta, 257 (1992) 129–133.

[27] A. Westland and C.J. Kantlpuly, Anal. Chim. Acta, 154 (1983) 355–358.

Adsorption behaviour of metal ions on hydroximate resins

Mamta Ahuja[a,*], A.K. Rai[a], P.N. Mathur[b]

[a]*Department of Chemistry, University of Rajasthan, Jaipur 302 004, India*
[b]*Department of Chemistry, J.N.V. University, Jodhpur 342 001, India*

Received 5 September 1995; revised 22 April 1996; accepted 29 April 1996

Abstract

Some new chelating ion-exchange resins containing a hydroxamic acid moiety attached to a divinylbenzene styrene (DVBS) copolymer. i.e. glycine hydroximate in DVBS (GH-DVBS), anthranilic acid hydroximate in DVBS (AAH-DVBS), malonic acid dihydroximate in DVBS (MAH-DVBS) and iminodiacetic acid dihydroximate in DVBS (IDAAH-DVBS). have been synthesized and their various physicochemical characteristics studied. The degree of retention of metal ions by the resins at equilibrium has been determined in terms of the molar distribution coefficient (K_d). In general. the resins having a dihydroximate moiety are found to be more efficient compared to monohydroximate resins. However, it is of interest to note that the monohydroximate derivative of amino acid (GH-DVBS) showed better metal retention capability than the dihydroximate of carboxylic acid (MAH-DVBS). The selectivity of the resins for transition and highly charged metal ions is quite high compared to that for alkaline earth metals. All the synthesized resins can be utilized for the separation of a mixture of metal ions because the differences in the distribution coefficient values are large enough to permit good separations on columns. However, the GH-DVBS resin was tried for the separation of copper cobalt and copper nickel mixtures at pH 5.5 using the column mode of operation.

Keywords: Adsorption; Hydroximate resins; Metal ions

1. Introduction

Chelating ion-exchange resins having specific chelating groups attached to a polymer have found extensive use in the separation and concentration of metal ions [1–4], as floataids, depressants, flocculants and collectors, and in the extraction and concentration of metals from sea water [5,6]. An important feature of the chelating ion exchangers is the greater selectivity which they offer compared to conventional types of ion exchangers.

Chelex-100 is the most widely-used functionalized polymer for the preconcentration and separation of rare earth and heavy metals [7]. However, one of the disadvantages of this resin is that its affinity for alkaline earth metals is almost the same as that for zinc or other transition metal ions [8]. Therefore, there is a need to develop those functionalized polymers which show better affinity for transition metal ions as compared to alkali and alkaline earth metals.

---

* Corresponding author.

With the aim of synthesizing selective ion-exchange resins which require no preconcentration of the samples, do not form stable complexes with alkaline earth metals and are useful in mineral processing industries, we have synthesized chelating resins containing hydroximates of carboxylic and amino carboxylic acids.

The choice of hydroxamic acids is based on their extensive use as collectors for various minerals containing Sn, Fe, W, Cu, La, Ce, Nb, and Y metal ions [9]. Hydroxamic acids have found a variety of commercial applications in mineral processing in the former Soviet Union [10] under the trade name IM-50. Various studies have been made with hydroximate collectors in the floatation of haematite [11], pyrolusite [12], cassiterite [13], chrysocolla and rare earth bastnaesite ores [14]. However, little work is reported on chelating resins incorporating hydroxamic acid as a functional group. Cellulose hydroximate was prepared by Maekawa et al. [15] and was selective for copper, iron, cobalt and nickel. Malonic acid dihydroximate in divinylbenzene styrene (DVBS) was reported [16] for the recovery of U(VI) from sea water. However, no reports are available for the separation of other metal ions on this resin.

2. Experimental

Chelex-100 was procured from John Baker Inc. (Colorado, USA). Chloromethylated DVBS with 4% cross linking was procured from Thermax Pvt. Ltd. Other chemicals used were of analytical grade.

2.1. Synthesis of resins

2.1.1. Synthesis of glycine hydroximate in DVBS

Glycine hydroximate was synthesized in two steps as shown in Scheme 1.

#### 2.1.1.1. Incorporation of glycine ester in DVBS.
The chloromethylated DVB styrene beads (0.028 mol) were soaked in DMF overnight to allow swelling to occur. Glycine methyl ester (0.14 mol) was taken in DMF, heated for 10 min and then transferred to the flask containing swollen DVBS

beads. The reaction mixture was refluxed for 6 h. The product thus formed was filtered, washed with 80% aqueous methanol containing a few drops of nitric acid and dried in vacuum.

2.1.1.2. Preparation of glycine hydroximate in DVBS.
A methanolic solution of hydroxylamine hydrochloride (0.14 mol) was added to the previously filtered beads of glycine ester in DVBS. The reaction mixture was refluxed for 4 h. It was then cooled and freshly prepared sodium ethylate solution was added to it to adjust the pH to 9.2–9.3. The reaction mixture was refluxed again for 5 h. The product formed was filtered and treated successively with 0.1 N HCl, 0.1 N NaOH and 0.1 N HCl. Finally, it was washed with absolute alcohol and dried in vacuum.

2.1.2. Synthesis of anthranilic acid hydroximate and malonic acid dihydroximate in DVBS

Anthranilic acid hydroximate in DVBS was synthesised following a similar procedure to that employed for the synthesis of glycine hydroximate in DVBS by taking methyl anthranilate in place of glycine methylester (Scheme 2).
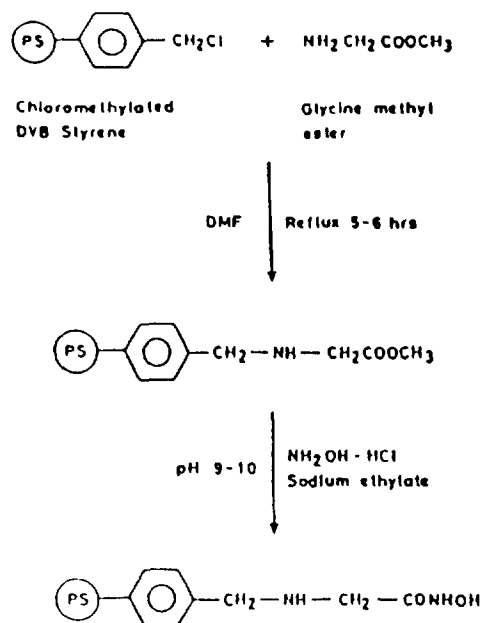
Scheme 1. Synthesis of glycine hydroximate in DVBS.
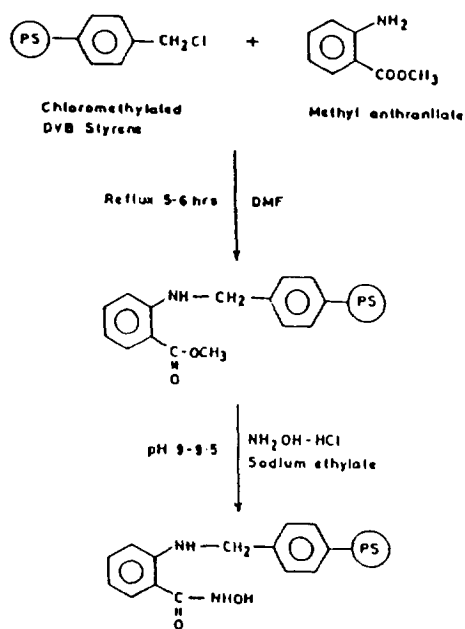
Scheme 2. Synthesis of anthranilic acid hydroximate in DVBS.

Malonic acid dihydroximate in DVBS was prepared by the reported method [17] as shown in Scheme 3.

2.1.3. Synthesis of iminodiacetic acid dihydroximate in DVBS

Iminodiacetic acid dihydroximate was prepared from Chelex-100, an iminodiacetic acid derivative of DVBS, as shown in Scheme 4.

2.1.3.1. Synthesis of the ester of Chelex-100. Chelex-100 (0.05 mol) was taken in methanol in a round-bottomed flask and dry HCl gas was passed through it until saturation was complete. The reaction mixture was refluxed for 3 h. The dimethylester of Chelex-100 was thus formed.

2.1.3.2. Synthesis of iminodiacetic acid dihydroximate in DVBS. A mixture of methyl ester of Chelex-100 (0.25 mol) and hydroxylamine hydrochloride (0.25 mol) in methanol was refluxed for 12 h. The pH of the reaction mixture was adjusted by sodium ethylate solution to 9.2. The product thus formed was filtered, washed with 80% ethanol and dried in vacuum.

2.2. Apparatus

Infrared spectra of the synthesized resins were recorded on a Shimadzu IR-400 spectrophotometer using KBr pellets. Nitrogen analysis was done using Kjeldahl's method. A Perkin-Elmer 2380 atomic absorption spectrophotometer was employed for the quantitative determination of metal ions.

2.3. Determination of distribution coefficients

A batch equilibration technique was employed for the investigation of metal uptake by the resins. The method involved equilibrating the H^+ form of resins with 1 ml of 1000 ppm metal ion solution and a known volume of sodium acetate–acetic acid buffer (pH range 4–7) for 1–10 h. Two phases were separated after equilibration and an aliquot of filtrate was analyzed for metal by atomic absorption spectrophotometery. The quantity of metal ion adsorbed by the resin was obtained by subtracting the concentration in the filtrate from the initial concentration.
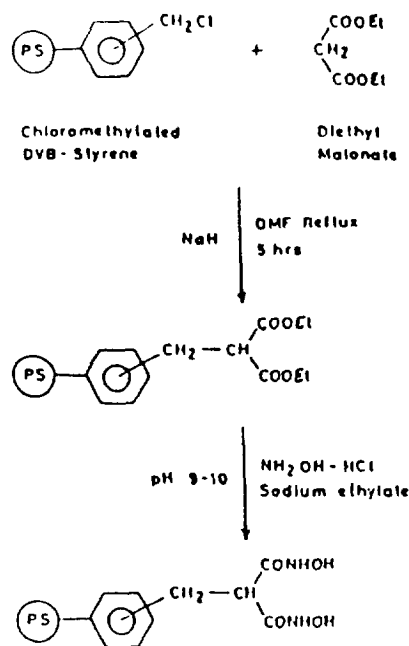
Scheme 3. Synthesis of malonic acid dihydroximate in DVBS.
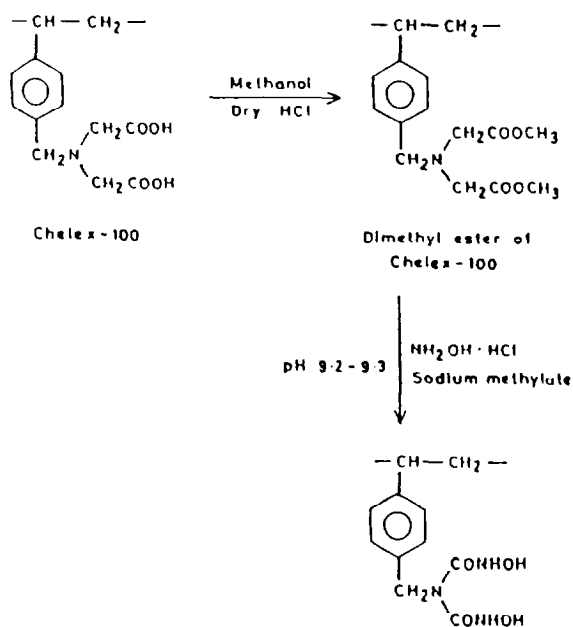
Scheme 4. Synthesis of iminodiacetic acid dihydroximate in DVBS.

The molar distribution coefficient (K_d) values were then calculated using the formula:

$$K_d =$$

$$\frac{\text{Amount of metal ion in resin per gram of resin}}{\text{Amount of metal ion in solution}}$$

$$\text{per milliliter of solution}$$

3. Results and discussion

The synthesized resins are highly stable in water and commonly used solvents in the pH range 4–7.

In the infrared spectra of hydroximate derivatives of DVBS, a band near 3450 cm^{-1} was assigned to ν(N–H) and another band near 1695–1650 cm^{-1} was assigned to C–O stretching vibrations of hydroxamic acid. The ν(C–O) band of carboxylic acids near 1580 cm^{-1} and the ν(C–O) band of esters near 1725 cm^{-1} disappeared in the spectra of hydroxamic acid derivatives.

The moisture content, bulk density, specific bulk volume, nitrogen content and degree of substitution of the resins are given in Table 1 and the pH titrations (determined by a batch method using 0.1 N NaOH) are represented in Fig. 1.

### 3.1. Uptake of metals by the resins

The molar distribution coefficient values of Fe(II), Co(II), Ni(II), Cu(II), Zn(II), Cd(II), U(VI) and W(VI) metal ions with GH-DVBS, AAH-DVBS, MAH-DVBS and IDAAH-DVBS are represented in Tables 2–5, respectively. The results indicate that the distribution coefficient values first increase, then attain a maximum and finally decrease with increasing pH.

Glycine hydroximate in DVBS shows maximum adsorption for Fe(II), Cu(II) and Zn(II) at pH 5.5, and for W(VI), U(VI), Co(II), and Ni(II) at pH 6.0. At pH 6.5, maximum adsorption of Cd(II) takes place whereas Ca(II) is adsorbed maximally at pH 4. At the pH of maximum adsorption, the selectivity order of various metal ions on this resin is as follows:

W(VI) > Fe(II) > U(VI) > Cu(II) > Zn(II)

> Cd(II) > Co(II) > Ni(II) > Ca(II)
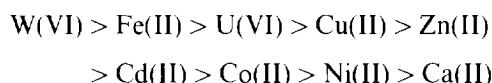
The resin exhibits high selectivity for tungsten ($K_d = 10\,861$) and iron ($K_d = 5822$) which can be easily separated from all other metal ions at pH 6 and 5.5 respectively. This resin can be utilized for the separation of copper ($K_d = 1995$) from cobalt ($K_d = 412$) and nickel ($K_d = 478$) at pH 5.5. It also shows marked adsorption for uranium ($K_d = 2879$).

The sorption studies of various metal ions on AAH-DVBS resin reveal that Fe(II), Co(II), U(VI), and W(VI) are adsorbed maximally at pH 6, Zn(II) and Ni(II) at pH 5.5, Ca(II) at pH 4 and Cu(II) at pH 5. The metal ions show the following adsorption pattern at the pH of maximum adsorption:

W(VI) > Zn(II) > Fe(II) > Cu(II) > Cd(II)

> U(VI) > Co(II) > Ni(II) > Ca(II)
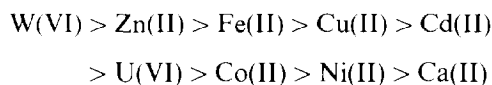
This resin is selective for tungsten, zinc, iron, and copper. The increased adsorption behaviour of anthranilic acid derivatives for zinc has already been discussed in our previous paper [18]. The separation of tungsten ($K_d = 4030$) from cobalt ($K_d = 572$), nickel ($K_d = 364$), copper ($K_d = 404$), cadmium ($K_d = 913$) and uranium ($K_d = 796$) can be achieved at pH 6.

Table 1
Resin characteristics

Resin	Moisture content (%)	Bulk density (g cm⁻³)	Specific bulk volume (cm³ g⁻¹)	Nitrogen content (%)	Degree of substitution (%)
GH-DVBS	11.80	0.60	1.66	1.86	20.66
AAH-DVBS	11.19	0.55	1.80	1.96	26.06
MAH-DVBS	10.11	0.89	1.12	2.73	34.51
IDAAH-DVBS	9.80	0.44	2.27	3.00	25.42

The distribution coefficient values of various metal ions, namely, Fe(II), Co(II), Ni(II), Cu(II), Zn(II), Cd(II), Ca(II), U(VI) and W(VI), with MAH-DVBS resin at the maximum adsorption pH are 1599, 546, 448, 904, 879, 843, 129, 1101 and 4030 respectively. The selectivity order is

$$W(VI) > Fe(II) > U(VI) > Cu(II) > Zn(II)$$

$$> Cd(II) > Co(II) > Ni(II) > Ca(II)$$
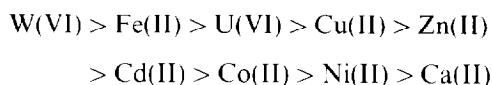
Sorption studies of various metal ions with IDAAH-DVBS resin suggest that it is the most
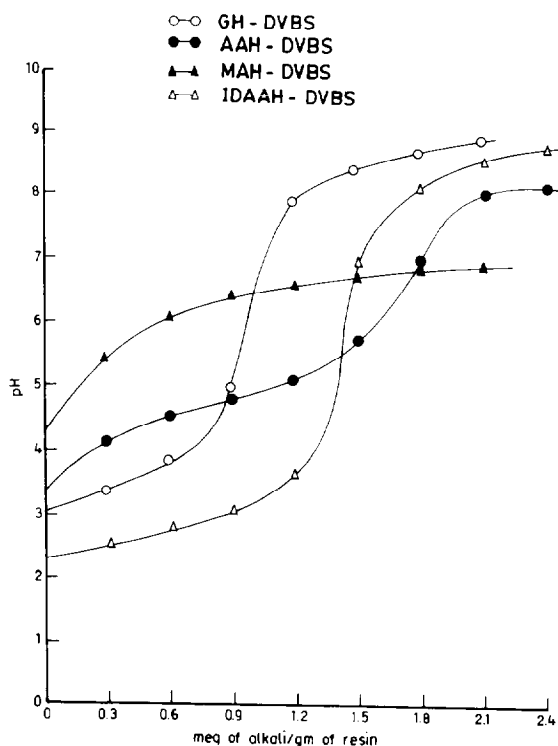
Fig. 1. pH titration curves for GH-DVBS, AAH-DVBS, MAH-DVBS and IDAAH-DVBS resins.

effective of the four synthesized resins for the selective adsorption of metal ions. At the pH of maximum adsorption, distribution coefficient values for Fe(II), Co(II), Ni(II), Cu(II), Zn(II), Cd(II), Ca(II), U(VI) and W(VI) are 36 489, 10 177, 7960, 32 483, 10 760, 8109, 395, 43 436 and 21 707 respectively and these values can be arranged in the following descending order of selectivity:

$$U(VI) > Fe(II) > Cu(II) > W(VI) > Zn(II)$$

$$> Co(II) > Cd(II) > Ni(II) > Ca(II)$$
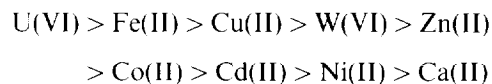
Thus, the selectivity of this resin for uranium, iron, copper and tungsten is quite high. This order is consistent with the metal stability order given by Bogdanov [19] for hydroxamic acids:

Alkaline earth metals	Transition < metals	Rare < earths	Fe, Cu and < highly charged cations
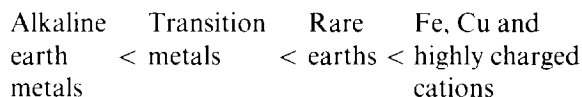
Hydroxamic acids form chelates with high stability constants when complexed with ferrous, non-ferrous and rare earth metals whereas those with low stability order complex with alkali and alkaline earth metals [20]. Hydroxamic acid exists in two tautomeric forms:

Form 1.
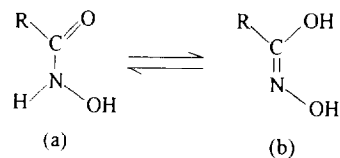
Metal complexes are formed via the hydroxamide functional group (a) and not through the hydroxyoxime structure (b). Thus there is a con-

Table 2
K_d values of different metal ions on GH-DVBS resin

pH	Fe(II)	Co(II)	Ni(II)	Cu(II)	Zn(II)	Cd(II)	Ca(II)	U(VI)	W(VI)
3.5	740	–	150	215	1011	900	120	650	990
4.0	865	–	204	231	1134	959	176	788	1035
4.5	1704	-	251	770	1205	975	155	1250	--
5.0	2289	330	289	1035	1430	1008	96	1676	1791
5.5	5822	412	478	1995	1816	1042	--	2264	2763
6.0	3884	713	689	708	1283	1076	–	2849	10861
6.5	3012	233	496	371	1181	1315	--	2134	7791
7.0	2140	150	310	140	540	610	--	1784	3891

Table 3
K_d values of different metal ions on AAH-DVBS resin

pH	Fe(II)	Co(II)	Ni(II)	Cu(II)	Zn(II)	Cd(II)	Ca(II)	U(VI)	W(VI)
3.5	160		–	150	940	551	95	--	220
4.0	250	--	125	253	1228	783	154	151	441
4.5	504	210	207	610	1635	804	125	203	698
5.0	756	404	377	1451	1691	829	70	253	1103
5.5	1117	469	510	1014	1794	845	.	501	1701
6.0	1701	572	364	404	1728	913	--	796	4030
6.5	1075	334	311	190	1705	833	--	562	2500
7.0	640	135	305	179	1690	805		540	1690

Table 4
K_d values of different metal ions on MAH-DVBS resin

pH	Fe(II)	Co(II)	Ni(II)	Cu(II)	Zn(II)	Cd(II)	Ca(II)	U(VI)	W(VI)
3.5	90	.	---		558	350	85	410	150
4.0	157	–	122	122	712	537	129	479	315
4.5	397		146	314	762	592	79	535	625
5.0	572	150	204	537	779	633	44	831	1019
5.5	934	221	325	904	837	748	--	923	2309
6.0	1599	546	448	623	879	843		1101	4030
6.5	1045	208	342	257	798	612	.	981	1572
7.0	515	–	142	–	440	550	–	612	1121

Table 5
K_d values of different metal ions on IDAAH-DVBS resin

pH	Fe(II)	Co(II)	Ni(II)	Cu(II)	Zn(II)	Cd(II)	Ca(II)	U(VI)	W(VI)
3.5	3140			5450	6101	3728	245	10550	1125
4.0	4354		2258	7228	6243	4719	395	11409	2701
4.5	10620	2230	2849	12668	7009	5027	289	14928	3229
5.0	14316	6481	4018	32483	7960	6287	188	21263	5077
5.5	36489	10177	5612	21475	8731	6635	–	23727	1062
6.0	16590	7009	7960	15970	10760	7186	–	43436	21707
6.5	3717	5809	4498	4962	5612	8109	–	26807	6925
7.0	2980	3550	4440	3961	4123	6387	–	14115	4125

siderable covalency in the bonds formed (compared with the ionic characteristic of the bonds formed with the carboxylic group) and this contributes to the high selectivity of the hydroximate interaction with metals. Hydroxamic acids are weaker donors than the carboxylic acids but are more selective.

A perusal of the results shows that the four synthesized hydroximate resins are selective towards transition and highly charged metal ions [U(VI) and W(VI)] in comparison to alkaline earth metals, i.e. calcium. Therefore, the disadvantage of Chelex-100 can be overcome by utilizing these resins, especially IDAAH-DVBS where the order of K_d values is comparable with those of Chelex-100. This resin can be effectively used in the recovery of uranium from sea water of pH 6–8 [K_d of U(VI) at pH 6 = 43 436].

Among the four chelating resins reported, the dihydroximate of amino carboxylic acid (IDAAH-DVBS) is more effective than the monohydroximate of amino carboxylic acid (GH-DVBS) because of the extra coordinating sites in

the IDAAH-DVBS resin. However, even the dihydroximate of carboxylic acid (MAH-DVBS) is a weaker donor compared to the monohydroximate of amino carboxylic acid (GH-DVBS) although the former has a high degree of substitution. This is because of the presence of nitrogen, which increases the electron density on the coordinating oxygen of the amino acid hydroximate resin. GH-DVBS is also found to be a stronger donor compared to AAH-DVBS, which has a higher degree of substitution compared to GH-DVBS. Assuming that the phenyl group is electron-withdrawing [21], the electron density on the donor oxygen atom is decreased. Thus, AAH-DVBS is a strong acid, weak donor but more selective while GH-DVBS is a weak acid, strong donor and less selective.

3.2. Separation of metal ions by the resin

A study of the K_d values of various metal ions with GH-DVBS resin reveals that separation of a mixture of metal ions can be achieved using this resin. Copper ($K_d = 1995$) was separated from cobalt ($K_d = 412$) and nickel ($K_d = 478$) at pH 5.5 by GH-DVBS using column chromatography.

A 10 cm long glass column of uniform diameter (1 cm) was used for the separation of metal ions. The resin in the H$^+$ form was kept overnight in DMF to allow swelling to occur. The swollen resin was poured into the column to a height of 2–3 cm. The column was equilibrated with sodium acetate–acetic acid buffer of pH 5.5. 20 ml of a mixture containing 10 ml of each metal ion was loaded onto the column at a flow rate of 2 ml min^{-1} which is the normal flow rate of the medium height column under atmospheric pressure. The column was washed with the same buffer solution and the sorbed metal ions were eluted with 0.1 N HCl. 5 ml fractions were collected and were analyzed for metal ion concentration by atomic absorption spectrophotometry.

The quantitative separation of copper–cobalt and copper–nickel at pH 5.5 is shown in Figs. 2 and 3 respectively. Cobalt and nickel ions, being less strongly held by the resin, move down the column more rapidly and are collected before copper.
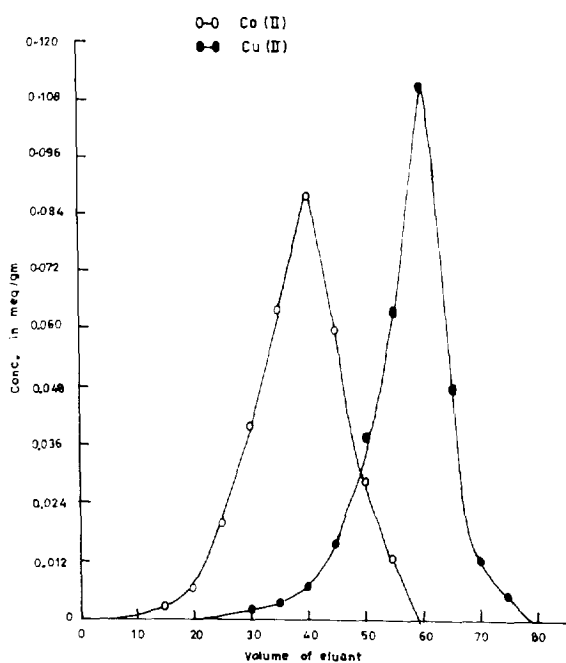

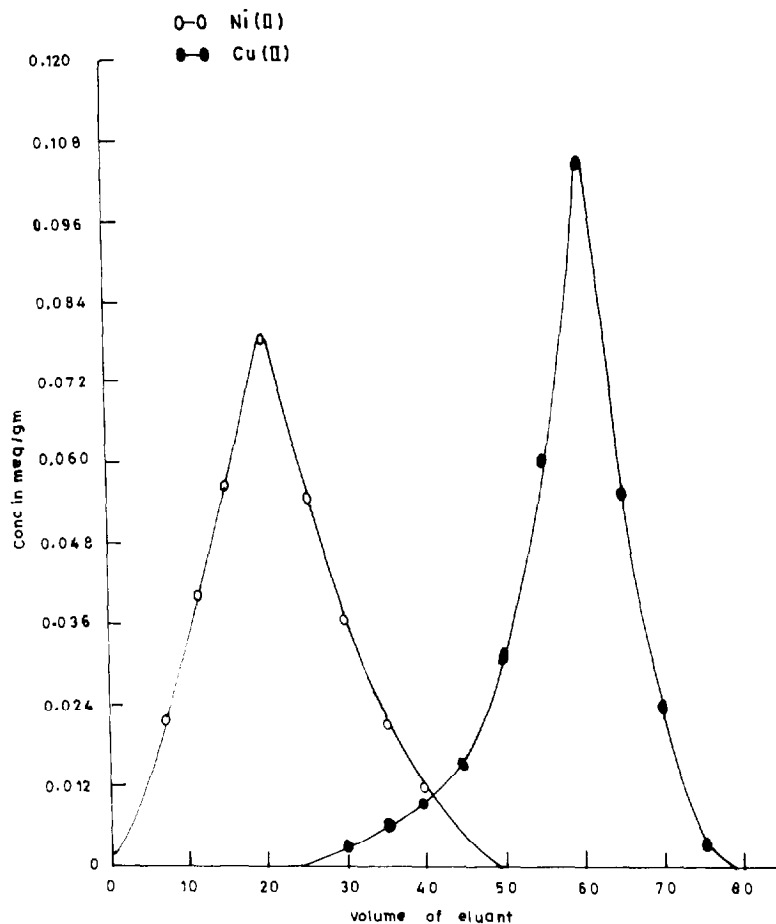Fig. 2. Column separation of Co(II) and Cu(II) on GH-DVBS resin.

Fig. 3. Column separation of Ni(II) and Cu(II) on GH-DVBS resin.

Acknowledgements

References

[1] J. Dingman, Jr., S. Siggia, C. Barton and K.B. Hiscock, Anal. Chem., 44 (1972) 1351.
[2] E.M. Moyers and J.B. Fritz. Anal. Chem. 49 (1977) 418.
[3] C.W. Blount, D.E. Leyden, T.L. Thomas and S.M. Guill, Anal. Chem., 45 (1973) 1045.

[4] S. Bohra, R. Mathur, N.K. Mathur and P.N. Mathur, J. Polym. Mater., 9 (1992) 101.
[5] Y.A. Attiya, Int. J. Miner. Proc., 4 (1977) 191.
[6] H.M. Kingston, I.L. Barnes, T.J. Bready, T.C. Rains and M.A. Champ, Anal. Chem., 50 (1978) 2064.
[7] A. Hirose, K. Kobori and D. Ishi, Anal. Chim. Acta, 97 (1978) 303.
[8] D.E. Leyden, T.A. Pattersons and J.J. Alberto, Anal. Chem., 47 (1975) 733.
[9] D.W. Fuerstenau and Pradip, in M.J. Jones and R. Oblatt (Eds.), Reagents in the Minerals Industry, The Institution of Mining and Metallurgy, London, 1984, pp. 161–168.
[10] O.S. Bogdanov, Proc. Xth Int. Minerals Processing Congress, The Institution of Mining and Metallurgy, London, 1974, pp. 553–564.
[11] M.C. Fuerstenau, R.W. Harper and J.D. Miller, Trans. Am. Inst. Min., Metall. Pet. Eng., 247 (1970) 69.
[12] R. Natarajan and D.W. Fuerstenau, Int. J. Miner. Process. 11 (1983) 139.

[13] H.D. Peterson, Trans. Am. Inst. Min., Metall. Pet. Eng. 232 (1965) 388.

[14] A. Rosenbaum, Freiberg. Forschungsh. A, 455 (1969) 35.

[15] E. Maekawa, T. Kousaki and T. Koshyima, Sen'i Gakkaishi, 42 (1986) 68.

[16] T.M. Suzuki, T. Tokoyama, H. Matsunager and I. Kimura, Bull. Chem. Soc. Jpn., 59 (1986) 865.

[17] T. Hirotsu et al., J. Polym. Sci., Part A: Polym. Chem., 24 (1986) 1953.

[18] M. Ahuja, S. Gupta and P.N. Mathur, J. Polym. Mater., 12 (1995) 257.

[19] O.S. Bogdanov, XIIth Int. Minerals Processing Congress, Sao Paulo, Brazil, 1977, pp. 3–7.

[20] K. Dekun, C. Jingqing and Z. Weizhi, in M.J. Jones and R. Oblatt (Eds.), Reagents in the Minerals Industry. The Institute of Mining and Metallurgy, London, 1984, pp. 169–172.

[21] B. Chatterjee, Coord. Chem. Rev., 26 (1978) 281.

ELSEVIER

Talanta

Speciation of chromium (VI) and total chromium determination in welding dust samples by flow-injection analysis coupled to atomic absorption spectrometry

Louise Girard[1], Joseph Hubert*

Chemistry Department, University of Montreal, P.O. Box 6128, Station Centre-Ville, Montreal, Que., H3C 3J7, Canada

Abstract

We have studied the speciation of chromium (VI) in stainless-steel welding dusts. The approach used for the analysis of Cr(VI) and total Cr relies on a flow-injection analyzer (FIA) equipped with two different sequential detectors. The system measures Cr(VI), by colorimetry (with 1,5-diphenyl carbohydrazide) and total chromium content by flame atomic absorption spectroscopy (AAS). The extraction of the samples of welding-fume dusts is achieved in a buffer solution (acetic acid and sodium acetate at pH 4). This extraction procedure gives a 96% recovery of chromium (VI). The FIA–AAS system that has been described is also more sensitive, has a lower detection limit (0.005 μg ml^{-1}) and gives a better precision (< 1%) than other equivalent systems that have been previously described.

Keywords: Atomic absorption spectrometry; Chromium; Flow-injection analysis; Speciation; Welding dust

1. Introduction

Industrial development has brought many problems of environmental pollution and has also increased the exposure of workers to several toxic substances. Toxicological studies have shown that some essential and non-essential elements become toxic at a certain level of concentration. It has also been demonstrated that the degree of toxicity depends on the chemical form in which the toxic agent is present. In particular, it has been shown that the negative effect of an element on health could depend on its state of oxidation [1,2]. Chemical speciation has consequently become important. This type of analysis is difficult since, on the one hand, many precautions are necessary to avoid a modification of the analyte during the storage, processing and analysis of the sample and, on the other hand, it is obvious that the concentration of an element present in a particular oxidation state will be lower than, or at the very most equal to, the total concentration of the analyte.

* Corresponding author. Fax: (+ 1) 514-343-2185.

[1] Present address: Chemistry and Biochemistry Department, University of Moncton, Moncton, N.B., E1A 3E9, Canada;

We have been particularly interested in the speciation of chromium. For this element, it is well known that the most toxic form is the hexavalent oxidation state. The high toxicity is related to its ability to cross the cell membrane and to its strong oxidation properties. Chromium (VI) compounds are widely used in industrial processes such as tanning, painting, plating, welding and metallurgy. Since welders are an important target group, we have chosen, as a typical sample, the welding dusts generated by the fumes of the stainless-steel welding process.

The chemical composition and physical form of this type of sample are extremely complex and variable. In addition, the solubility of the species found in welding-fume dusts is variable according to its chemical form and can change in a few hours or months following the time of sampling [3]. For chromium (VI) speciation several studies on extraction procedures have been reported. They rely on extractions under acidic [4–6], neutral [7] or basic conditions [8,9].

Several methods have been investigated for the speciation of Cr(VI): liquid chromatography, solvent extraction, flow-injection analysis, etc. [10,11]. The approach that we have used for the analysis relies on a flow-injection analyzer (FIA) equipped with two different sequential detectors. In this work, we will determine Cr(VI) and total chromium content in samples of welding fume dusts. The system will measure Cr(VI) by colorimetry and total chromium content by flame atomic absorption spectroscopy (AAS).

The reaction of Cr(VI) with 1,5-diphenyl carbohydrazide (DPC) is one of the best colorimetric methods for the determination of hexavalent chromium. The reaction is rapid and specific and, under proper acidic conditions, the ligand reacts little with the other transition metals. Furthermore, elements that are complexed by DPC have a different color to the Cr(VI) complex and this minimizes the risks of interference during the colorimetric determination. In acidic solution, DPC reacts with Cr(VI) to form an intense violet complex according to

$$2\,CrO_4^{2-} + 3\,H_4L + 8\,H^+ \rightleftharpoons$$

$$[Cr(III)(HL)_2]^+ + Cr^{3+} + H_2L + 8\,H_2O$$
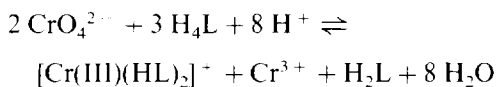
where H_4L represents the DPC and H_2L the 1,5-diphenyl carbazone. The colored complex is believed to be a chelate of Cr(III) and 1,5-diphenyl carbazone [12]. The molar absorptivity of the chromium complex is of the order of 84 000 1 M $^{-1}$ cm $^{-1}$ at 540 nm. The direct reaction of the chromium (III) with H_2L is difficult in an aqueous medium and should not form another complex that could interfere in the analysis [12,13]. When the reaction is used for quantitation, it is necessary to study the possible interferences that can result from the reactions between the ligand and other elements or by a secondary reaction with the ligand under its oxidized form. The colorimetric reaction with DPC is the method used by Occupational Health Agencies in Canada and in the USA. The sequential determination of chromium (VI) and chromium (III) by FIA–AAS was described by Lynch et al. [14].

In this paper, we describe the FIA system that we have developed. The original system was based on the prototype developed by Lynch et al. [14]. This system has been modified and highly optimized to allow the speciation of chromium (VI) in stainless-steel welding-fume dust samples. The system has been fully automated, and its analytical performance and potential interferences were assessed. Finally, the method has been used for the analyses of welding-fume dusts.

2. Experimental

2.1. Instrumentation

The FIA set-up used by Lynch et al. [14] and our system are shown in Fig. 1. The peristaltic pump is an eight-channel pump (Gilson, Villers-Bel, France) that has been modified to allow microcomputer control. The computer can also control the injection via a three-way pneumatic rotary valve (Rainin, Woburn, MA). The sampling loop can be filled either by a second peristaltic pump or with an automatic sampler. Two detectors are used: a UV–visible spectrophotometer (model 100-20, Hitachi, Tokyo, Japan) equipped with flowthrough micro-cell (Model 178.12 QS, Helma, Forest Hill, NY) and an
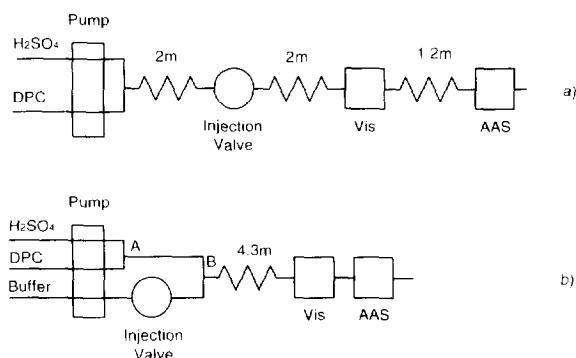
Fig. 1. Schematic representation of the FIA configurations: (a) used by Lynch et al. [14]. (b) used in this paper.

atomic absorption spectrometer (Model 2380, Perkin-Elmer, Norwalk, CT). An IBM-XT computer controls the pump and the injector and ensures instrument control and data acquisition. Control and data acquisition are done through a parallel digital interface (Model PI012, Metrabyte Corp., Taunton, MA). All the control and data acquisition hardware and software were developed in our laboratory. The optimized operating conditions are given in Table 1.

2.2. Reagents and solutions

All chemical products and solvents are of analytical grade. A 1000 μg ml⁻¹ standard solution

Table 1
Optimized operating conditions of the FIA system

FIA	
H_2SO_4 0.2 M flow rate (ml min⁻¹)	1
DPC 0.0060 M flow rate (ml min⁻¹)	1
Acetate buffer solution (pH 4) flow rate (ml min⁻¹)	1.6
Total flow rate (ml min⁻¹)	3.6
Volume of the injection (μl)	300
Length of the reactor (m)	4.3
Temperature of the reactor (°C)	40
Stopped flow time (s)	35
Analytical wavelength (nm)	540

AAS	
Analytical wavelength (nm)	357.9
Spectral bandwidth (nm)	0.7
N_2O C_2H_2 molar ratio	3
Observation height (mm above the burner head)	5

in Cr(VI) is freshly prepared from potassium dichromate, while the 1000 μg ml⁻¹ standard solution of Cr(III) comes from BDH (Montreal, Que., Canada). Diluted standard solutions are freshly prepared before each analysis. Solutions of potential interfering ions are prepared from 1000 μg ml⁻¹ standard solutions (BDH) or from the chloride or nitrate of the element of interest. The concentrated sulfuric acid ("Instra-analyzed"; Baker, Montreal, Que., Canada) is certified to contain < 0.0002 μg ml⁻¹ chromium. Solutions of DPC are obtained by dissolving the appropriate quantity of products in 100 ml of acetone. The volume is then completed to 1 l with the purified water (deionized, filtered on a carbon bed and with a Millipore filter 10 μm). The solutions are kept in the dark to avoid their decomposition. All containers are cleaned by soaking in a 50% nitric acid solution for at least 24 h and thoroughly washed with purified water before use.

2.3. Choice of the sampling membrane

Two membranes are usually used for sampling of the welding-fume dusts. The first is a filter made of mixed cellulose ester (FECM) and the other is a polyvinyl chloride membrane (PVC). Both membranes have a 8 μm porosity. The effect of membrane composition on the chromium speciation was evaluated using diluted standard solutions as samples. The solution containing the analyte is deposited on the different membranes and is dried overnight. The samples contain 2 and 20 μg of Cr(VI). Three successive extractions are performed with volumes of 5, 3 and 3 ml of an acetate buffer solution (pH 4). During the extractions the solution and membrane are first shaken manually and then placed in an ultrasonic bath for 5 min. The three extracts are then mixed, filtered and analyzed.

2.4. Generation of the welding-fume dust samples

The welding-fume dust samples are generated under rigorously controlled conditions to obtain deposits which are similar in terms of mass and composition. A special dust generation hood is used. The welding fumes are generated from a

Table 2
Typical composition of a stainless-steel welding rod[a]

Element	Fe	Cr	Ni	Mo	Mn	Si	C	P	S	Cu	V
Composition[b] ($\%$ w/w)	65.4	18.8	11.5	2.4	1.5	0.3	0.04	0.03	0.01	0.01	<0.01

[a] Stainless-steel welding rod. Arcweld Model E316-16, diameter 2.4 mm, coating LIM, $CaCO_3$.
[b] Values provided by the manufacturer.

welding rod and are aspirated through a membrane to collect the fine dust particles. The system is built to produce the same flow rate over the whole surface of the membrane to insure the uniformity of the deposit. A stainless-steel welding rod with a 2.4 mm diameter (Model E316-16, Arcweld) is used. The description and composition of the welding rod used are presented in Table 2. The diameter of the membrane is 293 mm and this allows collection of a sample with a large surface that can be subdivided into several smaller identical sub-samples. A system of rings is used to maintain the membrane and to mask its external part. This masked section is not in contact with generated fumes and serves as a blank for weightings and analyses. From the membrane several samples are punched in both the exposed and non-exposed zones. Approximately 20 blanks and 40 samples are thus obtained from one membrane. The position of each of these small membranes is noted to allow us to group the samples coming from different parts of the membrane in order to minimize the error that could be produced by heterogeneity of the deposit. The dust particle mass for each sample is obtained by subtracting the average mass of the blanks from the sum of the sample and filter masses.

2.5. Preparation of the welding dust samples

For the preparation of the standards, samples and blanks, all the glassware, polyethylene containers and pipette tips are cleaned by soaking in nitric acid (20% (v/v)) for at least 24 h and rinsed with purified water. Each membrane is inserted in a sample tube to which an 8 ml aliquot of an acetate buffer solution (pH 4) is added. The sample tube is hermetically closed, vigorously shaken by hand and, then left in an ultrasonic bath for an

hour. The solution is then filtered (0.45 μm filter, Millipore, Bedford, MA) to eliminate residual particles. Some of the samples are digested according to the standard analytical method 6-1 of the "Institut de Recherche en Santé et Sécurité" (IRSST) of Québec [15]. This method used a hot digestion with concentrated nitric acid followed by concentrated hydrochloric acid for complete dissolution of the sample.

2.6. Interference studies

To evaluate the level of interference, a series of solutions is prepared at three concentrations (10, 50 and 200 μg ml^{-1}) of the potential interfering ion and with a Cr(VI) concentration of 0.1 μg ml^{-1}. The potential interfering species examined are Co(II), Cr(II), Fe(II), Fe(III), Ni(II), Pb(II), V(V) and Mo(VI). The molar ratio of DPC to Cr is approximately 3200.

3. Results and discussion

3.1. FIA development and optimization

In the initial system proposed by Lynch et al. [14] (Fig. 1a) the injection valve is located directly in the reagent channel. Consequently, the reaction begins at both ends of the sample plug, then progresses towards the central part of the sample plug. In our system (Fig. 1b) we have modified the FIA configuration, firstly to allow for a more efficient (turbulent) mixing of the reagents and the sample, and secondly to prevent the problems related to the difference in refractive index between the carrier and the sample plug. A third tube is used to bring the sample or the blank to point B where the solutions are more efficiently

Table 3
Analytical performances of the FIA systems

Parameter	System[a]			
	A	B	C	D
Sensitivity (ml g⁻¹)	0.020	0.244	0.369	0.490
Dynamic range (g ml⁻¹)	0.1 20	0.01–2	0.01 2	0.01 1.5
Detection limit (g ml⁻¹)		0.005	0.005	0.002
Precision (%)[b]	1.6 (8)	0.8 (0.5)	0.6 (0.5)	1.3 (0.4)
Reproducibility	4 (8)	0.2 (0.5)	0.6 (0.5)	1.3 (0.4)
Number of measurements	16	10	3	5

[a] A, Lynch et al. [14]. B–D, this work. B, manual system. C, automated system. D, automated system with stopped flow.
[b] Values in parentheses are the chromium concentrations (g ml⁻¹).

mixed. This channel provides a more constant composition for the carrier flow and therefore avoids the problems related to the change in refraction index.

A standard optimization procedure of the FIA was performed. The reaction coil length (2.3–5.3 m), the reagent concentrations (H_2SO_4:0.036–0.2 M, DPC:0.016–0.057 M), the reagent flow rate ratio, the total flow rate, the coil temperature (20–60°C), the sample volume (30–400 μl) and the stopped flow time (0–60 s) were optimized. The range of the experimental parameters that has been investigated was limited by instrumental constraints (coil length), solubility problems (DPC concentration), Cr(VI) stability (H_2SO_4 concentration) and solvent boiling point (temperature). The optimized operating conditions of the FIA system are given in Table 1.

3.2. Analytical performances

The analytical performances were evaluated on synthetic samples to allow their comparison with previously reported data. The results obtained after optimization are reported in Table 3. The calibration curves were obtained from six standard solutions. For manual operation, the analytical sensitivity and reproducibility are higher than those reported by Lynch et al. [14]. The increase in sensitivity can be explained by a combination of several factors: a smaller dispersion obtained with a tube of smaller inside diameter, a different manifold and a careful optimization resulting in a

higher reagent concentration, the optimization of the ratio of the flow rates, reactor length and the increase in temperature. Since the sensitivity is increased by a factor of 10, the linear range is shifted toward lower concentrations from 0.01 to 2.00 μg ml⁻¹. The spectrophotometric detector is saturated if the concentration of Cr(VI) is raised to 3 μg ml⁻¹. The detection limit is 0.005 μg ml⁻¹ and the precision is excellent with a relative standard deviation of 0.8% at a concentration of 0.5 μg ml⁻¹. This represents a significant improvement compared to a value of 1.6% at 8 μg ml⁻¹ observed by Lynch et al. [14].

Microprocessor control of the pumping system allows a more precise and complex flow control and results in improved analytical performances (Table 3, columns C and D). The use of a stopped flow mode allows an increase of a factor of two in sensitivity. With a dynamic range up to 1.5 μg ml⁻¹, the sensitivity is 0.49 ml μg⁻¹. The precision is 0.5% at a concentration level of 0.4 μg ml⁻¹ and the limit of detection is 0.002 μg ml⁻¹ of chromium (VI). The sensitivity has increased by a factor of 25 compared to the results of Lynch et al. and the detection limit has decreased from 0.01 to 0.002 μg ml⁻¹. In addition, the sample-to-sample reproducibility is excellent.

3.3. Interference studies

Interferences can originate from two sources. The first type occurs when another element is complexed by DPC and the resulting complex has

an absorption band located at the same wavelength as the chromium complex. In this case, a positive interference occurs which will increase the absorption of the solution. This type of interference is a function of the concentration of the interfering elements and ther relative stability of their complexes with DPC. The second type of interfering species reacts with Cr(VI) and reduces it to Cr(III). Since chromium(III) has a small affinity for DPC the analytical signal will decrease. This interference is not only a function of the concentration levels, but also a function of pH and reaction time.

In our case, we wish to analyze stainless-steel welding-fume dusts and the elements that might be present in the sample are [4,6]: Fe, Ni, Mo, Mn, Si, Cu, Ca, Na, Ti, Co and V. According to the type of welding rod used, the concentrations and chemical forms of these elements can vary from sample to sample. The known interfering elements for the Cr–DPC system are Fe(III), Cu(II), Ni, V(VI), Pb, Cr(III), Sn(IV), Mo and Hg [16]. To assess the level of interference, a series of solutions of the interfering element are prepared at three concentrations (10, 50 and 200 μg ml^{-1}) with a constant Cr(VI) concentration of 0.1 μg ml^{-1}. The molar ratio of DPC to Cr is approximately 3200. The results obtained from the interference studies are given in Table 4.

For the trace elements (Co, Cu, Pb, V) present in stainless-steel welding rod the interferences are absent or negligible. Among the major elements (Cr, Fe and Mo), the effect of Mo(VI) can be neglected since this element will be present at low concentrations in the sample. In the case of Cr(III), a positive deviation of 20% is observed when its concentration is 500 times higher than that of Cr(VI). This ratio represents an extreme case which is not found in 'real' stainless-steel welding dusts. At lower levels (100 times or more) the interference is 2% or less. Iron(II) is a particular case since its shows a strong negative influence at molar ratios up to approximately 500 and a positive interference at higher molar ratios (1800). The effect of iron(II) can be explained in two ways: (i) Fe(II) can easily reduce Cr(VI) and induce a decrease in

absorbance; and (ii) Fe(III) obtained by oxidation, or the excess of Fe(II), can react with DPC and absorb moderately at the wavelength of analysis, producing a positive interference. Fortunately, high concentrations of iron(II) are not found in stainless-steel welding dusts [4]. Iron(III) also gives interferences and therefore the presence of iron could cause significant problems for the determination of Cr(VI) if present at high concentration. Fortunately iron is poorly extracted from the sample and the analysis is manageable (see Section 3.5.3).

Table 4
Interference studies for the chromium (VI) analysis

Species	Concentration (mg l^{-1})	Mass ratio	Molar ratio	Interference factor[a]
Co(II)	10	100	90	0.96
	50	500	440	1.00
	200	2000	1770	1.02
Cu(II)	10	100	80	0.97
	50	500	410	0.96
	200	2000	500	0.92
V(V)	10	100	100	1.27
	50	500	510	2.60
	200	2000	2040	2.83
Cr(III)	10	100	100	1.27
	50	500	510	2.60
	200	2000	2000	1.51
Fe(II)	10	100	100	1.02
	50	500	470	0.85
	200	2000	1860	1.84
Fe(III)	10	100	90	0.91–1.28
	50	500	470	1.50
	200	2000	1860	3.00
Ni(II)	10	100	90	0.95
	50	500	440	1.01
	200	2000	1770	0.74
Mo(VI)	10	100	50	0.95
	50	500	270	1.55
	200	2000	1060	8.61

[a] Mean of three measurements with a relative standard deviation of 2.5%.

3.4. Sequential determination of chromium (VI) and total chromium by FIA–AAS

The coupling of the FIA system to AAS imposes a certain number of constraints. To avoid interferences of acids and other elements in the AAS determination of chromium a nitrous oxide–acetylene flame is used and the optimal conditions are reported in Table 1. From previous studies, it was shown that the signal intensity in AAS is different for chromium (VI) and chromium (III). To verify the importance of this effect, several solutions containing a total chromium concentration of 20 μg ml^{-1} made up of varying amounts of chromium (III) and chromium (VI) have been prepared. The maximum deviation is less than 2% under our optimal conditions, and consequently no effects of the oxidation state of chromium on the signal are observed. The coupling of the FIA to the AAS nebulizer sets the uptake rate of the nebulizer to 3.7 ml min^{-1}, without any loss in signal compared to a free uptake. The precision obtained for the peak height measurements is satisfactory: 0–1.8% for a concentration range of 0–32 μg ml^{-1}.

The calibration curves obtained for the sequential determination of chromium (VI) and total chromium are shown in Fig. 2.

3.5. Analysis of welding-fume dust samples

3.5.1. Comparison of the membranes used for the sampling

Two membranes are used to sample the welding-fume dusts: a filter of FECM and a PVC membrane. The first membrane is normally used with an acidic digestion for total dissolution of the whole sample and the membrane. In Table 5 the recoveries obtained with the two membranes are presented. The results obtained with the FECM membrane are very poor in terms of recovery. The loss of Cr(VI) can result from the filtration of the solution or loss by reduction of Cr(VI) [5]. The recoveries on the PVC membrane are excellent; they show that the membrane has no particular affinity for the analyte and the former can then be entirely recovered. This membrane is stable and chemically inert but is difficult

to wet. The extraction has therefore to be undertaken with care to ensure that the sample is in good contact with the extraction solution. The best extraction method consists of introducing the membrane in a sample tube that can be closed and to shake manually followed by shaking in an ultrasonic bath. The sample is then filtered.
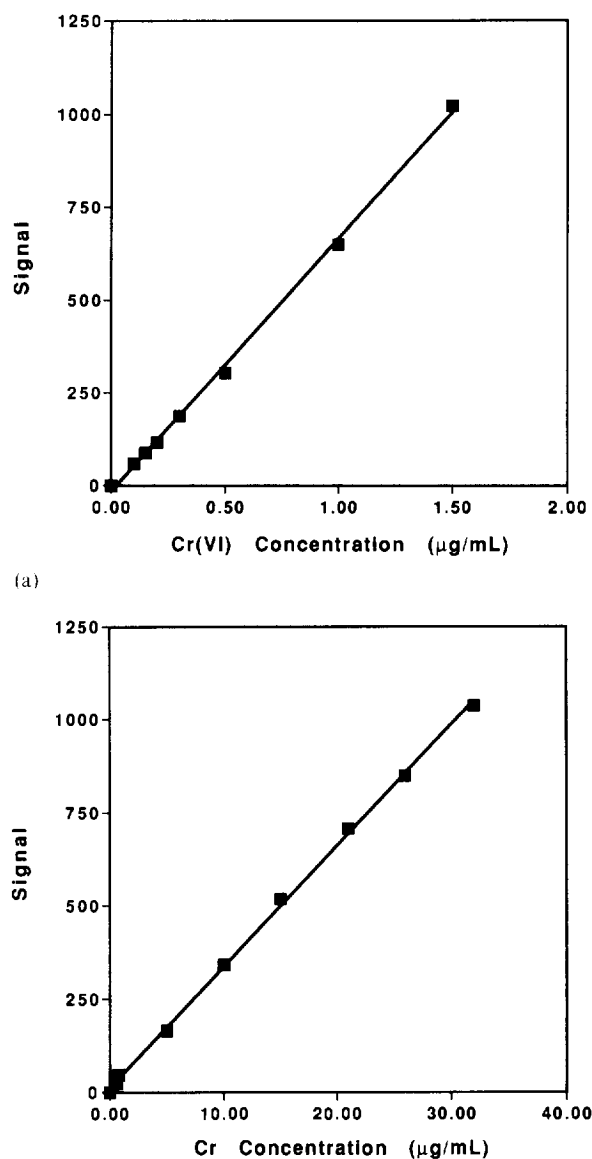
Fig. 2. Calibration curves for (a) Cr (VI); (b) total Cr.

3.5.2. Extraction from the welding-fume dusts

A stainless-steel welding rod allows generation of a sample containing chromium and iron together; iron being the element that presents the greatest potential for interference. The composition of the welding rod is given in Table 2. To accomplish the speciation of Cr(VI) it is essential that this oxidation state be preserved during the entire analytical procedure. In addition, a complete extraction of chromium with minimal extraction of elements that could interfere with the analysis is also desirable.

The solubility of the different chemical forms of chromium depends on the pH. At very acidic pH (< 1), the majority of species are soluble, but Cr(VI) is reduced to Cr(III) at any pH lower than 4 [4,6]. Furthermore, the solubility of Cr(III) is at its maximum at a pH value less than 5. The optimum extraction pH range is therefore between 4 and 5. at this value, the major metals present in fume dusts, such as Fe, Mn and Ni, are slightly soluble [4] and will be extracted only slightly. Several solutions were evaluated for the extraction and the results obtained are shown in Table 6. A recovery of 100% is obtained with a total digestion in HNO_3–HCl. In this series of samples, the chromium is extracted with a recovery of ≥ 91% in all tested solutions and, as indicated by the standard deviation, no method of extraction is superior to the other methods in terms of the quantity of extracted analyte. However, extraction with an acetic acid and sodium

Table 5
Chromium (VI) recovery

Membrane	Cr(VI) (μg)	Recovery[a] (%)	Standard deviation (%)
PVC	2.0	100	1
	2.0	102	4
	20.0	90	1
	20.0	100	1
FECM	2.0	36	1
	2.0	29	1
	20.0	88	1
	20.0	89	1

[a] Mean of three measurements.

Table 6
Comparison of the extraction methods

Extraction solution	Analyte	Recovery (%)[a]
HNO_3 HCl[b]	Cr	100 (8)
H_2O	Cr(VI)	91 (7)
H_2O	Cr	93 (6)
Na_2CO_3 (1%)	Cr (VI)	97 (7)
NaOH (2%)	Cr (VI)	99 (6)
H_2SO_4 (0.5 M)	Cr (VI)	99 (6)
H_2SO_4 (0.5 M)	Cr	100 (7)
Acetate buffer	Cr (VI)	96 (6)[c]

[a] Recovery and (standard deviation).
[b] Total digestion.
[c] All the recoveries were measured on five samples with this exception where three samples were measured.

acetate buffer at pH 4 is far more advantageous in terms of extract stability. A study of the stability of Cr(VI) in this acetate buffer has shown that the concentration of the analyte is stable for more than 24 h. In addition, the same buffer is used as the matrix for the standard solutions and as the FIA carrier flow.

The detection limit for the determination of Cr(VI) by FIA is excellent (0.005 μg ml^{-1} or 1.5 μg); the dynamic range is from 0.005–1.5 μg ml^{-1}. The detection limit with AAS is poorer than normally observed (0.3 μg ml^{-1} or 85 μg), which can be explained by the sample dilution and the small sample volume (300 μl). The short-term precision is 0.5% and the reproducibility of a series of five measurements is 1.3% at a concentration level of 0.4 μg ml^{-1}. The precision for the total chromium determination by AAS does not exceed 2%.

To demonstrate that the method developed can be used in occupational health, Table 7 shows the concentrations of chromium in air equivalent to the lower limit of quantification and to the upper limit of the dynamic range for different sample volumes. Generally volumes of 180–600 l of air are sampled for the determination of total Cr and Cr(VI) respectively. Obviously an increase in the volume of air sampled will result in a lower quantification limit. The legal norms for total chromium and hexavalent chromium concentrations generally accepted by the Canadian and

Table 7
Equivalent chromium concentration in air

Air volume (L)	Lower limit of Quantification (mg m^{-3})	Legal norm (mg m^{-3})	Upper limit of linearity (mg m^{-3})
600	0.037	0.5 Cr	0.67
600	0.00067	0.05 Cr(VI)	0.020
180	0.12	0.5 Cr	2.2
180	0.0022	0.05 Cr(VI)	0.067

[a] The quantification limit is 10 × the detection limit.
[b] All the calculations were made assuming a final solution volume of 8.0 ml and sampling volumes of 180 and 600 l of air.

American Occupational Health Organizations are given and are well within the range of quantification of the FIA system.

3.5.3. Determination of Cr(VI), total Cr and Fe in samples of welding-fume dusts

The analyses of Cr(VI), total Cr and Fe have been performed by different techniques to obtain a good estimate of the potential of the FIA system for the determination of the total chromium, extractable chromium and hexavalent chromium contents of samples. The results obtained are shown in Table 8. Two processing procedures are used for the samples: (i) a complete digestion that allows the determination of the total chromium content; and (ii) an extraction with an acetate buffer (pH 4) which allows the determination of the extractable chromium.

First, the results obtained by FIA are compared with those obtained by well-known method for the speciation of chromium by complexation of

Table 8
Welding-fume dust analyses

Analyte	Concentration (mg g^{-1})	Measurement method
Total Cr after digestion	30 (6)[a]	AAS
Total Cr after extraction	25 (4)[b]	AAS
Extractable Cr(VI)	22.5 (0.6)[b]	DPC-FIA
Total Fe after digestion	34 (7)[a]	AAS
Extractable Fe	7.5 (3)[a]	AAS

[a] Mean and (standard deviation) for five samples.
[b] Mean and (standard deviation) for three samples.

Cr(VI) with ammonium pyrrolidine dithiocarbamate (APDC) followed by an extraction with 4-methylpentan-2-one (MIBK) and determination by AAS [16]. The concentration found by FIA in welding-fume dusts for Cr(VI) is 22.5 mg g^{-1} and is within the range of the value found by complexation with APDC (23 ± 3 mg g^{-1}). However, the precision obtained by the DPC-FIA method is better than that obtained by the other method.

The average quantity of total chromium is of the order of 30 mg g^{-1}. The greatest part of this chromium is in an extractable form (25 mg g^{-1}) and, as expected, the extractable chromium is mainly in its hexavalent form (22.5 mg g^{-1}).

From these measurements, it appears that only 83% of chromium is extracted from the sample. The proportion of extractable chromium varies with the fume samples and gives an indication of the variability of the composition of the welding-fume dusts. In our case, the two series of fume dust samples (Tables 7 and 8) have been generated at different times, and in different amounts, but from the same welding rod. Thus it is not suprising to find that the chemical composition varies not only with the composition of the welding rod but also as a function of the welding parameters used (voltage, current intensity, etc.) [17].

To be able to judge the quality of the extraction conditions used in terms of their potential to produce iron interferences, we have measured the portion of iron that is extracted. The quantity of iron contained in the sample is 34 mg g^{-1} and the amount of iron that is extracted in only 7.5 mg g^{-1}. This amount of iron would not cause any serious interference problem since, as indicated earlier, this interference is only important when the concentration of iron is about 100 times greater than that of Cr(VI) and when iron is in its divalent form (which is not the case here).

4. Conclusion

Elemental speciation requires a great specificity of the method of analysis and control of the chemical form of the analytes during the whole analytical procedure. The method and analyzer

that we have developed meet these demands. The extraction of the samples of welding-fume dusts in a buffer solution (acetic acid and acetate of sodium at pH 4) has proven comparable to that with other extraction solutions. The main advantage of this buffer is that it minimizes the extraction of iron and avoids the reduction of Cr(VI). The FIA–AAS system that has been described is also more sensitive, has a lower detection limit and gives a better precision than the system that developed by Lynch et al. [14].

Acknowledgements

References

[1] P.L. Williams and J.L. Burson, Industrial Toxicology, Van Nostrand Reinhold, New York, 1985, pp. 197–210.

[2] American Conference of Governmental Industrial Hygenists, Supplemental documentation, Cincinnati, OH, 1983, pp. 98–100.

[3] R.M. Stern and E. Thomsen, Scand. J. Work Environ. Health, 79 (1983) 1.

[4] D. Naranjit, Y. Thomassen and J.C. Van Loon, Anal. Chim. Acta, 110 (1979) 307.

[5] G. Blooquist, C.A. Nilsson and O. Nygren, Scand. J. Work Environ. Health, 9 (1983) 489.

[6] M.T. Abell and J.R. Calberg, Am. Ind. Hyg. Assoc. J., 35 (1974) 229.

[7] NIOSH, Manual of Analytical Methods, Chromium (VI) in Air, 2nd edn., US Dept. of Health, Education and Welfare Publishers, P & CAM182, 1977.

[8] V.J. Zatka, Am. Ind. Hyg. Assoc., J., 46 (1985) 327.

[9] R. Milacie, J. Stupar, N. Kozuh and J. Korosin, Analyst, 117 (1992) 125.

[10] C.M. Andrle and J.A.C. Broekaert, Fresenius' J. Anal. Chem., 346 (1993) 653.

[11] J.F. Jen, G.L. Ou-Yang, C.S. Chen and S.M. Yang, Analyst, 118 (1994) 1281.

[12] E.B. Sandell and H. Onishi, Determination of Traces of Metals, Part I, Photometric Detemination of Traces of Metals, 4th edn., John Wiley, New York, 1978, pp. 390–391.

[13] H. Onishi, Photometric Determination of Traces of Metals, Part II, Individual Metals, Aluminium to Lithium, 4th edn., John Wiley, New York, 1986, pp. 412–423.

[14] T.P. Lynch, N.J. Fernoghan and J.N. Wilson, Analyst, 109 (1984) 839.

[15] Institut de Recherche en Santé et Sécurité du Travail du Québec, Analytical Methods, Vol. 1, Method 6-1, Montreal, Que., 1982 (in French).

[16] M.R. Midgett and M.J. Fishman, At. Absorpt. Newsl., 6 (1967) 128.

[17] Commission de la sAntLk et de la Sécurité du Travail, Environmental Monitoring of Workers Exposed to Gases and Welding fumes, Report, Montreal, Que., 1983, pp. 91.

Aqueous complexing of nickel and zinc with 3-(N-morpholino)propanesulfonic acid and the solubility products of nickel and zinc hydroxides

Simon R. Poulson*, James I. Drever

Department of Geology & Geophysics, University of Wyoming, Laramie, WY 82071-3006, USA

Abstract

Phosphate and carbonate buffers serve as excellent pH buffers at circumneutral values of pH, except for systems requiring significant concentrations of heavy metals, which are severely restricted by the low solubilities of heavy metal phosphates and carbonates. 3-(N-morpholino)propanesulfonic acid (MOPS; pK_a 7.2) is a suitable replacement buffer at circumneutral values of pH. However, only limited data are available concerning aqueous complexing involving MOPS. Aqueous complexing of nickel and zinc with MOPS has been investigated by the solubility method, using the sparingly soluble solids $Ni(OH)_2$ and $Zn(OH)_2$. Log K_{sp} values of -15.9 and -16.6 have been determined for $Ni(OH)_2$ and $Zn(OH)_2$ respectively. Experiments with MOPS indicate that there is negligible complexing between Zn and MOPS, but that significant Ni–MOPS complexing occurs, such that $Ni^{2+} + OH^- + MOPS^- \rightleftharpoons Ni(OH)MOPS^\circ$; log $K = +7.0$.

Keywords: Aqueous complexing; 3-(N-morpholino)propanesulfonic acid; Nickel; Solubility products; Zinc

1. Introduction

Carbonate and phosphate buffers have long been used as buffers for circumneutral values of pH. Correspondingly, a large database of aqueous complexation constants exists for carbonate and phosphate species, which has been incorporated into aqueous speciation programs such as MINTEQA2 [1] and WATEQ4F [2]. However, carbonate and phosphate buffers are not suitable for all experiments. In particular, the low solubilities of

heavy metal carbonates and phosphates (Table 1) severely limit the range of heavy metal concentrations that can be used in experiments buffered with either carbonate or phosphate buffers. This problem is particularly acute for researchers investigating the toxicity of heavy metals for various biological organisms, which frequently require circumneutral values of pH for growth. Alternative pH buffers with suitable values of pK_a have been made available by Good and co-workers [3–5]. However, only limited data are available concerning aqueous complexation between these buffers and metal cations.

* Corresponding author. Fax: + 1 307-766-6679.

The objective of this study is to evaluate aqueous complexation constants for nickel and zinc with the buffer 3-(N-morpholino)propanesulfonic acid (MOPS; $pK_a = 7.2$). The method employed to determine the aqueous complexation constants involved measurement of the solubilities of nickel and zinc hydroxides in the presence and absence of MOPS. Hence, the solubility products of nickel and zinc hydroxides were also determined during the course of the experiments.

2. Experimental

Values of aqueous complexation constants are commonly derived by potentiometric titration [3,6]. However, the low solubilities of heavy metal hydroxides (Table 1) at circumneutral pH demand low metal concentrations, which would lead to reduced sensitivity during titration. The approach used in this study was to compare the solubility of nickel and zinc hydroxides with and without the presence of MOPS. Increased solubility in the presence of MOPS is attributed to metal-MOPS complexing, while decreasing solubility in the presence of MOPS is attributed to precipitation of a metal-MOPS phase.

All experiments were designed to avoid the presence of carbonate in experimental solutions, in order to simplify the experimental system, to avoid possible metal-carbonate complexing, and to prevent the possible precipitation of metal carbonates. All solutions were prepared with water which had been purged of CO_2 by boiling and gassing with N_2 [7]. All experiments, pH measurements, and sampling of solutions were conducted

Table 1
Solubility products (log K_{sp} at 25°C) of selected heavy metal phosphates and carbonates [12]

Phosphate	log K_{sp}	Carbonates	log K_{sp}
$Ni_3(PO_4)_2$	−30.3	$NiCO_3$	−8.2
$Zn_3(PO_4)_2$	−32.0	$ZnCO_3$	−10.8
$Cd_3(PO_4)_2$	−32.6	$CdCO_3$	−11.3
$Pb_3(PO_4)_2$	−42.1	$PbCO_3$	−13.1
$Co_3(PO_4)_2$	−34.7	$CoCO_3$	−12.8
$Cu_3(PO_4)_2$	−36.9	$CuCO_3$	−9.9

in a glove bag purged with N_2. The solubilities of nickel hydroxide (Johnson Matthey Chemical Co.) and zinc hydroxide (Aldrich Chemical Co.) were determined at 22°C over a pH range of approximately 7–8.5, with $NaNO_3$ present in concentrations between 0.002 and 0.2 molal. pH was adjusted by the addition of HNO_3. Similar experiments were conducted with MOPS concentrations between 0.0008 and 0.2 molal. Experiments were conducted in 60 ml polyethylene bottles. pH was measured with an Orion Ross Sure-Flow combination electrode and a Beckman Φ21 pH meter, which was calibrated using pH 7 and 10 buffers. Samples were taken using a syringe, and filtered through a 0.45 μm syringe filter. Samples were acidified with HNO_3, and diluted where appropriate. Nickel concentrations were measured using a Thermo Jarrell Ash 3000 inductively-coupled plasma spectrophotometer, and zinc concentrations were measured using a Perkin-Elmer 2380 atomic absorption spectrophotometer. Samples were periodically sampled until repeated sampling indicated negligible changes in pH and metal concentration between sampling events. Equilibration time was approximately 70 days.

The activities of Ni^{2+}(aq) and Zn^{2+}(aq) were calculated using the program MINTEQA2 [1] for all experiments conducted in the absence of MOPS. A comparison of the MINTEQA2 and WATEQ4F [2] databases revealed that the relevant data used in these calculations are the same in each case. Combined with pH measurements, these data permit calculation of K_{sp} values for nickel and zinc hydroxides, which were added to the MINTEQA2 database, together with the K_a value for MOPS [4]. Measured metal concentrations in experiments conducted in the presence of MOPS were compared with calculated metal concentrations assuming no metal-MOPS interaction.

MINTEQA2 speciation calculations performed in this study require the activity of H^+ (provided by pH measurement), and do not require a conversion into H^+ concentration values. Equilibrium constants calculated in this study are thermodynamic constants. Aqueous activities have been calculated using the MINTEQA2 speciation program for a reference state of infinite dilution, accounting for speciation and correcting for ionic strength using the Davies equation.
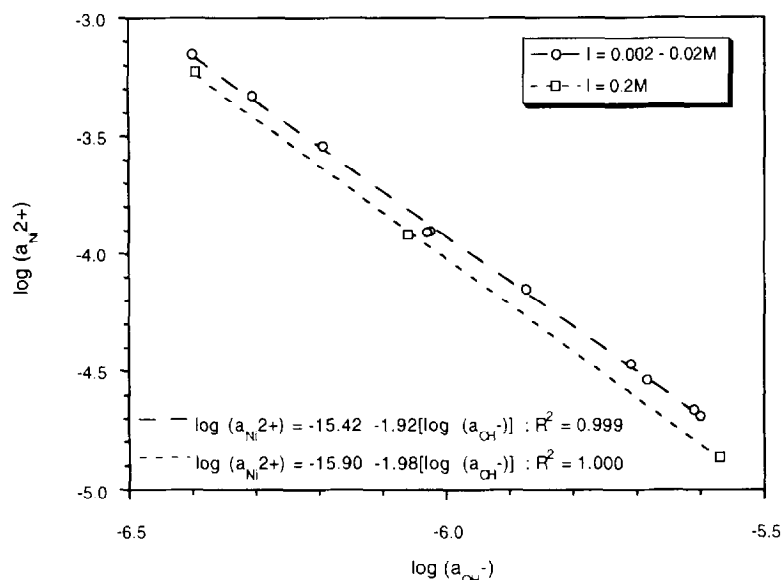
Fig. 1. Calculated values of $\log a_{Ni^{2+}}$ vs. $\log a_{OH^-}$ for solutions saturated with $Ni(OH)_2$. Ionic strength $NaNO_3 = 0.002–0.2$ M.

3. Results

3.1. Solubility products

Values of $\log a_{Ni^{2+}}$ vs. $\log a_{OH^-}$ for Ni hydroxide solubility experiments conducted in the absence of MOPS are presented in Fig. 1. A linear least-squares fit for experiments with ionic strength between 0.002 and 0.02 molal yields:

$$\log a_{Ni^{2+}} = -15.42 - 1.92(\log a_{OH^-}) \tag{1}$$

with a correlation coefficient $R^2 = 0.999$. Using Eq. (1) for a value of $\log a_{OH^-} = -6.5$ gives $\log K_{sp}[Ni(OH)_2] = -15.9$. Data from experiments with an ionic strength of 0.2 molal yield systematically lower values of $a_{Ni^{2+}}$ for a given value of $\log a_{OH^-}$, although a linear least-squares fit yields an excellent correlation coefficient ($R^2 = 1.000$). The different values obtained from the high ionic strength experiments are attributed to incorrect modelling of activity coefficients using the Davies' equation in MINTEQA2 at these ionic strengths.

Values of $\log a_{Zn^{2+}}$ vs. $\log a_{OH^-}$ for Zn hydroxide solubility experiments conducted in the absence of MOPS are presented in Fig. 2. A linear least-squares fit for experiments with ionic strength between 0.002 and 0.02 molal yields:

$$\log a_{Zn^{2+}} = -16.70 - 2.01(\log a_{OH^-}) \tag{2}$$

with a correlation coefficient $R^2 = 0.999$. Using Eq. (2) for a value of $\log a_{OH^-} = -6.5$ gives $\log K_{sp}[Zn(OH)_2] = -16.6$. As in the case of the Ni hydroxide experiments, data from experiments with an ionic strength of 0.2 molal yield systematically lower values of $\log a_{Zn^{2+}}$ for a given value of $\log a_{OH^-}$, although a linear least-squares fit again yields an excellent correlation coefficient ($R^2 = 0.998$).

These values of K_{sp} compare favorably with previous measurements of K_{sp}. Compiled measurements [8,9] of $\log K_{sp}[Ni(OH)_2]$ have a range of values between -13.8 and -18.0, and an averaged $\log K$ value of -15.6, compared to a value of -15.9 measured in this study. Compiled measurements [8,9] of $\log K_{sp}[Zn(OH)_2]$ have a range of values between -13.2 and -18.0, and an averaged $\log K$ value of -16.3, compared to a value of -16.6 measured in this study.

3.2. Complexing with MOPS

Solution speciation calculations were performed for experiments conducted in the presence of MOPS and in equilibrium with Ni or Zn hydrox-
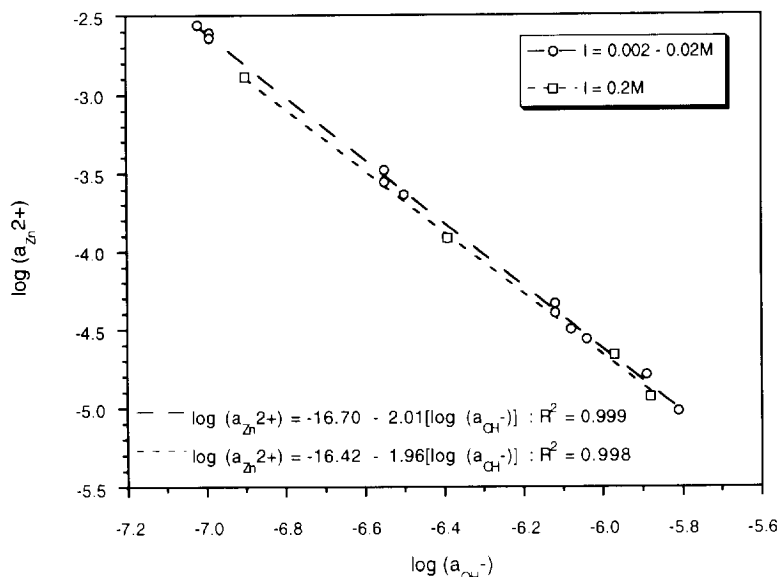
Fig. 2. Calculated values of $\log a_{Zn^{2+}}$ vs. $\log a_{OH}$ for solutions saturated with $Zn(OH)_2$. Ionic strength $NaNO_3 = 0.002$–0.2 M.

ide solid. Calculations at $I = 0.2$ molal were amended with an empirical correction factor to account for the inability of MINTEQA2 to accurately model activity coefficients at this ionic strength, although this correction factor was small. Using the values K_{sp} measured previously, calculated values of the saturation index with respect to $Zn(OH)_2$ are plotted vs. $a_{Zn^{2+}}$ in Fig. 3, and the calculated values of the saturation index with respect to $Ni(OH)_2$ are plotted vs. $\log a_{Ni^{2+}}$ in Fig. 4. The saturation index of $M(OH)_2$ is given by
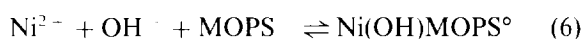
Saturation index

$$= \log\{a_{M^{2+}} \cdot (a_{OH})^2 \, K_{sp}[M(OH)_2]\} \qquad (3)$$

Fig. 3 demonstrates that there is no systematic deviation of the value of the saturation index with respect to $Zn(OH)_2$ for experiments conducted in the presence of MOPS. The spread of saturation indices around zero (i.e. perfectly measured equilibrium) is similar for experiments conducted with or without MOPS. This indicates that the solubility of $Zn(OH)_2$ is not affected by the presence of MOPS, which implies that negligible Zn–MOPS complexing is taking place.

In contrast to Zn, Fig. 4 demonstrates that there is a deviation towards positive values of the saturation index with respect to $Ni(OH)_2$ for experiments conducted in the presence of MOPS, with the most positive values of the saturation index being associated with the highest concentration of MOPS. This indicates that the solubility of $Ni(OH)_2$ is increased by the presence of MOPS, and suggests that significant Ni–MOPS complexing is taking place. The measured Ni concentrations in the presence of MOPS are compared with the calculated Ni concentrations assuming no nickel–MOPS interaction, and the value of excess nickel is defined as

$$C_{Excess \, Ni} = C_{Measured \, Ni} - C_{Calculated \, Ni} \qquad (4)$$

Likely Ni–MOPS complexes include the simple 1:1 complex $NiMOPS^+$, and also the complex $Ni(OH)MOPS°$, as Ni forms a number of Ni–OH complexes. These complexes are formed accordingly:

$$Ni^{2+} + MOPS^- \rightleftharpoons NiMOPS^+ \qquad (5)$$

$$Ni^{2+} + OH^- + MOPS^- \rightleftharpoons Ni(OH)MOPS° \qquad (6)$$
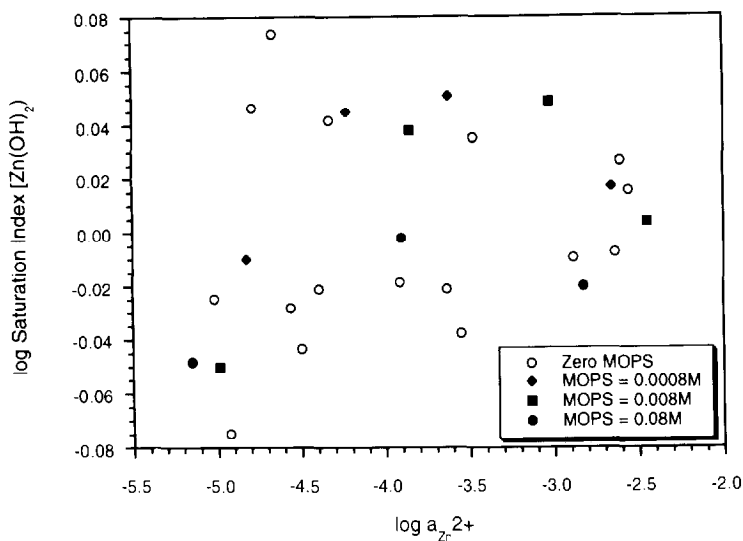
If $NiMOPS^+$ is responsible for the increase in Ni concentration, then:

Fig. 3. Calculated values of log [saturation index $Zn(OH)_2$] for solutions with MOPS concentrations = 0–0.08 M.

$$a_{Excess\ Ni} = C_{Excess\ Ni} \cdot \gamma_{1\pm} \tag{7}$$

and a plot of $\log a_{Excess\ Ni}$ vs. $\log(a_{Ni^{2+}} \cdot a_{MOPS^-})$ should result in a straight line. If $Ni(OH)MOPS°$ is responsible for the increase in nickel concentration, then:

$$a_{Excess\ Ni} = C_{Excess\ Ni} \cdot \gamma_0 \tag{8}$$

and a plot of $\log a_{Excess\ Ni}$ vs. $\log(a_{Ni^{2+}} \cdot a_{OH^-} \cdot a_{MOPS^-})$ should result in a straight line. Values

of $a_{Ni^{2+}}$ and a_{MOPS^-} have been calculated using MINTEQA2, assuming that the fractions of Ni and MOPS present as the Ni–MOPS complex are small, i.e. values of $a_{Ni^{2+}}$ and a_{MOPS^-} are assumed to be unaffected by Ni–MOPS complexing. $\log(a_{Excess\ Ni})$ is plotted vs. $\log(a_{Ni^{2+}} \cdot a_{MOPS^-})$ and $\log(a_{Ni^{2+}} \cdot a_{OH^-} \cdot a_{MOPS^-})$ in Figs. 5 and 6. Linear least-squares fits give respectively:
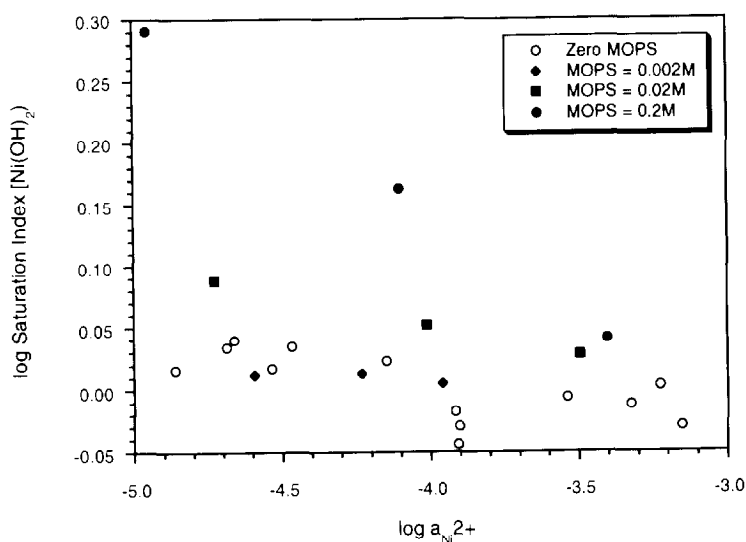

Fig. 4. Calculated values of log [saturation index $Ni(OH)_2$] for solutions with MOPS concentrations = 0–0.2 M.
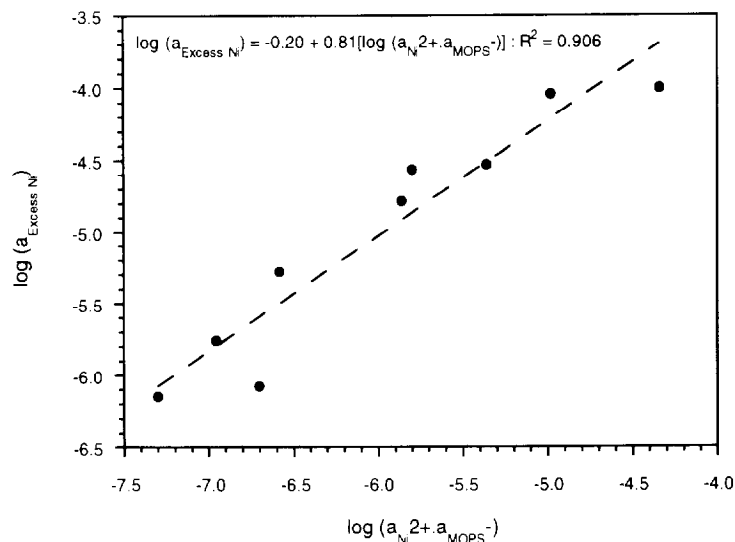
Fig. 5. Calculated values of $\log(a_{\text{Excess Ni}})$ vs. $\log(a_{\text{Ni}^2+} \cdot a_{\text{MOPS}^-})$.

$$\log(a_{\text{Excess Ni}}) = -0.20 + 0.81[\log(a_{\text{Ni}^2+} \cdot a_{\text{MOPS}^-})];$$

$$R^2 = 0.906 \qquad (9)$$

$$\log(a_{\text{Excess Ni}})$$

$$= 7.32 + 1.03[\log(a_{\text{Ni}^2+} \cdot a_{\text{OH}^-} \cdot a_{\text{MOPS}^-})];$$

$$R^2 = 0.969 \qquad (10)$$

The higher value of R^2, and the value of the slope

being very close to the expected value of one, both suggest that formation of the complex Ni(OH)MOPS° provides the best explanation of the experimental data, assuming that only one significant Ni–MOPS complex is formed. Hence:

$$K_{\text{Ni(OH)MOPS}°} = (a_{\text{Ni(OH)MOPS}°})/(a_{\text{Ni}^2+} \cdot a_{\text{OH}^-}$$
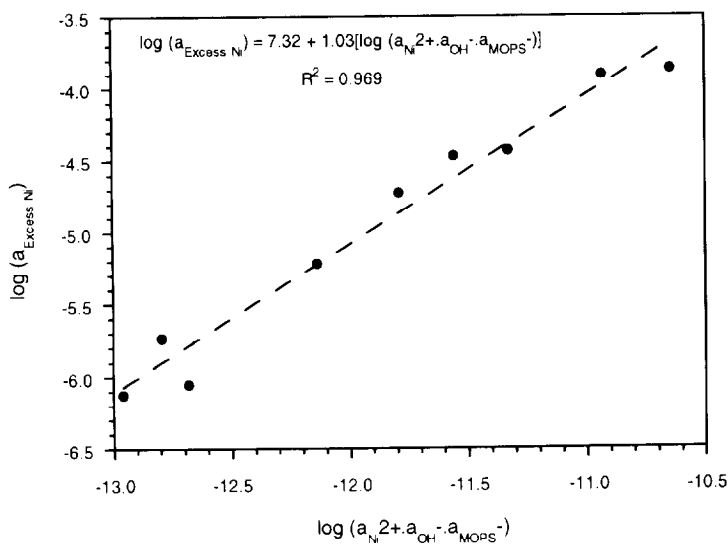
$$\cdot a_{\text{MOPS}^-}) \qquad (11)$$

Fig. 6. Calculated values of $\log(a_{\text{Excess Ni}})$ vs. $\log(a_{\text{Ni}^2+} \cdot a_{\text{OH}^-} \cdot a_{\text{MOPS}^-})$.

and substituting an intermediate value of $\log(a_{Ni^{2+}} \cdot a_{OH^-} \cdot a_{MOPS^-}) = -12$ into Eq. (10) yields a value of $\log K_{Ni(OH)MOPS^=} = +7.0$.

4. Discussion and conclusions

The extent of aqueous complexing between MOPS and Ni^{2+} and Zn^{2+} has been experimentally measured. Complexing between Zn and MOPS is negligible. Although complexing between Ni and MOPS is measurable, the extent of complexing is minor, especially for concentrations of MOPS used for the majority of biological experiments. An example calculation for a solution of 1 μM $Ni(NO_3)_2$ + 20 mM NaMOPS at pH 7 indicates that only 0.5% of the total Ni is present in solution as $Ni(OH)MOPS^\circ$.

The nature of the Ni–MOPS complex has not been determined, but is likely that complex formation is due to interaction of Ni^{2+} with the amine functional group present in MOPS. A systematic variation of metal–amine equilibrium constants across the transition metal series has long been known (the Irving–Williams order [10]). This results in the formation of stronger Ni–amine complexes than Zn–amine complexes, due to the crystal field/molecular orbital stabilization energy associated with the $3d^8$ electron configuration of Ni^{2+}, and the lack of any stabilization energy associated with the $3d^{10}$ electron configuration of Zn^{2+} [11]. This may explain why negligible Zn–MOPS complexing has been identified, while weak Ni–MOPS complexing has been measured.

References

[1] J.D. Allison, D.S. Brown and K.J. Novo-Gradac, U.S. Environmental Protection Agency, Cincinnati, OH, EPA/600 3-91 021, 1991.

[2] J.W. Ball and D.K. Nordstrom, U.S. Geological Survey, Reston, VA, Open File Rep., (1991) 91–183.

[3] N.E. Good, G.D. Winget, W. Winter, T.N. Connolly, S. Izawa and R.M.M. Singh, Biochemistry, 5 (1966) 467.

[4] N.E. Good and S. Izawa, Methods Enzymol., 24B (1972) 53.

[5] W.J. Ferguson, K.I. Braunschweiger, W.R. Braunschweiger, J.R. Smith, J.J. McCormick, C.C. Wasmann, N.P. Jarvis, D.H. Bell and N.E. Good, Anal. Biochem., 104 (1980) 300.

[6] A.E. Martell and R.J. Motekaitis, Determination and Use of Stability Constants, VCH, New York, 1988, p. 216.

[7] I.B. Butler, M.A.A. Schoonen and D.T. Rickard, Talanta, 41 (1994) 211.

[8] L.G. Sillén and A.E. Martell, Chem. Soc. Spec. Publ., 17 (1964) 754.

[9] L.G. Sillén and A.E. Martell, Chem. Soc. Spec. Publ., 25 (1971) 865.

[10] H. Irving and R.J.P. Williams, J. Chem. Soc., (1953) 3192.

[11] F.A. Cotton and G. Wilkinson, Advanced Inorganic Chemistry, 4th edn., Wiley, New York, 1980, p. 1396.

[12] J.A. Dean (Ed.), Lange's Handbook of Chemistry, 13th edn., McGraw-Hill, New York, 1985, p. 1792.

Fluorimetric trace determination of cerium(III) with sodium triphosphate

Ayçiçek Akseli*, Yener Rakicioğlu

Department of Chemistry, Science and Letter Faculty, Istanbul Technical University, 80626 Maslak, Istanbul, Turkey

Abstract

Sodium triphosphate acts as a specific reagent for enhancing the fluorescence intensity of cerium(III). The purpose of this study was to investigate the spectrofluorimetric determination of trace amounts of Ce(III) in sodium triphosphate solution. The excitation and emission wavelengths are 303.5 nm and 353 nm respectively. Optimum sodium triphosphate concentration is found to be 0.074 g l^{-1} at room temperature. The fluorescence varies linearly with the concentration of cerium(III) in the range $0.001-45 \ \mu\text{g ml}^{-1}$. The detection limit is $9.4 \times 10^{-4} \ \mu\text{g ml}^{-1}$. The relative standard deviations for $30 \ \mu\text{g ml}^{-1}$ and $0.05 \ \mu\text{g ml}^{-1}$ Ce(III) in 0.074 g l^{-1} sodium triphosphate solution are 1.1% and 0.72% respectively. Quenching effects of other lanthanides and some inorganic anions are described. This method is a direct and rapid analytical method for the determination of Ce(III) in rare earth mixtures and cerium concentrates.

Keywords: Cerium determination; Fluorimetry; Molecular luminescence spectrometry; Sodium triphosphate

1. Introduction

The chemical properties of the rare earth elements are very similar. Consequently, it is difficult, and important, to find specific reactions for individual ions, especially in their mixtures.

The direct methods described in the literature for the fluorimetric determinations of cerium(III) are the fluorescence of Ce(III) in sulphate and chloride solutions at different pH [1–17], in perchloric acid and sulfuric acid medium [18], in perchloric acid [19] and phosphoric acid medium

[20], and the formation of Ce(III) complexes with hydroxyethylidenediphosphonic acid [21] and sulphonaphtholazo resorcinol [22], in hexametaphosphate solutions [23]. The indirect methods are the chemiluminescent reaction of lucigenin with hydrogen peroxide in the presence of cerium(III) [24], the decomposition of 2-[(8-hydroxy-5-sulpho-7-quinonyl)azo]-1,8-dihydroxy naphthalene-3,6-disulphonic acid with cerium(III) [25], and the oxidative reaction of cerium(IV) with an organic reagent [26–30]. In contrast, fluorimetric determinations of Ce(IV) with an organic reagent [31,32] and determinations of some inorganic and organic compounds with the cerium(IV)–cerium(III) system have been reported [33–35].

* Corresponding author. Fax: +90 212 285 6386.

In this paper, the fluorescence properties of cerium(III) triphosphate are reported and a rapid and sensitive method for the determination of trace amounts of Ce(III) in solution is described.

2. Experimental

2.1. Apparatus

The fluorimetric measurements were carried out on a Perkin Elmer 204 fluorescence spectrophotometer with a 150 W xenon arc lamp. The fluorescence intensities of solutions were measured in 10 mm quartz cells. The excitation and emission slitwidths were 10 nm. The amplifier gain was adjusted according to the fluorescence intensity.

2.2. Reagents

Standard solutions of Ce(III) were prepared by dissolving $Ce(NO_3)_3 \cdot 6H_2O$ (Merck, "Extra Pure") and sodium triphosphate solution was prepared by dissolving $Na_5O_{10}P_3$ (Merck). Other reagents used were of analytical-reagent-grade and were at least 99.5% pure. All solutions were prepared by simply weighing and dissolving the undried chemicals. Ultrapure deionised water (Milli Q Millipore System) was employed for all dilutions.

2.3. Procedure

Apparent fluorescence excitation and emission spectra were measured at room temperature and optimum excitation and emission wavelengths were found from these spectra. A known amount of Ce(III) and 0.1 ml of 7.4 g l^{-1} sodium triphosphate were pipetted onto a 20 ml test tube. The mixture was diluted to 10 ml with deionized water. The fluorescence measurements were made at excitation and emission wavelengths of 303.5 and 353 nm respectively.

3. Results and discussion

3.1. Fluorescence spectra

Ce(III) fluoresces strongly in triphosphate solution when irradiated with ultraviolet light, and is the only lanthanide ion which is appreciably fluorescent under these conditions. Other lanthanide ions do not show any measurable fluorescence in this solution.

Fig. 1 shows the excitation and emission spectra of Ce(III) ion in 0.074 g l^{-1} sodium triphosphate solution. Maximum excitation and emission wavelengths are observed at 303.5 nm and 353 nm respectively.

Experimental results showed that Ce(III) in sodium triphosphate solution is more fluorescent than in solutions without sodium triphosphate, with sulfuric and hydrochloric acids. For sulfuric and hydrochloric acid solutions, we used optimum acid concentrations given in the literature [8,13]. These results are given in Table 1.
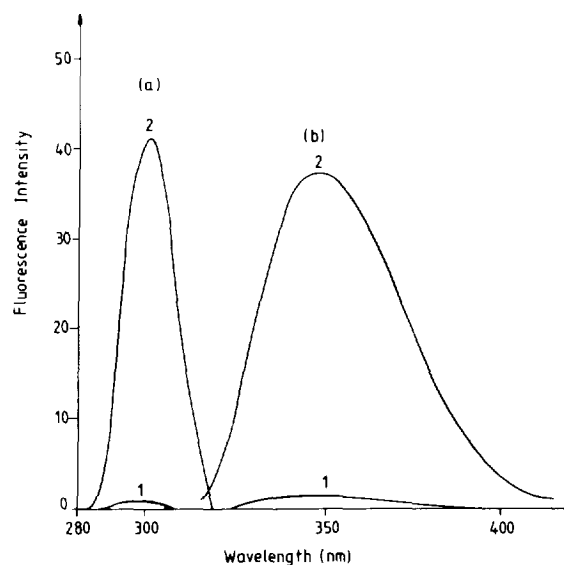

Fig. 1. Fluorescence spectra: (a) excitation; (b) emission. Curves (1): without sodium triphosphate; curves (2): with sodium triphosphate. Conditions: 30 μg ml^{-1} Ce(III) in 0.0074 g l^{-1} sodium triphosphate.

Table 1
Comparison of the fluorescence intensities of Ce(III) in different solutions. Excitation and emission wavelengths are 303.5 nm and 353 nm respectively

Concentration of Ce(III) (μg ml^{-1})	Fluorescence intensity			
	In pure aqueous solutions	In 39.2 g l^{-1} H$_2$SO$_4$ solution	In 255.5 g l^{-1} HCl solution	In 0.074 g l^{-1} sodium triphosphate solution
7.5	75	150	260	1800
15.0	150	300	520	3760
22.5	225	450	780	5760

3.2. Concentration of sodium triphosphate

The effect of sodium triphosphate concentration on the fluorescence intensity was studied for two different Ce(III) concentrations (30 μg ml^{-1} and 0.05 μg ml^{-1} Ce(III) respectively). Fig. 2 shows that maximum fluorescence intensity was obtained for 0.074 g l^{-1} sodium triphosphate.

3.3. Stability of fluorescence with time

The effect of time on the fluorescence intensity was investigated with 30 μg ml^{-1} and 0.05 μg
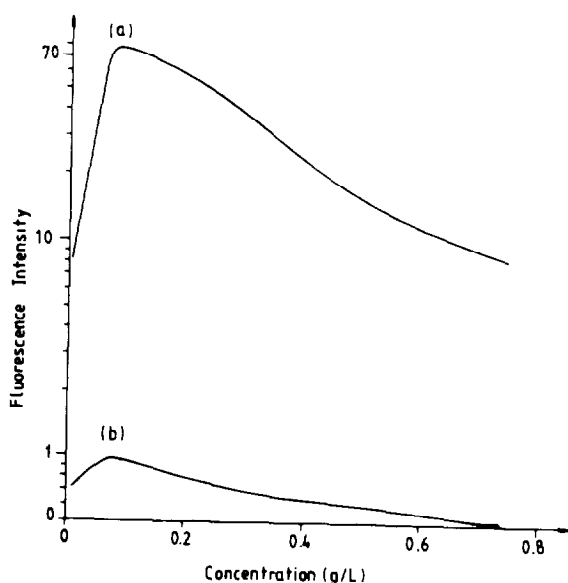
Fig. 2. Variation of fluorescence intensity with sodium triphosphate concentration. Conditions: (a) 30 μg ml^{-1} Ce(III); (b) 0.05 μg ml^{-1} Ce(III). Excitation wavelength: 303.5 nm; emission wavelength: 353 nm.

ml^{-1} Ce(III) in 0.074 g l^{-1} sodium triphosphate solutions. Fig. 3(a; curve 1) and Fig. 3(b; curve 1) show that the solutions were allowed to stand under normal laboratory conditions. Continuous irradiation (Fig. 3(a; curve 2) and Fig. 3(b; curve 2)) for 1 h causes reductions in the fluorescence intensity of 14.63% and 13.64% respectively.

3.4. Effect of pH

pH effect was studied in the range 1.35–10.80 by adjusting the pH with sulfuric acid or sodium hydroxide solution. The results shown in Fig. 4 indicate that the optimum pH range is 5.70–9.35. After studying a series of different buffer systems, it was found that only borax–hydrochloric acid buffer can be successfully used without causing any quenching. Nevertheless, in this study no
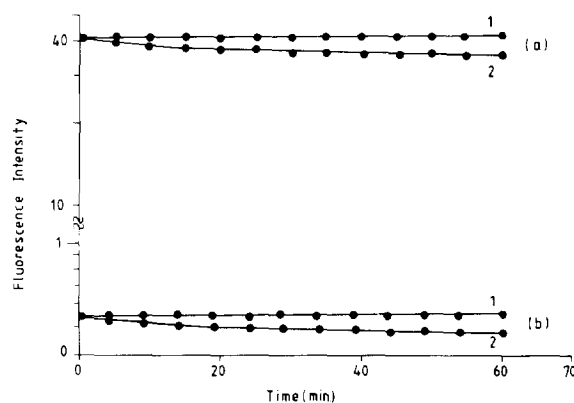
Fig. 3. Fluorescence intensity as a function of time. Conditions: 0.074 g l^{-1} sodium triphosphate solution. (a) 30 μg ml^{-1} Ce(III); (b) 0.05 μg ml^{-1} Ce(III). Curves (1): standing under normal laboratory conditions. Curves (2): continuous irradiation at 303.5 nm.
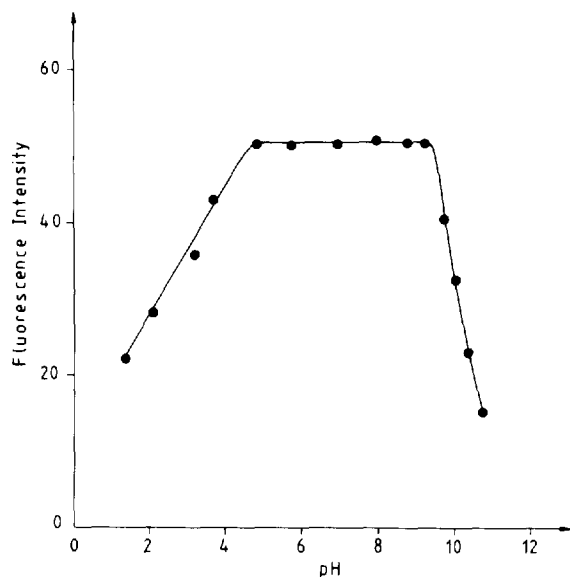
Fig. 4. Effect of pH on the fluorescence intensity. Conditions: 7.5 μg ml⁻¹ Ce(III) in 0.074 g l⁻¹ sodium triphosphate solution.

buffer was used because the pH of the solutions was always in the optimum range 5.70–9.35 during the entire procedure.
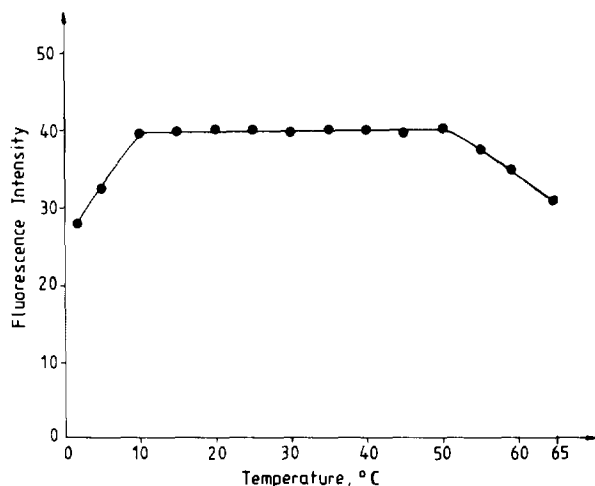
Fig. 5. Effect of temperature on the fluorescence intensity. Conditions: 15 μg ml⁻¹ Ce(III) in 0.074 g l⁻¹ sodium triphosphate solution.

3.5. Effect of temperature

As can be seen from Fig. 5, temperature effect is not pronounced between 10–50°C and room temperature is recommended.

3.6. Calibration graph

The calibration graph for the determination of Ce(III) was constructed under the optimum conditions. Excellent linearity was obtained over the range 0.001–45 μg ml⁻¹ Ce(III). The limit of detection is 9.4 × 10⁻⁴ μg ml⁻¹. It was calculated by multiplying the standard deviation of 16 blank measurements by three and dividing by the slope of the linear calibration curve. Table 2 lists the results of several methods used previously for the spectrofluorometric determination of cerium. It can be seen that the method proposed in this paper is the most sensitive.

3.7. Interferences

As can be seen from Table 3, when other lanthanides are present in relatively low concentrations in the sample no significant interference was observed.

The effects of La(III), Ho(III) and Lu(III) were also investigated. The amount of Ce(III) used is 15 μg ml⁻¹ in 0.074 g l⁻¹ sodium triphosphate solution. 20 μg ml⁻¹ La(III) did not show any interference, whereas 40.90% and 43.18% interferences were shown by 20 μg ml⁻¹ Ho(III) and 20 μg ml⁻¹ Lu(III) respectively.

The interference effects of diverse anions on the fluorescence intensity of 15 μg ml⁻¹ Ce(III) in 0.074 g l⁻¹ sodium triphosphate solution were also investigated. No interference was observed for 300 μg ml⁻¹ sulfate, nitrate, or chloride ions, whereas 30% interference was observed in the presence of 15 μg ml⁻¹ phosphate ions.

3.8. Application of the method

The procedure was applied to the determination of trace amounts of cerium in some synthetic mixtures. The results given in Table 3 indicate that the proposed method is suitable and can be successfully applied.

Table 2
Summary of several methods for the fluorimetric determination of cerium

Reagent	Limit of detection (μg ml^{-1})	Linear range (μg ml^{-1})	Ref.
H$_2$SO$_4$	–	$1.0 \times 10^{-3} - 1.0 \times 10^{-1}$	8
HCl	–	$1.4 \times 10^{-2} - 1.4 \times 10^{-1}$	13
Sulphonaphtholazoresorcinol	5.0×10^{-2}		22
Sodium hexametaphosphate	–	$1.0 \times 10^{-3} - 60$	23
Lucigenin (I)–H$_2$O$_2$ system		$8.0 \times 10^{-1} - 1.2$	24
Oxine-5-sulfonic acid		$1.0 \times 10^{-2} - 3.0$	26
Sodium-4.8-diamino-1,5-dihydroxyan-thraquinone-2,6-disulfonate		$2.0 \times 10^{-2} - 3.7 \times 10^{-1}$	27
1-amino-4-hydroxyanthraquinone		$1.0 \times 10^{-1} - 9.0 \times 10^{-1}$	28
Paracetamol	1.4×10^{-3}	$2.8 \times 10^{-2} - 1.12$	30
Sodium triphosphate	9.4×10^{-4}	$1.0 \times 10^{-3} - 45$	Present method

Table 3
Analysis of the synthetic mixtures in 0.074 g l^{-1} sodium triphosphate solutions

Mixture number	Mixture composition (μg ml^{-1})	Ce(III) found (μg ml^{-1})	Error (%)
1[a]	Ce(7.50), La(2.50), Pr(0.68), Nd(2.50), Sm(0.26), Eu(0.0075), Gd(0.30), Tb(0.10), Dy(0.12), Ho(0.03), Er(0.06), Yb(0.03), Lu(0.015), Tm(0.001)	7.43	0.93
2	Ce(10.00), Nd(5.00), Sm(2.00), Gd(2.00)	9.91	0.90
3	Ce(15.00), Sm(5.00), Tm(1.00), Yb(2.00)	14.85	1.00
4	Ce(22.50), Gd(5.00), Tm(2.00), Yb(2.00)	22.28	0.98
5	Ce(30.00), Dy(3.00), Sm(2.00), Nd(2.00)	29.73	0.90

[a]This mixture was prepared on the basis of relative concentrations of rare earths in Monazite mineral.

3.9. Precision

The precision was determined by measuring 16 solutions of the same sample 16 different times. The relative standard deviations of these measurements were 1.1% for 30 μg ml^{-1} and 0.72% for 0.05 μg ml^{-1} Ce(III) in 0.074 g l^{-1} sodium triphosphate solutions.

4. Conclusion

From the results presented it can be concluded that sodium triphosphate is a very suitable reagent and that the fluorimetric trace determination of Ce(III) with sodium triphosphate is a very easy, rapid, sensitive and inexpensive new method.

References

[1] A.N. Filippov, Ya Larionov and A. Zaidel, C. R. (Dokl.) Acad. Sci. URSS 20 (1938) 351.
[2] P.C. Mukherji. Z. Phys. 109 (1938) 573.
[3] A. Zaidel, Ya Larionov and A.N. Filippov, J. Gen. Chem. USSR. 8 (1938) 943.
[4] A.N. Zaidel, Ya. I. Larionov and A.N. Filippov, Bull. Acad. Sci. USSR. Cl. Sci. Math. Nat. Ser. Phys., 3 (1938) 334.
[5] L. Mazza, Ann. Chim. Appl., 30 (1940) 47.
[6] A.N. Zaidel and Ya. I. Larionov, Bull. Acad. Sci. USSR. Ser. Phys., 4 (1940) 25.
[7] Ya. I. Larionov, Vestn. Leningr. Univ., 7 (1947) 18.
[8] W.A. Armstrong, D.W. Grant and W.G. Humpreys, Anal. Chem., 35 (1963) 1300.
[9] G.F. Kirkbright, T.S. West and C. Woodward, Talanta, 12 (1965) 517.
[10] N.S. Polucktov, A.I. Kirillov, M.A. Tishchenko and Yu. V. Zelyukova, Zh. Anal. Khim., 22 (1967) 707.
[11] F. Masamichi. S. Shozo and N. Ryozo, Nagoya Kogyo

Gijutsu Shikensho Hokoku. 17 (1968) 251.

[12] B. Herbert, Nature, 222 (1969) 161.

[13] G.F. Kirkbright, C.G. Saw and T.S. West, Talanta, 16 (1969) 65.

[14] T. Shigematsu, Y. Nishikava, H. Keizo, G. Shiro and T. Yoshimori, Bunsegi Kagaku, 20 (1971) 575.

[15] V.P. Kazakov and A.I. Laphsin, Teor. Eksp. Khim., 7 (1971) 133.

[16] D.P. Shcherbov, O.D. Inyutina, R.N. Plotnikova and V.I. Kosianenko, Zh. Anal. Khim., 27 (1972) 1407.

[17] Z. Yulun, Yanshi Kuangwu Ji Ceshi, 3 (1984) 344.

[18] P. Cukor and R.P. Weberling, Anal. Chim. Acta, 41 (1968) 404.

[19] R.I. Cazotti, Report INIS-mf-1571, INIS Sect., Int. At. Energy Agency, Vienna, Austria, 1973.

[20] Z. Holzbecher, Collect. Czech. Chem. Commun., 54 (1989) 616.

[21] D.V. Demeshko, V.A. Perfilev and V.T. Mishchenko, Vysokochist Veshchestva., 2 (1992) 162.

[22] C.T. Hjeu, A.I. Volkova and T.E. Getman, Zh. Anal. Khim., 24 (1969) 688.

[23] A. Akseli and Y. Rakicioğlu, Fresenius. J. Anal. Chem., 354 (1996) 424.

[24] L.I. Dubuvenko, M.M. Tananaiko and V.G. Drokov, Ukr. Khim. Zh., 40 (1974) 758.

[25] Y. Yuan, J. Zhiqin and H. Jianfeng, Fenxi Huaxue, 21 (1993) 53.

[26] B.K. Pal, F. Toneguzzo and A. Corsini, Anal. Chim. Acta, 88 (1977) 353.

[27] A. Navas, F.S. Rojas and F.G. Sanchez, Mikrochim Acta, Part 1, (1982) 175.

[28] F. Salinas, C. Genestar and F. Grases, Microchem. J., 27 (1982) 32.

[29] F. Grases, C. Genestar and J.G. March, Microchem. J., 29 (1984) 237.

[30] J. Nianqin, Y. Jinghe and L. Tao, Talanta, 41 (1994) 415.

[31] G. Yaxian, S. Shuju, W. Qingxun, L. Hongmei and N. Fenglan, Jilin Daxue Ziran Kexue Xuebau, 3 (1989) 89.

[32] J. Nianqin and D. Zhihang, Yejin Fenxi, 11 (1991) 51.

[33] G.F. Kirkbright, T.S. West and C. Woodward, Anal. Chim. Acta, 36 (1966) 298.

[34] G. Amann, G. Gubitz, R.W. Frei and W. Santi, Anal. Chim. Acta, 116 (1980) 119.

[35] E.E. Elbashier and G.M. Greenway, J. Micronutr. Anal., 8 (1990) 311.

Calorimetry and potentiometry of chemical oscillations in Briggs–Rauscher reactions with simultaneous measurements of the produced oxygen volume[1]

Shuko Fujieda*, Hideko Ogata

Department of Chemistry, Ochanomizu University, Bunkyo-ku, Tokyo 112, Japan

Abstract

The Briggs–Rauscher reaction is known as a nonlinear and non-equilibrium chemical oscillation reaction. The reaction solution is composed of malonic acid as organic substrate, hydrogen peroxide and iodate in sulphuric acid as oxidizing agent, and manganese (II) as metal catalyst. The calorimetric behaviour, in terms of the total heat Q and the heat evolving rate q for each chemical oscillation, was followed with the use of a heat exchange calorimeter of the batch type assembled by the authors. Simultaneously, the concentration of iodide ions produced as the intermediate species was measured as the potential difference E by the common potentiometric cell incorporated in the calorimeter and the released oxygen volume G was also observed by a simple flowmeter. The starting point of the peak on the curve of q against time t coincided with that in the curve of E against t. The switching concentration of iodide between radical and nonradical paths was calculated from literature values of rate constants. The heat evolving period of Q coincided with the period in the radical path. The curve of Q against t also coincided with that of G against t. The total volume of released oxygen was larger than that calculated from the stoichiometric reaction formula.

Keywords: Briggs–Rauscher reactions; Calorimetry; Chemical oscillations; Potentiometry; Produced oxygen volume

1. Introduction

The Belousov–Zhabotinskii (BZ) reaction is typical of nonlinear and non-equilibrium oscilla-

tion reactions and the reaction mechanism has been well studied [1]. In the best known BZ reaction, the oxidation of malonic acid by acidic bromate is catalyzed by the cerium (IV) salt or by ferroin (tris(1,10-phenanthroline) iron (II) complex).

The Briggs–Rauscher (BR) reaction was discovered in 1973 [2]. A mixture of hydrogen peroxide and iodate is used in sulphuric acid as the oxidizing agent, and manganese (II) ion is used as

---
* Correspoding author. Tel.: +813 5978 5347; Fax: +813 5978 5716; e-mail: fujieda@chem.ocha.ac.jp.

the catalyst. Malonic acid (MA) is also used as the organic reaction substrate. The detailed reaction mechanism was studied in a series of reports [3–5]. The reaction process is more complex than that of the BZ reaction, as the BR reaction is composed of 30 elementary reactions which are divided into six steps. MA was expressed generally as RH [5].

In the stoichiometry, only reaction (1) may be relevant:

$$IO_3^- + 2H_2O_2 + RH + H^+ \rightarrow RI + 2O_2 + 3H_2O \tag{1}$$
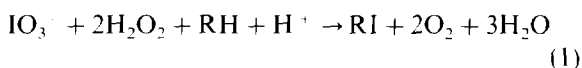
However, reaction (1) is divided into reaction (2), reduction of iodate, and reaction (3), organic iodination:

$$IO_3^- + 2H_2O_2 + H^- \rightarrow HOI + 2O_2 + 2H_2O \tag{2}$$

$$HOI + RH \rightarrow RI + H_2O \tag{3}$$
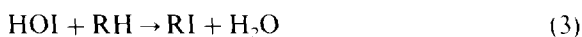
Reaction (2) is derived from (I3) + (I2) + 2(D1) in Ref. [5] as a nonradical path, and also from 2(I5) + 4(M1) + 4(M2) + 2(O2) + (I4) as a radical path. The chemical oscillations may be caused by switching between these two paths. Reaction (3) is derived from (I1) + (C3) + (C4).

De Kepper and Epstein [6] demonstrated the phase diagrams of complicated intermediate compounds and distinguished the existence of oscillation and bistable steady states.

Nakanishi and Fujieda [7] developed heat exchange calorimetry [7]. Two vessels were fixed differentially in the water bath. Heat released in the reaction vessel was exchanged freely with the ambient water. The temperature change in each vessel was monitored via thermistors used as temperature sensors, and then converted to electric signals. The analogue computation was followed on line to obtain total heat effect Q and heat evolving rate q. As the bath water is controlled precisely within a narrow temperature range, chemical reactions can be conducted at almost constant temperature. Therefore, heat exchange calorimetry may be a very suitable method to follow the thermal behaviour in the BZ and BR reactions. Calorimetric studies using batch-type [8,9], flow-type [10] and continuous stirred tank reactors (CSTRs) have been reported for BZ reactions.

It appears that the reproducibility commonly used in analytical chemistry may be poor with respect to the period and amplitude of each chemical oscillation owing to delicate differences in experimental conditions, such as initial concentrations of each component, temperature and stirring rate. Therefore, simultaneous observations of chemical and physical quantities as far as possible are desired for an oscillation run.

In the present report, BR reactions of the batch type were studied to compare with the results of the BZ reactions. The heat exchange calorimeter was assembled, the fundamental concept and essential parts being almost the same as those reported previously [8]. The common potentiometric cell was incorporated. The Q and q values for every oscillation were observed. Simultaneously, the oscillation behaviour of the iodide ion produced as the intermediate species was monitored potentiometrically as E. The evolving rate of produced oxygen G and the total amount of released oxygen were measured with a simple apparatus.

2. Experimental

2.1. Reagents

All the reagents were of guaranteed grade and were used without further purification. The chemical oscillation systems were composed of potassium iodate, hydrogen peroxide, sulphuric acid, MA and manganese(II) sulphate, of which initial concentrations were in the ranges 0.040–0.080 M, 0.20–1.44 M, 0.018–0.071 M, 0.030–0.12 M and 0.0040–0.010 M respectively. As usual, deionized water was used after distillation. Solid MA was selected to start the oscillation reaction because of its rapid dissolution and ease of handling.

2.2. Apparatus

The block diagram of the assembled calorimeter system is shown in Fig. 1. An acryl box of 42 × 27 × 28 cm³ was used as the water bath and all surfaces were covered with thermal insulator boards 3 cm thick. About 28 dm³ of water was used in the bath, the temperature of the bath water being controlled by the previously reported
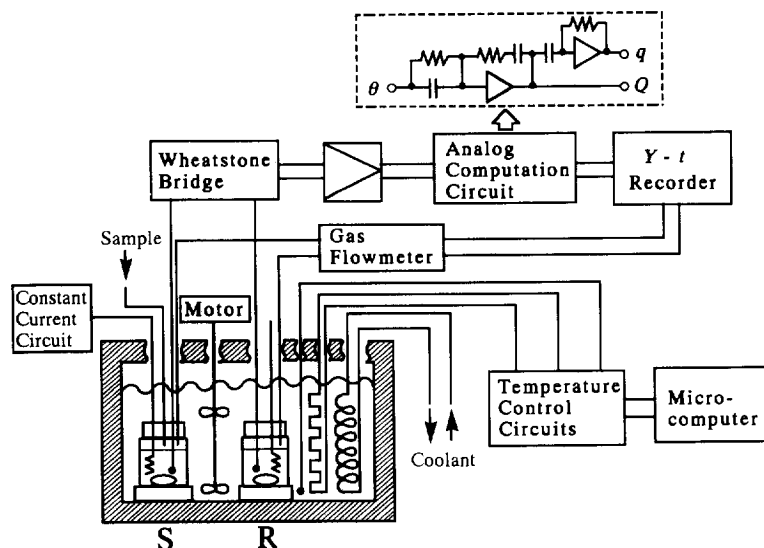
Fig. 1. Schematic diagram of the heat exchange calorimeter system for the batch run.

method [11] within ≤0.001°C at 25.0°C. Detailed illustrations of the sample and reference vessels denoted S and R respectively in Fig. 1 are shown in Fig. 2. The Ag–AgI indicating electrode (A) was made of a silver rod 2 mm in diameter. The salt bridge contained approximately 2% potassium nitrate in agar. The electric heater (H) was made from a metal-wound resistor (1/8 W, 49.98
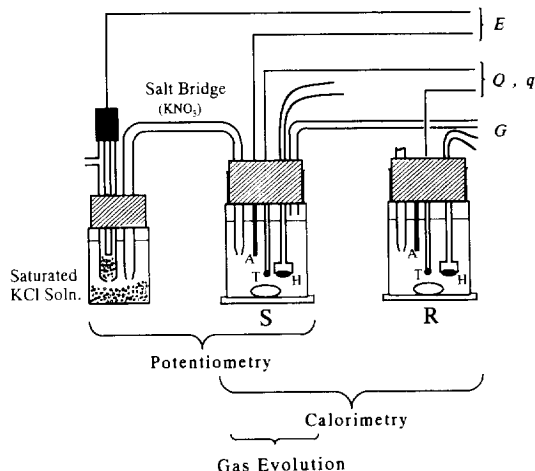
Fig. 2. Details of the sample and reference vessels: S, sample; R, reference; E, potential difference; Q, total heat; q, heat evolving rate; G, oxygen evolving rate; A, Ag–AgI electrode; T, thermistor; H, electric heater element.

Ω) coated with epoxy resin. In the reference vessel, A, H, T and one end of the salt bridge were also installed to compensate for the effective heat capacity. The thermistors (MB, Technoseven Co., Yokohama, Japan) were installed in the S and R vessels as shown by T in Fig. 2. The B and R constants of the thermistor are defined by $R = A \exp(BT^{-1})$. The B constants were observed to be 3377.5 K and 3377.7 K and the resistances (R) to be 5.639 kΩ and 5.625 kΩ respectively, for S and R at 25.0°C. Magnetic stirrers of submarine type (M-3, Iuchi Seieido Co., Tokyo, Japan) were used for each vessel. The electric signals obtained as the unbalanced voltage of the Wheatstone bridge, which is proportional to the temperature observed as the difference between the two vessels, were converted to output voltages which are proportional to Q and q using the analogue operational amplifier (Op Amp) circuit. The output signals were recorded against time with two strip-chart recorders (R-02, Rika Denki Co., Tokyo, Japan).

The potentiometric cell was constructed in the usual manner. The potential difference E of iodide ions against the reference electrode, which was a commerically available saturated Ag–AgCl electrode, was monitored with a digital voltmeter and the strip-chart recorder.

The evolving rate of oxygen produced during the BR reaction was monitored by a simple flowmeter (Floweye 3850 MS, Kojima Seisakusho, Kyoto, Japan), and the output voltage G proportional to the released rate of oxygen was recorded against time. The total volume released by a run was measured primitively with glass burettes as usual in fundamental experiments.

2.3. Procedures

The temperature of the bath water was set to 25.0°C on the control panel. The required amount of water at a temperature near to 25°C was introduced into the water bath and the temperature control system controlled by an 8-bit small microcomputer (M5, SORD Co., Tokyo, Japan) was turned on. 50.0 g of water was used in the reference vessel. The required volumes of the stock solutions of hydrogen peroxide, potassium iodate in sulphuric acid and manganese sulphate were placed in the sample vessel which was fixed with the reference vessel in the water bath. After 40 or 50 min. temperature equilibrium in the water bath was attained and most of the electrical instruments, including the Wheatstone bridge and preamplifier (PM-16, Toa Dempa Co., Tokyo, Japan), were warmed up. Then, the offset voltage of the Op Amp in the analogue computation circuit was adjusted carefully to obtain an output voltage small enough to record horizontal baselines. Time constants in the analogue circuit were fitted to corresponding constants of the calorimeter by adjusting variable resistors on the circuit panel in the course of electrical heating. The Joule heat was accurately measured for the conversion from temperature to heat. To start the BR reaction, MA was added directly to the solution in the sample vessel, which was composed of iodate, sulphuric acid, hydrogen peroxide and Mn(II) salt, from the outside of the calorimeter and the outlet opened to the air was closed at the same time. The output voltages corresponding to Q, q, E and G were recorded on two two-pen recorders. After the chemical oscillation had finished, Joule heat was again observed.

3. Results and discussion

The BZ reactions comprise bromine chemistry and the BR reactions comprise iodine chemistry. Potentiometry of intermediate species, such as bromide and iodide, is commonly used to analyze the reaction mechanism of their chemical oscillations and to study the nature of their reactions. Both reactions are very sensitive to temperature in terms of their oscillation behaviour. Therefore, the execution of chemical oscillation reactions at a strictly constant temperature may be indispensable for precise estimations of chemical and physical properties. With heat exchange calorimetry, chemical reactions can be conducted within a very narrow range of temperatures.

In the calorimetry of chemical oscillation reactions, rapid thermal response may be indispensable. The calorimetric data of BZ reactions were presented by several researchers [12–14] but data for BR reactions are more scarce [15]. In heat exchange calorimetry, the response delay in the measuring system including a pair of thermistors can be expressed via a relation between the real temperature and the observed temperature in each vessel S and R using a constant β (see Ref. [7]). The delay constant can only be estimated experimentally, because it depends upon the assembled calorimeter and may be impossible to express mathematically. With this form of calorimetry, the response delay can be compensated for by on-line analogue computation. The speedy response to sudden thermal changes such as a step function was examined in a previous study [16]. Therefore, in the present work, the advantages of the calorimetric method were applied to study chemical oscillations of BR reactions at constant temperature and without a significant response delay.

The assembled calorimeter of the batch type shown in Fig. 1 was examined by electric heating prior to chemical reactions. The evolved heat was monitored from 1.023 J to 11.531 J by changing the electric current and the operating time. The heat range was selected in connection with each oscillation of the BR reactions. The standard deviation for 10 runs was 0.39% of the mean (mJ mm $^{-1}$ on the recorder used), which was precise
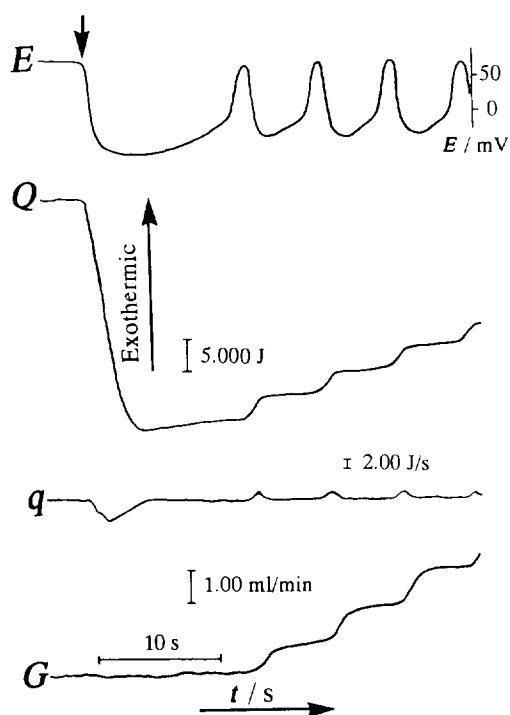
Fig. 3. Typical curves observed against time for the BR reaction in the solution composed of $[H_2O_2]_0 = 1.0$ M, $[KIO_3]_0 = 0.040$ M, $[MnSO_4]_0 = 0.010$ M, $[H_2SO_4]_0 = 0.020$ M and $[MA]_0 = 0.040$ M: E, potential difference; Q, total heat; q, heat evolving rate; G, oxygen evolving rate. At the position of the down arrow, an aliquot of solid MA was added to start the reaction.

enough to measure the heat evolution in every chemical oscillation.

Typical traces of simultaneous measurements for potential difference E, total heat Q, heat evolving rate q and oxygen evolving rate G are shown in Fig. 3 for a batch run. The pen differences on recorder charts were corrected. The initial concentrations of each species were $[H_2O_2]_0 = 1.0$ M, $[KIO_3]_0 = 0.040$ M, $[MA]_0 = 0.040$ M, $[MnSO_4]_0 = 0.010$ M and $[H_2SO_4]_0 = 0.020$ M. The start of the reaction by adding MA is indicated by a down arrow in curve E of Fig. 3. Endothermic curves in Q and q were observed as the heat of solution of MA to the acidic mixture of the other three components and some heat effect by iodination [17] as well, because it is possible that some iodine formation may take place. Detailed estimations of these heat effects

will be discussed separately in relation to minimal oscillation reactions. The induction period was then followed for ≈ 10 s. Heat and gas evolutions became more active after a time lapse of 1 min, and then gas evolution decreased to some extent. Heat evolution was 4.23 J in one cycle 1 min after the start, and corresponded to ≈ 105.8 J mol^{-1} KIO_3 in 0.020 M sulphuric acid. After the duration of the chemical oscillations, a fairly large heat evolution was maintained for about 20 min. At the end of heat evolution, the release of gas gradually finished. The ending patterns of E (obtained from the trace of the E versus time curve in the final stage of chemical oscillations and the final voltage of E at which the oscillation finished) in BR reactions may be more complex than those in BZ reactions and depend upon many factors including each initial concentration. A detailed discussion using a chemometrics approach may be presented separately.

The effect of stirring rate on the oscillation was examined. The influence on E was significant, maximum differences being about 55 mV 40 s after the start of the reaction with a change in the stirring rate from 200 to 700 rev min^{-1}. However, the effect on the oscillation period was small. In the present work, the rate was fixed at 400 rev min^{-1} due to calorimetric restrictions.

The oscillation behaviour was influenced largely by the initial concentration of MA. In the solution with $[MA]_0 = 0.060$ M, the oscillation period was almost constant at 8–11 s and Q was 5–10 J for six runs, for which reaction solutions were composed of $[H_2O_2]_0 = 0.72$ M, $[KIO_3]_0 = 0.080$ M, $[MnSO_4]_0 = 0.0040$ M and $[H_2SO_4]_0 = 0.018$ M. However, with the solution of $[MA]_0 = 0.030$ M, the period was gradually prolonged and Q was also enlarged slowly. For the BZ reaction, similar results were reported in the literature [1,8].

For discussing more explicit relations between potentiometric and calorimetric behaviour, q may be preferred to Q. One cycle of oscillation in E and q curves is shown in Fig. 4. The broken lines in the vertical direction correspond to the starting point and the maximum in the q curve. The maximum of q was not coincident with that of E. The switching concentration [5] was calculated using the literature values of rate constants [5,18].

The critical concentration of iodide, [I $^-$]$_{crit}$, can be obtained as $(k_{15}/k_{12})[KIO_3]_0$ from switching between (I2) and (I5) from Ref. [5]. The E_{crit} relation observed at [I $^-$]$_{crit}$ was obtained from fundamental knowledge of potentiometry to be $E_{crit} = E_s - E_r = (-0.15 - 0.059 \log[I^-]) - 0.2221$ at 25°C, where E_s and E_r are the potentials of the indicating and reference electrodes respectively. As a matter of course, nernstian response was examined with known potassium iodide solutions under experimental conditions as similar as possible. The response time was also rapid enough in comparison with the oscillation period. Increase in E corresponded to a decrease in the concentration of iodide ion. E_{crit} corresponding to [I $^-$]$_{crit}$ was calculated to be (1) -5.0 mV for $[KIO_3]_0 = 0.07919$ M using rate constants [18] of $k_{12} = 2.0 \times 10^9$ M^{-2} s^{-1} and $k_{15} = 1.516 \times 10^4$.

Fig. 4. One cycle of oscillation to compare E and q against time. The initial concentrations were as follows: [H$_2$O$_2$]$_0$. 0.7171 M; [KIO$_3$]$_0$, 0.07919 M; [MA]$_0$, 0.02998 M; [MnSO$_4$]$_0$. 0.009001 M; [H$_2$SO$_4$]$_0$, 0.07094 M. Switching concentrations calculated [18]: (1) from Noyes and Furrow; (2) from De Kepper and Epstein.

M $^{-2}$ s $^{-1}$ from Noyes and Furrow (1982), as shown in Fig. 4. However, for the same concentration of potassium iodate, E_{crit} was (2) 72.7 mV using rate constants [18] of $k_{12} = 2.0 \times 10^{10}$ M^{-2} s^{-1} and $k_{15} = 7.3 \times 10^3$ M^{-2} s^{-1} from De Kepper and Epstein (1982). In the case of $[KIO_3]_0 = 0.03959$ M, E_{crit} was obtained similarly as (1) 13.4 mV and (2) 91.3 mV. Since each initial concentration in this work was not adjusted to the literature values, agreement between experimental and calculation is not necessarily expected. Roughly speaking, when E is larger than the value (1), reactions in the radical path may be in the active state, and when E is smaller than (1), those in the nonradical path may be in the active state. The starting point of the peak on the E curve coincided with that of q. This means that heat evolution may begin instantaneously on switching to the radical path. In BZ reactions a fairly large heat evolution in each oscillation was observed in batch runs [8] and with a CSTR [10]. However, with minimal oscillations in solutions composed of Ce(III), bromate, bromide and sulphuric acid, heat evolution was not detected [17]. Of special interest here is the absence of MA. As for BR reactions, heat evolution may be involved in the process including the MA, even if an exothermic reaction is not included in the radical path.

The maximum q observed in Fig. 3 was 1.88 J s^{-1} (or 37.62 m W cm^{-3}) for a sample volume of 50.0 cm^3. Lamprecht [15] also measured the heat evolving rate and estimated it to be 2 m W cm^{-3} in the same volume of a mixture of [H$_2$O$_2$]$_0$ = 3.6 M, [KIO$_3$]$_0$ = 0.20 M, [MnSO$_4$]$_0$ = 0.020 M, [HClO$_4$]$_0$ = 0.15 M, [MA]$_0$ = 0.15 M and 0.01% of starch. In the present work, the corresponding value was much larger than that of Lamprecht. However, there were several differences between the methods such as experimental technique, initial concentrations of species, inclusion of starch, and the use of perchloric acid instead of sulphuric acid.

Roelofs [19] estimated the reaction enthalpy as $\Delta H = -565$ kJ mol^{-1} IO$_3^-$ for IO$_3^-$ + 6H$_2$O$_2$ + RH + H$^+$ → RI + 4O$_2$ + 7H$_2$O, instead of reaction (1). In the present study, the total Q from the beginning to the end of oscillations
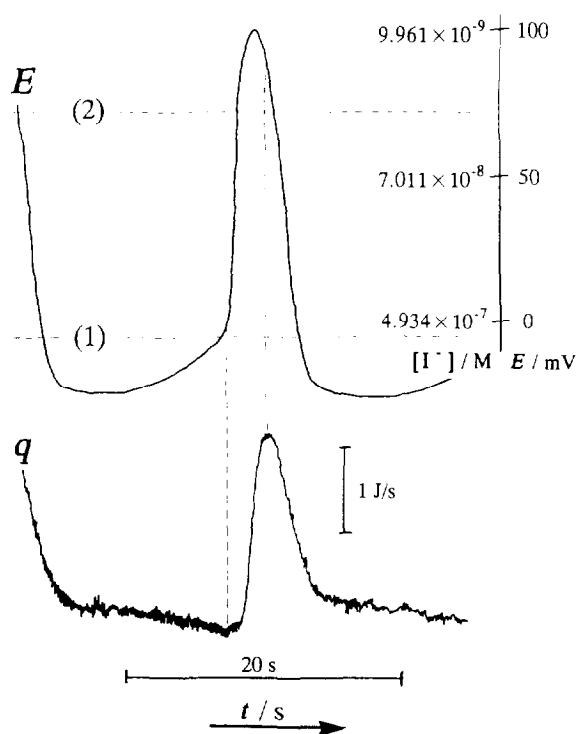
amounted to 2.0 kJ or 1.0×10^3 kJ mol^{-1} IO$_3^-$, which was almost twice that found by Roelofs.

The maximum of E corresponded to the minimum of G. The most active period in the radical reaction may correspond to the period of lowered gas evolution.

Accurate estimation of the released oxygen volume was considered to be necessary for the correction of heat released by oxygen evolution. The total volume of oxygen released was measured for several combinations of three concentrations of hydrogen peroxide (0.36, 0.72 and 1.44 M) and MA (0.030, 0.060 and 0.120 M) with 0.079 M [IO$_3^-$]$_0$. All the observed volumes were larger than those calculated from reaction (1) at 25.0°C. However, some elementary reactions involving oxygen production exist which were not included in the fundamental equations [5]. Therefore, the observed volume may be larger than those calculated. Unfortunately, however, the correction for heat released was impossible due to the lack of the heat of gas evolution. Degn [20] also reported the released volume of carbon dioxide in the BZ reaction with simultaneous measurement of the potential differences of platinum and platinized platinum electrodes. The oscillations of oxygen release observed for the BR reaction in the present study were essentially similar to those for the BZ reaction given in the literature.

References

[1] R.J. Field, E. Koros and R.M. Noyes, J. Am. Chem. Soc., 94 (1972) 8649.

[2] T.S. Briggs and W.C. Rauscher, J. Chem. Educ., 50 (1973) 496.

[3] S.D. Furrow and R.M. Noyes, J. Am. Chem. Soc., 104 (1982) 38.

[4] S.D. Furrow and R.M. Noyes, J. Am. Chem. Soc., 104 (1982) 42.

[5] R.M. Noyes and S.D. Furrow, J. Am. Chem. Soc., 104 (1982) 45.

[6] P. De Kepper and I.R. Epstein, J. Am. Chem. Soc., 104 (1982) 49.

[7] M. Nakanishi and S. Fujieda, Anal. Chem., 44 (1972) 574.

[8] S. Fujieda and J. Kawahito, Thermochim. Acta, 183 (1991) 153.

[9] J. Kawahito and S. Fujieda, Thermochim. Acta, 210 (1992) 1.

[10] S. Fujieda and W. Zhang, Thermochim. Acta, 267 (1995) 95.

[11] S. Fujieda and J. Kawahito, Thermochim. Acta, 190 (1991) 175.

[12] I. Lamprecht and C. Meggers, Z. Naturforsch., Teil B, 24 (1969) 1205.

[13] H.G. Busse, Nature (London), Phys. Sci., 233 (1971) 137.

[14] E. Koros, M. Orban and Zs. Nagy, Nature (London), Phys. Sci., 242 (1973) 30.

[15] I. Lamprecht, Indian J. Technol., 30 (1992) 578.

[16] S. Fujieda and M. Nakanishi, Thermochim. Acta, 92 (1985) 245.

[17] S. Fujieda and W. Zhang, personal communication, 1995.

[18] R.J. Field and M. Burger (Eds.), Oscillations and Travelling Waves in Chemical Systems. Wiley, Chichester, UK, 1985, p. 190.

[19] M.G. Roelofs, J. Chem. Phys., 88 (1988) 9.

[20] H. Degn, Nature, 213 (1967) 589.

Near-infrared tetra-substituted aluminum 2, 3-naphthalocyanine dyes for optical fiber applications

Guillermo A. Casay, Narasimhachari Narayanan, Lawrence Evans III,
Tibor Czuppon, Gabor Patonay*

Department of Chemistry, Georgia State University, Atlanta, GA 30303, USA

Abstract

The synthesis and spectral characterization of several tetra-substituted aluminum 2, 3-naphthalocyanine dyes for the determination of metal ions is reported. The synthesis is done by means of a homogeneous phase reaction, replacing the previously used heterogeneous method. The new scheme allows for improved product yields, higher purity, better product reproducibility and can be monitored at different stages using UV–Vis–near-infrared spectroscopy. The incorporation of electron-donating or -withdrawing groups was found to influence the product yield and to cause a shift in the absorbance maximum. The typical shift in the excitation maximum (of up to 27 nm) enables the dye to match the output of semiconductor laser diodes. In addition the tetra-substituted groups were capable of undergoing an ion-exchange process with the metal ions which produced a change in the fluorescence signal of the dye. Similar results were achieved using an optical fiber metal probe. The detection of metal ions using the near-infrared dyes was accomplished via steady-state fluorescence using both a commerically available instrument and a fiber optic system and also via the fluorescence lifetime technique.

Keywords: Fluorescence; Fluorescence lifetime; Metal ions; NIR; Probes

1. Introduction

The development of a rapid method to determine metal ions in the environment has become the major priority of many health organizations [1,2]. Optical fiber chemical detectors (OFCDs)

have been shown to be a good method for the rapid determination of metal ions [3–8]. Compared to the conventionally used methods (atomic absorption, inductively-coupled plasma (ICP) emission and ICP–MS), OFCDs are smaller and more cost efficient [9,10]. The principle behind the OFCD is the ability to excite a molecular dye and then detect its emission signal via fiber optics. In the present study the authors have synthesized

* Corresponding author

several molecular dyes with the ability to bind metal ions through an ion-exchange process.

Most OFCDs reported in the literature was UV–Vis fluorophores such as rhodamine, fluorescein and their derivatives [4,11–14]. However, many of these probes suffer from spectral interferences either from other molecules with similar properties to the molecular probe or by direct interference [15–17]. For instance, many different polyaromatic hydrocarbons have emission spectra in the 200–600 nm region where many UV–Vis fluorophores also exhibit absorbance or fluorescence [18]. Also, assuming the fluorescence has been sufficiently quenched, the Raman shift (especially in water) may interfere with the fluorescent signal. The near-infrared (NIR) region (700–1000 nm) can be used as an alternative region of analysis for the application and developement of optical fiber metal probes. This particular region exhibts low background interference from many molecules and is ideal when laser diode excitation is coupled with silicon photodiode detectors to allow for a very sensitive detection system [10,19].

We are currently interested in the synthesis and development of new near-infrared dyes (NIRDs) that can be used in optical fiber applications, especially for the determination of metal ions [19–21]. The aluminum naphthalocyanine family of dyes characteristically exhibits a sharp Q-band at ≈ 780 nm which was found to be well suited for laser diode excitation. The Q-band is also well separated from a stronger band at ≈ 340 nm which minimizes band overlap [22,23]. The Stokes' shift exhibited by the dyes is very small, and can cause broadening of the emission band due to scattered light [24]. However, this can be resolved by exciting the NIRD at a wavelength blue-shifted with respect to the absorbance maximum or by using a bandpass filter. Exciting at a wavelength blue-shifted with respect to the absorbance maximum will cause the intensity of the emission band to be slightly lower but can be enhanced by increasing the output power of the light source.

We report in this paper the synthesis and spectroscopic characteristics of several new tetra-substituted aluminum 2,3-naphthalocyanine (AlNc) dyes synthesized in homogeneous phase which can

be followed by using UV–Vis–NIR spectroscopy. In earlier reports, the synthesis of AlNc dyes in a hetergeneous phase involved several disadvantages, such as low yields, complicated steps and random reproducibility [22,23]. The procedure reported here permits better control of the synthesis of the dye and significantly improves the final yield of the product. Also, the effect of the substituent moiety and the use of different solvents in the preparation of the NIR dyes will be examined to show their effect on the final product. The tetra-sulfonated AlNc derivative was used since its absorbance maximum (781 nm) was a good match for the wavelength output of the laser diode (780 nm). Results comparing the changes in the photochemical properties of the unbound and metal-bound tetra-sulfonated AlNc dye will be presented.

To determine the utility of the tetra-sulfonated dye in optical fiber probe applications, the dye was entrapped in a permeable polymer and the polymer attached to the probe support. As the metal ions move towards the dye, the metal ions exchange with the H^- on the HSO_3 inside the polymer matrix and, upon laser diode excitation, the fluorescence is acquired. Assuming a 1:1 ratio and that no other interfering ions take part in the equilibrium, the association of metal ions, M^+, with the NIRD can be represented as

$$[M^+] + [D^-] \rightleftharpoons [DM]$$

where the square brackets indicate molar concentrations of the metal ions, the NIR dye (D^-) and the dye–metal complex (DM) formed. At equilibrium, the binding of the metal ions to the dye (entrapped by the polymer at the end of the fibers), can be expressed as the optical fiber association constant K_{op}, where $K_{op} = [DM]/[M][D]$.

The optical fiber association constant of the dye can be determined by

$$\frac{1}{I_f} = \frac{1}{kD_T} + \left(\frac{1}{kD_T K_{op}}\right)\frac{1}{[M]} \qquad (1)$$

where I_f is the intensity of fluorescence measured, k is a constant dependent upon the quantum efficiency of the fluorescent process and D_T is the total concentration of the dye [25]. At low concentration, a plot of $1/I_f$ vs. $1/[M]$ produces a straight

Table 1
Selection of organic solvent for the reaction of the naphthalocyanine compounds

Solvent	Boiling point (°C)	Reaction		Solubility
		Time (h)	Yield (%)	
Tetralin	207	4	0	Low solubility of $AlCl_3$
Anisole	154	2	0	Strong complex formation
Quinoline	238	2	12	Sodium complex formation
1-Chloronaphthalene	259	2	35	Moderate solubility
Nitrobenzene	211	2	65	Very good solubility
1,3,5-Trichlorobenzene	208	4	63	Solid at room temperature
1,2,4-Trichlorobenzene	214	4	5	
1,2-Dichlorobenzene	180	7	88	
Benzonitrile	188	12	27	Competition with starting material

line which can be used to calculate the optical fiber association constant. K_{op}, from the slope.

2. Experimental

2.1. Synthesis of the unsubstituted AlNc

A solution of 5.0 g (28.0 mmol) of 2,3-dicyanonaphthalene and 100 ml of 1,2-dichlorobenzene was refluxed. Then 14 ml (14.0 mmol) of 1 M $AlCl_3$ in nitrobenzene (about twice the amount stoichiometrically required) was added. The reaction mixture was refluxed for 7 h and monitored every 30 min by a UV–Vis–NIR spectrometer for product formation and by TLC to check the starting material. The reaction mixture was cooled to room temperature and the solvents removed by steam distillation. The suspension obtained was filtered under pressure and washed thoroughly with acetone. The purity of the product was verified by ¹H NMR and C, H analysis (Table 1). The residue was extracted with acetic acid in a Soxhlet extractor and reprecipitated from concentrated sulfuric acid. The dark-green product was dried sat 125°C (yield 4.80 g, 88%).

2.2. Synthesis of the substituted AlNc

The initial step of the synthesis of the substituted AlNc dyes began with ortho-xylenes 1 (Aldrich). All other intermediates (2, 3, and 4)

and the final dyes 5 were purified by a column chromatography on silica gel. A scheme of the reaction steps used in this synthesis is shown in Fig. 1 and some of the substituted AlNc NIR dyes prepared using this scheme are shown in Table 2. The final products were characterized by traditional ¹H NMR, IR and C, H analysis (which had shown agreement in the ranges C ± 0.3 and H ± 0.1) and purified by reverse-phase HPLC, using RPC18 were aqueous solvents. Fig. 1 also shows a typical structure of the AlNc dyes with the tetrasubstituted groups located in the outer benzene ring.

2.3. Reagents and Methods

All starting materials were obtained from Sigma. All other organic and inorganic reagents: sodium hydroxide, sodium chloride, lithium hydroxide, lithium chloride, potassium hydroxide, potassium chloride, tetralin, anisole, quinoline, 1-chloronaphthalene, benzonitrile, 1,3,5-trichlorobenzenethanol, 1,2,4-trichlorobenzene, 1,2-dichlorobenzene, nitrobenzene, cadmium chloride, and ammonium hydroxide were obtained from Fisher Scientific. Spectragrade methanol was obtained from Aldrich.

For the metal ion investigations, stock solutions of 1000 ppm were prepared to provide suitable metal ion solutions. All successive dilutions were made from the stock solution in 5 ml vials using ultrapure water provided by a Nanopure water

Table 2
Synthesis and properties of substituted AlNc

1	R¹	A: ref.	2	R₅²	R_{//}²	4	Time (h)	Yield (%)	5	λ_{max}^a (nm)	B: ref.	6	R³	λ_{max}^{a,b} (nm)
				H	H	a	7	88	a	788	27	a	HO_3S-	783
				O_2N-	H	b	4	91	b	776	28	b	H_2N-	825
			c	H	O_2N	c	25	0	c					
			d	NC-	H	d	5	79	d	770	f	d	HOOC-	780
			e	H	NC	e	25	0	e					
f	H_2N-	29	f	CF_3CONH	H-	f	5	51	f	787	30	b	H_2N-	825
	H_2-N	29		H	CF_3CONH-		5	32		794	30		H_2N-	830
	HO-	c		H	PhCOO		18	25		797				
	HO-	c		CH_3COO	H		16	0						
				H	CH_3O		25	54		808				
				Br-	H		3	67		785				
				F	H-		3	58		783				
f	H_2N	31		SCN	H		4	55		793				
	HOOC-	32		H-	CH_3OOC-		20	0						
	HOOC-	d		PhOOC-	H-		18	51		790	f	d	HOOC-	780
	HOOC-	d		Ph_2NOC	H-		10	7-		788	f	d	HOOC-	780
	H_2N-	33		H	Phth = N- c		13	42		805	33		H_2N-	830
	H_2N-	34		H	DPM = N-e		8	59		797	33		H_2N-	830

a The spectra were recorded in MeOH (or with <2% DMSO to induce dilution).
b Absorbance maximum of 6 is pH dependent, reported wavelength is for pH 7.
c PhCOCl or MeCOCl respectively, Et_3N, CH_2Cl_2, 0°C.
d PhOH or Ph_2NH respectively, $POCl_3$, toluene, reflux.
e Phth: phthaloyl-, DPM: 2,3-diphenylmaleoyl-.
f Reflux in a mixture of 48% HBr and 100% AcOH.

purification system (Barnstead/Thermolyne Corp., Dubuque IA). Fresh dye samples were prepared as necessary using a 10^{-4} M stock solution of the NIR dye. Each sample of dye was dissolved in methanol unless otherwise specified. Some of the dyes required the addition of small amounts of DMSO (<2%) as a co-solvent to increase solubility in methanol. Solutions of 10^{-1} M metal ion with 10^{-4} M NIRD were prepared and stored in a freezer only for the duration of the experiments. All data reported were obtained at 20°C.

2.4. Apparatus

A Perkin-Elmer Lambda 2 UV–Vis–NIR spectrometer was used for the absorption measurements. The spectrometer was interfaced to a Zenith 286 computer equipped with a PECSS program to store data and control the spectrophotometer. Quartz cuvettes (Fisher) were used to house the samples for absorbance measurements.

Samples were prepared for relative comparison by diluting the dye stock solution to an absorbance intensity of 0.1. Under the conditions used in these experiments, reproducible absorbances of 0.25% ± 0.08% were obtained. Fluorescence measurements were conducted on a SLM8000 Aminco spectrofluorometer using an external laser diode excitation source. Laser diodes (Toshiba or Sharp) of 750–830 nm output wavelengths were used as the excitation source. The spectrofluorometer detector was operated in the photon counting mode at 1000 V. A PS/2 PC system controlled the data acquisition and stored the data automatically for later analysis. Slit widths of 4 mm were used during the experiments. A $12.5 \pm 10 \times 1$ mm³ Herasil (near-UV Silica) cell with all sides optically polished (3.5 ml) was purchased from Starna for fluorescence investigations.

The fluorescence lifetimes were measured on an ISS K2 multifrequency phase fluorometer (Champaign, IL). The light source was a 350 W Xenon

Table 3
R^2 group selectivity for compound 5 in Fig. 1

Reaction	R_x^2	R_p^2	Duration of reaction (h)	Yield (%)
(a)	Withdrawing	H	3-10	51-91
(b)	H	Donating	8-25	25-59
(c)	Donating	H		No product
(d)	H	Withdrawing		No product
(e) A single exception to this observation exists in the case of 4f and 4g, which behave similarly to 4a. However, their sensitivity towards $AlCl_3$ allows only moderate yields.				

arc lamp and the signal was modulated by a Marconi model 2022D frequency synthesizer. The emitted light was modulated and detected via the combination of a second Marconi 2022D frequency synthesizer and a ENI 525LA amplifer coupled to a Hamamatsu R928 photomultiplier tube. Glycogen in water was used as the reference scattering solution for all observations. In cases where the emission band was close to the excitation band, excitation and emission polarizers were set at 0° and 55° respectively to maximize the signal.

2.5. Optical fiber apparatus

The optical fiber apparatus used for the detection of metal ions has been discussed previously and only major characteristics will be presented here [26]. Fig. 2. shows a cross-section diagram of the probe that has been used in these investigations. The unit was composed of two plastic fibers, one connected to the laser diode (Toshiba LTO23MFO) and the other to the detector (silicon photodiode). The ends of the fiber not attached to the detector or laser diode were fused together with poly (methyl methacrylate) (PMMA). The PMMA served as a support for the dye entrapped in the permeable polymer, poly (2-hydroxyl ethyl methacrylate) (PHEMA). A solution of dye with PHEMA polymer was coated onto the support and allowed to air dry. A 1.5:1 polymer:dye ratio was sufficient to collect the fluorescence signal. The optical probe was interfaced to the instrument using the fiber attachment of the instrument to the emission port. The optical fiber was positioned perpendicular to the

opening of the fiber bundle and a collecting lens (Melles Griot) was used to focus the signal from the excitation fiber.

Prefabricated probes were allowed to soak for 10 min in distilled water. Sampling was done of controlled concentrations from lowest to highest. The fluorescence signal was then recorded after immersion for 2 min to allow for ion equilibration. The probe was then removed, rinsed with distilled water and sampling of the next ion concentration was done.

3. Results and Discussion

The use of a homogenous reaction phase allowed for better product yields and a faster overall synthesis time (Table 2). The use of different solvents significantly minimized the reaction times. The results of these investigations are summarized in Table 3. The number and amount of isomers formed as final product were found to be solvent dependent. In some solvents, the formation of several isomers were unavoidable and could not be controlled, making the purification process and isolation of the desired dye more tedious. The purification of compound 5 was found to be dependent on the properties of R^2 which indicated what solvents were appropriate for the synthesis. Compound 5 (if $R^2 \neq H$) symbolized the structures of the four possible isomers that may have been introduced as by-products.

The nature of the R^2 moiety was found to significantly influence the physical and photochemical properties of the molecular dye. The data suggest that better product yields were ob-

Table 4

Spectroscopic characteristics of the 2,3-AlNc derivates

A1-2,3-Nc	λ_{max}		Φ ($\%$)	Log(ε) (l mol^{-1} cm^{-1})	τ (ns)	χ^2
	Ex (nm)	Em (nm)				
(5-O$_2$N)$_4$	765	773	6.80	4.31	1.75 ± 0.001	6.49
(5-NC)$_4$	762	766		4.15	4.05 ± 0.001	2.87
(5-F)$_4$	781	787	48.9	4.18	3.47 ± 0.004	8.61
(5-HOOC)$_4$	794	803		3.76	3.13 ± 0.011	10.35
(5-TFA-NH)$_4$	772	777	45.2	4.10	3.45 ± 0.066	3.62
(5-PhOOC)$_4$	786	790	28.1	n.a.	3.21 ± 0.001	3.95
(5-Ph$_2$NCO)$_4$	784	785	20.3	4.21	3.54 ± 0.039	3.62
(HO$_3$S)$_4$	781	784	33.5	5.09	2.92 ± 0.010	5.47
(6-H$_2$N)$_4$	831	n.f.	n.f.	n.a.	n.f.	n.f.
(6-DPM = N)$_4$	793	801	17.7	3.66	2.46 ± 0.001	4.20

tained when R_x^2 was an electron-withdrawing group and R_β^2 was a hydrogen substituent than when R_x^2 was a hydrogen substituent and R_β^2 was an electron-donating group. No final product was obtained when R_x^2 was an electron-donating group and R_β^2 was a hydrogen substitutent or when R_x^2 was a hydrogen substituent and R_β^2 was an electron-withdrawing group (Table 3). The introduction of electro-withdrawing and-donating moieties also caused shifts in the absorbance maxima.

During the synthesis of the naphthalocyanine compounds, we also observed that if 4 contains an oxygen link to a carbon, an extra equimolar amount of AlCl$_3$ per oxygen was needed to compensate for complexation losses (reaction time 4 h). Also, some polyaromatic by-products (λ_{max} = 400–600 nm) resulted from the interaction of AlCl$_3$ and 1,2-dichlorobenzene if excess AlCl$_3$ was used or the reaction time was too long (more than 10 h). This method was also successful with AlBr$_3$ and GaCl$_3$. The photochemical properties of the tetra-substituted dyes are found in Table 4.

Most of the spectral changes that we have observed using the sulfonated NIRD in the presence of metal ions were blue shifts of the Q-band at ≈783 nm. In the presence of Cd^{2+}, the absorbance maximum shifted to 755 nm. With Mg^{2+} present in solution, the fluoresence signal decreased without a blue shift in the wavelength of the emission band. Similar results were observed with Ba^{2+} and Cd^{2+}. Of the ions investigated, Pb^{2+} and Li$^+$ had the strongest effect on

the photophysical properties of the dyes. The effects of PbCl$_2$ and PbAc$_2$ were almost identical and the changes occurring in the dye resulted soley from the presence of Pb^{2+} and not the counter ion. Similar results were obtained with lithium.

Even though the presence of the counter ions using lead and lithium was not significant, other counter ions showed an effect in the absorbance maximum of the dye, namely OH$^-$. A greater blue shift is observed in very basic (OH$^-$) solutions than with Cl$^-$ ions, as shown in Fig. 3. The presence of OH$^-$ in the microenvironment of the dye increased the $\pi \to \pi^*$ transition gap of the molecule as measured by the larger blue shift of the Q-band. This may have been due to small pH
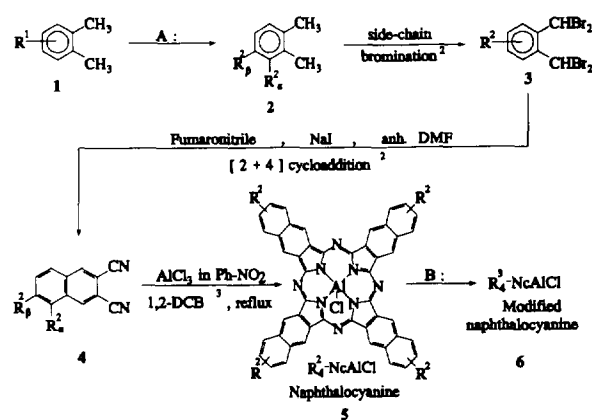

Fig. 1. General procedure used in the synthesis of tetra-substituted AlNc dyes where R represents different moieties.
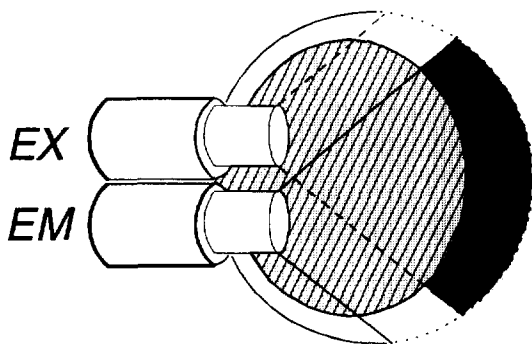
Fig. 2. Cross-section diagram of an optical fiber probe used in this investigation. One fiber is used for excitation and the other is used to collect the fluorescence signal. The darker region represents the area where the optical fiber is collecting most of the fluorescence signal. In one set-up the detector was part of an in-house unit and in the other the probe was interfaced to an ISS K2 fluorometer.

changes in the microenvironment of the dye due to the strong stretching and bending modes of the OH^- groups in the NIR region. If the OH^- group was interacting only through ionic interactions at the peripheral rings, a red shift would have been produced; however, this was not observed since the OH^- groups were acting in a different dye location. Another strong possibility is the effect of the OH^- groups on the central atom, aluminum. The observed changes may be attributed to the effect of the extra orbital of the central atom, that disturbs the electron cloud of the inner nitrogens. The increased Van der Waals forces between the OH^- groups and the metal may have increased the $\pi \rightarrow \pi^*$ transitions gap, especially for the $a_{1u} \rightarrow e_g$ energy transition, thus producing the observed shift. The Van der Waals forces were the result of a strong hydrogen bond between the two center nitrogen atoms that are only partially bonded to the central atom. Steric hindrance by electrostatic repulsion between the extra molecules then changes the symmetry of the structure of D_{2h}. Further evidence of the effect of pH was observed at extreme levels (pH = 3 or pH = 9) where the absorbance maximum increased, therefore also affecting the molar absorption coefficient. Under neutral conditions, the molar absorption coefficients were 78 000 and 5000 for the $(HO_3S)_4$ $(5-O_2N)_4$ dyes respectively.

Under basic conditions (0.1 M NaOH) the absorption coefficient increased to 340 000 for the $(HO_3S)_4$ dye and 7000 for the $(5-O_2N)_4$ dye. A similar increase was observed under acidic conditions when using 0.05 M HCl where the molar absorption coefficient increased to 105 000 $(HO_3S)_4$ and 6600 $(5-O_2N)_4$ respectively.

Using laser diode excitation, the dye was detectable at the picomolar level. At low metal ion concentrations (1–5 ppm) a plot of the fluorescence signals versus the metal ion concentrations produced straight lines with correlation values of around $R = 0.9$. However, beyond 5 ppm the signal began decreasing as linearity diminished. This phenomenon was due to a blue shift of the absorbance band, which caused a mismatch with the wavelength output of the laser diode allowing for excitation on the right side of the absorbance band which gave a lower fluorescence signal.

The fluorescence stability of these NIR dyes was excellent when left at room temperature or stored at 4°C with no special treatment. The excitation source was applied to the NIR dye solution only when the fluorescence intensity was to be measured, to circumvent the possibility of photobleaching. A plot of the measured fluorescence signal for several of these dyes remained unchanged during these investigations. The average normalized intensity, after 28 measurements (30 min intervals), was 1.02 with a standard deviation of 0.01, which may have been due to solvent evaporation.

The fluorescence lifetime of the tetra-sulfonated dye with no metal ions present is 2.92 ns, as shown in Fig. 4. The fluorescence lifetime of the other naphthalocyanine derivatives varied from 1.75 ns to 4.00 ns, as shown in Table 4. In the presence of metal ions (Li^+, Na^+, K^+ and Rb^-), the fluorescence lifetime of the tetra-sulfonated dye decreased. The lifetimes were measured to be 1.56 ns, 1.53 ns, 1.50 ns and 1.43 ns respectively. This trend was found to be consistent with the ionic radii of the metal ions. As the ionic radii increased, the fluorescence lifetime of the dye decreased.

Typical response times of the probe (to 95% of the steady-state response) varied between 10 and 80 s. The longer times measured were at higher
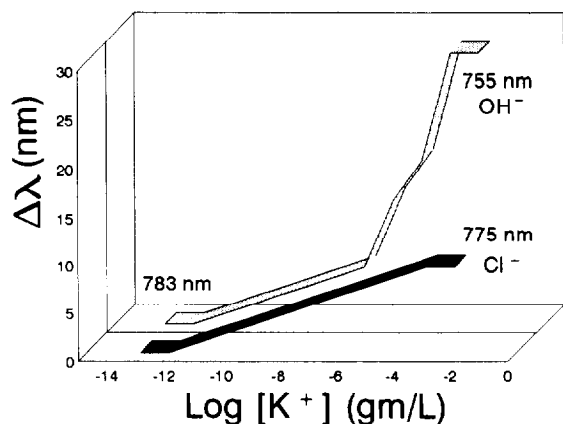
Fig. 3. Blue shift of the absorbance maximum of a sulfonated dye. The nature of the counter ion produced different shifts. A larger shift was observed using OH⁻ rather than Cl⁻ counter ions.

metal ion concentrations. This difference may be attributed to a decrease in free volume in the polymer matrix or saturation of either of the binding sites of the dye. As the metal ions penetrated the matrix there was less free volume for the ions to move inside the matrix and therefore they became concentrated at the surface of the probe.

To determine the dynamic range of the optical probe, several controlled concentrations of metal ions were prepared. The tetra-sulfonated dye showed a good response to changes in metal ion
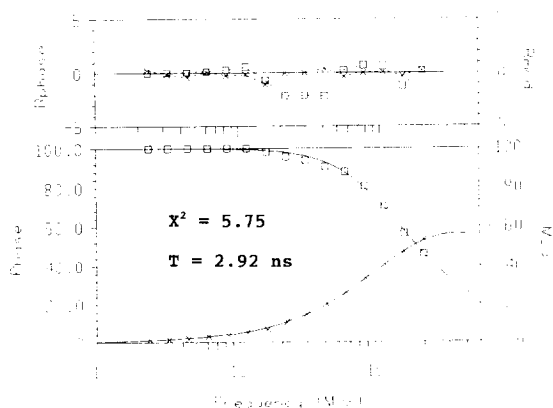

Fig. 4. Frequency-dependent demodulations and phase shifts for the tetrasulfonated AlNc dye taken in methanol using an excitation wavelength of 783 nm. The measured fluorescence lifetime of the dye is 2.92 ns.

concentration. Probes prepared with 1:1 and 3:2 polymer:dye ratios produced linear responses from 0 and 10 ppm and optical constants of 1.93×10^6 M^{-1} and 2.27×10^6 M^{-1}. The small difference between the two probes may have been the result of the difference in the amount of dye loaded.

4. Conclusion

The synthesis of tetra-substituted AlNc dyes in a homogenous phase was successfully accomplished and followed by UV–Vis–NIR spectroscopy. The photochemical properties of the dyes were determined and were applicable for the determination of metal ions. The data shown here demonstrate the use of a NIRD for the detection of metal ions comparable to the dyes used in the UV–Vis region. We have also demonstrated a very practical synthesis scheme with improved product yields. Additional work in this area will be directed towards the development of NIRDs that can be made more sensitive to specific metal ions by introducing crown moieties. There are many potential applications of NIR OFCDs for the determination of metal ions and their utility for the detection of metal ions may not be their only application. Investigations are also currently under way to evaluate their efficacy as pH probes.

Acknowledgment

References

[1] World Health Organization. Guidelines for Drinking-Water Quality, Vol. 1, Geneva, 1984.

[2] U.S. Environmental Protection Agency and Office of Water and Hazardous Materials, Quality Criteria for Water, Washington, DC, 1976.

[3] D.C. Sundberg, Z. Zhujun, Y. Zhang, M. Wangbai, R. Russell, Z.M. Shakhsher, C.L. Grant and W.R. Seitz, Anal. Chem., 61 (1989) 202–205.

[4] Z. Zhujun and W.R. Seitz, Anal. Chim. Acta, 171 (1985) 251 258.

[5] J. Janata, Anal. Chem., 64 (1992) 921A 927A.

[6] J. Janata, Anal. Chem., 64 (1992) 196R 219R.

[7] E. Koller, in O.S. Wolfbeis (Ed.), Fiber Optic Chemical Sensors and Biosensors, Vol. 1, CRC Press, Boca Raton, FL, 1991, pp. 319–322.

[8] T. Vo-Dinh, G.D. Griffin and M.J. Sepaniak, in O.S. Wolfbeis (Ed.), Fiber Optic Chemical Sensors and Biosensors, Vol. 2, CRC Press, Boca Raton, FL, 1991, p. 217 257.

[9] M.A. Arnold, Anal. Chem., 64 (1992) 1015A 1025A.

[10] J.O.W. Norris, Analyst, 114 (1989) 1359 1372.

[11] Y. Kawabata, R. Tahara, T. Kamichika, T. Imasaka and N. Ishibashi, Anal. Chem., 62 (1990) 1528 1531.

[12] Y. Kawabata, T. Kamichika, T. Imasaka and N. Ishibashi, Anal. Chem., 62 (1990) 2054 2055.

[13] K.S. Litwiler, P.M. Kluczynski and F.V. Bright, Anal. Chem., 63 (1991) 797 802.

[14] L.A. Saari and W.R. Seitz, Anal. Chem., 54 (1982) 821 823.

[15] Y. Kubota, Y. Motoda, Y. Shigemune and Y. Fujisaki, Photochem. Photobiol., 29 (1979) 1099.

[16] R. Huttenrauch, S. Fricke and K. Matthey, Pharmazie, 37 (1982) 225 230.

[17] T. Ando and H. Miyata, Anal. Biochem., 129 (1983) 170 175.

[18] T. Vo-Dinh, G.D. Griffin, K.R. Ambrose, and M.J. Spaniak, in M. Cooke and A.J. Dennis (Eds.), Polyaromatic Hydrocarbons: A Decade of Progress, Battelle Press, Columbus, OH, 1988, p. 885.

[19] G. Patonay and M.D. Antoine, Anal. Chem., 63 (1991) 321A 327A.

[20] J.-M. Zen, M. Lipowska and G. Patonay, J. Appl. Polym. Sci., 46 (1992) 1167 1176.

[21] G. Patonay, J.-M. Zen and T. Czuppon, SPIE OE/Environmental and Process Monitoring Technologies, Los Angeles, CA, January 20 22, 1992, 1637 (1992) pp. 142 150.

[22] M. Matsuoka, Infrared Absorbing Dyes, Plenum Press, New York, 1990, pp. 1 212.

[23] P.G. Edelman and J. Wang, Biosensors and Chemical Sensors: Optimizing Performance Through Polymeric Materials, ACS Publications, Washington, DC, 1992, pp. 276 291.

[24] G.A. Casay, T. Czuppon, N. Narayanan, J. Lipowski and G. Patonay, J. Process Control Qual., 5 (1993) 35–44.

[25] G.A. Casay, D.B. Shealy and G. Patonay, in J. Lakowicz (Ed.), Topics in Fluorescence Spectroscopy, Vol. 4, Plenum Press, New York, 1994.

[26] G.A. Casay, T. Czuppon, N. Narayanan and G. Patonay, Proc. SPIE Int. Soc. Opt. Eng., 1976 (1993) 76–86.

[27] B. Paquette, H. Ali, R. Langlois and J.E. Van Lier, Photochem. Photobiol., 51 (1990) 313

[28] E.I. Kovshev and E.A. Luk'yanets, Zh Obshch. Khim., 42 (1972) 1593.

[29] R.J. Bergeron and J.J. McManis, J. Org. Chem., 53 (1988) 3108.

[30] F. Weygand and E. Frauendorfer, Chem. Ber., 103 (1970) 2437.

[31] R.B. Mujumdar, L.A. Ernst, S.R. Mujumdar and A.S. Waggoner, Cytometry, 10 (1989) 11 19.

[32] S. Danishefsky, M. Hirama, K. Gombatz, T. Harayama, E. Berman and P. Schuda, J. Am. Chem. Soc., 100 (1978) 6536.

[33] T. Saski, K. Minamoto and H. Itoh, J. Org. Chem., 43 (1978) 2320.

[34] G. Barany and R.B. Merrifield, J. Am. Chem. Soc., 99 (1977) 7363.

Permselectivity of neurotransmitters at overoxidized polypyrrole-film-coated glassy carbon electrodes

Tian-Fang Kang*, Guo-Li Shen, Ru-Qin Yu

Department of Chemistry and Chemical Engineering, Hunan University, Changsha 410082, People's Republic of China

Abstract

The permselectivity of neurotransmitters such as dopamine, epinephrine, and norepinephrine at overoxidized polypyrrole (OPPY)-film-coated glassy carbon electrodes has been investigated. The chemically-modified electrodes exhibit attractive permselectivity and antifouling properties of rejecting anionic species, e.g. ascorbate, etc. Compared with the response of neurotransmitters at modified electrodes overoxidized in phosphate buffer solution (pH 7.4), higher sensitivity and reversibility response can be obtained at modified electrodes overoxidized in sodium hydroxide solution. The effect of film thickness on the permselective response was tested. Rotating disk electrode experiments were used to determine the apparent diffusion coefficients of several electroactive solutes in the OPPY films. The influence of the hydrophobicity of the organic ions on the permeability within the polymer films was discussed. Dopamine and epinephrine were determined at the 1×10^{-6}–1×10^{-4} M level by means of voltammetry after an exposure period of 2 min in 0.1 M phosphate buffer (pH 7.4) with detection limits of 8×10^{-7} M and 6×10^{-7} M respectively.

1. Introduction

In recent years there has been extensive interest in the field of polymer-modified electrodes [1,2]. Such sensors hold great promise for increasing the selectivity, sensitivity, and reproducibility of voltammetric measurements [3,4]. Chemically-modified electrodes have also been developed for the electrochemical determination of neurotrans-

mitters both in vivo and in vitro [5,6]. The voltammetric responses of the neurotransmitters, however, usually suffer from the interference of ascorbic acid which usually coexists in vivo as anions in high concentration.

Overoxidized polypyrrole OPPY-film-modified electrodes have been studied previously [7–9]. These electrodes are easily prepared by electropolymerization of pyrrole monomer with subsequent overoxidation treatment. It is known that the electrical conductivity is lost upon irreversible

* Corresponding author.

oxidation of polypyrrole at quite positive potentials [10,11], although the films still possess ionic conductivity. The OPPY films have been shown to possess excellent cation permselectivity. To our knowledge, although there have been several reports [12,13] of the electrochemical properties of dopamine (DA) at OPPY-film-coated electrodes prepared by different procedures, the permselectivity and voltammetric behaviour of other catecholamines, e.g. epinephrine (EP) and norepinephrine (NE), at the modified electrodes have not been reported. The biogenic amines co-exist with dopamine, ascorbic acid (AA) and uric acid (UA) in vivo. Clarifying their permselectivity and voltammetric properties at OPPY-film-coated electrodes is desirable for the development of the polymer-film-modified electrodes as neurotransmitter sensors. In this paper, the voltammetric responses of the OPPY-film-modified glassy carbon (GC) electrodes for DA, EP and NE as well as AA at physiological pH are evaluated. The apparent diffusion coefficients of DA, EP, etc. are determined by rotating disk electrode (RDE) experiments. The results of the study show that the OPPY-film-modified electrodes exhibit attractive permselective and antifouling properties.

2. Experimental

2.1. Apparatus and Reagents

All electrochemical experiments were performed with an EG&G PARC Model 273 potentiostat galvanostat and a Hewlett Packard X–Y recorder. An electrochemical cell with three electrodes was used for both the electropolymerization and electrochemical determinations. A bare or OPPY-film-coated GC disc electrode with an area of 0.20 cm^2 (Beijing Institute for Artificial Crystals) was used as working electrode, a platinum foil was used as auxiliary electrode and a saturated calomel electrode (SCE) as the reference electrode. All potentials were recorded relative to the SCE.

Pyrrole (Fluka) was purified by double distillation and was stored in a refrigerator. DA hydrochloride, NE hydrochloride, UA (Sigma), EP (Fluka), catechol and AA (Fisher) were used as received. All chemicals were of reagent grade. All solutions were prepared with doubly-distilled water and were degassed with high purity nitrogen for 10 min. Nitrogen was passed over the solution during the electrochemical measurements.

2.2. Preparation of OPPY-film-modified electrodes

The GC electrode was polished with 0.5 μm alumina paste for 5 min, and then ultrasonicated for 5 min in distilled water before use.

Polypyrrole films were electropolymerized on the GC electrode in a degassed solution of 0.1 M pyrrole and 0.1 M $NaClO_4$ with a constant current of 1 mA cm^{-2}. The thickness was controlled [14] by the amount of charge passed and was estimated to be ≈ 0.2 μm by passing 48 mC cm^{-2}. Polypyrrole films on the surface of GC electrodes were overoxidized at +1.0 V vs. SCE in 0.2 M NaOH solution, unless stated otherwise. The overoxidation process was monitored by following the current decay until the current levelled off. This took about 6 min for a 0.2 μm thick film.

2.3. RDE experiments

RDE experiments were carried out using a Model EG & G PARC 616 RDE system with a GC disk working electrode with an area of 0.13 cm^2, a platinum wire auxiliary electrode and a Ag/AgCl (KCl saturated) reference electrode.

2.4. Procedure for voltammetric assay

A 20 ml aliquot of 0.1 M phosphate buffer pH 7.4 was placed in a voltammetric cell, and the required volumes of standard solutions were added. The modified electrode was immersed in the solution with stirring to expose it to the analytes. After a given period of exposure, a potential scan was performed.

3. Results and Discussion

3.1. Voltammetric behaviour of neurotransmitters and other species at OPPY film electrodes

During overoxidation of polypyrrole in NaOH solution, nucleophilic attack of the radical cationic pyrrole units in the polymer by hydroxide ions takes place, resulting in loss of the conjugated structure and electrical conductivity. Meanwhile, the doping ions (ClO_4^-) are also expelled from the polymer film [11], forming a porous structure on the film. Electroactive species and electrolyte can still diffuse through the porous film to the underlying electrode surface. However, carbonyl groups and carboxylic groups are also produced in the polymer when the oxidation is taking place [15]. The diffusion of anions in the film is hindered by the carbonyl groups of high electron density and the ionized carboxylic groups.

It was reported that the optimum conditions for electrochemical activation of GC electrodes in the analysis of dopamine were a pH range of 13–14 and a potential of 1.2 V (vs. SCE) [16]. Similar conditions are used in this report for activation of a polypyrrole-film-coated GC electrode to be overoxidized. In order to estimate the activation of the underlying electrode surface arising from the treatment of a polypyrrole-film-coated GC electrode, a bare GC electrode was also treated under the same conditions as the polypyrrole-film-coated GC electrode. The treated bare GC electrode was also used as a working electrode to perform cyclic voltammetric experiments. Fig. 1 shows the cyclic voltammograms for a series of biologically important cationic, nonionic, and anionic species at OPPY-film-coated and bare GC electrodes.

Although both AA and UA were in the form of monovalent anions at pH 7.4, AA was more efficiently repelled from an OPPY-film-coated electrode surface than UA (Fig. 1). AA (1×10^{-3} M) was oxidized at the bare GC electrode, producing a large current peak, while its current response was almost completely suppressed at the OPPY-film-coated GC electrode. The response of UA (5×10^{-5} M) was also suppressed, although

not so completely, at the OPPY-film-coated electrode compared to the response at the bare GC electrode. UA is a more hydrophobic species than AA judging from the much lower solubility of UA in aqueous solution. The hydrophobicity difference between UA and AA is probably one of the reasons why there is an obvious difference in permeability between the two species within OPPY films. The voltammetric responses of UA and AA at OPPY-film-coated or bare GC electrodes were investigated in phosphate buffer solutions of different pH. It was found that the suppression of the OPPY films electrodes for the response of UA was obviously weaker than that for the response of AA over the pH range 7–9. A similar phenomenon, i.e. hydrophobic interaction between the monoanionic species, e.g. 3, 4-dihydroxyphenylacetic acid, and the OPPY film, which is favourable for permeation of these species into the OPPY film, was also observed by Palmisano et al. [15]. The large permeability of the cationic neurotransmitters DA, EP and NE, which are protonated at the physiological pH,
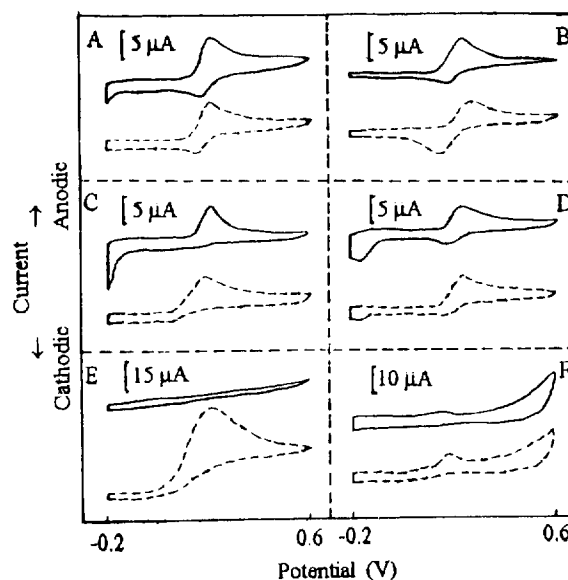
Fig. 1. Cyclic voltammograms for 1×10^{-4} M DA (A), catechol (B), EP (C), NE (D), 1×10^{-3} M AA (E), and 5×10^{-5} M UA (F) at OPPY-film-coated (solid lines) and bare GC electrodes (broken lines). Conditions: scan rate, 20 mV s^{-1}; electrolyte, 0.1 M phosphate buffer (pH 7.4); exposure time, 2 min.

results in faradaic responses significantly higher than that of the anionic species. The faradaic response obtained is close to that obtained with a bare GC electrode. The neutral catechol exhibits a similar behaviour. The voltammetric responses of the neurotransmitters usually suffer from the interference of AA which may coexist in vivo in the anionic form on high concentrations. For example, large overlapping oxidation peaks of neurotransmitters and other species tested were observed at the bare GC electrode. Therefore, the selective retardation of the electroactive anion ascorbate is of great significance for the development of neurochemical sensors. It has been shown [12] that if polypyrrole-film-coated GC electrodes are treated by overoxidation of polypyrrole in sodium hydroxide solution, rather than in other supporting electrolyte solutions, highly sensitive and reversible voltammetric responses for DA will be obtained. In the present investigation, it was also observed that the voltammetric responses of both EP and NE at the OPPY-film-modified electrodes overoxidized in strongly alkaline medium were of higher sensitivity and reversibility than those at the modified electrodes overoxidized in, say, a phosphate buffer solution (pH 7.4). In sodium hydroxide solution, the overoxidation of polypyrrole film proceeds faster than in median pH buffer solutions because hydroxide ions in sodium hydroxide solution act as nucleophilic reactants which are stronger than anionic species present in buffer solutions [11]. The highly sensitive and reversible voltammetric responses for catecholamines can be attributed to the activation of the matrix surface of the underlying GC electrodes. The electrochemical oxidation of the matrix surface will occur when the polypyrrole film coated at the surface of the GC electrode is overoxidized in sodium hydroxide solution at quite a positive potential, for example +1.0 V or +1.2 V vs. SCE [16].

Study of the effect of scan rate on the anodic peak height of DA and EP at the OPPY film electrode was performed by linear scan voltammetry. The peak height increased linearly with the square root of the scan rate. The results show that the electrochemical processes involving DA and EP at OPPY film electrodes are all diffusion-controlled [17].

Table 1
Effect of film thickness on permselective response at the 1×10^{-3} M level[a]

Thickness (μm)	$i_{p,DA}/i_{p,AA}$	$i_{p,EP}/i_{p,AA}$	$i_{p,NE}/i_{p,AA}$
0	2.43	2.26	2.12
0.2	52.8	51.5	50.2
0.4	87.6	82.4	79.8
0.6	284	273	265

[a] Other conditions as in Fig. 1.

3.2. Effect of OPPY film thickness

The permselective transport is strongly affected by the film thickness (Table 1). The sensitivity of a 0.2 μm OPPY-film-coated electrode for neurotransmitters was close to that of a bare electrode. However, the selectivity of the OPPY-film-coated electrode for neurotransmitters with respect to AA was much higher than that of the bare electrode. As film thickness increases, the sensitivity decreases but the neurotransmitter selectivity with respect to AA increases substantially.

A plot of linear scan voltammetric peak height as a function of the exposure time (Fig. 2) shows that the peak height of EP increased sharply with exposure time up to 3 min. With longer exposure times, up to 6 min, the slope decreased. Meanwhile, the slope for the 0.2 μm OPPY film de-
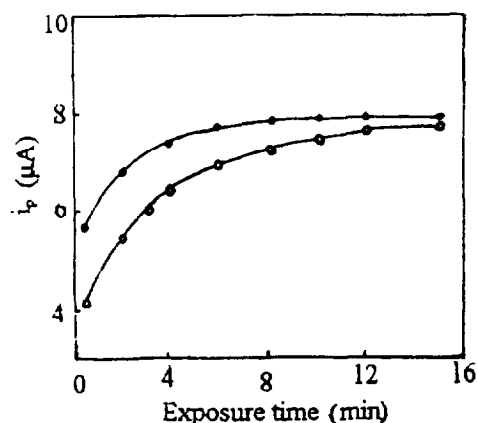

Fig. 2. Effect of exposure time on oxidation peak height of EP at OPPY film electrodes of (●) 0.2 and (○) 0.4 μm thickness. EP concentration: 1×10^{-4} M; phosphate buffer concentration: 0.1 M (pH 7.4); scan rate: 50 mV s^{-1}.

creased more quickly than that of a 0.4 μm OPPY film. This is not surprising, since prolonged exposure allows a larger quantity of analyte to diffuse into the film and saturation occurs more quickly for thinner films. When a polymer-film-coated electrode is exposed to an aqueous solution containing analyte, the response sensitivity depends on the film thickness [18]. Thicker film, for example 0.4 μm, results in a lower response sensitivity but, with an exposure time of, say, 3 min a wider linear response range. Because of the expected faster response time and higher sensitivity, it is more advantageous for the voltammetric determination of catecholamines to employ a thin, say 0.1 μm or 0.2 μm, OPPY film than a thicker one.

3.3. Determination of apparent diffusion coefficients

The apparent diffusion coefficients of DA, EP, UA and AA in OPPY film were determined by OPPY-film-coated RDE voltammetry in pH 7.4 phosphate buffer solution in order to evaluate the permeability of the solutes in the polymer film. In the permeability studies, the limiting current, i_l for the electrochemical reaction of a solute which partitions with partition coefficient α and diffuses into a RDE through a film barrier with diffusion constant D_m is described by the following equation [19,20]:

$$\frac{1}{i_l} = \frac{1}{nFA\alpha D_m C\delta_m^{-1}} + \frac{1}{0.62nFAD_s^{2/3}\nu^{-1/6}\omega^{1/2}C} \quad (1)$$

where A is the electrode area, δ_m is the film thickness, ω is the rotation speed of the electrode (rad s^{-1}) C and D_s are the bulk concentration and diffusion coefficient of the solute in solution respectively, and the other symbols have their usual meanings. The two terms on the right-hand side of Eq. (1) represent the reciprocal of the current that would be measured without the diffusion layer, and the reciprocal of the current without a film. The Koutecky–Levich plots are obtained by measuring the limiting current at different rotation speeds and plotting $1/i_l$ vs. $\omega^{-1/2}$. From the intercept the apparent diffusion coefficient αD_m can be obtained.

Table 2
Apparent diffusion coefficients measured with the RDE in 0.1 M phosphate buffer solution (pH 7.4) for some species[a]

Solute	pK_a[b]	Change	C (mM)	αD_m (10^{-9} cm^2 s^{-1})
DA	8.92	+1	0.10	21
EP	8.88	+1	0.10	16
UA	5.40	−1	0.10	2.8
AA	4.20	−1	4.0	0.42

[a] Polypyrrole film was overoxidized in 0.4 M phosphate buffer (pH 7.4). OPPY film thickness: 0.40 μm. Scan rate: 10 mVs^{-1}.
[b] References for pK_a values: DA and EP [21]; UA [22]; AA [23].

Table 2 lists the values of αD_m obtained for the solutes at different electrodes. The errors in the αD_m values are less than 20%. AA showed a small voltammetric response at a concentration of 4 mM but it is almost indistinguishable from the background signal at 0.5 mM levels. UA possesses a small solubility in neutral aqueous solutions. Therefore, concentrations of 4.0 mM AA and 0.10 mM UA were adopted in the RDE experiments. The results show that DA possesses a slightly higher permselectivity than EP at the OPPY-film-coated GC electrodes. However, the αD_m value of UA is higher by a factor of about seven than that of AA, which further confirms that UA possesses higher permeability than AA. The αD_m value of DA is about double that reported by Witkowski and Brajter-Toth [7]. This is probably due to the different preparation conditions of the OPPY film, i.e. different doping ions were applied during the electropolymerization of pyrrole monomer, etc.

3.4. Analytical applications

In order to evaluate the possibility of applying the OPPY film electrodes to the determination of neurotransmitters in practical samples, mixtures of DA or EP, AA and UA were prepared. The concentrations of AA and UA were 1×10^{-4} M and 1×10^{-5} M respectively. Linear scan voltammetry was adopted in the experiments. The results are shown in Table 3. The limit of detection was calculated as three times the noise of the determination of a low level of DA or EP. EP was

Table 3
Linear range and detection limit of DA and EP determinations[a]

Species	Linear range (M)	Correlation coefficient	Detection limit (M)
DA	1×10^{-6} 1×10^{-4}	0.999	8×10^{-7}
EP	1×10^{-6} 1×10^{-4}	0.998	6×10^{-7}

[a] Scan rate: 50 mV s^{-1}. Other conditions as in Fig. 1.

determined 12 times at the 5×10^{-5} M level with a 2 min exposure time. The relative standard deviation was 3.9%.

The stability of the OPPY film on GC was also tested. There were no obvious changes observed in the response of the OPPY film electrodes after the electrodes were stored in phosphate buffer for 8 days. This indicates that the OPPY film electrodes are stable in a quiescent solution. However, after repeated voltammetric determinations, for example over a period of 5 h, about 15% decrease in current sensitivity for 1×10^{-5} M EP was observed. This was obviously superior to the results obtained at an untreated bare GC electrode which was prone to contamination by EP oxidation products, resulting in reduction of response sensitivity.

4. Conclusions

OPPY films demonstrate large permeability for cationic and neutral catechols, for example DA. EP. NE or catechol, and very effective and selective retardation of electroactive anionic species such as ascorbate anions. The thinner the thickness of the OPPY film, the shorter the response time. Uniform thickness of OPPY films and stable adherence to the GC electrode surface are easily obtained by electropolymerization of pyrrole monomer. In contrast, neurotransmitters and catechols tested displayed excellent electrochemical reversibility at a polymer-film-coated GC electrode which had been treated in strong basic solution at +1.0 V vs. SCE. Therefore, high voltammetric response sensitivity for these species can be obtained. In particular, the enhanced selectivity obtained as a result of excluding anionic species could be very valuable in the development of neurochemical sensors.

References

[1] R.W. Murray (Ed.), Molecular Design of Electrode Surfaces, Wiley-Interscience, New York, 1992.
[2] S.A. Wring and J.P. Hart, Analyst, 117 (1992) 1215.
[3] J. Janata, Anal. Chem., 64 (1992) 196R.
[4] J. Ye and R.P. Baldwin, Anal. Chem., 60 (1988) 1979.
[5] D.J. Wiedemann, K.T. Kawagoe, R.T. Kennedy, E.L. Ciolkowski and R.M. Wightman, Anal. Chem., 63 (1991) 2965.
[6] J. Wang, P. Tuzhi and T. Golden, Anal. Chim. Acta, 194 (1987) 129.
[7] A. Witkowski and A. Brajter-Toth, Anal. Chem., 64 (1992) 635.
[8] C. Hsueh and A. Brajter-Toth, Anal. Chem., 66 (1994) 2458.
[9] Z. Gao, M. Zi and B. Chen, Anal. Chim. Acta, 286 (1994) 213.
[10] A. Haimerl and A. Merz, J. Electroanal. Chem., 220 (1987) 55.
[11] F. Beck, P. Braun and M. Oberst, Ber. Bunsenges. Phys. Chem., 91 (1987) 967.
[12] M. Freund, L. Bodalbhai and A. Brajter-Toth, Talanta, 38 (1991) 95.
[13] Z. Gao and A. Ivaska, Anal. Chim. Acta, 284 (1993) 393.
[14] A.F. Daiz and J.I. Castillo, J. Chem. Soc., Commun., (1980) 397.
[15] F. Palmisano, C. Malitesta, D. Centonze and P.G. Zambonin, Anal. Chem., 67 (1995) 2207.
[16] D.M. Anjo, M. Kahr, M.M. Khodabakhsh, S. Nowinski and M. Wanger, Anal. Chem., 61 (1989) 2603.

[17] A.J. Bard and L.R. Faulkner, Electrochemical Methods, Wiley, New York, 1980.

[18] L.D. Whiteley and C.R. Martin, Anal. Chem., 59 (1987) 1746.

[19] D.A. Gough and J.K. Leypoldt, Anal. Chem., 51 (1979) 439.

[20] T. Ikeda, R. Schmehl, P. Denisevich, K. Willman and R.W. Murray, J. Am. Chem. Soc., 104 (1982) 2683.

[21] M.D. Hawley, S.V. Tatawawadi, S. Piekarski and R.N. Adams, J. Am. Chem. Soc., 89 (1967) 447.

[22] J.A. Dean, Lange's Handbook of Chemistry, McGraw-Hill, New York, 1985, p. 560.

[23] S. Steenken and P. Neta, J. Phys. Chem., 83 (1979) 1134.

Talanta

Nafion-coated mercury thin film electrodes for batch-injection analysis with anodic stripping voltammetry

Christopher M.A. Brett[a,*] Ana Maria Oliveira Brett[a,*], Frank-Michael Matysik[a], Silke Matysik[a], Sunita Kumbhat[b]

[a]Departamento de Química, Universidade de Coimbra, 3049 Coimbra, Portugal
[b]Department of Chemistry, Urbu-Jodhi University, Jodhpur 342001, India

Abstract

Batch-injection analysis exhibits the advantages of rapid and simple electroanalysis of microlitre samples. Nafion-coated mercury thin film electrodes have been evaluated for use in batch-injection analysis with anodic stripping voltammetry (BIA-ASV). The advantages of Nafion-coated electrodes in reducing electrode contamination by components of complex matrices are combined with the analysis of small microlitre sample volumes. The measurement of traces of lead and cadmium is used to illustrate the approach. An optimised procedure for formation of Nafion-coated mercury thin film electrodes is evolved. The relative sensitivity for BIA-ASV at electrodes with and without Nafion coatings is 0.9 and 0.8 for cadmium and lead respectively; detection limits are 2×10^{-9} M and 4×10^{-9} M. Studies were done concerning the influence of surfactants and their effect was found to be much less with the Nafion film coating. Applications to real environmental samples are demonstrated.

Keywords: Batch-injection analysis; Mercury film electrodes; Nafion-coated electrodes; Stripping voltammetry; Trace metals

1. Introduction

The batch-injection analysis (BIA) technique [1] was developed to enable the analysis of small ($\leqslant 100$ μl) volumes of liquid samples whilst retaining the advantage of convection in continuous flow systems. Recent work involving electrochemical detection has demonstrated the similarities between amperometric detection in BIA and the response obtained at wall-jet electrodes in continuous flow [2]. This similarity arises because in both techniques a fine jet of solution (in the BIA case from a micropipette tip) impinges on the centre of a disc electrode immersed in electrolyte solution; this configuration means that memory

* Corresponding author. Fax: (+351) 39-35295.

effects are almost zero. The advantages of the use of a programmable, motorised electronic micropipette have been shown [2,3]. BIA with voltammetric detection has also been demonstrated [4]: consecutive injections during a slow potential sweep lead to a point-by-point voltammetric curve, and cyclic voltammetry and square wave voltammetry can be done during the injection itself.

BIA with stripping voltammetry is also an exciting possibility. After initial studies showing its viability [5], BIA with anodic stripping voltammetry (BIA-ASV) has been explored in detail and nanomolar detection limits were reached with good sensitivity using square wave stripping [6]. The mercury thin film electrode (MTFE) was formed *in situ* and the influences of injected volume, preconcentration time, and micropipette dispension rate were investigated.

A particular benefit of the small sample volumes injected in BIA is that the contact time between sample and electrode is small. Problems of electrode fouling are thus reduced compared with continuous flow systems. Nevertheless, for complex matrices such as waste water with high surfactant levels and blood serum it is often necessary to reduce contamination even further, which can be done by suitable modification of the electrode surface.

Permselective electrode coatings have found use in reducing interference and contamination. Amongst those with applications in stripping voltammetry are Nafion (see e.g. Refs. [7-9]), cellulose acetate (see e.g. Ref. [10]) and dialysis membranes (see e.g. Ref. [11]). An additional benefit is the fact that any problems with adhesion of the mercury film to the glassy carbon substrate [12], which can occur under convective conditions, are removed.

Concerning Nafion films, the signal stability for differential pulse ASV was examined in detail for a number of Nafion-coated thin mercury film preparation methods [7], involving Nafion coating followed by mercury film deposition. Other work involved mixing a ligand specific for the metal ion to be determined, lead [8] and copper [9], with the solution of Nafion before coating.

The objective of this study was to reduce the interferences from complex matrices in the BIA-ASV technique through coating of the glassy carbon electrode with a thin Nafion film. Optimum experimental parameters are examined and comparison with results using a simple MTFE is presented. Application to trace metal determinations in environmental samples is described.

2. Experimental

A modified large open wall-jet cell constructed of perspex and filled with inert electrolyte was used as described previously [2]. The micropipette tip (internal tip diameter 0.47 mm) was fixed exactly over the centre of a glassy carbon (Tokai, GC-20) disc electrode, diameter 5 mm, at a distance of 2-3 mm. The cell also contained a platinum gauze counter electrode and a saturated calomel reference electrode.

A 5% solution of Nafion in low weight alcohols (Aldrich) was diluted with ethanol to prepare appropriate working solutions for forming the Nafion coatings. N,N-dimethylformamide (DMF) was of analytical grade (99.5%) and purchased from Fluka. The preparation of the Nafion-coated (NC) electrode is discussed below. Mercury films were made *in situ* by injection of 10 μl of a 10^{-1} M Hg(II) solution at -1.0 V applied potential. Unless stated otherwise the cell contained 0.1 M KNO_3/0.002 M HNO_3 supporting electrolyte. Injections were performed using a programmable motorised electronic micropipette (EDP Plus 100 EP-100, Rainin Instrument Co. Inc.). This micropipette, of maximum dispensing volume 100 μl, has three dispensing rates; the BIA-ASV measurements were conducted at the slowest dispensing rate, which was calibrated in this study as 22.7 μl s^{-1}.

A computer-controlled EG&G PAR273A potentiostat with M270 Research Electrochemistry Software was used for running the electrochemical experiments.

Solutions were prepared from analytical-grade chemical reagents and Millipore Milli-Q ultrapure water (resistivity $\geqslant 18$ MΩ cm). Stock solutions of 10^{-3} M Pb^{2+} and Cd^{2+} were prepared and di-

luted on the day as appropriate. The protein standard solution (Sigma) containing 0.5 g l^{-1} albumin and 0.3 g l^{-1} globulin; Triton X-100 (Sigma) and sodium dodecyl sulphate (SDS; Aldrich) were used as received in the corresponding studies after appropriate dilution. Experiments were conducted at room temperature (25 ± 1°C) and without deoxygenation.

2.1. Preparation of NCMTFE for BIA-ASV

Prior to polymer coating the glassy carbon electrode was polished using polishing foils with 0.3 μm alumina particles (Hirschmann, Germany), rinsed with Milli-Q water and allowed to dry.

The optimised procedure for forming the Nafion coating was as follows. First, 5 μl of 0.25% (w v) Nafion solution was applied, followed immediately by 3 μl of DMF, to the electrode surface with a micropipette. The solvents were evaporated in a warm air stream from an air gun while the electrode was rotated at 50 rev min^{-1}. The polymer film was then cured for 60 s in a hot air stream (about 70°C), holding the gun just a few millimetres above the electrode surface. The studies which led to this procedure are described in the next section.

The NC electrode was then placed in the BIA cell and mercury deposition was done in situ by injecting 10 μl of a solution of 0.1 M Hg^{2+} in 0.1 M KNO$_3$ 0.002 M HNO$_3$ and applying a deposition potential of -1.0 V during injection (≈ 0.4 s) and a further 60 s after the end of the injection period. As previously shown [6], continuing to apply a potential corresponding to the electrode deposition reaction after the end of the injection itself significantly increases the electrolysis efficiency. The NCMTFE was then ready for use in ASV experiments.

3. Results and discussion

3.1. Optimisation of preparation methods of NCMTFEs

The procedure of Nafion coating and mercury deposition onto a glassy carbon electrode for use in conjunction with BIA was studied with respect to practicality, the stability of the coating under the hydrodynamic conditions of BIA and the maximum attainable sensitivity for trace metal determinations.

There are two principal ways of preparing NCMTFEs. One possibility is to deposit mercury first followed by removal of the electrode from the plating solution and covering of the thin mercury film with a Nafion membrane under air [13]. Alternatively, the procedure can be reversed and the Nafion film prepared first followed by mercury deposition through the Nafion film [14]. The latter approach was found to be more convenient, particularly in a BIA arrangement; this is due to the fact that the mercury deposition can be performed in situ utilising the BIA approach [6]. In addition, covering a bare glassy carbon electrode with a Nafion film offers more freedom for varying the curing procedure parameters than in the presence of mercury, which may evaporate at higher temperatures.

Thus, the procedure of preparing the Nafion film first and then depositing mercury through the polymer film in the BIA cell was studied in detail with a view to optimisation of the relevant parameters. Initial studies used Nafion solutions alone for film formation, which led to films with a tendency to crack and have low adhesion. Previous studies suggested that the addition of a casting solvent can modify the properties of Nafion [15]. This was explored and it was found to be advantageous to employ DMF casting solvent and to heat during the formation of the Nafion film in order to improve its mechanical properties. In addition, preparing the Nafion film by spin-coating resulted in a more uniform polymer layer than under stationary conditions; a rotation speed of 50 rev min^{-1} was employed. For the size of the glassy carbon electrode used, 0.20 cm^2 area, 5 μl Nafion solution and 3 μl DMF were found to be appropriate.

The thickness of the Nafion film was varied using Nafion solutions of different concentration in the range 0.1–0.5% (w/v). The thinnest Nafion film made from 0.1% Nafion solution was found, after mercury deposition, to be insufficiently stable for BIA-ASV experiments. In contrast, using the

0.5% Nafion solution a stable Nafion film was obtained. but a substantial decrease in sensitivity for cadmium and lead determinations occurred in comparison with a MTFE without Nafion coating. As a compromise, employing a 0.25% Nafion solution yielded a film with sufficient stability under BIA conditions and acceptable relative sensitivities of 0.9 for cadmium and 0.8 for lead when compared with that for an uncovered MTFE (see below). Visually, the Nafion coating appeared transparent and uniform over the whole electrode surface, and resulted in homogeneous films without cracks, which was not possible without the addition of DMF casting solvent.

The above results led to the optimised procedure described in detail in Section 2.

3.2. Performance characteristics of BIA-ASV with NCTMFE

The determination of traces of cadmium and lead ions using square wave ASV was chosen in order to characterise the analytical features of the NCMTFE when incorporated in a BIA arrangement. Fig. 1 shows typical responses obtained for cadmium determinations in the concentration range $10^{-8}-10^{-7}$ M. For both cadmium and lead the calibration plots were highly linear as expressed by the linear regression data given in Table 1 for the the ions analysed separately and as a mixture. Fig. 2 illustrates the good reproducibility of repetitive trace metal determinations. No memory effects were observed providing that between successive measurements an injection of electrolyte was done at a conditioning potential of
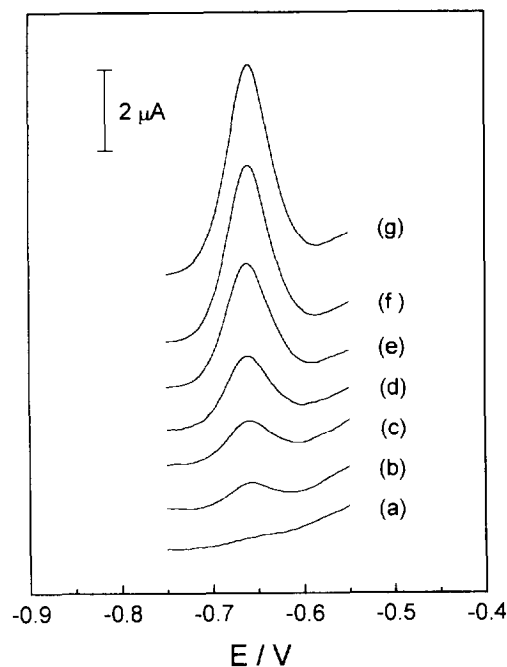

Fig. 1. Concentration dependence of the BIA-ASV response obtained for cadmium determinations with a NCMTFE. Experimental conditions: injection volume. 50 μl; preconcentration, 30 s at -1.0 V vs. SCE; stripping mode, square wave voltammetry with amplitude 25 mV, scan increment 2 mV and frequency 100 Hz. Cadmium concentrations: (a) background; (b) 10^{-8}; (c) 2×10^{-8}; (d) 3×10^{-8}; (e) 5×10^{-8}; (f) 8×10^{-8}; (g) 10^{-7} M.

-0.2 V to ensure the removal of electroactive species from the vicinity of the electrode surface. This potential was applied constantly between determinations. Detection limits were determined on the basis of the 3σ criterion related to the baseline noise level and amounted to 5×10^{-9} M

Table 1
Results of linear regression of calibration data for cadmium and lead determinations by BIA-ASV using a NCMTFE (Pb^{2+}: $1 \times 10^{-8}-1 \times 10^{-7}$ M; Cd^{2+}: $5 \times 10^{-9}-1 \times 10^{-7}$ M)

Analyte	Slope (μA nM^{-1})	Intercept (μA)	Regression coefficient
Cd^{2+}	0.052	-0.07	0.9992 ($n = 7$)
Pb^{2+}	0.022	-0.01	0.9975 ($n = 6$)
Cd^{2+} (Pb^{2+})[a]	0.042	0.09	0.9976 ($n = 5$)
Pb^{2+} (Cd^{2+})[b]	0.023	0.05	0.9958 ($n = 5$)

[a] Cadmium determinations in the presence of equal amounts of lead.
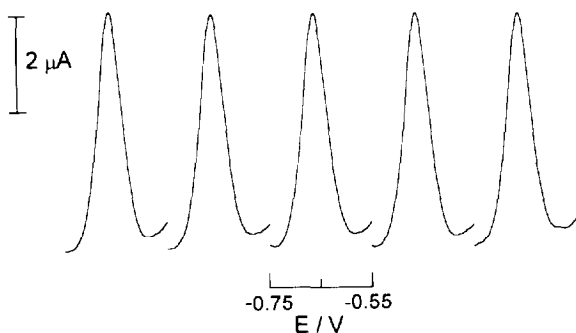[b] Lead determinations in the presence of equal amounts of cadmium.

Fig. 2. Reproducibility of BIA-ASV determinations at a NCMTFE for a cadmium concentration of 10⁻⁷ M. Other conditions as in Fig. 1.

and 1×10^{-8} M for cadmium and lead respectively.

The stripping peaks corresponding to cadmium and lead using a NCMTFE appear at potentials 12 mV more negative than in the case of measurements at a MTFE without Nafion coating. This probably reflects the cation exchanging behaviour of the Nafion coating which favours the oxidised state of the test species. However, there was only a slight effect on the shape of the signals, the peak width at half height increasing from 52 to 55 mV, suggesting that any kinetic limitations due to the Nafion film are not important.

The above results are based on injections of 50 μl of analyte solution and accumulation times of 30 s as suggested previously for BIA-ASV using an uncoated MTFE [6]. This was because, in the preconcentration step, the profile of signal height vs. injection volume reaches a maximum for this injection volume, due to the important contribution from diffusion to the electrode after the end of the injection itself of species remaining in the zone of the electrode. It was found during the course of this study that multiple injections of fractions of the total injection volume can lead to a further improvement in sensitivity using the multiple-dispense mode of the programmable micropipette without removing the pipette from the BIA cell. For example, four successive injections of 25 μl analyte with short periods in between yielded about 2.5 times higher signals in comparison to a single injection of 50 μl (note that an injection of 50 μl gives the same signal as injec-

tion of 100 μl, as explained above). The higher electrolysis efficiency obtainable via this multiple-injection approach is illustrated in Fig. 3 for BIA experiments using $K_4[Fe(CN)_6]$ oxidation as model reaction.

The multiple-injection technique was applied to trace metal determinations when the concentrations of the analyte species were close to the detection limit. In this way, the detection limit is reduced by a factor of 2.5 to 2×10^{-9} M and 4×10^{-9} M for cadmium and lead respectively. The analytical utility of this approach is demonstrated in Section 3.4.

3.3. Influence of matrix constituents on the BIA-ASV response

The effects of various organic surfactants on the response of the NCMTFE in BIA-ASV measurements were studied using cadmium as test analyte. Some common surface-active compounds, such as Triton X-100, and a protein

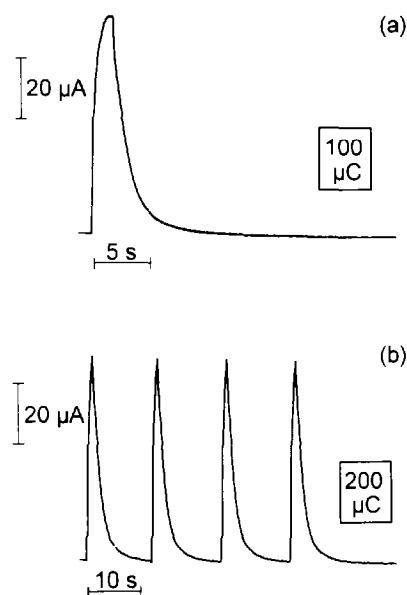Fig. 3. BIA response for amperometric detection at +0.6 V vs. SCE for oxidation of 2 mM $K_4[Fe(CN)_6]$ in 0.4 M K_2SO_4 electrolyte using a bare glassy carbon electrode. The amperometric transient (a) corresponds to an injection of 50 μl of $K_4[Fe(CN)_6]$ solution while (b) represents the response for four consecutive injections of 25 μl analyte solution. The dispensing rate is 22.7 μl s⁻¹ in both cases.

Table 2
Effects of surface-active compounds on the BIA-ASV response for 50 μl injections of 10^{-7} M Cd^{2-} at a MTFE and a NCMTFE

Surface-Response active compound		c(mg l^{-1})				
		1	2	5	11	22
Triton X-100	ΔI_p (%) MTFE	-12	-21	-37	-81	-91
	ΔI_p (%) NCMTFE	-14	-17	-24	-37	-76
SDS [a]	ΔI_p (%) , MTFE	-14	-19	-24	-26	-27
	ΔI_p (%) NCMTFE	-3	-9		-20	-23
Protein standard	ΔI_p (%) MTFE		-8	-15	-20	-68
	ΔI_p (%) NCMTFE		-5	-6	-6	-6

[a] The measurements were performed in 0.1 M acetate buffer (pH 4.5).

standard, were chosen as representing different types of interference with faradaic electrode processes. The effects of the individual surfactants on the BIA-ASV response were examined with both the MTFE and the NCMTFE in order to obtain a direct comparison under identical conditions. The experimental approach used was to inject first a sample containing 10^{-7} M cadmium ions (without the surfactant) onto a newly prepared electrode. Next, samples containing the same concentration of metal ions but in the presence of increasing concentrations of surfactant were injected consecutively. Table 2 summarises the relevant results of these measurements. In all cases, the NCMTFE was clearly less susceptible to peak depression than the MTFE. As an example, Fig. 4 illustrates the different extent of signal depression due to the presence of Triton X-100 for (A) a MTFE and (B) a NCMTFE. In particular, the results obtained for samples with a matrix containing proteins indicate that the Nafion coating is an effective barrier to the transport of these potential interferents towards the mercury surface. which agrees with data found previously by other authors [14,16-18]. The slight decrease in the BIA-ASV signal of 5 or 6% obtained with the NCMTFE after additions of protein standard to the sample was even independent of the protein concentration in the range studied up to 22 mg l^{-1}. Thus, it can be speculated that the measured decrease in signal results from complexation of the analyte [19] rather than from electrode blocking effects.

3.4. Practical applications

The analytical utility of the NCMTFE in conjunction with BIA-ASV was investigated by applying it to the analysis of heavy metal traces, lead and cadmium, in environmental samples with complex matrices, using the standard addition method.

Fig. 5 illustrates the results obtained for an undiluted waste water sample using the technique of multiple standard additions and the evaluation of cadmium concentration—these samples were found not to contain lead at a detectable concentration. The rather low concentration of 5.0 ± 0.1
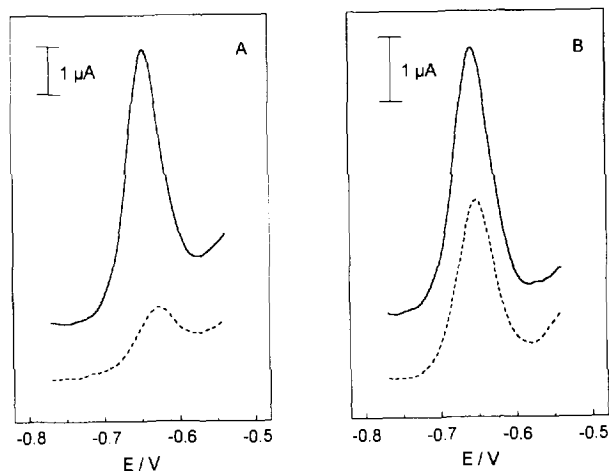

Fig. 4. BIA-ASV signals obtained with (A) MTFE and (B) NCMTFE for injections of samples containing 10^{-7} M Cd^{2+} in the absence (solid line) or in the presence (broken line) of 11 mg l^{-1} Triton X-100 surfactant. Other conditions as in Fig. 1.
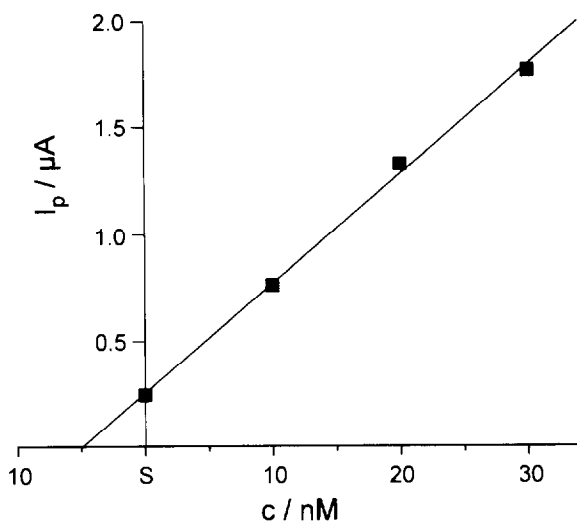
Fig. 5. Evaluation of the cadmium determination in an undiluted waste water sample by BIA-ASV with a NCMTFE using the standard addition method. The signals for the original sample (S) and that obtained after standard addition correspond to a multiple-injection preconcentration of four consecutive injections of 25 μl within a total preconcentration period of 60 s.

nM (0.56 ± 0.1 ppb) cadmium showed the advantages of using the multiple-injection preconcentration procedure described above in order to increase electrolysis efficiency. Repetitive measurements showed almost no changes in the voltammetric response, which indicates effective protection of the NCMTFE against interfering matrix constituents.

In addition, a sample was taken from a car wash, which obviously contained a high amount of detergents. In this case, lead traces were quantified in this sample using multiple-injection preconcentration but no detectable traces of cadmium were encountered. The NCMTFE was not completely insensitive to the matrix constituents as indicated by a progressive signal decrease of the BIA-ASV response of a few percent for repetitive measurements. However, the technique of standard addition requires just a limited number of measurements and the contact time of the sample matrix with the electrode surface in the BIA mode is very short. Consequently, a lead concentration of 15.5 ± 0.9

nM (3.2 ± 0.2 ppb) was determined on the basis of measuring the signal from the sample solution and performing two standard additions for which the electrode characteristics can be assumed to remain constant.

Confirmation of the values was obtained by AAS with electrothermal atomization. The waste water sample led to 0.6 ppb and <0.05 ppb and the car wash sample to 0.15 ppb and 3.0 ppb for cadmium and lead respectively. The levels of lead in the first case and cadmium in the second are below BIA-ASV detection limits. Since electrochemical methods probe the amount of labile species in a given oxidation state rather than the total amount of the element as in AAS, the agreement between BIA-ASV with standard addition and AAS shows that in the samples tested all the metal ions are present in a labile form. In other cases, where a fraction of the metal ions is not labile, the electrochemical response will be lower, and standard addition will measure the concentration of these labile species.

For the environmental samples studied the performance characteristics of the NCMTFE were far superior to those of the MTFE with regards to fouling of the electrode surface by contaminants in complex matrices and the improved stabilisation of the mercury film. In fact, it was impossible to obtain meaningful results concerning the lead concentration in the car wash sample when using a bare MTFE.

4. Conclusions

It has been shown that NCMTFEs offer significant advantages compared to ordinary MTFEs for square wave ASV using the BIA technique, and these are particularly evident in the analysis of environmental sample containing high surfactant levels. The technique for the formation of the NCMTFE is simple. This, combined with the easy and rapid BIA-ASV procedure, demonstrates that it will be an important method for the determination of small (microlitre) volumes of traces of heavy metals in complex matrices.

References

[1] J. Wang and Z. Taha. Anal. Chem., 63 (1991) 1053.

[2] C.M.A. Brett, A.M. Oliveira Brett and L. Costel Mitoseriu. Electroanalysis, 7 (1995) 225.

[3] J. Wang, L. Chen, L. Angnes and B. Tian, Anal. Chim. Acta, 267 (1992) 171.

[4] C.M.A. Brett, A.M. Oliveira Brett and L. Costel Mitoseriu, Anal. Chem., 66 (1994) 3145.

[5] J. Wang, J. Lu and L. Chen, Anal. Chim. Acta, 259 (1992) 123.

[6] C.M.A. Brett, A.M. Oliveira Brett and L. Tugulea, Anal. Chim. Acta, 322 (1996) 151.

[7] B. Hoyer and N. Jensen, Talanta, 41 (1994) 449.

[8] J.-M. Zen and S.-Y. Huang, Anal. Chim. Acta, 296 (1994) 77.

[9] J.-M. Zen, N.-Y. Chi, F.-S. Hsu and M.-J. Chung, Analyst, 120 (1995) 511.

[10] B. Hoyer and N. Jensen, Talanta, 42 (1995) 767.

[11] J.H. Aldstadt, D.F. King and H.D. Dewald, Analyst, 119 (1994) 1813.

[12] W. Frenzel, Anal. Chim. Acta, 273 (1993) 123.

[13] R.D. Guy and S. Namarante, Can. J. Chem., 65 (1987) 1133.

[14] B. Hoyer and T.M. Florence, Anal. Chem., 59 (1987) 2839.

[15] Z. Fan and D.J. Harrison, Anal. Chem., 64 (1992) 1304.

[16] B. Hoyer, T.M. Florence and G.E. Batley, Anal. Chem., 59 (1987) 1608.

[17] J.C. Vidal, R.B. Viñao and J.R. Castillo, Electroanalysis, 4 (1992) 653.

[18] M.E.R. Dam, K.N. Thomsen, P.G. Pickup and K.H. Schroder, Electroanalysis, 7 (1995) 70.

[19] J.C. Vidal, G.C. Cepria and J.R. Castillo, Anal. Chim. Acta, 259 (1992) 129.

Book reviews

Understanding Medications: What the Label Doesn't Tell You, by A. Burger, American Chemical Society, Washington, DC, 1995, xiv + 206 pp., ISBN 0-8412-3210-5.

The author of the book, Dr Alfred Burger, founded the Journal of Medicinal Chemistry in 1959 in collaboration with Arnold H Beckett. His inspiration for this book stems from the requirement to "satisfy and stimulate the curiosity of educated lay people who, on the whole, lack the biochemical and pharmacological background for the study of medicinal agents." The themes of the book are also described by the author as "the history, discovery, manufacture, action, acceptance and rejection of drugs".

Contained in the 21 small chapters is a wealth of information on drugs, albeit in a limited form, which indeed will satisfy most lay people. I found the text enjoyable and very easy to read–in a relaxed style somewhat similar to that found in Reader's Digest. Of course, whole books could have been written on each of the chapters so it will be very easy for a reviewer to criticise the oversimplicity of some of the contents. In the chapter on naming drugs it is interesting that not all trade names in the USA are the same as elsewhere, for example, the most common over-the-counter drug in the UK is paracetamol but the word paracetamol does not occur anywhere in the book. This is because the drug is known in the USA by the trade name Tylenol and the book correctly gives another corresponding nonproprietary name for the same drug as acetominophen.

The chapters devoted to drug categories are: neurohormones and drugs that affect the central nervous system, drugs for the relief of pain, local anesthetics, antispasmodics and antihistamines, drugs that act on the blood pressure and the heart, intestinal medications, hormones and vitamins, drugs for the treatment of cancer, drugs affecting the immune response, drugs for infectious diseases, antiparasitic drugs and antiviral drugs. There is also a chapter on research and a glossary of some chemical and medical terms. I found the explanation of X-ray diffraction in the glossary as "A method of determining the chemical structure of a compound by measuring the distances between it atoms" somewhat vague. I was also surprised to read under a heading on Diuretics that the concentration of salts (especially sodium chloride) for the mammalian body is one-fourth that of seawater, namely about 0.23%. It has been my understanding that the concentration of sodium chloride which is isotonic with blood is 0.9% w/v and this should be the value used in the book.

Overall, an interesting book which achieves its stated aims. A little more on the need for different dosage forms (i.e., tablets, capsules, injections, suppositories, etc.,) would be useful to satisfy the curiosity of the lay person.

P.J. Cox

Flow Injection Atomic Absorption Spectrometry, by Zhaolun Fang, Wiley, Chichester, 1995, xii + 306 pp., £60.00. ISBN 0-471-95331-8.

Book reviews

Understanding Medications: What the Label Doesn't Tell You, by A. Burger, American Chemical Society, Washington, DC, 1995, xiv + 206 pp., ISBN 0-8412-3210-5.

The author of the book, Dr Alfred Burger, founded the Journal of Medicinal Chemistry in 1959 in collaboration with Arnold H Beckett. His inspiration for this book stems from the requirement to "satisfy and stimulate the curiosity of educated lay people who, on the whole, lack the biochemical and pharmacological background for the study of medicinal agents." The themes of the book are also described by the author as "the history, discovery, manufacture, action, acceptance and rejection of drugs".

Contained in the 21 small chapters is a wealth of information on drugs, albeit in a limited form, which indeed will satisfy most lay people. I found the text enjoyable and very easy to read–in a relaxed style somewhat similar to that found in Reader's Digest. Of course, whole books could have been written on each of the chapters so it will be very easy for a reviewer to criticise the oversimplicity of some of the contents. In the chapter on naming drugs it is interesting that not all trade names in the USA are the same as elsewhere, for example, the most common over-the-counter drug in the UK is paracetamol but the word paracetamol does not occur anywhere in the book. This is because the drug is known in the USA by the trade name Tylenol and the book correctly gives another corresponding nonproprietary name for the same drug as acetominophen.

The chapters devoted to drug categories are: neurohormones and drugs that affect the central nervous system, drugs for the relief of pain, local anesthetics, antispasmodics and antihistamines, drugs that act on the blood pressure and the heart, intestinal medications, hormones and vitamins, drugs for the treatment of cancer, drugs affecting the immune response, drugs for infectious diseases, antiparasitic drugs and antiviral drugs. There is also a chapter on research and a glossary of some chemical and medical terms. I found the explanation of X-ray diffraction in the glossary as "A method of determining the chemical structure of a compound by measuring the distances between it atoms" somewhat vague. I was also surprised to read under a heading on Diuretics that the concentration of salts (especially sodium chloride) for the mammalian body is one-fourth that of seawater, namely about 0.23%. It has been my understanding that the concentration of sodium chloride which is isotonic with blood is 0.9% w/v and this should be the value used in the book.

Overall, an interesting book which achieves its stated aims. A little more on the need for different dosage forms (i.e., tablets, capsules, injections, suppositories, etc.,) would be useful to satisfy the curiosity of the lay person.

P.J. Cox

Flow Injection Atomic Absorption Spectrometry, by Zhaolun Fang, Wiley, Chichester, 1995, xii + 306 pp., £60.00. ISBN 0-471-95331-8.

The combination of flow injection (FI) and atomic absorption spectrometry (AAS) has undergone a spectacular development within the past decade as reflected in the exponentionally increasing number of publications (more than 600 are included in the book). In fact, the effects are in the words of the author "so dramatic" that it has brought "new vitality to a technique [AAS] which otherwise seemed to be confronted by a period of stagnancy". Most of these novel developments have taken place since Burguera in 1989 edited the first monograph on FI-AAS, and for this reason it seems highly appropriate that Fang, who is one of the foremost authorities in the field, has undertaken to scrutinize, compile and communicate the current knowledge in this rapidly growing area.

His book is composed of twelve chapters. Chapter 1 gives a brief introduction to the basic principles of FI and some general aspects of FI-AAS, where it is noteworthy that Fang warns that "flow injection techniques are not as simple as they appear", implying that it is important to direct attention to technical and operational details to avoid detours and pitfalls. The core, mission and justification of his book is to assist the reader to design optimal systems for dedicated purposes. Chapter 2 deals with general instrumentation, where the author generously shares his wealth of practical experience, discusses advantages and disadvantages of the individual components (pumps, valves, tubings, etc.) and offers numerous useful operational hints. In fact, these aspects are characteristically manifested throughtout the text, where one is constantly reminded that this is a book written by a person who truly has hands-on experience with his subject. These introductory chapters (and sections of the following ones) inevitably imply recycling of material from his previous book on Flow Injection Separation and Preconcentration. This should not, however, be taken as a derogatory remark, because if one is not the fortunate owner of that book the material included here is essential prerequisites for sufficient appreciation of the ensuing chapters. The various modes of FI sample introduction used in AAS are treated in Chapter 3—detailed appropriately because it is well recog-

nised that this feature is indeed the 'Achilles heel' of atomic spectrometric techniques—followed by separate chapters on FI techniques for on-line dilution (Chapter 4) and sensitivity enhancement (Chapter 5), all used mainly in connection with flame spectrometry. For this reviewer, who has constantly advocated the exploitation of the potentials which are inherent in the concentration gradient created in FI, it is most satisfying to see that Fang stresses this point, which has been much overlooked in conjunction with FI-AAS. Chapter 6 is devoted to FI vapor generation methods, that is, hydride generation (HGAAS) and cold vapor (CVAAS), where advantage can not only be taken of separating the gaseous analyte species from possible interfering matrix constituents, but where one can also exploit kinetic discrimination to enhance the analytical signal in favour of the sample constituent. Chapter 7 treats the so-called indirect methods, that is, conversion techniques where a sample consitiuent via intelligent chemistry is converted into a species detectable by AAS. FI on-line preconcentration systems for flame and vapor generation AAS are discussed separately in Chapter 8, which relies heavily on the author's previous book, but also contains much new material in this rapidly expanding field and is a most illuminating section comprising much valuable information which will no doubt be of great value for the reader. In Chapter 9 FI techniques (including preconcentration techniques) used for electrothermal AAS are treated. Not surprisingly, this section draws heavily on the author's own results, where he, undisputably, has been one of the pioneers, and which area promises to be one of the most exciting ones in the future. Chapters 10 and 11 are devoted to FI calibration (by exploiting the concentration gradient of FI) and on-line digestion techniques. The last chapter (12) deals with the application of FI-AAS methods to the environmental, agricultural, clinical, pharmaceutical, geological and metallurgical fields, a compilation which should prove most useful for practising analytical chemists.

In the preface it is stated that the book may be used "both as a reference source and a laboratory manual, but some of the chapters may also be

used as textbook material". I am not sure that the author has managed to achieve all these goals satisfactorily (and it would, admittedly, also be virtually impossible to do so). While the book constitutes a homogenous entity when read as a whole, it is somewhat problematic to extract specific information on a certain subject (as guided from the otherwise detailed index) unless several sections are consulted simultaneously. Although Fang has tried to eliminate this shortcoming with a fine-masked net of cross references, it does in instances create more confusion than overview. On the other hand, it should be added that the book inevitably compels the reader to continue reading, which is a commendable asset. Some subjects, which to the AAS-practitioner might be termed to be rather exotic, are treated in unnecessary detail (e.g. thermospray and high pressure sample deposition), while others are mentioned merely superficially. This is especially true for the subject of speciation to which only half a page is devoted. To the excuse of the author it should be added that this area has received particular attentiion in the very recent past, and since the manuscript for Fang's book was concluded in late 1994, he really cannot be blamed. A neat detail which deserves to be mentioned is the way that Fang has compiled and combined the references and the FI-AAS bibliography at the end of his book. While the references are quoted in the "normal" fashion (i.e., without titles), the bibliographic ones include the full title of the individual papers which is most helpful.

Altogether Fang has written an authoritative book on a subject of vital interest, but also on a subject on which there is an expanding growth and practical interest. Therefore, I am sure that his book will stand out as a milestone, firstly because it is written by one of the foremost specialists in the field, and secondly because it contains a wealth of applicable information. Both for the beginner in the area of FI-AAS and for the experienced analyst the book should prove most useful and, what I find important, inspirational. The concluding chapter is virtually a gold mine as a reference source as well a practical guide for determining various elements in different matrices. Here the book not only proves its merits as

a handbook for the analytical chemist, but also as a viable practical tool. For all these reasons I am of the firm conviction that the book is a very good investment.

E.H. Hansen

Special Trends in Thermal Analysis, by F. Paulik, Wiley, Chichester, 1995, xvii + 459 pp., £90.00. ISBN 0-471-95769-0.

Can there be anyone who worked in the field of thermal analysis who has failed to notice one name recurring time and again with amazing frequency over the last thirty years— the name Paulik? Indeed, there were usually two Pauliks, the brothers Ferenc and Jenö, who make their name in the field of differential thermal analysis, designing and building their own apparatus in the 1950's, and applying it, and its later developments, to the investigation of countless materials of both synthetic and natural origin, so that this has come to be widely recoginsed as an essential tool in materials testing and chemical analysis.

This book— by Ferenc Paulik— is dedicated to the memory of his collaborator for over thirty years—his younger brother Jenö who died in 1988. It is a survey of the applications of these instruments, and in principle of any similar instruments operating in simultaneous measurement mode. This survey includes a comprehensive bibliography of over 2800 papers, spanning the years from the description of the original instrument in 1954 up to the present day (1995).

Part I of the book is concerned with experimental methodology, including dilatometry, thermogas titrimetry and evolved gas analysis. Part II reflects the Pauliks' view that recording thermal analysis data for a substance was just a beginning—they always pursued the interpretation of the curves in terms of chemical and physical changes, aided by evolved gas analysis or X-ray methods. So this part is concerned with the kinetics and mechanism of the processes occurring during heating of samples.

used as textbook material". I am not sure that the author has managed to achieve all these goals satisfactorily (and it would, admittedly, also be virtually impossible to do so). While the book constitutes a homogenous entity when read as a whole, it is somewhat problematic to extract specific information on a certain subject (as guided from the otherwise detailed index) unless several sections are consulted simultaneously. Although Fang has tried to eliminate this shortcoming with a fine-masked net of cross references, it does in instances create more confusion than overview. On the other hand, it should be added that the book inevitably compels the reader to continue reading, which is a commendable asset. Some subjects, which to the AAS-practitioner might be termed to be rather exotic, are treated in unnecessary detail (e.g. thermospray and high pressure sample deposition), while others are mentioned merely superficially. This is especially true for the subject of speciation to which only half a page is devoted. To the excuse of the author it should be added that this area has received particular attentiion in the very recent past, and since the manuscript for Fang's book was concluded in late 1994, he really cannot be blamed. A neat detail which deserves to be mentioned is the way that Fang has compiled and combined the references and the FI-AAS bibliography at the end of his book. While the references are quoted in the "normal" fashion (i.e., without titles), the bibliographic ones include the full title of the individual papers which is most helpful.

Altogether Fang has written an authoritative book on a subject of vital interest, but also on a subject on which there is an expanding growth and practical interest. Therefore, I am sure that his book will stand out as a milestone, firstly because it is written by one of the foremost specialists in the field, and secondly because it contains a wealth of applicable information. Both for the beginner in the area of FI-AAS and for the experienced analyst the book should prove most useful and, what I find important, inspirational. The concluding chapter is virtually a gold mine as a reference source as well a practical guide for determining various elements in different matrices. Here the book not only proves its merits as

a handbook for the analytical chemist, but also as a viable practical tool. For all these reasons I am of the firm conviction that the book is a very good investment.

E.H. Hansen

Special Trends in Thermal Analysis, by F. Paulik, Wiley, Chichester, 1995, xvii + 459 pp., £90.00. ISBN 0-471-95769-0.

Can there be anyone who worked in the field of thermal analysis who has failed to notice one name recurring time and again with amazing frequency over the last thirty years— the name Paulik? Indeed, there were usually two Pauliks, the brothers Ferenc and Jenö, who make their name in the field of differential thermal analysis, designing and building their own apparatus in the 1950's, and applying it, and its later developments, to the investigation of countless materials of both synthetic and natural origin, so that this has come to be widely recoginsed as an essential tool in materials testing and chemical analysis.

This book—by Ferenc Paulik—is dedicated to the memory of his collaborator for over thirty years—his younger brother Jenö who died in 1988. It is a survey of the applications of these instruments, and in principle of any similar instruments operating in simultaneous measurement mode. This survey includes a comprehensive bibliography of over 2800 papers, spanning the years from the description of the original instrument in 1954 up to the present day (1995).

Part I of the book is concerned with experimental methodology, including dilatometry, thermo-gas titrimetry and evolved gas analysis. Part II reflects the Pauliks' view that recording thermal analysis data for a substance was just a beginning—they always pursued the interpretation of the curves in terms of chemical and physical changes, aided by evolved gas analysis or X-ray methods. So this part is concerned with the kinetics and mechanism of the processes occurring during heating of samples.

Part III of the book discusses the more recent topic of quasi-isothermal TG and DTA, which permits greatly improved resolution of decomposition steps by raising the temperature very slowly through the regions of change, maintaining a tiny but constant temperature difference between the sample and its environment, and thus overcoming the problem associated with earlier instruments that thermal analysis curves from different laboratories could vary significantly due to the use of different heating rates.

This unique, readable and well illustrated volume is authoritative. It is the voice of the master, or, rather, the voice of the master brothers, a fitting tribute, and an excellent handbook of the state of the art of thermal analysis.

I. Marr

Capillary Electrophoresis Guidebook: Principles, Operation and Applications, edited by K.D. Altria, Humana, Totawa, 1996, xi + 349 pp., US$74.50. ISBN 0-896-03315-5.

This book in two parts, is volume 52 in the series on Methods in Molecular Biology. Part 1 is ideal for those lacking in, or with limited knowledge of, the theory and the practice of capillary electrophoresis (CE). It is an excellent, easy-to-follow, instructive text, particularly on the practicalities of the methods and instrumentation involved in CE. By the frequent use of flow diagrams, clear figures and tables and the use of smaller print in the text to highlight important aspects of the instrumentation or essential steps in the methodology, the author guides the reader in a logical fashion from start up to the final step of running a successful, validated, separation. The text communicates to the reader the author's obvious enthusiasm and knowledge of CE.

The contents of Part 2 are more geared towards those with current or future research interests in CE. It reviews the methods and technologies which are commonly used at present, for example, chiral separations by CE, micellar electrokinetic chromatography, capillary gel electrophoresis, and capillary electrochromatography. The final chapter reviews the less common uses of CE and in so doing illustrates amply the potential of CE for the analysis of a very diverse range of subject matter. Though different authors contribute to Part 2, the high, uniform, standard of presentation of the text, as seen in Part 1, is maintained throughout Part 2. As per Part 1, up-to-date, appropriate references are included at the end of each of the chapters.

Though CE is a comparatively recent addition to available chromatographic separation techniques, its importance as a widely used separation method with a very diverse range of applications is encapsulated in this very worthwhile, well written, and referenced text.

R.R. Moody

Part III of the book discusses the more recent topic of quasi-isothermal TG and DTA, which permits greatly improved resolution of decomposition steps by raising the temperature very slowly through the regions of change, maintaining a tiny but constant temperature difference between the sample and its environment, and thus overcoming the problem associated with earlier instruments that thermal analysis curves from different laboratories could vary significantly due to the use of different heating rates.

This unique, readable and well illustrated volume is authoritative. It is the voice of the master, or, rather, the voice of the master brothers, a fitting tribute, and an excellent handbook of the state of the art of thermal analysis.

I. Marr

Capillary Electrophoresis Guidebook: Principles, Operation and Applications, edited by K.D. Altria, Humana, Totawa, 1996, xi + 349 pp., US$74.50. ISBN 0-896-03315-5.

This book in two parts, is volume 52 in the series on Methods in Molecular Biology. Part 1 is ideal for those lacking in, or with limited knowledge of, the theory and the practice of capillary electrophoresis (CE). It is an excellent, easy-to-follow, instructive text, particularly on the practicalities of the methods and instrumentation involved in CE. By the frequent use of flow diagrams, clear figures and tables and the use of smaller print in the text to highlight important aspects of the instrumentation or essential steps in the methodology, the author guides the reader in a logical fashion from start up to the final step of running a successful, validated, separation. The text communicates to the reader the author's obvious enthusiasm and knowledge of CE.

The contents of Part 2 are more geared towards those with current or future research interests in CE. It reviews the methods and technologies which are commonly used at present, for example, chiral separations by CE, micellar electrokinetic chromatography, capillary gel electrophoresis, and capillary electrochromatography. The final chapter reviews the less common uses of CE and in so doing illustrates amply the potential of CE for the analysis of a very diverse range of subject matter. Though different authors contribute to Part 2, the high, uniform, standard of presentation of the text, as seen in Part 1, is maintained throughout Part 2. As per Part 1, up-to-date, appropriate references are included at the end of each of the chapters.

Though CE is a comparatively recent addition to available chromatographic separation techniques, its importance as a widely used separation method with a very diverse range of applications is encapsulated in this very worthwhile, well written, and referenced text.

R.R. Moody

Talanta

Polarographic determination of loratadine in pharmaceutical preparations

J.A. Squella*, J.C. Sturm, M.A. Diaz, H. Pessoa, L.J. Nuñez-Vergara

Bioelectrochemistry Laboratory, Chemical and Pharmaceutical Sciences Faculty, University of Chile, P.O. Box 233, Santiago 1, Chile

Abstract

Loratadine, a potent antihistamine drug, is not directly electroreducible at a dropping mercury electrode; however, by means of a nitration procedure it is possible to obtain a nitro-loratadine derivative which has been identified as 4-(8-chloro-7-nitro-5,6-dihydro-11H-benzo-[5,6]-cyclohepta-[1,2-b]-pyridin-11-ylidene)-1-piperidine carboxylic acid ethyl ester. The electrochemical reduction of this derivative at different pHs and concentrations using polarography and cyclic voltammetry was studied. The derivative exhibits a differential pulse polarographic peak due to the reduction of the nitro group. This peak was used in order to develop an analytical procedure for determining loratadine in pharmaceutical dosage forms.

The recovery study shows adequate accuracy and precision for the developed assay and the excipients do not interfere in the determination.

Keywords: Loratadine; Polarography; Drug analysis; Nitrated loratadine

1. Introduction

Loratadine (Fig. 1) is a potent, long-acting antihistamine which has a high selectivity for peripheral histamine H_1-receptors in the central nervous system (CNS) in vitro or in vivo. The drug displays little activity at acetylcholine or α_1-adrenergic receptors, and is inactive in animal models of assessing anticholinergic effects. Loratadine penetrates poorly into the CNS [1].

The therapeutic efficacy of loratadine has been investigated in allergic rhinitis, both seasonal and perennial, acute coryze (common cold) and chronic idiopathic urticaria. The recommended adult dosage of loratadine is 10 mg once daily while that of the combination tablet (5 mg loratadine plus 120 mg pseudoephedrine) is one tablet twice daily [2].

Radioimmunoassay and high performance liquid chromatography, with detection limits of 0.3 $\mu g\ l^{-1}$ and 0.6 $\mu g\ l^{-1}$ respectively, have been used to quantitate loratadine and its chief metabolite, descarboethoxy-loratadine, in plasma [3]. However, no analytical assays for pharmaceutical forms of loratadine have been reported to date.

* Corresponding author.

Modern computer-based electrochemical instru-
mentation has increased the usefulness of electro-
chemical methods in pharmaceutical analysis and
there are several examples where electrochemical
determinations of drugs in pharmaceutical forms
have been developed [4–6]. A practical advantage
of polarography and voltammetric methods in the
determination of drugs in pharmaceutical forms is
that undissolved excipients or colored solutions
do not interfere to the extent that they do in other
methods. The prerequisite for direct determina-
tion without prior separation is that the drug is
more strongly adsorbed onto the electrode surface
than the excipients present in the formulation [7].

The purpose of this work is to investigate some
of the electrochemical properties of loratadine
and to work out a new method for loratadine
determination using principally differential pulse
polarography (DPP), for both the pure drug and
for commercial preparations.

2. Experimental

2.1. Apparatus

DPP, Tast polarography and cyclic voltammet-
ric experiments were carried out in an Inelecsa
assembly containing a PDC1212 potentiostat–
generator attached to an Acer 500 + PC computer
with suitable software for totally automated con-
trol of the experiments and data acquisition. A 50
ml thermostated cell equipped with a three-elec-
trode system was used. The working electrode was
a dropping mercury electrode (DME) and a hang-
ing mercury drop electrode (HMDE), Metrohm
model EA-290, for polarographic and cyclic
voltammetric experiments respectively. A satu-
rated calomel electrode (SCE) as a reference elec-
trode and a platinum wire as an auxiliary
electrode were also used.

Spectrophotometric measurements were carried
out with a Perkin-Elmer model 551 spectrophoto-
meter using 1 cm quartz cells. Spectra were
recorded between 200 and 400 nm, and quantita-
tive sample measurements were made at 270 nm.

A Varian XL-100 nuclear magnetic resonance
spectrometer, a Bruker AM-200 nuclear magnetic

resonance (NMR) spectrometer and a Perkin-
Elmer model 1310 IR spectrophotometer were
used. The IR spectra were obtained in 1% potas-
sium bromide pellets, and the NMR spectra were
carried out in deuterated chloroform with TMS as
internal standard.

2.2. Materials and reagents

Loratadine,   4-(8-chloro-5,6-dihydro-11H-
benzo-[5,6]-cyclohepta-[1,2-b]-pyridin-11-ylidene)
-1-piperidine carboxylic acid ethyl ester, was
obtained from Schering-Plough Laboratories
(Santiago, Chile; 99.7% chromatographically
pure). Clarityne® tablets containing 10 mg of
loratadine were commercially obtained. All
reagents and solvents were of analytical grade.

2.3. Procedures

2.3.1. Nitration mixture

A previously reported [8] modified mixture was
used. 500 mg of sodium nitrate was accurately
weighed and dissolved in 50 ml concentrated sul-
furic acid.

2.3.2. Nitration procedure

An accurately weighed amount of the drug (10
mg) was transferred to a 10 ml tube and treated
with 1 ml of nitration mixture. The drug was
solubilized in an ultrasonic bath for 1–5 min,
cooled over ice and diluted with 10 ml distilled
water. Then the solution was transferred to a 50
ml calibrated flask and diluted to volume with
distilled water in order to obtain a 5×10^{-4} M
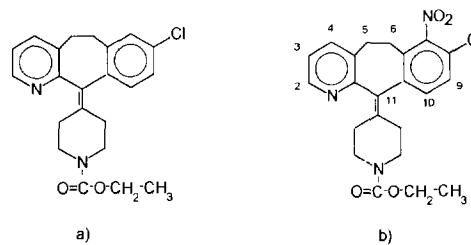standard solution of nitrated loratadine (NO_2-
loratadine).

Fig. 1. Chemical structures of (a) loratadine, (b) nitro-lo-
ratadine derivative.

2.3.3. Isolation of nitrated derivative

After the nitration procedure the solution was chromatographed on a silica column with chloroform:ethyl acetate (50:50) as eluant. The obtained solutions from the column were concentrated to give an oily yellow substance that was analyzed by IR and NMR.

2.3.4. Buffer solutions

To study the effect of pH on the electrochemical behavior of the nitrated loratadine, 0.1 M Britton–Robinson buffer with a pH range of 1.5–13.5 was used. 30% ethanol as a co-solvent was also used. For analytical studies a pH 12 buffer solution was prepared as follows: add 10 ml 5 M NaOH, 30 ml 0.4 M H_3BO_3 and 30 ml acetone and then make up to volume with distilled water.

2.3.5. Calibration curve

Solutions for the calibration curve were individually prepared by diluting the standard solution with pH 12 buffer to obtain solutions which varied from 1×10^{-5} M to 1×10^{-4} M.

2.3.6. Synthetic samples

Synthetic samples from recovery studies were prepared by weighing 10 mg plus suitable excipients according to the manufacturer's batch formulas for 10 mg loratadine tablets. The excipients tested were magnesium stearate, starch and lactose. The pure loratadine plus excipients mixture was homogenized and then the above nitration procedure was followed. Following the nitration procedure and suitable dilutions, the solutions were directly assayed by polarography and spectrophometry.

2.3.7. Tablet assay

Each loratadine tablet (Clarityne®, Lab. Schering, Santiago, Chile) was finely ground and then nitrated and diluted according to the above nitration procedure. After the nitration procedure and adequate dilutions the solutions were directly assayed by polarography and spectrophometry.

2.3.8. Polarography

Before the polarographic experiments all the solutions were purged with pure nitrogen for 5

min. All the potentials are referenced to the SCE. The operating conditions were (a) DPP mode: pulse amplitude, 50 mV; potential scan rate, 5 mV s^{-1}; drop time, 1 s; potential range, 0 to -1000 mV; current range, 1–10 μA full scale; (b) d.c. mode: potential scan rate, 5 mV s^{-1}; drop time, 1 s; potential range, 0 to -1000 mV; current range, 0.5–5 μA full scale.

2.3.9. Spectrophotometry

The same solutions as for the polarographic measurements were filtered and measured with the spectrophotometer at 269 nm. As a reference a buffer solution of pH 12 was used.

3. Results and discussion

Loratadine is not polarographically reducible as evidenced by the absence of waves in the available potential range. Consequently, in order to obtain a polarographic signal we tried a derivatization method in order to transform the drug into an electroactive moiety, in this case a nitration procedure. According to the described nitration procedure we have obtained a very well-defined polarographic peak, or wave (Fig. 2), with peak potential or half wave potential of -770 mV vs. SCE by differential pulse or d.c. polarography respectively. In addition, by following the limiting current of this peak, or wave, it is possible to control the nitration procedure. Specifically, this procedure is very sensitive to the following parameters: concentration of the nitration mixture, time of reaction and temperature. In Fig. 3 the dependence of the nitrate concentration of the nitration mixture on the peak current of the NO_2-loratadine derivative is shown. It can be concluded that above 7 mg sodium nitrate per ml H_2SO_4 the quantity of the NO_2-loratadine derivative remains constant. In order to obtain suitable nitration conditions we recommend a concentration of 10 mg sodium nitrate per ml H_2SO_4. The nitration procedure is only slightly dependent on reaction time. However, in order to secure both a complete dissolution of the drug and adequate reproducibility in terms of the extent of the reaction, a reaction time of 10 min is recommended.
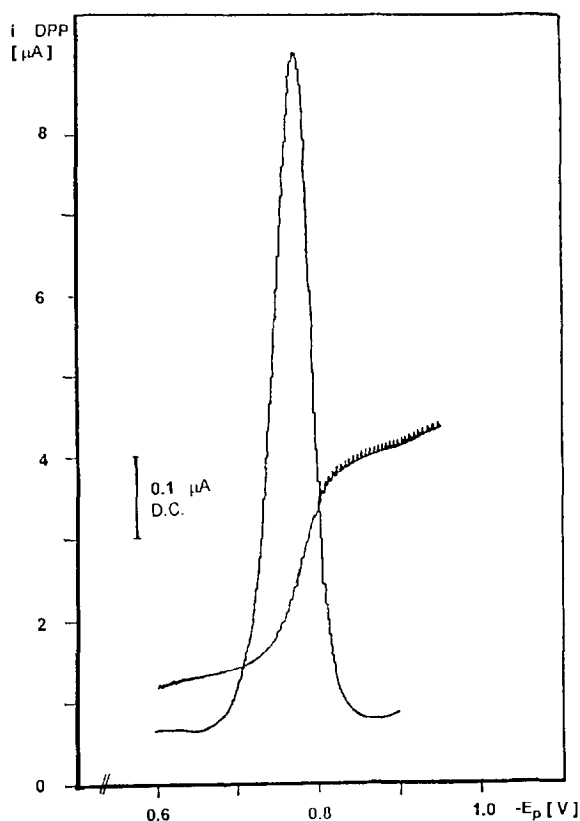
Fig. 2. DP and d.c. polarograms of 5×10^{-5} M solution of treated loratadine in buffer, pH 12, aqueous buffer:acetone (70:30, v/v).

Furthermore, the nitration procedure is strongly dependent on temperature. In Fig. 4 the effect of increasing reaction temperature on the differential pulse polarogram of the reaction product is shown. From this behavior it can be concluded that at temperatures > 30°C a second peak appears, at approximately − 540 mV.

In order to confirm the nitration procedure and to identify the nitrated derivative we have used IR and NMR spectroscopy. Firstly, we have confirmed that nitration occurs by comparison of the IR spectrum of loratadine with the IR spectrum of the nitrate derivative. The latter spectrum shows two bands, at 1530 cm^{-1} and 1350 cm^{-1}, that do not appear in the loratadine IR spectrum. These bands are characteristic of nitro groups [9], thus confirming the nitration of loratadine. Secondly, considering the structural analysis of the

molecule, there are two main possibilities for nitration, namely the pyridine and chlorobenzene moieties (Fig. 1). However, the ^{1}H-NMR spectrum of the nitrated derivative shows the following signals: δ: 7.20 (d,d 1H, 3-H, $J = 8$ Hz); 7.50 (d,d, 1H, 4-H, $J = 8$, $J = 4.5$ Hz) and 8.47 (d,d, 1H, 2-H, $J = 8$, $J = 4.5$ Hz), indicating that there is not substitution in the pyridine moiety. Consequently, the nitro substitution occurs in position 7 of the chlorobenzene moiety, producing the nitro-loratadine derivative (Fig. 1). Furthermore, the second polarographic peak that appears at more anodic potential (Fig. 4) may be explained by considering a side product of the nitration reaction when the reaction temperature is > 30°C. This side product is a quinone derivative produced due to the further oxidation of the nitro derivative, according to Scheme 1. The quinone group was confirmed by the green color obtained in the presence of ammonia and the reduction peak at more anodic potentials can be ascribed to the reduction of the quinone moiety.

As a result of our selected temperature conditions (cooling over ice) only one peak due to the reduction of the NO_2-loratadine was observed. Specifically, the electroactivity is due to the four-electron reduction of the nitro-aromatic moiety
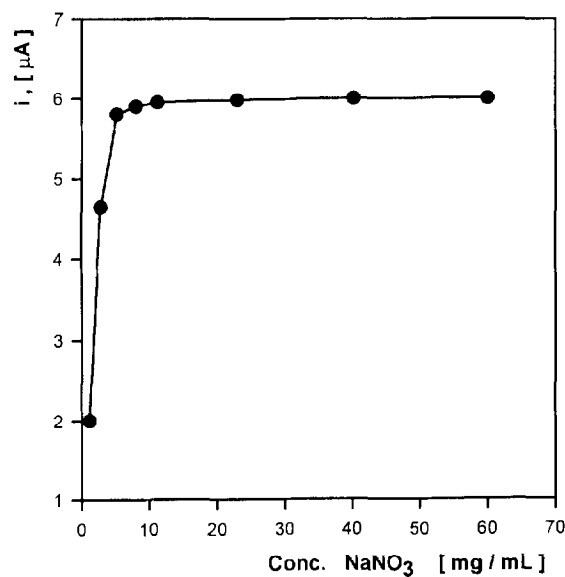

Fig. 3. Effect of the nitrate concentration in the nitration mixture on the nitro-loratadine derivative formation.
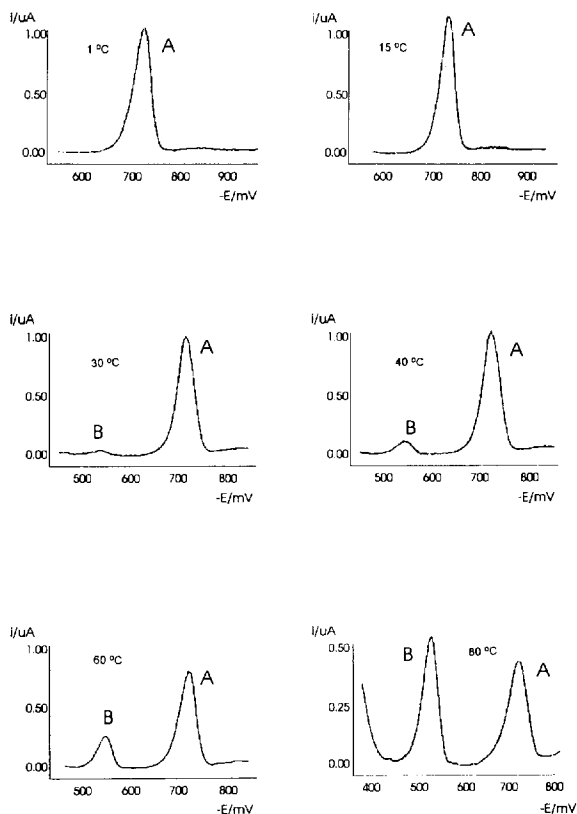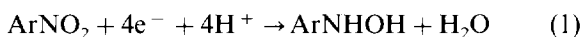
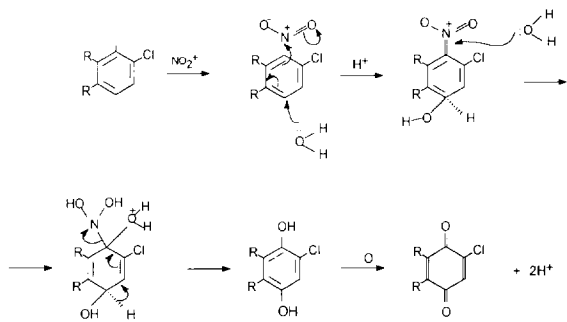Fig. 4. Effect of increasing temperature on the nitration reaction.

Fig. 5. pH dependence of the DPP peak potentials in nitrated loratadine solutions.

according to the well-known global mechanism [10]:

$$ArNO_2 + 4e^- + 4H^+ \rightarrow ArNHOH + H_2O \qquad (1)$$

To examine the effect of pH on the limiting current and peak potential, a series of d.c. and DP

Scheme 1. Mechanism of the loratadine nitration and further oxidation at higher temperatures.

polarograms were recorded for 5×10^{-5} M loratadine solutions in a 0.1 M Britton–Robinson buffer with 30% ethanol as a cosolvent. The behavior of the peak potential with pH is given in Fig. 5. As can be seen the peak potential was shifted to more negative values, showing a linear dependence between pH 1.5 and pH 10.5, with a break at approximately pH 5. Above pH 10.5 the potential peak is pH-independent, suggesting that no protons are involved previously or in the rate-determining step. This fact implies that in a strongly alkaline medium the rate-determining step is the transfer of the first electron, without previous protonation. This pH behavior is typical for nitroaromatic compounds [11]. Furthermore, linear sweep voltammetric experiments reveal the presence of a very sharp asymmetric peak indicating both the irreversible character of the reduction process and the weak adsorption of the electroactive species [12].

In contrast, the limiting current of the NO_2-loratadine derivative in DPP remains practically constant over all the pH range. However, in DPP the peak current shows a distinct change with pH (Fig. 6). This change is because in DPP mode the peak current is strongly dependent on the reversibility of the process, i.e. irreversible redox

systems result in lower and broader current peaks compared with those predicted for reversible systems [13]. In our case we have a distinct change in the reversibility of the electrode process with pH, with a greater degree of reversibility at basic pHs. To obtain better resolution and reproducibility we have selected pH 12 for further studies. In order to clarify the nature of the electrode process that controls the limiting current, we studied the limiting current behavior as a function of the height of the mercury column. From this study we obtained a linear relation between the limiting current and the square root of the height of the mercury column (corrected for back pressure), showing diffusion control of the electrode process. Consequently, we have also obtained a linear relation between the peak current and loratadine concentrations with a linear range between 1×10^{-7} M and 1×10^{-4} and a detection limit of 1×10^{-7} M by DPP at pH 12. The determination of the detection limit was effected by comparison with a blank signal, being positive when the signal surpassed the signal-to-noise ratio by a factor of three. In order to quantify the drug, we have used the calibration curve method with concentrations ranging between 1×10^{-5} M and 1×10^{-4} M. The calibration curve is described by the follow-
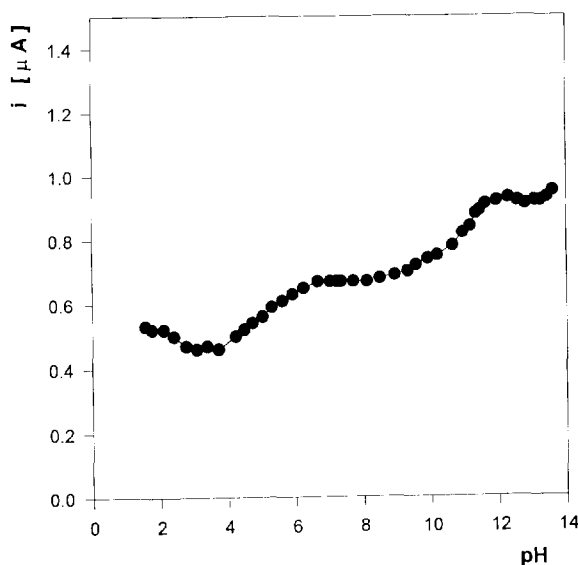
ing regression curve:

$$i_p(\mu A) = 80.02 \times 10^3 C(M) + 0.199 \qquad (2)$$

(correlation coefficient = 0.999, $n = 10$, pH = 12, $T = 25°C$), where i_p is the peak current and C is the loratadine concentration. The reproducibility of the method was calculated from ten independent runs of a 5×10^{-5} M loratadine solution, obtaining an RSD of 1.4%. In order to check the accuracy and precision of the developed method, we have also carried out a recovery study, obtaining a recovery of 98.97% with an RSD of 1.81%. From these results we can conclude that the method is sufficiently accurate and precise in order to be applied to pharmaceutical forms. The result for the individual tablet assay for commercial tablets containing 10 mg of loratadine shows a mean of 10.02 mg with an RSD of 1.67% for 10 individual tablets. Furthermore, to obtain comparative results a UV spectrophotometric method was also developed. Loratadine adsorption spectra exhibit two poorly-resolved absorption maxima at 240 and 280 nm; however, the NO_2-loratadine absorption spectrum exhibits a well-defined UV absorption maximum with a higher absorbance at 269 nm. The maximum exhibits a linear relation between absorbance and drug concentration. For analytical determination the calibration curve method, with concentrations ranging between 1×10^{-5} M and 1×10^{-4} M, was used. This curve is described by the following regression line:

$$A = 13.5 \times 10^3 C(M) - 3.8 \times 10^{-5} \qquad (3)$$

(correlation coefficient = 0.999, $n = 10$), where A is the absorbance of NO_2-loratadine solution at 269 nm. The results of the recovery study (99.9% recovery, 1.82% RSD) and individual tablet assay (10.08 mg, 1.83% RSD) are in accord with the polarographic results.

Although both the developed methods showed similar accuracy and precision, the principal advantage of the proposed polarographic method over the spectrophotometric method is that the excipients do not interfere and consequently the filtration procedure is not necessary.

The proposed polarographic method proved to have adequate precision and accuracy to enable

Fig. 6. Peak current dependence of the DPP peak in nitrated loratadine solutions.

reliable analysis of loratadine and is therefore recommended as a useful tool for the analysis of loratadine in pharmaceutical forms. Although it is an indirect method, it is not time consuming as the derivatization process is easy. Consequently, the present contribution is a good example of the fact that the availability of electrochemical techniques is not restricted to molecules with electroactive groups.

Acknowledgements

References

[1] W. Kreutner, R.W. Chapman, A. Gulbenkian and M.I. Siegel, Allergy, 42 (1987) 57.
[2] S. Clissold, E. Sorkin and K. Goa, Drugs, 37 (1989) 42.
[3] E. Radwanski, V. Hilbert, S. Symchowicz and N. Zampaglione, J. Clin. Pharmacol., 27 (1987) 530.
[4] J.M. Kauffmann and J.C. Vire, Anal. Chim. Acta, 273 (1993) 329.
[5] R.K. Gilpin and L.A. Pachla, Anal. Chem., 65 (1993) 117R.
[6] P.M. Bersier and J. Bersier, Electroanalysis, 6 (1994) 171.
[7] P.M. Bersier and J. Bersier, Crit. Rev. Anal. Chem., 16 (1985) 81.
[8] M.A. Brooks, J.A.F. Silva and R.M. Hackman, Anal. Chim. Acta, 64 (1973) 165.
[9] R.M. Silverstein and G.C. Bassler, in Spectrometric Identification of Organic Compounds, John Wiley, New York, 2nd edn., 1968, p. 99.
[10] J.T. Browne in W.F. Smyth (Ed.), Polarography of Molecules of Biological Significance, Academic Press, London, 1979, p. 111.
[11] P. Zuman, Z. Fijalek, D. Dumanovic and D. Suznjevic, Electroanalysis, 4 (1992) 783.
[12] R.H. Wopschall and I. Shain, Anal. Chem., 38 (1967) 1514.
[13] J. Wang, in Analytical Electrochemistry, VCH, New York, 1994, p. 38.

Spectrophotometric determination of periodate or iodate ions by liquid–liquid extraction as an ion-pair using tetramethylammonium iodide

M.S. El-Shahawi[*,1], F.A. Al-Hashemi

Chemistry Department, Faculty of Science, UAE University, Al-Ain, P.O. Box 17551, United Arab Emirates

Abstract

A simple and accurate extractive spectrophotometric procedure was developed for the microdetermination of periodate and iodate in aqueous media. The determination of periodate was based upon the extraction of the ion-pair formed between the periodate and tetramethylammonium iodide at pH 4 in chloroform followed by direct spectrophotometric measurements at 509, 358 and 288 nm. The optimum concentration range evaluated by Ringbom's plot, the molar absorptivity, the Sandell's sensitivity and the stoichiometry of the formed ion-pair were critically determined. Iodate could be determined quantitively by the proposed procedure after oxidation to periodate with potassium persulphate. The effect of the diverse ions on the determination of the periodate and/or iodate by the proposed procedures was also investigated. The application of the method for the analysis of iodate or periodate in the artificial fresh water was successfully carried out.

Keywords: Determination; Iodate; Ion-pair; Periodate

1. Introduction

Because iodate and periodate exclusively associate with oxidation of metal ions [1–6], polyhydroxylated compounds [6,7] and catalytic applications [8] at trace levels, sensitive methods are required for their reliable quantitification. Several spectrophotometric methods for the determination of both ions have been reported [9–13]. The existing methods for spectrophotometric determination of these ions were unsatisfactory for routine analysis as the procedures required direct maintenance of the experimental conditions (e.g. a strictly fixed pH, standing of the samples before the determination and low stability of the compound formed) and suffer from the lack of selectivity, sensitivity, the requirement of a laborious enrichment step and a low tolerance limit [12,13].

* Corresponding author.

[1]Permanent address: Chemistry Department, Faculty of Science at Damiatta, Mansoura University, Mansoura, Egypt.

The oxoanions are the least investigated species that form a liquid–liquid extractable ion-pair with onium cations [14–18]. The aim of the present study was to develop a simple and sensitive extraction spectrophotometric analytical procedure for the determination of periodate or iodate ions in aqueous matrices. The method we suggest is superior to some of the reported methods in sensitivity, and stability of the associate obtained [11–13].

2. Experimental

2.1. Reagents and materials

All the chemicals and solvents used were of analytical reagent grade. Britton–Robinson (B–R) buffer (pH 2.2–11.5) was prepared from boric, acetic and phosphoric acids and sodium hydroxide in double distilled water. Stock solutions of potassium periodate (BDH) and potassium iodate (1 mg ml^{-1}) were prepared separately by dissolving the extract weight of the corresponding salt in hot distilled water. The reagent tetramethylammonium iodide (Fluka, Purum > 98%) was used without further purification. Tetramethylammonium iodide (TMA$^+$I$^-$) (0.5% w/v) and potassium persulphate (2% w/v) were prepared in distilled water.

2.2. Apparatus

A Pye-Unicam Sp 8-400 double beam UV-visible spectrophotometer was used for recording the absorption spectra and the absorbance measurements with a quartz cell of 10 mm path length. A Phillips 9418 digital pH-meter was used for the pH measurements.

2.3. Recommended procedures

2.3.1. Determination of periodate ion

An aliquot (1–5 ml) of the aqueous solution of potassium periodate containing 1–50 μg of periodate ion was transferred to a 100 ml separating funnel. A volume of 10 ml of Britton–Robinson buffer (pH 4), 5 ml of water and 5 ml of te-

tramethylammonium iodide (0.5% w/v) were added and mixed. This was extracted twice with 5 ml of chloroform (2 × 2.5) and the extracts were collected in a 50 ml beaker containing anhydrous sodium sulphate (1 g). The beaker was swirled to mix the contents. The extract was transferred to a 10 ml volumetric flask, the residue was washed with 5 ml CHCl$_3$ and transfered to the volumetric flask. The solution was made up to the mark with the solvent. The absorbance of the organic phase was measured at 509, 358 and 288 nm against a reagent blank prepared under the same experimental condition.

2.3.2. Determination of iodate ion

A known volume (1–10 ml) of sodium iodate solution (containing 1–50 μg of iodate ions) was transferred to a 100 ml Erlenmeyer conical flask. A volume of 10 ml of potassium persulphate (2% w/v) and 10 ml of water were added to each flask, the solution was boiled for 10 min and the reaction mixture was allowed to cool. The pH of the solution was adjusted (pH 4) with 10 ml buffer followed by the addition of 5 ml of the reagent (TMA$^+$I$^-$). The reaction mixture and the washing solution of the flask were transferred to a 100 ml separating funnel. The formed ion-pair was extracted with 5 ml chloroform (2 × 2.5) and the recommended procedure for periodate determination was followed. A blank prepared under the same experimental conditions in the presence of potassium persulphate was run.

3. Results and discussion

The technique suggested for the determination of the periodate ions was based on its interaction in acidic medium with an excess of tetramethylammonium iodide. The solubility of the produced ion associate of the periodate with (TMA$^+$I$^-$) was investigated in the following solvents: dichloromethane, n-hexane, dichloroethane, isobutylether, benzene, nitrobenzene, tetrachloromethane, chloroform and toluene. The highest absorbance of the produced ion-associate was obtained in chloroform and toluene in a very short time. In chloroform the extraction was com-

plete and a better separation of phases was obtained. Therefore, chloroform was selected as a proper solvent for these reasons and because its greater density allows a better separation of the layers. The absorption spectrum of the formed yellow-violet ion-pair in chloroform extracted from the aqueous solution at pH 4 is given in Fig. 1(a). The coloured ion associate formed has three absorption maxima at 509, 358 and 288 nm in the UV-visible region whilst no peaks were found in this range in the spectra of $(TMA^+ I^-)$ and the periodate in chloroform. Therefore, the absorbance measurements for the ion-associate formed from the reaction of $(TMA^+ I^-)$ and IO_4^- were measured at 509, 358 and 288 nm. In Fig. 1(b) the absorption spectrum of iodine in chloroform is also given which differs from the spectrum of the postulated ion-pair.

The extraction of the formed ion-associate into chloroform was rapid and a shaking time of 2 min was selected in the subsequent work. The absorbance of the pink-coloured associate in chloro-

Fig. 2. Influence of pH of the aqueous phase on the absorbance of the extracted ion-pair in chloroform at 509 nm.

form was found to be constant up to 2 h for samples containing 0.05–10 μg ml^{-1} periodate in aqueous solution at pH 4 and $\lambda = 509$ and 358 nm. The addition of sodium chloride in the concentration range 0.01–0.5 mol l^{-1} did not improve the amount of the ion-associate extracted at 5 μg ml^{-1} periodate aqueous phase at pH 4 suggesting that the reaction is quantitative without salt effect.

To optimize the reaction conditions we studied the effect of the pH of the aqueous phase upon the interaction of the periodate with $(TMA^+ I^-)$ by measuring the absorbance of the produced ion-associate in chloroform. The final pH of each aqueous solution was measured before the extraction. The experimental data (Fig. 2)[1] showed that the maximum absorption of the produced ion-pair was obtained at pH 4. In strong (pH < 4) or weak acidic solution (4 < pH) the absorbance of the extracted species decreased owing to the incomplete dissociation of the periodate salt or the hydrolysis of the ion-associate formed. When HCl
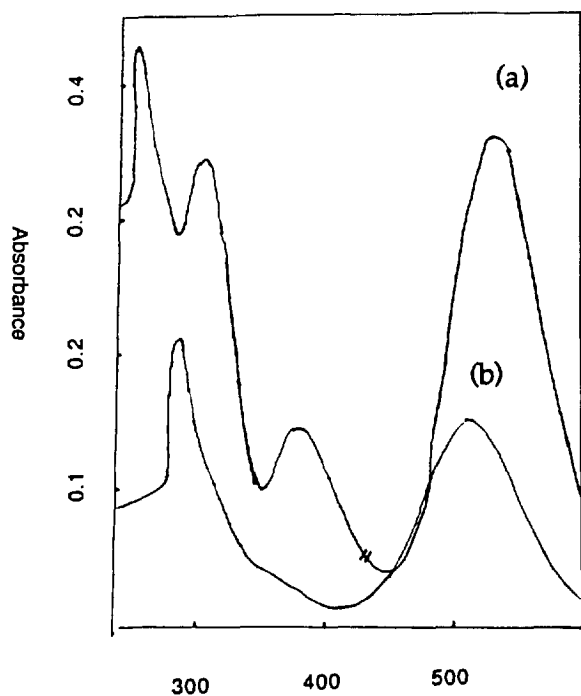

Fig. 1. Absorption spectra of the extracted ion-pair formed between $(TMA^+ I^-)$ and periodate ions (a) at pH 4 or the aqueous phase and iodine (b) in chloroform.
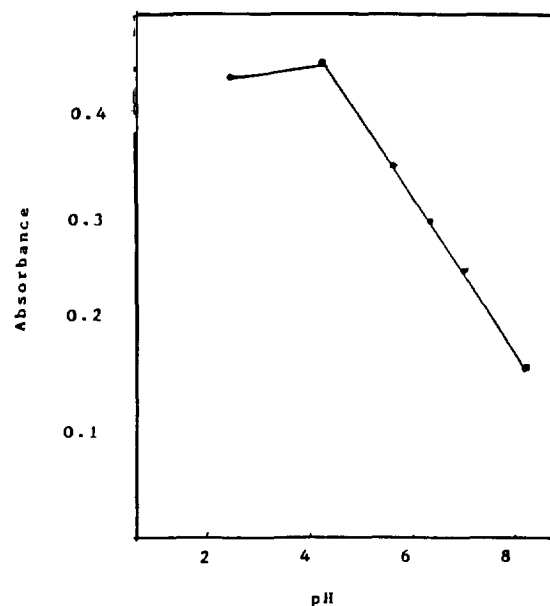
[1] Each point in the figures represents an average of five measurements.

or $HClO_4$ was used instead of Britton–Robinson buffer (pH 3–4) no significant differences in the absorbance values were observed. Thus a B–R buffer solution of pH 4 was finally chosen and employed as described in the recommended procedures.

Tetramethylammonium hexafluorophosphate, tetraphenylphosphonium chloride, tetramethylammonium iodide, tetramethylammonium bromide, tetramethylammonium chloride and tetraphenylarsonium chloride were investigated at the optimum pH. Good results were obtained with tetramethylammonium iodide and the highest absorbance of the coloured associate was obtained in chloroform from an aqueous solution of pH 4. The effect of (TMA^+I^-) concentration upon the determination of periodate was studied. The absorbances of the extracted species in chloroform for a series of solutions containing 10–20 μg of periodate and various amounts of the reagent (TMA^+I^-) up to 1.2% (w/v) in water at pH 4 was examined. It was found that 5 ml of (TMA^+I^-) at a concentration of $\leqslant 0.5\%$ (w/v) was sufficient to form the ion-associate for 20 μg or less of periodate ion (Fig. 3).
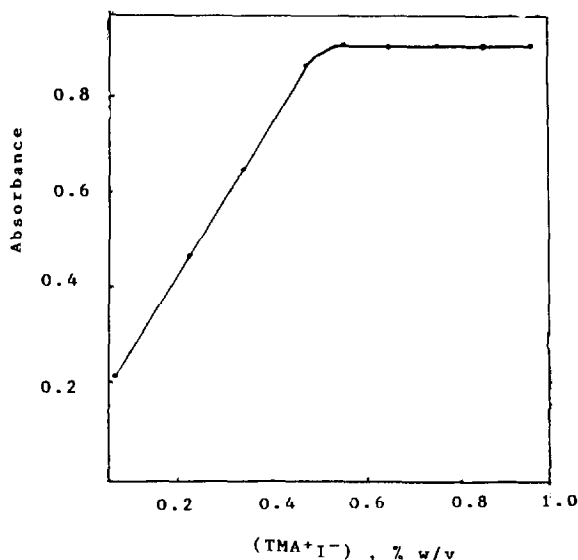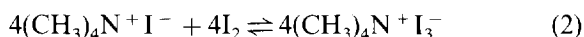

Fig. 3. Dependence of the absorbance (at $\lambda = 509$ nm) of the formed ion-pair in chloroform with (TMA $^+$ I $^-$) concentration (% w/v) in aqueous solution.

The mechanism of the produced ion-associate was critically investigated. It appears from Fig. 1 that the extracted product is not iodine nor an ion-pair between periodate ion and TMA^+. Actually, the reaction of (TMA^+I^-) with periodate ions gave quasi-immediately a red-orange precipitate which was readily extracted in chloroform (in yellow-violet colour). This reaction appears to proceed in two successive steps: (1) a rapid one involving the liberation of some iodine and subsequently (2) formation of the precipitate. These results suggest the possible formation of the complex ion I_3^- which subsequently may interact with the tetramethylammonium cation. These results were also confirmed by reacting the triiodide ion I_3^- (prepared from $I_2 + KI$) with the tetramethylammonium cation followed by extracting the produced species in chloroform. The electronic spectrum of this species was exactly similar to the spectrum of the produced ion associate from the reaction of (TMA^+I^-) with periodate ions. Thus a possible mechanism of the produced ion-associate $(CH_3)_4N^+I_3^-$ is proposed as follows:

$$7(CH_3)_4N^+I^- + IO_4^- + 8H^+$$
$$\rightleftharpoons 4I_2 + 4H_2O + 7(CH_3)_4N^+ \qquad (1)$$

$$4(CH_3)_4N^+I^- + 4I_2 \rightleftharpoons 4(CH_3)_4N^+I_3^- \qquad (2)$$

and the overall reaction is

$$11(CH_3)_4N^+I^- + IO_4^- + 8H^+$$
$$\rightleftharpoons 4(CH_3)_4N^+I_3^- + 7(CH_3)_4N^+ + 4H_2O \qquad (3)$$
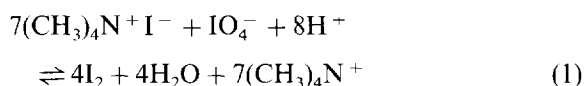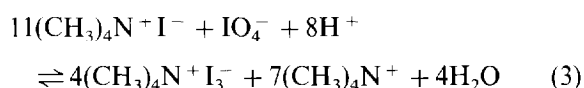
These results also explain why only $(CH_3)_4N^+I_3^-$ gives good results since there is a need to have an excess of iodide ion in solution to form the complex ion I_3^-, as indicated in Eqs. (1)–(3). For instance, with tetramethylammonium chloride periodate gives iodine at a slow rate but there is no iodide to form the complex ion I_3^-. However, on reacting periodate ions with tetramethylammonium bromide no colour is formed.

3.1. Photometric characteristics

The comoposition of the ion-pair $(CH_3)_4N^+I_3^-$ was established spectrophotometrically by the Job's method. Equimolar solutions of potassium

Fig. 4. Determination of the composition of the extracted ion-associate by the Job's method; $[IO_4] = 0.002$ (1 ml) and $[(TMA^+I^-)] = 0.001$ at 509 nm.

periodate and the (TMA^+I^-) reagent of a concentration of 0.001 M were mixed in complementary proportions to a fixed total volume and the pH of the solutions was adju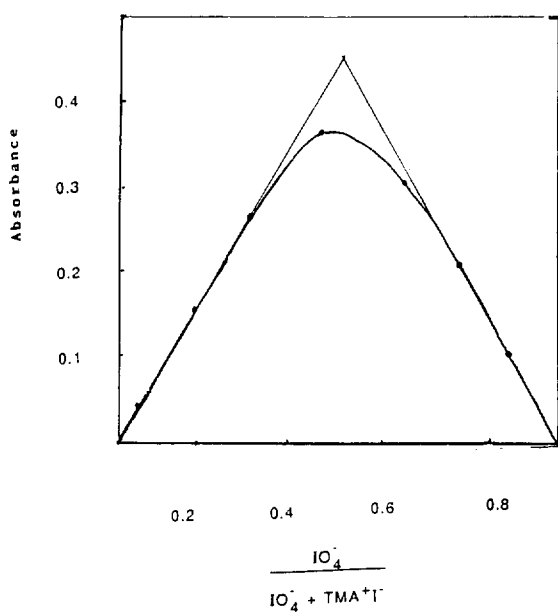sted to pH 4. The mixture was allowed to stand for 5 min for completion of the reaction. The ion-associate was then extracted with 5 ml chloroform and the absorbance was measured against a blank obtained by extraction of the reagent containing no periodate. A plot of absorbance of the extracted ion-associate in chloroform versus $[IO_4^-]/[IO_4^-] + [TMA^+I^-]$ produced a graph (Fig. 4) that indicated the formation of an associate having a periodate to a reagent ratio of 1:1.

Linear graphs at 509, 358 and 288 nm were obtained by recording the absorbance of the associate $(CH_3)_4N^+I_3^-$ in organic phase as a functionof periodate ion concentration. Beer's law was obeyed between 0.05–10 mg 1^{-1} periodate in aqueous solution of pH 4. The effective concentration of periodate as evaluated by Ringbom's plot [19] was found to be 0.2–7 mg 1^{-1}. The molar absorptivity calculated from Beer's law and

the Sandell [20] sensitivity index of the associate $(CH_3)_4N^+I_3^-$ at 509 and 358 nm was found to be 6.4×10^4 and 1.2×10^5 1 mol^{-1} cm^{-1} and 0.0003 and 0.0006 μg cm^{-2}, respectively. The selectivity and sensitivity of the spectrophotometric measurement is far better than the recent spectrophotometric procedure developed by Kamburova [13] and Fernandez-Gutierre et al. [21] since in the present work the measurements were carried out in the visible region while in the reported method [13] all the absorbance data were recorded in the UV region. The relative standard deviations of five measurements with 10 μg periodate, (at 95% confidence limit) of the method were 0.8% and 1.2% at 509 and 358 nm, respectively. Detection limits [22] of 0.016 and 0.03 μg ml^{-1} of periodate and regression coefficients of 0.996 and 0.942 were achieved by the proposed procedure at 358 and 509 nm, respectively. Regression analysis of the Beer–Lambert plot of the absorbance at 358 nm (A_{358}) and the concentration of periodate (C) in mg ml^{-1} in the range of 1–10 μg ml^{-1} gave the following linear regression equation:

$$A_{358} = 0.026 + 0.035C \qquad (n = 5) \qquad (4)$$

This equation has a slope of 0.035 with an intercept of 0.021.

3.2. Determination of iodate ions

Preliminary experiments showed interference of iodate with the proposed procedure of periodate determination. The reaction of the iodate ions with the reagent $(CH_3)_4N^+I_3^-$ is slow and possibly proceeds to produce the ion-associate $(CH_3)_4N^+I_3^-$ as follows:

$$5(CH_3)_4N^-I^- + IO_3^- + 6H^+$$

$$\rightleftharpoons 3I_2 + 5(CH_3)_4N^+ + 3H_2O \qquad (5)$$
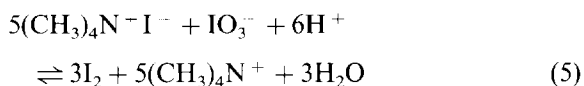
The produced iodine may react with the iodide ion of the excess reagent $(CH_3)_4N^+I^-$ to form the complex ion I_3^- which subsequently reacts with the tetramethylammonium cation to form the ion-associate $(CH_3)_4N^+I_3^-$. Therefore different attempts involving oxidation of iodate to periodate were carried out. A series of oxidizing agents, e.g. $K_2S_2O_8$, H_2O_2 and $KMnO_4$ were used

for the possible oxidation of IO_3^- → IO_4^-. Boiling the iodate ions for 10 min with potassium persulphate (2% w/v) in water was found to be the most convenient procedure for the oxidation of the iodate to periodate without interference of the unreacted persulphate. The determination of various levels (1–50 μg ml^{-1}) of iodate in aqueous solution was carried out and satisfactory results with absolute standard deviations ($n = 5$) in the range 0.2–0.35 were achieved. A linear correlation ($r = 0.967$) was found between the absorbance at 509 nm (A_{509}) and concentration of iodate (C) in μg ml^{-1} in the range 1–20 μg ml^{-1}. Regression analysis of Beer's plot gave the following linear regressin equation:

$$A_{509} = 0.035 + 0.039C \qquad (n = 5) \qquad (6)$$

3.3. Effect of diverse ions

The selectivity of the proposed method in the presence of a relatively high excess (2 mg) of some ions, e.g. NO_3^-, Br^-, SO_4^{2-}, CO_3^{2-}, HCO_3^-, $S_2O_8^{2-}$, AsO_2^-, SbO_2^-, $EDTA^{2-}$, $C_2O_4^{2-}$, $S_2O_3^{2-}$, SCN^-, SeO_3^{2-}, TeO_4^{2-}, PO_4^{3-}, BiO_3^-, WO_4^{2-}, SeO_3^{2-}, BrO_3^- and MoO_4^{2-} upon the extraction equilibrium in the determination of 10 μg of periodate (or iodate) by the proposed procedure was studied. Good recoveries in the range 100 ± 2% were obtained with all the ions except $S_2O_3^{2-}$, and BiO_3^- ions interfered seriously. The tolerance limits of various cations (0.1 mg), e.g. NH_4^+, Al^{3+}, Cd^{2+}, Zn^{2+}, Pt^{2+}, Au^+, Pb^{2+}, Co^{2+}, Fe^{3+}, Bi^{3+}, Sn^{2+}, Ni^{2+}, Mg^{2+}, Ba^{2+} and Li^+, were also examined. All these ions did not interfere with the proposed method and a good recovery percentage (100 ± 1.5%) was achieved. The ions Mn^{2+}, Cr^{6+}, Cr^{3+}, Mn^{7+} and Ru^{3+} interfered seriously even at very low concentrations. The reason for these interferences is possibly attributed to the ability of periodate ions in the aqueous media to oxidize Mn^{2+}, Cr^{3+}, Ru^{3+} and $S_2O_3^{2-}$ producing MnO_4^-, $Cr_2O_7^{2-}$, RuO_4 and IO_3^- ions, respectively, at the developed experimental conditions as previously reported [4–6,23]. The produced species and the trioxobismuthate BiO_3^- are possibly able to oxidize the iodide ion in the reagent (TMA^+I^-)

producing iodine. A representative reaction possibly proceeds as follows:

$$Cr_2O_7^{2-} + 6(CH_3)_4N^-I^- + 14H^+$$

$$\rightleftharpoons 2Cr^{3+} + 6(CH_3)_4N^+ + 3I_2 + 7H_2O \qquad (7)$$
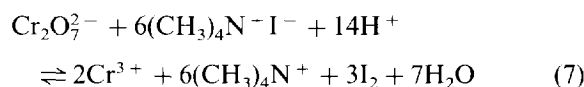
The produced iodine subsequently reacts with the iodide ion in the reagent (TMA^+I^-) forming the ion-associate ($(CH_3)_4N^+I_3^-$ as given in Eq. (2). On the other hand, the $S_2O_3^{2-}$ ions were found able to reduce the produced ion-associate $(CH_3)_4N^+$ I_3^- to the iodide ion.

The determination of 10 μg of periodate or iodate by the proposed procedure in artificial fresh water containing 10 mg l^{-1} of sodium, calcium, chloride, sulphate and bicarbonate together was carried out against a blank. The periodate or iodate concentrations were determined by the preconstructed standard curves. The precision was 0.7% and the percentage error was in the range −1.1%–1.3%.

4. Conclusion

The proposed procedure for periodate or iodate determination is superior as compared to most of the reported procedures. It offers many advantages, e.g. good precision, accuracy, the obtained associate is very stable and no standing time is needed before determining the ions. The clear advantages of the method are that it is applicable for IO_4^- (or IO_3^-) determination in artificial sea water. The determination of IO_4^- besides IO_3^- or iodate besides IO_4^- is not possible.

References

[1] M.S. El-Shahawi and A.B. Farag, Anal. Chim. Acta, 307 (1995) 139.
[2] A.B. Farag, M.S. El-Shahawi and E.M. El-Nemma, Fresenius Z. Anal. Chem., 346 (1993) 455.
[3] A.M. El-Wakil, A.B. Farag, M.S. El-Shahawi, Talanta 36 (1989) 783.
[4] A.M. El-Wakil, A.B. Farag, M.S. El-Nahas, Talanta 40 (1993) 841, and references cited within.
[5] A.M. El-Wakil, A.B. Farag, M.S. El-Shahawi, Fresenius Z. Anal. Chem., 337 (1990) 886.
[6] A. Townshend and D.T. Burns, Talanta, 39 (1992) 715.

[7] A. Gaikwad, M. Silva and D. Perez-Bendito, Analyst, 119 (1994) 1819.

[8] P.S. Radhakrishnamurti and H.P. Panda, React. Kinet. Catal. Lett., 14 (1980) 193.

[9] Z. Marczenko, Separation and Spectrophotometric Determination of Elements, Ellis Horwood Limited, Chichester, 1986, p. 319.

[10] M. Romàn Ceba, J.C. Jimènez Sànchez Sànchez and T. Galeano Diaz, Microchem. J., 31 (1985) 256.

[11] A. Hareez and W. Bashir, Microchem. J., 31 (1985) 375.

[12] M. Callejon Mochon and J.A. Munoz Leyva, Microchem. J., 34 (1986) 83.

[13] M. Kamburova, Talanta, 39 (1992) 997.

[14] D.T. Burns, M. Harriott and S.A. Barakat, Anal. Chim., 258 (1992) 325.

[15] M.S. El-Shahawi, A.Z. Abu Zuhri and S.M. Al-Daheri,

Fresenius Z. Anal. Chem., 350 (1994) 874.

[16] D.T. Burns, S.A. Barakat, M. Harriott and M.S. El-Shahawi, Anal. Chim. Acta, 270 (1992) 213.

[17] D.T. Burns, S.A. Barakat, M. Harriott and M.S. El-Shahawi, Fresenius Z. Anal. Chem., 344 (1992) 131, and references cited within.

[18] D.T. Burns, M. Harriott and S.A. Barakat, Anal. Chim. Acta, 259 (1992) 33.

[19] A. Ringbom, Fresenius Z. Anal. Chem., 115 (1939) 332.

[20] E.B. Sandell, Colorimetric Determination of Trace Metals, Interscience, New York, 1959.

[21] A. Fernandez-Gutierrez, A. Munoz de la Pena and J.A. Murillo, Anal. Lett., 16 (1983) 759.

[22] J.E. Barmey, Talanta, 14 (1967) 1363.

[23] M.S. El-Shahawi and S.A. Barakat, Talanta, 42 (1996) 277, and references cited within.

ELSEVIER

Talanta

Cyanide thermodynamics
2. Stability constants of copper(I) cyanide complexes in aqueous acetonitrile mixtures[1]

K. Kurnia, D.E. Giles, P.M. May, P. Singh, G.T. Hefter*

Department of Chemistry, Murdoch University, Murdoch, WA 6150, Australia

Abstract

The stability (formation) constants of the binary $Cu(I)–CN^-$ complexes have been measured in five aqueous mixtures containing from 10% to 70% v/v acetonitrile (MeCN) by glass electrode potentiometry at 25°C and an ionic strength of 1 M ($NaClO_4$). The constants show monotonic increases with MeCN concentration, the changes being greatest for the higher order complexes, consistent with the unfavourable solvation of CN^- in these mixtures. The sparing solubility of CuCN(s) prevented determination of the stability constant for $CuCN^0$ (soln.) at low MeCN concentrations.

1. Introduction

In the absence of complexing agents Cu(I) is unstable in aqueous solution, disproportionating to metallic copper and the more common Cu(II) state [1]:

$$2Cu(I) \rightleftharpoons Cu(s) + Cu(II) \qquad K \approx 10^6$$
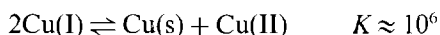
Accordingly, the complexation chemistry of Cu(I) in aqueous solutions is rather poorly understood compared with that of Cu(II). However, there is mounting evidence that Cu(I) may be the more important oxidation state in some biological systems [2,3] and in ore genesis and mineral transport processes [4]. In cyanide media Cu(I) is certainly predominant because, at least thermodynamically, Cu(II) is reduced by CN^-, forming cyanogen [5] in a reaction which may be notionally represented as

$$2Cu(II) + 2CN^- \rightleftharpoons 2Cu(I) + (CN)_2$$
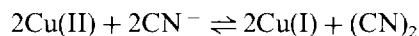
This process is assisted by the very strong complexation [6,7] of Cu(I) by CN^-, presumably arising from the well-known $d_\pi–p_{\pi^*}$ 'back-bonding' of the d^{10} Cu(I) orbitals to the low-lying π^* orbitals of CN^-.

Despite their considerable importance in a variety of hydrometallurgical and environmental

---

* Corresponding author. Fax: (+61) 9-310-1711; e-mail: hefter@chem.murdoch.edu.au
[1] For Part 1 see K. Kurnia, D.E. Giles, P.M. May, P. Singh and G.T. Hefter, J. Coord. Chem., 38 (1996) 183.

situations [7] the stability constants of the $Cu(I)/CN^-$ complexes have not been well characterized in aqueous solution. There are seveal reasons for this, including the difficulty of detecting the $CuCN^0(aq)$ species on account of the instability of $Cu(I)$ at low CN^- concentrations, the sparing solubility of $CuCN(s)$, the very high stability of the $Cu(CN)_3^{2-}(aq)$ species and its similarity in strength to $Cu(CN)_4^{3-}(aq)$.

Copper(I) can also be stabilized in aqueous solution by the addition of certain miscible non-aqueous solvents, the best known of which are the nitriles [8–10]. Stabilization of $Cu(I)$ in aqueous acetonitrile has been exploited by Parker [11,12] to develop novel hydrometallurgical processes and by several workers [8,9] to study the complexation of $Cu(I)$ by acetonitrile (MeCN). Consequently, it seemed worthwhile to attempt a precise study of the $Cu(I)/CN^-$ system in aqueous MeCN solu-

2. Experimental

All reagents were analytical grade, used without further purification. All solutions were made with high purity water (Millipore Milli-Q system) boiled and purged with nitrogen gas to remove CO_2 and O_2. A stock solution of ≈ 0.2 M $Cu(I)$ was prepared by dissolving copper(I) cyanide (Fluka, 99%) in excess sodium cyanide (BDH, 97%) to give a final solution with $CN^-/Cu(I) \approx 4$. This solution was quite stable but was standardized from time to time against commercial 20.00 mM thiosulphate (BDH, concentrated volumetric standard) using the procedure described by Vogel [16]. Other reagents and methods of standardization were identical to those discussed in detail elsewhere [14,15].

Stability constants were obtained by glass electrode potentiometry at $25.0 \pm 0.005°C$ and with an ionic strength (I) of 1.00 M, maintained with $NaClO_4$. The cells used may be represented as

Reference half-cell	Salt bridge	Test solution	
$Ag|AgCl|0.95$ M $NaClO_4$	1 M $NaClO_4$	$(1-z)$ M $NaClO_4$	GE
0.05 M $NaCl$	$v\%$ MeCN/H_2O	x M $NaCN$, y M $NaOH$	
$v\%$ MeCN/H_2O		z M $CuClO_4$	
		$v\%$ MeCN/H_2O	
	E_{j1}	E_{j2}	

tions. Such data are also useful for optimizing a recently developed ion-exchange chromatographic procedure which employs MeCN/H_2O as the mobile phase to determine 'active' cyanide in complex metal/cyanide mixtures [13–15]. Such mixtures are typically encountered in the lixiviant solutions used for the recovery of gold from its ores and in effluents from electroplating and gold extraction plants [4].

The present paper therefore reports the stability constants of the cyanide complexes of $Cu(I)$ in aqueous acetonitrile mixtures containing up to 70% v/v MeCN, obtained by high precision glass electrode potentiometry. These data complement those previously reported for $Cd(II)$ and $Zn(II)$ cyanide complexes under the same conditions [14].

where v is the volume percentage of MeCN (in ml MeCN per 100 ml solution) in the aqueous solvent mixture, GE is a glass electrode and E_{j1} and E_{j2} are liquid junction potentials (LJPs). The glass electrodes (three separate GE/reference electrode combinations were used) were calibrated in terms of $[H^+]$. Since the cell is of the constant ionic strength type and $x, y, z \ll 1$ M the LJPs can be assumed to be constant [17].

The apparatus and general procedures for the titrations are given elsewhere [14,18]. Particular precautions were taken to minimize the volatilization of HCN and MeCN during the titrations. All titrations commenced at high pH (i.e. $-\log[H^+]$) ≈ 12.5, with varying total $Cu(I)$ concentrations (2.5–5.0 mM) and (total) $CN^-/Cu(I)$ ratios of four and five. The titrant was ≈ 50 mM $HClO_4$ in

$I = 1$ M $NaClO_4$ in the appropriate $MeCN/H_2O$ mixture.

During the course of the titrations a white precipitate was usually observed at pH ≈ 4.5 except at MeCN concentrations $\geqslant 50\%$ v/v. These precipitates were identified by X-ray diffraction to be CuCN ($K_{S0} = 3.2 \times 10^{-19}$ in water) [19]. Unlike the Cd(II) and, to a lesser extent, the Zn(II)/CN$^-$ systems [14,15,18], these precipitates did not in general re-dissolve at low pH. This made the determination of the lower order stability constants difficult in mixtures not rich in MeCN.

Complex formation in the Cu(I)/CN$^-$ system can be represented by the general equilibrium (omitting charges for simplicity):

$$pCu + qCN + rH_2O \rightleftharpoons Cu_p(CN)_q(OH)_r + rH$$
(1)
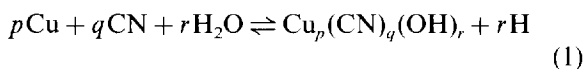
for which the corresponding overall stability (formation) constant of the complex $Cu_p(CN)_q(OH)_r$ is

$$\beta_{pqr} = \frac{[Cu_p(CN)_q(OH)_r]K_w^r}{[Cu]^p[CN]^q[OH]^r}$$
(2)

where

$$K_w = [H][OH] = \beta_{00-1}$$
(3)

is the ion product of water under the conditions of the experiment. Since HCN is a very weak acid [6,19] it is also necessary to know its association constant, K_{ass}:

Table 1
Formation constants of water and HCN in MeCN/H$_2$O mixtures at 25°C and $I = 1$ M (NaClO$_4$)[a]

%MeCN	pK$_w$	log K$_{ass}$ (HCN)
0.0	13.7518(8)	9.0330(10)
10.0	13.9162(10)	9.1209(15)
20.0	14.1920(10)	9.2844(11)
30.0	14.4184(7)	9.4260(20)
50.0	14.9705(9)	9.9338(24)
70.0	15.9189(17)	10.8531(26)

[a] Data from Ref. [15,20]. Values in parentheses are standard deviations in the last significant figure of the constant and refer to the internal precision of the computer calculations; the maximum uncertainties are generally an order of magnitude larger.

$$K_{ass} = \frac{[HCN]}{[H][CN]} = \beta_{011}$$
(4)

The determination of K_w and K_{ass} under conditions identical to the present study is described in detail elsewhere [20] but for convenience the values used in the determination of the Cu(I)/CN$^-$ complexes are listed in Table 1.

Stability constants for the Cu(I)/CN$^-$ system were obtained from the potentiometric data using the ESTA suite of programs [21–23]. Model selection was based on minimization of an objective function in total analytical hydrogen ion concentration with unit weights as defined in Ref. [21]. Species were generally considered acceptable only if the objective function was significantly reduced ($\geqslant 50\%$) by their inclusion, along with a consideration of the formation curves, and the standard deviations and chemical reasonableness of the complexes detected.

For a metal–cyanide system the metal–ion formation function, $\bar{Z}_M$, can be formulated (again omitting charges) as

$$\bar{Z}_M = [T_{CN} - A(1 - [H]\beta_{011})]/T_M$$
(5)

where T_i is the total (analytical) concentration of the species i (CN or M) and

$$A = [(T_H - [H] + K_w[H]^{-1})/\beta_{011}[H]]$$
(6)

When only mononuclear complexes (i.e. $p = 1$ in Eq. (1)) are formed, as in the present study, A is the free ligand concentration and $\bar{Z}_M$ can be considered as the average number of ligands bound per metal ion. When the most likely set of species was determined, the precision of the calculated formation constants was determined using a Monte-Carlo procedure as described previously [18,23].

3. Results and discussion

Typical titration data at low and high MeCN concentrations are shown in Figs. 1 and 2 respectively and require comment. Both curves exhibit the 'curl-backs' at high pH (low pA) characteristic of the presence of ternary complexes $Cu_p(CN)_q(OH)_r^{(p-q-r)+}$ and/or metal hydroxo complexes $Cu_p(OH)_r^{(p-r)+}$. However, as for the
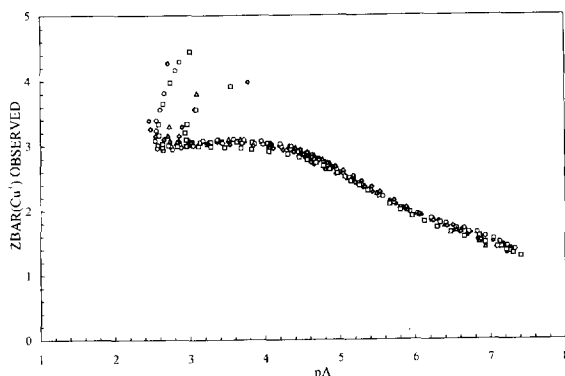
Fig. 1. Observed formation function $\bar{Z}_M$ for the Cu(I)/CN$^-$ system in 30% v/v MeCN, typical of lower (⩽ 30% v/v) MeCN concentrations plotted against pA over the approximate pH range 5–12; the different symbols refer to differing values of T_{CN} and T_{Cu}. For discussion of the shapes of these curves see text.

Cd(II) and Zn(II) systems studied previously [14,18], these data had to be excluded from the analysis because of the unavailability of the formation constants for the Cu(I)/OH$^-$ complexes [19]. Attempts to measure the Cu(I)/OH$^-$ complexes by glass electrode potentiometry were unsuccessful due to precipitation of the sparingly soluble CuOH(s). Consequently, only the formation constants for the binary Cu(I)/CN$^-$ complexes could be determined.

The curves in Figs. 1 and 2 also share two other common features. First, they were independent of T_{Cu}, indicating that no 'polynuclear' ($p > 1$ in Eq.
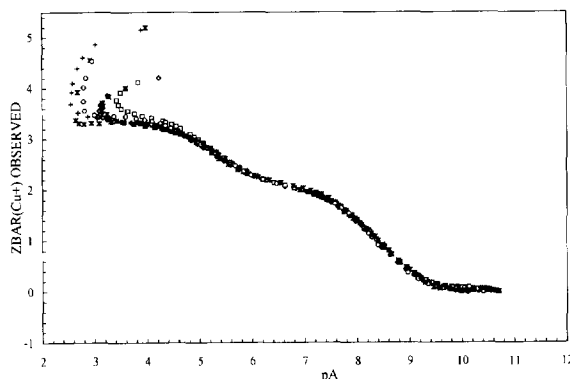
Fig. 2. Observed formation function $\bar{Z}_M$ in 70% v/v MeCN, typical of higher (⩾ 50% v/v) MeCN concentrations, plotted against pA over the approximate pH range 2–12; the different symbols refer to differing values of T_{CN} and T_{Cu}. For discussion of the shapes of these curves see text.

(1)) species are formed over the concentration range studied. Secondly, $\bar{Z}_M$ barely rises above 3.0, which indicates that Cu(CN)$_3^{2-}$ is the predominant species and that, over the concentration ranges studied, Cu(CN)$_4^{3-}$ forms only to a very limited degree.

As noted above, precipitation of CuCN(s) at lower MeCN concentrations prevented the investigation of complexation at low free cyanide concentrations (high pA, low pH) so the formation function curves in Fig. 1 are limited to $\bar{Z}_M > 1.0$. Consequently it was not possible to evaluate β_{110}(CuCN^0) in these solutions. At higher MeCN concentrations no precipitation occurred and $\bar{Z}_M$ was determined down to zero (Fig. 2). As the measurements at high MeCN concentrations (⩾ 50% MeCN) were more straightforward they will be discussed first and in some detail.

3.1. 50–70% MeCN

At these relatively high MeCN concentrations no precipitation of CuCN(s) occurs and it was possible to obtain data over the pH range from 2 to 13. The plateaux at $\bar{Z}_M = 2.0$ and 3.0 (Fig. 2) indicate that the complexes Cu(CN)$_2^-$ and Cu(CN)$_3^{2-}$ were formed to a significant degree. Thus, model selection commenced with Cu(CN)$_2^-$ and Cu(CN)$_3^{2-}$. As it was possible to cover the low pH (high pA) region, the system could be studied where $\bar{Z}_M \rightarrow 1.0$ (Fig. 2). The lack of a plateau at $\bar{Z}_M = 1$ indicates that CuCN^0 never becomes predominant. Nevertheless, evidence for CuCN^0 was conclusive in both 50% and 70% MeCN/H$_2$O mixtures on the basis of our specified criteria: the objective function (OBJT) decreased by 94% and 99% in 50% and 70% MeCN respectively and the standard deviations for the other constants also improved. Consistent with the fact that $\bar{Z}_M > 3.0$ at high CN$^-$ concentration (low pH in Fig. 2), the addition of Cu(CN)$_4^{3-}$ had similar effects and was therefore accepted into the model. The 'best estimates' of the formation constants in these two media are summarized in Table 2. The low values of the objective function (especially in 70% MeCN) and the standard deviations on the β_{1q0} values are pleasing. It should be noted that the values listed

Table 2
Formation constants of Cu(I)/CN⁻ complexes in 50% and 70% MeCN at 25°C and $I = 1$ M (NaClO₄)[a]

MeCN (% v/v)	Species			log β_{pqr}	Standard deviation[b]	OBJT	Number of titrations	Number of data points
	p	q	r					
50	1	1	0	8.760	0.011	1.04×10^{-8}	8	297
	1	2	0	16.521	0.009			
	1	3	0	22.215	0.012			
	1	4	0	25.948	0.015			
70	1	1	0	8.714	0.005	3.06×10^{-9}	8	334
	1	2	0	16.769	0.004			
	1	3	0	22.422	0.006			
	1	4	0	26.438	0.012			

[a] Species and stability constants as defined in Eqs. (1) and (2) respectively.
[b] Standard deviations refer to the internal precision of the computer calculations; maximum uncertainties are generally an order of magnitude larger.

in Table 2 represent the first time it has been possible to fix with any precision a value for β_{110} for the formation of the CuCN⁰ complex in any medium. This is undoubtedly a reflection of the stabilization of Cu(I) at low T_{CN} in the presence of high MeCN concentrations by complexation (i.e. solvation) of the CuCN⁰ complex by MeCN molecules in the solvent mixture. That is to say, the CuCN⁰ species detected here is better represented as $[Cu(NC)(NCCH_3)_n]^0$ (soln.) where n could be 1, 2, 3 or more (the CH₃CN molecules, being part of the solvent, are potentiometrically 'invisible'). This species is likely to have quite different characteristics to $[Cu(NC)(OH_2)_x]^0$ (aq), if such a species exists at all. Such considerations are probably best resolved by NMR spectroscopy but this is beyond the scope of the present study.

3.2. 10–30% MeCN

The 'best estimates' for the formation constants of the Cu(I)/CN⁻ complexes in 10–30% MeCN/H₂O mixtures are given in Table 3. As noted above, the accessible pH range in these solvent mixtures was limited by the precipitation of CuCN(s). Thus, as can be seen in Fig. 1, it was not possible to investigate below $\bar{Z}_M \approx 1.2$. Consequently, in 10% and 20% MeCN, β_{110}(CuCN⁰) was omitted and model selection was based on the two complexes for which the evidence (from the

inflection point at $\bar{Z}_M = 2.0$ and the plateau at $\bar{Z}_M = 3.0$) is clearcut: Cu(CN)₂⁻ and Cu(CN)₃²⁻. Inclusion of Cu(CN)₄³⁻ resulted in only small improvements in the unweighted objective function. However, as its incorporation lowered the standard deviations of β_{120} and β_{130} without significantly altering the optimized stability constants themselves, Cu(CN)₄³⁻ was retained in the final model. The difficulty of detecting Cu(CN)₄³⁻ is reflected in the $\bar{Z}_M$ values (Fig. 1), which barely rise above 3.0, and the large standard deviations for β_{140} (Table 3). Similar difficulties have been reported by previous workers [6].

In 30% MeCN (Fig. 1), where $\bar{Z}_M$ clearly falls below 2 at low pH values, indicating less than complete formation of Cu(CN)₂⁻, it was necessary to fix the value of β_{110} (CuCN⁰) to obtain a satisfactory fit. The value chosen, log $\beta_{110} = 8.76$, was that measured for 50% MeCN. Numerical attempts to simultaneously evaluate β_{110} with the other species in the model failed to converge.

3.3. The variation of $Cu(CN)_q^{(1-q)+}$ stabilities with solvent composition

The variation of the stability constants expressed as the change in log β_{1q0} between H₂O and MeCN/H₂O, of the three higher order cyanide complexes of Cu(I) is plotted in Fig. 3 as a function of MeCN concentration. The first complex is omitted because of the detection difficulties

Table 3
Formation constants of Cu(I)/CN⁻ complexes in 10%, 20% and 30% MeCN at 25°C and $I = 1$ M (NaClO₄)[a]

MeCN/H₂O (% v/v)	Species			log β_{pqr}	Standard deviation[b]	OBJT	Number of titrations	Number of data points
	p	q	r					
10	1	1	0	–	–	2.93×10^{-8}	8	188
	1	2	0	14.432	0.024			
	1	3	0	19.750	0.025			
	1	4	0	21.602	0.111			
20	1	1	0	.	–	3.16×10^{-8}	7	168
	1	2	0	14.819	0.027			
	1	3	0	20.088	0.031			
	1	4	0	21.574	0.396			
30	1	1	0	$(8.76)^c$	–	1.83×10^{-8}	9	230
	1	2	0	15.468	0.011			
	1	3	0	20.667	0.012			
	1	4	0	22.991	0.055			

[a,b] As for Table 2.
[c] Fixed value, see text.

at low MeCN concentrations. Given the instability of uncomplexed Cu(I) in aqueous solution and the fact that β_{1q0} values cannot be measured in NaClO₄ media in water [6], it is not possible at present to rationalise the results in terms of the solvation characteristics of each species. Nevertheless, some general observations can be made.
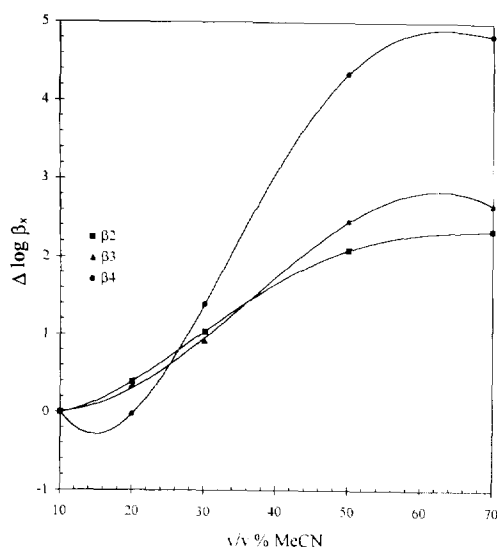
Fig. 3. Variation of the stability constants of $Cu(CN)_q^{(1-q)+}$ in MeCN H₂O mixtures:

$\Delta \log \beta_x = \{(\log \beta_{1q0})_{MeCN/H_2O} - (\log \beta_{1q0})_{H_2O}\}$ where $x = q$

Cu(I) is very strongly preferentially solvated by MeCN in MeCN/H₂O mixtures and its coordination sphere is likely to be fully occupied by MeCN molecules even in 10% MeCN/H₂O solutions [10-12]. Thus the increased stability of the $Cu(CN)_q^{(1-q)+}$ species is almost certainly due to the increasingly unfavourable solvation of CN⁻ as the MeCN concentration increases. This might at first seem surprising: the 'soft' MeCN might be expected to solvate the 'soft' CN⁻ quite well. Nevertheless, it is consistent with the data of Muir et al., [24] which show that $\Delta_t G(CN^-)$ is positive for transfer from H₂O to 70% MeCN. This interpretation is also consistent with the value of β_{140} showing the greatest increase (Fig. 3).

This can be seen more clearly by considering the (hypothetical) transfer of the reaction

$$Cu^+ (soln.) + xCN^- (soln.) \rightleftharpoons$$

$$Cu(CN)_x^{(1-x)+} (soln.) \qquad (7)$$
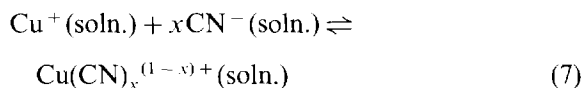
from H₂O to MeCN/H₂O mixtures. It is readily shown [25] that

$$\Delta_{r,t} G = -2.303 RT \Delta \log \beta_x$$

$$= \Delta_t G(Cu(CN)_x^{(1-x)+}) - \Delta_t G(Cu^+)$$

$$- x\Delta_t G(CN^-) \qquad (8)$$

where G is the Gibbs energy and the subscripts r and t refer to reaction (7) and the transfer process $(H_2O \rightarrow MeCN/H_2O)$ respectively. Strictly speaking, Eq. (8) should be expressed in terms of standard state (infinite dilution) values; however, activity effects should not be large in these significantly aqueous solutions. Assuming approximately equal changes in solvation for the transfer of the various $Cu(CN)_x^{(1-x)+}$ complexes, and given that $\Delta_t G(CN^-)$ is positive [24], Eq. (8) predicts that $\Delta \log \beta_x$ will become increasingly positive as x increases. The apparent flattening out of the curves at higher MeCN concentrations is probably related to the subtle interplay of the relative values of the solvation energies of each of the species involved in Eq. (7).

It is interesting that the variation of $\Delta \log \beta_x$ with solvent composition is rather similar to those observed for Zn(II) and Cd(II) [14,15]. On the basis of Eq. (8) and the expectation that Zn(II) and Cd(II) and (to a lesser extent) their cyanide complexes are significantly different from Cu(I), this is perhaps a little surprising. It is probably a reflection of the dominance of CN^- solvation in determining the strength of cyanide complexation in mixed solvents. A similar effect has been reported for the $ZnCl_n^{(2-n)+}$ complexes in MeCN/ H_2O mixtures [25].

References

[1] N.N. Greenwood and A. Earnshaw, Chemistry of the Elements, Pergamon, Oxford, 1984.

[2] M.N. Hughes, The Inorganic Chemistry of Biological Processes, Wiley, New York, 1981.

[3] D.L. Rabenstein, R. Guevremont and C.A. Evans, in H.Siegel (Ed.), Metal Ions in Biological Systems, Marcel Dekker, New York, Vol. 9, 1973, p. 103.

[4] J. Marsden and I. House, The Chemistry of Gold Extraction, Ellis Horwood, New York, 1993.

[5] A.G. Sharpe, The Chemistry of Cyano Complexes of the Transition Metals, Academic Press, London, 1976.

[6] M.T. Beck, Pure Appl. Chem., 59 (1987) 1703.

[7] G.T. Hefter and P.M. May, Proc. 5th AUSIMM Extractive Metall. Conf., Perth, Australia, October, 1991, p. 139–146.

[8] A. Zuberbuhler, Helv. Chim. Acta, 53 (1970) 473.

[9] P. Hemmerich and C. Sigwart, Experientia, 19 (1963) 488.

[10] B.G. Cox, A.J. Parker and W.E. Waghorne, J. Phys. Chem., 78 (1974) 1731.

[11] A.J. Parker, in N. Tanaka, H. Ohtaki and R. Tamamushi (Eds.), Ions and Molecules in Solution, Elsevier, Amsterdam, 1983, pp. 313–324.

[12] A.J. Parker, Pure Appl. Chem., 53 (1981) 1437.

[13] D.E. Giles and K. Kurnia, Abstracts 11th Austral. Symp. Anal. Chem., RACI, Hobart, Australia, July, 1991, p. 137.

[14] K. Kurnia, D.E. Giles, P.M. May, P. Singh and G.T. Hefter, J. Coord. Chem., 38 (1996) 183.

[15] K. Kurnia, Ph.D. Thesis, Murdoch University, 1995.

[16] A.I. Vogel, A Textbook of Quantitative Inorganic Analysis, 3rd edn., Longmans, London, 1961.

[17] G.T. Hefter, Anal. Chem., 54 (1982) 2518.

[18] P. Verhoeven, P.M. May and G.T. Hefter, J. Coord. Chem., 22 (1990) 7.

[19] L.G. Sillén and A.E. Martell, Stability Constants of Metal–Ion Complexes, Special Publications Nos. 17 and 25, Chemical Society, London, 1964, 1971.

[20] K. Kurnia, D.E. Giles, P.M. May, P. Singh and G.T. Hefter, in preparation.

[21] P.M. May, K. Murray and D.R. Williams, Talanta, 32 (1985) 483.

[22] P.M. May and K. Murray, Talanta, 35 (1988) 927.

[23] P.M. May and K. Murray, Talanta, 35 (1988) 933.

[24] D.M. Muir, P. Singh, C.C. Kenna, N. Tsuchida and M.D. Benari, Aust. J. Chem., 38 (1985) 1079.

[25] B.W. Clare, P. Singh and G.T. Hefter, Aust. J. Chem., 43 (1990) 257.

Flow-injection analysis for hypoxanthine in meat with dissolved oxygen detector and enzyme reactor[1]

Manami Numata[a], Naomi Funazaki[a], Satoshi Ito[a], Yasukazu Asano[a,*], Yukio Yano[b]

[a]*Research Center, DKK Corporation, Kitamachi, Kichijoji, Tokyo 180, Japan*
[b]*Central Research Institute, Itohamu Food Inc., Kubogaoka, Moriya-machi, Kitasoma-gun, Ibaragi 302-01, Japan*

Received 7 November 1995; revised 9 February 1996; accepted 9 February 1996

Abstract

A low cost flow-injection analysis (FIA) with a dissolved oxygen (DO) detector and a xanthine oxidase immobilized column for the analysis of hypoxanthine as an index to determine degree of aging in meat was developed for quality control in the food industry. In this system, hypoxanthine is oxidized by an enzyme reaction with xanthine oxidase immobilized on the column to produce xanthine. Then the catalytic reaction between hypoxanthine and DO with xanthine oxidase proceeds with the DO concentration decreasing in the stream of the flow system. Decrease in the DO concentration was monitored by a DO detector located downstream of the flow system. This decrease in DO concentration was proportional to the hypoxanthine concentration. For detecting the decreased DO concentration efficiently a flow-through cell with a polarographic-type DO sensor was specially designed. As a result, a linear working curve was obtained from 3.68×10^{-5} to 1.84×10^{-3} M hypoxanthine concentrations with this FIA system. We applied the present system with a DO detector for the determination of hypoxanthine in meat samples and compared the results with those obtained by the conventional HPLC method. The data obtained with the present FIA method were in fairly good agreement with those obtained by the conventional HPLC method for the meat samples. Correlation factor and regression line between the two methods were 0.998 and $Y = 1.51X-32.64$ respectively. We concluded that the present FIA system with a DO detector was suitable as a simple, easy to handle and reliable instrument for quality control in the food industry.

Keywords: Aging of meat; DO detector; Enzyme reactor; Flow-injection; Hypoxathine

1. Introduction

Recently, quality control of meat has become increasingly important worldwide with the need to protect consumers from food poisoning using the directives ISO-9000 and HACCP [1]. When meat is not frozen during storage, bacterial distribution progresses and decays the meat, making it unsuitable for eating.

Therefore, there is a need to develop a simple meat aging sensing system based on the scientific background in knowing the period when the meat companies supply it to the customers.

---

* Corresponding author. Tel.: (+81) 422-53-511; Fax: (+81) 422-52-2042.
[1] Presented at the Seventh International Conference on Flow Injection Analysis (ICFIA'95), held in Seattle, WA, USA, August 13-17, 1995.

Many indexes for aging in meat have been proposed, such as share force value [2], myofibrillar fragmentation index [3], disappearance of Troponin T, and 300 Da component [4] Mg–Ca-enhanced ATpase activity [5]. However, as these methods lack simplicity, rapidity and cost-effective performance, they were not suitable for routine use in quality control in meat-packing factories. Accordingly, quality control of aging in meat has been done by an organoleptics test by experts until now.

In previous papers, we found that hypoxanthine, which is a product of ATP as an energy source [6,7], is an aging-determining index for meat. There have been some reports on determination methods for hypoxanthine such as HPLC [8], amperometric detection [9,10], enzyme sensor [11], flow-injection analysis (FIA) systems with a biosensor [6,7] and optical detection [12]. Although there are advantages in constructing a measurement system using sensors and FIA, such as small amount of sample, simplicity, reduction of measurement time, selectivity, ease of handling and so on, there have been no practical studies on the application of a FIA system with a dissolved oxygen (DO) sensor for the determination of hypoxanthine as an index of aging in meat. Therefore, the development of a meat aging sensing system using a DO sensor as a detector in FIA which can measure hypoxanthine more simply and more rapidly is demanded because it is stable, selective, simple and easy to use over a long period.

Hypoxanthine is oxidized by the catalytic reaction of xanthine oxidase immobilized on the column, reducing the concentration of oxygen:

$$Hypoxanthine + O_2 \rightarrow Xanthine + H_2O$$

$$\uparrow$$

Xanthine oxidase
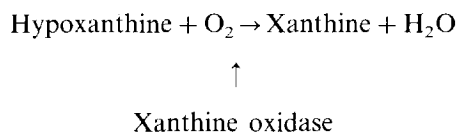
Accordingly, simple determination of hypoxanthine becomes possible by detecting the decrease in oxygen concentration electrochemically.

Based on this concept, we developed a simple FIA system for hypoxanthine using a DO detector and a enzyme reactor with immobilized xanthine oxidase to detect consumption of DO for fast quality control of meat aging. The DO sensor with an oxygen-selective permeable PTFE membrane was stable over a long period because it is durable to contamination from substances such as lipids and proteins in the meat samples. The sensor is also easy to handle and hypoxanthine oxidase is specific for hypoxanthine.

2. Experimental

2.1. Reagents

All chemicals used were of analytical-reagent grade. Xanthine oxidase from butter milk was obtained from Sigma. Pure water treated with a 0.45 μm membrane filter to give an electrical conductivity of less than 0.1 μS cm^{-2} was used throughout the work. A 0.1 M phosphate buffer (pH 7.0) was used as a carrier solution.

2.2. Preparation of xanthine oxidase immobilized column

A xanthine oxidase immobilized column was prepared by the following procedure.

(1) The porous silica beads, aminopropyl CPG (CPG Inc.), with a pore size of 500 Å and 200/400 mesh, were packed into a column (108 mm × 3 mm i.d.).

(2) A 0.1 M carbonate solution was circulated in the column for 30 min with a peristaltic pump.

(3) A 4% glutaraldehyde solution was circulated for 30 min in the same manner as above.

(4) After these procedures, the column was washed with pure water by the same procedure for 2 h.

(5) A solution of xanthine oxidase (5 units) was circulated for 2 h to immobilize the enzyme onto the porous silica beads.

(6) After circulating a 0.1 M glycine solution for 2 h, the column was filled with a 0.1 M phosphate buffer solution.

(7) The xanthine oxidase immobilized column solution thus prepared was stored in a refrigerator at 4°C.
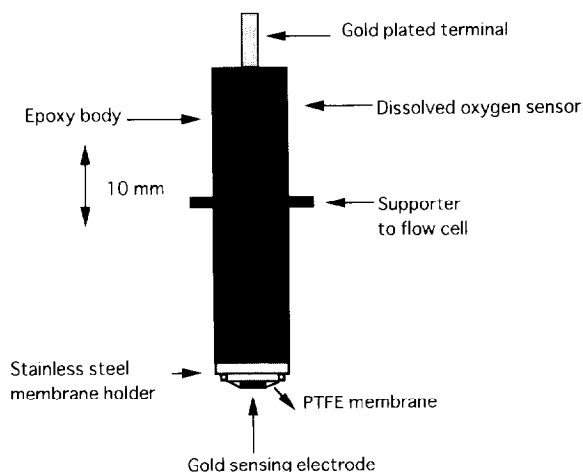
Fig. 1. Outline of DO sensor for FIA system.

2.3. Fabrication of the DO detector

A DO sensor and a flow cell for FIA are shown in Figs. 1 and 2.

The detector was fabricated by assembling a small DO sensor (11 mm i.d. × 42 mm length) specially designed for a FIA system and a flow cell [26 mm × 40 mm × 30 mm (height × width ×
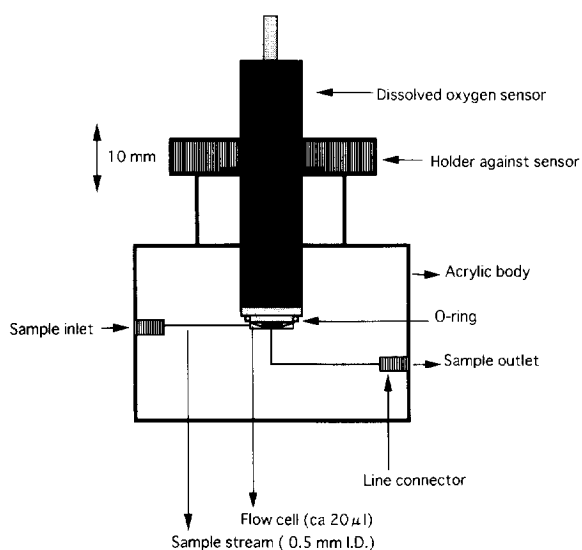
Fig. 2. DO detector for FIA system.
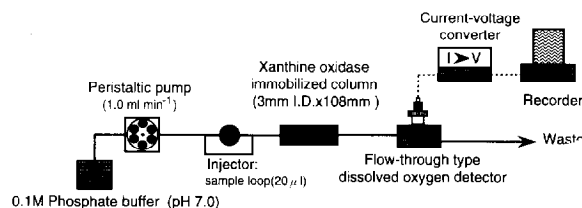
Fig. 3. FIA system with DO detector and xanthine oxidase immobilized column for hypoxanthine.

2.4. FIA system with DO detector

The one-channel FIA system consisted of a peristaltic pump (XV type; Alitea AB, Sweden), an injector (Rheodyne 7125; Rheodyne; Cotati, CA) a xanthine oxidase immobilized column, a DO detector, a current–voltage converter (ILO-50; DKK, Japan) and a recorder (250-F; Sekonic, Japan) as shown in Fig. 3. The flow rate of the pump was 1 ml min^{-1}. The 10 cm long PTFE tube (0.5 mm i.d.) from the mixing point and sample to the detector was determined experimentally. The phosphate buffer and sample were initially saturated with oxygen throughout this work.

By injecting a 20 μl sample into the buffer stream saturated with oxygen, the decreased oxygen content based on the enzyme reaction in the detector. Then, the decrease in the DO concentration in the stream was monitored by a detector located downstream of the flow system. This current intensity from the detector was amplified by the current–voltage converter and its signal was fed to the recorder. The concentration of hypoxanthine was determined by the change in the detector output which is observed as a peak-shaped signal (FIA signal) on the recorder. The height of the FIA signal is proportional to the hypoxanthine concentration.

3. Results and discussion

3.1. Optimum conditions for FIA system

Optimum conditions for this system were determined after varying the pH, flow rate of the pump, sample volume and column length.

Fig. 4 shows the effect of the pH of the samples on the FIA signal. The tests were carried out by changing the pH of the samples from 5 to 9 under the conditions of 1.47×10^{-4} M hypoxanthine and 108 mm $\times$ 3 mm i.d. column size. As a result, the maximum value was obtained at pH 7.0. This means that measurement at pH 7.0 was desirable to raise the activity of the immobilized hypoxanthine oxidase. Therefore, 0.1 M phosphate buffer (pH 7.0) was chosen as a carrier buffer for subsequent experiments.

Similarly, optimum values of flow rate, sample volume and column length were investigated. The results are shown in Table 1. It became apparent that determining the optimum values of pH, flow rate, sample volume and column length was very important for the determination of hypoxanthine with the present FIA system as decomposition and diffusion of hypoxanthine took place on the column as revealed by the stability and intensity of the FIA signal and the measurement range of the system.

3.2. Calibration curve for hypoxanthine

We prepared several standard solutions of hypoxanthine and investigated the relationship between the concentration and the peak height of the FIA signal with the analytical conditions

Table 1
Optimum conditions of FIA system with DO detector

Parameter	Optimum value	Range investigated
pH	7.0	5-9
Flow rate (ml min^{-1})	1	0.5-1.5
Sample volume (μl)	20	5-30
Column length (3 mm; mm i.d.)	108	63-126

shown in Table 1 which were determined experimentally. A linear calibration curve was obtained from 3.68×10^{-5} to 1.84×10^{-3} mol l^{-1} hypoxanthine as shown in Fig. 5. This shows that enzyme-catalytic conversion to xanthine by reaction of hypoxanthine and oxygen proceeds efficiently on the column. The lower detection limit was 1.84×10^{-3} mol l^{-1} for an S/N ratio of the FIA signal of three. The repeatability of the FIA signals was 1.6% in terms of the RSD for five injections of the same sample with a concentration of 1.10×10^{-3} M. The sampling rate was about 20 h^{-1}. This shows that the DO detector is suitable as a new simple FIA detector for hypoxanthine. The change in the baseline of the FIA system was about 1.8% of the peak height for the

Fig. 4. Effect of pH on FIA signal.
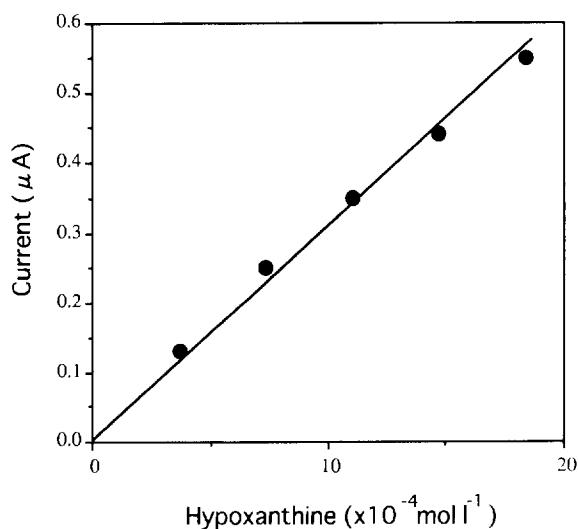
Fig. 5. Calibration curve for hypoxanthine.

measurement of 3.68×10^{-5} M hypoxanthine. The slope of the calibration curve in the range 3.68×10^{-5}–1.84×10^{-3} M hypoxanthine was 3.06×10^{-1} μA mmol l^{-1}.

3.3. Stability of xanthine oxidase immobilized column

The long term stability of the xanthine oxidase immobilized column was investigated. The column, stored at 4°C, was tested periodically for a 10^{-4} M hypoxanthine sample. After 1 month, the output signal from the detector had decreased by about 20% compared to the initial value. The column performance was checked at the same hypoxanthine concentration every 2 weeks. The signal from the detector was stable within $\pm$10% relative error for 5 months. The column performance after 1 year showed that the activity had decreased by 50% of the initial value. This means that the xanthine oxidase immobilized column was durable for 1 year. 150 measurements for meat samples were possible for one column.

3.4. Selectivity

The specificity of the present FIA system for hypoxanthine using the DO detector and the immobilized xanthine oxidase reactor was studied for several substances which often coexist in food samples. Peak height for a sample containing 10^{-4} M hypoxanthine was compared with those for 10^{-3} M concentrations of substances such as L-glutamic acid, L-lactate, glucose, pyruvic acid, inosine 5'-monophosphate, inosine, guanosine and guanine. No current from the detector was observed with any of these substances and they did not interfere with the determination of hypoxanthine because the enzyme reaction with xanthine oxidase was specific to hypoxanthine. However, the detector output with 10^{-4} M xanthine was 54% of that of hypoxanthine. This means that xanthine is also oxidized by xanthine oxidase. However, the hypoxanthine content was higher than that of xanthine in meat samples. Therefore, interference of xanthine in the FIA system can be ignored in this work.

Table 2
Analytical conditions of HPLC method for hypoxanthine

| Instrument:	Shimadzu LC-6A
Elution:	0.05 M phosphate buffer
Column:	Shim-pack CLC-ODS
	(6 mm i.d. × 15 cm)
Flow rate (ml min^{-1}):	0.7 (15 min) → 1.2 (15 min)
Column temperature °C:	40
Measurement pressure (atom cm^{-2}):	150
Wavelength (nm):	254 UV
Sample volume (μl):	20

3.5. Correlation between the present FIA method and the conventional HPLC method

We applied the present FIA system for the determination of hypoxanthine in six meat samples. The results were compared with data obtained by the conventional HPLC method with a UV detector. The 1 g meat samples for analysis were extracted into 20 ml of 10% perchloric acid and diluted with pure water to within the determination range of this system after neutralization of the meat extracts and elimination of perchlorate ion as potassium perchlorate. The analytical conditions for the HPLC method are shown in Table 2.

The correlation of the analytical results between the two methods is fairly good, as shown in Fig. 6. From these data, we obtained the regression line $Y = 1.02X$-4.54 and a correlation factor of 0.993. This seems to confirm that the present FIA system with a DO detector can be applied for the determination of hypoxanthine in meat samples.

3.6. Changes in amounts of hypoxanthine in meat samples

We applied the present FIA system to monitor the aging course of meat samples. Specimens of sirloin steak stored at 2°C were used for experiments conducted at regular time intervals. The result is shown in Fig. 7. We compared the
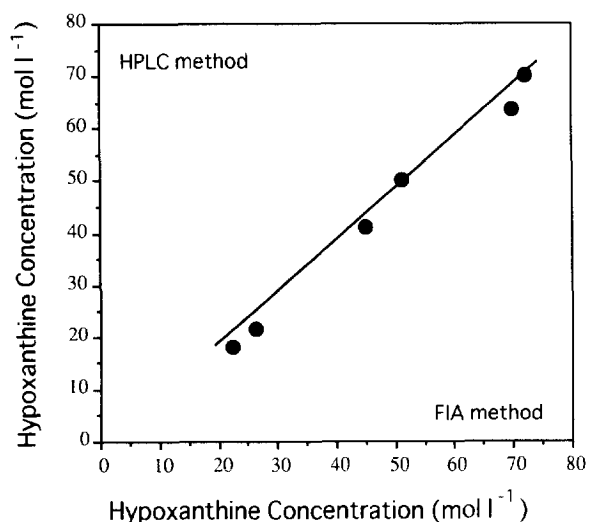
Fig. 6. Correlation between HPLC method and FIA method for determination of hypoxanthine.

change in the data obtained with the present method and the conventional method for the same storage period. The data from both methods showed the same tendency with the passing of time.

From these data it is clear that hypoxanthine is a good index for evaluating the aging time and the present FIA system is useful for the quality control of meat samples.
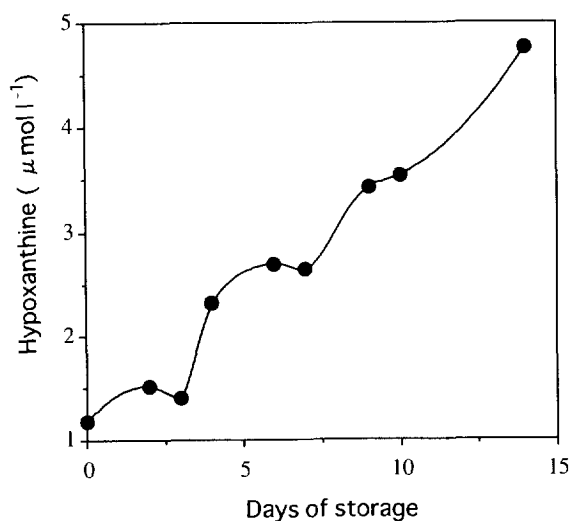
Fig. 7. Change in amount of hypoxanthine in meat stored at 10°C.

4. Conclusion

We have developed a FIA system with a DO detector for the determination of hypoxanthine in meat samples. The present FIA system has the specifications shown in Table 3. We conclude that the present FIA system has the advantages of simplicity, low cost, ease of maintenance, low consumption of reagents, ease of use and no need for a chemical analysis expert. The system is suitable as a quality control technique for the determination of hypoxanthine during the manufacturing process in the food industry. However, it is necessary to calibrate the system before every measurement because the activity of xanthine oxidase changes gradually over the course of a year. Therefore, it would be better to determine the more stable xanthine oxidase from the viewpoint of quality control online in the food industry.

The basic concept described in this paper would appear to be applicable to evaluate other taste-determining substances in food samples.

Table 3
Specifications of present FIA system for hypoxanthine

Detector:	DO detector with 20 μl cell volume
Sample (μl):	20
Carrier solution:	0.1 M phosphate buffer
pH:	7.0
Flow rate (ml min^{-1}):	1
Coil length:	10 cm from column to detector
Measurement temperature (°C):	25
Enzyme:	Xanthine oxidase (Sigma)
Column size (mm):	3 (i.d.) × 108
Measurement range:	3.68×10^{-5}–1.84×10^{-3} M hypoxanthine
Analysis rates (h^{-1}):	20
Repeatability:	1.6% (RSD) for 1.10×10^{-3} M hypoxanthine
Correlation factor with HPLC for 6 samples:	0.993
Regression line with HPLC for 6 samples:	$Y = 1.02X$-4.54
Sample:	Beef

References

[1] ICMSF, Microorganisms in Foods 4. Application of the Hazard Analysis Critical Point (HACCP) system to Ensure Microbiological Safety and Quality, Blackwell Scientific, London, 1988.

[2] F.C. Parrish Jr., R.B. Young, B.E. Miner and L.D. Andersen, J. Food Sci., 38 (1973) 690-695.

[3] D.G. Olson, F.C. Parrish and M.H. Storomer, J. Food Sci., 41 (1976) 1036-1046.

[4] R.A. Macbridge and F.C. Parrish Jr., J. Food Sci., 31 (1977) 1627-1629.

[5] A. Ouali, Meat Sci., 11 (1983) 79-88.

[6] Y. Yano and Y. Asano, Japanese Technology Reviews (On-Line Sensors for Food Processing), Gordon and Breach Science, Switzerland, Vol. 4, No. 2, 1994, pp. 36-43.

[7] Y. Yano, N. Kataho, M. Watanabe, T. Nakamura and Y. Asano, Food Chem., 52 (1995) 439-445.

[8] M. Yoshimura, T. Iwamoto and K. Iriyama, Jikeikai Med. J., 33 (1986) 37.

[9] T. Yao, Y. Kobayashi and S. Musha, Anal. Chim. Acta, 138 (1982) 81.

[10] H. Okuma, T. Takahashi, S. Sekimukai, K. Kawahara and R. Akahoshi, Anal. Chim. Acta, 224 (1990) 161-164.

[11] E. Watanabe, K. Ando, I. Karube, H. Matsuoka and S. Suzuki, J. Food Sci., 48 (1983) 496-500.

[12] K. Hayashi, E. Tamiya and I. Karube, 59th Spring Annual Meeting, The Chemical Society of Japan, Yokahama, Kanagawa, 1990, Abstract I, 160.

Studies of the chlorpheniramine solid-state ion-selective electrode

Chao-Lun Huang, Ju-Jie Ren, Da-Feng Xu*

Department of Pharmacy, Hebei Medical University, Shijiazhuang, People's Republic of China

Abstract

An Ag/AgCl solid-state electrode was prepared by using urea–formaldehyde resin as the frame material and KCl powder as the active material. Using the prepared Ag/AgCl solid-state electrode as substrate and chlorpheniramine tetraphenylborate ion-pair complex as the active component, a new type of solid-state chlorpheniramine ion-selective electrode was constructed. The properties of the electrode were studied in detail. The electrode shows a rather good stability and can be used in the potentiometric determination of chlorpheniramine.

1. Introduction

Many all-solid-state drug ion-selective electrodes have been reported [1–3]. Most of them were prepared by using graphite rod or inert metals as the substrate of the electrode. The shortcoming of this kind of electrode is that they usually show poor stability. The stability of a electrode is the key to obtaining precise results. Therefore, methods to raise the stability of a electrode are very important. Using urea–formaldehyde resin as the frame material and KCl powder as the active component, a Ag/AgCl solid-state electrode was prepared at first. By using the prepared Ag/AgCl solid-state electrode as the substrate, a new type of all-solid-state chlorpheniramine ion-selective electrode was constructed.

* Corresponding author. Fax: (86) 311-6048177.

2. Experimental

2.1. Apparatus and reagents

The apparatus used for the measurement of the electrode potential was a PXJ-1B model digital pH/mV meter (Jiangsu Electroanalytical Instrument Factory). Chlorpheniramine ($C_{16}H_{19}ClN_2 \cdot C_4H_4O_4$) was supplied by the Pharmaceutical Factory of Hebei Medical University. Atropine sulfate (($C_{17}H_{23}NO_3)_2 \cdot H_2SO_4 \cdot H_2O$), sulfanilamide ($H_2NC_6H_4SO_2NH_2$), dicaine hydrochloride ($CH_3(CH_2)_3NHC_6H_4COOCH_2$-$CH_2N(CH_3)_2 \cdot HCl$), streptomycin sulfate (($C_{21}H_{39}N_7O_{12})_2 \cdot 3H_2SO_4$) and vitamin B_1 ($C_{12}H_{17}ClN_4OS \cdot HCl$) were kindly supplied by the manufacturers. Other reagents used were analytical grade.

2.2. Preparation of the active component

Chlorpheniramine tetraphenylborate was prepared by mixing 50 ml of 0.02 M chlorpheniramine and 50 ml of 0.02 M sodium tetraphenylborate solution. The resulting precipitate was filtered out on a porosity-4-sintered-glass crucible and washed several times with water, and then dried under vacuum at 313 K.

2.3. Preparation of the Ag/AgCl wire

A silver wire with a diameter of 0.5 mm was twisted into a spiral with a diameter of 3 mm and was then washed with acetone to remove the pollutants on its surface. Using the silver spiral as the cathode and a platinum wire as the anode, a thin sheet of pure silver was electroplated on the surface of the silver spiral with an electric current of 10 mA for 0.5 h in a electrolyte, which was prepared by mixing 3 g AgNO$_3$, 60 g KI and 7 ml 25% ammonia water and diluting to 100 ml with water. The electroplated silver spiral was washed with KI solution, ammonia water and water successively. Using the electroplated silver spiral as the anode and a platinum wire as the cathode, a thin sheet of AgCl was coated on the surface of the silver spiral by electrolyzing in 1 M HCl with a 3 mA electric current for 1 h. An Ag/AgCl wire was prepared after removing the silver spiral coated with a sheet of AgCl from the electrolysis bath and washing with water. The prepared Ag/AgCl wire was preserved in a KCl or HCl solution and kept away from light.

2.4. Preparation of the solid-state Ag/AgCl electrode

A mass of 60 g (1 mol) urea and 142 g (1.8 mol) formaldehyde were mixed in a 500 ml Wolff bottle, which was equipped with a stirrer and a reflux condenser. A 2 M KOH solution was added to the Wolff bottle until the pH of the mixture was 7–8. The mixture was reflux heated for 2 h. Then, between the Wolff bottle and the reflux condenser, an oil–water separator was fitted. Syrupy urea–formaldehyde resin polymer was obtained after about 40 ml water was separated by the separator.

A previously prepared Ag/AgCl wire was put in a polythylene molded pipe with a diameter of 1.4 cm.

A mass of 2 g KCl powder, which had been previously ground carefully, and 8 g syrupy urea–formaldehyde resin polymer was mixed thoroughly. Under the condition of stirring 1 M HCl solution was added until the pH of the mixture was 4–5, then, the mixture was transfered quickly to the polyethylene pipe. The Ag/AgCl solid-state electrode was obtained after keeping the mixture at room temperature for 24 h and removing from the pipe. Finally, the side wall of the prepared electrode was sealed with a thermoplastic pipe.

2.5. Preparation of chlorpheniramine solid-state electrode

The above prepared Ag/AgCl solid-state electrode was put in 10^{-3} M chlorpheniramine solution for 1 h. The water on the surface of the electrode was removed with filter paper.

Chlorpheniramine tetraphenylborate (5 mg) dissolved in 0.4 g dibutylphthalate was mixed with 4 g of 5% PVC solution in tetrahydrofuran. A solid-state chlorpheniramine ion-selective electrode was prepared by immersing one end of the prepared Ag/AgCl solid-state electrode in the above solution five or six times and drying at room temperature for 48 h. This electrode was called electrode A.

2.6. Preparation of electrode B

One end of a graphite rod of 99.99% purity, with a diameter of 1 cm was mechanically polished with emery paper to a mirror finish. Electrode B was prepared in a similar way to electrode A except the polished end of the graphite rod was used as the substrate of the chlorpheniramine solid-state electrode.

2.7. Preparation of the electrode C

Electrode C was prepared the same as electrode A except by using the prepared Ag/AgCl wire as the substrate of chlorpheniramine solid state electrode.

Table 1
Comparison of the stability of the three different chlorpheniramine electrodes

Electrode	Drifts in 8 h[a] (mV h^{-1})	Potentials[b] (mV)						
		1d	2d	3d	5d	10d	15d	20d
A	0.2	−27.0	−26.8	−26.8	−26.8	−26.5	−26.4	−26.1
B	12.0	70.8	67.4	63.5	60.8	59.2	54.3	53.6
C	10.0	−75.4	−63.4	−42.0	−7.4	3.9	9.9	16.4

[a] Potentials measured continuously in 10^{-3} M chlorpheniramine solutions for 8 h.
[b] Potentials measured in 10^{-3} M chlorpheniramine solution after preserving for different times and the electrode was kept dry after each measurement.

2.8. Preparation of the solutions

Total ionic strength adjustment buffer (TISAB): 0.05 mol $NaNO_3$ and 0.05 mol NaOAc (sodium acetate (CH_3COONa)) was dissolved in 0.05 mol AcOH (acetic acid (CH_3COOH)) and the mixture was diluted to 1000 ml with water. The ionic strength and pH of the buffer were 0.1 and 4.6 respectively.

Standard chlorpheniramine solution: chlorpheniramine (3.9080 g) was dissolved in 20 ml TISAB, and diluted to the mark in a 100 ml volumetric flask with TISAB, to give a 0.1 M standard solution. Series of standards were prepared by successive dilution to 10^{-2}–10^{-6} M with TISAB.

2.9. Measurements of electromotive force

The electromotive force (emf) measurements were made at a constant ionic strength, and the junction potential was kept constant. The cell can be expressed as Chlorpheniramine electrode |sample, $I = 0.1$|0.1 M $NaNO_3$|SCE.

3. Results and discussion

3.1. The stability of the electrode

The potential drift of the electrode was studied in 0.001 M chlorpheniramine solution when the emf of the cell had been measured for 8 h. The electrode potentials were measured after preserving the electrode for different times. The repro-

ducibility of the electrode stability was investigated by the reported method [4]. At first, the electrode potential was measured in a 0.001 M solution; when the electrode was transferred to a 0.01 M solution another potential was measured. The potential was measured again after transferring the electrode from the 0.01 M to 0.001 M solution. By repeating the transferring process five times, the greatest potential deviation obtained from the measurements was defined as the reproducibility of the electrode. The results (Tables 1 and 2) indicate that electrode B showed poor stability due to the irreversible state between the graphite rod and the PVC membrane [5]. Electrode C showed poor stability because the Ag/AgCl wire lacks chloride ions. Electrode A exhibits excellent stability and reproducibility due to the use of Ag/AgCl solid-state electrode as the substrate of the chlorpheniramine electrode. The substrate of electrode A was composed of urea–formaldehyde resin together with some water. Urea–formaldehyde resin has a three-dimensional

Table 2
Comparison of the reproducibility of the three different chlorpheniramine electrodes (five measuring times)

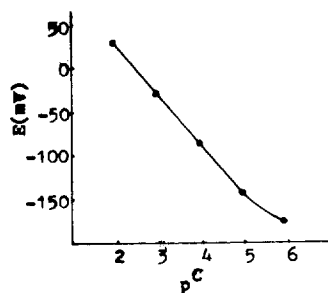| Electrode	Chlorpheniramine concentration (M)	Mean value (mV)	RSD (%)	Reproducibility (mV)
A	0.01	31.3	0.18	0.2
	0.001	−27.1	0.33	
B	0.01	120.8	0.97	3.1
	0.001	63.6	2.02	
C	0.01	−24.0	2.72	1.5
	0.001	−82.3	0.78	

Fig. 1. Calibration curve of the all-solid-state chlorpheniramine electrode.

net structure. It can contain some water and provide ionic passage. The substrate was immersed in chlorpheniramine solution before being coated with PVC membrane; therefore, the pores of the urea–formaldehyde resin had some chlorpheniramine cations. Due to the existence of the exchangeable chlorpheniramine cation in the interface between the urea–formaldehyde resin and PVC membrane, the whole electrode was in a thermodynamic reversible state; as a result the stability of the electrode was greatly improved. Electrode A was used in subsequent studies.

3.2. Electrode calibration

The linear range of the electrode was measured. The results (Fig. 1) show that the linear range of the electrode is from 1.0×10^{-2} to 5.0×10^{-5} M with a slope of 58.2 mV per decade and a detection limit of 2.5×10^{-5} M.

3.3. Effect of pH

The influence of pH on the response of the chlorpheniramine electrode was studied by adjusting the pH of the chlorpheniramine solution with 0.1 M HCl or 0.1 M NaOH. The results (Fig. 2) show that the pH range, where the potential of the electrode remains constant, is 4–8.

3.4. Selectivity of the electrode

The selectivity coefficients for nine substances were determined by the mixed-solution method. The experimental data were treated by the reported method [6]. The method can be outlined as

follows: the response potential of a electrode measured in dilute solution with two kinds of coexisting ions can be expressed by Eq. (1)

$$E = E_o + S \ln(C_i + K_{ij}C_j^{Z_i/Z_j}) \tag{1}$$

where i is the measured ion, j is the interferential ion, Z_i is the electric charge number of i ions, Z_j is the electric charge number of j ion, S is the Nernst slope and K_{ij} is the selectivity coefficient. The appearance of Eq. (1) can be arranged to form Eq. (2)

$$e^{E/S} = e^{E_o/S}(C_i + K_{ij}C_j^{Z_i/Z_j}) \tag{2}$$

which is the equation of a straight line of slope $(e^{E_o/S})$ and intercept $e^{E_o/S} \cdot K_{ij}C_j^{Z_i/Z_j}$ when C_j was fixed. A series of solutions were prepared by fixing the concentration of j ions $(10^{-3}$ M) and changing the concentration of i ions from 10^{-2}–10^{-6} M. The electrode potentials of the series of solutions were measured and $e^{E/S}$ was plotted against C_i. From the slope and the intercept of the straight line K_{ij} can be obtained. All the calculations were completed by a computer. The results (Table 3) show that the electrode has a very good selectivity for chlorpheniramine except with dicaine hydrochloride.

3.5. Internal resistance, response time and life-span of the electrode

The internal resistance of the electrode was measured and the result was 2×10^5 Ω. The response time of the electrode in 10^{-1}–10^{-4} M concentration is less than 30 s and in 10^{-4}–10^{-6} M it is less than 2 min. The life-span of the electrode is 6 months.
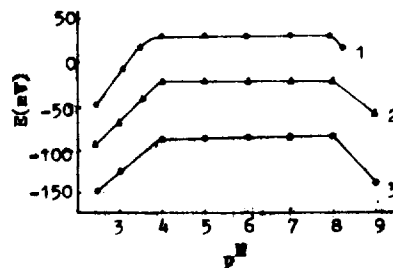

Fig. 2. Effect of pH on the potential of the chlorpheniramine ion-selective electrode. Chlorpheniramine solution: curve 1, 10^{-2} M; 2, 10^{-3} M; curve 3, 10^{-4} M.

Table 3
Selectivity coefficients (mixed-solution procedure)

Interferent	K_{ij}
K^+	7.09×10^{-3}
Na^+	1.14×10^{-2}
Cu^{2+}	2.24×10^{-4}
Al^{3+}	9.50×10^{-5}
Vitamin B_1	1.02×10^{-2}
Sulfanilamide	2.01×10^{-3}
Atropine sulfate	6.79×10^{-2}
Dicaine hydrochloride	9.60×10^{-1}
Streptomycin sulfate	5.59×10^{-4}

Table 4
Recovery of chlorpheniramine (standard addition method)

Chlorpheniramine taken (mg)	Chlorpheniramine found (mg)	Recovery (%)
3.91	3.89	99.5
7.82	7.69	98.3
19.5	19.5	100.0
39.1	39.2	100.3
58.6	58.5	99.8
78.2	78.4	100.3
117	117	100.0

3.6. Advantages of the solid-state chlorpheniramine electrode

Ishibashi et al. [7] have reported a chlorpheniramine electrode based on a liquid or a PVC membrane containing the chlorpheniramine–tetraphenylborate ion pair. This needed the poisonous solvent nitrobenzene or an internal reference solution and an internal reference electrode. The internal reference solution must be changed periodically in order to ensure the precision of the measurement. The solid-state chlorpheniramine electrode in this paper can be prepared, used and preserved conveniently due to the fact that it does not need internal reference solution. The stability of the solid-state chlorpheniramine electrode is much better than the reported [7] liquid or PVC membrane chlorpheniramine electrode.

3.7. Applications to chlorpheniramine determination

The recovery test was carried out with the standard addition method. The results (Table 4) indicate that the average recovery is 99.7% and the coefficient of variation is 0.7%.

The electrode was applied to the actual determination of chlorpheniramine in chlorpheniramine tablets (labeled amount 4 mg per tablet) with the standard addition method. The results indicate that the average content of chlorpheniramine, when measured ten times, is 3.86 mg per tablet and the coefficient of variation is 1.2%. This agrees well with the Pharmacopoeia of the PR China. The electrode can, therefore, be applied to the rapid determination of chlorpheniramine.

References

[1] L.Z. Cai and H. Ren, Chinese J. Anal. Chem., 16 (1988) 991.
[2] L.H. Nie, W.L. Ma, X.C. Xiang and S.Z. Yao, Acta Pharm. Sinica, 24 (1989) 458.
[3] H. Tamura, K. Kimura and T. Shono, Anal. Chem., 54 (1982) 1224.
[4] D.P. Huang, Z.C. Shen and G.L. Wu, The Principle and Application of the Ion-Selective Electrode, New Times Press, Beijing, 1982, p. 64.
[5] X.Y. Hu and Z.Z. Leng, Chinese J. Appl. Chem., 6 (1989) 97.
[6] C.L. Huang, Chinese J. Anal. Chem., 17 (1989) 1039.
[7] K. Kina, N. Maekawa and N. Ishibashi, Bull. Chem. Soc. Jpn., 46 (1973) 2772.

Talanta

Stopped-flow kinetic determination of aluminum in Chinese tea leaves by fluoride ion-selective electrode potentiometry

Huaisheng Wang, Zihong Zhang, Ailing Sun, Daojie Liu, Renmin Liu*

Department of Chemistry, Liaocheng Teachers College, Liaocheng, Shandong, People's Republic of China

Abstract

A stopped-flow kinetic potentiometric method for the determination of aluminum is described, based on monitoring the reaction between aluminum and fluoride at pH 3.0 using fluoride ion-selective electrode. The initial rate of the reaction is proportional to the concentration of aluminum present in the solution. The method is simple and rapid and has been applied to the determination of aluminum in Chinese tea leaves after microwave digestion.

Keywords: Aluminum determination; Fluoride ion-selective electrode; Kinetic potentiometric method; Microwave digestion; Tea leaf analysis

1. Introduction

Aluminum is the third most abundant element in the Earth's crust. It is commonly found in living organisms consumed as food by human beings. Aluminum and the role it plays in the human body have been topics of interest over the past decade. Experimental evidence shows that aluminum is potentially toxic, expecially on accumulation in the human body, where it can damage various tissues and cells in the central nervous system [1,2]. Abnormal accumulation of aluminum in certain tissues of the human body was associated with abnormal skeletal metabolism [3] and various diseases, such as Alzheimer's disease [4], Osteomalacia[5] and Parkinsonism dementia [6].

There has been much interest in the possible biological function of aluminum in recent years. Hence, the development of a simple and reliable method for the determination of aluminum is urgently required for future surveys and for use in routine monitoring.

Many methods have been used for the determination of aluminum in food. The most widely used methods are electrothermal atomization atomic absorption spectrometry [7,8], inductively-coupled plasma optical emission spectrometry [9], and spectrophotometry [10,11].

The fluoride ion-selective electrode (ISE) can be used for the indirect determination of aluminum [12–15]. The method most commonly used is potentiometric titration of aluminum with

fluoride. Radic and Bralic [16] studied the kinetics of the $AlF_j^{(3-i)+}$ formation reaction in acidic solution using a fluoride ISE, and found that the initial formation, rate of the aluminum–fluoride complex was proportional to the amount of aluminum.

In the present work, a stopped-flow kinetic method for the determination of aluminum has been developed using a fluoride ISE. The proposed method is simple and useful. It has been applied to the determination of aluminum in Chinese tea leaves and of aluminum extracted from tea leaves by immersion in boiling water.

2. Experimental

2.1. Apparatus

Fig. 1 shows the flow system used in this experiment. Two two-channel peristaltic pumps (Jiangsu Electroanalytical Instrument Plant) controlled by a T1200XE computer (Toshiba) were used. The detector cell used is shown in Fig. 2. A 201 fluoride ISE (Jiangsu Electroanalytical Instrument Plant) was used as the sensor. The electrode potential was measured with an Orion SA720 pH/mV meter which is connected to the computer.

2.2. Reagents

All chemicals used were of analytical-reagent grade and the solutions were prepared with distilled–deionised water.

Fluoride solution. 0.1 M sodium fluoride solu-

Fig. 2. Schematic diagram of the detector cell: S and B, sample and buffer; W, waste; 1, 1.0 min i.d. conduit; 2, PTFE sleeve; 3, rubber O-ring.

tion was prepared with sodium fluoride (Beijing Chemical Plant). Solutions of other concentrations were prepared by diluting with deionised water.

Aluminum standard solution (0.0100 M). This was prepared by dissolving the appropriate amount of aluminum wire (99.99%); (Shanghai Chemical Reagent Plant) in 10 ml of 6 M hydrochloric acid. The solution was transferred to a 250 ml calibrated flask and diluted to the mark with deionised water. A series of aluminum working solutions were prepared by diluting the standard solution with buffer solution.

Buffer solution. A solution containing 0.1 M sodium dihydrogen orthophosphate (Shanghai Chemical Reagent Plant), 2.3 mM 1, 10-phenanthroline and 0.45 M hydroxylammonium was used as a buffer solution. The pH was adjusted with 5M sulfuric acid and 1 M sodium hydroxide. 1, 10-Phenanthroline and hydroxylammonium were used to overcome the interference of Fe^{3+}.

Nitric acid. Concentrated nitric acid (Jinan Chemical Reagent Plant), was used. Perchloric acid. 70% perchloric acid (Shanghai Taopu Chemical Plant) was used.

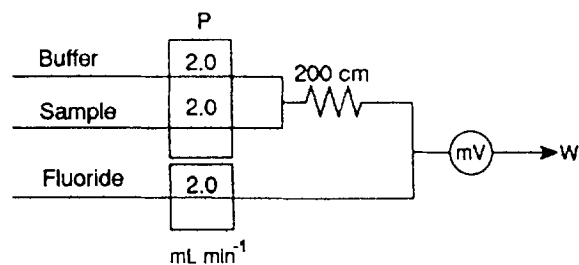

Fig. 1. Flow system for determination of aluminum: P, pump; mV, pH/mV meter detector; W, waste.
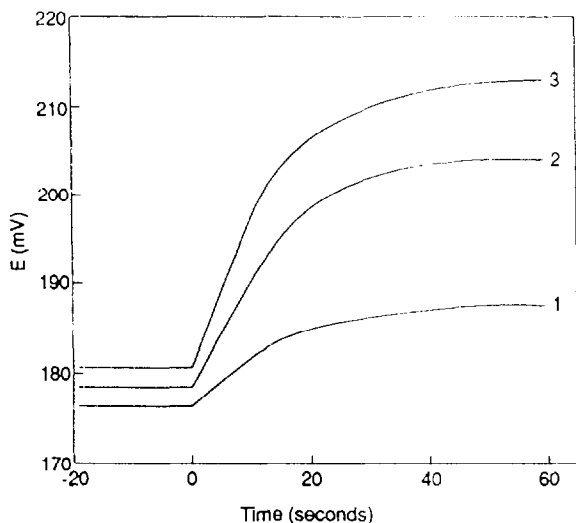
Fig. 3. Typical record curve: F . 50 μM; pH, 3.0; Al^{3+}: (1), 20 μM; (2), 50 μM; (3), 100 μM.

2.3. Measurement procedure

2.3.1. General Procedure

The flow system was connected with PTFE tubing (1.0 mm i.d.) according to Fig. 1. Pumps were started and the flow rate of every channel was adjusted to 2.0 ml min^{-1}. The electrode potential was recorded using the pH/mV meter. When the electrode potential reached equilibrium and a flat E–t line was observed, the pumps were stopped and the potential changes were recorded over a period of 1 min. The initial slope of the curve, $\Delta E/\Delta t$, is used as a measure of aluminum.

The standard solutions of aluminum were also analyzed by the same procedure. A calibration graph was constructed of logarithmic concentration of aluminum versus initial slope ($\Delta E/\Delta t$).

2.3.2. Digestion of tea sample

A Xianhua E-32 microwave oven (total microwave power 650 W) was used for the digestion of tea leaves. The digestion procedure was as follows. 0.2 g of tea leaves was heated (65 W, 10%) with 5 ml of nitric acid for 10 min. Then 2 ml of water was added. After 5 min of heating, 1 ml of 70% perchloric acid was added and the solution heated for another 5 min. Then 5 ml of water was added and heating was resumed for 15

min. The solution was diluted to 50 ml with water after cooling.

2.3.3. Determination conditions of the graphite-furnace atomic absorption spectometry (GFAAS)

A Hitachi 180-80 polarized Zeeman atomic absorption spectrophotometer (Hitachi Ltd., Tokyo, Japan) was used for GFAAS determination of aluminum. The instrumental conditions are as follows:

Light source:	Al hollow cathode lamp
Wavelength:	309.3 nm
Slit:	1.3 nm
Lamp current:	10 mA
Cuvette:	Tube type
Sample volume:	10 μl
Carrier gas flow:	200 ml min^{-1}

Graphite furnace program:

Step	Temperature (°C)	Time(s)
Drying	120	30
Ashing	1000	20
Atomization	2900	10
Cleaning	3000	5

3. Results and discussion

In aqueous solution aluminum ions are present as $Al[(Al(H_2O)_6]^{3+}$, which can be hydrolyzed to form $Al[(Al(H_2O)_5OH]^{2+}$, $Al[(Al(H_2O)_4(OH)_2]^+$ and $Al[(Al(H_2O)_3(OH)_3]$. Then reaction equations are as follows [17]:

$$[Al(H_2O)_6]^{3+} + H_2O$$
$$\rightleftharpoons [Al(H_2O)_5(OH)]^{2+} + H_3O^+$$

$$[Al(H_2O)_5(OH)]^{2+} + H_2O$$
$$\rightleftharpoons [Al(H_2O)_4(OH)_2]^+ + H_3O^+$$
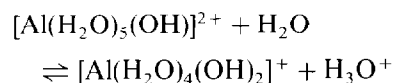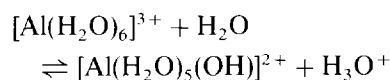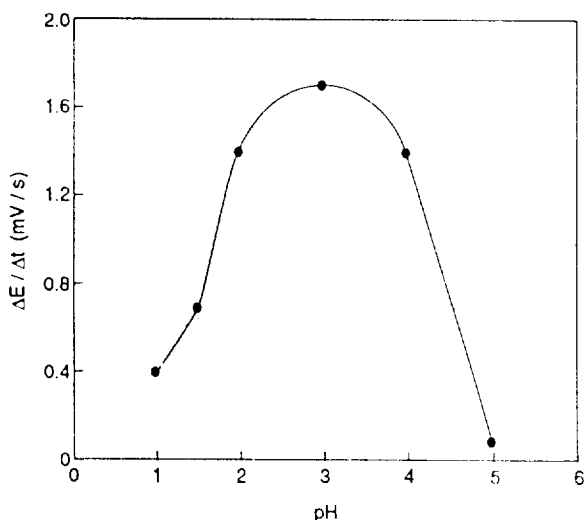
Fig. 4. Influence of pH on determination of Al^{3+}: Al^{3+}, 50 μM; F^-, 50 μM.

$$[Al(H_2O)_4(OH)_2]^+ + H_2O$$
$$\rightleftharpoons [Al(H_2O)_3(OH)_3] + H_3O^+$$
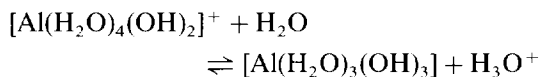
Only in acidic medium can aluminum species be present mainly in the form of Al^{3+} (co-ordinated water has been omitted for simplicity). Al^{3+} can react with F^- to form the AlF^{2+} complex. This reaction can be monitored using a fluoride ISE.

Fig. 3 shows the typical potential–time curve of the fluoride ISE when fluoride was used for measuring (1) 20 μM, (2) 50 μM and (3) 100 μM Al^{3+}. The initial slope of the curve, $\Delta E/\Delta t$, is proportional to the concentration of aluminum present in the solution.

3.1. The influence of pH

The influence of pH on the determination of aluminum was investigated. Fig. 4 shows the change in the initial slope of the potential curve of the fluoride ISE with the pH of the solution in the range 1.0–5.0. The highest sensitivity is obtained at pH 3.0. An obvious decrease in the initial rate was found when the pH was altered from 3 to 5 and from 3 to 1. This may be due to the following reactions:

$$F^- + H^+ \rightleftharpoons HF$$

$$Al^{3+} + iOH^- \rightleftharpoons Al(OH)_i^{(3-i)+}$$
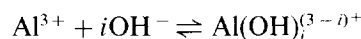
In highly acidic medium, F^- reacts with H^+ to form HF, leading to a decrease in the rate of complexation of Al^{3+} with F^-. In the solution of pH higher than 3.0, the hydrolysis reaction of Al^{3+} to $Al(OH)_i^{(3-i)+}$ reduces the free Al^{3+} concentration and the complexation rate is decreased.

Fig. 5. Influence of pH on determination of Fe^{3+}: Fe^{3+}, 100 μM; F^-, 100 μM.
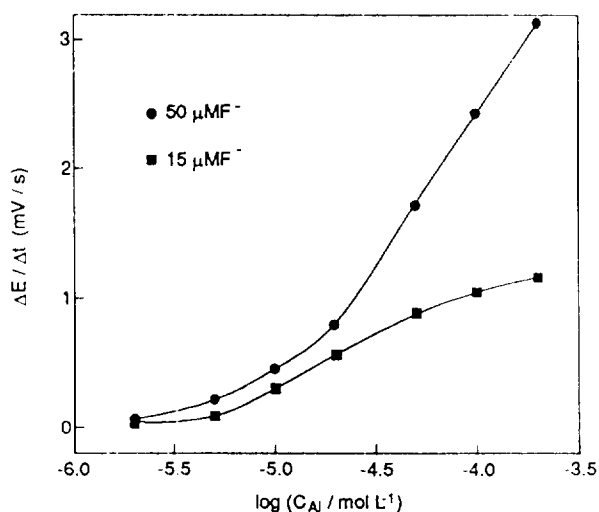
Fig. 6. Calibration graph: (1), 15 μM F^-; (2), 50 μM F^-.

Table 1
Determination of aluminum in Chinese tea leaves

Sample	Proposed method (μg g^{-1})	GFAAS method (μg g^{-1})	Relative error (%)
1. Jasmine tea (Zhenghe, Fujian)[a]	526.4	544.2	−3.3
2. Xian Yin oolong tea (Fuzhou, Fujian)[a]	474.6	466.3	1.8
3. Ti Kun Yin (Anxi, Fujian)[a]	618.6	609.7	1.5
4. Early-spring band jasmine tea (You County, Hunan)[a]	708.2	717.8	−1.3

[a] The names in parentheses are the areas producing the tea leaves.

3.2. Interferences

Because the reaction of Fe^{3+} with F^- is similar to that of Al^{3+}, Fe^{3+} interferes with the determination of aluminum when using the fluoride electrode as the sensor. The initial slope, $\Delta E/\Delta t$, of the reaction of Fe^{3+} with fluoride in different pH buffer solutions is shown in Fig. 5. Although the highest value of $\Delta E/\Delta t$ is observed at pH 1.5, the value of the initial slope pH 3.0 is significant and has an intense effect on the determination of aluminum. Attempts to overcome the Fe^{3+} interference by a kinetic method (difference between the reactions of Fe^{3+} and Al^{3-} with F^-) are not feasible and an iron masking reagent must be used to remove the Fe^{3+} interference. A mixture of 1, 10-phenanthroline and hydroxlammonium was often used to mask Fe^{3+} in Al determination by spectrophotometry. We have found that this kind of solution is suitable for masking Fe^{3+} in the proposed method. In this study, the masking reagent used is a mixture of 2.5 mM 1, 10-phenanthroline and 0.45 M hydroxylammonium in the buffer solution. Using this masking reagent, no interference was found with 2.0 mM Fe^{3+} for the determination of 20 μM aluminum.

3.3. Effect of concentration of F^-

The effect of the concentration of F^- was also

investigated. The results indicate that only when the concentration of F^- is higher than 10 times the actual detection limit of the electrode can a linear calibration graph be obtained. The results also indicate that the concentration of F^- has a great effect on the linear range and the signal. The linear range of the calibration graph is about 0.3–4 times the concentration of F . When the concentration of F is low, a calibration graph with a gentle slope is obtained. When the concentration of F^- is high, a calibration graph with a steep slope is obtained.

3.4. Calibration graph

The standard aluminum solutions were analyzed by the proposed method. The calibration graphs were constructed by plotting the initial $\Delta E \Delta t$ versus $\log C_{Al}$. Fig. 6 shows the calibration graphs of Al^{3+} with fluoride concentrations of 15 μM and 50 μM. When the 15 μM fluoride solution was used, the linear range of the calibration graph for aluminum was 5–50 μM. The linear regression equation is

$$\Delta E/\Delta t = 0.816 \log C + 4.405 \quad (n = 6, r = 0.9991)$$
$$(C \text{ mol L}^{-1})$$

A linear calibration graph for 20–200 μM aluminum was obtained when 50 μM fluoride solution was . The linear regression equation is

Table 2
Percentage of aluminum extracted from tea leaves by immersion in boiling water

Sample[a]	Content after 1st extraction (μg g^{-1})	Content after 2nd extraction (μg g^{-1})	Degree of 1st extraction (%)	Degree of 2nd extraction (%)
1	332.7	261.5	36.8	24.4
2	383.0	349.3	19.6	8.8
3	486.2	424.9	21.4	12.6
4	478.7	258.3	32.4	21.4

[a] The samples are the same as those in Table 1.

$$\Delta E/\Delta t = 2.352 \log C + 11.908 \quad (n = 6, r = 0.9997)$$
$$(C \text{ mol L}^{-1})$$

The precision of the proposed method was investigated by using 15 μM fluoride solution. The 8 μM aluminum standard solution was determined seven times and relative standard deviation was 3.8%.

3.5. Applications

The proposed method has been applied to the determination of aluminum in Chinese tea leaves after microwave digestion. The samples were analyzed by the proposed method and by the GFAAS method. The results are shown in Table. 1

The percentage of aluminum extracted from tea leaves by boiling water was also investigated. Tea leaves were immersed in boiling water and the percentage of aluminum extracted was determined as follows 2.0 g of tea leaves was immersed in 100 ml of boiling water for 5 min, the solution was poured off and aluminum was determined in the residue by the proposed method. After a second immersion in boiling water the aluminum in the residue was determined again. The results are listed in Table 2. It can be seen that a certain amount of aluminum can be ingested by drinking tea made from Chinese tea leaves. According to the results given by Greger et al. [18], aluminum cannot be accumulated in the human body, if the total amount of aluminum absorbed is less than 125 mg/per day. Therefore, although the amount of aluminum in tea water exceeds the limit for the maximum allowable concentration of aluminum in drinking water, no accumulation of aluminum occurs for people drinking tea.

References

[1] H. D. Belitz and W. Crosh, Food Chemistry, Springer-Verlag, New York, 1987.
[2] E. Berman, Toxic Metals and Their Analysis, Heyden & Son Ltd., London, 1980.
[3] A. Lione, Food Chem. Toxical., 21, (1983) 103.
[4] L. Finberg, H.S. Dweck, F. Holmes, N. Kretchmer, A.M. Maurer, J.W. Raynolds, R.M. Suskind and S. Hellerstein, Pediatrics, 78, (1986) 1150.
[5] B.F. Boyce, H.Y. Elder, H.L. Ellio, I. Fogelman, G.S. Fell, B.J. Juners, G. Beastall and I. T. Boyle, Lancet, 2 (1982) 1009.
[6] D.P. Perl, D.C. Gajdusek,R.M. Garruto, R.T. Yanagihara and C.J. Gibbs, Science, 217 (1982) 1053.
[7] Y. Wang, C. Lu.; Z. Xiao, S.S. Kuan and E.J. Rigsby. J. Agric. Food Chem., 39 (1991) 724.
[8] D.M. Sullivan, D.F. Kehoe and R.L. Smith, J. Assoc. Off. Anal. Chem., 70 (1987) 118.
[9] K.R. Koch, M.A.B. Pougnet and S. De Villiers, Analyst, 114 (1989) 911.
[10] M. Froede and J. Rollin, Nahrung, 26 (1982) 409.
[11] D. Liu, Fenxi Huaxue, 9 (1991) 705.
[12] B. Jeselskis and M.K. Bandemer. Anal. Chem., 41 (1969) 855.
[13] E.W. Baumann, Anal. Chem., 42 (1970) 110.
[14] Nj Radic, D. Prugo and M. Bralic, J. Electroanal. Chem., 248 (1988) 87.
[15] Nj. Radic, Analyst, 101 (1976) 657.
[16] Nj. Radic and M. Bralic, Analyst, 115 (1990) 737.
[17] Teaching and Research Section of Inorganic Chemistry of Beijing Normal University, Huazhong Teachers College and Nanjing Teachers College, Inorganic Chemistry, Vol. 1 People's Education Press, Beijing, 1981, p. 202.
[18] J.L. Greger and M.J. Baier Food Chem. Toxicol, 21 (1983) 473.

Solubility, dissociation and complexation with Nd(III) and Th(IV) of oxine, thenoyltrifluoroacetone and 1,10-phenanthroline in 5.0 m NaCl

Yuan-Xian Xia, Jian-Feng Chen, Gregory R. Choppin*

Department of Chemistry, The Florida State University, Talahassee, FL 32306-3006, USA

Abstract

Equilibria in the system of Nd(III) and Th(IV) with 8-hydroxyquinoline (oxine), thenoyltrifluoroacetone (HTTA) and 1,10-phenanthroline (phen) in 5.0 m NaCl solution have been investigated by spectroscopy and potentiometry. The solubility and deprotonation constants of the three organics were measured to be: $pK_s = 3.09 \pm 0.01$, $pK_{a1} = 5.82 \pm 0.02$, $pK_{a2} = 10.00 \pm 0.01$ for oxine; $pK_s = 2.49 \pm 0.01$, $pK_{a1} = 6.47 \pm 0.03$ for HTTA; $pK_s = 2.86 \pm 0.02$, $pK_{a2} = 5.82 \pm 0.05$ for phen. The stabilities of the corresponding metal complexes are in the order M(oxine) > M(TTA) > M(phen), where M = Nd(III), Th(IV). For all three organic ligands, the Th(IV) complexation is stronger than that of Nd(III).

Keywords: Complexation; Dissociation; HTTA; Neodymium(III); Oxine; 1,10-Phenanthroline; Solubility; Thorium(IV)

1. Introduction

Research into the methods of permanent disposal of the nuclear fission and activation products from nuclear reactor operation is being conducted in a number of countries. Underground salt beds are among the geological systems being investigated as sites for disposal of nuclear wastes. In order to be able to assess the effects of release of the long-lived actinide elements into the environment from such repositories, it is necessary to understand their chemistry under conditions encountered in brine solutions. In non-vitrified wastes the organic compounds present from the processing systems are not destroyed and may be a significant factor in increased solubilities and migration of the actinide cations. 8-Hydroxyquinoline (oxine or HOxn), thenoyltrifluoroacetone (HTTA) and 1,10-phenanthroline (phen) have been identified as three of the organics likely to be present in the nuclear wastes planned for disposal in the Waste Isolation Pilot Plant (WIPP) under study near Carlsbad, NM [1]. Although these organic compounds are sparingly soluble in aqueous systems, their complexation reactions with metal ions can compete with other chemical processes in the aqueous phase or at the aqueous–solid interface.

---

* Corresponding author. Fax: (+1) 904 644 8281.

The published investigations of the heterogeneous equilibria of these organics in water or in aqueous electrolyte media have been limited to ionic strengths ≤ 2.0 m [2–4] and no data have been reported for more concentrated electrolyte solutions. The structures of these compounds are presented in Form 1.

The purpose of this study was to investigate the solubilities, proton dissociation and complexation interactions of Am(III) and Th(IV) with oxine, HTTA and phen in 5.0 m NaCl solution. Since the use of the solvent extraction technique for determining metal ion–ligand complexation is limited by the significant solubility of the three acids in organic solvents, a spectroscopic method, based on the spectral properties of the three ligands in the UV region, was used. As the spectroscopic technique required macro concentrations, Nd(III) was used as a chemical analog of Am(III) to avoid use of a macro amount of radioactive Am(III).

2. Experimental

2.1. Reagents

HTTA (Aldrich, A.C.S.) was purified by sublimation at 45°C. Oxine (Aldrich, A.C.S.) and phen (Aldrich, A.C.S.) were used without purification. All the other chemicals used were of A.C.S. grade unless specified. Stock solutions of the three compounds (1.0×10^{-4} M) were prepared by dissolving the required amount of solid in 5.0 m NaCl solution. The concentrations of the compounds were standardized by spectroscopy. A stock buffer solution consisting of 1.0 M acetate and 1.0 M hydroxylamine was prepared by dissolving the required amounts of soldium acetate and hydroxylamine with deionized water and adjusting to pH_m 4.1 (pH_m denotes pH meter reading).

A standard thorium stock solution of 0.10 M in 5.0 m NaCl at pH_m 1.0 was prepared by dissolving a weighed amount of anhydrous thorium chloride (99.9%, Stem Chemical) in 5.0 m NaCl, and adjusting to the desired pH_m with NaOH solution. A standard neodymium stock solution of 0.32 M in 5.0 m NaCl at pH_m 4.81 was
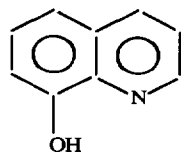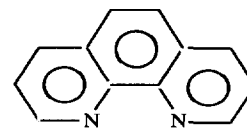
8 - hydroxyquinoline   **1,10 - phenanthroline**
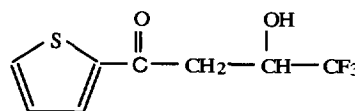
thenoyltrifluoroacetone

Form 1

prepared by dissolution of the proper amount of Nd_2O_3 (99.9%, Aldrich) in 3–6 M HCl, followed by evaporation to dryness and dissolution of the solid in 5.0 m NaCl solution with adjustment to the desired pH_m. The concentrations of Nd and Th were standardized by titration with EDTA.

2.2. pcH measurement

A Corning Semimicro-Combination glass electrode/Accumet 950 pH/ion meter assembly was used in which the KCl solution of the electrode was replaced with a saturated NaCl solution. The electrode was calibrated using two standard pH buffer solutions: 0.05 M potassium biphthalate buffer pH 4.00 at 25°C (Fisher) and 0.05 M potassium phosphate monobasic–sodium hydroxide buffer pH 7.00 at 25°C (Fisher). The meter reading, pH_m, was converted to pcH ($= -\log$ [H^+]) using the following calibration equation [5,6]:

$$pcH = s\, pH_m + b \tag{1}$$

where $s = 1$ and b is the electrode parameter whose value for 5.0 m NaCl solution has been determined to be 1.06 ± 0.01 [6].

2.3. Spectrophotometric measurements

The absorption spectra were recorded on a Cary-14 UV–VIS spectrophotometer (upgraded by On-Line Instrument System) interfaced to a Zenith 248 computer in the wavelength range 200–400 nm. The spectra were measured against 5.0 m NaCl solution as the blank unless specified. The molar absorptivities calculated from calibrations with solutions of known concentration are 4.22×10^4 cm^2 mole^{-1} (253 nm) for oxine, 5.12×10^3 cm^2 mole^{-1} (263 nm) for HTTA and 2.76×10^4 cm^2 mole^{-1} (267 nm) for phen.

2.4. Solubility

For each organic compound, 12 portions (0.10 g each) of solid samples were placed in separate 25 ml glass vials and dissolved in 20.0 ml of 5.0 m NaCl stock solution. After shaking for 24 h, the solutions in the 36 vials were adjusted to the required pcH values by adding sodium hydroxide or hydrochloric acid. The vials were shaken vigorously for 7 days at $25.0 \pm 0.1°C$. The establishment of the dissolution equilibrium in each vial was confirmed when the same solubility was obtained for 7 days as after 1 month. The concentrations of the three organic compounds were measured by spectrophotometry.

2.5. Potentiometric titrations

The potentiometric titrations were conducted using a 50 ml water-jacketed vessel controlled to $25.0 \pm 0.1°C$ with an Isotemp constant temperature circulator. For each experiment, 10.0 ml of test solution was titrated with a standardized solution of 0.030 M NaOH in 5.0 m NaCl. The titrant was delivered to the cell via Teflon tubing by a Schott Gerate automatic buret. Nitrogen gas was bubbled through the solution to remove dissolved carbon dioxide. A differential graphical technique described elsewhere [6] was used to analyze the titration data. The method is based on the use of a differential quantity, Γ (equivalent to the buffer capacity), and a second quantity, Q, which are defined and related to each other as follows:

$$\Gamma = \frac{[(m - \tilde{n})C_{HmL} + C_H + C_{OH}]V_0}{2.303(V + V_0)^2} \cdot \frac{dV}{dpH_m} \qquad (2)$$

$$Q = \Gamma - [H^+] - [OH^-] = \sum_{i=1}^{m} \frac{K_{ai}[H^+]}{(K_{ai} + [H^+])^2} \cdot C_{HmL} \qquad (3)$$

where V_0 is the initial volume of test solution and V the volume of the titrant added, C_{HmL}, C_H and C_{OH} are respectively the initial concentrations of the ligand and the proton in the test solution and the concentration of the hydroxide ion in the titrant and $\tilde{n}$ is the protonation number defined as

$$\tilde{n} = \frac{\sum_{i=1}^{m} i[H_iL]}{C_{HmL}} \qquad (4)$$

Q is a quasi-parabolic function of pcH in which each peak in a Q vs. pcH plot corresponds to a dissociation sequence and the maximum value of the peak of Q_{max} ($= 0.25\ C_{HmL}$) occurs at pcH $=$ pK_{ai}.

2.6. Complexation

The complexation of each metal–ligand system was investigated by measuring the spectra of the ligand in the presence of varying amounts of the metal ion at constant pH$_m$. Six series of spectra were recorded for each combination of the two metal ions and three ligands. For Nd(III), pcH values for all three ligands were maintained at 5.87 by using a mixture of 0.010 M acetic and 0.010 M hydroxylamine as pcH buffer (the necessary corrections were made for the complexation competition by the two ligands). For Th(IV), a lower pcH range was chosen to avoid hydrolysis and difference spectra (against ligand solutions as blank) were recorded to detect the small amounts of the complexes formed.

Secondary stock solutions of the ligands of desired concentrations (depending on the molar absorptivities) were prepared by diluting the original ligand stock solutions with 5.0 m NaCl solution and adjusting to the required pcH. Ligand + metal stock solutions were prepared by mixing aliquots of the ligand stock solutions and the metal stock solutions,
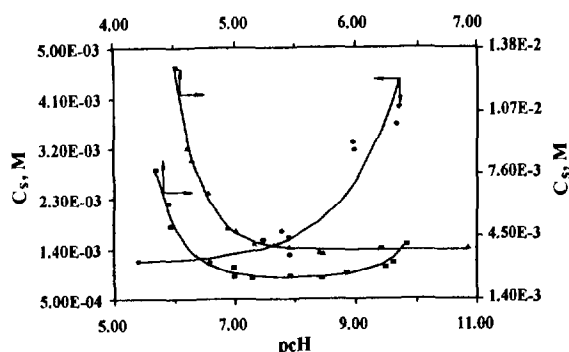
Fig. 1. The stoichiometric solubilities of the three organic compounds as a function of pcH in 5.0 m NaCl solution: (■) oxine; (▲) phen; (●) HTTA.

diluting with 5.0 m NaCl solution and adjusting to the desired pcH. Final samples were prepared by mixing a variable volume of the secondary ligand stock solutions with a volume of the ligand–metal stock solution.

3. Results and discussion

3.1. Solubility

The stoichiometric solubilities of oxine, HTTA and phen in 5.0 m NaCl solution in the pcH range 5.0–11.0 are shown in Fig. 1. The solubility of oxine increases above $pcH \approx 8.5$ and below $pcH \approx 7$ with a minimum in the middle of the pcH region. This solubility pattern is consistent with that observed by Janjic et al. [2], who rationalized it quantitatively by a heterogeneous dissolution equilibrium with two stepwise proton dissociations. The stoichiometric solubility of phen decreases with pcH to ≈ 7.5, above this value it is constant. The opposite pattern was observed for HTTA, indicating that different protonation or deprotonation mechanisms may be involved for these two organics. The following equilibria were used to model quantitatively the solubility behavior:

$$H_nL(s) \xrightleftharpoons{K_s} H_nL(aq)$$

$(n = 1$ for oxine and HTTA, $n = 0$ for phen$)$ (5)

$$H_2Oxn^- \xrightleftharpoons{K_{a1}} HOxn + H^+ \xrightleftharpoons{K_{a2}} Oxn^- + 2H^-$$

(6)

$$Hphen^- \xrightleftharpoons{K_{a2}} phen + H^-$$

(7)

$$HTTA \xrightleftharpoons{K_{a1}} TTA^- + H^+$$

(8)
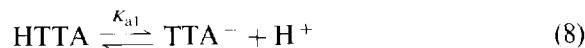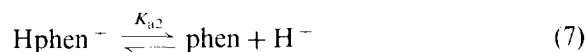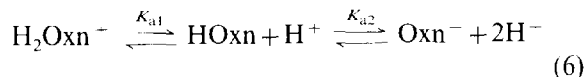
The stoichiometric solubilities, C_s, can be expressed as

(a) oxine:

$$C_s = \left(\frac{K_{a2}}{[H^+]} + 1 + \frac{[H^+]}{K_{a1}}\right) \cdot K_s$$

(9)

(b) HTTA:

$$C_s = \left(\frac{K_{a1}}{[H^+]} + 1\right) \cdot K_s$$

(10)

(c) phen:

$$C_s = \left(1 + \frac{[H^-]}{K_{a2}}\right) \cdot K_s$$

(11)

The corresponding equilibrium constants were calculated by least-squares analysis of the stoichiometric solubility data using Eqs. (9)–(11) with the results listed in Table 1. The solubility constants of oxine and phen are much lower than the reported values at low ionic strength, reflecting the 'salting out' effect of the ionic medium. Oxine has the lowest solubility among the three compounds, which may be due to the formation of an inner hydrogen bond $N \cdots H–O$ in the molecule.

3.2. Acid constants

The absorption spectra of oxine exhibit a shift of the peak at 253 nm to 236 nm as the pcH decreases from 12 to 8 (see Fig. 2a), while the shift is in the reverse direction from pcH 8 to 4. This is consistent with the dissociation mechanism deduced from the solubility study. The absorbances of oxine at 236 nm and 253 nm are plotted vs. pcH in Fig. 2b, indicating the existence of three species of the ligand. Accordingly, the expression to correlate the absorbance variation with the proton concentration can be written as [7]

$$\frac{1}{\varepsilon_i - \varepsilon_{i(L)}} = \frac{1}{\varepsilon_{i(HL)} - \varepsilon_{i(L)}} \cdot \left(1 + \frac{K_{a2}}{[H^+]}\right)$$

(12)

Table 1
Equilibrium constants of oxine, HTTA and phen in 5.0 m NaCl solution at 25°C

Ligand	Method	pK_s	pK_{a1}	pK_{a2}	pK_s	pK_{a1}	pK_{a2}
		Present work			Literature values		
Oxine	Sol.	3.09 ± 0.01		–	$2.42[2]^a$	$5.30[2]^a$	$9.63[2]^a$
	Pot.	–	5.82 ± 0.02	10.00 ± 0.01	–	$5.22[2]^a$	$9.60[2]^a$
	Spec.	–	5.87 ± 0.03	10.05 ± 0.03	–	–	–
TTA	Sol.	2.49 ± 0.01	–	–	–	–	–
	Pot.	–	6.47 ± 0.03	–	–	$6.53[3]^b$	–
	Spec.	–	6.37 ± 0.04	–	–	–	–
Phen	Sol.	2.86 ± 0.02		–	$1.89[9]^c$	–	$4.96[9]^c$
	Pot.	–		5.82 ± 0.05	–	–	$4.77[4]^d$
	Spec.	–		5.81 ± 0.07	–	–	$4.88[9]^c$

[a] $\mu = 1.0$ M NaCl.
[b] $\mu = 1.0$ (unknown medium).
[c] $\mu = 0$.
[d] $\mu = 0.1$ M (KCl).

or

$$\frac{1}{\varepsilon_i - \varepsilon_{i(H_2L)}} = \frac{1}{\varepsilon_{i(HL)} - \varepsilon_{i(H_2L)}} \cdot \left(1 + \frac{[H^+]}{K_{a1}}\right) \qquad (13)$$

where ε_i is the observed absorptivity. $\varepsilon_{i(H_2L)}$, $\varepsilon_{i(HL)}$ and $\varepsilon_{i(L)}$ are the absorptivities of the species H_2Oxn^+, $HOxn$ and Oxn^- respectively. From the linear plots of $1/(\varepsilon_i - \varepsilon_{i(L)})$ vs. $1/[H^+]$ and $1/(\varepsilon_i - \varepsilon_{i(H_2L)})$ vs. $[H^+]$, the corresponding equilibrium constants were calculated to be $pK_{a1} = 5.78 \pm 0.03$ and $pK_{a2} = 10.11 \pm 0.03$ respectively from the absorbance data at pcH > 8 (using Eq. (12)) and at pcH < 8 (using Eq. (13)). Potentiometric titrations yielded values of $pK_{a1} = 5.82 \pm 0.02$ and $pK_{a2} = 10.00 \pm 0.01$, in good agreement with the result of the spectroscopic analysis.

The protonation of phen is evident from its absorption spectra at different pcH values. As shown in Fig. 3, five isobestic points were observed at 224, 239, 268, 284 and 292 nm. Schilt and Dunhar [8] assigned the first to the dissociation equilibrium of the biprotonated species, H_2phen^{2+}, the last three to the dissociation of the monoprotonated species, $Hphen^+$, and that at 239 nm to both reactions. The value of $pK_{a1} = -1.8-1.95$ given by some authors [8,9] for the first dissociation indicates the absence of

H_2phen^{2+} in the high pH_m region (pcH > 4.8), which agrees with the fact that the change of the spectra in Fig. 3 is a monotonic function of pH_m and with the solubility measurement described in the previous section. Following the procedure used for oxine, the deprotonation constant, pK_a, of $Hphen^+$ was calculated to be 5.81 ± 0.07, while potentiometric titration resulted in a value of 5.82 ± 0.05. This result, when compared with the reported value of 5.00(2) [10] at zero ionic strength, shows the 'salting out' effect of the ionic medium on acid dissociation. The existence of the species H_2phen^{2+} and $Hphen^+$ has been proposed [11] and their thermodynamic data were reported from calorimetric [12] and potentiometric titrations [13]. Although no evidence was found in the spectroscopic measurement, our potentiometric titration supported the existence of the species $Hphen^+$ since a significant improvement in the fit of the calculation resulted by inclusion of this species. In this study the single dissociation model as described in Eq. (7) was used in the modeling of the metal–ligand interactions.

The deprotonation of HTTA is reflected in an isobestic point at 310 nm as the pcH is varied. In the spectra, peaks at 269 and 292 nm and at low pcH can be assigned to the protonated keto form
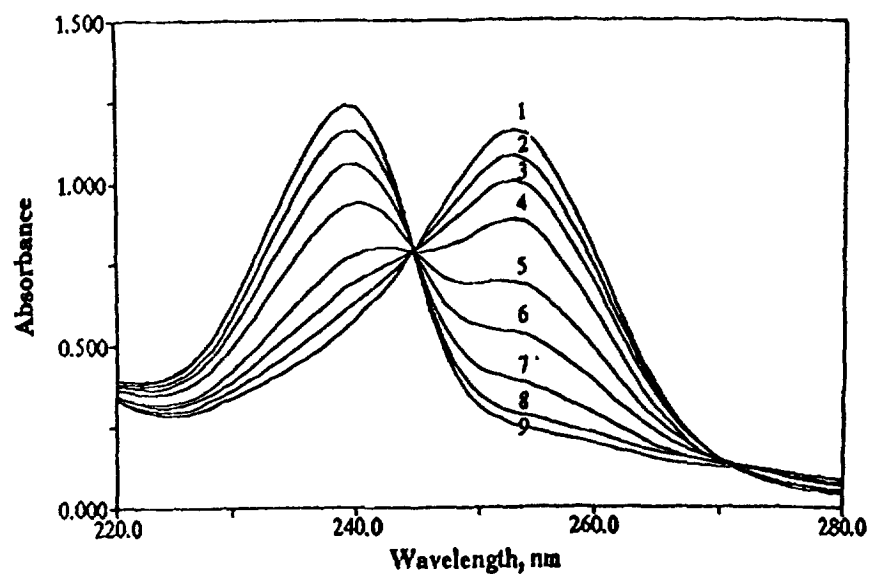
Fig. 2(a)
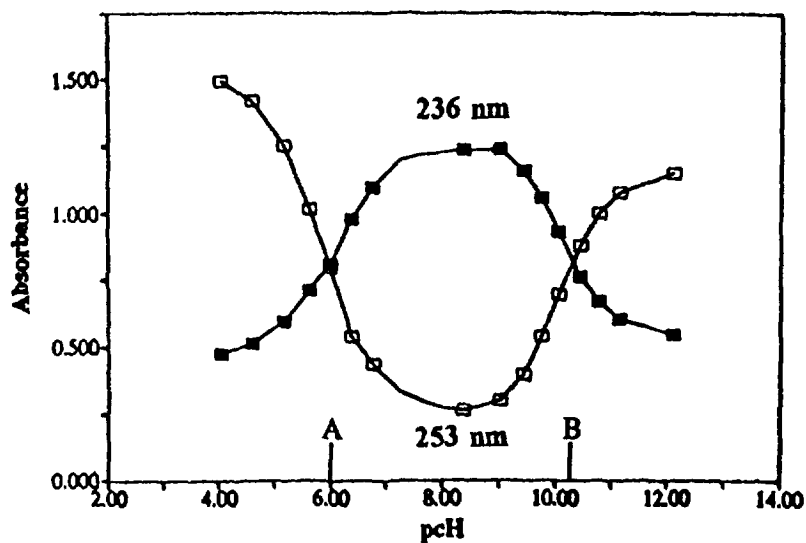
Fig. 2(b)

Fig. 2. (a) The spectra of 4.0×10^{-5} M oxine in 5.0 m NaCl solution. The corresponding pcH values are: (1) 12.13; (2) 11.15; (3) 10.80; (4) 10.46; (5) 10.08; (6) 9.78; (7) 9.47; (8) 9.03; (9) 8.39. (b) The absorbances of oxine at 236 and 256 nm as functions of pcH: (A) $[H_2Oxn^+] = [HOxn]$; (B) $[HOxn] = [Oxn^-]$.

of HTTA, and the peak at 350 nm can be assigned to the ionized enolate form, TTA⁻. The deprotonation constant, pK_{a1}, calculated from the absorbances using Eq. (12) has a value of 6.37 ± 0.04, which agrees with that from poten-

tiometric titration of $pK_{a1} = 6.47 \pm 0.03$.

Fig. 4 shows the speciation diagrams of oxine, phen and HTTA calculated using the pK_a values from the potentiometric titration experiment.
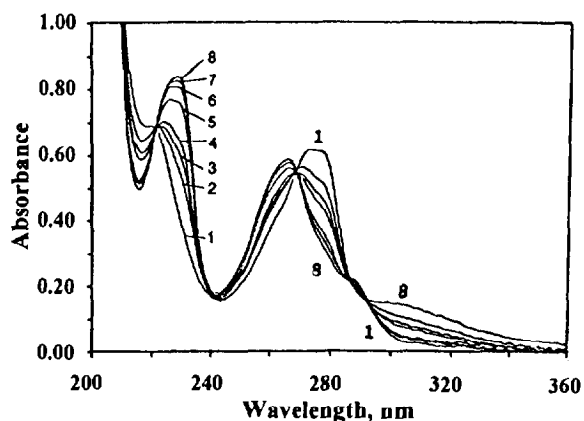
Fig. 3. The spectra of 2×10^{-5} M phen in 5.0 m NaCl. The corresponding pcH values are: (1) 4.85; (2) 5.51; (3) 5.74; (4) 5.83; (5) 6.26; (6) 6.67; (7) 7.36; (8) 7.98.

3.3. Complexation with Nd(III) and Th(IV)

Complexation of the three ligands with Nd(III) and Th(IV) cations was studied by spectrophotometry. Since low ligand concentrations were used to obtain a suitable absorbance in these experiments, a large excess of metal ion was added to give an observable amount of complex. Under such a condition, the following 1:1 metal–ligand complexation reactions may be dominant:

$$M^{n+} + L^{m-} \underset{}{\overset{\beta_1}{\rightleftharpoons}} ML^{(n-m)+}$$

($m = 0$ for phen, $m = 1$ for oxine and HTTA)

(14)
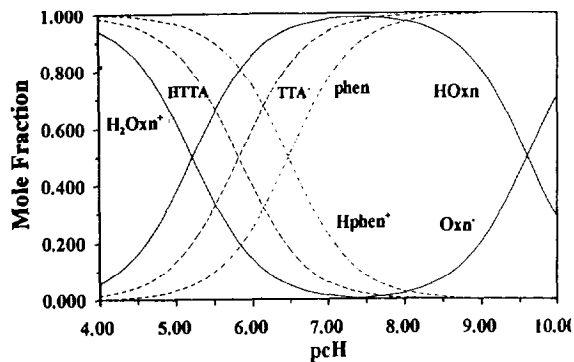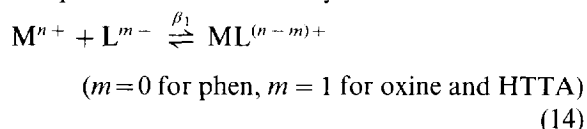
Fig. 4. The speciation diagram of oxine/HTTA/phen in 5.0 m NaCl solution: (——) oxine; (- - -) phen; (- • -) HTTA.

where M represents Nd(III) or Th(IV). The expression relating the change in absorbance and the metal concentration (C_M) can be simplified to [14]

$$\frac{1}{\varepsilon_i - \varepsilon_{i0}} = \frac{1}{\varepsilon_{i(ML)} - \varepsilon_{i0}} \cdot \left[1 + \frac{1 + \sum_{i=1}^{m} \frac{[H^+]^i}{K_{a1} \cdots K_{ai}}}{\beta_1 C_M} \right]$$

(15)

where ε_i and ε_{i0} are the observed absorbances of the ligand in the presence and the absence of the metal ion respectively, and $\varepsilon_{i(ML)}$ and β_1 are the absorbance and the stability constant of the complex formed respectively. The stability constant, β_1, can be calculated from a linear plot of $1/(\varepsilon_i - \varepsilon_{i0})$ vs. $1/C_M$ and from the dissociation constants, K_{ai}.

Plots of $1/(\varepsilon_i - \varepsilon_{i0})$ vs. $1/C_M$ were linear in all cases, confirming the formation of 1:1 complexes. Table 2 lists the stability constants calculated from the slopes and intercepts of the plots. Also included in the Table are values of log β_1 from the analysis of the data with the computer program SQUAD [15]. Corrections for the competition of the acetate buffer as a complexant of Nd were made using the values pK_a (acetic) = 5.130 [6] and log β_1(Nd–acetate) = 2.20. This value of β_1 is for AmAc$^-$ complexation [16] since data for NdAc$^-$ were unavailable. This correction increased the stability constants by 0.11. The complexation competition from hydroxylamine was neglected as no visible change in the hypersensitive spectrum of Nd(III) was observed upon addition of hydroxylamine up to a concentration of 0.01 M.

Complexation of actinide cations with these three ligands has not been investigated extensively. Skorik [17] reported the first stability constant data for the trivalent rare earth Sc(III) and Th(IV) complexes with oxine in 0.1 M NaClO$_4$ (measured by the potentiometric titration method). The values reported for Nd(III) and Th(IV) are: log β_1(Nd) = 6.66 ± 0.09 and log β_1(Th) = 11.70 ± 0.13. Considering that different ionic media and ionic strengths are involved, our values do not seem to disagree with those of Skorik. A value of log $K = 0.30$ was reported for the equilibrium constant of the Th(IV)–TTA complexation, [Th^{4+}][HTTA]/[ThTTA^{3+}][H$^+$], in

Table 2
Stability constants, log β_1, of Nd(III) and Th(IV) complexes with oxine, TTA and phen in 5.0 m NaCl at 25°C

Ligand	From Eq. (15)		From SQUAD program	
	Nd(III)	Th(IV)	Nd(III)	Th(IV)
Oxine	7.41 ± 0.02[a]	10.46 ± 0.09[b]	7.29 ± 0.01	
	7.52 ± 0.02[c]		7.40 ± 0.01[c]	
Phen	2.72 ± 0.06[d]	3.81 ± 0.05[e]	2.15 ± 0.06	3.24 ± 0.05
	2.83 ± 0.06[c]		2.26 ± 0.06[c]	
TTA	3.68 ± 0.02[f]	7.14 ± 0.05[g]	3.60 ± 0.05[c]	6.57 ± 0.01
	3.79 ± 0.02[c]		3.71 ± 0.05[c]	

Solutions prepared for measurements are:
[a] 3.2×10^{-5} M oxine at pcH 5.87 with Nd(III) from 0 to 0.018 M.
[b] 2.4×10^{-5} M oxine at pcH 3.62 with Th(IV) from 0 to 0.038 M.
[c] Corrected for the buffer competition.
[d] 4×10^{-5} M phen at pcH 5.87 with Nd(III) from 0 to 0.015 M.
[e] 4.0×10^{-5} M phen at pcH 3.53 with Th(IV) from 0 to 0.079 M.
[f] 8.0×10^{-5} M TTA at pcH 5.87 with Nd(III) from 0 to 0.0010 M.
[g] 8.0×10^{-5} M TTA at pcH 3.09 with Th(IV) from 0 to 0.014 M.

2.0 M (H, Na)ClO$_4$ from solvent extraction measurements [18]. Our value, calculated from pK_a data measured by potentiometric titration, is 0.67.

The complexation interactions of both metal ions follow the order: oxine > HTTA > phen, which is consistent with the basicities of the three ligands as reflected by their acid constant values. The strong interaction with oxine probably reflects formation of a chelate structure. The interactions of phen with Nd^{3+} and Th^{4+} are weaker than those with soft divalent cations, such as Ni^{2+} (log $\beta_1 = 8.60$), Cu^{2+} (log $\beta_1 = 9.08$ and Zn^{2+} (log $\beta_1 = 6.04$) [11], but stronger than those with the hard divalent cations Mg^{2+} (log $\beta_1 = 1.55$) and Ca^{2+} (log $\beta_1 = 1.09$) [19]. This suggests that phen behaves as a soft ligand.

4. Summary

The solubilities of the organic compounds studied in the neutral pcH range of natural waters are in the millimolar range. In the pcH 7-8 region, dissolved TTA is present as an anion, phen as a neutral species and oxine as a cation. Consequently only TTA and phen form complexes with actinide cations. The complexation of Nd(III) by

TTA at pcH 7 could compete with hydrolysis to increase the solubility of Nd(III) by 1-10%. However, the competition with hydrolysis of Th(IV) would provide an insignificant increase in Th(IV) solubility. The weaker complexation constants of phen indicate that this ligand would have even less effect on the solubilities of Nd(III) and Th(IV). Oxine would have no effect in the pcH 7-8 range.

References

[1] L.H. Brush, Test Plan for Laboratory and Modeling Studies of Repository and Radionuclide Chemistry for

the Waste Isolation Pilot Plant, Report # SAND90-0266, Sandia National Laboratories, Albuquerque, New Mexico, 1990.

[2] T.J. Janjic, L.B. Pfendt and M.B. Aleksic, Talanta 39 (1992) 55-62.

[3] W.M. Peshkova and P. Ang, Russ. J. Inorg. Chem., 7 (1962) 765-766.

[4] C.R. Krishnamoorthy, S. Sunil and K. Ramalingam, Polyhedron, 4 (1985) 1451.

[5] A. Avdeef, J.E.A. Comer and J. Thomson, Anal. Chem., 65 (1993) 42-49.

[6] J.F. Chen, Y.X. Xia and G.R. Choppin, submitted to Anal. Chem.

[7] V.M. Peshkova, J. Anal. Chem., USSR 20 (1965) 442.

[8] A.A. Schilt and W.E. Dunhar, Tetrahedron, 30 (1974) 401.

[9] R.H. Linnell and A. Kacymarcyk, J. Phys. Chem., 65 (1961) 1196.

[10] P.G. Daniele, C. Rigano and S. Sammartano, Talanta, 32 (1985) 78-80.

[11] M.J. Fahsel and C.V. Banks, J. Am. Chem. Soc., 88(5) (1966) 878.

[12] P. Dei, A. Paoletti and A. Vacca, J. Chem. Soc. A, (1971) 2656.

[13] M.J. Fahsel and C.V. Banks, J. Am. Chem. Soc., 88 (1966) 878.

[14] I.M. Gnutonva, R.A. Maier, Yu.S. Maslennikov and N.A. Skorik, Russ. J. Inorg. Chem., 23(6) (1978) 827-828.

[15] D.J. Leggett, Computation Method for the Determination of Formation Constants, Plenum, New York, 1988, Chapter 6, p. 159.

[16] J.F. Chen, O.S. Pokrovsky, M. Borkowski, Y.X. Xia and G.R. Choppin, in preparation.

[17] N.A. Skorik, Russ. J. Inorg. Chem., 22(5) (1977) 776.

[18] W.C. Waggener and R.W. Stoughton, J. Phys. Chem., 56 (1952) 1.

[19] S. Capone, A. De Robertis, C. De Stefano and R. Scanrcella, Talanta, 32 (1985) 675.

Evaluation of dithiocarbamates and β-diketones as chelating agents in supercritical fluid extraction of Cd, Pb, and Hg from solid samples

C.M. Wai[a,*], Shaofen Wang[a], Yan Liu[b], Viorica Lopez-Avila[b], Werner F. Beckert[c]

[a]*Department of Chemistry, University of Idaho, Moscow, ID 83843, USA*
[b]*Midwest Research Institute, California Operation, 625-B Clyde Avenue, Mountain View, CA 94043, USA*
[c]*U.S. Environmental Protection Agency, 944 East Harmon Avenue, Las Vegas, NV, 89119, USA*

Abstract

The use of four dithiocarbamates and three fluorinated β-diketones as potential chelating agents for three transition metal ions (Cd^{2+}, Pb^{2+}, and Hg^{2+}) extracted from spiked sand and filter paper samples by supercritical fluid extraction (SFE) was investigated. The extractions were performed at 45°C and 250 atm for spiked sand samples and at 60°C and 200 atm for filter paper samples using supercritical carbon dioxide modified with 5% methanol. At 250 atm and using carbon dioxide modified with 5% methanol, the recoveries of Cd^{2+}, Pb^{2+}, and Hg^{2+} ions from spiked sand samples were $\geq 95\%$ with lithium bis(trifluoroethyl)dithiocarbamate (LiFDDC) as the chelating agent; they ranged from 83–97% with diethylammonium diethyldithiocarbamate and from 87–97% with sodium diethyldithiocarbamate as chelating agents, and from 68–96% with trifluoroacetylacetone, hexafluoroacetylacetone, and thenoylfluoroacetone as chelating agents. Ammonium pyrrolidinedithiocarbamate was not effective in the chelation SFE of Cd^{2+}, Pb^{2+}, and Hg^{2+} ions from either spiked sand or spiked filter paper samples under the extraction conditions used. Supercritical carbon dioxide alone gave consistently lower analyte recoveries than supercritical carbon dioxide modified with 5% methanol. The results suggest that the solubility of the metal chelate in the supercritical fluid plays a more important role than the solubility of the chelating agent in the supercritical fluid, as long as sufficient chelating agent is present in the fluid phase. Fluorination of the chelating agent, as in the case of LiFDDC, increases the solubility of the metal chelate, and subsequently enhances the extraction efficiency for the metal ions.

Keywords: Cd; Chelating agents; Hg; Pb; Supercritical fluid extraction

* Corresponding author. Fax: (+1) 208-885-6173, e-mail: wchien@sprey.csrv.uidaho.edu

1. Introduction

Supercritical fluid extraction (SFE) of organic compounds has gained acceptance as an alternative sample preparation technique in recent years [1–3]. Compared with conventional solvent extractions techniques, SFE offers several advantages including relatively high sample throughput and the reduction in both solvent usage and solvent waste generation, whilst still achieving analyte recoveries that are comparable to those achieved by Soxhlet and sonication techniques. Although most of the SFE studies published so far have focused on organic compounds, there is an increasing interest in extracting metal ions by SFE from solid samples [4–12]. Direct extraction of metal ions with supercritical CO_2 is not possible because of the charge neutralization requirement and the weak solvent–solute interactions. To extract metal ions with supercritical carbon dioxide it is necessary that metal ions be converted into neutral metal complexes that are soluble in supercritical carbon dioxide or supercritical carbon dioxide modified with small amounts of organic solvents.

The selection of suitable chelating agents is critical in the chelation–SFE of metal ions. Important requirements include high stability constants of the metal complexes, high solubilities of the chelating agents and their metal complexes in pure or modified supercritical carbon dioxide, fast chelation kinetics, and complexing specificity to allow selective extraction of a metal ion or a group of metal ions. We have recently demonstrated that lithium bis(trifluoroethyl)dithiocarbamate (LiFDDC) is an effective chelating agent for extracting several transition metal ions, including Cd^{2+}, Co^{2+}, Cu^{2+}, Zn^{2+}, and Hg^{2+} ions, from solid and aqueous samples by SFE [6–8]. The successful use of LiFDDC as chelating agent is largely due to the fact that the solubilities of metal–FDDC complexes in supercritical carbon dioxide are generally 2–3 orders of

magnitude greater than those of the non-fluorinated analogues [4,5]. Wang and Marshall [9] reported recently that tetrabutylammonium dibutyldithiocarbamate (DBDTC) was effective in extracting Cd^{2+}, Pb^{2+}, and Zn^{2+} from aqueous matrices by SFE with carbon dioxide. Our other recent SFE studies indicated that several fluorinated β-diketones were effective chelating agents for thorium, uranium, lanthanide, and actinide metal ions [10–12]. Obviously, the successful use of chelation–SFE techniques for routine extraction metal ions also depends on the availablity of these chelating agents. LiFDDC and DBDTC are not available commercially; therefore, their routine use in SFE is currently limited because they are costly to synthesize in small quantities.

As part of a continuing development and evaluation program of new sample preparation techniques, conducted by the U.S. Environmental Protection Agency (EPA) through the Environmental Monitoring Systems Laboratory-Las Vegas (EMSL-LV), we investigated the use of several commercially available dithiocarbamates and fluorinated β-diketones as chelating agents for extracting metal ions by SFE. In this paper, we report the evaluation of four dithiocarbamates [LiFDDC, diethylammonium diethyldithiocarbamate (Et_2NH_2DDC), sodium diethyldithiocarbamate (NaDDC), ammonium pyrrolidinedithiocarbamate (APDC)] and three fluorinated β-diketones [trifluoroacetylacetone (TFA), hexafluoroacetylacetone (HFA), thenoyltrifluoroacetone (TTA)] as chelating agents for three transition metal ions (Cd^{2+}, Pb^{2+}, and Hg^{2+}) that were extracted from spiked sand and cellulose filter paper by SFE.

2. Experimental

2.1. Reagents and materials

The chelating agents Et_2NH_2DDC, NaDDC,

APDC, TFA, HFA, and TTA were purchased from Aldrich (Milwaukee, WI). LiFDDC was synthesized according to a procedure outlined in the literature [13]. The starting material, bis(trifluoroethyl)amine, was obtained from PCR Chemicals (Gainesville, FL) and other chemicals used in the synthesis, including n-butyllithium (2.5 M in hexane), carbon disulfide, and isopentane were obtained from Aldrich.

Stock solutions of Cd^{2+}, Pb^{2+}, and Hg^{2+} ions at 1000 μg ml^{-1} were obtained from J.T. Baker Inc. (Phillipsburg, NJ). Spiked solutions were prepared from the stock solutions as needed. Deionized water from a Millipore Milli-Q system (Bedford, MA) was used for the preparation of all aqueous solutions.

Methylisobutylketone (MIBK) and nitric acid were Ultrex-grade ultrapure reagents from J.T. Baker Inc. All other reagents and solvents used in this study were of analytical grade and were obtained from Aldrich or Baxter Scientific (Mc-Gaw Park, IL). Purified sand was obtained from J.T. Baker Inc. Cellulose filter paper (Whatman 42) was obtained from Baxter Scientific. A local soil sample was obtained from a soil laboratory at the University of Idaho. SFC-grade carbon dioxide and carbon dioxide modified with 5% methanol (Scott Speciality Gases, Plumsteadville, PA) were used in all experiments reported here.

2.2. SFE apparatus

All experiments were performed with a laboratory-built SFE system. A 3.5 ml stainless-steel vessel obtained from Dionex (Sunnyvale, CA) was used as the extraction vessel. The extraction vessel was fitted with two two-way stainless-steel needle valves (Supelco, Inc., Bellefonte, PA) as the inlet and outlet valves, which were manually adjusted to perform the static and dynamic extractions. The extraction vessel was maintained at the desired temperature by placing it in a thermostated oven. The extraction fluid (SFC-grade carbon dioxide or carbon dioxide modified with 5% methanol) was delivered to the extraction vessel using a microprocessor-controlled high-pressure

pump (Haskel Inc., Burank, CA). The extraction pressure was controlled to ± 5 psi using a Setra Systems (Acton, MA) pressure transducer. Fused-silica tubing (50 μm i.d. $\times$ 20 cm length) was used as a restrictor. The flow rate of the extraction fluid was about 2.0 ml min^{-1} (as a liquid). The restrictor and the collection solvent were at room temperature before extraction. No attempt was made to control the temperature of the collection solvent during extraction.

2.3. SFE procedures

The spiked sand and filter paper samples were prepared as follows. A known amount (5 μg) of each element was spiked onto a pre-washed cellulose-based filter paper (Whatman 42) or onto sand (300 mg). The spiked samples were air-dried at room temperature overnight prior to extraction. To perform chelation–SFE, the spiked sample was placed in a sample holder made of a glass tube (0.9 cm o.d. $\times$ 0.7 cm i.d. $\times$ 3 cm length), which was plugged at one end with a piece of glass wool. After the sample was wetted with 10 μl of deionized water, the open end of the sample holder was plugged with a piece of glass wool. The sample holder was then placed into the extraction vessel. The chelating agent (50 mg) was placed into another glass tube (0.65 cm o.d. $\times$ 0.5 cm i.d. $\times$ 2 cm length), with the middle portion of the tube blown to a bulb-like shape to hold the chelating agent. The chelating agent holder was then partially inserted into the upstream end of the sample holder in the extraction vessel and the vessel was closed (Fig. 1). This arrangement is suitable for handling liquid ligands such as TFA and HFA. The chelation and extraction process
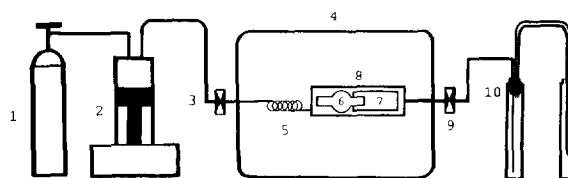
Fig. 1. Schematic diagram of the experimental system used for the SFE of metal ions: (1) CO_2 cylinder; (2) pump; (3) inlet valve; (4) oven; (5) pre-heat coil; (6) ligand holder; (7) sample holder; (8) extraction cell; (9) outlet valve; (10) collection vials.

was conducted in the static mode for 15 min, followed by dynamic extraction for an additional 15 min. The extracted metal chelates were collected in chloroform (4 ml each) and placed in two glass vials (1.2 cm i.d. × 10 cm length) connected in series.

2.4. Solubility measurement

The approximate solubilities of the three dithiocarbamates (NaDDC, Et_2NH_2DDC, and APDC) in supercritical carbon dioxide and carbon dioxide modified with 5% methanol were measured as follows. A known amount of the dithiocarbamate chelating agent was placed in the special holder described above. The holder was plugged with glass wool at both ends and inserted into an extraction vessel. The extraction vessel was heated to 60°C and pressurized to 200 atm using either supercritical carbon dioxide or carbon dioxide modified with 5% methanol. After a 30 min static step, the inlet valve of the extraction vessel was closed and its outlet valve was opened; the dissolved chelating agent was collected by immersing the restrictor outlet in a vial containing 4 ml of chloroform. After the extraction vessel was completely depressurized, the chelating agent holder was removed from the extraction vessel and the empty extraction vessel was re-installed in the oven. To recover any chelating agent that might have precipitated inside the extraction system during the depressurization step, the extraction vessel was extracted again with either supercritical carbon dioxide or carbon dioxide modified with 5% methanol at 60°C and 200 atm in the dynamic mode. The dynamic flushing step may contribute up to 10% of the total chelating agents collected in the collection vial. Precipitation of the chelating agent on the surface of the ligand holder may contribute to the uncertainties in solubility measurements. This source of error is probably small because the surface area of the ligand holder is small compared with the total surface of the SFE system. The concentration of the dithiocarbamate in the chloroform solution was measured with a spectrophotometer. The solubility was then calculated from the amount of dithiocarba-

mate recovered in the chloroform and the volume of the extraction vessel.

2.5. Analysis of extracted solid samples and SFE extracts

The concentrations of Cd^{2-} and Hg^{2+} in sand and cellulose-based filter paper samples and chloroform extracts were determined by neutron activation analysis (NAA). The details of the NAA system used have been reported previously [14]. The solid samples were placed in polyethylene vials; the vials were then sealed by heat and subjected to neutron irradiation. Standards were irradiated and counted under the same condition as samples. To determine the concentrations of mercury and cadmium complexes in the chloroform extracts, a known volume of the extract was transferred to polyethylene vials and evaporated to dryness in the vials prior to NAA. The samples and standards were irradiated for 1 h in a 1 MW TRIGA nuclear reactor at a steady flux of 6×10^{12} n cm^{-2} s^{-1} and counted on a large-volume ORTEC Ge(Li) detector with a resolution (FWHM) of about 2.3 keV at the 1332 keV ^{60}Co peak. The activities at the 336 and 279 keV gamma peaks from ^{115}Cd and ^{203}Hg respectively were used for the quantification of Cd^{2+} and Hg^{2+}. If sufficient ligand is present in the extraction system, quantitative recovery of extracted metal chelates can be achieved. Under our experimental conditions, the amount of metal collected generally agrees with that remaining in the sample to within a few percent.

The concentration of Pb^{2-} in chloroform extracts was determined by atomic absorption spectrophotometry (IL VIDEO 12 AAS) or inductively-coupled plasma mass spectrometry (ICP-MS) (Sciex Elan model 250). The metal chelate in the chloroform solutions was back-extracted with 5 ml of 50% (v/v) Ultrex HNO_3 for 1 h using a wrist-action mechanical shaker (Burrell model 75). After phase separation, the acid solutions were transferred to 10 ml volumetric flasks and diluted to volume for AAS or ICP-MS analysis.

Table 1
Percent recoveries of Cd^{2+}, Pb^{2+} and Hg^{2-} ions from spiked sand samples by SFE using dithiocarbamates as chelating agents[a]

Chelating agent	Cd (%)		Pb (%)		Hg (%)	
	100 atm	250 atm	100 atm	250 atm	100 atm	250 atm
Carbon dioxide						
LiFDDC	90	92	84	91	92	93
	92	91	81	90	93	94
Et_2NH_2DDC	61	66	70	81	75	91
	58	70	71	80	78	93
NaDDC	35	81	40	86	60	95
	36	82	43	85	55	92
APDC	16	21	18	42	24	27
	10	17	20	44	21	24
Carbon dioxide with 5% methanol						
LiFDDC	92	97	91	97	94	97
	90	96	89	95	90	98
Et_2NH_2DDC82	80	85	92	83	97	90
	88	83	86	93	89	95
NaDDC	53	92	84	91	89	97
	52	87	83	90	84	96
APDC	32	53	53	65	47	54
	34	52	52	63	43	59

[a] Extractions were performed in duplicate at 45°C and 100 atm or 250 atm, 15 min static followed by 15 min dynamic. The samples were 300 mg of sand spiked with 5 μg of each metal ion. The amount of chelating agent used was 50 mg per sample.

The paper samples were digested with concentrated nitric acid in beakers that were covered with glasses and heated on hot-plates to temperatures slightly below the boiling points of the sample solutions. The spiked metals in sand were extracted using 5% nitric acid. The acid solution from each sample was transferred to a 10 ml volumetric flask and diluted to volume for AAS or ICP-MS analysis.

3. Results and discussion

The recoveries of Cd^{2+}, Pb^{2+}, and Hg^{2+} ions from spiked sand samples are summarized in Table 1. When extractions were performed with LiFDDC and supercritical CO_2 at 45°C and 100

atm, the recoveries from the spiked sand samples ranged from 90-93% for Cd^{2+} and Hg^{2+} ions and were 81% and 84% for Pb^{2+} ions. Et_2NH_2DDC and NaDDC were less effective than LiFDDC in extracting these metal ions; with Et_2NH_2DDC, recoveries from 70-78% for Pb^{2+} and Hg^{2+} ions and were 58 and 61% for Cd^{2+} ions; with NaDDC, recoveries of Pb^{2+}, Hg^{2+}, and Cd^{2+} were between 35 and 60%. APDC was the least effective chelating agent; none of the metal ions could be extracted with recoveries above 24%.

Higher recoveries were obtained with supercritical carbon dioxide modified with 5% methanol. When the extractions were performed with LiFDDC at 45°C and 100 atm, the recoveries of Cd^{2+}, Pb^{2+}, and Hg^{2+} ions ranged from 89-94%;

Table 2
Percent recoveries of Cd^{2+}, Pb^{2+} and Hg^{2+} ions from spiked filter paper samples by SFE using dithiocarbamates as chelating agents[a]

Chelating agent	Cd (%)	Pb (%)	Hg (%)
Carbon dioxide			
LiFDDC	91	83	95
	90	88	95
Et_2NH_2DDC	29	62	94
	30	64	95
NaDDC	38	68	91
	36	71	94
APDC	4	9	13
	6	11	18
Carbon dioxide with 5% methanol			
LiFDDC	96	96	96
	96	95	97
Et_2NH_2DDC	72	92	96
	70	90	95
NaDDC	75	91	92
	71	90	91
APDC	16	51	35
	18	49	44

[a] Extractions were performed in duplicate at 60°C and 200 atm, 15 min static followed by 15 min dynamic. The amount of chelating agent used was 50 mg per sample.

with Et_2NH_2DDC and NaDDC, recoveries ranged from 82–89% (except that the recovery of Cd^{2+} was only about 53% with NaDDC). Recoveries obtained with APDC as the complexing agent were also higher than those obtained with supercritical carbon dioxide alone.

When the pressure was increased from 100 atm to 250 atm (the temperature was maintained at 45°C), the recoveries increased noticeably. The increases were more pronounced with supercritical carbon dioxide modified with 5% methanol than with supercritical carbon dioxide along (Table 1). For example, the recoveries were 95% or greater for the three metal ions using LiFDDC, and they ranged from 83–97% with Et_2NH_2DDC or NaDDC. APDC was still not effective even with the increased extraction pressure.

The results for the spiked filter paper samples (Table 2) indicate that supercritical carbon dioxide modified with 5% methanol was also a more effective extraction fluid than supercritical carbon dioxide alone. When extraction was performed at 60°C and 200 atm with supercritical carbon dioxide modified with 5% methanol, the recoveries from spiked filter paper samples were ≥95% for the three metal ions when using LiFDDC, and ranged from 90–96% for Pb^{2+} and Hg^{2+} ions and from 70–75% for Cd^{2+} ions when using Et_2NH_2DDC and NaDDC. APDC was not effective in the chelation–SFE of Cd^{2+}, Pb^{2+}, and Hg^{2+} ions from spiked filter paper samples under the extraction conditions used (recoveries ranged 16–51%).

The results in Tables 1 and 2 indicate that the fluorinated chelating agent LiFDDC is more ef-

Table 3
Solubilities of various dithiocarbamates in supercritical carbon dioxide and modified carbon dioxide at 60°C and 200 atm[a]

Chelating agent	Fluid phase	Solubility (mole l^{-1})
Et_2NH_2DDC	Carbon dioxide with 5% methanol	24×10^{-2}
		17×10^{-2}
Et_2NH_2DDC	Carbon dioxide	6×10^{-2}
		2×10^{-2}
NaDDC	Carbon dioxide with 5% methanol	0.4×10^{-2}
		0.3×10^{-2}
NaDDC	Carbon dioxide	0.2×10^{-2}
		0.1×10^{-2}
APDC	Carbon dioxide with 5% methanol	0.04×10^{-2}
		0.04×10^{-2}
APDC	Carbon dioxide	0.02×10^{-2}
		0.02×10^{-2}

[a] Duplicate determinations.

fective than its non-fluorinated analogues. This finding may be explained by the fact that the fluorinated metal–dithiocarbamate chelates have higher solubilities in supercritical carbon dioxide than their non-fluorinated analogues. It is known that fluorine substitution in metal chelates tends to enhance their solubilities in supercritical carbon dioxide significantly [6]. For example, the solubility of $Hg(FDDC)_2$ in supercritical carbon dioxide at 50°C and 150 atm has been determined to be $(5.0 \pm 0.4) \times 10^{-3}$ M, which is about 600 times greater than the non-fluorinated analogue $Hg(DDC)_2$ [5]. The solubility of $Hg(FDDC)_2$ in supercritical carbon dioxide modified with 5% methanol at the same temperature and pressure is about a factor of two higher than its solubility in supercritical carbon dioxide alone at 50°C and 150 atm [5]. The solubilities of $Pb(FDDC)_2$, $Pb(DDC)_2$, $Pb(PDC)_2$ in CO_2 at 50°C and 150 atm were determined by this study to be $(2.3 \pm 0.6) \times 10^{-4}$ M, $(1.2 \times 0.3) \times 10^{-6}$ M, and $(5.1 \times 0.2) \times 10^{-7}$ M respectively, i.e. the fluorinated complex is about 200 times more soluble than the non-fluorinated complex. APDC, which forms the $Pb(PDC)_2$ complex with a low solubility in supercritical CO_2, is also the least effective ligand for SFE of Pb. The solubility of $Cd(FDDC)_2$ has not

been measured because of the difficulties involved in preparation of the pure compound. However, based on the available solubility data of metal dithiocarbamates in supercritical CO_2, we expect the fluorinated $Cd(FDDC)_2$ to be more soluble than its non-fluorinated analogue.

We determined the approximate solubilities of three dithiocarbamates (Et_2NH_2DDC, NaDDC and APDC) in supercritical carbon dioxide and carbon dioxide modified with 5% methanol (Table 3). The results indicate that the solubilities of these dithiocarbamates in supercritical carbon dioxide modified with 5% methanol were approximately 2–5 times higher than those in supercritical carbon dioxide alone, and the solubilities of Et_2NH_2DDC in the supercritical fluids were approximately 25 times higher than that of NaDDC in supercritical carbon dioxide alone and approximately 60 times higher than that in supercritical carbon dioxide modified with 5% methanol. Although Et_2NH_2DDC was much more soluble than NaDDC, the recoveries of Cd^{2+}, Pb^{2+} and Hg^{2+} ions from the solid matrices were similar with either Et_2NH_2DDC or NaDDC because the chelates formed with Et_2NH_2DDC and NaDDC were identical. This suggests that the solubility of the metal chelate in the supercritical fluid plays a

Table 4
Percent recoveries of Cd^{2+}, Pb^{2-} and Hg^{2+} ions from spiked sand samples by SFE using β-diketones as chelating agents[a]

Chelating agent	Amount	Cd (%)		Pb (%)		Hg (%)	
		100 atm	250 atm	100 atm	250 atm	100 atm	250 atm
Carbon dioxide							
TFA	50 μl	65	76	71	70	72	85
		51	65	68	66	63	83
TFA	100 mg	21	67	51	70	50	72
		24	58	62	74	56	75
HFA	50 μl	62	69	68	65	67	66
		77	60	71	68	62	73
Carbon dioxide with 5% methanol							
TFA	50 μl	93	95	88	72	91	94
		84	90	80	68	82	93
TTA	100 mg	77	96	75	86	86	96
		82	93	80	81	92	91
HFA	50 μl	82	96	87	77	92	74
		67	95	81	74	93	82

[a] Extractions were performed in duplicate at 45°C and 100 atm or 250 atm, 15 min static followed by 15 min dynamic. The samples were 300 mg of sand spiked with 5 μg of each metal ion.

more important role than the solubility of the chelating agent, as long as sufficient chelating agent is present in the fluid phase.

The recoveries of Cd, Pb, and Hg from spiked sand samples by SFE using fluorinated β-diketones (TFA, HFA, and TTA) as chelating agents are summarized in Table 4. When the extractions were performed with carbon dioxide alone at 45°C and 100 atm or 250 atm, the recoveries of Cd^{2+}, Pb^{2+}, and Hg^{2+} ions ranged from 50–85% (21 and 24% for Cd^{2+} with TTA as chelating agent). When the extractions were performed with carbon dioxide modified with 5% methanol at 45°C and 100 atm or 250 atm, the recoveries ranged from 67–96% with TFA, HFA, and TTA as the chelating agents. The results indicate that the three fluorinated β-diketones are also effective chelating agents for Cd^{2+}, Pb^{2+}, and Hg^{2+} ions.

Table 5 shows the extraction of spiked Cd and Hg (5 μg each) from a real soil sample (300 mg) using LiFDDC, NaDDC, and HFA as chelating agents. This soil sample, obtained from Latah

County, ID, contains low levels of Cd and Hg (< 0.1 ppm) and hence is suitable for Cd and Hg spike experiments. According to Table 5, at 45°C and 250 atm LiFDDC can quantitatively extract all spiked Cd and Hg from the soil under the specified SFE conditions. NaDDC shows slightly lower extraction efficiencies for Cd and Hg in the real soil sample compared with the results observed from sand. HFA also shows lower extraction efficiencies for Cd and Hg in the real soil sample. The matrix appears to play a role in lowering metal extraction efficiencies from the real soil sample for some chelating agents.

4. Conclusions

The results of this study show that diethyldithiocarbamates (LiFDDC, Et_2NH_2DDC and NaDDC) and fluorinated β-diketones (TFA, HFA, and TTA) are effective chelating agents for extracting transition metal ions such as Cd^{2+}

Table 5
Extraction of spiked Cd^{2+} and Hg^{2+} from a soil sample using carbon dioxide with 5% methanol

Chelating agent	Cd (%)		Hg (%)	
	100 atm	250 atm	100 atm	250 atm
LiFDDC	85	97	86	103
	89	100	88	100
NaDDC	54	90	84	87
	50	84	82	90
HFA	40	53	68	81
	42	64	64	73

[a] SFE conditions: 300 mg of soil spiked with 5 μg of Cd^{2+} and Hg^{2+} each, 50 mg of LiFDDC or NaDDC or 50 μl of HFA, 200 μl of H_2O, 15 min static and 15 min dynamic extraction.

Pb^{2+}, and Hg^{2+} from solid matrices, including sand and filter paper, by SFE. The use of supercritical CO_2 modified with 5% methanol gave higher metal ion recoveries compared to those obtained with supercritical carbon dioxide alone. The results also suggest that the solubility of the metal chelate in the supercritical fluid plays a more important role than the solubility of the chelating agent for recovering metal ions, as long as sufficient chelating agent is present in the fluid phase. Fluorination of the chelating agent (as in the case of LiFDDC) increases the solubility of metal chelate and subsequently enhances the extraction recoveries of the metal ions. In real soil samples, LiFDDC is the most effective chelating agent for extracting spiked Cd and Hg ions. The native soil matrix appears to lower metal extraction efficiencies for the chelating agents. This study presents preliminary method development data concerning the effectiveness of some commercially available chelating agents for SFE of metals in simulated solid samples. Further studies of these and other chelating agents for SFE of metal ions in real soil samples are currently in progress.

Acknowledgments

References

[1] S.B. Hawthorne, Anal. Chem., 62 (1990) 633A.
[2] V. Janda, K.D. Bartle and A.A. Clifford, J. Chromatogr. 642 (1993) 283.
[3] S.A. Westwood, Supercritical Fluid Extraction and its Use in Chromatographic Sample Preparation, Blackie Academic and Professional/Chapman and Hall, Boca Raton, FL, 1993.
[4] K.E. Laintz, C.M. Wai, C.R. Yonker and R.D. Smith, J. Supercrit. Fluids, 4 (1991) 194.
[5] K.E. Laintz, J.J. Yu and C.M. Wai, Anal. Chem., 64 (1992) 311.
[6] K.E. Laintz, C.M. Wai, C.R. Yonker and R.D. Smith, Anal. Chem., 64 (1992) 2875.
[7] C.M. Wai, Y.H. Lin, R.D. Brauer and S. Wang, Talanta, 40 (1993) 1325.
[8] Y. Liu, V. Lopez-Avila, M. Alcaraz, W.F. Beckert and E.M. Heithmar, J. Chromatogr. Sci., 31 (1993) 310.
[9] J. Wang and W.D. Marshall, Anal. Chem., 66 (1994) 1658.
[10] Y. Lin, R.D. Brauer, K.E. Laintz and C.M. Wai, Anal. Chem., 65 (1993) 2549.
[11] Y. Lin, C.M. Wai, F.M. Jean and R.D. Brauer, Environ. Sci. Technol., 28 (1994) 1190.
[12] Y. Lin and C.M. Wai, Anal. Chem., 66 (1994) 1971.
[13] L. Sucre and W. Jennings, Anal. Lett., 13 (1980) 497.
[14] W.M. Mok and C.M. Wai, Anal. Chem., 59 (1987) 233.

Solid-phase extraction of metal ions and their estimation in vitamins, steel and milk using 3-hydroxy-2-methyl-1,4-naphthoquinone-immobilized silica gel

B.S. Garg*, J.S. Bist, R.K. Sharma*, N. Bhojak

Department of Chemistry, University of Delhi, Delhi 7, India

Abstract

3-Hydroxy-2-methyl-1,4-naphthoquinone-immobilized silica gel has been used for the adsorption and estimation of copper, cobalt, iron and zinc by both batch and column techniques. The distribution coefficient D determined for each metal ion was as follows (ml g^{-1}): Fe, 3.6×10^2; Cu, 3.9×10^2; Co, 3.8×10^2; Zn, 4.1×10^2. Methods have been developed to estimate zinc, copper and cobalt in milk, steel and vitamin samples respectively.

Keywords: 3-Hydroxy-2-methyl-1,4-naphthoquinone-immobilized silica gel; Metal ions; Milk; Solid-phase extraction; Steel; Vitamins

1. Introduction

Metal chelating resins (adsorbed or chemically-bonded chelates) have been found to be of great utility for the preconcentration and separation of trace metals from different matrices. Alkylamines [1], diamine [2], xanthate [3], dimethylglyoxime [4], n-butylamide [5], amidoxime [6], dithizone [7], 8-hydroxyquinoline [8], dithiocarbamates [9], propylenediamine tetraacetic acid [10], 3(1-imidazolyl)propyl [11], thiazolylazo anisole [12], salicyldehyde [13], 8-hydroxyquinone [14], 2,5-dimercapto [15], quinolylazo [16] and didecylamino tridecylammonium iodide [17] have been immobilized on various substrates. Chelex 100 [18,19],

Dionex [20], cyanex [21,22] and Amberlite [23,24] have also been used for the determination of various metal ions. The use of supports loaded with chelating reagents is particularly convenient because it is easy to prepare such resins, although their stabilities and collection abilities may be inferior to those of the chelating resins containing the various functionalized groups [25]. However, these modified sorbents have shown a lack of stability in high ionic strength media and low recovery if more than 300 ml of solution is used. Another disadvantage is the partial elution of the chelating reagent with perchloric or hydrochloric acid solutions of the concentration required for elution of metals forming very stable chelating complexes, which makes the use of the column impossible for several sorption–elution processes.

---

* Corresponding authors. Fax: (+91) 11-7257-336.

Chelex is also found to be ineffective for quantitative separation of many metal ions from water samples containing appreciable amounts of naturally occuring fulvic and humic acids [26,27]. This natural organic matter binds metals and competes with the Chelex, making it necessary to use an additional sample treatment such as irradiation with ultraviolet light [28]. Although many materials, such as silica, polystyrene and cellulose, have been used as solid supports for chelating groups, silica shows the fast metal ion-exchange kinetics and the good mechanical strength and swelling stability required for use in high-performance liquid chromatography [29]. Such columns are superior to conventional columns because of their high sorption efficiency even at very high flow rates. 3-Hydroxy-2-methyl-1,4-naphthoquinone and its derivatives are of considerable interest due to their widespread applications in the biological and analytical fields. Sharma and Sindhwani [30-32] have demonstrated the strong chelation behaviour of 3 - hydroxy - 2 - methyl - 1,4 - naphthoquinone (HMNQ) with transition and lanthanide metal ions. Higher sensitivity and selectivity of HMNQ derivatives towards the determination of metal ions have already been reported by Sharma and co-workers [33–37].

The present work describes the application of silica-based HMNQ complexing agent to the batch and column adsorption of various transition metals and its application in the estimation of metal ions in various samples.

2. Experimental

2.1. Apparatus

A digital (ECIL model) pH meter 5651A and a Schimadzu AA-640-13 atomic absorption spectrometer were used. A glass tube of 100 mm length and 7 mm i.d. was used as a chromatographic column.

2.2. Preparation

HMNQ was prepared from 2-methyl-1,4-naphthoquinone (Sigma) by the method of Fieser [38]. Its purity was checked by TLC and it was characterized by elemental analysis.

Preparation of immobilized silica gel was done as reported by Kubota and Moreira [13]. Immobilization of the organofunctional group on the silica gel was performed in two steps.

2.2.1. Step 1

Activated silica gel (silica was activated before modification in a high vacuum) was suspended in 10% v/v 3-amino propyl triethoxy silane in dry toluene. The mixture was refluxed for 12 h in a nitrogen atmosphere with constant stirring. The resulting product amino propyl silica gel (APSG) was filtered, washed consecutively with toluene, ethanol and acetone and then heated at 75°C for 10 h in a vacuum line.
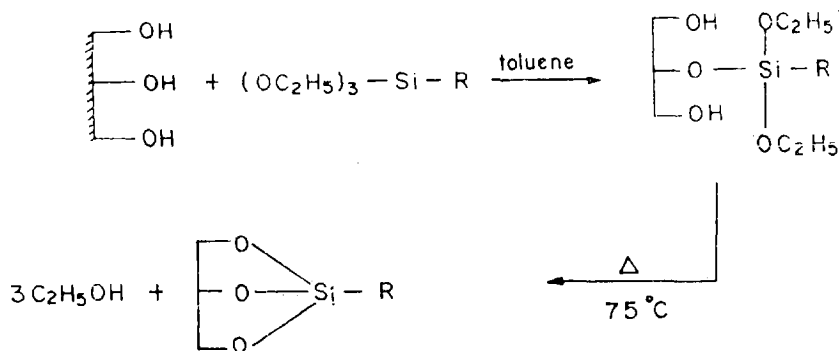
R = Aminopropyl group

2.2.2. Step 2

The APSG was reacted with HMNQ in anhydrous diethyl ether with constant stirring. The mixture was filtered and washed and then solid, modified silica was heated at 55°C in a vacuum line.

$$Y - (CH_2)_3 - NH_2 + O = \overset{HO}{\underset{}{\bigcirc}}\overset{CH_3}{\underset{}{}} = O$$

$$Y - (CH_2)_3 - N = \overset{HO}{\underset{}{\bigcirc}}\overset{CH_3}{\underset{}{}} = O$$

Y = Solid support

The infrared spectrum confirmed the occurrence of the coupling reaction. The band at 1640 cm^{-1} is due to the C–N stretching frequency of the imino group.

2.3. Procedure

2.3.1. Batch experiment

The chelating silica gel was equilibrated with a suitable amount of metal ions for a certain period of time. The unextracted metal ions were determined by atomic absorption spectroscopy (AAS).

2.3.2. Column experiment

This study was carried out using a glass column packed with 1 g of immobilized silica gel through which 100 ml of solutions of individual metal ions were percolated at a flow rate of 3 ml min^{-1}. The metal ions were then eluted from the column using 1 N HCl/HNO$_3$ and determined by AAS. Each metal experiment was carried out in triplicate in order to determine the precision of the method.

2.3.3. Optimization of adsorption time

The time required for the solid liquid system to attain the equilibrium condition was determined by placing the solution of metal ions in a conical flask and shaking with modified silica gel. The supernatant from each flask was separated off at different time intervals and metal ions were determined. The amount of metal ions adsorbed by the solid phase was determined by the equation

$$N_f = (X - Y)/Z \tag{1}$$

where X is the initial amount of metal ion, Y is the amount of metal ions in the supernatant, N_f is the amount of metal ion adsorbed and Z is the mass of modified silica gel (g).

3. Results and discussion

3.1. Optimization of adsorption time

The time taken for the adsorption of the metal ion and the attainment of the equilibrium condition by the immobilized silica gel is of considerable importance. The time taken for the system to reach equilibrium is found to be about 10 min in the case of Zn, Fe and Cu, and 12 min in the case of Co (Fig. 1).
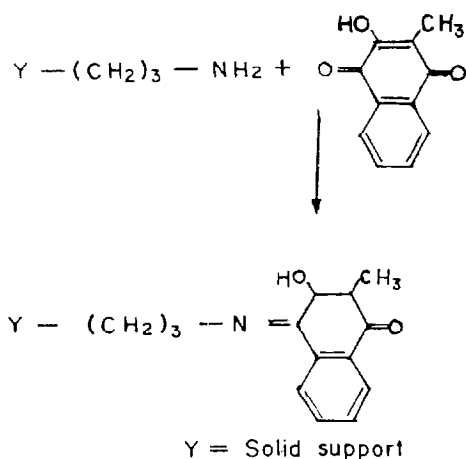
3.2. Effect of amount of modified silica gel

The percentage retention of metal ions on modified silica gel was determined by using different amounts of silica gel. The percentage retention of metal ion on modified silica gel was best when 0.1 g of modified silica gel was employed.

3.3. Effect of pH

Metal solutions were adjusted to the required pH and passed at a flow rate of 1 ml min^{-1}. Then the metal ions were eluted from the column. Subsequent atomic absorption analysis gave the percentage recoveries of the eluted metals at various pH. The pH range studied was between 2 and 9. This study of effect of pH on modified silica gel shows that maximum adsorption in the case of Fe occurs in the pH range 5–7. In the case of Co it occurs in the pH range 4.5–6.5. Cu shows maxi-
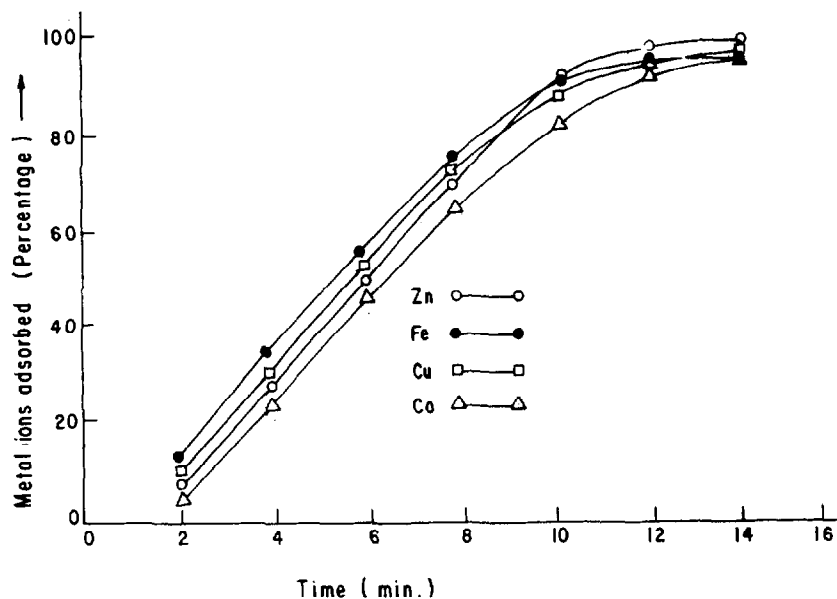
Fig. 1. Effect of time on adsorption.

mum adsorption in the pH range 3-7. In the case of Zn maximum adsorption occurs in the pH range 5-8 (Fig. 2).

3.4. Effect of flow rate

The dependence of the uptake of the transition metals on the flow rate was studied for Cu, Co, Fe and Zn at the pH of the aqueous metal ion solutions chosen for maximum complexation, the solution flow rate being varied from 0.5 to 5 ml min^{-1}. Adsorption was quantitative and reproducible in this range. The flow rate was maintained at 2 ml min^{-1} throughout the experiment.

3.5. Adsorption isotherms

The adsorption isotherms were determined using the batch techniques at 25°C. Solutions of metal ion in the concentration range 2×10^{-5}–2×10^{-3} mol l^{-1} were shaken for 45 min with modified silica gel. The supernatant from each flask was separated off, metal ions were determined using AAS and the amount of metal adsorbed was calculated using Eq. (1). The distribution coefficient, D is defined as $D = N_f/c$. Here N_f is expressed in mmol g^{-1} and c is in

mmol ml^{-1}. The average values of D calculated for each metal (ml g^{-1}) in the concentration range 2×10^{-5}–2×10^{-3} mol l^{-1} are found to be Fe, 3.6×10^2; Co, 3.8×10^2; Cu, 3.9×10^2; and Zn, 4.1×10^2 (Fig. 3).

3.6. Effect of temperature

Adsorption of metal ion is affected by the temperature, with the equilibrium constant decreasing as the temperature is lowered. Studies have shown that adsorption increases with temperature up to 40°C but remains constant after that.

3.7. Effect of electrolytes

Various electrolytes, such as sodium chloride, potassium nitrate and potassium chloride, caused no improvement in the adsorption.

3.8. Preconcentration and recovery of metal ions

The results of the preconcentration and recovery of the metal ions using the column method are shown in Table 1. It can be seen that in each instance the recovery is almost 96%. The volume of eluent was 10 ml in every case.
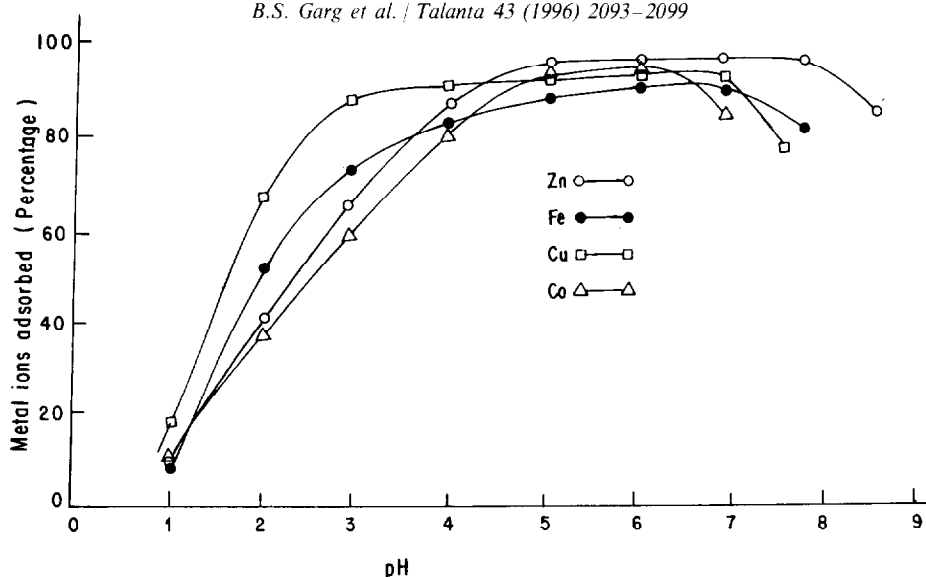
Fig. 2. Effect of pH on recovery of metal ion.

3.9. Determination of Cu in steel solution A and B

0.2 g of steel was added to a 250 ml calibrated flask. 10 ml of water and 4 ml of concentrated H_2SO_4 were then added. This solution was then boiled with 2.5 ml of nitric acid. Any solid that

Fig. 3. Adsorption isotherms of metal ion at 298 K.

appearing at this point redissolved in the next step. The flask was cooled and then 5 ml of concentrated H_2SO_4, 5 ml of 85% phosphoric acid, 2 ml of 0.1 m silver nitrate and 60 ml of H_2SO_4 were added in that order. Following this 5 g of potassium persulphate was then added. This solution was swirled until most of the salt had dissolved. The solution was boiled again for 5 min, cooled, and then 0.5 g of potassium periodate was added. This solution was boiled again, cooled to room temperature and diluted to 250 ml. Copper solution then passed through the column filled with silica gel. Copper ion was eluted from the column using 0.01 N HCl. The amount of copper ion was then determined by AAS. The results in Table 2 show that Cu in steel solution is completely recovered by immobilized silica gel. The recovery is almost 95%.

Table 1
Preconcentration and recovery of metal ions

Ion	Conc. of metal ions (mg l^{-1})	Vol. of eluent (ml)	Recovery (mg l^{-1})	Recovery (%)
Fe	5	10	4.85	97
Co	5	10	4.8	96
Cu	5	10	4.8	96
Zn	5	10	4.8	96

Table 2
Determination of Cu in steel solutions A and B

Sample	Certified composition	Cu taken	Cu found
A	Cu = 0.22, C = 0.24, Mn = 0.74, Si = 0.31, Cr = 1.17, Mo = 0.51	0.22	0.21
B	Si = 0.06, Zn = 0.045, Al = 7.50, Mn = 0.24, Cu = 0.04	0.04	0.031

3.10. Determination of Zn in milk sample

The required amount of the powdered sample (6.0 g) was mineralized in a kjeldahl flask with a sulphuric acid–nitric acid mixture. Most of the acid was neutralized with sodium hydroxide. The solution was then transferred to a 100 ml calibrated flask and diluted to volume with water. 10 ml aliquots of the sample solution were added to five conical flasks which contained 2 ml of stock solution, 5 ml of the buffer solution and 8 ml of distilled water. This solution was then passed through the column filled with modified silica gel. The metal ions were then eluted from the column using 0.01 N HCl/HNO_3 and determined using AAS. The results for determination of Zn in the milk sample are given in Table 3. The standard deviation was found to be 0.57.

3.11. Determination of cobalt in vitamins

The contents of 2 ml ampoules of Macraberin Forte injection were decomposed in a covered beaker by heating with concentrated nitric acid, first at low temperature to avoid violent reaction, then more strongly (with more acid) until the acid had evaporated. Finally, the residue was heated to

Table 3
Determination of zinc in milk samples (powdered milk)

Sample	Amount of Zn present $(\mu g\ g^{-1})$	Amount of Zn found $(\mu g\ g^{-1})$	Standard deviation
Sample 1	56	53	
Sample 2	56	54	0.57
Sample 3	56	54	

Table 4
Determination of cobalt in vitamin

Sample	Co present (mg l^{-1})	Co found (mg l^{-1})	Co found (%)	Standard deviation
1	22	21.0	95.5	
2	22	21.0	95.5	0.11
3	22	21.2	96.0	

about 400°C on a hot-plate, cooled to room temperature and dissolved in nitric acid(1 + 1) to give a solution which was slowly evaporated (1–2 h) on a steam bath. The residue was taken up in water (25 ml) to which concentrated nitric acid was added in 0.25 ml portions until a clear solution was obtained on gentle heating. This solution was then passed through the column containing modified silica gel. The metal ions were then eluted from the column using 0.01 N HCl/HNO_3. The cobalt content of this solution was determined using AAS. This method resulted in 95.5% recovery of cobalt in vitamins. The results are given in Table 4.

4. Conclusions

In conclusion, using a new type of HMNQ-immobilized silica gel iron, copper, cobalt and zinc can be readily determined. This solid-phase extraction method shows fast ion-exchange kinetics and high sorption efficiency. The proposed method is widely applicable for the measurement of trace copper, cobalt and zinc in a variety of samples such as steel, milk and vitamins.

Acknowledgements

References

[1] D.E. Leyden, G.H. Luttrel and N.J. Deangellis, Anal. Chim. Acta, 84 (1976) 97.

[2] D.E. Leyden, G.H. Luttrel, W.K. Nonidez and D.B. Werho, Anal. Chem., 46 (1976) 67.

[3] D.E. Leyden and G.H. Luttrel, Anal. Chem., 47 (1975) 1612.

[4] D.W. Lee and M. Halman, Anal. Chem., 48 (1976) 2214.

[5] G.M. Orf and J.S. Fritz, Anal. Chem., 50 (1978) 1328.

[6] B. Colella, S. Siggla and R. Barnes, Anal. Che., 52 (1980) 2347.

[7] K. Lorber, H. Spitzy and K. Muller, Mikrochim. Acta, (1975) 603.

[8] D.M. Hercules, L.E. Cox, G.D. Nichols and J.C. Carver, Anal. Chem., 45 (1983) 1973.

[9] E.M. Moyers and J.S. Fritz, Anal. Chem., 49 (1977) 418.

[10] J.C. Moreira and Y. Gushikem, Anal. Chim. Acta, 176 (1985) 263.

[11] A. Kettrup, Anal Chim. Acta, 169 (1985) 331.

[12] J.C. Moreira and Y. Gushikem, Anal. Chim. Acta, 191 (1987) 134.

[13] L.T. Kubota and J.C. Moreira, Analyst, 114 (1989) 13.

[14] R.E. Sturgeon and S.S. Beeman, Talanta, 29 (1982) 167.

[15] K. Terada, K. Matsumoto and Y. Nanao, Anal. Sci., 1 (1985) 145.

[16] M.J. Haron, M.D. Yunus and A. Kassim, Talanta, 41 (1991) 799.

[17] O.A. Zapozhees and O. Nadzhapova, Talanta, 41 (1994) 2067.

[18] R. Bonoforti and R. Ferraorli, Anal. Chim. Acta, 162 (1984) 33.

[19] A.J. Paulson, Anal. Chem., 58 (1986) 183.

[20] P. Pakalns, Anal. Chim. Acta, 120 (1980) 289.

[21] B.R. Reddy and P.V.R. Bhaskara Sarma, Talanta, 41 (1994) 1335.

[22] K.S. Pansar, O.V. Singh and S.N. Tandon, Talanta, 41 (1994) 1341.

[23] S. Hoshi, H. Fujisama, K. Nakamura and K. Akatsu, Talanta, 41 (1994) 503.

[24] A.N. Masi and R.A. Olsina, Talanta, 40 (1994) 931.

[25] C. Kantipury, S. Katragadda, A. Chow and H.D. Gesser, Talanta, 37 (1990) 491.

[26] T.M. Florence and G.E. Batley, Talanta, 23 (1976) 179.

[27] P. Figura and B. McDuffie, Anal. Chem., 49 (1977) 1950.

[28] E. Leyden, J.T. Cronin and A.T. Ellis, Int. J. Environ. Anal. Chem., 11 (1982) 105.

[29] R. Van Grieken, Anal. Chim. Acta, 143 (1982) 3.

[30] R.K. Sharma and S.K. Sindhwani, Bull. Soc. Chim. Fr., 5 (1986) 700–702.

[31] R.K. Sharma and S.K. Sindhwani, Monatsh. Chem., 117 (1986) 459–463.

[32] R.K. Sharma and S.K. Sindhwani, Proc. Indian Acad. Sci., 103(5) (1991) 607–612.

[33] R.K. Sharma and S.K. Sindhwani, Analyst, 112 (1987) 175.

[34] R.K. Sharma, K. Sharvah and S.K. Sindhwani, Talanta, 35 (1988) 661.

[35] R.K. Sharma and S.K. Sindhwani, Fresenius' Z. Anal. Chem., 332 (1988) 819.

[36] R.K. Sharma, Anal. Chem., 64 (1992) 220A.

[37] R.K. Sharma, Bull. Chem. Soc. Jpn., 66 (1993) 1084.

[38] L.F. Fieser, J. Biol. Chem., 133 (1940) 391.

Enhanced decompositions of some cyano complexes during diode array spectrophotometric measurements

Guillermo López-Cueto[a], José F. Rodríguez-Medina[b], Carlos Ubide[b],*

[a] *Departamento de Química Analítica, Facultad de Ciencias, Universidad de Alicante, Apdo. 99, 03080 Alicante, Spain*
[b] *Departamento de Química Aplicada, Facultad de Química, Universidad del País Vasco, Apdo. 1072, 20080 San Sebastián, Spain*

Abstract

Acidic solutions of the Fe(III), Mo(V), W(V) and Mn(IV) cyano complexes are known to decompose photochemically. These reactions do not take place to an appreciable extent when the cyano complexes are subjected to spectrophotometric measurements by means of conventional spectrophotometers, but they do take place when diode array spectrophotometers are used. The reactions are autoaccelerated, at least in the cases of Mo(V), W(V) and Mn(IV), and consist of photoinduced reductions of the metal ion. This effect should be taken into account in all cases where the measured signal has to be used for quantitative purposes, but its significance must be emphasized mainly in the field of kinetic analysis, where it can lead to large errors. The extent of these reactions, and therefore the size of the errors, can be lowered by using UV cut-off filters and by taking discontinuous measurements with suitable integration times. All these possibilities, which are of general application, are discussed.

1. Introduction

Diode array spectrophotometers are able to acquire data at a rate of several spectra per second [1]. This makes them especially well suited to follow, in the UV–Visible region, systems moving to equilibrium (kinetic runs, chromatography, flow injection, etc.) [2], but they are also used instead of conventional spectrophotometers with systems at equilibrium. One of the key features of diode array spectrophotometers is that light of all energies in the UV–Visible region impinges simultaneously on the sample at any time, whilst in a conventional spectrophotometer only a narrow band of wavelengths does this. As a result, undesirable photochemical reactions happen much more easily in diode array spectrophotometers. The extent of these photochemical reactions, in each case, is usually related to the time the sample stays in the light beam. These reactions can be a significant source of errors, mainly in kinetic analysis, where reaction rates or any other kinetic variable are measured for quantitative analytical

* Corresponding author. Fax: (+34)43-21-22-36.

purposes. However, few specific cases of photochemical reactions have been reported to take place in diode array spectrophotometers [3].

A number of cyano complexes of the transition metals are known to undergo photolytic reactions [4,5]. The redox potentials for $Mn(CN)_6^{2-}$, $Mo(CN)_8^{3-}$, $W(CN)_8^{3-}$ and $Fe(CN)_6^{3-}$ are, (vs. NHE) 1.04 V [6], 0.725 V [7], 0.457 V [8] and 0.361 V [9] respectively. Accordingly, all these compounds have oxidizing properties, and some of them have been used as slow oxidizing reagents with inorganic as well as organic substrates in kinetic determinations [10–12]. Some of these cyano complexes can undergo thermal as well as photochemical decomposition, as has been reported for $Fe(CN)_6^{3-}$ [13] and $Mn(CN)_6^{2-}$ [14]. During study of the oxidation of aminophenols by octacyanomolybdate(V) (in order to propose a method for the simultaneous kinetic determination of aminophenol isomers) [12] we observed that the Mo(V) cyano complex underwent photolytic reduction if the reaction was monitored with a diode array spectrophotometer. In that particular case the photochemical reaction did not result in a problem; however, in general, if the reaction is going to be followed through the cyano complex concentration, high errors can be produced in the presence of photochemical reactions. The present paper shows that all the aforementioned complexes undergo photolytic decomposition to appreciable extents when exposed to the light beam of a diode array spectrophotometer; however, this problem can be reduced or even avoided by using suitable instrumental conditions, although a price may have to be paid for it.

2. Experimental

2.1. Apparatus

A Shimadzu UV-260 spectrophotometer with 1.0 cm pathlength fused-silica cells and constant temperature cell-holders was used as the conventional spectrophotometer. The temperature in the cell was continuously monitored by means of a small Pt 100 temperature probe installed just before the water entrance in the cell-holder, and

kept constant ($\pm 0.2^\circ C$) by circulating water from a Haake F3 K thermostat controlled by the probe. A microcomputer HP vectra ES/12, coupled to the spectrophotometer, controlled it, acquired the data and processed them via home-made programs. A diode array Hewlett Packard HP 8452A spectrophotometer with 1.0 cm pathlength fused-silica cell was also used. The cell temperature was controlled by the HP 89090A Peltier temperature control accessory ($\pm 0.2^\circ C$). To obtain reliable and reproducible measurements the solution in the cell was continuously stirred with a small magnetic stirrer incorporated into the Peltier system. A filters kit (HP part number 08451-60302) was sometimes used; because the kit is not compatible with the Peltier system, a water-circulating thermostatic bath was used in these cases. All the data were acquired with a Hewlett Packard HP vectra 386/25N coupled to the spectrophotometer.

Volumes <0.1 ml were added with Eppendorf micropipettes.

2.2. Reagents

Caesium octacyanomolybdate(V) dihydrate [15], caesium octacyanotungstate(V) dihydrate [15] and potassium hexacyanomanganate(III) [16] were prepared according to the procedures previously reported.

Hexacyanomanganate(IV) solution (2×10^{-4} M) was obtained by fast disproportionation of hexacyanomanganate(III) in 0.1 M H_2SO_4 according to the procedure previously reported [11]. Other cyano complex solutions (5×10^{-4} M unless otherwise stated) were prepared from the caesium or potassium salts in 0.1 M H_2SO_4.

Other chemicals as (potassium hexacyanoferrate(III) (Merck) and sulphuric acid (Riedel de Häen) were of analytical-reagent-grade and were used as received. Doubly-distilled water was used throughout.

2.3. Procedure

To a 1.0 cm cell 2.5 ml of 0.1 M H_2SO_4 was added and the cell was left to stand for 5 min in the controlled temperature cell-holder of the spec-

trophotometer (blank solution). A volume of 0.1 ml of the cyano complex solution was added (zero time) and the change of absorbance with time was followed either at a fixed wavelength (conventional) or along a part of the UV–Visible spectrum (diode array).

3. Results and discussion

Acidic solutions of $Mo(CN)_8^{3-}$ and $W(CN)_8^{3-}$ are stable in the dark, but $Fe(CN)_6^{3-}$ and $Mn(CN)_6^{2-}$ undergo thermal decomposition [13,14]; nevertheless, only $Mn(CN)_6^{2-}$ decomposes at an appreciable rate at room temperature (Fig. 1). These decompositions are apparently insensitive to the light levels present in a conventional spectrophotometer (corresponding to the wavelengths of their absorption maxima in the visible or near-UV regions) and therefore, the reactions proceed to the same extent both in the spectrophotometric cell and in the dark, indicating that only thermal reactions take place under these conditions. In contrast, when the cyano complexes are placed in the cell-holder of a diode array spectrophotometer significant differences in the reaction profiles are found (Fig. 2): $Mo(CN)_8^{3-}$ and $W(CN)_8^{3-}$ now decompose at a noticeable rate, the reaction being autoaccelerated
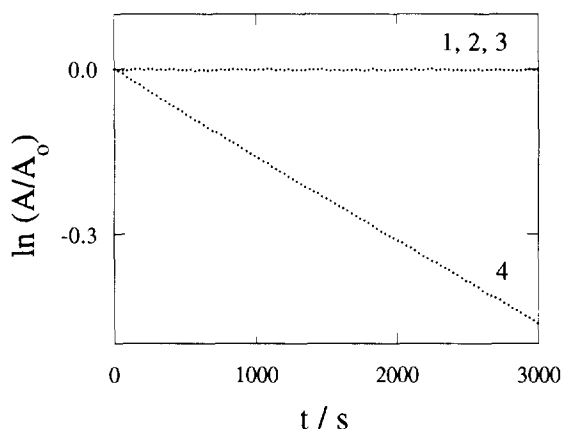
Fig. 1. Kinetic runs for the decomposition of cyano complexes in a conventional spectrophotometer: (1), Fe(III) (422 nm); (2) W(V) (388 nm); (3), Mo(V) (388 nm); (4), Mn(IV) (387 nm). H_2SO_4, 0.1 M. T, 40°C.
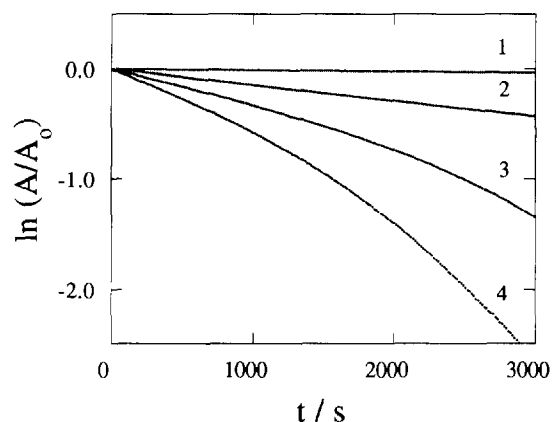
Fig. 2. Kinetic runs for the decomposition of cyano complexes in a diode array spectrophotometer: (1), Fe(III) (422 nm); (2), W(V) (388 nm); (3), Mo(V) (388 nm); (4), Mn(IV) (388 nm). H_2SO_4, 0.1 M. T, 25°C.

in both cases; the $Fe(CN)_6^{3-}$ decomposition is now perceptible and $Mn(CN)_6^{2-}$ decomposes at a much faster rate (the initial rate increases by a factor of about 3.5 in the latter case). This seems to indicate that, in additioin to the thermal decomposition, a parallel photodecomposition takes place in the cell of the diode array spectrophotometer. For instance, the reaction profile of the $Mn(CN)_6^{2-}$ decomposition shows an autoacceleration behaviour clearly different from the pseudo-first-order kinetics shown when a conventional spectrophotometer is used (Fig. 1). These differences can be attributed, therefore, to a photochemical effect caused by UV radiation of certain wavelengths present in the light beam of the diode array spectrophotometer. This is illustrated in Fig. 3, where the behaviour of a $Mo(CN)_8^{3-}$ solution subject to alternating periods of irradiation and darkness in a diode array spectrophotometer is shown.

As has been remarked on in the case of $Mn(CN)_6^{2-}$ solutions, the effect of irradiation is not only in terms of quantity but also in terms of quality. That is to say, the observed changes seem to affect both reaction rate and mechanism since the initial rate as well as the reaction propfiles change significantly. The autoaccelerated kinetic profile is a quite frequent feature of photoinitiated reactions, in which the absorption of a photon of

relatively high energy (UV region) leads to the formation of an electronically excited species which suffers subsequent reactions. These reactions can include dissociations accompanied by redox processes with participation of free radicals, which usually lead to chain mechanisms which are responsible for the autoacceleration kinetics. In these stepwise photoinduced reactions unusually high values of the quantum yield can be attained [17].

The reaction products under the conditions of Fig. 2 were not completely identified in the case of $Fe(CN)_6^{3-}$ and no attempt was made to elucidate the mechanism of its photodecomposition. It seems quite probable that free cyanogen radicals could be involved. In fact, it has been suggested that the photoinitiated aquation of hexacyanomanganate(III) is followed by the oxidation of released cyanide by unchanged $Fe(CN)_6^{3-}$ [18], and it has been proposed that this reaction proceeds via the formation of cyanogen radical as an intermediate species [19]. In the case of $Mo(CN)_8^{3-}$ and $W(CN)_8^{3-}$ the reaction products were identified as $Mo(CN)_8^{4-}$ and $W(CN)_8^{4-}$. This seems to support reaction mechanisms occurring via OH radicals [20] instead of via CN radicals [21]. In the case of $Mn(CN)_6^{2-}$ the reaction products were the same as those obtained in the thermal decomposition and so the stoichiometry of both the thermal and the photochemical reactions
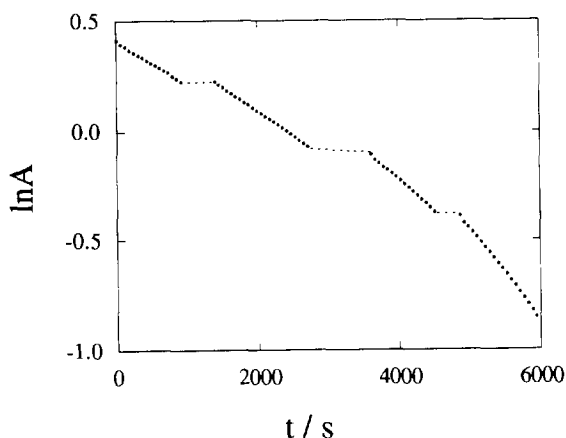
Fig. 3. Decomposition of 10^{-3} M $Mo(CN)_8^{3-}$ in a diode array spectrophotometer and in the dark. H_2SO_4, 0.1 M. The sloping sections correspond to lighting times.
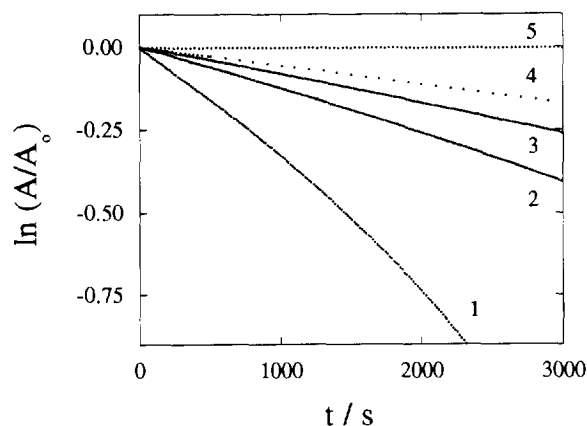
Fig. 4. Effect of filters and shutter on the photoinduced reduction of octacyanomolybdate (V). Curves (1)–(4) obtained in a diode array spectrophotometer. (1), No filter; (2), 265 nm cut-off filter (at 50% T); (3), 295 nm cut-off filter (at 50% T); (4), no filter but shutter active (measurements every 15 s; integration time, 2 s). Curve (5) obtained in a conventional spectrophotometer.

should be the same: the reduction of the metal ion by the coordinated cyanide [14].

Photochemical reactions produced in a diode array spectrophotometer can be an important source of errors, especially if the sample has to be in the light beam for a long time (kinetic runs). Therefore some tentative procedures were tested to prevent these disadvantages:

(1) The use of UV filters. Photochemical reactions are usually initiated by UV radiation which is more energetic than visible radiation, and so they can be prevented by the use of cut-off filters for the UV region. The effect of UV filters on the photoinduced reduction of $Mo(CN)_8^{3-}$ is shown in Fig. 4. The extent of the reaction is lower when a 265 nm cut-off filter is used (curve 2) than in the absence of a filter (curve 1); however, a 295 nm cut-off filter is more efficient (curve 3) because it cuts off a wider wavelength region. Even so, the prevention of the photochemical reaction is not complete (with curve 5, obtained by means of a conventional spectrophotometer).

(2) The use of the couple shutter–integration time. The reaction kinetics in a diode array spectrophotometer can be monitored discontinuously and the signal is integrated over short, fixed time intervals. When undesired photochemical reac-

tions can take place the shutter should be kept active (closed) whenever measurements are not being taken. The question is how long the shutter should be open for (integration time) in order to take reliable measurements. Obviously, very short integration times would not allow the photochemical reaction to go very far, but the value of the signal-to-noise ratio could become excessively low. Consequently the integration time should be optimized as the longest time that still makes the photochemical reaction negligible. In Fig. 4, it can be seen that a measurement every 15 s with an integration time of 2 s (curve 4) does not completely prevent the photochemical reduction of $Mo(CN)_8^{3-}$ but the result is better than the one obtained using the 295 nm cut-off filter (curve 3). Nonetheless, if the instrumental conditions used in curves (3) and (4) are combined (filter + shutter) no apparent photochemical reaction occurs and a profile similar to curve 5 is found.

4. Conclusion

From a general point of view it can be said that photochemical reactions are much more frequently originated by the light beam of a diode array spectrophotometer than by that of a conventional one. Kinetic analysis is especially subject to errors due to these effects. To avoid this drawback, some instrumental precautions can be taken, namely: UV cut-off filters, discontinuous measurements, use of the shutter, and short integration times. Though all these precautions can result in certain limitations (for instance the use of UV filters does not allow measurements to be taken in that region) and poorer precision will be obtained (fewer experimental points can be acquired, decreased signal/noise ratio, etc.), their use frequently allows one to take advantage of the instrumental possibilities of diode array spectrophotometers in unfavourable cases.

References

[1] D.G. Jones, Anal. Chem., 57 (1985) 1057A.

[2] D.G. Jones, Anal. Chem., 57 (1985) 1207A.

[3] A.J. Owen, Diode-array spectroscopy, in A. Townshend (Ed.), Encyclopedia of Analytical Science, Academic Press, London, 1995, p. 5314.

[4] V. Balzani and V. Carassiti, Photochemistry of Coordination Compounds, Academic Press, London, 1970.

[5] A.G. Sharpe, The Chemistry of Cyano Complexes of the Transition Metals, Academic Press, London, 1976.

[6] G. López-Cueto and C. Ubide, Can. J. Chem., 69 (1991) 2112.

[7] N. Stolica, in A.J. Bard, R. Parsons and J. Jordan (Eds.), Standard Potentials in Aqueous Solution. M. Dekker, New York, 1985, p. 478.

[8] A.T. Vas'ko, in A.J. Bard, R. Parsons and J. Jordan (Eds.), Standard Potentials in Aqueous Solution, M. Dekker, New York, 1985, p. 502.

[9] K.E. Hensler and W.J. Lorenz, in A.J. Bard, R. Parsons and J. Jordan (Eds.), Standard Potentials in Aqueous Solution, M. Dekker, New York, 1985, p. 408.

[10] G. López-Cueto and J.A. Casado-Riobó, Talanta, 26 (1979) 151.

[11] G. López-Cueto and C. Ubide, Talanta, 37 (1990) 849.

[12] G. López-Cueto, S. Maspoch, J.F. Rodríguez-Medina and C. Ubide, Analyst, 121 (1996) 407.

[13] A.G. Sharpe, The Chemistry of Cyano Complexes of the Transition Metals, Academic Press, London, 1976, p. 113.

[14] G. López-Cueto and C. Ubide, Can. J. Chem., 64 (1986) 2301.

[15] L.D.C. Bok, J.G. Leipoldt and S.S. Basson, Z. Anorg. Allg. Chem., 415 (1975) 81.

[16] J.A. Lower and W.C. Fernelius, Inorg. Synth., 2 (1946) 213.

[17] M.J. Pilling and P.W. Seakins, Reaction Kinetics, Oxford University Press, Oxford, 1995.

[18] A.G. Sharpe, The Chemistry of Cyano Complexes of the Transition Metals, Academic Press, London, 1976, p. 115.

[19] G. López-Cueto and J.A. Casado-Riobó, Talanta, 26 (1979) 127.

[20] A.G. Sharpe, The Chemistry of Cyano Complexes of the Transition Metals, Academic Press, London, 1976, p. 63.

[21] G.W. Gray and J.T. Spence, Inorg. Chem., 10 (1971) 2751.

Simultaneous spectrophotometric determination of drugs in pharmaceutical preparations using multiple linear regression and partial least-squares regression, calibration and prediction methods

R.D. Bautista, F.J. Aberásturi, A.I. Jiménez, F. Jiménez*

Department of Analytical Chemistry, Nutrition and Food Science, Faculty of Chemistry, University of La Laguna, E-38071 La Laguna, Tenerife, Spain

Abstract

Two new methods for the simultaneous determination of acetylsalicylic acid, acetaminophen and caffeine based on total absorbance measurements and their processing by multiple linear regession and partial least-squares regression are proposed. The concentration ranges used to construct the calibration matrix were 4.0–12.0, 2.0–10.0 and 0.9–6.0 μg ml^{-1} for acetylsalicylic acid, acetaminophen and caffeine respectively. The proposed methods were validated by using a set of synthetic sample mixtures and subsequently applied to the determination of the three active principles in three different pharmaceutical preparations.

Keywords: Acetaminophen; Acetylsalicylic acid; Caffeine; Multiple linear regression; Partial least-squares; Simultaneous determination

1. Introduction

Multideterminations of analytes that exhibit absorbance signals in the UV–Vis region have become commonplace tasks in most analytical laboratories (clinical, food control, pharmaceutical, etc.), which address them in different—but not always effective—ways.

*Corresponding author.

The greatest difficulties with UV–Vis multidetermination methods arise when the analytes to be determined give partly or fully overlapped spectra, as is the case with the ingredients of most pharmaceutical preparations. As a result, the methods to be used in quality control analyses should be highly reliable as regards processing of calibration data and predicting the absorbance signals for the target analytes. The many choices available in this respect include univariate calibra-

tion [1,2] and multivariate calibration methods such as multiple linear regression (MLR) [3], partial least-squares regression (PLS) [4,5], iterative target transformation factor analysis (ITTFA) [6] and evolving factor analysis (EFA) [7].

This paper demonstrates the high potential of MLR and PLS-2 calibration–prediction methodologies for processing absorbance signals of drugs (specifically acetylsalicylic acid, acetaminophen and caffeine). Based on the results obtained, the multideterminations performed are not influenced by the prevailing strong spectral overlap throughout the absorption wavelength range.

Acetaminophen (AAP) and caffeine (CAF) have previously been determined in mixtures by use of derivative spectrophotometry [8] and PLS [9]. Also, these two drugs and acetylsalicylic acid (ASA) have been quantified jointly by HPLC [10–12] and spectrophotometry (using Kalman filtering) [13,14].

The proposed methods were validated by resolving synthetic mixtures of the three drugs, which were also subsequently determined in the three most widely used pharmaceutical preparations in Spain.

2. Theory

The theory and uses of multivariate calibration as applied to analytical chemistry are by now solidly established and have been the subject of several reviews and monographs [15,16], therefore only a brief outline of the methods used in this work is provided below.

2.1. Multiple linear regression method (MULTI3), using several standards of the analytes and their mixtures

If absorbance measurements for several solutions containing mixtures of the analytes are made in numbers exceeding the number of mixture components, then the system composed of the absorbance and concentration matrices will be overdimensioned and take the following matrix form:

$$A = KC$$

where A is the data absorbance calibration matrix, K is the matrix form which the proportionality constants are calculated from spectra for standard solutions of the pure analytes and/or their mixtures, and C is the concentration matrix. The C prediction concentration matrix can be calculated from the following equation:

$$C = (K'K)^{-1}K'A$$

where K' is the transpose of K and A is the absorbance matrix of unknown samples. Matrix K can be obtained in various ways. We calculated K values by MLR of data for mixtures of analytes of known composition. Mathematically, this entails solving an equation system of the following form at each wavelength:

$$a(\lambda, s) = e(\lambda) + \sum_{i=1}^{n} k(\lambda, i)c_{si}; \quad \forall s = 1 \ldots n_s$$

where a is the signal for mixture s at wavelength λ, $e(\lambda)$ is the independent fitting term at each λ value and c_{si} is the concentration of component i in mixture s. This equation can be solved by MLR when the number of mixtures exceeds the number of components. The deviation of the fit at each wavelength, $d(\lambda)$, can be calculated from:

$$d(\lambda) = \sqrt{\frac{\sum_{s=1}^{n_s} [a(s, \lambda) - \hat{a}(s, \lambda)]^2}{n_s - n}}$$

$d(\lambda)$ values are reused, after weighting (those wavelengths with the higher deviations are assigned smaller weights than the rest), in the initial fitting.

$$\frac{a(\lambda)}{d(\lambda)} = k'_0 + \sum_{i=1}^{n} \frac{k(i, \lambda)}{d(\lambda)} c_i; \quad \forall \lambda = 1 \ldots n_\lambda$$

2.2. PLS method

PLS analysis resolves matrices X and Y into the product of smaller matrices, namely P (the X loading matrix, which contains the directions of the principal components or axes) and T (the scores matrix, which includes the coordinates for the new axes) and Q (the Y loading matrix):

$$X = TP + E$$

$$Y = TQ + F$$

In our case, matrix X (the absorbance matrix) was composed of objects as rows $(1 \ldots N)$ and variables as columns $(1 \ldots K)$ (the calibration solutions and absorption wavelengths at which measurements were made respectively). Matrix Y (the concentration matrix) consisted of the calibration solutions as rows $(1 \ldots N)$ and the analyte concentrations as columns $(1 \ldots J)$. Finally, matrices E and F (the residual matrices) contained the model error and random noise respectively.

Scheme 1 shows the calibration and prediction processes, where W is the so-called "loadings weight matrix" or "PLS weights matrix".

3. Experimental

3.1. Apparatus

Spectra were recorded on a Hewlett-Packard HP 8452A diode array spectrophotometer furnished with quartz cuvettes of 1 cm pathlength that was interfaced to a Vectra ES computer and a Think Jet printer, also from Hewlett-Packard. The spectrophotometer measures each even wavelength.

A Radiometer PHM-84 digital pH-meter furnished with a combined glass–saturated calomel electrode was used for pH measurements. The meter was calibrated with at least two buffer solutions at pH 4.02 and 7.00.

An ultrasonic bath was also employed.

3.2. Computer hardware and software

Absorbance and derivative spectra were acquired and processed using the spectrophotometer's bundled software. Additional software used included a MLR programme (MULTI3) [17] and Unscrambler v. 5.0 [18] for calibration–prediction and experimental design. Exported data from the spectrophotometer were converted into MULTI3 and Unscrambler formats using the word processor WordPerfect 5.1 for filing in ASCII format. All software was run on a PC/AT 486 DX2 66 MHz computer.

3.3. Reagents

Standard solutions containing 100 μg ml^{-1} ASA, AAP and CAF were made by direct weighing of the required amount of commercially available reagent (Merck) and then dissolving in 0.1 M HCl.

An HAcO/NaAcO buffer (pH 5.5; 1.0 M) was also prepared.

All reagents and solvents used were of analytical grade and the water was doubly-distilled.

3.4. Analysis of synthetic mixtures

Ternary mixtures of ASA, AAP and CAF were prepared in triplicate as follows. A 25 ml flask was filled with 3 ml of HAcO/NaAcO buffer at pH 5.5, an appropriate volume of drug solution to obtain final concentrations of 4.0–12.0 μg ml^{-1} ASA, 2.0–10.0 μg ml^{-1} AAP and 0.9–6.0 μg ml^{-1} CAF, and bidistilled water to the mark.

Mixed spectra were recorded over the wavelength range 220–310 nm using a blank prepared in the same way as the mixtures but containing none of the analytes. An integration time of 1 s was employed in every experiment.

3.5. Simultaneous determination of ASA, AAP and CAF in pharmaceutical preparations

The contents of a pharmaceutical tablet or capsule, and/or 5 g of accurately weighed granules, were dissolved in doubly-distilled water with ultrasonication for 15 min. Then, the solutions were filtered through a Whatman No. 41 paper and the filtrates transferred to 1000 ml volumetric flasks and made up to volume with doubly-distilled water. Aliquots of these solutions were used in such a way that the concentration of each drug obtained upon dilution to 25 ml lay within the range of the calibration matrix. The dilute solutions were analysed in quintuplicate as described in the previous section.

4. Results and discussion

Fig. 1 shows the absorption spectra for aqueous solutions of ASA, AAP and CAF at pH 5.5. As

can be seen, ASA gave two absorption maxima (a stronger one at 224 nm and a weaker one at 288 nm), CAF also gave two (at 222 and 274 nm, the intensity of the latter band is higher) and AAP a single maximum (at 244 nm).

The simultaneous determination of these drugs in mixtures by conventional spectrophotometric methods is hindered by strong spectral overlap throughout the wavelength range. Such a determination could theoretically be facilitated by the use of a multivariate calibration method.

In order to establish the optimal measurement conditions for the joint determination, we used the univariate method to investigate the effect of experimental variables on the absorption spectra for the drugs studied.

We first checked the stability of the three analytes in aqueous solution. For this purpose, we recorded the UV absorbance spectra for solutions of the three drugs as a function of time and found that the spectra for AAP and CAF did not vary appreciably over a period of a few days provided that the solutions were

kept at room temperature in the dark. In contrast, the spectrum for ASA exhibited signs of instability 6 h after the solution was prepared, even under the same experimental conditions used for the other two drugs. The instability probably arose from hydrolysis in solution and compelled use to use freshly made solutions of ASA in subsequent experiments.

The influence of pH on the absorption spectrum for each drug was studied over the range 1.0–12.0; pH values were adjusted by addition of small volumes of dilute solutions of HCl and/or NaOH. The spectrum for ASA was found to be markedly affected by the pH of the medium: the absorbance signal increased with decreasing acidity as a new absorption maximum gradually appeared at 300 nm due to the hydrolysis product. In contrast, the signal for AAP was increased by highly acid or alkaline media and decreased over the pH range 4.0–8.0, coinciding with a hypsochromic shift in the absorption maximum. Finally, the spectrum for CAF exhibited no significant changes at any pH. In order to avoid the potential hydrolysis of the drugs by too acid or too alkaline a medium, pH 5.5 was adopted as optimal for subsequent experiments.

Of the different buffering solutions tested HAcO/NaAcO was found to result in signals coinciding with those obtained in its absence, and so was chosen for subsequent work. In order to determine the optimal buffer concentration, a series of experiments was conducted in the range 0.05–0.25 M. Such concentrations were found to have no effect on the spectra for the three drugs so an intermediate buffer concentration, 0.12 M, was adopted.

The temperature was found to have no appreciable effect on the spectra of the analytes, so 25°C was chosen for subsequent work.

4.1. Determination of ASA, AAP and CAF by MLR

The ASA–AAP–CAF mixture was resolved with the aid of the programme MULTI3. The calibration matrix was constructed according to a
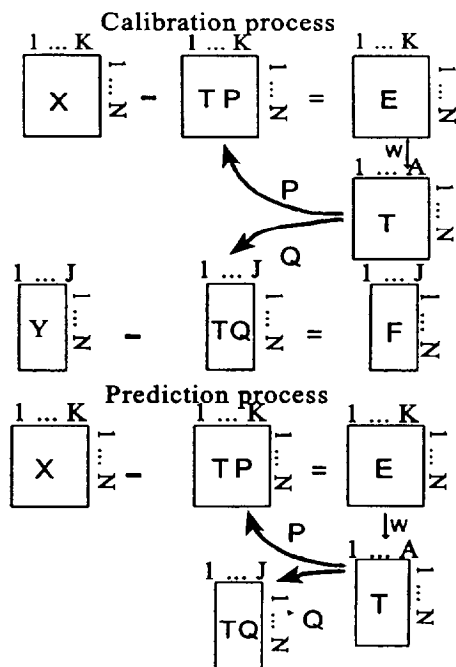
Scheme 1.

$(2^n + 1)$ experimental design. The composition of the calibration solution used was as follows:

Analyte/solution	1	2	3	4	5	6	7	8	9
ASA	+	+	+	−	−	−	+	−	~
AAP	+	+	−	+	−	+	−	−	~
CAF	+	−	+	+	+	−	−	−	~

Level (+): ASA 12.0 μg ml^{-1}, AAP 10.0 μg ml^{-1}, CAF 6.0 μg ml^{-1}.
Level (−): ASA 4.0 μg ml^{-1}, AAP 2.0 μg ml^{-1}, CAF 0.9 μg ml^{-1}.
Level (~): ASA 8.0 μg ml^{-1}, AAP 6.0 μg ml^{-1}, CAF 3.5 μg ml^{-1}.

The method was validated using eight solutions encompassing the concentration range of the calibration matrix.
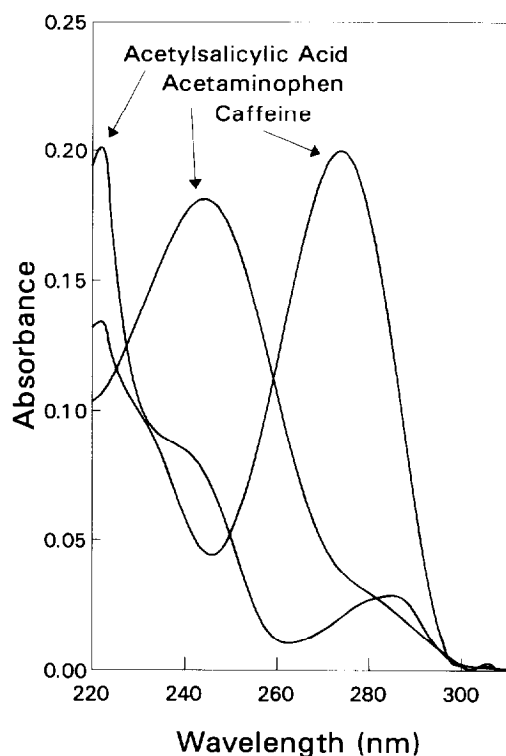
Fig. 1. Absorption spectra of ASA (8.0 μg ml^{-1}), AAP (3.0 μg ml^{-1}) and CAF (2.0 μg ml^{-1}) at pH 5.5, HAcO/NaAcO buffer.

-1

4.2. PLS

The same mixtures were employed as calibration matrix for applying PLS-2 using the software Unscrambler v.5.0.

Fig. 2 shows the variation of the residual variance with the number of factors used. As can be seen, the proposed model accounts for 100% of the data variance with only three factors. The first factor accounts for the variance of AAP, the second for that of CAF and the third for that of ASA.

Fig. 3 shows a plot of model scores against analyte concentrations in each calibration solution. As can be seen in Fig. 3a, a plot of score 2 vs. score 1, the solutions arranged themselves horizontally within each group according to the AAP concentration (i.e. an increase in the first and second scores led to an increase in the concentrations of AAP and CAF respectively). The third score (Fig. 3b) is related to the concentration of ASA: the solutions grouped vertically according to its concentration, an increase in which increased the third score.

The relationship between the scores and analyte concentrations confirms the hypothesis made in studying the variance of the residuals for the analyte solutions.

Fig. 4 shows the model loadings, each of which is related to one or more of the analytes in
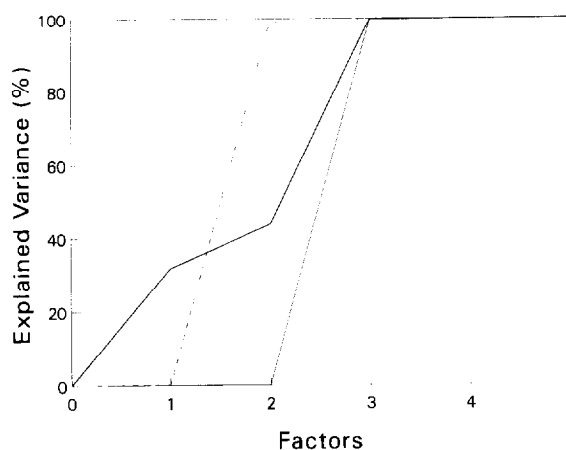
Fig. 2. Explained variance in the calibration process as a function of the number of factors for (—) total variance of data, (- - -) variance of AAP data, (– – –) variance of CAF data and (—) variance of ASA data.
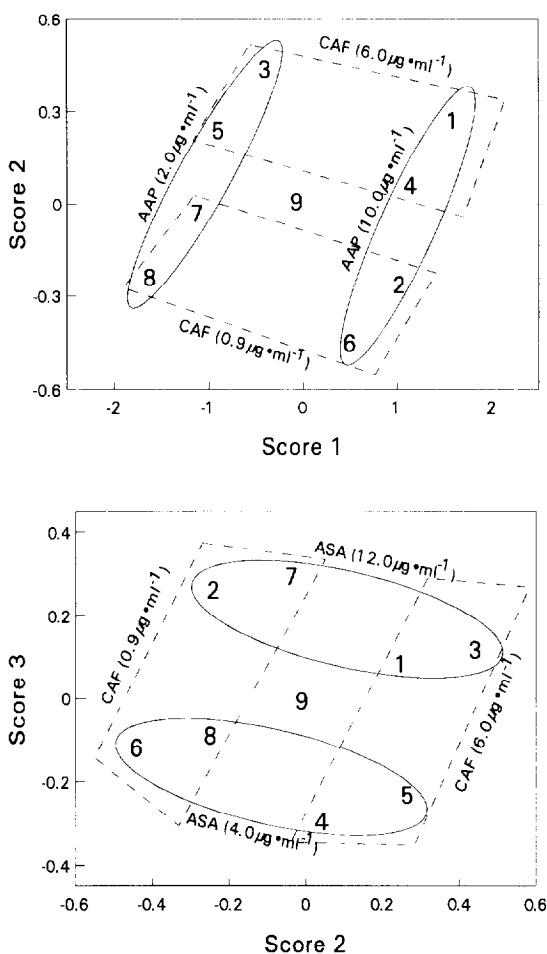
Fig. 3. Scores plot for the calibration set, showing the positions of the different solutions used (see text).

solution. The relationship is reflected in the spectral shape, which may coincide with that of one of the analytes or a combination of two or more. In our case, the first loading accounts for the variance of AAP, the second for that of CAF and the third for that of ASA. Finally, including a fourth loading lacks chemical significance.

4.3. Resolution of synthetic mixtures

In order to test the proposed methods, a set of synthetic mixtures containing the three analytes in variable proportions was prepared and analysed. Table 1 shows the results obtained using MLR. As can be seen, the errors made never exceeded 3.7%. The analyte resulting in the largest errors
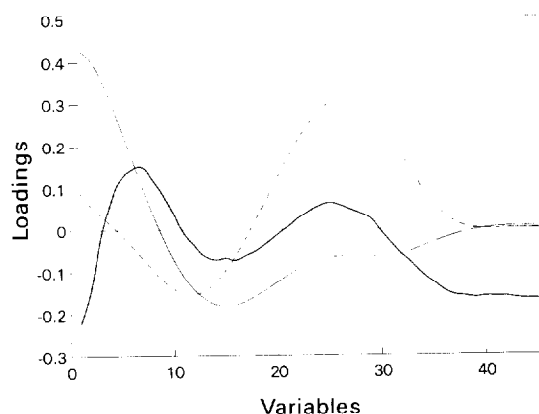
Fig. 4. Loadings plot as a function of the wavelength (variables): (– – –) first loading (related to AAP); (———) second loading (related to CAF); (—) third loading (related to ASA); (—) fourth loading (lacks chemical significance).

was ASA, possibly because it was also that giving the lowest signals; the errors for the other two drugs were quite similar.

The results obtained by applying PLS-2 to the same sample set are listed in Table 2. As can be seen, the errors were also quite acceptable as they never exceeded 3.6%.

The predictive ability of a model can be defined in different ways. The most common is probably the standard error of prediction (SEP), which compares the concentration found by the model with the added concentration, and is given by

$$SEP = \sqrt{\frac{\sum_{i=1}^{N} (C_i^{Added} - C_i^{Found})^2}{N}}$$

where C_i^{Added} is the added concentration of the analyte, C_i^{Found} is the concentration found and N is the number of synthetic samples. Tables 1 and 2 show the errors made in the resolution of different synthetic mixtures.

4.4. Accuracy and precision

In order to check the goodness of the results, the amounts added and found in each synthetic solution were subjected to a statistical test aimed at discarding systematic errors. For this purpose, the mutual confidence region test, developed by Mandel and Linnig [19], was applied to slopes and

Table 1
Simultaneous determination of ASA, AAP and CAF in different synthetic mixtures using the MLR prediction method

Amount added (μg ml^{-1})			Amount found[a] (μg ml^{-1})			Error (%)		
ASA	AAP	CAF	ASA	AAP	CAF	ASA	AAP	CAF
10.00	7.00	5.40	9.68	7.01	5.31	−3.2	+0.1	−1.7
10.00	6.00	4.80	9.88	6.00	4.77	−1.2	0.0	−0.6
8.00	5.00	4.50	7.80	4.98	4.51	−2.5	−0.4	+0.2
6.00	4.00	4.20	5.78	4.01	4.18	−3.7	+0.3	−0.5
7.00	8.00	3.00	6.87	7.91	2.99	−1.9	−1.1	−0.3
9.00	8.00	2.40	9.00	7.94	2.39	0.0	−0.8	−0.4
11.00	5.00	2.40	10.61	4.97	2.37	−3.6	−0.6	−1.3
5.00	5.50	4.80	5.04	5.38	4.76	+0.8	−2.2	−0.8
					SEP:	0.22	0.06	0.04

[a] Mean values of five determinations.

intercepts. The test revealed the absence of systematic errors in the determination of ASA by either method at a significance level of $p = 0.01$. Also, no systematic error was detected in the determination of AAP by MLR at $p = 0.1$ or by PLS-2 at $p = 0.01$. Finally, no systematic error was found for CAF as determined by MLR ($p = 0.05$) or PLS-2 ($p = 0.01$).

The precision of the proposed methods was determined by one-way ANOVA of six replicates processed on three consecutive days. Snedecor's F values were all below the tabulated value ($F = 3.68$, $n_1 = 2$, $n_2 = 15$), so there were

no significant differences between the results obtained in the determination of each pharmaceutical in the presence of the other two on different days.

4.5. Interferences

In order to apply these methods for the analysis of a pharmaceutical dosage form, the influences of commonly used excipients and tablet additives for these drugs were investigated. No interferences could be observed when up to a 100-fold excess of saccharose, glucose, cellulose,

Table 2
Simultaneous determination of ASA, AAP and CAF in different synthetic mixtures using PLS-2 prediction method

Amount added (μg ml^{-1})			Amount found[a] (μg ml^{-1})			Error (%)		
ASA	AAP	CAF	ASA	AAP	CAF	ASA	AAP	CAF
10.00	7.00	5.40	9.69	6.98	5.26	−3.1	−0.3	−2.6
10.00	6.00	4.80	9.87	5.97	4.73	−1.3	−0.5	−1.5
8.00	5.00	4.50	7.80	4.97	4.49	−2.5	−0.6	−0.2
6.00	4.00	4.20	5.79	4.00	4.15	−3.5	0.0	−1.2
7.00	8.00	3.00	6.88	7.89	2.97	−1.7	−1.4	−1.0
9.00	8.00	2.40	9.00	7.94	2.39	0.0	0.8	−0.4
11.00	5.00	2.40	10.61	4.95	2.34	−3.6	−1.0	−2.5
5.00	5.50	4.80	5.05	5.37	4.74	+1.0	−2.4	−1.3
					SEP:	0.21	0.07	0.06

[a] Mean values of five determinations.

Table 3
The results of standard additions method applied to commercial pharmaceutical determinations[a]

Pharmaceutical preparation	Amount from pharmaceutical[b] (mg ml⁻¹)			Amount found (mg ml⁻¹)			Recovery ± SD[c]		
	ASA	AAP	CAF	ASA	AAP	CAF	ASA	AAP	CAF
MLR method									
Fiorinal Sandoz oral	20.0	30.0	4.0	42.3	59.1	7.7	106 ± 1	98.5 ± 0.8	96 ± 2
Cerebrino Mandri	25.0	20.0	2.0	53.9	43.2	4.1	100 ± 2	108 ± 1	102 ± 1
Neocibalena	20.0	15.0	5.0	37.7	31.2	11.4	94 ± 2	104 ± 2	114 ± 1
PLS method									
Fiorinal Sandoz oral	20.0	30.0	4.0	41.3	58.8	7.8	103.3 ± 0.8	98 ± 1	97.5 ± 0.8
Cerebrino Mandri	25.0	20.0	2.0	52.8	40.8	4.1	105.6 ± 0.9	102 ± 1	103 ± 1
Neocibalena	20.0	15.0	5.0	41.1	32.0	10.9	102.8 ± 0.6	106.7 ± 0.9	109 ± 1

[a] The amount added was equal to the declared content of the pharmaceutical preparations.
[b] Obtained by dilution of commercial preparations.
[c] Mean of five determinations.

lactose or starch was added to the synthetic mixtures to be analysed, for either of the methods.

Concerning the degradation products of the drugs, salicylic acid is the major degradation product interference, probably as a result of ASA hydrolysis into salicylic acid and acetic acid, but this effect is observed 10 h after the ASA solution was prepared. In order to avoid the hydrolysis of ASA, all experiments were made using fresh solutions.

4.6. Applications

The proposed methods were used to determine the three drugs in various pharmaceutical preparations: Fiorinal Sandoz Oral (capsules), Cerebrino Mandri (granules) and Neocibalena (tablets). These preparations are administered to patients with rheumatic or neuralgic pain (with or without concomitant fever).

The impurities and degradation products which may be encountered in pharmaceutical dosages, besides ASA, are: acetylsalicylic anhydride (0.0012–0.024%) and acetylsalicylsalicylic acid (0.03–0.1%); acetaminophen, p-aminophenol ($\not> 0.025\%$), p-chloroacetanilide (≤ 10 ppm), o-acetylacetaminophen (1.1–1.3%), inorganic chloride ($\not> 0.014\%$), inorganic sulfate (0.02%) and water ($\not> 0.5$). None of these impurities are in quantities to be of significant interference in the determination of the drugs. Moreover, the pharmacopeia limits for these drugs in the pharmaceutical preparations are between 90 and 110%.

Recovery studies of standard additions to commercial pharmaceuticals were also carried out to provide further support for the validity of the

Table 4
Simultaneous determination of ASA, AAP and CAF in pharmaceutical preparations using the MLR prediction method

Pharmaceutical preparations	Label claim (mg)			Amount found (mg)[a]			Error (%)		
	ASA	AAP	CAF	ASA	AAP	CAF	AAP	AAP	CAF
Fiorinal Sandoz oral	200	300	40	201.5	289.1	39.7	+0.8	−3.6	−0.8
Cerebrino Mandri	250	200	20	280.8	203.3	21.0	+12.3	+1.7	+5.0
Neocibalena	200	150	50	190.3	153.0	52.5	−4.9	+2.0	+5.0

[a] Mean values of five determinations.

Table 5
Simultaneous determination of ASA, AAP and CAF in pharmaceutical preparations using the PLS-2 prediction method

Pharmaceutical preparations	Label claim (mg)			Amount found (mg)[a]			Error (%)		
	ASA	AAP	CAF	ASA	AAP	CAF	ASA	AAP	CAF
Fiorinal Sandoz oral	200	300	40	201.8	288.8	39.1	+0.9	−3.7	−2.3
Cerebrino Mandri	250	200	20	280.8	203.3	21.0	+12.3	−1.7	+5.0
Neocibalena	200	150	50	203.4	150.9	54.3	+1.7	+0.6	+8.6

[a] Mean values of five determinations.

proposed methods. The related data are given in Table 3; the mean percentage recoveries and their standard deviations. The results also confirm the precision and validity of the proposed methods.

Tables 4 and 5 show the results obtained in the simultaneous determination of the three drugs in the above-mentioned pharmaceutical preparations using MLR and PLS-2. As can be seen, all were consistent with the manufacturer's certified contents and the results are with the limits allowed by the Spanish Pharmacopeia.

5. Conclusions

Based on the results obtained in this work, application of multivariate calibration to the absorbance signals produced by drugs during their simultaneous determination in pharmaceutical preparations is an effective means for quality control of their manufacture. The ensuring methods are simple, precise and affordable; also, they require no complex pretreatment or chromatographic separation of the samples containing the active principles to the determined. Overall, they make a viable alternative to existing analytical methods for routine analyses.

Acknowledgements

References

[1] T.C. O'Haver, Anal. Chem., 51 (1979) 91A.
[2] F. Salinas, J.J. Berzas and A. Espinosa, Talanta, 37 (1990) 347.
[3] M. Blanco, J. Coello, F. González, H. Iturriaga and S. Maspoch, Anal. Chim. Acta, 226 (1989) 271.
[4] H. Wold, Perspectives in Probability and Statistics, Academic Press, London, 1975.
[5] H. Martens and T. Naes, Multivariate Calibration, John Wiley & Sons, New York, 1989.
[6] B.G.M. Vandeginste, W. Derks and G. Kateman, Anal. Chim. Acta, 173 (1985) 253.
[7] H. Gampp, M. Maeder, Ch. Meyer and A.D. Zuberbühler, Anal. Chim. Acta, 193 (1987) 287.
[8] F. Onur and N. Acar, FABAD Farm. Bilimler Derg, 14(1) (1989) 1.
[9] Y. Wang, G. Lio, Z. Wang and G. Zhou, Gaodeng Zuexiao Huaxue Xuebao, 10(10) (1989) 990.
[10] V. Das Gupta, J. Pharm. Sci., 69(1) (1980) 110.
[11] M.G. Mamolo, L. Vio and V. Maurich, Farmaco, Ed. Prat., 40(4) (1985) 111.
[12] A.A. Mustafa, E.A. Mohamed and A.I. El-Sebai, Anal. Lett., 22(2) (1989) 365.
[13] Y. Wang, J. Yang, S. Dong and G. Luo, Nanjing Yauxueyuan Xuebao, 17(4) (1984) 270.
[14] A. Van Loosbroek, H.J.G. Debets and P.M.J. Coenegracht, Anal. Lett., 17(B9) (1984) 779.
[15] D.L. Massart et al., Chemometric: A Textbook, Elsevier Science, Amsterdam, 1988.
[16] J. Havel, in J. Havel and M. Holík (Eds.), Proc. Chemometrics II, 2nd Czech. Chemometrics Conf., Brno, Czechoslovakia, 1990.
[17] V. Cerdá, J.M. Estela, R. Forteza, A. Cladera and E. Gómez y M.T. Oms, Int. J. Environ. Anal. Chem., 52 (1993) 159.
[18] Unscrambler v.5.0, Computer-Aided Modelling A/S, Trondheim, Norway, 1993.
[19] J. Mandel and F.J. Linnig, Anal. Chem., 29 (1957) 743.

Extraction and determination of crown ethers from water samples using a membrane disk and gas chromatography

Yadollah Yamini[a], Mojtaba Shamsipur[b,*]

[a]Department of Chemistry, Tarbiat Modarres University, Tehran, Iran
[b]Department of Chemistry, Razi University, Kermanshah, Iran

Abstract

A method for rapid extraction and determination of some crown ethers in aqueous matrices using octadecyl-bonded silica membrane disks and gas chromatography is presented. Extraction efficiency and the influence of vacuum pressure, pH, and type and least amount of eluting solvent used to extract the crown ethers from the membrane disks were evaluated. Extraction efficiencies > 95% were obtained for benzo-15-crown-5, benzo-18-crown-6 and dicyclohexyl-18-crown-6 using 5 ml of acetonitrile as eluting solvent. The limit of detection of the proposed method for the determination of the crown ethers is reported.

Keywords: Crown ethers; Gas chromatography; Membrane disk; Solid-phase extraction

1. Introduction

Macrocylic crown ethers, first synthesized by Pedersen [1], have been extensively used to selectively separate metal ions from their mixtures by solvent extraction [2–8] or by liquid membranes [9–15]. However, bleeding of crown ethers from the organic phase of the liquid membranes or solvent extraction systems, even at low levels, into the aqueous phases [14,16] causes complications in the separation process.

The problem of crown bleeding can be overcome by covalently attaching the macrocylces to

silica gel [17,18] or by using polycrown ethers [19,20]. Moreover, the precipitates of crown ethers with phosphomolybdic acid and phosphotungstic acid [21] and the coating of macrocyclic ligands on hydrophobic silica gel [7] have also been used to reduce the leaching of crown ethers during separation processes. However, even in these cases, crown ether bleeding can occur to some extent when aqueous samples containing metal ion or mineral acids as stripping agents are passed through the separation columns. Thus, to evaluate the efficient age of the columns, the development of methods for preconcentration and determination of low levels of crown ether bleeding into aqueous phases is of great importance.

---

* Corresponding author.

The use of classical methods of extraction for this purpose are usually time-consuming, labor-intensive and require large amounts of high purity solvents for extraction. Nevertheless, it is possible to extract the components of interest in the aqueous samples with minimal usage of organic solvents by means of solid-phase extraction (SPE) techniques [22]. In this method, the aqueous sample first passes through a cartridge or tube containing an adsorbent that retains the analytes. Then the analytes are eluted from the adsorbent using a minimal amount of a suitable organic solvent. The main limitation of the SPE cartridges and tubes is the tendency for fine particulates to plug the frits holding the adsorbent in place. However, this problem can be overcome by using flat disks with high cross-sectional area (SPE disks). The decreased back pressure encountered with the SPE disks makes much higher flow rates possible, and their wide bed decreases the chance of plugging. Recently, the SPE disks have been utilized for the extraction and determination of many different environmental matrices, such as pesticides, linear alkylbenzenesulfonates, polyaromatic hydrocarbons, etc. [23–30].

The aim of this work was the development of a rapid and efficient method for the extraction and determination of low levels of some crown ethers in aqueous media using a membrane disk and gas chromatography. Different experimental conditions, e.g. the type of eluting solvent, the effect of pH, the effect of vacuum pressure on extraction time and efficiency and the minimum amount of eluting solvent necessary to wash the disk, have been studied.

2. Experimental

2.1. Reagents

HPLC-grade methanol, acetonitrile, ethylacetate and dichloromethane (all from Aldrich) were used without any further purification. Reagent-grade 12-crown-4, 15-crown-5 (15C5), benzo-15-crown-5 (B15C5), 18-crown-6 (18C6), benzo-18-crown-6 (B18C6) and dicyclohexyl-18-crown-6 (DC18C6) were of the highest purity available

from Merck and were used as received. Standard solutions of crown ethers were prepared by dilution of different volumes of their 1000 ppm solutions to 500 ml with deionized water.

2.2. Sample extraction

Extractions were performed with 47 mm diameter × 0.5 thickness Empore membrane disks containing octadecyl-bonded silica (8 μm particles, 60 Å pore size) from J.T. Baker. The typical composition of the disks was 90% w/w octadecyl-bonded silica and 10% w/w PTFE fibers. The disks were used in conjunction with a standard Millipore 47 mm filtration apparatus.

Before extraction, each membrane was washed with 10 ml of eluting solvent to remove all contaminants arising from the manufacturing process and from the environment. After placing the membrane in the filtration apparatus and drawing air through the disk for several min, 10 ml of methanol was introduced into the reservoir of the apparatus and drawn slowly through the disk by applying a slight vacuum until a thin layer of methanol was left on the surface of the disk. Finally, a 10 ml portion of deionized water was used to rinse methanol. This step pre-wets the surface of the disk prior to extraction of crown ethers from water.

Immediately after completion of the washing process, 500 ml of water containing 2 mg of each crown ether was passed through the disk for about 10–22 min by applying a suitable vacuum. After drawing the aqueous sample through the disk, the vacuum was applied for an additional 5 min to remove the residual water from the disk. It is important to note that the surface of disk was not allowed to dry from the time the methanol was added until the extraction of crowns from water was completed.

After complete drying of the disk, the extraction funnel was transported to a second vacuum filtration flask containing a 25 mm × 200 mm test tube and the extracted crowns were eluted into the test tube by application of the eluting solvent. Then, the extract was completely transferred into a graduated cylinder and the solvent was evaporated to a final volume of 2 ml. 1 μl of this

solution was then injected onto the gas chromatograph. To demonstrate the efficiency of extraction of the membrane disk, the same concentration of crown ethers was prepared in 2 ml of the eluting solvent and a 1 μl portion of it was injected onto the gas chromatograph.

2.3. Apparatus

Gas chromatography was performed with a Philips Scientific model 4410 chromatograph equipped with a flame ionization detector and split/splitless injection, and fitted with a 25 m × 0.25 mm i.d. fused silica column coated with an immobilized film of BP-5. Nitrogen was used as the carrier gas at a flow rate of 1.5 ml min^{-1}. The injector and detector temperatures were 320°C and 300°C respectively. The oven temperature was 100°C for 0.5 min after injection and was then programmed at a rate of 20°C min^{-1} up to 300°C, where it was held for 5 min. The split ratio was 1:14. The pH measurements were carried out with a Metrohm pH-meter using a combined glass electrode.

3. Results and discussion

In this work octadecyl-bonded silica was evaluated for the extraction of crown ethers from their water samples. Deionized water spiked with low concentrations of crown ethers (4 mg l^{-1}) was extracted using membrane disks and the results obtained were compared with those from direct measurement of concentrated crown ethers using GC. Fig. 1 shows GC-flame ionization detection (FID) analysis of a crown ether mixture containing 12C4, 15C5, B15C5, 18C6, B18C6 and DC18C6, after membrane disk extraction and elution by acetonitrile. The elution order of the crowns used is the order of increasing molecular weight.

The membrane disk construction is similar to that of a reversed-phase column with a large diameter and short length. The use of smaller particles (8 μm, 60 Å pore diameter) and uniform packing in the disk results in a reasonable flow without excessive back pressure. The retention

mechanism of the SPE disk is based on the same sorption-desorption phenomena as in reversed-phase LC. In fact, the capacity factor determines whether a given compound can be quantitatively retained by the hydrophobic disk in an aqueous mobile phase, and whether it can be quantitatively eluted by an organic solvent. Also, as with LC columns, the efficiency of the extraction by membrane disks is a function of the particulate packing density and the linear velocity of the mobile phase through the stationary phase.

Table 1 illustrates the recovery data obtained for different crown ethers in water at a concentration of 4 mg l^{-1} using 10 ml of various eluting solvents. As can be seen, the capacity factor for 12C4 is almost zero and the amount of crown retained on the disk is negligible. 15C5 and 18C6 are retained on the disk very loosely and are easily washed off with water. However, for B15C5, B18C6 and DC18C6, due to their high lipophilic
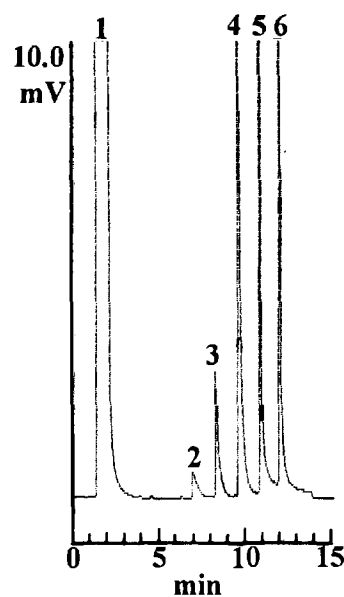
Fig. 1. GC–FID chromatogram obtained for 4 mg l^{-1} aqueous solutions of the crown ethers used after following the proposed procedure: (1) solvent; (2) 15C5; (3) 18C6; (4) B15C5; (5) B18C6; (6) DC18C6. Conditions: initial volume of aqueous solution, 500 ml; volume of acetonitrile, 10 ml; final volume of the eluted solution, 1 ml; injection volume, 1 μl split; oven temperature, 100°C for 0.5 min after injection, then programmed at 20°C min^{-1} to 300°C which was held for 5 min.

Table 1
Percent recovery of crown ethers from membrane disk using 10 ml of different solvents at pH 6.8 and a vacuum pressure of 510 mmHg

Crown ether	Solvent			
	Methanol	Acetonitrile	Ethylacetate	Dichloromethane
12C4	0	0	0	0
15C5	4.2(1.1)[a]	4.4(5.7)	4.5(16.0)	5.2(6.5)
18C6	16.6(6.0)	19.5(5.8)	12.9(8.9)	15.9(5.0)
B15C5	72.4(12.4)	96.8(0.2)	84.0(7.4)	87.8(3.7)
B18C6	90.7(1.8)	98.6(4.8)	90.4(2.3)	91.8(4.5)
DC18C6	92.0(2.5)	101.3(5.7)	98.3(4.0)	99.0(2.8)

[a] %RSD based on three replicate analyses.

character, the k' values are high and they are retained by the membrane disk very tightly. The data given in Table 1 represent the influence of the properties of the eluting solvent on the recovery of crown ethers. It is seen that, among the four different organic solvents used, acetonitrile possesses the highest elution efficiency. It is noteworthy that, since the injector and detector temperatures were quite high and the initial column temperature (i.e. 100°C) was also much higher than the boiling point of acetonitrile, the use of acetonitrile as the eluting solvent resulted in no practical problem in GC measurements.

The influence of vacuum pressure (flow rate) on the percentage recoveries of the crown ethers used was studied in the range 560–710 mmHg. It was found that there is no recognizable correlation between flow rate and percentage recoveries of 2 mg of crown ether from 500 ml of deionized water. Similar results have been reported before [23,27,31].

It is well known that the packing density and linear velocity through membranes are two important factors in determining the effectiveness of reversed-phase interactions. An LC column of 4.6 mm i.d. at a flow rate of 1.5 ml min^{-1} possesses a linear velocity of 0.15 cm s^{-1} [23]. An SPE cartridge of 10.0 mm i.d. when used to process 1000 ml of water in 2 h, as recommended in the EPA Method 525 [32], has approximately the same linear velocity of 0.18 cm s^{-1}. The 47 mm i.d. EPA disk used in this study under a linear velocity of 0.18 cm s^{-1} has

a flow rate of 187.4 ml min^{-1}; thus, the optimum time for the extraction of crown ethers will be some 3 min. Obviously, for longer periods of time, the efficiency of extraction (and also the percentage recovery) is expected to be affected by the vacuum pressure only slightly.

In order to investigate the effect of pH on the SPE of crown ethers, the pH of aqueous samples was varied from 3 to 7, using perchloric acid, and the recommended procedure was followed at a vacuum pressure of 510 mmHg using 10 ml of acetonitrile as eluting solvent. It was found that, especially for more lipophilic crown ethers, the percentage recovery is nearly independent of pH. It is interesting to note that a similar pH effect has already been reported for the solvent extraction separation of different metal ions with crown ethers [4,33]. The results indicate that due to the negligible degree of protonation of crown ethers, their lipophilicity will remain unaffected by the existence of protons in solutions, even at an acid concentration of 10^{-3} M.

The least amount of acetonitrile necessary for the quantitative elution of crown ethers from the disk was studied and the results are given in Table 2. It is seen that 5.0 ml of acetonitrile seems to be adequate for the complete elution of crown ethers from the membrane disk. Under such conditions a pre-concentration factor of 100 will be obtained in transferring the crown ethers from the initial aqueous phase into the acetonitrile as eluting solvent.

Table 2
Percent recovery of crown ethers from membrane disk using different volumes of acetonitrile at pH 6.8 and 510 mmHg

Crown ether	Volume of acetonitrile (ml)			
	2.5	5.0	7.5	10.0
15C5	1.3(3.0)	1.4(0.5)	3.4(0.8)	4.4(5.7)
18C6	6.5(4.1)	9.7(6.0)	16.0(1.4)	19.5(5.8)
B15C5	71.4(1.6)	95.8(5.0)	95.3(2.1)	96.8(0.2)
B18C6	74.3(2.9)	104.7(4.1)	102.7(0.8)	98.6(4.8)
DC18C6	79.9(4.5)	103.4(4.1)	101.5(2.3)	101.3(5.7)

The limit of detection (LOD) of the proposed method for the determination of crown ethers with quantitative extraction efficiencies (i.e. B15C5, B18C6 and DC18C6) was studied under the optimal experimental conditions discussed. The LOD values obtained for B15C, B18C6 and DC18C6 are 0.07, 0.17 and 0.29 μg ml^{-1} respectively. It is interesting to note, however, that by using a 100 μl portion of the samples and a 4 min delay after injection (instead of 0.5 min) the LOD could be easily reduced to a part per billion level.

The results of this study demonstrate that the SPE using a membrane disk produces acceptable precision and accuracy data for the lipophilic crown compounds. This extraction–GC technique provided advantages in terms of analysis time, solvent use and solvent disposal. The basis of extraction is similar to reverse-phase LC. The capacity factor is very small for the more hydrophilic macrocycles 12C4, 15C5 and 18C6 so that these compounds could not be retained completely by the disk. In contrast, the more lipophilic crowns B15C5, B18C6 and DC18C6 with high capacity factors were retained completely by the disk. Finally, 5 ml of acetonitrile is enough for complete elution of the crown ethers B15C5, B18C6 and DC18C6 from the membrane disk. These crown ethers could be determined at sub microgram per milliliter levels.

References

[1] C.J. Pedersen, J. Am. Chem. Soc., 89 (1967) 7017.
[2] M. Yoshio and H. Noguchi, Anal. Lett., 15 (1982) 1197.
[3] L.M. Tsay, J.S. Shih and S.C. Wu, Analyst, 108 (1983) 1108.
[4] B.S. Mohite and S.M. Khopkar, Talanta, 32 (1985) 565.
[5] H. Koshima and H. Onishi, Analyst, 111 (1986) 1261.
[6] Y.Y. Vin and S.M. Khophar, Ind. J. Chem., 24A (1988) 458.
[7] B.S. Mohite, C.D. Jadage and S.R. Pratap, Analyst, 115 (1990) 1367.
[8] E.P. Horwitz, M.L. Dietz and D.E. Fisher, Anal. Chem., 63 (1991) 552.
[9] M. Dozol, in C. Cecille, M. Casarci and L. Pietrelli, (eds.), New Separation Chemistry Techniques for Radioactive Waste and other Specific Applications, Elsevier, New York, 1991.
[10] R.M. Izatt, G.A. Clark, J.S. Bradshaw, J.D. Lamb and J.J. Christensen, Sep. Purif. Methods, 15 (1986) 21.
[11] R.M. Izatt, R.L. Bruening, W. Geng, M.H. Cho and J.J. Christensen, Anal. Chem., 59 (1987) 2405.
[12] T. Delloye, M. Burgard and M.J.F. Leroy, New J. Chem., 13 (1989) 139.
[13] H. Parham and M. Shamsipur, J. Membr. Sci., 86 (1994) 29.
[14] H. Parham and M. Shamsipur, J. Membr. Sci., 95 (1994) 21.
[15] M. Akhond and M. Shamsipur, Sep. Sci. Technol., 30 (1995) 3061.
[16] L.F. Lindoy and D.S. Baldwin, Pure Appl. Chem., 61 (1989) 909.
[17] J.S. Bradshaw, K.E. Karakowiak, B.J. Tarbet, R.L. Bruening, J.F. Biernat, M. Bochenska, R.M. Izatt and J.J. Christensen, Pure Appl. Chem., 61 (1989) 1619.
[18] S.L. Da, W.G. Wu, Y.F. Wen, H.L. Da and Z.H. Weng, Anal. Chim. Acta, 299 (1994) 239.
[19] B.S. Mohite, J.M. Patil and D.N. Zambare, Talanta, 40 (1993) 1511.
[20] B.S. Mohite, D.N. Zambare and B.E. Mahadik, Analyst, 119 (1994) 2033.
[21] D.L. Tzeng, J.S. Shih and Y.C. Yeh, Analyst, 112 (1987) 1413.
[22] R. Majors, LC–GC, 4 (1989) 972.
[23] D.F. Hagen, C.G. Markell, G.A. Schmitt and D.D. Blevins, Anal. Chim. Acta, 236 (1990) 157.
[24] E.R. Brouwer, H. Lingeman and U.A. Th. Brinkman, Chromatographia, 29 (1990) 415.
[25] S. Chiron, A.F. Alba and D. Barcelo, Environ. Sci. Technol., 27 (1993) 2352.
[26] I.J. Barnabas, J.R. Dean, S.M. Hitchen and S.P. Owen, Anal. Chim. Acta, 291 (1994) 261.
[27] Y. Yamini and M. Ashraf-Knorasani, J. High Resolut. Chromatogr., 17 (1994) 634.
[28] J.S. Ho, P.H. Tang, J.W. Eichelberger and W.L. Budde, J. Chromatogr. Sci., 33 (1995) 1.
[29] D.C. Messer and L.T. Taylor, J. Chromatogr. Sci., 33(1995) 290.
[30] T.S. Thompson and L. Morphy, J. Chromatogr. Sci., 33 (1995) 393.
[31] J.J. Richard and G.A. Clark, Mikrochim. Acta, (1986) 387.

[32] J.W. Eichelberger, T.D. Behymer and W.L. Budde, Determination of Organic Compounds in Drinking Water by Liquid–Solid Extraction and Capillary Column Gas Chromatography/Mass Spectrometry, EPA Method 525, Environmental Monitoring Systems Laboratory, U.S. Environmental Protection Agency, Cincinnati, OH, 1988.

[33] B.S. Mohite and S.M. Khopkar, Anal. Chem., 59 (1987) 1200.

Spectrophotometric and polarographic investigation of the ofloxacin–Cu(II) complexes

V. Kapetanović*, Lj. Milovanović, M. Erceg

Faculty of Pharmacy, University of Belgrade, Belgrade, Yugoslavia

Received 10 October 1995; revised 23 February 1996; accepted 15 May 1996

Abstract

By means of spectrophotometric methods it was found that ofloxacin reacts with copper(II) ions to form complexes with molar ratios of ofloxacin: Cu(II) of 1:1 at pH 4.00, 2:1 at pH 7.02 and 3:1 at pH 8.30. The stability constants of the complexes were determined. The formation of ofloxacin:Cu(II) 1:1 and 3:1 complexes was confirmed by a polarographic method and the corresponding overall stability constant was evaluated.

Keywords: Cu(II)–Ofloxacin complexes; Polarography; Spectrophotometry; Stability constants

1. Introduction

Ofloxacin, [9-fluoro-2,3-dihydro-3-methyl-10-(4-methyl-1-piperazinyl)-7-oxo-7H-pyrido-[1,2,3-de]-1,4-benzoxazine-6-carboxylic acid], is one of the 4-quinolone synthetic antibiotics (Fig. 1). As can be seen, ofloxacin possesses two relevant ionizable functional groups: a basic piperazinyl group in the 4'-position ($pK_{a,2} = 8.22$ [1] and 7.90 [2]) and a carboxylic acid group in the 6-position ($pK_{a,1} = 6.05$ [1] and 5.70 [2]). Ofloxacin belongs to the quinolone class of broad spectrum antibiotics developed during the last decade [3]. Quinolones are active against many gram-positive and gram-negative bacteria [4–6]. All quinolones possess a carboxylic acid moiety and the carbonyl group required for antimicrobial activity that is also thought to be a site of chelation interaction with various cations. A potential problem with the increasing use of quinolone-type antibiotics for treatment of systematic illness is the chelation and interaction of these compounds by several cations [7]. One outcome of these potential interactions could be a reduction in the bioavailability and effectiveness of quinolone compounds. This is especially emphasized when these drugs are co-administered with antacids or with vitamin preparations.

Quinolones also effect trace metal metabolism, being potent inhibitors of some copper- and zinc-dependent enzymes [8]. For this reason the complexing ability of these ligands with some essential bioelements in serum (Fe(III), Cu(II) etc.), as well as with Al(III) and Mg(II) ions in antacids is of special interest. The complexation of lomefloxacin with Al(III), Ca(II), Mg(II), Bi(III) and Fe(III) ions commonly found in antacid or vitamin

---

* Corresponding author.

NALIDIXIC ACID

CIPROFLOXACIN   OFLOXACIN

ENOXACIN   NORFLOXACIN

LOMEFLOXACIN   CINOXACIN
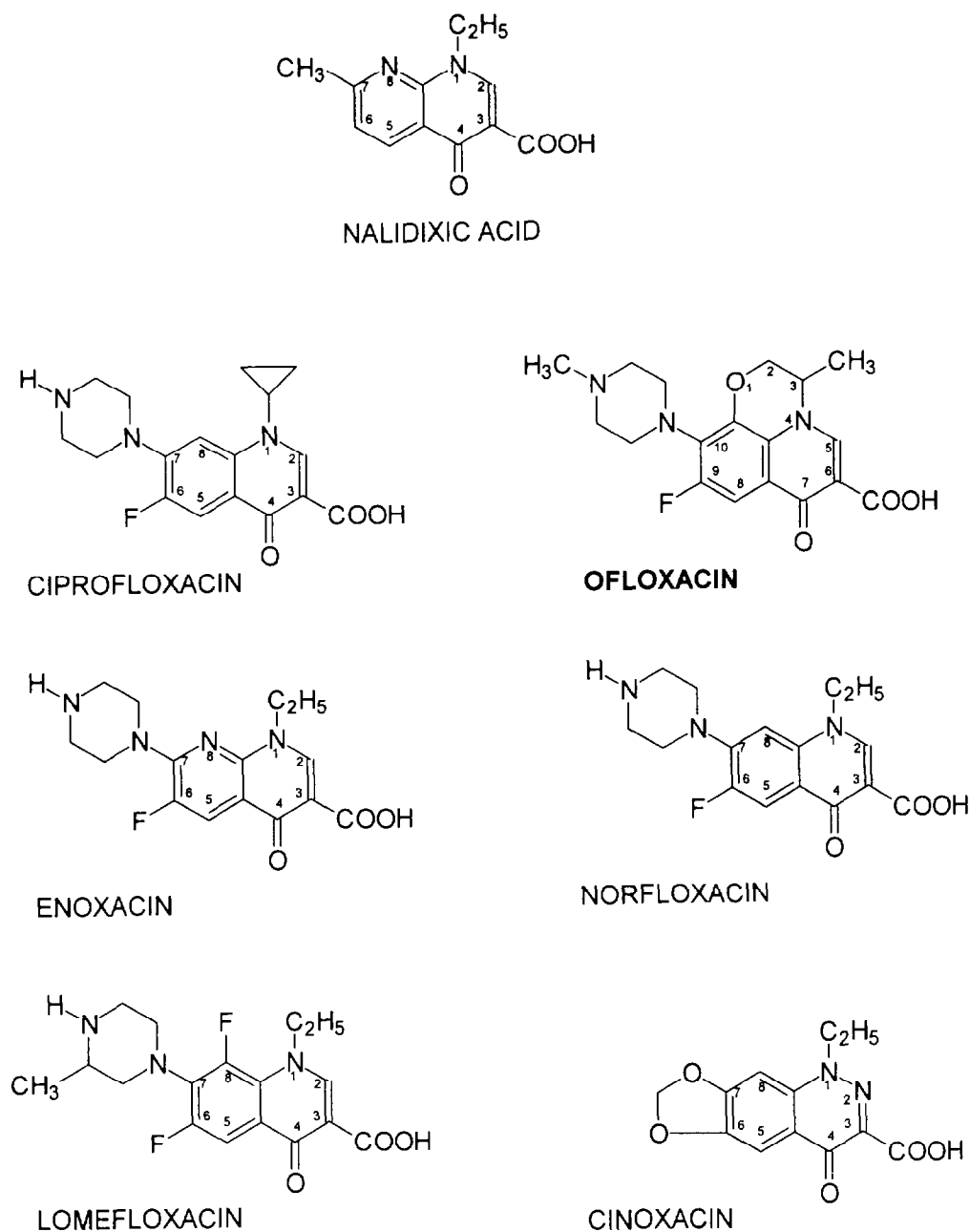
Fig. 1. Structures of selected quinolones.

preparations was studied [9]. Two complexes, proposed to have stoichiometries of 2:1 and 3:1 (drug to metal), were observed. The metal complexes of cinoxacin with Ni(II) and Zn(II) ions were synthesized and isolated [10]. The crystal and molecular structures of the complexes were determined by X-ray structure analysis. It was shown that two cinoxinate ligands bind metal ions through one carboxylate oxygen atom and the exocyclic carbonyl oxygen atom. The complexation of two model compounds, lomefloxacin and norfloxacin, with Al(III) ions was studied using NMR [11].

Two complexes, proposed to have stoichiometries of 2:1 and 3:1 (drug:metal), were observed.

The reactions of ciprofloxacin and ofloxacin with Al(III), Mg(II), Ca(II) and Fe(II) ions in aqueous medium were studied using different spectroscopic techniques [12]. Formation constants of the 1:1 Fe(III) complexes of ciprofloxacin, enoxacin and ofloxacin [13] were determined by spectrophotometry. The optimum pH for complexation was found to be 3.8. The stability constant of the Oflx–Fe(III) complex was found to be $\log \beta_1 = 6.98$. The stability constants of lomefloxacin with Al(III), Ca(II), Mg(II), Mn(II), Fe(II), Co(II), Ni(II), Zn(II) and Cu(II) ions were determined by potentiometry [14]. Three complexes, with drug:metal molar ratios of 1:1, 2:1 and 3:1, were found in all cases except Ca(II) and Fe(II), where the formation of only 1:1 complexes was established. The stability constants for Cu(II)–lomefloxacin complexes were: $\log \beta_1 = 6.16$, $\log \beta_2 = 10.96$ and $\log \beta_3 = 13.41$. The same authors reported the stability constants for ofloxacin complexes of Ca(II), $\log \beta_1 = 2.12$; Mg(II), $\log \beta_1 = 2.82$, $\log \beta_2 = 5.48$; and Al(III), $\log \beta_1 = 7.13$, $\log \beta_2 = 12.53$ and $\log \beta_3 = 17.87$. No literature date were found for Cu(II)–ofloxacin complexes.

In this work the equilibria of ofloxacin–Cu(II) complexes were studied by applying spectrophotometric and polarographic methods.

2. Experimental

2.1. Apparatus

The following equipment was used: a PHM-62 Radiometer (Denmark) pH-meter with combined GK 2401B electrode, a UV–Vis Varian Super Scan 3 spectrophotometer with 1 cm quartz cells and a PAR-174A polarograph connected to a three-electrode cell (dropping mercury electrode, DME, saturated calomel electrode, SCE and Pt auxilary electrode). Differential-pulse polarography (DPP) was performed under the following conditions: forced drop time, 2 s; modulation amplitude, 25 mV; scan rate 2 mV s^{-1}; and mercury column height, 81 cm.

2.2. Reagents

All chemicals were of analytical-reagent grade and demineralized distilled water was used throughout. Ofloxacin working standard and Visiren tablets were from Jugoremedija (Zrenjanin, Yugoslavia). $Cu(NO_3)_2$, NaOH and $NaNO_3$ were p.a. grade (Merck).

2.3. Ofloxacin (oflx) stock aqueous solution

A 4×10^{-3} M solution was prepared by dissolving the appropriate amount of ofloxacin standard in demineralized water. 10^{-1} M $Cu(NO_3)_2$ stock solution was standardized by a complexometric method. Britton–Robinson buffer [15] (0.08 M) was used for investigations in the pH range 4.02–10.02. 2 M $NaNO_3$ solution was used to maintain constant ionic strength.

2.4. Procedure for calibration graph

Oflx solution, 2×10^{-3} M (0.25–2.5 ml), $Cu(NO_3)_2$ solution, 2×10^{-2} M (0.5 ml), and Britton–Robinson buffer pH 4.5 (5 ml) were pipetted into a 10 ml volumetric flask. After addition of 1 ml of 2 M sodium nitrate solution, the reaction mixture was diluted to 10 ml with water. The solution was mixed and the absorbance was measured at a wavelength of 360 nm against Oflx as the reagent blank. All measurements were performed at room temperature (25 ± 0.5°C).

2.5. Procedure for determination of oflx in pharmaceutical formulations

Sample amounts equivalent to the average weight of one 200 mg tablet of Oflx were weighted from a combined amount of 10 Visiren tablets. This procedure was used to compensate for any variation in the weights of individual tablets. Each sample was transferred with water to a 500 ml volumetric flask to make the final concentration of the solution approximately the same as that of the standard stock solution. An aliquot of the tablet sample was used in the same procedure as that described in Section 2.4.

3. Results and discussion

3.1. Absorption spectra

The reaction of Oflx with Cu(II) ion was investigated over the pH range 4.02–10.02 in Britton–Robinson buffer. The spectra were recorded at 350–450 nm. Since Cu(II) ion had no absorbance in this wavelength range and Oflx showed a high absorbance value with a λ_{max} value of 330 nm (Fig. 2, curve 14), the spectra denoted 1–13 are due to the formation of a complex between Oflx and the Cu(II) ion.

3.2. Effect of pH

The absorption spectra of a mixture of 6×10^{-4} M Oflx and 1×10^{-4} M Cu(II) solutions were recorded at constant ionic strength, $I = 0.2$ M, and are shown in Fig. 2 (curves 1–13). On increasing the pH of the solution from 4.00 to 8.50 the peak corresponding to the maximum of the complex

Fig. 3. Job's curves of equimolar solution at pH 7.02 (a), 8.30 (b) and 4.00 (c). $C_{Cu(II)} + C_{Oflx} = 4 \times 10^{-4}$ M (a,b); $C_{Cu(II)} + C_{Oflx} = 6 \times 10^{-4}$ M (c).

absorbance underwent a slight bathochromic shift ($360 \rightarrow 366$ nm). The complex was found to exhibit a maximum absorbance in the pH range 4.00–5.52 ($\lambda_{max} = 360$ nm), 6.01–7.53 ($\lambda_{max} = 363$ nm) and 8.00–9.00 ($\lambda_{max} = 365$ nm). Further increase in the pH to pH 9.00 resulted in a slight decrease in the absorbance of the complex. At pH > 9.00, a pronounced decrease in the absorbance of the complex can be observed due to the hydrolytic processes (curves 12 and 13). The spectra obtained in the investigated pH range show that more than one complex species is formed in the solution.

Further investigations were performed at the pHs where λ_{max} was constant, i.e. pH 4.00, 7.02 and 8.30.

3.3. Composition of the complexes

Job's method [16] of equimolar solution showed that 1:1, 2:1 and 3:1 Oflx:Cu(II) complexes were formed at pH 4.00, 7.02 and 8.30 respectively (Fig. 3a, 3b and 3c respectively). The Bent–French method [17] was used to find the number of Cu(II) ions in the complex. It was found that one Cu(II) ion participates in the formation of the complexes (the slope of $-\log A$ versus $-\log$ Cu(II) ion was 0.94).
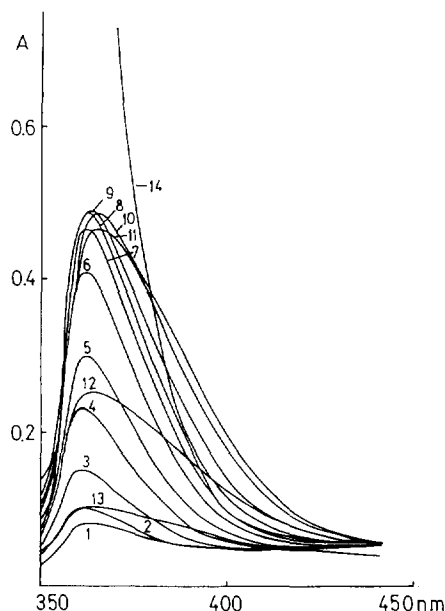

Fig. 2. Absorption spectra of the system Oflx–Cu(II) at different pH values: (1) 4.02, (2) 4.50, (3) 5.00, (4) 5.52, (5) 6.01, (6) 6.50, (7) 7.02, (8) 7.53, (9) 8.00, (10) 8.50, (11) 9.00, (12) 9.52, (13) 10.02, (14) absorption spectrum of 6×10^{-4} M Oflx.
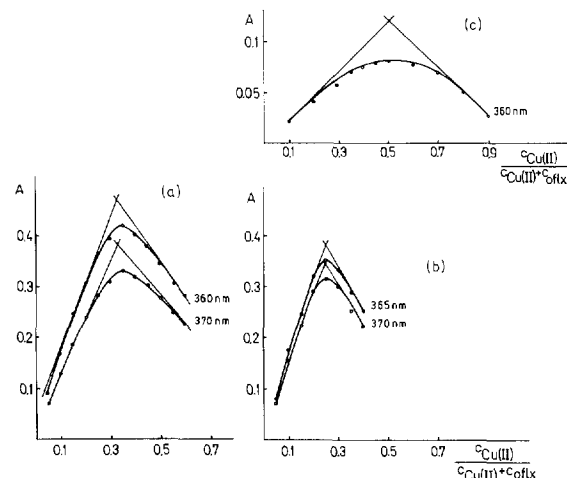
Table 1

Stability constants of Oflx–Cu(II) complexes obtained by different methods ($I = 0.2$ M, Britton–Robinson buffer, room temperature)

Method	pH 4.00		pH 7.02		pH 8.30	
	$\log \beta'_1$	$\log \beta_1$	$\log \beta'_2$	$\log \beta_2$	$\log \beta'_3$	$\log \beta_3$
Sommer and Tsin-Jao [18][a]	4.15	6.34 ± 0.07	9.68	10.31 ± 0.05	15.90	15.90 ± 0.07
Asmus [19]	4.35	6.54 ± 0.06	9.80	10.44 ± 0.04	16.20	16.20 ± 0.07
Lingane [21][b] (polarography)					16.30	16.30 ± 0.10
Leden [22][b] (polarography)	4.23	6.42 ± 0.09		–		

[a]Mean value of three determinations.
[b]Mean value of five determinations.

3.4. Stability constants of the complexes

The relative stability constants of the complexes were calculated according to the methods of Sommer and Tsin-Jao [18] and Asmus [19] and are presented in Table 1. Taking into account the following equilibria:

$$M + L \rightleftharpoons ML \tag{1}$$

$$\beta_1 = [ML]/[M][L] \tag{1'}$$

$$HL \rightleftharpoons H + L \tag{2}$$

$$K_{a,1} = [H][L]/[HL] \tag{2'}$$

where equilibrium (1) denotes the reaction of complex formation and (2) the reaction of ligand dissociation, the stability constant obtained under experimental conditions will be a conditional one and can be defined as

$$\beta'_1 = [ML]/[M][HL] \tag{3}$$

As Oflx is a weak acid, the concentration of L (according to equilibrium (2)) is strongly influenced by pH due to the protonation of the ligand. For this reason the real stability constant β_1 can be calculated using the following equation [20]:

$$\beta_1 = \beta'_1(1 + [H^+]/K_{a,1}) \tag{4}$$

where $[H^+]$ represents the hydrogen ion concentration (calculated from the activity at $I = 0.2$ M) and $K_{a,1} = 8.91 \times 10^{-7}$ is the first ionisation constant of Oflx [1]. As can be seen, the values of the stability constants obtained by different methods are in good agreement.

3.5. Polarographic investigations of the Oflx–Cu(II) complex

The peaks for Oflx ($E_p = -1.41$ V, curve 1), Cu(II) ion ($E_p = -0.06$ V, curve 2) and Oflx–Cu(II) mixture ($E_p = -0.29$ V, curve 3) obtained under the same experimental conditions of pH 7.50 (Britton–Robinson buffer, $I = 0.2$ M), are
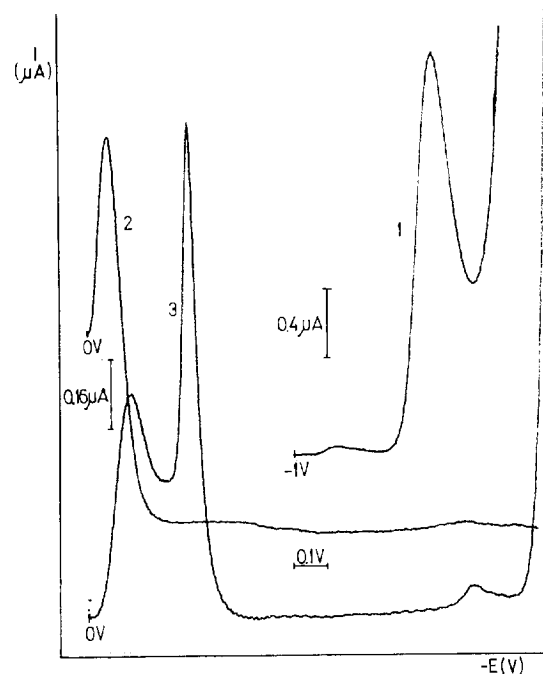

Fig. 4. DP polarograms of (1) 1×10^{-4} M Oflx, (2) 5×10^{-5} M Cu(II) and (3) Oflx–Cu(II) mixture (5×10^{-5} M Cu(II) and 3×10^{-4} M Oflx); pH 7.50 (Britton–Robinson buffer); $I = 0.2$ M (NaNO₃).
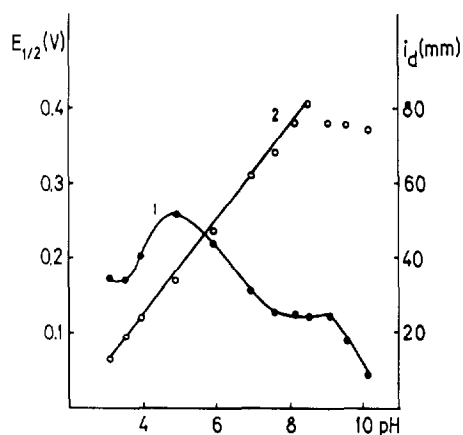
Fig. 5. Dependence of the Oflx-Cu(II) complex diffusion current (curve 1) and $E_{1/2}$ (curve 2) on pH.

shown in Fig. 4. The appearance of a new peak at $E_p = -0.29$ V is due to the reduction of the polarographically active complex formed between Oflx and the Cu(II) ion.

3.6. pH dependence of the Oflx-Cu(ii) ion

The dependence of the diffusion current and $E_{1/2}$ value of the Oflx-Cu(II) complex on pH is shown in Fig. 5. The Cu(II) ion and Oflx concentrations were constant: 1×10^{-4} M and 6×10^{-4} M respectively. As can be seen, the diffusion current of the complex increases on going from pH 3.15 to 5.00, where its maximum is attained. It then slowly decreases until pH 7.65, where it becomes constant. From pH 9.10 the complex current decreases abruptly. A plot of $E_{1/2}$ vs. pH (from 3.15-8.60) was a straight line with a slope of 0.062 V, showing that two hydrogen ions were involved in the electrode process. The shape of the plot of the diffusion current vs. pH can be explained by the presence of different ionic species in the solution, i.e. different complex species (the first from pH 3.15-5.00; the second from 5.00-7.65 and the third from 7.65-9.10). This effect is a consequence of different diffusion coefficients of the ionic species present in the solution. By logarithmic analysis of d.c. polarograms of log $\bar{i}_d - i/\bar{i}$ vs. E throughout the pH range investigated, the slope of the straight line of 62 mV was obtained, indicating a two-electron reversible electrode process.

3.7. Composition and stability constants of the complex

The metal-to-ligand ratio in the complex was determined by amperometric titration of a 1×10^{-4} M Cu(II) solution with Oflx (at concentrations of 1×10^{-4}–8×10^{-4} M) in Britton–Robinson buffer at pH 8.30. The stoichiometric ratio of Oflx to Cu(II) in the complex and the stability constant were determined by Lingane's method [21]. By plotting the dependence of the peak potential difference between the complexed and free Cu(II) ions, ΔE_p, against the logarithm of the Oflx concentration, a coordination number of three ($p = 2.7$) and a conditional stability constant, log β'_3, were calculated from the slope and intercept of the straight line ($r = 0.9921$). The average value of the stability constant from five titrations is presented in Table 1. The results obtained by applying both spectrophotometric and polarographic methods show that Oflx forms very stable complexes with Cu(II) ions. By applying Lingane's polarographic method it was possible to calculate the overall stability constant of the complex with the maximum coordination number.

The stability constant of the Cu(II)–Oflx complex at pH 4.00 was determined by Leden's method [22]. Amperometric titrations of 1×10^{-4} M Cu(II) ion with Oflx, in the concentration range 4×10^{-5}–1×10^{-4} M, were done at pH 4.00, $I = 0.2$ M (NaNO$_3$). A lower pH was used to follow the free Cu(II) wave height, i.e. by calculating the free metal ion concentration. Equilibrium concentrations of the metal, M, and complex, ML, were determined from the wave height of the free copper(II) ion, [Cu^{2+}], while equilibrium concentrations of the free ligand, [Oflx], were calculated from its analytical concentration and the concentration of the complex. According to Leden's equation:

$$F_{[\text{oflx}]} = \beta_1 + \beta_2[\text{Oflx}] \tag{5}$$

where F is $C_{Cu}^{2+} - [Cu^{2+}]/[Oflx]$ and C_{Cu}^{2+} represents the total analytical concentration of Cu(II) ion. By applying the method of least-squares or by plotting the dependence of Leden's function, F vs. [Oflx], a straight line parallel with the x axis

was obtained with an intercept of $\beta'_1 = 1.71 \times 10^4$. This finding suggests the formation of a 1:1 Cu(II): Oflx complex at pH 4.00. By applying the method of continuous variations at pH 4.00, 7.02 and 8.30 it was clearly shown that the ratio of Oflx:Cu(II) was 1:1, 2:1 and 3:1 respectively.

Since no literature data were found on Oflx–Cu(II) complexes, comparison of the results can be made with the stability constants of the metal complexes of other quinolones, i.e. lomefloxacin [14]. According to these authors, the stability constants of the three complexes of lomefloxacin with Cu(II) ion were established as $\log \beta_1 = 6.16$, $\log \beta_2 = 10.96$ and $\log \beta_3 = 13.41$. The same authors give the stability constants for Oflx–Al(III) complexes as $\log \beta_1 = 7.13$, $\log \beta_2 = 12.53$ and $\log \beta_3 = 17.87$. Our experimental results show good agreement with literature data for ofloxacin–Al(III) complexes ($\log \beta_1$), while the stability constants of higher complexes differ, particularly the $\log \beta_3$ values. By comparing the stability constants obtained with Cu(II)–lomefloxacin complexes, a good agreement is obtained with β_1 and β_2, while the stability constant β_3 is higher.

From a critical review [23] relating to the dissociation and complexation of fluoroquinolones it is seen that stability constants studied to date differ by less than two orders of magnitude. The carbon NMR spectrum of lomefloxacin [11] and Al(III) ion revealed that the carboxylic acid carbon and keto carbon signals both showed upfield shifts in the presence of Al(III) ion due to the direct binding of the C3 and C4 oxygens of carboxylic and carbonyl groups to Al(III) ion. The structure of the 3:1 (drug:Al(III)) complex was proposed to consist of three drug molecules bound to the quinolone molecule with an octahedral geometry about the Al(III) ion.

Although there is no definite evidence in the literature concerning the possibility of metal ion coordination through the N'-piperazinyl group, NMR and spectral data given by Okabayashi et al. [14] showed little change of the piperazine group by addition of the Al(III) and Mg(II) ions to lomefloxacin. Since the piperazinyl group was protonated under the conditions of measurement the authors considered that the chelation of the ligand occurred between the carbonyl and car-

boxyl groups. Bearing in mind that our complexation studies were carried out over a wide pH range there is no doubt that the N'-piperazinyl group is available for complexation because at higher pH this atom is not protonated (at pH 8.30 about 60% of the anionic form of ofloxacin is present in the solution).

There is also clear evidence for the existence of three complexes formed between Oflx and Cu(II) ion and good reason to suppose that the site of binding of the Cu(II) ion is at the two carboxylic groups. This can be supported by the fact that two hydrogen ions were involved in the reduction process at the DME (results obtained by polarography). Taking into account the literature data, the experimental parameters obtained and the great affinity of copper(II) ion for nitrogen it can be supposed that the N'-piperazine atom is involved in the complexation. The polarographic method applied enabled us to prove that the polarographic activity of Oflx itself (the reduction of the double bond of the azinone ring [24]) is distorted by the presence of Cu(II) ion. The same height and position of the polarographic waves obtained by scanning the samples of Oflx in the absence and presence of Cu(II) ion showed that the double bond of the azinone ring was not involved in coordination. Similar results were reported by Mendozza-Diaz and Pannell [25] relating to the coordination of Cu(II) ion with nalidixic acid.

An attempt was made to use the Oflx–Cu(II) complex for the analytical determination of Oflx by applying a spectrophotometric method at pH 4.5, where the effects of hydrolytic processes of the Cu(II) ion were minimized.

3.8. Quantification of linearity of calibration graph

Beer's law was tested at pH 4.5 ($I = 0.2$ M). A linear dependence between the absorbance of the complex and the Oflx concentration is observed over the range of 18–180 mg ml^{-1} Oflx. The regression equation is $y = 2.2062 + 589.36x$ and the correlation coefficient, $r = 0.9998$ ($n = 5$), shows good linearity.

Table 2
Spectrophotometric and polarographic determination of Oflx in Visiren tablets (200 mg)

Method	Sample ($n = 6$)			
	Expected (mg)	Found ($\bar{x}$, mg)	Recovery (%)	RSD (%)
Spectrophotometric	200	197.18	98.59	0.072
Polarographic	200	197.40	98.70	0.043

3.9. Applications to tablets

The proposed method was successfully applied to the assay of Oflx in Visiren tablets. The results obtained by the spectrophotometric method were compared with the results obtained by the direct polarographic method for the determination of ofloxacin previously described [26] and presented in Table 2. The method is simple and gives accurate and reproducible results.

References

[1] D.L. Ross and C.M. Riley, Int. J. Pharm., 63 (1990) 237.

[2] R.K. Chohen, Quinolone Bull., 3 (1987) 7.

[3] M. Neuman, Clin. Pharmacokinet. 14 (1988) 96.

[4] J. Joos, B. Ledergerber, M. Flepp, S.D. Bettex, R. Luthy and W. Siegenthaler, Antimicrob. Agents Chemother., 27 (1985) 353.

[5] J. Smith, Pharm. J., 233 (1984) 299.

[6] K. Sato, Y. Inoue, T. Fujii, H. Aoyama and M. Inoue, Antimicrob. Agents Chemother., 30 (1986) 777.

[7] M. Nakano, M. Yamamoto and T. Arita, Chem. Pharm. Bull., 26 (1978) 1505.

[8] J. Wagner, P. Vitali, J. Schoun and E. Giroux, Can. J. Chem., 55 (1977) 4028.

[9] D.L. Ross and C.M. Riley, Int. J. Pharm., 87 (1992) 203.

[10] M. Ruiz, R. Ortiz, L. Perello, A. Castineiras and M. Quiros, Inorg. Chim. Acta, 211 (1993) 133.

[11] C.M. Riley, D.L. Ross, D. Vandervelde and F. Takusagawa, J. Pharm. Biomed. Anal., 11 (1993) 49.

[12] B.M. Sanchez, M.M. Cabarga, A.S. Navarro and A.D.G. Hurle, Int. J. Pharm., 106 (1994) 229.

[13] D.S. Lee, H.J. Hau, K. Kim, W.B. Park, J.K. Cho and J.H. Kim, J. Pharm. Biomed. Anal., 12 (1994) 157.

[14] Y. Okabayashi, F. Hayashi, Y. Terui and T. Katagawa, Chem. Pharm. Bull., 40 (1992) 692.

[15] J.A. Coch-Frugoni, Gazz. Chim. Ital., 87 (1957) 403.

[16] P. Job, Ann. Chim., 9 (1928) 13.

[17] H. Bent and C. French, J. Am. Chem. Soc., 63 (1941) 568.

[18] L. Sommer and J. Tsin-Jao, Chem. Listy, 55 (1961) 574.

[19] E. Asmus, Z. Anal. Chem., 183 (1961) 321.

[20] J. Inczwdy, Analytical Applications of Complex Equilibria, 1st edn., Ellis Horwood, UK, 1976, p. 140.

[21] J.J. Lingane, Chem. Rev., 29 (1941) 1.

[22] J. Leden, Z. Phys. Chem., Abt. A, 188 (1941) 160.

[23] D.L. Ross and C.M. Riley, J. Pharm. Biomed. Analy., 12 (1994) 1325.

[24] W.J. Van Oort, R.H.A. Sorel, D. Brussee, P. Zuman and J. Den Hartgh, Anal. Chim. Acta, 149 (1983) 175.

[25] G. Mendozza-Diaz and K. Pannell, Inorg. Chim. Acta, 77 (1988) 152.

[26] V. Kapetanovič, Lj. Milovanovič, M. Erceg, D. Dumanovič and D. Sužnjevič, Extended Abstracts, 13th Yugoslav Symposium on Electrochemistry, Vrnjačka Banja, Yugoslavia, June, 1995, pp. 383–385.

Determination of autoprotolysis constants of some non-aqueous solvents using coulometric titration

R. Mihajlović*, Z. Simić, Lj. Mihajlović, M. Vukićević

Department of Chemistry, Faculty of Sciences, University of Kragujevac, R. Domanovića 12, Kragujevac, Yugoslavia

Abstract

Autoprotolysis constants of acetonitrile, propionitrile, nitromethane, ethylene carbonate and dimethyl sulphoxide were determined using a coulometric–potentiometric method with a hydrogen/palladium electrode as generator. The method is based on the titration of a strong base, tetrabutylammonium hydroxide, with H^+ ions generated by anodic oxidation of hydrogen dissolved in palladium. The titration was carried out in a galvanic cell with glass and calomel electrodes at 25°C. The pK_s values for the investigated solvents are: acetonitrile, 28.8; propionitrile, 24.6; nitromethane, 23.7; ethylene carbonate, 21.5; and dimethyl sulphoxide 29.1. These data are in accordance with those reported in the literature.

1. Introduction

Dipolar aprotic solvents (DAS) are widely used in the analytical chemistry of non-aqueous solvents.

Dimethyl sulphoxide (DMSO) is one of the best solvents in the DAS group as it dissolves well numerous inorganic and organic substances (hydrocarbons, sugar, starch, cellulose, proteins, polyamides and various heterocyclic compounds). It has a high dielectric constant ($\varepsilon = 47$), in the range 18–189°C it is in the liquid state, and its autoprotolysis constant is 33.3 [1]. Since many inorganic salts dissolve well in DMSO, there are many electrolytes which can be used for electrolysis in this solvent, such as $NaClO_4$, $LiCl$, $NaNO_3$, NH_4PF_6, NH_4SCN, tetraalkyl ammonium salts, etc. The range of working potentials in the cathode compartments determines the potential of cation reduction (tetraalkyl ammonium ions are reduced at -2.8 V with respect to the saturated calomel electrode) [2] while the limit in the anodic compartments is the oxidation potential of DMSO. Calomel, modified calomel and some amalgam electrodes (Tl(Hg)/TlCl [3], Li(Hg)/LiCl [4]) are used as reference electrodes, DMSO shows the characteristics of a base ($pK = 0.91–1$) [5] because it reacts with strong acids to produce the corresponding salts

---

* Corresponding author

The autoprotolysis constant (pK_s) is an important physicochemical characteristic of a solvent because it indicates the conditions for acid–base titrations in the given solvent to a great extent. Therefore, interest in the determination of the above-mentioned characteristic of a solvent has been demonstrated in the literature.

The K_s value is a function of numerous parameters such as the acidity (K_a) and basicity (K_b) of the solvent, the dielectric permeability, the polarity of molecules, etc.

$$K_s = a_{H_{2S}} + a_S = F(K_a, K_b, \epsilon, E_s, \ldots)$$

If the solvent is more ionized, the autoprotolysis constant and the solvation ability of the substances dissolved by the solvent are increased, which causes stronger dissociation of the dissolved electrolyte. The solvents with higher K_s values have a weaker differentiating effect on the titration of multicomponent compounds.

K_s is one of the basic thermodynamic constants of solvents by which we can make a choice of the solvent for acid–base titrations. The relationship between the autoprotolysis constant (K_s) and the dissociation constant of the acid (or base) defined as the constant of titration is important when choosing the solvent for titration.

Different methods for the determination of the autoprotolysis constant of non-aqueous solvents are described in the literature and the obtained values for particular solvents differ to a great extent, indicating the difficulties encountered in the course of the determination.

Kreshkov et al. [6] determined potentiometrically the autoprotolysis constants of numerous non-aqueous solvents.

Bykova and Petrov [7] showed that the pK_s values of the solvents could be calculated on the basis of measuring the relative scale of acidity of the solvents (E_s). According to these authors the determination of the relative scale of acidity of non-aqueous solvents by the method of measuring the potentials of polyneutralization of $HClO_4$ and R_4NOH showed that the pH interval which could be used for acid–base titrations in many cases corresponded to a higher scale of acidity than could be calculated from K_s.

Coetze and Padmanabhan [8] determined the pK_s value of acetonitrile by determining the dissociation constants (K_b^d) of 1,3-diphenylguanidine conductrimetrically and potentiometrically ($K_{BH^+}^d$ and obtained the value of 28.5. Similarly, using the stronger base tetramethylguanidine (TMG), Kolthoff and Chantooni [9] obtained the value of 33.3 pK_s units.

The difference in pK_s values of different solvents obtained by various authors ranges from 3 pK_s units for ethanol [10,11] to 16 pK_s units for dimethyl sulphoxide [1,12]. One of the difficulties encountered in the determined of pK_s is the impossibility of producing an absolutely non-aqueous solvent. The presence of even the smallest amounts of water causes an increase an K_s; however, there are many factors that may also lead to an error such as an incomplete dissociation of the electrolytes used, the use of different methods for the determination of dissociation constants of the base and the corresponding conjugated acid, the impossibility of precise measurement of diffuse-phase potentials in the cell, etc.

The classical potentiometric method for the determination of the autoprotolysis constant is based on the addition of a titrant to the solution

Table 1
Determination of the autoprotolysis constant of acetonitrile ($V = 40$ ml, $I = 5$ mA, supporting electrolyte = 0.025 M tetrabutylammonium perchlorate. $Q_{EP} = 11\,640$ C)

Charge (mC)	EMS (mV)	E_b° (mV)	E_a° (mV)
2400	−823	−983.8	
3600	−820	−984.4	
4800	−816	−984.5	
6000	−810	−983.5	
7200	−805	−984.6	
8400	−797	−984.7	
13 800	531		729.1
15 000	544		730.8
16 200	551		729.8
17 400	558		730.9
18 600	563		731.1
19 800	566		730.0
Average		−984.3	730.3

$$pK_s = \frac{730.3 - (-984.3)}{59.16} = 28.98.$$

Table 2

Determination of the autoprotolysis constant of DMSO ($V =$ 40 ml, $I = 5$ mA, supporting electrolyte $= 0.025$ M tetrabutylammonium perchlorate, $Q_{EP} = 12\,120$ C)

Charge	EMS (mV)	E_b° (mV)	E_a° (mV)
2400	1145	1304.5	
3600	1141	1303.8	
4800	1137	1303.8	
6000	1133	1304.4	
7200	1127	1303.9	
8400	1120	1304.2	
15 000	−220		−410.7
16 200	−229		−410.8
17 400	−236		−411.2
18 600	−241		−410.9
19 800	−245		−410.5
21 000	−249		−410.8
	Average	1304.1	−410.8

$$pK_s = \frac{1304.1 - (-410.8)}{59.16} = 28.99$$

(strong acid or strong base), which causes difficulties since a certain amount of water is introduced into the investigated solution together with the titrant. To avoid the introduction of water with the titrant and to simplify the procedure for the determination of the pK_s of acetone and methylethyl ketone, in our previous work we determined the pK_s values of these solvents by titration with H^+ ions generated by hydrogen oxidation at a H_2/Pd anode [13]. In this paper we applied the same electrode for the determination of the pK_s values of acetonitrile, propionitrile, nitromethane, ethylene carbonate and dimethyl sulphoxide.

2. Experimental

2.1. Reagents

All chemicals used were of analytical-reagent grade and were obtained from Merck and Fluka. Before use, some solvents were purified as described elsewhere [14]. Dimethyl sulphoxide and ethylene carbonate were used without previous purification. Tetrabutylammonium hydroxide (0.1 M solution) was dissolved in an isopropanol–

methanol mixture. The standardization of this solution was carried out by coulometric titration with H^+ ions generated by anodic oxidation of hydrogen dissolved in palladium. A 0.025 M solution of tetraethylammonium perchlorate in the corresponding solvent was used as the supporting electrolyte.

2.2. Apparatus

The apparatus used for coulometric–potentiometric titration was described in the previous paper [13]. In the course of the titration the potential was measured by means of a Radiometer pHM-86 pH-meter with a Radiometer G202B glass electrode and a Radiometer K201 modified calomel electrode. The aqueous solution of KCl in the SCE is replaced by a methanolic solution of KCl. Before use of the glass electrode was kept in the corresponding solvent for 48 h. A constant temperature was maintained with a U 15C thermostat (NBE; Dresden, Germany).

2.3. Procedure

The procedure for the determination of the pK_s values of the investigated solvents was described in the previous paper.

Table 3

Determination of the autoprotolysis constant of propionitrile ($V = 40$ ml, $I = 5$ mA, supporting electrolyte $= 0.25$ M tetrabutylammonium perchlorate, $Q_{EP} = 11\,050$ C)

Charge	EMS (mV)	E_b° (mV)	E_a° (mV)
2400	830	992.5	
3600	827	993.3	
4800	822	992.8	
6000	817	993.3	
7200	810	993.3	
8400	800	992.9	
13 800	−264		−455.9
15 000	−273		−455.6
16 200	−280		−455.8
17 400	−285		−455.4
18 600	−290		−456.0
19 800	−294		−456.2
	Average	993.0	−455.8

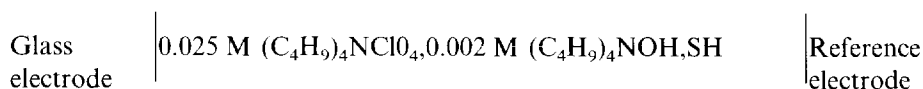$$pK_s = \frac{993.0 - (-455.8)}{59.16} = 24.49$$

Table 4
Determination of the autoprotolysis constant of nitromethane ($V = 40$ ml, $I = 5$ mA, supporting electrolyte = 0.025 M tetrabutylammonium perchlorate, $Q_{EP} = 11\ 720$ C)

Charge	EMS (mV)	E_b^o (mV)	E_a^o (mV)
2400	669	829.6	
3600	666	830.1	
4800	662	830.2	
6000	657	830.1	
7200	651	830.2	
8400	643	830.1	
13 800	−376		−575.1
15 000	−387		−574.4
16 200	−395		−574.4
17 400	−402		−575.3
18 600	−407		−575.4
19 800	−411		−575.2
	Average	830.4	−575.6

$$pK_s = \frac{830.4 - (-575.6)}{59.16} = 23.76$$

3. Results and discussion

Autoprotolysis constants of the investigated solvents were determined by E^o titration [15,16] in the following cell:

| Glass electrode | 0.025 M $(C_4H_9)_4NClO_4$, 0.002 M $(C_4H_9)_4NOH$.SH | Reference electrode |

In order to eliminate the introduction of a standard solution of mineral acid as the titrating agent, the base was titrated with protons generated by anodic oxidation of hydrogen dissolved in palladium in perchlorate medium. The titration was continued even after the equivalence point until twice the amount of protons required for the neutralization of the base was obtained. The e.m.f. of the cell at 25°C, at a constant ionic strength, is given by the following equations:

$$E = E_a^o + 0.05916 \log c_S -$$ (1)

$$E = E_b^o - 0.05916 \log c_{SH_2^+}$$ (2)

E_a^o and E_b^o are the specific cell constants for the basic and acidic regions respectively, and $c_S -$ and $c_{SH_2^+}$ denote molar concentrations of the lyate and lyonium ions respectively. The autoprotolysis constant of the solvent, $K_s = c_{SH} + c_S -$, is calcu-

lated from the expression:

$$pK_s = \frac{E_b^o - E_a^o}{59.16}$$ (3)

The value for the potential of the cell constant in the basic region E_b^o (mV) is calculated from the relation:

$$E_b^o = E - 59.16 \log \frac{Q_{EP} - Q}{FV}$$ (4)

where Q denotes the amount of charge used after the equivalence point, Q_{EP} is the amount of charge needed up to the equivalence point, V is the solution volume (ml) and F is Faraday's constant (96 500 C). In a similar manner, E_a^o in the acidic region was calculated from the equation:

$$E_a^o = E + 59.16 \log \frac{Q - Q_{EP}}{FV}$$ (5)

An example of the calculation of the pK_s value of acetonitrile on the basis of experimental data obtained in one titration is given in Table 1. As can be seen constant values of E_a^o and E_b^o are obtained at the titration points in the basic and acidic regions by Eqs. (3) and (4) respectively. The

Table 5
Determination of the autoprotolysis constant of ethylene carbonate ($V = 40$ ml, $I = 5$ mA, supporting electrolyte = 0.025 M tetrabutylammonium perchlorate, $Q_{EP} = 12\ 200$ C)

Charge	EMS (mV)	E_b^o (mV)	E_a^o (mV)
2400	690	849.3	
3600	687	849.6	
4800	683	849.5	
6000	679	850.0	
7200	673	849.6	
8400	666	849.6	
15 000	−230		−421.5
16 200	−240		−422.3
17 400	−246		−421.5
18 600	−252		−422.2
19 800	−256		−421.8
21 000	−260		−422.0
	Average	849.6	−421.9

$$pK_s = \frac{849.6 - (-421.9)}{59.16} = 21.49$$

Table 6
Autoprotolysis constants of solvents (pK_s) at 25°C, obtained by coulometry

Solvent	Present work	Literature			
		Found	Ref.	Calcd.	Ref.
Acetonitrile	28.8 ± 0.6	33.3	[9]	33.2	[7]
Propionitrile	24.6 ± 0.1				
Nitromethane	23.7 ± 0.1	24.0	[17]		
Ethylene carbonate	21.5 ± 0.4				
DMSO	29.0 ± 0.3	33.3	[1]	31.8	[7]

constant values (E_a° and E_b°) obtained in the intervals 20%–80% and 120%–180% respectively in the course of titration show that tetrabutylammonium hydroxide in this solvent is a strong base which dissociates into S^- and HS^+ ions. Constant values of E_a° and E_b° obtained in a wide titration range in the basic and acidic regions respectively, may serve as a criterion for the application of a strong base in the determination of pK_s using the E° titration method (Tables 2–5).

The pK_s values for the investigated non-aqueous solvents obtained coulometrically using a H_2/Pd generator electrode and a 0.025 M tetrabutylammonium perchlorate supporting electrolyte, as well as the data found in the literature obtained by other experimental techniques, are listed in Table 6. These data show that pK_s values obtained by the coulometric–potentiometric method (E° titration) differ from those reported in the literature. Even the pK_s values for certain solvents obtained by different authors differ widely. This can be explained by the fact that different authors used different experimental methods and therefore different conditions for the determination, or different calculation methods on the basis of the acidity scale for 'pure' solvents (the solvents without any additives).

The pK_s value is strongly influenced by the conditions of determination (the purity of the solvent, the strength of the base, the value of the diffuse potential, the type of electrolyte, etc.).

The pK_s values of the investigated solvents are somewhat lower than those reported in the literature (obtained either experimentally or by calcula-

tion), which can be explained by different conditions of investigation in the present work in comparison with those applied by other authors. The obtained pK_s values are concentration constants (at a concentration of 0.025 M tetrabutylammonium perchlorate) since in the medium of these solvents the ionic strength of the solution cannot be calculated accurately.

4. Conclusion

Using the coulometric–potentiometric method and a H_2/Pd electrode as a source of hydrogen ions for the titration of a strong base, the use of a standard acid solution as well as the water present in the acid solution are avoided. Thus the effect of water, one of the main causes of the lowering of pK_s values of non-aqueous solvents, is eliminated. In addition, the procedure for the determination of pK_s values is simplified by the application of coulometry since the change of the volume of the solution in the course of titration is eliminated as well.

References

[1] J. Courtot-Coupez and M. Le Demezet, Bull. Soc. Chim. Fr., (1969) 1033.
[2] K.I. Evstratova and N.A. El Rabbat, Zh. Fiz. Khim., 45 (1971) 2320.
[3] A.P. Kreshkov and L.G. Yarmarkovkaya, Zh. Fiz. Khim., 47 (1973) 464.

[4] A.P. Kreshkov, L.P. Senezkaia and T.A. Malikova, Zh. Fiz. Khim., 42 (1968) 284.

[5] K.K. Andersen, J. Org. Chem., 31 (1966) 2859.

[6] A.P. Kreshkov, N. Sh. Aldarova and B.B. Tanganov, Zh. Fiz. Khim., 44 (1970) 2089.

[7] L.N. Bykova and S.I. Petrov. Zh. Anal. Khim., 27 (1972) 1076.

[8] J.F. Coetze and G.R. Padmanabhan, J. Phys. Chem., 69 (1965) 3193.

[9] I.M. Kolthoff and M.K. Chantooni, J. Phys. Chem., 72 (1968) 2270.

[10] L.M. Mukherjee, J. Phys. Chem., 60 (1956) 1019.

[11] B. Gutberahl and E. Grundvald, J. Am. Chem. Soc., 66

(1962) 1708.

[12] I.M. Kolthoff and T.B. Reddy, Inorg. Chem., 7 (1962) 189.

[13] R.P. Mihajlović, R.M. Džudović and V.J. Vajgand, Talanta, 40 (1993) 649.

[14] A.P. Kreskov, L.N. Bykova and N.A. Kazaryan, Kislotno-osnovnoe titrovanie v Nevodnikh, Khimia, Moscow, 1967.

[15] L. Pehrsson, F. Ingman and A. Johansson, Talanta, 23 (1976) 769.

[16] A. Johansson and S. Johansson, Analyst, 103 (1978) 305.

[17] E.I. Matrosov and A.G. Kazačenko, Izv. Akad. Nauk SSSR, Ser. Khim., 2 (1977) 313.

Spectrophotometric estimation of rhenium with 5-chloro-2-hydroxythiobenzhydrazide after its extraction separation using n-octylaniline

S.S. Sawant, M.A. Anuse, M.B. Chavan*

Department of Chemistry, Shivaji University, Kolhapur 416004, India

Received 8 April 1993; revised 20 May 1996; accepted 23 May 1996

Abstract

A solution of n-octylaniline in chloroform extracts rhenium selectively from 0.12–0.16 M nitric acid medium. Rhenium from the organic phase is backstripped with 5% aqueous ammonia solution and estimated spectrophotometrically with 5-chloro-2-hydroxythiobenzhydrazide (5-Cl-2-OHTBH). 5-Cl-2-OHTBH forms a blue complex with rhenium on heating in the acidity range 0.40–3.5 M HCl. The complex is extracted into chloroform and its absorbance is measured at 580 nm. The complex is stable for more than 12 h with a molar extinction coefficient of $9.0 \times 10^3 \, 1 \, \text{mole}^{-1} \, \text{cm}^{-1}$ and a Sandell sensitivity of 0.019 μg cm^{-2}.

Keywords: 5-Chloro-2-hydroxythiobenzhydrazide; Extraction separation; n-Octylaniline; Rhenium

1. Introduction

n-Octylaniline has been employed as an extractant for noble metals [1–5]. It has also been applied successfully for the extraction separation and determination of indium(III), gallium(III) and thallium(III) [6]. Other high molecular weight amines such as TBA [7], Adogen 464 [8], Hostarex A 327 [9] and Aliquat 336 [10], and oxygenated solvents such as mesityl oxide [11], acetylacetone [12], diethyl ether [13], cyclohexanone [14] and ethylmethyl ketone [15] have been reported for the extraction separation of rhenium. However, some of these methods require preliminary separation of molybdenum.

The use of thiohydrazides in the spectrophoto-

metric determination of rhenium and platinum group metals has been described in a number of papers [16–24]. However, alcoholic solutions of some of these reagents need to be stored below 15°C. The complexes of rhenium with naphthalenethiocarboxhydrazide (NTH) [23] and 2-pyrrolethiocarboxhydrazide (PTH) [23] are not suitable for the colorimetric estimation of rhenium due to the lack of a suitable solvent while those with 2-furanthiocarboxhydrazide [23] and 2-thiophenethiocarboxhydrazide [23] are less sensitive and selective compared to 5-Cl-2-OHTBH.

Although the tin(II) chloride-thiocyanate [25] is a well-established spectrophotometric reagent for rhenium, the method suffers from: (i) limited acid range for complexation; (ii) dependence of colour intensity on the chloride concentration of the

* Corresponding author.

aqueous phase; (iii) occurrence of λ_{max} in the near-UV region; and (iv) difficulties in the colour development caused by the presence of multiple species in a given valence state.

Therefore, we recommend n-octylaniline as a selective extractant and 5-Cl-2-OHTBH as a colorimetric reagent for rhenium.

2. Experimental

2.1. Apparatus

A Carl Zeiss (Jena, Germany) spectrophotometer with 1 cm glass cells was used for absorbance measurements.

2.2. Reagents

Standard rhenium(VII) solution was obtained by dissolving potassium perrhenate (JM 99.9% pure) in doubly-distilled water and standardised by the nitron method [26].

Other standard solutions of different metals used to study the effect of diverse ions were prepared by dissolving weighed quantities of their salts in distilled water or dilute hydrochloric acid. Solutions of anions were prepared by dissolving the respective alkali metal salts in water. All the chemicals used were of A.R. grade.

2.3. Preparation of reagents

n-Octylaniline was synthesised from aniline and n-octanol by the method of Pohlandt [4].

5-Cl-2-OHTBH was synthesised according to the method of Jensen and Pedersen [27] and purified by recrystallisation from hot water by adding activated charcoal to obtain the colourless product.

2.4. Reagent solutions

10% n-octylaniline solution was prepared in doubly-distilled chloroform.

A 6.0×10^{-3} M solution of 5-Cl-2-OHTBH was prepared in doubly-distilled ethyl alcohol. The solution remains stable for 1 week.

2.5. Procedure

2.5.1. Extraction separation of rhenium using n-octylaniline

To an aliquot of solution containing 200 μg of rhenium(VII) in a 100 ml separatory funnel, sufficient nitric acid and water were added to give a final concentration of 0.12 M with respect to nitric acid in a total volume of 25 ml. The aqueous phase was equilibrated once with 10 ml of 10% n – octylaniline solution in chloroform for 45 s. The phases were allowed to separate, the metal from the organic phase was backstripped with two 10 ml portions of 5% aqueous ammonia solution and finally estimated spectrophotometrically with 5-Cl-2-OHTBH.

2.5.2. Spectrophotometric estimation of rhenium with 5-Cl-2-OHTBH

The aqueous ammonia solution containing rhenium was shaken with 5 ml of chloroform in order to remove traces of dissolved amine and then neutralised with HCl. Tin(II) chloride solution (1 ml, 10% in 2 M HCl) was added to reduce the metal, the solution was adjusted to 0.8 M HCl and then 5 ml of the reagent solution was added. It was then heated on a water bath for 30 min, cooled to room temperature, and the metal complex was extracted with two 10 ml portions of chloroform containing traces of pyridine. The chloroform extract was dried with anhydrous sodium sulphate, diluted to 25 ml with chloroform and the absorbance measured at 580 nm against the solvent blank.

3. Results and discussion

3.1. Extraction separation of rhenium with n-octylaniline

3.1.1. Effect of acidity

The extraction of rhenium with 10 ml of 10% n-octylaniline in chloroform was carried out from solutions in nitric, hydrobromic, hydrochloric and hydroidic acid media varying in the range 0.04–5.0 M.

Table 1
Effect of diverse ions on the determination of Re(VII) (0.200 mg)

Diverse ion added	Amount tolerated (mg)	Diverse ion added	Amount tolerated (mg)	Diverse ion added	Amount tolerated (mg)
Mn(II)	20	Cu(II)	1	Ca(II)	5
Hg(II)	5	Sn(II)	5	Ba(II)	5
V(V)	5	Th(IV)	5	Tartrate	25
U(V)	5	W(VI)	5	Citrate	100
Ni(II)	5	Se(IV)	1	Acetate	100
Pd(II)	1	Te(IV)	1	Thiocyanate	100
Os(VIII)	1	Rh(III)	1	Phosphate	25
Au(III)	1	Pt(IV)	1	Thiourea	25
Mo(VI)	2	Zn(II)	5	Oxalate	100
Bi(VIII)	5	Pb(II)	20	EDTA	100
Cd(II)	20	Ru(III)	1	Ascorbate	100
Tl(III)	5	Ti(IV)	1	Fluoride	100
Mg(II)	20	As(III)	5	Hydroxyamine hydrochloride	100
Fe(III)	20	Ag(II)	5		
Cr(VI)	1	Zr(IV)	1	H_2O_2 30% (100 v/v)	2 ml
Co(II)	5	Be(II)	5		
Ce(IV)	5				

The extraction was found to be quantitative from nitric acid (0.12–0.16 M) and hydrobromic acid (0.2 M), 50% from hydrochloric acid (2 M)

Fig. 1. Absorbance curves for Re-5-C-2-OHTBH complexes in chloroform. Re(VII): I, 4 ppm; II, 8 ppm; III, 12 ppm; IV, 16 ppm; V, 20 ppm.
-1

and 0% from hydroiodic acid. In the nitric acid system no emulsion is formed, and hence the use of the nitric acid system is recommended for further studies.
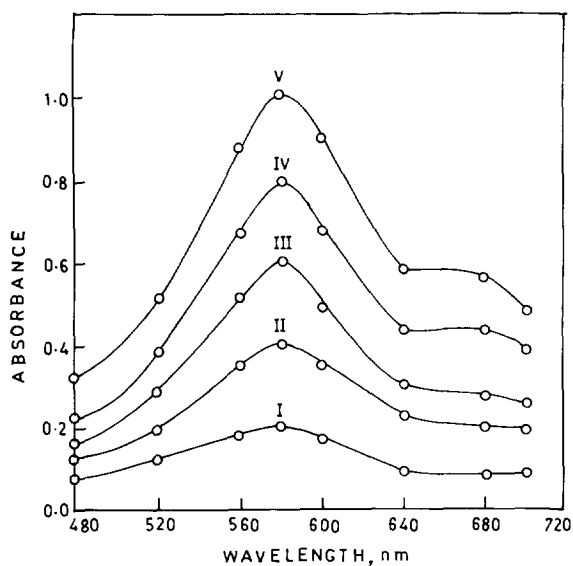
3.1.2. Distribution ratio as a function of n-octylaniline concentration

The concentration of n-octylaniline in chloroform was varied from 3–15% over the acidity range 0.04–0.5 M nitric acid. It was observed that extraction increases with the increase in acidity of the aqueous solution, becomes quantitative at 0.12–0.16 M and again decreases with a further increase in acidity. With 10% n-octylaniline in chloroform, the extraction was quantitative from 0.12–0.16 M nitric acid. There was no adverse effect with higher n-octylaniline concentrations.

3.1.3. Nature of the extracted species

The extraction mechanism may be formulated as shown below:

$$ReO_{4(aq)}^{-} + RNH_3^{+} NO_{3(org)}^{-}$$

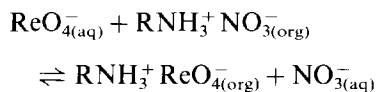$$\rightleftharpoons RNH_3^{+} ReO_{4(org)}^{-} + NO_{3(aq)}^{-}$$

Table 2
Determination of rhenium in synthetic mixtures: results of three determinations of each sample

Diverse elements taken (mg)	Re(VII) added (μg)	Re(VII) found (μg)
Mo(VI) 1, V(V) 5,	200	199.8
W(VI) 5, Fe(III) 5		200.0
		200.0
Co(II) 10, Cr(VI) 1,	200	200.2
Ni(II) 5, U(VI) 5,		200.0
Se(IV) 1, Te(IV) 1,		
Pt(IV) 1		
Mo(VI) 1, V(V) 4,	200	200.0
W(VI) 5, Os(VIII) 1,		199.5
Ru(III) 1, Rh(III) 1,		200.0

The equilibrium constant for the reaction is given by

$$K_c = \frac{[RNH_3^+ ReO_4^-]_{org}[NO_3^-]_{aq}}{[ReO_4^-]_{aq}[RNH_3^+ NO_3^-]_{org}}$$

The distribution ratio (K_D) for rhenium is given by the equation

$$K_D = \frac{[RNH_3^+ ReO_4^-]_{org}}{[ReO_4^-]_{aq}}$$

Therefore:

$$K_c = K_D \frac{[NO_3^-]_{aq}}{[RNH_3^+ NO_3^-]_{org}}$$

Taking logarithms of both sides and rearranging the terms, the equation at a constant concentration of nitrate ion in the aqueous solution becomes

$$\log K_D = x \, \log[RNH_3^+ NO_3^-]_{org}$$

$$+ (\log K_c - \log[NO_3^-]_{aq})$$

where x represents the number of amine molecules associated with each extracted metal atom.

The log–log plots of distribution ratio versus n-octylaniline concentration at 0.04 and 0.08 M nitric acid concentrations gave slopes of 1.0 and 1.1 respectively, indicating that the amine-to-metal ratio in the extracted species is 1:1 and that the probable extracted species is $RNH_3^+ ReO_4^-$.

Extraction was found to be more than 99.9% complete in 30 s; therefore a 45 s shaking period is recommended for quantitative extraction.

3.1.4. Effect of diverse ions

Several ions were examined for interference (Table 1). An error of $\pm 1.5\%$ in analyte recovery was considered tolerable. Only thiosulphate affected the extraction of rhenium.

3.2. Spectrophotometric estimation of rhenium with 5-Cl-2-OHTBH

3.2.1. Absorption spectrum

The absorption spectrum of the rhenium-5-Cl–2-OHTBH complex showed a maximum at 580 nm (Fig. 1). The reagent blank under similar conditions showed no absorption over the entire wavelength range.

3.2.2. Optimal conditions and spectral properties

The variation of the acidity of the aqueous phase revealed that the complex formation remained maximal and constant over the acidity range 0.40–3.5 M HCl. Different solvents were studied for extraction. Benzene, MIBK and chloroform were found to be good extractants; however, in benzene the complex is less stable and with MIBK it becomes turbid. Hence chloroform is recommended for extraction.

Under optimum conditions Beer's law is obeyed over the range 1–17 μg Re ml^{-1} and an apparent molar absorptivity of 9.0×10^3 l mole^{-1} cm^{-1} was obtained.

Table 3
Analysis of alloy steels: results of triplicate analysis

Type of alloy	Composition of alloy (%)							Re(VII) added (μg)	Re(VII) found (μg)
33b	C	2.24,	Si	2,	S	0.035		200	198.99
	P	0.11,	Mn	0.64,	Ni	2.24,			199.20
	Cr	0.61	Mo	0.40					199.60
33d	V	2.30,	Si	1.63,	S	0.023		200	199.80
	P	0.026,	Mn	0.63	Ni	2.38			199.20
	Cr	0.52	Mo	0.48,	Cu	1.54			199.90
320	C	0.22	Si	0.02,	Mn	0.19,		200	
	P	0.019,	S	0.009,	Cr	0.13,			200.00
	Sb	0.003,	Mo	0.22,	Ni	0.022,			199.8
	Al	0.013,	As	0.031,	Sn	0.095,			199.8
	Al	0.013,	As	0.031,	Sn	0.085,			
	Ti	0.021	V	0.004	W	0.17			

3.2.3. *Determination of rhenium in synthetic mixtures and alloy steels*

Tables 2 and 3 show the results for analysis of synthetic mixtures and alloy steel samples containing added rhenium.

Three samples of alloy steel (Nos. 33b, 33d and 320 from The Bureau of Analysed Samples Ltd., UK) were analysed separately.

A known weight (1 g) of alloy steel was dissolved in a mixture of 9 ml of concentrated sulphuric acid and 50 ml of water. After the initial reaction was over the solution was heated with 5 ml portions of nitric acid until white fumes were observed, boiled to dissolve soluble matter, filtered to remove silica and diluted to 100 ml with distilled water. An aliquot of this solution was analysed by the recommended procedure.

References

[1] A.A. Vasilyeva, I.G. Yudelevich, L.M. Gindin, T.V. Lan-
bina, R.S. Shulman, I.L. Kotlarevsky and V.N. Andrievsky, Talanta, 22 (1975) 745.
[2] C. Pohlandt, Report No. 1881, National Institute of Metallurgy, Johannesburg, 1977.
[3] C. Pohlandt and M. Hegetschweller, Report No. 1940, National Institute of Metallurgy, Johannesburg, 1978.
[4] C. Pohlandt, Talanta, 26 (1969) 199.
[5] R.N. Gedye, J. Bozict, P.M. Durbano and B. Williamson, Talanta, 36 (1989) 1055.
[6] S.R. Kuchekar and M.B. Chavan, Talanta, 35 (1988) 357.
[7] M. Ziegler and H. Schroeder, Z. Anal. Chem., 212 (1965) 395.
[8] B.W. Budesinsky, Analyst, 105 (1980) 278.
[9] H.B. Pietsch, Symp. Ion Exch. Solvent Extr., Oslo, 1982, pp. V/1 V/14. Available from Chem. Abstr., 98 (1983) Abstr. No. 183135P.
[10] Kh. Vasilev, L. Karagosov, M. Chimbulev and D. Kunev, God. Vissh. Khimikotekhnol. Inst., Sofia, 24 (1978) 127.
[11] M.B. Chavan, Z. Anal. Chem., 70 (1975) 276.
[12] V. Yatirajan and L.R. Kakkar, Anal. Chim. Acta, 42 (1969) 468.
[13] L.B. Koval, Zavod. Lab., 52 (1986) 7.
[14] N. Irdanov, M. Pavlova and D. Boikova, Talanta, 23 (1976) 463.
[15] M.B. Shiryaeva, L.N. Lyubimova, Yu.P. Salmin, K.N. Ryamina and M.A. Tatarkin, Zavod. Lab., 50 (1984) 3.
[16] S. Gangopadhyay, P.K. Gangopadhyay and S.C. Shome, Anal. Chim. Acta. 83 (1976) 409.
[17] S.C. Shome, P.K. Gangopadhyay and S. Gangopadhyay, Talanta, 23 (1976) 603.
[18] S. Gangopadhyay, P.K. Gangopadhyay and S.C. Shome, Z. Anal. Chem., 281 (1976) 143.
[19] S.C. Shome and P.K. Gangopadhyay, Anal. Chim. Acta, 65 (1973) 216.
[20] P.K. Gangopadhyay, H.R. Das and S.C. Shome, Anal.

Chim. Acta, 66 (1973) 460.

[21] P.K. Gangopadhyay and S.C. Shome, Anal. Chim. Acta 75 (1975) 235.

[22] P.K. Gangopadhyay and S.C. Shome, Mikrochim. Acta, Part I, (1977) 173.

[23] S.C. Shome, S. Nandy, A. Guhathakurta, N.C. Ghosh, H.R. Das and P.K. Gangopadhyay, Mikrochim. Acta, Part II, (1978) 347.

[24] N.A. Mote, M.A. Anuse and M.B. Chavan, Curr. Sci. 52 (1983) 69.

[25] E.B. Sandell, Colorimetric Determination of Traces of Metals, 3rd edn., Interscience, New York, p. 754.

[26] W.W. Scott, Standard Methods of Chemical Analysis, Vol. 1, Van Nostrand, New York, 1939, p. 771.

[27] K.A. Jensen and C. Pedersen, Acta Chem. Scand., 15 (1961) 1097.

X-ray ionization and fragmentation for use with time-of-flight mass spectrometry

Robert T. Pogue[1], Vahid Majidi*

Department of Chemistry, University of Kentucky, Lexington, KY 40506, USA

Abstract

In this paper, we introduce laser desorption X-ray ionization for producing ions from the previously undetected neutral species present during laser desorption mass spectrometry. Studies involving the laser desorption of simple sugars were conducted to illustrate the differences between spectra with and without the X-ray source. Ionization was made possible by placing a 200 mCi Am X-ray source directly into the ionization chamber of a time-of-flight mass spectrometer.

Keywords: Fragmentation; Laser desorption mass spectrometry; Sugars; X-ray ionization

1. Introduction

Numerous methods are known for producing ions from neutral molecules in all states of matter. The ion production process can be accomplished through the use of electrons, ions, photons, fission fragments, and electric fields. Until now, ionizing radiation in the form of X-rays has been mostly overlooked as a possible method for producing ions within a mass spectrometer.

Laser desorption/ionization (LDI) [1] is commonly employed in the analysis of solid materials because it is a soft ionization technique, capable of producing molecular ions for most analytes.

Work by Karas et al. [2] has extended the usefulness of LDI by making it applicable to very high molecular weight compounds through the use of absorbing matrices. From its inception, however, it has been known that the laser desorption process produces gas-phase neutrals as well as ions. [1] Studies have shown not only that neutrals are produced during laser desorption, but that these neutrals may be produced in greater abundance, and for a longer period of time, than the ions. [3] Cotter [4] showed that neutrals may be emitted for as long as 10 ms after the cessation of the laser pulse.

Vertes et al. [5] have provided hydrodynamic models to explain the temperature, density and velocity distributions of laser plumes with time. Their models illustrate that the plume density is greatest directly above the target at the end of

---

* Corresponding author.
[1] Present address: University of Dayton Research Institute, 300 College Park, Dayton, OH 45469-0131, USA.

laser irradiation. Later, after the cessation of the laser pulse, the desorbed packet begins to expand and drift away from the target surface.

Due to the large abundance of neutrals, and the extended time frame available, new methods have been introduced for post-desorption ionization of neutral species [3,4,6–8]. One of these methods, multi-photon ionization (MPI), involves the use of two distinct laser beams. These beams may be produced by separate lasers [8], or by splitting the output of a single laser [7]. MPI may be used either non-selectively, or as a selective tool for ionizing specific molecules [9]. The literature indicates that non-resonant (non-selective) ionization requires a high photon energy due to its inefficiency. One can then conclude that X-ray sources, due to their energetic nature, are ideally suited to fulfill this need. Several studies [10–12] have previously shown that soft X-rays produced by synchrotron sources can be used in combination with mass spectrometry. The use of natural sources, however, has largely been avoided due to safety, and other, concerns. With careful adherence to safety precautions, natural X-ray sources can be useful for mass spectrometric applications.

A typical radioactive X-ray source is capable of providing a high flux of X-rays at energies from approximately 3 to 30 keV. X-ray tubes have the added benefits of higher photon flux, user control of the wavelength at which the X-rays are emitted, and better shielding. The interaction of X-rays with gaseous materials has been previously exploited in the production of gas-filled detectors [13]. Veigele [14] and others have shown that the absorption cross-section for X-rays decreases as the photon energy increases. Evidence also indicates that the photoionization cross-section makes up a large percentage of the total cross-section at low photon energies.

Lasers have been used almost exclusively for producing the photons necessary for non-resonant MPI. In this paper, however, we introduce the use of X-rays for non-resonant ionization of neutral molecules produced in the laser desorption of sugar molecules. In addition, we have included evidence of ion production in a stream of aniline gas using only 241 Am X-rays as the ionization source. Although there are many possible expla-nations to describe the interactions between X-rays and gas-phase species, some of these explanations are more plausible than others. A few of these will be proposed, and their applicability and limitations discussed.

2. Experimental

2.1. Instrumental

The third harmonic frequency (355 nm) of a pulsed Nd:YAG laser (Spectra-Physics GCR-3, Mountain View, CA) was employed for desorption of sugar samples. Laser output was attenuated using neutral density filters in order to provide a suitable signal for analysis. The linear time-of-flight (TOF) mass analyzer was designed and built at the University of Kentucky; it consists of a 1.3 m flight tube typically held at 5×10^{-6} Torr. The repeller voltage was maintained at 2.5 kV and the microchannel plate detector (Chevron Assembly, Model 3025, Galileo Electro-Optics Corp., Sturbridge, MA) was biased at -2.0 kV. The signal was digitized using a Lecroy 8013A digitizer (Lecroy, Chesnut Ridge, NY) and transferred to an IBM-PC by software written with Asyst 3.0 (Asyst Software Technologies, Rochester, NY). Ten individual spectra were co-added in order to obtain the desired profiles. A 200 μCi ^{241}Am source was placed into a Delrin sheath which was attached directly to a blank vacuum flange. This X-ray source holder could then be easily inserted in, or removed from, the ionization chamber through an unused arm of a six-way cross. The orientation of the Am source with respect to the sample surface is illustrated in Fig. 1. For these experiments, the extraction plate and lens openings were 0.125 in. Care was taken to place the X-ray source as close as possible (approximately 0.40 in) to the sample surface to provide the maximum solid angle overlap of the X-rays with the dense laser plume that is present directly following the cessation of the laser pulse [5]. Data collection was initiated by the laser pulse to allow ions produced both from the laser pulse, and from the interaction of X-rays and neutrals, to be detected simultaneously.

Aniline profiles were collected using a magnetic mirror ion trap placed inside the ionization chamber of the TOF. Rare earth cobalt magnets (0.8 T, Edmund Scientific) replaced the extraction plate and electrostatic lenses shown in Fig. 1. The repeller was pulsed at 2.4 kV. Approximately 1×10^{-5} Torr of aniline was leaked directly into the trapping region. The X-ray source was placed perpendicular to the magnetic trap.

It is important to note that a radioactive source was used in these experiments, and that care must be taken when using an X-ray source of this type. The ^{241}Am source was placed in a lead-lined canister when not in use and covered with a lead foil. It is also suggested that the operator monitor his or her dosage regularly using radiation film badges. Additionally, proper authorization and certification must be obtained when using certain radioactive sources.

2.2. Samples

Saturated solutions of glucose and sucrose (unpurified) were prepared in deionized water. Aliquots of these solutions were placed on dry stainless-steel substrates (≈ 0.3 mm thick), and the solutions were allowed to dry. The substrates were then affixed to the center of the repeller plate. Aniline (Baker) was distilled prior to use.
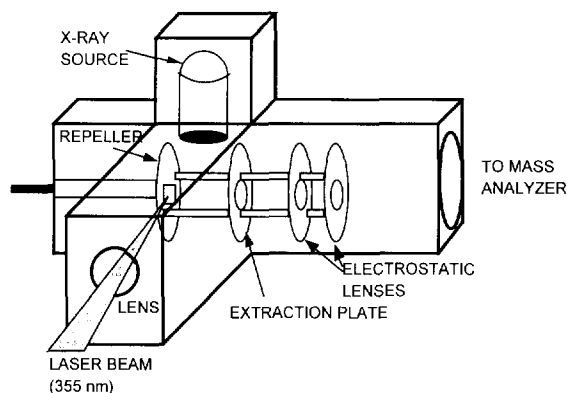

Fig. 1. Three-dimensional view of the ionization chamber used in LD-XRI. Note that the desorption beam and ^{241}Am source are perpendicular to the direction of ion travel, and that the X-ray source is placed as close as possible to the sample surface.

Table 1
Photons emitted from ^{241}Am source

Energy(keV)	Intensity(%)	Assignment
59.5	36	γ
26.3	2.4	γ
20.8	4.9	L_γ
17.8	20	L_β
13.9[a]	13.3	L_α

[a] Not observed with our source.

3. Results and discussion

3.1. X-ray flux

The energies of the photons emitted from the source used for this set of experiments are given in Table 1. Not all of the photons emitted from the ^{241}Am source are within the useful region for ionization of carbon as described by Veigele [14]. It is important to note that the photons which have higher energies may also be absorbed by the laser generated plume; however, the probability of such interactions is less than for the lower energy X-ray photons. We determined, using experimental parameters, that approximately 1450 X-ray photons will be emitted from the 200 mCi source during the 195 ns residence time of ions in the ionization region (based on m/z 144). By approximating the interaction volume as that contained within the column defined by the repeller and the extraction orifice we calculated that approximately 25 photons can be expected to pass through the interaction region during the time that the laser plume is in residence. The number of photons which would react with the plume was determined using the equation $(N_a/N_0 = e^{-\mu x})$, where N_a/N_0 is the number of photons which will pass through the plume without interaction, and μ and x describe the interaction cross-section and the sample depth respectively.

From these calculations, it is apparent that an average of 4% of the X-ray photons will interact with the laser plume. By adding the resultant spectra from several events it is possible to obtain the profiles given in Figs. 2 and 3. Although several series of samples were analyzed and the results found to be reproducible, only representa-
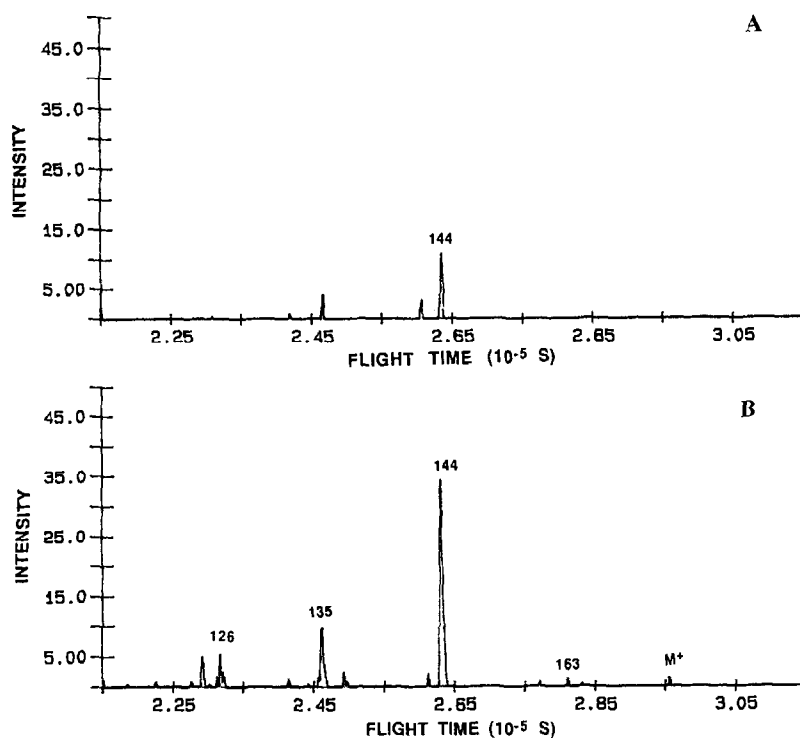
Fig. 2. (A) Laser desorption TOF profile of glucose. (B) Laser desorption X-ray ionization profile of glucose: 355 nm desorption beam.

tive spectra are included. Additionally, as explained below, the primary interaction of a single photon results in a large number of secondary interactions and collisions which multiply the effect of the initial event.

3.2. Laser desorption mass spectrometry of sugars

Laser desorption profiles of glucose both with and without the presence of the X-ray source in the ionization chamber are displayed in Fig. 2. The base peak in Fig. 2A (m/z 145) is a dehydration product of the levoglucosan fragment. Noticeably absent are ions with $m/z > 145$. In the laser desorption X-ray ionization (LD-XRI) profile given in Fig. 2B, the molecular ion is present with a signal-to-noise ratio (S/N) of approximately 10. Peak broadening (30 ns at m/z 145), clearly visible when comparing Figs 2A and 2B, is most probably due to the lateral distribution of the X-ray-produced ions at the time of

ionization by the X-ray photons. As the lateral distribution of ions, with respect to the ion repeller, increases the kinetic energy, distribution of ions with the same mass-to-charge ratio will also increase. Although the intensity of the molecular ion is only a small fraction of that of the base peak, opportunities exist for improving the amount of interaction, and thus the intensities of desired ions, by using instrumental X-ray sources.

Similar spectra for the laser desorption of sucrose appear in Fig. 3. Note, again, the increase in peak width in the LD-XRI profiles, which indicates that neutral/photon interactions are occurring. Also important to note is the strong presence of ions at $m/z > 160$ in the LD-XRI profile. The molecular ion, in this profile, is of relatively high intensity compared with the corresponding glucose profile. The base peak in Fig. 3A (m/z 131) is most likely due to a simple cleavage reaction leaving the six-membered ring and its proton and hydroxyl substituents. Due to the structure of this compound and the repetitiveness of its sub-
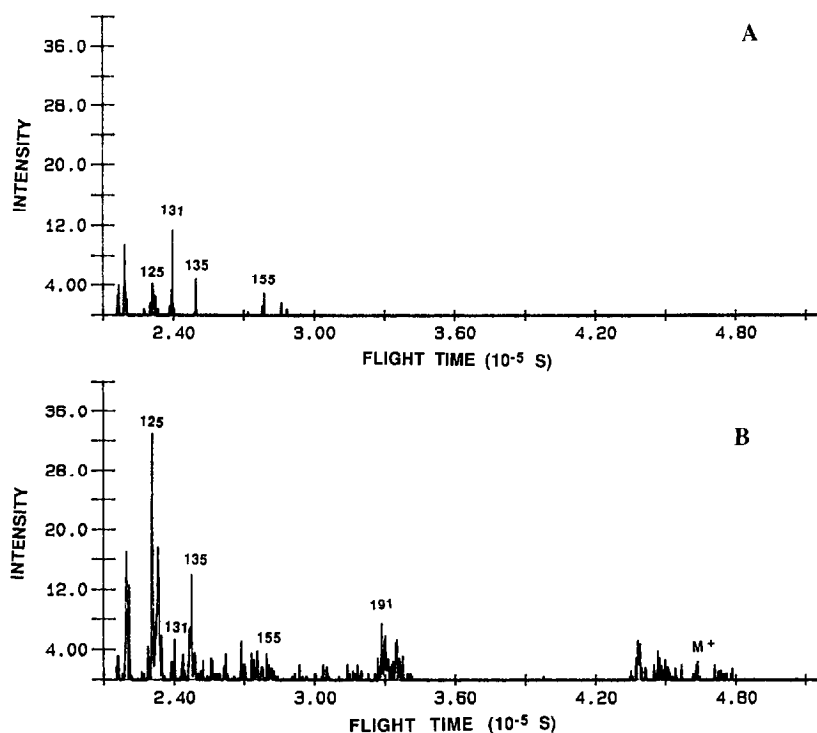
Fig. 3. (A) Laser desorption TOF profile of sucrose. (B) Laser desorption X-ray ionization profile of sucrose: 355 nm desorption beam.

stituents, it is difficult to assign specific fragmentation pathways leading to the base peak. Because the same sample is used in Figs. 3A and 3B without removal from the ion source, it is surprising that the peak at this mass-to-charge ratio is weaker in Fig. 3B relative to the rest of the spectrum. This fact may point to selective ionization or fragmentation, during desorption or X-ray ionization, or to the presence of mechanisms which are not clearly evident from the information obtained in these experiments.

LDI experiments were conducted prior to the introduction of the [241]Am source, and after it had been removed from the ionization chamber, so that X-ray/solid interactions could be ruled out as a possible explanation for the observed effects.

3.3. Production of aniline ions in a magnetic ion trap

While conducting experiments using a mag-

netic mirror ion trap, we observed that the presence of the X-ray source in the ionization chamber of our mass spectrometer causes ion formation in gas-phase neutrals. It is important to note that ions were only visible, above the background, when the magnetic mirror was in place. This indicates that the high plume density present during laser desorption is a necessary condition for creating a useful ion signal. The ion storage property of the magnetic mirror allows the signal to be enhanced; however, the resolution is substantially degraded with respect to the LD-XRI profiles. These experiments also indicate that even at high pressure the background signal caused by the continuous X-ray source is not intense enough to cause significant changes in the background profile. For this reason, ionization events which occur after the passage of the laser plume will not cause spurious peaks in the mass profile or significantly affect peak shape.

3.4. Mechanisms of X-ray/neutral interaction

The major difficulty in determining the method of interaction between the X-rays and the gas-phase neutrals, in the TOF ionization chamber, is the high energy of the incident ionizing photons. Typical lasers used for ionization are the vacuum ultraviolet (VUV), ultraviolet (UV), or visible ranges, which encompass the region of the electromagnetic spectrum from 10–800 nm (130–2 eV). X-rays emitted from the 241 Am source have a minimum energy of 13.9 keV. Electrons at 70 eV are commonly used for electron impact ionization are considered a "hard" ionization source. LD XRI, as developed in this laboratory, exhibits soft ionization characteristics even though the ionizing radiation has several orders of magnitude more energy to transfer during a collision. It is our belief that this occurs via a multiple-step mechanism whereby the products of direct collision are involved in secondary collisions which produce the ions visible in the TOF profile. This mechanism is supported by ion counting calculations made by determining the current collected from the micro-channel plate detector. These calculations indicate that the highest number of primary collisions possible in the given time frame cannot account for the total number of ions which are being detected. In order to understand the processes which we believe are making up the total X-ray/neutral interaction mechanism, it is useful to treat direct and indirect processes separately.

3.4.1. Direct interaction

Models suggest that as the time following the cessation of the laser pulse and the distance above the target surface approach zero, the density of the laser-induced plume approaches that of the condensed phase [5]. Although it is not possible to claim that all of the collisions occur within these time and space boundaries, we can understand some of the collision processes better by using these constraints. A typical X-ray detector may be effective as a model for these interactions. As the X-ray passes through a gas-filled detector, interactions with the detector gas produce a large number of ion–electron pairs. Following the initial collision, a photoelectron is emitted with a kinetic energy equal to the energy of the photon minus the binding energy. If this primary collision is the only process which is occurring, the ions produced would then be repelled down the flight tube and detected by the microchannel plate. In a similar manner, ions may be produced which can be detected using TOF mass spectrometry. Spectra caused by direct interaction only would have low signal-to-noise ratios and would contain a large number of low molecular weight fragments of poor resolution. These fragments would result from vibrational dissociation of the primary ions, and could be produced throughout the ionization region and flight tube.

3.4.2. Indirect ionization by energetic fragments and secondary electrons

In the previous section, we considered only those interactions caused by direct collision with an X-ray photon. We may also assume that the products of primary collisions sufficient energy to ionize and/or fragment addition gaseous neutrals. As described in the previous section, a photoelectron may be emitted from the primary collision. This photon would have less energy the the primary photon, and therefore have a higher collision cross-section than its predecessor. Through additional collisions, the energy of the photon would decrease. The outcome would be similar to the Townsend Cascade which is the basis for gasfilled radiation detectors (see Ref. [13])

In addition to the photoelectrons which may be formed during X-ray neutral interaction, fragments formed due to vibrational excitation may be sufficiently energetic to cause secondary reactions. These fragments would have higher cross sections and lower kinetic energies than the photoelectrons and could be the source of the soft ionization processes which are observed.

Clearly, additional studies are necessary to determine what role each of the proposed mechanisms plays in the overall reaction mechanism. High sensitivity, and MS/MS, measurements may shed light on how each of the pathways contributes to cause the changes observed in the spectra. Additional work in this area is presently being conducted on these and other classes of compounds.

4. Conclusions

The use of X-rays as a supplemental ionization source for laser desorption mass spectrometry has been illustrated. For this study, a natural (radioactive) X-ray source was employed. The presence of molecular ion peaks in the LD-XRI spectra, which were not present in the LDI spectra, indicates that LD-XRI has the characteristics of a soft ionization source; however, the ionization mechanism is not clear.

Acknowledgements

References

[1] R.E. Honig and J.R. Woolston, Appl. Phys. Lett., 2 (1963) 138-139.
[2] M. Karas, D. Bachmann, U. Bahr and F. Hillenkamp, Int. J. Mass Spectrom. Ion Processes, 78 (1987) 53-68.
[3] R.B. Van Breemen, M. Snow and R.J. Cotter, Int. J. Mass Spectrom. Ion Phys., 49 (1983) 35-50.
[4] R.J. Cotter, Anal. Chem., 52 (1982) 1767.
[5] A. Vertes, G. Irinyi and R. Gijbels, Anal. Chem., 65 (1993) 2389-2893.
[6] U. Boesl, J. Grotemeyer, K. Walter and E. W. Schlag, Anal. Instrum., 16 (1987) 151-171.
[7] J.R. Appling and D.D. Bland, Talanta, 39 (1992) 883-886.
[8] N. Winograd, J.P. Baxter and F.M. Kimock, Chem. Phys. Lett., 88 (1982) 581-584.
[9] D.M. Lubman, Anal. Chem., 59 (1987) 31A-40A.
[10] M. Simon, M. Lavollee, P. Morin and I. Nenner, J. Phys. Chem., 99 (1995) 1733-1740.
[11] U. Boesl, J. Grotemeyer, K. Muller-Dethlefs, H.J. Neusser, H.L. Selzle and E.W. Schlag, Int. J. Mass Spectrom. Ion Processes, 118/119 (1992) 191-220.
[12] K. Ueda, E. Shigemasa, Y. Sato, S. Nagaoka, I. Koyano, A. Yagishita and T. Hayaishi, Chem. Phys. Lett., 166 (1990) 391-396.
[13] W.D. Ehmann and D.E. Vance, Radiochemistry and Nuclear Methods of Analysis, John Wiley and Sons, New York, 1991, pp. 207-220.
[14] W.M.J. Veigele, At. Data, 5 (1973) 67.